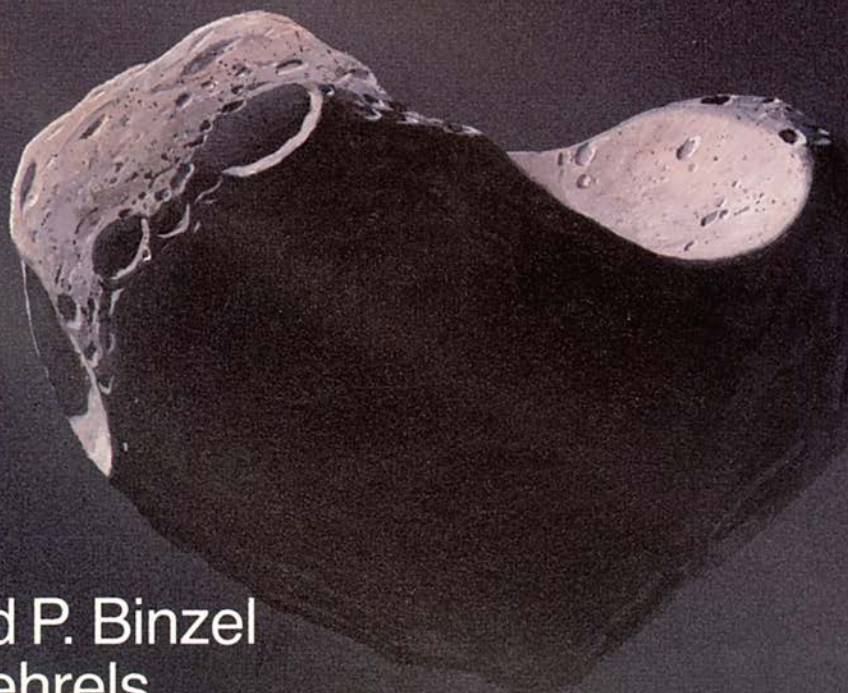# ASTEROIDS II

Richard P. Binzel
Tom Gehrels
Mildred Shapley Matthews

Editors

SPACE SCIENCE SERIES

Tom Gehrels, General Editor

Planets, Stars and Nebulae, Studied with Photopolarimetry
Tom Gehrels, editor, 1974, 1133 pages
Jupiter
Tom Gehrels, editor, 1976, 1254 pages
Planetary Satellites
Joseph A. Burns, editor, 1977, 598 pages
Protostars and Planets
Tom Gehrels, editor, 1978, 756 pages
Asteroids
Tom Gehrels, editor, 1979, 1181 pages
Comets
Laurel L. Wilkening, editor, 1982, 766 pages
Satellites of Jupiter
David Morrison, editor, 1982, 972 pages
Venus
D. M. Hunten, L. Colin, T. M. Donahue, and V. I. Moroz,
editors, 1983, 1143 pages
Saturn
Tom Gehrels and Mildred S. Matthews,
editors, 1984, 968 pages
Planetary Rings
Richard Greenberg and André Brahic,
editors, 1984, 784 pages
Protostars & Planets II
David C. Black and Mildred S. Matthews,
editors, 1985, 1293 pages
Satellites
Joseph A. Burns and Mildred S. Matthews,
editors, 1986, 1021 pages
The Galaxy and the Solar System
Roman Smoluchowski, John N. Bahcall, and Mildred S. Matthews,
editors, 1986, 485 pages
Meteorites and the Early Solar System
John F. Kerridge and Mildred S. Matthews,
editors, 1988, 1269 pages
Mercury
Faith Vilas, Clark R. Chapman, and Mildred S. Matthews,
editors, 1988, 794 pages
Origin and Evolution of Planetary and Satellite Atmospheres
S. K. Atreya, J. B. Pollack and M. S. Matthews,
editors, 1989, 881 pages
Asteroids II
Richard P. Binzel, Tom Gehrels, and Mildred S. Matthews,
editors, 1989, 1258 pages

ASTEROIDS II

ASTEROIDS II

Richard P. Binzel
Tom Gehrels
Mildred Shapley Matthews

Editors

With 100 collaborating authors

THE UNIVERSITY OF ARIZONA PRESS
TUCSON

About the cover:

A small Apollo asteroid approaches within 0.01 A.U. of the Earth-Moon system. Its extremely irregular shape, and the highlights of sunlight on craters and slopes, hint at the complexity of its rotational lightcurve. The asteroid is silhouetted against the inner zodiacal light, and is only 15° from the Sun. The Earth, Moon and Venus all appear in the background, with the Earth subtending about 0°.5 from 0.01 AU. This "telephoto" view has an angular height of 20°. Painting by William K. Hartmann.

Back cover: Plane view of the positions of approximately 5059 asteroids on 8 March 1988 15:30 UT, the starting date and time of the Asteroids II conference. Circles and tick marks represent the orbits and positions of the major planets Mercury through Jupiter. Aten, Apollo and Amor asteroids are seen in the inner solar system. In the main belt, orbital eccentricities tend to smear out the Kirkwood gaps, making the 3:1 and 2:1 gaps barely discernible. At Jupiter's orbit, the preceding and following Trojan clouds are clearly evident. (Figure courtesy of L. McFadden, J. Bytof and D. Tholen.)

CONTENTS

Part V—SPACE STUDIES

Part VI—TABULATION

COLLABORATING AUTHORS

PREFACE

The whole is greater than the sum of its parts. This philosophical, rather than mathematical, expression describes what we have tried to accomplish in bringing together a large number of authors to prepare a new source book describing our knowledge about the asteroids. During the week of March 8–11, 1988 over 160 scientists from 14 countries gathered in Tucson for the Asteroids II conference. In this setting, amidst invited reviews and contributed presentations on current research, teams of authors having a wide variety of backgrounds and viewpoints began the work of compiling the chapters for this book and papers for the April 1989 special Asteroids issue of the journal *Icarus*. This process in itself has led to a new level of understanding as authors worked together over several months to establish presentations of what is known and unknown throughout the broad field of asteroid science. The collective magnitude of this task cannot be underestimated. We are indebted to the authors and referees for their efforts to produce the parts that form this book as a whole.

Asteroids II is not a sequel, *per se,* to the 1979 book *Asteroids.* It is a fresh new treatment intended to stand on its own as a complete description of the current understanding of the field. We are proud of the large international collaboration in this volume, a sign of an active and growing discipline. All authors were given the charge to write their chapters at the graduate-student level and to keep in mind that their readers would most likely be students and researchers who are not experts in their specialty. The subjects in each chapter are concisely introduced and references are given to additional background material when necessary. The reviews contain extensive references to the original literature and cross-references to other chapters. For each chapter, authors were also asked to highlight problems and uncertainties for which future work might lead to significant advances. It is these areas that will probably be of most interest to students and outside researchers. The styles and presentation levels vary somewhat from chapter to chapter, as can be expected for a volume with such a large number of contributors. Given infinite time and patience among the authors and editors, additional iterations could have produced a highly homogeneous (but less interesting) final product.

This book is structured in the order in which a new reader might approach the field, beginning with an introduction to the asteroids, a description of exploration techniques, details on their physical properties, discussions of

their origin and evolution, an examination of their interrelations with meteorites and comets followed by an attempt at a "Big Picture" framework for our current knowledge. A look to the future is given in the section on space studies. The tabulation in Part VI is intended to serve as a useful resource for students and researchers alike. An extensive glossary has been compiled which reflects the growing interdisciplinary nature of asteroid science between astronomers, meteoriticists and geologists. New students will want to examine the glossary and refer to it frequently.

Asteroids II appears at a time when the field is at a major crossroad. Barring misfortune, the first spacecraft encounter with an asteroid will occur in the early 1990s. How will the paradigms presented here stand up in the wake of *in situ* observations and what new questions will arise to challenge asteroid researchers over the next decade? It is hoped that this book will serve as a foundation for stimulating continued growth in asteroid research as we approach January 1, 2001, the 200th anniversary of the first asteroid's discovery.

It is a pleasure to thank Melanie Magisos for her tireless efforts and invaluable assistance in producing this book.

<div style="text-align: right">

Richard P. Binzel
Tom Gehrels
Mildred Shapley Matthews

</div>

PART I
Introduction

AN OVERVIEW OF THE ASTEROIDS

RICHARD P. BINZEL
Massachusetts Institute of Technology

An introduction and overview of the field of asteroid science is presented, high-lighting the accomplishments of the 1980s. The development and application of many observational techniques and data from the Infrared Astronomical Satellite have greatly increased our knowledge of asteroid physical properties. New scenarios for understanding the chemical diversity and dynamical structure of the asteroids have emerged. New insights have been gained toward understanding their origin and interrelations with meteorites and comets. Suggestions and speculations are offered on future research directions. Extensive references to other chapters are provided to serve as a "road map" to this book.

I. INTRODUCTION

Why study the asteroids? Asteroids (and comets) represent the only existing remnant planetesimals dating back to the formation of the solar system. The asteroids occupy the transition region between the rocky terrestrial planets and the outer gas giants. It is generally believed that perturbations by Jupiter led to the failure of planet formation in that region. Although asteroids have probably undergone substantial collisional evolution since their formation, most have experienced relatively little geological, thermal or orbital evolution. Thus the asteroids provide us with a blueprint to the conditions in the early solar system. The collisional disruption of those asteroids that have experienced significant thermal evolution gives us a rich diversity of chemical compositions and provides us with a means to study the interiors of differentiated bodies.

The asteroids are also of interest because they are the source for most meteorites; the study of asteroids, meteorites and solar system formation are

all closely intertwined. Dynamical evolution of some asteroid orbits can lead
them to trajectories that intersect the orbits of the terrestrial planets, thus
leading to the delivery of meteorite-sized bodies as well as larger ones that
result in major cratering events. A likely extraterrestrial signature in the
Cretaceous-Tertiary boundary (Alvarez et al. 1980) and their potential use as
space resources (O'Leary 1977) has heightened interest in asteroids through-
out many disciplines.

We are now approaching the bicentennial anniversary of Piazzi's discov-
ery of Ceres in 1801 and William Herschel's naming of these bodies as "as-
teroids" in 1802. For a brief history of the field, the reader is referred to the
chronology in Gehrels (1979*b*). Cunningham (1988*a,b*) gives some additional
historical insights to the previously little-known efforts of Franz von Zach and
a group of astronomers who called themselves the "celestial police" in search-
ing for the missing planet between Mars and Jupiter during the late eighteenth
century.

The beginning of the modern era of asteroid research is usually linked to
the *Physical Studies of Minor Planets* conference held in Tucson in March
1971 and the resulting publication (Gehrels 1971). Figure 1 shows the rapid
growth of the field during the 1970s. With the *Asteroids* meeting and book
(Gehrels 1979*a*), the activity of asteroid research during the 1980s has re-
mained at a high level. The large attendance and broad international participa-
tion at the *Asteroids II* conference in March 1988 shows great potential for
continued growth in the 1990s, especially with the prospects for Hubble
Space Telescope and spacecraft flyby observations of asteroids.
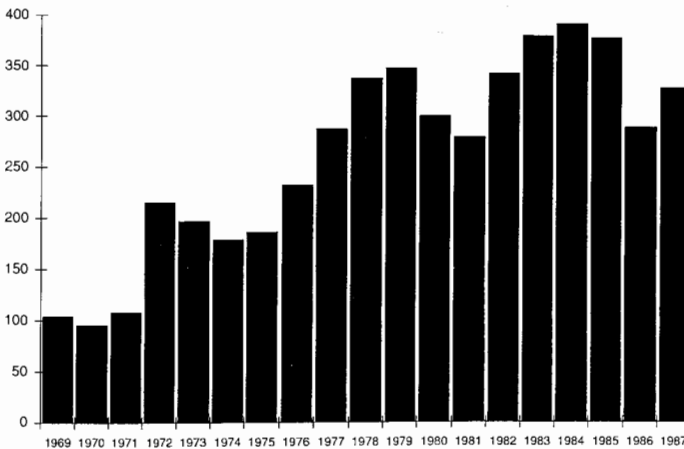
Fig. 1. Annual number of asteroid publications vs time showing the rapid growth in the field
during the 1970s and 1980s. Data are from Cunningham (personal communication, 1989)
based on *Astronomy and Astrophysics Abstracts* and other literature searches.

This chapter attempts to provide a brief introductory overview to the field of asteroid science, concentrating on the highlights of the 1980s. A second goal is to serve as a road map to the other chapters within this book, wherein more extensive background and references to the original literature can be found. The final section of this chapter gives some suggestions for future research and offers some speculations on future directions. For a popular level introduction to the asteroids (and asteroid scientists), the book by Cunningham (1988b) is recommended. A synthesis of current dynamical, mineralogical and structural data into a coherent paradigm is presented in the chapter by Bell et al.

II. A SURVEY OF THE ASTEROIDS

The number of asteroids, also called minor planets, that have received permanent designations (i.e., numbers) has nearly doubled during the 1980s owing largely to programs conducted at Lowell Observatory and the Crimean Astrophysical Observatory. (See the chapter by Bowell, Chernykh and Marsden. Names and discovery circumstances are given by Pilcher in Part VI of this book.) Figure 2 shows the heliocentric distribution of semimajor axes for nearly 4000 numbered asteroids. Most are located in the main belt between 2.1 and 3.3 AU from the Sun. A few have greater or lesser semimajor axes or have large orbital eccentricities such that they are not contained within this region.

The innermost asteroids are called the Atens (groups of asteroids are often named after their first discovered member, in this case 2062 Aten), having semimajor axes inside the Earth's orbit. Apollo asteroids have orbits that cross the Earth's; Amor asteroid orbits have perihelia between the Earth's orbit and 1.3 AU. Many Apollo and Amor asteroids have semimajor axes that fall within the main belt (and correspondingly large orbital eccentricities), so the regions labeled in Fig. 2 do not fully denote these populations. Collectively, the Aten-Apollo-Amor objects are often referred to as AAAO, near-Earth asteroids, or planet crossing asteroids. Dedicated AAAO photographic surveys, most notably work on Palomar Mountain, California by Helin and associates and by Eugene and Carolyn Shoemaker, have more than doubled the number of discoveries in the 1980s to a total of over 120 objects. A new technique using charge-coupled devices to scan for asteroids and comets has been developed by Gehrels (1981; McMillan et al. 1986) and associates at the "Spacewatch Telescope" in Arizona. This instrument uses charge-coupled devices both in the standard "stare mode" (chapter by French and Binzel) and also in a "scanning mode" whereby the charges are transferred at the same rate as the telescope scans the sky.

Dynamical lifetimes for the planet crossing asteroids are short ($\sim 10^7$ yr) compared to the age of the solar system due to gravitational interactions leading to their ejection from the solar system or to planetary impacts. What is the
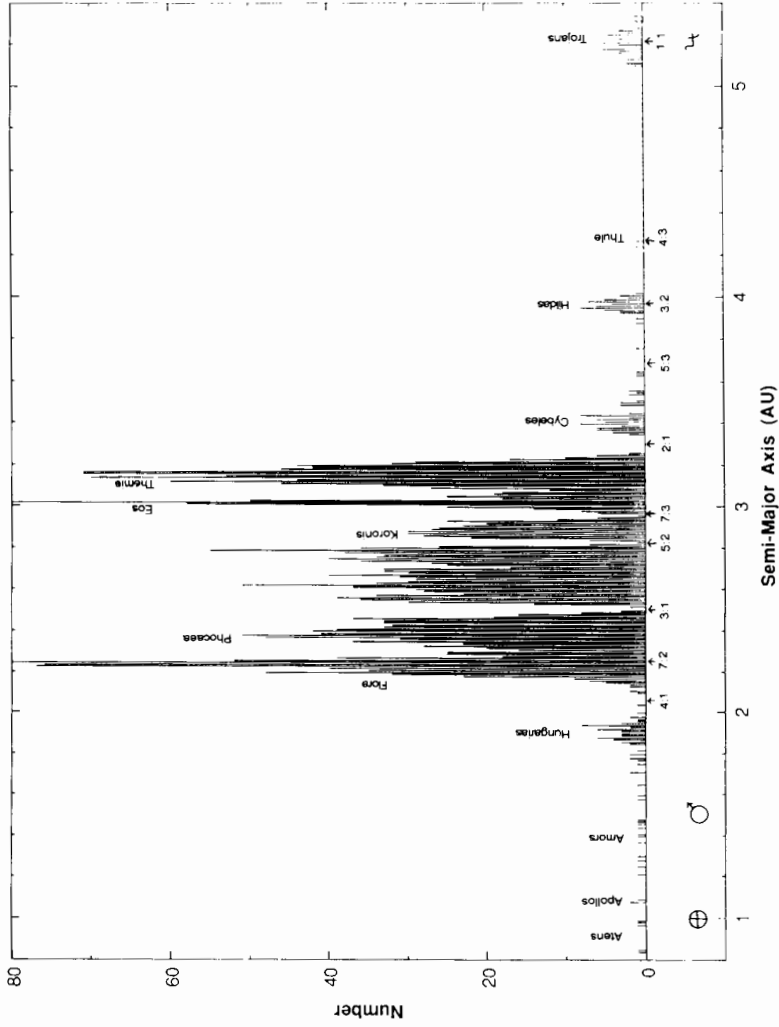
Fig. 2. Heliocentric distribution of orbital semimajor axes for nearly 4000 numbered asteroids. Commonly referred to regions and the major Jovian resonances are labeled. Other frequently referred to zones (such as those defined by Zellner et al. 1985a) and their eccentricity and inclination boundaries are listed in Table I of the chapter by Gradie et al. Compare this diagram with that on the back cover (which depicts the actual asteroid positions at a given moment in time) to see how orbital eccentricities tend to "smear" this distribution.

source of resupply? To address this question we turn our attention to the main belt. Figure 2 clearly shows a nonuniform distribution with distinct breaks called the "Kirkwood gaps," named after Daniel Kirkwood who in 1867 noted depletions at the positions of resonances with Jupiter. (The mean orbital motion of an asteroid located at a resonance is an exact integer ratio of Jupiter's; e.g., at the 3 : 1 resonance an asteroid completes exactly three revolutions for every one of Jupiter.) Although the correspondence of the resonances and the gaps have long indicted Jupiter, a physical explanation for clearing gaps at some resonances (e.g., at 3 : 1 and 2 : 1) while leaving concentrations at others (e.g., 3 : 2) has eluded astronomers for over a century.

A solution to this problem and the identification of a significant source region for the near-Earth asteroids now appears to be in hand thanks to recent work by Wisdom. Wisdom (1983, 1987; see the chapter by Froeschle and Greenberg) has shown that chaotic orbit zones occur at the 3 : 1 and 2 : 1 resonances while quasi-periodic solutions occur at the 3 : 2 resonance. Quasi-periodic orbits allow concentrations to occur while chaotic orbits lead to increased eccentricities, allowing asteroids to cross the orbit of Mars where they are removed by gravitational interactions or collisions. Wisdom (1985) and Wetherill (1985) showed that chaotic dynamics can serve as a transportation route to resupply meteorites and asteroids to the inner solar system from the central main belt. While the transport methods now appear to be established, there is less agreement on how processes such as asteroid collisions inject bodies into resonance zones for delivery. (See the chapter by Greenberg and Nolan and the discussion following it.) This represents an area open for continued active research.

The physical properties of AAAO (described in the chapter by McFadden et al.) show a wide diversity comparable to that seen across the entire main belt, consistent with their being supplied from more than one resonance region. Wetherill (1988) models the AAAO population as being supplied from the 3 : 1 resonance in the central main belt and the ν_6 secular resonance (see the chapter by Scholl et al.) in the inner belt. Wetherill (1988) also proposes that an additional significant source for near-Earth asteroids may be extinct cometary nuclei. The probable evolution of comets into asteroids is discussed in the chapter by Weissman et al.

Significant clumpings of asteroids in orbital element space were first noted by K. Hirayama in 1918 who called them "families" because he believed they are the result of the disruption of large parent bodies. Families are identified using statistical analyses of so-called proper orbital elements, i.e., orbital elements that are independent of planetary perturbations. In a series of papers spanning more than a decade, Hirayama identified a number of families. Contemporary researchers have continued the process of family identifications, and those by Williams (1979; also see his tabulation in Part VI) have been widely adopted as a standard over the last decade. However, not all researchers have always agreed on family memberships because there are a

variety of techniques for proper element computation and family identifica-
tion, as reviewed in the chapter by Valsecchi et al. Figure 1 of their chapter
shows clearly the clustering of three of the original Hirayama families:
Themis, Eos and Koronis. Other groupings are apparent (in their figure and in
Fig. 2 here) that are not considered families. Instead these are usually called
"groups" and they represent regions that are isolated by mean motion and/or
secular resonances. Examples are the Hungarias, Phocaeas, Cybeles, Hildas
and Trojans. The Flora region at 2.2 AU may be composed of several small
dynamical families.

   It is widely believed that families result from the breakup of larger parent
asteroids by catastrophic collisions. However, it remains an open question as
to whether all of the clusters that have been identified dynamically as families
are "real" in the sense that they formed in this way. Physical observations of
asteroids within many purported families have shown that only a few of the
most populous ones (e.g., Themis, Eos, Koronis) have members whose com-
positions make cosmochemical sense in trying to reconstruct a parent body
from the pieces. These unresolved problems in the areas of family identifica-
tion, origin and evolution are discussed in the chapter by Chapman et al.

   In the 1980s there has been greatly increased interest in the asteroids
located beyond the main belt: the Cybeles located between the 2:1 and 5:3
resonances, the Hildas at the 3:2 resonance, 279 Thule at the 4:3 resonance
with Jupiter, the Trojans (located at the 1:1 resonance, occupying two
swarms librating about the L4 and L5 Lagrangian points 60 deg preceding and
following Jupiter), 944 Hidalgo which is likely to be an extinct comet, and
2060 Chiron which may be an active comet. The count of numbered Trojans
more than doubled during the 1980s (to a total of > 50 objects) with signifi-
cant improvements in their orbits so that some structure as well as the popula-
tions of the L4 and L5 clouds can now be estimated (see the chapter by
Shoemaker et al.). Evidence for dynamical groupings suggests that the L_4
cloud may contain families produced by collisions. The dynamics of the out-
ermost asteroids are discussed in Nobili's chapter.

   Recent physical observations of distant asteroids are summarized in the
chapter by French et al. It has been found that the Trojans (and perhaps Hil-
das) have more elongated shapes than their main belt counterparts which may
be due to differences in their formation or collisional evolution. Some of the
most exciting news in 1988 were reports of Chiron's observed brightening by
0.6 mag, possibly due to outbursts of volatile material on its surface. Chiron
(semimajor axis = 13.7 AU) is heading toward perihelion (8.5 AU) in 1997
and is likely to be intensively scrutinized by observers over the next few
years. The first detection of what may be a coma was reported by Meech and
Belton (1989).

   Although the orbital structure of the asteroids has been known for most
of this century, a clear picture of the compositional structure has emerged only
recently. Bobrovnikoff (1929) was the first to note different spectral colors
between Ceres and Vesta but more diagnostic multifilter spectrophotometric

techniques were not extensively applied to the asteroids until the 1970s. Two broad groups were recognized: neutrally colored low-albedo objects were labeled "C types" and more reddish objects with moderate albedos were labeled "S types." The letters were chosen as mnemonics for spectral similarities seen with carbonaceous and stony meteorites (although no specific mineralogical link was implied). By 1979 two other major classes, E (enstatite) and M (metallic) were added and U denoted unusual or unclassifiable objects. Since that time we have seen a boom in asteroid classifications from spectrophotometry starting with the Eight-Color Asteroid Survey (ECAS) conducted at the University of Arizona (Zellner et al. 1985b) and the taxonomic system derived by one of the survey's key workers (Tholen 1984). Tholen's taxonomy employs an alphabet soup of types A, B, C, D, E, F, G, M, P, Q, R, S, T, V which are described in the chapter by Tholen and Barucci (see their Table I and Fig. 1 for a quick synopsis). Additional taxonomies have been developed utilizing ECAS and results from the Infrared Astronomical Satellite. These systems are described and compared in the chapters by Tholen and Barucci and by Tedesco et al. (See also the taxonomic tabulations in Part VI.)

Since the earliest development of taxonomies, it was also recognized that there was some correlation with heliocentric distance. C types appear more prevalent in the outer main belt while S types are more common in the inner belt. Using preliminary ECAS and radiometry data, a landmark paper by Gradie and Tedesco (1982) showed distinct heliocentric distributions for various compositional classes. These distributions are described in the chapter by Gradie et al. and their Fig. 1 shows how the distributions of E, R, S, M and C types, respectively, reach their peaks with increasing heliocentric distances and how P and D types dominate beyond the main belt. It is possible that this distribution may reflect a varying degree of thermal processing across the asteroid belt with the innermost objects being the most processed and the outermost ones being the most primitive (unprocessed). Various thermal processing mechanisms have been proposed for the asteroids (see the chapter by Scott et al.) with the main contenders being radioactive heating by ^{26}Al and electrical induction heating driven by a T-Tauri type solar wind from the pre-main-sequence Sun. Current views tend to favor electrical induction heating. This mechanism is also consistent with the thermal evolution paradigm discussed in the chapter by Bell et al. Bell has proposed three "superclasses" of asteroids: igneous, metamorphic and primitive. Asteroids are placed in one of these classes based solely on their mineralogical interpretations (chapter by Gaffey et al.; see Sec. IV below). Figure 1 of Bell et al. shows a consistent heliocentric distribution with the igneous objects dominant in the inner belt and the primitive (unheated) bodies dominant in the outer belt.

III. OBSERVATIONS OF ASTEROIDS

The Infrared Astronomical Satellite (IRAS) was launched into orbit in 1983 and its nearly year-long mission provided a bonanza of data on asteroid

albedos and diameters (see the tabulation by Tedesco in Part VI). Nearly 2000 numbered and many more unnumbered asteroids were measured as part of the IRAS Asteroid and Comet Survey. This survey and the resulting IRAS Asteroid and Comet Catalog are described in the chapter by Matson et al. One of the results of this survey (see the chapters by Veeder et al. and Tedesco et al.) is that the largest asteroids show a different albedo distribution than the smallest ones. Do these smaller asteroids represent fragments of larger bodies and can the albedo difference be explained if they are composed of material from asteroid interiors?

Some important new discoveries in the field of asteroid science were made by IRAS. First was that of dust bands within the asteroid belt, which are likely associated with asteroid collisions and may be the source of zodiacal dust. As discussed in the chapter by Sykes et al., there is an apparent association of the dust bands with some of the major Hirayama families, although random collisions may also be involved. A second IRAS discovery was of the Apollo asteroid 1983 TB (subsequently numbered and named 3200 Phaethon), which Whipple (1983) noted lies in the orbit of the Geminid meteor stream. As discussed in the chapter by Weissman et al., this object may be an extinct comet.

The 1980s have seen many groundbased exploration techniques come of age, most notably radar (see the chapter by Ostro). This technique can yield diagnostic information on asteroid sizes, shapes, spin vectors and surface characteristics. Among the most important radar results has been the determination of very high metal contents for the M-type asteroids 16 Psyche and 1986 DA, the latter being an Amor and a possible source for some iron meteorites. Radar observations currently can only be made of inner belt and near-Earth asteroids, although a proposed upgrade for Arecibo could make the entire belt available. Radar ranging can also yield precise astrometric measurements and echoes from Mars (to measure orbit perturbations) have been used by Standish (1989) to determine asteroid masses (see also the chapter by Hoffmann). This may prove to be an increasingly important and widely utilized astrometric technique in the future.

As asteroids rotate, their changing surface areas cause measurable brightness variations and the resulting lightcurves can be used to study their shapes and spin-vector orientations. Notwithstanding these being well-established techniques, many refinements are still being made to lightcurve observing methods and the chapter by Harris and Lupishko describes the current state of the art. Pole determination techniques have come of age since the pioneering work of Taylor, and significant progress has been made in the modeling of asteroid shapes (see the chapter by Magnusson et al. and the tabulation by Magnusson in Part VI). Systematic lightcurve studies over a range of aspect angles, such as in the work of Weidenschilling et al. (1987), are providing an important resource for continuing progress in these modeling efforts.

Work by Drummond and Hege (see their chapter) has significantly advanced speckle interferometry techniques for shape and pole determinations and image reconstructions. Observations of stellar occultations still remain the only direct Earth-based means of measuring an asteroid's profile in detail and great improvements have been made in accurately predicting locations where these events can be observed (see the chapter by Millis and Dunham). Their Table I lists 40 successfully observed occultation events, where three-fourths have been obtained since 1979. For every one successful observation there are probably more than an equal number of unsuccessful attempts where despite careful planning and often lengthy travel to the location of the shadow path, bad weather prevails. Thus their table is a tribute to a decade of dedicated effort.

Using a comparison between observed intensities at visible and thermal-infrared wavelengths, radiometry is the most widely applied method for asteroid diameter and albedo determinations. (This remains true even if IRAS measurements are excluded.) As described in the chapter by Lebofsky and Spencer, radiometric diameter determinations are, however, model dependent and size determinations from occultations have been extensively used for calibrations. Considerable refinements have been made to the various models to achieve more accurate physical representations. The increase in radiometric measurements, combined with the advances in spectrophotometry described in Sec. II, have led to the growth in the number of asteroids for which taxonomic classifications are now available.

An additional technique as applied to asteroids that has grown from infancy in the 1980s is radio observations, which can yield information on the depths and structures of surface materials. As of 1979, only two asteroids had been measured at a single wavelength. Webster and Johnston (see their chapter) have recently succeeded in detecting six additional asteroids over a range of five wavelengths between 1.3 to 200 mm using the Very Large Array (VLA) radio telescope. They find the surfaces to be composed of finely divided dust with a range of depths from 1 to 8 cm. Many uncertainties remain in understanding the regolith formation mechanisms as discussed in the chapter by McKay et al.

One opportunity for detailed study of the regolith of a small and perhaps asteroid-like body was unrealized with the unfortunate loss of contact with both Phobos spacecraft in 1989. This was a serious setback to many aspects of our studies of small bodies, particularly the detailed study of their surfaces and the data that can only be obtained from low orbit and surface sampling. Our best knowledge of Phobos and Deimos remains the data obtained on them by the Viking spacecraft, as summarized by Veverka and Thomas (1979).

Related to our understanding of surfaces is the manner in which an asteroid's brightness varies with changing solar phase angle, independent of rotational variations. The most dramatic effect is a nonlinear surge in brightness at low phase angles that is referred to as the "opposition effect." Dedi-

cated observational efforts by Harris and Young at Table Mountain Observatory and others elsewhere (chapter by Harris and Lupishko) have substantially increased the number of phase-curve observations available for study. Interpretation of phase curves has been the subject of much debate over recent years; two models that succeed in fitting the observed behavior are presented in the chapter by Bowell et al. Although these models represent significant progress, it is difficult to constrain many of their parameters for inferring regolith properties. These constraints on photometric analysis are discussed in the chapter by Helfenstein and Veverka. The two photometric models described in the chapter by Bowell et al. have as their major difference the treatment of surface roughness and its corresponding effect on multiple scattering. Additional theoretical and laboratory investigations may be able to distinguish this effect. Photopolarimetry of asteroids (see the chapter by Dollfus et al.) is also diagnostic of their surface properties; unfortunately there have been relatively few recent observations.

The improved characterization of asteroid phase curves has had an important consequence for observers. A new two-parameter magnitude system for the prediction and reduction of asteroid magnitudes was adopted by the IAU in 1985. A description of this new system may be found as an appendix to the chapter by Bowell et al.

Perhaps the most notable observation that was *not* made during the last decade was the indisputable detection of an asteroid satellite, despite concentrated efforts to confirm such bodies through stellar occultation observations (chapter by Millis and Dunham). Suggestive evidence for such bodies has continued to accumulate: extremely slow rotations for asteroids 288 Glauke (Harris 1983) and 1220 Crocus (Binzel 1985) possibly resulting from tidally despun binaries; bifurcated radar echoes from 216 Kleopatra (chapter by Ostro); and an analysis of the occurrence of double craters (Hut and Weissman 1985). However, as pointed out in the chapter by Weidenschilling et al., all evidence for satellites of asteroids remains indirect or inconclusive. Their dynamical modeling of satellite collisional formation and orbital evolution argues that relatively few asteroids are likely to have satellites.

IV. ORIGIN, EVOLUTION AND INTERRELATIONS

The origin of the asteroids is intimately tied to the formation of the solar system as a whole. Slow but steady progress in cosmogony has been made, and various scenarios are reviewed in the chapter by Wetherill. Particular progress has been made in identifying the conditions under which "runaway growth" can occur, a process in which the rapid growth of a few large bodies dominates accretion zones. In this scenario, rapid growth of Jupiter and Saturn and their resulting resonances could have pumped up relative velocities in the asteroid zone sufficiently to prevent further accretion into a single planet. Some additional mechanism(s), such as the scattering of large planetesimals

by Jupiter and their passing through the asteroid zone, is needed to remove much of the mass from the asteroid belt and to boost the average relative velocities to the current value near 5 km s^{-1}. The question of how a large fraction of the mass in the asteroid zone could be depleted without mixing the compositional gradient (discussed in the above Sec. II) is examined in the chapter by Ruzmaikina et al.

Meteorites represent direct samples of materials from the asteroid belt (the dynamics of which are outlined in Sec. II above) and their compositions can be used to infer the cosmochemistry of the solar nebula. A complete interpretation, however, requires knowledge of the evolutionary processes that occurred in the asteroid belt, including heating, melting, aqueous alteration and impact processing as described in the chapter by Scott et al. Thus the study of geology of asteroids and the study of meteorites are closely related fields. For a broad overview from the perspective of meteoritics, the treatment by Wetherill and Chapman (1988) is recommended.

No specific meteorite has as yet been linked to a specific asteroid despite modest increases in the number of high resolution spectra of asteroids and a great expansion in our meteorite collections resulting from increased field work in Antarctica. Based on laboratory studies, some mineralogical interpretations of asteroid spectra can be made and these are described in the chapter by Gaffey et al. Their Table III lists proposed mineralogical correlations between asteroid taxonomic types as well as possible meteorite analogs. Identifying meteorite parent bodies among the asteroids is also the topic of the chapter by Lipschutz et al. One of the most puzzling (and frustrating) aspects in comparing the observed samples of asteroids and meteorites is that they appear to represent partially mismatched sets. The meteorites are an unrepresentative sample of the interpreted mineralogy for the asteroids and in fact the most common meteorite type, the ordinary chondrites, may have no observed analog in the main belt. These chapters discuss the debate as to whether the S-type asteroids are the parent bodies of the ordinary chondrites. Qualitatively they have the same mineralogy although quantitatively the interpreted proportions of the constituents differ. Observationally the S-types appear more closely related to the stony-iron meteorites. One object, 1862 Apollo (taxonomic type Q), appears to be mineralogically consistent with the ordinary chondrites although this single near-Earth asteroid is much too small to be a sufficient source.

What is the resolution of the ordinary chondrite paradox? Various possibilities are discussed in these chapters, including the prospect that our mineralogical interpretations are completely wrong owing to some not understood regolith altering process on main belt asteroids or some altering process suffered by meteorites upon entering the Earth's atmosphere. An alternative possibility arises from the paradigm described in the chapter by Bell et al. If the post-accretionary heating mechanism had a size cutoff, below which objects remained unheated, the ordinary chondrite parent bodies in the main belt may

have simply escaped spectroscopic detection to date because of their small sizes and faint apparent magnitudes. The chapter by Lipschutz et al., however, points out that there is significant meteoritical evidence that implies large ($\sim$100 km) sizes for the ordinary chondrite parent bodies.

Collisions are another evolutionary process that has occurred among the asteroids since the time when accretion was halted and relative velocities were increased. An understanding of asteroid collisional evolution is therefore another important ingredient in deciphering the primordial structure of the asteroid belt. The current state of collisional modeling is described in the chapter by Davis et al. It is estimated that since the time when relative velocities were pumped up, the total asteroidal mass has decreased by a factor of 3 to 5. Many large asteroids may have suffered shattering collisions and are now held together only by their self-gravity. The expected degree of collisional evolution raises a paradox. If the M-class asteroids (like 16 Psyche) represent the metallic cores of differentiated parent bodies that have been disrupted, then there is an apparent shortage of olivine mantle material (which should have been stripped from around the core) observed among the asteroids (A-class objects). Perhaps comminution of these bodies also places them below the current observational size cutoff? However, as pointed out in the chapter by Davis et al., if such a large degree of collisional evolution has occurred, then it is difficult to understand how Vesta could have remained unshattered and preserved its basaltic crust.

Since collisions involve an exchange of rotational angular momentum, important constraints on collisional evolution models are derived from statistics on asteroid rotation rates and shapes obtained from asteroid lightcurves (see the chapter by Binzel et al. and the tabulation by Lagerkvist et al. in Part VI). Observed distributions of asteroid rotation rates show distinct differences above and below diameters of 125 km. A possible explanation is that this size represents a transition between larger primordial bodies and their collision fragments. Laboratory collision experiments (see the chapter by Fujiwara et al.) and the Hirayama families (chapter by Chapman et al.) provide other constraints on asteroid collisional evolution. While the laboratory results on the distributions of shapes of fragments from catastrophic disruption events are in generally good agreement with the observed shapes of asteroids, fragmental velocity and size distributions are not. In addition, scaling the impact strengths for laboratory targets upward by 7 orders of magnitude to asteroid-sized bodies has not yet yielded results consistent with the major families.

V. SUMMARY AND FUTURE DIRECTIONS

Significant progress has been made in established areas and many new lines of research that were only emerging (or even nonexistent) before the 1980s have seen dramatic advancements. What is in store for the 1990s? This section takes a speculative look at possible future directions and lists some of the outstanding research problems.

Astrometric surveys are likely to push to fainter magnitudes resulting in the continued rapid growth in new asteroid discoveries and permanent designations. New faint surveys must be careful to make multiple observations over several nights to establish reliable preliminary orbits for these difficult to recover objects. Charge-coupled devices (CCDs) will continue to emerge in a variety of applications over the next decade, particularly in astrometry, spectroscopy and photometry (see the chapter by French and Binzel). Although photographic plates may remain the old-fashioned workhorse for astrometry in the 1990s, CCDs will become increasingly dominant. Larger CCDs in the telescope focal plane will allow survey and astrometric programs such as Spacewatch to increase their effective sky coverage and discovery rates. A Tektronix 2048×2048 CCD has been put into use by the Spacewatch program in 1989. Although much progress has been made, technical problems remain in achieving real-time processing of such large data rates and this presents a challenge for astronomically minded computer scientists.

The giant leap forward in dynamics in identifying chaotic orbital zones as responsible for the Kirkwood gaps will open up many new areas of investigation. For example, the dynamics of the $2:1$ resonance remain to be completely described. Although chaotic dynamics provide an apparent delivery route for meteorites (and near-Earth asteroids), significant problems remain in reconciling their characteristics with the mineralogy interpreted from asteroid spectra. The problem of the ordinary chondrites remains an enigma. Will spectra of fainter and smaller asteroids reveal the parent bodies for these meteorites or will the resolution require new insights into dynamical or thermal alteration processes? Bell predicts that there will be size dependence to the composition of asteroids in the inner belt.

Much of the data from the IRAS Asteroid and Comet Survey remains an untapped resource. Searches for new asteroids need to be performed on the few deep scans with the goal of investigating the number density of small asteroids. Such studies will require careful consideration of bias corrections. Groundbased radiometry is needed to follow up some of the systematic trends in the IRAS data set and new spectrophotometry observations will allow taxonomic classifications to be made for many asteroids for which only the IRAS albedo is known. Further analysis of the IRAS dust bands is needed to investigate their origin and evolution and the identification of additional bands may broaden our understanding of this process.

Asteroid spectroscopy has the potential for significant growth in the next decade both in terms of improved resolution and pushing to fainter limits and smaller diameters through the use of CCD detectors. This may bring about solutions to the ordinary chondrite problem and to the case of the missing (A class) olivine mantle material. Improved spectral resolution, especially in the near infrared, will need corresponding laboratory work to yield enhanced diagnostic information on asteroid mineralogy. Increasing sophistication of spectral measurements may lead to the introduction of new taxonomic classes or may perhaps show clear subdivisions among existing classes, such as the S class.

Radar, radio and speckle observational techniques have undergone significant advancement in the 1980s largely through the efforts of individuals or small research groups. Much of the groundwork has now been laid and there is the potential to apply these techniques to many additional asteroids, especially if some of the proposed system improvements are made. Participation by larger teams or additional researchers are needed to realize this new potential.

Much work remains to be done in understanding the origin and evolution of the asteroids. Runaway growth models for planetary accretion show many promising aspects, but the factors allowing such growth for Jupiter while preventing it in the asteroid zone need to be more fully investigated. Mechanisms that pumped up relative velocities among the asteroids to their current state and removed much of the mass (while preserving a compositional gradient) are still not completely understood. New studies of the populations and physical properties of the outermost asteroids have yet to be fully incorporated into solar system formation models and further observations are needed to confirm the recent findings. Improved models are also essential for understanding the evolution of pre-main-sequence stars and the corresponding effects on planetary formation.

Continued effort is required for obtaining a complete understanding of asteroid collisional evolution and the origins of asteroid families. Models of coupled collision and spin evolution show promise and additional lightcurve observations (particularly of small asteroids) are needed for shape and rotation statistics to constrain these models. The scaling of laboratory collisions to asteroid sizes appears to be a challenging problem. Asteroid families have great value for constraining models if they indeed represent large natural collision experiments; additional observational (photometric and spectroscopic) data are needed to characterize specific families. Improved proper element determinations and studies of the time scales for the dispersion of proper element clusters are necessary to resolve some of the problems in identifying possible families. Researchers should take care to distinguish carefully between dynamical families—clusters of asteroids identified solely on the basis of proper elements: and "true" families—clusters of asteroids in orbital-element space for which physical observations are consistent with their having originated in a common parent body.

Physical studies of the innermost asteroids are likely to see continued advancement in the 1990s with one focus being on the possible link between asteroids and comets. Studies of the primitive outermost asteroids and particularly 2060 Chiron (with its probable volatile activity) as it approaches perihelion in 1997 will also be important in establishing an asteroid-comet connection. Increased interest in the near-Earth asteroids is also likely for characterizing their detailed mineralogy as a precursor to plans for utilizing them as space resources. Also as illustrated by the March 1989 close Earth approach of 1989 FC to within 0.0046 AU, their population and potential hazard must be more extensively evaluated.

The 1990s may be called the decade of space studies of asteroids. Observations with the Hubble Space Telescope could have a giant impact across a broad range of topics because of its potential to survey and spatially resolve many asteroids. (See the chapter by Zellner et al.) Will asteroids conform to the canonical view of being individual rocky/dusty bodies or will we find some accompanied by satellites or surrounded by debris clouds? Direct observations of asteroid shapes and spin-vector orientations will allow verification and refinement of existing groundbased techniques. The Space Telescope, however, will not supplant these methods since its utilization will be in high demand by all areas of astronomy and only a very limited amount of time is likely to be devoted to asteroids. Thus, systematic groundbased observing programs should continue and expand into the 1990s. Radiometry (and analysis of IRAS data) should continue to be the dominant method for diameter determinations. The planned launch of SIRTF in the late 1990s may open a new era in providing radiometric and infrared spectral data on the asteroids over a wide range of wavelengths.

The Hubble Space Telescope also may provide the first preliminary reconnaisance of asteroid surface geology, by mapping compositional units on the surfaces of the largest asteroids. Such mapping could greatly complement the tremendous results that can only be accomplished through spacecraft encounters (see the chapter by Veverka et al.), which will be necessarily limited to far fewer objects than can be surveyed by Space Telescope. During the 1990s we should at last achieve our first *in situ* measurements of an asteroid beginning with encounters by the Galileo spacecraft enroute to Jupiter. Such data may revolutionize our understanding of asteroid surface chemistry, geology, structure and morphology. Consequently, there may be a significant impact on our theories for asteroid origin and evolution.

Finally, and perhaps most importantly, there will be additional unexpected advances through new imaginative ideas and techniques. In a large part, these advancements and innovations will be brought about by new generations of students of asteroids.

REFERENCES

Alvarez, L. W., Alvarez, W., Asaro, F., and Michel, H. V. 1980. Extraterrestrial cause for the Cretaceous-Tertiary extinction. *Science* 208:1095–1108.
Binzel, R. P. 1985. Is 1220 Crocus a precessing binary asteroid? *Icarus* 63:99–108.
Bobrovnikoff, N. T. 1929. The spectra of minor planets. *Lick Obs. Bull.* 14:18–27.
Cunningham, C. J. 1988a. The baron and his celestial police. *Sky and Telescope* 75:271–272.
Cunningham, C. J. 1988b. *Introduction to Asteroids* (Richmond: Willmann-Bell).
Gehrels, T., ed. 1971. *Physical Studies of Minor Planets,*NASA SP-267.
Gehrels, T., ed. 1979a. *Asteroids* (Tucson: Univ. of Arizona Press).
Gehrels, T. 1979b. The asteroids: History, surveys, techniques, and future work. In *Asteroids,* ed. T. Gehrels (Tucson: Univ. of Arizona Press), pp. 3–24.

Gehrels, T. 1981. Faint comet searching. *Icarus* 47:518–522.

Gradie, J., and Tedesco, E. F. 1982. Compositional structure of the asteroid belt. *Science* 216:1405–1407.

Harris, A. W. 1983. Slowly rotating asteroids: Evidence for binary asteroids? *Bull. Amer. Astron. Soc.* 15:828 (abstract).

Hut, P., and Weissman, P. 1985. Double craters on the Earth and planets: Evidence for binary asteroids and comets? *Bull. Amer. Astron. Soc.* 17:690 (abstract).

McMillan, R. S., Scotti, J. V., Frecker, J. E., Gehrels, T., and Perry, M. L. 1986. Use of a scanning CCD to discriminate asteroid images moving in a field of stars. In *Instrumentation in Astronomy—VI, Proc. S.P.I.E.*, ed. D. L. Crawford, vol. 627, pp. 141–154.

Meech, K., and Belton, M. 1989. (2060) Chiron. *IAU Circ.* No. 4770.

O'Leary, B. 1977. Mining the Apollo and Amor asteroids. *Science* 197:363–366.

Standish, E. M. 1989. Mass determinations of asteroids. *Icarus,* in press.

Tholen, D. J. 1984. Asteroid Taxonomy from Cluster Analysis of Photometry. Ph.D. Thesis, Univ. of Arizona.

Veverka, J., and Thomas, P. 1979. Phobos and Deimos: A preview of what asteroids are like? In *Asteroids,* ed. T. Gehrels (Tucson: Univ. of Arizona Press), pp. 628–651.

Weidenschilling, S. J., Chapman, C. R., Davis, D. R., Greenberg, R., Levy, D. H., and Vail, S. 1987. Photometric geodesy of main-belt asteroids. I: Lightcurves of 26 large, rapid rotators. *Icarus* 70:191–245.

Wetherill, G. W. 1985. Asteroidal source of ordinary chondrites. *Meteoritics* 20:1–22.

Wetherill, G. W., and Chapman, C. R. 1988. Asteroids and meteorites. In *Meteorites and the Early Solar System,* eds. J. F. Kerridge and M. S. Matthews (Tucson: Univ. of Arizona Press), pp. 35–67.

Wetherill, G. W. 1988. Where do the Apollo objects come from? *Icarus* 76:1–18.

Whipple, F. L. 1983. 1983 TB. *IAU Circ.* No. 3881.

Williams, J. G. 1979. Proper elements and family memberships of the asteroids. In *Asteroids,* ed. T. Gehrels (Tucson: Univ. of Arizona Press), pp. 1040–1063.

Wisdom, J. 1983. Chaotic behavior and the origin of the 3/1 Kirkwood gap. *Icarus* 56:51–74.

Wisdom, J. 1985. Meteorites may follow a chaotic route to Earth. *Nature* 315:731–733.

Wisdom, J. 1987. Urey Prize Lecture: Chaotic dynamics in the solar system. *Icarus* 72:241–275.

Zellner, B., Thirunagari, A., and Bender, D. 1985a. The large scale structure of the asteroid belt. *Icarus* 62:505–511.

Zellner, B., Tholen, D. J., and Tedesco, E. F. 1985b. The eight-color asteroid survey: Results for 589 minor planets. *Icarus* 61:355–416.

PART II
Exploration

DISCOVERY AND FOLLOW UP OF ASTEROIDS

E. BOWELL
Lowell Observatory

N. S. CHERNYKH
Crimean Astrophysical Observatory

and

B. G. MARSDEN
Harvard-Smithsonian Center for Astrophysics

After a summary of the increasing activity in asteroid discovery during the past few years, we discuss the importance of carefully thought out observing strategy, in particular with regard to target selection, observing frequency and the time distribution of observations. Problems of cataloguing and orbit linkage are outlined, inasmuch as they affect individual observers and orbit computers as well as the work of the Minor Planet Center. There is some discussion of appropriate two-way communication between observers and the Minor Planet Center.

It is our premise that the aim of asteroid discovery is to augment the set of numbered asteroids, and that this set should comprise asteroids with orbits that are sufficiently well determined, not only to provide a satisfactorily detailed and reasonably unbiased delineation of the structure of the whole asteroid belt, but also to permit the ready observation of a specific member at any subsequent time. Our opinion may not be entirely unbiased, for after the long-defunct Heidelberg program, the observing programs directed by the first two authors have been the most productive in achieving the above aim, while as director of the Minor Planet Center the third author has overseen a

[21]

plurality of the actual asteroid numberings. Nevertheless, as time goes on, it is clear, not only that the orbital data for the numbered asteroids are becoming progressively more accurate, but also that the totality of orbital data is providing an ever more complete description of asteroid orbits as a whole. The actual astrometric process is not discussed here. For this, appropriate reference can be made, for example, to papers by Roemer (1971) and Gibson (1984).

I. NUMBERED ASTEROIDS

A. Growth

The acquisition of new numbered asteroids obviously tends to progress to objects of greater apparent magnitude. However, as has been noted before (see, e.g., Jaschek 1978), there have been unusual departures from the constant exponential growth that the accumulation of observational data generally seems to involve. This is demonstrated in Table I, where the column of dates on the left-hand side shows dramatic variations in the time required for the successive doubling of the number of numbered asteroids. Although the number of objects is currently just over 4000, the doubling period from 2048 to 4096 is clearly going to be the shortest since that from 64 to 128 and is significantly shorter than the mean doubling period of 16 years. The two excessively long doubling periods, 41 years from 4 to 8 and 53 years from 1024 to 2048, are readily explained, in the former case by the unavailability of star charts, and in the latter by a combination of the disruption of World War II and the overtaxing of human computers, followed by a rather cautious postwar recovery and the introduction of automated computers.

Table I also shows the mean photographic opposition magnitude, the values listed being the average for the $2^{n/2}$ objects around each specified 2^n. There are indications that the difference between the magnitudes corresponding to 4096 and 2048 will be less than the mean 0.8 magnitude fading between earlier doublings.

B. Orbital Accuracy

Cohn (1911) largely succeeded in his plan that the ephemerides of the numbered asteroids should not be in error by more than 30' to 60'. Such was often far from the case during the rapid growth of the 1930s and the collapse of the 1940s, however, and by the end of World War II as many as 13% of the asteroids then numbered were effectively lost. Thanks to Herget's (1971) direction of the reconstruction effort, the situation had dramatically improved by the time of the first of this series of conferences and books (*Physical Studies of Minor Planets* [Gehrels 1971]), although even then only 64% of the ephemerides were accurate to within 3' (Marsden 1971), and perhaps 3% of the objects were still lost. Eight years later at the "Asteroids" colloquium (and

TABLE I
Exponential Data Growth

No.	Numbered			Discoveries	
	Date	Diff.	Mag.	Date	Diff.
1	1801.0		7.9	1801.0	
		1.2			1.2
2	1802.2		8.5	1802.2	
		5.0			5.0
4	1807.2		8.3	1807.2	
		40.6			40.6
8	1847.8		9.9	1847.8	
		4.4			4.4
16	1852.2		10.7	1852.2	
		2.6			2.6
32	1854.8		11.8	1854.8	
		6.4			6.4
64	1861.2		12.7	1861.2	
		11.7			11.6
128	1872.9		12.9	1872.8	
		13.4			12.4
256	1886.3		14.4	1885.2	
		17.2			13.7
512	1903.5		14.2	1898.9	
		21.5			7.8
1024	1925.0		15.6	1906.7	
		53.2			10.6
2048	1978.2		16.7	1917.3	
		(11.6)			14.3
4096	(1989.8)		(17)	1931.6	
					16.8
8192				1948.4	
					12.8
16384				1961.2	
					17.9
32768				1979.1	
					(14 ?)
65536				(1993 ?)	

in the subsequent book *Asteroids*), it could be reported (Marsden 1979) that 98% of the ephemerides were off by less than 5′, while the lost objects had been reduced to the 1% level. Figure 1 illustrates the continuing improvement of accuracy, to the extent that orbits are now routinely improved when ephemerides are found to be off by 1′, and 98% of the ephemerides are now good to 7″; the lost objects, specifically the two asteroids 719 Albert and— alas for one of the editors of this book—878 Mildred, now account for only 0.05% of the whole.

C. Bias

It is sometimes hard to imagine that no Apollo asteroid was numbered before the post-war reconstruction and that there was no numbered Aten asteroid until after the Minor Planet Center moved from Cincinnati. Only during the past two years have there been numberings of asteroids that experience the chaotic effects of close encounters with Jupiter, e.g., 3360 1981 VA and 3552 1983 SA (Hahn and Lagerkvist 1988).

In spite of the increasing interest in unusual objects, every effort is made to ensure that each batch of new numberings also contains an overwhelming sample of main-belt asteroids. A predominance of discoveries during the clear nights of the northern hemisphere autumn has long been known to produce a directional bias for main-belt objects, although recent increased activity at
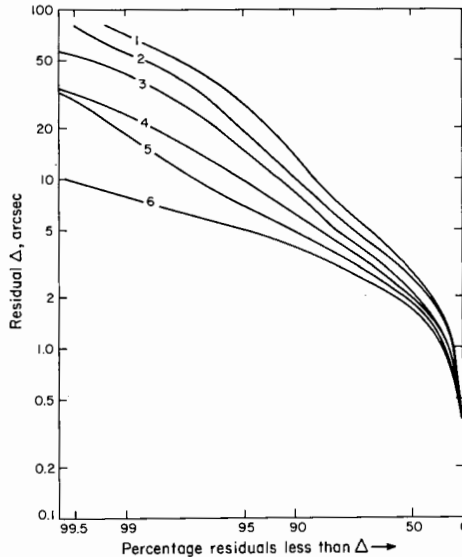
Fig. 1. Log-log plot of the great-circle residual $\triangle$ (absolute observed minus computed) in positions of numbered asteroids observed at the Lowell Observatory since 1979 vs the percentage less than $\triangle$. The dates and numbers of observations corresponding to the various lines are: (1) 1983 Apr. 21: 8673; (2) 1984 Jan. 1: 10,700; (3) 1985 Jan. 4: 14,516; (4) 1986 Feb. 13: 17,531; (5) 1987 Feb. 21: 19,583; (6) 1988 Apr. 14: 21,420.

other times of the year and at southern hemisphere sites is helping to reduce this effect.

II. UNNUMBERED ASTEROIDS

A. Growth

The introduction a century ago of photography to the discovery of asteroids made it necessary to introduce preliminary designations for new discoveries. Since 1925 these preliminary designations have basically consisted of the year of observation and two letters, the first indicating the half-month of the year and the second the order of announcement during the half-month; if necessary, the second letter is recycled and numerals are added. Asteroids have been given permanent numbers only after really satisfactory orbits were obtained, although the required standards for such orbits were considerably lower before World War II than afterward. The dates on the right-hand side of Table I show the rate of doubling of the actually reported discoveries, which do exhibit rather constant exponential growth. This count of total discoveries consists of the standard post-1925 preliminary designation system, supplemented by 1562 designations in the same system for pre-1925 discoveries, the

1046 asteroids that were numbered before 1925, the 2403 PLS (Palomar-Leiden Survey) discoveries of 1960 and the 1422 discoveries of the Third Palomar-Leiden Trojan Survey (T3S) of 1977; the dates corresponding to 32,768 and the estimate for 65,536 will obviously be modified when the results of the other Palomar-Leiden Trojan Surveys become available.

The current total number of discoveries, 49,466 following the batch of *Minor Planet Circulars* (MPCs) issued in February 1988, is known to include 14,970 entries for the numbered asteroids, or 4.0 per object. The number of different identifications for the 100 most recently numbered asteroids averaged as high as 4.3 at the time of numbering. Since searches for identifications have become rather thorough in recent years, these ratios are presumably greater than the average number of repetitions that must exist among the objects that have not yet been numbered. For example, there are only an average of 2.6 different designations for the 1200 unnumbered asteroids for which observations have been linked at more than one opposition. Even this ratio must be too high for most of the remainder, which includes, for example, the bulk of the discoveries from the PLS and T3S, as well as most of the 1257 UCAS (U.K. Schmidt-California Institute of Technology Asteroid Survey) objects—which were given standard preliminary designations—and a number of other faint recent discoveries that are scarcely likely to have been recorded more than once. There must still be some duplication of entries among the 7779 available single-opposition orbits, however, and furthermore, 315 preliminary designations are known to refer to comets and satellites of Jupiter or have otherwise been eliminated.

B. Bias

In a given photographic field, the sample of asteroids actually observed is biased by factors that arise from observing strategy and that are imposed by the true distribution of asteroids. If a small area of sky is sampled, the distribution of asteroid orbital elements is usually heavily biased. Obviously, a high-latitude field cannot contain low-inclination asteroids. But even a small displacement from the ecliptic can produce a strong bias in the longitude of the ascending node. This is quite evident in UCAS, for example. Limiting magnitude clearly depends on trail length. Using the Metcalf method, in which the telescope is usually tracked according to the motion of a typical asteroid in the region of the sky being observed, there is a bias in favor of asteroids moving at average rates, causing the sampling of a preferred orbital semimajor axis to fainter absolute magnitudes.

As for a bias imposed by the true distribution, inner-belt asteroids are clearly sampled to smaller sizes than outer-belt asteroids, and all main-belt asteroids are preferentially discovered near perihelion. There are more subtle effects, however. For example, high-latitude fields tend to sample a greater proportion of outer-belt asteroids because of the correlation of mean orbital

inclination with semimajor axis, yet these same distant asteroids are observationally discriminated against because of their lower average surface albedo.

C. August–November 1986 and 1987

The two northern hemisphere autumns of 1986 and 1987 have been remarkable for their discoveries made essentially in real time. The 713 discoveries (of which 7 were omitted or deleted) during August–November 1986 already announced in the mid-December MPCs were twice as many as had previously been reported so quickly from an interval of four consecutive months. The count from August–November 1987 by the MPCs of early January 1988, 681 (with 10 omitted or deleted), was only slightly less (Marsden 1987,1988). Since this feverish rate of reporting appears to be setting a trend for the future, it is useful to examine these reported discoveries in more detail. This is conveniently accomplished using the pie chart shown in Fig. 2, where the upper semicircle refers to the discoveries made in 1986, the lower to those of 1987, and the widths of the sectors show the distribution according to the length of the orbital arcs (in days) over which the various discoveries were observed.
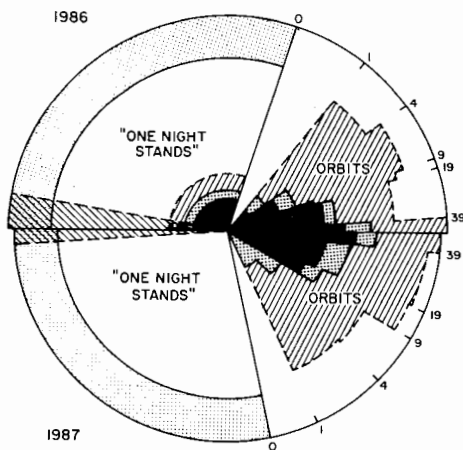
Fig. 2. The various areas show the distribution of asteroid discoveries by arclength and whether orbit computations could be made. The upper semicircle refers to Aug.–Nov. 1986, the lower semicircle to Aug.–Nov. 1987. The areas of the large sectors labeled "one-night stands" from the left to 0 show that most of the asteroids were observed on a single night. The hatched areas at the left indicate single observations and the outer dotted region the contribution of a single observatory. Areas corresponding to 0–1, 2–4, 5–9, 10–19, 20–39, and 40 and more days are also indicated. For arcs of more than 2 days the fraction of general orbit determinations (i.e., the availability of observations on 3 or more nights) is shown, the dotted region indicating cases of identifications, and the black region that the discoveries were principal ones. The corresponding shadings in the 1986 sector of one-night stands refer to the situation with regard to the same discoveries as of February 1988.

The largest sectors, covering about 60% of each semicircle and extending from the left-hand edge to the radius labeled 0, illustrate that in each year a majority of the discoveries were observed on only a single night. The hatched sectors at the extreme left, about twice as large in 1986 as in 1987, indicate objects for which there was only a single observation and hence no information whatsoever about motion. Eleven different observatories (most of which generally conduct highly successful observing programs) contributed to the "one-night stands," but in both 1986 and 1987 some 35% of such discoveries (shown by the stippled area near the peripheries) were reported by the same observatory, an observatory that also failed to include magnitude estimates with its observations.

The remaining sectors in Fig. 2 are categorized by orbital arclength in days, as given around the peripheries. Those extending from 0 to 1 illustrate the fraction of discoveries observed on two consecutive nights. As is discussed in more detail below (see Sec. III.C), two observations of an asteroid can be conveniently represented in terms of "*Väisälä orbits*." Although Väisälä orbits can be fitted to multiply observed one-night stands, arcs of a day or more are far preferable, as they also allow the possibility of making an unequivocal identification of a newly discovered asteroid with one for which an orbit of only poor-to-moderate quality has been determined from observations at just one other opposition.

The right-hand sectors in Fig. 2 break the discoveries into arclengths of 2–4, 5–9, 10–19, 20–39, and 40 or more days, respectively. More often than not, objects with such arclengths are observed on three nights or more, in which case general orbit determinations are attempted. The hatched area on the right-hand side of Fig. 2 indicates these orbit solutions, made for 20% of all the discoveries in 1986 and 25% of those in 1987.

It is important to note that fully 32% of the 1986 orbits and 23% of the 1987 orbits were based on observations spanning only 2 to 4 days. Except for unusual objects discovered in the vicinity of the Earth, general orbit solutions from arcs as short as these are of negligible value. Many short-arc general orbit solutions give completely spurious results, so it has become the custom to make an orbit solution appear acceptable by arbitrarily forcing the eccentricity (and perhaps also the semimajor axis) to have a reasonable value. Usually, one might just as well ignore the observations on the middle night and fit a Väisälä orbit to the first and last observations (Sec. III.C).

For a measure of the utility of the general orbit solutions, it is instructive to examine the inner sections in the orbits sectors of Fig. 2. These sections, 4.4% of the whole in 1986 and 6.4% in 1987, illustrate the cases where the orbit solutions have permitted identifications with observations at previous oppositions. The black area (3.0% in 1986 and 3.3% in 1987) shows the subset in which the current discoveries are the "principal" discoveries. Since it is these principal discoveries that count when asteroids are given permanent numbers, the black area is directly related to the success of the whole observa-

tional enterprise in terms of the premise stated in the introductory paragraph to this chapter. Few orbits with arcs of less than 10 days yield identifications, and in 1987 no object with an arc this short counted as the principal discovery.

The chance of success increases significantly when an arc exceeds 20 days, but there is not necessarily more to be gained by observing an object for more than 40 days. Once a new identification has been clearly established, there is little need for more observations at the current opposition (unless the arc happens to be very short). Any additional effort is best expended at the next favorable opposition, when a light spread of observations over another 20 to 40 day arc will probably ensure that the object will be numbered. Arcs in excess of 40 days are generally necessary only when there are no past identifications. To guarantee the recovery of an object without identifications at some future opposition, the current arc should of course be as long as possible, at least 60 days, say, and preferably 80 or even more than 100 days.

The final feature in Fig. 2 to be discussed is the inner portion of the left-hand sector of the 1986 semicircle that is hatched, dotted or black. This shows the orbit and identification situation, as of February 1988, for the one-night stands of 1986. Of course, the fact that general orbits have been calculated means that further observations of these objects have now become available. For the most part, the additional observations were supplied by other observers who accidentally discovered the same objects. In several cases, these other observers followed the objects for more than 10 days themselves, and in combination with the positions on the discovery nights sometimes yielded arcs of more than a month. It is important to realize that the situation with regard to specific discoveries is continually changing, both as further observations become available, and as further computations—perhaps after a lapse of decades—yield identifications.

III. MODUS OPERANDI

A. Qualification for Provisional Designations

When the measurement of a photographic plate meant that one had to write down long sequences of numbers at the measuring engine, the reduction process required scanning the pages of printed star catalogues as well as time-consuming work on a mechanical calculator, and the uncertainties in the ephemerides of the known asteroids were frequently large, it was customary for the Minor Planet Center to supply a provisional designation on the basis of a single approximate positional observation of a supposed new asteroid discovery.

As astrometric procedures have become automated, and as ephemerides have improved, the Minor Planet Center has insisted that accurate positions (or at least "semiaccurate" positions, good to ~5″ to 6″) be provided—although an exception might be made in the case of a fast-moving asteroid

discovered in the vicinity of the Earth. On the receipt of such observations, the Center routinely attempts to make an immediate check for the more obvious identifications (e.g., with the orbits of asteroids observed at more than one opposition). An accurate position tends to make a suspected identification more definite; some indication of motion and magnitude in addition can be even more helpful.

It is now proposed, in general, to supply provisional designations only when accurate (or good semiaccurate) positions have been measured on *two different nights*. Observers are urged also to indicate the magnitude and to delay even reporting their discoveries until they have measurements on two nights. Again, an exception may be made for an asteroid near the Earth, and one-night stands will eventually be processed if no other observations become available after a lapse of, say, four to six months (by which time some of them will have been credited instead to independent discoverers who *do* make observations on two nights). This new procedure should (a) make immediate identifications even more definite; (b) permit more reliable Väisälä orbits; and (c) be more fair to those careful observers who conduct extensive observing programs far from home base and who may therefore not be able to complete their measurements for some months.

It is also useful if the observer can provide two positions on *each* night, for a Väisälä orbit might then reveal any gross inconsistency. These two positions may refer to trail ends, but measurements of breaks in a gated exposure or of two separate images (perhaps even on two separate plates, although this would cost more in time and money) are preferable. If the Metcalf method is used, it is necessary to vary the gating or the duration of the exposures so that the sense of motion relative to the tracking is unambiguous. The measurement of three (or more) positions of a main-belt asteroid on the same night is usually a waste of time.

B. The Follow Up

After recording a new asteroid on a second night, the discoverer needs to decide whether to abandon it or to follow it up further in the hope that an orbit can be computed and that the object will eventually be numbered with the principal discovery credited to him. From the statistics in Sec. II.C, it is clear that this credit is rarely assured simply by obtaining another observation on the next clear night. If he wants to go about the task efficiently, he should in fact wait a while and then repeat the earlier process of observing the object on two more nights in rather quick succession. Clouds and telescope availability may not cooperate, and interference from the Moon is inevitable, but the observer should at least attempt to spread the two pairs of nights over an arc of more than ten days, say, around new Moon.

A more experienced observer, particularly one who is able to calculate his own Väisälä orbits, will choose instead to span full Moon with the pairs of nights, and this can clearly yield arcs that are well in excess of 20 days. Since

the brightness of an asteroid generally peaks near opposition, there is merit in conducting the first month's observations an hour or so to the east of the opposition point, so that the follow-up observations a month later are made a comparable amount to the west of opposition, and the object is of similar brightness on each occasion. As already noted, if an identification is to be found, there is a very good chance that observations during two consecutive dark runs will reveal it, and observations during a third dark run will then be unnecessary. Frequently, a correct month-to-month linkage can be made on the basis of a pair of observations on a single night in the second month. A second night would clinch the matter, however, and if the linkage fails, the second month's observations would then immediately qualify as another new discovery.

Observations made on a single night at a particular opposition are not entirely useless, for they can give valuable additional support to identifications that are already moderately well established. Inspection of the orbits in the MPCs will show the importance, in this connection, of many observations made at the Crimean Astrophysical Observatory during the past quarter of a century. Processing one-night stands is clearly not an urgent matter, however, and chances are that these identifications will not be found until many years after the observations have been made.

C. Väisälä Orbits

The observed motion vector of an asteroid at discovery usually suffices to indicate its approximate position in the sky for a number of days by linear extrapolation. Exceptional cases are observations made well away from opposition, when the motion can be highly nonlinear, and deep plates containing images of hundreds of unknown asteroids whose identity can easily be confused on a second night. For secure identification, however, it is always preferable to calculate Väisälä orbits for new discoveries.

First developed by Väisälä (1939), and well described in English by Dubyago (1961), the method plausibly assumes that the asteroid is at perihelion (or, rather less plausibly, at aphelion) at the time of the second observation. It remains to specify just one more of the five other orbital elements, usually the semimajor axis or the eccentricity, in order to calculate a unique apsidal orbit. In the present treatment, we have generalized Väisälä's original method in two ways: first, we calculate a family of apsidal orbits using the geocentric distance as argument; and second, we allow for nonapsidal orbits by examining the region in the sky plane where a newly discovered asteroid is likely to be at the time of the next proposed observation.

An example, using observations of 1985 FZ made at the Lowell Observatory, shows how the method works. Having observed the asteroid twice on each of two nights (1985 March 21 and 24), we wished to find it on a plate taken during the subsequent lunation (on April 14). Figure 3 summarizes the results. The locus of Väisälä orbits is a shallow curve in right ascension-
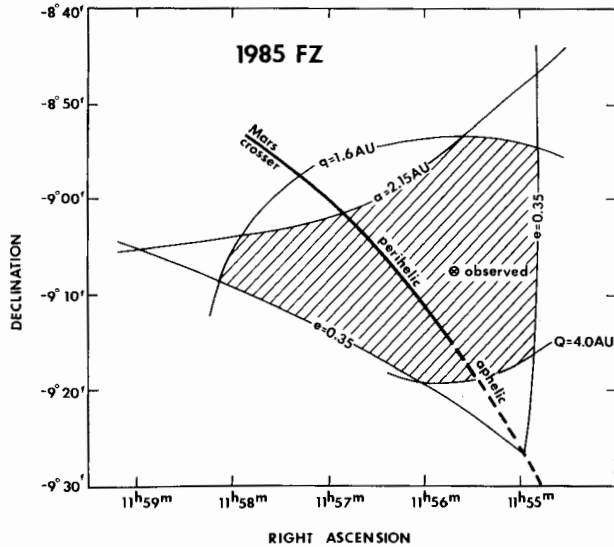
Fig. 3. Position prediction by means of the generalized Väisälä method. The bold curve is the locus of apsidal Väisälä orbits (solid indicates perihelic orbits, dashed aphelic). The hatched region constrains the possible location of 1985 FZ on 1985 Apr. 14, twenty-one days after it was last observed, assuming the asteroid to be a main-belt object. The observed position is indicated, and bounds to the hatched region (in terms of eccentricity e, semimajor axis a, perihelion distance q and aphelion distance Q) are explained in the text. Note that the right ascension and declination are not to scale.

declination space, bounded at one end by the orbit becoming Mars crossing (q = 1.6 AU) and at the other by it becoming Jupiter-approaching (Q = 4.0 AU). Nonapsidal cases are considered by introducing fictitious positions of the asteroid near the Väisälä locus and examining the likelihood of the resulting orbits. The other bounds in the Fig. 3 example are set by a reasonable upper limit on the eccentricity; the minimum main-belt semimajor axis also has a small effect. In general, it is sufficient to restrict attention to main-belt orbits, for which elements should be within the approximate bounds given in Table II. However, not all the bounds come into play in a particular case. In our example, the inclination does not provide a useful constraint. The hatched area in Fig. 3 indicates that the asteroid should be sought in a region about 45′ × 25′ in greatest extent. In fact, it was found 8′ from the Väisälä locus, and in almost all acceptable orbits, the mean anomaly was between 330° and 30°.

The orbits of unusual asteroids are easily revealed by the generalized Väisälä method, so it is possible, at least near opposition, to recognize Hilda and Trojan asteroids, and even to distinguish Hungarias from Phocaeas. The case of Earth-approaching asteroids is more difficult to deal with because the orbital elements are poorly constrained. It is notable, however, that the instan-

TABLE II
Bounds on Main-Belt Orbital Elements

Element	Lower Limit	Upper Limit
Inclination (deg)	0	30
Eccentricity	0.00	0.35
Semimajor axis (AU)	2.15	3.3
Perihelion distance (AU)	1.6	3.3
Aphelion distance (AU)	2.15	4.0

taneous motion near opposition is frequently sufficient to determine the semimajor axis of a main-belt asteroid to within 0.2 AU.

D. Very Faint Objects

A particular problem does exist with observations of very faint objects, say, where the blue magnitude is much greater than 18, or about one magnitude fainter than the mean opposition magnitude of asteroids currently being numbered. Very faint objects are of course extremely numerous, and it is relatively unlikely that they can be linked with asteroids that have been noted at past oppositions. In applying the Väisälä method to deep fields, where there may be confusion from many asteroid images, it is useful to calculate the motion and magnitude of the target asteroid at each predicted location.

An observer who wants to do useful work with very faint asteroids should be prepared to make really extensive follow-up observations, for the likelihood that observations can be secured at another opposition will depend on the availability of a very good orbit at the first. The PLS was of course the pioneering enterprise on faint asteroids and provided a wealth of data on asteroids as faint as magnitudes 20 to 21. The best PLS arcs were only 32 days, however, so direct recoveries have been rather rare. It is also true that 40% of the PLS orbits covered arcs of only four days (van Houten et al. 1984).

Future surveys for faint objects should therefore plan to meet the exacting standards of the more recent UCAS (vintage 1981). Fully 75% of the UCAS arcs exceeded 70 days, and 90% exceeded 20 days; four-day arcs were entirely eliminated. The long arcs have so far led to the identification or recognition of images of 26% of the UCAS objects at other oppositions. They therefore constitute the best pool of km-sized asteroids having reasonably accurate orbits. LUKAS (the Lowell Observatory-U.K. Schmidt Asteroid Survey) is to be conducted on the same general lines as UCAS but will address the bias problem of UCAS mentioned in Sec. II.B.

Current image-processing technology is such that the comparison of two deep Schmidt plates of the same field can be accomplished electronically, and it is quite feasible nowadays to take a quite large collection of plates, to separate asteroid images/trails from the true "vermin of the skies" (stars, gal-

axies and the like), and to store the asteroid data on tape. On the other hand, the Schmidt plates are themselves very convenient repositories for observations of asteroids. Some researchers are instead making automatic correlations of plate centers and dates with the ephemerides of faint asteroids. It was in this manner that Bus (1982) was able to extend a significant part of UCAS to another opposition, and that Schmadel and West (1986) could confirm the recovery of the lost asteroid 1179 Mally.

IV. OTHER OBSERVATIONAL TECHNIQUES

Photography has provided the means for making 98% of the asteroid discoveries, and it is likely to remain the dominant agent for serious discovery work for some time to come. A CCD-based project such as Spacewatch (Gehrels 1981) obviously has considerable potential for such work, but the unavailability of a sufficiently large CCD has so far precluded its being used for a significant program of discovery and appropriate follow up. However, CCD observations are becoming increasingly valuable in following up faint objects.

The IRAS project in 1983 (Matson 1986; see the chapters by Matson et al. and Veeder et al.) made many thousands of detections of asteroids, and the signals at different infrared wavelengths contain potentially useful physical data. Attempts to link these detections with photographic observations of unnumbered asteroids have been disappointing, however, except for the few fast-moving IRAS discoveries that were reported in real time.

The discovery of asteroids by television techniques (Taff 1981) has yielded more results, but neither the astrometric accuracy nor the follow up has been particularly satisfactory.

V. FOLLOW UP AT ADDITIONAL OPPOSITIONS

The problem of recovering an asteroid at a second opposition is not considered here, except to say that searches are normally made along the line of variation, the locus of changing orbital longitude projected on the plane of the sky. It is remarkable, however, that there exists no analytical method for predicting the accuracy of a recovery ephemeris for an asteroid observed at just one opposition, particularly in the face of observational error. Such a formulation is sorely needed.

In practice, even wide-field searches become very difficult when the original arcs are less than about 30 days. So, although the long UCAS arcs have led to successful, deliberate searches for images of asteroids at a second opposition (and LUKAS is likely to involve even more of this activity), most second-opposition observations of asteroids are currently found as the result of the establishment of identifications with images already found and catalogued as asteroids. By specifying observations of a new discovery on two

nights, rather than one, the possibility of establishing identifications is greatly facilitated. This is true whether one is using the technique of comparing specific orbits with all the available observations or the inverse of comparing specific observations with all the available orbits. For a review of the various identification procedures, see Marsden (1985).

A. Definition of Principal Discoveries

If elliptical orbits are available at two (or more) of the oppositions involved in an identification, the principal discovery has traditionally been defined as that at the chronologically earlier (or earliest) opposition, provided that individual elliptical orbit bears some resemblance to the final linked result. It can be argued that precedence should instead be given to the earliest orbit *to be computed* that shows resemblance; but the definition of resemblance can be subjective.

Another suggestion, quantification in terms of observational coverage (particularly arclength), would be difficult to enact, particularly when one realizes that the resemblance can be greater when some of the observations are erroneous than when all appear to be satisfactory. In any case, if multiple designations are involved at some of the oppositions, it can make a difference whether the multiple designations are found before or after the identifications.

Furthermore, thanks notably to some interesting work by the Canadian amateur astronomer Lowe, there is an increasing number of identifications in which observations have been made on no more than two nights at any opposition (see, e.g., Lowe 1987). With such identifications, the practice has been to select the earliest opposition with observations on two nights, although the situation can be confused by the discovery of unsuspected multiple designations or by the possible existence of a bad (but not so bad that it is an obvious misidentification) observation on a third night.

Although circumstances might conspire to deny credit for a particular discovery to a particular observer, it is probably true that the relative contributions of the various observers have been appropriately recognized statistically in the total set of numbered asteroids.

B. Qualification for Asteroid Numbering

The decision by the Minor Planet Center to assign a permanent number to a new asteroid has in recent times been made, in the case of a main-belt object, when there is good to moderate coverage at three oppositions, or from moderate to poor coverage at four oppositions. Earth-approaching objects are often numbered when there is good coverage at only two oppositions. Until a decade or so ago, newly numbered asteroids tended to have the most accurately determined orbits. Increased attention during the past decade to the orbits of older numbered asteroids makes this no longer the case, however, so there is now a tendency to defer decisions on numbering until further oppositions have been covered. In any case, an object observed at only three opposi-

tions will automatically be included in the "critical list," which is conventionally taken to refer to numbered asteroids that have not been observed in ten years or at four or more oppositions altogether.

VI. COMMUNICATION

An important factor in the successful execution of a real-time asteroid search program is the rapid communication of data. Modern communication by computer, specifically using networks such as SPAN and BITNET, as well as the computer service operated since early 1984 in part by the Minor Planet Center, has dramatically changed the way in which observers—those in the countries of the first world, at least—and the Minor Planet Center interact. With just a few additional keystrokes, an observer can transmit his observations (of numbered and unnumbered as well as of unidentified asteroids) as soon as they emerge from the computer program that performs the reduction, and the data are received by the Minor Planet Center in a form that is immediately usable. In return, the Minor Planet Center can quickly respond to the observer with a straightforward identification for a supposedly new object or perhaps the news that the object has been independently detected elsewhere.

Rapid communication of such information, as well as of appropriate orbital elements and/or ephemerides (and occasionally of suspect residuals), is obviously useful if the observer wishes to plan his course efficiently. Exchanges of this type have been particularly effective in connection with highly successful observing programs conducted by an ever-increasing number of Japanese amateur astronomers. Here the communication is between Syuichi Nakano (currently at the Minor Planet Center) and Takeo Kobayashi (in Tokyo), who between them are responsible for establishing a majority of all the asteroid identifications currently being made. When the absence of identifications renders it desirable to extend arcs far from opposition, by which time an asteroid may have become too faint for detection by its discoverer, the Minor Planet Center sometimes requests further follow up by observers with small-field, long-focus reflectors. Unfortunately, the scarcity of such observers and available telescopes means that these observations are not always possible. Autumn and winter discoveries (in either hemisphere) can be best followed up with instruments in the same hemisphere, where the ecliptic rides high in the winter and spring evening sky.

Other observers, particularly in the second and third worlds, communicate with the Minor Planet Center by telex, although this can be expensive. Telex communication is therefore generally restricted to objects the observers believe to be new—and sometimes only to objects that seem to be unusual. Several of these observers communicate the bulk of their data (after some delay, of course) on magnetic tapes or diskettes. There are still a number of observers, however, even in parts of the first world, who submit their observations in the form of computer printout or even typescript. Because of the need

to respond adequately to the observers in regular electronic communication, the Minor Planet Center has sometimes had to give lower priority to the processing of data provided in printed or handwritten form.

Direct rapid communication between observers can often be useful, particularly when one observer has discovered a new fast-moving object (cf., e.g., Helin 1988). In view of the new requirement for observations on two nights, some collaboration of this type can be anticipated for main-belt objects, most of which are discovered in the course of observing programs on known asteroids. Observers do not have to be coordinated so as not to overlap, and it is still true that the number of duplicate discoveries is not particularly great.

VII. CONCLUDING REMARKS

In summary, we conclude that the act of asteroid discovery is currently succeeding admirably, if one registers that success in terms of new asteroid numberings on the basis of photographic observations and appropriate searches for observations at other oppositions. However, there is clearly a disproportionate effort on discoveries observed on a single night or on three or more nights too close together in time to yield a satisfactory general orbit solution. Observers should try to plan their programs so that the objects they discover are observed on two nights in quick succession, with the possibility then of observing the objects on additional pairs of nights after enough time has elapsed that a reliable orbit can be determined. Attention should be given to very faint discoveries only if the observer is prepared to make extensive follow up.

New discoveries are frequently a by-product of photographic astrometric programs on known asteroids. In conducting such programs observers should note that numbered asteroids on the critical list and all unnumbered asteroids for which ephemerides are published in the MPCs are especially in need of observation. Many of these unnumbered asteroids are not receiving the little additional astrometric attention they really require in order to be numbered, and the rate at which new two-opposition identifications are established is fully three times that of new numberings. Measurements of the new objects, as well as of known asteroids that may appear on the same plates, should be carried out in a way that allows the results to be reproduced, and magnitudes should be estimated for asteroids that are unidentified. Global reductions (i.e., involving the least-squares determination of plate constants, using reference stars that cover most or all of the plate area), rather than dependences, should also be carried out in a reproducible manner, using all the terms appropriate for the particular telescope, and (until suitable new catalogues are available covering the whole sky) with respect to a star catalogue capable of yielding B1950 asteroid positions to $2''$ or better. Accurate timing of the exposures to

within a few seconds is essential. Too many observers persist in making errors of an integral number of hours (or days) in reporting their observations.

The communication of observations to the Minor Planet Center should be in some kind of machine-readable form, if this is at all possible. Since the Minor Planet Center generally updates the orbit determination for each new discovery whenever a new observation is reported, it is also helpful if an observer would report all his observations of it during a particular dark run in no more than two communications (and all the observations on a particular night at once): the observations on the first two nights establish priority for the discovery and a Väisälä orbit, and those on the other nights a single general orbit. Any subsequent minor adjustments of the observations should be avoided, and (except perhaps in the case of a fast-moving object near the Earth) semi-accurate positions should not be provided if the observer later intends to attempt accurate measurements. When observations are communicated electronically in near-real time, the Minor Planet Center attempts to advise the observer in the same way on potential identifications and thus on the appropriate degree of follow up.

The growth in the number of numbered asteroids is impressive but still quite manageable. This could cease to be the case, however, if the Minor Planet Center has to put a disproportionate effort into attending to large numbers of isolated discoveries and to observations that are made and reported in a thoughtless manner. Cooperative and intelligent follow up is eminently preferable to an indiscriminate increase in one-night stands and indeterminate short-arc general orbit determinations.

In the case of the numerous very faint asteroids that are not to be well followed up, it may be sufficient that images of them exist on photographic plates and can easily be retrieved if and when that becomes desirable. Alternatively, measurements could be made available via machine-readable files but not published in print. In either case, considerations might be given to the publication of dates, plate centers and sizes, and approximate limiting magnitudes. However, as those involved in identification work well know, there is nothing so frustrating as encountering a possible critical identification with an old approximate position, so plate centers should be listed only if there exists the immediate prospect that an identifier could acquire the necessary measurements.

Nonphotographic methods of asteroid discovery have so far not been particularly productive, principally because of the difficulty otherwise of securing sufficiently accurate measurements with an appropriate distribution in time. The production of larger CCD chips may or may not change this situation in the foreseeable future. The past decade or so has seen the welcome introduction of devices such as PDS microdensitometers into the process of plate measurement, however, and even more dramatic capabilities for automatic and rapid plate measurement are clearly to be expected by the time the "Asteroids III" book is made.

REFERENCES

Bus, S. J. 1982. Observations made with the U.K. Schmidt at Siding Spring. *Minor Planet Circ.* Nos. 7087–7104.

Cohn, F. 1911. Konferenz zur Beratung gemeinsamer Massnahmen in betr. der Ephemeriden Sammlungen. *Astron. Nachr.* 189:433–440.

Dubyago, A. D. 1961. *The Determination of Orbits* (New York: Macmillan), pp. 192–199.

Gehrels, T., ed. 1971. *Physical Studies of Minor Planets,* NASA SP-267.

Gehrels, T. 1981. Faint comet searching. *Icarus* 47:518–522.

Gibson, J. 1984. Measuring—the quantifying art. In *Cometary Astrometry,* eds. D. K. Yeomans, R. M. West, R. S. Harrington and B. G. Marsden (Pasadena: Jet Propulsion Laboratory), pp. 125–149.

Hahn, G., and Lagerkvist, C.-I. 1988. Orbital evolution studies of planet-crossing asteroids. Presented at Humboldt Colloquium on Celestial Mechanics, Ramsau, Austria.

Helin, E. 1988. Discovery, recovery and physical observations of (3757) 1982 XB. In Asteroids II Abstract Booklet, 8–11 March, Tucson, Arizona.

Herget, P. 1971. The work at the Minor Planet Center. In *Physical Studies of Minor Planets,* ed. T. Gehrels, NASA SP-267, pp. 9–12.

Jaschek, C. 1978. Data growth in astronomy. *Q. J. Roy. Astron. Soc.* 19:269–276.

Lowe, A. 1987. Orbital elements. *Minor Planet Circ.* Nos. 12324–12325.

Marsden, B. G. 1971. Precision of ephemerides for space missions. In *Physical Studies of Minor Planets,* ed. T. Gehrels, NASA SP-267, pp. 639–642.

Marsden, B. G. 1979. The work of the Minor Planet Center. In *Asteroids,* ed. T. Gehrels (Tucson: Univ. of Arizona Press), pp. 77–83.

Marsden, B. G. 1985. Identifications of minor planets. In *Asteroids, Comets, Meteors II,* eds. C.-I. Lagerkvist, B. A. Lindblad, H. L. Lundstedt and H. Rickman (Uppsala: Uppsala Univ.), pp. 3–12.

Marsden, B. G. 1987. Annual report of the Minor Planet Center 1986. *IAU Inf. Bull.* No. 58, pp. 13–14.

Marsden, B. G. 1988. Report of the Minor Planet Center 1987. *IAU Inf. Bull.* No. 59, pp. 16–17.

Matson, D., ed. 1986. *IRAS Asteroid and Comet Survey* (Pasadena: Jet Propulsion Laboratory).

Roemer, E. 1971. Astrometric observations. In *Physical Studies of Minor Planets,* ed. T. Gehrels, NASA SP-267, pp. 3–7.

Schmadel, L. D., and West, R. M. 1986. (1179) Mally. *IAU Circ.* No. 4278.

Taff, L. G. 1981. Observations made at the Lincoln Laboratory ETS. *Minor Planet Circ.* Nos. 5964–5967.

Väisälä, Y. 1939. Eine einfache Methode der Bahnbestimmung. *Astron.-Opt. Inst. Univ. Turku Informo* No. 1.

van Houten, C. J., Herget, P., and Marsden, B. G. 1984. The Palomar-Leiden survey of faint minor planets: Conclusion. *Icarus* 59:1–19.

PHOTOMETRIC LIGHTCURVE OBSERVATIONS AND REDUCTION TECHNIQUES

A. W. HARRIS
Jet Propulsion Laboratory

and

D. F. LUPISHKO
Khar'kov University Observatory

Photoelectric lightcurves are used to determine the period of rotation, estimate shape and pole orientation, and define the phase relation, or brightness as a function of solar phase angle, of asteroids. We discuss methods of taking and reducing observations that lead to a high level of accuracy and productivity of lightcurves for these purposes. We also recommend the essential elements that should be included in a report of lightcurve observations.

The variation in brightness of an asteroid can be separated into three components: (1) that due to changing distances from the Earth and Sun; (2) that due to rotation, causing a periodic variation of the area and/or average albedo of the visible surface; and (3) that due to the changing solar phase angle, or angle between the lines of illumination and viewing. The first effect is trivial, and is commonly removed by reducing magnitudes from the observed values to those that would be observed if the asteroid were at 1 AU from both the Earth and Sun. We refer to such magnitudes as "reduced magnitudes" and reserve the term "absolute magnitude" to imply a measure of the intrinsic brightness of an asteroid, e.g., $V(1,0)$, or H in the new IAU magnitude system. The second and third effects are both of interest for studies of asteroid rotation rates, shapes and pole orientations, and studies of the phase

relations (see the chapters by Binzel et al., Magnusson et al., and Bowell et al.). The goal of lightcurve observations is to map out and separate these two variations as completely and accurately as possible.

Space does not permit a complete discussion of photometric observational procedures. Hardie (1962) gives a thorough, although somewhat dated, discussion. Harris and Young (1983) discuss some procedures specific to the problem of asteroid lightcurves. In the following sections, we discuss the correction for atmospheric extinction, including color and time variability, and the use of Fourier analysis in constructing composite lightcurves and phase relations. We emphasize the analysis of errors and the planning of observation sequences to yield the best results as efficiently as possible.

I. CORRECTION FOR ATMOSPHERIC EXTINCTION

The effect of atmospheric extinction on the measured magnitude of a star is generally modeled (see, e.g., Hardie 1962) by

$$v = v_o + k_v X \qquad (1)$$

where v is the magnitude as seen from the ground, v_o is the magnitude which would be observed from above the atmosphere, k_v is the extinction coefficient and X is the air mass, which is the amount of air along the line of sight compared with that of a vertical line of sight. Because many error sources cancel for differenced magnitudes, it is common to treat only one color band in an absolute sense, and additional colors differentially, for example,

$$(b - v) = (b_o - v_o) + k_{b-v} X \qquad (2)$$

where $(b - v)$ is the magnitude difference in the two color bands, k_{b-v} is the differential extinction coefficient (note that the total extinction coefficient for the blue band is $k_v + k_{b-v}$), and X is the air mass, as before. We use lower-case v and b to denote instrumental magnitudes in the two color bands. (While most of our work is carried out in the visual and blue color bands, the treatment is the same for any pair of color bands and can easily be generalized for more than two colors.) An instrumental magnitude is just the number of photon counts N_v converted to a magnitude scale: $v = -2.5\log(N_v)$. The extinction coefficient is a function of color; that is, bluer light is, in general, absorbed more heavily than redder light. Thus, k_{b-v} is generally a positive quantity. Since most photometric systems employ filter bands of significant width, the extinction coefficient for a given color band depends somewhat on the color of the object observed; that is, a bluer object will suffer more atmospheric extinction than a redder one, observed in the same passband, because more of the energy within the passband is near the blue end. To account for this, it is common to introduce a second-order extinction which is propor-

tional to the color index $(b_o - v_o)$. It should be noted that the whole formulation of first- and second-order extinction coefficients is an approximation, since the rate of further extinction of light decreases as the surviving light becomes more reddened. However, in the b and v color bands and for low to moderate air mass, the approximation is sufficient for 0.001 magnitude accuracy. We introduce a further refinement, allowing the extinction to be time variable

$$k_v = \sum_{i=0}^{n} E_i(t - t_o)^i + (b_o - v_o)k_v'' \tag{3}$$

$$k_{b-v} = F_o + (b_o - v_o)k_{b-v}'' \tag{4}$$

where E_o and F_o are the constant extinction coefficients, k_v'' and k_{b-v}'' are the second-order extinction coefficients, and the coefficients $E_1 \ldots E_n$ define a power-series representation of the time-variable component of the extinction. The constant terms, E_o and F_o, are the first-order extinction coefficients traditionally denoted k_v' and k_{b-v}' (see, e.g., Hardie 1962). We introduce the notation E and F in order to avoid the cumbersome addition of another sub- or superscript when these quantities become a polynomial series of terms. We choose the units of time, and the zero point of the time scale t_o so that time runs from about -1 to $+1$ from dusk to dawn. This minimizes round-off errors and correlations between terms in the solution. Note that this formulation implies that the time-variable component of extinction does not depend on color, and that the color-dependent component (F_o, k_v'', k_{b-v}'') is not a function of time. The physical reason for this choice is that the primary color dependence is due to Rayleigh scattering from atmospheric molecules, which is rather constant. The principal variable component, absorption and scattering by particulate matter (air pollution), is more or less "gray."

For the case of constant extinction, one can solve for k_{b-v} and $(b_o - v_o)$ by simple linear regression (Eq. 2), and then using $(b_o - v_o)$ from that solution, solve for v_o and k_v by another linear regression (Eq. 1). For the case of time-variable extinction, the problem becomes more complicated, because v_o and $k_v(t)$ are correlated in such a way that they cannot be separated from observations of a single star. The problem is physical in nature, not mathematical: the assumption of constant extinction can lead to completely wrong values of k_v and v_o, if in fact k_v varies even a small amount during the night.

The difficulty can be reduced by observing more than one star during the night. Consider two stars well separated in the sky, such that they are at significantly different air masses most of the time, but pass through the same air mass (elevation in the sky) at some time. If one observes them at the same air mass, then the atmospheric extinction is the same for both, and the ob-

served magnitude difference is the true difference, $(v_{o1} - v_{o2})$. Then, at any other time, the extinction can be found to be

$$k_v = \frac{(v_1 - v_2) - (v_{o1} - v_{o2})}{X_1 - X_2} . \qquad (5)$$

The above equation and discussion illustrate the essential requirements to obtain a good solution for the time-variable extinction. In practice, a least-squares estimation procedure is used that includes all observations of all stars for the night, and does not require strict observance of the above conditions. However, a better solution is obtained if one strives to observe stars over a range of air masses at all times, and to observe pairs of stars near the times of equal air mass.

It should be emphasized that one need not use standard stars for the determination of extinction. Indeed, it is better to use many observations of unknown (local-comparison) stars, than just a few observations of standards. Only a few observations of standards suffice to place all stars on a standard magnitude system, once the extinction function is known.

It must be kept in mind, however, that this technique requires that extinction be the same in the directions of both (or all) stars at the same time. There are situations, such as smog over Los Angeles, as seen from Table Mountain, where extinction is in fact not the same in all directions. One clue to this condition is when the extinction appears to change on a time scale shorter than an hour or so, which is the typical time scale of motion of the troposphere where most of the extinction occurs, over an observing site. By employing a time-variable extinction model, one can improve the quality of reductions, to salvage a marginal night or make a good night even better. However, there is still no substitute for good observing conditions, and the all-sky observations used to place local comparison stars on a standard magnitude system, or to derive color transformation terms, should be saved for nights of very high quality.

To solve for the time-variable extinction, we write one equation for each v observation (1), or $(b - v)$ differential observation (2). $(b - v)$ observations of asteroids can be used as well, since asteroids show almost no variation in color with rotational phase. The resulting system of equations contains the unknowns, v_o and $(b_o - v_o)$, for each star observed (or just $b_o - v_o$ for an asteroid), the extinction coefficients F_o, k''_v, k''_{b-v}, and the time-series coefficients $E_o \ldots E_n$. In fact, the program we have written allows for a time series in k_{b-v} (F_o, F_1, . . .) as well, but in confirmation of our hypothesis that color variability is small, we have found only slight variation in k_{b-v} on any night. The v and $(b - v)$ equations are only weakly coupled, through the coefficient k''_v, which is very small, of the order of 0.01. In order to achieve a reduction accuracy of <0.001 magnitude, it is only necessary to know $(b - v)$ to about 0.1 magnitude. Hence, for single-color photometry, one can be very

casual about taking only a few blue observations. It is possible to select the degree n of the time series (even zero is allowed, for a constant assumed value of extinction), as well as to hold constant any of the other parameters, F_o, k_v'' and k_{b-v}''. Figure 1 is a plot of the extinction at Table Mountain Observatory (TMO) on the night of 26 March, 1987. This night was devoted to calibration and determination of nominal extinction values. It was not a particularly good night, as can be seen from the value of the v extinction coefficient (0.12 corresponds to excellent transparency from TMO). The general clearing in the course of the night is typical from this observatory, as the air pollution from Los Angeles moves out of the basin. Note the near constancy of the $b - v$ extinction in spite of the considerable variation of the v extinction. This was the only night with sufficient observations to determine reliably the color terms, k_v'' and k_{b-v}''. The values found are -0.012 ± 0.005 and -0.025 ± 0.008, respectively. The second-order extinction coefficients can be calculated for a system of known spectral response using a nominal extinction vs wavelength function (see, e.g., Hardie 1962). For Table Mountain Observatory, we obtain expected values of -0.005 and -0.018, in fair agreement with the measured values above.

II. REDUCTION TO A STANDARD MAGNITUDE SYSTEM

In order to minimize errors from variable extinction, it is customary to observe asteroids relative to nearby comparison stars. If the asteroid observation is followed quickly by an observation of a nearby star, then the relative
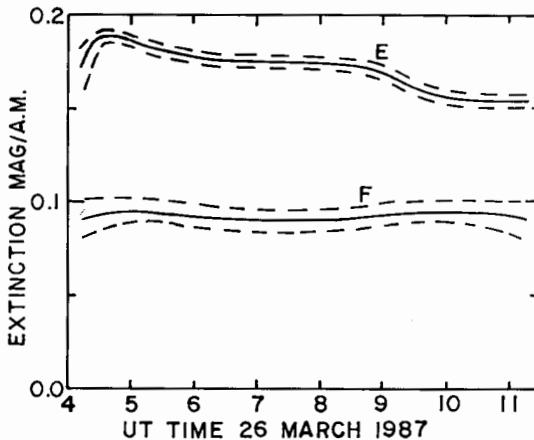
Fig. 1. First-order extinction coefficients E and F (k_v' and k_{b-v}'), measured at Table Mountain Observatory. The $\pm 1\sigma$ error envelopes are indicated. The rapid change in E early in the night is not significant, as indicated by the error range; however, the general decrease in E during the night is highly significant, and typical as the smog clears out of the Los Angeles basin. F does not vary significantly from a constant value all night long.

magnitude can be determined by simply differencing the two instrumental magnitudes. The differential magnitude outside the atmosphere is

$$dv = v_a - v_c - k_{va}X_a + k_{vc}X_c \qquad (6)$$

where subscripts a and c refer to the asteroid and comparison-star measurements, respectively. In the simplest case, where k_v does not depend on color or time, $k_{va} = k_{vc}$, and the correction for extinction depends only on the difference in air mass between the asteroid and star. However, since k_v actually depends on color, the correction depends on total air mass to the extent that a and c differ in color, and if k_v changes appreciably between the times of the two measurements, another correction arises which depends on the total air mass. In order to make the best correction possible, we compute k_{va} and k_{vc} separately from the extinction solution of the last section, thus allowing for both time and color variation of the extinction. The colors $(b_o - v_o)$ for asteroids or standard stars can be obtained from the extinction solution, or from known values transformed from a standard magnitude system to the instrumental system.

One further small correction which we apply is to remove the slow trend in brightness due to changing phase angle and distances to the Earth and Sun. To do this, we assume a linear rate of change of magnitude dm/dt due to the effects of changing distances and changing phase angle. Usually, we take dm/dt to be simply the difference from one night to the next of the predicted magnitude, from the ephemeris. The above relative magnitudes are then corrected by $-(t - t_o)dm/dt$, thus removing the linear trend in the lightcurve. The reference time t_o is best chosen near the middle of the time span of the lightcurve, but can often be chosen to be at 0^h UT for convenience, without introducing significant error.

In order to make full use of the observations, it is desirable to transform observations to a standard magnitude scale, so that observations from different observatories or different apparitions can be compared. In taking the observations for the extinction solution described above, one should include both local comparison stars, which are observed with the asteroids, and some standard stars, with magnitudes that are known on a standard magnitude system. The lists of standards along the equator by Landolt (1973,1983) are particularly useful. In general, a simple linear transformation suffices to relate instrumental magnitudes (v_o,b_o) to an absolute system (V,B)

$$V = v_o + \epsilon(b_o - v_o) + \zeta_v \qquad (7)$$

$$(B - V) = \mu\,(b_o - v_o) + \zeta_{b-v} . \qquad (8)$$

The transformation constants ϵ, μ, ζ_v and ζ_{b-v} are found by linear least-squares fit between the measured v and $b - v$, and tabular V and $B - V$ values

for the standard stars. The V and $B - V$ values for comparison stars can then be computed from Eqs. (7) and (8). In general, the transformation constants ϵ, μ, and ζ_{b-v} are fairly constant for a given system from night to night, so it is only necessary to rederive them occasionally, on nights of particularly good conditions and complete observations. The constant ζ_v defines the system sensitivity, which generally changes any time the high voltage to the photomultiplier tube is changed or cycled off and on. Thus, it should be redetermined for each night of observation. The other constants should be redetermined any time a significant change in the system is made, such as cleaning or recoating the optical surfaces. As noted above, this should be reserved if possible for a night of exceptional photometric quality.

The transformation equation for converting the asteroid magnitudes from the instrumental to standard system can be derived by combining equations of the form of Eq. (7) for asteroid and comparison readings

$$V_a = dv - (t - t_o)dm/dt + v_c - 5\log(r\Delta) + \zeta_v + \epsilon(b_o - v_o)_a \quad (9)$$

where dv is the magnitude difference from Eq. (6), the next term is the small correction for changing distances and phase, v_c is the instrumental magnitude of the comparison star (v_o from the previous section), the log term is the reduction to unit Earth and solar distances, and the remaining terms are the transformation to the standard color system. Note that t_o is not necessarily the same as that in Eq. (3), although they both refer to reference times chosen near the middle of the time span of observations.

III. ERROR ANALYSIS

Each measurement of an asteroid, star or background sky should consist of several readings so that the standard error can be computed from the dispersion among readings. Since the random fluctuation in count rate sets a minimum uncertainty of $N^{1/2}$ on a reading of N counts, the standard error σ is the larger of that from the measured dispersion or $N^{1/2}$. The total uncertainty of dv is

$$\sigma_{dv}^2 = 1.17 \left[\frac{\sigma_a^2 + \sigma_s^2}{(N_a - N_s)^2} + \frac{\sigma_c^2 + \sigma_s^2}{(N_c - N_s)^2} \right]$$
$$+ [\sigma_E^2 + \sigma_E^{\cdot 2}(t_a - t_c)^2](X_a - X_c)^2. \quad (10)$$

The subscripts a, c and s refer to asteroid, comparison and sky readings, respectively, σ_E is the uncertainty in the value of the extinction coefficient, and $\sigma_E^{\cdot}$ is the uncertainty in the time variation of extinction. These latter quantities can be estimated from the plot of extinction and its error envelope.

In spite of the many errors combined into Eq. (10), σ_{dv} often turns out to be quite small, perhaps only a few thousandths of a magnitude. This is espe-

cially true when dealing with relatively bright asteroids where the intention is to derive a very high-precision lightcurve. On the other hand, the formal error on v_c and on the transformation coefficients are often much larger, perhaps one or a few hundredths of a magnitude. For this reason, it is useful to report three separate error quantities:

1. The uncertainty of the magnitude level with respect to the local comparison star (either derived from the values of σ_{dv} for the night or the dispersion of the points in an individual lightcurve from the fitted composite);
2. The uncertainty of the magnitude of each comparison star used with respect to the others used on different nights;
3. The uncertainty in the transformation of the comparison star magnitudes to a standard magnitude system.

For some purposes, such as the uncertainty in the shape of a composite lightcurve or the phase relation when the same comparison star was used on successive nights, only the smaller error bar σ_{dv} applies. On the other hand, when comparing absolute magnitudes from one observatory to another or from one apparition to another, the full uncertainty must be allowed.

IV. COMPOSITE LIGHTCURVES

It is not necessary, and often impossible, to cover the complete rotational phase of the lightcurve on a single night. Since the variation is nearly periodic, one can superimpose coverage on successive nights to form a composite lightcurve. This can be done efficiently with a Fourier analysis fitting procedure (see, e.g., Harris et al. 1989a). The lightcurve is represented by the following function

$$V(\alpha,t) = \bar{V}(\alpha) + \sum_{l=1}^{n} \left[A_l \sin \frac{2\pi l}{P} (t - t_o) + B_l \cos \frac{2\pi l}{P} (t - t_o) \right] \quad (11)$$

where $V(\alpha,t)$ is the computed reduced magnitude at phase angle α and time t, $\bar{V}(\alpha)$ is the mean absolute magnitude at phase angle α, A_l and B_l are Fourier coefficients, P is the rotation period, and t_o is a zero-point time chosen near the middle of the time span of the observations. The above function can be fitted with a linear least-squares formulation for a fixed value of the period, and fixed degree n. In practice, it is efficient to grid search the solution space to determine the optimum degree n and period or periods P, and the uncertainty of P. If only one acceptable value of P is found, then the period determined can be assumed to be the correct rotation period. Occasionally, more than one acceptable value of P is found, either because of a limited data set, or because the lightcurve is of low amplitude so that it may have more or less than the usual two extrema per rotation cycle.

Figures 2 and 3 illustrate a typical result of Fourier analysis of a set of lightcurve data. Figure 2 is the composite lightcurve of 44 Nysa, based on 23 individual lightcurves. Figure 3 is the phase relation, or mean magnitude as a function of solar phase angle, for the 23 nights of observation. The solid line is the least-squares fit of the $H - G$ magnitude relation. There is clearly a deviation of the fitted function from the data. This is an example of the opposition surge observed on high-albedo objects, and is discussed more fully in the chapter by Bowell et al. The full documentation of the observations is reported by Harris et al. (1989*b*).

The rate of change in brightness dm/dt used in the initial reductions, depends in part on the phase relation (e.g., Fig. 3), which is often not known exactly in advance. Thus, to achieve maximum accuracy, an iterative procedure can be adopted. After deriving a first estimate of the phase curve, new values of dm/dt can be derived from that curve, and those values used to improve the reductions of the individual lightcurves. This was done for the 44 Nysa observations shown here. Because of the unexpectedly steep phase relation near zero phase, dm/dt turned out to be about three times greater than the initial estimates on the nights of lowest phase angle, exceeding 0.1 magnitude/day.

In the above fitting procedure, it is assumed that the lightcurve is exactly periodic, and does not change form over the time span covered. In fact, the
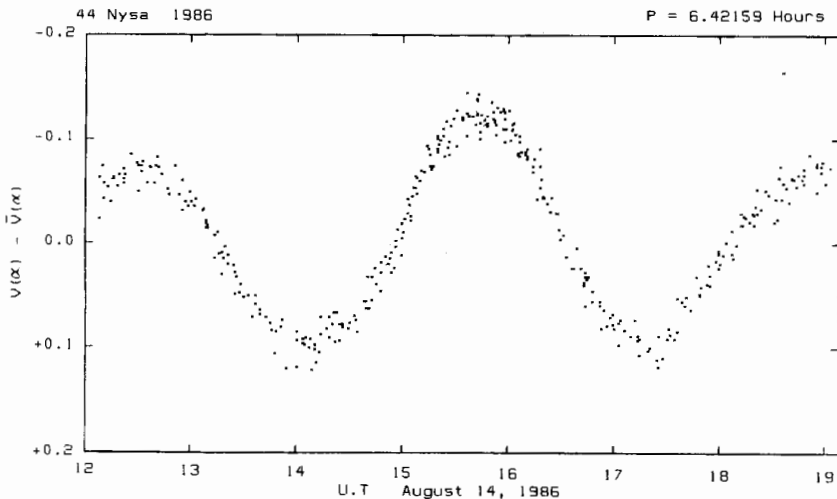
Fig. 2. The composite lightcurve of 44 Nysa, obtained on 23 nights from June to October, 1986. There are 340 individual observations in this plot. The lightcurve was constructed with the Fourier-analysis method described in the text. There was some slight change in lightcurve form over the course of the observations, as revealed by the strings of deviant points near the extrema at 14ʰ and 15ʰ5.
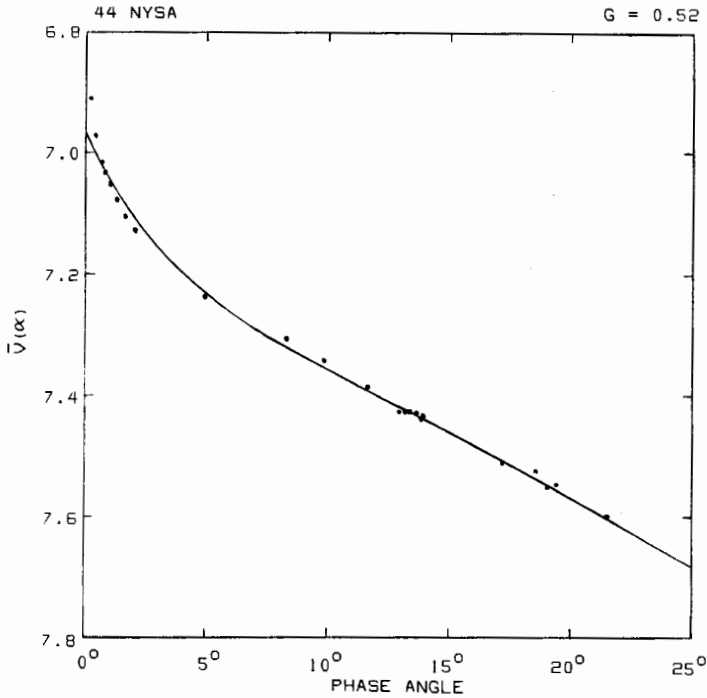
Fig. 3. The phase relation of 44 Nysa, obtained from the same Fourier analysis as the lightcurve in Fig. 2. The computation of the Fourier fit, including machine plotting of both figures, required only a few minutes, and was done on a personal computer.

lightcurve may change form slowly, due to changing aspect or solar phase angle, and the observed synodic period is likely to differ slightly from the constant sidereal rate. The presence of these effects can be detected by fitting shorter spans of data and comparing the results to the long-span fit. In extreme cases, the changes in form and period can be traced in detail by a succession of short-arc solutions (see, e.g., Hahn et al. 1989).

In planning observations, one may wish to obtain a very detailed light-curve on one or within a few cycles; or at the opposite extreme, composite coverage over a more extended period of time. Often factors of telescope scheduling, weather and the period of rotation of the asteroid limit the choices. In general, one should not depend on a single coverage to yield a reliable, detailed lightcurve, because of the danger of confusing background stars, atmospheric effects, etc. As with any good scientific procedure, results should be based on repeated observations. Thus, even a lightcurve designed to be a detailed "snapshot" at one epoch in time should be a composite of at least two redundant coverages. On the other extreme, for maximum accuracy of period determination, or for defining the phase relation, it may be desirable to

fit observations from the longest possible span of time to a single composite lightcurve. In this case, one must be careful to obtain enough data over a short time span to eliminate possible ambiguity in the period determination, and repeat detailed coverage often enough to evaluate deviations from strict periodicity over the range of time spanned. Generally, these effects are negligibly small over times of a week or two, or a phase angle range of a few degrees. Thus even when obtaining a detailed "snapshot," one can often count on a full two week "dark run" over which to obtain full coverage. For purposes of determining a rotation period or defining the mean phase relation, one can often make composite observations spanning the entire apparition, over several months, into a single lightcurve. Exceptions are observations of near-Earth asteroids, where the aspect may be changing rapidly, and observations at very low phase angle, where the form of the lightcurve may change significantly within the range of the "opposition effect," for only a few degrees of phase angle. Thus, one should not combine incomplete coverage over more than a few degrees of solar phase angle in the opposition-effect range, less than about 5 or 6 degrees phase angle.

Having defined the time one has to obtain complete coverage, the next question is, what constitutes "complete" coverage? Consider a sphere which is painted with alternate sectors of black and white. For the two-sector case (hemispherical sectors), viewed equatorially, the lightcurve amplitude is equal to the full contrast between black and white. For increasing numbers of sectors, the lightcurve amplitude becomes less, because the variation in total white vs black area visible becomes less and less. The same effect occurs for higher-order variations in the shape of the object, where the resulting variation in the cross-sectional area becomes less and less, even for very large-scale but high-order variation in the shape. Russell (1906) calculated the amplitudes of the harmonic coefficients which result from large-scale variations in either the albedo or the surface curvature (which is an equivalent expression of the shape). He found that, even for unit variations in albedo (or curvature), the 10th harmonic should have an amplitude of only 0.005 magnitude, and by the 20th harmonic, the amplitude would be only 0.0008 magnitude. Thus, if one wants to define the lightcurve of an asteroid to <0.01 magnitude, a 10th-degree fit should be entirely sufficient, and a 20th-degree fit should define the curve to 0.001 magnitude. In practice, we find that these are, if anything, over estimates of amplitudes which occur on real asteroids. We have found no terms exceeding a few thousandths of a magnitude above the 10th order.

It appears, then, that all of the information in a lightcurve, down to the typical noise level of a few thousandths of a magnitude, can be expressed in terms of about 20 harmonic coefficients. In principle, 20 perfectly spaced and error-free data points would suffice to define the curve. We also need one additional point per individual lightcurve, to define the mean magnitude level for each lightcurve. It is prudent to oversample the lightcurve by a factor of two or so to allow for imperfectly spaced data points and occasional errors in

observation. Thus, a composite lightcurve of about 50 data points, well spaced, should suffice to define the lightcurve down to the noise level. A fairly high density of data points on one or two nights will help to resolve any possible ambiguity, but otherwise it is desirable to spread the observations over a longer time span in order better to determine the period and the phase curve. At Table Mountain Observatory, we attempt to obtain about 10 data points per night on a given asteroid, and alter our observing strategy as appears necessary based on preliminary reductions of the data.

Some words of caution are in order regarding the physical interpretation of the harmonic coefficients obtained from the above procedure. Just as it is necessary to sample the function at least twice per cycle of the highest frequency component present (the sampling theorem), it is also necessary that there be no gaps in coverage greater than one half cycle of the highest frequency present; that is, if we have only the minimum necessary number of points, they must be equally spaced. If we have oversampled, then the points can be unequally spaced, so long as there are no gaps longer than in the case of the minimum number of equally spaced points. If this condition is met, then the coefficients can be taken as physically meaningful, e.g., for interpretation of shape and pole orientation calculations (but see the next paragraph). If the condition is not met, the Fourier analysis may still have value for defining the period, an "epoch of extremum," or light level of maximum or minimum brightness, so long as the relevant part of the lightcurve is not the part with the gap in coverage. In this case, the Fourier analysis is just a convenient curve-fitting tool, and the coefficients cannot be given physical significance, as for example, the presence of odd harmonics which might otherwise be interpreted as evidence for albedo variations.

A second note of caution is that harmonic coefficients in magnitude space are not simply related to shape, or albedo, for that matter. A more fundamental basis would be a harmonic analysis in units of intensity squared, where a geometrically scattering ellipsoid at zero phase angle would yield only a single second harmonic term (see, e.g., Pospieszalska-Surdej and Surdej 1985). In magnitude space, the same lightcurve would yield an infinite series of even harmonics. On the other hand, it is difficult to deal with the changing brightness level of an asteroid with phase angle, and an unknown period, in computing Fourier coefficients in intensity-squared units. Thus we recommend the magnitude formulation above for the purpose of constructing the composite and assessing the suitability of the resulting lightcurve for physical interpretation, but the composite should be re-analyzed in intensity-squared units for shape and pole studies.

V. REPORTING OF ASTEROID LIGHTCURVE DATA

Recent theoretical progress in the analysis of asteroid shapes and pole orientations, and in the interpretation of phase relations, has given cause to re-

analyze data from earlier publications. Recognizing that one cannot fully anticipate the use to which observations may someday be put, we feel it would be useful to make some comments regarding the essential contents of a report of lightcurve observations. It is not our intention to promote a specific format, but only to call attention to the necessary data which must be given in order to allow future researchers to reconstruct accurately the original observations.

The most important information which must be contained in a complete report are quantities that cannot be found out or inferred otherwise: the instrumental characteristics which may influence the accuracy of the results; the identifications of the objects observed (asteroids, comparison stars and standard stars); the magnitudes and colors of comparison stars and asteroids used to compute final magnitudes; and the error estimates on all quantities. The actual observations should be presented in a form such that full accuracy is preserved. We prefer a table of times (light-time corrected), reduced magnitudes, and error estimates for each measurement. If such a table is too lengthy to publish in printed form, it should be made available by the author, either privately or, better, through an established data archive. We cannot emphasize too strongly that this is the most important element of the publication. The original data must be recoverable, either from figures, tables or a public data archive.

Of less importance is information which can be reconstructed, namely the aspect data. Nevertheless, it is convenient to list at least a summary of the position in the sky, phase angle range observed, etc. in the written report. A more detailed tabulation of aspect might well be deferred to a machine readable table, along with the observations. We prefer to list in a summary table the ecliptic coordinates of the phase-angle bisector (the mean of the geocentric and heliocentric positions) on one reference date (opposition, or near the middle of the interval of observations), and in the more detailed aspect table, the geocentric right ascension and declination, as well as the longitude and latitude of the phase-angle bisector, for each date of observation. Also, the phase angle on each night should be included. Geocentric and heliocentric distances have traditionally been included in aspect tables, but these are unnecessary if times reported are light-time corrected, and magnitudes are reduced to unit distances.

Generally, presenting individual lightcurves, or composites in sufficient detail to allow one to reconstruct the original observations, is not very space efficient. We recommend instead presenting figures in only such detail as necessary to illustrate the points of discussion, and encourage those wishing to reanalyze the data to use tabular data of full accuracy, rather than attempting to reconstruct original data from a figure. Again, however, we must note the importance of being able to retrieve the original data, so if it is not provided in any other form, then the figures must be of sufficient quality and clarity that the individual data points can be extracted.

In reporting results of lightcurve observations, care should be taken to

provide estimates of uncertainty for the period and the magnitude level of each individual lightcurve, and an appraisal of the reliability of the period given—that is, are there any other possible periods, completely different from the stated range of uncertainty? The reliability scale used in the lightcurve data base (Part VI) should be used for this purpose.

For phase relations, two conventions have been used in reporting magnitudes: either the mean light level or the maximum light level. The mean level follows naturally from the Fourier analysis above, but in the case of incomplete lightcurve coverage, the mean level is not well defined, so there will be cases where the maximum light, or some other reference level, may be more appropriate. Furthermore, if the lightcurve changes amplitude or shape in the course of observations, then neither level may be a good choice. However, for the more common case where there is no discernible change in the lightcurve structure in the course of observations, either level can be used equally well. We encourage reporting of both levels, or just a difference between the levels, along with a statement of the total range of variation. The three error quantities mentioned in Sec III should be reported: the uncertainty in magnitude level for each night; the uncertainty in relative magnitudes between the local comparison stars used; and the uncertainty in the transformation of magnitudes to a standard scale. In reporting the absolute magnitude and phase relation, we follow the IAU magnitude system (Bowell et al. 1989), but for comparison with earlier work, it is useful to give also the linear constants $V(1,0)$ and β_V. We obtain these by transformation of the H and G values as described by Bowell et al. (1989). It is important in reporting phase-relation solutions to provide the quantities necessary to reconstruct the error envelope for magnitude as a function of phase angle. For the approximation given by Bowell et al. (1989), one needs to specify the mean phase angle of the observations $\langle\alpha\rangle$, the uncertainty in magnitude at that phase angle, and the uncertainty in the slope of the phase relation. These quantities can be determined by a linear regression of the residuals to the fit, and should be included in a report of a fit of the $H - G$ magnitude relation to a set of observations.

VI. AVAILABILITY OF COMPUTER PROGRAMS

Computer programs that solve the two principal problems discussed above, the determination of the time-variable extinction function for a night, and the construction of the composite lightcurve by Fourier analysis, are available from A. W. Harris by sending a blank 5 1/4 inch (DS/DD or DS/HD) diskette. The programs are in Microsoft Fortran, and will be provided in IBM DOS format. Because of the large array sizes and volume of calculations involved, a machine of the IBM/AT class, with floating point coprocessor, is advisable. Unfortunately, the plotting routines are quite specific to one (rather uncommon) printer, and are not included. Commercially available plotting routines could be used instead. All programs are in the public domain (un-

copyrighted), and are development versions, in which a few bugs may still be present. They are offered with no warranty or liability assumed.

Dedication and Acknowledgments. This chapter is dedicated to James W. Young, the Resident Observer at Table Mountain Observatory. It is a tribute to the high quality of his observations that such refined methods of analysis have been possible, and the quantity of his observations are directly responsible for the development of the automated methods of analysis reported here. The research reported in this chapter was supported at the Jet Propulsion Laboratory, California Institute of Technology, under contract from the National Aeronautics and Space Administration.

REFERENCES

Bowell, E., Harris, A. W., and Lumme, K. 1989. A two parameter magnitude system for asteroids. *Icarus,* to be submitted.

Hahn, G., Magnusson, P., Harris, A. W., Young, J. W., Belkora, L. A., Fico, N. J., Lupishko, D. F., Shevchenko, V. G., Velichko, F. P., Burchi, R., Ciunci, G., Di Martino, M., and Debehogne, H. 1989. Physical studies of Apollo-Amor asteroids: UBVRI photometry of 1036 Ganymed and 1627 Ivar. *Icarus,* in press.

Hardie, R. H. 1962. Photoelectric reductions. In *Stars and Stellar Systems, Vol. II, Astronomical Techniques,* ed. G. P. Kuiper (Chicago: Univ. of Chicago Press), pp. 178–208.

Harris, A. W., and Young, J. W. 1983. Asteroid rotation IV. 1979 observations. *Icarus* 54:59–109.

Harris, A. W., Young, J. W., Bowell, E., Martin, L. J., Millis, R. L., Poutanen, M., Scaltriti, F., Zappalà, V., Schober, H.-J., Debehogne, H., and Zeigler, K. W. 1989a. Photoelectric observations of asteroids 3, 24, 60, 261, and 863. *Icarus* 77:171–186.

Harris, A. W., Young, J. W., Contreiras, L., Dockweiler, T., Belkora, L., Salo, H., Harris, W. D., Bowell, E., Poutanen, M., Binzel, R. P., Tholen, D. J., and Wang, S. 1989b. Phase relations of high-albedo asteroids: 44 Nysa and 64 Angelina. *Icarus,* in press.

Landolt, A. U. 1973. UBV photoelectric sequences in the celestial equatorial Selected Areas 92–115. *Astron. J.* 78:959–1020.

Landolt, A. U. 1983. UBVRI photometric standard stars around the celestial equator. *Astron. J.* 88:439–460.

Pospieszalska-Surdej, A., and Surdej, J. 1985. Determination of the pole orientation of an asteroid. The amplitude-aspect relation revisited. *Astron. Astrophys.* 149:186–194.

Russell, H. N. 1906. On the light-variations of asteroids and satellites. *Astrophys. J.* 24:1–18.

CCD PHOTOMETRY OF ASTEROIDS

LINDA M. FRENCH
Air Force Geophysics Laboratory

and

RICHARD P. BINZEL
Massachusetts Institute of Technology

Since their advent in 1976, charge-coupled devices (CCDs) have provided astronomers with the ability to make observations which were virtually impossible only a few years ago. A practical discussion is presented on the relative merits and disadvantages of charge-coupled device detectors in their application to asteroid photometry. We briefly describe the necessary calibration steps for CCD data, and suggest strategies for optimal observing efficiency. The primary methods of CCD data reduction are outlined, and two sample asteroid lightcurves which were determined with CCDs are shown.

I. INTRODUCTION

Charge-coupled device (CCD) detectors have revolutionized astronomy since the early 1980s. Degewij and van Houten (1979) pointed out the unavailability of sufficient observing time with large telescopes to make extensive lightcurve studies for distant objects. The increased quantum efficiency and two-dimensional nature of CCDs has remedied this situation by making possible precise photometric studies of objects with V magnitudes in the range of 15 to 20 using small to moderate-sized telescopes, on which large amounts of observing time are more readily available. In this chapter, we discuss the application of CCDs to asteroid photometry, give a very basic outline of the reduction process for CCD images, and demonstrate that this new technique

can be used to obtain scientifically useful information on previously "unobser-vable" faint asteroids. We do not attempt here anything more than a brief introduction to the operating characteristics of CCDs; excellent overviews are given by Janesick et al. (1987) and Mackay (1986). Tyson (1986) reviews the astronomical uses of CCDs.

The advantages of photometry from two-dimensional images have been recognized as long as photographic plates have been used for quantitative measurements. With careful reduction, the photometric precision of CCDs is far superior to that attainable by the photographic technique. The first advan-tage of two-dimensional photometry is that many objects such as the target asteroid and several comparison stars can be recorded within a single ex-posure, thereby making more efficient use of telescope time. Second, in stan-dard photoelectric aperture photometry, one must use a relatively large aperture to avoid systematic errors due to telescope tracking deviations and seeing variations. With a CCD image, one chooses an aperture size during data reduction after observing; therefore, it is often possible to use smaller apertures and hence obtain more precise measurements for faint objects. Howell (1989) discusses the determination of an optimum aperture. Third, contamination due to nearby field stars and cosmic rays can be easily detected and often removed from the images. Fourth, sky measurements are made simultaneously with those of program objects, thereby reducing photometric errors caused by short-term variability of the atmosphere. Finally, for long exposures (>5 min), less-than-perfect photometric conditions (e.g., thin cirrus) can yield useful data for many purposes, since the asteroid and com-parison stars are all imaged simultaneously and transparancy variations are averaged out over the small field of the image.

The merits of CCD photometers are great, but they are somewhat offset by the increased complexity of CCDs over photoelectric photometers. CCDs are kept at a stable operating temperature above that of liquid nitrogen by means of an electronic servo system; if that system malfunctions and the de-tector gets either too warm or too cold, the performance deteriorates markedly. The complex electrical contacts within a CCD detector are easily jarred loose by trips up and down mountain roads and by frequent instrument changes. On several occasions, CCD systems have continued to function with one or more such contacts broken, but with performance degraded in strange, not immediately recognizable ways. For these reasons, most high-performance CCD systems are maintained by engineering staffs with specialized training.

In addition, data analysis for the astronomer is time consuming and the computation is expensive. Enormous amounts of data are generated: a single CCD frame containing an asteroid and a few comparison stars contains ap-proximately one-half a megabyte of information, although only a small frac-tion of this is typically utilized in the reduction. A single night of observing can easily produce more than 100 frames, making a dedicated computer with a large storage device essential. Also, for projects where images are needed

more frequently than once per 30 s or so, most CCD photometers are at a disadvantage because of the long time required for readout of the image from the chip and the transfer to the storage device on the computer. However, a high-speed CCD photometer has been developed as described by Stover (1986). While their expense and complexity make it unlikely that CCD instruments will soon replace photomultiplier tubes as the photometric detectors in small observatories, they are ideal for systematic photometric, spectroscopic and astrometric studies of faint asteroids of great scientific interest. We close this chapter with two examples of such photometric studies; for an example of the application of CCD spectroscopy to the study of asteroids, the reader is referred to Vilas and Smith (1985). Gehrels (1981) and Gehrels et al. (1986) describe the use of CCDs for asteroid survey and astrometric work.

II. CCD DETECTORS AND THEIR ADVANTAGES

Fundamentally, a CCD is a two-dimensional solid-state detector, in the structure of a grid (rows and columns) of picture elements, or pixels. Each pixel is composed of a photoelectrically sensitive material and held at a slight positive potential, so that incoming photons are converted to electrons and trapped within the pixel's potential well during the exposure time. When the exposure is completed, a computer reads out the image one pixel at a time: typically, the lowest row is read, pixel by pixel, then the voltages on the second row are varied to allow the photoelectrons to move down to the first row where they are read out pixel by pixel and so on until the entire task is completed. The readout process and the analog to digital conversion of the electrons is described more fully in Mackay (1986). This readout introduces a source of noise typically amounting to 5 to 70 electrons per pixel, independent of exposure time.

A major advantage of CCD photometry is apparent immediately: one retains spatial information about the asteroid and its surroundings during each observation. Faint stars which would contaminate the photometry might not be visually apparent to an observer while centering the aperture of a photoelectric photometer; with a CCD such stars are apparent in the image and their effects can be removed (if they are not too close to the asteroid).

The processing of CCD data is facilitated by the intrinsic stability of the devices: each pixel reacts to light in a repeatable fashion and careful processing can remove virtually all the systematic instrumental effects. A final advantage for lightcurve observing is instant data analysis; one would like to know in the middle of a night's observing whether a new target is varying on a time scale of minutes, hours or days. Although the reduction process for CCD frames is complicated, the multi-tasking computers in use at observatories such as Kitt Peak and Cerro Tololo make on-line data reduction possible during a night of observing. With such a system and a little practice, one can plot a lightcurve during the first night for a short-period object.

Many types of CCD chips are currently in use. Reviews of RCA CCDs are given by Fowler et al. (1981) and Geary and Kent (1981), while Blouke et al. (1987) review TI 800 × 800 chips. A useful comparison of RCA, GEC and Thomsen CCDs is given by Thorne et al. (1986). Most chips have their highest quantum efficiencies in the V to R part of the spectrum; this is ideal for the red slopes generally seen in asteroid spectra. CCD quantum efficiencies usually fall off into the blue and ultraviolet, and although U and B filters still may provide useful compositional information if no other observations are available, long integration times are needed with a small telescope for good signal-to-noise ratio observations in the U bandpass. The low quantum efficiency of the CCD and the sharp variation in quantum efficiency for most chips across the ultraviolet region of the spectrum make accurate color transformations extremely difficult; for this reason we do not recommend CCDs for ultraviolet studies of asteroids. For blue and ultraviolet observations, the thinned RCA chips or a thick chip which has been ultraviolet-flooded to improve the quantum efficiency at short wavelengths are most suitable. At the other end of the visible spectrum, thinned CCD chips such as the RCA devices show significant interference fringes (with pixel-to-pixel variations of ~25% in some cases) due to night-sky emission lines within the I bandpass (Thorne et al. 1986). Such fringes cannot be easily removed by standard calibration frames; instead a more complicated flattening process using long-exposure sky frames must be employed. For these reasons, we recommend using V and R filters if a transformation to magnitudes in a standard photometric system is desired.

III. REDUCTION AND ANALYSIS OF CCD DATA

A. Systematic Effects

Ultimately, of course, the scientific goal of CCD photometry and more traditional methods is the same: a precise record of an object's intrinsic brightness variation as a function of time in one or more colors. To reach that goal, one must convert the raw initial images produced at the telescope into images with a linear intensity scale. Several systematic effects must be removed from CCD data prior to analysis. These are:

1. *Removal of DC offset.* The positive voltage used to hold the photoelectrons in their potential wells during the exposure will cause a nonzero direct current (DC) signal when the chip is read out. This offset level can be determined from an overscan region which usually consists of rows or columns masked off at the edge of each frame. Removal usually consists of averaging the overscan pixels to form a single constant and subsequently subtracting that constant from the image. The overscan regions are then discarded.

2. *Bias-frame subtraction.* In addition to the individual DC level for each frame, a low spatial frequency variation in the amplifiers across the chip may remain. The variation occurs in both rows and columns, necessitating a two-dimensional subtraction of a frame showing the structure of the chip. (See Gilliland and Brown [1988] and Mackay [1986] for a complete discussion of this effect.) The simplest method of measuring the bias is by means of a zero-second exposure with the dark shutter closed. Because subtracting only a single bias frame would introduce readout noise from that frame, it is usually advisable to average many bias frames before subtraction. In systems where the DC level remains constant throughout the night, a series of bias frames taken in the evening and in the morning, suitably filtered and averaged, will suffice for determining the bias level. Consultation with an expert user of the CCD photometer one is planning to use is recommended for choosing the optimal method of removing the DC offset and bias subtraction.

3. *Flat-field correction.* All chips retain pixel-to-pixel variations in sensitivity, which can be removed by dividing the data frames by a high signal-to-noise flat-field frame. A normalization factor is introduced to preserve the original count rates as closely as possible. Typically, the signal level for the flat-field exposure should be about one-half the full potential well depth. Averaging and median filtering several flats will reduce the readout noise from this step as well. Dome flats will be sufficient for broadband photometry of many point sources; the best arrangements use internal projectors and color-balanced lamps so that the flat fields are closely repeatable within an observing run. To attain the best precision ($<1\%$), it may be necessary to use twilight sky flats or even long-exposure astronomical images minus stars and galaxies. The subtleties of flat fielding are discussed by Baum et al. (1981).

4. *Dark-current subtraction.* Dark currents on most professionally maintained CCDs are very low and at worst add a uniform, though noisy, background level. When obtaining images, it is best if objects of interest are placed in the field so as to avoid any "hot" pixels which have very high dark counts. Because modern CCDs usually have very low dark-count levels, it is better not to subtract a dark frame because the procedure adds noise; additionally, cosmic rays present in the dark frame are introduced into the data. Occasional dark frames taken in the afternoon (from 30 to 60 min in length) help to verify that the dark level is indeed low.

5. *Check for cosmic-ray events.* Meaningful photometry of point sources, such as asteroids, will not be possible if one is unlucky enough to have a cosmic-ray event within the image profile. (Some asteroids seem to be virtual cosmic-ray magnets.) For a cosmic-ray strike on the asteroid profile, one can only discard the image. Use of multiple comparison stars (see Sec. II.D) allows a differential magnitude for the asteroid to be derived even if one comparison star is unusable due to a cosmic-ray event.

Care also must be taken to insure that a cosmic-ray event also does not occur in the region where sky measurements are made. In this case, use of an alternate sky location or an interpolation and replacement of the contaminated pixels can often allow successful photometric measurements.

The above steps can be expressed mathematically. If one denotes the initial raw image by I, the direct current level for each frame by DC, the bias structure frame value by B, and the flat-field frame by FF, the final processed image value for each pixel will be

$$\text{Final Image} = \frac{(I - \text{DC}_I) - \langle B - \text{DC}_B \rangle}{N \langle (\text{FF} - \text{DC}_{\text{FF}}) - \langle B - \text{DC}_B \rangle \rangle} \tag{1}$$

where $\langle \rangle$ indicate a quantity which is an average over many frames and N is a normalization factor so that the average pixel value in the denominator is unity.

B. A Basic Cookbook for CCD Calibration and Reductions

Obtaining the calibration frames is a vital part of a successful night of observing and thankfully these can be obtained during the afternoon without taking away from one's observing time. An afternoon's preparation for a night's observing might proceed as follows: Take 10 to 30 bias frames, subtract the DC offset from each, and average and median filter them. The resulting bias-correction frame corresponds to the quantity $<B-\text{DC}_B>$ in Eq. (1) above. Take 10 to 30 flat fields in each filter, checking that the exposure time gives the signal level as explained in Sec. III.A. Subtract the DC offset and the bias-correction frame from each flat-field image. Average and median filter the resulting flats for each color to obtain the corrected flat-field frame corresponding to the quantity $\langle (\text{FF}-\text{DC}_{\text{FF}})-\langle B-\text{DC}_B \rangle \rangle$ in Eq. (1). If we denote the average pixel value in the corrected flat-field frame by A, then the normalization factor N is simply equal to A^{-1}. Check the dark current with a 30 to 60 min dark frame to verify that it is indeed low. When finished averaging bias and flat frames, delete the individual frames from the disk and store the averaged frames to a raw data tape or other archival storage device. During the night's observing, each new image can be saved to the raw data tape; many observatory computers allow the images to be processed in the background while observing. After saving the raw image (I) on tape, each can then have the DC offset (DC_I) and the bias-correction frame subtracted and then be divided by the appropriate corrected flat-field frame and normalization factor. This yields the processed "Final Image" denoted in Eq. (1) which should be stored on magnetic tape.

C. Strategies for CCD Observing

One's observing strategy will largely be dictated by the telescope and instrument capabilities and the goals of the observing run. Generally, a field several arcmin across is desired for the CCD image with an optimal scale being on the order of one arcsec per pixel; such a scale may require the use of a reducing lens in the optical system. This relatively wide field has the advantage (one hopes) that many viable comparison stars will be located within the field. If the field can be rotated, the long axis of the chip should be aligned in the predominant direction of the asteroid's motion (usually east-west). This will allow chosen comparison stars to remain on the chip longer before the asteroid's motion forces them out of the field.

Finding charts are not always needed to locate the target asteroid amid the clutter of background stars and galaxies ("the vermin of the sky" for asteroid observers), although their use can increase the observer's efficiency. An asteroid's motion will usually reveal its identity even for relatively uncertain ephemerides. If the imaging system displays new images by scrolling across the display screen and directly replacing the old image, then two short exposures (without moving the telescope) can be used in a blink-comparator method. By carefully watching the new image as it is displayed, star images will reappear on top of themselves while the asteroid image will appear to jump. The exposures must be long enough to reach beyond the expected magnitude of the asteroid and should be separated by about 5 min. The second option for locating the target asteroid through its motion is simply to take an old-fashioned time exposure of about 10 min, guiding at the sidereal rate. The asteroid's trail in the image will reveal its presence.

Placement of the asteroid's image in the frame for systematic observing is a critical step. The asteroid should be imaged in a "clean" region, free of hot pixels, bad columns, etc. It is advisable to adjust the pointing of the telescope periodically to keep the asteroid image in the same region, while allowing the star field to advance across the image. This keeps the flat-field characteristics of the asteroid images nearly constant. On the other hand, flat-field uncertainties will affect the comparison stars. However, by using several comparison stars and averaging them, such sources of error are reduced. It is best to choose comparison stars ahead of the asteroid's direction of motion so that they remain on the chip for the longest possible time. New comparison stars can be chosen as the old ones drift out of the field.

Exposure times will depend on the telescope aperture, instrument sensitivity and the magnitude of the object. Typical exposures to achieve 1% precision in a broad filter on a 17th magnitude asteroid may be in the range of 3 to 5 min for a 1 m telescope. During this time, most main-belt asteroids will display trails if the telescope is tracked at the sidereal rate. For aperture photometry (discussed in Sec. III.D), this is unlikely to have a large systematic effect if the photometric aperture necessary for the asteroid is the same as that required for the comparison stars.

An advantage of wide-field imaging, where lightcurves are derived from on-chip differential magnitudes between an asteroid and comparison stars, is that observations can be obtained in less than ideal photometric conditions, e.g., through thin cirrus clouds. Limitations arise if the added extinction becomes so severe that insufficient photons can be gathered on the object for the desired photometric precision or if the background light level increases significantly (such as by cloud-scattered moonlight). (See Howell et al. 1988 for a more detailed discussion of these limitations.) Exposures taken under conditions of variable extinction should be at least 5 to 10 min long so as to average out variations over the entire field.

Finally, photometric calibrations on nights of good quality can be made in much the same way as normal photoelectric photometry (see the chapter by Harris and Lupishko). Photoelectric standard stars can be used, although the brighter standards will saturate in the shorter exposure times needed with CCDs. We recommend the standards of Landolt (1983), all located within $10°$ of the celestial equator. *BVRI* colors for southern standards have been published by Graham (1982), and a new fainter extension of that list is in preparation at Cerro Tololo (D. Terndrup, personal communication). Optimally, one should locate a small grouping of standard stars with "asteroidal colors" (0.6 $< B - V <$ 0.9) that can all be imaged within the CCD field. Because extinction coefficients are not often well determined when performing differential photometry, it is best to try to image the standard stars at times when they are at the same air mass as the asteroid to be observed in order to minimize transformation errors. If a transformation to a standard photometric system is needed (for determination of phase curves, for example), one should also include some stars of extreme color (bluer and redder than the asteroid) among the standards.

D. Photometry with CCD Data

The great majority of CCD photometric reduction programs perform functions essentially equivalent to simple aperture photometers; the precise details are dependent on the particular reduction software used. Typically, one sets a radius for the stellar image, in pixels, and an inner and outer radius for the extent of sky around the object. This annulus is then used to determine the sky level for the star. The program then measures the total counts within the stellar aperture, subtracts the expected number of sky counts based on the annulus measurement, and computes an instrumental magnitude for the star. Variation in an asteroid's brightness can be monitored through differential instrumental magnitudes between the asteroid and one or several comparison stars on each frame. The use of several comparison stars per frame is advised as a means of judging the observational errors and also providing for a "hand-off" as comparison stars traverse the chip throughout the night. Observational errors for on-chip differential photometry are more fully discussed by Howell et al. (1988).

Asteroids show a perverse tendency to move through crowded star fields exactly when we would most like to observe them—on the nights when a lightcurve extremum which would resolve an alias is expected, or very close to zero phase angle, for example. Because spatial information is retained, one can often continue observing in crowded fields longer than would be possible with standard photometers. As long as the asteroid's "stellar" radius is not contaminated by a nearby star, one can safely overwrite the contaminated sky region for the asteroid with sky determined from nearby. In this manner, one may lose only a few minutes to a close appulse, as opposed to nearly an hour.

More complicated photometry algorithms than the simple aperture method described above make fuller use of the spatial information available. The most widely used such program, DAOPHOT by Stetson, is designed for photometry of extremely crowded fields, such as the central regions of globular clusters. Given initial values of the mean sky level in the frame and the full width at half maximum of a stellar image, the program determines point-spread-functions (PSF) for a number of bright, relatively isolated stars in the field. These are then averaged to produce a model PSF which is then used to fit and subtract close stellar images. The total time required to set up the initial parameters is perhaps 2 to 4 hr for a frame containing several thousand stars; the computer time required for such a frame may be tens of hours (Stetson 1987). Even for the small number of objects per frame which are typically of interest to asteroid observers, DAOPHOT reductions must be run in batch mode; thus it cannot provide the rapid analysis which is ideal for asteroid lightcurves. In addition, most typical asteroid motions will produce anomalous point-spread functions and the program will not produce good results for these objects. In certain cases, however, such as close satellites of the slow-moving outer planets, DAOPHOT has proven useful for removing a sloping sky gradient. For an example of this, see the work of Klavetter (1989) on Saturn's satellite Hyperion.

IV. SAMPLE CCD PHOTOMETRIC OBSERVATIONS OF ASTEROIDS

In this section we give two examples of asteroid lightcurves which would have been difficult or impossible to obtain photoelectrically. It should be remembered that it is not merely the intrinsic faintness of these asteroids which make them difficult for photoelectric photometers, but also their motion through often-crowded star fields.

The physical properties of small main-belt asteroids are essentially unknown. Knowledge of these properties is central to our understanding of the origin of near-Earth asteroids of similar size and to the investigation of asteroid collisional evolution. Figure 1 shows the lightcurve of asteroid 1981 ED35, a 2.7 km main-belt asteroid. These observations were obtained in November 1987, using the Perkins 1.8-m telescope and an RCA CCD at
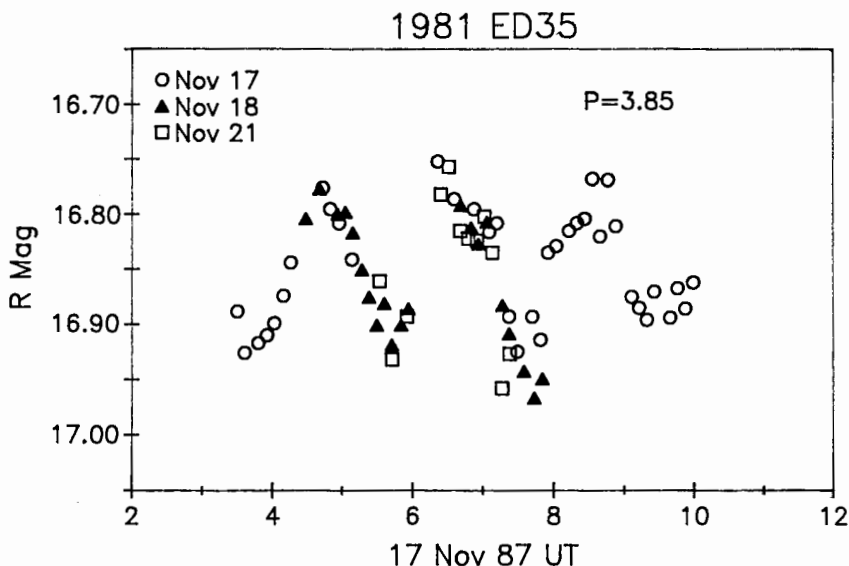
1981 ED35

Fig. 1. Lightcurve of 1981 ED35, a main-belt asteroid with an estimated diameter of 3 km. Observations were made with the Lowell Observatory 1.8-m telescope and an RCA CCD detector (figure from Binzel et al. 1989).

Lowell Observatory (Binzel et al., in preparation). The period of 3.85 ± 0.05 hr is relatively short, as would be expected for a collisionally evolved population or collision fragments (see the chapter by Davis et al.). The amplitude of the lightcurve, 0.18 mag., is relatively low. A CCD photometric survey of many small main-belt asteroids is being conducted by one of us (RPB) and if such low amplitudes prevail in a larger sample, it would indicate that collisional erosion processes may be active in the main belt (see the chapter by Binzel et al.). Also, if small main-belt asteroids exhibit relatively regular shapes, this would contrast with the generally more elongated shapes of the near-Earth asteroids of similar size.

Figure 2 shows the lightcurve of Trojan asteroid 1173 Anchises. This lightcurve was obtained during July 1986 with the Cerro Tololo 0.9-m telescope and a GEC CCD (French 1987). The period of 11.56 ± 0.01 hr is unremarkable, but the amplitude of 0.56 mag is much larger than the average for main-belt asteroids. This is part of an evident trend among Trojan asteroids, indicating that these objects also may have a different collisional history from the main-belt objects. A more extensive discussion will be found in the chapter on distant asteroids by French et al. and in the paper by Hartmann et al. (1988).

Both sets of data shown here have been transformed to standard photometric systems. We note that the photometric precision, 1 to 2%, is typical
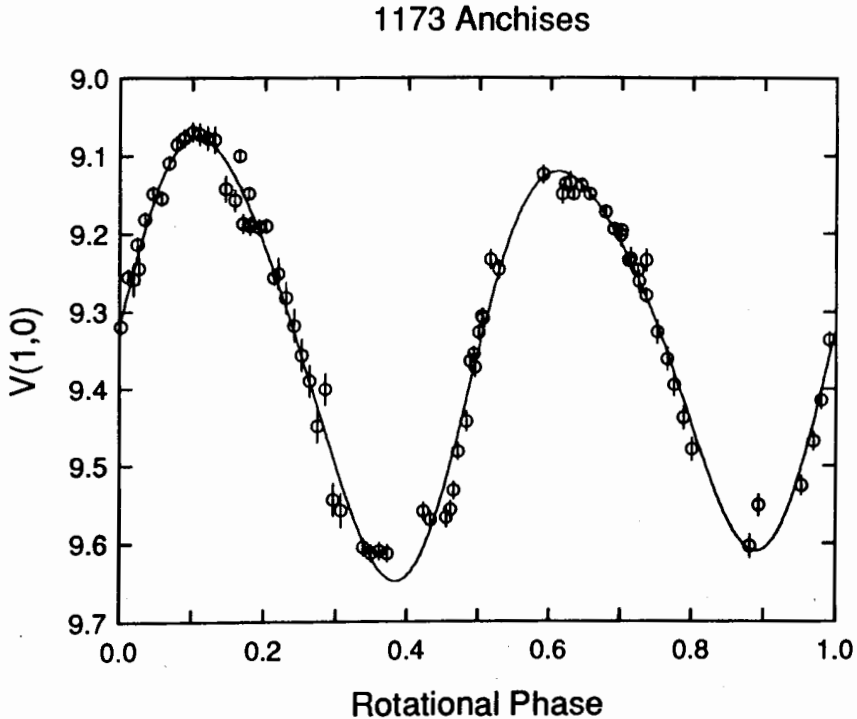
1173 Anchises

Fig. 2. Lightcurve of Trojan asteroid 1173 Anchises, corrected for distance and solar phase-angle effects. Observations were made with the Cerro Tololo 0.9-m telescope and a GEC CCD detector. The smooth curve is a four-component Fourier series used to remove the effects of the mean lightcurve in modeling the phase properties (figure from French 1987).

of what one could attain with most standard photoelectric photometers and is entirely adequate for most purposes.

V. CONCLUSIONS AND FUTURE TRENDS

With CCDs, observations which would have been on the cutting edge 10 yr ago have become routine, and the frontiers are still expanding. CCDs will allow physical measurements to be made of smaller and more distant asteroids and thus provide new information for the investigation of a variety of problems. The availability of blue and infrared sensitive arrays will allow extended spectrophotometric studies for fainter asteroids. Chips with large formats, 2048 × 2048 pixels, are being developed and these devices will be especially valuable for asteroid searches and recovery. As even larger formats are developed in the future, faster computers and advanced software will be needed to handle the increased data rates. Over the next decade, the capabilities of CCDs will continue to challenge astronomers with new opportunities.

REFERENCES

Baum, W. A., Thomsen, B., and Kreidl, T. J. 1981. Subtleties in the flat-fielding of CCD images. *Proc. SPIE* 290:24–27.

Blouke, M. M., Janesick, J. R., Elliott, T., Hall, J. E., Cowens, M. W., and May, P. J. 1987. Current status of the 800 × 800 charge-coupled device image sensor. *Opt. Eng.* 26:864–874.

Degewij, J., and Van houten, C. J. 1979. Distant asteroids and outer Jovian satellites. In *Asteroids,* ed. T. Gehrels (Tucson: Univ. of Arizona Press), pp. 417–435.

Fowler, A., Waddell, P., and Mortara, L. 1981. Evaluation of the RCA 512 × 320 charge-coupled device (CCD) imagers for astronomical use. *Proc. SPIE* 290:34–44.

French, L. M. 1987. Rotation properties of four L5 Trojan asteroids from CCD photometry. *Icarus* 72:325–341.

Geary, J. C., and Kent, S. M. 1981. Imaging characteristics of the RCA 512 × 320 charge-coupled device. *Proc. SPIE* 290:51–57.

Gehrels, T. 1981. Faint comet searching. *Icarus* 47:518–522.

Gehrels, T., Marsden, B. G., McMillan, R. S., and Scotti, J. V. 1986. Astrometry with a scanning CCD. *Astron. J.* 91:1242–1243.

Gilland, R. L., and Brown, T. M. 1988. Time-resolved photometry of an ensemble of stars. *Publ. Astron. Soc. Pacific* 100:754–765.

Graham, J. A. 1982. UBVRI standard stars in the E-regions. *Publ. Astron. Soc. Pacific* 94:244–265.

Hartmann, W. K., Tholen, D. J., Goguen, J., Binzel, R. P., and Cruikshank, D. P. 1988. Trojan and Hilda asteroid lightcurves I. Anomalously elongated shapes among Trojans (and Hildas?) *Icarus* 73:487–498.

Howell, S. B. 1989. Two-dimensional aperture photometry: S/N of point source observations and optimal data extraction techniques. *Publ. Astron. Soc. Pacific,* in press.

Howell, S. B., Mitchell, K. J., and Warnock, A. 1988. Statistical error analysis in CCD time-resolved photometry with applications to variable stars and quasars. *Astron. J.* 95:247–256.

Janesick, J. R., Elliott, T., Collins, S., Blouke, M. M., and Freeman, J. 1987. Scientific charge-coupled devices. *Opt. Eng.* 26:692–714.

Klavetter, J. J. 1989. Rotation of Hyperion I. Observations. *Astron. J.* 97:570–579.

Landolt, A. U. 1983. UBVRI photometric standard stars around the celestial equator. *Astron. J.* 88:439–460.

Mackay, C. 1986. Charge-coupled devices in astronomy. *Ann. Rev. Astron. Astrophys.* 24:255–275.

Stetson, P. 1987. DAOPHOT: A computer program for crowded-field stellar photometry. *Publ. Astron. Soc. Pacific* 99:191–222.

Stover, R. J. 1986. High-speed charge-coupled device (CCD) imaging stellar photometer. *Proc. SPIE* 627:195–200.

Tyson, J. A. 1986. Low-light-level charge-coupled device imaging in astronomy. *J. Opt. Soc. Am.* 3:2131–2138.

Thorne, D. J., Jordan, P. R., Waltham, N. R., and Van Breda, I. G. 1986. Laboratory and astronomical comparisons of RCA, GEC, and Thomsen CCDs. *Proc. SPIE* 627:530–542.

Vilas, F., and Smith, B. A. 1985. Reflectance spectroscopy (0.5-1.0 micron) of outer-belt asteroids: Implications for primitive, organic solar system material. 64:503–516.

DETERMINATION OF POLE ORIENTATIONS AND SHAPES OF ASTEROIDS

PER MAGNUSSON
Uppsala Universitet

M. ANTONIETTA BARUCCI
Observatoire de Paris

JACK D. DRUMMOND
University of Arizona

KARI LUMME
University of Helsinki

STEVEN J. OSTRO
Jet Propulsion Laboratory

JEAN SURDEJ
Universite de Liège

RONALD C. TAYLOR
University of Arizona

and

VINCENZO ZAPPALÀ
Osservatorio Astronomico di Torino

The principles of asteroid lightcurve inversion and the information available from photometry are carefully reviewed. General tools as well as specific techniques for shape and pole determinations are summarized and their advantages and shortcomings are discussed. We also present the results obtained so far in this very active field and discuss their significance in the general context of asteroid research and planetary formation.

I. INTRODUCTION

Is there any correlation between pole directions and asteroid sizes, shapes, families, spin rates or the population as a whole? If so, what would such findings mean in terms of collisional histories and basic physical properties of the asteroids? What can asteroid shapes reveal about their physical nature and evolutionary regimes? It is widely accepted that answers to these questions are essential and fundamental to reaching an understanding of the origin and evolution of the solar system.

Asteroids have been studied by a wide variety of observational techniques. Polarimetry, radiometry, radar observations and photometry are all available, but their interpretations and modeling are often tightly coupled to pole direction and/or shape. In many cases, our present characterization of an asteroid is contingent upon the validity of assumptions of spherical shape and isotropic distribution of reflected solar radiation.

We cannot ignore Russell's (1906) demonstration that lightcurve data are not sufficient to determine the three-dimensional shape of an asteroid. However, in the last forty years we have made both observational and theoretical advances which provide opportunities to set limits and/or constraints on an asteroid's pole and shape. We now have speckle interferometry, informative numerical and laboratory simulation studies, pole determination methods which are not extremely model dependent, photoelectric detectors which give photometric magnitudes, thermal infrared lightcurves (which when compared with simultaneous visual lightcurves may reveal albedo features), occultation measurements that can reveal an asteroid's silhouette and radar echoes that often provide one-dimensional images and, increasingly, two-dimensional images or projections. Thus, the tools are available to constrain asteroid poles and shapes in a reliable manner. Once a significant number of high-quality results exist, statistically meaningful studies can be performed which address the fundamental questions posed above.

In this chapter, we outline the current state of the art of deriving asteroid pole and shape constraints. We discuss the theoretical limits of geometric constraints for both the pole and shape from lightcurve data alone and from numerical and laboratory simulation studies. Within this context, we describe and compare the merits of various pole determination techniques. Nomenclature used throughout the chapter is given in Table I (see Sec. IV).

II. THEORY OF LIGHTCURVE INVERSION

In increasing order of difficulty the purpose of lightcurve inversion is to derive information on (1) an asteroid's spin axis, sense of rotation and sidereal period; (2) its shape; and (3) its light-scattering properties (including photometric function and albedo variegation) from disk-integrated photometry. In a classic paper, Russell (1906) offered the first analysis of this problem, investigating in fine detail the information content of lightcurves taken at opposition, i.e., with the solar phase angle $\alpha = 0°$. We follow Russell's thoughts rather closely in this section.

Let $B(\theta_s, \phi_s)$ be the brightness of a surface element with topocentric coordinates (θ_s, ϕ_s) in a spherical coordinate system (r, θ, ϕ) fixed to the asteroid. We assume convex shape and let $C(\theta_s, \phi_s)$ be the Gaussian curvature of the surface. Now, the integrated light observed from any distant position in space will depend on the distribution of the ratio B/C across the surface and not on B and C separately. For any convex shape $C(\theta_s, \phi_s)$, we can always find a brightness distribution $B(\theta_s, \phi_s)$ such that B/C is equal to a predefined function, thus *it is impossible to determine the three-dimensional shape of the asteroid from photometry.*

Russell expanded the B/C ratio as a spherical harmonics series

$$\frac{B(\theta_s, \phi_s)}{C(\theta_s, \phi_s)} = Y_0 + Y_1(\theta_s, \phi_s) + Y_2(\theta_s, \phi_s) + Y_3(\theta_s, \phi_s) \ldots \qquad (1)$$

where

$$Y_n(\theta_s, \phi_s) = \sum_{k=1}^{n} P_n^k[\cos(\theta_s)][\alpha_{nk}\cos(k\phi_s) + b_{nk}\sin(k\phi_s)] \qquad (2)$$

and derived the luminosity $L(\theta, \phi)$ (corrected to unit distance) that would be received at a distant point with *zero solar phase* assuming *geometric scattering*:

$$L(\theta, \phi) = 2\pi \sum_{n=1}^{\infty} Y_n(\theta, \phi) \int_0^1 P_n(x)x\,dx. \qquad (3)$$

The first terms in this series are explicitly

$$L(\theta, \phi) = \pi \left(Y_0 + \frac{2}{3}Y_1(\theta, \phi) + \frac{1}{4}Y_2(\theta, \phi) - \frac{1}{24}Y_4(\theta, \phi) + \frac{1}{64}Y_6(\theta, \phi) \ldots \right).$$

Note that the coefficients decrease quickly for increasing order n, thus high spatial information on B/C is difficult to retrieve even if the observed lightcurves have high time resolution. Furthermore, the coefficients for all odd
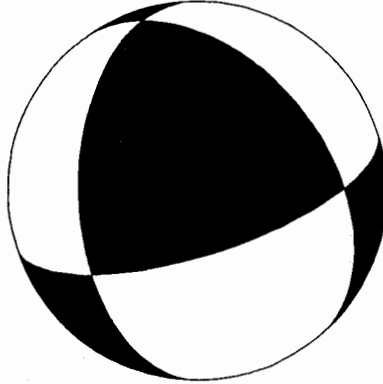
Fig. 1. A spherical object with the eight octants colored alternately black and white, capable of giving zero-amplitude opposition lightcurves if it scatters light geometrically.

orders except one is zero. If the brightness $B(\theta_s, \phi_s)$, is constant, also the first order term will be zero. Some information on B/C is therefore absent in zero phase lightcurves. As an example, Fig. 1 shows a sphere with strong albedo contrasts, dominated by the $P_3^2[\cos(\theta)]\cos(2\phi)$ term, which will look equally bright from all directions if it is geometrically scattering. Nonopposition lightcurves might help in determining the odd harmonics, but this would be very difficult because then L would be a function of two more angles and the unknown but presumably nongeometric light-scattering properties of the regolith would be more pronounced.

The above-mentioned loss of information made Russell quite skeptical toward prospects for lightcurve inversion. He did, however, give some useful diagnostic tools for testing certain hypotheses about shape, scattering law and albedo distribution. For example, if two opposition lightcurves obtained in opposite directions are different, then either the scattering is not geometric or the albedo is not uniform, or both; if the difference is not sinusoidal, then the asteroid's shape is not convex. He further showed that *it is always possible (theoretically) to determine the position of the asteroid's equator,* (except that the sign of the inclination remains unknown). It follows from Eq. (4) that the Fourier expansion of an opposition lightcurve ($\alpha = 0°$) observed at equatorial aspect ($\theta = 90°$) cannot have odd harmonics higher than the first if the scattering is geometric; it cannot have any odd harmonics if the albedo distribution is uniform and the light scattering is geometric.

III. LABORATORY AND NUMERICAL SIMULATIONS

Laboratory simulations, numerical experiments and analytical descriptions have been carried out to clarify the role of shape, viewing geometry, surface morphology and composition in shaping an asteroid lightcurve.

Analytical approaches (Surdej and Surdej 1978; Barucci and Fulchignoni 1982; Ostro and Connelly 1984; Karttunen 1989) with regularly shaped objects allow the understanding of the influence of the orientation parameters. Numerical experiments make it easier to take into account the physical and chemical properties of the asteroid surfaces by varying the scattering laws (Thompson and Van Blerkom 1982; Argentini et al. 1986), and facilitates systematic studies of nonellipsoidal shapes (Cellino et al. 1987a, 1988). Laboratory simulations (Dunlap 1971; Barucci et al. 1982, 1983, 1984, 1985) using both regularly and irregularly shaped models are significant in investigating the effects of body shape and surface morphology. The main results of work to date are briefly summarized here.

The viewing geometry primarily affects the amplitude of a lightcurve, which usually becomes larger for aspects approaching the equatorial view and for increasing phase angles. Fulchignoni et al. (1988) found a linear amplitude-phase relationship in the phase range 2° to 30° with slopes depending on surface properties, shape and the viewing geometry. The amplitude increase is less evident for more irregularly shaped models than for smooth ellipsoidal ones. The effects of the variation of the obliquity angle are practically negligible for solar phases <30°, thus simplifying the interpretation of main-belt asteroid lightcurves.

The model proposed by Cellino et al. (1987a), formed by combining eight octants of different ellipsoids to a body with a continuous surface, offers an interesting set of smooth objects whose lightcurves may easily be computed and investigated at different aspect angles. Cellino et al. (1988) showed that the shapes of this set of objects, even for zero phase-angle and geometric scattering, can cause the majority of the features commonly observed in asteroid lightcurves, such as different shapes and magnitudes of the extrema, extrema inversion and switching of primary and secondary extrema at different aspects, flat maxima and/or sharp minima, number of equatorial extrema twice that at more polar aspects, etc. Similar results were obtained earlier by Barucci et al. (1984) from analysis of very irregular fragments from laboratory hypervelocity impacts.

At phase angles <30°, the effects of large structural features (chosen in the dimension range of those observed on the smaller satellites) are negligible within the lightcurve accuracy, while the albedo variations strongly affect the lightcurve shape. Small/medium scale irregularities in a lightcurve are mainly due to the albedo variation of an asteroid surface which can be studied only as an integrated effect (Cellino et al. 1987a). In general, it is very difficult to infer information on the geological structures of an asteroid from its lightcurve.

The scattering of sunlight by the surface material affects the behaviour of the asteroid lightcurves: higher amplitudes are obtained for laboratory models compared to those obtained analytically using geometric scattering, and these effects are amplified for larger phase angles. Estimates of the elongation of asteroids obtained from the maximum lightcurve amplitude therefore have to

be corrected for scattering effects (Barucci et al. 1984; Magnusson 1988; Fulchignoni et al. 1988; Poutanen et al. 1981).

A detailed study of how magnitudes, amplitudes and lightcurve shapes depend on the scattering law at various solar phases have been carried out by Karttunen and Bowell (1988) using the numerical integration method of Karttunen (1988). They demonstrated that lightcurves and phase curves have ambiguous interpretations. The lightcurves of the Earth-crossing asteroids obtained at very high phases have to be carefully interpreted because all the effects due to viewing geometry and scattering properties are amplified, and the effects of the various parameters can no longer be separated.

A general conclusion to be drawn from the laboratory and numerical simulations is that essentially all characteristics of asteroid lightcurves can be recreated with simple and physically plausible models. But these techniques cannot prove uniqueness and we are reminded that *any* photometrically derived shape can just as well be attributed *solely* to albedo variegation or to any mixture of shape and albedo effects (see Sec. II for refinement of this statement). However, the present results make it possible to check theoretical models of asteroid properties, and permit qualitative statements about relations among model parameters.

Many of the above results were obtained by Barucci and co-workers using the SAM (System of Asteroid Model), located at the Laboratorio di Scienze Planetarie of the Osservatorio di Teramo in Italy (Barucci et al. 1982). This instrument makes it possible to construct synthetic lightcurves of laboratory models at a wide range of viewing geometries (0° to 90° for the aspect and obliquity angles, 2° to 45° for the solar phase angle, and full rotational phase coverage). The light source consists of an astrograph with a light bulb at the focal point of a 16-cm aperture three-lens system which can give both parallel and divergent light beams. A set of gears allows the model and its support to attain any orientation. A photometer is mounted at the end of a horizontal arm which can rotate around the model support, thus providing changing phase angles. A computer drives both the observing sequence and the data acquisition.

IV. TECHNIQUES

This section describes the basic principles inherent to the major approaches for deriving asteroid poles and shape parameters. The nomenclature used for parameters in common to several techniques is shown in Table I. The characteristics of the methods described in this section are summarized in Table II. We start with methods based on photometric lightcurves, the most abundant data source, and proceed further with techniques based on other kinds of observations that can provide valuable checks on the photometric results as well as give additional information.

The geometrical considerations may be explained as follows. The geometry of photometric observations is characterized by two optical axes, Sun-

TABLE I

Nomenclature

A	Amplitude of photometric lightcurve (mag.)
$H(\alpha)$	Reduced V-magnitude ($H(\alpha) = V_{obs} - 5\log(r\Delta)$)
L	Reduced luminosity ($L = 10^{0.4H(\alpha)}$)
a, b, c	Semimajor axes of a triaxial ellipsoid model ($a \geq b \geq c$)
λ_0	Ecliptic longitude of asteroid spin vector
β_0	Ecliptic latitude of asteroid spin vector
α	Solar phase angle (Sun $-$ asteroid $-$ Earth)
ϕ	Rotational phase (arbitrary zero point)
θ	Aspect angle (angle between observers' line of sight and asteroid spin vector)
γ	Photometric obliquity (co-angle to angle between light scattering plane and aspect plane, i.e., planes containing α and θ, respectively)
PAB	Phase angle bisector (see Sec. IV)
PGC	Photometric great circle (see Sec. V.A)

asteroid and asteroid-Earth. The situation is simplified when these axes are equal ($\alpha = 0°$) since the observed absolute magnitude then depends on two angles only, the rotational phase ϕ and the aspect angle θ. For nonzero solar phases ($\alpha \neq 0$) two additional parameters are required, e.g., α and the photometric obliquity γ. Since the solar phase angle is small for main-belt asteroids ($\alpha \leq 30°$) the effect of the obliquity is usually neglected and the effects of α and θ are assumed to be independent (no cross terms). Furthermore, it is natural to use a representation which is symmetric with respect to interchange of the Sun and the Earth. This is usually achieved by defining the rotational phase and the aspect angle with respect to the phase angle bisector (PAB) instead of the line of sight (see, e.g., Harris et al. 1984). This use of the PAB is of critical importance for the epoch methods (Sec. IV.B), but may be ignored for amplitude and magnitude methods applied at small phase angles $\alpha < 15°$ (see below) (Zappalà and Di Martino 1986).

A. Amplitude and Magnitude Methods

One easily understands that, if light variations of a minor planet are primarily caused by the changing projected surface area of a smooth and regular object, the observed lightcurve amplitude and maximum/minimum brightness will be more or less complex functions of the aspect angle θ, of gross shape parameters and of the phase-angle effect (see Vesely 1971 for early applications). In particular, for a triaxial ellipsoidal shape (semi-axes $a \geq b \geq c$) and rotation about the c axis, the projected area is a simple analytical function (Connelly and Ostro 1984) of the rotational phase ϕ, the aspect angle θ and the axial ratios a/b and b/c (see below). Most techniques take advantage of this fact by assuming uniform and geometric scattering and use various approaches to extrapolate the data to zero solar phase angle. In order to preserve the physical meaning of the derived axis ratios, one must also consider the effects of nongeometric scattering (see Sec. III; Magnusson 1988).
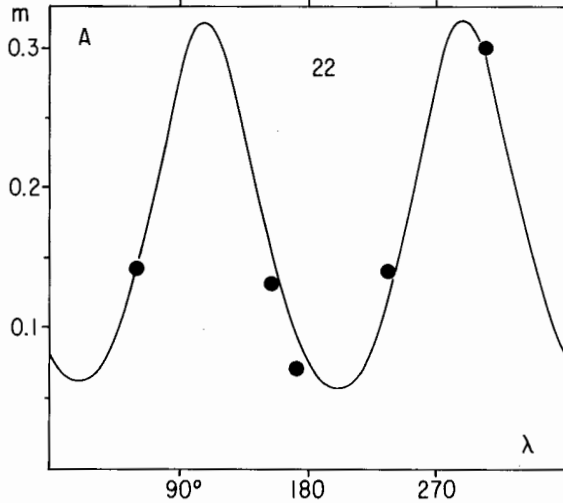
Fig. 2. Relationship between the amplitude (corrected to $\alpha = 10°$ for each opposition) and the observed longitude for 22 Kalliope based on five apparitions. Figure adapted from Zappalà and Knežević (1984).

In a frequently used method developed by Zappalà (1981), and refined by Zappalà et al. (1983) and Zappalà and Knežević (1984), the axis ratios are determined from amplitude-longitude (Fig. 2) and magnitude-amplitude plots. Since the maximum possible opposition amplitude (corresponding to "equatorial" view) can always be reached in principle, a set of amplitude data collected during different oppositions conveniently spread in longitude can help to infer a good estimate of the a/b ratio. More difficult is the determination of the b/c ratio because the "pole-on" view cannot generally be observed from Earth. However, using both amplitudes and absolute magnitudes, an approximate b/c ratio is obtained (the magnitude at lightcurve maximum rather than, e.g., mean magnitude is usually used since the former is independent of the a/b ratio). Once the model shape is determined, it is easy to derive an approximate aspect angle for each observed opposition. The pole solution may be obtained from the intersections of the resulting "aspect circles" (circles with the aspect as radii and the lines of sight, or PAB's, as centers).

More recent solutions that simultaneously relate the dependence of the amplitudes and magnitudes to both the aspect and phase angles and to the asteroid shape parameters have been proposed independently by Drummond and Hege (1986), Magnusson (1986) and Surdej et al. (1986). The last approach uses a general relationship between the reduced magnitude $H(\alpha_i)$ and the rotational phase ϕ for an ellipsoid model scattering uniformly and geometrically

$$L^2 = 10^{-0.8H(\alpha_i)} = B_i\cos^2\phi + C_i. \tag{5}$$

TABLE II

Summary of Pole and Shape Techniques

Section	Technique	Observational Input	Derivable Results	Assumptions
IV.A	amplitude and magnitude methods	lightcurve amplitudes and/or magnitudes	axis of rotation, triaxial model	uniform and geometric scattering, triaxial shape
IV.B	epoch methods (photometric astrometry)	times of a lightcurve feature	axis of rotation, sense of rotation, sidereal period	lightcurve feature at constant rotational phase
IV.C	numerical integration method	individual photometric observations	axis of rotation, sense of rotation, sidereal period, triaxial model	predefined scattering law, triaxial shape
IV.C	spherical harmonics method	amplitude terms of lightcurve's Fourier expansion	axis of rotation	very short spherical harmonics expansion is adequate
IV.D	convex-profile inversion	equatorial lightcurve	mean equatorial cross section	uniform and geometric scattering, convex shape, predefined spin axis

		pre- and post-opposition radiometry	sense of rotation	rotationally symmetric thermal properties
IV.E	infrared	polarization	axis of rotation, sense of rotation, thermal inertia	spherical shape, uniform albedo, theoretical model
		simult. thermal and optical lightcurve	separation of shape and albedo effects	known thermal inertia
IV.F	radar	distribution of echo power in Doppler frequency and/or time delay	axis of rotation, sense of rotation, 1-D or 2-D images	
IV.G	occultation	immersion and emersion times	silhouette	
		same for three different occultations	axis of rotation, triaxial model	triaxial shape
IV.H	speckle interferometry	spatial power spectra	axis of rotation, sense of rotation, triaxial model	uniform and geometric scattering, triaxial shape
		complex visibility functions	reconstructed image of asteroid	
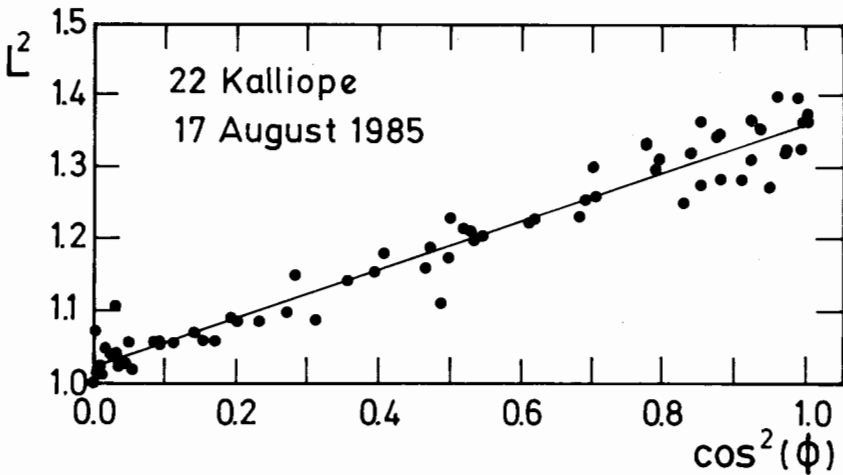
Fig. 3. Example of a reduced lightcurve. The dots correspond to photometric observations of 22 Kalliope (see Surdej et al. 1986), reduced in accordance with Eq. (5). The straight continuous line represents the least-squares linear fit to the data from which the values of B_i and C_i have been estimated.

Reduction of the photometric observations of a minor planet according to Eq. (5) leads to a so-called "reduced lightcurve." An example is shown in Fig. 3. The coefficients B_i and C_i are expressed by

$$B_i = \left[\frac{\pi bc}{g(Q,\alpha_i)p(0°)} \right]^2 [(a/b)^2 - 1]\sin^2\theta_i \qquad (6)$$

$$C_i = \left[\frac{\pi bc}{g(Q,\alpha_i)p(0°)} \right]^2 \{1 + [(a/c)^2 - 1]\cos^2\theta_i\} \qquad (7)$$

and they show a simple, although nonlinear, dependence on the unknown parameters λ_0, β_0, a/b, b/c, $bc/p(0°)$ and the multiple scattering factor Q (Lumme and Bowell 1981) where $p(0°)$ is the zero-phase geometrical albedo. They also depend on the observed quantities λ_i, β_i and α_i pertaining to the ith opposition of the asteroid under study. Expressions for the function $g(Q,\alpha_i)$ have been given by Lumme and Bowell (1981) and Bowell et al. (1988). The classical amplitude-aspect relation is given by the normalized slope $(B/C)_i$ of the reduced lightcurve i while the classical magnitude-aspect relation, for the maximum brightness, is obtained by setting $\phi = 0°$ in Eq. (5), i.e. $L^2_{max} = (B + C)_i$; compare with Fig. 4. A minimum number of $N = 4$ lightcurves $i = 1,..., N$ recorded at distinct (different λ_i) oppositions is required in order to solve the system of N nonlinear amplitude equations for the four unknown parameters λ_0, β_0, a/b and b/c. If the N magnitude equations are added to the
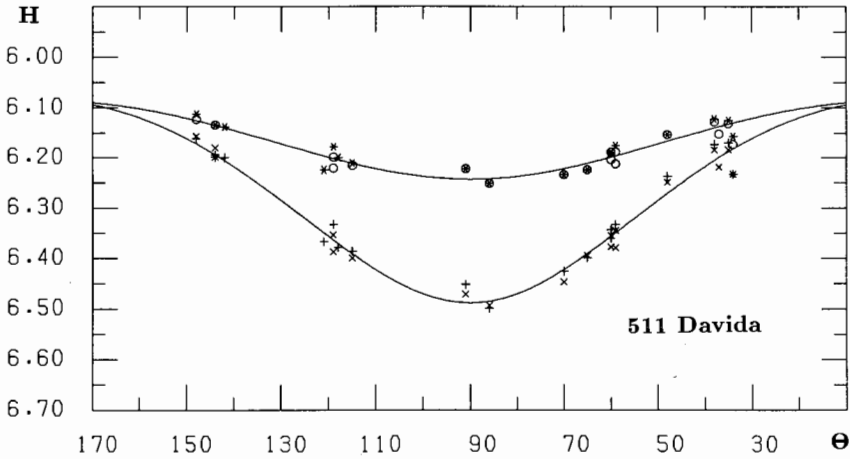
Fig. 4. The changing brightness of 511 Davida as a function of aspect. Two maxima and two minima from lightcurves at several oppositions, corrected to $\alpha = 0°$ with the Lumme-Bowell scattering function fit to the set of maxima and minima independently, are plotted against the aspect angle θ. The asterocentric latitude of the sub-Earth point is $90° - \theta$. Note that both the maximum and minimum are faintest and the amplitude (the difference between the two) is greatest in the equatorial plane, characteristics of a triaxial ellipsoid rotating about its shortest axis. Davida appears to be a good candidate for a relatively smooth and featureless triaxial ellipsoid, with a well-determined rotational pole and set of axial ratios (see Sec. VII). Figure adapted from Drummond et al. (1988b).

system, we may solve also for $bc/p(0°)$ and Q using only $N = 3$ oppositions. Such systems are conveniently solved by a least-squares method which also gives error estimates of the parameters and checks for the existence of correlations between them. Let us further insist here that the applicability of Eq. (5) to asteroid lightcurves presupposes that these were obtained at small phase angles $\alpha_i < 15°$ (because only then does the scattering law approach the geometric approximation close enough for our purposes [Pospieszalska-Surdej and Surdej 1985]) and that there should be no signs of color or albedo variation in the lightcurve. Note, however, that absence of any visible signs of albedo variegation does not imply uniform albedo (see Sec. II). Furthermore, the trend of the reduced lightcurve should be as linear as possible (see Fig. 3).

One should be very cautious about assuming a nearly pole-on view for minimum and low amplitude observations; the amplitude of a lightcurve is quite insensitive to changing aspect near polar views. For instance, a triaxial ellipsoid with axis ratios $a/b = 1.5$ and $b/c = 1.5$ gives an amplitude smaller than $0^m.02$ for aspects in the range $0°$ to $20°$. Hence, uncritically assuming zero aspect for small amplitudes can introduce serious errors in the computed pole. Another often misunderstood point is that an asteroid reaches minimum aspect at a longitude very close to the pole longitude. In fact, this is true only
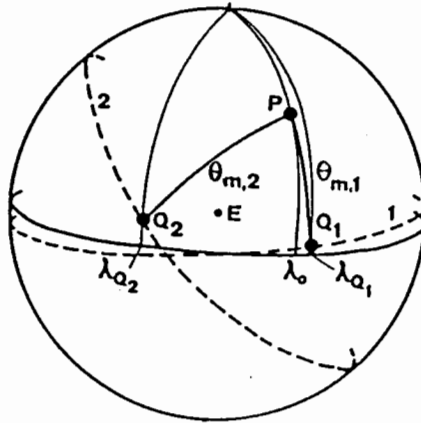
Fig. 5. An object that follows a path in the sky (dashed curve 2) which is highly inclined to the ecliptic (solid circle) is seen at minimum aspect (distance $\theta_{m,2}$ to pole P) at a point Q_2 with longitude λ_{Q2} far from the pole longitude λ_0. Approximation of the pole longitude with the longitude λ_{Q1} of minimum opposition amplitude is valid only for low-inclination paths (object 1).

for asteroid paths parallel to the ecliptic, and large discrepancies can arise for highly inclined orbits (see Fig. 5).

B. The Epoch Method

The epoch method (also known as photometric astrometry) involves measuring time intervals between a lightcurve feature observed at different viewing geometries, usually over several apparitions. The feature, whether a lightcurve extremum, "notch" or phase of a Fourier component, should be identifiable to a moment in time (epoch) within about 2% of the rotation period. How can such epochs of a lightcurve feature give us information on the axis and sense of rotation of an asteroid?

Figure 6 demonstrates how an observer on a ship can determine the rotation sense of the revolving beam(s) from a lighthouse simply by noting the changing flash frequency as he travels about the lighthouse with varying angular velocity. In the asteroid case the observer's motion is generally not confined to the equatorial plane of the asteroid (sea-level in Fig. 6) and the orientation of this plane is one of the unknowns to be determined. We must therefore make the basic assumption that the lightcurve feature occurs at the same rotational phase for all aspect angles and phase angles. Without knowledge of the optical properties of an asteroid's surface, the rotational phase is naturally measured with respect to the midpoint of the great circle arc between the sub-Earth and sub-solar points, i.e., the sub-PAB (phase angle bisector) point. Nevertheless, due to shadowing effects, there may be a shifting in the arrival time of the epoch. Therefore, it is prudent to select more than one
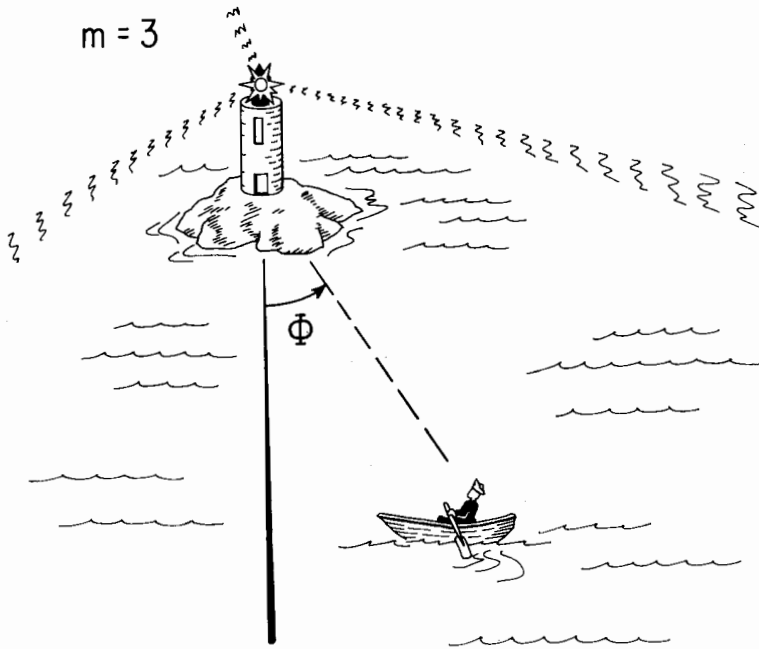
Fig. 6. A cartoon illustrating how by noting the "synodic" flash frequency f_{syn} of the lighthouse changes with the angular velocity $d\Phi/dt$ of the ship, an observer on board may determine the sense of rotation of the light source and the number of light beams m from the formula $f_{syn} = f_{sid} \pm m d\Phi/dt$.

lightcurve feature, to use time intervals from epochs with a similar longitude or lightcurve shape (to decrease the likelihood of violation of the basic assumption), and to work with a data set providing homogeneous solar phase angle coverage (to decrease systematic error due to shadowing effects).

There are four similar approaches to the epoch method, or photometric astrometry. Two use a synodic reference frame and two a sidereal reference frame. Authors, and their most recent references are: for synodic, Taylor et al. (1988) and Lambert (1985); and, for sidereal, Magnusson (1986) and Drummond et al. (1988b). Both Taylor and Lambert count the synodic cycles between epochs and correct them to a sidereal frame of reference by applying a correction term that is roughly equivalent to the fractional part of a rotation cycle that the PAB has moved. The two methods differ mainly in how the number of revolutions made by the PAB is accounted for. Magnusson and Drummond, using sidereal cycles, determine the sidereal period directly with the least-squares method. All four methods scan the celestial sphere with a grid of trial poles and use various measures to determine which pole gives the best fit.

Knowledge of the number of rotational cycles over long intervals is naturally essential for extraction of information from the changing synodic spin frequency. Taylor and Lambert first determine the number of synodic cycles and then search for the pole, while Magnusson and Drummond make simultaneous searches for rotation cycles and pole. The search must generally include half cycles since the lightcurve primary maximum at one opposition often becomes a secondary maximum at another opposition (a switch). This procedure is also essential for modeling of asteroid shapes.

The epoch method is a powerful tool in that it is not strongly model dependent and is an "orthogonal" pole routine from the amplitude-aspect and magnitude-aspect techniques. Furthermore, it has so far been our most reliable tool for obtaining asteroid senses of rotation.

C. Recent Photometric Methods

Here we present a few interesting new developments in deriving accurate information from photometry with a minimum number of approximations and assumptions. These methods have not yet been described in the literature in such detail that their merits and faults can be assessed properly, and we naturally have discordant opinions among ourselves in this respect, but they probably reflect important techniques of the future.

A Numerical Integration Method.   Uchida and Goguen (1987) have developed a versatile technique that uses all photometric data points for simultaneous extraction of both "amplitude-magnitude-like" and "epoch-like" information on an asteroid's pole and shape. They compare the observed magnitudes of every point, for all lightcurves, with the corresponding magnitudes of ellipsoidal models with various spin vectors. The integrated flux of the model is computed by adding up the contributions from a large number of plane facets (see also the integration technique by Karttunen [1989]). The axis ratios and the spin vector of the model are varied until a simultaneous fit to all lightcurves is achieved. The technique has been tested for 624 Hektor. A main advantage of this method is that it can easily be applied with any scattering law and generalized to other parameterized shape and albedo distribution models.

Lightcurve Inversion using Spherical Harmonics.   In light of the beautiful results by Russell (1906) concerning spherical harmonics expansions, in rotational phase and aspect angle, of geometrically scattered light (see Sec. II), it is natural to examine routes to derive pole and shape/albedo information through such expansions. In particular, the coefficients for odd orders larger than one should vanish for a geometrically scattering object observed at zero solar phase when computed for the correct spin state, but are likely to deviate from zero for erroneous pole coordinates or rotation periods. This is the key to a method proposed by Lumme et al. (1986) in which a search is made for the

asteroid pole and spin rate that minimize the coefficients mentioned above. The method has so far proved difficult to apply in practice.

Spherical Harmonics Method. Provided that an asteroid's lightcurves have either been observed at, or properly reduced to, zero solar phase ($\alpha = 0°$), the integrated brightness can be given by a spherical harmonics expansion

$$L(\theta,\phi) = \sum_{n=0}^{\infty} \sum_{k=0}^{n} P_n^k(\mu)[x_{kn}\cos(k\phi + \delta_n) + y_{kn}\sin(k\phi + \delta_n)] \quad (8)$$

where $\mu = \cos\theta = \sin\beta_0\sin\beta + \cos\beta_0\cos\beta\cos(\lambda - \lambda_0)$. Here δ_n are the unknown absolute rotational phases (epochs) which are functions of the pole position, x_{kn} and y_{kn} are some unknown coefficients related to the asteroid's shape and albedo variegations, and P_n^k are the associated Legendre functions.

The absolute phases δ_n, which are not needed for pole determination with the spherical harmonics method, can be eliminated by constructing the power spectrum or squared amplitude terms of Eq. (8). The second-order-squared amplitude (usually the dominating term for asteroids) is explicitly given by

$$A_2^2(\mu) = \left[\sum_{n=2}^{\infty} x_{2n}P_n^2(\mu) \right]^2 + \left[\sum_{n=2}^{\infty} y_{2n}P_n^2(\mu) \right]^2 \equiv (1 - \mu^2)^2 M_2(\mu) \ . \ (9)$$

Note that $P_n^2(\mu)$ are polynomials, with $(1 - \mu^2)$ as a factor. The only approximation needed in this method arises from the finite number of available apparitions which forces a truncation of the power series of M_2. There are good reasons to believe (see Lumme and Karttunen, in preparation) that the resulting polynomial is fairly rapidly converging, thus the finite expansion should be a good approximation to the actual infinite power series.

The key idea in the current spherical harmonics method lies in the fact that, regardless of truncation order N, the $2N$th degree polynomial for A_2^2 provides $2N + 1$ known quantities from the nonlinear least-squares fit to data (as a function of λ and β) while there are only $2N - 1$ unknowns, pole coordinates λ_0, β_0 and $2N - 3$ coefficients in M_2. The method itself does not require M_2 to be an even polynomial of μ although both the "Russell conditions" (Sec. II) and actual data seem to indicate this. The pole solution can be sought in an iterative way; start with $M_2 = b_0$ (=constant) and solve for λ_0 and β_0 using at least three reasonably well-separated apparitions. Then set $M_2 = b_0 + b_2\mu^2$ and solve for the pole again. The procedure can be continued up to the point where the number of unknowns equals to the number of apparitions. It is possible to linearize Eq. (9) after the first iteration, thus allowing the use of linear least-squares fitting and giving a convenient method to estimate the formal errors of λ_0 and β_0. The method has been put forward by Lumme and Karttunen

(in preparation) who have successfully applied it to synthetic, computer-generated data and to one asteroid, 44 Nysa.

We expect the recent Fourier expansion of the photometric asteroid data base (Barucci et al. 1988; Lagerkvist and Magnusson, in preparation) will make application of techniques like the above easier and stimulate development of new methods that make full use of the photometric data.

D. Convex-Profile Inversion

Ostro and Connelly (1984) showed that any lightcurve can be inverted to yield a convex profile, and that, under certain ideal conditions the profile represents a two-dimensional *average* of the three-dimensional shape. That average is called the mean cross section C and it is defined as the convex set equal to the average of the convex envelopes on all surface contours parallel to the asteroid's equatorial plane. A convex profile can be represented by a radius-of-curvature function or by that function's Fourier series. Deletion of a profile's odd harmonics "symmetrizes" the profile. For example, an asteroid's symmetrized mean cross section C_S has the same even harmonics as C but no odd harmonics. Figure 7 gives a practical illustration from a real case.

The following ideal conditions pertain to estimation of C from a lightcurve:

1. The scattering is uniform and geometric;
2. The viewing/illumination geometry is equatorial, i.e., the Sun and the Earth are in the asteroid's equatorial plane;
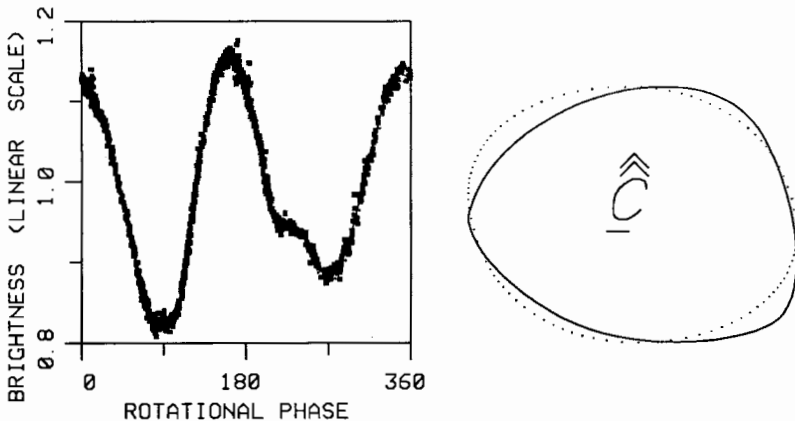
Fig. 7. Convex-profile inversion of a lightcurve obtained at $\alpha = 26°$ for 164 Eva by Schober et al. (1982). Think of the solid profile (right) as a two-dimensional, geometrically scattering asteroid. As this asteroid rotates, it generates a model lightcurve (tiny dots at left) which is almost completely obscured by the actual Eva data (large symbols). If conditions (1), (2) and (3) were satisfied, the profile would be an unbiased estimate of Eva's mean cross section C. The dotted profile (right) is C_S (see text). Figure from Ostro et al. (1988).

3. All surface contours parallel to the equatorial plane are convex;
4. The solar phase angle α does not equal $0°$ or $180°$.

These conditions are necessary and sufficient for the three-dimensional light-curve inversion problem, which cannot be solved uniquely, to "collapse" into a two-dimensional inversion problem that can.

Convex-profile inversion builds on the canonical work of Russell (1906) by (i) identifying the mean cross section as the optimal shape constraint available from a lightcurve; (ii) defining the difference between the potential information contained in opposition lightcurves and that in nonopposition lightcurves; and (iii) specifying the conditions that determine the accessibility of that information. For example, we cannot estimate $\underline{C}$'s odd harmonics from an opposition lightcurve, but we can estimate its even harmonics and hence its symmetrization $\underline{C}_S$.

The methodology for estimating $\underline{C}$ and $\underline{C}_S$ was introduced by Ostro and Connelly (1984). Ostro et al. (1988) assess the nature, severity and predictability of systematic error (due to violation of ideal conditions) and statistical error (due to lightcurve noise). The most severe obstacle to estimating the mean cross section stems from violation of the first condition (uniform and geometric scattering). Simulations suggest that even for optimum solar phase angles (near $20°$), violation of this condition introduces systematic distortion in the estimated mean cross section. However, this distortion is not necessarily severe, and, at least for fairly regular shapes, estimates of the salient characteristics of $\underline{C}$ might not be severely biased.

E. Infrared Techniques

Infrared radiometric observations of an asteroid before and after opposition can reveal which of those geometries presents the cooler morning terminator, and hence can distinguish prograde from retrograde rotation (Hansen 1977; Morrison 1977). The degree of linear polarization of emitted thermal radiation will depend on the viewing/illumination geometry as well as on the asteroid's shape and thermal properties, so infrared polarimetry can, at least in principle, constrain asteroid pole directions (Johnson et al. 1983).

Infrared lightcurves, where emitted light dominates over reflected, provide powerful constraints on albedo distribution. If an asteroid's visible lightcurve is caused primarily by shape and only mildly modulated by albedo features, then the infrared and visible lightcurves will be in phase with each other. However, if an albedo feature has a major influence on the lightcurve, then the two lightcurves will be out of phase because, for example, a cool region, being darker, will produce greater flux at infrared wavelengths than in the visible where a minimum flux would be detected. The classic examples of the application of this technique are the findings of Murphy et al. (1972) that Iapetus' lightcurve is caused by hemispheric albedo differences, and the findings of Hartmann and Cruikshank (1978; Hartmann 1979) that Hector's light-

curve is caused by shape. Similar analysis has led to the rejection of one albedo model for Herculina (Taylor et al. 1987; Lebofsky et al. 1988). In short, complementary infrared and visible lightcurves can separate the contributions of albedo and shape if an asteroid possesses strong albedo markings.

F. Radar

Radar observations can constrain an asteroid's pole direction because the echo's bandwidth B depends on the aspect angle θ, as well as on the asteroid's size and apparent rotation period. For example, for a spherical object with known diameter D and known rotation period P, the bandwidth is given by

$$B = \frac{4\pi D}{\lambda_r P} \sin\theta \tag{10}$$

so a measurement of bandwidth provides the aspect angle, and hence constrains the pole direction (modulo 180°) to an "aspect circle." Radar observations of the asteroid at widely separated sky positions yield aspect circles intersecting at pole solutions (compare the analogous situation for the amplitude-magnitude method in Sec. IV.A).

If D is unknown, a bandwidth measurement couples the diameter to the aspect angle, and sets a lower bound on D corresponding to the most "efficient" geometry for achieving high bandwidth, namely equatorial aspect ($\theta = 90°$). A sequence of solutions with aspect angles (and circles) that shrink and asteroid diameters that increase as the pole-on view is approached are obtained. A second radar observation at a different sky position will yield a second set of circles, and possible pole directions are intersections of aspect circles corresponding to the same diameter D (Fig. 8).

Most asteroids are unlikely to be spherical. However, the echo bandwidth will generally be proportional to the breadth $D(\phi)$ of the asteroid's polar silhouette at rotational phase ϕ (Ostro et al. 1988), and by sampling B during at least half a rotation cycle, the above analysis can be applied to nonspherical objects.

Proposed improvements to the Arecibo radio telescope could make multiple-apparition observations routine and make feasible echo bandwidth observations over a wide range of viewing geometries, to reveal the sense of rotation as well as the pole direction (see the chapter by Ostro for discussion of radar constraints on asteroid shapes).

G. Occultations

Stellar occultations provide a powerful direct method of checking, and under the right circumstances of independently determining asteroid poles and shapes. The chapter by Millis and Dunham provides the details, but one sim-
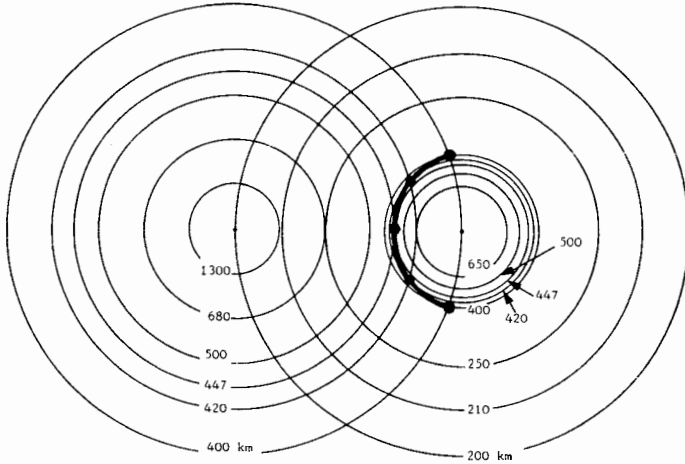
Fig. 8. Constraints on θ and *D* from two radar observations of a spherical asteroid. Each observation results in a sequence of possible aspect circles (the corresponding diameters *D* are marked). The loci of pole positions where aspect circles with the same diameter intersect (heavy curve) constitute the solution set. It will generally collapse to a unique pole (except for ambiguous sense of rotation) if a third observation is added.

ple modeling approach is to fit an ellipse to timings of immersions and emersions for a particular rotational phase. The shape and orientation of this ellipse can serve to discriminate between ambiguous poles from other methods. Lambert (1985) and Magnusson (1986) have done this for Pallas, Juno and Hebe. For each occultation, six unknown parameters collapse into three observable ones. Three angles (pole coordinates λ_0 and β_0, and rotational phase ϕ) and three axes' dimensions (a,b,c) project onto the plane of the sky as two dimensions and a position angle of the ellipse for each occultation. With two occultations there are seven unknowns $(a,b,c,\lambda_0,\beta_0,\phi_1,\phi_2)$ and six observables. Thus additional information is required to solve for the model, e.g., a sidereal period accurate enough to give $\phi_2 - \phi_1$. Pallas has had two occultations, from which it is easy to develop at least a few good constraints. For instance, it can be shown that the model parameters (pole location and three dimensions) used by Wasserman et al. (1979) and Magnusson (1986), or the model itself, must be incorrect at some point. That is, either the long axis *a* must be greater than they find and/or the shortest axis *c* must be smaller (Drummond and Cocke 1988) or the homogenous ellipsoid model is invalid. Finally, occultation data is our most reliable source of information on shape or surface roughness on intermediate scales (km-sized "mountains").

H. Speckle Interferometry

The high angular resolution technique of speckle interferometry is described by Worden (1979), and as applied specifically to the study of as-

teroids, by Drummond et al. (1985*a,b,* 1988*a*; Drummond and Hege 1986; see also their chapter). Two approaches are possible, one involving generally the same assumptions as used in photometric techniques (i.e., that asteroids can be treated as uniformly bright, smooth, featureless triaxial ellipsoids) and another approach, image reconstruction, that makes no specific assumptions about the object. In the first case, by following the two-dimensional power spectra or autocorrelation of the resolved ellipse projected by the ellipsoid as it rotates, the model's dimensions and the orientation of the rotational pole may be estimated by least-squares with only a two-fold ambiguity in the position of the pole. The analysis is the same as would be used for an imaginary series of stellar occultations of an ellipsoid in one evening that provides a series of elliptical outlines as a function of rotational phase. Twice each period (at maximum light under the above assumptions) the long axis would be seen unprojected on the plane of the sky, and twice the intermediate axis (at minimum light) could be directly measured. When the long axis is seen, the pole is approximately in a direction perpendicular to this axis. The other parameters, two angles and the dimension of the short axis, can then be calculated. Controlling instrumental systematics and calibrating the point spread function are essential to successful analysis, but apparently the biggest obstacle involves violation of the photometric assumptions, particularly regarding albedo uniformity.

Still in its infancy with respect to extended (resolved) objects, image reconstruction is an immediate goal that holds immense potential. Proper reconstruction would obviate the need for any assumptions about the object, and would provide literal pictures of asteroids. Currently, the problem is to identify the best algorithm that is the least sensitive to calibration errors and noise. The first attempts at image reconstruction have resulted in scientifically useful glimpses of Vesta's surface (Drummond et al. 1988*a*) that reveal dark and bright patterns. It can be expected that clearer images obtained in the near future will serve as checks and calibrations for other techniques and will open new avenues of asteroid research.

V. LIMITATIONS

A. Symmetry Properties and Pole Ambiguities

A problem often misunderstood in the literature is the ambiguity of pole solutions. Figure 9 demonstrates the effects of the various symmetry properties inherent to photometric and speckle interferometric observations. The solutions obtained from photometric data are subject to two symmetry properties:

1. Model amplitudes and magnitudes are symmetric about equatorial aspect ($\theta = 90°$) which makes it impossible to determine the direction of rotation around the spin axis from observed amplitudes and magnitudes;
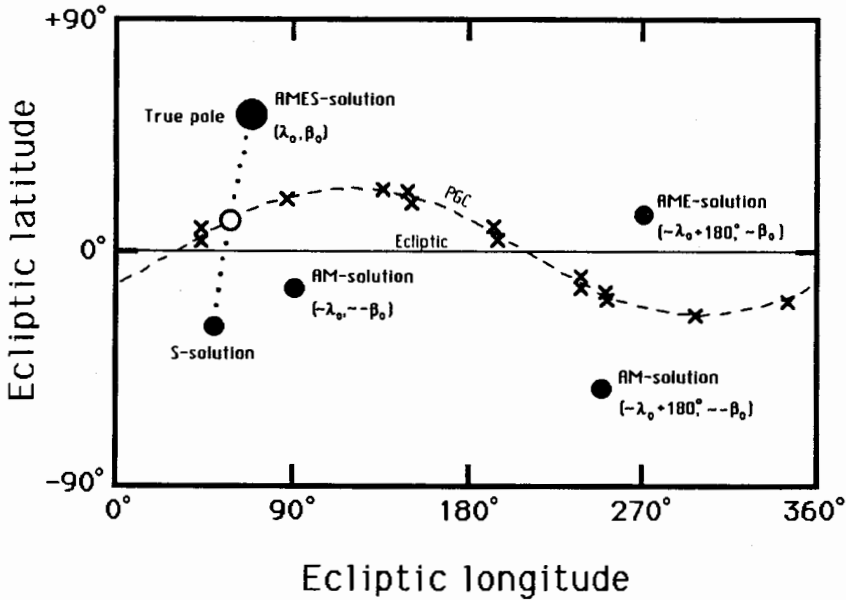
Fig. 9. Map of the celestial sphere showing spin-vector solutions obtained using amplitudes A, magnitudes M, epochs E, and speckle interferometry ellipsoid silhouettes S. Crosses mark PABs of hypothetical photometric observations. The two-fold and four-fold ambiguities are due to two symmetry properties (see text). A speckle observation (open circle) gives two solutions with the line of sight as their bisector. Figure adapted from Magnusson (in preparation).

2. Symmetry of the observations about the "photometric great circle" (PGC), defined as the great circle which departs as little as possible (in least-squares sense) from the directions of the PABs of individual photometric observations (see Fig. 9). The photometric great circle has ascending node $\Omega_{PGC} \approx \Omega$ and inclination $i_{PGC} \approx i(1 + 1/2a)$ (Magnusson, in preparation), where Ω, i and a are standard orbital elements of the asteroid. For zero-inclination objects, the PGC will coincide with the ecliptic and give an exact symmetry of the observations with respect to reflection in the ecliptic plane. The pole solutions will have this same symmetry property. A typical main-belt asteroid, with $a = 2.8AU$, $i = 10°$ and small eccentricity, observed at solar elongations exceeding $90°$, will produce PABs departing on average $2°$ from the PGC ($i_{PGC} \approx 12°$). It is difficult in practice to resolve the pole ambiguity resulting from a symmetry broken by such a small amount. However, for certain objects with unusual orbits, e.g., Earth-approaching objects, we may not find a good PGC and the ambiguity will not occur.

The effect of these symmetries is to create a four-fold ambiguity for amplitude-magnitude methods, but only a two-fold ambiguity for epoch

methods. The two pole solutions in the latter case will be symmetrically placed on one side of the orbital plane (think of what happens when you make a mirror reflection of the right-hand rule for the spin vector), thus resolving the prograde/retrograde ambiguity (Fig. 9). By combining the solutions from amplitude-magnitude and epoch methods, it is sometimes possible to get a unique solution even though the individual methods failed to achieve this.

Speckle interferometric data obtained at a specific longitude, yielding an elliptical approximation to the projected shape, but not individual surface markings, gives two pole solutions symmetric about the line of sight (see Drummond et al. 1985a). Elimination of the pole ambiguity may therefore be obtained with speckle data from at least two longitudes, with images reconstructed from speckle data showing features moving across the disk, or with speckle and photometric data combined. Occultation observations have the same ability to resolve the photometric ambiguity (Magnusson 1986). Radar observations at fewer than 3 longitudes give symmetries similar to photometry (see Sec. IV.F).

B. Uncertainties

Most of the methods discussed in the previous sections use very idealized models of asteroids, e.g., a triaxial ellipsoid with a uniform surface reflectivity. When albedo variegation is included, it is usually in the form of one or two circular spots. Other hypothetical contributions to the light variation, e.g., binarity/satellites (Tedesco 1979; Cellino et al. 1985; Binzel 1985) and free precession (Sher 1971; Barsuhn 1983), have been ignored.

Shape and Albedo Variegation. Our limited knowledge of the optical properties of asteroid surfaces and the inherent inversion ambiguity of disk-integrated scattered light (see Sec. II) make most lightcurve-based determinations of shapes and albedo variegation uncertain. The determined deviations from sphericity, e.g., the $(a/b) - 1$ and $(b/c) - 1$ parameters for triaxial ellipsoids and the departure from circularity of mean convex hulls (Sec. IV.D), may be uncertain at the 25% level (Barucci et al. 1984). All published models with albedo spots and craters must be regarded as one of an infinite number of possible models that can fit the data equally well.

Pole Position. Can we compensate for the simplifying assumptions of current pole methods with good input data? Let us assume that we have photometric data with an isotropic distribution of observations in ecliptic longitude and solar phase. Would systematic errors due to departure from our assumptions cancel out because of symmetry of data about the pole longitude? Such a symmetry protection exists for λ_0 obtained with amplitude-magnitude methods and β_0 obtained with epoch methods for zero-inclination orbits (approximately valid also for moderately inclined orbits if pole coordinates are based on the PGC instead of the ecliptic). On the other hand, β_0 from amplitude-magnitude methods and λ_0 from epoch methods may show large

systematic errors no matter how well distributed and accurate the input data is. The obvious resolution to the above error susceptibilities is to combine the amplitude-magnitude and epoch methods as have been done by, e.g., Magnusson (1986) and Drummond et al. (1988b). (See Fig. 4 in the former paper for an illustration of the complementarity of the methods.)

In the light of the above limitations, caution is advised in using the collection of pole solutions obtained to date (see the table of pole positions in *Part VI* of this book).

VI. REVIEW OF RESULTS

A. Shape Constraints

Whereas a general knowledge of the distribution of asteroidal shapes would certainly provide interesting clues on the collisional evolution of the solar system, not a single close-up picture of a minor planet is yet available. However, various observational and theoretical approaches have enabled one to set up interesting constraints on asteroidal shapes.

Asteroid silhouettes are sometimes derived from stellar occultations (Millis and Elliot 1979; chapter by Millis and Dunham). Although these results are aspect dependent, they seem to indicate that the gross shapes of the largest asteroids are close to spherical or ellipsoidal, while radar delay-Doppler images of small objects show more irregular and elongated shapes (see the chapter by Ostro). Under certain ideal conditions, we have seen in Sec. IV.D that convex-profile inversion allows one to constrain the average equatorial cross section of an asteroid with a known pole orientation; a few examples are given in Ostro et al. (1988).

There is no doubt that the largest homogeneous sets of asteroidal shape parameters presently available come from the application of the amplitude and magnitude, and speckle interferometric techniques (see Magnusson 1988; Drummond et al. 1988b). As explained in Secs. IV.A and IV.H, these techniques rely upon the fitting of observations with a geometrically scattering ellipsoid model. The resulting two-parameter representation $(a/b, b/c)$ provides a first approximation to the real shape of an asteroid, and facilitates comparison with the shapes of rotating bodies in hydrostatic equilibrium (see Fig. 10). Note that there is a considerable uncertainty in the size of the correction for nongeometric scattering (see Sec. III) for the most elongated objects. Furthermore, the sample is biased towards objects with (1) large size, (2) high amplitude, (3) fast spin and (4) small heliocentric distance. Among the consequences of these biases, we can expect a strong overrepresentation of objects far from the Maclaurin curve. A few tentative conclusions can nevertheless be drawn from the present distribution:

1. Asteroids like 39 Laetitia, 45 Eugenia and 107 Camilla constitute candidates for quasi-equilibrium rubble piles (cf. Farinella et al. 1981,1982).
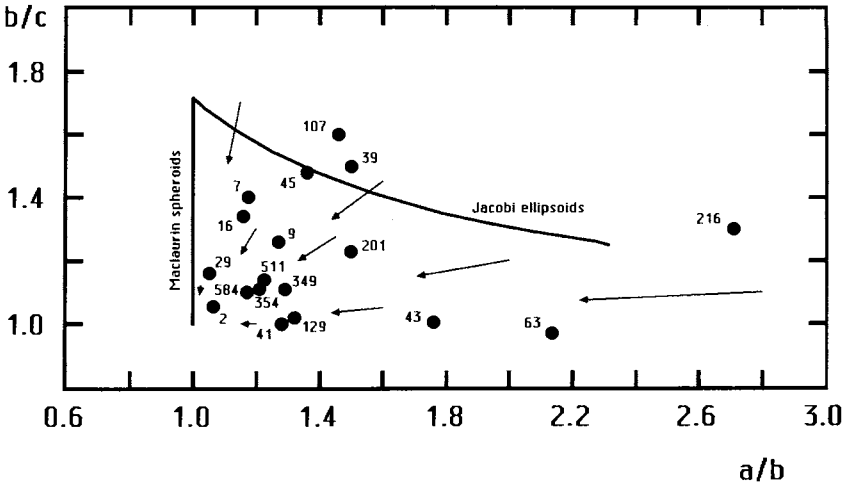
Fig. 10. A homogeneous set of ellipsoidal model parameters (a/b, b/c) for large main-belt asteroids. The loci of Maclaurin spheroids and Jacobi ellipsoids are also shown for comparison (Chandrasekhar 1969). Because of known observational biases, the number of asteroids near the Maclaurin spheroid curve is probably underestimated. Geometric scattering was assumed in the shape determination. The arrows indicate the shift to be applied in order to correct for nongeometric scattering (according to Barucci et al. 1984). The data comes from Magnusson (1986,1988). See also a similar figure by Drummond et al. (1988b).

Abnormally elongated ($a/b > 2$) asteroids such as 216 Kleopatra and 624 Hektor remain possible examples of binary fission (cf. Weidenschilling 1980);

2. Most of the asteroids are located far from the Maclaurin and Jacobi curves, suggesting evidence of significant internal strengths responsible for large deviations from equilibrium. The objects identified in (1) might well be the extremes of a distribution with little or no correlation with equilibrium figures;

3. Laboratory catastrophic impact experiments by Fujiwara et al. (1978) gave a very disperse shape distribution of the fragments, with average "axis ratios" $a : b : c$ near the simple ratio $2 : \sqrt{2} : 1$. The shape distribution of large asteroids seems to be dominated more by objects closer to spherical shape, especially considering nongeometric scattering, with a probable underrepresentation of objects near the Maclaurin line in Fig. 10;

4. There is a weak correlation between the axis ratios in Fig. 10 and the spin frequency. Natural explanations may be flattening and elongation due to centrifugal forces, and high angular momentum transfer to oddly shaped debris of catastrophic collisions. A larger sample of reliable asteroid shapes is needed in order to improve upon the conclusions drawn from amplitude - spin rate statistics (see Tedesco and Zappalà 1980; Farinella et al. 1982; and the chapter by Binzel et al.).

B. Spin-Vector Distribution

The preferential prograde rotation of the eight major planets is sometimes attributed to collisional spin up during the accretion phase of the solar system (see discussions by Harris [1977] and Schofield [1981]). It is therefore natural to seek complementary information on this process by studying the spin-vector distribution of a probable remnant population of planetesimals, namely asteroids. Planetesimal accretion, accompanied by a hypothetical spin alignment process, probably occurred in a dynamically well-ordered system with low interparticle velocities (compare with preferential particle spins in ring systems [Salo 1987]). The subsequent collisional evolution of the asteroids has probably tended to randomize the spin vectors through very high-speed (~ 5 km s^{-1}) collisions with randomly oriented impact parameters (see numerical simulations by Barucci et al. 1986). Therefore, if any anisotropy is found in the spin-vector distribution today, we can conclude that a more enhanced anisotropy probably existed in the past. However, the degree of randomization depends on the past size of the asteroid population, which is unknown (see Farinella et al. 1985).

What do the observations tell us? The longitudes of the poles probably contain no evolutionary information since the precessional frequency is high enough to erase any original anisotropy. Fig. 11 shows the distribution of spin-vector latitudes β_0 based on confirmed pole determinations. The distinct bimodality was first noticed by Zappalà and Knežević (1984) and Barucci et al. (1986) as a clustering at intermediate pole latitudes. Magnusson (1986) suggested that part of this effect is due to a systematic error introduced by an amplitude-magnitude method and Magnusson (1988) hypothesized that a bias has been introduced by the epoch method's inability to use the near-zero-amplitude lightcurves often obtained for objects with the spin axis near the ecliptic plane. Although Drummond et al. (1988b) suggest that the bimodality is more obvious with respect to the orbital planes, the reality of the bimodality is an open question.

A quantity not influenced by any known bias or systematic effect is the ratio of prograde to retrograde rotators. That asteroids have spin vectors that are more isotropically distributed than the major planets is now well documented. There is a small dominance of prograde rotators in the available sample that is more pronounced for the very largest objects (> 200 km). The statistical significance of a majority of prograde rotators is 80 to 90% (Magnusson 1988). If confirmed by future observations, this tendency would provide more credit to the accretional spin alignment process and further constrain theories of asteroid evolution.

Hypotheses of spin alignment for specific classes of asteroids have been put forward. Binzel (1988) found statistically higher lightcurve amplitudes for Koronis family members than for comparable field asteroids. He noted that if the Koronis parent body had a spin vector at high ecliptic latitudes and the
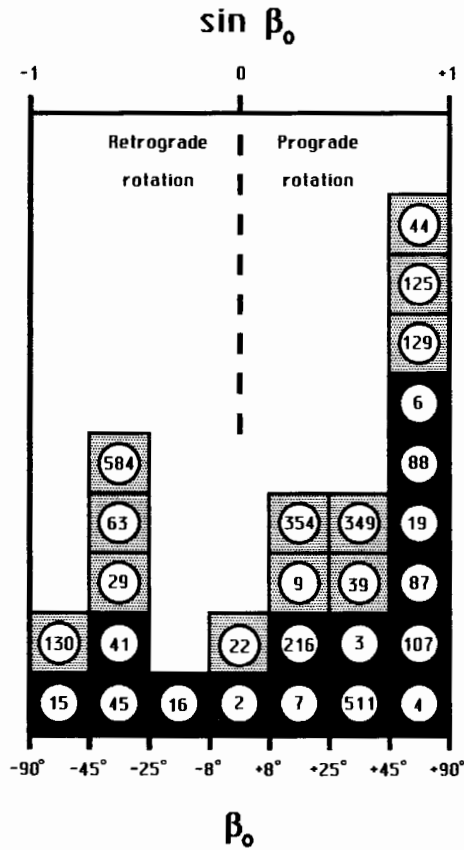
Fig. 11. Distribution of pole latitudes for a set of large main-belt asteroids. Black boxes indicate objects larger than 200 km and gray boxes, smaller objects. See also an alternative representation, where the distribution of the spin-vector components perpendicular to the ecliptic plane is given by Magnusson (1988).

subsequent fragmentation partially conserved spin orientation, we would observe preferentially high-amplitude equatorial lightcurves, but other explanations are possible. Weidenschilling has suggested that the more dramatic lightcurve amplitudes of several Trojan asteroids might be due to an alignment of their spin axes perpendicular to the ecliptic plane (Hartmann et al. 1988).

VII. STATE OF THE ART AND FUTURE PROSPECTS

With roots as far back as the works of I. Groeneveld, G. Kuiper, T. Gehrels, Y. Chang, and C. Chang in the 1950s and 1960s, pole and shape determinations have come a long way over the last decade. Most of the tech-

niques described in this chapter have appeared on the scene during the last decade, and the observational material has increased enormously, both in quantity and diversity. Asteroid pole and shape determination still requires detailed attention to peculiarities of individual objects. An understanding of the sources of error and the difficulties of acquisition and data reduction is essential. Judicious selection of data from the heterogeneous sample in the literature is required in order to derive useful information. A few examples will illustrate the diversity of objects and problems.

The large asteroid *4 Vesta* has long been suspected of having hemispherical albedo differences, which have prompted the introduction of techniques to monitor and model it. Cellino et al. (1987*b*) fitted a model with circular albedo markings to the photometric data. Drummond et al. (1988*a*) have reconstructed the first asteroidal surface images from speckle observations of Vesta.

Theoretical and laboratory studies (Secs. II and III) have a bearing on the plausibility and consistency of a derived formal solution for an asteroid. For example, the switches between primary and secondary extrema occurring in some solutions for *16 Psyche* and *201 Penelope* constitute a matter of debate (Tedesco and Taylor 1985; Magnusson 1986; Drummond et al. 1988*b*).

The problem of properly treating scattering becomes acute for extreme high-amplitude objects like *216 Kleopatra* and *624 Hektor* (see Fig. 10). Calibration of the dimensions of one of these objects with a nonphotometric method would put shape determinations on a much sounder footing.

The Earth-approaching asteroid *433 Eros* is really the object for which asteroid lightcurve analysis started off early this century, and its light variation has been monitored regularly ever since. Eros is the prime test for any method which attempts to model and extract information about highly elongated asteroids at large phase angles ($\sim 60°$). Additional lightcurve data on Earth-approaching objects are mainly in the form of single apparitions, for which decoupling of solar phase angle and aspect effects is difficult.

The large C-type asteroid *511 Davida* is the object for which the various techniques have given the most consistent results and it is a good candidate for calibration of other techniques. The pole is accurately determined to be close to $\lambda_0 = 299°$ and $\beta_0 = +34°$, and the usual ambiguity of photometric data (Sec. V.A) has been resolved by speckle interferometry (Drummond and Hege 1986). The lightcurves span a wide range in asterocentric latitudes (Fig. 4) and solar phase angles, and since they are smooth and nearly sinusoidal, indicate that Davida is nearly uniform in albedo and topography. The derived ellipsoid model, $a/b = 1.24$ and $b/c = 1.14$, is therefore probably valid to the extent that the geometric scattering approximation applies.

And finally, *532 Herculina,* an asteroid that has a great number of lightcurves in both the visible and infrared and has also been studied with speckle interferometry, still defies a reliable pole and shape determination (Taylor et al. 1987; Lebofsky et al. 1988; Drummond et al. 1988*c*). Perhaps this is a demonstration of the limitations of present techniques.

New Tendencies

Large uniform observation programs have been carried out recently by Binzel (1987) and Weidenschilling et al. (1987). The latter project, called "Photometric Geodesy" involves some 257 lightcurves for 26 main-belt asteroids, and was planned and executed primarily with pole and shape determinations in mind. Collaboration to present data in uniform and accessible form is another important development (see *Asteroid Photometric Catalogue* by Lagerkvist et al. 1987). Fourier analysis of this data base is in progress. The production of uniform data sets on asteroid poles and shapes with standardized techniques (see, e.g., Zappalà and Kneževič 1984; Magnusson 1986; Drummond et al. 1988b) is essential for statistical analysis. The very good consistency between the results by Drummond et al. (1988) and Magnusson (1988) for the Photometric Geodesy data indicates that the field is maturing. Perhaps most important of all, new observing techniques like radar, speckle interferometry, infrared polarimetry and occultations have opened up new avenues for deriving poles and shapes. The continuing effort to combine the different techniques holds great potential for the future.

Future progress in this field requires interactive development in two directions: (1) continued collaborative efforts to achieve a large, uniform (observations isotropically distributed in α, θ and ϕ) data set of photometric observations (perhaps also combined with radar, infrared and speckle); and (2) detailed studies of a small number of representative asteroids using a wide range of observational techniques, including dedicated space missions, with the aim of producing a few reference objects that could be used as calibration standards for the larger data base.

REFERENCES

Argentini, S., Barucci, M. A., Fulchignoni, M., Guerriero, L., and Salvatori, R. 1986. Peculiar shaped asteroids: Some laboratory results. In *Asteroids, Comets, Meteors II*, eds. C.-I. Lagerkvist, B. A. Lindblad, H. Lundstedt and H. Rickman (Uppsala: Uppsala Univ.), pp. 63–66.

Barsuhn, J. 1983. The lightcurves of a freely precessing spheroidal minor planet. *Astron. Astrophys.* 122:237–240.

Barucci, M. A., and Fulchignoni, M. 1982. The dependence of asteroid lightcurves on the orientation parameters and the shapes of asteroids. *Moon and Planets* 27:47–57.

Barucci, M. A., Casacchia, R., Fulchignoni, M., Burchi, R., Dipaoloantonio, A., Giuliani, C., Milano, L., Scaltriti, F., and Zappalà, V. 1982. Laboratory simulation of photometric light curves of the asteroids. *Moon and Planets* 27:387–395.

Barucci, M. A., Capaccioni, F., Cerroni, P., Flamini, E., and Fulchignoni, M. 1983. Laboratory simulation of asteroid lightcurves from fragments obtained from hypervelocity impacts. In *Asteroids, Comets, Meteors*, eds. C.-I. Lagerkvist and H. Rickman (Uppsala: Uppsala Univ.), pp. 95–100.

Barucci, M. A., Fulchignoni, M., and Zappalà, V. 1984. On the estimate of the shape of regular asteroids. *Bull. Amer. Astron. Soc.* 16:700 (abstract).

Barucci, M. A., Fulchignoni, M., Burchi, R., and D'Ambrosio, V. 1985. Rotational properties of ten main belt asteroids: Analysis of the results obtained by photoelectric photometry. *Icarus* 61:152–162.

Barucci, M. A., Bockelee-Morvan, D., Brahic, A., Clairemidi, S., Lecacheux, J., and Roques, F. 1986. Asteroid spin axes: Two additional pole determinations and theoretical implications. *Astron. Astrophys.* 163:261–268.

Barucci, M. A., Capria, M. T., Harris, A. W., and Fulchignoni, M. 1988. Fourier analysis of about 400 asteroid lightcurves. *Icarus,* submitted.

Binzel, R. P. 1985. Is 1220 Crocus a precessing binary asteroid? *Icarus* 63:99–108.

Binzel, R. P. 1987. A photoelectric survey of 130 asteroids. *Icarus* 72: 135–208.

Binzel, R. P. 1988. Collisional evolution in the Eos and Koronis asteroid families: Observational and numerical results. *Icarus* 73:303–313.

Bowell, E., Harris, A. W., and Lumme, K. 1988. A two-parameter magnitude system for asteroids. *Icarus,* submitted.

Cellino, A., Pannunzio, R., Zappalà, V., Farinella, P., and Paolicchi, P. 1985. Do we observe light curves of binary asteroids? *Astron. Astrophys.* 144:355–362.

Cellino, A., Zappalà, V., and Di Martino, M. 1987a. Effects of non-triaxial shape on the determination of the asteroid spin axis direction via the amplitude-magnitude method. In *10th European Regional Meeting of the IAU, Proceedings, Vol. 2. Interplanetary Matter,* eds. Z. Ceplecha and P. Pecina (Ondřejov, Astronomical Institute of Czechoslovak Academy of Sciences), pp. 121–124.

Cellino, A., Zappalà, V., Di Martino, M., Farinella, P., and Paolicchi, P. 1987b. Flattening, pole, and albedo features of 4 Vesta from photometric data. *Icarus* 70:546–565.

Cellino, A., Farinella, P., and Zappalà, V. 1988. Asteroid shapes and lightcurve morphology. *Icarus,* submitted.

Chandrasekhar, S. 1969. *Ellipsoidal Figures of Equilibrium* (New Haven: Yale Univ. Press).

Connelly, R., and Ostro, S. J. 1984. Ellipsoids and lightcurves. *Geometriae Dedicata* 17:87–98.

Drummond, J. D., and Cocke, W. J. 1988. Triaxial ellipsoid dimensions and rotational pole of 2 Pallas from two stellar occultations. *Icarus,* submitted.

Drummond, J. D., and Hege, E. K. 1986. Speckle interferometry of asteroids. III. 511 Davida and its photometry. *Icarus* 67:251–263.

Drummond, J. D., Cocke, W. J., Hege, E. K., Strittmatter, P. A., and Lambert, J. V. 1985a. Speckle interferometry of asteroids. I. 433 Eros. *Icarus* 61:132–151.

Drummond, J. D., Hege, E. K., Cocke, W. J., Freeman, J. D., Christou, J. C., and Binzel, R. P. 1985b. Speckle interferometry of asteroids. II. 532 Herculina. *Icarus* 61:232–240.

Drummond, J. D., Eckart, A., and Hege, E. K. 1988a. Speckle interferometry of asteroids. IV. Reconstructed images of 4 Vesta. *Icarus* 73:1–14.

Drummond, J. D., Weidenschilling, S. J., Chapman, C. R., and Davis, D. R. 1988b. Photometric geodesy of main-belt asteroids. II. Analysis of lightcurves for poles, periods, and shapes. *Icarus* 76:19–77.

Drummond, J., Taylor, R., Greenberg, R., and Lebofsky, L. 1988c. The mysterious case of 532 Herculina. Asteroids II Abstract Booklet, 8–11 March, Tucson, Arizona.

Dunlap, J. L. 1971. Laboratory work on the shapes of asteroids. In *Physical Studies of Minor Planets,* ed. T. Gehrels, NASA SP-267, pp. 147–154.

Farinella, P., Paolicchi, P., and Zappalà, V. 1981. Analysis of the spin rate distribution of asteroids. *Astron. Astrophys.* 104:159–165.

Farinella, P., Paolicchi, P., and Zappalà, V. 1982. The asteroids as outcomes of catastrophic collisions. *Icarus* 52:409–433.

Farinella, P., Paolicchi, P., and Zappalà, V. 1985. Original abundance of asteroids from their present rotational properties. *Mon. Not. Roy. Astron. Soc.* 216:565–570.

Fujiwara, A., Kamimoto, G., and Tsukamoto, A. 1978. Expected shape distribution of asteroids obtained from laboratory impact experiments. *Nature* 272:602–603.

Fulchignoni, M., Barucci, M. A., and Zappalà, V. 1988. Asteroid lightcurves: The amplitude-phase relationships. *Icarus,* submitted.

Hansen, O. L. 1977. On the prograde rotation of asteroids. *Icarus* 32:458–460.

Harris, A. W. 1977. An analytical theory of planetary rotation rates. *Icarus* 31:168–174.

Harris, A. W., Carlsson, M., Young, J., and Lagerkvist, C.-I. 1984. The lightcurve and phase relation of the asteroid 133 Cyrene. *Icarus* 58:377–382.

Hartmann, W. K. 1979. Diverse puzzling asteroids and a possible unified explanation. In *Asteroids*, ed. T. Gehrels (Tucson: Univ. of Arizona Press), pp. 466–479.

Hartmann, W. K., and Cruikshank, D. P. 1978. The nature of Trojan asteroid 624 Hektor. *Icarus* 36:353–366.

Hartmann, W. K., Tholen, D. J., Goguen, J., Binzel, R. P., and Cruikshank, D. P. 1988. Trojan and Hilda asteroid lightcurves. I. Anomalously elongated shapes among Trojans (and Hildas?). *Icarus* 73:487–498.

Johnson, P. E., Kemp, J. C., Lebofsky, M. J., and Reike, G. H. 1983. 10 μm polarimetry of Ceres. *Icarus* 56:381–392.

Karttunen, H. 1989. Modelling asteroid brightness variations I. Numerical methods. *Astron. Astrophys.* 208:314–319.

Karttunen, H., and Bowell, E. 1988. Modelling asteroid brightness variations I. On the uninterpretability of lightcurves and phase curves. *Astron. Astrophys.*, submitted.

Lagerkvist, C.-I., Barucci, M. A., Capria, M. T., Fulchignoni, M., Guerriero, L., Perozzi, E., and Zappalà, V. 1987. *Asteroid Photometric Catalogue* (Roma: Consiglio Nazionale della Ricerche).

Lambert, J. V. 1985. Occultation and lightcurve analysis: The figure of 2 Pallas. Ph.D. Thesis, New Mexico State Univ., Las Cruces.

Lebofsky, L. A., Greenberg, R., Tedesco, E. F., and Veeder, G. J. 1988. Infrared lightcurves of asteroids 532 Herculina and 45 Eugenia: Proof of the absence of significant albedo markings. *Icarus* 75:518–526.

Lumme, K., and Bowell, E. 1981. Radiative transfer in the surfaces of atmosphereless bodies. II. Interpretation of phase curves. *Astron. J.* 86:1705–1721.

Lumme, K., Karttunen, H., Bowell, E., and Poutanen, M. 1986. Inversion of asteroid lightcurves using spherical harmonics. In *Asteroids, Comets, Meteors II*, eds. C.-I. Lagerkvist, B. A. Lindblad, H. Lundstedt and H. Rickman (Uppsala: Uppsala Univ.), pp. 55–59.

Magnusson, P. 1986. Distribution of spin axes and senses of rotation for 20 large asteroids. *Icarus* 68:1–39.

Magnusson, P. 1988. Spin vectors of 22 large asteroids. *Icarus*, submitted.

Millis, R. L., and Elliot, J. L. 1979. In *Asteroids*, ed. T. Gehrels (Tucson: Univ. of Arizona Press), pp. 98–118.

Morrison, D. 1977. Asteroid sizes and albedos. *Icarus* 31:185–220.

Murphy, R. E., Cruikshank, D. P., and Morrison, D. 1972. Radii, albedos, and 20 micron brightness temperature of Iapetus and Rhea. *Astrophys. J.* 177:L93–L96.

Ostro, S. J., and Connelly, R. 1984. Convex profiles from asteroid lightcurves. *Icarus* 57:443–463.

Ostro, S. J., Connelly, R., and Dorogi, M. 1988. Convex-profile inversion of asteroid lightcurves: Theory and application. *Icarus* 75:30–63.

Pospieszalska-Surdej, A., and Surdej, J. 1985. Determination of the pole orientation of an asteroid. The amplitude-aspect relation revisited. *Astron. Astrophys.* 149:186–194.

Poutanen, A., Bowell, E., and Lumme, K. 1981. A physically plausible ellipsoidal model of Hektor? *Bull. Amer. Astron. Soc.* 13:725 (abstract).

Russell, H. N. 1906. On the light-variations of asteroids and satellites. *Astrophys. J.* 24:1–18.

Salo, H. 1987. Numerical simulations of collisions between rotating particles. *Icarus* 70:37–51.

Schober, H. J. 1982. A revised rotation period for the asteroid 164 Eva. *Astron. Astrophys. Suppl.* 48:57–62.

Schofield, N. 1981. On the formation of the Earth and Moon by gravitational accretion in a dust disc. *Mon. Not. Roy. Astron. Soc.* 197:1031–1047.

Sher, D. 1971. On the variation in light of tumbling bodies. *Astrophys. Space Sci.* 11:222–231.

Surdej, A., and Surdej, J. 1978. Asteroid lightcurves simulated by the rotation of a three-axes ellipsoid model. *Astron. Astrophys.* 66:31–36.

Surdej, J., Pospieszalska-Surdej, A., Michalowski, T., and Schober, H. J. 1986. Photoelectric photometry of 22 Kalliope during the 1985 opposition and the determination of its pole orientation: The "magnitude-aspect" relations revisited. *Astron. Astrophys.* 170:167–173.

Taylor, R. C., Birch, P. V., Drummond, J., Pospieszalska-Surdej, A., and Surdej, J. 1987. Asteroid 532 Herculina: Lightcurves, pole orientation and a model. *Icarus* 69:354–369.

Taylor, R. C., Birch, P. V., Pospieszalska-Surdej, A., and Surdej, J. 1988. Asteroid 45 Eugenia. Lightcurves and the pole orientation. *Icarus* 73:314–323.

Tedesco, E. F. 1979. A photometric investigation of the colors, shapes, and spin rates of Hirayama family asteroids. Ph.D. Thesis, New Mexico State Univ., Las Cruces.

Tedesco, E. F., and Taylor, R. C. 1985. Pole orientation of 16 Psyche by two independent methods. *Icarus* 61:241–251.

Tedesco, E. F., and Zappalà, V. 1980. Rotational properties of asteroids: Correlation and selection effects. *Icarus* 43:33–50.

Thompson, W. T., and Van Blerkom, D. 1982. A Monte Carlo approach to scattering off surfaces of triaxial ellipsoids. *Icarus* 49:387–397.

Uchida, K., and Goguen, J. D. 1987. A new method for determining asteroid shapes and rotation poles from lightcurves and its application to 624 Hektor. *Bull. Amer. Astron. Soc.* 19:842 (abstract).

Vesely, C. D. 1971. Summary on orientations of rotation axes. In *Physical Studies of Minor Planets*, ed. T. Gehrels, NASA SP-267, pp. 133–140.

Wassermann, L. H., Millis, R. L., Franz, O. G., Bowell, E., White, N. M., Giclas, H. L., Martin, L. J., Elliot, J. L., Dunham, E., Mink, D., Baron, R., Honeycutt, R. K., Henden, A. A., Kephart, J. E., A'Hearn, M. F., Reitsema, H. J., Radick, R., and Taylor, G. E. 1979. The diameter of Pallas from its occultation of SAO 85009. *Astron. J.* 84:259–268.

Weidenschilling, S. J. 1980. Hector: Nature and origin of a binary asteroid. *Icarus* 44:807–809.

Weidenschilling, S. J., Chapman, C. R., Davis, D. R., Greenberg, R., Levy, D. H., and Vail, S. 1987. Photometric geodesy of main-belt asteroids. I. Lightcurves of 26 large, rapid rotators. *Icarus* 70:191–245.

Worden, S. P. 1979. Interferometric determinations of asteroids. In *Asteroids*, ed. T. Gehrels (Tucson: Univ. of Arizona Press), pp. 119–131.

Zappalà, V. 1981. A semi-analytic method for pole determination of asteroids. *Moon and Planets* 24:319–325.

Zappalà, V., and Di Martino, M. 1986. Rotation axes of asteroids via the amplitude-magnitude method: Results for 10 objects. *Icarus* 68:40–54.

Zappalà, V., and Kneževič, Z. 1984. Rotation axes of asteroids: Results for 14 objects. *Icarus* 59:435–455.

Zappalà, V., Di Martino, M., Farinella, P., and Paolicchi, P. 1983. An analytical method for the determination of the rotational direction of asteroids. In *Asteroids, Comets, Meteors,* eds. C.-I. Lagerkvist and H. Rickman (Uppsala: Uppsala Univ.), pp. 73–76.

REFLECTANCE SPECTROSCOPY AND ASTEROID SURFACE MINERALOGY

MICHAEL J. GAFFEY
Rensselaer Polytechnic Institute

JEFFREY F. BELL
University of Hawaii

and

DALE P. CRUIKSHANK
NASA-Ames Research Center

Asteroid surface mineralogy is a function of the initial composition of the parent planetesimal modified to a greater or lesser extent by endogenic processes (e.g., heating, metamorphism, partial or complete melting, magmatic differentiation and aqueous alteration) and exogenic processes (e.g., regolith processes, excavation during cratering events and collisional disruption to expose internal layers). Detailed mineralogical characterizations of asteroidal objects permit their evolutionary history to be, at least partially, deciphered. Analysis of visible and near-infrared spectral reflectances and spectral albedos provide our primary means of characterizing the surface mineralogy and petrology of asteroidal bodies. Such mineralogical analysis of asteroidal reflectance spectra is based in quantum physics but employs a series of empirically derived interpretive calibrations and methodologies. The last decade has seen significant improvements in both the interpretive procedures and in the observational data base. This has resulted in a greatly improved understanding of the nature of individual asteroids, of the asteroid population and of the early solar system processes which have produced and modified these objects. This chapter provides an overview of the current asteroid spectral interpretive procedures and of our present understanding of the nature and history of these minor planets. Several very important, but still unresolved, issues are discussed, such as the source of the ordinary chondrites.

I. MINERALOGICAL INFORMATION IN REFLECTANCE SPECTRA

Introduction

Electromagnetic radiation interacts with matter by a coupling process between the electrical fields of the photon and the electrons or charges in the material. The details of the interaction depend upon the wavelength of the radiation and the physical state of the matter. At thermal or mid-infrared (>3 μm) wavelengths, this interaction is primarily with the oscillating charges in vibrating molecules. Photons are absorbed or emitted with energies corresponding to the fundamental vibrational frequencies of the molecules, or at the overtones and combinations of these fundamentals (Herzberg 1945). For asteroidal surface temperatures, emission is negligible at visible and near-infrared ($\sim$0.35 to 3 μm) wavelengths, and absorption features are produced by vibrational, crystal field (Burns 1970a), and charge transfer mechanisms (Burns 1981). At near-ultraviolet ($\sim$0.25 to 0.35 μm) wavelengths, absorptions are produced primarily by charge-transfer mechanisms. At vacuum ultraviolet ($<$0.25 μm) wavelengths, absorption results from exciton (electron-hole pair) formation, the solid-state analogue of ionization (Nitsan and Shankland 1976).

For objects illuminated by the Sun, the maximum incident flux is in the mid-visible region of the spectrum, while the maximum emission due to thermal processes depends on surface temperature and ranges from <3 μm for the central sunlit hemisphere of Mercury to nearly 100 μm for the pre-sunrise portions of icy bodies in the outer solar system. For bodies in the asteroid belt, the emission peak lies between 5 and 20 μm depending upon the surface albedo (proportion of incident flux reflected), emissivity and thermophysical properties.

There are several major reasons why visible and near-infrared reflectance spectroscopy has been the most heavily exploited technique of asteroid surface material characterization. First, the detectable flux is maximized at visible and near-infrared wavelengths because the illuminating solar flux peaks in the visible region, and because the Earth's atmosphere is relatively transparent at these wavelengths compared to either the ultraviolet or mid-infrared. But more importantly, in the visible and near-infrared spectral region, mineralogy is the primary first-order determinant of spectral properties. By contrast, the features in mid-infrared spectra are simultaneous functions of composition, texture and temperature. For planetary surfaces, where properties such as particle-size distribution cannot be controlled, the mid-infrared spectra provide a potentially rich but bewilderingly complex, and largely unexploited, source of information (Logan et al. 1973,1975; Salisbury et al. 1987; Christensen and Luth 1987). At ultraviolet wavelengths, the absorptions are very intense and tend to suppress the diagnostic features in the spectra of particulate surfaces (Hapke et al. 1978).

The unresolved complexity of mid-infrared spectral features and the weakness of ultraviolet features, combined with the general difficulty of obtaining calibrated photometry from groundbased telescopes in these spectral regions, have retarded their use in characterizing asteroid surface materials. Fortunately, many cosmically significant (e.g., meteoritic) mineral phases exhibit absorption features in visible and near-infrared reflectance spectra which are diagnostic of the presence, composition and abundance of those specific mineral phases. The subsequent discussion, except as noted, will pertain solely to visible and near-infrared reflectance spectroscopy. These reflectance curves of a number of important or potentially important asteroid minerals are shown on Figs. 1 and 2A.

Electronic Absorption Features

The most common visible and near-infrared electronic absorption features in minerals arise from the presence of iron and/or other transition metal cations (e.g., nickel, cobalt, copper, titanium, etc.) in specific crystallographic sites within the mineral species. The symmetry and dimensions of these crystallographic sites (e.g., the M1 and M2 sites in olivines) are characteristic of the particular mineral type in which they are located. The electrostatic field resulting from the particular coordination and dimensions of the anion array which forms the cation site produces a distinctive energy level pattern among the electronic orbitals of the d-shell or valence electrons of the cations (see, e.g., Burns 1970a,b). A photon can be absorbed by an electron which occupies a ground-state orbital (energy level) separated from a vacant orbital by an energy difference equal to the energy (hν) of the photon. For transition metal-bearing minerals, spectral features can be used: (a) to identify the mineral species; (b) to establish which transition metal cations are present; and (c) to determine the mineral chemistry and/or transition metal abundance.

Different mineral species have different crystallographic sites resulting in distinct patterns of crystal field splitting in the d-shell electrons of any particular transition metal cation. This produces distinct visible and near-infrared absorption-band positions for most transition metal-bearing minerals (see, e.g., Adams 1975). Examples of the diversity of Fe^{2+} absorptions are seen in Fig. 1. The orthopyroxene spectrum exhibits two symmetric absorption features near 1 and 2 μm. The olivine exhibits a broad asymmetric feature, a combination of three overlapping absorptions, near 1 μm. Feldspar exhibits a weak band near 1.25 μm from its trace content of Fe^{2+}. Spinel shows a broad absorption feature longwards of 1.5 μm. The geologically important transition metal species (e.g., Fe, Ni, Co, Cu, Ti, Mn, etc.) and their various cations (e.g., Fe^{2+}, Fe^{3+}, etc.) have different ionic radii, and therefore undergo different degrees of crystal field splitting in any particular crystallographic site. Absorption-band position is thus also diagnostic of the specific absorbing cation species (Burns 1970a,b,1981). (See Adams [1975] or Gaffey and McCord [1978,1979] for additional discussion of the spectra of meteoritic minerals.)
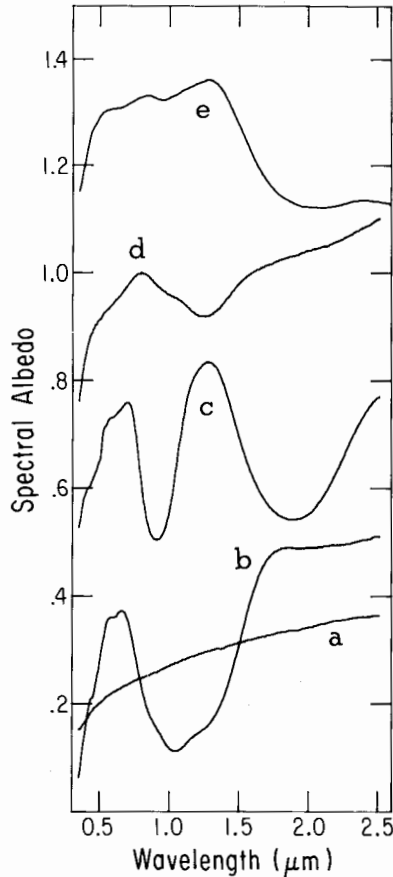
Fig. 1. The spectral albedo curves of five anhydrous mineral species that are spectrally important in meteoritic and asteroid assemblages: (a) nickel-iron metal (Gaffey 1986); (b) olivine (*Chassigny*: Gaffey 1976); (c) orthopyroxene (the diogenite Johnstown: ibid.) [offset by +0.4]; (d) plagioclase feldspar (lunar sample 12063,79 - J.B. Adams) [offset by +0.4]; (e) spinel-bearing Allende inclusion (Rajan and Gaffey 1984, and in preparation) [offset by +1.0].

Substitution of a large cation for a smaller one in a solid solution series [e.g., Fe^{2+} or Ca^{2+} replacing Mg^{2+} in olivine or pyroxene) systematically expands and/or distorts the entire crystal structure. The resulting change in the crystal field splitting of the transition metal cations produces a correlated shift in the wavelength position of the associated absorption features. Absorption-band position is thus diagnostic of phase composition in solid-solution series (e.g., the olivine suite: Burns 1970*b;* the pyroxene suite: Adams 1974).

Charge transfer absorptions involve electronic transitions between different shells in a particular cation or between adjacent cations or cation-anion

pairs. These generally occur at shorter wavelength and are significantly stronger than the crystal-field absorptions. An overlapping series of such charge-transfer features produces the strong blue-ultraviolet absorption edges in many silicate and oxide minerals (Burns 1981). The extremely strong absorptions in iron oxides (e.g., the hematite spectral curve on Fig. 2A) shortwards of 0.6-0.7 μm represent such charge transfer absorptions (Morris et al. 1985). In the Fe-bearing phyllosilicates of the CI/CM meteoritic assemblages, several different combinations of charge-transfer features are present and are characteristic of the particular clay mineral species (see, e.g., Gaffey 1980; King 1986). Note the difference in the 0.5-1.3 μm spectral regions between lizardite and antigorite, two different serpentine-group phyllosilicates shown in Fig. 2A.

Organic molecules can also provide the coordination sites for transition metal cations. For example, the organic porphyrin structures incorporate transition metal ions into the center of their square planar units producing intense narrow features (Baker and Louda 1986). The geologically common nickel- and vanadium-bearing porphyrins exhibit a strong band (the Soret band) near 0.40 μm and 0.41 μm, respectively, as well as pairs of weaker bands between 0.55 and 0.60 μm. Metal-bearing porphyrins are a common constituent of biological materials (e.g., iron-bearing heme-porphyrin is the basic building block of hemoglobin, and Mg-porphyrin is the basis of chlorophyll). Porphyrins are also produced by abiotic synthesis processes. Such metal-bearing porphyrins are quite stable against thermal degradation which permits their long-term survival upon and within asteroids.

Hodgson and Baker (1969) reported the presence of porphyrins in samples of CI1 (Orgueil) and CM2 meteorites (Murray, Cold Bokkeveld, Mokoia) but not in samples of CV3 (Vigarano), E6 (Indarch), L6 (Peace River, Bruderheim) chondrites. Although terrestrial contamination as a source of these porphyrins cannot be ruled out, their absence in the carbon-poor meteorites and their production as a part of most abiotic synthesis processes, such as those which produced the other organic compounds in the CI and CM meteorites, argue that these are plausible candidates for asteroid surface-material components. Holden and Gaffey (1987) suggested that absorptions in the spectrum of Orgueil were due to a porphyrin phase.

For conductors, such as metals, two spectrally significant electronic interactions are important for the present discussion. Electrons can be excited from the ground state to the conduction band (delocalized electrons) by photons with energies in excess of the band gap. This produces strong absorption edges and the colors seen in metals such as gold and copper. For the meteoritic nickel-iron alloys, there is no ground-state conduction band gap corresponding to visual and near-infrared wavelengths. In such materials the spectral reflectance is controlled primarily by the wavelength-dependent conductivity. A photon incident upon a perfect conductor produces electron oscillations at the photon frequency. In a real metal, the finite conductivity limits the effi-
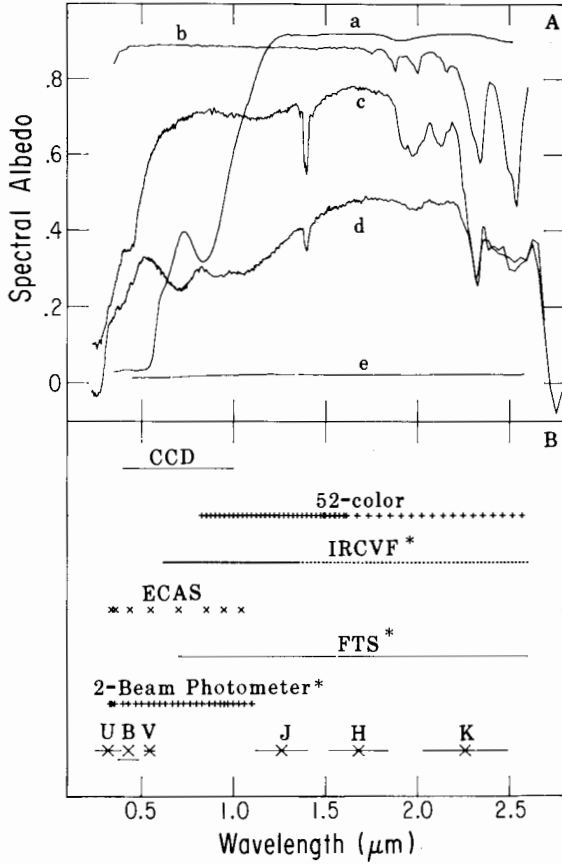
Fig. 2. (A) Spectral albedo curves of additional spectrally important or potentially important asteroidal mineral species: (a) hematite (alpha-Fe_2O_3: R.H. Huguenin); (b) calcite (var. Icelandic spar: S.J. Gaffey 1986); (c) serpentine (var. Lizardite: King, 1986); (d) serpentine (var. Antigorite: ibid.) [Offset by -0.1]; (e) carbonaceous residue from Murchison (Cruikshank et al. 1983).

(B) Wavelength coverage and resolution for various asteroid data sets are plotted at the same wavelength scale as the mineral spectra in Fig. 2A. Spectral bandpasses for the UBVJHK filters are indicated by the horizontal lines. Wavelength sampling positions are indicated by "+", "x" or dots for the 2-beam photometer, ECAS (eight color asteroid survey), IRCVF and 52-color data. Spectral resolution for the CCD and Fourier Transform Interferometer data are approximately 20 Å and 1 Å, respectively. [An asterisk (*) indicates that asteroid data is no longer regularly being obtained with this system or that the system is no longer operational.]

ciency of the electron response. At higher frequencies (shorter wavelengths) the conductivity decreases and the reflectivity as well. For the NiFe alloys, the visible and near-infrared reflectance decreases approximately linearly with photon frequency (inverse wavelength), as shown by the NiFe reflectance curve in Fig. 1. (See Gaffey [1986] for additional discussion and references to NiFe spectral properties.) Britt and Pieters (1988) note that geometry can affect the spectral reflectance curve of NiFe, but also indicate that this will be, at most, a very minor effect for particulate surfaces.

Visible and Near-Infrared Vibrational Absorption Features

Several molecular species which are common in the CI/CM meteoritic assemblages produce important or potentially important visible and near-infrared absorption features. These include water and OH-bearing minerals, the carbonate minerals and the organic hydrocarbons.

Water. Water in the form of bound water, structural OH or fluid inclusions is found in various hydrated silicates, oxides and salts common or present in the CI and CM assemblages. The water molecule (it can be visualized as a V-shaped configuration with the oxygen atom at the apex and hydrogen atoms at the end of the arms) undergoes three types of vibrations: a bend (the V-opening and closing) with a fundamental frequency corresponding to a wavelength of 6.08 μm; a symmetric stretch (both arms lengthening or shortening together) at 3.05 μm; and an asymmetric stretch (one arm lengthening or shortening) at 2.87 μm. An OH^- radical can only undergo the asymmetric stretch mode of vibration. The wavelengths of the fundamentals undergo small shifts depending upon mass of attached (or nearest-neighbor) ions and hence upon the mineral species which contains the water or OH molecule.

The 3.05 μm and 2.87 μm fundamentals combine with the first overtone (twice the frequency) of the bend fundamental at 3.04 μm to produce a broad and extremely intense absorption feature in the 3 μm region. The presence of a 3 μm feature in asteroidal spectra thus indicates water-bearing phases such as hydrated silicates (see, e.g., Lebofsky 1980; Lebofsky et al. 1981; Jones 1988). However, the feature is normally so intense (saturated) in reflectance spectra of water-bearing species that the actual positions of the fundamentals cannot be accurately determined. Even under laboratory conditions, the 3 μm feature can generally be used to distinguish clay mineral species only in nearly monomineralic assemblages with a very fine and uniform particle size (Farmer 1974), or in the case of essentially anhydrous silicates, to detect small traces of water (Aines and Rossman 1984a,b). Thus paradoxically because of its strength, the 3 μm feature has provided only minor mineralogical information—beyond the detection of hydrated species—in asteroid studies.

Combination and overtone features of the water fundamentals are present at shorter wavelengths, with the 1.9 μm and 1.4 μm features of particular importance. These are much weaker than the fundamentals, but are relatively

strong in clay mineral species (e.g., in the lizardite and antigorite spectra in Fig. 2A). In particular the 1.4 μm appears to be a sensitive discriminator of clay mineralogy (King 1986). In CI/CM spectra, these overtone and combination features are relatively weak (<10% below the background continuum: Gaffey 1976; Larson et al. 1979). Weak features near these wavelengths are difficult to observe with groundbased telescopes since the atmospheric water-vapor absorptions interfere. The weaker overtone features are also much more readily masked by opaque phases in intimate mixtures, so that surface petrology will play an important part in whether they are detected. However, these weaker bands do provide much better mineralogic discriminators than the 3 μm region, so additional effort is justified to exploit their potential. Tantalizingly, the CI specimen Alais exhibits a pronounced 1.9 μm feature (Gaffey 1976), which may represent a particular type of alteration environment. Additionally, the processes of aqueous alteration evident in the CI/CM suite and invoked to explain the spectrum of asteroid 1 Ceres (see, e.g., Gaffey 1978; Feierberg et al. 1981) can reasonably be expected to suppress the spectral effect of the opaque phases which decrease the apparent intensity of these overtone features in meteorite and asteroid spectra.

Carbonates. The carbonate minerals are common accessory phases in the CI meteorites (Richardson 1978; Fredriksson and Kerridge 1988) and could be concentrated wherever aqueous alteration has taken place on asteroid bodies. The relatively strong overtones of the fundamental vibrational modes of the CO_3 radical occurs longwards of 1.6 μm (see the calcite spectrum in Fig. 2A), the exact positions depending on the crystal system (rhombohedral [calcite] or orthorhombic [aragonite] group) and on the dominant cation species (calcium, magnesium, iron, etc). Transition metal-bearing carbonates such as the dolomite and breunnerites present in the CI chondrites (Fredriksson and Kerridge 1988) also exhibit crystal field bands in the 1 μm region and shortward. See S.J. Gaffey (1986,1987) for a more detailed discussion of carbonate spectra. Although no features in CI/CM spectra have yet been assigned to carbonate minerals, the aqueous processes which modified those assemblages may well have produced significant carbonate concentrations on or within individual asteroids. The surficial evaporite deposits proposed for Io by Fanale et al. (1974) prior to the 1979 Voyager encounter, may well be found on Ceres or Pallas based upon what we presently believe about the nature and evolution of these asteroids.

Hydrocarbons. Vibrations of the C-H pair which forms the basis for hydrocarbon compounds gives rise to a relatively strong feature near 3.4 μm in the spectra of organic compounds. The exact position of this feature is a function of the specific organic compound, and has long been utilized in analytical chemistry to identify compounds (e.g., the infrared correlation charts in the *Handbook of Physics and Chemistry* 1975). In the spectra of CI and CM

meteorites, the C-H stretch feature is relatively weak, generally having an intensity of 10% or less (see, e.g., Larson et al. 1979; Sandford 1984; Cruikshank and Brown 1987; Jones 1988). It is located on the edge of the intense 3 μm terrestrial atmospheric absorption feature, so that its detection requires particularly careful observational procedures and extinction calibrations (see, e.g., Cruikshank and Brown 1987; Jones 1988; Piscitelli 1988, personal communication).

II. GENERAL CLASSES OF ASTEROID SPECTRAL REFLECTANCE DATA

The available data base of asteroid reflectance spectra has improved significantly during the 1980s, both in number and quality, although this growth has fallen well below the estimates that one would have derived by extending the Chapman and Zellner (1978) graph of growth for the 1970-1979 period. Activity has actually decreased significantly in several areas, particularly polarimetry and *UBV* photometry. In some cases these shortfalls or declines derive from the relative expansion of a competing technique or from the increasing difficulty of pushing to fainter magnitudes, but in many cases arise because of the decrease in real funding for this kind of work. Table I lists the various spectral and spectrophotometry data sets and the number of asteroids available for each as of early 1988.

Ideally one desires broad wavelength coverage, high spectral resolution, and low noise data for asteroid investigations. Realistically we are limited to existing instrumental capabilities. Figure 2 compares the wavelength coverage and spectral resolution for several of the VNIR data sets to the wavelength position and width of the features in the spectral curves of some candidate asteroidal mineral species.

In addition to sophisticated instruments and access to telescope time, careful definition of the research problem and the availability of high-quality interpretative calibrations are necessary conditions for any sophisticated asteroid investigation. Although enhanced instrumental capabilities are highly desirable, careful problem definition can often overcome, or at least ameliorate, limited instrumental capabilities and telescope time. Examples of the importance of interpretive calibrations and problem definition in asteroid investigations are discussed below.

III. ANALYSIS OF ASTEROID REFLECTANCE SPECTRA

The procedures to derive asteroid properties or surface material characterizations from asteroid color and spectral data can be divided into four major approaches: classification, curve matching, feature matching and quantitative analysis of spectral parameters. These represent a series of increasingly sophisticated methodologies, with progressively greater demands on both the

<div align="center">

TABLE I
Asteroid Data from Various Spectral Techniques

</div>

No. of Objects	Technique
	Broad-Band VNIR Color Data
920	UBV filters (see TRIAD index in Part VI)
589	8-color subvwxpz filters (Zellner et al. 1985)
88	JHK filters (Johnson et al. 1975; Chapman and Morrison 1976; Matson et al. 1977; Leake et al. 1978; Larson and Veeder 1979; Veeder et al. 1982,1983a,b,1984)
	Medium-Resolution (1–5%) VNIR Spectra
290	2-beam photometer, 24-filter data (0.33–1.1 μm) (Chapman and Gaffey 1979; McFadden et al. 1984)
11	1% CVF data (0.6–2.6 μm) (Gaffey 1983,1984; Gaffey and Ostro 1987; and Gaffey, unpublished)
119	52-color 3% CVF data (0.8–2.5 μm) (Bell et al. 1988, and in preparation)
46	3% CVF data, CGAS and filters (2.5–5 μm) (Lebofsky et al. 1981; Eaton et al. 1983; Feierberg et al. 1985; Cruikshank and Brown 1987; Jones 1988; Piscitelli, unpublished)
	Higher-Resolution (<1%) VNIR Spectra
14	FTS spectra (0.8–2.8 μm) (Feierberg et al. 1981,1982)
>75	CCD spectra (0.4–1.0 μm) (Vilas and Smith 1985; Vilas and McFadden 1989; Sawyer, unpublished)
	Mid-Infrared Spectra
19	8–13 μm, 2% resolution (Feierberg et al. 1983; Green et al. 1985; Gillett and Merrill 1975)
31	8–13 μm and 8–24 μm, 10% resolution (Hansen 1976)
	Broadband Mid- and Far-Infrared Photometry
1811	12,25,50,100 μm IRAS fluxes (not all channels for all objects)
	Albedos
>250	Earth-based mid-infrared photometry (Brown and Morrison 1984, and references therein)
1811	IRAS (large uncertainties for faintest sources)

observational data and the interpretive calibrations. Any particular asteroid investigation may incorporate several of these techniques in the analysis of a data set.

Classifications

Classification is the sorting of a suite of available parameters by simple or sophisticated means. Classification techniques tend to be of two general types: inclusive (lumpers) or exclusive (splitters). Any data set can be sorted into a series of classes or pigeonholed, but the relevance of the sorted parameters will determine whether the derived groupings are physically meaningful. The asteroid color-albedo classes [C, S, M, etc.] have evolved significantly

over the past decade. The reader is referred to the chapter by Tholen and Barucci for a detailed review of the origin and evolution of the asteroid taxonomic classifications.

With the parameters presently used, the asteroid classes should lump grossly similar types of materials together and can be used to investigate problems such as the general patterns of asteroid distribution (Gradie and Tedesco 1982; see also the chapter by Gradie et al.) or the nature of asteroid families (Gradie et al. 1979; Tedesco 1979; see also the chapter by Chapman et al.). However, since the classification procedures do not specifically employ compositionally diagnostic criteria, the assignment of an asteroid to a class should not be construed as a compositional interpretation. Although some of the designations for asteroid classes are compositionally suggestive (e.g., C, carbonaceous; M, metallic), the classification of an asteroid as a member of that type does not actually establish the presence of any particular surface assemblage. Moreover, the very nature of the binning process includes diverse assemblages within the same class. It must be constantly borne in mind that the classes, while useful for many purposes, may often comprise quite heterogeneous groups of asteroid assemblages.

Matching Spectral Curves

The form of an asteroid's spectral reflectance curve is determined by the various molecular and ionic absorption features from mineral phases on its surface. The curve-matching approach involves comparison of the asteroid spectral curve with a catalog of spectral curves for some reference suite, most commonly meteorite samples (see, e.g., McCord et al. 1970; Chapman and Salisbury 1973; McCord and Gaffey 1974; Chapman 1975,1976; Matson et al. 1976; Miyamoto et al. 1982). This method provides a relatively rapid identification of possible analogous assemblages. As albedos have become more available, the matches increasingly have been made to spectral albedo curves (the wavelength-dependent albedo), a practice which significantly reduces ambiguities.

The major uncertainty with this technique lies in the question of just what constitutes a good match and what such a match really means. This is complicated by the incompleteness of the comparison library. Ideally the comparison library should include spectra for all materials which might plausibly be found on asteroid surfaces. The selection should include not only all of the different mineral assemblages (phase abundances, phase compositions) and petrologies (particle sizes, petrographic relations, etc.), but also the effects of mixing at all scales, and the effects of space weathering and regolith processes. The compilation of a complete library of comparison spectra is probably a transfinite task.

Any spectral matching effort quickly runs up against this limit. In the absence of an ideal comparison library, one has to guess at the significance of discrepancies between the observational and comparison spectra. A basic un-

derstanding of the various molecular and ionic processes which affect spectral curves, and of the effects of physical state, space weathering and regolith processes can provide guidelines for estimating when a deviation between the observational curve and the comparison curve is significant. These issues are discussed in more detail by Gaffey and McCord (1978,1979).

Matching Spectral Features

Significant variations in the spectral albedo curve of an assemblage may arise from variations in physical properties which are of little or no geologic or cosmologic consequence. The isolation and matching of individual spectral features exploits a much more direct relationship with the mineralogical and compositional properties of a surface. For assemblages with well-defined absorption features, such as the pyroxene bands in Vesta's spectrum, the interpretation of such features is relatively unambiguous. For overlapping features such as those found in the spectra of olivine-pyroxene mixtures, there can be considerably more ambiguity.

Both the curve-matching and the feature-matching approaches require a catalog of comparison spectra, but the feature-matching catalog can consist primarily of representative samples of plausible mineral suites. The creation of such a comparison library is thus merely an extremely large, and not a transfinite, task. However, the feature-matching technique places more stringent requirements on the observational data, which must have sufficient spectral resolution, wavelength coverage and photometric precision to permit identification of the individual spectral features. The specific requirements depend on the spectral properties of the surface assemblage, as can be seen by an examination of Figs. 1 and 2A. For example, narrow features require higher spectral resolution, while weaker features require higher signal-to-noise ratios.

Interpretations derived from matching spectral features are less subject to questions of uniqueness than the curve-matching technique, since the interpretation focused primarily on mineralogically significant parameters. The spectral-feature-matching technique provides a much more detailed characterization, in which the presence and, to some extent, the composition of mineral phases can be determined. The limitations include the more severe observational requirements and the omission of species without significant visible and near-infrared spectral features.

Quantitative Spectral Interpretation

This approach is the logical outgrowth of the feature-matching technique, and to some extent no sharp boundary can be defined between these two. The real distinction is the decreased dependence upon the personal expertise of the interpreter. Instead, specific spectral parameters such as band area, band position, relative depth, relative slope are quantitatively extracted from the spectrum by means of a prescribed procedure and these parameters

are compared to quantitative calibrations of similar parameters developed from laboratory spectral study of meteoritic and asteroid analogue assemblages. For example, the pyroxene composition in the surface material of Vesta can be determined by correlating the absorption-band positions in Vesta's spectrum to the Adams (1974) calibration between pyroxene composition and band position. The attainable levels of sophistication in the detection and quantitative characterization of phase abundance and/or composition depend on the sophistication of the available interpretive calibrations and upon the precision and accuracy with which the appropriate spectral parameters can be determined for the particular asteroid.

The requirement for reasonably precise absorption-feature parameters places significant spectral resolution, wavelength coverage and photometric precision requirements on asteroid observational data. While the pyroxene feature might be detectable in relatively noisy or low-resolution data, its position would be poorly defined. Useful determination of the diagnostic spectral parameters requires observational data with both low-noise and moderately high spectral resolution.

Several improved methods of spectral analysis or spectral feature extraction have recently been proposed. These include mathematical analysis (Johnson et al. 1983; Huguenin and Jones 1986) and spectral modeling (Clark and Roush 1984; Nelson and Clark 1988).

Interpretation of the derived spectral parameters requires appropriate calibrations, the development of which often involve major laboratory efforts. The work of Adams (1974) on pyroxene composition, and the work of Cloutis et al. (1986) on phase abundance in olivine-orthopyroxene mixtures are good examples of such efforts. A basic calibration also exists for pyroxene-feldspar assemblages such as found in the basaltic achondrites (McFadden and Gaffey 1978). Each of these quantitative calibrations employs a specific procedure to extract the appropriate diagnostic spectral parameters from the observational spectra. Table II outlines these procedures, as well as their attainable accuracy and limitations, for three of the available interpretive calibrations.

However, in the area of calibrations much remains to be done. Qualitative or semi-quantitative studies of spectral systematics have been carried out for a number of asteroidally plausible mineral assemblages or physical parameters (see, e.g., Adams and Filice 1967; Nash and Conel 1974; Feierberg et al. 1982; Rajan and Gaffey 1984; Roush and Singer 1986; Crown and Pieters 1987; Bell and Keil 1988). But, the need for quantitative interpretive calibrations is still very acute. Of particular need for asteroid studies are calibrations for olivine-orthopyroxene-clinopyroxene assemblages, metal-mafic silicate mixtures, feldspar-bearing, magnetite/spinel-bearing, and phyllosilicate-bearing assemblages. Additionally, although physical properties (e.g., particle size) generally have only second-order effects on the spectra of meteoritic-type assemblages, their importance varies with different assemblages and their specific effects need to be better defined.

TABLE II
Quantitative Spectral Interpretive Calibrations

1. Pyroxene Composition (Adams 1974)

Primary Spectral Parameter: 1 μm(BI) and 2 μm(BII) band centers measured relative to a linear continuum tangent to the maxima in the reflectance curve on either side of the bands.

Parameters Determined: Molar abundance of Fe(Fs) and Ca(Wo) in pyroxenes.

Calibration:	Fs = Fe/(Fe + Mg + Ca) = (BII − 1.78 μm)/0.0036
Uncertainty:	±5 to 10%
Restrictions:	Ca(Wo) < 10% (orthopyroxenes and low calcium clinopyroxenes)
Calibration:	Wo = Ca/(Fe + Mg + Ca) = (BI − 0.899 μm)/0.00154
Uncertainty:	±5 to 10%

2. Olivine-Orthopyroxene Abundance (Cloutis et al. 1986)

Primary Spectral Parameter: Relative areas of 1 and 2 μm (bands I and II) below linear continua tangent to reflectance curve shortwards, between, and longwards of bands. Band areas in units of reflectance or albedo times wavelength (e.g., from plots with scales of wavelength and reflectance or spectral albedo).

Parameters Determined: Relative abundance (wt. %) of olivine [Ol] and orthopyroxene [Opx] in binary mixtures, or when mixed with species not having discrete absorption features between 0.5 and 2.6 μm.

Calibration:	Opx(wt.%) = [Opx/(Opx + Ol)] = 41.7 × [(BII/BI) + 0.125]
Uncertainty:	±5% for Opx = 10% to 90%

3. Plagioclase-Pyroxene Abundance (McFadden and Gaffey 1978)

Primary Spectral Parameter: Relative areas of 1 μm (band I) pyroxene and 1.25 μm plagioclase feldspar absorption features. Pyroxene band area below a linear continuum tangent to relative maxima in curve near 0.7 and 1.5 μm. Plagioclase band area below a fitted pyroxene curve. Band area units in reflectance × wavelength or albedo × wavelength.

Parameters Determined: Relative abundance (normative or vol. %) of plagioclase feldspar to pyroxene.

Calibration:	Plag/Py (Vol. %) = 3.46 × [(Plag band/Py band) + 0.017]
Uncertainty:	±10 to 20%
Restrictions:	Derived for basaltic achondrites

Spectral modeling techniques (Nelson and Clark 1988) could significantly increase the efficiency of such laboratory calibration efforts, by providing a means of extrapolating the spectra of assemblages intermediate between the measured samples. Such models derive the relevant optical constants from measured spectra of end-member and a few intermediate samples, and then use those constants to compute the spectra of assemblages with varying abundances of the same phases in similar petrographic relationships. Because of the complexity of chemical and petrologic relationships in real geologic as-

semblages, the theoretical spectral modeling techniques compliment but do not replace the empirical laboratory mixing calibrations. For example, despite major progress in crystal-field and charge-transfer models of the optical properties of minerals, there is no reliable means of extrapolating the optical constants between end-members of the solid solution series to the required degree of precision. Thus, the necessary optical constants must continue to be derived from measured spectra of controlled mixtures or actual samples.

Currently, characterizations of asteroid surface material are limited to the identification of mafic assemblages, metal-rich assemblages and the clay mineral assemblages. Particular molecular absorptions due to hydrocarbons, porphyrins, water and OH-bearing phases, and carbonates (CO_3) are or should be present in the spectra of certain asteroids. To date, only the broad water fundamental near 3 μm has been unambiguously detected (Lebofsky, 1980; Lebofsky et al. 1981; Feierberg et al. 1981; Jones 1988). Cruikshank and Brown (1987) report that they have identified the 3.4 μm CH-stretch of hydrocarbon compounds in the spectrum of 130 Elektra.

Quantitative determinations of phase abundance are presently limited to determinations of pyroxene-phase composition in pyroxene-dominated assemblages (e.g., Vesta), and to pyroxene, olivine and feldspar abundances in olivine-orthopyroxene and pyroxene-feldspar assemblages (e.g., ordinary chondrites, the silicate component of stony irons and basaltic achondrites).

Overcoming Sources of Uncertainty in Asteroid Characterizations

There are several means of overcoming the limitations of current asteroid surface-material characterizations. Some are obvious such as expanding the availability and sophistication of quantitative interpretive calibrations, and in improved wavelength coverage, spectral resolution and photometric precision to provide data appropriate to those calibrations. There are two additional means of improving asteroid surface-materials characterizations that are often given short shrift. These can be termed *problem definition* and *observational methodology.*

Much of the available asteroid data has been obtained as part of various spectral survey programs. Such survey data provide a valuable overview of the asteroid population, but it often is not appropriate to address specific issues. For example, the question of whether S-type asteroids include (or are primarily) undifferentiated ordinary-chondritic assemblages cannot be addressed by simply identifying the phases present. The general olivine-pyroxene-metal assemblage indicated by the S-type spectra is found among both differentiated and undifferentiated meteorite assemblages. However, a diagnostic test can be formulated by utilizing the basic definition of "chondrite," which stipulates that the bulk chemistry is fixed within a small range. The chondritic system has well-defined covariations in the composition and abundance of the mineralogic phases. This approach was used by Gaffey (1984) to show that the variation in pyroxene composition relative to the

olivine/pyroxene abundance ratio was inconsistent with an undifferentiated assemblage on the surface of 8 Flora.

It is very important to define properly the problem or question being addressed in an asteroid investigation. As in the example above, the proper definition of the problem can often provide a means of testing the issues involved. The determination of spectral parameters that are most relevant to particular issues being addressed is a critical part of problem definition. A standardized set of measurements will not be appropriate to every problem. For the Flora example discussed above, the appropriate rotational phase coverage was a critical parameter in establishing the reality and determining the nature of spectral differences across the surface.

Equally important is the utilization of an instrumental system and observational methodology appropriate to the determination of the critical spectral parameters. There may be significantly different requirements for a survey program vs the problem-oriented investigation of a single object or class of objects. It is important to realize that no matter how sophisticated any particular instrument system may be, it is not appropriate to the investigation unless it can provide data to determine the relevant spectral parameters.

The rotationally resolved spectral-reflectance studies that established the differentiated, nonchondritic nature of asteroids 8 Flora (Gaffey 1984) and 15 Eunomia (Gaffey and Ostro 1987) took advantage of the fact that the relative spectral variations of a rotating asteroid can be determined with a very high degree of *precision* even though the *accuracy* of the spectra may be significantly lower due to uncertainties in the standard-star spectral-flux calibrations. Such rotational studies effectively use the asteroid itself as a calibration standard, permitting a comparison of the predicted variability to the observed variability.

IV. ASTEROID SURFACE MATERIAL CHARACTERIZATIONS

The status of asteroid surface material characterizations at the time of the 1979 Asteroids meeting was reviewed by Gaffey and McCord (1979). The present discussion concentrates on the advances made since 1979.

The Asteroid Taxonomic Classes

Although the classification of asteroids into the taxonomic groups is not specifically an interpretative procedure, the classes do have some general compositional significance. While objects of the same class may not be mineralogically similar, objects in different classes are likely to be mineralogically different.

The general types of meteoritic analogues for each asteroid class are listed in Table III. These interpretations are derived from analysis of the spectral albedo data of selected members of each class. The compositional homogeneity and heterogeneity varies considerably between the individual asteroid

TABLE III
Asteroid Classes: General Mineralogic Characterizations
and Meteoritic Analogues

Type	No.[a]	Inferred Surface Mineralogy	Possible Meteoritic Analogues
A	4	olivine or olivine-metal	olivine achondrite or pallasite
B	6 ⎫		⎧ CI1-CM2 assemblages and as-
C	88 ⎪	hydrated silicates + carbon/	⎪ semblages produced by aqueous
F	13 ⎬	organics/opaques	⎨ alteration and/or metamorphism
G	5 ⎭		⎩ of CI/CM precursor materials
D	26 ⎫	carbon/organic-rich sili-	⎰ organic-rich cosmic dust grains?
P	23 ⎭	cates?	⎱ CI1-CM2 plus organics?
E	8	enstatite or possibly other iron-free silicates	enstatite achondrites
M	21	metal (poss. trace silicates) metal + enstatite?	irons (poss. with silicate incl.) enstatite chondrite?
Q	1	olivine + pyroxene + metal	ordinary chondrites
R	1	pyroxene + olivine	pyroxene-olivine achondrite
S	144	metal ± olivine ± pyroxene	pallasites with accessory py. olivine-dominated stony-iron ureilites and primitive achondrites CV/CO chondrites
V	1	pyroxene ± feldspar	basaltic achondrites
T	4	possibly similar to types P/D	

[a]The number of asteroids classified as this type by Tholen (1984).

types. For example, the S type includes a wide range of assemblages including (but not limited to) analogues of olivine-dominated stony irons, ureilites, CV3 and CO3 chondrites (Bell et al. 1987; Bell 1988; see also the chapter by Bell et al.), and perhaps a small component of ordinary chondrites. Moreover, the proportions of olivine, pyroxene and metal vary considerably from one end of the S field to the other on the principal component diagram of Tholen (1984; see also the chapter by Tholen and Barucci). It is probable that upon careful examination, similar diversity will be discovered within all of the larger asteroid classes.

Characterizations of Individual Asteroids

A number of individual asteroids have been studied in detail and relatively unambiguous and sophisticated surface material characterizations have been derived. Table IV lists these objects along with a brief discussion of each. Figure 3 shows the normalized spectral-reflectance curves of selected asteroids, and Fig. 4 shows the spectral albedo curves for the same asteroids.

TABLE IV
TABLE IV
Mineralogic Characterizations of Specific Asteroids

Asteroid[a]	Surface Assemblage and/or History
1 Ceres [G]	Phyllosilicate (relatively iron-poor) with magnetite and/or carbonaceous opaque phase(s) resulting from extensive aqueous alteration of CI/CM precursor material (Gaffey 1978; Lebofsky et al. 1981; Feierberg et al. 1981).
2 Pallas [B]	Similar to Ceres (Gaffey 1978; Lebofsky et al. 1981).
4 Vesta [V]	Spectrum (Fig. 3A and 4A) exhibits strong 1 and 2 μm pyroxene features, with weaker 1.25 μm plagioclase feldspar absorption. Surface is a pyroxene-plagioclase assemblage analogous to eucritic basaltic achondrites over most of surface with several regions of diogenetic (feldspar-poor) basaltic material. Minor olivine in at least one small region (excavated by large impact?). Nearly intact crust of differentiated body (Gaffey 1983, and references therein).
8 Flora [S]	Spectrum (Figs. 3A and 4B) shows broad shallow 1 and 2 μm absorptions and reddish spectral slope, indicating metal and olivine with minor pyroxene (ol/px $\sim$ 2.8, with considerable abundance variations across the surface). Present surface represents an internal metal-enriched shell or mantle-core boundary region of differentiated parent body with the crust removed (Gaffey 1984).
15 Eunomia [S]	Spectrum (Figs. 3A and 4B) indicates metal and olivine with minor ortho- and clinopyroxene (ol/px $\sim$ 3.4). Elongated shape appears to sample range of depths from core-mantle region to crust within a differentiated parent body (Gaffey and Ostro 1987).
16 Psyche [M]	Spectrum (Figs. 3A and 4B) exhibits no mafic silicate features. High radar reflectivity indicates a metallic or metal-dominated surface. Exposed core of differentiated body (Ostro et al. 1985, and references therein).
29 Amphitrite [S]	Metal with pyroxene ($\sim$Fs$_{40}$, $\sim$ Wo$_5$) and olivine with (ol/px $\sim$ 0.66). Exposed metal-rich internal shell or core-mantle region of differentiated body (Bell et al. 1985).
44 Nysa [E]	Relatively featureless, high albedo spectrum indicates a surface dominated by a nonabsorbing, spectrally neutral phase such as enstatite, forsterite or some other iron-poor silicate. Recent data (Figs. 3B and 4A) indicate a weak 0.85–0.9 μm pyroxene band consistent with the low-iron enstatite seen in meteorites. Nysa's surface is the crust or exposed mantle of a differentiated parent body with E-chondrite bulk composition (Zellner et al. 1977).
113 Amalthea [S]	Spectrum (Fig. 3B) shows a strong olivine feature with weak 2 μm pyroxene absorption. Spectral albedo (Fig. 4B) is significantly lower than for a nearly pure

TABLE IV   (continued)

Asteroid[a]	Surface Assemblage and/or History
	olivine assemblage. Surface is dominated by olivine with minor metal and pyroxene, and may have significant spatial variations. Assemblage represents the lower-most mantle region in a highly differentiated parent body (Gaffey et al. in preparation).
246 Asporina [A]	An essentially pure olivine assemblage derived from the mantle of a well differentiated parent body (Cruikshank and Hartmann 1984). IRAS albedo is lower than expected.
289 Nenetta [A]	Similar to 246 Asporina (Cruikshank and Hartmann 1984). IRAS albedo is similarly low.
349 Dembowska [R]	Spectrum (Figs. 3B and 4A) shows strong 1 and 2 μm pyroxene features. The 1 μm band is broadened to longer wavelengths than that of Vesta (Fig. 4A) and the 2 μm band occurs at shorter wavelengths than in Vesta. Spectrum indicates a signficant olivine and a less iron-rich pyroxene and a pyroxene-olivine assemblage with little or no metal, probably the silicate residue left by the partial melt extraction of metal from the upper mantle of an incompletely differentiated parent body (Feierberg et al. 1980; Veeder et al. 1983b; Gaffey et al. in preparation).
354 Eleonora [S]	Spectrum (Fig. 3B) shows a strong olivine feature and a lower spectral albedo than Amalthea. No 2-μm pyroxene feature. An olivine-rich olivine-metal assemblage, probably derived from the core-mantle boundary region of a completely differentiated parent body.
446 Aeternitas [A]	Spectrum and spectral albedo (Figs. 3B and 4B) indicate an essentially pure olivine assemblage derived from the mantle of a well differentiated parent body (Bell et al. 1984).
1866 Apollo [Q]	Olivine and pyroxene features. Current spectral albedo data is indistinguishable from that of an ordinary chondrite (McFadden et al. 1985; chapter by Bell et al.).

[a] Asteroid types in brackets.

V. THE PRESENT ASTEROID POPULATION AS METEORITE SOURCE BODIES

The relationship between meteorites and the present asteroid population is subject to considerable controversy. However, during the past decade telescopic spectral studies of the minor planets have provided significant constraints upon this relationship, several of which are discussed below.
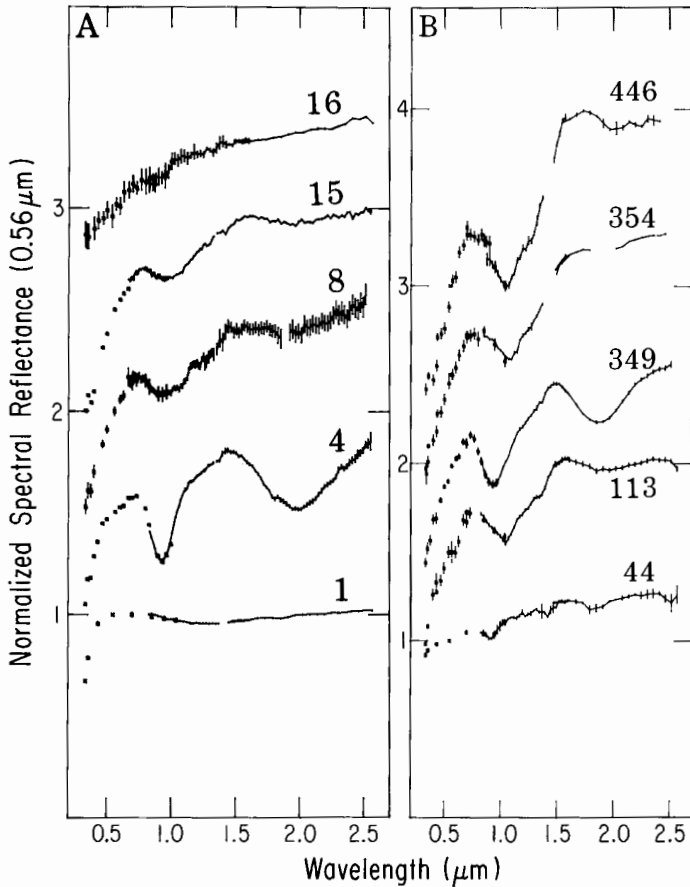
Fig. 3. (A and B) Normalized (0.56 μm) spectral reflectance curves of asteroids. For purpose of clarity, the curves are offset vertically from each other by 0.5. Data and sources: [1] Ceres: ECAS (Zellner et al. 1985) and 52-color (Bell et al. 1988, and in preparation); [4] Vesta: 2-beam photometer and IRCVF (Gaffey 1983, and in preparation); [8] Flora: 2-beam photometer and IRCVF (Gaffey 1984); [15] Eunomia: 2-beam photometer and IRCVF (Gaffey and Ostro 1987, and in preparation); [16] Psyche: 2-beam photometer (Chapman and Gaffey 1979) and 52-color (Bell et al. 1988, and in preparation); [44] Nysa: ECAS (Zellner et al. 1985) and 52-color (Bell et al. 1988, and in preparation); [113] Amalthea: ECAS (Zellner et al. 1985); 2-beam photometer (Chapman and Gaffey 1979) and 52-color (Gaffey, February 1988, unpublished); [349] Dembowska: 2-beam photometer (Gaffey, unpublished) and 52-color (Bell et al. 1988, and in preparation); [354] Eleonora: ECAS (Zellner et al. 1985); 2-beam photometer (Chapman and Gaffey 1979) and 52-color (Bell et al. 1988, and in preparation); [446] Aeternitas: ECAS (Zellner et al. 1985); 2-beam photometer (Chapman and Gaffey 1979) and 52-color (Bell et al. 1988, and in preparation).
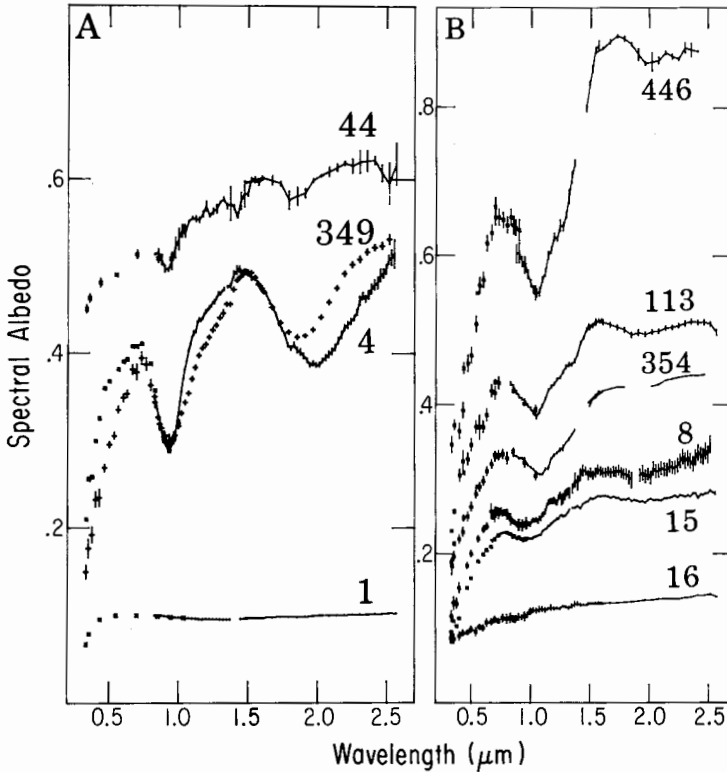
Fig. 4. (A) Spectral albedo curves of asteroids: [1] Ceres, [4] Vesta, [44] Nysa, and [349] Dembowska ("+"). Data and sources are the same as in Fig. 3 multiplied by the IRAS albedos. (B) Same as Fig. 4A for asteroids: [8] Flora, [15] Eunomia, [16] Psyche, [113] Amalthea (offset by +0.1), [354] Eleonora (offset by +0.1), and [446] Aeternitas (offset by +0.2).

Are the Asteroids and the Meteorite Source Bodies Incongruent Sets?

If, as seems probable, a major fraction of the terrestrial meteorite flux is derived directly or indirectly (e.g., near-Earth asteroids as intermediate source bodies) from the asteroid belt, then the relative proportions of various asteroid and meteorite types indicate that the meteorite flux is both a biased and an incomplete sample of the materials present in the belt. For example, there is a discrepancy of a factor of approximately 400 in the ratio of basaltic achondrites to olivine achondrites in meteorite falls and the Antarctic collections (about 100:1) compared to the ratio of the V to A types that are their asteroidal analogues (about 1:4). Since the S asteroids should be contributing much more to the olivine achondrite flux than to the basaltic achondrite flux, the actual discrepancy is most probably even greater (see, e.g., Gaffey 1984; Gaffey and Ostro 1987; see also the chapters by Lipschutz et al. and Green-

berg and Nolan). Since only the larger main-belt asteroids are well observed and since our understanding of the fragmentation process is imperfect, the size difference between the members of the V and A types alone may cause significant bias (see also the chapter by Bell et al.).

Other assemblages, such as the aqueously altered surface materials of Ceres and Pallas, or the apparently organic-rich materials of the D- and P-type asteroids have not been found among the meteorites at all. The rarity of these inferred weak assemblages can be explained by the atmospheric entry selection against weak and fast moving meteoroids. The examination of cosmic dust particles collected at high altitudes helps to overcome this source of bias. Even allowing for such selection effects, the discrepancies suggest that the meteorite flux at any point in time is dominated by a relatively few source bodies. Wetherill (1985) suggests that these favorably located source bodies are adjacent to the 3:1 Kirkwood gap at 2.5 AU. Greenberg and Chapman (1983) suggested that the meteorite flux is affected by size and strength considerations, and hence ejection velocity, in the source bodies. A major meteorite source from bodies in Earth-crossing orbits has also been invoked, but since these objects are in short-lived orbits, they too must be regularly replenished from some reservoir.

In any case, it is clear that the meteorites are neither a complete nor a representative sample of the asteroid assemblages. Any model of meteoritic sources must incorporate or reconcile this incompleteness. Asteroids do not contribute equally to the meteorite flux, and some do not appear to contribute at all. It is difficult to escape the conclusion that the present asteroid bodies and the source bodies of the present meteorite population are, to some unknown extent, incongruent sets. Caution should be exercised since perfectly valid conclusions drawn from meteorite studies simply may not be relevant to the observed asteroids, and *vice versa*.

Where are the Ordinary Chondrite Parent Bodies?

One of the most puzzling aspects of current asteroid investigations is the apparent absence (or extreme rarity) among the larger asteroids of the belt, of the ordinary chondrite-like assemblages which dominate the present meteorite flux. Dynamical models and meteoritical studies would suggest that these meteorites should derive from a common asteroid type, probably in the region of the chaotic zone associated with the 3:1 Kirkwood gap at 2.5 AU (Wetherill 1985). The presence of the ordinary chondrite-like Q objects in the Earth-crossing population provides a set of intermediate source bodies, but leaves unanswered the question of the original parent bodies.

Several testable solutions to this apparent paradox have been suggested. One suggestion is simply that the asteroid spectral interpretations are wrong and that some unknown regolith process is modifying an ordinary chondrite-type substrate to produce the S spectra. The observational evidence, where it

shows any preference, overwhelmingly indicates that most of the larger S-type asteroids must be differentiated. The most carefully studied S asteroids (Flora: Gaffey 1984; Eunomia: Gaffey and Ostro 1987) are differentiated surface assemblages irrespective of plausible calibration uncertainties or regolith processes. Moreover, Flora was chosen for study precisely because it had been identified as the most likely candidate for an ordinary chondrite assemblage among eleven S asteroids (Feierberg et al. 1982). There is simply no observational evidence to support the interpretation that the S types should be the parent bodies for the ordinary chondrites, although the data does not exclude the possibility of a small component of undifferentiated bodies within the S population.

Alternate resolutions of the paradox include the model proposed by Bell (1986; see also the chapter by Bell et al.) in which the post-accretionary heating mechanism had a lower size cut-off below which objects escaped heating. The original ordinary chondrite parent bodies would have been somewhat smaller than the S-type parent bodies and have escaped significant heating. Being relatively weak, like the silicate crusts and mantles of the proto-S and proto-M objects, the ordinary chondrite parent bodies would have suffered significant collisional fragmentation. In this model, the ordinary chondrite parent bodies would be small (i.e., below current observation limits) inner-belt objects which now dominate the terrestrial meteorite flux because of a favorable location, perhaps adjacent to the 3:1 Kirkwood gap or in Earth-crossing orbits.

Gaffey (1984) suggested two additional models to reconcile the paradox. For planetesimals subjected to a surface-heating event, an unheated core could be preserved below a melted and differentiated mantle. The metal-rich surface layers of some S asteroids could be strong metallic shells protecting ordinary chondritic cores (Bell's "armour-deck" model). Complete disruption of such a body could release a horde (hoard) of small ordinary chondritic fragments. Such ordinary chondrite assemblages might dominate the smaller size range of the inner main-belt population.

Gaffey (1984) also suggested that ordinary chondrite assemblages might be absent from the main belt at any size, and instead were expelled from the inner solar system by very early dynamical processes to an external reservoir. Comets are considered to be expelled outer solar system bodies, which are now returning from such an external reservoir, the Oort cloud. The processes of dynamical expulsion should not depend upon whether the body is rock or ice, although the efficiency of expulsion to external reservoirs may vary with initial heliocentric distance. Subsequent perturbation into orbits with small perihelia will not depend on material type. Even in the absence of non-gravitational forces, returning rocky bodies could be captured by Jupiter into short-period orbits just as cometary nuclei are, or be involved in collisions with main-belt objects injecting some fraction of their fragments in short-period orbits.

The apparent absence of ordinary chondritic assemblages in the main belt places a strong constraint on the asteroid-meteorite relationship. Any model for this relationship must reconcile the asteroidal and meteoritic evidence. The four models described above all attempt to do this by various *ad hoc* means. None are as yet generally accepted, but all have the virtue of being testable.

Incomplete Characterization of the Asteroid Population

Although the characterization of individual asteroids has become both more reliable and more sophisticated, work has concentrated upon the larger asteroids. And even for the larger members of the population, our coverage is incomplete. Almost nothing is known about the compositional nature of the main-belt population below diameters of about 20 km. It is not known whether the properties of the smaller main-belt asteroids are, or even should be, similar to those of the larger asteroids.

The choice of asteroid targets in observational programs is often biased toward the brighter objects in any particular group or class. Normally this selects for larger bodies at smaller heliocentric distances. Bias corrections can be applied to population studies (e.g., the S : C ratio with semimajor axis), but not to individually characterized objects. There is a possibility of real systematic differences between the larger and smaller members of any class. The variety and range of asteroid assemblages continues to expand as our data improve.

Asteroids as Meteorite Source Bodies

With the exception of the ordinary chondrites, there are plausible source bodies for all significant meteorite types in the belt. However, no specific genetic links have yet been established between individual asteroids and meteorite specimens or groups. In terms of diversity of assemblages, the meteorite flux is dominated by differentiated assemblages. There must be, or recently have been, at least one inner solar system outcrop for each different meteorite type. Current observational evidence is consistent with the meteoritic requirement for many more outcrops of differentiated assemblages than of undifferentiated assemblages.

However, it is important to maintain the distinction between the asteroids we see today and the parent bodies whose nature and conditions were recorded in the meteorites. The regolith processes that produced, and the xenolithic inclusions that are present within, the ordinary chondritic breccias provide an early record of some region of the solar system. Care must be taken in extending the conclusions from that remote time and uncertain location to the asteroid belt in the present epoch. The seeming contradictory meteorite and asteroid data may simply be different, but basically correct perceptions of blindmen feeling different parts of the same elephant.

VI. ASTEROID PERSPECTIVES ON THE EARLY SOLAR SYSTEM

Quite independently of their uncertain role as the provenance of meteorite specimens, the asteroids provide significant constraints on early solar system processes and conditions. Two such constraints are discussed below.

Thermal Evolution

The first mineralogical analysis of the Vesta spectrum indicated that even very small bodies could undergo heating sufficiently intense to produce at least partial melting and magmatic activity. Until recently, it has generally been assumed that Vesta was an anomaly, and that the variation in asteroid types from an S-dominated inner belt to a C-dominated outer belt represented the fossil signature of the compositional gradient in the solar nebula (Gradie and Tedesco 1982). Recent work has shown that large S asteroids are predominantly differentiated assemblages and that there was a strong post-accretionary temperature gradient across the asteroid belt (Gaffey 1984,1988; Gaffey and Ostro 1987). At the inner edge of the belt (1.8 to 2.0 AU), essentially all of the objects have experienced heating sufficient to produce some significant degree of melting. The proportion of strongly heated bodies decreases almost linearly with semimajor axis to 0% at 3.5 AU.

The small size of plausible asteroid parent planetesimals and the ages of similar events in the meteorites constrain the heating mechanisms to short-lived radioisotopes, or to the T Tauri or superluminous periods of solar evolution. The pattern preserved within the asteroid population may permit specific identification of the mechanism.

Missing Bits

Collisional models suggest that the present asteroid population is a small remnant of the original planetesimal population in that region of the early solar system. The interpretation of the larger S asteroids as the exposed cores of numerous disrupted differentiated bodies is consistent with such models. This interpretation also implies the release of a multitude of fragments from the overlying metal-depleted mantles or surface layers. However, instead of being very common, the olivine (A-type) and olivine-pyroxene (R-type) asteroids are rare. If the smaller members of the present population were derived from the collisional breakup of larger members, then large amounts of silicate-rich material derived from these surface and mantle layers have been removed from the belt. Where has this material gone?

Conversely, the preservation of an intact or nearly intact crustal layer on Vesta implies that the collisional disruption was dominated by single events, rather than by cumulative erosion from an evolved population size distribution. Is Vesta really a unique intact body among the main-belt objects or should Ceres and Pallas be included in this category? Was their initial large size combined with chance, the primary determinant of survival?

VII. FUTURE DIRECTIONS

The ideal means of addressing these questions would be a series of asteroid missions to a representative selection of the minor planets either with sophisticated *in situ* mineralogic and petrologic measurements or with sample returns. It seems unlikely that more than a few such missions will be carried out within the professional lifetimes of most current asteroid scientists.

In lieu of such missions, Earth-based remote sensing will remain our major source of new information. In particular, visible and near-infrared reflectance spectroscopy, given a sufficient level of support, promises to provide major increments in our understanding of this ancient population and of the early period in solar system history. Visual and near-infrared spectroscopy is still within the linear portion of the curve of growth both in terms of its capabilities and in the availability of asteroid targets. The last decade has shown clearly that each increment in observational capability (e.g., sensitivity, resolution, wavelength coverage, etc.) when coupled with parallel increases in the sophistication of interpretive calibrations and methodologies has produced a corresponding increment in the level of our understanding of the asteroids.

VIII. SUMMARY

The asteroids exhibit surface assemblages consistent with their being the present-day outcrops from which most types of meteorites are chipped. The irons, stony irons, achondrites, primitive achondrites (e.g., Lodran, etc.), C(O/V)3 and CI1/CM2 assemblages have plausible sources in the main belt. The lack of identified ordinary chondrite parent bodies in the asteroid belt is a major issue, but several testable, if *ad hoc*, models have been proposed to resolve this dilemma.

The asteroids themselves tell of a strong post-accretionary heating event in the very early inner solar system. They also suggest that a very large amount of material has been lost from the belt, with preferential depletion of certain types of assemblages.

Much of the input from the meteoritical, the dynamical and the asteroid spectroscopy communities is seemingly contradictory. These apparent paradoxes almost certainly arise from a too narrow perception of the real elegance, complexity and subtlety of the system. The relationships between asteroids and meteorites are likely to be less simple, and hence, more interesting than presently believed. We all have a part of the elephant, but none have the complete picture.

in part by NASA grants. L.A. McFadden and F. Vilas provided detailed and helpful reviews of the original manuscript.

REFERENCES

Adams, J. B. 1974. Visible and near-infrared diffuse reflectance spectra of pyroxenes as applied to remote sensing of solid objects in the solar system. *J. Geophys. Res.* 79:4829–4836.

Adams, J. B. 1975. Interpretation of visible and near-infrared diffuse reflectance spectra of pyroxenes and other rock-forming minerals. In *Infrared and Raman Spectroscopy of Lunar and Terrestrial Minerals,* ed. C. Karr (New York: Academic Press), pp. 91–116.

Adams, J. B., and Filice, A. L. 1967. Spectral reflectance 0.4 to 2.0 microns of silicate rock powders. *J. Geophys. Res.* 72:5705–5715.

Aines, R. D., and Rossman, G. R. 1984a. Water content of mantle garnets. *Geology* 12:720–723.

Aines, R. D., and Rossman, G. R. 1984b. Water in minerals? A peak in the infrared. *J. Geophys. Res.* 89:4059–4071.

Baker, E. W., and Louda, J. W. 1986. Porphyrins in the geologic record. In *Biological Markers in the Sedimentary Record* (New York: Elsevier) pp. 125–225.

Bell, J. F. 1986. Mineralogical evolution of the asteroid belt. *Meteoritics* 21:333–334 (abstract).

Bell, J. F. 1988. A probable asteroidal parent body for the CV or CO chondrites. *Meteoritics* 23:256–257 (abstract).

Bell, J. F., and Keil, K. 1988. Spectral alteration effects in chondritic gas-rich breccias: Implications for S-class and Q-class asteroids. *Proc. Lunar Planet. Sci. Conf.* 18:573–580.

Bell, J. F., Hawke, B. R., Singer, R. B., and Gaffey, M. J. 1984. The olivine asteroids: Discovery, mineralogy, and relationship to meteorites. *Lunar Planet. Sci.* XV:48–49 (abstract).

Bell, J. F., Gaffey, M. J., Gradie, J. C., Hawke, B. R., and McCord, T. B. 1985. Asteroid 29 Amphitrite: Surface mineralogy and heterogeneity. *Lunar Planet. Sci.* XVI:47–48 (abstract).

Bell, J. F., Hawke, B. R., and Owensby, P. D. 1987. Carbonaceous chondrites from S-type asteroids. *Bull. Amer. Astron. Soc.* 19:841 (abstract).

Bell, J. F., Owensby, P. D., Hawke, B. R., and Gaffey, M. J. 1988. The 52-color asteroid survey: Final results and interpretation. *Lunar Planet. Sci.* XIX:57–58 (abstract).

Britt, D. T., and Pieters, C. M. 1988. Bidirectional reflectance properties of iron-nickel meteorites. *Proc. Lunar Planet. Sci. Conf.* 18:503–512.

Brown, R. H., and Morrison, D. 1984. Diameters and albedos of thirty-six asteroids. *Icarus* 59:20–24.

Burns, R. G. 1970a. *Mineralogical Applications of Crystal Field Theory* (New York: Cambridge Univ. Press).

Burns, R. G. 1970b. Crystal field spectra and evidence of cation ordering in olivine minerals. *Amer. Min.* 55:1608–1632.

Burns, R. G. 1981. Intervalence transitions in mixed-valence minerals of iron and titanium. *Ann. Rev. Earth Planet. Sci.* 9:345–383.

Chapman, C. R. 1975. The nature of asteroids. *Sci. Amer.* 232(1):24–33.

Chapman, C. R. 1976. Asteroids as meteorite parent-bodies: The astronomical perspective. *Geochim. Cosmochim. Acta* 40:701–719.

Chapman, C. R., and Gaffey, M. J. 1979. Reflectance spectra for 277 asteroids. In *Asteroids,* eds. T. Gehrels and M. S. Matthews (Tucson: Univ. of Arizona Press), pp. 655–687.

Chapman, C. R., and Morrison, D. 1976. J,H,K Photometry of 433 Eros and other asteroids. *Icarus* 28:91–94.

Chapman, C. R., and Salisbury, J. W. 1973. Comparisons of meteorite and asteroid spectral reflectivities. *Icarus* 19:507–522.

Chapman, C. R., and Zellner, B. H. 1978. The role of Earth-based observations of asteroids during the next decade. In *Asteroids: An Exploration Assessment,* eds. D. Morrison and W. C. Wells, NASA CP-2053, pp. 183–191.

Christensen, P. R., and Luth, S. J. 1987. Thermal-infrared spectral observations of Martian candidate materials in emission. In *Lunar Planet. Sci.* XVIII:169–170 (abstract).

Clark, R. N., and Roush, T. L. 1984. Reflectance spectroscopy: Quantitative analysis techniques for remote sensing applications. *J. Geophys. Res.* 89:6329–6340.

Cloutis, E., Gaffey, M. J., Jackowski, T. L., and Reed, K. L. 1986. Calibrations of phase abundance, composition, and particle size distribution for olivine-orthopyroxene mixtures from reflectance spectra. *J. Geophys. Res.* 91:11641–11653.

Crown, D. A., and Pieters, C. M. 1987. Spectral properties of plagioclase and pyroxene mixtures and the interpretation of lunar soil spectra. *Icarus* 72:492–506.

Cruikshank, D. P., and Brown, R. H. 1987. Organic matter on asteroid 130 Elektra. *Science* 238:183–184.

Cruikshank, D. P., and Hartmann, W. K. 1984. The meteorite-asteroid connection: Two olivine-rich asteroids. *Science* 223:281–283.

Cruikshank, D. P., Bell, J. F., Gaffey, M. J., Brown, R. H., Howell, R., Beerman, C., and Rognstad, M. 1983. The dark side of Iapetus. *Icarus* 53:90–104.

Eaton, N., Green, S. F., McCheyne, R. S., Meadows, A. J., and Veeder, G. J. 1983. Observations of asteroids in the 3- to 4-μm region. *Icarus* 55:245–249.

Fanale, F. P., Johnson, T. V., and Matson, D. L. 1974. Io: A surface evaporite deposit? *Science* 186:922–925.

Farmer, V. C. 1974. The layer silicates. In *The Infrared Spectra of Minerals,* ed. V. C. Farmer (London: Mineralogical Society), pp. 331–364.

Feierberg, M. A., Larson, H. P., Fink, U., and Smith, H. A. 1980. Spectroscopic evidence for two achondrite parent bodies: Asteroids 349 Dembowska and 4 Vesta. *Geochim. Cosmochim. Acta* 44:513–524.

Feierberg, M. A., Lebofsky, L. A., and Larson, H. P. 1981. Spectroscopic evidence for aqueous alteration products on the surfaces of low-albedo asteroids. *Geochim. Cosmochim. Acta* 45:971–981.

Feierberg, M. A., Larson, H. P., and Chapman, C. R. 1982. Spectroscopic evidence for undifferentiated S-type asteroids. *Astrophys. J.* 257:361–372.

Feierberg, M. A., Witteborn, F. C., and Lebofsky, L. A. 1983. Detection of emission features in the 8- to 13-μm spectra of main belt asteroids. *Icarus* 56:393–397.

Feierberg, M. A., Lebofsky, L. A., and Tholen, D. J. 1985. The nature of C-class asteroids from 3-μm spectrophotometry. *Icarus* 63:183–191.

Fredriksson, K., and Kerridge, J. F. 1988. Carbonates and sulfates in CI chondrites: Formation by aqueous activity in the parent body. *Meteoritics* 23:35–44.

Gaffey, M. J. 1976. Spectral reflectance characteristics of the meteorite classes. *J. Geophys. Res.* 81:905–920.

Gaffey, M. J. 1978. Mineralogical characterizations of asteroid surface materials: Evidence for unsampled types. *Meteoritics* 13:471–473 (abstract).

Gaffey, M. J. 1980. Mineralogically diagnostic features in the visible and near-infrared reflectance spectra of carbonaceous chondrite assemblages. In *Lunar Sci.* XI:312–313 (abstract).

Gaffey, M. J. 1983. The asteroid (4) Vesta: Rotational spectral variations, surface material heterogeneity, and implications for the origin of the basaltic achondrites. In *Lunar Planet. Sci.* XIV:231–232 (abstract).

Gaffey, M. J. 1984. Rotational spectral variations of asteroid (8) Flora: Implications for the nature of the S-type asteroids and for the parent bodies of the ordinary chondrites. *Icarus* 60:83–114.

Gaffey, M. J. 1986. The spectral and physical properties of metal in meteorite assemblages: Implications for asteroid surface materials. *Icarus* 66:468–486.

Gaffey, M. J. 1988. Thermal history of the asteroid belt: Implications for accretion of the terrestrial planets. In *Lunar Planet. Sci.* XIX:369–370 (abstract).

Gaffey, M. J., and McCord, T. B. 1978. Asteroid surface materials: Mineralogical characterizations from reflectance spectra. *Space Sci. Rev.* 21:555–628.

Gaffey, M. J., and McCord, T. B. 1979. Mineralogical and petrological characterizations of asteroid surface materials. In *Asteroids,* ed. T. Gehrels (Tucson: Univ. of Arizona Press), pp. 688–723.

Gaffey, M. J., and Ostro, S. J. 1987. Surface lithologic heterogeneity and body shape for asteroid (15) Eunomia: Evidence from rotational spectral variations and multi-color lightcurve inversions. In *Lunar Planet. Sci.* XVIII:310–311 (abstract).

Gaffey, S. J. 1986. Spectral reflectance of carbonate minerals in the visible and near infrared (0.35-2.55 microns): Calcite, aragonite, and dolomite. *Amer. Min.* 71:151–162.

Gaffey, S. J. 1987. Spectral reflectance of carbonate minerals in the visible and near infrared (0.35-2.55μm): Anhydrous carbonate minerals. *J. Geophys. Res.* 92:1429–1440.

Gillett, F. C., and Merrill, K. M. 1975. 7.5-13.5 micron spectra of Ceres and Vesta. *Icarus* 26:358–360.

Gradie, J. C., Chapman, C. R., and Williams, J. G. 1979. Families of minor planets. In *Asteroids*, ed. T. Gehrels (Tucson: Univ. of Arizona Press), pp. 359–390.

Gradie, J., and Tedesco, E. 1982. Compositional structure of the asteroid belt. *Science* 216:1405–1407.

Green, S. F., Eaton, N., Aitken, D. K., Roche, P. F., and Meadows, A. J. 1985. 8- to 13-μm spectra of asteroids. *Icarus* 62:282–288.

Greenberg, R., and Chapman, C. R. 1983. Asteroids and meteorites: Parent bodies and delivered samples. *Icarus* 55:455–481.

Handbook of Physics and Chemistry 1975. R. C. Weast ed. (Boca Raton, FL: CRC Press), 55th ed.

Hansen, O. L. 1976. Thermal emission spectra of 24 asteroids and the Galilean satellites. *Icarus* 27:463–471.

Hapke, B. W., Partlow, W. D., Wagner, J. K., and Cohen, A. J. 1978. Reflectance measurements of lunar materials in the vacuum ultraviolet. In *Proc. Lunar Planet. Sci. Conf.* 9:2935–2947.

Herzberg, G. 1945. *Molecular Spectra and Molecular Structure II. Infrared and Raman Spectra of Polyatomic Molecules* (New York: Van Nostrand Reinhold Co.).

Hodgson, G. W., and Baker, B. L. 1969. Porphyrins in meteorites: Metal complexes in Orgueil, Murray, Cold Bokkeveld, and Mokoia carbonaceous chondrites. *Geochim. Cosmochim. Acta* 33:943–958.

Holden, P. N., and Gaffey, M. J. 1987. The detection of porphyrin-like features in reflectance spectra of carbonaceous chondrites. *Meteoritics* 22:412 (abstract).

Huguenin, R. L., and Jones, J. L. 1986. Intelligent information extraction from reflectance spectra: Absorption band positions. *J. Geophys. Res.* 91:9585–9598.

Johnson, P. E., Smith, M. O., Taylor-George, S., and Adams, J. B. 1983. A semiempirical method for analysis of the reflectance spectra of binary mineral mixtures. *J. Geophys. Res.* 88:3557–3561.

Johnson, T. V., Matson, D. L., Veeder, G. J., and Loer, S. J. 1975. Asteroids: Infrared photometry at 1.25, 1.65, and 2.2 microns. *Astrophys. J.* 197:527–531.

Jones, T. D. 1988. An Infrared Reflectance Study of Water in Outer Belt Asteroids: Clues to Composition and Origin. Ph.D. Thesis, Univ. of Arizona.

King, T. V. V. 1986. Contributions Toward a Quantitative Understanding of Reflectance Spectroscopy: Phyllosilicates, Olivine, and Shocked Materials. Ph.D. Thesis, Univ. of Hawaii.

Larson, H. P., and Veeder, G. J. 1979. Infrared spectral reflectances of asteroid surfaces. In *Asteroids*, ed. T. Gehrels (Tucson: Univ. of Arizona Press), pp. 724–744.

Larson, H. P., Feierberg, M. A., Fink, U., and Smith, H. A. 1979. Remote spectroscopic identification of carbonaceous chondrite mineralogies: Applications to Ceres and Pallas. *Icarus* 39:257–271.

Leake, M., Gradie, J., and Morrison, D. 1978. Infrared (JHK) photometry of meteorites and asteroids. *Meteoritics* 13:101–120.

Lebofsky, L. A. 1980. Infrared reflectance spectra of asteroids: A search for water of hydration. *Astron. J.* 85:573–585.

Lebofsky, L. A., Feierberg, M. A., Tokunaga, A. T., Larson, H. P., and Johnson, J. R. 1981. The 1.7- to 4.2-μm spectrum of asteroid 1 Ceres: Evidence for structural water in clay minerals. *Icarus* 48:453–459.

Logan, L. M., Hunt, G. R., Salisbury, J. W., and Balsamo, S. R. 1973. Compositional implications of Christiansen frequency maximums for infrared remote sensing applications. *J. Geophys. Res.* 78:4983–5003.

Logan, L. M., Hunt, G. R., and Salisbury, J. W. 1975. The use of mid-infrared spectroscopy in remote sensing of space targets. In *Infrared and Raman Spectroscopy of Lunar and Terrestrial Minerals*, ed. C. Karr (New York: Academic Press), pp. 117–142.

Matson, D. L., Fanale, F. P., Johnson, T. V., and Veeder, G. J. 1976. Asteroids and comparative planetology. In *Proc. Lunar Sci. Conf.* 7:3603–3627.

Matson, D. L., Johnson, T. V., and Veeder, G. J. 1977. Asteroid infrared reflectances and compositional implications. In *Comets, Asteroids, Meteorites—Interrelations, Evolution, and Origins*, ed. A. H. Delsemme (Toledo, Ohio: Univ. of Toledo Press), pp. 229–241.

McCord, T. B., and Gaffey, M. J. 1974. Asteroids: Surface composition from reflection spectroscopy. *Science* 186:352–355.

McCord, T. B., Adams, J. B., and Johnson, T. V. 1970. Asteroid Vesta: Spectral reflectivity and compositional implications. *Science* 168:1445–1447.

McFadden, L. A., and Gaffey, M. J. 1978. Calibration of quantitative mineral abundances determined from meteorite reflection spectra and applications to solar system objects. *Meteoritics* 13:556–557 (abstract).

McFadden, L. A., Gaffey, M. J., and McCord, T. B. 1984. Mineralogical-petrological characterizations of near-Earth asteroids. *Icarus* 59:25–40.

McFadden, L. A., Gaffey, M. J., and McCord, T. B. 1985. Near-Earth asteroids: Possible sources from reflectance spectroscopy. *Science* 229:160–163.

Miyamoto, M., Mito, A., and Takano, Y. 1982. An attempt to reduce the effects of black material from the spectral reflectance of meteorites or asteroids. In *Proc. of the Seventh Symp. on Antarctic Meteorites* (Tokyo: Natl. Inst. of Polar Research), pp. 291–307.

Morris, R. V., Lauer, H. V., Lawson, C. A., Gibson, E. K., Nace, G. A., and Stewart, C. 1985. Spectral properties of well-characterized, sub-micron powders of hematite (α-Fe$_2$O$_3$), maghemite (γ-Fe$_2$O$_3$), magnetite (Fe$_3$O$_4$), goethite (α-FeOOH), and lepidocrocite (γ-FeOOH). *J. Geophys. Res.* 90:3126–3144.

Nash, D. B., and Conel, J. E. 1974. Spectral reflectance systematics for mixtures of powdered hypersthene, labradorite, and ilmenite. *J. Geophys. Res.* 79:1615–1621.

Nelson, M. L., and Clark, R. N. 1988. Application of radiative transfer theory to the spectra of mineral mixtures. In *Lunar Planet. Sci.* XIX:846–847 (abstract).

Nitsan, U., and Shankland, T. J. 1976. Optical properties and electronic structure of mantle silicates. *Geophys. J. Roy. Astron. Soc.* 45:59–87.

Ostro, S. J., Campbell, D. B., and Shapiro, I. I. 1985. Mainbelt asteroids: Dual-polarization radar observations. *Science* 229:442–446.

Rajan, S., and Gaffey, M. J. 1984. Spectral reflectance characteristics of Allende white inclusions. In *Lunar Planet. Sci.* XV:284–285 (abstract).

Richardson, S. M. 1978. Vein formation in the CI carbonaceous chondrites. *Meteoritics* 13:141–159.

Roush, T. L., and Singer, R. B. 1986. Gaussian analysis of temperature effects on the reflectance spectra of mafic minerals in the 1-μm region. *J. Geophys. Res.* 91:10301–10308.

Salisbury, J. W., Hapke, B., and Eastes, J. W. 1987. Usefulness of weak bands in midinfrared remote sensing of particulate planetary surfaces. *J. Geophys. Res.* 92:702–710.

Sandford, S. A. 1984. Infrared transmission spectra from 2.5 to 25 μm of various meteorite classes. *Icarus* 60:115–126.

Tedesco, E. F. 1979. The origin of the Flora family. *Icarus* 40:375–382.

Tholen, D. J. 1984. Asteroid Taxonomy from Cluster Analysis of Photometry. Ph.D. Thesis, Univ. of Arizona.

Veeder, G. J., Matson, D. L., and Kowal, C. 1982. Infrared (JHK) photometry of asteroids. *Astron. J.* 87:834–839.

Veeder, G. J., Matson, D. L., Hoover, G., and Kowal, C. 1983a. Infrared (JHK) photometry of asteroids. II. *Astron. J.* 88:1060–1063.

Veeder, G. J., Matson, D. L., and Tedesco, E. F. 1983b. The R asteroids reconsidered. *Icarus* 55:177–180.

Veeder, G. J., Kowal, C., and Matson, D. L. 1984. The earth-crossing asteroid 1983 TB. In *Lunar Planet. Sci.* XV:878–879 (abstract).

Vilas, F., and McFadden, L. A. 1989. CCD reflectance spectra of selected asteroids: Presentation and data analysis considerations. *Icarus,* submitted.

Vilas, F., and Smith, B. A. 1985. Reflectance spectrophotometry ($\sim$0.5-1.0 μm) of outer-belt asteroids: Implications for primitive, organic solar system material. *Icarus* 64:503–516.

Wetherill, G. W. 1985. Asteroidal sources of ordinary chondrites. *Meteoritics* 20:1–22.

Zellner, B., Leake, M., Morrison, D., and Williams, J. G. 1977. The E asteroids and the origin of the enstatite achondrites. *Geochim. Cosmochim. Acta* 41:1759–1767.

Zellner, B., Tholen, D. J., and Tedesco, E. F. 1985. The eight-color asteroid survey: Results for 589 minor planets. *Icarus* 61:355–416.

RADIOMETRY AND THERMAL MODELING OF ASTEROIDS

LARRY A. LEBOFSKY
University of Arizona

and

JOHN R. SPENCER
University of Hawaii

Measurement of thermal emission from asteroids, when coupled with a determination of their visual magnitudes, is a powerful technique for the determination of asteroid diameters and albedos. In recent years, thanks to stellar occultations, asteroid thermal models which assume a mature surface regolith (dusty, with low thermal inertia), have been refined so that model diameters are now consistent with the occultation diameters. When applied to main-belt asteroids the derived diameters now are probably accurate to better than 10%. In some cases, however, these models have been found to fail for a variety of reasons. In particular, they fail to characterize the shape, surface roughness, rate and sense of rotation and maturity of the surface regolith all of which affect the observed thermal flux. A variety of more sophisticated theoretical models can be used to determine the importance of the variables. Such models suggest that Ceres and Pallas, at least, have much smaller thermal inertias than does the Moon. Thermal polarimetry and spectroscopy can also be used to obtain physical and mineralogical information about asteroid surfaces.

Infrared observations of asteroids have been used to study a number of problems in the interpretation of the physical and mineralogical properties of asteroids. For asteroids, which are illuminated by the Sun, the spectral region beyond 5 μm is dominated by radiation thermally emitted from the asteroids

themselves. Below 2.5 μm, their flux is dominated by reflected solar radiation, and between 2.5 and 5 μm is a transition region (Fig. 1). The wavelength where this transition occurs is strongly dependent on the asteroid's albedo, solar distance and thermophysical properties.

In this chapter, we discuss the region beyond 5 μm, where thermal emission dominates. We limit our discussion to wavelengths $\lesssim$ 100 μm. Sub-mm- and mm-wavelength studies are discussed in a paper by Redman and Feldman (1989, in preparation), while the radio region is discussed in the chapter by Webster and Johnston. IRAS observations are discussed in the chapters by Matson et al., Veeder et al. and Tedesco et al. The model used for the reduction of the IRAS data, the standard thermal model, is the same as that discussed in Sec. II below.
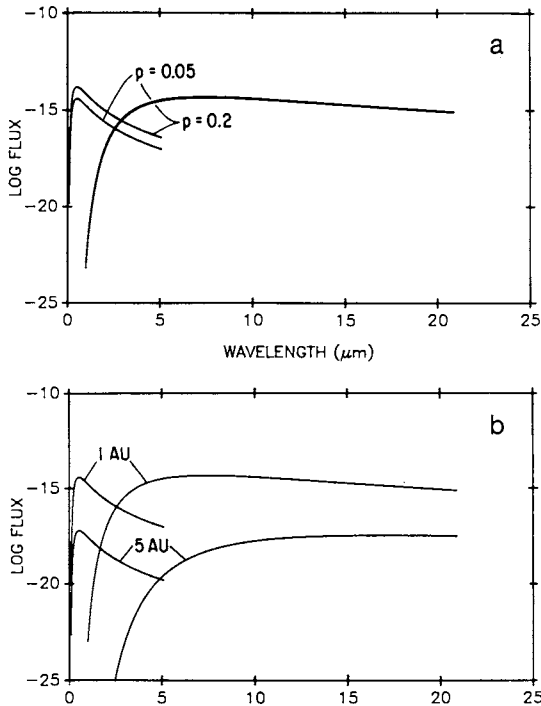
Fig. 1. A comparison of the reflected and thermal flux from two 100-km radius asteroids. (a) Both asteroids at 1 AU from the Sun, one with a geometric albedo of 0.05 and one with a geometric albedo of 0.20, typical of C- and S-class asteroids, respectively. While the reflected fluxes differ, the thermal fluxes are indistinguishable at the scale of this figure. However, the crossover from reflected to thermal shifts about 0.4 μm. (b) One asteroid at 1 AU and the other at 5 AU, both with geometric albedos of 0.05. The crossover from reflected to thermal shifts by about 2.5 μm.

I. RADIOMETRIC DIAMETER DETERMINATION AND
THERMAL MODELS

Thermal infrared observations of asteroids (5 to 20 μm) have been used for the determination of asteroid diameters and albedos for nearly two decades (Allen 1970,1971; Matson 1971a,b). Radiometric diameter determination involves finding a diameter and albedo that will simultaneously match the observed reflected sunlight and thermal emission from an object. A given visual magnitude can be matched by a large dark object or a small bright one, but the former will be warmer as well as larger than the latter and so will show much greater thermal emission. To make the technique quantitative, various assumptions are needed to determine a bolometric albedo from a visual magni-
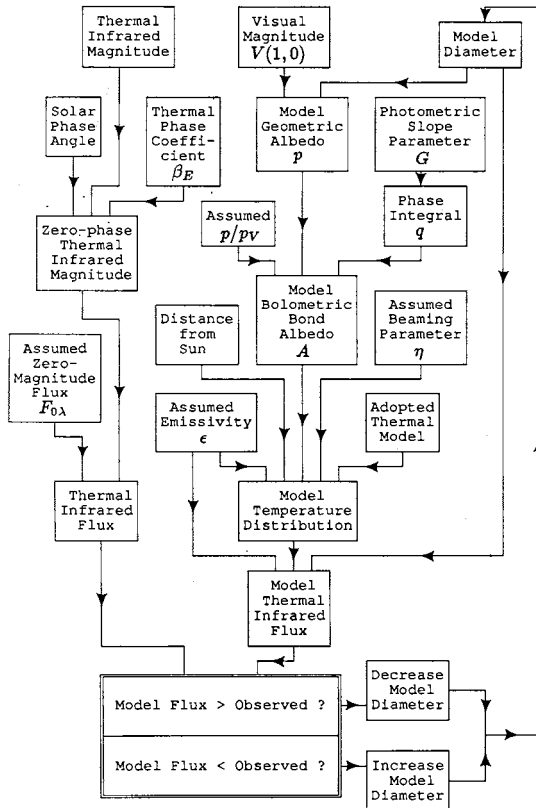
Fig. 2. The steps required to determine a radiometric diameter from observations of a body's visual and thermal radiation. $V(1,0)$ is the V magnitude corrected to zero phase and to distances from the Sun and Earth of 1 AU. An initial guess at the model diameter is required, and the process is iterated until the thermal flux of the model converges on the observed value, using Newton/Raphson or similar techniques.

tude and diameter, and a thermal model is required to predict the emission expected from a body of given size and bolometric albedo. The flow chart in Fig. 2 summarizes the steps required; each is discussed below.

Three basic models have been developed for the reduction of radiometric observations: the nonrotating or *standard* thermal model, the fast-rotating (*rocky or isothermal latitude*) thermal model, and the *thermophysical* model. As we discuss below, all three models assume a balance of solar insolation with re-emitted thermal radiation. For simplicity, the asteroid is assumed to be spherical. This can be generalized in the form

$$\pi R^2 (1 - A)S = \eta \epsilon \sigma R^2 \int_{-\pi}^{\pi} \int_{-\pi/2}^{\pi/2} T^4(\theta,\phi)\cos\phi \, d\phi d\theta \qquad (1)$$

where R is the radius of the asteroid, A is the bolometric Bond albedo, S is the solar flux at the distance of the asteroid, η is a normalization constant for adjusting the surface temperatures to compensate for the angular distribution of the thermal emission (infrared beaming) so that the correct flux is obtained at zero phase angle, ϵ is the wavelength-independent emissivity, σ is the Stefan-Boltzmann constant and $T(\theta,\phi)$ is the model temperature at longitude θ and latitude ϕ. Figure 3 illustrates the generalized model, with the spherical asteroid being illuminated by the Sun and rotating about some arbitrary axis. T_{SS} represents the subsolar temperature. Note that η has been called β in previous papers. We have renamed it because, as we shall see below, β is often used to represent several other parameters, leading to confusion.

The nonrotating and fast-rotating models (Fig. 4) are idealized end members of the thermophysical model which assumes certain properties of the asteroid: rotation rate and direction, pole orientation, and thermophysical properties of the surface material. Discussions of these models may be found
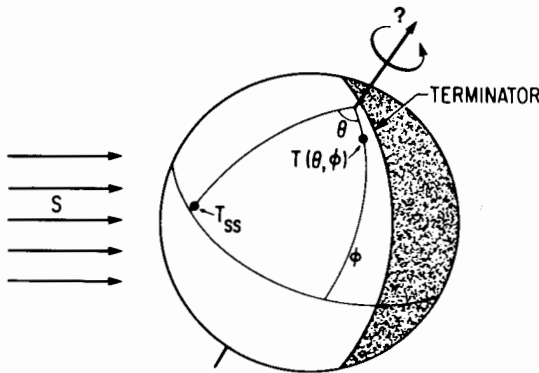
Fig. 3. Illustration of the generalized thermal model with a spherical asteroid illuminated by the Sun and rotating about some arbitrary axis.
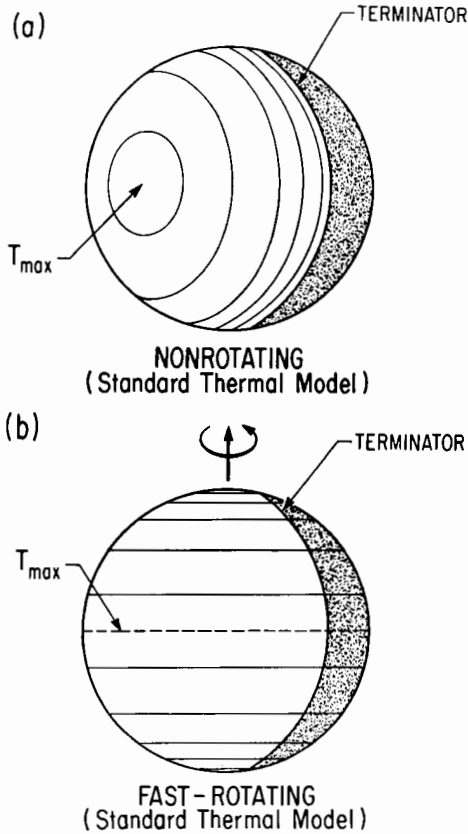
Fig. 4. Illustration of the two end-member thermal models. (a) The standard thermal (nonrotating) model, with the temperature dependent only on the solar incidence angle. (b) The fast-rotating (isothermal-latitude) model, with the temperature dependent only on the distance from the equator.

in Matson et al. (1978), Morrison and Lebofsky (1979), Lebofsky et al. 1985,1986*b* and Spencer et al. (1989). We discuss all of these models in detail below.

II. THE STANDARD (NONROTATING) THERMAL MODEL

The Standard Thermal Model (STM) for asteroids is a simplistic thermal model that has been evolving over the last 20 yr (Morrison and Lebofsky 1979; Lebofsky et al. 1986*b*). Specifically, the model assumes the ideal situation of a nonrotating spherical asteroid in instantaneous equilibrium with solar insolation. It also assumes that the asteroid is observed at 0° solar phase angle,

i.e., the subsolar and sub-Earth points on the asteroid coincide. In reality, observations are never made at exactly 0° phase, so the observed fluxes must be adjusted to 0° phase (see discussion below). However, given the uncertainties of telescopic observations, and the usually limited data sets, more sophisticated models have not been warranted for most asteroid observations.

Since the surface is in instantaneous equilibrium with insolation, $T(\theta,\phi)$ takes the form

$$T(\theta,\phi) = \begin{cases} T_{SS}\cos^{1/4}\theta \, \cos^{1/4}\phi & \text{if } \theta < \pi/2 \\ 0 & \text{if } \theta \geq \pi/2 \end{cases} \tag{2}$$

or, because of the symmetry about the subsolar point

$$T(\Omega) = \begin{cases} T_{SS}\cos^{1/4}\Omega & \text{if } \Omega < \pi/2 \\ 0 & \text{if } \Omega \geq \pi/2 \end{cases} \tag{3}$$

where T_{SS} is the subsolar temperature and Ω is the subsolar/Earth angle, i.e., the solar zenith angle (Fig. 4a).

Thus, from Eq. (1) we have

$$T_{SS} = \left[\frac{(1 - A)S}{\eta\epsilon\sigma} \right]^{1/4}. \tag{4}$$

Parameters and Assumptions in the Standard Thermal Model

There are a number of parameters and assumptions that go into the STM which we now discuss: these are summarized in Table I.

Thermal Phase Coefficient. Matson (1971b) observed that asteroids had solar phase coefficients β_E in the thermal infrared that ranged from about 0.005 to 0.017 mag deg^{-1}. Therefore, a mean value of 0.01 mag deg^{-1} has been used in all standard thermal modeling as a typical phase coefficient to correct the observed thermal fluxes to the zero phase assumed in the thermal models. Recently, Lebofsky et al. (1984,1986a,b) showed that in the case of Ceres, the phase coefficient may be different before and after opposition. They determined that this was due to the effects of rotation, the so-called morning/evening effect. We will return to this point later. However, the mean phase coefficient that they observed was still about 0.01 mag deg^{-1}, as was the phase coefficient for several other well-observed asteroids (see Fig. 8 below).

Relationship Between Visual Geometric and Bolometric Bond Albedo. The relationship between the visual magnitude and the thermal flux is used to determine the diameter and albedo. The visual magnitude is a function of the

TABLE I
Parameter Values

Parameter	Value	Source
η	0.756	Lebofsky et al. 1986
ϵ	0.9	Lebofsky et al. 1986
p/p_V	1.0	Morrison and Lebof-sky 1979
β_E	0.01 mag deg^{-1}	Matson 1971a,b
S	0.1373 Wcm^{-2}	Neckel and Labs 1984
V_{sun}	-26.76	Campins et al. 1985
N (0 mag flux at 10.6 μm)	9.6×10^{-17} W cm$^{-2}\mu$m^{-1}	Rieke et al. 1985
Q (0 mag flux at 21.0 μm)	6.4×10^{-18} W cm$^{-2}\mu$m^{-1}	Rieke et al. 1985
Q (0 mag flux at 20.2 μm)	7.5×10^{-18} W cm$^{-2}\mu$m^{-1}	Lebofsky et al. 1986b

asteroid's diameter and the visual geometric albedo, and the visual solar magnitude. As shown in Eqs. (1) and (4), the thermal flux is a function of asteroid diameter, the bolometric Bond albedo, and the solar flux. The geometric and Bond albedos are related by the equation

$$A = pq \qquad (5)$$

where p is the bolometric geometric albedo and q is the bolometric phase integral. All recent thermal models also incorporate the absolute magnitude system for asteroids adopted by IAU Commission 20 at the November 1985 General Assembly. This system is described in the appendix to the chapter by Bowell et al. and uses zero phase magnitudes which include the opposition effect (see the tabulation by Tedesco in Part VI). The magnitude system is based on an empirical phase function for the scattering of light from solid surfaces developed by Bowell et al. (see the chapter by Bowell et al.). The phase function can be used to estimate the bolometric phase integral q

$$q = 0.29 + 0.684 \, G \qquad (6)$$

where G is the slope parameter. Since the absolute visual magnitude at zero phase (within the uncertainty of the lightcurve variation), total radiated flux of the Sun and q are known or calculable, then the observable thermal flux uniquely determines the diameter and bolometric geometric albedo of an asteroid.

Finally, since most reflected light observations are reported in the broadband Johnson V filter, while determination of the bolometric geometric albedo requires knowledge of the entire reflectance spectrum, one other assumption is generally made

$$p_V = p \qquad (7)$$

where p_V is the magnitude at V (band center at 0.56 μm). This simplifying assumption leads to errors in the determination of A that are only a few percent (Hansen 1977) and small in comparison to the other uncertainties that go into the determination of A.

The Factor η

The STM does not predict accurately the thermal emission from solar system objects of known size, unless the beaming factor η is included. As shown by Eq. (4), η is effectively an adjustment to the subsolar temperature T_{SS}; it was first introduced in that form by Jones and Morrison (1974). η is needed for two reasons: (1) no real rotating asteroid radiates all its heat on the day side, as the STM (without η) assumes, and (2) individual points on the surface radiate their heat preferentially in the sunward direction, and not isotropically, again as the STM assumes.

The anisotropy of thermal emission was first noticed on the Moon by Petit and Nicholson (1930). The disk-integrated flux from the full Moon is enhanced due to a combination of two effects: first, the subsolar brightness temperature as seen at low phase angles is enhanced compared to the calculated equilibrium surface temperature for vertical solar incidence, and second, the brightness temperature away from the subsolar point falls off towards the limb more slowly than the $\cos^{1/4} \Omega$ dependence expected for equilibrium temperatures, so that brightness temperatures toward the limb are even more enhanced than subsolar brightness temperatures (Saari and Shorthill 1972; Mendell and Lebofsky 1982). Both these effects are reproduced more or less successfully by a rough-surface thermal model: depressions are warmer than their surroundings because they receive thermal radiation and scattered sunlight from the surrounding walls as well as direct solar radiation, and they radiate their heat preferentially in the sunward direction (Winter and Krupp 1971; Spencer 1989). Because the Moon's rotation period is so long, these presumed roughness effects are the dominant cause of departures from the equilibrium temperatures on the Moon, and the above-mentioned effects of rotation are negligible. Asteroids, on the other hand, rotate much more rapidly, and the emission from the night side has a potentially important influence on η (Hansen 1977; Spencer et al. 1989), a fact that has sometimes been forgotten.

The factor η modifies the STM by multiplying surface temperatures by the factor $\eta^{-1/4}$. The total sunward thermal emission is increased by $1/\eta$ (Eq. 1), but because of the nonlinearities of the Planck curve, the increase at any given wavelength is a more complex function of η. For a smooth, nonrotating body, $\eta \equiv 1.0$. Surface roughness tends to decrease η by enhancing the sunward emission, and rotation of a body with nonzero thermal inertia increases η.

The key to radiometric diameter determinations is the equating of the solar flux intercepted by the body with the sum of its reflected and thermally radiated fluxes. Asteroids are generally dark objects, and most of the flux they intercept (97% in the case of Ceres, for which $A = 0.03$) is absorbed and re-radiated thermally rather than reflected. It is therefore more critical to model accurately the total thermal emission than the total reflected flux, and most of the uncertainty in asteroid radiometric diameters is due to uncertainty in η and β_E rather than in p/p_V or q.

It should be emphasized that the beaming factor η is applicable only for zero solar phase angle. Since flux is enhanced at low phase angles, energy conservation requires that it must decrease with increasing phase angle at a rate faster than predicted by Lambertian emission models. This is where the thermal phase coefficient β_E fits in. The Lambertian model predicts a fall off of only about 0.002 mag deg^{-1}, but what is observed is about 0.01 mag deg^{-1}. Thus, the greater fall off in flux with phase angle should eventually compensate for the enhanced flux used at zero phase. Clearly, this is not an ideal model, but it does appear to be valid out to at least 20° phase.

Attempts to Determine η

Early attempts to determine the appropriate value of η for asteroids, for the purpose of diameter determinations, are summarized in Morrison and Lebofsky (1979). Typically, a value of η was chosen that yielded the correct diameters for the Galilean satellites, or gave asteroid diameters consistent with polarimetric determinations (see, e.g., Jones and Morrison 1974). Others (Hansen 1976, 1977) used theoretical arguments to determine the appropriate choice of η. The consensus in 1979 was that $\eta = 0.85$ to 0.90 was appropriate for normal asteroids, though exceptions were known (see Sec. III below).

Since 1979, there have been two attempts to improve the calibration of asteroid radiometric diameter determinations, using the occultation diameters of various asteroids. Though initial comparisons of radiometric and occulta-tion diameters were made by Morrison and Lebofsky (1979), the first detailed effort to use occultation diameters for calibration was made by Brown et al. (1982), using the asteroids Pallas and Juno, as well as the Galilean satellite Callisto. Their approach was not to determine η directly but to define an adjusted 10- and 20-μm flux for a zero-magnitude object $F'_{0\lambda}$ so that when the observed asteroid magnitudes are converted into fluxes using this zero point, the fluxes agree with the predictions of the standard thermal model with the assumption of $\eta = 1$.

The advantage of this approach is that it sidesteps any uncertainty in the absolute 10- and 20-μm calibration (as expressed by the true flux for a zero-magnitude object $F_{0\lambda}$). Errors in the absolute calibration will not affect diame-ters determined using the Brown et al. technique, provided that their magni-tude system is used. At a particular wavelength, the ratio of the actual to the (standard) model flux is given by $F_{0\lambda}/F'_{0\lambda}$, so $F'_{0\lambda}$ can be related to the actual

sunward enhancement of asteroid thermal emission (η), if $F_{0\lambda}$ is known. A limitation of the approach is that it cannot easily be generalized to other wavelengths, for instance the wavelengths of the IRAS asteroid data. Table II includes a summary of the Brown et al. flux enhancement factors. Spencer et al. (1989) have taken the thermal observations of Brown et al. (1982) and Lebofsky et al. (1986b) (discussed below) and re-reduced them using improved parameters where appropriate. Table II also shows the results of the re-reduction, in the form of both flux ratios and η values so that the two sets of observations can be compared.

The second attempt to use occultation diameters to calibrate radiometric diameter determinations was that of Lebofsky et al. (1986b). They used the absolute calibration of Rieke et al. (1985) and determined the value of η that resulted in radiometric diameters for Ceres and Pallas in agreement with the observed occultation diameters. Table II compares their results with those of Brown et al. It is interesting to note that Brown et al., who expressed their results in terms of flux enhancement at each wavelength, determined a very similar flux enhancement at 10 and 20 μm for each object, while the data of

TABLE II
Comparison of Standard Thermal Model Calibrations

| | | 10 μm | | | | 20 μm | | | |
| | | F/F_1 [a] | | η | | F/F_1 [a] | | η | |
Workers[e]	Object	Orig.[b]	Recal.[c]	Orig.	Recal.	Orig.	Recal.	Orig.	Recal.
Brown et al.	1 Ceres	—	1.45	—	0.79	—	1.52	—	0.59
(1982)	2 Pallas[d]	1.43	1.60	—	0.73	1.42	1.60	—	0.55
	3 Juno	1.48	1.46	—	0.76	1.44	1.43	—	0.61
	J_{IV} Callisto	1.43	1.37	—	0.87	1.37	1.34	—	0.77
Lebofsky et al.	1 Ceres	—	1.53	0.75	0.75	—	1.36	—	0.69
(1986b)	2 Pallas	—	1.60	0.77	0.74	—	1.41	—	0.68
Spencer (1989)[f]	rough-surface model	1.41		0.80		1.22		0.78	

[a]F/F_1 is the observed flux ratioed to the flux from the standard thermal model with the assumption $\eta = 1.0$.
[b]These columns refer to values given in the original publication (or in the case of Brown et al. 1982, obtained by ratioing the given $F'_{0\lambda}$ values to the 0-mag fluxes of Rieke et al. 1985, correcting for the difference in magnitude system).
[c]These columns refer to values recalculated from the observed magnitudes by Spencer et al. (1989), using improved values for diameter and albedo where appropriate.
[d]The large difference between the original and recalculated values for the Brown et al. Pallas observations is due to an error in the solar phase angle in their original calculations.
[e]The absolute 10- and 20-μm calibration of Rieke et al. (1985) is assumed throughout. Brown et al. data are converted to the Rieke magnitude system using the difference in assumed magnitudes for α Boo. Wavelengths are 10.0 and 20.0 μm throughout except for the Lebofsky et al. data, which use 10.6 and 20.2 μm.
[f]The Spencer (1989) rough-surface model assumes a thermal inertia of 3×10^4 erg cm^{-2} s$^{-1/2}$ K^{-1}, an albedo of 0.0, and a surface entirely covered in hemispherical depressions (rms slope = 49°), at 3.0 AU from the Sun.

Lebofsky et al., who expressed their results in terms of a temperature enhancement (which is what η describes), shows a more similar η (and therefore a different flux enhancement) at each wavelength. However, the two methods are in broad agreement at 10 μm, and indicate larger sunward flux enhancements (smaller values of η) for typical asteroids than was supposed when *Asteroids* (Gehrels 1979) was published. The largest tabulated 10-μm η is for Callisto, and probably indicates a real difference in thermal properties between this large, icy, slowly rotating satellite and typical asteroids. This underscores the dangers involved in using objects other than asteroids to calibrate asteroid radiometry. At 20 μm, the situation is more uncertain and the values of η or F/F_1 determined from the Brown et al. and Lebofsky et al. data for the same objects differ significantly. This is probably due to the greater uncertainty in both absolute calibration and the relative magnitudes of standard stars at 20 μm.

Lebofsky et al. (1986*b*) averaged their 10-μm η values for Ceres and Pallas to obtain a mean value of 0.756 ± 0.014. Because η represents a temperature adjustment, there is some physical justification for assuming that a similar value applies over a large wavelength range, and the rough-surface thermophysical model of Spencer (1989) predicts little variation in η with wavelength, as shown by the sample result in Table II. The value of 0.756 was assumed to apply at IRAS wavelengths and was used for determination of the diameters in the IRAS asteroid catalog. However, note that even the Lebofsky 20-μm data, as re-reduced by Spencer et al. (1989), shows η values of 0.69 and 0.68, significantly smaller than the 10-μm value. Recent results for Ceres have cast doubt on its suitability as a standard for radiometric diameter determinations. In the IRAS data set (see the chapter by Matson et al.), Ceres is anomalous when derived diameters at different wavelengths are compared. Also, the work of Ostro (see his chapter) has shown that most asteroids have higher radar reflectivities than does Ceres. Radar reflectivity increases with regolith compaction and metal content, both of which will increase thermal inertia, so Ceres may have atypical thermal properties.

A further potential problem with using *any* asteroids as calibration objects is that their spin-axis orientations and thermal inertias are rarely known with any accuracy. This is discussed in the upcoming section on thermophysical modeling.

III. OTHER THERMAL MODELS

The question of the generality of the standard thermal model and its associated value of η is difficult to tackle observationally, because we have accurate occultation diameters for only a few asteroids, and for these only at a few select cross sections. Some small Earth-approaching asteroids show obvious deviation from standard behavior, and sufficiently detailed observations of a few asteroids such as Ceres also show emission inconsistent with the

standard model. Departures from standard-model behavior will result in significant errors in the radiometric diameters so derived. Theoretical thermal models that relax some of the assumptions of the standard model can be used to test the generality of the standard model, and to deal with the special cases. These topics are discussed next.

Ellipsoidal Shape

Brown (1985) explored the effects of nonspherical shape on asteroid thermal emission. He calculated the ratio of the thermal flux from an ellipsoidal asteroid to that from a spherical body with the same instantaneous projected area, assuming the standard thermal model. The flux ratio varies wildly depending on the shape and orientation of the ellipsoid, but for approximately spherical bodies, the deviations are relatively small. For instance, at 2.5 AU, if a spherical asteroid is assumed to have $\eta = 1$, then an ellipsoidal body with axial ratios $a/b = 1.5$, $c/b = 1.0$, and the a axis pointed at the observer and the Sun, will have a flux ratio ellipsoid/sphere of ~ 0.77 at 10 μm and 0.85 at 20 μm, yielding $\eta = 1.19$ and 1.23, respectively. Because the effects of nonsphericity are different at 10 and 20 μm, discrepant 10- and 20-μm diameters for an asteroid may be one indicator of an aspherical shape.

The Fast-Rotating (Isothermal-Latitude) Model

For small, Earth-approaching asteroids, the standard thermal model sometimes gives albedos which imply compositions inconsistent with those inferred from visual spectroscopy. In all cases, the model albedos are high by as much as a factor of two over the albedos expected from the spectrally determined compositions (Lebofsky et al. 1978,1979). The derived albedos are more consistent with the other data if a fast-rotating thermal model is used.

The fast-rotating model differs from the standard thermal model in that it assumes the extreme case of a spherical asteroid whose surface is extremely rocky (high thermal inertia) and/or executes relatively rapid rotation, and/or is very cold. Such an object has a very large thermal parameter Θ as defined in the following section. This results in a temperature distribution that is isothermal in longitude (temperature constant through the day and night) and depends only on latitude, so the model is also called the isothermal-latitude model. If the Sun is in the equatorial plane, temperature decreases with latitude due to the decreased solar insolation

$$T(\theta,\phi) = T_{MAX} \cos^{1/4} \phi \qquad (8)$$

where

$$T_{MAX} = \left[\frac{(1 - A)S}{\pi \epsilon \sigma} \right]^{1/4} \qquad (9)$$

(cf. Eq. 4 and Fig. 4b). There is assumed to be no beaming due to roughness, as supported by the models of Spencer (1989) which show that the thermal effects of roughness disappear for very large Θ.

The Thermophysical Model

In reality, most asteroids probably lie somewhere between the two extreme cases just discussed. The appropriateness of the equilibrium (STM) or isothermal-latitude models can be described by the thermal parameter Θ which is defined by

$$\Theta = \frac{\Gamma\sqrt{\omega}}{\epsilon\sigma T_{SS}^3} \tag{10}$$

(Spencer et al. 1989). Γ is the thermal inertia, ω the angular velocity of rotation and T_{SS} is the subsolar equilibrium temperature, from Eq. 4 with $\eta = 1$. For the standard thermal model, where temperatures are always in equilibrium with sunlight, $\Theta = 0$; $\Theta \to \infty$ for the isothermal-latitude model. Values of Θ between about 0.1 and 10.0 are poorly described by either model, and a thermophysical model, which numerically calculates the diurnal flow of heat between the surface and subsurface, is required. For the Moon, $\Theta = 0.025$, but $\Theta = 1.04$ for Ceres if it has the Moon's thermal inertia, because of its lower temperature and much faster rotation. Thermophysical models are thus likely to be necessary to understand the thermal emission of many asteroids.

Spencer et al. (1989, Appendix) describes the simplest form of thermophysical model in detail. The model numerically solves the one-dimensional thermal-diffusion equation with the surface boundary condition determined by the diurnal variations in insolation, and assumes constant thermal parameters with depth and temperature, and absorption of all insolation at a smooth surface with albedo independent of solar incidence angle. Relaxation of any of these assumptions produces more complex and potentially more realistic models (see, e.g., Winter and Saari 1969; Brown and Matson 1987; Spencer 1989).

The thermophysical model was first discussed by Matson (1971b). Thermophysical models were next applied to observations of the Apollo asteroid Eros (Morrison 1976; Lebofsky and Rieke 1979). Lebofsky et al. applied a similar model to infrared observations from 10 to 1100 μm of asteroid 10 Hygiea, but the data were not of sufficiently high quality to distinguish between a thermal inertia of zero and the lunar value.

Spencer et al. (1989) give a detailed description of the effects of Θ on thermal emission for spherical bodies, as determined by a numerical thermophysical model. One important result is that spin-axis orientation should have a significant effect on thermal emission unless Θ is very small. If the spin axis points at the Sun, temperatures are always in equilibrium with sunlight, regardless of Θ. However if the Sun is in the equator, there is significant

nightside thermal emission, and daytime thermal emission decreases with increasing Θ. As a result, the sunward thermal emission from an asteroid whose spin axis is not perpendicular to its orbit should vary around the orbit. However, the data so far available show no such variations. Figure 5 shows the beaming parameter η for Pallas as a function of subsolar latitude, using the pole orientation from Magnusson (1986). The lack of variation in emission with subsolar latitude is most easily explained if Pallas has a thermal inertia 20% of the lunar value or smaller. The situation for Ceres is very similar, though the pole position is less reliable. If most asteroid thermal inertias are this small, the STM is more nearly appropriate for modeling the thermal emission of asteroids, and the effects of spin-axis orientation are reduced. Note, however, that the thermal inertia of the asteroid-like Martian moon, Phobos is similar to the Earth's Moon (Lunine et al. 1982).

Another implication of the thermophysical models of Spencer et al. (1989) is that because of the T^3 term in the expression for Θ, bodies at large distances from the Sun radiate a larger percentage of their flux from the night side, resulting in reduced sunward thermal emission and thus smaller radiometric diameters than otherwise identical warmer bodies at smaller heliocentric distances. Standard radiometric methods are thus subject to a systematic bias, in that the diameters of distant, cold asteroids such as the Trojans tend to be overestimated (Fig. 6). For instance, a 50-km diameter Trojan at 5.2 AU with a 10-hr rotation period, a thermal inertia of 1×10^4 erg cm^{-2} s$^{-1/2}$ K^{-1} (the value for Ceres suggested by Spencer 1989), an albedo
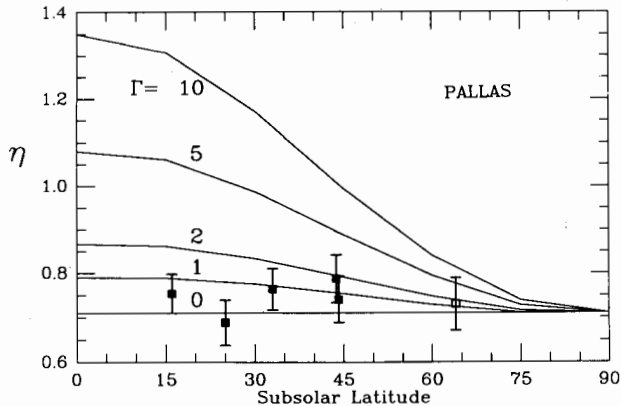
Fig. 5. Observed STM beaming parameter η for Pallas as a function of subsolar latitude, assuming the pole of Magnusson (1986): filled squares from Lebofsky et al. (1986); open squares from Brown et al. (1982). Also shown is the variation expected from a thermophysical model with thermal inertias of 1, 2, 5 and 10 × 10^4 erg cm^{-2} s$^{-1/2}$ K^{-1}, and assuming a surface roughness equal to the lunar value. A thermal inertia much lower than the lunar value of 5 × 10^4 is suggested for Pallas (figure from Spencer et al. 1989).
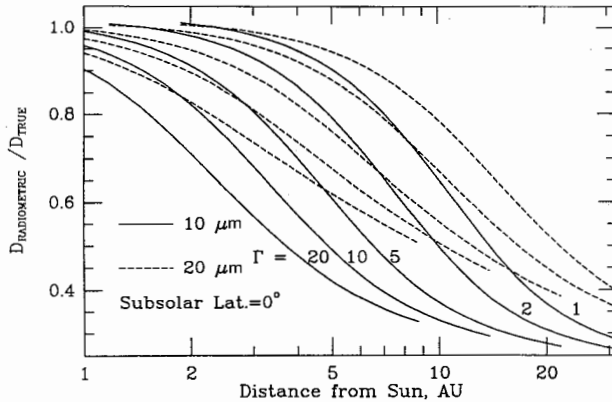
Fig. 6. The error in radiometric diameter as a function of distance from the Sun R, for various assumed thermal inertias, an albedo of 0.03, a 10-hr rotation period, and the Sun in the equatorial plane. This is derived from a smooth thermophysical model with a roughness correction that assumes lunar surface roughness (see text). Results are shown for wavelengths of 20 and 10 μm. For each wavelength, the five curves, from uppermost to lowermost, refer to thermal inertias of 1, 2, 5, 10 and 20 × 10⁴ erg cm⁻² s⁻¹/² K⁻¹. Depending on thermal inertia, there are likely to be considerable systematic errors in diameters and albedos determined by standard radiometric methods, especially as a function of AU (figure from Spencer et al. 1989).

of 0.030 and a subsolar latitude of 0° would yield a diameter of 45 km and an albedo of 0.038 using standard radiometric techniques at 10 μm, and 47 km and 0.034 at 20 μm. If the Trojan had a lunar thermal inertia of 5×10^4, the 10-μm diameter and albedo would be 30 km and 0.09, and the 20-μm values would be 38 km and 0.053. Unfortunately, as can be seen from this example, it is difficult to quantify and thus correct for the bias as it depends so much on the assumed thermal inertia, which as discussed previously is poorly known for asteroids.

Rough-surface Thermophysical Models

None of the above models include the effects of surface roughness which, as discussed above, tends to increase the sunward thermal emission from an asteroid. Hansen (1977) modeled temperatures on a rough surface and the consequent thermal emission from a rough asteroid, but he did not consider simultaneously the effects of thermal inertia, and had to make non-physical assumptions about the global temperature distribution. Recently, Spencer (1989) has constructed a more general asteroid thermal model which, like Hansen's, calculates temperatures on a surface covered in spherical-section indentations and thus attempts to model physically the sunward beaming of the thermal radiation, but which also includes the effect of thermal inertia and multiply scattered sunlight. The model calculates the value of η

required in the STM to obtain the same sunward flux, for various combinations of surface roughness, obliquity and the thermal parameter Θ. This value of η is used as a measure of the model thermal emission. The most important simplification of this model is the assumption of a spherical asteroid, so it is complementary to that of Brown (1985).

Figure 7 summarizes some results, showing that the calculated value of η varies greatly with surface roughness and Θ. However, η varies little with surface albedo for fixed roughness and Θ. The thermal emission from the Moon requires an rms slope of about 40° at cm or larger scales according to this model. If Ceres has the same roughness as the Moon, Ceres' observed 10-μm η value of 0.76 (Lebofsky et al. 1986b) implies a thermal inertia much smaller than the Moon's, consistent with the lack of variation of emission with subsolar latitude discussed in the thermophysical model section.

The rough surface model can for the first time, also model the variation in asteroid thermal emission with solar phase angle. Figure 8 shows a fit by Spencer (1989) to the thermal phase curve for Ceres obtained by Lebofsky et al. (1986b). The difference in the thermal emission of Ceres before and after opposition is matched with a rough-surface thermophysical model that has prograde rotation and thermal inertia 20% of the lunar value. This is consistent with the other evidence for very low thermal inertias already mentioned (the small η values and lack of variation in emission with subsolar latitude) but it provides a measurement of the thermal inertia rather than just an upper limit.
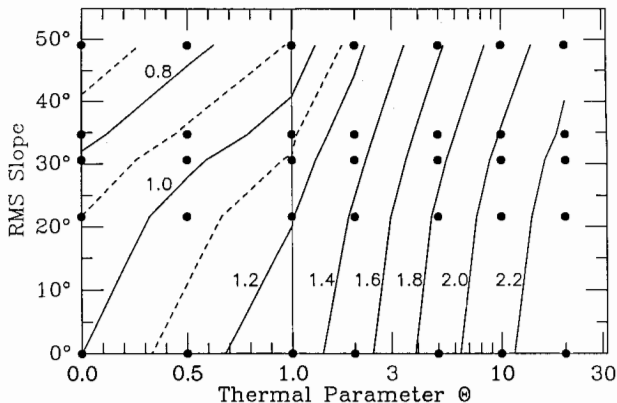
Fig. 7. Beaming parameter η as a function of thermal parameter Θ and rms slope, from the Spencer (1989) rough-surface thermophysical model. Subsolar latitude and albedo of zero are assumed. Dots show the points at which the model was run to generate the contours. Note that the Θ axis is logarithmic for $\Theta > 1.0$ and linear for $\Theta < 1.0$.
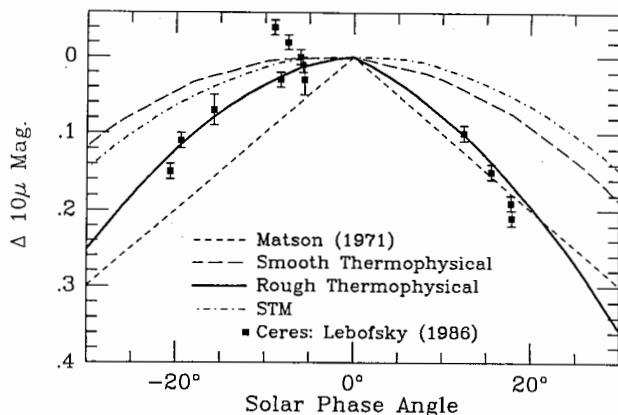
Fig. 8. Rough thermophysical model fit to the 10-μm phase curve of Ceres. The vertical axis shows the difference in 10 μm magnitude from zero phase. Data are from Lebofsky et al. (1986b), corrected to uniform geocentric and heliocentric distance. The rough thermophysical model has an rms slope of 44°, prograde rotation about an axis normal to the orbital plane, and a thermal inertia of 1×10^4 erg cm^{-2} s$^{-1/2}$ K^{-1}. The smooth thermophysical model is similar but with a smooth surface; STM is the standard thermal model (zero thermal inertia), and (Matson 1971) refers to the standard empirical thermal phase curve of 0.01 mag deg^{-1} (figure from Spencer 1989).

IV. OTHER THERMAL OBSERVATIONAL TECHNIQUES

Distinguishing the Effects of Shape and Albedo

The visual lightcurves of asteroids can be caused by one of two effects (or a combination of both): nonspherical shape or albedo spots. Thermal infrared measurements, when coupled with visual or near-infrared reflected measurements of the lightcurve, can be used to discriminate as to whether its variations are due to shape or albedo. A spotted, spherical asteroid will have reflected and thermal lightcurves that are out of phase. At reflected wavelengths, maxima occur when high-albedo areas are visible, while minima occur when dark areas are in view. Conversely, in the thermal infrared, maxima occur when warmer dark areas are visible. However, if the lightcurve is due to nonspherical shape, both the reflected and thermal lightcurves will be in phase, peaking when the largest cross section is presented. For asteroids 433 Eros (Lebofsky and Rieke 1979) and 624 Hektor (Hartmann and Cruikshank 1980), the reflected and thermal lightcurves are distinctly in phase, implying a varying cross-sectional area (nonspherical shape). More recently, Lebofsky et al. (1988) investigated a model which implied a spotted surface for Herculina (Taylor et al. 1987). Lebofsky et al. modified the STM to account for a spotted surface, and this model predicted out-of-phase thermal and reflected light-

curves. However, they observed in-phase lightcurves, demonstrating that the lightcurve was due to shape, not albedo spots.

Thermal Polarimetry

This is a relatively unexplored technique which shows some potential. Surface thermal emission in directions away from the local surface normal is polarized, to a degree that depends on the emission angle, the surface roughness and the dielectric constant. The disk-integrated emission from a nonrotating body seen at zero phase is unpolarized, by symmetry, but if the object is rotating, the warmest region moves into the afternoon, away from the subsolar point, and is no longer seen with zero emission angle. The disk-integrated emission, dominated by the warmest region, thus becomes polarized, and by observing at several different epochs, it is possible to determine both the pole orientation and the thermal inertia. So far, this has only been done for Ceres, by Johnson et al. 1983, who gave the first estimate of Ceres' pole position and sense of rotation, and also determined that the thermal inertia is similar to the Moon's. However, this pole position and thermal inertia are inconsistent with the thermal observations of Ceres by Lebofsky et al. (1986b), as interpreted by Spencer et al. (1989) and discussed in the previous section on thermophysical models. Also, Millis et al. (1987) show lightcurve evidence that the pole position of Ceres is almost normal to its orbit, not highly inclined as the Johnson et al. polarimetry suggests. However, if these conflicts can be reconciled, the technique may eventually prove useful in determining asteroid pole positions and thermal inertias.

Thermal Spectroscopy

Thermal radiation carries compositional as well as temperature information, in the form of discrete spectral features resulting from variations in emissivity with wavelength. The Moon shows emission features in the 10-μm region due to silicates (Murcray et al. 1970), and extensive laboratory measurements have investigated the dependence of thermal-emission spectra on composition, surface structure and surface temperature distribution (see, e.g., Conel 1969; Salisbury et al. 1987). However, the only published observations of discrete features in asteroid thermal-emission spectra have been those of Feierberg et al. (1983). They observed six main-belt asteroids and found probable silicate emission features in the spectra of two of them (19 Fortuna and 21 Lutetia) centered at 10 and 11 μm, respectively. The spectra of the others (11 Parthenope, 14 Irene, 349 Dembowska and 64 Angelina) were featureless to within the precision of the observations. Lutetia is an M type and the presence of the silicate feature rules out a pure metal-surface model for that body. There therefore appears to be some useful compositional information in thermal-emission spectra of asteroids, and there is room for much more work in this area.

V. SUMMARY AND CONCLUSIONS

Thermal models of asteroids have come a long way over the past two decades. From the early models that ignored (or at least avoided) many of the physical properties of asteroids have come more sophisticated models that more closely represent physically realistic asteroid models. In many ways even these new models still represent simplifications, but more and more they are helping us understand the true nature of asteroids and their surfaces.

REFERENCES

Allen, D. A. 1970. The infrared diameter of Vesta. *Nature* 227:158–159.

Allen, D. A. 1971. The method of determining infrared diameters. In *Physical Studies of Minor Planets,* ed. T. Gehrels, NASA SP-267, pp. 41–44.

Brown, R. H. 1985. Ellipsoidal geometry in asteroid thermal models: The standard radiometric model. *Icarus* 64:53–63.

Brown, R. H., and Matson, D. L. 1987. Thermal effects of insolation propagation into the regoliths of airless bodies. *Icarus* 72:84–94.

Brown, R. H., Morrison, D., Telesco, C. M., and Brunk, W. E. 1982. Calibration of the radiometric asteroid scale using occultation diameters. *Icarus* 52:188–195.

Campins, H., Rieke, G. H., and Lebofsky, M. J. 1985. Absolute calibration of photometry at 1 through 5 μm. *Astron. J.* 90:896–899.

Conel, J. E. 1969. Infrared emissivities of silicates: Experimental results and a cloudy atmosphere model of spectral emission from condensed particulate mediums. *J. Geophys. Res.* 74:1614–1634.

Feierberg, M. A., Witteborn, F. C., and Lebofsky, L. A. 1983. Detection of silicate emission features in the 8- to 13-μm spectra of main belt asteroids. *Icarus* 56:393–397.

Gehrels, T., ed. 1979. *Asteroids* (Tucson: Univ. of Arizona Press).

Hansen, O. L. 1976. Radii and albedos of 84 asteroids from visual and infrared photometry. *Astron. J.* 81:74–84.

Hansen, O. L. 1977. An explication of the radiometric method for size and albedo determination. *Icarus* 31:456–482.

Hartmann, W. K., and Cruikshank, D. P. 1980. Hektor: The largest highly elongated asteroid. *Science* 207:976–977.

Johnson, P. E., Kemp, J. C., Lebofsky, M. J., and Rieke, G. H. 1983. 10 μm polarimetry of Ceres. *Icarus* 56:381–392.

Jones, T. J., and Morrison, D. 1974. Recalibration of the photometric/radiometric method of determining asteroid sizes. *Astron. J.* 79:892–895.

Lebofsky, L. A., and Rieke, G. H. 1979. Thermal properties of 433 Eros. *Icarus* 40:297–308.

Lebofsky, L. A., Veeder, G. J., Lebofsky, M. J., and Matson, D. L. 1978. Visual and radiometric photometry of 1580 Betulia. *Icarus* 35:336–343.

Lebofsky, L. A., Lebofsky, M. J., and Rieke, G. H. 1979. Radiometry and surface properties of Apollo, Amor, and Aten objects. *Astron. J.* 84:885–888.

Lebofsky, L. A., Sykes, M. V., Tedesco, E. F., Veeder, G. J., Matson, D. L., Nolt, I. G., Radostitz, J. V., Ade, P. A. R., Gear, W. K., Griffin, M. J., and Robson, E. 1. 1984. Thermal properties of the regolith of asteroid 1 Ceres. *Bull. Amer. Astron. Soc.* 16:698 (abstract).

Lebofsky, L. A., Sykes, M. V., Nolt, I. G., Radostitz, J. V., Veeder, G. J., Matson, D. L., Ade, P. A. R., Griffin, M. J., Gear, W. K., and Robson, E. I. 1985. Submillimeter observations of the asteroid 10 Hygiea. *Icarus* 63:192–200.

Lebofsky, L. A., Matson, D. L., Veeder, G. J., and Tedesco, E. F. 1986a. The IRAS asteroid thermal model. In *Infrared Astronomical Satellite Asteroid and Comet Survey: Preprint Version No. 1,* ed. D. L. Matson, JPL Internal Doc. D-3698, pp. 7:1–7:34.

Lebofsky, L. A., Sykes, M. V., Tedesco, E. F., Veeder, G. J., Matson, D. L., Brown, R. H., Gradie, J. C., Feierberg, M. A., and Rudy, R. J. 1986b. A refined "standard" thermal model for asteroids based on observations of 1 Ceres and 2 Pallas. *Icarus* 68:239–251.

Lebofsky, L. A., Greenberg, R., Tedesco, E. F., and Veeder, G. J. 1988. Infrared lightcurves of asteroids 532 Herculina and 45 Eugenia: Proof of the absence of significant albedo markings. *Icarus* 75:518–526.

Lunine, J. I., Neugebauer, G., and Jakosky, B. M. 1982. Infrared observations of Phobos and Deimos from Viking. *J. Geophys. Res.* 87:10297–10305.

Magnusson, P. 1986. Distribution of spin axes and senses of rotation for 20 large asteroids. *Icarus* 68:1–39.

Matson, D. L. 1971*a*. Infrared observations of asteroids. In *Physical Studies of Minor Planets*, ed. T. Gehrels, NASA SP-267, pp. 45–50.

Matson, D. L. 1971*b*. I. Astronomical Photometry at Wavelengths of 8.5, 10.5, and 11.6 μm. II. Infrared Emission from Asteroids at Wavelengths of 8.5, 10.5, and 11.6 μm. Ph.D. Thesis, California Institute of Technology.

Matson, D. L., Veeder, G. J., and Lebofsky, L. A. 1978. In *Asteroids: An Exploration Assessment*, eds. D. Morrison and W. C. Wells, NASA CP-2053, pp. 127–144.

Mendell, W. W., and Lebofsky, L. A. 1982. Lunarlike thermal emission and the standard asteroid radiometric model. *Bull. Amer. Astron. Soc.* 14:726 (abstract).

Millis, R. L., Wasserman, L. H., Franz, O. G., Nye, R. A., Oliver, R. C., Kreidl, T. J., Jones, S. E., Hubbard, W., Lebofsky, L., Goff, R., Marcialis, R., Sykes, M., Frecker, J., Hunten, D., Zellner, B., Reitsema, H., Schneider, G., Dunham, E., Klavetter, J., Meech, K., Oswalt, T., Rafert, J., Strother, E., Smith, J., Povenmire, H., Jones, B., Kornbluh, D., Reed, L., Izor, K., A'Hearn, M. F., Schnurr, R., Osborn, W., Parker, D., Douglas, W. T., Beish, J. D., Klemola, A. R., Rios, M., Sanchez, A., Piironen, J., Mooney, M., Ireland, R. S., and Leibon, D. 1987. The size, shape, density, and albedo of Ceres from its occultation of BD+8°471. *Icarus* 72:507–518.

Morrison, D. 1976. The diameter and thermal inertia of 433 Eros. *Icarus* 28:125–132.

Morrison, D., and Lebofsky, L. A. 1979. Radiometry of asteroids. In *Asteroids*, ed. T. Gehrels (Tucson: Univ. of Arizona Press), pp. 184–205.

Murcray, F. H., Murcray, D. G., and Williams, W. J. 1970. Infrared emissivity of lunar surface features 1. Balloon-borne observations. *J. Geophys. Res.* 75:2662–2669.

Neckel, H., and Labs, D. 1984. The solar radiation between 3300 and 12500 Å. *Solar Phys.* 90:205–258.

Pettit, E., and Nicholson, S. B. 1930. Lunar radiation and temperatures. *Astrophys. J.* 71:102–135.

Rieke, G. H., Lebofsky, M. J., and Low, F. J. 1985. An absolute photometric system at 10 and 20 μm. *Astron. J.* 90:900–906.

Saari, J. M., and Shorthill, R. W. 1972. The sunlit lunar surface. I. Albedo studies and full Moon temperature distribution. *The Moon* 5:161–178.

Salisbury, J. W., Hapke, B., and Eastes, J. W. 1987. Usefulness of weak bands in mid infrared remote sensing of particulate planetary surfaces. *J. Geophys. Res.* 92:702–710.

Spencer, J. R. 1989. A rough-surface thermophysical model for airless planets. *Icarus*, submitted.

Spencer, J. R., Lebofsky, L. A., and Sykes, M. V. 1989. Systematic biases in radiometric diameter determinations. *Icarus* 78, in press.

Taylor, R. C., Birch, P. V., Drummond, J., Pospiezalska-Surdej, A., and Surdej, J. 1987. Asteroid 532 Herculina: Lightcurves, pole orientation and a model. *Icarus* 73:354–369.

Winter, D. F., and Krupp, J. A. 1971. Directional characteristics of infrared emission from the Moon. *The Moon* 2:279–292.

Winter, D. F., and Saari, J. M. 1969. A particulate thermophysical model of the lunar soil. *Astrophys. J.* 156:1135–1151.

PRECISE MEASUREMENT OF ASTEROID SIZES AND SHAPES FROM OCCULTATIONS

R. L. MILLIS
Lowell Observatory

and

D. W. DUNHAM
International Occultation Timing Association

Occultations of stars by asteroids provide opportunities to measure asteroid dimensions with an accuracy not currently achievable in other ways from Earth-based observatories. During the past decade, significant progress has been made in the identification, prediction, and observation of asteroid occultations. As a result, several such events have been well observed, and important information concerning the size, shape, density and internal structure of asteroids has been learned. Prospects for continued effective application of the occultation technique to asteroid studies are good, but additional properly equipped observers would be helpful.

I. INTRODUCTION

Precise measurement of the size and shape of an asteroid is one of the more challenging tasks confronting groundbased astronomers. The angular diameter of the largest minor planet never exceeds 0.84 arcsec, a value comparable to the seeing disk at even the best observing sites; most asteroids subtend significantly smaller angles. Consequently, direct diameter measurements made with filar micrometers or similar devices have been published for only a few asteroids (Dollfus 1971), and these were admittedly very inaccurate. Given that useful measurements of the dimensions of asteroids and other

small solar system bodies are not possible using classical methods, indirect techniques based on polarimetry (see the chapter by Dollfus et al.) and infrared radiometry (see the chapter by Lebofsky and Spencer) were devised. Both methods have been widely applied to asteroids, but the accuracy of the resulting diameters depends on the validity of the assumptions inherent in each. Speckle interferometry also has been used to measure the size and shape of a few asteroids (see the chapter by Drummond and Hege). This method appears to hold significant promise, but the processing of speckle data is complex, and an objective assessment of the uncertainties in the resulting size determinations is difficult at present. The same is true of diameter determinations based on radar data (see Ostro's chapter).

There is an additional way of measuring directly the dimensions of an asteroid which requires few assumptions, is capable of very high accuracy, and can be carried out with modest instrumentation. This method, which is the subject of this chapter, is based on observation of occultations of stars by asteroids. In the course of such a chance passage of a minor planet across an observer's line of sight to a distant star—which, incidentally, is a common occurrence (see Millis and Elliot 1979)—the asteroid will be seen to approach the star, block it from view for a time, and then move away on the other side. By simply measuring the time interval during which the star is occulted, one can easily calculate the length (in linear, rather than angular, units) of one chord across the asteroid. Because of horizontal parallax, observers at different locations in general will see the star pass behind different portions of the asteroid. With enough appropriately located observers, one can map the apparent limb profile of the asteroid as closely as desired.

While the applicability of occultation observations to measurement of the dimensions of asteroids was understood as early as 1952 (Taylor 1962), significant success in actual use of the technique was slow in coming. In the early years, predictions realistically could be made for only a fraction of the potentially observable occultations. Furthermore, observers were not yet well organized and equipped, and reliable methods of predicting the location of the narrow stripe across the globe, within which a particular occultation would occur, had not been worked out. Between 1952, when Taylor began issuing occultation predictions, and the end of 1974, only three asteroid occultations were observed: one by Juno and two by Pallas. None of the three had sufficient observational coverage to permit determination of more than lower limits on the diameters of these objects. In 1975 a widely publicized occultation by 433 Eros was seen by eight observers (O'Leary et al. 1976), but the uncertainty in these visual timings was too great to permit other than a crude measurement of the figure of this small, fast-moving body.

The potential of the occultation technique for measuring asteroid dimensions was finally realized in May 1978, when Pallas occulted SAO 85009 (Wasserman et al. 1979). That occultation was observed photoelectrically at six sites on the ground and from the Kuiper Airborne Observatory. Based on

these observations, it was possible to determine the dimensions of Pallas' apparent profile with an uncertainty of less than 2%, which, in turn, permitted the asteroid's density to be computed with sufficient accuracy to be interesting. The successful observation of the Pallas occultation and nearly contemporaneous reports by occultation observers of possible minor planet satellites (see, e.g., Bowell et al. 1978) resulted in greatly heightened interest in asteroid occultations. The state of this research area at the time of the 1979 Tucson Asteroids Conference was reviewed by Millis and Elliot (1979). Here we will emphasize primarily developments which have occurred in the intervening years.

II. OCCULTATION PREDICTIONS

Star Catalog Searches

The most common means of identifying upcoming occultations of stars by asteroids has been comparison of asteroid ephemerides with the positions of stars given in star catalogs. As noted before, this work was initiated by Taylor, who carried it on virtually single-handedly for nearly three decades. Initially, the comparison was necessarily done by hand, a painstaking and time-consuming task. With the advent of electronic computers, the process could be automated and, as a result, occultation searches have been steadily expanded to include more asteroids and larger star catalogs. A recent search conducted by Wasserman et al. (1987), for example, is complete for all numbered asteroids (within certain constraints on angular diameter) and spans a composite star catalog containing 326,000 stars. Complementary searches have been performed by Goffin (1988) and others. Because of these vastly extended searches, one can say with confidence that virtually all occultations of stars in the major astrometric catalogs (SAO, AGK3, Perth 70 and Lick-Voyager) are being identified with adequate time for planning observations. Dunham (1988) has extended the searches to fainter stars in the astrographic catalogs, but the accuracy of these predictions is degraded by the lack of proper motions and the early epoch (often over 75 yr old) of these positions.

Photographic Searches

A more complete inventory of stars which may be occulted can be had by taking plates covering the future paths of asteroids of interest. The path of each asteroid across the relevant plates is traced using a microdensitometer under computer control. Stars falling near the path are tagged, and their positions subsequently measured relative to a network of astrometric catalog stars. The positions of these stars are then input to star catalog search routines, as discussed above, to identify those stars that will actually be occulted. Since recent plates are normally used, errors introduced by lack of proper motions are insignificant and the overall prediction accuracy is better than that of

catalog searches. Additionally, occultation candidate stars too faint to be included in the star catalogs, but bright enough to produce detectable occultations, will be found. Photographic searches for asteroid occultations are very time consuming compared to catalog searches, and only a few have been published (see, e.g., Millis et al. 1984c). Nevertheless, the very successfully observed occultation by Ceres on 13 November 1984 was first identified in this way (Millis et al. 1983b).

Prediction Refinement

Orbital elements of the low-numbered asteroids have been improved considerably in recent years, but ephemeris errors of typically 0.5 arcsec remain. The SAO and AGK3 star catalogs, from which the bulk of occultations are identified, contain zonal and random errors often greater than 1 arcsec. However, an accuracy of ± 0.1 arcsec is commonly needed to locate the narrow occultation paths accurately enough to insure that a majority of the observers will be within the actual path. As a consequence, catalog predictions must be refined before observations of an occultation can be attempted with any reasonable chance of success. In practice, the necessary astrometric accuracy usually can be achieved with astrographs having plate scales of about 60 arcsec mm^{-1} or less. It is important that the plates be taken when the target star and asteroid are close enough in the sky to be contained within a single plate. For that reason, fields of view of at least 1°5 are needed for most occultations to allow enough time for coordination and notification of observers, and fields of 3° or more are preferred to permit utilization of the more accurate but less dense AGK3R, SRS or Perth 70 reference catalogs. An alternative approach which has worked well has involved use of the automatic photoelectric meridian circle at Bordeaux Observatory. With this instrument, it sometimes has been possible to produce precise predictions with greater lead time than is typically the case with plates.

III. OBSERVATIONAL TECHNIQUES

Due to the narrowness of asteroid occultation ground tracks and the need to accommodate changes in weather and path predictions, adequate observational coverage of these events invariably requires the augmentation of fixed observatories with portable telescopes. Well over half of all observations of asteroid occultations have been obtained by mobile observers. Furthermore, because the instrumental requirements are modest, occultation research represents one of the few areas in which students, amateur astronomers and teachers at small colleges and universities can contribute effectively to planetary research.

When observing an occultation, one is simply trying to detect the change in the brightness of the blended star-asteroid image at the moments of disappearance and reappearance of the star and to establish accurately the times of

these two events. Actually, depending on the signal-to-noise characteristics and time resolution of the observations and the angular diameter of the occulted star, immersion and emersion sometimes will not occur instantaneously and a Fresnel diffraction pattern may be resolved in the lightcurve (Millis 1986). In such cases, the angular diameter of the occulted star can sometimes be derived by fitting models to the occultation lightcurve (see, e.g., Reitsema et al. 1981). Modeling is also required to determine the precise time of geometric occultation but, in general, it will occur when the starlight has been reduced to between 50% and 25% of its unocculted level, depending on the star's angular diameter (Nather and Evans 1970).

Because a typical asteroid occultation lasts from 10 to 20 s and we wish to establish the object's diameter with an uncertainty of 1% or 2%, one should strive for timing that is accurate to 0.1 s or better. However, less accurate data can often be useful. Three observational techniques, as described below, have been used to record asteroid occultations.

Photoelectric Observations

In most instances, the preferred way of recording an occultation is with a photoelectric photometer and a high-speed data recording system. With such equipment, it is routinely possible to determine the times of immersion and emersion to an accuracy of a few millisec. Photoelectric equipment also produces a tangible, objective observational record which can be scrutinized at leisure in order to assess the accuracy of the timing and the reality of various features of the lightcurve. Moreover, photoelectric equipment is capable of detecting significantly smaller brightness changes than is the eye or video equipment, which means that many occultations involving comparatively faint stars will be observable in no other way. These will include almost all occultations involving bright asteroids such as Vesta and Ceres. Signal-to-noise considerations in photoelectric detection of occultations have been thoroughly discussed by Millis and Elliot (1979). Descriptions of photoelectric photometers and data systems especially designed for observing occultations with small portable telescopes have been published by Baron et al. (1983) and Hubbard et al. (1985). Completely satisfactory observations are possible with photometers substantially more rudimentary than those described by these authors, but it is nevertheless true that the primary disadvantages of the photoelectric method are the cost and complexity of the equipment.

Television Recordings

Video recording of occultations is less common than photoelectric recording, but the popularity of this method is growing. A low-light-level camera is attached to the telescope so that the focus falls on the camera vidicon. The video signal from the camera is recorded with a VCR along with time signal and verbal comments on the audio track. Times accurate to within the 0.03 s frame rate can be obtained by slow playback of the videotape with a

0.01 s time display. Since the video field of view is generally several arcmin, requirements for polar alignment and guiding are much less stringent than for photoelectric observations. Moreover, video equipment is more compact than most currently used portable photoelectric systems, making the former easier to transport, especially by airplane. Although not nearly as accurate as in photoelectric records, photometric information can be derived from video records, and relatively shallow events that would be missed by a visual observer can be detected. Several individuals have successfully observed a variety of asteroid occultations with video equipment (D. W. Dunham et al. 1983; E. W. Dunham et al. 1984; Manly 1984).

Visual Methods

Since most amateur observers are not equipped to record occultations photoelectrically or with video equipment, many occultation observations consist of simple visual timings. Normally, a tape recorder is used to record shortwave radio time signals, verbal comments and often a manually generated signal to mark immersion and emersion. While visual occultation observations are generally less accurate and sometimes less reliable than photoelectric and video observations, they are still often quite useful (see Millis and Elliot 1979).

The record shows that visual observers can routinely detect events involving stars at least as bright as the asteroid. Experienced individuals can establish the times of immersion and emersion to within a few tenths of a second, but almost invariably, visual timings will be systematically late—often by substantially more than the expected reaction time. This systematic error can be allowed for in the analysis of the data, as will be discussed later. Furthermore, near the edges of a ground track, timing errors are less serious since a moderate timing error translates into only a small error in the radial dimension of the asteroid. Consequently, visual observers can play a particularly important role in defining the precise track boundaries.

IV. ANALYSIS TECHNIQUES

The methods of analysis appropriate to occultation data are well developed and have been discussed by several authors (see, e.g., Smart 1960; Wasserman et al. 1979; Millis and Elliot 1979; Reitsema et al. 1981; Dunham et al. 1984). We give only a brief outline here. In an occultation, the shadow which the asteroid casts in the light of the occulted star sweeps across the surface of the Earth along the occultation ground track. Because the star is effectively at infinity, the cross section of the shadow, when cut by a plane instantaneously perpendicular to the line connecting the asteroid and star, has the same size and shape as the apparent profile of the asteroid at the time of occultation. By convention, this plane is referred to as the fundamental plane and is defined to pass through the center of the Earth. One then defines an x,y

coordinate system in this plane which moves such that its origin is always at the center of the shadow. The coordinates of an observer at the time of immersion or emersion, projected onto the moving coordinate system, defines a point (ξ', η') on the edge of the shadow. ξ' and η' are given by

$$\xi' = \rho \cos \phi' \sin H - \Delta \cos \delta_a \sin(\alpha_a - \alpha_*) \tag{1}$$

and

$$\eta' = \rho[\cos \delta_* \sin \phi' - \sin \delta_* \cos \phi' \cos H]$$
$$- \Delta[\sin \delta_a \cos \delta_* - \cos \delta_a \sin \delta_* \cos(\alpha_a - \alpha_*)] \tag{2}$$

where α_a, δ_a, α_*, δ_* are the right ascensions and declinations of the asteroid and star, respectively; Δ is the asteroid's geocentric distance in units of the Earth's equatorial radius; ρ is the observer's distance from the center of the Earth (in the same units); ϕ' is the observer's geocentric latitude; and H is the hour angle of the star. By computing ξ' and η' for all observers at both immersion and emersion, one obtains a map of the asteroid's limb profile. Usually an asteroid will rotate only a negligible amount during the time required for its shadow to sweep across all observers. However, combinations of circumstances are possible (rapid rotation, events occurring near stationary points or long ground tracks) for which this effect is significant. In these cases, the derived limb profile is in some sense an average over those faces of the asteroid presented to the Earth during the interval spanned by the total data set.

The completeness of the limb profile map from a particular occultation data set obviously depends on the number of observers and their distribution across the occultation ground track. The degree of coverage can be so dense that the occultation data practically give the limb profile directly, as was the case for the 29 May 1983 occultation by Pallas (Fig. 1). At the other extreme, one has observations from a single site, which give only a lower limit on the asteroid's longest dimension. More typically, one must work with observations from an intermediate number of sites scattered across the track. One such "typical" data set, from an occultation by Ceres (Millis et al. 1987), is shown in Fig. 2. In order best to represent the asteroid's profile, a circle or ellipse is fitted by least squares to the data points. The diameter of the best-fitting circular profile or the lengths and orientation of the semimajor and semiminor axes, if an elliptical profile is assumed, are derived from the least-squares fit, as are corrections in right ascension and declination to the asteroid's ephemeris.

Either the radial residuals or the timing residuals can be minimized in the least-squares solution. Which approach is better depends on the character of the particular data set under consideration. If all the observed times of immer-
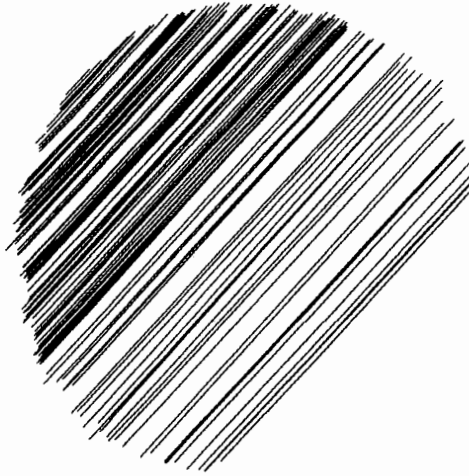
Fig. 1. Chords across 2 Pallas derived from observations of the 29 May 1983 occultation of 1 Vulpeculae (D. W. Dunham et al. 1983).
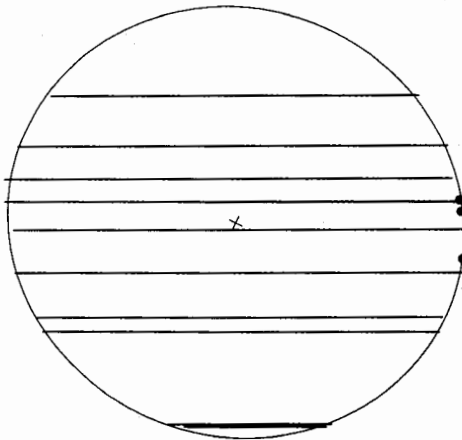
Fig. 2. An elliptical limb profile fitted by least-squares to observations of the 13 November 1984 occultation by 1 Ceres (Millis et al. 1987). Straight lines represent chords across the asteroid derived from sites where both immersion and emersion were recorded. Filled circles are points from sites where only immersion was successfully observed.

sion and emersion are believed to be sufficiently accurate that the residuals primarily reflect real limb irregularities, then minimization of radial residuals is preferred (see, e.g., Millis et al. 1987). If, on the other hand, timing errors are believed to be the dominant cause of departures from the fitted profile, then minimization of timing residuals is appropriate (see, e.g., E. W. Dunham et al. 1984). Additionally, there may be instances, such as the Ceres occultation illustrated in Fig. 2, where observations near the edge of the ground track are critical in distinguishing between a circular and an elliptical limb profile. Because observations near the edge of the track could have large timing errors and still produce comparatively small radial residuals, one may wish to do the solution both ways for such cases (Millis et al. 1987).

Analysis of occultation data is often complicated by the probable presence of systematic timing errors in some of the observations. As was mentioned earlier, visual observers, for example, are able to measure the duration of an occultation more accurately than the absolute times of immersion and emersion (Millis et al. 1985). Accordingly, when combining visual observations with photoelectric and video data, the response times of the individual visual observers have often been included as additional free parameters in the least-squares solution (see, e.g., Millis et al. 1983a). This procedure has the effect of allowing the visual chords to slide in time relative to the photoelectric and video data while holding the lengths of the visual chords constant. A better fit to the data is obtained, but the result must be evaluated critically to insure that the magnitudes of the shifts are reasonable and that they are justified by the surrounding photoelectric or video measurements. One must bear in mind that large timing errors are sometimes present in photoelectric and video data because of blunders by the observer, equipment malfunction or misidentification of the features in the occultation lightcurve that correspond to immersion and emersion.

Observations of a single occultation yield only the dimensions of that face of the asteroid seen at the time of the occultation. (The same is true of a single measurement by any other technique, though this fact is often not stressed.) Ideally, one would like to observe several occultations by the same minor planet at a variety of aspects, but only for Pallas have even two occultations been well observed (see Drummond and Cocke 1988). Usually one must resort to other means of evaluating how representative the results of a single event are of the body's overall three-dimensional figure. The rotational lightcurve is one piece of information that is available for many asteroids which provides a clue to an asteroid's shape (see the chapter by Magnusson et al.). If the body displays the same low-amplitude lightcurve regardless of ecliptic longitude, then its shape is very likely to be approximately that of a sphere or an oblate spheroid with small obliquity. In either case, a single well-observed occultation gives directly a good representation of the asteroid's overall figure. If the lightcurve amplitude is large, then estimation of the three-dimensional shape is less certain. However, a model can be constructed based

on the occultation profile, the phase of the lightcurve at the time of occultation, and the shape and amplitude of the lightcurve.

V. RESULTS

Diameter Determinations

Table I summarizes those asteroid occultations for which two or more chords have been observed. Consequently, the table includes virtually all confirmed events, although, in some cases, meaningful diameter determinations were not possible because the chords were too closely spaced. We are excluding single-chord events because they give no information about an asteroid's shape and give only a lower limit for the mean diameter. However, single-chord occultations are astrometrically useful, and sometimes a lower limit has some value. For a complete list of observed events, including those with only one chord, see D. W. Dunham et al. (1989).

The dates of occultation and names of the asteroids involved are given in the first two columns of Table I. The taxonomic classes of the asteroids, taken primarily from Tholen (1984), are listed in column 3, followed in the next column by their orbital zones. Zones I through IV span the main belt, progressing from the inner edge outward (see Zellner [1979] for exact definitions of zone boundaries). All asteroids for which accurate occultation data exist have typical main-belt orbits except Pallas, whose orbit has an abnormally large inclination. The numbers of photoelectric/video (p) and visual (v) observations of each occultation are given in column 5. Column 6 contains the asteroids' diameters as derived from the occultation data. The quoted uncertainties are taken from the original papers listed in the last column or are estimates based on the least-squares solutions, the completeness of observational coverage and the amplitude of the objects' rotational lightcurve. An indication of the quality of the occultation diameter determination is given in column 7. Only for quality A and some B events are the diameters firmly established from the occultation observations. The asteroids' published radiometric diameters are listed in column 8. Where possible, we have quoted results from IRAS and those values are accompanied by error estimates (Matson et al. 1986). Otherwise, TRIAD (Bowell et al. 1979) values are given.

One of the primary objectives of measuring asteroid diameters by the occultation technique has been to permit a better calibration of the radiometric method of size determination. Indeed, two recalibrations have been performed based on occultation data (Brown et al. 1982; Lebofsky et al. 1986). One might conclude, on the basis of the generally satisfactory agreement between the two types of diameters in Table I, that this task has been completed. In fact, there is room for very significant improvement. Brown (1985) has shown that the standard thermal model will yield effective radiometric diameters which are substantially in error for asteroids that are significantly aspherical,

TABLE I

Asteroid Occultation Results

Date	Asteroid	Class[a]	Zone[b]	No. Obs.	Occ. Diam. (km)	Quality[c]	IR[d] Diam. (km)	Reference
19 Feb 61	2 Pallas	B	Z	1p/1v	>430	E	538 ± 12	Sinvhal et al. 1962
24 Jan 75	433 Eros	S	A	8v	17 ± 5	B	20	O'Leary et al. 1976
5 Mar 77	6 Hebe	S	I	2v	186.9 ± 9	C	192 ± 4	Taylor and Dunham 1978
29 May 78	2 Pallas	B	Z	7p	538 ± 12	A	523 ± 20	Wasserman et al. 1979
7 Jun 78	532 Herculina	S	II	1p/2v	217 ± 15	C	231 ± 4	Bowell et al. 1978
19 Jul 78	3 Juno	S	II	2v	>256	E	267 ± 5	Sheffer 1979
11 Dec 78	18 Melpomene	S	I	6p/2v	148 ± 10	A	148 ± 3	Dunham 1979a
17 Aug 79	51 Nemausa	CU	I	2p	153 ± 8	B	153 ± 3	Kristensen 1981
17 Oct 79	65 Cybele	P	IV	1p/2v	230 ± 16	B	245 ± 6	Taylor 1981
11 Dec 79	3 Juno	S	II	15p/3v	267 ± 5	A	244 ± 12	Millis et al. 1981
11 Dec 79	9 Metis	S	I	2v	>141	E	168	Dunham 1979b
4 Sep 80	78 Diana	C	II	10v	116 ± 18	D	125 ± 3	Dunham 1981a
10 Oct 80	216 Kleopatra	M	II	4p/5v	137 ± 15	A	140 ± 5	Dunham 1981a
24 Nov 80	134 Sophrosyne	C	II	5v	107 ± 5	B	122 ± 21	Dunham 1981a
19 Mar 81	48 Doris	CG	III	3v	219 ± 25	D	225 ± 11	Dunham 1982
7 Aug 81	18 Melpomene	S	I	1p?/2v	>126	E	148 ± 3	Dunham 1981b
7 Oct 81	88 Thisbe	CF	II	3p/9v	232 ± 12	A	214	Millis et al. 1983a
23 Mar 82	386 Siegena	C	III	2p	>160	E	173 ± 3	Stamm 1986
14 Nov 82	690 Wratislavia	CPF	III	2v	>156	E	140 ± 4	Marsden 1982
15 Nov 82	375 Ursula	C	III	2p/3v	216 ± 10	A	—	Millis et al. 1984a
22 Nov 82	93 Minerva	CU	II	5p/5v	170.8 ± 1.4	B	146 ± 5	Millis et al. 1985

Date	Asteroid							Reference
19 Jan 83	106 Dione	G	III	8v	147 ± 3	B	152 ± 3	Kristensen 1984a
3 Feb 83	19 Fortuna	G	I	1p/1v	>137	E	226	Marsden 1983
11 Mar 83	19 Fortuna	G	I	3v	$149? \pm 50?$	B	226	Dunham and Bode 1984
26 Apr 83	52 Europa	CF	III	1p?/5v	278 ± 30	D	312 ± 7	Unpublished
29 May 83	2 Pallas	B	Z	26p/114v	523 ± 5	A	523 ± 20	Dunham et al. 1983
15 Jun 83	83 Beatrix	X	I	2p	>68	E	84 ± 2	Bash 1984
11 Sep 83	51 Nemausa	CU	I	{ 6p	151.6 ± 6	A	153 ± 3	Dunham et al. 1984
				{ 6p/26v	137 ± 8	A	153 ± 3	Dunham and Dunham 1988
19 Feb 84	9 Metis	S	I	1p/6v	190 ± 19	B	168	Kristensen 1984b
11 May 84	230 Athamantis	S	I	4v	125 ± 5	E	113 ± 2	Stamm 1984
16 Sep 84	47 Aglaja	C	III	3p/10v	137.2 ± 1.4	B	133 ± 8	Millis et al. 1984b
13 Nov 84	1 Ceres	G	II	13p	932.6 ± 5.2	A	913 ± 43	Millis et al. 1987
11 Apr 85	129 Antigone	U	III	3p/2v	113 ± 4	D	125 ± 4	Wasserman et al. 1986
15 Apr 85	275 Sapientia	X	II	1p/1v	103 ± 12	B	121 ± 4	Stamm 1985a
24 Oct 85	2 Pallas	Z	I	3v	>485	E	523 ± 20	Stamm 1985b
24 Jan 87	471 Papagena	S	III	2p/3v	127 ± 8	B	139 ± 3	Stamm 1988
16 Mar 87	511 Davida	C	III	1p/1v	>241	E	337 ± 5	Stamm 1988
8 Dec 87	324 Bamberga	C	II	4p/9v	228.2 ± 2.0	B	242 ± 7	Millis et al. 1988
8 Mar 88	121 Hermione	C	IV	3v	>140	E	217 ± 4	Blow 1988
				2v				

[a] From Tholen (1984) if available, otherwise from TRIAD (Bowell et al. 1979).

[b] As defined by Zellner (1979).

[c] A: Same as B, but combined with known pole orientation and/or lightcurve to obtain average three-dimensional shape; B: Coverage more than half the asteroid. Quoted diameter is derived from least-squares fit to the occultation data; C: Like D, but elliptical shape determined from pole orientation and lightcurve fitted to data; D: Coverage is less than half of asteroid. Size and shape are quite uncertain; E: Average length of closely spaced chords.

[d] From IRAS (Matson et al. 1986), if available, otherwise from TRIAD (Bowell et al. 1979).

while Spencer (1988) has suggested that errors as large as 40% can result from failure of the standard thermal model to account adequately for the effects of surface roughness, rotation and heliocentric distance. Consequently, accurately measured effective diameters are needed for a much broader sample of asteroids in order to assess the dependence of the radiometric method on these various parameters. The asteroids in Table I clearly are not a representative sample of the entire asteroid population. Most of the well-observed events involve C (or related) types. There are no E types listed in Table I, and the two events involving M types suffered from either poor observational coverage or an unfavorable aspect (minimum of a large-amplitude lightcurve). Only three observations were made of each of the two occultations by outer-belt (zone IV) asteroids.

Shape

While radar, speckle interferometry and photometry do give clues to an object's shape, occultation observations without question provide the most accurate measures of asteroid shape which are currently possible short of a flyby or rendezvous mission. In view of the violent collisional history of main-belt asteroids, pronounced departures from symmetric limb profiles might be expected for many minor planets. However, evidence of global-scale limb irregularities has been seen in the occultation data for very few objects. In all cases in Table I for which there are accurately timed observations from sites well distributed across the ground track, it has been possible to fit the data satisfactorily with either a circular or elliptical limb profile. In the case of Ceres, for example, the observed limb profile agrees well with that expected for a body in hydrostatic equilibrium (Millis et al. 1987).

On the other hand, it should be emphasized that the occultation data do give conclusive evidence of real limb irregularities. Typically, in well-observed occultations, radial residuals between the fitted profile and the observations have been a few (i.e., 0 to 5) km. Most authors have argued that these residuals are primarily due to asteroidal topography and not to timing errors in the observations or uncertainties in the locations of the observers (see, e.g., Millis et al. 1981,1987; Dunham et al. 1983). Hence, an important result which has emerged from occultation observations is that asteroids in the diameter range from 100 to 1000 km apparently are rough on a scale of a few km. In fact, the residuals derived from occultation data place only a lower limit on the vertical scale of the topography, because the measurements sample only relatively widely spaced points around the limb, because the limb profile itself is simply the envelope of the higher terrain near the limb (Thomas 1988) and because often some chords are allowed to slide as discussed in Sec. IV.

It is of interest to compare the degree of limb irregularity observed for the asteroids with that seen in other solar system objects of comparable size.
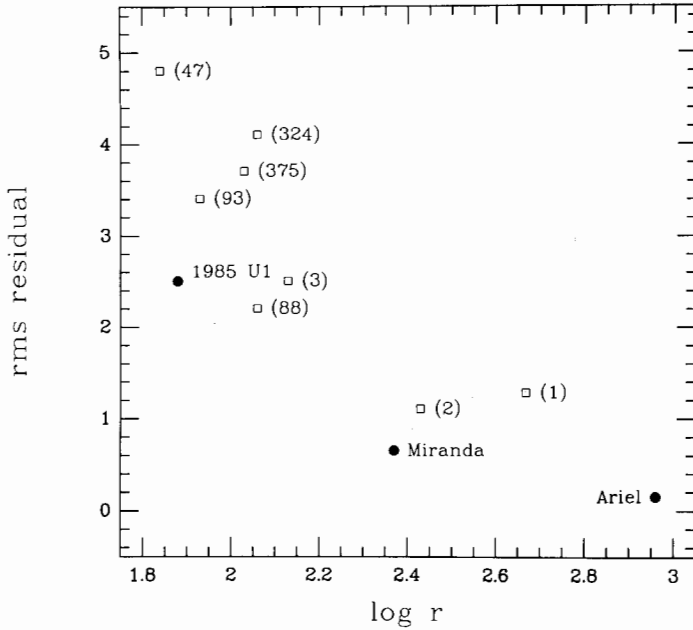
Fig. 3. Mean residuals of the observed limb, with respect to the best-fitting circular or elliptical limb profile, plotted as a function of the log of the mean radius of the body. Filled circles are for three of the Uranian satellites; squares are for the asteroids whose numbers are indicated.

In Fig. 3, rms radial residuals for several asteroids (expressed as a percent of the object's mean radius) are plotted as a function of the log of the object's mean radius. The rms residuals were derived from data given in the papers referenced in Table I. Also plotted are comparable data for 1985 U1, Miranda and Ariel from Thomas and Veverka (1987) and Thomas (1988) who have fitted smooth limb profiles to Voyager images of the Uranian satellites. The degree of limb irregularity appears to be greater for the asteroids than for the icy satellites of Uranus, which no doubt reflects the greater structural strength of the former class of objects. When expressed as a percentage of the radius, the rms residual increases as the size of the body decreases, but the absolute vertical scale of limb irregularities seen on those asteroids plotted in the figure is on the order of a few km, regardless of the size of the object.

Possible indications of very large limb irregularities exist in the occultation data set for two asteroids. In these two cases, 93 Minerva (Millis et al. 1985) and 324 Bamberga (Millis et al. 1988), visual observers, who, on the basis of the least-squares solution for the asteroid's limb profile, should have been in the ground track, reported that no occultation occurred. Because these

observers were closer to the expected edge of the track than all successful observers, their negative reports cannot be discounted. If they are correct, both Minerva and Bamberga have substantial chunks missing, presumably as a result of past major collisions.

Density

Another major goal of occultation research has been to make possible density determinations of useful accuracy for those minor planets whose masses are known. Because density provides clues to both composition and origin, it is extremely important to measure this parameter for asteroids. Unfortunately, the masses of only a few asteroids are known. Vesta's mass has been derived from this body's perturbations of the orbit of 197 Arete. Similarly, the masses of Ceres and Pallas have been determined from their mutual perturbations and from the action of Vesta on Ceres (see Schubart and Matson 1979). Scholl et al. (1987) measured the mass of 10 Hygiea from its effect on the orbit of 829 Academia, but the value they derived is uncertain by 50%. Most recently, Standish (1989; see also the chapter by Hoffman) has used Earth–Mars ranging data to derive the masses of Ceres, Pallas and Vesta. The results of Schubart and Matson and of Scholl et al. are summarized in Table II. Standish finds that Ceres is 10 to 20% less massive and Pallas 20 to 40% more massive than do Schubart and Matson; the mass of Vesta, he finds to be nearly the same.

The diameters of Pallas and Ceres are known from occultations (Wasserman et al. 1979; Millis et al. 1987). Densities based on these diameters and the masses determined by Schubart and Matson are given in Table II. If Standish's values for the masses of these two objects are adopted, the densities would, of course, change proportionally. Additionally, Drummond and Cocke (1989), based on two occultation data sets, have derived smaller dimensions for Pallas than did Wasserman et al. The corresponding density is about 20% greater than the figure quoted in Table II. Three values for the density of Vesta

TABLE II
Asteroid Density

Object	Mass (10^{-10} $M_\odot$)	Density (g cm^{-3})	Reference
1 Ceres	5.9 ± 0.3[a]	2.7 ± 0.14	Millis et al. 1987
2 Pallas	1.08 ± 0.22[a]	2.6 ± 0.5	Millis and Elliot 1979
4 Vesta	1.38 ± 0.12[a]	3.62 ± 0.35	Drummond et al. 1988
		3.3 ± 1.5	Schubart and Matson 1979
		2.4 ± 0.3	Cellino et al. 1987
10 Hygiea	0.47 ± 0.23[b]	2.05 ± 1	Scholl et al. 1987

[a]From Schubart and Matson 1979.
[b]From Scholl et al. 1987.

are listed in the table: one based on the Drummond et al. (1988) diameter determination from speckle observations, one based on the average of the radiometric and polarimetric diameters and one based on analysis of rotational lightcurves by Cellino et al. (1987). The latter figure is dependent on the rather dubious assumption that the shape of Vesta is determined wholly by self gravitation. The density quoted for 10 Hygiea is from Scholl et al., who adopted the radiometric diameter from the TRIAD file (Bowell et al. 1979). Except, perhaps, for Vesta, the uncertainty in the densities of the asteroids listed in Table II is determined primarily by the uncertainty in the masses, not by the uncertainty in the diameters. In any case, the densities of Ceres and Pallas are sufficiently well constrained to conclude that these two bodies are primarily rocky in composition. Vesta also is probably rocky, but a well-observed occultation would permit the actual value of its density to be more firmly established.

Minor Planet Satellites

In their chapter, Weidenschilling et al. outline the evidence that some asteroids may have satellites. While we will not repeat the details here, we note that some of the evidence and much of the impetus for renewed interest in this topic has come from occultation observations in which observers usually outside the main ground track reported that the target star was briefly occulted by objects other than the asteroid itself (see, e.g., Bowell et al. 1978; Williamon 1980; Arlot et al. 1985). Regrettably, in the late 1970s several satellite detections were claimed which were not well justified by the underlying occultation observations. While this brief outbreak of "satellite fever" quickly passed, it left the perception that occultation observations are inherently unreliable means of detecting minor planet satellites and, therefore, will not play a significant role in establishing the reality and frequency of minor planet satellites. This perception is in error.

Clearly, the best hope of gaining incontrovertible evidence of the existence of a contact-binary-type asteroidal system in the forseeable future will be from a densely observed occultation. Likewise, densely monitored occultations in which no secondary events are seen further constrain, in a statistical sense, the frequency of occurrence of satellites. It is worth noting that occultation observations are capable of detecting satellites which are too faint and/or too close to their primary to be found by either the speckle or direct-imaging techniques. We wish to emphasize that photoelectric occultation observations made at a single site under good sky conditions are capable of establishing, without independent confirmation, whether a particular feature in the photometric record results from a true occultation of the star rather than from an obscuration of both star and asteroid. In an occultation, the signal will fall to the level of the sky plus asteroid, while in a total or partial obscuration due to clouds, airplanes, guiding errors, etc., it almost certainly will fall to some other level. If the star and asteroid are significantly different in color and the

observations are made in two widely separated passbands with a two-channel photometer, the reality of lightcurve features can be doubly confirmed. Therefore, occultation observers equipped with photoelectric photometers should establish accurately the contributions to their observed signal from the sky, the star and the asteroid, and they should extend their coverage of an occultation from many minutes before to many minutes after the predicted time of the event. In this way, either a minor planet satellite eventually will be unequivocally detected, or it will be established through continued failure to find them that such bodies, if they exist at all, are inconsequential freaks.

VI. THE FUTURE

Observational Strategy

There are two sets of criteria that must be addressed when deciding which of the large number of potential asteroid occultations identified each year to pursue seriously. One set is pragmatic in nature (i.e., what are the chances that the occultation can be observed with sufficient coverage to realize the scientific objectives of the enterprise). The other set of criteria addresses the scientific potential of the occultation (i.e., is the object interesting and important).

Many practical matters must be considered in evaluating a future occultation including the duration of the occultation, the relative brightnesses of star and asteroid, the proximity of the Moon, the probability of clear sky and the availability of appropriate observing sites. At least as important as these, however, is the accuracy to which the location of the occultation ground track can be predicted. If an adequate number of observers cannot with certainty be located within the track, then the occultation usually should not be given serious consideration. Millis and Elliot (1979) introduced a parameter Q as a measure of the predictability of an occultation. This parameter is given by $Q = 2\sigma\Delta/d$, where σ is the expected uncertainty in the predicted angular separation of the star and asteroid at closest approach (expressed in radians), Δ is the geocentric distance of the asteroid (in km), and d is the estimated diameter of the asteroid (km). Stated another way, Q is twice the ratio of the angular uncertainty in the predicted separation of star and asteroid at closest approach to the angular diameter of the asteroid. Predictions from Lowell Observatory (see, e.g., Wasserman et al. 1987) have routinely included a tabulation of this parameter. These investigators, by convention, have assumed σ to be 0.1 arcsec, a value consistently achieved in predictions based on plates taken with the Carnegie Double Astrograph at Lick Observatory. Past efforts to observe events for which Q was greater than 2 usually have not been successful, and almost all of the truly well-observed asteroid occultations have had values of Q less than 1. The lesson from the past decade of concerted effort to observe asteroid occultations, then, is "concentrate on small-Q events" (i.e., large angular diameter asteroids).

Preparation of a list of asteroids whose occultations are important on astrophysical grounds is a subjective undertaking. Nevertheless, there are some obvious candidates for such a list. Vesta is the one remaining asteroid whose mass is accurately known, but whose diameter has not been measured by the occultation technique. Obviously, it would be desirable to compute with certainty the density of this spectrally unique minor planet. Other intrinsically interesting objects are those for which radar observations and/or photometry indicate unusual shape. 624 Hektor (Hartmann 1979) and 216 Kleopatra (Ostro et al. 1986) are prime examples, though Hektor's angular diameter is so small as to render prediction of its occultations difficult. As has been noted earlier, we need to observe occultations involving asteroids spanning a broad range in taxonomic class and orbital zone. One can list other criteria by which important target asteroids can be identified. However, it is probably premature to select occultation targets primarily on the basis of the intrinsic importance of the asteroid involved. We have only begun to study the asteroids by the occultation technique. Of the 18 asteroids listed by Millis and Elliot in 1979 as high-priority candidates for occultation measurements, occultation data of sufficient quality to warrant inclusion in Table I have since been obtained for only 7. Too few minor planets have been probed at the very high resolution possible with occultations to identify with confidence in advance those that will yield important results. Many surprises no doubt await us, but we can discover those surprises only by efficiently and thoroughly observing as many events as possible. In the opinion of the authors, that means concentrating observational efforts on those occultations for which circumstances indicate the highest probability of success.

Potential for Improving Predictions

The major astrometric catalogs described in Sec. II do not include hundreds of thousands of 10th- to 12th-magnitude stars, occultations of which could be readily observed. The Space Telescope Guide Star Catalog that is expected to become available in 1989 will include recent positions of all of these stars accurate to 1 arcsec or better. This promises to result in many more predicted asteroid occultations and will obviate the need for astrographic catalog and special photographic searches. The other astrometric catalogs will be needed since the Guide Star Catalog will not include stars brighter than 9th magnitude, and because the astrometric catalogs are more accurate. The U.S. Naval Observatory's Zodiacal Zone (ZZ) Catalog, expected to become available also in 1989, will be a considerable improvement over AGK3 and SAO data. The ZZ Catalog, constructed to support the Galileo mission, seeks to improve the positions and proper motions of all SAO stars within 13° of the ecliptic. These two catalogs, combined with recently improved orbital elements of the asteroids, will result in more accurate preliminary predictions from catalog searches.

With more comprehensive and improved searches, we will know better

which events should be refined with last-minute astrometry. The ZZ Catalog will provide a much better reference frame for astrometrists than the SAO or AGK3R. Using the former, plates of the asteroid (and target star, if it is not in the ZZ Catalog) taken a month or more in advance should locate the path within about 300 km, allowing plenty of time to organize observers. The ZZ Catalog, being much denser than AGK3R or SRS/Perth 70, will also allow use of astrometric telescopes with smaller fields of view for both preliminary and last-minute astrometry. If more astrometrists who currently observe asteroids routinely would devote a small fraction of their effort to photographing particular asteroids at times needed to improve occultation predictions, this work would greatly benefit.

Nothing is more disheartening to an observer than to succeed in deploying equipment under clear skies only to see the asteroid miss the star because of errors in the predictions. Disillusionment caused by one or two such experiences undoubtedly has depleted the ranks of occultation observers. Is there hope of achieving significant improvement in the astrometry on which final occultation predictions are based? Perhaps. Experiments, stimulated by the work of Monet and Dahn (1983), are currently in progress at the Massachusetts Institute of Technology and the Lowell Observatory aimed at using CCD's for obtaining high-precision measurements of the relative position of a star and asteroid during the last few days prior to an occultation. This approach avoids problems inherent in the photographic process but has others of its own. For example, in order to cover a sufficiently large area, the CCD must be operated in a strip-scanning mode (see Gehrels et al. 1986), and overlapping scans must be carefully registered. It remains to be seen what level of astrometric precision will be possible with CCD strip-scanning astrometry.

The Hubble Space Telescope is another potential source of very high-accuracy astrometry. According to Duncombe et al. (1982), positional measurements with an uncertainty of only 0.002 arcsec rms will be possible with the Fine Guidance Sensors on H.S.T. Obviously, the Space Telescope will not be used routinely for occultation predictions, but this long-awaited facility could contribute in a powerful way to the prediction of especially important events.

The Need for More Observers

It would be incorrect to conclude from the preceding section that the quality of available predictions is the factor primarily limiting progress in asteroid occultation studies. Such may have been the case a decade ago, but, at present, progress is contrained mostly by an inadequate number of appropriately equipped observers—particularly outside the North American continent. Visual observers have contributed importantly to occultation research and will continue to do so. However, it is important that more individuals equip themselves with the photoelectric or video equipment required for precise timing of occultations. Wider use of such instruments, which are now available com-

mercially at relatively modest cost, holds the key to a major advance in asteroid occultation research. Our goal should be a feasible number of occultations densely and accurately observed, not large numbers of events recorded at one or two random sites.

REFERENCES

Arlot, J. E., Lecacheux, J., Richardson, C. H., and Thuillot, W. 1985. A possible satellite of (146) Lucina. *Icarus* 61:224–231.

Baron, R. L., Dunham, E. W., and Elliot, J. L. 1983. A portable telescope, photometer, and data-recording system. *Publ. Astron. Soc. Pac.* 95:925–937.

Bash, F. N. 1984. Observatory report, University of Texas at Austin. *Bull. Amer. Astron. Soc.* 16:333–356.

Blow, G. L. 1988. Solar system occultations and appulses. *Roy. Astron. Soc. New Zealand, Occultation Section Circular* CQ87/4, pp. 5–10.

Bowell, E., McMahon, J., Horne, K., A'Hearn, M. F., Dunham, D. W., Penhallow, W., Taylor, G. E., Wasserman, L. H., and White, N. M. 1978. A possible satellite of Herculina. *Bull. Amer. Astron. Soc.* 10:594 (abstract).

Bowell, E., Gehrels, T., and Zellner, B. 1979. Magnitudes, colors, types, and adopted diameters of the asteroids. In *Asteroids,* ed. T. Gehrels (Tucson: Univ. of Arizona Press), pp. 1108–1129.

Brown, R. H. 1985. Ellipsoidal geometry in asteroid thermal models: The standard radiometric model. *Icarus* 64:53–63.

Brown, R. H., Morrison, D., Telesco, C. M., and Brunk, W. E. 1982. Calibration of the asteroid scale using occultation diameters. *Icarus* 52:188–195.

Cellino, A., Zappalà, V., Di Martino, M., Farinella, P., and Paolicchi, P. 1987. Flattening, pole, and albedo features of 4 Vesta from photometric data. *Icarus* 70:546–565.

Dollfus, A. 1971. Diameter measurements of asteroids. In *Physical Studies of Minor Planets,* ed. T. Gehrels, NASA SP-267, pp. 25–31.

Drummond, J. D., and Cocke, W. J. 1989. Triaxial ellipsoid dimensions and rotational pole of 2 Pallas from the two stellar occultations. *Icarus,* in press.

Drummond, J., Eckart, A., and Hege, E. K. 1988. Speckle interferometry of asteroids IV. Reconstructed images of 4 Vesta. *Icarus* 73:1–14.

Duncombe, R. L., Benedict, G. F., Hemenway, P. D., Jefferys, W. H., and Shelus, P. J. 1982. Astrometric observations with the Space Telescope. In *The Space Telescope Observatory,* ed. D. N. B. Hall, NASA CP-2244, pp. 114–120.

Dunham, D. W. 1979a. Duplicity of both (18) Melpomene and SAO 114159 discovered during occultation. *Occultation Newsletter* 2:12–16.

Dunham, D. W. 1979b. Juno occultation best-observed yet, even visually; Soviets claim satellite of Cybele; first international asteroidal occultation expedition (for Metis) partly successful; other late 1979 occultation attempts. *Occultation Newsletter* 2:75–77.

Dunham, D. W. 1981a. Recently observed planetary occultations. *Occultation Newsletter* 2:139–143.

Dunham, D. W. 1981b. IOTA news. *Occultation Newsletter* 2:177–178.

Dunham, D. W. 1982. Observations of asteroidal occultations and appulses. *Occultation Newsletter* 2:201.

Dunham, D. W. 1988. Planetary occultations of stars in 1988. *Sky and Telescope* 75:70–71.

Dunham, D. W., and Bode, H. J. 1984. IOTA/ES news. *Occultation Newsletter* 3:162.

Dunham, D. W., Van Flandern, T. C., Millis, R. L., Chapman, C. R., Maley, P. D., and Poven-mire, H. 1983. The size and shape of (2) Pallas from its occultation of 1 Vulpeculae on 1983 May 29. *Bull. Amer. Astron. Soc.* 15:822 (abstract).

Dunham, D. W., Dunham, J. B., and Maley, P. M. 1989. Observed asteroidal occultations. In *Tables of Minor Planets*, eds. E. Tedesco and F. Pilcher. In preparation.

Dunham, E. W., Baron, R. L., Conner, S., Dunham, D. W., Dunham, J. B., Schneider, G., Cohen, H. L., Helms, V. T., Croom, M., and Safko, J. 1984. Results from the occultation of 14 Piscium by 51 Nemausa. *Astron. J.* 89:1755–1758.

Gehrels, T., Marsden, B. G., McMillan, R. S., and Scotti, J. V. 1986. Astrometry with a scanning CCD. *Astron. J.* 91:1242–1243.

Goffin, E. 1988. 1988 asteroidal occultation supplement for North American observers. *Occultation Newsletter* 4, 88NAAOS-1-88NAAOS-36.

Hartmann, W. K. 1979. Diverse puzzling asteroids and a possible unified explanation. In *Asteroids,* ed. T. Gehrels. (Tucson: Univ. of Arizona Press), pp. 466–479.

Hubbard, W. B., Frecker, J. E., Gehrels, J.-A., Gehrels, T., Hunten, D. M., Lebofsky, L. A., Smith, B. A., Tholen, D. J., Vilas, F., Zellner, B., Avey, H. P., Mottram, K., Murphy, T., Varnes, B., Carter, B., Nielsen, A., Page, A. A., Fu, H. H., Wu, H. H., Kennedy, H. D., Waterworth, M. D., and Reitsema, H. J. 1985. Results from observations of the 15 June 1983 occultation by the Neptune system. *Astron. J.* 90:655–667.

Kristensen, L. K. 1981. The size of 51 Nemausa. *Astron. Astrophys. Suppl.* 44:375–377.

Kristensen, L. K. 1984a. The diameter of (106) Dione. *Astr. Nachr.* 305:207–211.

Kristensen, L. K. 1984b. (9) Metis okkultationen den 19 februar 1984. *Astronomi & Rumfart* Maj-Jun 1984, pp. 76–78.

Lebofsky, L. A., Sykes, M. V., Tedesco, E. F., Veeder, G. J., Matson, D. L., Brown, R. H., Gradie, J. C., Feierberg, M. A., and Rudy, R. J. 1986. A refined "standard" thermal model for asteroids based on observations of 1 Ceres and 2 Pallas. *Icarus* 68:239–251.

Manly, P. L. 1984. Television in amateur astronomy. *Astronomy* 12:50–53.

Marsden, B. G. 1982. Occultation of BD + 24°522 by (690) Wratislavia. *IAU Circ.* No. 3747.

Marsden, B. G. 1983. Occultation of AGK3 + 11°201 by (19) Fortuna. *IAU Circ.* No. 3776.

Matson, D. L., Veeder, G. J., Walker, R. G., Fowler, J. W., Chillemi, J. R., Lebofsky, L. A., and Tedesco, E. F. 1986. IRAS asteroid and comet catalogs. In *IRAS Asteroid and Comet Survey,* Preprint Version No. 1, Part III, ed. D. L. Matson (Pasadena: Jet Propulsion Laboratory), pp. 1–84.

Millis, R. L. 1986. Occultation studies with small telescopes. In *Instrumentation and Research Programmes for Small Telescopes,* eds. J. B. Hernshaw and P. L. Cottrell (Dordrecht: D. Reidel), pp. 199–211.

Millis, R. L., and Elliot, J. L. 1979. Direct determination of asteroid diameters from occultation observations. In *Asteroids,* ed. T. Gehrels (Tucson: Univ. of Arizona Press), pp. 98–118.

Millis, R. L., Wasserman, L. H., Bowell, E., Franz, O. G., White, N. M., Lockwood, G. W., Nye, R., Bertram, R., Klemola, A., Dunham, E., Baron, R. L., Elliot, J. L., Harris, A., Young, J. W., Faulkner, J., Stanton, R., Reitsema, H. J., Hubbard, W. B., Zellner, B., Lebofsky, L., Cruikshank, D. P., Macknik, L. S., Becklin, E. E., Morrison, D., Lonsdale, C. J., Kunkle, T. D., Lee, T., Gatley, I., A'Hearn, M. F., DuPuy, D. L., Nolthenius, R., Ford, H., McKenna, D., Placova, Z., Horne, K., Sandmann, W., Taylor, G. E., and Tucker, R. 1981. The diameter of Juno from its occultation of AG + 0°1022. *Astron. J.* 86:306–313.

Millis, R. L., Wasserman, L. H., Franz, O. G., White, N. M., Bowell, E., Klemola, A., Elliott, R. C., Smethells, W. G., Price, P. M., McKay, C. P., Steel, D. I., Everhart, E., and Everhart, M. 1983a. The diameter of 88 Thisbe from its occultation of SAO 187124. *Astron. J.* 88:229–238.

Millis, R. L., Wasserman, L. H., Bowell, E., Franz, O. G., and Klemola, A. 1983b. Asteroid occultations—progress and prospects. *Bull. Amer. Astron. Soc.* 15:882 (abstract).

Millis, R. L., Wasserman, L. H., Bowell, E., Franz, O. G., Klemola, A., and Dunham, D. W. 1984a. The diameter of 375 Ursula from its occultation of AG + 39°303. *Astron. J.* 89:592–596.

Millis, R. L., Wasserman, L. H., Williamon, R. M., Dunham, D. W., Manly, P. L., Olson, R. W., Baggett, W. E., Maley, P. D., Zeigler, K. W., and Klemola, A. R. 1984b. The occultation diameter of 47 Aglaja. *Bull. Amer. Astron. Soc.* 16:1027 (abstract).

Millis, R. L., Wasserman, L. H., Franz, O. G., Bowell, E., and Klemola, A. 1984c. Occulta-

tions of stars by solar system objects. V. A photographic search for occultations by selected asteroids in 1984. *Astron. J.* 89:698–701.

Millis, R. L., Wasserman, L. H., Bowell, E., Franz, O. G., Nye, R. A., Osborn, W., and Klemola, A. 1985. The occultation of AG + 29°398 by 93 Minerva. *Icarus* 61:124–131.

Millis, R. L., and 41 others. 1987. The size, shape, density, and albedo of Ceres from its occultation of BD + 8°471. *Icarus* 72:507–518.

Millis, R. L., Wasserman, L. H., Franz, O. G., Bowell, E., Nye, R., Thompson, D. T., White, N. M., Hubbard, W. B., Eplee, R. E., Lebofsky, L. A., Marcialis, R. L., Greenberg, R. J., Hunten, D. M., Reitsema, H. J., Dunham, D. W., Maley, P., Klemola, A. R., Yeomans, D. K., and Qian Bochen. 1988. Observations of the 8 December 1987 occultation by 324 Bamberga. Asteroids II, Abstract Booklet, 8–11 March, Tucson, Arizona.

Monet, D. G., and Dahn, C. C. 1983. CCD astrometry. I. Preliminary results from the 4-M/CCD parallax program. *Astron. J.* 88:1489–1507.

Nather, R. E., and Evans, D. S. 1970. Photoelectric measurement of lunar occultations. I. The process. *Astron. J.* 75:575–582.

O'Leary, B., Marsden, B. G., Dragon, R., Hauser, E., McGrath, M., Backus, P., and Robkoff, H. 1976. The occultation of K Geminorum by Eros. *Icarus* 28:133–146.

Ostro, S. J., Campbell, D. B., and Shapiro, I. I. 1986. Detection of 12 asteroids from Arecibo. *Bull. Amer. Astron. Soc.* 18:796 (abstract).

Reitsema, H. J., Hubbard, W. B., Zellner, B. H., and Lebofsky, L. A. 1981. High-speed photometry of the 11 December 1979 Juno occultation. *Astron. J.* 86:121–126.

Scholl, H., Schmadel, L. D., and Roser, S. 1987. The mass of the asteroid (10) Hygiea derived from observations of (829) Academia. *Astron. Astrophys.* 179:311–316.

Schubart, J., and Matson, D. L. 1979. Masses and densities of asteroids. In *Asteroids*, ed. T. Gehrels (Tucson: Univ. of Arizona Press), pp. 84–97.

Sheffer, Y. 1979. More on Juno. *Occultation Newsletter* 2:27.

Sinval, S. D., Sanwal, N. B., and Pande, M. C. 1962. Observations of the occultation of BD5°5863 by Pallas. *The Observatory* 82:16–17.

Smart, W. M. 1960. *Textbook in Spherical Astronomy*, 4th ed. (London: Cambridge Univ. Press).

Spencer, J. R. 1988. A realistic asteroid thermal model, including the effects of surface roughness and thermal inertia. Asteroids II Abstract Booklet, 8–11 March, Tucson, Arizona.

Stamm, J. 1984. Observations of asteroidal appulses and occultations. *Occultation Newsletter* 3:185–187.

Stamm, J. 1985a. Observations of asteroidal appulses and occultations. *Occultation Newsletter* 3:249–253.

Stamm, J. 1985b. Observations of asteroidal appulses and occultations. *Occultation Newsletter* 3:296–299.

Stamm, J. 1986. Observations of asteroidal appulses and occultations. *Occultation Newsletter* 3:325.

Stamm, J. 1988. Reports of asteroidal appulses and occultations. *Occultation Newsletter* 4:159–164.

Standish, E. M. 1989. A determination of the masses of Ceres, Pallas and Vesta from their perturbations upon the orbit of Mars. *Icarus*, in press.

Taylor, G. E. 1962. The diameters of minor planets. *J. British Astron. Assoc.* 72:212–214.

Taylor, G. E. 1981. The size of the minor planet 65 Cybele. *J. British Astron. Assoc.* 92:13–15.

Taylor, G., and Dunham, D. W. 1978. The size of minor planet 6 Hebe. *Icarus* 34:89–92.

Tholen, D. J. 1984. Asteroid Taxonomy from Cluster Analysis of Photometry. Ph.D. Thesis, Univ. of Arizona.

Thomas, P. 1988. Radii, shapes, and topography of the satellites of Uranus from limb coordinates. *Icarus* 73:427–441.

Thomas, P., and Veverka, J. 1987. Voyager observations of 1985U1. *Icarus* 72:79–83.

Wasserman, L. H., Millis, R. L., Franz, O. G., Bowell, E., White, N. M., Giclas, H. L., Martin, L. J., Elliot, J. L., Dunham, E., Mink, D., Baron, R., Honeycutt, R. K., Henden, A. A., Kephart, J. E., A'Hearn, M. F., Reitsema, H. J., Radick, R., and Taylor, G. E. 1979. The diameter of Pallas from its occultation of SAO 85009. *Astron. J.* 84:259–268.

Wasserman, L. H., Millis, R. L., and Franz, O. G. 1986. The occultation of AG + 20°1138 by 129 Antigone on 11 April 1985. *Bull. Amer. Astron. Soc.* 18:797 (abstract).

Wasserman, L. H., Bowell, E., and Millis, R. L. 1987. Occultations of stars by solar system

objects. VII. Occultations of catalog stars by asteroids in 1988 and 1989. *Astron. J.* 94:1364–1372.

Williamon, R. M. 1980. Observation of a secondary extinction during the occultation of SAO 114159 by (18) Melpomene. *Astron. J.* 85:174–176.

Zellner, B. 1979. Asteroid taxonomy and the distribution of the compositional types. In *Asteroids*, ed. T. Gehrels (Tucson: Univ. of Arizona Press), pp. 783–806.

SPECKLE INTERFEROMETRY OF ASTEROIDS

JACK D. DRUMMOND and E. KEITH HEGE
University of Arizona

We summarize Steward Observatory's two-dimensional power spectrum signature analysis of speckle interferometry observations. Results for six asteroids are presented. The poles and triaxial ellipsoid dimensions of 4 Vesta, 433 Eros, 511 Davida and 532 Herculina have been previously reported. New results for 2 Pallas and 29 Amphitrite are given, as well as further results for Vesta. Image reconstruction is ultimately required to minimize biasing effects of asteroid surface features on the simpler power spectrum analysis. Preliminary imaging results have been achieved for Vesta and Eros, and images for these two are displayed. These results show great promise for further resolving ambiguities from conventional measurements, as well as for providing insights into the nature of surface features of asteroids. Speckle interferometry and radiometry diameters are compared, and diameters from the two occultations of Pallas are also addressed.

I. INTRODUCTION

Speckle interferometry is a high angular resolution technique first suggested in the form used here by Labeyrie (1970,1978). To overcome the approximately one arcsec limit to resolution imposed by the Earth's atmosphere, and to approach the theoretical resolving power of large telescopes according to the Rayleigh criterion ($\approx \lambda/D$), short exposure ($\Delta t \approx 0.01$ to 0.05 s) narrowband (≈ 10 to 30 nm) images of an object are recorded. These short exposures (specklegrams) can then be combined (Fourier transformed) to obtain information down to the resolution limit of the telescope. Worden (1979) gives an introduction and some intuition-building illustrations of the phenomenon. For more comprehensive reviews of speckle interferometry and related

[171]

methods, see Bates (1982), Bates and McDonnell (1986) and most recently Roddier (1988).

Since the angular sizes of all asteroids are <1 arcsec, but many are greater than the resolution limit of large telescopes, they are suitable candidates for speckle techniques. The Fourier moduli of the specklegrams of the *resolved* asteroids contain diffraction limited information. This information can be obtained from either the image power spectrum or its autocorrelation function, but it is necessary to calibrate these observations of extended sources by inverse filtering with similar observations of a point source in order to calibrate residual seeing effects as well as the effects of the combined telescope and speckle camera optical transfer function. Furthermore, the effect of individual photons must also be calibrated. These calibrations are usually (most easily) made in the power spectrum domain.

In Worden's overview of speckle interferometry, he also gave a description of an atmospherically compensated image-intensified speckle camera. Present cameras are similar except that digital video readout (or photoelectron event coordinate readout in the newest systems) replaces the original photographic recordings of specklegrams.

Worden's simple summary of speckle interferometric data processing did not treat seeing calibration and photon noise bias effects, which we will address in this chapter. In speckle interferometry it is assumed that image perturbing processes in the atmosphere acting on the object irradiance function $o(\mathbf{r})$ can be represented by a linear convolution with an instantaneous point spread function $s_m(\mathbf{r})$ valid over the quasi-stationary exposure time Δt, at time t_m. Specifically, $s_m(\mathbf{r})$ is the speckle pattern of a point source at t_m.

Let $\mathbf{r} = x\hat{\mathbf{i}} + y\hat{\mathbf{j}}$ represent a two-dimensional vector in image space (x,y) and $\mathbf{f} = u\hat{\mathbf{i}} + v\hat{\mathbf{j}}$ the corresponding vector in frequency space (u,v). Then, representing the two-dimensional specklegram by $i_m(\mathbf{r}) = o(\mathbf{r}) * s_m(\mathbf{r})$, and its Fourier transform by $I_m(\mathbf{f}) = O(\mathbf{f})S_m(\mathbf{f}) = FT(i_m(\mathbf{r}))$, the speckle interferometric power spectrum PS is the biased estimate

$$PS = E\{PS \ (\mathbf{f})\} = <|I(\mathbf{f})|^2>_M = |O(\mathbf{f})|^2<|S(\mathbf{f})|^2>_M \qquad (1)$$

for the ensemble of specklegrams $m = 1,2,\ldots,M$. The average of the ensemble of M observations is denoted by $< \ldots >_M$, where typically $M = 10^3$ to 10^5 for speckle interferometric observations of asteroids.

The speckle photon-statistics biased estimate of Eq. (1) can be written

$$PS = \{|\ O(\mathbf{f})|^2<|S(\mathbf{f})|^2> + <S(0)>\}|D(\mathbf{f})|^2 \qquad (2)$$

where $<S(0)> = \bar{N}$ is the mean number of photons per specklegram, independent of the object, after averaging over M frames. For a perfect detector, this is a constant bias but for the Steward Observatory speckle interferometer system (Hege et al. 1982) it is colored by the detector's photon detection

transfer function $D(\mathbf{f})$. This is explained further by Christou (1988), who also discusses methods for calibrating and removing the biasing effects of the detector $D(\mathbf{f})$ and of the photon statistics $S(0)$.

The unbiased PS estimate of the object $o(\mathbf{r})$ is then

$$PS_o = \frac{\langle|I(\mathbf{f})|^2\rangle_M}{|D(\mathbf{f})|^2} - \bar{N} = |O(\mathbf{f})|^2 \langle|S(\mathbf{f})|^2\rangle. \tag{3}$$

This unbiased estimate contains both seeing information as well as diffraction limited imaging information. In speckle interferometry the seeing information is calibrated with reference to a point source, effectively an unresolvable $\delta(\mathbf{r})$. M_* specklegrams of the point source are similarly observed for which the biased estimate $<|I_*(\mathbf{f})|^2>_{M_*}$ yields the unbiased seeing estimate

$$PS_* = \frac{\langle|I_*(\mathbf{f})|^2\rangle_{M_*}}{|D(\mathbf{f})|^2} - \bar{N}_* = |\Delta(\mathbf{f})|^2 \langle|S_*(\mathbf{f})|^2\rangle = \langle|S_*(\mathbf{f})|^2\rangle. \tag{4}$$

If the seeing statistics for both measurements are identical (i.e., the seeing is stationary), then $<|S_*(\mathbf{f})|^2> \doteq <|S(\mathbf{f})|^2>$, and in the photon counting case, the unbiased, seeing calibrated speckle interferometric power spectrum estimate of $o(\mathbf{r})$ is

$$|O(\mathbf{f})|^2 \doteq \frac{PS_O}{PS_*} \doteq \frac{\{\langle|I(\mathbf{f})|^2\rangle_M / |D(\mathbf{f})|^2\} - \bar{N}}{\{\langle|I_*(\mathbf{f})|^2\rangle_{M_*} / |D(\mathbf{f})|^2\} - \bar{N}_*}. \tag{5}$$

The effects of variable seeing are discussed by Christou et al. (1985,1987). Methods for applying the seeing calibration in this more likely observational circumstance are discussed by them, and by Hege et al. (1986).

In practice, the linear deconvolution (Eq. 5), hereafter referred to as PS, is to be applied with strict attention to the following caveat: both PS_o and PS_* approach zero at the diffraction limit cutoff of the telescope, $f_c = D/\lambda$, and both contain (unbiased) measurement noise. Therefore, the ratio (Eq. 5) becomes unreliable near $|\mathbf{f}| \approx f_c$ where the quotient of small noisy numbers becomes erratic.

The foregoing assumes that the data integrations are performed in the power spectrum domain, but the observed quantities $<|I(\mathbf{f})|^2>_M$ and $<|I_*(\mathbf{f})|^2>_{M_*}$ can also be accumulated in the image domain as the Fourier transforms of averages of autocorrelation functions,

$$\langle|I(\mathbf{f})|^2\rangle_M = FT \left\{ \left\langle \int_{\mathbf{f}} i_m(\mathbf{r}) i_m(\mathbf{r} - \mathbf{f}) d\mathbf{f} \right\rangle_M \right\} \tag{6}$$

and similarly for the reference point source. In the faint object limit (which includes all asteroid observations) for which the specklegrams $i_m(\mathbf{r})$ are observed as sets of N_m photon responses with point spread function $d(\mathbf{r})$,

$$i_m(\mathbf{r}) = \sum_{j=1}^{N_m} d(\mathbf{r}) * \delta(\mathbf{r} - \mathbf{r}_j). \tag{7}$$

The autocorrelation integral collapses to a histogram of image pixel vector differences (Nisenson and Papaliolios 1983; Hege and Vokac 1986),

$$ACF = \left\langle \int_{\mathbf{f}} i(\mathbf{r})i(\mathbf{r} - \mathbf{f})d\mathbf{f} \right\rangle_M = \left\langle N_m \sum_{j,k}^{N_m} \delta(\mathbf{r}_j - \mathbf{r}_k - \mathbf{r}) \right\rangle_M$$

$$= \frac{\bar{N}}{M} \sum_{m=1}^{M} \sum_{j,k}^{N_m} \delta(\Delta\mathbf{r}_{j,k} - \mathbf{r}). \tag{8}$$

The average vector autocorrelation (Eq. 8), for all vector address differences $\Delta\mathbf{r}_{j,k} = \mathbf{r}_j - \mathbf{r}_k$ in each frame, is the quantity accumulated in the Steward Observatory asteroid speckle interferometry program. In the ideal detector case, where $d(\mathbf{r}) = \delta(\mathbf{r})$, the unbiased estimate of ACF obtains if the terms for which $i = j$ are omitted from Eq. (8). This unbiased ACF can be accumulated from data obtained with, e.g., the Stanford MAMA detector (Timothy and Morgan 1986). The quotient of $FT(ACF)$, divided by a similar $FT(ACF_*)$ for a point source, yields directly the unbiased power spectrum estimate (Eq. 5), $|O(\mathbf{f})|^2$. The results with the PAPA detector (Papaliolios et al. 1985) are not so cleanly unbiased, and flat-field corrections are required.

II. AUTOCORRELATION/POWER SPECTRUM ANALYSIS

A. Background

To interpret the two-dimensional autocorrelation (Eq. 8) of an asteroid image, more particularly its seeing calibrated Fourier inverse, the two-dimensional object PS (Eq. 5), we extract asteroid image signatures as follows. A triaxial ellipsoid asteroid would project a series of ellipses onto the plane of the Earth's sky as the asteroid rotates, as can be seen during a stellar occultation (see the chapter by Millis and Dunham). The observed major and minor axes, and position angle, will vary in a unique fashion as a function of rotation. Drummond et al. (1985a) derive the equations relating these potentially observable parameters back to triaxial ellipsoid axes dimensions and to three Euler angles then used to locate the spin axis direction. The lengths of the major and minor axes, and the position angle of the major axis, for the

two-dimensional elliptical *PS* projections (Eq. 5) are fit to the same parameters for the power spectra of uniform disks using a nonlinear least-squares routine. The image power spectrum signature is sufficiently elliptical and uniform that the parameters required to fit for the two projected axial dimensions and position angle can be extracted from them.

The model of an asteroid as an ellipsoid is a mathematically tractable, first-order approximation to the actual shape of an asteroid. Since for most purposes any body can be described by its principal axes, the ellipsoid assumption is a very general and powerful abstraction. Departures from a true ellipsoid (and perhaps from other simplifying assumptions) are sometimes evident as secondary effects that bias the first-order approximation. A triaxial ellipsoid rotating about its shortest axis ($a \geq b \geq c$) is widely used in asteroid work (see, e.g., the chapter by Magnusson et al.), and has been found to be appropriate for the Saturnian satellite Mimas (Dermott and Thomas 1988), and for the Uranian satellites Miranda and Ariel (Thomas 1988). An ellipsoid shape would be a natural stable outcome for a body in gravitational and/or hydrostatic equilibrium, such as would be formed by either coalescence or catastrophic collisions resulting in so-called rubble piles (Davis et al. 1979, and their chapter in this book; Farinella et al. 1981; Catullo et al. 1984; Zappalà et al. 1984). Rotation about the short axis is the most stable configuration, and even precession induced by perturbations and collisions is expected to be damped out for asteroids over a small fraction of the lifetime of the solar system (see the chapter by Binzel et al.).

For dark atmosphereless bodies observed at low solar phase angles, uniform brightness is to be expected for reasonable scattering laws (see the chapter by Bowell et al.). Moreover, limb darkening, which may be 5 to 10% for completely smooth bodies, is shown to be reduced to <5% in meteorites by roughness (French and Veverka 1983). Deformation of a triaxial ellipsoid shape by the presence of mountains, craters, etc., may be important for smaller bodies, but should be much less severe for larger asteroids. Even with a random distribution of such deformations, it is still possible to treat the object as a triaxial ellipsoid with noise (irregularities of outline). Unless a deformation has a different albedo, it has no effect on speckle interferometric measurements until it lies on the limb. Similarly, Fulchignoni and Barucci (1984) have shown that even for the largest craters known (in terms of the body diameter), for Phobos, Mimas and Tethys, the presence of a crater with the same albedo as the surrounding asteroid material cannot be detected in a lightcurve. See also the chapter by Magnusson et al. for further justification and use of the adopted assumptions.

B. Results from Power Spectrum Signature Analysis

433 Eros. Key to the development of the present form of speckle interferometer power-spectrum signature analysis (PSSA) is the well-observed small Earth-approaching asteroid Eros. Observations of Eros taken a month
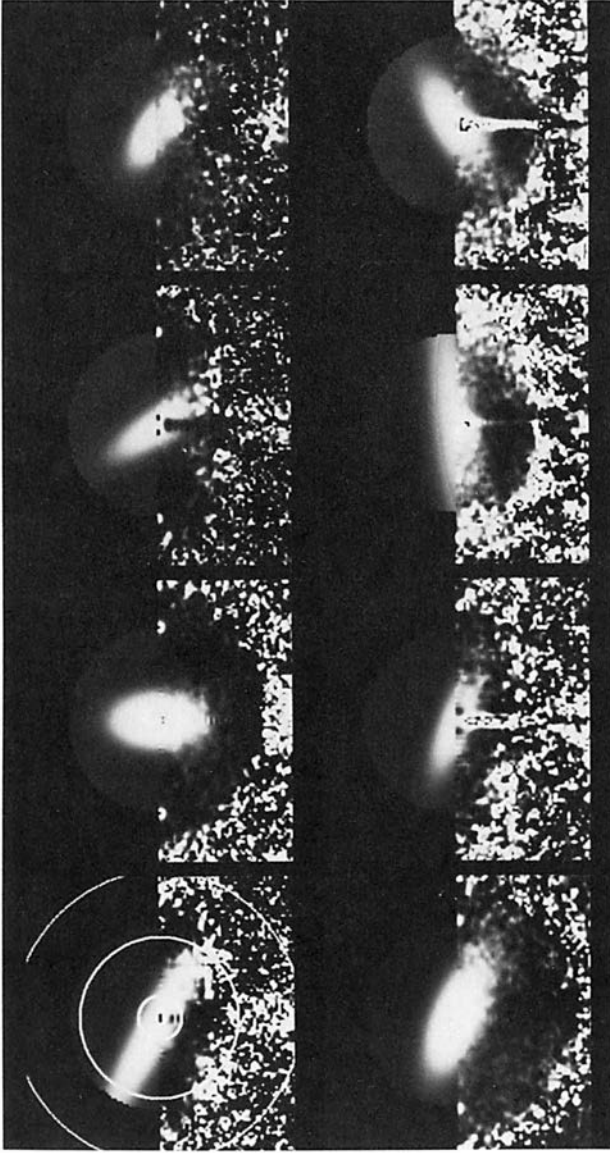
Fig. 1. Two dimensional power spectra of 433 Eros from 17,18 December 1981. The upper part of each frame is the centro-symmetric elliptical fit to the centro-symmetric data shown in the lower half. The first figure contains rings, in outward order, of 1/0.3, 1/0.1, and 1/0.06 arcsec^{-1}, increasing in spatial frequency in power spectra domain, used for scaling illustrations. The data in the region 1/0.3 to 1/0.1 were fit to obtain the elliptical signature parameters.

TABLE I
Diameters and Poles from Speckle Interferometry

Asteroid	a	b	c	Ecliptic Pole (1950)
2 Pallas	537 ± 29	488 ± 11	485 ± 11	100 − 22 ± 8
				295 + 16 ± 8
4 Vesta	566 ± 15	531 ± 15	467 ± 15	311 + 67 ± 18
29 Amphitrite	186 ± 18	152 ± 15	144 ± 10	134 − 36 ± 12
				303 + 35 ± 12
433 Eros	41 ± 3	15 ± 2	14 ± 2	23 + 37 ± 14
511 Davida	465 ± 90	358 ± 58	258 ± 356	196 − 12 ± 29
				291 + 37 ± 29
532 Herculina	263 ± 14	218 ± 12	215 ± 12	132 − 59 ± 7
				128 + 74 ± 7

apart, with substantially different geometries at high solar phase angles, spurred derivations of equations expressing the projection of triaxial ellipsoids to ellipses. This permitted the use of a nonlinear variance minimization method to relate the observed two-dimensional major and minor axes and position angle signatures back to the three-dimensional triaxial ellipsoid figure and rotational pole of the model asteroid (Drummond et al. 1985a). Figure 1 shows 7 two-dimensional power spectra of Eros from two nights in December 1981, arranged in order of rotational phase. The lower half of each frame is the actual seeing calibrated power spectrum (Eq. 5), and the upper half is the ellipse fit to that *PS*. Since *PS* are centro-symmetric, it is sufficient to fit and display a half plane. If Eros were a smooth triaxial ellipsoid, these elliptical *PS* signatures would have the same shape as the ellipses projected onto the plane of the sky. At the very least, Fig. 1 clearly shows signatures of an elongated object spinning in space with the sub-Earth point close to the rotational pole. (Hereafter, the term SI will specifically designate the speckle interferometry PSSA process. As used at Steward Observatory, SI is a specific and well-calibrated application of the specific and well-defined model just described.)

The results from the two runs for Eros are summarized in Table I. The two-fold ambiguity for the pole is resolved from SI alone because of the differing geometries of the two runs. This pole is consistent with the pole derived from photometric methods. Table II gives the average of the 8 most recent pole determinations (including the SI pole) listed in Part VI of this book. The dimensions in Table II are the averages and standard deviations from SI, radiometry (Lebofsky and Reike 1979), radar (Jurgens and Goldstein 1976), and the consensus model of Zellner (1976), all listed by Drummond et al. (1985a). The biggest discrepancy between SI and other results appears to be in the pole, but given the smallness of the target, the large (40 and 52°) solar phase angles involved in the SI observations and the distinctly nonellipsoidal shape of the reconstructed image shown in Sec. III.C, the agreement is actually quite good.

TABLE II
Diameters and Poles from Combining SI and Others

Asteroid	a	b	c	Ecliptic Pole (1950)
2 Pallas	570 ± 22	525 ± 4	482 ± 15	74 − 17 ± 24
4 Vesta	566 ± 15	531 ± 15	467 ± 15	311 + 67 ± 18
29 Amphitrite	210 ± 30	188 ± 39	174 ± 19	138 − 33 ± 16
433 Eros	38 ± 2	15 ± 1	14 ± 1	17 + 16 ± 11
511 Davida	417 ± 48	333 ± 25	292 ± 34	299 + 34 ± 9
532 Herculina	? ± ?	? ± ?	? ± ?	? ± ?

2 Pallas. The first asteroid studied with SI by Steward Observatory was 2 Pallas in 1979 (Hege et al. 1980a,b). Its extremely elongated signature was initially interpreted (plausibly) as an indication for a large Pallas satellite, but was later found to be the product of incomplete calibration. This led to our present observing methods, where we measure the asteroid (and two calibration stars) throughout its rotation, and to our PSSA methods, which properly interpret changing signatures of the projected image. This has enabled us to derive the dimensions and pole of Pallas from a later run.

On 9 and 10 April 1982, 9 observations were made at Steward Observatory's 2.3 m telescope with the Steward Observatory intensified video speckle camera (Hege et al. 1982). The results from these Pallas observations (previously unpublished) are given in Table I. Substantial, systematic departures from a triaxial ellipsoid model are evident as a nonrandom distribution of residuals to the fit of the major and minor diameters and position angles. We have come to realize that such departures are characteristic of the impact of albedo features on our PSSA.

Pallas is the only asteroid with two well observed stellar occultation outlines (which are free from albedo effects) that give very reliable direct measurements of its size and shape at the two epochs. In considering these occultations, and the two models of the triaxial ellipsoid shape and rotational pole derived from them by Wasserman et al. (1979) and Magnusson (1986), it can be shown that neither model yields the exact occultation outlines as represented by the observed chords. Drummond and Cocke (1988) show that with the ellipsoid equations derived by Drummond et al. (1985a), the two occultations give a narrowly defined pole (to within a two-fold sense-of-rotation ambiguity) and triaxial dimensions. For the nominal occultation parameters for Pallas, they found that the c axis could be no greater than 120 km. Since this is unrealistically small, and since the first occultation had much larger uncertainties on the measured parameters than the second, Drummond and Cocke examined a range in solutions found by varying the first occultation parameters by their uncertainties. Evidently, the size of the outline on the first occasion was (only slightly) overestimated, since only smaller dimensions yield

better (larger c) solutions. Taking the average and standard deviations for the various possible realistic ($c \geq 300$ km) solutions, they give a pole for Pallas at $(71; -19)$ or $(251; +19)$ with a $10°$ radius error circle, and dimensions of $583(\pm 18) \times 527(\pm 3) \times 409(\pm 52)$.

The weighted averages between the direct techniques of SI and occultations are given for the axial dimensions in Table II. Because of the geometries of the observations, SI determines the c axis better than the occultations, but the occultations define the b axis more precisely. Lebofsky et al. (1986) have recently revised the radiometric scale with Ceres and Pallas occultation results and derive an average diameter of 532 km for Pallas. The IRAS diameter (Matson et al. 1986) is 523 ± 20 km. The mean diameter $(abc)^{1/3}$ of the model of Pallas from SI and the occultations given in Table II is 524 km, with a range of 503 km for the minimum average diameter seen at equatorial aspects to 547 km for the maximum cross section seen at polar aspects. The pole in Table II is the average between the speckle pole at $(100; -22)$, the occultation pole from the mean of the possible solutions at $(71; -19)$, and the pole at $(54; -6)$ from lightcurve analyses by Magnusson (1986).

4 Vesta. Retiring our traditional intensified video speckle detector in favor of Harvard's PAPA and Stanford's MAMA two-dimensional photon counting arrays, we have obtained excellent observations of 4 Vesta. As reported by Drummond et al. (1988a), 10 observations were made with the PAPA detector over two nights in November, 1983. Triaxial ellipsoid dimensions and the usual two poles were obtained from PSSA. In addition, the superior characteristics and geometric fidelity of the detector allowed successful image reconstructions, discussed further in the next section. Three years later, over three nights in October, 1986, we obtained some 65 observations with the MAMA detector, which generally corroborated the results from the earlier run. The two-fold ambiguity inherent to SI leads to a two-fold ambiguity in the location of the rotational pole, but comparing the two possible poles from each run, it was found that the prograde poles were slightly closer than the retrograde poles, and were located in one of the two possible prograde regions as determined from lightcurve analysis. Thus the pole of Vesta seems to be rather well located. The two possible poles from the PAPA run were $(336; +55)$ and $(209; -50)$, while the two from the MAMA run were around $(278; +71)$ and $(145; -60)$. Treating the results from each of the three nights of the MAMA run independently, the weighted average of four pole determinations involving 10, 17, 23, and 25 observations from the two runs is given in Table I, and since it can be regarded as definitive (with the assumptions and to within the uncertainties involved), is repeated in Table II.

The weighted average for the triaxial ellipsoid dimensions determined on four nights by SI are given in both Tables I and II. The mean diameter of Vesta's projected disk would vary between extremes of 498 and 548 km, with $(abc)^{1/3} = 520$ km. This is much closer to the radiometrically determined 530

km in the TRIAD file than the 579 km from polarimetry. (These diameters were inadvertently attributed to the opposite techniques by Drummond et al. [1988a].) Brown et al. (1982) have suggested that the radiometric diameters in the TRIAD file should be reduced by 5% on the average, which would yield 504 km for Vesta's radiometric diameter. The IRAS diameter is listed as 501 ± 24 km. It appears that most of the radiometric observations were made near Vesta's equatorial plane, where the average projected diameter would range between 498 and 514 km.

29 Amphitrite.   Previously unpublished results from PSSA of 5 observations of Amphitrite on 1 July 1985 are given in Table I. It is well known from its irregular photoelectric lightcurves that Amphitrite must possess either substantial albedo variations over its surface or higher-order shape parameters, making conclusions and interpretations of SI signatures somewhat dangerous. On the other hand, with the large number of available lightcurves and with the converging consensus of axial ratios from photometric analysis, the shape and pole of this asteroid appear to be well determined.

From the photometric determinations of the rotational axis listed in Part VI of this book, two ambiguous poles emerge, at (139; −33) and (328; −40), both with about 15° errors. The two possible poles from SI are listed in Table I, only one of which is consistent with the photometric determinations. Thus, the pole ambiguity is resolved in favor of the first listed pole. The average from the 6 photometric and one SI determination is listed in Table II.

The mean a/b ratio for Amphitrite from 6 photometric determinations in Part VI of this book is 1.11 ± 0.04 and from 4 determinations, the average b/c ratio is 1.09 ± 0.07. The ratios from SI are $a/b = 1.22 ± 0.17$ and $b/c = 1.06 ± 0.13$. In light of the good agreement between the photometric and SI axial ratios, it is surprising to find that the mean TRIAD polarimetric and radiometric diameters of 197 and 200 km, respectively, and the IRAS value of 219 ± 5 km do not agree well with the mean SI diameter of 160 km, with an extreme range of 148 to 168 km corresponding to $(bc)^{1/2}$ and $(ab)^{1/2}$, respectively. The reason for the discrepancy undoubtedly lies in the surface albedo structure inferred from the lightcurves, but it is not clear whether this influences SI or radiometry more. Adopting a mean diameter of 190 km, midway between the SI and the IRAS values, and adopting the consensus (photometric plus SI results) axial ratios of 1.21 : 1.08 : 1.00, the best estimates of the dimensions are given in Table II, where the adopted uncertainties are the vector sum of the uncertainties in Table I and the differences between the dimensions in the two tables.

511 Davida.   From only 5 observations in one night, covering only a quarter of a rotation, the results given in Table I were derived from PSSA (Drummond and Hege 1986). Although it was suggested that the difficulty in finding a triaxial ellipsoid solution was perhaps due to albedo features, subsequent photometric analysis strongly suggests the contrary, that Davida is very

smooth and uniform. In fact, Magnusson et al. (see their chapter) offer it as a possible "standard." Despite the large associated error, SI does resolve the ambiguity in the photometric pole determinations. Part VI in this book shows that the two possible poles are located around $(95;+30)$ and $(300;+35)$, but considering the two possible poles from SI in Table I, we identify the latter as being the correct one (see Table II).

Because of the small number of observations and the low albedo of the object, the SI diameters have large associated errors. Yet, it is still surprising that the mean SI diameter of 350 km, with a range of $(bc)^{1/2} = 304$ km to $(ab)^{1/2} = 408$ km, differs so much from the TRIAD radiometric diameter of 323 km or the downward revised 307 km. However, the IRAS diameter of 337 $\pm$ 5 km stands in much better agreement with the SI mean diameter. For our best estimate of the diameters in Table II, we use the well-determined axial ratios from the Magnusson et al. chapter and a mean diameter midway between the IRAS and SI values. The adopted uncertainties are the difference between the diameters in Tables I and II.

532 Herculina. Herculina presents a peculiar case. Its sometimes single max/min and sometimes double max/min lightcurves have proven difficult to explain. The first attempt to develop a model was given by Drummond et al. (1985b) to explain the SI observations. The pole and dimensions from SI are given in Table I. In order to account for peculiar SI measurements at certain rotational phases, and to account for the lightcurve history, a bright spot was postulated. However, with a photometric astrometry method, Taylor et al. (1987) found an entirely different pole, and offered a spherical model with two dark spots. Nevertheless this model was, in turn, rejected because Lebofsky et al. (1988) showed from thermal lightcurves that the visible lightcurve amplitude was caused by changing cross sectional area and therefore Herculina could not be a sphere. Current modeling efforts (Drummond et al. 1988b) to help interpret its lightcurves are concentrating on a triaxial ellipsoid shape with major albedo or topographic (crater) features. Even low-resolution images from speckle data should be very helpful in understanding Herculina.

It would be premature to list parameters with any degree of confidence in Table II. While the original TRIAD radiometric diameter of 220 km is in good agreement with the SI mean diameter of 231 km, the revised diameter of 209 km falls outside the range inferred from SI of 216 to 239 km. However, the IRAS diameter of 231 $\pm$ 4 km agrees exactly with the SI mean diameter. Further observations of Herculina with all techniques are needed before anything definitive can be said about its shape, but its average size seems well determined and the pole from Taylor et al. (1987) at $(96;-1)$ derived from the timings of lightcurve features appears firm.

C. Comparison of SI to Other Diameters

Figure 2 shows the mean diameters $(abc)^{1/3}$ from Table I plotted against the radiometric diameters from the IRAS file (Matson et al. 1986). The verti-
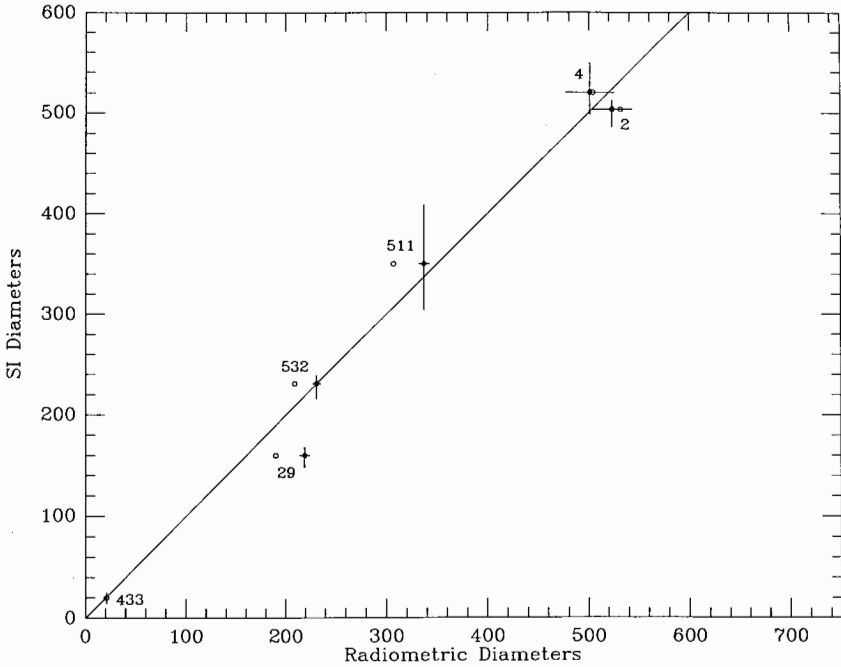
Fig. 2. SI vs IRAS radiometric mean diameters. The vertical bars giving the range of allowable SI diameters, from $(bc)^{1/2}$ to $(ab)^{1/2}$, are not error bars but correspond to the minimum and maximum possible mean diameters according to Table I. The dots and their horizontal error bars are from the IRAS file (Matson et al. 1986), and the open circles, also plotted with ordinates corresponding to SI diameters, are TRIAD diameters reduced by 5%, except for 2 Pallas which comes from Lebofsky et al. (1986).

cal lines on the mean diameters are not error bars, but represent the extreme possible range of mean diameters, from $(bc)^{1/2}$ in the equatorial plane to $(ab)^{1/2}$ at polar aspects according to the SI values in Table I. Observations should statistically tend to occur near the bottom of this range since an asteroid's orbit guarantees that the Earth will cross the equatorial plane every sidereal period, but only in the exceptional circumstance where the rotational pole lies nearly in its orbital plane could a polar view be provided. The horizontal lines are error bars from the IRAS list. For comparison, the diameters from the TRIAD file (Morrison and Zellner 1979), reduced by the 5% suggested by Brown et al. (1982), are shown as open circles. The Pallas diameter, however, is from Lebofsky et al. (1986), where a refined thermal model was used. Also note that Eros does not have an IRAS measurement, so only a reduced TRIAD diameter is used.

Except for 29 Amphitrite, the agreement between the SI and radiometric diameters is quite good. Pallas' radiometric diameter has been considerably

reduced from the original TRIAD diameter of 589 km. For two asteroids (511 and 532), the agreement between the SI and IRAS diameters is much better (moved to the right in Fig. 2) than the TRIAD diameters with the indiscriminate 5% reduction. The direct correlation (slope = 1) of SI with IRAS diameters stands convincingly, and with no worse scatter than the former consensus (TRIAD) diameters.

In cases where surface-structure effects are significant, SI is known to produce biased estimates. When unresolvable surface structure dominates, SI yields an underestimate of the size of the object. This appears to be the case for Pallas and Amphitrite. Large dark regions could have the opposite effect. Analysis of reconstructed images is expected to be less sensitive to these biasing effects. One of the strong points about the PSSA results is that all three axes diameters are derived at once, so that the vertical lines on the filled points in Fig. 2 can be drawn in the first place. With SI, each asteroid is treated independently; SI yields a complete analysis involving no indeterminable parameters.

III. IMAGE RECONSTRUCTION

A. Background

The image of an object, $o(\mathbf{r})$, can be reconstructed from measurements of the object's complex visibility function by inverse Fourier transform

$$o(\mathbf{r}) = FT^{-1}[V(\mathbf{f})] \tag{9}$$

where, as in Sec. I, $\mathbf{r}$ and $\mathbf{f}$ represent image ordinary space (x,y) and image frequency space (u,v), respectively. The complex visibility, $V(\mathbf{f})$, is conveniently represented, after Euler, in terms of its amplitude and phases

$$V(\mathbf{f}) = A(\mathbf{f})e^{i\phi(\mathbf{f})}. \tag{10}$$

The image amplitude $A(\mathbf{f})$ is just the square root of the image PS (Eq. 5) calibrated as described in Sec. I.

The image phase measurements in the Knox-Thompson method are obtained from the same set of M Fourier transformed specklegrams as required for the image PS (Eq. 1), the complex quantities $I_m(\mathbf{f}) = FT[i_m(\mathbf{r})]$, $m = 1,2,...M$. Knox and Thompson (1974) showed that phase differences, and hence by numerical integration the phases, can be accumulated from two quite similar complex cross spectrum accumulations in the two-dimensional $\mathbf{f} = (u,v)$ plane

$$CS_u(\mathbf{f}) = <I_m^*(u,v)I_m(u+1,v)>_M \tag{11a}$$

and

$$CS_v(\mathbf{f}) = <I_m^*(u,v)I(u,v + 1)>_M . \qquad (11b)$$

An initial estimate of the image phases $\phi(\mathbf{f})$ can be obtained by starting with $\phi(0) = 0$, as it is always possible to assume that the reconstructed image is to be centered in the data frame. To avoid problems in averaging phases with $\pm 2\pi n$ periodic ambiguity, it is necessary to work with *phasors*, two-dimensional vector-like quantities which are *not* influenced by such ambiguity. To visualize the problem, consider two noisy quantities, $\phi_1 = \pi + \epsilon_1$ and $\phi_2 = -\pi + \epsilon_2$. The simple average produces $0 + 1/2(\epsilon_1 + \epsilon_2)$, whereas the correct average is π (or $\pi + 2\pi n$, but not 0) $+1/2(\epsilon_1 + \epsilon_2)$. We use a normalized phasor $Ph(\mathbf{f})$ defined such that its argument is the required $\phi(\mathbf{f})$. Thus we begin with the complex normalized phasor

$$Ph(0) = (1,0) \qquad (12)$$

The phases at all other points in the (u,v) plane within the diffraction limit $|\mathbf{f}| < f_c$ are then integrated from the measured phase differences by iteration of Eq. (12) using the complex cross spectra Eq. (11) according to the rules

$$Ph(\mathbf{f} + \hat{\imath}) = CS_u(\mathbf{f})/Ph(\mathbf{f}) \qquad (13a)$$

and

$$Ph(\mathbf{f} + \hat{\jmath}) = CS_v(\mathbf{f})/Ph(\mathbf{f}) . \qquad (13b)$$

By successively stepping in $\hat{\imath}$ and $\hat{\jmath}$, any arbitrary frequency $\mathbf{f}$ can be reached from 0.

The frequency $\mathbf{f} + \hat{\imath} + \hat{\jmath}$ is the same as the frequency $\mathbf{f} + \hat{\jmath} + \hat{\imath}$, but the path specified by the order of the terms is different. The path integral along the two paths may produce different results due to measurement errors. Results are averaged for the two numerical integration paths at each step in the iteration of Eq. (12) by Eqs. (13),

$$Ph_a(\mathbf{f} + \hat{\imath} + \hat{\jmath}) = 1/2[Ph(\mathbf{f} + \hat{\imath} + \hat{\jmath}) + Ph(\mathbf{f} + \hat{\jmath} + \hat{\imath})] . \qquad (14)$$

The phase estimate $\phi(\mathbf{f})$ is then obtained from the argument of $Ph_a(\mathbf{f})$, the two path phasor averages,

$$\phi(\mathbf{f}) = \arg[Ph_a(\mathbf{f})] . \qquad (15)$$

This is only the first estimate since there are an increasingly large number of paths from 0 to $\mathbf{f}$ as $|\mathbf{f}|$ increases. What is desired is a method which finds the properly weighted least squares solution for $Ph_a(\mathbf{f})$ for all possible paths to

f. Such general methods are only now being investigated (Takajo and Takahashi 1988; Freeman et al. 1988).

In order to improve the phase approximation, the two-path average (Eq. 14) can be subjected to an iterative relaxation algorithm (such as that used in adaptive optics image-compensation systems by Hardy et al. 1977). This is accomplished by starting at the DC point, $Ph_a(0) = (1,0)$, and spiraling around it toward higher spatial frequencies. Again, the spiral has two senses depending on whether the first step is along $\hat{\imath}$ and then $\hat{\jmath}$, or the converse. Because of (unbiased) measurement noise, the two senses give different results, which are again averaged. The quantity computed at each step, $\mathbf{f} \neq 0$, of this spiral smoothing involves 4 complex quotients describing the 4 nearest-neighbor phase relationships

$$Ph_s(\mathbf{f}) = 1/4 \left\{ \left(\frac{CS_u(\mathbf{f})}{Ph_a(\mathbf{f} + \hat{\imath})} \right)^* \right.$$

$$\left. + \left(\frac{CS_v(\mathbf{f})}{Ph_a(\mathbf{f} + \hat{\jmath})} \right)^* + \frac{CS_u(\mathbf{f} - \hat{\imath})}{[Ph_a(\mathbf{f} - \hat{\imath})]^*} + \frac{CS_v(\mathbf{f} - \hat{\jmath})}{[Ph_a(\mathbf{f} - \hat{\jmath})]^*} \right\} \quad (16)$$

where $(...)^*$ denotes complex conjugate. This average ensures that locally at $\mathbf{f}$ the value of the new phase estimate $\phi(\mathbf{f}) = \arg(Ph_s(\mathbf{f}))$ is consistent with the measured phase differences $CS_u(\mathbf{f})$ and $CS_v(\mathbf{f})$ for its nearest neighbors $\phi(\mathbf{f} \pm \hat{\imath})$ and $\phi(\mathbf{f} \pm \hat{\jmath})$.

This process converges, for $|\mathbf{f}| < f_c$, after several iterations of Eq. (16) in which $Ph_a(\mathbf{f})$ is replaced by its new estimate $Ph_s(\mathbf{f})$ after each iteration. Convergence is achieved when the "variance" of the iteration

$$\epsilon = \sum_{|\mathbf{f}| < f_c} [Ph_a(\mathbf{f}) - Ph_s(\mathbf{f})]^2 \quad (17)$$

decreases significantly, typically after 20 to 200 iterations. This is not, however, a "least squares" solution, but it is nevertheless a weighted solution since the complex cross spectra CS_u and CS_v contain the image amplitudes.

Just as there is an image plane analog of the PS (the ACF), there are equivalently image plane analogs to the two phase difference cross spectra (Eqs. 11), the two corresponding unbiased complex cross correlation functions, similar to Eq. (8)

$$XC_x(\mathbf{r}) = \frac{1}{M} \sum_{m=1}^{M} \frac{1}{N_M} \sum_{j,k=1; j \neq k}^{N_M} \exp(-i2\pi x_k/L)\delta(\Delta\mathbf{r}_{j,k} - \mathbf{r}) \quad (18a)$$

and

$$XC_y(\mathbf{r}) = \frac{1}{M} \sum_{m=1}^{M} \frac{1}{N_M} \sum_{j,k=1;\, j\neq k}^{N_M} \exp(-i2\pi y_k/L)\delta(\Delta\mathbf{r}_{j,k} - \mathbf{r}) \quad (18b)$$

where L is the size of the data domain. The cross spectra (Eqs. 11) are then obtained from these complex weighted cross correlations (Eqs. 18) by Fourier transformation. Hence the complex visibility measurements can be made in either data domain.

The phases $\phi(\mathbf{f})$, obtained from Eq. (16), and amplitudes $A(\mathbf{f})$, obtained from Eq. (5), can be combined (Eq. 10) to retrieve the image of the object (Eq. 9). Further refinement of the image estimate given by Eq. (9) can be obtained using methods developed by Feinup (1978,1979,1986) and co-workers (Feinup et al. 1982; Feinup and Wackerman 1986). This image estimate refinement effectively imposes the additional physical constraints that an image is positive definite and, for finite objects, bounded by its support.

In summary, the reconstructed image is positive definite, with a finite support, and is consistent with its observed seeing calibrated image amplitudes and its observed image phase differences (see Drummond et al. [1988a] for descriptions of further calibration procedures as applied to Vesta).

B. Images of 4 Vesta

Ten images of Vesta were reconstructed and discussed by Drummond et al. (1988a). The data were taken with Harvard's PAPA detector (Papaliolios et al. 1985), and with the close cooperation of C. Papaliolios, P. Nisenson and S. Ebstein. The images are due to A. Eckart. A problem with multiple detection of photons, yielding biased estimates of amplitudes (Eq. 8) and phase differences (Eqs. 18), (which has since been corrected) produces an artificially bright central spot in all of these images. Ignoring this known artifact, the images were sufficient to reveal dark and bright areas on the surface. A model of surface spots was developed based on the images. When combined with the triaxial ellipsoidal shape derived from the PSSA, this model can reproduce all low solar phase-angle lightcurves ever taken, down to the rotational phase and amplitude.

From theoretical considerations of its inferred basaltic crust, it could be argued that the derived triaxial shape (Drummond et al. 1988a), where $a/b = 1.10 \pm 0.04$ from 10 observations, cannot be correct, that a/b must be 1.0, and that Vesta has an equilibrium shape (Cellino et al. 1987). It should be pointed out that the SI results are observational, with the model being driven by the images, and not vice versa. However, estimates of figures obtained as fits to images with surface structure can also be biased. The possibility certainly exists that Vesta's a/b ratio may be closer to unity, with the observed spots dominating the lightcurves more than the unequal axes. Some 65 later observations with Stanford's MAMA detector, provided through the courtesy of J. Morgan and J. G. Timothy, and reduced at Steward Observatory by R.
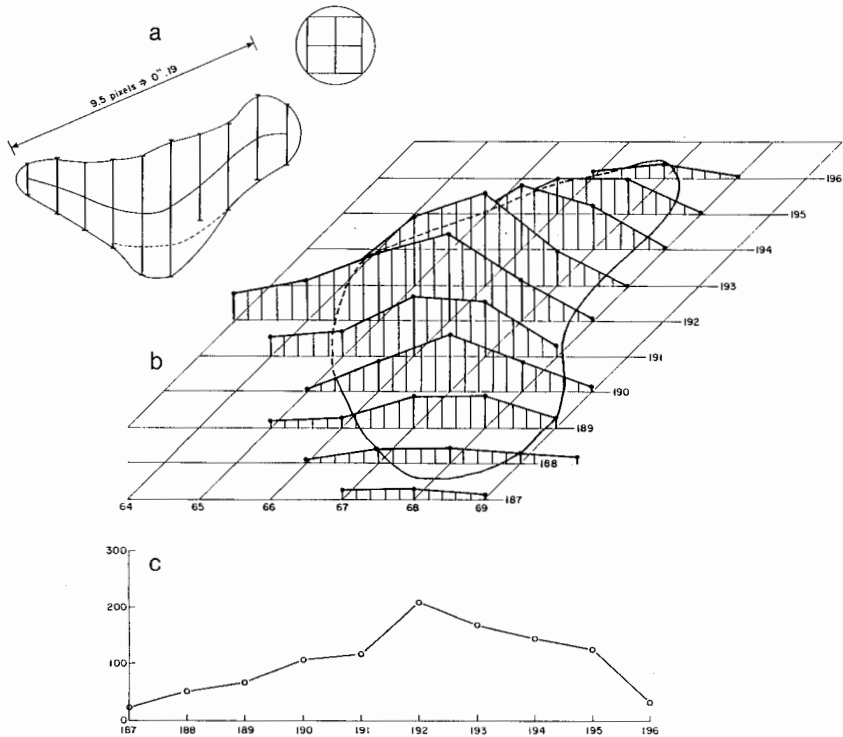
Fig. 3. Intensity profiles from a reconstructed image of 433 Eros. (a) is the outline of the as-
teroid's reconstructed image, and (b) and (c) are intensity profiles of the same image from
different perspectives. The image was reconstructed from the *PS* shown third from the right in
the top row of Fig. 1.

Watkins, are shown to produce unbiased estimates of amplitudes, yielding a
PSSA *a*/*b* ratio nearer to unity, 1.07 ± 0.04, as reported in Table I.

C. Image Phase Reconstructions for 433 Eros

In collaboration with the speckle group at Steward Observatory, Bates
and coworkers at the University of Canterbury in New Zealand (Bates and
Fright 1983,1984; Bates and Lane 1987) have obtained a reconstructed image
of the second observation of Eros on 18 December 1981, which corresponds
to the third *PS* from the right in the top row in Fig. 1. (In Drummond et al.
[1985a], the observation is the sixth point in their Figs. 2 and 3, the third
frame in Fig. 9 and the sixth drawing in Fig. 10.) This previously unpublished
image was produced from the *PS* amplitudes only, and therefore involved
reproducing the phases from the amplitudes as well.

Line drawings of the image are given in Fig. 3a, and intensity profiles are
presented in two different perspectives in 3b and 3c. The intensities between

the dotted and solid line in the projected image and exterior to the dotted line in the intermediate perspective are biased because of known instrumental artifacts along these rasters. The solar phase angle at the time was 40° and the latitude of the sub-Earth point was −74° according to the pole in Table I, or −62° with the pole from Table II. The projected image reveals that Eros is shaped more like a peanut than a strict triaxial ellipsoid, and the intensity profiles suggest that the brightness distribution across the small asteroid is not uniform at 40° solar phase angle. Both of these points would contribute to the difference between the poles in the two tables. Does this picture suggest that Eros may be a "chip" off a larger body or does Eros look more like the nucleus of a comet?

D. The Future

The question is now how to obtain unbiased estimates of an asteroid's figure from noisy images modulated by observable surface structure. One
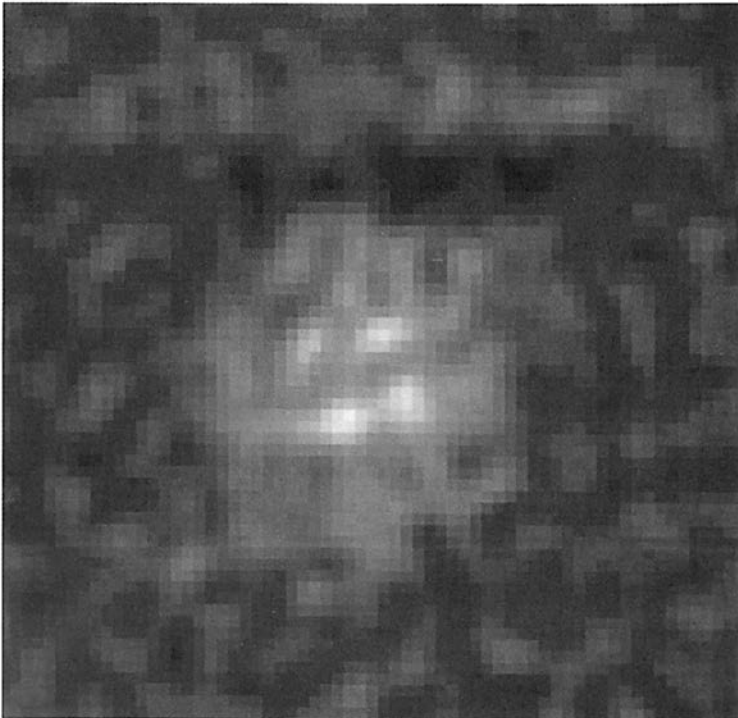
Fig. 4. Reconstructed image of 4 Vesta. This reconstruction of an image was made with the Knox-Thompson algorithm applied to the first Vesta observation of 14 Nov. 1986. The size of Vesta at this time was 0.50 by 0.47 arcsec with the position angle of the long axis oriented 50° West (counterclockwise) of North (left) as determined from PSSA.

image of Vesta from the set of 65 currently being constructed from data taken with the MAMA detector is shown in Fig. 4 and illustrates the problem. The improvements obtained by Takojo and Takahashi (1988) with least-squares phase retrieval from phase-difference measurements in computer simulations lead us to expect similar improvements will be forthcoming in our Vesta mapping project.

REFERENCES

Bates, R. H. T. 1982. Astronomical speckle imaging. *Phys. Rept.* 90:203–297.

Bates, R. H. T., and Fright, W. R. 1983. Composite two-dimensional phase restoration procedure. *J. Opt. Soc. Amer.* 73:358–365.

Bates, R. H. T., and Fright, W. R. 1984. Reconstructing images from their Fourier intensities. In *Advances in Computer Vision and Image Processing*, vol. 1, ed. T. S. Huang (Greenwich, Conn.: JAI Press), pp. 227–264.

Bates, R. H. T., and Lane, R. G. 1987. Automatic deconvolution and phase retrieval. *Proc. SPIE* 828:157–164.

Bates, R. H. T., and McDonnel, M. J. 1986. *Image Restoration and Reconstruction* (Oxford: Clarendon Press).

Brown, R. H., Morrison, D., Telesco, C. M., and Brunk, W. 1982. Calibration of the radiometric asteroid scale using occultation diameters. *Icarus* 52:188–195.

Catullo, V., Zappalà, V., Farinella, P., and Paolicchi, P. 1984. Analysis of the shape distribution of asteroids. *Astron. Astrophys.* 138:464–468.

Cellino, A., Zappalà, V., Di Martino, M., and Paolicchi, P. 1987. Flattening, pole and albedo features of 4 Vesta from photometric data. *Icarus* 70:546–565.

Christou, J. C. 1988. Application of speckle interferometry techniques: Working with real data. In *Proc. NOAO/ESO Conf. on High Resolution Imaging by Interferometry*, 15–18 March, Garching, FRG, Part 1:97–111.

Christou, J. C., Cheng, A. Y. S., Hege, E. K., and Roddier, C. 1985. Seeing calibration of optical astronomical speckle interferometric data. *Astron. J.* 90:2644–2651.

Christou, J. C., McCarthy, D. W., and Cobb, M. C. 1987. Image selection and binning for improved atmospheric calibration of infra-red speckle data. *Astron. J.* 94:516–522.

Davis, D. R., Chapman, C. R., Greenberg, R., and Weidenschilling, S. J. 1979. Collisional evolution of asteroids: Populations, rotations, and velocities. In *Asteroids*, ed. T. Gehrels (Tucson: Univ. of Arizona Press), pp. 528–577.

Dermott, S. F., and Thomas, P. C. 1988. The shape and internal structure of Mimas. *Icarus* 73:25–65.

Drummond, J. D., and Cocke, W. J. 1988. Triaxial ellipsoid dimensions and rotational pole of 2 Pallas from two stellar occultations. *Icarus*, in press.

Drummond, J. D., and Hege, E. K. 1986. Speckle interferometry of asteroids. III. 511 Davida and its photometry. *Icarus* 67:251–263.

Drummond, J. D., Cocke, W. J., Hege, E. K., Strittmatter, P. A., and Lambert, J. V. 1985a. Speckle interferometry of asteroids. I. 433 Eros. *Icarus* 61:132–151.

Drummond, J. D., Hege, E. K., Cocke, W. J., Freeman, J. D., Christou, J. C., and Binzel, R. P. 1985b. Speckle interferometry of asteroids. II. 532 Herculina. *Icarus* 61:232–240.

Drummond, J. D., Eckart, A., and Hege, E. K. 1988a. Speckle interferometry of asteroids. IV. Reconstructed images of 4 Vesta. *Icarus* 73:1–14.

Drummond, J., Taylor, R., Greenberg, R., and Lebofsky, L. 1988*b*. The mysterious case of 532 Herculina. Asteroids II Abstract Booklet, 8–11 March, Tucson, Arizona.

Farinella, P., Paolicchi, P., Tedesco, E. F., and Zappalà, V. 1981. Triaxial equilibrium ellipsoids among the asteroids? *Icarus* 46:113–123.

Feinup, J. R. 1978. Reconstruction of an object from the modulus of its Fourier transform. *Opt. Lett.* 3:27–29.

Feinup, J. R. 1979. Space object imaging through the turbulent atmosphere. *Opt. Eng.* 18:529–534.

Feinup, J. R. 1986. Phase retrieval using boundary conditions. *J. Opt. Soc. Amer. A* 3:284–288.

Feinup, J. R., and Wackerman, C. C. 1986. Phase retrieval stagnation problems and solutions. *J. Opt. Soc. Amer. A* 3:1897–1907.

Feinup, J. R., Crimmins, T. R., and Holsztynski, W. 1982. Reconstruction of the support of an object from the support of its autocorrelation. *J. Opt. Soc. Amer.* 72:610–624.

Freeman, J. D., Christou, J. C., Roddier, F., McCarthy, D. W., and Cobb, M. L. 1988. Application of bispectrum analysis for phase recovery from one-dimensional infrared speckle data. *J. Opt. Soc. Amer. A* 5:406–415.

French, L. M., and Veverka, J. 1983. Limb darkening of meteorites and asteroids. *Icarus* 54:38–47.

Fulchignoni, M., and Barucci, M. A. 1984. The effect of the large crater on the asteroid's lightcurve. *Bull. Amer. Astron. Soc.* 16:699 (abstract).

Hardy, J. W., Lefebvre, J. E., and Koliopoulos, C. L. 1977. Real-time atmospheric compensation. *J. Opt. Soc. Amer.* 67:360–369.

Hege, E. K., and Vokac, P. R. 1986. Real-time amplitude and phase integration for diffraction limited imaging. *Proc. SPIE* 627:780–786.

Hege, E. K., Cocke, W. J., Hubbard, E. N., Christou, J., and Radick, R. 1980*a*. Possible secondaries of asteroids found by speckle interferometry. *Bull. Amer. Astron. Soc.* 12:662 (abstract).

Hege, E. K., Cocke, W. J., Hubbard, E., Gesham, M., Strittmatter, P. A., Radick, R., and Worden, S. P. 1980*b*. Speckle interferometric observations of 2 Pallas. *Bull. Amer. Astron. Soc.* 12:509 (abstract).

Hege, E. K., Hubbard, E. N., Strittmatter, P. A., and Cocke, W. J. 1982. The Steward Observatory speckle interferometry system. *Optica Acta* 29:701–715.

Hege, E. K., Eckart, A., and Christou, J. 1986. The noise bias problem in optical speckle interferometry: Experience with a real detector. *Proc. SPIE* 627:772–779.

Jurgens, R. F., and Goldstein, R. M. 1976. Radar observations at 3.5 and 12.5 cm wavelength of asteroid 433 Eros. *Icarus* 28:1–15.

Knox, K. T., and Thompson, B. J. 1974. Recovery of images from atmospherically degraded short exposure photographs. *Astrophys. J.* 193:L45–L48.

Labeyrie, A. 1970. Attainment of diffraction limited resolution in large telescopes by Fourier analyzing speckle patterns in star images. *Astron. Astrophys.* 6:85–87.

Labeyrie, A. 1978. Stellar interferometry methods. *Ann. Rev. Astron. Astrophys.* 16:77–102.

Lebofsky, L. A., and Reike, G. H. 1979. Thermal properties of 433 Eros. *Icarus* 40: 297–308.

Lebofsky, L. A., Sykes, M. V., Tedesco, E. F., Veeder, G. J., Matson, D. L., Brown, R. H., Gradie, J. C., Feierberg, M. A., and Rudy, R. J. 1986. A refined "standard" thermal model for asteroids based on observations of 1 Ceres and 2 Pallas. *Icarus* 68:239–251.

Lebofsky, L. A., Greenberg, R., Tedesco, E. F., and Veeder, G. J. 1988. Infrared lightcurves of asteroids 532 Herculina and 45 Eugenia: Proof of the absence of significant albedo markings. *Icarus* 75:518–526.

Magnusson, P. 1986. Distribution of spin axes and senses of rotation for 20 large asteroids. *Icarus* 68:1–39.

Matson, D. L., Veeder, G. J., Walker, R. G., Fowler, J. W., Chillemi, J. R., Lebofsky, L. A., and Tedesco, E. F. 1986. IRAS asteroid and comet catalogs. In *IRAS Asteroid and Comet Survey,* Preprint Version 1, Part III, ed. D. L. Matson (Pasadena: Jet Propulsion Laboratory) pp. 1–84.

Morrison, D., and Zellner, B. 1979. Polarimetry and radiometry of the asteroids. In *Asteroids,* ed. T. Gehrels (Tucson: Univ. of Arizona Press), pp. 1090–1097.

Nisenson, P., and Papaliolios, C. 1983. Effects of photon noise bias on speckle image reconstruction with the Knox-Thompson algorithm. *Opt. Comm.* 47:91–96.

Papaliolios, C., Nisenson, P., and Ebstein, S. 1985. A new two dimensional photon counting camera. *Appl. Opt.* 24:287–292.

Roddier, F. 1988. Interferometric imaging in optical astronomy. *Phys. Rept.*, 170(2):97–166.

Takajo, H., and Takahashi, T. 1988. Least-squares phase estimation from the phase difference. *J. Opt. Soc. Amer. A* 5:416–425.

Taylor, R. C., Birch, P. V., Drummond, J., Pospieszalska-Surdej, A., and Surdej, J. 1987. Asteroid 532 Herculina: Lightcurves, pole orientation, and a model. *Icarus* 69:354–369.

Thomas, P. C. 1988. Radii, shapes, and topography of the satellites of Uranus from limb coordinates. *Icarus* 73:427–441.

Timothy, J. G., and Morgan, J. S. 1986. Imaging by time-tagging photons with the muti-anode microchannel array detector system. *Proc. SPIE* 627:654–659.

Wasserman, L. H., Millis, R. L., Franz, O. G., Bowell, E., White, N. M., Giclas, H. L., Martin, L. J., Elliott, J. L., Dunham, E., Mink, D., Baron, R., Honeycutt, R. K., Hendon, A. A., Kephart, J. E., A'Hearn, M. F., Reitsema, H. J., Radick, R., and Taylor, G. E. 1979. The diameter of Pallas from its occultation of SAO 85009. *Astron. J.* 84:259–268.

Worden, S. P. 1979. Interferometric determinations of asteroid diameters. In *Asteroids,* ed. T. Gehrels (Tucson: Univ. of Arizona Press), pp. 119–131.

Zappalà, V., Farinella, P., Knezevic, Z., and Paolicchi, P. 1984. Collisional origin of the asteroid families: Mass and velocity distributions. *Icarus* 59:261–285.

Zellner, B. 1976. Physical properties of asteroid 433 Eros. *Icarus* 28:149–153.

RADAR OBSERVATIONS OF ASTEROIDS

STEVEN J. OSTRO
Jet Propulsion Laboratory

Echoes from 33 main-belt asteroids (MBAs) and 19 near-Earth asteroids (NEAs) have provided a wealth of new information about these objects such as sizes, shapes, spin vectors, and such surface characteristics as decimeter-scale morphology, topographic relief, regolith porosity and metal concentration. On average, small NEAs are much rougher at decimeter scales than MBAs, comets or the terrestrial planets. Some of the largest MBAs (e.g., 1 Ceres and 2 Pallas) are smoother than the Moon at decimeter scales but much rougher than the Moon at some much larger scale. There is at least a five-fold variation in the radar albedos of MBAs, implying substantial variations in the surface porosities or metal concentrations of these objects. The highest MBA albedo estimate, for 16 Psyche, is consistent with a metal concentration near unity and lunar porosities. The diversity of NEA radar signatures is extreme. The radar albedo of 1986 DA is twice that of Psyche and strongly suggests that this Earth-approacher is a ~2-km metallic fragment with hardly any regolith; it might be the source of some of our iron meteorites. NEA polar silhouettes range from slightly noncircular to highly elongated and distinctly nonelliptical. Delay-Doppler images of 1627 Ivar show this ~7-km object to be elongated, irregular, nonconvex and bifurcated. The radar signatures of NEAs often seem extraordinarily complex compared to those of large MBAs, and suggest an abundance of exotically shaped objects in the near-Earth population. Echoes from 1986 JK, detected at 11 lunar distances from Earth three weeks after its discovery, yielded Doppler-frequency measurements adequate to ensure future optical recovery of this asteroid. "Radar astrometry" of NEAs is important even for asteroids with an extensive optical astrometric history, because a handful of delay-Doppler measurements can shrink the positional error ellipsoid of the prediction ephemeris by a factor ≥2 for decades.

I. INTRODUCTION

Radar observations of asteroids have increased exponentially since this book's predecessor was published (Gehrels 1979) (Fig. 1 and Table I; cf. Pettengill and Jurgens 1979, their table). This chapter reviews the relatively small portion of the results already reported in the literature, but its primary emphasis is on techniques, observational strategies and physical interpretation of radar signatures.

Radar observations of asteroids are powerful for a variety of reasons, the most prominent being the high degree of control exercised by the observer on the signal transmitted to illuminate the target. This illumination is an intense, coherent radio signal whose polarization and time/frequency modulation are designed by the astronomer to match particular scientific objectives. By comparing the echo's characteristics to those of the transmitted waveform, one can deduce the asteroid's radar properties. Thus, the astronomer is intimately involved in an active observation and, in a very real sense, conducts a controlled laboratory experiment on the asteroid.

As discussed below, resolution of echoes in Doppler frequency and/or time delay provides one-dimensional or two-dimensional images of an asteroid, even though the target's angular extent is miniscule compared to that of the radar beam. Because of the macroscopic wavelengths employed, radar is sensitive to near-surface structure at "human" as well as much larger, "to-

CUMULATIVE # OF RADAR-DETECTED ASTEROIDS
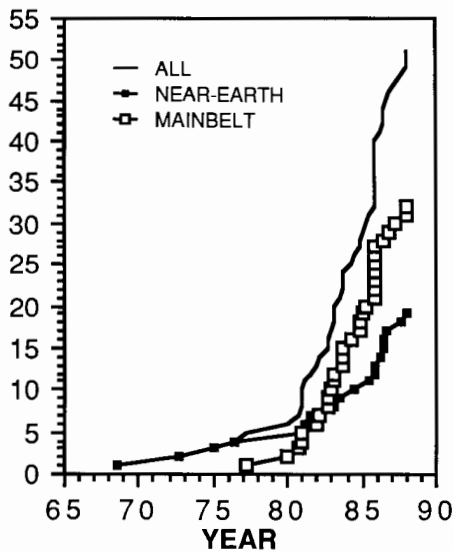
Fig. 1. Cumulative number of radar-detected asteroids. See Table I.

TABLE I
History of Asteroid Radar Detections[a]

Year	Main-Belt	Reference[b]	Near-Earth	Reference[b]
1968			1566 Icarus	1 (λ13 single) [G]
			"	2 (λ3.8 single) [H]
1972			1685 Toro	3 (λ13 single) [G]
1975			433 Eros	4 (λ3.5, λ13) [G]
			"	5 (λ70 single)
1976			1580 Betulia	6 (λ13 single)
1977	1 Ceres	7 (λ13 single)		
1979	4 Vesta	8 (λ13 single)		
1980	7 Iris	9	1685 Toro[c]	10
	16 Psyche	9	1862 Apollo	11
			"	12 (λ3.5 single) [G]
1981	97 Klotho	9 (λ13 single)	1915 Quetzalcoatl	11
	4 Vesta[c]	9	2100 Ra-Shalom	13
	8 Flora	9		
1982	2 Pallas	9		
	12 Victoria	9		
	19 Fortuna	9		
	46 Hestia	9		
1983	5 Astraea	9	1620 Geographos	11
	139 Juewa	9	2201 Oljato	11
	356 Liguria	9		
	80 Sappho	9		
	694 Ekard	9		
1984	9 Metis	9	2101 Adonis	11
	554 Peraga	9	2100 Ra-Shalom[c]	11
	144 Vibilia	9		
	1 Ceres[c]	9		
	7 Iris[c]	14		

Year	Main-belt	λ	Near-Earth	λ
1985	6 Hebe	9	1627 Ivar	11
	41 Daphne	9	1036 Ganymed	15
	21 Lutetia	15	1866 Sisyphus	15
	33 Polyhymnia	15		
	84 Klio	15		
	192 Nausikaa	15		
	230 Athamantis	15		
	216 Kleopatra	15		
	18 Melpolmene	15		
	16 Psyche[c]	14		
1986	1 Ceres[d]	14	1986 DA	15
	393 Lampetia	15	1986 JK	16 (λ3.5) [G]
	27 Euterpe	14	3103 (1982 BB)	15
	19 Fortuna[c]	14	3199 Nefertiti	14
	9 Metis[c]	14		
1987	5 Astraea[c]	14	1981 Midas	17 (λ3.5) [G]
	532 Herculina	14	3757 (1982 XB)	14
	2 Pallas[c]	14		
	20 Massalia	14		
1988	654 Zelinda	14		
	4 Vesta[c]	14		
	105 Artemis	14		
Totals:	33 main-belt		19 near-Earth	

[a] Most of the observations are from Arecibo, λ13-cm, and dual-polarization. Exceptions are flagged by the wavelength in cm, by "single" to denote single polarization, and/or by [G] for Goldstone or [H] for Haystack.

[b] References: 1: Goldstein 1969a,b; 2: Pettengill et al. 1969; 3: Goldstein et al. 1973; 4: Jurgens and Goldstein 1976; 5: Campbell et al. 1976; 6: Pettengill et al. 1979; 7: Ostro et al. 1979; 8: Ostro et al. 1980; 9: Ostro et al. 1985a; 10: Ostro et al. 1983; 11: Ostro et al. 1985b; 12: Goldstein et al. 1981; 13: Ostro et al. 1984; 14: Ostro, Campbell, Shapiro et al. (unpublished); 15: Ostro et al. 1986a; 16: Ostro et al. 1989; 17: Ostro, Yeomans, Goldstein and Jurgens (unpublished).

[c] Second apparition yielding radar detection.

[d] Third apparition yielding radar detection.

pographic" scales, and to regolith porosity and metal abundance. Moreover, since radar measurements are "line of sight," radar constraints on asteroid orbits, dimensions and spin vectors are distinct from, and complementary to, optical "plane of sky" constraints on those quantities. The principal limitations of asteroid radar astronomy arise because of insufficient echo strength; most asteroids rarely, if ever, pass within the detectability windows of current planetary radar telescopes.

II. TECHNIQUES

Echo Detectability

What factors determine an asteroid's radar echo strength? Let P_T be the transmitted power, λ the radar wavelength, G the antenna gain, $A_e = G\lambda^2/4\pi$ the antenna's effective aperture, R the target's distance and σ the target's radar cross section, defined as 4π times the backscattered power per steradian per unit incident flux at the target. Then the received power will be (see, e.g., Ostro 1987a)

$$P_R = P_T G A_e \sigma / (4\pi)^2 R^4. \qquad (1)$$

The receiver noise power can be written $P_N = kT_s\Delta f$, where k is Boltzmann's constant, T_s the receiver system temperature and Δf the data's frequency resolution. Since we can determine and remove the mean background noise level P_N, the echo power P_R is detectable as long as it dwarfs the random fluctuations in P_N. Those fluctuations are chi-square distributed, but for values of Δf and the integration time Δt satisfying $\Delta f \cdot \Delta t >> 10$, the distribution is approximately Gaussian with standard deviation $\Delta P_N = P_N/(\Delta f \cdot \Delta t)^{1/2}$. (See, e.g., Jenkins and Watts 1968.) We can maximize the signal-to-noise ratio, $SNR = P_R/\Delta P_N$, by picking a frequency resolution matched to the echo spectrum, whose bandwidth will be proportional to $D/\lambda P$, where D and P are the target's diameter and rotation period. Defining the target's radar albedo as $\hat{\sigma} = \sigma/(\pi D^2/4)$ and substituting, we have

$$SNR \simeq (\text{system factor}) \times (\text{target factor}) \times (\Delta t)^{1/2} \qquad (2)$$

where

$$\text{system factor} \simeq P_T G^2 \lambda^{5/2} /T_s \qquad (3)$$

and

$$\text{target factor} = \hat{\sigma} D^{3/2} P^{1/2} /R^4. \qquad (4)$$

A signal-to-noise ratio > 5 normally indicates a detection, but useful resolution of the echo demands much larger values. For example, interesting delay-Doppler imaging is difficult if SNR is much less than ~ 100. Propagation of noise into error in estimates of such echo characteristics as spectral bandwidth is examined by Jurgens and Bender (1977).

Radar Systems

The two radar facilities active in asteroid studies are the National Astronomy and Ionosphere Center's Arecibo Observatory in Puerto Rico and the Jet Propulsion Laboratory's Goldstone Radar in California. Wavelengths for all asteroid radar observations during the past decade have been 13 cm at Arecibo and 3.5 cm at Goldstone. Order-of-magnitude values of each system's characteristics during recent asteroid work are $P_T = 400$ kw, $G = 10^{7.1}$ and $T_s = 25$ K.

The Arecibo instrument, located at $18°3$ N latitude, consists of a fixed, 305-m, spherical reflector (Fig. 2). Movable line feeds, suspended from a triangular structure some 130 m above the dish, correct for spherical aberration and can be pointed in altitude and azimuth, enabling the telescope to track asteroids within $20°$ of the zenith, i.e., for durations up to ~ 2.9 hr. Goldstone, located at $34°$ N latitude, consists of a parabolic antenna with horn feeds (Fig. 3). It is fully steerable and has access to the entire sky north of declination $-50°$, a capability that compensates for its peak sensitivity during recent asteroid observations being almost an order of magnitude less than Arecibo's. Among the 51 radar-observed asteroids, Goldstone obtained the only detection in two cases and the strongest echoes in two others. However, improvements being made in Goldstone, including enlargement of the dish's diameter from 64 m to 70 m, will leave it $\sim 1/3$ as sensitive as Arecibo's, so 3.5-cm asteroid studies should expand sharply during the next few years.

Measurements: Time Delay and Doppler Frequency

In a typical radar experiment, a signal is transmitted toward the target for a duration near the roundtrip light travel time to the target, and then echoes are received for a comparable duration. During reception, the maser-amplified signal is mixed to lower frequencies and filtered, and then digital samples of the signal's voltage are either recorded directly or, depending on the nature of the radar experiment and the transmitted waveform's time/frequency structure, first Fourier transformed or decoded using online hardware into a format more amenable to post-real-time processing (Ostro 1987a).

The time delay τ between transmission of a pulse and reception of the echo from a target at distance R is of order $2R/c$, where c is the speed of light. Among the radar-detected asteroids, echo time delays have ranged from 29 seconds for 1986 JK at 0.029 AU (Ostro et al. 1989) to 35 minutes for a recent Arecibo observation of Pallas at 2.1 AU.

For a target whose velocity component in the direction of the radar is
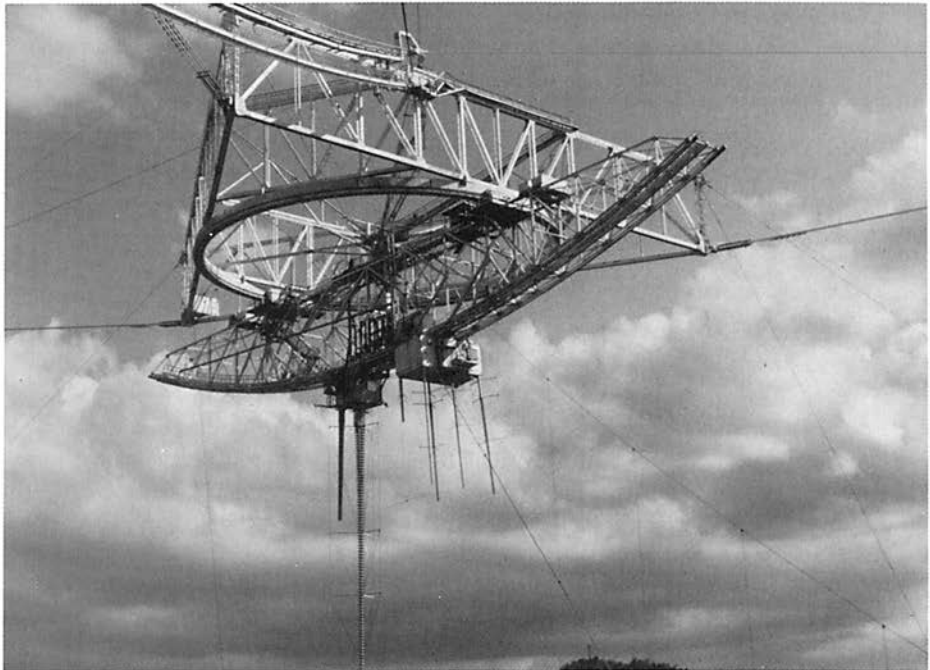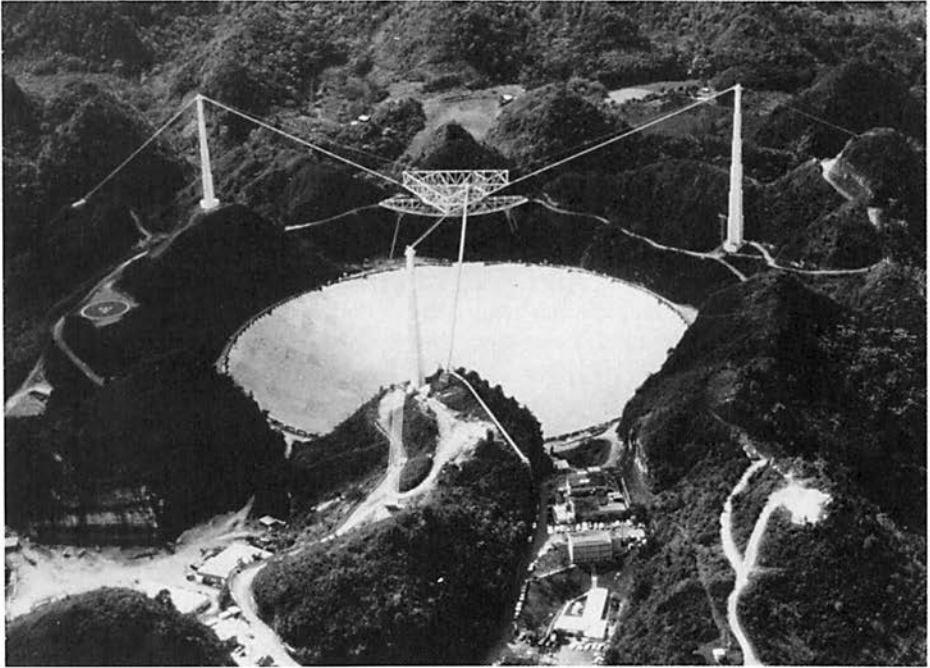
Fig. 2. The Arecibo telescope in Puerto Rico. *Top:* an aerial view of the entire instrument; *bottom:* a close-up of the structure suspended above the spherical reflector. The λ13-cm feed, used for asteroid radar observations, extends from the middle, uphill part of the carriage house closest to the viewer.
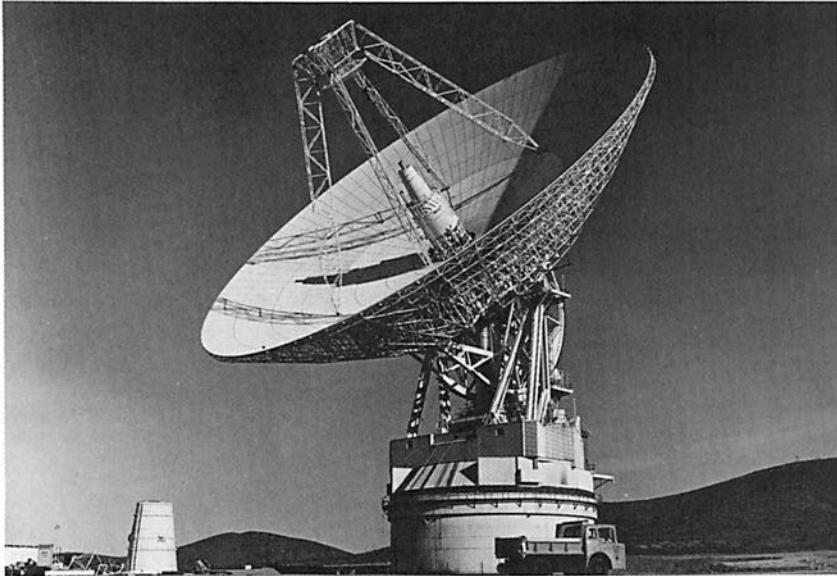
Fig. 3. The Goldstone antenna in California.

v_{RAD}, echoes are Doppler shifted by a frequency given, to first order in v_{RAD}/c, by $\nu = 2v_{RAD}f_{TX}/c$; a 1-Hz Doppler shift corresponds to a radial velocity of a half wavelength per second. Asteroid radial velocities can be as large as several tens of kilometers per second, causing Doppler frequencies on the order of a MHz at $\lambda = 3.5$ cm. Asteroid Doppler shifts have been reported with quoted errors as low as 0.05 Hz at $\lambda = 13$ cm, or 3 mm s^{-1}, while recent observations (Ostro, Shapiro, Campbell and Hine, unpublished results) have yielded time-delay measurements with intrinsic precisions on the order of a few microseconds for near-Earth asteroids and several tens of microseconds for main-belt asteroids.

Radar Astrometry

Because line-of-sight radar astrometric measurements have much finer intrinsic fractional precision than their optical plane-of-sight counterparts, they are potentially valuable for refining our knowledge of asteroid orbits. Noting that reliable prediction ephemerides tend to be more difficult to develop for near-Earth asteroids than for MBAs, Yeomans et al. (1987) performed a series of uncertainty analyses to assess quantitatively the degree to which radar astrometry can improve the accuracy of NEA ephemerides. They studied a variety of possible optical and radar data histories to explore how

errors in predicted plane-of-sky asteroid positions vary as a function of time after a series of optical astrometric measurements, and how radar delay and Doppler estimates can improve the predictions. Radar provided only a modest absolute reduction in ephemeris uncertainty for a numbered asteroid with a half-century-long optical astrometric history and a well established orbit, but dramatic improvement in future ephemerides of various asteroids with optical astrometric histories only a few months long.

For a newly discovered NEA, a few radar observations could easily mean the difference between successfully recovering the object during its next close Earth approach and losing it entirely. However, even for a numbered NEA with a secure orbit, a few delay-Doppler measurements can shrink the positional error ellipsoid by a factor of two for at least a decade. Such modest refinement could prove critical in planning stellar occultation observations and would certainly be valuable for asteroids targeted for spacecraft flyby and rendezvous missions. Figure 4 illustrates results of the Yeomans et al. (1987) error analysis for 1986 DA, an object with a good astrometric history.

Delay-Doppler Dispersion of Echo Power

Each backscattering element on an asteroid's surface returns an echo with a particular time delay τ and Doppler frequency ν, and we use $\sigma(\tau,\nu)$ to denote the asteroid's delay-Doppler distribution of echo power. Contours of constant delay are equidistant from the radar. The asteroid's delay depth, or the dispersion $\Delta\tau$ in $\sigma(\tau,\nu)$, is the time difference between the shortest and longest delays, i.e., between arrival times for echoes from the subradar point and the limb.

The echo's Doppler frequency dispersion $\Delta\nu$, or simply the bandwidth B, depends on the asteroid's size and spin rate as well as on the viewing geometry. An asteroid's instantaneous echo bandwidth can be expressed as

$$B = (4\pi D/\lambda P) \sin \alpha \qquad (5)$$

where P is the synodic rotation period, α the aspect angle (between the spin vector and the line of sight) and D the sum of the distances from the plane containing the radar line of sight and the asteroid's apparent spin vector Ω to the backscattering surface elements with the greatest positive (approaching) and greatest negative (receding) radial velocities. Figure 5 shows geometric relationships between an asteroid's shape and its echo power spectrum. The view along Ω shows the asteroid's pole-on projection, i.e., its "polar silhouette." D is this silhouette's width, or breadth, measured normal to the line of sight. Equivalently, D is the breadth of the silhouette's convex envelope or "hull." Ostro et al. (1988) show how the hull can be estimated from a collection of echo spectra with adequate rotational phase coverage, frequency resolution and signal-to-noise ratio.

We can think of the hull H either as the shape of a rubber band stretched
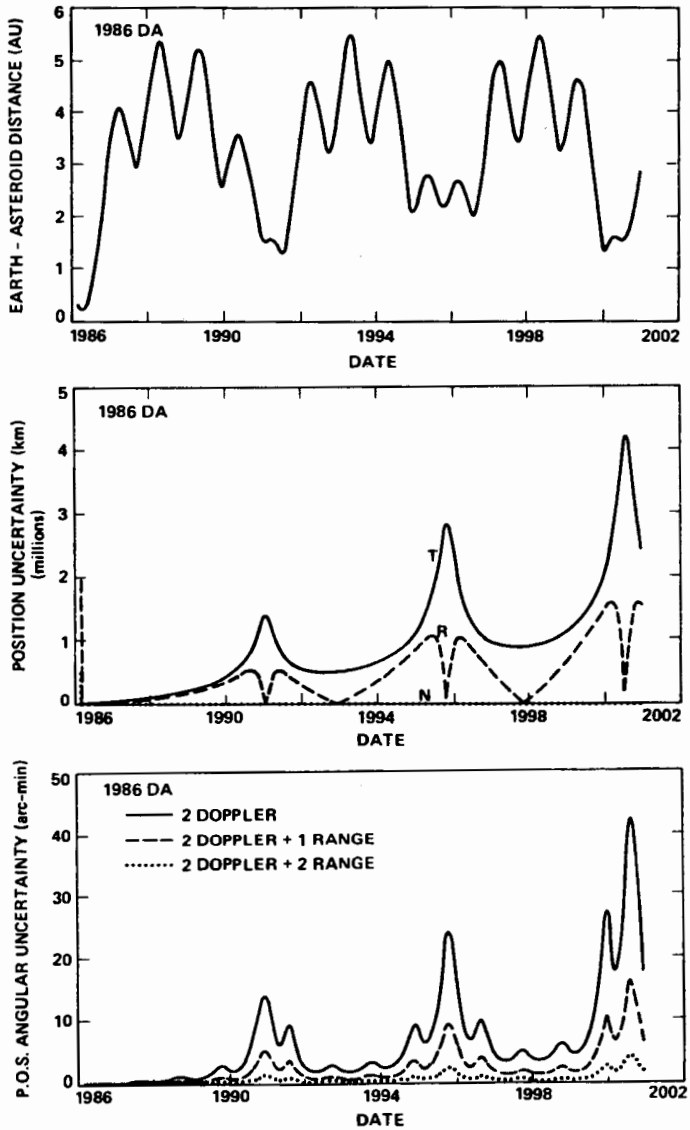
Fig. 4. Radar astrometric study of asteroid 1986 DA by Yeomans et al. (1987). *Top:* geocentric distance vs date. *Middle:* position uncertainties vs date. The asteroid-centered coordinate system is defined by the Sun-asteroid unit vector **R,** the unit vector **N** normal to the orbital plane, and **T** = **N** × **R.** *Bottom:* Plane-of-sky (P.O.S.) uncertainty in the prediction ephemeris vs date, for two radar Doppler measurements combined with 0, 1 or 2 range measurements.
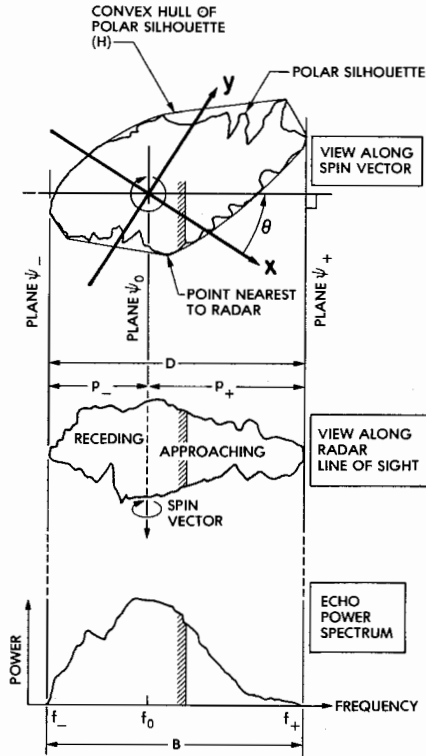
Fig. 5. Geometric relationships between an asteroid's shape and its echo power spectrum. The plane ψ_0 contains the line of sight and the asteroid's spin vector Ω. Echo from any portion of the asteroid intersecting ψ_0 has Doppler frequency f_0. The cross-hatched strip of power in the spectrum corresponds to echoes from the cross-hatched strip on the asteroid. The convex hull H on the asteroid's polar silhouette can be estimated from echo spectra adequately distributed in rotational phase (figure from Ostro et al. 1988).

around the polar silhouette or as the pole-on projection of the asteroid's three-dimensional convex envelope. In simpler words, H furnishes a pole-on view of the asteroid with concavities "filled in" and with dimensions in units of kilometers/sin α. Thus H sets a lower bound on the asteroid's dimensions and pole-on projected area, which in turn can be used to refine albedo estimates. Furthermore, by treating the center-of-mass frequency (f_0 in Fig. 5) as a free parameter, one can optimize estimation of Doppler frequencies for asteroids with unknown and potentially irregular shapes, minimizing systematic error in radar astrometric measurements.

For very large, main-belt asteroids, prior knowledge of sizes and spin periods often is very good, so here echo bandwidth measurements are most valuable as pole-direction constraints. This topic is discussed in the chapter by Magnusson et al.

Albedo and Polarization Ratio

In most modern asteroid radar observations, we transmit a circularly polarized signal and use two parallel receiving channels to receive echoes in the same circular polarization sense as transmitted (the SC sense) as well as in the opposite (OC) sense. Coherent, single back reflections from dielectric interfaces whose sizes and radii of curvature greatly exceed the wavelength would produce echoes almost entirely in the OC populations. SC echo power can arise from multiple scattering, from single backscattering from interfaces with wavelength-scale radii of curvature (e.g., rocks) or from subsurface refraction effects. Therefore, the circular polarization ratio, $\mu_c = \sigma_{sc}/\sigma_{oc}$, serves as a useful gauge of the asteroid's generalized, wavelength-scale complexity, or roughness, within the radar penetration depth of the surface. Measurement of the disk-integrated radar quantities μ_c and the "radar albedo" $\hat{\sigma}_{oc}$ comprise primary objectives of most asteroid radar observations. [The geometric albedo, used in optical astronomy, equals $(1 + \mu_c)\hat{\sigma}_{oc}/4$.]

For targets with very low μ_c, the ratio's physical interpretation is unique, because the surface must be smooth at all scales within about an order of magnitude of the wavelength and the subsurface material must be virtually devoid of wavelength-scale structure to depths of several $1/e$ power absorption lengths L. If we know the asteroid's gross shape, its spin period and the aspect angle, then we can determine the asteroid's radar backscattering law, which can be modeled to yield the *rms* slope of surface elements with respect to the gross shape as well as the backscatter gain, $g = \hat{\sigma}_{oc}/\rho$, where ρ is the Fresnel power-reflection coefficient for normal incidence. That coefficient depends on the electrical properties of the asteroid surface. If the upper few meters are homogeneous, porous, dry, unconsolidated regolith consisting of particles no larger than $\sim\lambda/100$, then ρ and L depend just on bulk density (Ostro et al. 1985a; Garvin et al. 1985). Bulk density is a function of the porosity and the volume fractions and specific gravities of the rock and metal phases. Thus, in principle, radar measurements let us estimate regolith characteristics that are poorly constrained by other methods. Metal concentration is of particular interest, since it bears on the asteroid's meteorite association and hence its thermochemical history, as well as on its potential economic value as a space resource.

Using $\hat{\sigma}_{oc}$ to estimate ρ may lead to overestimation of the Fresnel coefficient, and hence to overestimation of bulk density, if $g > 1$. The gain would be unity for a smooth sphere, but larger for larger *rms* slopes. However, at least for applicable rough-surface scattering models compatible with μ_c near zero, gains closer to two than to unity seem very unlikely; a sphere with an *rms* slope of $0°$ would have $g = 1$, and one with *rms* slope comparable to the angle of repose for particulates ($\sim35°$) would have $g \sim 1.1$. Moreover, although taking $\hat{\sigma}_{oc}$ to estimate ρ may inflate estimates of regolith bulk density, we expect this positive bias to be offset by an "artificial" reduction in ρ if the regolith density near the surface is not constant, but instead increases gradu-

ally down to depths $>\lambda/4$. Such a configuration creates an impedance match between the regolith and free space, severely attenuating the reflected power (Simpson 1976).

III. RESULTS FOR MAIN-BELT ASTEROIDS

This section summarizes results obtained by Ostro et al. (1985a) for 20 main-belt asteroids. Figure 6 shows the dual-polarization radar signatures for 15 of those objects, averaged over the observed rotational phases and filtered to the indicated frequency resolutions. Asteroid echoes obtained to date lack the sharply peaked *OC* spectral signature seen for the Moon and the inner planets. That signature arises because single back reflections from smooth surface elements dominate the echo and the *rms* surface slope is very small
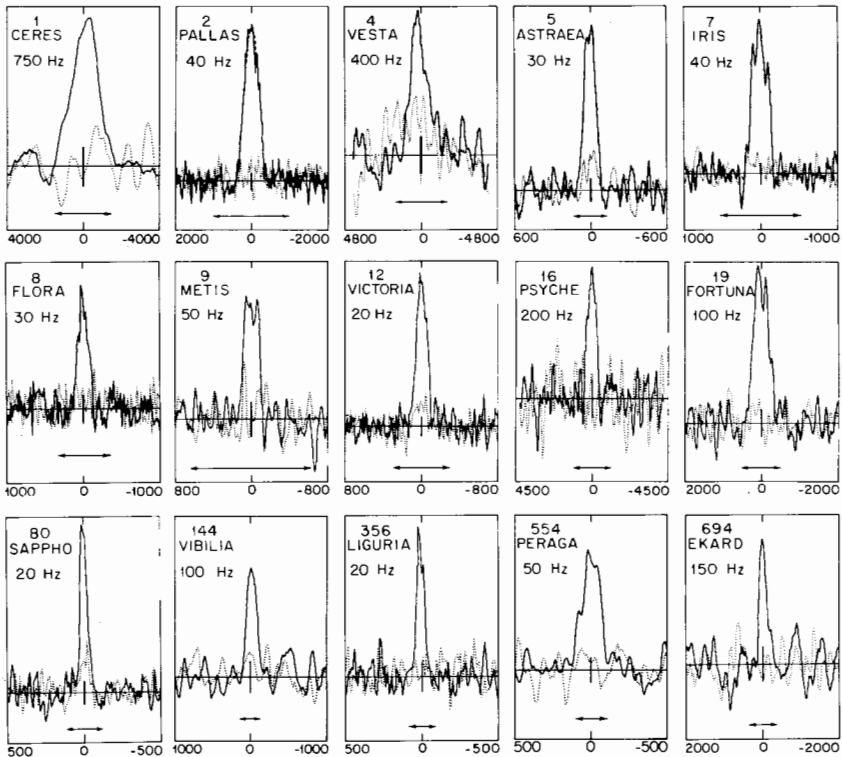
Fig. 6. Dual-polarization radar echo spectra obtained for 15 asteroids by Ostro et al. (1985a). *OC* and *SC* spectra (solid and dotted curves, respectively) are filtered to the indicated frequency resolution. Echo power is plotted against Doppler frequency. Central vertical bars represent ±1 standard deviation of the receiver noise. Horizontal arrows show the maximum echo bandwidth expected.

(~6°); most of the echo comes from a region within ~6° of the subradar point. In contrast, asteroid echo spectra are very broad (that is, there is very little limb darkening), so we know that asteroids are rougher than the Moon at some scale(s) no smaller than a few cm. As can be seen in Figs. 6 and 7, most MBAs tend to have low circular polarization ratios, indicating that single back reflection from smooth surface elements is the dominant scattering mechanism. For such objects, the roughness scale responsible for the broad *OC* spectral shapes must exceed many m, and the severity of that roughness must exceed the Moon's.

Exploiting the high signal-to-noise ratio of their *OC* echo for Pallas and the existence of outstanding stellar-occultation chords and a reliable spin period for that object, Ostro et al. (1985a) performed model fits which argue strongly for *rms* slopes ≥20°. (Those estimations also yielded an aspect angle estimate consistent with optical constraints on the pole direction.) Therefore,
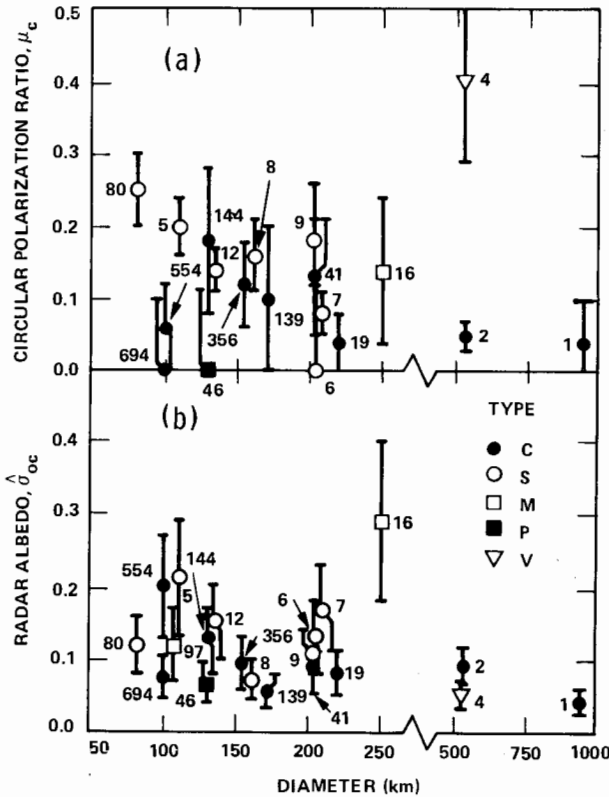
Fig. 7. Main-belt asteroid radar albedos and circular polarization ratios, plotted vs asteroid diameter (figure from Ostro et al. 1985a).

Pallas appears to be smooth at "human" scales but topographically rough. Given the available constraints on spin vectors, dimensions, and hence maximum echo bandwidths of other MBAs, Ostro et al. (1985a) deduced that most MBAs appear rough at some scale no smaller than a few m. Note that km-sized residuals between stellar-occultation chord ends and elliptical models (see, e.g., Millis et al. 1987; Wasserman et al. 1979) argue for the presence of topography at scales monumental compared to the minimum scale dictated by the radar data.

Additional evidence for large-scale structure on asteroids comes from radar spectra obtained for 9 Metis (Fig. 8). The presence of a huge spike on one side of the spectrum taken over a narrow rotational phase interval, but not in spectra at other phases, suggests that the source of the spike is a major topographic construct. An even more extreme example is provided by echoes from the large M-class object 216 Kleopatra (Fig. 9; Ostro et al. 1986a). Spectra taken about 90° apart indicate that Kleopatra is two to three times longer than it is wide. The spectrum presenting the maximum breadth is bifurcated, supporting the conjecture (Weidenschilling 1980, and references
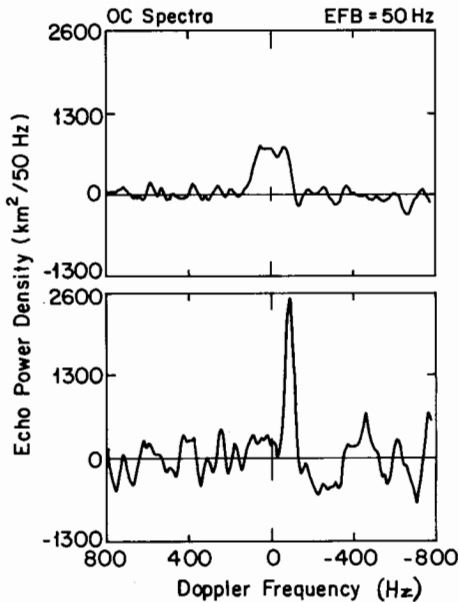
Fig. 8. Radar echo spectra obtained for 9 Metis. *OC* echo power is plotted vs Doppler frequency. The top spectrum, which is plotted on a different scale in Fig. 6, is a 15-run sum of all data obtained by Ostro et al. (1985a) in March 1984. Those data span 300° of rotational phase. The bottom spectrum, from a single run, spans about 28° of rotational phase; its severe asymmetry may be due to a huge flat area on the receding side of Metis, oriented almost normal to the line of sight during this run.
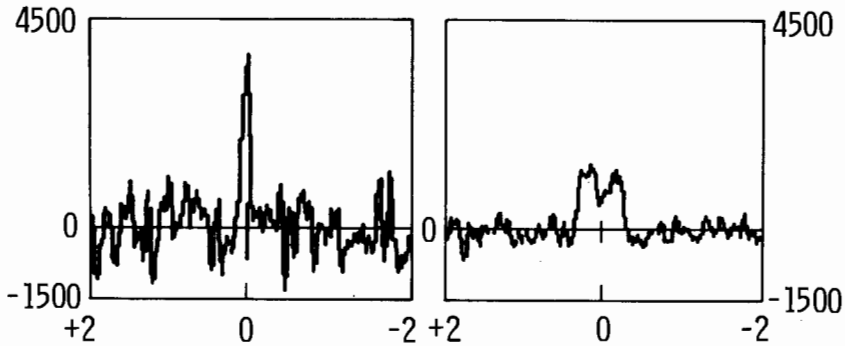
Fig. 9. Echo spectra obtained for 216 Kleopatra at rotational phases ~90° apart (Ostro et al. 1986a). Echo power, in km² of radar cross section per 75-Hz resolution cell, is plotted vs Doppler frequency (kHz). The bar at (0,0) shows ±1 standard deviation of the receiver noise.

therein) that Kleopatra is a "dumbbell-shaped" asteroid. Thorough observation of a stellar occultation by Kleopatra on 14 August 1989, predicted by Wasserman et al. (1987), might elucidate this object's shape and possible duplicity.

Figure 7 demonstrates that MBA circular polarization ratios range from near zero to ~0.3. Whereas the mean value of μ_c for S-class objects might be slightly larger than that for the C class, the two distributions clearly overlap. The figure also suggests the possible tendency for the S-class objects' decimeter-scale roughness to increase with decreasing size.

Combining estimates of radar cross section with occultation or radiometric diameters, Ostro et al. (1985a) estimated the radar albedos of 20 asteroids, finding them to range from 0.047 for Ceres to 0.29 for Psyche. The dispersion implies substantial variations in regolith porosity or metal abundance, or both. Psyche's albedo estimate is consistent with porosities comparable to the typical lunar value (~0.5) and metal concentrations near unity, but it also is consistent with a bare-rock surface and a metal concentration typical of enstatite chondrites. The first hypothesis seems preferable because we expect any asteroid as large as Psyche to possess a thick regolith. Still, we must remember that the premises for the two hypotheses are dictated by Psyche's taxon (M) and by the absence in our meteorite sample of enstatite chondrites with metal concentrations near 0.7. Taken by themselves, the radar results are quite consistent with such a mineralogy and a porosity (~0.3) near the low end of lunar values. The issue of Psyche's meteoritic affiliation is not closed, but if the first hypothesis is correct, Psyche might be the collisionally stripped core of a differentiated asteroid, and by far the largest piece of refined metal in the solar system.

For S-class MBAs, the radar albedos provide joint constraints on porosity and metal abundance, but the metal abundances for the candidate meteorite

analogs ($\sim$0.5 for stony irons vs $<$ 0.2 for ordinary chondrites) are too close to each other to let us choose reliably between the two hypotheses.

IV. RESULTS FOR NEAR-EARTH ASTEROIDS

Whereas the largest MBAs might have nearly spherical shapes, few prior constraints apply to configurations of asteroids much smaller than 100 km. For this reason, a prime goal of NEA radar investigation is to obtain concrete dimensional information. Jurgens and Goldstein (1976) pioneered this effort, applying techniques developed by Jurgens (1982) to model the 3.5-cm *OC* spectra of 433 Eros in terms of a homogeneously scattering ellipsoid. Their post-fit residuals led them to conjecture that this $\sim$20-km object might be more egg-shaped than ellipsoidal. Ostro et al. (1983) applied the same method to 13-cm echoes from 1685 Toro and noted significant departures from the simplified model, possibly including a surface feature with enhanced radar brightness and μ_c. Combining their radar and photoelectric measurements for 2100 Ra-Shalom with infrared-radiometric size information, Ostro et al. (1984) developed joint constraints on its dimensions, pole direction and spin period, again finding it difficult to reconcile the radar data with a homogeneous, axisymmetric model.

Ostro et al. (1985*b*) list spectral bandwidths for eight NEAs, noting that for Toro, Ra-Shalom, 1627 Ivar, 1862 Apollo and 2201 Oljato, differences between bandwidths measured at different rotational phases indicate that the polar silhouettes of those objects are not circular. They report that Oljato's spectra were double-peaked on 1 July 1983 but not on three other nearby dates, possibly indicating a complex shape. For Ivar (Fig. 10), the fractional
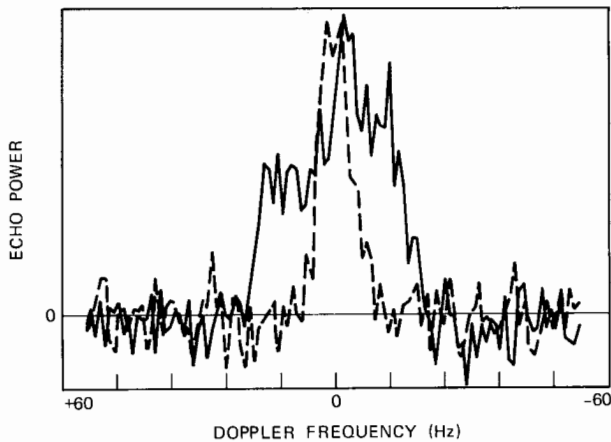
Fig. 10. Echo spectra obtained for 1627 Ivar at rotational phases $\sim$90° apart. *OC* echo power is plotted vs Doppler frequency.

variation in B is twice that in σ_{oc}, suggesting an aspect far from equatorial. Ostro et al. (1986b) describe first results of efforts to estimate the hulls of the polar silhouettes of Ivar and Apollo. Both asteroids are distinctly nonelliptical, with Ivar the more elongated. The same authors report that delay-Doppler images of Ivar show a bimodal, asymmetrical distribution of echo power and suggest a bifurcated shape. For 1986 DA, the spectra are strongly bimodal for each of two rotational phase intervals $\sim180°$ apart, while spectra at other phases range from fairly symmetrical to extremely asymmetrical.

Circular polarization ratios of NEAs tend toward larger values than those of MBAs. For most of the objects observed by Ostro et al. (1985b), μ_c varies with rotational phase, suggesting substantial surface heterogeneity. For Apollo, μ_c varies dramatically across the disk; polarization features exist, but only for tiny (<0.1) fractions of a rotation, and the features' rotational dependence suggests considerable structure at m-to-decameter scales.

The radar properties of 1986 DA are unique among planetary radar targets: a very low circular polarization ratio but an enormous radar albedo. Ostro et al. (1987) report that delay-Doppler images of this object show it to be 1 to 2 km in size, and that the radar albedo is at least twice as large as Psyche's and about ten times that of the Moon. The most plausible interpretation of this radar signature is that 1986 DA's composition is very rich in metal, and that there is little coverage of the surface by porous regolith thicker than a few cm. Hence this object might contribute some of our iron meteorites, or perhaps might share a common origin with them.

In summary, the radar signatures of NEAs often seem extraordinarily complex compared to those of large MBAs. Given the small size of the NEA radar sample, the results strongly suggest an abundance of exotically shaped objects in the NEA population.

V. FUTURE PROSPECTS

Upgrades recently proposed for the Arecibo and Goldstone radars would dramatically extend their reach, permitting major advances in asteroid exploration. At present, Arecibo can barely skim the inner edge of the main belt, but an upgraded instrument would have access to asteroids throughout the belt (Fig. 11; Ostro 1987b). The number of detectable asteroids would increase by two orders of magnitude; those asteroids easy to observe with the current telescope would be observable at signal-to-noise ratios greater than those achieved to date for any asteroid. During its first decade of operation, an upgraded Arecibo could provide valuable delay-Doppler images ($>>10$ pixels on target) of two dozen MBAs and two dozen NEAs, plus accurate hulls for over 100 objects. It could estimate albedos and polarization ratios for some 600 MBAs and half of the currently numbered NEAs.

An upgraded Goldstone would be as sensitive as today's Arecibo, but
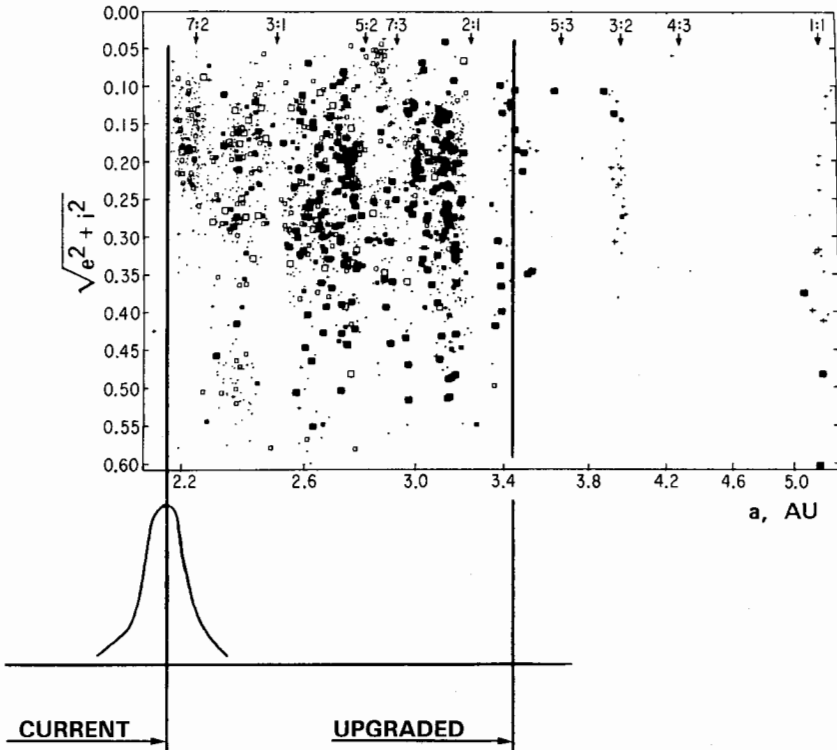
Fig. 11. Effects of the proposed Arecibo upgrade on radar detectability of main-belt asteroids (Ostro 1987*b*). This overview of the main belt, from Chapman (1979), shows some 2000 objects coded for size and taxon. Class-C asteroids are shown as solid boxes, class S as open boxes, other classes as crosses, and unclassified objects as dots. The larger boxes and crosses indicate sizes >80 km. Vertical lines are means of the distributions (approximate form sketched at left) of the range of the Arecibo radar today and after completion of proposed upgrade.

fully steerable. It could reveal the 3.5-cm properties of the same objects Arecibo has seen at 13 cm, permitting stronger constraints on scales of surface structure. Unlike Arecibo, Goldstone could take advantage of close approaches in the southern sky; the list of accessible targets would increase by several tens of percent, and we would have considerably greater geometric leverage in determining pole directions.

With the upgraded instruments, most newly discovered NEAs would be observable, and the resulting delay-Doppler astrometry could secure their orbits and thereby enlarge the pool of space mission candidates. Radar measurements could also assist asteroid missions navigationally, e.g., with high-precision ranging to targets of MBA flybys.

REFERENCES

Campbell, D. B., Pettengill, G. H., and Shapiro, I. I. 1976. 70-cm radar observations of 433 Eros. *Icarus* 28:17–20.

Chapman, C. R. 1979. The asteroids: Nature, interrelations, origins, and evolution. In *Asteroids*, ed. T. Gehrels (Tucson: Univ. of Arizona Press), pp. 25–60.

Garvin, J. B., Head, J. W., Pettengill, G. H., and Zisk, S. H. 1985. Venus global radar reflectivity and correlations with elevation. *J. Geophys. Res.* 90:6859–6871.

Gehrels, T., ed. 1979. *Asteroids* (Tucson: University of Arizona Press).

Goldstein, R. M. 1969a. Radar observations of Icarus. *Icarus* 10:430–431.

Goldstein, R. M. 1969b. Radar observations of Icarus. *Science* 162:903–904.

Goldstein, R. M., Holdridge, D. B., and Lieske, J. H. 1973. Minor planets and related objects. XII. Radar observations of 1685 Toro. *Astron. J.* 78:508–509.

Goldstein, R. M., Jurgens, R. F., and Yeomans, D. K. 1981. Radar observations of Apollo. *Icarus* 48:59–61.

Jenkins, G. M., and Watts, D. G. 1968. *Spectral Analysis and its Applications* (San Francisco: Holden-Day), pp. 79–81 and 230–233.

Jurgens, R. F. 1982. Radar backscattering from a rough rotating triaxial ellipsoid with applications to the geodesy of small asteroids. *Icarus* 49:97–108.

Jurgens, R. F., and Bender, D. F. 1977. Radar detectability of asteroids: A survey of opportunities for 1977 through 1987. *Icarus* 31:483–497.

Jurgens, R. F., and Goldstein, R. M. 1976. Radar observations at 3.5 and 12.6 cm wavelength of asteroid 433 Eros. *Icarus* 28:1–15.

Millis, R. L., Wasserman, L. H., Franz, O. G., Nye, R. A., Oliver, R. C., Kreidl, T. J., Jones, S. E., Hubbard, W., Lebofsky, L., Goff, R., Marcialis, R., Sykes, M., Frecker, J., Hunten, D., Zellner, B., Reitsema, H., Schneider, G., Dunham, E., Klavetter, J., Meech, K., Oswalt, T., Rafert, J., Strother, E., Smith, J., Provenmire, H., Jones, B., Kornbluh, D., Reed, L., Izor, K., A'Hearn, M. F., Schnurr, R., Osborn, W., Parker, D., Douglas, W. T., Beish, J. D., Klemola, A. R., Rios, M., Sanchez, A., Piironen, J., Mooney, M., Ireland, R. S., and Leibow, D. 1987. The size, shape, density, and albedo of Ceres from its occultation of BD+8°471. *Icarus* 72:507–518.

Ostro, S. J. 1987a. Planetary radar astronomy. In *The Encyclopedia of Physical Science and Technology*, Vol. 10, ed. R. A. Meyers (San Diego: Academic Press), pp. 611–634.

Ostro, S. J. 1987b. Benefits of an upgraded Arecibo Observatory for radar observations of asteroids and natural satellites. In *Proceedings of the Arecibo Upgrading Workshop*, eds. J. H. Taylor and M. M. Davis (Arecibo, P.R.: National Astronomy and Ionosphere Center, Box 995, Arecibo, Puerto Rico 00613), pp. 233–240.

Ostro, S. J., Pettengill, G. H., Shapiro, I. I., Campbell, D. B., and Green, R. R. 1979. Radar observations of asteroid 1 Ceres. *Icarus* 40:355–358.

Ostro, S. J., Campbell, D. B., Pettengill, G. H., and Shapiro, I. I. 1980. Radar detection of Vesta. *Icarus* 43:169–171.

Ostro, S. J., Campbell, D. B., and Shapiro, I. I. 1983. Radar observations of asteroid 1685 Toro. *Astron. J.* 88:565–576.

Ostro, S. J., Harris, A. W., Campbell, D. B., Shapiro, I. I., and Young, J. W. 1984. Radar and photoelectric observations of asteroid 2100 Ra-Shalom. *Icarus* 60:391–403.

Ostro, S. J., Campbell, D. B., and Shapiro, I. I. 1985a. Mainbelt asteroids: Dual-polarization radar observations. *Science* 224:442–446.

Ostro, S. J., Campbell, D. B., and Shapiro, I. I. 1985b. Radar properties of near-Earth asteroids. *Bull. Amer. Astron. Soc.* 17:729–730 (abstract).

Ostro, S. J., Campbell, D. B., and Shapiro, I. I. 1986a. Radar detection of 12 asteroids from Arecibo. *Bull. Amer. Astron. Soc.* 18:796 (abstract).

Ostro, S. J., Campbell, D. B., and Shapiro, I. I. 1986*b*. Near-Earth asteroids: Radar evidence for extremely irregular, nonconvex shapes. *Eos: Trans. AGU* 67:1078 (abstract).

Ostro, S. J., Campbell, D. B., and Shapiro, I. I. 1987. Radar echoes from asteroid 1986 DA indicate a metallic composition. *Bull. Amer. Astron. Soc.* 19:840 (abstract).

Ostro, S. J., Connelly, R., and Belkora, L. 1988. Asteroid shapes from radar echo spectra: A new theoretical approach. *Icarus* 73:15–24.

Ostro, S. J., Yeomans, D. K., Chodas, P. W., Goldstein, R. M., Jurgens, R. F., and Thompson, T. W. 1989. Radar observation of asteroid 1986 JK. *Icarus*, in press.

Pettengill, G. H., and Jurgens, R. F. 1979. Radar observations of asteroids. In *Asteroids*, ed. T. Gehrels (Tucson: Univ. of Arizona Press), pp. 206–211.

Pettengill, G. H., Shapiro, I. I., Ash, M. E., Ingalls, R. P., Rainville, L. P., Smith, W. B., and Stone, M. L. 1969. Radar observations of Icarus. *Icarus* 10:432–435.

Pettengill, G. H., Ostro, S. J., Shapiro, I. I., Marsden, B. G., and Campbell, D. B. 1979. Radar observations of asteroid 1580 Betulia. *Icarus* 40:350–354.

Simpson, R. A. 1976. Reflection and transmission from interfaces involving graded dielectrics with applications to planetary radar astronomy. *Proc. IEEE AP* 24:17–24.

Wasserman, L. H., Millis, R. L., Franz, O. G., Bowell, E., White, N. M., Giclas, H. L., Martin, L. J., Elliot, J. L., Dunham, E., Mink, D., Baron, R., Honeycutt, R. K., Henden, A. A., Kephart, J. E., A'Hearn, M. F., Reitsema, H. J., Radick, R., and Taylor, G. E. 1979. The diameter of Pallas from its occultation of SAO 85009. *Astron. J.* 84:259–268.

Wasserman, L. H., Bowell, E., and Millis, R. L. 1987. Occultations of stars by solar system objects. VII. Occultations of catalog stars by asteroids in 1988 and 1989. *Astron. J.* 94:1364–1372.

Weidenschilling, S. J. 1980. Hektor: Nature and origin of a binary asteroid. *Icarus* 44:807–809.

Yeomans, D. K., Ostro, S. J., and Chodas, P. W. 1987. Radar astrometry of near-Earth asteroids. *Astron. J.* 94:189–200.

PASSIVE MICROWAVE OBSERVATIONS OF ASTEROIDS

WILLIAM J. WEBSTER, JR.
NASA Goddard Space Flight Center

and

KENNETH J. JOHNSTON
Naval Research Laboratory

This chapter reviews the advances in the quantity and quality of the radio obser-
vations of asteroids and in the understanding of the physics of the asteroidal
microwave emission since the first Asteroids *volume in 1979. The data now*
cover the four largest asteroids (Ceres, Pallas, Vesta and Hygiea) at several
wavelengths and four smaller asteroids (Interamnia, Eunomia, Euphrosyne and
Bambergia) at one wavelength. The spectra show that most asteroids are cov-
ered by a layer of material with the physical properties of finely divided dust and
that there is a marked change in physical properties at a depth of a few cm.
Spectral analysis shows that this surface material is in layers of variable depth
(typically a few cm) and has dielectric properties which vary somewhat from
asteroid to asteroid. Disk-resolved observations of Ceres and Vesta (resolution
typically 7 or so pixels along a diameter) provide no evidence of strong (≥30%
of peak brightness) microwave surface markings implying a nearly uniform spa-
tial distribution of the microwave properties of the material. The future avail-
ability of mm wavelength synthesis arrays and large single antennas with good
performance in the mm wavelength range should allow observations of the
smaller asteroids which will complement both the infrared and cm wavelength
observations. The planned improvements to the Very Large Array will also add
to the available data. Together with sub-mm wavelength, infrared and radar
data, these data will provide valuable insights to the appropriate physics for a
general thermophysical model for the prediction of asteroidal emission. Such a
model will be of great value in the future study of surface properties.

I. INTRODUCTION

Since the publication of *Asteroids* (Gehrels 1979), the observation and analysis of the microwave continuum emission from asteroids has experienced extensive growth. This can be attributed to both an increase in the knowledge of the physics of microwave emission from natural surfaces and the completion of new observing instruments. The bulk of the growth in knowledge of the physics of the emission has been abstracted from work on the interpretation of satellite and aircraft observations of the Earth. The major new observing system is the Very Large Array (VLA) of the National Radio Astronomy Observatory.

The recognition that the physical characteristics of the asteroidal surface have an effect on the infrared emission different from the effect on the microwave emission has allowed a significant advance in the understanding of the physics of the radio emission. It appears that the dielectric properties of finely divided materials dominate the microwave spectrum. This insight was made possible by the ability of the VLA to measure the continuum emission of the largest asteroids over a wavelength range from 6 cm (and in the case of Ceres 20 cm) to 1 cm. At the same time, single antenna mm wavelength measurements have improved to the point that 3.3 mm wavelength measurements of the largest asteroids now have a useful signal-to-noise ratio for spectral inversions and, at least in the case of Ceres, valuable measurements have been made at wavelengths as short as 1.32 mm.

Table I lists the number of currently available measurements of cm and mm wavelength emission of asteroids. In those cases where an analysis of the continuum spectrum has been undertaken, the reference is to the spectral analysis rather than the publication of the individual measurements. Note that half of the objects listed have been observed only at wavelengths near 2 cm. This

TABLE I
Radio Continuum Observations of Asteroids[a]

Asteroid	Wavelengths Observed					Reference
	1.3 mm	3.3 mm	2 cm	6 cm	20 cm	
Ceres	1	2	3	3	1	Webster et al. 1988
Pallas			3	3		Johnston et al. 1989
Vesta		1	1	2		Johnston et al. 1989
Hygiea			3	1		Johnston et al. 1989
Interamnia			1			Webster et al. 1987
Eunomia			1			Webster et al. 1987
Euphrosyne			1			Dickel 1979
Bambergia			1			Dickel 1979

[a]The numbers in each column are the numbers of published or in press observations at each wavelength as of January 1989.

is due to the intrinsic strength of the signal and to the sensitivity of the receivers used at the single antennas and the VLA.

II. PHYSICS OF MICROWAVE EMISSION FROM ASTEROIDS

Clearly a complete model of the microwave emission of asteroids is a formidable task. First, as in the case of the infrared emission, one requires a model temperature distribution. This model should take into account the variation of thermal parameters with depth as well as the nature of the surface. It should be evolved to equilibrium with the insolation and must be oriented properly with respect to both the insolation direction and the direction of observation. In the microwave region there are, of course, no spectral lines or bands from solid materials. However, the greater penetration depth of microwave radiation requires a radiative transfer calculation which uses the dependence of dielectric properties on depth to at least a few 10s of cm.

Many of the factors influencing the temperature distribution are as important in the microwave as in the infrared. For example, the rotation rate, pole position and cross section for insolation and its time dependence all contribute to the equilibrium of the microwave and infrared energy balance. One also needs to treat the thermal conductivity and emissivity and properly use the bolometric albedo or an appropriate analog to connect the thermal distribution with the observed emitted radiation.

Other factors make a more important contribution to the emitted microwave radiation than to the emitted infrared radiation. Even for simple two layer models (Webster 1987), the depth dependences of porosity, dielectric constant and loss tangent (more properly, the real and imaginary parts of the dielectric vector) can yield microwave brightness temperatures very different from those of an equivalent blackbody. In addition, surface physical structure both on size scales much larger than (topography) and on the order of (conventional roughness) a wavelength make significant changes to the overall level of the continuum spectrum (Keihm 1984).

Some recent literature can provide valuable insights into the problem of calculating the microwave spectrum of asteroidal bodies. Keihm (1984), in an analysis of the factors influencing the determination of heat flow from microwave measurements of the Moon, demonstrates the crucial importance of near-surface dielectric properties in calculating the expected brightness temperatures. His analysis clearly shows the increasing dominance of the loss tangent as the wavelength decreases. He also finds that near-surface porosity can be responsible for as much as a 10% gradient in the lunar brightness temperature between 5 and 30 cm wavelength. Webster (1987) has shown that these considerations carry over to calculations of the microwave spectra of asteroids. In particular, most of the current controversy over whether the microwave spectra of asteroids can be matched to the properties of known materials is resolved by noting that finely divided materials have loss tangents

which increase strongly as the wavelength of observation decreases. For wavelengths shorter than 2 cm, this effect can limit the depth influence to values near to those typical of the infrared.

In addition to the astrophysical literature, investigators concerned with the interpretation of passive microwave observations of the Earth have been forced to consider many of the same physical processes that concern us here. The literature in this field is scattered through several journals including the *IEEE Transactions on Geosciences and Remote Sensing*, the *Remote Sensing of the Environment* and the *Journal of Geophysical Research: Solid Earth and Planets*. Some of the most useful material (e.g., dielectric properties measurements) can be difficult to find. However, the three volume treatise by Ulaby et al. (1981,1982,1986) is a valuable starting place. In particular, several levels of sophistication in the calculation of microwave emission are described in detail in vol. 2. In adapting the work from terrestrial observations to the radio astronomical case, it is important to note that the terrestrial observers are normally concerned with thermodynamic temperatures much higher than the asteroidal case. Further, the accuracy of the terrestrial measurements is much higher than the radio astronomical case due both to the much higher signal-to-noise ratio of the data and to the better absolute calibration of the observing instruments.

III. RESULTS ON INDIVIDUAL ASTEROIDS

Before discussing the detailed interpretations of the individual continuum spectra, we will review those features of the physical structure of an asteroid which can be discerned in the microwave continuum spectra without a model analysis. We will only give a schematic discussion here. The interested reader should consult Dickel (1979), Keihm (1984) and Webster (1987) for additional details. As an example, we will use the measurements of Ceres analyzed by Webster et al. (1988). The model-based analysis will be reviewed later in this section.

In Fig. 1, we plot the observed brightness temperatures of Ceres published in Table 1 of Webster et al. (1988). A diameter of 950 km was adopted and the observed brightness temperatures have been normalized to a heliocentric distance equal to the semimajor axis of Ceres' orbit (2.766 AU). We have fitted a horizontal line to the observations shortward of 6 mm wavelength and a separate horizontal line to the observations longward of 6 mm. Note that the expected brightness temperature for a rapidly rotating blackbody is <2 K different from the line fitted to the region shortward of 6 mm wavelength. Also, the difference between the fitted line at 1.32 mm and the observations is an effect of the phase at which the asteroid was observed (see below and Webster et al. 1988).

The two brightness temperature regimes imply that the surface material has a very strong dependence of loss tangent (more properly, the imaginary
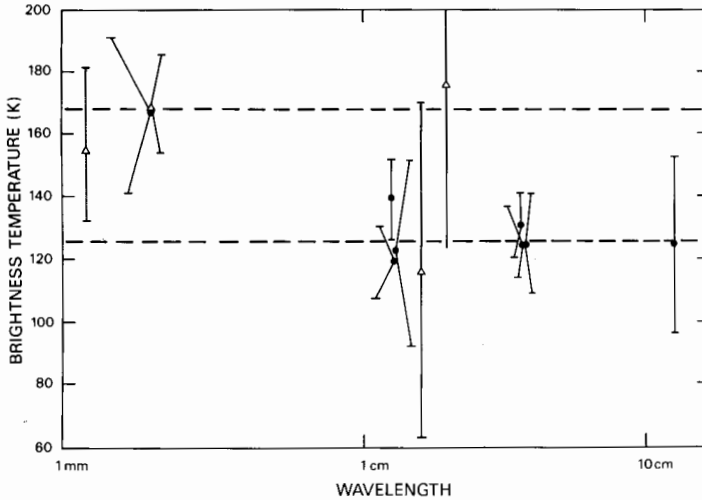
Fig. 1. Radio continuum spectrum of Ceres. The data points and error bars are taken from Table 1 of Webster et al. (1988). Although the fitted horizontal lines are carried across the figure for clarity, the upper line was fitted only to the mm wavelength data and the lower line was fitted only to the cm wavelength data.

part of the dielectric vector) on wavelength. The high short-wavelength brightness temperature shows that the radio penetration depth is much less than the thermal depth and implies a large loss tangent. At longer wavelengths, the low brightness temperature shows that the radio penetration depth is much greater than the thermal depth and implies a small loss tangent. Materials with this behavior are finely divided powders or dusts (see Ulaby et al. 1986, Appendix E). The surface of Ceres is therefore covered by finely divided material. The physical properties of this material are the same as dust.

The excellent fit of the horizontal line to the brightness temperatures longward of 6 mm and the much lower value of the fitted brightness temperature show that the microwave emission is predominantly from a depth region whose physical properties are relatively uniform and are different from the properties of the surface material. The abruptness of the variation between the short-wavelength data and the long-wavelength data is a measure of the abruptness of the transition between the two depth regimes. Thus, there is a near discontinuity (on the scale of a few mm) in the bulk physical properties of the material a few cm (about 3 cm from the gradient and the difference between 3 mm and 2 cm) within Ceres.

The simplest model consistent with the data is a two-layer model without lateral heterogeneity (Webster 1987). Because the brightness temperatures are averages over more than one rotation (especially at cm wavelengths), the apparent structure reflected in the spectrum cannot show any evidence of lateral

heterogeneity. The model analysis thus allows the objective determination of the average apparent dielectric properties of the surface material and the average depth of the discontinuity. If the signal-to-noise ratio of the longest wavelength data is high enough, the dielectric and physical properties of the material below the apparent discontinuity can also be estimated. Although the determination of the dielectric properties of the substrate is, to a degree, model dependent, the determination of the surface dielectric properties and the depth to the discontinuity uses the two-layer model as a mechanism of convenience. Additional discussion of the consequences of various limitations in our knowledge of the physics of the emission for any model analysis, whether two-layer or more complex, can be found in the last two sections of this review.

The bulk of the results discussed here are published model analyses for the largest four asteroids (Ceres, Pallas, Vesta and Hygiea); see Webster et al. (1988) for the details of the procedure employed. Results are summarized in Table II. The concentration on the four largest asteroids is, of course, due to the relative ease of observing these asteroids compared with the smaller ones. One 11 hr observing run on Ceres at 2-cm wavelength gave a signal-to-noise ratio of nearly 50 while one 11 hr observing run on 704 Interamnia (diameter about 340 km) yielded a signal-to-noise ratio of 11.5. The need for relatively long observing time to obtain high quality flux densities even with the VLA

TABLE II
Summary Results of Detailed Analysis of Asteroid Radio Continuum Spectra

Ceres. A finely divided layer about 3 cm deep overlying a much more compact layer. The transition between the two layers is relatively sharp. The surface layer dielectric properties are best matched by a water-poor clay. The substrate dielectric properties may differ significantly.

Vesta. A finely divided layer about 6 cm deep overlying a much more compact layer. The surface and substrate dielectric properties are best matched by basaltic dust and basalt, respectively.

Pallas. A finely divided layer at least 6 cm deep. It is not possible from the existing data to determine the dielectric properties of the substrate with any confidence. The surface dielectric properties are closer to basalt than clay.

Hygiea. A finely divided surface layer at least 8 cm deep. The surface dielectric properties are closer to basalt than clay. No effects of the substrate can be found in the data.

Interamnia. A finely divided surface layer much more than 3 cm deep.

Eunomia. A 1 cm deep surface layer which is either porous with 10% voids (most probable) or dust-like.

will necessarily limit the rate of growth of the existing data base rather se-
verely. This is also true for longer-wavelength observations of the largest as-
teroids. One 11 hr observing run on Ceres at 20 cm wavelength gave a signal-
to-noise ratio of 8. For the other larger asteroids, the ratio is proportionally
less. For Vesta, the expected ratio would be <4.

Webster et al. (1988) have analyzed the microwave continuum spectrum
of Ceres (Fig. 2). This spectrum extends from 1.32 mm wavelength to 20.12
cm wavelength and includes observations at 2 cm and 6 cm for a large range
of phase angles. At cm wavelengths (20, 6 and 2 cm) the observed brightness
temperature was found to be roughly constant and much lower than the bright-
ness temperature at 3.3 mm and 1.32 mm wavelength. Given the occultation
diameter, it was found that this spectrum is consistent with a finely divided
surface layer composed of water-poor clay about 3 cm deep. This layer over-
lies a substrate which may be chemically different from the surface layer and
is physically distinct from the surface layer. The data show that the substrate
is denser than the surface layer. Disk-resolved observations at 2 cm (Fig. 3),
while degraded by the low declination of Ceres, showed no evidence of limb
brightening or darkening. Some hint of low-intensity surface brightness fea-
tures was present but the low declination of Ceres has made it difficult to
confirm the reality of the features.

Although the data for Vesta are not as extensive as for Ceres, the contin-
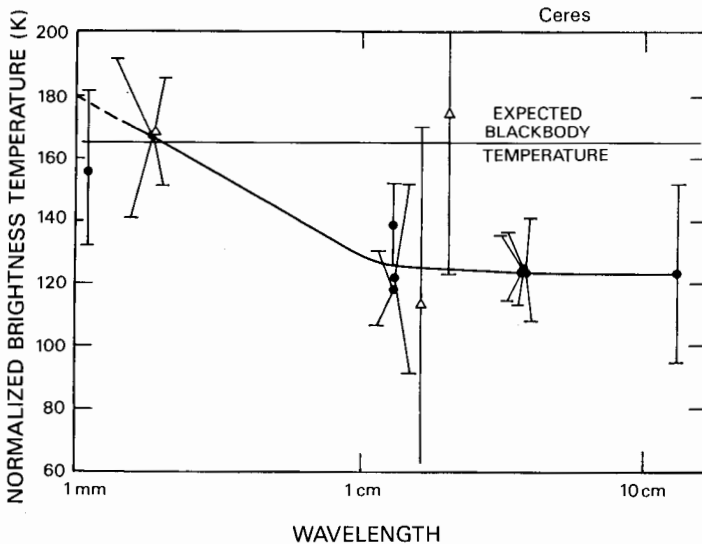
Fig. 2. Radio continuum spectrum of Ceres, after Webster et al. 1988. See reference for details
on the individual measurements. The solid line (dashed for wavelengths shorter than 2 mm) is
the calculated spectrum at 0 deg phase angle for the model structure discussed in the reference.
Error bars are based on the observations and do not include diameter errors.
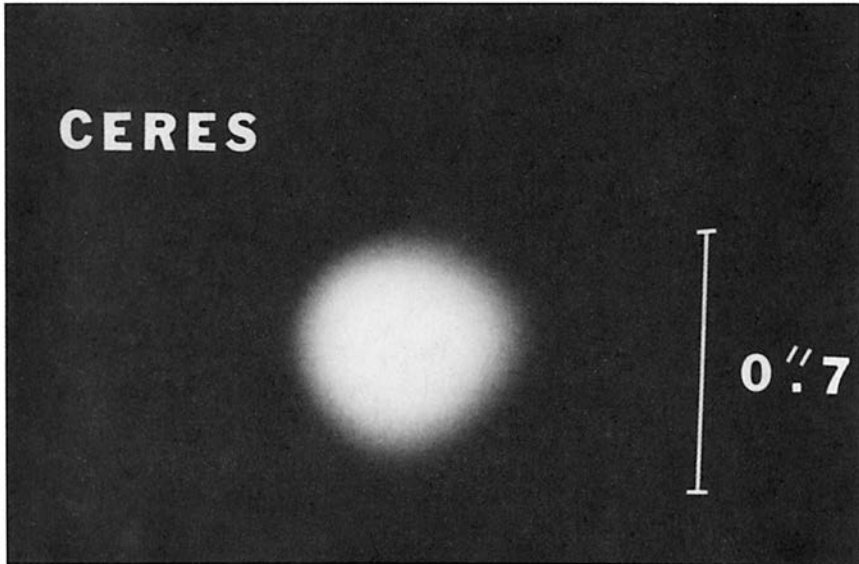
Fig. 3. Synthesis image of Ceres at 2 cm wavelength. Data set of 19 May 1981. The resolution is about 7 pixels per diameter (~135 km per pixel). Angular size marks are separated by 1 arcsec.

uum spectrum of Vesta (Fig. 4) has a similar shape to that of Ceres (Johnston et al. 1989). In this case, we inferred a layer depth of about 6 cm and found dielectric properties which resemble those reported for basaltic dust (Dickel 1979). Because we only have observations at 3 wavelengths (3.3 mm, 2 cm and 6 cm), the properties of the substrate are less well determined than in the case of Ceres. However, it is possible to eliminate water ice as a constituent of either the surface layer or the substrate (<5% by volume). The substrate dielectric constant was found to be near 7.2 (2 cm wavelength) while the loss tangent was found to be near 0.54 (also 2 cm wavelength). These values are consistent with those previously reported for basalt (Dickel 1979). Note that the formal errors are at the 20% level. Disk resolved observations at 2 cm wavelength (Fig. 5) show a featureless disk with a sharp edge.

In the cases of Pallas and Hygiea, the data set is restricted to observations at 2 cm and 6 cm. Accordingly, we have no sensitivity to the dielectric properties of the substrate. For both asteroids, the lower cm wavelength brightness temperatures compared to the infrared (Pallas) or sub-mm (Hygiea) are diagnostic of a finely divided surface layer. If we adopt basalt dielectric properties for the surface material, a surface layer depth of ≥8 cm results for Hygiea while a depth of >6 cm results for Pallas. These results are principally determined by the gradient between the two values. Although it was not possible to determine the dielectric properties to a high accuracy, we were able to estab-
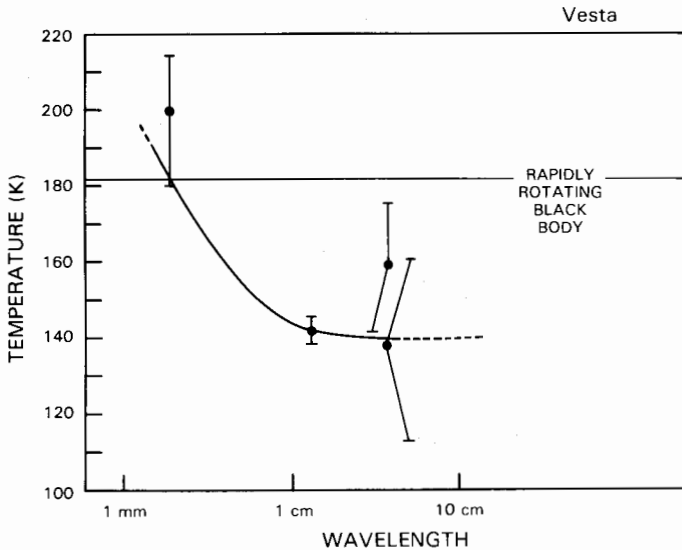
Fig. 4. Radio continuum spectrum of Vesta, after Johnston et al. 1988. See Fig. 1 for additional details.

lish that the dielectric constant is nearer to 7 than to 2 and that the loss tangent is as strong a function of wavelength as is observed in the case of Ceres and Vesta.

As Table I shows, all of the smaller asteroids detected in the microwave have been observed at only one wavelength. In most cases, the pre-VLA data does not have sufficient signal-to-noise ratio to do much beyond comparing the observed brightness temperature to the expected blackbody value. This comparison suggests the possibility of a "standard model" type of analysis for the determination of photometric diameters in the radio. Only in two cases is it possible to carry the analysis much beyond this. For Eunomia and Interamnia (Webster et al. 1984,1987), the availability of high accuracy sub-mm flux density measurements allows at least a crude analysis of the kind done for the major asteroids. As would be expected, the surfaces of these asteroids do not appear to have the physical characteristics of bare rock. These asteroids appear to be covered by a dust-like layer of at least one cm and perhaps more. Clearly, this layer can only be the upper part of a more extensive regolith which cannot be detected in microwave observations above 8 GHz due to loss tangent effects. VLA observations at a wavelength of 6 cm would require observing times of the order of 24 hr to produce a signal-to-noise ratio of 10 for Eunomia while times of the order of 12 hr would be required for Interamnia. Note that these times were calculated for the best of all possible observing geometries (opposition at minimum Earth-asteroid distance). It will thus be extremely difficult to add to these results with the present technology.
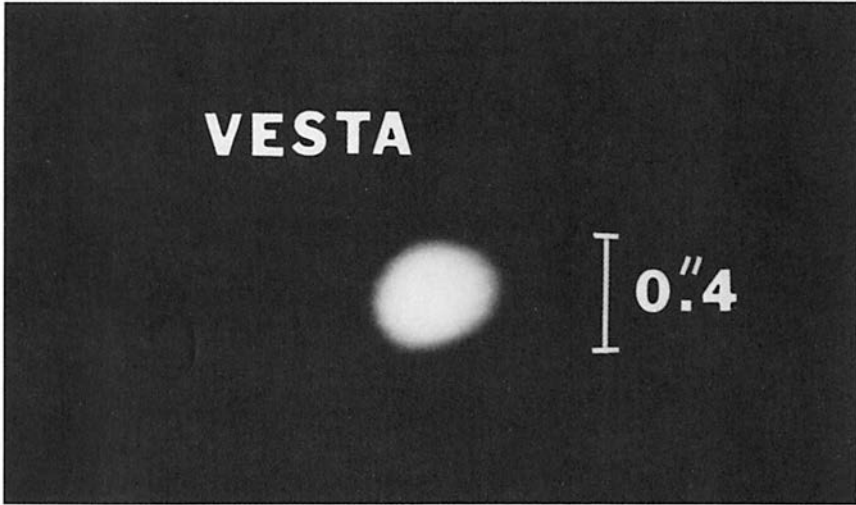
Fig. 5. Synthesis image of Vesta at 2 cm wavelength, after Johnston et al. 1988. The disk of Vesta is fully resolved with 8 pixels per diameter (~65 km per pixel). Note the uniformity of the brightness distribution. The apparent ellipticity of the image is not an artifact of the elliptical beam.

Independent of model analyses, it seems possible to draw some general conclusions from the admittedly limited data concerning the microwave "appearance" of asteroids. Bare surfaces, that is, surfaces with the physical properties of solid rock, must be the exception for asteroids with diameters above about 200 km. Regardless of the dielectric properties of the material, emission at wavelengths shorter than 3 cm seems to be dominated by the very near surface due to the strong increase in loss tangent with decreasing wavelength. A dusty surface appears to be the rule for larger asteroids. Water ice, which has a unique spectral signature, does not appear to be a major (<15% by volume) contributor to the microwave emission of any of the asteroids observed. The high observed brightness temperatures (>100 K) eliminate free metals as a constituent of the surface material (<<2% by volume).

IV. THE EFFECTS OF INSTRUMENTATION
ON THE INTERPRETATION

It is important to note that, as is often the case, the improvement in the technology of observing systems has made these new results possible. In the mm range, the technology is only just reaching the point that major observing programs of asteroid flux density measurements are possible with single antennas. Aperture synthesis at mm wavelengths has lagged behind that in the cm region because of the technical difficulty of implementing high sensitivity

aperture synthesis at wavelengths shorter than 1 cm. Although mm wavelength arrays are beginning to make their presence felt in other aspects of radio astronomy, it will be a little time yet before such systems are able to observe even Ceres with the kind of high signal-to-noise ratios which are needed. For the present, the improvement of the quality of the apertures of the single-antenna mm wavelength telescopes as evidenced by the new 30 m telescope at Pico Velata and the corresponding developments in receiver technology appear to offer the best hope for new data.

In the cm range, it is clear that VLA-class instruments are the key to new data. The large equivalent collecting area and the ability to track a moving source by shifting the phase tracking center are powerful tools in the fight to increase signal-to-noise ratio and eliminate the influence of confusing sources on the measurements. The largest single antennas either do not have a sufficiently large aperture to obtain the high signal-to-noise ratios required or do not allow tracking over a sufficient range of hour angle to permit the accumulation of the long (8 hr or more) integration time required in a reasonable amount of observing time. As it stands now (1989), the true performance of the VLA as an imaging tool has not been pressed except for the 2 cm observations of Vesta reported by Johnston et al. (1989). For the other large asteroids, there are some formidable observational problems to overcome. At 2 cm, a VLA observer is faced by the problem of correction for atmospheric effects on fringe phase at the very low declinations of especially Ceres and by an extreme sensitivity to the stability of the atmosphere. For the past four oppositions of Ceres, we have attempted to improve on the map published by Webster et al. (1988) without success. The atmospheric perturbations on the 2 cm data obtained more than compensated for the higher signal strength due to instrumental improvements. Only further motion along Ceres' orbit (to a higher declination) or much improved atmospheric stability will improve this situation.

The brightness temperatures which result from the employment of the best of the current systems are of sufficient quality to allow the use of interpretive schemes which have traditionally been the province of satellite and aircraft-based observations of the Earth. As the treatise by Ulaby et al. (1981,1982,1986) shows, the relatively high accuracy of the terrestrial data has allowed the interpretation techniques to reach a high level of sophistication. Although we cannot, as yet, make full use of these techniques due to the limited accuracy of the radio astronomical data, major portions of the formalisms can be adapted with success. In particular, a somewhat simplified version of the simultaneous estimation technique has enabled us to estimate objectively layer depths and dielectric properties with a high degree of confidence. However, in making the identification of the dielectric properties with material types, we are faced with a formidable problem. Due to the lack of good published short-wavelength laboratory measurements of dielectric properties, it is necessary to make extreme extrapolations in wavelength. In the

case of the Ceres observations discussed by Webster et al. (1988), the di-
electric properties of clay had to be extrapolated from 10 GHz to 200 GHz.
The improvement in the laboratory state-of-the-art evidenced in Appendix E
of Ulaby et al. (1986) gives us hope that valuable laboratory data will be
published soon.

    With the improvement in data quality, the importance of ancillary data in
the interpretation has grown. It is now clear that the circumstances of the
observation are essential elements in the interpretation. In particular, as the
wavelength decreases, the phase of the asteroid at the time of observation is
crucial. Although this effect can be negligible at long wavelengths (i.e., <1 K
at 20 cm for the structure derived for Ceres by Webster et al. 1988), at mm
wavelengths this effect can be of major significance (20 K at 1.32 mm wave-
length for a phase angle of -21 deg). The data now require consideration of
this and such parameters as rotation period and pole position.

    Although the improvement in data quality is clear, it is important to
recognize the limits to the model interpretation set by the accuracy of the data.
The most sophisticated of the interpretative formalisms developed by the ter-
restrial and lunar observers require data quality which is still beyond the state
of the art for asteroid observations. The complex calculations of emitted radi-
ation and the full inversion schemes are still not applicable here. Webster
(1987) has shown that the current state of the observations is still satisfied by
two-layer models 8 yr after Dickel (1979) made the same point. At present,
the information content of the spectra is restricted to homogenous layer depth,
surface dielectric properties and substrate dielectric properties, and compac-
tion of the material (ie, dust vs solid).

V. THOUGHTS ON FUTURE DIRECTIONS

    The recent developments in single antenna technology and in aperture
synthesis at mm wavelengths hold great promise for very high signal-to-noise
ratio observations of asteroidal brightness tempertures. These data are crucial
as they provide the link between the infrared and cm wavelength regions.
Future improvements in this wavelength regime promise to allow two major
efforts. The first is a general survey of the radio emission of a statistically
significant sample of asteroids. This will be made possible by a combination
of the improvements in observing systems and the fact that the asteroid emis-
sion is intrinsically stronger in the mm compared to the cm wavelength re-
gion. Second, the technology is on the threshold of being able to measure the
variation of mm wavelength brightness temperature as a function of rotation
for the largest asteroids. These efforts will be made possible not only by the
improvement of receiver technology and antenna surface quality (which also
applies to single antennas as well) but also by the increased understanding of
mm wave aperture synthesis which comes from the use of aperture synthesis
arrays.

One important problem faced by the single antenna observers which is crucial to their success at mm wavelengths is the need for high quality ephemerides for the smaller asteroids. Although the existing ephemerides predict the short term (daily) motion well enough to allow fringe phase tracking at cm wavelengths, the mm wavelength observers using single antennas require positions accurate to an arcsec in both coordinates. Even with 30 m antennas, current technology mandates significant integration times merely to detect the emission at 3.3 mm wavelength. Thus, relatively precise positions are mandatory for successful high signal-to-noise measurements. The observations reported by Webster et al. (1984,1987) suggest that the current standard ephemerides are accurate to no better than 5 arcsec for all but the largest asteroids and a few special cases among the smaller asteroids. Unless this is improved for a large number of cases, single antenna observers working at mm wavelengths will be restricted to the four or so largest asteroids and a very few smaller asteroids. Clearly, ephemerides incorporating recent position measurements and detailed numerical integrations can produce predicted positions of the required accuracy. However, for a survey of the mm wavelength emission of a statistically meaningful sample of asteroids (which could easily include asteroids whose diameters are around 75 km), the amount of specialized ephemeris preparation required could be formidable. We encourage those who are pursuing improvements in the quality of standard ephemerides to continue this crucial effort with vigor. The alternatives are to wait for mm system performance which allows observers to find the asteroidal source by the "peaking up" procedures used with other radio sources or to engage in a considerable and specialized ephemeris improvement activity before undertaking any extensive observing programs.

In the cm wavelength region, we can look forward to the construction of additional spectra and the extension of existing spectra to other, especially longer, wavelengths. Although the technical problems (strength of signal, confusion, etc.) are formidable, these data provide the best means of gaining an indication of the dielectric properties of the material which underlies the surface. In addition, the continued refinement of the cm wavelength parameters as more occultation diameters become available promises to allow the development of a radio version of the "standard model." At present, it seems likely that such a model will have an emissivity of about 0.8 at 2 cm wavelength and will show a wavelength dependence which corresponds to a dust-like surface layer at least 1.5 cm deep. With a reliable "standard radio model," it should be possible to determine photometric diameters from microwave data of sufficient quality to allow the easy recognition of objects with unusual microwave properties.

Lebofsky et al. (1985) have pointed out that the current state of thermophysical modeling does not allow a single description of the emission characteristics of asteroids that covers the entire wavelength range from the thermal infrared to the microwave. In part, this lack can be ascribed to the

differing accuracy of the observations in the individual wavelength regions. However, the difficulty of recognizing the appropriate physics for such a general description is the most important factor. The observations themselves must be the guide to the appropriateness of the physical processes which should be included. In particular, observations in the mm wavelength range are likely to be of crucial importance in linking the very near-surface characteristics of the infrared observations with the much deeper ones of the microwave observations. In this context, the radar observations assume a pivotal role because these data give the passive observers the means for deconvolving the influence of surface roughness from the influence of topography.

We are still just beginning the effort to understand the physical structure of the asteroids. Already, one fundamental result has emerged: various studies have shown that Pallas, Vesta and Hygiea have dust layers of similar depth. However, infrared, radar and microwave data all point to very different structures and perhaps compositions. Some explanations of this difference have suggested that it is primarily a result of differing evolutions occurring at different locations within the asteroid belt. Does this current understanding (limited though it is) of the possible causes of the divergence of the structures of Pallas, Vesta and Hygiea carry over to all asteroids? One would expect so; proving this will be an important and difficult task.

In the more general context, it is important to know whether it is meaningful to ask what the near-surface properties of a "typical" main-belt asteroid are. If differing structure is the rule and not the exception, a full understanding of the structure and of the evolution of asteroids will probably require the analysis of many different varieties of small bodies. It is also perhaps obvious that the surface physics of asteroids is dominated by the impact history. However, it is necessary to consider what we can learn from the observations about the physics of small-body formation and whether this understanding can be translated to improvements in the theory of planet formation.

REFERENCES

Dickel, J. R. 1979. Radio observations of asteroids. In *Asteroids,* ed. T. Gehrels (Tucson: Univ. of Arizona Press), pp. 212–221.

Gehrels, T., ed. *Asteroids* (Tucson: Univ. of Arizona Press).

Johnston, K. J., Webster, W. J., Jr., Wade, C. M., Hobbs, R. W., Kaplan, G. K., Seidelmann, P. K., and Lowman, P. D., Jr. 1989. Microwave observations of Vesta, Pallas and Hygiea. *Astron. J.,* in press.

Keihm, S. J. 1984. Interpretation of the lunar microwave brightness temperature spectrum: Feasibility of orbital heat flow mapping. *Icarus* 60:568–589.

Lebofsky, L. A., Sykes, M. V., Nolt, I. G., Radostitz, J. V., Veeder, G. J., Matson, D. L., Ade, P. A. R., Griffin, M. J., and Gear, W. K. 1985. Submillimeter observations of the asteroid 10 Hygiea. *Icarus* 63:192–200.

Ulaby, F. T., Moore, R. K., and Fung, A. K. 1981. *Microwave Remote Sensing: Active and Passive,* Vol. 1 (Reading: Addison Wesley).

Ulaby, F. T., Moore, R. K., and Fung, A. K. 1982. *Microwave Remote Sensing: Active and Passive,* Vol. 2 (Reading: Addison Wesley).

Ulaby, F. T., Moore, R. K., and Fung, A. K. 1986. *Microwave Remote Sensing: Active and Passive*, Vol. 3 (Dedham: Artech).

Webster, W. J., Jr. 1987. On the simple models for the interpretation of centimeter-wavelength radio observations of asteroids. *Publ. Astron. Soc. Pacific* 99:1009–1013.

Webster, W. J., Jr., Hobbs, R. W., and Lowman, P. D., Jr. 1984. Detection of $\lambda = 2$cm emission from minor planet 15 Eunomia. *Icarus* 60:538–540.

Webster, W. J., Jr., Hobbs, R. W., and Lowman, P. D., Jr. 1987. Detection of $\lambda = 2$cm emission from minor planet 704 Interamnia. *Icarus* 69:29–32.

Webster, W. J., Jr., Johnston, K. J., Hobbs, R. W., Lamphear, E. S., Wade, C. M., Lowman, P. D., Jr., Kaplan, G. H., and Seidelmann, P. K. 1988. The microwave spectrum of asteroid Ceres. *Astron. J.* 95:1263–1268.

ASTEROID MASS DETERMINATION: PRESENT SITUATION AND PERSPECTIVES

MARTIN HOFFMANN

Observatorium Hoher List der Universitäts-Sternwarte Bonn

Basic methods for asteroid mass determinations and their errors are discussed. New results and some current developments in the astrometric method are reviewed. New methods and techniques, such as electronic imaging, radar ranging and space probes are becoming important for asteroid mass determinations. Mass and density estimations based on rotational properties and possible satellites are also discussed.

I. INTRODUCTION

A mass determination of any celestial object requires gravitational interaction and known absolute kinematic data. The most efficient gravitational interactions for asteroids are long-lasting encounters at small distances. They can either be very efficient single encounters or repeated encounters with similar geometries, thereby accumulating the gravitational effects. To determine masses one must have the following:

1. A good knowledge of the kinematic behavior of the perturbing asteroid to define the geometric conditions during the interaction;
2. An excellent knowledge of the kinematic behavior of the perturbed object to derive even marginal deviations from unperturbed conditions (e.g., its orbit);
3. An excellent knowledge of further gravitational interactions with the major planets (which are generally much stronger than the perturbing asteroid);
4. An excellent coordinate reference system;
5. A good estimate of the errors involved in the measuring process.

There are two ways of measuring gravitational perturbations: (1) in the line of sight by radar ranging and radial motion determinations; (2) perpendicular to the line of sight by the measurement of celestial coordinates and their comparison with theoretical orbits. In some cases, further information is needed, for example, rotation lightcurves. The material collected for this chapter preferentially covers publications subsequent to the review by Schubart and Matson (1979).

II. THE ASTROMETRIC METHOD

The astrometric method seeks to obtain asteroid mass determinations by analyzing the motion resulting from gravitational interactions with other asteroids. Observed residuals of positions with respect to ephemerides are attributed to perturbations from insufficiently known masses. For all known asteroid-asteroid encounters, the encounter distance is large compared with the radii of their spheres of action (where their gravity dominates over that of the Sun). Therefore, only residuals in excess of 1 arcsec, resulting from permanent changes of the orbital elements, can be observed with sufficient precision and utilized by the astrometric method. The strength of an interaction can be characterized by the deflection angle, which is inversely proportional to the encounter distance and the square of the encounter velocity. It can also be described by the transfer of momentum which is inversely proportional to the encounter distance and the (linear) encounter velocity (Bender personal communication, 1988). In these cases, two-body approximations are used for a time interval near the closest encounters. The differences between a three- or n-body integration are usually small, but they may be dependent on the three-body geometry at the moment of the encounter, especially if the orbits are nearly tangential (Carusi and Valsecchi 1980; Greenberg et al. 1988).

The astrometric method yields a mass determination by iteratively comparing the observed positions of a perturbed asteroid with an ephemeris computed by numerical integration taking into account all other known perturbing masses (e.g., the major planets). Then, equations of condition for the mass of the perturbing body are solved (numerically) and the initial orbital elements of the perturbed asteroid are improved (as an example, see Scholl et al. 1987). Depending on the formal accuracies of the available observations and the precision requirements in the analysis, the following factors are important:

1. The right ascension and declination measurements should be weighted according to their precision.
2. There may be a magnitude equation for right ascensions with respect to clock stars (meridian observations), and possibly a color equation due to refraction.
3. Corrections may be necessary for different (older) catalogs, e.g., precession corrections or local catalog errors.

4. Minor resonance effects by other large objects may need to be taken into account, e.g., in the case of Ceres that by Vesta.
5. There are astrometric position errors due to phase and rotational effects such as spots and shapes (Sec. II.D).
6. A calculation for slightly different masses of the major planets should be tried to evaluate the solution's sensitivity to these uncertainties.
7. If there is a possibility for adding new observations, some care should be taken on the distribution of the data over the orbit of the test asteroid.
8. Relativistic effects may become significant for highest accuracy.
9. If necessary (old) observations should be corrected for light time.

This method may be modified by replacing right ascension and declination by range data. Obviously the greatest residuals will occur for main-belt objects at perihelion oppositions.

A. New Asteroid Mass Determinations by the Astrometric Method

During the last decade improved or new results could only be determined for two objects: 1 Ceres (Landgraf 1988; Schubart, personal communication 1988), and 10 Hygiea (Scholl et al. 1987). Landgraf reconsidered the perturbations on the orbit of 2 Pallas from Ceres. By adding numerous new observations and a careful treatment of previous error influences, his new result is 5.2×10^{-10} $M_\odot$. Schubart (personal communication, 1988) compared some recent sets of observations of Pallas and of 197 Arete with ephemerides based on the last differential corrections produced together with the mass determinations of Ceres and Vesta, respectively. The recent observations of Arete are well represented so that Schubart's (Schubart and Matson 1979) last determination of the mass of Vesta appears to be reliable. The recent observations of Pallas, especially those obtained at perihelion oppositions, show a small systematic deviation from the ephemeris of Schubart (1976). That systematic effect indicates that Schubart's (1974) mass of Ceres may be too large by a small amount. Scholl et al. considered a single very close encounter of 829 Academia with the fourth largest asteroid, Hygiea, in 1927, and derived for the latter a mass of 4.7×10^{-11} $M_\odot$.

B. Further Opportunities for the Astrometric Method

Several attempts have been made to identify further very close encounters between asteroids. Lists of such events were compiled by Davis (personal communication, 1988), Hoffman (1988), Kuzmanoski (personal communication, 1988) and Scholl (1988, unpublished). These are summarized in Table I. Searches for close encounters are tedious unless a preference for close encounters can be derived easily from the orbital elements, such as:

1. A close encounter that has been found for one epoch, and there is a commensurability of the revolution periods of the involved objects;

TABLE I
List of Very Close Encounters Between Asteroids

Large Asteroid	Target Asteroid	Reference	Year of Close Encounter
1 Ceres	with 91 Aegina	(Davis 1988)	1973
3 Juno	with 1767 Lampland	(Kuzmanoski 1988)	1982
10 Hygiea	with 395 Delia	(Davis 1988)	1966
15 Eunomia	with 1284 Latvia	(Scholl 1987)	1964
15 Eunomia	with 1313 Berna	(Scholl 1987)	1955
16 Psyche	with 1725 Crao	(Davis 1988)	1984
65 Cybele	with 526 Jena	(Kuzmanoski 1988)	1984
92 Undina	with 2950 1974VQ2	(Kuzmanoski 1988)	1985
324 Bamberga	with 1939 Loretta	(Kuzmanoski 1988)	1988
704 Interamnia	with 993 Moultona	(Davis and Bender 1977; Landgraf 1988)	1973
804 Hispania	with 1002 Olbersia	(Hoffmann 1988a)	1982

2. Pairs of objects that have very similar inclinations and longitudes of the ascending node;
3. Pairs of objects that have nearly equal semimajor axes and very low eccentricities.

Each of these three cases reduces the number of degrees of freedom of the encounter geometry by one. The first case has been used by Davis and Bender (1977), the second by Kuzmanoski (personal communication, 1988) and the third case by Hoffman (1989, in preparation).

Among these searches and selections, the question of the equality of the distribution of orbital elements is always inherent. In particular, the influence of the resonant structure of the belt and the existence of families must leave their signature on the distribution of close encounters. This problem was touched empirically in some detail by Hoffmann (1988). The actually identified close encounters of all available lists do not show a preference for family members. On the other hand, the available sample of close encounters shows considerable deviations in the distribution of orbital elements from the average belt population. If this effect turns out to be real, it may have consequences for the internal dynamical processes in the asteroid belt. Assuming equal densities, the histogram of mass ratios of asteroid encounter pairs with mutual distances < 0.01 AU is given in Fig. 1. Obviously, the lack of extreme mass ratios is caused by the incompleteness of the number of known small asteroids. This is also evident in Table II, showing the diameter frequency of individual objects. There is a search bias that increases the number of the largest objects because almost all searches for very close encounters have dealt only with encounters involving at least one large asteroid (e.g., Table I). A completeness of known asteroids can be assumed down to the diameter bin
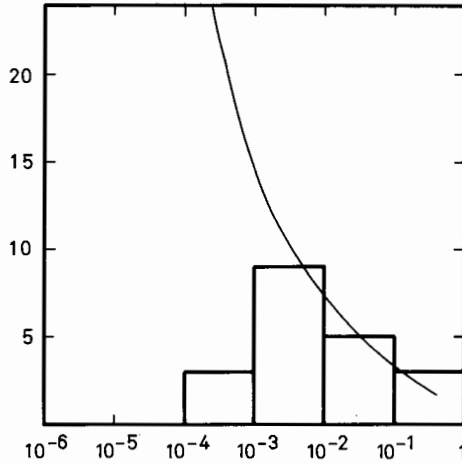
Fig. 1. Mass ratio frequency among the 20 closest encounter pairs of known asteroids, assuming equal densities. The curve shows the expected distribution from the currently known mass function of asteroids.

of 46 km. For smaller asteroids, the difference between the numbers of identified and expected encounter objects increases sharply, indicating the potential opportunities for an amplification of mass determinations. Furthermore, the list of very close encounters may not be free of selection effects, as the number of these events is surprisingly high (Fig. 2).

More distant encounters of asteroids may only be useful for mass determinations if they are very long lasting, and involve very large objects. For example, the similarity of the semimajor axes of 31 Euphrosyne and 511 Davida, two 300-km sized objects, may look promising, but their very differ-

TABLE II
Asteroid Diameter Frequency

Diameter (km)	Number of Encountering Asteroids	
	Observed	Expected
>220	4	
100–220	4	
46–100	8	
22–46	8	≈20
10–22	8	≈40
4.6–10	8	≈80
2.2–4.6	0	
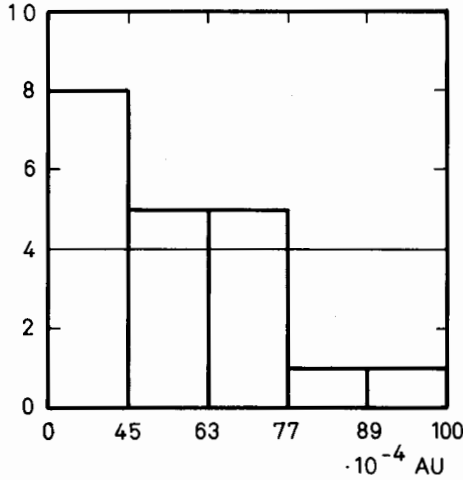
Fig. 2. Frequency of encounter distances of the 20 closest asteroid encounters as a function of the cross section (AU²). For each cross section interval, 4 of the 20 encounter distances should be expected, as indicated by the line.

ent inclinations and eccentricities allowed only one high-velocity encounter within 0.1 AU, a little more than a century ago.

C. Advanced Technologies for the Astrometric Method

Astrometric observations of asteroids are still primarily made by classic photographic methods—mostly because no other method is able to rival the information capacity of large, wide-field plates. For single objects, which can be located in a moderately small field, the astrometric accuracy of various electronic detectors are replacing photographic plates. The higher quantum efficiency for electronic cameras leads to a faster detection of the program objects, and each pixel can be calibrated with respect to its position. This is very important for moving objects like asteroids. Therefore, general improvements over data obtained by photography can be expected from the application of two-dimensional electronic detectors, in particular, CCD cameras. Recent accuracy determinations are of the order 0″.01, about a factor of 10 better than can be obtained with photographic plates.

Improvements may also be expected from extracting the astrometric content from occultation observations. This is valid both for occultations of asteroids by the Moon and of stars by asteroids. To estimate the expected accuracy, two examples are given: first, 1-m telescope, with the Moon at first or third quarter and asteroid magnitude 10. This means a total visual sky background brightness of 10th magnitude (approximately) within a diaphragm of 15 arcsec diameter. A detection of the object with a signal-to-noise ratio of 5 can be obtained by a photomultiplier within 2×10^{-3}s, neglecting scintilla-

tion. This can provide an accuracy of 4×10^{-3} arcsec mainly in right ascension for a central occultation track if the position of the limb of the Moon is known with infinite accuracy. Second, a 1-m telescope with a moonless dark sky and star and asteroid magnitude 12, daily motion $0°25$: timing the stellar occultation to within 0.1 s, yields a signal-to-noise ratio of 100, corresponding to a motion of 10^{-3} arcsec. No star position is known with such accuracy.

Still another improvement over photographic method is high-resolution speckle interferometry of asteroids in close vicinity to reference stars, e.g., an asteroid located in front of a dense star field or star cluster. The astrometric accuracy will depend on the aperture of the telescope.

Finally space astrometry is promising. In the near future this will be the domain of the Hubble Space Telescope, and the HIPPARCOS satellite which may have a much longer lifetime.

The HIPPARCOS mission will have a strong mutual interaction with the determination of asteroid masses. Its position measurements of asteroids will enable an accurate determination of the dynamically defined fundamental system. On the other hand, this fundamental system is needed for the determination of asteroids relying on the residuals of their positions. Control observations (groundbased and by the HST) are planned (Duncombe et al. 1984). Some basic consequences of HIPPARCOS are the following:

1. The astrometry will be homogeneous and directly related to the fundamental system;
2. It should be possible to detect trends of residuals on the order of $0''01$ over 2 yr;
3. Accurate pre-encounter positions and orbital elements can be obtained for close asteroid encounters of the future;
4. It should be possible to detect mass effects of smaller objects, objects with larger encounter distances, and higher relative velocities. However, this improvement will call for the inclusion of a multitude of minor (so far neglected) effects in the reductions and there may not be enough observations per object for their separation. One example of such effects is the resolution of surface details for the largest asteroids.
5. The observations will unfortunately be restricted to bright-test objects only.

For higher-precision data the combined effects of all asteroids within individual zones may need to be reconsidered similarly to the reduction approach of Mayo (1979). Williams (1984) preferred to assume the mass structure of the asteroid belt as lumpy because of the dominant mass concentrations in large objects. However, our observational evidence on smaller asteroids (and their mass law) is still far from complete.

D. Center of Light vs the Center of Mass

The displacement of the photocenter of an asteroid with respect to its center of mass due to phase effects is in general not negligible. This phase

effect not only includes the light defect (nonilluminated part of the disk) but also the scattering properties and limb darkening of each surface element, in particular close to the terminator. Opposite to the geometric effect of light defect, the scattering properties are closely related to the integrated phase curve (brightness vs phase angle) and must be treated for each asteroid individually (see the chapter by Bowell et al.). The contribution of this phase effect is significant especially for typical moderate asteroid phase angles, when the geometric light defect is small. Usually this phase-dependent displacement of the light center will exceed 10% of the diameter. Arlot (1982) discussed this phenomenon for photographs of Jupiter and its satellites.

Displacements of the photocenter due to irregular shape and albedo spots are of a similar order of magnitude. In this case, a detailed knowledge of the geometric conditions of the shape and rotational phase and spot positions is
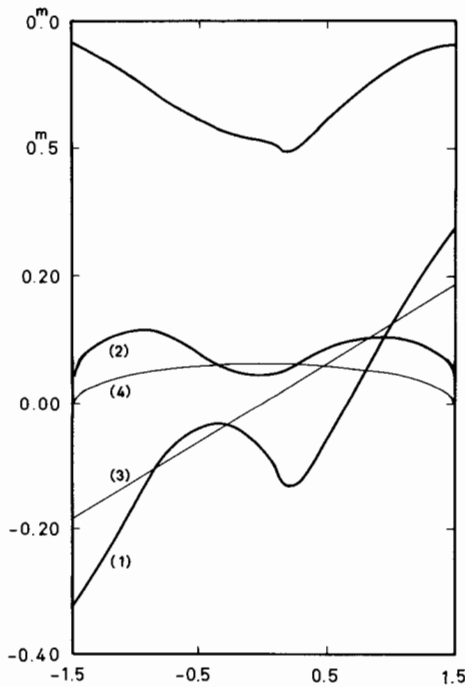
Fig. 3. The displacement of the center of light of two spheres of a constant surface brightness in contact with each other. The x-axis denotes the apparent separation of the centers (in units of the primary's radius) along the observer's line of sight. The displacement is also in units of the primary's radius. Model parameters are ratio of radii: 0.5; aspect angle: 60°; phase angle 15°; illumination angle 45°. The secondary component is assumed to be in front of the primary. Curve (1) shows the displacement along the semimajor axis of the projected circular orbit; curve (2) that for the displacement perpendicular to curve (1). Curves (3) and (4) show the respective displacements of the center of mass, assuming equal densities. The resulting light-curve is shown at the top (arbitrary zero magnitude).

important because the combination of both effects tends to increase asymmetries of magnitude and light-displacement graphs. In the case of drastic changes in the geometric conditions (e.g., a highly irregular shape or an albedo spot crossing the terminator), a critical treatment of the conditions during one longer integration may even be required. Fortunately, large asteroids are of fairly regular shape and there are only a very few clear-cut cases of distinct albedo spots, Vesta being the most well known (Drummond et al. 1988). A first attempt to detect the displacement of the photocenter of Vesta due to spots was made by Geffert and Hoffmann (1981).

There is a multitude of other possible complicating influences which might arise for at least some asteroids. These include: limb effects (multiple reflection); color effects; the center of mass $\neq$ the geometrical center; contact or orbiting binaries.

Computing the center of light may follow analytic lines as shown by Drummond et al. (1985), or it can be done by numerical integrations of the illuminated surface elements of individually defined components (e.g., polyhedric models [Cellino et al. 1987], which may even include larger craters). An example of a displacement model is given in Fig. 3, where a contact-binary asteroid is treated, but with several simplifying assumptions. The shape of the contact zone of a contact-binary asteroid is difficult to predict, and the phase effect of its surface elements may even be dependent on the illumination angle (nonsymmetrically). It will be useful to check the model by a comparison with the resulting and observed lightcurves, whose fine structures may be diagnostic (as shown by the peculiar nose-shaped light minimum in Fig. 3).

III. THE RADAR METHOD

Radar techniques are expected to improve asteroid mass determinations dramatically in the near future. An astrometric observation is an angular observation, and the actual position of an object in space is determined with an accuracy depending on the distance (like proper motions of stars). This is not the case for radar observations, which are absolute data (like radial velocity data of stars). Details for the applications of radar astrometry can be found in Yeomans et al. (1987) and in the chapter by Ostro. Range data with respect to Mars of basically any kind (with explicit application to Viking data) were discussed by Williams (1984). Standish (1989) analyzed a large collection of Mars range data including radar observations for effects of the masses particularly of the three largest asteroids. The mass of Ceres was found in close agreement with the previous results by Landgraf (1988).

IV. SPACE PROBES

Several proposals have been brought forward to measure the masses of asteroids *in situ*. These missions include the projects ASTEREX, CRAF,

GALILEO, CASSINI, VESTA and PIAZZI. Their common theme is a flyby of one or several asteroids. Mass effects may then be detected, depending on encounter distance and velocity, by Earth-bound or star sensor checks of the changes of the spacecraft's orbit; active radar ranging by the probe; or observations of released test objects in the vicinity of the asteroid.

V. ASTEROID SYSTEMS: ROTATIONS AND SATELLITES

Masses of asteroids may also be estimated by their intrinsic gravitational effects. These will, depending on the internal structure and the rotation velocity, evoke approximations to hydrodynamic equilibrium figures. Additionally, the structure of the surface is a consequence of the erosional interactions of the asteroid's environment under specific conditions of rotation, internal strength and gravity. Reactions to torques may also be indicative for the mass of asteroids. Each of these methods requires an accurate knowledge of the dimensions and the shape of the asteroid. This subject is discussed in detail in several other chapters (see, e.g., Millis and Dunham; Drummond and Hege; Magnusson et al.). This relation of shapes and rotation was discussed for 1566 Icarus by Gehrels et al. (1970), and for 433 Eros by Zellner (1976). They assumed densities of 3 g cm^{-3} and 4 g cm^{-3}, respectively. Cellino et al. (1987) deduced a density of 2.4 g cm^{-3} for Vesta as a homogeneous body with a flattening as a consequence of a rotational equilibrium figure. Comparing the observed rotation periods of asteroids with possible triaxial equilibrium ellipsoids, Farinella et al. (1981) find densities of 1.1 to 1.4 g cm^{-3} for objects of 100 to 300 km diameter with periods of 6 hr, and 2.4 to 3.2 g cm^{-3} for similar objects with periods of 4 hr. Weidenschilling (1981) finds by similar considerations densities of 2 to 3 g cm^{-3} for objects with rotation periods of 4 hr. There is also a prolonged discussion concerning the dependence of asteroid rotation rates on their taxonomic types, that would influence the consideration of densities with respect to equilibrium figures (see Lagerkvist 1983 and the chapter by Binzel et al.).

Precession will in general play no important role among asteroids, although it may be present in some special cases and then may be useful for mass determinations. Burns and Safronov (1973) discussed free precession of an asteroid after a collision; details on forced precession among asteroids can be found in the discussion of 1220 Crocus by Binzel (1985). Lightcurves for precessing spheroidal asteroids were calculated by Barsuhn (1983).

Although some doubt has now arisen for some previously announced detections of binary systems among asteroids, this possibility should be mentioned. Binary configuration seems to be the most important condition for mass determination in the universe. In the case of asteroids, there are two configurations to be considered: *tidally evolving binaries* and *contact binaries*.

Details on the binary phenomenon among asteroids can be found in the chapter by Weidenschilling et al.; therefore, only remarks concerning the

masses of binary asteroid components are given here. Binary asteroids may contribute in this respect as an extension of the implications by rotating single asteroids, and by analyzing the "Keplerian content" of the binary motion. Both methods are applicable for each of the two configurations mentioned above. Equilibrium models of binary asteroids were discussed by Leone et al. (1984) and applied to 624 Hektor and 216 Kleopatra by Weidenschilling (1980), who found densities of 2.5 g cm^{-3} and 3.9 g cm^{-3}, respectively. Assuming a single-body model for Kleopatra, a density of only 1.7 g cm^{-3} would result (Zappalà et al. 1983). Wijesinghe and Tedesco (1979) discussed the lightcurve of 171 Ophelia, and concluded that it could be modeled by an eclipsing-binary asteroid system with a mean density of 1.7 g cm^{-3}. Cellino et al. (1985) derived densities for possible binary asteroids ranging from 1.1 to 5.0 g cm^{-3}.

VI. SUMMARY

The accuracy of current mass determinations have only slightly improved from the attempts 20 years ago. They are still not much different from the order of magnitude that one would reach just by reasonable assumptions. Technological progress has improved the precision for a few massive objects and shows promise for the next decade. The variety of different new approaches to the problem clearly indicates a common interest in these basic data which are sometimes closely related to very different phenomena.

REFERENCES

Arlot, J. E. 1982. The determination of the center of gravity of a planet from photographic plates. *Celest. Mech.* 26:199–205.

Barsuhn, J. 1983. The light curves of a freely precessing spheroidal minor planet. *Astron. Astrophys.* 122:237–240.

Binzel, R. P. 1985. Is 1220 Crocus a precessing, binary asteroid? *Icarus* 63:99–108.

Burns, J. A., and Safronov, V. S. 1973. Asteroid nutation angles. *Mon. Not. Roy. Astron. Soc.* 165:403–411.

Carusi, A., and Valsecchi, G. B. 1980. Planetary close encounters: Importance of nearly tangent orbits. *Moon and Planets* 22:113–124.

Cellino, A., Pannunzio, R., Zappalà, V., Farinella, P., and Paolicchi, P. 1985. Do we observe light curves of binary asteroids? *Astron. Astrophys.* 144:355–362.

Cellino, A., Zappalà, V., Di Martino, M., Farinella, P., and Paolicchi, P. 1987. Flattening, pole, and albedo features of 4 Vesta from photometric data. *Icarus* 70:546–564.

Davis, D. R., and Bender, D. F. 1977. Asteroid mass determinations: A search for further encounter opportunities. *Bull. Amer. Astron. Soc.* 9:502–503 (abstract).

Drummond, J. D., Cooke, W. J., Hege, E. K., and Strittmatter, P. A. 1985. Speckle interferometry of asteroids. I. 433 Eros. *Icarus* 61:132–151.

Drummond, J., Eckart, A., and Hege, E. K. 1988. Speckle interferometry of asteroids. IV. Reconstructed images of 4 Vesta. *Icarus* 73:1–14.

Duncombe, R. L., Hemenway, P. D., and Whipple, A. L. 1984. Minor planet observations and the fundamental reference system. *Celest. Mech.* 34:19–36.

Geffert, M., and Hoffmann, M. 1981. Observations of asteroid 4 Vesta. *Minor Planet. Bull.* 8:17–18.

Gehrels, T., Roemer, E., Taylor, R. C., and Zellner, B. H. 1970. Minor planets and related objects. IV. Asteroid (1566) Icarus. *Astron. J.* 75:186–195.

Greenberg, R., Carusi, A., and Valsecchi, G. B. 1988. Outcomes of planetary close encounters: A systematic comparison of methodologies. *Icarus* 75:1–29.

Hoffmann, M. 1988. Impactless asteroid collisions: Opportunities for mass determinations and implications from actual close encounters. *Icarus*, submitted.

Lagerkvist, C.-I. 1982. Asteroids: Spins and shapes. *Highlights Astron.* 6:371–376.

Landgraf, W. 1988. The mass of Ceres. *Astron. Astrophys.* 191:161–166.

Leone, G., Farinella, P., Paolicchi, P., and Zappalà, V. 1984. Equilibrium models of binary asteroids. *Astron. Astrophys.* 140:265–272.

Mayo, A. P. 1979. Analytical method for the effect of the asteroid belt on planetary orbits. *Celest. Mech.* 19:317–333.

Scholl, H., Schmadel, L. O., and Röser, S. 1987. The mass of the asteroid (10) Hygiea derived from observations of (820) Academia. *Astron. Astrophys.* 170:311–316.

Schubart, J. 1974. The masses of the first two asteroids. *Astron. Astrophys.* 30:289–292.

Schubart, J. 1976. New reduction and collection of meridian observations of Ceres and Pallas. *Astron. Astrophys. Suppl.* 26:405–413.

Schubart, J., and Matson, D. L. 1979. Masses and densities of asteroids. In *Asteroids,* ed. T. Gehrels (Tucson: Univ. of Arizona Press), pp. 84–97.

Standish, E. M., Jr. 1989. A determination of the masses of Ceres, Pallas, and Vesta from their determinations upon the orbit of Mars. *Icarus* 80:326–333.

Weidenschilling, S. J. 1980. Hektor: Nature and origin of a binary asteroid. *Icarus* 46:124–126.

Weidenschilling, S. J. 1981. How fast can an asteroid spin? *Icarus* 46:124–126.

Wijesinghe, M. P., and Tedesco, E. F. 1979. A test of the plausibility of eclipsing binary asteroids. *Icarus* 40:383–393.

Williams, J. G. 1984. Determining asteroid masses from perturbations on Mars. *Icarus* 57:1–13.

Yeomans, D. K., Ostro, S. J., and Chodas, P. W. 1987. Radar astrometry of near-Earth asteroids. *Astron. J.* 94:189–200.

Zappalà, V., Di Martino, M., Scaltriti, F., Djurasevic, G., and Kneževic, Z. 1983. Photoelectric analysis of asteroid 216 Kleopatra: Implications for its shape. *Icarus* 53:458–464.

Zellner, B. 1976. Physical properties of asteroid 433 Eros. *Icarus* 28:149–153.

EXPERIMENTS AND SCALING LAWS FOR CATASTROPHIC COLLISIONS

A. FUJIWARA
Kyoto University

P. CERRONI
Istituto di Astrofisica Spaziale

D. DAVIS, E. RYAN
Planetary Science Institute

M. DI MARTINO
Osservatorio Astronomico di Torino

and

K. HOLSAPPLE, K. HOUSEN
Boeing Aerospace Company

Experimental data on catastrophic disruption experiments are the starting point for understanding larger-scale asteroidal collisions. We review the existing data on shattering impacts using natural silicate, ice and cement-mortar targets. A comprehensive data base containing the most important parameters describing these experiments was prepared. The collisional energy needed to shatter consolidated homogeneous targets and the ensuing fragment size distributions have been well studied experimentally. However, major gaps exist in the data on fragment velocity and rotational distributions, as well as collisional energy partitioning for these targets. Current scaling laws lead to predicted outcomes of asteroid collisions that are inconsistent with interpretations of astronomical data. This scaling problem is a major deterrent to constructing more plausible models of large asteroidal collisions.

I. INTRODUCTION

Asteroids, as well as many planets and satellites, have evolved to their present state through various classes of collisional events. Many properties of asteroids such as the distributions of sizes, shapes and rotation periods should be interpreted in the context of studies of collisional phenomena. Hence, understanding the collisional processes of two solid bodies is indispensable for the study of asteroids and other solar system bodies. In this chapter we treat only catastrophic processes, which have played a crucial role in the collisional evolution of asteroids and small satellites.

Our goal in studying the process of catastrophic disruption is to understand the outcomes of collisional events. We must clarify how the fragmentation modes, size distributions, fragment shapes, velocity distributions, spin periods of fragments, energy partitioning, and so on, depend on the many possible combinations of parameters specifying the impact condition, such as: size, shape, density, strength of both projectile and target, impact velocity, impact geometry and target spin rate. The usual starting point for studies of asteroidal collisions is the laboratory. Many experiments that shatter cm-scale targets to varying degrees by impacting small projectiles have been carried out. Unfortunately, the experimental data base cannot readily be extended to substantially larger sizes due to our inability to accelerate massive projectiles to km s^{-1} impact speeds. This is in contrast to cratering studies, where data exist for a wide range of sizes starting with laboratory cratering experiments, and going to chemical and nuclear explosion tests in the field, and finally up to natural impact craters. However, there are up to 7 orders of magnitude difference in size between laboratory fragmentation experiments and asteroid impacts. The only way to connect the experimental data with asteroid size bodies is through scaling theories. Application of scaling laws to asteroids and small satellites is needed not only to understand their collisional evolution, but also to test what effect changing the scaling-theory parameters has on the observed physical properties of these bodies.

In Sec. II.A, the experimental results obtained to date are presented. These data include information on the collisional classification of destruction mode (fracture pattern); mass fractions of the largest fragments; fragment size and shape distributions; rotation periods and velocities of fragments; and energy partitioning. In Sec. III, theoretical approaches to the construction of scaling rules are introduced, and some problems that arise in applying the scaling to asteroid families are pointed out. Finally in Sec. IV, future research areas are suggested.

II. LABORATORY EXPERIMENTS

A. Experimental Methods

The experimental techniques used in low- and high-velocity impact experiments for accelerating macroscopic projectiles are summarized in Table I.

TABLE I
Experimental Techniques

Accelerating Technique	Max. Velocity (m s^{-1})	Typical Operating Velocities (m s^{-1})	References
Drop method	~50	—	Hartmann 1978 Nakamura et al. 1983
Single-stage gas gun	~1500	~1000	Curtis 1962
Powder gun	~2000	~1000	Mizutani et al. 1981 Matsui et al. 1982
Two-stage light gas gun	~10000	3000–5000	Seigel 1965
Modified explosive-shaped charge	~10000	6000–10000	Martelli and Newton 1977

Our purpose here is to focus on the experiments themselves; therefore only an overview of the characteristics of each method is provided. For further details on the accelerating techniques, the interested reader is directed to the references given in Table I.

B. Summary of Experiments

A large number of catastrophic fragmentation experiments have been performed covering a wide range of impact velocities (from 50 m s^{-1} to 9 km s^{-1}), target materials (natural rocks, cement mortar, glass, ice, ice-silicate mixtures, etc.) and shapes, projectile materials, impact geometries, etc. Data from all available experiments have been organized into a computer-compiled data table for comparison and analysis (this data base can be obtained from DRD). The main results to be inferred from the experiments done to date are outlined in the following subsections.

C. Classification of Collisional Outcomes

The outcomes of a collisional event can be classified in order of increasing destruction based on the collisional energy density (E/M_T) of the event, where E is the projectile kinetic energy and M_T the target mass (Fujiwara et al. 1977). The possible outcomes, ranging from rebound and cratering to catastrophic fragmentation for rocky targets, are shown in Table II for two empirically defined velocity regimes: v $\lesssim$ 1 km s^{-1} (low velocity) and v $\gtrsim$ 1 km s^{-1} (high velocity).

It is interesting to note that depending on the impact speed for silicate and mortar materials, two different fragmentation modes occur. In the high-velocity regime, the outer layers of the target are spalled off leaving a large central core (core shattering), while in the low-velocity regime the target is shattered into cone-shaped fragments, pointing towards the impact point

TABLE II

Classification of Collisional Outcomes for Low- and High-Velocity Experiments onto Rocky Targets[a]

Low Velocity ($v \lesssim 1$ km s^{-1})		High Velocity ($v \gtrsim 1$ km s^{-1})	
Energy Range (erg g^{-1})	Outcome	Energy Range (erg g^{-1})	Outcome
$\lesssim 5 \times 10^6$	rebound with radial fissuring	$\lesssim 1 \times 10^6$	cratering
$\gtrsim 5 \times 10^6$	rebound: longitudinal splitting	$1 \times 10^6 \lesssim (E/M_T) \lesssim 1 \times 10^7$	larger, well-defined crater; spalling from the edges
$5 \times 10^6 \lesssim (E/M_T) \lesssim 5 \times 10^7$ $\gtrsim 5 \times 10^7$	cone shattering catastrophic fragmentation	$1 \times 10^7 \lesssim (E/M_T) \lesssim 1 \times 10^8$ $\gtrsim 1 \times 10^8$	core shattering catastrophic fragmentation

[a]References: Matsui et al. 1982, 1984; Takagi et al. 1984; Fujiwara et al. 1977; Fujiwara and Tsukamoto 1980.

(cone shattering). Core shattering and cone shattering are sketched in Fig. 1a and b.

A few exceptions to the fragmentation modes listed in Table II have been reported. In the high-velocity regime no core-type fragmentation was observed by Fujiwara and Asada (1983) for clay targets, or by Capaccioni et al. (1986) for basalt and mortar targets, who instead observed longitudinal splitting similar to cone-type destruction. On the other hand, no cone-type destruction was observed by Matsui et al. (1982) in low-velocity experiments into cubic basalt targets. For icy targets, neither cone- nor core-type destruction has been observed. Rather, an intermediate stage where the target is broken into a few large pieces separates the cratering regime from catastrophic fragmentation. This intermediate stage occurs at $E/M_T \sim 5 \times 10^5$ erg g^{-1} (Lange and Ahrens 1981; Kawakami et al. 1983).
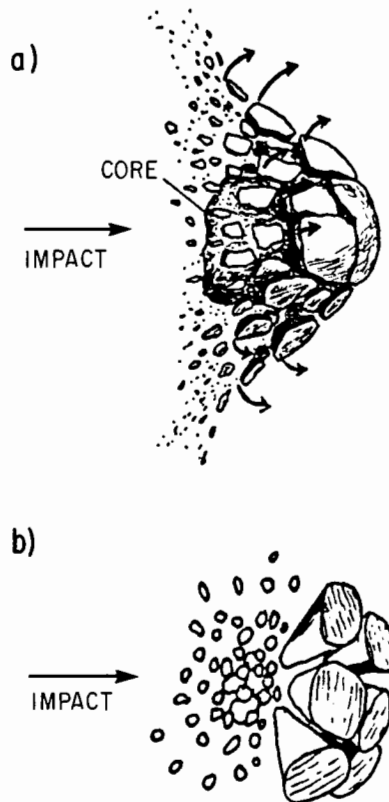
Fig. 1. The two modes of catastrophic disruption of a spherical rocky target by high-velocity impact are schematically illustrated. (a) shows core-type shattering while (b) depicts the cone type of fragmentation. Arrows show the sense of the rotation of the fragments (figure from Fujiwara 1986).

The degree of fragmentation undergone by the target is usually quantified by the parameter M_L/M_T, where M_L is the mass of the largest remaining fragment after collision. This parameter is equal to 1 for simple rebound and is defined here to be between 0.5 and 1.0 for cratering outcomes and ≤ 0.5 for catastrophic fragmentation. Of special interest is the transition threshold between cratering and shattering, when $M_L/M_T = 0.5$, which is called a barely catastrophic outcome. A fundamental concept in describing catastrophic fragmentation is the threshold collisional specific energy $Q^* = (E/M_T)^*$, defined as the kinetic energy per unit mass of the target required to produce a barely catastrophic outcome. (Related to Q^* is the impact strength S_o defined to be Q^*/ρ, where ρ is the target density.) This parameter is principally a function of material type and physical state, although it is also affected by the impact speed and geometry, target and projectile shape and relative sizes, and partitioning of the collisional kinetic energy between target and projectile. Values of Q^* for glass, basalt and granodiorite targets (Gault and Wedekind 1969; Fujiwara et al. 1977; Cintala and Hörz 1984) have been determined to be ~ 7 to 8×10^6 erg g^{-1}, while for ice targets they lie ~ 2 to 3×10^5 erg g^{-1} (Hartmann 1978; Cintala et al. 1985). To illustrate the range of collisional outcomes for different target materials, the ratio M_L/M_T is shown as a function of the collisional specific energy (see Fig. 2) for a wide range of experimental conditions.

There is a power-law relationship between M_L/M_T and E/M_T (linear in the log-log plot of Fig. 2) for different target materials. Furthermore, a similar slope is observed for rocky as well as ice targets; however, a given degree of destruction will be obtained in an ice target with only a few percent of the specific energy required for rocks. This is in qualitative agreement with the difference in tensile strength for the two materials. Data for ice-silicate targets follow a similar trend, but the energy required for a given degree of fragmentation is ~ 3 to 5 times that for pure ice. The wide scatter in the data points out that the relation between M_L/M_T and E/M_T may depend on other parameters, such as impact velocity and the size and physical properties of the projectile (Matsui et al. 1982; Cintala and Hörz 1984). While most of the data in Fig. 2 are for central impacts, a few data points from impacts at oblique incidence are shown. As a general trend, M_L/M_T seems to increase with increasing impact angle (as measured from the normal to the target surface) for a constant specific energy (Fujiwara and Tsukamoto 1980). However, this trend is not very straightforward, and it is masked by large uncertainties at large angles, and by the dearth of experimental points.

The effect of decreasing the target temperature on fragmentation was investigated for icy, ice-silicate and rocky targets (Smrekar et al. 1986; Lange and Ahrens 1981,1982). No effect was observed for rocky targets, while ice-silicate and icy targets were affected in opposite ways. The critical energy required to obtain a given degree of fragmentation increased with decreasing temperature for icy targets, but decreased for the case of the ice silicates. The
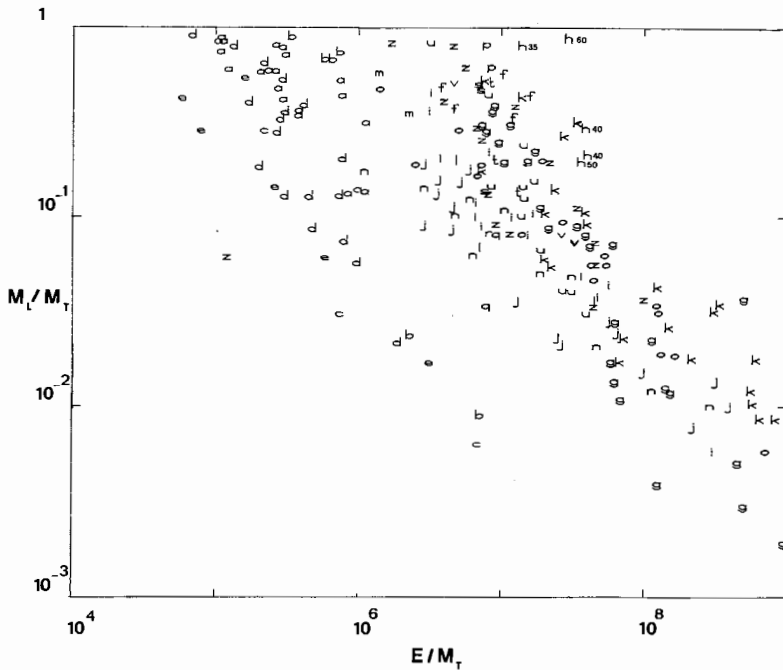
Fig. 2. M_L/M_T vs E/M_T (in erg g^{-1}) for various experimental conditions. For the case of oblique impacts, the numbers shown near the experimental points "h" indicate the angle of incidence of the impact, measured from the normal to the target surface. ICE: a—Hartmann, 1978; b,c— Lange and Ahrens, 1981 (257, 81 K); d—Cintala and Hörz, 1985; e—Kawakami et al., 1983. BASALT: f—Hartmann, 1978; g—Fujiwara et al., 1978; h—Fujiwara and Tsukamoto, 1980 (oblique); i,j—Matsui et al., 1982,1984 (cube, sphere); k—Takagi et al., 1984. DIFFERENT MATERIALS: l,m,n,o—Matsui et al., 1982 (granite, dunite, tuff); p,q,r—Gault and Wedekind, 1969 (synthetic tektites, glass); s,t—Smrekar et al., 1985 (granodiorite, warm, cold); u—Cintala and Hörz, 1984 (granodiorite); v—Takagi et al., 1984 (pyrophyllite); z— Davis et al., 1986 (mortar cement).

effects of different parameters, such as the target shape, projectile material, impact geometry, temperature, etc.; the collisional outcomes are not well understood at present and must be more thoroughly investigated.

D. Size Distribution of Fragments

The size (mass) distributions of the fragments produced during the catastrophic disruption of targets of different composition impacted by low- and high-velocity projectiles have been investigated by many authors (Gault and Wedekind 1969; Hartmann 1969; Fujiwara et al. 1977; Hartmann 1980; Lange and Ahrens 1981,1982; Matsui et al. 1982,1984; Kawakami et al. 1983; Nakamura et al. 1983; Takagi et al. 1984; Bianchi et al. 1984; Cintala and Hörz 1984; Hörz and Cintala 1985a,b; Capaccioni et al. 1986; Davis et al.

1986). The size distribution curve is well represented by a power law that is usually presented in one of three forms:

(a) Cumulative Mass Distribution:

$$M(<s) \sim s^k \tag{1}$$

defined as the total mass M of fragments smaller than a given size s; the exponent k is the power index.

(b) Cumulative Frequency Distribution:

$$N(>s) = A_s \, s^{-\alpha} \tag{2}$$

or

$$N(>M) = B_m \, M^{-\beta} \tag{3}$$

where $N(>s)$ and $N(>M)$ are the cumulative number of fragments larger than size s and mass M, respectively; A_s and B_m are constants; α and β are the indices of the distribution.

(c) Incremental Frequency Distribution:

$$dN(s) = C_s \, s^{-\gamma} \, ds \tag{4}$$

or

$$dN(M) = D_m \, M^{-\delta} \, dM \tag{5}$$

which represent the linear incremental relationships for the number of fragments dN within linear increments ds and dM, respectively. C_s, D_m are constants; γ and β are the power indices.

The relationships between the exponents of these distributions are:

$$\gamma = 3\delta - 2; \quad \alpha = \gamma - 1; \quad \beta = \delta - 1; \quad k = 3(1-\beta).$$

The value of the exponent depends on the amount of shattering of the target; the greater the degree of fragmentation, the steeper the exponent becomes. This fact simply reflects the increasing preponderance of small fragments from highly shattered targets. It is interesting that a variety of target materials, (silicates, glass, ice and ice silicate) when fragmented to the same degree, present quite similar size (mass) distributions which can be represented by Eqs. 1 to 5. However, the whole range of measurable fragment sizes usually cannot be well represented by a single exponent for the power law (Fujiwara et al. 1977; Matsui et al. 1982,1984; Bianchi et al. 1984; Takagi et al. 1984;

Capaccioni et al. 1986). Rather, the size distributions are usually divided into two or three segments with the slope of the distribution being generally steeper for larger fragments (see Fig. 3). The change in slope between large and small fragments generally occurs at fragment sizes ~1/10 that of the original target. With decreasing impact specific energy, there is a possible small shift in the position of the inflection point towards larger fragment sizes, indicating a predominance of small fragments. This behavior seems to indicate that the fracturing process occurs in two stages, possibly correlated to the pressure at which the change from plastic to elastic flow occurs in the target (Fujiwara et al. 1977; Di Martino et al. 1989), although the possibility that the mass distributions have been somewhat affected by further fracturing of small fragments after the main impact (e.g., collisions with the walls of the experimental chamber) cannot be excluded.

A useful way of representing the fragment distribution in the large-size range was introduced by Kresák (1977). In the Kresák log-log diagram,
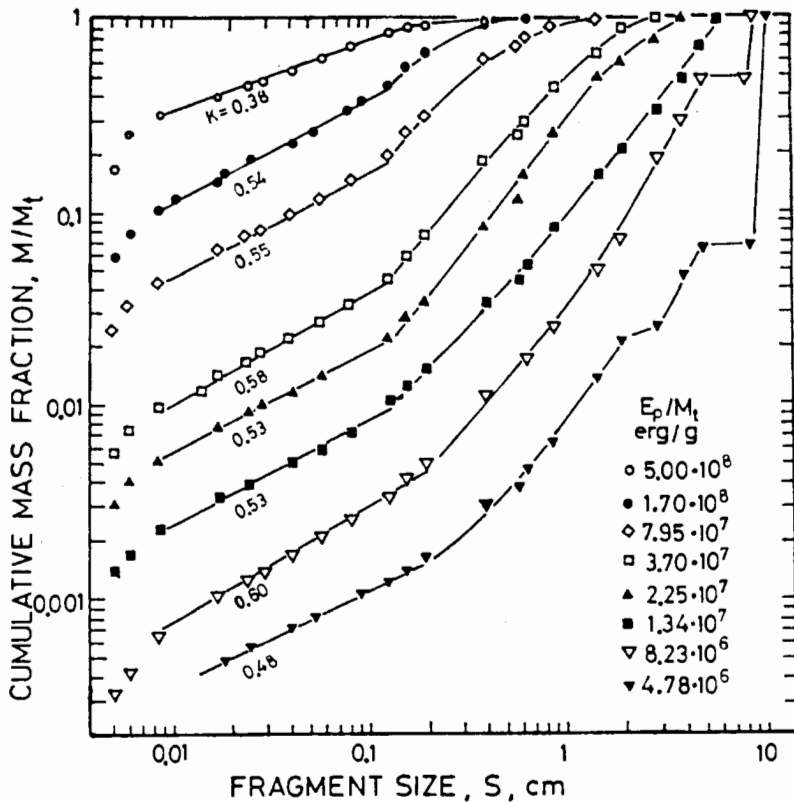
Fig. 3. Size distribution of fragments from catastrophic fragmentation of basalt targets illustrating the change in slope between large and small fragments (figure from Fujiwara et al. 1977).

M_j/M_T is plotted versus $(2j-1)$, where M_j is the mass of the jth fragment (ordered by mass). In Fig. 4(a), fragments with sizes >15 mm, obtained in the experiments by Capaccioni et al. (1986) are presented in a Kresák plot, while in Fig. 4(b) the same plot is shown for some well-known asteroid families (Zappalá et al. 1984). In the Kresák plot, one can see that after the few largest fragments, these distributions become nearly linear. While there are differences in the slopes of the distributions, the similarity between the plots representing the experimental data and those for the asteroid families is striking.
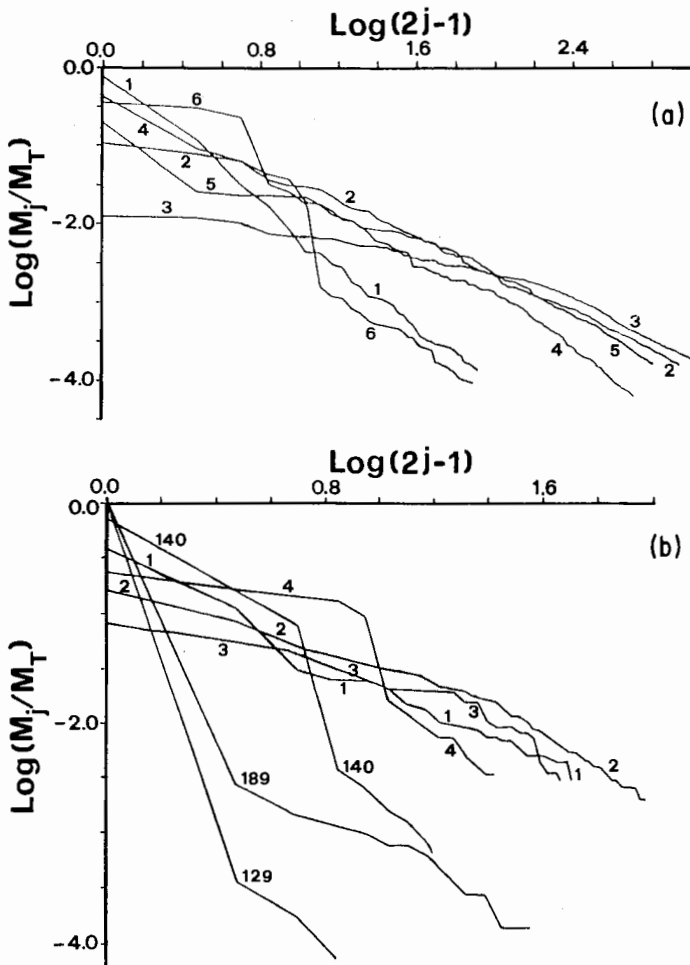
Fig. 4. (a) Log-log plot of the mass of the single fragments normalized to the target mass and ordered by their size (M_j is the mass of the jth fragment); (b) the same as in (a), but for several asteroid families numbered according to Williams' (1979) classification.

Low-velocity experiments produce fragmental size distributions that are not significantly different from those found in high-velocity impacts (Matsui et al. 1982). Hartmann (1980) shot low-velocity projectiles against artificial conglomerates. An interesting result was found in that the size distribution of fragments from the conglomerate was similar to that of fragments produced from competent targets. This result suggests that the fragmentation model can be applied to bodies ranging from loosely bound aggregates to solid coherent bodies.

In ice-fragmentation experiments performed at temperatures of 81 K and 275 K, Lange and Ahrens (1981) found that ice shatters in a manner similar to rocks with a single power-law fragment size distribution (for masses $\lesssim 0.1$ M_T), where the exponent increases with increasing specific energy. Decreasing temperature increases the strength of ice, such that the relative abundance of large fragments increases for constant impact-energy density. Kawakami et al. (1983) carried out experiments on ice at a temperature of 265 K and added a power-law fit for the 15 largest fragments, whose slope increases with increasing energy density to a single power-law fit for the smaller fragments.

The effects of multiple impacts against targets of different materials (glass, gypsum, granodiorite, plagioclase, pyroxene and olivine) were analyzed by Gault and Wedekind (1969), Nakamura et al. (1983) and Hörz and Cintala (1985a,b). They concluded that multiple impacts produce the same degree of shattering and fragmental size distribution as single impacts when the same total energy is applied.

E. Shape Distribution

The shapes of fragments from catastrophic collisions as defined by axes a, b and c, these being the maximum dimensions of the fragment in three mutually orthogonal planes ($a \geq b \geq c$), have been found to behave in a very regular way (Fujiwara et al. 1978; Fujiwara 1986). In Fig. 5 the distribution of b/a vs c/a is plotted for the collisional fragments from a basalt target (Capaccioni et al. 1984). There are no extreme shapes among these fragments, most being grouped in the central region with b/a and $c/a > 0.2$. Figure 6 depicts histograms of b/a and c/a showing that the axial ratios are quasi-normally distributed around mean values of the axial ratios $b/a \sim 0.7$ and $c/a \sim 0.5$, i.e., corresponding to $a:b:c$ in the simple proportion $2:\sqrt{2}:1$. This result is particularly intriguing because it seems to indicate a general property of collisional fragments which is repeated with great regularity in widely different experimental conditions (Fujiwara et al. 1978; Matsui et al. 1982,1984; Bianchi et al. 1984; Capaccioni et al. 1984,1986). Furthermore, this result has been found to be valid for fragments as small as ~ 100 μm (Capaccioni et al. 1986). The only exception has been observed for ice by Lange and Ahrens (1981) who found that fragment shapes depend both on temperature and on E/M_T; results from ice at 81 K are similar to the results described above, while
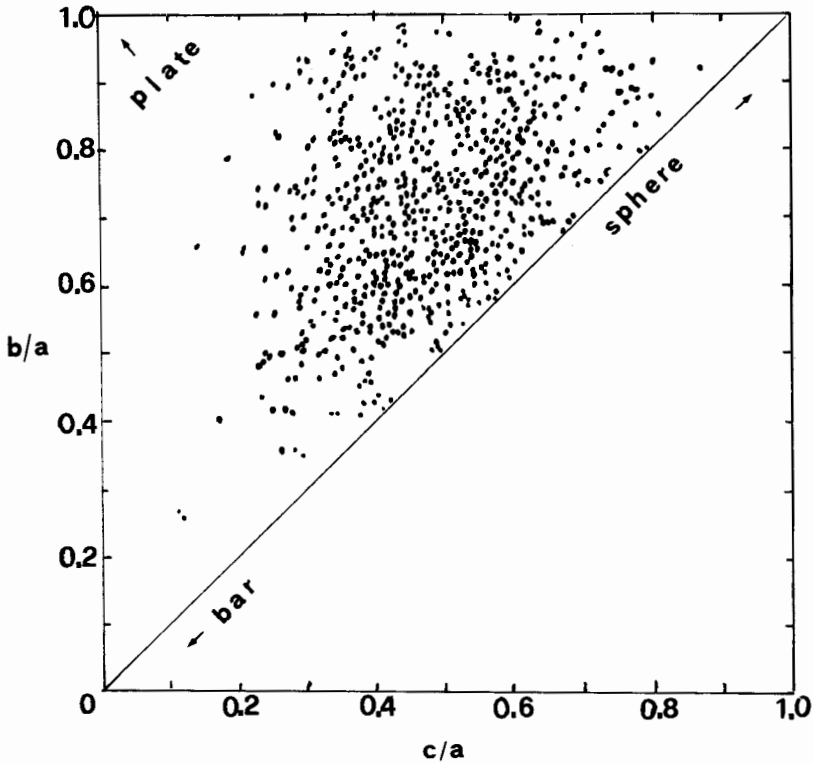
Fig. 5. Shape distribution of concrete fragments (after Capaccioni et al. 1984). *a*, *b* and *c* are the three orthogonal axes ($a \geq b \geq c$).

at 257 K, the axial ratios are lower and increase with increasing specific energy (i.e., the fragments are more plate-like).

The surface geometry of collisional fragments has been investigated using fractal analysis techniques (Fujimura et al. 1986). That is, irregularities in the fracture surfaces of dunite and basalt fragments from catastrophic collisions have been quantitatively expressed by "fractal dimensions" and compared with analogous data for fragments from static compression tests. The fractal dimension of collisional fragments was found to be consistently lower (i.e., their surfaces are rougher) than that of fragments from static compression tests; thus, fractal analysis could turn out to be a powerful tool to discriminate between different fracturing modalities.

F. Velocity of Fragments

Fragment velocity data from catastrophic disruption experiments are still quite sparse, and are limited to the velocities of selected fragments from basalt
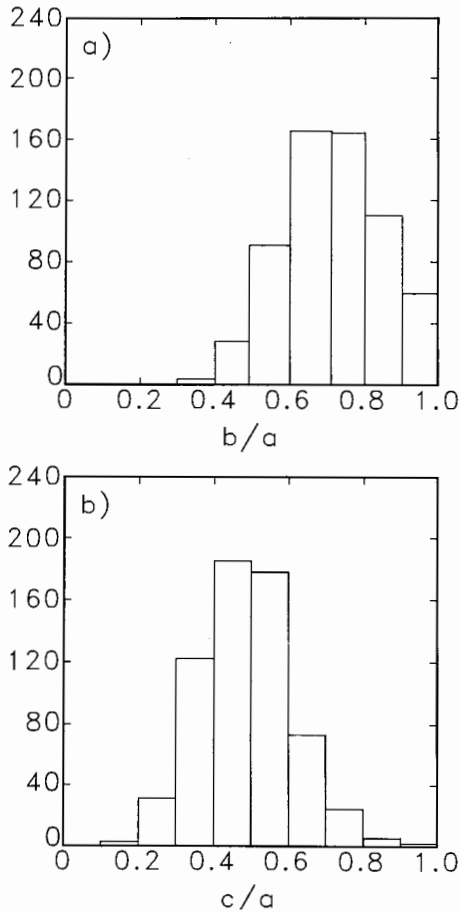
Fig. 6. Histograms for *b/a* and *c/a* corresponding to Fig. 3 (after Capaccioni et al. 1984). Mean values are 0.72 and 0.48, respectively.

targets which could be seen in the filmed records of the experiments. Analysis of high-speed movies (Gault and Wedekind 1969; Fujiwara and Tsukamoto 1980; Fujiwara 1987) shows that fragment velocities are highest near the impact point and decrease with increasing distance from the impact point. The fragments fly away successively from the surface to the interior, and generally do not collide with one another. In a core-type impact, the core fragment is traveling at a very low velocity. As a representative velocity, the velocity V_a of fragments from the antipodal point of the spherical basalt target was determined to be (Fujiwara and Tsukamoto 1980):

$$V_a = 3.2 \times 10^{-5}(E/M_T)^{0.76} \qquad (6)$$

(cgs units) for the high impact-velocity range. Takagi et al. (1984) plotted their own V_a obtained in the lower impact-velocity region, together with Fujiwara and Tsukamoto's data, as a function of the scaling parameter called the nondimensional impact stress $P_I = PV_p/YV_t$ (where P, V_p, Y and V_t are impact pressure, projectile volume, target compressive strength and target volume, respectively). In this representation, both data sets agree well in spite of the differing impact conditions (Fig. 7).

G. Rotation of Fragments

Rotation of fragments is commonly observed except for the core and antipodal fragments. Generally, the fastest rotators originate near the impact point. Figure 8 shows that while many fragments rotate with very short periods, they are still longer than the rotational bursting limit. The minimum rotation period is expected to be proportional to the size (Fujiwara and Tsukamoto 1981) and fit to the data (solid line in Fig. 8). The sense of rotation of the fragments from catastrophic collisions is illustrated in Fig. 1a (Fujiwara and Tsukamoto 1981; Fujiwara 1987). It should be noted that if the expected lower bound line is extrapolated to asteroid sizes, the predicted rotation rates agree with observed rates (to within a factor of 2 or so) for 100 km-sized asteroids. The physical basis for this extrapolation must be studied in future investigations.

H. Energy Partitioning

Partitioning of the impact energy into various energy modes (translational and rotational kinetic energy of fragments, comminution energy, heat, etc.) is the most physically fundamental quantity for understanding the whole process of catastrophic disruption. Experimental determination of energy par-
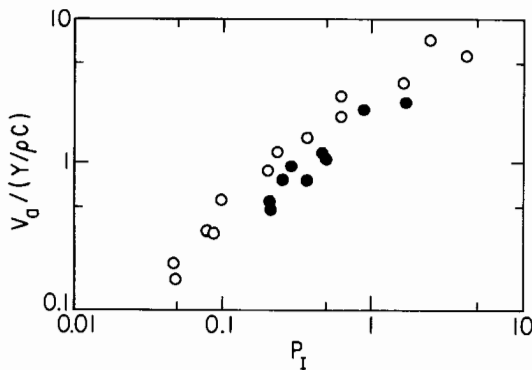
Fig. 7. Velocity of fragments from the antipodal point V_a as a function of P_I (see text). Y, ρ and c are, respectively, strength, density and sound velocity of the target material. The Fujiwara and Tsukamoto data (open circles) are in the high-velocity regime (2.7 km s^{-1}), while that of Takagi and Mizutani (filled circles) are for the low-velocity regime (<1 km s^{-1}).
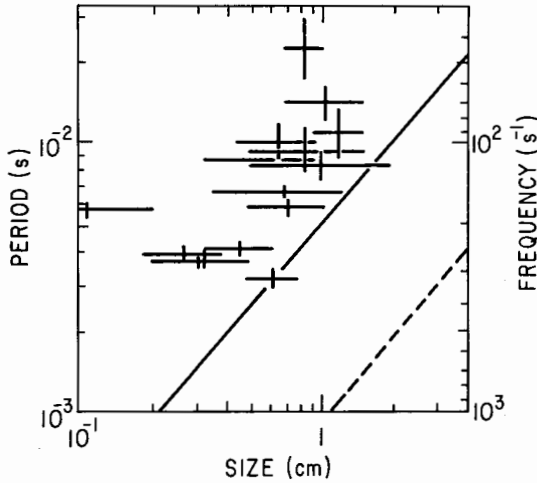
Fig. 8. Rotation period (frequency) as a function of fragment size. The horizontal and vertical bars represent the errors in the determination of the fragment size and frequency, respectively. Solid line: apparent minimum rotation period; broken line: rotational bursting limit of a basalt sphere (figure from Fujiwara 1987).

titioning for three core-type impacts (Fujiwara and Tsukamoto 1980) showed that the total kinetic energy imparted to larger fragments having 70 to 80% of the target mass is only about 0.3 to 3% of the impact energy, and the comminutional energy for this mass fraction is of the order of 0.1% of the impact energy. For catastrophic disruption by high-velocity impact into finite basalt targets, most of the collisional energy goes into kinetic energy of the finer fragments near the impact site, comminution and heat (Asada 1985). A similar energy partitioning is found from high-velocity cratering impacts into semi-infinite basalt (Gault and Heitowit 1963). They also found that 1% or less of the impact energy propagates into the whole target as an elastic wave; this is the energy we expect to be available for catastrophic fragmentation and ejection of the fragments. This result, too, is consistent with that of Fujiwara and Tsukamoto (1980) for catastrophic disruption.

At lower impact velocities, a smaller fraction of the impact energy is expended in the kinetic energy of fine fragments, comminution and heat, and a larger fraction is available for catastrophic fragmentation and ejection of the bulk of the target mass. Waza et al. (1985) shows that in the splitting and cone-type disruption of basalt and tuff targets, about 10 to 20% of the impact energy is transferred to the large fragments.

Partitioning of projectile kinetic energy into translational and rotational motion for individual fragments was determined by Fujiwara (1987). The results show the maximum ratio of rotational energy to translational energy for individual fragments to be on the order of 10^{-2} or less.

III. SCALING THEORY

A. General Scaling Law

The purpose of a scaling theory is to provide a rigorous framework that allows experiments to be extrapolated or scaled to other conditions that may either be impractical or impossible to attain experimentally. A complete scaling law would allow suitably designed experiments to be used to predict the distribution of sizes, velocities, shapes and rotational states of collisional fragments. Although significant progress has been made in recent years, there remains a large gap which separates the current state of collisional scaling from this ideal case. In this section, we review scaling theories, identify some of the difficulties and summarize areas where additional research is needed.

Explicit scaling theories have been developed only recently. However, collisional experiments have been performed and used in discussions of asteroidal evolution for nearly two decades. The application of laboratory results to asteroid collisions implicitly involves certain (sometimes unstated) scaling assumptions. The most popular assumption has been that, for a given type of target material, collisional outcomes depend only on the specific energy E/M_T of the event. The specific energy was referred to in some of the early fragmentation studies (Gault and Wedekind 1969; Fujiwara et al. 1977; Hartmann 1978). One of the concepts that grew out of these initial studies is that the fragmentation threshold is a function of the specific energy alone. Since that time, models of asteroid evolution have commonly assumed that other variables, such as fragment size distributions and velocities, are determined by E/M_T, independent of the size of the event (see, e.g., Dohnanyi 1969; Housen et al. 1979; Fujiwara 1982).

Davis et al. (1979) developed a model based on the above assumption regarding collisional fragmentation. However, they recognized the fact that sufficiently large asteroids would re-accumulate some of their collisional debris. Compared to their small laboratory counterparts, these asteroids would require a larger specific energy to cause fragmentation *and* dispersal of the fragments. Hence, while this model did not allow for a dependence of the fracturing process on size scale, it did include the effects of debris re-accumulation at large sizes.

Fujiwara (1980) first suggested that the fragmentation threshold for small bodies might depend on target size. In essence, he assumed that the threshold specific energy is proportional to the tensile strength of the target which, in turn, was assumed to be proportional to $R^{-1/2}$, where R is the target radius. The size-dependent strength stems from earlier suggestions by Moore et al. (1965) and Gault et al. (1972) that fragmentation is governed by the growth and coalescence of cracks and the assumption that the size of the largest crack is proportional to the size of the target. According to the Griffith model of crack growth, cracks of length L begin to grow when the stress exceeds a threshold value that is proportional to $L^{-1/2}$. Thus, if the largest cracks (which

are the first to initiate growth because they activate at the lowest stress) control the failure of the target, then the fracture stress would be proportional to $R^{-1/2}$. Under these assumptions, the threshold specific energy is proportional to $R^{-1/2}$ and therefore should decrease as target size increases, at least for bodies small enough that gravitational forces are not important.

Farinella et al. (1982) and Paolicchi et al. (1983) constructed a model based on the idea that the energy required to fragment a body depends not on the volume of the body, but rather on the area of the surfaces created. By adopting a power-law size distribution for the fragments, they showed that the energy required to initiate fragmentation Q^* is proportional to the $-1/6$ power of the target mass, or $R^{-1/2}$. This is the same result as obtained by Fujiwara (1980) by different assumptions.

Davis et al. (1983,1985) noted that large asteroids should be significantly strengthened by the effects of gravitational self-compression. The idea was that fracture would only occur if tensile stresses due to the passage of the shock wave in the asteroid exceeded the combined effects of the material strength and the self-compressive loading. They calculated the fragmentation threshold for large gravity-dominated bodies by adding a term representing the average compressive stress to the specific energy required to overcome the material strength. As a result, the threshold specific energy in their model is constant for small, strength-dominated bodies, and is proportional to R^2 for large bodies. Davis et al. found that the increased strength of large asteroids helped to reconcile previous discrepancies between the observed size distributions of asteroid family members and model calculations.

Holsapple and Housen (1986) approached the scaling question in a more general way using dimensional analysis. Some of the scaling results from their work are shown in Table III. One advantage of their approach is that it permits complex (and unknown) relationships among variables to be expressed more simply in terms of a reduced number of nondimensional parameters. This scaling model includes two specific generalizations over previous models. First, the impactor is described by both its size and velocity (or equivalently, its energy and velocity) whereas previous studies were based on the energy alone. The inclusion of both the energy and velocity is motivated by scaling studies of impact cratering (see, e.g., Holsapple and Schmidt 1987) which have shown that for cratering, analyses based on energy considerations alone are not valid. These studies have also shown that a variety of impact phenomena are well described by a particular combination of the impactor energy E and velocity U given by $E\ U^{(3\mu-2)/2}$, where μ is a constant determined primarily by the porosity of the target material. Note that when $\mu = 2/3$, the additional velocity dependence vanishes resulting in energy scaling of the impactor. However, for nonporous materials such as hard rocks, μ has been found to be about 0.55, which is distinctly lower than the energy scaling limit.

The second generalization included in the Holsapple and Housen (1986)

TABLE III
Dimensional Analysis Scaling

	Strength Regime[a]	Gravity Regime[b]
Mass of Fragments with Masses $\leq m$	$M_m/M = F[m/M, \Pi_s]$ [c]	$M_m/M = F[m/M, \Pi_G]$
Mass of Largest Fragment	$m_1/M = F[\Pi_s]$	$m_1/M = F[\Pi_G]$
Fragmentation Threshold[d]	$\overset{*}{Q} \propto (S/\rho)^{-3\mu/(B-2)} R^{3\mu(A+B)/(B-2)} U^{2-3\mu}$	$Q^* \propto (\rho G)^{3\mu/2} R^{3\mu} U^{2-3\mu}$
Mass of Fragments with Velocity $> v$	$M_v/M = F[v \bar{Q}^{1/3\mu} U^{(2-3\mu)/3\mu}, \Pi_s]$	$M_v/M = F[v \bar{Q}^{1/3\mu} U^{(2-3\mu)/3\mu}, \Pi_G]$
Characteristic Velocity[e]	$v_c = Q^{1/3\mu} U^{(3\mu-2)/3\mu} F[\Pi_s]$	$v_c = Q^{1/3\mu} U^{(3\mu-2)/3\mu} F[\Pi_G]$
Characteristic Vel at Fragmentation	$v_c^* \propto (S/\rho)^{-1/(B-2)} R^{(A+B)/(B-2)}$	$v_c^* \propto (\rho G)^{1/2} R$

Notes: (a) The strength parameter, Π_s, is defined as $\Pi_s = Q (S/\rho)^{3\mu/(B-2)} R^{-3\mu(A+B)/(B-2)} U^{3\mu-2}$
   (b) The gravity parameter, Π_G, is defined as $\Pi_G = Q (\rho G)^{-3\mu/2} R^{-3\mu} U^{3\mu-2}$
   (c) F represents a generic functional dependence, which differs from one equation to the next.
   (d) The threshold is defined such that $m_1/M = $ constant
   (e) The characteristic velocity is defined such that $M_v/M = $ constant

Variables:

M = Target mass	U = Impactor speed
R = Target radius	G = Gravitational constant
ρ = Target density	μ, A, B are scaling exponents
S = Target strength measure	(see text)
(see text)	

model is that the target material is described by a generalized mechanical property S^* which has dimensions of (stress) (length)^A(time)^B, where A and B are constants. Any material model characterized by any single-strength measure can be realized by suitable choices of A and B. For example, if A and B are both zero, S^* simply has units of stress. In this case, S^* represents the fracture strength of a material whose strength is constant. If one assumes energy scaling ($\mu = 2/3$) together with $A = B = 0$, then the specific energy Q^* at the fragmentation threshold is constant in the strength regime (Table III). In this case, $Q^* = S_o/\rho$, where S_o is defined as the impact strength with units of energy density (ergs cm^{-3}). This represents the model of Davis et al. On the other hand, $A = 10$ and $B = -13$ results in Q^* proportional to $R^{-1/2}$, corresponding to the model of Fujiwara (1980) and Farinella et al. (1982). Holsapple and Housen adopted as a nominal case a rate-dependent material model in which the fracture strength is proportional to the 1/4 power of the strain rate. This behavior has been observed in dynamic measurements of the tensile strength of rock (see, e.g., Grady and Lipkin 1980; Cohn and Ahrens 1981). Under the nominal strain-rate model, Q^* should decrease as target size increases, according to $R^{-0.24}$ (Holsapple and Housen 1986). The physical basis for this is the fact that the strain rate of loading processes effectively decreases with increasing target size.

As noted by Davis et al. (1983,1985), fracture of large bodies will only occur if the stress wave caused by the impact can overcome the combined effects of the material fracture strength and the gravity-induced compressive loading. In the approach of Holsapple and Housen (1986) the view is that the stress pulse caused by the impact event must overcome both that initial compressive stress and the strength of the material. Therefore, there is an effective local strength that is simply the sum of that pre-stress and the material fracture strength for their general model. Note that Davis et al. add the gravity stress to the *specific energy* required for fracture. For the Holsapple and Housen approach, the result for sufficiently large bodies where the gravity stresses dominate the material strength, gives Q^* proportional to $R^{3\mu}$. This agrees with the Davis et al. model under their assumed energy scaling. It increases with R because of the gravitational self-compression which increases with size.

Holsapple and Housen also derived scaling relations for fragment size and velocity distributions. For example, they defined a characteristic fragment velocity v_c. At the fragmentation threshold, v_c can be shown to be independent of size for the constant fracture stress model ($A = B = 0$). On the other hand, for the strain-rate model, v_c is proportional to $R^{-1/7}$, so that fragment velocities should decrease with increasing target size. This is due to the fact that the target effectively becomes weaker (because the strain rate decreases) as R increases. In the gravity regime, the characteristic velocity is proportional to R.

Takagi et al. (1984) introduced a different approach to scaling laws for fragmentation and compared them to experimental results. In their analysis, as discussed in Sec. II.F, they suggest that many aspects of collisions should be correlated by the nondimensional impact stress parameter P_I. According to this model, fragmentation occurs above a threshold value of P_I. This can be shown to be equivalent to $Q^* \propto U^\theta$ for a given target material. The exponent θ depends on the collision speed: for large U, θ approaches 0 and for small U it approaches -1. Thus, while this model allows a dependence of the fragmentation threshold on encounter velocity, it does not include a dependence on size scale.

Figure 9 presents a comparison of the scaling predictions for the threshold specific energy Q^* as a function of target size. There are clearly significant differences between the scaling estimates. Attempts to use the existing laboratory data to discriminate the theories are inconclusive at present due to the limited size scale and velocity regimes of the experiments (Holsapple and Housen 1986).

B. Scaling With Material Types

The strength parameter (S_o or Q^*) characterizing the target material needed in the scaling theory described above is usually determined by impact experiments in the laboratory. While the experimental data base has grown significantly in the past decade, it is still far from complete. A methodology is
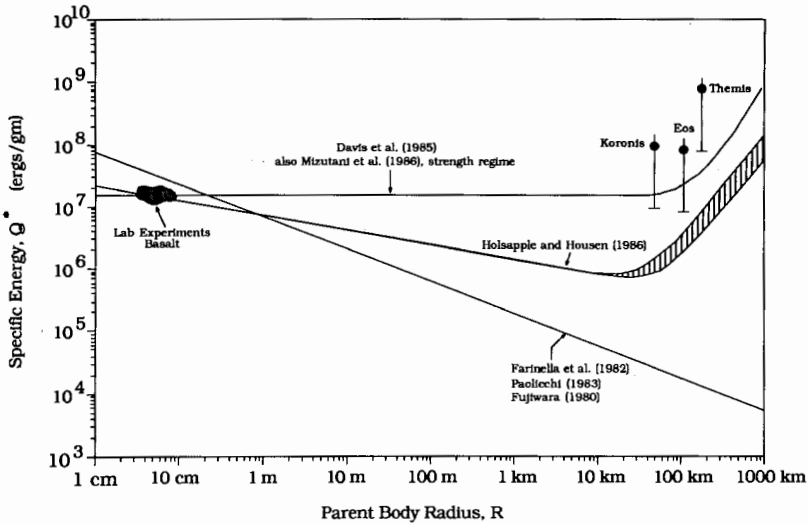
Fig. 9. The specific energy at the fragmentation threshold as a function of target size for rocky materials. The curve from Davis et al. represents the scaling for a material whose fracture stress is independent of size or strain rate in the strength regime but increases in the gravity regime due to self-compression. Holsapple and Housen developed their estimate for a material whose strength is strain-rate dependent in the strength regime. The Farinella et al. curve is based on the hypothesis that fragmentation is governed by the energy required to create new surfaces. Typical values of the specific energy are shown for laboratory experiments. Three points are shown for asteroid families, as estimated by Fujiwara (1982), and adjusted as described in the text.

required to enable us to extend the experimentally determined values of impact strength to new material types and structures.

The simplest scaling law for impact strength is to assume that it is proportional to the compressive or, better yet, the tensile strength of the body. This law was assumed by earlier workers, e.g., Davis et al. (1979,1985), in order to calculate collisional outcomes for materials on which there were no available experimental data. Davis and Ryan (1989) tested the proportionality scaling law for impact strength using the compiled experimental data base mentioned earlier in Sec. II.B. Figure 10 shows the experimental data on impact strength as a function of the laboratory-measured value of compressive strength. Compressive strength, which is generally proportional to tensile strength, was adopted because it is available for a wider variety of materials. The experimental data lends support to the assumption that strength is the dominant factor in determining the energy needed to fracture a body. However, strength is not the whole story; refined analysis of the data shows that a strain-rate dependent strength is a superior law to that of strength alone (Davis and Ryan 1989).
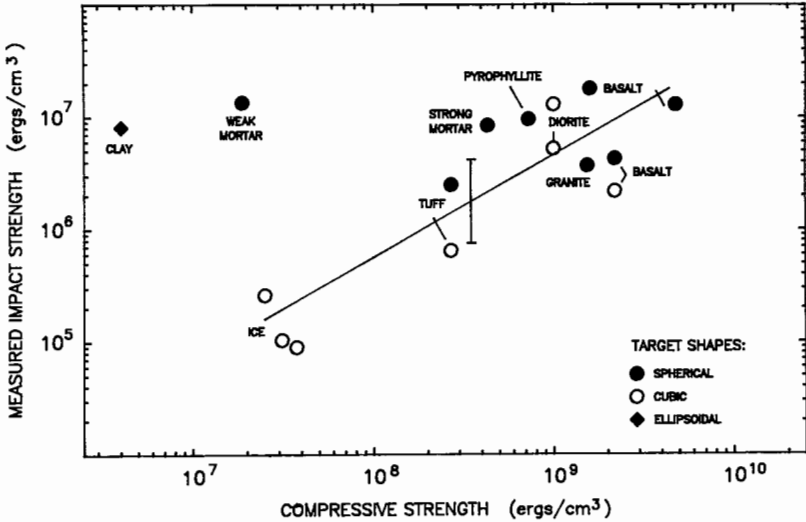
Fig. 10. A log-log plot of impact strength vs compressive strength for natural silicates, cement mortar and ice. The solid line is the fit to the data but excluding the clay and 500 psi targets (see text). The error bar shown at the center of the plot represents the 1σ scatter variance.

The only significant exceptions to the above scaling laws were found from experiments using clay targets by Fujiwara and Asada (1983) and those using weak mortar targets (Davis and Ryan 1989). These materials have impact strengths that are about 1.5 to 2 orders of magnitude larger than predicted using static compressive strengths. The reason for this large impact strength is not clear, but may relate to the granular, nonhomogeneous nature of these materials. Perhaps such structures do not propagate the impact-stress pulse efficiently, but dissipate much of the collisional energy close to the impact site. Hence, much higher collisional energies would be needed to shatter such bodies as compared with competent targets.

C. Comparison of Scaling-Law Predictions with Astronomical Data

We may test the validity of scaling theories by comparing their predictions for size and velocity distributions of collisional fragments with those observed within asteroid families assuming, of course, a collisional origin of these families (see the chapter by Chapman et al.). Strain-rate scaling (Sec. III.A) predicts that in the strength regime, the energy required to shatter a body decreases as target size increases (Fig. 9). This implies that large-scale asteroid collisions with an impact speed of 5 km s^{-1} are low-strength, low-strain-rate events. For example, if the collisional strain rate $\dot{\epsilon}$ can be approximated by V/D_p, where V is the impact speed and D_p the projectile diameter, then for asteroid collisions $\dot{\epsilon} \simeq (5/D_p)$ s^{-1}, where D_p is in km. An asteroid

impact involving a 5-km diameter projectile would occur under strain rates comparable to those of machine-measured (static loading) laboratory conditions (~ 1 s^{-1}) in striking contrast to laboratory impact studies which involve high rates of strain ($\sim 10^4$ s^{-1}). Thus, the laboratory measured impact strength can be significantly larger ($\sim$ a factor of 10 if the 1/4 power scaling for the strain rate is correct) than the low strain-rate value.

However, strain-rate dependent scaling fails to yield satisfactory results when used in algorithms for collisional evolution for the formation of asteroid families. When incorporated in the numerical model described by Davis et al. (1985) and starting with the "best" initial population from that paper, the weaker asteroid strengths lead to more collisional grinding, and a depleted asteroid population in the size range ~ 80 to 150 km (see the chapter by Davis et al.). Also, the existence of large fragments in the populous asteroid families, each thought to have originated from the disruption of a parent body, certainly suggests a strength-dominated fracture regime. The large diameter (up to ~ 300 km) of the parent bodies demands very large impact strengths in order to form sizeable fragments, up to $\sim 10^9$ ergs cm^{-3} according to this model. However, strain-rate scaling predicts a much lower strength at these sizes when based upon laboratory measurements for strong basalt. Either the material composing the parent bodies responds to impacts as if it were very strong or the strain-rate scaling is incorrect.

Fujiwara (1982) used the proper elements for the Themis, Eos and Koronis families to calculate the relative velocities of family members. He estimated the total energy that the observed fragments would have had following the breakup of the parent asteroid. The impactor energy can then be calculated if one assumes a value for the fraction f_{KE} of kinetic energy which is transferred from the impactor to the debris. The data points shown in Fig. 9 for the three families represent the specific energy based on Fujiwara's nominal value of $f_{KE} = 0.1$. Lower limits are also shown. These were calculated by assuming that all of the impactor energy is transferred to the fragments (i.e., $f_{KE} = 1$). The nominal estimates of Q^* for the three families are significantly higher than the values measured for rock in the laboratory. This is consistent with the observations of Davis et al. (1985) that large asteroids must behave as if they are considerably stronger than the targets typically used in fragmentation experiments.

In addition to the above contradictions to observational evidence that strain-rate scaling implies, there is also a problem with characterizing fragment velocities. Ejection velocities determined for family members (based on the dispersion of their orbital elements) are typically greater by a factor of 5 to 10 than those exhibited in laboratory impact experiments. It is suspected though, that this is simply a consequence of the strength scaling difficulties, since for bodies dominated by solid-state strength, fragment velocities are likely to scale with the square root of the specific binding energies (Holsapple and Housen 1986). Therefore, if impact strengths appear to be too low by a

factor of 25 or so, it is not surprising to find observationally determined fragment velocities are approximately 5 times too slow as well.

There is better agreement, however, between experimental results and asteroid observations for sizes and shapes. We have already noted similarities, particularly in the low-mass tail of the distribution, between plots for collisional fragments and distributions of some representative asteroid families (see Fig. 2b). A second interesting comparison can be drawn for the shape distribution. As discussed in Sec. II.E, the shape distribution of collisional fragments is fairly regular over a wide range of impact conditions. These can be directly compared with asteroid shapes inferred from lightcurves (Capaccioni et al. 1984; Catullo et al. 1984). The average value of b/a for 194 main-belt asteroids with $D < 100$ km was found to be in good agreement with the experimental results, thus supporting the hypothesis that they are of collisional origin. However, a much more spherical shape, with average b/a values closer to one, was shown by larger asteroids, where self-gravitation effects could be expected to be relevant and act to smooth out large-scale irregularities. An intriguing discrepancy emerges when considering Apollo-Amor objects, a significant fraction ($\sim 1/4$) of which are elongated to a level very rarely encountered among fragments ($b/a \lesssim 0.4$). Some physical explanation is required for this puzzling feature, possibly related to a peculiar origin or evolution of these Earth-approaching objects.

IV. AVENUES FOR FUTURE RESEARCH

To develop scaling theory further, systematic acquisition of more data for a wide variety of parameters for both the projectile and the target is necessary. Available data on kinematical behaviors are still limited. The velocity distribution as a function of size has not yet been determined for the full size range of fragments, in spite of the fact that this is essential for realistic modeling of asteroid collisional evolution. It must be remembered that most of the present experimental data have been obtained in normal-incidence impact experiments, while most of the natural impacts among asteroids are oblique. Therefore, more data are needed to cover collisions at a variety of impact angles.

Tailoring experiments to take into account more realistic situations for actual asteroids is important. Asteroids may have structures such as mantles and cores, and may have suffered repeated impacts, resulting in the body having either many pre-existing fractures or a rubble-pile structure. The question as to how the gravitational self-stress combines with the material strength could in principle be addressed with experiments using a pre-stress imposed by an external pressure loading. Impact experiments using significantly larger targets cannot be conducted due to our inability to launch very large projectiles. However, large-scale catastrophic disruption experiments using explosively-generated stresses are a possibility. There is literature from the mining and

nuclear tests industries on the breakup of rocky materials, which might give guidance on the appropriate scaling in the strength regime. Finally, numerical code calculations cannot be used to choose unambiguously between the theories because, as demonstrated by the approach of Holsapple and Housen (1986), the very choice of the strength measure dictates much of the resulting scaling. However, such calculations would be useful to study the appropriate measure of strength of impact events, and to determine results in the gravity regime.

REFERENCES

Asada, N. 1985. Fine fragments in high-velocity impact experiments. *J. Geophys. Res.* 90:12445–12453.

Bianchi, R., Capaccioni, F., Cerroni, P., Coradini, M., Flamini, E., Hurren, P., Martelli, G., and Smith, P. N. 1984. Experimental simulation of asteroidal fragmentation by macroscopic hypervelocity impacts against free falling bodies. *Astron. Astrophys.* 139:1–6.

Capaccioni, F., Cerroni, P., Coradini, M., Farinella, P., Flamini, E., Martelli, G., Paolicchi, P., Smith, P. N., and Zappalà, V. 1984. Shapes of asteroids compared with fragments from hypervelocity impact experiments. *Nature* 308:832–834.

Capaccioni, F., Cerroni, P., Coradini, M., Di Martino, M., Farinella, P., Flamini, E., Martelli, G., Paolicchi, P., Smith, P. N., Woodward, A., and Zappalà, V. 1986. Asteroidal catastrophic collisions simulated by hypervelocity impact experiments. *Icarus* 66:487–514.

Catullo, V., Zappalà, V., Farinella, P., and Paolicchi, P., 1984. Analysis of the shape distribution of asteroids. *Astron. Astrophys.* 138:464–468.

Cintala, M. J., and Hörz, F. 1984. Catastrophic rupture experiments: Fragment-size analysis and energy considerations. *Lunar Planet. Sci.* XV:158–159 (abstract).

Cintala, M. J., Hörz, F., Smrekar, S., and Cardenas, F. 1985. Impact experiments in H_2O ice, II: Collisional disruption. *Lunar Planet. Sci.* XVI:129–130 (abstract).

Cohn, S. N., and Ahrens, T. J. 1981. Dynamic tensile strength of lunar rock types. *J. Geophys. Res.* 86:1794–1802.

Curtis, J. S. 1962. An Accelerated Reservoir Light-Gas Gun. NASA TN D-1144.

Davis, D. R. 1987. Summary Report on the Second International Workshop on Catastrophic Disruption of Small Solar System Bodies, Belgrade, Yugoslavia.

Davis, D. R., and Ryan, E. V. 1989. Collisional disruption: Experimental results and scaling laws. *Icarus,* submitted.

Davis, D. R., Chapman, C. R., Greenberg, R., Weidenschilling, S. J., and Harris, A. W. 1979. Collisional evolution of asteroids: Populations, rotations and velocities. In *Asteroids,* ed. T. Gehrels (Tucson: Univ. of Arizona Press), pp. 528–557.

Davis, D. R., Chapman, C. R., Greenberg, R., and Weidenschilling, S. J. 1983. Asteroid collisions: Effective body strength and efficiency of catastrophic disruption. *Lunar Planet. Sci.* XIV:146–147 (abstract).

Davis, D. R., Chapman, C. R., Weidenschilling, S. J., and Greenberg, R. 1985. Collisional history of asteroids: Evidence from Vesta and Hirayama families. *Icarus* 62:30–53.

Davis, D. R., Weidenschilling, S. J., Ryan, E. V., and Williams, B. L. 1986. Experimental studies of catastrophic disruption. *Lunar Planet Sci.* XVII:156–157 (abstract).

Di Martino, M., Martelli, G., Woodward, A., and Smith, P. N. 1989. Astrophysical implications of the time evolution of the catastrophic fragmentation by hypervelocity impacts of freefalling bodies. In preparation.

Dohnanyi, J. W. 1969. Collisional model of asteroids and their debris. *J. Geophys. Res.* 74:2531–2554.

Farinella, P., Paolicchi, P., and Zappalà, V. 1982. The asteroids as outcomes of catastrophic collisions. *Icarus* 52:409–433.

Fujiwara, A. 1980. On the mechanism of catastrophic destruction of minor planets by high-velocity impact. *Icarus* 41:356–364.

Fujiwara, A. 1982. Complete fragmentation of the parent bodies of Themis, Eos, and Koronis families. *Icarus* 52:434–443.

Fujiwara, A. 1986. Results obtained by laboratory simulation of catastrophic impact. *Mem. S. A. It.* 57:47–64.

Fujiwara, A. 1987. Energy partition into translational and rotational motion of fragments in catastrophic disruption by impact: An experiment and asteroid cases. *Icarus* 70:536–545.

Fujiwara, A., and Asada, N. 1983. Impact fracture patterns on Phobos ellipsoids. *Icarus* 56:590–602.

Fujiwara, A., and Tsukamoto, A. 1980. Experimental study on the velocity of fragments in collisional breakup. *Icarus* 44:142–153.

Fujiwara, A., and Tsukamoto, A. 1981. Rotation of fragments in catastrophic impact. *Icarus* 48:329–334.

Fujiwara, A., Kamimoto, G., and Tsukamoto, A. 1977. Destruction of basaltic bodies by high-velocity impact. *Icarus* 31:277–288.

Fujiwara, A., Kamimoto, G., and Tsukamoto, A. 1978. Expected shape distribution of asteroids obtained from laboratory impact experiments. *Nature* 272:602–603.

Fujimura, A., Takagi, Y., Furumoto, M., and Mizutani, H. 1986. Fractal dimensions of fracture surfaces of rock fragments. *Mem. Natl. Inst. Polar Res., Spec. Issue* 41:348–357.

Gault, D. E., and Heitowit, E. D. 1963. The partition of energy for hypervelocity impact craters formed in rock. *Proc. 6th Hypervelocity Impact Symp.*, vol. 2 (Cleveland, OH: Firestone Rubber Co.), pp. 419–456.

Gault, D., and Wedekind, J. A. 1969. The destruction of tektites by micrometeoroid impact. *J. Geophys. Res.* 74:6780–6794.

Gault, D. E., Hörz, F., and Hartung, J. B. 1972. Effects of microcratering on the lunar surface. *Proc. Lunar Planet Sci.* Conf. 3:2713–2734.

Grady, D. E., and Lipkin, J. 1980. Criteria for impulsive rock fracture. *Geophys. Res. Lett.* 7:255–258.

Greenberg, R., Wacker, J. E., and Hartmann, W. K. 1979. Impact strength: A fundamental parameter of collisional evolution. *Bull. Amer. Astron. Soc.* 9:455 (abstract).

Greenberg, R., Hartmann, W. K., and Chapman, C. R. 1978. Planetesimals to planets: Numerical simulation of collisional evolution. *Icarus* 35:1–26.

Hartmann, W. K. 1969. Terrestrial, lunar and interplanetary rock fragmentation. *Icarus* 10:201–213.

Hartmann, W. K. 1978. Planet formation: Mechanism of early growth. *Icarus* 10:201–213.

Hartmann, W. K. 1980. Continued low-velocity impact experiments at Ames vertical gun facility: Miscellaneous results. *Lunar Planet. Sci.* XI:404–406 (abstract).

Holsapple, K. A., and Housen, K. R. 1986. Scaling laws for the catastrophic collisions of asteroids. *Mem. S. A. It.* 57:65–85.

Holsapple, K. A., and Schmidt, R. M. 1987. Point source solutions and coupling parameters in cratering mechanics. *J. Geophys. Res.* 92:6350–6376.

Hörz, F., and Cintala, M. J. 1985a. Collisional fragmentation of granodiorite targets by multiple impact events. *Lunar Planet.* XVI:364–365 (abstract).

Hörz, F., and Cintala, M. J. 1985b. Experimental regolith evolution: Differential comminution of plagioclase, pyroxene and olivine. *Lunar Planet.* XVI:362–363 (abstract).

Housen, K. R., Wilkening, L. L., Chapman, C. R., and Greenberg, R. 1979. Asteroidal regoliths. *Icarus* 39:317–351.

Kawakami, S., Mizutani, H., Takagi, Y., Kato, M., and Kumazawa, M. 1983. Impact experiments on ice. *J. Geophys. Res.* 88:5806–5814.

Kresák, L. 1977. Mass content and mass distribution in the asteroid system. *Bull. Astron. Inst. Czech.* 28:65–82.

Lange, A., and Ahrens, T. J. 1981. Fragmentation of ice by low-velocity impact. *Proc. Lunar Planet. Sci. Conf.* 12:1667–1687.

Lange, M. A., and Ahrens, T. J. 1982. Impact fragmentation of ice-silicate bodies. *Lunar Planet. Sci.* XIII:417–418 (abstract).

Martelli, G., and Newton, G. 1977. Hypervelocity cratering and impact magnetization of basalt. *Nature* 269:478–480.

Matsui, T., Waza, T., Kani, K., and Suzuki, S. 1982. Laboratory simulation of planetesimal collisions. *J. Geophys. Res.* 87:10968–10982.

Matsui, T., Waza, T., and Kani, K. 1984. Destruction of rocks by low velocity impact and its implications for accretion and fragmentation processes of planetesimals. *Proc. Lunar Planet. Sci. Conf.* 14, *J. Geophys. Res. Suppl.* 89:B700–B706.

Mizutani, H., Kumazawa, M., Kato, M., Masuda, T., Kawakami, S., Takagi, Y., and Kani, K. 1981. A performance test of the low velocity shock gun with a novel sabot stopper. *Proc. ISAS Lunar Planet. Symp.* 14:267–277.

Mizutani, H., Takagi, S., and Kawakami, S. 1986. New scaling law on impact fragmentation. Preprint.

Moore, H. J., Gault, D. E., and Heitowit, E. D. 1965. Change in effective target strength with increasing size of hypervelocity impact craters. In *Proc. of 7th Hypervelocity Impact Symp.* 4:341.

Nakamura, H., Ito, K., Fujii, N., Takeuchi, H., Miyamoto, M., and Kobayashi, Y. 1983. Effects of velocity, size, and repeated fragmentation on the mass distribution in low-velocity impact experiment. *Proc. ISAS Lunar Planet. Symp.* 16:55–59.

Paolicchi, P., Farinella, P., and Zappalà, V. 1983. The critical energy density and the inelasticity coefficient for asteroidal catastrophic collisions. *Adv. Space Res.* 82:235–238.

Seigel, A. E. 1965. The theory of high speed guns. *AGARDograph* 91.

Smrekar, S., Cintala, M. J., Hörz, F., Cardenas, F., and Thompson, T. D. 1985. Impact experiments in cold rock. II: Collisional fragmentation. *Lunar Planet. Sci.* XVI:795–796 (abstract).

Smrekar, S., Cintala, M. J., and Hörz, F. 1986. Small-scale impacts into rocks: An evaluation of the effects of target temperature on experimental results. *Geophys. Res. Lett.* 13:745–748.

Takagi, Y., Mizutani, H., and Kawakami, S. 1984. Impact fragmentation experiments of basalts and pyrophyllites. *Icarus* 59:462–477.

Waza, T., and Matsui, T. 1983. Size distribution of fine fragments produced from destruction of rocks in low velocity impact. *Lunar Planet. Sci.* XIV:838–839 (abstract).

Waza, T., Matsui, T., and Kani, K. 1985. Laboratory simulation of planetesimal collision. 2. Ejecta velocity distribution. *J. Geophys. Res.* 90:1995–2011.

Williams, J. G. 1979. Proper orbital elements and family membership of the asteroids. In *Asteroids*, ed. T. Gehrels (Tucson: Univ. of Arizona Press), pp. 1040–1063.

Zappalà, V., Farinella, P., Knežević, A., and Paolicchi, P. 1984. Collisional origin of asteroid families: Mass and velocity distributions. *Icarus* 59:261–285.

PART III
Structure and Physical Properties of the Asteroids

THE IRAS ASTEROID AND COMET SURVEY

DENNIS L. MATSON, GLENN J. VEEDER, EDWARD F. TEDESCO
Jet Propulsion Laboratory

and

LARRY A. LEBOFSKY
University of Arizona

Observations made by the Infrared Astronomical Satellite (IRAS) during 1983 constitute the largest, most complete and least biased of the asteroid surveys to date. 1811 asteroids and 25 comets with known orbits were measured. Thermal flux densities at 12, 25, 60 and 100 µm, as well as (in the case of asteroids) their derived radiometric albedos and diameters have been compiled in the IRAS Asteroid and Comet Survey. Useful low-resolution spectra were obtained for 47 numbered asteroids. There is evidence in the IRAS data base for a large population of asteroids with unknown orbits. The methods of observation are outlined. The survey strategy and the data reduction are discussed. The rationale is given for the various IRAS asteroid and comet data products. Some directions for future research using IRAS data are suggested.

I. INTRODUCTION

In 1983 the Infrared Astronomical Satellite (IRAS) was launched into Earth orbit for the purpose of mapping the infrared sky. From January to November, it observed sources of infrared radiation on the celestial sphere. In the course of the mission it returned the data which constitute the basis for the IRAS Asteroid and Comet Survey. This survey is the largest, most complete and least biased survey of asteroids and comets yet conducted. It is largest because of the number of objects observed. Its completeness arises from the

fact that the whole sky was surveyed (though, by no means were all known asteroids observed). It is least biased because the space environment permits more uniform observing conditions than obtainable from the Earth's surface and because the observations were of thermal emission rather than of reflected sunlight. This latter advantage is due to the fact that (for the observed range of minor planet and comet albedos) the detection of an object at thermal wavelengths is a less sensitive function of albedo than it is in the visual.

Measurements of thermal emission from small bodies are required for our present method of estimating the fundamental properties of size and albedo. Knowledge of these properties is the key to the study of asteroids as individual bodies. Effective diameter is perhaps the most important parameter in the physical and thermal modeling needed for comparative planetological study of asteroids, and their comparison with satellites, planets and the parent bodies of the meteorites. Albedos are also needed in order to scale properly relative spectral reflectance data and obtain spectral albedos, the required data for discrimination between a number of asteroid classes. Albedo is also key to the determination of the surface temperature.

The work of the asteroid and comet survey was carried out with broad participation of researchers active in the field. Initial thinking about the possibilities of such a survey occurred as early as the spring of 1976, when a number of informal discussions occurred in Pasadena. By late summer, the importance of such a survey was widely discussed at IAU Colloquium No. 39 in Lyon, France. It was recognized that such a survey could easily be the most important survey yet undertaken, and might provide a new basis for studying the relationships between asteroids, comets and meteorites. Serious planning started in the spring of 1980 when the first IRAS Asteroid Workshop was held in Asilomar, California. Here an overall assessment, from both scientific and practical points of view, was made and the detailed planning for the implementation of this survey was initiated. Shortly thereafter, the planning function for the survey was assumed by the IRAS Project and an Asteroid Advisory Group (AAG) was formed at Jet Propulsion Laboratory as an element of the Project. A series of periodic Asteroid Workshops was initiated and through these the scientific community at large assisted by providing technical advice and independent assessments of the work performed (IRAS Asteroid Workshops No. 1–4, 1983–1985). At these meetings the matters of completeness and reliability were studied and it was decided that the data products should, above all, be reliable—even at the expense of completeness.

The purpose of this chapter is to present a brief overview of the IRAS Asteroid and Comet Survey. First, the actual observing of asteroids by IRAS is discussed. In addition to the spacecraft and its telescope, this includes the temporal and spatial strategy for the execution of observations. In the IRAS data stream, the recognition of asteroid data was not trivial. Many real asteroid observations were left behind as each of the filtering steps were applied in order to achieve the needed reliability. Later, these lower-quality data were

gathered together in a "reject" file available for statistical studies. The asteroid data were processed into a number of data products which now reside at the National Space Sciences Data Center (NSSDC) at the Goddard Spaceflight Center in Greenbelt, Maryland.

Next, our attention is turned to those asteroids whose orbital elements are not known. Several approaches were developed for the study of these objects; these are discussed in Sec. IV. By far the greatest value of these data is for retrieval of radiometry of asteroids whose orbital elements have been determined since the survey. The IRAS asteroid data remain a rich scientific resource; this chapter closes with some suggestions for future research. Some of the first-order scientific results from the survey are discussed in the chapter by Veeder et al. The use of the IRAS survey results to classify asteroids is discussed in the chapter by Tedesco et al.

The scope of this book does not permit a discussion of the IRAS comets. For that part of the survey, the reader is referred to papers by Walker (1986) and Walker et al. (1986). Near-real-time analysis of IRAS data is another subject beyond the scope of this book; it was carried out at the Preliminary Analysis Facility (PAF) in the United Kingdom where attention was focused on the unique opportunity to discover fast-moving (i.e. near-Earth) asteroids and new comets. Such timely discoveries have permitted additional observations both from IRAS and from groundbased observatories. Descriptions of these discoveries and activities at PAF have been written by Davies et al. (1984), Stewart et al. (1984) and Green et al., (1985*a,b*).

II. OBSERVING ASTEROIDS WITH THE INFRARED ASTRONOMICAL SATELLITE

The satellite was launched into an approximately circular orbit of 900 km altitude. The inclination was set at 99° with the orbit plane precessing about 1° per day so that it was Sun-synchronous (see Fig. 1). Thus, the satellite orbited approximately above the Earth's terminator, with the telescope pointed outward scanning the sky. The telescope can be thought of as projecting a virtual image of the focal plane array (Fig. 2) upon the sky, to be swept in turn across all of the sources observed and yielding the survey data stream.

The focal plane of the IRAS telescope contained an array of 62 infrared detectors (Fig. 2). Their spectral coverage was divided into four wavelength bandpasses: 12, 25, 60 and 100 μm. The relative spectral response for each of the IRAS bandpasses is shown in Fig. 3. The effective wavelength of these passbands for asteroid work has been calculated by Lebofsky et al. (1986) who present tabular data useful for interpreting IRAS asteroid observations.

The survey observing mode consisted of many scans of the sky such as that illustrated in Fig. 1. The positioning of the satellite orbit over the terminator and the outward-looking scan paths led to an observing geometry for the asteroids as sketched in Fig. 4. On a typical observation, the asteroid was
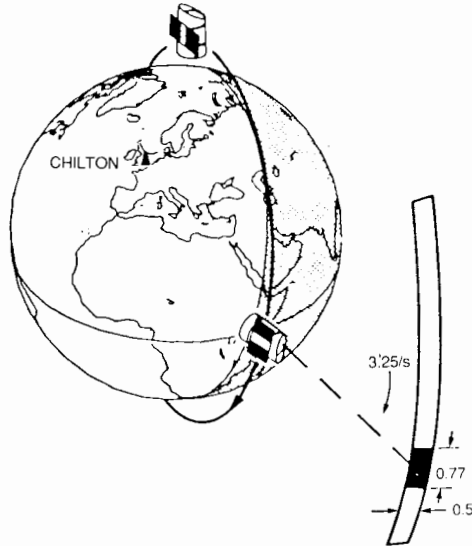
Fig. 1. The orbit of IRAS. A typical scan is indicated. The dark patch represents that portion of the sky imaged on the focal plane at a particular instant of time (figure from Kia and Fowler 1987).

closer to quadrature than to opposition. This geometry is a systematic difference between the IRAS observations and the usual norm for groundbased observations. For asteroids, the IRAS geometry has two disadvantages which reduce the observed flux: most asteroids were not near their closest approach to the Earth and, because of the angle, the terminator as well as part of the cooler night-time surface was visible on the disk.

The strategy of the survey was to sample the sky both spatially and temporally. The spatial objective was to observe the whole sky and this was 95% realized. The temporal sampling procedure enabled the separation of signals from sources fixed on the sky from transients such as asteroids, comets and noise. The procedure consisted of rescanning the same strip of sky after several different time intervals in order to check which sources yielded repeatable observations. Time scales were seconds, hours and months (which were typically 10 days to several months). The check for repeatability on the time scale of seconds was carried out using the data from different detectors in the focal plane. Objects traversed the focal plane in a straight line, as indicated in Fig. 2, and yielded a predictable pattern of detections. Sources which did not match this template, both in direction across the focal plane and in arrival times at each detector, were not processed further. Thus, signals produced in the detectors by very fast moving, close objects (e.g., other satellites or debris in Earth orbit) were rejected at the first step in the processing.

WAVELENGTH BANDS, μm
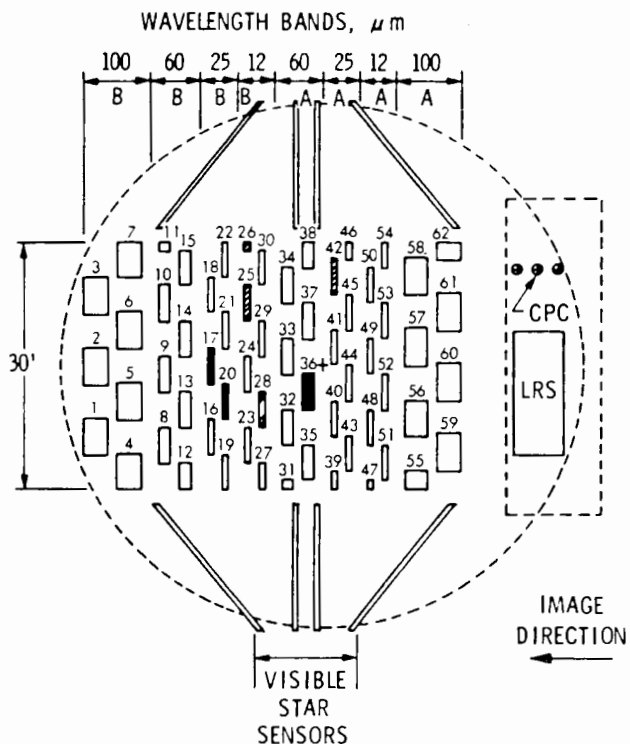
Fig. 2. The IRAS focal plane. The numbered rectangles represent the field of view of a detector assembly. Images of sources cross the focal plane from right to left, as indicated. Solid rectangles indicate detectors that did not work. Cross-hatched rectangles identify detectors that showed degraded performance during the mission. While 25 μm was the best bandpass for asteroid observations, it suffered most from degraded detector performance, resulting in significant loss of data. (IRAS Catalogs and Atlases, Explanatory Supplement 1985, Fig. 11.C.6).
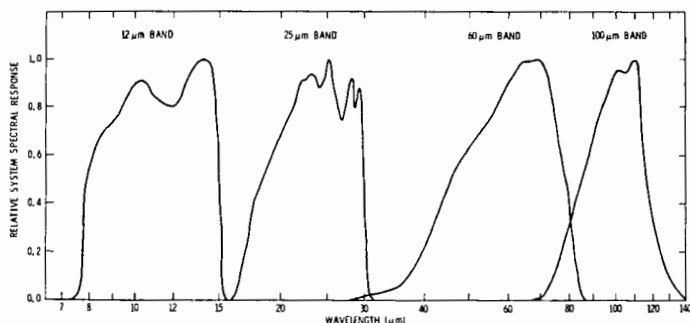
Fig. 3. IRAS bandpasses. The relative spectral response of IRAS as a function of wavelength. In addition to these survey bandpasses, the Low Resolution Spectrometer (LRS) recorded spectra from 8 to 22 μm for bright sources. (IRAS Catalogs and Atlases, Explanatory Supplement 1985, Fig. 11.C.9).
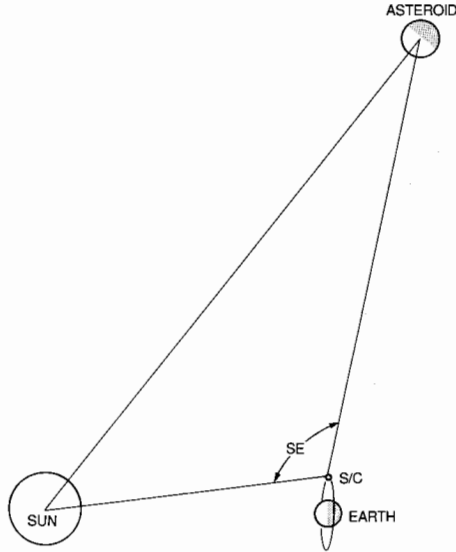
Fig. 4. Typical geometry for IRAS asteroid observations. Solar elongations (angle SE) were generally about 90°, and were restricted to between 60° and 120°. By comparison, most groundbased asteroid observations are made between 160° and 180° of solar elongation.

The next check was made after a period of hours when data were available from a subsequent orbit and when the scan path would be shifted by 0°25 (at the Earth's equator). The data from the two scans of the same sky region were compared. Objects fixed upon the sky, if their signals were great enough, should repeat. Objects that failed this hours-confirmation test were flagged. The faster moving asteroids were one class of objects which usually failed the hours-confirmation test.

About two weeks to months later, the same region of sky was again scanned twice and the new hours-confirmed sources were compared with those previously found. This, then, was the "months-confirmation" test and a positive result was a necessary condition for entry into the *IRAS Point Source Catalog*. A class of objects which failed this test were the slow moving asteroids.

All sources which failed hours-confirmation were tested for a simple and very broadly construed "asteroid-like" color. Those passing this test were written to special files to be used later as a prime data source for the IRAS Asteroid Data Processing System (ADAS) (*IRAS Asteroid and Comet Survey 1986*).

III. ASTEROID RECOGNITION AND ASSOCIATION

The chief difference among the asteroids and comets and the other IRAS sources was their motion on the sky. Asteroidal ephemerides were computed

and compared with the paths of the IRAS sky scans. Spatial coincidence at the same epoch was the indication that a particular asteroid would be in the IRAS field of view. It was necessary for the asteroid trajectory to come within 15 arcmin of the telescope boresight trajectory during a single sky scan. This is shown schematically in Fig. 5.

Once a candidate asteroid was found, its position as observed by IRAS was compared to the ephemerides predictions. In making this comparison, it was necessary to take into account likely uncertainties in orbital elements as well as all the uncertainties in the observed position. Comparison was then made between these two probability density functions. Passing this test with a score above a predetermined threshold, allowed the observed source to be identified with a particular asteroid (Kia and Fowler 1987; Fowler and Chillemi 1986; Chillemi and Fowler 1986; Fowler and Rolfe 1982). At the time when the candidate asteroid sightings were separated from the bulk of the IRAS data, orbital elements were available only for the first 3318 numbered asteroids. Also, good orbits were available for 135 additional asteroids and 21 of these were measured by IRAS.

While the sky-scanning strategy assured an accurate mapping of the fixed sources on the sky, it did not guarantee that all of the asteroids would be observed. In one case, 9 Metis, the asteroidal rate of motion was relatively slow but, by chance, all of the scan patterns fell such that not a single observation of Metis was obtained. Another example of an asteroid that slipped through the scan pattern was 1983 LC, an Amor asteroid, which was moving rapidly in an apparent retrograde trajectory on the sky (Green et al., 1985a).
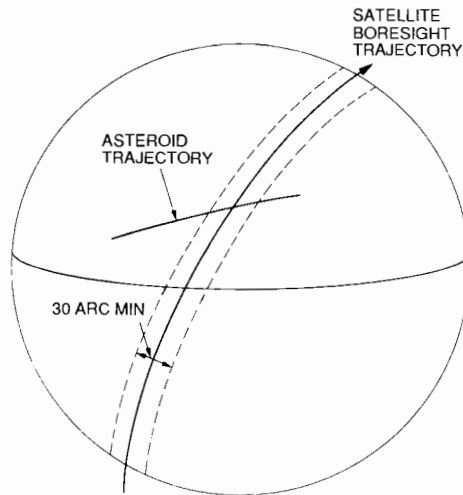
Fig. 5. Projection on the celestial sphere of the trajectory intersection between an asteroid and an IRAS scan (figure from Kia and Fowler 1987).

IV. ASTEROIDS WITH UNKNOWN ORBITS

In addition to the numbered asteroids discussed thus far, the IRAS data contain many observations of asteroids whose orbital elements are not known. These data are of value for several purposes. First, as orbital elements become available for new asteroids, these IRAS data can be searched for observations of the same asteroids. If flux measurements were obtained, then diameters and albedos can be calculated. Secondly, the data can be used to draw some statistical conclusions about asteroids as a whole.

We have tried a number of approaches toward collecting these asteroids into a catalog. Using signal-to-noise, color and other tests, we have produced a number of tabulations. However, the reliability of any given sighting appears to be relatively low. Thus, we were faced with the prospect of a product which perhaps contained fewer asteroids than other sources. We did not regard this as a useful data product because it offered only a marginal refinement over the original input file itself. This is to be contrasted with the reliability in excess of 96% that we obtained for the released data products.

We have estimated the numbers of additional asteroid sightings that may be available in the Survey data. These estimates are tabulated in Table I. The first column indicates the data type. In the second column the number of asteroid sightings is estimated. In the right-most column, we estimate the number of asteroids that are responsible for the sightings. The first entry is for all of the data at hand. The remaining entries are for various subsets of the data. The reliability of the observations in these tracks remains to be determined.

IRAS asteroid tracks are defined as a series of sightings of the same asteroid. These sightings are offset both spatially (on the sky) and in time. An example of a track produced by an uncatalogued asteroid is shown in Fig. 6. The length of the track is about $0°.4$. Many tracks exist in the data. If the region about the galactic center is rejected and if known debris streams are masked off, then there are approximately 550 sightings that group into about 260 tracks.

TABLE I
Estimates for Additional Asteroid Candidates within the Survey

Detections at Bandpasses	Number of Sightings	Number of Asteroids
Input total	2.5×10^6	10^4
25 μm (only)	3.5×10^4	3500
12 & 25 μm	5000	500
25 & 60 μm	2000	200
12, 25 & 60 μm	600	100
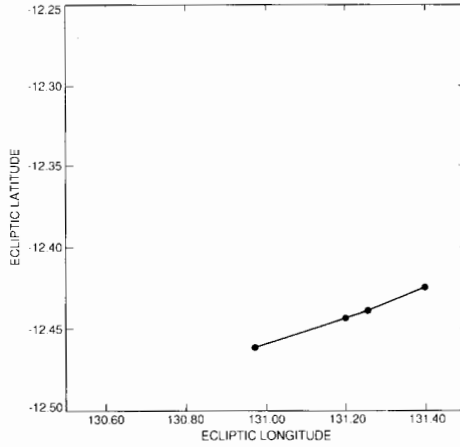
Fig. 6. The track of an unknown asteroid.

V. ASTEROID DATA PRODUCTS

The detailed definitions of these products are to be found in the *IRAS Asteroid and Comet Survey* (1986, Ch. 8, App. B). A summary is listed here in Table II. The system of software used for the production of these asteroid data was called the Asteroid Data Processing System (ADAS). A block diagram and description of ADAS is presented in Fig. 7.

The final data products (FDP) are discussed here in order of subject grouping: asteroids, comets, probable asteroids/comets, survey analysis and
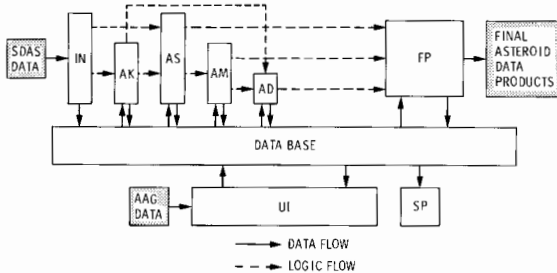
Fig. 7. Block diagram of the Asteroid Data Processing System (ADAS). This was the system that produced the final asteroid data products (shaded box on the right). The system utilized two sets of data as its input (shaded boxes to the left): candidate asteroid sightings from SDAS (Scientific Data Analysis System) and files of groundbased photometric and orbital data supplied by the IRAS Asteroid Advisory Group (AAG). The various modules are: IN: input and database production; AK: known asteroid processor (i.e., asteroids with known orbital elements); AS: asteroid sighting processor; AM: asteroid motion processor; AD: asteroid diameter and albedo calculation; and FP: final products format processor. The data base could interact with the user (user interface: UI) and used to produce special products, SP, such as tabulations, graphs and other specified output.

TABLE II
IRAS Asteroid and Comet Final Data Products

Name	Type[a]
Possible Asteroids/Comets (FDP 1)	Data base
Catalog of Asteroid Sightings (FDP 2)	Data base
Probable Asteroids/Comets (FDP 3)	Data base
Asteroid Names and Pointers (FDP 12)	Data base
Asteroid Groundbased Data (FDP 13)	Data base
Asteroid Statistics (FDP 6)	Data base
Comet Catalog	Data base
Asteroid and Comet LRS Spectra (FDP 9)	Data base
Asteroid and Comet Supplement (FDP 16), which contains all of the documentation for the above as well as the following: Asteroid Catalog (FDP 4) Graphic Data (FDP 5) Asteroid Statistics (FDP 6) Fast Moving Objects (FDP 7) Asteroid and Comet LRS Spectra (FDP 9) Rejected Sightings (FDP 15)	Book

[a]Data base refers to a machine readable medium only while others have been presented in the printed format indicated.

archive. The names for the final products are accompanied by their original FDP numbers. These numbers have been used consistently throughout all of the documentation, whereas some of the descriptive names have evolved. The final asteroid data products consist of a summary catalog, a catalog of sightings, a collection of Low-Resolution-Spectrometer (LRS) spectra and various files of groundbased data that were prepared for use in reducing the IRAS data. In all, there are a total of five products.

The Asteroid Catalog (FDP No. 4) is a distillation of the IRAS asteroid results, organized by asteroid number. One value is given for each property, such as albedo and diameter. The Catalog of Asteroid Sightings (FDP No. 2) is a listing of the reliable asteroid sightings. It is replete with all of the detail of observational circumstances, detection qualities, position accuracies and the quantities computed from orbital geometry and the asteroid thermal model. The Asteroid and Comet LRS Spectra (FDP No. 9) is a catalog of 47 useful spectra of asteroids. The Asteroid Ground-Based Data (FDP No. 13) is a catalog of the various groundbased data on asteroids that were needed in order to reduce the IRAS observations and derive quantities such as diameters and albedos. Contained herein are data on 24-color spectrophotometry, the eight-color asteroid survey, lightcurves, polarimetry and *UBV* photometry. Asteroid Names and Pointers (FDP No. 12) is a file that contains the asteroid names, provisional designations and pointers. The pointers identify the types of data available for each asteroid in FDP No. 13. Thus, this product is essentially an index.

All of the foregoing data products have been released and are available from the National Space Science Data Center (NSSDC) and the affiliated European Data Center in Strasburg, France (see Appendix A in the *IRAS Asteroid and Comet Catalog* [1986] for information on how to obtain data). There are other sets of data which have not yet been released and reside at the Infrared Processing and Analysis Center at Caltech. These include working versions of FDP's 1 and 3. The information in FDP's 5, 6, 8 and 15 is printed in the *IRAS Asteroid and Comet Catalog, Preprint No. 1* (1986).

VI. FUTURE WORK

While the present IRAS Asteroid and Comet Survey is the fruit of a tremendous amount of work, there is much more research that can be done. Below we discuss some of the opportunities for future work.

A. Serendipitous Survey

Throughout the course of the survey, pointed observations were made of many objects of interest. In this mode a small region of the sky (typically $\sim 1°$ in greatest dimension) was repeatedly scanned. Thus, there are often many sightings of the same source available for co-addition to improve the signal-to-noise ratio. These data have been collected into the IRAS Serendipitous Survey Catalog (SSC) (Kleinmann et al. 1986). It contains some 43,866 point-like sources which lie in 1813 fields. The limiting magnitude is typically a factor of 4 better than for the survey mode. The effective sky coverage is 1108 deg². We estimate that the number of asteroid observations to be recovered from the pointed observations amount to about 10% of the number in the survey data. These data have the advantage that fainter sources can be recovered and thus provide a means to study a population of smaller asteroids.

B. Update and Reprocessing

At the time when the asteroid and comet survey was processed, known asteroids up to No. 3318 were included. At this writing, almost a thousand additional asteroids have been numbered. Many observations of these asteroids reside in the IRAS data and thus it is possible to compute diameters and albedos for them. Also, many new and/or better visual magnitudes have become available for the asteroids included in the survey. Thus, ADAS can be rerun in order to produce a more extensive and a more accurate set of data products. While quantitative improvement can be realized ($\sim 25\%$ in the number of asteroids and improved groundbased photometry for $\sim 20\%$), the potential research value is even higher. Most of the asteroids which have been added are smaller objects. The IRAS albedo data have provided the basis for supposing that some unique compositional asteroid classes may have only small asteroids (Tedesco et al 1988; also the chapter by Tedesco et al.). Updating and reprocessing the IRAS asteroid data will yield a data base suitable for

research on this question. Thus, there is much more to be gained than just numerical improvement in reprocessing the final data products.

C. New Processing Strategies

In a fundamental sense there may be much to be learned by trying new processing strategies on the IRAS data. In the Asteroid and Comet Survey, we required that all of the sources be detected at 25 μm. However, there are many sources which were detected at 60 μm but do not show up well enough at 25 μm to be included in the survey. Also, there were many sources whose 12 μm to 60 μm flux ratios were asteroid-like, but were not detected at 25 μm due to noisy or dead detectors. These and other subsets of the observations have not yet been studied and can be made available for research by using different acceptance criteria in ADAS or other processor and producing a new data base or catalog.

There is a significant overabundance of faint 25 μm point source detections toward the plane of the ecliptic. Most of these sources failed to meet the acceptance criteria that we used for the Asteroid and Comet Survey. However, the symmetric distribution of these detections about the ecliptic and their increasing density as the ecliptic is approached suggest that they are solar system sources. A detailed investigation of these data should be carried out.

D. Sky-Flux Images

IRAS sky-flux images are $16°\!.5 \times 16°\!.5$ regions of the sky which have been produced by mosaicing survey scans. Mosaics are then made available as hard copy. Many faint features, especially large extended sources, can be recognized. For example, Sykes et al. (1986) have made use of these and similar products to identify debris trails from comets.

E. Types of Processing That Can be Done at the Infrared Processing and Analysis Center

The Infrared Processing and Analysis Center (IPAC) is the prime site for the processing and study of IRAS asteroid data. In addition to the several unreleased asteroid data products, all of the IRAS data are available as well as all of the software which is tailored to the handling of asteroid data. One example of specialized software is the blinker. The blinking method of asteroid recognition became available too late for use in the Asteroid and Comet Survey. The blinker software emulates a blink plate comparator by plotting data from the individual sources on a computer screen. Data from successive scans over a given region on the sky are alternately displayed on the plot, permitting a visual determination by inspection of which sources are stationary, which are moving, and which are probably noise. Other types of customized processing can be designed and implemented for specific research problems. The facilities of IPAC are available to astronomers who have been selected as participants of approved guest investigator programs.

REFERENCES

Chillemi, J. R., and Fowler, J. W. 1986. The Asteroid Data Analysis System (ADAS). In *IRAS Asteroid and Comet Survey: Preprint Version No. 1*, ed. D. L. Matson, JPL Document No. D-3698, pp. 6-1-6-24.

Davies, J. K., Green, S. F., Stewart, B. C., Meadows, A. J., and Aumann, H. H. 1984. The IRAS fast-moving object search. *Nature* 309:315-319.

Fowler, J. W., and Chillemi, J. R. 1986. Asteroid processing in SDAS. In *IRAS Asteroid and Comet Survey: Preprint Version No. 1*, ed. D. L. Matson, JPL Document No. D-3698, pp. 5-1-5-12.

Fowler, J. W., and Rolfe, E. G. 1982. Position parameter estimation for slit-type scanning sensors. *J. Astronaut. Sci.* 30:385-402.

Green, S. F., Davies, J. K., Eaton, N., Stewart, B. C., and Meadows, A. J. 1985a. The detection of fast-moving asteroids and comets by IRAS. *Icarus* 64:517-527.

Green, S. F., Meadows, A. J., and Davies, J. K. 1985b. Infrared observations of the extinct cometary candidate minor planet (3200) 1983TB. *Mon. Not. Roy. Astron. Soc.* 214:29-36.

IRAS Asteroid and Comet Survey: Preprint Version No. 1. 1986. Ed. D. L. Matson, JPL Document No. D-3698.

IRAS Asteroid Workshop Number 1: Report and Recommendations. 1983. JPL Document No. D-803.

IRAS Asteroid Workshop Number 2: Report and Recommendations. 1983. JPL Document No. D-8399.

IRAS Asteroid Workshop Number 3: Report and Recommendations. 1984. JPL Document No. D-1617.

IRAS Asteroid Workshop Number 4: Report and Recommendations. 1985. JPL Document No. D-2176.

IRAS Catalogs and Atlases, Explanatory Supplement, 1985. Eds. C. A. Beichman, G. Neugebauer, H. J. Habing, P. E. Clegg and T. J. Chester. (Washington DC: U. S. Government Printing Office).

Kia, T., and Fowler, J. W. 1987. IRAS known asteroid prediction and association. *J. Astronaut. Sci.* 35:287-299.

Kleinmann, S. G., Cutri, R. M., Young, E. T., Low, F. J., and Gillett, F. C. 1986. *Explanatory Supplement to the IRAS Serendipitous Survey Catalog* (Pasadena: Infrared Processing and Analysis Center).

Lebofsky, L. A., Matson, D. L., Veeder, G. J., and Tedesco, E. F. 1986. The IRAS asteroid thermal model. In *IRAS Asteroid and Comet Survey: Preprint Version No. 1*, ed. D. L. Matson, JPL Document No. D-3698, pp. 7-1-7-18.

Stewart, B. C., Davies, J. K., and Green, S. F. 1984. IRAS fast mover program. *J. Brit. Interplanet. Soc.* 37:348-352.

Sykes, M. V., Lebofsky, L. A., Hunten, D. M., and Low, F. 1986. The discovery of dust trails in the orbits of periodic comets. *Science* 232:1115-1117.

Tedesco, E. F., Williams, J. G., Matson, D. L., Veeder, G. J., Gradie, J. C., and Lebofsky, L. A. 1988. A three-parameter asteroid taxonomy. *Astron. J.*, submitted.

Walker, R. G. 1986. IRAS Comets. In *IRAS Asteroid and Comet Survey: Preprint Version No. 1*, ed. D. L. Matson, JPL Document No. D-3698, pp. 3-1-3-22.

Walker. R. G., Matson, D. L., and Veeder, G. J. 1986. IRAS observations of comets. *Adv. Space Res.* 6:56-66.

ASTEROID RESULTS FROM THE IRAS SURVEY

GLENN J. VEEDER, EDWARD F. TEDESCO
and
DENNIS L. MATSON
Jet Propulsion Laboratory

The IRAS Asteroid and Comet Survey yielded a data base of infrared flux densities for 1811 individual asteroids. Albedos and diameters for these have been derived via a standard thermal model. IRAS sampled a large number of small asteroids and detected many dark asteroids in the outer belt. High-albedo asteroids remain rare. Observations of the brighter asteroids at multiple wavelengths show the expected range of color temperatures through the main belt.

The production of the IRAS Asteroid and Comet Survey (1986) is described in the chapter by Matson et al. This large data base resulted from the association of infrared sources detected against the sky by IRAS with the predicted positions of asteroids whose orbital elements were well known at the time of final processing. The dynamical parameters of these numbered asteroids as well as their absolute visual magnitudes are the result of many groundbased photographic discovery and photometric followup programs. These inputs were then combined with the infrared flux densities for each asteroid observed by IRAS to derive physical properties such as albedos and diameters. The size and uniformity of the IRAS survey yields good statistics on trends within various subpopulations of asteroids. These fundamental results may then be cross correlated with other data sets. Some implications for spectral-albedo classification and interpretation of composition are described in the chapter by Tedesco et al.

This chapter presents an overview of some of the first-order results of the IRAS asteroid survey. The variation of color temperatures within the main

belt are discussed. Other expected trends due to intrinsic properties of asteroids are highlighted. The spatial distribution of asteroids observed by IRAS will be examined for how both visual and infrared sampling and peculiarities of the IRAS processing may bias the results. The future of the survey and some of its limitations will also be mentioned.

I. COLOR TEMPERATURES OF ASTEROIDS

For those candidate asteroid sources which were bright enough to be detected by IRAS at more than one wavelength, the flux density ratios of adjacent bands were used as a powerful discriminant against confusion with background fixed sources. For example, most stars have stronger emission at 12 μm than at longer wavelengths because they are hot whereas cold dust clouds become more prominent in the galactic plane at 60 and 100 μm than at shorter wavelengths. In contrast, the spectra of main-belt asteroids peak within the IRAS 25-μm bandpass.

A color-color plot of all the sightings of asteroids detected at 12, 25 and 60 μm shows a great deal of scatter (cf. Veeder 1986, Fig. 2–10). Many of these sightings include hits in only a single pair of detectors at 12 and/or 60 μm due to an emphasis on completeness over reliability during the first cut. Figure 1 shows the result of a straightforward co-addition of flux density ratios for those asteroids with at least four accepted sightings during separate scans each of which included detections in all of the three shortest wavelength IRAS channels. The scales have been expanded such that hot ($T > 280$ K) stars plot off the figure to the upper right and cold ($T < 175$ K) molecular dust clouds plot off the figure to the lower left. The scatter of the asteroid ratios is improved as much as may be expected within the photometric accuracy of the IRAS system. In both dimensions, the color temperatures observed for asteroids are a relatively weak function of albedo. The correlation with heliocentric distance is much stronger. The color temperatures of thermal models for asteroids thus range along a narrow diagonal. About 3 bands of color temperatures for asteroids are resolved across the main belt such that hotter ones are seen in the inner belt closer than 2.5 AU (towards the upper right) and the colder ones are found in the outer belt beyond 3 AU (towards the lower left).

II. SPATIAL DISTRIBUTION OF ASTEROIDS

The IRAS survey considered all asteroids whose orbital elements were known at the time of final processing. These asteroids were previously discovered during photographic surveys to some limiting magnitude. As a function of size, this visual sample is strongly biased towards high albedos as well as small perihelion distances (cf. Zellner 1979; Gradie and Tedesco 1982). Detection in the thermal infrared (slightly) favors those asteroids with low al-
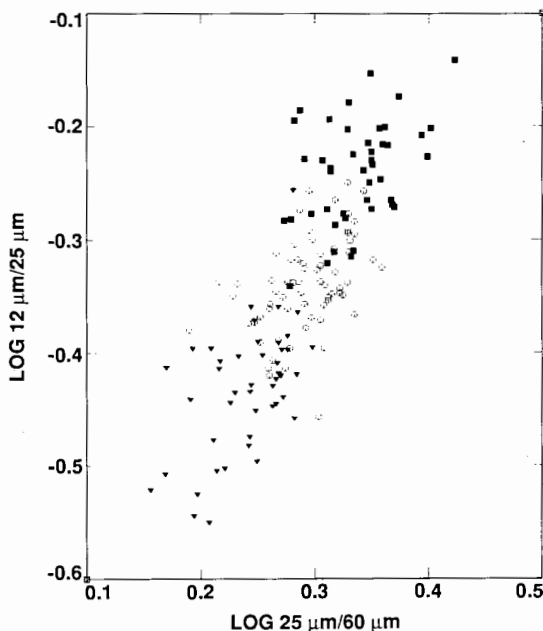
Fig. 1. Infrared colors of asteroids with known orbital elements and more than 4 IRAS sightings plotted as flux density ratios. Effective temperatures increase towards the upper right. Inner-belt asteroids (■) have subsolar temperatures as warm as ~ 300 K. Outer-belt asteroids (▼) have subsolar temperatures as cold as ~ 200 K even though they are also dark. Main-belt asteroids with heliocentric distance between 2.5 and 3 AU are plotted as open circles (○).

bedos because they are warmer for a given size at a given heliocentric distance. However, the more relevant effect here for IRAS is again the decrease of observed flux density with heliocentric and geocentric distance as well as size. As expected from the combination of the IRAS and stronger visual bias, small asteroids remain incompletely sampled in the outer belt. The largest main-belt asteroid, 1 Ceres, is a very strong infrared source at all IRAS wavelengths. IRAS was sufficiently sensitive at 25 μm to detect objects as small as 2201 Oljato (whose diameter is about 2 km) if they happened to be near the Earth. IRAS also detected many other objects whose orbits have not yet been determined. These asteroid candidates remain relatively uncharacterized for the present but eventually may be associated with future groundbased discoveries.

Figure 2 shows the diameters derived for high-albedo ($p_V > 0.1$) asteroids plotted against their heliocentric distance at the time they were observed by IRAS. The results from multiple sightings of individual asteroids tend to scatter vertically due to lightcurve variations and photometric uncer-
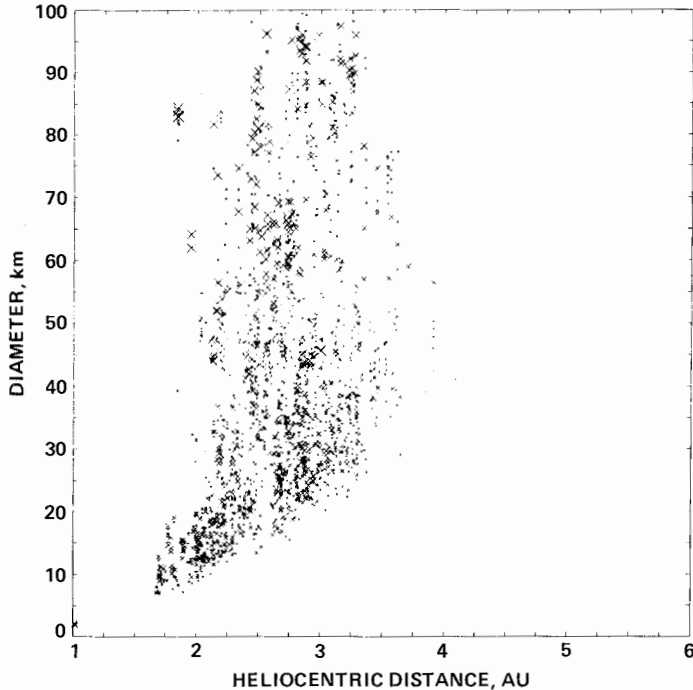
Fig. 2. Diameter plotted against heliocentric distance for IRAS asteroids with high visual geo-
metric albedos ($p_V > 0.1$). Separate model diameters have been derived from the observed flux
density at 25 μm for each accepted observation.

tainties between different scan tracks across the focal plane array. The well-
known Kirkwood gaps in the distribution of asteroid semimajor axes map into
depleted areas at the expected distances in this figure. Only a few asteroids
were detected in the Hungaria region (near 1.8 AU) because these objects not
only tend to be small but also tend to have very high albedos ($p_V > 0.3$); they
are therefore relatively cold and faint in the infrared even though they are in
the inner belt.

Figure 3 shows the diameters derived for low-albedo ($p_V < 0.1$) asteroids
plotted against their heliocentric distance at the time they were observed by
IRAS. Their general size and spatial distributions are similar to those of the
high-albedo asteroids in Fig. 2. Low albedos are somewhat more common in
the outer main asteroid belt to the extent that all asteroids detected by IRAS
beyond 4 AU are dark despite the visual bias against the discovery of such
objects. IRAS also detected several Trojan asteroids near the Lagrangian
points both preceding and trailing Jupiter because those with known orbital
elements tend to be relatively large.
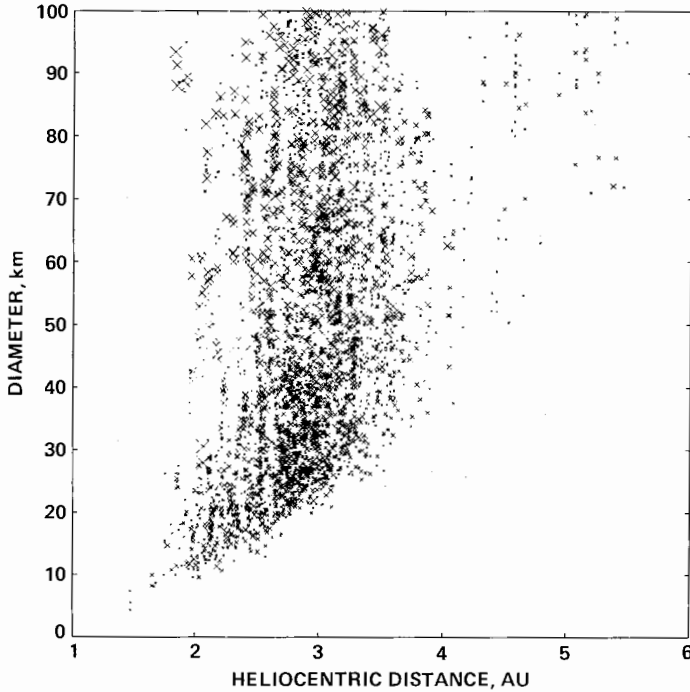
Fig. 3. Diameter plotted against heliocentric distance for IRAS asteroids with low visual geo-
metric albedos ($p_V < 0.1$). Separate model diameters have been derived from the observed flux
density at 25 μm for each accepted observation.

III. THERMAL MODELS FOR ASTEROIDS

 The "standard" thermal model used to reduce the IRAS asteroid sightings
has been described by Morrison and Lebofsky (1979), Lebofsky et al. (1986*a*,
b) and in the chapter by Lebofsky and Spencer . Since the IRAS data stream
did not include any simultaneous visual observations, visual magnitudes had
to be assumed. This ignores the problem of the changing cross section of
asteroids with rotation as seen in their lightcurves. Moreover, the derived
albedos and diameters for each asteroid are then not independent. Since multi-
ple wavelength coverage overdetermines the model solution for bright as-
teroids, the results of each detection at each wavelength for each sighting were
averaged with equal weight. The range of albedos extends up to a value of
0.49 for 44 Nysa and the range of diameters extends up to a value of 913 km
for Ceres.

 Figure 4 shows the average diameters for asteroids with multiple sight-
ings (i.e., two or more) plotted against their average visual geometric albedos
from the IRAS thermal model. The scale of this figure has been expanded to
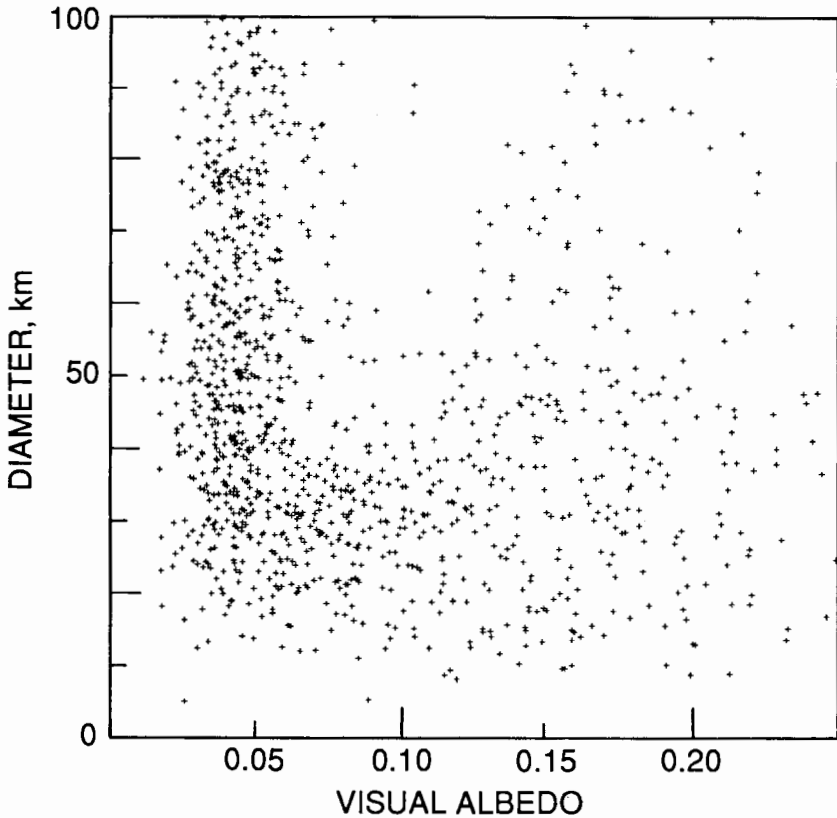
Fig. 4. Average model diameter vs average model visual geometric albedo for IRAS asteroids with multiple accepted observations. A few large and/or bright asteroids are outside the range of this plot.

show detail at small sizes and low albedos. Veeder (1986) includes comparisons of sightings showing the largest and brightest asteroids. Large asteroids are concentrated at values of ~0.05 and ~0.15 for their albedos; this trend is seen here to continue down below 100 km. Relatively more dark asteroids are represented in the IRAS results than in the similar distribution observed within the groundbased TRIAD data (cf. Zellner 1979; Morrison and Zellner 1979). Large asteroids whose albedos are ~0.1 remain rare among IRAS observations and all sizes of asteroids with very high albedos (i.e., $p_V > 0.3$) are also very rare. A few albedos < 0.01 were rejected as not physically real. There are few diameters found smaller than ~10 km due to incompleteness in the list of known orbital elements and the signal-to-noise limit of the IRAS survey. A significant number of small asteroids appear to have derived model albedos near a value of 0.1 in contrast to the relative absence of large asteroids in this range (cf. the chapter by Tedesco et al.).

Whether this effect is physically meaningful or an artifact of the asteroid processing system is still an open question.

IV. CAVEATS

Although the IRAS survey sampled the sky uniformily (Matson 1986), there are subtle variations within the IRAS asteroid products. Veeder (1986) details several characteristics of the IRAS asteroid data for consideration by the serious user. Some of the more obvious complications are a direct result of the strong correlation of size with flux density and of the requirement for relative completeness in a sample limited by background noise. In particular, the signal-to-noise ratio decreases with flux density which in turn results in a corresponding decrease in the relative reliability near the asteroid survey cutoff. It should be remembered that single asteroid sightings by IRAS are not confirmed by definition and deserve low weight during further analysis compared to those asteroids which yielded multiple sightings. In addition, sightings which include detections at more than one wavelength are more reliable than those that only have detections at 25 μm. A few of the faint asteroid sightings at 25 μm may be confused with background sources near the galactic center.

The IRAS point-source sky survey was limited by a signal-to-noise cutoff of 3. Therefore, as a statistical consequence, the flux densities of sources fainter than one Jansky were systematically overestimated as a function of flux density down to the cutoff (~ 0.5 Jy at 25 μm). During asteroid product generation, this led to overestimating the derived cross sections and underestimating the derived albedos for such faint asteroids by up to a factor of about 2 at the cutoff. Since size is strongly correlated with observed flux density, the diameters produced may be systematically too large by a few to tens of percent for the smallest asteroids depending upon the details of selecting such a subset. The fact that asteroids changed their positions between IRAS scans complicates correcting for this effect which may also be an inverse function of the number of accepted sightings.

A few asteroid associations generated very low values for their derived albedos. Such results are probably due to confusion with faint background sources rather than an intrinsic physical property of the asteroids in question; they were therefore rejected from the final products by selecting a value of p_V equal to 0.01 as an otherwise arbitrary cutoff. These rejected sightings tend to be concentrated toward the galactic center (see Veeder [1986] for further discussion of additional caveats).

V. FUTURE PROSPECTS

The IRAS asteroid data base will continue to support additional analyses. The issues concerning small asteroids with albedos near a value of 0.1 will be addressed further. The possibility that such objects might be fossil metallic cores left over from catastrophic disruptions needs to be tested. All the small

asteroids within the IRAS data base will be thoroughly examined to see if they are in fact similar to the well-characterized large asteroids and whether the trends within the size distributions of different classes of asteroids continue down to the survey cutoff. Subpopulations of the members of dynamical families detected by IRAS will be intercompared.

Groundbased infrared observations will also be used to follow up some IRAS omissions and discrepancies. IRAS did not scan all the asteroids and many additional ones with new orbital elements are now available. Another outstanding issue is the case of several asteroids which have S classifications based upon visual spectra but low albedos reported by IRAS. Veeder et al. (1987, 1989) have already checked the near-Earth asteroids 1685 Toro and 1980 Tezcatlipoca which seem in fact to have moderate albedos well within the range expected but contrary to their IRAS results. Other dark main-belt S asteroids remain to be investigated in greater detail. Some should clearly be observed again at visual wavelengths. In any case, there are a large number of IRAS asteroids that only have far-infrared data and now need visual and near-infrared colors in order to classify them satisfactorily and take advantage of cross correlations between various data sets in order to study the asteroid population as a whole.

REFERENCES

Gradie, J. C., and Tedesco, E. F. 1982. Compositional structure of the asteroid belt. *Science* 216:1405–1407.

Infrared Astronomical Satellite Asteroid and Comet Survey; Preprint Version No. 1. 1986. ed. D. L. Matson, JPL Document No. D-3698.

Lebofsky, L. A., Matson, D. L., Veeder, G. J., and Tedesco, E. F. 1986a. The IRAS asteroid thermal model. In *Infrared Astronomical Satellite Asteroid and Comet Survey: Preprint Version No. 1,* ed. D.L. Matson JPL Document No. D-3698, pp. 7–1-7–18.

Lebofsky, L. A., Sykes, M. V., Tedesco, E. F., Veeder, G. J., Matson, D. L., Brown, R. H., Gradie, J. C., Feierberg, M. A., and Rudy, R. J. 1986b. A refined "standard" thermal model for asteroids based on observations of 1 Ceres and 2 Pallas. *Icarus* 68:239–251.

Matson, D. L. 1986. Introduction. In *Infrared Astronomical Satellite Asteroid and Comet Survey: Preprint Version No. 1,* ed. D. L. Matson, JPL Document No. D-3698, pp. 1–1-1–10.

Morrison, D., and Lebofsky, L. A. 1979. Asteroid radiometry. In *Asteroids,* ed. T. Gehrels (Tucson: Univ. of Arizona Press), pp. 184–205.

Morrison, D., and Zellner, B. 1979. Polarimetry and radiometry of the asteroids. In *Asteroids,* ed. T. Gehrels (Tucson: Univ. of Arizona Press), pp. 1090–1097.

Veeder, G. J. 1986. Characteristics of the IRAS asteroid data. In *Infrared Astronomical Satellite Asteroid and Comet Survey: Preprint Version No. 1,* ed. D. L. Matson, JPL Document No. D-3698, pp. 2–1-2–53.

Veeder, G. J., Matson, D. L., and Tedesco, E. F. 1987. Physical properties of near-Earth asteroids. *Bull. Amer. Astron. Soc. 19:* 840 (abstract).

Veeder, G. J., Hanner, M. S., Matson, D. L., Tedesco, E. F., Lebofsky, L. A. and Tokunaga, A. T. 1989. Radiometry of near-Earth asteroids. *Astron. J.* 97:1211–1219.

Zellner, B. 1979. Asteroid taxonomy and the distribution of the compositional types. In *Asteroids,* ed. T. Gehrels (Tucson: Univ. of Arizona Press), pp. 783–806.

CLASSIFICATION OF IRAS ASTEROIDS

EDWARD F. TEDESCO, DENNIS L. MATSON
and
GLENN J. VEEDER
Jet Propulsion Laboratory

Albedos and spectral reflectances are essential for classifying asteroids. For example, classes E, M and P are indistinguishable without albedo data. Colorometric data are available for about 1000 asteroids but, prior to IRAS, albedo data was available for only about 200. IRAS broke this bottleneck by providing albedo data on nearly 2000 asteroids. Hence, excepting absolute magnitudes, the albedo and size are now the most common asteroid physical parameters known.

In this chapter we present the results of analyses of IRAS-derived asteroid albedos, discuss their application to asteroid classification, and mention several studies which might be done to exploit further this extensive and unique data set.

I. RESULTS FROM ANALYSES OF IRAS ASTEROID ALBEDO DATA

It has been known for over a decade that the albedo distribution of the asteroids is bimodal (cf., Morrison and Lebofsky 1979). As demonstrated in Fig. 1, the albedo distribution for large (i.e., diameters $\geqslant 60$ km), well-observed IRAS asteroids is also bimodal (Tedesco et al. 1987b), in agreement with the results of earlier studies utilizing groundbased data. Figure 2, however, shows that the distribution for small, well-observed IRAS asteroids is
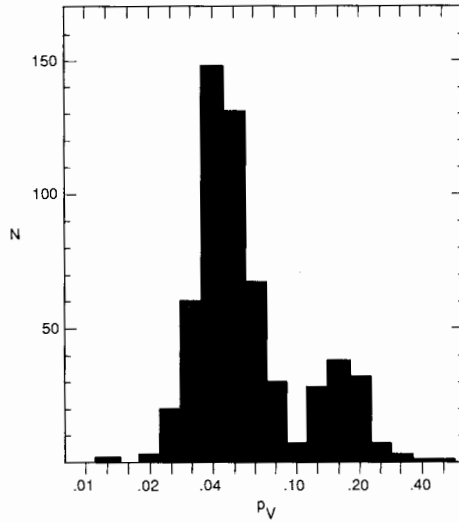
Fig. 1. Albedo histogram for large, well-observed IRAS asteroids. (Large means IRAS diameter > 56.2 km and well-observed means having two, or more, accepted sightings, at least two of which were obtained within 36 hours of one another.)
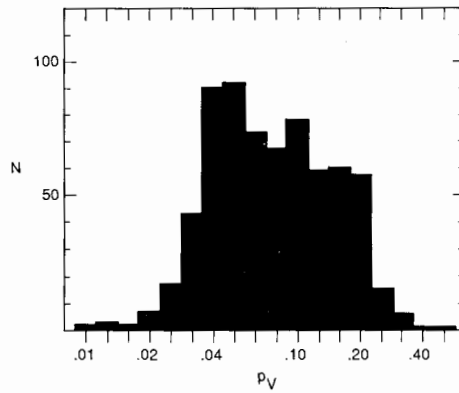
Fig. 2. Albedo histogram for small, well-observed IRAS asteroids. (Small means IRAS diameter ≤ 56.2 km and well-observed means having two, or more, accepted sightings, at least two of which were obtained within 36 hours of one another.)
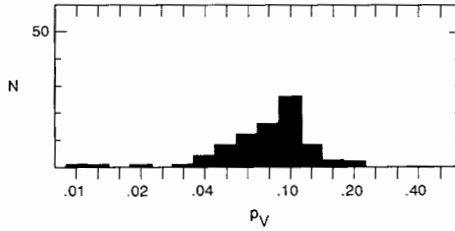
Fig. 3. Albedo histogram for small, well-observed IRAS asteroids belonging to the Themis and Eos dynamical families. (Small and well-observed have the same meaning as in Fig. 2.)

much different; the prominent gap in the distribution for the large asteroids at albedos near 0.1 is filled in when only the smaller asteroids are considered. Even if most of this effect is attributable to flux overestimation (cf., the chapter by Veeder et al.), the possibility exists that the albedo distribution of small asteroids may differ from that of the larger asteroids.

To illustrate this point, consider the albedo distribution for asteroids belonging to the Themis and Eos dynamical families (Fig. 3). Here, the distribution resembles that for the small IRAS asteroids. (Most of the Themis and Eos asteroids observed by IRAS have diameters < 60 km.) This result is in agreement with groundbased studies of these families (Gradie 1978; Gradie and Tedesco 1982a). Hence, there is independent evidence to support the idea that at least certain groups of small asteroids have albedo distributions which peak in the vicinity of 0.1.

II. TAXONOMIES EXPLICITLY INCORPORATING IRAS ALBEDO DATA

Barucci et al. (1987) were the first to incorporate IRAS asteroid albedos into a classification scheme. These authors used all 489 asteroids for which both eight-color photometry (Zellner et al. 1985) and IRAS albedos (IRAS Asteroid and Comet Survey, 1986) were available. (See the chapter by Tholen and Barucci for additional details.)

Most IRAS-derived albedos are reliable but a substantial fraction lack needed corrections (e.g., for flux-overestimation) and a few may be erroneous (Veeder 1986; Tedesco et al. 1987a,b). For this reason care must be exercised when incorporating IRAS-albedo data into asteroid classification schemes.

The flux overestimation problem was recognized after the publication of the IRAS photometry for point sources (IRAS Point Source Catalog, 1985). The second version of this catalog (IRAS Point Source Catalog V.2, 1986) contained a statistical correction for the fainter sources. However, the "flux overestimation correction" applied to stars in this catalog is not directly applicable to asteroids. For asteroids thus affected, the thermal model underestimates the albedos and overestimates the diameters (cf., Veeder 1986).

The taxonomic system introduced by Tedesco et al. (1989) mitigates this problem by using only albedos based on well-observed IRAS asteroids. Clearly, this approach is only a "work-around" but, as of this writing, the problem of how to validate the less-well-observed IRAS asteroids has not been resolved. In the near term, each researcher must assess the probable accuracy of each IRAS-derived albedo before using it. The key to recognizing possibly spurious results lies in looking at the 25 μm flux density and its signal-to-noise ratio, together with the number of realized vs expected sightings. If the flux density is below 1 Jy and/or the number of expected sightings greatly exceeds the number of sightings realized, then the accuracy of the average albedo given in IRAS Asteroid and Comet Survey (1986, Final Product Number Four) is probably significantly lower than the formal uncertainty.

The system introduced by Tedesco et al. is a convenient, pragmatic scheme which will be useful for classifying large numbers of asteroids observed in surveys. The rationale for this *three-parameter* taxonomy lies in the fact that the most readily measured, physically meaningful parameters for an asteroid are its spectrum and its albedo. Asteroid spectra show, at most, strong absorption features in two regions of the spectrum between 0.3 and 1.1 μm. In addition, these two features, which may be blends of overlapping bands, are located in the same spectral region from class to class. One of these features is located longward of 0.7 μm and, whenever that band is present, another located shortward of 0.55 μm is also present. The shorter wavelength absorption feature, however, may be present alone. In cases where no feature is present, the 0.3 to 1.1 μm reflectivity either remains constant or increases with increasing wavelength. Given these facts, it is clear that, in most cases, three parameters are sufficient to characterize asteroid spectral-albedo data, *viz.*, the strengths of the short- and long-wavelength features and the albedo. The U-V color index (0.36 to 0.55 μm) is a measure of the strength of the short-wavelength absorption feature while the eight-color *v-x* (0.55 to 0.85 μm) color index provides a measure of the strength of the long-wavelength feature (Tedesco et al. 1982). Both Tholen (1984) and Barucci et al. (1987) reached similar conclusions; namely that these three parameters are sufficient to identify the most important classes.

The three-parameter method begins by generating a six-sided error box for each asteroid formed by the three parameters and their uncertainties. Each of the previously defined volumes in the three-dimensional parameter space are searched in turn. If the error box, in its entirety, is found to be included in one of them then it is assigned as a member of that class. If part of the error box lies outside the class volume, but not within the class volume of another class, then a question mark is appended to the single-letter class. If the error box intersects two class volumes then a two-letter class is assigned. When an error box intersects three or more class volumes all class labels are concatenated. In practice, only one of the 357 asteroids in the high-quality classification data set generated a three-letter class and none were assigned four or more letters. Finally, if the error box is found to lie wholly outside of all class

volumes then it is considered to be unclassifiable in this system. Fourteen such asteroids were found.

Figure 4 displays histograms for each of the 11 classes recognized in the three-parameter system. It is based on the 303 asteroids (85% of the defining sample) with single-letter, i.e., "certain," classifications.

Four classes (A, D, E and P) have albedos which fall well outside of the
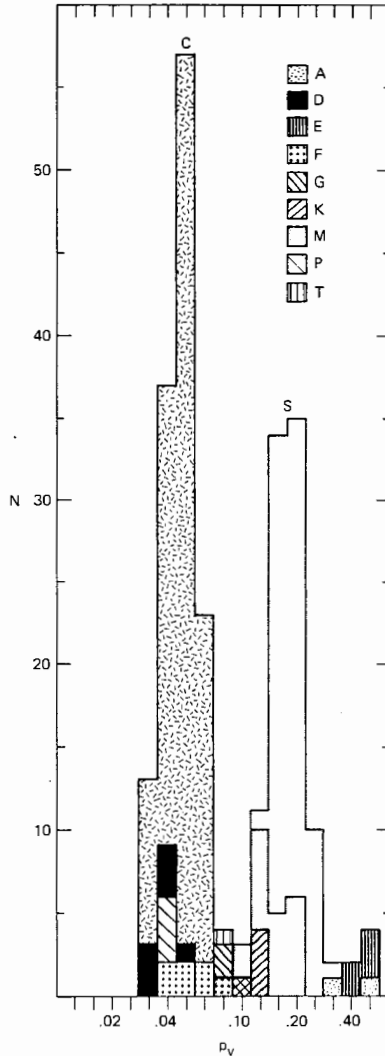
Fig. 4. Albedo histogram for certain matches to the eleven taxonomic classes defined in the three-parameter asteroid taxonomy. The individual class histograms are overlaid, not stacked.

three bins centered on 0.1. (These bins include albedo values between 0.072 and 0.141, inclusive.) Of the remaining classes the C, F and S classes have 5%, 11%, and 14% of their members, respectively, with albedos in this gap; 62% of the M class and 83% of the G class are found in the gap while this is true for 100% of the K and T classes.

None of the K or T class members has a diameter > 110 km. Two of the six K class asteroids in the defining sample are members of the Eos family, one is a member of Williams (1979) family 148, and the others are not family members. None of the five T-class asteroids belong to a Williams family.

There are 581 well-observed numbered IRAS asteroids with IRAS diameters > 56.2 km. About 12% of these have IRAS albedos between 0.072 and 0.141, inclusive (i.e., which lie in a broad gap centered near an albedo of 10%), and about 1.4% have albedos between 0.090 and 0.112, inclusive (i.e., which lie in a narrower gap centered near 10%). There are 673 well-observed asteroids with diameters ≤ 56.2 km. Thirty percent of these lie in the broad 10% gap and 8.4% in the narrow 10% gap. Hence, it appears that asteroids with albedos near 0.1, (and, hence, presumably primarily of classes G, K, M and T) are about 2.5 to 8.4 times more common among asteroids with diameters < 56.2 km than among larger asteroids. The result for diameters < 56.2 km, however, is uncertain because the numbered asteroid population is complete only down to about this size.

To overcome the incompleteness problem, and until such time as a reliable bias-corrected sample of smaller asteroids is available, we can do the following. Consider two albedo bins, one in the 10% gap (0.090 to 0.112, inclusive) and one just above the gap (0.142 to 0.178, inclusive). Other factors being equal, the higher albedo group should be the more complete at smaller diameters. Hence, the ratio of the number of asteroids in the lower-albedo bin to the number in the higher-albedo bin should remain constant until incompleteness in the numbered population begins to set in, at which point it should begin to *decrease* as preferentially more higher-albedo asteroids are discovered. For the samples of asteroids used above, this ratio is 0.21 for the larger asteroids but *increases* to 1.30 for the smaller asteroids. Hence, the increase in the proportion of asteroids in the 10% gap with decreasing size is apparently real.

Without knowledge of the composition of the G, K, M and T classes, little of substance can be said concerning the reason for this increase. One is tempted to speculate, however, that here we may be seeing the (relatively small) interior pieces or, possibly, cores of disrupted asteroids.

III. FUTURE WORK

In the immediate future the classification-related applications of IRAS albedo data include the following.

1. Generate preliminary classifications for asteroids lacking v-x data but with U-V data and for asteroids with U-V and v-x data but lacking any albedo data. (Fortunately, this latter group is small.)

2. For the approximately 1000 asteroids with an IRAS albedo but lacking color data, one can eliminate a number of classes. For example, if the albedo is < 0.07, classes A, E, M and S are not allowed, while for albedos >0.33, all classes other than A and E are excluded. Of course, before attempting this exercise, the reliability of the IRAS albedo must first be established. Since flux overestimation, from whatever cause, will result in a systematically low albedo, one must be especially careful in excluding moderate- to high-albedo classes on the basis of a low IRAS albedo.

3. The most efficient approach to increase the number of asteroids with reliable classifications is to obtain colorimetry for those with good-quality IRAS albedos. This should serve to keep visual observers busy for some time.

4. A follow-up groundbased radiometry program is needed to help better understand the low-flux IRAS results and to complete the coverage for important individual asteroids not observed by IRAS. Such a program is already under way using the NASA Infrared Telescope Facility at the Mauna Kea Observatory.

5. Once we understand how to interpret the low flux IRAS results a bias-corrected distribution of the taxonomic classes, similar to that given by Gradie and Tedesco (1982b) but to smaller sizes, can be determined.

Clearly, the application of IRAS-albedo data to the area of taxonomic classification has only begun. Applications employing this data base and follow-up ground and space-based observing programs should prove to be fertile fields of investigation for decades.

REFERENCES

Barucci, M. A., Capria, M. T., Coradini, A., and Fulchignoni, M. 1987. Classification of asteroids using G-mode analysis. *Icarus* 72:304–324.

Gradie, J. C. 1978. An Astrophysical Study of the Minor Planets of the Eos and Koronis Asteroid Families. Ph.D. Thesis, Univ. of Arizona.

Gradie, J., and Tedesco, E. F. 1982a. The diameter-albedo relationship among Themis family members. Variations in regolith thickness? *Bull. Amer. Astron. Soc.* 14:621 (abstract).

Gradie, J., and Tedesco, E. F. 1982b. The compositional structure of the asteroid belt. *Science* 216:1405–1407.

Infrared Astronomical Satellite Asteroid and Comet Survey: Preprint Version No. 1. 1986. Ed. D. L. Matson, JPL Internal Document No. D-3698.

IRAS Point Source Catalog. 1985. Joint IRAS Science Working Group (Washington DC: U.S. Government Printing Office).

IRAS Point Source Catalog, V.2. 1986. Joint IRAS Science Working Group (Washington DC: U.S. Government Printing Office).

Morrison, D., and Lebofsky, L. A. 1979. Asteroid radiometry. In *Asteroids,* ed. T. Gehrels (Tucson: Univ. of Arizona Press), pp. 184–205.

Tedesco, E. F., Matson, D. L., Veeder, G. J., and Lebofsky, L. A. 1987a. IRAS observations of asteroids. In *Comets to Cosmology,* ed. A. Lawrence (Berlin: Springer-Verlag), pp. 19–26.

Tedesco, E. F., Matson, D. L., Veeder, G. J., and Lebofsky, L. A. 1987b. IRAS albedos for faint asteroids. *Bull. Amer. Astron. Soc.* 19:839 (abstract).

Tedesco, E. F., Tholen, D. J., and Zellner, B. 1982. The eight-color asteroid survey: Standard stars. *Astron. J.* 87:1585–1592.

Tedesco, E. F., Williams, J. G., Matson, D. L., Veeder, G. J., Gradie, J. C., and Lebofsky, L. A. 1989. A three-parameter asteroid taxonomy. *Astron. J.* 97:580–606.

Tholen, D. J. 1984. Asteroid Taxonomy from Cluster Analysis of Photometry. Ph.D. Thesis, Univ. of Arizona.

Veeder, G. J. 1986. Characteristics of the IRAS asteroid data. In *Infrared Astronomical Satellite Asteroid and Comet Survey: Preprint Version No. 1,* ed. D. L. Matson, JPL Internal Document No. D-3698, pp. 2–1:2–53.

Zellner, B., Tholen, D. J., and Tedesco, E. F. 1985. The eight-color asteroid survey: Results for 589 minor planets. *Icarus* 61:355–416.

ASTEROID TAXONOMY

DAVID J. THOLEN
University of Hawaii

and

M. ANTONIETTA BARUCCI
Observatoire de Paris

The spectral reflectivity of asteroid surfaces over the wavelength range of 0.3 to 1.1 μm can be used to classify these objects into several broad groups with similar spectral characteristics. The three most recently developed taxonomies group the asteroids into 9, 11 or 14 different classes, depending on the technique used to perform the analysis. The distribution of the taxonomic classes shows that darker and redder objects become more dominant at larger heliocentric distances, while the rare asteroid types are found more frequently among the small objects of the planet-crossing population.

I. INTRODUCTION

In many ways, asteroid taxonomy is analogous to the stellar spectral classification system. With just a single letter, the color and principal spectral features of a star can be described. An asteroid spectral classification performs a similar function, indicating the color, albedo and major spectral features of the object. In many cases, the classification also suggests a likely mineralogy for the asteroid as well as its thermal history, although the actual taxonomic class definitions are divorced from any mineralogical considerations.

It is not the purpose of this chapter to review the evolution of asteroid taxonomy. Instead, the reader is referred to a fairly thorough history provided

by Tholen (1984) and two landmark papers by Chapman et al. (1975) and Bowell et al. (1978).

The introduction, removal and re-introduction of the letter designations for the various asteroid classes has been a continuing source of confusion for many asteroid, comet and meteorite researchers. An ingenious figure devised by Bell and first published by Tholen and Bell (1987) summarizes the evolution of asteroid taxonomic class letter designations through 1984. We reproduce that figure here as Fig. 1.

Although other asteroid classifications have been performed that recognize even finer distinctions between objects (see, for example, Table IV of Chapman and Gaffey [1979] or Table I of Gaffey and McCord [1979]), the most popular taxonomies have been the ones based on a few broad classes of objects, as pioneered by Chapman et al. (1975). Since that classic work, four more taxonomic schemes have evolved along these same lines. The first of these was produced by Bowell et al. (1978) using essentially the same kind of data and somewhat more mature techniques than its predecessor. A substantial amount of additional colorimetry led to a major revision by Tholen (1984), and additional radiometry was utilized by both Barucci et al. (1987) and Tedesco et al. (1989) for yet another pair of variations. For the remainder of this chapter, we shall refer to these five systems as the CMZ, Bowell, Tholen, Barucci and Tedesco taxonomies, respectively.

An important augmentation of the Tholen taxonomy has been prepared
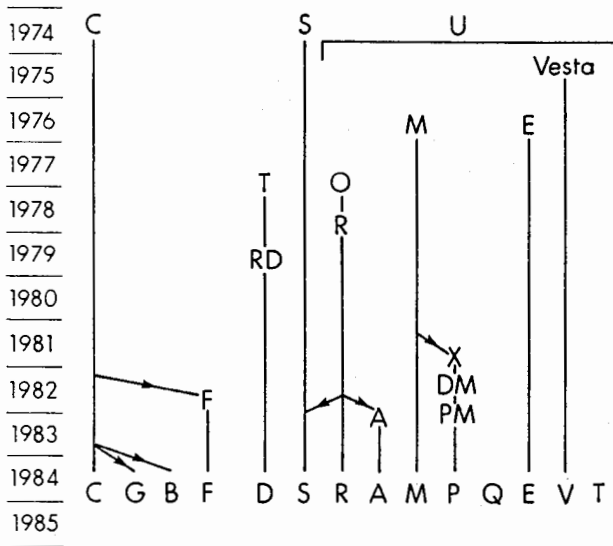
Fig. 1. Evolution of letter designations used by the main asteroid taxonomies through 1984.

by Chapman (1989). We call the reader's attention to this work because of its importance, but because it does not represent an independent, newly defined taxonomy, we will not discuss it here in the same context as the other taxonomies.

II. OBSERVATIONAL DATA

All asteroid taxonomies involve an analysis of the distribution of values in some parameter space. This process necessarily involves the observational data for a large number of objects, if statistically significant results are to be achieved. Thus the observational techniques that have been applied to the largest number of objects are the ones whose resulting data have been used to generate asteroid taxonomies.

The most widely available observational parameter for the asteroids is the brightness, or apparent magnitude, which, when corrected for distance and phase angle, becomes the absolute magnitude. Most of these measurements are crude estimates made from the photographic plates utilized for the majority of modern discoveries. By itself, however, the magnitude is not a useful taxonomic parameter. During the course of the Infrared Astronomical Satellite (IRAS) all-sky survey, the thermal emission from thousands of asteroids was measured (see the chapters by Matson et al. and Veeder et al.). By comparing the amount of light reflected by an object with the amount of light emitted, and balancing these against the amount of light received from the Sun, one can deduce the effective diameter and mean albedo (reflectivity) of the asteroid (see the chapter by Lebofsky et al.). Because the reflectivity of asteroid surface materials can range from a few % to as high as 50% at visible wavelengths, the albedo is quite useful for taxonomic purposes and now represents the most commonly available taxonomic parameter. Only recently has this situation become the case, however.

Prior to the 1983 IRAS survey, the observational technique most widely applied to the asteroids was standard Johnson *UBV* photometry, which yielded *U-B* and *B-V* color indices. The earliest two-color plots clearly separated the C and S asteroids recognized in the CMZ taxonomy, but the M and E classes defined in the Bowell taxonomy were poorly separated in *UBV* space.

Because some of the absorption features of the common meteoritic minerals pyroxene and olivine occur at near-infrared and infrared wavelengths, it became clear that important compositionally diagnostic information could be obtained from observations at wavelengths longer than those covered by standard *UBV*. Such observations were carried out primarily by Chapman and Gaffey (1979) using as many as 25 medium-band filters covering the wavelength range of 0.3 to 1.1 μm. Rather than attempting to work in a 24-dimensional space, they extracted four useful parameters (BEND, DEPTH, IR and R/B) from these spectra, two of which were used for defining the C

and S classes in the CMZ taxonomic system. All except the IR parameter were utilized in the Bowell taxonomic system.

The advantages of wavelength coverage and resolution provided by the 24-color system were partially offset by the system's inability to obtain high-quality data on the fainter asteroids. Thus a broadband variant of the 24-color system was developed that utilized just 8 filters covering the same wavelength range. The project was known as the Eight-Color Asteroid Survey (ECAS) and produced reflectance spectra for 589 different asteroids between 1979 and 1983 (Zellner et al. 1985). Whereas the "first generation" taxonomies (CMZ and Bowell) were based on radiometry, polarimetry, *UBV* colors and the parameters from the 24-color spectrophotometry, the "second generation" taxonomies (Tholen, Barucci and Tedesco) are based on ECAS data and radiometry.

III. METHODS OF CLASSIFICATION

Of the five taxonomies mentioned in the previous section, all have essentially the same goal, namely to group the asteroids into a few broad classes, yet the techniques used to arrive at that goal are strikingly different. In this section, we only briefly describe the methods used for the CMZ and Bowell taxonomies, given that they were already developed a decade ago at the time of the *Asteroids* book (Gehrels 1979), and present in somewhat more detail the techniques used for the more recent Tholen, Barucci and Tedesco taxonomies.

A. CMZ and Bowell Taxonomies

The CMZ taxonomy recognized only the C and S classes. Natural hiatuses in the distributions of five optical parameters were used to define the two classes; those objects that did not clearly fall into one of the two groups were designated U (unclassifiable). The five parameters included the radiometric albedo, the minimum value of the polarization phase curve, the *B-V* color and the spectrophotometric parameters DEPTH and R/B. (see Table II of Chapman et al. [1975] for the class definitions.)

Once the observational techniques used for the CMZ taxonomy were applied to a larger number of objects, it became clear that two asteroid classes were inadequate to describe the sampled population. Numerous two-parameter plots enabled Bowell et al. (1978) to recognize three new classes of objects: M, E, and R. To the five parameters utilized in the CMZ taxonomy, they added the *U-B* color and the BEND spectrophotometric parameter. The Bowell taxonomy was then defined in terms of strict limits on these seven observational parameters. (See Table I of Bowell et al. [1978] for the class definitions.)

B. Tholen Taxonomy

The Tholen taxonomy is based on the minimal tree algorithm with the results displayed on a principal components plot. Before going into the details

of the minimal tree algorithm, a brief discussion of principal components analysis is appropriate.

Consider a sample of objects for which two quantities have been measured, x and y. If x and y are correlated, then we may rotate the coordinate system so that one of the two axes coincides with the best-fit line; the other axis remains orthogonal to the first axis. With this rotation, the variance along the first axis has been maximized, and the variance along the second axis has been minimized. The first axis is then called the first principal component and the second axis is called the second principal component.

This simple two-dimensional case can be easily generalized to the seven dimensions of the ECAS data. In the case of the ECAS data, 68% of the sample variance is represented by the first principal component, and another 27% is represented by the second principal component. The remaining 5% of the sample variance is distributed among the other five component axes. Thus a single two-parameter plot is capable of displaying 95% of the variance in the ECAS data. Figure 2 shows the first and second principal components for the 405 asteroids with the highest-quality ECAS data.

The reason why 95% of the variance is contained in just two principal
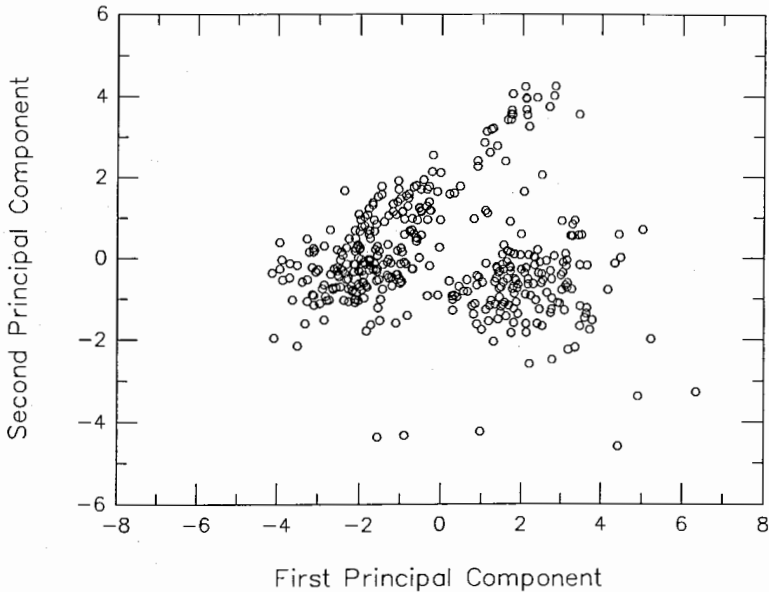
Fig. 2. First and second principal component plot for 405 asteroids with high-quality ECAS data. Note that the centroid in *subvwxpz* space has been subtracted from the asteroid data so that the centroid in principal component space would fall at 0 for all components. The scale is arbitrary and was chosen so that the eigenvalues would add up to the number of dimensions, which is 7 in this case.

components is because asteroid reflectance spectra have just two major features in the 0.3 to 1.1 μm wavelength range covered by the ECAS data, one in the ultraviolet and one in the infrared. The ultraviolet feature is the stronger of the two and therefore shows the highest correlation with the first principal component. For example, the asteroids with the strongest ultraviolet absorption feature, the A class, fall in the lower right corner while the objects with the weakest ultraviolet absorption features fall along the upper left edge of the distribution.

The principal-components analysis was performed primarily to provide a means of displaying the ECAS data and the taxonomic classes that resulted from the analysis of the data in as efficient and compact a manner as possible. The actual taxonomy itself was produced in several steps which we shall describe here rather briefly; for complete details, see Tholen (1984). First, a minimal tree was produced using the highest-quality asteroid data. The resulting tree is shown in Fig. 3. Normally, such a tree is displayed as a dendrogram, but such a diagram for 405 objects would be particularly unwieldy.

For a given sample, the minimal tree is unique, a definite advantage over most of the other clustering techniques examined. On the other hand, the cutoff for an asteroid to be included in the high-quality sample is arbitrary, and the minimal tree will certainly change as the sample size is changed.

The longest branches of the minimal tree (relative to the lengths of the
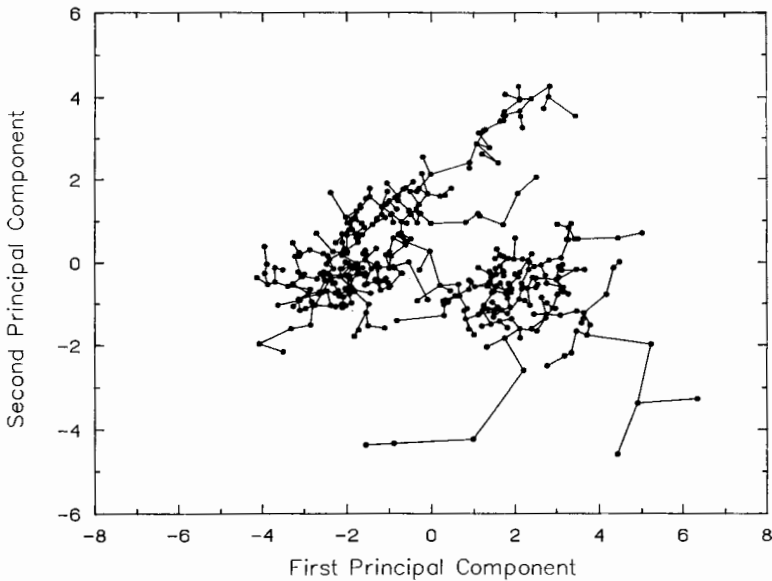
Fig. 3. Minimal tree diagram for the same sample of asteroids plotted in Fig. 2. The sum of the lengths of all branches in this tree is a minimum for this particular sample.

neighboring branches) were then cut to produce the initial clusters. The number of clusters produced at this stage is somewhat arbitrary. Certainly, shorter branches could have been cut, resulting in a greater number of classes with fewer members each. Only a few broad classes were created, however, as in the popular CMZ and Bowell taxonomies. These classes were assigned the letter designations A, C, D, S and T. Single-member classes were created for the unique objects 4 Vesta (V), 349 Dembowska (R), and 1862 Apollo (Q). Note that cutting only the longest branches of the minimal tree is analogous to identifying the natural hiatuses in the distribution, as done in the CMZ and Bowell taxonomies.

The C-asteroid population differed from the other classes in that it had a densely populated core with some isolated branches dangling away from the core in three distinct directions. By cutting somewhat shorter branches, three subgroups were created, namely the B, F, and G classes. In some applications, these subclasses are significant (see Sec. V); in other applications, however, it is entirely appropriate to reabsorb these classes into the C class.

Some researchers have recommended subdividing the S class in the same fashion. To do so, however, phase reddening effects would need to be taken into account. Objects with multiple observations, such as 433 Eros and 3199 Nefertiti, have clearly demonstrated the effects of phase reddening on the position of an object in eight-color parameter space. In most cases, however, insufficient data exist to determine and remove phase reddening. Note that the neutral spectra of the C asteroids seem to be more immune to phase reddening effects, and because of their typically greater distances, the range of phase angles at which C asteroids have been observed is smaller than for typical S asteroids.

At this stage of the analysis, the measurement uncertainties were introduced, and each object's classification was compared with the classfications of from one to three (depending on their error bars) of its nearest neighbors in seven-dimensional space. Not only did this step account for measurement uncertainties, it also made the resulting classifications less sensitive to the initial choice of the high-quality sample size. If the nearest neighbors fell in different clusters, multiple classifications were introduced. The process was repeated until all the classifications stabilized. This set of objects was then used as the basis of comparison for all other objects (the ones not in the high-quality sample), whether or not they had been observed through the entire set of eight filters.

Up to this point, the albedos of the objects had not been taken into consideration. The asteroids were classified according to their colors only. Once separated by their colors, however, the albedo distribution for each class was examined for consistency. One particular class of objects split into high, moderate and low albedo groups, the first two of which became the E and M classes. The low-albedo objects formed a subset of the C class and became the P class. Although the initial cluster forming process did not recognize distinct

C and P classes on the basis of colors alone, the objects in the P class did fall at one end of the C distribution, between the D class and the dense core of the C class, and therefore they were permitted to exist as a separate class. It is important to recognize that in this taxonomic system, the P asteroids *by defini-tion* occupy the same color space as the M and E classes and that they represent the reddish end of a nearly continuous distribution of reflectance spectra of objects that had previously been classified entirely as C.

Figure 4 shows the domains of the various asteroid taxonomic classes in principal components space. The letter designation X is used in this figure to represent either E, M or P objects, which are spectrally degenerate.

C. Barucci Taxonomy

The G-mode method (Coradini et al. 1977) is a multivariate statistical method that allows the user to classify automatically a set of N samples described by M variables. The samples are clustered in homogeneous taxonomic classes without the need for any *a priori* criteria. The method takes into account the measurement errors and looks for the true number of degrees of freedom characterizing the groupings. The original M variables are collapsed into one new variable, whose distribution is the superposition of as many quasi-Gaussian components as there are homogeneous classes. The criteria for assigning each sample to a given class are based on the rules of statistical
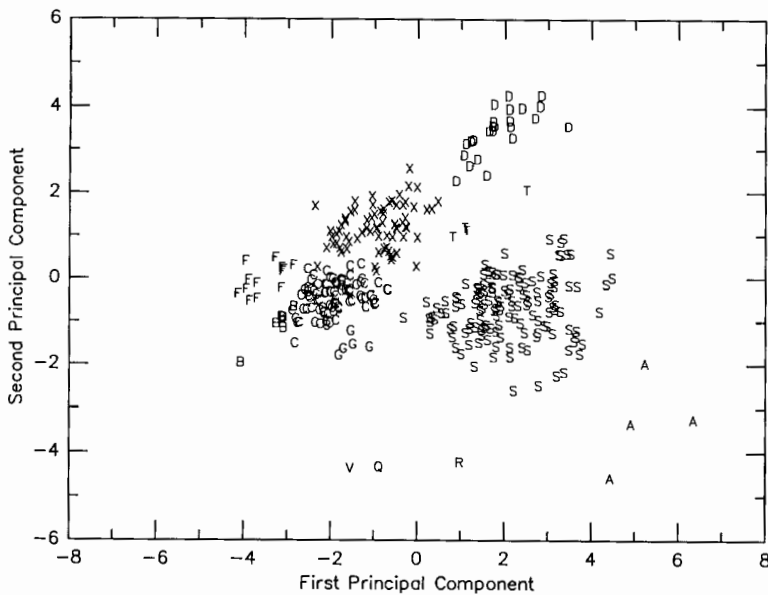
Fig. 4. Domains of the asteroid classes. The letter designation X represents an abbreviation for the spectrally degenerate E, M, and P classes.

inference. The confidence level of the decision is the only *a priori* choice, which defines the level of detail in the classifications (analogous to the decision of what length branch to cut in the minimal tree method). When the samples are grouped into homogeneous classes, a check on the role of each variable in determining the classification permits one to eliminate the useless variables (those that do not distinguish any class). In that way the "noise" in the classification is reduced and the nondiscriminating variables can be disregarded in the acquisition of data. For more details about the G-mode method and its application to the asteroid data, the reader is referred to the paper by Barucci et al. (1987).

D. Tedesco Taxonomy

The Tedesco taxonomy utilizes only three observational parameters, namely the Johnson U-V color, the ECAS v-x color and the IRAS albedo. By choosing color indices that sample different absorption features and are therefore not strongly correlated, Tedesco et al. (1989) have succeeded in utilizing substantially more than $3/8$ of the information available in the ECAS plus IRAS data, despite the fact that they used only 3 out of the 8 available parameters.

Clusters were identified by direct visual examination of stereo pairs of two-dimensional plots containing the three-dimensional data. Preliminary boundaries were created around each of the visually identified clusters and then later refined when only localized regions were examined stereoscopically. They identified 11 classes of objects, although these 11 classes are not sufficient to classify all the observed asteroids; certain unique objects, such as 2 Pallas, 4 Vesta, and 349 Dembowska were not classified in their system.

Subsequent classification of the entire sample of objects with all three parameters available was performed by comparing the volumes occupied by the 11 classes with the three-dimensional error box for each object. Classifications consisting of multiple letter designations were generated when an error box overlapped the volume of more than one class.

E. Advantages and Disadvantages of Each Method

The principal advantage of the CMZ and Bowell taxonomies is the ease with which newly observed objects can be classified. All one needs is Table II from Chapman et al. (1975) or Table I from Bowell et al. (1978) and the new data to determine the classification. New classifications in the Tedesco taxonomic system are almost as easy to generate, with the principal complication being the slanted plane tests made necessary by the close spacing of certain classes.

Both the Tholen and Barucci methods are somewhat more difficult to apply to a newly observed object than either the CMZ, Bowell or Tedesco methods. To generate a classification in the Tholen system, one must deter-

mine the three nearest neighbors (taken from the 405 objects in the high-quality ECAS set) and assign the newly observed object the designation of the nearest neighbor, plus additional designations of the second and third nearest neighbors, if their classifications differ from that of the nearest neighbor, and only if measurement uncertainties warrant the comparison with the more-distant neighbors. The albedo, if available, must then be checked for consistency with class norms, or in the case of the X class (an abbreviation used for the E, M, and P objects in their common color space), the class ambiguity can be resolved.

To classify rigorously a newly observed object in the Barucci system, one must repeat the entire G-mode analysis. Another disadvantage of the G-mode method is that a complete set of variables is required. In the case of the asteroids, both the ECAS data and the IRAS albedos are available for only 438 objects at this time. An advantage of Barucci's implementation of the G-mode method is that both the colors and the albedo are considered simultaneously.

Because of the larger data bases they had to work with, the Tholen, Barucci and Tedesco taxonomies recognize additional classes consisting of objects that had previously been either misclassified or grouped together with other dissimilar objects. Note that the Bowell taxonomy was superior to the CMZ system for this same reason.

The minimal tree algorithm as applied by Tholen is more forgiving of measurement errors than either the CMZ, Bowell or Tedesco taxonomies. For example, if a noisy measurement caused an object to fall just outside the boundary defined for a particular class, that object was designated as U (unclassifiable) in the Bowell taxonomy; 80 Sappho is a good example. The Tholen taxonomy does not have "brick-wall" boundaries; objects are classified according to their distance from the nearest neighboring asteroids and cluster centers, and Sappho indeed retains an S classification. If the distance of an object from a cluster center is sufficiently greater than the mean distance of the other cluster members, a U could be appended to the classification to call attention to its unusual character.

Another advantage of the Tholen, Barucci and Tedesco systems is the homogeneity of the data used in the classification process. The seven parameters utilized by the Bowell method were available for very few objects, which meant that the parameter space had not been as thoroughly explored as the eight-color parameter space.

It is important to remember that the Bowell taxonomy worked on the basis of exclusion; all recognized types were initially allowed and the observed physical parameters were used to eliminate those classes whose characteristics did not match those of the observed object. The Tholen taxonomy works by inclusion; the object is assigned the classification of the nearest neighbors in their common parameter space. Note that this technique permits the classification of objects even if they have not been observed using the full

set of filters. As the reader can imagine, there are advantages and disadvantages to both the exclusion and inclusion techniques. Obviously, exclusion works best when there are only a few classes to deal with; only six letter designations were utilized in the Bowell taxonomy, and never more than four appeared in a classification, thus the exclusion method was appropriate. With the large number of classes recognized by all of the newer taxonomies, inclusion represents the preferred method.

A weakness of the Tedesco method lies in the limited number of parameters utilized by the algorithm. Because the three principal distinguishing characteristics of asteroid spectra are described by only one parameter each, random errors could easily cause misclassifications. If multiple parameters are utilized, as in the Tholen and Barucci taxonomies, random errors will tend to average out, thus lowering the likelihood of a misclassification. Another limitation of the Tedesco taxonomy is its inability to classify all the observed asteroids. Should someone stumble across another Dembowska-like asteroid in the future, there is no classification in the Tedesco system that can be assigned to this hypothetical object. This scenario is similar to the situation that actually occurred in late 1983, following Tholen's discovery that the five-color spectrum of 3551 1983 RD was indistinguishable from that of Vesta. Fortunately, the V class had just been created, and therefore a meaningful classification for 1983 RD was immediately available. Note that the V class now consists of four objects (Tholen et al. 1988; Cruikshank et al. 1989).

IV. RESULTS OF CLASSIFICATION

Applying the methods described in Sec. III to the data described in Sec. II results in classifications for several hundred astroids. These classifications are tabulated in Part VI of this book. Classifications in the Barucci system are available for only those objects with a complete set of ECAS data and IRAS albedo, while classifications in the Tholen system are given for objects with either ECAS or just *UBV* data. Nonrigorous classifications are also provided for a handful of objects observed only in the 24-color system; the classifications were arrived at by a direct visual comparison of the 24-color reflectance spectra with the mean eight-color reflectance spectra for the various classes. Classifications in the taxonomic system of Tedesco et al. (1989) appear in a separate tabulation in Part VI of this book.

The results of the taxonomy developed by Tholen are summarized in Table I. The table presents all of the letter designations and other symbols currently in use, and a short description of the reflectance spectrum and albedo for each class. Mean spectra are shown for the various classes in Fig. 5.

The Barucci taxonomy is based on the analysis of a sample of 438 asteroids described by the ECAS data and the IRAS albedo. The taxonomy has been obtained by choosing the 97.7% confidence level, which corresponds to an expected number of 10 misclassified asteroids. The asteroids are grouped
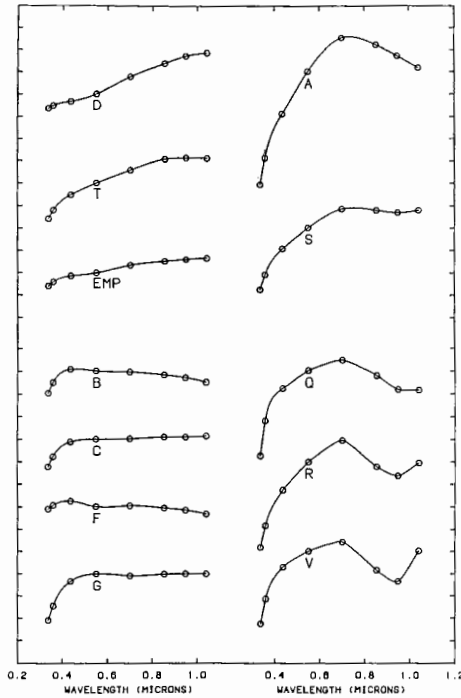
Fig. 5. Mean reflectance spectra for the asteroid classes. Tick marks on the ordinate are spaced 0.2 magnitudes apart. These spectra are based on the Tholen taxonomic classifications. For the mean spectra based on the Barucci classifications, see Fig. 1 of Barucci et al. (1987).

into 9 principal classes, some of which are divided into subclasses having the same general trend of the variables even if there is some significant difference among the subclasses. To avoid increasing the entropy of the nomenclature, the 9 principal classes have been given letter designations as in the Tholen taxonomy (i.e., B, C, E, M, G, D, S, A, and V). A number following the letter of each class indicates the subdivision: 0 is used for the main class, and successive integers indicate the subclasses, ordered according to increasing albedo values. The Tholen F class is absorbed into the B class of this system, the T class is included in the D class, the P class is joined with the C class, and the Q, R, and V objects in the Tholen system are lumped together into the V class.

Five percent of the asteroids have been classified as B in four subclasses, characterized by low albedos (0.04 to 0.08) and a quasi-flat spectrum with a maximum at the ECAS *b* band and decreasing toward the infrared bands. The largest class is the C class, with a flat spectrum slightly increasing from the *s* to *z* band, and albedo range of 0.04 to 0.06, which includes 41% of the

TABLE I
Asteroid Classes

Letter Designation	Albedo	Spectrum
A	moderately high	extremely reddish shortward of 0.7 microns; strong absorption feature longward of 0.7 microns, centered near the 1.05 micron filter
B	moderately low	higher albedo variant of the C class with a tendency toward lower reflectivities at the red end of the spectrum (subclass of the C class)
C	low	ultraviolet absorption feature shortward of 0.4 microns, generally flat to slightly reddish longward of 0.4 microns
D	low	generally featureless spectrum; neutral to slightly reddish shortward of 0.55 microns, very red longward of 0.55 microns; some objects' spectra tend to flatten longward of 0.95 microns
E	high	featureless spectrum; flat to slightly reddish over entire 0.3 to 1.1 micron wavelength range; differs from the spectrally identical M and P classes in albedo only
F	low	featureless spectrum; flat to slightly bluish over entire 0.3 to 1.1 micron wavelength range; differs from the C class in the weakness of the ultraviolet absorption feature (subclass of the C class)
G	low	very strong ultraviolet absorption feature shortward of 0.4 microns, flat longward of 0.4 microns; differs from the C class in the strength of the ultraviolet absorption feature (subclass of the C class)
M	moderate	featureless spectrum; flat to slightly reddish over entire 0.3 to 1.1 micron wavelength range; differs from the spectrally identical E and P classes in albedo only
P	low	featureless spectrum; flat to slightly reddish over entire 0.3 to 1.1 micron wavelength range; differs from the spectrally identical E and M classes in albedo only; spectra are intermediate between C and D classes

Q	moderately high	strong absorption features shortward and longward of 0.7 microns; band center between those of A and V classes (1862 Apollo is the type example)
R	moderately high	strong absorption features shortward and longward of 0.7 microns; band center between those of A and V classes (349 Dembowska is the type example)
S	moderate	moderate to strong absorption feature shortward of 0.7 microns, and moderate to nonexistent absorption feature longward of 0.7 microns
T	low	moderate absorption feature shortward of 0.85 microns, and generally flat longward of 0.85 microns
V	moderately high	strong absorption feature shortward of 0.7 microns and strong absorption feature longward of 0.7 microns, centered near the 0.95 micron filter

other letters and symbols used in the classifications

I	used for inconsistent data (e.g. a low albedo but an A-type spectrum); such a designation would be used only in the case of unconfirmed data; should high-quality data confirm such a combination, then a new asteroid class should be introduced
K	this letter has been reserved to represent a class of objects similar to 221 Eos; at this time, no formal definition for this class exists in the taxonomic system described above
U	appended to the classifications of those objects that fall far from the cluster center, indicating an unusual spectrum for that class
X	in the absence of albedo information, the E, M, and P classes are spectrally degenerate; X is used to represent the spectrum shared by these three classes and should be replaced by E, M, or P once a high-quality albedo becomes available
:	indicates noisy data and a classification of lower quality
::	indicates extremely noisy data and a classification of dubious quality
—	indicates that physical data do exist but are useless for classification purposes due to excessive noise

sample. The E (1%), M (9%) and G (1%) groups have spectra similar to the C asteroids but the albedos are distinctively higher: 0.38, 0.12 and 0.09, respectively. D asteroids (7%) are divided into 4 subclasses and have a spectrum with high values in the infrared region increasing from w to z and albedos in the range of 0.04 and 0.07. Four subclasses contain the S asteroids (33%), which have albedos ranging from 0.14 to 0.17 and a spectrum increasing from the u band and then generally flat in all the redder bands. A (1%) asteroids have a high albedo and a spectrum with a maximum in the w band decreasing toward both the ultraviolet (steeply) and the z band. 4 Vesta, 192 Nausikaa, and 349 Dembowska are included in the V class, which has the same characteristics as the S group in the s, u, b, v and w bands but shows lower values in the red portion of the spectrum where there is a deep absorption band due to olivines and pyroxenes.

It is very important to remember that asteroid taxonomy is defined in terms of the observational data used in the analysis. The taxonomic systems currently in use are based on the reflectivity of asteroid surfaces between 0.3 and 1.1 μm. Therefore, one cannot take *JHK* data, for example, and rigorously classify an asteroid according to the 0.3 to 1.1 μm scheme. Similarly, one cannot rigorously classify an asteroid as an M type, simply because a high radar reflectivity implies a high metal content.

V. DISCUSSION

That S-type asteroids are found more frequently in the inner part of the main asteroid belt and C-type asteroids more frequently in the outer part of the belt has been known for some time. See Zellner (1979) and the chapter by Gradie et al. for a review. With the extensive surveys since that time, however, the spatial distributions of the less populous asteroid classes have also been examined. One such study was performed by Gradie and Tedesco (1982). They found that some of the other classes also showed pronounced peaks in their distributions, notably the P and D classes. This work preceded the new taxonomic class definitions produced by Tholen (1984), however, so the reader will find no mention of the A class asteroids, and the E+R peak at the inner edge of the belt should now be recognized as containing no R asteroids, at least as defined in the Tholen taxonomy.

The raw distribution of taxonomic types as observed by the Eight-Color Asteroid Survey was shown in tabular form by Tholen (1984, Table X). Bell has reproduced this table in graphical form, and it appears as Figure 1a in the chapter by Bell et al. Unlike the earlier graph by Gradie and Tedesco and Figure 1 in the chapter by Gradie et al., no attempt has been made to correct this distribution of taxonomic type vs distance for observational bias. For a more detailed discussion of the distribution of taxonomic types vs heliocentric distance and diameter, see Chapman (1989) and the chapter by Gradie et al.

Until 1983, Vesta was the only known example of an object with a basal-

tic achondritic surface, which led to some questions about how commonly asteroids were differentiated. In that year, however, an Earth-approaching asteroid designated as 1983 RD (later numbered as 3551 but not yet named at the time of this writing) was found to have a reflectance spectrum indistinguishable from Vesta's at visible and near-infrared wavelengths. Medium resolution spectrophotometry over the wavelength range 0.8 to 2.5 μm during the object's favorable apparition in 1986 confirmed the presence of the two pyroxene bands and its compositional similarity to Vesta. Since that time, two more Earth-approaching asteroids have been discovered with similar surface compositions: 3908 1980 PA and 4055 1985 DO2 (Tholen et al. 1988; Cruikshank et al. 1989). These small objects are most likely the crustal fragments of some collisionally disrupted Vesta-like parent body, although we cannot rule out the possibility that they represent chips off the surface of Vesta itself.

Similarly, the reflectance spectrum of 1862 Apollo has been observed a couple of other times among the Earth-approaching population, though not unambiguously, but no counterpart has been found among the main-belt asteroids. Are such surface materials unique to the planet-crossing population, or to the objects with small diameters?

As mentioned in Sec. III, the B, F, and G subclasses of the C class can be significant in some applications. For example, Feierberg et al. (1985) noticed a correspondence between those objects classified as G and those objects having 3.0 μm absorption features due to water of hydration. Similarly, many of the objects without water of hydration features were classified as F. This discovery led to a more detailed comparison of the U-B color and the depth of the water of hydration absorption feature for a set of 14 C-type asteroids (including the F and G subclasses). A highly significant correlation was found. Because the ultraviolet absorption feature is caused by the Fe^{2+} to Fe^{3+} charge transfer absorption, the correlation indicates that the lower temperatures that permitted the formation of hydrated minerals also promoted higher oxidation states of the iron. For more details, see the paper by Feierberg et al. (1985).

The analysis of the distribution of taxonomic classes has led to some important hypotheses regarding the formation and evolution of the asteroids. For more details, see the chapter by Bell et al.

VI. FUTURE WORK

Asteroid taxonomy is still in its adolescent stages. We have witnessed tremendous growth in the sophistication of asteroid taxonomy commensurate with the growth in the available observational data. We can certainly expect the observational data base to continue growing, so it stands to reason that asteroid taxonomy will continue to mature in the forseeable future.

Perhaps the biggest problem facing those who utilize these taxonomic systems is the confusion created by the proliferation of asteroid taxonomies. There are now three "second generation" taxonomies, all of which use many

of the same letter designations as their predecessors. Although the mean class characteristics in each system are fairly similar, which is one reason why the same letter designations have been retained, the classification for any individual object could be quite different in the three systems. All three systems are likely to coexist for some time, so nobody should expect any immediate solution to the confusion. For now, we can only recommend that those who make reference to the classifications of asteroids also make clear reference to the system in which they are working.

The most significant change to the current asteroid taxonomic schemes will likely occur after a large sample of homogeneous infrared (longward of 1.1 μm) spectral reflectance data has been incorporated into the class definitions. As an example, Bell et al. (1988) has already sampled all (except Q) of the recognized taxonomic classes at 52 wavelengths between 0.8 and 2.5 μm. Eos family members stand out in this sample as being distinctly different from typical S asteroids.

That Eos family members are unusual is nothing new. Their $B-V$ colors have long been known to straddle the gap between the C and S asteroid classes (Gradie 1978). The observation of their reflectance spectra further into the infrared showed somewhat greater similarity to the S asteroids, however, and as a result these objects have been classified as S asteroids in both the Tholen and Barucci taxonomies. Bell's infrared data is rather compelling, however, and we have confidence that a new taxonomy that includes observational data longward of 1.1 μm will split these objects from the S asteroids. In anticipation, we have already discussed the letter designation for this class, and chose the letter K, simply because it falls midway between C and S in the alphabet, much in the same way the $B-V$ colors fell midway between those of C and S asteroids. We do want to emphasize, however, that the K class has not yet been formally defined in either the Tholen or Barucci taxonomic systems. Coincidentally, Tedesco et al. (1989) independently created a K class to represent some Eos-like asteroids, choosing the same letter designation for the same reasons.

Even without the addition of infrared data, undoubtedly others will apply different classification algorithms to the existing data bases. There is no "right" or "wrong" approach when it comes to assigning asteroids to classes. The overall similarity of the Tholen, Barucci and Tedesco taxonomies does indicate that strikingly different methods will recognize the same basic patterns in the data, and so we can anticipate that other methods will do likewise, assuming that approximately the same number of broad classes are created.

Finally, advances in detector technology will permit the observation of even fainter, and therefore smaller, objects in the main asteroid belt. These observations will enable us to examine the distribution of taxonomic classes among the smaller asteroid population. Given the apparent differences between the Earth-approaching small-asteroid population and the main belt, we can expect some interesting discoveries to be made.

REFERENCES

Barucci, M. A., Capria, M. T., Coradini, A., and Fulchignoni, M. 1987. Classification of asteroids using G-mode analysis. *Icarus* 72:304–324.

Bell, J. F., Owensby, P. D., Hawke, B. R., and Gaffey, M. J. 1988. The 52-color asteroid survey: Final results and interpretations. *Lunar Planet. Sci.* XIX:57–58 (abstract).

Bowell, E., Chapman, C. R., Gradie, J. C., Morrison, D., and Zellner, B. 1978. Taxonomy of asteroids. *Icarus* 35:313–335.

Chapman, C. R. 1989. Compositional structure of the asteroid belt and its families. In preparation.

Chapman, C. R., and Gaffey, M. J. 1979. Reflectance spectra for 277 asteroids. In *Asteroids*, ed. T. Gehrels (Tucson: Univ. of Arizona Press), pp. 655–687.

Chapman, C. R., Morrison, D., and Zellner, B. 1975. Surface properties of asteroids: A synthesis of polarimetry, radiometry, and spectrophotometry. *Icarus* 25:104–130.

Coradini, A., Fulchignoni, M., Fanucci, O., and Gavrishin, A. I. 1977. A Fortran V program for a new classification technique: The G-mode central method. *Comp. Geosci.* 3:85–105.

Cruikshank, D. P., Tholen, D. J., Hartmann, W. K., Bell, J. F., and Brown, R. H. 1989. Three basaltic asteroids and the source of the eucrites. In preparation.

Feierberg, M. A., Lebofsky, L. A., and Tholen, D. J. 1985. The nature of C-class asteroids from 3-μm spectrophotometry. *Icarus* 63:183–191.

Gaffey, M. J., and McCord, T. B. 1979. Mineralogical and petrological characterizations of asteroid surface materials. In *Asteroids*, ed. T. Gehrels (Tucson: Univ. of Arizona Press), pp. 688–723.

Gehrels, T., ed. 1979. *Asteroids* (Tucson: Univ. of Arizona Press).

Gradie, J. C. 1978. An Astrophysical Study of the Minor Planets in the Eos and Koronis Asteroid Families. Ph.D. Thesis, Univ. of Arizona.

Gradie, J. C., and Tedesco, E. F. 1982. Compositional structure of the asteroid belt. *Science* 216:1405–1407.

Tedesco, E. F., Williams, J. G., Matson, D. L., Veeder, G. J., Gradie, J. C., and Lebofsky, L. A. 1989. A three-parameter asteroid taxonomy. *Astron. J.* 97:580–606.

Tholen, D. J. 1984. Asteroid Taxonomy from Cluster Analysis of Photometry. Ph.D. Thesis, Univ. of Arizona.

Tholen, D. J., and Bell, J. F. 1987. Evolution of asteroid taxonomy. *Lunar Planet. Sci.* XVIII:1008–1009 (abstract).

Tholen, D. J., Hartmann, W. K., and Cruikshank, D. P. 1988. 1980 PA and 1985 DO2. *IAU Circ.* 4655.

Zellner, B. 1979. Asteroid taxonomy and the distribution of the compositional types. In *Asteroids*, ed. T. Gehrels (Tucson: Univ. of Arizona Press), pp. 783–806.

Zellner, B., Tholen, D. J., and Tedesco, E. F. 1985. The eight-color asteroid survey: Results for 589 minor planets. *Icarus* 61:355–416.

DISTRIBUTION OF TAXONOMIC CLASSES AND THE COMPOSITIONAL STRUCTURE OF THE ASTEROID BELT

JONATHAN C. GRADIE
University of Hawaii

CLARK R. CHAPMAN
Planetary Science Institute

and

EDWARD F. TEDESCO
Jet Propulsion Laboratory

The distribution of asteroid taxonomic classes and, presumably, actual composition varies systematically with heliocentric distance and is seen qualitatively in the results of a variety of taxonomy methods. In general, the distribution of taxonomic classes is characterized by moderate-albedo asteroids dominant in the inner belt with low-albedo asteroids prevalent in the outer belt and beyond. If the differences in taxonomic classes are assumed to be due to differences in composition, then the asteroid belt can be divided into many compositionally distinct regions defined by peaks and troughs in the distributions of the various classes. Unfortunately, differences in the class definitions used by different classification methods are manifested in the bias-corrected distribution of the classes, which makes detailed interpretation of these trends difficult. UBV color differences among members of the moderate-albedo S class show a distribution in semimajor axis which indicates subgroups in the S class. Explanations of the causes of the overall trends range from primarily dynamical to primarily in situ arrangements of igneous, metamorphic and unaltered primitive material, but a combination of several of these factors may be more likely. Size distributions which probably reflect collisional evolution, differ for different classes; S, M and P are approximately power laws, while C types are deficient at ~60 km diameter relative to the number at 100 to 150 km diameter.

[316]

The present spatial, compositional and size distribution of the asteroids appears to have been determined by both primordial and evolutionary processes. The heliocentric distribution of the orbits of asteroids which must be in part a primordial imprint and in part an evolutionary artifact shows, quite clearly, the dominance of dynamics by Jupiter. Studies of the physical properties of individual asteroids, i.e., the albedo, spectral reflectance, radar and polarization properties, which must also contain a primordial as well as an evolutionary imprint, provide clues about composition and geochemical evolution of the asteroids and the solar system in general. Interpretations of studies of the physical properties of the asteroids rely heavily upon the idea of an asteroid taxonomy, i.e., the clumping together of objects into classes with similar physical properties. Once classes are defined, distributions in space, composition and size can be studied in a statistically meaningful manner.

The intent of this chapter is to review previous studies of the distribution of the asteroid taxonomic classes and to analyze the techniques, results and interpretations of these studies. We provide an overview of previous studies in an attempt to identify the strong and weak points, point out important caveats for the interpretation of results, and most important, provide some insight into the problem that will be used as a starting point for future investigations.

I. HISTORICAL PERSPECTIVE

Early studies of the *UBV* colors of asteroids (Fisher 1941; Kitamura 1959; Wood and Kuiper 1963; cf. review by Chapman et al. 1971) noted that outer-belt asteroids ($a > 3.0$ AU) have systematically bluer *UBV* colors than do the inner-belt asteroids ($a < 2.3$ AU). Unfortunately, the significance of this finding could not be appreciated due to the small sample of asteroids studied and the lack of corresponding theoretical and geochemical studies of meteorites.

The realization that the physical properties of asteroids vary significantly with heliocentric distance developed as the result of systematic spectrophotometric, thermal-radiometric and polarimetric surveys of the asteroids in the 1970s. Chapman et al. (1975) analyzed the physical properties (radiometric and polarimetric albedos combined with near-infrared spectrophotometry) of 110 asteroids and came to the conclusion that, at least for asteroids with diameters > 90 km, the low-albedo objects (called C class in their study) became more prevalent, in an absolute as well as a relative sense, in the outer belt. Although the C class of Chapman et al. has subsequently been subdivided into several classes, the basic trend of increasing proportions of lower-albedo objects with increasing heliocentric distance remains unchanged.

Different Taxonomies

Variations in the heliocentric distribution of the physical properties of asteroids have been studied in a variety of ways. Perhaps the most useful method has been the development of asteroid taxonomies, which allows for

the statistical analysis of hundreds or thousands of asteroids. In most tax-
onomies, small variations in physical properties of observations are ignored
so that groups of asteroids with nearly identical or, at least, very similar physi-
cal properties (albedo, color, etc.) can be identified.

   Not all classification schemes are identical and hence do not necessarily
produce identical results. Not only is there a distinction between a pattern-
recognition-classification method and a mineralogic-classification method,
but there are different approaches in each method which in turn affect the
results. It is wise not to assume that class identifiers used by one scheme are
the same in all other schemes. There is not yet, nor is there likely to be, an
accepted well-defined set of class definitions because, depending upon the
data one has and the specific problem to be addressed, one scheme may be
more applicable than another (see also the chapters by Tholen and Barucci,
Tedesco et al., and Chapman et al.).

   The pattern-recognition-classification method was first used by Chapman
et al. (1975) who introduced single letters which identified asteroids with
similar albedo and spectrophotometric properties. This was the beginning of
the C, S, M, etc., taxonomic system. This method, used on larger and larger
samples of asteroids by Bowell et al. (1978), Zellner (1979a) and in a variety
of other studies of specific groups of asteroids, relied upon the demarcation of
subjectively defined boundaries around well-separated groupings of observ-
able parameters. Reliance on the interpretation of the physical properties of
the asteroids is not required for this group-identification process. In fact, com-
plete ignorance of any physical interpretation is desired because this addi-
tional information, if used to draw boundaries or identify groupings, would
make the classes somewhat contrived. The latest scheme using this approach
is that of Tedesco et al. (1988).

   The application of cluster-analysis methods to the asteroid classification
process has led to a classification system different from those previously de-
scribed. Tholen (1984) and Barucci et al. (1987) have produced new sets of
classifications that, for the most part, include the major classes identified by
the previous method (see the chapter by Tholen and Barucci). Unfortunately,
there is not a one-to-one correspondence in class memberships defined by
these various approaches. Attempts such as Chapman (1989), to classify
newly observed asteroids into extensions of the classes identified by cluster
analysis have been made using a "boundary method" (placing boundaries
around the clusters defined by another technique).

   The "mineralogical" or physical classification, which relies upon the
geochemical interpretation of the spectrophotometric and albedo properties of
each asteroid, is best exemplified by the approach of Gaffey and McCord
(1978,1979). Extensive mineralogical interpretations of the 0.4 to 1.1 μm
spectrum combined with the albedo of individual asteroids were used to iden-
tify a number of types of asteroids. Subtle differences in the spectral proper-
ties of asteroids were exploited to relate individual asteroids to individual
meteorites or meteorite types. The interpretations of results of this method are

highly dependent upon the validity of the association of an asteroid with a specific meteorite type. Any error in the identification of minerals or composition would certainly influence greatly any analysis of the distribution of asteroid compositions, using such classes.

A variation on this method has been used by Bell (1985; see also the chapter by Bell et al.) who has divided the asteroids into three basic groups or "superclasses" interpreted as being primitive, metamorphic and igneous. Whether an asteroid falls into one or another superclass is dependent upon Bell's interpretation of the physical and compositional properties of the arbitrarily defined classes.

The reader is cautioned that a discussion of the distribution in space and size of the compositional classes of the asteroids and the study of the large-scale structure of the asteroid belt becomes controversial if classes from the various methods and schemes are mixed indiscriminately. As an example, consider the case of the P-class asteroids first recognized as a separate class of asteroids by Gradie and Tedesco (1982). This class of asteroids is described by Gradie and Tedesco as being of low albedo yet spectrally similar to the M-class asteroids. The application of cluster analysis technique by Tholen (1984) quantified the definition of the class and the letter P was retained as the class identifier. This new quantification changes the number of objects falling into the class originally labeled P by Gradie and Tedesco (1982). Subsequently, Barucci et al. (1987) classified 438 asteroids using G-mode analysis which failed to isolate a separate P class; instead classic P types became part of other classes, in particular, their classes C and M. Chapman (1989) refined the P class as defined by Tholen (1984) using the spectral parameters "bend" and "IR" which again changed the number of objects in the class. Recently, Tedesco et al. (1989) have redefined the P class according to a two-color plus albedo scheme nearly identical to the original method used by Gradie and Tedesco (1982). Although all of the various investigations have varied the definition or boundaries of the P class which in essence changed the class itself, the class identifier P has remained the same throughout, which results in some confusion.

Bias Corrections

The true, rather than the apparent, distribution of compositional classes is of interest since the apparent distribution is affected by a variety of observational biases. These biases include (1) the incomplete inventory of the asteroid population; (2) the tendency to observe brighter asteroids (hence closer, larger, higher albedo asteroids) in the case of many groundbased observations; (3) the underestimation of albedo for some small IRAS-observed asteroid due to the flux overestimation at low signal-to-noise (see chapter on Classification of IRAS Asteroids by Tedesco et al. and the chapter on Asteroid Results from IRAS Survey by Veeder et al.); and (4) the selection of certain dynamically interesting regions (e.g., families) of the asteroid belt.

Several approaches have been used to eliminate observational biases in the asteroid sample due to inventory and faintness biases. Zellner and Bowell (1977) and Gradie and Tedesco (1982) used the semimajor axis zones defined by Kiang (1971) to define bias factors (estimated ratio of total number to observed number of a particular compositional class) based on a mean opposition magnitude cutoff of $B(a,0) < 16.5$ mag. Zellner (1979a) modified the definitions of these zones, in essence creating new zones, to account for eccentricity and inclination factors before doing a bias analysis. This method necessarily causes the cutoff at small diameters to be a function of heliocentric distance and the bias analysis for the total population is limited to diameters larger than the cutoff diameter in the most distant zone.

The bias corrections for asteroids observed by IRAS are very different, because the detections are a function of infrared brightness, not apparent visual magnitude (cf. chapter by Matson et al.) which favors low-albedo asteroids (the opposite of groundbased optical surveys). In addition, the bias (3) discussed above must be taken into account. Bias due to asteroid families can be lessened by removing family members from the analysis and replacing the family by a single asteroid of a given taxonomic type, at least for those families (Koronis, Eos and Themis) which we suspect are caused by the collisional disruption of a single homogeneous parent asteroid.

The most recent analysis of the dynamical morphology of the asteroid belt for use in bias analysis is that of Zellner et al. (1985a). The distribution in orbital inclination, eccentricity and semimajor axis of 2888 numbered asteroids was used to define 19 zones. These zones, given in Table I, account for major family groups, such as the Koronis, Eos and Themis families, as well as dynamically isolated regions such as the Phocaea group of asteroids. Unfortunately, as noted by Zellner et al., the zones for the families were defined using osculating elements rather than proper orbital elements which means that the zones are not as tightly constrained as they might be.

The number of asteroids in Zellner et al.'s analysis, 2888, represents an 80% increase in sample size compared with Kiang's (1971) analysis. In some cases, such as for Kiang's M (Mars-crossing) zone, a six-fold increase (95 in the combined zones AAA, HU and MC of Zellner et al. [1985a] vs 15 in Kiang's [1971]) in numbered objects permits a better definition of the zones in the inner asteroid belt and the terrestrial planet-crossing region. Since the Zellner et al. (1985a) analysis, the numbered asteroids have been augmented by 35%, similar in numbers to the increase between the analysis of Kiang (1971) and Zellner et al. (1985a). Any future attempt at bias analysis should incorporate all available data on orbital elements.

II. DISTRIBUTION OF TAXONOMIC CLASSES

Studies of the distribution of taxonomic classes are limited by the availability of observational data. Class assignments, which require that certain

TABLE I
Osculating Element Zones for the Minor Planets[a]

Zone	Description	Number	Mean a (AU)	Limits for a (AU)	Limits for e	Limits for i
AAA	Apollo-Amor-Aten	36	1.831	—	$q = a(1 - e) \leq 1.30$	—
HU	Hungaria Group	30	1.900	$1.78 \leq a \leq 2.00$	$e \leq 0.18$	$16° \leq i \leq 34°$
MC	Mars crossers	29	2.285	—	$q \leq 1.666$	—
FL	Flora Family	421	2.230	$2.10 \leq a \leq 2.30$ (limited by MC)	$i \leq 11°$	—
PH	Phocaea Group	62	2.368	$2.25 \leq a \leq 2.50$	$e \leq 0.10$	$18° \leq i \leq 32°$
NY	Nysa Family	44	2.448	$2.41 \leq a \leq 2.50$	$0.12 \leq e \leq 0.21$	$1.5° \leq i \leq 4.3°$
I	Main belt	316	2.391	$2.30 < a \leq 2.50$	(limited by MC)	$i < 18°$
PAL	Pallas zone	4	2.755	$2.500 < a < 2.82$	(limited by MC)	$33° \leq i \leq 38°$
IIa	Main belt	455	2.614	$2.500 < a \leq 2.706$	(limited by MC)	$i < 33°$
IIb	Main belt	298	2.761	$2.706 < a \leq 2.82$	(limited by MC)	$i \leq 33°$
KOR	Koronis zone	86	2.873	$2.83 < a \leq 2.91$	$e \leq 0.11$	$i \leq 3.5°$
EOS	Eos zone	144	3.014	$2.99 \leq a \leq 3.03$	$0.01 \leq e \leq 0.13$	$8° \leq i \leq 12°$
IIIa	Main belt	189	2.933	$2.82 < a \leq 3.03$	$e \leq 0.35$	$i \leq 30°$
THE	Themis zone	165	3.145	$3.08 \leq a \leq 3.24$	$0.09 \leq e \leq 0.22$	$i \leq 3°$
GR	Griqua Group	3	3.243	$3.10 \leq a \leq 3.27$	$e \leq 0.35$	(no test)
IIb	Main belt	480	3.140	$3.03 < a \leq 3.27$	$e < 0.35$	$i \leq 30°$
CYB	Cybele Group	51	3.431	$3.27 < a \leq 3.70$	$e \leq 0.30$	$i \leq 25°$
HIL	Hilda Group	34	3.952	$3.70 < a \leq 4.20$	$e \leq 0.30$	$i \leq 20°$
T	Trojan Group	35	5.203	$5.05 \leq a \leq 5.40$	(no test)	(no test)
Z	No zone	6	—	—	none of the above	—

[a] Defined by Zellner et al. (1985a).

spectrophotometric, albedo or other data of a specified quality are available for the classification process, are frequently based on incomplete physical observations.

The first attempt to derive bias-corrected frequency distributions of taxonomic classes by Chapman et al. (1975) demonstrated that the heliocentric distribution of types was not uniform. The more detailed analysis of the TRIAD data base by Zellner (1979a) using the classification system of Bowell et al. (1978) confirmed the previous results of Chapman et al. and of Zellner and Bowell (1977) that the general configuration of the belt was of moderate albedo S-class objects, predominantly in the inner belt ($a < 2.4$ AU) and low-albedo objects (clumped together in the Bowell et al. [1978] C class) dominant in the outer belt ($a > 2.4$ AU). Apparent in the distribution was the local enhancement of moderate-albedo objects at 3.017 AU due to the Eos family.

Gradie and Tedesco (1982) used a set of observational data, namely the preliminary results of the Eight-Color Asteroid Survey (ECAS) (Zellner et al. 1985b) and the preliminary results of a groundbased 10- and 20-μm radiometric survey (Gradie and Tedesco 1989), that was more complete in terms of available observations and the extent of the asteroid belt observed. That study was aimed specifically at outer regions of the belt that had been poorly observed in early surveys and had excessively large bias factors in Zellner's (1979a) study. The bias factors in the Gradie and Tedesco (1982) study were reduced significantly in many areas, some to order unity for diameters > 50 km. For example, among the outer-belt asteroids, 38 of the 51 Cybele members numbered at the time were sampled.

The class definitions for the major classes C, S, M, E and R used by Gradie and Tedesco (1982) are essentially those defined by Zellner (1979a) for inclusion in the Tucson revised index of asteroid data (Zellner 1979b). Qualitative descriptions (only) of the properties of the classes F, D and P were offered by Gradie and Tedesco (1982). The lack of quantitative descriptions of class boundaries has led to confusion over the qualifications for membership in the P class, as discussed above. In spite of this shortcoming, the significant increase in asteroids sampled with semimajor axes < 2.2 AU and > 3.0 AU, the increase in asteroids with both reliable albedo and spectrophotometric observations, and the recognition of these new classes of asteroids has led to a significant new view of the heliocentric distribution of the asteroids.

Figure 1 shows the bias-corrected heliocentric distribution of classes defined by Gradie and Tedesco (1982). This figure should not be compared directly with the heliocentric distribution of classes drawn from alternate taxonomies without first understanding the caveats and differences associated with each taxonomy (see the chapter by Tholen and Barucci, Sec. III). Such figures represent the distribution of taxonomic classes (of a particular definition) with heliocentric distance. Before one can interpret these distributions in
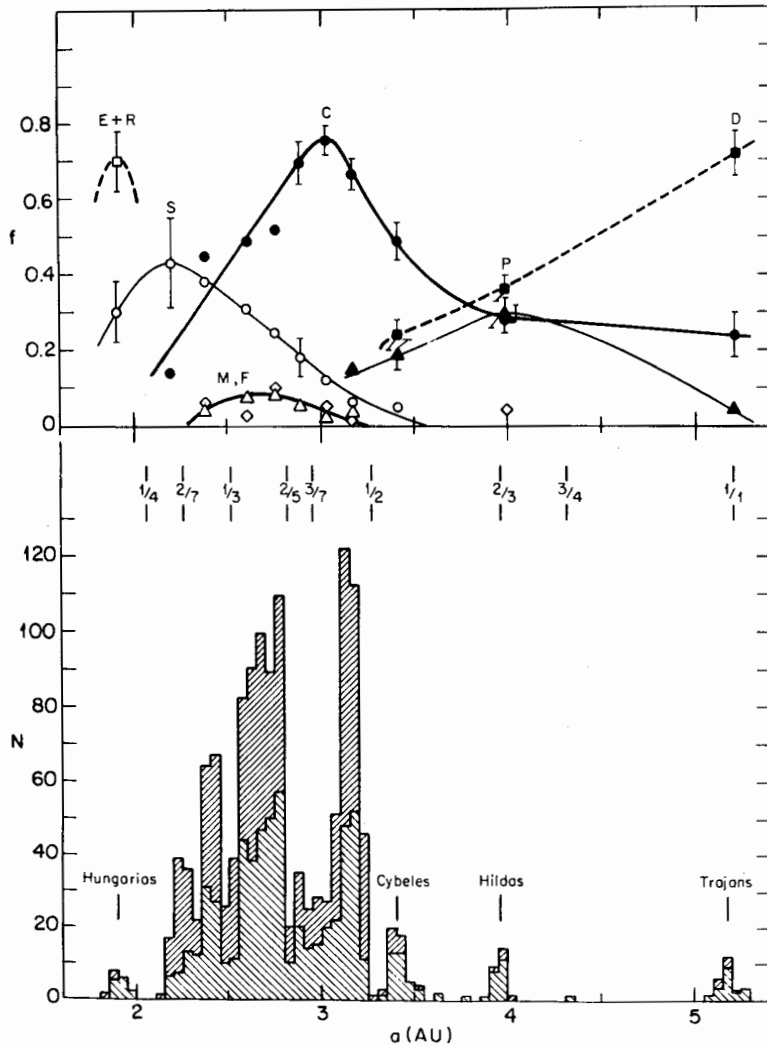
Fig. 1. *Top:* plot showing the observed relative type distribution of the bias-corrected sample for the types E, R, S, M, F, C, P and D defined by Gradie and Tedesco. Smooth curves are drawn through the data points for clarity. *Bottom:* plot showing the number distribution in semimajor axis for the 1373 asteroids in the bias-corrected sample used by Gradie and Tedesco (1982). The darkly shaded portion is the fraction of the bias-corrected sample for which taxonomic types existed for their study. Major resonances with Jupiter are indicated. (Figure adapted from Gradie and Tedesco 1982.)

terms of cosmochemical models, one must first understand the relationship between a taxonomic class and mineralogy. Although a preliminary interpretation is offered in the chapter by Bell et al., a thorough understanding of this relationship at the level of detail required for a full cosmochemical interpretation does not yet exist.

The general character of the belt as seen in earlier studies (the moderate-albedo S objects most populous in the inner belt and the low-albedo object classes [C, P and D] most populous in the outer belt) has been confirmed by subsequent studies. In terms of both absolute and relative numbers, the peak in the distribution of the C class near 3 AU, the P class near 4 AU, and the D class at 5.2 AU must be considered real. Also, there is an apparent concentration of M-class objects in the middle of the belt between 2.5 and 3.0 AU.

Subtle structure exists within the large-scale trends presented in Fig. 1. For example, Dermott et al. (1985) found that the mean U-V color of S-class asteroids varied noticeably and systematically with heliocentric distance. Figure 2 shows how the mean U-V color of nearly 200 S-class asteroids decreases as a function of increasing semimajor axis. S-class asteroids closer to the Sun are significantly redder than those farther away. This bend in U-V color cannot be due to observational effects such as phase reddening since the difference in average phase angle of observation between the "inner" and "outer" asteroids is only $2°13$. This small difference in mean phase angle corresponds to a U-V change of only 0.004 magnitude. A possible interpretation suggested by Dermott et al. is that there are at least two subclasses of S-class asteroids with two different mean locations, the redder objects clustering at 2.2 AU with the rest possibly being distributed evenly from 2 to 3.2 AU.

Significant improvement in the study of the distribution of taxonomic classes has been possible since the completion of the IRAS Asteroid and Comet Survey (1986), which yielded albedos for more than 1700 numbered asteroids. Chapman (1989) has used the IRAS albedos (IRAS Asteroid and Comet Survey 1986) in conjunction with a variety of groundbased data sets to develop an augmented taxonomy. Since this taxonomy uses a significantly broader set of physical observations—including intermediate-band spectrophotometry and polarimetry, which were used in the original Chapman et al. [1975] and Bowell et al. [1978] taxonomies—then was used by Gradie and Tedesco (1982), one must be careful in comparing the heliocentric distributions.

Chapman has used unique "best-guess" classes for 939 asteroids with additional constraints on the taxonomy for a total of 1721 asteroids to produce an eighteen-class taxonomy (Tholen's classes augmented by a subdivision of the S class). IRAS Asteroid Survey albedos were used in conjunction with other groundbased observations (spectrophotometry, polarimetry, etc.) whenever groundbased albedos were not available. The letter identifiers are identical to those used by earlier workers but the meanings may be subtly different.
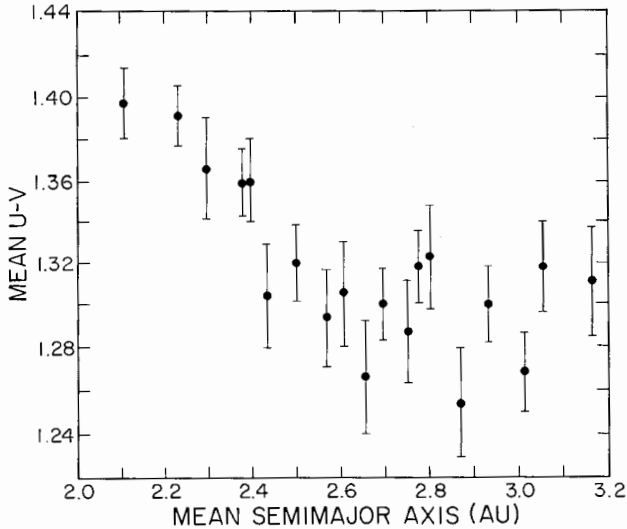
Fig. 2. Variation in the mean *U-V* color for 191 S-class asteroids with semimajor axis as computed by Dermott et al. (1985). The asteroids were sorted in order of increasing semimajor axis and then separated into independent samples of 10 asteroids. The error bars were estimated from the variance of each sample.

Chapman's approach was designed to bootstrap from, and extend, Tholen's (1984) taxonomy and should not differ appreciably from Tholen's analysis for most classes but may differ more for poorly sampled minor classes (e.g., G, B, F, etc.). The bias analysis of Chapman uses the 19-zone system of Zellner et al. (1985a) given in Table I rather than the Kiang (1971) system used by Gradie and Tedesco (1982). The subgroups of the S class defined by Chapman demonstrate, in agreement with Dermott et al. (1985), that there are different preferred heliocentric distances for different S subgroups.

Figures 3 and 4 show the results of Chapman's analysis of the bias-corrected distributions of classes. The general characteristic of moderate-albedo objects dominant in the inner belt and low-albedo objects dominant in the outer belt has not changed. The concentration of M-class objects in the middle belt is still apparent. However, important differences are apparent and must be explained. For example, the dominance of the C-class objects in the main belt, seen by Gradie and Tedesco (1982) as a distinct peak in the distribution is diminished in Chapman's distribution.

One significant difference is the apparently greater predominance of P-class objects in the middle belt than was found by Gradie and Tedesco
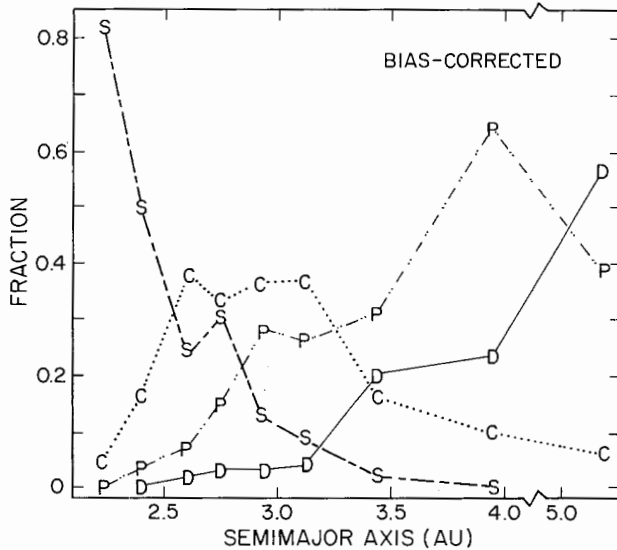
Fig. 3. Percentage of bias-corrected asteroids as a function of semimajor axis from 2.1 to 5.2 AU for the major classes S, C, P and D defined by Chapman (1989). Percentages apply to cumulative numbers of asteroids with diameters larger than the completeness limits of total numbered asteroids, for albedos ~3%, for each zone. Note the break in the semimajor axis scale.

(1982). It is clear that the change in the apparent distribution of the P class is driven more by the change in the class definition than by the discovery of more P-class objects. Tedesco et al. (1989) point out that from the same high-quality data set, they find 15 P-class objects, Tholen (1984) finds 47 P-class objects, and Barucci et al. (1987) find none at all. Such differences must be due to the different definition of the P class by each investigator, not by better estimates of membership in a well-defined unique P class. Chapman's results, in addition may reflect better sampling of P types (as defined by Tholen) as well as inadequate correction for biases in IRAS albedos.

One change in the distribution found in the Chapman study, which is probably not due to the changes in class definitions, is the apparently steeper gradient in S-class abundance with increasing heliocentric distance than was seen by Zellner (1979a) or Gradie and Tedesco (1982). The change in gradient may reflect the true relative abundance of small S- and C-class objects in the near-to-middle regions of the belt because earlier groundbased studies were biased against small low-albedo objects in any particular heliocentric zone. However, differences in the bias-correction analysis, i.e., using Zellner et al.'s (1985a) zones rather than Kiang's (1971) zones could influence the bias-corrected relative abundances. For example, inclusion of small Flora-family
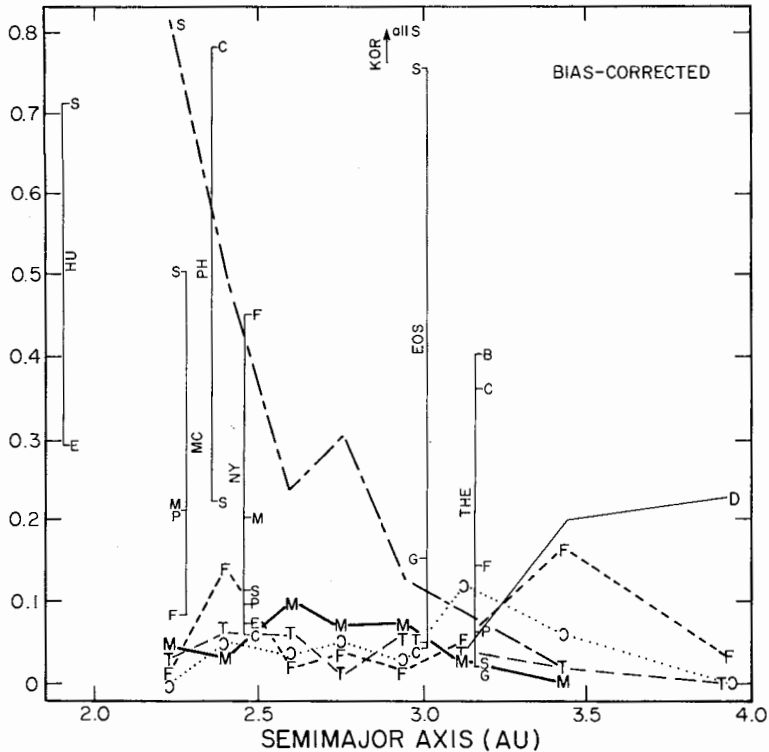
Fig. 4. Percentage of bias-corrected asteroids as a function of semimajor axis from 2.1 to 5.2 AU for the minor classes M, F, T and B+G (shown as a backwards "C") defined by Chapman (1989). For reference, the distributions for S and D (see Fig. 3) are indicated. Along vertical lines are the percentage by class for the special zones HU, MC, PH, NY, KOR, EOS and THE defined in Table I.

members in the analysis will cause the S-class distribution to appear to have a steeper gradient than in a study that omits the Floras.

The availability of new observations encourages the development of more sophisticated taxonomy schemes. It is apparent that as the number, types and precision of physical observations increases, so will the number of asteroid classes. In essence, the "arbitrary" classification method, which tends to group asteroids into large classes, will approach the "physical" classification method, which tends to find each asteroid unique. Chapman's division of the S-class asteroids into seven subgroups is one such example. It is likely that these subgroups bear a relationship to some of the asteroids classes developed by Gaffey and McCord (1979) from the narrowband spectrophotometric observations. The fact that the S class displays a broad dispersion in parameter

space is beyond doubt. Interpretation of the reasons (i.e., mineralogy, composition, surface properties, space weathering, etc.) is another matter.

Gaffey and McCord (1978) grouped the 65 asteroids classified in their system into either primitive assemblages or thermalized assemblages which are not too different from the terms primitive and metamorphic used by Bell (1988). In spite of their small sample of asteroids, Gaffey and McCord (1978) concluded that the thermalized bodies concentrate toward the inner part of the belt.

A completely different approach to studying the distribution of asteroid compositions has been undertaken by Bell (1985) who uses three "superclasses" interpreted as primitive, metamorphic and igneous. Bell's study was driven by the limited number of objects used in the Gaffey and McCord (1979) study relative to the large data set available in the broadband photometric studies. The relationship between Tholen (1984) classes and Bell's superclasses is given in the chapter by Bell et al. Heliocentric distributions of the nonbias-corrected relative abundances of these superclasses are shown in their Fig. 1. The merit of this superclass approach is that it emphasizes the most general trends in the asteroid belt, which perhaps tell about the largest-scale processes operating during the formation and evolution of the asteroids.

III. SIZE DISTRIBUTION

The size distribution of the asteroids is a statistical characterization of an inherent property of the population. In fact, as we will show, there are a variety of size distributions, significantly different from each other, which characterize subgroups of the asteroid population, such as different taxonomic classes, members of different families, and so on. This property of the population is very significant for understanding the origin and collisional history of the asteroids. An extensive literature, commencing with the classic paper of Piotrowski (1953), has developed concerning asteroid collisional physics and the generation of size distributions through collisional evolution. The motivations for this work include asteroid cosmogony, the generation of meteorites, interpretations of size distributions for crater populations on planetary and satellite surfaces, and assessment of hazards to spacecraft flying through interplanetary space.

Collisional physics is discussed in the chapters by Fujiwara, et al. and Davis et al. Here we briefly summarize some salient points so that we can have a physical context for our discussions of observed size-frequency populations. Under a number of simplifying assumptions, a population of particles collisionally interacting and fragmenting should evolve toward a power-law size distribution with an exponent of -3.5 (incremental; equivalent to the alpha $= 1.833$ of Dohnanyi [1971]). However, more sophisticated numerical models of asteroid collisional evolution (see, e.g., Davis et al. 1979,1985,

and their chapter) show that the picture is rather more complicated, due in part to the role of gravity. The exponent that results from the simulations is closer to −2.5, in the size range of 20 to 200 km, for evolved populations. It may steepen to −3.5 at still smaller sizes (Davis et al. 1985). A slope of −4.0 has the property that equal masses are contained in equal logarithmic intervals of size. All shallower slopes imply domination in mass by the largest bodies. A slope of −3.0 has the property that there are equal areas in equal logarithmic intervals; thus, for example, a crater field produced by the impact of a population of asteroidal projectiles with a slope steeper than −3.0 (e.g., −3.5) will saturate first at small sizes, whereas if the slope is shallower than −3.0, the largest craters will dominate the crater field.

A bump in the size distribution is not normally expected for an evolved population. Thus, evidence of such bumps have been taken, in the past, to indicate a remnant of an original, perhaps Gaussian-shaped, population (cf. Kuiper et al. 1958; Anders 1965; Hartmann and Hartmann 1968; Chapman 1974). Numerical simulations of incomplete collisional evolution from initial Gaussian-shaped distributions illustrate this behavior (cf. Davis et al. 1985, his Fig. 8).

Initial attempts to compare observation with theory (see, e.g., Kuiper et al. 1958; Dohnanyi 1971) were largely invalid due to the fact that it was not recognized until the 1970s that there is a complex mixture of asteroids of very different albedos in the asteroid population; therefore, there were significant biases in deduced diameter distributions. A significant step was taken by Zellner (1979a), who published bias-corrected size distributions for several different taxonomic classes in several different annular zones of the asteroid belt; his Figs. 6 and 7 show that the size distributions, for different subsets of asteroids, are very dissimilar. C-class objects in the outer belt had a nearly linear (i.e., power-law) shape, whereas those in the middle of the belt showed a prominent hump near 150-km diameter (alternatively, a major dearth near 50-km diameter), reminiscent of an incompletely evolved initially Gaussian population.

Zellner's graphs must now be regarded as obsolete, since the C class he was using (essentially all low-albedo asteroids) has since been subdivided. As described above and in the chapter by Tholen and Barucci, the C class now refers to a more narrowly defined low-albedo class, and there are numerous other subclasses, most notably the P class. Chapman's (1989) new, preliminary study of asteroid taxonomic types is the first set of bias-corrected statistics that addresses the question of asteroid size distributions since completion of the new taxonomy. As described earlier, he used a groundbased sample of asteroids—in order to perform the well-known procedures for correcting for biases in a groundbased sample (Zellner 1979a)—but he also used IRAS data to improve knowledge about the albedos. Since the cataloged IRAS albedos have some biases of their own (cf. Tedesco et al. 1987), the work should be regarded as preliminary.

J.C. GRADIE ET AL.

Figure 5 shows the bias-corrected size distribution of Chapman's (1989) classes on a log-log plot. Note the striking difference between the shape of the C class, which has a major deficit of bodies about 60 km in diameter, and the nearly linear relationships for the S, M and P classes. When the size distributions are plotted for the different annular zones, and the heliocentric variation in mix of types is taken into account, the new results help us understand Zellner's (1979a) original results. Zellner did not recognize the distinctions between P, B, G, F and some D classes and included all those objects in the C class, so his statistics for the outer main belt were heavily affected by the presence of other classes in his sample. Chapman's (1989) new results confirm Zellner's (1979a) conclusion that there is a bump in the distribution for C classes in the middle of the belt, but it is also evident for C-class objects (with Chapman's P-class objects now excluded) in the outer belt, as well. The size distribution for Chapman's main-belt P-class objects can be well characterized only in the outer main belt, where the log-log size distribution is fairly linear.

We have already mentioned that linear slopes are interpreted in terms of
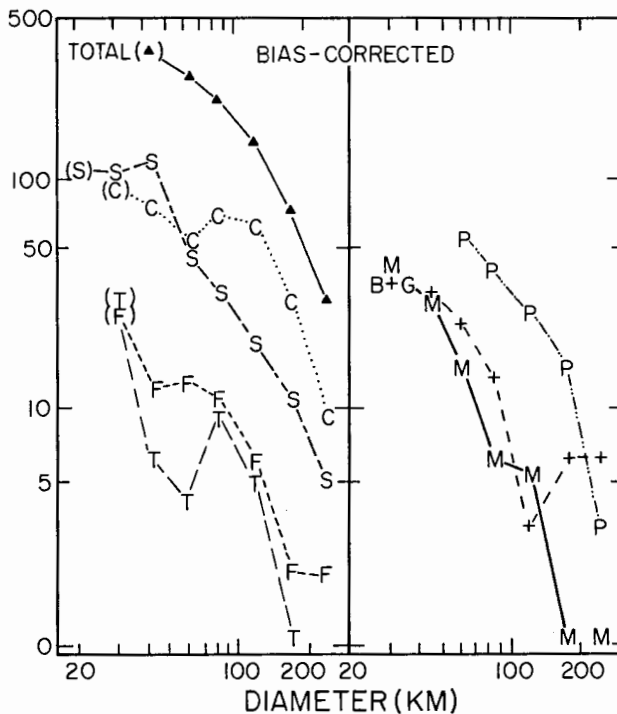
Fig. 5. Diameter-frequency relationship for all the asteroids (total) and the classes C, S, F, T, D, P, M and B+G (shown as a backwards "C") as defined by Chapman (1989). Data plotted are bias-corrected counts in equal logarithmic intervals of diameter.

extensive collisional evolution, while distributions in size like that exhibited by the C class imply little collisional evolution. However, since all of these asteroids are collisionally interacting with each other, there must be some other explanation. Perhaps C-class objects about 100 km or more in size are preferentially protected by gravity strengthening, while smaller C-class objects are extensively depleted by collisions; in a general sense, the numerical simulations of Davis et al. (1985) yield just such a distribution. The S and M classes, on the other hand, may be dominated by inherent strength to larger sizes, assuming they are of stony-iron and iron compositions, respectively. Still there remains the question of why the P-class objects, which are thought to be ultra-primitive carbonaceous types, show a more S-like size distribution; they would not be expected to be physically strong. Actually, the slopes of the linear distributions are shallower than predicted by Dohnanyi (1971) for a strength-dominated, collisionally evolved population; the slopes are shallow for the S-class objects and, especially, for the P-class objects (see the chapter by Chapman et al. for further discussion). When refinements are made to the IRAS data set, it should be possible to extend more reliably studies of size distributions to smaller diameters as well as to larger heliocentric distances, where the P's predominate. We may hope that they will help us address these perplexing questions.

The chapter by Bell et al. offers predictions about the compositional mix of small asteroids. In particular, it suggests that there should be a number of A-class objects at sizes of $\leq$ 30 km diameter, and an abundance of Q-class objects at < 10 km diameter. At this point, we lack sufficient data about small main-belt asteroids to confirm these predictions. Three of the nine possible or probable A-class objects that have been identified so far are in Mars-crossing or Amor-like orbits, and all of the Q-class objects are, as well. It remains to be seen whether this is simply an observational selection bias—so that small A- and Q-class objects will eventually be found in the main belt as well—or whether the chief difference is truly in the distribution with semimajor axis.

In conclusion, there are important differences in the size distributions for different groups of asteroids. In the broadest sense, they match the outcomes of numerical simulations that take gravity into account. But it is difficult to interpret the size distributions as resulting from evolution to a steady state at all diameters. The size distribution for the P-class objects requires further analysis.

IV. DISCUSSION

Most of the observed differences in physical properties among the asteroids are surely due to differences in composition. In spite of the differences in class definition, the rather ordered heliocentric distribution of the compositional classes is real and must be due to either primordial, evolutionary or dynamical processes, or to a combination of all three.

Primordial processes imply those processes that operated before the end of planetary formation and are suggestive of those events that were controlled primarily by the temperature, pressure and composition of the nebular dust and gas. Gradie and Tedesco (1982) suggested that the process is a vestige of the thermal and geochemical processes operating in the solar nebula during the formation of the original asteroids. If it is true that asteroids are remnant planetesimals that "remember" their original distribution in space and physical and chemical properties, then detailed chemical analysis of asteroids of each type should provide insight into the temperatures, pressures and chemistry of the nebula during planetary formation.

The combination of the observed heliocentric distribution in the S and C classes and the implied differences in composition between the S asteroids (moderate-temperature siliceous condensates) and the C asteroids (low-temperature siliceous condensates) as suggested by Gaffey and McCord (1979), is qualitatively consistent with the predictions of some solar system chemical-condensation models (Larimer 1967; Lewis 1974; Grossman and Larimer 1974). The concentration of S objects between 2 and 2.75 AU and the concentration of C objects between 2.5 and 3.5 AU suggest a source region for the formation of S objects closer to the Sun than for the C objects.

The low albedo and spectral characteristics of the P and D classes suggest a composition of low-temperature, carbonaceous-rich, silicate materials (Gradie and Veverka 1980). Gradie and Tedesco (1982) speculated that the differences between the observed physical properties of the P and D objects and those of the C objects are most likely due to differences in the temperature, pressure and composition of the solar nebula, since the P and D asteroids peak in frequency near 4 AU and 5.2 AU, respectively. It must be remembered that this interpretation is highly speculative since very little, if anything, is known about the compositions of the P and D asteroids.

The inner part of the belt, 2.0 AU, is dominated by the highly reflective, specially neutral, E-class asteroids suggested by Zellner et al. (1977) to be consistent with higher temperature, spectrally neutral (or oxidized iron-free) silicates. Gradie and Tedesco (1982) interpreted this accumulation of objects to be indicative of a warmer inner belt, at least compared to the region beyond 3.0 AU where the C-, P- and D-class objects predominate.

Post-formation evolutionary processes most definitely operated to modify the compositional structure of the asteroid belt. Vesta is considered a primary, if not unique, example of extensive post-formation modification of an asteroid exterior and, most probably, interior. Evidence from meteorites, presumed to have originated from asteroids, points to the fact that both high-temperature processes (melting of iron and subsequent slow cooling) and low-temperature metamorphic processes (formation of aqueous-alteration products in some carbonaceous chondrites) occurred.

The issue of post-formation evolution is one of degree—how much did post-formation evolution change the observed compositional characteristics of

the asteroids? Bell et al. address this issue. The metamorphic and igneous classes involve substantial alteration of the original compositions perhaps due to internal heating by ^{26}Al or externally induced electromagnetic heating from a T-Tauri phase solar wind (Sonett and Reynolds 1979). To what degree these post-formation alterations mask the original distribution of compositions is unknown. However, it may be possible to unravel some of these effects since external heating due to a solar wind could be size- and heliocentric-dependent, at least for objects of identical composition.

Post-formation reshuffling of the asteroids by dynamical means cannot be overlooked as a possible cause for some of the nonrandom structure in the distribution of compositions. Wasson and Wetherill (1979) noted the possibility that bodies formed initially in the outer solar system can be transferred into orbits between Mars and Jupiter having long-term stability. Short-period comets perturbed by nongravitational forces are notable examples of objects moved from the outer solar system into stable orbits in the inner solar system. Likewise, bodies may be removed from the innermost part of the solar system and caught in metastable Mars-crossing orbits (Wetherill 1979) where they provide fragments for subsequent capture into orbits in the main belt. If the present location of an asteroid does not necessarily correspond to the heliocentric distance at which it was formed, then the interpretation of the compositional distribution of the asteroid belt becomes exceedingly complex. However, the existence of the nonrandom distribution may mean that whatever reshuffling of objects occurred has been done in a systematic manner. It cannot be discounted that detailed chemical analysis of the various asteroid types may shed considerable light on the role of celestial dynamics as well as the role of thermodynamics during the formation of the asteroid belt.

REFERENCES

Anders, E. 1965. Fragmentation history of asteroids. *Icarus* 4:399–409.

Barucci, M. A., Cupria, M. T., Coradini, A., and Fulchignoni, M. 1987. Classification of asteroids using G-mode analysis. *Icarus* 72:304–324.

Bell, J. F. 1985. The stratigraphy of the asteroid belt: An outline model. In *Rept. Planet. Geol. Geophys. Principal Invest. Program,* NASA TM-4041, pp. 66–68.

Bowell, E., Chapman, C. R., Gradie, J. C., Morrison, D., and Zellner, B. 1978. Taxonomy of asteroids. *Icarus* 35:313–335.

Chapman, C. R. 1974. Asteroid size distribution: Implications for the origin of the iron asteroids. *Geophys. Res. Lett.* 1:341–344.

Chapman, C. R. 1989. Compositional structure of the asteroid belt and its families. *Icarus,* to be submitted.

Chapman, C. R., Johnson, T. V., and McCord, T. B. 1971. A review of spectrophotometric studies of asteroids. In *Physical Studies of Minor Planets,* ed. T. Gehrels, NASA SP-267, pp. 51–65.

Chapman, C. R., Morrison, D., and Zellner, B. 1975. Surface properties of asteroids using a synthesis of polarimetry, radiometry and spectrophotometry. *Icarus* 25:104–130.

Davis, D. R., Chapman, C. R., Greenberg, R., Weidenschilling, S. J., and Harris, A. W. 1979. Collisional evolution of asteroids: Populations, rotations and velocities. In *Asteroids,* ed. T. Gehrels (Tucson: Univ. of Arizona Press), pp. 528–557.

Davis, D. R., Chapman, C. R., Weidenschilling, S. J., and Greenberg, R. 1985. Collision history of asteroids: Evidence from Vesta and the Hirayama families. *Icarus* 62:30–53.

Dermott, S. F., Gradie, J., and Murray, C. D. 1985. Variation of the UBV colors of S class asteroids with semimajor axis and diameter. *Icarus* 62:289–297.

Dohnanyi, J. S. 1971. Fragmentation and distribution of asteroids. In *Physical Studies of Minor Planets,* ed. T. Gehrels, NASA SP-267, pp. 263–295.

Fisher, H. 1941. Farbmessungen an kleinen planeten. *Astron. Nachr.* 272:127–147.

Gaffey, M. J., and McCord, T. B. 1978. Asteroid surface materials: Mineralogical characterizations from reflectance spectra. *Space Sci. Rev.* 21:555–628.

Gaffey, M. J., and McCord, T. B. 1979. Mineralogical and petrological characterizations of asteroid surface materials. In *Asteroids,* ed. T. Gehrels (Tucson: Univ. of Arizona Press), pp. 688–723.

Gradie, J., and Tedesco, E. F. 1982. Compositional structure of the asteroid belt. *Science* 216:1405–1407.

Gradie, J., and Tedesco, E. F. 1989. Albedos and diameters for 350 asteroids from the IRTF 10 and 20 μm radiometric survey. *Astron. J.,* submitted.

Gradie, J., and Veverka, J. 1980. The composition of the Trojan asteroids. *Nature* 283:840–842.

Grossman, L., and Larimer, J. W. 1974. Early chemical history of the solar system. *Rev. Geophys. Space Phys.* 12:71–101.

Hartmann, W. K., and Hartmann, A. C. 1968. Asteroid collisions and evolution of asteroidal mass distribution and meteoritic flux. *Icarus* 8:361–381.

IRAS Asteroid and Comet Survey: Preprint Version No. 1. 1986. Ed. D. L. Matson, JPL Internal Document No. D-3698.

Kiang, T. 1971. The distribution of asteroids in the direction perpendicular to the ecliptic plane. In *Physical Studies of Minor Planets,* ed. T. Gehrels, NASA SP-267, pp. 187–195.

Kitamura, M. 1959. A photoelectric study of colors of asteroids and meteorites. *Publ. Astron. Soc. Japan* 11:79–89.

Kuiper, G. P., Fujita, Y., Gehrels, T., Groeneveld, I., Kent, J., Van Biesbroeck, G., and van Houten, C. J. 1958. Survey of asteroids. *Astrophys J. Suppl.* 3:289–428.

Larimer, J. W. 1967. Chemical fractionations in meteorites—I. Condensation of the elements. *Geochim. Cosmochim. Acta* 31:1215–1238.

Lewis, J. S. 1974. The temperature gradient in the solar nebula. *Science* 186:440–443.

Piotrowski, S. I. 1953. The collisions of asteroids. *Acta Astron. Ser.* A6:115–138.

Sonett, C. P., and Reynolds, R. 1979. Primordial heating of asteroidal parent bodies. In *Asteroids,* ed. T. Gehrels (Tucson: Univ. of Arizona Press), pp. 822–848.

Tedesco, E. F., Matson, D. L., Veeder, G. J., and Lebofsky, L. A. 1987. IRAS albedos for faint asteroids. *Bull. Amer. Astron. Soc.* 19:839 (abstract).

Tedesco, E. F., Matson, D. L., Veeder, G. J., and Lebofsky, L. A. 1988. IRAS observations of asteroids. In *Comets to Cosmology,* ed. A. Lawrence (Berlin: Springer-Verlag), pp. 19–26.

Tedesco, E. F., Williams, J. G., Matson, D. L., Veeder, G. J., Gradie, J. C., and Lebofsky, L. A. 1989. A three-parameter asteroid taxonomy. *Astron. J.,* 97:580–606.

Tholen, D. 1984. Asteroid Taxonomy from Cluster Analysis of Photometry. Ph. D. Thesis, Univ. of Arizona.

Wasson, J. T., and Wetherill, G. W. 1979. Dynamical, chemical and isotopic evidence regarding the formation locations of asteroids and meteorites. In *Asteroids,* ed. T. Gehrels (Tucson: Univ. of Arizona Press), pp. 926–974.

Wetherill, G. W. 1979. Steady-state populations of Apollo-Amor objects. *Icarus* 37:96–112.

Wood, J. H., and Kuiper, G. P. 1963. Photometric studies of asteroids. *Astrophys. J.* 137:1279–1285.

Zellner, B. 1979a. Asteroid taxonomy and the distribution of compositional types. In *Asteroids,* ed. T. Gehrels (Tucson: Univ. of Arizona Press), pp. 783–806.

Zellner, B. 1979b. The Tucson revised index of asteroid data. In *Asteroids,* ed. T. Gehrels (Tucson: Univ. of Arizona Press), pp. 1011–1013.

Zellner, B., and Bowell, E. 1977. Asteroid compositional types and their distributions. In *Comets, Asteroids, Meterorites: Interrelations, Evolution and Origins*, ed. A. H. Delsemme (Toledo: Univ. of Toledo Press), pp. 185–197.

Zellner, B., Leake, M., Morrison, D., and Williams, J. G. 1977. The E asteroids and the origin of the enstatite achondrites. *Geochim. Cosmochim. Acta* 41:1759–1767.

Zellner, B., Thirunagari, A., and Bender, D. 1985a. The large-scale structure of the asteroid belt. *Icarus* 62:505–511.

Zellner, B., Tholen, D. J., and Tedesco, E. F. 1985b. The eight-color asteroid survey: Results for 589 minor planets. *Icarus* 61:355–416.

DUST BANDS IN THE ASTEROID BELT

MARK V. SYKES, RICHARD GREENBERG
University of Arizona

STANLEY F. DERMOTT, PHILIP D. NICHOLSON, JOSEPH A. BURNS
Cornell University

and

T. N. GAUTIER, III
California Institute of Technology

In 1983 the Infrared Astronomical Satellite discovered three bands of dust: one above, one below and one approximately in the plane of the ecliptic. These bands are located in the asteroid belt and are believed to arise from collisional activity. Debris from an asteroid collision, over time, fills a torus having peaks in particle number density near its inner and outer corners, corresponding to the locus of perihelia and aphelia, respectively. As a consequence of this geometry, such a swarm should produce two pairs of bands that straddle the ecliptic— a perihelion band pair and an aphelion band pair (which generally overlap along the line of sight from Earth). Indeed, processing of the IRAS data now resolves the band structure into at least three such band pairs, with indications of several more pairs distributed over a large range of ecliptic latitudes. Some of these bands appear to be associated with major Hirayama asteroid families, while others are not. Possible origins of the observed dust bands include: (1) the gradual comminution of the asteroid belt as a whole, in which the local dust population is maximum where the concentration of asteroids is greatest (e.g., families); (2) one or a few large random asteroid collisions enhancing the local population of small debris, which in turn is comminuted into dust; and (3) the disintegration of one or more large comets. Dust bands are not necessarily constant features of the solar system. They form, gradually fade, and may be

replenished, but estimates of the time scale and frequency are model dependent. Also, within the context of a given model, observations of dust bands may constrain the collisional history of the asteroid belt, including asteroid family ages, and may provide information on small-particle dynamics. Interpretation of the distribution of bands suggests that collisions in the asteroid belt are a principal source of zodiacal dust, transported to the vicinity of the Earth by Poynting-Robertson drag.

I. INTRODUCTION

A. The Discovery of the Zodiacal Dust Bands

One of the major discoveries of the Infrared Astronomical Satellite (IRAS) was of three parallel bands of dust roughly straddling the plane of the ecliptic (Low et al. 1984). Zodiacal dust bands were first noticed in the IRAS data as a pair of symmetrically placed bumps of 12 and 25 μm emission superimposed on the smooth zodiacal background (Fig. 1). The same emission could be seen in the 60 and 100 μm data at a lower intensity, indicating a fairly high temperature (about 200 K) for the emitting material.

During its All-Sky Survey, the IRAS telescope scanned the sky in circles of constant solar elongation, its nearly polar orbit precessing by ~ 1° a day in order to remain above the terminator on the Earth. (See the chapter by Matson et al., Fig. 1.) The entire sky can be mapped over a period of six months in this way. More specifically, for the first two-thirds of its ten-month life, IRAS used elongations between 80° and 100° to scan nearly the entire sky 4 times (Neugebauer et al. 1984; IRAS Explanatory Supp. 1988). Each scan had a width of 0°.5, and was shifted in longitude by about 0°.25 on the subsequent orbit, observing by overlapping scans the same location twice after ~ 103 minutes. This was called an "hours-confirmed" observation or HCON. The initial observing strategy was to allow the telescope to map a section of sky in this fashion by slowly changing its solar elongation for about one week (HCON 1), after which the telescope was repositioned and the same section of sky was observed a second time (HCON 2).

As the sky survey unfolded, the emission bumps were found to be distributed more or less completely around the solar system. The initial impression was that two disks or belts of material had been found, presumably in the inner solar system because of their geometry and high color temperature. Such independent bands would, at some longitude, cross each other and the ecliptic. However, as the mapping became more complete the emission was found to form parallel bands above and below the ecliptic plane. They did not cross. This configuration was difficult to explain at first, because the upper and lower bands were thought *a priori* to be composed of separate groups of material which would have to cross the mid-plane given the Sun's central force. IRAS Science Team member D. Beintema suggested the correct explanation: A band pair can arise from a single distribution of material with an
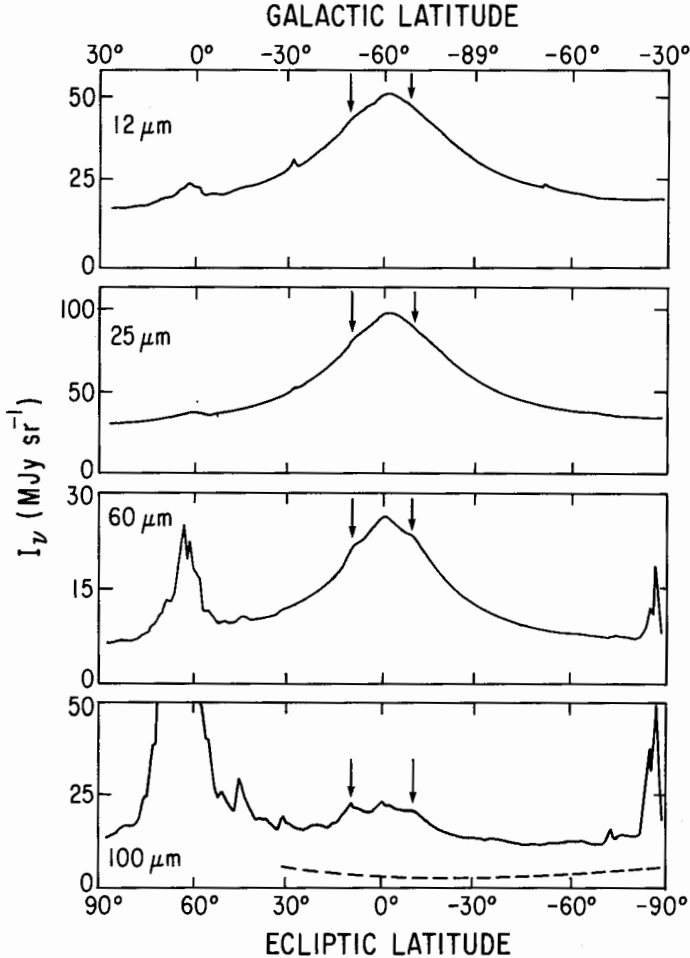
Fig. 1. Brightness profiles for an IRAS scan on 24 June 1983 at elongation 91°.1 (Hauser et al. 1984). The ecliptic plane is crossed at longitude 1°.3. The galactic plane is crossed near ecliptic latitude +60° and galactic longitude $\ell = 96°.8$. All discrete features are from real sources. The prominent source near the south ecliptic pole at 60 and 100 μm is the Large Magellanic Cloud. At 12 μm and 25 μm, the thermal emission is dominated by a broad zodiacal component while galactic emission dominates at the longest wavelengths. The arrows indicate bumps in the profile corresponding to the γ bands.

ensemble of orbits which shared a common inclination, but whose nodes were uniformly distributed over all ecliptic longitudes. This distribution produces a band pair because each individual particle spends most of its time at its extreme separation from the ecliptic, traveling roughly parallel to the plane, much like a pendulum is preferentially found at its maximum amplitude. A
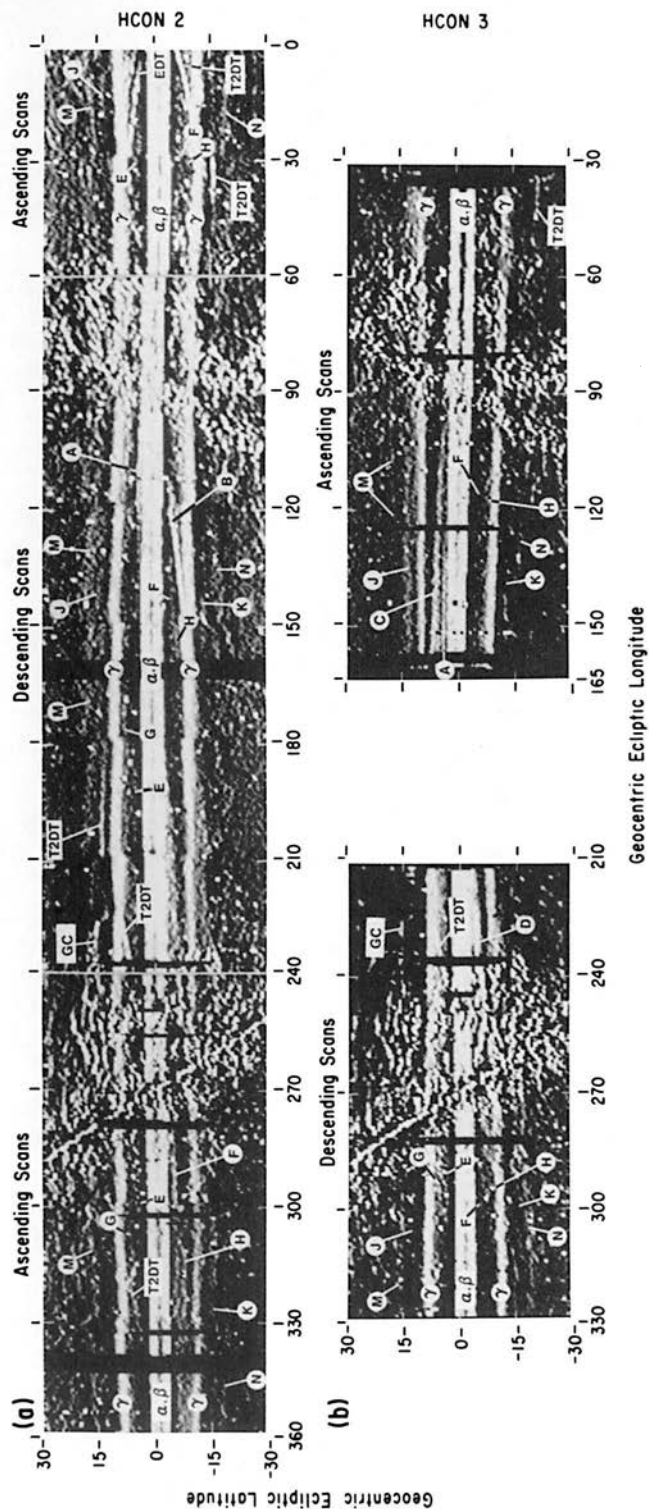
Fig. 2. The 25 μm IRAS scans segregated into (a) HCON 2 and (b) HCON 3, and zero-sum high-pass filtered along the in-scan direction using a filter width of 3°.5. The data has been binned into 0°.5 × 0°.5 pixels and mapped in ecliptic cylindrical coordinates. Because of the separation of only ~ 10 days, HCON 1 (not shown) and HCON 2 images are nearly identical. The dust-band structures are described in Table I. A − D are Type II dust trails, T2DT and EDT denote the Tempel 2 and Encke dust trails, respectively, and GC indicates galactic cirrus. The galactic plane is seen crossing the ecliptic near 90° and 270° ecliptic longitude (Sykes 1988).

TABLE I
Dust Band Pairs

Name	Geocentric Ecliptic Latitude (HCON 1 and 2) (deg)	Comments
α	$\pm(0$ to $2.5)$	Unresolved with β (Low et al. 1984). Resolved and associated with Themis family (Sykes 1986).
β	$\pm(1$ to $3.5)$	Unresolved with α (Low et al. 1984). Resolved and associated with Koronis family (Sykes 1986).
γ	$\pm(8.5$ to $11.5)$	(Low et al. 1984). Associated with Eos family (Dermott et al. 1984).
E	4 to 6	Possible pair with F (Sykes 1988).
F	-4 to -6.5	Possible pair with E (Sykes 1988).
G	6.5 to 8	Possible pair with H (Sykes 1988).
H	-5.5 to -8.5	Possible pair with G (Sykes 1988).
J	12.5 to 15	Probable pair with K (Sykes 1988). Associated with Io family (Sykes 1989).
K	-13 to -16	Probable pair with J (Sykes 1988). Associated with Io family (Sykes 1989).
M	15 to 17.5	Probable pair with N (Sykes 1988).
N	-17 to -20	Probable pair with M (Sykes 1988).

particle spends little time near the ecliptic plane because there it has a large velocity component normal to the plane.

A high-pass spatial filter can be employed to remove the smooth zodiacal background from the IRAS survey scans, revealing many details of the zodiacal dust bands. This process was used to produce the emission maps shown in Fig. 2. The originally recognized band pair is seen $\sim 10°$ above and below the ecliptic. Part of the central band is due to the peak in the smooth zodiacal emission near the plane leaking through the high-pass filter, but there is also clearly another pair of bands similar to the $10°$ bands, but spaced only one or two degrees from the ecliptic plane. These inner bands were later separated further into two pairs of bands (Sykes 1986).

Further analysis of the IRAS data has suggested that four additional pairs of bands may also exist (Table I) (Sykes 1988), and that these bands extend over $40°$ of ecliptic latitude. In the IRAS skyflux maps, the central bands (α and β) have apparent widths of $< 0°.5$. The other bands, particularly the γ bands, are several degrees in apparent width (Sykes 1988). As will be seen later, the broad morphology of most dust bands has a significant impact on the number of bands which are possible to observe. So, from the original three bands reported by Low et al. (1984), as many as 14 bands (7 pairs) have now been detected.

B. Initial Analysis

During its last months of operation, IRAS surveyed the sky a last time (HCON 3), but changed its scanning pattern to begin at extreme solar elongations of 60° and 120°, and smoothly approach 90° elongation from both sides, and then reverse the procedure until the whole sky was covered (Fig. 2b). This map includes only 72% of the sky because the survey was prematurely terminated by liquid helium exhaustion aboard the satellite. The bands, in particular, show clear variation in their separation corresponding to changes in viewing geometry, and can be readily understood if the density enhancements giving rise to the bands are confined to a small range in distance from the Sun, maintain a constant linear separation around their circumference, and lie outside the orbit of the Earth. This variation in parallactic separation yielded heliocentric distances and proper inclinations for the observed band material of 2.3 AU and 8°7 (Gautier et al. 1984), 2.5 AU and 8°1 (Hauser et al. 1985) and 2.44 AU and 8°4 (Dermott et al. 1989). None give error estimates, but the values seem to be reasonably consistent.

Color-temperature calculations by Low et al. (1984) produced values between 165 and 200 K. A rapidly rotating gray body of this temperature would be located between 3.2 and 2.2 AU, well within the main asteroid belt, and is consistent with the locations determined by parallax. Consequently, it was suggested that the dust bands arose from small particles generated by collisions among asteroids (Low et al. 1984). This idea was reinforced by an apparent association between the latitudes of the bands and the proper inclinations of some major Hirayama asteroid families (Dermott et al. 1984), which are believed to have been produced by the catastrophic disruptions of large asteroids (Table II; see the chapters by Chapman et al. and by Valsecchi et al.). At the same time, Sykes et al. (1984) calculated that the random catastrophic disruption of a small asteroid ($\sim$ 10 km in diameter) could possibly generate sufficient debris to be observed by IRAS as a band pair.

Models for the asteroidal origin of the dust bands have since followed two general paths which will be examined in more detail in Section III. The first path (Dermott et al. 1984,1985,1986,1988,1989) assumes the asteroid belt to be in collisional equilibrium, and that the size distribution of the particle population at all locations within the asteroid belt is characterized by a power law with a single index over all sizes from tens of km to tens of μm. The surface area of dust at any given location thus increases monotonically with the local volume of asteroids. Since asteroid families represent concentrations of asteroids in a—sin i space, there should be corresponding peaks in the dust population. Hence, dust bands should be associated with asteroid families.

The second path (Sykes and Greenberg 1986; Sykes 1986,1988,1989) is a nonequilibrium theory of dust-band origin which asserts that occasional random catastrophic disruptions of asteroids result in debris whose subsequent comminution products give rise to the dust bands. In this case, dust bands are

TABLE II

Asteroid Family Proper and Forced Orbital Elements

Family	a	δa	e	δe	e_f	i	δi	i_f	Ω_f	$\bar{\omega}_f$
Themis	3.137	0.025	0.153	0.009	0.038	1.420	0.223	1.22	97.8	8.7
Koronis	2.875	0.018	0.049	0.006	0.037	2.118	0.081	1.16	96.1	6.2
Nysa	2.446	0.020	0.162	0.009	0.036	3.205	0.154	0.93	86.9	351.7
Flora	2.193	0.008	0.138	0.006	0.048	5.024	0.452	0.61	43.4	338.2
Eos	3.015	0.006	0.071	0.008	0.037	10.12	0.710	1.19	97.1	7.6
Io	2.650	0.035	0.143	0.009	~0.06	13.36	0.240	1.06	93.9	~32
Maria	2.550	0.013	0.089	0.009	0.035	15.21	0.170	1.03	91.0	354.2

not associated with known asteroid families *a priori* and may be found at other locations. This model predicts that dust bands should fade with time, and that the population of dust bands is replenished by new collisions. Though focusing on the more frequent disruptions of asteroids tens of km in diameter, this model predicts that bands arising from disruptions large enough to create the largest Hirayama families should be detectable by IRAS for ≥ 1 Gyr.

An alternative theory for dust-band origin is the disintegration of a large comet, which will be considered separately in this chapter (Sec. III.C). This comes about from the fact that the potentially most prominent cometary suppliers of the zodiacal cloud have similar inclinations to dust bands (Dermott et al. 1984).

In the next section a mathematical model of a dust-band torus will be presented to provide some insight into what we are studying in terms of a spatial distribution of particles. The effects of secular gravitational perturbations and dispersions in orbital elements on this spatial distribution are then considered, which provide additional means of determining dust-band locations as well as determining the effects of different physical processes on the small-particle population comprising a dust band. The different origin scenarios described above are presented, along with their observational consequences. Within the context of the (nonequilibrium) random-collision hypothesis, we examine how dust bands form, how their surface areas decrease with time, and how many dust bands are likely to be seen as old bands are replaced by newer ones from more recent catastrophic disruptions.

II. THE DUST BAND TORUS

A. An Analytical Model

The spatial distribution of the dust we see as a dust band pair can be idealized by considering an ensemble of dust particles whose orbits have identical semimajor axes a, proper eccentricities e and proper inclinations i, but perihelia and nodes distributed over all longitudes. For purposes of exposition here, we neglect, for the moment, the effects of secular gravitational perturbations. The material fills a torus whose particle number density is (Sykes 1989)

$$\rho(r,\beta) = R(r)\Theta(\beta) \tag{1}$$

where

$$R(r) = \frac{C_r}{r^2 a} \left(\frac{r}{2a - r}\right)^{1/2} \left\{1 + \frac{a^2(1 - e^2)^2}{e^2 r^2 - [a(1 - e^2) - r]^2}\right\}^{1/2} \tag{2}$$

$$\Theta(\beta) = (2\pi^2)^{-1}(\cos^2\beta - \cos^2 i)^{-1/2} \tag{3}$$

within the limits

$$a(1 - e) \leq r \leq a(1 + e), \tag{4}$$

$$-i \leq \beta \leq i. \tag{5}$$

Here C_r is a constant of normalization, r is heliocentric distance and β is the heliocentric latitude with respect to the plane of symmetry (which is close to the ecliptic plane).

These equations describe a spatial distribution that is a torus with a squarish cross section (Fig. 3a), centered on the Sun, whose radial extent is bounded by the perihelion and aphelion distances, and whose latitudinal extent is bounded by the proper inclination of particle orbits. Maxima in volume density occur at the "corners" of the torus. The latitudes of the maxima, seen from the Sun, correspond to the proper inclination of the particle orbits. That is why, from the Earth, these concentrations appear as pairs of bands straddling the ecliptic. The geometry is such that maxima in volume density at perihelion and aphelion give rise to both perihelion and aphelion band pairs (see Dermott et al. 1985), which overlap each other when seen from the Earth. However, IRAS detects more flux from perihelion bands for two reasons: larger particle number densities and higher temperatures.

B. The Effects of Dispersions in Orbital Elements

Particles that make up a dust band torus do not have identical a, e and i; there must be some dispersion in orbital elements. This significantly affects the spatial density of dust-band particles (Fig. 3b), and hence the locations at which their flux is seen. Two mechanisms by which the orbital elements of dust-band particles are distributed will be examined. The first mechanism is the collisional production of dust, considered in the next subsection. The second, considered in the section following, is Poynting-Robertson drag.

Collisional Dispersion. Studies of collision ejecta indicate that smaller particles tend to have larger ejection velocities (Melosh 1989), which yields a greater dispersion in orbital elements for small particles than for large ones. Moreover, in a plausible particle-size distribution (steeper than 1/diameter), small particles experience more collisions with other objects of comparable size than do large particles. The orbital elements of small particles will spread, consequently, more rapidly than large particles. The most obvious effects are associated with a distribution in orbital inclinations, which primarily determines the angular separation of the bands we observe. For a Gaussian distribution with fixed mean values, increasing the dispersion in proper inclination, results in (a) increased band widths and (b) shifting peak emission of the latitudinal profile to lower latitudes (Sykes 1989; Fig. 4a). Thus, in the case of an asteroid family, a pair of bands consisting of associated dust having
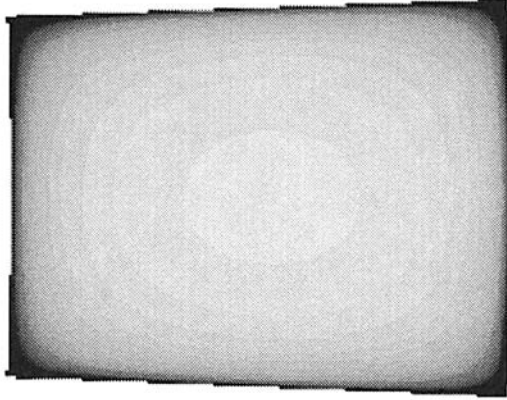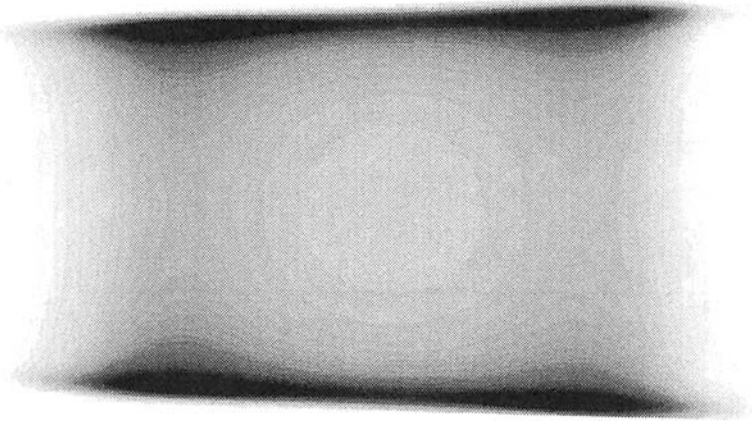
Fig. 3. (a) The particle number density distribution in a radial cross section of a Koronis dust band torus whose particles have orbital elements equal to the mean values of the Koronis asteroid family (with no dispersion in elements). The Sun is to the left. The jagged edges are an artifact of sampling. (b) Convolution by Gaussian dispersions in proper inclinations (1σ) and semimajor axis (2σ) of the model Koronis torus increases the volume of the torus, particularly in the radial direction, while separations between peak densities at perihelion and aphelion decrease both radially and in latitude. (Sykes 1989).
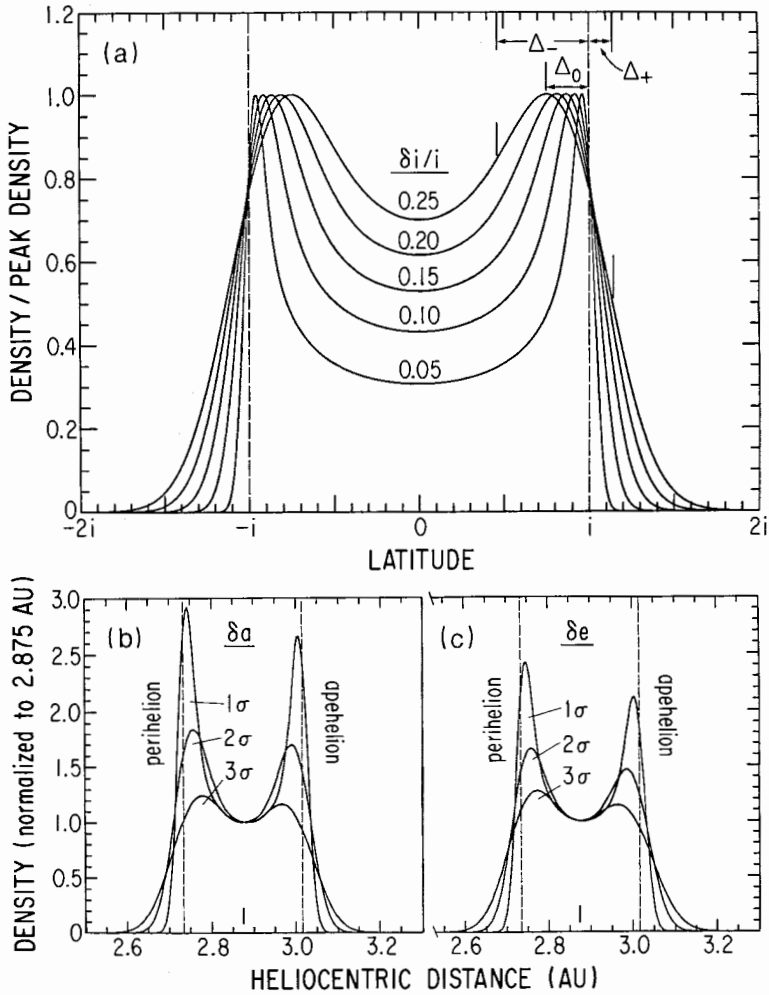
Fig. 4. (a) The latitudinal profile of the dust bands shown after being convolved with a Gaussian distribution of orbital inclinations with standard deviation δi. Increasing dispersion in inclination results in decreasing latitudinal separation of the dust bands and decreasing contrast between the band peaks and centers. Δ_o, Δ_+, and Δ_- indicate the shift of peak and band edge latitudes, respectively, and are defined in the text. The mean elements of the particles remain unchanged. (b) Radial profiles of the particle number density of a model torus associated with the Koronis asteroid family are shown for different dispersions in semimajor axis and (c) eccentricity. Densities are normalized to the value at $a = 2.875$ AU. The 1σ values correspond to the standard deviation of those terms over the orbits of known family members (Table II calculated from Williams 1979). Increasing dispersion in both terms results in a decrease in the radial separation of the perihelion and aphelion bands, as well as a decrease in their contrast. The mean elements of the particles are unchanged (Sykes 1989).

submillimeter diameters would be expected to be observed at lower latitudes than if the dust-band particles had a distribution of orbital inclinations identical to kilometer and larger family members.

The outer edge of an individual band (defined as the latitude where peak flux drops by half) increases slightly (Δ_+) with respect to the mean inclination of particle orbits with increasing dispersion in inclination δi. Similarly, the latitude of the peak flux and inner band edge (defined as the latitude where the flux equals the average of the values at the midplane and peak) are displaced away from the mean inclination towards the midplane by Δ_o and Δ_-, respectively. The empirical relations describing these shifts are (Sykes 1989):

$$\frac{\Delta_+}{i} \approx 0.48 \left(\frac{\delta i}{i} \right)^{0.89} \tag{6}$$

$$\frac{\Delta_0}{i} \approx 1.16 \left(\frac{\delta i}{i} \right)^{1.13} \tag{7}$$

$$\frac{\Delta_-}{i} \approx 1.73 \left(\frac{\delta i}{i} \right)^{0.84}. \tag{8}$$

Another effect that can be seen in Fig. 4 is the decreasing contrast of the inner edges of the bands with increasing dispersion in inclination. The ratio of peak flux (F_P) to the flux at the midplane (F_C) is approximated by

$$\frac{F_p}{F_c} \approx 0.71 \left(\frac{\delta i}{i} \right)^{0.5} \tag{9}$$

a factor of 2 lower than the upper limit of $1.414/\sqrt{\delta i/i}$ determined by Dermott et al. (1985). The relations (6) through (9) are good to within a few % for $i < 20°$ and $\delta i/i \lesssim 0.25$.

Dispersions in semimajor axis and eccentricity act to increase the heliocentric distance of the peak flux from the perihelion bands while decreasing it for the aphelion bands (Figs. 4b and c). Perihelion and aphelion bands associated with asteroid families overlap along the line of sight when observed from the Earth, since the latitudinal displacement of their peaks is small. Increasing dispersion in semimajor axis and eccentricity thus decreases an already small peak-to-peak separation.

Dispersion Due to Poynting-Robertson Drag.   The thermal flux from the dust bands is due principally to those particles in the 10 to 100 μm size range because of their greater surface area (Sykes and Greenberg 1986; Dermott et al. 1986), and it is possible that the orbits of these particles decay significantly due to Poynting-Robertson drag before they are either dynamically scattered (Dermott et al. 1986) or are comminuted to sizes which are ejected from the immediate vicinity by radiation pressure (Sykes 1989). If

orbital decay is significant, then the particles in the dust bands will have a wide range of semimajor axes, and may show significant dispersions in proper eccentricity and inclination, forced inclination, and forced ascending node (these "forced" elements are functions of semimajor axis and will be discussed more fully in Sec. II.C below). These dispersions arise from two causes: (1) Passage through various resonances, particularly the 1 : 3 gap at 2.5 AU, results in a dispersion of the proper eccentricities and inclinations (Dermott et al. 1989). (2) If the particles have a range of semimajor axes, then they must also have a range of forced orbital elements (cf. Fig. 5). This may
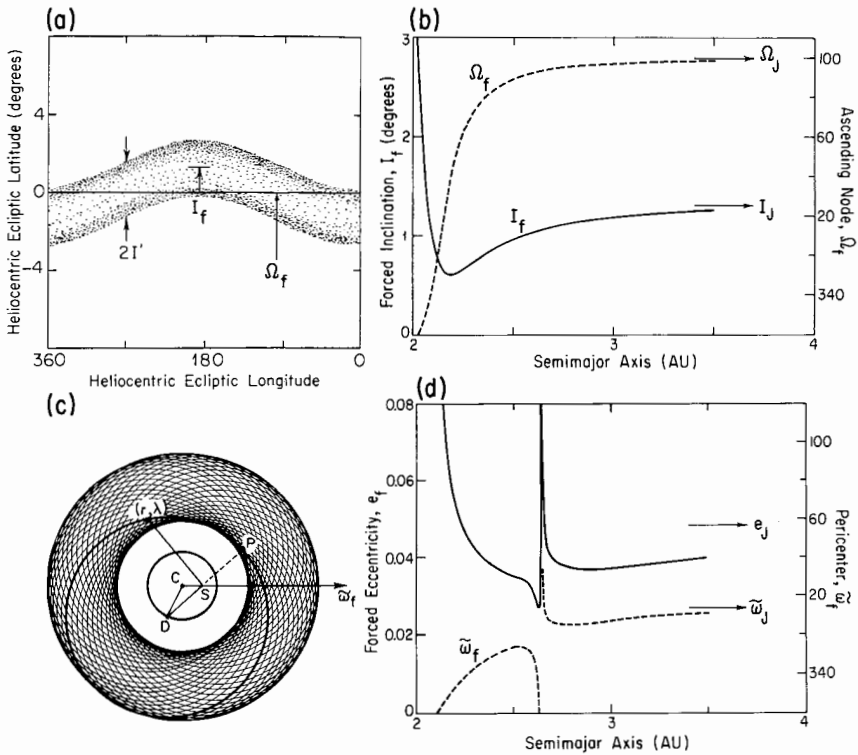
Fig. 5. (a) Variation of the ecliptic latitude of a dust band with ecliptic longitude, as measured in a Sun-centered coordinate system. The latitudinal width of the band at all longitudes is $2i'$, twice the proper inclination of the dust particle orbits. The amplitude of the apparent sinusoidal variation is determined by the forced inclination i_f. (b) Variation of the forced inclination i_f and the corresponding longitude of the ascending node Ω_f with semimajor axis. The elements with subscript J are the present orbital elements of Jupiter. (c) Plane view of the distribution of elliptical particle orbits in a dust band. To order e, the figure is circularly symmetric about the point C which is displaced from the Sun by an amount ae_f in a direction opposite to that of the forced pericenter $\tilde{\omega}_f$. (d) The variation of the forced eccentricity e_f and the corresponding longitude of the forced pericenter $\tilde{\omega}_f$ with semimajor axis (Dermott et al. 1985).

be particularly important for those particles close to the inner edge of the asteroid belt ($a < 2.5$ AU), and it may be that the dispersion of the orbital elements in this region of the belt defines the inner edges of the dust bands if the particle orbits have decayed (Dermott and Nicholson 1989).

The effect of dispersion due to Poynting-Robertson drag is not the same as collisional dispersion (where the mean orbital elements are unchanged). In the former case, the shift in the peak dust-band emission to higher or lower ecliptic latitudes is a function of the longitude of observation (Sykes 1989). Also, a simple decrease in the heliocentric distance of dust pericenters results in an increase in the apparent angular separation of a band pair as a consequence of parallax.

C. The Effects of Secular Gravitational Perturbations

A careful examination of the dust-band images in ecliptic coordinates (Fig. 2) shows that they are not symmetric about the plane of the ecliptic. The orbits of the dust-band particles are perturbed by Jupiter and other planets whose orbits are slightly inclined to the ecliptic. Ensembles of particles with the same semimajor axes will precess about a common plane where the torques produced by these gravitational perturbations vanish. This defines the plane of symmetry of the dust-band torus which has an inclination (relative to the ecliptic) i_f and ascending node Ω_f which vary with semimajor axis (Figs. 5a and b). These gravitational perturbations also act to distort particle orbits, introducing a "forced" component to their eccentricities. Some of the effects of this on the dust-band torus are shown in Dermott et al. (1985). The torus shifts away from its Sun-centered position by an amount ae_f in a direction opposite to that of $\tilde{\omega}_f$ (Fig. 5c), which now defines the longitude of pericenter of the torus. Figures 5b and d show the variations in these parameters as a function of semimajor axis. We see that as the semimajor axis moves closer to Jupiter (the dominant perturber) beyond 2.6 AU, these forced element components approach values for Jupiter's orbit. The shifting of the torus center gives rise to a longitudinal temperature variation in a band pair which is diagnostic of its distance (Dermott et al. 1985).

The existence of these various effects allows for the potential extraction of all the orbital elements of the dust-band particles. The semimajor axis can be determined by the direct measurements of Ω_f and $\tilde{\omega}_f$. The use of Ω_f in this way is described for the β bands in Sec. III.A. The apsidal longitude $\tilde{\omega}_f$ is that at which dust-band temperatures are highest. Given the semimajor axis of the torus-particle orbits, their proper eccentricity and forced eccentricity can be decoupled through the longitudinal variation of dust-band temperature (Dermott and Nicholson 1989). The proper inclination and forced inclination of the dust bands can be decoupled from measurements of band-center latitudes and band separation as a function of longitude (Dermott et al. 1989; Sykes 1989). Secular gravitational perturbations also result in the distortion of the dust-band torus, resulting in the north and south bands no longer being exactly

plane parallel. Determining the angle between the planes containing the individual bands making up a band pair provides another means of calculating the forced eccentricity (Sykes 1989).

III. THE ORIGIN OF THE DUST BANDS

A. The Collisional Equilibrium (Asteroid Family) Hypothesis

This hypothesis assumes that the dust population at a given location is related to the population of observable asteroids at that same location. This has been examined by assuming that, at each point in the asteroid belt, all sizes of particles are characterized by a single equilibrium size distribution arising from the general comminution of the asteroid belt through mutual collisions. This model predicts that prominent dust bands are associated with known concentrations of asteroids such as the asteroid families. By demonstrating a relationship between dust bands and asteroid families, the equilibrium hypothesis provides one vehicle by which dust production can be understood in the asteroid belt as a whole, as well as its relationship to the observed zodiacal dust complex.

The relationship between the Hirayama asteroid families and the prominent dust bands has been a central question in the study of the latter since it was first posed by Dermott et al. (1984). In the following, the consistency between the calculated surface areas and volumes of the dust bands and the major Hirayama asteroid families is examined. Two basic approaches are then taken to determine whether the dust bands derive from asteroid families. The first method is the direct (or indirect) measurement of some of the orbital elements of the dust bands. These can then be compared with the corresponding elements of the asteroid families. The second method is the generation of predictive models which are then compared with the IRAS dust band observations.

Estimating Dust Band Volume. The surface optical depth of the prominent dust bands was estimated to be $\sim 10^{-8}$ (Low et al. 1984), corresponding to a total surface area of $\sim 2 \times 10^{19}$ cm^2 (Dermott et al. 1984). It is assumed that the size-frequency distribution of the dust-band particles is described by a single power law of the form

$$dN(m) = Km^{-q}dm \qquad (10)$$

where dN is the number of particles having masses between m and $m + dm$, K is a constant and q is the mass index. Following Dermott and Nicholson (1989), this converts to the following cumulative power law in radius,

$$N(r) = \frac{1}{3(q-1)} \left(\frac{r_0}{r} \right)^{3(q-1)} \qquad (11)$$

where $N(r)$ is the number of asteroids with radii $>r$ and r_0 is a constant, similar in magnitude to the largest particle (in this case asteroid) radius. The total area A of the particles is then given (for $q > 5/3$) by

$$A = \frac{\pi r_{min}^2}{(3q - 5)} \left[\frac{r_0}{r_{min}} \right]^{3(q - 1)}$$ (12)

where r_{min} is the lower cut-off in the size distribution, while the total volume of the particles V can be obtained from the radius R_e of a sphere with the same volume. $V = (4/3)\pi R_e^3$ and, to a good approximation (for $q < 2$),

$$R_e = r_0[3(2 - q)]^{-1/3}.$$ (13)

Values of R_e that are needed to account for the observed areas are shown in Fig. 6 for a range of values of r_{min} and q. The theoretical equilibrium solution
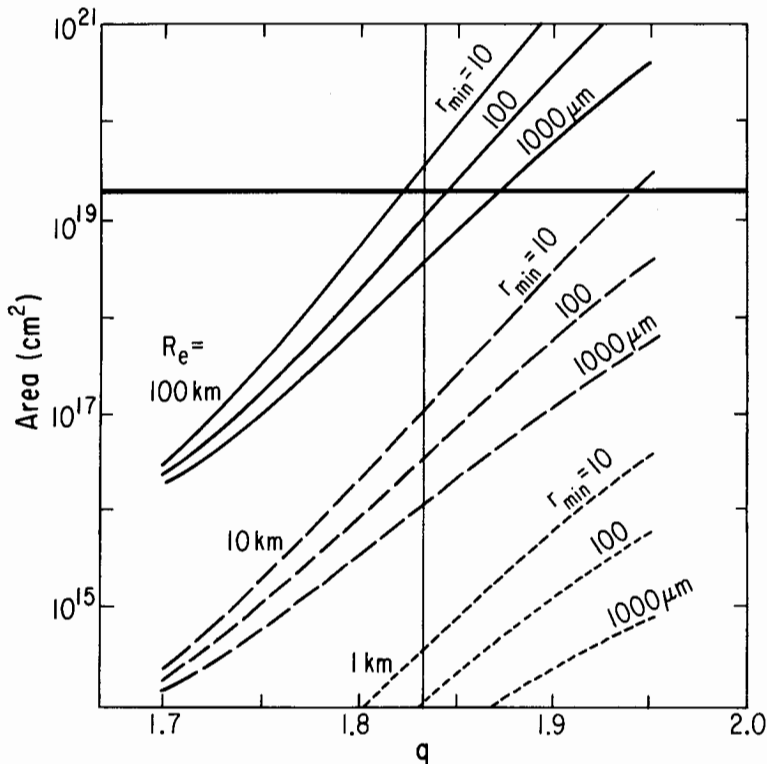
Fig. 6. The total surface area of particles contained within a sphere of equivalent radius R_e shown for a range of power-law distribution index q and the lower cut-off in the particle-size distribution, r_{min}. The horizontal line shows the area for the central dust band, inferred from Low et al. (1984) (figure from Dermott and Nicholson 1989).

for asteroids (Dohnanyi 1978) has a population index $q = 1.837$ (indicated by the vertical line in Fig. 6). If q is in the vicinity of this value, and the size distribution extends down to ~ 10 μm, then we can conclude from Fig. 6 that spheres containing the inferred volume of dust band particles (up to asteroids tens of kilometers in radius) must have equivalent radii of ~ 100 km. The equivalent radii shown in Fig. 6 are similar to the radii of Hirayama family progenitors (Gradie et al. 1979; Dermott et al. 1984). Assuming a single size-frequency index, however, does result in large variations in surface area produced by a given mass of material if the index or minimum particle size is varied. In a nonequilibrium case (Sec. III.B.; Sykes and Greenberg 1986), though the initial population index may be close to $q = 2$, subsequent collisional evolution calculated by Sykes and Greenberg (1986) shows that the population quickly changes from the initial power law. The result is that much smaller bodies (with equivalent radii of ~ 10 km) could be dust band parents, and numerical experiments indicate that the theory is not very sensitive to the initial value of q.

Measuring Dust Band Orbital Elements. The simplest means of determining the semimajor axes of dust band particles is to determine the orientation and/or the inclination of their plane of symmetry relative to the ecliptic. Utilizing different methods, contradictory results have been obtained for the central dust bands.

Using the 0°5 IRAS Zodiacal History File (see IRAS Explanatory Suppl. 1988), Dermott et al. (1988) separated dust-band profiles from the broad zodiacal background utilizing a Fast Fourier Transform and high-pass filtering with a Parzen window. Plotting the latitude of the central dust band (Fig. 7), in which the α and β bands are not resolved, it was estimated that the forced inclination of the composite central band is 1°2 and that the longitude of the associated ascending node is 52°. The forced inclination clearly differs from that of the zodiacal cloud (1°5) and is what one would expect for the Themis (at α = 3.1 AU) and Kornis (at a = 2.9 AU) asteroid families (see Fig. 5). However, the node is the same as that of the background cloud and disagrees with the expected longitude of ~97° for particles at a distance of 3 AU (Fig. 5).

A parallactic measurement (Fig. 8) of the resolved β band pair was obtained by Sykes (1989) using the IRAS skyflux maps (IRAS Explanatory Suppl. 1988). The proper inclination of the particle orbits measured was 2°1, consistent with the Koronis asteroid family. Sykes found the ascending node for this band pair to be 90° ± 6°, reasonably consistent with the value of 96° expected for particles with the semimajor axes of the Koronis family. The discrepancy with the earlier measurement is thought by Sykes (1989) to arise from the contamination of the Fourier-filtered dust-band profiles of Dermott et al. (1988) by a possible cusp-like high-spatial frequency component of the broad zodiacal emission.
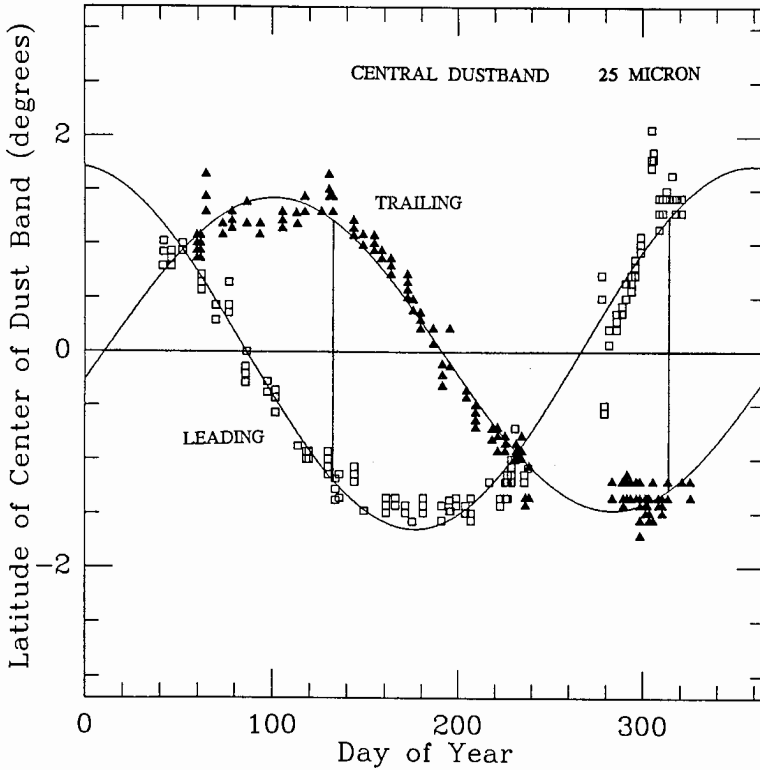
Fig. 7. Variation of the latitude of the center (measured between the half-power points) of the central dust band as with day of the year, as seen at 25 μm in the IRAS Zodiacal History File. Data obtained when IRAS was in the leading or ascending leg of its motion around the Earth are represented by squares, while the data from the trailing or descending leg are represented by triangles. The vertical lines give the forced inclination of the central band and the location of the nodes (Dermott et al. 1988).

Comparison with Family Dust-Band Models. Dermott and Nicholson (1989) have constructed a three-dimensional numerical model that permits the calculation of the distribution of night-sky brightness that would be produced by any particular distribution of dust-particle orbits. This model includes the effects of planetary perturbations on the dust-particle orbits, reproduces the exact viewing geometry of the IRAS telescope, and allows for the eccentricity of the Earth's orbit. The result is a model for the variation with ecliptic latitude of the brightness observed in a given waveband as the line of sight of the telescope sweeps through the model dust bands at a constant elongation angle. The models assume the same dispersion in orbital elements as that displayed by the known family members. In Fig. 9, this model is used to generate a predicted profile for the Eos and Themis asteroid families and is compared
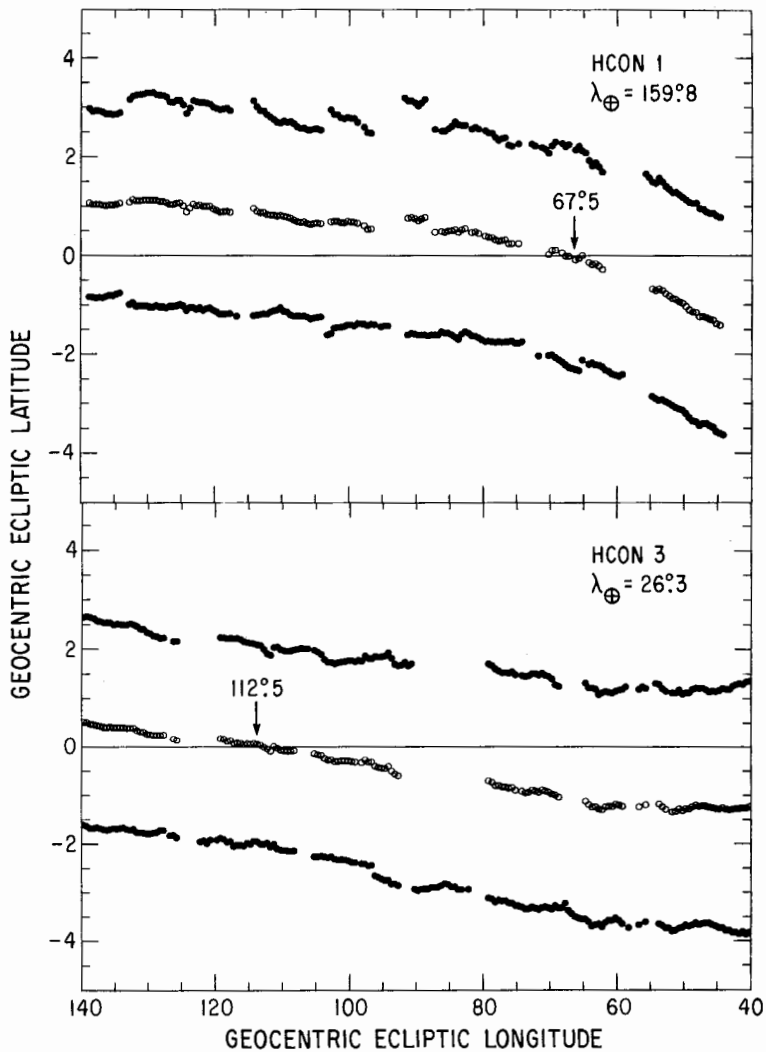
Fig. 8. Geocentric ecliptic coordinates of the north and south β bands as measured from un-
filtered IRAS skyflux plates (25 μm). The latitude of each band-pair component was binned
and averaged every 0°.5 in longitude (filled circles). North and south component values were
then averaged (open circles) in order to determine the geocentric ecliptic longitude of the
ascending node as seen in both HCON 1 and HCON 3 roughly eight months apart. This
corresponds to the longitude at which the average latitude crosses the ecliptic plane. The
Earth's longitude λ⊕ is given for the times of plane-crossing observations. HCON 1 observa-
tions plotted were made in the direction opposite to the Earth's motion, while the HCON 3
observations plotted were made in the direction of the Earth's motion (Sykes 1989).
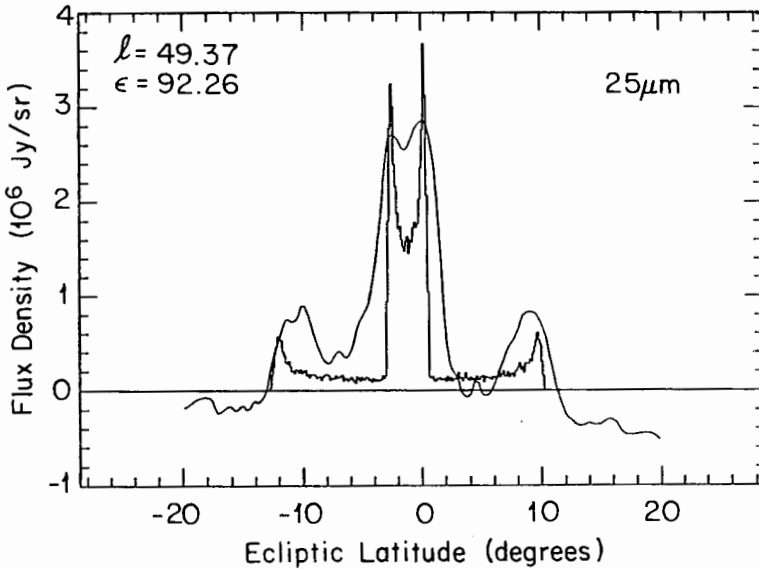
Fig. 9. An observed dust band profile (smooth curve), after high-pass filtering, compared with the prediction of a model based on the distribution of orbits in the Eos and Themis families (Dermott and Nicholson 1989).

with a high-pass filtered scan from the Zodiacal History File. The model distributions for the asteroid families are too sharply peaked to account for the observed profiles. Dermott and Nicholson then examine the effects of dispersion due to evolution under Poynting-Robertson drag, and this yields some improvement in the comparison of model and filtered profiles. However, while the agreement between observed dust bands and specific models of orbitally evolved particles originating in the prominent Hirayama families is suggestive, definitive results from this approach are not yet available.

Sykes (1989) utilizes the dust-band model of Sec. II and maps the inner and outer edges of the latitudinal profile of the dust bands as well as the location of peak emission onto the two-dimensional IRAS skyflux maps. This allows the α and β bands to be individually studied (Fig. 10a), whereas they are indistinguishable at the lower resolution of the Zodiacal History File. Like Dermott and Nicholson (1989), Sykes initially assumes that the mean orbital elements of the dust-band particles are the same as the corresponding family members. The only parameter varied is the dispersion in proper inclination which is assumed to be Gaussian. Separations between perihelion and aphelion bands are found to be small, and increasing dispersions in semimajor axis and eccentricity only makes that separation smaller. Mapping routines fully reproduce the IRAS pointing geometry.
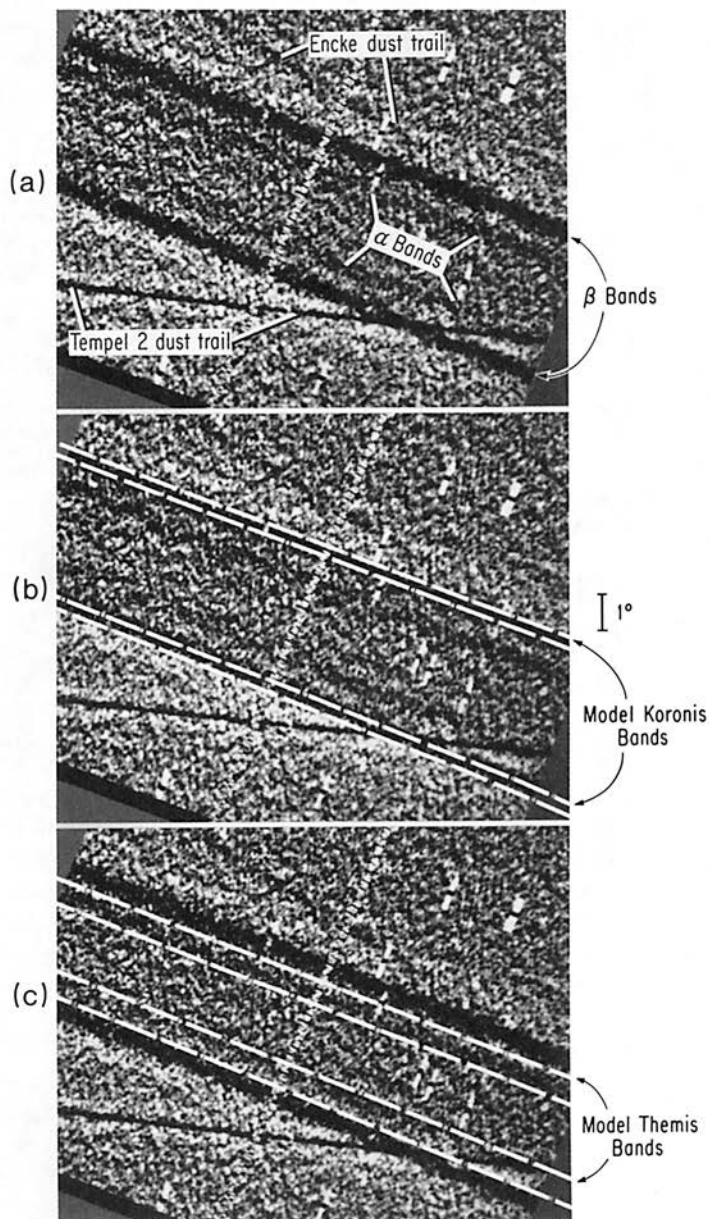
Fig. 10. (a) An IRAS skyflux map (Plate 95, 25 μm) boxcar high-pass filtered, using a filter width of 1° along the scan direction, allowing the α and β bands to be distinguished. The edges of model (b) Koronis and (c) Themis dust bands are then projected onto the skyflux map for comparison with the observed bands (Sykes 1989).

Comparison of Koronis and Themis models with the β and α bands, respectively, yields excellent fits to the data as observed in the IRAS skyflux maps at all longitudes (Fig. 10b,c). This assumes dispersions in proper inclinations equal to those of the Koronis and Themis family members. Modifying the Koronis and Themis family models by decreasing the semimajor axis and other associated orbital elements (including forced components) consistent with orbital decay by Poynting-Robertson drag, results in significant divergence from the observed locations of the α and β bands. At $a = 2.4$ AU, the discrepancy can be as large as $1°\!.5$ in latitude. This compares with a width of $\sim 0°\!.25$ for the β bands in the IRAS skyflux plates.

The γ bands are very closely tracked by the model Eos bands in the filtered Zodiacal History File images (cf. Fig. 1), indicating an orientation and inclination of the γ torus that may be similar to that of the Eos family. However, the nominal Eos family band model yields a latitude of peak emission which is systematically greater by $\sim 1°$ than that observed for the γ bands. Also, the pericenter distances of the bands determined by parallax (Sec. I.B) indicate a value ~ 0.4 AU smaller than that of Eos family members. The former may be resolved by increasing the dispersion in proper inclinations of the model Eos bands by a factor of ~ 2. This also results in significant broadening of the bands (Fig. 3), which seems to agree with the several degree width of the individual γ bands. Dispersion due to Poynting-Robertson drag (Sec. II.B) may also account for band broadening and a decrease in apparent latitude (Dermott et al. 1989), though such effects are viewing-geometry dependent and may not occur at all longitudes observed (Sykes 1989). On the other hand, the apparent discrepancy in pericenter distances may be explained by the Poynting-Robertson drag. An alternative explanation in both cases is that the γ bands and Eos asteroid family are not causally related.

In addition to the more prominent α, β and γ bands, fainter dust bands reported by Sykes (1988) (Table I) were compared to model bands associated with several other known asteroid families (Table II). This resulted in a possible correlation between the Io family and the J/K bands (Sykes 1989). However, no bands were detected in association with the Flora, Nysa or Maria families. Flora and possible Maria bands had been predicted previously on the basis of the collisional equilibrium hypothesis (Dermott et al. 1985). Their absence, coupled with the apparent existence of bands not associated with any prominent asteroid families, presents a challenge to the collisional equilibrium hypothesis of dust-band origin.

B. The Nonequilibrium (Random Collision) Hypothesis

The asteroid belt contains tens of thousands of objects in mutual-crossing orbits. On average, the population of particles may be described by some equilibrium size-frequency distribution as discussed in the previous section. However, when two asteroids collide, a small area of orbital element space will be filled with their debris. As this debris experiences further collisions

with background interplanetary dust particles, the local dust population will be enhanced. If the collision is large enough, the resultant dust population deriving from the comminution of its debris, may have enough surface area to be detected by an instrument such as IRAS. Eventually, removal of dust through radiation forces and the continual erosion of the debris population results in the decline of the surface area of dust. Then at another location, another collision takes place and the process is repeated.

The nonequilibrium, or random collision, hypothesis of dust-band origin views dust bands as the product of a stochastic process in which they are created and destroyed over geologic time, while maintaining a certain average population whose spatial distribution may be different at different times. This is in contrast to the equilibrium hypothesis, in which the dust-band population and spatial distribution is effectively steady state.

In the following subsections, some of the consequences of the nonequilibrium model are examined: band pairs must form on finite time scales; their surface area changes with time as mass is collisionally redistributed from larger sizes to smaller; a pseudo-equilibrium population of bands must be maintained due to constant "gain" and "loss" rates. Finally, predictions grounded in the nonequilibrium hypothesis must be tested against the IRAS data.

Dust-band Formation. The collisional disruption of an asteroid results in fragments having a dispersion in semimajor axes that is likely small compared with the semimajor axis of the parent body. For example, the major Hirayama families (see also the chapter by Valsecchi et al.) have a dispersion of semimajor axes corresponding to relative orbital velocities of ~ 100 m s^{-1}, compared with absolute orbital velocities of ~ 17 km s^{-1}. In fact, it is a mystery how even a value as great as 100 m s^{-1} could have been achieved. Such a small dispersion in semimajor axes results in these debris being distributed around the orbit of the parent body on time scales of $\sim 10^3$ yr.

The orbits of asteroids (and therefore debris in the asteroid belt) experience secular precession of their apsides and nodes as a consequence of gravitational perturbations by Jupiter and the other planets. The dust-band torus is formed as the orbits of collisional debris precess at different rates due to small differences in their orbital elements, primarily semimajor axis, so that with time their nodes spread around the ecliptic relative to each other. Two mechanisms operate simultaneously to distribute the nodes of particle orbits. The first is differential precession due to the differences in semimajor axes for particles of a given size. The second is a mass fractionation of the nodes arising from the size-dependent variation of semimajor axes with time due to Poynting-Robertson drag on smaller particles (Sykes and Greenberg 1986).

Increasing the dispersion in semimajor axes increases the rate at which band pairs are formed by this mechanism, as does increasing the mean semimajor axis of the particle orbits. This last is a consequence of the stronger

gravitational effects of Jupiter as the particle orbits approach Jupiter's orbit. From Fig. 11, minimum formation time scales range between 10^5 and $\sim 10^7$ yr, with dust bands associated with the Themis, Koronis and Eos families forming in less than 10^6 yr.

Mass fractionation of the orbital nodes occurs as Poynting-Robertson drag decreases the semimajor axis of small particles with time, relative to large
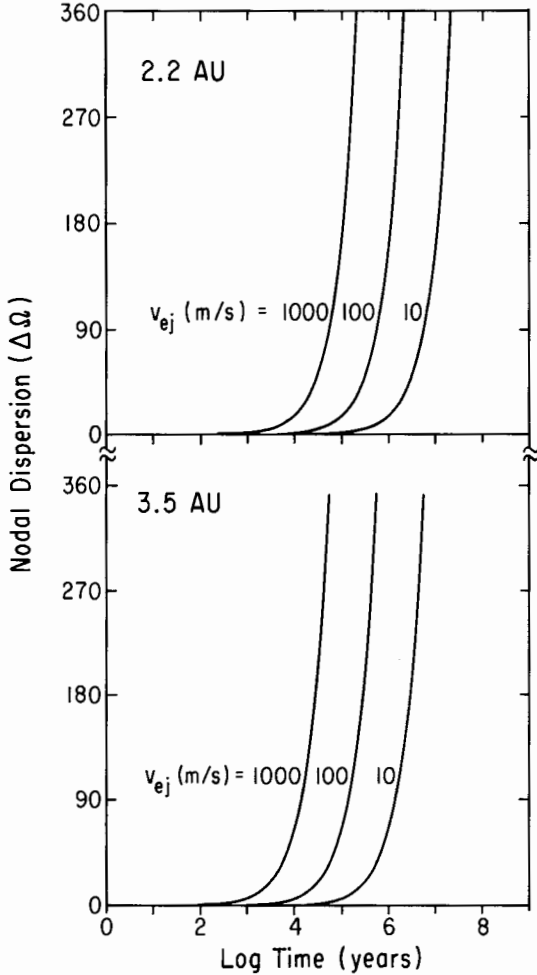
Fig. 11. The longitudes of the ascending nodes of an ensemble of collisional debris orbits increasingly dispersed due to differences in semimajor axes among the debris after ejection. Nodal dispersion as a function of time is shown for different mean ejection velocities in the inner (a) and outer (b) part of the asteroid belt. When the nodes have been distributed over 360°, band formation is complete. Band formation is more rapid in the outer belt due to the closer proximity of Jupiter (Sykes and Greenberg 1986).

particles. Small particles consequently precess at increasingly lower rates with respect to large particles. Depending on the size-frequency distribution of particles created in the initial catastrophic disruption, this mechanism can potentially result in more rapid band-pair formation ($\sim 10^5$ to 10^6 yr) than differential precession due to the initial dispersion in semimajor axes (Fig. 12).

Surface Area Evolution. The debris that comprises a dust-band torus will not maintain its original mass distribution. Particles are comminuted by collisions with background interplanetary dust particles, both cometary and asteroidal in origin. Catastrophic fragmentation, rather than gradual erosion, dominates the comminution (Dohnanyi 1978), and the breakup of larger particles into smaller particles increases the surface area of the dust bands, tending to increase their brightness. Mass (and surface area) from the torus is even-
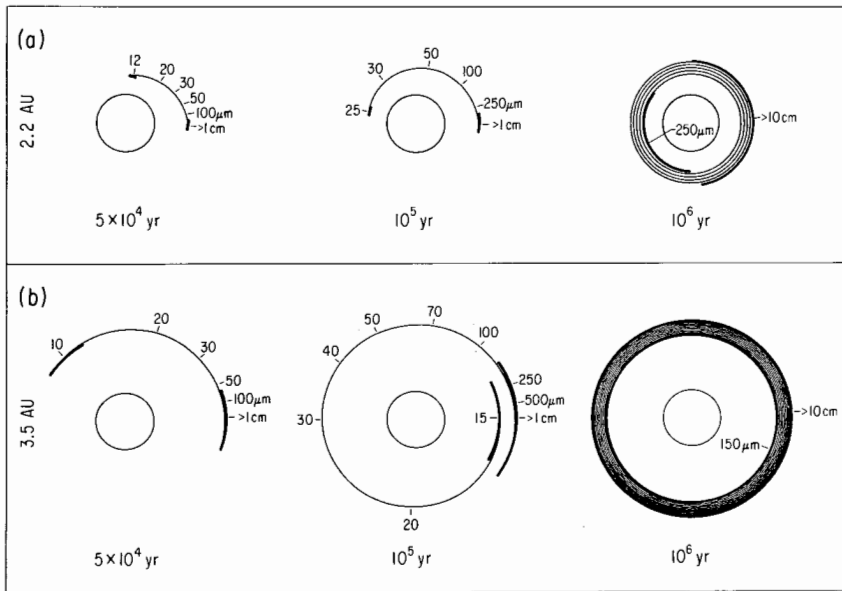
Fig. 12. The ascending nodes of debris orbits from a single collisional event shown as a function of time. Poynting-Robertson drag coupled with Jovian gravitational perturbations acts to decrease the rate of orbital precession by small particles relative to large particles by decreasing their semimajor axes with time. This results in band-pair formation by mass fractionation of debris orbits. The distribution of ascending nodes by this mechanism (thin curves) and by the initial dispersion of semimajor axes (thick curves) are shown at different times for a single collision in the inner (a) and outer (b) part of the asteroid belt. Particle mass densities of $\rho = 3$ g cm^{-3} are assumed, and a dispersion in ejection velocities of 100 m s^{-1}. For reference, the inner circle represents the orbit of the Earth. As in Fig. 11, band-pair formation in the outer belt is more rapid than the inner belt due to the closer proximity of Jupiter (Sykes and Greenberg 1986).

tually lost when the debris is comminuted into small enough fragments that they are swept away by Poynting-Robertson drag or radiation pressure (Fig. 13). For most meteoritic compositions this corresponds to particle diameters between approximately 0.08 and 4 μm (Burns et al. 1979).

In the competition between production and loss rates of surface area in a dust-band torus, gradual loss eventually wins out with time (Fig. 13c). Thus, the eventual fate of any band pair in the nonequilibrium model is to fade away (Sykes and Greenberg 1986).

How Many Dust Bands Should We See? According to the nonequilibrium model, the population of bands above a limiting surface area will be determined by two quantities: the mean time between collisions which generate more than the minimum required surface area (the gain term), and the lifetime of bands before they fade below this limit (the loss term). The ratio of the gain-to-loss terms determines the number of bands one would expect to observe at any given time. Based on their models, Sykes and Greenberg (1986) calculated that there should be on the order of 2 pairs of bands with surface areas equal to or exceeding that estimated for the bands reported by Low et al.
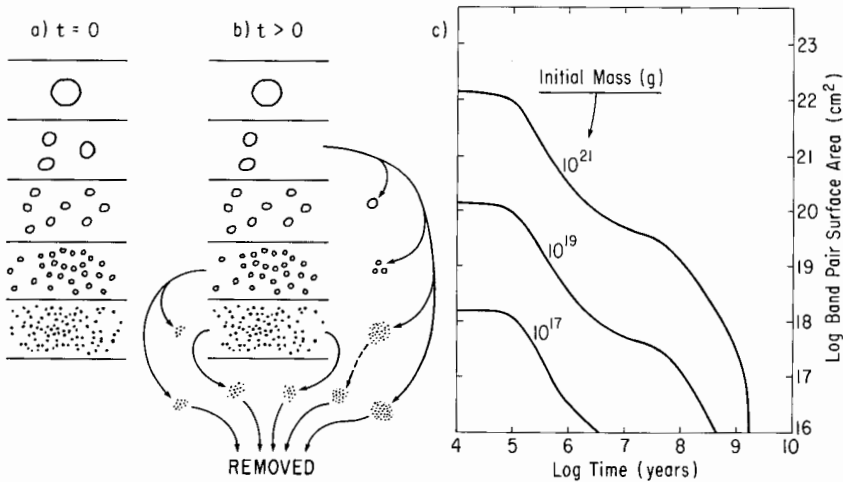
Fig. 13. (a) Debris from the catastrophic disruption of an asteroid indicating an initial size-frequency distribution which subsequently (b) undergoes collisional redistribution of its mass from larger to smaller particles. Eventually, particles are small enough that they are rapidly removed by radiation forces from the ensemble comprising a dust-band torus. (c) The surface area of dust-band tori gradually diminishes with time. The differing rates of change in surface area at different times is a consequence primarily of particle collision lifetimes which change with particle size. As time progresses, larger particles begin to be comminuted, supplying the smaller particle population at different rates (Sykes and Greenberg 1986).

(1984) and ~30 pairs of bands an order of magnitude fainter. This agreed nicely with the number of bands at the bright end (Low et al. 1984), but seemed to conflict with the smaller number of faint bands detected by Sykes (1988). The problem was resolved when it was found that the dust bands are not sharp features, but have typical widths of a few degrees (the exception being the α and β bands). Assuming Gaussian profiles, Sykes (1988) showed that the superposition of so many faint and bright bands would produce something of a continuum above which only 2 to 5 bands (or clusters of bands) could be detected in addition to the α, β and γ bands. Thus, the non-equilibrium model is consistent with the numbers of bands now detected.

The dust bands predicted by Sykes and Greenberg (1986) were disruption products of asteroids tending to have diameters between 5 and 10 km. A significant fraction of these bands also arose from the disruption of 30 to 90 km diameter bodies. Thus, the prominent α, β and γ bands (with the possible exception of the β bands), assuming association with the Themis, Koronis and Eos families, respectively, were not predicted by Sykes and Greenberg (1986). Bodies large enough to form the Themis and Eos asteroid families disrupt so infrequently (on time scales of the age of the solar system) that they were not included in the collision statistics. However, the Sykes and Greenberg model can explain the observation of these bands in the event of such large collisional disruptions. This is due to their long observational lifetimes. At the other end of the size scale, asteroids much smaller than 5 km in diameter would not produce enough debris to form a detectable band pair.

The mean time between catastrophic collisions generating a mass of debris equivalent to a 5 to 10 km asteroid was found to be between 10^5 and 10^6 yr—on the order of both the dust-band formation time and lifetime (for surface areas exceeding 10^{18} cm^2, ~ 1/10 that of the prominent bands). Consequently, it was thought that faint partial band pairs might be observed whose nodes were not distributed over all longitudes. One such partial band was reported to be detected (Sykes 1986,1987), but later evidence suggested that the structure had moved over a period of eight months, indicating that it may actually be a debris trail of a type not previously observed (Sykes 1988).

C. The Comet Hypothesis

It cannot be concluded *a priori* that because the zodiacal dust bands are located in the asteroid belt, that they have an asteroidal origin. Numerous short-period comets have low inclinations; the peak in the distribution of the observed inclinations is actually close to 10°. Many of the observed short-period comets also have perihelion distances between 2 and 4 AU and, because of selection effects, there is probably a large number of such comets with perihelia within the asteroid belt that remain undetected (Burns et al. 1984; Dermott et al. 1989).

IRAS discovered that many short-period comets have associated dust trails detected over large portions of their orbits (Sykes et al. 1986a). In Fig.

1, the dust trails associated with P/Tempel 2 and P/Encke are clearly seen. This represents a possible significant increase in the contribution of cometary dust to the zodiacal dust complex, particularly in the submillimeter and millimeter size ranges (Sykes et al. 1986b). Another source of zodiacal dust of possible cometary origin are the Type II dust trails (A to D in Fig. 1) (Sykes 1988). These recently detected structures may arise from the ejection of large particles at high velocities ($\sim$ 100 m s^{-1}) from a comet nucleus during a perihelion passage, in comparison to the lower velocities ($<$ 10 m s^{-1}) associated with the originally detected Type I trails. They may also represent the breakup of cometary nuclei. In either case, the dust trail particles will tend to evolve into a dust band torus as described in Sec. III.B, though with a much greater radial width than for asteroidal debris due to the larger typical cometary eccentricities.

As a torus forms, the cometary material is spread out over a substantially larger volume, tending to decrease the surface brightness of the dust observed unless it is increased through comminution of the larger particles or the emission of additional material from the parent comet. In the case of the latter, emissions from short-period comets are expected to last only about 10,000 orbits (the nominal lifetime of a short-period comet), which is smaller than the dust band formation time scales. Unless the comet itself is disrupted, the population of large particles whose comminution provides the observed dust population is likely to be minimal. Therefore, dust bands associated with cometary emission are likely to be very short lived. There remains the possibility, however, that emissions from a large number of small, undetected short-period comets of similar inclination could superpose to yield an observable dust-band torus.

The disruption of a cometary nucleus might allow for a dust band to be formed as bright as any detected by IRAS. Though highly uncertain, the size-frequency distribution of the large-particle population of comets is thought to have a size index $q \sim 2.1$ (Sekanina 1979). This is similar to the initial size distribution assumed for a catastrophically disrupted asteroid by Sykes and Greenberg (1986). From Fig. 6, such breakup would require an initial cometary radius of only $\sim$ 10 km, similar to that observed for Halley (Sagdeev et al. 1986; Keller et al. 1986). The frequency with which such cometary disruptions occur would then determine the probability of the resultant band pair being observed.

One means of distinguishing between asteroidal and cometary models of the bands is probably a combination of the forced orbital element and parallax methods (Dermott et al. 1989). The forced orbital element method determines the semimajor axis of the particles, whereas the parallax method determines an "effective distance" which is probably closely related to the pericenter distance, $a(1-e)$. Thus, it should be possible, in principle, to determine the proper eccentricities of the particle orbits, thereby indicating whether the particles derive from comets.

IV. DISCUSSION

Neither the equilibrium nor nonequilibrium models of dust-band origin, as currently formulated, present a complete picture of the IRAS dust-band observations. The equilibrium model fails to explain the existence of bands at nonfamily locations and the absence of bands associated with the Flora, Nysa and Maria families. Both theories can explain the α, β and γ bands and their respective relationships to the Themis, Koronis and Eos families. The non-equilibrium model of Sykes and Greenberg (1986) overestimates the surface brightness of bands arising from the disruption products of small asteroids (unless it eventually turns out that γ bands are not associated with the Eos family). It also predicts the detection of partial bands, which have yet to be unambiguously observed.

On the other hand, the equilibrium model led to the initial correlation between the prominent bands and the major Hirayama asteroid families (Dermott et al. 1984), and the nonequilibrium model inspired the search for and detection of zodiacal structures including additional dust bands (Sykes 1988). Both models predicted that a significant fraction of the zodiacal dust complex derives from the asteroid belt.

If the asteroid belt is a principal source of zodiacal dust, then that dust must be transported to the inner solar system by Poynting-Robertson drag. Initially, it seems contradictory that the previous statement be true while the dust bands—regions where dust is obviously being generated—evidence little if any orbital decay (Hauser et al. 1985; Dermott and Nicholson 1989; Sykes 1989). Sykes (1989) interprets these observations as indicating particle sizes whose collisional lifetimes are short in comparison with their Poynting-Robertson decay times, and that the removal of their comminution products from the ensemble of dust-band particles must be rapid. This does not mean that the particles simply disappear, rather that they are no longer distinguishable from the broad zodiacal background depicted in Fig. 1. One possibility is that a significant fraction of the smaller particles are comminuted into sizes sensitive to radiation pressure, resulting in large semimajor axis orbits. These particles are then essentially removed from the ensemble of dust-band particles on time scales of an orbital period. These particles eventually decay by Poynting-Robertson drag, but their surface area is spread over a large volume and hence contribute little to the local dust-band surface brightness.

Dermott and Nicholson (1989) believe that Poynting-Robertson drag will turn out to explain the broadness of the bands and the apparent displacement of parallactic distances of the dust bands inward from the pericenters of their associated families.

The association of dust bands with asteroid families may help to shed some light on the nature and evolution of the latter. The major Hirayama families are thought to have originated with the breakup of large parent asteroids (Kuiper 1950; see the chapter by Valsecchi et al.). That the dust bands

have orbital elements consistent with the mean elements of the corresponding families indicates (from the perspective of the nonequilibrium model) that we probably are looking at comminution products of debris from the original family-forming collision, rather than from the random disruption of a smaller family member (which would likely have a different inclination). Thus, the dust-band, surface-area evolution model can be utilized in an attempt to constrain the ages of asteroid families. This was done by Sykes (1986) utilizing the dust-band, surface-area evolution model of Sykes and Greenberg (1986). A total surface area of 2×10^{19} was assumed for bands associated with the Themis, Koronis and Eos families, which is probably something of an overestimate, particularly for the Themis family which has a relatively low surface brightness in the IRAS skyflux maps. A surface area of 10^{18} cm^2 was assumed as an upper limit to the dust in the Nysa family. The calculated times elapsed since the disruption of the family parent bodies are listed in Table III, and should be considered as very model dependent. If the calculated values are correct, this model indicates that the Koronis family is younger than both the Themis and Eos families. This result is consistent with rotational studies of family members (see the chapter by Binzel et al.). If the Nysa family was the product of a catastrophic disruption, then its lack of an associated dust band suggests that a family-forming collision was indeed ancient.

The Sykes and Greenberg model says that dust bands deriving from the disruption of an asteroid on the order of a few 100 km in diameter should be detectable by a detector like IRAS for at least 1 Gyr. Also, according to this model, the probability of any such event occurring in the last several Gyr is very small. The fact that two such events occurred (Themis and Eos) and that other families with similar-sized parents arose from even earlier collisions suggests two things: (1) collisional activity was much greater in the asteroid belt more than 1 Gyr ago, or (2) many families may not have derived from a single collisional event, but that they may be associations arising from segregation or lumping (in orbital element space) as a consequence of dynamical resonances, such as the Phocaea family (Williams 1971).

TABLE III
Asteroid Family Formation Estimates

Family	Minimum Parent Body Diameter (km)	Minimum Age (yr)
Themis	300	1.5×10^6
Koronis	90	1.3×10^8
Nysa	200	1×10^9
Eos	189	5.8×10^8

IRAS first detected the dust bands in 1983, providing a new data base and phenomenology against which models of asteroid collisional activity and small particle dynamics could be tested. A wealth of more information is yet to come as more spacebased infrared telescopes are launched (beginning with the Cosmic Background Explorer (COBE) in the fall of 1989, to be followed by the Infrared Space Observatory (ISO) in the 1990s, and the Space Infrared Telescope Facility (SIRTF) early in the next century). The instruments being launched will allow not only for more detailed studies along lines reviewed here, but also will allow spectroscopy studies to be undertaken, opening whole new areas of investigation to link dust to asteroids and comets and link dust in the asteroid belt to extraterrestrial dust collected in the Earth's atmosphere and elsewhere.

REFERENCES

Burns, J. A., Lamy, P., and Soter, S. 1979. Radiation forces on small particles in the solar system. *Icarus* 40:1–48.

Burns, J. A., Dermott, S. F., Nicholson, P. D., and Houck, J. R. 1984. IRAS' solar system dust rings: Collisional debris from asteroids or comet dust. IAU Colloquium 85, Properties and Interactions of Interplanetary Dust, Marseille, p. 72 (abstract).

Dermott, S. F., and Nicholson, P. D. 1989. IRAS dust bands and the origin of the zodiacal cloud. *Highlights of Astronomy,* in press.

Dermott, S. F., Nicholson, P. D., Burns, J. A., and Houck, J. R. 1984. Origin of the solar system dust bands discovered by IRAS. *Nature* 312:505–509.

Dermott, S. F., Nicholson, P. D., Burns, J. A., and Houck, J. R. 1985. An analysis of IRAS' solar system dust bands. In *Properties and Interactions of Interplanetary Dust,* eds. R. Geise and P. Lamy (Dordrecht: D. Reidel), pp. 395–409.

Dermott S.F., Nicholson, P.D., and Wolven, B.A. 1986. Preliminary analysis of the IRAS solar system dust data. In *Asteroids, Comets, Meteors.* eds. B.A. Lagerkvist, H. Lindblad, H. Lundstedt and H. Rickman. (Uppsala: Uppsala Univ.), pp. 583–594.

Dermott, S. F., Nicholson, P. D., Kim, Y., Wolven, B. A., and Tedesco, E. F. 1988. The impact of IRAS on asteroid science. In *Comets to Cosmology,* ed. A. Lawrence (Berlin: Springer-Verlag), pp. 3–18.

Dermott, S. F., Nicholson, P. D., Gomes, R. S., and Malhotra, R. 1989. Modelling the IRAS solar system dust bands. *Adv. Space Res.,* in press.

Dohnanyi, J. S. 1978. Particle dynamics. In *Cosmic Dust,* ed. J. A. M. McDonnell (New York: Wiley), pp. 527–625.

Gautier, T. N., Hauser, M. G., and Low, F. J. 1984. Parallel measurements of the zodiacal dust bands with the IRAS Survey. *Bull. Amer. Astron. Soc.* 16:442 (abstract).

Gradie, J. C., Chapman, C. R., and Williams, J. G. 1979. Families of minor planets. In *Asteroids,* ed. T. Gehrels (Tucson: Univ. of Arizona Press), pp. 359–390.

Hauser, M. G., Gillett, F. C., Low, F. J., Gautier, T. N., Beichman, C. A., Neugebauer, G.,

Aumann, H. H., Baud, B., Boggess, N., Emerson, J. P., Houck, J. R., Soifer, B. T., and Walker, R. G. 1984. IRAS observations of the diffuse infrared background. *Astrophys. J.* 278:L15–L18.

Hauser, M. G., Gautier, T. N., Good, J., and Low, F. J. 1985. IRAS observations of the interplanetary dust emission. In *Properties and Interactions of Interplanetary Dust,* eds. R. Giese and P. Lamy (Dordrecht: D. Reidel), pp. 43–48.

IRAS Explanatory Supplement, eds. G. Neugebauer, H. J. Habing, P. E. Clegg and T. Chester. 1988. (Washington, DC: Government Printing Office).

Keller, H., Arpigny, C., Barbieri, C., Bonnet, R., Cazes, S., Caradini, M., Cosmovici, C., Delamare, W., Huebner, W., Hughes, D., Jamar, C., Malaise, D., Reitsema, H., Schmidt, H., Schmidt, W., Siege, P., Whipple, F., and Wilhelm, K. 1986. First Halley Multicolor Camera imaging results from Giotto. *Nature* 321:320–326.

Kuiper, G. 1950. On the origin of asteroids. *Astron. J.* 55:164.

Low, F. J., Beitema, D. A., Gautier, T. N., Gillett, F. C., Beichman, C. A., Neugebauer, G., Young, E., Aumann, H. H., Boggess, N., Emerson, J. P., Habing, H. J., Hauser, M. G., Houck, J. R., Rowan-Robinson, M., Soifer, B. T., Walker, R. G., and Wesselius, P. R. 1984. Infrared cirrus: New components of the extended infrared emission. *Astrophys. J.* 278:L19–L22.

Melosh, H. J. 1989. *Impact Cratering* New York: Oxford University Press.

Neugebauer, G., Beichman, C. A., Soifer, B. T., Aumann, H. H., Chester, T. J., Gautier, T. N., Gillett, F. C., Hauser, M. G., Houck, J. R., Lonsdaley, C. J., Low, F. J., and Young, E. T. 1984. Early results from the Infrared Astronomical Satellite. *Science* 224:14–21.

Sagdeev, R. Z., Blamont, J., Galeev, A., Moroz, V. I., Shapiro, V., Shevchenko, V., and Szego, K. 1986. Vega spacecraft encounters with comet Halley. *Nature* 321:258–262.

Sekanina, Z. 1979. Expected characteristics of large dust particles in periodic comet Halley. In *Comet Halley Micrometeorite Hazard Workshop,* ed. N. Longdon, ESA SP-153 (Noordwijk: ESA), pp. 25–34.

Sykes, M. V. 1986. IRAS Observations of Asteroid Dust Bands and Cometary Dust Trails. Ph.D. Thesis, Univ. of Arizona.

Sykes, M. V. 1987. Evidence for a recent catastrophic asteroid collision. *Bull. Amer. Astron. Soc.* 19:825 (abstract).

Sykes, M. V. 1988. IRAS observations of extended zodiacal structures. *Astrophys. J.* 334:L55–L58.

Sykes, M. V. 1989. Zodiacal dust bands: Their relation to asteroid families. *Icarus,* submitted.

Sykes, M. V., and Greenberg, R. 1986. The formation and origin of the IRAS zodiacal dust bands as a consequence of single collisions between asteroids. *Icarus* 65:51–69.

Sykes, M. V., Greenberg, R., and Hunten, D. 1984. Formation of the zodiacal dust bands in the asteroid belt. *Bull. Amer. Astron. Soc.* 16:690 (abstract).

Sykes, M. V., Lebofsky, L. A., Hunten, D. M., and Low, F. J. 1986*a*. The discovery of dust trails in the orbits of periodic comets. *Science* 232:1115–1117.

Sykes, M. V., Hunten, D. M., and Low, F. J. 1986*b*. Preliminary analysis of cometary dust trails. *Adv. Space. Res.* 6:67–78.

Williams, J. G. 1971. Proper elements, families and belt boundaries. In *Physical Studies of Minor Planets*, ed. T. Gehrels NASA SP-267, (Washington, DC: Government Printing Office), pp. 177–181.

Williams, J. G. 1979. Proper elements and family memberships of the asteroids. In *Asteroids*, ed. T. Gehrels (Tucson: Univ. of Arizona Press), pp. 1040–1063.

IDENTIFICATION OF ASTEROID DYNAMICAL FAMILIES

G. B. VALSECCHI, A. CARUSI
Istituto di Astrofisica Spaziale

Z. KNEŽEVIĆ
Astronomical Observatory, Belgrade

Ľ. KRESÁK
Astronomical Institute of the Slovak Academy of Sciences

and

J. G. WILLIAMS
Jet Propulsion Laboratory

A satisfactory solution of the problem of the identification of asteroid dynamical families, apart from its intrinsic interest, represents a prerequisite for a meaningful study of the more general problems such as the collisional evolution of the asteroid belt and the origin of compositional inhomogeneities or trends in it. Unfortunately, published studies on this subject are in disagreement for many families, though not for the major ones found by Hirayama. The various aspects of this complex issue are reviewed and discussed, and some methodological guidelines are presented.

I. INTRODUCTION

A. Review of Asteroid Family Classifications

The idea of asteroid concentrations in the space of orbital parameters dates back to 1918, when Hirayama found that the distribution of asteroids in

the *a-e-i* space (osculating orbital semimajor axis, eccentricity and inclination) is not uniform, even taking into account the discontinuities due to the mean motion resonances with Jupiter (Kirkwood gaps). In a series of papers, Hirayama (1918,1919,1920,1923,1928,1933) was able to single out the existence of a number of clusterings, that he called families, some of which were very well defined and included many members, whereas other clusterings had more confused boundaries and only a few members. The Hirayama families Themis, Eos and Koronis are evident in Fig. 1.

After Hirayama's work there have been many other studies dedicated to the identification of asteroid families (Brouwer 1951; Arnold 1969; Lindblad and Southworth 1971; Carusi and Massaro 1978; Williams 1979; Kozai 1979). Van Houten et al. (1970) have also looked for asteroid families in the Palomar-Leiden Survey (PLS) but the absence of the numbered objects in their sample makes any comparison of their work with that of most other researchers difficult. The so-called proper elements (see Sec. III for a definition of proper elements) were used as parameters in all classifications of as-
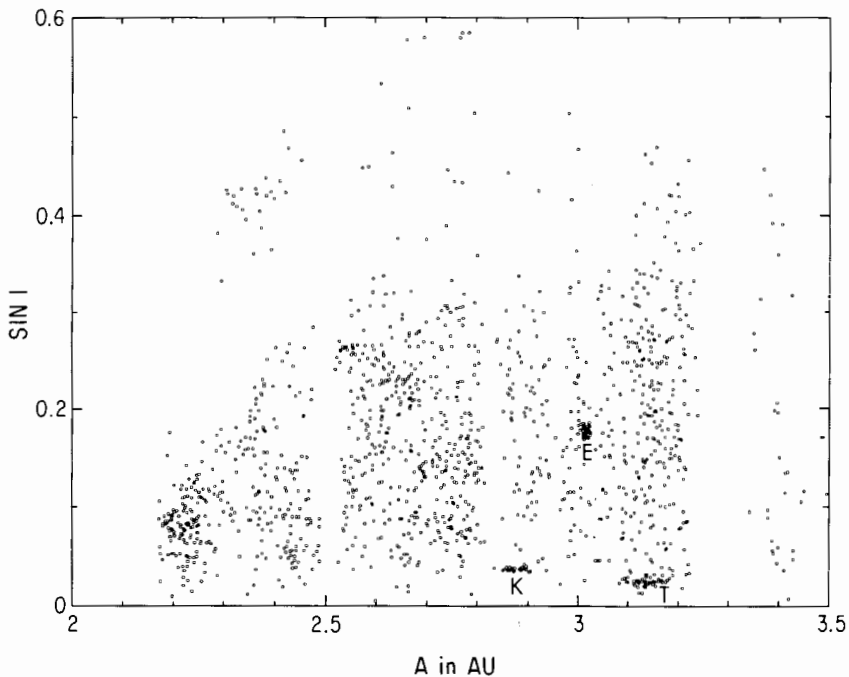
Fig. 1. Distribution of the proper sine of inclination vs semimajor axis for the first 1500 numbered asteroids. The Hirayama families Themis (T), Eos (E) and Koronis (K) are marked. Kirkwood gaps are visible. The detached Phocaea region is at the upper left.

teroids into families carried out so far (Carusi and Valsecchi 1982; Froeschlé et al. 1988).

Table I lists the main characteristics of the published classifications. As can be seen, there are differences in the size of the asteroid sample, in the method for proper-elements computation, and in the method for identifying families; moreover, only in some cases have statistical checks been made. Particularly noteworthy is this difference in the sizes of the samples, caused by not only the increase of numbered asteroids with time, but also by the inclusion by some authors of the best orbits from the PLS, whose selection effects are different from those affecting the sample of numbered asteroids (see Sec. II for a discussion).

Looking at the column of Table I which shows how many families were identified by each author, it is easy to see that the range spanned by this important number is of an order of magnitude, and illustrates a basic controversy that must be resolved, i.e., whether there are only a few heavily populated families or whether there are also many less populated ones.

The differences among the classifications are discussed in Carusi and Valsecchi (1982); we only mention here that, given these differences, it is not surprising that there is less agreement among the results of the various classifications than one would expect. There is general agreement on the populous families Themis, Eos and Koronis; there is less agreement on the clusters of lower population, and they suspect that most of the low-population families are spurious.

While some researchers doubt that the less populated families are real and Table I shows that there is a disconcertingly large spread in the number of families found by different investigators, it should not be thought that there is total disagreement. Lindblad and Southworth (1971) singled out five of Brouwer's families of low population as significant. They also recovered some of the clusterings of van Houten et al. (1970). Arnold (1969) found it necessary to alter or rearrange (with new numbers) nearly all of Brouwer's low-population families. Of the families first discovered by other investigators and little altered by Williams (1979), five were from Lindblad and Southworth and two each from Brouwer and Arnold. All investigators except Carusi and Massaro found the Maria family. Detailed examination shows that there are complicated regions of clustering in the proper-element space found by several recent investigators. While one investigator may give a single family identification to the large-scale group, others may break it down into smaller groups. Such cases exhibit failures of uniqueness when comparing the families of different investigators, but they need not be failures of statistical significance. Thus the large spread in the number of families exhibited in Table I tells us something about uniqueness, but nothing about statistical significance.

After the peak of studies aimed at the identification of asteroid families between 1969 and 1979, in the last decade there has been only the work by Williams and Hierath (1987), concerning PLS asteroids. In a slightly different

TABLE I
Published Asteroid Classifications

Author(s)	Year	Numbered Ast. Used	PLS Incl.	Number of Families	Pertbn. Theory	Method of Identif.	Stat. Check
Hirayama	1933	1223	no	5	Stockwell	visual	no
Brouwer	1951	1563	no	28	Brouwer & van Woerkom	visual	no
Arnold	1969	1735	no	37	Brouwer & van Woerkom	boxes in a-e-i space	yes
Lindblad & Southworth	1971	1735	yes	34	Brouwer & van Woerkom	Southworth criterion	not applic.
Carusi & Massaro	1978	1861	yes	15	Brouwer & van Woerkom	z^2	yes
Williams	1979	1796	yes	104	Williams	visual	yes
Kozai	1979	2125	no	72	Yuasa	visual	no
Williams	1989	2065	yes	117	Williams	visual	yes
van Houten et al. [a]	1970	none	yes	14	Brouwer & van Woerkom	visual	no

[a]This classification is included for completeness, but is not directly comparable to the others because of the absence of numbered objects.

context, i.e. focusing only on the four major classical Hirayama families Themis, Eos, Koronis and Flora, Klačka (1989) has examined the sample of numbered asteroids currently available (a total of 3720 objects), looking for new members of those families.

B. Problems Arising from the Comparison of Existing Classifications

The rapid acquisition of data on the physical properties of asteroids makes available a huge amount of information useful for reconstructing the history of the belt and for understanding its present state. Studies on the collisional evolution of asteroids and on the origin of compositional inhomogeneities in the belt can greatly benefit from a deeper understanding of the origin and evolution of dynamical families and, in fact, this understanding appears to be a necessary condition for those studies. On the other hand, dynamical families will be better understood when the general picture of the collisional evolution becomes clearer.

The reasons for the discrepancies among published classifications should be related to the fact that these classifications differ in many respects (data sample, method for proper-element computation, method for family identification and rejection criteria for family membership; see Carusi and Valsecchi [1982]), each of which, in principle, may be significant in determining the results. Unfortunately, although things such as sizes of statistical samples of orbital elements should lend themselves to quantitative treatment, in practice it is difficult to quantify the effects of these methodological differences because each of the published classifications differs from the others in more than one (if not in all) of the respects mentioned above.

Furthermore, there is a fundamental question for which the various authors have given different answers or no explicit answer (see Carusi and Valsecchi 1982), namely what is an asteroid family and how does it differ from a clumping of asteroids in phase space. The commonly accepted view is that an asteroid family is constituted by a group of asteroids whose proper elements a, e and i appear to form a cluster distinguishable from the background and, in addition, that these asteroids are genetically related because they come from the disruption of a larger parent body. Groupings that are due to lack of asteroids in nearby volume elements of the phase space should not be termed families: an example of this is Phocaea (Fig. 1), which Williams showed to be isolated by secular resonances and a Kirkwood gap (Williams 1971; Gradie et al. 1979; see also the discussion in Sec. II.A). Incidentally, one could speculate that there could be a third type of cause for the grouping, if there existed some dynamical process "pushing" asteroids in specific zones of the phase space. Currently we do not have proof that any asteroid groupings have been formed in this way, but this is a possibility that should be kept in mind.

Once one accepts that dynamical families can be composed of genetically related bodies, it is natural to examine the taxonomy to see if family members differ from background asteroids. This problem is reviewed in the chapter

by Chapman et al. Table I shows a large spread in the number of families found by recent researchers and the disagreements add an additional uncertainty to the interpretation of physical-properties data for the controversial families. It is necessary to have clear in mind the distinction between dynamical considerations and physical ones, at least until we are able to identify asteroid families *from the dynamical point of view only* in a way less controversial than in the past. Physical evidence should not substitute, but rather corroborate, dynamical evidence for identifying families. Physical observations are therefore very important for interpreting plausible mechanisms of formation.

II. OBSERVATIONAL SELECTION

A. Resolution of Asteroid Families from their Background

As stated in the introduction, asteroid families are identified as clusters of objects in three-dimensional phase space of proper elements: semimajor axis a, eccentricity e and inclination i. The background makes it essentially impossible to identify all the family members with certainty. The difficulties, affecting not only family membership but also the assessment of the reality of less populated families, tend to increase with increasing density of the background and decreasing degree of concentration of the family. The nonrandomness of the background in all proper elements makes it impossible to apply simple and uniform criteria for their resolution.

Ninety-four % of numbered objects fall into three semimajor axis zones separated by mean motion resonances with Jupiter: 4/1 ($a = 2.065$), 3/1 ($a = 2.501$), 5/2 ($a = 2.825$) and 2/1 ($a = 3.278$). The mean numbered population per unit of a is nearly the same, within $\pm 5\%$, for these three zones, so that there is no general trend on a large scale. On smaller scales, however, definite irregularities appear. Around the zone limits, there are the major Kirkwood gaps, where the population drops nearly to zero. Additional irregularities are due to less effective resonances, but mainly just to the presence of asteroid families.

Other zones of avoidance, produced by secular resonances (Williams and Faulkner 1981; chapter by Scholl et al.), appear in the a-i plane (Fig. 1). Most important are those produced by the secular precession of the orbital axis at the mean rate of Jupiter, running through the whole belt between $i = 25°$ and $30°$, and by an analogous effect with the mean rate of Saturn, starting at $i = 0°$, $a = 2.0$ and rising at a decreasing rate up to $i = 21°$ in the outer part of the belt. In the a-e plane there are no additional gaps. Only the upper boundary of e is slowly rising and then declining, as the perihelia recede from the orbit of Mars and the aphelia approach to within 1 AU of the orbit of Jupiter.

The distributions in inclination and eccentricity are rather similar, somewhat resembling a Poisson distribution (for histograms of their osculating

values see, e.g., Scholl [1987]). The overall medians are 7° and 0.14, respectively. The distribution does not deviate very much from a random one for 2° $< i < 10°$ and $0.05 < e < 0.20$. A slow progressive decline at higher values of i and e is tied with the general structure of the asteroid system, preferring motions parallel to those of the major planets. A steep drop at very small inclinations, approaching a direct proportionality to the inclination angle, is due to the fact that a random dispersion of orbital planes corresponds to a random dispersion of their poles, rather than to that of the inclination angles. An analogous effect applies to the eccentricities.

The operation of the background irregularities can be illustrated on the already mentioned example of the Phocaea region, which was among the first seven families discovered by Hirayama (1918), and is still included in the list of Kozai (1979) as a broadly dispersed family of 34 members. Its concentration is indeed well recognizable when mapping the population of the asteroid belt. However, as pointed out by Williams (1971), its boundaries are set by the 3/1 Kirkwood gap and three secular resonance gaps, so it appears that we are not dealing with a family of objects produced by collisional disintegration of a common parent body, but with an island which remained there after its surroundings had been depleted by perturbations.

B. Effects of Observational Selection

Our information on asteroid families is strongly biased by observational selection. Since accurate orbit computations are a prerequisite for the determination of family membership, the list of numbered objects serves as the primary data base. The difference of this sample from the total number of asteroids down to a given size (or mass) limit is appreciable, and manifests itself in three aspects: in the discernibility of the families, their relative population, and internal structure.

The variety of observational selection effects is discussed in detail by Kresák and Klačka (1988). Here only some implications concerning the asteroid families will be summarized and illustrated for the four major families: Flora (without divisions into smaller groupings which have been suggested by several authors), Koronis, Eos and Themis. The relative population of these families in different samples is intercompared in Table II. All the values are percentages of the whole asteroid population consisting of: all asteroids numbered by the end of 1987 (3720 objects); all numbered asteroids detected by the IRAS Survey (1811 objects); asteroids of semimajor axis $a < 5$ AU and absolute magnitude $H < 10.0$ (684 objects); asteroids of $a < 5$ AU and diameter $D > 50$ km (711 objects); asteroids of $a < 5$ AU and $D > 100$ km (232 objects).

The classification of family membership is taken from Klačka (1989); the orbital elements and absolute magnitudes from Minor Planet Ephemerides for 1988 (Batrakov et al. 1987) up to No. 3516, and from Minor Planet Circulars (Marsden et al. 1986,1987) for Nos. 3517-3720. The listing of IRAS sight-

TABLE II
Population of Main Families (percentages)

	Flora	Koronis	Eos	Themis	Sum
Numbered asteroids	13.4	3.1	4.1	5.4	26.0
IRAS asteroids	5.3	1.9	5.3	5.7	18.3
$H < 10.0$ mag	1.0	1.0	2.0	2.0	6.1
$D > 50$ km	0.7	0.0	0.8	2.4	3.9
$D > 100$ km	0.4	0.0	0.4	1.7	2.5

ings is from Matson et al. (1986), with diameters based on the thermal model by Lebofsky et al. (1986). Only for the objects missed by the IRAS Survey (7% at $D > 50$ km, 5% at $D > 100$ km), the TRIAD data by Bowell et al. (1979) are adopted. In the statistics of absolute magnitudes and diameters, the Trojans and 2060 Chiron are omitted because, for these types of objects, our present record is still incomplete below $H = 10.0$ and above $D = 50$ km. Also, they are far outside the main asteroid belt.

Table II shows that the striking prevalence of the Flora family among the numbered asteroids is not matched by the IRAS Survey. At a given apparent magnitude, the infrared satellite had a stronger signal from the darker, larger asteroids than from the brighter ones, so that families of dark asteroids, such as Themis, were sampled with higher efficiency than families with brighter members, such as Flora. When passing to the absolute brightness scale, the share of these families among all asteroids decreases considerably: from 26% of numbered objects to 6% at $H < 10.0$. The effects of heliocentric and geocentric distance are removed, but those of the albedo are still present. In the size distribution, the representation of the four major families becomes still smaller: only 2.5% for $D > 100$ km. This is also the approximate fraction of the total mass of the asteroid system falling in these families.

In addition to the concentration in the a-e-i space, defining the families, some authors have found significant irregularities in the distribution of the other two proper elements, perihelion longitude and nodal longitude. Such concentrations were interpreted by Alfvén (1969) and others as asteroid jet streams, features of fundamental significance for the problems of asteroid origin and evolution. Later, it was shown that the presence of such concentrations is just a result of selection effects. Since asteroids are, with very few exceptions, discovered near opposition, each position of the Earth on its annual orbit favors some osculating perihelion longitudes. Thus the selection is strongest in time-limited search programs like the Palomar-Leiden Survey (van Houten et al. 1970), where the latitude limitation of the exposed area introduces an additional selection according to the nodal longitudes (Kresák 1971). Even in the total current data set, the selection effects are quite significant due to the annual variation of asteroid discovery rates. This is a com-

posite effect of the perturbational alignment of the asteroid orbital axes to that of Jupiter; variations of the galactic latitude of the opposition point (producing considerable periodic changes in the density of the stellar background, and thereby in the detectability of faint asteroids); variations of the declination of the opposition point (affecting its culmination altitude and night length at observatories which are very unevenly distributed in geographic latitude); and seasonal variations of the weather conditions at principal northern hemisphere observatories. The resulting annual variations in discovery reach an amplitude as high as $1:6$ between the minimum in June and maximum in October (see also the chapter by Bowell, Chernyk and Marsden). They can be approximately modeled and fully explain the irregularities once attributed to the presence of jet streams (Kresák and Klačka 1988).

III. THEORIES OF SECULAR PERTURBATIONS OF ASTEROIDS AND THE DERIVATION OF PROPER ELEMENTS

A. Classical Linear Theory

Within the formalism of the analytical theories of secular perturbations, proper elements are defined as constants of integration of the differential equations of variation of orbital elements; proper eccentricity and inclination appear in the solutions as amplitudes, while proper longitudes of perihelion and node represent phases of the corresponding free oscillation terms. The linear theory of asteroid secular perturbations (also called Laplace-Lagrange theory) has been most frequently used for derivation of the proper elements; in it (see Brouwer and Clemence 1961), eccentricities and inclinations appear in the first power in the differential equations, but in the second degree in the disturbing function.

Let us consider an asteroid of negligible mass perturbed by n planets, and the second-degree expansion of the disturbing function in the nonsingular variables

$$h = e \sin \tilde{\omega}$$

$$k = e \cos \tilde{\omega}$$

$$P = \sin i \sin \Omega$$

$$Q = \sin i \cos \Omega. \tag{1}$$

The solutions of the differential equations of motion are obtained in the form of sums of free and forced oscillations of h, k, P and Q; these solutions depend on known frequencies and phases of planetary motions and on constants dependent, in their turn, on the masses of the perturbing planets and on the ratios between the semimajor axis of the perturbed asteroid and those of the planets. In practice, one substitutes in these solutions the asteroid osculat-

ing elements for a particular epoch, and taking the corresponding forced oscillation values from tables (see, e.g., Brouwer and van Woerkom 1950), one easily derives the proper elements.

The linear theory has some important drawbacks that prevent the derived proper elements from being as accurate as one could wish for reliable family classification:

1. It does not eliminate the short-periodic perturbations;
2. It does not account for resonance effects, apart from a couple of the most important secular resonances;
3. It does not include terms in the disturbing function of higher order/degree, etc.

Although it has long been clear that the accuracy and long-term stability of the proper elements are of crucial importance for the reliability of asteroid-family classification, only recently has this problem been investigated in greater detail. The accuracy and long-term stability of the proper elements derived from linear theory of secular perturbations were analyzed by Carpino et al. (1986). They have numerically integrated the orbits of a number of real asteroids as well as those of a swarm of fictitious objects in the frame of the elliptic restricted three-body problem. By filtering out the short-periodic perturbations by means of a suitable numerical filter, they monitored the behavior of the proper eccentricities and inclinations computed from the linear theory. As expected, significant short- and long-periodic variations with amplitudes ranging from few thousandths to few hundredths were found, even for objects of moderate eccentricities and inclinations; moreover these variations were strongly amplified in the proximity of mean-motion resonances. The obvious conclusion that can be inferred from these results is that the proper elements derived from linear theory suffer from significant "noise," which in some cases can seriously affect the family membership assignment.

B. Williams' Theory

Analytical theories which, like the linear one just discussed, use expansions in terms of the eccentricity and inclination of the asteroid must lose accuracy for large values of either. Kozai (1962) showed that a fourth-degree term in the disturbing function (proportional to $e^2 i^2 \cos 2\omega$) can give rise to sizable perturbations for many known asteroids and he demonstrated that there is a libration region for large values of e or i. Kozai showed that 1373 Cincinnati was such an argument of perihelion librator; several such librators are known today. For ordinary (nonlibrating) asteroids this perturbation has half of the period of the argument of perihelion circulation and it causes the eccentricity to have maxima at $\omega = 90°$ and $270°$, minima at $0°$ and $180°$, while the inclination has its maxima and minima the reverse of the eccentricity. The secular perturbation term that Kozai first investigated does not appear in the Laplace-Lagrange theory since that theory is truncated at

second-degree terms in the disturbing function. Any improvement to the Laplace-Lagrange theory proper elements would have to incorporate Kozai's effect in a new theory.

The theory of Williams (1969) combined the argument-of-perihelion dependent terms with those driven by the eccentricities and inclinations of the major planets. Because the planetary eccentricities and inclinations, particularly Jupiter's, are small compared to those of most asteroids, they were retained to first degree in the differential equations analogous to Laplace-Lagrange theory. A conventional expansion was not used for the asteroid's eccentricity and inclination. An expansion is made about a reference proper a, e and $\sin i$ for a hypothetical reference asteroid near to the asteroids of interest. The differential equations are separated into the part dependent on the planetary eccentricities and inclinations and the part which depends on planetary perturbations from circular, uninclined orbits. The reference asteroid's eccentricity and inclination are retained in closed form in the latter part and the changes in the eccentricity and inclination caused by the planetary eccentricity and inclination terms are expanded out of the former. The differential equations are split into zero- and first-order parts. Gauss averaging (which is equivalent to calculating the perturbation on one elliptical ring by another, where the line density of the rings is inversely proportional to the velocity of the body at that location) is performed numerically for each asteroid-planet pair and summed.

The averaged differential equations for the zero-order state, the partial derivatives of the zero-order state with respect to proper a, e and $\sin i$, and the first-order terms for each of the 17 nonzero frequencies of Brouwer and van Woerkom's secular theory of the planets (1950) are then simultaneously numerically integrated over an argument of perihelion range of $0°$ to $90°$. Symmetry and periodicity properties can then be used to extend the solution to any value of argument of perihelion.

The tabulated solution is used to derive the proper elements of any asteroid near to the reference proper elements. Several hundred boxes are used to cover the asteroid belt. Though not part of the secular perturbation theory, several of the more important short-period terms are subtracted from the osculating elements of each asteroid before applying the secular perturbation theory to get proper elements.

Proper elements computed with this theory have been published for asteroids numbered through 1796 (Williams 1979), through 2065 (Williams, table in Part VI) and the 1227 Palomar-Leiden survey minor planets with better-quality orbits (Williams and Hierath 1987).

The accuracies of these proper elements are generally better away from secular resonances (Williams and Faulkner 1981) and away from commensurabilities (which abound in the outer belt). Improvements can be made. Secular perturbation theory for the planets has advanced in recent years (Applegate et al. 1986; Carpino et al. 1987; Laskar 1988) and could replace the

theory of Brouwer and van Woerkom. This would particularly help objects near the sixth and tenth secular resonances which are slightly displaced in the older theory. The most useful improvement would be the addition of secular terms which arise from second-order effects of short-period terms. These terms are strong next to major mean-motion resonances and have some significant influence beyond 3 AU. The strongest effect is on the perihelion rate and hence on the location of the secular resonances (Williams and Faulkner 1981; Froeschlé and Scholl 1987).

C. The Higher Order/Degree Theory of Yuasa

The higher order/degree theory of asteroid secular perturbations of Yuasa (1973) completely avoids or at least considerably reduces the major drawbacks of the linear theory mentioned above (Sec.III.A). The most important characteristics of Yuasa's theory in that sense are:

1. The short-periodic terms are analytically eliminated and the mean elements are derived. For the semimajor axis this is also the final, proper value that can be used as a parameter for family classification purposes;
2. In the disturbing function, which is obtained after elimination of the short-periodic terms, one takes into account terms of up to the fourth degree in eccentricity and inclination in the first order with respect to the perturbing mass, and of the second degree in the second order;
3. Low-order mean-motion and secular resonances are accounted for; however, the results in the vicinity of resonances are still unsatisfactory.

Solutions of the secular equations in Yuasa's theory have the same form of the sum of free and forced oscillations, but this time Poincare's canonical variables, freed from the short- and long-periodic perturbations, appear on the left-hand side of the solutions. On the right-hand side, as amplitudes of the oscillations of Poincare's variables (thus in the place of proper eccentricity and inclination of linear theory), we have

$$v = \{2\,[1 - (1 - e^2)^{1/2}]\}^{1/2} \tag{2}$$

and

$$\mu = [2\,(1 - e^2)^{1/2}(1 - \cos i)]^{1/2}. \tag{3}$$

Note that these proper elements do not exactly correspond to proper eccentricity and inclination, but the differences are really small, and from the practical point of view, negligible (v and the proper eccentricity as defined in the linear theory, for example, differ by $<1\%$ up to 0.4).

In practical use, however, Yuasa's theory in its original form cannot be directly employed in the common heliocentric ecliptical coordinate system, because it is necessary to take into account terms coming from the indirect

part of the disturbing function and because there are several errors in the main part of the second-order Hamiltonian derived by Yuasa. A revised version of that part of the theory is given in Knežević (1989) and with it, the proper elements of asteroids up to number 3859 have been computed. (See the table of proper elements by Knežević and Milani in Part VI.)

The accuracy of the mean elements obtained by elimination of the short-periodic terms has been examined by Knežević et al. (1988). A comparison with the results of a suitable numerical procedure shows a very good agreement (within 0.001 to 0.002) of the results for the eccentricities and inclinations for the four largest Hirayama families, thus giving a clear indication of their accuracy and long-term reliability. For the semimajor axis, the remaining variation of the mean (i.e., proper) semimajor axis derived using Yuasa's theory (even in the case of the nearly commensurable orbits of Themis' family) is always better than $\Delta a/a \cong 0.001$ (Δa stands here for the difference of the highest- and lowest-mean semimajor axis value in the observed time span).

Critical eccentricities and inclinations above which the theory of Yuasa, due to the truncation errors, cannot supply mean semimajor axes of good accuracy have been determined by Knežević and Jovanović (1987), who found that the "safe" region in the inner part of the main belt extends up to 0.5 in eccentricity, provided that the inclination is small, and up to 50° in inclination when the eccentricity is small; in the outer main belt these values gradually drop reaching finally something like 0.2 and 25°. In the proximity of commensurabilities, however, especially the 2:1, the critical values are significantly affected, and the critical eccentricity at 3.2 AU, for example, amounts to only 0.05.

Regarding the accuracy of the procedure of elimination of the long-periodic perturbations, and of the derived proper elements, there are at the moment just some preliminary estimates. As reported by Farinella et al. (1988), in the elliptic restricted three-body problem (Sun-Jupiter-asteroid), the remaining variations of the proper values of the amplitudes of Poincare's canonical variables υ and μ of Flora, Koronis and Eos are considerably reduced with respect to their linear theory counterparts (for Eos the reduction of the remaining variation of υ reaches an order of magnitude); for Themis, however, the opposite is found. Although seemingly surprising, this result is easy to understand. Themis is close to the strong 2:1 resonance, and the linear-theory frequency of the free oscillation is wrong by about 50%. Since it appears in the divisors of the higher-order long-periodic terms in Yuasa's theory, this value spoils the final results as one adds more terms in order to improve the accuracy.

In conclusion, one can state that the second-order/fourth-degree theory of Yuasa supplies, in general, data of significantly better accuracy than the linear theory. In order to find out definitely whether this accuracy is enough for a reliable classification of asteroids into families, various, more numerous and more refined analyses are needed.

D. Commensurate Asteroids and Planet Crossers

None of the secular-perturbation techniques for deriving proper elements of main belt asteroids work for strongly commensurate objects such as the Trojans and Hildas. Direct numerical integration and empirical removal of the periodic terms has been used to derive proper elements for the Hildas (Schubart 1982) and the Trojans (Bien and Schubart 1987; see also the chapter by Shoemaker et al.).

Planet-crossing asteroids are on chaotic orbits (see Hahn and Rickman 1985; Milani et al. 1989, for examples) and proper elements can no longer be considered constant for the age of the solar system; they may have some use only for short time scales.

IV. DISCUSSION

The discrepancies among the published classifications mentioned in Sec. I could be interpreted as showing that in fact only very few "real" asteroid dynamical families exist. However, to draw a conclusion like this is probably just simplistic, unless the evidence leading to it is better justified. The methodological differences certainly play a major role, but to quantify this role, explaining each discrepancy as due to this or that difference in the methods of the various researchers, appears to be a too difficult task. But we can still make some qualitative general statements.

A. Method for Proper-Elements Computation

Almost all the classifications, with the notable exceptions of Williams' (1979; also table in Part VI) and Kozai's (1979), have used proper elements coming from the linear theory; as discussed in Sec. III.A, recent work has shown that the inaccuracy of such elements can be large enough to prevent reliable family assignments. On the other hand, for the higher order/degree theory of Yuasa (as corrected by Knežević), we have numerical evidence of more reliable proper elements. One can reasonably expect that better proper elements should give better resolution of real families from the background.

B. Linearity and the Choice of Parameters

Small increments in the orbital velocities are linearly related to small increments in the elements a, e and i. A multitude of combinations of these three parameters, both linear and nonlinear, can be defined. The linear combinations preserve the linear mapping of small velocity increments and will map similar-sized velocity distributions into similar-sized families in the three parameters. Nonlinear combinations of the three parameters, particularly e and i, will map similar-sized velocity distributions into different-sized families. When hunting families in a three-parameter space one should be aware that impacts would give similar-sized velocity distributions and the choice of parameters, search technique, and classification criteria should be able to rec-

ognize the resulting families. Because it is a conserved quantity for Kozai's 2ω perturbation, Kozai (1979) used $(1-e^2)^{1/2} \cos i$ as one of his parameters, along with the minimum i value during the 2ω perturbation, and a. The first of these parameters is a nonlinear function of both e and i. It has the property that when e becomes small and i is not, it will be mainly a function of i which is already a separate parameter. Thus, for small e, clusters of asteroids in i and a, but not e, can appear as clusters in the three parameters because two of the parameters are not sufficiently independent.

C. Size of the Asteroid Sample

Numbered asteroids are rapidly approaching 4000, more than triple the sample available to Hirayama; the more recent classifications, even those that have included PLS asteroids, actually used a smaller total data sample. Such a large sample of numbered asteroids means, of course, better statistics, and can therefore have a positive influence, improving the reliability of the results of statistical methods and checks of Table I.

D. Identification of Families

Different investigators have used several automatic and visual techniques and sometimes mixes. The automatic techniques have adjustable parameters and the visual techniques have explicit or implicit criteria. There is normally agreement between investigators on the major families; there is agreement between some of the investigators on some of the minor families; and there are considerable differences between different investigators on many minor clusters. The differences between investigators are partly due to differences in their samples and partly due to different techniques. If the problem of family identification was simple, we would expect more agreement so these differences point up the complexity of the problem. Various techniques and criteria should be explored.

E. Identification of Interlopers

Here, a reasoning in part similar to that of the previous point applies; the problem is inherently of a statistical nature, since we can at most infer what is the probable number of interlopers in a well-established family, but cannot identify them only on the basis of statistical and dynamical information. Consideration of physical characteristics, taxonomy and the like can be of help in this respect, after the dynamical and statistical aspects of the problem are clearly settled.

F. Future Work

We see that, beyond a modest number of families, the problem of asteroid families is controversial. Published works in the field show discrepancies in the results, and important ingredients like the theories for computing

proper elements, are still being refined. Given the importance of the issue (that represents a key to understanding the evolution of the asteroid belt), it is desirable that future classifications incorporate, as much as possible, what has been learned from past work, in order to give more reliable results. In this respect, a viable approach could be to carry out future classifications using more than one procedure for those aspects that can meaningfully be dealt with by alternative methods. In practice, a future work in which the best available proper elements were used on the larger sample of asteroids available today, using a variety of techniques to find the clusterings, would hopefully improve our understanding of controversial families. If also the proper elements coming from the linear theory were used, for comparison purposes only, then we could also understand some of the discrepancies among the published classifications, thereby removing some old controversies. Once the goal is accomplished from the dynamical point of view, then further studies, taking into account physical characteristics and the possible mechanisms of family formation, should give a check of the results based on independent evidence.

REFERENCES

Alfvén, H. 1969. Asteroidal jet streams. *Astrophys. Space Sci.* 4:84–102.
Applegate, J. F., Douglas, M. R., Gursel, Y., Sussman, G. J., and Wisdom, J. 1986. The outer solar system for 200 million years. *Astron. J.* 92:176–194.
Arnold, J. R. 1969. Asteroid families and "jet streams." *Astron. J.* 74:1235–1242.
Batrakov, Yu. V., et al., eds. 1987. *Ephemerides of Minor Planets for 1988* (Leningrad: Nauka Press).
Bien, R., and Schubart, J. 1987. Three characteristic orbital parameters for the Trojan group of asteroids. *Astron. Astrophys.* 175:292–298.
Bowell, E., Gehrels, T., and Zellner, B. 1979. Magnitudes, colors, types and adopted diameters of the asteroids. In *Asteroids,* ed. T. Gehrels (Tucson: Univ. of Arizona Press), pp. 1108–1129.
Brouwer, D. 1951. Secular variations of the orbital elements of minor planets. *Astron. J.* 56:9–32.
Brouwer, D., and Clemence, G. M. 1961. *Methods of Celestial Mechanics* (New York: Academic Press), p. 526.
Brouwer, D., and van Woerkom, A. J. J. 1950. The secular variations of the orbital elements of the principal planets. In *Astron. Papers Amer. Ephemeris* 13, Part 2, pp. 85–107.
Carpino, M., Farinella, P., Froeschlé, C., Gonczi, R., Paolicchi, P., and Zappalà, V. 1986. The accuracy of proper orbital elements and the properties of asteroid families: Comparison with the linear theory. *Icarus* 68:55–76.
Carpino, M., Milani, A., and Nobili, A. M. 1987. Long-term numerical integrations and synthetic theories for the motion of the outer planets. *Astron. Astrophys.* 181:182–194.
Carusi, A., and Massaro, E. 1978. Statistics and mapping of asteroid concentrations in the proper elements' space. *Astron. Astrophys. Suppl.* 34:81–90.
Carusi, A., and Valsecchi, G. B. 1982. On asteroid classifications in families. *Astron. Astrophys.* 115:327–335.

Farinella, P., Froeschlé, C., and Knežević, Z. 1988. The puzzle of asteroid families. In *Long-Term Dynamical Behaviour of Natural and Artificial N-Body Systems,* ed. A. E. Roy (Dordrecht: Kluwer Academic Publishers), pp. 237–244.

Froeschlé, C., and Scholl, H. 1987. Orbital evolution of asteroids near the secular resonance ν_6. *Astron. Astrophys.* 179:294–303.

Froeschlé, C., Farinella, P., Carpino, M., Froeschlé, C., Gonczi, R., Paolicchi, P., Zappalà, V., and Knežević, Z. 1988. Asteroid families. In *The Few-Body Problem,* ed. M. J. Valtonen (Dordrecht: D. Reidel), pp. 101–116.

Gradie, J. C., Chapman, C. R., and Williams, J. G. 1979. In *Asteroids,* ed. T. Gehrels (Tucson: Univ. of Arizona Press), pp. 359–390.

Hahn, G., and Rickman, H. 1985. Asteroids in cometary orbits. *Icarus* 61:416–442.

Hirayama, K. 1918. Groups of asteroids probably of common origin. *Astron. J.* 31:185–188.

Hirayama, K. 1919. Further notes on the families of asteroids. *Proc. Phys.-Math. Soc. Japan* 3(1):52–59.

Hirayama, K. 1920. New asteroids belonging to new families. *Proc. Phys.-Math. Soc. Japan* 3(2):236–240.

Hirayama, K. 1923. Families of asteroids. *Japan J. Astron. Geophys.* 1:55–93.

Hirayama, K. 1928. Families of asteroids. Second paper. *Japan J. Astron. Geophys.* 6:137–162.

Hirayama, K. 1933. Present state of the families of asteroids. *Proc. Imp. Acad. Japan* 9:482–485.

Klačka, J. 1989. The population of large asteroid families. In preparation.

Knežević, Z. 1989. Asteroid long-periodic perturbations: the second order Hamiltonian. *Cel. Mech.,* in press.

Knežević, Z., and Jovanović, B. 1987. Asteroid short-periodic perturbation: Critical eccentricity and inclination for analytically derived mean semimajor axes. In *Interplanetary matter,* eds. Z. Ceplecha and P. Pecina (Prague: Publ. of Astron. Inst. of Czech. Acad. of Sciences), pp. 107–110.

Knežević, Z., Carpino, M., Farinella, P., Froeschlé, C., Froeschlé, C., Gonczi, R., Jovanović, B., Paolicchi, P., and Zappalà, V. 1988. Asteroid short-periodic perturbations and the accuracy of mean orbital elements. *Astron. Astrophys.* 192:360–369.

Kozai, Y. 1962. Secular perturbations of asteroids with high inclination and eccentricity. *Astron. J.* 67:591–598.

Kozai, Y. 1979. The dynamical evolution of the Hirayama family. In *Asteroids,* ed. T. Gehrels (Tucson: Univ. of Arizona Press), pp. 334–358.

Kresák, L'. 1971. Orbital selection effects in the Palomar-Leiden asteroid survey. In *Physical Studies of Minor Planets,* ed. T. Gehrels, NASA SP-267, pp. 197–210.

Kresák, L'., and Klačka, J. 1988. Selection effects of asteroid discoveries and their consequences. *Icarus,* submitted.

Laskar, J. 1988. Secular evolution of the solar system over 10 million years. *Astron. Astrophys.* 198:341–362.

Lebofsky, L. A., Matson, D. L., Veeder, G. J., and Tedesco, E. F. 1986. The IRAS asteroid thermal model. In *Infrared Astronomical Satellite Asteroid and Comet Survey,* ed. D. L. Matson, JPL D-3698, Preprint Version No. 1, pp. 7.1–7.18.

Lindblad, B. A., and Southworth, R. B. 1971. In *Physical Studies of Minor Planets,* ed. T. Gehrels, NASA SP-267, pp. 337–352.

Marsden, B. G., ed. 1986 and 1987. *Minor Planet Circulars* Nos. 11375–12624.

Matson, D. L., ed. 1986. *Infrared Astronomical Satellite Asteroid and Comet Survey,* JPL D-3698, Preprint Version No. 1, Section III-1.

Milani, A., Carpino, M., Hahn, G., and Nobili, A. M. 1989. Project Space-guard: Dynamics of planet-crossing asteroids. Classes of orbital behaviour. *Icarus,* in press.

Scholl, H. 1987. Dynamics of asteroids. In *The Evolution of the Small Bodies of the Solar System,* eds. M. Fulchignoni and L'. Kresák (Amsterdam: North-Holland), pp. 53–78.

Schubart, J. 1982. Three characteristic parameters of orbits of Hilda-type asteroids. *Astron. Astrophys.* 114:200–204.

van Houten, C. J., van Houten-Groeneveld, I., Herget, P., and Gehrels, T. 1970. The Palomar-Leiden survey of faint minor planets. *Astron. Astrophys. Suppl.* 2:339–448.

Williams, J. G. 1969. Secular Perturbations in the Solar System. Ph.D. Thesis, Univ. of California at Los Angeles.

Williams, J. G. 1971. Proper elements, families, and belt boundaries. In *Physical Studies of Minor Planets,* ed. T. Gehrels, NASA SP-267, pp. 177–181.

Williams, J. G. 1979. Proper elements and family memberships of the asteroids. In *Asteroids,* ed. T. Gehrels (Tucson: Univ. of Arizona Press), pp. 1040–1063.

Williams, J. G., and Faulkner, J. 1981. The positions of secular resonance surfaces. *Icarus* 46:390–399.

Williams, J. G., and Hierath, J. 1987. Palomar-Leiden minor planets: Proper elements, frequency distributions, belt boundaries, and family memberships. *Icarus* 72:276–303.

Yuasa, M. 1973. Theory of secular perturbations of asteroids including terms of higher orders and higher degrees. *Publ. Astron. Soc. Japan* 25:399–445.

ASTEROID FAMILIES: PHYSICAL PROPERTIES AND EVOLUTION

CLARK R. CHAPMAN
Planetary Science Institute

PAOLO PAOLICCHI
Università di Pisa

VINCENZO ZAPPALÀ
Osservatorio Astronomico di Torino

RICHARD P. BINZEL
Massachusetts Institute of Technology

and

JEFFREY F. BELL
Hawaii Institute of Geophysics

Asteroid families are considered to be the fragments from collisional destruction of precursor bodies. As such, they offer the potential for examining the disassembled interiors of large bodies and for studying individual catastrophic collisions of much larger scale than can be done in the laboratory. Now that augmented lists of family members are available, and now that much data exists on the inferred mineralogy, size distributions and spins of family members, we should be in a position to realize this potential. However, results do not confirm the expectations of the simple, traditional model. Only a handful of nearly 100 proposed families (mostly the populous families) have distributions of inferred mineralogies consistent with simple cosmochemical models for parent bodies. Size distributions appear to indicate less thorough fragmentation than expected from collisional physics. Apparent ejection velocities show systematic asymme-

tries and have other differences from expectations. Doubt is cast on the physical reality of many of the less populous families; if they are real, then our understanding of asteroid spectral reflectances, meteorite parent bodies, asteroid cosmogony and dynamics, and collisional physics must be re-evaluated. We suggest one possible resolution: most catastrophic collisions (depending on target properties) may not result in observable families, but rather in a spray of smaller particles, thus accounting for the small number of confirmed and consistent families despite evidence for extensive collisional evolution of the asteroids. Most large family members may be rubble piles, and many families may be of comparatively recent origin. Implications for the size distribution of the whole asteroid population are also discussed.

I. INTRODUCTION

Asteroid families, first recognized by Hirayama (1918), are groupings of asteroids significantly clustered in three orbital elements, semimajor axis a, eccentricity e, and inclination i. Hirayama considered that asteroids in a particular family were genetically related. In recent decades, as the pervasive role of inter-asteroidal collisions has become recognized, the predominant hypothesis for the origin of families is by collisional disruption of a precursor parent body. This conjecture remains unproven. The hypothesis seems plausible for some families, and may well be true for all of them. Nevertheless, there are serious technical problems with understanding many of the families as products of collisional breakup, both in terms of their size distributions and their inferred compositions. In this chapter, we describe the problems and speculate on solutions to many of them.

The subject of physical properties of family members is potentially very important. Modern understanding of the asteroids suggests that they are remnant planetesimals from the crucial period of planetary formation some 4.5 Gyr ago. The dominant process that has modified asteroids since those primordial epochs has been collisions. If families can be understood in terms of collisions, then they provide great insight to the collisional processes that have affected all asteroids to a greater or lesser extent, and thus we may hope to "see through" the collisional evolution to understand better the primordial properties of the asteroids. Many questions about the partition of collisional energy into kinetic and rotational energy, about problems of scaling collisional processes from laboratory to asteroidal dimensions, and about fragmentation modes and fragment size distributions can, in principle, be studied directly from Hirayama families.

Another important issue, related to the first, is that families provide the only potential opportunity for planetary scientists to observe planetary interiors directly. Some families may represent the collisional disruption of parent bodies many hundred km in diameter. Thus a family may consist of fragments from the core, mantle and crust of a geochemically differentiated parent body. Alternatively, the parent body may have been undifferentiated and ho-

mogeneous; or, it may have been differentiated but homogenized by cycles of breakup and re-accretion into a rubble-pile structure (Davis et al. 1979). In principle, study of the remaining fragments of a disruption can enable us to reconstruct the original parent body and study its physical and compositional structure in three dimensions. Such reconstructions can then be compared with model asteroids derived by cosmochemists for the parent bodies of suites of meteorites.

The potential utility of families for these purposes can be achieved only if families are truly the result of collisional breakups and if they have not been altered significantly by subsequent evolution. In the simplest view, a family is created instantaneously by a single catastrophic collision. In the typical case, the projectile contributes negligible mass compared with the target parent body, for two reasons: (1) due to the asteroid size distribution, the most common projectile/target mass ratio for breakup is only a little larger than threshold values, which are usually under 1% (see the chapter by Fujiwara et al.); and (2) it is a well-known result of cratering mechanics that the projectile is subject to far greater stresses than the target, it is much more thoroughly fragmented (if not actually pulverized or melted), and it is ejected at very high velocities. Thus the recognizable fragments that compose a family are effectively derived only from the target.

The trajectories of ejection for the separate target fragments translate directly into dispersed orbital elements, as calculated by straightforward celestial mechanics. Subsequent orbital evolution of the fragments involves the well-understood short time-scale randomization of longitude and epoch of perihelion and longitude of the nodes, plus more subtle—but still understood—secular oscillations of e and i. Finally, in the simplest view, subsequent collisional evolution of family members has been slight, so a family is assumed to present a complete view of the precursor body, disassembled, with the orbital differences between fragments and the size distribution reflecting the specific conditions of breakup.

The real picture is much more complex. There are two general types of problems. First, the collisional and dynamical evolution of family members subsequent to formation must certainly be more complex than in the simple view; some progress has been made in understanding those issues. For an older family, many of the fragments may have undergone subsequent collisional evolution; indeed, much of the original mass may be lost, and the loss process may be both size-dependent and composition-dependent (e.g., iron fragments would last longer than weaker rock fragments), which could bias our attempts to reconstruct the mineralogy of the precursor body. In addition, the history of our understanding of the orbital dynamics of asteroids provides little confidence that we fully understand all of the orbital modification processes over time scales much longer than 1 Myr (e.g., due to subtle, or even chaotic, effects of resonances). Therefore we do not know the degree to which

subsequent evolution has dispersed the original fragmental velocity distribution implied by the distribution of a, e and i. Indeed, it is conceivable that unknown dynamical effects may even concentrate genetically unrelated asteroids into groups (e.g., the "jet streams" of Alfvén [1969]), or appear to do so by creating a network of resonance gaps within the general distribution of asteroids (cf. Patterson, personal communication 1988; Bell 1989).

This raises the second general problem: are the family groupings identified by various researchers composed of "true," genetically related asteroids—are the families "real"? Since the first papers by Hirayama, there has been a succession of studies by Brouwer (1951), Arnold (1969), Carusi and Massaro (1978), Kozai (1979), Williams (1979) and others. As noted by various authors (see, e.g. Carusi and Valsecchi 1982), there is rather poor agreement between the separate lists of families. There are two obvious reasons for some of the differences: first, the number of known asteroids has increased dramatically over the decades, both numbered asteroids and Palomar-Leiden Survey (PLS) asteroids with orbits known well enough to incorporate into searches for family clusterings. The later lists are based on a much larger sample than the early ones. Since the last study by Williams, the list of numbered asteroids has nearly doubled. Updated lists based on new proper elements by Knežević et al. (see table in Part VI) are now becoming available. Second, there are differences in family lists because dynamical theories used in calculating so-called proper elements have improved. Proper elements may be thought of as the underlying orbital elements once all short- and long-periodic effects have been removed. Although this field of research remains a lively one with areas of contention, all would agree that the theories applied by Williams and by Knežević et al. are more complete than that applied long ago by Hirayama. This topic is treated in detail in the chapter by Valsecchi et al.

Beyond the obvious reasons for the differences, there remain other uncertainties. There are concerns about the completeness and even validity of the theories that have been used to determine proper elements; and the theories are known to be more reliable or less reliable in various parts of orbital phase space. Also, different investigators have applied different approaches to estimating the statistical confidence of proposed family clusterings, and they have not always been rigorously explained. Subjective criteria have been applied for identifying the "boundaries" of the families. Kozai's families are obviously larger and more inclusive than those of Williams, who has often subdivided large clusters into several separate families. These choices of statistical thresholds and boundary definitions result in a greater or lesser propensity for separate families to be mixed together, or for a certain fraction of supposed family members to be accidental interlopers (background objects).

One approach to addressing these dilemmas is to reverse the logic of family studies. Instead of assuming some or all of the family lists to be correct and using them to understand asteroid collisional processes and precursor

body structures, we may analyze proposed families in terms of observable or inferred physical properties, considered in the light of modern knowledge about asteroids and meteorites, and deduce which of the dynamical families make physical sense. This approach has been used by Chapman (1989) and Bell (1989), who have studied composition-related taxonomic classifications of asteroid family members and have concluded that many, or even most, of the proposed families may not be real by this criterion. To the degree that the proposed families do not make compositional sense, one or more of the following conclusions must be true:

1. The family lists are bogus, due to either theoretical or methodological errors, or due to as-yet-not-understood dynamical complexities;
2. The interpretation of asteroid mineralogy from astronomical observations of reflectance spectra (as summarized in taxonomic classifications) is erroneous;
3. Cosmochemical models for meteorite parent bodies in the asteroid belt are grossly in error.

We will discuss alternative (1) later in this chapter (see also the chapter by Valsecchi et al.). Alternative (2) is addressed by Wetherill and Chapman (1988); see also the chapters by Gaffey et al., Bell et al. and Lipschutz et al. Alternative (3) is beyond the scope of this book, but meteoriticists should take heed.

There have been many advances since the last review on the physical properties of asteroid families (Gradie et al. 1979). Many more asteroids have been studied for physical properties, such as spin period and taxonomic class. There has been much more research on asteroid collisional evolution, some of it based substantially on analysis of families. Furthermore, the lists of families published in 1979 have now been interpreted in physical terms by a variety of authors. Some progress has been made in trying to identify indicators of family evolution, so that "new" and "old" families may be recognized. Finally, there has been the recognition of asteroidal dust belts in the Infrared Astronomical Satellite (IRAS) data (see the chapter by Sykes et al.), some of which are probably associated with asteroid families and are presumably related to them by collisional processing.

In this chapter, we first treat the interpretation of family-member compositions from analysis of taxonomies, and consider them in terms of cosmochemical models for parent bodies. We then treat the physical and orbital properties of family asteroids, especially their mass distributions and implied fragmental velocity distributions, as they are related to our understanding of collisional processes. A related physical trait, rotational-lightcurve properties, of family members is discussed in the chapter by Binzel et al. In the final section, we discuss preliminary work on the evolution of asteroid families, and speculate on the implications of family studies for the nature and evolution of the asteroid population as a whole.

II. TAXONOMY AND COMPOSITIONS OF FAMILY MEMBERS

Based on the Triad taxonomic classifications available (Bowell et al. 1979), Gradie et al. (1979) discussed the inferred compositions, including homogeneity vs heterogeneity, for 47 of Williams' (1979) families for which two or more family members were classified. They concluded, on the basis of the limited classifications available, that many of the more populous families are homogeneous, and consistent with the breakup of a homogeneous parent body. Of the less populous, smaller families, many were found to be homogeneous, but a significant fraction were not. And those families composed of dissimilar members were often difficult to explain in terms of the prevailing interpretations of mineralogy and cosmochemical models for parent bodies. Gradie et al. noted that the sampling of classified asteroids was poor for the smaller families, and generally could not be considered to be different from a random sampling of asteroids at the semimajor axis of each family. They posed the possibility that the smaller families might not be *physically real,* although they preferred the conclusion that they were, ascribing their similarities with nonfamily asteroids as reflecting the same prevailing processes of formation and collisional evolution that affect both family and nonfamily asteroids.

More recent studies have taken advantage of the refinements in asteroid taxonomy and of the much larger data base that has been compiled over the past decade. Bell (1989) has used a relatively recent list of asteroid taxonomic types provided by Tholen; it is somewhat augmented from the published list by Tholen (1984). He has compared the mix of taxonomic classes in families defined by Hirayama (1933), Brouwer (1951), Arnold (1969), Carusi and Massaro (1978), Kozai (1979) and Williams (1979). Bell has adopted some mineralogical interpretations for the various classes, including noncontroversial assignments (e.g., V class = basaltic achondrites) and controversial ones (e.g., S class = stony-irons). He has judged how sensible the proposed families seem to be from a cosmochemical perspective. He concludes that there are only five families that seem to be well established and composed of genetically related asteroids: the Eos, Koronis, Themis and Flora families, plus a subset of the Nysa/Hertha families consisting of the small F-type asteroids, but not the others, which he interprets as interlopers. All five families are fairly homogeneous.

Bell doubts the reality of a large fraction of the remaining families, because they often contain combinations of types which are either geochemically incompatible, or imply low-temperature primitive mineral assemblages co-existing in the same parent body with high-temperature igneous melts. Particularly puzzling is the common association of S types and C types in the same family. This is equally unlikely in terms of both of the competing hypotheses for the composition of S-type asteroids, since neither stony-iron-like nor ordinary-chondrite-like mineralogies are likely to occur in the same parent

body with CM/CI-like material. Bell notes that the boundary between real and doubtful families found in his study corresponds approximately to the distinction between families whose membership is agreed upon by most dynamicists and families about which disagreement exists (see Carusi and Valsecchi 1982). He considers several explanations for this effect, and concludes that the most likely one is that many of the smaller families are *statistically* real (as defined by their orbital elements): their members are *not* fragments of the same parent body but, instead, have been grouped by selective removal of asteroids from adjacent regions of the belt by poorly understood dynamical processes, perhaps analogous to the known secular resonances. The Phocaea group is cited as an example of this process which is already recognized by current dynamical theory. (The Phocaeas were considered a family by all early workers in this area, but were deleted by Williams from his family lists due to the discovery that their region of orbital-element space was isolated from the rest of the belt by secular resonances.)

As others have done, Bell also wonders about the statistical procedures used for identifying families, their boundaries and their statistical significance. While such issues are important for minimizing the frequency of interlopers, the statistical clusters in proper orbital elements are probably real, although Williams has not rigorously demonstrated this. A recent extension of Williams' work to more than a thousand PLS asteroids (Williams and Hierath 1987) confirms the existence of the earlier clusters.

Chapman (1985, 1986a,b) performed preliminary analyses similar to Bell's and reached similar conclusions. Subsequently, Chapman (1987,1989) performed an augmented study which arrives at somewhat different conclusions. In the more complete study, Chapman devised an augmented taxonomy, based on the Tholen (1984) criteria but utilizing a wide variety of data sets, including IRAS albedos (Matson 1986), to obtain constraints on the classifications for 1721 asteroids, including unique best-guess classes for 939 objects. While further refinements on this work can be made, and are underway, Chapman's work provides the largest data base for assessing the compositional make-up of proposed families. Chapman ignored the older family listings of Hirayama, Brouwer and Arnold, and chose to concentrate on the modern work of Williams (1979), Kozai (1979) and Carusi and Massaro (1978). He considered, for example, 83 Williams families for which 2 or more members are classified; this is nearly twice the number in the Gradie et al. (1979) study.

In order to compare whether the mix of taxonomies found within each family was similar or dissimilar to the general asteroid population, Chapman also plotted the ratios of asteroids of each taxonomic class at each semimajor axis. In defining the background distribution, the most populous families were omitted. Chapman then attempted to determine whether or not the mix of taxonomic classes in a family was significantly different from the background distribution at the particular semimajor axis of the family in question. Being "distinct" does *not* necessarily mean homogeneity in Chapman's study. For

example, a mixture of types including low-albedo types would be deemed distinct in the inner asteroid belt, where the background is almost wholly S types. A family might not be distinct, by Chapman's criterion, for a variety of reasons: (a) a homogeneous family is located in a part of the belt where the background has similar homogeneity; (b) a heterogeneous family happens to share the same heterogeneity as its own environs in the belt; and (c) the sampling statistics are too poor to tell that a family is truly distinct. Thus a distinct family is genetically "real," but one that is not distinct in Chapman's sense may or may not be genetically real.

From this study, Chapman confirms that the classical families (Nysa, Maria, Koronis, Eos and Themis, plus subsets of the Flora family) are distinct and thus real. Furthermore, Chapman finds that several additional Williams families are compositionally distinct, and a dozen more are probably distinct (although statistics are poor). Chapman believes that it is possible that *all* of the Williams families are real and genetically related, on the grounds that those that are not distinct are either homogeneous in a zone where the background is the same as the family, or the statistics are inadequate to tell. Unlike Bell, Chapman does not apply cosmochemical criteria to reject a family.

An interesting result of Chapman's studies is that Williams' criteria for defining a family are certainly better than Kozai's. As earlier authors have noted, Kozai adopted much bigger, more inclusive boundaries for his families. From comparisons of taxonomies with the related Williams families, it is clear that the homogeneous families are much more pure in the case of Williams' families than for Kozai's. Kozai's liberal boundaries have introduced innumerable interlopers. An example is Kozai's Parthenope family, which consists of Nysa family members (very distinctly recognizable because they are F types) plus roughly equal numbers of background objects. Carusi and Massaro were much more conservative than the other authors in defining families. Chapman's study shows that those they did identify do not suffer from the problems of Kozai's definitions; about half of their families appear to be distinct. A summary of Chapman's results on "distinctness" are given in Table I (question-marks indicating "probably not distinct" and "probably distinct").

It will be important to augment the data base in order to confirm or deny Chapman's conclusion that some of the smaller Williams families are distinct, and his suggestion that they all might be real. For if that is true, the dilemma raised by Gradie et al. and Bell remains: many of the families do not appear to consist of a plausible mix of mineralogies, in the context of cosmochemistry.

Let us consider some specific families from Williams' lists (his numbers are preceded by "W" below), including some that seem to be real and make good sense, others that might make sense with some changes, and still others that are apparently distinct and real but which have strange compositional mixes. We include illustrations for most of the families discussed, showing the best estimates of sizes and taxonomic classes for family members (Fig.

TABLE I
Number of Distinct Families[a]

Family Source	Distinct?:	Number of Families			
		No	No?	Yes?	Yes
Williams ($N>=5$)		6	13	8	11
Williams ($2<=N<=4$)		37	5	4	0
Williams ($N>=12$)		1	0	3	6
Kozai ($N>=5$)		36	13	6	5
Kozai ($2<=N<=4$)		9	1	1	0
Kozai ($N>=12$)		19	2	4	4
Carusi & Massaro ($N>=5$)		7	3	3	6
Carusi & Massaro ($N>=12$)		3	2	2	4

[a]Question-marks indicate "probably not distinct" and "probably distinct."

1a,b,c,d). The asteroids are plotted on a projection of their three proper elements. Percentages tabulated in each figure give the approximate distribution of taxonomic classes in the background population at the family's indicated semimajor axis.

Examples of Families that Make Cosmochemical Sense

W1+W1A (Themis). This family is entirely composed of low-albedo classes related to the old C class (C, B and F), with many objects appearing to have intermediate properties. The close association of Themis family members both in spectral parameter space and in orbital element space suggests that they are metamorphic grades of carbonaceous chondritic material. The Themis parent body may have originally been of uniform CM-like composition. Upon heating, it developed internal zones of differing metamorphic grades due to the internal temperature gradient. These zones were then spread out for our study by collisional disruption.

W2 (Eos). Gradie and Zellner (1977) found that the *UBV* colors of the Eos family clustered tightly on the boundary between the S and C fields, and that their radiometric albedos were also intermediate to these two classes. This led to the apparently contradictory situation in which the Eos family was thought to be homogenous in composition, while the individual objects were classed as C, S or U based on very small variations in color and albedo (see Gradie 1978, Table 15). The classification scheme of Tholen (1984) eliminated this discrepancy by putting almost all Eos family objects into an enlarged S class. The several Eos family members that have been observed in the 1 to 2.5 μm spectral region exhibit flat reflectance curves with very shallow or nonexistent silicate absorption bands (Bell et al. 1987). These spectra are totally atypical of other S-type asteroids, and more closely resemble classical C-type spectra. Bell (1989) has suggested adoption of a new "K"

class to identify the unique combination of spectral characteristics in the W2 family asteroids. Comparison of the asteroid data with the available meteorite spectra reveals a close similarity with CV and CO chondrites; ureilites cannot be ruled out either. It is possible that either CV's or CO's (but not both) are actually derived from the Eos family. This family now seems established as a product of a homogenous parent body, despite its checkered past. (The picture is complicated only slightly by a few C-like types and by 639 Latona, which has a spectrum and albedo very close to the average for normal S asteroids. One or more of these may be examples, we suggest, of interlopers or background objects.)

Examples of Families that Make Cosmochemical Sense with Minor Modifications to the List of Actual Members

W24/W160 (Nysa/Hertha). See Fig. 1a. Zellner et al. (1977) and Gradie et al. (1979) considered this family (a twin family in Williams' list) as an example of a fragmented fully differentiated enstatite-achondrite parent body, with M-type 135 Hertha the core, and E-type 44 Nysa a surviving fragment of the mantle. This model was disproved by the eight-color asteroid survey, which revealed that all the smaller members of the subfamily W24 are of the otherwise rare F type. (Unfortunately there are no useful data for any of the smaller members of the Hertha subfamily, W160.) The only way to incorporate these objects into the traditional model is to postulate a thin surface layer of metamorphosed chondritic material on the parent body that was never melted or covered over by enstatitic volcanism, despite the complete melting and core formation that occurred in the interior. Furthermore, many fragments of this layer must survive the catastrophic destruction of the parent body, while no similar fragments other than Nysa survive from the mantle. Together these considerations make it seem highly improbable that either Nysa or Hertha is a genuine fragment from the same parent body that produced the smaller F-class objects. In order to make sense of this family, it is necessary to accept W160 as an unrelated family and reject Nysa as an interloper in a family of F-class objects. The extreme rarity of F-class asteroids elsewhere in the belt demands some such interpretation which preserves a common origin for the F's in W24.

W67 (Ceres). See Fig. 1b. This family seems distinct, compared with the background of 2.8 AU, where low-albedo types outnumber S types by about 2 to 1. Four of the 7 members are S types, another is an M type (normally M's are not even 10% of the population), another an even rarer A type, and the final member is the largest asteroid in the belt, Ceres, itself a somewhat unusual G type (perhaps a metamorphosed C type). Models for asteroid collisional evolution demonstrate that Ceres has probably never been disrupted (Davis et al. 1985). How, then, do we explain its physically implausible association with 156-km diameter 39 Laetitia and other S types (thought
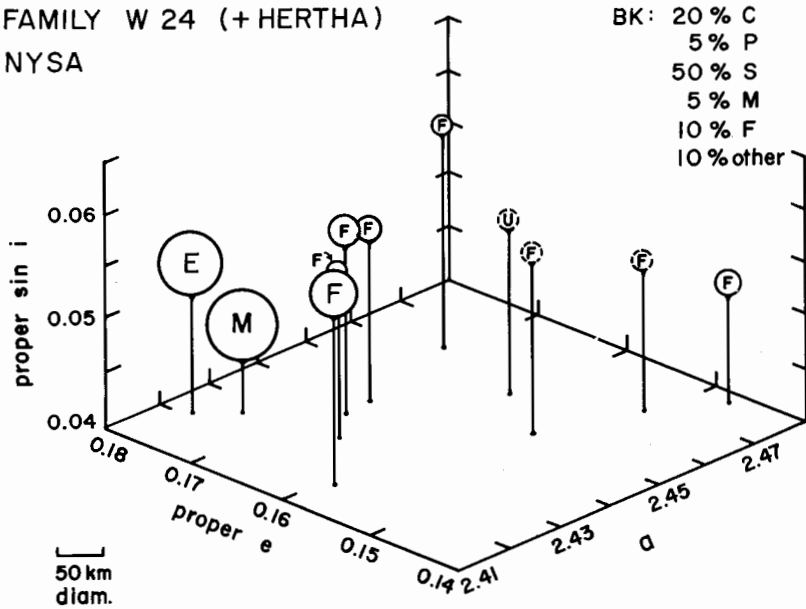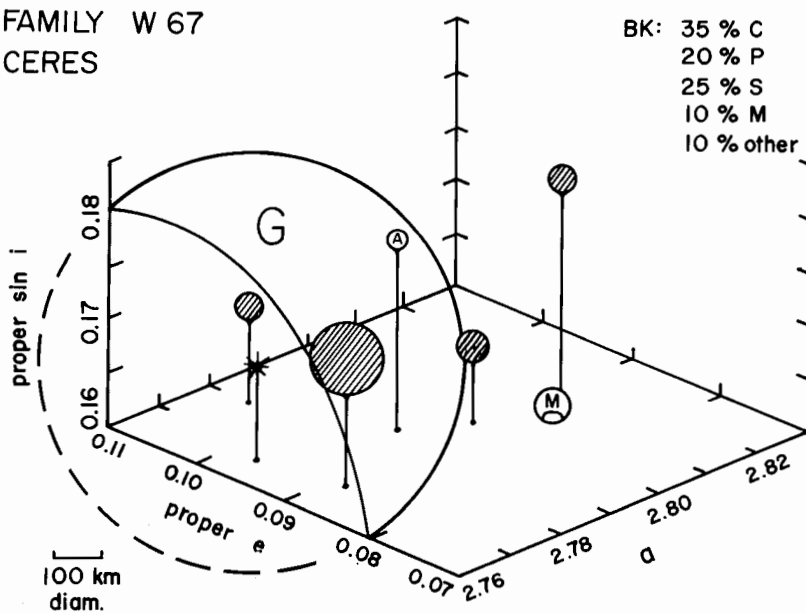
Fig. 1. Perspective plots for four of the families discussed in *a*-proper-*e*-proper sin *i* space. The sizes of the family members are shown to approximate scale (one-half sizes for Ceres family), with dashed outlines if uncertain. The probable taxonomic types are indicated by letters or as follows: cross-hatched = S, solid black = C, solid black with central white = low albedo (e.g., C, P, F, etc.), question-mark = unknown. The listing under BK gives the approximate (bias-corrected) proportions of taxonomic types for background asteroids at the semimajor axis

FAMILY W 124
BUDROSA

BK: 30 % C
30 % P
20 % S
10 % M
10 % other

proper sin i

0.14
0.13
0.12

0.06
0.05
proper e
0.04
0.03
0.02 2.89

2.91
2.93
2.95
a

50 km
diam.

FAMILY W 132
CONCORDIA

BK: 30 % C
15 % P
30 % S
10 % M
15 % other

proper sin i

0.10
0.08
0.07

0.12
0.11
proper e
0.10
0.09
0.08 2.69

2.71
2.73
2.75
a

50 km
diam.
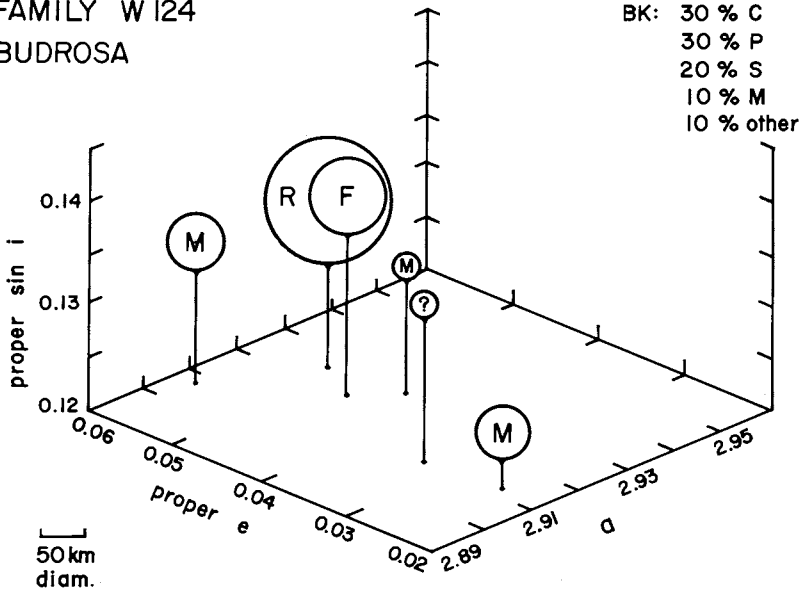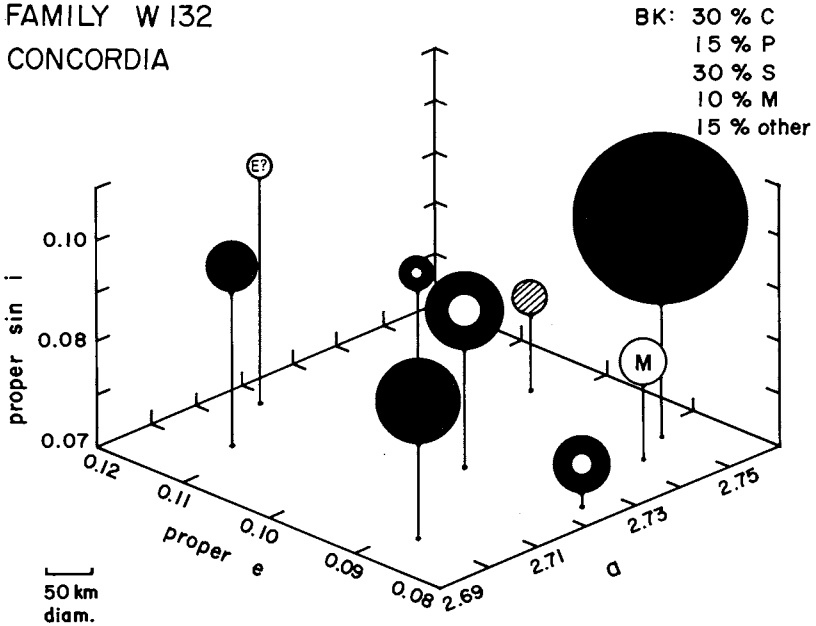
of the family, according to Chapman's analysis; the catalogued-and-classified family members
may be expected to be under-represented in low-albedo asteroids relative to these proportions,
by an uncertain amount. For the Nysa family, 7 additional known family members are not
plotted because proper elements are not available; 4 of these are probable F types, while the
other 3 have not been classified.

to be stony-iron cores or ordinary chondrites)? Must we consider Ceres an interloper in its own family? It would be the second case (Nysa is the first) of two prominent families in which the largest member is considered an interloper. The other members of the Ceres family, considered in the absence of Ceres, could represent the broken-up core and lower-mantle fragments of a precursor body previously stripped of its upper mantle and crust, although few other families, if any, share this cosmochemically plausible mix.

Examples of Families that Make Little Sense

W124 (Budrosa). See Fig. 1c. This family was previously considered by Chapman (1979). The family is dominated by 349 Dembowska, a large, olivine-rich asteroid bearing a unique taxonomic classification, R. At least two (and probably three) family members are rare M types (between 30 and 60 km diameter), thought to be composed of metal. One 80-km diameter member has a very low albedo and is probably a rare F type. The last member has a relatively low IRAS albedo, although it was poorly sampled by IRAS. If the collision was energetic enough to shatter the metal core of the precursor body into three pieces, how could the olivine-rich mantle be represented by a single, much larger object? The canonical model would have the mantle and crustal rocks, which originally surrounded the metal core, thoroughly shattered into much smaller pieces than the strong central core. Also what is the origin of the presumably carbon-rich F-type object? Although F's may be metamorphosed C's, the canonical model of a differentiated parent body with iron core and olivine mantle would not retain any sizeable volumes of carbon-rich mineral assemblages, even if the original body had been carbonaceous.

W132 (Concordia). See Fig. 1d. This is a typical heterogeneous Williams family. With 6 of its 9 classified members being C's or having low albedo, and with only 1 S, this family is somewhat rich in dark asteroids where S's should be outnumbered by only 3 to 2 (although this difference is not statistically significant); the other two members are an M and a possible E. If low-albedo asteroids are primitive carbonaceous objects, how do we account for an associated metal-core body and an S type (whether one believes S types to be ordinary chondrites or stony-irons)? This family illustrates the major problem with the common heterogeneous families: the typical mix of asteroid classes (including C's and S's) is most readily interpreted as being derived from different pots of nebular condensates, not as fragments of differentiated bodies. Even the disfavored onion-shell model for meteorite parent bodies, containing low-albedo material on the outside and a traditional assemblage of high-temperature silicates and metal on the inside, would seem unlikely to fragment into mineralogically "clean" fragments of C's, S's and M's with the numbers and dimensions observed in many of Williams' families.

Let us summarize some conclusions. The compositions of asteroid fam-

ilies shed light on the reality of the family listings; in this regard, Williams' criteria are better than those of Kozai. We must conclude that the question remains open about whether: (a) Bell is correct that most of the smaller Williams families are genetically unrelated clusterings of asteroids, possibly separated by as-yet-unidentified resonance gaps; or (b) Chapman is correct that some of the smaller Williams families are compositionally distinct from the background, suggesting genetic connections despite the frequent incompatibility with cosmochemical parent-body models. In either case, there is more research to be done by both dynamicists and cosmochemists. Of course, it would help if even better and more objective criteria were identified for defining family boundaries and memberships (minimizing interlopers), if the family lists could be extended to all numbered asteroids, and if many more observations of reflectance spectra and albedos could be obtained for family members.

III. MASS DISTRIBUTION

To investigate collisional scenarios, it is crucial to determine the mass distribution (or, equivalently, size distribution) of family members, because it allows direct comparison with laboratory experiments as well as numerical simulations of both the individual breakup process and the overall collisional evolution.

Anders (1965) first studied size distributions of asteroid families. Gradie et al. (1979) made the first comprehensive attempt to reconstruct the precursor bodies for some selected families. Fujiwara (1982) performed a detailed study of the mass distribution of the three classical Hirayama families (Koronis, Eos and Themis). Estimating the kinetic and gravitational energies of the fragmented bodies, he concluded that the three families were completely fragmented at specific impact energies of 10^8 erg g^{-1} or more. However, due to the low relative velocities, most of the fragments should have re-accumulated by mutual gravitation, while the larger members could have rubble-pile structures, roughly fitting hydrostatic equilibrium figures. Similar results were found by Zappalà et al. (1984), who extended the analysis to the whole set of Williams' (1979) families. Although the latter study is more comprehensive, as with all studies of families, it is only as meaningful as the family assignments; as discussed earlier, both the reality and the inferred collisional origin of the major Hirayama families are thought to be more secure for the most populous families than for the smaller Williams families.

The first goal is to reconstruct the total mass of a family and, as a consequence, the mass of its parent body, assuming little mass has been lost. Such reconstruction is useful for defining the approximate minimum size of the parent asteroid, and consequently for a comparison of its size with that of the fragments. As is well known, direct estimates of asteroid masses are extremely rare (Schubart and Matson 1979; see also the chapter by Hoffmann),

while estimates of diameters are more frequent and based on different observational techniques (Bowell et al. 1979; see the compilation by Tedesco in Part VI). In the case of a "true" family, all asteroids *must* be of common origin, assuming target fragments dominate over those from the projectile, which is usually the case. Thus, we might assume the same density for all members (disregarding possible internal differentiation of the parent body) and obtain, instead of a "total mass," an "equivalent size" of the parent body. When direct information on individual diameters is not available, an estimate of the sizes could be made by adopting a certain albedo for each member of a given family, based either on the most common albedo observed within the family (Fujiwara 1982) or, more simply, on their position in the belt (Zappalà et al. 1984), unless other taxonomic data invalidates the assumption of homogeneity. The catalogued population must then be corrected for incompleteness for asteroids with apparent magnitudes fainter than the limits of the family lists (about 15). To complete the cumulative size spectra, Fujiwara (1982) applied the detection bias factor tabulated by Kuiper et al. (1958) and then extrapolated to smaller sizes with a power function. Zappalà et al. (1984) computed the missing mass of the unobserved smaller components using a differential mass distribution, with an assumed exponent of 1.8 as suggested on theoretical grounds by Dohnanyi (1971) for the whole sample of asteroids. Obviously, these procedures yield only a crude estimate of the lower limit for the total mass of each individual precursor body, but they can be usefully employed in statistical analyses. Gradie et al. (1979) tried to reconstruct the sizes of precursor bodies in a somewhat different way, by considering a three-dimensional "jigsaw puzzle" of the largest existing fragments.

In order to analyze detailed mass distributions of specific families, Zappalà et al. (1984) represented the data in terms of the "discrete mass distribution" introduced by Kresàk (1977)

$$M_j/M_0 = (2j\text{-}1)^{[1/(1\text{-}k)]} \tag{1}$$

where M_0 is the mass of the parent body, M_j is the mass of the j-th largest fragment, and k is the exponent of the differential mass distribution. The M_j/M_0 vs j plot for some selected Williams families is given in Fig. 2, where the lines indicate power laws with some different k values.

We can compare the distribution tails, the best-fit exponents, the mass ratios among the largest fragments, and the total masses of the parent bodies. It appears that for large j, the trend is quite similar among most of the families and it can be roughly fit by the usual exponent of ~1.8. A comparison of the results of laboratory experiments on hypervelocity breakups (Fujiwara 1986; chapter by Fujiwara et al.) is particularly instructive. Figure 3 refers to mass distributions of some laboratory experiments plotted as for Fig. 2. The typical k values are similar to those found for the families, although the physical significance is uncertain because of the large difference in scale, ranging from
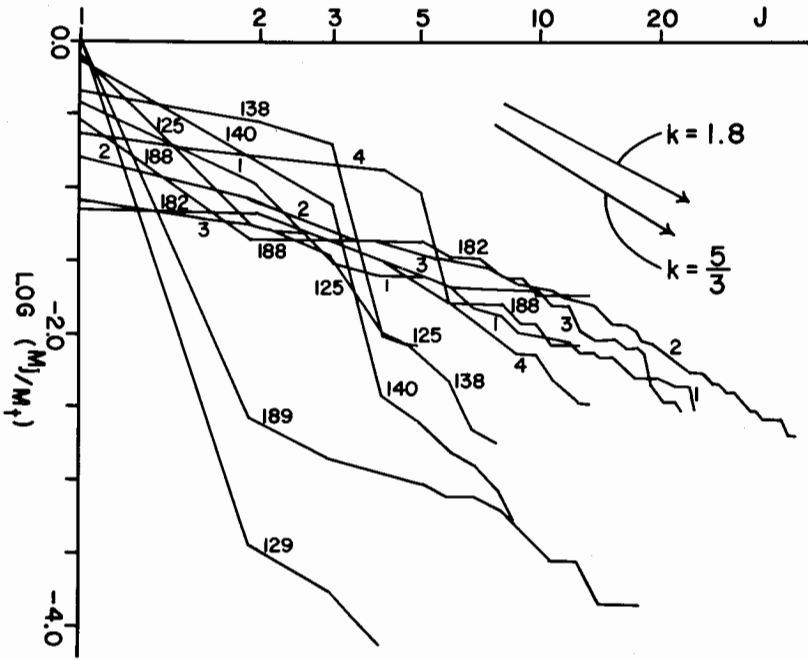
Fig. 2. Log-log plot of the mass of the single fragments for some Williams asteroid families, normalized to the target mass and ordered by their size (M_j is the mass of the j-th fragment).

cm in the case of laboratory experiments up to hundreds of km for major asteroid collisions (cf. Holsapple and Housen 1986; Davis et al. 1985; see also the chapters by Fujiwara et al. and Davis et al.). Also, the values of k are known to vary at least over the range from 5/3 for barely catastrophic impacts to about 2 for supercatastrophic breakups (Matsui et al. 1982,1984).

The behavior of the mass distribution among the largest bodies, in particular the mass ratios among the parent body, the largest fragment and the second largest fragment, deserve further scrutiny. As shown in Figs. 2 and 3, both asteroid families and experiments exhibit a wide range of M_1/M_0 values, but a few families (such as W129 and W189) show an unusual behavior, with a sudden mass drop from the largest to the second largest remnant, which is completely absent among catastrophic fragmentation experiments. Williams (1987,1988) interprets such families to result from subcatastrophic or cratering impacts, which leave most of the precursor body's mass intact as the largest family member; the small family members are interpreted by Williams as crater ejecta. Williams also points out that the largest body is often near the edge of a family in orbital phase space (see below), so that the family members could be thought of as asymmetric cratering ejecta. An alternative expla-
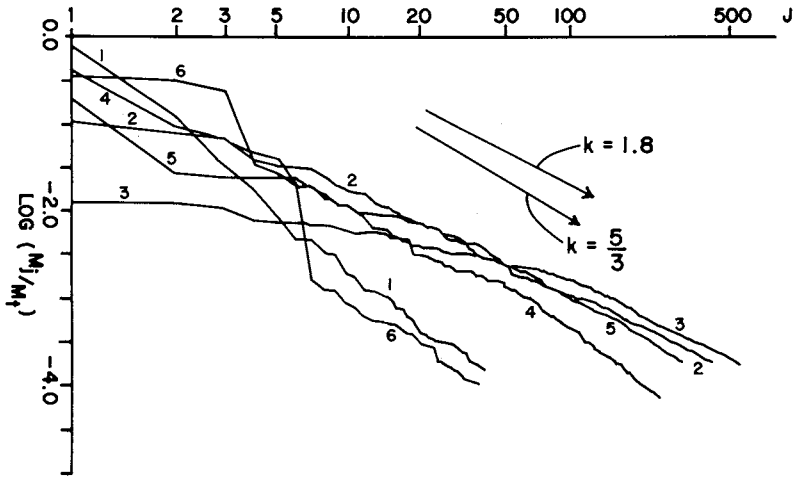
Fig. 3. Same as for Fig. 2, except for 6 laboratory experiments.

nation (Zappalà et al. 1984) for such families, if they are real, involves self-gravitational effects leading to recapture of the slowest escaping fragments onto the largest remnant, forming a single, large rubble pile, accompanied by some smaller pieces that failed to re-accumulate into the main body.

We have analyzed the cumulative distribution of M_2/M_1 for families belonging to different size ranges. We have compared families whose largest remnant is >100 km, intermediate size, or <50 km with typical power laws (Kresák 1977). An excess of small M_2/M_1 is evidently correlated with size, which is consistent with re-accumulation onto the largest fragment, but not onto the other smaller fragments (see the chapter by Weidenschilling et al.). This effect is clearly shown in Fig. 4: M_1/M_0 increases with size, although M_2/M_0 does not.

Unless self-gravitational recapture is also effective in re-accumulating fragments other than the largest one, there is a major discrepancy between the mass distributions for most families and the laboratory results: a scaling of specific energy (E/M) from laboratory experiments to asteroidal sizes predicts much more fragmentation for the asteroids than is seen. In fact, the specific energy necessary to disperse the fragments to infinity, overcoming the gravitational binding of the parent body, is considerably higher than the critical value for breakup observed in the laboratory. The problem is that any reasonable partition of impact energy into breaking the material bonds would break a target body into innumerable tiny pieces, if the impact were sufficiently energetic to provide the kinetic energy necessary to disperse the fragments into a family. Thus we should not expect such similarity between the mass distributions for the laboratory experiments and the asteroid families as we, in fact,
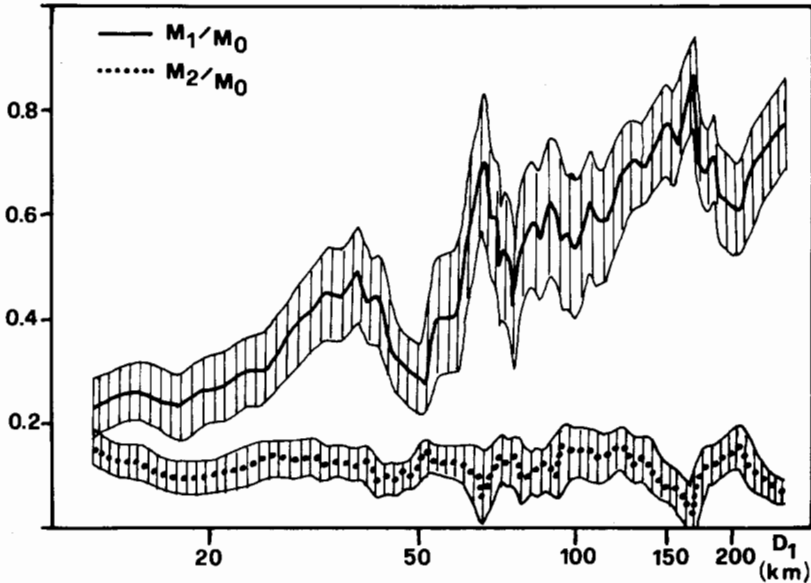
Fig. 4. Running-box plot of M_1/M_0 and M_2/M_0 vs the diameter of the largest remnant.

observe. Davis et al. (1985) suggest that the dilemma could be resolved if the effective strengths for asteroids were exceptionally high. We will return to this dilemma again, and suggest some possible solutions, in Sec. V (also see the chapter by Davis et al.).

IV. INFERRED EJECTION VELOCITY DISTRIBUTIONS

Another aspect of asteroid families which can be compared with experimental data is the apparent ejection velocities of fragments. Of course, precise knowledge of the original ejection velocities depends on unknown geometrical parameters associated with the moment of breakup. Nevertheless, interesting estimates of ejection velocities can be made in terms of the differences between the Williams proper elements (a, e', i') of the family asteroids and those of the largest remnants (cf. Brouwer 1951; Ip 1979; Zappalà et al. 1984). There are at least three inescapable difficulties: (1) we must correct for the retardation of an ejected fragment due to the self-gravitation of the disrupted body; (2) we must assume that there has been no further dispersion due to subsequent orbital evolution of family members; and (3) the velocities depend on two unknown angles at the moment of breakup.

The lack of information about the angles makes it impossible to obtain the actual ejection velocities for individual families. However, for statistical purposes, the problem can be partially overcome by using some mean value of

the trigonometric functions or by exploring the resulting velocities with various assumptions. This was the approach of Zappalà et al. (1984), who studied the proper elements of Williams' (1979) families. The velocity distributions were found to be far from isotropic (even with the most favorable assumptions about the unknown angles) since the implied *rms* values of velocity components in two directions exceed by a factor of 4 or 5 that in the third orthogonal direction. This trend exists even for the three largest classical families (Themis, Koronis and Eos). There is no obvious physical explanation for this result within the collisional theory. Patterson (personal communication, 1988) suggests the problem is an indication of cosmogonic rather than strictly collisional origin for families.

Within the collisional theory, it is possible to ascribe the asymmetry to poor reliability of the proper elements e' and i' for Brouwer's linear-theory proper elements. This was shown by Carpino et al. (1986) by means of numerical integration for 10^4 yr of some "synthetic" families, each of whose central body was taken to correspond to the largest remnant of the most reliable Hirayama families, and with "fragments" taken to be isotropically ejected with the same velocity in all directions. The results were that e' and i', as computed with the aid of the linear theory, fluctuate widely in time. Carpino et al. suggested that uncertainties in the definition of proper elements can cause a systematic "noise" in e' and i', artificially increasing the resulting differences; such effects cannot be completely removed, even within more refined perturbation theories (Knežević et al. 1988).

Based on these considerations, Zappalà et al. (1984) restricted their interpretation of family velocities to the velocity component that depends on the most stable and reliable orbital parameter, the semimajor axis. The resulting value was multiplied by a factor of $\sqrt{3}$ to account for the other two neglected components, assuming overall isotropy. The ejection velocity was then computed by correcting the above velocity at infinity v_∞ for the gravitational slowing down of the fragments escaping from the parent body

$$v = (v_\infty^2 + v_e^2)^{0.5} \tag{2}$$

where v_e is the escape velocity *from the surface of the largest remnant;* more refined computations in Farinella et al. (1988) lead to similar values. Assuming a power-law distribution for the fragment mass vs velocity, provided only that the escape velocity exceeds the minimum allowed value (i.e. that some fragments are gravitationally recaptured), we obtain (Zappalà et al. 1983)

$$dM = Cv^{-\gamma} dv = C (v_e^2 + v_\infty^2)^{-(\gamma + 1)/2} v_\infty dv_\infty = f(v_\infty) dv_\infty. \tag{3}$$

We can easily see how the maximum of f is at $v_\infty = v_e/\gamma^{1/2}$, where γ is not too different from unity. The result is confirmed by Fig. 5, representing the mean value of v (for several Williams families) vs the diameter of the largest
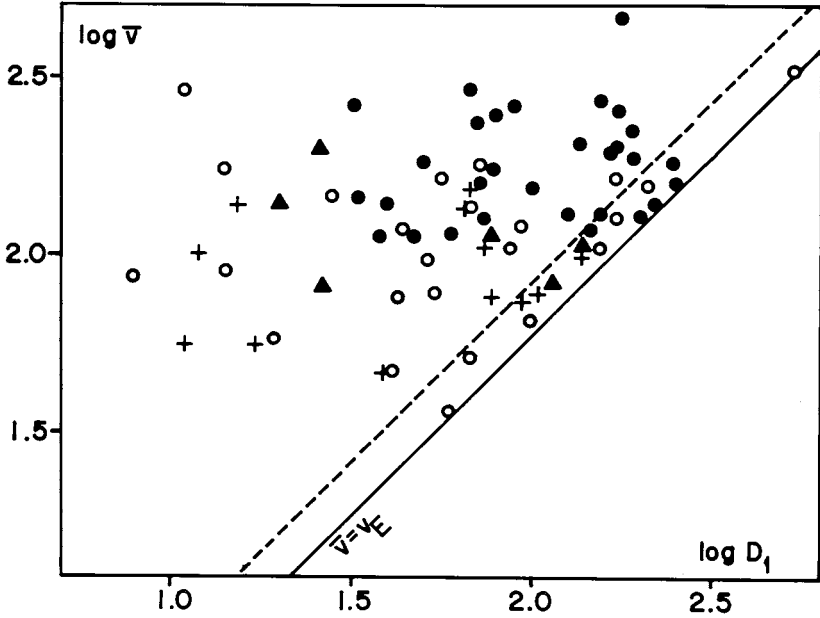
Fig. 5. Log-log plot of mean ejection velocity, in m s⁻¹, vs diameter (km) of the largest remnant.
Solid dots = asymmetric families, open symbols = dispersed, triangles = intermediate cases
and crosses = families with only three members. Diagonal lines bound the region diagnostic of
self-gravitational re-accumulation (figures adapted from Zappalà et al. 1984).

remnant. The solid line represents the obvious limitation $v = v_e$, while the
dotted line corresponds to $v_e = v_\infty$. These considerations are consistent with
the v values found for large, gravity-dominated bodies. It is less easy to under-
stand the large inferred ejection velocities for small target bodies (there are no
velocities lower than 60 m s⁻¹), for which gravitational re-accumulation
should be negligible. This result seems discrepant from experimental break-
ups, for which fragment velocities are generally lower for the same degree of
fragmentation. Similar evidence about larger ejection velocities consistent
with a moderate degree of fragmentation, among solar system bodies, has
been discussed in terms of the supposed catastrophic breakup of the Saturnian
satellite Hyperion (Farinella et al. 1983). This problem of velocity scaling
may be related to the E/M scaling problem mentioned above: in both cases,
the apparent degree of fragmentation seems inadequate for the evident energy.

Ip (1979) first showed that the distribution of Δa within a family can
provide insights on the symmetry of the ejection velocity field, and thus on the
qualitative modalities of the actual breakup. To extend this analysis, Zappalà
et al. (1984) introduced a quantitative symmetry parameter

$$C = \langle v^2 \rangle / \langle v \rangle^2 \qquad (4)$$

where $\langle\rangle$ indicates mean value taken among all fragments except the largest remnant, and the velocities are computed with respect to the center of mass. C distinguishes between the so-called "dispersed" families (i.e., with isotropic velocities $C > \sim N$; N is the number of fragments) and "asymmetric" ones (with most fragments on the same "side"; $1 \leq C < N$). The criterion appears promising, and can be applied also to experiments and numerical simulations. For the families, it was applied only in the single, most reliable dimension. (We have already noted that most families are distributed asymmetrically when considered in 3 dimensions, probably for spurious reasons.) It was concluded
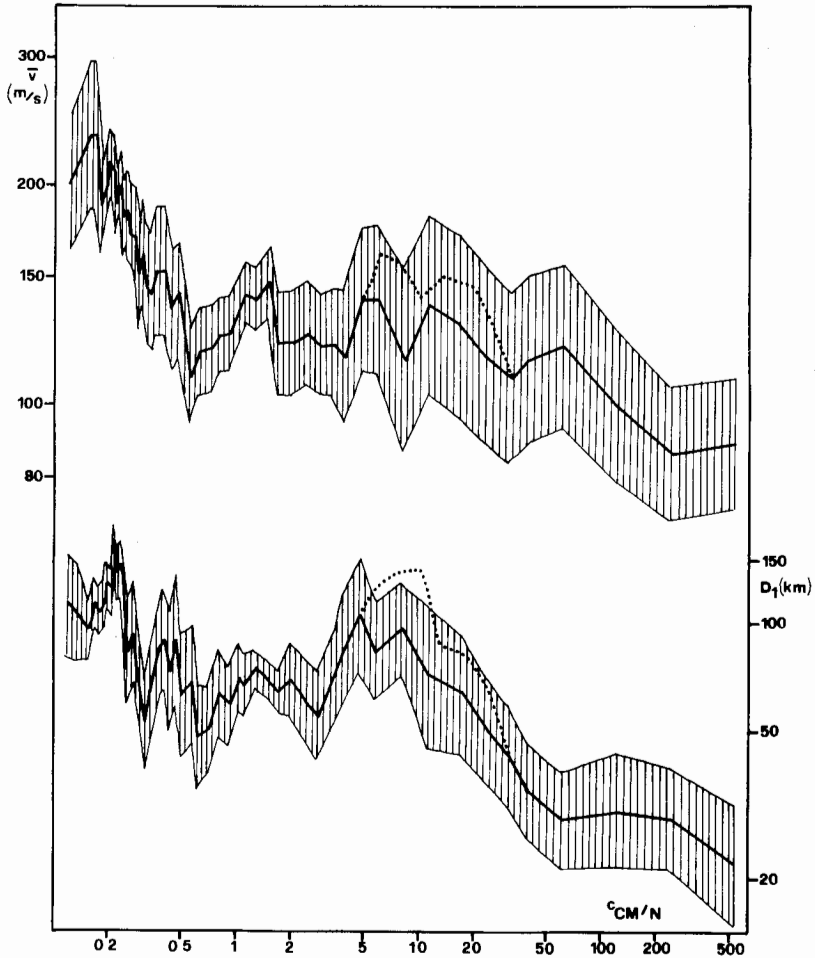
Fig. 6. Running-box diagram of the mean ejection velocity (top) and of the diameter of the largest remnant (bottom) vs the symmetry parameter C/N (where N is the number of objects in the family). The dotted lines are obtained when 1 Ceres is also taken into account.

that asymmetric families generally correspond to larger ejection velocities and larger objects (Fig. 6). Possibly this is related to self-gravitation effects, which could amplify any initial anisotropy of the velocity field.

Recently, Paolicchi et al. (1989) have studied the breakup processes by a simple semi-empirical approach, based on the assumption that fragments are ejected with an explosion-like velocity field and that the rupture criterion is expressed in terms of the derivatives of this field with respect to the position within the target. They derived some average physical properties of the fragments formed in different zones of the target, and analyzed the most important correlations among them for a number of different choices of free parameters of the model. Some correlations seen both in the observations and in the experiments were at least qualitatively confirmed, including increasing spin rates for decreasing sizes, larger ejection velocities for smaller objects, and an almost constant ratio between translational and rotational energies.

Inferred fragmental velocities from orbital elements of asteroid families permit interesting kinematic comparisons. However, a complete understanding of the mass distributions, fragmental shapes, etc. will require much more research. For instance, the geometry of fractures analyzed in the experiments (Fujiwara and Asada 1983; Capaccioni et al. 1986) have not yet been taken into account.

V. EVOLUTION OF FAMILIES AND RELATIONSHIP TO MAIN BELT STRUCTURE

Rather than providing us with clearer insight about the interiors of large broken-up asteroids and about asteroid collisional processes, our analyses of asteroid families are casting some doubts on the reality of many of the families themselves, at least in terms of the paradigm that families are collisional products. To be sure, some families seem to be composed of genetically related bodies, but the mix of compositions and the size distributions are difficult to explain in many cases. Further analysis may well re-affirm the paradigm, but the difficulties must be addressed first.

Particularly troublesome, if only a handful of the most populous families are real, is why there are not more families. A variety of lines of evidence suggests that the asteroids are highly collisionally evolved. For example, the existence of 16 Psyche as a 250-km diameter metallic body (and there are other fairly large M types, too) implies prodigious collisional evolution. As Chapman (1986b) has noted, there is contradictory evidence about the true extent of collisional evolution of the asteroids, but analyses of size distributions, spin rates, elementary particle-in-a-box estimates of collision frequencies, meteoritical evidence, etc.—much of it discussed in other chapters of this book—point to considerable collisional evolution. How can it be that there are only a handful of recognizable families?

If most of Williams' families are indeed real, then there are a number of

problems that must be solved. First, we must understand why the families are so asymmetric in *a-e-i* space; because the asymmetry is systematic (families are "squashed" in the radial direction from the Sun), the explanation must be in terms of either calculation of proper elements or in terms of dynamical evolution. Second, we must understand in more than a hand-waving sense how inter-asteroid collisions can result in size distributions that resemble laboratory experimental results on either catastrophic breakup or subcatastrophic cratering, without invoking physically unrealistic strengths. Third, we must understand the perplexing fact that most asteroid families are cosmochemically unrealistic. Perhaps the solutions to some of these problems will turn out to reflect other cosmogonic and evolutionary processes that are not yet understood. Let us consider some possible ways to approach these problems, in terms of family evolution.

So far, the paradigm for interpreting families has wholly involved collisional processing. Perhaps because of the discrediting some years ago of Alfvèn's (1969) ideas about cosmogonic (jet-stream) processes for formation of families, alternative cosmogonic approaches have been unjustly ignored. But they may play some role. For example, Patterson (personal communication, 1988) has suggested that both families and large asteroids may be located at preferential distances from the Sun, due to primordial resonance effects. This could partly explain the association between large, possibly unrelated interlopers and cosmochemically real families, such as those found in the Nysa and Ceres families, discussed above. It is not yet understood how resonance effects might either concentrate asteroids into clusters in *a-e-i,* or alternatively clear asteroids away from clusters, following the Phocaea analogy; but that remains a logical possibility for understanding most of Williams' families as statistically real clusters (though even that has not been rigorously demonstrated) but not as genetically related asteroids. We worry, however, that any such processes yet to be identified should just happen to form apparent families having just the dispersion expected for collisionally brokenup fragments (ejection velocities of hundreds of m s^{-1}).

Whether families were formed by cosmogonic processes or by collisional breakup, they must continue to evolve. Although such evolution has not been studied thoroughly, there is a general presumption that on some time scale shorter than the age of the solar system, asteroid orbits may evolve away from their original locations. If so, older families would gradually disperse. The characteristic mixing distance indicated by the overlapping distributions of the various taxonomic classes when plotted as a function of distance from the Sun (~1 AU) could be an indication of the general mixing scale. On the other hand, it may be that different types of asteroids were originally formed at identical solar distances, for instance, if asteroid accretion took place episodically or sequentially over a period of time in which the nebula was changing characteristics. Some researchers even believe that the heliocentric distribution of types reflects not primordial zonation but rather the processes that

implanted asteroids into the belt from other locations in the solar system (cf. Wasson 1988). But if asteroid orbits do generally evolve and move over distances of 1 AU, then families should disperse and become unrecognizable. Then the families that are recognized would have to be either the most recently created families, or those somehow especially protected from such dispersal. Although it is difficult to be certain, it is our impression that families do not disperse in this manner for two reasons: (a) we do not see a complete range of apparent ejection velocities for different families, and (b) we do not see more widely, partially dispersed examples of such families as the Nysa and Eos families, which would be readily recognizable—even if quite widely dispersed—due to their nearly unique colors (taxonomic classes).

Another way in which families must evolve is collisionally. All aspects of collisional evolution are potentially recognizable, including generation of a collisionally evolved size distribution and generation of collisionally evolved spins. In general, little work has been done to study such indicators of collisional evolution, partly because of incomplete data. Binzel (1988) did study the spins of members of the Eos and Koronis families and compared them with a control sample. Workers in this field assume that collisional evolution should generate something approaching a Maxwellian distribution of spin periods and axis orientations (see the chapter by Binzel et al.). Although that hypothesis is model dependent itself, Binzel nevertheless adopted it and concluded that while the Eos family had generated such an evolved distribution, the Koronis family had not. In essence, many Koronis family members may "remember" the original spin of the precursor body and have not collided enough to have their spins randomized. Binzel is very uncertain, however, of the time duration that separates the two families. For instance, different original conditions of an impact event can generate very different outcomes, both in terms of mass and of spin rate distributions (see Paolicchi et al. 1989). Also perhaps related to collisional evolution and relative youth are the degrees to which families have had time to generate and dissipate an associated dust belt (see the chapter by Sykes et al.).

Let us now offer some speculations on (a) why family size distributions resemble laboratory experiment results despite the role of gravity, and (b) why there is an apparent absence of families (particularly assuming Williams' smaller families are not real products of breakups), despite abundant evidence for pervasive collisional evolution of the asteroid population. In particular, we will suggest why it may be that only a minority of collisions produce observable families at all, and why families, once produced, may be collisionally destroyed on a short time scale.

We suggest that, in principle, production of families by collisional fragmentation may be a common process, but that a typical collision does not generally yield individual, coherent fragments of observable sizes (i.e., diameter >20 km) so that most produced families are not detectable. As we will describe, there may be particular parent-body structures or collisional circum-

stances that do yield observable families, though even some of these may be dispersed by subsequent collisional and/or dynamical evolution.

As we have discussed (see also the chapter by Davis et al.), model calculations imply that, for unshattered targets, collisions sufficiently energetic to disperse fragments into a family are necessarily supercatastrophic, and they will generate a size distribution with many unobservably small fragments, but no large observable fragments. The only way to produce large fragments may be if an asteroid is made of materials stronger than metal, which is inappropriate for the rocky and carbonaceous objects that comprise much of the asteroid population (even taking into account the increased strength due to self-compression). A tempting but speculative scenario is suggested at the top of Fig. 7. As discussed, an unshattered target might yield size and velocity distributions similar to those of observed families only (a) if the strength is exceptionally large, or (b) if, after the impact event, some fragments somehow regroup into larger bodies with rubble-pile structures. Obviously, the re-accumulation of bodies from the escaping fragments requires that they be grouped in very concentrated jets. We do not know if such a phenomenon could ever really happen, and this intriguing possibility is not yet supported by any explicit laboratory or astronomical evidence (see the chapter by Fujiwara et al.; also Zappalà et al. 1984).

If it is difficult to form families from strong targets, it is even more difficult to produce large, observable family members from weak targets. Therefore, we expect that no observable families can be produced from impacts into weak target bodies for *any* value of the specific energy for shattering (Fig. 7, case 2).

The case of a rubble-pile target body, already re-accumulated following previous catastrophic events, is more complicated (Fig. 7, case 3). Impacts into rubble-pile targets have never been investigated by laboratory experiments. In particular, we have little idea about the effective strength of such a body and no idea about the fraction of impact energy converted into kinetic energy of the fragments. Therefore, we can only suggest some very speculative hypotheses. For instance, it could happen that the impact disperses such a body into a spray of very small pieces. On the other hand, it could happen that only the elements of the rubble-pile that are close to the impact point would be broken into still smaller pieces, while the remaining elements of the rubble-pile might survive, possibly being ejected at rather high velocities. Such a scenario could yield an observable family whose size distribution is like that of a less energetic event but decoupled from the velocity distribution. The usual modeling in terms of impact strength and the fraction of impact energy partitioned into kinetic energy of the fragments (cf. the chapter by Davis et al.) would be meaningless in this case.

Finally, the bottom of Fig. 7 shows the possible collisional outcomes for a parent body with differentiated structure (strong core and weaker mantle). High-energy impacts could disperse the mantle completely and shatter the
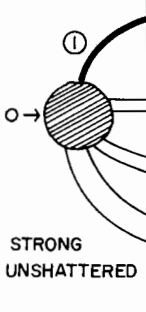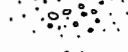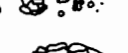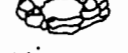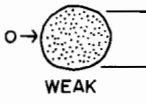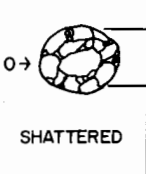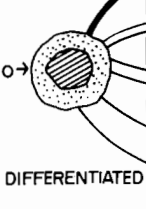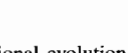
TARGET	E/M_T	OUTCOMES OF SINGLE IMPACT	IS A FAMILY OBSERVABLE ?	POST-IMACT EVOLUTION
① STRONG UNSHATTERED	HIGH		NO (even for very strong target)	—
	MEAN		YES (but for very strong target)	⟹ GO TO ①
			YES (but for peculiar ejection of frag.)	⟹ GO TO ③
	LOW		NO	⟹ GO TO ③
	VERY LOW		NO	⟹ GO TO ①
② WEAK			NO	—
③ SHATTERED			NO	—
			YES	⟶ GO TO ① AND ③
			NO	⟹ GO TO ④
			NO	⟹ GO TO ③
④ MULTIPLY SHATTERED			NO	—
⑤ DIFFERENTIATED	HIGH		YES	⟹ GO TO ①
	MEAN		NO	⟹ GO TO ①
	LOW		YES	⟶ GO TO ① AND ②
	VERY LOW		NO	⟶ GO TO ⑤ AND/OR ①

Fig. 7. Speculations on the collisional evolution of families. Five cases show large initial asteroids, about to be struck by projectiles. Initial outcomes and subsequent evolution proceed to the right. The smallest asteroid fragments are too small to be seen; any family composed solely of such small family members (apart from a single large-target remnant) would not be observable as a family. Collisional outcomes are different depending on relative size and velocity of the projectile (subcases are indicated for high-to-low values of E/M_T).

core, yielding a size distribution of core fragments similar to that expected for an impact into an exceptionally strong target. In fact, the real strength of the core could be augmented by the overburden of the mantle.

According to our speculation, it is most difficult to produce large family members from weak materials. In that connection, it is interesting to note that the most secure families are invariably composed of what are inferred to be relatively strong materials. The following are all of the Williams families with 5 or more members that are deemed to be distinct from the background by Chapman (1989) and are of fairly homogeneous composition: Hungaria (E type), Nysa (chiefly F type), Maria (S type), Leto (S type), Koronis (S type), Eos (K type) and Themis (many C's, but more than half B's and F's). None of these families are composed of the C or P types, which are the two most populous classes of asteroids and the two thought to be of most primitive composition. We assume here that the F and B types represent metamorphism of a C-type body. K type (proposed by Bell 1989) could be a ureilite (differentiated), or CO or CV type chondrites which are primitive (although meteorite samples are quite hard). The other types listed above all indicate metamorphism or differentiation. In fact, the remaining three Williams families ($N \geq 5$) regarded by Chapman (1989) as certainly distinct but *not* homogeneous (the Eugenia, Lydia and Budrosa families) are all composed predominantly of M's, S's, F's, T's and R's, but again contain no C's or P's. It may be that primitive types are inherently weak and that when the larger ones are broken up, they simply do not yield large fragments. This has some observational support, at least in the case of the C types, since the observed size distribution for C types shows a major deficit of asteroids in the size range 40 to 100 km diameter, compared with an extrapolation of the power law for sizes larger than 150-km diameter (see the chapter by Gradie et al.). Low-impact energies might yield a large preserved core plus a mantle completely dispersed into unobservable small pieces, or a preserved core with a few relatively large mantle fragments. Such possibilities could explain the unexpectedly large abundance of metallic bodies in families and, perhaps, the nature of some of the families that are composed of members of different taxonomic types.

We cannot be sure which of the elements of the traditional paradigm are necessarily wrong. There are warnings in our review for those who calculate proper elements, devise family lists, work on asteroid collisional physics, interpret asteroid spectra, and devise meteorite parent-body models. One or more of these disciplines may require serious revision. It is possible that asteroid families are actually of cosmogonic origin, with collisions having played a minimal role. We believe, however, that some of the families—and possibly all of those identified by Williams, but not by Kozai—may be real products of precursor breakup. We suggest, however, that many catastrophic collisions do not yield families. Those families that do exist may evolve rapidly and have short lifetimes before dispersing through collisional evolu-

tion (and possibly also dynamical dispersion). Koronis may be a particularly young family. Families may not be volumetrically representative of their precursor bodies, and may consist chiefly of rubble piles. The nature of such families sheds light on the modality of asteroid collisions, necessary for understanding the large-scale structure of the asteroid belt, discussed in chapters by Gradie et al. and Bell et al., including, (a) the relative lack of middle-size C-type asteroids, and (b) the relationship between main-belt asteroids and their smaller collisional products that get transferred into Earth-crossing orbits, the Apollo/Amors and the meteorites.

REFERENCES

Alfvén, H. 1969. Asteroidal jet streams. *Astrophys. Space Sci.* 4:84–102.

Anders, E. 1965. Fragmentation history of asteroids. *Icarus* 4:398–408.

Arnold, J. R. 1969. Asteroid families and "jet streams." *Astron. J.* 74:1235–1242.

Bell, J. F. 1988. Mineralogical clues to the origins of asteroid dynamical families. *Icarus* submitted.

Bell, J. F., Hawke, B. R., and Owensby, P. D. 1987. Carbonaceous chondrites from S-type asteroids? *Bull. Amer. Astron. Soc.* 19:841 (abstract).

Binzel, R. 1988. Collisional evolution in the Eos and Koronis families: observational and numerical results. *Icarus* 73:303–313.

Bowell, E., Gehrels, T., and Zellner, B. 1979. Magnitudes, colors, types and adopted diameters of the asteroids. In *Asteroids*, ed. T. Gehrels (Tucson: Univ. of Arizona Press), pp. 1108–1129.

Brouwer, D. 1951. Secular variation of the orbital elements of the minor planets. *Astron. J.* 56:9–32.

Capaccioni, F., Cerroni, P., Coradini, M., DiMartino, M., Farinella, P., Flamini, E., Martelli, G., Paolicchi, P., Smith, P. N., Woodward, A., and Zappalà, V. 1986. Asteroidal catastrophic collisions simulated by hypervelocity impact experiments. *Icarus* 66:487–514.

Carpino, M., Gonczi, R., Farinella, P., Froeschlé, C., Froeschlé, C., Paolicchi, P., and Zappalà, V. 1986. The accuracy of proper orbital elements and the properties of asteroid families: Comparison with the linear theory. *Icarus* 68:55–76.

Carusi, A., and Massaro, E. 1978. Statistics and mapping of asteroid concentrations in the proper element space. *Astron. Astrophys. Suppl.* 34:81–90.

Carusi, A., and Valsecchi, G. B. 1982. On asteroid classification in families. *Astron. Astrophys.* 115:327–335.

Chapman, C. R. 1979. The asteroids: Nature, interrelations, origin, and evolution. In *Asteroids*, ed. T. Gehrels (Tucson: Univ. of Arizona Press), pp. 25–60.

Chapman, C. R. 1985. Compositions of Hirayama family members. *Bull. Amer. Astron. Soc.* 17:730 (abstract).

Chapman, C. R. 1986a. Do observations of Hirayama families tell us about parent-body interiors? *Meteoritics* 21:345–346 (abstract).

Chapman, C. R. 1986b. Implications of the inferred compositions of the asteroids for their collisional evolution. *Mem. Soc. Astron. Italiana* 57:103–114.

Chapman, C. R. 1987. Distributions of asteroid compositional types with solar distance, body diameter, and family membership. *Meteoritics* 22:353–354 (abstract).

Chapman, C. R. 1989. Compositional structure of the asteroid belt and its families. *Icarus*, to be submitted.

Davis, D. R., Chapman, C. R., Greenberg, R., Weidenschilling, S. J., and Harris, A. W. 1979. Collisional evolution of asteroids: Populations, rotations, and velocities. In *Asteroids,* ed. T. Gehrels (Tucson: Univ. of Arizona Press), pp. 528–557.

Davis, D. R., Chapman, C. R., Weidenschilling, S. J., and Greenberg, R. 1985. Collisional history of asteroids: Evidence from Vesta and the Hirayama families. *Icarus* 62:30–53.

Dohnanyi, J. S. 1971. Fragmentation and distribution of asteroids. In *Physical Studies of Minor Planets,* ed. T. Gehrels NASA SP-267, pp. 263–295.

Farinella, P., Milani, A., Nobili, A. M., Paolicchi, P., and Zappalà, V. 1983. Hyperion: Collisional disruption of a resonant satellite. *Icarus* 54:353–360.

Farinella, P., Paolicchi, P., Cellino, A., and Zappalà, V. 1988. Escape velocity for fragments of collisionally shattered solar-system bodies. *Bull. Obs. Astron. Belgrade* 138:88–90.

Fujiwara, A. 1982. Complete fragmentation of the parent bodies of Themis, Eos, and Koronis families. *Icarus* 52:434–443.

Fujiwara, A. 1986. Results obtained by laboratory simulations of catastrophic impact. *Mem. Soc. Astron. Italiana* 57:47–64.

Fujiwara, A., and Asada, N. 1983. Impact fracture patterns on Phobos ellipsoids. *Icarus* 56:590–602.

Gradie, J. C. 1978. An Astrophysical Study of the Minor Planets in the Eos and Koronis Asteroid Families. Ph.D. Thesis, Univ. of Arizona.

Gradie, J. C., and Zellner, B. 1977. Asteroid families: Observational evidence for common origins. *Science* 197:254–255.

Gradie, J. C., Chapman, C. R., and Williams, J. G. 1979. Families of minor planets. In *Asteroids,* ed. T. Gehrels (Tucson: Univ. of Arizona Press), pp. 359–390.

Hirayama, K. 1918. Groups of asteroids probably of common origin. *Proc. Phys.-Math. Soc. Japan,* series 2, 9:354–361.

Hirayama, K. 1933. Present state of the families of asteroids. *Proc. Imp. Acad. Japan* 9:482–485.

Holsapple, K. A., and Housen, K. R. 1986. Scaling laws for the catastrophic collisions of asteroids. *Mem. Soc. Astron. Italiana* 57:65–85.

Ip, W. 1979. On the three types of fragmentation processes observed in the asteroid belt. *Icarus* 40:418–422.

Knežević, Z., Carpino, M., Farinella, P., Froeschlé, C., Froeschlé, C., Gonczi, R., Jovanovic, B., Paolicchi, P., and Zappalà, V. 1988. Asteroid short-periodic perturbations and the accuracy of mean orbital elements. *Astron. Astrophys.* 192:360–369.

Kozai, Y. 1979. The dynamical evolution of the Hirayama families. In *Asteroids,* ed. T. Gehrels (Tucson: Univ. of Arizona Press), pp. 334–358.

Kresák, L. 1977. Mass content and mass distribution of the asteroids system. *Bull. Astron. Inst. Czech.* 28:65–82.

Kuiper, G. P., Fujita, Y., Gehrels, T., Groeneveld, I., Kent, J., Van Biesbroeck, G., and van Houten, C. J. 1958. Survey of asteroids. *Astrophys. J. Suppl.* 3:289–428.

Matson, D., ed. 1986. *Infrared Astronomical Satellite Asteroid and Comet Survey: Preprint Version No. 1,* JPL Doc. D-3698.

Matsui, T., Waza, T., Kani, K., and Suzuki, S. 1982. Laboratory simulation of planetesimal collision. *J. Geophys. Res.* 87:10968–10982.

Matsui, T., Waza, T., and Kani, K. 1984. Destruction of rocks by low velocity impact and its implications for accretion and fragmentation processes of planetesimals. *Proc. Lunar Planet. Sci. Conf.* 14, *J. Geophys. Res.* 89:B700–B706.

Paolicchi, P., Cellino, A., Farinella, P., and Zappalà, V. 1989. A semiempirical model of catastrophic breakup processes. *Icarus* 77:187–212.

Schubart, J., and Matson, D. L. 1979. Masses and densities of asteroids. In *Asteroids,* ed. T. Gehrels (Tucson: Univ. of Arizona Press), pp. 84–97.

Tholen, D. J. 1984. Asteroid Taxonomy from Cluster Analysis of Photometry. Ph.D. Thesis, Univ. of Arizona.

Wasson, J. T. 1989. The building stones of the planets. In *Mercury,* eds. F. Vilas, C. R. Chapman and M. S. Matthews (Tucson: Univ. of Arizona Press), pp. 622–650.

Wetherill, G., and Chapman, C. R. 1988. Asteroids and meteorites. In *Meteorites and the Early Solar System,* eds. J. F. Kerridge and M. S. Matthews (Tucson: Univ. of Arizona Press), pp. 35–67.

Williams, J. G. 1979. Proper elements and family memberships of the asteroids. In *Asteroids*, ed. T. Gehrels (Tucson: Univ. of Arizona Press), pp. 1040–1063.

Williams, J. G. 1987. Less well known asteroid families. *Bull. Amer. Astron. Soc.* 19:824 (abstract).

Williams, J. G. 1988. Asteroid families. Asteroids II, Abstract Booklet, 8–11 March, Tucson, AZ.

Williams, J. G., and Hierath, J. E. 1987. Palomar-Leiden minor planets: Proper elements, frequency distributions, belt boundaries, and family memberships. *Icarus* 72:276–303.

Zappalà, V., Farinella, P., and Paolicchi, P. 1988. Collisional origin of asteroid families: Effects of the target's gravity. In *Dynamical Trapping and Evolution in the Solar System,* eds. V. V. Markellos and Y. Kozai (Dordrecht: D. Reidel), pp. 177–188.

Zappalà, V., Farinella, P., Knežević, and Paolicchi, P. 1984. Collisional origin of asteroid families: Mass and velocity distributions. *Icarus* 59:261–285.

Zellner, B., Leake, M., Morrison, D., and Williams, J. G. 1977. The E asteroids and the origin of the enstatite achondrites. *Geochim. Cosmochim. Acta* 41:1759–1767.

ASTEROID ROTATION RATES: DISTRIBUTIONS AND STATISTICS

RICHARD P. BINZEL
Massachusetts Institute of Technology

PAOLO FARINELLA
Università di Pisa

VINCENZO ZAPPALÀ and ALBERTO CELLINO
Osservatorio Astronomico di Torino

Within the last decade the data base of asteroid rotation parameters (rotation rates and lightcurve amplitudes) has become sufficiently large to identify some definite trends and properties which can help us to interpret asteroid collisional evolution. Many significant correlations are found between rotation parameters and diameter, with distinct changes occurring near 125 km. This size range, which is also the diameter above which self-gravity may become important, perhaps represents a division between surviving primordial asteroids and colli- sional fragments. A Maxwellian is able to fit the observed rotation rate distribu- tions of asteroids with D > 125 km, implying that their rotation rates may be determined by collisional evolution. Asteroids with D < 125 km show an excess of slow rotators and their non-Maxwellian distributions suggests that their rota- tion rates are more strongly influenced by other processes, such as the distribu- tion resulting from their formation in catastrophic disruption events. Other correlations observed in the data set include different mean rotation rates for C, S and M type asteroids implying that their surface spectra are indicative of different bulk properties. No correlation is found between orbital and rotational parameters, although such an investigation is hampered by bias and selection effects. A comparison of rotational parameters between family and nonfamily asteroids suggests that the Koronis and Eos families exhibit noticeable differ-

ences possibly due to different impact conditions and/or to a relatively younger age for the Koronis family. Near-Earth asteroids display significantly higher maximum lightcurve amplitudes than small main-belt asteroids, although this is probably the result of their being observed over a wider range of phase and aspect angles. However, the lack of data for similar-sized main-belt asteroids makes a meaningful comparison difficult.

I. INTRODUCTION

Among the fundamental observable parameters of the asteroids is their rotation rates. Because rotational angular momentum is gained or lost through collisions, characterizing the properties of asteroid rotation rates is essential for achieving an understanding of their collisional evolution. The shapes of most asteroids are also affected by collisions and approximate shapes can be inferred from observed lightcurve amplitudes. In this chapter we analyze the measured distributions of asteroid rotation rates and lightcurve amplitudes. The observational techniques for determining these parameters are described in the chapter by Harris and Lupishko. Although some implications of these results are discussed here, a more detailed treatment of asteroid collisional evolution is presented in the chapter by Davis et al.

In the past decade there has been a tremendous increase in the number of asteroids for which rotation rates and lightcurve amplitudes have been determined owing to systematic programs by Harris, Binzel, Zappalà and others. Figure 1 shows the sampling completeness of these rotational parameters as a function of diameter for the numbered main-belt asteroids. Asteroids larger than 200 km have been fully sampled while only about one half of the 100-km asteroids have measured rotational parameters. For our analysis of rotational periods and lightcurve amplitudes, we have used the compilation prepared by Lagerkvist et al. (1988); see Part VI of this book. Certain selection effects are present in such a data base. For example, it is observationally easier to determine reliable and publishable parameters for an asteroid that displays a short rotation period with a large lightcurve amplitude. In our analysis we attempt to eliminate bias effects as much as possible by including all asteroids for which Lagerkvist et al. have assigned reliability codes ≥1 (see Part VI). We have directly checked that excluding poor reliability objects of class 1 results into overweighing asteroids with large amplitudes and short periods, introducing a significant bias in the results of the statistics (see also bias analysis in Binzel [1987, Fig. 2]). In addition, we exclude altogether results from photographic photometry which have been shown to have inherent selection effects against periods >12 hr and amplitudes <0.2 mag, as discussed by Binzel and Mulholland (1983).

Diameters and taxonomic types have been taken from the compilations by Tedesco and by Tholen in Part VI of this book. If diameters are not listed by them, we used the taxonomic type of the asteroid to infer its likely albedo and to compute its diameter from its absolute magnitude. In the few
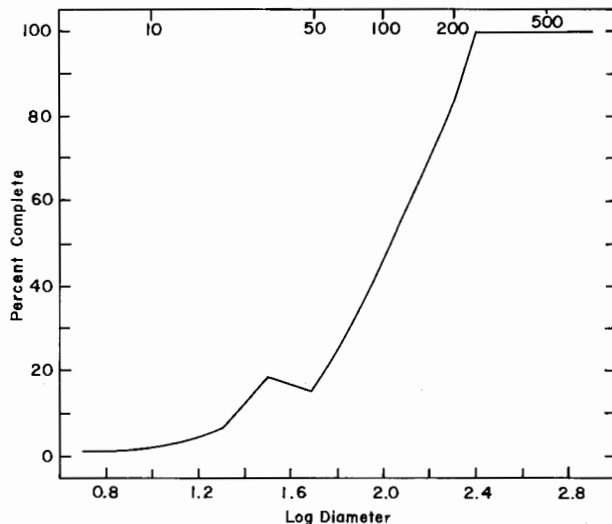
Fig. 1. Completeness of asteroid rotation data as a function of log diameter for numbered main-belt asteroids. Data are from the compilation by Lagerkvist et al. in Part VI. The peak near 30 km is due to dedicated photoelectric surveys within that size range (Binzel and Mulholland 1983; Binzel 1987).

cases where not even the taxonomic type was available, the latter has been guessed from the most abundant observed type at that heliocentric distance. We adopted S type for $a < 2.7$ AU and C type for $a > 2.7$ AU. This procedure is obviously rough; however, it should not introduce serious errors in the statistics, since it was generally applied to very faint objects for which even a large difference in albedo cannot change the inferred diameter drastically in absolute terms.

II. ANALYSIS OF ROTATION RATES

In our analysis, we assume that an asteroid is in a simple state of rotation about its principal axis. If an asteroid can be approximated by a triaxial ellipsoid having semiaxes $a \geq b \geq c$, then the moments of inertia about these axes are $I_a \leq I_b \leq I_c$. Because rotational energy E is described by

$$E = L^2/2\,I \tag{1}$$

the lowest energy state for a given angular momentum L occurs for rotation about the maximum moment of inertia axis c. Although off-center collisions tend to misalign the rotation axis from this principal axis and induce a free precession or wobble, Burns (1971) and Burns and Safronov (1973) have

shown that damping from internal stresses returns the asteroid to its lowest rotational energy state in a relatively short time scale (e.g., $\sim 10^5$ yr for a 100-km asteroid). Because this time scale is inversely proportional to diameter, small asteroids ($D < \sim 1$ km) are the best candidates for observing free precession. Sher (1971) and Barsuhn (1983) have illustrated how lightcurves from such tumbling bodies might appear, but no certain cases of free precession have been observed to date. Future detection and lightcurve measurements of such bodies could place important constraints on the interior structure of asteroids. A second type of precession, forced precession due to the presence of an external torque, has perhaps been detected for two asteroids with extremely long rotational periods, 288 Glauke (Harris 1983) and 1220 Crocus (Binzel 1985), where the external torque is applied by a hypothetical satellite (see the chapter by Weidenschilling et al.).

Figure 2a shows the distribution of rotation rate Ω (revolutions/day) vs log diameter for the whole data set except for the planet-crossing Aten-Apollo-Amor (AAA) asteroids and members of the Themis, Eos, Koronis and Maria families. Family asteroids and planet-crossing are discussed separately in this chapter (Sec. V and VI; see also the chapters by McFadden et al. and Chapman et al.). The interesting lightcurve properties of the Trojan and Hilda asteroids are covered in the chapter by French et al.

The most notable structure in what otherwise appears to be a scatter diagram is a marked increase in the dispersion of rotation rates towards smaller diameters. A useful illustrative technique which was first applied to asteroid rotation data by Dermott et al. (1984) is the "running-box" mean. Figure 2b is a running-box diagram for the same data set where a box size of $n = N/10$ was used while shifting through the sample one object at a time. (For the smaller samples in subsequent figures, we have used $n = N/3$ or $n = N/5$). The envelope depicts plus and minus one standard deviation from each mean. It must be stressed that for a data set of size N and a box size n, there are only N/n independent measurements, plotted in such a diagram. Although the small-scale features in this diagram cannot be considered meaningful, the overall V-shape first noted by Dermott et al. (1984) is significant. There appears to be a steady decrease in rotation rate from the smallest asteroids up to about $D = 100$ km. A classical explanation for this effect as suggested by McAdoo and Burns (1973) is that, because of their lower intrinsic moments of inertia and the increasing number of small projectiles, small asteroids more frequently undergo collisions which significantly affect their rotational angular momenta. Since the vector components of the incoming angular momentum are added quadratically to the existing angular momentum, collisions tend to spin-up a body's rotation rate in a random-walk fashion. Therefore the expected observational result is a trend for increasing spin rates with decreasing diameters. However, it is now being recognized (see the chapter by Davis et al.) that this spin-up towards smaller sizes might also be a natural result of equipartition of energy among these bodies if they are fragments resulting
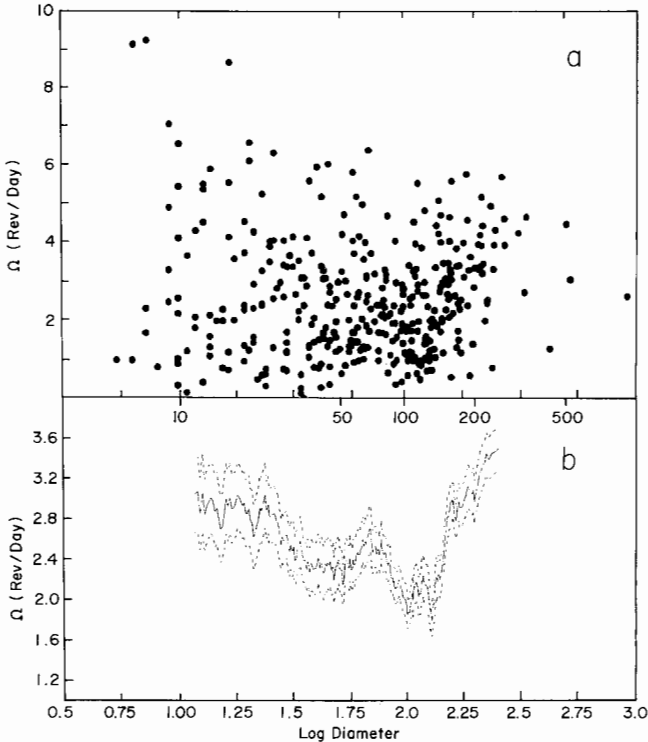
Fig. 2.(a) Plot of rotation rates (rev/day) vs log diameter from the data base in Part VI, excluding
the planet-crossing asteroids and members of the major families. (b) Running-box diagram for
the same data set. The solid line gives the mean for a box size of $n = N/10$, shifted one value at
a time over the entire diameter range. One sigma uncertainties are shown above and below the
mean (dashed lines). The overall V-shape of the distribution is a real characteristic of the data
set. The greater dispersion of rotation rates for smaller asteroids is apparent in both plots.

from catastrophic disruption events. Further, the survival times for small
asteroids (before they also are disrupted) may be too short for significant
random-walk increases in spin rates.

The minimum at 100 to 125 km and the steep increase of Ω between
~125 km and ~200 km, first noticed by Farinella et al. (1981a), is an inter-
esting feature which may be the result of an effect called "angular momentum
drain" proposed by Dobrovolskis and Burns (1984). For cratering impacts on a
rotating body, ejecta traveling in the prograde direction are preferentially lost
due to their additional rotational velocity component. The corresponding
drain effect on the rotation rate is

$$\Delta\Omega \sim \Omega_o \, (M_{loss}/M_o) \qquad\qquad (2)$$

where Ω_o and M_o are the asteroid's initial rotation rate and mass and M_{loss} is the mass which preferentially escapes from the asteroid in the prograde direction. M_{loss} is a function of the asteroid's escape velocity and the ejecta's velocity distribution. For the largest asteroids, the escape velocity is high and no ejecta escape. For small asteroids, the escape velocity is low and all of the ejecta escape. Thus angular momentum drain has its greatest effect on asteroids in the intermediate size range. Further collisional modeling is needed to verify whether this effect can fully account for the observed minimum of Ω in this size range. It should also be noted that at about 70 km there is a peak in the rotation rate curve. Even though the validity of small-scale features is very uncertain for this kind of representation, this peak is also reproduced in the amplitude-diameter plot (see Fig. 7b below) and therefore could be connected with a real physical effect.

Figure 3 presents running-box diagrams of rotation rate vs diameter for the three main compositional classes of asteroids from Tholen's tabulation in Part VI of this book (see also the chapter by Tholen and Barucci). Qualitatively, the curves all show the characteristic V-shape although there is a noticeable offset between the three types. For a given diameter, C asteroids show slightly slower rotation rates than S asteroids. This difference may only be truly significant for the M asteroids which show distinctly faster rotation rates. Interestingly, a similar $C > S > M$ trend may be seen in the diameter at which the inflection point of the V-shaped distribution occurs. Tholen's C asteroids turn up at larger diameters than S asteroids which turn up at larger diameters than M asteroids (whose sample, however, is so small that adding even one object might appreciably change the shape of the curve). An interpretation of these trends is that there may be different relative bulk properties for the different asteroid classes. M class asteroids probably have higher bulk densities and impact strengths than S and C asteroids. This is consistent with the spectroscopic interpretation that M asteroids have relatively higher metal abundances and that C asteroids are more primitive. S class asteroids may have intermediate bulk properties. (See the chapter by Bell et al.) Bodies with higher impact strengths would display faster rotation rates because they are able to survive longer and undergo more energetic collisions (without being disrupted) thus significantly increasing their rotational angular momentum.

We now examine the histogram distribution of rotation rates. This distribution has been frequently compared with Maxwellian distributions (see, e.g., Harris and Burns 1979; Farinella et al. 1981a), for which a sufficient condition is that all three components of Ω are distributed according to a Gaussian with zero mean values and equal dispersions. In fact, it is plausible to expect that this is the typical outcome for a collisionally evolved system (see Salo 1987). However, asteroids are not a gas composed of equal mass, elastically colliding particles, and there are many physical reasons why discrepancies from the Maxwellian outcome might be generated. For instance, a population of "young" (collisionally unrelaxed) fragments might tend to "re-
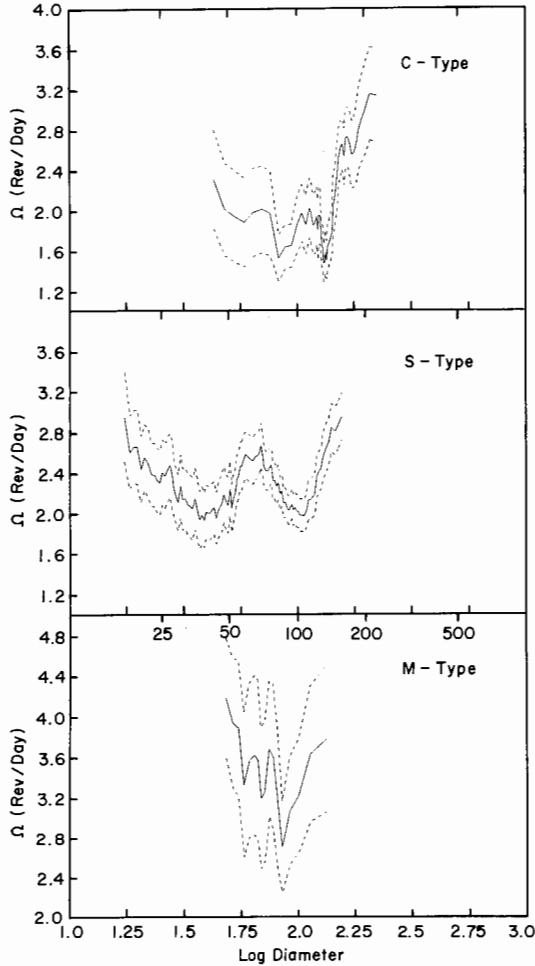
Fig. 3. Running-box diagrams of rotation rate vs log diameter for C, S and M compositional classes as defined by Tholen (1984) and listed in Part VI. Note that the ordinate for the M asteroids is significantly offset. Differences between the compositional classes may imply different bulk properties. Similar trends are observed for the compositional classes defined by Barucci et al. (1987) except that there is no apparent shift in the diameters at which the minima occur.

member" the spin rate of the parent body, and in this case one would expect a distribution narrower than Maxwellian about the spin rate of the parent; or, alternatively, "young" fragments could include a large fraction of slow rotators, yielding a distribution wider than Maxwellian (which tends to zero proportionally to Ω^2 for values of Ω much less than the mean). But a "wide"

distribution might also result from an inhomogeneous sample, namely from the superposition of two or more (or a continuous range) of Maxwellian functions, and in this case it is impossible to invert uniquely the observed distribution to derive the makeup of the dispersion. Notice, moreover, that assuming the same (zero-mean, Gaussian) distribution for the three components of Ω implies also that asteroid rotation poles are isotropically distributed on the celestial sphere (see the chapter by Magnusson et al.). Even taking into account these considerations, a comparison of observed distributions with a Maxwellian may give some insight as to whether or not the asteroids represent a collisionally evolved population.

The Maxwellian distribution has the form

$$f(\Omega) = \sqrt{\frac{2}{\pi}} \frac{N\Omega^2}{\sigma^3} \exp\left(\frac{-\Omega^2}{2\sigma^2}\right) \tag{3}$$

where $f(\Omega) \, d\Omega$ is the fraction of objects in the range $(\Omega, \Omega + d\Omega)$ and

$$\Omega_\mu = \sqrt{\frac{8}{\pi}} \, \sigma \tag{4}$$

is the mean. Figure 4 shows a histogram distribution for the entire sample of rotation rates and its best-fit Maxwellian made by a least-squares estimate of σ after having split the distribution into 20 equal bins over the range of 0 to 10
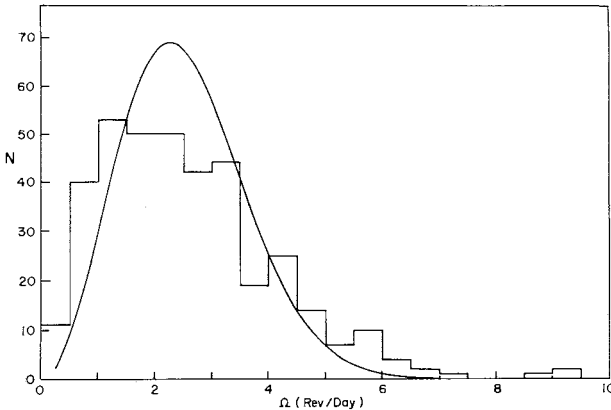
Fig. 4. A histogram distribution of rotation rates for the entire data set where the range of 0 to 10 rev/day has been divided into 20 equal bins. Cases where data values listed as upper or lower limits tied with bin boundaries have been adjusted in the proper direction. The solid curve gives the best fit Maxwellian distribution although the data show a relative excess of slow and fast rotation rates and the fit is formally rejected. For the chi-squared tests for goodness of fit in Table I, the high Ω bins with few objects were grouped together.

rev/day. Table I lists σ and also gives the result of a chi-squared test of the fit to the distribution. We use standard hypothesis testing techniques and take as the null hypothesis, H_o: "the sample is fit by a Maxwellian distribution." The confidence level criteria as to whether or not we should reject H_o are: <90% cannot reject H_o; 90 to 95% can marginally reject H_o; >95% can reject H_o.

A clear excess of slowly rotating asteroids is apparent in Fig. 4, as has been noted by Farinella et al. (1981a). For a Maxwellian with $\sigma = 1.595$ only 11 out of 375 asteroids would be predicted to have $\Omega < 1.0$ ($P > 24$ hr); our sample has 51. For $\Omega < 0.5$, only 2 asteroids would be predicted and 11 are observed. There also appears to be an excess tail of fast rotators and the results of the chi-squared test formally reject the fit of the entire data set by a Maxwellian.

We investigate the Ω distribution further by breaking it down into four diameter groups divided around 125 km, which is the minimum in Fig. 2. A Maxwellian fit is shown for each sample in Fig. 5, and the chi-squared test results (Table I) show that an acceptable fit is obtained only for the two largest-diameter groups. An interesting interpretation of this fit may be that $D > 125$ km asteroids may have reached an evolved state of collisional evolution by having long survival lifetimes (against catastrophic disruption) compared to the age of the solar system. However, preliminary collision models such as described by Davis et al. find that the largest asteroids do not evolve significantly from their primordial rotation rates.

Asteroids with $D < 125$ km clearly show the most non-Maxwellian dis-

TABLE I
Maxwellian Fits of the Distribution of Ω

Sample	N	σ	χ^2	Degrees of Freedom	Conf. Level	Interpretation
All	375	1.595	121.5	9	>99%	reject
$D < 50$ km	134	1.734	158.0	9	>99%	reject
$50 \leq D < 125$	136	1.325	27.2	7	>99%	reject
$125 \leq D < 200$	75	1.622	9.9	7	<90%	cannot reject
$D \geq 200$	30	2.179	8.6	9	<90%	cannot reject
C (Tholen)	62	1.421	26.5	7	>99%	reject
C (Barucci)	68	1.366	17.1	7	~99%	reject
S (Tholen)	125	1.538	22.4	7	>99%	reject
S (Barucci)	71	1.604	8.0	7	<90%	cannot reject
M (Tholen)	24	2.493	6.7	9	<90%	cannot reject
M (Barucci)	22	2.478	7.8	9	<90%	cannot reject
AAA	28	3.600	209.2	9	>99%	reject
$D \leq 15$	23	1.681	24.5	7	>99%	reject
Eos	23	2.303	10.4	9	<90%	cannot reject
Koronis	22	1.416	20.5	7	>99%	reject
Nonfamily	21	1.264	22.6	7	>99%	reject
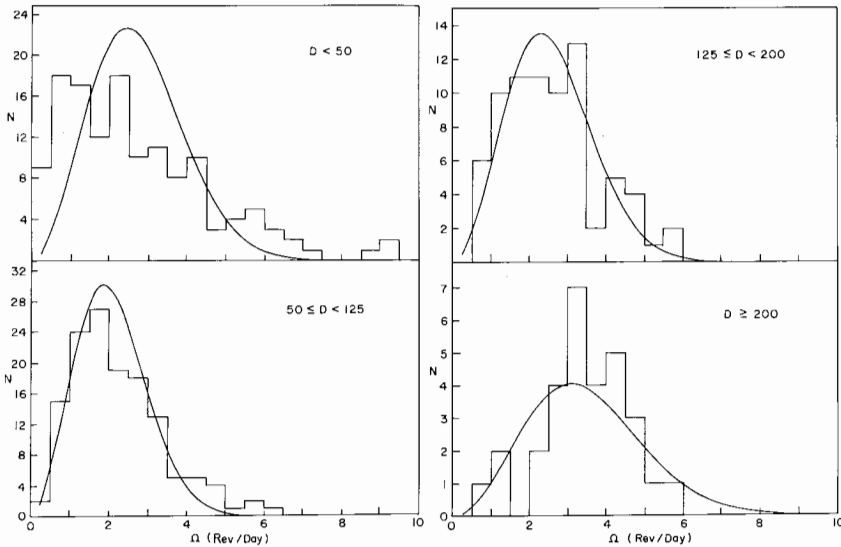
Fig. 5. Histogram distributions of rotation rates broken down into four groups defined by $D < 50$ km, $50 \leq D < 125$ km, $125 \leq D < 200$ km and $D \geq 200$ km. Acceptable Maxwellian fits (given in Table I) are obtained only for the two largest diameter groups.

tribution which also leads to an interesting interpretation that despite their intrinsically lower moments of inertia and low angular momenta compared to that carried in frequent collisions, the spin rates of small asteroids may not be highly evolved by collisions. Lifetimes of these bodies may not be long enough (before being destroyed) for them to reach an evolved state. The distribution of rotation rates among $D < 125$ km asteroids possibly more dominantly reflects the angular momentum partitioning resulting from the formation of these bodies as collisional fragments. Some studies of the distribution of rotation rates among disruption fragments have been performed (Fujiwara and Tsukamoto 1981; Paolicchi et al. 1989); however, more laboratory and theoretical studies are needed in this area. Indeed, as discussed earlier, a broad spin-rate distribution might be derived from the superposition of several narrow ones, centered at different values of Ω. An excess of slow rotators is most clearly seen among the smallest asteroids and might be explained by tidal despinning due to satellites (Zappalà et al. 1980; see also the chapter by Weidenschilling et al.) or due to the observational measurements being precessional rather than due to rotational periods.

Histogram distributions of Ω for the main compositional types show that C and S type asteroids have similar distributions, although the S asteroids display more of a high frequency tail and the C's show the clearest overabundance of slow rotators. These characteristics may be related to possibly differ-

ent strengths of C and S type material. The M asteroids show a distinctly different (much broader) distribution. Table I shows that a Maxwellian fit can be rejected for the C types, but not for the M types. For the S types, a Maxwellian fit cannot be rejected for the sample based on the Barucci et al. (1987) classification, but it has to be rejected for the sample of Tholen (1984). If M asteroids do indeed have higher impact strengths, then a Maxwellian fit may be consistent with their longer survival times allowing them to reach a higher degree of collisional evolution.

In addition to the collisional evolution of angular momentum, there are most likely other processes (such as angular momentum partitioning and tidal despinning) affecting the Ω distribution, and an asteroid sample may represent the superposition of two (or more) populations. As a means for investigating such possibilities, we attempt to fit several samples with a linear combination of two Maxwellians having dispersions $\sigma 1$ and $\sigma 2$ which were scaled by the factors α and $1-\alpha$, respectively. For several of the above cases where the fit to a single Maxwellian distribution was poor, Fig. 6 shows our attempt to fit the observed distributions with a bi-Maxwellian. Table II lists the Maxwellian parameters and also gives the results of the chi-squared tests of these fits. In all cases, the chi-squared statistic is significantly reduced and the fit is greatly improved (as is to be expected), although even a bi-Maxwellian fit is still formally rejected for the entire sample and for the $D < 50$ km subset. For the whole sample, a combination with 25% of the sample being due to a slowly rotating population ($\Omega_\mu \sim 1.2$ rev/day) gives a much better overall fit except for an excess of fast rotators in the tail. Clearly, there are multiple processes affecting the entire asteroid population. Separate slow and fast distributions are most strongly implied in the curve fit to the $D < 50$ km subset.

Further work is needed to determine if this sample can be fully modeled as collisional fragments or whether a second mechanism is needed to account for the two apparent populations. A very good fit is achieved for the 50 to 125 km sample by a combination of two Maxwellians having relatively close mean Ω's. Clearly, however, these good fits are not unique, and other model functions could well be tested by comparison with the observed distributions.

III. ANALYSIS OF LIGHTCURVE AMPLITUDES

Lightcurve amplitudes (defined as the peak-to-peak variation) provide a crude indicator for asteroid shapes. For a triaxial ellipsoid rotating about the c axis, the lightcurve amplitude may be given by

$$A(\theta) = 2.5 \log \left(\frac{a}{b} \right) - 1.25 \log \left(\frac{a^2\cos^2\theta + c^2\sin^2\theta}{b^2\cos^2\theta + c^2\sin^2\theta} \right) \qquad (5)$$

where θ is polar aspect viewing angle. If an asteroid is viewed pole-on ($\theta = 0$), then no change in projected surface area is seen and the expected ampli-
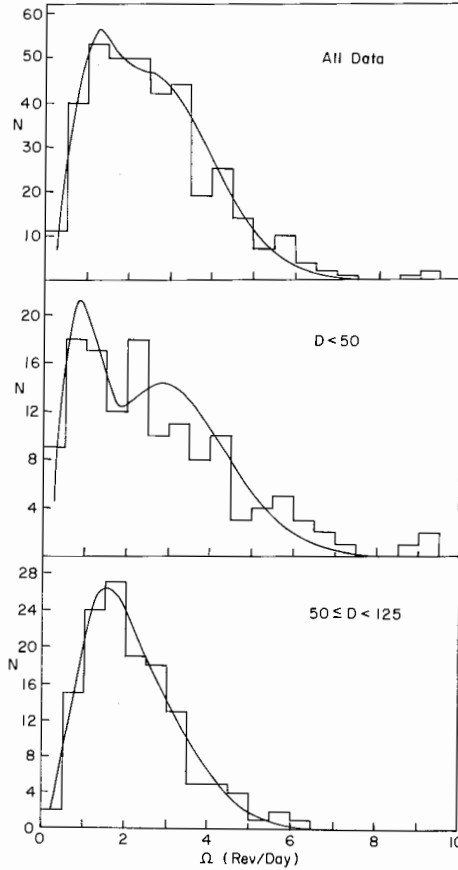
Fig. 6. Fits to the histogram distributions rotation rates using a linear combination of two Maxwellian distributions having the parameters listed in Table II. Fits are shown for the whole data set, the $D < 50$ km subset and the $50 \leq D < 125$ km subset.

tude is zero. If an asteroid is viewed at an equatorial aspect ($\theta = 90$) such that the rotation axis is perpendicular to the line of sight, then the second term in the above equation is zero and the maximum amplitude would be expected as the projected surface area varies from πac to πbc.

Laboratory impact experiments (see the chapter by Fujiwara et al.) have found that over a wide range of energies and target strengths, the shapes of fragments over a broad size range tend to be distributed about an $a : b : c$ ratio of $2 : \sqrt{2} : 1$. If real asteroids are roughly ellipsoidal and follow this ratio, then at an equatorial aspect we would expect to find $A(90) = 0.38$ magnitude. However, for an asteroid observed during only one apparition, its aspect angle is unknown. (See the chapter on pole determinations by Magnusson et al.) If

TABLE II
Bi-Maxwellian Fits of the Distribution of Ω

Sample	N	$\sigma 1$	$\sigma 2$	α	χ^2	Degrees of Freedom	Confidence Level	Interpretation
All	375	0.717	1.835	0.240	13.0	7	~95%	marg. rejected
$D < 50$ km	134	0.582	1.998	0.273	16.4	7	~98%	reject
$50 \leq D < 125$	136	0.888	1.643	0.353	3.9	7	<90%	cannot reject
AAA	28	1.095	3.776	0.183	28.9	7	>99%	reject
$D < 15$	23	1.122	3.482	0.448	6.7	7	<90%	cannot reject

we assume an isotropic distribution of asteroid spin vectors, the probability of observing an asteroid at aspect θ is proportional to sin (θ) and the expected mean amplitude can easily be computed from Eq. (5), which for the given axial ratios yields $\langle A \rangle = 0.20$ mag.

Figure 7a shows the observed distribution of lightcurve amplitudes where we have taken the maximum observed amplitudes from Lagerkvist et al. (1988; see also Part VI). Because high phase angles can significantly increase observed amplitudes (due to scattering and shadowing effects), when possible we have preferentially taken values for the maximum amplitude observed at low phase angles. We have also excluded four objects with very high amplitudes (>0.9 mag) which would have caused sudden jumps in the running-box diagram shown in Fig. 7b.
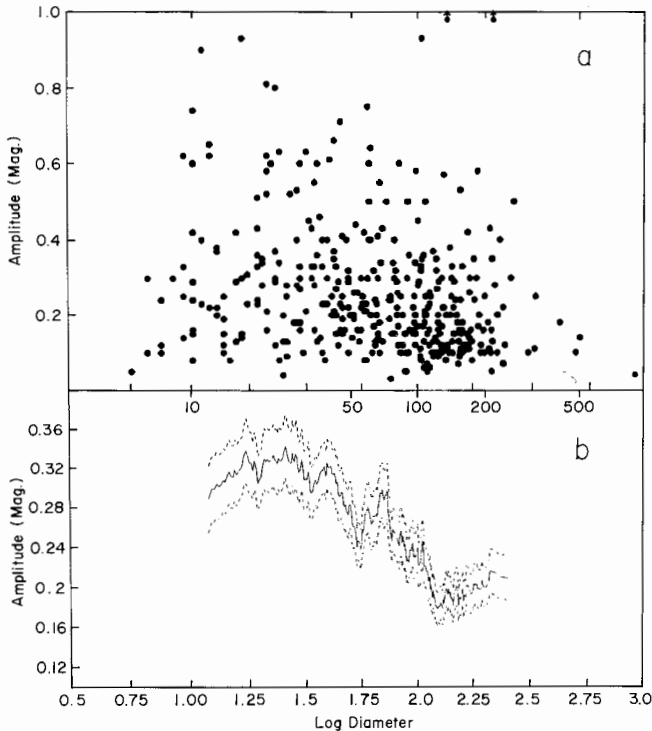
Fig. 7.(a) Plot of lightcurve amplitudes (magnitudes) vs log diameter from the data base in Part VI. (b) Running-box diagram for the same data set using a box size of $n = N/10$. Small asteroids show higher amplitudes and a greater dispersion about the mean. The minimum mean amplitudes observed for the largest asteroids occur at the same diameter as the minimum of the V distribution in Fig. 2. Breaking down the amplitude-diameter diagram into different taxonomic types shows no significant differences in the amplitude distributions for C, S and M type asteroids.

As already found by Catullo et al. (1984), the distribution shows that the smallest asteroids have higher mean amplitudes (and greater dispersion about the mean). The nearly constant mean amplitude for $D < 50$ km asteroids may be evidence that shapes in this size range are determined by a single process, perhaps the catastrophic disruption of parent bodies. The largest asteroids ($D > 125$) show the lowest mean amplitudes, where this minimum occurs at about the same diameter as the minimum of the V-shaped distribution in Fig. 2. This correspondence also occurs at the size range where self-gravity may become an important factor in constraining asteroid shapes, since, of course, large departures from axisymmetric shapes could cause significant internal stresses (Farinella et al. 1982). Over most of the diameter range, the observed mean amplitudes are higher than expected for a random distribution of ellipsoidal fragments. Apart from the uncertainty in scaling laboratory results up to asteroid sizes, nonellipsoidal shapes, scattering, shadowing and albedo effects at nonzero phase angles may be enhancing the observed amplitudes. More laboratory and observational studies of these effects are needed.

We now examine the correlation between amplitude and rotation rate. Figure 8 presents running-box diagrams for the entire data set and subsets larger and smaller than 125 km. The interesting features are the upturns towards higher amplitudes for fast and very slowly rotating asteroids. We believe the latter feature is probably an observational selection effect due to the difficulty in obtaining results for long-period and low-amplitude asteroids. The upturn toward higher amplitudes for Ω between 4 and 6 rev/day is precisely the range in which Farinella et al. (1981b) pointed out that triaxial (Jacobian) ellipsoids are possible equipotential figures for self-gravitating spinning bodies with negligible strength and constant density, provided the latter quantity is in the range 2 to 3 g cm^{-3}. This upturn is especially sharp for the $D > 125$ km subset and these bodies may be gravitationally bound rubble piles, i.e., asteroids composed of fragments which are held together in part by their mutual gravity (see the chapter by Davis et al.). The high-amplitude large Ω objects in the $D < 125$ km sample are perhaps collision fragments which obtained their elongated shapes and fast rotation rates in disruption events. A second interesting feature seen for this $D < 125$ km sample is the secondary peak at $\Omega = 2.7$ which corresponds to the expected rotation period for nearly contact binaries with comparable mass components (Leone et al. 1984). Larger amplitudes would indeed be expected for such bodies.

IV. CORRELATION WITH ORBITAL PARAMETERS

In examining the observed distributions with respect to orbital parameters, caution must be exercised to avoid misleading conclusions due to systematic effects. For example, in Fig. 9a, which is a running-box diagram of rotation rates vs semimajor axis, it is intriguing to note that the rotation rates
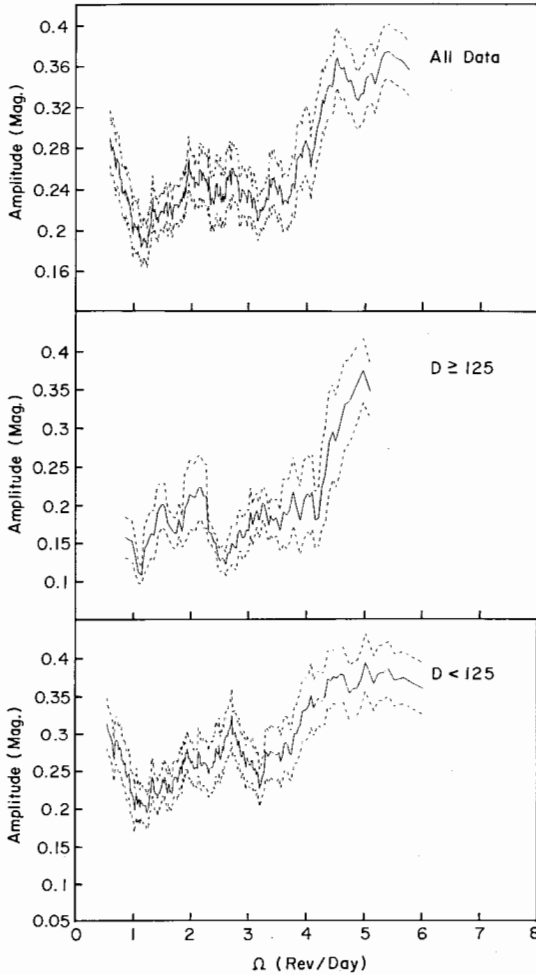
Fig. 8. Running-box diagram for lightcurve amplitude vs rotation rate using a box size of $n = 10$ for the entire data set, the subset of $D \geq 125$ km and the subset $D < 125$ km. There is a strong upturn towards larger amplitudes for faster rotation rates. Among the larger asteroids these may be gravitationally bound rubble piles whose shapes are determined by self-gravitational forces. The high Ω, large-amplitude bodies in the $D < 125$ km sample are perhaps collision fragments.

reach relative maxima in proximity to the primary Jovian resonances. This tendency, previously noticed by Tedesco and Zappalà (1980), can probably be explained by a correlation between diameter and semimajor axis as shown in Fig. 9b (see also Dermott and Murray 1981). In addition to the smaller mean diameters in the vicinity of the 1 : 3 resonance, it is also apparent that diameter is correlated with semimajor axis due to observational selection effects and the
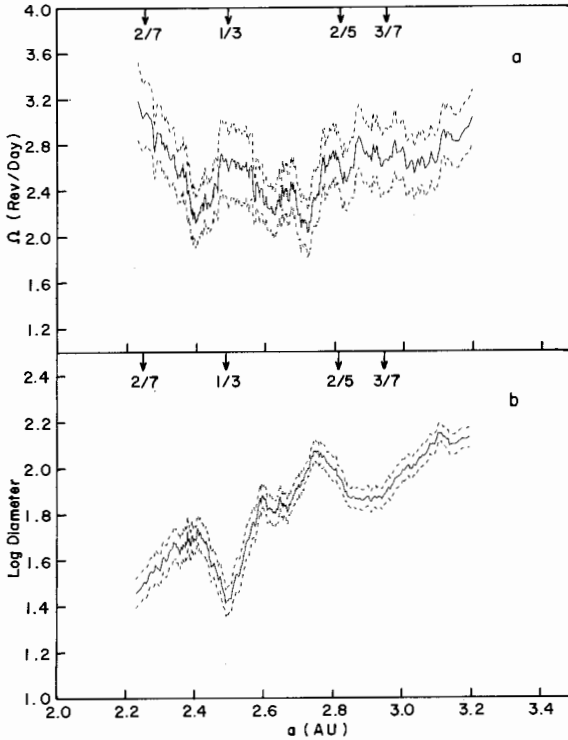
Fig. 9.(a) Running-box diagram for Ω vs semimajor axis (AU) for asteroids inside the 1 : 2 Jovian resonance. Other low-order resonances are noted. The relative maxima in rotation rates near resonances may be due to a correlation between diameter and semimajor axis as shown in (b). Observational selection effects and a compositional gradient in the asteroid belt strongly affect this observed distribution.

correlation of compositional types with heliocentric distance (see the chapter by Gradie et al.). Lagerkvist et al. (1987) found different results on this issue (see their Fig. 30), but their sample was more limited than the present one (e.g., it did not include the small asteroids observed in the program of Binzel (1987) and non-C/S/M objects). As a consequence, they also did not observe the upward trend in the Ω vs D curve at small sizes.

Next we seek to examine the correlation with respect to a measure of the average energy of the collisions undergone by an asteroid. From Opik (1976), the parameter ψ is proportional to the square of the average relative velocity of the asteroid with respect to a circular orbit and is given by

$$\Psi = \frac{\sin^2 i + 0.625 e^2}{a} \tag{6}$$

where a, e and i are the semimajor axis, eccentricity and inclination, respectively. For small values of Ψ, the collision energy is probably dominated by the average Ψ of the projectiles available in the same region. At large values of Ψ, no strong correlation is seen for either Ω or amplitude (Fig. 10). Further work in collisional modeling is needed to examine more fully the utility of the average energy in examining collisional outcomes.

V. ANALYSIS OF ASTEROID FAMILIES

Because asteroid families are believed to be the recognizable outcomes of specific catastrophic disruption events (see the chapters by Fujiwara et al. and Chapman et al.), they have been of particular interest for studies of rotational parameters. If a family is the result of a recent breakup, then the observed distribution of rotation rates would be indicative of the partitioning of rotational angular momentum among the fragments. Such observations would provide useful constraints for collisional evolution models. However the ages
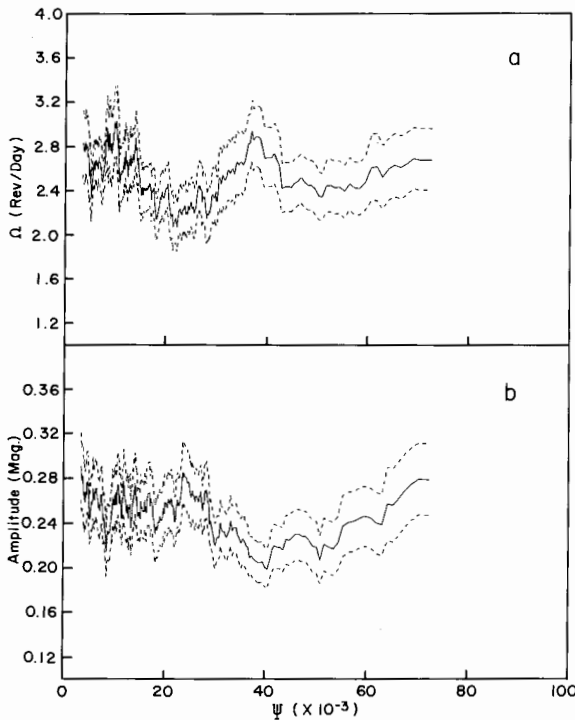
Fig. 10. Running-box diagrams for Ω and lightcurve amplitude vs the parameter ψ (Opik 1976), which is proportional to the square of the average relative velocity and is a measure of the expected average collisional energy. No significant correlation is evident.

of the families are uncertain and some interpretation is required before obser-
vational results can be applied to the models. In addition, except for the
largest families (e.g., Themis, Eos, Koronis), there is no universal agreement
on the determination of family membership (see the chapter by Valsecchi
et al.).

The preceding caveats have only recently been realized and previous
studies (see, e.g., Burns and Tedesco 1979) which globally compared the
properties of all family vs all nonfamily asteroids have not given a clear under-
standing of the rotation-rate distributions in families. The main reason was
that in these studies all the family asteroids were grouped together in the same
sample, neglecting any possible family-dependent feature such as a record of
the parent's rotation. Recently, investigations by Binzel (1986,1988) at-
tempted to overcome these limitations by extensively studying rotation prop-
erties within two individual families.

Figure 11 shows histogram distributions of rotation rates for the Eos and
Koronis families and a group of similar diameter ($D < 30$ km) nonfamily
asteroids located at the same semimajor-axis distance as the two families (Bin-
zel 1986). Eos family asteroids display faster rotation rates and their distribu-
tion can be fit by a Maxwellian. However, Koronis family and nonfamily
asteroids clearly display slower mean rotation rates and non-Maxwellian dis-
tributions. Because studies by Fujiwara (1982) and others imply that similar
disruption energies formed both families, Binzel (1988) has interpreted their
differences to imply that Eos is an older family that has undergone a large
degree of collisional evolution subsequent to its formation. A first-order
Monte Carlo collisional evolution model suggests an age for the family dating
back to the early solar system. On the other hand, modeling the rotation-rate
distribution for the Koronis family suggests that it may be relatively young
and that its members have not been significantly affected by subsequent colli-
sional evolution. Therefore the observed Koronis family distribution may still
resemble that resulting from its catastrophic formation. However, we cannot
rule out that the differences found in the rotation-rate distributions of the two
families might be due to different conditions of the impact events (Paolicchi et
al. 1989).

An additional result from the observed Eos and Koronis spin-rate dis-
tributions is that the largest members within each family appear to have rela-
tively similar rotation rates and that the dispersion increases with decreasing
diameter. In Fig. 11, the shaded boxes depict the rotation rates of the largest
family members. Binzel (1988) has interpreted these similar rotation rates to
imply that the largest bodies may "remember" the spin rate of their parent
body. Their larger moments of inertia make it less likely that their rotation
rates have been significantly altered since their formation and thus their spin
rates may more closely represent that of their parent body.

The Eos and Koronis families also display different distributions for
lightcurve amplitudes as shown in Fig. 12. The Eos family and nonfamily
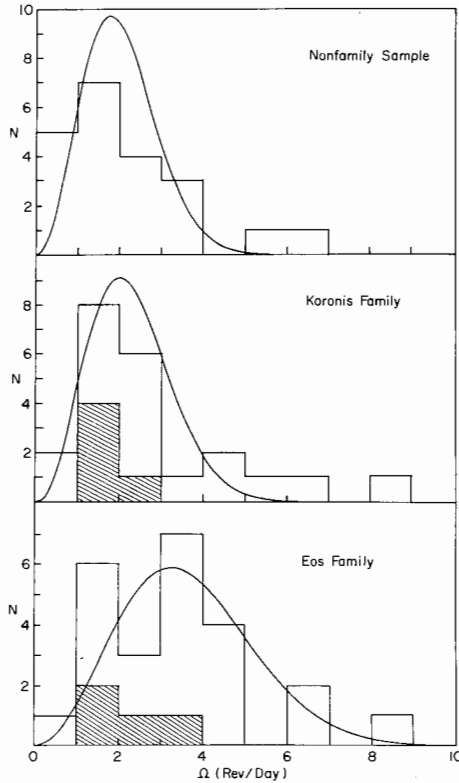
Fig. 11. Histogram distributions of rotation rates and Maxwellian fits for the Koronis and Eos families and a set of nonfamily asteroids with similar diameters and orbital properties (Binzel 1986). Eos family asteroids display faster mean rotation rates and give a plausible fit to a Maxwellian distribution. The Koronis family and nonfamily asteroids have similar non-Maxwellian distributions. The shaded blocks denote the largest members in each family.

asteroids both have similar distributions that are consistent with the shapes of laboratory fragments assuming random aspect angles. However, the Koronis family shows significantly higher lightcurve amplitudes and its distribution is best fit by assuming a nonrandom aspect angle of 90°. Binzel (1988) has proposed that spin vectors in the Koronis family may be preferentially aligned perpendicular to the ecliptic, where this direction reflects the orientation of the Koronis family parent body. Additional observations of Koronis family asteroids over a range of ecliptic longitudes are underway to test this hypothesis. If correct, this would strongly imply a relatively recent formation for the Koronis family since subsequent collisions have not had time to orient their spin vectors randomly. However, this interpretation should be taken with caution, since the distribution of the fragment spin vectors after a catastrophic
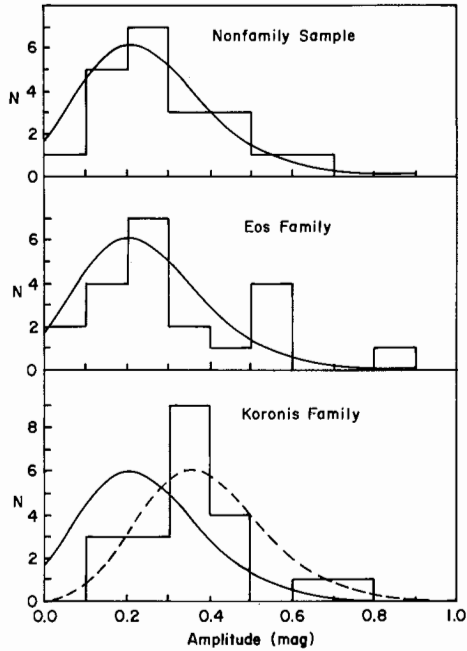
Fig. 12. Histogram distribution of lightcurve amplitudes for Eos, Koronis and nonfamily asteroids. The solid curves represent the shapes of laboratory fragments assuming a random orientation of their principal axes. The Eos family and nonfamily asteroids show similar histograms which are well fit by the fragment distribution. The Koronis family, however, shows a higher mean lightcurve amplitude and is much better fit by a fragment distribution assuming a preferential alignment of the principal axes normal to the observer's line of sight (dashed curve).

impact is at present very poorly understood. A young age for the Koronis family may be consistent with observations of the IRAS dust bands (see the chapter by Sykes et al.).

The distinctly different properties observed in these two families underscore the need for future investigations focused on specific families. Although it appears that rotation studies may be able to suggest relative ages for families, additional supporting dynamical studies (such as that done by Carpino et al. [1986]) of the time scales for the dispersion of families in proper element space are also needed.

VI. NEAR-EARTH ASTEROIDS

In this final section, we examine the rotational properties of the near-Earth population of Apollo-Amor-Aten (AAA) asteroids (see the chapter by McFadden et al.). Because these asteroids have short dynamical lifetimes

(compared to the age of the solar system) before they are removed by a grav-
itational encounter or collision, a source for these bodies must be identified.
Possible sources from the asteroid belt and from extinct cometary nuclei are
discussed in the chapters by Greenberg and Nolan and by Weissman et al. as
well as in Wetherill (1988).

Figure 13 compares the distribution of rotational frequencies for the
AAA asteroids and the subset of main-belt asteroids having diameters <15
km. The average diameters for the samples are 3 and 11 km, respectively.
(The two largest Amor asteroids, 433 Eros and 1036 Ganymed, with diame-
ters of ~25 and ~40 km have been excluded.) The AAA sample consists of
data from Part VI and also unpublished data (A. W. Harris, personal com-
munication) which are given in Table IV of the chapter by McFadden et al.

Both the AAA and small main-belt samples have broad dispersions of
rotation rates and Table I shows that neither distribution can be fit by a single
Maxwellian, where the poor fit is largely due to an excess of slowly rotating
bodies. A bi-Maxwellian (Table II) provides a better (but still not statistically
acceptable) fit to the AAA sample. The AAA and small main-belt samples
show very similar values for $\sigma 1$ and $\sigma 2$ and the bi-Maxwellian fit is rejected
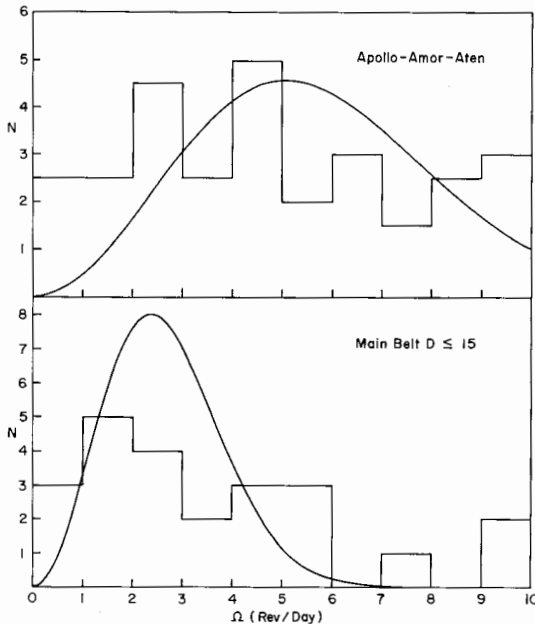
Fig. 13. Distributions of rotation rates for Apollo-Amor-Aten asteroids and main-belt asteroids
with diameters <15 km. The curves depict the best fit Maxwellian distributions which are both
rejected due to an excess of slowly rotating asteroids.

TABLE III
Comparison of AAA and Small Belt Asteroids

Sample	N	Mean Diam. (km)	Mean Amp. (mag)	σ	t	Confidence Level	Interpretation
Maximum amplitudes Apollo–Amor–Aten	31	3	0.496	0.086	1.518	94%	Significant
Maximum amplitudes Main belt $D \leq 15$ km	23	11	0.334	0.044			
Corrected amplitudes Apollo–Amor–Aten	31	3	0.390	0.066	0.713	<90%	Not significant
Corrected amplitudes Main belt $D \leq 15$ km	23	11	0.330	0.042			

for the AAA sample due to one very long-period object. Interestingly, studies of the rotational properties of cometary nuclei (see, e.g., Jewitt and Meech 1988, Table 8) suggest that they have relatively slow rotation rates ($\Omega < 2$ rev/day). More nuclei rotation measurements are needed before a meaningful comparison can be made.

We now compare the mean observed lightcurve amplitudes for the AAA and small main-belt samples. Because of their proximity, AAA asteroids are often observed over a wide range of phase and aspect angles. Both of these factors can significantly enhance the maximum value for their observed light-curve amplitudes. In contrast, small main-belt asteroids typically only have observations at low phase angles over a narrow aspect range during one opposition. To account for the enhancement of amplitudes, we assume that for an asteroid observed over a wide range of aspect angles, the maximum observed lightcurve amplitude corresponds to $A(90)$ in Eq. 5. This equation is then used to correct this maximum amplitude to what would be measured for a single random-aspect $A(60)$ observation.

Table III gives the mean for the maximum observed amplitudes and for the corrected amplitudes. Student's t-test is applied to compare the sample means and finds that there is a statistically significant difference between the maximum amplitudes observed in the two samples. However, after applying a correction for aspect-related amplitude enhancement, this difference is no longer significant, implying that the previously reported differences (see, e.g., Binzel 1984) may be due to the wider range of viewing geometries for the AAA asteroids. Moreover, we have to take into account that amplitudes of AAA asteroids could still be enhanced by phase effects, which cannot be quantified with the present knowledge of the amplitude-phase relationship. More studies of amplitude-aspect and amplitude-phase relations are needed for small asteroids. In addition, a proper comparison between AAA and small main-belt asteroids is difficult because the samples compared here differ by a factor of ~4 in diameter and a factor of ~64 in mass. Future studies of the rotational properties of similar-sized ($D < 5$ km) asteroids in the main belt are needed.

REFERENCES

Barsuhn, J. 1983. The light curves of a freely precessing spheroidal minor planet. *Astron. Astrophys.* 122:237–240.

Barucci, M. A., Capria, M. T., Coradini, A., and Fulchignoni, M. 1987. Classification of asteroids using G-mode analysis. *Icarus* 72:304–324.

Binzel, R. P. 1984. The rotation of small asteroids. *Icarus* 57:294–306.

Binzel, R. P. 1985. Is 1220 Crocus a precessing binary asteroid?. *Icarus* 63:99–108.

Binzel, R. P. 1986. Collisional Evolution in the Asteroid Belt: An Observational and Numerical Study. Ph.D. Thesis, Univ. of Texas.

Binzel, R. P. 1987. A photoelectric survey of 130 asteroids. *Icarus* 72:135–208.

Binzel, R. P. 1988. Collisional evolution in the Eos and Koronis asteroid families: Observational and numerical results. *Icarus* 73:303–313.

Binzel, R. P., and Mulholland, J. D. 1983. A photoelectric lightcurve survey of small main belt asteroids. *Icarus* 56:519–533.

Burns, J. A. 1971. The alignment of asteroid rotation. In *Physical Studies of Minor Planets*, ed. T. Gehrels, NASA SP-267, pp. 257–262.

Burns, J. A., and Safronov, V. S. 1973. Asteroid nutation angles. *Mon. Not. Roy. Astron. Soc.* 165:403–411.

Burns, J. A., and Tedesco, E. F. 1979. Asteroid lightcurves: Results for rotations and shapes. In *Asteroids*, ed. T. Gehrels (Tucson: Univ. of Arizona Press), pp. 257–262.

Carpino, M., Gonczi, R., Farinella, P., Froeschlé, C., Froeschlé, C., Paolicchi, P., and Zappalà, V., 1986. The accuracy of proper orbital elements and properties of asteroid families: Comparison with linear theory. *Icarus* 68:55–76.

Catullo, V., Zappalà, V., Farinella, P., and Paolicchi, P. 1984. Analysis of the shape distribution of asteroids. *Astron. Astrophys.* 138:464–468.

Dermott, S. F., and Murray, C. D. 1981. Resonant structure in the asteroid belt. *Nature* 290:664–668.

Dermott, S. F., Harris, A. W., and Murray, C. D. 1984. Asteroid rotation rates. *Icarus* 57:14–34.

Dobrovolskis, A. R., and Burns, J. A. 1984. Angular momentum drain: A mechanism for despinning asteroids. *Icarus* 57:464–476.

Farinella, P., Paolicchi, P., and Zappalà, V. 1981*a*. Analysis of the spin rate distribution of asteroids. *Astron. Astrophys.* 104:159–165.

Farinella, P., Paolicchi, P., Tedesco, E. F., and Zappalà, V. 1981*b*. Triaxial equilibrium ellipsoids among the asteroids? *Icarus* 46:114–123.

Farinella, P., Paolicchi, P., and Zappalà, V. 1982. The asteroids as outcomes of catastrophic collisions. *Icarus* 52:409–433.

Fujiwara, A. 1982. Complete fragmentation of the parent bodies of the Themis, Eos and Koronis families. *Icarus* 52:434–443.

Fujiwara, A., and Tsukamoto, A. 1981. Rotation of fragments in catastrophic impact. *Icarus* 48:329–334.

Harris, A. W. 1983. Slowly rotating asteroids: Evidence for binary asteroids? *Bull. Amer. Astron. Soc.* 15:828 (abstract).

Harris, A. W., and Burns, J. A. 1979. Asteroid rotation. I. Tabulation and analysis of rates, pole positions, and shapes. *Icarus* 40:115–144.

Jewitt, D. C., and Meech, K. J. 1988. Optical properties of cometary nuclei and a preliminary comparison with asteroids. *Astrophys. J.* 328:974–986.

Lagerkvist, C.-I., Hahn, G., Magnusson, P., and Rickman, H. 1987. Physical properties of asteroids XVI: Photoelectric photometry of 17 asteroids. *Astron. Astrophys. Suppl.* 70:21–32.

Lagerkvist, C.-I., Harris, A. W., and Zappalà, V. 1988. Asteroids II machine-readable data base: March 1988 floppy disk version.

Leone, G., Farinella, P., Paolicchi, P., and Zappalà, V. 1984. Equilibrium models of binary asteroids. *Astron. Astrophys.* 140:265–272.

McAdoo, D. C., and Burns, J. A. 1973. Further evidence for collisions among asteroids. *Icarus* 18:285–293.

Öpik, E. J. 1976. In *Interplanetary Encounters* (Amsterdam: Elsevier), pp. 27–29.

Paolicchi, P., Cellino, A., Farinella, P., and Zappalà, V. 1989. A semiempirical model of catastrophic breakup processes. *Icarus* 77:187–212.

Salo, H. 1987. Numerical simulations of collisions between rotating particles. *Icarus* 70:37–51.

Sher, D. 1971. On the variation in light of tumbling bodies. *Astrophys. Space Sci.* 11:222–231.

Tedesco, E. F., and Zappalà, V. 1980. Rotation properties of asteroids: Correlations and selection effects. *Icarus* 43:33–50.

Tholen, D. J. 1984. Asteroid Taxonomy from Cluster Analysis of Photometry. Ph.D. Thesis, Univ. of Arizona.

Wetherill, G. W. 1988. Where do the Apollo objects come from? *Icarus* 76:1–18.

Zappalà, V., Scaltriti, F., Farinella, P., and Paolicchi, P. 1980. Asteroidal binary systems: Detection and formation. *Moon and Planets* 22:153–162.

PHYSICAL PROPERTIES OF ATEN, APOLLO AND AMOR ASTEROIDS

LUCY-ANN MCFADDEN
University of California, San Diego

DAVID J. THOLEN
University of Hawaii

and

GLENN J. VEEDER
Jet Propulsion Laboratory

The physical properties of Aten, Apollo and Amor objects including their taxonomy, composition, size, rotation rate, shape and surface texture, are derived from observations using spectrophotometry, reflectance spectroscopy, broadband photometry, radiometry, polarimetry and radar. Our current understanding of this population is that it is diverse in terms of all physical properties that can be studied from the ground and consists of contributions from more than one source region. Almost all taxonomic types found in the main belt are present among this population. Class Q objects are unique to the AAAO population. Both low-temperature assemblages, which are dark and probably carbonaceous-rich, and high-temperature, differentiated assemblages of olivine, pyroxene and metallic phases, are found among the AAAO. These asteroids have experienced a range of different thermal regimes in the past. Discovery biases probably create the high abundance of bright objects. A bimodal distribution of rotation rates indicates that the population is not collisionally evolved. Most AAAO have been modeled as aspherical objects with a variety of surface textures and roughness. There is more diversity in their roughness at the cm-to-m scale than observed among the main-belt asteroids. All this evidence indicates that multiple source regions contribute to the population of planet-crossing asteroids.

[442]

I. INTRODUCTION

A group of planet-crossing asteroids, the Aten, Apollo and Amor objects (AAAO) have orbits carrying them outside of the main asteroid belt. The Atens are defined as asteroids having a semimajor axis less than that of the Earth (1.0 AU). The Apollos, by definition, have orbits that cross that of the Earth; their perihelion distance q is on average less than the Earth's semimajor axis. The Amors approach the Earth, passing inside the semimajor axis of Mars but not inside of the Earth's orbit. Amors are sometimes referred to as Earth-approachers as distinguished from the Apollos, referred to as Earth-crossers. The aphelion distance of all AAAO ranges from just beyond the Earth's orbit, to beyond that of Jupiter. Shoemaker et al. (1979) estimate that the population, to magnitude $V(1,0) = 18$, consists of approximately 100 Atens, 700 ± 300 Apollos, and 1000 to 2000 Amors, although the total number of known objects is currently in the 100s. Members of this group are listed, where available, with their orbital elements and taxonomic classification in Table I. The mean lifetime of AAAO against collision with a planet or ejection from the solar system is calculated to be on the order of 10^7 to 10^8 yr (Arnold 1964), as opposed to the main-belt asteroids that have stable orbits over the lifetime of the solar system.

The short lifetime of these asteroids requires the existence of a replenishing source. One of the major objectives of the study of their physical properties is to determine their source regions and the dynamical mechanisms which produce this group. Because Apollo asteroids are in orbits similar to the meteorites that collide with the Earth, they are likely to be the parent bodies of some meteorites. Thus, we also study these asteroids to determine the relationship between meteorites and asteroids. Comets, also in Earth-crossing orbits, are a possible source of some AAAO. Those with anomalous physical characteristics and in comet-like orbits are discussed as possible extinct cometary nuclei in the chapter by Weissman et al. The close proximity of AAAO to the Earth makes them remarkable both for their potential usefulness for space-borne activities (habitation and manufacturing) and their possible destructiveness resulting from collisions with the Earth.

The high-quality observations of the previous decade (Shoemaker et al. 1979) are still valued for their contribution toward assessing the characteristics of the AAAO population. In a previous review (Shoemaker et al. 1979), 14 were classified based on *UBV* data and albedo. Polarimetric and radiometric measurements, from which diameters and albedos are derived, were available for 10 members of this group, and spectral reflectance and radar measurements were available for a few AAAO, but no compilation of their physical properties existed. There are now independent taxonomic classifications for 43 AAAO, diameter calculations for 35 (Veeder et al. 1989), and reflectance spectra for 20. Polarimetric measurements are available for 11, and rotation periods and shapes (derived from lightcurves) have been mea-

sured for 30. Radar measurements constrain the size, shape and surface roughness at cm-to-m scales and exist for 19 objects.

The population of planet-crossing asteroids appears to be extremely diverse in all aspects of their physical properties. With available information, we observe no interrelationships among their known properties. For example, there are both large and small asteroids with both fast and slow rates of rotation over a wide range of surface composition. If we compare one physical property with another, we see no systematic relationships. Some AAAO have physical properties similar to those dominating the inner asteroid belt, the S types (see the chapter by Tholen and Barucci), and they probably originated in that region. The first predominantly metallic asteroids (Tedesco and Gradie 1987; Ostro et al. 1987) among this population have been found, making them likely parent bodies for metallic meteorites. The best candidates for the parent bodies of the ordinary chondrite meteorites (see the chapter by Lipschutz et al.) are currently found among the AAAO and not in the main asteroid belt. Whether or not these parent bodies exist only in the near-Earth environment or are also in the main belt, below our detection limits, remains to be determined. The association of an asteroid, 3200 Phaethon, with the orbit of the Geminid meteor shower raises the question as to whether asteroids can have debris trails or whether this particular asteroid is an extinct cometary nucleus. This subject is addressed in the chapter by Weissman et al. We review here the physical properties of the AAAO: their taxonomy, mineralogical surface composition, albedo and diameter, their rotation rate and shape and surface roughness.

II. TAXONOMY

The taxonomy of asteroids is based on photometric colors and albedo and is discussed in the chapter by Tholen and Barucci. It is a powerful tool for studying the distribution of photometric types of asteroids, information which, when compared with other asteroids and objects in the solar system, reveals the history and source regions of the AAAO. Through study of reflectance spectra of asteroid types, the mineralogical differences between the types can be determined, as discussed in the chapter by Gaffey et al. Forty-three AAAO have been classified by two different classification schemes. Tholen (1984a,b, 1988) uses cluster analysis and the Eight Color Asteroid Survey (ECAS; Zellner et al. 1985). The other major classification scheme applied to AAAO is designed by Chapman, Morrison and Zellner (CMZ; Chapman et al. 1975). All taxonomic types except classes B and P are found among the AAAO (Table I). Measurements made at low signal-to-noise levels cause an object's position in color space to overlap more than one class, giving rise to the multiple classifications designated in Table I.

TABLE I
Orbital Elements and Taxonomy

Asteroid	q	a	e	i	Class	Reference[a]
			ATENS $a < 1.0$ AU, $Q > 0.983$ AU			
2062 Aten	0.79	0.97	0.182	18.9	S	1
2100 Ra-Shalom	0.47	0.83	0.436	15.8	C	2
2340 Hathor	0.46	0.84	0.450	05.9	CSU	3
3362 Khufu	0.53	0.99	0.469	09.9		
3554 Amun	0.70	0.97	0.280	23.4	M	4
3753 1986 TO	0.48	1.00	0.515	19.8		
1954 XA	0.51	0.78	0.345	03.9		
			APOLLOS $a > 1.0$ AU, $q < 1.017$ AU			
1566 Icarus	0.19	1.08	0.827	22.9		
1620 Geographos	0.83	1.24	0.336	13.3	S	2
1685 Toro	0.77	1.37	0.436	09.4	S	5
1862 Apollo	0.65	1.47	0.560	06.3	Q	2
1863 Antinous	0.89	2.26	0.607	18.4	SU	2
1864 Daedalus	0.56	1.46	0.615	22.2	SQ	6
1865 Cerberus	0.58	1.08	0.467	16.1	S	2
1866 Sisyphus	0.87	1.89	0.539	41.2		
1981 Midas	0.62	1.78	0.650	39.8		
2063 Bacchus	0.70	1.08	0.349	09.4		
2101 Adonis	0.44	1.87	0.764	01.4		
2102 Tantalus	0.90	1.29	0.298	64.0		
2135 Aristaeus	0.80	1.60	0.503	23.0		
2201 Oljato	0.63	2.18	0.711	02.5		
2212 Hephaistos	0.36	2.16	0.835	11.9	SG	7
2329 Orthos	0.82	2.40	0.658	24.4		
3103 1982 BB	0.91	1.41	0.355	20.9	E	8
3200 Phaethon	0.14	1.27	0.890	22.1	F	9
3360 1981 VA	0.63	2.46	0.744	22.0		
3361 Orpheus	0.82	1.21	0.323	02.7		
3671 Dionysius	1.01	2.20	0.541	13.6		
3752 1985 PA	0.99	1.41	0.303	55.5		
3838 1986 WA	0.45	1.50	0.701	29.3		
1937 UB Hermes	0.62	1.63	0.622	06.2		lost
1950 DA	0.84	1.68	0.502	12.1		
1959 LM	0.72	1.98	0.637	06.8		
1973 NA	0.88	2.43	0.638	68.0		
1974 MA	0.42	1.77	0.762	37.8		
1978 CA	0.88	1.12	0.215	26.1	S	10
1979 VA	1.00	2.64	0.623	02.8	CF	2
1979 XB	0.65	2.26	0.714	24.9		
1982 DB	0.95	1.49	0.360	01.4		
1982 TA	0.52	2.30	0.773	12.2		
1983 LC	0.76	2.63	0.710	01.5		
1983 TF2	0.66	2.45	0.732	14.8		

TABLE I   **(continued)**
Orbital Elements and Taxonomy

Asteroid	q	a	e	i	Class	Reference[a]
1983 VA	0.81	2.61	0.692	16.2		
1983 VB	0.96	1.87	0.488	17.6		lost
1984 KB	0.52	2.22	0.764	04.8	S	11
1986 JK	0.90	2.80	0.680	02.1	C	12
1986 PA	0.59	1.06	0.444	11.2		
1987 KF	0.59	1.84	0.679	11.9		
1987 OA	0.61	1.49	0.593	09.0		
1987 QA	0.88	1.65	0.469	40.7		
1987 SB	0.75	2.20	0.661	03.0		
1987 SY	0.60	1.44	0.587	05.5		
1988 EG	0.64	1.27	0.499	03.5		
1988 TA	0.79	1.64	0.518	02.7	C	13
1988 VP4	0.79	2.26	0.653	11.7		
1988 XB	0.76	1.46	0.476	03.1		
1989 AC	0.90	2.60	0.654	00.5		
1989 AZ	0.86	2.00	0.570	12.3		
5025 P-L	0.45	4.21	0.894	06.3		
6344 P-L	0.97	2.63	0.631	04.5		
6743 P-L	0.80	1.68	0.523	07.9		

AMORS
$a > 1.0$ AU, 1.017 AU $< q < 1.3$ AU

Asteroid	q	a	e	i	Class	Reference[a]
433 Eros	1.13	1.46	0.223	10.8	S	2
719 Albert	1.17	2.58	0.545	11.2		lost
887 Alinda	1.10	2.49	0.559	09.3	S	2
1036 Ganymed	1.23	2.66	0.537	26.5	S	2
1221 Amor	1.08	1.92	0.435	11.9		
1580 Betulia	1.12	2.19	0.490	52.1	C	14
1627 Ivar	1.12	1.86	0.396	08.4	S	2
1915 Quetzàlcoatl	1.08	2.54	0.574	20.5	SMU	2
1916 Boreas	1.25	2.27	0.450	12.8	S	3
1917 Cuyo	1.06	2.15	0.505	24.0		
1943 Anteros	1.06	1.43	0.256	8.7	S	2
1951 Lick	1.30	1.39	0.062	39.1	A	15
1980 Tezcatlipoca	1.09	1.71	0.365	26.8	SU	3
2059 Baboquivari	1.26	2.65	0.526	11.0		
2061 Anza	1.05	2.26	0.538	03.7	TCG	16
2202 Pele	1.12	2.29	0.512	08.8		
2368 Beltrovata	1.24	2.10	0.413	05.3	SQ	3
2608 Seneca	1.04	2.49	0.582	15.4	S	10
3102 1981 QA	1.19	2.15	0.449	08.4	QRS	2
3122 1981 ET3	1.02	1.77	0.422	22.2		
3199 Nefertiti	1.13	1.57	0.284	33.0	S	2
3271 1982 RB	1.27	2.10	0.394	25.0		
3288 Seleucus	1.10	2.03	0.458	05.9	S	2
3352 McAuliffe	1.19	1.88	0.369	04.8		
3551 1983 RD	1.07	2.09	0.487	09.5	V	17

TABLE I (continued)
Orbital Elements and Taxonomy

Asteroid	q	a	e	i	Class	Reference[a]
3552 1983 SA	1.21	4.23	0.713	30.8	D	18
3553 Mera	1.12	1.64	0.321	36.8		
3691 1982 FT	1.27	1.77	0.284	20.4		
3757 1982 XB	1.02	1.84	0.446	03.9	S	2
3908 1980 PA	1.04	1.93	0.459	02.2	V	17
3988 1986 LA	1.06	1.54	0.317	10.8		
1972 RB	1.10	2.15	0.486	05.2		
1977 VA	1.13	1.86	0.394	03.0	XC	3
1979 QB	1.30	2.33	0.441	03.6		
1980 AA	1.05	1.89	0.444	04.2		
1980 WF	1.08	2.23	0.514	06.4	QU	2
1980 YS	1.23	1.82	0.321	02.3		
1981 QB	1.08	2.24	0.518	37.2		
1982 YA	1.12	3.71	0.698	34.6		
1983 LB	1.19	2.29	0.479	25.4		
1983 RB	1.09	2.22	0.507	19.4		
1985 DO2	1.23	1.82	0.326	23.2	V	17
1985 TB	1.11	2.58	0.567	26.8		
1985 WA	1.13	2.85	0.602	09.7		
1986 DA	1.17	2.82	0.585	04.3	M	4
1986 NA	1.17	2.13	0.451	10.4		
1986 RA	1.23	3.35	0.631	19.0		
1987 PA	1.21	2.74	0.557	16.1	C	12
1987 QB	1.14	2.80	0.594	3.5		
1987 SL	1.15	2.97	0.612	19.4		
1987 SF3	1.05	2.25	0.535	3.3		
1987 UA	1.22	1.73	0.297	16.4		
1987 WC	1.04	1.36	0.234	15.8		
1988 NE	1.21	2.18	0.444	9.9		
1988 PA	1.28	2.16	0.407	8.2		
1988 SM	1.09	1.67	0.347	11.0		
1988 TJ1	1.14	1.37	0.168	15.7		
1988 VN4	1.23	1.81	0.320	17.9		
4788 P-L	1.18	2.63	0.550	11.0		

[a]References: 1: Gradie 1976; 2: Tholen 1984*a*; 3: data from Degewij et al. 1978, classified by Tholen 1988; 4: Tedesco and Gradie 1987; 5: data from Dunlap et al. 1973, classified by Tholen 1988; 6: data from Zellner et al. 1975, classified by Tholen 1988; 7: data from Bowell et al. 1978, classified by Tholen 1988; 8: taxonomy inferred by Veeder et al. 1989, from high albedo and neutral colors of Wisniewski 1987; 9: Tholen 1985; 10: Degewij 1978; 11: Bell et al. 1988; 12: Wisniewski 1987; 13: Tholen 1988; 14: Tedesco et al. 1978; 15: Wisniewski, personal communication; 16: data from Rakos 1960, classified by Tholen 1988; 17: Tholen et al. 1988; 18: Tholen 1984*b*; Tholen 1988.

The true distribution of taxonomic types among the near-Earth population is masked by observational biases due to discovery circumstances. The observational limits of telescopes used to search for AAAO combined with their large orbital eccentricity of these asteroids and, their small size makes it difficult to assess the true nature of this population. It is clear from Fig. 1 that the majority of the *observed* AAAO are of type S. Tedesco and Gradie (1987) attempted to make a bias correction and assumed the number of dark asteroids discovered is directly proportional to the ratio of dark to bright asteroids in the main belt, about 4:1. With this reasoning, they suggest that there should be four times more dark asteroids among the true population of AAAO than have been discovered to date. This is probably a lower limit, as this reasoning does not assess the bias in terms of eccentricity and size. If we assume at least a ratio of dark to bright asteroids equivalent to the main asteroid belt, then it is a fact that dark asteroids are still under represented in the near-Earth population.

Four of the seven known Aten asteroids have been classified. One member of each of the three most populous classes in the main belt, types S, C and M, is found among the Atens. Another one, 2340 Hathor, has a multiple classification, CSU. The significance of the taxonomic distribution of the Atens will be determined when a larger population is known.

A notable exception to the frequent occurrence of S-type objects among the Apollo asteroids is the parent body of the Geminid meteor shower, 3200 Phaethon, which is classified type F (Tholen 1985). Members of this class have neutral-to-bluish colors and a low albedo. The prototype Q-type asteroid, 1862 Apollo, and four other possible members of class Q are all found among the AAAO. No Q types have been found in the main asteroid belt. Note, however, that the Q classifications for all members (except 1862 Apollo), are part of multiple designations (Table 1), meaning that with improved data, they may be classified into different groups. Based on its albedo (Veeder et al. 1989) and colors (Wisniewski 1987), 3103 1982 BB is the first E type found among the AAAO.
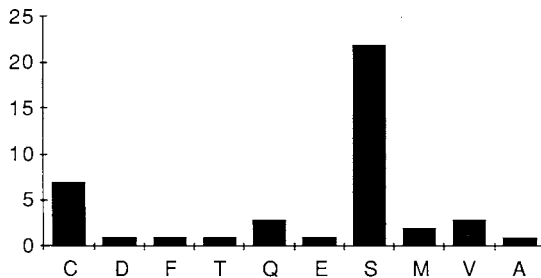
Fig. 1. Histogram of taxonomic types as defined by Tholen with the eight-color asteroid system. The observed population is not corrected for observational bias.

The Amors are mostly S types as currently observed. Members of most of the other classes are observed but represented only in small numbers. One D type, 3552 1983 SA (Tholen 1988), is found among the Amors. The existence of this asteroid in the inner solar system is curious because most D types are found beyond the 2:1 resonance with Jupiter, at 3.28 AU, where asteroids are in stable orbits. It has been suggested that D types might be related to comets (Hartmann et al. 1987); this possibility is discussed in the chapter by Weissman et al. There is one M-type asteroid among the Amors (Tedesco and Gradie 1987), a likely candidate for the parent body of some metallic meteorites. All three V types in the near-Earth population are Amors with photometric colors similar to the main-belt asteroid, 4 Vesta, a basaltic achondrite meteorite analogue. Members of the V class include 3551 1983 RD, 3908 1980 PA, and 1985 DO2 (Tholen 1988). Vesta is the only main-belt asteroid in this class.

The variety of taxonomic types found among the AAAO indicates that the population is diverse in terms of composition and origin. The mixture of compositional types among the three subgroups, Apollos, Amors and Atens, supports the dynamical observation that the populations are continuously mixing through orbital evolution (Shoemaker et al. 1979).

III. MINERALOGICAL SURFACE COMPOSITION

Knowledge of mineralogical surface composition is extracted from reflectance spectroscopy and albedo measurements (see the chapter by Gaffey et al.; Gaffey and McCord 1978). This knowledge provides constraints on formation mechanisms and the thermodynamic conditions in their formation regions. Mineralogical information exists for 20 AAAO from reflectance spectra, and can be inferred for 24 others from ECAS spectra and the older CMZ classification. Interpretation of these reflectance spectra reveals assemblages consisting of both low-temperture and high-temperature phases. Changes in the abundance of carbonaceous material, consisting of clay-like hydrous silicates, Mg- and Ca- sulphates, magnetite, carbonates and complex organic compounds (Sears and Dodd 1988), and of high-temperature mafic silicates and metal, are inferred from variations in spectral properties. A sequence of four groups in which the albedo, spectral contrast and spectral slope all increase with decreasing abundances of low-temperature assemblage and increasing abundance of high-temperature phases, defines the range of surface mineralogy found among the AAAO. This sequence is shown in Fig. 2. The AAAO with similar spectral characteristics and the data used to place them in these groups are listed in Table II. The spectral characteristics and mineralogical interpretation of each of these four spectral groups relies heavily on an analogy between meteorites and asteroids.

The lowest-temperature assemblages, presumed to have a considerable abundance of carbonaceous material, is represented by the spectrum of 1580
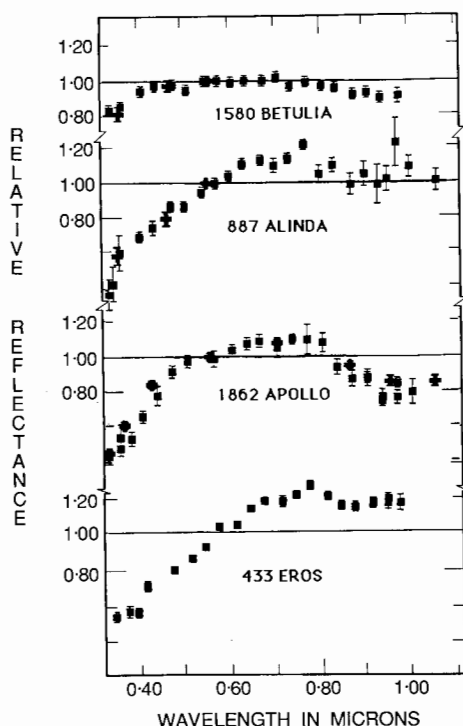
Fig. 2. Representative reflectance spectra for members of the AAAO population falling into four groups: A: low temperature, carbonaceous-rich; B: low temperature, carbonaceous-poor; C: moderate temperature, carbonaceous-poor and D: differentiated assemblages.

Betulia (Fig. 2). This asteroid has weak ultraviolet and 1.0-μm absorption bands and a low albedo (0.03). We interpret these features in laboratory studies, as due to the presence of mafic silicates and carbonaceous material which results in both low albedo and subdued absorption bands in the 1.0 μm region (see, e.g., Johnson and Fanale 1973). In carbonaceous chondrite meteorites, < 3% of elemental carbon, which is opaque in the visible, results in an albedo at 0.56 μm of 0.03 to 0.04 and a very weak absorption band at 1.0 μm (Gaffey 1976). The ultraviolet absorption band in the spectrum of 1580 Betulia and the other C-type asteroids is attributed to the presence of low-temperature phases such as phyllosilicates (clay minerals) which have strong charge-transfer absorption bands in the ultraviolet persisting in laboratory mixtures containing opaques. The phyllosilicates are hydrous phases. Their presence is further supported by spectra of some main-belt C-type asteroids which have absorption bands at 3 μm due to water of hydration (Jones 1988; Feierberg and Lebofsky 1985).

Additional asteroids inferred to have similar surface mineralogy to that of Betulia are: 1979 VA, 1986 JK, 1986 RA and 1988 TA. These are all C-types according to photometric taxonomy (Table I). An additional low-temperature assemblage is 3552 1983 SA, classified as type D. According to current interpretations, D-type asteroids consist most probably of phyllosilicates, an organic polymer, and possibly an opaque material (Jones 1988; Gradie and Veverka 1980; see the chapter by French et al.). Asteroids with the above-described spectral properties are the most carbonaceous-rich asteroids.

The next compositional group in the sequence probably consists of an assemblage of higher-temperature mafic silicates, poor in carbonaceous material. The spectrum of 887 Alinda (Fig. 2) represents this group which has a strong and linear ultraviolet absorption band, a moderate-to-weak 1.0 μm band and an albedo of 0.16 (Zellner and Gradie 1976). These features and its albedo (Gaffey and McCord 1979) are consistent with those of the matrix-poor, CV and CO carbonaceous chondrite meteorites (see Sears and Dodd [1988] for definition of meteorite types). By comparison with the CM carbonaceous chondrite spectra (Gaffey 1976; Johnson and Fanale 1973), which are darker and have weaker absorption bands, asteroids with these spectral features probably contain less carbonaceous material and more crystalline olivine grains. These two factors would account for their higher albedo and stronger ultraviolet and 1.0 μm absorption bands. The contribution to the spectrum of either metallic iron (see, e.g., McCord and Chapman 1975) or hydrous phyllosilicates is not determinable with available spectra. The presence of these minerals has cosmochemical implications that will affect the sequencing of the spectral types presented here. Additional near-infrared measurements would constrain interpretations related to the abundance and composition of olivine and the presence or absence of metallic iron or phyllosilicates. The higher albedo, 0.23, listed in Table III could imply a high metal abundance; this albedo, however, assumes a dusty regolith.

Two other AAAO, 2100 Ra-Shalom and 3102 1981 QA, have similar spectral features as 887 Alinda; that is, a strong and linear ultraviolet band and moderate-to-weak 1.0 μm band (McFadden et al. 1984). The linear ultraviolet absorption band distinguishes this group from spectra of the differentiated group in which the minerals have been melted and the elements repartitioned relative to their initial composition. The albedo of 2100 Ra-Shalom is low (0.09; Veeder et al. 1989) compared to 887 Alinda. It is lower than CV and CO chondrites, yet its spectrum contains more spectral contrast than CM meteorites. 2100 Ra-Shalom might represent a composition between these two meteorite types. There is no meteoritic analogue to 2100 Ra-Shalom because of its unusual combination of low albedo and relatively pronounced spectral contrast (McFadden 1983). Additionally, there is no albedo measurement for 3102 1981 QA; it is included in this group because of the similarity of its spectral features to those of 887 Alinda (McFadden et al. 1984). These as-

TABLE II
AAAO Compositions

Asteroid	Composition	Class	Technique	Reference
Atens				
2100 Ra-Shalom	Low Temp, Carb-poor	C	Reflectance Spectroscopy	1
3554 Amun	Differentiated, Metal	M	CMZ classification	2
Apollos				
1566 Icarus	Differentiated	S	Reflectance Spectroscopy	3
1620 Geographos	Differentiated	S	Reflectance Spectroscopy	3
1685 Toro	Differentiated	S	Reflectance Spectroscopy	1,4
1862 Apollo	Mod Temp, Carb-poor	Q	Ref Spect, ECAS Photometry	1,5
1865 Cerberus	Differentiated	S	ECAS Photometry	5
1866 Sisyphus	Differentiated	S	Reflectance Spectroscopy	6
1979 VA	Low Temp, Carb-rich	CF	ECAS Photometry	5
1984 KB	Differentiated	S	Reflectance Spectroscopy	7
1986 JK	Low Temp, Carb-rich	C	ECAS Photometry	8
1988 TA	Low Temp, Carb-rich	C	ECAS Photometry	9
Amors				
433 Eros	Differentiated	S	Reflectance Spectroscopy	1,10
887 Alinda	Low Temp, Carb-poor	S	Reflectance Spectroscopy	1,11,12

1036 Ganymed	Differentiated	S	Reflectance Spectroscopy	1,3,13
1580 Betulia	Low Temp, Carb-rich	C	Reflectance Spectroscopy	1,3
1627 Ivar	Differentiated	S	Reflectance Spectroscopy	13
1915 Quetzálcoatl	Diff, pyroxene-rich	S	Reflectance Spectroscopy	1
1943 Anteros	Differentiated	S	ECAS Photometry	5
1951 Lick	Diff, olivine-rich	A	ECAS Photometry	14
3102 1981 QA	Low Temp, Carb-poor	QRS	Reflectance Spectroscopy	1
3199 Nefertiti	Diff, olivine-rich	S	Reflectance Spectroscopy	15
3288 Seleucus	Differentiated	S	Reflectance Spectroscopy	16
3551 1983 RD	Diff, pyroxene-plag	V	ECAS Photometry	17
3552 1983 SA	Low Temp, Carb-rich	D	ECAS Photometry	5
3757 1982 XB	Differentiated	S	ECAS Photometry	5
3908 1980 PA	Diff, pyroxene-plag	V	ECAS Photometry	17
1980 AA	Mod Temp, Carb-poor	S	Reflectance Spectroscopy	1
1980 WF	Diff, olivine-rich	QU	ECAS Photometry	18
1985 DO2	Diff, pyroxene-plag	V	ECAS Photometry	17
1986 DA	Differentiated, Metal	M	ECAS Photometry	2,8
1986 RA	Low Temp, Carb-rich	C	ECAS Photometry	8

References: 1: McFadden et al., 1984; 2: Tedesco and Gradie, 1987; 3: Chapman and Gaffey, 1979; 4: Chapman et al., 1973; 5: Tholen, 1984a; 6: Vilas and McFadden, 1985; 7: Bell et al., 1988; 8: Wisniewski, 1987; 9: Tholen, 1988; 10: Pieters et al., 1976; 11: Gaffey and McCord, 1978; 12: McCord and Chapman, 1975; 13: Bell et al., 1987; 14: Wisniewski, personal communication; 15: Cruikshank et al., 1985; 16: Vilas et al., 1985; 17: Tholen et al., 1988; 18: Zellner et al., 1985.

teroids have probably been subjected to a thermal event that has driven off much of the carbonaceous material.

Moderate-temperature, carbonaceous-poor assemblages are next in the sequence. The spectrum of 1862 Apollo, representing this group, has the same band position, band depth and continuum characteristics as laboratory measurements of powdered, ordinary chondrite meteorites of type LL4 (McFadden et al. 1984). The continuum of 1862 Apollo, as measured in the visible (to 1.0 μm), is flat as is the reflectance of metallic iron extracted from ordinary chondrites (Gaffey 1986). Based on the position of the 1.0 μm absorption band, the surface composition of this asteroid contains olivine and pyroxene of the same chemical composition as ordinary chondrite meteorites, compositions that are diagnostic of these assemblages. Ordinary chondrites have been exposed to temperatures ranging from 400 to 950°C (McSween et al. 1988).

Among the asteroids with high-quality ECAS data, 1862 Apollo is unique, thus Tholen (1984a) defines a single-member class, Q, to represent these colors. Additional objects with lower-quality data have somewhat similar colors including 1864 Daedalus, 2368 Beltrovata, 3102 1981 QA and 1980 WF. They receive less-definite, multiple classifications including Q. A logical assumption is that all Q-type asteroids are ordinary chondrite analogues. However, other members of class Q are placed in different compositional groups when their spectral features, instead of their photometric statistics, are analyzed in terms of their mineralogy. 3102 1981 QA was placed among the lower-temperature assemblages and 1980 WF belongs among the differentiated assemblages. Another ordinary chondrite analogue, which was measured at 24 bandpasses, is 1980 AA (McFadden et al. 1984) whose spectral features are similar to those of shocked, black chondrites with a lower albedo and weaker absorption bands than the ordinary chondrites (McFadden et al. 1984). This interpretation is based on a spectral match to laboratory spectra of meteorites.

The highest-temperature assemblages have been heated to the melting point of silicates (1000°C) and differentiated. 433 Eros is a typical member of this group whose spectrum is shown in Fig. 2. We interpret reflectance spectra with strong ultraviolet and 1.0 μm bands, a high near-infrared reflectance (> 1.0 relative to 0.56 μm) and a moderate-to-high albedo (>0.15) as differentiated assemblages. These asteroids contain olivine and pyroxene in varying proportions and have a metallic component that is probably present in discrete chunks as opposed to being uniformly dispersed in fine particles (see the chapter by Gaffey et al.). It is expected that spectra of most of these asteroids, given data of adequate spectral resolution and signal-to-noise, would have absorption band positions indicating mineral chemistry that is outside of the range of the undifferentiated, ordinary-chondrite assemblages. The stony-iron meteorites are the best meteoritic analogue of these asteroids.

Most of the observed AAAO for which there is mineralogical informa-
tion are differentiated assemblages by analogy with well-studied main-belt
objects (see, e.g., Gaffey 1985; also see Table II). Three special members of
this group appear to have monomineralic silicate phases. 1915 Quetzàlcoatl
appears to have little to no olivine and is a good meteoritic analogue to di-
ogenite meteorites (McFadden et al. 1985). 3199 Nefertiti contains little to no
pyroxene and is a meteoritic analogue to the stony-iron meteorites called pal-
lasites (Cruikshank et al. 1985). 1980 WF, according to its ECAS spectrum
(Zellner et al. 1985; Tholen 1984a) is most likely composed predominantly of
olivine. Two purely metallic asteroids have been found among this popula-
tion, 3554 Amun (Tedesco and Gradie 1987) and 1986 DA (Ostro et al. 1987)
which are also probably close to being monomineralic.

Finding members of this population that have come from both low-tem-
perature and high-temperature thermal regimes indicates that there is more
than one source mechanism responsible for injecting these asteroids into their
current orbits. The true distribution of low- to high-temperature assemblages
is not presently known because the effects of discovery biases have not been
adequately evaluated.

IV. ALBEDOS AND DIAMETERS

Albedos and diameters are derived from radiometric, polarimetric and
radar measurements. Radiometric models are discussed in the chapter by
Lebofsky and Spencer; polarimetry is discussed in the chapter by Dollfus et
al.; and Ostro in his chapter discusses radar measurements and techniques.
The albedo of an object places constraints on its composition, photometric
properties and surface texture. From diameters, aspects of the asteroids' colli-
sional history can be derived. Radiometry of the AAAO is reported by Veeder
et al. (1989); eleven AAAO have polarimetric diameters and albedos (see
Zellner et al. 1974), while radar measurements have been obtained for 19.

Radiometric measurements of AAAO pose special analysis problems. In
many cases, the observations are acquired at high phase angles which must be
accounted for in the models. The asteroids' rotation rate and shape can also
affect the results of the derived quantities and must be incorporated into the
models. Some AAAO must be modeled with a high thermal inertia (i.e., bare
rock) to eliminate unusually high albedos, disagreement between different
wavelengths (10 μm vs 20 μm measurements) or measurement techniques
(radiometry vs polarimetry). However, some small AAAO, 1862 Apollo (1.4
km), for example, have thermophysical properties consistent with a particu-
late surface as derived from both radiometry (Lebofsky et al. 1981) and polar-
imetry (Tedesco, personal communication). From this, we conclude that the
controlling factors of regolith properties and processes are not simply due to

TABLE III
Diameters and Albedos

Asteroid	Diam (km)	P_v	Model	References[a]
Atens				
2062 Aten	0.9	0.20	1	3
2100 Ra-Shalom	2.4	0.09	2	4
3362 Khufu	0.7	0.16	1	4
3554 Amun	2.0	0.17	1	5
Apollos				
1566 Icarus	0.9	0.42	1	4
1620 Geographos	2.0	0.19	1	4
1862 Apollo	1.5	0.21	1	6
1685 Toro	5.2	0.14	2	4
1863 Antinous	1.8	0.18	1	4,5
1865 Cerberus	1.0	0.26	1	4
1866 Sisyphus	8.2	0.18	1	4
2201 Oljato	1.4	0.42	2	4
3103 1982 BB	1.4	0.63	1	4
3200 Phaethon	6.9	0.08	2	7
3360 1981 VA	1.8	0.07	1	4
1978 CA	1.9	0.06	1	8
1982 TA	1.7	0.33	1	4
1984 KB	1.4	0.16	1	9
Amors				
433 Eros	22	0.18	1	10
887 Alinda	4.2	0.23	1	4
1036 Ganymed	38.5	0.17	1	4
1580 Betulia	7.4	0.03	2	11
1627 Ivar	8.1	0.12	1	4
1915 Quetzàlcoatl	0.3	0.29	1	4
1943 Anteros	1.8	0.22	1	4
1980 Tezcatlipoca	4.3	0.21	1	4
2368 Beltrovata	2.3	0.13	1	4
2608 Seneca	0.9	0.16	1	8
3199 Nefertiti	2.2	0.26	2	4
3288 Seleucus	2.8	0.17	2	4
3551 1983 RD	0.8	0.40	1	4
3552 1983 SA	18.7	0.02	1	4
3757 1982 XB	0.5	0.15	1	12
1980 WF	0.6	0.18	1	4,5
1986 DA	2.3	0.12	1	5

[a]References: 1: "standard" nonrotating thermal model; 2: "nonstandard" fast-rotating thermal model; 3: Morrison et al. 1976, Cruikshank and Jones 1977; 4: Veeder et al. 1987,1988; 5: Tedesco and Gradie 1987; 6: Lebofsky et al. 1981; 7: Veeder et al. 1984; 8: Lebofsky et al. 1979; 9: Bell et al. 1988; 10: Lebofsky and Rieke 1979; 11: Lebofsky et al. 1978; 12: Helin et al. 1983, recalculated in Veeder et al. 1989.

NEAR EARTH ASTEROIDS
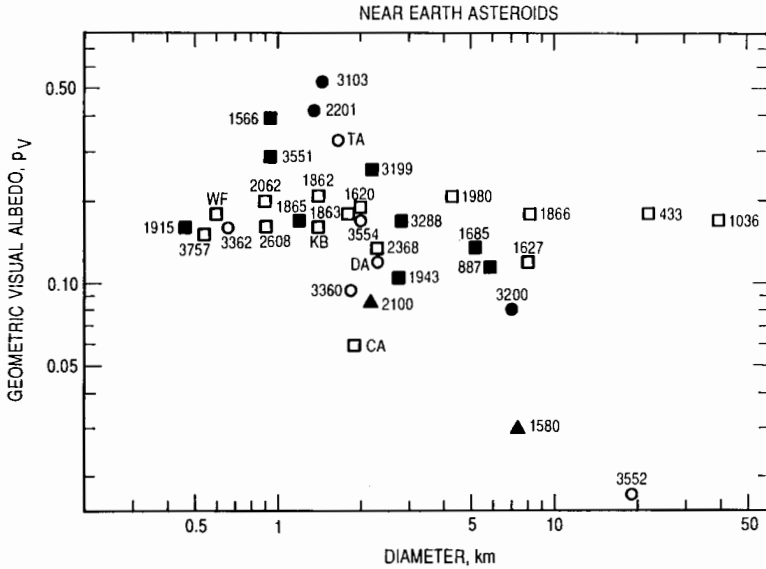
Fig. 3. Albedo of the AAAO as a function of diameters (figure from Veeder et al. 1989).

scaling with size and gravity. Table III and Fig. 3 summarize the available data for albedos and diameters of AAAO as discussed in detail by Veeder et al. (1989).

The range of AAAO albedos sampled so far appears to span that seen across the main belt. Due to discovery biases, most of the known AAAO have moderate-to-high albedos typical of type S. 3552 1983 SA (0.02) is the darkest AAAO so far observed. 3103 1982 BB (0.63) appears to have the highest albedo of any observed AAAO, although acquiring radiometric observations without simultaneous visible measurements might account for this high albedo. Veeder et al. (1987,1989) have confirmed the IRAS albedos in Matson (1986) for 1036 Ganymed (0.17) and 2201 Oljato (0.42) but not the low values reported for 1685 Toro and 1980 Tezcatlipoca (Matson 1986). The latter two are incorrect associations due to confusion at low signal-to-noise levels in the IRAS asteroid catalogue (see the chapter by Veeder et al.).

The range of diameters of AAAO is smaller than that of main-belt asteroids. 1036 Ganymed (38.5 km) appears to be the largest known AAAO whereas main-belt asteroids have diameters ranging up to 1000 km. 1915 Quetzàlcoatl (0.3 km) is the smallest recorded diameter. The absence of objects > 40 km indicates that the AAAO are perturbed into planet-crossing orbits after collisional fragmentation from larger asteroids. Collisional processes play an important role in creating this population, otherwise larger members of this population would exist.

V. ROTATION RATES AND SHAPES

Rotation rates and asteroid shapes are determined from photometric lightcurves and radar measurements. From these, constraints are derived on their collisional evolution. Table IV lists the rotation rates which have been measured for AAAO to date. Binzel et al. discuss rotation rates in more detail in their chapter.

There is a bimodal distribution of rotation rates $><$ 15 hr, among the AAAO. Additional information is needed to determine whether this distribution is a function of the asteroids' size (AAAO form a population of the smallest asteroids observed), their source region or their collisional history. The geometric mean of the rotation rates is 7.32 hr which is shorter than the mean of 9.91 hr, calculated from 347 rotation rates for all asteroids (Harris 1986). For those with periods <15 hr, the mean is 4.94 hr, and 52 hr for the five asteroids with periods > 15 hr. There is no clear correlation between rotation rate and taxonomic type or albedo; however, such a relationship might be masked by observational biases or incomplete data sets. The distribution of rotation rates among the AAAO cannot be fit by a Maxwellian function (see the chapter by Binzel et al.) indicating that the population is not collisionally evolved. Such a population would have a smoothly varying range of rotation rates. The bimodal distribution again suggests a population with multiple origins having different collisional evolutions.

Asteroid shapes are modeled from lightcurve measurements on the premise that the projected cross-sectional area is proportional to the measured brightness. The shapes of small asteroids are probably irregular if they are collisional fragments. Phase effects, the variation in brightness as a function of phase angle, are due to multiple scattering and the surface properties of the asteroid. Lightcurves measured at large phase angles can have large amplitudes depending on their surface composition and texture. When large-amplitude lightcurves are assumed to be controlled by shape alone, without taking into account surface scattering properties, the result is an extremely elongated shape which might be erroneous (see, e.g., Harris et al. 1987).

All available photometric and radar measurements model the AAAO as nonspherical objects except for 1566 Icarus. This small (0.9 km) and bright (0.42) asteroid is apparently close to being spherical. Miner and Young (1969) derive a shape which deviates from a sphere by 5%. Analysis by Gehrels et al. (1970) indicates a 10% deviation from a sphere.

Roach and Stoddard (1938) model the lightcurve of 433 Eros as a triaxial ellipsoid of dimensions $35.0 \times 15.6 \times 7.2$ km. Drummond et al. (1985) used speckle interferometry to determine dimensions of $40.5 \pm 3.1 \times 14.5 \pm 2.3 \times 14.1 \pm 2.4$ km. Radar cross sections (Jurgens and Goldstein 1976) yielded radii 18.6×7.9 km in the rotational equator. The third-axis dimension could not be determined. Other nonspherical shapes for Eros were modeled using photometric lightcurves by Millis et al. (1976) who considered it a cylinder

TABLE IV
Rotation Rates of Near-Earth Asteroids

Name	Period (hr)	Reference[a]
Atens		
2100 Ra-Shalom	19.79	1
Apollos		
1566 Icarus	2.273	2
1620 Geographos	5.227	3
1685 Toro	10.196	4
1862 Apollo	3.065	5
1863 Antinous	4.02	6
1864 Daedalus (1971 FD)	8.57	7
1865 Cerberus	6.80	8
1866 Sisyphus	2.4	9
2201 Oljato	>24.	10
3103 1982 BB	5.71	11
1978 CA	3.748	12
1979 VA	3.6	10
Amors		
433 Eros	5.27	13
887 Alinda	73.97	14
1036 Ganymed	10.308	15,16
1580 Betulia	6.130	17
1627 Ivar	4.798	15,18
1915 Quetzàlcoatl	4.9	19
2061 Anza (1960 UA)	11.50	20
2368 Beltrovata (1977 RA)	5.9	21
2608 Seneca (1978 DA)	8.0	12
3102 1981 QA	148	22
3199 Nefertiti (1982 RA)	3.0	15
3288 Seleucus (1982 DV)	75.	23
3551 1983 RD	4.930	15
3757 1982 XB	9.012	15
1980 AA	2.70	24
1984 KD	2.4	15
1986 DA	3.58	11

References: 1: Ostro et al. 1984; 2: Veverka and Liller 1969, Miner and Young 1969; 3: Dunlap, 1974; 4: Dunlap et al., 1973; 5: Hahn, 1983; 6: Binzel, 1987; 7: Gehrels et al., 1971; 8: Harris personal communication, Harris and Young in prep.; 9: Hahn and Harris personal communication; 10: Harris and Young, 1983; 11: Wisniewski, 1987; 12: Degewij, 1978; 13: Taylor, 1985; 14: Dunlap and Taylor, 1979; 15: Harris and Young, 1985; 16: Lupishko et al, 1987; 17: Tedesco et al, 1978; 18: Lupishko et al., 1986; 19: Binzel and Tholen, 1983; 20: Rakos, 1960; 21: Bowell, 1977; 22: Harris personal communication, Harris, Young and Gibson in prep.; 23: Debehogne et al., 1983; 24: Harris, 1985.

with rounded ends of axial ratio 2.3:1, and Dunlap (1976) who assumed the same shape and derived dimensions of 12 ± 1 km $\times$ 12 ± 1 km $\times$ 31 ± 3 km. Observations of Eros were extensive enough to remove phase effects so the shape analyses are probably realistic.

Lightcurve measurements of 1580 Betulia (Tedesco et al. 1978) indicate that it is close to an irregular, prolate spheroid with a topographic feature on one of its broad sides and an axial ratio of 1:1.21. 1620 Geographos has also been modeled as a cylinder with rounded ends from optical lightcurves. It is 1.50 ± 0.15 km wide and 4.0 ± 0.5 km long (Dunlap 1974). Vilas et al. (1985) model an ellipsoid of dimensions $3.5 \times 1.4 \times 1.4$ km to data from 3288 Seleucus (1982 DV). Radar measurements of 1685 Toro (Ostro et al. 1983) modeled as an ellipsoid with semi-axes equal to 2.60 ± 0.10 and 1.68 ± 0.17 km, have reasonable fits to the data as do the results of modeling of photometric lightcurves (Dunlap et al. 1973; axis radii of 2.8 and 1.6 km). These results are consistent with a technique applied to 1685 Toro by Ostro and Connelly (1984) which uses integral geometry to invert lightcurves to convex profiles describing shapes. There is evidence for irregular shapes of unspecified dimensions for asteroids 1627 Ivar (Lupishko et al. 1986; Ostro et al. 1985), 1862 Apollo (Lebofsky et al. 1981; Hahn 1983; Ostro et al. 1985), 2201 Oljato (see the chapter by Ostro; Ostro et al. 1985) and 2100 Ra-Shalom (Ostro et al. 1984).

The irregular shapes that have been determined for AAAO are consistent with their derivation as collisional fragments. Whether or not these collisions occurred near their present orbits, previous orbits, or both, remains to be answered.

VI. SURFACE ROUGHNESS

Information on the surface texture and larger-scale topographic roughness is derived from photometric phase relations, polarimetry, radiometry and radar measurements. Photometry and polarimetry provide information on the small-scale texture of the surface. Radiometric models are functions of the thermophysical properties of the regolith, and present constraints on the presence and porosity of the regolith. Radar measurements are sensitive to the cm-to-m-scale variation of the asteroids. There is evidence, from both radar and photometry, of heterogeneity across the surface of some AAAO.

Radar (Goldstein et al. 1981) and radiometry (Lebofsky et al. 1981) measurements of 1862 Apollo support a modeled dusty-regolith surface for this asteroid. Its phase coefficient (Harris et al. 1987) is consistent with that of other bright, main-belt asteroids, a fact which also supports the concept of the existence of an asteroid regolith. Polarimetric measurements for 1862 Apollo (Tedesco, personal communication) also support independent data indicating that this km-sized body has a dusty regolith.

Lebofsky and Rieke (1979) model the thermal properties of 433 Eros varying multiple parameters. The best fit of their observed thermal data involves parameters of a rocky material covering 10 to 50% of the surface, or a rocky substrate with a thin, dusty regolith less than a few cm thick. These parameters are unlike the lunar regolith. Jurgens and Goldstein (1976) and Campbell et al. (1976) also determine that the surface of Eros is rougher than the Moon or any planets at 3.5 and 12.6 cm, and 70 cm, respectively.

Goldstein (1969) presents evidence for a change in surface roughness at the 12.5-cm scale as a function of latitude across the surface of 1566 Icarus. The surface of this asteroid becomes rougher at higher latitude. Its phase coefficient is consistent with that of the Moon (Gehrels et al. 1970) indicating a similar surface roughness at optical wavelength scales.

The lightcurve shape of 1580 Betulia is indicative of a variation in roughness across this asteroid's surface at optical wavelength scales (Tedesco et al. 1978). In order to reconcile radiometric and polarimetric diameter measurements, the radiometry of Betulia has to be modeled as a bare rocky surface, thus indicating that its surface is different from those modeled for the larger, main-belt asteroids (Lebofsky et al. 1978).

From radar cross sections and circular polarization ratios, the radar reflectivity and surface density of 2100 Ra-Shalom is constrained. Ostro et al. (1984) model this asteroid's surface as having a two-fold variation in surface density at the observed rotational phases. In spite of a number of unconstrained parameters, it is difficult to reconcile the radar and photoelectric observations of Ra-Shalom with a surface of uniform roughness. Radiometric data of Ra-Shalom (Lebofsky et al. 1979,1983) require invoking the high thermal inertia, bare-rock model in order to derive consistent albedos from polarimetry and radiometry at both 10 and 20 μm.

The surface of 1685 Toro, on the other hand, is relatively smooth at the 13-cm scale based on the ratio of polarized echo power. Ostro et al. (1983) claim that *rms* slopes are <10 deg at 10-to-100-cm scales, but that there is considerable roughness at 10-to-100-m scales. Earlier radar measurements by Goldstein et al. (1973) support this description in qualitative terms. At optical-wavelength scales, the surface, with a higher phase factor than the Moon and comparable polarization characteristics, is rougher than the Moon (Dunlap et al. 1973).

Among the asteroids that must be modeled with a high thermal inertia in order to produce consistent results with radar and visual data are: 1580 Betulia, 1685 Toro, 2100 Ra-Shalom, 2201 Oljato, 3199 Nefertiti, 3200 Phaethon and 3288 Seleucus (1982 DV; Vilas et al. 1985; Veeder et al. 1989). These objects probably have less regolith than those asteroids with radiometric properties which fit the standard thermal model.

1984 KB (Bell et al. 1988) along with 1862 Apollo and others (see Table III) have a dusty regolith with a low thermal inertia. Most of these asteroids are quite small, illustrating that some small AAAO apparently have retained a

regolith, or at least the same thermal properties as some of the main-belt asteroids (Veeder et al. 1989).

Ostro (1985) concludes that the surface of 2101 Adonis is unlike that of other near-Earth, main-belt asteroids, or active comets. Unusual radar echo spectra have been measured for 1866 Sisyphus as well (Ostro 1988). Radar observations by Ostro et al. (1987) indicate that 1986 DA, classified as type M by Tedesco and Gradie (1987), has a surface which is more metallic than asteroid 16 Psyche. However, the infrared radiometry does not show any anomalous elevation of surface temperature above that expected from the standard model which might be expected for the implied low emissivity of a metallic surface (Veeder et al. 1989). Its regolith may be only a few cm deep and/or very heterogeneous.

From circular polarization ratios of radar measurements, the AAAO are rougher on a cm-to-m scale than the large, main-belt asteroids (see the chapter by Ostro). The observed variations in this ratio as a function of rotational phase for individual asteroids also indicates that the surface roughness at these scales is not homogeneous.

VII. DISCUSSION

Due to discovery biases, conclusions about the true nature of the population of AAAO cannot presently be made. Our discussion of their physical properties is based on the observed population and is not corrected for these biases. Examination of the relationships of different data sets to each other has not revealed any systematic results. Both the largest and the smallest AAAO are S-type asteroids, and the few C types span a considerable range in diameter. The rare taxonomic types have a range of rotation rates as do the abundant S types. Knowledge of the shapes of the AAAO is not precise enough to examine as a function of taxonomy at this time. There is no correlation between radar parameters and taxonomy indicating that the roughness at radar scales is not controlled by composition alone.

The complete range of cosmochemical assemblages that are found in the main belt are found in the AAAO population, indicating that their compositions, and therefore source regions, are diverse in terms of their location within the asteroid belt. It is reasonable to expect that the S-type AAAO originated from the inner regions of the main asteroid belt where most of the S-type asteroids are located (see, e.g., Gradie and Tedesco 1985; Matson 1986).

Analysis of main-belt asteroid reflectance spectra indicates the presence of few ordinary chondrite analogues in the main belt. The absence of Q-type asteroids in the main belt is consistent with spectral reflectance data. However, it is not known whether their absence in the main belt is real and controlled by dynamics, or if the Q's (and ordinary chondrites parent bodies as well), are too small to be observed in the main belt. Visible and near-infrared

reflectance spectroscopy of those ambiguously classified Q-type asteroids should be made to test their relationship to ordinary chondrite analogues. Caution must be taken in using taxonomy alone to make mineralogical inferences.

The need to invoke the rapidly rotating, high thermal inertia, radiometric model for some AAAO and not for the main-belt asteroids must be investigated further. Since some of the small AAAO can be fit by the standard thermal model, the issue is not merely one of size. Knowledge of the controlling factors of regolith coverage is likely to tell us something of their history and origins.

In spite of the large amplitude lightcurves observed for many of the AAAO, conclusions about their shape relative to the main-belt asteroids cannot be drawn at this time. Most of those with lightcurves from which their shape can be determined are irregular, with the notable exception of 1566 Icarus. Accounting for the phase-amplitude effect may change some of the results but probably not to the extent of making them close to spherical. 1566 Icarus is spherical in spite of the high phase-angle measurements.

Radar measurements reveal a larger range of surface properties than found for large main-belt asteroids and also support the conclusion that the source and history of the AAAO is quite diverse. Combined observations including radar, radiometry and photometry have resulted in the discovery of the first mostly metallic AAAO. Until this time, the presence of metallic material, cited as important as a space resource, has been inferred only through the existence of iron meteorites. There is now observational evidence in support of this.

It is clear that the population of the AAAO is diverse in all of their physical characteristics. For purposes of utilization of asteroidal material, any needed material will probably be found. This physical diversity implies that the AAAO come from multiple sources, and have had different evolutionary histories. It is only recently that enough information has been available to consider more than one physical property of an asteroid in the context of the whole population of AAAO. The next step in the analysis of AAAO is to evaluate the bias correction for this population and to determine which asteroids originated from which region of the asteroid belt or solar system. Determination of source regions for specific asteroids begins in the chapter by Weissman et al., where the physical properties of possible extinct cometary nuclei are discussed. A carefully organized program of coordinated analysis and observations of the AAAO at their discovery apparition would improve our understanding of these objects significantly.

REFERENCES

Arnold, J. R. 1964. The origin of meteorites as small bodies. In *Isotopic and Cosmic Chemistry,* ed. H. Craig, S. L. Miller and G. J. Wasserburg, (Amsterdam: North-Holland Publ. Co.), pp. 347–364.

Bell, J. F., Brown, R. H., and Hawke, B. R. 1988. Composition and size of Apollo asteroid 1984 KB. *Icarus* 73:482–486.

Bell, J. F., Hawke, B. R., Owensby, P. D. and Gaffey, M. J. 1987. Atlas of Asteroid Infrared Reflection Spectra (0.8-2.5 Microns). unpublished.

Binzel, R. P. 1987. A photoelectric survey of 130 asteroids. *Icarus* 72:135–208.

Binzel, R. P., and Tholen, D. J. 1983. The rotation, color, phase coefficient and diameter of 1915 Quetzàlcoatl. *Icarus* 55:495–497.

Bowell, E. 1977. 1977 RA. *IAU Circ.* 3111.

Bowell, E., Chapman, C. R., Gradie, J. C., Morrison, D., and Zellner, B. 1978. Taxonomy of asteroids. *Icarus* 35:313–335.

Campbell, D. B., Pettengill, G. H., and Shapiro, I. I. 1976. 70-cm radar observations of 433 Eros. *Icarus* 28:17–20.

Chapman, C. R., Morrison, D., and Zellner, B. 1975. Surface properties of asteroids: A synthesis of polarimetry, radiometry, and spectrophotometry. *Icarus* 25:104–130.

Cruikshank, D. P., and Jones, T. J. 1977. The diameter and albedo of Asteroid 1976 AA. *Icarus* 31:427–429.

Cruikshank, D. P., Hartmann, W.K., Tholen, D., and Bell, J. 1985. An olivine-rich Earth-crossing asteroid: Source of pallasites? *Lunar Planet. Sci.* XVI:160 (abstract).

Debehogne, H., De Sanctis, G., and Zappalà, V. 1983. Photoelectric photometry of Asteroids 45, 120, 776, 804, 814 and 1982 DV. *Icarus* 55:236–244.

Degewij, J. 1978. The sizes of 1978 CA and 1978 DA. *Messenger* 13:5.

Degewij, J., Gradie, J., and Zellner, B. 1978. Minor planets and related objects: XXV. UBV photometry of 145 faint asteroids. *Astron. J.* 83:643–650.

Dollfus, A., and Zellner, B. 1979. Optical polarimetry of asteroids and laboratory samples. In *Asteroids,* ed. T. Gehrels (Tucson: Univ. of Arizona Press), pp. 170–183.

Drummond, J. D., Cocke, W. J., Hege, E. K., and Strittmatter, P. A. 1985. Speckle interferometry of asteroids. *Icarus* 61:132–151.

Dunlap, J. L. 1974. Minor planets and related objects. XV. Asteroid (1620) Geographos. *Astron. J.* 79:324–332.

Dunlap, J. L. 1976. Lightcurves and the axis of rotation of 433 Eros. *Icarus* 28:69–78.

Dunlap, J. L., and Taylor, R. C. 1979. Minor planets and related objects. XXVII. Lightcurves of 887 Alinda. *Astron. J.* 84:269–273.

Dunlap, J. L., Gehrels, T., and Howes, M. L. 1973. Minor planets and related objects. IX. Photometry and polarimetry of (1685) Toro. *Astron. J.* 78:491–501.

Feierberg, M. A., Lebofsky, L. A., and Tholen, D. J. 1985. The nature of C-class asteroids from 3-μm spectrophotometry. *Icarus* 63:183–191.

Gaffey, M. J. 1976. Spectral reflectance characteristics of the meteorite classes. *J. Geophys. Res.* 81:905–920.

Gaffey, M. J. 1985. Rotational spectral variations of Asteroid (8) Flora: Implications for the nature of the S-type asteroids and for the parent bodies of the ordinary chondrites. *Icarus* 60:83–114.

Gaffey, M. J. 1986. The spectral and physical properties of metal in meteorite assemblages: Implications for asteroid surface materials. *Icarus* 66:468–486.

Gaffey, M. J., and McCord, T. B. 1978. Asteroid surface materials: Mineralogical characterizations from reflectance spectra. *Space Sci. Rev.* 21:555–628.

Gaffey, M. J., and McCord, T. B. 1979. Mineralogical and petrological characterizations of asteroid surface materials. In *Asteroids,* ed. T. Gehrels (Tucson: Univ. of Arizona Press), pp. 687–723.

Gehrels, T., Roemer, E., Taylor, R. C., and Zellner, B. H. 1970. Minor planets and related objects. IV. Asteroid (1566) Icarus. *Astron. J.* 75:186–195.

Gehrels, T., Roemer, E., and Marsden, B. G. 1971. Minor planets and related objects. VII. Asteroid 1971 FA. *Astron. J.* 76:607–608.

Goldstein, R. M. 1969. Radar observations of Icarus. *Icarus* 10:430–431.

Goldstein, R. M., Holdridge, D. B., and Lieske, J. H. 1973. Minor planets and related objects. XII. Radar observations of (1685) Toro. *Astron. J.* 78:508–509.

Goldstein, R. M., Jurgens, R. F., and Yeomans, D. K. 1981. Radar observations of Apollo. *Icarus* 48:59–61.

Gradie, J. C. 1976. Physical observations of object 1976 AA. *Bull. Amer. Astron. Soc.* 8:458 (abstract).

Gradie, J., and Tedesco, E. 1985. Compositional structure of the asteroid belt. *Science* 216:1405–1407.

Gradie, J. C., and Veverka, J. 1980. The composition of the Trojan asteroids. *Nature* 283:840–842.

Hahn, G. 1983. UBVRI and JHK photometry of the near-Earth Asteroid 1862 Apollo. In *Asteroids, Comets, Meteors,* eds. C.-I. Lagerkvist and H. Rickman (Uppsala: Uppsala Univ.), pp. 35–44.

Harris, A. W. 1985. 1980 AA. *IAU Circ.* 3450.

Harris, A. W., and Young, J. W. 1983. Asteroid rotation IV. 1979 observations. *Icarus* 54:59–109.

Harris, A. W. 1986. Asteroid lightcurve studies. In *Asteroids, Comets, Meteors II,* eds. C.-I. Lagerkvist, B. A. Lindblad, H. Lundstedt and H. Rickman (Uppsala: Uppsala Univ.), pp. 35–44.

Harris, A. W., and Young, J. W. 1985. Photometric results for Earth approaching asteroids. *Bull. Amer. Astron. Soc.* 17:726 (abstract).

Harris, A. W., Young, J. W., Goguen, J., Hammel, H. B., and Hahn, G. 1987. Photoelectric lightcurves of the asteroid 1862 Apollo. *Icarus* 70:246–256.

Hartmann, W. K., Tholen, D. J., and Cruikshank, D. P. 1987. The relationship of active comets, "extinct" comets, and dark asteroids. *Icarus* 69:33–50.

Helin, E. F., Harris, A. W., Young, J. W., Tedesco, E. F., Lebofsky, L. A., Tholen, D., Binzel, R. P., and Hulkower, N. D. 1983. A new Earth-approaching asteroid, 1982 XB. *Lunar Planet. Sci.* XIV:297 (abstract).

Johnson, T. V., and Fanale, F. P. 1973. Optical properties of carbonaceous chondrites and their relationships to asteroids. *J. Geophys. Res.* 78:8507–8518.

Jones, T. 1988. An Infrared Reflectance Study of Water in Outer Belt Asteroids: Clues to Composition and Origin. Ph.D. Thesis, Univ. of Arizona.

Jurgens, R. F., and Goldstein, R. M. 1976. Radar observations at 3.5 and 12.6 cm wavelength of asteroid 433 Eros. *Icarus* 28:1–15.

Lebofsky, L. A., and Rieke, G. H. 1979. Thermal properties of 433 Eros. *Icarus* 40:297–308.

Lebofsky, L. A., Veeder, G. J., Lebofsky, M. J., and Matson, D. L. 1978. Visual and radiometric photometry of 1580 Betulia. *Icarus* 35:336–343.

Lebofsky, L. A., Lebofsky, M. J., and Rieke, G. H. 1979. Radiometry and surface properties of Apollo, Amor and Aten Asteroids. *Astron. J.* 84:885–888.

Lebofsky, L. A., Veeder, G. J., Rieke, G. H., Lebofsky, M. J., Matson, D. L., Kowal, C., Wynn-Williams, C. G., and Becklin, E. E. 1981. The albedo and diameter of 1862 Apollo. *Icarus* 48:335–338.

Lebofsky, L. A., Veeder, G. J., and Matson, D. L. 1983. 2100 Ra-Shalom: A rocky asteroid? *Bull. Amer. Astron. Soc.* 15:824 (abstract).

Lupishko, D. F., Velichko, F. P., and Shevchenko, V. G. 1986. Asteroid 1627 Ivar. UBV photometry, period and sense of rotation. *Kinematika Fiz.* 2:39–43.

Lupishko, D. F., Velichko, F. P., Kazakov, V. V., and Shevchenko, V. G. 1987. 1036 Ganymed: Light curves, period and sense of rotation. *Kinematika Fiz.* 3:92–93.

Matson, D. L. 1986. IRAS asteroid and comet survey, Preprint version No. 1, JPL D-3698.

McCord, T. B., and Chapman, C. R. 1975. Asteroids: Spectral reflectance and color characteristics. II. *Astrophys. J.* 197:781–790.

McFadden, L. A. 1983. Spectral Reflectance of Near-Earth Asteroids: Implications for Composition, Origin and Evolution. Ph.D. Thesis, Univ. of Hawaii.

McFadden, L. A. Gaffey, M. J., and McCord, T. B. 1984. Mineralogical-petrological characterization of near-Earth asteroids. *Icarus* 59:25–40.

McFadden, L. A., Gaffey, M. J., and McCord, T. B. 1985. Near-Earth asteroids: Possible sources from reflectance spectroscopy. *Science* 229:160–163.

McSween, H. Y., Sears, D. W. G., and Dodd, R. T. 1988. Thermal metamorphism. In *Meteorites and the Early Solar System*, eds. J. F. Kerridge and M. S. Matthews (Tucson: Univ. of Arizona Press), pp. 102–113.

Millis, R. L., Bowell, E., and Thompson, D. T. 1976. UBV photometry of asteroid 433 Eros. *Icarus* 28:53–67.

Miner, E., and Young, J. 1969. Photometric determination of the rotation period of 1566 Icarus. *Icarus* 10:436–440.

Morrison, D., Gradie, J., and Rieke, G. H. 1976. Radiometric diameter and albedo of the remarkable asteroid 1976AA. *Nature* 260:691.

Ostro, S. J. 1985. Radar observations of asteroids and comets. *Publ. Astron. Soc. Pac.* 97:877–884.

Ostro, S. J., and Connelly, R. 1984. Convex profiles from asteroid lightcurves. *Icarus* 57:443–463.

Ostro, S. J., Campbell, D. B., and Shapiro, I. I. 1983. Radar observations of asteroid 1685 Toro. *Astron. J.* 88:565–576.

Ostro, S. J., Harris, A. W., Campbell, D. B., Shapiro, I. I., and Young, J. 1984. Radar and photoelectric observations of asteroid 2100 Ra-Shalom. *Icarus* 60:391–403.

Ostro, S. J., Campbell, D. B., and Shapiro, I. I. 1985. Radar properties of near-Earth Asteroids. *Bull. Amer. Astron. Soc.* 17:729–730 (abstract).

Ostro, S. J., Campbell, D. B., Hine, A., and Shapiro, I. I. 1987. Radar echoes from asteroid 1986 DA indicate a metallic composition. *Bull. Amer. Astron. Soc.* 19:840 (abstract).

Pieters, C., Gaffey, M. J., Chapman, C. R., and McCord, T. B. 1976. Spectrophotometry (0.33 to 1.07 μm) of 433 Eros and compositional implications. *Icarus* 28: 105–115.

Rakos, K. D. 1960. Light variations of the fast-moving minor planet, 1960 UA. *Lowell Obs. Bull.* 5(109):28–29.

Roach, F. E., and Stoddard, L. G. 1938. A photoelectric lightcurve of Eros. *Astrophys. J.* 88:305–312.

Sears, D. W. G., and Dodd, R. T. 1988. Overview and classification of meteorites. In *Meteorites and the Early Solar System*, eds. J. F. Kerridge and M. S. Matthews (Tucson: Univ. of Arizona Press), pp. 3–31.

Shoemaker, E. M., Williams, J. G., Helin, E. F., and Wolfe, R. F. 1979. Earth-crossing asteroids: Orbital classes, collision rates with Earth and origin. In *Asteroids*, ed. T. Gehrels (Tucson: Univ. of Arizona Press), pp. 253–282.

Taylor, R. C. 1985. The pole orientation of asteroid 433 Eros determined by photometric astrometry. *Icarus* 61:490–496.

Tedesco, E. F., and Gradie, J. 1987. Discovery of M class objects among the near-Earth asteroid population. *Astron. J.* 93:738–746.

Tedesco, E. F., Drummond, J., Candy, M., Birch, P., Nikoloff, I., and Zellner, B. 1978. 1580 Betulia: An unusual asteroid with an extraordinary lightcurve. *Icarus* 35:344–359.

Tholen, D. J. 1984a. Asteroid Taxonomy from Cluster Analysis of Photometry. Ph.D. Thesis, Univ. of Arizona.

Tholen, D. J. 1984b. Photometry of Earth-approaching asteroids. *Bull. Amer. Astron. Soc.* 16:690–691 (abstract).

Tholen, D. J. 1985. (3200) 1983 TB. *IAU Circ.* 4034.

Tholen, D. J. 1988. Asteroids II machine-readable data base: March 1988 floppy-disk version.

Tholen, D. J., Hartmann, W. K., and Cruikshank, D. P. 1988. 1980 PA and 1985 DO2. *IAU Circ.* 4655.

Veeder, G. J., Kowal, C., and Matson, D. L. 1984. The Earth-crossing asteroid 1983 TB. *Lunar Planet. Sci.* XV:878–879 (abstract).

Veeder, G. J., Matson, D. L., Tedesco, E. F., Lebofsky, L. A., and Gradie, J. 1987. Physical properties of near-Earth asteroids. *Bull. Amer. Astron. Soc.* 19:840 (abstract).

Veeder, G. J., Hanner, M. S., Matson, D. L., Tedesco, E. F., Lebofsky, L. A., and Tokunaga, A. T. 1989. Radiometry of near-Earth asteroids. *Astron. J.*, submitted.

Veverka, J., and Liller, W. 1969. Observations of Icarus: 1968. *Icarus* 10:441–444.

Vilas, F. and McFadden, L. A. 1985. Spectral studies of possible sources of near-Earth asteroids-CCD reflectance spectra. *Bull. Amer. Astron. Soc.* 17: 732 (abstract).

Vilas, F., Tholen, D. J., Lebofsky, L. A., and Campins, H. 1985. Physical parameters of near-Earth asteroid 1982 DV. *Icarus* 63:201–205.

Wisniewski, W. Z. 1987. Photometry of six radar target asteroids. *Icarus* 70:566–572.

Zellner, B., and Gradie, J. 1976. Minor planets and related objects. XX. Polarimetric evidence for the albedos and compositions of 94 asteroids. *Astron. J.* 81:262–280.

Zellner, B., Gehrels, T., and Gradie, J. 1974. Minor planets and related objects. XVI. Polarimetric diameters. *Astron. J.* 79:1100–1110.

Zellner, B., Wisniewski, W., Andersson, L., and Bowell, E. 1975. Minor planets and related objects. XVIII. UBV photometry and surface composition. *Astron. J.* 80:986–995.

Zellner, B., Tholen, D. J., and Tedesco, E. F. 1985. The eight-color asteroid survey: Results for 589 minor planets. *Icarus* 61:355–416.

DISTANT ASTEROIDS AND CHIRON

LINDA M. FRENCH
Air Force Geophysics Laboratory

FAITH VILAS
Johnson Space Center

WILLIAM K. HARTMANN
Planetary Science Institute

and

DAVID J. THOLEN
University of Hawaii

Knowledge of the physical properties of distant asteroids ($a > 3.3$ AU) has grown dramatically over the past five years, due to systematic compositional and lightcurve studies. Most of these objects have red, dark surfaces, and their spectra show a reddening in spectral slope with heliocentric distance implying a change in surface composition. Trojans for which near-opposition phase curve information is available appear to show little or no opposition effect, unlike any other dark solar system objects. The lightcurve amplitudes of Trojan and Hilda asteroids imply significantly more elongated shapes for these groups than for main-belt asteroids of comparable size. These recent observations are reviewed in the context of their implications for the formation and subsequent evolution of the distant asteroids, and their interrelations with the main belt, Chiron and comets.

Because of their great heliocentric distance and their corresponding faintness, little was known about the physical properties of distant asteroids until

very recently. For the purposes of this chapter, we define distant asteroids to be those whose orbits have semimajor axes outside the 2 : 1 resonance with Jupiter at about 3.3 AU. With a few exceptions, asteroids beyond the main belt are found in three distinct zones. The Cybeles are located between the 2 : 1 and 5 : 3 Jovian resonances (mean semimajor axis $a = 3.4$ AU). The Hildas are found at the 3 : 2 resonance ($a = 4.0$ AU), and the Trojan asteroids are located at the L4 and L5 Lagrangian points of Jupiter's orbit at $a = 5.2$ AU. Asteroid 279 Thule is the sole object known to occupy the 4 : 3 resonance of Jupiter's orbit, while 944 Hidalgo and 2060 Chiron have semimajor axes farther beyond the orbit of Jupiter. The dynamical structure of this part of the solar system is discussed in the chapter by Nobili.

The past ten years have seen an increasing number of systematic studies of the spectral and lightcurve parameters of distant asteroids. Emerging evidence indicates several intriguing differences between main-belt asteroids and more distant objects. Because they are isolated from most interactions with other asteroids by Jovian resonances, the collisional and rotational history of the distant asteroids may differ significantly from the main-belt objects. The major taxonomic types found among the distant asteroids are quite rare in the main belt and are not currently represented in terrestrial meteorite collections. An understanding of the nature and original formation location of these objects is essential for a complete understanding of the mechanisms of solar system formation.

I. NUMBER AND DISTRIBUTION OF TROJANS

The stability of the L4 and L5 equilateral points was first demonstrated by Lagrange in 1772. These points are often referred to as potential minima, but in fact are maxima in the gravitational potential field, as demonstrated by Greenberg and Davis (1978). Objects near L4 and L5 are stabilized and kept near the Lagrange points by Coriolis forces. However, they do not remain perfectly fixed within a Sun-Jupiter reference frame but undergo a complex libration which can be described by a combination of two periods, one equal to the orbital period of the asteroids (and Jupiter), 11.86 yr, and one of order 200 yr (Rabe 1961). The libration amplitudes are typically up to $\pm 30°$ on either side of the Lagrange points. However, there is no dynamical limit to the libration amplitude; theoretically, even larger amplitudes are permitted (Yoder 1979; E. Shoemaker, personal communication).

The allowed eccentricities of Trojan orbits are dynamically limited by secular resonances (Rabe 1967; Yoder 1979) to an upper limit of about 0.19. Their inclinations, however, are not dynamically constrained and a large proportion of the known Trojans are in high-inclination orbits (see Fig. 1). The combination of large libration amplitudes and a wide range of orbital inclinations means that the known Trojans are not tightly grouped together in the sky, but span an area of thousands of square degrees. Fields chosen for initial
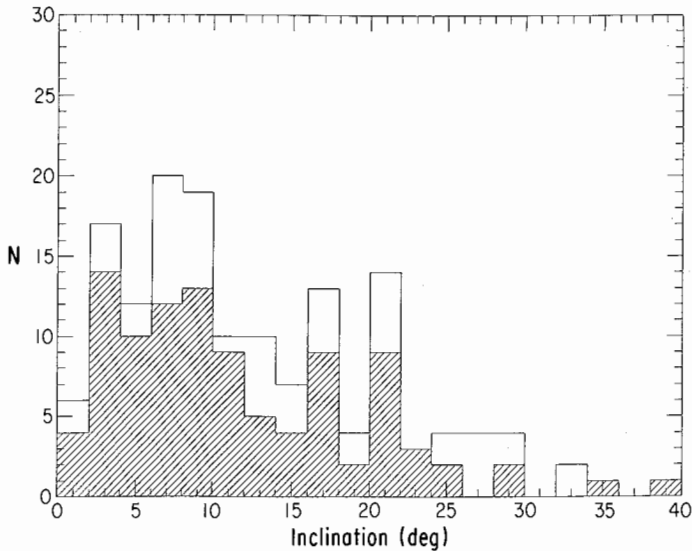
Fig. 1. Histogram of orbital inclinations for all multiple-opposition Trojan orbits as of mid-1988. The cross-hatched subset represents the inclinations of L4 asteroids; the higher curve describes the total (L4 + L5) population.

surveys of the Trojan regions were limited to regions near the ecliptic (van Houten et al. 1970a,b), so that high-inclination Trojans, at least, may be severely underrepresented in these surveys (Degewij and van Houten 1979). van Houten et al. (1970a) found a large discrepancy in the numbers of Trojans in the two groups: they estimated 700 Trojans brighter than magnitude 20.9 in the L4 group, with only 200 in L5 to the same magnitude limit.

Recently Shoemaker et al. (1989) have begun a photographic search for L5 Trojans which samples a wider range of inclinations and libration amplitudes than previous surveys. C. and E. Shoemaker are using the Palomar 46-cm Schmidt to survey most of the known Trojan region down to $B = 18.5$ (~35 km) (see their chapter). L. French, S. Bus and E. Bowell are using the Cerro Tololo 61-cm Curtis Schmidt to sample several fields over an area of 200 square degrees spaced in ecliptic latitude and longitude centered on L5; their magnitude limit is $B = 20$ (~15 km). E. Bowell and K. Russell are using the 1.2-m UK Schmidt telescope to obtain plates (70 deg^2) of the L5 region down to $B = 21.5$ (~10 km). Two-month long orbital arcs will be obtained for most of the Trojans found, thus enabling their recovery at future oppositions. To date, 20 new Trojans have been found from the Palomar plates. Additionally, three objects from the Palomar-Leiden Survey of van Houten et al. (1970a) have been re-observed, providing new opposition orbits for these objects. The

Cerro Tololo plates have resulted in 32 new Trojans, and the UK Schmidt plates have revealed 20 to 50 new Trojans per plate. As of this writing, Shoemaker et al. (1989) conclude the following: (1) The number of known Trojans in the L5 cloud will probably triple as a result of this survey; (2) Down to a diameter of about 50 km, the populations of L4 and L5 are about equal; (3) Down to 15 km diameter, the total Trojan population (L4 + L5) seems to be comparable with that of the main belt (about 2500 objects each); (4) There is preliminary orbital evidence for family structure in L4 (see the chapter by Shoemaker et al.). The implications of families among the Trojans are discussed in connection with their rotational properties (Sec. III).

II. COMPOSITION

The three major classes of dark asteroids (C, P and D) are all represented among the distant asteroids. Because of their suspected composition, these classes of asteroids are also referred to as primitive asteroids. Two additional S-class asteroids have been identified as well (Tholen 1984; see the chapter by Tholen and Barucci). The D class, first identified by Degewij and van Houten (1979), have reddish spectra in the visible region; the spectra may either flatten slightly in the near-infrared or continue to increase into the infrared. The D objects have extremely low geometric albedos (~0.03). Gradie and Tedesco (1982) first recognized the P-class asteroids, whose spectra are linear and reddish with a smaller slope than those of D's, and whose albedos are similarly low. Figure 2 shows spectral data for sample C, P and D asteroids located among the distant asteroids.

A gradual shift in dominant compositional class with heliocentric distance was first identified by Chapman et al. (1975). Further revisions have been added by Zellner (1979), Gradie and Tedesco (1982), Tholen (1984), Vilas and Smith (1985), Zellner et al. (1985) and Hartmann (1987); see also the chapters by Gradie et al. and by Bell et al. The recent work shows the P objects to be more prominent than originally thought. They are widely spread in semimajor axis, making up 15% of the bias-corrected asteroid population at 2.76 AU and 37% in the Trojan region at 5.2 AU. P objects also attain a higher maximum percentage (~65% among the Hildas) than previously believed. The Trojan region is dominated by objects of the D class, which comprise more than 60% of the asteroids in that area.

The surface composition of the D-class asteroids was first investigated by Gradie and Veverka (1980), who mixed organic polymers, clay silicates and an opaque to simulate the reddened slope seen in the D-class spectra. Bell et al. (1985) investigated the composition of the dark material on the leading edge of Iapetus and suggested that a combination of clay silicates and organics alone would produce the red-sloped spectra common to both Iapetus and D-class asteroids. The addition of organics to clays in the simulated spectra of Bell et al. lowers the overall absolute reflectance of the mixtures and masks
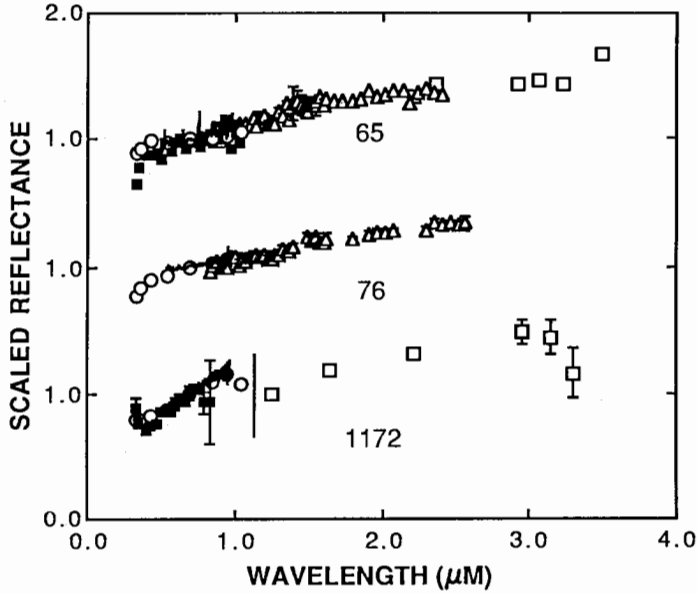
Fig. 2. Sample distant asteroid spectra: 65 Cybele (C or P class), 76 Freia (P), 1172 Aneas (D). Data are from different observational programs: ○ Zellner et al. (1985); △ Bell et al. (1988); ——— Vilas and Smith (1985), Vilas and McFadden 1987; ☐ Lebofsky et al. (1989); ■ Chapman and Gaffey (1979). Data are scaled 1.0 at 0.7 μm. The 1172 Aneas data are partitioned where no overlapping spectral region allowed scaling of the infrared data to visible data. These infrared data are scaled 1.0 at 1.25 μm.

some of the features seen in the clay silicate spectra. Sill's (1973) reflectance spectra of two hydrocarbon separates show a simple hydrocarbon to have a spectrum with a redder slope than that of a more complex hydrocarbon. Vilas and Smith (1985) inferred from Sill's work that simpler hydrocarbons might form at increasing heliocentric distances, producing the increased spectral slope seen in the distant asteroid spectra. Spectra of bituminous tar sands (composed of clays, hydrocarbons, quartz grains, water and accessory minerals [Cloutis 1989]) also appear to be reasonable analogs for these dark objects.

Compositional information about the distant asteroids is obtained from remote sensing studies of how the reflected sunlight is affected by the composition of the top surface layers, usually a few micrometers thick (see the chapter by Gaffey et al.). Using Tholen's (1984) classification of Eight-Color Asteroid Survey photometry and thermal radiometry as a guide for selecting target asteroids, various researchers have undertaken compositional studies of the primitive asteroids, concentrating on data acquired in different spectral ranges. It should be noted that the large heliocentric distances and low albedos

of these objects make them challenging targets for existing astronomical instrumentation. In particular, spectral resolution is often sacrificed in order to improve the signal-to-noise ratio for these faint objects. With further developments in instrumentation, these problems (and the asteroid spectra) will be resolved.

High-resolution (16 to 20 Å) spectrophotometry of distant asteroids and main-belt primitive asteroids is underway to search for compositional information in the ~0.5 to 1.0-μm spectral range (Vilas and Smith 1985; Vilas 1986; Vilas and McFadden 1987). Based upon a small number of spectra, Vilas and Smith (1985) proposed that discrete changes in spectral slope seen among the Cybele, Hilda and Trojan asteroids can be correlated with the discrete heliocentric distances represented by these groups of asteroids. They suggested that these distant asteroid groups formed *in situ* with surface compositions for which one element changed continuously with increasing heliocentric distance, manifesting itself in a continuous change in spectral slope. Vilas and Smith (1985) found support for their view in the spectral studies of the material on the dark side of Saturn's satellite, Iapetus, by Bell et al. (1985). Iapetus is redder than any D asteroid known, consistent with a trend in reddening with solar distance. Removal of asteroids from the outer-belt regions due to the dynamical clearing of material which many think occurred during the formation of Jupiter (Fernández 1978) has left only the groups of asteroids seen today. Vilas and Smith suggested that the distant asteroids are remnants of this once-continuous compositional change. Additional high-resolution spectra have been obtained in order to test this hypothesis (Vilas and McFadden 1989).

Vilas and Gaffey (1988,1989) have found absorption features with depths of a few percent among their high-resolution spectra of distant asteroids which match features seen in CM2 carbonaceous chondrite material and terrestrial chlorites (King 1986). These features have been attributed to $Fe^{2+} - Fe^{3+}$ charge transfers occurring in the iron oxides found in phyllosilicates. Features seen in the spectra of distant primitive asteroids are weaker than those seen in main-belt asteroids of the same taxonomic type. The cause of the change in the depth of these features is not presently understood.

The progression of primitive objects beginning with the concentration of C-class asteroids near 2.5 AU and continuing through the outer solar system have been the targets of a search for the absorption feature from 2.6 to 4.0 μm due to bound water of hydration (see, e.g., Lebofsky 1978; Feierberg et al. 1985; Jones 1988; Lebofsky et al. 1989). This deep absorption is a combination of a sharp drop in reflectance near 2.6 μm due to structural OH coupled with a steadily decreasing absorption due to H_2O. The water of hydration feature is seen in the main-belt C-class asteroids and in most subsets of the C class. The P- and D-class asteroids, however, do not show the water of hydration absorption (Jones 1988; Lebofsky et al. 1989). The low mean albedos of these taxonomic classes suggest that they contain more opaques than C asteroids. However, the laboratory studies of Jones (1988) demonstrated that

large amounts of opaques do not mask this hydrated silicate feature. Thus, the lack of detection suggests that the C asteroids, concentrated in the outer portion of the main asteroid belt, contain hydrous silicates, while asteroids at greater heliocentric distances do not (Lebofsky et al. 1989). Lebofsky et al. and Jones formulate a scenario in which chemical equilibrium was not attained in the solar system region where the P- and D-class asteroids are concentrated. They suggest that all asteroids began as combinations of ice and rock. In the region where C-class asteroids are dominant, moderate heating occurred, resulting in ice melting and subsequent aqueous alteration (see the chapter by Scott et al.). Distant asteroids, however, were not sufficiently heated for these reactions to occur, and their water was lost to sublimation over the age of the solar system.

In conclusion, the compositional information about the distant P- and D-class asteroids is constrained more by what is *not* seen in spectral data than by what *is* seen. The "canonical" model includes dark organic material with some workers favoring the presence of clay silicates. No observational evidence, however, suggests that clay silicates are present in the surface material of the distant P- and D-class asteroids. Lebofsky et al. (1989) make a strong argument against clay silicates being present but spectrally masked through some physical process. This is in contrast to the case for Iapetus, where the deep water of hydration absorption feature characteristic of hydrated silicates is observed (Bell et al. 1985). This difference suggests that Iapetus may *not* be the next example of a continuous compositional gradation in the solar system. However, the Iapetus dark material is probably not native to the surface of the satellite from the epoch of solar system formation (see, *e.g.*, Bell et al. 1985). The Iapetus dark material has had a complicated history, and whatever processes brought it to its current location could have been responsible for spectral alteration as well.

Gradie and Tedesco (1982) suggested that the P-class asteroids are, in composition, a transitional class between the C and D asteroids. However, the absence of the water of hydration absorption band and the near ultraviolet absorption band, in P and D asteroids suggests that the formation histories of the main-belt C objects and that of the more distant P and D asteroids may have been quite different, with the P's and D's escaping any melting episodes. Important clues to the conditions existing during the formation of the outer solar system may well be found here.

III. ROTATION PROPERTIES

Prior to the early 1980s, a well-determined lightcurve existed for only one distant asteroid, Trojan 624 Hektor (Dunlap and Gehrels 1969). That lightcurve has a maximum amplitude of 1.09 mag; if due to projected area variations alone, this implies an axial ratio of almost 3:1. Hektor's extreme brightness variation, its large size (the dimensions were estimated to be ap-

proximately 150 × 300 km by Hartmann and Cruikshank [1978]), and its relatively short rotation period of 6.92 hr have led many to suspect that the asteroid is not a single elongated body held together by internal material strength, but is either a figure of hydrostatic equilibrium or a binary asteroid. The models proposed include a re-assembled brecciated ellipsoid (Cook 1971; Poutanen et al. 1981), a dumbbell-shaped object formed by the partial coalescence of two nearly spheroidal asteroids of equal size (Hartmann and Cruikshank 1978), and a binary system of two Darwin ellipsoids nearly in contact (Weidenschilling 1980; Farinella et al. 1981). Thus, studies of the largest Trojan alone led to a variety of intriguing models and unresolved problems.

Motivation for lightcurve studies of additional distant asteroids involves the dynamical isolation of the distant asteroid groups. One can estimate the relative collision frequencies for each group of asteroids from a knowledge of the number density of asteroids and their mean encounter velocity (Wetherill 1967; Hartmann and Cruikshank 1978; Davis and Weidenschilling 1981; see also the chapter by Shoemaker et al.). During most of the history of the solar system, the collision probabilities among Hildas and Trojans, for example, are much lower than those in the main belt. Thus, the rotation properties of the distant asteroids could be little altered by collisions with other asteroids since the late bombardment stage of solar system formation, while each main-belt asteroid has typically undergone several catastrophic collisions.

At present, some lightcurve information is available for ~30 Trojans and Hildas (Taylor et al. 1976; Lagerkvist and Sjölander 1979; French et al. 1986; French 1987; Hartmann et al. 1987,1988). For the majority of objects, only the lightcurve amplitude at a single epoch is available; in general, this will give a lower limit to the asphericity since asteroid polar axes can have any orientation. Observations over several oppositions are needed to establish the pole direction. Not enough rotation periods are well determined for meaningful statistical analysis, although those which are known are in the 6 to 12 hr range typical of main-belt asteroids (Dunlap and Gehrels 1969; French 1987; see the chapter by Binzel et al.). Figure 3 shows the amplitude measured at a single epoch for Trojans and Hildas compared with that for main-belt asteroids of equal diameter. Trojans and Hildas have higher amplitudes, on the average, than their main-belt counterparts; statistical analysis of the data indicates that the higher mean amplitudes are significant at the 97 to 99% confidence level (Hartmann et al. 1988).

A possible conclusion is that Trojans and Hildas have more elongated shapes than belt asteroids; however, one can imagine scenarios which would produce this observed effect, while maintaining identical shape distributions for main-belt and distant asteroids. For example, the poles of the Trojans and Hildas could be preferentially aligned nearly perpendicular to the plane of the ecliptic. Then the viewing aspect, not shape, would explain the observed amplitude difference. This scenario is unlikely because the rotational pole for the

MAX. OBS'D AMPLITUDES $42 \leq \bar{D} \leq 188$ KM
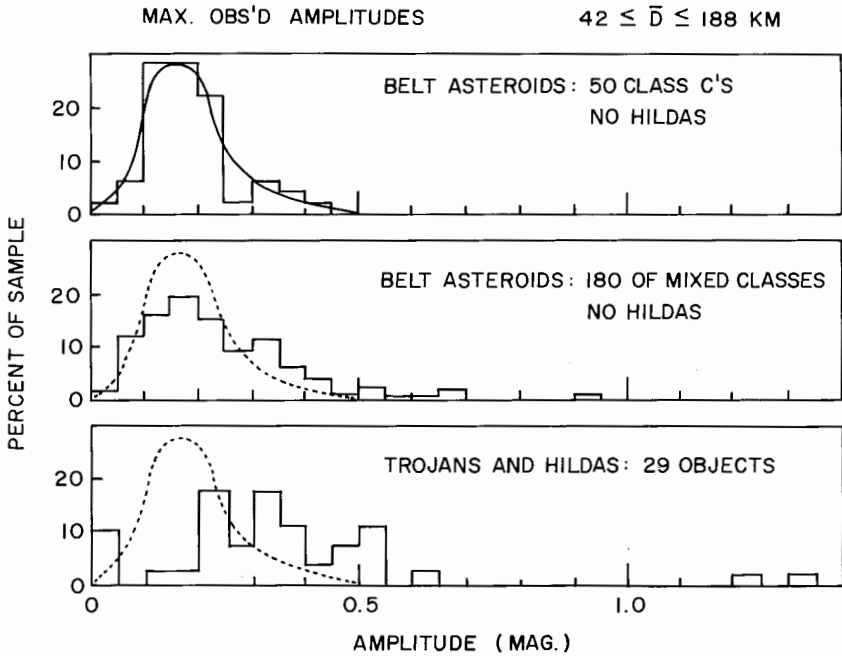
Fig. 3. Histograms of amplitudes of two samples of belt asteroids, compared with a sample of 29 Trojans and Hildas in the same size range. The diagram shows maximum observed amplitudes for each object (most Trojans and Hildas are observed at only one random epoch). A tight clustering of low amplitudes is found for class C belt asteroids, indicated schematically by the bell curve which is reproduced for reference in the other diagrams. Trojans and Hildas appear to have a greater incidence of high amplitudes (figure from data sets discussed by Hartmann et al. [1988], with three additional new lightcurve observations by Tholen and Hartmann).

largest Trojan, 624 Hektor, was determined by Dunlap and Gehrels to lie only $12° \pm 10°$ from the ecliptic plane.

French (1987) and Hartmann et al. (1987,1988) believe that the shapes of the Trojans and Hildas are indeed more elongated than those of main-belt asteroids of comparable size. What this is telling us about the collision history of the distant asteroids, or about the effects of collisions on asteroid shape, is not yet clear. Perhaps the Trojans are more irregular because they are more highly fragmented than main-belt asteroids—an idea which follows from the intuitive notion that fragmentation leads to elongated shapes. Shoemaker et al. (see their chapter) propose that the size distribution of L4 Trojans suggests a large degree of collisional evolution. As we have seen, however, the isolation of the distant asteroids suggests that these groups may have undergone less fragmentation due to collisions with other asteroids since the end of heavy bombardment than the asteroids of the main belt.

French (1987) and Hartmann et al. (1987,1988) proposed that the Trojans are more pristine remnants of the early epochs of solar system formation; Hartmann et al. consider the Hildas to be pristine objects as well. In this view, the asteroids preserve primordial shapes which are more irregular than those found in the collisionally evolved main belt. The irregular shapes could be due to one or both of the following reasons. First, relative collision velocities between distant asteroids are lower than for main-belt objects, simply because their Keplerian velocities are lower. Especially for the Trojans, Hartmann and Cruikshank (1978) proposed that low relative velocities (on the order of <1 km s^{-1}) might produce elongated shapes such as that of Hektor by the inelastic collision of two smaller planetesimals. Typical relative velocities in the Trojan region are $\sim$3.5 km s^{-1} as opposed to $\sim$5 km s^{-1} in the main belt. In order to obtain the low velocity needed to make a Hektor, Hartmann and Cruikshank postulated a low-velocity "tail" on the velocity distribution curve, at least in early times. Such a tail would be caused by the complicated librational motions of Trojans. The currently observed wide range of inclinations and libration amplitudes among Trojan orbits suggests that such low-velocity collisions may not be common today. Alternatively, as main-belt asteroid velocities increased and accretion ceased, higher-speed collisions in the main-belt region could either have rounded off those objects, or allowed reassembly of collisional fragments into zero-strength rubble piles, which adopt more rounded equilibrium shapes than the most extreme objects seen among the Trojans and Hildas. Interesting support for irregular primordial shapes comes from the theoretical work of Donn and Hughes (1986), who show that the fractal geometry of primordial bodies accreting randomly at low speeds produces very elongated shapes.

In contrast to the "pristine remnant" idea, Shoemaker et al. (see their chapter) argue that the Trojans should be at least as evolved collisionally as main-belt asteroids of comparable size. They believe the Trojans are Uranus-Neptune planetesimals which were scattered inward from the outermost solar system during the late heavy bombardment stage of solar system formation. Shoemaker et al. suggest that a possible mechanism for capturing such objects is still active among Jupiter family comets. Encounters with Jupiter drive short-period comets into temporary 1:1 libration in approximately 2% of the known short-period orbits; in such cases, a very small impulse would be required to capture such a temporary librator as a permanent Trojan. At an epoch of heavy bombardment, Shoemaker et al. suggest both such temporary captures and subsequent collisions could have been sufficiently numerous to create the observed population of Trojans and cause extensive collisional modification. Thus, the current low collision rates would be irrelevant. They are currently searching for Hirayama-type families among the Trojans (chapter by Shoemaker et al.; Shoemaker et al. 1989). Since main-belt Hirayama families are generally believed to be collisional fragments of a few original parent bodies (Gradie et al. 1979; see the chapter by Chapman et al.), identification

of such families would support their view that Trojans may be strongly collisionally evolved. This, in turn, would argue against the view that the Trojans are pristine bodies which "remember" their primordial shapes.

IV. SURFACE PROPERTIES

Once the rotational lightcurve of an asteroid is well determined, one can remove its effects to determine the phase curve. Recent years have seen much theoretical and empirical work devoted to systems of photometric parameters which will give information diagnostic of the albedo and surface texture for asteroid surfaces (see the chapter by Bowell et al. for more information about phase functions). To date, only one Trojan, 1173 Anchises, has a well-determined phase curve near zero phase angle (French 1987). Anchises is classified as a P object by Tholen (1984); its geometric albedo has been determined by both IRAS and from groundbased radiometric data to be < 0.05 (Tedesco 1986; Cruikshank 1977). The phase curve observations were made at phase angles ranging from $0°3$ to $2°0$; all other dark solar system objects studied to date show a strong opposition effect at such small phase angles. Figure 4 shows the typical dark object phase curve from the model of Bowell
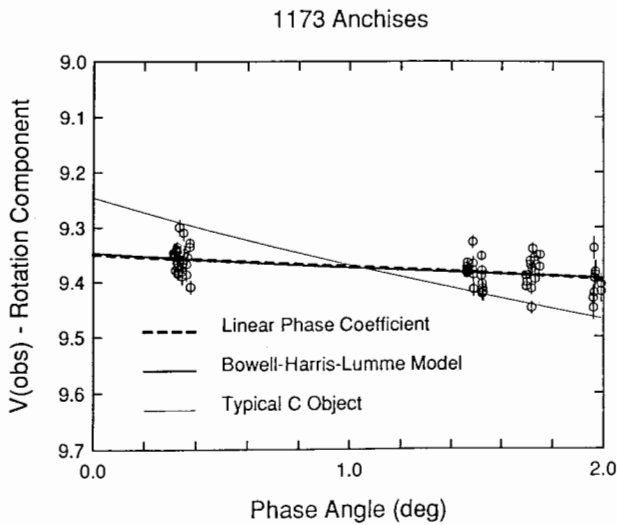
Fig. 4. Phase curve of Trojan asteroid 1173 Anchises. The four clusters of data represent observations from four different nights; a Fourier model was fit to the rotational component of the lightcurve to remove its effects. The difference between the observed V magnitude and the model is plotted; this gives the phase curve of the asteroid. The best-fit straight-line phase function, the best fitting model of Bowell et al. and the Bowell et al. phase curve typical for most dark C asteroids are superimposed on the data. The C-object curve is clearly a poor match, making Anchises the first dark asteroid observed to show no opposition effect (Fig. from French 1987).

et al. (see their chapter) and the observed data for 1173 Anchises. Clearly the Trojan's brightness surge near zero phase is much less pronounced than that of other dark asteroids. The phase curve is similar to what one would expect for bare rock rather than for a regolith-covered surface with a large amount of particle shadowing. One other Trojan, 2674 Pandarus, was observed by French (1987) on three nights very close to zero phase angle; the range was not large enough to derive a significant fit to the phase function. However, the lightcurves from the three nights suggest that a large opposition effect cannot be present, and imply that the phase curve of Pandarus, too, will be poorly matched by standard models.

Possible explanations for this unique behavior include:

1. Lack of a regolith, due to infrequent collisions between asteroids in the Trojan regions;
2. Unusual single particle scattering functions;
3. An unusual surface texture; perhaps a slightly more fluid-like surface than for other asteroids, thereby allowing surface features to relax.

A complete absence of regolith is not likely; impacts from comets alone should be sufficient to provide some regolith. Possibilities (2) and (3) seem more likely and merit further investigation, since they imply possible further differences between the "ultraprimitive" P and D material and the materials which are common in the main belt.

V. CHIRON

2060 Chiron is the most distant of the objects classified as asteroids. Its orbital semimajor axis of 13.7 AU is more than twice that of the next most distant asteroid, 944 Hidalgo. Oikawa and Everhart (1979), Scholl (1979) and Kowal et al. (1979) have all investigated the orbital evolution of Chiron. The present orbit is chaotic and subject to strong perturbations due to Saturn; Chiron is most likely slowly evolving toward the inner part of the solar system. The uniqueness of its orbit and the probability that it originated in the outer solar system (perhaps even in the Oort cloud) have made Chiron the subject of intense interest.

Early visual-band photometry of Chiron gave discrepant results: Kowal (1979) quotes early unpublished magnitudes of Bowell and Hewitt which gave $B(1,0) = 7.0$, while the *Ephemeris of Minor Planets* for 1980 listed $B(1,0)$ as 6.0. Hartmann et al. (1981) reported the first *VJHK* photometry of Chiron. The results indicated relatively neutral, approximately solar colors similar to those of C-type asteroids and distinctly unlike those of bright icy materials. Thus, a surface similar to those of the bright icy satellites of Saturn was ruled out.

Lebofsky et al. (1984) reported both visual and thermal infrared data, obtained approximately three weeks apart. The visual photometry yielded a

flat spectrum from 0.3 to 0.9 μm, with a derived $B(1,0)$ of 7.60, 1.6 mag fainter than the brightest earlier reported measurement. A related problem arose when the data sets were combined to derive a diameter and albedo: both the visible and infrared photometry of Lebofsky et al. individually indicated neutral colors, but the combined data suggested a major discontinuity in the spectrum between 0.9 μm (the end of the visible data) and 1.2 μm (the beginning of the infrared data). Lebofsky et al. noted that the discrepancy was most likely due to some sort of brightness variation between the times of the two sets of observations. They suggested either a periodic variation due to a rotational lightcurve, or nonperiodic-lightcurve behavior.

The lightcurve of Chiron was investigated in late 1986 by Bus et al. (1989). Nine nights of CCD photometry obtained yielded a lightcurve amplitude of only 0.09 mag and a rotational period of 5.9 hr; both values are typical for main-belt asteroids. Their R magnitude is consistent with the fainter of the earlier magnitude determinations. The low amplitude rules out rotational variation as a cause for the discrepancy observed by Lebofsky et al. The Bus et al. data from 1986 show no signs of nonperiodic brightness variations although their observations spanned only about one month.

That large, nonperiodic changes in Chiron's brightness do occur was demonstrated conclusively by Tholen et al. (1988). Three consecutive nights of near-simultaneous *VRIJHK* photometry in early 1988 all yielded V magnitudes 0.6 mag brighter than the values previously reported by Lebofsky et al. The spectrum is indeed flat between the visible and infrared regions and appears similar to that of a C-type asteroid. The 1978 measurements of Bowell and Hewitt (now incorporated into the 1989 paper of Bus et al.) also are 0.6 ± 0.1 mag brighter than those of Lebofsky et al. (1984) and Bus et al. (1989). It thus appears that such brightening events have occurred before. Since Chiron has been found on photographic plates taken as long ago as 1895, photographic photometry of those plates may well be informative about past outbursts, and such work is planned at Lowell Observatory (E. Bowell, personal communication). It seems likely that the current brightening is part of a trend: by late 1988, Chiron was almost a magnitude brighter than had been observed in the early 1980's (W. Hartmann, personal communication). One would expect such behavior from a comet nearing perihelion.

The observed brightening suggests that Chiron may be experiencing cometary-like outbursts of volatile material. Recent observations (Bus et al. 1988) lend support to that hypothesis: Chiron's lightcurve amplitude had decreased to only 0.04 mag by October 1988. Such a reduction in amplitude would be expected from a comet "turning on," due to light from the unresolved coma diluting the variations in the light reflected from the nucleus. Searches for visible evidence of a coma in CCD images have been undertaken, but have been unsuccessful to date (Bus et al. 1988,1989; W. Hartmann, personal communication).

What are the possible mechanisms for comet-like behavior in an object at

Chiron's distance from the Sun? Stern (1989) has calculated sublimation rates for likely volatile materials, and concludes that the detection of surface volatiles or outgassing from Chiron would indicate a relatively short time of residence in its present orbit and hence a likely formation region in the outer solar system or the Oort cloud. He finds that such materials as CH_4, CO and CO_2 could have lasted for less than a few times 10^6 yr. CO^+ emission has been detected in the spectrum of P/Schwassmann-Wachmann 1, which has a heliocentric distance of 6 AU, suggesting that CO or CO_2 could be the volatile responsible for its outbursts (Cruikshank and Brown 1983). Chiron is currently more than twice that distance from the Sun, however, so the same mechanism may not be at work in Chiron. Spectra of Chiron reported by Cochran (1988) showed no gaseous emission, although upper limits on the column densities of C_2, C_3, and CN were derived.

Chiron is currently approaching its next perihelion passage in early 1996, when its heliocentric distance will be ~8 AU. Increasing activity is therefore likely; the next few years offer excellent opportunities to establish the nature of the outburst mechanism.

VI. RELATIONSHIPS TO OTHER SOLAR SYSTEM OBJECTS

The observed trend in compositional class with solar distance provides provocative clues to possible relationships between distant asteroids and other small solar system objects. At least two other classes of small bodies appear to be relevant. First, comets: Cruikshank et al. (1985) determined broadband *BVJK* colors for P/Halley to be consistent with the colors of D asteroids, and suggested that the nucleus of the comet could have a low albedo similar to that of the D objects. This is supported by spacecraft observations of P/Halley (Keller et al. 1986), as well as by physical studies of the nuclei of relatively inactive comets (Campins et al. 1987; Millis et al. 1988). These studies yield albedos and colors for the nuclei of P/Halley, P/Neujmin 1, P/Tempel 2 and P/Arend-Rigaux which appear to overlap the observed albedos and colors of C, P and D asteroids, but none of the higher-albedo classes. Generally, the similarity is greatest between cometary nuclei and the D class, which are predominant among the Trojan asteroids; Campins et al. note that P/Neujmin 1 is even redder than most Trojans. More observations are needed to confirm the apparent spectral similarities, since little is known about the extreme ultraviolet colors of D asteroids (L. McFadden, personal communication). Of course, the distant asteroids need not be extinct or dormant comets to have comet-like compositions.

The other group to be compared with distant asteroids comprises the natural satellites which appear to be captured. Most notable are Jupiter's outer eight moons and Saturn's moon S9 Phoebe; Phobos and Deimos are included in this group by many. If the Trojans, for example, formed *in situ*, one might predict from the condensation hypothesis that the captured Jovian moons

would be members of the same taxonomic class as the Trojans. In fact, however, the outer Jovian satellites for which accurate photometric data are available are not P's or D's, but C's (Tholen and Zellner 1984). Tholen and Zellner proposed that either (1) the captured Jovian moons are fragments of what were originally C-type main-belt asteroids and that the P- and D-type Trojans are the indigenous objects at 5.2 AU; or (2) objects composed of D material formed at a greater heliocentric distance than that of Jupiter and have been transported inward by some mechanism. Hartmann (1987) presents an argument for scenario (1). He hypothesizes that a large flux of C asteroids was scattered out of the main belt as Jupiter reached its present mass and accreted an extended proto-atmosphere. Any original D-type satellites which formed near Jupiter would have spiraled in toward Jupiter due to atmospheric drag and been lost. The extended proto-atmosphere would help capture the scattered C objects, which became the outer Jovian satellites we see today. The identification of material in the Saturnian system (Bell et al. 1985) and in some cometary nuclei which is even redder than the D asteroids is intriguing, but cannot be taken as evidence in favor of either scenario at the present, since D material is found from the main belt to comets. More observational work on spectral properties of primitive asteroids (both in the main belt and beyond), satellites and cometary nuclei is needed to quantify the similarities and differences of the various D-like spectra and to determine whether a genetic relationship exists between the different types of bodies.

VII. ORIGIN OF DISTANT ASTEROIDS

The various lines of research described in this chapter have led to two very distinct models of distant asteroid origin; at present, both are in the general discussion stage rather than formally developed theories. In Model I, groups such as the Trojans formed *in situ*; in Model II, they formed much farther from the Sun, were scattered gravitationally after formation, and were later captured into their present locations.

Figure 5 illustrates these two hypotheses with sketches of the putative primordial distribution of planetesimal classes during planet formation in the solar nebula. In Model I, the observed change in dominant taxonomic class from C objects around 2.5 AU to P's in the Cybele region and D's at 5.2 AU is due to a change in composition or formation conditions with distance in the solar nebula, or to some combination of the two. The Trojans, Hildas, Cybeles and 279 Thule are all viewed as remnants of the native primordial population at their respective solar distances trapped by stabilizing resonances with Jupiter. The classes native to more distant regions are unknown, possibly including still redder materials such as the Iapetus dark material and the P/Neujmin 1 nucleus. This model allows for comets and satellites of Trojan-like or redder material to be formed among the outer planets, and implies that the captured C-type satellites of Mars, Jupiter and Saturn originated in the
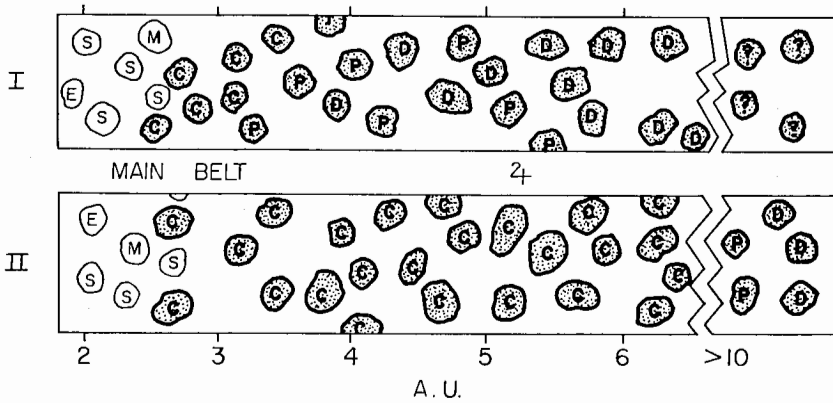
Fig. 5. Schematic illustration of two possible primordial planetesimal distributions. In both, the most dramatic transition is near 2.5 AU where the higher-albedo types give way to much darker objects. In both, also, there is a reddening with distance, at least as far as the present position of Saturn. In Model I, however, present asteroids are near their original locations, with C objects native to the outer main belt and D objects most abundant beyond, possibly in the Jovian region. In Model II, the C objects originally extended beyond Jupiter, with P's and D's native to more distant regions, from which they have been gravitationally scattered inward.

outer main belt. The observed trends of spectral slope with solar distance for P and D objects argue in favor of this view.

In Model II, the C objects extended initially at least as far out as Saturn, with P and D types formed at a greater distance. This model accounts naturally for the C composition of the captured satellites of Jupiter and Saturn by making them the indigenous bodies at their respective distances. Current models for comet formation (Fernández 1978; see also the Monte Carlo simulations of Shoemaker and Wolfe [1985]) are consistent with both models. However, gravitational scattering by Jupiter and Saturn of a large population of Uranus-Neptune planetesimals into the regions closer to the Sun offers a natural mechanism for transporting such planetesimals into regions where they could be captured into resonance with the recently formed Jupiter.

The discovery of a much larger population of Jovian Trojans than was previously known (Shoemaker et al. 1989; see the chapter by Shoemaker et al.) leads to the question of whether Saturn, Uranus or Neptune Trojans exist. Recent numerical modeling has shown that such objects should be stable against perturbations from Jupiter for long time scales (Zhang and Innanen 1988a,b). Previous searches, described by Gehrels (1979), of the Saturnian Lagrange points have detected none. Of course, the observational problems merely detecting such objects are formidable. Even at Saturn's distance, Hektor, the largest Jovian Trojan, would have $B \sim 18$. Thus, the largest Schmidt telescopes would be needed for adequate aperture and area coverage. The discovery and subsequent physical studies of more distant Trojan groups,

however, could offer the prospect of distinguishing between the two models discussed here: if today's Jovian Trojans were the early solar system's Uranus-Neptune planetesimals, the composition of all groups of outer solar system Trojans should be much the same. If the Jovian (and other) Trojans formed *in situ,* then other groups at larger solar distances than Jupiter's might be composed of material yet more primitive than the Jovian Trojans.

Other hypotheses are possible; we focus on these two broad scenarios to suggest areas for future observational and theoretical work. They demonstrate the need for more fundamental data on distant asteroids, for a better understanding of their composition, and for a deeper understanding of the dynamical processes which have shaped this region of the solar system.

REFERENCES

Bell, J. F., Cruikshank, D. P., and Gaffey, M. J. 1985. The composition and origin of the Iapetus dark material. *Icarus* 61: 192–207.

Bell, J. F., Owensby, P. D., Hawke, B. R., and Gaffey, M. J. 1988. The 52-color asteroid survey: final results and interpretation. *Lunar Planet. Sci.* XIX:57–58 (abstract).

Bus, S. J., Bowell, E., and French, L. M. 1988. 2060 Chiron. *IAU Circ.* No. 4684.

Bus, S. J., Bowell, E., Harris, A. W., and Hewitt, A. V. 1989. 2060 Chiron: CCD and electronographic photometry. *Icarus* 77:223–238.

Campins, H., A'Hearn, M., and McFadden, L. A. 1987. The bare nucleus of comet P/Neujmin 1. *Astrophys. J.* 316:847–857.

Chapman, C. R., and Gaffey, M. J. 1979. Reflectance spectra for 277 asteroids. In *Asteroids,* ed. T. Gehrels (Tucson: Univ. of Arizona Press). pp. 655–687.

Chapman, C. R., Morrison, D., and Zellner, B. 1975. Surface properties of asteroids: A synthesis of polarimetry, radiometry, and spectrophotometry. *Icarus* 25:104–130.

Cloutis, E. A. 1989. Spectral reflectance properties of hydrocarbons: Remote sensing implications. *Science,* submitted.

Cochran, A. L. 1988. (2060) Chiron. *IAU Circ.* No. 4586.

Cook, A. F. 1971. 624 Hektor: A binary asteroid? In *Physical Studies of Minor Planets,* ed. T. Gehrels, NASA-SP 267, pp. 155–163.

Cruikshank, D. P. 1977. Radii and albedos of four Trojan asteroids and Jovian satellites 6 and 7. *Icarus* 30:224–230.

Cruikshank, D. P., and Brown, R. H. 1983. The nucleus of comet P/Schwassmann-Wachmann 1. *Icarus* 56:377–380.

Cruikshank, D. P., Tholen, D. J., and Hartmann, W. K. 1985. Color, albedo, and nuclear size of Halley's comet. *Nature* 315:122.

Davis, D. R., and Weidenschilling, S. J. 1981. Avoiding close encounters: Collisional evolution of Trojan asteroids. *Lunar Planet. Sci.* XII:199–201 (abstract).

Degewij, J., and van Houten, C. J. 1979. Distant asteroids and outer Jovian satellites. In *Asteroids,* ed. T. Gehrels (Tucson: Univ. of Arizona Press), pp. 417–435.

Donn, B., and Hughes, D. 1986. A fractal model of a cometary nucleus formed by random accretion. In *20th ESLAB symposium on the Exploration of Halley's Comet,* vol. 3, eds. B. Battrick, E. J. Rolfe and R. Reinhard, ESA SP-250 (Noordwijk: ESA), pp. 523–534.

Dunlap, J. L., and Gehrels, T. 1969. Minor planets, III: Light curves of a Trojan asteroid. *Astron. J.* 74:796–803.

Farinella, P., Paolicchi, P., and Zappalà, V. 1981. The asteroids as outcomes of catastrophic collisions. *Icarus* 52:409–433.

Feierberg, M. A., Lebofsky, L. A., and Tholen, D. J. 1985. The nature of C-class asteroids from 3-μm spectrophotometry. *Icarus* 63:183–191.

Fernández, J. A. 1978. Mass removed by the outer planets in the early solar system. *Icarus* 34:173–181.

French, L. M. 1987. Rotation properties of four L5 Trojan asteroids from CCD photometry. *Icarus* 72:325–341.

French, L. M., Kramer, D. M., and Vargas, H. 1986. Rotation properties of Trojan asteroids. *Bull. Amer. Astron. Soc.* 18:796–797 (abstract).

Gehrels, T. 1979. The asteroids: History, surveys, techniques, and future work. In *Asteroids*, ed. T. Gehrels (Tucson: Univ. of Arizona Press), pp. 3–24.

Gradie, J. C., Chapman, C. R., and Williams, J. G. 1979. Families of minor planets. In *Asteroids*, ed. T. Gehrels (Tucson: Univ. of Arizona Press), pp. 359–390.

Gradie, J., and Tedesco, E. F. 1982. The compositional structure of the asteroid belt. *Science* 216:1405–1407.

Gradie, J., and Veverka, J. 1980. The composition of the Trojan asteroids. *Nature* 283:840–842.

Greenberg, R. J., and Davis, D. R. 1978. Stability at potential maxima: The L4 and L5 points of the restricted 3-body problem. *Amer. J. Phys.* 46:1068–1070.

Hartmann, W. K. 1987. A satellite-asteroids mystery and a possible early flux of scattered C-class asteroids. *Icarus* 71:57–68.

Hartmann, W. K., and Cruikshank, D. P. 1978. The nature of Trojan asteroid 624 Hektor. *Icarus* 36:353–366.

Hartmann, W. K., Cruikshank, D. P., Degewij, J., and Capps, R. W. 1981. Surface materials on unusual planetary object Chiron. *Icarus* 47:333–341.

Hartmann, W. K., Tholen, D. J., Cruikshank, D. P., Goguen, J., and Binzel, R. P. 1987. Trojan asteroid lightcurve survey: Unusually elongated shapes? *Bull. Amer. Astron. Soc.* 19:850 (abstract).

Hartmann, W. K., Tholen, D. J., Cruikshank, D. P., Goguen, J., and Binzel, R. P. 1988. Trojan and Hilda asteroid lightcurves I. Anomalously elongated shapes among Trojans (and Hildas?) *Icarus* 73:487–498.

Jones, T. D. 1988. An Infrared Reflectance Study of Water in Outer Belt Asteroids: Clues to Composition and Origin. Ph. D. Thesis, Univ. of Arizona.

Keller, H. U., Arpigny, C., Barbieri, C., Bonnet, R. M., Cazes, S., Coradini, M., Cosmovici, C. B., Delamere, W. A., Huebner, W. F., Hughes, D. W., Jamar, C., Malaise, D., Reitsema, H. J., Schmidt, H. U., Schmidt, W. K. H., Seige, P., Whipple, F. L., and Wilhelm, K. 1986. First Halley multicolor camera imaging results from Giotto. *Nature* 321:320–326.

King, T. V. V. 1986. Contributions Toward A Quantitative Understanding of Reflectance Spectroscopy: Phyllosilicates, Olivine, and Shocked Materials. Ph.D. Thesis, Univ. of Hawaii.

Kowal, C. T. 1979. Chiron. In *Asteroids*, ed. T. Gehrels (Tucson: Univ. of Arizona Press), pp. 436–439.

Kowal, C. T., Liller, W., and Marsden, B. G. 1979. The discovery and orbit of (2060) Chiron. In *Dynamics of the Solar System. IAU Symp. No. 81*, ed. R. L. Duncombe (Dordrecht: D. Reidel), pp. 245–250.

Lagerkvist, C.-I., and Sjölander, N.-G. 1979. Photographic photometry of asteroids with Schmidt telescopes. II. Observations of 11 asteroids during 1977 and 1978. *Acta Astron.* 29:455–461.

Lebofsky, L. A. 1978. Asteroid 1 Ceres: Evidence for water of hydration. *Mon. Not. Roy. Astron. Soc.* 182:17P–21P.

Lebofsky, L. A., Jones, T. D., Owensby, P. D., Feierberg, M. A., Consolmagno, G. J. 1989. The nature of low albedo asteroids from 3 μm spectrophotometry. *Icarus*, submitted.

Lebofsky, L. A., Tholen, D. J., Rieke, G. H., and Lebofsky, M. J. 1984. 2060 Chiron: Visual and thermal infrared observations. *Icarus* 60:532–537.

Millis, R., A'Hearn, M., and Campins, H. 1988. An investigation of the nucleus and coma of comet P/Arend-Rigaux. *Astrophys. J.* 324:1194–1209.

Oikawa, S., and Everhart, E. 1979. The past and future orbit of 1977 UB, object Chiron. *Astron. J.* 84:134–139.

Poutanen, M. E., Bowell, E., and Lumme, K. 1981. A physically plausible ellipsoidal model of Hektor. *Bull. Amer. Astron. Soc.* 13:725 (abstract).

Rabe, E. 1961. Determination and survey of periodic Trojan orbits in the restricted problem of three bodies. *Astron. J.* 66:500–513.

Rabe, E. 1967. Third order stability of the long-period Trojan librations. *Astron. J.* 72:10–17.

Scholl, H. 1979. History and evolution of Chiron's orbit.*Icarus* 40:345–349.

Shoemaker, E., and Wolfe, R. 1985. Evolution of the Uranus-Neptune planetesimal swarm. *Lunar Planet. Sci.* XV:780–781 (abstract).

Shoemaker, E. M., Bowell, E., Bus, S. J., French, L. M., Russell, K. S., and Shoemaker, C. S. 1989. A search for Trojans in the L5 cloud. In *Comets, Meteors, Asteroids III*, submitted.

Sill, G. T. 1973. Reflection spectra of solids of planetary interest. *Comm. Lunar Planet. Lab.* 10:1–7.

Stern, S. A. 1989. Implications of volatile release from object 2060 Chiron. *Publ. Astron. Soc. Pacific*, in press.

Taylor, R. C., Gehrels, T., and Capen, R. 1976. Minor planets and related objects. XXI. Photometry of eight asteroids. *Astron. J.* 81:778–786.

Tedesco, E. 1986. Ground-based data for asteroids and comets. In *IRAS Asteroid and Comet Survey: Preprint Version No. 1*, ed. D. L. Matson, JPL Document No. D-3698, pp. 9:1–9:42.

Tholen, D. J. 1984. Asteroid Taxonomy from Cluster Analysis of Photometry. Ph.D. Thesis, Univ. of Arizona.

Tholen, D. J., Hartmann, W. K., and Cruikshank, D. P. 1988. (2060) Chiron. *IAU Circ.* No. 4554.

Tholen, D. J., and Zellner, B. 1984. Multicolor photometry of outer Jovian satellites. *Icarus* 58:341–347.

van Houten, C. J., van Houten-Groenveld, I., and Gehrels, T. 1970a. Minor planets and related objects. V. The density of Trojans near the preceding Lagrangian point. *Astron. J.* 75:659–662.

van Houten, C. J., van Houten-Groenveld, I., Herget, P., and Gehrels, T. 1970b. The Palomar-Leiden Survey of faint minor planets. *Astron. Astrophys. Suppl.* 2:339–448.

Vilas, F. 1986. Continued studies of outer belt asteroids—New CCD reflectance spectra. *Lunar Planet. Sci.* XVI:540–541 (abstract).

Vilas, F., and Gaffey, M. J. 1988. Correlation of absorption features present in CCD reflectance spectra of asteroids, the CI-CM carbonaceous chondrite group, and serpento-chlorite minerals. *Bull. Amer. Astron. Soc.* 20:1126 (abstract).

Vilas, F., and Gaffey, M. J. 1989. Identification of iron-bearing phyllosilicate absorption features in high-precision narrowband reflectance spectra of primitive asteroids. *Science*, submitted.

Vilas, F., and McFadden, L. A. 1987. New CCD reflectance spectra of outer belt asteroids. *Bull. Amer. Astron. Soc.* 19:825 (abstract).

Vilas, F., and McFadden, L. A. 1989. CCD reflection spectra of selected asteroids: Presentation and data analysis considerations. *Icarus*, submitted.

Vilas, F., and Smith, B. A. 1985. Reflectance spectrophotometry (~ 0.5–1.0 μm) of outer-belt asteroids: Implications for primitive, organic solar system material. *Icarus* 64:503–516.

Weidenschilling, S. J. 1980. Hektor: Nature and origin of a binary asteroid. *Icarus* 44:807–809.

Wetherill, G. W. 1967. Collisions in the asteroid belt. *J. Geophys. Res.* 72:2429–2444.

Yoder, C. F. 1979. Notes on the origin of Trojan asteroids. *Icarus* 40:341–344.

Zellner, B. 1979. Asteroid taxonomy and the distribution of the compositional types. In *Asteroids*, ed. T. Gehrels (Tucson: Univ. of Arizona Press), pp. 783–806.

Zellner, B., Tholen, D. J. and Tedesco, E. F. 1985. The eight-color asteroid survey: Results for 589 minor planets. *Icarus* 61:355–416.

Zhang, S.-P., and Innanen, K. A. 1988a. A numerical investigation of the stability of Saturn's triangular Lagrangian points. *Astron. J.* 96:1983–1988.

Zhang, S.-P., and Innanen, K. A. 1988b. A numerical investigation of the stability of the triangular Lagrangian points of the planets. *Astron. J.* 96:1989–1994.

Note added in proof: Continued CCD imaging of 2060 Chiron has finally revealed visible evidence for a substantial coma (Meech and Belton, 1989, *IAUC* 4770). Thus it appears that Chiron is indeed experiencing cometary-like outbursts of volatile material.

TROJAN ASTEROIDS: POPULATIONS, DYNAMICAL STRUCTURE AND ORIGIN OF THE L4 AND L5 SWARMS

EUGENE M. SHOEMAKER, CAROLYN S. SHOEMAKER,
and
RUTH F. WOLFE
U. S. Geological Survey

A total of 157 Trojans had been discovered as of mid-1988, 52 of which were numbered. Two-thirds of the known Trojans are in the L4 swarm, where discovery is estimated to be complete to $B(1,0) = 9.75$. The L4 population to $B(1,0) = 14$ is estimated to be 1000 ± 200. Bright Trojans are about as numerous in the L5 swarm as in L4, but faint L5 Trojans appear to be only 50% as numerous. The total population of Trojans > 15-km diameter is roughly half that estimated for main-belt asteroids. Similarity of characteristic orbital parameters (libration amplitude, proper eccentricity and proper inclination) among certain Trojans with accurately determined orbits suggests the presence of 5 and possibly as many as 8 collisional groups in the L4 swarm. Further, the magnitude distribution of L4 Trojans probably is a result of strong collisional evolution. The observed distribution of characteristic orbital parameters is most readily explained by collisional diffusion of orbital elements and capture into stable 1:1 resonance of bodies previously on Jupiter-crossing orbits. Capture probably was the result of collisional impulses received by bodies librating in temporary horseshoe orbits. We suggest that the present Trojans are chiefly fragments of Jupiter planetesimals that were captured during an episode of heavy flux near Jupiter during dispersal of the planetesimal swarm.

I. INTRODUCTION

In October 1906, Max Wolf, the founding director of the Heidelberg Observatory, discovered an unusually distant asteroid. At that time, Heidelberg was the premier center for asteroid discovery. Wolf's new asteroid

turned out to have a semimajor axis close to 5 AU; subsequent studies proved that the object was librating about the Sun-Jupiter L4 Lagrange point, which is 60° ahead of the mean orbital longitude of Jupiter on a circle with a radius equal to the semimajor axis of Jupiter. Wolf's discovery was a spectacular empirical confirmation of the theoretical work of J. L. Lagrange, who had proved, more than a century before, that regions of stable libration exist around the triangular equilibrium points in the so-called restricted three-body problem. The finding of the new asteroid further proved that regions of stability exist when the orbit of the small third body is inclined to the orbit of the planet, when both orbits are eccentric, and when both bodies are subject to secular perturbations by other planets in the solar system. Wolf's discovery sparked a resurgence of theoretical work on the three-body problem (see, e.g., Brown 1911). He called the new asteroid Achilles, thus starting a tradition of naming objects in the stable libration regions after the heroes of the Trojan War. In subsequent years the tradition was modified at Heidelberg: objects librating about the preceding point (L4) were named for Greek heroes and those librating about the following point (L5) were named for Trojan heroes. For simplicity, the Greek and Trojan asteroids are referred to collectively as Trojans.

In a few years, several more Trojans were discovered at Heidelberg. A. A. Kopff found 617 Patroclus in the L5 libration region in November 1906 and 624 Hektor in the L4 region the following year. (These famous objects were named before L4 and L5 asteroids, respectively, were given the names of Greek and Trojan heroes; hence each is librating in the "camp" of its mythical enemy.) Wolf discovered 659 Nestor near L4 in 1908 and 884 Priamus near L5 in 1917. The next seven Trojans were discovered at Heidelberg by Karl Reinmuth between 1919 and 1949. During this early period, Heidelberg employed the best equipment in a dedicated search for asteroids and utterly dominated the field. Because the Trojans are so distant and have very low albedos, their apparent magnitudes were close to the detection threshold at the time of their discovery.

Two Trojans were discovered in the 1950s, one by S. Arend at Uccle, the other by S. B. Nicholson at Mt. Wilson. Then a batch of 24 mostly very faint Trojans was discovered in the L4 region by C. J. van Houten and I. van Houten-Groenveld from plates taken by T. Gehrels for the Palomar-Leiden Survey (PLS) in 1960. Two of the PLS Trojans are now numbered (1868 and 1869), and multiple opposition orbits have been obtained for four others as a result of independent rediscoveries, chiefly by E. Bowell. The somewhat serendipitous discovery of the PLS Trojans led the van Houtens, in collaboration with Gehrels, to carry out further searches for faint Trojans with the Palomar 1.2-m Schmidt. First, a study was conducted with plates taken near the L4 point in 1965 to estimate the population of L4 Trojans brighter than $B(1,0) \approx 14$. Then, the L5 region was photographed in March 1971; four of the brightest objects detected were followed for orbit determination and were numbered. A relatively bright Trojan was found in the same month by C.

Cesco at El Leoncito. Next, the van Houtens obtained short-arc orbits for 35 faint Trojans in the L4 region from plates taken in 1973; one of these has become numbered. In 1977, Gehrels took new plates near the L5 point from which the van Houtens obtained short-arc orbits for 26 faint Trojans. (New asteroids reported from the 1977 plates have been designated T-3 in the *Minor Planet Circulars*.)

Since the early 1970s, there has been a veritable burst of discoveries and determinations of accurate orbits for relatively bright Trojans. Altogether, about 43 new Trojans equal to or brighter than $H = 10$ $[B(1,0) \approx 11]$ have been found. Many observers contributed to these discoveries, among them E. Bowell, at Lowell Observatory, and C. S. and E. M. Shoemaker, observing with the 46-cm Schmidt at Palomar. The total of numbered Trojans has risen from 22 to 52 since 1979; multiple opposition orbits are available for an additional 11 Trojans. This increase in our knowledge opens the way to a reassessment of the L4 and L5 Trojan populations. Perhaps more significant, the number of accurate orbits enables us, for the first time, to examine the detailed dynamical structure of the L4 swarm and to pose or attempt to answer some critical questions bearing on the origin of the Trojan asteroids.

II. POPULATIONS OF THE L4 AND L5 SWARMS

As of mid-1988, 157 Trojans had been discovered. Of these, 105 are in the swarm librating around the L4 point, and 52 are in the L5 swarm. It appears to be an accident of history that the L4 region has been more thoroughly explored. In 1985, there were equal tallies of numbered asteroids in the L4 and L5 regions, and the numbers of known, relatively bright asteroids in the two libration regions were about the same. But the most recent discoveries have been made in the L4 region, when the L5 point was unfavorably located near the Milky Way and low in the summer sky of northern hemisphere observers. A rough balance in discoveries may be restored as L5 rises and moves into the clear opposition region of the fall months.

Because most discoveries of both bright and faint Trojans have been made in the L4 region, our understanding is currently most complete for the L4 swarm. The most recent history of L4 Trojan discoveries is reflected in the magnitude-frequency distributions shown in Fig. 1. Magnitudes were taken from the IRAS catalogue (Matson 1986) for the brightest Trojans (Table I) and from the *Minor Planet Circulars* (MPC's) and the PLS survey (van Houten et al. 1970a, 1984) for the remainder. Absolute magnitudes reported in the IRAS catalogue probably are correct in most cases to within ±0.2 mag, whereas absolute magnitudes from the MPC's, derived almost entirely from photographic observations, may have errors on the order of ±0.5 mag. It can be seen that the number of known L4 Trojans up to $B(1,0) = 9.75$ has remained steady for the last few years, but the number up to $B(1,0) = 10.25$ has increased. (We use $B(1,0)$ rather than H in Fig. 1 in order to maintain easy

TABLE I

Proper Elements and Absolute Magnitudes of L_4 Trojans with Multiple Opposition Orbits[a]

Trojan	D B&S[b] (°)	D Eq. (5&6)[c] (°)	e_p B&S[b]	e_p Eq. (7a)[c]	i_p B&S[b] (°)	i_p i(trans.)[c] (°)	H	B(1,0)
588 Achilles	13	16	0.103	0.103	11.4	11.4	8.59	9.66
624 Hektor	38	38	0.054	0.052	19.0	18.9	7.47	8.65
659 Nestor	20	20	0.130	0.132	5.0	5.1	8.80	9.82
911 Agamemnon	34	32	0.021	0.027	22.7	22.6	7.88	8.95
1143 Odysseus	20	20	0.052	0.051	4.0	4.0	8.43	9.53
1404 Ajax	40	38	0.076	0.086	19.1	18.9	9.07	10.17
1437 Diomedes	57	57	0.017	0.007	22.0	21.7	8.30	9.30
1583 Antilochus	49	48	0.018	0.024	29.1	29.2	8.66	9.71
1647 Menelaus	16	17	0.058	0.054	6.7	6.7	10.20	11.31
1749 Telemon	27	25	0.068	0.067	6.8	6.8	10.10	11.20
1868 Thersites	46	45	0.098	0.102	16.9	17.0	9.6	10.7
1869 Philoctetes	43	43	0.056	0.064	3.4	3.4	11.2	12.3
2148 Epeios	9	9	0.024	0.027	8.9	8.9	11.1	12.2
2260 Neoptolemus	8	8	0.019	0.022	16.4	16.5	8.95	10.04
2456 Palamedes	33	36	0.029	0.031	14.9	14.8	9.20	10.30
2759 Idomeneus	21	19	0.087	0.089	21.5	21.6	9.77	10.87
2797 Teucer	46	47	0.073	0.066	21.0	21.2	8.51	9.61
2920 Automedon	44	47	0.016	0.018	21.9	21.9	8.83	9.93
3063 Makhaon	25	26	0.055	0.051	13.5	13.5	8.70	9.80
3391 Sinon	25	37		0.038		15.6	10.3	11.3

3540 Protesilaos		35		0.108	23.0	9.0	10.0
3548 1973 SO		39		0.044	7.5	9.7	10.7
3564 Talthybius		20		0.082	15.2	9.0	10.0
3596 Meriones		35		0.030	23.9	9.5	10.5
3709 Polypoites		23		0.016	19.6	9.5	10.5
3793 Leonteus		22		0.053	21.2	8.8	9.8
3794 Sthenelos		9		0.127	6.8	9.9	10.9
3801 Thrasymedes		48		0.026	29.0	11.3	12.3
1973 SM		23		0.045	2.8	9.8	10.8
1973 SW		25		0.065	17.2	9.5	10.5
1973 SA2		30		0.023	4.7	11.5	12.5
1985 TQ		24		0.074	2.9	10.0	11.0
1985 TG3		29		0.035	12.9	10.0	11.0
1985 VK2		41		0.082	20.9	9.0	10.0
1986 WD		30		0.011	13.1	9.5	10.5
6541 PL		40		0.028	7.4	11.5	12.5
6591 PL		34		0.042	7.4	11.5	12.5
9507 PL		25		0.081	4.6	10.5	11.5
9602 PL		27		0.038	6.3	12.5	12.5
2146 Stentor[d]	(8)	(13)	(0.06)	(0.067)	(38.1)	10.4	11.5
1986 TT6[e]		(15)		(0.076)	(36.3)	9.0	10.0

[a] D is libration amplitude, e_p is proper eccentricity and i_p is proper inclination.

[b] Proper elements derived from numerical integration by Bien and Schubart (1987).

[c] Proper elements estimated from Eqs. (5), (6) and (7a) and from transformation of orbits to orbit plane of Jupiter.

[d] Integration of the motion of Stentor by Bien and Schubart failed to yield secure proper elements; the elements shown should be regarded as rough approximations.

[e] 1986 TT6 is included for comparison with Stentor; orbit is based on a 31-day arc of observations; estimated proper elements are uncertain.
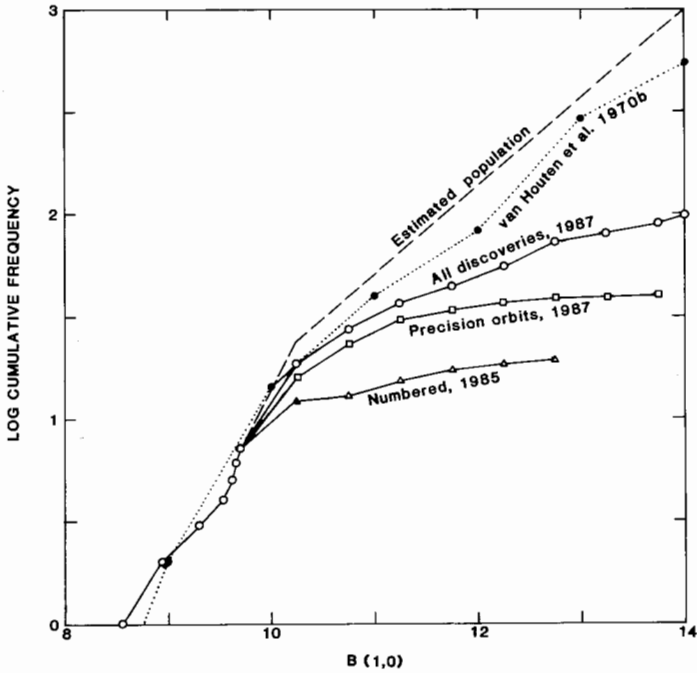
Fig. 1. Cumulative magnitude-frequency distributions and estimated population for L4 Trojans.

comparability with the published work on faint Trojans by van Houten et al. (1970*b*); broadly, $H \approx B(1,0) - 1$ mag.) We infer that the discovery of L4 Trojans probably is complete to about $B(1,0) = 9.75$. This is supported by a search that we conducted in the fall of 1985 of a major fraction of the L4 libration region. Our brightest new L4 Trojan is 3793 Leonteus, at $B(1,0) = 9.8$. Several L4 Trojans with magnitudes near $B(1,0) = 10.0$ have been discovered subsequently, and we expect that a few brighter than mag 10.25 remain to be found.

By combining observations of faint Trojans close to L4 made in 1965 with PLS discoveries, the sparse data on bright numbered Trojans known at the time, and observations of bright Trojans detected in the McDonald Survey (Kuiper et al. 1958), van Houten et al. (1970*b*) estimated the magnitude-frequency distribution of L4 Trojans to $B(1,0) = 14$. Their results are presented in cumulative distribution form in Fig. 1. The curve based on their 1970 estimates reflects the number of presently discovered Trojans rather well to $B(1,0) = 9.75$. The cumulative number reported by the end of 1987 to $B(1,0) = 10.25$ also lies on the van Houten curve, but two Trojans estimated to be brighter than mag 10.25 have since been reported. It now appears fairly certain that the L4 population exceeds the van Houten curve at $B(1,0) =$

10.25, and we suspect that the estimates of van Houten et al. are low by about 40% for most fainter L4 objects because of underestimation of observational selection effects.

A basic difficulty in determining the population of faint Trojans from observations made close to the libration points, or close to the ecliptic, lies in estimating the observational selection effects due to the large dispersion in inclination of the Trojan orbits. Known relatively bright Trojans have a much larger mean orbital inclination than numbered main-belt asteroids. Moreover, inasmuch as the discovery of Trojans is incomplete at magnitudes fainter than $B(1,0) \approx 10$, the true mean inclination of relatively bright Trojans is almost certainly higher than that of objects already discovered. This is so because most searches for asteroids have been carried out close to the ecliptic, whereas high-inclination asteroids are located far from the ecliptic most of the time. An example of this selection effect is the delayed discovery of two bright L5 Trojans. The brightest known L5 Trojan, 3451, was found by Mrkos and Vavrova at Klet in May 1984; C. S. and E. M. Shoemaker discovered the fourth brightest, 3317 Paris, in the following month. Both of these discoveries were made incidentally in the course of surveys carried out for other objectives. These relatively bright asteroids had escaped earlier discovery because they have inclinations greater than 24° and are located near the ecliptic during only a small fraction of their orbital period.

The discovery of 3317 Paris prompted our re-examination of the magnitude and inclination statistics for Trojans and our decision to begin a systematic search for new Trojans at the next favorable opportunity. Paris was, in fact, at high ecliptic latitude when it was found, and we anticipated that many fairly bright, high-inclination Trojans remained to be discovered. In our survey for planet-crossing asteroids and comets (Shoemaker and Shoemaker 1988), we normally photograph the opposition region up to northern ecliptic latitudes of about 45°; thus we could add a search for Trojans, including the high-inclination objects, with minimal additional effort. This addition would allow us to determine the threshold magnitude of completeness for both the L4 and L5 swarms and, indeed, to extend that threshold to fainter magnitude.

The frequency distributions of orbital inclination for Trojans discovered by the van Houtens and for all Trojans discovered independently of the van Houten surveys are illustrated in Fig. 2. Van Houten Trojans that were independently recovered (rediscovered) are included in the histogram for independent discoveries. The mode of the inclinations for Trojans discovered in the van Houten surveys is between 8° and 10° and the median is 8°, whereas the mode for independent discoveries is between 20° and 22° and the median 17°. This demonstrates the strong selection against high-inclination asteroids, when the search fields are constrained to lie close to the ecliptic. A strong selection against Trojans with high libration amplitude also occurs when search fields are concentrated around the libration points.

Over an interval of 6 yr (half the orbital period), all Trojans must pass

through the ecliptic, and in an interval of about 100 yr (about two-thirds the typical libration period), most Trojans must also pass the longitude of the libration point. The latter interval corresponds to two successive observational careers of long-lived astronomers. Systematic searches for Trojans, moreover, generally are not sustained on an annual basis even for 6 yr, because the libration regions become difficult to survey when they pass through the Milky Way or move to unfavorable declinations. Given enough time, of course, the collective efforts of asteroid observers can lead to completeness of discovery to progressively fainter magnitudes. The alternative, which we have adopted, is to survey most or all of an entire libration region in a single season, when it moves into a favorable part of the sky. Reasonable completeness to a magnitude somewhat brighter than our detection threshold can be then achieved in a few seasons. This requires an intermittent but intensive effort with a fast, wide-field telescope.

Through January 1988, our search over a broad range of ecliptic latitudes yielded 8 new Trojans with magnitudes in the range $9.4 < B(1,0) < 11.0$; 7 are in the L4 region. The majority of these Trojans have inclinations above 20° (Fig. 2); their mean inclination of 19°.5 is 4° higher than the mean for other discoveries made independently of the van Houten surveys. There is a subtle bias in this result, because a significant fraction of the Trojan population in our magnitude range of discovery had already been found; thus the number of low-inclination Trojans remaining to be discovered was preferentially reduced. From a curve for the estimated population presented in Fig. 1 (obtained as described below), we calculate that about 45% of the Trojans brighter than $B(1,0) = 11.0$, exclusive of the Shoemaker Trojans, have been found. On this basis, a weighted mean of the inclinations of the Shoemaker Trojans and the inclinations of the other independently discovered Trojans may give the best estimate for the mean inclination of the Trojan population, i.e., $0.45 \times 15°.5 + 0.55 \times 19°.5 = 17°.7$.

If we normalize the frequency of all independent discoveries by setting their cumulative frequency up to 12° inclination equal to the frequency of the van Houten Trojans (Fig. 3), a rough first estimate can be made of the relative deficiency of high-inclination objects among the Trojans discovered in the van Houten surveys. The difference in total frequency between the normalized independent discoveries and the van Houten Trojans is a factor of 2.0; it is 2.2 when we account for the small bias in the inclination distribution of all independent discoveries (mean inclination of 16°.0 vs our best estimate of 17°.7 for the population). The latter factor is precisely the correction adopted by van Houten et al. (1970b) to calculate the population of faint Trojans from combined observations of the PLS and two fields close to L4 examined in 1965. This close agreement is fortuitous, however, as the correction derived by van Houten et al. is based partly on results for PLS main-belt asteroids and partly on the very limited set of orbits of numbered Trojans known in 1970.

The mean inclination of PLS Trojans is 7°.4, somewhat lower than the 9°.8
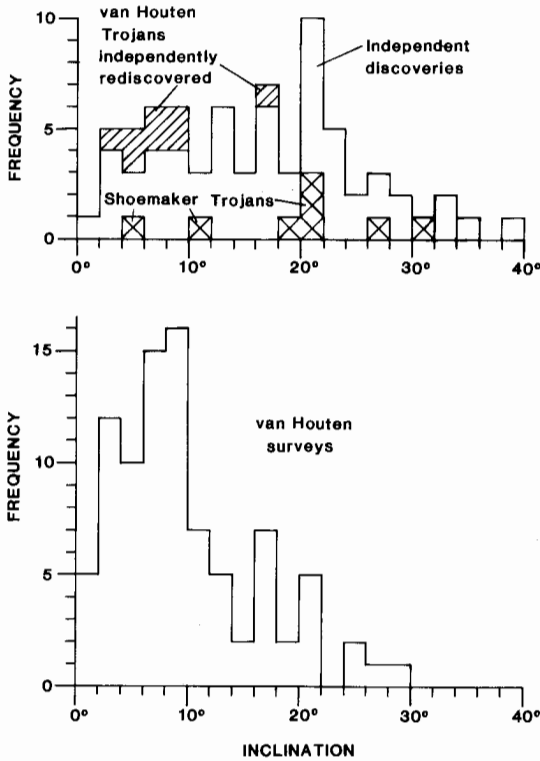
Fig. 2. Inclination-frequency distributions for Trojans discovered through mid-1988. Upper histogram shows distribution of all Trojans discovered independently of the van Houten surveys; lower histogram shows all Trojans discovered in the van Houten surveys.

mean for all van Houten Trojans (see distribution in Fig. 4). If we normalize the frequency of independent discoveries to the cumulative frequency of PLS Trojans at 12° inclination, the correction factor obtained for PLS Trojans is 2.6. A larger correction would be found if we normalized at the mode of inclinations for PLS Trojans.

   An explicit solution for the inclination selection factor for the PLS Trojans can be obtained as follows. If we assume a circular orbit, the fraction of time t_o that an asteroid spends outside a heliocentric ecliptic latitude limit $|l|$ of the PLS is given by

$$t_0 = \frac{\pi/2 - \sin^{-1}\left(\frac{|l|}{i}\right)}{\pi/2}, \qquad i > |l| \qquad (1)$$
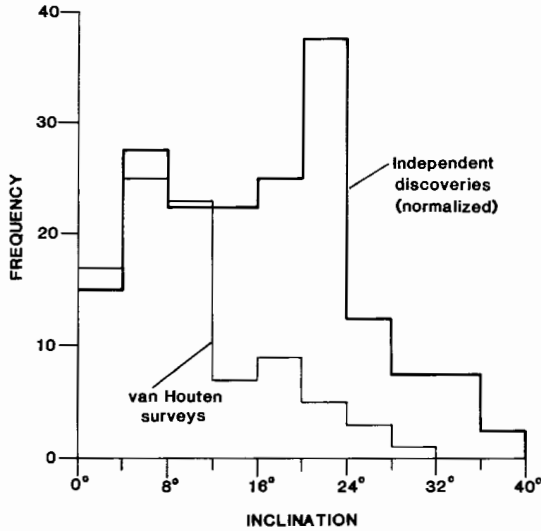
Fig. 3. Comparison of the inclination-frequency distribution of Trojans discovered independently of the van Houten survey with that of the van Houten Trojans. The number of independent discoveries is normalized so that the cumulative frequency to 12° inclination is equal to that of the van Houten Trojans.

and, conversely, the fraction of time t_i it spends inside $|l|$ is given by

$$t_i = \frac{2\sin^{-1}\left(\frac{|l|}{i}\right)}{\pi}, \qquad i_{,} > |l|. \qquad (2)$$

(See van Houten et al. [1970a] for derivation of related formulae.) For $i < |l|$, t_i and its reciprocal, the selection factor, is 1. The angular height of the Palomar 1.2-m Schmidt plates is $6°7$, and the PLS was based on six fields arranged in two rows of three each placed about equally on either side of the ecliptic. The plate fields were slightly overlapped; van Houten et al. (1970b) adopted $6°5$ as the mean angular half height of the PLS, which is taken to be effectively centered on the ecliptic. At a heliocentric distance of 5.203 AU (the semimajor axis of Jupiter's orbit), the distance above or below the ecliptic subtended by a geocentric angle of $6°5$, when the plate field is near opposition, is 0.48 AU, and the mean heliocentric ecliptic latitude of the plate boundaries $|l|$ at this distance is $5°3$.

    A direct estimate of the inclination-selection effect for PLS Trojans can be made from their observed inclination distribution by applying Eq. (2) to derive t_i for each discovered object. The correction factor obtained by this method is 2.1_9, virtually identical with that used by van Houten et al. (1970b).
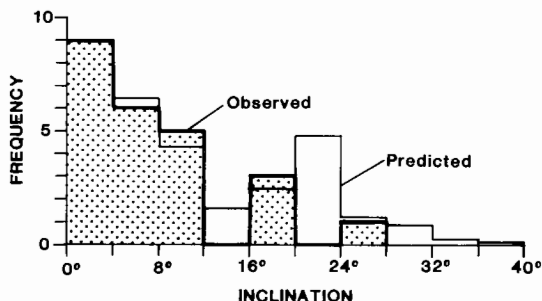
Fig. 4. Predicted inclination-frequency distribution for discovered PLS Trojans compared with the observed distribution. The predicted distribution is derived from the observational selection effect given by Eq. (2) applied to a model of the true inclination distribution estimated from discoveries independent of the van Houten surveys. The predicted frequency is normalized to the observed cumulative frequency at 4°.

However, because the PLS Trojans number just 24, and only 4 have inclinations greater than 12° (where the selection effect is strongest), a much more reliable estimate of the inclination selection effect can be made from the independently discovered Trojans.

If we evaluate t_i from Eq. (2) for 64 independently discovered Trojans (exclusive of Shoemaker Trojans), we find a mean t_i of 0.360, which yields a correction factor of $1/\bar{t_i} = 2.78$ to be applied to the PLS Trojans. For 8 Shoemaker Trojans, $\bar{t_i}$ is 0.277; the estimated correction factor is 3.62. The weighted mean t_i for independent discoveries combined with Shoemaker Trojans is $0.45 \times 0.360 + 0.55 \times 0.277 = 0.314$; thus our best estimate of the correction for the PLS inclination selection effect is $1/$(weighted mean t_i) $= 3.2$

The predicted distribution of inclinations for PLS Trojans, normalized to the observed frequency from 0° to 4°, is compared with the observed distribution in Fig. 4. The predicted frequency is 29% higher than observed, chiefly because of the deficiency of observed PLS Trojans with inclinations > 20°. Although this difference may be due chiefly to the statistical uncertainty of small observed numbers both of high-inclination PLS Trojans and the Shoemaker Trojans, a small additional bias in the PLS may also contribute. About half the high-inclination asteroids near the north and south margins of the PLS fields tended to move either off or onto the fields during the period when the plates were taken. Thus 5 to 10% of the high-inclination objects may not have been followed long enough to obtain even short-arc orbits and are missing from the statistics.

If we apply our best estimate of the correction factor, we find that the corrected number of faint L4 Trojans shows an increase of about 45% above that estimated by van Houten et al. (1970b), i.e., $3.2/2.2 = 1.45$. A further

correction should be made, however, because only 19 of the 24 PLS Trojans had been recognized and reported by them in 1970. Hence the final corrected number of faint PLS Trojans is $1.45 \times 24/19 = 1.8$ times the number estimated in 1970.

The estimate of van Houten et al. (1970b) of the population of faint L4 Trojans was based chiefly on observations from two fields near L4 photographed in 1965; the PLS provided observations of the libration region at a distance about 22° to 38° from L4. The 1965 fields were approximately centered on the ecliptic, and the mean heliocentric ecliptic latitude limit $|l|$ for Trojans in these fields is effectively half that of the PLS. Applying Eq. (2) to derive the weighted correction factor from the inclination statistics for independently discovered and Shoemaker Trojans, we find that the weighted mean t_i is 0.146 and the correction factor is 6.85. The correction for the inclination selection effect is 1.56 times that used by van Houten et al. (1970b).

A further correction must be made to the 1965 material because presumed Trojans were identified solely by their motion; orbits were not obtained. In the 1973 survey of the region around L4, van Houten found 43 slow-moving objects thought to be Trojans; astrometry and orbit determination revealed that seven of these objects were Hildas and one was a Mars-crossing asteroid (see *Minor Planet Circulars* 4285–4292). If we apply the ratio of 35/43 to estimate the true number of Trojans among 45 candidates found on the 1965 plates, the estimated number of Trojans must be reduced by a factor of 0.81_4. Hence our final correction to the estimates van Houten based on the 1965 plates is $0.814 \times 1.56 = 1.27$. This final correction applies to about 70% of the estimated population of faint L4 Trojans; about 30% of the estimate is based on the PLS. Our estimate of the L4 population is $0.7 \times 1.27 + 0.3 \times 1.8 = 1.43$ times higher than the estimate of van Houten et al. (1970b). The result is shown in Fig. 1, where we have drawn a smooth curve for the cumulative frequency parallel with the mean curve of van Houten et al. but a factor of 1.43 times higher. The equation for this curve is

$$\log_{10} F = 1.375 + 0.433[B(1,0) - 10.25], \qquad B(1,0) \geq 10.25 \qquad (3)$$

or

$$F = 23.7 \; e^{0.998[B(1,0) - 10.25]}, \qquad B(1,0) \geq 10.25 \qquad (4)$$

where F is the cumulative number to absolute magnitude $B(1,0)$. When observational selection effects have been appropriately accounted for, this curve is consistent with the number of L4 Trojans found by van Houten from the 1973 plates to about $B(1,0) = 12.75$. At $B(1,0) = 14$, the estimated population is 1000 ± 200.

Degewij and van Houten (1979) suggested, from comparison of results from search fields photographed in 1971 and 1973, that the number of faint L5 Trojans is about 3.5 times smaller than the number of faint L4 Trojans. Al-

though positions and orbits for 35 L4 Trojans found in 1973 have been published in the *Minor Planet Circulars,* no analysis or comparison of the 1971 and 1973 observations has yet been presented. Orbits for 26 new Trojans found by van Houten in the 1977 survey of the L5 region were published in *Minor Planet Circulars* 12538 to 12560 in 1987. Comparison of these data with the results from the 1973 observations near L4 suggests that the number of faint L5 Trojans is about 50% of the L4 population. On the other hand, the number of L5 Trojans brighter than $B(1,0) = 10.25$ discovered through 1984 was slightly greater than that found in the L4 swarm; subsequent discoveries have pushed the known number of bright L4 Trojans only slightly ahead. If the population of L5 Trojans to $B(1,0) = 14$ is only half the L4 population, the form of the cumulative magnitude distribution of Trojans in the L5 swarm must be somewhat different from that of L4.

The magnitude distribution of faint L4 Trojans was shown by van Houten et al. (1970*b*) to be similar to the distribution of main-belt asteroids. Because the size and magnitude distributions of belt asteroids <100 km in diameter are now understood to be the result of collisional evolution (see, e.g., chapter by Davis et al.), the inference is strong that the magnitude distribution of faint L4 Trojans is also a result of collisions. It is equally probable that faint L5 Trojans are collisionally evolved. We anticipate that the slope of the magnitude distribution of faint L5 Trojans will be similar to that found for the faint objects in the L4 swarm, but it may intercept the steep curve for bright L5 Trojans at a somewhat lower magnitude and lower cumulative number. Part of the difference in numbers of faint objects observed near L4 and L5 might be due to differences in the dynamical structure of the two swarms. As we suggest in the following section, there may be a somewhat diffuse, low-inclination, low-libration-amplitude dynamical group among the bright L4 Trojans. Any strong irregularities in the distribution of characteristic orbital elements, which might have have evolved from collisions, pose difficulties in estimating the population of faint Trojans from small observational samples.

In view of the paucity of evidence, we surmise that the L5 population to $B(1,0) = 14$ probably lies somewhere in the range of $\sim$500 to $\sim$1000. Adding the L5 and L4 swarms together, we roughly estimate the total population of Trojans to $B(1,0) = 14$ at 1750 $\pm$ 300. From data presented in the IRAS catalogue (Matson 1986; see the tabulation by Tedesco in Part VI), we find that the mean geometric albedo of Trojans in the V band (based on H) is 0.0400 $\pm$ 0.0046 and the mean B-V is 0.76. The average diameter of Trojans at $B(1,0) = 14$, calculated on the basis of these data (assuming mean $[V(1,0)-H] = 0.3$), is 17.1 ($+1.0$, -0.9) km. The estimated population of Trojans extrapolated to 15-km diameter is about 2300 $\pm$ 500. From extrapolation of the bias-corrected size distributions of the various taxonomic classes of asteroids given by Zellner (1979), the number of belt asteroids > 15 km in diameter is roughly estimated at about 5000. Within the rather large uncertainties of the estimates, the population of Trojans > 15-km diameter is about half that of main-belt asteroids. It is appropriate to think of the Trojan swarms

as a largely unexplored second asteroid belt, very roughly comparable with the main asteroid belt in number of bodies and probably in importance to our understanding of the solar system.

III. DYNAMICAL STRUCTURE OF THE TROJAN SWARMS

Orbits based on two or more oppositions were available for 40 L4 Trojans and 23 L5 Trojans by mid-1988. These numbers are large enough that we can begin a meaningful assessment of the dynamical structure of the swarms. Sufficient work has been done to enable determination of three characteristic orbital parameters of the Trojans with accuracy adequate for reconnaissance study. These parameters, here called proper elements, are the libration amplitude, the proper eccentricity and the proper inclination. Bien and Schubart (1987) have carried out numerical integrations, in most cases extending over ±73,000 yr, to determine these proper elements for 41 numbered Trojans, 20 in the L4 swarm and 21 in L5. One L4 Trojan with very high inclination, 2146 Stentor, failed to yield secure proper elements. The results of Bien and Schubart provide a standard against which approximate analytical methods for deriving proper elements can be checked. This comparison shows that proper elements can be obtained from relatively simple theory with an accuracy adequate for our reconnaissance purposes.

The libration amplitude can be calculated from the theory of Yoder et al. (1983). The motion in mean longitude of a Trojan with respect to Jupiter is described approximately by

$$E = \frac{1}{6} \left(\frac{d\phi}{dt} \right)^2 - \frac{\epsilon^2 \eta_0^2}{2 \left| \sin \frac{\phi}{2} \right|} \left[1 + 4 \left(\sin \frac{\phi}{2} \right)^3 \right]$$

$$\frac{d\phi}{dt} = \eta - \eta_0 = \frac{1}{a^{3/2}} - \frac{1}{a_0^{3/2}}$$

(5)

where E = equivalent energy constant; ϕ = mean difference in longitude between the Trojan and Jupiter; ϵ = (mass of Jupiter)$^{1/2}$ = 0.0309; η_0 = mean motion of Jupiter = 0.084260 rev yr^{-1}; η = mean motion of Trojan; a = semimajor axis of Trojan; a_0 = semimajor axis of Jupiter = 5.203 AU.

To solve for E, we obtain ϕ from the difference of the mean anomalies of the Trojan and Jupiter at a given epoch and a from the osculating Trojan orbit at this epoch. Solutions for the minimum and maximum values of ϕ (Yoder et al. 1983) are then given by

$$\sin \frac{\phi_{min}}{2} = \frac{\sin(\alpha/3)}{(3A)^{1/2}}, \qquad \sin \frac{\phi_{max}}{2} = \frac{\sin(\alpha/3 + 120°)}{(3A)^{1/2}}$$

(6)

where $A = \epsilon^2 \eta_0^2 / 2E$ and $\sin\alpha = (3A)^{3/2}$.

The libration amplitude D is here defined as $\phi_{max} - \phi_{min}$, consistent with the usage of Bien and Schubart (1987). It can be seen from Eq. (5) that an accurate value of a is required to derive a secure estimate of the libration amplitude. In general, only orbits based on observations over two or more oppositions are sufficiently accurate to derive useful estimates of D.

The proper or free eccentricity e_p can be estimated for L4 Trojans from

$$e_p^2 = [e \cos\tilde{\omega} - e_o\cos(\tilde{\omega}_o + 60°)]^2 + [e \sin\tilde{\omega} - e_o\sin(\tilde{\omega} + 60°)]^2 \quad (7a)$$

and for L5 Trojans from

$$e_p^2 = [e \cos\tilde{\omega} - e_o\cos(\tilde{\omega}_o - 60°)]^2 + [e \sin\tilde{\omega} - e_o\sin(\tilde{\omega} - 60°)]^2 \quad (7b)$$

where e and $\tilde{\omega}$ are the osculating eccentricity and longitude of perihelion of the Trojan at epoch, and e_o and $\tilde{\omega}_o$ are the osculating eccentricity and longitude of perihelion of Jupiter at the same epoch. Proper inclination i_p can be estimated simply by referring the osculating Trojan orbit to the orbit plane of Jupiter (which is currently inclined $1°307$ to the ecliptic) for $i \lesssim 30°$.

Proper elements derived for L4 Trojans from Eqs. (5) to (7) and the transformation of the Trojan orbits to Jupiter's orbital plane are compared in Table I with proper elements derived by numerical integration. The largest deviations are 3° for libration amplitude, 0.010 for proper eccentricity and $0°3$ for proper inclination; the *rms* deviations are $1°7$ for D, 0.0050 for e_p and $0°11$ for i_p.

The *rms* deviations correspond to peak differences in velocity (with respect to a circular orbit) of 4 m s^{-1} for D, 66 m s^{-1} for e_p and 25 m s^{-1} for i_p. It can be seen that the largest uncertainties in velocity are due to errors in e_p. Uncertainties in velocity due to errors in D are negligible. The uncertainties in velocity are well within the observed dispersion of velocity for the best defined Hirayama families in the main asteroid belt (several 100 m s^{-1}). Hence we conclude that the approximate proper elements are suitable for an initial search for candidate dynamical groups of collisional origin among the Trojans.

Libration amplitudes for all Trojans for which we have multiple opposition orbits range from 2° to 63°. The extreme values of D are found in the L5 swarm, which seems to have a somewhat flatter distribution of libration amplitude than the L4 swarm (Fig. 5). The mean D for L5 Trojans, $28°8$, is not statistically discriminable from the mean for L4 Trojans, $29°9$. All but a small fraction of the Trojans with accurate orbits were discovered in the course of general asteroid search programs. These general searches have not been restricted to the neighborhoods of the L4 and L5 points; hence there has been comparatively little bias with respect to libration amplitude in the discovery circumstances. A small selection effect might be anticipated from inclusion of 8 van Houten Trojans discovered near the libration points. Rather than lower
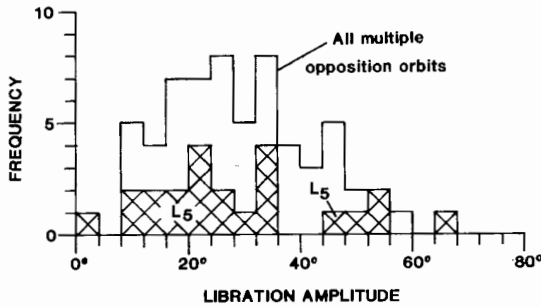
Fig. 5. Frequency distribution of libration amplitude calculated for all Trojans with multiple opposition orbits. The distribution for the subset of L5 Trojans is shown with cross hatch. Libration amplitudes were calculated from Eq. (5) and (6); the amplitudes so derived deviate up to a maximum of 5° from the amplitudes found by Bien and Schubart (1987).

as expected, however, the mean libration amplitude for these Trojans is 33°, somewhat higher than the mean for all 63 Trojans with multiple opposition orbits.

It is of interest that an increase in the number of multiple opposition orbits by more than a factor of 2 in the last 10 years has not extended the observed upper limit of libration amplitude. For decades, the Trojan with the largest known libration amplitude ($D = 57°$) was 1437 Diomedes, a relatively large, bright object in the L4 swarm. The range of known libration amplitudes was extended to 63° (68° as estimated from Eqs. 5 and 6) with the discovery of 2594 (1978 TB), a faint L5 Trojan; no objects with larger libration have since been found. As pointed out by Yoder (1979), the limited range of libration amplitudes of the Trojan swarms is a dynamical feature that remains to be explained.

Proper eccentricities for the 63 Trojans with multiple opposition orbits range from about 0.014 to 0.130. Mean e_p, as calculated from Eqs. (7a) and (7b), is 0.055 for L4 Trojans and 0.063 for L5 Trojans. Within the combined uncertainties of statistics and estimation, the differences in the means and in the observed distributions in the two swarms (Fig. 6) may not be significant. As a consequence of eccentricity limits for stable libration of the Trojans, the mean proper eccentricity of Trojans is much less than that of main-belt asteroids. The maximum observed e_p, however, is below the limit suggested by Rabe (1965,1967).

The distribution of proper inclination of the Trojans, corrected for observational selection effects, should match the distribution of their osculating inclinations fairly closely. Maximum deviation between i_p and osculating i is about 1°.6, except in cases of $i > 30°$, and the mean deviation should be close to 0°. Thus mean i_p for all Trojans, corrected for observational bias, is estimated to be close to 18°. The observed distribution of i_p is similar in the L4
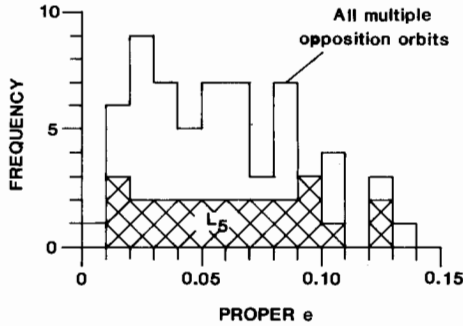
Fig. 6. Frequency distribution of proper eccentricity calculated for all Trojans with multiple opposition orbits. Distribution for subset of L5 Trojans is shown with crosshatch. Proper eccentricities were calculated from Eqs. (7a) and (7b).

and L5 swarms. Compared with the main asteroid belt, the Trojan swarms are characterized by exceptionally large dispersion in proper inclination.

The number of accurate orbits for L4 Trojans has reached a threshold that invites close examination of the L4 swarm for pairs or larger dynamical groups of possible collisional origin. Schubart and Bien (1987) conducted such a search among 19 Trojans in the L4 swarm and 21 in the L5 swarm but failed to identify pairs that they felt were convincing. On the other hand, Schubart (1982) found pairs among 34 Hildas (asteroids in libration about the 3:2 commensurability with Jupiter) with very similar proper elements. We now have 40 L4 Trojans to examine (or 39, if we neglect 2146 Stentor). Doubling the set of proper elements for the L4 swarm has revealed a number of candidate pairs that could not have been found from the smaller set available to Schubart and Bien. The distribution of L4 Trojans in proper element phase space is illustrated in Fig. 7, where candidate dynamical pairs and larger associations are identified. Proper elements and absolute magnitudes for these pairs and associations are listed in Table II.

An appropriate measure of the similarity of proper elements for any pair or group is the dispersion in encounter velocity U relative to a particle in some reference circular orbit with a and i_p equal to one member of the pair or group. For Trojans, we use a at times when the asteroid is passing the libration point, as these are the times of maximum differences in a and in the tangential component of velocity U_y. An expression for a at libration point passing can be obtained from Eq. (5) by setting $\phi/2 = 30°$. Substituting $A = \epsilon^2 n_0^2/2E$, we have

$$a = \left\{ \frac{1}{a_0^{3/2}} - \left[3 \epsilon^2 \eta_0^2 \left(\frac{1}{A} - 3 \right) \right]^{1/2} \right\}^{-2/3}. \qquad (8)$$
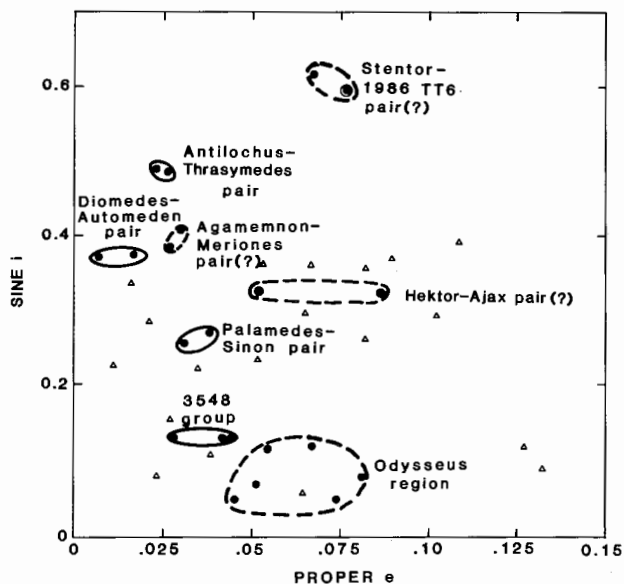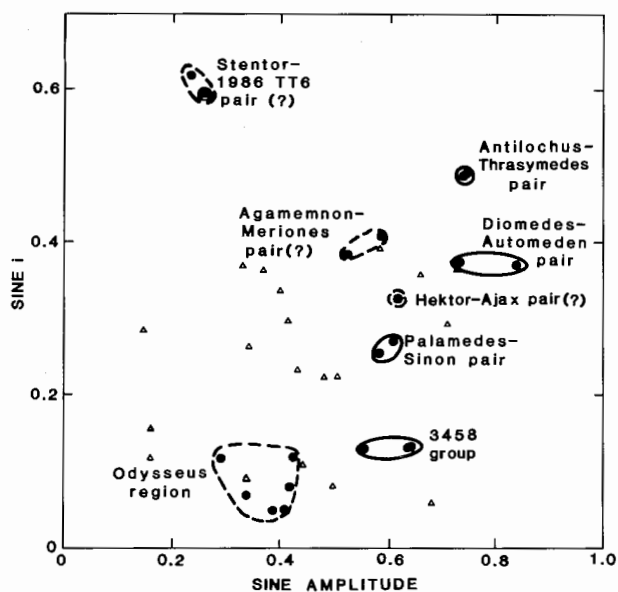
Fig. 7. Distribution of L4 Trojans in proper element phase space. Distribution of sine proper *i* vs sine libration amplitude is shown in Eq. (7a), and of sine *i* vs proper eccentricity in Eq. (7b). Proper elements, calculated from Eqs. (5), (6) and (7) and from transformation of the orbits to the orbit plane of Jupiter, are shown for all L4 Trojans with multiple opposition orbits. Candidate dynamical pairs and larger dynamical groups are shown with solid dots enclosed within oval lines. Dynamical associations that are considered less certain or questionable are enclosed with broken lines. Trojans not linked with dynamical groups are shown with triangles.

The two solutions of Eq. (8) for a correspond to passages interior to and exterior to a circle with radius a_0. For convenience, we use the solution for interior passage (corresponding to the positive root of the second term on the right hand of Eq. 8). The difference in encounter velocity ΔU for two closely similar orbits (equivalent to the mutual encounter velocity when the nodes and apsides are nearly aligned) is given with close approximation by

$$(\Delta U)^2 = (\Delta U_x)^2 + (\Delta U_y)^2 + (\Delta U_z)^2$$

$$\Delta U_x = \Delta e$$

$$\Delta U_y = (a_2/a_1)^{1/2} - 1$$

$$\Delta U_z = \sin \Delta i \tag{9}$$

where ΔU_x, ΔU_y and ΔU_z are the differences in the radial, tangential and normal components of velocity, respectively, normalized to the circular orbital velocity at $a_1 \approx a_2$; a_1 and a_2 are the semimajor axes of the two orbits; Δe is the difference in eccentricity; and Δi is the difference in inclination. For comparison of Trojan dynamical pairs and groups with main-belt families, we multiply ΔU, ΔU_x, ΔU_y and ΔU_z by the mean orbital velocity of Jupiter to obtain the corresponding differences of velocity and velocity components, Δv, Δv_x, Δv_y and Δv_z, in m s^{-1} (Table III).

A pair of Trojans that appear from initial inspection of Fig. 7 and Table II to have the most similar sets of proper elements consists of 1583 Antilochus and 3801 Thrasymedes. Libration amplitudes for this pair are the same to the nearest degree, as calculated from Eqs. (5) and (6); proper eccentricities match within 0.002, as calculated from Eq. (7a); proper inclinations match within 0°2. Because the osculating elements for these two asteroids are also closely similar, refined estimates of the proper elements probably will reveal nearly the same differences. Libration amplitude and i_p obtained by Bien and Schubart (1987) for Antilochus are close to the values obtained analytically, while their e_p is 0.006 lower. Using the approximate proper elements obtained analytically, we find $\Delta v \approx 60$ m s^{-1}. This velocity difference is small in comparison with the velocity dispersion in well-established main-belt families. The Antilochus-Thrasymedes pair occurs on the margin of the distribution of elements in proper element phase space (Fig. 7) and is very unlikely to have arisen by chance. We conclude that Antilochus and Thrasymedes probably were once united in a single object. Antilochus is about 2.4 mag brighter than and probably nearly 3 times the diameter of Thrasymedes, so the latter can be viewed as a "chip" off Antilochus (diameter ≈ 110 km) or the Antilochus parent body.

The dynamical pair formed by 1437 Diomedes and 2920 Automedon may have lower Δv than the Antilochus-Thrasymedes pair. The Diomedes-Automedon pair was overlooked by Schubart and Bien (1987) because of the

TABLE II

Candidate Dynamical Groups in the L4 Swarm[a]

	D		e_p		i_p		Diameter
	B&S (°)	Eq. 5&6 (°)	B&S	Eq. 7a	B&S (°)	i(trans.) (°)	(km)
Antilochus–Thrasymedes pair							
1583 Antilochus	49	48	0.018	0.024	29.1	29.2	110
3801 Thrasymedes		48		0.026		29.0	(35)
Diomedes–Automedon pair							
1437 Diomedes	57	57	0.017	0.007	22.0	21.7	170
2920 Automedon	44	47	0.016	0.018	21.9	21.9	125
3548 group							
3548 1973 SO		39		0.044		7.5	(70)
6541 PL		40		0.028		7.4	(35)
6591 PL		34		0.042		7.4	(35)
Palamedes–Sinon pair							
2456 Palamedes	33	36	0.029	0.031	14.9	14.8	100
3391 Sinon		37		0.038		15.6	(60)

Agamemnon-Meriones pair(?)							
911 Agamemnon	34	32	0.021	0.027	22.7	22.6	175
3596 Meriones		35		0.030		23.9	(85)
Hektor-Ajax pair(?)							
624 Hektor	38	38	0.054	0.052	19.0	18.9	(150 × 300)
1404 Ajax	40	38	0.076	0.086	19.1	18.9	90
Stentor-1986 TT6 pair(?)							
2146 Stentor	8	13	0.06	0.067		38.1	(60)
1986 TT6		15		0.076		36.3	(110)
Odysseus region							
1143 Odysseus	20	20	0.052	0.051	4.0	4.0	135
1647 Menelaus	16	17	0.058	0.054	6.7	6.7	70
1749 Telemon	27	25	0.068	0.067	6.8	6.8	115
1973 SM		23		0.045		2.8	(75)
1985 TQ		24		0.074		2.9	(70)
9507 PL		25		0.081		4.6	(55)

[a] See Table I for explanation of headings for proper elements D, e_p, and i_p. Diameters, rounded to the nearest 5 km, are taken from the IRAS catalogue (Matson 1986) or, where shown in parentheses, are calculated from H using the mean estimated albedo of the Trojans.

E. M. SHOEMAKER ET AL.

TABLE III
**Relative Separation Velocities within Candidate Dynamical Groups
in the L4 Swarm[a]**

	Δv_x (m/s^{-1})	Δv_y (m/s^{-1})	Δv_z (m/s^{-1})	Δv (m/s-1)
Antilochus-Thrasymedes pair	35 ± 15	2(+4,−2)	45 ± 25	60 ± 30
Diomedes-Automedon pair	15 ± 15	26 ± 4	25 ± 25	35 ± 30
3548 group				
3548-6541 PL	210 ± 65	2(+4,−2)	5(+25,−5)	210 ± 70
3548-6591 PL	25(+65,−25)	15 ± 4	10(+25,−10)	30(+70,−30)
Palamedes Sinon pair	90 ± 65	5 ± 4	180 ± 25	200 ± 70
Agamemnon-Meriones pair(?)	50(+65,−50)	10 ± 4	270 ± 25	275 ± 70
Hektor-Ajax pair(?)	290 ± 15	7 ± 4	25 ± 25	290 ± 30
Odysseus region				
Menelaus-Telemon pair	130 ± 15	24 ± 4	25 ± 25	135 ± 30

[a]Velocity differences are calculated from proper elements using Eqs. (8) and (9).

separation in D. As noted above, substantial differences in D correspond to modest differences in the tangential component of velocity. For easier assessment of the velocity differences, the scales of the coordinates for sine amplitude and proper e in Fig. 7 should be compressed. The difference in D does account for the largest component of Δv between Diomedes and Automedon, but because Δe_p and Δi_p are very small (Table II) Δv is only ~35 ± 30 m s^{-1}. This pair, on the high D-low e_p margin of proper element phase space (Fig. 7), is also very unlikely to be an accidental pair. In contrast to Antilochus and Thrasymedes, Diomedes and Automedon are subequal in size, with estimated diameters of ~170 and ~125 km. Within the uncertainties of estimation, the albedos of these two bodies are the same. We suspect that many fainter dynamical companions of this pair of large asteroids remain to be discovered.

A third dynamical pair with very low estimated Δv occurs within a group of three rather faint Trojans with similar proper elements (Table II). These three asteroids were discovered in the van Houten surveys; one of them, 3548 (1973 SO), has been numbered but not named. We refer to them as the 3548 group. Estimated Δv for the pair 3548 − 6591 PL is 30(+70,−30) m s^{-1}. All three asteroids in the group have similar D and i_p, but 6541 PL appears to be somewhat separated from the other two in e_p. The estimated Δv for the pair 3548 − 6541 PL is 210 ± 70 m s^{-1}. This higher Δv is within the range found for main-belt families, but the estimate could be spuriously high, owing to the inaccuracy of Eq. (7) used to derive e_p. The *rms* Δv for the 3548 group

(determined with respect to the brightest member) is ~ 150 m s^{-1}, which is fairly typical of main-belt families. It is of interest that this group was detected among Trojans discovered in searches for faint asteroids; many additional dynamical groups can be expected to be found with deep Trojan surveys, provided that the objects are observed on multiple oppositions so that accurate orbits are obtained.

Other dynamical pairs of possible collisional origin are 2456 Palamedes-3391 Sinon, 624 Hektor-1404 Ajax and 911 Agamemnon-3596 Meriones. Estimated Δv's are of the order of 200 to 300 m s^{-1} (Table III). The latter velocity difference is near the upper end of the range for large members of main-belt families; thus a collisional relation is suggested only tentatively for the Agamemnon-Meriones pair. For our reconnaissance study, we have taken a difference in i_p of $1°3$ ($\Delta v_z = 300$ m s^{-1}) as an approximate upper bound for dynamical pairs of large asteroids that may have originated from single events of collisional disruption. A tentative pair noticed by Schubart and Bien (1987), 1404 Ajax-2797 Teucer, has a difference in i_p of $1°9$ and substantially exceeds this bound. Members of another pair noticed by these authors, Hektor-Ajax, are closely similar in D and i_p but are separated by 0.022 in e_p (Table II). The Δv for this pair is 290 ± 30 m s^{-1} (Table III), just within the range we consider likely for dispersal in a single impact event. If we entertain the possibility that Hektor is a binary asteroid whose components are perhaps in contact, as suggested by Cook (1971), these components, together with Ajax, could be thought of as a related group of collision fragments (or possibly clumps of collision debris) of subequal size.

Near the low i_p margin of the proper element distribution of the L4 swarm is a cluster of six Trojans with small dispersion in D and moderate dispersion in i_p and e_p (Table II). We refer to this region of proper element phase space as the Odysseus region, after the brightest and earliest numbered member of the cluster. The spread of the cluster in estimated i_p is $4°$, much greater than observed in well-defined main-belt families but comparable with that of a region of high asteroid density near the main-belt asteroid Flora. The complex distribution of asteroids in the Flora region, which seems to contain several close-spaced families, may be the consequence of a sequence of collisional events. At least one good dynamical pair, 1647 Menelaus-1749 Telemon ($\Delta v = 135 \pm 30$ m s^{-1}), is present in the Odysseus region; we speculate that the apparent cluster originated from multiple collisions in a manner similar to that postulated for the Flora region. It is also possible that the occurrence of several asteroids in the Odysseus region is due to chance. Much larger statistics are needed to test the viability of the cluster and the multiple-collision hypothesis.

Finally, we draw attention to the possible dynamical pair 2146 Stentor-1986 TT6, two asteroids with the highest osculating inclinations among all known Trojans. They have similar proper elements, as obtained from Eqs. (5)–(7) and from transforming the osculating orbits to the orbit plane of Jupi-

ter, and they are far removed from all other L4 Trojans in proper element phase space (Fig. 7). It is improbable that this pair is an accidental association. The transformed inclinations are separated by $1°8$, higher than the limit we adopted for accepting other pairs. However, in their study of Stentor, Bien and Schubart (1987) found that the inclination showed a tendency to increase from the starting transformed value; hence they were unable to estimate i_p from an integration over their standard time interval. It appears that simple transformation to the orbit plane of Jupiter does not provide a satisfactory estimate of i_p for these very high-inclination Trojans. Integrations much longer than 73,000 yr evidently will be required to obtain reliable proper elements. A further uncertainty about the similarity of proper elements of the pair stems from the fact that the orbit of 1986 TT6 is based on an observed arc of only 31 days; this uncertainty can be removed readily by deliberate recovery of this relatively bright Trojan.

In summary, we find that possibly as many as 8 dynamical pairs or groups of Trojans can be identified from the presently available statistics on the L4 swarm. A few of these pairs might be chance associations, but it is highly probable that the majority are asteroids that have separated from common parent bodies. The most likely cause of separation is collisional disruption. About half the L4 Trojans for which we have accurate orbits belong to the tentatively identified pairs or dynamical groups. A similar fraction of main-belt asteroids belong to recognizable families (Williams 1979), suggesting that they and the L4 swarm have undergone somewhat similar collisional evolutions. Because statistics are fewer for the L5 swarm, it is too early to assess the number of its dynamical groups. Nonetheless, at least 3 candidate pairs, 2207 Antenor-2594 (1978 TB) ($\Delta v = 170 \pm 25$ m s^{-1}), 1208 Troilus-2363 Cebriones ($\Delta v = 190 \pm 25$ m s^{-1}) and 2895 Memnon-3317 Paris ($\Delta v = 210 \pm 25$ m s^{-1}) can be identified among the presently numbered L5 Trojans.

IV. ORIGIN OF THE TROJAN ASTEROIDS

A satisfactory theory for the origin of the Trojans should provide an explanation for their abundance and size distribution, the dynamical structure of the L4 and L5 swarms, and the taxonomic relations of Trojans to other small bodies in the solar system. We might also hope to explain peculiarities of the distributions of their shape and spin state, although this may be asking too much, given our present rudimentary knowledge.

Many students of asteroids feel that these bodies were formed close to the regions where they are now found (see, e.g., Gradie and Tedesco 1982; Vilas and Smith 1985) and that the Trojan swarms are rather empty, quiet regions, where collisions are rare and not much has happened (e.g., Hartmann 1979; Davis and Weidenschilling 1981; Hartmann et al. 1988). Thus it is commonly believed that the Trojans were formed near 5.2 AU, perhaps locked

in the 1:1 commensurability with Jupiter from near the time of their birth, and that large individual Trojans may be pristine bodies whose features, including shapes and spin states (French 1987; Hartmann et al. 1988), may reflect configurations acquired at or near the time of their accretion. This perspective is derived from an application to the asteroids of Lyell's doctrine of uniformitarianism—the assumption that present conditions and processes hold for the past.

Against the uniformitarian view is the evidence for a violent past in the solar system, first recognized from the heavily cratered surfaces of the Moon, Mars and Mercury. From the exploration of the Moon (Wilhelms 1987), we know that heavy bombardment, at least in the vicinity of one terrestrial planet, extended nearly 1 Gyr beyond the time of accretion of meteorite parent bodies (small bodies like asteroids). Exploration of the outer planets by the Voyager spacecraft has revealed heavily cratered surfaces on several satellites of each planet visited. This cratering cannot have been produced by bombardment over solar system time at the estimated present rates (Shoemaker and Wolfe 1982; Smith et al. 1982,1986). An episode or episodes of heavy bombardment are indicated in the vicinity of each outer planet, at least out to the orbit of Uranus. Whether heavy bombardment in the outer solar system was related to that in the terrestrial planet region remains an open question.

The pairs of probable collisional origin in the Trojan swarms provide independent evidence for an episode of heavy flux of small bodies near the orbit of Jupiter. Mutual collisions between Trojans does not satisfactorily account for breakup of the largest objects, although it does contribute importantly to collisional evolution of the faint Trojans. Davis and Weidenschilling (1981) analyzed the probability of catastrophic disruption by mutual collision among the present L4 Trojans and found a mean time to breakup for 100-km bodies in the range ~ 10 to ~ 100 Gyr. From a simple particle-in-a-box calculation, they found a mean lifetime for 100-km bodies of 200 Gyr, assuming that collision of a body at least 25 km in diameter is required for disruption. The number of Trojans >25 km diameter in the L4 swarm was taken to be ~ 250, consistent with the estimate of the population by van Houten et al. (1970b). From our revised population estimate (Eqs. 3 and 4) and the mean albedo determined from IRAS observations, we find the number of L4 objects >25 km diameter to be ~ 440. Further, our estimate of the mean inclination of the Trojans is twice the mean of the orbits used by Davis and Weidenschilling. Increasing the estimated mean inclination from 9° to 18° doubles the estimate of the mean collision speed without seriously changing the mean collision probability. (Contrary to the conclusions of Hartmann and Cruikshank [1978] and Davis and Weidenschilling [1981], the mean collision speed among Trojans is greater than the mean collision speed in the main belt, owing to the large dispersion of Trojan inclinations.) The mean energy of the impactors should be increased by $\sim \sqrt{2}$ and the mean times to disruption reduced approximately by $440\sqrt{2}/250 \approx 2.5$. The revised mean disruption time of 100-

km diameter Trojans is ~100 Gyr for the particle-in-a-box calculation and ~5 Gyr for the most favorable disruption conditions assumed in a detailed Monte Carlo simulation by Davis and Weidenschilling. Minimum mean time to disruption of 150-km-diameter Trojans is ~16 Gyr. Breakup of precursors of the largest Trojans, Hektor (~150 × 300 km), Agamemnon (~175 km diameter) and Diomedes (~170 km diameter) would indicate a fluence of smaller bodies at least an order of magnitude greater than the present flux of small Trojans integrated over solar system time. That the three largest Trojans are members of possible dynamical pairs suggests a period of heavy bombardment.

The present small Trojans evidently were formed chiefly from collisions among Trojans following heavy bombardment. Correcting the results of Davis and Weidenschilling (1981) by the factor 2.5, we find the maximum mean time to disruption of 50-km Trojans is about the age of the solar system, and the minimum is an order of magnitude less. Most L4 Trojans fainter than $B(1,0) = 12$ (diameters <43 km) probably are fragments formed by collisions among Trojans within the last 2 Gyr. Similarity of the magnitude distribution of faint L4 Trojans to that of the collisionally evolved main belt, therefore, should come as no surprise. However, the steep slope of the magnitude distribution at B magnitudes brighter than 10.25, which reflects a peculiarly low relative abundance of Trojans larger than ~100-km diameter, does call for special explanation.

A principal key to understanding the origin of the Trojan swarms is their broad dynamical structure. Limits to the eccentricities of Trojans for stable libration about the Lagrange points have long been recognized. Similarly, there are limits to libration amplitudes. These limits are very broad for orbits of sufficiently low eccentricity. Horseshoe orbits in which the libration exceeds 280° are theoretically stable. Yoder (1979) noted the restricted observed range of Trojan libration amplitudes and explored a variety of mechanisms by which libration might have been damped. Damping of libration probably has occurred, but an alternative explanation for the distribution both of libration amplitude and of eccentricity follows directly from recognition of the collisional evolution of the Trojan swarms.

The joint distribution of proper eccentricity and libration amplitude for the combined Trojan swarms is illustrated in Fig. 8. The frequency tapers off with increasing e_p and increasing D, and the observed range of e_p decreases with increasing D. The observed distribution is roughly consistent with a limit for stable libration derived by Rabe (1967) from the theory of the planar, restricted, three-body problem. At $D > 45°$, however, a few Trojan orbits lie outside a limit extrapolated from Rabe's results; the true stability limit must lie beyond the observed range of e_p and D. We infer that it lies a short distance beyond the observed points at $D = 45°$, $e_p = 0.102$ and $D = 68°$, $e_p = 0.057$, as shown in Fig. 8, and that it may approach Rabe's theoretically calculated limit for $D < 20°$.

To test the validity of our inferred stability limit, as drawn in Fig. 8, we
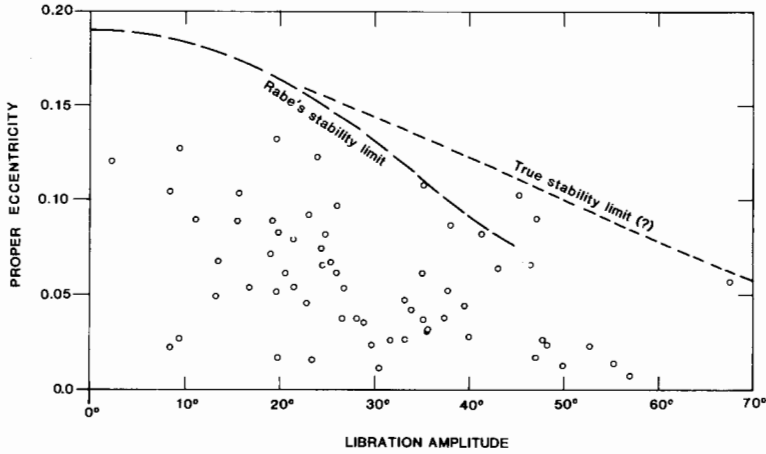
Fig. 8. Distribution of proper eccentricity vs proper libration amplitude for all Trojans with multiple opposition orbits. Proper elements are calculated from Eqs. (5) and (7). The theoretical limit of stable libration derived by Rabe (1967) and the true limit of stable libration inferred from the observed distribution are shown with dashed lines.

integrated orbital motion for starting orbits with a range of eccentricities but otherwise identical with the orbit of 2594 (1978 TB), the Trojan with the highest observed libration amplitude. The integration program yielded stable libration when started with observed Trojan orbits, as expected. When starting e was increased from 0.0854 (the observed e at epoch for 2594) to 0.1322, corresponding to an initial free eccentricity of 0.100, the libration amplitude gradually increased with time. At +14,080 yr, the modified "Trojan" began librating in a horseshoe orbit, and at +14,605 yr it escaped entirely from the 1 : 1 commensurability. In other words, an impulse sufficient to change e by 0.047 would lead to rather prompt escape of 2594 (1978 TB). A large number of long integrations of trial starting orbits are required to map the precise stability limit, but the limiting e_p clearly must decrease with increasing D. Our few numerical experiments suggest that the stability limit is in the neighborhood of the line drawn in Fig. 8.

Within a distance of ~0.05 Δe_p from the inferred stability limit, the density of Trojan orbits drops off markedly. This depletion near the boundary has a simple explanation in terms of the collisional history of the Trojan swarms. Trojans near the boundary tend to escape as a result of increases either in e_p or D due to collisional impulses. For the boundary as drawn, the smallest impulses required for escape from the orbits nearest the boundary correspond primarily to changes in D. Fairly large changes in D are produced by modest impulses. The width of the depleted region in ΔD, ~30°, is equivalent to an escape impulse on the order of 100 m s^{-1}, comparable with the

mean Δv both of the dynamical pairs found in the L4 swarm and of main-belt Hirayama families. The loss from multiple collisions is analogous to diffusion, and the gradient in number density near the boundary roughly resembles a diffusion gradient, as measured in the coordinate of Δv to escape.

Extrapolating the inferred stability limit shown in Fig. 8 beyond about 70° libration amplitude, we find the width of the stable region is comparable with or less than that of the zone of strong depletion. Hence few Trojans are expected to be found there. Although horseshoe orbits of very low eccentricity are theoretically stable, the Δv to escape probably is so low that nearly all objects on initial horseshoe orbits have been lost as a result of collisional impulses.

Under certain conditions of the collisional diffusion model, small bodies can also be captured into stable libration. If the region beyond the stability boundary is occupied by bodies moving in temporary unstable libration, collisional diffusion can transfer objects into the stable region. With a high enough number of objects orbiting just beyond the stable region of proper element phase space, the net transfer can be into the Trojan swarms rather than out of them. We will argue that this was the situation early in the period of heavy bombardment.

The most remarkable feature of the Trojan swarms is their large dispersion in inclination. Because their planetesimal precursors probably formed from particles concentrated near the central plane of the solar nebula and had low initial orbital inclinations, the present high mean inclination of the Trojans is an important clue to their dynamical history. Only two mechanisms are known that might account for the observed high inclinations: (1) drift through a secular resonance; or (2) encounters with very massive bodies, i.e., the major planets or very large protoplanets.

Yoder (1973,1979) has pointed out a secular resonance in the Trojan libration region near near $D = 60°$, where the free precession rate of the node is $-26\overset{\circ}{.}3$ yr^{-1}. Yoder further showed that, if there were a slow drift of D through this resonance, the inclination would be pumped up to $\sim 20°$. Possible causes of drift in D are a secular decrease in Jupiter's semimajor axis or a large flux of small particles in the Trojan region, both of which seem likely. Thus, it is of interest that a strong sharp node in the inclination distribution is observed between 20° and 22° (Fig. 2), which can be regarded as fairly good evidence that drift in D has indeed occurred. The Diomedes-Automedon pair and 1985 VK2 (Table I) are examples of L4 Trojans with i_p near 20° that are not far removed from the resonance. On the other hand, if drift or damping of D were the principal cause of high Trojan inclinations, we might expect to find a correlation between i_p and D and perhaps also between e_p and D (Yoder 1979). The proper elements are uncorrelated both in the L4 swarm (Fig. 7) and in the L5 swarm. Moreover, about 20% of the Trojans have higher inclinations than can be explained by resonance pumping. We conclude that a large part of the dispersion of inclinations of the Trojans probably is due to

their encounter with one or more massive bodies prior to their capture in the 1:1 commensurability.

A further clue to the origin of the Trojans is provided by their taxonomy. On the basis of spectrophotometric observations of Zellner et al. (1985) and albedos derived from IRAS observations (Matson 1986), it appears that the majority of Trojans are D-type (very red, low albedo) objects. Other D-type objects are found librating about the 3:2 and 4:3 commensurabilities, and a few occur in the main asteroid belt. It seems particularly significant that three Jupiter-crossing asteroids, 944 Hidalgo, 3552 (1983 SA) and 1984 BC, are D-type objects (Hartmann et al. 1987). These asteroids have short-lived chaotic orbits like those of Jupiter-family comets, and it is highly probable that they are extinct comets. The nuclei of a few nearly inactive to weakly active comets that have been well observed also resemble the D-class asteroids (Hartmann et al. 1987). The distinctive dark, reddish color of the D-type objects probably is due to the presence of kerogen-like polymerized organic compounds (Gradie and Veverka 1980), the presence of which appears to have been detected directly as grains (CHON particles) in the coma of P/Halley (Kissel et al. 1986). Commonality of spectral class between Trojans and extinct comets suggests that they may be closely related, and it is pertinent to inquire whether Trojans and comets can have been derived from the same region of the solar system. In other words, are Trojans extinct comets captured in the 1:1 commensurability?

A large fraction of the mass of solid material derived from the solar nebula that aggregated into planetesimals in the neighborhood of the giant planets was ejected from the solar system (Safronov 1972). From Monte Carlo studies of the scattering of Uranus and Neptune planetesimals (UNP's), Shoemaker and Wolfe (1984) found that no more than a few percent collided with these planets as they approached their final masses. Over the history of planetary growth, the fraction of UNP's accumulated by Uranus and Neptune probably was close to 5%. This low fraction implies an initial mass of the UNP swarm in the neighborhood of Uranus and Neptune of about 600 $m_\oplus$. Approximately 20% of the UNP's were scattered into the region of the Oort comet cloud, where stellar perturbations controlled their subsequent dynamical evolution. About 1/4 to 1/2 the mass initially injected into the Oort cloud (30 to 60 $m_\oplus$) may remain there at the present time; hence UNP's appear to be an adequate source to account for Oort cloud comets. Roughly 30% of the UNP's were ejected from the solar system by perturbations from Uranus and Neptune, and the remainder (about half) became Jupiter crossing. Thus, the mass of planetesimal material passed down to Jupiter from the Uranus-Neptune region can be estimated at about 300 $m_\oplus$, roughly equal to the mass of Jupiter. All but a tiny fraction of this mass was ejected from the solar system by Jupiter.

Several implications bearing on the origin of the Trojans follow from the enormous mass flux in Jupiter's neighborhood inferred from the study of UNP

scattering. First, it was found that depletion of the UNP swarm was protracted in time (Fig. 9). About half the swarm was lost in the first 130 Myr, but 4% remained 1 Gyr after the beginning of accretion of the planets (Shoemaker and Wolfe 1984). In contrast, all but a small fraction of the planetesimals that formed in the neighborhood of Jupiter probably were ejected from the solar system within a few Myr after collapse of nebular gas onto Jupiter. Jupiter's planetesimals that may have been captured as Trojans at that time were subjected to collisional fragmentation and depletion by collisional diffusion, owing to the later huge flux of small bodies.

A secular decrease in Jupiter's semimajor axis by about 25% is another consequence of the large UNP flux. According to a formula presented by Yoder (1979), this decrease would tend to reduce the libration amplitudes of objects captured early by a factor of ~60%. After accounting for collisional trimming of the distributions of D and e_p, one might expect that most of the surviving fragments of Jupiter planetesimals among the Trojans would be librating $\leq 45°$. A heavy flux of small particles accompanying the larger UNP's would tend to damp further libration and would also decrease e_p (see Yoder 1979). However, continuing collisional diffusion would lead to dispersion of D and e_p and would offset, to some extent, the effects of damping.

The large UNP flux might also have been a source for some Trojans. On the basis of studies by Duncan et al. (1988) of the capture of comets to short-period orbit, we estimate that ~20% of the Jupiter-crossing UNP's were captured by a succession of Jupiter encounters into orbits comparable with those
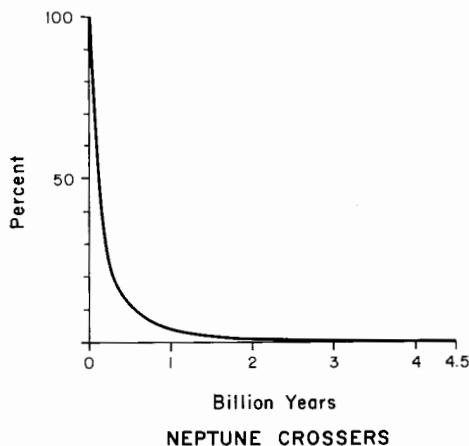
NEPTUNE CROSSERS

Fig. 9. Depletion of the Uranus-Neptune planetesimal swarm obtained from Monte Carlo studies of planetesimal scattering (see Shoemaker and Wolfe 1984). The fraction of planetesimals remaining on Neptune-crossing orbits is shown as a function of time from the beginning of scattering.

of present short-period comets (periods <20 yr). If we assume comparable mean periods of the short-period UNP's and present short-period comets (7.9 yr), their flux at the orbit of Jupiter slightly exceeded that of the longer period UNP's. Short-period UNP's generally were expelled from the solar system by further Jupiter encounters in periods of <1 Myr. But while they were trapped in short-period orbits, their semimajor axes were subject to random walk from Jupiter perturbations, and a substantial number must have entered temporary 1 : 1 libration in horseshoe orbits.

Integration of the motion of 113 short-period comets by Carusi et al. (1985) has shown that four comets become temporary horseshoe librators during a 821-yr interval from AD 1585 to 2406. (Because of inevitable small errors in determination of the present orbits, the integrations do not demonstrate that each of these four comets has been or will become a librator but that objects with closely similar orbits will do so.) The mean fraction of time spent librating in horseshoe orbits, for all the short-period comets studied, is 0.5%. Two comets, P/Whipple and P/Russell 3, entered horseshoe orbits with eccentricities well within the Trojan range. These comets could have been captured into stable 1 : 1 libration (tadpole orbits) with moderate impulses, about 250 m s^{-1} in the case of P/Whipple and 270 m s^{-1} in the case of P/Russell 3. The impulses for capture are comparable with the Δv's of separation for some of our candidate Trojan dynamical pairs. We do not suppose that an entire comet could be captured by a collisional impulse, but a fragment impelled with the appropriate Δv could be. Similarly, collisional disruption of UNP's librating in temporary horseshoe orbits could have led to the capture of UNP fragments in stable tadpole orbits during the period of intense planetesimal flux near Jupiter.

The mass of UNP fragments captured as Trojans can be very roughly estimated as follows. During the first 130 Myr of planetesimal scattering, we estimate that about 150 $m_\oplus$ of UNP's were delivered to Jupiter-crossing orbits at an average rate of ~ 1.2 $m_\oplus$ per Myr. About 20% of this mass was captured in short-period orbits with estimated lifetimes averaging $\sim 2 \times 10^5$ yr. The mean mass residing in short-period orbits was about $(0.2)(1.2\ m_\oplus\ \text{Myr}^{-1})$ $(2 \times 10^5\text{yr}) \approx 0.05\ m_\oplus$. To estimate the number of bodies represented by this mass, we assume a size distribution of UNP's similar in form to that of the present short-period comets but extended to larger sizes.

Shoemaker and Wolfe (1982) found that the size distribution of short-period comets can be fairly well represented by a function of the form

$$N = Kd^\lambda \tag{10}$$

where N is cumulative frequency and d is diameter; their estimate of the size index λ is -1.97, consistent with observations of nuclear magnitudes of comets by E. Roemer and with the size distribution of young craters on Ganymede, which are inferred to have been formed chiefly by impact of short-

period comets. The majority of comets that are presently on short-period or-
bits are extinct, as shown by Shoemaker et al. (1986), who estimated the total
population of active and extinct comets at ~1460 to a nuclear magnitude
$B(1,0) = 18$. Observations of active and extinct comets show that they have
low mean geometric albedos. At a mean B albedo of 0.03, the diameter of a
comet nucleus at $B(1,0) = 18$ is 2.5 km (Shoemaker and Wolfe 1982); this
diameter, together with the estimated population, yields a value for K of 1.0
$\times$ 10^4km$^{-\lambda}$ for the present short-period comets. When $|\lambda|<3$, the total vol-
ume V of bodies distributed according to Eq. (10) is given approximately by

$$V = \frac{\pi}{6} K \left(\frac{-\lambda}{\lambda + 3} \right) d_{max}^{\lambda + 3} \qquad (11)$$

where d_{max} is the diameter of the largest body. Setting $N = 1$, we calculate from
the estimated values of K and λ that the most probable diameter of the largest
short-period comet is ~110 km, about twice the probable diameter of 949
Hidalgo; this undiscovered comet, if it exists, presumably is extinct. The total
volume of short-period comets estimated from Eq. (11) is 1.3×10^6 km^3. At an
assumed density of 1 g cm^{-3}, their mass would be ~2×10^{-7} m$_\oplus$.

We wish to compare UNP's, whose maximum diameter probably greatly
exceeded 100 km, with the short-period comets. Provisionally, we assume
that d_{max} for UNP's was ~1000 km. Probably larger UNP's existed (e.g.,
Pluto), but we assume that their number was sufficiently low that they did not
contain the bulk of the volume. If we take the density of UNP's to be the same
as that of the comets, the volume of 0.05 m$_\oplus$ of UNP's is 3.3×10^{11} km^3. The
value of K in Eq. (11) that corresponds to this volume, when $\lambda = -1.97$ and
$d_{max} = 1000$ km, is 2.6×10^8 km$^{-\lambda}$. Hence the estimated ratio of the mean
number of UNP's residing in short-period orbits, during the first ~130 Myr of
planetesimal scattering, to the present number of short-period comets is $2.6 \times
10^8$ km$^{-\lambda}$/1.0×10^4 km$^{-\lambda} = 2.6 \times 10^4$. With the above assumptions, the
average number of 1000-km-diameter UNP's orbiting with short periods at
any given time was ~300; about 1300 had diameters >500 km, of which
~0.5%, or about 6 objects on average, are estimated to have been librating in
temporary horseshoe orbits.

Probabilities of collision among the short-period UNP's can be derived
from the detailed study of the collision of short-period comets with the
Galilean satellites by Shoemaker and Wolfe (1982). The mean probability of
collision P_c of short-period comets with Callisto was found to be $4.56 \times
10^{-11}$yr^{-1}. If a body of the same size and density were far removed from
Jupiter, the collision probability would be reduced by a factor $\bar{F} = 34.2$, the
mean enhancement of the comet flux by the gravitational field of Jupiter at the
orbital radius of Callisto. A further reduction by a factor of 1.32, the ratio of
the mean capture cross section to the physical cross section of Callisto, should
be made to obtain collision probabilities for much smaller bodies. In addition,

P_c should be reduced by a factor of ~ 1.04 to correct for the dispersion of i and e of the target UNP's. The final mean probability for collision with a massless sphere the diameter of Callisto is $9.7 \times 10^{-13} \text{yr}^{-1}$; if we multiply by $(500/4820)^2$, the probability of collision with a 500-km UNP is $1.05 \times 10^{-14} \text{yr}^{-1}$.

For purposes of illustration, we assume that collision of a 100-km UNP projectile will catastrophically disrupt a 500-km target UNP with a density near 1.0 g cm^{-3} and low strength. Grazing collisions probably would not lead to disruption, so the increase in collision probability due to the finite diameter of the 100-km projectile will be neglected. From the value of K derived above for the short-period UNP's, we find that there were $\sim 3 \times 10^4$ projectiles with $d > 100$ km revolving on short-period orbits at any one time in the first 130 Myr, and the probability of their colliding with a single 500-km target was $\sim 3 \times 10^{-10} \text{yr}^{-1}$. Over one 130-Myr interval, the probability of collisional disruption of a >500-km UNP librating in a temporary horseshoe orbit is $\sim 6 \times (3 \times 10^{-10} \text{yr}^{-1}) \times (1.3 \times 10^8 \text{yr}) \approx 0.2$. Integrating over the 1 Gyr heavy bombardment period, we obtain a probability of disruption of ~ 0.3. When we add collisions by the long-period, Jupiter-crossing UNP's, which were 5 times as numerous but had a substantially longer mean period, the total probability comes to ~ 0.6.

Not all collisional disruptions could deliver fragments into stable Trojan orbits. Only about half the temporary horseshoe librators may have had sufficiently low e for capture of fragments to occur, and they dwelt only $\sim 25\%$ of the time in the range of ϕ where capture was likely. When e and ϕ were favorable, perhaps $\sim 10\%$ of the mass in a typical disruption event was imparted, the velocity required for capture. The odds appear to be no better than ~ 0.08 for disruption of a 500-km UNP that might have led to capture of a 200- to 250-km fragment. The odds improve approximately with the inverse square of the diameter of the target UNP. About two 100-km UNP's might have been disrupted under conditions leading to capture in stable libration of perhaps two ~ 50-km fragments and smaller debris. Many smaller bodies probably were captured during disruption events, but their contribution to the total mass of Trojans was negligible.

We conclude that UNP's cannot account for most of the Trojans; the precursors of the large majority of Trojans probably were Jupiter planetesimals. The efficiency of the capture mechanism we have described increases with the square of the population of objects in short-period orbits. It is likely that at least several tens of $m_\oplus$ of Jupiter's planetesimals remained on orbits in Jupiter's neighborhood just at the onset of collapse of nebular gas onto Jupiter. Most of these objects would have been quickly ejected from the solar system as Jupiter grew to its near-final mass. But during the few hundred thousand to million years before most were lost, their number and mass in short-period orbit may have been several hundred to ~ 1000 times our estimates for the UNP's during the following ~ 100 Myr. If so, the rate of collisional disruption

of the Jupiter planetesimals would have been $\sim 10^5$ to $\sim 10^6$ times higher; the duration of this intense collision episode, however, was $\sim 10^2$ to 10^3 times shorter. If ~ 50 $m_\oplus$ of Jupiter planetesimals survived a mean time of $\sim 2 \times 10^5$yr before ejection, about 50 planetesimals >500 km in diameter might have been collisionally disrupted while librating in temporary horseshoe orbits. Disruptions of about 6 of these may have resulted in capture of fragments $\gtrsim 200$ km diameter as Trojans and may have transferred a total of $\sim 10^{-5} m_\oplus$ into stable Trojan orbits. Another $\sim 10^{-5} m_\oplus$ may have been captured into Trojan orbits from disruption of smaller bodies, but a comparable amount may have been lost from subsequent collisional diffusion. Both the suggested number of large Trojan precursors and the estimated final mass are consistent with the observed Trojan swarms. We find the present volume of the L4 swarm to be $(5\pm1)10^6$km^3, and we estimate the combined L4 and L5 volume to be $(8\pm2)10^6$km^3; at a density of 1 g cm^{-3}, this volume is equivalent to $(1.4\pm0.4)10^{-5}m_\oplus$.

We draw the following conclusions with regard to the collisional capture model for the origin of the Trojans.

1. The model provides an explanation for the large dispersion of Trojan inclinations. In particular, because the model allows for many close encounters with Jupiter before capture in Trojan orbits, we can understand how very high inclinations ($i_p >25°$) may have been achieved. Resonance pumping due to drift in D, which is a corollary of the model, probably explains the high frequency of i_p near 20°.

2. Collisional capture can also explain the peculiar low frequency and steep size-frequency distribution of the largest Trojans. The absence of Trojans $\gtrsim 300$ km follows from the low probability of collisions with still larger precursors. Even if very large (>1000-km diameter) bodies could be disrupted, too few were trapped in horseshoe orbits for capture of very large (e.g., 500-km) fragments to be likely.

3. For a plausible mass of Jupiter planetesimals, the model leads to about the right number of large Trojans and an appropriate total mass of the Trojan swarms. The bulk of the mass in each swarm probably is derived from a modest number of captured large objects; the apparent difference in the population between the L4 and L5 swarms may simply reflect chance fluctuation in the number of largest bodies captured, from which most of the present Trojans probably have been formed by further collisional evolution. About 8 to 12 modest to large captured bodies may be required to explain the inclination distribution in the L4 swarm.

4. A minimum of about 60 $m_\oplus$ (~ 10 $m_\oplus$ of which accreted to form the core of Jupiter) appears to have been required for the Jupiter planetesimal swarm in order to account for the observed mass of Trojans. If a major fraction of the planetesimal mass was distributed in bodies larger than 1000-km diameter, then a correspondingly larger total mass was required.

5. Inward migration of Jupiter from about 8 AU is implied (from conservation of orbital energy) by the combined scattering of ~ 50 $m_\oplus$ of Jupiter planetesimals and ~ 300 $m_\oplus$ of Uranus-Neptune planetesimals. (This drift in a_0 may have been partly offset by dispersal of the solar nebula.)

6. The source region of the Trojans probably was broad. The Jupiter planetesimals captured may have originated at solar distances from about 5 to 9 AU. A trace amount of the total mass of the Trojans ($\lesssim 1\%$) probably consists of Uranus-Neptune planetesimals and probably also of Saturn planetesimals.

7. The spectrophotometric similarity of Trojans to inactive comet nuclei suggests that both are coated with similar material, possibly grains of kerogen-like organic matter (CHON grains?). The composition of planetesimals formed at solar distances of about 5 to 9 AU may have been roughly similar to those formed at ~ 15 to 35 AU (UNP's), which are inferred to be a primary source of Oort cloud comets.

8. The D-type Hildas and Thule may be fragments of Jupiter planetesimals captured in the $3:2$ and $4:3$ commensurabilities by collisions; the efficiency of capture in these resonances remains to be studied.

9. Impacts of Uranus-Neptune planetesimals were primarily responsible for collisional evolution of the Trojan swarms after capture of the Jupiter planetesimal fragments.

10. Conditions for collisional capture of planetesimals in Trojan-type orbits may also have been favorable near the orbits of Saturn, Uranus and Neptune, but, by analogy with the capture process of Jupiter, we do not expect any such Trojans to be much larger than 200 km. Only surveys with faint limiting magnitudes are likely to find them.

REFERENCES

Bien, R., and Schubart, J. 1987. Three characteristic orbital parameters for the Trojan group of asteroids. *Astron. Astrophys.* 175:292–298.

Brown, E. W. 1911. On a new family of periodic orbits in the problem of three bodies. *Mon. Not. Roy. Astron. Soc.* 71:438–454.

Carusi, A., Krešak, Ĺ., Perozzi, E., and Valsecchi, G. B. 1985. Long-Term Evolution of Short-Period Comets. (Bristol, England: Adam Hilger Ltd.).

Cook, A. F. 1971. 624 Hektor: A binary asteroid? In *Physical Studies of Minor Planets*, ed. T. Gehrels, NASA SP-267, pp. 155–163.

Davis, D. R., and Weidenschilling, S. J. 1981. Avoiding close encounters: Collisional evolution of Trojan asteroids. *Lunar Planet. Sci.* XII:199–201 (abstract).

Davis, D. R., Chapman, C. R., Greenberg, R., Weidenschilling, S. J., and Harris, A. W. 1979. Collisional evolution of asteroids: Populations, rotations, and velocities. In *Asteroids,* ed. T. Gehrels (Tucson: Univ. of Arizona Press), pp. 528–557.

Degewij, J., and van Houten, C. J. 1979. Distant asteroids and outer Jovian satellites. In *Asteroids,* ed. T. Gehrels (Tucson: Univ. of Arizona Press), pp. 417–435.

Duncan, M., Quinn, T., and Tremaine, S. 1988. The origin of short-period comets. *Astrophys. J.* 328:L69–L73.

French, L. M. 1987. Rotation properties of four L5 Trojan asteroids from CCD photometry. *Icarus* 72:325–341.

Gradie, J., and Tedesco, E. 1982. Compositional structure of the asteroid belt. *Science* 216:1405–1407.

Gradie, J., and Veverka, J. 1980. The composition of the Trojan asteroids. *Nature* 283:840–842.

Hartmann, W. K. 1979. Diverse puzzling asteroids and a possible unified explanation. In *Asteroids,* ed. T. Gehrels (Tucson: Univ. of Arizona Press), pp. 466–479.

Hartmann, W. K., and Cruikshank, D. P. 1978. The nature of Trojan asteroid 624 Hektor. *Icarus* 36:353–366.

Hartmann, W. K., Tholen, D. J., and Cruikshank, D. P. 1987. The relationship of active comets, "extinct" comets, and dark asteroids. *Icarus* 69:33–50.

Hartmann, W. K., Tholen, D. J., Goguen, J., Binzel, R. P., and Cruikshank, D. P. 1988. Trojan and Hilda asteroid lightcurves. *Icarus* 73:487–498.

Kissel, J., Brownlee, D. E., Buchler, K., Clark, B. C., Fechtig, H., Grun, E., Hornung, K., Igenbergs, E. B., Jessberger, E. K., Krueger, F. R., Kuczera, H., McDonnell, J. A. M., Morfill, G. M., Rahe, J., Schwehm, G. H., Sekanina, Z., Utterback, N. G., Völk, H. J., and Zook, H. A. 1986. Composition of comet Halley dust particles from Giotto observations. *Nature* 321:336–337.

Kuiper, G. P., Fujita, Y., Gehrels, T., Groeneveld, I., Kent, J., van Biesbroeck, G., and van Houten, C. J. 1958. Survey of asteroids. *Astrophys. J. Suppl.* 3:289–428.

Matson, D. L., ed. 1986. *IRAS Asteroid and Comet Survey: Preprint Version No. 1,* JPL Internal Document No. D-3698.

Rabe, E. 1965. Limiting eccentricities for stable Trojan librations. *Astron. J.* 70:687–688 (abstract).

Rabe, E. 1967. Third-order stability of the long-period Trojan librations. *Astron. J.* 72:10–17.

Safronov, V. S. 1972. Ejection of bodies from the solar system in the course of the accumulation of the giant planets and the formation of the cometary cloud. In *Motion, Evolution of Orbits, and Origin of Comets, Proc. IAU Symp. No. 45,* eds. G. A. Chebotarev, E. I. Kazimirchak-Polonskaya and B. G. Marsden (Dordrecht: D. Reidel), pp. 329–334.

Schubart, J. 1982. Three characteristic parameters of orbits of Hilda-type asteroids. *Astron. Astrophys.* 114:200–204.

Schubart, J., and Bien, R. 1987. Trojan asteroids: Relations between dynamical parameters. *Astron. Astrophys.* 175:299–302.

Shoemaker, C. S., and Shoemaker, E. M. 1988. The Palomar Asteroid and Comet Survey (PACS), 1982–1987. *Lunar Planet. Sci.* XIX:1077–1078 (abstract).

Shoemaker, E. M., and Wolfe, R. F. 1982. Cratering time scales for the Galilean satellites of Jupiter. In *The Satellites of Jupiter,* ed. D. Morrison (Tucson: Univ. of Arizona Press), pp. 277–339.

Shoemaker, E. M., and Wolfe, R. F. 1984. Evolution of the Uranus-Neptune planetesimal swarm. *Lunar Planet. Sci.* XV:780–781 (abstract).

Shoemaker, E. M., Wolfe, R. F., and Shoemaker, C. S. 1986. Extinct Jupiter-family comets and cratering rates on the Galilean satellites. *Lunar Planet. Sci.* XVII:799–800 (abstract).

Smith, B. A., Soderblom, L., Batson, R., Bridges, P., Inge, J., Masursky, H., Shoemaker, E., Beebe, R., Boyce, J., Briggs, G., Bunker, A., Collins, S. A., Hansen, C. J., Johnson, T. V., Mitchell, J. L., Terrile, R. J., Cook, A. F., II, Cuzzi, J., Pollack, J. B., Danielson, G. E., Ingersoll, A. P., Davies, M. E., Hunt, G. E., Morrison, D., Owen, T., Sagan, C., Veverka, J., Strom, R., and Suomi, V. E. 1982. A new look at the Saturn system: The Voyager 2 images. *Science* 215:504–537.

Smith, B. A., Soderblom, L. A., Beebe, R., Bliss, D., Boyce, J. M., Brahic, A., Briggs, G. A., Brown, R. H., Collins, S. A., Cook, A. F., II, Croft, S. K., Cuzzi, J. N., Danielson, G. E., Davies, M. E., Dowling, T. E., Godfrey, D., Hansen, C. J., Harris, C., Hunt, G. E., Inger-

soll, A. P., Johnson, T. V., Krauss, R. J., Masursky, H., Morrison, D., Owen, T., Plescia, J. B., Pollack, J. B., Porco, C. C., Rages, K., Sagan, C., Shoemaker, E. M., Sromovsky, L. A., Stoker, C., Strom, R. G., Suomi, V. E., Synnott, S. P., Terrile, R. J., Thomas, P., Thompson, W. R., and Veverka, J. 1986. Voyager 2 in the Uranian system: Imaging science results. *Science* 233:43–64.

van Houten, C. J., Herget, P., and Marsden, B. G. 1984. The Palomar-Leiden Survey of faint minor planets: Conclusion. *Icarus* 59:1–19.

van Houten, C. J., van Houten-Groeneveld, I., Herget, P., and Gehrels, T. 1970a. The Palomar-Leiden Survey of faint minor planets. *Astron. Astrophys. Suppl.* 2:339–448.

van Houten, C. J., van Houten-Groeneveld, I., and Gehrels, T. 1970b. Minor planets and related objects. V. The density of Trojans near the preceding Lagrangian point. *Astron. J.* 75:659–662.

Vilas, F., and Smith, B. A. 1985. Reflectance spectrophotometry (~0.5–1.0 μm) of outer-belt asteroids: Implications for primitive, organic solar system material. *Icarus* 64:503–516.

Wilhelms, D. E. 1987. *The Geologic History of the Moon,* U.S. Geol. Surv. Prof. Paper 1348.

Williams, J. G. 1979. Proper elements and family memberships of the asteroids. In *Asteroids,* ed. T. Gehrels (Tucson: Univ. of Arizona Press), pp. 1040–1063.

Yoder, C. F. 1973. On the Establishment and Evolution of Orbit-Orbit Resonances. Ph.D. Thesis, Univ. of California, Santa Barbara.

Yoder, C. F. 1979. Notes on the origin of the Trojan asteroids. *Icarus* 40:341–344.

Yoder, C. F., Colombo, G., Synnott, S. P., and Yoder, K. A. 1983. Theory of motion of Saturn's coorbiting satellites. *Icarus* 53:431–443.

Zellner, B. 1979. Asteroid taxonomy and the distribution of the compositional types. In *Asteroids,* ed. T. Gehrels (Tucson: Univ. of Arizona Press), pp. 783–806.

Zellner, B., Tholen, D. J., and Tedesco, E. F. 1985. The eight-color asteroid survey: Results for 589 minor planets. *Icarus* 61:355–416.

APPLICATION OF PHOTOMETRIC MODELS TO ASTEROIDS

EDWARD BOWELL
Lowell Observatory

BRUCE HAPKE, DEBORAH DOMINGUE
University of Pittsburgh

KARI LUMME, JOUNI PELTONIEMI
University of Helsenki

and

ALAN W. HARRIS
Jet Propulsion Laboratory

The way an asteroid or other atmosphereless solar system body varies in brightness in response to changing illumination and viewing geometry depends in a very complicated way on the physical and optical properties of its surface and on its overall shape. We summarize the formulation and application of recent photometric models by Hapke and by Lumme and Bowell. In both models, the brightness of a rough and porous surface is parametrized in terms of the optical properties of individual particles, by shadowing between particles, and by the way in which light is scattered among collections of particles. Both models succeed in their goal of fitting the observed photometric behavior of a wide variety of bodies, but neither has led to a very complete understanding of the properties of asteroid regoliths, primarily because in most cases the parameters in the present models cannot be adequately constrained by observations of integral brightness alone over a restricted range of phase angles.

I. INTRODUCTION

Since the last decade, several models of light scattering in planetary regoliths have been developed. It is our purpose in this chapter to summarize and compare results from two of these models, one by Hapke and one by Lumme and Bowell. The primary aim of such models is to understand the physical properties of the surfaces of asteroids and other atmosphereless bodies by analyzing disk-resolved and disk-integrated photometric observations. To this end, parametrization in terms of optical and physical quantities is attempted. We have also collected in one place all the principal formulae relating to the two models, so that recipes for fitting photometric data are available to interested readers. First, however, it will be useful to sketch some of the progress made during the last ten years.

In the photometric model developed by Hapke and described by Hapke (1981,1984,1986) and Hapke and Wells (1981), it is assumed that geometric optics is valid. The contribution from singly scattered rays is derived exactly. The opposition effect is assumed to be due to hiding of the shadow of one particle on another and is derived by an approximation to the Seeliger-Irvine formulation (Irvine 1966), with significant differences that allow for a distribution of particle sizes and also include a more rigorous derivation of the extinction, scattering and absorption coefficients (Hapke 1986). The multiple-scattering contribution is calculated from a modified two-stream solution of the radiative transfer equation for isotropic scatterers and with a collimated source, which results in an analytic approximation to the Chandrasekhar H functions (Chandrasekhar 1950).

In Lumme and Bowell's model, given in its first form by Lumme and Bowell (1981a; hereafter LBa), it is also assumed that geometric optics is valid. Single and multiple components of light scattered in particulate surfaces are treated separately. In single scattering, a number of phase functions, due specifically to single particles, shadowing and roughness, are combined, whereas multiple scattering is calculated using an approximate theory developed by Lumme and Reitsema (1978). In LBa, it was concluded that the opposition effect was controlled by porosity. However, in this chapter, recent work by Muinonen et al. (1989) on backscattering by crystalline particles is invoked to explain what Lumme et al. (1987) have termed an *opposition spike*, apparent at phase angles smaller than a degree or two and present mainly in the phase curves of icy satellites. Such an explanation for sharp opposition spikes was apparently first proposed by Trowbridge (1978). Working along similar lines, and following Morozhenko and Yanovitsky (1971), Shkuratov (1983) has imputed what he calls an optical concentration of light toward the source; he includes the effects of focusing, glory and interference.

Neither Hapke's nor Lumme and Bowell's model allows for the effects of

linear polarization of light from planetary surfaces. Although the degree of linear polarization may exceed 30% for low-albedo surfaces observed in the ultraviolet at large phase angles, that of most asteroids, the Moon and Mercury is less than 10% in the V band and at the generally smaller phase angles at which photometric observations are available. Wolff (1981) has derived an equation to compute the amount of light scattered from a surface consisting of irregular particles, and has applied it to an interpretation of the polarization slope-albedo law.

Both Hapke's and Lumme and Bowell's work have spawned applications, too numerous to detail here, aimed at fitting and interpreting photometric data on solar system bodies and laboratory samples. Discussions by Helfenstein and Veverka (1987) and Helfenstein (1988) give good summaries of work using Hapke's model on Mercury and the Moon (Hapke 1984; Buratti 1985; Veverka et al. 1989), Jovian and Saturnian satellites (Buratti 1983,1985; Helfenstein 1986; Simonelli and Veverka 1987), Uranian satellites and rings (Smith et al. 1986; Hapke 1986), and laboratory samples (Goguen 1981; Hapke and Wells 1981; Johnson et al. 1983; Mustard and Pieters 1987; Clark et al. 1989). Domingue and Hapke (1989) and Helfenstein and Veverka (see their chapter) have used Hapke's model to fit asteroid phase curves; these works may be regarded as extensions of our review. Lumme and Bowell's model was first applied to asteroids in a preliminary way by Bowell and Lumme (1979), and then more fully to a variety of atmosphereless bodies by Lumme and Bowell (1981b), although no detailed exposition on the derivation of model parameters has been published. Further work on asteroids has concerned pole and shape determination (cf. Poutanen et al. 1981; Lumme et al. 1986; chapter by Magnusson et al.), the effects of shape and albedo features on lightcurves and phase curves (Karttunen 1989; Karttunen and Bowell 1989) and the derivation of a two-parameter system for calculating magnitudes (Marsden 1986a; Bowell et al. 1989). Other applications have been made to the Moon (Lumme and Irvine 1982), Phobos and Deimos (Pang et al. 1983b), Jovian and Saturnian satellites (Lockwood et al. 1980a,b; Pang et al. 1981; Pang et al. 1983a), the zodiacal cloud (Lumme and Bowell 1985) and laboratory samples (Lumme et al. 1980).

In the following two sections, we outline Hapke's and Lumme and Bowell's photometric models. On the whole, we have chosen to adhere to the nomenclature and notation used in the original publications of the models, and have accordingly separately defined all the quantities used in each section. Although this has led to some repetition and some slightly different terminology for a few parameters, it has allowed each of the two treatments to be internally complete and consistent. In Sec. IV, we present fits to a selection of disk-resolved and disk-integrated data. Then, in Sec. V, we compare and contrast the two models, and give some thoughts on possible future developments. In an Appendix, we summarize the equations for the IAU two-parameter magnitude system for asteroids, and outline its use.

II. HAPKE'S PHOTOMETRIC MODEL

A. Photometric Relations for a Smooth Surface

The reflectances are functions of the angle of incidence i, the angle of emergence (viewing angle) e, the phase angle α and the azimuth angle between the planes of incidence and emergence φ. These are related by

$$\left\{ \begin{array}{l} \cos \alpha = \mu_0 \mu + \sin i \sin e \cos \varphi \\ \mu_0 = \cos i \\ \mu = \cos e. \end{array} \right. \tag{1}$$

What is termed the *bidirectional reflectance r* is given by

$$r(i,e,\alpha) = \frac{w}{4\pi} \frac{\mu_0}{\mu_0 + \mu} \{[1 + B(\alpha)]p(\alpha) + H(\mu_0)H(\mu) - 1\} \tag{2}$$

in which w is the average single-scattering albedo, $B(\alpha)$ is the opposition-effect function, $p(\alpha)$ is the average single-particle scattering function, and H is an analytical approximation to Chandrasekhar's H function for isotropic scatters [cf. Eq. (7)] below.

For a mixture of particles of albedos w_i, densities ρ_i, diameters D_i, and mass fractions M_i,

$$w = \left(\sum_i M_i w_i / \rho_i D_i \right) \bigg/ \left(\sum_i M_i / \rho_i D_i \right) . \tag{3}$$

Thus the reflectance of a mixture may be calculated from the reflectances of the end members. The opposition-effect function is

$$\left\{ \begin{array}{l} B(\alpha) = B_0/[1 + \tan(\alpha/2)/h] \\ h = n \dfrac{\ln P^{-1}}{1 - P} \langle\sigma\rangle\langle r\rangle \\ \langle r\rangle = \sqrt{\langle\sigma\rangle/\pi}. \end{array} \right. \tag{4}$$

Here, h is the angular width of the opposition effect, n is the number of particles per unit volume, P is the porosity, and $<\sigma>$ is the average extinction cross section weighted by number. B_0 is the amplitude of the opposition effect. If the opposition effect is due only to the hiding of shadows between regolith particles, then $B_0 \le 1$, and B_0 is the fraction of $wp(0)$ scattered from the portion of a particle surface that faces the source. However, individual particles can also be rough, composite, or behave like corner reflectors, and can thereby contribute to the opposition effect; this is taken into account by allowing B_0 to exceed unity. [Rigorously, another term of the same form as

$B(\alpha)$ multiplying $p(\alpha)$ is required, but that would introduce two more parameters. Hence, $B(\alpha)$ should be interpreted as a composite opposition effect that may involve both the soil porosity and individual particle complexity.] The single-particle scattering function $p(\alpha)$ is empirically expressed either as an N-term Legendre polynomial expansion,

$$p(\alpha) = 1 + \sum_{n=1}^{N-1} a_n P_n(\alpha) \tag{5}$$

where a_n are constants and $P_n(\alpha)$ is the Legendre polynomial of degree n, or by a Henyey-Greenstein function of the form

$$p(\alpha) = (1 - b^2)/(1 - 2b \cos \alpha + b^2)^{3/2} \tag{6}$$

as convenient. Here, b is the asymmetry factor. Usually, two or three terms suffice in the Legendre expansion. Since diffraction is not appropriate for particles in intimate contact, $p(\alpha)$ does not include a diffraction term. Finally,

$$\begin{cases} H(x) = (1 + 2x)/(1 + 2\gamma x) \\ \gamma = \sqrt{1 - w}. \end{cases} \tag{7}$$

Note that H is a function of both angle and single-scattering albedo.

The so-called *bihemispherical reflectance* r_0 is calculated from

$$r_0 = (1 - \gamma)/(1 + \gamma). \tag{8}$$

The *directional-hemispherical reflectance* for a two-term $p(\alpha)$ of the form

$$p(\alpha) = 1 + a \cos \alpha \tag{9}$$

is given by

$$A_H(i) = r_0 \frac{1 + \gamma}{1 + 2\gamma\mu_0} + a \frac{w}{4} \frac{\mu_0}{1 + \mu_0}. \tag{10}$$

For a spherical planet of uniform albedo, with $p(\alpha)$ given by Eq. (9), the *Bond albedo* for a two-term $p(\alpha)$ is

$$A_B = r_0 \left[1 - \frac{1}{3} \frac{\gamma}{1 + \gamma} + 0.69a(1 + \gamma)^2 \right]. \tag{11}$$

The *physical* or *geometric albedo* is

$$A_P = (w/8)[(1 + B_0)p(0) - 1] + (r_0/2 + r_0^2/6). \tag{12}$$

The *integral phase function* is given by

$$\Phi(\alpha) = (1/A_P)\{\left[(w/8)[(1 + B(\alpha))p(\alpha) - 1]\right.$$
$$+ (r_0/2)(1 - r_0)][1 - \sin(\alpha/2)\tan(\alpha/2)\ln[\cot(\alpha/4)]\left.\right]$$
$$+ (2r_0^2/3\pi)[\sin\alpha + (\pi - \alpha)\cos\alpha]\}. \tag{13}$$

B. Photometric Relations for a Rough Surface

The derivation of the photometric functions of a macroscopically rough surface takes into account two major effects: (1) *Shadows*: One part of the surface can prevent another part from being illuminated or from being seen by the detector. (2) *Effective surface tilt:* Portions of the surface tilted away from the source or detector have a greater probability of not being illuminated or seen than portions of the surface tilted toward the source or detector, resulting in the average surface being tilted toward the source and detector.

It is assumed in the model that the surface is made up of unresolved facets tilted at various angles. The angles of tilt are assumed to be distributed uniformly in azimuth and described by a function $A(\theta)$, where θ is the angle between the normal to the facet and the normal to the mean surface. In Hapke (1984), $A(\theta)$ was assumed to be given by a Gaussian distribution in $\tan\theta$. The sizes of the facets are large compared to the extinction mean free path $1/n\sigma$, but small compared to the detector footprint on the surface of the body. Double and higher-order reflections between facets are ignored. However, multiple scattering between grains of soil within each facet is allowed for.

The roughness is described by a characteristic slope angle $\bar{\theta}$, defined by

$$\tan\bar{\theta} = (2/\pi) \int_0^{\pi/2} \tan\theta A(\theta) d\theta. \tag{14}$$

Shadowing is described by a shadow function $S(i, e, \alpha)$ and surface tilt by replacing μ and μ_0 by effective cosines μ_e and μ_{oe}, respectively.

The *bidirectional reflectance of a rough surface* is given by

$$r(i,e,\alpha) = \frac{w}{4\pi} \frac{\mu_{oe}}{\mu_{oe} + \mu_e} \{[1 + B(\alpha)]p(\alpha) + H(\mu_{oe})H(\mu_e) - 1\}S(i,e,\varphi). \tag{15}$$

Let

$$\begin{cases} f(\varphi) = e^{-2\tan(\varphi/2)} \\ C(\bar{\theta}) = (1 + \pi\tan\bar{\theta})^{-1/2} \\ E_1(x) = e^{-(2/\pi)\cot\bar{\theta}\cot x} \\ E_2(x) = e^{-(1/\pi)\cot^2\bar{\theta}\cot^2 x}. \end{cases} \tag{16}$$

Then S, μ_e, and μ_{oe} have slightly different forms depending on the relative values of i and e. If $i \leq e$:

$$
\left\{
\begin{array}{l}
\mu_{oe}(i,e,\varphi) = C(\bar{\theta}) \left[\mu_0 + \sin i \tan \bar{\theta} \, \dfrac{\cos \varphi E_2(e) + \sin^2(\varphi/2)E_2(i)}{2 - E_1(e) - (\varphi/\pi)E_1(i)} \right] \\[12pt]
\mu_e(i,e,\varphi) = C(\bar{\theta}) \left[\mu + \sin e \tan \bar{\theta} \, \dfrac{E_2(e) - \sin^2(\varphi/2)E_2(i)}{2 - E_1(e) - (\varphi/\pi)E_1(i)} \right] \\[12pt]
S(i,e,\varphi) = \dfrac{\mu_e(i,e,\varphi)}{\mu_e(0,e,0)} \dfrac{\mu_0}{\mu_{oe}(i,0,\pi)} \, C(\bar{\theta}) \left\{ 1 - f(\varphi) \left[1 - C(\bar{\theta}) \dfrac{\mu_0}{\mu_{oe}(i,0,\pi)} \right] \right\}^{-1}.
\end{array}
\right.
$$

$$\tag{17}$$

If $i \geq e$:

$$
\left\{
\begin{array}{l}
\mu_{oe}(i,e,\varphi) = C(\bar{\theta}) \left[\mu_0 + \sin i \tan \bar{\theta} \, \dfrac{E_2(i) - \sin^2(\varphi/2)E_2(e)}{2 - E_1(i) - (\varphi/\pi)E_1(e)} \right] \\[12pt]
\mu_e(i,e,\varphi) = C(\bar{\theta}) \left[\mu + \sin e \tan \bar{\theta} \, \dfrac{\cos \varphi E_2(i) + \sin^2(\varphi/\pi)E_2(e)}{2 - E_1(i) - (\varphi/\pi)E_1(e)} \right] \\[12pt]
S(i,e,\varphi) = \dfrac{\mu_e(i,e,\varphi)}{\mu_e(0,e,\pi)} \dfrac{\mu_0}{\mu_{oe}(i,0,0)} \, C(\bar{\theta}) \left\{ 1 - f(\varphi) \left[1 - C(\bar{\theta}) \dfrac{\mu}{\mu_e(0,e,\pi)} \right] \right\}^{-1}
\end{array}
\right.
$$

$$\tag{18}$$

The *physical albedo of a rough surface* is given by

$$
A_P = (w/8)[(1 + B_0)p(0) - 1] + (r_0/2 + r_0^2/6)C(w,\bar{\theta}) \tag{19}
$$

where

$$
C(w,\bar{\theta}) = 1 - (0.048\bar{\theta} + 0.0041\bar{\theta}^2)r_0 - (0.33\bar{\theta} - 0.0049\bar{\theta}^2)r_0^2. \tag{20}
$$

And the *integral phase function of a spherical body with a rough surface* is derived from

$$
\begin{aligned}
\Phi(\alpha) = & \{(w/8)[(1 + B_0)p(0) - 1] + r_0/2 + r_0^2/6\}^{-1} \\
& \times \{[(w/8)[(1 + B(\alpha))p(\alpha) - 1] \\
& + (r_0/2)(1 - r_0)][1 - \sin(\alpha/2)\tan(\alpha/2)\ln[\cot(\alpha/4)]] \\
& + (2r_0^2/3\pi)[\sin \alpha + (\pi - \alpha) \cos \alpha]\} \, K(\alpha,\bar{\theta})
\end{aligned} \tag{21}
$$

where $K(\alpha,\bar{\theta})$ is given in Table I. For $\alpha < 60°$, an analytical approximation is

$$
K(\alpha,\bar{\theta}) \approx e^{-[0.32\sqrt{\tan \bar{\theta} \, \tan(\alpha/2)} + 0.52 \tan \bar{\theta} \, \tan(\alpha/2)]\bar{\theta}}. \tag{22}
$$

An excellent discussion of $\bar{\theta}$ has been given by Helfenstein (1988).

TABLE I

Hapke's Integral Phase Function Roughness Correction Factor $K(\alpha,\bar{\theta})$

α	$\bar{\theta}$						
(°)	0°	10°	20°	30°	40°	50°	60°
0	1.00	1.00	1.00	1.00	1.00	1.00	1.00
2	1.00	0.997	0.991	0.984	0.974	0.961	0.943
5	1.00	0.994	0.981	0.965	0.944	0.918	0.881
10	1.00	0.991	0.970	0.943	0.909	0.866	0.809
20	1.00	0.988	0.957	0.914	0.861	0.797	0.715
30	1.00	0.986	0.947	0.892	0.825	0.744	0.644
40	1.00	0.984	0.938	0.871	0.789	0.692	0.577
50	1.00	0.982	0.926	0.846	0.748	0.635	0.509
60	1.00	0.979	0.911	0.814	0.698	0.570	0.438
70	1.00	0.974	0.891	0.772	0.637	0.499	0.366
80	1.00	0.968	0.864	0.719	0.566	0.423	0.296
90	1.00	0.959	0.827	0.654	0.487	0.346	0.231
100	1.00	0.946	0.777	0.575	0.403	0.273	0.175
110	1.00	0.926	0.708	0.484	0.320	0.208	0.130
120	1.00	0.894	0.617	0.386	0.243	0.153	0.094
130	1.00	0.840	0.503	0.290	0.175	0.107	0.064
140	1.00	0.747	0.374	0.201	0.117	0.070	0.041
150	1.00	0.590	0.244	0.123	0.069	0.040	0.023
160	1.00	0.366	0.127	0.060	0.032	0.018	0.010
170	1.00	0.128	0.037	0.016	0.0085	0.0047	0.0026
180	1.00	0	0	0	0	0	0

III. LUMME AND BOWELL'S PHOTOMETRIC MODEL

A. Disk-Resolved Brightness

In their original work (LB*a*), Lumme and Bowell gave the reflection coefficient πr in the form

$$\frac{I}{F} \equiv \pi r = \pi r_1 + \pi r_m \tag{23}$$

where πF is the incident flux, πI the emergent flux, πr_1 the contribution from single scattering, and πr_m that from multiple scattering. Explicitly,

$$\begin{cases} \pi r_1 = \dfrac{\varpi_0}{2} P(\alpha)\Phi_S(\alpha,\lambda) \dfrac{\mu_0}{\mu + \mu_0} \left(\dfrac{\sigma}{1 + \rho\xi} + 1 - \sigma \right) \\[2ex] \pi r_m = \dfrac{\varpi_0^*}{4} [h(\mu,\varpi_0^*)h(\mu_0,\varpi_0^*) - 1] \end{cases} \tag{24}$$

where ϖ_0 is the single-scattering albedo, ϖ_0^* is the single-scattering albedo according to the "similarity relations" approximation, P is the single-particle

phase function, Φ_S is the mutual shadowing function (normalized to unity at $\alpha = 0°$, as all Φ's have been in the following), σ is the fraction of the surface covered with "holes" (called q in LBa; σ is used here to avoid confusion with the symbol conventionally used for the phase integral), ρ is a measure of the surface roughness (roughly, the tangent of the mean surface slope at the mm scale), and h is a multiple-scattering function (approximated by Chandrasekhar's H function for isotropic scatterers). In addition,

$$
\begin{cases}
\xi = \dfrac{\sqrt{\mu^2 + \mu_0^2 - 2\mu\mu_0\cos\alpha}}{\mu\mu_0} \equiv \dfrac{\sin\alpha}{\cos\beta\,\cos\lambda\,\cos(\lambda - \alpha)} \\[2ex]
\mu = \cos\beta\,\cos\lambda \\[1ex]
\mu_0 = \cos\beta\,\cos(\lambda - \alpha) \tag{25}
\end{cases}
$$

where β is the photometric latitude and λ the longitude. The shadowing function is given by the expression

$$
\begin{cases}
\Phi_S(y) = ye^y \displaystyle\int_0^1 x^{2y\,-\,1} e^{-\,xy}dx \equiv \dfrac{1}{2}\,_1F_1(1,1 + 2y;y) \\[3ex]
y = \dfrac{\ln\dfrac{1}{1 - D}}{2.4}\;\dfrac{\cos\lambda + \cos(\lambda - \alpha)}{\sin\alpha} \tag{26}
\end{cases}
$$

in which $_1F_1$ is a degenerate hypergeometric function and D is the volume density of the regolith, here assumed constant with depth. Eqs. (23–26) summarize Lumme and Bowell's model for surface brightness.

Before studying the consequences and results of Lumme and Bowell's model, the following should be noted: (1) The singly scattered component πr_1 does not tend to zero at the limb ($\mu \to 0$). (2) The principle of conservation of energy is not seriously violated. A straightforward check may be made by directly integrating I/F to yield the Bond albedo for the case of conservative scattering, i.e., $\varpi_0 = 1$, with the result that there is a slight underestimate. (3) Regarding the shadowing function Φ_S, after Eq. (17) (LBa), an approximation $\ln(1 - x) \approx -x$ is given and stated to be valid only for small volume densities, but if D is large, the correct expression, Eq. (26), should be used.

B. Single-Particle Phase Function

Both Hapke and Lumme and Bowell have used a physical model to parametrize most of the effects that play a role in light scattering by regoliths, with the exception of the single-particle phase function $P(\alpha)$. Appropriate specification of this function is essential for the interpretation of the integral-brightness data, which are also functions of the same variable. Even for disk-resolved data at a fixed α, $P(\alpha)$ is important because it determines the absolute scale for single scattering; but only if there exist disk-resolved data at several

widely separated phase angles, can one hope to solve for $P(\alpha)$ independently. Hitherto, Lumme and Bowell have been using either isotropic scattering ($P \equiv 1$) or a single Henyey-Greenstein phase function, the latter being an analytical representation having no physical basis. Hapke has on occasion chosen to use a three-term Legendre expansion (having two free parameters), which also lacks physical justification.

To provide deeper insight into P, two further sources have been called upon: microwave analog measurements made by Giese et al. (1978) on realistic nonspherical particles, and theoretical ray-tracing calculations for statistically rough particles by Peltoniemi et al. (1989). All four of the absorbing fluffy or irregular particles measured by Giese et al. have refractive indices in the range $1.45 \leq n \leq 1.65$, and the imaginary part times the size parameter (a descriptor of absorption) on the order of unity, making them well suited for treatment of the photometry of low-albedo bodies (Mercury, for example). When properly normalized (the integral of P over 4π equals one), the measurements indicate that all four particles have small, roughly linear backward scattering for $0° \leq \alpha \leq 90°$, strong forward scattering for $\alpha \geq 120°$, and P is similar for all particles. The data can be well represented (Fig. 1) by an empirical function, somewhat different from that used by Peltoniemi et al. of the form

$$\left\{ \begin{array}{l} P(\alpha) = Be^{-b\alpha} + Ce^{-f(\pi - \alpha)} \\[2mm] C = \dfrac{1 + f^2}{1 + e^{-\pi f}} \left[2 - \dfrac{B}{1 + b^2} (1 + e^{-\pi b}) \right] \end{array} \right. \tag{27}$$

where the expression for C comes from normalization and

$$\left\{ \begin{array}{l} B = P(0°) = 0.95 \\ C = P(180°) = 16.15 \\ b = 0.4 \ \text{rad}^{-1} \\ f = 4.0 \ \text{rad}^{-1}. \end{array} \right. \tag{28}$$

Diffraction is not included in this function. A two-term Henyey-Greenstein function does not give such a good fit, and a high-degree Legendre function would be required to provide an equally good fit. Equation (27) suggests that, in the backward regime,

$$P(\alpha) \approx B - Bb\alpha. \tag{29}$$

Using geometric optics, Peltoniemi et al. (1989) have theoretically studied light scattered by statistically deformed spheres. They assumed a log-normal distribution of the particle radius vector, and varied both the amount of
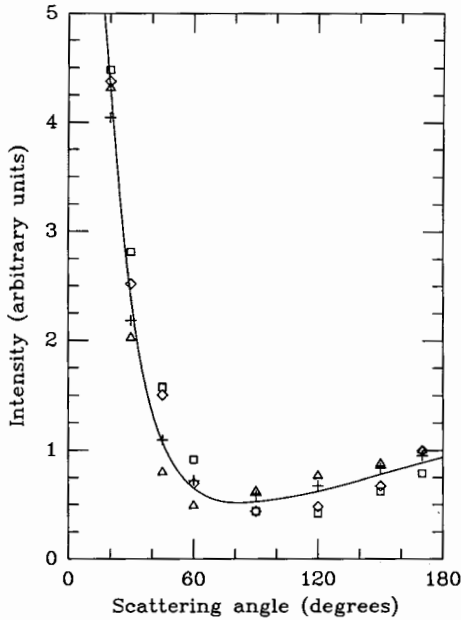
Fig. 1. The single-particle phase function $P(\alpha)$. Intensity (arbitrary units) is plotted as a function of scattering angle ($= 180° - \alpha$) for four nonspherical particles (Giese et al. 1978). Squares: size parameter $x = 27$, refractive index $n = 1.45-0.05i$, fluffy particles; triangles: $x = 31.2, n = 1.65-0.25i$, irregular; pluses: $x = 31.2$, $n = 1.65-0.25i$, fluffy; diamonds: $x = 27, n = 1.45-0.05i$, fluffy. The fitted curve is from Eq. (27).

deformation and the optical parameters. It is clear from their work that Eq. (27) is a good approximation, with values in the range of Eq. (28). In the forward regime, it is not yet known whether the sharply peaked $P(\alpha)$ for single particles should be used for regoliths because the latter may comprise particle aggregates (see the chapter by Helfenstein and Veverka). Laboratory experiments are called for.

A recently discovered sharp opposition effect, here termed the *opposition spike*, has been observed in the phase curves of some high-albedo objects at very small phase angles. It has led to the addition here of another component to P. Obviously, single-particle scattering of the type characterized by Eq. (27) is suitable only for irregular particles. However, ices and regolith-forming minerals can exist in crystalline form. Some of these crystals have right-angle troughs, making them very effective backscatterers (retroreflec-tors). Muinonen et al. (1989) have calculated the light-scattering properties of a number of common crystal forms by using ray-tracing techniques, allowing the optical constants to vary. The resulting calculated phase curves can be well fitted in the important phase angle range $0°1 \le \alpha \le 10°$ by

$$P(\alpha) = Ae^{-\alpha/(0.333 + 0.231\alpha)} \equiv A\Phi_c(\alpha) \tag{30}$$

where α is in degrees. A more rigorous but more complicated approximation has been given by Muinonen et al. (1989). The unknown scale factor $A \geq 10$ results from the use of geometric optics, which breaks down at $\alpha = 0°$, where the rigorous theory of physical optics should be used. Such a theory does not exist for nonspherical particles, however. Equations (27) and (30) can now be combined as a plausible mean single-particle phase function. If v is the fractional volume occupied by crystals and $1 - v$ that occupied by irregular particles, then, for $\alpha \lesssim 100°$,

$$\left\{ \begin{array}{c} P(\alpha) = vA\Phi_c(\alpha) + (1 - v)Be^{-b\alpha} \\[2ex] \Phi_P(\alpha) = \dfrac{P(\alpha)}{P(0)} = c\Phi_c(\alpha) + (1 - c)e^{-b\alpha} \\[2ex] c = \dfrac{va}{vA + (1 - v)B}. \end{array} \right. \tag{31}$$

Henceforth, we term c the opposition-spike parameter.

C. Disk-Integrated Brightness

The disk-integrated brightness of a spherical body of unit radius can be calculated from

$$L(\alpha) = \pi F \int_{-\pi/2}^{\pi/2} d\beta \, \cos^2 \beta \int_{\alpha - \pi/2}^{\pi/2} r(\lambda,\beta,\alpha)\cos \lambda \, d\lambda \equiv \pi F R(\alpha). \tag{32}$$

The classical integrated descriptors of brightness, p the geometric albedo, q the phase integral, and A the Bond albedo, can be conveniently expressed in terms of $R(\alpha)$:

$$\left\{ \begin{array}{c} p = \dfrac{L(0°)}{\dfrac{1}{\pi} \pi^2 F} = R(0°) \\[3ex] q = 2 \displaystyle\int_0^\pi \dfrac{R(\alpha)}{R(0°)} \sin \alpha \, d\alpha \\[3ex] A = pq = 2 \displaystyle\int_0^\pi R(\alpha) \sin \alpha \, d\alpha. \end{array} \right. \tag{33}$$

It might be a good policy to refer to $R(\alpha)$ as the *pseudoalbedo* of a body fixed phase angle α lest there be confusion with p.

Equation (32) can be transformed into the form

$$\begin{cases} \Phi_{obs}(\alpha) = (1 - Q)\Phi_1(\alpha) + Q\Phi_M(\alpha) \\[6pt] \quad \Phi_1 = \Phi_P[\sigma\Phi_R + (1 - \sigma)\Phi_0] \\[6pt] \quad \Phi_0 = \Phi_R(\rho = 0) \\[6pt] \quad \Phi_R = \dfrac{1}{2\cos(\alpha/2)} \displaystyle\int_0^{1/2(\pi - \alpha)} \dfrac{(2\cos^2\varphi - z_0)^2}{2\cos^2\varphi - z_1,} \ \dfrac{y_0 + \cos\varphi}{2y_0 + \cos\varphi} \ \dfrac{d\varphi}{\cos\varphi} \\[10pt] \quad \Phi_M = \dfrac{R_M(\alpha)}{R_M(0°)} \\[10pt] R_M(\alpha) = \dfrac{\varpi_0^*}{2\pi} \displaystyle\int_0^{\pi/2} d\beta \cos^2\beta \int_{\alpha - \pi/2}^{\pi/2} [h(\cos\beta \cos\lambda)h(\cos\beta \cos(\lambda - \alpha)) - 1] \\[10pt] \qquad\qquad \times \dfrac{\cos\lambda \cos(\lambda - \alpha)}{\cos\lambda + \cos(\lambda - \alpha)} \ d\lambda \\[10pt] \quad y_0 = \dfrac{1.8}{\ln\dfrac{1}{1 - D}} \sin(\alpha/2) \\[14pt] \quad z_0 = 1 - \cos\alpha \\[6pt] \quad z_1 = z_0 - \dfrac{\rho}{0.6} \sin\alpha \end{cases} \qquad (34)$$

where Φ_P is given by Eq. (31). In deriving the expression for Φ_R, two approximations have been used:

$$\begin{cases} \displaystyle\int_0^{\pi/2} \dfrac{\cos^3\beta \ d\beta}{z + \cos\beta} \approx \dfrac{\pi/4}{1 + 1.2z} \\[10pt] \qquad \Phi_S(y) \approx \dfrac{y + 3/4}{y + 3/2} \end{cases} \qquad (35)$$

both of which are accurate at the 1% level.

Since Φ_1 and Φ_M are not known, Φ_1 and Φ_2 as defined by Bowell et al. (1989) are adopted [cf. Eq. (A4)]. For Φ_1, the best nonlinear least-squares solution was sought with the four parameters b, D, ρ and σ. Because the opposition spike was not manifestly present in the data set used by Bowell et al., it is natural to set c [cf. Eq. (31)] equal to zero. However, properly determined h functions are not yet available to explain the empirical function Φ_2 (or Φ_M), which is in any case somewhat steeper than would be derived from classical radiative transfer theory. This matter is currently under investigation. Solution values for the parameters in Φ_1 are

$$\begin{cases} b = 0.21 \text{ rad}^{-1} \\ D = 0.24 \\ \rho = 1.34 \\ \sigma = 1.00 \end{cases} \qquad (36)$$

for which the relative *rms* error is 1.3%. It must be emphasized that the solution, Eq. (36), is not unique, except for *D*, and that a strong correlation exists between parameters. To see this explicitly, *b* and σ can be constrained to be consistent with the disk-resolved data for Mercury ($b = 0.38$ rad^{-1}, $\sigma = 0.71$; cf. Sec. 4.B). Whence, solving only for *D* and ρ, one obtains

$$\begin{cases} D= 0.22 \pm 0.04 \\ \rho= 1.7 \pm 0.3 \end{cases} \tag{37}$$

with a slightly larger *rms* error.

To explain the opposition-spike data, the effect of crystals is taken into account by rewriting Eq. (34) in three-parameter form:

$$\begin{cases} 10^{-0.4V_{\text{obs}}(\alpha)}= a_1\Phi_1(\alpha) + a_2\Phi_2(\alpha) + a_3F_c(\alpha) \\ F_c= \Phi_1\Phi_c \\ a_1= (1 - c)(1 - Q)10^{-0.4H} \\ a_2= Q \cdot 10^{-0.4H} \\ a_3= c(1 - Q)10^{-0.4H} \end{cases} \tag{38}$$

where V_{obs} is a reduced observed magnitude, Φ_1 and Φ_2 are given by Eq. (A4), Φ_c is given by Eq. (30), and $H \equiv V (0°)$. In LB*a*, *Q* was termed the *multiple-scattering factor;* it is the ratio of multiple- to single-scattering light at zero phase angle. Note that one cannot uniquely determine the fractional volume of crystals v [Eq. (31)] from values of *c* because geometric optics does not provide a means of estimating the brightness of a crystal at $\alpha = 0°$. However, a crude estimate *can* be made because one can be almost certain that $A \geq 10$ when $v \leq c/(10 - 9c)$ (Muinonen et al. 1989). This implies that an admixture of just a few percent of material in the form of crystals could explain observed opposition spikes.

IV. MODEL FITS TO SELECTED PHOTOMETRIC DATA

Usually, the integral phase curve of an asteroid is known only over a small range of phase angles: $\alpha < 25°$, say. Over this restricted portion of the phase curve, some of the parameters in both Hapke's and Lumme and Bowell's formulations have similar effects on $\Phi(\alpha)$, and it is usually very difficult to disentangle them. Hence, *a unique interpretation of the phase curve in terms of the physical properties of the asteroid is usually not possible from the integral phase curve alone.* Furthermore, it is not possible to obtain the single-scattering albedo, which determines the ratio of multiple- to single-scattering light, from the integral phase curve alone, although the single-scattering albedo can sometimes be constrained by measurements of the geometric albedo.

However, if the integral phase curve is known over a wide range of phase angles (from $< 2°$ to $> 90°$, say) and if the geometric albedo is known, then it

is sometimes possible to obtain a unique fit and physical interpretation. If disk-resolved data are available over a wide range of phase angles, then it is possible to separate these effects and thereby obtain unique values of the photometric parameters and to interpret them in terms of physical properties of the surface.

A. Disk-Resolved Data

Disk-resolved photometry of Mercury has been taken from Mariner 10 orange-filter image FDS 2577. It consists of radiances observed at $\alpha = 77°$ and normalized to those of a Lambert surface illuminated vertically and observed at 0 phase angle.

In Fig. 2, the data have been fitted using Hapke's model with parameter values as given in Table IV below.

To model the Mercury data using Lumme and Bowell's formulation, Eq. (24) is written in the following form, noting that $\Phi_S = 0.5$, since $\alpha >> 0°$:

$$\left\{ \begin{aligned} &\pi r = a_1 f_1 + a_2 f_2 + f \\[6pt] &a_1 = \frac{\varpi_0}{4} P(77°)\sigma \\[6pt] &a_2 = \frac{\varpi_0}{4} P(77°)(1 - \sigma) \\[6pt] &f_1 = \frac{\mu_0}{\mu + \mu_0} \\[6pt] &f_2 = \frac{f_1}{1 + \rho\xi} \\[6pt] &f = \frac{\varpi_0^*}{4} f_1 [h(\mu,\varpi_0^*)h(\mu_0,\varpi_0^*) - 1]. \end{aligned} \right. \qquad (39)$$

Using the Mariner 10 data both for $\beta = 0°$ (photometric equator) and $\lambda = 50°$ (meridian), the free parameters a_1, a_2, ρ and ϖ_0^* were calculated by nonlinear least squares, with the result that χ^2 was most sensitive to ϖ_0^*, thus imposing the constraint $0.44 \leq \varpi_0^* \leq 0.52$ by the 2-σ criterion. The dependence on ρ is relatively weak because both a_1 and a_2 are small quantities. From the derived values of a_1 and a_2, one can deduce that

$$\left\{ \begin{aligned} &\frac{\varpi_0}{4} P(77°) = 0.051 \\[6pt] &\qquad\quad \sigma = 0.71 \\[6pt] &\quad 1.0 \leq \rho \leq 1.5. \end{aligned} \right. \qquad (40)$$
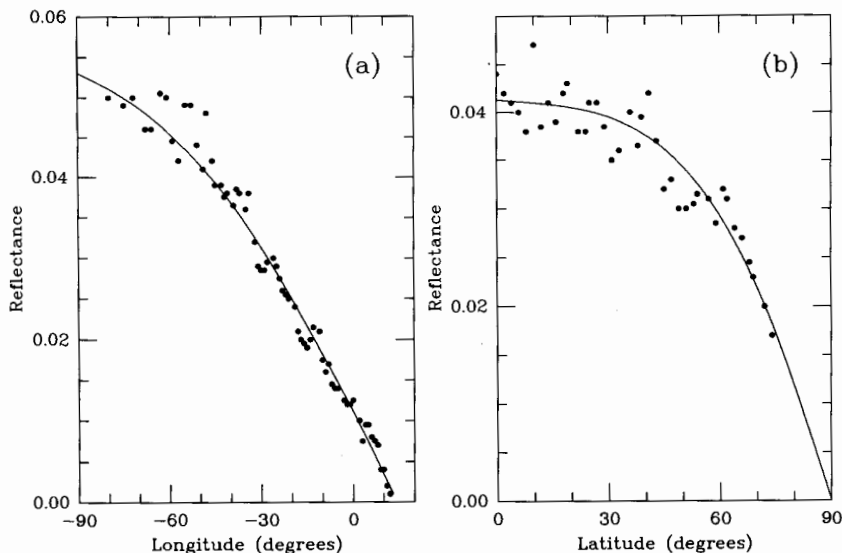
Fig. 2. Fits to disk-resolved photometry of Mercury using Hapke's model. (a) Reflectance as a function of longitude along the photometric equator. (b) Reflectance as a function of latitude along the meridian $\lambda = 50°$.

As can be seen from Tables II and III and Fig. 3, the fits are good.

It is notable that, with no further information, one can solve only for σ, the fraction of the surface covered with "holes." If one accepts the value derived for the asymmetry factor g that results from the single-particle phase function suggested above (namely $g = 0.04$), one can solve for ϖ_0 and $P(77°)$, obtaining $\varpi_0 = 0.46$ and $P(77°) = 0.44$, a result that is in remarkably

TABLE II
Lumme-Bowell Model: Fit to Mariner 10 Data Along Mercury's Photometric Equator ($\beta = 0°$)

$\lambda(°)$	πr_{obs}	πr_{calc}
80	0.050	0.047
60	0.046	0.047
40	0.038	0.038
20	0.025	0.026
0	0.011	0.011
−5	0.007	0.006

TABLE III
Lumme-Bowell Model: Fit to Mariner
10 Data Along a Meridian
of Mercury ($\lambda = 50°$)

$\beta(°)$	πr_{obs}	πr_{calc}
0	0.044	0.043
20	0.041	0.041
40	0.037	0.038
60	0.030	0.030
70	0.023	0.024
75	0.018	0.021

good agreement with the value obtained by means of the phase function de-
fined in Eq. (34). (Note that g alone does not constrain P, so a circular argu-
ment is not being invoked.) If the geometric albedo p and multiple-scattering
factor Q of the body are also known, as is the case for Mercury (for which $p =$
0.13 and $Q = 0.23$), one can not only derive additional information but can
also check some of the conclusions. Unfortunately, the integral-brightness
data for Mercury are very noisy, particularly when $\alpha \leq 20°$. Therefore, use
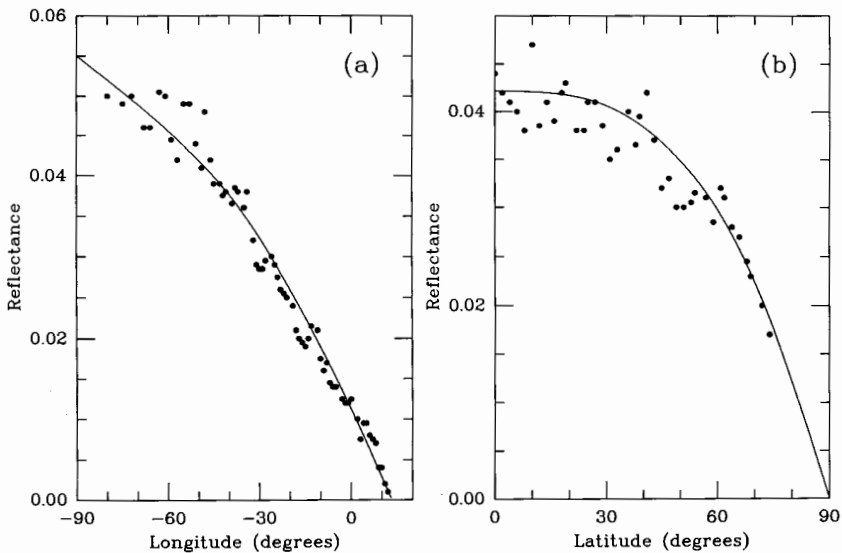
Fig. 3. As Fig. 2, using Lumme and Bowell's model.

has instead been made of the much less noisy data for the Moon (Rougier 1933), which are almost indistinguishable. Now

$$p_1 = (1 - Q)p = \frac{\varpi_0}{4} P(0°) = 0.10 \tag{41}$$

and

$$p_M = Qp = \frac{\varpi_0}{4} \int_0^1 [H^2(\mu,\varpi_0) - 1]\mu \, d\mu = 0.03 \tag{42}$$

where p_1 is the geometric albedo of a single particle and p_M is the multiple-scattering contribution to the geometric albedo. From Eq. (41), one can calculate that $P(0°) = 0.89$, which agrees remarkably well with the value of B in Eq. (28). Inserting $\varpi_0 = 0.46$ in Eq. (42), one finds that $p_M = 0.024$, a value that is certainly within the observational error of p.

Although it is true that, by analyzing the disk-resolved brightness, disk-integrated brightness and microwave analog measurements, an internally consistent picture of Mercury's light-scattering properties has been arrived at using Lumme and Bowell's model, a caveat is in order: disk-resolved photometry is available at only one phase angle, and use has been made of several approximations for the true radiative transfer process in a rough regolith made up of closely packed particles. This situation, of course, violates the requirements of classical radiative-transfer theory and, therefore, the corrections for multiple scattering could be prone to error.

B. Disk-Integrated Data

In this section, fits to the phase curves of atmosphereless bodies (mainly asteroids) are illustrated and described. In Figs. 4 through 11, the ratio of the ordinates to abscissae is constant, so slopes of the phase curves can be readily intercompared.

An integral phase curve of Mercury derives from Danjon (1949), and is constrained to have a geometric albedo of 0.14. A comparison of Hapke's model with the data is given in Fig. 4a; a three-term Legendre expansion was used for $p(\alpha)$. Because of the noisiness of Danjon's data, Lumme and Bowell have chosen to fit whole-disk photometry of the Moon, as mentioned above; the fit is shown in Fig. 4b.

V-band photometric data for asteroids were selected for their reliability, and for their variety of taxonomic classes and phase-curve shapes. The data derive from the following sources: 24 Themis (taxonomic class C according to Tholen 1984), pertaining to brightness averaged over rotation (Harris et al. 1989a); 44 Nysa (E), mean brightness (Harris et al. 1989b); 69 Hesperia (M), brightness at primary maximum (Poutanen et al. 1985); 82 Alkmene (S), max-
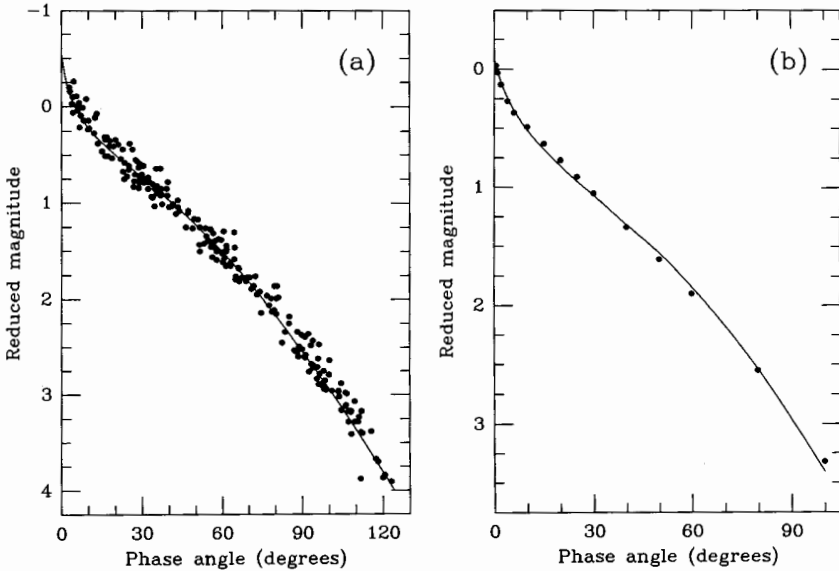
Fig. 4. Fitted phase curves for (a) Mercury, using Hapke's model, and (b) the Moon, using Lumme and Bowell's model.

imum brightness (Harris et al. 1984*b*); 133 Cyrene (SR), maximum brightness (Harris et al. 1984*a*); 419 Aurelia (F), mean brightness (Harris and Young 1989); and 1862 Apollo (Q), maximum brightness (Harris et al. 1987).

For the integral phase curves of the asteroids, the Henyey-Greenstein expression for $p(\alpha)$ given by Eq. (6) was used for Hapke's model. Then $\Phi(\alpha)$ contains five parameters: w, B_0, h, b and $\bar{\theta}$. Fits of the model to observed photometric data on the selected asteroids are shown in Figs. 5a through 11a. The fits were made by trial-and-error variation of the five parameters, values for which are given in Table IV. The parameters are not necessarily the optimum ones; however, in almost all cases, the goodness of fit is consistent with the quality of the observations.

In Lumme and Bowell (1981*b*), there was discussion of the indeterminacy of model parameters, in particular the roughness ρ and the asymmetry factor g. It was found, however, that mean values of the volume density D and surface roughness sufficed to represent the entire data set of 74 asteroid phase curves, all of which could be well fitted by varying only the multiple-scattering factor Q. In accordance with the rather similar findings given in Sec. III.C, and incorporating the opposite-spike parameter c, least-squares fits of Eq. (38) were made to the asteroid data sets (in the relative sense, to give equal weight in magnitude space). Fitted phase curves are shown in Figs. 5b through 11b, and the resulting values of H, Q and c, together with the *rms* magnitude residuals, are given in Table V.
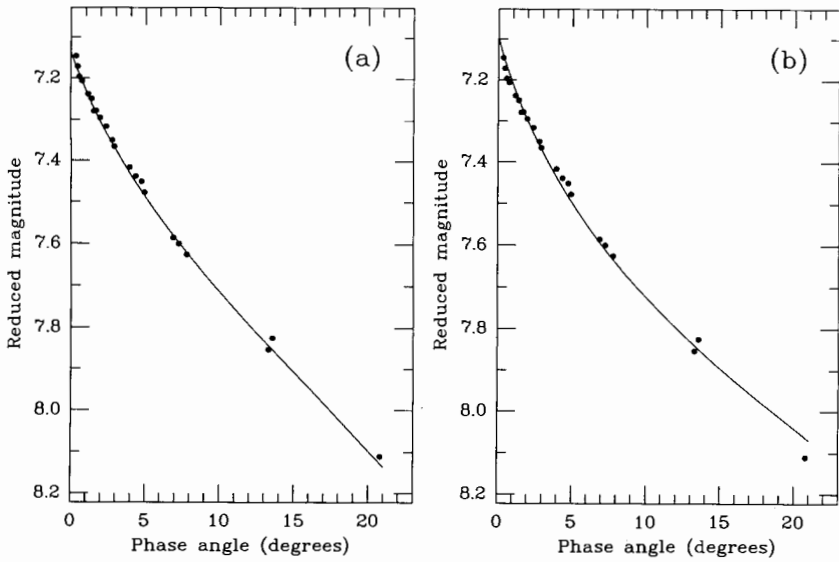
Fig. 5. Fitted *V*-band phase curves for 24 Themis, using (a) Hapke's model, and (b) Lumme and Bowell's model.
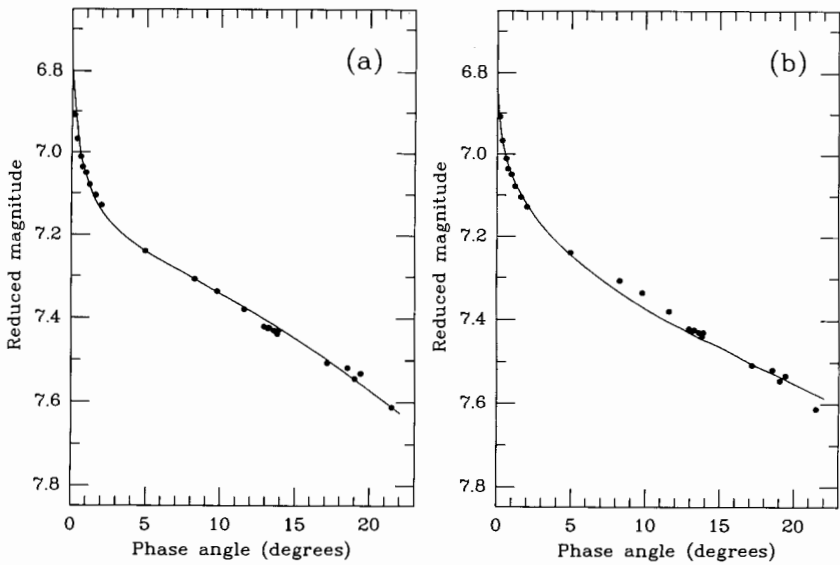
Fig. 6. As Fig. 5, for 44 Nysa.
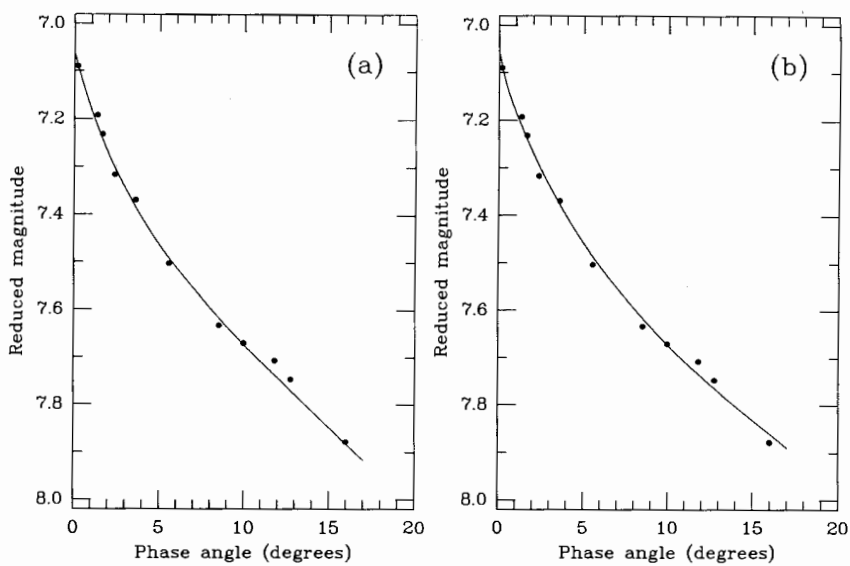
Fig. 7. As Fig. 5, for 69 Hesperia.
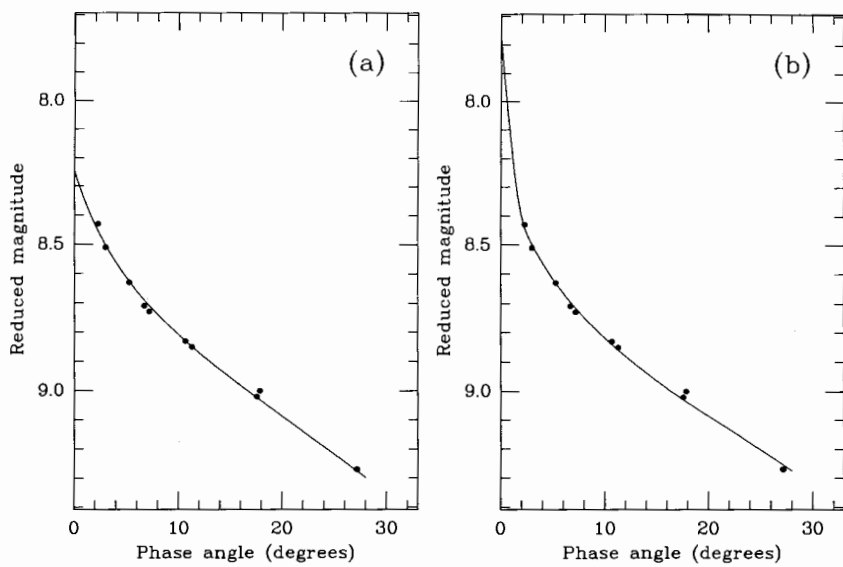
Fig. 8. As Fig. 5, for 82 Alkmene.
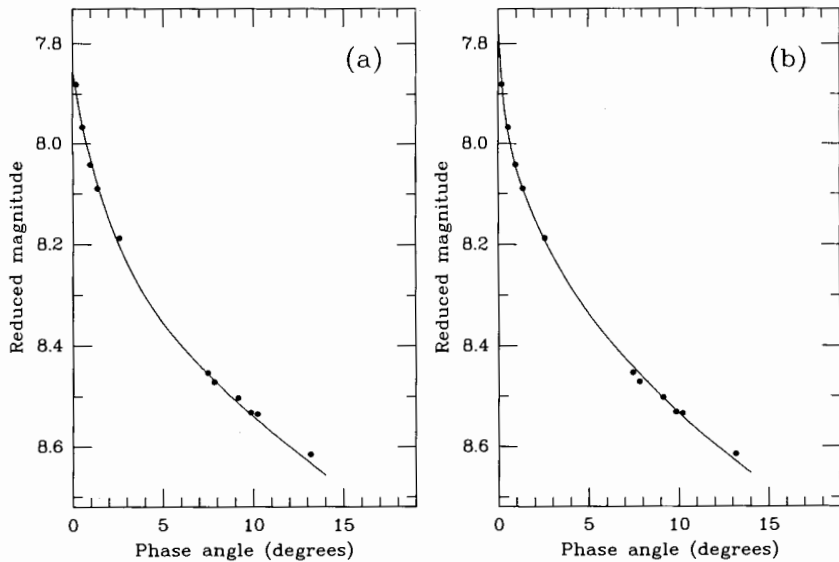
Fig. 9. As Fig. 5, for 133 Cyrene.
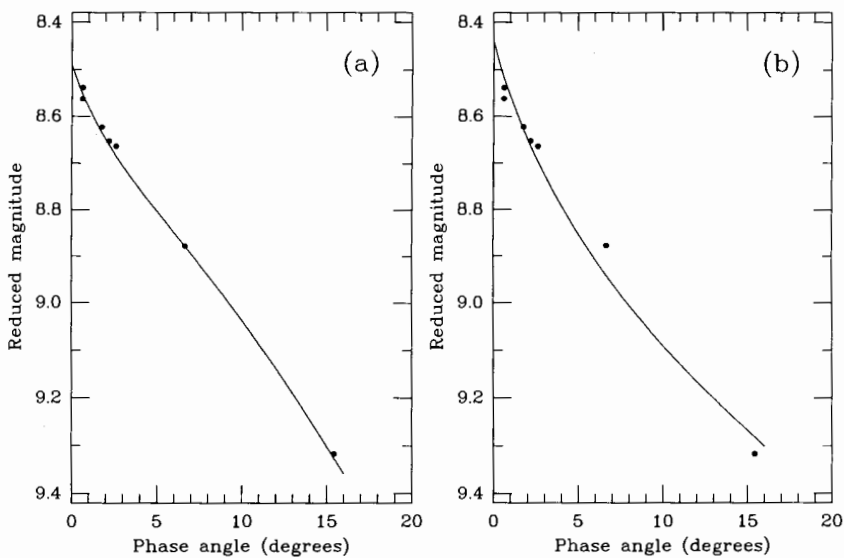
Fig. 10. As Fig. 5, for 419 Aurelia.

[545]
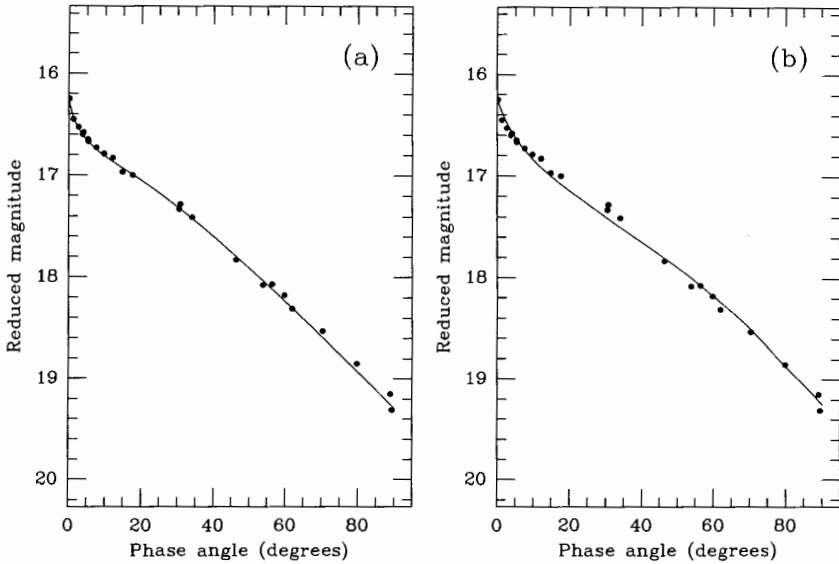
Fig. 11. As Fig. 5, for 1862 Apollo.

Most of the fits in Figs. 4 through 11 are very good, as can be seen from values of the *rms* residuals in Tables IV and V. We comment specifically as follows. The phase curve of 24 Themis is less steep than those of the majority of C asteroids. That of 44 Nysa exhibits a pronounced opposition spike at phase angles $\lesssim 2°$. The fit using Hapke's model appears to be superior to that using Lumme and Bowell's because it matches the downturn of the phase curve at phase angles $\gtrsim 10°$. Observations of 82 Alkmene are lacking at phase angles $< 2°29$, with the consequence that Lumme and Bowell's model re-

TABLE IV
Hapke's Model: Parameters for Fitted Phase Curves

Body	*w*	B_0	*h*	*b*	$\bar{\theta}$	*rms* Residual (mag)	Geometric Albedo
24 Themis	0.048	1.6	0.060	0.40	5°	0.011	0.061
44 Nysa	0.58	0.6	0.0055	0.40	27	0.014	0.492
69 Hesperia	0.154	0.94	0.036	0.40	35	0.017	0.147
82 Alkmene	0.183	1.4	0.047	0.28	5	0.017	0.138
133 Cyrene	0.204	1.19	0.022	0.383	10	0.012	0.21
419 Aurelia	0.204	0.47	0.030	0.60	25	0.011	0.044
1862 Apollo	0.28	0.98	0.026	0.325	2	0.042	0.21
Mercury[a]	0.21	1.85	0.030	0.40	20	0.12	0.14

[a] A three-term Legendre polynomial was used for $p(\alpha)$ [cf. Eq. (5)] with c = 0.4.

TABLE V
Lumme-Bowell Model: Constrained ($0 \leq c \leq 1$) Least-Squares
Fits to Phase-Curve Data

Body	H (mag)	Q	c	rms Residual (mag)
24 Themis	7.097	0.201	0.000	0.016
44 Nysa	6.844	0.522	0.311	0.024
69 Hesperia	7.054	0.240	0.026	0.013
82 Alkmene	7.778	0.201	0.469	0.013
133 Cyrene	7.763	0.254	0.252	0.007
419 Aurelia	8.438	0.170	0.000	0.028
1862 Apollo	16.232	0.225	0.000	0.050
Moon	−0.089	0.233	0.000	0.023

quires a very large opposition spike to optimally fit the data. Of course, the spike may not be real, and the unconstrained model solution serves to point up the importance of observations at small phase angles. For 133 Cyrene, the opposite situation may prevail. Hapke's model seems slightly to underestimate the opposition spike. 419 Aurelia's phase curve has no significant opposition effect, and its slope of about 0.05 mag deg^{-1} is among the largest known. The phase curve can be better fitted by a straight line than by using either of the two models. In Hapke's model, the small opposition effect is accounted for by a small value of B_0 and a large value of b (cf. Table IV). The best-fit phase curve from Lumme and Bowell's model, at least in the three-parameter form used here, seriously fails to represent the observations. However, an improvement can be made by increasing the volume density D. One must be cautious of the parametrization of 1862 Apollo's phase curve, which was most likely distorted both by large changes in the amplitude and shape of the lightcurve with increasing phase angle and by changes in aspect angle during the long intervals spanned by the observations. Note, however, that for highly nonspherical asteroids, it is best to fit phase curves defined by light-curve maxima (see the chapter by Helfenstein and Veverka).

V. COMPARISON, CONTRAST AND FUTURE WORK

Although the mathematical formalisms of the two models are somewhat different, both rest on similar assumptions. The major difference is in the treatment of roughness. In Lumme and Bowell's model, roughness affects only the single-scattering terms, it being implicit that the major contribution to shadowing occurs on scales on the order of that of the extinction mean free path—a few particle diameters. In Hapke's model, by contrast, roughness affects both the single- and multiple-scattering terms, thus assuming that

shadowing is important on all scales. Lumme and Bowell's model overestimates the brightness for surfaces of low albedo, and is most nearly exact for high-albedo surfaces; whereas Hapke's model is more correct for surfaces of low albedo, and underestimates the brightness for high-albedo surfaces.

In both Hapke's model and Lumme and Bowell's model, it is agreed that the classical opposition effect at phase angles $2° \lesssim \alpha \lesssim 7°$ is caused by mutual shadowing. Hapke's model achieves a narrow opposition effect by taking account of the effects of particle size distribution and predicts lunar soil porosities consistent with those measured for Apollo samples (Hapke 1986). Lumme and Bowell's model leads to volume densities that are typical of those seen in particulate laboratory samples (Lumme et al. 1980).

Another difference between the two models as presented here is the parametrization of the newly discovered opposition spike. Hapke allows the amplitude of the opposition effect B_0 to exceed unity. Lumme and Bowell believe that the opposition spike may be caused by the presence of a few percent crystalline particles, which act as retroreflectors. To account for the effect in their model, the single-particle phase function is modified.

In both models, the parameters in the mathematical expressions for the geometric albedo and integral phase function can be associated with physical properties of asteroid surfaces, such as porosity and roughness, and with the light-scattering properties of individual soil particles. Thus, one may hope to obtain information about asteroid surfaces from observations of the integral brightnesses. For instance, in the original formulation of Lumme and Bowell's model, the opposition effect was taken to be controlled by porosity and the linear part of the phase curve by roughness. Unfortunately, we now realize that, at the present state of development of the models (c. 1988), unique values of the parameters cannot be determined because different parameters may have similar effects on the phase curves (cf. Domingue and Hapke 1989; chapter by Helfenstein and Veverka). Hence, the associated physical properties of asteroid surfaces cannot be assigned with any confidence. If the models are to be fully useful, a major task for the future will be to find ways of constraining the parameters that will allow unique fits to observational data. In the same way, it is clear from the model fits described above that available observational data sets are almost all deficient; in particular, observations at very small and very large phase angles and covering a variety of wavelengths are called for.

Another important task for the future will be to generalize the classical radiative transfer theory to include the effects of (1) a statistically rough upper boundary instead of smooth, plane-parallel geometry; (2) the conditional propagation probability for a photon whose entire history is known (this becomes important in close packing); (3) a discrete, finite-size and closely packed medium, rather than the continuous medium required by classical theory. First steps towards solving these questions have been taken by Muinonen et al. (1989) and Peltoniemi et al. (1989).

APPENDIX

THE IAU TWO-PARAMETER MAGNITUDE SYSTEM FOR ASTEROIDS

The description of the magnitude system for asteroids given here has been adapted from Bowell et al. (1989). Termed the H, G magnitude system, it was adopted by IAU Commission 20 in 1985 (Marsden 1986a). An essential complement to it is a tabulation of magnitude parameters for individual asteroids, and a preliminary list for numbered asteroids has been compiled by Tedesco (1986) and Marsden (1986b). Since 1986, usage of the system has been extended to all asteroids, numbered and unnumbered, for which orbits have been derived; the tabulation by Tedesco in Part VI lists these values of H and G for numbered asteroids. It is planned that magnitude parameters for the numbered population be updated and published annually in *Ephemerides of Minor Planets* (Institute of Theoretical Astronomy, Leningrad), beginning with the 1990 edition.

The mean V-band magnitude of an asteroid (that is, in the absence of rotational or aspect variations) can be calculated from the formula

$$H(\alpha) = H - 2.5 \log [(1 - G) \, \Phi_1(\alpha) + G \, \Phi_2(\alpha)] \qquad (A1)$$

where $H(\alpha)$ is the V-band magnitude, at solar phase angle α, reduced to unit heliocentric and geocentric distances; H is the *absolute magnitude*: that is, the reduced magnitude explicitly at mean brightness and at $\alpha = 0°$. G is termed the slope parameter; indicative of the gradient of the phase curve, it has been scaled in such a way that $G \approx 0$ for steep phase curves (low-albedo bodies, generally) and $G \approx 1$ for shallow phase curves (high-albedo bodies), although $G < 0$ and $G > 1$ are not formally excluded. Φ_1 and Φ_2 are two specified phase functions, described below, that are normalized to unity at $\alpha = 0°$. Stated in another way, the phase curve for a given asteroid results from partitioning the phase functions Φ_1 and Φ_2 in the ratio $1 - G : G$. Equation (A1) is related to the first member of Eq. (34).

Reduced magnitudes $V(\alpha)$ may be derived from observed magnitudes $V_{obs}(\alpha)$ by means of

$$V(\alpha) = V_{obs}(\alpha) - 5 \log r\Delta \tag{A2}$$

where r is the heliocentric distance and Δ the geocentric distance of the asteroid, both in AU.

H and G are the two fundamental photometric parameters for each asteroid. They may be calculated by linear least squares (see below) from the reduced observed magnitudes using

$$\begin{cases} 10^{-0.4V(\alpha)} = a_1\Phi_1(\alpha) + a_2\Phi_2(\alpha) \\ H = -2.5 \log (a_1 + a_2) \\ G = \dfrac{a_1}{a_1 + a_2}. \end{cases} \tag{A3}$$

In this equation, similar to the first member of Eq. (38), a_1 and a_2 are auxiliary constants for a given asteroid. Optimally, $V(\alpha)$ are magnitudes averaged over rotation, but in practice they may be individual magnitudes (sometimes of widely differing quality) observed without prior knowledge of an asteroid's rotational brightness variation, or a mixture of both. The $V(\alpha)$ may even pertain to more than one apparition, though it will not usually be prudent to combine observations over long intervals because of aspect changes. In wave bands other than V, it is conventional to subscript H and G: for example, H_B, G_B.

To *calculate* H and G for asteroids, and to predict asteroid magnitudes that should well represent the observations, use is made of

$$\begin{cases} \Phi_i = W\Phi_{iS} + (1 - W)\Phi_{iL}; \qquad i = 1,2 \\[4pt] W = \exp\left(-90.56 \tan^2 \dfrac{1}{2}\alpha \right) \\[4pt] \Phi_{iS} = 1 - \dfrac{C_i \sin \alpha}{0.119 + 1.341 \sin \alpha - 0.754 \sin^2 \alpha} \\[4pt] \Phi_{iL} = \exp\left[-A_i \left(\tan \dfrac{1}{2}\alpha \right)^{B_i} \right] \\[4pt] A_1 = 3.332 \qquad A_2 = 1.862 \\ B_1 = 0.631 \qquad B_2 = 1.218 \\ C_1 = 0.986 \qquad C_2 = 0.238. \end{cases} \tag{A4}$$

To predict asteroid magnitudes according to the precepts adopted by the IAU, the simpler, more symmetric, but slightly less accurate expression can be used:

$$\begin{cases} \Phi_i = \exp\left[-A_i \left(\tan \frac{1}{2}\alpha \right)^{B_i} \right]; \quad i = 1,2 \\ A_1 = 3.33 \quad A_2 = 1.87 \\ B_1 = 0.63 \quad B_2 = 1.22. \end{cases} \tag{A5}$$

Equations (A4) and (A5) are valid for phase angles $0° \leq \alpha \leq 120°$, and for $0 \leq G \leq 1$.

Since H is defined explicitly at $\alpha = 0°$, the ensuing geometric albedo is also so defined, but since the latter quantity is an estimate rather than a measurement of p, we prefer to call it p_H. We have recommended above that geometric albedos at nonzero phase angles or from extrapolation to zero phase angle [such as those resulting from $B(1,0)$ or H] be referred to as *pseudoalbedos*. From Bowell and Lumme (1979) and Gehrels (1986 and personal communication):

$$\begin{cases} \log p_H = 6.259 - 2 \log d - 0.4 \, H_v \\ \log p_{H_b} = 6.521 - 2 \log d - 0.4 \, H_B \end{cases} \tag{A6}$$

where d is the diameter of an asteroid in km.

The phase integral [cf. Eq. (33)] is given by numerical integration of Eq. (A4)

$$q = 0.290 + 0.684 \, G; \quad 0 \leq G \leq 1. \tag{A7}$$

Extrapolation of the integration beyond $\alpha = 120°$ should not have led to significant error, and Eq. (A7) should be accurate to about 1%.

Geometric albedos calculated from H_m are on average about one-third larger than the pseudoalbedos that result from $m(1,0)$. Phase integrals calculated from Eq. (A7) are correspondingly smaller, however, so Bond albedos [calculated from Eq. (33)] are not rescaled. Lebofsky et al. (1986) have remarked on the way the modeling of asteroid infrared flux data is carried out using the H,G magnitude system.

Marsden (1986a) has recommended that $B(1,0)$ absolute magnitudes be converted to H by means of

$$H = B(1,0) - 1.0 \text{ mag} \tag{A8}$$

although more accurate formulae exist in which the last (constant) term is a function of β or G, and differences in asteroid color indices are allowed for.

The least-squares solution of Eq. (A3) is carried out as follows. Given n reduced magnitudes $V_i(\alpha_i)$ and their associated errors ϵ_i, we compute

$$\begin{cases} I_i = 10^{-0.4V_i(\alpha_i)} \\[2mm] h_{jk} = \Sigma \dfrac{\Phi_j(\alpha_i)\Phi_k(\alpha_i)}{\epsilon_i^2 I_i^2}\,; \qquad j,k = 1,2 \\[2mm] g_j = \Sigma \dfrac{\Phi_j(\alpha_i)}{\epsilon_i^2 I_i^2} \\[2mm] D = h_{11}h_{22} - h_{12}^2 \end{cases} \qquad (A9)$$

where the sums are over $i = 1,n$; and Φ_1 and Φ_2 are given by Eq. (A4), setting $W = 0$ at large α to avoid underflow. The auxiliary constants a_1 and a_2 are given by

$$\begin{cases} a_1 = (h_{22}g_1 - h_{12}g_2)/D \\ a_2 = (h_{11}g_2 - h_{12}g_1)/D \end{cases} \qquad (A10)$$

whence H and G from Eq. (A3). Note that a_1 and/or a_2 are of order $10^{-0.4H}$, which may be computationally inconvenient. If so, they may be scaled to order unity by setting

$$H(\alpha) = m - 2.5 \log (a_1\Phi_1 + a_2\Phi_2) \qquad (A11)$$

where m is one of the reduced magnitudes $V_i(\alpha_i)$ (that at smallest α, for instance).

A linear error analysis is recommended as being computationally convenient. While approximate, the method gives results quite similar to a more rigorous formulation. Three quantities are required to compute the magnitude error as a function of phase angle. Those chosen are α_0 the weighted mean phase angle of observation, $\Delta H(\alpha_0)$ the error in the reduced magnitude at α_0, and ΔG the error in G. First, magnitude residuals r_i are computed from

$$\begin{cases} r_i = V_i(\alpha_i) - H - \Delta m(\alpha_i) \\ \Delta m(\alpha_i) = -2.5 \log [(1 - G)\,\Phi_1(\alpha_i) + G\,\Phi_2(\alpha_i)] \end{cases} \qquad (A12)$$

where $\Delta m(\alpha_i)$ is the calculated magnitude drop from zero phase angle. Then

$$\begin{cases} \alpha_0 = \Sigma(\alpha_i/\epsilon_i^2)/\Sigma(1/\epsilon_i^2) \\[2mm] \sigma_{H(\alpha_0)}^2 = 1/\Sigma(1/\epsilon_i^2) \\[2mm] \sigma_\beta^2 = 1/[\Sigma(\alpha_i^2/\epsilon_i^2) - \alpha_0^2\Sigma(1/\epsilon_i^2)] \\[2mm] s^2 = \dfrac{1}{n-2}\,\Sigma(r_i/\epsilon_i)^2 \\[2mm] \Delta H(\alpha_0) = \pm\, s\sigma_{H(\alpha_0)} \\[2mm] \Delta\beta = \pm\, s\sigma_\beta \\[2mm] \Delta G = \pm\, \Delta\beta/(0.0673 - 0.1132\,G + 0.0615\,G^2). \end{cases} \qquad (A13)$$

Here, s^2 is the bias-corrected mean squared residual, or χ^2 per degree of freedom. It is the dimensionless ratio of the fit achieved compared to that expected.

Given the error in the asteroid's diameter Δd, the error in the albedo Δp_H is

$$\Delta p_H = \pm p_H \left[\frac{2|\Delta d|}{d} + 0.921|\Delta H(0°)| \right]. \qquad (A14)$$

Finally, the error envelope of the fitted phase curve [the uncertainty in $H(\alpha)$] results from

$$\Delta H(\alpha) = \pm [\Delta H^2(\alpha_0) + \Delta\beta^2(\alpha - \alpha_0)^2]^{1/2}. \qquad (A15)$$

It is clear from the work of Tedesco (1986) and Harris and Young (1988), as well as from earlier work by Bowell and Lumme (1979) and Lumme and Bowell (1981b), that, in the absence of large aspect variations, values of G for asteroids span the range $0 \lesssim G \lesssim 0.5$. If G lies outside this range, is indeterminate, or in the face of noisy magnitude estimates such as those from photographic photometry, it may be assigned a fixed value. In such cases, Tedesco (Part VI) has assigned three mean values of G according to major groupings in taxa, and hence geometric albedo: $G = 0.15$ for low-albedo C, D, F, G, P or T types; $G = 0.25$ for moderate-albedo A, B, M, Q or S types; and $G = 0.40$ for high-albedo E, R or V types (the taxa have been defined by Tholen 1984). Harris and Young have derived four such groupings: $G = 0.09 \pm 0.09$ (rms dispersion) for B, C, D, F, G, P or T types; $G = 0.21 \pm 0.06$ for M types; $G = 0.23 \pm 0.11$ for S or Q types; and $G = 0.42 \pm 0.08$ for E, R or V types. In the Minor Planet Circulars, however, it is conventional to assign $G = 0.25$ to all newly discovered and newly numbered asteroids. It is a task for the future to agree on a protocol for choosing G.

For a fixed G and estimated error ΔG,

$$H = \frac{\Sigma\{[V_i(\alpha_i) - \Delta m(\alpha_i)]/\epsilon_i^2\}}{\Sigma(1/\epsilon_i^2)}. \qquad (A16)$$

Equation (A3) is used to calculate a_1 and a_2, and the error analysis [Eqs. (A12) through (A15)] proceeds as before, except that $\Delta\beta$ is calculated from the last member of Eq. (A13) using the specified G and ΔG.

As a numerical example, consider fitting the phase-curve data for 69 Hesperia (Fig. 7). Assuming equal magnitude errors $\epsilon_i = \pm0.01$ mag, the following parameter values are obtained: $H = 7.058$ mag, $G = 0.210$, $\alpha_0 = 6°.71$, $\Delta H(\alpha_0) = \pm0.005$ mag, and $\Delta G = \pm0.020$. Also, $s^2 = 2.6$, so either the magnitude errors were underestimated on the fit is unsatisfactory. (However, increasing the ϵ_i by a factor of $\sqrt{2.6}$ to ±0.016 mag—a not unreason-

able value, given the nature of the data—removes the poorness of fit.) Since the phase-curve data are rather uniformly distributed between $\alpha = 0°$ and $\alpha = 16°$, one would not anticipate great changes in the width of the error envelope $\Delta H(\alpha)$ over that range, as is indeed the case: $\Delta H(0°) = \pm 0.008$ mag and $\Delta H(16°) = \pm 0.010$ mag. At larger phase angles, the envelope does widen: $H(50°) = 8.797 \pm 0.041$ mag and $H(100°) = 10.551 \pm 0.088$ mag. Fixing inappropriate values of $G = 0.09$ and $\Delta G = \pm 0.09$ (as for an average C asteroid, according to Harris and Young [1988]), leads to different $H = 6.992$ mag, $\Delta H(\alpha_0) = \pm 0.015$ mag, and $s^2 = 26.0$, the last indicating a very much poorer fit. The error envelope is far wider, too, especially outside the range of the observations: $H(50°) = 8.987 \pm 0.130$ mag and $H(100°) = 10.764 \pm 0.280$ mag. FORTRAN code for the solution and error analysis of asteroid observations according to the H, G magnitude system is available from the first author.

REFERENCES

Bowell, E., and Lumme, K. 1979. Colorimetry and magnitudes of asteroids. In *Asteroids,* ed. T. Gehrels (Tucson: Univ. of Arizona Press), pp. 132–169.

Bowell, E., Harris, A. W., and Lumme, K. 1989. A two-parameter magnitude system for asteroids. *Icarus,* submitted.

Buratti, B. J. 1983. Photometric Properties of Europa and the Icy Satellites of Saturn. Ph.D. Thesis, Cornell Univ.

Buratti, B. J. 1985. Applications of a radiative transfer model to bright icy satellites. *Icarus* 61:208–217.

Clark, R. N., Kierein, K. S., and Swayes, G. A. 1989. Experimental verification of the Hapke reflectance theory. 1. Computation of reflectance as a function of grain size and wavelength based on optical constants. *J. Geophys. Res.,* in press.

Danjon, A. 1949. Photométrie et colorimétrie des planètes Mercure et Vénus. *Bull. Astron.* 14:315–345.

Domingue, D., and Hapke, B. 1989. Fitting theoretical photometric functions to asteroid phase curves. *Icarus* 78:330–336.

Gehrels, T. 1986. On the feasibility of observing small asteroids with Galileo, Venera, and Comet-Rendezvous-Asteroid-Flyby missions. *Icarus* 66:288–296.

Giese, R. H., Weiss, K., Zerull, R. H., and Ono, T. 1978. Large fluffy particles: A possible explanation of the optical properties of interplanetary dust. *Astron. Astrophys.* 65:265–272.

Goguen, J. 1981. A Theoretical and Experimental Investigation of the Photometric Functions of Particulate Surfaces. Ph.D. Thesis, Cornell Univ.

Hapke, B. 1981. Bidirectional reflectance spectroscopy. 1. Theory. *J. Geophys. Res.* 86:3039–3054.

Hapke, B. 1984. Bidirectional reflectance spectroscopy. 3. Correction for macroscopic roughness. *Icarus* 59:41–59.

Hapke, B. 1986. Bidirectional reflectance spectroscopy. 4. The extinction coefficient and the opposition effect. *Icarus* 67:264–280.

Hapke, B., and Wells, E. 1981. Bidirectional reflectance spectroscopy. 2. Experiments and observations. *J. Geophys. Res.* 86:3055–3060.

Harris, A. W., and Young, J. W. 1988. Observations of asteroid phase relations.*Bull. Amer. Astron. Soc.* 20:865 (abstract).

Harris, A. W., and Young, J. W. 1989. Photoelectric lightcurves of asteroids: 1980 observations from Table Mountain Observatory. *Icarus,* submitted.

Harris, A. W., Carlsson, M., Young, J, W., and Lagerkvist, C.-I. 1984a. The lightcurve and phase relation of the asteroid 133 Cyrene. *Icarus* 58:377–382.

Harris, A. W., Young, J. W., Scaltriti, F., and Zappalà, V. 1984b. Lightcurves and phase relations of the asteroids 82 Alkmene and 444 Gyptis. *Icarus* 57:251–258.

Harris, A. W., Young, J. W., Goguen, J., Hammel, H. B., Hahn, G., Tedesco, E. F., and Tholen, D. J. 1987. Photoelectric lightcurves of the asteroid 1862 Apollo. *Icarus* 70:246–256.

Harris, A. W., Young, J. W., Bowell, E., Martin, L. J., Millis, R. L., Poutanen, M., Scaltriti, F., Zappalà, V., Schober, H. J., Debehogne, H., and Zeigler, K. W. 1989*a*. Photoelectric observations of asteroids 3, 24, 60, 261, and 863. *Icarus*, in press.

Harris, A. W., Young, J. W., Contreiras, L., Dockweiler, T., Belkora, L., Salo, H., Harris, W. D., Poutanen, M., Bowell, E., Binzel, R. P., Tholen, D. J., and Sichao Wang. 1989*b*. Phase relations of high albedo asteroids: 44 Nysa and 64 Angelina. *Icarus*, submitted.

Helfenstein, P. 1986. Derivation and Analysis of Geological Constraints on the Emplacement and Evolution of Terrains on Ganymede from Applied Differential Photometry. Ph.D. Thesis, Brown Univ.

Helfenstein, P. 1988. The geological interpretation of photometric surface roughness. *Icarus* 73:462–481.

Helfenstein, P., and Veverka, J. 1987. Photometric properties of lunar terrains derived from Hapke's equation. *Icarus* 72:342–357.

Irvine, W. 1966. The shadowing effect in diffuse reflectance. *J. Geophys. Res.* 71:2931–2937.

Johnson, P. E., Smith, M. O., Taylor-George, S., and Adams, J. B. 1983. A semi-empirical method for analysis of the reflectance spectra of binary mineral mixtures. *J. Geophys. Res.* 88:3557–3561.

Karttunen, H. 1989. Modelling asteroid brightness variations. I. Numerical methods. *Astron. Astrophys.*, in press.

Karttunen, H., and Bowell, E. 1989. Modelling asteroid brightness variations. II. On the uninterpretability of lightcurves and phase curves. *Astron. Astrophys.*, in press.

Lebofsky, L. A., Sykes, M. V., Tedesco, E. F., Veeder, G. J., Matson, D. L., Brown, R. H., Gradie, J. C., Feierberg, M. A., and Rudy, R. J. 1986. A refined "standard" thermal model for asteroids based on observations of 1 Ceres and 2 Pallas. *Icarus* 68:239–251.

Lockwood, G. W., Lumme, K., and Thompson, D. T. 1980*a*. The recent photometric variability of Io. *Icarus* 44:240–248.

Lockwood, G. W., Thompson, D. T., and Lumme, K. 1980*b*. A possible detection of solar variability: Photometry of Io, Europa, Callisto, and Rhea, 1976–1979. *Astron. J.* 85:961–968.

Lumme, K., and Bowell, E. 1981*a*. Radiative transfer in the surfaces of atmosphereless bodies. I. Theory. *Astron. J.* 86:1694–1704.

Lumme, K., and Bowell, E. 1981*b*. Radiative transfer in the surfaces of atmosphereless bodies. II. Interpretation of phase curves. *Astron. J.* 86:1705–1712.

Lumme, K., and Bowell, E. 1985. Photometric properties of zodiacal light particles. *Icarus* 62:54–71.

Lumme, K., and Irvine, W. M. 1982. Radiative transfer in the surfaces of atmosphereless bodies. III. Interpretation of lunar photometry. *Astron. J.* 87:1076–1082.

Lumme, K., and Reitsema, H. J. 1978. Five-color photometry of Saturn and its rings. *Icarus* 33:288–300.

Lumme, K., Bowell, E., and Zellner, B. 1980. Interpretation of laboratory sample photometry by means of a generalized radiative transfer theory. *Lunar Planet. Sci.* XI:637–639.

Lumme, K., Karttunen, H., Bowell, E., and Poutanen, M. 1986. Inversion of asteroid lightcurves using spherical harmonics. In *Asteroids, Comets, Meteors II*, eds. C.-I. Lagerkvist, B. A. Lindblad, H. Lundstedt and H. Rickman (Uppsala: Uppsala Univ.), pp. 55–59.

Lumme, K., Muinonen, K., Peltoniemi, J., Karttunen, H., and Bowell, E. 1987. A possible explanation for anomalously sharp opposition effects. *Bull. Amer. Astron. Soc.* 19:850 (abstract).

Marsden, B. G. 1986*a*. Notes from the IAU General Assembly. *Minor Planet Circ.* Nos. 10193 and 10194.

Marsden, B. G. 1986*b*. Magnitude parameters for the numbered minor planets. *Minor Planet Circ.* Nos. 11095–11108.

Morozhenko, A. V., and Yanovitsky, E. G. 1971. Optical properties of the surface layer of the Moon. *Astron. Zh.* 48:172–183.

Muinonen, K., Lumme, K., Peltoniemi, J., and Irvine, W. M. 1989. Light scattering by randomly oriented crystals. *Appl. Optics*, submitted.

Mustard, J. F., and Pieters, C. M. 1987. Quantitative abundance estimates from bidirectional

reflectance measurements. *Proc. Lunar Planet. Sci. Conf.* 17, *J. Geophys. Res. Suppl.* 92:E617–E626.

Pang, K. D., Lumme, K., and Bowell, E. 1981. Microstructure and particulate properties of the surfaces of Io and Ganymede: Comparison with other solar system bodies. *Proc. Lunar Planet. Sci. Conf.* 12:1543–1553.

Pang, K. D., Ajello, J. M., Lumme, K., and Bowell, E. 1983*a*. Interpretation of whole-disk photometry of Callisto and Ganymede. *Proc. Lunar Planet Sci. Conf.* 13 *J. Geophys. Res. Suppl.* 88:A569–A576.

Pang, K. D., Rhoads, J. W., Hanover, G. A., Lumme, K., and Bowell, E. 1983*b*. Interpretation of whole-disk photometry of Phobos and Deimos. *J. Geophys. Res.* 88:2475–2484.

Peltoniemi, J., Lumme, K., Muinonen, K., and Irvine, W. M. 1989. Scattering of light by stochastically rough particles. *Appl. Optics,* submitted.

Poutanen, M., Bowell, E., and Lumme, K. 1981. A physically plausible ellipsoidal model of Hektor? *Bull. Amer. Astron. Soc.* 13:725 (abstract).

Poutanen, M., Bowell, E., Martin, L. J., and Thompson, D. T. 1985. Photoelectric photometry of asteroid 69 Hesperia. *Astron. Astrophys. Suppl.* 61:291–297.

Rougier, G. 1933. Photométrie photoélectrique globale de la Lune. *Ann. Obs. Strasbourg* 2:205–339.

Shkuratov, Yu. G. 1983. Model of the Heiligenschein of atmosphereless cosmic bodies. *Astron. Zh.* 60:1005–1008.

Simonelli, D. P., and Veverka, J. 1987. Phase curves of materials on Io: Interpretation in terms of Hapke's function. *Icarus* 68:503–521.

Smith, B. A., Soderblom, L. A., Beebe, R., Bliss, D., Boyce, J. M., Brahic, A., Briggs, G. A., Brown, R. H., Collins, S. A., Cook, A. F., II, Croft, S. K., Cuzzi, J. N., Danielson, G. E., Davies, M. E., Dowling, T. E., Godfrey, D., Hansen, C. J., Harris, C., Hunt, G. E., Ingersoll, A., Johnson, T. V., Krauss, R. J., Masursky, H., Morrison, D., Owen, T., Plescia, J. B., Pollack, J. B., Porco, C. C., Rages, K., Sagan, C., Shoemaker, E. M., Sromovsky, L. A., Stoker, C., Strom, R. G., Suomi, V. E., Synnott, S. P., Terrile, R. J., Thomas, P., Thompson, W. R., and Veverka, J. 1986. Voyager 2 in the Uranian system: Imaging science results. *Science* 233:43–64.

Tedesco, E. F. 1986. Ground-based data for asteroids and comets. In *IRAS Asteroid and Comet Survey: Preprint Version No. 1.* Ed. D. L. Matson, JPL Document No. D-3698, pp. 9:1–9:42.

Tholen, D. J. 1984. Asteroid Taxonomy from Cluster Analysis of Photometry. Ph.D. Thesis, Univ. of Arizona.

Trowbridge, T. S. 1978. Retroreflection from rough surfaces. *J. Opt. Soc. Amer.* 68:1225–1245.

Veverka, J., Helfenstein, P., Hapke, B., and Goguen, J. 1989. Photometry and polarimetry of Mercury. In *Mercury,* eds. F. Vilas, C. R. Chapman and M. S. Matthews (Tucson: Univ. of Arizona Press), pp. 37–58.

Wolff, M. 1981. Computing diffuse reflection from particulate planetary surface with a new function. *Appl. Optics* 20:2493–2498.

PHYSICAL CHARACTERIZATION OF ASTEROID SURFACES FROM PHOTOMETRIC ANALYSIS

P. HELFENSTEIN and J. VEVERKA
Cornell University

Rigorous photometric models, like Hapke's equation, can be applied to the analysis of disk-integrated phase curves in order to estimate a variety of regolith physical properties (average particle single-scattering albedo, particle transparency, soil compaction and large-scale roughness). Unfortunately, unambiguous interpretation is difficult due to uncertainties introduced by the irregular shapes of many asteroids and because Earth-based observations are often restricted to small phase angles (< 30°). In this chapter, we explore in detail how incomplete phase-angle coverage and nonsphericity of asteroids limits the reliable determination of Hapke's photometric parameters from asteroid phase curves. From obtainable Earth-based observations, it is possible to derive useful relative comparisons of single-scattering albedos, opposition-surge amplitudes, and regolith compaction states for different asteroids. Such comparisons demand that high-quality (low-noise) data be obtained in small increments of phase angle, especially very close to opposition. Laboratory studies of the photometric properties of meteorite powders and lunar soil samples are needed to characterize particle phase function behavior at large (~ 170°) phase angles and may help resolve ambiguous interpretations of particular asteroid phase curves. The macroscopic roughnesses of asteroids cannot be determined without observations at large phase angles (> 60°); the most reliable estimates require disk-resolved data, obtainable only from spacecraft observations.

I. INTRODUCTION

Asteroid photometry has a long tradition going back to the work of Müller (1893) in the late 19th century on the phase curves of some of the brighter asteroids. More recent years have seen a sustained growth in our

ability to interpret photometric observations in general, with a major impetus coming in the 1960s as part of the then increased interest in lunar studies. From that era come the initial extensions of the classical Lommel-Seeliger theory as developed by Hapke (1963,1966) and Irvine (1966). These early photometric models, that neglected multiple scattering, were adequate to deal with the typical asteroid data then available (see, e.g., Veverka 1971). Considerable progress both in photometric theory and in asteroid observations has occurred since then. Hapke (1981,1984,1986) and Lumme and Bowell (1981*a,b*) developed independent models to deal more realistically with actual regoliths, by including effects of microstructure, multiple scattering and large-scale roughness. An excellent review of the status of asteroid photometry in the 1970s is contained in Bowell and Lumme (1979). One of the important conclusions reached by Bowell and Lumme was that the two major types of asteroids recognized at the time, the S's and the C's, had distinct phase curves. Bowell and Lumme suggested that a major difference between the two types derived from a significant difference in $\tilde{\omega}_o$ (the single scattering albedo) rather than to differences in other parameters (e.g., surface roughness). This fundamental conclusion has been supported by subsequent work (see, e.g., Gradie and Veverka 1986).

It was recognized early on that most asteroids show strong opposition effects indicative of very porous surface textures (see, e.g., Gehrels 1956,1967; Gehrels et al. 1964). Only recently have several objects been discovered whose phase curves appear to lack an opposition surge (see, e.g., French 1987). To interpret such observations in terms of regolith properties requires a model. In recent years, there have been two extensive formulations of photometric models which aim to reproduce the scattering of light from a typical planetary, satellite or asteroid surface. These two models (those of Hapke and of Bowell and Lumme) are compared and contrasted insofar as they apply to asteroids, in the chapter by Bowell et al. Our own investigation in this chapter concentrates on applications of the Hapke theory.

The application of any photometric model can have several distinct aims. Observations are often available over very restricted geometries; also, different geometries obtain for different objects observed. Thus, one aim of photometric theory is to interpolate and extrapolate photometric data to geometries for which observations are not available. Such procedures may be necessary to define essential photometric parameters such as geometric albedo, phase integrals, Bond albedos, etc. They may also be needed to bring data sets for different objects into a comparable format to search for similarities or differences. For these purposes, all we require of any photometric theory is that it fit all available data well with a small number of free parameters. The danger exists, however, that if the model is unphysical, extrapolation beyond the range of observational data may lead to grief.

A more demanding requirement of photometric theory is not only to fit the data well, but that it be based on parameters related to physical and

TABLE I
Hapke Parameters and Component Functions

Hapke Parameters

$\tilde{\omega}_0$	Single scattering albedo which characterizes the efficiency of an average particle to scatter and absorb light
h	Characterizes the width of the opposition surge in terms of soil structure (porosity, particle-size distribution and rate of compaction with depth)
$S(O)$	Opposition surge amplitude term which characterizes the contribution of light scattered from near the front surface of particles at zero phase
g	Asymmetry factor in the Henyey-Greenstein particle phase function; $g = 0$ for isotropic scattering, $g > 0$ for forward scattering and $g < 0$ for backward scattering particles
$\bar{\theta}$	Average topographic slope angle of macroscopic roughness

Component Functions

Opposition Surge:

$$B(\alpha, h, S(O)) = \frac{B_0}{1 + \frac{1}{h} \tan\left(\frac{\alpha}{2}\right)}$$

where total amplitude $B_0 = \dfrac{S(O)}{\tilde{\omega}_0} \dfrac{(1 + g)^2}{(1 - g)}$

Particle Phase Function (Henyey-Greenstein)

$$P(\alpha, g) = \frac{(1 - g^2)}{(1 + 2g \cos\alpha + g^2)^{3/2}}$$

Multiple Scattering Functions (Hapke's Approximation):

$$H(\tilde{\omega}_0, x) = \frac{(1 + 2x)}{[1 + 2x(1 - \tilde{\omega}_0)^{1/2}]}$$

geological properties of the regolith. Such properties fall into two general categories: (1) *optical properties* having to do with the albedos, transparency and scattering patterns of individual regolith grains or clumped aggregates; (2) *structural properties* both on small and large scales, including properties related to the microstructure of the regolith (particle size and shape distribution, porosity, etc.), as well as properties related to the slope distribution (topography) of the surface itself.

In what follows we are concerned primarily with how Hapke's photometric theory can deal with characterizing regolith structural and optical properties in the context of typical asteroid data. The form of Hapke's equation (Hapke 1981,1984,1986) that we consider is described in detail in the accompanying chapter by Bowell et al.; the definitions of the five model parameters are summarized in Table I. This bidirectional reflectance equation describes the intensity of reflected light relative to the incident flux as a func-

tion of incidence angle i, emission angle ϵ and phase angle α. Note that for $\bar{\theta} = 0°$, the complicated form of Hapke's equation reduces to

$$r(i,\epsilon,\alpha) = \frac{\bar{\omega}_0}{4} \frac{\mu_0}{\mu_0 + \mu} \ [\{1 + B[\alpha,h,S(O)]\}P(\alpha,g) + \cdots$$

$$\cdots H(\mu_0, \bar{\omega}_0)H(\mu, \bar{\omega}_0) - 1] \qquad (1)$$

the expression for the bidirectional reflectance of a macroscopically smooth particulate surface.

Given the success of applying Hapke's photometric theory to a wide variety of planets and satellites (see, e.g., Buratti 1985; Simonelli and Veverka 1987; Helfenstein 1986; Helfenstein et al. 1988, 1989; Verbiscer and Veverka 1989; Efford and Wilson 1988; Regner et al. 1988; Veverka et al. 1987,1988; Thomas et al. 1987; Helfenstein and Veverka 1987; McEwen 1989; McEwen et al. 1988), it is of interest to ask to what extent the theory can yield fundamental data about asteroid regoliths. The observational base for asteriods is constrained in that only disk-integrated data are available, and often only over a restricted range of phase angles around opposition. The experience accumulated in the analysis of Voyager satellite observations suggests that disk-resolved data over a significant range of phase angles (available only from spacecraft observations) are needed to constrain possible solutions and determine some regolith photometric parameters uniquely (see, e.g., Helfenstein 1986; Veverka et al. 1987,1988; Domingue and Hapke 1989). In addition, unlike most large satellites, many asteroids have irregular shapes which cannot be deduced uniquely from current observations. Without an accurate knowledge of shape, one cannot determine the effective photometric angles (i and ϵ) accurately.

To illustrate the first part of this problem in a preliminary fashion, we consider data for two well-observed asteroids, Ceres and Vesta, neither of which has a highly nonspherical shape (thus obviating the second difficulty), and address the basic question: can the available observations be interpreted unambiguously?

A. Ceres and Vesta

The two asteroids selected, 1 Ceres and 4 Vesta, are not only well observed, but span a wide range of albedos. Ceres is a relatively dark object; Vesta is one of the brighter asteroids. Available data indicate that Ceres is almost spherical (Millis et al. 1987). The situation from Vesta is more ambiguous; interpretations of Vesta's lightcurve still vary from ones involving shape effects alone, albedo spots alone or a combination of both. Recent speckle interferometry data according to Drummond et al. (1988) suggest that Vesta may have a moderately triaxial shape (584 km $\times$ 531 km $\times$ 467 km).

For both asteroids, observations extend from opposition to about 25° phase, and can be fitted extremely well using Hapke's model (Fig. 1). The fits
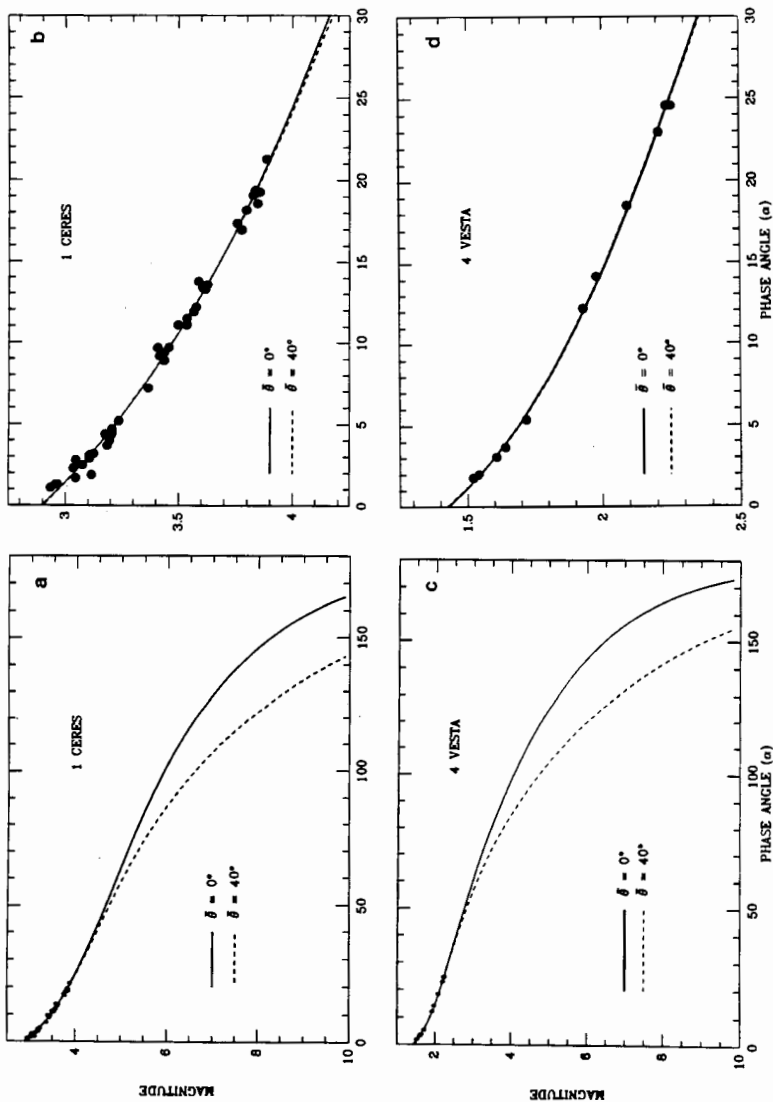
Fig. 1. Observations of 1 Ceres (Tedesco et al. 1983) and 4 Vesta (Gehrels 1967) compared with predicted phase curves from trial Hapke parameter fits (Table V) using two different values of $\bar{\theta}$ (0° and 40°). (a) Phase curve for Ceres plotted to large phase angles; (b) enlarged Ceres plot for $\alpha < 30°$; (c) phase curve for Vesta plotted to large phase angles; (d) enlarged Vesta plot for $\alpha < 30°$.

TABLE II
Nominal Hapke Parameters for Selected Asteroids[a]

Object	$\bar{\omega}_0$	h	$S(O)$	g	$\bar{\theta}$
1 Ceres	0.057 ± 0.004	0.059 ± 0.006	0.35 ± 0.01	-0.40 ± 0.01	$(20°)$
Average C-type asteroid	0.037 ± 0.003	0.025 ± 0.001	0.20 ± 0.01	-0.47 ± 0.01	$(20°)$
Average S-type asteroid	0.23 ± 0.02	0.020 ± 0.001	0.97 ± 0.03	-0.35 ± 0.01	$(20°)$
1862 Apollo	0.318 ± 0.004	0.034 ± 0.007	0.82 ± 0.02	-0.32 ± 0.01	$15° \pm 1°$
4 Vesta	0.40 ± 0.03	0.044 ± 0.010	1.09 ± 0.10	-0.30 ± 0.03	$(20°)$

[a] Values in parentheses are assumed.
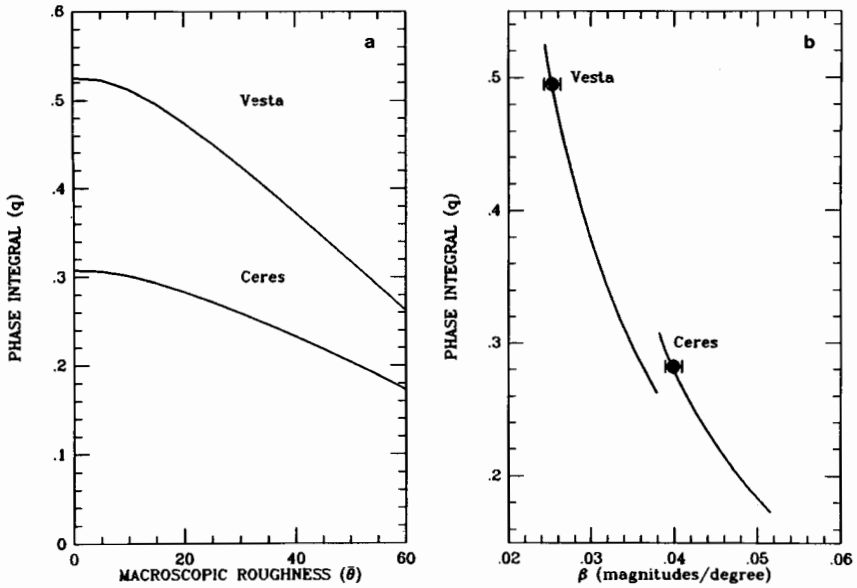
Fig. 2. (a) Predicted values of phase integral q as a function of various assumed surface rough-nesses $\bar{\theta}$ given nominal values of $\bar{\omega}_o$, h, $S(O)$ and g for Ceres and Vesta (Table II). (b) q as a function of predicted phase coefficient β evaluated over $10° < \alpha < 30°$. Observed values of β for Ceres and Vesta are indicated.

shown were obtained by the methods outlined in the Appendix at the end of this chapter; the parameters are listed in Table II.

As excellent as the fits are, it is demonstrated in Secs. II and III that the solutions shown are not unique because the observed data sets are too limited to constrain all of the Hapke parameters. This fact can be demonstrated quickly by noting that the available data are not sufficient to constrain the macroscopic roughness parameter θ. As the four plots in Fig. 1 illustrate, one can change θ from 0° to 40° without affecting significantly the fit to available data, all restricted to phase angles below 25°. Figure 1 also suggests that observations at large phase angles are needed to constrain $\bar{\theta}$. However, one must be careful not to misinterpret Fig. 1; it does not follow that just because data at large phase angles are available, it is always possible to determine $\bar{\theta}$ uniquely. As explained in detail in Sec. II, the situation is more complicated and trade-offs with other parameters must be considered.

While it is true that typical asteroid phase curves such as those in Fig. 1 do not constrain the value of $\bar{\theta}$, one should not forget that accurate knowledge of $\bar{\theta}$ is essential for many purposes. As shown in Fig. 2ab, possible changes in $\bar{\theta}$ can change the phase integral q by $\pm 50\%$, with correspondingly large changes in the Bond albedo, A_B (similar effects can also result from changes
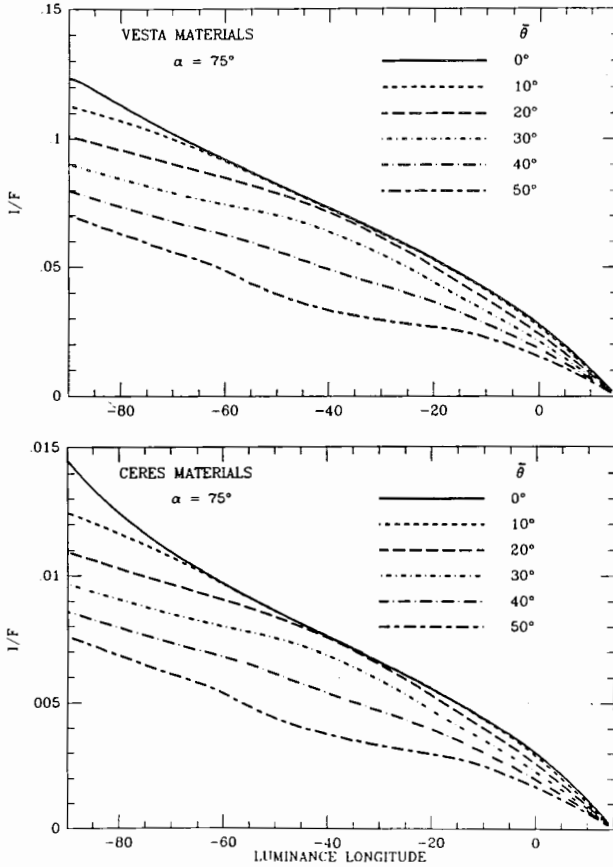
Fig. 3. Predicted scans of disk-resolved brightness I/F along the photometric equator of hypo-
thetical spherical asteroids whose surfaces differ only in macroscopic roughness $\bar{\theta}$. The as-
sumed values of $\bar{\omega}_0$, h, $S(O)$ and g are nominal values (Table II) for Vesta (top) and Ceres
(bottom).

in g). Unfortunately, as documented in Sec. II (cf. Fig. 6 below), phase coeffi-
cients (β: mag/deg) determined between phase angles of 10° and 30° do not
provide useful constraints on $\bar{\theta}$. However, we note that unless $\bar{\theta}$'s for Vesta
and Ceres differ significantly, the phase integral for Vesta must be considera-
bly higher than that of Ceres (Fig. 2a).

So far, high phase-angle observations are available for only some Earth-
approaching asteroids. Unfortunately, many of these objects have severely
nonspherical shapes, making photometric interpretation more difficult (see the
case of 1862 Apollo; Sec. IV.B). In the future, one can expect that spacecraft
such as Galileo will obtain whole-disk photometry of the brighter main-belt
asteroids at large phase angles not available from Earth (see the chapter by

Veverka et al.). Galileo and other missions to the outer solar system will also involve close flybys of individual asteroids, at which time disk-resolved photometry can be obtained. Figure 3ab illustrates the point that disk-resolved photometry of asteroids can constrain the range of possible photometric solutions. For example, at phase angles away from opposition (in this case $\alpha = 75°$), the brightness profiles across an asteroid's disk are extremely sensitive to the value of the roughness parameter $\bar{\theta}$. Disk-resolved observations have already been successfully applied to constrain $\bar{\theta}$ in the majority of recent efforts to derive Hapke parameters for planet and satellite surfaces (see references cited earlier).

Our Ceres and Vesta examples demonstrate that we cannot make totally unambiguous interpretations of available asteroid data. The situation is not hopeless, however, for some ambiguity can be eliminated by realizable improvements in observational data. Also, as we show next, it is possible to take advantage of the fact that only a few of Hapke's model parameters are poorly constrained by available asteroid phase-curve coverage.

II. CONSTRAINTS ON PHOTOMETRIC ANALYSIS

Meaningful solutions to Hapke's equation require adequate observational constraints. Two major limitations for most asteroid observations are that the data are restricted to small phase angles and refer to whole disk measurements (no spatial resolution). Can such observations constrain simultaneously *all* of the parameters in Hapke's equation? And if not, can estimates of *any* of them be derived with confidence? Satisfactory answers to these questions depend critically upon (1) how changes in each Hapke parameter affect the predicted shape and amplitude of a given disk-integrated phase curve; (2) the extent to which noisy data restrict our ability to choose among solutions which produce slightly different, but almost similar phase curves; (3) the ability of rigorous statistical analysis techniques to identify unique solutions or at least to isolate a family of plausible (statistically nonunique) fits; and (4) knowledge of physical criteria that can be used to exclude statistically valid but physically unrealistic fits from a family of candidate solutions. We begin by exploring the sensitivity of disk-integrated phase curves with respect to independent changes in each Hapke photometric parameter. In other words, for a given change in a particular Hapke parameter, how much does the phase curve change in shape and in amplitude?

A. Sensitivity of Phase Curves to Photometric Parameters

Investigators who have used Hapke's equation to analyze disk-integrated observations of planets, satellites and asteroids have noted (with some concern) that different combinations of the parameters can predict remarkably similar phase curves (see, e.g., Buratti 1985; Simonelli and Veverka 1987; Helfenstein 1986,1988; Helfenstein and Veverka 1987; Veverka et al.
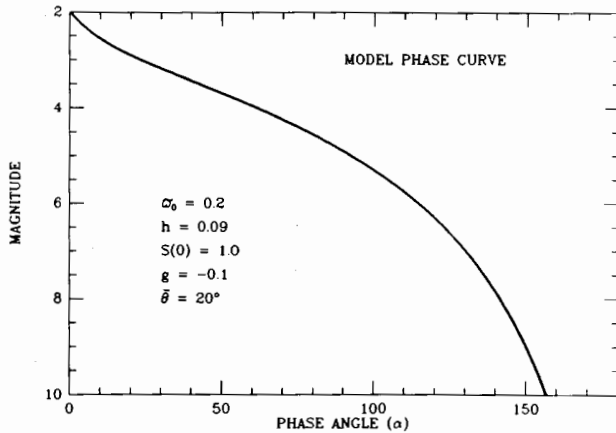
Fig. 4.   Predicted phase curve for a hypothetical spherical asteroid with $\bar{\omega}_o = 0.2$, $h = 0.09$, $S(O) = 1.0$, $g = -0.1$ and $\bar{\theta} = 20°$. Magnitudes are normalized so that, at $\alpha = 0°$, magnitude $= -2.5\log(p)$ where p is the geometric albedo. This phase curve is used as the basis of the sensitivity studies shown in Figs. 5 and 6.

1987,1988; McEwen 1989; Domingue and Hapke 1989). The range of possible solutions increases as the data become more noisy and as the coverage in phase angle is more restricted. Although the parameters of Hapke's equation are strongly coupled, each plays a different role in describing the phase-angle behavior of disk-integrated brightness. If we understood the range of phase angles over which a given parameter has its dominant influence, and how strongly it affects predicted photometric behavior relative to the other parameters, we could determine which observations are most critical to constraining that parameter. Furthermore, such information would provide an idea about how effectively that parameter can be decoupled from others.

The sensitivity of a phase curve to each Hapke parameter can be studied by choosing typical parameter values and showing how modest perturbations of the assumed values affect the amplitude and shape of the predicted phase curve at each phase angle. For the purposes of this demonstration, we assume average lunar values of $\bar{\omega}_0 = 0.20$, $\theta = 20°$ and $g = -0.1$ (Helfenstein and Veverka 1987) and $h = 0.09$ reported for 69 Hesperia (Hapke 1986). We arbitrarily set $S(O) = 1.0$. The phase curve predicted for this set of parameters is shown in Fig. 4; the amount by which each of the assumed parameters must be perturbed to cause a 1% change in the predicted disk-integrated phase curve is shown in Fig. 5 as a function of phase angle. Outside of the opposition surge region, $\bar{\omega}_0$ need be changed by only about 1% to cause a 1% change in disk-integrated brightness (Fig. 5a). The inverse proportionality of the total amplitude of the opposition surge (B_0) to $\bar{\omega}_0$ causes the phase curve to be slightly less sensitive to $\bar{\omega}_0$ within the surge region ($\alpha < 20°$) itself than at
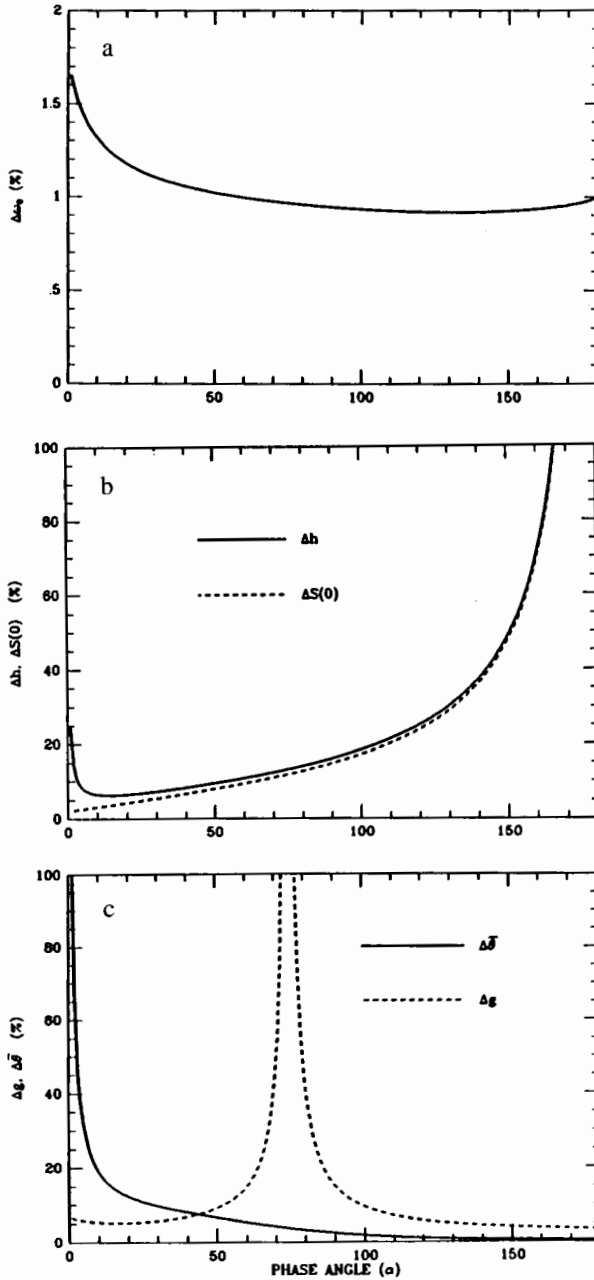
Fig. 5. Sensitivity of the phase curve in Fig. 4 to independent changes in each Hapke parameter. Plots show the percent change in each parameter required to cause a 1% change in brightness of the phase curve at each phase angle. (Plot a): $\Delta\tilde{\omega}_o$ vs α; (Plot b): $\Delta S(O)$ vs α; (Plot c): Δg and $\Delta\theta$ vs α.

larger phase angles. As expected, the phase curve is most sensitive to the opposition surge parameters h and $S(O)$ at phase angles near opposition (Fig. 5b). While the sensitivity to $S(O)$ increases continuously with decreasing phase angle, the disk-integrated brightness is influenced most strongly by h over phase angles that define the shoulder of the opposition surge, that is, for the phase angles over which the curvature of the surge changes most quickly with increasing phase angle. The phase curve is insensitive to the roughness parameter $\bar{\theta}$ at small phase angles, but becomes strongly sensitive to $\bar{\theta}$ as α increases beyond about 90° (Fig. 5c). In contrast, the phase curve is about equally sensitive to the particle phase function parameter g at small ($\alpha < 40°$) and at large ($\alpha > 110°$) phase angles. The phase curve is generally insensitive to g over the range of phase angles for which the backward-scattering lobe of the particle phase function transitions to the forward-scattering lobe.

The patterns of sensitivity displayed in Fig. 5 depend to some extent on the specific initial values assumed for the Hapke parameters and upon the mathematical form of the constituent functions of Hapke's equation, but they can be considered as representative of the trends involved. In summary:

1. Opposition surge parameters are best constrained by data at small phase angles ($\alpha < 20°$);
2. Particle phase function behavior, at least within the Henyey-Greenstein formulation, can be constrained by data both at small and large phase angles, but not by data near 90°;
3. Macroscopic roughness is poorly constrained by data at small phase angles, but is very well constrained by large phase-angle data.
4. The single-scattering albedo $\bar{\omega}_0$ can be constrained by data within almost any phase angle range.

Figure 5c suggests that it should be possible to distinguish the effects of roughness $\bar{\theta}$ and particle phase function g in phase curves for which data are available at both small and large phase angles. This possibility arises because the phase curve is much more sensitive to $\bar{\theta}$ than to g at large phase angles, whereas the converse is true at small phase angles.

Thus far, we have focused upon the sensitivity of the absolute value of the phase curve (the brightness). The shape of the phase curve, particularly the slope at moderate phase angles (the phase coefficient), is also sensitive to parameter changes. Our assumed parameters correspond to a value of $\beta = 0.02$ mag deg^{-1} evaluated between $\alpha = 10°$ and 30°. Figure 6 shows how much of a change in each parameter is required to alter β by specified amounts. As before, when one parameter is varied, all others are kept fixed at their nominal value. The effects of changes in h, $S(O)$, g and $\bar{\theta}$ are qualitatively similar: β increases as these parameters are increased. Conversely, β is decreased by increasing $\bar{\omega}_0$. It is evident that any particular change in β cannot be interpreted uniquely. For example, a 10% decrease in β can be achieved by a 60% decrease in $S(O)$, or a 75% decrease in either g or h, or an 80% increase
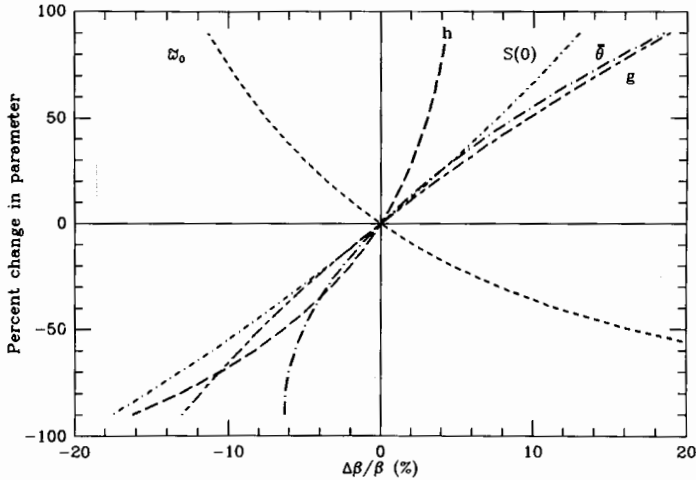
Fig. 6. Sensitivity of the phase coefficient β to independent changes in each Hapke parameter for the hypothetical spherical asteroid of Fig. 4. Vertical axis is the percent change in each parameter needed to cause a particular change, $\Delta\beta/\beta$, in the phase coefficient. The predicted value of β for the model phase curve in Fig. 4 is 0.02 mag deg^{-1}. In this chapter, β is evaluated between α = 10° and 30°.

in $\tilde{\omega}_0$; it cannot be accomplished by changing $\bar{\theta}$ alone. On the other hand, a 10% increase in β could result from a 35% decrease in $\tilde{\omega}_0$, or a 50 to 60% increase in either g or $\bar{\theta}$, or a 90% increase in $S(O)$; it cannot be achieved with a change in h of under 100%.

For very small values of $\Delta\beta/\beta$, the relative sensitivity of each parameter is approximately linear and inversely proportional to the slope of the curves in Fig. 6 near $\Delta\beta/\beta = 0$. As might be expected, β in the range of 10° < α < 30° is least sensitive to the opposition angular width h; a 12% change in h is needed to cause only a 1% change in β. The sensitivity of β to the remaining parameters does not vary greatly. A 5 to 6% change in either $\tilde{\omega}_0$, g or $S(O)$ or a 7% change in $\bar{\theta}$ will cause a 1% change in β. As previously noted, the phase coefficient is strongly coupled to nearly all of the Hapke parameters: *thus differences in β can be interpreted in terms of differences in specific photometric parameters only if some can be constrained independently.* For example, as shown below, observations at phase angles < 10° can be used to constrain $S(O)$ and h so that their contribution to β can be estimated. For most asteroids, $\bar{\theta}$ is probably nonzero and not likely to exceed 45° (Helfenstein 1988). Within these constraints, there is only a limited range of $\tilde{\omega}_0$ and g which can produce an observed β.

On the basis of the preceding discussion (see also Domingue and Hapke 1988; Lumme and Bowell 1981b), it is evident that some parameters (i.e., $\bar{\theta}$
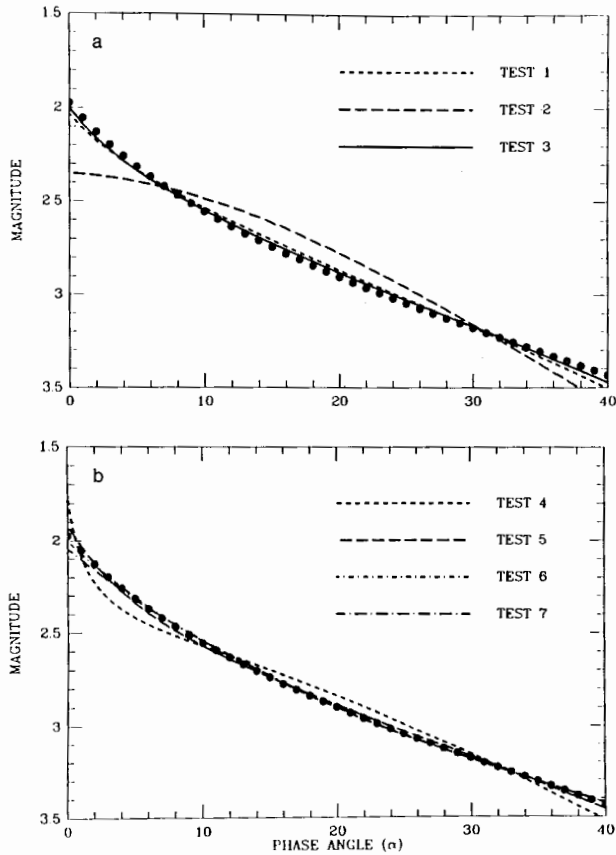
Fig. 7. (a) Trial solutions to an idealized phase curve (dots) for which the opposition surge function of Hapke's equation is ignored. The simulated data is sampled from Fig. 4 in 1° increments of α and restricted to $\alpha = <40°$. Best-fit Hapke parameters for each solution are listed in Table III. (b) Trial fits to phase curve data at top for which h has been fixed at different test values and $\bar{\omega}_o$, h, $S(O)$ and g allowed to vary. $\bar{\theta} = 20°$ for tests 4 through 7. See Table III and text for discussion.

and g) are poorly constrained by typical asteroid photometric data which consist of whole-disk observations made over a limited range of phase angles. Does the inability to constrain some photometric parameters prevent the reliable determination of the remaining parameters? To properly address this question, we must now shift to the inverse problem, that is, investigate how well one can actually constrain a particular parameter from an actual phase curve by the usual fitting techniques. For that purpose we use the hypothetical data in Fig. 4 as an idealized asteroid phase curve from which we derive photometric parameters by the fitting procedure outlined in the Appendix. The

TABLE III
Trial Fits to Idealized Asteroid Phase Curve[a]

	$\bar{\omega}_0$	h	$S(O)$	g	$\bar{\theta}$
Actual Values	0.20	0.09	1.0	−0.10	20°
Fitted Values					
Test 1	0.64	(0.0)	(0.0)	(−0.1)	75°
Test 2	0.17	(0.0)	(0.0)	−0.47	(20°)
Test 3	0.84	(0.0)	(0.0)	+0.23	77°
Test 4	0.19	(0.01)	0.80	−0.40	(20°)
Test 5	0.20	(0.05)	0.88	−0.25	(20°)
Test 6	0.18	(0.13)	1.14	+0.19	(20°)
Test 7	0.0001	(0.17)	1.22	+0.80	(20°)

[a] Values in parentheses were held constant during the trial.

hypothetical curve (Fig. 7ab; dots) was derived from Fig. 4 by sampling in 1° increments in phase between $\alpha = 0°$ and 40°.

In our first three tests, we explored whether we can completely neglect (i.e., ignore) h and $S(O)$ and find combinations of $\bar{\omega}_0$, g and $\bar{\theta}$ which fit the restricted phase curve. If we fix $S(O) = 0$, then the opposition surge function $B(\alpha)$ of Hapke's equation is effectively turned-off and h has no effect on the predicted phase curve. In Test 1, we fixed $S(O) = 0$, $g = -0.1$, fitted for $\bar{\omega}_0$ and $\bar{\theta}$. In Test 2, we fixed $S(O) = 0$, $\bar{\theta} = 20°$, and attempted to fit for $\bar{\omega}_0$ and g. Finally, in Test 3, we fixed $S(O) = 0$, and simultaneously adjusted $\bar{\omega}_0$, g and $\bar{\theta}$ to fit the phase curve. The results are displayed in Table III and Fig. 7a. Test 1 shows that we can very nearly fit the phase curve by adjusting $\bar{\omega}_0$ and $\bar{\theta}$. However, the best-fit value of $\bar{\theta} = 75°$ is physically unrealistic and must be rejected. Test 2 demonstrates that the restricted phase curve cannot be fit satisfactorily simply by adjusting $\bar{\omega}_0$ and g. Test 3 shows that only a slight improvement over Test 1 is realized by simultaneously adjusting $\bar{\omega}_0$, g and $\bar{\theta}$. This solution is also excluded because of its unrealistic value of $\bar{\theta} = 77°$. We conclude that, while h and $S(O)$ are not needed to fit the shape of typical asteroid phase curves, the resulting solutions are physically invalid. Meaningful solutions cannot be found without invoking h and $S(O)$.

In Tests 4 through 7, we arbitrarily fixed h at 0.01, 0.05, 0.13 and 0.17, respectively, held $\bar{\theta} = 20°$, and sought best-fit solutions by simultaneously adjusting $\bar{\omega}_0$, $S(O)$ and g (Table III and Fig. 7b). Test 4 shows that we cannot satisfactorily adjust $\bar{\omega}_0$, g and $S(O)$ to compensate for a value of h that is much smaller than its true value ($h = 0.09$). *This result implies that we can at least identify lower limits for* h *from asteroid phase curves.* The fits from Tests 5, 6 and 7 all deviate significantly from the data only at phase angles $\lesssim \alpha = 2°$, underscoring the fact that accurate observations very close to $\alpha = 0°$ are needed to constrain h well. Table III shows that the solution for $h = 0.17$ (Test 7) can be excluded because of its unrealistically small value of $\bar{\omega}_0 = 0.0001$
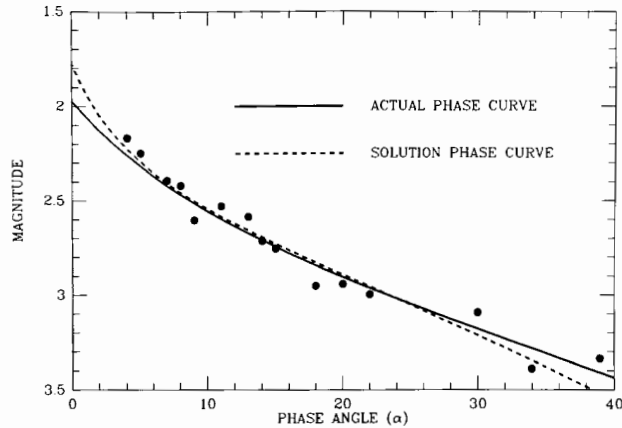
Fig. 8. Effects of simulated random noise and irregular sampling with phase angle on the re-
liability Hapke parameters solutions. The baseline curve is that in Fig. 7. Dashed curve: pre-
dicted phase curve for the best-fit parameters ($\tilde{\omega}_o = 0.18$, $h = 0.04$, $S(O) = 1.01$, $g = -0.33$
with fixed $\bar{\theta} = 20°$). Solid curve: phase curve predicted from the true values of Hapke parame-
ters ($\tilde{\omega}_o = 0.2$, $h = 0.09$, $S(O) = 1.0$, $g = -0.1$, $\bar{\theta} = 20°$). See text for discussion.

and implausible value of $g = +0.80$. *Thus, we are able to identify upper as
well as lower limits on* h.

The parameters for the remaining acceptable solutions (Tests 5 and 6)
bracket the true values of the input phase curve. This fact demonstrates that, if
we are given the accurate estimates of h and $\bar{\theta}$, there is only one combination
of $\tilde{\omega}_o$, g and $S(O)$ that describes the actual phase curve.

The exercise above is idealized in that fits were performed on hypotheti-
cal data exhibiting no noise and sampled in uniform small increments of α.
The adverse effects of noise and irregular sampling are seen in Fig. 8. Here,
we have resampled half of the hypothetical data of Fig. 7ab in random inter-
vals of phase angle and added artificial random noise in brightness between
$\pm 10\%$. We then fixed $\theta = 20°$ and solved for the remaining Hapke parame-
ters. The best-fit values of $\tilde{\omega}_o = 0.18$, $h = 0.04$, $S(O) = 1.01$ and $g = -0.33$
deviate substantially from the values used to create the hypothetical data.
While the values of $\tilde{\omega}_o$ and $S(O)$ are acceptably close to their "true" values ($\tilde{\omega}_o$
$= 0.2$, $S(O) = 1.0$), g and h are radically different (-0.33 vs -0.1 and 0.04
vs 0.09, respectively). Further aspects of the detrimental effects of noise and
irregular sampling are explored in Sec. III.

B. Laboratory Constraints on Hapke Parameters

We have established that, for realistic values of $\bar{\theta}$, the opposition surge
parameters h and $S(O)$ (or B_o) are well constrained by observations at small
phase angles available for asteroids. It is also clear that, while $\tilde{\omega}_o$ is sensitive

to data at small phase angles, different combinations of $\tilde{\omega}_o$, g and $\bar{\theta}$ can produce remarkably similar phase curves. Much needed additional constraints could be obtained from laboratory measurements on appropriate asteroid-surface analogs (i.e., meteorites). While such measurements cannot give information on $\bar{\theta}$, they could provide useful constraints on $\tilde{\omega}_o$ and g. Ideally, our analogs should model the texture, particle microstructure and particle-size distributions in asteroid regoliths. At present, we lack the knowledge to simulate any of these variables well; however, detailed study of lunar soil samples could help considerably.

Measurements of crushed meteorite samples can at least tell us whether the one-term Henyey-Greenstein representation of the particle phase function is satisfactory, or whether more elaborate forms, such as the two-term Henyey-Greenstein function or Legendre polynomial representations are needed. In what follows, we carry out this test on two meteorite powders: Murchison, a carbonaceous chondrite which can be considered as an approximate analog to C-type asteroids, and the ordinary chondrite Bruderheim, an approximate analog for S asteroids. The Murchison data were obtained by French (1980); the Bruderheim measurements are those of Egan et al. (1973).

Given observations of the reflectances of these powders over a large range of i, ϵ, and α, we can use the following procedure to make good estimates of g and of the opposition surge parameters h and $S(O)$ independently of $\tilde{\omega}_o$. First, note that Eq. (1) can be inverted to solve for the quantity $F(\alpha)$:

$$F(\alpha) = [1 + B(\alpha,h,S(O))]P(\alpha,g) = \tag{2}$$

$$\frac{4}{\tilde{\omega}_0} \frac{\mu_0 + \mu}{\mu_0} r(i,\epsilon,\alpha) - H(\mu_0,\tilde{\omega}_0)H(\mu,\tilde{\omega}_0) + 1.$$

For particulate, macroscopically smooth laboratory samples, we assume that $\bar{\theta} = 0$. In the case of low albedo particles, like those in Murchison, and for at least one size fraction of Bruderheim, multiple scattering of light between particles is negligible (Egan et al. 1973) and $\tilde{\omega}_o$ is low enough so that $H(\mu_o,\tilde{\omega}_o)H(\mu,\tilde{\omega}_o) \sim 1$. Then the equation above simplifies to

$$F(\alpha) = \frac{4}{\tilde{\omega}_0} \frac{\mu_0 + \mu}{\mu_0} r(i,\epsilon,\alpha). \tag{3}$$

If $F(\alpha)$ is normalized to its value at some reference phase angle, say $\alpha = 4°$ for Murchison (after French 1980) and $\alpha = 3°6$ for Bruderheim (after Egan et al. 1973), we can solve for g, h and the total amplitude of the opposition surge B_o (but not for $S(O)$).

French (1980) and Egan et al. (1973) provide plots of $F(\alpha)$ for their samples over phase angles from about $4° < \alpha < 120°$. Values of g, h and B_o obtained from a subset of French's data using a nonlinear least-squares solution for Eq. (3) are listed in Table IV. An example plot of our fit to French's data is shown in Fig. 9. In Table IV values of h and B_o appear to vary with λ,

TABLE IV

Fitted Hapke Parameters for Murchison Meteorite Powder[a]

Wavelength (μm)	h	B_0	g	residual
0.388	0.231	5.03	0.0965	0.00097
0.449	0.213	3.31	0.0663	0.00049
0.514	0.185	2.98	0.0651	0.00062
0.583	0.202	2.97	0.0651	0.00131
0.657	0.231	2.77	0.0746	0.00069
0.779	0.183	1.87	0.0561	0.00133
0.902	0.277	2.82	0.1047	0.00136
1.025	0.203	1.70	0.0681	0.00200

[a]Particle diameter < 74 μm.

but this may be an artifact, since few observations were made within the opposition surge region. Values of g, however, are all similar to the mean value of 0.075 ± 0.016, suggesting that average particles in the Murchison powder (particle size $\sim$ 74 μm) are consistently slightly forward scattering over these wavelengths.

Our fit to the Bruderheim data of Egan et al. (1973) is shown in Fig. 10. Our solution gives $g = -0.085$, indicating particles that are, on average, slightly backward scattering.

Figures 9 and 10 show that the one-term Henyey-Greenstein function is adequate for modeling particle phase behavior out to phase angles of at least
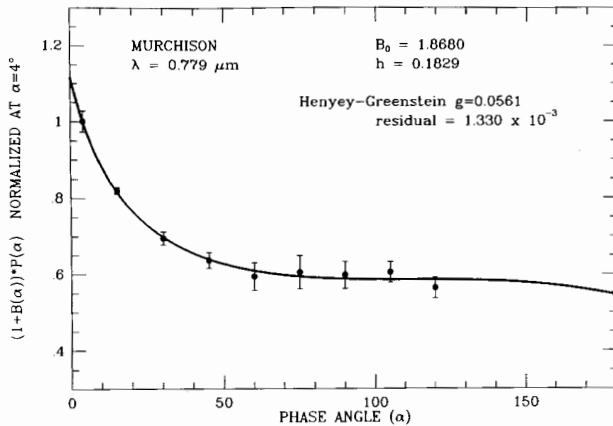
Fig. 9. Example fit of h, B_0 and g to laboratory photometric measurements of crushed Murchison meteorite powder (from French 1980). Dots with 1σ error bars are observed values of $F(\alpha)$ (see text for definition) and solid curve is predicted from the best-fit solution. The sample consists of particles having mean diameters < 74 μm.
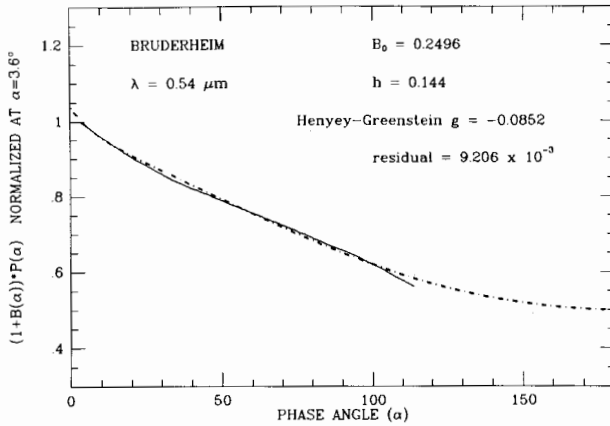
Fig. 10. Fit of h, B_0 and g to laboratory photometric measurements of Bruderheim meteorite particles (from Egan et al. 1973). Solid curve represents observations; the dashed curve is predicted from best-fit parameters.

120°: At phase angles closer to the forward-scattering direction more complicated phase functions may be required (cf. Fig. 1 of the Bowell et al. chapter). Unfortunately, there is a serious lack of data on the scattering behavior of powdered surfaces at large phase angles; laboratory observations of soil analogs at $\alpha > 120°$ are needed badly. Accurate descriptions of particle phase functions over a wide range of phase angles for analog materials of a variety of candidate asteroid would constrain the range of possible particle phase functions and would improve our chances of extracting meaningful estimates of $\bar{\omega}_0$, h, $S(O)$ and especially $\bar{\theta}$. Such laboratory results could also be useful for distinguishing the most likely solution to Hapke's equation when a variety of nonunique solutions are found for a given asteroid phase curve.

III. HAPKE PARAMETERS FOR SPHERICAL ASTEROIDS

In this section, we make use of the methods outlined above and in the Appendix to estimate Hapke parameters for several asteroids. We begin with a more thorough discussion of Ceres and Vesta and continue with an analysis of the phase curves for average C and S asteroids published by Bowell and Lumme (1979).

A. Ceres and Vesta

In Sec. I.A, we noted that of all the Hapke parameters, $\bar{\theta}$ is least constrained by Earth-based observations of main-belt asteroids such as Ceres and Vesta. To quantify this assertion, we performed a series of fits of $\bar{\omega}_0$, h and $S(O)$ to the Ceres and Vesta data in which g was set arbitrarily to our labora-

TABLE V

Values of $\bar{\omega}_0$, h, $S(O)$ for Various Assumed $\bar{\theta}$ for Ceres and Vesta[a]

$\bar{\theta}$	$\bar{\omega}_0$	h	$S(O)$	residual
Ceres (g = +0.0746)				
0.0	0.0517	0.1146	0.5127	0.02767
5.0	0.0495	0.1163	0.5139	0.02771
10.0	0.0536	0.1163	0.5112	0.02775
15.0	0.0542	0.1194	0.5102	0.02776
20.0	0.0582	0.1220	0.5067	0.02778
25.0	0.0653	0.1239	0.5007	0.02781
30.0	0.0619	0.1329	0.5016	0.02780
35.0	0.0776	0.1323	0.4891	0.02778
40.0	0.0760	0.1437	0.4885	0.02781
Vesta (g = −0.0852)				
0.0	0.435	0.0959	1.4221	0.00101
5.0	0.436	0.0965	1.4202	0.00102
10.0	0.440	0.0979	1.4108	0.00102
15.0	0.448	0.1001	1.3922	0.00102
20.0	0.464	0.0998	1.3590	0.00102
25.0	0.483	0.1000	1.3187	0.00101
30.0	0.506	0.0990	1.2673	0.00099
35.0	0.534	0.0973	1.2055	0.00095
40.0	0.566	0.0944	1.1311	0.00091

[a] g is fixed at values shown.

tory estimates for Murchison (g = +0.075) and Bruderheim (g = −0.085) samples, respectively. For each trial, $\bar{\theta}$ was held constant at an assumed value which was incremented by 5° from trial to trial. The results of the fits are summarized in Table V.

The sensitivity of the solutions to $\bar{\theta}$ is apparent from comparison of residuals over the entire range of $0° < \bar{\theta} < 45°$. For Ceres, the worst and best residuals differ by only 0.5%, emphasizing the need for rigorous fitting techniques when applying Hapke's model. For Vesta, the maximum difference in residuals is about 10%; however, the statistically best solutions occur for the largest, and possibly most unrealistic values of $\bar{\theta}$. Figure 1 (Sec. I.A), demonstrates that the actual difference between the best ($\bar{\theta}$ = 40°) and worst ($\bar{\theta}$ = 0°) solutions for Vesta is negligible. We conclude that $\bar{\theta}$ is not constrainable from existing observations of Ceres or Vesta.

It is worth pointing out that, while the residuals do not differ strongly between trials, values of $\bar{\omega}_0$, h and $S(O)$ do change appreciably. This phenomenon is a consequence of the coupling between parameters by which variations in one parameter can be compensated by changes in another. The adverse effects of coupling between parameters are reduced greatly when phase

TABLE VI
Values of $\bar{\omega}_0$, h, $S(O)$ for Various Assumed g for Ceres and Vesta[a]

g	$\bar{\omega}_0$	h	$S(O)$	residual
Ceres				
−0.50	0.0510	0.0286	0.3008	0.02900
−0.45	0.0544	0.0437	0.3249	0.02621
−0.40	0.0565	0.0586	0.3538	0.02588
−0.35	0.0575	0.0720	0.3824	0.02614
−0.30	0.0581	0.0830	0.4079	0.02648
−0.25	0.0580	0.0926	0.4302	0.02679
−0.20	0.0575	0.1006	0.4492	0.02705
−0.15	0.0567	0.1071	0.4652	0.02726
−0.10	0.0566	0.1119	0.4779	0.02742
−0.05	0.0541	0.1176	0.4905	0.02755
0.00	0.0517	0.1222	0.5010	0.02767
+0.05	0.0528	0.1238	0.5072	0.02774
+0.10	0.0605	0.1221	0.5084	0.02783
+0.15	0.0586	0.1252	0.5151	0.02787
+0.20	0.0498	0.1306	0.5241	0.02791
+0.25	0.0540	0.1305	0.5260	0.02794
+0.30	0.0772	0.1248	0.5204	0.02810
+0.35	0.0791	0.1263	0.5236	0.02810
+0.40	0.0867	0.1263	0.5247	0.02815
+0.45	0.1016	0.1247	0.5236	0.02827
+0.50	0.1115	0.1246	0.5241	0.02831
Vesta				
−0.50	0.277	0.0046	1.0124	0.02452
−0.45	0.311	0.0073	1.3051	0.00676
−0.40	0.345	0.0153	1.1321	0.00152
−0.35	0.374	0.0282	1.0623	0.00030
−0.30	0.397	0.0438	1.0849	0.00023
−0.25	0.417	0.0592	1.1448	0.00042
−0.20	0.433	0.0738	1.2140	0.00065
−0.15	0.447	0.0867	1.2820	0.00083
−0.10	0.460	0.0971	1.3428	0.00098
−0.05	0.473	0.1060	1.3959	0.00109
0.00	0.484	0.1139	1.4427	0.00118
+0.05	0.496	0.1204	1.4819	0.00124
+0.10	0.507	0.1261	1.5157	0.00129
+0.15	0.523	0.1282	1.5363	0.00133
+0.20	0.538	0.1299	1.5531	0.00136
+0.25	0.553	0.1315	1.5671	0.00138
+0.30	0.563	0.1343	1.5828	0.00139
+0.35	0.577	0.1347	1.5895	0.00140
+0.40	0.586	0.1364	1.5992	0.00140
+0.45	0.594	0.1385	1.6092	0.00141
+0.50	0.607	0.1376	1.6087	0.00140

[a] $\bar{\theta}$ is fixed at 20°.
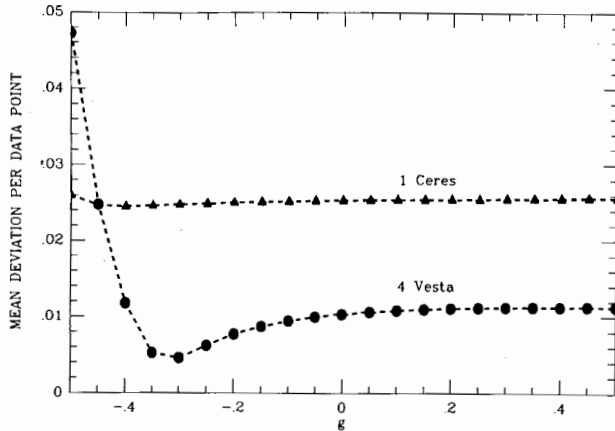
Fig. 11. Discriminability of best-fit Hapke solutions from actual asteroid phase curves for 1 Ceres and 4 Vesta for different fixed values of g (see Table VI). Mean deviation per data point is equivalent to the *rms* residual for the solution.

angle coverage is uniform and data exhibit little scatter, as discussed at the end of this section.

We also examined whether the Ceres and Vesta observations are sensitive enough to place limits on g. In these trials, we sought best-fit values of $\bar{\omega}_o$, h and $S(O)$ for which g was held fixed at assumed values which were incremented by 0.05 between trials. Since the solutions are not especially sensitive to $\bar{\theta}$, we fixed $\bar{\theta}$ at a plausible value of 20° for all trials. Our results are shown in Table VI.

For Vesta, significant systematic variations between residuals for different assumed values of g are apparent and the optimal solution of $g = -0.30$ is defined by a clear minimum in Fig. 11. For Ceres, changes in the residual with increasing g are much less pronounced, differing only by about 10% over the entire range. The optimal solution for Ceres ($g = -0.40$) is barely distinguishable from nearby solutions. The optimal solution for Vesta is better defined than that for Ceres because Vesta observations contain less scatter. Since the residuals for Ceres are about 20 times more sensitive to g than to $\bar{\theta}$, we will take the $g = -0.40$ solution as our best and choose the obvious $g = -0.30$ solution for Vesta. Note that these g's are significantly more backscattering than are the values for the meteorite analogs discussed in Sec. II.C.

The preceding examples illustrate that reliable estimates of Hapke parameters from Earth-based observations of asteroids require high-quality data. Reasonable estimates of $\bar{\omega}_o$, h, $S(O)$ and limits on g can be successfully derived from Earth-based observations provided that several conditions are satisfied:

1. Observations span the widest range of obtainable phase angles;
2. Observations are made in small increments of phase angle, especially within the opposition surge;
3. Observations contain minimal scatter (noise).

If the Vesta and Ceres data sets are taken as representative, we can conclude that for a typical asteroid even more observations are needed before we can place strong confidence in estimates of photometric parameters. Additional observations are needed to extend phase angle coverage closer to $\alpha = 0°$, to provide more uniform coverage with increasing phase angle, and to reduce data scatter by providing multiple observations at each phase angle. Finally, in spite of all this effort, it will not be possible to constrain $\bar{\theta}$ for main-belt asteroids until observations at higher phase angles, or better still, disk-resolved observations are available from space.

B. Average C and S Asteroids

Bowell and Lumme (1979) combined observations of 166 C asteroids and 132 S asteroids to construct mean phase curves for C and S type asteroids. In a related study (with A. Verbiscer), we have used the Bowell and Lumme data (see Fig. 12) to derive Hapke parameter fits. In a series of trials, $\bar{\theta}$ was fixed at different assumed values while $\bar{\omega}_o$, h, $S(O)$ and g were allowed to adjust. $\bar{\theta}$ was incremented by 5° between trials over a range of $0° < \bar{\theta} < 60°$. Table VII lists the results for C and S asteroids, respectively. As in our trials for Ceres and Vesta, residuals do not change significantly as $\bar{\theta}$ is varied, again because the available phase curves are *not* sensitive to the value of $\bar{\theta}$. How-
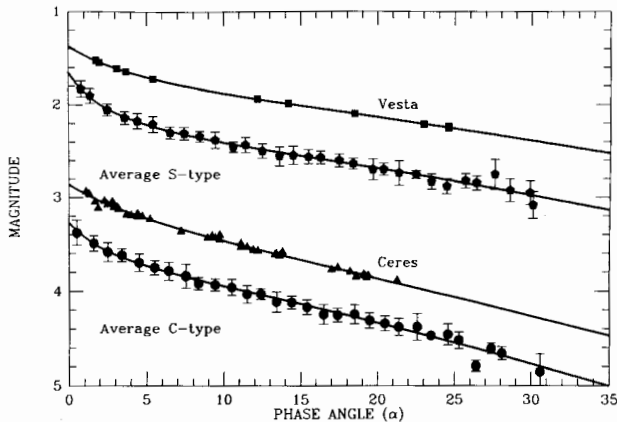
Fig. 12. Observed asteroid phase curves compared with model phase curves derived from nominal Hapke parameters in Table II. The points for average C and S type asteroids are averages from Bowell and Lumme (1979); the Ceres data are from Tedesco et al. (1983); Vesta, from Gehrels (1967).

TABLE VII
Trial Hapke Parameters for Average C and S Type Asteroids

$\bar{\theta}$	$\tilde{\omega}_0$	h	$S(O)$	g	Residual
C Type					
0.0	0.0341	0.0258	0.209	−0.478	15.45
5.0	0.0341	0.0263	0.207	−0.478	15.45
10.0	0.0346	0.0262	0.205	−0.477	15.43
15.0	0.0354	0.0262	0.202	−0.475	15.43
20.0	0.0365	0.0256	0.198	−0.473	15.43
25.0	0.0379	0.0252	0.193	−0.470	15.43
30.0	0.0397	0.0243	0.189	−0.466	15.43
35.0	0.0418	0.0239	0.183	−0.460	15.44
40.0	0.0444	0.0230	0.177	−0.454	15.44
45.0	0.0475	0.0222	0.169	−0.446	15.44
50.0	0.0513	0.0210	0.160	−0.437	15.42
55.0	0.0565	0.0196	0.151	−0.424	15.40
60.0	0.0636	0.0180	0.138	−0.408	15.41
S Type					
0.0	0.213	0.0211	1.002	−0.359	3.898
5.0	0.213	0.0212	0.995	−0.360	3.899
10.0	0.215	0.0206	0.990	−0.361	3.897
15.0	0.221	0.0208	0.977	−0.356	3.899
20.0	0.227	0.0198	0.965	−0.357	3.894
25.0	0.237	0.0193	0.951	−0.351	3.893
30.0	0.248	0.0183	0.938	−0.346	3.890
35.0	0.264	0.0183	0.912	−0.333	3.892
40.0	0.283	0.0174	0.891	−0.323	3.891
45.0	0.305	0.0160	0.875	−0.310	3.889
50.0	0.335	0.0150	0.852	−0.291	3.892
55.0	0.374	0.0139	0.816	−0.267	3.898
60.0	0.427	0.0118	0.787	−0.238	3.905

ever, the remarkable feature of the data in Table VII is that the values of $\tilde{\omega}_0$, h, $S(O)$ and g indicated do not vary much over realistic ranges of $\bar{\theta}$ ($0° < \bar{\theta} < 35°$). The uniform phase angle coverage and relatively small scatter in the averaged data effectively reduce the adverse effects of coupling between Hapke parameters by smoothly and accurately defining the shapes of the phase curves. If $\bar{\theta} = 35°$ is taken as a reasonable upper limit, then we may average $\tilde{\omega}_0$, h, $S(O)$ and g over $0° < \bar{\theta} < 35°$ to obtain our best estimates of Hapke parameters for average C and S asteroids. The standard deviation of each parameter about its mean should provide a good approximation to formal error bars for the individual parameters. These optimum values, as well as those for Ceres and Vesta, are summarized in Table II (Sec. I.A). Several trends are apparent.

First, as might be expected, the darker asteroids have lower values of $\bar{\omega}_o$ and $S(O)$. There is also a suggestion that the phase functions are slightly more backscattering for Ceres and the C asteroids than for Vesta and the S asteriods. The values of h show wide scatter; it is noteworthy that the phase curves for the two individual asteroids yield significantly higher values of h than do the phase curves for the "average" C and S asteroids. This systematic difference is almost certainly due to differences in data coverage. The "average" curves are defined much better near opposition than are those of the individual asteroids Ceres and Vesta. Consequently, we do not believe that this systematic differ- ence in h is a real effect. By the same token, we believe that the "average" phase curves provide the best available estimates of h for asteroids; hence, we find it significant that closely similar values of h result for both C and S asteroids.

IV. NONSPHERICAL ASTEROIDS: ROTATION AND PHASE CURVES

A. Lessons from an Ellipsoidal Model

To date, all fits of Hapke's equations to phase curves have been per- formed by comparing the observed whole-disk brightness at each phase angle to that predicted for a sphere for a given set of Hapke parameters. Since many asteriods are irregular in shape, it is important to assess the effects of this simplification. We note that in the case of the Bowell-Lumme phase function such a study is being carried out by Karttunen (1989) and by Karrtunen and Bowell (1989).

In this preliminary effort, we restrict our attention to the photometric characteristics of hypothetical biaxial ellipsoids which rotate about the minor axis, $2c$, perpendicular to the observer's line of sight (Fig. 13). (It should be understood that this approach is determined by simplicity and not by any conviction that ellipsoidal asteroids really exist.) In what follows, we examine how the disk-integrated brightness of two model ellipsoids changes as a func- tion of rotation angle ψ and phase angle α. We define $\psi = 0°$ as the angle for which semimajor axis a is perpendicular to the observer's line of vision and $\psi = 90°$ for the counterclockwise rotation angle when it points toward the ob- server (Fig. 13). The nominal Hapke parameters for 1 Ceres from Table II are used to model the photometric properties of the surface.

Figure 14 shows the numerically calculated rotation curves for the two biaxial ellipsoids at a variety of phase angles. The curve of larger amplitude corresponds to an ellipsoid with axial ratio $a:c = 2:1$; the curves of smaller amplitude are for $a:c = 1.3:1$. The solid horizontal lines represent the light- curves of a sphere of cross section $\pi r^2 = \pi ac$. The magnitudes in each rota- tion curve are based on a normalization to the disk-integrated brightness at zero phase of a perfect Lambert disk of cross section πac. A noteworthy
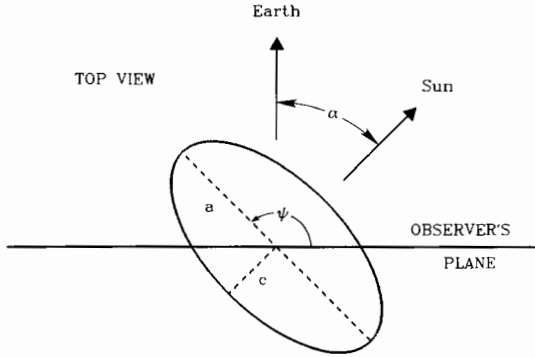
Fig. 13. Geometry used for computing simulated rotation curves for model biaxial ellipsoids. ψ is the ellipsoid rotation angle and α is the phase angle. Also shown, semimajor axis *a* and semiminor axis *c* of the biaxial ellipsoid.
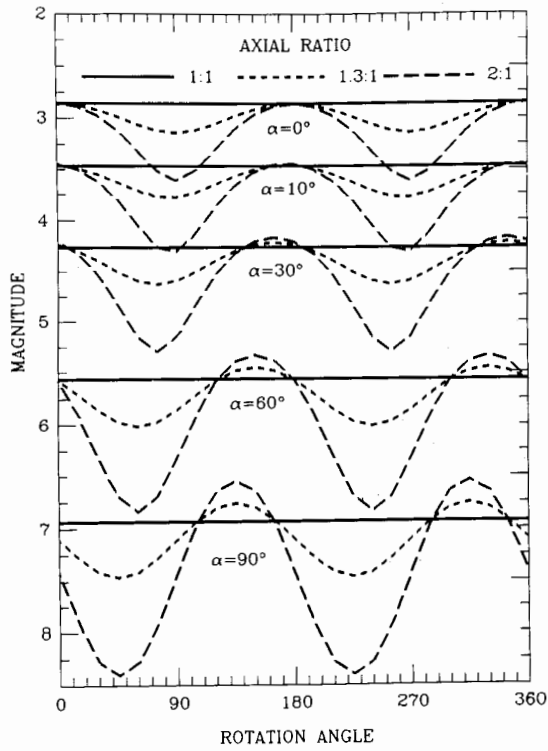
Fig. 14. Simulated lightcurves for biaxial ellipsoids having different axial ratios over a range of different phase angles. See text for discussion.
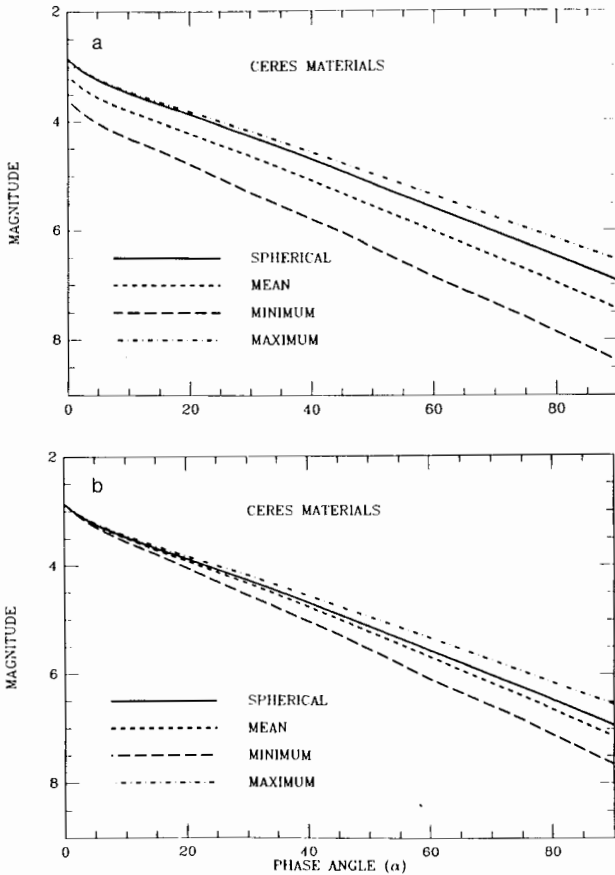
Fig. 15. (a) Phase curves constructed from simulated lightcurves for an ellipsoid of axial ratio of 2:1. The solid curve is phase curve predicted for a sphere of cross section $\pi a c$. The mean curve is derived from average lightcurve magnitudes; the minimum is from minima of lightcurves and the maximum from maxima of lightcurves. (b) Same as (a), except that magnitudes of all curves are adjusted to be the same as for the sphere at $\alpha = 0°$.

aspect of these curves is that both the maxima and minima shift systematically in rotation angle with increasing phase angle.

Several interesting implications arise from the shift in extrema with increasing phase angle. First, since asteroid rotation periods are derived from the time intervals between consecutive patterns of extrema, estimates of the rotation period may be in error if observations at very different phase angles are employed. A more important implication is that extrema at different phase angles do not correspond to identical regions of an asteroid's surface. For example, the projected cross section of the asteroid at $\psi = 135°$, where a

maxima occurs at $\alpha = 90°$, is considerably smaller than at $\psi = 0°$, where a maxima occurs at $\alpha = 0°$. The differences in projected cross section between extrema at different phase angles can affect the shapes of phase curves derived from asteroid rotation curves.

In Fig. 15a, we show phase curves constructed from lightcurves for our biaxial 2:1 ellipsoid under several assumptions:

1. Plotting the magnitude corresponding to maximum brightness as a function of phase angle;
2. The magnitude corresponding to minimum brightness;
3. The mean magnitude.

For comparison, the phase curve for a sphere covered with the same material is also provided (solid curve). All of the curves are superficially similar in appearance, but have different slopes. Note that the vertical offset of some of the curves from that for the sphere is due to the normalization used; the differences would disappear if the mean lightcurve brightnesses are normalized to the mean projected cross section, $\pi(ac + c^2)/2$, rather than to the maximum area πac.

The shapes of phase curves in Fig. 15a are compared more easily if they are adjusted to have the same magnitude of $\alpha = \psi = 0°$. The result is that the phase curve obtained from the mean magnitudes is most similar in shape to that of a sphere (Fig. 15b). We conclude that the phase curve derived from the mean lightcurve magnitudes is the best approximation to the sphere and offers the best hope of deriving valid Hapke parameters within the spherical shape approximation usually employed.

A fit of Hapke's equation to the mean magnitude phase curve of the 2:1 ellipsoid yields $\tilde{\omega}_o = 0.55$, $h = 0.056$, $S(O) = 0.35$, $g = -0.42$ and $\bar{\theta} = 25°$, compared to $\tilde{\omega}_o = 0.57$, $h = 0.059$, $S(O) = 0.35$, $g = -0.40$ and $\bar{\theta} = 20°$ for the nominal parameters. Despite the ellipsoid's rather extreme axial ratio, acceptable estimates of the photometric parameters are obtained by the standard spherical procedure. For ellipsoids with smaller axial ratios, the agreement is expected to be even better.

Strong cautionary comments are in order. While ellipsoids may represent asteroid shapes better than spheres, they may themselves be poor models of real asteroids. At any given phase angle, the distribution of incidence and emission angles for highly irregular asteroids will differ substantially from those predicted from an equivalent model ellipsoid. The occurrence of shadows cast by topographic features whose scales approach that of an asteroid will add considerable uncertainty. Finally, the difficulties introduced into the analysis by asteroids which do not have spin axes perpendicular to the line of sight remain to be explored within the context of Hapke's model.

B. Nonspherical Asteroids: Applications to 1862 Apollo

Earth-crossing asteroids afford the opportunity to obtain data at phase angles large enough to estimate $\bar{\theta}$. An excellent series of observations span-
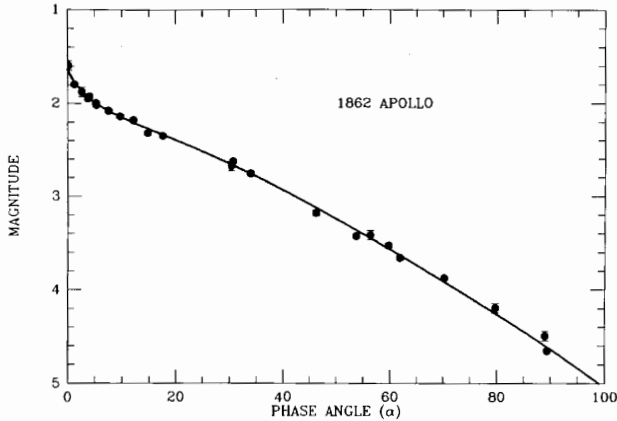
Fig. 16. Observations (points with 1σ error bars) of 1862 Apollo from Harris et al. (1987) and predicted phase curve for best-fit Hapke parameters from Table II.

ning phase angles $0°.2 < \alpha < 89°.4$ has recently been published by Harris et al. (1987) for the S-type asteroid 1862 Apollo. The phase curve for Apollo constructed by Harris et al. (see Fig. 16) was derived from the mean magnitudes of the lightcurve of this small ($d = 1.5$ km) irregular ($\Delta m = 0.5$ mag) body.

Following the approach used to fit phase curves for average S and C type asteroids, we obtained independent fits of $\bar{\omega}_o$, h, $S(O)$ and g for values of $\bar{\theta}$ in the range of $0° < \bar{\theta} < 45°$, in $5°$ increments (Table VIII). Unlike the situation for our previous examples, the residuals for 1862 Apollo change significantly for different values of $\bar{\theta}$ indicating that the solution is indeed sensitive to roughness. The optimal fit occurs for $\bar{\theta} = 15°$. We used the $\bar{\theta} = 15°$ solution as a first guess in another trial for which all of the photometric parameters were free to adjust simultaneously. The result, summarized in Table II, is not significantly different from the first guess. The observed phase curve is compared with our best fit in Fig. 16.

We note that the $\bar{\theta} = 15°$ for 1862 Apollo is slightly lower than lunar and Mercurian values, $20° < \bar{\theta} < 25°$ (Helfenstein and Veverka 1987; Veverka et al. 1987; Efford and Wilson 1988), but comparable with values derived for some outer planet satellites (e.g., $\bar{\theta} = 16°$ for Rhea by Verbiscer and Veverka [1989]).

Applying the lessons of Fig. 15b to the case of Apollo, one suspects that the value of $\bar{\theta}$ given here may be a slight overestimate (since the slope of the "mean" curve exceeds that of the "spherical" curve, fitting the mean curve will involve a larger value of $\bar{\theta}$ than the true nominal value). But such refinement may be unwarranted, given that 1862 Apollo is almost certainly not an ellipsoid.

Large topographic relief on irregular objects will result in projected

TABLE VIII

Hapke Parameters for 1862 Apollo for Various Assumed $\bar{\theta}$

$\bar{\theta}$	$\tilde{\omega}_0$	h	$S(O)$	g	χ^2
0	0.305	0.0313	0.844	−0.324	7.242
5	0.306	0.0320	0.837	−0.323	7.217
10	0.311	0.0333	0.830	−0.318	7.131
15	0.320	0.0359	0.820	−0.309	7.049
20	0.332	0.0410	0.813	−0.293	7.153
25	0.347	0.0513	0.812	−0.268	7.611
30	0.361	0.0745	0.838	−0.227	8.390
35	0.335	0.1461	0.948	−0.138	9.136
40	0.326	0.2200	1.1566	−0.036	9.480
45	0.334	0.2595	1.2233	+0.039	9.625

shadows that cover a larger portion of the surface than would be expected for a spherical object with equivalent macroscopic roughness. Consequently, phase curves for irregular objects can be expected to decrease (darken) more rapidly with increasing phase angle than spherical objects with identical roughness properties. Thus, while we have shown that disk-integrated observations at large phase angles are sensitive to macroscopic roughness, the value of $\bar{\theta}$ obtained from disk-integrated analysis may not be representative of the roughness which would be measured with disk-resolved photometry (cf. Veverka et al. 1987; Helfenstein 1988; Helfenstein et al. 1988). One should beware of the possibility that it may not be meaningful to compare values of $\bar{\theta}$ derived from phase curves for asteroids of different irregular shapes even if large phase-angle observations are available from which solutions of $\bar{\theta}$ can be calculated.

V. DISCUSSION

What can we conclude confidently about the surface properties of asteroids on the basis of Hapke parameters? A major limitation results from the restricted range of phase angles available for most asteroid observations. One consequence of the limited phase angle coverage is that the particle phase function cannot be determined accurately. In fact, except for the indications derived from laboratory analogs (Sec. II.C) we cannot be sure that the particular form of the phase function used here (the Henyey-Greenstein) is appropriate; hence, we cannot be sure that our values of g are very accurate. Uncertainties in g translate into uncertainties in other parameters such as $\tilde{\omega}_0$ (clearly, a lower value of $\tilde{\omega}_0$ can be compensated by a more backscattering g, and vice versa).

It should also be clear that, except perhaps for cases such as 1862 Apollo (but here we must beware of the irregular shape of this small asteroid), we cannot say anything about $\bar{\theta}$ for most asteroids, again largely due to the lack of data at large phase angles.

Within these limitations, we can compare relative values of $\tilde{\omega}_o$, g, $S(O)$ and h and identify trends among the asteroids investigated in this chapter (Table II). Several significant points emerge. The first is that there is a general similarity among the parameters (other than h) derived for similar objects: average C asteroids and Ceres; average S asteroids, 1862 Apollo and Vesta. In general terms, $\tilde{\omega}_o$ and $S(O)$ are lower and g is more backscattering for the first category than for the second. This dichotomy of derived properties indicates that the fits *are* producing meaningful solutions. The second is the wide scatter in derived values of h. We believe (see above) that the phase curves for "average" C and S asteroids are defined well enough to constrain h: thus we accept the result shown in Table II that, on average, C and S asteroids seem to have the same values of the regolith compaction parameter. The fact that the values for the three individual asteroids in Table II differ from each other and are systematically higher (more compact regoliths?) than those for the "average" classes, may reflect the fact that the phase curves for individual objects have fewer data points in the all-important region of phase angle between $0°$ and $2°$. It may also indicate a real difference in the regolith structure of individual asteroids. Only very high-quality observations of individual objects (dense phase angle coverage and abundant data near $0°$) will resolve this important question.

A strong correlation of $S(O)$ with $\tilde{\omega}_o$ is also evident in Table II: that is, $S(O)$ increases with increasing values of $\tilde{\omega}_o$. Helfenstein and Veverka (1987) noted a similar trend among Hapke parameters for different lunar terrains, but could not attribute it uniquely to a specific physical property of lunar soils because several physical factors can influence $S(O)$. According to Hapke (1986), $S(O)$ represents the contribution to the total amplitude of the opposition effect of singly scattered light from near-first surface reflections off regolith crystal facets. In the limiting case of a regolith composed of ideally euhedral crystals, $S(O)$ is equivalent to the Fresnel reflections of the crystals at normal incidence. $S(O)$ should be larger for high-albedo (S-type) asteroids than for lower-albedo (C-type) asteroids if S-type regoliths contain larger amounts of reduced metal than do C-type regoliths. Such a trend would be consistent with the fact that ordinary chondrites are more metal rich than carbonaceous chondrites.

VI. SUMMARY

Useful characterizations of asteroid surface properties can be achieved from the analysis of disk-integrated phase curves. High-quality observations can yield meaningful comparisons of relative single-scattering albedos, oppo-

sition-surge amplitudes and regolith compaction states. Crude inferences may also be drawn about particle phase function behavior at modest phase angles. Unfortunately, except perhaps in the case of Earth-crossing asteroids which can be observed at large phase angles, nothing can be said about the photometric roughness of most asteroids until disk-resolved observations become available from spacecraft. Such observations are needed not only to extend the phase coverage for main-belt asteroids, but in specific cases to provide much needed disk-resolved data.

A variety of related studies will enhance the value and reliability of photometric analyses of asteroid phase curves:

1. Laboratory studies of the photometric properties of meteorite powders and lunar soil samples are needed to define the detailed shapes of particle phase functions out to large ($\sim 170°$) phase angles. These studies should also yield useful limits on values of $\tilde{\omega}_o$ that can be used to distinguish between possible nonunique solutions of Hapke's equation for specific phase curves.
2. High-quality observations of asteroid phase curves, sampled in small increments of phase angle, (especially near $\alpha = 0°$) are needed to place tight constraints on values of h and $S(O)$.
3. Computer modeling of phase curves for topographically complex objects, such as Phobos and Deimos, should help to define the best way to analyze phase curves for irregular-shaped asteroids.
4. Continued efforts to measure asteroid diameters and shapes are needed to allow more precise calibrations of the absolute brightnesses of particular asteroid surfaces.

The next major step in asteroid photometry will occur when spacecraft data become available in the 1990s. High-resolution images returned from spacecraft, such as Galileo and the proposed CRAF mission, at moderate-to-high phase angles will provide data which can be used to determine photometric roughness and test the reliability of Earth-based estimates of surface physical properties.

In Sec. I, we pointed out that the macroscopic roughness of a surface could be constrained from disk-resolved photometry for which brightness variations with incidence and emission angles (as well as phase angle) can be characterized. On irregular objects, however, local angles of incidence and emission cannot be determined without an accurate knowledge of topographic shape. Thus, even the benefits for photometry of disk-resolved data returned by spacecraft may be limited if these observations are not coupled with accurate topographic measurements.

APPENDIX
OPTIMAL APPROACHES FOR DERIVING PHOTOMETRIC
PARAMETERS FROM OBSERVATIONS

Solutions to Hapke's equation cannot be found in closed form. Numerical methods must be employed to find optimal values of the parameters from any given data set. The task is made difficult by the possibility that a given solution may not be unique and by the known strong coupling among the parameters in Hapke's equation.

The most rigorous algorithms for solving Hapke's equation seek values of the parameters which minimize the summed squares of differences between observed magnitudes or disk-integrated brightnesses R_n and those predicted from Hapke's equation $R(\alpha_n, \bar{\omega}_o, h, S(O), \bar{\theta}, g)$ at corresponding phase angles α_n. When observational uncertainties σ_n are given, it is best to seek parameters which minimize χ^2, defined as

$$\chi^2 = \sum_n \frac{[R_n - R(\alpha_n, \bar{\omega}_0, h, S(O), \bar{\theta}, g)]^2}{\sigma_n^2} \tag{A1}$$

where the summation is over all $n = 1, N$ observations. If the minimization is carried out in terms of χ^2, it is not especially important whether observations are expressed on a magnitude or on an intensity scale. Unfortunately, rigorous values of σ_n are often lacking in standard asteroid photometry; therefore it is difficult to carry out the normalization required to obtain χ^2 without arbitrary assumptions. Without the normalization to σ_n, the quantity computed from Eq. (2) (Sec. II.B) is equivalent to the variance times the number of degrees of freedom in the fit. When Hapke parameters must be obtained from observations lacking error estimates, it is vital that the phase curve be expressed on a magnitude scale because of an implicit statistical weighting of the fit that depends upon how relative brightnesses at different phase angles are represented. Generally, observations at large phase angles correspond to small intensities compared with those at smaller phase angles and, on an intensity scale, low-intensity observations contribute negligibly to computed values of χ^2. In Sec. II, we showed that $\bar{\theta}$ is constrained best by disk-integrated observations at large phase angles, making it essential that these low-intensity observations are given adequate statistical weight in the fit. When observations are expressed on a magnitude scale, high phase angle (low-intensity) observations automatically receive a statistical weighting comparable to that given to data at smaller phase angles.

By far the most reliable numerical approach for minimizing χ^2 is the brute-force grid-search method (cf. Bevington 1969). In this method, the admissible range of each parameter is divided into small increments which define a grid in parameter space. χ^2 is computed for every possible combination of the parameters on the hypergrid. The parameter values corresponding to the smallest value of χ^2 are either taken to represent the solution values, or are assumed to be nearest the actual solution which can be found by grid-searching a smaller parameter hypercube surrounding these values in successively finer parameter increments. Despite its inherent reliability, the grid-search method is often impractical for use on modest computers due to the large number of computations needed to fit five (or more) parameters to numerous data points.

A faster way to minimize χ^2 is the gradient-follower method (see, e.g., Marquardt 1963). In this approach, χ^2 is computed for a first guess of parameter values; incremental improvements to the first guess are determined from the gradient of the χ^2 hypersurface (the locus of χ^2 as a function of all parameter combinations) in the immediate vicinity of the assumed parameter values. Each incrementally improved estimate of the parameters serves as a starting point for the next iteration. The process of incrementally following the steepest downward slope of the χ^2 hypersurface is repeated until a minimum is located. The major disadvantage of the gradient follower is its susceptibility to local minima, which may occur frequently for equations containing many mathematically coupled parameters. If the gradient-follower method is used by itself to find best-fit Hapke parameters, then many trials with different first guesses must be performed in order to insure that the absolute minimum has been found.

While either of the methods above can be used by itself, it is advantageous to devise a hybrid method which combines the reliability of the grid search with the speed of the gradient follower. A logical strategy is to perform a grid search only over the most closely coupled parameters, and to carry out a gradient search over the remaining parameters at each point in the grid. For example, it is often adequate to perform a grid search only over $\bar{\theta}$ space while using a gradient follower to find best-fit values of $\bar{\omega}_o$, g, h, $S(O)$ for each assumed $\bar{\theta}$ increment. As we show in Sec. III.A and B, this technique can also be used to identify when a particular parameter is not constrained by available data.

The distribution of observations over phase-angle influences which approach is best to determine parameter values. For example, if observations are available only for phase angles far outside of the opposition surge ($\alpha > 30°$), then h and $S(O)$ are completely unconstrained and it is only necessary to search on $\bar{\omega}_o$, g and $\bar{\theta}$. If phase angle coverage is relatively complete, one can solve for $\bar{\omega}_o$, h and $\bar{\theta}$ using the moderate-to-high phase angle observations ($\alpha > 30°$) and obtain h and $S(O)$ from observations at small phase angles ($0° < \alpha < 30°$).

Once Hapke solutions are found for a given phase curve, it is desirable to determine a formal measure of uncertainty. If values of σ_n are given, one can estimate uncertainties in best-fit Hapke parameters from the matrix of all second partial derivatives of χ^2 with respect to every parameter combination, that is, the curvature matrix

$$C_{jk} = \frac{1}{2} \frac{\partial^2 \chi^2}{\partial X_j \partial X_k} \tag{A2}$$

where X_j and X_k refer to the jth and k^{th} Hapke parameter, respectively. The inverse of the above matrix is known as the error matrix, whose diagonal terms are roughly equivalent to the square of the uncertainty in the corresponding Hapke parameters. Specifically

$$\sigma_{x_j}^2 \simeq C_{jj}^{-1} \tag{A3}$$

where σ_{x_j} is the uncertainty in the jth Hapke parameter and the superscript $^{-1}$ is used to identify the matrix inverse. If rigorous values of σ_n are not available, then all σ_n must be set equal to 1 in Eq. (A1) and the resulting error matrix in Eq. (A3) must be multiplied by the variance given by Eq. (A1) divided by the number of degrees of freedom to obtain estimates of σ_{x_j}.

REFERENCES

Bevington, P. R. 1969. *Data Reduction and Error Analysis in the Physical Sciences* (New York: McGraw-Hill).

Bowell, E., and Lumme, K. 1979. Colorimetry and magnitudes of asteroids. In *Asteroids* ed. T. Gehrels (Tucson: Univ. Arizona Press), pp. 132–169.

Buratti, B. J. 1985. Applications of a radiative transfer model to bright icy satellites. *Icarus* 61:208–217.

Domingue, D., and Hapke, B. 1989. Fitting theoretical photometric functions to asteroid phase curves. *Icarus*, submitted.

Drummond, J., Eckart, A., and Hege, E. K. 1988. Speckle interferometry of asteroids. IV. Reconstructed images of Vesta. *Icarus* 73:1–14.

Efford, N. D., and Wilson, L. 1988. Photometric characterisation of the lunar surface using Hapke's equation. *Lunar Planet. Sci.* XIX:295–296 (abstract).

Egan, W. G., Veverka, J., Noland, M., and Higelman, T. 1973. Photometric and polarimetric properties of the Bruderheim chondritic meteorite. *Icarus* 19:358–371.

French, L. M. 1980. Photometric Properties of Carbonaceous Chondrites and Related Materials. Ph.D. Thesis, Cornell Univ.

French, L. M. 1987. 1173 Anchises: A dark Trojan asteroid with no opposition effect. *Bull. Amer. Astron. Soc.* 19:850 (abstract).

Gehrels, T. 1956. Photometric studies of asteroids. V. The lightcurve and phase function of 20 Massalia. *Astrophys. J.* 123:331–338.

Gehrels, T. 1967. Minor planets. I. The rotation of Vesta. *Astron. J.* 72:929–938.

Gehrels, T., Coffeen, T., and Owings, D. 1964. Wavelength dependence of polarization. III. The lunar surface. *Astron. J.* 69:826–852.

Gradie, J., and Veverka, J. 1986. The wavelength dependence of phase coefficients. *Icarus* 66:455–467.

Hapke, B. W. 1963. A theoretical photometric function for the lunar surface. *J. Geophys. Res.* 68:4571–4576.

Hapke, B. W. 1966. An improved theoretical photometric function. *Astron. J.* 71:333–339.

Hapke, B. W. 1981. Bidirectional reflectance spectroscopy. I. Theory. *J. Geophys. Res.* 86:3039–3054.

Hapke, B. W. 1984. Bidirectional reflectance spectroscopy. III. Correction for macroscopic roughness. *Icarus* 59:41–59.

Hapke, B. W. 1986. Bidirectional reflectance spectroscopy. IV. The extinction coefficient and the opposition effect. *Icarus* 67:264–280.

Harris, A. W., Young, J. W., Goguen, J., Hammel, H. B., Hahn, G., Tedesco, E. F., and Tholen, D. J. 1987. Photoelectric lightcurves of the asteroid 1862 Apollo. *Icarus* 70:246–256.

Helfenstein, P. 1986. Derivation and Analysis of Geological Constraints on the Emplacement and Evolution of Terrains on Ganymede from Applied Differential Photometry. Ph.D. Thesis, Brown Univ.

Helfenstein, P. 1988. The geological interpretation of photometric surface roughness. *Icarus* 73:462–481.

Helfenstein, P., and Veverka, J. 1987. Photometric properties of lunar terrains derived from Hapke's equation. *Icarus* 72:342–347.

Helfenstein, P., Veverka, J., and Thomas, P. C. 1988. Uranus satellites: Hapke parameters from Voyager disk-integrated photometry. *Icarus* 74:231–239.

Helfenstein, P., Thomas, P. C., and Veverka, J. 1989. Early resurfacing of Umbriel: Evidence from Voyager II photometry. *Nature,* 338:324–326.

Irvine, W. 1966. The shadowing effect in diffuse reflectance. *J. Geophys. Res.* 71:2931–2937.

Karttunen, H. 1989. Modelling asteroid brightness variations. I. Numerical methods. *Astron. Astrophys.,* in press.

Karttunen, H., and Bowell, E. 1989. Modelling asteroid brightness variations. II. On the uninterpretability of lightcurves and phase curves. *Astron. Astrophys.,* in press.

Lumme, K., and Bowell, E. 1981a. Radiative transfer in the surfaces of atmosphereless bodies. I. Theory. *Astrophys. J.* 86:1694–1704.

Lumme, K., and Bowell, E. 1981b. Radiative transfer in the surfaces of atmosphereless bodies. II. Interpretation of phase curves. *Astrophys. J.* 86:1705–1721.

Marquardt, M. A. 1963. An algorithm for least-squares estimation of non-linear parameters. *J. Soc. In. Appl. Math.* 11:431–441.

McEwen, A. S., 1989. Photometric functions for photometry and other applications. *Icarus,* submitted.

McEwen, A. S., Matson, D. L., and Soderblom, L. A. 1988. The global distribution, abundance, and stability of SO_2 on Io. *Icarus* 75:450–478.

Millis, R. L., Wasserman, L. H., Franz, O. G., Nye, R. A., Oliver, R. C., Kreidl, T. J., Jones, S. E., Hubbard, W., Lebofsky, L., Goff, R., Marcialis, R., Sykes, M., Frecker, J., Hunten, D., Zellner, B., Reitsema, H., Schneider, G., Dunham, E., Klavetter, J., Meech, K., Oswalt, T., Rafert, J., Strother, E., Smith, J., Povenmire, H., Jones, B., Kornbluh, D., Reed, L., Izor, K., A'Hearn, M. F., Schnurr, R., Osborn, W., Parker, D., Douglas, W. T., Beish, D., Klemola, A. R., Rios, M., Sanchez, A., Piironen, J., Mooney, M., Ireland, R. S., and Leibow, D. 1987. The size, shape, density and albedo of Ceres from its occulation of BD +8°471. *Icarus* 72:507–518.

Müller, G. 1893. Helligkeitsbestimmungen der grossen Planeten und einiger Asteroiden. *Publ. Astrophys. Obs. Potsdam* 8(92):197–398.

Regner, P., Kamp, L., and Neukum, G. 1988. Multispectral photometric classification and mapping of the martian surface in the Oxia Palus region. *Lunar Planet. Sci.* XIX:968–969 (abstract).

Simonelli, D. P., and Veverka, J. 1987. Phase curves of materials on Io: Interpretation in terms of Hapke's function. *Icarus* 68:503–521.

Tedesco, E. F., Taylor, R. C., Drummond, J., Harwood, D., Nickoloff, I., Scaltriti, F., Schober, H. J., and Zappalà, V. 1983. Worldwide photometry and lightcurve observations of 1 Ceres during the 1975–1976 apparition. *Icarus* 54:23–29.

Thomas, P., Veverka, J., Helfenstein, P., Brown, R. H., and Johnson, T. V. 1987. Titania's opposition effect: Analysis of Voyager observations. *J. Geophys. Res.* 92:14911–14917.

Verbiscer, A., and Veverka, J. 1989. Albedo dichotomy of Rhea: Hapke analysis of Voyager photometry. *Icarus,* submitted.

Veverka, J. 1971. The physical meaning of phase coefficients. In *Physical Studies of Minor Planets* ed. T. Gehrels, NASA SP-267, pp. 79–90.

Veverka, J., Helfenstein, P., Hapke, B., and Goguen, J. 1988. Photometry and polarimetry of Mercury. In *Mercury* eds. F. Vilas, C. R. Chapman and M. S. Matthews (Tucson: Univ. of Arizona Press), pp. 37–58.

Veverka, J., Thomas, P., Helfenstein, P., Brown, R. H., and Johnson, T. V. 1987. Satellites of Uranus: Disk-integrated photometry from Voyager imaging observations. *J. Geophys. Res.* 92:14895–14904.

PHOTOPOLARIMETRY OF ASTEROIDS

A. DOLLFUS
Observatoire de Paris

M. WOLFF
Technotran

J. E. GEAKE
UMIST Manchester

D. F. LUPISHKO
Khar'kov University Observatory

and

L. M. DOUGHERTY
UMIST Manchester

*The history of optical polarimetry for planetary surfaces is summarized begin-
ning with the discovery of the polarization of moonlight by Arago in 1811 and
Lyot's realization in 1929 that detailed investigation of polarization characteris-
tics of the Moon, Mercury and Mars could give important information about the
nature of their surfaces. The present state of the art as relevant to asteroids is
reviewed and some recent telescopic polarimetric observations of asteroids are
described. Mathematical models that attempt to explain the polarization of light
by a rough surface are reviewed; a new refinement of the theory based on
Fresnel reflection extended to include Rayleigh scattering effects is treated in
some detail.*

I. INTRODUCTION

When unpolarized light is scattered by a rough surface it becomes par-
tially polarized. The polarization produced is usually found to be linear
(Stokes parameters Q and U), with the circular polarization (Stokes parameter
V) usually negligible. The azimuth of the linear polarization is usually found
to be either normal to the plane containing the incident and observation rays
(Q positive and $U = 0$), or parallel to this plane (Q negative and $U = 0$). If the
scattered light has intensities $I_\perp$ and $I_\parallel$ polarized in planes normal and parallel
to the ray plane, then the proportional polarization is defined as $P = (I_\perp -
I_\parallel)/(I_\perp + I_\parallel)$, usually expressed as a percentage, or in parts per thousand,
where P corresponds to Q/I. P is found to change with the angle between the
incident and observation rays, usually known as the phase angle and denoted
by V, G or α by different workers. A plot of P against V is found to give a
curve characteristic of the surface. Figure 1 gives an example for asteroid 1
Ceres (see also Fig. 8 for 4 Vesta). This curve is typical of a rough surface,
and defines the parameters P_{min}, V_{min}, V_0 (inversion angle) and h (slope near
V_0) whose measured values are found to be diagnostic of the surface texture
and optical properties.
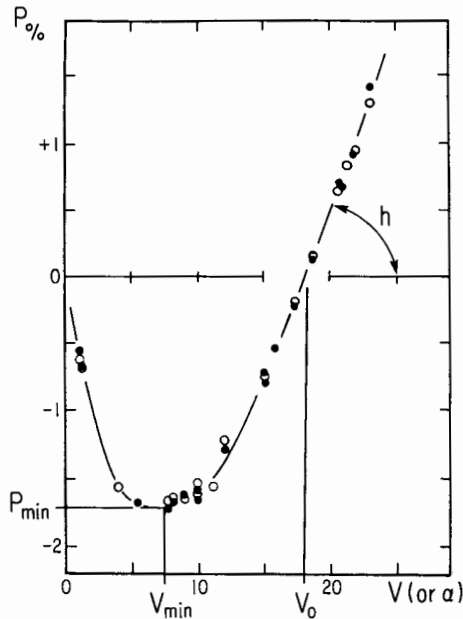
Fig. 1. Curve of polarization showing degree of linear polarization as a function of solar phase
angle, for asteroid 1 Ceres. Definitions are shown for the polarization parameters P_{min}, V_0 and
h (figure adapted from Zellner et al. 1974).
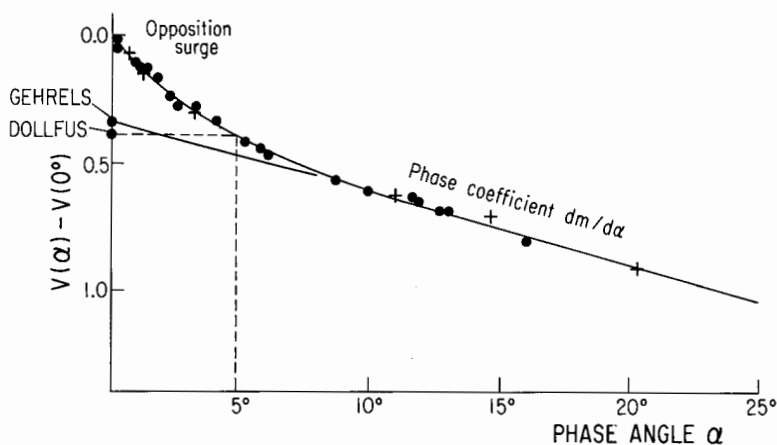
Fig. 2. Photometric phase curve showing magnitude reduced to 1 AU from Earth and Sun as a function of solar phase angle, for asteroids 69 Hesperia (dots) and 20 Massalia (crosses). Definitions are shown for the photometric parameters. Telescopic observations are by T. Gehrels and laboratory measurements by A. Dollfus.

The nomenclature and parameters relevant to photometry are discussed in the chapter by Bowell et al. and are summarised in Fig. 2 which refers to 69 Hesperia (dots) and 20 Massalia (crosses). The photometric visual albedo has special relevance to polarimetry, in view of the complication of the opposition spike or surge effect at zero phase angle. There are different practices to allow for this. Gehrels used the magnitude extrapolated to zero phase angle for photometry at the telescope. Dollfus has adopted the value at the phase angle of 5° for comparative laboratory measurements. The results are almost the same, as shown in Fig. 2.

II. HISTORICAL BACKGROUND

A. Polarimetric Remote Sensing of Planetary Surfaces

Telescopic Observations.   Arago's original observations in 1811 (Arago 1858) were made for eight regions on the lunar surface, but the modern use of the technique really started with Lyot (1929) who used a much more sensitive polarimeter, of his own design. He discovered the negative polarization, and was the first to realize that the complex curve of polarization vs phase angle provided a method of discerning remotely the surface texture of planetary bodies, and other rough surfaces. Lyot's telescopic work at Meudon Observatory was continued by Dollfus, and developed at the Lunar and Planetary Laboratory of the University of Arizona by Gehrels and Zellner, and at Kiev Observatory USSR by Morozenko. An early use of the method was the successful prediction of the nature of the lunar surface, which was found to be

simulated in the laboratory by powdered igneous rock (Lyot 1929; Dollfus 1955). The surface of Mars was similarly identified as resembling powdered limonite (Dollfus 1958).

Only planetary objects with visible surfaces are considered here. Polarization maps of the visible surface of Mercury were produced by Dollfus and Aurière (1974); similar mapping of Mars has been made over a large range of wavelengths (Gehrels et al. 1964; Dollfus and Bowell 1971; Bowell 1973), and a detailed polarimetric atlas was published by Dzapiashvili and Korol (1982). Measurements of the Galilean satellites of Jupiter have also been made (Veverka 1971a; Gradie and Zellner 1973) and interpreted (Dollfus 1975; Mandeville et al. 1980). Asteroid observations are reported in Sec. III.B.

Some key papers, reporting planetary surface polarimetric observations, are those by Lyot (1929), Dollfus (1957,1961,1985,1986) and Gehrels (1974).

Laboratory Interpretation. In order to interpret the observations of asteroids and other atmosphereless solar system objects, extensive laboratory studies of solid, rough surfaces have been conducted in a coordinated program involving Observatoire de Meudon, the University of Manchester and the University of Arizona. The bulk of these results can be found in Dollfus (1956,1961,1971,1985), Dollfus et al. (1977,1979), Zellner et al. (1977a,b, Dollfus and Geake (1975,1977), Dollfus and Zellner (1979), Geake et al. (1984) and Geake and Dollfus (1986).

Measurements on a variety of rocks, meteorites, lunar and artificial samples, both solid and pulverized, have produced empirical relationships between the polarimetric parameters, which can be understood by simple physical processes. It has been demonstrated experimentally that the polarization parameters P_{min} and V_0, as defined in Fig. 1, are related to the surface texture. Laboratory measurements on bare chips or large fragments of rocks, from the Moon or Earth, are confined to domain I on the left in Fig. 3a, whereas very finely divided silicaceous powders and lunar fines are grouped in domain II on the right. Pulverized rocks with grain sizes between 30 and 300 μm come in between these two domains, as shown in Fig. 3b. The discrimination is clear, and such plots have been used for the remote analysis of microtextures on the surfaces of planetary bodies.

It has also been found that the slope h of the polarization curve is directly related to the albedo A of the sample, irrespective of the nature of the surface (Fig. 4). There is a saturation effect for very low-albedo surfaces, which is produced on dark surfaces because the degree of polarization reaches very large values, close to total polarization. This empirical calibration offers an accurate method of determining the surface albedo of a planetary object, and hence the average diameter of the body, even if it is too small to be resolved telescopically. This method has been used extensively for asteroids, and the results have been compared with diameter determinations by the infrared
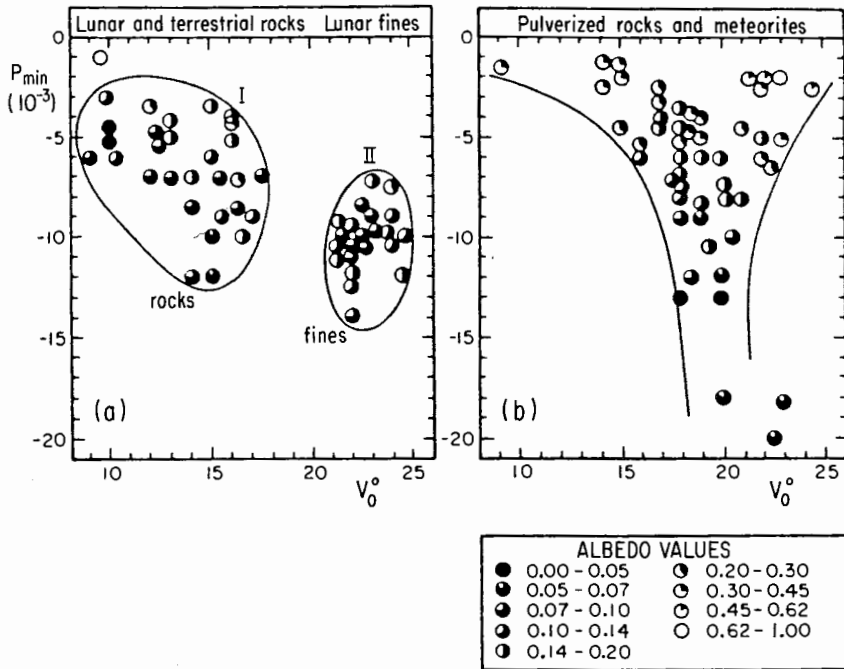
Fig. 3. The P_{min}–V_0 diagrams describing, by two parameters, the shape of the negative branch of the polarization curve. The albedo is indicated for each sample by a sector symbol in the plot. Plot (a): the zones occupied by lunar fines and by solid pieces of rocks are completely separated. Plot (b): pulverized rocks with grains between 30 and 300 μm are in between the two zones for the solid rocks and for the lunar fines. The values of P_{min} appear to be related to the albedo (figure from Geake and Dollfus 1986).

method (see Zellner et al. 1974; Chapman et al. 1975; Dollfus and Zellner 1979).

Theoretical Explanation. The polarization produced by a cloud of small spherical particles or droplets not exceeding a few wavelengths in size is amenable to computation by the extended Mie theory. However, the light entering into the intricate structure of a rough surface is subjected to more complex optical processes. At first, the cause of the negative polarization for small phase angles was unclear. It was shown that the negative polarization observed on a pile of sand grains disappeared when the same sand was in a stream falling past the polarimeter (Dollfus 1956), suggesting that complex-multiple reflections between closely neighboring grains were involved. Ohman (1955) pointed out that light from retro-reflectors may be negatively polarized, and he suggested that this mechanism could explain the negative polarization which is observed. McCoyd (1967) suggested that negative polar-
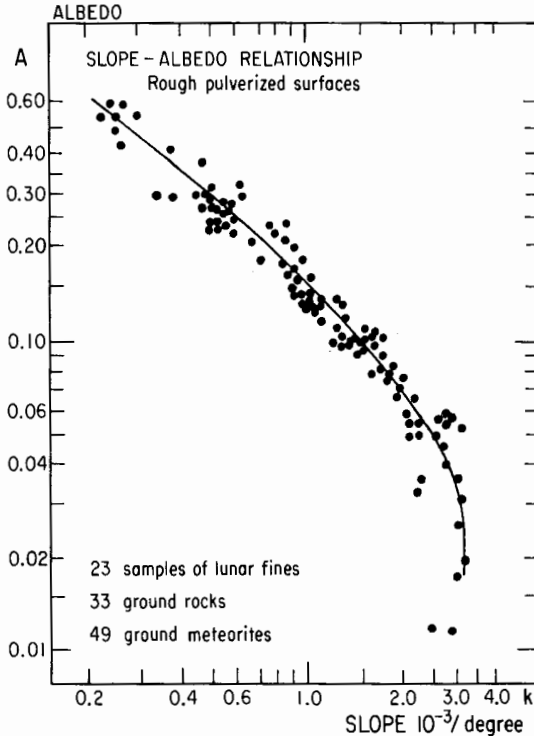
Fig. 4. The slope-albedo relationship. The albedo A is expressed by the luminance of the sample illuminated at normal incidence and observed at a phase angle of 5°, normalized to the case of a white magnesium oxide surface (see Fig. 2) (figure adapted from Geake and Dollfus 1986).

ization might be produced by total internal reflection within a crystal with two layers.

The geometrical theory by Wolff (1975) used the retro-reflector concept and traced singly and doubly reflected rays for the grains of a rough surface, using a computer program to sum the rays for different phase angles. His first theory did not deal with the diffuse unpolarized component of the scattered light, but later refinements included this, to produce the model which is described in Sec. III.B (Wolff 1980, 1981).

B. Optical Polarimetry of Asteroids

Available Telescopic Observations. The polarimetric analysis of asteroids was also pioneered by Lyot who, in 1934, recorded polarization curves for 1 Ceres and 4 Vesta, using a photographic technique. Lyot discovered that, like the Moon, Mars and Mercury, these small bodies also produce negative polarization at small phase angles. This was confirmed on 1 Ceres, 2

Pallas and 7 Iris by Provin, with the first use of a photoelectric polarimeter in 1954. These early works have been reviewed by Dollfus (1971).

Later Veverka (1971*b,c*, 1973) produced polarization curves for 4 Vesta, 8 Flora, 9 Metis, 15 Eunomia and 86 Julia; Veverka and Liller (1969) obtained measurements for 1566 Icarus; Dunlap (1974) measured the Earth-crossers 1620 Geographos and 1685 Toró (Dunlap et al. 1973).

Gehrels at the University of Arizona then initiated a major coordinated program of asteroid polarimetry, led by Zellner who produced extensive data on 94 asteroids (Zellner and Gradie 1974,1976; Bowell and Zellner 1974; Zellner et al. 1974); 53 objects were documented for several of the parameters P_{min}, V_0 or h. These measurements are available in Table V of the Tucson Revised Index of Asteroid Data (Morrison and Zellner 1979) which has 111 entries on polarimetry, and are also found in Chapman et al. (1975).

Interpretation of Asteroid Observations. Polarimetry is essentially a method of sensing the texture of a surface. In a $P_{min}-V_0$ plot such as Fig. 3, large bodies such as Mercury, the Moon and Mars are within domain II, corresponding to a fine grained powder, whereas the asteroids are located between domains I and II, and correspond to pulverized rock with coarse grains (Fig. 5). The two classes of asteroids S (circles) and C (crossed circles) are clearly separated and both types are characterized by a coarse-grained surface.

Planetary surface analysis by telescopic photopolarimetry, complemented by surface landings on the Moon and Mars, have already demonstrated that all the atmosphereless planetary objects in the solar system are subjected to the formation on their surfaces of a thick layer of small grains and debris. This layer, termed the regolith of fines, is produced by meteoritic impacts which accumulate a layer of ejected fragments, periodically gardened by new impacts that produce further ejecta. For impacts on lunar-sized objects with average impact velocities of several tens of kilometers per second, the cumulative effect of impacts working is shown in Fig. 6, and this eventually produces a thick layer of 10 μm size grains (Gault et al. 1974; Langevin and Arnold 1977). Some liquid droplets of silicate are produced on impact, and these freeze and break to produce dark fragments of agglutinates intermixed with the regolith grains (Rajan et al. 1974). The effect of solar proton bombardment is also to darken the regolith, thus producing an almost uniform low-albedo surface (Rosenberg and Wehner 1964; Matson et al. 1977; Hapke 1973).

Asteroid Vesta, with a diameter of 550 km, is the largest of the noncarbonaceous asteroids. Reflectance spectroscopy indicates an eucritic composition. Telescopic polarimetry indicates a regolithic layer made up of a broad mixture of particle sizes, mainly > 50 μm, but mixed and partially coated with small particles of ≤ 10 μm (Le Bertre and Zellner 1980). The depletion of small grains, compared to the Moon, results from the escape velocity of 0.34 km s^{-1} which is 7 times lower than for the Moon, as explained in the
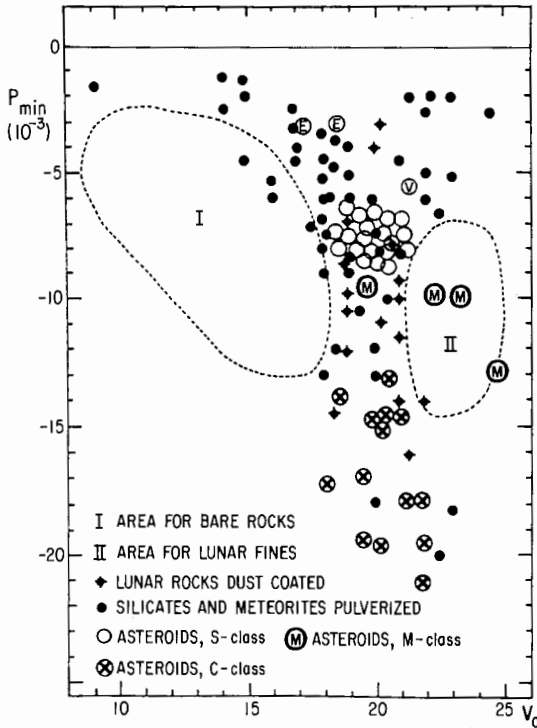
Fig. 5. Polarization of asteroids in the P_{min}–V_0 diagram of Fig. 3. Asteroids are in the zone between the area I, corresponding to large rock fragments and area II for fine powders such as lunar samples. Both S (circles), E and V asteroids and C asteroids (crossed circles) appear to be covered with a coarse-grained regolith (figure from Dollfus et al. 1977). M asteroids occupy area II (Dollfus et al. 1979).

caption to Fig. 7. The average impact velocity of 5 km s^{-1} in the asteroid belt releases 15 times less energy at impact than for the Moon, and apparently is not sufficient to melt the ejected fragments (Housen et al. 1978,1979). The optical properties of the surface are not modified by this process.

For the smaller asteroids, the polarimetric signature is consistent with a coarse regolith still more depleted in the smallest particles. This depletion is understood, because the small grains are ejected at impact with a higher speed than the escape velocity (O'Keefe and Ahrens 1977; Cintala et al. 1978,1979). There is no significant accumulation of dark agglutinate fragments, because the average impact energy is insufficient to produce molten droplets. The escape of the smallest grains into space at impact permits a continuous renewal of the regolith, which therefore does not accumulate much evidence of an optical aging effect, such as that produced by proton
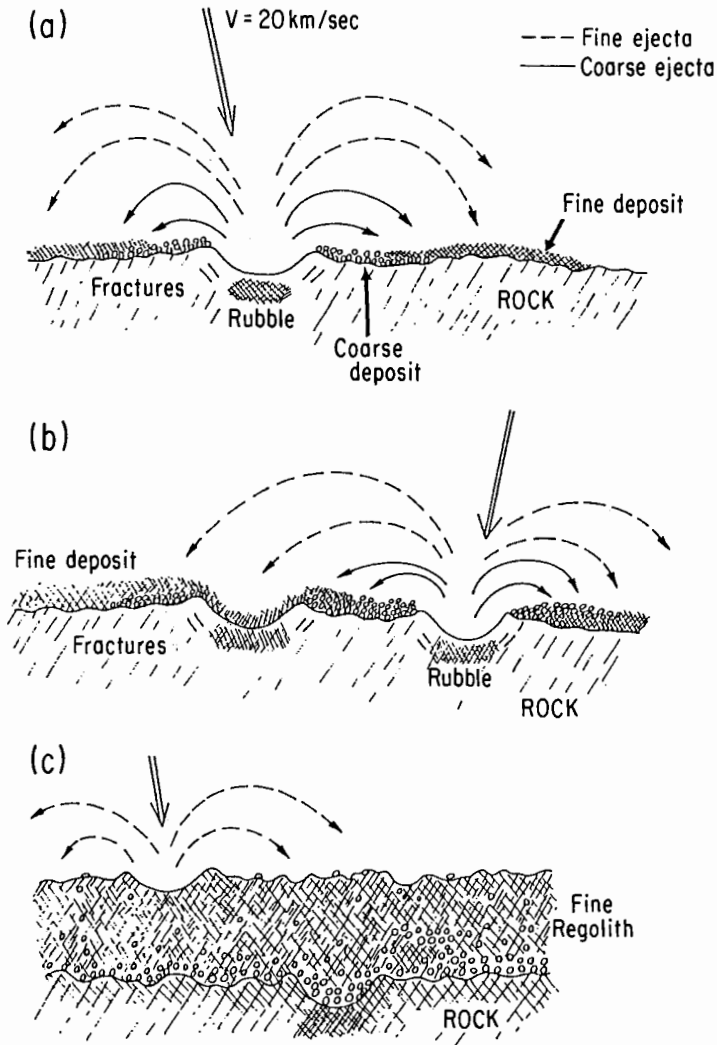
Fig. 6. Formation of the regolith at the surface of the Moon and Mercury. (a) high-velocity meteoroid impacts (typically 20 km s^{-1}) ejects coarse fragments at low velocity and small dust grains at higher velocity, plus some melted droplets of silicates. All the ejected matter returns to the surface. (b) new impacts mantle the older layer with new deposits, and produce an enrichment in small grains and in dark vitrious pieces resulting from the droplets. (c) accumulation of impacts eventually produces a thick layer of fine regolith, made of typically 10 μm size grains. There is almost no matter lost into space; the darkening is the cumulative effect of long exposure to high-energy radiation, and to the dark agglutinates resulting from melted ejecta, thus modifying the spectral reflectance of the surface (figure adapted from Dollfus 1986).
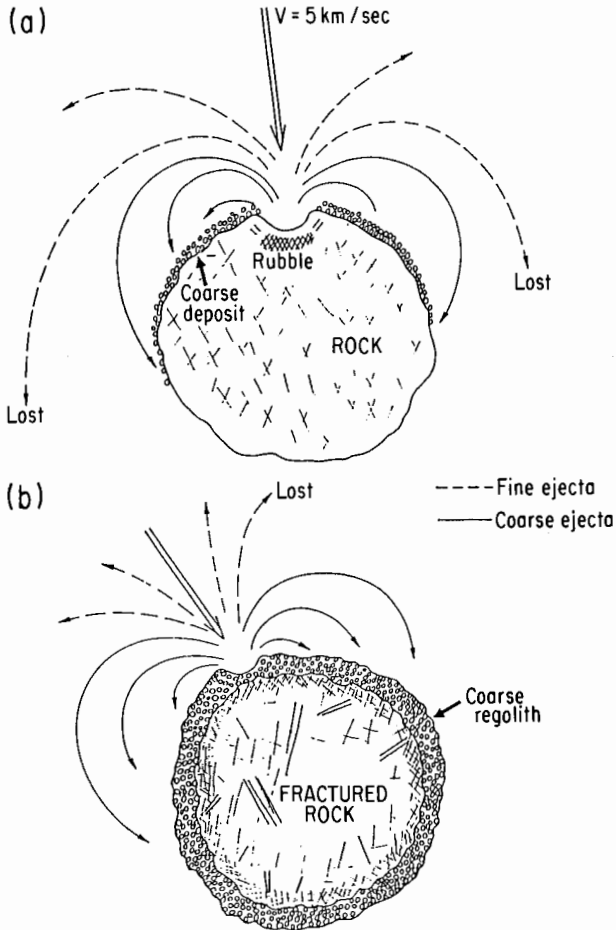
Fig. 7. Formation of the regolith at the surface of an asteroid. (a) low-velocity meteoroid impacts (typically 5 km s^{-1}) eject coarse fragments at low velocity, which return to the surface, and small dust grains at a velocity higher than the escape velocity, which are lost into space. There is not enough energy to produce a significant number of molten droplets. (b) an accumulation of such ejecta ends up as a thick layer of coarse fragments; the smaller grains disappear into space. There are neither dark agglutinates nor any accumulation of the high-energy radiation effects. The spectral reflectance of the surface therefore remains representative of the core material (figure adapted from Dollfus 1986).

bombardment. Accordingly, the regolith surface apparently preserves the optical and spectral properties of the underlying core, an important fact for remote sensing.

The polarization curves for M-type asteroids are specific. They are not reproduced by coarse-grained silicate rocks, nor do they correspond to fract-

ured metallic surfaces. Their symbols (M) in the plot of Fig. 5 depart from the silicaceous asteroids trend. They do fit with metallic powders with 20 to 40 μm fragments. Impacts by meteoroids on metallic bodies are able to produce a superficial coating of small metallic debris because, at the lower temperature of asteroids (about 150 K), nickel-iron metals are no longer ductile but brittle (Dollfus et al. 1979).

In summary, these results indicate that, for all the atmosphereless planetary objects, the formation of a surface regolith by meteoritic bombardment is ubiquitous. All bodies larger than 1500 km in diameter retain the impact ejecta and build up a thick layer of very small fines everywhere on the surface; this is then subjected to the effect of impact and irradiation from space. For smaller objects, represented by the asteroids, the escape velocity is lower and the smallest grains, which are produced by impacts at the highest velocity, are ejected into space and lost; only the larger grains remain and the regolith is continuously rejuvenated because subsequent impacts produce further losses of material into space (Housen et al. 1978,1979; Duraud et al. 1979).

This scenario, which emerges from the presently available polarization results, is over simplified. The presence of patches, spots and albedo variations at the surface of the large asteroids, plus anomalous polarization, suggest unexpectedly complex effects. These could be analyzed by more extended photopolarimetric work, including measurements from flyby spacecraft, if one wishes to assess the true physical nature of the asteroid surfaces on which more elaborate exploration or exploitation is contemplated.

More details of the polarization results for asteroids are given in the papers by Bowell and Zellner (1974), Zellner et al. (1974), Chapman et al. (1975), Geake and Dollfus (1986), Zellner and Gradie (1976), Dollfus and Zellner (1979), Le Bertre and Zellner (1980) and Dollfus (1986).

III. RECENT WORK

A. Recent Polarimetry of Asteroids

Since the review published in *Asteroids* (Dollfus and Zellner 1979), new telescopic analyses of asteroids by optical polarization have been conducted in the USSR. These investigations began in 1983 at the Astronomical Observatory of the Kharkov State University (Belskaya et al. 1985,1987*a,b*; Lupishko and Belskaya 1988; Lupishko et al. 1988*a,b*). Observations were also made with the 125-cm reflector at the Crimean Astrophysical Observatory, equipped with the five-color polarimeter of Helsinki Observatory, designed by V. Piirola (1973); in addition observations were carried out with the 100-cm Zeiss reflector of Sanglok Observatory in Dushambe, Tadjik SSR, with the 125-cm reflector in Abastumani, Georgia SSR, and with the 60-cm reflector of the Soviet-Bolivia Observatory near Tarikh, Bolivia.

Figure 8 shows the phase dependence of the polarization for 4 Vesta. The new measurements (circles) by Lupishko et al. (1988*b*) complement the pre-
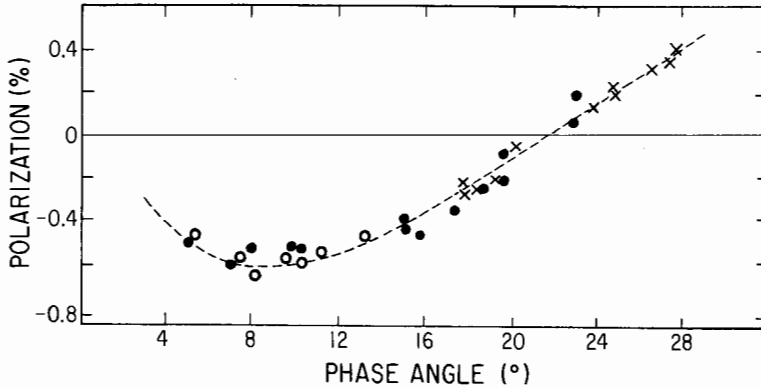
Fig. 8. Polarization phase curve of 4 Vesta in green light. Dots are data from Veverka (1971*b*); crosses are data from Zellner and Gradie (1976); and circles are new observations by Belskaya et al. (1987*a*) (Figure adapted from Lupishko et al. 1988*b*).

vious data (dots) by Veverka (1971*b*) and those (crosses) by Zellner and Gradie (1976) and produce the Vesta polarization parameters $P_{min} = -0.61\%$ $\pm 0.03\%$, $V_{min} = 9° \pm 1°$, $V_0 = 21°9 \pm 0°5$, $h = 0.065 \pm 0.004\%$ deg^{-1}. The value of P_{min} was recorded at the Bolivian station for more than 6 consecutive hr, to cover a full rotation of the body about its spin axis (Fig. 9). An amplitude variation for P_{min} of 0.1% is observed, with a maximum of the negative value of P_{min} in coincidence with the lightcurve minimum; this is to be expected if Vesta's lightcurve is assumed to be entirely caused by albedo features over its surface, rather than by an elongated shape. The presence of
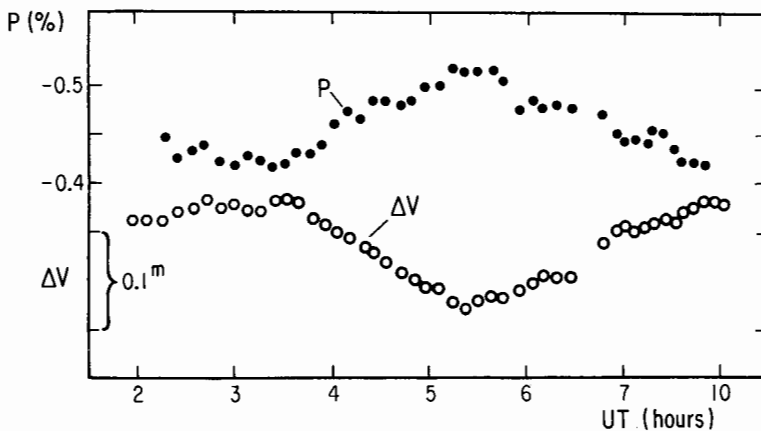
Fig. 9. Lightcurve and polarization curve of 4 Vesta in green (Lupishko et al. 1988*b*).

large dark and light patches covering extended portions of the surface is im-
plied here, and this result agrees with the speckle interferometry and radar
results (see the chapters by Drummond and Hege and by Ostro), as well as
with reflectance spectroscopy variations. Polarimetry supports a rotation
period of 5.342 hr, for a nearly spherical body with different reflectivities at
opposite edges.

   UBVRI polarimetry of the 260-km diameter, M-type asteroid 16 Psyche
was carried out with the 125-cm Crimean reflector on June 4–5, 1983, at the
phase angle 9°.6 corresponding to P_{min}, and repeated during several hours
covering a complete rotation of the body (Belskaya et al. 1985). The spin axis
pointed towards the Earth. There was no significant variation of the linear
polarization Stokes parameters Q/I and U/I, either in the ultraviolet or in the
red. The indication is that there is no preferential orientation of the surface
particles (which are assumed to be metallic) other than with symmetry about
the polar axis.

   Measurements of P_{min} have been recorded at the Sanglok Observatory
for 10 asteroids presumed to be of the metallic M type (Belskaya et al.
1987*a*). The values of P_{min} are related to the color $U-B$ and to the albedo A as
shown in Figs. 10 and 11, which also show the regions representing the tax-
onomic types E, M, C and S according to Bowell et al. (1978). Asteroids 55,
125, 201, 216, 325, 347, 441 and 796 are found to be M type, and 259 and
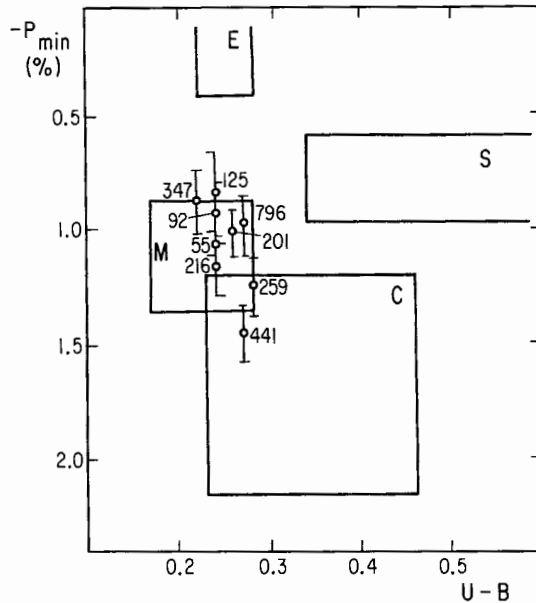
Fig. 10. Position of asteroids in the diagram P_{min}–color ($U-B$), with the main compositional
types indicated (Lupishko and Belskaya 1988).
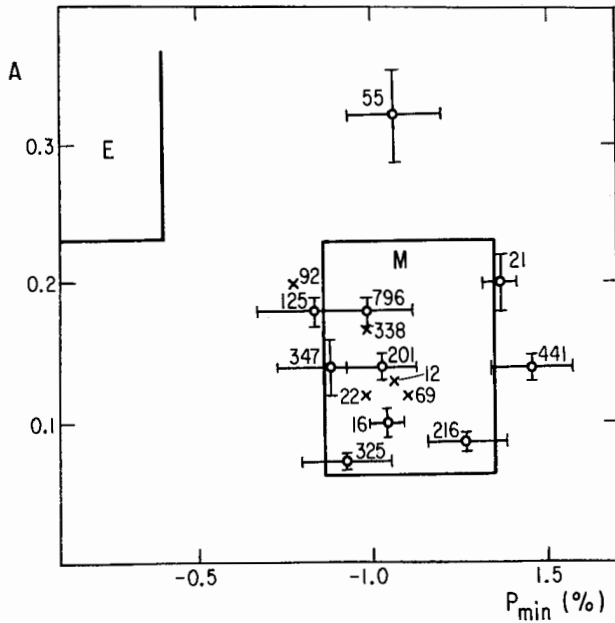
Fig. 11. Position of asteroids in the diagram albedo-P_{min} (Lupishko et al. 1988).

412 resemble C type. When comparisons are feasible with the recent eight-color photometry and radiometry classification of Tholen (1984), the results agree. Asteroids 441 Bathilde and 21 Lutetia have very deep negative branches of polarization (Fig. 11) which suggests an unusually complex surface.

55 Pandora, on the basis of the IRAS albedo of $P_v = 0.32$, was classified by Barucci et al. (1987) as E type. However, a very deep polarization minimum was found (Fig. 11), with a $P_{min} = -1.06\%$ which is inconsistent with a classical E type. The reflectance spectrum is consistent with either E or M type. Pandora either has a unique type of surface in its mineralogy or structure, or it has a metallic composition which would bias the interpretation of the IRAS data.

When all the values of P_{min} now available for asteroids are plotted vs albedo, the major types are clearly isolated; however, within each group there is a large dispersion of the P_{min} values, particularly for the M type, suggesting a variety of surface textures for all types.

B. Work on Surface Models

Two different types of mathematical model have evolved, in attempts to explain the observed photometric and polarimetric properties of planetary surfaces.

Radiative Transfer Theory for Photometry. This method adapts the work of Chandrasekhar (1950); using this approach, Hapke (1981,1986; chapter by Bowell et al.) has created a surface model which adequately explains the phase function of lunar-type surfaces. This model, for which an iterative method of computation has been developed by Helfenstein (1986), recently updated by Helfenstein and Veverka (see their chapter), uses five physical parameters; three of these refer to individual particles, namely the particle albedo for single scattering, the Henyey-Greenstein asymmetry factor and the back-scattering surge amplitude; the other two represent the overall surface microstructure in a general way, namely the compaction factor (or surface porosity), and the mean slope angle of the surface roughness. A somewhat similar mathematical approach has been proposed by Lumme and Bowell (1981; also see the chapter by Bowell et al.), and applied to the photometry of asteroids.

Models based on this approach are adequate for photometry, but fundamentally unable to explain the polarization properties of a surface, especially the observed negative polarization. This is because, as discussed below, negative polarization can only be explained by a detailed consideration of the geometry of individual multiple reflections within the complex grain structure of the surface, whereas the radiative-transfer type of theory deals only with single scattering or average multiple effects.

Geometrical Optics Methods for Polarimetry. The models that have been successful in explaining the observed positive and negative polarization by a rough surface have been those based on Fresnel reflection. An earlier theory by Hopfield (1966), was based on polarization by diffraction at grain edges; however, experiments showed that the effect is far too weak to explain the amount of polarization observed for a rough surface.

Several workers have produced models based on Fresnel reflection. Bandermann et al. (1972) and Steigmann (1978) modeled the rough surface as a smooth surface with cylindrical flat-bottomed pits. Steigmann used four parameters: the proportion of light reflected from unpitted/pitted surface (R_1), the proportion of unpolarized diffuse light (R_2), the *hole* diameter and the real refractive index. R_1 and R_2 are difficult to estimate for a real surface, but it is possible to choose values empirically that result in calculated polarization curves in general agreement with those observed. The most advanced of the models based on Fresnel reflection is that due to Wolff (1975,1980,1981); he considers the more general case of a granular surface with rough pits or intergrain interstices, and allots statistical weighting factors to the different types of reflection that can occur. He represents the surface by five parameters: the first represents the proportion of unpitted surface (EXT); the other four represent the average width/depth ratio of the pits (WID), the average grain size in wavelengths (XTL) and the real and imaginary parts of the complex refractive index (MR and MI). Again, two of these (EXT and WID) are difficult to

quantify for a real surface, but values can be found that give calculated polarization curves that fit with observations over a wide range of conditions. The physical basis of the Wolff model, and laboratory tests of it, are discussed by Geake et al. (1984); it is shown that it does broadly represent the behavior of real surfaces.

An essential feature of these models based on Fresnel reflection is that negative polarization depends on sideways double reflections. An objection has been made that, for surfaces of low albedo, those rays that have undergone two reflections would be exceedingly weak and could not contribute enough light to provide the observed intensity of negative polarization. However, the intensity of reflections from grain surfaces is independent of the albedo, and depends mainly on the real component of the complex refractive index. A low albedo is mainly due to absorption of transmitted light within opaque grains, which depends on the imaginary component of the refractive index. It is therefore only the light that enters the grains which is lost, and this has the effect of reducing the intensity of the diffuse unpolarized light. For a low-albedo surface, the polarized component is therefore relatively stronger than the unpolarized background; this is the physical explanation of Umov's law, which states that the proportional polarization is reciprocal with albedo.

A serious limitation of the Wolff model in its present form is that it takes no account of diffraction effects, which would be expected to become more important for small grain sizes. Experimental evidence for these effects is discussed below, and work is now in progress to extend the Wolff model by incorporating a Rayleigh scattering term.

Application of the Wolff Model to Asteroids. The Wolff model has been used to compute plots of the slope h vs albedo, simulating the experimental curve shown in Fig. 4. The case is presented in Fig. 12 (Wolff 1980; Dougherty 1986). This plot is computed for EXT = 0.1 and XTL = 20 wavelength and is in practice a two-dimensional diagram of the real (MR) and imaginary (MI) components of the complex refractive index of the surface particles. The data points for asteroids form a narrow band with a nearly constant MR and MI from 0.001 to 0.004 for the S type, and from 0.008 to 0.03 for the C type asteroids. A plot of P_{min} vs albedo (Fig. 13) shows similar results.

Figures 14 and 15 show computed plots of P_{min} vs the inversion angle V_0, simulating those shown in Figs. 3 and 5. These computations are developed as a function of the parameter EXT, the proportion of unpitted surfaces which, for the case of a powder, is related to the grain size XTL. Figure 14 is computed for MI = 0.006, which represents silicaceous minerals. The Moon, Mercury and Mars, which are covered with a layer of fine regolith, are shown on the plot; they give values of EXT around 0.14. Rocks and chips in large fragments, measured at the laboratory, (crossed circles) give EXT larger than 0.3. Typical S-type asteroids lie in the shaded rectangle, and give EXT around 0.2, a value representative of coarse-grained regoliths. Figure 15 is for MI =
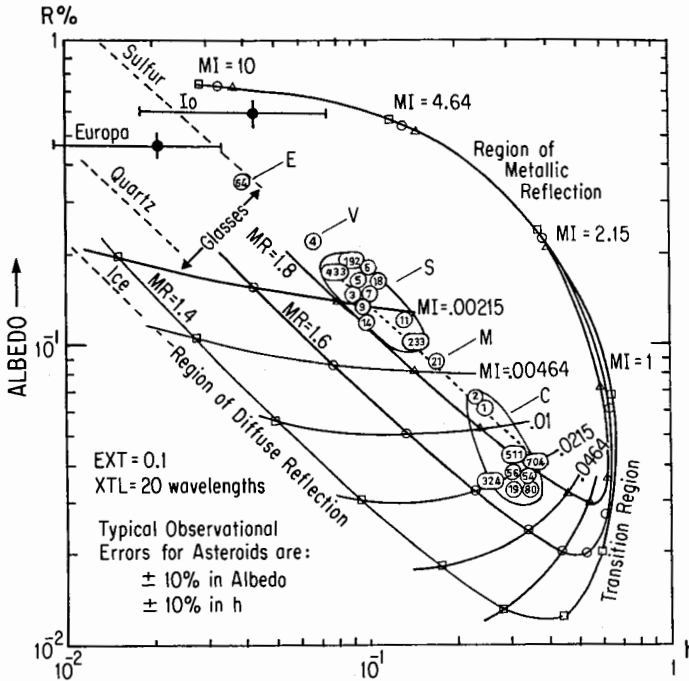
Fig. 12. Theoretical calculation of the slope-albedo diagram in the Wolff model. Plot of typical asteroids for each of the taxonomic classes E, V, S, M and C. Uncertainties in the albedo definitions do not permit a safe definition of the real index MR, but estimates of MI are given (figure from Dougherty 1986).

0.024, corresponding to the C-type asteroids; they are plotted together with samples of coarse-grained pulverized carbonaceous chondrites; EXT values are centered around 0.16, and may indicate grain sizes slightly smaller than for the S-type asteroids.

C. Recent Laboratory Work

Recent work in the laboratory has been mostly aimed at testing, evaluating and calibrating mathematical models of the way in which light becomes polarized when scattered by a planetary regolith. Using the polarimeter Minipol at the Lunar and Planetary Laboratory of the University of Arizona, Geake devised experiments to evaluate the different theoretical models, and concluded that those based on Fresnel reflection best explained the effects observed for planetary surfaces. The Wolff model was explored by computer and then tested experimentally (Geake et al. 1984). The effect of varying each of the five parameters in turn was demonstrated by computed polarization curves. It was shown experimentally that sideways double reflections were
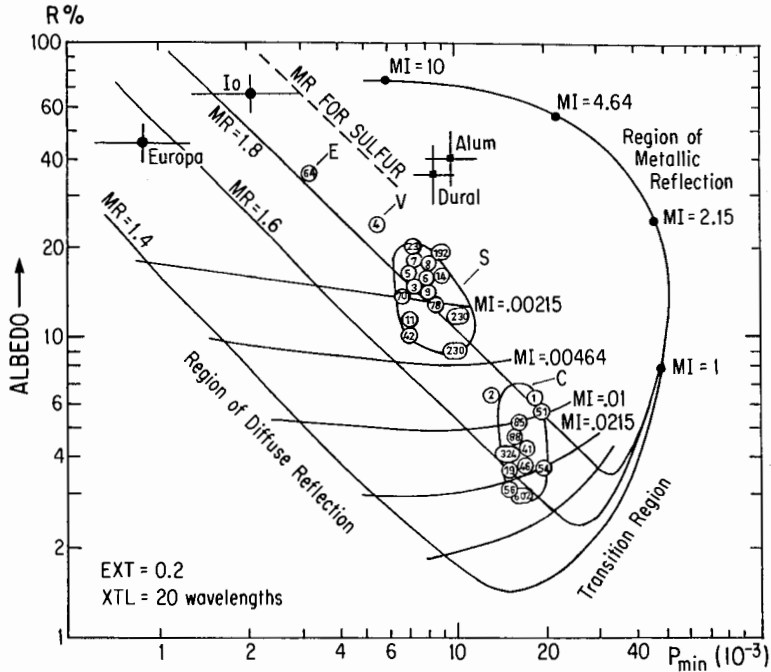
Fig. 13. Theoretical calculation of the P_{min}-albedo diagram in the Wolff model. See caption for Fig. 14 (figure from Dougherty 1986).

indeed necessary to produce negative polarization, and, following the earlier work of Dollfus, it was confirmed by different methods that surface grains must have near neighbors for this mechanism to be effective. The consequences of varying the surface albedo, and the size range and opacity of the grains, were also explored experimentally.

In later work at the Lunar and Planetary Laboratory (LPL), Geake set out to investigate the limitations of the existing theory. He explored the effect of using very small grains, down to sizes smaller than the wavelength, and discovered that the shape of the polarization curve changed in a very distinctive manner when the grain size was comparable to the wavelength (Geake, in preparation). As discussed earlier, this has now resulted in an extension of the Wolff model by the introduction of a Rayleigh scattering term (Wolff, in preparation). This work looks promising.

Laboratory work by Dougherty and Geake at the University of Manchester Institute of Science and Technology has involved the construction of a new photoelectric polarimeter, and its intercomparison with the Meudon and LPL instruments. The UMIST work has mainly concerned the exploration of samples of very high imaginary refractive index (opacity). Special glasses loaded
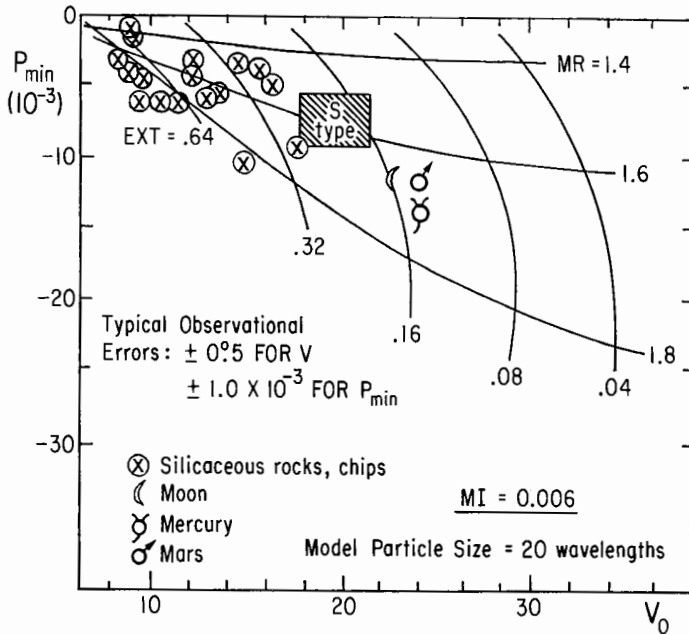
Fig. 14. Theoretical calculation of the $P_{min}-V_0$ diagram in the Wolff model. Case of powders of grains, where the parameter EXT is related to the average grain size. This plot is for MI = 0.006 corresponding to silicaceous material. Laboratory measurements on crushed rock samples are plotted (crossed circles) and give values of EXT larger than 0.3. The Moon, Mercury and Mars (see symbols) are covered with a fine grained layer and give EXT around 0.14. The S-type asteroids are within the rectangle with EXT values around 0.2, corresponding to a powder made of coarse grains (50 to 200 μm).

with cobalt oxide have been prepared by Sheffield University. These are probably the most optically dense glasses ever made, and this process has been pursued to the point where uniformity is difficult to achieve. Measurements of these samples have been carried out by Dougherty (1986) at UMIST and Meudon, and by Geake at LPL (in preparation). The real and imaginary components of refractive index are measured by using Fresnel reflection and attenuated total internal reflection methods.

Further refinements of the Wolff model have included attempts to improve the estimated values of the coefficients representing the probabilities of the different possible types of reflection within the grain structure of a rough surface. An attempt has been made to determine these coefficients by developing a computer model in which each reflected ray within a smooth pit departs in a random direction, thus simulating the effect of a more realistic rough pit (Dougherty 1986).
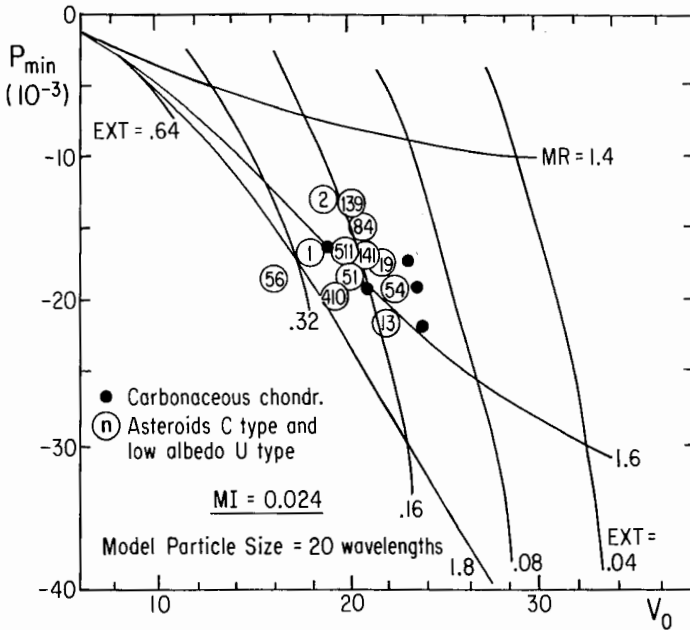
Fig. 15. Same as in Fig. 14, but for MI = 0.024 corresponding to dark material. Laboratory measurements on carbonaceous chondrites pulverized in coarse grains (dots) and C-type asteroids (circles) are intermixed with EXT value around 0.16.

REFERENCES

Arago, F. 1858. *Astronomie Populaire* 2:99–105.

Bandermann, L. W., Kemp, J. C., and Wolstencroft, R. D. 1972. Circular polarization of light scattered from rough surfaces. *Mon. Not. Roy. Astron. Soc.* 158:291–304.

Barucci, M. A., Cafria, M. T., Coradini, A., and Fulchignoni, M. 1987. Classification of asteroids using G. Mode analysis. *Icarus* 72:304–324.

Belskaya, I. N., Efimov, J. S., Lupishko, D. F., and Shakhovskoj, N. M. 1985. Five color polarimetry of the asteroid 16 Psyche. *Soviet Astron. Lett.* 11:286–291.

Belskaya, I. N., Kiselev, N. N., Lupishko, D. F., and Chernova, G. P. 1987a. Polarimetry of CMEU asteroids. I—Number of M-type asteroids. *Kinematics and Physics of Celestial Bodies* 3:19–22.

Belskaya, I. N., Lupishko, D. F., and Shakhovskoj, N. M. 1987b. Spectral dependence of negative polarization of some asteroids. *Soviet Astron. Lett.* 13:530–534.

Bowell, E. 1973. Analyse polarimétrique de la Lune, des roches terrestres et des échantillons lunaires avec application aux astéroïdes et satellites. Thèse Univ. Paris VI.

Bowell, E., and Zellner, B. 1974. Polarizations of asteroids and satellites. In *Planets, Stars and Nebulae Studied with Photopolarimetry,* ed. T. Gehrels (Tucson: Univ. of Arizona Press), pp. 381–404.

Bowell, E., Chapman, C. R., Gradie, J. C., Morrison, D., and Zellner, B. 1978. Taxonomy of asteroids. *Icarus* 35:313–335.

Chandrasekhar, S. 1950. *Radiative Transfer* (Oxford: Clarendon).

Chapman, C. R., Morrison, D., and Zellner, B. 1975. Surface properties of asteroids: A synthesis of polarimetry, radiometry, and spectrophotometry. *Icarus* 25:104–130.

Cintala, M. J., Head, J. W., and Veverka, J. 1978. Characteristics of the cratering process on small satellites and asteroids. *Proc. Lunar Sci. Conf.* 9:3803–3830.

Cintala, M. J., Head, J. W., and Wilson, L. 1979. The nature and effects of impact cratering on small bodies. In *Asteroids,* ed. T. Gehrels (Tucson: Univ. of Arizona Press), pp. 579–600.

Dollfus, A. 1955. Study of the planets by means of the polarization of their light. Thesis, Univ. Paris, English trans. NASA TT F-188, 1964.

Dollfus, A. 1956. Polarisation de la lumière renvoyée par les corps solides et les nuages naturels. *Ann. Astrophys.* 19:83–113.

Dollfus, A. 1957. Etude des planètes par la polarisation de leur lumière. Thèse Paris. English trans. NASA-TTF-188, 1964.

Dollfus, A. 1958. The nature of the surface of Mars. *Publ. Astron. Soc. Pacific* 70:56–64.

Dollfus, A. 1961. Polarization studies of planets. In *Planets and Satellites,* eds. G. P. Kuiper and B. M. Middlehurst (Chicago: Univ. of Chicago Press), pp. 343–399.

Dollfus, A. 1971. Physical studies of asteroids by polarization of the light. In *Physical Studies of Minor Planets,* ed. T. Gehrels, NASA SP-267, pp. 95–116.

Dollfus, A. 1975. Optical polarimetry of the galilean satellites of Jupiter. *Icarus* 25:416–431.

Dollfus, A. 1985. Photopolarimetric sensing of planetary surfaces. In *Venus, Mars, and Satellites of the Outer Planets,* eds. R. W. Shorthill and A. T. Basilevsky, *Adv. Space Res.* 5(8):47–58.

Dollfus, A. 1986. Analyse des propriétés des sols planétaires par polarimétrie télescopique. *Revista d'Investigacions Geologiques,* Univ. of Barcelona 42/43.

Dollfus, A., and Aurière, M. 1974. Optical polarimetry of planet Mercury. *Icarus* 23:465–482.

Dollfus, A., and Bowell, E. 1971. Polarimetric properties of the lunar surface and its interpretation. Part I—Telescopic observations. *Astron. Astrophys.* 10:29–53.

Dollfus, A., and Geake, J. E. 1975. Polarimetric properties of the lunar surface and its interpretation. Part VII: Other solar system objects. *Proc. Lunar Science Conf.* 6:2749–2768.

Dollfus, A., and Geake, J. E. 1977. Polarimetric and photometric studies of lunar samples. *Phil. Trans. Roy. Astron. Soc. London,* 285:397–402.

Dollfus, A., and Zellner, B. 1979. Optical polarimetry of asteroids and laboratory samples. In *Asteroids,* ed. T. Gehrels, (Tucson: Univ. of Arizona Press), pp. 170–183.

Dollfus, A., Geake, J. E., Mandeville, J. C., and Zellner, B. 1977. The nature of the asteroid surfaces, from optical polarimetry. In *Comets, Asteroids, Meteorites,* ed. A. H. Delsemme (Toledo: Univ. of Toledo Press), pp. 243–261.

Dollfus, A., Mandeville, J. C., and Duseaux, M. 1979. The nature of the M-type asteroids from optical polarimetry. *Icarus* 37:124–132.

Dougherty, L. 1986. Ph.D. Thesis, Univ. of Manchester.

Dunlap, J.L. 1974. Asteroid 1620 Geographos. *Astron. J.* 79:324–332.

Dunlap, J. L., Gehrels, T., and Howes, M. L. 1973. Photometry and polarimetry of 1685 Toro. *Astron. J.* 78:491–501.

Duraud, J. P., Langevin, Y., and Maurette, M. 1979. An analytical model for the regolith evolution of small bodies in the solar system. *Lunar Sci.* X:323–325 (abstract).

Dzapiashvili, V. P., and Korol, A. N. 1982. *Polarimetric Atlas of the Moon* (Tbilisi, Georgia: Publisher Metsniereba). In Russian.

Gault, D. E., Horz, F., Brownlee, D. E., and Hartung, J. B. 1974. Mixing of the lunar regolith. *Proc. Lunar Sci. Conf.* 5:2365–2386.

Geake, J. E., and Dollfus, A. 1986. Planetary surface texture and albedo from parameter plots of optical polarization data. *Mon. Not. Roy. Astron. Soc.* 218:75–91.

Geake, J. E., Geake, M., and Zellner, B. 1984. Experiments to test theoretical models of the polarization of light by rough surfaces. *Mon. Not. Roy. Astron. Soc.* 210:89–112.

Gehrels, T. 1974. Introduction and overview. In *Planets, Stars and Nebulae Studied with Photopolarimetry,* ed. T. Gehrels (Tucson: Univ. of Arizona Press), pp. 3–34.

Gehrels, T., Coffeen, D., and Owings, D. 1964. Wavelength dependence of polarization. III. The lunar surface. *Astron. J.* 69:826–852.

Gradie, J., and Zellner, B. 1973. A polarimetric survey of the galilean satellites. *Bull. Amer. Astron. Soc.* 5:404 (abstract).

Hapke, B. 1973. Darkening of silicate rock powders by solar wind sputtering. *The Moon* 7:342–355.

Hapke, B. 1981. Bidirectional reflectance spectroscopy. 1—Theory. *J. Geophys. Res.* 86:3039–3054.

Hapke, B. 1986. Bidirectional reflectance spectroscopy. 4—The estimation coefficient and the opposition effect. *Icarus* 67:264–280.

Helfenstein, P. 1986. Derivation and Analysis of Geological Constraints on the Emplacement and Evolution of Terrains on Ganymede from Applied Differential Photometry. Ph.D. Thesis, Brown Univ.

Hopfield, J. J. 1966. Mechanism for lunar polarization. *Science* 151:1380–1381.

Housen, K. R., Wilkening, L. L., Greenberg, R. J., and Chapman, C. R. 1978. Regolith evolution on small bodies. *Lunar Sci.* IX:546–548 (abstract).

Housen, K. R., Wilkening, L. L., Chapman, C. R., and Greenberg, R. J. 1979. Regolith development and evolution on asteroids and the moon. In *Asteroids,* ed. T. Gehrels (Tucson: Univ. of Arizona Press), pp. 601–627.

Langevin, Y., and Arnold, J. R. 1977. The evolution of the lunar regolith. *Ann. Rev. Earth Planet. Sci.* 5:449–489.

Le Bertre, T., and Zellner, B. 1980. Surface texture of Vesta from optical polarimetry. *Icarus* 43:172–180.

Lumme, K., and Bowell, E. 1981. Radiative transfer in the surface of atmosphereless bodies. II—Interpretation of phase curves. *Astron. J.* 86:1705–1721.

Lupishko, D. F., and Belskaya, I. N. 1988. Asteroids of M-type: Optical properties, rotation and composition. Presented at Asteroids II, 8–11 March, Tucson, AZ.

Lupishko, D. F., Velichko, F., and Shevchenko, V. 1988*a*. UBV photometry of Amor asteroids 1036 Ganymed, 1139 Atami, 1627 Ivar. Presented at Asteroids II, 8–11 March, Tucson, AZ.

Lupishko, D. F., Belskaya, I. N., Kvaratskhelia, O. I., Kiselev, N. N., Morozhenko, A. V., and Shakhovskoj, N. M. 1988*b*. Polarimetry of Vesta during the 1986 opposition. *Soviet Astron. Vestrik* 22:142–146.

Lyot, B. 1929. Recherches sur la polarisation de la lumière des planètes et de quelques substances terrestres. *Ann. Obs. Paris* 8(1). English trans. Research on the polarization of light from planets and from some terrestrial substances. NASA TTF-187, 1964.

Mandeville, J. C., Geake, J. E., and Dollfus, A. 1980. Reflectance polarimetry of Callisto and the evolution of the galilean satellites. *Icarus* 41:343–355.

Matson, D. L., Johnson, T. V., and Veeder, G. J. 1977. Soil maturity and planetary regolith: The Moon, Mercury and the asteroids. *Proc. Lunar Sci. Conf.* 8:1001–1011.

McCoyd, G. C. 1967. Polarization properties of a simple dielectric rough-surface model. *J. Opt. Soc. Amer.* 57:1345–1350.

Morrison, D., and Zellner, B. 1979. Polarimetry and radiometry of the asteroids. In *Asteroids,* ed. T. Gehrels (Tucson: Univ. of Arizona Press), pp. 1090–1097.

Ohman, Y. 1955. A tentative explanation of the negative polarization in diffuse reflection. *Stockholm Obs. Ann.* 18(8):3–10.

O'Keefe, J. D., and Ahrens, T. J. 1977. Meteorite impact ejecta: Dependence of mass and energy lost on planetary escape velocity. *Science* 198:1249–1251.

Piirola, V. 1973. A double image chopping polarimeter. *Astron. Astrophys.* 27:383–388.

Rajan, R. S., Brownlee, D. E., Heiken, G. H., and McKay, D. S. 1974. Glassy agglutinate-like objects in the Bununu howardite. *Meteoritics* 9:394–397.

Rosenberg, D. L., and Wehner, G. K. 1964. Darkening of powdered basalt by simulated solar-wind bombardment. *J. Geophys. Res.* 69:3307–3308.

Steigmann, G. A. 1978. A polarimetric model for a dust-covered planetary surface. *Mon. Not. Roy. Astron. Soc.* 185:877–888.

Tholen, D. J. 1984. Asteroid Taxonomy from Cluster Analysis of Photometry. Ph.D. Thesis, Univ. of Arizona.

Veverka, J. 1971*a*. Polarization measurements of the galilean satellites of Jupiter. *Icarus* 14:355–359.

Veverka, J. 1971*b*. Polarization curve and the absolute diameter of Vesta. *Icarus* 15;11–17.

Veverka, J. 1971*c*. Polarimetric observation of the minor planet Flora. *Icarus* 15:454–458.

Veverka, J. 1973. Polarimetric observation of 9 Metis, 15 Eunomia, 89 Julia and other asteroids. *Icarus* 19:114–119.

Veverka, J., and Liller, W. 1969. Observations of Icarus: 1968. *Icarus* 10:441–444.

Wolff, M. 1975. Polarization of light reflected from rough planetary surface. *Appl. Opt.* 14:1395–1405.

Wolff, M. 1980. Theory and application of the polarization albedo rules. Icarus 44:780–792.

Wolff, M. 1981. Computing diffuse reflection from particulate planetary surface with a new function. *Appl. Opt.* 20:2493–2497.

Zellner, B., and Gradie, J. 1974. Polarization of the reflected light of asteroid 433 Eros. *Icarus* 28:117–123.

Zellner, B., and Gradie, J. 1976. Polarimetric evidence for the albedos and compositions of 94 asteroids. *Astron. J.* 81:262–280.

Zellner, B., Gehrels, T., and Gradie, J. 1974. Polarimetric diameters. *Astron. J.* 79:1100–1110.

Zellner, B., Leake, M., Le Bertre, T., Duseaux, M., and Dollfus, A. 1977a. The asteroid albedo scale. I—Laboratory polarimetry of meteorites. *Proc. Lunar Sci. Conf.* 8:1091–1100.

Zellner, B., Le Bertre, T., and Day, K. 1977b. The asteroid albedo scale. II—Laboratory polarimetry of dark carbon-bearing silicates. *Proc. Lunar Sci. Conf.* 8:1111–1117.

ASTEROIDAL REGOLITHS: WHAT WE DO NOT KNOW

D. S. McKAY

NASA Johnson Space Center

T. D. SWINDLE and R. GREENBERG

University of Arizona

Most of our knowledge of asteroidal regoliths is indirect. It comes primarily from extensive studies of the lunar regolith and meteorite regolith breccias, and from theoretical models which try to match some characteristics of these two types of samples. By making comparisons with the well-characterized lunar regolith, the differences in location (affecting impactor flux and velocity) and gravity (affecting ejecta distribution) lead to predictive qualitative differences in the properties of asteroidal regolith. However, since the detailed distribution and flux of impactors in the main belt is a source of debate, there remain quantitative uncertainties. Comparisons can be made with meteorite regolith breccias, but we lack the detailed geological information we have for the lunar case. More to the point, we do not know with certainty whether any meteorite breccias are samples of modern regoliths. There is evidence that at least some were assembled in their present form more than 4 Gyr ago. Also, since regoliths can change with time because of changes in the flux and velocity of impactors, the properties of meteorite breccias may not reflect those of modern asteroidal regoliths. In addition, some meteorite breccias may come from either accretional regoliths or the megaregoliths predicted to result from catastrophic disruption of an asteroid followed by re-accretion.

I. INTRODUCTION

Since we have never been to an asteroid, we really do not know what their surfaces are like. We can, however, make some educated guesses. Because of their small sizes, asteroids are unlikely to have an atmosphere or

geologic processes driven by internal heating. The most important process acting on an asteroid's surface at present is impact cratering. Any asteroid with significant gravity is probably covered by regolith, a layer of incoherent fragmentary debris produced by these impacts. In addition to impacts which may produce craters and significant gardening, low velocity or gentle impacts may occur as dust and larger particles are accreted from material in similar orbits. Other processes not related to impact likely also occur on asteroidal surfaces including solar-wind implantation, sputtering and radiation damage.

In the absence of *in situ* knowledge of the properties of any asteroidal regolith, we must try to infer these properties from what we do know. One source of knowledge is the well-characterized lunar regolith. However, there are likely to be significant differences between lunar and asteroidal regoliths as a result of the differences in size and location of the bodies involved. Another source of knowledge is meteorites, particularly those inferred to contain components that were once part of asteroidal regoliths. Again, there might be differences between the properties of these meteorites and their host asteroidal regoliths, because these meteorites may have been in a regolith at a time in the past when conditions were very different. In addition, the meteorites have certainly been through a process that converted the incoherent material expected to be at the surface into a breccia, a recemented rock, solid enough to withstand ejection into space, transit to Earth, and passage through its atmosphere. Therefore, we can attack the problem from two different logical directions although there are significant uncertainties inherent in each approach.

In this chapter, we will approach our task by first describing the properties of the materials we know, the lunar regolith, lunar breccias and meteoritic breccias. We will then consider the processes involved in regolith formation and evolution and breccia formation. By then considering how those processes may have changed through time, or might be different on asteroids than they are on the Moon, we can extrapolate to asteroidal regoliths, and consider what they might be like. Finally, we will consider how we can corroborate the predictions of these models with spacecraft observations.

Before we begin our descriptions, we want to digress briefly to discuss some definitions. First, although we have used a rather standard definition of regolith (cf. the glossary), there are other similar terms that might be important for asteroids. For example, if asteroids accreted from smaller fragments (see the chapter by Wetherill), then during this accretion some (if not all) of any given asteroid was probably an accretionary regolith, consisting of incoherent material that was not necessarily fragmentary. Another type of regolith structure that probably exists is a megaregolith, a structure of fractured, if not fragmented, material throughout much or all of the body. Megaregolith can be formed in two ways: (1) a near-catastrophic collision might result in extensive fracturing, while (2) a slightly larger collision might result in disruption that would be followed by re-accretion (see the chapter by Fujiwara et al.). Breccias could in principle form from any kind of regolith. If we want to

understand the surficial regoliths on modern asteroids, we need to know which of these environments the meteoritic breccias come from, a task that is not trivial.

The Lunar Regolith

The lunar regolith consists of the fragmental unconsolidated debris layer that overlies more coherent rock nearly everywhere on the Moon. It is primarily very fine-grained material. At the Apollo sites, about 80 to 90% of the mass of the sampled regolith is finer than 1 mm. While some coarser-grained samples were collected, a typical sample has a mean grain size of about 60 to 80 μm (Heiken 1975). The finest-grained sample has a mean grain size of about 45 μm. Rocks and even boulders are considered part of the regolith, but sub-mm soil makes up by far the bulk of the lunar regolith. In the mare regions, the lunar regolith is typically 5 to 10 m deep.

The lunar regolith is made of rock fragments from broken-up or comminuted bedrock of various kinds including basalts, and coherent breccias and impact glass forms of various types. Lunar regolith shows considerable variation from place to place in chemical composition, constituent rock and mineral fragments, and properties related to maturity (duration of surface exposure). As maturity increases, the average grain size decreases and the content of volatiles directly implanted by the solar wind (including H, C, N and the noble gasses) increases. In addition, there is also an increase in the abundance of agglutinates, delicate glass forms in which impact glass from micrometeorite impacts welds together aggregates of small soil grains (Fig. 1). The amount of reduced iron, as measured by the ferromagnetic resonance index, I_s/FeO, is commonly used as a quantitative reproducible measurement of maturity of specific lunar soil samples (see, e.g., Morris 1978). Use of I_s/FeO as a maturity indicator is based on the principle that oxidized iron is reduced to metallic iron in micrometeorite impacts aided by the presence of implanted solar-wind hydrogen. These maturity properties strongly influence the optical properties of lunar soils including albedo and strength of mineral absorption bands (Adams and McCord 1973).

Lunar Breccias

The Moon contains a rich array of breccia types. In the lunar literature, breccia refers to any coherent rock made up of fragments of various sizes. Larger fragments are generally called clasts and below a generally arbitrary size, say 20 μm, the fragments are considered to be matrix. The terminology is complex and was not particularly standardized until the attempt by Stoffler et al. (1979) to define a set of breccia terms, particularly for highland rocks. Common breccia types include fragmental breccias, which consist entirely of fragments; glassy and melt matrix breccias or melt rocks, in which the matrix has obviously melted; granulitic or metamorphosed breccias, in which some solid-state recrystallization of the matrix has occurred; and a variety of crys-
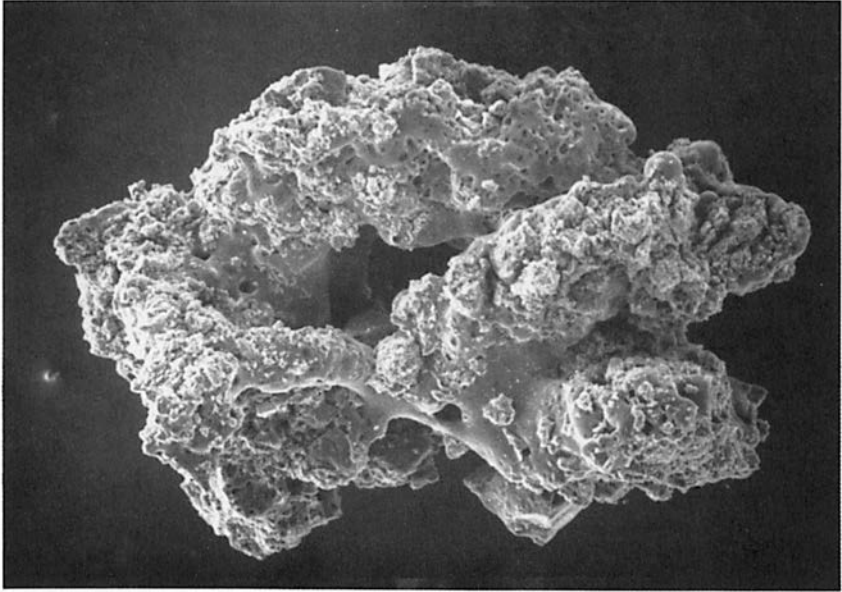
Fig. 1. A scanning electron microscope photograph of a typical lunar agglutinate. This object consists of impact glass which has engulfed small soil fragments and welded them together in an irregular aggregate. Width of particle is 1mm.

talline breccias, which result from the crystallization of a fragment-laden melt. Some lunar breccias are made entirely of one rock type, but most contain a variety of rock types. We emphasize that most of the accessible rocks on the Moon are breccias. The exceptions are the mare basalts and the relatively rare pristine crystalline highland rocks which have not obviously been through breccia-forming events.

The term "regolith breccia" is restricted to coherent rocks which have a detectable regolith component known to be produced near the lunar surface such as agglutinates or impact glass spherules (Stoffler et al. 1979). Regolith breccias always contain detectable solar-wind gases. These rocks are made from material which has been part of the surficial regolith at some time during its pre-compaction history. Regolith breccias are generally a subclass of fragmental breccias, but regolith breccias having glassy matrices also exist. Regolith breccias were originally considered to be "instant rock" or simply very local shock-compressed soil (Short 1970).

Meteorite Breccias

The use of the term breccia has been more limited in the meteorite literature. While it was realized early that many meteorites were breccias, the term

has been used mainly for achondrites showing obvious angular fragmental textures. More recently, attempts have been made to apply the lunar breccia terminology to meteorite breccias so that comparisons could be made (Keil 1982). Many breccia types have been identified among both lunar breccias and meteoritic breccias, but there are some significant differences. There are some meteoritic breccias, primitive or accretionary breccias, that do not have lunar analogs. These breccias, which have primitive components found in type 3 chondrites as well as clasts of other meteorite types, may have formed by mixing of rock fragments with unconsolidated primitive material during disruption and re-assembly of asteroids (Keil 1982). Also, the strict lunar usage of the term "regolith breccia" is not exactly applicable to meteorite breccias because meteorite breccias generally lack agglutinates or impact glass obviously produced by small-scale impact. However, "regolith breccia" has been used for both brecciated achondrites and chondrites which contain significant trapped solar wind in their interiors. The lack of features indicative of small-scale impact might be the result of differences in the cratering environment, as discussed in Sec. III.

Meteorite breccias have never really been discussed in terms of maturity properties the way lunar regolith and regolith breccias have, although the concept is probably appropriate for many kinds of meteorite breccias. It is therefore difficult to compare such properties between lunar and meteorite materials. For example, although abundant grain-size data exist on lunar regolith samples including lunar regolith breccias, few data exist for meteorites. However, enough information is available to say that meteorite breccias appear to be less mature than the lunar regolith. The grain-size data of Bhattacharya et al. (1975) indicate that at least some meteorite breccias are coarser grained than typical lunar regolith materials, and the abundances of solar-wind-implanted noble gases in gas-rich meteorites are far less than those typical of the lunar regolith (the difference is larger than can be explained by the difference in distance from the Sun). As discussed later, other major maturity indices commonly used for lunar regolith materials such as agglutinate abundances or the ferromagnetic resonance maturity index either do not apply to meteorite breccias, or the abundances and index are so low as to be undetectable in most meteorites. Consequently, it is very difficult to make quantitative comparisons in terms of maturity between the two kinds of material. Additional efforts should be made to look for maturity parameters developed for lunar materials in meteorites. Perhaps most meteorites are simply at the very low end of the lunar scale so that greater sensitivity is required. Alternatively, identification of some other maturity index more applicable to meteorites might be appropriate. The use of maturity concepts for lunar regolith materials has been so useful in providing insight into the formation and evolution of the lunar regolith that its application to meteorites would undoubtedly provide some new insights into asteroid evolution.

Age of the Regolith

Lunar soils typically have concentrations of spallogenic noble gases corresponding to cosmic-ray exposure ages (i.e., time in the upper ~1 m) of about 400 Myr, although fragments within the soils have ages ranging from <100 Myr to as much as 1700 Myr (see, e.g., Kirsten et al. 1972). The comparable quantity in breccias is the pre-compaction exposure age. This is defined as the amount of time the individual components spent in a regolith before becoming a breccia. Although difficult to separate this irradiation from the recent irradiation (post-compaction) that usually provides the bulk of the spallogenic noble gases for either lunar or meteoritic breccias, a separation can be done in some cases. Pre-compaction exposure ages ranging from 0 to 500 Myr, comparable to exposure ages of modern lunar soils, have been calculated for components of various lunar breccias and soils by Bernatowicz et al. (1977,1980) and Eugster et al. (1983a,b,1984; Eugster, 1985). In meteorites, the magnitude of pre-compaction irradiation effects has only recently become apparent. As tabulated in Table I, clasts from several meteorites apparently have pre-compaction exposure ages on the order of 10 to 20 Myr, and individual grains from some meteorites seem to require 100 to 200 Myr of irradiation if exposed in a regolith setting. Alternatively, if some or all of the pre-compaction exposure did not occur in a regolith (Caffee et al. 1987; Ped-

TABLE I
Pre-Compaction Exposure Ages of Meteorites

Meteorite	Excess $^{21}Ne_c$ (10^{-8} STP g^{-1})	T (Myr)	Reference
Clasts[a]			
Djermaia	2–3	15	Lorin and Pellas 1979
Fayetteville	2	15	Wieler et al. 1988
Kapoeta	1.4–7.6	10–60	Pedroni et al. 1988
St. Mesmin	1	5	Schultz and Signer 1977
Weston	3	20	Schultz et al. 1972
Matrix[a]			
Fayetteville	1.0–2.5	10–20	Wieler et al. 1988
Kapoeta	1.1–1.9	10–20	Pedroni et al. 1988
Sets of irradiated grains[b]			
Fayetteville	5–19	20–75	⎫
Kapoeta	5–17	60–110	⎬ Caffee et al. 1987
Murchison	3–4	15–50	⎪
Weston	4–5	20–40	⎭

[a]Pre-compaction exposure ages for clasts and matrix are calculations given by Wieler et al. assuming maximum production rate in 2-pi geometry.
[b]For irradiated grains, "regolith" ages of Caffee et al. have been divided by 2, corresponding to an assumption of maximum production rate.

roni et al. 1988), other regolith features of these meteorites may not have occurred either.

II. PROCESSES OF REGOLITH AND BRECCIA FORMATION

The currently dominant geologic process on asteroids is impact by other asteroids. These impacts can produce and modify the unconsolidated material that we call regolith. Samples of regolith can never reach the Earth as meteorites unless they undergo lithification. By lithification, we mean compression and cementation into cohesive rocks that are strong enough to survive excavation and the hazards of transport. All meteorites in the collection have been lithified to some degree and therefore cannot be exactly like an assumed loose asteroidal regolith. However, some of the interplanetary dust particles collected in the Earth's stratosphere may have originally come from unconsolidated asteroid regoliths. Many of these dust particles are quite weak and friable and survive entry into the Earth's atmosphere only by virtue of their very small size (generally <50 μm). Bradley et al. (1988) have reviewed the arguments for asteroidal or cometary sources of interplanetary dust.

Lunar meteorites recovered in Antarctica provide some insight into differences between meteorites made from regolith and the original regolith. These Antarctic lunar meteorites are very tough and compact and lack the typical intergranular porosity of both unconsolidated lunar regolith (soil) and consolidated but porous regolith breccias. Examples of tough compact regolith breccias do exist in the returned lunar collection, but these regolith breccias do not resemble closely typical lunar soil. Agglutinates are very common in lunar regolith and the abundance of agglutinates is an indication of the exposure age or maturity of a particular sample of lunar regolith. These agglutinates tend to be destroyed in compact regolith breccias, and agglutinates are also mostly lacking in the lunar meteorites. Porosities on lunar regolith breccias range from 16 to 30% with the most common porous and subporous varieties generally above 25% (McKay et al. 1986). Figure 2 shows a comparison between a typical porous lunar regolith breccia and a compact one. Unconsolidated lunar regolith is even more porous than this porous breccia. On the other hand, measured porosities for chondrites are nearly all lower than 20% (Fujii et al. 1981; Hamano and Yomogida 1982). Although it has not yet been quantitatively measured, the glassy (ALHA 81005) or extremely dense (Y-82192 and Y-82193) matrix texture of lunar meteorite breccias (see, e.g., Marvin 1983; Bischoff et al. 1987) suggests that these breccias are also less porous than typical porous regolith breccias. In the case of lunar material, it is likely that a selection process prevents the more typical porous regolith material from surviving ejection from lunar gravity and entry into the Earth's atmosphere. A similar effect could prevent us from sampling as meteorites some kinds of asteroid regolith materials.
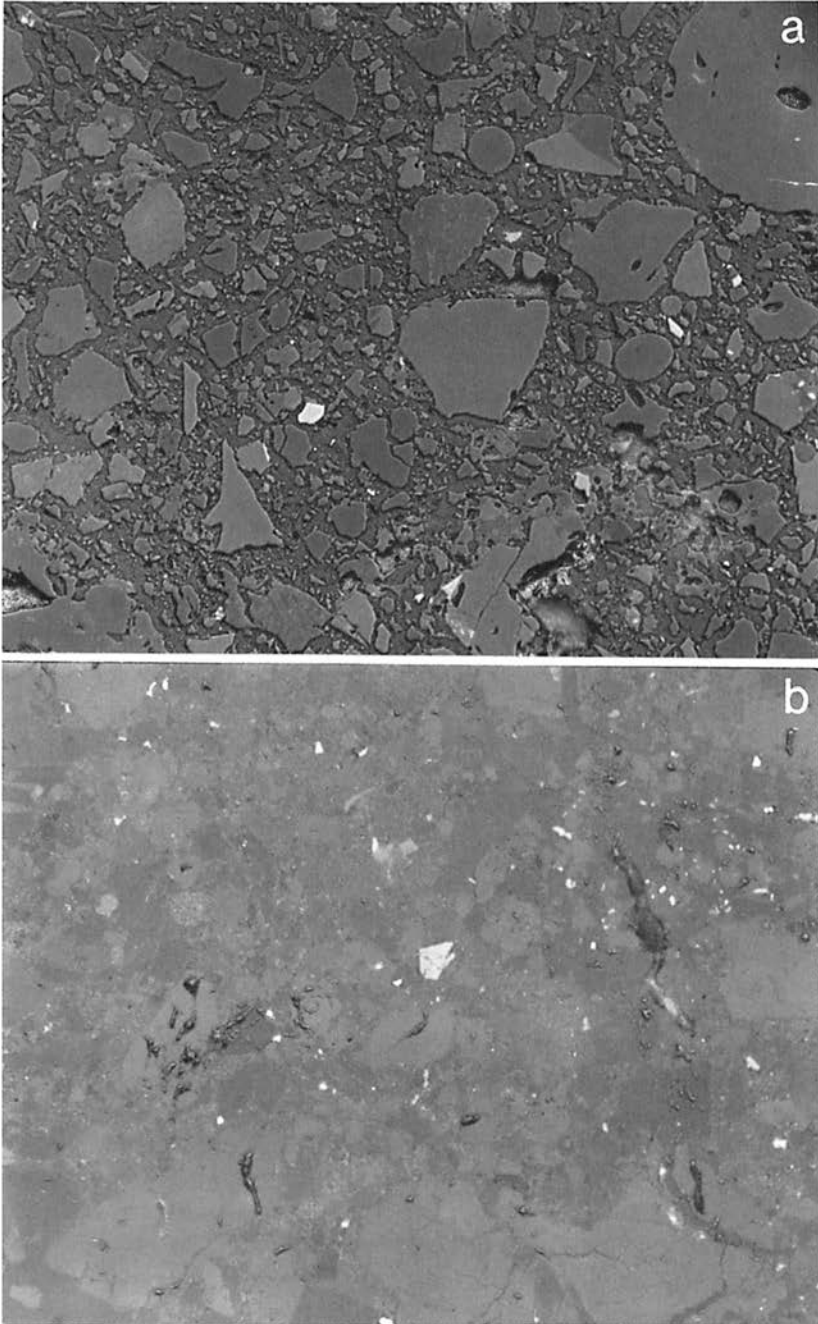
Fig. 2. Reflected light photomicrograph of (a) a porous lunar regolith breccia (15086) showing lithic and mineral fragments, glass droplets and agglutinate fragments, and (b) a compact lunar regolith breccia (15505) containing similar type of lithic and mineral clasts but lacking any significant agglutinates. Width of field for both photos: 250 μm.

As discussed earlier, the maturity of lunar regolith samples as measured by the ferromagnetic resonance maturity index I_s/FeO is derived from the fine-grained metallic iron formed mostly in agglutinates. The maturity index of lunar regolith samples ranges from about 1 unit to >100 units. While this maturity index has proved to be extremely useful for lunar soils and regolith breccias, it apparently cannot be applied on meteorites, even the gas-rich ones which have clearly had surface exposure during their history. While the data are sparse, no non-lunar meteorite has been shown to contain a detectable ferromagnetic resonance corresponding to the band used to indicate the I_s/FeO maturity index of lunar regolith materials (Morris 1983). By contrast, the first lunar meteorite, ALHA 81005, shows a clear ferromagnetic resonance corresponding to an I_s/FeO maturity index of about 5 units, that of an immature regolith sample (Morris 1983). This observation shows that the fine-grained iron which causes this resonance can survive the shock and heating processes which may accompany the ejection of the meteorites from parent bodies and the entry through the Earth's atmosphere. Thus the explanation for the lack of the ferromagnetic resonance signal in nonlunar meteorites must be found elsewhere. The general lack of agglutinates in meteorites, coupled with the related lack of significant ferromagnetic resonance effects at the appropriate frequency, is evidence that micrometeorite or small-scale, high-velocity impacting was not a significant process, at least for the meteorites in our collections. This conclusion has implications for the size distribution of impacting objects which is discussed in Sec. III.

An accretional regolith probably formed on growing planetesimals as small particles accreted via gravitational collapse and impacts. Rock could have formed later by lithification of this accretional and impact gardened regolith, or by more complete metamorphism due to heating, and perhaps, aqueous alteration. In this sense, all chondrites are essentially lithified regolith, and in principle could exhibit a continuous range of modification from those that retain the physical structure of the regolith to rocks that have lost all evidence of earlier structure. Few, if any, clearly accretional breccias exist in the meteorite collections (Keil 1982). Any low metamorphic class chondrite could be considered a kind of breccia. In fact, nearly all classes of meteorites contain identifiable examples of breccias (Keil 1982). However, meteorites are generally not called breccias unless they exhibit angular fragments embedded in a finer ground mass. Such breccias must have formed from regolith that either (a) underwent gardening that comminuted chondrules and other fragments, or (b) regolith that itself formed from an earlier generation of solid (metamorphosed chondritic or differentiated) rock.

Regolith can also form when the solid rock of an asteroid is fragmented by impacts. Unless the impact is energetic enough to fragment catastrophically the entire target body, the effect is local crater formation. Ejecta from the crater has many times the mass of the impacting projectile and considerable kinetic energy. Some ejecta (the dominant component for asteroids

smaller than ~10 km) escapes from the body. A lower velocity component is spread globally over the surface; and the slowest (most of the ejecta on larger asteroids) is deposited in the immediate vicinity of the crater. Emplacement of such ejecta begins the process of formation of a layer of regolith. In addition, the fragmented material below the base of a crater also contributes to the regolith inventory.

Once a substantial regolith layer develops on an asteroid's surface, subsequent cratering events (except for the most energetic that penetrate to solid rock) serve to excavate and redistribute pre-existing regolith. This process has been called gardening. The regolith layer is thinned at the crater site, and thickened wherever ejecta is deposited. Although there can be a net removal of material resulting from escape of the higher-velocity component, ejecta velocities are much lower for impact into regolith than for impact into solid rock. Even though gardening does not, by itself, create regolith, it can affect the nature of meteorites that later form, by exposing new layers to the surface for solar irradiation and gas implantation, by comminuting regolith grains, and by compressing the deeper layers under the crater to promote lithification.

Study of lunar regolith cores has produced an extensive discussion of the details of the gardening process. The concept of maturity profiles has been developed for lunar cores. Material in the cores, if left undisturbed by large impacts for a while, will develop a systematic increase in maturity toward the surface (Morris 1978b). The detailed shape and length of this maturity profile is determined by the exposure time of the core section and the starting maturity of the core soils. Larger impacts can overturn this profile so that deeper layers may be more mature than shallow layers. Maturity may vary by an order of magnitude over centimeter distances as a result of the random mixing and stirring effects of impacts. One of the more striking features of the lunar regolith is the variability from place to place both vertically and laterally over sometimes short distances. However, homogeneous cores and areas also exist. Asteroid regoliths subjected to gardening and reworking may also show significant differences in maturity properties over short distances, both vertically and horizontally. However, such differences have not been documented in any meteorite.

Systematic differences in the quantity of regolith produced on asteroids as a function of asteroid size occur because larger asteroids retain a larger fraction of impact ejecta and because their longer lifetimes against collisional disruption permit greater accumulation. Attempts to model these differences have been made by groups in Tucson (Housen et al. 1979a,b; Housen 1981a,b; Housen and Wilkening 1982) and Orsay (Langevin and Maurette 1976,1980,1981; Dran et al. 1979; Duraud et al. 1979; Langevin 1982, 1986). Some of their results are compared to the lunar regolith in Table II. As with many aspects of asteroid work, calculations are not straightforward because the dominant events are infrequent and stochastic. This follows from the size-frequency distribution of impacting bodies. The distribution is such

TABLE II
Comparison of Lunar Regolith with Model Asteroidal Regoliths

	Lunar[c]	Asteroid models	
		Orsay[c]	Tucson[c]
Depth	5–10 m(mare)		
10 km asteroid		70 m–0 m[a]	8 m–0 m[a]
100 km asteroid		15–500 m[a]	16–230 m[a]
500 km asteroid		12–250 m[a]	28–4600 m[a]
Exposure in top 1 m	400 Myr	1–10 Myr[b]	0–4 Myr
		100–500 Myr[b]	
Mean grain size	60–80 μm	"fine"–1 mm[a]	
Agglutinate abundance	up to 60%	1%	

[a]First number is for a weak asteroid, second for a strong asteroid.
[b]Smaller number from Langevin and Maurette (1980), larger calculated from erosion rate given by Dran et al. (1979).
[c]References: Lunar petrology: Heiken 1975; Orsay model: Langevin and Maurette 1980,1981; Dran et al. 1979; Duraud et al. 1979; Tucson model: Housen 1981a.

that the largest impacting projectiles excavate, distribute and eject more material than all the smaller impacts combined. Besides introducing major, stochastic changes in the time evolution of regolith, these larger impacts also create anomalous regions. At the impact site, the regolith may be thin or nonexistent, and in the neighborhood of the crater the ejecta deposits may be anomalously thick.

Housen (1981a,b; Housen and Wilkening 1982) has shown that quantitative differences between results of his group and of the French group are primarily due to the respective definitions of the "typical" portion of the surface over which average regolith parameters (e.g., regolith depth) were evaluated. It is not clear what definition is most appropriate, and the differences can be as large as the calculated values. Housen also has showed that the irregular, stochastic time variation results in regolith thickness can vary by ±100%, even for a single asteroid's nonanomalous regions. Thus systematic differences calculated for types, sizes and locations of asteroids can only be taken as suggestive of trends, and not necessarily applicable to any particular body.

Another theoretical result obtained since 1979, that has to do with stochastic variations, is Housen's (1981a,b) conclusion, based on Monte Carlo studies, that irradiation histories and regolith maturity are independent of asteroid size. Housen did find that these theoretical irradiation histories are consistent with the fraction of irradiated grains found in gas-rich meteorites.

Housen (1981a,b) also compared his theoretical results with the fraction of breccia among achondrites and among chondrites. He concluded that any differentiated asteroid of diameter >150 km could have contributed the quan-

tity of brecciated material observed in achondrites, and any weak chondritic asteroid >20 km could produce the correct fraction of brecciated chondrites. Here again, the ambiguous use of the word brecciated reveals a conceptual problem: while Housen's models indicate the amount of regolith on a body, they do not address the problems of either how or how much of that broken-up material is lithified into breccias strong enough to reach the Earth. Any quantitative interpretation of amounts of breccia among meteorites requires some model of how, where and how much lithification occurs.

Lithification and Alteration Processes

Lithification, the formation of rock from regolith, can occur in several different ways. Some lunar breccias were clearly made by direct shock compression of fragmental material, generally accompanied by heating, glass formation and welding. These breccias have relatively low porosity. This class of breccia includes the compact variety (Fig. 2b) of regolith breccia (Wentworth and McKay 1984). Other regolith breccias, while coherent, show no obvious evidence of shock and may be lithified by a thermal welding process in which the heat is originally generated by impact. Some of the more porous lunar regolith breccias appear to have been welded rather than shocked. Many lunar breccias, while coherent, show no obvious shock effects or no obvious welding, melting and glass formation. It is thus not clear how they were lithified.

A common type of lunar breccia has an obviously melted and finely recrystallized matrix. These melt-rock breccias combine impact-melted material with clastic or fragmental material. Still other lunar breccias are not melted but are clearly metamorphosed and these have apparently recrystallized at moderate depths in the lunar megaregolith. The heat source for this metamorphism and recrystallization may be (1) the lunar thermal gradient, or (2) impact thermal energy trapped in thick ejecta blankets. Except for the porous regolith breccias, analogous examples of all of these breccia types have been found among meteorites. On the other hand, lunar breccias do not include anything resembling an accretional breccia.

Deducing details about the lithification process has been very difficult for lunar breccias. Even where much is known about the regional and local geology, the lithification processes which made regolith breccias still remains a controversial subject (Chao et al. 1971; McKay and Morrison 1971; Simonds 1973; Phinney et al. 1976; Schaal and Horz 1980; Bischoff et al. 1987). While similar processes should operate on asteroids, it is even more difficult to constrain or deduce these lithification processes without any geologic information whatever on the structure of asteroids.

Lunar breccias have not been subjected to aqueous alteration whereas many meteorites, both carbonaceous chondrites and low-grade chondrites, have clearly undergone this kind of alteration. One effect of aqueous alteration may be to cement and lithify the regolith into coherent rock. This topic is covered more fully in the chapter by Scott et al.

III. CHANGES OF REGOLITH PROPERTIES WITH TIME

As long as there are impactors and energetic particles, regolith formation and evolution are continuous. Therefore, a modern regolith will not necessarily be the same as the regolith at some time in the past, even on the same body. In this section, we will consider how regoliths might be expected to change with time, as well as estimate when the regolith samples we have actually were part of a regolith.

Changes Intrinsic to the Processes of Regolith Formation and Evolution

If asteroids accreted from smaller bodies, they probably would have had an accretionary regolith, consisting of unconsolidated (though not necessarily fragmented) material. Chondritic meteorites, which contain mixtures of primitive components such as chondrules and metal grains, could probably be thought of as breccias formed in an accretionary regolith; however, even this accretionary regolith may have been reworked and altered by impact processes as it was accreting so that our samples of it may not be pristine accretion material. These impact alteration processes would likely be limited to mechanical comminution during an early regime when relative velocities were low.

For asteroids that underwent differentiation, evidence for this regolith may have been destroyed, and regolith formation resumed when the surface solidified. Some asteroids may have undergone resurfacing with differentiated material so that the original accretional regolith surface was either destroyed or perhaps buried.

For the undifferentiated asteroids (chondrite parent bodies), the character of the regolith would have begun to change when relative velocities among asteroids became high enough that impacts caused net erosion, rather than accretion; however, these regoliths would have started with a less cohesive target than those on differentiated bodies. In either case, fragmentation and redistribution of existing material would become increasingly important and, depending on the relative importance of burial and turnover, grain size distribution and maturity might change considerably. Impact thermal effects would become more common and melting might occur locally. At some point, agglutinates might start to form, although mechanical mixing, gardening and reworking would serve to dilute agglutinates and keep their abundance very low. Over a long period of geologic time, asteroid regoliths would become more mature on the average, although regoliths of small asteroids may have never reached significant maturity because of a net loss of the regolith layer nearest the surface. In addition, xenoliths from more distant locations might become more common. At any time during the evolution of either type of body, a large impact may have fractured and brecciated a significant part of the asteroid. Even larger impacts may have disrupted the asteroid, leading to re-accretion and the formation of a highly brecciated asteroid. Both of these

processes form a megaregolith structure. After such large impacts, near-surface regolith development would basically start over, although some of the material would already have a regolith history. More than one cycle of disruption and re-accretion may have occurred leading to very complex histories for some asteroids. Breccias could thus form under a variety of conditions. Some breccias may be entirely or mostly early primarily accretionary regolith breccias, while others may be considerably evolved and reworked. Yet others would be mostly "restarted" regolith breccias and contain little or none of the early accretionary regolith. Keil (1982) has pointed out examples of meteorites that indicate breccia formation during many of the steps listed above. Aqueous and thermal alteration (see the chapter by Scott et al.) could be occurring simultaneously with regolith development, which might lead to slightly different breccias (see Kerridge and Bunch 1979).

Changes in Cratering Rate and Size Distribution

The cratering rate on the Moon was much higher in the past than it is now (Hartmann 1980). Because the macroscopic properties of a regolith are determined by impacts, a change in the flux would change the rate of evolution of the regolith and the average duration of exposure to solar or galactic cosmic-ray effects. However, unless the change in flux was accompanied by a change in crater size distribution, it would not change the impact-related maturity indices.

There is some evidence for changes in the crater size distribution over time. Younger surfaces in the inner solar system (e.g., the lunar mare) have a steeper crater size distribution than older surfaces for craters 5 to 100 km (Strom 1987). Although it is extremely difficult to find micrometeorite craters (0.1 to 1 μm) in meteorite breccias, the sparse data available suggest that the cratering rate differed from the present lunar rate by a factor of 10 or less (Brownlee and Rajan 1973; Goswami et al. 1976), and when coupled with the steep decline in large craters (Hartmann 1980), our data suggest that the difference extends to smaller size ranges as well. Data on lunar regolith breccias also suggest a significant change in the size distribution of impacting objects. Ancient regolith breccias, while they are well comminuted and include glass from larger impacts, they contain few agglutinates or other indicators of micrometeorite reworking (McKay et al. 1986). This suggests that larger impacts greatly dominated micrometeorite impacts during the time when these materials were exposed at the lunar surface and before these regolith breccias were closed to further processing (about 4000 Myr ago).

In the absence of competing effects, this dominance of larger impactors would tend to make the rate of turnover relative to burial lower in the past, leading to a less mature regolith. However, since it is not certain when (or where) the meteorites' micrometeorite craters were acquired, it is harder to compare with the known lunar flux of large craters. Also, the size distribution of the micrometeorite craters themselves in the gas-rich meteorites seems

comparable to the lunar size distribution (Brownlee and Rajan 1973; Goswami et al. 1976).

Changes in Solar Behavior over Geologic Time

Changes in solar behavior would not affect the macroscopic properties of a regolith, since these are determined by impact. However, since features related to solar activity are used to determine regolith maturity, any changes can affect our interpretations.

The possibility of secular changes is considered from several perspectives in Pepin et al. (1980). Evidence for variations in the solar-flare energy spectrum and the solar-wind flux and elemental composition is equivocal (see, e.g., Crozaz 1980; Pepin 1980). There is, however, convincing evidence for a change in the isotopic composition of the solar wind, particularly for nitrogen. The $^{15}N/^{14}N$ ratio in lunar soils and drill cores decreases as parameters related to age (maturity, exposure age, depth within core) increase, suggesting a secular change in the solar wind with time (Kerridge 1975). The Apollo 11 and 17 soil breccias are consistent with the observed trend if they are assumed to reflect surface exposure more than 2000 Myr ago (Clayton and Thiemens 1980). Although there is no convincing explanation of why the nitrogen isotopic composition of the solar wind should vary with time (Kerridge 1980,1985), explanations involving mechanisms on the lunar surface are even less satisfying (Kerridge 1975,1985).

Similar secular changes have been suggested for He and Ne, because the $^3He/^4He$ and $^{20}Ne/^{22}Ne$ ratios are progressively lower in the modern lunar soils, lunar breccias and meteorite breccias (in this order) (Eberhardt et al. 1972; Pepin 1980). This effect is probably related to a variation in the abundance of two isotopically distinct solar components with different energy spectra (Wieler et al. 1983). Arguments for secular changes in solar behavior based on the noble gases are less convincing than those based on nitrogen. For one thing, the effect could be explained by variations in the amount of loss of the lower-energy component, a plausible effect (although minerals with different retention properties within the same soil have the same ratio of the two components [Benkert et al. 1988]). Furthermore, the argument for a secular change hinges on the assumption that the lunar breccias and meteorite breccias are ancient, an assumption not totally proven (see below).

Changes in solar behavior associated with a T-Tauri phase could be much more dramatic. Currently, the strongest argument for T-Tauri behavior comes from studies of individual grains from gas-rich meteorites (Caffee et al. 1987). In several gas-rich meteorites, sets of grains with solar-flare tracks (i.e., grains that have had a surface exposure to the Sun) contain substantially more spallogenic noble gases than grains without solar-flare tracks, corresponding to exposure ages (under regolith conditions) of as much as 200 Myr. Caffee et al. (1987) have argued that the duration of the exposure and the lack of grains with spallogenic noble gas but no solar-flare tracks are both implausible for

grains within such an immature regolith, and therefore suggest a higher flux of solar flares with a harder energy spectrum than contemporary flares. Pedroni et al. (1988) have criticized this interpretation, arguing that the longest exposures are just the extreme end of a continuum of pre-compaction exposure histories, but the correlation of tracks and spallogenic noble gas remains a problem. For our purposes, the important point is this: if the Sun did go through a T-Tauri phase while asteroidal regoliths existed (as accretionary regoliths?), the estimates of the duration of regolith exposure based on spallogenic noble gases could be in error by many orders of magnitude.

Age of Formation of Lunar and Meteorite Breccias

Since regoliths may change substantially with time, it is important to try to define the ages of the breccias available.

An upper limit to the age of a breccia can be set by finding the ages of clasts, since the breccia must have formed at least as late as any of the clasts within it. In lunar samples, most studies of breccias find ages of about 4000 Myr, generally interpreted as representing major (breccia-forming) impacts (cf. review by Turner 1977), although there is some evidence for clasts with ages as young as 2900 Myr (Megrue 1973). Based on ^{40}Ar-^{36}Ar data, formation or closure ages for lunar regolith breccias may span the time from the present back to about 4000 Myr (McKay et al. 1986). Several meteorite breccias have clasts with ages between 3500 and 4500 Myr (see summary in Keil 1982), while one xenolith in St. Mesmin has concordant K-Ar, U-Th-He, and (possibly) Rb-Sr ages of about 1300 Myr (Schultz and Signer 1977; Minster and Allègre 1979).

In addition, ^{40}Ar-^{39}Ar studies indicate that many meteorites have experienced shock events in the last Gyr (Bogard 1979). These shock events are presumably related to the kind of impacts that drive regolith evolution and perhaps cause lithification of regolith material into breccias. However, most of the shocked meteorites are not regolith breccias, so this does not necessarily mean that any of the meteorites we have were in a regolith in the last Gyr.

Constraints on times of breccia formation can also be set by studying decay-produced noble gases resulting from surface or near-surface exposure. For example, most gas-rich lunar highland breccias contain grain surface-sited xenon produced by fission of ^{244}Pu (82 Myr halflife), accompanied by variable amounts of ^{129}Xe from the decay of even shorter-lived (16 Myr halflife) ^{129}I. Also, lunar breccias and soils usually contain surface-sited ^{40}Ar, almost certainly implanted by interactions with the solar wind (Manka and Michel 1970). None of these components was produced by *in situ* decay, but their abundances probably closely track the lunar production. If so, analyses of ^{129}Xe/fission Xe (Swindle et al. 1986) suggest extremely old times (up to 4500 Myr ago) of surface exposure for some breccias. Also, ratios of surface-sited ^{40}Ar to solar-wind-derived ^{36}Ar in breccias and soils suggest times of

exposure ranging from the recent past to more than 4000 Myr ago (see, e.g., Yaniv and Heymann 1972; Kerridge 1980; Eugster et al. 1980,1983b; McKay et al. 1986). Eugster et al. (1983a) have also used the fact that cosmic-ray-produced neutrons can induce fission of ^{235}U at depth of about 1 m, and have used analyses of neutron-induced fission abundances coupled with depth-dependent isotopic ratios to calculate times of near-surface exposure, and frequently find ages of 3000 to 4000 Myr.

The identification of comparable effects in meteorites might be taken as confirmation of the ancient nature of meteoritic regolith breccias, but so far there are only hints of such behavior. Some gas-rich meteorites release excess heavy (potentially fission-produced) Xe isotopes at low temperatures (Manuel 1967; Shukolyukov et al. 1983; Swindle et al. 1989), consistent with surface siting, but the isotopic spectra have not been precise enough to identify the source as ^{244}Pu or ^{238}U. In addition, ^{40}Ar and ^{36}Ar correlate in some grain-size separate experiments (Gopalan et al. 1976), but this appears to be the result of fortuitous chemical variations with grain size.

Another way to use ^{244}Pu as a chronometer for samples older than 4000 Myr involves analyzing fission tracks. Macdougall and Kothari (1976) used the track densities in actinide-poor olivine grains adjacent to actinide-bearing matrix to determine compaction ages of 4300 Myr or more for five CM carbonaceous meteorites. This provides the most direct evidence that some meteorites are samples of ancient regoliths, but it can be argued that gas-rich carbonaceous chondrites do not come from the same environment as gas-rich achondrites or ordinary chondrites (Goswami et al. 1984), i.e., that they are not analogous breccias. However, Kothari and Rajan (1982) used the ^{244}Pu fission track densities within easily annealed phosphates to conclude that the chondrite Bhola had not been significantly heated since about 4100 Myr ago. Because metallographic cooling-rate determinations suggest a common history from a high temperature, they concluded that this represents a lower limit to the time of lithification.

Finally, if one accepts the assertions of secular changes in solar-wind isotopic ratios with time, these could potentially be used to determine time of exposure. Unfortunately, solar-wind-implanted nitrogen in gas-rich meteorites cannot be unambiguously distinguished from spallogenic and indigenous nitrogen (Murty and Marti 1986; Grady and Pillinger 1988). For the noble gases, much of the argument for secular variation is based on the assumption that meteoritic breccias are old, so it would be circular reasoning to argue that the isotopic variations prove an old breccia age.

In summary, there is strong evidence that many lunar breccias contain evidence of regolith exposure 3000 Myr or more ago. For meteorites, there is some evidence (particularly from fission tracks) that some breccias are quite old and no evidence that any record regolith exposures in the last 1 Gyr. Thus, we may not have a meteoritic sample of a typical modern asteroidal regolith. Since maturity, as the name implies, tends to increase with time, modern

asteroidal regoliths might be more mature than we would suspect from analysis of meteorite regolith breccias. This may present a problem if we try to correlate remote spectral data on asteroids too closely with meteorites in the collection; it has been well demonstrated from lunar studies that maturity can have a major effect on spectral properties of the regolith.

IV. CHANGES OF REGOLITH PROPERTIES WITH LOCATION

Having considered how regoliths might change with time, let us now consider how modern regoliths might differ from one place to another. The two most important differences between the Moon and the typical main-belt asteroid are the location in the solar system and the strength of the local gravity field.

Effects of a Different Location in the Solar System

The flux of impactors is almost certainly higher in the main asteroid belt than at 1 AU. Housen and Wilkening (1982) have briefly reviewed estimates of the cratering flux in the main asteroid belt, and argue that the flux of large bodies is greater by a factor of 100 to 1000 in the main asteroid belt compared to that at 1 AU. On the other hand, Shoemaker (1984) calculated an increase by a factor of <10, so there is substantial uncertainty in the actual flux. A higher flux will speed up regolith evolution, increasing the depth of regolith for a given time of evolution. However, the maturity of the regolith is also determined by the crater size distribution, which is even harder to infer. It would not be surprising if the size distribution differed substantially from that at 1 AU, since Strom (1987) has found different crater size distributions at different locations in the solar system. In the most detailed attempt to find the overall size distribution in the main asteroid belt, Housen et al. (1979a) tied telescopic observations to observations of dust and inferred a size distribution that has a lower ratio of small to large impactors than is found at 1 AU.

Impact velocities will tend to be lower on asteroids than on the Moon, both because relative velocities are lower and because acceleration just before impact (as a result of gravity) is less. Lunar impacts have an extra 2.4 km s^{-1} added just from this effect. A lower velocity will result in a smaller crater, again leading to slower regolith evolution. A lower velocity will also result in a lower magnitude of thermal effects, including agglutinate formation (but see Horz and Schaal [1981]). Langevin and Maurette (1981) have suggested that the lack of agglutinates in meteoritic regolith breccias can be explained by a combination of the lower impact velocity and a different size distribution of impactors in the main asteroid belt.

Finally the difference in location will lead to a difference in the flux of solar particles, because the flux falls off as r^{-2}. This means, for example, that it would take an order of magnitude longer to acquire a given density of solar-flare tracks at 3 AU than it would at 1 AU. In addition, since the galactic

cosmic-ray flux changes little with distance, the ratio of galactic cosmic ray to solar effects should be higher in the asteroid belt. Assuming that the ratio of time spent in the solar-active zone to that spent in the galactic cosmic-ray-active zone remained constant and that the solar-wind gases were not saturated, Anders (1975) suggested that by comparing the ratio of solar-wind-implanted gases to galactic cosmic-ray-produced spallation products (from pre-compaction only) in gas-rich meteorites to that in lunar samples, it might be possible to constrain locations of exposure. Although the number of assumptions involved seems formidable, the calculation often suggests main-belt exposure locations (Anders 1975; Wieler et al. 1988).

Effects of Reduced Gravity

The differences in cratering expected between the Moon and asteroids are reviewed in the chapter by Davis et al. (see also Cintala et al. 1979).

Asteroids have smaller gravity fields than the Moon, which makes a substantial difference in the ejecta pattern. A far greater proportion of ejecta is lost than on the Moon (although some may temporarily go into orbit, only to re-accrete). Also, the ejecta that is retained tends to travel farther, making many ejecta blankets global, rather than local, phenomena. These effects should all make loss or burial of material more important and turnover less important on asteroids compared to that on the Moon. Thus, asteroidal regoliths should be less mature than the lunar regolith.

For small asteroids which tend to lose a significant proportion of ejecta, the net effect may be to limit the thickness of the regolith involved in gardening and reworking. This, in turn, will limit maximum maturity which the reworked regolith can attain and may set an upper limit on both agglutinate production and solar-wind gas acquisition. Thin regoliths cannot become very mature because they are easily diluted by fresh subregolith material (McKay and Basu 1983).

There are also effects related to the transition from strength to gravity scaling. This occurs at an energy inversely proportional to the local acceleration due to gravity, and hence occurs earlier for larger bodies. Since gravity-scaled craters tend to be smaller for a given energy, smaller bodies will tend to have larger craters for comparable impacts, leading to more ejecta. For bodies small enough, this effect is overcome by the tendency to lose ejecta.

The low gravity and small body sizes might make it more likely that surface material far from the crater would be lofted ("spalled") by impact-generated shock waves. This process could be important, but has not been modeled in detail. If most of the material affected is fine grained, this could lead to more stirring of an asteroidal regolith and to "ponding" of fine-grained regolith material in topographic lows (Cintala et al. 1979). Horz and Schaal (1981) have suggested even more dramatic differences: they argue that the spall volume might exceed the crater ejecta volume in many cases, which could lead to a much different regolith than that envisioned based on ejecta properties.

V. CONSTRAINTS FROM SPACECRAFT OBSERVATIONS

A number of constraints on the properties of asteroid regoliths have been created by groundbased observations of spectral and radar properties. These observations are covered elsewhere in this book (e.g., see the chapters by Gaffey et al. and by Ostro) and will not be discussed further here. We will only point out some of the observations which have been made from spacecraft and which may be made on possible future missions.

The major reason our knowledge of the lunar regolith is so much more detailed than our knowledge of asteroidal regoliths is that we have been there. We not only know a wealth of detail about the chemical and physical properties of the lunar regolith, we also know much about the geologic setting, both locally at the collection sites and globally. This setting gives us a context in which to interpret the lunar regolith. This first-hand knowledge of one regolith also provides a crucial constraint to models of asteroidal regoliths. Therefore, on-site knowledge of other regoliths, obtainable only by spacecraft missions, can help us both recognize and separate out the effects which are caused by the Moon's size or location.

Martian Satellite Missions

Other than the lunar regolith, the most detailed observations of regoliths are for the Martian satellites, Phobos and Deimos, as a result of the Viking mission. It will be many years before we can dramatically increase our knowledge of the regolith of these bodies as a result of the unfortunate loss of the Soviet mission to the Martian satellites. Both Phobos, the primary mission target, and Deimos are obviously more similar to main-belt asteroids in terms of size and solar system location than is the Moon. While Phobos and Deimos have been interpreted as being like carbonaceous chondrites in composition, direct analysis of their composition must await the results of spacecraft missions to them.

The Viking observations of Phobos and Deimos, and their implications for asteroidal regoliths, are discussed by Veverka and Thomas (1979). One important first-order observation is that the surfaces of the two moons are qualitatively different from one another: Phobos has extensive grooves that Deimos lacks, as evidenced by fill within craters and bright albedo markings, while Deimos apparently has more fine debris. This observation serves as a warning that there may not be a "typical" asteroidal regolith. Another important observation is that the regolith on Phobos appears to be at least 100 m thick in some places, about an order of magnitude greater than predicted for a comparable-sized asteroid by Housen et al. (1979a). However, models specifically designed for Phobos, and the expected local environment rather than an asteroid (in particular, including the effects of re-accretion of ejecta as a result of Martian influences) predict a thicker regolith (Veverka et al. 1986), more consistent with the observations. Thus the Phobos regolith may not be a much better analog for an asteroidal regolith than is the Moon.

However, since Phobos and the Moon are at the opposite end of the size range of interest, the detailed knowledge of the Phobos regolith that could come from a spacecraft mission would provide important points for comparison. For regolith studies, the important components of a mission will include: (1) chemistry experiments, yielding information on lateral mixing and maybe detecting implanted solar-wind species (Eugster and Geiss 1986); (2) the radar, which may be able to determine the depth and vertical structure of the regolith; (3) the imaging; and (4) the experiments on landers, which could determine several important properties (chemistry, grain size, bearing strength, thermal conductivity, etc.) at specific locations.

Comet Missions

The various missions to Comet Halley in 1986 provided some information that is potentially relevant to studies of asteroid regoliths. For example, computer-enhanced images show signs of a crater and other rather large topographic features (Keller et al. 1988). The next comet mission could be NASA's proposed Comet Rendezvous-Asteroid Flyby (CRAF). Since it involves a rendezvous rather than a flyby, it could provide much more detail on the comet it studies. However, the surfaces of comet nuclei are probably extensively modified by the release of volatiles, a process that is not applicable to impact-dominated asteroid surfaces.

Asteroid Missions

The ideal mission to learn about an asteroidal regolith would involve a sample return or at least a landing. Although such missions have been proposed, none is underway at the time of this writing (see the chapter by Veverka et al.). The most detailed near-term exploration of the main belt in the near future will be limited to asteroid flybys by Galileo and perhaps CRAF.

Depending on the instrumentation, such flyby missions can enhance our knowledge of the regolith in several ways. Photographs can be used to determine the crater size distribution and ejecta distribution, two of the most important parameters in regolith models (along with the absolute cratering flux). The depth of the regolith might be constrained by photographs (e.g., if bedrock can be observed) or radar observations. Radar studies can also determine surface roughness, and can be used to calibrate groundbased radar observations.

Other important data collected by flyby missions will include reflectance spectra, X-ray emission analysis, and gamma-ray analysis. Such data can be used to infer the physical and chemical properties of the regolith.

VI. CONCLUSIONS

Our experience with lunar samples has taught us quite a bit about what processes are important to the production and evolution of regolith. However, we do not know enough about how these processes operate on asteroids to be

able to say much about asteroidal regoliths with any certainty. In particular, there are large uncertainties associated with estimates of the flux and size distribution of crater-forming impactors in the main belt. Trying to deduce how those varied in the past is even more uncertain.

Models of asteroidal regoliths have shown that stochastic variations make it difficult to define a typical regolith depth, even for a single asteroid. However, it does appear that, for main-belt asteroids, regoliths will tend to be much thicker than the lunar regolith for strong asteroids that have regoliths (those $\gtrsim 100$ km diameter) and slightly thicker than the lunar regolith for weak asteroids ($\gtrsim 10$ km diameter).

In terms of the microscopic properties of regoliths (maturity), models typically produce regoliths that are less mature than the lunar regolith in properties ranging from agglutinate content to surface exposure age, in agreement with the observation that meteoritic regolith breccias, which presumably sample asteroidal regoliths, are apparently less mature than lunar regolith breccias. However, there are reasons to think that asteroidal regoliths might be more mature than suggested by meteorites. First, since we have no evidence that any meteorites are sampling modern asteroidal regoliths, the asteroidal regoliths might have matured since the time of compaction of meteorite breccias. Second, lunar meteorites show fewer signs of maturity than the regolith or typical lunar regolith breccias, suggesting that the process of compaction might reduce the apparent maturity. Furthermore, because of the different cratering environment, asteroidal regoliths may not mature in the same way that the lunar regolith does—for example, agglutinate formation may be a rare occurrence on an asteroid.

Although spacecraft missions to objects like comets and the Martian satellites will no doubt increase our knowledge of regolith formation under different conditions, we may not really understand asteroidal regoliths until we have had missions to actual asteroids.

REFERENCES

Adams, J. B., and McCord, T. B. 1973. Vitrification darkening in the lunar highlands and identification of Descartes material at the Apollo 16 site. *Proc. Lunar Sci. Conf.* 4:163–177.

Anders, E. 1975. Do stony meteorites come from asteroids? *Icarus* 24:363–371.

Benkert, J. P., Baur, H., Pedroni, A., Wieler, R., and Signer, P. 1988. Solar He, Ne and Ar in regolith minerals: All are mixtures of two components. *Lunar Planet. Sci.* XIX:59–60 (abstract).

Bernatowicz, T., Drozd, R. J., Hohenberg, C. M., Lugmair, G., Morgan, C. J., and Podosek, F. A. 1977. The regolith history of 14307. *Proc. Lunar Sci. Conf.* 8:2763–2783.

Bernatowicz, T. J., Hohenberg, C. M., Hudson, B., Kennedy, B. M., Laul, J. C., and Podosek, F. A. 1980. Noble gas component organization in 14301. *Proc. Lunar Planet. Sci. Conf.* 11:629–668.

Bhattacharya, S. K., Goswami, J. N., Lal, D., Patel, P. P., and Rao, M. N. 1975. Lunar regolith and gas-rich meteorites: Characterisation based on particle tracks and grain size considerations. *Proc. Lunar Sci. Conf.* 6:3509–3536.

Bischoff, A., Palme, H., Weber, H. W., Stöffler, D., Braun, O., Spettel, B., Begemann, F., Wänke, H., and Ostertag, R. 1987. Petrography, shock history, chemical composition and noble gas content of the lunar meteorites Yamato-82192 and -82193. In *Proc. Eleventh Symp. Antarctic Meteorites*, pp. 21–42.

Bogard, D. D. 1979. Chronology of asteroid collisions as recorded in meteorites. In *Asteroids*, ed. T. Gehrels (Tucson: Univ. of Arizona Press), pp. 558–578.

Bradley, J. P., Sandford, S. A., and Walker, R. M. 1988. Interplanetary dust particles. In *Meteorites and the Early Solar System*, eds. J. F. Kerridge and M. S. Matthews (Tucson: Univ. of Arizona Press), pp. 861–895.

Brownlee, D. E., and Rajan, R. S. 1973. Micrometeorite craters discovered on chondrule-like objects from Kapoeta meteorite. *Science* 182:1341–1344.

Caffee, M. W., Hohenberg, C. M., Swindle, T. D., and Goswami, J. N. 1987. Evidence in meteorites for an active early Sun. *Astrophys. J.* 313:L31–L35.

Chao, E. C. T., Boreman, J. A., and Desborough, G. A. 1971. The petrology of unshocked and shocked Apollo 11 and 12 microbreccias. *Proc. Lunar Sci Conf.* 2:797–816.

Cintala, M. J., Head, J. W., and Wilson, L. 1979. The nature and effects of impact cratering on small bodies. In *Asteroids*, ed. T. Gehrels (Tucson: Univ. of Arizona Press), pp. 579–600.

Clayton, R. N., and Thiemens, M. H. 1980. Lunar nitrogen: Evidence for secular change in the solar wind. In *The Ancient Sun: Fossil Record in the Earth, Moon and Meteorites*, eds. R. O. Pepin, J. A. Eddy and R. B. Merrill (New York: Pergamon Press), pp. 463–473.

Crozaz, G. 1980. Solar flare and galactic cosmic ray tracks in lunar samples and meteorites: What they tell us about the ancient Sun. In *The Ancient Sun: Fossil Record in the Earth, Moon and Meteorites*, eds. R. O. Pepin, J. A. Eddy and R. B. Merrill (New York: Pergamon Press), pp. 331–347.

Dran, J. C., Duraud, J. P., Langevin, Y., and Maurette, M. 1979. The predicted irradiation record of asteroidal regoliths and the origin of gas-rich meteorites. *Lunar Planet. Sci.* X:309–311 (abstract).

Duraud, J. P., Langevin, Y., and Maurette, M. 1979. An analytical model for the regolith evolution of small bodies in the solar system. *Lunar Planet. Sci.* X:323–325 (abstract).

Eberhardt, P., Geiss, J., Graf, H., Grogler, N., Mendia, M. D., Morgeli, M., Schwaller, H., Stettler, A., Krahenbuhl, U., and von Gunten, H. R. 1972. Trapped solar wind noble gases in Apollo 12 lunar fines 12001 and Apollo 11 breccia 10046. *Lunar Sci. Conf.* 3:1821–1856.

Eugster, O. 1985. Multistage exposure history of the 74251 soil constituents. *Proc. Lunar Planet. Sci. Conf. 15, J. Geophys. Res. Suppl.* 90:D95–D102.

Eugster, O., and Geiss, J. 1986. Observation and processes in the lunar regolith and implications for the surface of Phobos. In *Proc. Intl. Workshop for the Phobos Mission* (Moscow: USSR Academy of Sciences), pp. 104–121.

Eugster, O., Grogler, N., Eberhardt, P., and Geiss, J. 1980. Double drive tube 74001/2: Composition of noble gases trapped 3.7 AE ago. *Proc. Lunar Planet. Sci. Conf.* 11:1565–1592.

Eugster, O., Eberhardt, P., Geiss, J., and Grogler, N. 1983a. Neutron-induced fission of uranium: A dating method for lunar surface material. *Science* 219:170–172.

Eugster, O., Geiss, J., and Grogler, N. 1983b. Dating of the early regolith exposure and the evolution of trapped $Ar/^{36}Ar$ with time. *Lunar Planet. Sci.* XIV:177–178 (abstract).

Eugster, O., Eberhardt, P., Geiss, J., Grogler, N., Jungck, M., Meier, F., Morgeli, M., and Niederer, F. 1984. Cosmic ray exposure histories of Apollo 14, Apollo 15, and Apollo 16 rocks. *Proc. Lunar Planet. Sci. Conf. 14, J. Geophys Res. Suppl.* 39:B498–B512.

Fujii, N., Miyamoto, M., Kobayashi, Y., and Ito, K. 1981. Differences of relative strength among chondrites measured by the vibrational fracturing rate. In Proc. Sixth Symp. Antarctic Meteorites, pp. 362–371.

Gehrels, T., ed. 1979. *Asteroids* (Tucson: Univ. of Arizona Press).

Gopalan, K., Rao, M. N., and Venkatesan, T. R. 1976. ^{40}Ar-^{36}Ar correlation in gas-rich meteorites. *Meteoritics* 11:291 (abstract).

Goswami, J. N., Hutcheon, I. D., and Macdougall, J. D. 1976. Microcraters and solar flare tracks in crystals from carbonaceous chondrites and lunar breccias. *Proc. Lunar Sci. Conf.* 7:543–562.

Goswami, J. N., Lal, D., and Wilkening, L. L. 1984. Gas-rich meteorites: Probes for particle environment and dynamical processes in the inner solar system. *Space Sci. Rev.* 37:111–159.

Grady, M. M., and Pillinger, C. T. 1988. Nitrogen in the Fayetteville breccia. *Meteoritics* 23:270–271 (abstract).

Hamano, Y., and Yomogida, K. 1982. Magnetic anisotropy and porosity of Antarctic chondrites. In *Proc. Seventh Symp. Antarctic Meteorites*, pp. 281–290.

Hartmann, W. K. 1980. Dropping stones in magma oceans: Effects of early lunar cratering. In *Proc. Conf. Lunar Highlands Crust*, eds. J. J. Papike and R. B. Merrill (New York: Pergamon Press), pp. 155–171.

Heiken, G. 1975. Petrology of lunar soils. *Rev. Geophys. Space Phys.* 13:567–587.

Hörz, F., and Schaal, R. B. 1981. Asteroidal agglutinate formation and implications for asteroidal surfaces. *Icarus* 46:337–353.

Housen, K. R. 1981*a*. The Stochastic Evolution of Asteroidal Regoliths and the Origin of Brecciated and Gas-Rich Meteorites. Ph.D. Thesis, Univ. of Arizona.

Housen, K. R. 1981*b*. The stochastic variability of asteroidal regolith depths. *Proc. Lunar Planet. Sci. Conf.* 12:1717–1724.

Housen, K. R., and Wilkening, L. L. 1982. Regoliths on small bodies in the solar system. *Ann. Rev. Earth Planet Sci.* 10:355–376.

Housen, K. R., Wilkening, L. L., Chapman, C. R., and Greenberg, R. J. 1979*a*. Asteroidal regoliths. *Icarus* 39:317–351.

Housen, K. R., Wilkening, L. L., Chapman, C. R., and Greenberg, R. J. 1979*b*. Regolith development and evolution on asteroids and the Moon. In *Asteroids*, ed. T. Gehrels (Tucson: Univ. of Arizona Press), pp. 601–627.

Keil, K. 1982. Composition and origin of chondritic breccias. In *Workshop on Lunar Breccias and Soils and Their Meteoritic Analogs*, eds. G. J. Taylor and L. L. Wilkening, LPI Tech. Rept. 82-02 (Houston: Lunar and Planetary Inst.), pp. 65–83.

Keller, H. U., Kramm, R., and Thomas, N. 1988. Surface features on the nucleus of comet Halley. *Nature* 331:227–231.

Kerridge, J. F. 1975. Solar nitrogen: Evidence for a secular change in the ratio of nitrogen-15 to nitrogen-14. *Science* 188:162–164.

Kerridge, J. F. 1980. Secular variations in composition of the solar wind: Evidence and causes. In *The Ancient Sun: Fossil Record in the Earth, Moon and Meteorites*, eds. R. O. Pepin, J. A. Eddy and R. B. Merrill (New York: Pergamon Press), pp. 475–489.

Kerridge, J. F. 1985. Nitrogen isotopes in lunar regolith: A continuing puzzle. *Lunar Planet. Sci.* XVI:430–431 (abstract).

Kerridge, J. F., and Bunch, T. E. 1979. Aqueous activity on asteroids: Evidence from carbonaceous meteorites. In *Asteroids*, ed. T. Gehrels (Tucson: Univ. of Arizona Press), pp. 745–764.

Kirsten, T., Deubner, J., Horn, P., Kaneoka, I., Kiko, J., Schaeffer, O. A., and Thio, S. K. 1972. The rare gas record of Apollo 14 and 15 samples. *Proc. Lunar Sci. Conf.* 3:1865–1889.

Kothari, B. K., and Rajan, R. S. 1982. Fission track studies of xenolithic chondrites: Implications regarding brecciation and metamorphism. *Geochim. Cosmochim. Acta* 46:1747–1754.

Langevin, Y. 1982. Evolution of an asteroidal regolith: Granulometry, mixing and maturity. In *Workshop on Lunar Breccias and Soils and Their Meteoritic Analogs*, eds. G. J. Taylor and L. L. Wilkening, LPI Tech. Rept. 82-02 (Houston: Lunar and Planetary Inst.), pp. 87–93.

Langevin, Y. 1986. Regolith evolution on small bodies: Formation, lateral transport and aging effects. In *Proc. Intl. Workshop for the Phobos Mission* (Moscow: USSR Academy of Sciences), pp. 86–96.

Langevin, Y., and Maurette, M. 1976. A Monte-Carlo simulation of galactic cosmic ray effects in the lunar regolith. *Proc. Lunar Sci. Conf.* 7:75–91.

Langevin, Y., and Maurette, M. 1980. A model for small body regolith evolution: The critical parameters. *Lunar Planet. Sci.* XI:602–604 (abstract).

Langevin, Y., and Maurette, M. 1981. Grain size and maturity in lunar and asteroidal regoliths. *Lunar Planet Sci.* XII:595–597 (abstract).

Lorin, J. C., and Pellas, P. 1979. Preirradiation history of Djermaia (H) chondritic breccia. *Icarus* 40:502–509.

Macdougall, J. D., and Kothari, B. K. 1976. Formation chronology for C2 meteorites. *Earth Planet. Sci. Lett.* 33:36–44.

Manka, R. H., and Michel, F. C. 1970. Lunar atmosphere as a source of argon-40 and other lunar surface elements. *Science* 169:278–280.

Manuel, O. K. 1967. Noble gases in the Fayetteville meteorite. *Geochim. Cosmochim. Acta* 31:2413–2431.

Marvin, U. 1983. The discovery and initial characterization of Allan Hills 81005: The first lunar meteorite. *Geophys. Res. Lett.* 10:775–778.

McKay, D. S., and Basu, A. 1983. The production curve for agglutinates in planetary regoliths. *Proc. Lunar Planet. Sci. Conf.* 14, *J. Geophys. Res. Suppl.* 88:B193–B199.

McKay, D. S., and Morrison D. A. 1971. Lunar breccias. *J. Geophys. Res.* 76:5658–5669.

McKay, D. S., Bogard, D. D., Morris, R. V., Korotev, R. L., Johnson, P., and Wentworth, S. J. 1986. Apollo 16 regolith breccias: Characterization and evidence for early formation in the mega-regolith. *Proc. Lunar Planet. Sci. Conf.* 16, *J. Geophys. Res. Suppl.* 91:D277–D303.

Megrue, G. H. 1973. Spatial distribution of $^{40}Ar/^{39}Ar$ ages in lunar breccia 14301. *J. Geophys. Res.* 78:3216–3221.

Minster, J. F., and Allègre, C. J. 1979. ^{87}Rb-^{87}Sr age of Saint Mesmin chondrite and dating of gas-rich polymict breccia. *Nature* 278:732–734.

Morris, R. V. 1978a. The surface exposure (maturity) of lunar soils: Some concepts and I_s/FeO compilation. *Proc. Lunar Sci. Conf.* 9:2287–2297.

Morris, R. V. 1978b. *In situ* reworking (gardening) of the lunar surface: Evidence from the 41 Apollo cores. *Proc. Lunar Planet. Sci. Conf.* 9:1801–1811.

Morris, R. V. 1983. Ferromagnetic resonance and magnetic properties of ALHA81005. *Geophys. Res. Lett.* 10:807–808.

Murty, S. V. S., and Marti, K. 1986. Pursuit of solar nitrogen: Nitrogen components in the Pesyanoe meteorite. *Lunar Planet Sci.* XVII:591–592 (abstract).

Pedroni, A., Baur, H., Wieler, R., and Signer, P. 1988. T-Tauri irradiation of Kapoeta grains? *Lunar Planet. Sci.* XIX:913–914 (abstract).

Pepin, R. O. 1980. Rare gases in the past and present solar wind. In *The Ancient Sun: Fossil Record in the Earth, Moon and Meteorites,* eds. R. O. Pepin, J. A. Eddy and R. B. Merrill (New York: Pergamon Press), pp. 411–421.

Pepin, R. O., Eddy, J. A., and Merrill, R. B., eds. 1980. *The Ancient Sun: Fossil Record in the Earth, Moon and Meteorites* (New York: Pergamon Press).

Phinney, W. C., McKay, D. S., Simonds, C. H., and Warner, J. L. 1976. Lithification of vitric- and clastic-matrix breccias: SEM petrography. *Proc. Lunar Sci. Conf.* 7:2469–2492.

Schall, R. B., and Hörz, F. 1980. Experimental shock metamorphism of lunar soil. *Proc. Lunar Planet. Sci. Conf.* 11:1679–1695.

Schultz, L., and Signer, P. 1977. Noble gases in the St. Mesmin chondrite: Implications to the irradiation history of a brecciated meteorite. *Earth Planet. Sci. Lett.* 36:363–371.

Schultz, L., Signer, P., Lorin, J. C., and Pellas, P. 1972. Complex irradiation history of the Weston chondrite. *Earth Planet. Sci. Lett.* 15:403–410.

Shoemaker, E. M. 1984. Large body impacts through geologic time. In *Patterns of Change in Earth Evolution,* eds. H. D. Holland and A. F. Trendall (New York: Springer-Verlag), pp. 15–40.

Short, N. M. 1970. Evidence and implications of shock metamorphism in lunar samples. In *Proc. Apollo 11 Lunar Sci. Conf.,* ed. A. A. Levinson (New York: Pergamon Press), pp. 865–872.

Shukolyukov, Yu. A., Minh, D. V., Skripnik, A. Ya., and Simonovskiy, V. I. 1983. ^{244}Pu fission xenon in achondrites. *Geochem. Int.* 20(5):96–110.

Simonds, C. 1973. Sintering and hot pressing of Fra Mauro composition glass and the lithification of lunar breccias. *Amer. J. Sci.* 273:428–439.

Stöffler, D., Knöll, H., and Maerz, U. 1979. Terrestrial and lunar impact breccias and the classification of lunar highland rocks. *Proc. Lunar Planet. Sci. Conf.* 10:639–675.

Strom, R. G. 1987. The solar system cratering record: Voyager 2 results at Uranus and implications for the origin of impacting objects. *Icarus* 70:517–535.

Swindle, T. D., Caffee, M. W., Hohenberg, C. M., and Taylor, S. R. 1986. I-Pu-Xe dating and the relative ages of the Earth and Moon. In *The Origin of the Moon,* eds. W. K. Hartmann, R. J. Phillips and G. J. Taylor (Houston: Lunar and Planetary Inst.), pp. 331–358.

Swindle, T. D., Hohenberg, C. M., Nichols, R., and Olinger, C. T. 1989. Parentless fission xenon in the meteorite Bholghati? In *Lunar Planet. Sci.* XX, in press.

Turner, G. 1977. The early chronology of the Moon: Evidence for the early collisional history of the solar system. *Phil. Trans. Roy. Soc. Lond.* A285:97–103.

Veverka, J., and Thomas, P. 1979. Phobos and Deimos: A preview of what asteroids are like? In *Asteroids,* ed. T. Gehrels (Tucson: Univ. of Arizona Press), pp. 628–651.

Veverka, J., Thomas, P., Johnson, T. V., Matson, D., and Housen, K. 1986. The physical

characteristics of satellite surfaces. In *Satellites,* eds. J. A. Burns and M. S. Matthews (Tucson: Univ. of Arizona Press), pp. 341–402.

Wentworth, S., and McKay, D. 1984. Density and porosity calculations for Apollo 15 and 16 regolith breccias. *Lunar Planet. Sci.* XV:906–907 (abstract).

Wieler, R., Etique, Ph., Signer, P., and Poupeau, G. 1983. Decrease of the solar flare/solar wind flux ratio in the past several aeons deduced from solar neon and tracks in lunar soil plagioclases. *Proc. Lunar Planet. Sci. Conf.* 13, *J. Geophys. Res. Suppl.* 88:A713–A724.

Wieler, R., Pedroni, A., and Signer, P. 1988. Excess of GCR-Ne in the solar-gas-rich matrix of the chondrite Fayetteville. *Lunar Planet. Sci.* XIX:1268–1269 (abstract).

Yaniv, A., and Heymann, D. 1972. Atmospheric Ar[40] in lunar fines. *Proc. Lunar Sci. Conf.* 3:1967–1980.

DO ASTEROIDS HAVE SATELLITES?

STUART J. WEIDENSCHILLING
Planetary Science Institute

PAOLO PAOLICCHI
Università di Pisa

and

VINCENZO ZAPPALÀ
Osservatorio Astronomico di Torino

A substantial body of indirect evidence suggests that some asteroids have satellites, although none has been detected unambiguously. Collisions between asteroids provide physically plausible mechanisms for the production of binaries, but these operate with low probability; only a small minority of asteroids are likely to have satellites. The abundance of binary asteroids can constrain the collisional history of the entire belt population. The allowed angular momentum of binaries and their rate of tidal evolution limit separations to no more than a few tens of the primary's radii. Their expected properties are consistent with failure to detect them by current imaging techniques.

I. INTRODUCTION

The first suggestion of the existence of binary asteroids was due to Andre (1901), who noted the similarity between lightcurves of 433 Eros and of some eclipsing binary stars. Bobrovnikoff (1929) made the prescient comment that "if an occasional asteroid were not a single body but consisted of several pieces . . . we could never tell the difference." In more recent years, Cook (1971) proposed a contact binary model to explain the lightcurve of 624 Hek-

tor. In the late seventies, the hypothesis was newly supported by occultation of a star by 532 Herculina, which exhibited at least one secondary event, apparently corresponding to a satellite of $\simeq$50 km size about 1000 km from the primary body (Bowell et al. 1978). Data from occulations of other asteroids also suggested possible satellites (Binzel and Van Flandern 1979). The existence of satellites was also supported by lightcurves of additional asteroids (Wijesinghe and Tedesco 1979; Tedesco 1979a,b) and the opinion was expressed that it was a rather common phenomenon (Van Flandern et al. 1979). Zappalà et al. (1980) discussed likely general features of lightcurves of eclipsing binary asteroids, and inserted the problem of their existence into the general debate on rotational properties and collisional evolution. Weidenschilling (1980) introduced a model for 624 Hektor and 216 Kleopatra based on twin equilibrium figures (Darwin ellipsoids). In the following years, the role of equilibrium self-gravitating figures (Farinella et al. 1981a; Weidenschilling 1981), the features of spin rate distributions (Farinella et al. 1981b; Dermott et al. 1984) and general aspects of collisional evolution (Farinella et al. 1982; Davis et al. 1985) were discussed. Despite these developments, no asteroidal satellite has been detected unequivocally, and the earlier enthusiasm is tempered with skepticism. Some ideas on the formation of binary asteroids are outlined in Sec. II. They appear to be a plausible by-product of collisional evolution although their abundance is probably low. Their physical and dynamical nature is analyzed in Sec. III. Their expected properties are consistent with the lack of direct, unquestionable observation of any binary asteroid to date. Still, many indirect or statistical hints support their existence (Sec. IV).

II. FORMATION OF BINARY ASTEROIDS

The various mechanisms proposed for the formation of binary asteroids all involve collisions. If binaries formed preferentially by low-velocity impacts during the early accretional phase, those now existing would be a surviving remnant of an original population, depleted by its later collisional evolution. If the high-velocity impacts now prevalent can produce binaries, they represent a steady-state population that is both created and destroyed by collisions. Both primordial and recent binaries may exist, just as the present belt population contains a mix of survivors and fragments (Davis et al. 1985; see also their chapter). Here we examine three possible mechanisms of binary formation and their implications for the expected properties of such systems.

A. Rotational Fission

An impact on a large asteroid may shatter the target body without dispersing the fragments, yielding a gravitationally bound "rubble pile" (Davis et al. 1979,1985; see also their chapter). It was suggested by Weidenschilling (1980) and Farinella et al. (1982) that off-center impacts could also deliver enough angular momentum to the target to exceed the threshold for binary

fission. This threshold is reached at specific angular momentum $\simeq 0.4$ $(GMR)^{1/2}$, where G is the gravitational constant, M the primary's mass and R the mean radius (Chandrasekhar 1969; Weidenschilling 1981). For a collision with a projectile of mass m, impact velocity V, and the mean expected impact parameter $R/\sqrt{2}$, the angular momentum is $mVR/\sqrt{2}$. The projectile/target mass ratio that delivers the critical angular momentum is $m/M \simeq 0.4(2GM/V^2R)^{1/2} = 0.4(V_e/V)$, where $V_e = (2GM/R)^{1/2}$ is the target's escape velocity. The gravitational binding energy of the target is $0.6\ GM^2/R = 0.3\ MV_e^2$, so a single impact capable of causing rotational instability has a ratio of impact energy to binding energy of $\simeq V/V_e$. At the present belt's mean impact velocity ~ 5 km s^{-1}, an asteroid with $R = 100$ km has $V/V_e \simeq 40$. To have a high probability of fission, such an asteroid would need to survive an impact involving a few tens of times its binding energy. Although the conversion of impact energy to kinetic energy of ejecta is not very efficient (see the chapter by Fujiwara et al.), this seems rather unlikely (we have not considered the possible loss of angular momentum carried off by escaping ejecta). Fission may require favorable circumstances, such as a lower-than-average impact velocity or a prograde impact on an already rapidly spinning target. Requirements are less stringent for larger asteroids (larger V_e), but they are less likely to have experienced a collision of that magnitude during the age of the solar system. Thus, rotational fission appears most probable in some intermediate size range, estimated at $100 \lesssim R \lesssim 140$ km by Farinella et al. (1982).

Fission without destruction of the target is more likely for smaller relative velocities, and may have been more common during accretion, when $V \sim V_e$. However, at such low velocities an impactor comparable in size to the target is needed to provide the required angular momentum. Such impacts must have occurred, but were rarer than collisions of unequal-sized bodies (Hartmann 1979a). If fission-produced binaries exist in the present belt, a significant fraction of them may be primordial survivors, but they cannot be a large part of the total population. Any such objects should have weak rubble-pile structures for both components. Their shapes will approximate ellipsoidal figures of hydrostatic equilibrium, distorted by their mutual gravitational attraction (Leone et al. 1984). The large satellite/primary mass ratio implies a stable tidal end state with small separation and synchronous rotation (see Sec. III, below).

B. Orbiting Ejecta

An oblique impact too small to cause rotational fission can still yield some fraction of ejecta with sufficient velocity to go into orbit about the target. If the target is spherically symmetric, the ejecta trajectories are Keplerian ellipses that re-impact after a single orbit. Irregularly shaped target bodies could yield complex orbits with longer lifetimes (Cintala et al. 1979), and highly eccentric orbits would be subjected to solar perturbations that might prevent immediate re-impact (Harris 1987), but it is unlikely that either case

would yield permanently stable orbits. In the related problem of the origin of the Moon by a giant impact, pressure gradients in the ejecta plume and viscosity in a debris disk are invoked to inject material into stable orbits (Stevenson 1987). For asteroidal impacts, the smaller scale and shorter cooling time for ejecta make such processes less effective, and the yield of mass placed into orbit is probably very low.

In order to attain orbit without escaping, the ejecta velocity must fall in the range $(GM/R)^{1/2} \lesssim V \lesssim (2\,GM/R)^{1/2}$. For material excavated near the target's surface, the maximum specific angular momentum is $\simeq VR \lesssim (2\,GMR)^{1/2}$, equal to that of a circular orbit at distance $a = 2\,R$. Initial orbits may be highly eccentric, but mutual collisions or accretion into a satellite must circularize this material at a distance corresponding to the mean angular momentum. Thus, except for transient conditions immediately following an impact, the debris cloud should be confined within a few radii of the asteroid. Any satellite formed by this process would initially be in a close orbit. It would be a rubble pile, and probably much smaller than the primary (which is not necessarily shattered).

As shown in Sec. III, the orbit of a satellite will evolve due to tidal dissipation. It will decay until the satellite collides with the primary or is tidally disrupted, unless two conditions are met: (1) its orbit must be prograde; this requires a chance alignment of the impact direction with the target's rotation, unless the impact is large enough to re-orient its spin axis; and (2) the initial orbit must lie outside the synchronous distance; this requires rapid rotation of the primary; a synchronous distance of $\simeq 2\,R$ implies a spin period $\lesssim 6$ hr. As shown below, a small satellite (mass ratio $\lesssim 0.01$) would evolve outward slowly, and would not despin the primary significantly. We would expect satellites formed from ejecta to be small, and found in prograde orbits near rapidly spinning primaries. Given the formidable obstacles, satellites formed by this mechanism may be rare or nonexistent. Systems with these properties may have other origins, such as collisional disruption of one component of a binary originally formed by rotational fission.

C. Fragmentation with Mutual Capture

An impact that destroys an asteroid may produce fragments that escape with relative velocities low enough to produce gravitationally bound pairs (Hartmann 1979b). We consider a simple model for this process suggested by P. Farinella (personal communication). Assume that a parent body of mass M and radius R is disrupted, with the swarm of fragments expanding radially. In order to escape without being re-accumulated, fragments originating near the surface must have velocities $V \geq V_e = (2\,GM/R)^{1/2}$. Two fragments of radius r, mass m, originally adjacent, have an angular separation $\sim 2r/R$ with respect to the center of the parent asteroid, therefore their relative velocity is of order $2\,Vr/R \gtrsim 2(2\,GM/R)^{1/2}r/R$. Their mutual escape velocity is $\sim (Gm/2r)^{1/2}$. Taking $m \sim M(r/R)^3$, their relative velocity is $\simeq 4(V/V_e)$ times their mutual

escape velocity. Thus, fragments that escape the parent body ($V/V_e > 1$) generally are not gravitationally bound to each other (this argument is not changed by assuming unequal fragment sizes).

This highly simplified model does not consider nonradial expansion of the debris cloud, unusual shapes of the target or fragments, mutual collisions of fragments, etc., so gravitationally bound pairs (or larger collections) of fragments cannot be ruled out. Some may yield re-accumulated rubble piles, others, binaries. Given the large number of fragments produced in a single disruption, the production of one or more binaries may be a common outcome of such an event. It is clear, however, that they must represent only a small fraction of the total number of fragments. Bound pairs are more likely for the ejecta fraction that barely escapes the parent body, and for barely catastrophic disruptions rather than for supercatastrophic impacts. Some hierarchical aggregation cannot be ruled out, but it is more probable that binaries produced in this manner will have components that are individual competent fragments. There is no preferred mass ratio, but because the gravitational potential binding the pair varies inversely with separation, close binaries are more likely than distant pairs.

III. DYNAMICS OF BINARY ASTEROIDS

A. Orbital Stability

It is generally recognized that satellites must orbit inside the sphere of influence of the primary, i.e., within a distance of a few hundred radii. The irregular shapes of asteroids, evident from their lightcurves, may also impose inner limits on orbital stability. Their smaller sizes allow them to support much larger gravitational harmonics than those of the planets. Nonsynchronous orbits within a distance of a few radii may be subject to significant periodic perturbations that may lead to collision with the primary (for this reason, rings around asteroids are unlikely). The orbital evolution of close satellites of irregularly shaped bodies is an interesting topic for future study.

Synchronous orbits may be stable, even for bodies of irregular shape. However, tidal dissipation will drive a satellite away from the synchronous distance unless the system meets the condition (Harris and Ward 1982)

$$\frac{mM}{(M + m)} \, a^2 > 3(C_p + C_s) \tag{1}$$

where C_p and C_s are the rotational moments of inertia of the primary and satellite, having masses M and m, and separation a. If this condition is not met, then a small exchange of angular momentum between the spin and orbital components is unstable. If the satellite moves slightly inside the synchronous distance, the primary's spin does not increase rapidly enough to

"catch up;" the orbit decays until the satellite collides with the primary. If the initial displacement is outward, the satellite lags behind the primary's spin, and it continues to evolve outward. If the primary and satellite have the same density, then Eq. (1) can be expressed as

$$\left(\frac{a}{R}\right)^2 > \frac{6}{5} \frac{(1 + q)(1 + q^{5/3})}{q} \tag{2}$$

where $q = m/M$ and R is the radius of the primary. This expression implies that only large satellites (large q) can have stable synchronous orbits close to their primaries. Small satellites can, in principle, evolve outward tidally until they meet the stability criterion, but the rate may be slow.

B. Tidal Evolution Time Scales

The tidal torque exerted on the primary by the satellite is (Harris and Ward 1982)

$$dH/dt = 3k \, Gm^2R^5/Qa^6 \tag{3}$$

where Q is the specific dissipation function. The Love number k is a measure of the response of the primary to the tidal potential due to its elasticity and its own self-gravity. For modulus of rigidity μ, density ρ,

$$k = \frac{3/2}{1 + 57\mu/8 \, \pi G\rho^2R^2} \cdot \tag{4}$$

For small rocky bodies, the second term in the denominator dominates, and

$$k \simeq 12 \, \pi G\rho^2R^2/57 \, \mu. \tag{5}$$

This is a good approximation for $R \lesssim 200$ km, even if μ is as low as $\sim 10^8$ dyne cm^{-2} (solid rock has $\mu \gtrsim 10^{11}$ dyne cm^{-2}). The rate of change of orbital angular momentum is $(q/2)[GM^3/(1 + q)a]^{1/2}(da/dt)$. Equating these and integrating,

$$\left(\frac{a_f}{R}\right)^{13/2} - \left(\frac{a_o}{R}\right)^{13/2} = \frac{312 \, \pi^{3/2}G^{3/2}\rho^{5/2}q(1 + q)^{1/2}R^2}{19\sqrt{3} \, \mu \, Q} \Delta t \tag{6}$$

where a_o and a_f are the initial and final separations. The elapsed Δt is insensitive to the starting distance, a_o/R.

Contours of a_f/R are shown in Fig. 1 for different values of Δt. We have assumed $\mu Q = 10^{12}$ dyne cm^{-2}, the value determined for Phobos by Yoder
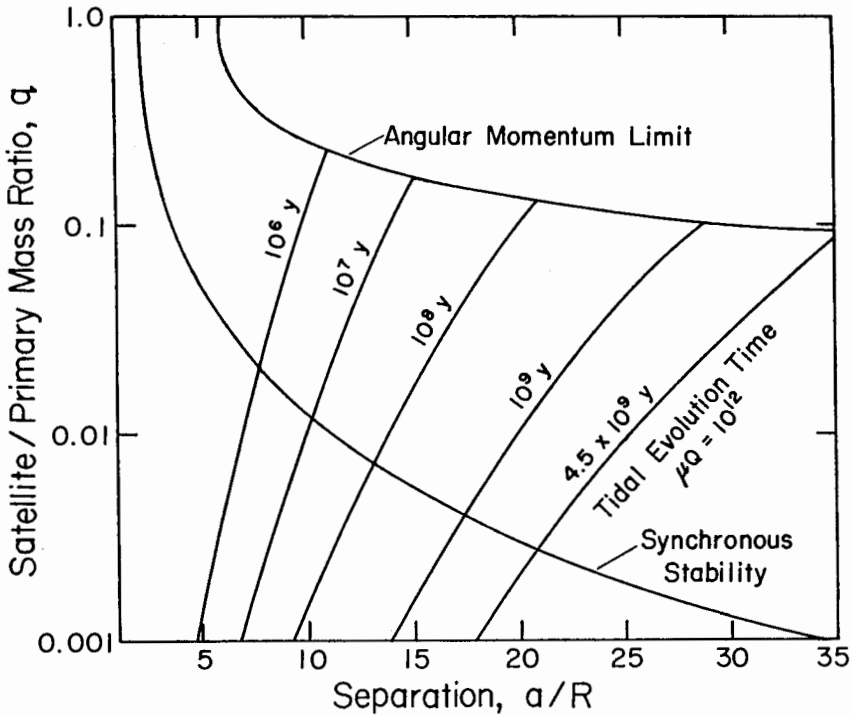
Fig. 1. Domains of separation a/R vs mass ratio q. Tidal evolution will cause binaries to move toward the right. Curve labeled Angular Momentum Limit shows maximum a/R attainable by conversion of initial spin to orbital angular momentum. Evolution times assume initial $a/R \simeq 1$, $\mu Q = 10^{12}$ dyne cm^{-2}, $\rho = 2.5$ g cm^{-3}, $R = 100$ km. Binaries to the left of the curve labeled Synchronous Stability cannot maintain spin-orbit synchronism. Those to the right may be synchronous, but are not required to be; their state depends on initial conditions and age.

(1981). As Q is generally $\sim 10^2$, this implies $\mu \sim 10^{10}$ dyne cm^{-2}, a value that may be appropriate to moderately fractured carbonaceous asteroids (Phobos may be a captured asteroid). Gravitationally bound rubble piles may have lower effective μ, but the computed separation depends only weakly on the assumed value. The final separation of large satellites ($q \gtrsim 0.1$) is limited by the initial spin angular momentum of the system. Even if both components initially have prograde spin just below the instability limit (Sec. II.A), the system must reach a despun synchronous end state below the curve labeled angular momentum limit. Small satellites are limited by their slow rate of tidal evolution. Figure 1 shows that separations greater than a few tens of radii of the primary, for *any* size satellite, are unlikely (larger separations could be caused by a major impact on the primary that removed a significant fraction of its mass, but such an event would usually disrupt the binary system).

C. Evolution of Eccentricity

Tidal evolution also can cause a secular change in a satellite's eccentricity. From Harris and Ward (1982), we have

$$\frac{de}{e} = \left[\frac{19}{8} \, \text{sign}(2\omega - 3\Omega) - \frac{7\rho_p{}^2 R Q_p k_s}{2\rho_s{}^2 r Q_s k_p} \right] \frac{da}{a} \tag{7}$$

where ω is the primary's spin rate, Ω the satellite's mean motion, and the subscripts p and s refer to the primary and satellite, respectively. The second term in brackets always causes damping of e. If the satellite's period is greater than 3/2 the primary's rotation period, the first term is positive, and e will increase if $19 \, \rho_s{}^2 r Q_s k_p > 28 \, \rho_p{}^2 R Q_p k_s$. Because $k \propto \rho^2 r^2/\mu$, if $\mu_p Q_p = \mu_s Q_s$, then $r/R < 19/28$, or $q \lesssim 0.31$ is necessary (but not sufficient) for $de/dt > 0$. Equation (7) integrates to $e/e_o = (a/a_1)^\alpha$, where e_o is the initial eccentricity at the separation a_1 where $2\,\omega - 3\,\Omega$ becomes positive. For $\mu_p Q_p = \mu_s Q_s$, $\alpha = 19/8 - (7/2)q^{1/3}$, varying from zero at $q = 0.31$ to 2.375 as $q \to 0$.

A satellite evolving outward from the synchronous distance will eventually reach a distance at which $2\,\omega - 3\,\Omega > 0$, provided that the primary is not despun too rapidly; this means that q cannot be too large. In order to have $\omega > 3\,\Omega/2$ for some range of a, it is necessary that $d\omega/da < (3/2)\,d\Omega/da$ at a_1, from which

$$q^{5/3} + \frac{35}{6} \frac{q}{(1 + q)} \left(\frac{a_1}{R}\right)^2 < \frac{3}{2} . \tag{8}$$

The limiting value of q depends on the primary's initial spin rate, but generally q must be $\lesssim 0.01$ to allow $de/dt > 0$. Tidal evolution time scales imply $a/a_1 \lesssim 10$, so $e/e_o \lesssim 10^2$. The initial eccentricity may be provided by gravitational harmonics of the primary, or an impact on either component. In cases with significant e_o, integration of Eq. (7) may formally predict $e \to 1$, but this relation is valid only in the limit of small e, and values of $e \gtrsim 0.7$ are not attainable by tidal evolution (Harris 1980). Thus, small asteroidal satellites may have modest eccentricities of a few tenths or less.

IV. EVIDENCE FOR BINARY ASTEROIDS

In the past decade, there have been many efforts to detect binary asteroids by various methods. Some of these have yielded strong hints or possible detections, but none has produced unambiguous and generally accepted evidence. Here we discuss these results (or lack thereof) and the prospects for future progress.

A. Occultations

Numerous occultations of stars by asteroids have been observed (see the chapter by Millis and Dunham). Reports of multiple events, or events well separated from the asteroid's occultation track, are not uncommon. Almost all of these are visual observations, with no permanent record. It is probable that many such reports are spurious (Reitsema 1979). Photoelectric records are more reliable, but for most occultations coverage is sparse. Detection of any distant satellite is essentially serendipitous and unlikely to be confirmed by other observers. There is a greater chance of detecting close binaries, but the geometry may be unfavorable, e.g., a well-observed occultation by the suspected contact binary 216 Kleopatra occurred near a minimum of the visual lightcurve when two components would have been superimposed. The best recent indication of a satellite by occultation is for 146 Lucina. Arlot et al. (1985) obtained a photoelectric record suggesting a satellite $\gtrsim 6$ km in size, about 1600 km from the primary $(a/R \sim 20)$.

B. Lightcurves

Lightcurve features of binary systems were analyzed by Leone et al. (1984) and Cellino et al. (1985). The lightcurve of a realistic binary asteroid should not fit a model with spherical components, since gravitationally bound rubble piles will be tidally distorted, while an almost spherical shape seems unlikely for solid fragments (see Capaccioni et al. [1984] for discussion of fragment shapes). These considerations rule out some previously suggested candidates (asteroids 46, 49, 111, 179; Tedesco 1979a), and increase the difficulties of the photometric detection of binary asteroids. Even if an eclipse is observed, its features can be confused with the effects of individual shapes.

The situation is more favorable when the components are dominated by self gravitation and their shapes are essentially equilibrium figures. Leone et al. discuss the geometrical properties of binaries, approximated by Roche equilibrium figures. The models are characterized by two nondimensional parameters, the mass ratio q and $\omega^2/\pi G\rho$ (proportional to the ratio of centrifugal and gravitational forces). For the observable parameters, lightcurve amplitude A and rotation rate ω, the unknown values of q and ρ can be constrained between minimum and maximum values (the same observables may be fitted by a denser system with larger q or by one with lower ρ and q). The region of possible binaries in the plane A-ω can be drawn assuming a realistic density range 1–4 g cm^{-3} (see Fig. 2 of Leone et al.). The binary ellipsoid model fixes also some characteristics of the lightcurve, in terms of observable parameters (e.g., amplitude of the eclipse and its duration).

Cellino et al. (1985) pointed out how some observed asteroid lightcurves could be fitted by synthetic lightcurves of eclipsing binaries with various assumptions on q and ρ. They derived binary models for 10 asteroids with large amplitudes and short periods. For asteroids 15 and 192, two different fits with

different lightcurves were performed, giving slightly different values. The fits are, in most cases, qualitatively good; nevertheless, there are a few difficulties. First, the computed density values—with a pair of exceptions—fall into two well-defined clusters, one with low-density values (1 to 2 g cm^{-3}), and the other with high densities (3.5 to 5 g cm^{-3}). It seems unlikely that both groups correspond to real binaries. The low-density systems appear consistent with values for rubble-pile structures due to breakup and partial re-accumulation. The high-density systems could be, more realistically, single elongated bodies with lower densities. Cellino et al. assumed geometric scattering in constructing these models, but showed that other scattering laws did not affect their parameters significantly, except to decrease the computed value of q.

Another difficulty is due to consideration of orbital stability. These models assumed synchronous satellites. Weidenschilling (1985) pointed out that half of them did not meet the criterion of Eq. (1). Those satellites would be driven out of synchronous orbits over short time scales, invalidating the models. Presumably, those asteroids are single bodies, with lightcurves due to shapes and/or albedo features (they do not correspond entirely to the high-density group mentioned above). Binary models for asteroids 43, 63, 192,
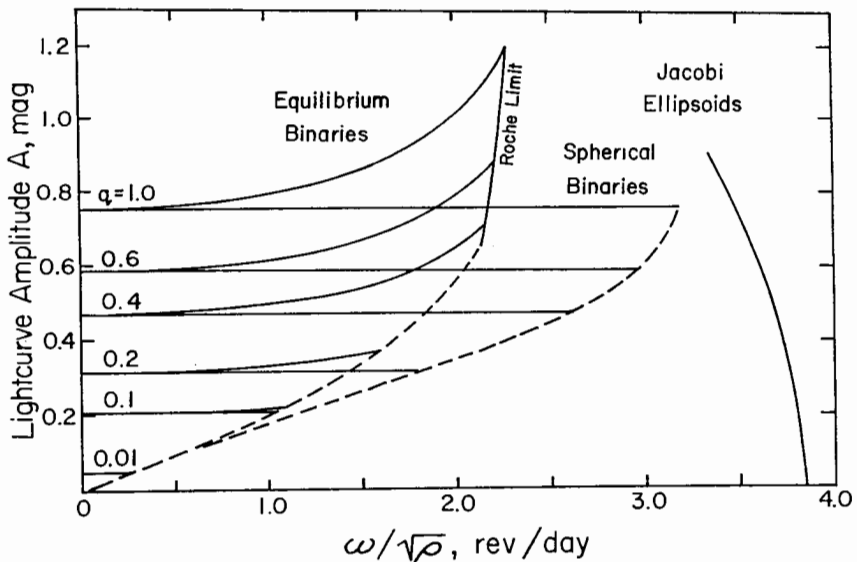
Fig. 2. Maximum lightcurve amplitude for eclipsing binaries viewed in their orbital plane vs normalized orbital frequency, with ρ in units of g cm^{-3}. Horizontal lines refer to binaries with spherical components, curved lines to tidally distorted equilibrium figures after Leone et al. (1984). Synchronous orbits are assumed. Binaries falling below the dashed lines are tidally unstable and will evolve away from synchroneity. Also shown is the A-ω locus for Jacobi ellipsoids. Because ρ is unknown, a given (A, ω) may refer to a low-density single body or a binary with higher ρ.

216 and 624 meet the tidal stability criterion. This result illustrates the general problem of the lack of uniqueness of lightcurves: it is usually possible to construct either a single or binary model to match the data (Cellino et al. 1988). Figure 2 shows the relationship of A and $\omega/\sqrt{\rho}$ for single bodies (Jacobi ellipsoids) and binaries that meet the tidal stability criterion.

In principle, a nonsynchronous satellite could be identified unambiguously, because features due to eclipses and transits would occur at regular intervals but at different parts of the lightcurve. However, such satellites are likely to be small, and will produce only subtle features that may be confused with the primary's intrinsic lightcurve. Separating the two would require observations at a time of favorable geometry, when the Earth is near the satellite's orbital plane, and spanning several complete revolutions under ideal conditions, in order to rule out other sources of variation, e.g., sky conditions or instrumental effects. Very few asteroids have been subjected to such scrutiny.

C. Rotation Rates

Support for the existence of binaries can be found in statistical analysis of rotations. The ω distribution presents a significant excess of slow rotators with respect to a Maxwellian behavior (Farinella et al. 1981b; see also the chapter by Binzel et al.). Dermott et al. (1984) list some very slow rotators, whose existence cannot be easily accounted for by any reasonable collisional model. Moderate periods of a few days may be due to tidal despinning by large ($q > 0.01$) satellites to synchronous end states. Harris (1983) and Binzel (1985) suggest that some very long periods of more than a month could correspond not to rotation, but to precession of the spin axis. Since free precession is very quickly damped (Burns and Safronov 1973), the presence of a "forcing" satellite is required. Harris claims this effect to explain the 2-month period of 288 Glauke. Binzel analyzed the 1-month lightcurve of 1220 Crocus, a possible binary system with ~20 km-sized components and an estimated age lower than 3×10^8 yr (1220 is a member of the Eos family, and might have captured a satellite during the breakup of the parent body). No different explanation is presently available for the excess of slow rotators, or for the existence of objects with such long observed periods.

D. Doublet Craters

Additional evidence for binary asteroids come from doublet craters, pairs formed by simultaneous impacts. On heavily cratered bodies, true doublets generally cannot be distinguished from separate impacts, and statistical arguments for their existence are disputed (Woronow 1978a,b; Oberbeck 1978). However, there are four recognized pairs of craters on the Earth, with matching ages and physical proximity: Clearwater Lakes (diameters 32 and 22 km), Ries/Steinheim (24 and 3.4 km), Kamensk/Gusev (25 and 3 km) and Kara/Ust-Kara (60 and 25 km) (Grieve 1987). Their sizes and separations make it

unlikely that they are due to tidal or atmospheric breakup of single bodies just before impact (Noerdlinger 1980) but can be readily explained by impacts of binary asteroids (Hut and Weissman 1985). Binaries would be expected to be more abundant than the fraction of craters that are recognizable as double. Close binaries would yield only single craters. More distant binaries may be separated by close encounters with a planet. During an encounter, the planet's tidal pull causes the sphere of influence of the asteroidal primary to shrink; its size, in asteroid radii, becomes comparable with the miss distance in planetary radii. For a planet-crossing body, near misses are more likely than impacts, so a distant satellite may be lost before the primary collides with the planet. With this consideration, the abundance of terrestrial doublet craters (a few percent of all impact structures with diameter >1 km, or $\sim 15\%$ of those with $D > 20$ km) is surprisingly large. Quantitative modeling of the evolution of binary orbits due to planetary encounters, and the expected separation of craters from impacting binaries, would be very useful.

E. Radar

Radar is a potentially powerful tool for detecting asteroidal satellites, but is limited by the small number of asteroids accessible by present equipment. The technique depends on the Doppler shift of the satellite's echo relative to the primary's, and so is best for close binaries. Radar has placed a stringent upper limit on the size of a possible satellite of 2 Pallas (Showalter et al. 1982). A radar spectrum of 216 Kleopatra (Ostro et al. 1986; see also the chapter by Ostro) shows definite bifurcation; the radar cross section *increases* with distance from the spin axis. While a single dumbell-shaped body cannot be ruled out, the most straightforward interpretation is a binary. This is probably the best evidence to date for a binary asteroid. The radar observations were made when Kleopatra's visual lightcurve had low amplitude, implying a nearly pole-on view. A more favorable equatorial aspect might show clear Doppler separation of the components, which would confirm its binary nature.

F. Imaging

Speckle interferometry has some promise for detecting asteroidal satellites, although early results indicating the presence of satellites of 2 Pallas and 12 Victoria (Hege et al. 1980) were apparently spurious. Its major limitation is its inability to detect very faint objects. The effective limiting magnitude of $\simeq +16$ corresponds to a diameter of a few tens of km in the main belt. Drummond et al. (1985) obtained only an upper limit of $\simeq 50$ km for a satellite of 532 Herculina. Drummond (personal communication, 1988) reports similar or larger size limits for asteroids 2, 4, 29 and 511, and an upper limit of 15 km for any satellite of asteroid 433. Interferometric techniques are most useful for systems with large satellites and moderate separations. As these would be tidally despun, the most promising targets would be slow rotators ($P \gtrsim 24$hr).

The clearest proof of asteroidal satellites would be direct images. There have been searches using CCD detectors and coronagraphic techniques to cut down scattered light from the primary (Gehrels et al. 1987; Gradie and Flynn 1988; total sample, 22 asteroids). These searches can detect very faint objects, only a few km in size, at sufficiently large separations. The inner limit for detection depends on observational circumstances, but is typically a few tens of radii of the primary. This is comparable to the maximum separation expected from consideration of their origins and tidal evolution, and does not rule out a substantial population of closer satellites. Further searches of this type should concentrate on those asteroids for which the inner search limits, in terms of a/R, are relatively small.

The pessimistic conclusion of Gehrels et al. that small satellites are virtually nonexistent was based on the lack of detections, and also on the collisional evolution model of Davis et al. (1985), who suggested that no asteroids smaller than ~ 30 km diameter are intact survivors from the primordial epoch. We note that a satellite is more resistant to disruption than an isolated asteroid of the same size, because fragments that remain in orbit around the primary can re-accrete. Also, satellites may be produced by collisions as well as destroyed by them, and some may be relatively young. Finally, collisional evolution models are still subject to considerable uncertainty (see the chapter by Davis et al.), and do not in themselves provide strong arguments for or against the existence of asteroidal satellites.

V. DISCUSSION

Of what significance are binary asteroids? As mentioned above, their expected properties, such as mass ratio, separation, etc., should depend on the mechanisms of their formation. Knowledge of these parameters for a significant sample of binaries, or even a reliable upper limit on their abundance, could provide a useful constraint on the collisional history of the asteroid belt. It might also yield insight on the outcomes of collisions and the validity of scaling laws, in addition to that provided by the properties of Hirayama families (Davis et al. 1985; see also their chapter).

Satellites could also be used to determine masses and densities of asteroids. In principle, the mean density of a binary system can be determined from lightcurves of satellite transits and occultations, even if the absolute sizes of the components are unknown (see the chapter by Hoffman). This technique has been applied to the Pluto-Charon system (Tholen et al. 1987). Any such analysis would be more complex for an asteroidal binary because of the unknown geometry of the system, in particular the possibility that the components have irregular shapes. If a system is resolved so that its separation can be measured, the total mass is found from Kepler's third law. The mass ratio could be estimated from the relative brightness of the components, or by astrometric determination of the primary's motion about the barycenter. The

accuracy of density determinations would probably be limited by uncertainties in the volumes of the components.

The belief of a decade ago that many asteroids possess satellites (Van Flandern et al. 1979) appears to have been too optimistic. Binary asteroids are rarer and harder to detect than had been concluded. The various mechanisms suggested for their origin appear to operate with low probability, so only a small fraction of asteroids may be binaries. Large satellites may exist in stable synchronous orbits close to their primaries; such systems cannot be easily distinguished from elongated single bodies. Tidal evolution will not produce separations greater than a few tens of primary's radii for any size of satellite. Our understanding of the predicted properties of binary asteroids is consistent with the failure to detect them by present techniques and the very limited number of asteroids examined. Nonetheless, there is strong indirect evidence in at least a few cases. In Table I, we list the most likely candidate binaries suggested to date; this is not an exhaustive list. We remain cautiously optimistic that future observations using the Space Telescope, radar and groundbased imaging techniques will soon allow a definite resolution of the intriguing problem of asteroidal satellites.

TABLE I
Suspected Binary Asteroids

Asteroid	Evidence[a]	Reference
43	L	Cellino et al. 1985
63	L	Cellino et al. 1985
146	O	Arlot et al. 1985
182	P	Dermott et al. 1984
192	L	Cellino et al. 1985
216	L,R	Weidenschilling 1980; Ostro et al. 1986
249	P	Binzel 1987
280	P	Binzel 1987
288	P	Harris 1983
385	P	Harris, unpublished
407	P	Weidenschilling, unpublished
437	P	Binzel 1987
508	P	Harris, unpublished
532	O	Bowell et al. 1978
624	L	Weidenschilling 1980
709	P	Dermott et al. 1984
1220	P	Binzel 1985
1481	P	Binzel 1987

[a]L: lightcurve; O: occultation; P: period > 40 hr; R: radar.

REFERENCES

André, C. 1901. Sur le système formé par la planète double (433) Eros. *Astron. Nachr.* 155:27–30.

Arlot, J., Lecacheux, J., Richardson, C., and Thuillot, W. 1985. A possible satellite of (146) Lucina. *Icarus* 61:224–231.

Binzel, R. 1985. Is 1220 Crocus a precessing, binary asteroid? *Icarus* 63:99–108.

Binzel, R. 1987. A photoelectric survey of 130 asteroids. *Icarus* 72:135–208.

Binzel, R., and Van Flandern, T. 1979. Minor planets: The discovery of minor satellites. *Science* 203:903–905.

Bobrovnikoff, N. 1929. The spectra of minor planets. *Lick Obs. Bull.* 14 (407):18–27.

Bowell, E., McMahon, J., Horne, K., A'Hearn, M., Dunham, D., Penhallow, W., Taylor, G., Wasserman, L., and White, N. 1978. A possible satellite of Herculina. *Bull. Amer. Astron. Soc.* 10:594 (abstract).

Burns, J., and Safronov, V. S. 1973. Asteroid nutation angles. *Mon. Not. Roy. Astron. Soc.* 165:403–411.

Cappacioni, F., Cerroni, P., Coradini, M., Farinella, P., Flamini, E., Martelli, G., Paolicchi, P., Smith, P., and Zappalá, V. 1984. Shapes of asteroids compared with fragments of hypervelocity impact experiments. *Nature* 308:832–834.

Cellino, A., Pannunzio, R., Zappalá, V., Farinella, P., and Paolicchi, P. 1985. Do we observe light curves of binary asteroids? *Astron. Astrophys.* 144:355–362.

Cellino, A., Di Martino, M., Farinella, P., Paolicchi, P., and Zappalá, V. 1988. Effects of non-ellipsoidal shapes on the lightcurves of asteroids. Asteroids II Abstract Booklet, 8–11 March, Tucson, Arizona.

Chandrasekhar, S. 1969. *Ellipsoidal Figures of Equilibrium* (New Haven: Yale Univ. Press).

Cintala, M., Head, J., and Wilson, L. 1979. The nature and effects of impact cratering on small bodies. In *Asteroids*, ed. T. Gehrels (Tucson: Univ. of Arizona Press), pp. 579–600.

Cook, A. F. 1971. 624 Hektor: A binary asteroid? In *Physical Studies of Minor Planets*, ed. T. Gehrels, NASA SP-267, pp. 155–163.

Davis, D. R., Chapman, C. R., Weidenschilling, S. J., and Greenberg, R. 1985. Collisional history of asteroids: Evidence from Vesta and the Hirayama families. *Icarus* 62:30–53.

Dermott, S., Harris, A. W., and Murray, C. 1984. Asteroid rotation rates. *Icarus* 57:14–34.

Drummond, J., Hege, E., Cocke, W., Freeman, J., Christou, J., and Binzel, R. 1985. Speckle interferometry of asteroids. II. 532 Herculina. *Icarus* 61:232–240.

Farinella, P., Paolicchi, P., and Zappalà, V. 1981a. Triaxial equilibrium ellipsoids among the asteroids? *Icarus* 46:114–123.

Farinella, P., Paolicchi, P., and Zappalà, V. 1981b. Analysis of the spin rate distribution of asteroids. *Astron. Astrophys.* 104:159–165.

Farinella, P., Paolicchi, P., and Zappalà, V. 1982. The asteroids as outcomes of catastrophic collisions. *Icarus* 52:409–433.

Gehrels, T., Drummond, J., and Levenson, N. 1987. The absence of satellites of asteroids. *Icarus* 70:257–263.

Gradie, J., and Flynn, L. 1988. A search for satellites and dust belts around asteroids: Negative results. *Lunar Planet Sci.* XIX:405–406 (abstract).

Grieve, R. A. F. 1987. Terrestrial impact structures. *Ann. Rev. Earth Planet. Sci.* 15:245–270.

Harris, A. W. 1980. A note on the tidal evolution of eccentric orbits. *Bull. Amer. Astron. Soc.* 12:744 (abstract).

Harris, A. W. 1983. Slowly rotating asteroids: Evidence for binary asteroids? *Bull. Amer. Astron. Soc.* 15:828 (abstract).

Harris, A. W. 1987. On the evolution of meteoroid collision debris in orbit about asteroids. *Bull. Amer. Astron. Soc.* 19:909 (abstract).

Harris, A. W., and Ward, W. R. 1982. Dynamical constraints on the formation and evolution of planetary bodies. *Ann. Rev. Earth Planet. Sci.* 10:61–108.

Hartmann, W. K. 1979*a*. A special class of planetary collisions: Theory and evidence. *Proc. Lunar Planet. Sci. Conf.* 10:1897–1916.

Hartmann, W. K. 1979*b*. Diverse puzzling asteroids and a possible unified explanation. In *Asteroids*, ed. T. Gehrels (Tucson: Univ. of Arizona Press), pp. 466–479.

Hege, E., Cocke, W., Hubbard, E., Christou, J., and Radick, R. 1980. Possible secondaries of asteroids found by speckle interferometry. *Bull. Amer. Astron. Soc.* 12:662 (abstract).

Hut, P., and Weissman, P. 1985. Double craters on the Earth and planets: Evidence for binary asteroids and comets? *Bull. Amer. Astron. Soc.* 17:690 (abstract).

Leone, G., Farinella, P., Paolicchi, P., and Zappalà, V. 1984. Equilibrium models of binary asteroids. *Astron. Astrophys.* 140:265–272.

Noerdlinger, P. 1980. Tidal disruption of impacting bodies. *Bull. Amer. Astron. Soc.* 12:829–830 (abstract).

Oberbeck, V. 1978. The expected frequency of doublet craters (a reply). *Icarus* 35:450–451.

Ostro, S., Campbell, D., and Shapiro, I. I. 1986. Radar detection of 12 asteroids from Arecibo. *Bull. Amer. Astron. Soc.* 18:796 (abstract).

Showalter, M., Ostro, S., Shapiro, I. I., and Campbell, D. 1982. Upper limit on the radar cross section of a Pallas satellite. *Bull. Amer. Astron. Soc.* 14:725 (abstract).

Stevenson, D. J. 1987. Origin of the Moon—the collision hypothesis. *Ann. Rev. Earth Planet. Sci.* 15:271–316.

Tedesco, E. 1979*a*. Binary asteroids: Evidence for their existence from lightcurves. *Science* 203:905–907.

Tedesco, E. 1979*b*. A photometric investigation of the colors, shapes, and spin rates of Hirayama family asteroids. Ph.D. Thesis, New Mexico State Univ.

Tholen, D., Buie, M., Binzel, R., and Frueh, M. 1987. Improved orbital and physical parameters for the Pluto-Charon system. *Science* 237:512–514.

Van Flandern, T., Tedesco, E., and Binzel, R. 1979. Satellites of asteroids. In *Asteroids*, ed. T. Gehrels (Tucson: Univ. of Arizona), pp. 443–465.

Weidenschilling, S. J. 1980. Hektor: Nature and origin of a binary asteroid. *Icarus* 44:807–809.

Weidenschilling, S. J. 1981. How fast can an asteroid spin? *Icarus* 46:124–126.

Weidenschilling, S. J. 1985. Stability of orbits of asteroidal satellites. *Bull. Amer. Astron. Soc.* 17:731 (abstract).

Wijesinghe, M., and Tedesco, E. 1979. A test of the plausibility of eclipsing binary asteroids. *Icarus* 40:383–393.

Woronow, A. 1978*a*. The expected frequency of doublet craters. *Icarus* 34:324–330.

Woronow, A., 1978*b*. A reply to V. R. Oberbeck's criticisms of "The Expected Frequency of Doublet Craters." *Icarus* 35:452–453.

Zappalà, V., Scaltriti, F., Farinella, P., and Paolicchi, P. 1980. Asteroidal binary systems: Detection and formation. *Moon and Planets* 22:153–162.

PART IV
Origin and Evolution

ORIGIN OF THE ASTEROID BELT

GEORGE W. WETHERILL
Carnegie Institution of Washington

Earlier work and concepts relevant to the origin of the asteroid belt are reviewed and considered in the context of the more general question of solar system origin. Several aspects of asteroidal origin by accumulation of smaller bodies have been addressed by new dynamic studies. Numerical and analytical solutions of the dynamical theory of planetesimal accumulation are characterized by a bifurcation into runaway and nonrunaway solutions. The differences in time scales resulting from runaway and nonrunaway growth can be more important than conventional time scale differences determined by heliocentric distances. This introduces new possibilities, e.g., planetary accumulation may be more rapid at the distance of Jupiter than in the asteroid belt, thus permitting Jupiter to control asteroidal growth. Although alternatives must be seriously considered, the most promising approach to asteroidal origin is one in which the initial surface density of the solar nebula varied smoothly between the terrestrial and giant-planet region. In the absence of external perturbations, it is found that runaway growth of excessively large asteroids would then occur in <1 Myr, but fairly modest external perturbations by Jupiter, Saturn or other perturbers, resulting in eccentricities ~0.01 may quench runaways, truncate asteroidal growth at their present size, and then initiate the necessary loss of asteroidal material by mutual fragmentation. For a gradual increase in velocity, most of the material in the asteroid belt could be lost before fragmentation of the larger asteroids becomes important. The role of Jupiter-scattered planetesimals in producing the present high relative velocities of the asteroids has been studied quantitatively. For some conditions that must be considered highly speculative, but not impossible, it is found that velocities comparable to those observed can be achieved thereby without excessive asteroidal mixing. It is also possible that long-range resonant perturbations may have been the principal cause of acceleration of asteroids to their present velocities.

I. INTRODUCTION

The absence of planets of significant size between the orbits of Mars and Jupiter has been the subject of conjecture for centuries (see, e.g., Kepler 1621; Kant 1755). The discovery of Ceres in 1801 by Piazzi was therefore not a surprise, and was widely welcomed as a second confirmation of the Titius-Bode law of planetary distances, the first having been the discovery of Uranus about twenty years earlier. The discovery of Pallas, Juno and Vesta within the next six years proved to be an embarrassment of riches, and led to the suggestion that the asteroids were fragments of a single disrupted planet, presumably thereby saving the law of Titius and Bode, as well as being in accordance with the generally accepted Kant-Laplace cosmogony in which the planets formed directly from the solar nebula. The multiplicity of asteroids discovered during the 19th century caused this hypothesis to become increasingly untenable, even though it has been revived from time to time (see, e.g., Ovenden 1972).

The origin of asteroidal bodies therefore appears to be more consistent with a "planetesimal" theory of planet formation, in which planets accumulated from smaller "meteoric bodies" (see, e.g., Chladni 1794; Proctor 1898; Chamberlin 1904). The growth of the asteroids by accumulation of smaller bodies was specifically addressed by Schmidt (1944), and most subsequent quantitative discussions of asteroidal origin have remained in the context of theories of planetary accumulation (Safronov 1969,1979). This approach will be followed in this chapter (Sec. II).

When considered in this way, the fundamental importance of asteroids and their origin to much more general problems of planetary science becomes apparent. The failure of a normal size planet to form in the asteroidal region is usually attributed to the prior formation of Jupiter (Proctor 1898; Safronov 1969). If so, the formation of the asteroids is intimately linked to the central unsolved problem of planetary formation, the time scale for growth of Jupiter and the other giant planets. Excess solid material, removed from the asteroid belt by the same processes that prevented the growth of full-scale planets, may be responsible for the "late veneer" on the Earth, proposed to explain its geochemical composition (see, e.g., Wänke 1981). Furthermore, we have in our meteorite collections actual samples of asteroidal fragments. These are known to bear the record of presolar events (see, e.g., Clayton 1981) as well as collisional events late in solar system history (Bogard 1979). Inevitably, they must also contain the imprint of events of intermediate age, 4.4 to 4.5 Gyr ago, at which time the asteroidal bodies formed. Thus, they provide fossil evidence of events relevant not only to the formation of the asteroids themselves, but for the reasons just mentioned, to the entire solar system.

Assuming that the asteroids grew from smaller bodies, it remains to be explained why only very small bodies, rather than full-size planets, were formed in that part of the solar system. From the most general point of view, there are two ways to explain the present 10^3- to 10^4-fold depletion of surface density material in the asteroid belt:

(1) There was never much material there, possibly because of a ring structure in the solar nebula. Present understanding of the solar nebula is inadequate to reject this hypothesis. Accumulation calculations of this kind discussed in Sec. II, have permitted estimation of the minimum surface density that will permit growth of asteroids on the time scale of <100 Myr inferred from meteoritic data. The lowest possible surface density found still requires subsequent loss of primordial asteroidal material by a factor of about 100, and therefore it does not seem that presence of a wide gap in the solar nebula can be the entire explanation of the observed deficiency in mass.

(2) There was a "normal" amount of material in the asteroid belt, but it was removed from the asteroid belt subsequent to the formation of the present larger asteroids. Two principal mechanisms have been proposed for removal of this material:

(a) Collisional fragmentation, followed by removal of the small fragments by nongravitational forces, e.g., inward spiralling under gas drag, or loss by entrainment during outflow of residual nebular gas. This is discussed in Sec. III. In order for asteroids to fragment, their collision velocity must be sufficient to overcome their mechanical strength and gravitational binding energy. Fragmentation of the largest asteroids requires relative velocities of >2 km s^{-1}. Present asteroidal collision velocities of ~5 km s^{-1} are therefore sufficient. Any complete theory of the origin of the asteroid belt must explain how the present asteroidal velocity distribution was achieved.

(b) External gravitational perturbations, whereby asteroidal material is accelerated into highly eccentric, dynamically short-lived, Jupiter- or Earth-crossing orbits.

These mechanisms are by no means mutually exclusive. More likely they interacted in a synergistic manner. For example, fragments ~100 m in diameter could spiral under gas drag into a resonant chaotic zone, followed by acceleration into eccentric orbits. On the other hand, high velocities produced by external gravitational perturbations would also be expected to cause fragmentation by mutual collisions.

It has often been proposed that residual planetesimals, scattered from the region of Jupiter, may have been responsible for loss of material from the asteroid belt, either as a result of collisional fragmentation or as a consequence of their gravitational perturbations. Jupiter-scattered planetesimals are discussed in Sec. IV. The effectiveness of both of these mechanisms for removal of material from the asteroid belt is closely linked to the time scale for the formation of Jupiter and Saturn. This problem will be addressed in Sec. V.

The author regards it fortunate that this is only a review chapter, and therefore he is not under obligation to actually report the solution of any of these problems, but only to discuss their present status. We are probably far from understanding what actually happened during the formation of the asteroids. To confine discussion to what is really known to be true would limit it to the trite. In such circumstances, it is preferable to consider what might

conceivably be true, in hope that it may at least prove interesting. Sec. VI identifies several problems that, in the author's opinion, are in particular need of attention if our present very rudimentary understanding of asteroidal origin is to improve.

II. GROWTH OF ASTEROIDS FROM PLANETESIMALS

Considerable quantitative work has been done on the processes by which planets like the Earth may have formed by the accumulation of much smaller (e.g., ~10 km diameter) bodies. It is worthwhile to apply the results of this work to the problem of forming asteroids in the same way.

A major uncertainty in this problem is the choice of initial planetesimal size at which the dynamical evolution of the planetesimals is primarily dominated by their gravitational perturbations and self-binding energy. Previous discussions of this problem in the terrestrial planet region have assumed initial planetesimals in the diameter range of 1 to 10 km. This is the size expected at 1 AU for bodies resulting from dust-layer gravitational instability in the central plane of the solar nebula (Safronov 1969; Goldreich and Ward 1973). Weidenschilling (1984) has identified reasons for believing that turbulence at the boundary layer between the dust in the central plane of the nebula and the much thicker gaseous disk may preclude the low velocities required to produce dust-layer gravitational instability. If so, the problem is more complex. Work of Donn and Meakim (1988) suggests that nongravitational accumulation may extend to diameters of >100 m.

In the first illustrative calculation reported here, a nominal size distribution at 2.5 AU is chosen identical to that used in recent previous work on the early stage of accumulation at 1 AU (Wetherill and Stewart 1989), together with a planetesimal and gas surface density inversely proportional to the semimajor axis. The midpoint mass of this nominal swarm is 4.5×10^{18} g, corresponding to a diameter of 14.2 km for a material density of 3.0 g cm^{-3}. As mentioned above, dust-layer gravitational instabilities may not prove to be physically realistic, and it may be that the size at which nongravitational growth of planetesimals ends is similar in both the terrestrial planet region and in the asteroid belt. The consequences of this assumption are explored below.

The results of the calculation of this nominal case are shown in Fig. 1. Following the earlier work at 1 AU, it is assumed that gravitational focusing was enhanced at low velocities in accordance with the work of Wetherill and Cox (1985) as extended to greater heliocentric distances and lower velocities by Lissauer and Greenzweig (1987; also personal communication of unpublished calculations). Again, in accordance with the earlier work at 1 AU, it was assumed that fragmentation caused the development of a tail of smaller bodies down to 1 m in diameter, similar to that described by Davis et al. (1979). Smaller fragmentation debris was assumed to be lost from the swarm
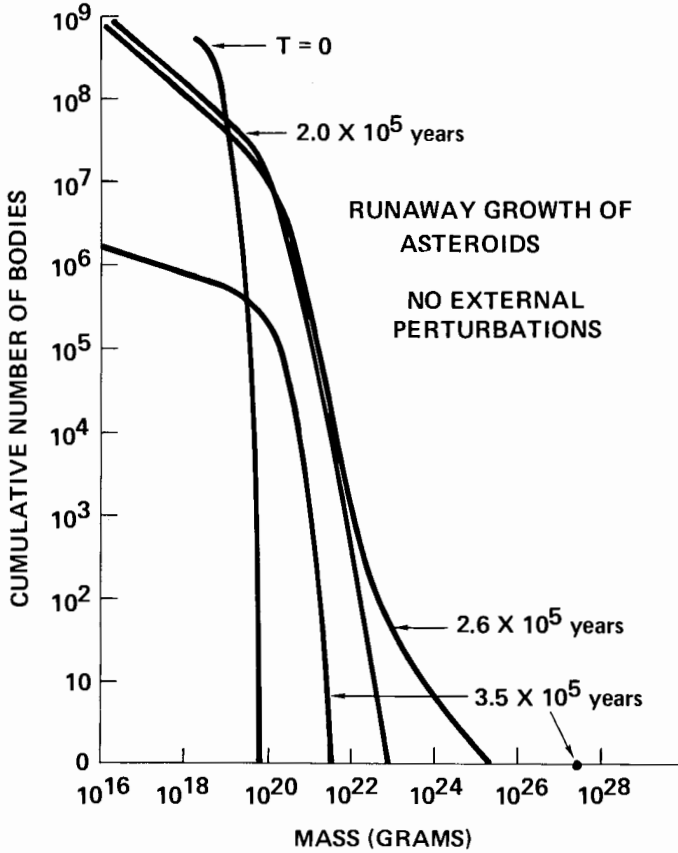
Fig. 1. Runaway growth of initial ~10 km diameter bodies in a zone 0.074 AU wide, centered at 2.5 AU in 3.5 × 10⁵ yr.

by nongravitational forces, e.g., infall by gas drag, or entrapment in radial outflow of gas associated with loss of the gaseous solar nebula.

The principal result of the calculation shown in Fig. 1 is that runaway growth of $>10^{27}$g asteroidal bodies in zones ~0.07 AU in width are predicted to form on a rapid time scale of ~3.5×10^5 yr. Although different choices of surface densities, etc. would alter the numerical results, the qualitative conclusions would be unchanged. The subsequent evolution of these bodies has been followed by the techniques used earlier for study of the final stages of terrestrial planet formation (Wetherill 1985,1986,1988a). The final outcome was the formation of an Earth-mass planet in the asteroid belt. While this might please devotees of the Titius-Bode law, it seems that pursuit of an otherwise plausible "nominal case" leads to a *reductio ad absurdum*, and that

alternatives should be sought if agreement with observation is to be found. If alternatives fail, then consideration can be given to ways of removing (e.g., resonances) unwanted planetary bodies of this kind.

Three alternatives are considered here:

(1) *Larger initial masses of the planetesimals.* In spite of the reservations expressed earlier regarding the formation of dust-layer gravitational instabilities, if, nevertheless, they did occur in the asteroid belt, they would be larger. Because the mass of these instabilities increases with the 6th power of the semimajor axis and only with the 3rd power of the dust surface density (Goldreich and Ward 1973), if the surface density varies as $1/a$, initial bodies of mass $\sim 7 \times 10^{19}$g will be expected at 2.5 AU. These larger initial planetesimals were found to inhibit the runaway, principally because the smaller number of bodies in the initial swarm reduced the tendency of early stochastic accumulation to generate a seed that ultimately became a runaway. (A corollary of this is that use of an initial swarm containing smaller bodies will increase the rate at which runaways occur.)

Nevertheless, after 1.5 Myr, a body of mass 7×10^{25}g was found to form, 20 times as large as the second largest body, indicating a continuing tendency for runaways to produce excessively large asteroidal bodies. (By comparison, Ceres has a mass of $\sim 10^{24}$g.) If some way were found to truncate the growth at ~ 1 Myr, the largest body would have a mass of only 8×10^{24}g. The problem with this is that truncation probably requires formation of Jupiter. It would therefore be necessary to assume that although dust-layer instabilities were large enough to delay runaway in the asteroid belt, that the even more massive instabilities expected at 5 AU did not occur. Otherwise, the growth of Jupiter would be delayed longer, and even larger bodies would form in the asteroid belt.

(2) *Collisional self-termination of the runaway.* In this case, it is assumed that an incipient runaway increased the velocities of the smaller bodies sufficiently to cause them to fragment by mutual collisions before the runaway went to completion, as proposed by Patterson and Spaute (1988). This requires assuming that the runaway body remains a fully effective gravitational perturber, despite the tendency of the Jacobi parameter (equivalent to the relative velocity of crossing orbits) to remain constant when gravitational perturbations are dominated by a single body. A calculation using the theory used by Wetherill and Stewart (1989), including this assumption, has been made. Qualitatively, the result of Patterson and Spaute is confirmed. At 7×10^5 yr, the runaway self-terminates at a mass of 3×10^{26}g, containing only 11% of the mass in the original accumulation zone. At this time, the midpoint mass of the swarm is only $\sim 2 \times 10^{21}$g and the relative velocity of bodies of this size is ~ 0.4 km s^{-1}, about a factor of 10 above their escape velocity, resulting in collisional fragmentation of the residual swarm.

Nevertheless, in our calculation, the mass of the runaway is found to be considerably greater than that of the largest presently observed asteroid, and

the proposed mechanism reduced the mass of the asteroid belt only by a factor of ~10. The results of these two calculations cannot be compared in detail because of a number of differences in the initial conditions and assumptions involved. Furthermore, self termination of runaway growth in this way would also inhibit the formation of terrestrial and giant planets.

(3) *Suppression of the runaway by external perturbations.* In all the preceding calculations, it was assumed that the increase in velocity of the planetesimal swarm was produced only by the mutual gravitational perturbations of the swarm bodies. Under these circumstances, the tendency towards equipartition of energy caused the largest body to have a markedly lower velocity than the smaller bodies, thereby increasing its gravitational capture cross section, and precipitating the runaway. If a process existed whereby this tendency would be inhibited, then the runaway could be avoided.

It is by no means certain that external perturbations of sufficient strength are possible. At the present time, the perturbations of the planets, particularly the giant planets, are capable of producing eccentricity variations as large as 0.05 in the asteroid belt even outside the present resonant regions and much larger increases in eccentricity in the vicinity of the secular and commensurability resonances. Relative velocities associated with eccentricities this high, if uncorrelated, would certainly preclude the runaway shown in Fig. 1, but because of correlations of perturbations in neighboring orbits and gravitational effects of nebular gas, it is unlikely that random velocities this large were present during the growth of the asteroids. It is possible, however, that much more modest relative velocities would also prevent runaway growth. A study has been made of the magnitude of the externally induced relative velocity changes required to effect this. Whether or not velocity changes of this magnitude might be expected to have been produced by early formation of Jupiter and loss of nebular gas will be left for future investigation.

The necessary degree of velocity enhancement has been studied by repeating the calculations shown in Fig. 1, but augmenting the expressions for velocity changes by gravitational perturbations, collisional damping and gas drag used by Stewart and Wetherill (1988) with an additional dv/dt term representing the effect of these external perturbations. For the first 2×10^5 yr, no external perturbations were introduced. Between 2×10^5 and 4×10^5 yr, the additional dv/dt term increased linearly from zero to 37.4 m s^{-1} per 10^5 yr. After 4×10^5 yr, a constant value of 37.4 m s^{-1} per 10^5 yr was used. As a result of these external perturbations, after 1 Myr, the largest body of the swarm had a velocity with respect to a circular orbit of 18 m s^{-1} and the midpoint mass of the swarm had a velocity of 192 m s^{-1}, corresponding to eccentricities at zero inclination of $\sim 10^{-3}$ and $\sim 10^{-2}$, respectively. These may be compared with even lower eccentricities of 6×10^{-7} and 2×10^{-3} at the end of the runaway growth shown in Fig. 1. The higher relative velocities eliminate the runaway, despite their being much lower than the eccentricities and inclinations of ~0.15 observed in the asteroid belt today.
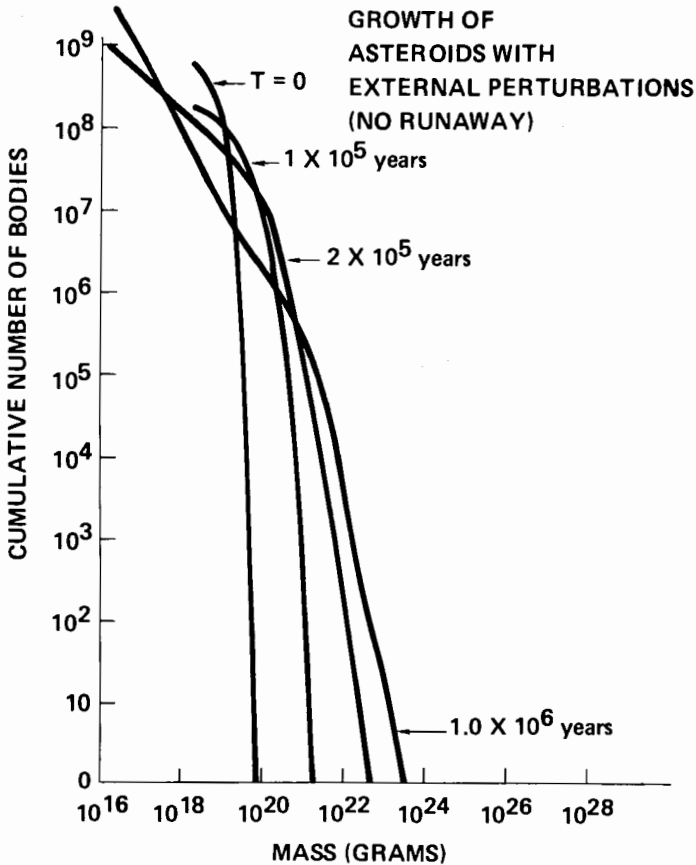
Fig. 2. Same initial conditions as Fig. 1. Here, however, "orderly" growth (without runaway) occurs because of external gravitational perturbations. This figure illustrates the growth regime. By ~1 Myr, the largest bodies cease to grow, and the smaller bodies are being destroyed by collisions.

The diameter reached by the largest body in a zone 0.074 AU wide at 2.5 AU was 624 km at 1 Myr (Fig. 2). This is in the general range of sizes of the largest present-day asteroids. Because of the low eccentricities associated with this growth phase, no significant radial mixing of material within the asteroid belt is expected during their growth.

III. REMOVAL OF MATERIAL FROM THE ASTEROID BELT BY FRAGMENTATION

Although the eccentricities of the bodies in the swarm shown in Fig. 2 at 1 Myr are very low in comparison with present asteroidal eccentricities, the associated relative velocities exceed twice the escape velocity for 94% of the

swarm mass. Only the bodies ≳200 km in diameter are safe from collisional destruction.

As a consequence, continuous fragmentation of smaller bodies accompanies the growth of the asteroids when a runaway does not occur. In the example shown in Fig. 2, after 1 Myr only 40% of the original mass of the zone remained in the original bodies of the swarm; 8% was in the tail consisting of bodies extending from the smallest ~10 km diameter bodies of the
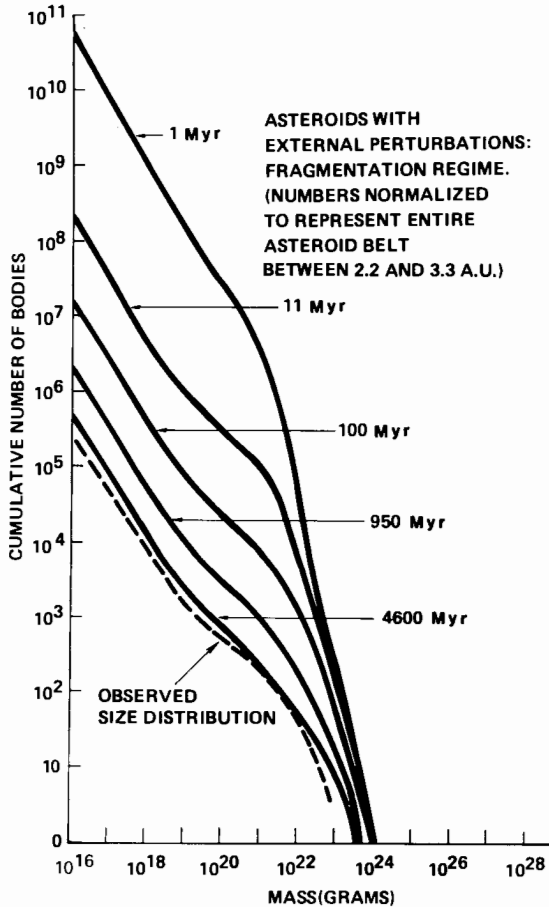
Fig. 3. Same initial conditions as Fig. 1, but "orderly" growth occurs because of external gravitational perturbations. This figure shows the fragmentation regime. After 11 Myr, fragmentation has reduced the mass of the zone by a factor of 80, by a factor of 4000 after 950 Myr, and by a factor of 1.3×10^4 during the history of the solar system. In this figure, the number of bodies is scaled upward by a factor of 15, in order to represent the number of bodies in the entire asteroid belt between 2.2 and 3.3 AU. The dashed curve represents the observed distribution of asteroids, assuming a mean albedo of 0.10 for asteroids smaller than 10^{22}g, and measured diameters for larger bodies.

original swarm down to objects 1 m in diameter. The remaining 52% has been reduced to smaller objects, and in accordance with the assumptions made in the calculation, lost from the system by nongravitational mechanisms. In Fig. 3, the calculation is continued into the fragmentation regime. The external perturbations were discontinued after 10 Myr, by which time the relative velocities achieved their present values. After 4.8 Myr, 95% of the material had been lost by fragmentation, and the eccentricity of the entire swarm has risen to ~0.07.

With the passage of time, collisions at velocities near their present value continued to remove material from the asteroid belt, leading to a distribution resembling that observed after 4.6 Gyr (dashed curve on Fig. 3).

Davis et al. (1979) have reported calculations of collisional evolution assuming a primordial asteroidal mass distribution resembling that of Figs. 2 and 3 at 1 Myr. In those calculations, the relative velocities of the asteroids were assumed to be the high ($\sim$5 km s^{-1}) velocities of the present asteroid belt. This differs from the collisional evolution described here, in that in the present work a large fraction of the asteroidal material is lost by quite *low*-velocity collisions before the present-day asteroidal velocities are reached. The method of calculation reported in the present work is insufficiently refined to discuss seriously important issues raised by these previous authors, such as the survival of a basaltic crust on Vesta. It would be valuable to evaluate more quantitatively such questions, including the effect of cratering collisions, in the case of more gradual increases of velocity.

IV. JUPITER-SCATTERED PLANETESIMALS

A concept that has played a major role in discussions of the evolution of the asteroid belt is that of Jupiter-scattered planetesimals, i.e., residual bodies from the formation of Jupiter (and possibly Saturn) scattered by Jupiter perturbations into the asteroid belt (Safronov 1969; Weidenschilling 1975; Kaula and Bigeleisen 1975; Ip 1987). The mass of these planetesimals varies considerably between authors, i.e., from $\sim$10^{24} to $\sim$6 $\times$ 10^{27}g. The effect of smaller planetesimals on the asteroidal belt would be primarily collisional, whereas the larger bodies would produce gravitational perturbations of the asteroidal bodies as well. These gravitational perturbations have sometimes been hypothesized to be simply sufficient to accelerate asteroidal material to their present eccentricities, followed by fragmentation, while in other cases it is proposed that the gravitational perturbations suffice to remove material directly from the asteroid belt.

Evaluation of the plausibility of this concept obviously depends on understanding how Jupiter was formed, as discussed in the next section. Anticipating the result of that discussion, it can be stated that there is at present no compelling reason to believe that the formation of Jupiter requires a significant flux of at least the larger planetesimals to penetrate the asteroid belt, but

neither is present understanding of the formation of Jupiter adequate to rule out this possibility.

Insofar as Jupiter-scattered planetesimals are relatively small ($<10^{26}$g), they would simply serve as asteroidal impactors, causing collisional fragmentation of the primordial asteroid population. Their effect will not be very different from that resulting from collisions between the asteroidal bodies themselves, particularly after the asteroid velocities have risen to their present values. Kaula and Bigeleisen (1975) considered the importance of Jupiter-scattered planetesimals as heat sources during the formation of the Earth and Moon, and concluded that if present in sufficient quantity, they should be considered to be a significant heat source. Weidenschilling (1975) pointed out that because of the approximate conservation of the Jacobi parameter in the Sun-Jupiter-planetesimal system, the influence of these planetesimals should be much greater in the asteroid belt and on Mars than at the Earth. Quantitative estimates of the effect of this on the asteroid belt are not given by these authors. Safronov (1979) also considered collisional destruction of asteroids by Jupiter-scattered planetesimals and concluded that a decrease in the asteroidal population of only about a factor of 3 would be achieved thereby, and that an alternative mechanism is required.

An alternative mechanism might be possible if the Jupiter planetesimals were large enough to perturb the asteroids gravitationally, resulting in their achieving velocities high enough to cause them to destroy one another by mutual collisions, or to transfer them into unstable orbits via resonances or by planet crossing. Safronov (1979) showed that for a favorable encounter a 1 to 2×10^{26}g body could accelerate an asteroid to typical asteroidal eccentricities. Davis et al. (1979) used the "kinetic theory of gas" program described by Greenberg et al. (1978) to study acceleration of asteroids by one-Earth-mass bodies, and concluded that the presence of about 5 such bodies in the asteroid belt for 3 Myr could provide the required eccentricities.

To my knowledge, the first work in which an attempt to follow the actual orbital evolution of the Jupiter-scattered planetesimals and asteroidal bodies is that of Ip (1987). In this work, Monte Carlo calculations based on the method of Arnold (1965) were used. The work was carried out in two stages. First, the orbital evolution of 1 and 3×10^{27}g Jupiter- and Saturn-crossing bodies were calculated. In the second stage, the calculated perturbed orbits and dynamical lifetime of 50 of these bodies were used to study the perturbations they would cause while traversing the asteroid belt. The mutual gravitational perturbations of the Jupiter-scattered bodies were not included. It was found that asteroidal velocities similar to those observed are produced only for the larger 3×10^{27}g bodies and only if Jupiter and Saturn were smaller, i.e., had only 0.1 their present mass for ~10 Myr. A full-size Jupiter and Saturn reduced the dynamical lifetime of the scattered planetesimals to such a degree that they were ineffectual asteroidal perturbers. It seems unlikely that a 30-Earth-mass Jupiter core could form and remain at that mass for 10 Myr with-

out capturing enough nebular gas to grow to its present mass. Therefore, the results of Ip do not really provide much support for believing that Jupiter-scattered planetesimals are primarily responsible for increasing asteroid eccentricities to their present high values.

The work of Ip is being extended by the present author using the program previously used to investigate terrestrial planet formation (see, e.g., Wetherill 1986). The simultaneous orbital evolution of 500 4×10^{24}g asteroids interacting with 100 Jupiter-scattered planetesimals has been studied. The Jupiter-scattered bodies are assumed to interact with one another, but mutual perturbations of the smaller bodies are ignored. Initially, only Jupiter is assumed to be present; Saturn is introduced after 2 Myr, Mars, Earth and Venus after 20 Myr. It is not claimed that this is an accurate way of determining the orbital evolution of material in the terrestrial planet region. Rather, it is simply a rough way of recognizing the possible importance of the presence of the terrestrial planets at an appropriate time in solar-system evolution, reflecting the time scale for terrestrial planet growth found in earlier work using this same program (see, e.g., Wetherill 1985).

A result of this investigation is shown in Fig. 4. Initially a swarm of 4×10^{27}g (2/3 Earth-mass) planetesimals were distributed randomly between 4.5
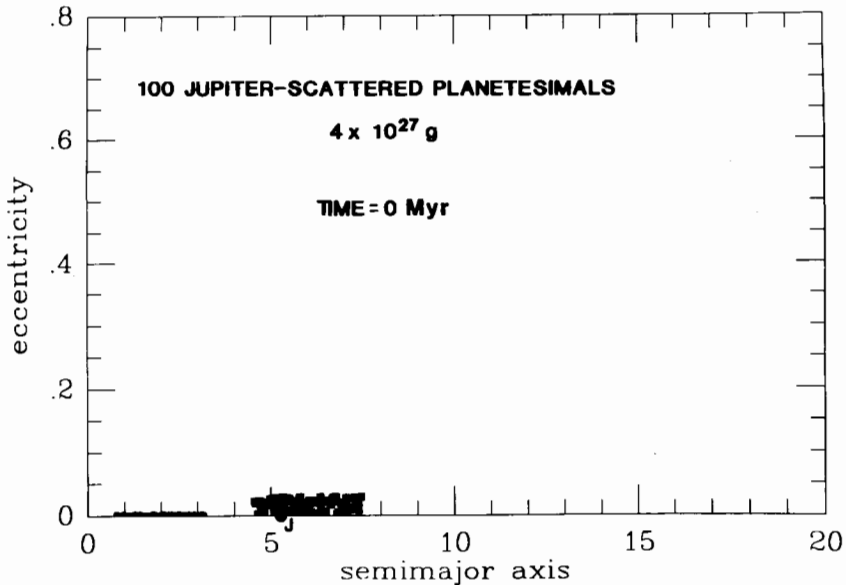
Fig. 4. Perturbation of small bodies in the asteroid belt and inner solar system by large (2/3 Earth-mass) bodies scattered by Jupiter and Saturn. The effects of resonances are not included. This figure shows the initial state. 100 large bodies are distributed between 4.5 and 7.5 AU, and 500 small bodies between 0.7 and 3.3 AU. The only planet-size body is Jupiter, with its present mass.

and 7.5 AU with random eccentricities and inclinations (in radians) between 0 and 0.03. A swarm of 500 much smaller (4×10^{24}g) bodies was distributed between 0.7 AU and 3.3 AU with initial eccentricities randomly distributed between 0 and 0.005, and inclinations over 1/2 that range. After 24 Myr (Fig. 5), a combination of Jupiter, Saturn and mutual perturbations scattered most of the original Jupiter-zone planetesimals into the large phase-space volume beyond the orbit of Saturn. Of the 205 smaller planetesimals originally in the present asteroidal region between 2.2 AU and 3.3 AU, 187 still remained at this time. Many of these bodies were accelerated to eccentricities comparable to those of the present asteroid belt. The manner in which this was accomplished was isolation by mutual perturbation of one Jupiter-zone planetesimal in the asteroid belt. This body was then perturbed into somewhat different orbits by other Jupiter-zone planetesimals with highly eccentric orbits that traversed the asteroid near their perihelia. This single isolated body migrated to different parts of the asteroid belt and scattered the asteroidal bodies to higher velocities. At these velocities, the mutual collisions of smaller asteroids with one another would destroy most of them on a time scale of ~10 Myr (see Figs. 2 and 3). The Jupiter-zone body isolated in the asteroid belt
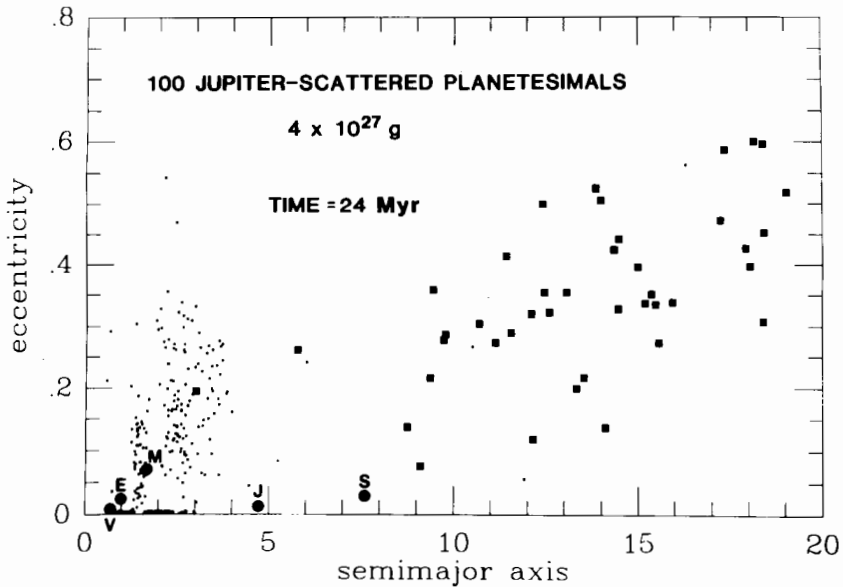
Fig. 5. This figure shows that after 24 Myr, mutual perturbations, together with those of Jupiter and Saturn (after 2 Myr) have transferred most of the large planetesimals to large semimajor axes, but one such body is isolated in the asteroid belt. Many of the "asteroids" have been accelerated to eccentricities similar to those in the present asteroid belt. Mars, Earth and Venus were introduced at 20 Myr.

continued to scatter larger asteroids on a longer time scale. After 318 Myr (Fig. 6), 52 bodies (25%) remained in the asteroid belt and 28 remained after 700 Myr. In these calculations, the effects of asteroidal resonances known to be effective in removing asteroidal material from the present asteroid belt (Williams 1973; Wisdom 1985; Wetherill 1988b) were not included. Perturbation of asteroids into these resonant regions should increase the rate at which the asteroid belt can be cleared by the isolated Jupiter-zone body. Finally, it is conceivable that the Jupiter-zone body itself could ultimately be removed by chance proximity to a resonance.

Similar calculations have been made for smaller Jupiter-zone bodies. An isolated body is always found; 1.8×10^{27}g and smaller bodies were found to be ineffectual in accelerating most of the asteroidal bodies to high velocities.

The following conclusions can be drawn from this rather preliminary investigation:

(1) Jupiter-zone planetesimals are capable of increasing asteroidal eccentricities significantly, even when Jupiter and Saturn have their present masses.
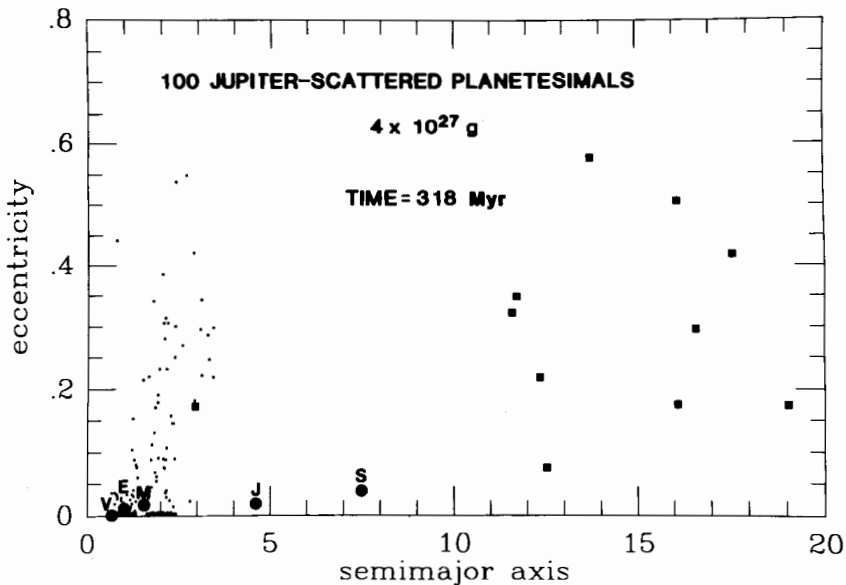
Fig. 6. This figure shows that after 318 Myr, most of the original large planetesimals have been transferred to semimajor axes beyond the present orbit of Uranus, and significant (75%) loss of asteroid bodies has taken place as well. A single one of the original 2/3 Earth-mass body remains "stranded" in the asteroid belt, and will remain there for the rest of solar system history unless removed by long-range resonant perturbations.

This is a consequence of the mutual scattering of the planetesimals by one another. The price that is paid for this success, however, is isolation of a planet-size object in the asteroid belt that requires fortuitous proximity to a resonance for its removal.

(2) In agreement with the results of Weidenschilling (1975), the effect of the scattered planetesimals decreases with decreasing heliocentric distance. In fact, the present work shows that the scattered planetesimals are very ineffectual in perturbing material interior to about 2.2 AU. In particular, they do not seem capable of causing the depletion of material required (Wetherill 1978, 1986) to prevent formation of Earth-mass terrestrial planets between 1 and 2 AU.

(3) In the next section, the plausibility of the necessary large number of very large Jupiter-scattered planetesimals will be questioned. Together with the question of removal of the isolated planetesimal that accomplishes the perturbations discussed above, it would seem excessively facile to place much reliance on Jupiter-scattered planetesimals having caused the asteroid belt to evolve to its present state, even though their possible importance cannot be ruled out. Scattering by large bodies does have the advantage of providing the observed mixing of semimajor axes of observed asteroidal compositional types, whereas long-range planetary perturbations cause velocity increases via changes in eccentricity and inclination. It is not out of the question that scattering of bodies originating in the terrestrial planet region may have had some influence on the asteroid belt, inasmuch as calculations have shown that some such material may penetrate and/or be transferred to the asteroid belt (Wetherill 1977,1985; Ip 1988).

An alternative to Jupiter-scattered planetesimals as the cause of high asteroidal velocities, is accomplishing this with long-range resonant outer-planet and residual solar-nebula perturbations, as proposed by several authors (Heppenheimer 1979; Ward 1980). At present, resonances appear to be effective over a limited portion ($\sim$15%) of the asteroid belt, but it may be that during the formation of the outer planets, the position of these resonances changed with time, causing the successive regions of the asteroid belt to be accelerated on the time scale for outer-planet formation. Ward (1980) proposed that this acceleration was limited to a "single sweep" through the asteroid belt. In view of our extremely incomplete understanding of the formation of the outer planets and the time scale on which this took place, it is possible that resonance sweeping was more complex. For example, Patterson (1987a) has described circumstantial evidence for imposition of the effects of commensurability resonances with Uranus at a late stage of asteroidal evolution. Further understanding of outer planet formation is required to evaluate whether or not resonant sweeping could supply the acceleration necessary to accomplish the velocity growth required to operate the asteroid growth and fragmentation model shown in Figs. 2 and 3.

V. GROWTH OF JUPITER AND SATURN

Much of the previous discussion involved the concept that possibly Jupiter and Saturn were formed on the time scales of ~ 1 Myr necessary to permit the modest accelerations required to prevent a runaway in the asteroid belt, and ultimately the major accelerations required to accelerate the asteroids to their present high velocities, well above their escape velocities, and thereby cause fragmentation and loss of most of the material originally in the asteroidal region. Effects related to the loss of gas from the solar nebula cannot significantly precede the formation of these planets that require nebular gas for their formation.

If Jupiter formed by accumulation of planetesimals without runaway, it seems certain that the necessary rapid growth will not be possible, and that time scales of >100 Myr are required for formation of the ~ 15-Earth-mass core necessary to trigger the collapse of nebular gas required to form the planet observed today. On the other hand, it has often been pointed out (Levin 1978; Greenberg et al. 1984) that runaways in the outer planet region could have reduced the time scales considerably. Lissauer (1987) proposed that a combination of runaway accumulation and high nebular surface densities may have permitted the Jupiter core to form directly by a single runaway, thereby eliminating the need to subsequently merge together smaller (i.e., ~ 1 Earth-mass) runaways on a longer time scale. It is not at all clear that the necessary surface densities existed to accomplish this. They may have been facilitated by a four-fold increase in density if H_2O ice is first condensed at the distance of Jupiter, or possibly by the "cold finger" hypothesis of Stevenson and Lunine (1987), whereby a high surface density is proposed to have occurred at 5 AU by diffusive concentration of condensible material at that distance.

An extensive discussion of the formation of the giant planets is beyond the scope of the present review. It will therefore be confined to results of a calculation that indicates the possibility that rapid formation of Jupiter may be included within the general framework of the formation of larger bodies by the accumulation of planetesimals.

In this calculation, the same program used to calculate the growth of planetary embryos at 1 AU (Wetherill and Stewart 1989), and used to calculate the growth of asteroidal bodies in Sec. II was employed, and the initial size distribution of the planetesimals was the same. The surface density in the asteroid belt was assumed to fall off as $1/a$, augmented by a four-fold increase in density at 5 AU caused by the condensation of H_2O ice. A material density of 2.0 g cm^{-2} was assumed, the 5 AU gravitational enhancement factors of Greenzweig and Lissauer were used; the effectiveness of the runaway body in perturbing the smaller bodies of the swarm was suppressed in the same way as before.

The results of this calculation are shown in Fig. 7. A 10-Earth-mass Jupiter core is formed by a runaway in 3.9 $\times$ 10^5 yr. Although somewhat
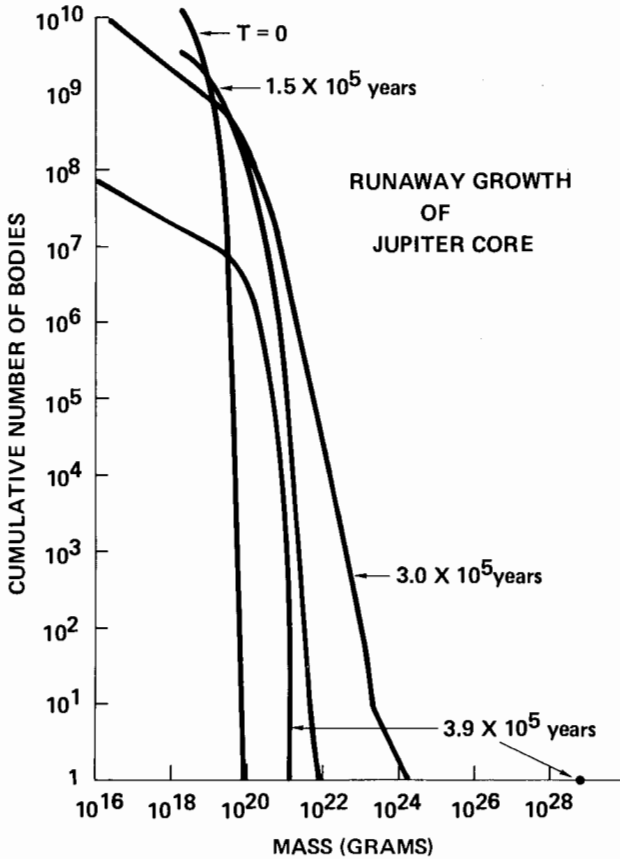
Fig. 7. Runaway growth of Jupiter core. Initial ~10 km diameter bodies grow in a rather orderly way until about 3×10^5 yr. At that time, rapid growth of a 10-Earth-mass body occurs during the next 10^5 yr.

different parameters were used, this result is in general agreement with that presented earlier (Wetherill and Chapman 1988) in which a "seed" at 5 AU was introduced. The present result supersedes this earlier work by including the effects of fragmentation and other phenomena in a manner identical to that used in Sec. II for the asteroid belt with, of course, the exception that no external perturbations would be expected if Jupiter were the first planet to be formed. The time scale for the formation of Jupiter's core is in the range for which modest external perturbations were assumed to begin in the asteroid belt. Rapid (<1 Myr) collapse of Jupiter's gaseous mantle would then correspond to the formation of the full-size Jupiter used in the calculations of Jupiter-scattered planetesimals.

The nebular zone cleared out by the formation of the Jupiter core, de-

fined by 4 Hill sphere radii, has a width of 0.42 AU. The same theory would predict formation of similar size cores at nearby heliocentric distances, unless growth of runaways is suppressed by perturbations during the formation of Jupiter. Calculations made at 6 AU lead to the result that the runaway of planetesimals of the same initial mass distribution to much larger bodies was delayed until 5×10^5 yr, in the absence of external perturbations. The largest bodies, formed at 6 AU at the time of the runaway of the Jupiter core, were only 10^{23}g, much smaller than the Jupiter-scattered planetesimals required to cause significant gravitational perturbations in the asteroid belt. Whether or not perturbations would be sufficiently large to truncate runaways at this distance is not known at present. The same calculations at 10 AU lead to growth of a Saturn core after 2 Myr, assuming it is sufficiently distant from Jupiter to permit a runaway core to grow. The role of resonances in facilitating and suppressing runaways in the outer solar system discussed by Patterson (1987b), may be relevant in this regard.

VI. CONCLUDING REMARKS AND FUTURE WORK

The combination of previous work and new calculations presented in this review show that there is promise that a theory of asteroidal accumulation consistent with work on the formation of the terrestrial planets, and the meteoritic record, may be possible. Nevertheless, it should be obvious that the account given here has more the character of an agenda for future work than a mature theory. Particularly important problems that need to be addressed are:

(1) The size of the initial gravity-dominated planetesimals formed at different heliocentric distances needs to be understood. Smaller bodies favor runaways. If the bodies in the asteroid belt are too small, external perturbations may be unable to prevent runaways in the asteroid belt. If the initial Jupiter-zone planetesimals are too large, a rapid Jupiter runaway may not take place.

(2) The magnitude of the relative asteroidal velocities that can be caused by external perturbations must be understood. These perturbations must be large enough to truncate asteroidal runaway in the face of the tendency of these external perturbations to be in phase with one another. Even though these requirements have been described as "modest," they cannot be too modest if they are to be effective.

(3) A theory of the magnitude and position of the sweeping commensurability and secular resonances in the asteroid belt requires much better understanding of the formation of the giant planets.

(4) Many aspects of the present discussion depend on the time scale and mechanism for the removal of the gas from the solar nebula. This must be linked with observation and theory of outflow from pre-main-sequence stars.

(5) A satisfactory theory of asteroidal origin must be developed in unison

with observational data obtained from laboratory studies of asteroidal meteorites, and Earth-based and *in situ* investigations of asteroids.

(6) It is possible that the asteroid belt may contain bodies not indigenous to that region, which "contaminated" this portion of the solar system after most of the indigenous asteroidal material was removed (Wetherill 1977; Wasson and Wetherill 1979). This may be important in connection with the observed mixing of asteroid compositional types, and requires further understanding of the early history of adjacent regions of the solar system, both internal and external to the asteroid belt.

REFERENCES

Arnold, J. R. 1965. The origin of meteorites as small bodies. III. General considerations. *Astrophys. J.* 141:1548–1556.

Bogard, D. D. 1979. Chronology of asteroid collisions as recorded in meteorites. In *Asteroids,* ed. T. Gehrels (Tucson: Univ. of Arizona Press), pp. 558–578.

Chamberlin, T. C. 1904. Fundamental problems of geology. *Carnegie Inst. of Washington Year Book* 3:195–258.

Chladni, E. F. F. 1794. *Über den Usprung der von Pallas gefundenen und anderer ihr ähnlicher Eisenmassen* (Riga: J. F. Hartknoch), pp. 56–59. Rpt. 1974, Meteoritical Society, with introduction by J. T. Wasson.

Clayton, R. N. 1981. Isotopic variations in primitive meteorites. *Proc. Roy. Soc. London* A303:339–341.

Davis, D. R., Chapman, C. R., Greenberg, R., Weidenschilling, S. J., and Harris, A. W. 1979. Collisional evolution of asteroids, populations, rotations, and velocities. In *Asteroids,* ed. T. Gehrels (Tucson: Univ. of Arizona Press), pp. 528–557.

Donn, B., and Meakim, P. 1988. Collisions of microscopic fluffy aggregates in the primordial solar nebula. *Lunar Planet. Sci.* XIX:281–282 (abstract).

Goldreich, P., and Ward, W. R. 1973. The formation of planetesimals. *Astrophys. J.* 183:1051–1061.

Greenberg, R., Wacker, J., Chapman, C. R., and Hartmann, W. K. 1978. Planetesimals to planets: Numerical simulation of collisional evolution. *Icarus* 35:1–26.

Greenberg, R., Weidenschilling, S. J., Chapman, C. R., and Davis, D. R. 1984. From icy planetesimals to outer planets and comets. *Icarus* 59:87–113.

Heppenheimer, T. A. 1979. Secular resonances and the origin of the eccentricities of Mars and the asteroids. *Lunar Sci.* X:531–533 (abstract).

Ip, W.-H. 1987. Gravitational stirring of the asteroid belt by Jupiter zone bodies. *Gerlangs Beitrag. Geophysik* 96:44–51.

Ip, W.-H. 1988. Dynamical injection of martian-sized planetoids into the asteroidal belt from the terrestrial planetary accretion zone. Preprint.

Kant, I. 1755. *Allgemeine Naturgeschichte und Theorie des Himmels* (Königsberg and Leipzig: J. F. Petersen), pp. 18ff, 163ff.

Kaula, W. M., and Bigeleisen, P. E. 1975. Early scattering by Jupiter and its collision effects in the terrestrial zone. *Icarus* 25:18–33.

Kepler, J. 1621. *Mysterium Cosmographicum*, 2nd ed., (Frankfurt: G. Tampachii). German trans. by M. Caspar, 1923 (Augsburg: B. Filser Verlag).

Levin, B. J. 1978. Relative velocities of planetesimals and the early accumulation of the planets. *Moon and Planets* 19:289–296.

Lissauer, J. J. 1987. Time scales for planetary accretion and the structure of the protoplanetary disk. *Icarus* 69:249–265.

Lissauer, J. J., and Greenzweig, Y. 1987. Protoplanet accretion rates in a disk of planetesimals with low random velocities. *Lunar Planet. Sci.* XVIII:556–557 (abstract).

Ovenden, M. W. 1972. Bode's law and the missing planet. *Nature* 239:508–509.

Patterson, C. W. 1987a. Three-body resonance trapping and the asteroid belt. *Lunar Sci.* XVIII:766–767 (abstract).

Patterson, C. W. 1987b. Resonance capture and the evolution of the planets. *Icarus* 70:319–333.

Patterson, C., and Spaute, D. 1988. Self-termination of runaway growth in the asteroid belt. Asteroids II abstract booklet, 8–11 March, Tucson, Arizona.

Proctor, R. A. 1898. *Other Worlds Than Ours* (New York: D. Appleton), pp. 220–229.

Safronov, V. S. 1969. *Evolution of the Protoplanetary Cloud and Formation of the Earth and Planets* (Moscow: Nauka). In Russian. Trans. NASA TT F-677, 1972.

Safronov, V. S. 1979. On the origin of asteroids. In *Asteroids*, ed. T. Gehrels (Tucson: Univ. of Arizona Press), pp. 975–993.

Schmidt, O. Yu. 1944. Meteoritic theory of the origin of the Earth and planets. *Doklady Acad. Nauk* 45:229–233.

Stevenson, D. J., and Lunine, D. J. 1987. Rapid formation of Jupiter by diffusive redistribution of water vapor in the solar nebula. *Icarus* 75:146–155.

Stewart, G. R., and Wetherill, G. W. 1988. Evolution of planetesimal velocities. *Icarus*, in press.

Wänke, H. 1981. Constitution of the terrestrial planets. *Phil. Trans. Roy. Soc. London* A303: 287–302.

Ward, W. R. 1980. Scanning secular resonances: A cosmogonical broom? *Lunar Planetary Sci.* XI:1199–1201 (abstract).

Wasson, J. T., and Wetherill, G. W. 1979. Dynamical, chemical, and isotopic evidence regarding the formation locations of asteroids and meteorites. In *Asteroids*, ed. T. Gehrels (Tucson: Univ. of Arizona Press), pp. 926–974.

Weidenschilling, S. J. 1975. Mass loss from the region of Mars and the asteroid belt. *Icarus* 26:361–366.

Weidenschilling, S. J. 1984. Evolution of grains in a turbulent solar nebula. *Icarus* 60:553–567.

Wetherill, G. W. 1977. Evolution of the Earth's planetesimal swarm subsequent to the formation of the Earth and Moon. *Proc. Lunar Sci. Conf.* 8:1–16.

Wetherill, G. W. 1978. Accumulation of the terrestrial planets. In *Protostars and Planets*, ed. T. Gehrels (Tucson: Univ. of Arizona Press), pp. 565–598.

Wetherill, G. W. 1985. Giant impacts during the growth of the terrestrial planets. *Science* 228:877–879.

Wetherill, G. W. 1986. Accumulation of the terrestrial planets and implications concerning lunar origin. In *Origin of the Moon*, eds. W. K. Hartmann, R. J. Phillips, and G. J. Taylor (Houston: Lunar and Planetary Inst.), pp. 519–550.

Wetherill, G. W. 1988a. Accumulation of Mercury from planetesimals. In *Mercury*, eds. F. Vilas, C. R. Chapman and M. S. Matthews (Tucson: Univ. of Arizona Press), pp. 670–691.

Wetherill, G. W. 1988b. Where do the Apollo objects come from? *Icarus*, in press.

Wetherill, G. W., and Chapman, C. R. 1988. Asteroids and Meteorites. In *Meteorites and the Early Solar System*, eds. J. F. Kerridge and M. S. Matthews (Tucson: Univ. of Arizona Press), pp. 35–67.

Wetherill, G. W., and Cox, L. P. 1985. The range of validity of the two-body approximation in models of terrestrial planet accumulation. II. Gravitational cross-sections and runaway accretion. *Icarus* 63:290–303.

Wetherill, G. W., and Stewart, G. R. 1989. Accumulation of a swarm of small planetesimals. *Icarus* 77:330–357.

Williams, J. G. 1973. Meteorites from the asteroid belt? *Eos: Trans. AGU* 54:233 (abstract).

Wisdom, J. 1985. Meteorites may follow a chaotic route to Earth. *Nature* 315:731–733.

RADIAL MIXING OF MATERIAL IN THE ASTEROIDAL ZONE

T. V. RUZMAIKINA, V. S. SAFRONOV
O. Yu. Schmidt Institute of Physics of the Earth

and

S. J. WEIDENSCHILLING
Planetary Science Institute

The asteroid belt shows radial zoning of compositional structure. The most abundant types are successively S, C and P types from the inner to the outer parts of the main belt, and D type in the Trojan clouds. Boundaries between compositional zones are not sharp, but show gradual transitions over scales ~1 AU in semimajor axis. We examine processes for producing this structure before, during and after the accretion of asteroids. The initial structure is established by temperature and composition gradients in the turbulent solar nebula during the collapse of the presolar cloud. The radial scale of the zoning, comparable to the disk thickness, favors disk models with relatively low turbulent viscosity. Radial decay of solid bodies due to gas drag during settling to the central plane and planetesimal formation probably causes only a small degree of mixing, due to the systematic nature of drag-induced motions. Formation of Jupiter causes scattering of massive planetesimals from that planet's zone through the asteroid zone. The present random velocities of asteroids resulting from that stirring process are consistent with the radial scale of transitions between compositional types.

The asteroid belt contains a collection of planetesimals from the early time of the solar system. Their compositions reflect cosmochemical and collisional processes that operated in the formation of planets. The asteroid belt has two remarkable properties: 10^3- to 10^4-fold depletion of surface density of material in the belt, and dependence of optical properties of asteroids on dis-

tance from the Sun (Gradie and Tedesco 1982; see also the chapter by Gradie et al.). Asteroids of S type with relatively high albedo dominate the inner part of the asteroid belt ($R \lesssim 2.5$ AU). Darker C asteroids are most abundant between 2.5 and 3.3 AU, and P types dominate in the main belt at distances > 3.3 AU. P asteroids are less abundant than D types in the Trojan clouds at heliocentric distances $\gtrsim 5$ AU. The D asteroids are dark and reddish, presumably because of the presence of a significant amount of organics; they may also contain ices (Chapman 1988). Thus, asteroid compositions reflect a trend from silicaceous objects in the inner part of the belt, through bodies of carbonaceous type, to even more primitive ones in the outer part.

It is likely that the trend of the chemical composition of the asteroids reflects differences in the thermal history of material in different parts of the belt before or during their formation. The boundaries between compositional zones are not sharp, but show gradual transitions in the proportions of the dominant types over scales of about 1 AU. The length scale of disorder in the chemical trend puts limits on the radial mixing of material in the asteroid belt. In this chapter, we discuss the processes associated with the formation of the asteroid belt and the apparent dependence of the chemical properties of asteroids on heliocentric distance, and we investigate restricting the intensity of radial mixing. We consider possible mixing processes before, during and after accretion of the asteroids.

I. FORMATION OF THE SOLAR NEBULA

We are interested in the formation of the solar nebula because the chemical inhomogeneity of the asteroid belt may result from the dependence of thermal history of solar-nebula material on the distance from the Sun. There are many different models of the solar nebula, with varying degrees of detail (Weidenschilling 1988a). Most of these examine the evolution of "generic" accretion disks, and do not attempt to produce the characteristic features of our solar system. In principle, it is possible to examine their implications for the structure and composition of the asteroid belt, but such an effort is beyond the scope of this chapter. Our analysis is based primarily on the model of Ruzmaikina and Maeva (1986), which attempts to match the parameters of the solar system. We offer it as an example of the present state of knowledge and the types of issues that must be discussed.

There are important reasons to believe that the Sun and solar nebula originated together as a result of the collapse of a molecular cloud core (presolar nebula): for example, the similarity of major elemental composition of the Sun, Earth and meteorites (Dodd 1981). Observations of extended (10^2 to 10^3 AU) low-mass disks around some very young solar-type stars (e.g., HL Tau) and main-sequence stars (β Pic; Backman 1987) suggest that they are a common result of stellar formation. The outcome of the collapse of a presolar cloud depends on its initial angular momentum and the processes of re-

distribution of angular momentum during collapse, as we will show in the section below.

A. Angular Momentum of the Presolar Nebula

A reconstruction of the solar nebula by augmenting the planets with H and He to restore solar composition results in a mass of 0.01 to 0.1 $M_\odot$, a distribution of the surface density with distance from the Sun as $R^{-3/2}$ to R^{-1}, and total angular momentum 3×10^{51} to 2×10^{52} g cm^{2}s^{-1} (Hoyle 1960; Weidenschilling 1977a). The angular momentum of the proto-Sun likely would not have exceeded 10^{51} g cm^{2}s^{-1}, which is about the value the Sun with present-day structure would have if rotating with the threshold velocity at the equator. Observational data on the rotation of most young stars (T Tau-type) reveal rates significantly slower, so the contribution of the Sun to the total angular momentum of the presolar nebula might be even smaller (Vogel and Kuhi 1981). Thus, a value of order 10^{51} to 10^{52} g cm^{2}s^{-1} is a reasonable minimal angular momentum acceptable for the presolar cloud. Stellar statistics support the idea that this interval of angular momentum (per 1 $M_\odot$) favored the formation of a single star with disk. It has been suggested that the solar system includes an inner Oort cloud with a total mass comparable to that of the planetary system (Weissman 1985). Weissman's estimate of the number of comets in the inner cloud yields an even higher total mass if one assumes as a representative mass that of Halley's nucleus (Marochnik and Mukhin 1988). The value of $\sim 3 \times 10^{17}$g derived from measurements of its nongravitational acceleration leads to a mass of $\sim 10^4$ $M_\oplus$ for the cometary cloud, correspond-ing to a presolar nebula of >2 $M_\odot$ with angular momentum $\gtrsim 10^{54}$ g cm^2 s^{-1}. A nebula with such parameters would require revision of our model for the origin of the solar system. It seems more likely that such a large angular momentum would lead to formation of a binary rather than a single star. A detailed study of the distribution of the angular momenta of spectroscopic binaries has revealed a gap between single and unevolved binary stars (Krai-cheva et al. 1978). A deficiency was found of very close binaries with separa-tions < 10 $R_\odot$ and hence angular momentum $< 10^{52}$ g cm^{2}s^{-1}. This value is an order of magnitude greater than the maximal angular momentum admiss-ible for a single star of solar mass (Ruzmaikina 1981). The interval for the solar nebula angular momentum approximately coincides with the gap be-tween the angular momenta of single stars and binaries.

In addition, recent observations with precision radial-velocity techniques of 16 solar-type stars reveal that 7 show evidence of long-term low-level varia-tions, which imply companions of a few Jupiter masses and reject the pres-ence of any companion with mass between 10 and 80 Jupiter masses (Camp-bell 1987). The observations suggest that the planets formed from a low-mass (and hence a low angular momentum) preplanetary disk that was stable against gravitational fragmentation of the gaseous component. These data and results of numerical simulations of the collapse of nonrotating and rotating gas

clouds have encouraged us to consider a relatively low angular momentum ($\sim 10^{52}$g cm^2 s^{-1}) as preferable for the presolar cloud.

B. Formation and Evolution of the Accretion Disk

Since the work of Larson (1969) there has been a great deal of progress on numerical simulation of the gravitational collapse of interstellar clouds. We now understand the process of 1-D collapse of nonrotating clouds and the relatively early stages of 2-D and 3-D collapse of rotating clouds (Boss 1987, and references therein). Numerical simulation reveals that the initial stage of collapse is characterized by free-fall contraction accompanied by increasing concentration of density toward the cloud center. It is important that the redistribution of the angular momentum is not effective at that stage. The collapse produces an increase of the ratio of rotational to gravitational energy β in the central part of cloud, which could fragment due to development of nonaxisymmetric instability if the cloud's initial rotation was fast enough.

In a slowly rotating cloud with initially uniform density and angular velosity, and the angular momentum considered ($J \simeq 10^{52}$g cm^{2}s^{-1}), a single hydrostatic star-like core is formed in the center of the cloud before β reaches the critical value for instability (Ruzmaikina 1980,1981). The threshold value of J below which a single core forms during collapse depends on the initial distribution of the angular momentum in the cloud. The threshold value of J could be significantly ($\sim 10^2$ times) greater for the uniformly rotating and strongly centrally condensed case (simple isothermal sphere). The initial mass and mean radius of the core are expected to be close to those for a nonrotating cloud ($M_c = 10^{-2}M_\odot$ and $R_c = 5 \times 10^{11}$ cm; Larson 1969). The core contracts slowly on a time scale which changes from 10^2 to 10^5 yr as the core mass grows from 10^{-2} to 1 $M_\odot$. Outward transport of the angular momentum in the core (e.g., by a magnetic field intensified during contraction of the cloud) could be effective on the time scale of its evolution. The transport could initiate outflow of the gas from the core equator to form the embryo disk and prevent core fragmentation (Ruzmaikina 1980; Safronov and Ruzmaikina 1985).

Another way to form the embryo disk is direct accretion of a rotating envelope at a distance from the rotational axis greater than the core's equatorial radius (Cassen et al. 1985). A mechanism for the simultaneous formation of the Sun and the extended solar nebula during the collapse of a cloud with $J \simeq 10^{52}$g cm^2 s^{-1} was suggested by Ruzmaikina (1980), and later in more detail by Cassen and Moosman (1981). When the cloud collapses with local conservation of angular momentum, all the streamlines intersect the equatorial plane at distances from the rotational axis that are not greater than some characteristic radius. This "centrifugal radius" is given by (Cassen and Summers 1983).

$$R_K = J^2/K^2GM^3 \tag{1}$$

where J and M are the angular momentum and mass of the presolar cloud, G is the gravitational constant, and k is a nondimensional quantity that depends on the distribution of the angular momentum inside the nebula ($k = 2/5$ corresponds to uniform rotation for $\rho = $ constant, and $k = 2/9$ to $\rho \propto R^{-2}$, which is the singular isothermal sphere). The presolar cloud with $J = 2 \times 10^{52}$ g cm^{2}s^{-1} collapses to $R_K = 0.3$ to 1 AU (for $k = 2/5$ to $2/9$, respectively). Formation of an extended disk with radius of the order of the present-day solar system or larger demands outward transport of the angular momentum.

It was recognized that an embryo disk could spread simultaneously with the growth of the core mass due to outward transfer of the angular momentum by turbulent stresses. The radius of the turbulent disk increases according to the diffusion law (Lynden-Bell and Pringle 1974)

$$R_D \simeq \sqrt{v_t t} \qquad (2)$$

where v_t is a turbulent viscosity. The belief that the disk should be turbulent in the accretional stage results from the large value of the Reynolds number (Re $\simeq 10^{10}$) associated with shear flow caused by accretion of the nebula gas onto the disk. This value of Re is much greater than the critical one ($\sim 10^3$ to 10^4) to excite turbulence in a wide class of shear flows (Monin and Yaglom 1971). Creation of a quantitative theory of turbulence in the disk is a matter for future investigation.

Shakura and Sunyaev (1973) parameterized v_t as $v_t = \alpha C_s h$ where C_s is the sound speed and h is the disk thickness. It follows from Relation (2) that a rather weak subsonic turbulence with $\alpha \sim 10^{-2}$ for $h \sim 0.1R$ is able to increase the disk radius to that of the present-day solar system in 10^5 yr, which is the time for formation of the central star. Only about 1% of the energy of the accreting material is needed to support the turbulence. Note that nearly sonic turbulence, $\alpha \sim 0.3$, results in a disk radius of order 10^3 AU, which is observed around β Pic.

Cassen and Summers (1983) found self-similar analytic solutions for the evolution of a thin Keplerian disk with either $v_t = $ constant or $v_t \propto R$ and $h \ll R$ in the accretion stage of the core growth, under the assumption that the material of the envelope accretes at a constant rate onto the core, while all the angular momentum of the accreting material is concentrated in the disk. In this case, the motion of material in the entire disk is directed away from the center (note that models such as that of Morfill [1983] that assume an inward flow require $R_K \gtrsim 30$ AU, with much higher total angular momentum).

However, these early models did not take into consideration that a considerable part of the accreting material must fall directly onto the disk. This is the material falling toward the center near the equatorial plane and impinging on the outer part of the disk, and material from somewhat higher latitudes that has an angular momentum too high to reach the core. The addition to the disk of material having a lower angular momentum must affect the rate of growth

of the disk and the flow pattern in it, and hence the thermal history of its material. The formation of a disk with allowance for material falling onto the disk has been considered by Ruzmaikina and Maeva (1986). The equations describing the evolution of the disk are solved in the approximation of a thin disk for v_t averaged vertically. At the same time, the finite thickness of the disk is taken into account when calculating the rate of flow of mass onto the faces. The onflow of material is described by a model function dependent on the thickness of the disk and allowing for the fact that material from low latitudes falls mainly onto the edge of the disk and is assimilated there, while that from high latitudes falls onto the core or onto the disk at $R < R_K$.

The boundary conditions were taken to be a specified finite tangential stress at the inner boundary (to describe the magnetic interaction between the disk and magnetosphere of the forming proto-Sun) and a small fixed value of the surface density at the edge of the disk. For viscosity they used $v_t \simeq$ (1 to 6)$10^{15} \left(\dfrac{M}{M_\odot} \dfrac{R}{1AU} \right)^{1/2}$ cm^{2}s^{-1}, where M is the core mass. The result was the formation of the solar nebula of radius $R \sim 24$ to 70 AU and mass ~ 0.1 M$_\odot$ in the period $\sim 10^5$ yr. This model is a bit more compact and massive than that predicted by models not taking into account accretion on the disk edge.

The most important thing introduced by accretion onto the disk is its influence on the radial-velocity distribution. In minimum-mass models without accretion, the disk's material flows outward at all distances from the proto-Sun (Cassen and Summers 1983). The flow pattern in the disk under consideration is more complicated. It is characterized by an inward mass flow in most of the disk at an early stage of its formation, and appearance of regions with both outward (at $R_K < R < 0.6 R_D$ and $R > 0.95 R_D$) and inward flow (at $0.6 R_D < R < 0.95 R_D$ and near the core, where R_D is the disk radius). The amplitudes of the radial velocity and details of evolution of the flow pattern depend on the distribution of viscosity in the disk and amount of material added to the outer part of the disk. The correct consideration of the mixing of the accreted material with the disk's material and the determination of the viscosity function seem the most significant problems for further investigation of 2-D or 3-D models of disk formation.

Since in the case we are considering, the angular momentum at the edge of the disk is higher than the angular momentum of the accreting material, $R_D \gg R_K$, the gas falling onto the outer part of the disk will flow around it toward the center. In the process of flowing around, the fallen material mixes with the disk material in a layer of thickness $\Delta h \sim (v\tau)^{1/2}$ where τ is the characteristic flow-around time. The gas accreting onto the surface of the disk at a low angle to the shock wave front has its velocity decreased only slightly; for it, therefore, $\tau \sim \Omega^{-1}$. Since for Keplerian rotation, the scale height of the atmosphere is $h \simeq C_s/\Omega$ while the turbulent viscosity is expressed through the

average velocity v_t of turbulent eddies and the mixing length l_t as $v_t = v_t l_t / 3$, we obtain

$$\frac{\Delta h}{h} \sim \left(\frac{v_t}{C_s} \frac{l_t}{h} \right)^{1/2} . \tag{3}$$

From this it follows that the mixing of accreted gas with disk gas will encompass the entire thickness of the disk only when the turbulence below the shock front is extremely strong: $v_t \sim C_s$, $l_t \sim h$. In the more likely regime of subsonic turbulence, with $\alpha \sim (10^{-2}$ to $10^{-1})$, the thickness of the mixing layer is small compared to h. Only a small fraction ($\sim \alpha^{1/2}$) of the accreting material penetrates into the deep layers (Ruzmaikina and Safronov 1985).

The material accreting onto the outer edge of the disk near the equator at distances less than the scale height of the disk must be added to the disk more efficiently, since in the shock it loses the radial-velocity component normal to it, and is trapped in the vicinity of $R = R_D$ for a time $t \gg \Omega^{-1}$. Moreover, an inversion of specific angular momentum j develops because of accretion onto the edge of the disk, $j(R_D) = (GMR_D)^{1/2} > j_K = (GMR_K)^{1/2}$ since $R_D > R_K$, which serves as an additional source of turbulence of the outer part of the disk (Rayleigh instability) and hence of mixing the accreting material with the disk material.

C. Thermal Evolution of Gas and Dust in the Forming Disk

The thermal evolution of the disk material is determined by the distribution of the temperature and radial flows within the disk, and heating of accreting gas and dust in the shock and shear layers at the surface of the disk. The radiation of the proto-Sun and of the shock, as well as the turbulent energy being dissipated, serve as sources of heating the disk. Cooling takes place through radiation from the surface. If turbulent dissipation dominates the heating, then the temperature at the disk's photosphere, as follows from the steady-state equation of the energy, is determined by the relation

$$T_S = \left(\frac{9}{8} \frac{GM}{\sigma_s} v_t \Sigma R^{1/2} \right)^{1/4} R^{-7/8} \tag{4}$$

where σ_s is the Stefan-Boltzmann constant and Σ is the surface density. The expression within the parentheses is approximately constant in the significant part of the disk, and $T_S \propto R^{-7/8}$. The $R^{-7/8}$ dependence results from the fact that the disk is expanding, in contrast to steady-state disks that result in $T \propto R^{-3/4}$ (Cassen et al. 1985).

A radius of the evaporation zone R_e for silicates ($T \sim 1500$ K) lies in the range of 0.3 and 0.5 AU when the disk is assumed to be isothermal vertically. It might be two times larger because of nonisothermality (Makalkin and Dor-

ofeeva 1987). However, the material which comes through the evaporation zone outward would be spread over a significantly larger area, due both to the mean outward flow at R_e (Ruzmaikina and Maeva 1986) and to turbulent mixing (Morfill 1983). It follows from Eq. (4) that $T_S \lesssim 400$ K and $T_S \lesssim 150$ K at $R \gtrsim 1$ to 2 AU and $R \gtrsim 4$ to 5 AU, respectively. Organic compounds of kerogen type and water ice can exist at these distances.

The infalling gas and dust particles also undergo brief heating in the shock front at the disk surface. The theory of heating of dust particles in the shock is discussed in detail by Hollenback and McKee (1979). Interstellar particles of radii $s \sim 10^{-2}$ to 1 μm, composed from graphite, silicate material, and water ice are heated up to temperatures (in Kelvin) $T_{gr} \simeq 370$ $A^{1/2}R^{-1/2}$; $460 A^{1/5} R^{-3/5}$; $440 A^{1/5} R^{-3/5}$ where $A = M/(st_a M_\odot)$ (s, t_a and R are measured here in microns, 10^5 yr and AU, correspondingly) (Ruzmaikina and Safronov 1985; Mukhin et al. 1988). The temperature of larger particles (radii much larger than the wavelength of the thermal infrared radiation that they emit) is $T_{gr} \simeq 600 R^{-3/4}$ K (Vityazev and Pechernikova 1985; Ruzmaikina and Safronov 1985).

It was assumed in their estimates that the normal (to the shock front) component of velocity of the infall is $v \simeq (GM/R)^{1/2}$, i.e., gas and dust are infalling approximately perpendicular to the shock front. It is true for the edge $R \simeq R_D$ of disk and near the core $R \lesssim R_K$. At $R_K << R << R_D$ the material infalls at small angles to the disk surface. It must be heated correspondingly to lower temperatures. It follows that organic and ice particles will survive both in the disk and in the shock front at the distances from the Sun $> R \simeq 2$ AU and 5 AU, respectively. Hence, the composition of the solid material at these distances might be remarkably different than that in the vicinity of the Sun. In addition, the accretion of material onto the edge of the disk (mentioned above) will progressively enrich the outer part with material that has not passed through the evaporation zone.

The radial transport of the gas and dust due both to mean flow and to the turbulence will mix material of different regions (Morfill 1983; Ruzmaikina and Maeva 1986). As a result, the gas and dust which came through the evaporation zone would be spread over a larger area to several AU, and also mixed with material that was never subjected to heating. However, the inner part of the disk is enriched to a greater degree with material subjected to the total vaporization and recondensation than is the outer part. One can expect that this tendency might be at least partly responsible for the radial gradient of the chemical composition in the asteroid belt (Ruzmaikina and Maeva 1986). Then the significant change of the chemical composition over $\Delta R \approx 1$ AU would put an essential restriction both on the intensity of the turbulence in the disk, at least in the central plane for $R \approx 2$ to 5 AU, and on the mixing of the solid material during the later history of the solar system.

Asteroids are classified as particular types (S, M, C, P, F, D, etc.) on the basis of their spectral properties. Some types may be the result of thermal and

collisional evolution; e.g., the S types may be collisionally stripped stony-iron cores rather than ordinary chondrites (see the chapter by Bell et al.). To some extent, the classification scheme obscures the fact that each class includes some range of spectral properties, hence compositions (Chapman 1988). Also, there are some intermediate types that do not fall into the main classes. The transitional types are relatively rare, and the distribution of types appears to be multimodal. This may be due to selective removal of asteroids at certain heliocentric distances (e.g., the gap between Hildas and Trojans). Still, the observed variety implies that the radial scale for mixing before accretion was not large compared with the length scale for significant variations in composition due to the thermal gradient in the disk, otherwise spectral properties would be blurred into a single type. Some of the variation may be due to condensation (e.g., H_2O) at a particular radial distance. Alternatively, one might conclude that material diffusing radially was chemically reprocessed on time scales shorter than that of mixing; however, this seems unlikely at the low temperatures in the outer belt.

The expected length scale for turbulent mixing is the size of the largest eddies. This is often taken to be of the order of the disk half-thickness, ~ 0.1 R. This is comparable to the observed scale of mixing of asteroid types, and would leave no room for later processes, discussed below (Sec. III). Also, the turnover time of these eddies is expected to be of the order of the Kepler period, so mixing would occur rapidly on a much larger scale than the eddy size. Such a model of turbulence would not produce the observed scale of radial zoning in the asteroid belt. One possible explanation for the zoning is found in the turbulence model of Cabot et al. (1987). They obtained small values of $\alpha \sim 10^{-2}$ to 10^{-3}, and pointed out that the largest eddies in a differentially rotating system are anisotropic, with radial extent several times smaller than their vertical scale. This implies radial scales of a few times 10^{-2} AU. The time to diffuse over a given distance varies inversely with the square of the eddy length scale, so the time to exchange material over $\Delta R \sim 1$ AU may be hundreds of times the Kepler period. This is compatible with the low value of viscosity (or α) assumed by Ruzmaikina and Maeva (1986). We conclude that the zoning in the asteroid belt indicates rather weak turbulence in the solar nebula. It is possible that other mechanisms for the transport of angular momentum, e.g., gravitational torques, also contributed to the evolution of the nebula (Larson 1989).

II. RADIAL TRANSPORT DURING PLANETESIMAL FORMATION

The formation of planetesimals requires that small solid grains settle to the central plane of the disk. This process cannot begin until turbulence decays to a low level after the cessation of infall from the presolar cloud. The disk has a radial pressure gradient, primarily due to the weakening of the Sun's gravity with distance (Weidenschilling 1988*b*), augmented by gradients

in surface density and temperature. The partial support of the gaseous disk by pressure forces causes its rotation to be slightly slower than Keplerian in order to maintain hydrostatic equilibrium (Whipple 1972). In a reference frame rotating with the gas, the residual gravity not compensated by centrifugal force is

$$\Delta_{\mathscr{E}} = \frac{1}{\rho} \frac{\partial P}{\partial R}. \tag{5}$$

We assume that $P \propto R^{-n}$, so that $\partial P / \partial R = -nP/R$. Then the fractional deviation of the gas velocity from the Kepler velocity V_K is (Weidenschilling 1977b)

$$\frac{\Delta V}{V_K} = -\frac{\Delta g}{2g} = \frac{nR_g T/\mu}{2GM_\odot/R} \tag{6}$$

where R_g is the gas constant and μ the molecular weight. From Eq. (6) we see that $\Delta V/V_K$ is approximately the ratio of thermal energy to gravitational potential energy in the gas, typically a few times 10^{-3}.

Bodies respond to gas drag on a characteristic time scale t_e, the ratio of a particle's momentum to the drag force. In the free molecular regime, $t_e = s\rho_s/\rho c$, where s is the particle radius, ρ_s its density, and c the thermal velocity of the gas molecules (t_e is more complex for irregularly shaped bodies [cf. Weidenschilling et al. 1989]). A body with $\Omega t_e \ll 1$ is small enough that its motion is controlled by the gas ($s \lesssim 10^2$ cm). It settles toward the central plane at the rate $dz/dt = -g_z t_e$, where $g_z = GM_\odot z/R^3 = \Omega^2 z$ is the vertical component of the solar gravity; it drifts radially at the rate $dR/dt = \Delta g t_e$. Its motion is predominantly vertical when $z/R > 2\Delta V/V_K$, and mainly radial at smaller values of z/R. Combining the expressions for vertical and radial motion, we can show that the distance traveled radially in a nonturbulent gas is

$$\frac{\Delta R}{R_o} = 1 - \left(\frac{z}{z_o}\right)^{2\Delta V/V_K}. \tag{7}$$

If the dust layer initially has a half thickness z_o equal to the scale height of the gas $\sim 0.1R$, it will reach the critical density for gravitational instability at $z/z_o \lesssim 10^{-5}$. For $\Delta V/V_K = 5 \times 10^{-3}$, Eq. (7) yields $\Delta R/R_o \simeq 0.1$. If there is some residual turbulence that delays settling, ΔR will be larger. If all particles are identical, there is no relative motion due to this drift, and hence no mixing. However, coagulation of grains is likely, with larger aggregates growing by sweeping up smaller particles. Such aggregates will collect grains over a range ΔR, which is the expected radial scale for mixing during settling. Unless R_o is near a major compositional boundary due to condensation or chemical reaction, there will be little variation of composition due to radial drift during this stage.

If planetesimals form by gravitational instability of the dust layer (Saf-

ronov 1969,1987; Goldreich and Ward 1973), then there is no further mixing until gravitational scattering becomes important (Sec. III). However, Weidenschilling (1988b; also Weidenschilling et al. 1989) argues that a very small degree of turbulence in the gas can prevent the dust layer from becoming dense enough to be gravitationally unstable. He suggests that collisional growth, driven by drag-induced relative velocities, would result in accretion of planetesimals. A large ($s \gtrsim 10^2$ cm) body with $\Omega t_e >> 1$ pursues a Keplerian orbit with a nearly constant "headwind" of magnitude ΔV relative to the gas. The orbit decays due to drag, and the body spirals inward at the rate

$$dR/dt = -2R(\Delta V/V_K)/t_e. \tag{8}$$

For Stokes drag, $t_e = 2s^2\rho_s/9\rho\nu$ where ν is the kinematic viscosity. If the body sweeps up mass in the form of small particles, it grows at the rate $ds/dt = \delta\Delta V/4\rho_s$ where δ is the space density of accretable matter. Combining these expressions, one can show that the body grows to an arbitrarily large size, such that orbital decay ceases, after it travels radially by an amount

$$\frac{\Delta R}{R} = 1 - \exp(-36\rho\nu/V_K\delta s_o) \tag{9}$$

where $s_o \sim 10^2$cm is the initial size at which Eq. (8) becomes valid. For plausible parameters in the asteroid belt (Weidenschilling 1988b), the growth rate ds/dt is a few cm yr^{-1}, and $\Delta R/R$ is a few tenths if $\delta \simeq \rho$, i.e., a dust/gas ratio of unity. Because of the exponential dependence on this ratio, the actual extent of radial transport during growth by this mechanism is highly model dependent and uncertain. If any meter-sized bodies form before the dust concentration exceeds the gas density near the central plane, there is the possibility that $\Delta R/R \rightarrow 1$; some material from the outer edge of the disk could be transported into the inner part. However, the small "seed" body would constitute only a small fraction of the mass accreted en route. If the radial displacement crossed a condensation boundary (most probably of H_2O), it is possible that planetesimals that might accrete in this manner would contain cores of volatile-rich material (or localized pockets of volatiles in larger bodies assembled from them). Such compositional variations would not be detectable on the meter-or-less size scale of meteorites. In general, transport by orbital decay due to aerodynamic drag is an orderly process that operates in one direction and varies smoothly with heliocentric distance. Therefore, it should not cause significant mixing between different parts of the asteroid zone.

III. INFLUENCE OF JUPITER

O. Schmidt (1954) considered Jupiter as the main perturber that prevented formation of a normal planet in the asteroid zone. The simplest assumption, that only gravitational perturbations by Jupiter could considerably

increase random velocities of asteroids to their present values of a few km s^{-1} and interrupt their further growth has not been confirmed. Numerical modeling by Lecar and Franklin (1973) and others has shown that presently Jupiter's perturbations can effectively remove asteroids from the outer part of their zone ($R \gtrsim 3.5$ AU) and in narrow bands where their periods of revolution are commensurable with that of Jupiter (Kirkwood gaps). Before accretion of gas onto Jupiter's solid core, its mass was many times smaller (less than 10 $M_\oplus$) and its perturbations were accordingly much smaller. According to Wetherill's chapter, even small eccentricities would slow down the growth of asteroids. Thus, Jupiter's core, if it formed early enough, might have delayed the accretion of an Earth-sized planet in the asteroid zone. However, it is not clear that this effect could have prevented its formation completely.

Resonances could play a more important role in the case of a massive initial solar nebula (Cameron and Pine 1973). During its mass loss, the positions of commensurabilities would scan across the asteroid belt and bring most of the asteroids into resonances. The loss of mass from the disk in this case should be comparable with the solar mass (Torbett and Smoluchowski 1980). However, the model of such a massive nebula encounters considerable difficulties in many respects. Such scanning of resonances would not occur during dissipation of a low-mass nebula. However, resonances could sweep through the asteroid zone due to radial motion of Jupiter during the stage of active accretion of gas onto its core (Safronov and Guseinov 1989), and also due to ejection of bodies from Jupiter's zone into the cometary cloud.

Stronger disturbances should have been produced in the asteroid region by bodies from Jupiter's zone when they began to penetrate the asteroid zone due to increased random velocities and eccentricities of their orbits (Safronov 1969,1979; Davis et al. 1979; Ip 1987). Jupiter planetesimals, being on average much larger than the asteroids, swept them out by collisions. The remaining asteroids acquired increased velocities by gravitational scattering at close encounters with the larger bodies from Jupiter's zone; these bodies are required to be large, perhaps Mars-sized. This explanation of a missing planet appears to be the most realistic. The efficiency of this mechanism depends on the initial properties of the nebula and on characteristic features of the accumulation process. It sets substantial constraints on important parameters of the system that are not yet well estimated—velocities of bodies, their relative rates of growth, and time scale of accumulation.

One can infer three stages of evolution of matter in the asteroid zone:

1. Initial stage of normal growth of preplanetary bodies without external intervention from neighboring zones;
2. The stage of active external disturbances, sweeping out of almost all asteroid bodies, increase of velocities of the remaining ones and in this way preventing their further accumulation (with, perhaps, the exception of the largest ones);

3. Subsequent disruptive collisional evolution of the asteroid belt, formation of families, removal of resonant asteroids.

There is no sharp boundary between stages 2 and 3. Stage 1 terminates when random velocities of bodies in Jupiter's zone reach 2 km s^{-1} and they penetrate to the middle of the belt, and 3 km s^{-1}, to its inner edge, eccentricities of their orbits being 0.3 and 0.4, respectively. Their velocities can be expressed through the mass m_J and the radius r_J of the largest body in the Jupiter zone (the core of Jupiter)

$$v_J = (Gm_J/\theta_J r_J)^{1/2}. \tag{10}$$

From this one can find the mass of the core m'_J at the beginning of Stage 2 if a reasonable value of the parameter θ_J can be estimated. We obtain a lower limit for θ_J as well as for m'_J by assuming nonrunaway accumulation. Then, taking, for example, $\theta_J = 4$ (Safronov 1969), we find that Stage 2 begins in the middle of the belt and at its inner edge when m'_J reaches 0.2 and 0.7 $M_\oplus$, respectively. These values of m'_J should really be diminished by several times because velocities of faster bodies are higher than the root-mean-square velocity given by Eq. (10). Decrease of velocities by the gas is small and can be neglected for bodies with $m > 10^{-3} M_\oplus$.

In recent years, the idea of a very rapid runaway accumulation has become popular (Wetherill and Stewart 1989; chapter by Wetherill). From Eq. (10), $\theta_J = V_e^2/V_J^2$, where $V_e = 2Gm_J/r_J$ is the embryo's escape velocity. The ratio of the gravitational cross section to the geometric cross section is $(1 + 2\theta_J)$, so low relative velocities imply large θ_J and rapid accretion. Lissauer (1987) suggests that the largest body m rapidly sweeps up all bodies moving near its orbit inside radial distance $\Delta R = (3 \text{ to } 4)r_H$, where $r_H = R(m/3M_\odot)^{1/3}$ is the radius of its Hill sphere. It is supposed that during this stage of growth, the velocities of bodies remain small, corresponding to very large values of $\theta \sim 400(R/1 \text{ AU})(\rho_J/4)^{1/3}$ where ρ_J is the density of the bodies in the Jupiter zone in g cm^{-3}. However, an increase of θ_J will increase $m'_J \propto \theta_J^{3/2}$. In that case, assuming for the Jupiter zone $\theta_J \sim 10^3$, one can find that for velocities to be high enough for bodies in the Jupiter zone to penetrate the asteroid zone, a much higher mass of the core m'_J is needed—more than twice the present mass of Jupiter. Stage 2 could begin before the beginning of rapid gas accretion onto the core ($m_J \sim 10\ M_\oplus$) only if $\theta_J < 55$. Otherwise, owing to the very rapid increase of m_J during accretion of gas, Stage 2 lasts such a short time that bodies in the Jupiter zone are unable to sweep out almost all of the asteroids before they themselves are accreted or ejected from the solar system by encounters with Jupiter (Ip 1987). This result can be considered as an argument against very rapid runaway accumulation.

Useful information can be obtained from a comparison of the increase of

the radius r_a of the largest body in the asteroid zone with the increase of r_J at Stage 1

$$\frac{dr_a}{dr_J} \approx \frac{(1 + 2\theta_a)\sigma_a\rho_J}{(1 + 2\theta_J)\sigma_J\rho_a} \left(\frac{R_J}{R_a}\right)^{3/2} \tag{11}$$

where σ_a and σ_J are surface densities of solid matter in the two zones. One can consider the following three possible cases:

1. Nonrunaway growth in the two zones. In this case, $\theta_J \approx \theta_a$ and $\rho_J < \rho_a$. Due to earlier dissipation of the gas in the asteroid zone, θ_a may be about two times smaller than θ_J. We have approximately

$$\frac{dr_a}{dr_J} \approx \frac{1}{2} (\rho_J\sigma_a/\rho_a\sigma_J)(R_J/R_a)^{3/2}. \tag{12}$$

If we take standard relations for the decrease of gas surface density with $R, \Sigma \propto R^{-3/2}$ (Weidenschilling 1977a), and increase the density of solids in the Jupiter zone by about 3 times (relative to the terrestrial planets zone) due to condensation of water ice, we obtain $dr_a/dr_J \approx (R_J/R_a)^3/6 \approx 1.0$ for the middle of the asteroid belt (2.85 AU) and ≈ 2.2 for $R_a \approx 2.2$ AU. Thus, in this case, Jupiter could not prevent the formation of a normal planet in the asteroid zone. Only violation of the relation $\Sigma \propto R^{-3/2}$ and the increase of the ratio σ_J/σ_a by several times can change the situation.

2. Runaway growth only in the Jupiter zone. In this case assume that only the core m_J in the Jupiter zone grows rapidly and that other bodies have the usual power-law mass distribution with the largest body (other than m_J) having mass m_{J1}. As long as the total mass in the power-law distribution is much larger than m_J, one can rewrite Eq. (10) in the form

$$v^2 \approx Gm_J/\theta_J r_J = Gm_{J1}/\theta_{J1} r_{J1} \tag{13}$$

where $\theta_{J1} \approx \theta_J r_{J1}^2/r_J^2$ is comparable with θ_a. Then

$$\frac{dr_a}{dr_{J1}} \approx \frac{\rho_J\sigma_a}{\rho_a\sigma_J} \left(\frac{R_J}{R_a}\right)^{3/2} /2. \tag{14}$$

Here the ratio r_a/r_{J1} is determined by a similar expression to Eq. (12) as the ratio r_a/r_J in the previous case. For efficient sweeping out of asteroids by Jupiter planetesimals, r_{J1} should be several times larger than r_a. This requires values of $\sigma_J \sim 15$ to 20 g cm^{-2}. Having $r_{J1} > r_a$ appears to be a necessary condition for sweeping out, but the above-mentioned arguments against large θ_J still apply.

3. Runaway growth in the two zones. In this case, relative growth of planet embryos is described by Eq. (11). Increase of the radii of the second

largest bodies dr_{a1}/dr_{J1} is described by the same equation, only θ_a and θ_J are changed to θ_{a1} and θ_{J1}. As the latter parameters are comparable, dr_{a1}/dr_{J1} equals approximately the right side of Eq. (14). In addition to the requirement of larger σ_J, there exists the problem of removal of an approximately Mars-sized embryo planet from the asteroid zone.

These considerations allow us to conclude that:

A. The hypothesis of rapid runaway growth at the stage of Earth-sized bodies with very high values of θ disagrees with the idea of bodies in the Jupiter zone sweeping out most of the solids from the asteroid zone. Arguments in favor of this hypothesis were suggested (see, e.g., Greenberg et al. 1978; Levin 1978; Lissauer 1987; Stevenson and Lunine 1988), as well as arguments against it (Safronov and Ruzmaikina 1978; Pechernikova and Vityazev 1979; Lecar and Aarseth 1986; Ipatov 1988; Hayakawa and Mizutani 1988). No considerable runaway is usually assumed for the late stage of accumulation. For the stage of asteroid removal, we would prefer quite moderate values of $\theta_J \lesssim 20$ to 30 in the Jupiter zone and $\theta_a < 10$ to 15 in the asteroid zone.

B. The initial mass of condensed matter in Jupiter's zone should have been higher than the mass of solids that entered Jupiter (the latter corresponds to $\sigma_J \approx 6$ g cm^{-2}). This requirement, obtained from the consideration of efficacy of removal of asteroids by solids in the Jupiter zone, agrees well with the fact that the giant planets, during their accumulation, ejected much material out of the solar system, as well as with the idea of Stevenson and Lunine (1988) that volatiles (mainly H_2O) replenished the Jupiter zone from the terrestrial planet zone (they were brought into Jupiter's zone by turbulent diffusion and after condensation remained there). This model implies that the surface density of solids in Jupiter's zone during accumulation was at least 20 g cm^{-2}. However, values of σ_J larger than 30 g cm^{-2} are hardly admissible: if Jupiter ejected that much mass from the solar system, it would lose angular momentum and its distance from the Sun would decrease significantly.

Moderate values of $\theta \sim 20$ to 30 in the Jupiter zone lead to a relatively long time scale of accumulation. With the values of θ_J and σ_J assumed above, we find that at Stage 1 the core of Jupiter grows in 10^7 yr to a few tenths of the Earth's mass when bodies from the Jupiter zone begin to penetrate the asteroid belt.

Some additional factors could probably shorten this time interval:

A. Due to a lower temperature and higher dust-to-gas ratio the turbulence in Jupiter's zone may have decayed earlier than in the asteroid zone. Accordingly, formation of the dust layer and the increase of its density would have taken place considerably earlier around Jupiter. If gravitational instability occurred in this layer, the initial masses of condensations ($\propto \sigma^3 R^6$) would be substantially higher than at smaller heliocentric distances. Their initial densities ($\propto R^{-3}$) were lower, and, for a longer time, they retained their increased cross sections and grew faster. Thus, solid bodies that formed in Jupiter's zone could have been from the very beginning larger than those in the asteroid zone.

B. Gas may have remained around Jupiter longer than in the asteroid region. It decreased random velocities of bodies and accelerated their growth. When the gas density in the asteroid zone became lower than that in the Jupiter zone, the sign of the radial pressure gradient could be reversed (this requires the gas surface density Σ to increase with R more rapidly than $\Omega T^{1/2}$ decreases, i.e., $\Sigma \propto R^{7/4} - R^2$). Then the radial gas-drag velocity v_R becomes positive and smaller bodies could move from the asteroid zone to the Jupiter zone and increase the surface density of solids there. Even if the pressure gradient did not reverse sign, it might have decreased enough to prevent shear-induced turbulence from occurring, thereby allowing gravitational instability in the particulate layer. Then the rapid formation of dust condensations would produce much larger bodies in Jupiter's zone than in the asteroid zone.

C. Transport of volatiles to Jupiter's zone from the terrestrial-planet region could increase the mass of solids around Jupiter by about 20 $M_{\oplus}$, i.e., only about 30%. Stevenson and Lunine (1988) find that this mass was concentrated in a narrow ring $\Delta R \approx 0.4$ AU during 10^5 yr. In such a case, the surface density of condensate in the ring increased almost ten times. However, for a rapid accumulation of a massive body capable of accreting the gas, Lissauer's runaway scenario with very high values of θ_J is needed; otherwise, many bodies that formed in the ring should be scattered over the whole Jupiter zone, slowing the growth of the core.

Jupiter-zone bodies scattered into the asteroid belt would play a different role depending on their relative size. These solids, being on the average much more massive than asteroids, would sweep out asteroids by many collisions. Smaller Jupiter planetesimals would erode and disintegrate asteroids by collisions. Large ones (of about Mars-mass or several times smaller if one takes into account that there are many more distant encounters) would increase random velocities of asteroids to their present values (Davis et al. 1979; Safronov 1979; Ip 1987). A fraction of asteroids perturbed into unstable orbits would leave the asteroid zone. Some of the expelled bodies might have been larger than Ceres. Owing to the considerable increase of relative velocities, the kinetic energy of colliding asteroids would become much higher than their potential (gravitational) energy, and they would not coalesce at collision. The process of accumulation would change to erosion and disintegration. The direct rotations of Ceres, Pallas and Vesta show that they were massive enough so that they did not experience catastrophic collisions.

There is much evidence in favor of extensive collisional evolution of asteroids: irregularities of shape, mass distribution, direction of spin axes, existence of families of asteroids, great variety of photometric, spectral and other characteristics, as well as types and structures of meteorites (chapter by Davis et al.). At the same time, the regular variation of average characteristics of asteroids with distance from the Sun shows that there was not mixing

throughout the belt. The compositional mixing length scale ΔR is <1 AU. Orbital characteristics of asteroids agree with this scale; eccentricities $\bar{e} \approx$ 0.15 give average radial oscillations $\overline{\Delta R}_e \approx 2\bar{a}\bar{e} \approx 0.85$ to 0.66 AU for the middle and inner parts of the belt, respectively. The chemical composition of asteroids should have been averaged over such ranges if they formed at their present values of eccentricities. Actually, they grew mainly at smaller eccentricities $e_{acc} < \bar{e}$, and the radial scale of their compositional mixing during accumulation $\Delta R = 2ae_{acc}$ should be considerably narrower than the present $\overline{\Delta R}_e$. In subsequent increases of e, the cumulative effect of small perturbations at distant encounters prevailed over the perturbations at close encounters. In such conditions, the variation of semimajor axes a should be considerably smaller than variations of e and i and should not increase appreciably the length scale of mixing.

The composition of the outer (regolith) layers of asteroids changed appreciably due to impact processing. The efficacy of this process depended on impact velocities and flux. In the inner part of the belt ($R \approx 2.2$ to 2.4 AU), impact velocities were higher than in the outer part due to higher eccentricity of bodies from the Jupiter zone (as also of bodies from the terrestrial zone) penetrating there, as well as due to higher Keplerian velocity at smaller R. Possibly, these high-velocity impacts produced S asteroids, which are now suspected to be stony-iron cores of larger parent bodies that have had their mantles stripped away by collisions (Gaffey 1988; chapter by Gaffey et al.).

IV. CONCLUSIONS

The compositional zoning of the asteroid belt may be explained in a general way as the result of the temperature gradient in the solar nebula, but many details are not yet understood (cf. the chapter by Bell et al.). The greatest paradox is the fact that the zoning persists despite the existence of more than one process that would tend to blur or destroy it. Turbulent mixing in the solar nebula plausibly could have yielded much greater length scales for compositional variations than are observed, unless stringent conditions were met. Velocity stirring and subsequent collisional evolution, as well as the unknown mechanism that depleted most of the initial mass in the asteroid zone, could have mixed this material even further. The original length scale for compositional variations must have been no more than the ~ 1 AU now observed. This is not much greater than the probable thickness of the nebula. How could composition vary significantly over such a short distance? Does it represent a nebular temperature gradient or relative proportions of primordial and reprocessed material, or both? How much variation in composition is needed to account for the spectral differences between, say, C, F and D types? Was there originally a continuum of compositions, with the present distinct classes due to selective removal of asteroids at specific distances? Could physical collisions with Jupiter-zone bodies remove $\sim 99\%$ of the original mass? If S types

were altered and stripped by bodies in the Jupiter zone, how did the largest asteroids, Ceres, Pallas and Vesta survive intact?

These questions, and many more, will continue to challenge theorists well into the future.

REFERENCES

Backman, D. 1987. IRAS statistics on IR-excesses and models of circumstellar disks. *Bioastronomy: The Next Steps, IAU Coll. No. 99,* Lake Balatan, Hungary, 22–27 June.

Boss, A. P. 1987. Protostellar formation in rotating interstellar clouds. VI. Nonuniform initial conditions. *Astrophys. J.* 319:149–161.

Cabot, W., Canuto, V., Hubickyj, O., and Pollack, J. 1987. The role of turbulent convection in the primitive solar nebula. I. Theory. *Icarus* 69:387–422.

Cameron, A. G. W., and Pine, M. 1973. Numerical models of the primitive solar nebula. *Icarus* 18:377–406.

Campbell, B. 1987. A search for brown dwarfs or planetary-mass companions to solar-type stars with precision radial velocities. *Bull. Amer. Astron. Soc.* 19:762 (abstract).

Cassen, P., and Moosman, A. 1981. On the formation of protostellar disks. *Icarus* 48:377–392.

Cassen, P., and Summers, A. 1983. Models of the formation of the solar nebula. *Icarus* 53:26–40.

Cassen, P., Shu, F., and Terebey, S. 1985. Protostellar disks and star formation: An overview. In *Protostars & Planets II,* eds. D. C. Black and M. S. Matthews (Tucson: Univ. of Arizona Press), pp. 448–483.

Chapman, C. R. 1988a. Structure of the asteroid belt and its families from bias-corrected studies of asteroid types and sizes. Asteroids II abstract booklet, March 8–11, Tucson, Arizona.

Chapman, C. R. 1988b. Compositional structure of the asteroid belt and its families. In preparation.

Davis, D. R., Chapman, C. R., Greenberg, R., Weidenschilling, S. J., and Harris, A. W. 1979. Collisional evolution of asteroids: Populations, rotations, and velocities. In *Asteroids,* ed. T. Gehrels (Tucson: Univ. of Arizona Press), pp. 528–557.

Davis, D. R., Chapman, C. R., Weidenschilling, S. J., and Greenberg, R. 1985. Collisional history of asteroids: Evidence from Vesta and the Hirayama families. *Icarus* 62:30–53.

Dodd, R. T. 1981. *Meteorites: A petrologic-chemical synthesis.* (Oxford: Cambridge Univ. Press).

Gaffey, M. 1988. The S-asteroid/ordinary chondrite controversy. Asteroids II abstract booklet, March 8–11, Tucson, Arizona.

Goldreich, P., and Ward, W. R. 1973. The formation of planetesimals. *Astrophys. J.* 183:1051–1061.

Gradie, J., and Tedesco, E. 1982. Compositional structure of the asteroid belt. *Science* 216:1405–1407.

Greenberg, R., Wacker, J., Hartmann, W. K., and Chapman, C. R. 1978. Planetesimals to planets: Numerical simulation of collisional evolution. *Icarus* 35:1–26.

Hayakawa, M., and Mizutani, H. 1988. Numerical simulation of planetary accretion process. *Lunar Planet. Sci.* XIX:465–466 (abstract).

Hollenback, D., and McKee, C. F. 1979. Molecular formation and infrared emission in fast interstellar shocks. 1. Physical processes. *Astrophys. J. Suppl.* 41:555–592.

Hoyle, F. 1960. Formation of the planets. On the origin of the solar nebula. *Quart. J. Roy. Astron. Soc.* 1:28–55.

Ip, W.-H. 1987. Gravitational stirring of the asteroid belt by Jupiter zone bodies. *Gerlands Beitr. Geophys.* 96:44–51.

Ipatov, S. I. 1988. Solid-body accumulation of the terrestrial planets. *Astron. Vestnik* 21:207–215.

Kraicheva, S. T., Popova, E. I., Tutukov, A. V., and Jungelson, L. P. 1978. Some properties of spectroscopic binaries. *Astron. Zh.* 55:1176–1189.

Larson, R. B. 1969. Numerical calculations of the dynamics of a collapsing protostar. *Mon. Not. Roy. Astron. Soc.* 145:271–295.

Larson, R. B. 1989. The evolution of protostellar disks. In *The Formation and Evolution of Planetary Systems,* eds. H. Weaver, F. Paresce and L. Danly (Cambridge: Cambridge Univ. Press), pp. 31–54.

Lecar, M., and Aarseth, S. I. 1986. A numerical simulation of the formation of the terrestrial planets. *Astrophys. J.* 305:564–579.

Lecar, M., and Franklin, F. 1973. On the original distribution of the asteroids. I. *Icarus* 20:422–436.

Levin, B. 1978. Some problems concerning the accumulation of planets. *Sov. Astron. Lett.* 4:54–57.

Lissauer, J. 1987. Timescales for planetary accretion and the structure of the protoplanetary disk. *Icarus* 69:249–265.

Lynden-Bell, D., and Pringle, J. E. 1974. The evolution of viscous disks and the origin of nebular variables. *Mon. Not. Roy. Astron. Soc.* 168:603–637.

Makalkin, A. B., and Dorofeeva, V. A. 1987. Temperature in the preplanetary disk: Results of new physical models, comparison with meteoritic data. XX. Soviet Meteoritic Conference abstracts, pp. 94–95.

Marochnik, L. S., and Mukhin, L. M. 1988. Missions "Vega" and "Giotto": New view on the structure of the solar system. *Pis'ma Astron. Zh.* 14:379–382.

Monin, A. S., and Yaglom, A. M. 1971. *Statistical Fluid Mechanics* (Cambridge: MIT Press).

Morfill, G. E. 1983. Physics and chemistry in the primitive solar nebula. In *The Birth and Infancy of Stars,* eds. R. Lucas, A. Omont and R. Stora (Amsterdam: North Holland), pp. 693–792.

Mukhin, L. M., Ruzmaikina, T. V., and Grechinskiy, A. 1988. Nature of dust of Halley's Comet. *Kosmicheskie Issledovanija,* in press.

Pechernikova, G. V., and Vityazev, A. V. 1979. Masses of the largest bodies and dispersion of velocities during accumulation of the planets. *Pis'ma Astron. Zh.* 5:54–59.

Ruzmaikina, T. V. 1980. On the role of the magnetic field and turbulence in the evolution of the presolar nebula. *Adv. Space Res.* 1:49–53.

Ruzmaikina, T. V. 1981. Angular momentum of protostars giving birth to protoplanetary disks. *Pisma Astron. Zh.* 7:188–192.

Ruzmaikina, T. V., and Maeva, S. V. 1986. Investigation of the process of the solar nebula formation. *Astron. Vestnik* 20:212–227.

Ruzmaikina, T. V., and Safronov, V. S. 1985. Premature particles in the solar nebula. *Lunar Planet. Sci.* XVI:720–721 (abstract).

Safronov, V. S. 1969. *Evolution of the Protoplanetary Cloud and Formation of the Earth and Planets* (Moscow: Nauka). Trans. NASA TTF-667, 1972.

Safronov, V. S. 1979. On the origin of asteroids. In *Asteroids,* ed. T. Gehrels (Tucson: Univ. of Arizona Press), pp. 975–991.

Safronov, V. S. 1987. Evolution of the dust components of the circumstellar protoplanetary disk. *Astron. Vestnik* 21:216–220.

Safronov, V. S., and Guseinov, K. M. 1989. Possible role of resonances in the formation of the asteroid belt. *Doklady Akad. Nauk Azerbaijan,* in press.

Safronov, V. S., and Ruzmaikina, T. V. 1978. On the angular momentum transfer and accumulation of solid bodies in the solar nebula. In *Protostars and Planets,* ed. T. Gehrels (Tucson: Univ. of Arizona Press), pp. 545–564.

Safronov, V. S., and Ruzmaikina, T. V. 1985. Formation of the solar nebula and the planets. In *Protostars & Planets II,* eds. D. C. Black and M. S. Matthews (Tucson: Univ. of Arizona Press), pp. 959–980.

Schmidt, O. Yu. 1954. On the origin of asteroids. *Doklady Akad. Nauk USSR* 96:449–452.

Shakura, N. J., and Sunyaev, R. A. 1973. Black holes in binary systems. Observational appearances. *Astron. Astrophys.* 24:337–355.

Stevenson, D. J., and Lunine, J. 1988. Rapid formation of Jupiter by diffusive redistribution of water vapor in the solar nebula. *Icarus* 75:146–155.

Torbett, M., and Smoluchowski, R. 1980. Sweeping of the Jovian resonances and the evolution of the asteroids. *Icarus* 44:722–729.

Vityazev, A. F., and Pechernikova, G. V. 1985. On the evaporation of dust during the preplanetary disk formation. *Lunar Planet. Sci.* XVI:885–886 (abstract).

Vogel, S. N., and Kuhi, L. V. 1981. Rotational velocities of pre-main-sequence stars. *Astrophys. J.* 245:960–976.

Weidenschilling, S. J. 1977a. The distribution of mass in the planetary system and solar nebula. *Astrophys. Space Sci.* 51:153–158.

Weidenschilling, S. J. 1977b. Aerodynamics of solid bodies in the solar nebula. *Mon. Not. Roy. Astron. Soc.* 180:57–70.

Weidenschilling, S. J. 1988a. Comparisons of solar nebula models. In *Workshop on the Origins of Solar Systems*, eds. J. Nuth and P. Sylvester, LPI Tech. Rept. 88-04 (Houston: Lunar and Planetary Inst.), pp. 31–37.

Weidenschilling, S. J. 1988b. Formation processes and timescales for meteorite parent bodies. In *Meteorites and the Early Solar System*, eds. J. F. Kerridge and M. S. Matthews (Tucson: Univ. of Arizona Press), pp. 348–371.

Weidenschilling, S. J., Donn, B., and Meakin, P. 1989. Physics of planetesimal formation. In *The Formation and Evolution of Planetary Systems*, eds. H. Weaver, F. Paresce and L. Danly (Oxford: Cambridge Univ. Press), pp. 117–136.

Weissman, P. 1985. Cometary dynamics. *Space Sci. Rev.* 41:299–349.

Wetherill, G. W., and Stewart, G. R. 1989. Accumulation of a swarm of small planetesimals. *Icarus* 77:330–357.

Whipple, F. L. 1972. On certain aerodynamic processes for asteroids and comets. In *From Plasma to Planet*, ed. A. Elvius (New York: Wiley), pp. 211–232.

CHEMICAL, THERMAL AND IMPACT PROCESSING OF ASTEROIDS

E. R. D. SCOTT, G. J. TAYLOR, H. E. NEWSOM
University of New Mexico

F. HERBERT
University of Arizona

M. ZOLENSKY
NASA Johnson Space Center

and

J. F. KERRIDGE
University of California, Los Angeles

We review the geological effects of impacts, heating, melting, core formation and aqueous alteration on asteroids. A review of possible heat sources appears to favor an important role for electrical induction heating. We consider the effects of each geologic process acting individually and in combination with others, and conclude that there is much evidence for impacts during alteration, metamorphism and melting. These interactions vastly increased the geologic diversity of the asteroid belt. Subsequent impacts of cool asteroids did not reduce this diversity. Instead new rock types were created by mixing, brecciation and minor melting.

In this chapter we discuss the major geologic processes that affected asteroids: heating, melting, aqueous alteration and impact. We consider each of these processes acting alone and the possible importance of more compli-

cated processes such as impact on hot objects. We intend this chapter to be a "guide to the geology of the asteroids," though we recognize our knowledge of this topic is woefully inadequate. Our evidence is derived largely from meteorite studies, though we use astronomical and experimental data as well. We realize that our interpretations rely heavily on our understanding of the origins of possible analogues from two vastly different bodies, *viz.*, the Earth and Moon.

Studies of meteorites indicate that asteroids in at least the inner asteroid belt accreted out of diverse proportions of chondrules, refractory inclusions, grains of metallic Fe-Ni, sulfides and matrix materials. In the outer parts of the belt, the matrix materials may have contained water ice and/or hydrated minerals. The proportion of matrix varied from < 1% for the most reduced enstatite chondrites to over 90% for the CI chondrites. Meteorite studies also suggest that each asteroid was rather homogeneous on the gram scale, except possibly for volatile elements. The degree of geologic processing of this material during accretion is not known with any certainty; we will assess what little evidence is available.

We believe that understanding the geology of asteroids is important for many reasons. We cannot correctly understand the origin of chondritic ingredients and their record of solar nebular processes until the effects of geologic processes in asteroids that affected all meteorites to some extent have been understood. If the asteroid belt has rather faithfully preserved a record of the approximate relative formation locations of diverse materials that existed in a zone of the solar nebula inside Jupiter's orbit, as many believe, then we can learn much about the composition and nature of planetesimals and how they accreted in this and other zones when we have understood the effect and timing of geologic processing on asteroids and meteorites. Finally, geological studies of asteroids can contribute towards our understanding of geologic processing on planets, moons and comets.

I. IMPACT PROCESSES

The existence of shock effects and brecciation in meteorites attests to the importance of impact processes on their parent asteroids. These events took place during accretion, during early metamorphism, alteration and melting in asteroids, and after the bodies had cooled. Impact velocities increased during accretion to hundreds of m s^{-1}. Since accretion ended, and inclinations and eccentricities of asteroids were drastically increased, impact velocities have been 5 $\pm$ 1 km s^{-1}. In this section, we consider mainly the effects of the higher-velocity impacts on asteroids after metamorphism and melting ended.

Shock and brecciation in meteorites

Many studies have been made of the effects of shock in meteorites; see Dodd (1981) and Stoffler et al. (1988) for concise summaries. Most mete-

orites are unshocked or only lightly shocked. Effects recorded in meteorites range from minor fracturing of silicate minerals to lattice deformation to complete melting. These effects indicate shock pressures ranging from a few tens of kb to almost 1 Mb. As shown by Taylor and Heymann (1971) and Smith and Goldstein (1977), the metallic minerals in shocked chondrites indicate post-shock cooling rates ranging from $100°C$ d^{-1} to $1°C$ 100 yr^{-1}. These cooling rates suggest burial depths of 0.5 m to 1 km (Taylor and Heymann 1971). The burial-depth calculations assume that the material cooled as a slab on the surface of the parent body, which may not be especially reasonable for the most rapidly cooled specimens. It is possible that the rapidly cooled chondrites were hot fragments that cooled by conduction in a predominantly cold, thick pile of ejecta or crater fall-back debris. The deeper burial depths of 1 km demonstrate the formation of relatively large craters on asteroids.

Breccias are clastic rocks composed of angular, broken rock fragments embedded in a finer-grained matrix. Other reviews of chondritic breccias are given by Wilkening (1977), Rubin (1985) and McKay et al. (see their chapter). We briefly review the types of breccias formed during impacts and, to provide geologic context, we describe where each type occurs in a crater. This is based on lunar and terrestrial work by Stoffler et al. (1979,1980) and Stoffler (1982, and references cited therein), and application to meteorites by Keil (1982) and Taylor (1982).

Cataclastic breccias.   These are monomict (composed of one rock type) breccias with textures showing crushed grains. Most are severely shocked. Some enstatite achondrites and shocked ordinary chondrites are in this category. Such rocks occur as clasts in the deposits that make up continuous ejecta blankets around craters, as clasts within impact-melt rocks, as clasts within breccias formed when material falls back into a crater cavity, or as part of the shocked bedrock beneath a crater (Stoffler et al. 1979). On asteroids, cataclastic breccias might also form during breakup and subsequent reassembly of their parent asteroids, or as a result of spallation (see below). The percentage of cataclastic breccias in a single crater is difficult to determine because some of the lithic fragments in the ejecta blanket, a large deposit of fragmental breccias (see below), have been shocked and are cataclastic. We infer from Stoffler (1982) that cataclastic rocks account for < 5% of the displaced rock, but account for considerable quantities of shocked rock beneath a crater; Stoffler (1982) estimates that cataclastic rocks account for five times as much material as do displaced rocks.

Dimict breccias.   These are composed of two distinct lithologies, one intruding the other. Examples of meteoritic dimict breccias are pallasites, in which molten metal seems to have been mixed with dunitic rock (Scott 1977). Chondrites with veins of melt throughout them or the eucrite Cachari (which has a vein of melt), might also be considered dimict, but the veins typically

have the same chemical composition as the host rock. Nevertheless, they might have formed in the same way as dimict breccias, which was either as dikes intruded into the shocked floor of a crater (Stoffler et al. 1979) or as blocks of rock intruded by melt and ejected from the crater (Spudis 1984). These breccias are not common in and around craters, accounting for < 1% of the crater materials.

Fragmental breccias.   These are composed of fragmental material derived from a variety of rock types. They may contain fragments of impact melt, but do not have a continuous matrix of impact melt. Almost all meteoritic breccias are of this type (see below). Examples are polymict eucrites, LL chondrites such as Kelly (Bunch and Stoffler 1974) and Siena (Kurat et al. 1969), the L chondrite Kendleton (Ehlmann et al. 1988), and the North Haig ureilite (Berkley et al. 1980; Prinz et al. 1987). Rubin et al. (1983) examined numerous hand specimens of ordinary chondrites and report that many are fragmental breccias, and Scott et al. (1985) suggest that many more are fragmental breccias because apparently unbrecciated samples commonly contain grains that could not have been metamorphosed *in situ*. Fragmental breccias form as ejecta blankets around craters, as breccia layers within a crater either below or intermingled with impact melt (Stoffler et al. 1979) when a parent asteroid is disrupted and then re-assembled, or as a result of spallation (see below). In the crater setting, fragmental deposits account for most of the displaced material, 85 to 90% (Stoffler 1982). However, not all this material is welded into fragmental breccias and much of it consists of large blocks of unshocked rocks. For example, Horz et al. (1983) show that the grain size of the ejecta at the Ries Crater, Germany, varies with distance from the crater center. Typically, on the Earth > 10% of the material consists of blocks > 1 m in size. Close to the rim, as much as 90% can be > 1 m and 80% > 10 m. Nevertheless, it is clear that the dominant displaced rock type produced during an impact is fragmental breccia.

Impact-melt breccias.   These rocks have clastic debris (both rock and mineral fragments) embedded in igneous-textured matrices. Examples are the mesosiderites Pinnaroo, Simondium and Hainholz (Floran et al. 1978), the L chondrite Point of Rocks (Scott et al. 1986) and numerous lithic fragments in ordinary chondrites, e.g., LL chondrites (Fodor and Keil 1975) and the Plainview H chondrite (Fodor and Keil 1976). Terrestrial impact melt rocks form in craters larger than 1 km (Dence 1971; Stoffler et al. 1979). They are found on the floors below the fragmental ejecta pile, as blobs or pods in the fragmental breccia deposit surrounding craters, and as dikes intruding the floor and walls of craters. Impact-melt rocks account for < 5% of the displaced material at terrestrial craters (Stoffler 1982).

Granulitic breccias.   These are metamorphosed, fragmental breccias. Their matrices have metamorphic textures; mineral compositions can be uni-

form throughout (i.e., totally equilibrated) or heterogeneous (unequilibrated). Possible meteoritic examples include most equilibrated LL chondrites (Mason and Wiik 1964; Fodor and Keil 1978), recrystallized mesosiderites such as Clover Springs, Emery and Bondoc (Floran 1978), and perhaps the IAB iron meteorite Landes (Bunch et al. 1972). Granulitic breccias are rare in individual terrestrial craters, which suggests that they formed in fundamentally different ways, perhaps when meteorite parent asteroids were disrupted and reassembled while still hot.

Regolith breccias.   These are much like fragmental breccias, but contain evidence that at least some material was exposed at the surface of the parent asteroid. The most telling evidence is the presence of solar-wind gases and solar-flare tracks. Meteorites like Kendleton, which have all the petrographic features of regolith breccias, but do not contain solar-wind gases, suggest that there is a continuous gradation between regolith breccias and fragmental breccias. McKay et al. (in their chapter) describe lunar and meteoritic regolith breccias and regolith processes in detail.

Asteroidal impacts

Much of our knowledge of impact phenomena comes from studies of terrestrial and lunar impact craters and their deposits, and from experiments done on the Earth (hence done at 1 *g*). However, impacts may have drastically different effects on small bodies such as asteroids than on larger ones such as the Earth and Moon. Factors driving those differences are gravitational field strength, radius of curvature, impact energy and velocity, physical characteristics of targets and projectiles, and the possibility of disruption of the target. Most of these factors have been discussed by Cintala et al. (1978,1979).

Gravity.   The smaller gravity on asteroid-sized bodies affects the cratering process in a number of ways. First, some ejecta escapes (O'Keefe and Ahrens 1977), and there is a net loss of material from the asteroid. Second, this loss results in the nonescaping ejecta containing a smaller percentage of shocked materials. This arises because, in general, shock level is proportional to ejection velocity. Consequently, as body size decreases, the percentage of high-velocity, shocked ejecta lost increases. Third, the smaller *g* allows ejecta to travel farther, hence continuous ejecta deposits (i.e., fragmental breccia deposits) are smaller on asteroids than they are on larger bodies. Fourth, the lower velocities of ejected particles result in formation of less pronounced secondary craters; perhaps none are formed on the smallest bodies. Fifth, the slower moving ejecta cause less overall crater degradation and because less ejecta remain in the excavated cavity, slumping of crater walls is less common.

Radius of curvature.   As Cintala et al. (1978,1979) point out, the more pronounced radius of curvature of small bodies places a free surface closer to

the point of impact. This results in a small component of the shock wave normal to the surface, causing ejection due to tensile failure. Hörz and Schaal (1981) have drawn attention to the possibility of spallation due to interaction of impact-induced seismic waves at the surface antipodal to the point of impact. Both processes produce unshocked debris on an asteroid's surface.

Impact velocities.   Asteroids experienced two basic regimes in impact velocity, slow (< 1 km s^{-1}) and fast (> 3 km s^{-1}). The slow regime occurs during accretion, when impact velocities in the asteroid belt had to be low to allow accretion. For accretion to take place, velocities must be less than about twice the escape velocity, which is only 280 km s^{-1} for a body 200 km in radius (assuming a density of 3.3 g cm^{-3}). Such slow velocities will cause extensive fragmentation and brecciation of incoming objects and the surface of the growing asteroid (Hartmann 1978), but will not cause shock effects (Stoffler et al. 1988). When velocities increased to the present 5 km s^{-1}, impacts would have produced shocked rocks and impact craters. Meteorites and the asteroids they come from record both epochs.

Physical characteristics.   In contrast to terrestrial impacts, many asteroidal impacts may have involved highly porous aggregates, which would lead to more extensive heating and shock than would impact into solid rock once impact velocities increased to > 3 km s^{-1} (Hörz and Schaal 1981; Stöffler et al. 1988). This might have produced some chondritic impact-melt fragments that apparently formed prior to chondrite metamorphism (Rubin 1985). A detailed assessment of the types of cratering products produced by impacts of weak, porous projectiles into weak, porous targets needs to be done.

Asteroid disruption.   Some asteroids may have been disrupted and gravitationally re-assembled (see, e.g., Hartmann 1979; Davis et al. 1985; Taylor et al. 1987). This could lead to the production of vast quantities of brecciated rock because the re-assembled object would basically be one large fragmental breccia. This mechanism of breccia formation is unique to asteroid-sized objects. A fragmentation and re-assembly event would not necessarily include production of much shocked or shock-melted rock (see below), but would lead to production of monomict and polymict fragmental breccias. More work is needed to develop criteria to distinguish these breccias from fragmental breccias formed in cratering events.

We have evaluated the abundances among meteorites of the various types of breccias (Table I). The abundance of regolith breccias varies from zero (EL chondrites) to 100% (CI chondrites). There are also large variations in the proportions of fragmental breccias and heavily shocked meteorites. These differences in the percentages of breccia types are partly due to poor sampling but may also reflect real differences in the impact velocities, fluxes and re-

TABLE I
Estimated Abundances (%) of Meteorites that Are Breccias or Heavily Shocked*

	Chondrites									Differentiated			
	EH	EL	H	L	LL	CI	CM	CO	CV	Aubrites	Basaltic[c]	Mesosiderites	Ureilites
Regolith breccias[a]	10	0	14	3	8	100	60	0	20	30	8	0	0
Fragmental breccias	20	25	10[d]	15[d]	50[d]	?	?	?	?	60	75	70	15
Heavily shocked[b]	0	0	15	50	?	0	0	0	0	0	~10	0	15
Impact melt breccias	0	0	<1	<1	<1	0	0	0	0	0	<1	30	0
No. of meteorites[c]	10	10	100s	100s	50	4	30	10	10	10	50	22	20

*Sources: Anders 1978; Basaltic Volcanism Study Project 1981; Binns 1967; Berkley 1986; Crabb and Schultz 1981; Dodd 1981; Heymann 1967; Kerridge and Bunch 1979; Rubin 1984; Rubin et al. 1983; Scott et al. 1985; Stöffler et al. 1988; Taylor and Heymann 1969.
[a] Contain solar-wind gases.
[b] Shocked >200 kb.
[c] Estimated number of meteorites studied.
[d] Probably lower limits (Scott et al. 1985).
[e] Howardites, diogenites and eucrites.

sponses of diverse meteorite parent asteroids. The differences may also be due in part to parent-body size: smaller bodies might retain less ejecta than larger bodies and because the more heavily shocked material moves faster, it might escape more readily from smaller bodies (Cintala et al. 1979). Thus, the absence of heavily shocked and impact-melted material among CI and CM chondrites could be due to preferential escape from their parent asteroids. It could also be due, of course, to hypervelocity impacts being rarer on these bodies.

Asteroid fragmentation

Highly energetic impacts can catastrophically disrupt an asteroid. Asteroid families may have formed in this way. However, there is a range in energy in which a body might be broken up but then re-assembled into gravitationally bound rubble piles (Davis and Chapman 1977). Data on the cooling rates of components in chondrite regolith breccias indicate that this process affected the parent asteroids of ordinary chondrites (Taylor et al. 1987). Such events apparently took place during chondrite metamorphism (Grimm 1985) and after the parent asteroids had cooled (Taylor et al. 1987).

Breakup and re-assembly might also have happened to other types of meteorite parent asteroids. Fragmentation and re-assembly events need not have involved the production of large quantities of shocked rock. If the colliding bodies are of roughly equal size, namely 20 to 100 km in diameter, and they collide with velocities of 1 to 0.1 km s^{-1}, then essentially none of the re-assembled asteroidal material will be significantly shocked (Taylor et al. 1987). If a small, high-velocity object hits a larger one, then some shock damage would result. Assuming conservatively that a velocity of > 3 km s^{-1} is required to produce some shock effects, Taylor et al. (1987) estimate that at that velocity a body 10 km in diameter could disrupt and re-assemble a body 100 km in diameter. The projectile would be heavily shocked, as would about ten times the projectile's mass, resulting in a re-assembled body containing only about 1% heavily shocked rock.

Mixing between asteroids

Several investigators have reported the presence of clasts of one type of meteorite in another (Wasson and Wetherill 1979). Many inclusions are carbonaceous chondrites, most of which resemble CM chondrites, but clasts of one type of ordinary chondrite in another type are also reported. However, these foreign clasts account for less than 1% vol of meteorites. Only two meteorites are known which contain abundant foreign materials: Cumberland Falls (aubrite and chondritic material) and Kaidun (CI-like, EH5 and EL3 chondritic clasts in a C2 matrix). The rarity of foreign xenoliths implies either that there is little transport across the asteroid belt or that impact velocities are high enough to render impacting projectiles unidentifiable. Both explanations

are probably correct, but apply to different times. During accretion, when impact velocities must have been relatively slow (< 100 m s^{-1}), objects impacting onto a growing asteroid would have survived. Because we do not observe great diversity of chemical composition within a given chondrite group, the accreting materials must have been compositionally similar, hence came from narrow zones in the asteroid belt. When eccentricities and inclinations were stirred up and relative velocities rose to the present 5 km s^{-1}, projectiles came from a much wider zone, perhaps from any location in the asteroid belt, but the high impact velocity ensured that they were almost entirely destroyed upon impact. The observed clasts of one type of meteorite in another represent either rare surviving fragments spalled off fast-moving impacting objects or fragments of projectiles that arrived during infrequent low-velocity impacts.

II. HEATING MECHANISMS

Classical Mechanisms

Heat Transfer Considerations.   The simplest rule of thumb for evaluating potential asteroidal heat sources is comparison of the global heat diffusion time scale τ_d with the lifetime τ_s of the heat source, which is assumed to be uniformly distributed. If the heat production integrated over time in the limiting case of complete heat retention is expressed as a net temperature increase ΔT_{max} above ambient, then the actual maximum rise in temperature is approximately given by the smaller of ΔT_{max} or $\tau_d \Delta T_{max}/\tau_s$. This approximation may be derived by approximating the temperature profile as a quadratic function of radius and solving the resulting ordinary differential equations for central temperature as a function of time.

Although this approximation is not accurate enough for calculating thermal models, it describes the behavior of heat diffusion well enough to clarify the issues to be discussed below. Sample values of τ_d and τ_s are given to the nearest half order of magnitude, commensurate with the approximations just made, in Tables II and III. The τ_d values assume representative values appropriate for asteroidal materials, but neglect the possibility of a very deep and porous regolith.

Thus heat sources with large τ_s such as long-lived radionuclides or accretional bombardment over time scales of order 100 Myr could only have been of importance for the larger asteroids. Sources with τ_s on the order of 1 Myr, such as ^{26}Al and induction heating could have been important for asteroids as small as a few km.

Heating by long-lived radionuclides.   The long-lived radionuclides ^{40}K, ^{232}Th, ^{235}U and ^{238}U are believed to have had a heat generation rate in

E.R.D. SCOTT ET AL.

TABLE II
Time Scales for Thermal Diffusion (τ_d)
as a Function of Radius

Radius (km)	Time scale (yr)
1	10^4
10	10^6
100	10^8
1000	10^{10}

chondritic material corresponding to a ΔT_{max} value of only 2000 to 3000 K, 4.5 Gyr ago (Kaula 1968, p. 110). If the heat of fusion is taken into account, this is not much more than that required for complete melting, so that the value of τ_d must be at least half that of τ_s for much melting to occur. The value of τ_s is about 1.8 Gyr (the e-fold life of ^{40}K), so for thermal diffusivities appropriate to consolidated material, a body radius of around 500 km is required. It has been suggested that a very fluffy regolith might materially increase τ_d, but an unrealistically large void fraction must be maintained against gravitational and impact compaction to depths comparable to the radius in order to relax materially the large radius constraint. Clearly, long-lived radionuclides are only of importance for the largest asteroids.

Impact heating. The heating due to impacts may be analyzed by comparing the energy density required to melt proto-asteroidal material (about half going to the 1000 to 1500 K temperature rise and half supplying the heat of fusion) to the velocity required for an equal kinetic energy density. Because impacts put a large fraction of their energy into ejecta kinetic energy, this velocity equivalent of melting (about 1.7 to 1.9 km s^{-1} for typical meteoritic materials) may usefully be compared to the asteroidal escape velocity (about 1.0 to 1.3 m s^{-1} for each km of radius). These velocities become equal at an asteroid radius of about 1500 km, or about 1000 km if only enough energy is to be supplied to reach the point where partial melting just begins. The largest apparently partially melted asteroid, Vesta, has an escape velocity equivalent

TABLE III
Time Scales of Heat Sources (τ_s)

Source	Time scale (yr)
Long-lived radionuclides	10^9
^{26}Al	10^6
Induction heating	10^4–10^7

to about 20% of the energy required to completely melt a projectile, while the equivalent energy fraction shrinks rapidly with radius (7% for a 100 km asteroid, 0.7% for 10 km, and so forth).

The point here is not that self-gravitational energy is insufficient to cause melting; relative orbit-crossing velocities might be supposed to suffice for that. Rather, the result of this simplified analysis is that when there is anything like equipartition of energy between melting and ejection of fragments at impact, the fragments will have velocities well above that required to escape. Thus it is to be expected that most impact-generated melt will escape and cool very rapidly as small particles. This material could be re-accreted by the original target asteroids (or others nearby) but the result would principally consist of glassy or microcrystalline fragments.

Wasson et al. (1987) have modeled heating effects in collisions between asteroids having radii of 200 to 300 km. From these calculations and their interpretations of the meteorite record, they infer that impact heating was an important and possibly dominant source of heat for asteroids. However, few details of their model assumptions have been published. Moreover, such calculations are extremely dependent on the assumed equation of state, which is poorly known for cold brittle rock.

^{26}Al Heating

^{26}Al has long been postulated to have been an important heat source in solar system bodies (Urey 1955; Fish et al. 1960). However, a search for evidence of primordial ^{26}Al (aluminum-correlated ^{26}Mg excesses) in meteoritic, lunar and terrestrial feldspar samples failed to find such evidence at the level of about ^{26}Al/Al $\leq$ 0.01 to 3 $\times$ 10^{-6}, depending on the sample (Schramm et al. 1970). These levels correspond variously to ΔT_{max} values in the range of 30 to 260 K, making reasonable assumptions about the ratio of Al to Si (*ibid.*). These values represent ^{26}Al concentrations and heating rates as of the time of solidification of the feldspars investigated. A recent search for indications of primordial ^{26}Al in a meteorite clearly showing evidence for melting, a mesosiderite, has also been negative at the ^{26}Al/Al $\leq$ 0.4 $\times$ 10^{-6} level (Papanastassiou et al. 1984).

It was thus of some interest when Lee et al. (1977) and Hutcheon et al. (1978) found inferred primordial ^{26}Al/Al values of about 50 $\times$ 10^{-6} in certain Ca/Al-rich inclusions from the CV3 chondrite Allende. This concentration, *if present in bulk material*, corresponds to a ΔT_{max} value over 5000 K and would still have produced melting in bodies a few km in radius after a delay (from the inclusion solidification epoch) of as much as three half-lives (or about 2 Myr). However, anorthites in type B2 Ca/Al-rich inclusions in Allende have inferred initial ^{26}Al/Al ratios that range from 50 $\times$ 10^{-6} to < 5 $\times$ 10^{-6} (Hutcheon 1982). Similarly, only 3 of 10 hibonites analyzed by Fahey et al. (1987a) show evidence for decay of ^{26}Al; a hibonite in an H3 chondrite gave an inferred ^{26}Al/Al ratio of 8.4 $\times$ 10^{-6} (Hinton and Bischoff 1984), and one

inclusion in Efremovka (CV3) had a rim with a higher inferred $^{26}Al/Al$ ratio than the core (Fahey et al. 1987*b*). The inclusions with evidence of a large original ^{26}Al content are a negligible volume fraction of their parental meteorites. Thus the inferred average ^{26}Al concentration was in all cases completely inadequate to produce bulk melting in the samples in which they were found. Petrographic evidence indicates that this chondritic material was not heated above 500°C.

The absence of evidence for live ^{26}Al in differentiated meteorites indicates that ^{26}Al was not a potent heat source. It might be argued that if ^{26}Al did melt asteroids, then the aluminous minerals might not have cooled below the Mg isotopic equilibration temperature until after the ^{26}Al had largely decayed away. However, any melt on such an asteroid that erupted to the surface would solidify and cool well before the ^{26}Al completely decayed. The absence of evidence for ^{26}Al in igneous meteorites, the heterogeneous distribution of minor amounts in chondrites, and the spectral evidence for preferential melting of inner asteroids (see the chapter by Bell et al.) tend to argue against a dominant role for ^{26}Al in melting asteroids.

Electrical Induction Heating

Another of the possible heat sources responsible for the melting and metamorphism of asteroids is electrical induction heating driven by a hypothesized dense solar-wind-like plasma outflow (often loosely termed a T-Tauri solar wind) from the pre-main-sequence Sun. This induction process, which is analogous to the induced currents driven through Io's ionosphere by Jupiter's corotating magnetospheric plasma, could have efficiently coupled the kinetic energy flux of the hypothetical primordial solar wind to the deep interiors of proto-asteroids.

Material dependence.   Induction heating is quite dependent on the electrical conductivity of the material to be heated. The conductivities of many candidate materials have been measured, but since the precise nature of the primordial chondritic materials that originally accreted into the asteroids is not known, their electrical characteristics are still mysterious. The great diversity of phases in chondrites favors conductivities higher than typical for igneous rocks and thus increases the likelihood of significant electric currents. Examples of candidate materials whose conductivities have been measured are carbonaceous chondrites (Schwerer et al. 1971; Brecher et al. 1975; Duba and Boland 1984) and ordinary chondrites (Evernden and Verhoogen 1956; Schwerer et al. 1971; Brecher 1973; Brecher et al. 1975). These possible analogues for surviving samples of primordial material have room-temperature conductivities varying over 10^{-8} to 10^{-2} s m^{-1}. Electrical conductivity is strongly dependent in most cases on temperature, oxygen fugacity and the presence of impurities such as water or carbon (Parkhomenko 1967; Duba and Boland 1984). The presence of a deep (with thickness more than a few % of

body size) regolith can further complicate the scenario; limitation of electrical current by the series resistance associated with porosity reduces heating but the thermal blanketing effect can help retain heat.

Solar dependence. Most work on primordial inductive heating has assumed a solar-wind plasma flux comparable to the large H fluxes (up to nearly 10^{-6} $M_\odot$ yr^{-1}) seen in T-Tauri stars (Kuhi 1964). Even larger outflows occur at FU Orionis stars, which appear to be T-Tauri stars in an outburst phase (Herbig 1977). Very massive outflows appear to occur frequently in what is believed to be the pre-T-Tauri stage of solar-mass stars, involving large electron densities (10^8 to 10^{11} cm^{-3}), mass losses in the range 10^{-7} to 10^{-6} $M_\odot$ yr^{-1}, and outflow velocities around 100 km s^{-1} (Lada 1985,1988). Edwards et al. (1987) have observed mass losses of 10^{-9} to 10^{-7} $M_\odot$ yr^{-1} with velocities up to 200 km s^{-1} in spectra of T-Tauri stars; they infer the presence of opaque protoplanetary accretion disks.

If such fluxes continue over time scales of the order 1 Myr, a large fraction of a solar mass can be lost. For the Sun to have lost more than about half of its original mass is unlikely (Weidenschilling 1978) and the limit may well be more stringent than that, but intense solar-wind fluxes such as those mentioned above, but of shorter duration, are not ruled out. Shorter time scales preferentially favor heating in smaller bodies. The actual outflow time is not well known; some theoretical treatments of the source of the flow (see, e.g., Shu et al. 1988) suggest that the flow could be driven by inflowing protoplanetary disk material and thus might be episodic. In such a case there could be significant energy input at a number of time scales.

Geometrical effects. As has often been pointed out, there are size- and distance-dependent variations in the efficiency of inductive heating (Sonett et al. 1968,1970; Herbert and Sonett 1978,1979,1980; Lebofsky et al. 1988). Naturally, induction is strongest nearer the Sun, and thermal conduction limits the temperature rise in smaller bodies. Moreover, the magnetic deflection of plasma by induced currents also reduces heating in larger-body sizes. Consequently, in any plasma environment there is some body size at which maximum temperature increase occurs (Herbert and Sonett 1978,1979,1980; Herbert 1989). This size and distance dependence of heating has been suggested (*ibid.*) as being responsible for the apparent igneous surface of Vesta (McCord and Gaffey 1974; Drake 1979) but unmelted surfaces of Pallas and Ceres (Chapman et al. 1975; Lebofsky 1978; Larson and Veeder 1979). More recent work by Gaffey (1984) has strengthened the notion that the S-type asteroids, which are concentrated toward the inner edge of the main belt (Zellner and Bowell 1977; Bowell et al. 1975) and in the size range $R \leq 40$ km (Chapman 1988; chapter by Gradie et al.), once melted.

This metamorphism pattern is suggestive of the heating pattern just described for electrical heating. The exact electrical heating pattern depends on

the conditions assumed, however. For example, if the solar mass lost is small but confined to a short time interval, such as 10^4 years, the size at which maximum temperature rise occurs is around 10 km (Herbert 1989). This contrasts with the 1 Myr-interval case with large solar mass loss assumed by Herbert and Sonett (1978,1979,1980), a model which yielded a 100 km radius of maximum temperature. The body size at which the maximum temperature rise occurs increases with induction epoch duration because conductive heat loss becomes increasingly important in small bodies at longer times. Models which assume the assembly of larger asteroids from already melted proto-asteroids lead to another interesting suite of possibilities analogous to scenarios investigated by Wood (1979).

Thus the electrical-induction model for asteroid heating may possibly explain the observed characteristics of asteroids and meteorites. Deduction of the important parameters and testing the hypothesis will require much more work, however.

III. THERMAL PROCESSING OF ANHYDROUS ASTEROIDS

Effects of Metamorphism

Material in many asteroids was heated up to temperatures of 300 to 900°C during the first 100 Myr of solar system history. Although the cause of heating is not known, the effects on the mineralogy and properties of the rocks are relatively well understood. It is commonly assumed that the asteroids were only heated after they accreted, but there are some indications in the meteorite record that heating may have started earlier (Taylor et al. 1987). Since the unknown heat source was probably active during the first few Myr of solar system history when asteroids probably formed, some heating in planetesimals is not implausible. Lipschutz et al. (see their chapter) find some evidence, however, in the H chondrites that maximum metamorphic temperatures were reached after the parent asteroid had largely accreted. Cooling of chondritic material through 400°C at rates of 10^{1-3} °C Myr^{-1} occurred after accretion had ended (Dodd 1981; Wasson 1985).

The effects of heating on the mineralogical, chemical and physical properties of chondritic asteroids are relatively well understood. Because chondritic asteroids that were heated above 400°C were probably fairly anhydrous, chemically homogeneous, and did not experience high pressures (< 1 to 2 kb) or attain temperatures high enough to cause even local melting (< 950°C), the effects of heating were relatively minor in comparison with, for example, those in terrestrial rocks. The principal ingredients of these asteroids, chondrules and matrix, were both largely composed of olivine, pyroxene, metallic Fe-Ni and troilite (FeS) prior to metamorphism. Heating to 500°C caused these minerals, especially the mafic silicates, to equilibrate and the grain size of the fine-grained matrix to coarsen from sub μm to μm size. Glass

in chondrules decomposed to feldspar and mafic silicates (Sears and Hasan 1987). Subsequent heating caused continued coarsening of mineral grains such that the outlines of chondrules were almost obliterated in rocks that reached 900°C (Dodd 1981).

The thermal history and mineralogical changes are best documented for ordinary chondrites. These chondrites were heated for $10^{7\text{-}8}$ yr: petrologic type-3 chondrites reached maximum temperatures of 400 to 600°C, type 4 600 to 700°C, type 5 700 to 750°C and type 6 750 to 950°C (Dodd 1981). It is probable that metamorphism in carbonaceous and enstatite asteroids followed broadly similar patterns, but the petrologic types are not well defined and corresponding metamorphic temperatures are more uncertain. Metamorphosed carbonaceous chondrites differ slightly in that their silicate grains contain numerous tiny grains of magnetite, and their feldspar is more heterogeneous (Scott and Taylor 1985). In enstatite chondrites, which have a unique set of opaque phases, sinoite Si_2N_2O and alabandite $(Mn,Fe)S$ formed during metamorphism while niningerite $(Mg,Fe)S$ disappeared (Keil 1968). The bulk compositions of chondrites were not affected by metamorphism, except that the volatile elements, Bi, In, Tl, C and the noble gases may have been depleted (Dodd 1981; Wasson 1985).

Many physical properties of chondrites show little or no correlation with petrologic type; spectral features may sharpen and albedos increase with increased metamorphism (Gaffey 1976). However, the porosity of ordinary and carbonaceous chondrites is not correlated with petrologic type, though there may possibly be a very weak inverse correlation among H chondrites (Sugiura and Strangway 1983; Yomogida and Matsui 1982). Strength too is probably not well correlated, as several weak chondrites of high petrologic type are known. Although recrystallization under hydrostatic pressure should increase the strength and decrease the porosity of rocks, the absence of these effects probably reflects the extensive impact processing of asteroids. Shocked chondrites may have lower porosity (Sugiura and Strangway 1983) and enhanced strength (Bischoff et al. 1983). But of equal importance, many chondrites are breccias of material with diverse metamorphic histories, which have been welded by shock (Scott et al. 1985). Thus, most ordinary chondrites are not, strictly speaking, metamorphosed rocks but breccias of materials which generally experienced similar degrees of metamorphism. A few ordinary chondrites are mixtures of all metamorphic grades.

For the ordinary chondrites, cosmic-ray exposure-age distributions are similar for all metamorphic grades of the same group (Crabb and Schultz 1981). Thus on their parent asteroids, material that had been heated to different temperatures was fairly well mixed on the km scale when meteoroids were ejected (Anders 1978). For the EH, EL, CO and CV groups of chondrites, our samples have, with few exceptions, experienced similar degrees of metamorphism (300 to 500°C), which are low except for the EL chondrites (900°C). But the small sizes of these groups preclude any deductions about the differ-

ences in metamorphic temperatures and extent of mixing of metamorphic grades in their parent asteroids.

Possible Effects of Impacts During Metamorphism

Impact itself was probably not a significant cause of metamorphism in meteorites, although a few mineralogical changes have been attributed to residual heat from impacts, e.g., in the Shaw chondrite (Taylor et al. 1979). Mesosiderites, which have ^{39}Ar- ^{40}Ar ages of 3.6 to 3.8 Gyr (Bogard et al. 1988), may be rocks that were strongly metamorphosed after a relatively recent, severe impact. Impacts between hot bodies will clearly produce more intense metamorphic effects than if they are cold, and deformation effects in minerals will be more easily erased following such collisions. Conceivably the diverse degrees of homogeneity of pyroxenes in eucrites may be partly controlled by impact heating.

At least one chondrite, Mezö-Madaras, is known to have been formed by mixing of diverse metamorphic grades of material before slow cooling through 400°C (Scott and Rajan 1981). Thus some impacts during metamorphism mixed material. If the L chondrite asteroid ever had concentric structure with metamorphic grade increasing with depth, this stratigraphy was destroyed by impacts even before the asteroid cooled through 400°C (see the chapter by Lipschutz et al.). Alternatively, maximum metamorphic temperatures may have been reached in the planetesimals that accreted to form the asteroids. Finally, the EH chondrites were quenched from 800 to 500°C faster than 0.1° C min^{-1} (Skinner and Luce 1971). Since breakup and re-assembly of asteroids and simple impacts are not expected to produce material with such uniformly rapid cooling rates (see the above discussion), the possibility exists that these chondrites were not metamorphosed in asteroids.

IV. ALTERATION AND METAMORPHISM OF HYDRATED ASTEROIDS

Reflectance spectra from most C-class asteroids show a 3 μm absorption feature caused by structural hydroxyl and interlayer and adsorbed water, and Ceres has a spectral feature characteristic of a thin layer of water ice (Lebofsky 1978; Jones et al. 1988; Lebofsky et al. 1988). The abundance of hydrated silicates in the asteroid belt decreases with increasing heliocentric distance: the outermost P- and D-class asteroids appear to be anhydrous. Lebofsky et al. (1988) suggest that C, P and D asteroids were originally composed of anhydrous silicates and water ice and that only certain C-class asteroids were heated sufficiently by electrical induction to melt the ice.

Our principle evidence for the nature of geologic processing on hydrous asteroids is derived from hydrous meteorites. These include the CI, CM, CO and CV carbonaceous chondrites and, to a much lesser extent, the type-3 ordinary chondrites. Alteration processes and metamorphic reactions span

temperatures from below 0°C (hydrocryogenic alteration; see Ugolini and Anderson 1972; Gooding 1984), through low temperatures (<100°C, essentially diagenetic processes), to traditional hydrothermal temperatures (>100°C) and, with increasing pressure, metamorphism.

All the hydrous chondrites are breccias with complex accretional histories, which are the subject of constant debate. Therefore, if we wish to consider the mineralogical evidence bearing on the chemical evolution of the hydrous asteroids we must be careful to exclude from discussion any hydrous minerals that may have condensed directly in the solar nebula. Water vapor would have been available for aqueous reactions in the solar nebula, and it is possible that hydrous phases could have either directly condensed here or formed through the interaction of pre-existing anhydrous phases with water vapor (Grossman and Larimer 1974; Barshay and Lewis 1976). However, experimental evidence for the former process is lacking, and recent theoretical work indicates that the latter reaction would have been kinetically inhibited (Prinn and Fegley 1987). Nevertheless, we shall limit discussion to meteoritical mineral assemblages that petrographic work has established as forming on asteroids (Zolensky and McSween 1988). The evidence for this includes: (1) alteration minerals bridging chondrules, aggregates and large crystals with matrix; (2) crystal morphologies that required crystallization from a gel or fluid phase; (3) relict chemical zoning or correlations within matrix and altered chondrules and aggregates; (4) alteration minerals lining fractures or forming veins within a meteorite; and (5) minerals which cannot have formed within the solar nebula (e.g., calcite and very pure magnetite) (Zolensky and McSween 1988; Fredriksson and Kerridge 1988). Table IV lists the products of hydrous alteration found within each hydrated meteorite type. Type-3 chondrites are the least altered (McSween 1979); CM2 and CI1 chondrites were derived from different primary materials by different alteration processes (Tomeoka and Buseck 1988). Whether CM2 and CI1 chondrites formed by alteration of type-3 materials, as McSween (1979) suggested, is not known; recent modeling by Zolensky et al. (1989) casts some doubt on this theory.

Mobilization of Water in Asteroids

Water ice that accreted into asteroids could have directly promoted hydrous alteration of silicates through hydrocryogenic processes involving interfacial water (Gooding 1984; Rietmeijer 1985). In laboratory experiments, this process is effective down to −11°C, and in nature it could have been effective at far lower temperatures considering the longer time available to asteroids.

Liquid water could have been produced by any or all of the heating processes discussed above. Heat from short-lived radionuclides would have produced a narrow zone of water that migrated towards the surface as heating continued (DuFresne and Anders 1962). This layer would have been trapped by a surficial icy layer, which could have existed for about 200 Myr on a 100 km radius asteroid. However, this calculation by DuFresne and Anders ne-

TABLE IV
Mineralogical Products of Alteration on Hydrated Asteroids[a]

Type	Group	Alteration Products
1	CI, CM	serpentines, smectites, carbonates, sulfates, elemental sulfur, magnetite, organics (?)
2	CM, CR	serpentines, smectites, carbonates, tochilinites, tochilinite-serpentine intergrowths, sulfates, organics (?)
3	CV, CO, H, L, LL	smectites, serpentines, calcite, melilite

[a]Sources: McSween and Richardson 1977; Grady et al. 1987; Zolensky and McSween 1988; Keller and Buseck 1988.

glects effects of regolith turnover. A surface layer of pure water ice would insulate the asteroid from electrical induction heating, but the likely presence of impurities would raise the electrical conductivity of the ice and permit heating to continue. Laboratory determinations of the electrical conductivities of meteoritic minerals and ices are required for further development of this model.

Lange et al. (1985) propose that repeated impacts during accretion of hydrous asteroids produced and transported water in the regolith layers. Water might have been released from hydrous minerals at relatively low shock pressures during repeated shocks. This model accounts for impact induced textural characteristics that Lange et al. infer are present in carbonaceous chondrites, and is favored by textural evidence in CI chondrites discussed below for repeated formation of veins during an extended period of impact brecciation (Richardson 1978). However, it is likely that the heat source that melted some asteroids, which was not impact, also mobilized water on some hydrous asteroids.

Alteration Conditions Inferred from Meteorites

Aqueous alteration in carbonaceous chondrites produced the following mineralogical changes: (1) transformation of anhydrous silicates (olivines, pyroxenes, etc.) to assemblages dominated by serpentines and smectites; (2) destruction of primary sulfides; (3) growth of secondary generation of sulfides and/or sulfates, and magnetite; (4) devitrification of chondrule glass; (5) nucleation and growth of carbonates; and probably (6) *in situ* development of complex organic compounds (Zolensky and McSween 1988). Results of this alteration are illustrated in Fig. 1.

The alteration minerals in CI and CM chondrites are sufficiently complex to permit some constraints to be placed on the *P-T* compositional characteristics of the alteration fluids themselves (DuFresne and Anders 1962; Bunch and

Chang 1980; Hayatsu and Anders 1981; Zolensky 1984; Clayton and Mayeda 1984; Zolensky et al. 1989). Aqueous fluids were characterized by values for the redox potential E_H of < 0 V, pH values of 8 to 12, and temperatures of about 25°C for the CM's and <150°C for the CI chondrites. The fluids must have contained NH_3, CO_2, H_2S and organic compounds at various times, but alteration appears to have been essentially isochemical for the other major species. Compared to the CI and CM chondrites, aqueous alteration in the CO, CV and ordinary chondrites is much less extensive. Modeling indicates that the alteration in these meteorites occurred below 25°C (Zolensky et al. 1989).

Most interplanetary dust particles (IDPs) may be derived from asteroids (Zook and McKay 1986), and some show effects of preterrestrial aqueous alteration that can be compared to those in chondritic meteorites (Zolensky and McSween 1988). In terms of alteration mineralogy, the serpentine group IDPs are similar to the CI and CV chondrites, and the smectite group IDPs are analogous to the CO, CV and LL chondrites (Zolensky and McSween 1988). However, these chondritic IDPs differ from chondritic meteorites in having higher carbon contents (Blanford et al. 1988) and far greater porosities (Bradley 1988). Chondritic IDPs might have originated from the organic-rich P and D classes of asteroids, or from comets.

Veins in the CI chondrites were deposited over a period of impact brecciation and leaching (Richardson 1978). Three generations of fracture-filling minerals dominated in turn by carbonates, calcium sulfate and magnesium sulfate, are visible (see Fig. 1a). This indicates that a complex scenario of aqueous alteration occurred contemporaneously with a period of pervasive fracturing on the CI parent asteroid. This fracturing most likely occurred near the asteroidal surface during a period of high-impact rates. These CI parent-body events are entirely consistent with the water-production scenarios presented above, which are all most efficient during and immediately following asteroid accretion.

The lack of analogous fracturing and shock effects in the other carbonaceous chondrites probably results from their moderate burial during alteration. Unfortunately, the observed alteration mineralogies and textures of chondrites and IDPs do not quantitatively constrain their burial depths during alteration. A weak preferred orientation of phyllosilicates in some CM chondrites (Fujimura et al. 1982,1983) indicates that these meteorites experienced compaction at moderate burial depths, but greater burial depths are precluded by the delicate cylindrical morphologies exhibited by tochilinite crystals in these same meteorites (Zolensky 1984). Some type 1-3 chondrites may have been heated and dehydrated to produce chondrites of higher metamorphic type (4-6) (see Fig. 1f,g,h). McSween (1977) has shown that the CO3 chondrites comprise a metamorphic series, with a peak temperature of 450°C. As in ordinary chondrites, some rocks were lithified after metamorphism (Van Schmus 1969). Metamorphic temperatures of at least 600°C are required by
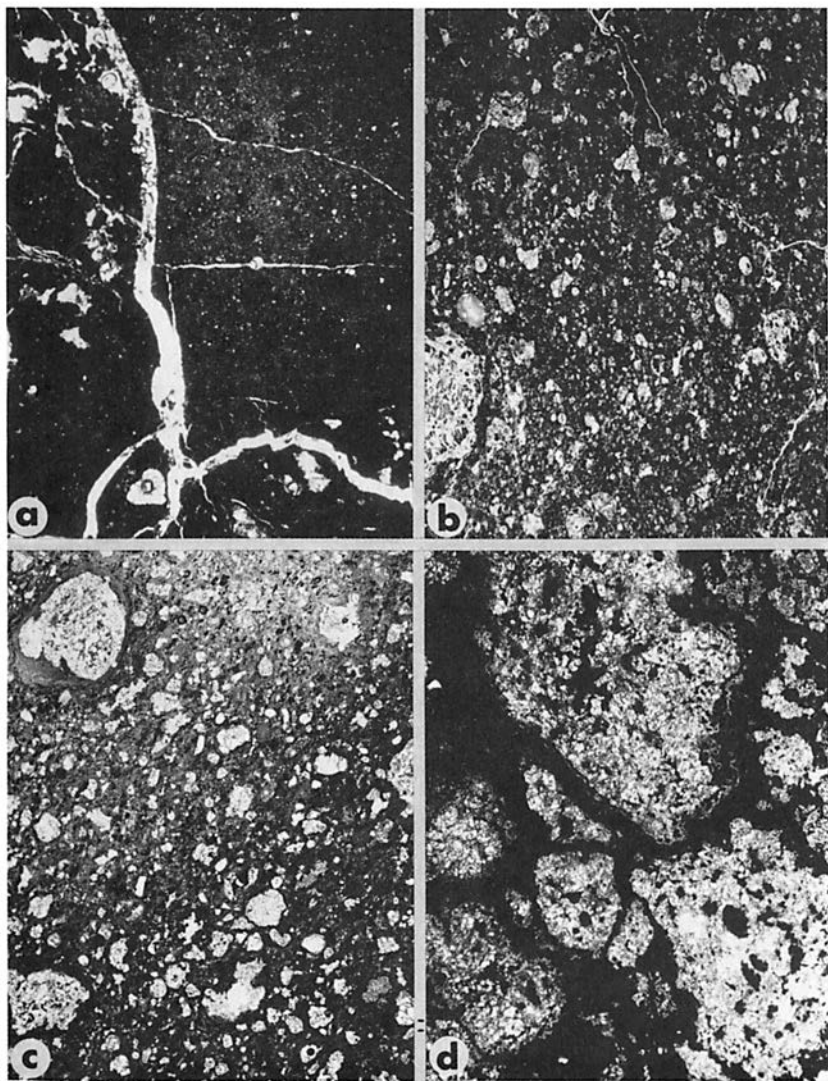
Fig. 1. Views of carbonaceous chondrite thin sections showing the effects of progressive aqueous alteration (a-d) and metamorphism (g and h), compared to relatively pristine type 3 chondrites (e and f). All views measure 4 mm high, and are in transmitted light. (a) Orgueil (CI1), showing fine-grained hydrous matrix and carbonates, cut by carbonate and sulfate veins; (b) EET 83334 (probably CM1: Zolensky and Barrett 1988), in which all chondrules and aggregates have been completely serpentinized, and opaque matrix is composed predominantly of serpentine and carbonates; (c) Murray (CM2), showing chondrules and aggregates (some ser-

pentinized) in an opaque matrix dominated by serpentine and tochilinite; (d) Renazzo (CR2), consisting of large chondrules and aggregates in an opaque phyllosilicate-rich matrix; (e) Vigarano (CV3), with large chondrules and aggregates in an opaque matrix of fine-grained anhydrous minerals; (f) Lancé (CO3) containing relatively small chondrules and aggregates in an opaque matrix of fine-grained anhydrous minerals; (g) Coolidge (CV4) showing translucent, recrystallized matrix and chondrules with blurred outlines; (h) PCA 82500 (C4), with a very coarsely recrystallized matrix containing nearly indistinguishable chondrules.
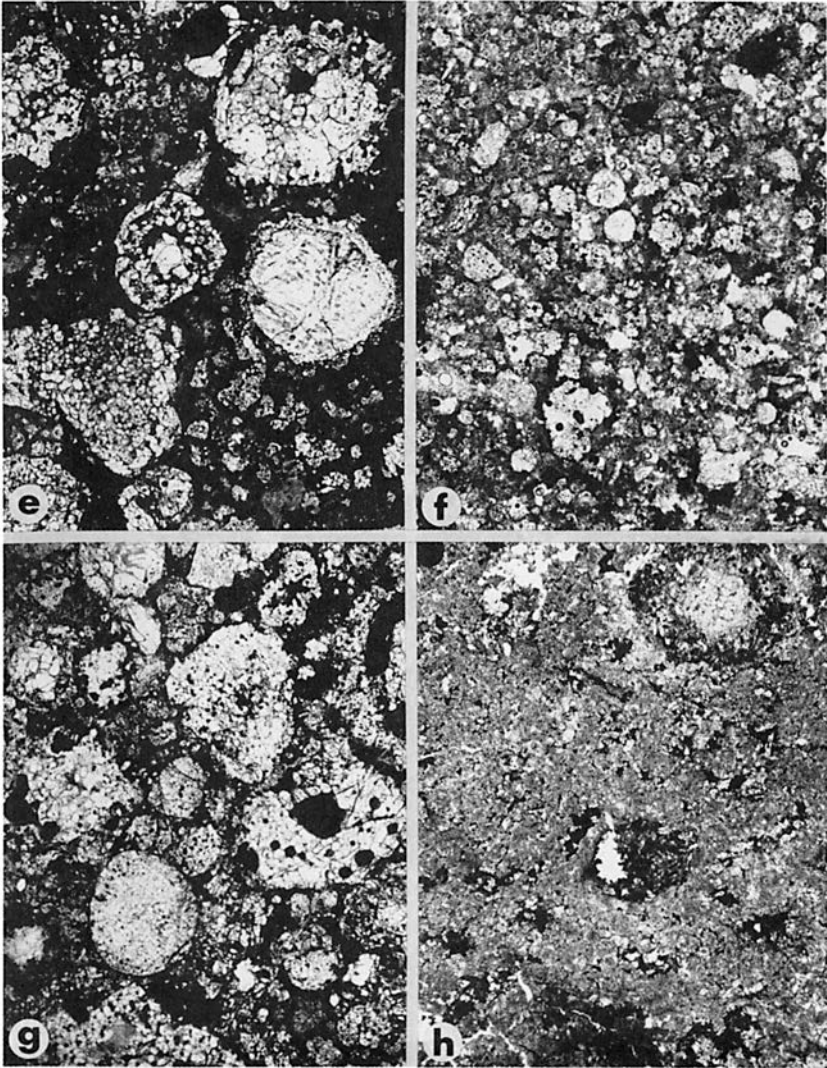
the mineralogy of the C4 chondrites (Scott and Taylor 1985). Many CV chondrites contain nonspherical chondrules with a preferred orientation, indicative of dynamic or shock metamorphism (Dodd 1981). However, the exact metamorphic processes responsible for these characteristics remain to be accurately characterized. Retrograde metamorphic reactions may also have contributed to the evolution of hydrous asteroids, although evidence for these processes (pseudomorphs of lower-temperature minerals after higher-temperature ones, etc.) have not been recognized.

A major problem in understanding geologic processes on the carbonaceous chondrite asteroids is our relative ignorance of the number of asteroids represented in our meteorite collection. Although CM and CV chondrites probably come from different asteroids (Zolensky et al. 1989), we do not know, for example, whether all CM2 chondrites come from one asteroid, or whether a CM1 chondrite (Grady et al. 1987; Zolensky and Barrett 1988) could be derived from a CM2 asteroid. And, due to their rarity, we cannot even be certain that the CV4 chondrites are samples of deeper regions of the CV3 parent asteroids. This situation is primarily due to the rarity of our samples of hydrous asteroids.

Chronology of Alteration and Irradiation on Carbonaceous Asteroids

The secondary mineralization caused by aqueous activity on the carbonaceous-chondrite parent asteroid, or asteroids, has been approximately dated by means of the Sr-isotopic composition of CI carbonates (Macdougall et al. 1984) and the I-Xe systematics of CI and CM magnetites (Lewis and Anders 1975). Both approaches suggest that the aqueous alteration occurred within approximately 100 Myr of the accretion of asteroids.

In reconstructing the earliest history of those asteroids, it would be useful to date the other events involved in their evolution, such as the epoch of impact-induced turnover and brecciation, and irradiation by solar wind and solar flares. These processes are less amenable to radiometric dating though ^{244}Pu-based breccia-compaction ages in the range 4.2 to 4.5 Gyr have been inferred (Macdougall and Kothari 1976), but petrographic relations within the CI and CM chondrites can be used to establish relative, if not absolute, chronologies.

This approach can be applied, for example, to the record of solar-wind and solar-flare irradiation carried, in the form of trapped and spallogenic noble gases and charged-particle tracks, by a population of euhedral olivines in CI and CM chondrites (Goswami and Macdougall 1983). This irradiation must have taken place after the grains acquired their present form and chemical composition and before final compaction of the meteorite. The latter event can presumably be established with increasing accuracy and precision as the ^{244}Pu-fission-track technique is further developed.

Our ability to date the formation of olivines is limited at present by un-

certainty as to the nature of the process, or processes, involved. Three possibilities are permitted by existing observations:

1. Alteration of previously formed silicates, possibly nebular condensates;
2. Crystallization from chondrule melts of variable initial composition;
3. Condensation from regions of nebular gas with variable, and nonsolar, fO_2 values.

The key features of the grains that might be used for discriminating between these possibilities are their contents and micro-distributions of a number of elements, notably Fe, Ca and Mn. Existing trends, such as correlated enrichments in Fe and Ca, appear to favor the first two possibilities, but calculations by Wood and Hashimoto (1988) suggest that the third possibility cannot yet be ruled out. The chronological consequences of this uncertainty are considerable. The third possibility does not usefully constrain the epoch of irradiation whereas the first two both constrain it to postdate the period of aqueous activity, required either to cause the alteration or to liberate euhedral grains from within chondrules.

Defining such a sequence of events would obviously improve our understanding of the history of C-type asteroids. Dating of the irradiation epoch has taken on added significance recently in light of evidence that the irradiation of the carbonaceous-chondrite olivines may be recording a period of enhanced solar activity (Caffee et al. 1987). Such early activity, the so-called T-Tauri phase, may characterize the pre-main-sequence behavior of solar-mass stars. Further analyses of the meteorites and more detailed modeling of the different possible processes are clearly needed.

V. IGNEOUS PROCESSES IN ASTEROIDS

Igneous Meteorites

Although chondrites are the most abundant type of meteorite to fall on the Earth, there are more types of differentiated, or igneous, meteorites than there are types of chondrites. Based on variations in chemical compositions (e.g., Ge and Ni concentrations), iron meteorites have been divided into 12 groups with 5 to 150 members in each group (Scott 1979). About 70 iron meteorites fall outside these groups and are related to 3 or fewer other irons. If the molten metal formed cores, as is probable for most groups, then most groups come from separate asteroids. These irons are probably samples of another 50 groups. The most abundant group of stony igneous meteorites consists of eucrites, which are basaltic rocks, diogenites, which are orthopyroxene-rich cumulates, and howardites, which are mixtures of the first two. (Cumulates are rocks that formed by accumulation of crystals in a magma.) Howardites, eucrites, and diogenites probably formed on the same parent asteroid. Many have properties that indicate a complicated origin with different

amounts of partial melting and fractional crystallization involved (Hewins and Newsom 1988); a few rock types seem to require formation by small amounts of partial melting of previously formed cumulates.

Aubrites consist mostly of FeO-free enstatite. These rocks are breccias and consist of mixtures of assorted enstatite-rich cumulates related by fractional crystallization of an ultramafic melt (Okada et al. 1988; Taylor et al. 1988). Aubrites are samples from at least two asteroids which probably formed in the vicinity of the EH and EL chondrite asteroids (Keil 1988). Ureilites are carbon-rich olivine and pigeonite cumulates which come from yet another, possibly carbonaceous asteroid. They have a complex origin that may have involved partial melting, fractional crystallization accompanied by reduction of FeO, alteration of trapped melt by mixing with another melt, and quenching from high magmatic temperatures (Goodrich et al. 1987). Finally, there are two achondrites, Angra dos Reis and Lewis Cliff 86010, composed mostly of fassaitic clinopyroxene (Ti,Al-rich pyroxene).

Although only two asteroids with basaltic crusts have been identified (V types), spectral observations indicate that there are numerous M asteroids (thought to be composed of metallic iron), many E types (possibly enstatite achondrites), and a few A types (olivine-rich achondrites) (see the chapter by Bell et al.). There are also a large number of S-type asteroids, which may be stony-iron differentiated meteorites, though some investigators favor a chondritic origin. Nevertheless, it is clear that igneous processes operated on many asteroids.

Igneous Processes on Asteroids

Igneous rocks form by one and usually more processes involving the production and modification of silicate melts. In general, the efficacy of igneous processes will be less in asteroids than in larger bodies such as the Moon and Earth (Walker et al. 1979). We illustrate this by a brief review of magmatic processes. The first step in magma genesis is partial melting of a source rock. On the Earth and Moon, this source is typically itself the product of previous episodes of magmatic activity, but on achondritic asteroids where the heating episode was of short duration, the melting usually (though not always) involved previously unfractionated, primitive materials. The percentage of partial melting can vary, producing an array of magma compositions. In general, the amount of melt needed to initiate melt migration out of the source region depends on the gravitational field; small asteroids required more melt than large ones (see, e.g., Walker et al. 1978). The amount of melt produced prior to magma migration also depends on the properties of the source region, including its grain size and composition. These features suggest that the primary melts produced in the interior of asteroids tended to be less fractionated than melts on large objects. Also, the lack of large pressures in the interiors of asteroids prevented high-pressure phases such as garnet

from participating in melting events, which also led to less fractionation by melting.

Once magmas are produced in a source region and begin to rise, there are several opportunities for differentiation to occur. One is fractional crystallization, the change in magma composition due to the crystallization and removal of a phase from the magma. This commonly takes place in magma chambers at depth in a body. This process was probably less efficient on asteroids than on larger bodies because the process is affected by gravitational forces. Early formed crystals tend to sink in a magma, forming cumulates on the bottom of a chamber. The settling velocity is inversely related to the gravitational acceleration, g. More likely than simple mineral settling is the flow of crystal-rich density currents (Irvine 1979), which will be slower at lower g. Finally, in terrestrial intrusions, crystallization takes place near the bottom as a result of adiabatic gradients in P-T that are much steeper than the P-T variations of silicate liquidus temperatures (see, e.g., Irvine 1970). The P-T gradients in an asteroidal-sized body would be small, so this mechanism would not have operated, leaving crystal settling and density currents as the main mechanisms of fractional crystallization in magma bodies. In spite of this inefficiency, however, some meteorites, such as diogenites, appear to have formed by crystal accumulation. As a magma chamber crystallizes, its composition can be altered by introduction of a fresh batch of magma (O'Hara 1977). This process, which on Earth can operate for many cycles, produces major and trace-element concentrations in the resulting magmas much different from those resulting from fractional crystallization alone. The extent to which this happened in asteroids is unknown, though the relatively short duration of asteroid magmatism and perhaps magma-chamber disruption by impact may have limited the number of replenishment cycles.

Assimilation is the digestion of solid rock by a magma. It may involve partial melting of the rock being assimilated and, to maintain heat balance, it almost always involves simultaneous fractional crystallization. This is unlikely to have been an important factor in altering asteroidal magmas because asteroids did not differentiate to the extent that larger bodies did. The Earth has a thick, granitic crust and the Moon contains areas rich in KREEP, a chemical component enriched in incompatible elements such as K, rare-earth elements and P. Both materials are highly evolved and have low melting temperatures, making them ripe for assimilation. The absence of such rocks in asteroids limited the extent to which assimilation could have operated, although some limited assimilation might have taken place; for example, pre-existing basalts might be assimilated partly by subsequent basaltic magmas, especially if the latter were richer in Mg.

Eruption processes would also be different on asteroids compared with that on larger planets. The velocity at which a magma rises is proportional to the square of the width of fissures. The fissure width is dependent on stress gradients within planets, which vary inversely with g (Wilson and Head

1988). Consequently, rise velocities are inversely proportional to g, and the mass eruption rate is much greater on smaller than on larger bodies. Wilson and Head (1988) estimate that the mass-eruption rate is 200 times greater on the Moon than on the Earth if no turbulence occurs (as for eruptions of magmas with low gas contents). Using Wilson and Head's (1988) results, we estimate that the mass eruption rate on an asteroid 200 km in radius was 10^5 times greater than on the Earth. Eruptions on the Earth have mass-effusion rates of 10^2 to 10^7 kg s^{-1} (Whitford-Stark 1982), so the range for asteroid eruptions might be 10^7 to 10^{12} kg s^{-1}. This extreme extrapolation needs to be evaluated. Because lengths of lava flows are controlled mostly by effusion rate (Walker 1973), flows on asteroids were probably extremely long. They would also be much thicker and wider, as these properties are inverse functions of g (Wilson and Head 1983). This could lead to substantial thicknesses (at least several km) of basaltic rock on asteroidal surfaces that experienced eruptive activity.

Core Formation

Evidence favoring the existence of metallic cores in some asteroids comes from iron meteorites, the lack of metal and the depletion of siderophile (metal-loving) elements in differentiated meteorites such as the eucrites (Newsom 1985; Hewins and Newsom 1988), and direct observation of large M-type asteroids with flat spectra that are interpreted to consist of Fe-Ni (see the chapter by Bell et al.). The evidence that most iron meteorites formed as parts of many large cores of asteroids, rather than as small isolated "raisins," comes from their lack of silicates and trace-element compositions which indicate that they formed by the igneous process of fractional crystallization (Scott 1979; Jones and Drake 1983). When a metallic liquid begins to crystallize and solidify, some elements are excluded from the solid metal and some are preferentially retained, resulting in fractionated compositions in iron meteorites from different portions of a fully solidified magma (Jones and Drake 1983; Narayan and Goldstein 1982). Assimilation of undifferentiated metal during the crystallization of one group of irons (IIIAB) has been inferred by Malvin (1988).

Three groups, IAB, IIICD and IIE, containing silicates, are less likely to have been cores and may have formed from impact-produced melt (Wasson and Wang 1986). But Kracher (1985) and Prinz et al. (1983) favor core origins for these groups. The sizes of metal cores compared to the silicate portions of asteroids are known only from the observed amounts of metal and sulfide (FeS) in primitive undifferentiated chondrites (8 to 20%Fe-Ni, and <1 to 15% FeS), and from the estimate of the core size in the eucrite parent body required to achieve the observed depletion of siderophile elements in the eucrites (20 to 40%Fe-Ni: Newsom 1985; Hewins and Newsom 1988).

The mechanism of core formation in asteroids has not been studied in detail. A preliminary assessment (Taylor 1989) indicates that metal segrega-

tion involved a large percentage of partial melting of the silicates. Experiments show that metal-sulfide melts do not readily wet silicates and, therefore, do not form interconnected networks of channels (Takahashi 1983; Walker and Agee 1988). Consequently, metal will not simply drain away by porous flow during melting. It must instead sink as globules, but this process is also inefficient as the globules must become large enough to overcome the significant yield strengths of crystal-bearing silicate melts. Yield strength, s, varies as a strong function of crystal content, or the fraction of melt present f, $s = 6500 (1-f)^{2.85}$ (Ryerson et al. 1988). Calculations by Taylor (1989) suggest that on bodies 100 km in radius, metal-sulfide globules will sink only if they are > 1 cm in radius and 90% of the silicate assemblage is molten. If the percentage of melting is only 50%, metal-sulfide globules must be 1 m in radius. (Minimum radii needed to sink are proportional to g^{-1}, so these values are 10 times larger for an asteroid 10 km in radius.) Although much more work needs to be done to understand metal segregation quantitatively, it appears that a core will not form until substantial percentages ($>50\%$) of the silicates have melted. This result is consistent with the calculations of Newsom (1985) and Hewins and Newsom (1988) based on siderophile element depletions, which suggest that metal segregation in the eucrite parent body occurred at 20 to 70% partial melting of the silicates.

Wasson (1985) argues that the low S contents of iron meteorites, generally less than 2 wt.% (Buchwald 1975), are best explained by removal of an early FeS-rich liquid from a chondritic precursor; this FeS-rich liquid did not mix with the denser S-poor metal that melted later. He envisages that the two cores would crystallize independently, the low-S interior core first. However, calculations (Taylor 1989) suggest that removal of the FeS-rich liquid is not possible unless the metal content is very high. Furthermore, the pallasites which are believed to represent the core-mantle boundary, are not, with one exception, rich in FeS. These rocks are believed to have formed when Fe-Ni metal was mixed with the olivine mantle as a result of cooling stresses, impacts, and the weight of the mantle (Scott 1984). Very rapid solidification of the metal must have occurred to prevent gravitational separation of olivine and metal.

A more complicated history is required to explain the mesosiderites, which are stony-iron meteorites that are mixtures of basaltic material and Fe-Ni metal. Suggestions include the foundering of a basaltic crust of an asteroid to the core-mantle boundary where it was intruded by metal from the core (Greenberg and Chapman 1984), or the low-velocity collision of an iron core of an asteroid, stripped by impacts of its silicate mantle, with the basaltic crust of another asteroid (Wasson and Rubin 1985).

Effects of Impact on Asteroids Undergoing Magmatic Activity

Many properties of individual groups of differentiated meteorites, such as trace-element concentrations, homogenization of zoned minerals and ages

cannot be explained by simple, one-stage heating of an asteroid. Although impact is unlikely to play a major role in providing heat to drive asteroid igneous activity, it might interact significantly with magmatic processes to produce products that magmatism alone could not. Impact could have complicated igneous processes in two ways: formation of thick regoliths and direct excavation of melts. These processes are illustrated in Figs. 2, 3 and 4.

Regoliths begin to develop almost as soon as a body begins to accrete. An incoming projectile with the strength of basalt breaks up if it arrives at > 25 m s^{-1} (Hartmann 1978), the escape velocity of a chondritic object about 20 km in radius. Less consolidated materials break up at even lower velocities. Allowing for compaction and sintering of the interior, the outer 10 km of an asteroid 100 to 200 km in radius will be a rubble pile as a consequence of accretion.

The presence of a thick regolith will affect the migration of magma. The regolith would have a lower density, perhaps as low as 2.5 g cm^{-3}, than the magmas moving through it (about 2.8 g cm^{-3} for eucritic magmas); this could arrest magma ascent, leading to the formation of intrusions rather than basalts. The lower temperature and blocky nature of the regolith would lead to rapid cooling of rising magmas, also causing arrested migration. Consequently, the earliest magmas probably formed intrusions, both dikes and plutons (Fig. 2). Continued magmatism would heat the crust and increase the average density, leading to eruptions. However, because impact rates were high early in solar system history, the upper crust would have continued to be reworked and fractured, causing magmas to engulf fragments of pre-existing
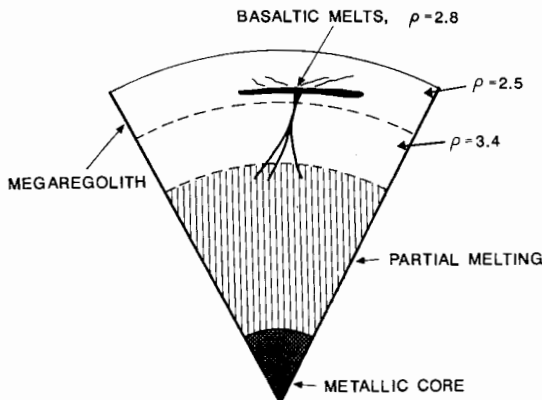
Fig. 2. Diagram showing how a thick regolith that develops during accretion of the asteroid may affect the migration of magma. When melting occurs, the magmas produced cannot reach the surface because of the lower density of the megaregolith, resulting in intrusions of basaltic magmas, rather than extrusion of lavas. This will continue until the crust becomes sufficiently dense to allow transport of magma through it.

rock and possibly thermally metamorphosing them. At first, the engulfed, metamorphosed rocks would have been primitive materials accreted to an asteroid. We have no known samples of such materials among achondrite breccias such as howardites. With time, however, as a basaltic crust built up, the rock fragments in an asteroidal regolith that were metamorphosed by entrapment in a lava would be basaltic.

Craters would be favored places for lava accumulation (Fig. 3) and could be quite deep: a crater 5 km in diameter would be 1 km deep. Furthermore, because individual flows might be exceptionally thick and effusion rates exceptionally high (see above), it is likely that such craters would be completely filled with lava. Thick flows or lava lakes in craters could provide the setting for equilibration of many eucritic basalts such as Juvinas, which need to be buried a few hundred meters; such metamorphism could also take place near dikes beneath the surface.

Magmas could be directly excavated by impacts over a wide range of depths on asteroids. Small impacts would excavate flows or lava lakes, mixing these lavas with solid rocks; this might provide another opportunity to equilibrate eucritic basalts. Larger impacts (craters 50 km across) could excavate magma chambers crystallizing at depths up to 10 km (Fig. 4). This could eject or expose crystal mushes to the surface, thereby quenching in their high-temperature characteristics. For example, ureilites contain high Ca in olivine and unexsolved pigeonites (Berkley et al. 1980; Goodrich et al. 1987); perhaps they were excavated by an impact while still containing intercumulus liquid. Impacts in this size range could also mix more-fractionated and less-fractionated magmas existing within a chamber or nearby chambers. Hewins
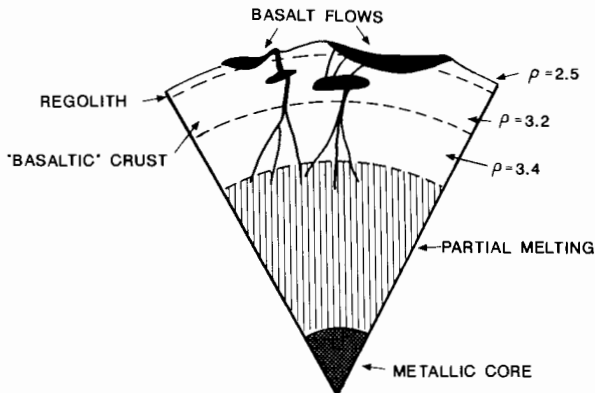
Fig. 3. Diagram showing how high extrusion rates due to low gravity on asteroids and the presence of large craters may allow asteroids to develop thick pools of lava and thick sequences of flows on their surfaces. This could account for the equilibration of many eucrite basalts.
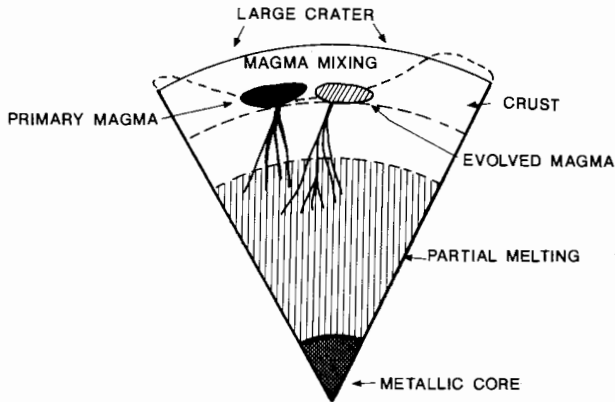
Fig. 4. Diagram showing how impacts on an asteroid undergoing magmatic activity can add twists to the course of petrologic events. A large crater could excavate magma chambers, thereby quenching them, or mix magmas of different composition. Extremely large craters could excavate down to the zone of partial melting, thus quenching in their high-temperature characteristics and possibly producing rocks that mimic igneous cumulates.

and Newsom (1988) suggest that some eucrites could have formed by mixing primary magmas poor in incompatible elements with fractionated magmas rich in them. It is also feasible that a large impact could mix impact-produced melt into a cumulate containing trapped liquids, as Goodrich et al. (1987) suggest happened during the genesis of ureilites. Parts of the projectile could be incorporated into the excavated melt, as proposed for Shallowater (Keil 1988).

Still larger impacts, those near the limit of an asteroid's strength, might excavate to the zone of partial melting; an asteroid 400 km in diameter might survive formation of a 200 km crater (Housen et al. 1979; Taylor et al. 1987), which would be 40 km deep. This could mix partial melts formed under a variety of conditions (source composition, percent of melting) or quench them. An impact during the early stages of partial melting, before metal segregated, might be responsible for the formation of nonmagmatic iron meteorites, such as groups IAB and IIICD. Finally, an extremely large event might disrupt a partly molten asteroid. If re-assembled by gravitational forces, the newly formed megabreccia would contain at great depth both surface lavas and cumulates formed in shallow intrusions. Hot, partially molten rock from the interior would cool partly during the several hours it would take to re-accrete the body, but fragments > 5 m in radius would cool negligibly. For example, using equations for the cooling of a sphere initially at a uniform temperature (Carlslaw and Jaeger 1959), it would take 33 days for the center of a sphere 5 m in radius to cool from 1250°C to 1100°C (certainly below the solidus of chondritic materials), ignoring the latent heat of crystallization.

Subsequent melting of the re-assembled but disorganized body, either by ^{26}Al returned to the interior in the buried basalts or by electromagnetic induction, might account for the rock types that appear to have formed by partial melting of previously formed cumulates. For example, Mittlefehldt (1979) and Delaney (1986) propose that eucrites rich in incompatible elements could have formed by remelting of plutons. Smith (1982) showed that the rare-earth-element patterns of eucrites could result from partial melting of differentiated crust.

VI. IMPLICATIONS AND CONCLUSIONS

We have illustrated some of the rich geologic diversity in the asteroid belt. This diversity is caused to some extent by compositional variations in the primordial chondritic materials, which reflect such factors as the abundance, oxidation state and volatile content of the matrix, the proportions of oxidized and reduced chondrules and refractory inclusions, and abundances of metal and sulfide. The existence of unique chondrites like Kakangari and Allan Hills 85085 shows that our sample of C, O and E chondrites is probably only a small part of the original spectrum of primordial compositions.

This primordial, chemical and mineralogical rainbow of rock types was diversified even more by the processes of heating (probably from several sources), alteration and impact, acting both individually and in concert. Even though these processes were most effective for a relatively short geologic epoch, < 200 Myr, the variety of rock types was multiplied many times.

We have several pairs of differentiated and chondritic meteorite types, such as IIE irons and H chondrites (Clayton et al. 1983), aubrites and enstatite chondrites (Brett and Keil 1986), that are sufficiently similar that they must have formed in the same part of the asteroid belt, yet different enough that they could not have formed in the same body. This proximity of melted and unmelted asteroids across the inner asteroid belt points to a highly selective heat source, possibly induction heating, that was capable of multiplying the geologic diversity within each narrow zone of primordial homogeneity, possibly throughout the asteroid belt.

Impacts between asteroids created or revealed a vast array of new rock types by mixing, melting and eroding asteroidal materials. The outcome of each asteroidal impact depended on the size, temperature, composition and physical state of each object and their angle of incidence and relative velocity. The range of shock and brecciation effects in meteorites (Table I) illustrates the diverse response of asteroids to their environment.

Even though impact heating was probably not the dominant heat source at most locations, the interaction of heating with impact was a major cause of geologic diversity. The low-gravity and highly fragmented, relatively porous nature of primordial asteroids ensured that melting processes on asteroids differed considerably from their planetary and lunar analogues. Evidence for re-

melting of some asteroidal materials may indicate an intermittent heat source that could have exaggerated these differences. The existence of a wide variety of stony-iron meteorites, such as pallasites, mesosiderites and irons with silicate inclusions, illustrates the significant stochastic effect impacts played in preventing the melting and solidification of asteroids from following an equilibrium path.

Impacts between warm or cold asteroids over the last 4 Gyr in no way homogenized this geologic diversity. Impacts created new rock types by intimately mixing strata from different depths (e.g., howardites) and occasionally from different bodies (e.g., Cumberland Falls), severely altering the physical properties of a few asteroidal materials (e.g., shock-blackened L chondrites) and eroding some, but not all, large and small asteroids to reveal the igneous and metamorphic rock types created earlier.

The carbonaceous asteroids that we have sampled were once thought to have escaped any geologic processing whatsoever. The chemical pristinity, especially of CI chondrites, was taken by many to indicate that carbonaceous chondrites had perfectly preserved the nebular components from which their parent bodies had formed. However, we now recognize that all sampled carbonaceous asteroids have experienced significant geologic processing, especially aqueous alteration, albeit generally at mild temperatures. Much more detailed petrology needs to be done to characterize the fine-grained materials in these rocks and to search for evidence for the nature and timing of the alteration processes on their parent asteroids. But existing studies suggest that on many carbonaceous asteroids, internal heating and impact gardening of hydrous materials were important geologic processes. Oxygen isotopic data suggest that a few carbonaceous asteroids probably melted to produce Eagle Station-type pallasites and ureilites, and we can infer the existence of equally diverse complementary differentiation products.

Laboratory experiments, lunar and terrestrial analogues and theoretical studies are poor guides for a good understanding of the geology of even well-sampled asteroids. But much more can be done with these tools to understand the origin of the samples we already have. Numerous, well-documented samples must be returned from many well-mapped locations in the asteroid belt before the geologic history of asteroids and small moons can be well understood. But, for the reasons outlined in the introduction, we believe these efforts will be well justified and richly rewarded.

REFERENCES

Anders, E. 1978. Most stony meteorites come from the asteroid belt. In *Asteroids: An Exploration Assessment,* eds. D. Morrison and W. C. Wells, NASA CP-2053, pp. 57–75.

Barshay, S. S., and Lewis, J. S. 1976. Chemistry of primitive solar material. *Ann. Rev. Astron. Astrophys.* 14:81–94.

Basaltic Volcanism Study Project. 1981. *Basaltic Volcanism on the Terrestrial Planets* (New York: Pergamon Press).

Berkley, J. L. 1986. Four Antarctic ureilites: Petrology and observations on ureilite petrogenesis. *Meteoritics* 21:169–189.

Berkley, J. L., Taylor, G. J., Keil, K., Harlow, G. E., and Prinz, M. 1980. The nature and origin of ureilites. *Geochim. Cosmochim. Acta* 44:1579–1597.

Binns, R. A. 1967. Structure and evolution of non-carbonaceous chondritic meteorites. *Earth Planet. Sci. Lett.* 2:23–28.

Bischoff, A., Rubin, A. E., Keil, K., and Stöffler, D. 1983. Lithification of gas-rich chondrite regolith breccias by grain boundary and localized shock melting. *Earth Planet. Sci. Lett.* 66:1–10.

Blanford, G. E., Thomas, K. L., and McKay, D. S. 1988. Microbeam analyses of chondritic interplanetary dust particles for carbon, oxygen, and major elements. *Lunar Planet, Sci.* XIX:102–103 (abstract).

Bogard, D. D., Jordan, J., and Mittlefehldt, D. 1988. ^{39}Ar-^{40}Ar dating of mesosiderites: Evidence for major parent body disruption less than 4 Ga ago. *Meteoritics* 22:258 (abstract).

Bowell, E., Chapman, C. R., Gradie, J. C., Morrison, D., and Zellner, B. 1975. Taxonomy of asteroids. *Icarus* 35:313–335.

Bradley, J. P. 1988. Analysis of chondritic interplanetary dust thin-sections. *Geochim. Cosmochim. Acta* 52:889–900.

Brecher, A. 1973. The electrical conductivity of carbonaceous meteorites. *Meteoritics* 8:330 (abstract).

Brecher, A., Briggs, P. L., and Simmons, G. 1975. The low-temperature electrical properties of carbonaceous meteorites. *Earth Planet. Sci. Lett.* 28:37–45.

Brett, R., and Keil, K. 1986. Enstatite chondrites and enstatite achondrites (aubrites) were not derived from the same parent body. *Earth Planet. Sci. Lett.* 81:1–6.

Buchwald, V. F. 1975. *Handbook of Iron Meteorites* (Berkeley: Univ. of California Press).

Bunch, T. E., and Chang, S. 1980. Carbonaceous chondrites—II. Carbonaceous chondrite phyllosilicates and light element geochemistry as indicators of parent body processes and surface conditions. *Geochim. Cosmochim. Acta* 44:1543–1577.

Bunch, T. E., and Stöffler, D. 1974. The Kelly chondrite: A parent body surface microbreccia. *Contrib. Mineral. Petrol.* 44:157–171.

Bunch, T. E., Keil, K., and Huss, G. I. 1972. The Landes meteorite. *Meteoritics* 1:31–38.

Caffee, M. W., Hohenberg, C. M., Swindle, T. D., and Goswami, J. N. 1987. Evidence in meteorites for an active early Sun. *Astrophys. J.* 313:L31–L35.

Carlslaw, H. S., and Jaeger, J. C. 1959. *Conduction of Heat in Solids* (London: Oxford Univ. Press).

Chapman, C. R. 1988. Compositional structure of the asteroid belt and its families. *Icarus*, submitted.

Chapman, C. R., Morrison, D., and Zellner, B. 1975. The surface properties of asteroids: A synthesis of polarimetry, radiometry, and spectrophotometry. *Icarus* 25:104–130.

Cintala, M. J., Head, J. W., and Veverka, J. 1978. Characteristics of the cratering process on small satellites and asteroids. *Proc. Lunar Planet. Sci. Conf.* 9:3803–3830.

Cintala, M. J., Head, J. W., and Wilson, L. 1979. The nature and effects of impact cratering on small bodies. In *Asteroids*, ed. T. Gehrels (Tucson: Univ. of Arizona Press), pp. 579–600.

Clayton, R. N., and Mayeda, T. K. 1984. The oxygen isotope record in Murchison and other carbonaceous chondrites. *Earth Planet. Sci. Lett.* 67:151–161.

Clayton, R. N., Mayeda, T. K., Olsen, E. J., and Prinz, M. 1983. Oxygen relationships in iron meteorites. *Earth Planet. Sci. Lett.* 65:229–232.

Crabb, J., and Schultz, L. 1981. Cosmic-ray exposure ages of the ordinary chondrites and their significance for parent body stratigraphy. *Geochim. Cosmochim. Acta* 45:2151–2160.

Davis, D. R., and Chapman, C. R. 1977. Collisional evolution of asteroid compositional classes. *Lunar Sci.* VIII:224–226.

Davis, D. R., Chapman, C. R., Weidenschilling, S. J., and Greenberg, R. 1985. Collisional history of asteroids: Evidence from Vesta and the Hirayama families. *Icarus* 62:30–53.

Delaney, J. S. 1986. Phase equilibria for basaltic achondrites and the basaltic achondrite plan-
    etoid. *Lunar Planet. Sci.* XVIII:164–167 (abstract).
Dence, M. R. 1971. Impact melts. *J. Geophys. Res.* 76:5552–5565.
Dodd, R. T. 1981. *Meteorites, A Petrologic-Chemical Synthesis.* (New York: Cambridge Univ.
    Press).
Drake, M. J. 1979. Geochemical evolution of the eucrite parent body: Possible nature and evolu-
    tion of asteroid 4 Vesta. In *Asteroids,* ed. T. Gehrels (Tucson: Univ. of Arizona Press), pp.
    765–782.
Duba, A. G., and Boland, J. N. 1984. High temperature electrical conductivity of the car-
    bonaceous chondrites Allende and Murchison. *Lunar Planet. Sci.* XV:232–233 (abstract).
DuFresne, E. R., and Anders, E. 1962. On the chemical evolution of the carbonaceous
    chondrites. *Geochim. Cosmochim. Acta* 26:1849–1862.
Edwards, S., Cabrit, S., Strom, S. E., Heyer, I., Strom, K. M., and Anderson, E. 1987. Forbid-
    den line and H alpha profiles in T Tauri star spectra: A probe of anisotropic mass outflows and
    circumstellar discs. *Astrophys. J.* 321:495–573.
Ehlmann, A. J., Scott, E. R. D., Keil, K., Mayeda, T. K., Clayton, R. N., Weber, H. W., and
    Schultz, L. 1988. Origin of fragmental and regolith meteorite breccias—evidence from the
    Kendleton L chondrite breccia. *Proc. Lunar Planet. Sci. Conf.* 19:545–554.
Evernden, J. F., and Verhoogen, J. 1956. Electrical resistivity of meteorites. *Nature* 178:106.
Fahey, A. J., Goswami, J. N., McKeegan, K. D., and Zinner, E. 1987a. ^{26}Al, ^{244}Pu, ^{50}Ti, REE,
    and trace element abundances in hibonite grains from CM and CV meteorites. *Geochim.
    Cosmochim. Acta* 51:329–350.
Fahey, A. J., Zinner, E. K., Crozaz, G., and Kornacki, A. S. 1987b. Microdistribution of Mg
    isotopes and REE abundances in a Type A calcium-aluminum-rich inclusion from Efremovka.
    Geochim. Cosmochim. Acta 51:3215–3229.
Fish, R. A., Goles, G. G., and Anders, E. 1960. The record in meteorites. III. On the develop-
    ment of meteorites in asteroidal bodies. *Astrophys. J.* 132:243–258.
Floran, R. J. 1978. Silicate petrography, classification, and origin of the mesosiderites: Review
    and new observations. *Proc. Lunar Planet. Sci.* 9:1053–1081.
Floran, R. J., Caulfield, J. B. D., Harlow, G. E., and Prinz, M. 1978. Impact-melt origin for the
    Simondium, Pinnaroo, and Hainholz mesosiderites: Implications for impact processes beyond
    the earth-moon system. *Proc. Lunar Planet. Sci.Conf.* 9:1084–1114.
Fodor, R. V., and Keil, K. 1975. Implications of poikilitic textures in LL-group chondrites.
    Meteoritics 10:325–340.
Fodor, R. V., and Keil, K. 1976. Carbonaceous and non-carbonaceous lithic fragments in the
    Plainview, Texas chondrite: Origin and history. *Geochim. Cosmochim. Acta* 48:177–189.
Fodor, R. V., and Keil, K. 1978. *Catalog of Lithic Fragments in LL-group Chondrites,* Spec.
    Publ. 19, Univ. of New Mexico Inst. of Meteoritics.
Fredriksson, K., and Kerridge, J. F. 1988. Carbonates and sulfates in CI chondrites: Formation by
    aqueous activity on the parent body. *Meteoritics* 23:35–44.
Fujimura, A., Kato, M., and Kumazawa, M. 1982. Preferred orientation of phyllosilicates in
    Yamato-74642 and -74662 in relation to the deformation of C2 chondrites. In *Proc. Seventh
    Symp. Antarctic Meteorites,* ed. K. Yanai (Tokyo: Natl. Inst. of Polar Research), pp. 207–
    215.
Fujimura, A., Kato, M., and Kumazawa, M. 1983. Preferred orientation of phyllosilicate [001]
    in matrix of Murchison meteorite and possible mechanisms of generating the oriented texture
    in chondrules. *Earth Planet. Sci. Lett.* 66:25–32.
Gaffey, M. J. 1976. Spectral reflectance characteristics of the meteorite classes. *J. Geophys. Res.*
    81:905–920.
Gaffey, M. J. 1984. Rotational spectral variations of asteroid (8) Flora: Implications for the nature
    of the S-type asteroids and for the parent bodies of the ordinary chondrites. *Icarus* 60:83–
    114.
Gooding, J. L. 1984. Aqueous alteration on meteorite parent bodies: Possible role of "unfrozen"
    water and the Antarctic meteorite analogy. *Meteoritics* 19:228–229 (abstract).
Goodrich, C. A., Jones, J. H., and Berkley, J. L. 1987. Origin and evolution of the ureilite parent
    magmas: Multi-stage igneous activity on a large parent body. *Geochim. Cosmochim. Acta*
    51:2255–2273.
Goswami, J. N., and Macdougall, J. D. 1983. Nuclear track and compositional studies of olivines

in CI and CM chondrites *Proc. Lunar Planet. Sci. Conf.* 13, *J. Geophys. Res. Suppl.* 88:A755–A764.

Grady, M. M., Graham, A. L., Barber, D. J., Aylmer, D., Kurat, G., Ntaflos, T., Ott, U., Palme, H., and Spettel, B. 1987. Yamato-82042: An unusual carbonaceous chondrite with CM affinities. In *Proc. Eleventh Symp. Antarctic Meteorites*, ed. K. Yanai (Tokyo: Natl. Inst. of Polar Research), pp. 162–178.

Greenberg, R., and Chapman, C. R. 1984. Asteroids and meteorites: Origins of stony-iron meteorites at mantle-core boundaries. *Icarus* 57:267–279.

Grimm, R. E. 1985. Penecontemporaneous metamorphism, fragmentation, and reassembly of ordinary chondrite parent bodies. *J. Geophys. Res.* 90:2022–2028.

Grossman, L., and Larimer, J. W. 1974. Early chemical history of the solar system. *Rev. Geophys. Space Phys.* 12:71–101.

Hartmann, W. K. 1978. Planet formation: Mechanisms of early growth. *Icarus* 33:50–61.

Hartmann, W. K. 1979. Diverse puzzling asteroids and a possible unified explanation. In *Asteroids*, ed. T. Gehrels (Tucson: Univ. of Arizona Press), pp. 466–479.

Hayatsu, R., and Anders, E. 1981. Organic compounds in meteorites and their origins. In *Cosmo- and Geochemistry*, vol. 99, *Topics in Current Chemistry* (Berlin: Springer-Verlag), pp. 1–37.

Herbert, F. 1989. Primordial electrical induction heating of asteroids. *Icarus*, in press.

Herbert, F., and Sonett, C. P. 1978. Primordial metamorphism of asteroids via electric induction in a T Tauri-like solar wind. *Astrophys. Space Sci.* 55:227–239.

Herbert, F., and Sonett, C. P. 1979. Electromagnetic heating of minor planets in the early solar system. *Icarus* 40:484–496.

Herbert, F., and Sonett, C. P. 1980. Electromagnetic inductive heating of the asteroids and moon as evidence bearing on the primordial solar wind. In *The Ancient Sun: Fossil Record in the Earth, Moon and Meteorites*, eds. R. O. Pepin, J. A. Eddy, and R. B. Merrill (New York: Pergamon Press), pp. 563–576.

Herbig, G. H. 1977. Eruptive phenomena in early stellar evolution. *Astrophys. J.* 217:693–715.

Hewins, R. H., and Newsom, H. E. 1988. Igneous activity in the early solar system. In *Meteorites and the Early Solar System*, eds. J. F. Kerridge and M. S. Matthews (Tucson: Univ. of Arizona Press), pp. 73–101.

Heymann, D. 1967. On the origin of hypersthene chondrites: Ages and shock effects of black chondrites. *Icarus* 6:189–221.

Hinton, R. W., and Bischoff, A. 1984. Ion microprobe magnesium isotope analysis of plagioclase and hibonite from ordinary chondrites. *Nature* 308:169–172.

Hörz, F., and Schaal, R. 1981. Asteroidal agglutinate formation and implications for asteroidal surfaces. *Icarus* 46:337–353.

Hörz, F., Ostertag, R., and Rainey, D. A. 1983. Bunte breccia of the Ries: Continuous deposits of large impact craters. *Rev. Geophys. Space Phys.* 21:1667–1725.

Housen, K. R., Wilkening, L. L., Chapman, C. R., and Greenberg, R. J. 1979. Asteroid regoliths. *Icarus* 39:317–351.

Hutcheon, I. D. 1982. Ion probe magnesium isotopic measurements of Allende inclusions. In *Nuclear and Chemical Dating Techniques: Interpreting the Environmental Record*, ed. L. A. Currie (Washington, DC: Amer. Chem. Soc.), pp. 95–128.

Hutcheon, I. D., Steele, I. M., Smith, J. V., and Clayton, R. N. 1978. Ion microprobe, electron microprobe and cathodoluminescence data for Allende inclusions with emphasis on plagioclase chemistry. *Proc. Lunar Planet. Sci. Conf.* 9:1345–1368.

Irvine, T. N. 1970. Heat transfer during solidification of layered intrusions. I. Sheets and sills. *Canadian J. Earth Sci.* 7:1031–1061.

Irvine, T. N. 1979. Rocks whose composition is determined by crystal accumulation and sorting. In *The Evolution of the Igneous Rocks: Fiftieth Anniversary Perspectives*, ed. H. S. Yoder, Jr. (Princeton: Princeton Univ. Press), pp. 244–306.

Jones, J. H., and Drake, M. J. 1983. Experimental investigations of trace element fractionation in iron meteorites. II: The influence of sulfur. *Geochim. Cosmochim. Acta* 47:1199–1209.

Jones, T. D., Lebofsky, L. A., and Lewis, J. S. 1988. The 3-μm hydrated silicate signature on C class asteroids: Implications for the origins of outer belt asteroids. *Lunar Planet. Sci.* XIX:567–568 (abstract).

Kaula, W. M. 1968. *An Introduction to Planetary Physics* (New York: Wiley).

Keil, K. 1968. Mineralogical and chemical relationships among enstatite chondrites. *J. Geophys. Res.* 73:6945–6976.

Keil, K. 1982. Composition and origin of chondritic breccias. In *Lunar Breccias and Soils and Their Meteoritic Analogs,* eds. G. J. Taylor and L. L. Wilkening, LPI Tech. Rept. 82-02, (Houston: Lunar and Planetary Inst.) pp. 65–83.

Keil, K. 1988. Enstatite meteorites and their parent bodies. *Meteoritics* 23:278–279 (abstract).

Keller, L. P., and Buseck, P. R. 1988. HRTEM study of the matrix mineralogy of the Lance CO(3) chondrite. *Lunar Planet. Sci.* XIX:595–596 (abstract).

Kerridge, J. F., and Bunch, T. E. 1979. Aqueous activity on asteroids: Evidence from carbonaceous meteorites. In *Asteroids,* ed. T. Gehrels (Tucson: Univ. of Arizona Press), pp. 745–764.

Kracher, A. 1985. The evolution of partially differentiated planetesimals: Evidence from iron meteorite groups IAB and IIICD. *Proc. Lunar Planet. Sci. Conf.* 15, *J. Geophys. Res. Suppl.* 90:C689–C698.

Kuhi, L. V. 1964. Mass loss from T Tauri stars. *Astrophys. J.* 140:1409–1433.

Kurat, G., Fredriksson, K., and Nelen, J. 1969. Der Meteorit von Siena. *Geochim. Cosmochim. Acta* 33:765–773.

Lada, C. J. 1985. Cold outflows, energetic winds, and enigmatic jets around young stellar objects. *Ann. Rev. Astron. Astrophys.* 23:267–317.

Lada, C. J. 1988. On the importance of outflows for molecular clouds and star formation. In *Galactic and Extragalactic Star Formation,* eds. R. E. Pudritz and M. Fich (Dordrecht: Kluwer Academic Publ.), pp. 5–24.

Lange, M. A., Lambert, P., and Ahrens, T. J. 1985. Shock effects on hydrous minerals and implications for carbonaceous meteorites. *Geochim. Cosmochim. Acta* 49:1715–1726.

Larson, H. P., and Veeder, G. J. 1979. Infrared spectral reflectances of asteroid surfaces. In *Asteroids,* ed. T. Gehrels (Tucson: Univ. of Arizona Press), pp. 724–744.

Lebofsky, L. A. 1978. Asteroid 1 Ceres: Evidence for water of hydration. *Mon. Not. Roy. Astron. Soc.* 182:17P–21P.

Lebofsky, L. A., Jones, T. D., and Herbert, F. 1988. Asteroid volatile inventories. In *Origin and Evolution of Planetary and Satellite Atmospheres,* eds. S. K. Atreya, J. B. Pollack and M. S. Matthews (Tucson: Univ. of Arizona Press), pp. 192–229.

Lee, T., Papanastassiou, D. A., and Wasserburg, G. J. 1977. Aluminum-26 in the early solar system: Fossil or fuel? *Astrophys. J. Lett.* 211:L107–L110.

Lewis, R. S., and Anders, E. 1975. Condensation time of the solar nebula from extinct [129]I in primitive meteorites. *Proc. Natl. Acad. Sci. U.S.* 72:268–273.

Macdougall, J. D., and Kothari, B. K. 1976. Formation chronology for C2 meteorites. *Earth Planet. Sci. Lett.* 33:36–44.

Macdougall, J. D., Lugmair, G. W., and Kerridge, J. F. 1984. Early solar system aqueous activity: Sr isotope evidence from the Orgueil CI meteorite. *Nature* 307:249–251.

Malvin, D. J. 1988. Assimilation-fractional crystallization modeling of magmatic iron meteorites. *Lunar Planet. Sci.* 19:720–721.

Mason, B., and Wiik, H. B. 1964. The amphoterites and meteorites of similar composition. *Geochim. Cosmochim. Acta* 28:533–538.

McCord, T. B., and Gaffey, M. J. 1974. Asteroids: Surface composition from reflectance spectroscopy. *Science* 185:352–355.

McSween, H. Y., Jr. 1977. Carbonaceous chondrites of the Ornans type: A metamorphic sequence. *Geochim. Cosmochim. Acta* 41:477–491.

McSween, H. Y., Jr. 1979. Are carbonaceous chondrites primitive or processed?—A review. *Rev. Geophys. Space Phys.* 17:1059–1078.

McSween, H. Y., Jr., and Richardson, S. M. 1977. The composition of carbonaceous chondrite matrix. *Geochim. Cosmochim. Acta* 41:1145–1161.

Mittlefehldt, D. W. 1979. The nature of asteroidal differentiation processes: Implications for primordial heat sources. *Proc. Lunar Planet, Sci. Conf.* 10:1975–1993.

Narayan, C., and Goldstein, J. I. 1982. A dendritic solidification model to explain Ge-Ni variations in iron meteorite groups. *Geochim. Cosmochim. Acta* 46:259–268.

Newsom, H. E. 1985. Molybdenum in eucrites: Evidence for a metal core in the eucrite parent body. *Proc. Lunar Planet. Sci. Conf.* 15, *J. Geophys. Res. Suppl.* 90:C613–C617.

O'Hara, M. J. 1977. Geochemical evolution during fractional crystallization of a periodically refilled magma chamber. *Nature* 266:503–507.

Okada, A., Keil, K., Taylor, G. J., and Newsom, H. E. 1988. Igneous history of the aubrite parent asteroid: Evidence from the Norton County enstatite achondrite. *Meteoritics* 23:59–74.

O'Keefe, J. D., and Ahrens, T. J. 1977. Meteorite impact ejecta: Dependence of mass and energy lost on planetary escape velocity. *Science* 198:1249–1251.

Papanastassiou, D. A., Wasserburg, G. J., and Marvin, U. B. 1984. Absence of excess ^{26}Mg in anorthite from the Vaca Muerta mesosiderite. *Meteoritics* 19:289–290 (abstract).

Parkhomenko, E. I. 1967. *Electrical Properties of Rocks*, ed. and tr. G. V. Keller (New York: Plenum Press).

Prinn, R. G., and Fegley, B. J. 1987. The atmospheres of Venus, Earth and Mars: A critical comparison. *Ann. Rev. Earth Planet. Sci.* 15:171–212.

Prinz, M., Nehru, C. E., Delaney, J. S., Weisberg, M., and Olsen, E. 1983. Globular silicate inclusions in IIE irons and Sombrerete: Highly fractionated minimum melts. *Lunar Planet. Sci.* 14:618–619 (abstract).

Prinz, M., Weisberg, M. K., Nehru, C. E., and Delaney, J. S. 1987. Black inclusions in carbonaceous chondritic matrix in polymict ureilites. *Meteoritics* 22:482–483 (abstract).

Richardson, S. M. 1978. Vein formation in the CI carbonaceous chondrites. *Meteoritics* 13:141–159.

Rietmeijer, F. J. M. 1985. A model for diagenesis in proto-planetary bodies. *Nature* 313:293–294.

Rubin, A. E. 1984. The Blithfield meteorite and the origin of sulfide-rich, metal-poor clasts and inclusions in brecciated enstatite chondrites. *Earth Planet. Sci. Lett.* 67:273–283.

Rubin, A. E. 1985. Impact melt products of chondritic material. *Rev. Geophys.* 23:277–300.

Rubin, A. E., Rehfeldt, A., Petterson, E., Keil, K., and Jarosewich, E. 1983. Fragmental breccias and the collisional evolution of ordinary chondrite parent bodies. *Meteoritics* 18:179–196.

Ryerson, F. J., Weed, H. C., and Piwinskii, A. J. 1988. Rheology of subliquidus magmas 1. Picritic compositions. *J. Geophys. Res.* 93:3421–3436.

Schramm, D. N., Tera, F., and Wasserburg, G. J. 1970. The isotopic abundance of ^{26}Mg and limits on ^{26}Al in the early solar system. *Earth Planet. Sci. Lett.* 10:44–59.

Schwerer, F. C., Nagata, T., and Fisher, R. M. 1971. Electrical conductivity of lunar surface rocks and chondritic meteorites. *The Moon* 2:408–422.

Scott, E. R. D. 1977. Formation of olivine-metal textures in pallasite meteorites. *Geochim. Cosmochim. Acta* 41:693–710.

Scott, E. R. D. 1979. Origin of iron meteorites. In *Asteroids*, ed. T. Gehrels (Tucson: Univ. of Arizona Press), pp. 892–925.

Scott, E. R. D. 1984. Origins of stony-iron meteorites. *Nature* 311:708.

Scott, E. R. D., and Rajan, R. S. 1981. Metallic minerals, thermal histories, and parent bodies of some xenolithic, ordinary chondrites. *Geochim. Cosmochim. Acta* 45:53–67.

Scott, E. R. D., and Taylor, G. J. 1985. Petrology of types 4–6 carbonaceous chondrites. *Proc. Lunar Planet. Sci. Conf.* 15, *J. Geophys. Res. Suppl.* 90:C699–C709.

Scott, E. R. D., Lusby, D., and Keil, K. 1985. Ubiquitous brecciation after metamorphism in equilibrated ordinary chondrites. *Proc. Lunar Planet. Sci. Conf.* 15, *J. Geophys. Res. Suppl.* 90:D137–D148.

Scott, E. R. D., Maggiore, P., Taylor, G. J., Keil, K., and Szuwalski, D. 1986. Chondritic impact melts and cratering processes on asteroids. *Lunar Planet. Sci.* 17:785–786 (abstract).

Sears, D. W. G., and Hasan, F. A. 1987. The type 3 ordinary chondrites: A review. *Surv. Geophys.* 9:43–97.

Shu, F. H., Lizano, S., Ruden, S. P., and Najita, J. 1988. Mass loss from rapidly-rotating magnetic protostars. *Astrophys. J.* 328:L19–L23.

Skinner, B. J., and Luce, F. D. 1971. Solid solutions of the type (Ca, Mg, Mn, Fe)S and their use as geothermometers for the enstatite chondrites. *Amer. Mineral.* 56:1269–1296.

Smith, B. A., and Goldstein, J. I. 1977. The metallic microstructure and thermal histories of severely reheated chondrites. *Geochim. Cosmochim. Acta* 41:1061–1072.

Smith, M. R. 1982. A Chemical and Petrologic Study of Igneous Lithic Clasts from the Kapoeta Howardite. Ph.D. Thesis, Oregon State Univ.

Sonett, C. P., Colburn, D. S., and Schwartz, K. 1968. Electrical heating of meteorite parent bodies and planets by dynamo induction from a pre-main sequence T Tauri "solar wind." *Nature* 219:924–926.

Sonett, C. P., Colburn, D. S., Schwartz, K., and Keil, K. 1970. The melting of asteroidal-sized

bodies by unipolar dynamo induction from a primordial T Tauri sun. *Astrophys. Space Sci.* 7:446–488.

Spudis, P. D. 1984. Apollo 16 site geology and impact melts: Implications for the geologic history of the lunar highlands. *Proc. Lunar Planet. Sci. Conf.* 15, *J. Geophys. Res. Suppl.* 89:C95–C107.

Stöffler, D. 1982. Terrestrial impact breccias. In *Lunar Breccias and Soils and Their Meteoritic Analogs,* eds. G. J. Taylor and L. L. Wilkening, LPI Tech. Rept. 82–02, (Houston: Lunar and Planetary Inst.), pp. 139–146.

Stöffler, D., Knöll, H.-D., and Maerz, U. 1979. Terrestrial and lunar impact breccias and the classification of lunar highland rocks. *Proc. Lunar Planet. Sci. Conf.* 10:639–675.

Stöffler, D., Knöll, H.-D., Marvin, U. B., Simonds, C. H., and Warren, P. H. 1980. Recommended classification and nomenclature of lunar highland rocks: A committee report. *Proc. Conf. Lunar Highlands Crust,* eds. J. J. Papike and R. B. Merrill (New York: Pergamon Press), pp. 51–70.

Stöffler, D., Bischoff, A., Buchwald, V., and Rubin, A. E. 1988. Shock effects in meteorites. In *Meteorites and the Early Solar System,* eds. J. F. Kerridge and M. S. Matthews (Tucson: Univ. of Arizona Press), pp. 165–202.

Sugiura, N., and Strangway, D. W. 1983. Magnetic anisotropy and porosity of chondrites. *Geophys. Res. Lett.* 10:83–86.

Takahashi, E. 1983. Melting of a Yamato L-3 chondrite (Y-74191) up to 30 kbar. In *Proc. Eighth Symp. Antarctic Meteorites* (Tokyo: Natl. Inst. of Polar Research), pp. 168–180.

Taylor, G. J. 1982. Petrologic comparison of lunar and meteoritic breccias. In *Lunar Breccias and Soils and Their Meteoritic Analogs,* eds. G. J. Taylor and L. L. Wilkening, LPI Tech. Rept. 82-02, (Houston: Lunar and Planetary Inst.), pp. 153–167.

Taylor, G. J. 1989. Metal segregation in asteroids. *Lunar Planet. Sci.* XX:1109–1110 (abstract).

Taylor, G. J., and Heymann, D. 1969. Shock, reheating and the gas retention ages of chondrites. *Earth Planet, Sci. Lett.* 7:151–161.

Taylor, G. J., and Heymann, D. 1971. Post shock thermal histories of reheated chondrites. *J. Geophys. Res.* 76:1879–1893.

Taylor, G. J., Keil, K., Berkley, J. L., Lange, P. E., Fodor, R. V., and Fruland, R. M. 1979. The Shaw meteorite: History of a chondrite consisting of impact-melted and metamorphic lithologies. *Geochim. Cosmochim. Acta* 43:323–337.

Taylor, G. J., Maggiore, P., Scott, E. R. D., Rubin, A. E., and Keil, K. 1987. Original structures and fragmentation and reassembly histories of asteroids: Evidence from meteorites. *Icarus* 69:1–13.

Taylor, G. J., Keil, K., Newsom, H. E., and Okada, A. 1988. Magmatism and impact on the aubrite parent body: Evidence from the Norton County enstatite achondrite. *Lunar Planet. Sci.* 19:1185–1186 (abstract).

Tomeoka, K., and Buseck, P. R. 1988. Matrix mineralogy of the Orgueil CI carbonaceous chondrite. *Geochim. Cosmochim. Acta* 52:1627–1640.

Ugolini, F. C., and Anderson, D. M. 1972. Ionic migration in frozen Antarctic soils. *Antarctic J. U.S.* 7:112–113.

Urey, H. C. 1955.The cosmic abundances of potassium, uranium and thorium and the heat balances of the Earth, the Moon, and Mars. *Proc. Natl. Acad. Sci. U.S.* 41:127.

Van Schmus, W. R. 1969. Mineralogy, petrology, and classification of types 3 and 4 carbonaceous chondrites. In *Meteorite Research,* ed. P. M. Millman (New York: Springer-Verlag), pp. 480–491.

Walker, D., and Agee, C. B. 1988. Ureilite compaction. *Meteoritics* 23:81–91.

Walker, D., Stolper, E. M., and Hays, J. F. 1978. A numerical treatment of melt/solid segregation: Size of the eucrite parent body and stability of the terrestrial low-velocity zone. *J. Geophys. Res.* 83:6005–6013.

Walker, D., Stolper, E. M., and Hays, J. F. 1979. Basaltic volcanism: The importance of planet size. *Proc. Lunar Planet Sci. Conf.* 10:1995–2015.

Walker, G. P. 1973. Lengths of lava flows. *Phil. Trans. Roy. Soc. London* A274:107–118.

Wasson, J. T. 1985. *Meteorites: Their Record of Early Solar-System History.* (New York: W. H. Freeman and Co.).

Wasson, J. T., and Rubin, A. E. 1985. Formation of mesosiderites by low-velocity impacts as a natural consequence of planet formation. *Nature* 318:168–170.

Wasson, J. T., and Wang, J. 1986. A nonmagmatic origin of group-IIE iron meteorites. *Geochim. Cosmochim. Acta* 50:725–732.

Wasson, J. T., and Wetherill, G. W. 1979. Dynamical, chemical and isotopic evidence regarding the formation locations of asteroids and meteorites. In *Asteroids*, ed. T. Gehrels (Tucson: Univ. of Arizona Press), pp. 926–974.

Wasson, J. T., Rubin, A. E., and Benz, W. 1987. Heating of primitive, asteroid-size bodies by large impacts. *Meteoritics* 22:525–526 (abstract).

Weidenschilling, S. J. 1978. A constraint on pre-main-sequence mass loss. *Moon and Planets* 19:279–287.

Whitford-Stark, J. L. 1982. Factors influencing the morphology of volcanic landforms: An Earth-Moon comparison. *Earth Sci. Rev.* 18:109–168.

Wilkening, L. L. 1977. Meteorites in meteorites: Evidence for mixing among the asteroids. In *Comets, Asteroids, Meteorites: Interrelations, Evolution and Origins*, ed. A. H. Delsemme (Toledo: Univ. of Toledo Press), pp. 389–396.

Wilson, L., and Head, J. W., III. 1983. A comparison of volcanic eruption processes on Earth, Moon, Mars, Io, and Venus. *Nature* 302:663–669.

Wilson, L., and Head, J. W., III. 1988. The influence of gravity on planetary volcanic eruption rates. *Lunar Planet. Sci.* XIX:1283–1284 (abstract).

Wood, J. A. 1979. Review of the metallographic cooling rates of meteorites and a new model for the planetesimals in which they formed. In *Asteroids*, ed. T. Gehrels (Tucson: Univ. of Arizona Press), pp. 849–891.

Wood, J. A., and Hashimoto, A. 1988. The condensation sequence under non-classic conditions ($P < 10^{-3}$ atm, non-cosmic compositions). *Lunar Planet. Sci.* XIX:1292–1293 (abstract).

Yomogida, K., and Matsui, T. 1982. Physical properties of some unequilibrated Antarctic ordinary chondrites. In *Proc. Seventh Symp. Antarctic Meteorites* (Tokyo: Natl. Inst. of Polar Research), pp. 308–318.

Zellner, B., and Bowell, E. 1977. Asteroid compositional types and their distributions. In *Comets, Asteroids, Meteorites: Interrelations, Evolution and Origins*, ed. A. H. Delsemme (Toledo: Univ. of Toledo Press), pp. 185–197.

Zolensky, M. E. 1984. Hydrothermal alteration of CM carbonaceous chondrites: Implications of the identification of tochilinite as one type of meteoritic PCP. *Meteoritics* 19:346–347 (abstract).

Zolensky, M. E., and Barrett, R. A. 1988. EET 83334: A CM1 chondrite with probable compaction textures. *Meteoritics* 23:314–315 (abstract).

Zolensky, M. E., and McSween, H. Y., Jr. 1988. Aqueous alteration. In *Meteorites and the Early Solar System*, eds. J. F. Kerridge and M. S. Matthews (Tucson: Univ. Arizona Press), pp. 114–143.

Zolensky, M. E., Gooding, G. L., and Bourcier, W. L. 1989. Aqueous alteration on hydrous asteroids: Results of computer simulations. *Icarus* 78, in press.

Zook, H. A., and McKay, D. S. 1986. On the asteroidal component of cosmic dust. *Lunar Planet. Sci.* XVII:977–978 (abstract).

METEORITIC PARENT BODIES: NATURE, NUMBER, SIZE AND RELATION TO PRESENT-DAY ASTEROIDS

MICHAEL E. LIPSCHUTZ
Purdue University

MICHAEL J. GAFFEY
Rensselaer Polytechnic Institute

and

PAUL PELLAS
Muséum National d'Histoire Naturelle

Data from meteorites provide strong constraints on the properties of their asteroidal parent bodies. Meteorites derive from a small number of parent bodies relative to the number of asteroids and their parent bodies seem to have been in the 100-km size range as determined by three chronometers of early cooling histories. The data relative to the internal structures of their parents can be interpreted in a variety of contradictory ways. Antarctica has proven to be a rich source of meteorites that mainly fell 0.1 to 1 Myr ago. The Antarctic meteorite population differs in many ways from the population of current falls. These differences lead to the highly controversial suggestion that the meteoroid flux sampled by Earth has varied on the Myr time scale, a suggestion that must be tested further. The spectral reflectance properties of meteorites and asteroid surfaces are similar in some cases, giving us confidence in our estimate of the nature of the surfaces of these asteroids. However, there is a major problem in the case of the most abundant meteorites, the ordinary chondrites and similar inclusions in meteorite breccias. Their spectral properties differ from those of the abundant S asteroids and no process is known that can reconcile these. Their closest spectral analogues are the rare near-Earth Q type asteroids. This leads to the uncomfortable question of why abundant meteorites have rare asteroidal

analogues and abundant asteroids have rare meteoritic analogues. These questions are clearly prime ones for study in the foreseeable future.

I. GENERAL METEORITE SOURCES

Before the manned Apollo missions, many researchers thought that meteorites come from the Moon, Apollo-Amor asteroids or degassed comets (Wetherill and Williams 1969 and references therein) since attempts to establish an asteroidal belt origin by orbital dynamics calculations were unsuccessful (Wetherill 1969). Other researchers continued to believe in an asteroidal belt origin for most meteorites (see, e.g., Anders 1964). In the past two decades, the evidence strongly favors an asteroidal (including Apollo-Amor objects) origin. While our picture of meteorite origin has clarified somewhat, it still presents many contradictory aspects and is the subject of much controversy.

The existence of lunar material on the Earth, returned by the Apollo and Luna programs, permits unambiguous identification of the lunar origin of six Antarctic meteorite samples (see, e.g., Dennison et al. 1987 and references therein). These six samples (one of which was recovered by the United States, the others by Japan) apparently originated from at least three separate large-scale impacts on the Moon (Dennison et al. 1987) but the location of these impacts, near- or far-side, is a matter of debate. Based in part on data from the Viking landers, the nine shergottites, nakhlites and the unique Chassigny (i.e., SNC) meteorites may well come from Mars (see Laul et al. 1986 and references therein) although there are difficulties in some cases (Ott and Begemann 1985; Vickery and Melosh 1987).

Carbonaceous chondrites have been suggested to be of cometary origin (Heymann 1978). However, some of these meteorites show evidence for effects of liquid water, which could not long survive on the surface of a cometary nucleus (McSween 1979). Moreover, a few highly unequilibrated ordinary chondrites, which are probably not of cometary origin, show evidence for the effects of liquid water (Hutchison et al. 1987; cf. chapter by Lebofsky and Spencer). Some interplanetary dust particles may have a cometary origin (Brownlee 1985) and a significant component of these and of the dust from Comet Halley have bulk carbon and nitrogen contents significantly higher than do the known chondrites (Brownlee et al. 1987). Hence, a meteorite-comet link is very doubtful. The distinction between extinct cometary nuclei and asteroids, however, is not always sharp (see the chapter by Weissman et al.).

The general asteroid-meteorite link is not debated because of direct orbital and spectral observations and a large body of indirect evidence. Three chondrites, Pribram (H5), Lost City (H5) and Innisfree (LL5), were photographed during fall (in 1959, 1970 and 1977, respectively) by camera networks so that their preterrestrial orbits and fall locations could be deter-

mined. The aphelion of each meteorite's orbit lay in the asteroid belt and the specimen, after recovery, appeared to be a normal member of its chemical-petrologic group. The other direct meteorite-asteroid link lies in the qualitative overall similarity between spectral reflectances of some meteorites and asteroid surfaces (Chapman 1977). This relationship is discussed in more detail below (Sec. III; also see the chapter by Gaffey et al.).

A decade after the first Asteroids volume (Gehrels 1979), some general conclusions concerning the asteroidal parents of meteorites can be made from indirect evidence.

1. Main-belt asteroids might be sources for many meteorite classes since mechanisms have been proposed allowing orbits of collisional debris to become Earth-crossing (Wetherill 1985).
2. From spectroscopic evidence, ordinary chondrite parent bodies are very rare or even absent in the asteroid belt (Gaffey and McCord 1977; McCord 1978; Bell 1987).
3. Ordinary chondrites could derive from Apollo-Amor asteroids if some mechanism can be devised to replenish the supply of these asteroids (Gaffey and McCord 1977; Chapman 1977; Wetherill 1977; McFadden et al. 1985; chapter by Bell et al.).
4. The very long cosmic-ray exposure ages of irons strongly indicate an asteroidal source (Wetherill 1977).
5. Cometary origins can be ruled out for all classes of stones that have gas-rich members (Anders 1978).
6. Solar-wind gases in gas-rich meteorites (regolith breccias) suggest that gas implantation took place between 1 and 8 AU from the Sun, in a region where the cratering rate was 10^2 to 10^3 times higher that at 1 AU (Anders 1978). The most recent data, for Fayetteville, indicate solar-wind implantation at 2 to 3 AU.

Wilkening (1977) and Anders (1978) noted that exotic inclusions ("xenoliths") trapped in meteoritic breccias were predominantly carbonaceous ($\sim$75%), while ordinary chondrites and related types made up $\sim$20%, in good agreement with the abundances of C and S type asteroids in the main belt. (However, the identification of S type asteroids as ordinary chondrite parents has been controversial and, as discussed later, Q type asteroids may be their parent.) This last observation is of great importance since it might be thought that abundances of asteroidal types would parallel abundances of meteorite types or collisional debris found as xenoliths in meteoritic breccias. Some evidence discussed later (Sec. III), however, suggests that this could not be so. Excellent reviews, now a decade old, have been given by Anders (1978) and Wasson and Wetherill (1979).

The Number of Meteorite Parent Bodies

The work of Clayton and coworkers (see, e.g., Clayton and Mayeda 1978) on oxygen isotopic signatures, and chemical distinctions between mete-

orite classes lead to a very conservative number of >20 different parent bodies for stony meteorites. Since different bodies can derive from the same nebular oxygen reservoir and share the same oxygen isotopic fingerprint (the Moon, enstatite E chondrites, aubrites and the unique Angra dos Reis achondrite lie on the terrestrial fractionation line), the number is probably much larger. There are 13 main groups of iron meteorites and ~50 smaller groups (Buchwald 1975; Wasson and Wetherill 1979). If these and a possible connection between irons and achondrites are taken into account, 60 to 70 different bodies are presently sampled in the world's collections. Antarctic meteorites might increase this number somewhat. Even if increased, the number of meteorite parent bodies is small compared with the number of known asteroids. On this basis alone, it seems likely that meteorites recovered on Earth are a biased sample of asteroidal objects.

The discrepancy between the most abundant meteorites, ordinary chondrites (i.e., H, L. and LL chondrites), which constitute 73% of observed falls, and their presumptive asteroid parents led to the suggestion that the current preponderance of ordinary chondrites captured by the Earth could be a very specific characteristic of the last Myr. Difficulties with this view were apparent even a decade ago.

Parents of Discrete Meteorites. Ordinary chondrites derive from at least 3 different bodies, each having its own chemical and oxygen isotopic signatures. This minimum number of parents is also confirmed by specific characteristics pertaining to each body.

 i. The H chondrites exhibit an 8 Myr cosmic-ray exposure age peak (Anders 1964; Crabb and Schultz 1981) although this peak is broad and may be complex.
 ii. Two-thirds of the L chondrites seem to have been outgassed in a massive disruptive collision around 500 Myr ago (Anders 1964; Heymann 1967).
iii. The LL chondrites exhibit a high percentage (~62%) of breccias (Binns 1967).

It seems unlikely that the special circumstances that "turned on" the ordinary chondrite flux would simultaneously affect debris from 3 spatially separated bodies of a very rare asteroid class, yet would spare debris from the more common classes.

Parents of Meteoritic Inclusions. Ordinary chondrite regolithic breccias may contain xenoliths, some of which are more or less outgassed of radiogenic gases (^{4}He, ^{40}Ar). This outgassing probably occurred because xenoliths correspond to projectile debris captured on asteroid surfaces. The survival of such exotic clasts indicates low relative velocities between the regolithic targets and collisional debris that makes up the projectiles (Wilkening 1977; Anders 1978; Wasson and Wetherill 1979). The largest abundance of these xenoliths are reported to be carbonaceous chondrites (mostly CM2).

Anders (1978) and Wasson and Wetherill (1979) considered that 23 of 27 (~85%) of these exotic clasts resembled carbonaceous chondrites. Since as many as 15% of the xenoliths were related to ordinary chondrites, the near absence of possible ordinary chondrite parent bodies in the main belt, inferred from spectral data, is peculiar. It would be strange indeed if no asteroidal counterparts of such collisional debris exist at their supposed source locations.

A decade later, many additional xenoliths have been detected in meteoritic surficial breccias. These xenoliths have been identified as ordinary chondrite-like by their distinctive mineralogy and petrology or by oxygen isotope

TABLE I
Foreign Ordinary Chondrite Type Clasts
in Meteorite Breccias

Host Meteorite (and Class)	Clast Type[a]
I. *From oxygen isotopic composition*	
ALHA 77015 (L3)	(H)
ALHA 76004 (LL3)	(H)(Chond.)
ALH 76005 (Polymict Eucrite)	(Chond.)
BARWELL (L5-6)	(H)
BOVEDY (L4)	(H)
BENCUBBIN (Mesosiderite)	(Chond.)
CUMBERLAND FALLS	(Chond.)
(Aubrite)	LL5
DIMMIT (H4-H5)	(Chond.)
EET 83309 (Ureilite)	L
FAYETTEVILLE (H3-H6)	(LL)
GUIN (Anom. Iron)	H
PLAINVIEW (H5)	EH or EL
ROOSEVELT CO. (L5)	H6
ST. MESMIN (LL4-6)	H
Y-75097 (L6)	(H)
Y-793241 (L6)	(H)
Y-790448 (LL3)	
II. *From chemistry and/or mineralogy*	
ALHA 78113 (Aubrite)	(Chond.)
CABEZO DE MAYO (L6)	(LL)
KAIDUN (C2V)	(EH or EL)
KAPOETA (Howardite)	(H)
NGAWI (LL3)	(H)
NILPENA (Ureilite)	(Chond.)
PARAGOULD (LL5)	(L)
ROMERO (H4)	(Chond.)
ROOSEVELT CO. (L5)	(H)
SUPUHEE (H6)	(E)
WASHOUGAL (Howardite)	(L)

[a]This assignment is to the meteorite type that the clast most resembles. It may be that the clast does not correspond to any known sort of meteorite.

TABLE II
Foreign Chondritic Clasts or Xenoliths in Meteorite Breccias

Meteorites		Asteroids	
Xenolith Type[a]	Number	Spectral Type	Percent
Anders (1978)			
Carbonaceous	20 (75%)	C	~55
Ord. chondrite	5 (20%)	S[b]	~40
Enst. achond.	2 (5%)	E	~1
This work			
Carbonaceous	≳40 (≥60%)	C	~60[c]
Ord. chondrite	24 (~36%)	S[b]	~25[c]
Enstatite	3 (~4%)	E	(very rare)[c]
Metal-rich	— —	M	~10[c]

[a]Classification is to the meteoritic type that the clast most resembles. It may be that clasts differ from known sorts of meteorites.
[b]For this purpose, S asteroids were assumed to be ordinary chondrite assemblages. See text for a discussion of this issue.
[c]From 2.5 to 3.0 AU (Gradie and Tedesco 1981).

measurements of Clayton and coworkers. Table I gives an up-to-date listing of noncarbonaceous chondrite, exotic clasts found in meteoritic breccias: 17 are ordinary chondrite-like, 8 others are of ordinary chondrite parentage and 3 are enstatite chondrite-like. Although not shown here, the large predominance (~60%) of carbonaceous xenoliths remains: some seem to be of CM2 types (Wasson and Wetherill 1979) while others are carbon-rich clasts related to ordinary chondrites (Scott et al. 1987). In Table II, the xenolith frequency is compared with that of possibly related main-belt asteroids at 2.5 to 3.0 AU. The distributions are similar but become dissimilar if S asteroids are not ordinary chondrite parents.

Xenoliths have been trapped by asteroid surfaces at all times between 4.6 Gyr and the present. One of the earliest of these xenoliths seems to be the H clast in Barwell which shows "I-Xe" and ^{40}Ar-^{39}Ar ages close to those of the L chondrite host, ~4.4 Gyr (Hutchison et al. 1988). The most recently trapped xenolith may be another H clast in St. Mesmin, whose age was reset during trapping 1.3 Gyr ago (Schultz and Signer 1977).

Parent-body Dimensions

Parent-body sizes also hint that meteorites come from asteroids. Three independent methods exist that can define parent-body dimensions, based on the relationship between the size of a heated solid body and the rate at which it cools (Wood 1967; Fricker et al. 1970). These are: (1) radiometric age determinations; (2) ^{244}Pu chrono-thermometry; and (3) metallographic cooling rates. The first two are based on radioactive decay, the third does not specify when cooling took place.

If a meteorite parent body is of the simple onion-shell type, these 3 size markers should yield concordant results. Disagreements could reflect the inapplicability of the model of a simple, stratified parent body or severe late heating such as, for example, might result from severe shock during asteroidal collision and disruption. We defer further discussion until after we review information conveyed by these size markers.

Absolute Radiometric Ages and Cooling Rates.   As closed-system conditions allowing reliable age determinations vary with the parent-daughter system used, it seems worthwhile to empirically define the starting times of the various absolute clocks in a given meteorite. Unfortunately, there are very few meteorites to which all radiometric methods have been applied together (Table III). One of these is the equilibrated chondrite St. Séverin (LL6). The oldest age is indicated by concordant U-Pb results which allow definition of a very precise ^{207}Pb-^{206}Pb age of 4.551 ± 0.003 Gyr on phosphate separates (Chen and Wasserburg 1981). The youngest ages are obtained by the ^{40}Ar-^{39}Ar method, 4.38 to 4.42 Gyr (Hohenberg et al. 1981): Rb-Sr data give intermediate values (Minster and Allégre 1981). A sequence of closure temperatures for the various chronometers is schematically shown in Fig. 1 for a chondritic parent body having a radius of 100 km.

Since we know that St. Séverin has never been molten, we can infer a peak metamorphic temperature of <1200 K (below the metal-troilite eutectic) which agrees rather well with equilibration temperatures obtained either by the Ca-pyroxene thermometer, ~1190 K (Olsen and Bunch 1984), or by oxygen isotopic data, 1200 ± 100 K (Onuma et al. 1972). From these results and

TABLE III
Concordant Absolute Ages (Gyr) of Meteorites

	^{207}Pb-^{206}Pb	^{87}Rb-^{87}Sr	^{40}Ar-^{39}Ar
Chondrites			
CAI	4.56–4.57(a,b)		
St. Séverin (LL6)	4.551 ± 0.003(b)	4.51 ± 0.15(c)	4.42 ± 0.01 D(d) 4.38 ± 0.01 L
LL (whole rock)	4.54–4.55(e)	4.49–4.51(c)	4.38–4.51(d,f)
H (whole rock)	4.55 ± 0.12(e)	4.48–4.52(g)	(4.44–4.52) ± 0.03(f)
Guareña (H6)		4.48(h)	4.44 ± 0.03(f)
Achondrites			
Angra dos Reis	4.551 ± 0.004(b)		
Ibitira (eucrite)	4.556 ± 0.006(i)		
Juvinas (eucrite)	4.539 ± 0.004(e)		

References: (a) Manhes et al. 1987; (b) Chen and Wasserburg 1981; (c) Minster and Allégre, 1981; (d) Hohenberg et al. 1981; (e) Manhes 1982; (f) Turner et al. 1978; (g) Minster and Allégre 1979; (h) Wasserburg et al. 1969; (i) Chen and Wasserburg 1985.
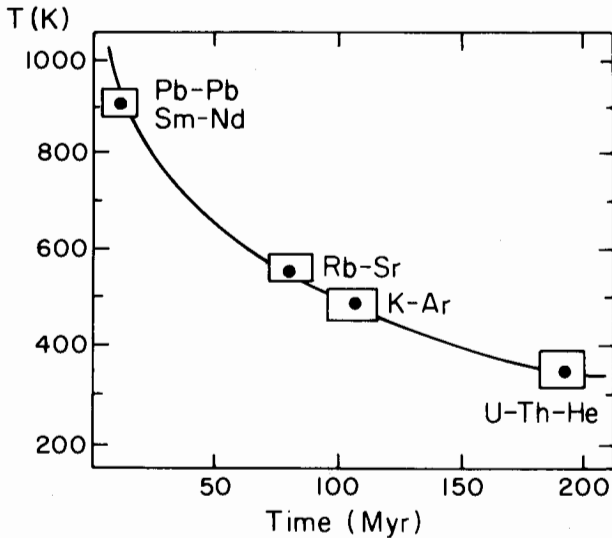
Fig. 1. Schematic representation of temperature variation vs time (in Myr) in the central zone $(r/R \leq 0.85)$ of a chondritic parent body (100 km radius). The corresponding approximate closure temperatures have been indicated for several chronometers.

assuming a peak metamorphic temperature of ~1150 K and a closure temperature for argon of ~640 K, calculated for the H6 chondrites Guareña and Kernouve (Turner et al. 1978), a mean cooling rate of ~3 K Myr^{-1} is obtained in the above temperature interval. The same method applied to Guareña (H6) gives a cooling rate of 4.5 K Myr^{-1}, distinctly faster than for St. Séverin. Within the temperature interval 870 to 670 K (applicable for metallographic cooling rates), the radiometric values are ~2.3 and ~4.0 K Myr^{-1}, for St. Séverin and Guareña, respectively. These compare favorably with metallographic data for the same meteorites, i.e., ~2 K Myr^{-1} for St. Séverin (Willis and Goldstein 1981) and 4.6 K Myr^{-1} for Guareña (Willis and Goldstein 1983). Radiometric cooling rates also agree with the ^{244}Pu fission track cooling rate of Guareña, ~3 K Myr^{-1}, if we adopt the most recent values of Pellas and coworkers for retention temperatures of ~900 K and ~385 K for fission xenon and fission tracks in whitlockite. In the temperature interval of 870 to 670 K, the Pu-fission track cooling rate of Guareña corresponds to ~4.5 K Myr^{-1}, in excellent agreement with both radiometric and metallographic methods. The agreement of results by the three methods for Guareña merit special notice, because for other meteorites (as we shall see below) data totally disagree: these disagreements must be explained. The above results show that St. Séverin cooled at a slower rate than Gaureña, probably because the LL chondrite parent was larger than the H parent.

Here, we may observe that the oldest and very precise (concordant) Pb-

Pb ages have been obtained on Allende CAIs: these cluster between 4.570 and 4.560 Gyr (Manhes et al. 1987). The Pb-Pb ages of H and LL chondrites cluster between 4.54 and 4.555 Gyr (Table III). Differentiated and unshocked achondrites like the Ibitira eucrite and Angra dos Reis also give very precise (concordant) Pb-Pb ages of 4.556 $\pm$ 0.006 and 4.551 $\pm$ 0.004 Gyr, respectively (Chen and Wasserburg 1981, 1985). For the Juvinas eucrite, which shows evidence of shock effects, closed-system conditions were achieved later, at 4.539 $\pm$ 0.004 Gyr (Manhes 1982). Therefore, Pb-Pb results strongly suggest that the most ancient meteorites became closed systems for Pb isotopes within a time interval of <20 Myr: this probably corresponds to the maximum formation time for asteroidal bodies. The observation that ordinary chondrites and achondrites give the same Pb-Pb ages, clustering between 4.540 and 4.555 Gyr also indicates that very fast fractionation processes occurred in some chondritic parents.

Significant information on internal structures and sizes of ordinary chondrite parent bodies is obtained by comparing $^{40}Ar-^{39}Ar$ ages of objects coming from the same parent source. Pellas and Fieni (1988) observed that for 11 out of 12 H chondrites, Ar-Ar ages overlap (whatever the petrologic type) at 4.48 $\pm$ 0.04 Gyr (Fig. 2). The reason apparently is that the H chondrite parent body was a rather small asteroid (radius <100 km), in which the Ar closure temperature for all portions was achieved within a spread of ~80 Myr. The Ar-Ar method is precise only to ±30 Myr, hence is not sensitive enough to establish whether various petrologic types were located at different depths in a small body. However, this is feasible for LL chondrites, which seem to come from a larger body. There appears to be a clear-cut difference between LL3 through LL5 and LL6 Ar-Ar ages, with almost no overlap (Fig. 2).This is the expected trend if LL3-6 chondrites derive from progressively greater depths in a rather large asteroid (radius: 130 to 150 km), assuming canonical parameters for thermal evolution (Fricker et al. 1970). An insulating regolith could decrease the radius (Wood 1979). More data are needed to confirm the observed trends for H and LL parents. For the L body, many data indicate that at around 4.45 Gyr a huge impact modified the internal structure, greatly perturbing all chronometers (Pellas 1981). A later event, ~500 Myr ago, perturbed it further making any additional chronological interpretation even more difficult and precluding further discussion of the L chondrite parent here.

No reliable data exist for absolute radiometric ages of pallasites which could give some hints to their early thermal histories. Recent Ar-Ar ages of mesosiderites give reasonably well-defined plateau ages of ~3.6 Gyr in some cases, suggesting disruption of their parent body and subsequent deep burial when mesosiderite debris gravitationally reassembled (Bogard et al. 1988).

The Ar-Ar ages of silicate inclusions in IAB irons range from 4.57 (Mundrabilla, Woodbine) to 4.54 (Pitts) and 4.50 Gyr (Copiapo) (Kirsten,
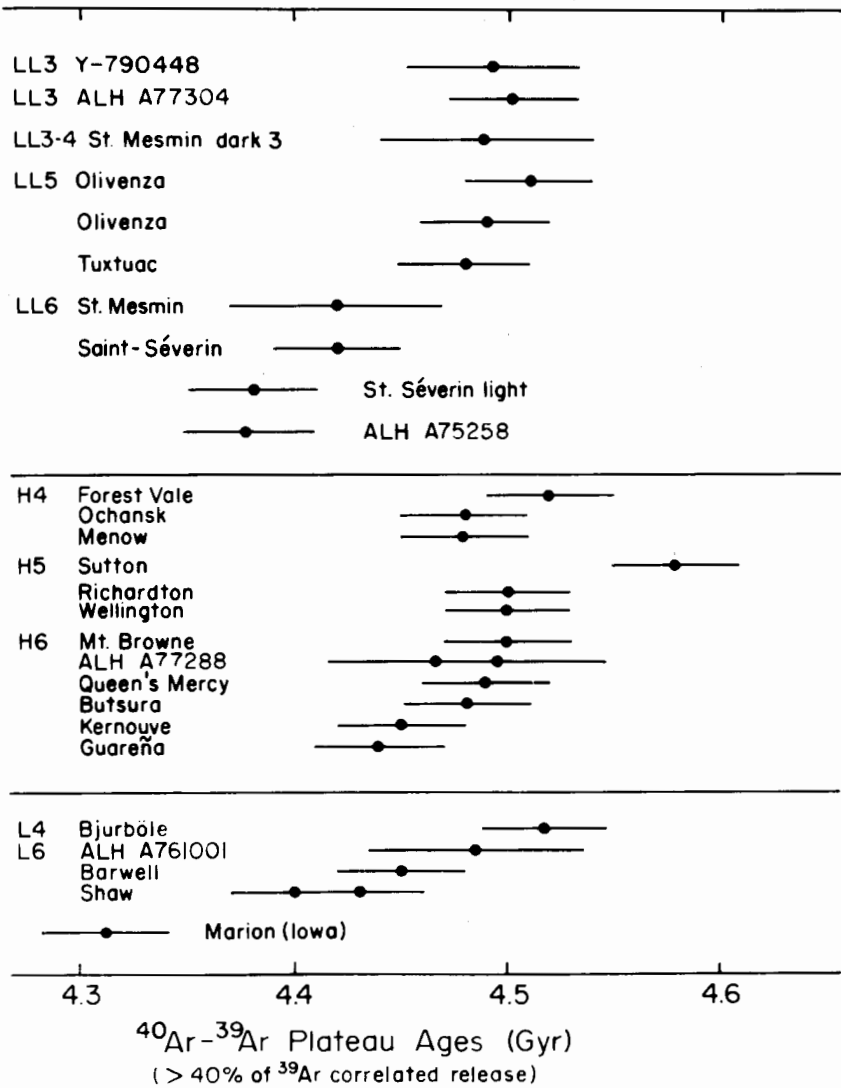
Fig. 2. Summary of ^{40}Ar-^{39}Ar plateau ages for unshocked ordinary chondrites (Shaw, recrystallized at high temperatures, is omitted). Ages of H chondrites (irrespective of petrographic type) overlap and cluster at 4.48 ± 0.04 Gyr, indicating a rather small (80 to 100 km radius) asteroid. Ar closure temperatures for H chondrite parent material were achieved at an earlier time than for LL6 chondrite parent material. For LL chondrites, a clear age difference is apparent for LL3-5 and LL6 parents, consistent with a near-surface origin for petrographic types 3-5 materials and a significantly deeper location for the LL6 samples. The size of the LL parent seems to have been relatively large (radius 130 to 150 km). Some L chondrites seem to have been severely shocked ~4.45 Gyr ago (e.g., Shaw), others have been shocked more recently. More data are needed to arrive at definite conclusions (see text). Data sources are: Bogard et al. (1976); Hohenberg et al. (1981); Kaneoka (1980, 1984); Takigami and Kaneoka (1987); Turner et al. (1978).

1973; Niemeyer 1979). These very old ages indicate that silicates intruded the irons very early, cooled very rapidly for Mundrabilla and Woodbine, and much more slowly for Pitts and especially Copiapo. The Pu-fission-track thermometry (Benkheiri et al. 1979) and/or metallographic results (Benkheiri 1984) agree well for slow-cooled Copiapo.

244Pu chronothermometry. This method, established by Pellas and co-workers since 1975, is based upon the ^{244}Pu ($T_{1/2}$ = 82 Myr) fission-track record in Pu-rich phosphates (whitlockite, apatite) and their adjacent mineral track detectors (olivine, pyroxene, feldspar) which are extremely depleted in actinides (Pellas and Störzer 1981). The adjacent mineral track detectors, having been in close contact with the phosphates since aggregation, registered and stored latent tracks originating from the phosphate fission fragment source. In a cooling environment, ^{244}Pu present in the phosphates, fissioned spontaneously and produced tracks. Hence, differences in Pu-fission-track densities observed today among the different track detectors are simply a function of the ^{244}Pu decay and the track-retention temperatures of the various minerals. They allow us to define the elapsed time until the fission tracks were retained in the respective minerals. The actual mineral, behaving as a thermometer, defines the temperature at which the fission-track clock started to run. In this respect, phosphates, olivines, orthopyroxenes, clinopyroxenes and feldspars, in that order, have different and increasingly higher fission-track-retention temperatures. Furthermore, ^{244}Pu fission xenon contents in phosphates, measured by mass spectrometry, can also be converted into equivalent fission-track densities. As the phosphates retain xenon at higher temperature than those at which mineral detectors retain tracks, the fission xenon content of phosphates gives the Pu abundance at a time before tracks were retained in their detectors. Thus, the fission xenon content in phosphates and the fission-track densities in the different mineral phases adjacent to phosphates (and in the phosphates themselves) in the best cases provide a 5-point cooling curve for meteoritic material, from the (assumed) Xe retention in phosphates (~900 K), down to the track retention in the same phosphates (~380 K), the intermediate temperature steps being defined by the fission-track densities in the adjacent feldspar, pyroxene and olivine. When comparison is possible (Table IV), the results agree with results by the metallographic method (Wood 1979; Willis and Goldstein 1981; Taylor et al. 1987). Most meteorites indicate slow cooling rates (1 to 25 K Myr^{-1}). However, many H4 chondrites give cooling rates >25 K Myr^{-1}, while most H6 chondrites give slow cooling rates of 5 to 9 K Myr^{-1} (Table IV). The sensitivity of the method, however, cannot resolve cooling rates >30 K Myr^{-1}. Furthermore, Pu-fission-track densities of whitlockites are reliable only for short (<5 Myr) exposure ages. For longer exposure ages, significant corrections must be made to account for spallation-recoil tracks (Crozaz and Tasker 1983).

The Pu-fission-track cooling rate of the Marjalahti pallasite (>5 K Myr^{-1})

TABLE IV

**Cooling Rates (K Myr^{-1}) in the 870-670 K Range Determined
by Various Techniques**

Ordinary Chondrites		Method		
		Metallography[a]	Fission Tracks[c]	Radiometry[d]
H6	Guareña	4.6	4.5	4.0
	Kernouve	10	5	(4)
	Estacado	10	9	
	Mt. Browne	10–30	(≳30)	(17.5)
H5	Allegan	15	(15)	
	Nuevo Mercurio	15		
	Richardton	20		(14.5)
	Nadiabondi	50	(15)	
H4	Ankober	(5)[b]	(≳25)	
	Sena	20		
	Kesen	20		
	Conquista	25		
	Ste. Marguerite	>1000		
	Beaver Creek	1000–5000	≳30	
	Forest Vale	>1000	(≳30)	(15)
LL6	Saint-Séverin	1–2	(1–10)	2.3
	Uden		(3)	
LL5	Tuxtuac		3.5	(6)
	Olivenza	4–16	3	(8)
LL3	Krymka	1		
	Chainpur	0.1–		
	Bhola	0.5		
Mesosiderites		0.1		
Pallasite, Marjalahti		0.5	>5	
IA iron				
	Copiapo	1 (Fe-Ni) ~10 (metal in	2.2	(10)
	Toluca	1.6 silicates)	5.5	

[a]Data from Wood (1979 and references therein), Willis and Goldstein (1981), Benkheiri (1984), Taylor et al. (1987), Goldstein and Short (1967) and Pellas et al. (unpublished).

[b]Some scatter in the result.

[c]Values extrapolated to 670-870 K assuming a monotonic cooling regime. Data in parentheses require further work to be definitely ascertained.

[d]See text for references to Guareña and Saint-Séverin. Tuxtuac and Olivenza references are from Bernatowicz et al. (1988) and Turner et al. (1978), respectively. Data for Copiapo are in Niemeyer (1979). It has been assumed that chondrites and IA irons formed at 4.55 Gyr and experienced a peak temperature of 1150 K; upon cooling, ^{40}Ar retention was effective at 650 K. Radiometric cooling rates in parentheses are indicative only. Approximate results for Kernouve, Mt. Browne, Richardton and Forest Vale are inferred from Turner et al. (1978).

(Pellas et al. 1983) strongly contrasts with the metallographic result (0.5 K Myr^{-1}) (Buseck and Goldstein 1969). It defines an upper limit for the radius of a fractionated asteroid of 110 km instead of 200 to 400 km.

Metallographic Method. The third independent way to estimate meteorite parent-body sizes is based on metallographic cooling rates, first determined on iron meteorites (Wood 1964; Goldstein and Ogilvie 1965), then chondrites (Wood 1967) and finally on stony irons (Powell 1969; Buseck and Goldstein 1969). The method is based on nickel distribution profiles at kamacite-taenite interfaces and models cooling rates through 773 K without, however, giving any direct information on the time when the cooling took place. By comparing metallographic cooling-rate data for all classes of meteorites with those from Ar-Ar and K-Ar ages, Wood (1979) proposed that metallographic cooling rates are systematically low by about a factor of 6. Willis and Goldstein (1981) concluded that for ordinary chondrites, cooling rates need to be increased only by a factor of 2. Recently Taylor et al. (1987) considered the data to be accurate within an order of magnitude. In fact, as indicated in Table IV, metallographic results agree well with radiometric and Pu-fission-track results for unshocked equilibrated meteorites (petrographic types 4, 5 and 6). However, disagreements exist indicating that, in specific cases, there are some flaws inherent in the metallographic method, perhaps related to secondary processes, possibly shock heating or reheating. One such example is the exceedingly slow metallographic cooling rates of mesosiderites, 0.1 K Myr^{-1} (Powell 1969) which appear rather unrealistic. If mesosiderites formed by partial melting of a pre-existing regolith (Wasson and Rubin 1985) or by catastrophic parent-body fragmentation and reassembly (Bogard et al. 1988), it seems difficult to believe that surficial mesosiderites would have cooled at such a low rate. A similar remark can be made regarding the slow cooling rates obtained for the unequilibrated (type 3) ordinary chondrites (Wood 1979) which are considered to be surficial materials affected slightly by post-accretionary metamorphism.

The above results show that there is general agreement between the three methods used to retrace the early cooling histories of meteorites (as shown in Table IV) that are essentially unshocked and unmodified by secondary processes.

Internal Structure of Meteorite Parent Bodies

In the last decade, suggestions about parent-body internal structures have been based upon data from either Earth-based observations of asteroids or metallographic cooling rates. One suggestion, that the original belt was substantially more populated in the past (by a factor of ~300 at 100 km diameter), presents the idea that S objects are exposed cores of fragmented parent bodies (Davis and Chapman 1977). This is questionable if S asteroids really are ordinary chondrite types (Feierberg et al. 1982), or if the fraction of exotic

ordinary chondrite-type clasts in the various meteorites (Table II) reflects the abundance of ordinary chondrite-type asteroids. However, these assumptions are arguable, as discussed in Section III. There also is some evidence that the actual number of asteroid families produced from disruption by a catastrophic impact is much smaller than considered before: the true number could be only 4 to 5 (Bell 1987). If so, this might argue that many asteroids escaped catastrophic fragmentation and reassembly, contrary to proposals by Davis et al. (1985) and Taylor et al. (1987). On the other hand, this argument can be circumvented by appropriate choices of reassembled asteroids/family ratios and/or estimated lifetimes of asteroid families.

The existence of an inverse relation between petrographic type and metallographic cooling rate for ordinary chondrites is a matter of considerable debate. Taylor et al. (1987) and earlier studies cited by them conclude that no such relationship exists and proposed a "fragmentation and reassembly" model. According to this model, disrupted fragments of an onion-shell-like parent re-accreted after or during metamorphism/automorphism at $\geq 500°C$ (cf. Grimm 1985). However, it is data for ordinary chondrite regolith breccias that underlie these arguments and such samples seem to have their own peculiar history compared with other ordinary chondrites. As a consequence of fragmentation and reassembly, regolith breccias should be found in contact with large chunks of homogeneous, equilibrated material. Such an association has not been observed.

If we disregard L chondrites, which experienced a very complex sequence of shock events that obscured many chronological interpretations (see above), and limit ourselves only to apparently *unshocked* H chondrites, a distinct order is apparent. As noted above, the data selection by Taylor et al. (1987) indicates no systematic effect. However, if the data listed in Table IV are used, 3 of 4 H6 chondrites give cooling rates in the range of 5 to 10 K Myr^{-1}, H5 chondrites of 15 to 50 K Myr^{-1} and H4 chondrites of 20 to 5000 K Myr^{-1} whatever method is used. These data agree well with a layered structure of the H chondrite parent asteroid, where the most metamorphosed H6 materials were located at greater depths ($r/R_0 \leq 0.85$) and types H5-H4 at shallower locations ($r/R_0 = 0.85$ to 0.97).

A sensitive method that gives a good indication of the original location of chondritic materials in their parent bodies is the ^{244}Pu abundance estimated from fission-track densities in chondritic whitlockites. This defines the approximate time at which each layer crossed the ~ 400 K isotherm where fission tracks are retained in these phosphates. Consequently, Pu-fission-track densities in whitlockites, if corrected for spallation-recoil tracks, roughly approximate the cooling histories of layers located at various depths in the original asteroid when Pu was still alive (e.g., between 4.6 and 4.2 Gyr ago). Data for H chondrites show that Pu-fission-track densities increase progressively from petrographic type 6 to type 4, in agreement with a layered internal structure (onion-shell model) of the parent asteroid (Pellas and Fieni 1988).

Volatile trace element contents in H chondrites also support a layered structure model (Lingner et al. 1987). Mean contents of 4 to 6 trace elements differ significantly with petrographic type with the lower concentration mainly being present in H chondrites of higher petrographic type because of primary or secondary thermal episodes (Lingner et al. 1987). Interpretation seems to be complicated by different degrees of ^{40}Ar outgassing in the various strata. Hence, the picture of the simple onion-shell model seems to be obscured somewhat by a later process. Whitlockites of LL chondrites also yield Pu-fission-track densities consistent with an onion shell model (Pellas and Fieni 1988). Finally, ^{40}Ar-^{39}Ar plateau ages of H and LL chondrites are consistent with (see above) the onion-shell model for the H and LL parent asteroids.

Why then are incoherent metallographic cooling rates obtained from re-golithic or fragmental breccias? A possible answer is given by the meso-siderites. If these objects indeed derive from metallic projectiles hitting pre-existing regoliths, as seems to be the case for the Bencubbin breccia (Kelly and Turner 1987), then the insulating properties of regoliths could perhaps explain the very large scatter (5 orders of magnitude!) observed in metal-lographic cooling rates of chondritic regolithic breccias (Taylor et al. 1987). Such an episode has nothing to do with the real depth inside a parent asteroid. More work is, however, needed to fully understand this and asteroid internal structures.

II. SOURCE CONSTANCY AND THE METEORITE FLUX

Until two decades ago, meteorite falls (essentially those falling within the last 200 yr) constituted our most valuable sampling of the near-Earth flux. Finds in temperate regions could have considerably older terrestrial ages and can be useful for some studies, but other studies can be affected by meteorite alteration during weathering. The discovery of large numbers of meteorites in Antarctica over the past two decades has extended our sampling of *well-preserved* meteorites back to about 1 Myr, possibly enhancing contributions from asteroids that no longer exist or that are in unusual orbits.

Meteorite occurrences in Antarctica are related to ice sheet dynamics on the continent so that a few words on this topic are appropriate (see summary reports and reviews prepared by Bull and Lipschutz [1982], Annexstad et al. [1986], Lipschutz and Cassidy [1986], Cassidy and Whillans [1988]). The Antarctic ice sheet is several km thick on the plateau near the Pole and rela-tively thin at the coast. Ice sheet motion toward the coast can be retarded or stopped by rock prominences even if they do not penetrate the ice surface to act as complete barriers to flow. Meteorites are generally found on the surface of such stagnant or near-stagnant, old "blue ice" regions upstream of barriers. Most of these represent samples entrained in the ice and transported by it, emerging onto the surface through some combination of upstream ice pressure and catabatic polar winds that evaporate the ice near the barrier. Hence, the

ice sheet generally acts as a meteorite collector, transporter, concentrator and preserver.

Meteorites are found in many parts of Antarctica, especially in Queen Maud Land and Victoria Land, because of extensive work by Japanese Antarctic Research Expeditions (JARE) and by U.S. Antarctic Search for Meteorites (ANSMET) personnel, respectively. In the last two decades, over 9000 specimens have been returned by annual JARE and/or ANSMET expeditions (Lipschutz and Cassidy 1986) but an unknown number of these are paired, clouding comparisons between Antarctic and non-Antarctic populations. For an estimated 4 ± 2 specimens per fall (Scott 1985), the 1500 to 4400 discrete Antarctic falls approximate the number of known non-Antarctic meteorites.

Actually, Antarctic meteorites may not constitute a single population. Samples from Queen Maud Land are, on average, considerably smaller than samples from Victoria Land (and non-Antarctic falls; cf. Fig. 2): they also differ in terrestrial age distribution (see Cassidy and Whillans 1988 and references therein). Samples from Queen Maud Land have a 0.2 Myr maximum age and become exponentially more numerous as terrestrial ages decrease, while meteorites from the Allan Hills region of Victoria Land are distributed randomly up to 1 Myr, averaging 0.3 Myr (Nishiizumi 1986).

Meteorite Types

Even at the grossest classificational level, meteorite type frequencies between Antarctic and non-Antarctic populations (Table V) differ. Taking a factor of 2 as significant, iron and stony-iron meteorites are underabundant relative to non-Antarctic falls, and groups common among non-Antarctic irons are rare in Antarctic samples. Antarctic aubrite and howardite achondrites seem underabundant while ureilites are overabundant (Table V). Representatives of some types unknown among non-Antarctic samples are found in Antarctica (e.g., lunar meteorites as already discussed) and *vice versa*. Meteorite types rare in the non-Antarctic population often differ petrographically from their Antarctic counterparts. For example, Antarctic eucrites are generally petrographically distinct from non-Antarctic eucrites (Takeda et al. 1983). In fact, eucrites from Victoria Land may differ petrographically from those in Queen Maud Land (Takeda 1986). The eucrites, with related howardites and diogenites (so-called HED achondrites), have spectral properties like those of 4 Vesta (McCord et al. 1970) and apparently derive from it or some similar asteroid.

It is relatively easy to identify paired meteorites of unusual types, and therefore estimate to what extent Antarctic and non-Antarctic populations differ in their complement of such meteorites. However, the statistical validity of the differences is questionable because of the necessarily small number of samples. The far more numerous ordinary chondrites overcome this problem but pairing of such meteorites is much more difficult. Dennison et al. (1986) point out that the proportions of very numerous equilibrated high-iron (H) and

TABLE V

Comparison of Numbers of Non-Antarctic Meteorite Falls and Classified Antarctic Specimens Collected by the U.S.

Meteorite Type	Falls[a]	U.S. Antarctic Collection[c]
Chondrites		
H	276	904
L	319	490
LL	66	83
E	13	9
C	35	29[b]
C1	*5*	*0*
C2	*18*	*14*
C30	*5*	*4*
C3V	*6*	*5*
C4	*0*	*5*
C5	*1*	*0*
TOTAL	709	1515
Achondrites		
Aubrites	*9*	*2*
Diogenites	*9*	*9*
Eucrites	*25*	*18*
Howardites	*18*	*4*
Lunar	*0*	*1*
Shergottites	*2*	*3*
Ureilites	*4*	*11*
TOTAL	69[b]	54[b]
Irons	42	21
Stony Irons		
Pallasites	*3*	*0*
Mesosiderites	*6*	*3*
TOTAL	10[b]	3
TOTAL CLASSIFIED	959	1593

[a]Graham et al. (1985).
[b]Includes unique, anomalous or unclassified specimens so that totals may exceed number of constituents (in italics).
[c]Corrected for pairing.

low-iron (L) chondrites differ, being about 1 : 1 in non-Antarctic falls (and finds) and 3 : 1 in well-characterized collections from Queen Maud Land and Victoria Land, Antarctica. More recent data might seem to indicate that the H : L chondrite ratio for samples collected by the U.S. is now about 2 : 1 (Table V). However, this decrease reflects sampling bias: essentially only L chondrites are currently being selected for classification so that the unbiased estimate of 3 : 1 for the Antarctic H : L proportion is probably correct. The non-Antarctic H and L chondrite mass distributions are virtually identical and

resemble the shape of the Antarctic H chondrite one (Fig. 3). The shape of the mass distribution for L chondrites is clearly very different (Harvey and Cassidy 1988).

Since there seems to be no *a priori* reason for such frequency differences to reflect terrestrial processes, the possibility exists that Antarctica has sampled a different meteoroid population in the past than is being sampled by contemporary, non-Antarctic falls (and finds). Qualitatively this is not surpris-
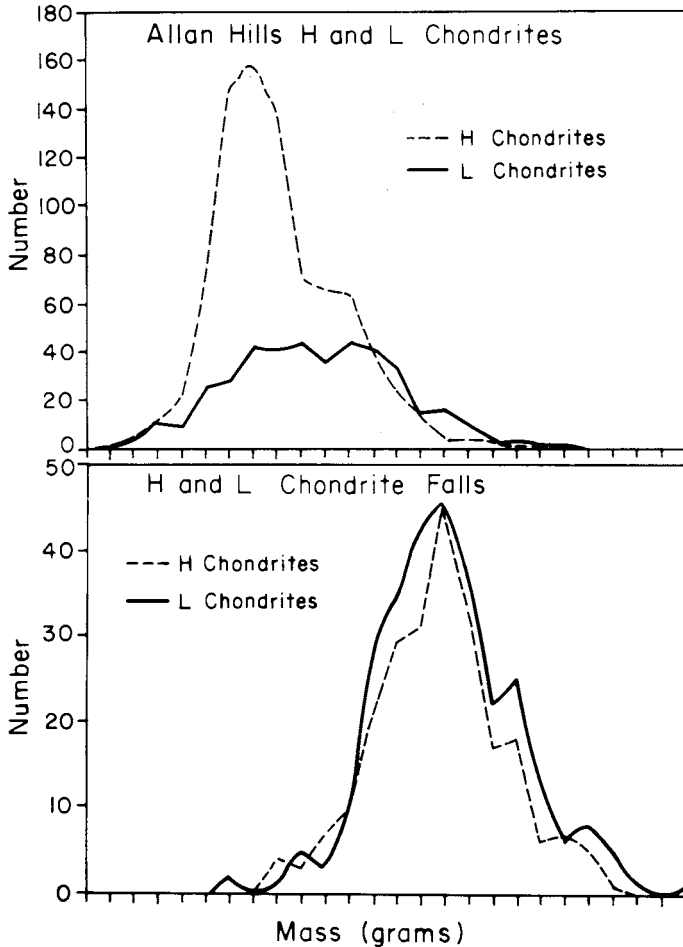
Fig. 3. Comparison of mass distributions (Harvey and Cassidy 1988) for Allan Hills, Antarctica, H and L chondrites (top) with non-Antarctic ones (bottom). The abscissa (identical for top and bottom) ranges from 0.06 to 4.2×10^6 g and each division represents a doubling of the previous one. Non-Antarctic shape distributions are virtually identical and resemble that of Antarctic H chondrites; the shape of the Antarctic L chondrite distribution is clearly unique. Antarctic samples are, on average, smaller than their non-Antarctic counterparts.

ing since it has long been recognized that the disparity in frequency between types of meteorites and asteroids implies a bias in the Earth's sampling of asteroidal debris. Hence, one might almost expect temporal or spatial variations in the extraterrestrial flux, but within the context of current statistical (Monte Carlo) orbital-dynamic models, there are quantitative problems with variations on time scales <20 Myr or so (Wetherill 1986).

At present, it seems clear that Antarctic and non-Antarctic meteorite populations differ in some of their chemical and physical properties. Whether these differences reflect preterrestrial genetic processes or result from terrestrial weathering of Antarctic meteorites is a current, highly controversial question. To resolve this question, it is necessary to establish what differences exist and determine whether these differences can reflect Antarctic weathering. If not, the differences must reflect preterrestrial processes. For the purposes of this review it is appropriate to summarize published results only. Cassidy and Whillans (1988) include a summary of results (even from ongoing studies) complete to mid-1988: we can expect additional information with time.

If Antarctic and non-Antarctic populations reflect variations of extraterrestrial source regions or derive from widely separated regions in the same parent asteroid, genetic differences should be most pronounced for the most sensitive markers of thermal history. So far, published data for thermally sensitive trace elements, thermoluminescence (TL) and $^{13}C/^{12}C$ ratios reveal such differences.

Physical and Chemical Comparisons

Trace elements are present in meteorites at ppm (or $\mu g/g$) to ppt (pg/g) levels and provide highly suitable markers for genetic processes, because in response to an external process, a small absolute concentration change is magnified into a large relative one. Obviously, not every trace element responds similarly to thermal stress and certain ones are considered volatile on theoretical grounds during primary nebular condensation and accretion (Larimer 1973). Many of these volatile elements, and some others, are mobile (easily volatilized and lost) in week-long laboratory heating experiments under temperature and ambient atmospheric conditions reasonable for post-accretionary processes (Ngo and Lipschutz 1980).

Palme et al. (1988) and Lipschutz and Woolum (1988) present a group-by-group discussion of labile (volatile and/or mobile) trace element trends in non-Antarctic chondrites. Date for these trace elements suggest solid-state metamorphic loss in enstatite chondrites, late shock heating in L chondrites and an early thermal fractionation when H chondrites formed. It seems clear that the thermal histories of H and L chondrites differ: conventional wisdom had previously assumed similar early histories for all ordinary chondrites. H and L chondrites are, by far, the meteorites most frequently encountered by Earth.

When contents of 13 trace elements in essentially unweathered H chondrites from Victoria Land are compared with those for non-Antarctic falls, at least half differ at statistically significant levels (Lingner et al. 1987; Dennison and Lipschutz 1987). Contents of most of these elements are *higher* in the Victoria Land population: Antarctic weathering (leaching) would result in *lower* concentrations in this population (Dennison and Lipschutz 1987). (Differences between Antarctic and non-Antarctic populations are not confined to H chondrites—see summary in Cassidy and Whillans [1988].) If, as the data suggest, the compositional differences reflect preterrestrial genetic effects, non-Antarctic H chondrite falls experienced higher average formation temperatures than did samples from Victoria Land or some early high-temperature episode that the Antarctic samples escaped. The trace-element data also hint at a compositional difference between H5 chondrites from Victoria Land and Queen Maud Land, Antarctica (Dennison and Lipschutz 1987), meteorite populations that differ in, e.g., terrestrial ages (see summary in Cassidy and Whillans [1988]). This hint of a time-dependent difference must be explored further.

Differences in TL properties, particularly peak temperatures and peak widths, for H (and perhaps L) chondrite falls compared with similar samples from Victoria Land argue for thermal history differences, probably metamorphic history differences (Haq et al. 1988; cf. Cassidy and Whillans 1988). Most of the TL properties studied by Haq et al. (1988) would not be affected by Antarctic weathering. Haq et al. (1988) also reported that the induced TL of H and L chondrite falls differ, the effects being consistent with the much higher degree of shock associated with L chondrites. The conclusions obtained from each comparison of TL in H or L chondrites are essentially consistent with those obtained from comparison of data for labile trace elements.

The only other published study comparing some indicator of thermal history in Antarctic and non-Antarctic populations of a single meteorite group are measurements of $^{13}C/^{12}C$ ratios in C2 chondrites (McGarvie et al. 1987). Isotopic ratios ($\delta^{13}C$) for carbon released from acid-treated residues of C1 and C2 chondrites heated for 1/3 to 1/2 hr at various temperature steps between 600° and 1300°C differ for Antarctic and non-Antarctic populations, particularly in high-temperature sites. McGarvie et al. (1987) concluded that "Antarctic C2 meteorites were found to be grossly similar to the non-Antarctic meteorites in their carbon release characteristics but to be significantly different in their $\delta^{13}C$ values." McGarvie et al. (1987) observed that the differences could be due to the Antarctic samples containing: (1) lower proportions of ^{13}C-rich material; (2) higher amounts of ^{12}C-rich component; (3) a ^{13}C-rich component less enriched in ^{13}C than are similar components of non-Antarctic samples. Any of these would indicate a difference in the origin or primary thermal history of members of the two populations. As a fourth alternative, McGarvie et al. (1987) hypothesized that isotopically heavy carbon could have somehow been leached out in Antarctica but did not suggest a mecha-

nism by which this might occur. Not every study reveals an Antarctic/non-Antarctic difference. McSween (1987) searched for but did not find a difference in the major element compositions of matrix in falls and Victoria Land CM2 chondrites. Matrix compositions of such samples apparently reflect aqueous alteration in the parent asteroid(s) so that the post-accretionary histories of parent regions for Antarctic and non-Antarctic CM2 chondrite populations apparently did not differ significantly (see note added in proof).

Implications

The available data suggest that neither a trivial explanation (such as data treatment models or chance) nor Antarctic weathering explain physical and chemical differences between Antarctic and non-Antarctic meteorite populations (Dennison et al. 1986; Dennison and Lipschutz 1987). Whether meteorite populations from Queen Maud Land and Victoria Land differ significantly is even less well established. The extent of these differences and the question of their preterrestrial origin will be studied extensively in the next few years. If, as a working hypothesis, we take these differences to be of preterrestrial origin, contemporary falls and Antarctic meteorites represent different extraterrestrial source regions or at least represent contributions from such regions in different proportions. However, this would imply at least partial preservation of differences in meteoroid launch parameters during their cosmic-ray exposure period, an idea at odds with the statistical Monte Carlo model for meteoroid derivation from the asteroid belt (Wetherill 1986). Furthermore, it would imply the existence of "meteoroid streams." The existence of such streams had been postulated by Wood (1982), and Oberst and Nakamura (1986) who claimed seismic detection of just such a stream striking the Moon in 1975. Further studies of this controversial topic are currently in progress.

A difference in the distribution of cosmogenic ^{53}Mn data for non-Antarctic H (but not L) chondrite falls and Victoria Land samples (Dennison and Lipschutz 1987) argues for orbital differences for meteoroids of the two populations (but, cf. Cassidy and Whillans 1988). Finally, near-Earth asteroids may have an enhanced importance as a meteoroid source on the time scale of Antarctic meteorite terrestrial ages, 0.1 to 1 Myr (Greenberg and Chapman [1983] and Greenberg as cited in Dennison and Lipschutz [1987]). As discussed below, Q type asteroids have spectral properties consistent with their being ordinary chondrite parent bodies and all four possible ones (1862 Apollo, 2368 Beltrovata, 1981 QA and 1980 WF) are near-Earth Apollo or Amor asteroids. For reasons discussed in Dennison and Lipschutz (1987), Oberst suggests that Antarctic meteorites may derive preferentially from asteroids in high-inclination orbits.

Clearly, the questions of whether and how meteoroids retain at least some distinctness in their orbit during derivation from Earth-crossing or Earth-approaching asteroid parents remain open. If HED meteorites derive

from Vesta, differences in the Antarctic and non-Antarctic populations of these achondrites argues that these questions might equally apply to belt asteroids.

III. ASTEROID SURFACE MATERIAL CHARACTERIZATIONS

This section outlines our present knowledge of asteroid surface assemblages, and considers the implications of these results for the nature and location of meteorite parent bodies. Many remote sensing techniques have been used to study the minor planets, and visible and near-infrared (VNIR) reflectance spectroscopy generally most directly characterizes the actual surface mineralogy and mineral chemistry. (See Gaffey and McCord [1979] and the chapter by Gaffey et al. and the references cited therein for a detailed discussion of techniques and calibrations used to characterize asteroidal surface material from spectral data.)

Various proposals have been made to classify asteroid color and albedo data; Tholen (1984; see the chapter by Tholen and Barucci) defines fourteen classes. Although this approach does not actually characterize the surface mineralogy, each class should comprise generally similar materials. A compositional description of each of the fourteen Tholen (1984) classes, derived from

TABLE VI
Asteroid Type, Surface Mineralogy and Meteoritic Analogues
from Reflectance Spectroscopy

Type	(No.)[a]	Surface Mineralogy	Meteoritic Analogues
A	(3)	olivine or olivine-metal	olivine achondrite or pallasite
B	(6)		CI1-CM2 assemblages with some
C	(41)	hydrated silicates and	additional alteration or meta-
F	(10)	carbon/organics/opaques	morphism (each group repre-
G	(5)		sents a different degree of modification)
D	(19)	carbon/organic-rich	organic-rich cosmic dust grains?
P	(23)	silicates?	CI1-CM2 plus organics?
E	(8)	iron-free enstatite, forsterite or other silicate	enstatite achondrites
M	(21)	metal (possibly trace silicates) metal + enstatite?	irons (possibly silicate inclusions) enstatite chondrite?
Q	(1)	olivine, pyroxene, metal	ordinary chondrites
R	(1)	pyroxene, olivine	pyroxene-olivine achondrite
S	(73)	metal, olivine, pyroxene	pallasites or olivine-dominated stony-iron
V	(1)	pyroxene, feldspar	basaltic achondrites
T	(1)	like BCFG group but possibly more altered	

[a]Number of asteroids classified as this type by Tholen (1984, tables 8 and 9).

detailed analysis of spectral reflectance data for individual members of each type are listed in Table VI with the mineralogical assemblages inferred for it.

Heterogeneity Within Asteroid Classes

As with any classification system, each spectral reflectance class containing more than one asteroid occupies an extended region on the Tholen (1984) principal component diagram and the class is likely to be heterogeneous. Although the significance of this spread in color and/or albedo within each class is not yet well understood, it clearly reflects significant diversity of generally similar assemblages. The apparent or possible heterogeneity in several major groups is discussed below.

S Class.   The S class exhibits significant variations in relative abundances of mafic and metallic phases and in mafic phase compositions (see, e.g., Feierberg et al. 1982; Gaffey 1984; Gaffey and Ostro 1987), but the present data permit no natural subdivisions of this class. Tholen (1984) suggested that subscripts could be used to indicate relative classification within the S class. Although surficial materials of S class asteroids appear dominated by assemblages analogous to igneous stony-iron meteorites, ranges of mafic features and of albedos within the S class suggest that a small fraction of meteoritic analogues as diverse as ureilites (igneous, carbon-bearing, olivine achondrites) and CV3/CO3 chondrites (undifferentiated, olivine-dominated assemblages) could also be present. As discussed below, a minor ordinary chondrite component within the S class population cannot be excluded based on present data.

C Class.   The older C class (Chapman et al. 1975; Bowell et al. 1978) was subdivided into the C, B, G and F classes by Tholen (1984). It is not clear just how these C subclass assemblages differ mineralogically from the others, although Bell (see the chapter by Bell et al.) suggests that the G, B and F classes are C-type parent materials altered or metamorphosed to different extents. Observational efforts are beginning to produce spectral data with the photometric precision, spectral resolution and wavelength coverage to permit sophisticated study of these dark asteroid types.

M Class.   Metal (most probably nickel-iron) is the sole or predominant spectrally active mineral phase on M asteroid surfaces. Their surface assemblages could range from pure NiFe metal to a mixture of reduced mafic silicates (iron-free phases such as enstatite or forsterite) with NiFe metal. Radar results (Ostro et al. 1985) have shown that 16 Psyche, the largest M type asteroid, must have a surficial layer almost entirely composed of metal. Radar returns for other M class objects are more ambiguous, and can be matched by iron or silicate-iron surfaces, depending upon model assumptions

of regolith density. The possible presence of a weak silicate feature near 0.9 μm and phase polarization behavior have led to suggestions that many M type asteroids have either iron-poor silicates (analogous to E chondrites) or trace abundances of mafic silicates (analogous to IAB iron meteorites with their silicate inclusions).

Surface Heterogeneity of Individual Asteroids

Although no asteroid exhibits the huge compositional and albedo contrasts of Saturn's satellite, Iapetus (Cruikshank et al. 1983 and references therein), careful spectrophotometry has shown that most asteroids have spectral (and presumably, albedo) variations at the several percent level. Rotational spectral variations demonstrate the presence of both diogenite and eucrite assemblages on Vesta's surface and show that it must have survived nearly intact from the end of igneous activity (Gaffey 1983 and references therein). For our purposes, rotational spectral variations are most important for testing whether individual S class asteroids could be (as suggested by many meteorite and some asteroid investigators) undifferentiated, ordinary chondrite-like assemblages whose spectral properties have been made S-like by space weathering or regolith processes.

The nature of S asteroids has led to considerable dispute and some friction between the asteroid spectroscopy and meteorite communities, who often reach opposite conclusions concerning their nature and meteoritic affinities. To explain the ordinary chondrite dominance in the terrestrial flux, meteorite investigators (see, e.g., Anders 1978; Greenberg and Chapman 1983; Wetherill 1985) generally argue that the abundant S type asteroids must be primarily undifferentiated, ordinary chondrite-like assemblages. Paradoxically, asteroid spectral studies now strongly indicate that most large S-type objects have stony-iron-like surfaces (see, e.g., Gaffey 1984,1986a,b; Bell 1986; Gaffey and Ostro 1987; and chapters by Gaffey et al., Greenberg et al., Bell et al.). Although conceptually possible, no well-defined, viable mechanism has been proposed to produce an S-type spectral albedo curve from an ordinary chondrite assemblage. This is clearly a research area that will continue to receive a great deal of attention in the foreseeable future.

In individual cases, reflectance spectra with adequate wavelength coverage, photometric precision and rotational coverage exist and the relative nature of rotational spectral variations can test for the presence of an undifferentiated surface assemblage. This approach utilizes the fundamental definition of chondritic material: an undifferentiated, fixed composition, or more accurately, a severely restricted compositional range, corresponding to the nonvolatile constituents of a solar gas. For a constant bulk composition (oxygen excepted), the oxidation state of iron simultaneously constrains the abundance and composition of mafic silicate and NiFe metal phases. An abundance or composition change of any individual mafic or metal phase within such an

undifferentiated assemblage must be accompanied by a series of compensating changes in abundance and composition of other phases.

Uncertainties, either known or possible, in the interpretive calibrations for reflectance spectra analyses limit the application of this approach. For a given S type spectrum, the accuracy of phase abundance or composition determination may be too low to establish reliably whether the surface material of that object is consistent with an undifferentiated assemblage. However, relative mineralogic changes across an asteroid surface that produce a set of rotational spectral variations can be determined with much higher precision (internal consistency) than can the absolute abundance or composition (accuracy). The relative sense of the variation in phase abundances and compositions is largely independent of uncertainties in either observational or interpretive calibrations.

Feierberg et al. (1982) studied twelve S asteroids and suggested that 8 Flora was the most chondrite-like. However, Gaffey (1984) showed that variations in pyroxene phase composition relative to the variation in the olivine/pyroxene abundance ratio exhibited the wrong sign for Flora to be undifferentiated. While an offset or slope mismatch could be attributed to uncertainties in the phase abundance calibration (Cloutis et al. 1986) or to the pyroxene composition calibration (Adams 1974), the sign of the slope could not be affected by any plausible calibration uncertainty. Flora is thus surfaced with an igneous, stony-iron-type metal-olivine-pyroxene assemblage. Similarly, Gaffey and Ostro (1987) showed that average surface material on 15 Eunomia, the largest S type asteroid, corresponds to a metal-olivine assemblage with a lesser proportion of pyroxene. Just as for Flora, the relative phase variation with rotation requires that Eunomia be a differentiated object rather than an undifferentiated chondritic body.

Limit of Current Asteroid Mineralogical Characterizations

The reliability and sophistication of available mineralogic characterizations of asteroid surface materials vary widely. Because of inherent limitations of telescopic systems, observations focus on larger, hence brighter, objects and sample completeness decreases with object size. Classification from 8-color data is virtually complete for main belt asteroids down to a diameter of 100 km and decreases to minuscule in the 10 to 20 km interval. Observations also are biased against darker and outer-belt asteroids. For any given data set or level of characterization, our sample is best for higher albedo, for larger and for inner-belt asteroids; the sample is smallest for the most sophisticated characterizations.

Moreover, asteroids are unresolved point sources for present spectral observations. With only a very few exceptions, e.g., Vesta (Gaffey 1983), Flora (Gaffey 1984), Eunomia (Gaffey and Ostro 1987), characterizations of asteroid surface materials are averaged over some large (>hemispheric) portion. Every solid, solar system surface investigated in any detail, possesses abun-

dant compositional and/or tectonic units on much smaller scales. From asteroid rotation studies, their surfaces are probably highly heterogeneous at small (<<hemispheric) scales, scales which present observational data cannot sample.

For individual asteroids investigated in detail, characterizations are both sophisticated and secure. The surface material of Vesta (Gaffey 1983 and references therein) is undoubtedly some combination of basaltic achondrite-like assemblages; that of 246 Asporina (Cruikshank and Hartmann 1984) nearly pure olivine; that of Flora (Gaffey 1984) a metal-olivine assemblage with accessory orthopyroxene formed by igneous processes; that of Eunomia (Gaffey and Ostro 1987) a metal-olivine assemblage with accessory ortho- and clinopyroxene phases also formed by igneous processes; and that of 16 Psyche (Ostro et al. 1985) which consists of nearly pure metal.

However, sophisticated characterizations depend upon the presence and detection of one or more mineralogically diagnostic parameters. Most asteroids have been studied in general survey programs and the available spectral reflectance data (see, e.g., Chapman and Gaffey 1979; Zellner et al. 1985; Bell et al. 1988) have neither the photometric precision to quantify weak features nor adequate spectral coverage of the mineralogically important wavelength interval. While such data are suggestive of particular spectral type(s), sometimes very strongly so, they do not permit sophisticated or unambiguous surface material characterizations.

IV. ASTEROID COMPOSITIONAL VARIATION WITH LOCATION

Chapman et al. (1975) noted that S-type asteroids are concentrated in the inner asteroid belt, and that C type asteroids dominate the outer belt. The distribution of E-, S-, M-, C-, P-, and D-asteroid types with semimajor axis demonstrates a definite compositional structure to the belt (Gradie and Tedesco 1982; see the chapter by Gradie et al.). Hence, Gradie and Tedesco (1982) suggested that the belt represented a transition zone between anhydrous and hydrous mineral assemblage in the late solar nebula, and that the distribution of the different asteroid types records the nebular composition gradient across this interval.

Dermott et al. (1985) showed that the *UBV* colors of S class asteroids vary with semimajor axis and suggested that this reflects a systematic variation in S asteroid surface mineralogy with semimajor axis. Gaffey (1986a; see also the chapter by Gaffey et al.) showed that this variation indicates decreasing olivine and increasing metal and pyroxene abundances in S asteroids with increasing semimajor axis.

The compositions of belt asteroids apparently differ significantly from those in the Earth-approaching population: the latter apparently includes contributions from both the asteroid belt and from the Oort cloud as extinct cometary nuclei (see the chapters by McFadden et al. and Weissman et al.). Q class

asteroids are of special interest: they are unique to the Earth-approaching population and have not been identified in the main belt. Within the limitations of the observational data, the best studied Q type object, 1862 Apollo, is identical to an ordinary chondrite assemblage, most closely resembling the LL4 chondrite Soko-Banja.

This identification emphasizes the dichotomy between the views of meteoriticists and asteroid spectroscopists. Apollo and the other 3 possible Q types are small and rare: data for ordinary chondrites suggest parent bodies that were larger and abundant. Where are these parent bodies today? On the other hand, S asteroids are common and may be large. If they are ordinary chondrite parents, what processes occurred that rendered their surfaces spectrally unrecognizable as ordinary chondrites, yet did not obscure links between other meteorite and asteroid types?

V. CONSTRAINTS ON THE EVOLUTIONARY HISTORY OF ASTEROIDS

The incompleteness in the sample of asteroids studied and in the sophistication level of asteroid surface-material characterizations allow considerable freedom for models of evolutionary histories of the asteroids. Despite the present limitations, important parameters of asteroidal evolution, meteoritic affinities and regolith processes can be significantly constrained by present data.

Asteroids Composed of Meteoritic Minerals

Asteroid surface assemblages deduced from remote observations are all consistent with some combination of mineral phases present in meteorites and cosmic dust particles or with reasonable extensions of known phases from these sources. No exotic, nonmeteoritic phases have been detected or need to be invoked to explain the observed spectral or other remote sensing data. The chemical and physical processes that produced the variety of meteoritic assemblages have also operated on and within asteroids.

Asteroid Surface Materials Representative of their Substrates

Optical wavelengths interact only with a thin surface layer, ranging from a few hundred μm to a few mm depending on the material's opacity. However, the available evidence strongly suggests that this is a representative sample of some average of subjacent lithologic units. In particular, we do not know very much about processes that can significantly modify mineralogic or chemical properties of the thin surface layer accessible to VNIR spectroscopy and to which the surface material characterizations apply. Such processes might include space weathering or regolith formation. Anders (1978) for example, suggested that the metal-rich surface of S asteroids might be produced from ordinary chondrite material by space erosion of brittle silicates, leaving

the surface enriched in malleable metal. However, Gaffey (1984) showed that ordinary chondrite material separated magnetically (and, therefore, metal-enriched) did not duplicate Flora's spectral features. Bell and Keil (1987) showed that reflection spectra of ordinary chondrite regolith-breccia regions that show shock and impact melting effects do not duplicate S asteroid spectra. It must be admitted however, that laboratory experiments have not yet absolutely simulated all possible space erosion processes. Until definitive experiments are designed and conducted, the nature of effects of space erosion upon asteroid spectra remain an open question.

With regard to regolith processes, Matson et al. (1977) showed that the spectrum of Vesta indicates the virtual absence of lunar surface-type space-weathering processes (solar-wind hydrogen implantation and subsequent reduction and vitrification during micrometeorite gardening of the surficial layer). Laboratory spectra of lunar meteorite powder does duplicate lunar spectral features and can even serve as a basis for suggesting a specific lunar feature as a source for the meteorite (McFadden et al. 1986).

An alternate form of space weathering, radiation damage of minerals in a long-lived surface layer, has been proposed for the less active asteroid regoliths. Sufficient irradiation by cosmic rays or by energetic photons could disrupt crystal structures, thus significantly altering spectral properties of the surficial layer. Several lines of evidence suggest that such a process is not effective in modifying spectral properties of present-day asteroid surfaces.

First, water-of-hydration features in the spectra of about two-thirds of the studied C-class asteroids should limit the degree of irradiation. Water and hydroxyl phases in hydrated silicates are much more weakly bound than are metal, oxygen or silicon in mafic silicates. If asteroid surface layers were irradiated sufficiently to disrupt mafic silicates (e.g., decreasing the intensity of the mafic silicate features and enhancing the apparent metal abundance to produce S-type spectra from ordinary chondritic substrates), the 3 μm water-of-hydration bands should be greatly weakened, radically altered or absent. The 3-μm water features of C types are similar in form and intensity to those present in CI1 and CM2 chondrite spectra, indicating no strong irradiation effect. A caveat here is that ions and/or radicals produced in this hypothesized disruption must be lost, by diffusion, say, before they recombine and rehydrate the mineral. The process has not been studied or simulated experimentally.

Second, asteroid regolith models and petrographic and spectral studies of meteoritic regolith breccias (see, e.g., Matson et al. 1977; Lorin and Pellas 1979; Housen and Wilkening 1982; McKay and Basu 1983; Bell and Keil 1987; and the chapter by McKay et al.) indicate that while asteroid and meteorite parent-body regoliths might conceivably be exposed on the surface longer than for lunar regolith, there is less gardening on asteroids, i.e., existing regolithic material is less subject to cycling back to the surface. Spectral effects seem dominated by shock effects rather than radiation damage. This

contrasts with the extensive spectral and chemical modification of carbon-bearing ices in the outer solar system and in the interstellar environment, where irradiation breaks C-H bonds, permitting loss of hydrogen, and production of carbon-rich polymers (see, e.g., Lanzerotti et al. 1985).

Observational data and theoretical models suggest that regolith processes, active on present-day asteroidal bodies, are generally comparable with those that operated on parent bodies of gas-rich meteorite breccias.

Asteroid Regolith and Collisional Processes

The apparently ubiquitous presence of discrete large-scale lithologic units on asteroid surfaces indicates that they do not "paint themselves gray." That is, the present asteroid surface layer is not simply ejecta from the last big impact. Ejecta from any large impact should be present over the entire surface but should not overwhelm the locally derived surface component everywhere. Surficial material in any location may be polymict, representing both local and distant contributions in varying proportions.

The apparent preservation of some internal stratigraphy in Eunomia (Gaffey and Ostro 1987) also suggests that megaregolith formation, the disruption and re-accretion of bodies, may strongly depend upon body strength or may be less common than suggested by proponents of fragmentation-reassembly models of meteorite parent bodies (Davis et al. 1985; see, however, Pellas and Fieni 1988).

Strong Post-Accretionary Heating of the Inner Belt

The basaltic surface of Vesta (McCord et al. 1970) provided the first direct evidence suggesting a high-temperature history for an asteroidal body. Up through the work of Feierberg et al. (1982), the consensus was that most asteroids escaped significant thermal evolution. In this view, the compositional gradient across the belt was the signature—smudged, to be sure—of the radial solar nebula compositional gradient during planetesimal growth (see, e.g., Gradie and Tedesco 1982).

Subsequent results (see, e.g., Gaffey 1984,1986a,b; Gaffey and Ostro 1987; Bell 1986 and the chapter by Bell et al.) are consistent with the interpretation that at least the larger, inner-belt objects experienced strong heating (>1000°C) and underwent at least partial melting and magmatic differentiation. While S class asteroids may be undifferentiated bodies, no direct evidence requires, or even prefers, that any such asteroid is undifferentiated (Gaffey 1986a,b,1988). In fact, numerous lines of observational evidence suggest that most large S asteroids are thermally evolved, magmatically differentiated bodies. Gaffey (1988) showed that the proportion of heated asteroid types (A, E, M, S, V, R) decreases almost linearly with semimajor axis from approximately 100% at 2 AU to 0% at 3.5 AU. This indicates a heliocentric post-accretionary heat source similar to that proposed for solar wind induction heating during the T-Tauri stage of stellar evolution.

The present composition pattern seen in the asteroid belt appears due to a combination of initial nebular compositional gradient with strong post-accretionary heating modifying the inner belt. If so, ordinary chondrites that show evidence for thermal metamorphism, must have come from objects that escaped the most intense heating either because of their greater distance from the Sun or because they were less susceptible to heating (see, e.g., the chapter by Bell et al.).

VI. ASTEROIDAL CONSTRAINTS ON THE ASTEROID-METEORITE RELATIONSHIP

The Meteorites, an Incomplete and Unrepresentative Sample of the Asteroid Belt

Probably, at least a major fraction of the terrestrial meteorite flux is derived directly from the asteroid belt, or from intermediate parent bodies (e.g., near-earth asteroids) coming from the belt. If so, the relative proportions of asteroid and meteorite types indicate that the meteorite flux is both a biased and an incomplete sample of belt materials. For example, the basaltic achondrite/ olivine achondrite ratio in meteorite falls and the Antarctic collections is approximately $100:1$ while the ratio of asteroidal analogues (the V and A classes) is about $1:4$, a factor of four hundred discrepancy. Since S class asteroids should contribute to the olivine achondrite flux much more than to the basaltic achondrite flux (see, e.g., Gaffey 1984; Gaffey and Ostro 1987), the discrepancy is probably even greater. This discrepancy suggests that the meteorite flux at any point in time is dominated by a few favorably located source bodies either in Earth-crossing orbits or adjacent to the $3:1$ Kirkwood gap (Wetherill 1985), a conclusion consonant with hypothesized preterrestrial differences in the Antarctic/non-Antarctic populations as discussed in Sec. II.

Other assemblages, such as the apparently extensively aqueously altered surface materials of asteroids Ceres and Pallas (Gaffey 1978; Hildebrand et al. 1987), the F-type or the apparently organic-rich D- and P-type asteroids, have not been found among the meteorites. Relatively low physical strengths of such assemblages may significantly decrease their survival probability during atmospheric entry: this, too, is a source of bias (see, e.g., Greenberg and Chapman 1983).

The Apparent Absence of Ordinary Chondrites in the Belt

One of the most puzzling aspects of current asteroid investigations is the apparent absence or extreme rarity of ordinary chondrite-like assemblages in the asteroid belt, at least among the larger bodies. Such assemblages dominate the present meteorite flux. Dynamical models and meteoritical studies suggest their origin from a common asteroid type, probably near the chaotic zone associated with the $3:1$ Kirkwood gap at 2.50 AU (see, e.g., Wetherill 1985).

One solution to this apparent paradox (*model 1*) is simply that asteroid spectral interpretations are wrong and that some unknown regolith process is modifying an ordinary chondrite-type substrate to produce S-type spectra. Such an explanation is clearly not viable for the most carefully studied S asteroids, Flora and Eunomia: less definitive observational data imply differentiated surface assemblages for most of the larger S types. It is important to note that Flora was studied precisely because it was the most likely candidate for an ordinary chondrite-assemblage among eleven S asteroids (Feierberg et al. 1982). The data do not exclude the possibility of a small component of undifferentiated bodies within the S population but no observational evidence supports this and no investigator actively involved in asteroidal compositional characterizations currently champions the "S asteroids are ordinary chondrites" model.

Alternate resolutions of the paradox include *model 2* of Bell (1986; see also the chapter by Bell et al.) in which the post-accretionary heating mechanism had a lower size cutoff below which objects escaped heating. In this model, ordinary chondrite source bodies would be small (i.e., below the current observation limit) inner-belt objects derived from the fragmentation of moderate-sized ($\sim$100 km) ordinary chondrite parent bodies and which now dominate the terrestrial meteorite flux because of a favorable location, perhaps adjacent to the 3 : 1 Kirkwood gap or in Earth-crossing orbits.

Gaffey (1984) suggested two additional models to reconcile the paradox. If post-accretionary heating is concentrated in the outer regions of asteroidal parent bodies, possible by solar-wind induction heating (Herbert and Sonett 1979; also see the chapter by Scott et al.) or during heating due to a superluminous stage of early solar evolution (Sonett and Reynolds 1979), a cool undifferentiated core could be preserved below a melted and differentiated mantle (*model 3*). The metal-rich surface layers of some S asteroids could be strong metallic shells protecting ordinary chondrite cores, what Bell calls the "armor deck" model. When such an object collides with sufficient energy to actually disrupt, its dispersal would release a hoard (and horde) of small ordinary chondrite fragments. Such ordinary chondrite assemblages (Q types?) might dominate the smaller-size range of the inner main-belt population. However, regolith breccias containing trapped solar-wind and other irradiation effects could not come from such a population. Another problem arises in the presence of numerous exposed cores of differentiated bodies (the larger S types) which imply release of a large number of bodies that comprised the overlying metal-depleted mantles or surface layers. These should have produced numerous olivine (A-type) and olivine-pyroxene (R-type) asteroids, but these are rare. Where has this material gone?

Gaffey (1984) also suggested that ordinary chondrite assemblages of any size might be absent from the main belt. In this *model 4*, Q-type ordinary chondrite sources in the Earth-approaching population are derived from an Oort cloud reservoir, to which they were expelled from the inner solar system

during late stages of terrestrial planet accretion. Perturbed from Oort cloud orbits into orbits with small perihelia, these rocky bodies could be captured by Jupiter into short-period orbits just as cometary nuclei are, or might be involved in collisions with main-belt objects injecting some fraction of the fragments in short-period orbits.

The apparent absence of ordinary chondrite assemblages in the main belt strongly constrains the asteroid-meteorite relationship and any model for this must reconcile evidence from both sources. The four models described above all attempt to do this by various *ad hoc* means. None is as yet generally accepted, but all have the virtue of being testable. An asteroid sample return, *in situ* characterization, definitive metal-abundance determinations, or the development of a plausible spectral-modification mechanism would critically test *model 1*. Spectral studies of small inner-belt objects would test *models 2 and 3*. Observations of objects in short-period comet-like orbits would test *model 4*.

It is also evident that these different models imply very different rates and magnitudes of temporal variations in the relative proportion of meteorite types in the terrestrial meteorite population, from negligible (*model 1*) through moderate (*models 2 and 3*) to large (*model 4*). As discussed above, some evidence suggests a significant variation in the meteorite type flux distribution within the last few hundred thousand years; however, this question must be studied further.

VII. ASTEROIDAL SOURCES OF METEORITES

During the past decade, telescopic spectral studies of the minor planets have significantly constrained the controversial meteorite-asteroid relationship. In particular, it is important to keep a number of concepts in mind.

1. Asteroid studies clearly show that meteorites provide a very biased and incomplete sample of material from the asteroid belt. Asteroids do not contribute equally to the meteorite flux, and some do not appear to contribute at all. It is difficult to escape the conclusion that the present asteroidal bodies and the source bodies of the present meteorite population are, to some unknown extent, incongruous sets. Great caution must be exercised in extending conclusions drawn from the study of either asteroids or meteorites to the other. Conclusions correct for meteorites simply may not be relevant to the observed asteroids, and *vice versa*.

2. Characterizations of asteroid surface assemblages are available only for larger asteroids. Almost nothing is known about properties of the population below diameters of about 20 km, in particular, whether properties of the smaller asteroids are, or even should be, similar to those of the larger asteroids.

3. Even for larger asteroids, much of our data is sketchy and tentative. The variety and range of asteroid assemblages continue to expand as our data

improve. However, the trend of the evidence with increasing data quality is uniformly against the S asteroids being the ordinary chondrite source.

4. Except for ordinary chondrites, there are plausible source bodies for all significant meteorite types in the belt. However, no specific genetic links have yet been established between individual asteroids and meteorite specimens or groups.

5. In addition to the relative proportions of meteorite types, models of asteroid-meteorite relationships should also consider the diversity within the meteorite flux. Meteorite diversity is dominated by undifferentiated assemblages. Asteroids at 2 to 3 AU seem to be dominated by differentiated assemblages. There must be, or recently have been, at least one inner solar system outcrop for each different meteorite type. Many more outcrops of differentiated assemblages are required than of undifferentiated assemblages to explain the present meteorite diversity.

6. It is important to maintain the distinction between the asteroids we see today and the meteorite parent bodies whose nature and conditions are recorded in the meteorites. Regolith processes that produced ordinary chondrite breccias and the xenolithic inclusions in them, record some early solar system region. Care must be taken in extending conclusions from that distant time and uncertain location to the asteroid belt today. The meteorite story and asteroid story may be different pages within the same book.

7. Collisional modeling studies suggest that the present asteroidal population represents something between a small and a minuscule fraction of the original population in that region of the early solar system. If smaller members of the present population derive from collision breakup of larger members, then large amounts of material have been removed from the belt. What was this material and where is it today? Has the composition, as well as the number of asteroids changed with time?

8. Probably, much of the seemingly contradictory input from the meteoritic, the dynamic and the asteroid spectroscopy communities is, in fact, approximately correct. It is important to recall this and maintain a balanced perspective while integrating these seemingly orthogonal views. The details of the meteorite-asteroid relationships are not likely to be as simple as we would prefer, and the solution to the apparent paradoxes almost certainly lie in our lack of an overview of their complexity and subtleness. In one or two more decades, after we have looked at asteroidal material close up, we will be able to answer some of these questions in *Asteroids III*, but it is clear that newer questions will take their place.

REFERENCES

Adams, J. B. 1974. Visible and near-infrared diffuse reflectance spectra of pyroxenes as applied to remote sensing of solid objects in the solar system. *J. Geophys. Res.* 79:4829–4836.

Anders, E. 1964. Origin, age, and composition of meteorites. *Space Sci. Rev.* 3:583–714.

Anders, E. 1978. Most stony meteorites come from the asteroid belt. In *Asteroids: An Exploration Assessment*, eds. D. Morrison and W. C. Wells, NASA CP-2053, pp. 145–157.

Annexstad, J. O., Schultz, L., and Wänke, H., eds. 1986. *International Workshop on Antarctic Meteorites*, LPI Tech. Rept. 86-01 (Houston: Lunar and Planetary Inst.).

Bell, J. F. 1986. Mineralogical evolution of the asteroid belt. *Meteoritics* 21:333–334 (abstract).

Bell, J. F. 1987. Mineralogical evolution of meteorite parent bodies. *Lunar Planet. Sci.* XVII:985–986 (abstract).

Bell, J. F., and Keil, K. 1987. Spectral alteration effects in chondritic gas-rich breccias: Implications for S-class and Q-class asteroids. *Proc. Lunar Planet. Sci. Conf.* 18:573–580.

Bell, J. F., Owensby, P. D., Hawke, B. R., and Gaffey, M. J. 1988. The 52-color asteroid survey: Final results and interpretation. *Lunar Planet. Sci* XIX:57–58 (abstract).

Benkheiri, Y. 1984. ^{244}Pu fission track and metallographic cooling rates of Toluca and Copiapo iron (IA) meteorites. *Meteoritics* 19:188 (abstract).

Benkheiri, Y., Pellas, P., and Störzer, D. 1979. The cooling histories of Copiapo and Landes (IA) irons. *Icarus* 40:497–501.

Bernatowicz, T. J., Podosek, F. A., Swindle, T. D., and Honda, M. 1988. I-Xe systematics in LL chondrites. *Geochim. Cosmochim. Acta* 52:1113–1122.

Binns, R. A. 1967. Structure and evolution of non-carbonaceous meteorites. *Earth Planet. Sci. Lett.* 2:23–28.

Bogard, D. D., Husain, L., and Wright, R. J. 1976. ^{40}Ar-^{39}Ar dating of collisional events in chondritic parent bodies. *J. Geophys. Res.* 81:5664–5678.

Bogard, D. D., Mittlefehldt, D., and Jordan, J. 1988. ^{39}Ar-^{40}Ar dating of mesosiderites: A case for parent body description less than 4.0 Gyr ago? *Lunar Planet. Sci.* XIX:112–113 (abstract).

Bowell, E., Chapman, C. R., Gradie, J. C., Morrison, D., and Zellner, B. 1978. Taxonomy of asteroids. *Icarus* 35:313–335.

Brownlee, D. E. 1985. Cosmic dust: Collection and research. *Ann. Rev. Earth Planet. Sci.* 13:147–173.

Brownlee, D. E., Wheelock, M. M., Temple, S., Bradley, J. P., and Kissel, J. 1987. A quantitative comparison of Comet Halley and carbonaceous chondrites at the submicron level. *Lunar Planet. Sci.* XVIII:133–134 (abstract).

Buchwald, V. F. 1975. *Handbook of Iron Meteorites* (Berkeley: Univ. of California Press).

Bull, C. B. B., and Lipschutz, M. E. 1982. *Workshop on Antarctic Glaciology and Meteorites*, LPI Tech. Rept. 82-03 (Houston: Lunar and Planetary Inst.).

Buseck, P. R., and Goldstein, J. I. 1969. Olivine compositions and cooling rates of pallasitic meteorites. *Geol. Soc. Amer. Bull.* 80:2141–2158.

Cassidy, W. A., and Whillans, I. 1988. *Workshop on Ancient Meteorite Stranding Surfaces*, LPI Tech. Rept. (Houston: Lunar and Planetary Inst.), in preparation.

Chapman, C. R. 1977. The evolution of asteroids as meteorite parent-bodies. In *Comets, Asteroids, Meteorites*, ed. A. H. Delsemme (Toledo, Ohio: Univ. of Toledo Press), pp. 265–274.

Chapman, C. R., and Gaffey, M. J. 1979. Reflectance spectra for 277 asteroids. In *Asteroids*, ed. T. Gehrels (Tucson: Univ. of Arizona Press), pp. 655–687.

Chapman, C. R., Morrison, D., and Zellner, B. 1975. Surface properties of asteroids: A synthesis of polarimetry, radiometry, and spectrophotometry. *Icarus* 25:104–130.

Chen, J. H., and Wasserburg, G. J. 1981. The isotopic composition of uranium and lead in Allende inclusions and meteoritic phosphates. *Earth Planet. Sci. Lett.* 52:1–15.

Chen, J. H., and Wasserburg, G. J. 1985. U-Th-Pb isotopic studies on meteorites ALH 81005 and Ibitira. *Lunar Planet. Sci.* XVI:119–120 (abstract).

Clayton, R. N., and Mayeda, T. K. 1978. Multiple parent bodies of polymict brecciated meteorites. *Geochim. Cosmochim. Acta* 42:325–327.

Cloutis, E., Gaffey, M. J., Jackowski, T. L., and Reed, K. L. 1986. Calibrations of phase abundance, composition, and particle size distribution for olivine-orthopyroxene mixtures from reflectance spectra. *J. Geophys. Res.* 91:11641–11653.

Crabb, J., and Schultz, L. 1981. Cosmic-ray exposure ages of the ordinary chondrites and their significance for parent-body stratigraphy. *Geochim. Cosmochim. Acta* 45:2151–2160.

Crozaz, G., and Tasker, D. R. 1983. Fission and spallation tracks in merrillite: Their annealing behavior and the recent thermal history of meteorites. *Meteoritics* 18:284–285 (abstract).

Cruikshank, D. P., and Hartmann, W. K. 1984. The meteorite-asteroid connection: Two olivine-rich asteroids. *Science* 223:281–283.

Cruikshank, D. P., Bell, J. F., Gaffey, M. J., Brown, R. H., Howell, R., Beerman, C., and Rognstad, M. 1983. The dark side of Iapetus. *Icarus* 53:90–104.

Davis, D. R., and Chapman, C. R. 1977. Collisional evolution of asteroid compositional classes. *Lunar Sci.* VIII:224–226 (abstract).

Davis, D. R., Chapman, C. R., Weidenschilling, S. J., and Greenberg, R. 1985. Collisional history of asteroids: Evidence from Vesta and the Hirayama families. *Icarus* 62:30–53.

Dennison, J. E., and Lipschutz, M. E. 1987. Chemical studies of H chondrites—II. Weathering effects in the Victoria Land Antarctic population and comparison of two Antarctic populations with non-Antarctic falls. *Geochim. Cosmochim. Acta* 51:741–754.

Dennison, J. E., Lingner, D. W., and Lipschutz, M. E. 1986. Antarctic and non-Antarctic meteorites: Different populations. *Nature* 319:390–393.

Dennison, J. E., Kaczaral, P. W., and Lipschutz, M. E. 1987. Volatile chalcophile, siderophile and lithophile trace elements in lunar meteorite Yamato-82192. In *Proc. Eleventh Symp. Antarctic Meteorites*, pp. 89–95.

Dermott, S. F., Gradie, J., and Murray, C. D. 1985. Variation of the UBV colors of S-class asteroids with semimajor axis and diameter. *Icarus* 62:289–297.

Feierberg, M. A., Larson, H. P., and Chapman, C. R. 1982. Spectroscopic evidence for undifferentiated S-type asteroids. *Astrophys. J.* 257:361–372.

Fricker, P. E., Goldstein, J. I., and Summers, A. L. 1970. Cooling rates and thermal histories of iron and stony-iron meteorites. *Geochim. Cosmochim. Acta* 34:475–491.

Gaffey, M. J. 1978. Mineralogical characterizations of asteroid surface materials: Evidence for unsampled meteorite types. *Meteoritics* 13:471–473 (abstract).

Gaffey, M. J. 1983. The asteroid (4) Vesta: Rotational spectral variations, surface material heterogeneity, and implications for the origin of the basaltic achondrites. *Lunar Planet. Sci.* XIV:231–232 (abstract).

Gaffey, M. J. 1984. Rotational spectral variations of asteroid (8) Flora: Implications for the nature of the S-type asteroids and for the parent bodies of the ordinary chondrites. *Icarus* 60:83–114.

Gaffey, M. J. 1986a. The spectral and physical properties of metal in meteorite assemblages: Implications for asteroid surface materials. *Icarus* 66:468–486.

Gaffey, M. J. 1986b. Evolution of the inner asteroid belt: Paradigms and paradoxes from spectral studies. *Meteoritics* 21:365–366 (abstract).

Gaffey, M. J. 1988. Thermal history of the asteroid belt: Implications for accretion of the terrestrial planets. *Lunar Planet. Sci.* XIX:369–370 (abstract).

Gaffey, M. J., and McCord, T. B. 1977. Asteroid surface materials from reflectance spectroscopy: A result. In *Comets, Asteroids, Meteorites,* ed. A. H. Delsemme (Toledo, Ohio: Univ. of Toledo Press), pp. 199–216.

Gaffey, M. J., and McCord, T. B. 1979. Asteroid surface materials: Mineralogical characterizations from reflectance spectra. *Space Sci. Rev.* 21:555–628.

Gaffey, M. J., and Ostro, S. J. 1987. Surface lithologic heterogeneity and body shape for asteroid (15) Eunomia: Evidence from rotational spectral variations and multi-color lightcurve inversions. *Lunar Planet. Sci.* XVIII:310–311 (abstract).

Gehrels, T., ed. 1979. *Asteroids* (Tucson: Univ. of Arizona Press).

Goldstein, J. I., and Ogilvie, R. E. 1965. The growth of the Widmanstätten pattern in metallic meteorites. *Geochim. Cosmochim. Acta* 29:893–920.

Goldstein, J. I., and Short, J. M. 1967. Cooling rates of 27 iron and stony-iron meteorites. *Geochim. Cosmochim. Acta* 31:1001–1023.

Gradie, J., and Tedesco, E. 1982. Compositional structure of the asteroid belt. *Science* 216:1405–1407.

Graham, A. L., Bevan, A. W. R., and Hutchison, R. 1985. *Catalogue of Meteorites,* 4th ed. (London: British Museum (Natural History) and Tucson: Univ. of Arizona Press).

Greenberg, R., and Chapman, C. R. 1983. Asteroids and meteorites: Parent bodies and delivered samples. *Icarus* 55:455–481.

Grimm, R. E. 1985. Penecontemporaneous metamorphism, fragmentation and reassembly of ordinary chondrite parent bodies. *J. Geophys. Res.* 90:2022–2028.

Harvey, R., and Cassidy, W. A. 1988. A statistical comparison of Antarctic finds and modern falls: Mass frequency distributions and relative abundance by type. *Meteoritics,* submitted.

Haq, M., Hasan, F. A., and Sears, D. W. G. 1988. Thermoluminescence and the shock and reheating history of meteorites—IV: The induced TL properties of type 4-6 ordinary chondrites. *Geochim. Cosmochim. Acta* 52:1679–1689.

Herbert, F., and Sonett, C. P. 1979. Electromagnetic heating of minor planets in the early solar system. *Icarus* 40:484–496.

Heymann, D. 1967. On the origin of hypersthene chondrites: Ages and shock effects of black chondrites. *Geochim. Cosmochim. Acta* 29:1203–1208.

Heymann, D. 1978. Solar gases in meteorites: The origin of chondrites and C1 carbonaceous chondrites. *Meteoritics* 13:291–303.

Hildebrand, A. R., Jones, T. D., and Lebofsky, L. A. 1987. Is Ceres differentiated? *Meteoritics* 22:410–411 (abstract).

Hohenberg, C. M., Hudson, B., Kennedy, B. M., and Podosek, F. A. 1981. Noble gas retention chronologies for the St. Séverin meteorite. *Geochim. Cosmochim. Acta* 45:535–546.

Housen, K. R., and Wilkening, L. L. 1982. Regoliths on small bodies in the solar system. *Ann. Rev. Earth Planet. Sci.* 10:355–376.

Hutchison, R., Alexander, C. M. O., and Barber, D. J. 1987. The Semarkona meteorite: First recorded occurrence of smectite in an ordinary chondrite, and its implications. *Geochim. Cosmochim. Acta* 51:1875–1882.

Hutchison, R., Williams, C. T., Din, V. K., Clayton, R. N., Kirschbaum, C., Paul, R. L., and Lipschutz, M. E. 1988. Our oldest basaltic rock? A pebble in the Barwell, L5-6, chondritic meteorite. *Earth Planet. Sci. Lett.*, 90:105–118.

Kaneoka, I. 1980. ^{40}Ar-^{39}Ar ages of Antarctic meteorites: Y-74191, Y-75258, Y-7308, Y-74450 and ALH 765. In *Proc. Fifth Symp. Antarctic Meteorites*, pp. 177–188.

Kaneoka, I. 1984. Characterization of Ar-degassing from Antarctic meteorites. In *Proc. Ninth Symp. Antarctic Meteorites*, pp. 272–284.

Kelly, S., and Turner, G. 1987. Laser probe ^{40}Ar-^{39}Ar investigation of the "unique" meteorite Bencubbin. *Meteoritics* 22:427 (abstract).

Kirsten, T. 1973. Isotope studies in the Mundrabilla iron meteorite. *Meteoritics* 8:400–403.

Lanzerotti, L. J., Brown, W. L., and Johnson, R. E. 1985. Laboratory studies of ion irradiations of water, sulfur dioxide, and methane ices. In *Ices in the Solar System*, eds. J. Klinger, D. Benest, A. Dollfus and R. Smoluchowski (Dordrecht: D. Reidel), pp. 317–335.

Larimer, J. W. 1973. Chemical fractionations in meteorites—VII. Cosmothermometry and cosmobarometry. *Geochim. Cosmochim. Acta* 37:1603–1623.

Laul, J. C., Smith, M. R., Wänke, H., Jagoutz, E., Dreibus, G., Palme, H., Spettel, B., Burghele, A., Lipschutz, M. E., and Verkouteren, R. M. 1986. Chemical systematics of the Shergotty meteorite and the composition of its parent body (Mars). *Geochim. Cosmochim. Acta* 50:909–926.

Lingner, D. W., Huston, T. J., Hutson, M., and Lipschutz, M. E. 1987. Chemical studies of H chondrites. I. Mobile trace elements and retention ages. *Geochim. Cosmochim. Acta* 51:727–739.

Lipschutz, M. E., and Cassidy, W. A. 1986. Antarctic meteorites: A progress report. *Eos: Trans. AGU* 67:1339–1341.

Lipschutz, M. E., and Woolum, D. S. 1988. Highly labile elements. In *Meteorites and the Early Solar System*, eds. J. F. Kerridge and M. S. Matthews (Tucson: Univ. of Arizona Press), pp. 462–487.

Lorin, J. C., and Pellas, P. 1979. Preirradiation history of Djermaia (H) chondritic breccia. *Icarus* 40:502–509.

Manhés, G. 1982. Développement de l'ensemble chronométrique U-Th-Pb. Contribution à la chronologie initiale du système solaire. Thèse, Univ. de Paris VII.

Manhes, G., Göpel, C., and Allègre, C. J. 1987. High resolution chronology of the early solar system based on lead isotopes. *Meteoritics* 22:453–454 (abstract).

Matson, D. L., Johnson, T. V., and Veeder, G. J. 1977. Soil maturity and planetary regoliths: The Moon, Mercury, and the asteroids. *Proc. Lunar Sci. Conf.* 8:1001–1011.

McCord, T. B. 1978. Asteroid surface mineralogy: Evidence from Earth-based telescope observations. In *Asteroids: An Exploration Assessment*, eds. D. Morrison and W. C. Wells, *NASA* CP-2053, pp. 109–124.

McCord, T. B., Adams, J. B., and Johnson, T. V. 1970. Asteroid Vesta: Spectral reflectivity and compositional implications. *Science* 168:1445–1447.

McFadden, L. A., Gaffey, M. J., and McCord, T. B. 1985. Near-Earth asteroids: Possible sources from reflectance spectroscopy. *Science* 219:160–163.

McFadden, L. A., Pieters, C. M., Huguenin, R. L., Hawke, B. R., King, T. V. V., and Gaffey, M. J. 1986. Reflectance spectroscopy of lunar meteorite Yamato-791197: Relation to remote sensing data bases of the moon. *Proc. Tenth Symp. Antarctic Meteorites*, pp. 140–151.

McGarvie, D. W., Wright, I. P., Grady, M. M., Pillinger, C. T., and Gibson, E. K., Jr. 1987. A

stable carbon isotopic study of types 1 and 2 carbonaceous chondrites. In *Proc. Eleventh Symp. Antarctic Meteorites,* pp. 179–195.

McKay, D. S., and Basu, A. 1983. The production curve for agglutinates in planetary regoliths. *Proc. Lunar Planet. Sci. Conf.* 14, *J. Geophys. Res. Suppl.* 88:B193–B199.

McSween, H. Y., Jr. 1979. Are carbonaceous chondrites primitive or processed? A review. *Rev. Geophys. Space Phys.* 17:1059–1078.

McSween, H. Y., Jr. 1987. Aqueous alteration in carbonaceous chondrites: Mass balance constraints on matrix mineralogy. *Geochim. Cosmochim. Acta* 51:2469–2477.

Minster, J. F., and Allègre, C. J. 1979. ^{87}Rb-^{87}Sr chronology of H chondrites: Constraints and speculations on the early evolution of their parent body. *Earth Planet. Sci. Lett.* 42:333–347.

Minster, J. F., and Allègre, C. J. 1981. ^{87}Rb-^{87}Sr dating of LL chondrites. *Earth Planet. Sci. Lett.* 56:89–106.

Ngo, H. T., and Lipschutz, M. E. 1980. Thermal metamorphism of primitive meteorites—X. Additional trace elements in Allende (C3V) heated to 1400°C. *Geochim. Cosmochim. Acta* 44:731–739.

Niemeyer, S. 1979. ^{40}Ar-^{39}Ar dating of inclusions from IAB iron meteorites. *Geochim. Cosmochim. Acta* 43:1829–1840.

Nishiizumi, K. 1986. Terrestrial and exposure histories of Antarctic meteorites. In *Workshop on Antarctic Meteorites,* eds. J. O. Annexstad, L. Schultz and H. Wänke, LPI Tech. Rept. 86-01 (Houston: Lunar and Planetary Inst.), pp. 71–73.

Oberst, J., and Nakamura, Y. 1986. Distinct meteoroid families identified on lunar seismograms. *Proc. Lunar Planet. Sci. Conf.* 17, *J. Geophys. Res. Suppl.* 92:E769–E773.

Olsen, E. J., and Bunch, T. E. 1984. Equilibration temperatures of the ordinary chondrites: A new evaluation. *Geochim. Cosmochim. Acta* 48:1363–1365.

Onuma, N., Clayton, R. N., and Mayeda, T. K. 1972. Oxygen isotope temperatures of "equilibrated" ordinary chondrites. *Geochim. Cosmochim. Acta* 36:157–168.

Ostro, S. J., Campbell, D. B., and Shapiro, I. I. 1985. Mainbelt asteroids: Dual-polarization radar observations. *Science* 229:442–446.

Ott, U., and Begemann, F. 1985. Martian meteorites: Are they (all) from Mars? *Nature* 317:509–512.

Palme, H., Larimer, J. W., and Lipschutz, M. E. 1988. Moderately volatile elements. In *Meteorites and the Early Solar System,* eds. J. F. Kerridge and M. S. Matthews (Tucson: Univ. of Arizona Press), pp. 436–461.

Pellas, P. 1981. Early thermal histories of L chondrites. *Lunar Planet Sci.* XII:825–827 (abstract).

Pellas, P., and Fiéni, C. 1988. Thermal histories of ordinary chondrite parent asteroids. *Lunar Planet. Sci.* XIX:915–916 (abstract).

Pellas, P., and Storzer, D. 1981. ^{244}Pu fission track thermometry and its application to stony meteorites. *Proc. Roy. Soc. London* A374:253–270.

Pellas, P., Perron, C., Crozaz, G., Perelygin, V. P., and Stetsenko, S. G. 1983. Fission track age and cooling rate of the Marjalahti pallasite. *Earth Planet. Sci. Lett.* 64:319–326.

Powell, B. N. 1969. Petrology and chemistry of mesosiderites. I. Textures and composition of nickel-iron. *Geochim. Cosmochim. Acta* 33:789–810.

Schultz, L., and Signer, P. 1977. Noble gases in the St. Mesmin chondrite: Implications to the irradiation history of a brecciated meteorite. *Earth Planet. Sci. Lett.* 36:363–371.

Scott, E. R. D. 1985. Pairing of meteorites found on Victoria Land, Antarctica. In *Proc. Ninth Symp. Antarctic Meteorites,* pp. 102–125.

Scott, E. R. D., Brearley, A. J., Keil, K., Grady, M. M., Pillinger, C. T., Clayton, R. N., Mayeda, T. K., Wieler, R., and Signer, P. 1987. Nature and origin of C-rich ordinary chondrites and chondritic clasts. *Proc. Lunar Planet. Sci. Conf.* 18:513–524.

Sonett, C. P., and Reynolds, R. T. 1979. Primordial heating of asteroidal parent bodies. *Asteroids,* ed. T. Gehrels (Tucson: Univ. of Arizona Press), pp. 822–848.

Takeda, H. 1986. Parent sources of Antarctic meteorites as inferred from pairing of the specimens. In *International Workshop on Antarctic Meteorites,* eds. J. O. Annexstad, L. Schultz and H. Wänke, LPI Tech. Rept. 86-01 (Houston: Lunar and Planetary Inst.), pp. 107–109.

Takeda, H., Mori, H., Delaney, J. S., Prinz, M., Harlow, G. E., and Ishii, T. 1983. Mineralogical comparison of Antarctic and non-Antarctic HED (howardites-eucrites-diogenites) achondrites. In *Proc. Eighth Symp. Antarctic Meteorites,* pp. 181–205.

Takigami, Y., and Kaneoka, I. 1987. Investigation of the effect of shock on the Antarctic Meteorites by the ^{40}Ar-^{39}Ar method. In *Proc. Eleventh Symp. Antarctic Meteorites*, pp. 133–143.

Taylor, G. J., Maggiore, P., Scott, E. R. D., Rubin, A. E., and Keil, K. 1987. Original structures and fragmentation and reassembly histories of asteroids: Evidence from meteorites. *Icarus* 69:1–13.

Tholen, D. J. 1984. Asteroid Taxonomy from Cluster Analysis of Photometry. Ph.D. Thesis, Univ. of Arizona.

Turner, G., Enright, M. C., and Cadogan, P. H. 1978. The early history of chondrite parent bodies inferred from ^{40}Ar-^{39}Ar ages. *Proc. Lunar Planet. Sci. Conf.* 9:989–1025.

Vickery, A. M., and Melosh, H. J. 1987. The large crater origin of SNC meteorites. *Science* 237:738–743.

Wasserburg, G. J., Papanastassiou, D. A., and Sanz, H. G. 1969. Initial strontium for a chondrite and the determination of a metamorphism or formation interval. *Earth Planet. Sci. Lett.* 7:33–43.

Wasson, J. T., and Rubin, A. E. 1985. Formation mesosiderites by low-velocity impacts as a natural consequence of planet formation. *Nature* 318:168–170.

Wasson, J. T., and Wetherill, G. W. 1979. Dynamical, chemical and isotopic evidence regarding the formation locations of asteroids and meteorites. In *Asteroids*, ed. T. Gehrels (Tucson: University of Arizona Press), pp. 926–974.

Wetherill, G. W. 1969. Relationships between orbits and sources of chondritic meteorites. In *Meteorite Research*, ed. P. M. Millman (Dordrecht: D. Reidel), pp. 573–589.

Wetherill, G. W. 1977. In *Comets, Asteroids, Meteorites*, ed. A. H. Delsemme (Toledo, Ohio: Univ. of Toledo Press), pp. 283–291.

Wetherill, G. W. 1985. Asteroidal source of ordinary chondrites. *Meteoritics* 20:1–22.

Wetherill, G. W. 1986. Unexpected Antarctic chemistry. *Nature* 319:357–358.

Wetherill, G. W., and Williams, J. G. 1969. Evaluation of the Apollo asteroids as sources of stone meteorites. *J. Geophys. Res.* 73:635–648.

Wilkening, L. L. 1977. Meteorites in meteorites: Evidence for mixing among the asteroids. In *Comets, Asteroids, Meteorites*, ed. A. H. Delsemme (Toledo, Ohio: Univ. of Toledo Press), pp. 389–395.

Willis, J., and Goldstein, J. I. 1981. A revision of metallographic cooling rate curves for chondrites. *Proc. Lunar Planet. Sci. Conf.* 12:1135–1143.

Willis, J., and Goldstein, J. I. 1983. A three-dimensional study of metal grains in equilibrated, ordinary chondrites. *Proc. Lunar Planet. Sci. Conf.* 14, *J. Geophys. Res. Suppl.* 88:B287–B292.

Wood, C. A. 1982. Fall statistics of H chondrites: Evidence of cometary origins for ordinary chondrites. *Lunar Planet. Sci.* XIII:873–874 (abstract).

Wood, J. A. 1964. The cooling rates and parent planets of several iron meteorites. *Icarus* 3:429–459.

Wood, J. A. 1967. Chondrites: Their metallic minerals, thermal histories, and present bodies. *Icarus* 6:1–49.

Wood, J. A. 1979. Review of the metallographic cooling rates of meteorites and a new model for the planetesimals in which they formed. In *Asteroids*, ed. T. Gehrels (Tucson: Univ. of Arizona Press), pp. 849–891.

Zellner, B., Tholen, D. J., and Tedesco, E. F. 1985. The eight-color asteroid survey: Results for 589 minor planets. *Icarus* 61:355–416.

Note added in proof: Recent data for CM2 chondrites from Queen Maud Land, Antarctica, demonstrate significant metamorphism, hence differences with falls. Reference: Paul, R. L. and Lipschutz, M. E. 1989. Labile trace elements in some Antarctic carbonaceous chondrites: Antarctic and non-Antarctic meteorite comparisons. *Zeit. Naturf.*, submitted.

DELIVERY OF ASTEROIDS AND METEORITES TO THE INNER SOLAR SYSTEM

RICHARD GREENBERG and MICHAEL C. NOLAN

University of Arizona

Critical observational constraints on the delivery of asteroids (including the very small ones, called meteorites, that land on the Earth) include orbital distributions, exposure ages and mineralogy. Orbital maturity in the inner solar system is indicated by the AM/PM distribution of meteorite falls and fireballs: orbits with perihelia at 1 AU are less mature and arrive preferentially in the PM. Ordinary chondrites have short exposure ages, but their AM/PM fall statistics indicate significant orbital maturity. Hence, many may be collisional offspring of slightly larger parents that emigrated from the main belt. The required size distribution, extrapolated up to multi-km-size bodies, would also yield numbers of planet-crossing asteroids comparable to those astronomically observed. However, such a distribution requires launch on Earth-bound trajectories by catastrophic disruption events, which probably cannot launch sufficient material at high enough velocities. Cratering events offer higher ejecta velocities, and if dominant would explain the abundance of basaltic meteorites relative to olivine, which should constitute the bulk of a differentiated parent body's volume. Whether cratering can produce enough meteorites, with the observed PM fraction, is not clear, but the possibility remains open, given uncertainties in the collisional and dynamical processes. Orbital clusters of both Amor-class asteroids and stony fireballs near a = 2.05 AU and 2.50 AU suggest significant contribution from the v_6 secular resonance as well as from the 3 : 1 resonance. How multi-km Apollo-Amor-Atens are launched from the main belt is a major outstanding problem, as is identification of a parent population for the ordinary chondrites now that S-type asteroids once again are considered to be different from this most common kind of meteorite on the basis of reflectance spectroscopy.

[778]

I. INTRODUCTION

Most meteorites probably come from the asteroid belt. With a few important but quantitatively small exceptions, there are no other likely sources. Moreover, as a population of rocky bodies in the process of smashing one another into pieces, the asteroids seem a most plausible source. This much was understood ten years ago when the predecessor volume *Asteroids* was published (Gehrels 1979). Beyond that, one would like to understand the relation between the various petrological/geochemical types of meteorites and the various astronomical classes of asteroids. Which meteorites are the same as which kinds of asteroids? Can we understand the mechanisms of formation of meteoritic material and its delivery to the Earth well enough to explain the absolute and relative amounts of the various types? Ultimately, can we hope to identify specific parent bodies for individual meteorites?

A decade ago there was a major obstacle to proceeding very far toward answering these questions. The most common type of meteorite, the ordinary chondrites, had no spectrally identified presence in the asteroid belt. And the most common kind of asteroid, the S type, seemed similar only to relatively rare meteorites: stony-irons, or perhaps enstatite chondrites.

This impasse seemed to be removed with the spectral study by Feierberg et al. (1982), which indicated that S asteroids might well be made of ordinary chondritic material. During the brief interval after 1982 when the S/ordinary chondrite identification was widely believed to be plausible, two major models of asteroid/meteorite demographics were published (Greenberg and Chapman 1983; Wetherill 1985).

However, the pendulum of popular opinion has now swung back, based on the work of Gaffey (1986; chapter by Gaffey et al.) to the identification of most S asteroids as differentiated material with a major metallic component, not ordinary chondrites. It is not clear that this conclusion is final or absolute; its merits are discussed in chapters by Lipschutz et al. and Bell et al. Wetherill (1985) guesses that surficial spectral data may misrepresent the bulk proportions of various materials; Larson (personal communication, 1988) also remains skeptical about Gaffey's conclusion; Bell points out that there are different kinds of S's and that some may be ordinary chondrite, while others are not. Thus, the S/ordinary chondrite identity remains a possibility, but seems to be contrary to the currently favored (Gaffey's) interpretation.

If the S's really are not ordinary chondrites, then the models of Greenberg and Chapman and of Wetherill are seriously undermined. In that case, both models would still have value as templates for future attacks on the problem. They both define critical processes and issues, and show how these relate to important observables. The models are complementary in the sense that each concentrates on a different subset of the relevant processes and addresses a different subset of the key observational constraints.

However, even if the S's are ordinary chondrites, which would satisfy the zeroth order assumption in both models, neither model is completely acceptable. Each tends to gloss over the central processes in the other, and each tends to ignore (and to some degree violate) the key observables that constrained the other. What remains to be done (and of course can only be done tentatively until the S identity is resolved), is to combine the ways of relating processes to observables that were demonstrated in the two models into a single model that contains all the important processes and fits all the observational constraints. Toward that goal, the objective of this chapter is to describe both models in a common framework, and to review both critically, highlighting the strong points of each.

II. OVERVIEW OF THE TWO MODELS

A. Collisional Model

The model by Greenberg and Chapman (1983; hereafter called G&C) concentrated on the collisional processes that liberate material from asteroidal parent bodies and launch it onto trajectories that can eventually reach the Earth. A key observational constraint for that model is the lack of any substantial representation of olivine on a volumetric basis among differentiated meteorites that reach the Earth. Any differentiated parent body with even approximately chondritic composition would have a concentration of basalt near the surface (~20% of the body's volume), which is the low-density silicate component, over a thick mantle of olivine (~70%), with a relatively small iron core (~10%). If this material were sampled on a volumetric basis by the processes of impact and delivery, one would expect to receive several times more olivine meteorites than basaltic ones, contrary to actual statistics.

Similarly, on a volumetric basis, iron from the core would be far more abundant than the tiny amount of stony-iron material at the core/mantle interface. But pallasites (olivine-iron meteorites) are considerably over-represented on the Earth.

The way around these difficulties, as proposed by G&C, is that the dominant collisional process for launching material onto Earth-bound trajectories is cratering. (The word cratering is used here to mean any process that tends to remove only surface material, and that launches this material at fairly high velocity. Cratering as used here could refer to chipping or spallation as well. We are not concerned here with the morphology of the hole left behind.) On a differentiated parent, this process preferentially samples surface layers (e.g., basalts) over deeper mantle material (Fig. 1(1)).

Catastrophic disruption events were assumed to be ineffective at getting material into our collections. There are a couple of arguments for that assumption. First, catastrophic events might not launch material at sufficiently high velocities to initiate trajectories to the Earth, although we know from labora-
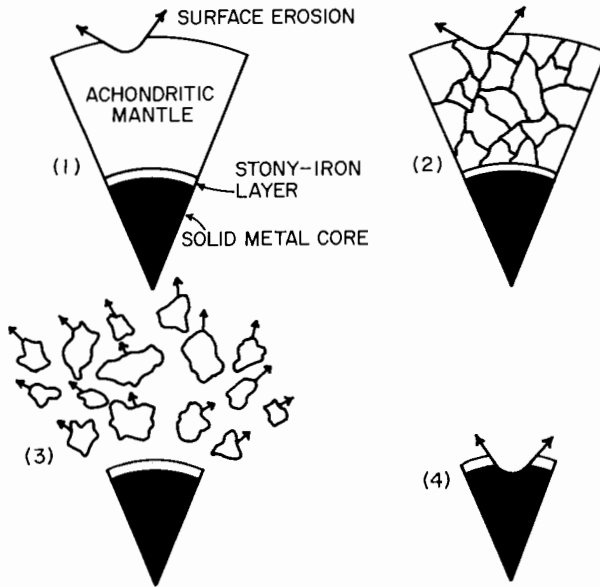
Fig. 1. Possible collision outcomes for differentiated parent bodies. (1) Cratering of an intact body samples the surface silicates, predominantly basalts. (2) A parent that has undergone catastrophic fragmentation, but remains gravitationally bound has its silicates jumbled; subsequent cratering liberates olivine. (3) Catastrophic disruption (fragmentation with fragments escaping) leaves the strong core with a stony-iron outer layer. (4) Subsequent cratering preferentially samples the stony-irons.

tory experiments and geological studies that cratering can. Second, such events would be relatively infrequent and might not happen to contribute at this time in solar system history.

Catastrophic disruption, when it occurred, was assumed to comminute olivine mantles while leaving strong metallic cores intact (Fig. 1(3)). Thus the olivine was subject to further fragmentation without much material being injected onto Earthward paths. The metal cores remain, and are subject to continuing cratering of their surfaces, which may liberate from the surface stony-iron and iron material for Earth-bound transport (Fig. 1(4)), while leaving the bulk of the iron behind intact in the asteroid belt.

Several quantitative elements of this story depended on unknown parameters, so G&C adopted the inductive approach of adjusting those parameters to make the model fit the observed statistics of meteorite and asteroid types (of course in the context of the S/ordinary chondrite identification). The model was constructed to explain not only the major classes of meteorites, but details about subclasses as well. For example, ordinary chondrites come from only a few parent bodies in that model, consistent with the three major kinds of ordinary chondrite. The fact that the data could be explained without outland-

ish choices of parameters for the various processes involved suggested that the model was on the right track.

On the other hand, not everyone has the same ideas of what is a physically plausible range of parameters. Wetherill (1985) objected that the increasing asteroid strength with size, which is necessary in the model so that only a few largest asteroids can contribute the bulk of each meteorite class, does not have a clear physical basis. In fact, by the inductive approach of G&C, this parameter choice was not an *a priori* assumption, but rather a requirement driven by the need to explain meteorite demographics in terms of asteroid sources. Its plausibility was rationalized by noting that collisional history within the main belt may have preferentially weakened smaller bodies.

Wetherill (1985) made two other explicit criticisms of that model. Greenberg and Chapman had assumed that roughly 20% of the material that entered resonance zones upon being ejected from parent bodies would impact the Earth. Again, in accord with the inductive approach, this number was largely selected to fit the observed flux of meteorites. Its plausibility was argued on the grounds that resonances might efficiently pump up orbital eccentricities, based on Wisdom's (1982) early reports of chaotic effects, and later reinforced as Wisdom's research continued (1983,1987). Wetherill (1985) criticized the 20% figure, comparing it with his own value 0.28%, which was based on his quantitative application of Wisdom's results to a Monte Carlo study of orbital evolution. Such a substantial difference would be potentially devastating to the G&C model.

Is it possible to reconcile these two values? First, we need to confirm that they do address the same efficiency. The 20% value from G&C refers to efficiency of impacts with planet Earth (above the atmosphere); on the other hand, the description of how the 0.28% value was obtained (Wetherill 1985) seems to suggest that it includes an atmospheric filtering factor. That difference would go a long way toward resolving the discrepancy. However, Wetherill now clarifies (personal communication) that the latter value (and all other efficiency values given in the tables of results in Wetherill [1985]) does refer to pre-atmospheric impact.

Actually these values can be reconciled in the context of the collision model. The G&C model yielded $\sim 1.2 \times 10^8$ g yr^{-1} of meteorite-size bodies at the Earth's surface. The fall rate estimated from fireball data (Halliday et al. 1984), and adopted by Wetherill (1985) as the best "observed" fall rate, is 3.9 $\times 10^7$ g yr^{-1}. Thus the efficiency assumed by G&C could be reduced to 6%, and it would only improve the agreement with observations. The G&C model also incorporated the assumption that the asteroid population is somewhat depleted below about 1 km in radius. This depletion allows for most meteorites to come from cratering of a few large asteroids so as to give the observed distribution of types. It is also the only way to preserve, in the context of the G&C model, a population of Apollo-Amors, which like all small asteroids were assumed to be very weak. The paucity of small asteroids would

increase the collision lifetime of small bodies en route to the Earth by an order of magnitude, so the relevant Earth-impact efficiency from Wetherill's (1985) Table 3 increases from 0.28% to about 2%, i.e., within a factor of three of the efficiency required in the G&C model. Given the significant uncertainty in all the calculations (as discussed in later sections), this constitutes good agreement.

Wetherill's (1985) other objection to the G&C model was that it assumes that all ejecta are meteorite-sized, while he believes that only about 10% is. This difference is due to the production of meteorites explicitly by cratering in the G&C model, as explained above, and the implicit assumption that catastrophic fragmentation is dominant in Wetherill's own model discussed below.

B. Orbital Evolution Model

The serious shortcoming of the G&C model is that it does not address the orbital distribution of meteorites arriving at the Earth. The orbital information is precisely what drives Wetherill's model. G&C concentrated on fitting asteroid types to meteorite classes by detailed modeling of collisional processes, while glossing over details of orbital evolution and ignoring orbital data on meteorites. On the other hand, Wetherill tried to fit the orbital data by constructing a detailed Monte Carlo simulation of orbital evolution, while glossing over details of collisional processes and not addressing many of the details of meteorite classification. In this way, as noted in the introduction, the two approaches are complementary, but neither is completely satisfactory by itself (even if S asteroids are ordinary chondritic).

Orbital information comes from trajectories of fireballs that are identified as ordinary chondrites (Wetherill and ReVelle 1981), from astrometry of three actual ordinary-chondrite falls, and from visual data on radiants of ordinary-chondrite falls (Simonenko 1975). Its relevance to the asteroid source issue is that statistical information on orbits indicates how long a given population has been en route from the asteroid belt. A particularly informative statistical parameter that describes this aspect of orbital statistics is the ratio of PM (i.e., noon to midnight) meteorite falls to total falls. This fraction is directly related to the degree of concentration of orbital perihelia near 1 AU.

The significance of the PM fraction as an indicator of orbital maturity follows from consideration of the stages of orbital evolution. A useful visualization (see, e.g., Kresák 1967) comes from a plot of orbital evolution on the semimajor axis a vs eccentricity e plane (Fig. 2). The shaded area shows the main belt (and Trojans, although not relevant to this discussion). Main-belt material injected into a resonance zone (especially the 3 : 1 and ν_6 resonances; see the chapters by Froeschlé and Greenberg and Scholl et al.) as debris or ejecta from a collision can have its eccentricity pumped up by chaotic effects. Earth-orbit crossing is first reached (in ∼1 Myr) with perihelion q near 1 AU, and subsequent evolution is predominantly controlled by gravitational encoun-

Orbital Elements of Fireballs
and Earth–Crossing Asteroids
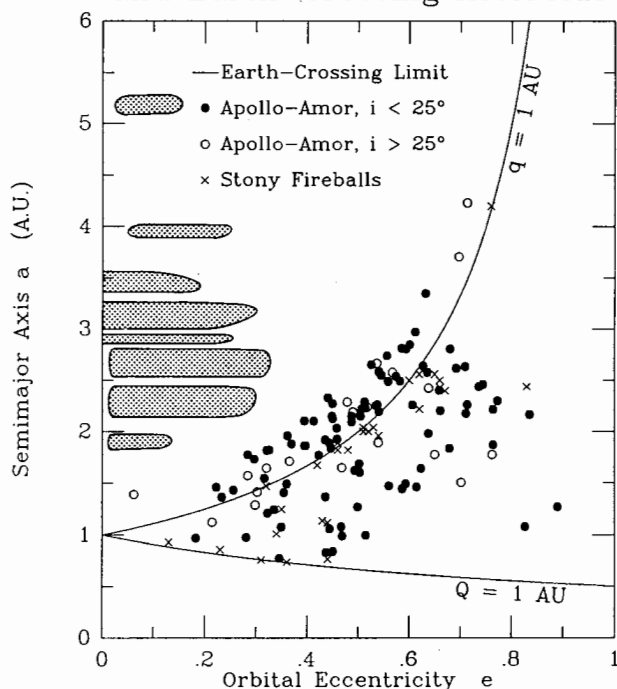
Fig. 2. A plot of semimajor axis a vs eccentricity e for asteroids. Main-belt and Trojan regions are shown by the shaded areas. The 3 : 1 and the low-inclination ν_6 resonances are at 2.5 and 2.05 AU, respectively. Limits of Earth crossing are where perihelion q or aphelion Q distance equal 1 AU (more precisely 1.017 and 0.983 AU when the Earth's e is taken into account). By definition, Amor class objects lie above the $q = 1$ line; Apollos lie between the $a = 1$ and $q = 1$ lines; Atens lie between $Q = 1$ and $a = 1$. Once an object becomes an Earth crosser, it evolves due to encounters with the Earth along surfaces of constant Tisserand invariant, which roughly parallel the $q = 1$ and $Q = 1$ lines, except at lower e where they cross from $q = 1$ to $Q = 1$ (Kresák 1967). After such evolution for $\sim$10 Myr, it may become a Venus crosser as well, and is then free to evolve rapidly over much of a,e space. (Asteroid data from E. Helin [personal communication]; fireball data from Wetherill and ReVelle [1981].)

ters with the Earth. For the next $\sim$10 Myr, encounters allow a random walk in a,e space, but confined close to the $q = 1$ AU line.

Only over a longer time scale can the random walk yield more "deeply" Earth-crossing orbits, spreading a population over the entire Earth-crossing zone. Figure 2 shows how the Apollo asteroids (plus the nearly Earth-crossing Amors) and the known meteorite orbits are distributed in this space. By a few 100 Myr, most trajectories lead to impact with a terrestrial planet (exponential decay time scale $\sim$100 Myr) or to Jupiter crossing with rapid ejection from

the solar system (~30 Myr). All these quoted time scales (see also the Appendix) come from the Monte Carlo experiments of Wetherill (1985,1989).

An object with $q \approx 1$ AU that hits the Earth does so on the trailing or PM side, where local time is after noon and before midnight, because the object's heliocentric orbital motion at perihelion is faster than, but in the same direction as, the Earth's. Such objects are generally less orbitally mature, in the sense of evolution from the main belt, than objects which have had more time to evolve into deep Earth crossers. A more mature population will have a more nearly equal AM/PM distribution of Earth-impact times.

From Monte Carlo modeling of orbital evolution, Wetherill (1985) showed that for a population that evolves for 20 Myr from orbits that are initially Earth-crossing near $a = 2.5$ AU (3 : 1 resonance) with $q \approx 1$ AU, 76% of the Earth impacts will be PM events. This value is quite reasonable, given that for the first 10 Myr the orbits must remain near $q = 1$ AU (100% PM falls) and for the second 10 Myr, they are deep Earth crossers (50% PM).

Most ordinary chondrites' cosmic-ray exposure ages are < 20 Myr. Presumably the limited exposure reflects a cut-off to their lifetimes imposed by impacts with other, even smaller, interplanetary particles (predominantly small asteroids encountered during apocentric passages through the main belt). The characteristic time scale before such catastrophic disruption is usually called the collision lifetime, as distinct from the other dynamical processes that terminate orbital evolution such as impact into a planet or ejection from the solar system. Ordinary chondrites that reached the Earth intact apparently were not exposed during transit to the Earth for > 20 Myr. Corresponding orbital immaturity might be expected to result in PM fall fractions >76%. In fact, however, ordinary chondrites have significantly smaller PM fractions of 65% ± 5%.

A plausible explanation for the lower observed PM fractions is that some portion of the ordinary chondrites left the asteroid belt as part of larger objects in which they were protected from cosmic-ray exposure. The larger bodies would have longer collisional lifetimes and could achieve greater orbital maturity before being disrupted. Part of the debris from these larger Earth crossers would be of meteoritic size (10^2 to 10^6 g is the estimated range for chondrite sizes before passing through the Earth's atmosphere). Such second- (or third- or fourth-) generation objects would have had orbits that would reflect the orbital maturity of their parents, even though their own collisional lifetimes are <10 Myr. Their contribution to fall-time statistics would tend to be more evenly distributed between AM and PM (although the PM fraction is never less than about 57% because the dynamical lifetime of all bodies is 100 Myr, during the first 10 Myr of which Earth impacts are about 100% PM). Thus a suitable mix of meteorite-size bodies, some direct from the asteroid belt and others from Earth-crossing asteroids, would give the observed PM/AM ratio.

Wetherill (1985) considered an assumed distribution of sizes of asteroids

injected into resonance and evaluated the expected quantity and PM fraction of meteorite-size bodies that hit the Earth. For material that came via the 3 : 1 resonance, these results were in reasonable agreement with observations for ordinary chondrites. The only other main-belt source that may contribute significant numbers of meteorites is the inner main belt near the ν_6 resonance (where oscillations resonate with the apsidal precession rate of Saturn). However, Wetherill (1987) has shown that a much lower PM fraction, about 50%, is achieved for material leaving the main belt via the latter resonance. This result has been given as evidence that achondrites come preferentially from this source, on the grounds that their falls are evenly divided between AM and PM (Wetherill 1987), although the fall-time statistics for achondrites are not compelling (see Sec. V).

In the remainder of this chapter we discuss the processes of delivery with special attention to the elements that remain uncertain, and the implications that these uncertainties have for the sources of meteorites. It will be demonstrated that the range of uncertainty is so great that no particular theoretical evaluation of delivery processes should be taken too literally from a quantitative point of view. However two qualitative conclusions seem difficult to avoid: (1) the PM fall fraction reflects a mix of bodies that have been able to reach varying degrees of orbital maturity since leaving the asteroid belt; and (2) parent bodies' crusts and core/mantle interfaces are preferentially sampled by the excavation and delivery process.

III. COLLISIONAL EXCAVATION AND INJECTION INTO RESONANCE

The asteroid belt is undergoing a process of comminution in which bodies are being ground down to ever smaller sizes by collisions. The same process sends some debris onto trajectories that ultimately reach the terrestrial planets. This material consists of bodies of a size too small (less than a few km) to be studied at their source from the Earth. We can guess about the population and collision rates there by invoking a steady-state model: at any given size, there may be a balance between collisional destruction of bodies and creation due to the breakup of larger bodies.

This equilibrium was evaluated in a detailed analysis by Dohnanyi (1969). Here we reproduce its essence in a more accessible form. First assume that the size distribution can be described by the power law

$$d_r N = C r^{-p} dr \tag{1}$$

where $d_r N$ is the number of main-belt bodies of radius r to $r + dr$. Bodies of this size are catastrophically disrupted by collision with any object of radius kr or greater, where we assume all impacts are at about the same speed. Most of these destructive projectiles are smaller than the r-size targets, so the rate of

destruction is proportional to the number of projectiles and the total cross-sectional area of target bodies

$$d(d_r N)/dt \propto N_{>kr} \, r^2 \, d_r N \tag{2}$$

where

$$N_{>kr} = \int_{kr}^{\infty} C \, r^{-p} \, dr = C(kr)^{1-p}/(1 - p) \tag{3}$$

so

$$d(d_r N)/dt = -\tau^{-1} \, d_r N \tag{4}$$

where $\tau \equiv Kr^{p-3}$ and K is a constant. If bodies of this size were not replenished, their numbers would decay exponentially on the time scale τ, which is their "collision lifetime."

When a larger body (radius r_b) breaks up, experiments show that it produces debris that follow a power law

$$d_r N = Br^{-q}dr \tag{5}$$

In general, excess impact energy yields greater comminution (smaller B and larger q), but the most probable breakup events have not much more energy than the minimum required for catastrophic fragmentation, in which case the largest fragment has a radius which is a certain fraction b of the original size r_b. In that case, the coefficient is

$$B = (1 - q)(br_b)^{q - 1} \tag{5a}$$

such that there is only one piece of debris as large as br_b. In any case, for the mass of debris to equal the mass of the fragmented body,

$$q = (b^3 + 4)/(b^3 + 1) \tag{5b}$$

so q is always less than 4, because the total mass of debris must be finite, and q must be substantially greater than 2.5, because $b < 1$.

The production rate of bodies of size r due to breakup of the larger bodies r_b is

$$d(d_r N)/dt = (Br^{-q}dr) \times (1/\tau(r_b)) \, dr_b N \tag{6}$$

and this rate integrated over all larger bodies ($r_b = r/b$ to ∞) is

$$d(d_r N)/dt = (C/K)[(1 - q)/(q - 2p + 3)] \, b^{2p-4} \, r^{3-2p} \, dr. \tag{7}$$

In fact, this expression is an overestimate because the integration should only be extended to the size r_{max} of the largest body in the population, but the estimate is not bad as long as $r_{max} \gg r/b$. In a steady state, Eq. (7) must balance the depletion rate (Eq. 4), which can be expressed as

$$d(d_r N)/dt = - (C/K) r^{3 - 2p} dr. \tag{8}$$

From Eqs. (7) and (8), a steady state (ss) requires

$$[(1 - q)/(q - 2p + 3)] b^{2p - 4} = 1 \tag{9}$$

or

$$p_{ss} = 3/2 + q/2 + b^{2p - 4} (q - 1)/2. \tag{10}$$

With substitution of q from Eq. (5b), we find that $p_{ss} = 3.5$ precisely satisfies Eq. (10), independent of the exact value of b.

The above discussion is somewhat simplified in a number of ways. The true steady-state value p_{ss} can differ (but remains in the mid-range between 3 and 4) when additional details are taken into account (cf. Dohnanyi 1969). For example, we have not included the effects of cratering impacts, which erode target bodies and create a population of much smaller debris. However, Dohnanyi showed that those events are unimportant relative to catastrophic disruption in this context.

How can a population that is undergoing overall continual comminution, like the asteroid belt, be in an equilibrium between destruction and creation of bodies in any given size increment? Suppose the population is in the steady state with $p = p_{ss}$. The equilibrium holds through most of the size range, but not near the limit of the largest bodies. There, the evaluation of the replenishment rate by integration of Eq. (6) as above becomes invalid. There simply are not enough even-larger bodies to supply the large end of the distribution with debris. Thus the largest bodies in the distribution will decrease in numbers at the rate given by Eq. (4). In turn, the entire population of smaller bodies decreases so as to maintain the steady-state power law (Fig. 3). In effect, in the steady state, the exponential decay time for numbers at all sizes is the lifetime τ of the largest body in the population.

One other aspect of the evolution of this type of idealized population needs to be understood. Suppose the distribution were a steeper power law, $p > p_{ss}$. In that case, at all sizes there is insufficient replenishment of numbers by debris from larger bodies. Numbers decay exponentially at rates given by Eq. (4) for each size. The shorter lifetimes for smaller bodies means that the size distribution flattens to the log/log slope p_{ss} at the small end before much change has occurred at the large end (Fig. 4). A bend develops where the two curves meet. As the number of bodies at that size decreases (at the rate given
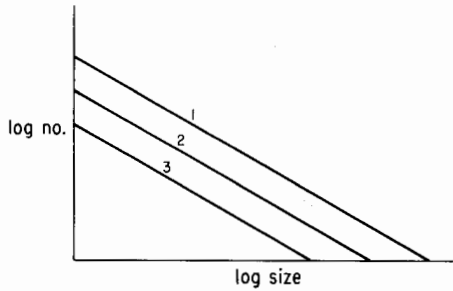
Fig. 3. Evolution of the size distribution of a population in a steady state. Slope in this log/log schematic plot is the steady-state power-law index p_{ss}. Numbers are diminishing from time 1 to 3, at a rate such that the intercept at the abscissa remains at a given size for as long as the collisional lifetime of the body of that size. The distribution would actually "wag" a bit due to the stochastic timing of destruction at the large end.
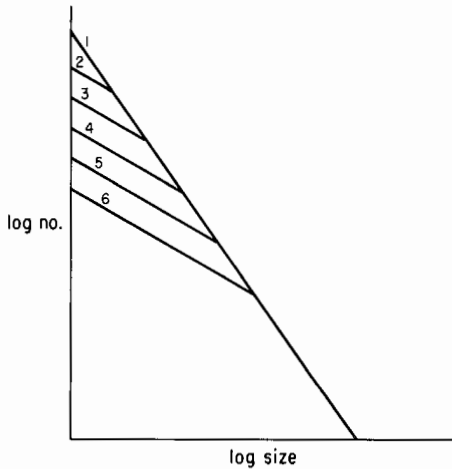
Fig. 4. Evolution of a size distribution initially steeper than p_{ss}, such as the collisional production assumed to be syphoned Earthward in the model of Wetherill (1985,1987). Such a population evolves toward equilibrium starting at the small-body end as shown. The position of the bend after any time t is given by the size for which the exponential-decay lifetime equals t. This evolution is less sensitive to stochastic timing than the example shown in Fig. 3, because there are so many bodies at the bend. The bend is actually less abrupt (more curved) than shown in this schematic.

by Eq. 4), the tail of the distribution (smaller bodies) decreases with it as shown in Fig. 4. Hence the numbers in the tail diminish at a rate given by the exponential decay lifetime of the size at the bend. And the number of small bodies remaining at any time t is given by extrapolation on the p_{ss} power law down from the number of bodies with $\tau(r)$ just greater than t (Fig. 4).

If we assume that the asteroids smaller than a few km are in a power-law steady state and that the same collisional production that replenishes numbers

of smaller bodies also injects a representative sample of those bodies into resonance zones for eventual delivery to planet-crossing orbits, then the injection rate is given by

$$d(d_r N)/dt \propto \tau^{-1} \, d_r N \propto r^{-4}. \tag{11}$$

This formalism implies that in every increment of time, a subpopulation of asteroids with a very steep size distribution ($p = 4 > p_{ss}$) embarks on the hazardous journey to the terrestrial planets. These bodies continue to be impacted by other asteroids, primarily those they encounter during continued passage through the main belt during parts of their orbits. Thus, each such subpopulation undergoes the collisional evolution expected for an initially steep size distribution (as shown in Fig. 4), while the orbits mature toward increased planet crossing (as described in the previous section). The number of bodies of meteorite size diminishes in accord with the lifetimes of much larger bodies. Individual meteorite size bodies of course have very short lifetimes, but are replenished by debris from the breakup of larger ones. The debris presumably reflects the degree of orbital maturity of the entire subpopulation, even if these individual later-generation particles are quite young as separate entities (short exposure ages).

Wetherill (1985,1987) in effect used this model to determine the proportion of meteorite-size bodies that survive collisions with other asteroids to reach various degrees of orbital maturity, although he did not describe his procedure in quite these same terms. By combining this model of the numbers of meteorites as a function of orbital time since leaving the main belt with Monte Carlo results on the orbital evolution of planet crossers, he found a theoretical value of the PM fall fraction (69%) that fit the ordinary-chondrite observation (65 ± 5%), if he started with orbits with semimajor axes near 2.5 AU, where there is a 3 : 1 commensurability with Jupiter's period.

That model assumes that material injected into resonance is characteristic of typical collisional production in the main belt. Thus, at all sizes the material is predominantly produced by catastrophic fragmentation events rather than by cratering, according to the results of Dohnanyi (1969). Moreover, in the size range from meters to ~10 km, which ultimately yields most of the meteoritic material in Wetherill's model, it is even more unlikely that material is injected to any significant degree by cratering. This implicit assumption thus contrasts with the G&C model in which predominance of cratering, perhaps mostly from a few of the largest events during the relevant time increment, was used to explain the relative abundances of the various meteorite types. G&C's model invoked experimental evidence (based primarily on Gault et al. 1963) regarding velocities of crater ejecta: substantial portions of excavated material can be ejected at speeds > 100 m s^{-1} if the target is solid basalt, for example.

Wetherill (1987) also referred to the debris-producing events in his model

as "cratering," and invoked the same experimental evidence as G&C did from cratering experiments as a basis for injections of debris into Earth-bound trajectories in the Monte Carlo experiments. However, as described above, a predominance of catastrophic disruption is implicit in Wetherill's adoption of typical main-belt production as the basis for the material injected into resonance.

The cited experimental results, specifically obtained for crater formation, cannot be applied to catastrophic disruption that must produce most debris in Wetherill's scenario. Gault et al. (1963) based their determination of velocity distributions on measurements of the expansion of the front of ejecta plumes. Extension of those results to a case of catastrophic fragmentation is not well justified. Moreover, it is not clear that competent, solid rock is the relevant material for the bulk of a target asteroid. Ejecta from weak material moves much more slowly, at least in the case of cratering (Stoffler et al. 1975), a phenomenon that was taken into account by G&C. In the case of catastrophic fragmentation, even ejecta from solid rock probably moves much more slowly than crater ejecta. Fujiwara and Tsukamoto (1980) found in laboratory experiments with impacts at nearly 3 km s^{-1} that most debris was launched at velocities < 10 m s^{-1}. (See the chapter by Fujiwara et al. on catastrophic fragmentation for more on this subject.) Such velocities would be too low to launch the required amounts of material into resonance in the Wetherill model.

The relevance of laboratory-scale experiments to collisions in the asteroid belt is always questionable. An interesting piece of evidence on velocities of debris from catastrophic disruption comes from the orbital distribution of members of Hirayama families (see the chapter by Valsecchi et al.). If these families do represent pieces of larger single bodies, their present orbital distributions required initial ejection of the pieces at speeds of ~ 150 m s^{-1}, consistent with Wetherill's model. On the other hand, invoking Hirayama families' orbits does not resolve the issue of debris velocity as much as it reminds us of another unsolved mystery of asteroid studies (Housen and Holsapple 1988). If debris velocities are generally $\lesssim 10$ m s^{-1}, how did the Hirayama members get their high relative velocities? In a recent preprint, Wetherill (1989) notes that the dispersion of family members may be due to some post-impact orbital diffusion process (Farinella et al. 1986), and thus identifies the issue of debris velocity as a possible problem with the delivery model.

While low velocities pose a problem with delivering enough catastrophic debris to the terrestrial planets, there may also be a problem with producing the correct PM fraction. Equipartition of energy suggests that smaller debris might have higher ejection velocities. This effect would enhance the relative proportion of small bodies injected into resonance compared with the size distribution of collisional production and thus tend to increase the fraction that hits the Earth in the PM. Since Wetherill's model gives a PM fraction (69%)

that is already near the greatest value consistent with observations, such an increase would not be acceptable.

Given the range of uncertainties regarding the impact processes, we can imagine a model which combines the desirable features of cratering (which yields the right kinds of differentiated material) with the constrained size distribution of material injected into resonance inferred from planet-crosser dynamics (which yields the correct PM fraction). G&C assumed that nearly all crater ejecta was in the meteorite-size range, which would give too large a PM fraction of ordinary chondrites. The correct PM fraction might be achieved if some of the ejecta were larger to supply material capable of reaching orbital maturity. The larger bodies might be from craters in a broad zone (~0.1 AU) near resonances, and from catastrophic disruption in a much narrower zone (~0.01 AU). The size distribution of such injected material would not be governed by the steep power law of the average main-belt production function assumed by Wetherill and found to give an acceptable PM fraction. However, it might be steepened to an appropriate degree by excess injection of small bodies due to their higher ejection velocities from the sites of impacts.

The point of this discussion is that there is great uncertainty about the nature of the collision processes that inject material into resonance. There remains a wide range of viable collision models that could yield the right mix of large and small bodies (which yield PM fractions of 57% to 75%, respectively) to give the observed PM fraction (65 ± 5%). Just because one model gives results consistent with the ordinary chondrite PM fraction is not strong evidence that it is the only possible model. Similarly, it may be that the distinction between the PM fractions of achondrites (about 53%) and of ordinary chondrites (if that difference is real) may be due to some degree by the nature of the impact launching process, rather than strictly a difference between locations of the sources.

IV. RESONANCES

Although resonances, especially that near the 3:1 commensurability with Jupiter, have now been shown to be plausible mechanisms for delivering asteroidal bodies to the terrestrial planets, there remains sufficient uncertainty about their effects that, as with collisional processes, scenarios for delivery remain subject to substantial revision. What we do know about behavior at resonance is described in Greenberg and Scholl (1979) and the chapters by Froeschlé and Greenberg and Scholl et al.

In order to investigate the delivery of material to Earth via the 3:1 resonance, Wetherill (1985) invoked some "typical" properties of the chaotic behavior computed by Wisdom (1983). Of course, as both Wisdom and Wetherill noted, chaotic behavior is by definition such that it is impossible to generalize about possible behavior from a limited set of examples. With that caveat, it

appears that orbital eccentricities increase to give Mars crossing ($e \approx 0.3$) in about 10^5 yr and to Earth crossing ($e \approx 0.6$) in about 10^6 yr (Fig. 5).

During a 1 Myr period of Mars crossing, encounters with Mars are likely to change the mean motion by more than 0.03 AU, enough to remove an orbit from resonance. That result comes from Monte Carlo experiments (Wetherill 1985); see also the Appendix. Thus Wetherill assumed that about half of the bodies will be on only Mars crossing orbits at the beginning of his Monte Carlo evolution calculations. Once the others become Earth crossing, Wisdom's typical cases show that e remains >0.6 for about 10^4 yr, just long enough for encounters with the Earth to uncouple them from the resonance (as shown in the Appendix). Therefore Wetherill started this other half of the population as Earth crossers in his Monte Carlo tests.

The half of the population that starts as only Mars crossers when leaving resonance takes about 100 Myr to become Earth crossers (see Appendix). Their dynamical evolution toward Earth is severely delayed. By the time they reach Earth crossing, their size distribution must be considerably evolved to substantially the steady-state form, without the substantial excess of short-lived meteorite-size bodies that the other half of the population has upon ar-
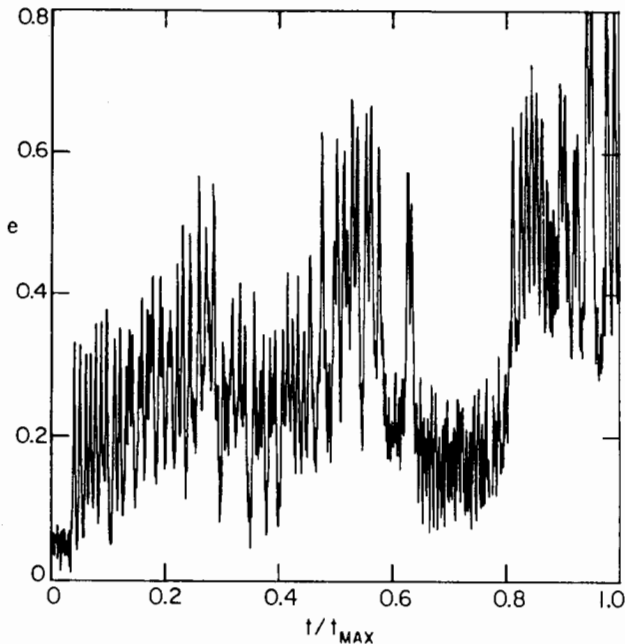
Fig. 5. Evolution of eccentricity for a chaotic trajectory in the 3 : 1 resonance (Wisdom 1983), with initial inclination of a few degrees. Earth crossing ($e = 0.6$) is reached in about 1 Myr ($t_{max} = 2.4$ Myr). Wetherill (1985) assumed that this value is typical and that, contrary to the behavior shown here, the asteroid is Mars crossing ($e > 0.3$) for most of that time.

rival at Earth crossing. Thus the hijacking of resonant bodies by Mars must substantially reduce the PM fraction of meteorites produced in this model.

It is possible that the extent of this hijacking has been significantly mis-estimated, but in which sense is hard to say. Inspection of Wisdom's typical case shows that during the 1 Myr before Earth crossing is reached, the orbit is only Mars crossing for about 10% of the time. If that is typical, the amount of material hijacked by Mars is negligible, the amount that reaches Earth may nearly double compared with the published model, and the PM fraction may substantially increase.

On the other hand, the typical case is based on an initial orbital inclination i of $5°$ or $10°$ (which value was used is uncertain). With $i = 0$, the resonance does not pump e above about 0.3 (Wisdom 1983). We do not yet know the i dependence in detail, but it may well be that a realistic range of initial inclinations might modify the orbital evolution of the population. More-over, the validity of Wisdom's calculations is questionable for e as large as 0.6, because the analysis was only done to third order in e. And even if the calculations of evolution of e performed to date are correct, there remains the question of how truly "typical" they are.

Any of these uncertainties could significantly affect both total numbers of delivered meteorites and their PM fraction. One could imagine ways in which true chaotic resonant behavior might give the observed PM fraction, even if all the bodies injected into resonances are meteorite-size. For example, suppose that most objects in the $3 : 1$ resonance reach Earth-crossing values of e in about 1 Myr, but they are uncoupled from the resonance typically when $e = 0.7$ (significant overlap of Earth's orbit), rather than when $e = 0.6$ (barely tangen-tial to Earth's orbit). In that case, the population could spread across the Earth-crossing portion of a,e space (Fig. 2) relatively quickly, yielding a much smaller PM fraction than the value (76%) from the assumption that initially $e = 0.6$.

The above example is hypothetical, but there is new evidence that, in fact, bodies on barely Earth-crossing orbits (i.e., those that give the greatest PM excess) may not impact the Earth before their orbits have significantly evolved. Numerical integration experiments by Tanakawa et al. (1987) sug-gest that perihelion distances must be < 0.9 AU (0.1 AU orbital overlap with the Earth) for impact to occur. That study was done only for zero-inclination orbits, so its implications are not definitive, but it does illustrate that the range of uncertainty about orbital behavior is still too great to support any particular detailed explanation of the measured PM fraction.

V. OTHER KINDS OF DELIVERED ASTEROIDS: ACHONDRITES AND APOLLOS

Most of the above discussion concentrated on delivery of ordinary chondrites, the most common kind of asteroid to land on the Earth. Next we address the delivery of other kinds as well.

Meteorites from differentiated asteroids include irons, stony-irons and the stone achondrites. The irons and stony-irons exhibit very long cosmic-ray exposure ages ($\sim$1 Gyr). Evidently their great strength allows them to survive collisions even as small bodies for much longer than stones. Such bodies clearly have survived to achieve complete orbital maturity before hitting the Earth or suffering one of the other dynamical demises. Therefore, issues of dynamics are less constraining than in the case of the ordinary chondrites. However, as mentioned above, the relative abundance of stony-irons requires a preferential excavation from differentiated asteroids. This constraint led to the conclusion by G&C that irons and stony-irons must be excavated and launched into resonance by cratering of strong iron cores that had been previously stripped of their silicate mantles.

Stone achondrites are nearly all basaltic, characteristic of the lowest-density silicates of a differentiated planet, the lavas that flow to the surface. The idea that cratering is the predominant way of excavating and launching meteorites toward Earth was largely motivated by this observation. The other interesting constraint offered by achondrites is the suggestion that their AM and PM falls may be more nearly equal than the chondrites'. Wetherill (1987) quotes an observed PM fraction of 53% and offers an ingenious explanation for this difference, based on calculations that indicate material reaching the Earth from the innermost edge of the asteroid belt.

Bodies near the inner edge of the main belt with typical orbital eccentricities are not very far from Mars crossing. With velocities similar to those assumed for the chondrites near the 3 : 1 resonance ($\sim$150 m s^{-1}, as discussed in the previous section), collisional debris can be injected close enough to the ν_6 resonance that it can undergo significant oscillations in e. These variations are qualitatively different from the behavior invoked at the 3 : 1 resonance. So far, no chaotic behavior has been demonstrated for secular resonance. Instead, the variations were assumed by Wetherill (1987) to follow analytically predictable oscillations of secular theory.

Such material spends a substantial fraction of its time in Mars-crossing orbits. Over $\sim$100 Myr it will random walk to Earth crossing (the same process and time scale for material in the 3 : 1 resonance that gets hijacked by Mars and delayed in its voyage to the Earth) and then to terrestrial-planet impact or ejection from the solar system. Of course, if its collision lifetime is shorter, it may not achieve such orbital maturity. By the time such a population reaches Earth crossing, its size distribution must have already flattened to the equilibrium power law $p = 3.5$, rather than the production power law $p = 4$, which a younger population would retain. Thus, the excess of small short-lived bodies that gave the significantly >50% PM fraction for Earth impactors from the 3 : 1 resonance does not exist for Earth impactors from the inner main belt. Wetherill (1987) concluded that achondrites must therefore come preferentially from that region. The other resonances farther out in the main belt are probably not important sources of Earth-crossing material, because bodies

there first become Jupiter crossers and are generally ejected from the solar system (Murray 1986).

The case for an inner-belt source of achondrites depends on the same implicit assumptions about collisional injection of material into resonance as did the model for ordinary chondrites at the 3:1 resonance. Thus, it suffers from the same uncertainties about the relevant collisional processes. Similarly, it depends on assumptions about behavior in resonance that are not fully explored or understood. Although there is a well-developed theory for motion near secular resonance, recent numerical experiments (Froeschlé and Scholl 1986,1987; see also the chapter by Scholl et al.) have shown that behavior at the ν_6 resonance can deviate from those predictions. Even though the motion is not chaotic, surprisingly high eccentricities can be achieved quickly (e.g., $e = 0.6$ in 1 Myr). Until this behavior is mapped out and understood, generalities about delivery of material from that region are speculative at best.

A final difficulty with that proposed source of the achondrites is the uncertainty about the significance of the statistics that yield the PM fraction. Histograms of the fall times of chondrites and achondrites (Fig. 6) show the shift toward the PM for the former, but any claim of AM/PM symmetry for the achondrites is questionable. The numbers involved are so small that the PM fraction has a very great uncertainty: 50% ± 15% (Wetherill 1968). Taking into account these large error bars, the achondrite PM fraction is not statistically distinguishable from the chondrites'. Perhaps the similarities are more striking: both groups have sharp peaks in the hour between 3 and 4 PM. The most striking feature of the achondrite distribution is the lunch-time gap.
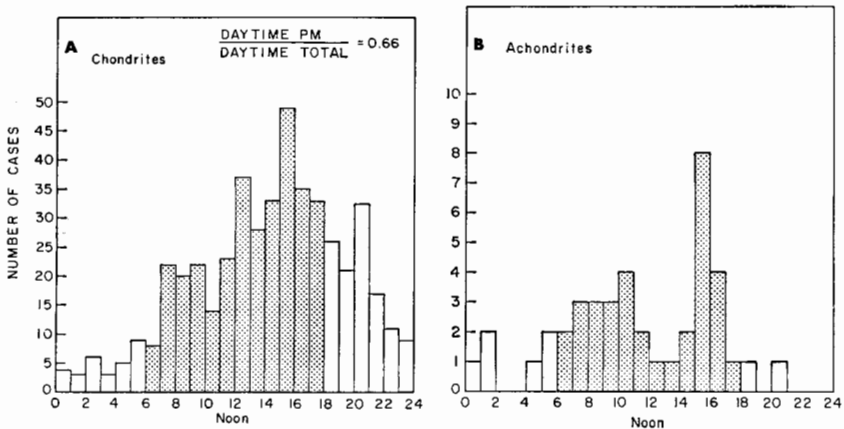
Fig. 6. Observed local times of fall of stone meteorites (Wetherill 1968). The numbers of achondrites are too small to show any significant difference in AM/PM ratio compared with the chondrites, so that datum is not a convincing way to discriminate among source regions. More intriguing, albeit of marginal statistical significance, is the achondrite lunch break: without this prominent minimum, the achondrite distribution would look much like the chondrites.

Do farmers tend to nap at lunch time when achondrites fall? Since achondrite falls are not clearly more symmetrical about noon than chondrites, there is no clear basis for any preferential inner-belt source.

The largest asteroids to become terrestrial-planet crossers are the Apollos, Atens and Amors, defined by their orbits as shown in Fig. 2. In a sense, all meteorites were tiny Apollo or Aten asteroids before they hit the Earth. But we will restrict these names to Earth-crossers large enough to be observed astronomically ($\gtrsim 1$ km). Each Apollo is more likely to hit the Earth than a given meteorite-size body. Fortunately for life on the Earth, the former are much less numerous and hit the Earth less frequently. Wetherill (1989) considers these larger bodies to be generated as part of the same continuous collisional production as he invoked to explain the ordinary chondrites' delivery rate and PM fall excess. With that rate of km-plus asteroids injected into potentially Earthward trajectories, the Monte Carlo calculations give a steady-state number of Apollos comparable to the number determined from observational surveys. Wetherill concludes that there is no difficulty populating the Apollos completely from the main belt, although he recognizes persuasive evidence that a large portion are extinct comets, as would also be consistent with his results to their level of precision.

Those calculations are certainly consistent with Wetherill's scenario for delivering the ordinary chondrites, but they are subject to all the same unknowns. Especially mysterious is how bodies as large as Apollos were ejected from impact sites at velocities exceeding 100 m s^{-1}. This problem exists for bodies only a little larger than meteorite size and seems to be even greater for objects larger than 1 km.

While in the above respect, planet-crossing asteroids are at least as difficult to understand as meteorites, there is additional information about their source that is not available for meteorites and has not yet been exploited. Recall that for the meteorites, orbital statistical information is almost entirely encoded in the PM fraction, which tells something about the orbital distribution in a,e space. For the Amor-Apollo-Atens, however, we have the actual distribution as shown in Fig. 2, which has some interesting structure, especially just outside the Earth-crossing zone (Amors). Amors are concentrated in orbits with a just beyond the 3:1 resonance ($a = 2.5$ AU) with a striking gap just inside the resonance (2.3 to 2.5 AU); similarly, there is a concentration at 2.1 AU (just outside the small-inclination ν_6 resonance at 2.05 AU and the 4:1 resonance at 2.06 AU), and a gap just inside the resonance location (1.9 to 2.05 AU).

Wetherill's (1989) Monte Carlo study does not reproduce these clusterings. In fact, it produces a strong concentration at 2.05 AU across the entire Earth-crossing space, a feature not seen in the real Apollos. Just as models of meteorite production and delivery are constrained by the PM fraction of meteorite falls, a successful model of asteroid delivery should be consistent with these other details of the orbital distribution.

Similarly, the fireball distribution must have something to tell us. As shown in Fig. 2, the fireball orbits of apparently stony bodies (Wetherill and ReVelle 1981) seem to be concentrated just inside the Earth-crossing zone with distinct clusters at 2 and at 2.5 AU, just the locations of the ν_6 and 3 : 1 resonances. The clusterings, if real, may be some indication of main-belt sources. Moreover, they suggest that many of the fireball bodies hit Earth within ~1 Myr of achieving Earth crossing, because in a longer time they would have random walked more smoothly over the space just inside $q = 1$. A problem to be resolved, however, is that the fireball orbits reported by Wetherill and ReVelle (1981) with 0.9 AU $< q <$ 1 AU lie in a forbidden zone according to the results of Tanikawa et al. (1987). Such orbits cannot be achieved by integrating backwards from the observed fireball trajectories as they hit the Earth. Apparently, some correction is required to the published orbits to account properly for the gravitational effect of the Earth as well as the Sun.

VI. DISCUSSION AND CONCLUSION

In this review, we have emphasized the uncertain elements that prevent definitive acceptance of any particular model for delivery of asteroidal material to the terrestrial region. These uncertainties are in several areas:

1. The identification of the various types of meteorites with observed classes of asteroids;
2. Collisional excavation of materials from asteroids;
3. Collisional launching of material onto trajectories that may lead to the Earth;
4. The full range of plausible kinds of resonant behavior that may control delivery.

Related fundamental questions remain unanswered except in tentative ways: Why are stony-irons and basalts so heavily represented among differentiated meteorites? Where are ordinary chondrites in the asteroid belt? Are chondrites and achondrites delivered in fundamentally different ways? Are statistics of the relevant data set (e.g., orbital or meteoritic demographics) governed by systematic processes or by random events? What is typical resonant evolution? How can objects as large as a few km be shot into resonance at >100 m s^{-1}?

These questions are amenable to solution, and progress in these areas during recent years has been significant as reported throughout this book. Some of the issues will not be resolved until a credible complete scenario is constructed. The Greenberg and Chapman model that focused on collisional processes cannot be accepted as truth until many dynamical and other issues are resolved. The orbital evolution models (Wetherill), now greatly advanced with the new results on resonant behavior, still have zeroth-order uncertain-

ties. Nevertheless, these synthetic models play an essential role in the search for understanding, as they demonstrate the various interconnections among the elements of the complete process. They provide a template for future synthesis that will be made possible as specific details are addressed.

This process is beautifully demonstrated in studying the work of Wetherill on asteroid and meteorite delivery, as we have done in preparing this review. In a remarkable series of papers since the 1960s, the scenario for delivery evolved in a very systematic way. As each new piece of observational evidence or theoretical insight became available, the logical structure of the previous synthesis served as a framework to incorporate the new ideas. Thus, while the overall scenario has changed in important ways, the logical process has ensured progress toward ever-greater understanding.

In this review we have identified remaining problems that must be faced, but thanks to the past efforts to synthesize what information does exist, as well as ongoing investigation of specific unknowns, we are optimistic that the process of delivery will be essentially understood in the near future.

APPENDIX

Time Scales for Steps in Delivery

In this chapter, we have cited a number of results from Monte Carlo numerical experiments that have given important time scales for consideration of the various steps in delivery of asteroids to the Earth, based on Monte Carlo experiments. In many cases, the same results can be derived analytically, which may help elucidate the underlying physical processes controlling the evolution. Here we summarize as "rules of thumb," some of these results that are useful in constructing models of asteroid and meteorite delivery. We also include some time scales that have been assumed to be typical of resonant behavior, based on limited numerical experiments; those less certain rules are indicated by an asterisk.

A*. Main-belt asteroids injected into the 3 : 1 resonance with Jupiter (at 2.5 AU) become Mars crossers in about 10^5 yr.

B. Once an asteroid becomes a Mars crosser via the 3 : 1 resonance, Mars encounters change its semimajor axis by about 0.03 AU (enough to remove it from resonance) in about 1 Myr.

C.   Mars crossers random walk, due to gravitational encounters with Mars, to Earth crossing ($q < 1$ AU) in about 100 Myr.

D*. Main-belt asteroids injected into the $3:1$ resonance become Earth crossers in about 1 Myr, if not removed from resonance first.

E*. Asteroids in the $3:1$ resonance that reach Earth crossing only stay that way for about 10^4 yr at a time, and are not very deeply Earth crossing (i.e., q is near 1 AU).

F.   Once an asteroid becomes an Earth crosser via the $3:1$ resonance, Earth encounters change its semimajor axis by about 0.03 AU (enough to remove it from resonance) in about 10^4 yr.

G.   Shallow Earth crossers (with q near 1 AU) random walk by Earth encounters, but for about 10 Myr their q remains near 1 AU, because evolution must follow contours of constant Tisserand invariant.

H.   After about 10 to 100 Myr, even initially shallow Earth crossers can random walk by Earth encounters to Venus crossing.

I.   After about 100 Myr, an Earth crosser's orbit will have evolved considerably; it is likely to have hit a terrestrial planet or, via combined encounters with the Earth and Venus, to have become a Jupiter crosser, all with comparable probability.

J.   A Jupiter crosser is likely to be ejected from the solar system in about 1 Myr.

The above dynamical time scales must be compared to the collisional lifetimes of small bodies limited by collisions with other (usually even smaller) bodies. From the short cosmic-ray exposure ages of meteorites, we infer that the collision lifetimes of that size, stony-body objects are limited to about 20 Myr. Scaling from that value, radii of tens of meters are required to survive for 100 Myr, the time for full maturation of orbital evolution according to the above rules; radii of >10 km would be required for collision lifetimes greater than 1 Gyr.

REFERENCES

Dohnanyi, J. S. 1969. Collisional model of asteroids and their debris. *J. Geophys. Res.* 74:2531–2554.

Farinella, P., Paolicchi, P., Froeschlé, C., Froeschlé, C., Gonczi, R., Carpino, M., Zappalà, V., and Knežević, Z. 1986. Numerical experiments on the orbital evolution of family asteroids. *Bull. Amer. Astron. Soc.* 18:792 (abstract).

Feierberg, M. A., Larson, H. P., and Chapman, C. R. 1982. Spectroscopic evidence for undifferentiated S-type asteroids. *Astrophys. J.* 257:361–372.

Froeschlé, C., and Scholl, H. 1986. The secular resonance ν_6 in the asteroid belt. *Astron. Astrophys.* 166:326–332.

Froeschlé, C., and Scholl, H. 1987. Orbital evolution of asteroids near the secular resonance ν_6. *Astron. Astrophys.* 179:294–303.

Fujiwara, A., and Tsukamoto, A. 1980. Experimental study on the velocity of fragments in collisional breakup. *Icarus* 44:142–153.

Gaffey, M. J. 1986. The spectral and physical properties of metal in meteorite assemblages: Implications for asteroid surface materials. *Icarus* 66:468–486.

Gault, D. E., Shoemaker, E. M., and Moore, H. J. 1963. Spray Ejected from the Lunar Surface by Meteoroid Impact. NASA TN-1767.

Gehrels, T., ed. 1979. *Asteroids* (Tucson: Univ. of Arizona Press).

Greenberg, R., and Chapman, C. R. 1983. Asteroids and meteorites: Parent bodies and delivered samples. *Icarus* 55:455–481.

Greenberg, R., and Scholl, H. 1979. Resonances in the asteroid belt. In *Asteroids,* ed. T. Gehrels (Tucson: Univ. of Arizona Press), pp. 310–333.

Halliday, I., Blackwell, A. T., and Griffin, A. A. 1984. The frequency of meteorite falls on the Earth. *Science* 223:1405–1407.

Housen, K. R., and Holsapple, K. A. 1988. Scaling problems in catastrophic collisions. *Lunar Planet. Sci.* XIX:509–510 (abstract).

Kresák, Ľ. 1967. Relation of meteor orbits to the orbits of comets and asteroids. In *Meteor Orbits and Dust,* ed. G. S. Hawkins, NASA SP-135, pp. 9–34.

Murray, C. D. 1986. Structure of the 2 : 1 and 3 : 2 Jovian resonances. *Icarus* 65:70–82.

Simonenko, A. N. 1975. *Orbital Elements of 45 Meteorites, Atlas* (Moscow: Nauka Press).

Stöffler, D., Gault, D. E., Wedekind, J., and Polkowski, G. 1975. Experimental hypervelocity impact into quartz sand. *J. Geophys. Res.* 80:4062–4077.

Tanikawa, K., and Manabe, S. 1987. On the origin of the planetary spin angular momentum by accretion of planetesimals. I. Property of collision orbits. *Proc. 20th Symp. Celest. Mech.,* eds. H. Kinoshita, H. Nakai and M. Yoshikawa (Tokyo: Tokyo Astron. Obs.), pp. 43–51: also *Icarus* 79: 208–222(1989).

Wetherill, G. W. 1968. Stone meteorites: Time of fall and origin. *Science* 159:79–82.

Wetherill, G. W. 1985. Asteroidal source of ordinary chondrites. *Meteoritics* 20:1–22.

Wetherill, G. W. 1987. Dynamical relations between asteroids, meteorites and Apollo-Amor objects. *Phil. Trans. Roy. Soc. Lond.* A323:323–337.

Wetherill, G. W. 1989. Where do the Apollo objects come from? *Icarus* 76:1–18.

Wetherill, G. W., and Revelle, D. O. 1981. Which fireballs are meteorites? *Icarus* 48:308–328.

Wisdom, J. 1982. The origin of the Kirkwood gaps: A mapping for asteroidal motion near the 3/1 commensurability. *Astron. J.* 87:577–593.

Wisdom, J. 1983. Chaotic behavior and the origin of the 3/1 Kirkwood gap. *Icarus* 56:51–74.

Wisdom, J. 1987. Chaotic dynamics in the solar system. *Icarus* 72:241–275.

DISCUSSION

G. W. Wetherill: In support of the intention of Greenberg and Nolan (G&N) to identify the source of differences between my work and that of Greenberg and Chapman (G&C) (1983), I feel that some further clarification will be of value. A more extensive discussion would be necessary in order to accomplish this in a complete manner. In the interest of brevity, I will confine my remarks to two points: (1) Contrary to statements made in G&N, my work neither implicitly nor explicitly assumes that catastrophic disruption is the dominant mode of asteroidal fragmentation responsible for the production of meteorites. Therefore, any differences between my work and that of G&C cannot be attributed to this. (2) The G&C model fails its own "inductive" criterion in that it does not provide an adequate flux of stony meteorites. These two issues are discussed in more detail below.

Point 1: The approach I have taken is to reduce as much as possible the major uncertainties that accompany reliance on the details of cratering mechanics such as evaluating the relative importance of cratering and catastrophic disruption. Instead, I have made use of the useful approximation that the asteroid belt can be thought of as a steady-state system in which the number of bodies in a given size range is determined by the balance between production of these bodies by collisional fragmentation of larger bodies (by all processes) and the destruction of these bodies by the same collisional processes. In analogy with "secular equilibrium" in radiochemistry, the larger asteroids can be thought of as the slowly decaying long-lived counterparts of uranium and thorium isotopes, and the smaller asteroids the counterparts of the steady-state assemblage of short-lived intermediate isotopes in the decay chains leading to stable isotopes of lead. In the case of the asteroids, the steady state will be punctuated by stochastic large collision events. This effect has not been studied in detail, but the effect of these stochastic events can be estimated to be less than a factor of two (probably much less) because of the smoothing effect of mixing many small events with a few large ones.

If the physical strength of the bodies is independent of size, the hierarchical assemblage of asteroids of various sizes then forms a self-similar system characterized by a differential power law (in terms of mass) with an exponent of $-11/6$. This was derived by Dohnanyi (1969) for the case of catastrophic disruption. A simple extension of Dohnanyi's approach to the case of cratering yields the same power law, and therefore, use of this result requires no assumption regarding the fragmentation process. Dohnanyi also discusses data from the Palomar-Leiden survey showing that the observed small asteroids obey a power law with this index.

This consistency between theory and observation provides the basis for my work on this problem. I have pursued the consequences of this model, assuming constant physical properties, and found that it is compatible with the observed orbits and mass flux of stony meteorites (Wetherill 1985, 1987—referred to subsequently as "GW"), the number and orbits of Apollo-Amor objects (Wetherill 1988), and the cratering rates on the terrestrial planets (Wetherill 1989). If the assumption of constant physical properties is not correct, a steady state will still develop, but the predicted values of all the observational quantities can be expected to differ. The sensitivity of these differences to variations in the physical model has not been studied in detail, and it would be of interest to do so. Inasmuch as the G&C model does assume variation in physical properties, a quantitative investigation in terms of that model would have facilitated comparison

G&N discuss the velocity distribution associated with asteroidal fragmentation. They are correct in stating that for my model the relevant asteroidal fragmentation must produce fragments with velocities ~ 100 m s^{-1}. If such velocities can be produced only by cratering, then my model implicitly assumes that *cratering* of asteroids of all sizes, not catastrophic disruption, is the dominant mechanism for producing asteroidal fragments that reach the Earth as meteorites. Attention should be drawn, however, to the meaning of the phrase "the relevant asteroidal fragmentation." In calculating meteorite production by asteroidal fragmentation, in order to be complete, production of meteorite size fragments by objects up to 20 km in diameter was included, bodies about as large as the largest Apollo-Amor objects. Repetition of these calculations assuming that the largest fragments actually injected at ~ 100 m s^{-1} toward the resonance regions were only 10 m in radius, yields a meteorite yield 80% as large as that published in GW. Therefore, as far as meteorite production is concerned, it is not necessary that ~ 1 km bodies are ejected at these moderately high velocities. In the case of Apollo objects, the velocities used in my work are based on the observed velocity distribution of the well-established Hirayama families, and therefore large objects will be transferred to the resonance regions, even if the mechanism whereby this is accomplished is not yet understood. Williams et al. (1989) and Williams (1988) have used the structure of asteroid families as evidence to support the position that the observed dispersion velocities are produced directly by asteroidal collisions. Paolicchi et al. (1989) discuss the differences between the observed velocity dispersion and that found in laboratory studies and in theoretical studies.

In summary, the principal difference between my model and that of G&C does not involve cratering vs catastrophic disruption, but rather the questions of whether meteorite production is a result of collisions between asteroidal bodies of all sizes or, as assumed "inductively" by G&C, only by large asteroids, and whether or not it is a useful approximation to consider the physical properties of smaller asteroids to be independent of size.

Point 2: A principal requirement of an adequate theory of meteorite production is that it provide a flux of meteorites similar to that observed. In the approach taken by G&C, that of estimating the mass ejected by cratering of large asteroids, it is necessary to multiply the total ejected mass by the fraction of the ejected mass that falls into the same size range that was used for calculating the observed flux. In my earlier work (Wetherill and Williams 1968; Wetherill 1976), the *cratering* (not catastrophic disruption) theory of Gault et al. (1963) was used to estimate the fraction of the ejecta that fell into the meteorite size range, defined to include preatmospheric masses in the range of 100 g to 10^6g. It was found that for the smaller (~ 1 km diameter) bodies, about 10% of the ejecta fell into this size range, whereas for larger bodies (~ 10 km diameter), the fraction fell to 5%. For cratering on the considerably larger bodies assumed by G&C to be the sole sources of meteorites, fractions $\sim 1\%$ would be obtained. For this reason, cratering theory provides no justification for assuming this fraction to be anywhere near 100%. In the discussion of G&C's meteorite flux in GW, a value of 10% was used in order to make a probably over-generous estimate of this fraction, taking into consideration uncertainties in cratering theory.

G&N draw a contrary conclusion by use of a meteorite size fraction of 100% and incor-

rectly attribute the lower values discussed above to an assumption of catastrophic disruption. They also say that further increase in the meteorite flux of G&C will result from lengthening collision lifetimes by an order of magnitude, said to be the consequence of the asteroid population being "somewhat depleted below about 1 km in radius."

In reviewing G&N, I was confused by this statement, because the observed cosmic-ray exposure ages of meteorites provides no evidence for this lengthening of lifetimes. In their reply to my comments, it was stated that the increase in flux is a consequence of meteorites being derived from somewhat larger Earth-crossing bodies, and that lengthening of the collisional lifetimes of these bodies increases the meteorite flux. These statements are too vague to be of value in quantitatively estimating the meteorite flux, and the authors provide no calculations to support their conclusion. One would think that any process that increases the meteorite yield by lengthening the collisional lifetimes of the larger bodies from which most of the meteorites are assumed to be derived would also decrease the production of meteorites by these same bodies by the same factor, because the collisional processes that destroy these larger bodies are the same as those that produce meteorites.

Although limited by the difficulty that it is not evident that the various inductively based assumptions made by G&C comprise an internally consistent model, one can use their stated cratering production rates to calculate an estimate for the pre-atmospheric flux. The flux that one might expect for their model will be

$$F = P \times f_1 \times f_2 \times f_3 \tag{1}$$

where P is the total asteroidal production rate of ordinary chondritic meteorites per year as given in G&C, f_1 is the Earth impact efficiency of random ejecta at their stated velocity of 200 m s^{-1} from Table 4 of GW, f_2 is the fraction of the asteroid belt accessible to the 3 : 1 resonance, on which the calculation of Table 4 is based, and f_3 is the fraction of the ejecta in the meteorite size range. Use of this value of f_1 includes the effect of producing meteorites by cratering of somewhat larger bodies. Inserting these factors, one obtains

$$F2 = (1.12 \times 10^{11} \text{ g yr}^{-1}) \times (1.106 \times 10^{-4}) \times \left(\frac{0.2}{1.2}\right) \times 0.1 = 2.06 \times 10^5 \text{ g yr}^{-1}. \tag{2}$$

This is smaller than the estimated pre-atmospheric flux of Halliday et al. (1984) by a factor of about 10^3, even using the probably overestimated value of f_3 of 10%.

The overall conclusion that I would like meteoriticists and asteroid observers to understand is that the production of meteorites by asteroid collisions only marginally provides an adequate flux. Any restriction on this flux by limiting the sources in any way, e.g., to only large asteroids, to rare smaller asteroids or to a particular disruption process, therefore tends simultaneously to introduce a problem with the flux. For this reason, the apparent paucity of ordinary chondrite parent bodies in the asteroid belt remains the principal problem in understanding the asteroidal sources of meteorites. This matter is discussed in detail by Wetherill and Chapman (1988) from both the dynamic and spectrophotometric point of view.

R. Greenberg and M. C. Nolan: This subject is important, exciting and still unresolved, as described in our chapter. Naturally, as a healthy part of the creative process, there remain differences of approach and perspective.

In response to Wetherill's first point, the population-distribution exponent $\alpha = -11/6 = 1.83$ is equivalent to the exponent $p_{ss} = 3.5$ that we derive in our chapter. Dohnanyi (1969) found that catastrophic fragmentation is dominant over cratering in the asteroid belt (cratering is not able to affect the exponent much), and he found that if cratering were the only comminution process, $\alpha = 1.92$, contrary to Wetherill's statement that it would be the same as for catastrophic fragmentation. More significantly, the production function for cratering would not likely produce the large bodies that are important contributors to the meteorite population (especially in determining the AM/PM ratio) in Wetherill's (1985) model. In his comments, Wetherill cites unpublished results that suggest that the larger bodies are not really necessary to get enough material. It will be interesting to see, in light of Wetherill's (1985) calculations, how the observed AM/PM ratio is achieved without the larger bodies, which come from catastrophic fragmentation.

In his second point, Wetherill argues that various production factors were overestimated in the G&C model. We note that one must be careful in applying a factor computed in the context of one model to the different context of another model. Most of the assertions made under that second point are debatable on those grounds.

This subject is very lively, complex and interdisciplinary. It is not the province of any one particular scientific specialty. Rather than try to identify a simple overall conclusion to our chapter and to this discussion, we prefer to encourage readers from a wide range of specialties to try to understand in some depth the issues and physical processes involved in meteorite delivery. Our objective has been to lay these issues out for consideration. We are confident that a variety of perspectives will ultimately lead to better understanding of this critical problem.

DISCUSSION REFERENCES

Dohnanyi, J. S. 1969. Collisional model of asteroids and their debris. *J. Geophys. Res.* 74:2531–2554.

Gault, D. E., Shoemaker, E. M., and Moore, H. J. 1963. Spray ejected from the lunar surface by meteoroid impact. NASA TN-1767.

Greenberg, R., and Chapman, C. R. 1983. Asteroids and meteorites: Parent bodies and delivered samples. *Icarus* 55:455–481.

Paolicchi, P., Cellino, A., Farinella, P., and Zappalà, V. A. 1989. Semiempirical model of catastrophic breakup processes. *Icarus* 77:187–212.

Wetherill, G. W. 1976. Where do the meteorites come from? A reevaluation of the Earth-crossing Apollo objects as sources of chondritic meteorites. *Geochim. Cosmochim. Acta* 40:1297–1317.

Wetherill, G. W. 1985. Asteroidal source of ordinary chondrites. *Meteoritics* 20:1–22.

Wetherill, G. W. 1987. Dynamical relations between asteroids, meteorites and Apollo-Amor objects. *Phil. Trans. Roy. Soc. London* A323:323–337.

Wetherill, G. W. 1989. Cratering of the terrestrial planets by Apollo objects. *Meteoritics* 24:15–22.

Wetherill, G. W., and Chapman, C. R. 1988. Asteroids and meteorites. In *Meteorites and the Early Solar System*, eds. J. F. Kerridge and M. S. Matthews (Tucson: Univ. of Arizona Press), pp. 35–67.

Wetherill, G. W., and Williams, J. G. 1968. Evaluation of the Apollo asteroids as sources of stone meteorites. *J. Geophys. Res.* 73:635–648.

Williams, J. G. 1988. The unusual Alexandra family. *Lunar Planet. Sci.* XIX:1277–1278 (abstract).

Williams, J. G., Shoemaker, E., and Wolfe, R. 1989. Structure in the Themis, Eos, and Koronis families. *Lunar Planet. Sci.* XX: 1207–1208 (abstract).

ASTEROID COLLISIONAL HISTORY: EFFECTS ON SIZES AND SPINS

DONALD R. DAVIS, STUART J. WEIDENSCHILLING
Planetary Science Institute

PAOLO FARINELLA, PAOLO PAOLICCHI
Università di Pisa

and

RICHARD P. BINZEL
Massachusetts Institute of Technology

Collisional evolution studies indicate that the total asteroidal mass has decreased only by a factor of ~3 to 5 since the time that asteroid velocities were pumped up to their present values of ~5 km s⁻¹. This primordial population had only a few more large (≳300 to 400 km diameter) bodies than does the current belt, with most of the additional mass residing in small (≲50 to 100 km) bodies. This estimate of the primordial population follows from the requirement that the assumed ancient basaltic crust of Vesta be preserved. Collisions have altered the spin rates of small bodies, but the largest asteroids may have retained their primordial rotation rates. Most asteroids larger than 100 km diameter have probably been shattered, but have gravitationally recaptured their fragments to form a rubble-pile structure. If the mass distribution of fragments implies a significant fraction of small particles, such bodies may have shapes determined by their rotation rates and mean density, similar to those of fluid bodies. Large angular momentum asteroids appear to have Maclaurian spheroidal or Jacobi-ellipsoid-like shapes; some of them may have fissioned into binaries. A major problem exists in understanding how large asteroids can collisionally break up into big fragments: current scaling laws predict that the energy required to disrupt gravitationally dominated bodies should result in the

bodies being shattered into tiny fragments. This prediction disagrees with the size distributions observed in the Hirayama families.

I. INTRODUCTION

The importance of collisional events in the evolution of the solar system, and especially of its minor bodies, has been increasingly recognized in the last decade. Although it has long been realized that asteroids occasionally collide with each other (and with the planets) at velocities of many km s^{-1} (Öpik 1951; Piotrowski 1953), several issues have recently emerged to focus growing attention on collisional processes: the megaimpact hypothesis for the origin of the Moon, collisional shattering of small satellites and the formation of planetary rings, the origin of the Hirayama families, the IRAS-discovered dust bands, and collisional evolution of asteroid sizes and spin rates.

Concerning the last topic, which is the subject of this chapter, ongoing studies have two basic goals. The first is to predict in a quantitative and reliable way the outcome of a collision with well-defined initial conditions (mass, shape, composition, structure, rotational state and relative velocity of the colliding bodies). This goal is addressed by collecting a large amount of experimental results for impacts carried out in the laboratory and by developing appropriate scaling relations to extrapolate these data to much larger (and possibly gravity-dominated) bodies (cf. chapter by Fujiwara et al.).

The second goal is to develop an integrated model capable of simulating the evolution of a population of colliding bodies with given initial properties (distribution of sizes, spin rates, relative velocities and impact response parameters). With this tool, we aim to determine the early asteroid population that led to the presently observed properties of asteroids. This procedure can provide insight to such basic mysteries as: how and when was some 99.9% of the condensed mass presumably present in the primordial solar nebula in the asteroid zone expelled from it (Weidenschilling 1977)? Do the presently observed bulk properties of asteroids reflect those of a swarm of accumulating planetesimals, or have disruptive collisions obliterated most memory (size distributions, rotation periods and pole directions, shapes, etc.) of this accretionary phase? For the purpose of this chapter, we restrict ourselves to analysis of the evolution under the current regime of high ($\sim$5 km s^{-1}) impact velocities, defining as "starting conditions" those established at the end of the earlier accumulation and velocity pumping phase. For the accumulation phase, and for the events which may have caused its premature interruption, see the chapter by Wetherill.

Fortunately, models which attempt to reach the above goals are constrained by different types of observational evidence, that drastically reduce the range of *a priori* unknown parameters. Many of these constraints are discussed in more detail in the following sections. To start we give just a schematic list, which includes:

1. Properties of asteroid surfaces, e.g., the preserved basaltic crust of Vesta, the existence of metal-rich asteroids (presumably stripped cores of differentiated parent bodies), the scarcity of olivine-rich asteroids which are widely interpreted as fragments from parent-body mantles;
2. The present features of the size and spin rate distributions, and the correlations between them and with taxonomic type and orbital parameters (see the chapter by Binzel et al.);
3. The existence of at least 8 and possibly over 100 distinct dynamical families, as well as any peculiar properties of their member bodies (see the chapter by Chapman et al.);
4. The existence of objects having rotational angular momenta much higher or much lower than the average, and of objects with nearly equilibrium shapes suggesting a low tensile strength of their material;
5. The existence of meteorites, Apollo-Amor-Aten objects, and dust bands, indicating that collisional evolution is an ongoing active process.

II. PREVIOUS STUDIES

Following the realization by Piotrowski (1953) that major collisions among asteroids occur on geologic time scales, researchers began to explore their effects. Dohnanyi (1971) argued that the present belt represents a collisionally relaxed distribution, which is essentially independent of the starting population. Numerical studies by Chapman and Davis (1975), incorporating more realistic collisional physics, supported this conclusion, although they found that not all starting populations would reproduce the present belt in detail. They pointed out the constraint that the initial distribution could not have contained many more bodies of Vesta's size (or larger) than exist now, because a significant fraction of such large bodies would have survived over the age of the solar system. However, they concluded that even a planetary mass initially in small-sized bodies could collisionally evolve to the present population.

Davis et al. (1979) studied effects of collisions on both sizes and rotation rates of asteroids and concluded that most asteroids $\gtrsim 100$ km diameter are probably fractured through much of their volume leading to the formation of gravitationally bound "rubble piles." However, the calculated mean spin rate of large asteroids (the equilibrium value between infrequent large collisions tending to spin up asteroids and numerous small collisions which damp rotation rates, according to the theory of Harris [1979]), agrees with the observed value if $\gtrsim 50\%$ of the collisional kinetic energy is converted into kinetic energy of ejecta. This is an extremely large fraction when compared with results from laboratory impact experiments and scaling laws (see the chapter by Fujiwara et al.). This kinetic energy partitioning parameter f_{ke} and the uncertainties in determining it are discussed in some detail in Sec. III.

Several aspects of the collisional evolution of asteroids, in particular

characteristics of their sizes and rotational distributions, have been clarified in the last decade. The existence of many large angular-momentum asteroids (LAMAs), with short rotation periods and high moments of inertia (due to elongated shapes), has been noted (Farinella et al. 1981,1985; Weidenschilling 1981). These have specific angular momenta up to twice that of spherical bodies with the same spin period, thus explaining in part the misfit between the observed values and the 2 to 3 hr periods predicted by Harris' (1979) theory for spherical bodies and choices of the relevant physical parameters consistent with the experimental evidence, i.e., $f_{ke} \approx 0.1$.

Farinella et al. (1982) outlined some general features of collisional outcomes in different size ranges. By calculating the effect of the most energetic collisions that bodies of different sizes are likely to have experienced over solar system history, they concluded that:

a. The largest asteroids may retain their primordial masses and spin rates;
b. Asteroids in the 150 to 300 km size range have been mostly shattered by very energetic collisions, but an important fraction of the fragments could be gravitationally re-accumulated into rubble piles having shapes approximated by biaxial Maclaurin spheroids, triaxial Jacobi ellipsoids or, in extreme cases of very efficient angular momentum transfer, Darwin binaries (see the chapter by Weidenschilling et al.). In this intermediate size range the formation of dynamical families is most likely due to the ejection of many fragments with velocities high enough to overcome the self-gravitation of the parent body, but small enough to yield clusters in orbital parameters (see the chapters by Valsecchi et al. and Chapman et al.).
c. At sizes smaller than 50 to 100 km, catastrophic impacts become more frequent, while gravitational re-accumulation is more difficult. Therefore, small asteroids are mostly expected to be just rocky fragments with irregular shapes, with their rotational states determined by angular momentum partitioning during breakup (see also Catullo et al. 1984; Paolicchi et al. 1989).

The observation that Vesta has a largely intact basaltic crust, together with the recognition of 8 significant dynamical families formed by breakup of parent bodies larger than 200 km diameter, was used by Davis et al. (1985) to constrain further asteroid collisional history. They investigated a wide variety of hypothetical initial asteroid populations, both in terms of total mass and the distribution of mass with size, and found that only a modest initial belt containing a few times the present mass could collisionally evolve to the present belt and still preserve Vesta's crust. Furthermore, a runaway-growth size distribution, with only Ceres, Vesta and Pallas at the large-size end and the additional mass at small diameters ($\leqslant 85$ km), best satisfied all constraints. This conclusion was confirmed by Farinella et al.'s (1985) analysis of the impact flux needed to convert into LAMAs $\sim 1/3$ of the bodies in the 200 to 300 km range.

However, interpretation of other asteroid observations suggests much more collisional evolution than the above scenarios allow. M asteroids almost certainly have high metal content (at least in the upper few meters) and are widely interpreted to be the collisionally exposed cores of differentiated parent bodies. It seems difficult to preserve the crust of Vesta, while completely demolishing other similar-sized bodies, leaving behind only the remnant cores. Furthermore, as pointed out by Chapman (1986), there are few olivine-rich A type asteroids, which should be produced in abundance from the shattered mantles of differentiated parent bodies. So, not only must the parent bodies be collisionally disrupted, but virtually all of the mantle material must be ground down to unobservable sizes or removed from the belt. (See the chapter by Chapman et al. for a further discussion of this problem, and of its possible [speculative] solutions.) Reconciliation of observations and geochemical interpretation of asteroid history with models of the collisional evolution is one of the major challenges in asteroid science.

III. OUTCOMES OF CATASTROPHIC COLLISIONS

A general model for predicting the outcome of an individual breakup event, i.e., the distribution of masses, ejection velocities, rotation rates and shapes of the fragments, is obviously a prerequisite for a quantitative theory of asteroid collisional evolution. For this purpose, laboratory impact experiments provide the necessary database with which to develop and test models of the fragmentation process (see the chapter by Fujiwara et al.). A comprehensive model for calculating collisional outcomes was developed at the Planetary Science Institute (Chapman and Davis 1975; Greenberg et al. 1978; Davis et al. 1979). *Fragmentation* or *shattering* is defined as the process of breaking part or all of the body by stress waves generated by collisions, and *disruption* as the process of fragmenting and dispersing a body. This distinction is important for large bodies with significant gravity fields in which case a target could be shattered, but not disrupted, provided most fragments were ejected with less than escape velocity. *Catastrophic fragmentation* is defined to occur when the largest piece resulting from the collision contains 50% or less of the initial target mass. Otherwise, collisions are defined as cratering events. The choice of the boundary between these two types of outcomes is not crucial as experiments show that the transition occurs in a narrow range of impact energy, and therefore borderline events are relatively rare.

In the collisional-outcome model described here, a projectile of mass m strikes a larger target asteroid of mass M, with a velocity V_p and kinetic energy $E = (1/2)mV_p^2$. The collisional energy is assumed to be partitioned equally into the target and projectile (Hartmann 1980; Hartmann 1988). However, assuming a different partitioning would just change the impact strength, as defined below. The mass of the largest fragment normalized to the mass of the original body, f_ℓ, is calculated using

$$f_\ell = 0.5 \left(\frac{SM}{\rho E/2} \right)^{1.24} \tag{1}$$

where ρ is the density of the target and S, the impact strength, is the energy density in the body needed to produce a barely catastrophic outcome $f_\ell = 0.5$ (Fujiwara et al. 1977). Of course, when $\rho E/2M < S$, the largest fragment contains more than 50% of the target mass and the cratering regime is assumed to hold. The numbers and sizes of smaller fragments can be calculated assuming that they have a power-law size distribution. The number of fragments with mass greater than m, $N(>m)$, is given by

$$N(>m) \propto m^{-q} \tag{2}$$

where the mass index q is determined by the size of the largest fragment and the condition of mass conservation (Greenberg et al. 1978). Also, the fragments are assumed to have a power-law distribution in velocity

$$f(>V) = (V/V_o)^{-k} \text{ for } V > V_o \text{ and } f(>V) = 1 \text{ for } V < V_o \tag{3}$$

where f is the fraction of the ejecta mass moving faster than V, and k is the velocity distribution index. The minimum ejecta velocity V_o is calculated from an energy partitioning coefficient f_{ke} defined to be the fraction of the collisional kinetic energy which goes into ejecta motion. The parameters f_{ke} and k are essential for calculating lifetimes of large asteroids, but they have not been well determined experimentally. The available laboratory and theoretical data suggest that f_{ke} is between 10^{-2} and $\sim 10^{-1}$ (see the chapter by Fujiwara et al.), while the value $k \simeq 9/4$ derived from cratering experiments is consistent with the very limited evidence from impact fragmentation experiments (see Fujiwara and Tsukamoto 1980, their Fig. 5). Of course, only fragments with V larger than the escape velocity of the parent body will avoid re-accumulation. A re-accumulated rubble pile can relax to a nearly equilibrium figure only if the irregular shape of the largest re-accreted fragments is smoothed out by a thick layer of finer debris. According to Eq. (2), the fraction of the total mass contributed by fragments of mean size less than γ times the size of the largest one is $\gamma^{(6-3q)}$. For $q = 1.8$, this yields 10% and 25% of the mass contributed by fragments with sizes $<1/50$ and $1/10$ times that of the largest body, respectively (for $q = 1.9$, these percentages grow to 31% and 50%). As noted by Shoemaker et al. (1979), the percentage of void space (or bulking factor) for assemblages of rocky ejecta from cratering experiments varies from 4% to 70%, with most values in the range of 20% to 30%. Thus, for a single shattering event, the amount of small fragments might not be sufficient to prevent the appearance of large irregularities on the surface of a rubble pile. However, for asteroids which can withstand many shattering events before being disrupted,

the accumulation of finely fragmented material should result into quasi-equilibrium shapes.

It has been sometimes observed that even finely fragmented bodies could maintain significant topographical features, because a loosely cohesive material can support static slopes, just as angles of repose maintain topography in a sand box. However, the rubble-pile asteroids would be continuously shaken by small-scale impacts, causing redistribution of debris towards depressed areas both by direct production of ejecta and by seismic disturbances favoring downslope movements of the loose material, as seen in the Viking images of Deimos (Veverka and Thomas 1979).

In addition to experimental determination of the critical parameters S and f_{ke}, we must know how they scale with target size. We use S_o for the laboratory measured impact strength (experimental S_o values are available for a variety of target materials and velocity regimes [see the chapter by Fujiwara et al.]), while S denotes the impact strength scaled to larger bodies. Davis et al. (1985) pointed out a crucial difficulty with the size distribution observed in asteroid families compared with that predicted by fragmentation models. If one assumes that the impact strength of asteroids corresponds to that measured in laboratory experiments on rocky targets, about 3×10^7 erg cm^{-3}, then Hirayama's dynamical families, such as the Themis and Eos family, should have been completely shattered into very small fragments. A disruptive event dispersing to infinity most of the mass of a 200-km diameter asteroid against its own self-gravity has to provide an energy density of $\sim 10^9$ erg cm^{-3}. In the laboratory, this high-energy density yields a largest fragment only about 10^{-3} of the target mass for rocky bodies. If self-gravitational re-accumulation is effective only for the largest fragment (see the chapter by Weidenschilling et al.), then the mass distribution of families should show a very wide gap between the largest body and the other family members. This is clearly inconsistent with most asteroid families including, in particular, Eos and Themis (Davis et al. 1982).

The same problem can also be considered from a different point of view: the existence of families generated from 200-km sized target asteroids implies a typical velocity for the ejected fragments somewhat larger than the escape velocities of the parent bodies, that are of the order of 100 m s^{-1}. Ejection velocities of this magnitude can indeed be derived from the distribution of proper elements of families (Zappalà et al. 1984), and are required to explain the properties of the Saturnian satellite Hyperion if it is a collisional fragment (Farinella et al. 1983). However, in laboratory experiments such velocities are observed only following super-energetic impacts, which cause complete disruption of the target and yield no sizeable fragments. For bodies dominated by solid-state strength, the fragment velocities for barely catastrophic collisions are likely to scale with the square root of the impact strength, which is a measure of the collisional energy needed to fracture material bonds (this result assumes that f_{ke} is independent of S). Thus, consideration of both the strength

vs size and the velocity vs size scaling issues suggest that asteroids, even neglecting gravity-related effects, are much more resistant to impacts than rocky laboratory targets, i.e., they behave as very strong bodies.

Theoretical considerations of scaling of impact strength with size lead to opposite conclusions. Farinella et al. (1982) assume that S is proportional to the energy required to break up the solid-state binding throughout all the fracture surfaces. On the basis of the observed mass distribution of the fragments, S should decrease with increasing target diameter D ($\propto D^{-1/2}$ for $q = 11/6$, in Eq. 2), because the overall fracture surface increases with a smaller power of the size than does the volume. On the other hand, Davis et al. (1985), on the basis of physical reasoning and laboratory evidence that a compressed body becomes more resistant to stresses, suggested that S should increase when gravitational forces become comparable to solid-state forces. The average value of S for a target of density ρ was assumed to be

$$S = S_0 + A \ (\pi/15) \ G \ (\rho D)^2. \tag{4}$$

The second term reflects the volume-averaged hydrostatic pressure, with an empirical parameter A of order unity. While laboratory results (in static loading conditions) indicate $A < 1$, for the compressed rocky material of the Earth's interior, the incompressibility (or bulk) modulus $K = \rho dP/d\rho$, measured from the propagation velocity of seismic waves, increases as $3.35 \ P$ (Stacey 1977, p. 173). If K is related to S, this may indicate that $A > 1$. With $A = 1$, a 300-km sized target such as the parent body of the Themis family, yields fragments that roughly match the observed mass distribution, and can be dispersed to "infinity" (i.e., to independent heliocentric orbits) provided $f_{ke} \geq 0.2$. This result can be shown by equating the collisional energy partitioned into ejecta kinetic energy ($f_{ke}E$) to a measure of the gravitational binding energy ($3/5 \ GM^2/R$) and further requiring that this energy be of the same order as that required to barely shatter the target ($S \ M/\rho$).

Holsapple and Housen (1986; see also the chapter by Fujiwara et al.) applied dimensional considerations and the coupling parameter concept to derive a fragmentation criterion including both an energy and a velocity dependence. This model is equivalent to including a strain-rate dependence on the impact strength and will hereafter be referred to as strain-rate dependent strength (see Fig. 9 in the chapter by Fujiwara et al.). They concluded that S should decrease with increasing size up to that where gravitational self-compression becomes important. In this theory, S should decrease to values smaller than the laboratory ones, implying again a misfit between the predictions of collisional evolution models and the observed size distribution of family asteroids. Moreover, the analysis of rotational properties for the smallest observed asteroids in the size range 1 to 10 km also suggest a smaller tensile strength than for cm-sized rocky bodies. Otherwise we would expect to see at least some fast rotators, having periods of 1 hr or less, based on simple

scaling considerations applied to experimental results on the spin rate of fragments. In fact, Harris' (1979) theory (strength regime), experiments reported by Fujiwara (1987), as well as the model of Paolicchi et al. (1989), indicate that spin rates vary inversely with size, possibly proportional to D^{-1}. It is interesting to note that such a scaling law fits well the spin rates of cm-sized fragments ($\approx 10^{-2}$ s) and those of 30-km sized asteroids (≈ 8 hr).

Different problems arise with the scaling of f_{ke}. Fujiwara and Tsukamoto's (1980) experimental results on the velocity of fragments imply that f_{ke} should increase approximately with the square root of E/M, the specific collisional energy

$$f_{ke} = K' (E/M)^a \tag{5}$$

with $K' = 2.2 \times 10^{-6}$ (cgs units) and $a = 0.52$ (Farinella et al. 1982; Paolicchi et al. 1983). While E/M ranges from 10^7 to 10^9 erg g^{-1}, f_{ke} increases from 0.01 to 0.11. The experimental uncertainties on K' and a can affect f_{ke} by a factor of ~ 2.

From observations we have two apparently conflicting constraints: one arising from the existence of families formed from large parent bodies and the other from the existence of LAMAs. The condition for having enough energy to disperse a large fraction of the mass and form a family requires that the collisional energy partitioned into ejecta exceed the gravitational binding energy, i.e.

$$f_{ke}(E/M) = K'(E/M)^{(a+1)} > 3/5 \, \frac{G\,M}{R} = 0.3 \, V_e^2 \tag{6}$$

where V_e is the escape velocity of the parent body. For a 200-km diameter target, with $\rho = 2.5$ g cm^{-3}, this relationship requires that $E/M > 5 \times 10^8$ erg g^{-1}, corresponding to a value of f_{ke} of $\simeq 0.08$.

A second constraint on f_{ke} is provided by the existence of LAMAs. As noticed by Farinella et al. (1985), in the diameter range from 200 to 300 km, photometric lightcurve observations imply that $\sim 1/3$ of all the existing objects are LAMAs, independently of every assumption on their shape (equilibrium vs irregular). If the high angular momentum of LAMAs, typically $H \simeq 0.1 \, M D \, V_e$, was imparted by a single large collision which did *not* disperse a large fraction of the target's mass, then

$$f_{ke} \, \frac{H V_p}{\sqrt{2}R} < 3/5 \, \frac{GM^2}{R}$$

or

$$f_{ke} < 2 \, V_e/V_p. \tag{7}$$

This implies an upper limit to f_{ke} of about 0.05 for 200 km diameter bodies, further decreased if the angular momentum transfer efficiency is <1. Clearly, the two constraints on f_{ke} can only be marginally consistent unless S is very high.

Could f_{ke} also depend on target size? One possibility is that f_{ke} scales with the effective impact strength S. In this case, we should assume that for barely catastrophic collisions f_{ke} is about 0.01, as observed in the laboratory. Then a collisional origin for LAMAs would be possible, but we would need a much higher energy to disperse the fragments in a family-forming event, and therefore an effective strength larger than the laboratory values by a factor $>10^2$.

The interplay among these physical and observational constraints is shown graphically in Fig. 1, using a 200-km diameter body as an example.
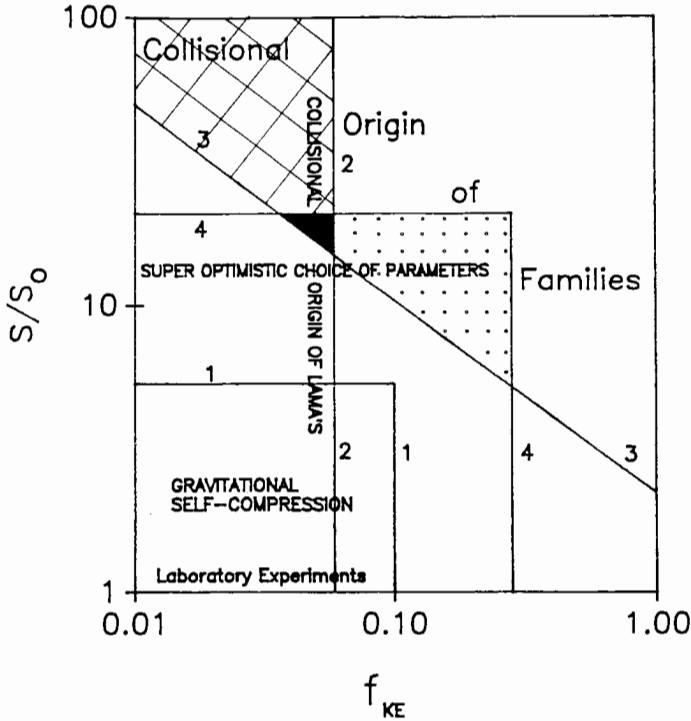
Fig. 1. Illustration in the S/S_o vs f_{ke} plane, of the various physical and observational constraints applied to asteroids with $D \simeq 200$ km, such as many LAMAs and family parent bodies. Laboratory impact experiments indicate values lying in the lower left corner, with higher S/S_o values possibly allowed by gravitational pressure strengthening (region within box labeled 1). The collisional origin of LAMAs gives a lower limit for f_{ke} (region left of line 2), while the collisional formation of families is only consistent with values above the oblique line (line 3). Only with a super-optimistic choice of parameters (region within box 4; also see text) can families and LAMAs be formed in this model (region within black triangle).

With the present status of our knowledge, we can choose among three alternative possibilities:

1. S is increased only by self-compression in the strongest way which makes sense (i.e., A not much larger than unity). The constraints can all be marginally fulfilled for a 200-km body, but only for a quite special choice of parameters (large S_o, $f_{ke} \lesssim 0.1$; filled central triangle in Fig. 1). Moreover, if S, apart from gravitational effects, decreases with increasing size as predicted by the current understanding of scaling, inconsistencies remain in the 10-km size range, i.e., bodies are predicted to be too weak.

2. We can relax the constraint arising from the assumption of a collisional origin of LAMAs (Eq. 7) by assuming they formed by low-velocity impacts during the accretionary era of asteroids. In this way, the dotted region of Fig. 1 becomes available for forming families; we can assume a more moderate self-compressional effect, and values of f_{ke} (≈ 0.5) larger than those derived from the experiments (even if we have no independent physical reason for that). We still have the above-mentioned problems concerning 10-km sized objects. The survival of LAMAs to the present day serves to constrain severely the collisional history of the asteroid belt.

3. f_{ke} remains small, S is increased well beyond the effects of self-compression by some other physical mechanism. This case (dashed region of Fig. 1) would work both at 100-km and at 10-km sizes. However, we need to understand how the impact strength can grow with size by as much as two orders of magnitude. Moreover, the comparatively slow rotation of very small asteroids would remain unexplained unless S is totally uncorrelated with tensile strength. There is currently no clear explanation for such an effect, though one could speculate (see, e.g., Paolicchi et al. 1982) that it may be the result of previous fracturing of the target asteroids. A mega-regolith structure could result in a different response to the final high-energy impact (e.g., with a more intense shattering process but confined to a small part of the target) than a solid body (see also the chapter by Chapman et al.). Future experiments should explore this hypothesis.

IV. COLLISIONAL CHANGES IN ASTEROID SIZE DISTRIBUTIONS

The scaling dilemma described above is reflected in current collisional evolution studies. The scenarios of asteroid collisional evolution presented in Davis et al. (1985), based on the impact strength given by Eq. (4) (with $A = 1$), showed that a small initial belt was most consistent with the observational constraints (see Sec. II). Recently, we have rerun a starting population similar to the "favored" initial population from Davis et al. (but smaller at sizes $\lesssim 30$ km), using a strain-rate dependent strength scaling algorithm. We also incor-

D.R. DAVIS ET AL.

porated a bin width spanning a factor of 2 rather than 4 in mass in order to get better resolution in the calculated distribution. Results of these calculations are shown in Fig. 2. The case without strain-rate effects is in reasonably good agreement with the current belt at sizes $\gtrsim$75 km diameter, but at 50 km the observed population is more abundant by a factor $\sim$2. The case with strain-rate strength shows no bump of the distribution between $\sim$80 and 150 km, while it appears to fit better the data for smaller sizes.

We also keep track of the types of bodies as a function of size in the population, i.e., the percentage that are survivors from the primordial population (defined as the bodies which have not moved to a smaller size bin, even if they may have been shattered), fragments from shattering or cratering collisions, eroded cores of cratered bodies, or partially dispersed cores ("cores" have been moved to a smaller size bin, as a result either of cratering erosion or
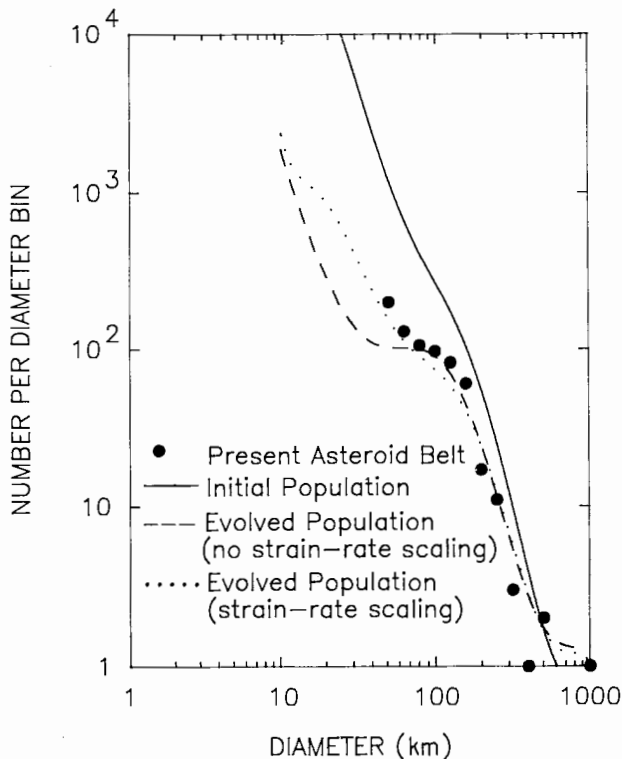
Fig. 2. Collisional evolution of an asteroid population similar to the "best" initial population distribution from Davis et al. (1985). This figure compares the case using the strength scaling of Eq. (4) with the same case using the current strain-rate dependent scaling. Both cases use bin width spanning a factor of 2 in mass rather than the factor of 4 used in Davis et al. (1985).

of an individual disruption event). Notice that this classification depends on the assumed bin width. Also, it only recognizes the last type of collision that changes the population of a bin. For example, a fragment produced by a shattering collision is recorded as such but if it is subsequently eroded by cratering collisions and moved into a smaller size bin, it is reclassified as an eroded core. We compare the distribution of types as a function of size for strength scaling both with and without strain-rate effects in Fig. 3a and b.

In the no strain-rate case (Fig. 3a), the Vesta/Pallas bin experiences 6 shattering collisions distributed between the two bodies; hence it is somewhat unlikely but not impossible that Vesta escaped being shattered. However, this case is a near-limiting one in terms of preserving Vesta's crust. The largest projectiles found to hit bodies in this size range were ~150 km in diameter— large enough to shatter the body with 30 times the minimum energy needed to barely fracture it. Clearly Vesta has not been hit by such a massive projectile since the time that its basaltic crust formed. At smaller sizes, there could be a few unshattered survivors also. For example, at 250 km diameter there were 11 survivors which had been hit with a total of 23 shattering impacts, making it likely that a few bodies of this size were not shattered. At sizes larger than 50 km, the population is dominantly composed of shattered survivors, eroded cores and partially dispersed cores; there are very few fragments at these sizes. Even at 25 km, less than one asteroid in 5 is a fragment from a shattering disruption of a larger body (but recall that at this size, many bodies classified as eroded cores may have been earlier generation fragments).

When strain-rate effects are included (Fig. 3b), bodies at all sizes are easier to smash up. In the Pallas/Vesta size bin, it only takes a ~17-km projectile to shatter the body whereas a ~50-km diameter projectile is needed in the strain-rate independent scenario. There are 23 shattering impacts into the weaker Pallas and Vesta; hence it is very improbable that Vesta would not be shattered. This case also predicts that there are essentially no discrete fragments down to sizes as small as 25 km. Disruption of large bodies produces very small fragments due to the inherent weakness of the body itself and, consequently, the collisional outcomes do not match the large fragments found in the Themis family.

The general conclusion from studies of large asteroid collisions is that they appear to respond to impacts as if they were quite strong. Gravitational self-compression works in the direction of strengthening large bodies, yet models using plausible parameters predict strengths that are just marginally large enough to produce the observed asteroid families. However, the strain-rate correction predicts substantially weaker bodies at large sizes than are found from laboratory experiments, a prediction at odds with the requirements obtained from asteroid observations. Clearly, further effort is needed to understand how large asteroids break apart due to massive collisions and how to relate this response to laboratory studies.

SHATTERED SURVIVORS   ERODED CORES   FRAGMENTS

UNSHATTERED SURVIVORS   PARTIALLY DISPERSED CORES $S_o = 3 \times 10^7$

NO STRAIN RATE

FRACTION OF FINAL POPULATION

1.0

.80

.60

.40

.20

0.0

25   50   100   200   400

DIAMETER (km)

b)

SHATTERED SURVIVORS   ERODED CORES   FRAGMENTS

UNSHATTERED SURVIVORS   PARTIALLY DISPERSED CORES $S_o = 3 \times 10^7$

STRAIN RATE INCLUDED

FRACTION OF FINAL POPULATION

1.0

.80

.60

.40

.20

0.0

25   50   100   200   400

DIAMETER (km)

Fig. 3. Predicted distribution of asteroid pedigrees as a function of size in the present belt. The distributions shown reflect the evolved populations shown in Fig. 2. (a) No strain rate; (b) Strain rate included.

V. COLLISIONAL EVOLUTION OF ASTEROID ROTATION RATES

A. A Physical Model for Changes in Spin Rates Due to Collisions

Collisions have affected not only the sizes and physical states of asteroids, but also their spin periods. In an effort to understand better asteroid collisional history, a model for calculating how collisions change spin periods has been incorporated into the numerical simulation code described above. This approach is a logical next step in understanding asteroid collisional evolution. Earlier work on asteroid spin changes due to collisions (Harris 1979; Farinella et al. 1982; Dobrovolskis and Burns 1984) focused on understanding the physical mechanisms that caused asteroid spins to change by impact. The evolution of the spin rates of the population was calculated parametrically using a simplified power-law size distribution. Binzel (1986) modeled the effect on rotational angular momentum by a Monte Carlo simulation of individual collisions. The interrelation between asteroid size and spin evolution was discussed by Davis et al. (1979); however, the actual calculations described there were done for the sizes and spins separately. Through an integrated approach, we hope to comprehend better the collisional history of the asteroids since the changes to spin rates depend on the total number and sizes of collisions that an asteroid has experienced. Below we outline our approach for developing an integrated model and discuss some preliminary results that are presented only as illustrative examples.

The model described here adopts the same mathematical approach to calculating spin-period changes that is used in calculating size changes, namely, that there is a large number of collisions involving particles in a size bin during a time step and that the effects of these collisions can be averaged to find the *mean* change to the *mean* particle spin rate in that bin. To do this, the *total (scalar) angular momentum of all particles in a size bin* is calculated assuming spherical shapes. The program keeps track of the changes in the total angular momentum due to particles being added to and removed from the bin, as well as changes caused by collisions leaving the particle in its original bin, i.e., cratering impacts and fragmentation events with more than half of the body re-accumulated. Spin angular momentum is not conserved in this approach, but neither is it conserved in real asteroid collisions. Of course, the total (vector) angular momentum of the system, including both rotational and orbital angular momentum, is strictly conserved. However, in collisions there is generally an exchange of angular momentum between the spin and orbital components. Since the orbital angular momentum far exceeds that due to rotations, it effectively acts as an infinite source or sink for asteroid spin angular momentum. We now describe the algorithm used for calculating the change in mean spin rate $\Delta\omega$ and associated angular momentum change for particles of various sizes as a function of type of collision.

Shattering Collisions. In this case, more than half the mass of the target is shattered (but not necessarily dispersed). The spin rates of fragments from such a collision are modeled as follows: Let ω_T be the spin rate (post-impact) of the target which is computed by adding quadratically the target's pre-impact angular momentum to a fraction β of the projectile's angular momentum with respect to the center of mass. Then the mean spin rate $\bar{\omega}$ of a fragment of mass m_f is

$$\bar{\omega} = \omega_T \qquad\qquad \text{if } m_f > 0.1\, M$$

$$= \frac{\omega_T}{\left(\dfrac{10 m_f}{M}\right)^\alpha} \qquad \text{if } m_f \le 0.1\, M. \tag{8}$$

A partially dispersed core is treated as a large fragment. This algorithm predicts that the large fragments have the same spin rate as the (post-impact) parent body, but that smaller fragments spin faster. This formulation is based on the experimental results of Fujiwara and Tsukamoto (1981) together with the semi-empirical model of Paolicchi et al. (1989). It implicitly assumes that some of the target's spin angular momentum is lost in a shattering collision (or rather, is imparted to the orbital angular momentum of fragments). The fraction of angular momentum retained by the fragments' spins (assuming aligned spin axes) is shown in Fig. 4 as a function of the degree of shattering and the exponent α. One concern with this model is that it would predict that a head-on impact into a nonspinning target would produce nonrotating fragments, a prediction not borne out by experiments. However, due to the quadratic addition of angular momenta, our numerical simulation never calculates that fragments are not rotating when computing the mean change to particle spins. Another problem is that the model never allows the largest bodies resulting from the collision to be slowed down, as would occur in the case of partial reaccumulation if the escaping fragments were preferentially those ejected in the prograde direction with respect to the rotation of the target. We are currently exploring model revisions to remove these deficiencies. Our choices for values of α and β are given in Subsec. B below, which describes some preliminary results.

Cratering Collisions. In this type of collision the target survives, with less than half of the original mass shattered. If the target body has a significant gravitational field with $V_e > V_o$ (see Eq. 3), then only a fraction of the ejecta escapes. We consider two subclasses of cratering collisions:

1. *All or none of the ejecta escapes:* Interestingly, the change in spin rate for a body is the same for the cases where all of the ejecta escapes or none of it escapes. The latter case is that of pure accretion which was studied by Harris (1979). His Eq. (7) in Davis et al. (1979) is
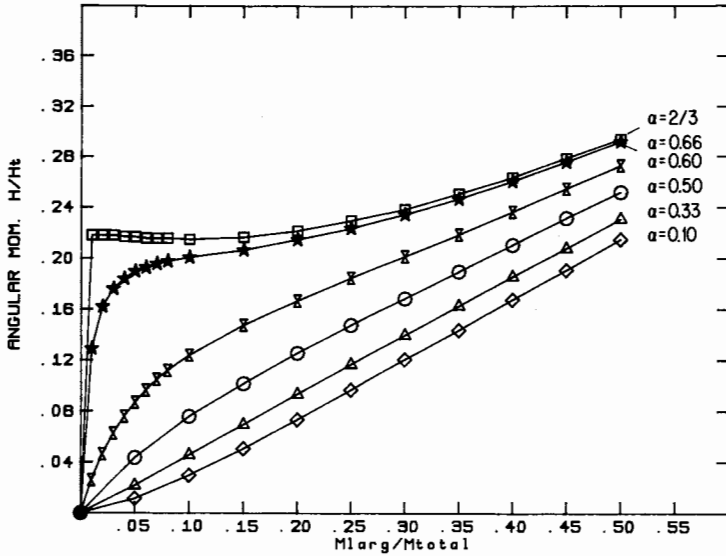
Fig. 4. The rotational angular momentum carried in collisional fragments normalized to the spin angular momentum of the post-impact target as a function of the degree of collisional shattering calculated from Eq. (8). Only the small values of α (≤ 0.33) lead to reasonable predicted spin rates for small (~ 1 km) sized asteroids.

$$\Delta\omega = \frac{25}{16} \left(\frac{m}{M} \right)^2 \frac{V_p^2}{\omega R^2} - \frac{5}{3} \left(\frac{m}{M} \right) \omega \qquad (9)$$

which gives the mean change ($\Delta\omega$) in the rotation rate (ω) of an asteroid of mass M and radius R due to a collision with a projectile having mass m at impact speed V_p. Equation 9 also describes the change in spin when all of the ejecta escapes ($V_o > V_e$). For this case, the escaping ejecta carry away the angular momentum (post-impact) of the surface *provided the ejecta are azimuthally symmetric*. This assumption is a good approximation for moderately oblique impacts, but breaks down for grazing impacts, in which ejecta may carry away some of the impactor's angular momentum. Thus, $\Delta\omega$ may be somewhat less than given by Eq. 9.

2. *Partial Ejecta Escape:* In this case the effect of angular-momentum drain, as discussed by Dobrovolskis and Burns (1984), is important. This effect causes a decrease in rotation rate due to loss of angular momentum by ejecta escaping preferentially in the prograde direction, and is given by

$$\Delta\omega = \frac{-5}{12} k \omega \frac{m}{M} \left(\frac{R}{R_a} \right)^{-k} \qquad (10)$$

where k is the exponent in the ejecta mass-velocity distribution (Eq. 3) and R_a is the critical radius above which the ejecta mass loss is smaller than the mass of the projectile, and the collisions are accretionary rather than erosive. All ejecta escape for $R \lesssim R_c = V_0/(8\pi G\rho/3)^{1/2}$. Since $R_c/R = V_0/V_e$, we get $R_a = R_c (M_{ej}/m)^{1/k}$, where the total ejecta mass $M_{ej} = C(mV_p^2/2)$ is assumed to be proportional to the impact energy through a proportionality factor C. To be consistent with Eq. (1) in the case when the fragmentation threshold is reached, we have to set $C \approx \rho/4S_0$. Then the total spin change of the target asteroid due to cratering collisions is the sum of Eqs. (9) and (10). One should note that the theory of Dobrovolskis and Burns (1984) assumes that the escaping ejecta originates at the target's surface near the impact point. Its applicability to large impacts in which a very large crater is formed is not clear. Again, oblique impacts could behave in a significantly different way. Further research into these effects is needed.

B. An Integrated Size and Spin Collisional Evolution Model

The algorithm described above was incorporated into the numerical simulation of asteroid collisional evolution. We report here on preliminary results using this integrated model. A limitation is that we model only the mean spin rate of a size bin; the dispersion about the mean is beyond the scope of the present program.

Two critical parameters for the spin evolution model are α (in Eq. 8), which determines the spin rates for small fragments resulting from a shattering collision, and β, the fraction of impact angular momentum that is retained by the target. For the former, simple physical arguments led Fujiwara and Tsukamoto (1981) and Paolicchi et al. (1989) to assume a cube-root dependence on mass ($\alpha = 1/3$); on the other hand, the very limited experimental data set provided by Fujiwara and Tsukamoto yields a best-fit value of $\alpha \simeq 0.18$. It is easy to see that values of $\alpha \gtrsim 1/3$ would lead to very short periods (fractions of an hour) for km-sized fragment asteroids, while observations (Binzel and Mulholland 1983; Binzel 1989, in preparation) suggest that such asteroids have typical periods of a few hours. We have thus adopted a value of $\alpha = 0.18$ for this study. The only experimental data on β come also from Fujiwara and Tsukamoto, who found that only $\sim$10% of the impact angular momentum reappears in the rotation of the most massive fragments, leading to β values of a few tenths. There is the possibility that for weakly consolidated rubble-pile asteroids the transfer of angular momentum is even less efficient than for the rigid experimental targets. Therefore, we have adopted values of β in the range from 0.01 to 0.3 for this study. We have also assumed that all asteroids were initially rotating with an 8 hr period. This is not intended to be a realistic choice; it just allowed us to test whether spin-up or spin-down effects predominate in different size ranges.

The rotation period as a function of size after 4.5 Gyr of evolution is shown in Fig. 5, for the same initial population and parameters ($S_o = 3 \times 10^7$erg cm^{-3}, $f_{ke} = 0.1$) used to generate Fig. 2, with and without strain-rate dependence. The spin period of Ceres has been changed little by collisions over solar system history, but with $\beta = 0.1$ already the 500-km diameter bin has been spun up to $\sim$5 hr. Likewise, at small sizes ($D \lesssim 100$ km, where nearly all the bodies have lost at least 50% of their original mass) the spin-up associated with fragmentation events is very effective, leading to rotational periods of the order of 1 to 3 hr at $D \simeq 10$ km. With $\beta = 0.3$, this is further reduced to $\sim$0.2 hr, a value comparable to the rotational burst limit. Real asteroids at these sizes are known to be strongly nonspherical, and we did not take into account relaxation of spin axes to principal axes of maximum moment of inertia (Burns and Safronov 1973). This probably leads to an underestimate of the periods by a factor of $\sim$1.5. However, our simulation clearly indicates that the choices $\alpha = 0.18$, $\beta = 0.1$ are indeed upper limits, and/or that some additional spin-down mechanism is effective (for instance, we have already noticed that our model does not include any angular momentum drain effect due to asymmetric escape of fragments after shattering events).

At intermediate sizes, with our choice of parameters ($C = 2 \times 10^{-8}$ s^2 cm^{-2} and $V_o = 20$ m s^{-1}, i.e., $R_c \simeq 17$ km and $R_a \simeq 600$ km), the slowing-down effect of the angular-momentum drain mechanism associated with cra-

$\overline{P}$ and associated $\overline{\omega}$
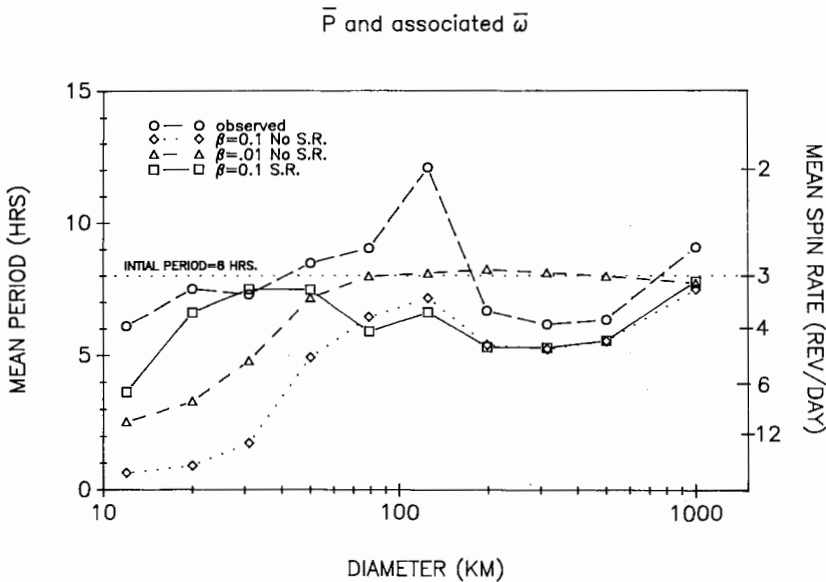
Fig. 5. Observed vs predicted mean rotation rates as a function of asteroid size in the collisional evolution case shown in Fig. 2. The deviations from the initial 8-hr rotation period show the effect of collisions in changing spin rates for asteroids of various size.

tering is very limited, resulting at most in a ~5% decrease of the spin rates with respect to the initial values even with $\beta = 0.01$. With $\beta = 0.1$, spin-up mechanisms prevail at all sizes. We must notice that the above-mentioned values of C and V_o yield an enhanced drain effect with respect to the values discussed by Dobrovolskis and Burns (1984). On the other hand, our choice of C is consistent with that of S_o (i.e., the largest crater cannot eject more than 50% of the target mass), while higher values of V_o (≈ 50 m s^{-1}), which would further enhance the effectiveness of the drain would result in a severe depletion of the final abundance of asteroids at $D \simeq 100$ km, due to mass loss from cratering. Again, it appears that the evolution of asteroid spin rates is dominated by catastrophic fragmentation events rather than by smaller-scale impacts. When the strain-rate scaling is included, the main effect is a significantly slower rotation for $D < 50$ km.

The observed distribution of asteroid rotation rates as a function of size does place meaningful constraints on the physics of asteroid collisions and on the whole collisional history of the belt. Further studies using this integrated model are planned.

VI. UNRESOLVED PROBLEMS

Preliminary results of an integrated size and spin evolution model can yield qualitative agreement with observations, but only with some arbitrary assumptions about impact outcomes and scaling. We have discussed the problem of the discrepancy between the laboratory data and scaling predictions that asteroids should behave as weak bodies, and some (although conflicting) observational evidence that they are strong in response to impacts. Much work is needed in the areas of experiments, scaling, modeling and observations. The prospects for improvements in the first two are discussed in the chapter by Fujiwara et al.; here we discuss unresolved issues in our modeling approach and associated observational needs.

As more experimental data become available, we can improve algorithms for rotational evolution. Equation (8) is in qualitative agreement with data showing that smaller fragments generally spin faster, but it seems likely that ω is not proportional to ω_T in the limit of high spin rates. We need to allow for lower efficiency of highly oblique impacts in imparting angular momentum to the target (cf. Eq. 9); some ejecta may escape preferentially in the direction of impact. The model for angular-momentum drain via partial ejecta escape (Eq. 8) has not been extended to very large impacts that shatter but do not entirely destroy the target. In general, asteroids are not spherical, and their shapes must be modeled to compare the calculated angular momentum with the observable property of spin rate.

Observations are needed to provide more complete statistics of rotation rates, especially for small asteroids. A more complete census of sizes, shapes and spin rates for members of several Hirayama families could provide better

constraints on large-scale collisional outcomes. By determinations of shapes, it may be possible to determine the fraction of large asteroids that are rubble piles (Drummond et al. 1988). Eventually, it may be shown by mass/density determinations, or remote or *in situ* compositional measurements, whether M type asteroids are remnant metal cores of shattered bodies. A more immediate prospect may be detection of very small olivine-rich fragments of the mantles of such bodies. Either would greatly increase the constraints on models of collisional evolution, and our understanding of the history of the asteroid belt.

REFERENCES

Binzel, R. P. 1986. Collisional evolution in the asteroid belt: An observational and numerical study. Ph.D. thesis, Univ. of Texas.

Binzel, R., and Mulholland, D. 1983. A photoelectric lightcurve survey of small main belt asteroids. *Icarus* 56:519–533.

Burns, J. A., and Safronov, V. S. 1973. Asteroid nutation angles. *Mon. Not. Roy. Astron. Soc.* 165:403–411.

Catullo, V., Zappalà, V., Farinella, P., and Paolicchi, P. 1984. Analysis of the shape distribution of asteroids. *Astron. Astrophys.* 138:464–468.

Chapman, C. R. 1986. Implications of the inferred compositions of asteroids for their collisional evolution. *Mem. S. A. It.* 57:103–122.

Chapman, C. R., and Davis, D. R. 1975. Asteroid collisional evolution: Evidence for a much larger early population. *Science* 190:553–556.

Davis, D. R., Chapman, C. R., Greenberg, R., and Harris, A. W. 1979. Collisional evolution of asteroids: Populations, rotations, and velocities. In *Asteroids,* ed. T. Gehrels (Tucson: Univ. of Arizona Press), pp. 528–557.

Davis, D. R., Chapman, C. R., Greenberg, R., and Weidenschilling, S. J. 1982. Hirayama families: Chips off the old block or collections of rubble piles? *Bull. Amer. Astron. Soc.* 14:720 (abstract).

Davis, D. R., Chapman, C. R., Weidenschilling, S. J., and Greenberg, R. 1985. Collisional history of asteroids: Evidence from Vesta and the Hirayama families. *Icarus* 62:30–53.

Dobrovolskis, A., and Burns, J. A. 1984. Angular momentum drain: A mechanism for despinning asteroids. *Icarus* 57:464–476.

Dohnanyi, J. 1971. Fragmentation and distribution of asteroids. In *Physical Studies of Minor Planets,* ed. T. Gehrels, NASA SP-267, pp. 263–295.

Drummond, J. D., Weidenschilling, S. J., Chapman, C. R., and Davis, D. R. 1988. Photometric geodesy of main-belt asteroids. II. Analysis of lightcurves for poles, periods, and shapes. *Icarus* 76:19–77.

Farinella, P., Paolicchi, P., Tedesco, E., and Zappalà, V. 1981. Triaxial equilibrium ellipsoids among the asteroids? *Icarus* 46:113–123.

Farinella, P., Paolicchi, P., and Zappalà, V. 1982. The asteroids as outcomes of catastrophic collisions. *Icarus* 52:409–433.

Farinella, P., Milani, A., Nobili, A. M., Paolicchi, P., and Zappalà, V. 1983. Hyperion: Collisional disruption of a resonant satellite. *Icarus* 54:353–360.

Farinella, P., Paolicchi, P., and Zappalà, V. 1985. *Mon. Not. Roy. Astron. Soc.* 216:565–570.

Fujiwara, A. 1987. Energy partition into translational and rotational motion of fragments in catastrophic disruption by impact: An experiment and asteroid cases. *Icarus* 70:536–545.

Fujiwara, A., and Tsukamoto, A. 1980. Experimental study on the velocity of fragments in collisional breakup. *Icarus* 44:142–153.

Fujiwara, A., and Tsukamoto, A. 1981. Rotation of fragments in catastrophic impact. *Icarus* 48:329–334.

Fujiwara, A., Kamimoto, G., and Tsukamoto, A. 1977. Destruction of basaltic bodies by high-velocity impact. *Icarus* 31:277–288.

Greenberg, R., Wacker, J. F., Hartmann, W. K., and Chapman, C. R. 1978. Planetesimals to planets: Numerical simulation of collisional evolution. *Icarus* 35:1–26.

Harris, A. W. 1979. Asteroid rotation rates. II. A theory for the collisional evolution of rotation rates. *Icarus* 40:145–153.

Hartmann, W. K. 1980. Continued low-velocity impact experiments at Ames Vertical Gun Facility: Miscellaneous results. *Lunar Planet. Sci.* XI:404–406 (abstract).

Hartmann, W. K. 1988. Impact strengths and energy partitioning in impacts into finite solid targets. *Lunar Planet. Sci.* XIX:451–452 (abstract).

Holsapple, K. A., and Housen, K. R. 1986. Scaling laws for the catastrophic collisions of asteroids. *Mem. S. A. It.* 57:65–86.

Öpik, E. J. 1951. *Proc. Roy. Irish Acad. Sec. A.* 54:165.

Paolicchi, P., Zappalà, V., and Farinella, P. 1982. Some ideas for a semiempirical theory of catastrophic impact processes among asteroids. *Harv. Obs. Bull.* 6(1):163–166.

Paolicchi, P., Farinella, P., and Zappalà, V. 1983. The critical energy and the inelasticity coefficient for asteroidal catastrophic collisions. *Adv. Space Res.* 2:235–238.

Paolicchi, P., Cellino, A., Farinella, P., and Zappalà, V. 1989. A semi-empirical model of catastrophic breakup processes. *Icarus* 77:187–212.

Piotrowski, S. I. 1953. The collisions of asteroids. *Acta Astron. Ser. A,* 6:115–138.

Shoemaker, E. M., Williams, J. G., Helin, E. F., and Wolfe, R. F. 1979. Earth-crossing asteroids: Orbital classes, collision rates with Earth, and origin. In *Asteroids,* ed. T. Gehrels (Tucson: Univ. of Arizona Press), pp. 253–282.

Stacey, F. D. 1977. *Physics of the Earth,* 2nd ed. (New York: J. Wiley & Sons), pp. 172–173.

Veverka, J., and Thomas, P. 1979. Phobos and Deimos: A preview of what asteroids are like? In *Asteroids,* ed. T. Gehrels (Tucson: Univ. of Arizona Press), pp. 628–651.

Weidenschilling, S. J. 1977. The distribution of mass in the planetary system and the solar nebula. *Astrophys. Space Sci.* 51:152–158.

Weidenschilling, S. J. 1981. How fast can an asteroid spin? *Icarus* 46:124–126.

Zappalà, V., Farinella, P., Knezevic, Z., and Paolicchi, P. 1984. Collisional origin of the asteroid families: Mass and velocity distributions. *Icarus* 59:261–285.

MEAN MOTION RESONANCES

Cl. FROESCHLÉ
Observatoire de Nice

and

R. GREENBERG
University of Arizona

Some recent work on the resonant structure of the asteroid belt is reviewed. After presenting the analytical and numerical methods available for investigating resonant motion, we review recent developments concerned with the formation of the Kirkwood gaps, especially within the framework of the so-called gravitational hypothesis. The problem seems to remain open for the 2 : 1 gap where the cosmogonic hypothesis is perhaps needed.

I. INTRODUCTION

Mean motion resonances are closely related both to gaps and to isolated clusters in the orbital distribution of asteroids (see Greenberg and Scholl 1979). They also introduce interesting complexities for the definition of the so-called proper elements used to define asteroid families (see the chapter by Valsecchi et al.; Froeschlé et al. 1987). These structural characteristics are related to the origin and evolution of the asteroid belt. The on-going processes that shaped the belt continue to deliver asteroidal material to the inner solar system, where some lands on the Earth as meteorites.

Besides these important planetological implications the study of mean motion resonances has attracted the attention of theoreticians concerned with general issues of nonlinear processes in mathematics and physics. In particu-

lar, the use of semi-computational (or semi-analytical) methods to study resonant behavior among asteroids has led to a better understanding of various phenomena of great current interest in modern dynamics: the homoclinic point, separatrix, ordered and chaotic motion, adiabatic invariant, etc.

An earlier review by Greenberg and Scholl (1979) on resonances in the asteroid belt still provides an excellent introduction both to the resonance mechanism through Greenberg's secular perturbation theory for low eccentric, planar orbits at the 2 : 1 resonance and to the four types of hypotheses (statistical, gravitational, collisional and cosmogonic) that have been invoked to try to explain the Kirkwood gaps. The statistical hypothesis assumes that asteroids librate around gaps and therefore are rarely seen crossing the exact resonances. The gravitational hypothesis supposes that asteroids that originally formed in the Kirkwood gaps were removed later by purely gravitational forces due to Jupiter. According to the collisional hypothesis, asteroids are removed from the gaps, either through destruction or change of mean motion, by collisions with neighboring asteroids. Finally, the cosmogonic hypothesis assumes that gaps represent regions where asteroids failed to form during the early history of the solar system.

Later reviews by Froeschlé and Scholl (1983) and Scholl (1985) update that of Greenberg and Scholl. The reviews by Wisdom (1987) and Froeschlé (1987) concentrate on chaotic dynamics. Of the four hypotheses previously invoked to explain the Kirkwood gaps, the gravitational hypothesis based on the elliptic Sun-Jupiter-asteroid restricted three-body problem has proven to be the most plausible thanks to recent theoretical breakthroughs. This chapter deals primarily with these numerical and analytical developments, although many more details about chaotic behavior can be found in the above-cited reviews. We do not describe the dynamics of the outer part of the asteroid belt or of secular resonances, as these topics are covered in the chapters by Nobili and by Scholl et al. We summarize the resonance mechanism (Sec. II) and describe both analytical and numerical models used to study mean motion resonant orbits (Sec. III). Then, after a brief discussion of the numerical results in Sec. IV and Sec. V, we show how fresh insight can be obtained by means of a new semi-analytical approach (Sec. VI and Sec. VII).

II. THE RESONANCE MECHANISM

A resonance occurs when the period of revolution of an asteroid is a multiple $p/(p + q)$ of Jupiter's period of revolution, where p and q are small integers. Traditionally, ratios of mean motions are considered and in the following these will be called $(p + q) : p$ resonances. If a conjunction (i.e., in the planar case, alignment of the Sun, Jupiter and the asteroid) occurs at some longitude L it will repeat at nearly the same value of L after a few revolutions of the asteroid around the Sun. For example, for the 5 : 2 resonance, conjunctions repeat after 5 revolutions of the asteroid and 2 of Jupiter. Repetition of

geometric configuration results in enhancement of perturbations. For instance, Jupiter may add orbital angular momentum to an asteroid's orbit for many periods before it later starts to take angular momentum out again. For a physical description of the resonance phenomenon, see Peale (1976) and Greenberg (1977).

It is convenient to introduce the resonance variable σ which describes the location of a conjunction with respect to the asteroid's longitude of perihelion $\tilde{\omega}$, i.e., $\sigma = L - \tilde{\omega}$. For $\sigma = 0$, conjunction occurs at the asteroid's perihelion (favors stability) but for $\sigma = \pi$, conjunction occurs at the asteroid's aphelion, in the case of the $2:1$ resonance. The latter case could be unstable if it allows close encounters with Jupiter, a situation prevented by any resonance that maintains σ at 0. Since σ changes slowly (for resonant motion), it is natural to use σ for theoretical purposes; e.g., Poincaré (1902) used σ as a canonical variable for the $2:1$ resonance in the planar problem. For the the nonplanar problem, an additional canonical variable is introduced which is critical for orbital stability. Schubart (1978) used the variable τ that measures the longitude of conjunction reckoned from the longitude of the ascending node of the asteroid's orbit. For $\tau = 0$, conjunction occurs in the orbital plane of Jupiter. Motion could therefore be destabilized: τ near $90°$ or $270°$ would prevent such a possibility.

III. ANALYTICAL MODELS FOR THE STUDY OF MEAN MOTION RESONANCES

The full equations of motion of an asteroid are nonintegrable even in the framework of the restricted three-body problem. The various approximations used represent treatment of the appropriate Hamiltonian or equivalently of the perturbing function R, in such a way as to reduce the problem to one degree of freedom.

The disturbing function R can be Fourier expanded into the general form

$$R = \Sigma \; \alpha(a, a_J, e, e_J, i, i_J) \cos(i\lambda + j\lambda_J + k\tilde{\omega} + l\tilde{\omega}_J + m\Omega + n\Omega_J) \quad (1)$$

where the coefficients α are functions of the semimajor axes, eccentricities and inclinations; $\tilde{\omega}$, Ω and λ, are respectively the longitude of pericenter, the longitude of the ascending node and the mean longitude of the asteroid; quantities with the subscript J refer to Jupiter's orbit. The summation is performed over all permissible values of the integers i, j, k, l, m, n and α is also a function of these integers. The following important mathematical properties of this expansion define it as a d'Alembert series : α is of the order $e^{|k|} e^{|l|}_J i^{|m|}$ $i^{|n|}_J$; the sum $m + n$ is even and $i + j + k + l + m + n = 0$. Therefore $|k| + |l| + |m| + |n| \geq |i + j|$. The terms with $i = 0$ and $j = 0$ are called secular since only slowly varying quantities are contained in the arguments of the cosine. However, if the ratio of the mean motions n and n_J are close to some

rational number, then the quantity $i\lambda + j\lambda_J$ can also be slowly varying and will dominate the motion of the asteroid because the remaining nonsecular terms are of short period. These short-period terms are usually eliminated using the averaging principle which assumes that if a particular resonant term is slowly varying, then the mean value of R and of its derivatives averaged over the resonant period only contains the secular and resonant terms which nevertheless are still given by a quadruple summation over k, l, m and n. Further truncations are of course performed and their validity depends on the location of the resonance and of the maximum eccentricity reached by the orbits since both a/a_J and $e^{|k|}$ appear in the coefficients of the cosine.

The number of terms that should be retained in the d'Alembert form of the disturbing function depends crucially on the value of q. For first-order resonances of the form $(p + 1): p$, terms proportional to a single power of the eccentricity are present while for the $3:1$ resonance ($q = 2$), the largest terms in the disturbing function are proportional to two powers of the eccentricities i.e., e_J^2, e^2 or $e_J e$ and the next terms which contribute are fourth order in the eccentricities. In all cases, the problem is to retain enough terms to obtain a good representation of the motion, but when terms of high order are included, an analytical description is extremely difficult. Greenberg (see Greenberg and Scholl 1979) developed such a secular perturbation theory for small eccentric planar orbits.

In addition to series expansions followed by truncation, changes into suitable canonical coordinates have lead to the two fundamental models for resonance: the pendulum model and the second fundamental model (Henrard and Lemaître 1983a). The pendulum has often been taken as the basic model for resonance (Lichtenberg and Lieberman 1983). It is the backbone of the so-called ideal resonance problem (Garfinkel 1966). As a matter of fact, many references about resonances mention the pendulum and use it implicitly or explicitly as a model. Quite often in celestial mechanics a resonance problem is reduced to that of a pendulum through the following steps: the Hamiltonian $H = H_0 + R$, where H_0 is the Hamiltonian of the unperturbed motion and is rewritten using canonical variables in such a way that after removing the short-period terms, the problem is reduced to a one degree of freedom Hamiltonian

$$K = K_0 (S) + \epsilon K_1 (S, \sigma) \qquad (2)$$

where K_1 is 2π periodic in σ and $\partial K_0/\partial S$ is small for $S = S^*$. Without loss of generality S^* can be taken equal to zero. For the restricted circular three-body problem (see Henrard and Lemaître 1983b), this form is obtained by using the resonance variable σ defined above, with L more specifically given by $L = (p + q)\lambda_J - p\lambda$. The conjugate variable S is given by $S = \sqrt{a/a_J}(1 - \sqrt{1 - e^2})$. ϵ is of the order of the Jupiter-to-Sun mass ratio. Then in the expansion of K_0

and K_1, only the most significant terms are retained. If $K_1(0,\sigma) \simeq \cos\sigma$, then K becomes

$$K' = \alpha S + \beta S^2 + \epsilon \cos\sigma \qquad (3)$$

which leads directly to the pendulum equation.

On the other hand, in many instances in celestial mechanics, the function K_1 possesses the d'Alembert characteristic in $\sqrt{S}, \sigma$). In other words, it is an analytic function in $x = \sqrt{2S} \sin\sigma$ and $y = \sqrt{2S} \cos\sigma$ at the origin (see Henrard 1974). This is the case in most orbit-orbit resonances where $\sqrt{2S}$ is proportional to the eccentricity or the inclination. In such cases, the analogous simplest form of the truncated Hamiltonian is

$$K'' = \alpha S + \beta S^2 + \epsilon \sqrt{2S} \cos\sigma \qquad (4)$$

where α is a measure of the closeness to the resonance and β is a constant of the order of the unity. The relation between the pendulum, Eq. (3), and the second fundamental model, Eq. (4) is no longer simple. For some values of the parameters (α, β, ϵ) and in some limited parts of the phase space, it is possible to define a nonzero mean value $\bar{S}$ of S. Expanding K'' around $\bar{S}$, it is possible to reduce Eq. (4) to Eq. (3) with ϵ replaced by $\epsilon\sqrt{2\bar{S}}$. Henrard and Lemaître (1983b) have studied in detail the Hamiltonian Eq. (4) as a model between the pendulum and the basic Eq. (2). In the case of the study of the $2:1$ resonance in the planar restricted problem, the topology exhibited by the second fundamental model is the same as that given by Schubart's numerical averaging process shown in Fig. 1.

Figure 1 shows various trajectories near the $2:1$ resonance which display the now well-known topology with an important feature which determines orbital behavior in near-resonant cases, namely a bifurcation point on the negative x-axis as well as bifurcation trajectory, which corresponds to the heavier line in Fig. 1. This bifurcation trajectory divides the S, σ space into three regions where orbits behave quite differently.

The first region corresponds to the inner portion of the bifurcation curve around the point a, where the apocentric librator occurs. Pericentric librators with banana-shaped trajectories occur around P in the second region. Finally, the outer circulators fill a third region outside of the bifurcation curve.

Schubart (1966) and Message (1966) have directly studied Hamiltonian Eq. (2), a one degree of freedom problem. Each resonance problem is treated in a particular way but the aim is always to reduce the number of degrees of freedom in order to obtain a problem susceptible to quadrature. For this reason, the assumption is often made that the perturbers move on circular orbits (see Kozai 1985).

Almost simultaneously, Henrard et al. (1986) and Wisdom (1986) proposed a canonical solution reducing the averaged planar planetary problem
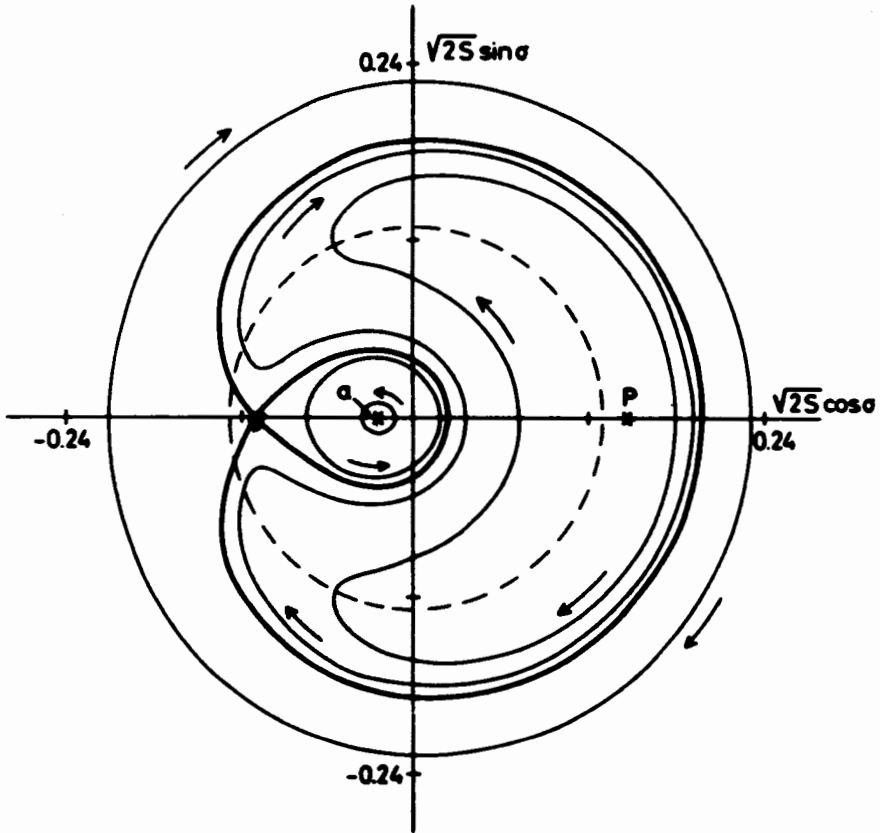
Fig. 1. Trajectories in σ vs $\sqrt{2S}$ space from Schubart's averaged circular model at the 2:1 commensurability for $A = 0.802$. The arrows indicate directions of motion in this space. The darker lines correspond to critical bifurcation trajectories. Paths immediately around point a are apocentric librators; those about p are pericentric librators. The dashed circle corresponds to the exact center of the resonance (figure from Greenberg and Scholl 1979).

near $(p + 1):p$ resonances to the standard, one critical argument problem. The basic step in the solution is based on the work of Sessin (1983) and Sessin and Ferraz-Mello (1984). But, with a more general intrinsic and elegant presentation, the Hamiltonian is reduced to the form of Eq. (4). An analogous canonical transformation simplifies the elliptic restricted problem. In the same spirit, Ferraz-Mello (1987a) derived a completely integrable system by averaging the elliptic asteroid problem near a first-order resonance and, in particular, used a Woltjer expansion to study the motion of high-eccentricity librators such as the Hildas and the Griquas (see Ferraz-Mello 1987b).

Let us emphasize that similar approaches to the solution of the motion of asteroids near the 3:1 or the 2:1 commensurabilities are bound to fail be-

cause numerical computations of orbits exhibit chaotic behavior (Wisdom 1983; Giffen 1973; Froeschlé and Scholl 1977). The integrability of the first-order Hamiltonian is spoiled by terms of higher order. In order to get some feeling for the appearance of stochasticity, let us go back again to the pendulum model (which is so useful in celestial mechanics and other nonlinear dynamical studies) because perturbations can be Fourier decomposed into a series of sinusoidal terms. Near resonance, for example, when an asteroid's period is near 1/3 of Jupiter's, one term may have a very long period and thus have a much greater effect than others. This effect corresponds to periodic repetition of geometric configurations which enhances perturbations. In many applications, the other weak, short-periodic terms are negligible. The dominant term introduces oscillations in orbital elements analogous to the behavior of a pendulum; both are governed by a sinusoidal force.

A simple pendulum has two distinct modes of behavior, oscillation and circulation, which can be separated by infinitesimal differences in initial conditions. The boundary is called the separatrix. The celestial system has analogous separatrices, where behavior can be grossly modified by the infinite number of small sinusoidal components and by small differences in initial conditions. The result is that over a significant range of initial conditions, long-term behavior may be unpredictable, or chaotic. The effect is exacerbated if changes in period during high-amplitude oscillations render otherwise short-period Fourier components to have long periods; this effect is sometimes called resonance overlap. Only by the use of clever computational techniques has chaotic behavior become possible to investigate. Wisdom (1985) and Henrard and Lemaître (1987) have developed semi-analytical theories to explain the qualitative features of the phase space near the $3:1$ and $2:1$ commensurabilities (see Sec. IV).

IV. METHODS FOR NUMERICAL STUDIES

Averaging

The perturbation theories described above use truncated power series and at large eccentricities, both analytical models and mappings (see Sec. V) break down and only numerical integration is possible.

Following an idea of Poincaré, Schubart (1968) developed a different approach. Modifying Poincaré's canonical equations for the planar-restricted Sun-Jupiter-asteroid problem, Schubart averaged the Hamiltonian over the corresponding commensurability period. Inserting the averaged Hamiltonian in Poincaré's equations, Schubart then integrated numerically the new set of differential equations. For the circular case, this set degenerates to a single implicit equation which can be solved without recourse to numerical integration. Orbits are represented by closed curves in S, σ space. Besides the aver-

aged Hamiltonian $\bar{H} = 1/2\pi(p + q) \int_0^{2\pi(p + q)} H d\lambda$, the quantity $A = \sqrt{a/a_J}$ $(2 - \sqrt{1 - e^2})$ which is a variable in the elliptic model, is also an integral of motion in the circular case. These two integrals exhibit the topology of the second fundamental resonance problem (see Fig. 1).

In the circular-averaged model with $e_J = 0$, orbits remain in their corresponding regions. In the more general model with $e_J = 0$ and without averaging, or even with $e_J \neq 0$ and with averaging, an orbit can cross the bifurcation curve and consequently can change its behavior. In particular, librators can become circulators and vice versa.

Schubart's averaging differs strongly from the above averaging principle: he does not drop short periodic terms and does not use a series expansion. Therefore, with Schubart's averaging there is no restriction for eccentricities or resonance type. The only price to pay with respect to the Henrard and Lemaître approach is that $\bar{H}$ is given implicitly.

It is clear that Schubart's topology as displayed in Fig. 1 is only valid for the circular planar-averaged model. Only in this model is the problem of resonant motion fully integrable. The critical bifurcation point is called a homoclinic point in modern dynamics (Arnold 1978). It is well known that integrable systems are not generic; i.e., as explained above for the pendulum, small perturbations can destroy the integrability, and the separatrix or homoclinic orbit can cause wild regions with chaotic behavior (Arnold 1978). This peculiar behavior for Schubart's topology was displayed by Froeschlé and Scholl (1977) in the elliptic averaged case.

Besides ellipticity, nonaveraging as well as noncoplanarity destroys the integrability. For the case of noncoplanarity, Schubart's topology displayed in Fig. 1 remains valid to some extent and can be regarded as a good example for understanding and describing the behavior of resonant orbits in the three-dimensional elliptic averaged case. Schubart (1978,1979) has extended the planar model to deal with this more general case. The six variables in his differential equation are:

$$G = \sqrt{a(1 - e^2)}$$

$$\mu = \lambda - \lambda_J(p + q)/p$$

$$\psi_1 = e \cos \tilde{\omega}$$

$$\psi_2 = e \sin \tilde{\omega}$$

$$\psi_3 = \tan(i/2) \cos \Omega$$

$$\psi_4 = \tan(i/2) \sin \Omega. \qquad (5)$$

The longitude Ω of the ascending node of the asteroid's orbit with inclination i relative to Jupiter's orbit, is reckoned from Jupiter's longitude of perihelion.

In addition to the quantity σ already defined, Schubart used the critical variable τ given by

$$\tau = -\Omega - \mu p/q \qquad (6)$$

with $p = q = 1$ for the $2:1$ resonance. Both σ and τ vary slowly for resonant motion.

Using Schubart's model, Froeschlé and Scholl (1982) have performed a systematic exploration of the three-dimensional asteroidal motion at the $2:1$ resonance. They have also shown (Froeschlé and Scholl 1986; Scholl and Froeschlé 1988) that the dynamical evolution of meteor-stream particles in resonance appears to be affected by the same resonance mechanisms as resonant asteroids. The crossing of separatrix-like zones appears to be crucial for the formation of arcs and for the dissolution of streams. Investigating the orbital evolution of known resonant meteor streams and of model streams, they have found examples for such a transitory arc formation. The orbital inclination of meteor streams appears to be a critical parameter for arc formation.

V. MAPPINGS

It is well known that through the introduction of a surface of section, the study of a Hamiltonian system with two degrees of freedom reduces to the study of a two-dimensional, area preserving mapping. Conversely, most of what is known about the qualitative properties of Hamiltonian systems has come from the study of arbitrarily chosen area preserving maps. The main reason is the speed of computation. On the other hand, for the study of a particular dynamical system, the formal equivalence is of no practical use since an explicit form for the map is rarely known and in order to compute the surface of section it is still necessary to integrate the orbit between the intersections. However, a very rapid method for numerically calculating resonant asteroidal orbits, i.e., a mapping, was introduced by Wisdom (1982) for the $3:1$ resonance. The idea of the method is due to Chirikov (1979).

Chirikov's Method

Let us consider the time dependent Hamiltonian

$$H = I^2/4\pi + K_0/2\pi \, cos \, V + \sum_{n \neq 0} K_n(I)\cos(V - nt) \qquad (7)$$

where I is the momentum and V its canonically conjugate coordinate. If the constants K_n are small, then the pendulum Hamiltonian H_o gives a good approximation to the system using the averaging principle. However, this averaging procedure is no longer valid near the separatrix which is replaced by a narrow chaotic band when the high-frequency terms are present. Therefore, in order to deal with this problem, Chirikov, instead of ignoring the high-frequency terms, made another approximation. He modified the high-frequency terms and got a new Hamiltonian

$$H_C = I^2/4\pi + K_0/2\pi \cos V + K_0/2\pi \sum_{n \neq 0} \cos(V - nt) \qquad (8)$$

which can be considered closer to H than H_o, since the new high-frequency terms allow chaos (see above).

Using the Fourier transform of the Dirac δ function with period 2π, H_C becomes

$$H_C = I^2/4\pi + K_0 \cos V \, \delta_{2\pi}(t). \qquad (9)$$

Then, by a straightforward integration, using the property that the delta function acts instantaneously, the standard map (see Lichtenberg and Lieberman 1983) is obtained

$$\begin{cases} I' = I + K_0 \sin V \\ V' = V + I' \, . \end{cases} \qquad (10)$$

Wisdom's Generalization

Wisdom has applied this method to the restricted elliptic three-body problem. From the Hamiltonian derived through a second-order expansion of the perturbing function: $H = -\mu_1/2a + H_{sec}(a, e, i, \omega, \Omega, a_J, e_J, i_J, \omega_J, \Omega_J)$ $+ H_{res}(---,3\lambda_J-\lambda,---) + H_{highfreq}$, he obtains the new Hamiltonian

$$H_W = -\mu_1/2a + H_{sec} + H_{res} \, \delta_{2\pi}(t) \qquad (11)$$

from which he derives his mapping. With this, orbits can be computed over millions of years. He found a surprising behavior, namely a test particle starting in the gap could remain on an orbit for 1 Myr with low eccentricity (<0.05) and then suddenly jump to a large eccentricity (>0.3), thus becoming a Mars crosser.

These results have led Murray and Fox (1984) to compute the motion of asteroids near the $3:1$ resonance using three numerical methods : (a) integration of the full equations of motion; (b) integration of the analytically averaged equations of motion; and (c) Wisdom's algebraic mapping. The agreement has been found to be good in the regular regions of phase space. No comparison has been made with Schubart's method.

The occurrence of these sudden jumps is related to chaotic motion as Wisdom has shown by computing maximum Lyapunov characteristic exponents at the $3:1$ resonance. Recall that the Lyapunov characteristic exponents of a given trajectory characterize the mean exponential rate of divergence of a neighboring trajectory, and that they provide a computable quantitative measure of the degree of stochasticity for a trajectory of a dynamical system with any number of degrees of freedom (see Froeschlé 1984). Froeschlé and Scholl (1981) have calculated maximum Lyapunov exponents at the $2:1$ resonance and found no clear evidence for chaotic motion, but their integrations typ-

ically spanned only 10,000 yr and new numerical integrations should be undertaken with greater time intervals.

Abrupt changes in orbital behavior have been known for some time, even before the work by Wisdom. Scholl and Froeschlé (1974,1975) thought that these were exceptional cases, but Wisdom has shown that such changes are to be expected for any orbit near the 3 : 1 resonance if one follows an orbit for a sufficiently long period of time. Wisdom's other great achievement was to demonstrate that the observed width of the 3 : 1 Kirkwood gap coincides with the size of the chaotic region.

But what about the other gaps? The same mapping methods have been applied by Murray (1986) for the 2 : 1 and 3 : 2 Jovian resonances. He determined the chaotic regions within these resonances by computing the largest Lyapunov exponent with the rescaling method. Like Wisdom, in the case of the 3 : 1 gap he found that both resonances have extensive chaotic regions. Figure 2 shows the isometric projection of the maximum eccentricity achieved during 7000 Jupiter periods (with the eccentricity of Jupiter taken equal to 0.048) for test asteroids at the 2 : 1 resonance.

Sidlichovsky and Melendo (1986) obtained similar mappings for the 5 : 2 resonance. They extended Scholl and Froeschlé's (1975) orbits to much longer time intervals (millions of years instead of 38,000) for 96 orbits, and found 53 orbits instead of 33 (Scholl and Froeschlé 1975) for which the eccentricities go beyond 0.3. They thus reproduced the V-shaped nature of the gap.
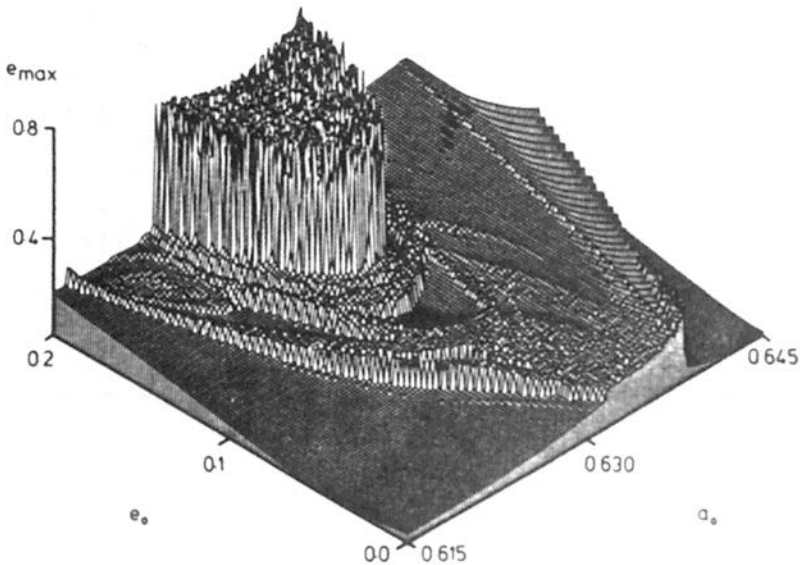
Fig. 2. Maximum eccentricity reached after 7000 Jupiter periods for test asteroids (figure from Murray 1986).

The Chirikov-Wisdom method may be used to solve any resonant problem provided that the problem which results from omitting the resonant term is (1) solvable analytically, and (2) the truncation does not change the topology of phase space too much.

A different approach for modeling the restricted three-body problem has been used by Hadjidemetriou (1986). Instead of solving approximately the perturbed equations of motion, he solved exactly the unperturbed equations and found the corresponding mapping on a surface of section. Then, he perturbed the mapping in such a way that some structure of the phase space known through numerical experiments (stability or instability of some families of periodic orbits for the given example of 3:1 commensurability) was included in the perturbed mapping. In this way, Hadjidemetriou was able to obtain qualitative results upon including additional perturbations, such as drag for example.

VI. INTERPRETATION AND CRITICISM OF THESE RESULTS: A SEMI-ANALYTICAL APPROACH

The impressive upsurge of challenging numerical results has called for new analytical interpretations. Wisdom (1985) developed a semi-analytic perturbation theory for motion near the 3:1 commensurability in the planar restricted three-body problem. Three natural time scales are considered: (i) the orbital period (a few years); (ii) the period of libration of the resonant argument (a few hundred years); (iii) the period of motion of the longitude of perihelion (several thousand years), i.e., the time scale for the slow evolution of the "guiding center" of σ and e. Taking advantage of these well-separated time scales, Wisdom approximated analytically the fastest oscillations; i.e., only terms which contain σ in the disturbing function were considered. Also terms beyond second order in the eccentricity were ignored. Then, the very long-period behavior was computed under the assumption that the action of the motion on the intermediate time scale is adiabatically conserved during the slow evolution.

The predictions of the theory are in good agreement with the features found on numerically generated surfaces of section as shown on Fig. 3. This figure shows clearly two large chaotic zones. A trajectory in the chaotic zone surrounding the origin enters the narrow part of the chaotic zone which extends to high eccentricity at irregular intervals, thus explaining the intermittent bursts of eccentricity. A new criterion for the existence of a large-scale chaotic zone is presented and shows that the eccentricity of Jupiter's orbit is at the source of chaos, which confirms the results obtained by Froeschlé and Scholl (1977) using the Schubart averaging procedure.

Following the same path as Wisdom (1985), Henrard and Lemaître (1987) have presented an analytical perturbation theory for the 2:1 resonance in the planar elliptic frame. The disturbing function is expanded in powers of
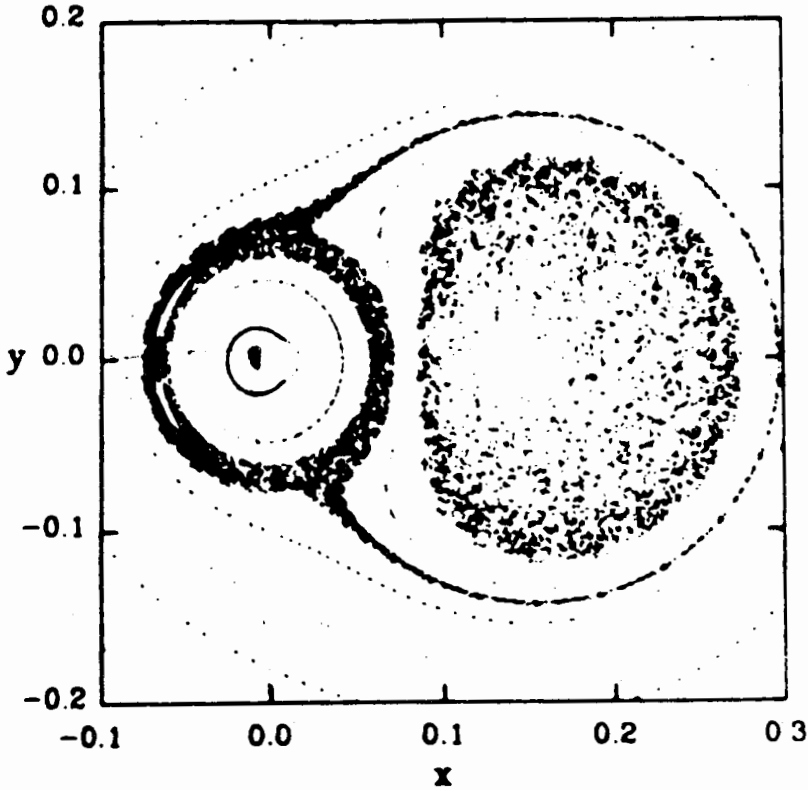
Fig. 3. Numerically generated surface of section computed with Wisdom's mapping. Large chaotic zones appear. The narrow region generates high eccentricities at irregular intervals (figure from Wisdom 1985).

the orbital eccentricities of both the asteroid and Jupiter and then averaged over the fast frequency in the vicinity of the 2:1 resonance. A system with two degrees of freedom is thus obtained in ω and σ. If the eccentricity of the test particle is not too small, the motion of σ is approximated by a pendulum equation and (except in the vicinity of the critical curve) the associated period is much smaller than the period associated with ω. Therefore, action-angle variables could be introduced for the pendulum and averaged again over the fast frequency (analytically and numerically). Then numerical averaging is performed. Of course the Hamiltonian is now parameterized by the action J which is an adiabatic invariant.

A very interesting result arises: for small values of J (small oscillations of the pendulum), the motion in ω,e is very sensitive to the order to which the initial problem has been truncated. Similarly, Murray (1986), in his numerical investigation of the same problem, truncated at order 2 in the eccentricities

and then found very large excursions in e. These disappeared at order 3 and then reappeared again at order 4, but for larger values of the eccentricity. Investigation up to order 8 shows that the problem of convergence is too severe for the method to give meaningful results for values of e larger than 0.3 or 0.4. For smaller initial values of e, the excursions in e are rather small. Thus Murray's central region (which exhibits these large excursions and could lead to collisions with Mars or Jupiter) is due to the early truncation of the perturbation function and not due to the three-body model.

These artifacts are not due to the mapping method itself, but rather to the fact that a low-order disturbing function does not well represent the problem. For larger values of J, the convergence problem is less severe. This means that at least qualitatively Murray's picture is correct for small values of e. This last point is confirmed by numerical explorations performed with the digital Orrery: a special purpose computer specifically designed to study problems in celestial mechanics (see Wisdom 1987). A sizeable chaotic zone near the 2 : 1 commensurability is shown. On the other hand, the region near the 3 : 2 commensurability where the Hildas are located is devoid of chaotic behavior.

Henrard and Lemaître investigated also the neighborhood of the critical curve where Wisdom's chaotic motion takes place. This region is rather small in the 2 : 1 resonance case. They found that in the elliptic restricted problem large portions of the 2 : 1 resonance zone are free from chaotic motions and from large perturbations in eccentricity. The Orrery survey also seems to show a discrepancy in the boundaries on the low semimajor-axis side for a low-eccentricity region.

In order to explain the Hecuba gap, do we still need some *Deus ex Machina*? Such a *Deus ex Machina* could operate during the accretion process (see Gonczi et al. 1982,1983) or perhaps during the removal of a protosolar nebula (see Torbett and Smoluchowski 1982,1983). We note that Henrard and Lemaître (1983), with roughly the same physical assumptions as Torbett and Smoluchowsky (1982,1983), have succeeded in depleting the 2 : 1 gap by making use of an adiabatic invariant. But as pointed out by Wisdom (1987), it is perhaps premature to be forced to assume a cosmogonic mechanism. The discrepancy may only reflect the inadequacy of the planar elliptic model. The three-dimensional elliptic problem and the variations of Jupiter's orbit arising from the perturbations of the other planets may be important.

For small eccentricities ($e < 0.2$) in the vicinity of the bifurcation at the entrance of the resonance zone, the one degree of freedom method is no longer valid. This is precisely the region of phase space where Murray (1986), using numerical integration, found an intricate pattern of chaotic and quasi-periodic motions. Then, instead of considering the usual one degree of freedom resonance problem (Eq. 2), Henrard and Lemaître (1987) considered a double resonance problem with two critical arguments. By applying a semi-numerical perturbation technique to a truncated Hamiltonian of the restricted three-body problem in the case of 2 : 1 resonance, these authors were able to

reproduce Murray's results. Another source of chaotic motion was identified: critical curves associated with the second degree of freedom, or with an interplay between the two degrees of freedom. A super-resonance (i.e., a $2:1$ resonance inside the $2:1$ resonance) is shown to be at the origin of the large chaotic region which crosses the entrance of the resonance zone in Murray's diagrams. Of course, since Murray's model is truncated at the second order in eccentricities, we still lack an exact picture of what happens in the $2:1$ asteroid-Jupiter resonance problem.

VII. ASTEROID FAMILIES: RESONANT PROPER ELEMENTS

Near commensurability the methods developed in order to define proper elements, which are fundamental for the definition of asteroid families, are not valid. Indeed, Dermott and Murray (1981) have found within the main families some narrow gaps corresponding to high-order resonances which indicate either post-formation instabilities or incorrect computations of proper elements. Some attempts have been made to define resonant proper elements: Carpino et al. (1986) have used a linear theory and Knežević et al. (1986, 1988) have used a more elaborate theory due to Yuasa (1973). These authors have shown by numerically simulating the dynamical evolution of families assumed to arise from the "explosion" of a parent object, that the proximity of mean motion commensurabilities adds a significant "noise" to the proper eccentricities and inclinations, and in some cases probably affects the derived memberships of families.

Schubart (1982) first provided, by numerical integration of 34 real Hilda-type orbits some characteristic parameters of these orbits. Bien and Schubart (1987), have given proper elements for the Trojan group of asteroids by using Labrouste's method, which eliminates all frequencies in a quasi-periodic process except in a given narrow or wide band. These parameters give the amplitude of libration, a proper eccentricity that characterizes the mean radius of the crescent described by the ψ_1, ψ_2 curve freed from the influence of Jupiter and Saturn [where $\psi_1 = e \cos(\bar\omega - \bar\omega_J)$, $\psi_2 = e \sin(\bar\omega - \bar\omega_J)$]. A numerical proper inclination is also found. Finally, Schubart and Bien (1987) have studied the distribution of these quantities as well as their relation to other dynamical parameters. They also have discussed the relation of $B(1,0)$, the absolute blue magnitude of the asteroids to their proper inclination.

VIII. SUMMARY AND CONCLUSION

Considerable progress has been made in the last decade mainly due to the new paradigm (Wisdom 1987) provided by the study of dynamical systems. It is now well established that nonlinear Hamiltonian systems with more than one degree of freedom almost always show chaotic behavior for some initial conditions while for other initial conditions the trajectories are quasi-periodic.

Moreover resonances are almost always accompanied by chaotic zones. Therefore, numerical experiments and mappings are the only way to determine the extent of chaotic motion, either through the use of surface of section techniques or, for problems with more than two degrees of freedom, by using Lyapunov characteristic exponents. Indeed, the 3 : 1 Kirkwood gap reflects the character of trajectories and the phase space boundary of the distribution of asteroids is in agreement with the outer boundary of the chaotic zone. For such studies one needs either a very fast computer like the Digital Orrery, specifically designed to study problems in celestial mechanics, or an explicit mapping to approximate the system. This latter approach has been used very successfully first for the 3 : 1 gap (Wisdom 1982) and for the 5 : 2 gap (Sidlichovsky and Melendo 1986).

However, mappings are less reliable for the 2 : 1 and 3 : 2 resonances because the low-order disturbing function does not well represent the problem. The 2 : 1 gap and the Hilda group are therefore not yet completely understood. If the qualitative difference in the distributions is reflected in the qualitative difference of the structure of the phase space, an analytic or semi-analytic explanation for this qualitative difference is not yet known. Moreover, we do not have a precise agreement between the distribution of asteroids and the boundaries of the chaotic zones for those resonances.

REFERENCES

Arnold, V. 1978. *Mathematical Methods of Classical Mechanics* (Heidelberg: Springer-Verlag).

Bien, R., and Schubart, J. 1987. Three characteristic orbital parameters for the Trojan group of asteroids. *Astron. Astrophys.* 175:292–298.

Carpino, M., Gonczi, R., Froeschlé, Ch., Froeschlé, Cl., Paolicchi, P., and Zappalà, V. 1986. The accuracy of proper orbital element and the properties of asteroid families: Comparison with the linear theory. *Icarus* 68:55–76.

Chirikov, B. V. 1979. A universal instability of many-dimensional oscillator systems. *Phys. Rept.* 52:263–379.

Dermott, S. F., and Murray, C. 1981. Resonant structure of the asteroid belt. *Nature* 290:664–668.

Ferraz-Mello, S. 1987a. Averaging the elliptic asteroidal problem near a first order resonance. *Astron. J.* 94:208–212.

Ferraz-Mello, S. 1987b. Expansion of the disturbing force-function for the study of high-eccentricity librations. *Astron. Astrophys.* 183:397–402.

Froeschlé, C. 1984. The Lyapunov characteristic exponents—Applications to celestial mechanisms. *Celest. Mech.* 34:95–115.

Froeschlé, C. 1987. Chaotic behaviour of resonant motion in the solar system. In *Proc. 10th Regional Meeting of the IAU*, eds. Z. Ceplecha and P. Pecina (Prague: Astron. Inst. Czech. Acad. Sci.), pp. 113–120.

Froeschlé, C., and Scholl, H. 1977. A qualitative comparison between the circular and elliptic Sun-Jupiter-Asteroids problem at commensurabilities. *Astron. Astrophys.* 57:33–39.

Froeschlé, C., and Scholl, H. 1981. The stochasticity of peculiar orbits in the 2/1 Kirkwood gap. *Astron. Astrophys.* 93:62–66.

Froeschlé, C., and Scholl, H. 1982. A systematic exploration of three-dimensional asteroidal motion at the 2/1 resonance. *Astron. Astrophys.* 111:346–356.

Froeschlé, C., and Scholl, H. 1983. The dynamical structure of the asteroidal belt. In *Asteroids, Comets, Meteors*, eds. C. I. Lagerkvist and H. Rickman (Uppsala: Uppsala Univ.), pp. 115–125.

Froeschlé, C., and Scholl, H. 1986. Gravitational splitting of quadrantid-like meteor streams in resonance with Jupiter. *Astron. Astrophys.* 158:259–265.

Froeschlé, C., Farinella, P., Carpino, M., Froeschlé, Ch., Gonczi, R., Paolicchi, P., Zappalà, V., and Knežević, Z. 1987. Asteroid families. In *The Few Body Problem, IAU Coll. No. 96*, ed. M. J. Valtonen (Dordrecht: D. Reidel), pp. 101–116.

Garfinkel, B. 1966. Formal solution in the problem of small divisors. *Astron. J.* 71:657–669.

Giffen, R. 1973. A study of commensurable motion in the asteroid belt. *Astron. Astrophys.* 23:387–403.

Gonczi, R., Froeschlé, Ch., and Froeschlé, C. 1982. Poynting-Robertson drag and orbital resonance. *Icarus* 51:633–654.

Gonczi, R., Froeschlé, Ch., and Froeschlé, C. 1983. Trapping time of resonant orbits in presence of Poynting-Robertson drag. In *Dynamical Trapping and Evolution in the Solar System, IAU Coll. No. 74*, eds. V. V. Markellos and Y. Kozai (Dordrecht: D. Reidel), pp. 397–410.

Greenberg, R. 1977. Orbit-orbit resonances in the solar system: Varieties and similarities. *Vistas in Astron.* 21:209–239.

Greenberg, R., and Scholl, H. 1979. Resonances in the asteroidal belt. In *Asteroids*, ed. T. Gehrels (Tucson: Univ. of Arizona Press), pp. 310–333.

Hadjidemetriou, J. D. 1986. A hyperbolic twist mapping model for the study of asteroid orbits near the 3/1 resonance. *J. Appl. Math. Phys. (Zamp)* 37:776–796.

Henrard, J. 1974. Virtual singularities in the artificial satellite theory. *Celest. Mech.* 10:437–449.

Henrard, J., and Lemaître, A. 1983*a*. A second fundamental model for resonance. *Celest. Mech.* 30:197–218.

Henrard, J., and Lemaître, A. 1983*b*. A mechanism of formation for the Kirkwood gaps. *Icarus* 55:482–494.

Henrard, J., and Lemaître, A. 1986. A perturbation method for problems with two critical arguments. *Celest. Mech.* 39:213–238.

Henrard, J., and Lemaître, A. 1987. A perturbative treatment for the 2/1 Jovian resonance. *Icarus* 69:266–279.

Henrard, J., Lemaître, A., Milani, A., and Murray, C. D. 1986. The reducing transformation and apocentric librator. *Celest. Mech.* 38:335–344.

Knežević, Z. 1986. Comparison of the asteroid proper elements obtained by various theories. In *Asteroids, Comets, Meteors II*, eds. C.-I. Lagerkvist, B. A. Lindblad, H. Lundstedt and H. Rickman (Uppsala: Uppsala Univ.), pp. 129–134.

Knežević, Z., Carpino, M., Farinella, P., Froeschlé, Ch., Froeschlé, C., Gonczi, R., Jovanovic, B., Paolicchi, P., and Zappalà, V. 1988. Asteroid short-periodic perturbations and the accuracy of mean orbital elements. *Astron. Astrophys.* 192:360–369.

Kozai, Y. 1985. Secular perturbation of resonant asteroids. *Celest. Mech.* 36:47–69.

Lichtenberg, A. J., and Lieberman, M. A. 1983. *Regular and Stochastic Motion* (Berlin: Springer-Verlag).

Message, P. J. 1966. On nearly commensurable periods in the restricted problem of three bodies. In *The Theory of Orbits in the Solar System and in Stellar Systems. IAU Symp. No. 25*, ed. G. Contopoulos (New York: Academic Press), pp. 197–222.

Murray, C. D., and Fox, K. 1984. Structure of the 3/1 Jovian resonance: A comparison of numerical methods. *Icarus* 59:221–223.

Murray, G. D. 1986. Structure of the 2/1 and 3/2 Jovian resonances. *Icarus* 65:70–82.

Peale, S. J. 1976. Orbital resonances in the solar system. *Amer. Rev. Astron. Astrophys.* 14:215–246.

Poincaré, H. 1902. Sur les planètes du type d'Hecube. *Bull. Astron.* 19:289–315.

Scholl, H. 1985. Resonances in the asteroidal belt. In *Motion of Planets, Satellites and Asteroids*, eds. S. Ferraz-Mello and W. Sessin (Saõ Paulo: Univ. de Saõ Paulo), pp. 129–141.

Scholl, H., and Froeschlé, C. 1974. Asteroidal motion at the 3/1 commensurability. *Astron. Astrophys.* 33:455–458.

Scholl, H., and Froeschlé, C. 1975. Asteroidal motion at the 5/2, 7/3 and 2/1 resonances. *Astron. Astrophys.* 42:457–463.

Scholl, H., and Froeschlé, C. 1988. Gravitational breaking of meteor streams in resonance with Jupiter. *Astron. Astrophys.* 195:345–349.

Schubart, J. 1966. Special cases of the restricted problem of the three bodies. In *The Theory of*

Orbits in the Solar System and in Stellar Systems, IAU Symp. No. 25, ed. G. Contopoulos (New York: Academic Press), pp. 187–193.

Schubart, J. 1968. Long-period effects in the motion of Hilda-type planets. *Astron. J.* 73:99–103.

Schubart, J. 1978. New results on the commensurability cases of the problem Sun-Jupiter-Asteroid. In *Dynamics of Planets of Satellites and Theories of Their Motion, IAU Coll. No. 48,* ed. V. Szebehely (Dordrecht: D. Reidel), pp. 137–143.

Schubart, J. 1979. Asteroidal motion at commensurabilities treated in three dimensions. In *Dynamics of the Solar System,* ed. R. L. Duncombe (Dordrecht: D. Reidel), pp. 205–215.

Schubart, J. 1982. Three characteristic parameters of orbits of Hilda-type asteroids. *Astron. Astrophys.* 114:200–204.

Schubart, J., and Bien, R. 1987. Trojan asteroids: Relations between dynamical parameters. *Astron. Astrophys.* 175:299–302.

Sessin, W. 1983. Lagrange variational equations from Hori's method for canonical systems. *Celest. Mech.* 29:361–366.

Sessin, W., and Ferraz-Mello, S. 1984. Motion of two planets with periods commensurable in the ratio 2/1. Solutions of the Hori Auxiliary System. *Celest. Mech.* 32:307–332.

Sidlichovsky, M., and Melendo, B. 1986. Mapping for 5/2 asteroidal commensurability. *Bull. Astron. Inst. Czech.* 37:65–80.

Torbett, M., and Smoluchowski, R. 1982. Motion of the Jovian commensurability resonance and the character of the celestial mechanics in the asteroid zone. *Astron. Astrophys.* 110:43–49.

Torbett, M., and Smoluchowski, R. 1983. Continuing investigation of sweeping Jovian resonances. The 7/3 and 3/2 resonances with further discussion of the 2/1 resonance. *Astron. Astrophys.* 127:345–348.

Wisdom, J. 1982. The origin of the Kirkwood gaps: A mapping for asteroidal motion near the 3/1 commensurability. *Astron. J.* 87:577–593.

Wisdom, J. 1983. Chaotic behaviour and the origin of the 3/1 Kirkwood gap. *Icarus* 56:51–74.

Wisdom, J. 1985. A perturbative treatment of motion near the 3/1 commensurability. *Icarus* 63:272–289.

Wisdom, J. 1986. Canonical solution of the two critical argument problem. *Celest. Mech.* 38:175–180.

Wisdom, J. 1987. Chaotic dynamics in the solar system. *Icarus* 72:241–275.

Yuasa, M. 1973. Theory of secular perturbations of asteroids including terms of higher order and higher degree. *Publ. Astron. Soc. Japan* 25:399–445.

SECULAR RESONANCES

H. SCHOLL, Ch. FROESCHLÉ
Observatoire de Nice

H. KINOSHITA, M. YOSHIKAWA
Tokyo Astronomical Observatory

and

J. G. WILLIAMS
Jet Propulsion Laboratory

The recent development of high-speed computers enables us to make a quantitative study of a new field of asteroidal dynamics, the secular resonances. Charlier's theory, at the beginning of the 20th century, allowed estimates for the evolution of low eccentricity and of low inclination orbits at secular resonances. Williams' theory coming nearly 70 yr later represents an improvement because it is valid for highly inclined and highly eccentric orbits as well. In addition, this theory yields the location of secular resonances in the asteroid belt. Modeling of orbital evolution at secular resonances leads to hypotheses concerning the importance of secular resonances for the delivery of meteorites and for the delivery of highly inclined Apollo asteroids. More advanced theories by Nakai and Kinoshita and by Yoshikawa allow us to model basic features of orbital evolution at the secular resonances v_{16} and v_6, respectively. The numerical experiments yield quantitative values for relevant orbital parameters which serve as a basis to test the hypotheses above. In addition, the numerical experiments allow us to investigate the topological structure of secular resonances and, in particular, the possible chaotic character of secular resonant motion.

I. BASIC DYNAMICS OF SECULAR RESONANCES

An asteroid is located in a secular resonance if its orbital precessional frequency $\dot{\varpi}$ or $\dot{\Omega}$ is equal to one of the eigenfrequencies of the system of

[845]

planetary orbits in the frame of secular perturbation theory; ϖ and Ω designate the longitude of perihelion and the longitude of ascending node, respectively.

The perturbations exerted by the planets on an asteroid's orbit can be divided up into terms depending directly (short periodic terms) and indirectly on time. Secular perturbation theories are concerned with the latter terms, the so-called secular terms (see, e.g. Brouwer and Clemence 1961). Due to secular perturbations, the secular orbital elements of an asteroid which are freed of short periodic effects, oscillate. It is convenient to decouple these oscillations into so-called free and forced oscillations. Free oscillations would result if all the perturbing planets were on circular and coplanar orbits. The forced oscillations result from the secular variations of planetary eccentricities and inclinations. The amplitudes of the forced oscillations are usually smaller than those of the free oscillations. An exceptional case is, for instance, the secular resonances where the forced oscillations may be dominant. This can be illustrated by considering the solutions of the linear secular theory for asteroidal motion. The linear theory considers only second-degree terms in the disturbing function. Time-dependent terms, i.e., terms that have the mean anomaly as an argument, are omitted. The resulting differential equations for asteroid motion perturbed by n planets can be integrated analytically. Using the variables: $h = e \sin \varpi$; $k = e \cos \varpi$; $p = \sin i \cos \Omega$; and $q = \sin i \sin \Omega$.

Brouwer and van Woerkom (1950) obtain the following solutions for the differential equations for the variations of asteroid orbital elements

$$
\begin{aligned}
h &= e_0 \sin(g_0 t + \varpi_0) + H(t) \\
k &= e_0 \cos(g_0 t + \varpi_0) + K(t) \\
p &= \sin i_0 \sin(-g_0 t + \Omega_0) + P(t) \\
q &= \sin i_0 \cos(-g_0 t + \Omega_0) + Q(t)
\end{aligned}
\tag{1}
$$

with

$$
H(t) = \sum_{l=1}^{10} \frac{G_l}{g_0 - \dot{\nu}_l} \sin(\dot{\nu}_l t + \nu_{0l})
$$

$$
K(t) = \sum_{l=1}^{10} \frac{G_l}{g_0 - \dot{\nu}_l} \cos(\dot{\nu}_l t + \nu_{0l})
$$

$$
\tag{2}
$$

$$
P(t) = \sum_{l=1}^{8} \frac{G_l'}{g_0 + \dot{\nu}_l'} \sin(\dot{\nu}_l' t + \nu_{0l}')
$$

$$
Q(t) = \sum_{l=1}^{8} \frac{G_l'}{g_0 + \dot{\nu}_l'} \cos(\dot{\nu}_l' t + \nu_{0l}')
$$

where t designates the time.

The theory of Brouwer and van Woerkom includes all the planets except Pluto. It also includes the two most important terms describing the great inequality of Jupiter and Saturn, which are in a 5/2 commensurability. We obtain 10 eigenfrequencies describing the variations of planetary eccentricities and longitudes of perihelia and 8 eigenfrequencies describing the variations of planetary inclinations and longitudes of nodes. One of the latter 8 eigenfrequencies, $\dot{v}'_5$ is equal to zero which corresponds to the fact that the invariable plane is fixed in space.

The variables e_0, ϖ_0, $\sin i_0$ and Ω_0 in Eq. (1) are constants of integration; they are called proper or free elements. These elements determine the free oscillations given by the first term on the right-hand side in each of the four solutions above. The proper longitude of perihelion precesses with the rate $\dot{\varpi}_0$ $= g_0$, and the proper node of the asteroidal orbit regresses with the rate $\dot{\Omega}_0 =$ $- g_0$. The second terms on the right-hand side are the forced oscillations. The quantities G_l and G'_l are functions of the planetary masses, the planetary semimajor axes and the asteroid's semimajor axis. The quantities $\dot{v}_l$ and $\dot{v}'_l$ are the eigenfrequencies of the planetary system in the frame of secular theory. It is obvious that the amplitudes of the forced oscillations become very large for

$$g_0 \simeq \dot{v}_l \quad or \quad g_0 \simeq -\dot{v}'_l. \tag{3}$$

This is the secular resonance case. Using the definition of g_0, we can say that a secular resonance occurs when either the rate of the proper longitude of perihelion or the rate of the proper longitude of ascending node of an asteroid's orbit is equal to one of the eigenvalues $\dot{v}_l$ of the planetary system, or if the rate of the longitude of ascending node $\dot{\Omega}$ matches any of the $\dot{v}'_l$ describing the variations of the planetary inclinations and nodes. The secular perturbation theory of Brouwer and van Woerkom yields the eigenvalues $\dot{v}_l, \dot{v}'_l$ and, hence, the characteristic time scales for secular resonances.

Up to this point, we have used only a linear theory to describe the phenomenon of secular resonances. Do secular resonances occur also in more general theories? In other words, are secular resonances physically relevant? A positive answer to this has been given by Williams (1969) who established a semi-analytical theory for secular asteroidal motion based on Gauss averaging. In particular, a mixture between analytical and numerical methods is used. Williams' theory is valid for large eccentricities and inclinations (i $< 40°$).

Additional terms appear in the Williams theory as compared to Brouwer and van Woerkom theory. In particular, in Williams' theory, h and k depend also on planetary inclinations and nodes and the variables p and q also depend on the planetary eccentricities and longitude of perihelion. The equations for h, k, p and q are coupled in his theory. Unlike in the linear theory of Brouwer and van Woerkom, where the amplitudes of the forced oscillations are inde-

pendent of the amplitudes of the free oscillations (Eq. 1 above), Williams takes into account an interaction between forced and free oscillations. In particular, the free oscillations are modulated by forced oscillations. Williams finds singularities in the amplitudes of forced oscillations for

$$\langle \dot{\varpi} \rangle = \dot{\nu}_l + 2\sigma \dot{\omega} \qquad l = 1,10$$
$$\langle \dot{\Omega} \rangle = \dot{\nu}_l + 2\sigma \dot{\omega} \qquad l = 11,14 \text{ and } 16,18 \qquad (4)$$

where σ is an integer. Because of the coupling of h, k, p and q in his theory, Williams uses one single set of eigenfrequencies $\dot{\nu}_l$. The index l runs from 1 to 18. The eigenfrequency $\dot{\nu}_{15}$ in Williams' theory corresponds to $\dot{\nu}_5'$ in Brouwer and van Woerkom's theory which can be omitted as explained above. The singularities for $\sigma = 0$, which define the principal secular resonances, correspond to the singularities in the linear theory.

Three principal secular resonances are dominant in the asteroid belt: ν_5, ν_6 and ν_{16}. Brouwer and van Woerkom's theory give rates of $\dot{\nu}_5 = 4\rlap{.}''30 \text{ yr}^{-1}$, $\dot{\nu}_6 = 27\rlap{.}''77 \text{ yr}^{-1}$ and $\dot{\nu}_{16} = -25\rlap{.}''3 \text{ yr}^{-1}$. These three terms are mainly due to the motions of Jupiter and Saturn. The frequencies $\dot{\nu}_5$, $\dot{\nu}_6$ and $\dot{\nu}_{16}$ are nearly equal to $\langle \dot{\varpi}_J \rangle$ and $\langle \dot{\varpi}_S \rangle$ and $\langle \dot{\Omega} \rangle$, respectively, where the notation $\langle \rangle$ indicates the averaged values with respect to the time; subscripts J and S refer to Jupiter and Saturn, respectively. There is an interpretation for these near equalities. Let us consider, for instance, the secular resonance ν_6. An asteroid is located in this secular resonance when the average rate of its longitude of perihelion is nearly equal to $\dot{\nu}_6$ which is nearly equal to the mean rate of the longitude of perihelion of Saturn's orbit. If only the frequency ν_6 would act, the perturbations from the eccentricity variations of Saturn's orbit would accumulate without cancelling.

What happens to an asteroid located in a secular resonance? In the case of the ν_{16} resonance, we can expect strong increases in the inclination of the asteroid's orbit according to the solutions of the linear theory and of Williams' theory. At the ν_5 and ν_6 resonance, strong variations in eccentricity can be expected. Due to the coupling between the variables h, k, p and q in the Williams theory, we can also expect additional inclination variations at the ν_5 and ν_6 resonance as well as additional eccentricity variations at the ν_{16} resonance which would not occur in the frame of linear theory. Corresponding numerical integrations can give a quantitative answer.

The dynamical nature of secular resonances is quite different from the one of mean-motion resonances that are related to the well-known Kirkwood gaps. In the case of mean-motion resonances, the resonance frequency is determined by the frequency of Jupiter's revolution around the Sun. In the case of secular resonances, we can imagine the planetary orbits replaced by elliptic mutually inclined rings. Gravitational attraction among these rings causes the rings to precess and causes the eccentricities and inclinations of the rings to oscillate. The major frequencies of these precessional motions and oscilla-

tions are the resonance frequencies for secular resonances. It is obvious from this picture that an asteroid's orbit in a secular resonance will show particularly strong eccentricity or inclination variations. Strong eccentricity variations can be expected at the resonances v_5 and v_6, while strong inclination variations can be expected at the resonance v_{16}.

II. THE ASTRONOMICAL IMPORTANCE OF SECULAR RESONANCES

Secular resonances are associated with depleted regions in the distribution of asteroids. In the late nineteenth century, Tisserand (1882) and twenty years later Charlier (1900,1902) noticed that the inner boundary of the main
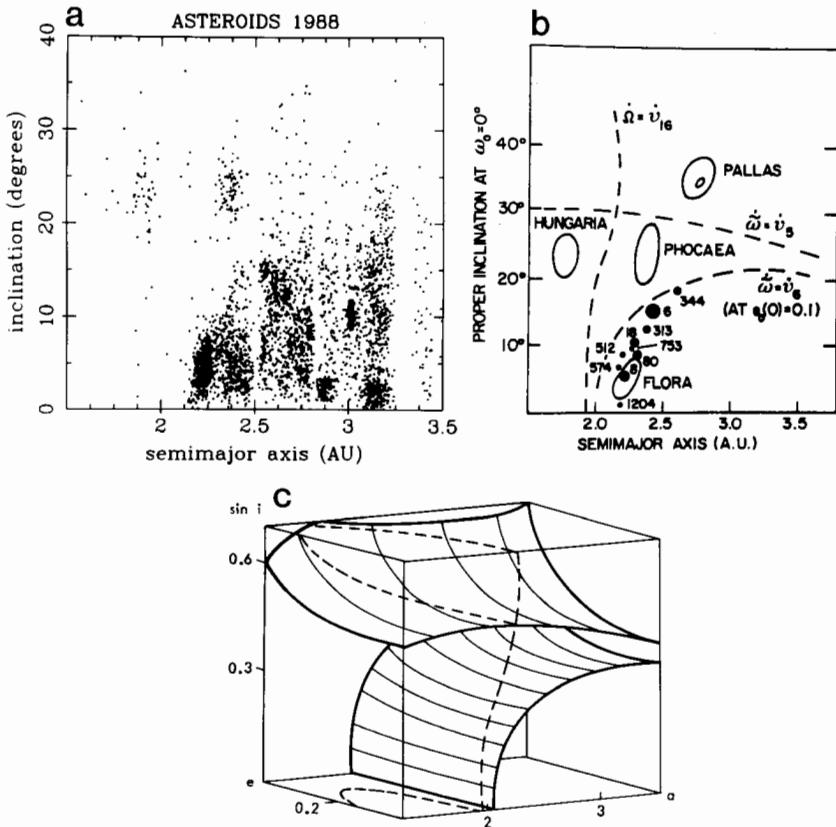
Fig. 1. (a) Semimajor axis vs inclination for 3510 numbered asteroids as of 1988. (b) The secular resonances v_5, v_6 and v_{16} in the asteroid belt according to Williams (1969). (c) The surfaces in proper a—e—$\sin i$ space corresponding to the v_5 (upper), v_6 (lower) and v_{16} secular resonances (dashed lines indicate where they intersect the box sides and upper surface).

belt near 2 AU coincides with the secular resonance ν_{16}. Williams (1971) showed that the surfaces of the three strongest resonances correspond to depopulated regions in the inner belt (see Fig. 1a,b). Hence, as in the case of mean-motion resonances, gaps are associated with resonances. It is interesting to note that no isolated group of asteroids is known to occur at a secular resonance such as the Hilda group at the 3/2 mean-motion resonance.

It is natural to ask for a cosmogonical explanation of the gaps related to secular resonances. The answer might contribute to the understanding of the evolution of the asteroid belt. It is also natural to ask for the history and future evolution of bodies known to be located in secular resonances. Already estimates based on Williams' theory (1969) showed strong increases in eccentricity and inclinations for secular resonant orbits. Mars crossers can be easily obtained. Williams (1973a,b) and Wetherill (1979) suggested the resonances ν_5 and ν_6 as sources for meteorites. In addition, Wetherill (1979) suggested the resonance ν_{16} as a source for highly inclined Apollo asteroids. According to Fig. 1b, the resonance ranges from 0° to 40° at about the same semimajor axis. The idea cannot be excluded that an asteroid entering this resonance at a low inclination may increase its inclination very strongly and finally after a close approach to Mars, for instance, may leave this resonance and finally become a highly inclined Apollo asteroid.

Secular resonances may have played an important role in pumping up eccentricities and inclinations of small bodies (Ward et al. 1976; Heppenheimer 1980). Any slow change of the mass distribution in the solar system slowly changes the values of the eigenfrequencies and, subsequently, causes a resonance sweeping in the asteroid belt.

III. THE POSITIONS OF SECULAR RESONANCES

The position of secular resonances can be mapped in proper a–e–i space (Williams 1969), where a,e,i designate, respectively, semimajor axis, eccentricity and inclination. Proper elements are obtained by first removing the short-period perturbations from all orbital elements. Furthermore, the forced and free variations for e,i,ϖ and Ω are removed. Forced oscillations result from the secular variations of the planetary eccentricities and inclinations. Free oscillations would appear even if all of the perturbing planets were on circular orbits and in the same plane. The proper elements e and i are defined by Williams (1969) to be equal to the elements of free oscillation at phase $\omega = 0°$. Proper e and i are equal to the free e and i at their respective minimum and maximum.

The secular theory of Williams (1969) based on Gauss averaging allows us to calculate precessional rates $\dot{\varpi}$ and $\dot{\Omega}$ for asteroid orbits in proper a–e–i phase space. Since the Gauss averaging technique leads to a replacement of planetary orbits by rings, planet-crossing asteroid orbits and orbits near mean-motion resonances cannot be treated accurately by this theory.

Williams and Faulkner (1981) calculated at grid points in proper $a-e-i$ space precession rates $\dot{\tilde{\omega}}$ and $\dot{\Omega}$. A suitable interpolation of $\dot{\tilde{\omega}}$ and $\dot{\Omega}$ in this three-dimensional grid yields the solutions for Williams' secular resonance Eqs. (4).

The resonant rates for the perihelion and node for the three principal resonances occur on surfaces in proper $a-e-i$ space. A projection of the resonance surfaces is given in Fig. 1b and a sketch of the resonance surfaces is given in Fig. 1c. The resonance ν_{16} occurs in the innermost part of the belt and in the Mars-crossing region for semimajor axes <2.3 AU with inclinations up to $40°$ and eccentricities up to 0.35. It passes near the Flora region and separates the Hungaria- and Phocaea-type asteroids (see Fig. 1a,b). The ν_5 resonance crosses the main belt and the Mars-crossing region at an inclination of about $30°$. Pallas lies close to this resonance. Passing closer to the more densely populated portions of the belt than the other two resonances, the ν_6 resonance emerges at $i = 0°$ near $a = 2$ AU and curves over as a increases to pass near $20°$ inclinations in the outer belt.

IV. SECULAR PERTURBATION THEORIES

A. The ν_{16} Resonance Case

Nakai and Kinoshita (1985) succeeded in deriving a simple system with one degree of freedom for the ν_{16} resonance in the frame of the Sun-Jupiter-Saturn-asteroid problem. The trajectory of an orbit in a system with one degree of freedom can usually be calculated easily by resolving an implicit equation with two variables. The trajectory of a secular resonant orbit is a closed curve around a libration center in the theory of Nakai and Kinoshita. Jupiter and Saturn are assumed to move on circular orbits. In a first step, the corresponding Hamiltonian K of the full problem is averaged over one period each of the asteroid and of the disturbing planets. This means that the orbits of the asteroid, Jupiter and Saturn are replaced by rings.

In a second step, the averaged Hamiltonian K is averaged over the circulation of the asteroid's argument of perihelion. This means that the ring representing the asteroid's orbit keeps a fixed eccentricity. Hence the following model is considered: two circular rings representing the orbits of Jupiter and Saturn rotate with the same speed in a coordinate system defined by the invariable plane and by the total angular momentum vector of the Sun-Jupiter-Saturn system.

The mass of each planet is uniformly distributed over its corresponding ring. A ring with constant eccentricity and constant semimajor axis, representing an asteroid's orbit, precesses with varying inclination due to planetary perturbations. The resulting system has one degree of freedom. The two variables are the inclination and the resonance variable $\Omega - \langle \Omega_J \rangle$ of the asteroid's orbit. The semimajor axis and mean eccentricity are parameters of the prob-
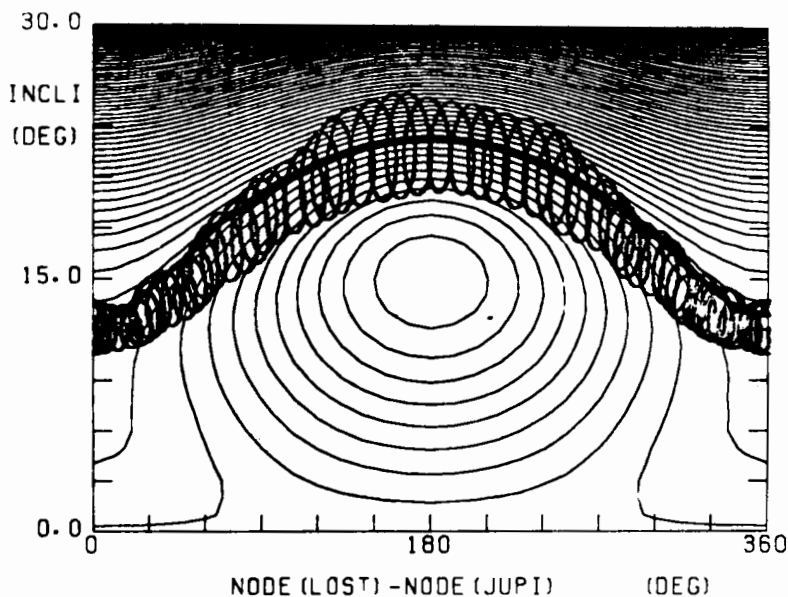
Fig. 2. The orbit of the Lost City meteorite in the model of Nakai and Kinoshita (1985).

lem. Figure 2 shows resulting contour lines and the trajectory of the Lost City meteorite integrated numerically in the nonaveraged problem. Obviously, Nakai and Kinoshita's model yield mean orbital evolutions.

B. The ν_6 Resonance

The principal parameters which affect orbital evolution at the resonance are the precessional motions of apsidal lines and the oscillations of eccentricities of the planetary and asteroidal orbits. Effects due to oscillations in i are comparatively weaker. Based upon this assumption, Yoshikawa (1987) finally established a simple theory for the ν_6 resonance; all the planets except Pluto are included in this model and are assumed to move in the same orbital plane. Following Yuasa's (1973) theory, Yoshikawa takes into account the terms of up to the third degree in the equations of motion. Short-period terms are, of course, omitted and only the forced terms of eigenfrequencies of $\dot{\nu}_5$ and $\dot{\nu}_6$ are considered. These forced terms are mainly due to Jupiter and Saturn. The model is the following: the planetary orbits are represented by eccentric rings all lying in the same plane. The eccentric rings representing Jupiter's and Saturn's orbit precess. The effects of the remaining planets, which are also taken into account, are not large in the main belt. The asteroid's orbit is represented by an eccentric ring with a fixed inclination but with varying eccentricity.

The corresponding dynamical system can be transformed into a system with two degrees of freedom, where angular variables are $\varpi - \langle \varpi_J \rangle$ and $\varpi - \langle \varpi_S \rangle$. The reduction to two degrees is possible because the Hamiltonian F can be made independent of the longitude of perihelion ϖ of the asteroid orbit. Of course, ϖ is not eliminated from the problem, but it is a linear part of two canonical variables.

The reduction to a system with one degree of freedom is carried out by averaging the Hamiltonian F over the variable $\varpi - \langle \varpi_J \rangle$. This averaging is possible because at the ν_6 resonance, the variable $\varpi - \langle \varpi_J \rangle$ moves much faster than the resonance variable $\varpi - \langle \varpi_S \rangle$ and, hence, can be considered as a fast moving variable. Closed trajectories in the plane e vs $\varpi - \langle \varpi_S \rangle$ represent resonant orbits as in the ν_{16} resonance case discussed above. Figure 3 shows such contour lines that represent the mean-orbital evolution of resonant orbits.

C. The ν_5 Resonance

After having succeeded in establishing a simple theory for the ν_6 resonance, Yoshikawa tried to apply the same idea to the ν_5 resonance. Instead of averag-
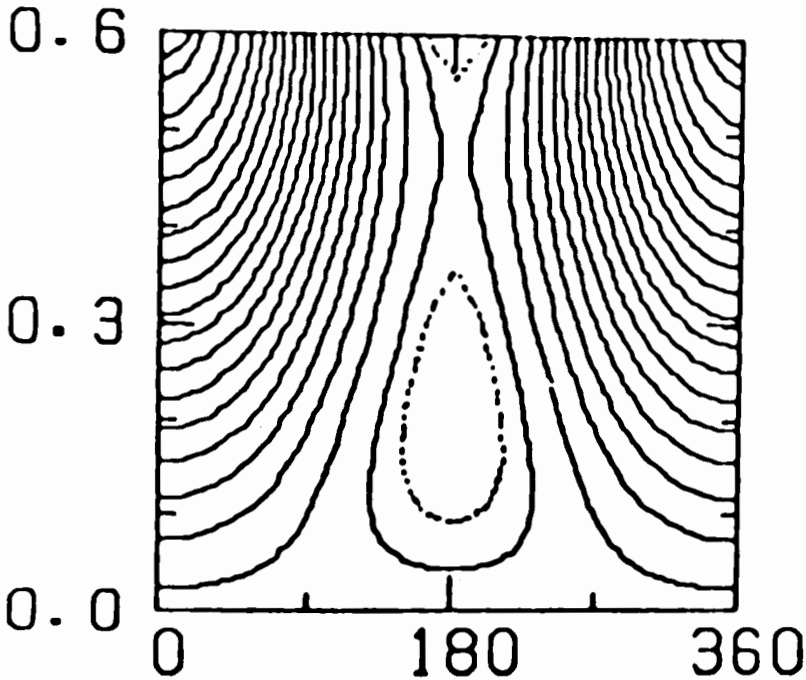
Fig. 3. Contour lines for the ν_6 resonance case at $a = 2.05$ AU, according to Yoshikawa's (1987) theory in a $\varpi - \langle \varpi_S \rangle$ vs l diagram.

ing over the variable $\varpi - \langle \varpi_J \rangle$ Yoshikawa averages over the variable $\varpi - \langle \varpi_S \rangle$. The resulting system shows the libration of $\varpi - \langle \varpi_J \rangle$ about 0°, which is consistent with numerical results obtained by Froeschlé and Scholl. However, the system does not yield quantitative agreement with numerical results.

Since the ν_5 resonance occurs at high inclinations, asteroid inclinations vary strongly as a function of the argument of perihelion. A suitable model including higher terms in the disturbing function and including a varying inclination must be established.

V. NUMERICAL EXPERIMENTS

Numerical integration experiments at secular resonances as carried out by Bien and Schubart (1984), Froeschlé and Scholl (1986,1987a,1987b, 1987c,1988) and Scholl and Froeschlé (1986) are for the most part based on the Sun-Jupiter-Saturn-asteroid model in three dimensions. The time interval covered in such model calculations is determined by the relevant libration periods of 10^5 to 10^6 yr.

A secular resonance case is indicated by the behavior of variables that approximate the resonance variables $\varpi - \langle \varpi_J \rangle$, $\varpi - \langle \varpi_S \rangle$ and $\Omega - \langle \Omega_J \rangle$. According to Williams (1969), the libration of a resonance argument around 0° or around 180° determines a resonance case. Numerical experiments try to yield preliminary answers to questions listed below. The motivations of these questions are given in parentheses.

1. Which known asteroids are located in secular resonances? (depletion at resonances);
2. Do asteroids leave secular resonance regions due to resonance perturbations? (stability of secular resonant motion);
3. How large are variations of inclinations and eccentricities? (meteorite source, highly inclined Apollo asteroids, Mars crossers);
4. Are there chaotic orbits at secular resonances? (dynamical topology, cosmogony).

A. Asteroids Located in Secular Resonances

The asteroids which were found to be secular-resonance cases in the frame of the Sun-Jupiter-Saturn model are listed in Table I. This table, of course, is not yet complete. We cannot exclude the fact that model calculations including all the planets might yield additional resonant asteroids which did not appear to be resonant in the Froeschlé and Scholl model. For instance, Froeschlé and Scholl (1987a) found asteroids to be nonresonant which are listed as resonant in Williams (1979) who included all the planets. The resonant objects in the latter reference are actually failures of the proper elements program to converge due to a resonance.

TABLE I
Asteroids Located in Secular Resonances According to Numerical
Experiments over 1 Myr

Asteroid	Resonance	Libration about	Semimajor axis (AU)	Mars crosser
759 Vinifera	ν_6	180°	2.62	no
945 Barcelona	ν_5	0°	2.64	grazing
1222 Tina	ν_6	180°	2.79	no
1580 Betulia	near ν_5	180°	2.19	yes
1864 Daedalus	ν_{16}	180°	1.46	yes
2335 James	ν_{16} and ν_5	0° and 180°	2.12	yes
2368 Beltovata	ν_6	180°	2.10	yes
1974 MA	ν_{16} and 5:1	0°	1.77	yes

B. Stability of Secular Resonances

The semimajor axes of resonant asteroids usually vary very little ($\Delta a <$ 0.1 AU) and remain in the resonance regions except in the case of overlapping resonances and, in particular, in the case of close approaches to a planet. Fictitious asteroids located at the border of resonance regions were found to enter and to leave temporarily resonance regions.

C. Variations of Eccentricities and Inclinations

Numerical experiments yield a large variety of oscillations in eccentricities and in inclinations with very different amplitudes. The resonances ν_5 and ν_6 affect mainly variations in eccentricity while the resonance ν_{16} is mainly related to strong variations in inclinations. This is due to the nature of these resonances: ν_5 and ν_6 are driven by planetary eccentricities when the precessional motion of the apsidal line matches discrete rates. The ν_{16} resonance, on the other hand, is driven by planetary inclinations when the precessional motion of the nodal line equals the planetary node rates.

Eccentricity and inclination variations depend strongly on starting values. At the ν_6 resonance, for instance, two orbits a and b with the same initial semimajor axis but different starting eccentricities show eccentricity variations between 0.05 and 0.6 (orbit a) or between 0.1 and 0.3 (orbit b) on a time scale of 1 Myr. At the ν_{16} resonance, the inclinations of 2 orbits c and d with the same semimajor axis but different initial inclinations range between 4° and 25° (orbit c) or between 15° and 20° (orbit d). It is natural to ask why such variations of eccentricity and inclination differ. The theories of Nakai and Kinoshita (Sec. IV.A) for the resonance ν_{16} as well as the theory of Yoshikawa (Sec. IV.B) for the resonance ν_6 serve as a basis for an explanation. Resonant orbits oscillate around a contour line about the resonance center. If an orbit is deeply in the resonance, it will follow a contour line that
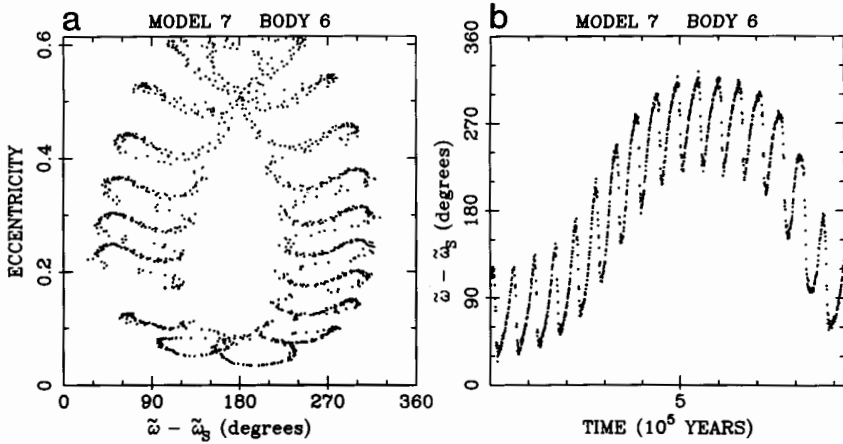
Fig. 4. (a) A numerical integration over 0.9 Myr of a fictitious asteroid in the ν_6 resonance. The orbit oscillates around a contour line as shown in Fig. 3. Starting values are $a = 2.05$ AU, $e = 0.17$, $i = 4°63$, $\varpi - \varpi_J = 180°$, $\Omega - \Omega_J = 335°$. (b) The resonance argument $\varpi - \varpi_S$ of the fictitious asteroid of plot (a) librates about 180°.

remains close to the resonance center. Hence, no strong variations in eccentricity or inclination can be expected. The farther away from the libration center a trajectory is located, the stronger are variations in eccentricity and inclination.

Figure 4 shows for a test asteroid located at the secular resonance ν_6, the variable $\varpi - \varpi_S$ as a function of time and as a function of eccentricity, respectively. This variable approximates the corresponding resonance variable. The trajectory in plot (a) follows, in accordance with Yoshikawa's theory, on the mean a contour line. This trajectory may leave the corresponding contour line and may even leave the resonance in the numerical experiment, due to effects not taken into account by theory; also, jumps from one contour line to a more distant one were found in numerical experiments.

D. Chaotic Orbits

The Sun-Jupiter-Saturn-asteroid system, which is used in numerical experiments, is a conservative Hamiltonian system. It is well known since the time of Poincaré (1892) that such systems may exhibit chaotic motion. The maximum Lyapunov characteristic exponent is a measure to determine chaotic motion. Froeschlé and Scholl (1981) were the first to introduce the calculation of the maximum Lyapunov characteristic exponent for the determination of chaotic motion at mean-motion resonances. Wisdom (1983) applied it exhaustively at the 3:1 mean-motion resonance demonstrating that the observed 3:1 Kirkwood gap is a chaotic region.

This method of determining chaotic motion calculates a number which is

a measure for the sensitivity of orbital evolution to the initial conditions. Chaotic motion means very strong separation and very different evolution of orbits with close initial values. It is clear from this concept of chaotic motion that bifurcations or overlapping resonances in the problem may lead to chaotic orbits. Bifurcations and overlapping resonances can be easily visualized just by using data produced by numerical experiments. The calculation of the maximum Lyapunov exponent, on the other hand, may be very time consuming because this exponent is defined for time going to infinity. Of course, the Lyapunov exponent is an objective measure for chaotic motion while the visualization of bifurcations and of overlapping resonances are only indications of chaotic motion.

The numerical experiments of Froeschlé and Scholl (1988a) and Scholl and Froeschlé (1986) show bifurcations which separate maximally up to three

MODEL 7   BODY 8
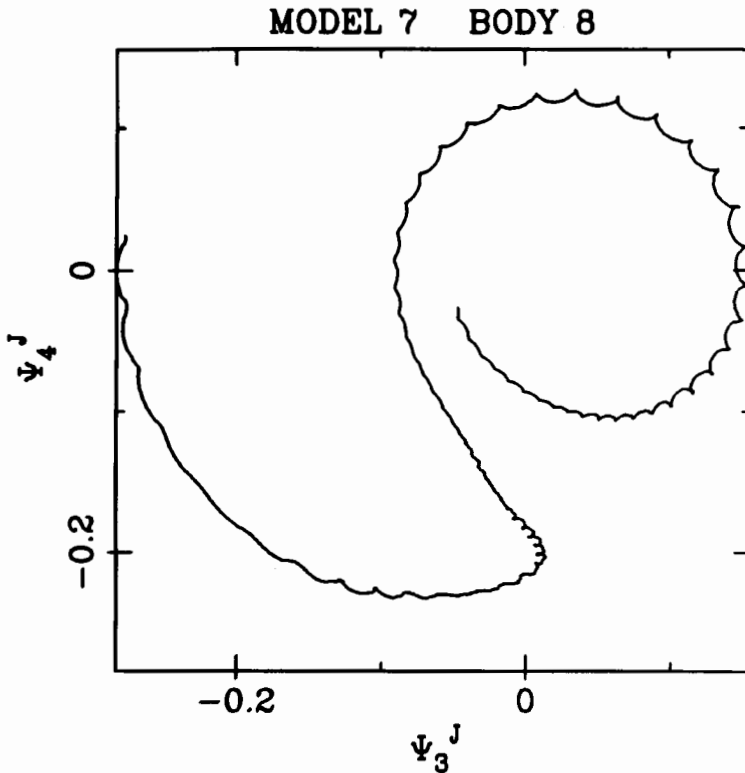
Fig. 5. Transition between inner circulation and libration for a ν_{16} resonant fictitious asteroid indicating chaotic motion. $\psi_3^J = [2(1 - e^2)^{1/2}(1 - \cos i)]^{1/2} \cos(\Omega - \Omega_J); \psi_4^J = [2(1 - e^2)^{1/2}(1 - \cos i)]^{1/2} \sin(\Omega - \Omega_J)$. Starting values are $a = 2.05$ AU, $e = 0.17$, $i = 4°63$, $\varpi - \varpi_J = 0°$, $\Omega - \Omega_J = 151°$.
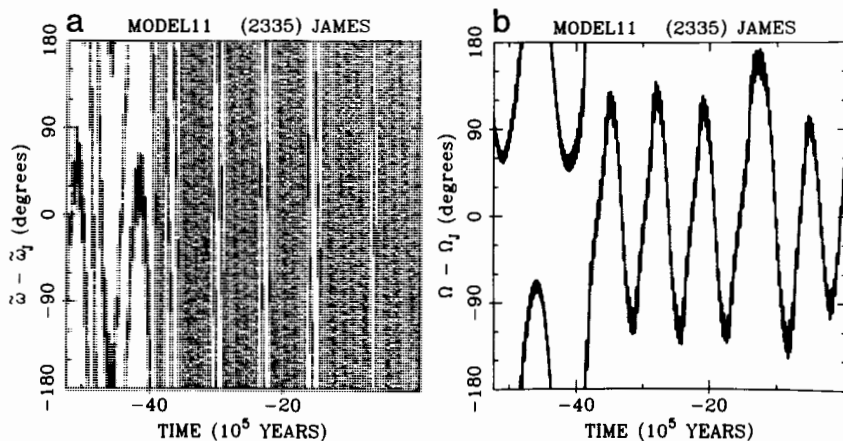
Fig. 6. (a) A backwards integration of the asteroid 2335 James over nearly 5 Myr in the Sun-Jupiter-Saturn model showing a switching libration center from 0° to 180°. (b) The switch of the libration center in plot (a) related to a temporary libration of 2335 James in the ν_5 resonance. James appears to be an overlapping resonance case, the first overlapping resonance case to be known in the solar system.

regions of motion: two libration regions and a so-called inner circulation region as in the case of mean-motion resonances. The two libration regions do not always occur simultaneously; transitions between these regions have been found. Figure 5 shows a transition between inner circulation and libration. Calculating another orbit with nearly the same initial values would yield an orbit crossing the bifurcation eventually at a different time. A strong separation of these two orbits and hence, chaotic motion can be expected.

Overlapping secular resonances might exist according to Williams and Faulkner's figures (1981) which show the locations of secular resonance surfaces. In addition, secular resonances may cross mean-motion resonances. Froeschlé and Scholl (1987b) discovered one asteroid, 2335 James, to be located in a region where the ν_5 and ν_{16} resonances overlap (Fig. 6). James alternates between these two resonances. The asteroid 1974 MA is located in a region where ν_{16} overlaps with the 5:1 mean-motion resonance (Froeschlé and Scholl 1986). In addition, this asteroid is near a ν_5 resonance case. It is interesting to note that these overlapping resonances yield much stronger variations in inclination than the ν_{16} resonance alone.

VI. RESONANT TRANSPORT OF METEORITES

For $a < 2.5$ AU, the secular resonances are populated only by planet-crossing asteroids, and the empty gaps in the inner belt which correspond to the ν_6 and ν_{16} resonances are quite obvious in Fig. 1a. Since the ν_6 resonance

passes close to densely populated regions such as the Flora region, some collision debris from asteroids in these regions must be thrown into this resonance. The resonant and near-resonant debris will have large eccentricity variations that will eventually bring it close to Mars. Figure 7 illustrates the results of a sequence of numerical integrations based on Gauss averaging (Williams 1973a,b). Plot a shows the secular variations of eccentricity vs $\varpi - \nu_6$ due to the ν_6 perturbation for 6 Hebe and two hypothetical examples of material ejected toward the resonance (considerable variations due to other terms have been smoothed out for the illustration). Hebe and the 230 m s^{-1}
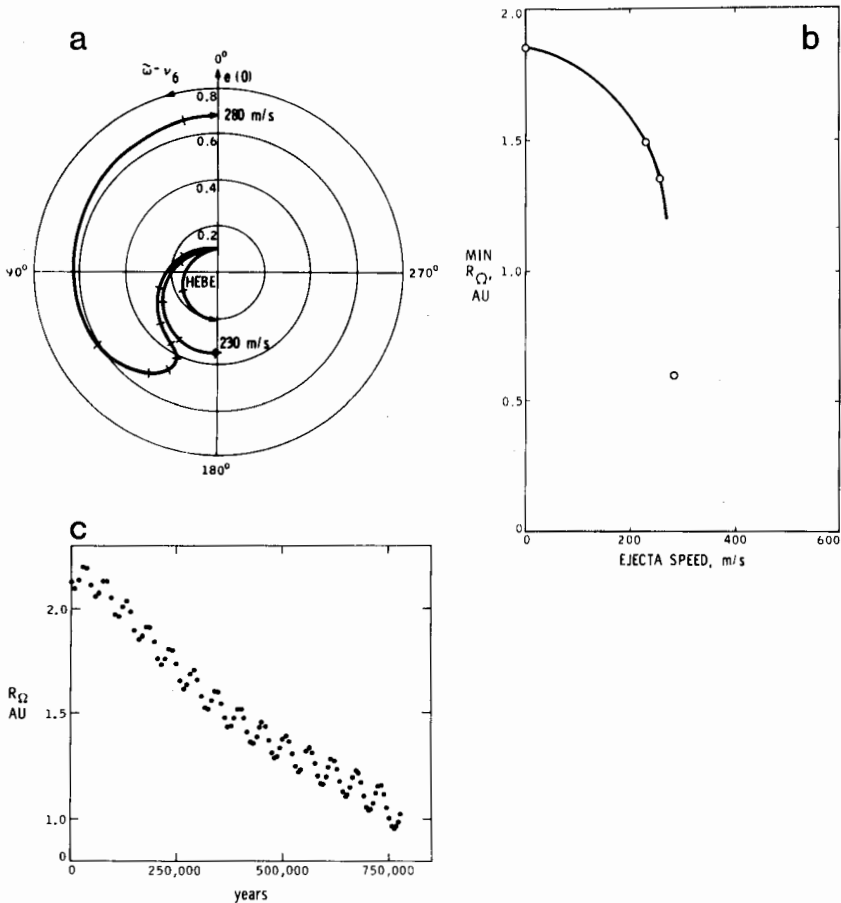
Fig. 7. (a) Polar plot of e vs ϖ - ν_6 for Hebe and hypothetical ejecta at two different speeds. The path is mirror symmetric and only half has been drawn. Higher-frequency variations have been smoothed out. (b) Minimum heliocentric distance at the nodes as a function of the ejecta speed for different integrations. (c) Minimum heliocentric distance at the nodes for each half cycle of the argument of perihelion circulation for the 280 m s^{-1} ejecta.

ejecta are close to the resonance, but not in it; the 280 m s^{-1} ejecta is librating in the resonance. Plot b shows the dependence of the minimum heliocentric distance at the node vs the ejecta speed. The phase of the ν_6 term (time of ejection) and the direction of ejection were chosen to maximize the eccentricity and perihelion variation. Plot c shows the evolution of the heliocentric distance at the node vs time for the 280 m s^{-1} case. The abundant, relatively low-speed ejecta can easily go into Mars-crossing orbits. Earth crossing only results for the less-abundant high-speed ejecta, unless the effects of close encounters with Mars are calculated.

The large e and i variations that secular resonances can induce, coupled with Mars' ability to knock material in and out of the resonances during close encounters, causes a diffusion of the orbits which can deliver some material into Earth-crossing orbits (Wetherill and Williams 1979; Wetherill 1979). While some material can go into Earth-crossing orbits in <1 Myr, the much longer time-scale diffusive process dominates the amount of material delivered into Earth-crossing orbits with the aid of secular resonances (see the chapter by Greenberg et al.). This path is one of two mechanisms identified for delivering sufficient amounts of belt-derived asteroids and meteoroids into Earth-crossing orbits (Wetherill 1987); the second mechanism uses chaotic behavior in the Kirkwood gaps (Wisdom 1983,1985).

REFERENCES

Bien, R., and Schubart, J. 1984. Trojan orbits in secular resonances. *Celest. Mech.* 34:425–434.
Brouwer, D., and Clemence, G. M. 1961. *Methods of Celestial Mechanics* (New York: Academic Press).
Brouwer, D., and van Woerkom, A. J. J. 1950. The secular variation of the orbital elements of the principal planets. *Astron. Papers U.S. Naval Obs.* 13:85–107.
Charlier, C. -Y. -L. 1900. Sur les points singuliers des inégalités séculaires des petites planètes. *Bull. Astron.* 17:209–219.
Charlier, C. -Y. -L. 1902. *Die Mechanik des Himmels* (Leipzig: Verlag Veit).
Froeschlé, Ch., and Scholl, H. 1981. The stochasticity of peculiar orbits in the 2/1 Kirkwood gap. *Astron. Astrophys.* 93:62–66.
Froeschlé, Ch., and Scholl, H. 1986. The secular resonance ν_6 in the asteroidal belt. *Astron. Astrophys.* 166:326–332.
Froeschlé, Ch., and Scholl, H. 1987a. Orbital evolution of asteroids near the secular resonance ν_6. *Astron. Astrophys.* 179:294–303.
Froeschlé, Ch., and Scholl, H. 1987b. A possible source for highly inclined Apollo-Amor asteroids: The secular resonance ν_{16}. In *The Few Body Problem*, ed. M. J. Valtonen (Dordrecht: Kluwer Academic Publishers), pp. 123–127.
Froeschlé, Ch., and Scholl, H. 1988a. Chaotic motion in secular resonances. In *Dynamics of the Solar System*, ed. M. Sidlichovsky (Publ. of the Astron. Inst. of the Czechoslovak Acad. of Sciences Publication No. 68, vol.3), pp. 125–128.
Froeschlé, Ch., and Scholl, H. 1988b. Secular resonances: New results. *Celest. Mech.*, submitted.

Heppenheimer, T. A. 1980. Secular resonances and the origin of eccentricities of Mars and the asteroids. *Icarus* 41:76–88.

Nakai, H., and Kinoshita, H. 1985. Secular perturbations of asteroids in secular resonances. *Celest. Mech.* 36:391–407.

Poincaré, H. 1892. *Les Méthodes Nouvelles de la Mécanique Céleste* (Paris: Gauthier Villars).

Scholl, H., and Froeschlé, Ch. 1986. The effects of the secular resonances ν_{16} and ν_5 on asteroidal orbits. *Astron. Astrophys.* 170:138–144.

Tisserand, M. F. 1882. Mémoire sur les mouvements séculaires des plans des orbites de trois planètes. *Ann. Obs. Paris* 16:E1–E57.

Ward, W. R., Colombo, G., and Franklin, F. A. 1976. Secular resonance, solar spin down and the orbit of Mercury. *Icarus* 28:441–452.

Wetherill, G. W. 1979. Steady state populations of Apollo-Amor objects. *Icarus* 37:96–112.

Wetherill, G. W. 1987. Dynamical relations between asteroids, meteorites, and Apollo-Amor objects. *Phil. Trans. Roy. Soc. Lond.* A323:323–337.

Wetherill, G. W., and Williams, J. G. 1979. Origin of differentiated meteorites. In *Origin and Distribution of the Elements,* ed. L. H. Ahrens (Oxford: Pergamon Press), pp. 19–31.

Williams, J. G. 1969. Secular Perturbations in the Solar System. Ph. D. Thesis, Univ. of California at Los Angeles.

Williams, J. G. 1971. Proper elements, families, and belt boundaries. In *Physical Studies of Minor Planets,* ed. T. Gehrels, NASA SP-267, pp. 177–181.

Williams, J. G. 1973a. Meteorites from the asteroidal belt? *Eos: Trans. Amer. Geophys. Union* 54:233 (abstract).

Williams, J. G. 1973b. Secular resonances. *Bull. Amer. Astron. Soc.* 5:363 (abstract).

Williams, J. G. 1979. Proper elements, families, and belt boundaries. In *Asteroids,* ed. T. Gehrels (Tucson: Univ. of Arizona Press), pp. 1040–1063.

Williams, J. G., and Faulkner, J. 1981. The positions of secular resonance surfaces. *Icarus* 46:390–399.

Wisdom, J. 1983. Chaotic behaviour and the origin of the 3/1 Kirkwood gap. *Icarus* 56:51–74.

Wisdom, J. 1985. Meteorites may follow a chaotic route to the Earth. *Nature* 315:731–733.

Yoshikawa, M. 1987. A simple analytical model for the secular resonance ν_6 in the asteroidal belt. *Celest. Mech.* 40:233–272.

Yuasa, M. 1973. Theory of secular perturbations of asteroids including terms of higher orders and higher degrees. *Publ. Astron. Soc. Pacific* 25:399–445.

DYNAMICS OF THE OUTER ASTEROID BELT

ANNA M. NOBILI
Università di Pisa

The dynamics of minor planets between Mars and Jupiter has long been a challenge for celestial mechanicians; gaps at some mean-motion resonances with Jupiter (3 : 1, 5 : 2, 7 : 3, 2 : 1), groups at others (3 : 2, 4 : 3, 1 : 1), and the depletion of the outer belt (a > 3.2 AU) are among the most extensively investigated problems so far. The outer belt is peculiar in that the distribution of objects in phase space shows no resemblance to the rest of the belt. Once the eccentricity of Jupiter is taken into account, the depletion is explained with no need to invoke nongravitational phenomena. Because of the longer time scale, collisions cannot have played a major role in the outer belt thus implying that big asteroids rather than families of small objects should be observed; this is confirmed by the data. Observed asteroids have particular dynamical configurations that minimize the strong perturbations by Jupiter; a sort of natural selection mechanism has operated in the outer belt, and as a result, only dynamically protected asteroids remain. There is no dynamical evidence so far that these protection mechanisms can last for a time span of ~ 1 Gyr. Spectral observations show a reddening in spectral slope with increasing heliocentric distance; if not due to weathering phenomena, this would suggest that outer-belt asteroids might be primordial objects. More work is required to prove that pure gravitation can also explain the 2 : 1 gap.

I. THE MODEL PROBLEM

Asteroids inhabit the region between Mars and Jupiter (see Fig. 1). At values of the semimajor axis for which the ratio of the asteroid's orbital period to the orbital period of Jupiter is very close to the ratio of two integer numbers, the *mean-motion resonances*, peculiar phenomena are known to occur (e.g. Wisdom 1982,1983; see the chapter by Froeschlé and Greenberg). The

Numbered Asteroids
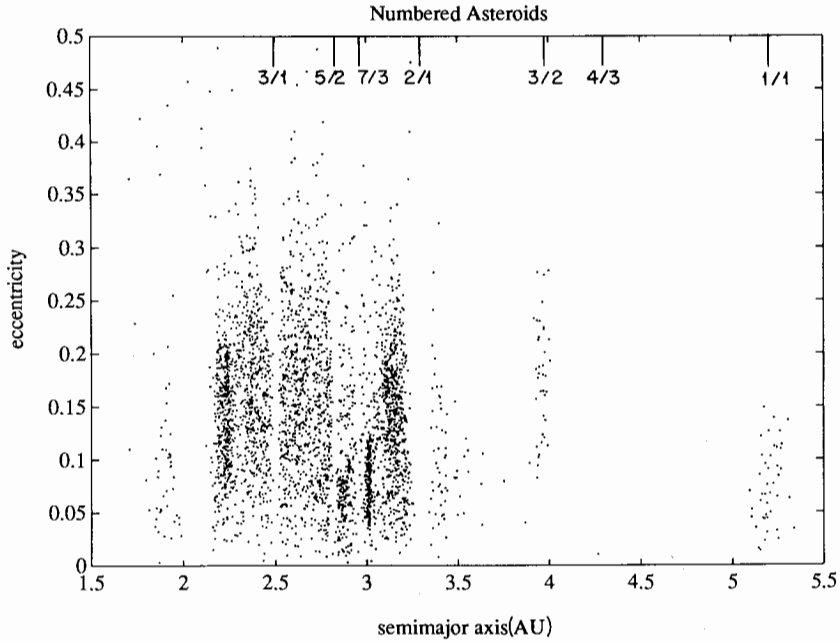
Fig. 1. Numbered asteroids (from the *Ephemerides of Minor Planets, 1987*) in the *a, e* plane. The locations of several mean-motion resonances are shown. The 3:1, 5:2, 7:3, 2:1 are associated with gaps, while there are groups of asteroids at the 3:2, 4:3, 1:1. The outer belt (*a* > 3.2 AU) is far less populated than the main belt and the distribution of objects is very uneven.

most apparent one is that some resonances ($3:1$, $5:2$, $7:3$, $2:1$) are almost clear of asteroids in comparison to well-populated nearby regions. They are known as the Kirkwood gaps. In contrast, at other resonances ($3:2$, $4:3$, $1:1$) asteroids are numerous while nearby regions are depleted. Also, gaps occur in the main belt (for $a < 3.2$ AU; a = the semimajor axis of the asteroid), while groups are located in the outer belt ($a > 3.2$ AU). It is remarkable that the largest gap in the asteroid belt (around $\simeq 2.1$ AU) is due to secular resonances (Williams and Faulkner 1981; see also the chapter by Scholl and Froeschlé). The peculiarity of the outer belt is shown very well in Fig. 1. The density of objects drops sharply and is extremely uneven. A relatively large number of asteroids is found just outside the $2:1$ resonance. Farther away, in the region 3.56 AU $< a <$ 3.87 AU there are only four numbered asteroids. Yet, it is not just getting closer to Jupiter that is responsible, as in correspondence of the $3:2$ resonance the density increases again (this is the Hilda group), with the asteroid eccentricities reaching values similar to those of short-period comets. Then the density drops to zero until 279 Thule is found at 4.29 AU, i.e., in the $4:3$ mean-motion resonance with Jupiter. There

are no asteroids beyond Thule apart from the Trojans, which move 60° ahead
or behind Jupiter along the same orbit in the vicinity of the L_4 and L_5 triangu-
lar equilibrium points. There is now sufficient evidence that most of these
features can be explained by pure gravitation. Dynamics provides important
insights into the origin, history and physical properties of these asteroids.

A mathematical model in which a problem is to be investigated should be
as simple as possible, and yet be able to reproduce the most important ob-
served features (see Milani [1988] for a discussion of the choice of the mathe-
matical model in asteroid dynamics). The first simplification is the so-called
gravitational hypothesis, namely the assumption that no force but pure Newto-
nian gravitation has shaped the outer belt as we observe it (see Fig. 2). Colli-
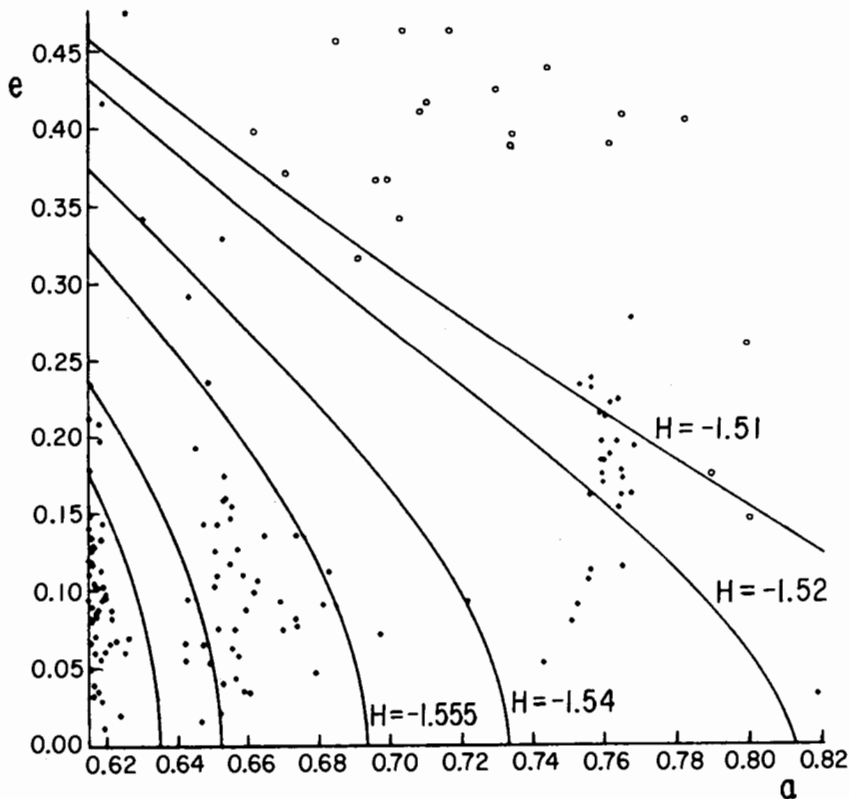
Fig. 2. Numbered asteroids (∗) from the TRIAD file (Bender 1979), and periodic comets with e
≤ 0.48 (o) from Marsden and Roemer (1982) in the a, e space (a is in units of Jupiter's
semimajor axis), 3.2 AU < a < 4.3 AU. The 2:1 gap (at 0.63) and the 3:2 group of Hilda
asteroids (at 0.763) are apparent, as well as a large region devoid of asteroids in between. The
curves are level lines of the Jacobi function H. The topological change, from closed to open
curves, occurs between $H = -1.52$ and $H = -1.51$ (at $H = -1.5193$). In the restricted
circular model, objects inside the closed curves are confined around the Sun indefinitely.

sions certainly dominated the early days of the solar system but we assume that, after this initial phase, the gravitational era began. Whether or not this assumption is correct, is possible to tell only *a posteriori* on the basis of how well it explains reality. If it fails, we should make certain that this is not because of an oversimplified gravitational model or because of our inadequate understanding of it.

The next important simplification is in the number of bodies whose gravitational attraction on an asteroid must be taken into account. In this respect, the outer belt is an easy problem since the two-body motion of the asteroid around the Sun is perturbed mostly by Jupiter. This is unlike the inner belt, planet-crossing asteroids which require that the effect of most of the planets be taken into account. The three-body Sun-Jupiter-asteroid model is thus a good model in the outer belt, and it can certainly be restricted in the sense of neglecting the gravitational attraction of the asteroid on Jupiter by modeling it as a massless body (the asteroid mass is smaller than the mass of Jupiter by at least 7 orders of magnitude). In the restricted circular model, the two primaries move around their common center of mass in circular coplanar orbits, while the asteroid moves with respect to the center of mass of the primaries under the gravitational attraction of them both.

It is well known that the three-body problem, even under the simplifying assumptions of being restricted, circular and planar, is nonintegrable; namely, it has no analytic solution, not even in the form of quadratures. It is actually the simplest nonintegrable problem, and the reason for this is that it does not have enough integrals of motion compared to the number of degrees of freedom (Poincaré 1893).

The restricted *circular* three-body problem, in two as well as in three dimensions, has only 1 integral of motion (which is not the energy) named after Jacobi. For a given binary with orbital angular velocity n and mass ratio μ ($\mu \simeq 10^{-3}$ in the Sun-Jupiter case), this integral of the motion depends only on the initial position and velocity of the third body. In a convenient system of units in which $G = 1$ (G is the universal constant of gravity), $m_1 + m_2 = 1$ (m_1, m_2 are the masses of the primaries), $D = 1$ (D, the mutual distance of the primaries), the orbital period of the primaries is 2π and $n = 1$. If the primaries move in the (x, y) plane of the $Oxyz$ Cartesian reference frame with origin O at their center of mass, the Jacobi integral is

$$H = E - J_z \tag{1}$$

where E is the asteroid's energy and J_z the component of its angular momentum perpendicular to the orbital plane of the primaries (each per unit mass).

The most important property of the Jacobi integral is that it confines the motion, i.e., it defines a topological stability criterion valid for all time; this is known as the Hill stability criterion (see Szebehely 1967). There exists a critical value H_2 of the Jacobi integral corresponding to the L_2 Lagrangian

equilibrium point. L_2 is the point along the conjunction line of the main bodies where the gravitational attraction of Jupiter equals the tidal effect of the Sun, namely the difference between the solar attraction plus the centrifugal force on Jupiter, and its corresponding value on the asteroid. L_2 marks the separation between the two Hill spheres of Jupiter and the Sun. Its distance from Jupiter (in units of the Sun-Jupiter distance) is $\simeq (\mu/3)^{1/3}$; thus the location of L_2 depends on the mass ratio μ only, and so does H_2. In the Sun-Jupiter case, with the units defined above, $H_2 = -1.5193$. Hill's criterion states that, if

$$H < H_2 \tag{2}$$

an asteroid inside the sphere of influence of the Sun with a value H of the Jacobi integral is trapped there indefinitely. The criterion is valid both in two and in three dimensions.

L_2 can be thought of as a "tap" in between the Hills spheres of the two primaries. For objects confined around either the Sun or Jupiter, namely having a value of the Jacobi integral which satisfies the Hill stability criterion (Eq. 2), the tap is closed. If an object has a value of H which equals H_2 the tap suddenly opens, and the larger the value of H, the greater the "flow" at the tap can be, the flow meaning the width of the hole which connects the two spheres of influence in such conditions. This does not mean that such an asteroid is certainly going to pass through that hole onto the other sphere. When the Hill criterion is not satisfied, we can only state that a continuous curve exists that connects the two spheres of influence. Whether or not the asteroid is going to follow that path at all, or how long it would take to do that, is impossible to tell from the value of H alone. We must necessarily resort to a direct computation of the orbit. Also, it should be recognized that, even when the Hill criterion is satisfied, we know nothing about the asteroid's motion except for the region in which it is trapped. For instance, we cannot tell whether the motion is regular or chaotic even if we know that it is trapped around the Sun indefinitely. An orbit is regular if it lies on a subset of half the dimension of the phase space (e.g., it is a curve in a two-dimensional phase space); it is chaotic if it fills a larger region of the phase space. As a matter of fact, the boundary between regular (also ordered) and chaotic motion is not very sharp, and ordered and chaotic regions of motion are not easy to locate; nonetheless identifying these regions has proved a useful tool (Sec. III).

A more difficult consideration is whether the eccentricity of Jupiter and the inclination of the asteroid can be neglected. Increasing the dimensionality of the problem certainly does increase the complexity of the phase space. However, what is essential to understand is whether one particular cause of increased complexity does, or does not, leave the main features unchanged. There are dimensions which play a major role and there are dimensions which are less important. As already mentioned, starting from the restricted planar circular model of three bodies, and then increasing the dimensionality by

allowing the asteroid's orbit to be inclined (the dimension of phase space increases from 4 to 6; in a rotating reference frame, the primaries are fixed and time is eliminated), the Jacobi integral still exists and defines regions of trapped motion. The basic structure of the level manifolds of the Jacobi integral in the phase space does not change. If we further increase the complexity by considering a third body with nonzero mass (this is the general three-body problem in which case the phase space has 12 dimensions), then after the number of dimensions is reduced by means of symmetries and changes of scale, we can again find an integral which turns out to play much the same role as the Jacobi integral in the restricted case (Milani and Nobili 1983, §6).

On the other hand, if we start from the restricted planar problem and simply allow a nonzero eccentricity to the orbits of the primaries (this is the restricted elliptic planar three-body problem), the situation changes dramatically. Being a time-dependent, two-degrees-of-freedom problem (even in the rotating frame the primaries move; we can keep them still, but then the unit of distance is not constant), it is equivalent to a time-independent problem with three degrees of freedom, so that the phase space, in the planar approximation, has six dimensions. This number is the same as in the restricted circular problem in three dimensions, yet it is well known that in the elliptic planar problem there is no stability criterion analogous to Hill's criterion. What then makes the elliptic planar problem basically different from the 3 D circular one, although the dimension is the same? Problems which look similar (in this case they both have three degrees of freedom and one time-independent integral, the Hamiltonian) can differ strongly depending on whether the dimension of the phase space can be reduced because of the symmetry properties of the problem. Both in the elliptic planar and in the circular 3 D problem, we start with a phase space of dimension six then reduce it to five using the constant Hamiltonian. The invariant tori of the *KAM* theory (see Arnold 1976, Appendix 8) on which the regular motion is confined have the same dimension as the number of degrees of freedom of the problem, three in this case, and therefore they cannot possibly confine the motion in a space of dimension five; they can do that only if the dimension of the phase space can be reduced to four. This is precisely where the main difference between our two problems is. In the circular 3 D problem one further dimension can be eliminated by projection onto the orbital plane of the binary, because in doing so the magnitude of the gravitational energy of the asteroid increases, and this increases the inequality which leads to the establishment of the stability criterion (Eq. 2) (Szebehely 1967). In the elliptic planar problem, no further reduction of dimensionality is possible so that the topology of the original problem remains unchanged.

Regarding the perturbations by the other planets, we must consider

1. Jupiter's eccentricity oscillates with a 54,000 yr period reaching a maximum value of 0.061, and its pericenter completes one revolution in about

300,000 yr; both of these effects are mostly due to Saturn and have often been taken into account;

2. Perturbations by Uranus and Neptune are usually neglected; however, the very presence of their perihelia and nodes generates a wealth of secular resonances which might be more responsible for chaotic motion than we would expect.

Since the complexity of the model should be increased only if the simpler one has failed, the main perturbations on the orbit of Jupiter can also be accounted for indirectly, in the framework of a restricted three-body problem in which Jupiter's orbit is no longer Keplerian (either circular or elliptic), but changes according to well-established results of secular perturbation theories (see, e.g., Nobili et al. 1989).

II. THE 2:1 GAP AND THE HILDA ASTEROIDS

Near a mean-motion commensurability with Jupiter, the elliptic problem has been simplified by numerical averaging (Schubart 1968), by retaining only the resonant and secular terms (to some order) and then introducing new high-frequency terms as delta functions such that it is possible to derive an algebraic map of the phase space onto itself (Wisdom 1982; Murray 1986; Šidlichovský and Melendo 1986), or by perturbative methods (Wisdom 1985a; Henrard and Lemaître 1986; Ferraz-Mello 1987). In no case can the Hamiltonian of the simplified problem be computed explicitly; furthermore, since all these methods rely on averaging, there is no rigorous proof that they retain the basic features of the original problem. In point of fact, because of the reduced dimensionality, equal to that of the circular planar problem, the tori where the regular orbits lie do bound the motion. Finding their location in the phase space is crucial to understanding whether the resonance should give rise to a gap or not. This requires us to investigate the topology of the level manifolds of the averaged Hamiltonian using the theory of critical points (which correspond to the periodic orbits of the original problem) (Milani et al. 1986).

The 2:1 and 3:1 resonances clearly demonstrate the difference. At the 2:1 resonance, the tori of the averaged problem bound the chaotic region at eccentricities of about 0.2 (Giffen 1973; Froeschlé and Scholl 1976; Grau Sanchez 1985). Henrard and Lemaître (1986) have developed an analytic perturbation theory for the 2:1 resonance in the elliptic planar model, and concluded that large parts of the phase space are preserved from chaotic motion or large increases in eccentricity. Thus the observation of only a few high-eccentricity ($e > 0.3$) asteroids in the 2:1 gap is unexplained. If the complexity of the problem is increased by adding the third dimension and taking into account the perturbations of Saturn, Uranus and Neptune, it seems that high-eccentricity values can be reached starting from low ones, passing first

through a phase of increasing inclination (Wisdom 1987). An increase in eccentricity is also found starting from high-amplitude librations and adding only the perturbations of Saturn; the inclination increases but does not exceed 9° (Yoshikawa 1988). Pure gravitation might possibly explain the 2 : 1 gap, but there is need to increase the dimensionality of the problem: whether it is necessary to add a third dimension or more perturbing bodies, or both, is an interesting question that remains to be answered.

In contrast, at the 3 : 1 resonance, the elliptic-averaged problem explains well the observed width of the gap; both regular and chaotic orbits become Mars crossers. The eccentricity of Jupiter is crucial to form the gap; the large increases in the asteroid's eccentricity as well as the extent of the chaotic region are preserved in the averaged problem even without reintroducing the high-frequency terms (Wisdom 1983, 1985a). Actually, one orbit was found to become an Earth crosser 3 times over an interval of 500,000 yr, thus suggesting that meteorites can be delivered to Earth directly from the 3 : 1 resonance with Jupiter (Wisdom 1985b). While in the three-body elliptic model this is an unlikely event, results from a numerical integration of planet-crossing asteroids for 200,000 yr including all planets except Mercury and Pluto (Milani et al. 1988) show that mean-motion resonances with Jupiter (not just the 3 : 1) are a common source of Earth-crossing objects. However, these results also show that asteroids in mean-motion resonances with Jupiter can come from (evolve into) cometary-type orbits. Therefore, although it is established that meteoritic material comes from the Kirkwood gaps, its composition might be representative of outer regions of the solar system.

The 3 : 2 Hilda asteroids are another example of the success of the averaged elliptic model. Schubart (1968, 1982) shows that, due to the libration of the critical argument around 0°, close approaches to Jupiter can never occur. In fact, Hilda asteroids never get closer to Jupiter than 1.4 AU (Marsden 1970). Numerical experiments in the elliptic restricted three-body model show no evidence of chaotic motion at the 3 : 2 resonance (Wisdom 1987). Schubart's earlier results are confirmed by Nakai and Kinoshita (1986) and by Schubart (1988) within a Sun-Jupiter-Saturn-asteroid four-body model. A suitable transformation to a new set of variables allows Schubart to answer a long open question about the two Hilda asteroids 334 Chicago and 1256 Normannia: Normannia is confirmed to librate while Chicago circulates and shows indication of non quasi-periodic behavior (Schubart 1988).

III. THE DEPLETION PROBLEM

If we apply the Hill criterion (Eq. 2) to a population of asteroids assumed to be initially uniformly distributed in circular Keplerian orbits around the Sun inside its sphere of influence, and wish to know how close to Jupiter the asteroid should orbit for its Jacobi integral to equal the critical value H_2, it is found that this occurs at about 0.81 of the Sun-Jupiter distance: all the as-

teroids that started closer to Jupiter have no stability guarantee whatsoever from the Hill criterion (Farinella and Nobili 1978). This is a nice result, since only 279 Thule is found inside the sphere of influence of the Sun slightly beyond 0.81, and Thule is known to avoid close approaches to Jupiter by libration in the 4 : 3 mean-motion resonance. This libration was confirmed in the four-body model (Nakai and Kinoshita 1986; Schubart 1988). However, the distribution of outer-belt asteroids in the semimajor axis/eccentricity plane shown in Fig. 2 needs a much deeper understanding. The continuous lines of Fig. 2 are the lines of constant Jacobi integral showing the topological change (from closed to open) across the critical value $H_2 = -1.5193$. The short-period comets are well outside the critical curve, and this is no surprise because we do not expect them to be confined. Most of the Hilda asteroids (with $a \simeq 0.763$) are also not confined by the Hill criterion, but are protected by the libration in the 3 : 2 resonance. However, Fig. 2 also shows a rather large region where the Jacobi integral is well below the critical value for asteroids to be confined by the Hill criterion, and yet it is largely depleted. It is apparent that the circular model must be abandoned.

Dermott and Murray (1983) have computed the width associated with mean-motion resonances taking into account the leading eccentricity term in the disturbing function. Figure 3, which is taken from their work, shows that the observed depleted region in between the 2 : 1 and the 3 : 2 resonances lies where mean-motion resonances overlap, and it is known that overlap of resonances gives rise to chaotic motion. However, early numerical experiments carried out within the elliptic model (either planar or in 3 D) did not give enough evidence that this region could be depleted within the pure gravitational hypothesis (Lecar and Franklin 1973; Froeschlé and Scholl 1979). Indeed, the elliptic planar model is enough to depopulate significantly the outer belt but it is very unlikely that escapes are found by integrating a random set of initial conditions for a limited span of time.

Milani and Nobili (1985) have found that objects escape, after only 10^2 to 10^3 yr, from well inside the Hill stability region of the circular model. This was done by first establishing regions of ordered and chaotic motion in the circular planar model on different-level manifolds of the Jacobi integral. Figures 4 and 5 are drawn for $H = -1.52$ (the phase space is reduced to dimension 2 by first fixing the value of H and then making a Poincaré surface of section); Fig. 4 shows several regular orbits; in Fig. 5 one single chaotic orbit fills large parts of the phase space beyond the 2 : 1 resonance. Figure 6 shows how ordered and chaotic regions look farther inside the stability region, on the level manifold $H = -1.54$. Although the chaotic orbits of Figs. 5 and 6 are confined by the Hill criterion, it is apparent that they get very close to Jupiter, and this is how they might be ejected if Jupiter were allowed a nonzero eccentricity. So, the eccentricity of Jupiter is introduced and escapes are searched for in the elliptic model. Instead of starting with a random distribution of objects, initial conditions are chosen inside the chaotic regions of the circular
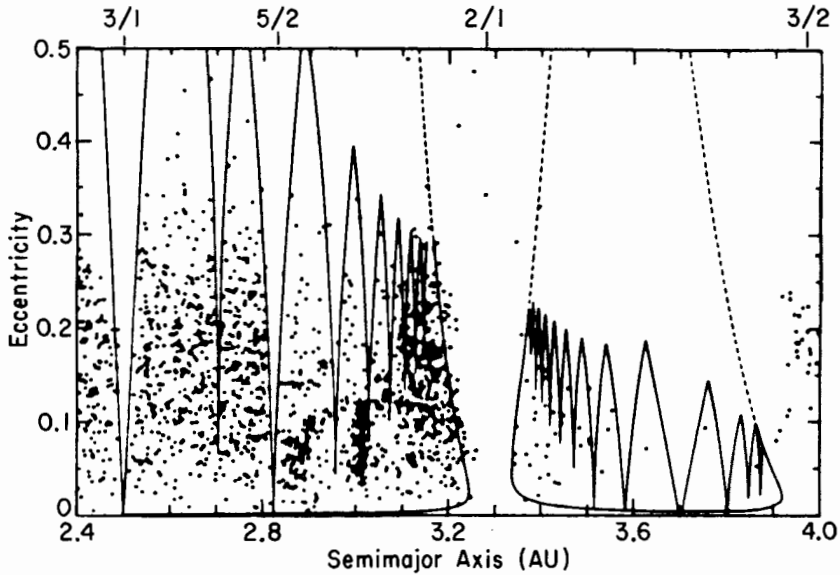
Fig. 3. All the numbered asteroids listed in the TRIAD file (Bender 1979) are plotted. The solid lines represent the libration width associated with the leading eccentricity term in the expansion of the perturbing function at the strongest Jovian resonances. Resonance overlap occurs where the solid lines meet. In the region of resonance overlap, the libration widths of the 2:1 and 3:2 resonances are represented by dashed lines (figure courtesy of Dermott and Murray 1983).

problem and with an initial angle $\varpi_A - \varpi_J$ (the pericenter of the asteroid minus the pericenter of Jupiter, which is the extra variable of the elliptic problem) close to π, the geometric configuration of the orbits in which the closest approach can happen. Since the period of the asteroid's pericenter is typically a few thousand years, there is no loss of generality in this choice. Because the initial conditions are in the chaotic zone, like the orbit of Fig. 5, a close approach to Jupiter occurs after a few synodic periods, long before the pericenter of the asteroid has moved away from the initial configuration.

Introducing the eccentricity of Jupiter is like opening a hole in a basin: although it is small (i.e., although the set of initial conditions giving rise to ejections is narrow), if the orbit is chaotic, it will pass through sooner or later. With the eccentricity of Jupiter at its maximum value of 0.061, escapes occur within a few thousand years. Considering the 54,000 yr period of Jupiter's eccentricity, a conservative conclusion is that the outer belt is largely depleted over a time scale of 10^6 yr. This leaves no time for significant collisional processes to occur and leads to the conclusion that an excess of large asteroids should be found in the outer belt in between the 2 : 1 and the 3 : 2 resonances where the gravitational depletion occurred. This is confirmed for both the numbered asteroids and the quality class 1 asteroids of the Palomar-Leiden
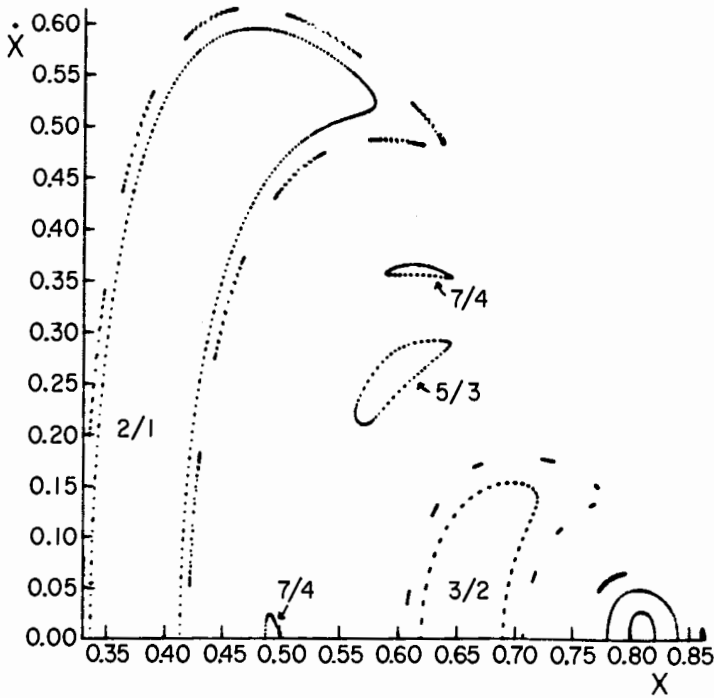
Fig. 4. Regular orbits in the phase space $(x, \dot{x})$ on the level manifold $H = -1.52$ ($y = 0, x > 0$ surface of section). The 2:1 and 3:2 librations are shown. Outside the librations, orbits which decompose into islands are plotted to give an idea of the size of the dubious region between the ordered and the chaotic region. All the stable regions of this figure are surrounded by a single connected chaotic region (see Fig. 5).

survey. The fact that the difference in size distribution is observed over a wide range of absolute magnitudes makes it unlikely that it is due to an observation selection effect (see Milani and Nobili 1985, p. 273).

IV. MECHANISMS OF DYNAMICAL PROTECTION

The motion of numbered asteroids in the outer belt shows a variety of dynamical behaviors, all of which appear to minimize the otherwise too strong Jovian perturbations. Over the past 30 yr, a number of authors have investigated the dynamics of these objects both analytically and with numerical experiments (see Milani and Nobili [1984] for a detailed discussion of many different mechanisms of dynamical protection and for a long list of references). Among the mechanisms which have been discovered, there is the libration of the critical argument in mean-motion resonances (such as 2:1, 3:2, 4:3, 1:1); there is a protection mechanism involving the angle ϖ_A −
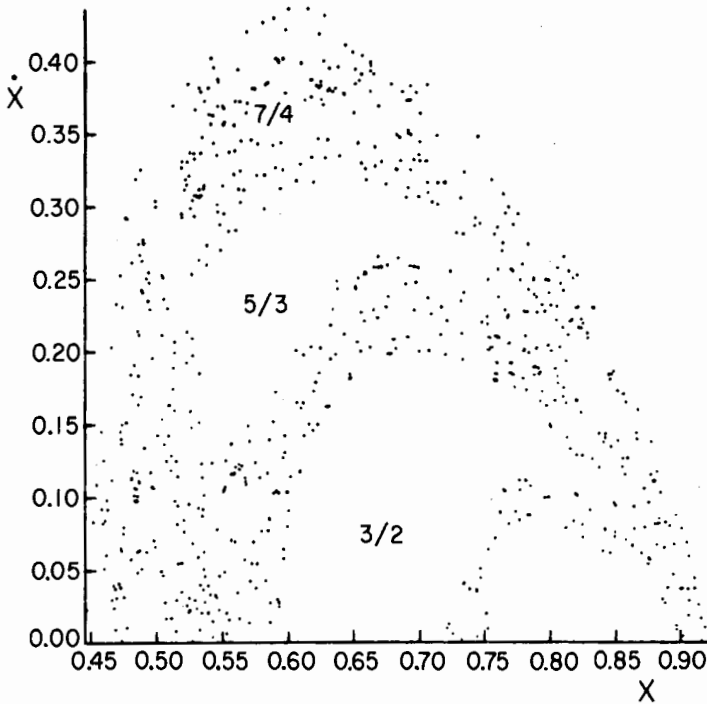
Fig. 5. One single chaotic orbit on the level manifold $H = -1.52$ fills a vast region of phase space, except for libration islands such as those of the 3:2, 5:3, 7:4 resonances. This plot refers to the region beyond the 2:1 libration island. Note that this object, wandering around chaotically in phase space can have very close approaches to Jupiter. However, as long as Jupiter has zero eccentricity, the object is confined to move around the Sun indefinitely.

ϖ_J; there is an alternation between the two; and there is a mechanism which protects inclined asteroids such as 1373 Cincinnati. Figure 7 shows how the angle $\varpi_A - \varpi_J$ in the cases of 1144 Oda and 522 Helga never gets close to π, which is the configuration of the orbits for which close approaches can occur. The motion of 1144 Oda is worth a brief discussion. The asteroid moves in an almost empty region very close to a highly chaotic region; yet, in spite of an eccentricity of 0.09, the motion is regular. Furthermore, at lower values of the eccentricity along the same level line of the Jacobi integral, there are no numbered asteroids, while one would expect them to be less perturbed by Jupiter (see Fig. 2). The answer to all these questions is found in the libration of the $\varpi_A - \varpi_J$ argument shown in Fig. 7 (top). The closer the angle $\varpi_A - \varpi$ is to zero, the safer the asteroid is, since the closest possible approach, with the asteroid at aphelion and Jupiter at perihelion, can only occur if $\varpi_A - \varpi_J = \pi$. In fact, the polar angle becomes $\simeq 70°$ at most. This libration mechanism also explains the present large value of Oda's osculating eccentricity. In Fig. 7, the
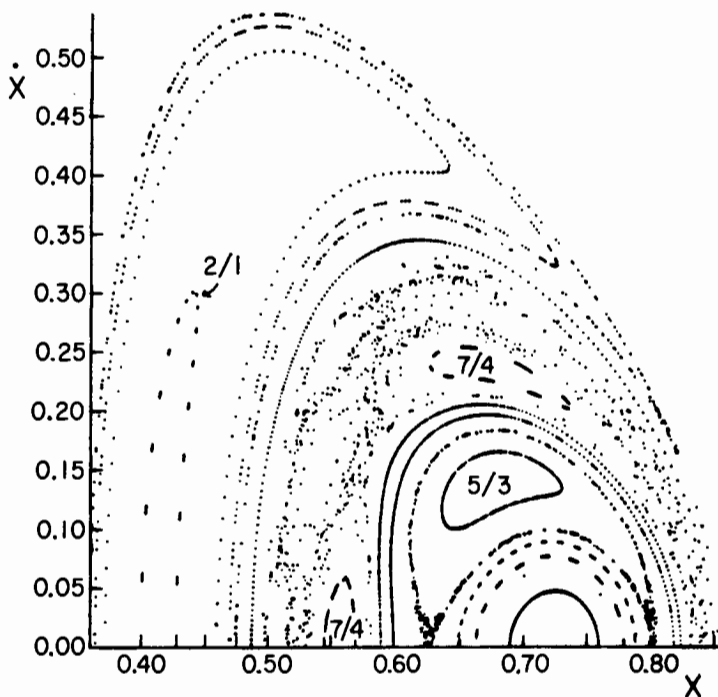
Fig. 6. Ordered and chaotic regions in the phase space $(x, \dot{x})$ on the level manifold $H = -1.54$ ($y = 0$, $x > 0$ surface of section). The chaotic region for $H = -1.54$ is smaller than that detected for $H = -1.52$ (Figs. 4 and 5) because $H = -1.54$ is deeper inside the Hill stability region (Fig. 2). Nevertheless, objects therein wander around chaotically and can get very close to Jupiter.

radius is the osculating eccentricity and the libration period of the argument $\varpi_A - \varpi_J$ is about 5000 yr. Since the annulus is off center (it is centered at the forced eccentricity), a region of osculating eccentricity between e and $e + \Delta e$ contains more points for a value of e close to the maximum. Therefore, finding Oda with an osculating eccentricity close to its maximum value is most likely. The eccentricity oscillates with a period of $\simeq 5000$ yr only and its present value has no special meaning. In Fig. 2, along the $H = -1.54$ level line of the Jacobi integral, 1144 Oda might well be at any point below the present one. Figure 8 shows the orbit of 319 Leona with two different mechanisms acting at the same time. As for the apocentric libration mechanism (discovered by Franklin et al. [1975]), recent analytic work has been done by Henrard et al. (1986) and Wisdom (1986).

Bien and Schubart (1984) have studied the combined effect of secular resonances and the 1:1 mean-motion resonance of the Trojan asteroids. A secular resonance occurs when a basic period which appears in the asteroid's
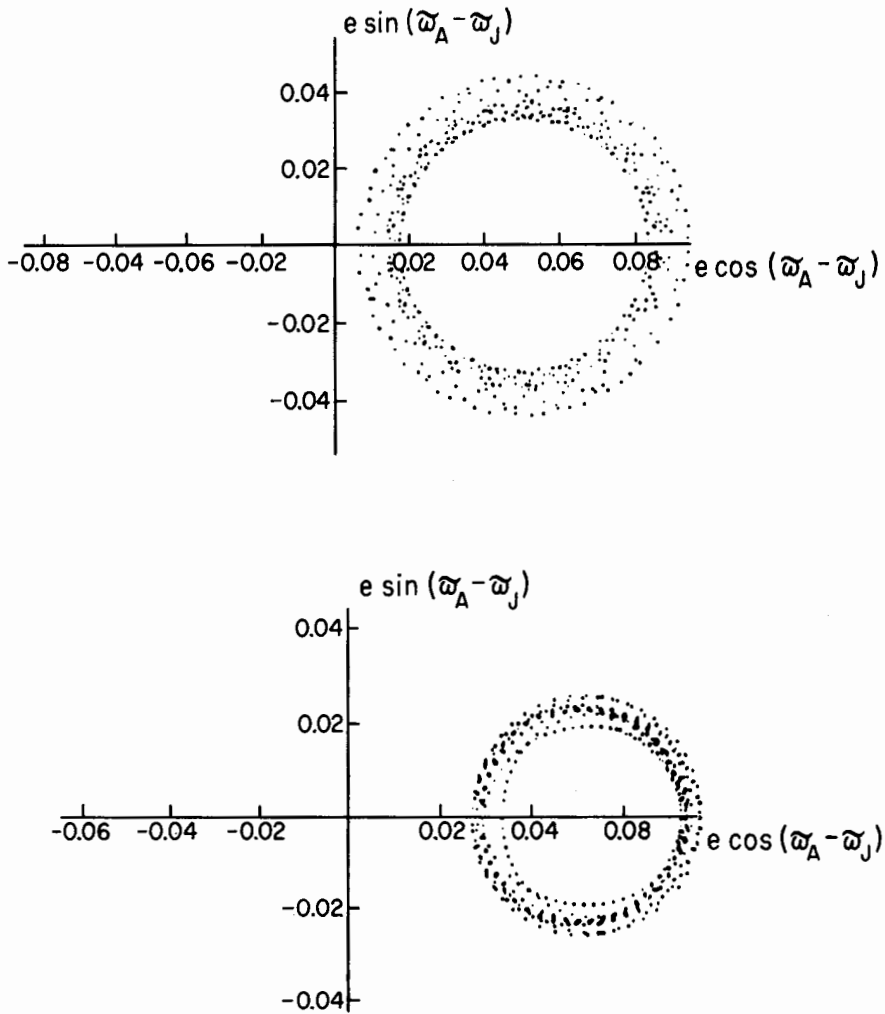
Fig. 7. The orbits of 1144 Oda (upper) and 522 Helga (lower) for 250 synodic periods (one for each point) in the planar elliptic three-body model. The polar angle $\varpi_A - \varpi_J$ (the pericenter of the asteroid minus the pericenter of Jupiter) librates around $0°$ within about $\pm 70°$. The $\varpi_A - \varpi_J = 180°$ geometrical configuration of the orbits, in which very close approaches can occur, is thus avoided.

motion is close to a secular period in the motion of the major planets. They find librations of the arguments $\Omega_A - \Omega_J$ and $\Omega_A - \varpi_J$ (Ω is the longitude of the node) with periods of some 10^6 yr. The Trojan asteroids inhabit the stability zone around the two Lagrangian equilibrium points of the Sun-Jupiter system, and Van Houten et al. (1970) point out that the leading Lagrangian
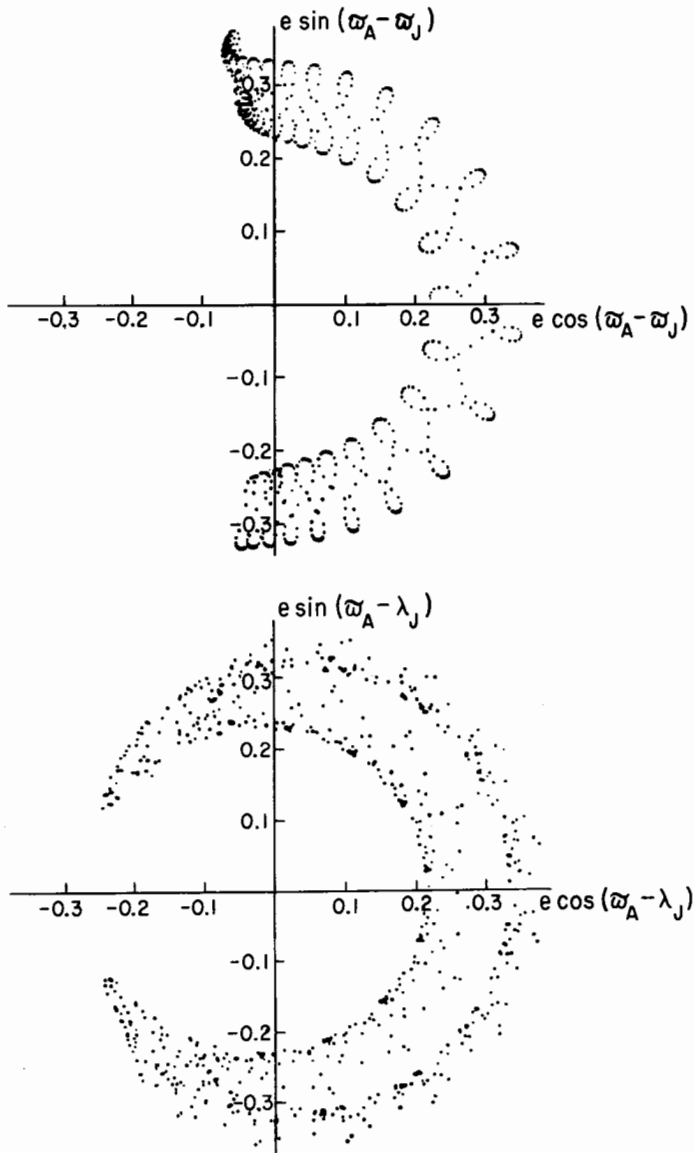
Fig. 8. The orbit of 319 Leona for 700 synodic periods (one for each point) in the planar elliptic three-body model. The upper diagram is in the same plane as in Fig. 7 while the lower one shows the libration in the 2:1 mean-motion resonance (λ_J is the longitude of Jupiter). The angle $\varpi_A - \varpi_J$ starts to come back towards $0°$ after reaching a value of about $110°$. Note that the closer $\varpi_A - \varpi_J$ is to $110°$, the smaller is the amplitude of the 2:1 libration. Vice versa, the amplitude of the 2:1 libration is very large when $\varpi_A - \varpi_J \simeq 0°$. Clearly, the two mechanisms alternate in protecting the asteroid from close approaches to Jupiter.

point has about 3.5 times more objects than the trailing one. However, recent work suggests that this is an observational bias (L. French, E. Bowell, S. J. Bus, K. S. Russell, C. S. Shoemaker and E. M. Shoemaker, personal communication).

Although a more systematic investigation of all the numbered asteroids in the outer belt would be very interesting, there is enough evidence that the majority of them are protected from close approaches to Jupiter by some dynamical mechanism (see Milani and Nobili 1984, their Fig. 1). If this is so, observed asteroids must have gone through a process of natural selection as a result of which all objects in unprotected orbits have been ejected from the system. Can we conclude that observed asteroids in the outer belt are the remnants of the original population? On the basis of the dynamical evidence alone, this conclusion is not legitimate unless we can also prove that the protection mechanisms are capable of maintaining the stability for a time span of the order of the age of the solar system. However, numerical experiments can only prove instability, since stable orbits such as those in Figs. 7 and 8 might become unstable if the integration were carried out for a longer interval of time. Schubart (1988) has found that the motion of 1144 Oda is regular, whereas 334 Chicago and 522 Helga show a non quasi-periodic behavior. Narrowband spectrophotometric observations of outer-belt asteroids show that there are four distinct slopes among the spectra (see the chapter by French et al.). The spectrum reddens with increasing heliocentric distance and the authors suggest that these asteroids are formed *in situ* and are the remnants of a gradation in composition of planetesimals in the outer solar system. Color observations also show a dependence with distance, although a rather weak one (Dermott et al. 1985). It is worth investigating the possibility that spectrum and color variations with distance from the Sun are due to weathering phenomena rather than to a difference in the primordial composition. In any case, to assess the long-term stability of outer-belt asteroids by pure Newtonian dynamics is an interesting open problem.

REFERENCES

Arnold, V. 1976. *Les Méthodes Mathématiques de la Mécanique Classique* (Moscou: Editions Mir).

Bender, D. F. 1979. Osculating orbital elements of the asteroids. In *Asteroids,* ed. T. Gehrels (Tucson: Univ. of Arizona Press), pp. 1014–1039.

Bien, R., and Schubart, J. 1984. Trojan orbits in secular resonances. *Celest. Mech.* 34:425–434.

Dermott, S. F., and Murray, C. D. 1983. Nature of the Kirkwood gaps in the asteroid belt. *Nature* 301:201–205.

Dermott, S. F., Gradie, J., and Murray, C. D. 1985. Variation of the UBV colors of S-class asteroids with semimajor axis and diameter. *Icarus* 62:289–297.

Ephemerides of Minor Planets. 1987. (Leningrad: Russian Academy of Sciences).

Farinella, P., and Nobili, A. M. 1978. A simple explanation of some characteristics of the asteroidal belt based on the restricted 3-body problem. *Moon and Planets* 18:241–250.

Ferraz-Mello, S. 1987. Averaging the elliptic asteroidal problem near a first-order resonance. *Astron. J.* 94:208–212.

Franklin, F. A., Marsden, B. G., Williams, J. G., and Bardwell, C. M. 1975. Minor planets and comets in libration about the 2:1 resonance with Jupiter. *Astron. J.* 80:729–746.

Froeschlé, C., and Scholl, H. 1976. On the dynamical topology of the Kirkwood gaps. *Astron. Astrophys.* 48:389–396.

Froeschlé, C., and Scholl, H. 1979. New numerical experiments to deplete the outer asteroid belt. *Astron. Astrophys.* 72:246–255.

Giffen, R. 1973. A study of commensurable motion in the asteroidal belt. *Astron. Astrophys.* 23:387–403.

Grau Sanchez, M. 1985. *Topologia y dynamica da asteroides en resonancia con Jupiter.* Thesis, Univ. de Barcelona, Spain.

Henrard, J., and Lemaître, A. 1986. A perturbative treatment of the 2 : 1 Jovian resonance. *Icarus* 69:266–279.

Henrard, J., Lemaître, A., Milani, A., and Murray, C. D. 1986. The reducing transformation and apocentric librators. *Celest. Mech.* 38:335–344.

Lecar, M., and Franklin, F. 1973. On the original distribution of the asteroids, 1. *Icarus* 73:422–436.

Marsden, B. G. 1970. On the relationship between comets and minor planets. *Astron. J.* 75:206–217.

Marsden, B. G., and Roemer, E. 1982. Basic information and references. In *Comets,* ed. L. L. Wilkening (Tucson: Univ. of Arizona Press), pp. 707–733.

Milani, A. 1988. Dynamique des astéroides: Exposé introductif. In *Développements récents en planétologie dynamique,* eds. D. Benest and C. Froeschlé (Nice, France: Observatoire de Nice), pp. 83–96.

Milani, A., and Nobili, A. M. 1983. On topological stability in the general 3-body problem. *Celest. Mech.* 31:213–240.

Milani, A., and Nobili, A. M. 1984. Resonant structure of the outer asteroid belt. *Celest. Mech.* 34:343–355.

Milani, A., and Nobili, A. M. 1985. The depletion of the outer asteroid belt. *Astron. Astrophys.* 144:261–274.

Milani, A., Murray, C. D., and Nobili, A. M. 1986. The Hilda group and the Hecuba gap. In *Asteroids, Comets, Meteors II,* eds. C. I. Lagerkvist, B. A. Lindblad, H. Lundstedt and H. Rickman (Uppsala: Uppsala Univ.), pp. 147–151.

Milani, A., Carpino, M., Hahn, G., and Nobili, A. M. 1988. Dynamics of planet crossing asteroids. Classes of orbital behavior; Project SPACEGUARD. *Icarus,* in press.

Murray, C. D. 1986. Structure of the 2 : 1 and 3 : 2 Jovian resonances. *Icarus* 65:70–82.

Nakai, H., and Kinoshita, H. 1986. The motion of numbered asteroids in resonance regions. In *Proceedings of the Nineteenth Symp. on Celestial Mechanics, Japan,* eds. H. Kinoshita and H. Nakai, pp. 1–9.

Nobili, A. M., Milani, A., and Carpino, M. 1989. Fundamental frequencies and small divisors in the orbits of the outer planets. *Astron. Astrophys.* 210:313–336.

Poincaré, H. 1893. *Méthodes Nouvelles de la Mécanique Céleste,* vol. 1 (Paris: Gauthiers-Villars).

Šidlichowský, M., and Melendo, B. 1986. Mapping for 5 : 2 asteroidal commensurability. *Bull. Astron. Inst. Czech.* 37:65–80.

Schubart, J. 1968. Long-period effects in the motion of Hilda-type planets. *Astron. J.* 73:289–310.

Schubart, J. 1982. Three characteristic parameters of orbits of Hilda-type asteroids. *Astron. Astrophys.* 114:200–204.

Schubart, J. 1988. Resonant asteroids between the main belt and Jupiter's orbit. *Celest. Mech.* 43:309–317.

Szebehely, V. 1967. *Theory of Orbits* (New York: Academic Press).

Van Houten, C. J., Van Houten-Groeneveld, I., and Gehrels, T. 1970. Minor planets and related objects. V. The density of Trojans near the preceeding Lagrangian point. *Astron. J.* 75:659–662.

Williams, J. G., and Faulkner, J. 1981. The positions of secular resonance surfaces. *Icarus* 46:390–399.

Wisdom, J. 1982. The origin of the Kirkwood gaps: A mapping for asteroidal motion near the 3 : 1 commensurability. *Astron. J.* 87:577–593.

Wisdom, J. 1983. Chaotic behavior and the origin of the 3 : 1 Kirkwood gap. *Icarus* 56:51–74.

Wisdom, J. 1985a. A perturbative treatment of motion near the 3 : 1 commensurability. *Icarus* 63:272–289.

Wisdom, J. 1985b. Meteorites may follow a chaotic route to Earth. *Nature* 315:731–733.

Wisdom, J. 1986. Canonical solution of the two critical argument problem. *Celest. Mech.* 38:175–180.

Wisdom, J. 1987. Urey Prize Lecture: Chaotic dynamics in the solar system. *Icarus* 72:241–275.

Yoshikawa, M. 1988. The survey of the motions of asteroids in the commensurabilities with Jupiter. *Astron. Astrophys.*, submitted.

EVOLUTION OF COMETS INTO ASTEROIDS

PAUL R. WEISSMAN
Jet Propulsion Laboratory

MICHAEL F. A'HEARN
University of Maryland

L. A. MC FADDEN
University of California, San Diego

and

H. RICKMAN
Uppsala University

Observational discoveries and theoretical developments in the past decade have led to a general consensus that at least some asteroids, in particular some Earth-crossing asteroids, may actually be extinct cometary nuclei. Theoretical developments include: exploration of dynamical mechanisms capable of delivering main-belt asteroids into Earth-crossing orbits (though these are still not enough to explain the estimated number of Apollo and Aten asteroids); and an understanding of possible processes which may affect comets during their long residence in the Oort cloud and lead to the formation of nonvolatile crusts before and after they enter the planetary system. The observations include: the discovery of a number of apparent asteroids in chaotic, Jupiter-crossing orbits; the IRAS discovery of 1983 TB (3200 Phaethon), an asteroid in the same orbit as the Geminid meteor shower; the apparent low activity levels determined for several short-period comet nuclei including Comet Halley, implying the existence of nonvolatile surface crusts; and anomalous observations of possible cometary activity in some Earth-crossing asteroids. Extinct nuclei may resemble primitive asteroid types such as C, P and D. Current best dynamical estimates

are that somewhat less than half the Apollo and Aten asteroids may be extinct cometary nuclei, though the uncertainty of that estimate is quite large. Further detailed physical studies of the Apollos, Atens and other unusual asteroids are clearly needed to help resolve these issues.

I. INTRODUCTION

The asteroids and the comets are each subsets of the full compositional spectrum of planetesimals which we believe formed in the solar nebula 4.5 Gyr ago. In the case of the main-belt asteroids, fortune or Nature has conspired to preserve one of the most interesting parts of that spectrum, the region where it changes from refractory dominated to volatile dominated bodies. In addition, the asteroids show evidence of a variety of modifying planetary processes including accretion, chemical differentiation, collisional disruption and re-assembly, and possibly short-lived internal heating.

In contrast, the comets represent a more distant, and possibly more compositionally uniform region of the solar nebula, the Uranus-Neptune zone and beyond. Until recently, it was widely believed that comets had experienced very little processing or modification from their original state, and had been stored in distant, cold orbits far from the Sun in the Oort cloud. Although a number of significant modifying processes have now been recognized (Weissman 1986a; Johnson et al. 1986; Stern 1986; Stern and Shull 1988), the comets have still undergone far fewer changes than the asteroids.

The question of whether or not comets can evolve to appear as asteroidal objects arises because of a desire to understand the source of the meteorites recovered on the Earth's surface. The meteorites must be fragments of objects already in near-Earth orbits, the Apollo, Amor and Aten asteroids, respectively; but such objects have dynamical lifetimes in those orbits of only 30 to 100 Myr (Wetherill 1975), far less than the age of the solar system. Either we must assume an immense original population of near-Earth asteroids, a concept that is physically unrealistic and not supported by cratering data, or there must be a replenishment source.

Historically, the identification of that source has been divided between asteroid observers (for example, see the review by Degewij and Tedesco 1982) who believed that the source must be asteroids, and dynamicists, (Öpik 1963; Wetherill 1971) who believed it must be comets. To the observers, the near-Earth asteroids showed no evidence of cometary activity, i.e., no observable coma, had surface compositions as determined by reflectance spectroscopy which mimicked the range (though not the statistics) of surface compositions for the main-belt asteroids, and in general had the aphelia of their orbits in the main belt. To the dynamicists, there were no known mechanisms for transferring the required flux of asteroids from the main belt into Earth-crossing orbits, whereas short-period comets were regularly thrown into small perihelion orbits by close encounters with Jupiter, and were sufficiently numerous to provide the needed flux.
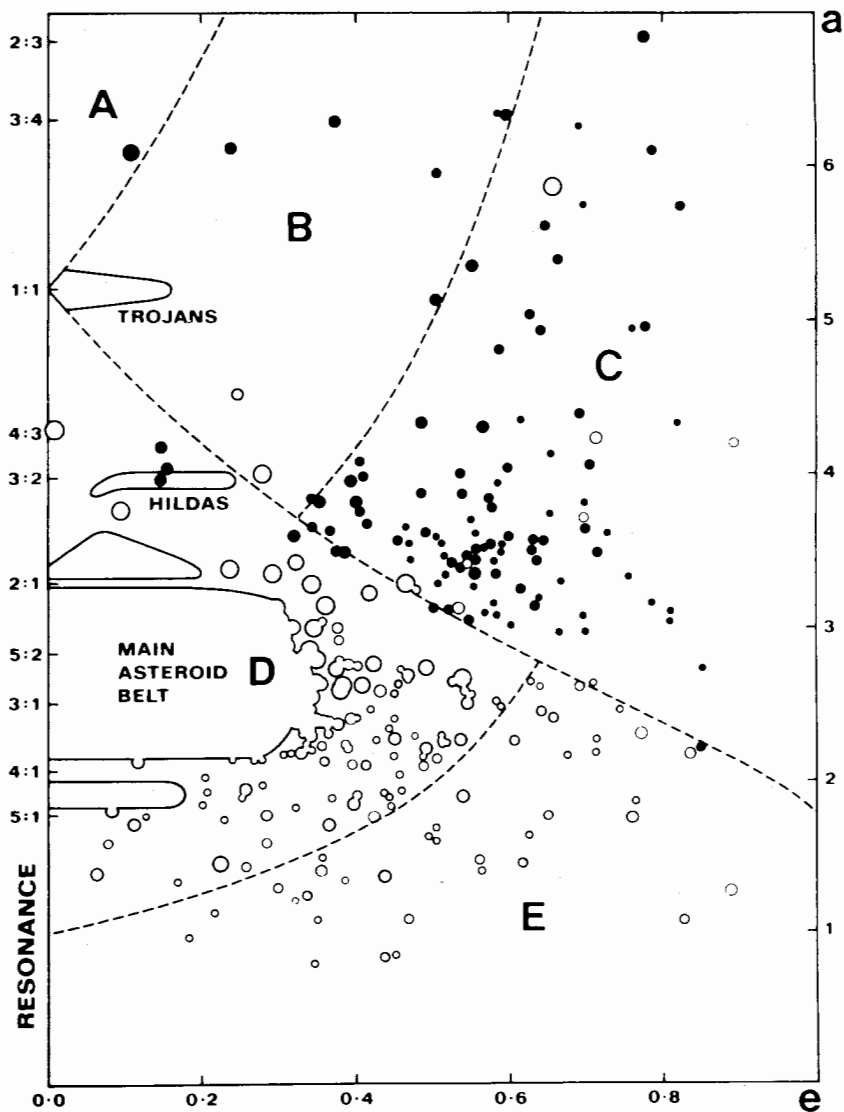
Fig. 1. Short-period comets (solid circles) and asteroids (open circles) plotted on a scatter dia-
gram of semimajor axis vs eccentricity (Kresák 1985). Increasing circle size indicates esti-
mated size of the objects: diameter < 1 km or lost, 1 to 3 km, 3 to 10 km, 10 to 30 km and >
30 km. Different regions identified within the diagram are: (A) transjovian region, (B) Jupiter
domain of weak cometary activity, (C) Jupiter domain of strong cometary activity, (D) minor
planets region, and (E) Apollo-Aten region. The dashed line going from upper left to lower
right corresponds to a Tisserand invariant of 3.0, the usual dividing line between comets and
asteroids. However, note the several asteroids above the line in the cometary region C; the
figure has been modified to include seven new asteroids in or near region C discovered since
Kresák's (1985) work was published.

The situation is illustrated, in part, by Fig. 1 (Kresák 1985) which is a scatter diagram of all the known short-period comet and asteroid orbits in semimajor axis a and eccentricity e. The diagram is divided into five major dynamical regions: (A) the transjovian region of objects with perihelia beyond Jupiter's semimajor axis; (B) the Jupiter domain of weak cometary activity where comets are Jupiter crossing but their perihelia are still relatively large; (C) the Jupiter domain of strong cometary activity where the cometary perihelia are sufficiently small to make them quite active; (D) the main-belt and Mars-crossing asteroids; and (E) the Earth-crossing asteroids.

The dashed line going from upper left to lower right in the diagram is defined by the Tisserand invariant T, a quasi-constant of the motion in the restricted three-body problem. Short-period comet orbits tend to evolve along lines of constant T. The Tisserand invariant was initially used to identify returning short-period comets even though their orbits may have been perturbed by a close encounter with Jupiter. The dashed line in the figure is for a value of $T = 3.0$. Note that virtually all short-period comets fall above the line where $T < 3.0$, and most asteroids fall below the line, $T > 3.0$. Only objects with $T < 3.0$ can be Jupiter crossing.

Before 1980 only two asteroids, other than the librating Trojans and Hildas, were known with a Tisserand invariant < 2.9: 944 Hidalgo, with $a = 5.76$ AU and $e = 0.656$, and 1373 Cincinnati with $a = 3.40$ AU and $e = 0.323$ (also, the unusual outer solar system asteroid 2060 Chiron is in a Saturn-crossing orbit with $a = 13.69$ AU and $e = 0.3786$). The small number of asteroidal objects in Jupiter-crossing orbits was used as an argument against the existence of extinct cometary nuclei transitioning to asteroidal orbits (Rickman and Froeschlé 1980). Typical estimates of the physical lifetimes of comets are less than the estimates of their dynamical lifetimes in Jupiter-crossing orbits. Thus, it was expected that if short-period comets did evolve to dormant or extinct objects, they would still be in Jupiter-crossing orbits, and would be observable as asteroidal objects.

Between 1981 and 1988 a substantial number of additional Jupiter-crossing and Jupiter-approaching asteroids were discovered; these are listed in Table I. They are also shown scattered through region C in Fig. 1; we have added seven objects to Fig. 1, in or near region C, discovered since Kresák's (1985) work was published. Dynamical studies of these asteroids have shown that several exhibit chaotic motion, interpreted as possibly implying a cometary origin. It is these Jupiter-crossing and Jupiter-approaching asteroids in chaotic orbits that can most easily be scattered into Earth-crossing orbits.

At the same time, dynamical studies have led to the conclusion that a larger fraction of the Earth-crossing objects, $\sim 60\%$, may be supplied from the asteroid belt through two mechanisms: secular resonances and chaotic motion at orbital commensurabilities. This provides a source for the differentiated near-Earth asteroids that are observed, and for the differentiated meteorite types. Thus, much of the previous conflict between asteroid observers

TABLE I
Recently Discovered Asteroids with $T \lesssim 3$ and Small Perihelia

Designation	Tisserand Invariant	q (AU)	Q (AU)	Protection Mechanism[a]	Current Classification
1981 FD	2.99	1.69	4.79	2:1 resonance	asteroidal
1981 VA	2.96	0.63	4.29	$(e - \omega)$ coupling	asteroidal
1982 TA	3.09	0.53	4.07	$(e - \omega)$ coupling	asteroidal
1982 YA	2.38	1.12	6.29	(5:3 resonance)	cometary (?)
1983 LC	2.98	0.77	4.50	ω - quasi-stable	asteroidal (?)
1983 SA	2.31	1.21	7.25	(4:3 resonance)	cometary
1983 TF2	3.02	0.64	4.23	?	? - not studied[b]
1983 VA	2.98	0.80	4.36	none - chaotic (?)	cometary (?)
1983 XF	2.98	1.45	4.78	(2:1 resonance)	cometary
1984 BC	2.78	1.55	5.30	none - chaotic	cometary
1985 TB	3.06	1.11	4.03	?	? - not studied[b]
1985 WA	2.99	1.13	4.57	5:2 resonance	asteroidal
1986 DA	3.04	1.17	4.47	5:2 resonance	asteroidal
1986 JK	2.94	0.90	4.71	5:2 resonance	asteroidal
1986 RA	2.76	1.23	5.31	2:1 resonance	asteroidal
1987 PA	3.08	1.21	4.27	?	? - not studied[b]
1987 QC	3.03	1.14	4.47	?	? - not studied[b]
1987 SL	2.88	1.15	4.76	?	? - not studied[b]

[a]Dynamical protection mechanisms in parentheses are temporary, and chaotic motion occurs within a short time. For a description of dynamical protection mechanisms, see Hahn and Rickman (1985) and Hahn and Lagerkvist (1988).
[b]Asteroids not yet studied are because aphelia were not Jupiter approaching or because discovery is too recent.

and celestial mechanicians has been resolved. However, at least one Earth-crossing asteroid, 3552 1983 SA, and one Mars-crosser, 1984 BC (both in chaotic Jupiter-crossing orbits) are spectral type D, typical of outer main-belt and Trojan asteroids. A dynamical mechanism for delivering objects to Earth-crossing orbits from these regions has not been identified.

The application of asteroid observing techniques to distant cometary nuclei during the past decade has yielded valuable new insights into the nature of these objects. The measured diameters of several short-period comet nuclei were found to be larger than expected, particularly when compared with the gas production rates for these comets. The implication is that only a very small fraction of the surface area of each nucleus is active, the rest being covered by an insulating, nonvolatile lag deposit of large grains and organics. This point was further demonstrated by the spacecraft images of Comet Halley which showed that only 20 to 30% of the sunlit surface of the comet nucleus was active, the rest covered by a dark, apparently inactive crust. This showed that even very active comets can develop nonvolatile crusts which might eventually transform them into dormant, asteroidal appearing objects.

Another new piece of evidence is the recognition that some Earth-crossing asteroids appear to be associated with meteor showers; most major meteor showers are associated with active short-period comets. This point was driven home particularly well by the discovery of 1983 TB by the Infrared Astronomical Satellite (IRAS). 1983 TB, now named 3200 Phaethon, is in an identical orbit with the Geminid meteor stream, one of the two largest meteor showers observed each year. Finally, new physical observations of Earth-crossing asteroids have revealed some with anomalous properties, including possible spectral emission features, possible outgassing debris in their orbits, and depolarized radar reflections.

In this chapter we examine the current state of these issues, and identify likely transitional candidates: both comets which have low activity and may be approaching an asteroidal appearance, and asteroids which for one reason or another appear anomalous and may be of cometary origin. In the following sections all of these points are discussed in more detail. We begin by stating our definitions and suggesting possible physical and dynamical discriminators between cometary and asteroidal objects (Sec. II). In Sec. III we discuss the possible dynamical paths by which cometary orbits can evolve to asteroidal ones, followed by the possible physical evolution of active cometary nuclei into dormant or extinct, asteroidal-appearing objects (Sec. IV). In Sec. V we discuss physical observations of cometary nuclei, and in Sec. VI compare them with observations of near-Earth asteroids and other possible candidates for extinct cometary nuclei.

II. DEFINITIONS AND DISCRIMINATORS

An important aspect of this task is first to define our terms. To do so, we adopt a slightly modified subset of the definitions stated by Hartmann et al. (1987) as follows:

Comet (or cometary nucleus): a body formed in the outer solar system containing volatiles in the form of ices and capable of developing a coma if its orbit brings it close enough to the Sun.

Active comet: a comet losing volatiles in a detectable coma.

Inactive comet: a comet nucleus that is active during part of its orbit, but presently is in a part of the orbit where volatile loss is negligible and there is no detectable coma.

Dormant comet: a comet nucleus which, although once active, has no detectable volatile loss and hence no detectable coma in any part of its present orbit. A dormant comet perturbed to lower semimajor axis (and/or lower perihelion distance) might be reactivated. There could be a range of cases: a body may be ice throughout but too far from the Sun to be active (Chiron is a possible example). Alternatively, a body may be closer to the Sun and contain ices in its interior, but has lost all the ices from its near surface layers, or had the ices covered over by a nonvolatile lag deposit.

Extinct comet: a comet that has lost its ices and thus is incapable of producing a coma.

Asteroid: an interplanetary body that formed without appreciable ice content, and thus never had or can have cometary activity.

We do not regard these definitions as perfect; any knowledgeable reader will certainly be able to find exceptions to them. As Hartmann et al. (1987) themselves noted, the definition of "asteroid" is particularly weak since many bodies which are classified as asteroids at present, such as the Trojan asteroids and Chiron, likely do have appreciable ice content. They also speculated on whether ice frosts could evolve on the surfaces of some of the larger C-type asteroids where water hydration bands have been observed. Note that the icy satellites of the outer solar system also do not fit well into these definitions. If one really wished to stretch the definitions to absurdity, the Earth would qualify as a comet since it contains ices and produces a detectable geocorona of escaped gases.

We next must describe how the definitions above translate into observables which allow us to discriminate comets from asteroids. For active comets vs asteroids, the classic discriminator is, as the definitions above state, the existence of detectable comae. For inactive comets one has to wait until the object reaches the active part of its orbit, as may now be happening for Chiron (Hartmann et al. 1989; see the chapter by French et al.). But for dormant or extinct comets the discriminator must be something else. For this, we look to what we know of the statistics of the different populations:

Shape.   The visual lightcurves of near-Earth asteroids (along with radiometric and radar data) show that many are irregularly shaped objects, as would be expected from the collisional disruption of larger planetesimals. For some time it was thought that cometary nuclei would be approximately spherical (Gehrels et al. 1970), as random accretion would not lead to substantially aspherical shapes, and subsequent sublimation would tend to round off extremities. However, the Vega and Giotto images of the Halley nucleus showed a body with axial ratios of 2:1:1 (Sagdeev et al. 1986a; Keller et al. 1986). And rotation lightcurves obtained for cometary nuclei such as Tempel 2 (Wisniewski 1988; Jewitt and Meech 1988) strongly imply substantial departure from a spherical shape. Thus, shape is no longer considered a valid discriminator between asteroids and comets.

Rotation Rate.   Rotation rates obtained for small asteroids are on the average faster than those found for cometary nuclei. However, the number of comets for which rotation rates have been determined is small, and thus, their statistics are poor. The presumed greater self-gravity (due to higher density) and higher internal strength of asteroidal materials may make asteroids more stable against very fast rotation rates than the lower-density, presumably

weaker cometary nuclei. However, there is considerable overlap in the ranges of determined rotation periods for comets and asteroids. Thus, rapid rotation tends to rule out a cometary source, whereas intermediate or slow rotation could be either cometary or asteroidal.

Size. The number of well-determined cometary diameters are too few to say very much about the population, other than that typical diameters are on the order of 6 to 10 km. The statistics of asteroid dimensions in the same size range are incomplete due to the difficulty of observing such small objects. For large asteroids the statistics are far more complete, but large comets or suspected comets, e.g., Schwassmann-Wachmann 1 and Chiron, are so few and, as yet, poorly understood, that it is not possible to make a valid comparison. Thus, size also appears to be a poor discriminator at the present time.

Albedo. Asteroidal albedos range from high reflectance objects such as 44 Nysa with an albedo of 0.49, to the very dark asteroids of the outer main belt and beyond, with albedos ~ 0.02. Although early expectations were that cometary nuclei had high albedos (Delsemme and Rud 1973), it is now recognized that most nuclei appear to be very dark objects (see Sec. V) as suggested by Shoemaker and Wolfe (1982) and others. The carbonaceous lag deposit that would develop on the surface of an extinct cometary nucleus is expected to preserve these very low albedos, typically < 0.05 (A'Hearn 1988). Whether or not further thermal and physical processing of the surface materials on an extinct nucleus could substantially change the albedo is unknown, but it seems unlikely. Thus, high albedo is likely a good test of asteroidal origin, but low albedo will not discriminate between dark asteroids and extinct cometary nuclei. However, coupled with other tests, low albedo would be suggestive of a cometary source.

Color. The more primitive asteroids of the outer main belt and beyond have either flat carbonaceous chondrite spectra with absorption in the blue and ultraviolet, or highly reddened spectra suggestive of hydrocarbons on their surfaces (Gradie and Veverka 1980). Observations of the nuclei and dust comae of active comets have found colors that are generally similar, although sometimes without the absorption in the blue characteristic of chondritic spectra, as shown in Fig. 2. On the other hand, the differentiated asteroids of the inner main belt have distinctly different spectra showing silicate and iron absorption features (Gaffey and McCord 1978). Thus, as with albedo above, the finding of reflectance spectra with strong features would tend to rule out a cometary source, whereas a featureless spectrum would be consistent with a cometary source, but not a conclusive proof.

Orbital Motion. All known short-period comets are in planet-crossing or planet-approaching orbits. As a result, the comets will occasionally make
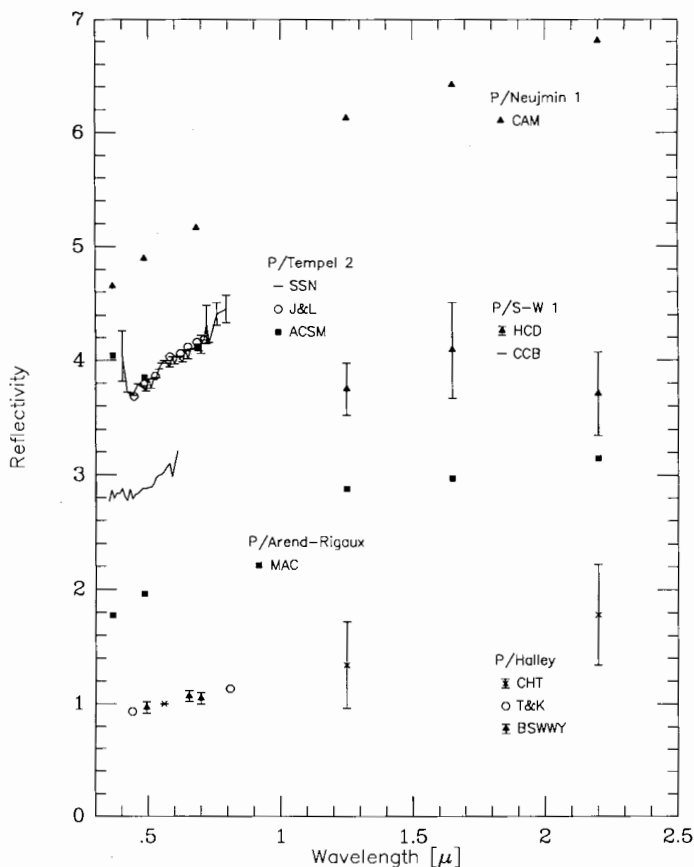
Fig. 2. Spectral reflectance of cometary nuclei; the data is normalized to unity at 0.56 μm. Data for Arend-Rigaux, Schwassmann-Wachmann 1, Tempel 2 and Neujmin 1 have been offset vertically by values of 1.0, 2.0, 3.0 and 4.0, respectively. References for the data: Neujmin 1: CAM = Campins et al. (1987); Tempel 2: ACSM = A'Hearn et al. (1989), SSN = Spinrad et al. (1979), J&L = Jewitt and Luu (1989); Schwassmann-Wachmann 1: CCB = adapted from Cochran et al. (1982), HCD = Hartmann et al. (1982); Arend-Rigaux: MAC = Millis et al. (1988); Halley: BSWWY = Belton et al. (1987), T&K = Thomas and Keller (1989), CHT = Cruikshank et al. (1985).

close approaches to the planets (with the exception of temporary librators which will be discussed in Sec. III) resulting in major changes in their orbital elements. Orbits which suffer such substantial and frequent random changes are referred to as chaotic and are not stable over the lifetime of the solar system. Jupiter-crossing objects are particularly short lived with a typical dynamical lifetime of 10^4 to 10^6 yr (Wetherill 1975). On the other hand, most main-belt asteroids are in stable orbits which do not approach that of any planet, or are trapped in librations (usually with Jupiter) which prevent them

from making close approaches to planets. Thus, chaotic motion might appear to be a fairly good discriminator of cometary vs asteroidal origin. However, Milani et al. (1989) showed that near-Earth asteroids can also evolve to chaotic orbits for some fraction of their dynamical histories, indistinguishable from that of typical short-period comets. Note that we do not include chaotic motion at orbital resonances, such as that found by Wisdom (1987), in our definition of chaotic orbits; that is a different form of chaos involving much longer time scales than for the short-period comets.

Meteor Stream Association. Until recently, most meteor showers were associated with active short-period comets. A number of Earth-crossing asteroids have now been identified as matching the orbits of other showers for which no parent comet is known (Drummond 1982; Olsson-Steel 1988). It may be that meteor showers can also be produced by debris from impacts on near-Earth asteroids, though large enough impacts to create sufficient debris for major meteor streams are not sufficiently probable within the dynamical lifetimes of the streams (Wetherill 1988). Also, in some cases, it has been shown that the distribution of meteor orbits in a particular shower are not consistent with an impact source (Hunt et al. 1985). On the other hand, the asteroid-meteor stream associations may in some cases be merely coincidental. We conclude that strong meteor-stream associations are highly suggestive of a cometary parent body, but not an absolute proof.

Dust Trails. The IRAS satellite discovered narrow dust trails composed of large grains in the orbits of several active short-period comets (Sykes et al. 1986). Over 100 trails were found in IRAS images, most of which could not be identified with any known periodic or long-period comets. However, none were identified with any known asteroids either. If a trail were to be identified with an asteroid, it would suggest a cometary origin, but for the moment, no such identifications exist.

Other Physical Parameters. Observers have attempted to determine various other physical parameters, such as thermal inertia, for both asteroids and comets. However, the number of objects for which this has been done is small and the error bars on the estimates are usually very large. Thus, there is presently little possibility of using these parameters as accurate discriminators. This situation may change in the future as improved observational and analytical techniques become available.

III. DYNAMICAL EVOLUTION OF COMETS TO NEAR-EARTH ASTEROIDS

Short-period comets and asteroids are fairly well separated dynamically, as seen in Fig. 1. Why then should one expect that comets would evolve

dynamically to asteroidal orbits? The answer lies in the existence of two dynamically short-lived families of objects: (1) interlopers, i.e., asteroids situated in the active cometary region C of the a,e plane as seen in Fig. 1; and (2) Earth-crossing and Earth-approaching asteroids, i.e., Apollo-Amor-Aten objects (AAAO; see the chapter by McFadden et al.) with typical dynamical lifetimes of only 30 to 100 Myr. We will discuss the dynamics of these two families in turn.

Most asteroids are protected from encountering Jupiter by aphelion distances much smaller than Jupiter's perihelion distance. In contrast, the short-period cometary population in Fig. 1 is characterized by clustering of aphelia near Jupiter's orbit. Orbital integrations for the short-period comets over several centuries (Carusi et al. 1985; Belyaev et al. 1986) indeed show that their dynamical evolution is governed by Jupiter's gravitational influence. Occasional cases of quasi-resonant behavior are seen for objects temporarily trapped near resonances with Jupiter, but on the whole, the evolutions appear chaotic and dominated by major perturbations at close Jupiter encounters.

Cometary orbital evolutions follow preferential paths in a,e,i space given by the Tisserand invariant:

$$T = a_j/a + 2\sqrt{(a/a_j)(1 - e^2)}\cos i \qquad (1)$$

where i is the inclination of the comet's orbit and a_j is Jupiter's semimajor axis. For the low inclinations typical of asteroids and short-period comets, Eq. (1) implies paths in the a,e plane as indicated by the $T = 3$ curve going from upper left to lower right in Fig. 1. Dynamical evolution is most rapid for $T \simeq 3$ since this implies low-velocity encounters with Jupiter (Carusi and Valsecchi 1987).

Although T is not conserved to high accuracy, either at cometary close encounters with Jupiter or in long-term asteroidal motion involving secular effects due to orbital eccentricities, it has been used as a discriminator between cometary and asteroidal orbits (Kresák 1979,1985). Comets typically have $T \leq 3$ while asteroids in general have $T \geq 3$. Most of those asteroids that approach or even overlap with the cometary domain (notably the Trojans and some Hildas along with the high-eccentricity Griqua group members) are characterized by regular motions where resonance librations prevent close approaches to Jupiter (Marsden 1970; Schubart 1979). Thus, they are dynamically distinct from comets.

However, in a few cases the asteroids also show the cometary property of chaotic orbital evolution. These appear to be real transitional cases with regard to the comet-asteroid classification: objects which are asteroidal in physical appearance and thus by convention classified as asteroids, but which are cometary in dynamical behavior. A number of these are included in Table I and an example is shown in Fig. 3. Most of the objects are recent discoveries, and new discoveries continue to be made at a high rate. These objects can be
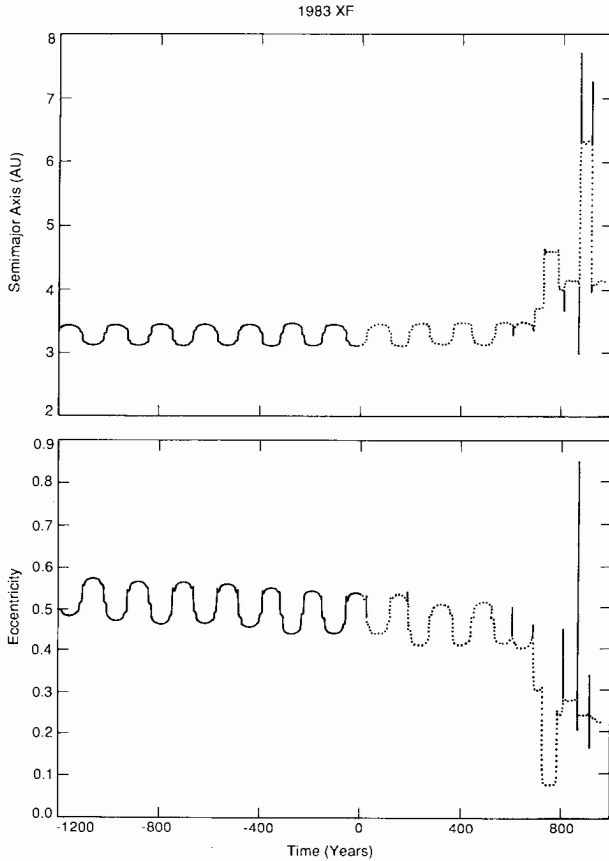
1983 XF

Fig. 3. Semimajor axis and eccentricity of asteroid 1983 XF according to an integration in a three-body model (Sun-Jupiter-asteroid) by Hahn and Rickman (1985). The object librates around the 2:1 resonance during most of the interval, but chaotic evolution appears at the end.

either extinct cometary nuclei or asteroids dynamically transferred from their usual stable orbits. Shoemaker and Wolfe (1982) have suggested that the second contribution is negligible due to arguments based on dynamical time scales. Thus, there is some reason to believe that the source of these objects is comets that have developed into dormant asteroidal objects.

Conversely, short-period comets can become trapped in resonant librations which keep them from making close approaches to Jupiter, greatly increasing their dynamical lifetimes (Marsden 1970). Two of the better known librators are comets Arend-Rigaux and Neujmin 1. Interestingly, these are also among the faintest short-period comets with very low activity levels and asteroidal appearances during a large fraction of their orbits (see Sec. IV). The

increased dynamical lifetime of the libration apparently affords the comets additional time to evolve to dormant-looking objects. In addition, the steady growth of nonvolatile crusts on the nucleus surfaces may be aided by the lack of drastic perihelion distance changes, a condition provided by the stable librations.

In general, the AAAO have orbits that do not approach that of Jupiter. The required influx of such objects to maintain a steady state population is 10^{-5} to 10^{-4} yr^{-1}, corresponding to a total number $\sim 10^3$ and a lifetime of 10 to 100 Myr (Wetherill 1979; Shoemaker et al. 1979). The loss mechanism yielding this lifetime is a collision or near-encounter with a terrestrial planet. The object will either be destroyed or, more likely, thrown into a Jupiter-crossing orbit. Jupiter will then eject it from the solar system with a mean lifetime of only 10^4 to 10^6 yr, or drastically increase its perihelion distance within an even shorter interval.

The near-Earth asteroids have a somewhat larger proportion of high-inclination objects than either of the two suspected parent populations, as shown in Fig. 4. The tail of their distribution appears compatible with a come-tary origin but also with one in the main asteroid belt, if the transfer mechanism from the main belt involves major increases of inclination or favors high-inclination objects.

Even though asteroidal dynamics appears basically regular, it is important to recognize that transfer of main-belt asteroids to near-Earth orbits can occur via chaotic routes. Chaotic zones have been shown to exist in phase space near mean motion resonances (Wisdom 1987; chapter by Froeschlé and Greenberg) where the orbital period of the asteroid is a small integer ratio of
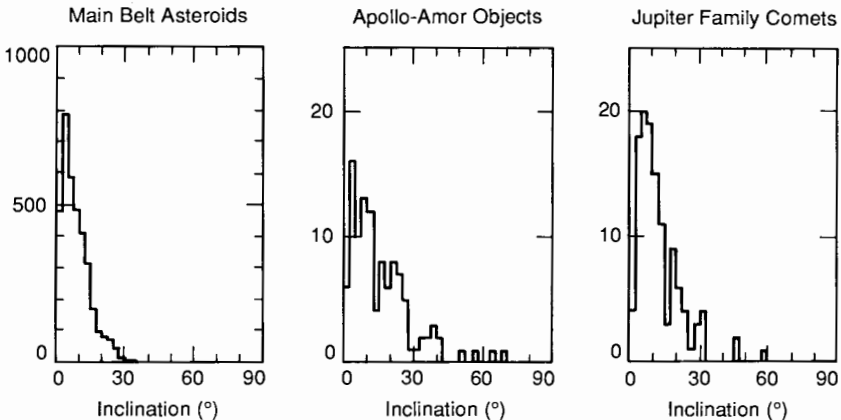
Fig. 4. Distributions of inclination i for the main-belt asteroids, the Apollo-Amor (near-Earth) asteroids and for the Jupiter family of short-period comets. Note the many high-inclination objects among the Apollo-Amor asteroids. No retrograde objects appear in any of the three groups.

the orbital period of Jupiter, i.e., $2:1$, $5:2$, $3:1$. If a main-belt asteroid enters one of the chaotic zones as the result of a collision, especially the large one at the $3:1$ resonance, it may reach an Earth-approaching orbit within a time scale of ~ 1 Myr (see the chapter by Greenberg et al.).

In addition, very large variations in orbital eccentricity might occur among asteroids in the inner belt due to secular resonances (see the chapter by Scholl et al.), perturbations due to secular terms in the motion of Jupiter. This appears to be another possible delivery mechanism of main-belt asteroids to Earth-approaching orbits. Interestingly, dynamical evolution of asteroids at the ν_6 resonance may favor high inclinations. Recent long-term orbital integrations for Earth-approaching asteroids by Hahn and Lagerkvist (1988) and Milani et al. (1989) have shown a few examples of the above-mentioned types of evolution.

Yet another means of supplying asteroids into high-eccentricity orbits is by exchange of angular momentum while conserving its normal component. If the semimajor axis of the asteroid is held constant according to Poisson's Law, then Eq. (1) permits evolutionary paths which oscillate between high-eccentricity/low-inclination and low-eccentricity/high-inclination end states. Particularly large amplitude librations of this type are sometimes found near mean motion resonances. Examples from Earth-approaching asteroids are 1983 VA (Hahn and Rickman 1985) and 2102 Tantalus (Hahn and Lagerkvist 1988).

According to Wetherill (1988) secular resonances and mean motion resonances can explain roughly 450 (56%) of the estimated 800 ± 300 Apollo and Aten objects, and about 1600 (80%) of the estimated 2000 Amor asteroids (these figures are for objects brighter than absolute visual magnitude 18.0, corresponding to diameters of 0.9 km for typical S-type asteroids, albedo $=$ 0.15, and 1.7 km for typical C-type asteroids, albedo $= 0.04$). Both secular resonances and mean motion resonances tend to favor asteroids inside 2.6 AU where the population of the main belt is dominated by differentiated asteroids (S, E and M types). Thus, most of the asteroids supplied to the zone of the terrestrial planets will be compositionally distinct from comets.

Wetherill also estimated that extinct comets could provide the remaining 40% of the near-Earth asteroids if one short-period comet evolved to an Encke type orbit every 5×10^4 yr, a not improbable figure. However, note that if the total number of AAAO is near the lower limit, then all the near-Earth asteroids can be supplied from the asteroid belt. On the other hand, if the total near-Earth asteroid population is near the upper limit, then an even larger cometary source is required.

For comets to evolve to Earth-crossing asteroids they must detach their aphelia from Jupiter's orbit. But that can not happen as a result of Jupiter perturbations. A different dynamical transfer mechanism must be invoked. One possibility is the gravitational "capture" of a comet due to an extremely close encounter with a terrestrial planet, whereby the aphelion distance can be

reduced sufficiently to decouple the comet from Jupiter's gravitational influence. A second mechanism involves consistent action by nongravitational forces (jetting of volatiles from the sunlit hemisphere of the cometary nucleus) during most of the active lifetime of the comet so that a net decrease of orbital energy occurs, leading to decoupling from Jupiter.

The cross section for dynamical capture due to close planetary encounters is similar to, though smaller than that yielding the dynamical lifetime of near-Earth asteroids. Thus, it seems reasonable to estimate a capture probability of $\sim 10^{-8}$ yr^{-1}. Knowledge of the steady-state number of extinct comets would then yield the cometary contribution to the AAAO, but unfortunately that number is difficult to estimate. Taking the number of active Mars-crossing Jupiter family comets as ~ 50 (Shoemaker and Wolfe 1982), Monte Carlo simulations (Froeschlé and Rickman 1980) indicate that $\sim 10^3$ extinct comets may exist in similar orbits, if all comets meet the fate of deactivation.

The problem is to estimate what fraction of the comets meet this fate rather than totally disintegrating into meteoroid streams. From the number and recent discovery rate of asteroids in Jupiter-crossing cometary orbits, it seems likely that a significant fraction of the comets develop into asteroidal bodies (Rickman 1985) but the statistics do not yet allow a more precise statement. Thus, tentatively, the cometary contribution to the generation of AAAO may be $\sim 10^{-6}$ to 10^{-5} yr^{-1}, approaching Wetherill's estimate, and significant in comparison with the required total influx rate, as quoted above.

Is there a further contribution to the number of near-Earth objects due to nongravitational captures? With a net gravitational capture rate of one new short-period comet per century into the Jupiter family (Fernández 1985) the nongravitational contribution would be significant if at least one comet out of 10^4 experiences such an evolution. The largest values of the nongravitational acceleration found among Jupiter-family comets (Marsden 1985) correspond to perturbations of the orbital period by ~ 0.1 day per orbit. Thus, $\sim 2 \times 10^3$ revolutions would be necessary with the nongravitational acceleration consistently negative in order to reduce the aphelion distance of a short-period comet by 0.5 AU — a minimum requirement for decoupling from Jupiter. However, nongravitational changes in orbital period are sometimes found to change from positive to negative values (and vice versa) for the same comet, apparently associated with a shift in the time of maximum brightness in the comet's lightcurve (Yeomans 1988), further lengthening the dynamical evolution.

Thus, a random walk picture may be more relevant, resulting in $\sim 10^5$ revolutions required to achieve the necessary aphelion decrease. Comparing this number with an active physical lifetime of ~ 500 revolutions (Kresák 1985; Fernández 1985), the likelihood for nongravitational capture of any particular short-period comet seems fairly small, probably $<< 10^{-4}$. On the other hand, Hadjuk (1985) and Weissman (1987a) have each argued for a

Halley age in excess of 2 x 10³ orbits, so active physical lifetimes of 10⁴ revolutions or more may not be unreasonable. In that case, some significant contribution from nongravitational captures may be feasible.

An important difference between the gravitational and nongravitational transfer mechanisms for bringing comets into near-Earth orbits is that the latter can only involve active comets while the former involves dormant and/or extinct ones as well. With an active lifetime $\sim 10^4$ yr (for $P < 10$ yr), it should be very unlikely at any moment to see a captured and still active object. Thus, the existence of comet Encke appears enigmatic. Possibly it was once an extinct Jupiter family comet that was decoupled from Jupiter long ago by an encounter with a terrestrial planet and more recently has been re-activated by a meteoroid impact (see Sec. IV). Such a scenario might also explain the abundance of asteroid-meteor stream associations, as described in Sec. II. Again, if the active physical lifetimes are substantially longer, the existence of comet Encke becomes far less problematical. Interestingly, three Earth-crossing asteroids, 1566 Icarus, 1685 Toro and 1862 Apollo, were cited for possible nongravitational effects in their orbital motion by Ziolkowski (1983), possibly indicative of cometary activity. However, these effects have not been substantiated under further investigation (Marsden 1985).

As a preliminary conclusion, in spite of the serious uncertainties in-volved, it seems that extinct comets can provide a significant contribution to
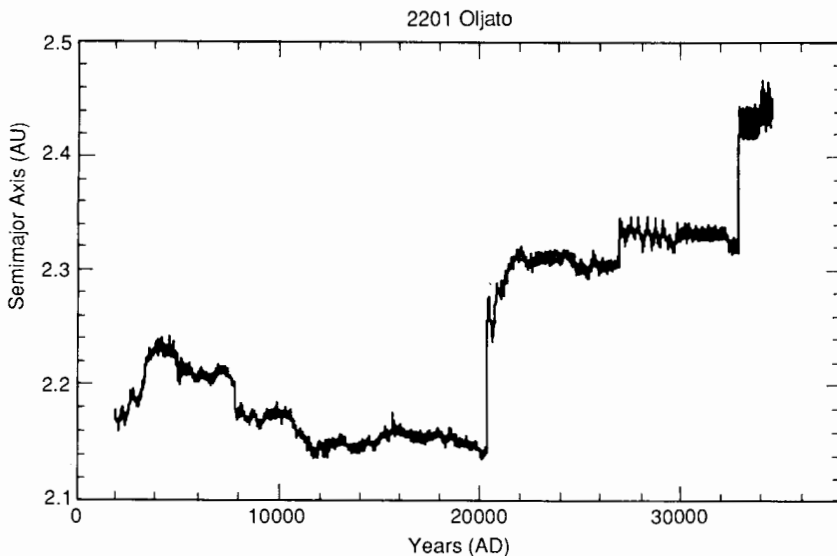
Fig. 5. Semimajor axis of asteroid 2201 Oljato according to an integration using a Venus to Neptune planetary system, by Hahn and Lagerkvist (1988). The evolution is chaotic due to many close encounters with Earth and Venus, and at the end of the interval, the asteroid can also make close approaches to Jupiter.

the Apollo-Amor-Aten population, notably by means of gravitational captures by the terrestrial planets. Such single-encounter captures are well known from cometary dynamics to give very little bias against high-inclination orbits (Newton 1893; Everhart 1969) and thus there appears to be no conflict with the relatively high inclinations of the Earth-crossing population. Recently captured objects would have a chaotic orbital evolution over $\sim 10^4$ yr, though near-Earth asteroids can also undergo such chaotic motions occasionally. It is likely significant that one of the prime candidates for an Apollo asteroid of cometary origin, 2201 Oljato (see Sec. VI), is dynamically the most chaotic one among the cases studied by Hahn and Lagerkvist (1988; see Fig. 5) and the archetype of the most chaotic dynamical class of AAAO defined by Milani et al. (1989).

IV. PHYSICAL EVOLUTION OF COMETS INTO ASTEROIDS

For a comet to evolve to appear physically as an asteroid, it must lose its ability to generate a detectable coma. This can occur through one of two possible mechanisms: (1) either the comet loses most or all of its volatiles so that there is simply little left to contribute to the generation of a coma, or (2) the comet nucleus surface is covered by a thick, nonvolatile lag deposit which effectively prevents the penetration of solar heating to frozen volatiles at depth, and also hinders the escape of those volatiles.

Loss of all volatiles is a fairly slowly acting mechanism because of the large amount of energy expended in sublimating water ice, the principal component of the cometary nucleus. Weissman (1980) determined a sublimation lifetime of ~ 600 perihelion passages for a 1 km radius nucleus with density of 0.6 g cm^{-3}, zero albedo, and with a perihelion distance of 1.0 AU. Lifetimes of larger nuclei would be proportionally longer; less dense nuclei would be proportionally shorter. Sublimation lifetimes would be greatly lengthened also by the formation of an insulating nonvolatile crust on the nucleus surface, since the crust reduces the sublimation rate of buried ice layers.

Comets may indeed be porous, loosely knit structures as suggested by the fractal model (Donn and Hughes 1985) or the primordial rubble pile model (Weissman 1986b), and indicated by the low-density estimates for Halley of 0.2 g cm^{-3} (Rickman 1986) and 0.6 g cm^{-3} (Sagdeev et al. 1987). In that case, it may be relatively easy for evolved gases to escape, leaving a low-density "fairy castle" structure of unpacked, nonvolatile grains. On the other hand, such a structure is a very effective insulator and it is difficult to see how solar energy would penetrate inward once the initial near-surface ices had sublimated. Gas transport of heat from inward diffusing gases may be a way around this difficulty. However, it is likely that this process would soon become self-defeating as the devolatilized outer layer thickened and heat conduction inward decreased. The icy core of a devolatilized cometary nucleus

would only warm very slowly, and the result may be a level of sublimation from the core that is too small to be detected by Earth-based observations. Thus, a comet may evolve to an asteroidal appearance while still retaining a volatile rich core, and may continue to outgas slowly for thousands of orbits or even more.

The above situation thus becomes essentially the same as the development of a nonvolatile insulating crust on the nucleus surface. Modeling efforts have shown that for typical short-period comets a residual dust layer only a few centimeters thick would develop over several orbits and quickly reduce sublimation rates sharply over that from an exposed ice surface (Brin and Mendis 1979; Fanale and Salvail 1984; Horanyi et al. 1984). Weissman (1979) showed that the lack of observed long-period comets with perihelia $<$ 0.4 AU and semimajor axes $\lesssim$ 350 AU could probably be explained by formation of nonvolatile crusts after an average of $\sim$ 20 perihelion passages. Fernández (1985) also demonstrated the need for a de-activating mechanism for comets.

Despite the fairly detailed and complex models which have been developed for cometary crust formation, it is still unclear how a crust actually forms. Is it simply a lag deposit of unbonded large particles, too heavy to be entrained in the evolving gas? Or does the large fraction of organics revealed by the Halley missions play a role, acting as a cometary glue to cement nonvolatile grains together? Is the crust porous, allowing evolved gases to diffuse through it, or do the organic glue and finer grains eventually seal the pores, creating a fairly impervious, high-strength crust? As gas pressure builds up beneath the crust, does it fail gradually or catastrophically, on small scales or large? Does a crust failure relieve the pressure from only the layers just below it, or is the nucleus sufficiently porous that an area much larger than the dimension of the surface failure will be relieved?

The Halley spacecraft encounters in 1986 did little to dispel these questions. Virtually all models of Halley had predicted that the comet would be so active near perihelion that any crust on its surface would be blown away. In fact, the Vega and Giotto images (Sagdeev et al. 1986a,b; Keller et al. 1986) showed a surface that was largely covered ($\sim$ 70% of the total area) by an inactive crust. By comparing expected ice sublimation rates from physical modeling with observed gas production rates, Weissman (1987b) showed that the average fraction of sublimating surface area was about 30% of the sunlit nucleus surface, in agreement with the results above, though this factor varied from a low of about 20% pre-perihelion to a physically unrealistic high (based on current concepts of cometary nuclei) of over 100% as the comet moved outward from the Sun beyond 2 AU. It was not possible to determine from the Giotto images if the apparently inactive crust might be participating in the gas production from the nucleus, particularly if only gas and not dust was escaping through the crust layer. However, the contribution is likely small, if it exists at all.

Nevertheless, the Halley images clearly demonstrated that crusts do form on cometary nuclei, even highly active ones. One possibility is that the initial crust forms as a result of irradiation of cometary nuclei by galactic cosmic rays during their long residence in the Oort cloud (Johnson et al. 1986). Cosmic rays are expected to polymerize all of the carbon within one to several meters of the nucleus surface (assuming a density of 1.0 g cm^{-3}; the depth of polymerization goes inversely as the density), creating complex hydrocarbons as well as free radicals, and sputtering away some fraction of the near-surface volatiles. Exactly how this highly processed surface layer behaves when the comet first makes its approach close to the Sun is a matter of some speculation. Prialnik and Bar-Nun (1987,1988) showed that the slow heating of an amorphous ice nucleus (presumably formed at low temperature, < 100 K) would cause a transition to crystalline ice at about 5 AU inbound. Since this is an exothermic reaction, an additional heat pulse would push inward converting a layer 10 to 20 m thick to crystalline ice (Prialnik and Bar-Nun showed that a chain reaction converting the entire nucleus to crystalline ice does not occur; the pulse is eventually dissipated as it reaches colder ice layers at greater depths and by the warming of nonvolatile dust mixed with the ice). The amorphous to crystalline ice transition may supply sufficient energy to blow off pieces of the primitive crust, resulting in the anomalously bright behavior at large solar distance often displayed by dynamically "new" long-period comets.

There are thus, two possible scenarios for crust formation. The comet may retain some or all of its original crust, and this serves as the foundation for additional crust growth. Or, the comet blows away all of its primitive crust, and then grows a new lag deposit of heavy grains, possibly glued together by complex organics.

The subsequent evolution is also a topic of considerable conjecture. Comets may eventually cover themselves over entirely with nonvolatile crusts which thicken asymptotically to some limit, and thus become dormant, asteroidal appearing objects. Or as gas pressure builds up within the core after many orbits, the crust may catastrophically fail and the comet will return to an active state (Kresák 1987), a process which may repeat many times before the comet disintegrates or becomes completely dormant. However, estimates of the expected thermal stresses on nucleus surfaces (Kührt 1984; Green 1986) indicate that any crust will repeatedly fracture due to the substantial thermal gradients across it. Dormant cometary nuclei might also be re-activated by sporadic meteoroid impacts blasting craters through the crust. Thus, there is some question as to whether a cometary nucleus can ever evolve to a completely dormant state at small to moderate perihelion distances, unless it loses all its volatiles.

During this complex physical evolution, the comet's orbit will also be evolving dynamically. For it to become a source of meteorites, it must evolve into an Earth-crossing orbit, though it may already be an Earth crosser. Typ-

ically, this evolution will also involve a decrease in the semimajor axis of the comet's orbit.

Herman and Weissman (1987) showed that the internal temperatures of cometary nuclei could be approximated by the "fast rotator" temperature for a given cometary orbit, to within ± 10%, by

$$T_i = 280 \ (1 - A)^{1/4} \ a^{-1/2} \ \varepsilon^{-1/4} \tag{2}$$

where T_i is the internal temperature in Kelvin, A is the nucleus surface Bond albedo, a is the semimajor axis of the comet's orbit in AU, and ε is the surface emissivity. Given the low expected thermal conductiviti~s of cometary surfaces, the heating to some equilibrium internal temperature may take hundreds or even thousands of orbits. This is longer than the typical time between significant changes in the comet's orbit due to close encounters with Jupiter or other planets. As a result, the internal temperature profile of the nucleus will be a complex function of its physical heating and its dynamical evolution.

Nevertheless, as the dormant nucleus' orbit evolves inward towards the Sun, it will continue to warm slowly, sublimating the ices within. The cometary crust may be sufficiently porous to vent slowly the evolved gases, allowing the nucleus to retain an asteroidal appearance to distant terrestrial observers; repeated cracking by thermal stresses may keep the crust from ever retaining significant gas pressure. In this fashion the nucleus may eventually sublimate away all of its volatile ices. Such an object might be recognized by its low density, if it were possible to measure accurately its mass and physical dimensions. On the other hand, if the crust is not porous, gas pressure will build up beneath the crust and it will eventually fail catastrophically, resulting in the dormant-active cycles described above.

What then will the final evolved object look like? It will likely have a dark surface of organics and refractory grains, similar perhaps to C- and D-type asteroids. It may have a fairly low density, some fraction of 1.0 g cm^{-3}, because of its porous structure, or slow compaction of the structure over time may allow it to approach the density of carbonaceous-type meteorites, 2.2 g cm^{-3}, though this seems unlikely in the comet's weak gravity field. The object may retain its original, possibly slow, cometary rotation rate, or it may have been spun up by collisions or by the compaction process suggested above.

The surface of an extinct comet may be far less cratered than a typical small asteroid since a comet spends most of its history in a low collision environment, the Oort cloud, versus the near-Earth asteroids which are almost certain to be collisional fragments. Also, craters on cometary surfaces may simply sublimate away. However,the only solar system objects of comparable size to cometary nuclei (other than Halley) that have been imaged in detail are Phobos and Deimos, two small satellites that may or may not provide repre-

sentative examples of asteroidal surfaces. Thus, any comparison of comet and asteroid surface morphologies is moot without additional data.

V. PHYSICAL OBSERVATIONS OF COMETARY NUCLEI

This section addresses the physical properties of cometary nuclei as observed, preparatory to a comparison with Earth-approaching asteroids. The observations have been reviewed in more detail by A'Hearn (1988) except for several very recent results. We concentrate on those nuclei which have been studied with several different techniques.

One must be careful of the possibly large selection effects in generalizing from the very few observations of cometary nuclei. Nevertheless, general properties that seem to apply to all nuclei of short-period comets include: very low visible albedos, geometric albedos of 0.02 to 0.05 being typical; elongated shapes, with axial ratios in excess of 1.5 apparently being common; moderately slow rotation periods, typically $\sim$ 10 hr or longer; and a low gas production per unit surface area, compared with that expected for exposed ice in sublimation equilibrium. Although there is a wide range, a "typical" effective diameter would seem to be $\sim$ 10 km. Colors of nuclei, like the diameters, appear to vary considerably. Table II presents values of these parameters for a number of comets, along with references to the original observations.

Visible albedos are directly measured only for short-period comets Neujmin 1, Arend-Rigaux and Tempel 2 (from simultaneous photometry and radiometry), Schwassmann-Wachmann 1 (photometry and radiometry but not simultaneous), and Halley (photometry of the spatially resolved nucleus). All five nuclei are clearly dark and the four best-determined values are among the darkest values in the solar system. On the other hand, two long-period comets, Tago-Sato-Kosaka 1969 IX and Bennett 1970 II, were found by Delsemme and Rud (1973) to have high albedos, $\sim$ 0.6; Delsemme and Rud compared the reflected brightness at large heliocentric distance with the total outgassing at small heliocentric distance. It is not clear whether the difference in derived albedos is due to a real evolutionary difference between long- and short-period comets or to a flaw in either the data or the assumptions of Delsemme and Rud, e.g., significant contamination by coma in the nucleus observations or outgassing from only a fraction of the surface. Given the fractional outgassing observed from all short-period comets, it is plausible that outgassing from only a fraction of the surface is also true for long-period comets; this invalidates Delsemme and Rud's assumptions and allows that the albedos of long-period comets are also quite low.

The spectral reflectance of cometary nuclei, i.e., the variation of albedo with wavelength, is very poorly known because the observations are very difficult. This is due to the difficulty of separating out the effect of dust in the coma and also of weak emission bands from gas in the coma. Overall, the cometary nuclei are reddish but there also appear to be significant differences

TABLE II
Well Studied Cometary Nuclei

Comet	D_{eff}[a] (km)	Axial Ratio	p_v	Color	P_{rot} (hr)	$Q(r)$[d] (s^{-1})	r (AU)	Active Fraction - %[e] Isothermal	Active Fraction - %[e] Pole-on
Halley (refs)	12.0[b] (1,2,3)	2.0[b] (1,2,3)	0.04 (4,5)	neutral red (6,25)	53?, 177? (7)	6×10^{29}	0.8	30.0[f]	7.0[f]
Arend-Rigaux (refs)	10.4 (8,9,10,11)	>1.6	0.03 (8,9)	neutral red (8,13)	13.5 (8,12,13)	2×10^{26} (8)	1.58	0.08	0.016
Neujmin 1 (refs)	20.8 (14)	>1.65 (12,13)	0.02 (14)	very red (14,15)	12.7 (12,13)	2×10^{26} (14)	1.68	0.1	0.023
Schwassmann-Wachmann 1 (refs)	80. (16)	small ?	0.13 (16)	red in near IR (26)					
Tempel 2 (refs)	11.2 (23)	1.9 (13,22,23)	0.02 (23)	very red (13,17)	8.9 (13,22,23)	2×10^{27} (24)	1.71	0.9	0.13
Encke (refs)	<4.4, 2.? (18,19)	>2.0 ?[c] (20)			22.4 ?[c] (20)	6×10^{28}	0.76	17.0	3.7
IRAS-Araki-Alcock	8.0 ? (20,21)					2×10^{28}	1.03	3.0	0.7

[a] $D_{eff} = 2\sqrt{ab}$ where a and b are projected semi-axes at maximum light.

[b] Actual Halley nucleus dimensions: $16 \times 8 \times 7$ km.

[c] See also discussion by Sekanina (1988).

[d] Production of H_2O based on Festou's (1981) vectorial model using observational data given in the references.

[e] Fraction of surface which must be "active" for vaporization of water in equilibrium to provide the observed gas assuming 5% albedo and either (a) incident heat distributed uniformly around an isothermal nucleus, or (b) incident heat in local equilibrium for a nucleus either pole-on to the Sun, or rotating very slowly.

[f] Directly observed value from Giotto (Keller et al. 1986): 10 to 15% of total surface or 20 to 30% of sunlit hemisphere.

Table II references: 1. Möhlmann et al. 1986; 2. Wilhelm et al. 1986; 3. Sagdeev et al. 1986a; 4. Sagdeev et al. 1986b; 5. Delamere et al. 1986; 6. Belton et al. 1987; 7. Sekanina 1988; 8. Millis et al. 1988; 9. Veeder et al. 1987; 10. Brooke & Knacke 1986; 11. Tokunaga & Hanner 1985; 12. Wisniewski et al. 1986; 13. Jewitt & Meech 1988; 14. Campins et al. 1987; 15. Hartmann et al. 1987; 16. Cruikshank & Brown 1983; 17. Spinrad et al. 1979; 18. Campins 1988; 19. Kamoun et al. 1982; 20. Goldstein et al. 1984; 21. Hanner et al. 1985; 22. Wisniewski 1988; 23. A'Hearn et al. 1988a and Campins et al. 1988; 24. A'Hearn et al. 1988b; 25. Thomas & Keller 1989; 26. Hartmann et al. 1982.

in color among the comets. Spectral reflectances in the visible and near infrared for five cometary nuclei are shown in Fig. 2, where all data are normalized to unity at 0.56 μm. Broadband infrared colors have been converted to reflectances using the calibration of solar colors by Campins et al. (1985); visual colors have been converted using a variety of sources. Although the data are from several sources and were obtained under a variety of circumstances, most of the data are thought to refer to the nuclei. This is particularly important in the light of recent studies of Tempel 2 which show that the color of the grains in the coma is very different from the color of the nucleus (Jewitt and Luu 1989; A'Hearn et al. 1989). The contribution by coma to the observations of Halley by Cruikshank et al. (1985) is unclear. Although the data were obtained while the comet was still very far from the Sun, they were obtained after the first signs of the onset of activity. Further details can be found in the original references.

One sees in Fig. 2 that the spectral reflectances vary markedly from one nucleus to another. In particular, the nuclei of Neujmin 1 and Tempel 2 differ dramatically in overall color from the other three nuclei. Furthermore, comparison with the spectral reflectance of near-Earth asteroids (Fig. 6; see the chapter by McFadden et al.) shows that the cometary data do not match well any single asteroid type. There are even features in many of the cometary spectra which do not appear in any asteroid spectra. For example, observations of Schwassmann-Wachmann 1 by Cochran et al. (1982) and of Tempel 2 both by Spinrad et al. (1979) and by A'Hearn et al. (1989) suggest that the reflectance increases shortward of 0.4 μm. No asteroid, with the exception of one observation of 2201 Oljato (an extinct cometary candidate) by McFadden et al. (1984a), shows this effect; in fact most asteroid types exhibit sharply decreasing reflectance shortward of 0.4 μm.

As with albedo, diameters have been directly measured for the same five comets: Schwassmann-Wachmann 1, Neujmin 1, Arend-Rigaux, Tempel 2 and Halley. If we assume that all cometary nuclei are as dark as these five, then infrared radiometry alone is sufficient to determine the size of any nucleus that can be separated from its associated coma. Comets Encke and IRAS-Araki-Alcock were both detected by radar which provides an estimate of the cross section times the radar albedo, though radar data of some comets seem to be contaminated by clouds of debris around the nuclei (Campbell et al. 1989). Thus, radar data alone is not enough to estimate a nucleus diameter. However, for both Encke and IRAS-Araki-Alcock there is independent infrared radiometry which yields consistent size estimates, although in the case of Encke the radiometric result is only an upper limit. These diameters are thus less well determined than the previously cited ones.

Axial ratios of cometary nuclei are known primarily from the amplitude of photometric variations except for Halley where they are known by direct imaging (see Table II). Since the photometric variation depends on the detailed geometry between the rotation axis, the body axes, and the plane of the
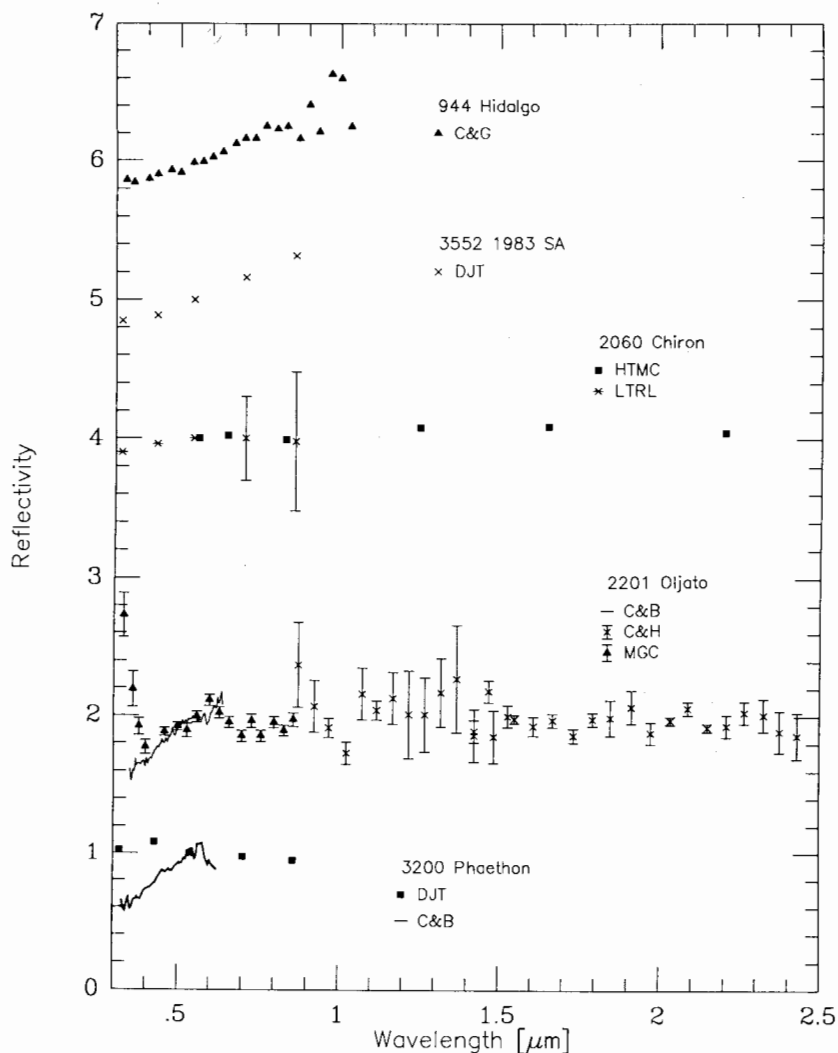
Fig. 6. Spectral reflectances of some comet-like asteroids; the data are normalized to unity at 0.56 μm. Data for Oljato, Chiron, 1983 SA and Hidalgo have been offset vertically by values of 1.0, 3.0, 4.0 and 5.0, respectively. References for the data: 944 Hidalgo: C&G = Chapman and Gaffey (1979); 3552 1983 SA: DJT = Tholen (unpublished); 2060 Chiron: LTRL = Lebofsky et al. (1984), HTMC = Hartmann et al. (1989); 2201 Oljato: MGM = McFadden et al. (1984*b*), C&B = Cochran and Barker (unpublished), C&H = Cruikshank and Hartmann (unpublished); 3200 Phaethon, C&B = Cochran and Barker (1984), DJT = Tholen (unpublished).

sky, these results are actually projected axial ratios and thus are lower limits to the true axial ratio. If part of the variability is due to outgassing from an active area rotating in and out of sunlight, the axial ratio could be overestimated but we believe that the results given in Table II, with the possible exception of that for Comet Encke, are reasonably free of these effects. The conclusion from an examination of those numbers is that cometary nuclei are highly elongated, more so than near-Earth asteroids.

Rotational periods have been determined for many comets in a variety of ways. Early determinations were reviewed by Sekanina (1981) and Whipple (1982), and were usually based on measurement of haloes and jets in the coma. Newer measurements have tended to rely on more direct photometric determinations (see references in Table II). Amazingly, despite more study than for any other comet, it is still not certain whether the rotation period of the Halley nucleus is 2.2 or 7.4 days (Sekanina 1988). This typifies the disagreement among different methods for determining rotation periods and even among different investigators using the same method. It also emphasizes the need for a cometary rendezvous mission in the near future to relate observed cometary phenomena to the actual rotation of the nucleus.

Photometric determinations of rotation periods are included in Table II. In all cases, except that of Halley, we have adopted a period corresponding to a double-peaked lightcurve, even where the original authors may have argued for one or four peaks in the lightcurve. The periods tend to be > 10 hr, with some periods much longer than that. The distribution is significantly different from the main-belt and near-Earth asteroids (see the chapters by Binzel et al. and by McFadden et al.).

Finally, we address the question of the gas production rate of the nucleus and a comparison with the values expected from equilibrium sublimation of ices. The abundance of OH has been measured in the comae of most of the comets in Table II. A uniform application of Festou's (1981) vectorial model yields production rates of H_2O at the times of observation which can be compared with the expected water ice sublimation.

Since the sublimation rate depends critically on the detailed geometry of the active area, we consider two simple, extreme examples. In the first case, we consider an isothermal (fast rotator) nucleus with albedo of 0.05 which minimizes the gas production per unit area. In the second case, we consider the opposite extreme, sublimation from the subsolar point on the nucleus of a comet which is not rotating, or slowly rotating and pole-on to the Sun. Dividing the observed H_2O production rate by the equilibrium sublimation rate yields the effective active area. Dividing this by the surface area of the appropriate spheroid (assumed to be prolate) yields the fraction of the surface which must be active, as given in Table II. These numbers are all uncertain by a factor of two or more due to long- and short-term temporal variations and model dependence. The value for Halley refers to the time of the Giotto encounter and it is seen that the range of active fractions includes the result

directly observed by Giotto that 10 to 15% of the total surface (20 to 30% of the sunlit surface) was active at that time. More detailed thermal models of Halley (Weissman 1987b) show that the simple calculations here yield an appropriate range of values for the active fraction. All other nuclei exhibit far lower rates of gas production per unit area. It seems clear then, that nearly all the nuclei that have been studied intensively must be covered with a relatively inert crust over much of their surface. Only Encke appears to have an active fraction comparable to that of Halley.

It is a reasonable inference from the observations, although clearly not yet shown conclusively, that crusts gradually cover more and more of the surface, rather than building up uniformly in thickness, until they choke off all active areas. Eventually only gases can leak through the crust. In this picture, Neujmin 1 which shows no detectable dust but significant gas, is probably entirely covered with a rigid though porous crust, while Arend-Rigaux, which still exhibits significant dust in its coma together with the gas, must still have some minute active areas. All of the other comets in our sample still have small but significant active surface fractions. It is the inert aspects of the nuclei, however, which must be compared with asteroids.

VI. PHYSICAL PROPERTIES OF COMET-LIKE ASTEROIDS

In Sec. II, we listed a variety of both physical and dynamical criteria which may be used to discriminate comets from asteroids. We have compiled a list of asteroids, given in Table III, which have been cited in the past as possibly cometary based on these criteria. In this section, we discuss recent physical observations of these asteroids and provide some judgment as to whether they are, in fact, likely cometary candidates.

A primary criterion for putting asteroids in Table III is chaotic motion with close approaches to Jupiter (or in the case of Chiron, to Saturn), making perturbation from cometary orbits statistically probable (Hahn and Rickman 1985; Hahn and Lagerkvist 1988). In addition to Chiron, this category includes asteroids 3552 1983 SA, 1983 XF and 1984 BC. Also, asteroids with orbits similar to existing short-period comets such as 944 Hidalgo and 2212 Hephaistos are included in this category.

A second important criterion for inclusion in Table III is strong association with meteor showers. This category includes asteroids 1685 Toro, 2101 Adonis, 2201 Oljato, 2212 Hephaistos (Drummond 1982) and 3200 Phaethon. Less certain associations have been made for 1566 Icarus, 1620 Geographos, 1862 Apollo, 1917 Cuyo, 2062 Aten, 1982 TA, 1984 KB, 1986 JK and 5025 P-L (see references in Table III). We give this latter group somewhat less weight because the match between their orbits and the known meteor showers is not as good.

Another, less definitive criterion for inclusion as a possible cometary candidate is a Tisserand invariant < 3 (as discussed in Sec. III) and lack of a

TABLE III
Possible Comet-like Asteroids

Name	Diameter (km)	p_v	Taxonomy	P_{rot} (hr)	Remarks	References
Strong Cometary Candidates:						
944 Hidalgo			D	10.06	Jupiter-crosser, orbit similar to comet P/Wild 1	1,2,3,4,5
2060 Chiron	198.0	.10	B		outer solar system cometary orbit	6,7,8,35,36
2101 Adonis					meteor-shower association, anomalous radar reflection	5,11,12,13,24
2201 Oljato	1.4	.42		24. ?	meteor-shower association, chaotic orbit	9,10,11,12,13,28
2212 Hephaistos			SG		meteor shower association, orbit similar to Comet P/Encke	4,11,12,13,14
3200 Phaethon	6.9	.08	F		parent body of Geminid meteor shower	9,27,28,29
3552 1983 SA	18.7	.02	D		chaotic orbit	9,15
1983 XF					chaotic orbit	15
1984 BC			D		chaotic orbit	15
Possible Cometary Candidates:						
1566 Icarus	0.9	.42		2.27	weak meteor shower association[a] large e, low q	3,9,12,13,16,17
1580 Betulia	7.4	.03	C	6.13	Tisserand invariant = 3.07, high inclination	5,18,19
1620 Geographos	2.0	.19	S	5.22	weak meteor-shower association	9,11,21
1685 Toro	5.2	.14	S	10.20	weak meteor-shower association[a]	9,11,14,23,32
1862 Apollo	1.5	.21	Q	3.06	weak meteor-shower association[a]	11,20,21,22,23,24

Name	D	albedo	Type		Notes	Refs
1866 Sisyphus	8.2	.18		2.4	ω-librator, $T = 3.51$	5,9,25,28
1917 Cuyo					weak meteor-shower association, high inclination	17
1981 Midas	0.9	.20	S		Tisserand invariant = 3.60 high inclination	5
2062 Aten					weak meteor-shower association, high inclination	11,33,34
1982 TA	1.7	.33			weak meteor shower association	9,13
1982 YA					$T = 2.38$, near 5:3 resonance	15
1983 VA					possible chaotic orbit	15
1984 KB	1.4	.16	S		weak meteor-shower association	13,30
1986 JK			C		weak meteor-shower association	13,31
1986 RA			C		dynamically protected	26,28
Hermes					weak meteor-shower association, lost	
1973 NA					lost[b]	
1974 MA					lost[b]	
1979 VA			CF	3.56	dynamically protected	10,15,21
5025 P-L					Jupiter-crosser, lost[b], weak meteor-shower association	13

[a]Suggested nongravitational motion by Ziolkowski (1983) but refuted by Marsden (1985).

[b]Poorly determined orbit, not worth considering further at this time.

Table III References: 1. Degewij and van Houten 1979; 2. Tedesco 1979; 3. Marsden 1970; 4. Kresák 1979; 5. Kresák 1977; 6. Kowal 1979; 7. Oikawa and Everhart 1979; 8. Scholl 1979; 9. Veeder et al. 1989; 10. Harris and Young 1983; 11. Drummond 1982; 12. Babadzhanov and Obrubov 1983; 13. Olsson-Steel 1988; 14. Tholen 1988; 15. Hahn and Rickman 1985; 16. Veverka and Liller 1969 and Miner and Young 1969; 17. Sekanina 1970; 18. Lebofsky et al. 1978; 19. Tedesco et al. 1978; 20. Lebofsky et al. 1981; 21. Tholen 1984b; 22. Hahn 1983; 23. Ziolkowski 1983; 24. Hoffmeister 1948 in Marsden 1970; 25. Hahn and Harris, personal communication; 26. Hahn and Lagerkvist 1988; 27. Veeder et al. 1984; 28. Tholen 1985; 29. Whipple 1983; 30. Bell et al. 1988; 31. Wisniewski 1987; 32. Dunlap et al. 1973; 33. Gradie 1976 and Morrison et al. 1976; 34. Cruikshank and Jones 1977; 35. Hartmann et al. 1989; 36. Lebofsky et al. 1984.

dynamical protection mechanism against close approaches to Jupiter (Kresák 1979; Hahn and Rickman 1985). Asteroids matching these criteria include 1580 Betulia (Marsden 1971; Kresák 1977), 1982 YA, 1983 VA and possibly 1983 LC (Hahn and Rickman 1985).

Hartmann et al. (1987) compiled a list of possible comet-like asteroids which included some asteroids dynamically protected from close encounters with Jupiter and with a Tisserand invariant ≃ 3. These are mostly outer-belt asteroids in mean motion resonances with Jupiter, and were rejected as cometary candidates by Kresák (1979). We have not included them in Table III.

We next review the physical properties of the candidate asteroids to the extent that they are known. The order of listing is by minor planet number or designation, within each of the two major groupings, Strong Candidates and Possible Candidates.

Strong Candidates

944 Hidalgo. This asteroid was observed for cometary emission features (Soderblom and Harlan 1976) with negative results, though at a heliocentric distance of 2.4 AU where many short-period comets are relatively inactive. Using broadband filters during its last favorable observing period, it was shown to have color variations across its surface of 0.1 magnitude in U-V (Degewij et al. 1979). Spectral reflectance measurements of Hidalgo indicate that it is similar to outer-belt asteroids classified as type D, as shown in Fig. 6 (Chapman and Gaffey 1979). The rotation period of Hidalgo is 10.06 hr (Tedesco 1979) and based on its lightcurve, it is expected to have an elongated shape. Speculation that nongravitational effects might be present in the orbital motion of Hidalgo as suggested by Marsden (1970) has not been supported by further analysis using a more accurate mass of Saturn, as Marsden himself originally suspected. Based on the reflectance spectrum of Hidalgo, we guess that its albedo is similar to D-type asteroids (see the chapter by French et al.), ~ 0.03, consistent with our current knowledge of cometary nuclei. This yields an estimated diameter of 51 km, quite large by typical cometary standards. The rotation rate of Hidalgo is similar to that for comets such as Tempel 2 and Neujmin 1, but there is no detailed knowledge of the axial ratios describing the shape of the asteroid. There is currently nothing about the physical properties of Hidalgo to indicate that it is any different from outer mainbelt asteroids. However, its orbit is similar to that of comet Wild 1 (Kresák 1977) and it makes moderately close approaches to Jupiter (Marsden 1970). Its next perihelion passage is in 1990 and additional physical studies should be made at that time.

2060 Chiron. Visible and infrared broadband photometry of Chiron, shown in Fig. 6 (Lebofsky et al. 1984; Hartmann et al. 1989), suggest that this object is spectrally neutral with no evidence of strong water absorption bands. Recent observations (Hartmann et al. 1989; chapter by French et al.) show

that the brightness of Chiron is variable and is increasing. These preliminary results are intriguing in that they may constitute the first physical evidence that this object is indeed cometary. Additionally, numerical integrations of Chiron's orbit indicate that it is evolving inward from the Uranus-Neptune zone (Scholl 1979). If Chiron is dark like other outer solar system asteroids, then it is quite large, ~ 200 km diameter, certainly near the upper end of the expected size distribution for cometary nuclei.

2101 Adonis. This asteroid was observable in the summer of 1984 mostly from the southern hemisphere. Drummond (1982) found a strong association with several of the Sagittarids meteor streams. Radar observations of Adonis acquired by Ostro et al. (1985) gave a polarization ratio of 1.0 ± 0.2, highly unusual and close to values obtained for Callisto, the outermost Galilean satellite of Jupiter. Ostro (1985) proposed that the surface structure of this asteroid and of Callisto might be controlled by sublimation of ice from a water-clay mixture. The radar properties of Adonis are not similar to those of active comets, nor are they similar to other asteroids. The combination of the meteor stream association and unusual physical properties suggest that Adonis is likely an extinct comet.

2201 Oljato. Extensive observations of 2201 Oljato have not resulted in a coherent picture for this asteroid. Data from its 1983 opposition, including spectroscopy, *JHK* photometry, and 10-μm radiometry show that it has a high albedo using both the standard and nonstandard thermal models (Matson 1986; Veeder et al. 1989), and has neutral to reddish colors with a strong ultraviolet absorption band (McFadden et al. 1984*a*). Few asteroids have these characteristics. This conflicts with spectral measurements taken in 1979 (shown in Fig. 6) where excess ultraviolet reflectance was measured on two nights (McFadden et al. 1984*b*). Yet *UBV* photometry taken a few weeks earlier in 1979 indicated normal colors of S-type asteroids (Bowell and Harris 1979). Radar observations (Ostro 1985) indicate an irregular shape and that Oljato may be bifurcated. They also indicate an inconsistency with the initial rotation period published in Harris and Young (1983) of 24 hr.

Independent of any knowledge of dynamical arguments associating Oljato with meteor streams or of groundbased measurements of its physical properties, Russell et al. (1984) found a statistical association with the position of this asteroid and interplanetary magnetic field perturbations measured by the Pioneer Venus Orbiter. Russell hypothesized, though not without criticism (Intrilligator 1985), that outgassing from debris in the orbit of this asteroid resulted in fluctuations in the solar magnetic field as measured near Venus. The unusual physical properties of Oljato compared to other asteroids, combined with its dynamical properties and association with several meteor streams make Oljato one of the strongest candidates for an extinct comet among the near-Earth asteroids. Note, however, that its high albedo is not

consistent with the albedos of comet nuclei measured to date, although its slow rotation period and irregular shape are characteristic of both cometary and asteroidal populations.

2212 Hephaistos.   Knowledge of the physical properties of this asteroid is limited to its *UBV* colors which indicate it is a C-type object (Shoemaker et al. 1979) based on the Chapman-Morrison-Zellner classification system (Bowell 1978), but is ambiguous according to the Eight Color Asteroid Survey classification (Tholen, Part VI of this book). Its orbit is very similar to that of Comet Encke and it is associated with the δ Cancrids meteor stream. Its next favorable apparition is in 1990 when this asteroid reaches $V = 16.0$ and in 1994 when $V = 15.1$ (Hahn 1988).

3200 Phaethon.   The similarity of the mean orbit of the Geminid meteor shower with that of 3200 Phaethon led Whipple (1983) to suggest that this is the parent body of that shower. Hunt et al. (1985) found that only a cometary nucleus could produce the observed distribution of aphelia for the Geminid shower. Also, Wetherill (1988) has stated that the mass of material in the Geminid stream is too great to have likely been produced by an impact within the dynamical lifetime of the stream. Halliday (1988) estimated particle densities of 0.7 to 1.3 g cm^{-3} for 12 fireballs associated with the Geminid shower, distinctly less than the higher densities found for fireballs associated with suspected meteorites; he concluded that they likely came from a compacted cometary surface crust.

   Observational efforts at detecting cometary activity by Phaethon have yielded negative results at visible wavelengths (Cochran and Barker 1984; Veeder et al. 1984; McFadden et al. 1985). Examination of IRAS data for evidence of a dust trail or any extended features at infrared wavelengths (Davies 1986) has also been negative. Cochran and Barker (1984) and Belton et al. (1985) classified Phaethon as an S-type asteroid based on spectroscopic measurements. However, subsequent precise broadband photoelectric photometry (Tholen 1985) and infrared photometry (Veeder et al. 1984; Green et al. 1985), as shown in Fig. 6, indicate that this object is spectrally blue at all wavelengths as opposed to the cometary nuclei measured to date, which are either neutral or red at most visible and infrared wavelengths. The lack of red colors and absence of evidence of an extended nature both suggest that this is not an extinct comet. However, its unusual colors, by asteroid standards, and strong meteor stream association must still be explained.

   3552 1983 SA and 1984 BC both have limited observational data. Eight-color photometry (shown in Fig. 6) classifies both as D-type asteroids (Tholen 1984*a;* Tholen, Part VI). 3552 1983 SA will not be brighter than $V = 17.2$ before the end of the century (Hahn 1988). 1984 BC will reach magnitude $V = 17.5$ in March, 1997. There are no physical measurements of *1983 XF;* it will reach its maximum brightness during the remainder of the century in

November, 1994 at $V = 16.0$ magnitudes. Given the limited knowledge of the physical properties of these asteroids, they cannot presently be distinguished from outer main-belt asteroids. However, their chaotic orbital motion is suggestive of a possible cometary connection.

Possible Candidates

The following objects, listed as possible candidates in Table III, have been cited for a variety of reasons. Although we find many of the arguments less compelling than those above, we discuss the possible candidates here in light of recent observations and our updated criteria.

1566 Icarus.   This is one of the few near-Earth asteroids that is nearly spherical in shape (Gehrels et al. 1970). Before evidence of the irregular shapes of cometary nuclei existed (see Sec. 5), the shape of Icarus was cited as evidence of its cometary nature. This belief is no longer valid. Icarus' high albedo (Veeder et al. 1989) and rapid rotation rate are inconsistent with our current knowledge of cometary nuclei. A weak association with the Arietids meteor stream may be coincidental. This asteroid is not likely to be an extinct comet.

1580 Betulia.   This high-inclination asteroid, $i = 52°$, was observed in 1976 during its last favorable apparition and has not been observed since (except for astrometric purposes). Polarimetric and radiometric albedo and diameter determinations require this asteroid to be modeled as a bare rocky surface with a high thermal inertia (Tedesco et al. 1978; Lebofsky et al. 1978). Its diameter of 7.4 km is of the same order of magnitude as the cometary nuclei studied to date (see Table II). The measured albedo is low (0.02 to 0.04) and its reflectance spectrum is flat (Chapman and Gaffey 1979; McFadden et al. 1984*b*), consistent with a taxonomic classification of type C. Whereas the size, albedo, color (neutral) and highly irregular shape inferred from the lightcurve (Tedesco et al. 1978) of Betulia are consistent with our current knowledge (and/or expectations) of cometary nuclei, its surface inertia and short rotation period of 6.13 hr are not. It may be possible that a completely extinct comet can evolve a bare surface with high thermal inertia; however, a physical mechanism for that transformation has not been proposed. We cannot say definitely whether or not this asteroid is an extinct cometary nucleus because its physical properties (except for its thermal inertia) are also typical of a main-belt asteroid.

1620 Geographos.   This asteroid has a weak association with the March Virginids meteor stream and has an elongated shape. However, it is spectrally classified as S type and has a rotation period of only 5.22 hr. It is not likely to be an extinct cometary nucleus.

1685 Toro.   This asteroid has been identified with the January Aquarids meteor shower by Drummond (1982). However, its S-type reflectance spectrum and high albedo argue against it as a likely cometary candidate.

1862 Apollo.   This asteroid is small, bright and rotates rapidly (Lebofsky et al. 1981; Harris et al. 1987), characteristics which are inconsistent with current statistics of cometary nuclei. In addition, its reflectance spectrum (McFadden et al. 1984*b*,1985) is characteristic of ordinary chondrite meteorites and its taxonomic classification Q (Tholen 1984*b*) is unique. However, it is weakly associated with the χ Scorpiids meteor stream. This asteroid is not likely to be a cometary nucleus.

1866 Sisyphus.   This asteroid is in a high-inclination orbit, $i = 41°$, and was cited as possibly cometary by Kresák (1977). Its reflectance spectrum shows strong ultraviolet and near-infrared absorption bands indicative of the presence of mafic silicates on its surface (Vilas and McFadden 1985). Whereas its size and albedo are not too different from those of the cometary nuclei studied to date, its reflectance spectrum indicates the presence of differentiated minerals which are not expected on comets in large quantities, nor with grain sizes > 50 μm, which are required to produce a significant absorption band. Hahn and Lagerkvist (1988) find an orbital evolution leading in the future to the Flora region; Sisyphus may have come from there in the past. Both physical and dynamical evidence make this asteroid a doubtful cometary candidate.

1917 Cuyo.   There is no physical information on 1917 Cuyo (1968 AA) for which Sekanina (1970) suggested a meteor shower association. This asteroid will be observable from the southern hemisphere in 1989.

1981 Midas.   This Apollo asteroid has a high inclination, $i = 40°$, orbit and was suggested as cometary by Kresák (1977). No physical observations exist for it. It will not be observable until March, 1992 (Hahn 1988).

2062 Aten.   This asteroid has a moderately high inclination, $i = 19°$, and is weakly associated with the ω Draconids meteor stream. However, it has a low eccentricity orbit and is classified as S type (Gradie 1976). We do not regard it as a good candidate for an extinct cometary nucleus.

1983 VA.   This object has a Tisserand invariant near 3 but has a poorly determined orbit which may or may not be chaotic; no physical observations exist for this asteroid. *1986 JK* also has a Tisserand invariant near 3, has been classified as C type (Wisniewski 1987) and has a weak meteor shower association, but will not be brighter than 21st magnitude through the end of the century. Ostro et al. (1989) detected *1986 JK* with radar and noted that its

radar albedo overlaps the range for observed short-period cometary nuclei, but also overlaps the low end of the radar albedo range for C-type asteroids. *1986 RA*, also classified as C type (Wisniewski 1987) and with $T < 3$ will brighten to magnitude $V = 18$ in October, 1992. *1982 TA* is smaller and brighter than observed cometary nuclei (Veeder et al. 1989). No physical observations of *1982 YA* exist. Too little is known about any of these objects to reach any meaningful conclusions as to their origin.

5025 P-L. This asteroid was discovered by the Palomar-Leiden survey in an eccentric, Jupiter-crossing orbit and has been identified with a meteor shower by Olsson-Steel (1988). However, it is currently classified as lost and no physical studies have been performed. Its comet-like orbit and meteor shower association are highly suggestive of a cometary origin.

The remaining objects are for the most part objects whose orbits are not well determined and which are classified as lost. Any decision about the nature of these objects must await their rediscovery and subsequent physical studies.

VII. DISCUSSION

There is, as yet, no conclusive evidence that any of the asteroids are extinct or dormant cometary nuclei. But there is a tantalizing body of evidence which we have presented here, which suggests that some of the near-Earth asteroids, plus several others, have cometary properties, either dynamical or physical. Of particular interest is the fact that many of the candidate asteroids are identified as cometary by two or more independent lines of evidence. It is highly unlikely that these could all be mere coincidence. We find these multiple, independent identifications to be compelling.

At the same time, many of the likely cometary candidates have physical properties which are inconsistent with our current understanding of cometary nuclei, such as high albedos and/or unusual spectra. Thus, it is not yet possible to put together a coherent picture of the evolution of cometary nuclei to asteroidal objects, or to conclusively identify any specific asteroid as an extinct cometary nucleus.

In addition, it is interesting that so many of the Apollo-Amor-Aten objects appear unusual, as compared with main-belt asteroids. It cannot simply be that these asteroids are often closer than main-belt objects and thus, better studied, since they are typically much smaller and thus fainter also. The heliocentric distance of the AAAO could be a factor, but the precise physical mechanism that might explain the differences remains a mystery.

The current dynamical estimates allow for $\sim 60\%$ of the Earth-crossing objects to be supplied from the main belt, leaving 40% to be supplied from some other reservoir(s). At present, the short-period comets are the only identified reservoir that can fill that gap. However, given the large uncertainty in

the actual population of near-Earth asteroids, the actual shortage of dynamical means for supplying near-Earth asteroids could be as little as zero, or as much as 70%. We think that either extreme is highly unlikely.

One problem, clearly illustrated by both Tables II and III, is the incompleteness in our detailed knowledge of both cometary nuclei and near-Earth asteroids. The sample of cometary nuclei which have been observed sufficiently to determine reasonably accurate shapes, diameters, rotation periods, albedos and colors is too small to say anything reliably about the statistics of the population. For the near-Earth asteroids the situation is somewhat better, though still far from complete, and is almost certainly still heavily biased towards high-albedo objects. The only solution to this problem is dedicated observing programs for the short-period comets and near-Earth asteroids to determine their basic physical parameters. We strongly encourage observers to pursue such programs.

An interesting example of what we have been talking about came to light just as we were completing this chapter. A new short-period comet, Parker-Hartley 1989i, was discovered in a fairly low eccentricity orbit, in a 4:3 Hilda-type resonance with Jupiter. Examination of the orbit (Nakano 1989) showed that the comet had previously been observed and catalogued as minor planet 1986 TF. The comet had been thrown into this orbit by a close approach to Jupiter (0.17 AU) in 1984. In addition, re-examination of the asteroid discovery plates (Jensen 1989) showed that the original images were slightly diffuse compared to other asteroid images on the plates.

We think that this example helps to illustrate our point: cometary objects can appear asteroidal in one part of their orbit, yet be clearly cometary in another part. In addition, without follow-up observations, the true nature of any object cannot be clearly identified. Thus, we not only urge observers to look at the many objects of interest we have pointed out in this chapter; we urge them to look at them very carefully.

Another valuable source of information on comets evolving into asteroids would be spacecraft missions to asteroids, in particular the Earth-crossing and Earth-approaching asteroids. Flybys of main-belt asteroids have been included in the Galileo mission (though Galileo's targets, Gaspra and Ida, are quite small) and in the designs of the Comet Rendezvous and Cassini (Saturn Orbiter/Titan Probe) missions. However, much more could be learned from dedicated asteroid missions. Current missions under consideration include: Near Earth Asteroid Rendezvous, Multiple Near Earth Asteroid Flybys, and Main Belt Asteroid Rendezvous. The proposed European-Soviet Vesta mission which includes main-belt asteroid flybys and penetrators is another interesting possibility. All of these would be quite valuable in increasing our knowledge and understanding of asteroids. However, flybys of the Earth-crossing asteroids, in particular some of those in Table III, would be most interesting in determining whether any of them are, in fact, extinct cometary nuclei. The CRAF mission will also be valuable in providing comparison data on an evolved short-period comet.

As with any field of study, our current views are a reflection of our current state of knowledge of cometary nuclei and asteroids. It is obvious that the general consensus on this question has changed considerably due to the observational and theoretical results of the past ten years. A decade ago direct physical observations of cometary nuclei were virtually nonexistent, the Halley spacecraft missions were still awaiting approval, and we were only just beginning to understand the complex, chaotic dynamics of both comet and asteroid orbital evolution. It will be most interesting to see what new light another decade of study will bring to this question.

REFERENCES

A'Hearn, M. F. 1988. Observations of cometary nuclei. *Ann. Rev. Earth Planet. Sci.* 16:273–293.

A'Hearn, M. F., Campins, H., and Schleicher, D. G. 1988*a*. Periodic comet Tempel 2 (1987g). *IAU Circ.* No. 4619.

A'Hearn, M. F., Feldman, P. D., Roettger, E., and Schleicher, D. G., 1988*b*. Periodic comet Tempel 2 (1987g). *IAU Circ.* No. 4622.

A'Hearn, M. F., Campins, H., Schleicher, D. G., and Millis, R. L. 1989. The nucleus of comet P/Tempel 2. *Astrophys. J.*, submitted.

Babadzhanov, P. B., and Obrubov, Y. V. 1983. Secular perturbations of Apollo, Amor and Aten asteroid orbits and theoretical radiants of meteor showers, probably associated with them. In *Asteroids, Comets, Meteors,* eds. C.-l. Lagerkvist and H. Rickman (Uppsala: Univ. of Uppsala), pp. 411–417.

Bell, J. F., Brown, R. H., and Hawke, B. R. 1988. Composition and size of Apollo asteroid 1984 KB. *Icarus* 73:482–486.

Belton, M. J. S., Spinrad, H., Wehinger, P. A., and Wyckoff, S. 1985. 1983 TB and comet Shoemaker (1984s). *IAU Circ.* No. 4029.

Belton, M. J. S., Spinrad, H., Wehinger, P. A., Wyckoff, S., and Yeomans, D. K. 1987. The spectral behavior of P/Halley at large heliocentric distance in light of the Giotto/Vega results. *Astron. Astrophys.* 187:569–574.

Belyaev, N. A., Kresák, L., Pittich, E. M., and Pushkarev, A. N. 1986. *Catalogue of Short-Period Comets* (Bratislava: Astron. Inst. Slovak Acad. Sci.).

Bowell, E. 1978. 1978 SB. *IAU Circ.* No. 3284.

Bowell, E., and Harris, A. W. 1979. 1947 XC = 1979 XA. *IAU Circ.* No. 3436.

Brin, G. D., and Mendis, D. A. 1979. Dust release and mantle development in comets. *Astrophys. J.* 229:402–408.

Brooke, T. Y., and Knacke, R. F. 1986. The nucleus of comet P/Arend-Rigaux. *Icarus* 67:80–87.

Campbell, D. B., Harmon, J. K., and Shapiro, I. I. 1989. Radar observations of comet Halley. *Astrophys. J.*, in press.

Campins, H. 1988. The anomalous dust production in periodic comet Encke. *Icarus* 73:508–515.

Campins, H., Rieke, G. H., and Lebofsky, M. J. 1985. Absolute calibration of photometry at 1 through 5 microns. *Astron. J.* 90:896–899.

Campins, H., A'Hearn, M. F., and McFadden, L.-A. 1987. The bare nucleus of comet Neujmin 1. *Astrophys. J.* 316:847–857.

Campins, H., A'Hearn, M. F., Schleicher, D. G., and Millis, R. L. 1988. The nucleus of comet P/Tempel 2. *Bull. Amer. Astron. Soc.* 20:835 (abstract).

Carusi, A., and Valsecchi, G. B. 1987. Dynamical evolution of short-period comets. In *Interplanetary Matter,* ed. P. Pecina, Publ. Astron. Inst. Czech. Acad. Sci. No. 67, pp. 21–28.

Carusi, A., Kresák, L., Perozzi, E., and Valsecchi, G. B. 1985. *Long-Term Evolution of Short-Period Comets* (Bristol: Adam Hilger).

Chapman, C. R., and Gaffey, M. J. 1979. Reflectance spectra for 277 asteroids. In *Asteroids,* ed. T. Gehrels (Tucson: Univ. of Arizona Press), pp. 655–687.

Cochran, A. L., and Barker, E. 1984. Minor planet 1983TB: A dead comet? *Icarus* 59:296–300.

Cochran, A. L., Cochran, W. D., and Barker, E. S. 1982. Spectrophotometry of comet Schwassmann-Wachmann 1. II. Its color and CO^+ emission. *Astrophys. J.* 254:816–822.

Cruikshank, D. P., and Brown, R. H. 1983. The nucleus of comet P/Schwassmann-Wachmann 1. *Icarus* 56:377–380.

Cruikshank, D. P., and Jones, T. J. 1977. The diameter and albedo of asteroid 1976AA. *Icarus* 31:427–429.

Cruikshank, D. P., Hartmann, W. K., and Tholen, D. J. 1985. Colour, albedo, and nucleus size of Halley's comet. *Nature* 315:122–124.

Davies, J. K. 1986. Are the IRAS-detected Apollo asteroids extinct comets? *Mon. Not. Roy. Astron. Soc.* 221:19–23.

Degewij, J., and Tedesco, E. F. 1982. Do comets evolve into asteroids? Evidence from physical studies. In *Comets,* ed. L. L. Wilkening (Tucson: Univ. of Arizona Press), pp. 665–695.

Degewij, J., and van Houten, C. J. 1979. Distant asteroids and outer Jovian satellites. In *Asteroids,* ed. T. Gehrels (Tucson: Univ. of Arizona Press), pp. 417–435.

Degewij, J., Tedesco, E. F., and Zellner, B. 1979. Albedo and color contrasts on asteroid surfaces. *Icarus* 40:364–374.

Delamere, W. A., Reitsema, H. J., Huebner, W. F., Schmidt, H. U., Keller, H. U., Schmidt, W. K. H., Wilhelm, K., and Whipple, F. L. 1986. Radiometric observations of the nucleus of Comet Halley. In *20th ESLAB Symp. on the Exploration of Halley's Comet,* vol. 2, eds. B. Battrick, E. J. Rolfe and R. Reinhard, ESA SP-250, pp. 355–357.

Delsemme, A. H., and Rud, D. A. 1973. Albedos and cross-sections for the nuclei of comets 1969 IX, 1970 II, and 1971 I. *Astron. Astrophys.* 28:1–6.

Donn, B., and Hughes, D. W. 1985. Characteristics and implications of a comet nucleus formed by random grain accretion. *Bull. Amer. Astron. Soc.* 17:689 (abstract).

Drummond, J. D. 1982. Theoretical meteor radiants of Apollo, Amor and Aten asteroids. *Icarus* 49: 143–153.

Dunlap, J. L., Gehrels, T., and Howes, M. L. 1973. Minor planets and related objects. IX. Photometry and polarimetry of (1685) Toro. *Astron. J.* 78:491–501.

Everhart, E. 1969. Close encounters of comets and planets. *Astron. J.* 74:735–750.

Fanale, F. P., and Salvail, J. R. 1984. An idealized short-period comet model: Surface insolation, H_2O flux, dust flux, and mantle evolution. *Icarus* 60: 476–511.

Fernández, J. A. 1985. Dynamical capture and physical decay of short-period comets. *Icarus* 64:308–319.

Festou, M. C. 1981. The density distribution of neutral compounds in cometary atmospheres. I. Models and equations. *Astron. Astrophys.* 95:69–79.

Froeschlé, C., and Rickman, H. 1980. New Monte Carlo simulations of the orbital evolution of short-period comets and comparison with observations. *Astron. Astrophys.* 82:183–194.

Gaffey, M. J., and McCord, T. B. 1978. Asteroid surface materials: Mineralogical characterization from reflectance spectroscopy. *Space Sci. Rev.* 21:555–628.

Gehrels, T., Roemer, E., Taylor, R. C., and Zellner, B. H. 1970. Minor planets and related objects. IV: Asteroid (1566) Icarus. *Astron. J.* 75:186–195.

Goldstein, R. M., Jurgens, R. F., and Sekanina, Z. 1984. A radar study of comet IRAS-Araki-Alcock 1983d. *Icarus* 89:1745–1754.

Gradie, J. C. 1976. Physical observations of object 1976 AA. *Bull. Amer. Astron. Soc.* 8:458 (abstract).

Gradie, J., and Veverka, J. 1980. The composition of the Trojan asteroids. *Nature* 283:840–842.

Green, J. R. 1986. Stress, fracture, and outburst in cometary nuclei. *Bull. Amer. Astron. Soc.* 18:800 (abstract).

Green, S. F., Meadows, A. J., and Davies, J. K. 1985. Infrared observations of the extinct cometary candidate minor planet (3200) 1983TB. *Mon. Not. Roy. Astron. Soc.* 214:29P–36P.

Hadjuk, A. 1985. The past orbit of comet Halley and its meteor stream. In *Dynamics of Comets: Their Origin and Evolution,* eds. A. Carusi and G. B. Valsecchi (Dordrecht: D. Reidel), pp. 399–403.

Hahn, G. 1983. UBVRI and JHK photometry of the near-Earth asteroid 1862 Apollo. In *Asteroids, Comets, Meteors,* eds. C.-I. Lagerkvist and H. Rickman (Uppsala: Univ. of Uppsala), pp. 35–44.

Hahn, G. 1988. A data base of observing conditions for Aten-Apollo-Amor objects II: First update (through February 1988). Uppsala Astron. Obs. Rept. No. 45.

Hahn, G., and Lagerkvist, C.-I. 1988. Orbital evolution of planet-crossing asteroids. *Celest. Mech.* 43:285–302.

Hahn, G., and Rickman, H. 1985. Asteroids in cometary orbits. *Icarus* 61:417–442.

Halliday, I. 1988. Geminid fireballs and the peculiar asteroid 3200 Phaethon. *Icarus* 76:279–294.

Hanner, M. S., Aitken, D. K., Knacke, R., McCorkle, S., Roche, P. F., and Tokunaga, A. T. 1985. Infrared spectrophotometry of comet IRAS-Araki-Alcock (1983d): A bare nucleus revealed? *Icarus* 62:97–109.

Harris, A. W., and Young, J. W. 1983. Asteroid rotation IV: 1979 observations. *Icarus* 54:59–109.

Harris, A. W., Young, J. W., Goguen, J., Hammel, H. B., and Hahn, G. 1987. Photoelectric lightcurves of the asteroid 1862 Apollo. *Icarus* 70:246–256.

Hartmann, W. K., Cruikshank, D. P., and Degewij, J. 1981. Surface materials on unusual planetary object Chiron. *Icarus* 47:333–341.

Hartmann, W. K., Cruikshank, D. P, and Degewij, J. 1982. Remote comets and related bodies: VJHK colorimetry and surface materials. *Icarus* 52:377–408.

Hartmann, W. K., Tholen, D. J., and Cruikshank, D. P. 1987. The relationship of active comets, "extinct" comets, and dark asteroids. *Icarus* 69: 33–50.

Hartmann, W. K., Tholen, D. J., Meech, K. J., and Cruikshank, D. P. 1989. 2060 Chiron: Colorimetry and possible cometary behavior. *Icarus,* submitted.

Herman, G., and Weissman, P. R. 1987. Numerical simulation of cometary nuclei, III. Internal temperatures of cometary nuclei. *Icarus* 69:314–328.

Hoffmeister, C. 1948. *Meteorstörme* (Leipzig, Werden und Wirken).

Horanyi, M., Gombosi, T. I., Cravens, T. E., Korosmezey, A., Kecskemety, K., Nagy, A., and Szegö, K. 1984. The friable sponge model of a cometary nucleus. *Astrophys. J.* 278:449–455.

Hunt, J., Fox, K., and Williams, I. P. 1985. Asteroidal origin for the Geminid meteor stream. In *Asteroids, Comets, Meteors II,* eds. C.-I. Lagerkvist, B. Lindblad, H. Lundstedt and H. Rickman (Uppsala: Univ. of Uppsala), pp. 549–553.

Intrilligator, D. S. 1985. New results on the Pioneer Venus orbiter February 10–11, 1982 events: A solar wind disturbance, not a comet. *Geophys. Res. Lett.* 12:187–190.

Jensen, P. 1989. Periodic comet Parker-Hartley (1987 XXXVI). *IAU Circ.* No. 4754.

Jewitt, D., and Luu, J. 1989. A CCD portrait of comet P/Tempel 2. *Astron. J.,* submitted.

Jewitt, D. C., and Meech, K. J. 1988. Optical properties of cometary nuclei and a preliminary comparison with asteroids. *Astrophys. J.* 328:974–986.

Johnson, R. E., Cooper, J. F., and Lanzerotti, L. J. 1986. Radiation formation of a non-volatile crust. In *20th ESLAB Symp. on the Exploration of Halley's Comet,* vol. 2, eds. B. Battrick, E. J. Rolfe and R. Reinhard, ESA SP-250, pp. 269–272.

Kamoun, P. G., Campbell, D. B., Ostro, S. J., Pettengill, G. H., and Shapiro, I. I. 1982. Comet Encke: Radar detection of nucleus. *Science* 216:293–295.

Keller, H. U., Arpigny, C., Barbieri, C., Bonnett, R. M., Cazes, S., Coradini, M., Cosmovici, C. B., Delamere, W. A., Huebner, W. F., Hughes, W. W., Jamar, C., Malaise, D., Reitsema, H. J., Schmidt, H. U., Schmidt, W. K., Seige, P., Whipple, F. L., and Wilhelm, K. 1986. First Halley multicolour camera imaging results from Giotto. *Nature* 321:320–326.

Kowal, C. T. 1979. Chiron. In *Asteroids,* ed. T. Gehrels (Tucson: Univ. of Arizona Press), pp. 436–442.

Kresák, L. 1977. Asteroid versus comet discrimination from orbital data. In *Comets, Asteroids, Meteorites: Interrelations, Evolution, and Origins,* ed. A. H. Delsemme (Toledo: Univ. of Toledo Press), pp. 313–321.

Kresák, L. 1979. Dynamical interrelations among comets and asteroids. In *Asteroids,* ed. T. Gehrels (Tucson: Univ. of Arizona Press), pp. 289–309.

Kresák, L. 1985. The aging and lifetimes of comets. In *Dynamics of Comets: Their Origin and Evolution,* eds. A. Carusi and G. B. Valsecchi (Dordrecht: D. Reidel), pp. 279–302.

Kresák, L. 1987. On the aging process of periodic comets. In *20th ESLAB Symposium on the Exploration of Halley's Comet* vol. 2, eds. B. Battrick, E. J. Rolfe and R. Reinhard, ESA SP-250, pp. 433–438.

Kührt, E. 1984. Temperature profiles and thermal stresses in cometary nuclei. *Icarus* 60:512–521.

Lebofsky, L. A., Veeder, G. J., Lebofsky, M. J., and Matson, D. L. 1978. Visual and radiometric photometry of 1580 Betulia. *Icarus* 35:336–343.

Lebofsky, L. A., Veeder, G. J., Rieke, G. H., Lebofsky, M. J., Matson, D. L., Kowal, C., Wynn-Williams, C. G., and Becklin, E. E. 1981. The albedo and diameter of 1862 Apollo. *Icarus* 48:335–338.

Lebofsky, L. A., Tholen, D. J., Rieke, G. H., and Lebofsky, M. J. 1984. 2060 Chiron: Visual and thermal infrared observations. *Icarus* 60:532–537.

Marsden, B. G. 1970. On the relationship between comets and minor planets. *Astron. J.* 75: 206–217.

Marsden, B. G. 1971. Evolution of comets into asteroids? In *Physical Studies of Minor Planets,* ed. T. Gehrels, NASA SP-267, pp. 413–421.

Marsden, B. G. 1985. Nongravitational forces on comets: The first fifteen years. In *Dynamics of Comets: Their Origin and Evolution,* eds. A. Carusi and G. B. Valsecchi (Dordrecht: D. Reidel), pp. 343–352.

Matson, D. L., ed. 1986. *IRAS Asteroid and Comet Survey: Preprint Version No. 1.* JPL Internal Document No. D-3698.

McFadden, L. A., Ostro, S. J., Barker, E. S., Cochran, A. L., Cruikshank, D. P., Hartmann, W. K., Soifer, B. T., and Veeder, G. J. 1984a. 2201 Oljato: An asteroid, a comet, or both? *Bull. Amer. Astron. Soc.* 16: 691 (abstract).

McFadden, L. A., Gaffey, M. J., and McCord, T. B. 1984b. Mineralogical-petrological characterization of near-Earth asteroids. *Icarus* 59:25–40.

McFadden, L. A., Gaffey, M. J., and McCord, T. B. 1985. Near-Earth asteroids: Possible sources from reflectance spectroscopy. *Science* 229:160–163.

Milani, A., Carpino, M., Hahn, G., and Nobili, A. M. 1989. Project SPACEGUARD: Dynamics of planet-crossing asteroids. Classes of orbital behaviour. *Icarus* 78:212–269.

Millis, R. L., A'Hearn, M. F., and Campins, H. C. 1988. The investigation of the nucleus and coma of comet P/Arend-Rigaux. *Astrophys. J.* 324:1194–1209.

Miner, E., and Young, J. 1969. Photometric determination of the rotation period of 1566 Icarus. *Icarus* 10:436–440.

Möhlmann, D., Börner, H., Danz, M., Elter, G., Mangoldt, T., Rubbert, B., and Weidlich, U. 1986. Physical properties of P/Halley derived from Vega images. In *20th ESLAB Symp. on the Exploration of Halley's Comet,* vol. 2, eds. B. Battrick, E. J. Rolfe and R. Reinhard, ESA SP-250, pp. 339–340.

Morrison, D., Gradie, J., and Rieke, G. H. 1976. Radiometric diameter and albedo of the remarkable asteroid 1976AA. *Nature* 260:691.

Nakano, S. 1989. Periodic comet Parker-Hartley (1989i = 1987 XXXVI) = 1986 TF. *IAU Circ.* No. 4752.

Newton, H. A. 1893. On the capture of comets by planets, especially their capture by Jupiter. *Mem. Natl. Acad. Sci.* 6:8–23.

Oikawa, S., and Everhart, E. 1979. Past and future orbit of 1977 UB, object Chiron. *Astron. J.* 84:134–139.

Olsson-Steel, D. I. 1988. Identification of meteoroid streams from Apollo asteroids in the Adelaide radar orbit surveys. *Icarus* 75:64–96.

Öpik, E. J. 1963. The stray bodies in the solar system. Part I. Survival of cometary nuclei and the asteroids. *Adv. Astron. Astrophys.* 2:219–262.

Ostro, S. J. 1985. Radar observations of asteroids and comets. *Publ. Astron. Soc. Pacific* 97:877–884.

Ostro, S. J., Campbell, D. B., and Shapiro, I. I. 1985. Radar properties of near-Earth asteroids. *Bull. Amer. Astron. Soc.* 17:729–730 (abstract).

Ostro, S. J., Yeomans, D. K., Chodas, P. W., Goldstein, R. M., Jurgens, R. F., and Thompson, T. W. 1989. Radar observations of asteroid 1986 JK. *Icarus* 78:382–394.

Prialnik, D., and Bar-Nun, A. 1987. On the evolution and activity of cometary nuclei. *Astrophys. J.* 313:893–905.

Prialnik, D., and Bar-Nun, A. 1988. The formation of a permanent dust mantle and its effect on cometary activity. *Icarus* 74:272–283.

Rickman, H. 1985. Interrelations between comets and asteroids. In *Dynamics of Comets: Their Origin and Evolution,* eds. A. Carusi and G. B. Valsecchi (Dordrecht: D. Reidel), pp. 149–172.

Rickman, H. 1986. Masses and densities of comets Halley and Kopff. In *Comet Nucleus Sample Return,* ed. O. Melita, ESA SP-249, pp. 195–205.

Rickman, H., and Froeschlé, C. 1980. A Monte Carlo estimate of the fraction of comets developing in to sizeable asteroidal bodies. *Moon and Planets* 22:125–128.

Russell, C. T., Aroian, R., Arghavani, M., and Nock, K. 1984. Interplanetary magnetic field enhancements and their association with the asteroid 2201 Oljato. *Science* 226:43–45.

Sagdeev, R. Z., Avanesov, G. A., Shamis, V. A., Szegö, K., Merenyi, E., Smith, B. A., Ziman, Ya. L., Krasikov, V. A., Tarnopolsky, V. A., and Kuzin, A. A. 1986a. TV experiment in Vega mission: Image processing technique and some results. In *20th ESLAB Symp. on the Exploration of Halley's Comet,* vol. 2, eds. B. Battrick, E. J. Rolfe and R. Reinhard, ESA SP-250, pp. 295–305.

Sagdeev, R. Z., Avanesov, G. A., Ziman, Ya. L., Smith, B., Toth, I., Moroz, V. I., Tarnopolsky, V. I., Zhukov, B. S., and Shamis, V. A. 1986b. TV experiment of the Vega mission: Photometry of the nucleus and inner coma. In *20th ESLAB Symp. on the Exploration of Halley's Comet,* vol. 2, eds. B. Battrick, E. J. Rolfe and R. Reinhard, ESA SP-250, pp. 317–326.

Sagdeev, R. Z., Elyasberg, P. E., and Moroz, V. I. 1987. Is the nucleus of comet Halley a low density body? *Nature* 331:240–242.

Scholl, H. 1979. History and evolution of Chiron's orbit. *Icarus* 40:345–349.

Schubart, J. 1979. Asteroidal motion at commensurabilities treated in three dimensions. In *Dynamics of the Solar System,* ed. R. L. Duncombe (Dordrecht: D. Reidel), pp. 207–215.

Sekanina, Z. 1970. Dynamics of meteor streams and new asteroid-meteor and comet-meteor associations. *Bull. Amer. Astron. Soc.* 2:217–218 (abstract).

Sekanina, Z. 1981. Rotation and precession of cometary nuclei. *Ann. Rev. Earth Planet. Sci.* 9:113–145.

Sekanina, Z. 1988. Rotation vector of Halley's Comet. In *Comet Halley 1986: Worldwide Investigations, Results, and Interpretations,* eds. J. Mason and P. Moore (Chichester, NY: Ellis Horwood), in press.

Shoemaker, E. M., and Wolfe, R. F. 1982. Cratering time scales for the Galilean satellites. In *Satellites of Jupiter,* ed. D. Morrison (Tucson: Univ. of Arizona Press), pp. 277–339.

Shoemaker, E. M., Williams, J. G., Helin, E. F., and Wolfe, R. F. 1979. Earth-crossing asteroids: Orbital classes, collision rates with Earth, and origin. In *Asteroids,* ed. T. Gehrels (Tucson: Univ. of Arizona Press), pp. 253–282.

Soderblom, D. R., and Harlan, E. A. 1976. 944 Hidalgo, *IAU Circ.* No. 3007.

Spinrad, H., Stauffer, J., and Newburn, R. L., Jr. 1979. Optical spectrophotometry of comet Tempel 2 far from the Sun. *Publ. Astron. Soc. Pacific* 91:707–711.

Stern, S. A. 1986. The effects of mechanical interaction between the interstellar medium and comets. *Icarus* 68:276–283.

Stern, S. A., and Shull, J. M. 1988. The influence of supernovae and passing stars in the Oort cloud. *Nature* 332:407–411.

Sykes, M. V., Lebofsky, L. A., Hunten, D. M., and Low, F. 1986. The discovery of dust trails in the orbits of periodic comets. *Science* 232:1115–1117.

Tedesco, E. F. 1979. Lightcurve parameters of asteroids. In *Asteroids,* ed. T. Gehrels (Tucson: Univ. of Arizona Press), pp. 1098–1107.

Tedesco, E. F., Drummond, J., Candy, M., Birch, P., Nikoloff, I., and Zellner, B. 1978. 1580 Betulia: An unusual asteroid with an extraordinary lightcurve. *Icarus* 35:344–359.

Tholen, D. J. 1984a. Photometry of Earth-approaching asteroids. *Bull. Amer. Astron. Soc.* 16:690–691 (abstract).

Tholen, D. J. 1984b. Asteroid Taxonomy from Cluster Analysis of Photometry. Ph.D. Thesis, Univ. of Arizona.

Tholen, D. J. 1985. (3200) 1983 TB. *IAU Circ.* No. 4034.

Tholen, D. J. 1988. Asteroids II Machine-readable database: March 1988. Floppy disk version.

Thomas, N., and Keller, H. U. 1989. The colour of comet Halley's nucleus and dust. *Astron. Astrophys.* 213:487–494.

Tokunaga, A. T., and Hanner, M. S. 1985. Does comet P/Arend-Rigaux have a large dark nucleus? *Astrophys. J.* 296:L13–L16.

Veeder, G. J., Kowal, C., and Matson, D. L. 1984. The Earth-crossing asteroid 1983 TB. *Lunar Planet. Sci.* XV:878–879 (abstract).

Veeder, G., Hanner, M. S., and Tholen, D. J. 1987. The nucleus of comet P/Arend-Rigaux. *Astron. J.* 94:169–173.

Veeder, G. J., Hanner, M. S., Matson, D. L., Tedesco, E. F., Lebofsky, L. A., and Tokunaga, A. T. 1989. Radiometry of near-Earth asteroids. *Astron. J.* 97:1211–1219.

Veverka, J., and Liller, W. 1969. Observations of Icarus: 1968. *Icarus* 10:441–444.

Vilas, F., and McFadden, L. A. 1985. Spectral studies of possible sources of near-Earth asteroids—CCD reflectance spectra. *Bull. Amer. Astron. Soc.* 17:732 (abstract).

Weissman, P. R. 1979. Physical and dynamical evolution of long-period comets. In *Dynamics of the Solar System,* ed. R. L. Duncombe (Dordrecht: D. Reidel), pp. 277–282.

Weissman, P. R. 1980. Physical loss of long-period comets. *Astron. Astrophys.* 85:191–196.

Weissman, P. R. 1986a. How pristine are cometary nuclei? In *Comet Nucleus Sample Return,* ESA SP-249, pp. 15–25.

Weissman, P. R. 1986b. Are cometary nuclei primordial rubble piles? *Nature* 320:242–244.

Weissman, P. R. 1987a. How typical is Halley's comet. In *Symp. on the Diversity and Similarity of Comets,* eds. E. J. Rolfe and B. Battrick, ESA SP-278, pp. 31–36.

Weissman, P. R. 1987b. Post-perihelion brightening of Halley's comet: Spring time for Halley. *Astron. Astrophys.* 187:873–878.

Wetherill, G. W. 1971. Cometary versus asteroidal origin of chondritic meteorites. In *Physical Studies of Minor Planets,* ed. T. Gehrels, NASA SP-267, pp. 447–460.

Wetherill, G. W. 1975. Late heavy bombardment of the Moon and terrestrial planets. *Proc. Lunar Sci. Conf.* 6:1539–1561.

Wetherill, G. W. 1979. Steady-state populations of Apollo-Amor objects. *Icarus* 37:96–112.

Wetherill, G. W. 1988. Where do the Apollo objects come from? *Icarus* 76:1–18.

Whipple, F. L. 1982. Rotation of comet nuclei. In *Comets,* ed. L. L. Wilkening (Tucson: Univ. of Arizona Press), pp. 227–250.

Whipple, F. L. 1983. 1983 TB. *IAU Circ.* No. 3881.

Wilhelm, K., Cosmovici, C. B., Delamere, W. A., Huebner, W. F., Keller, H. U., Reitsema, H., Schmidt, H. U., and Whipple, F. L. 1986. A three-dimensional model of the nucleus of Comet Halley. In *20th ESLAB Symposium on the Exploration of Halley's Comet,* vol. 2, eds. B. Battrick, E. J. Rolfe and R. Reinhard, ESA SP-250, pp. 367–369.

Wisdom, J. 1987. Chaotic dynamics in the solar system. *Icarus* 72:241–275.

Wisniewski, W. Z. 1987. Photometry of six radar target asteroids. *Icarus* 70:566–572.

Wisniewski, W. Z. 1988. Periodic comet Tempel 2. *IAU Circ.* No. 4603.

Wisniewski, W. Z., Fay, T., and Gehrels, T. 1986. Light variations in comets. In *Asteroids, Comets, Meteors II,* eds. C.-I. Lagerkvist, B. Lindblad, H. Lundstedt and H. Rickman (Uppsala: Univ. of Uppsala), pp. 337–339.

Yeomans, D. K. 1988. A new look at cometary nongravitational forces. *Bull Amer. Astron. Soc.* 20:841–842 (abstract).

Ziolkowski, K. 1983. Do nongravitational effects exist in the motion of asteroids? In *Asteroids, Comets, Meteors,* eds. C.-I. Lagerkvist and H. Rickman (Uppsala: Univ. of Uppsala), pp. 171–174.

Note added in proof: Meech and Belton (*IAU Circular 4770,* 1989) have detected visible coma associated with 2060 Chiron at a heliocentric distance of 11.8 AU, confirming that this object is a comet. Chiron (or should we say, "periodic Comet Kowal-Meech-Belton") is moving towards perihelion at 8.51 AU. Given its present distance, the activity may be driven by the sublimation of CO_2 ice from the nucleus surface.

ASTEROIDS: THE BIG PICTURE

JEFFREY F. BELL
University of Hawaii

DONALD R. DAVIS, WILLIAM K. HARTMANN
Planetary Science Institute

and

MICHAEL J. GAFFEY
Rensselaer Polytechnic Institute

During the past 15 yr much progress has been made in the study of the asteroids with optical, infrared, and radar telescopes. Simultaneously a vast body of petrologic, chemical and isotopic data has been acquired for meteorites, which are actual samples of asteroids. This work has demonstrated that asteroids vary widely in composition and thermal history in a systematic but complex way with orbital position and size. It appears that these variations can be explained to first order by a simple model invoking three principal mechanisms: (1) condensation of various known and unknown classes of chondritic material at radial locations in the nebula controlled by the temperature and composition; (2) intense metamorphic heating after accretion which declined rapidly with both increasing solar distance and smaller planetesimal size, producing complete differentiation in some inner belt objects, incomplete differentiation in many more, and extensive metamorphism and aqueous alteration in middle-belt objects; and (3) complex collisional fragmentation often controlled by internal strength gradients due to irregular distribution of metal. While inconsistent with some specific fragments of current knowledge, this conceptual model explains the great mass of raw data in a coherent manner, and makes many specific testable predictions which may serve to guide future investigations.

The remark "All observations must be considered suspect until confirmed by theory," sometimes attributed to Sir Arthur Eddington, is one that many scientists privately agree with to some extent. Asteroid scientists of the 1980s have been occasionally accused of being mere technicians who have lost sight of the forest in their intense study of the various kinds of trees. There is a grain of truth to this charge. The many new research techniques which have become available in the last 20 yr, combined with the vast number and variety of the asteroids themselves, have resulted in a period of rapid data collection without much progress in fitting the individual facts together into a unified paradigm for the history of the asteroids.

In this chapter we attempt to construct a simple model of the evolution of the asteroid belt from the vast amount of data available about the individual asteroids (Sec. IV). What we will present is not a theory in the sense that Eddington meant; i.e., an elaborate mathematical analysis deriving all the observed parameters of the system under consideration from basic physical laws. History teaches us that this is a methodology appropriate for simple systems composed of gases and fluids, not for the extremely complex systems of solids and semisolids involved in the evolution of rocky planetary bodies. All we can attempt is to outline a blurry quantitative picture of the major stages in the evolution of the asteroid belt, and point out how they might have produced the observed features of today's asteroid and meteorite populations.

Even with such modest goals, the task is difficult. Indeed, some who have attempted it in the recent past have concluded that the current majority opinions in the several subdisciplines of asteroid science are in direct conflict, and cannot be reconciled by any simple scenario (see, e.g., Chapman 1986; Wetherill and Chapman 1988). We agree with Eddington that this is one of the principal values of the exercise; when the puzzle is nearly fitted together in a satisfying way, the pieces which will not fit into the remaining space can be identified as suspect, despite their plausibility when examined in isolation.

II. REVIEW OF RELEVANT DATA

Most of the information we need to reconstruct the history of the asteroid belt is derived from petrographic, geochemical and isotopic studies of meteorites. We do not consider most of this in detail as a recent Space Science Series volume covers this subject (Kerridge and Matthews 1988). However, it is necessary to review the purely asteroidal data, and make some hard choices as to which subset of it we will use in working out our model.

The Meaning of Taxonomic Types

The most important datum available for a typical asteroid is its taxonomic type or spectral class. The system as standardized by Tholen (1984) employs principal component analysis of the Arizona Eight-Color Asteroid Survey (ECAS) spectra (Zellner et al. 1985; see the chapter by Tholen and Barucci), plus radiometric model albedos based on IRTF observations at 10

and 20 μm (Gradie and Tedesco 1989). There are several later variations of this classification. Two popular changes are to use albedos derived from the IRAS asteroid data instead of telescopic observations, and to incorporate older spectral data sets. Both these approaches enlarge the number of asteroids which are theoretically classifiable, at the cost of introducing a greater number of erroneous classifications which may obscure the systematics of the asteroid belt. Therefore, for the purposes of this chapter we will retain the 1984 Tholen classifications, with the addition of the possible new class K which has recently been separated from the old S class (Bell 1988,1989; Tedesco et al. 1989).

The true value of classification can only be realized if a class name can be firmly linked with a surface chemical composition. Since the classes are entirely based on the shape of the reflectance curve, and this shape is controlled by fairly well-understood physical processes in the regolith, there should be a direct correspondence between taxonomic type and composition. This correspondence is not always obvious from the 0.3 to 1.1 μm data alone. The principal supplementary data sets are:

1. 0.8 to 2.5 μm spectra which allow one to determine the presence or absence of the second pyroxene band near 1.9 μm and the degree to which the continuum is reddened;
2. Spectra in the 2.5 to 3.6 μm region which determine the presence or absence of bound water in phyllosilicates;
3. Radar reflectivities which can provide a relatively unambiguous identification of very metal-rich bodies (Ostro et al. 1985).

With the aid of these recent additions to the data, it is possible to infer the composition of most asteroid types with varying degrees of reliability. The principal limitation at present is the complete absence of meteorites with properties matching those of several important asteroid classes. In Table I, we summarize the current interpretations of the Tholen classes. The evidence supporting these interpretations is reviewed in the chapter by Gaffey et al.

The number of question marks in Table I is intended to indicate the relative reliability of the various interpretations. The most important controversy concerns the abundant S class asteroids. A significant number of scientists still associate these objects with the ordinary chondrites on the basis of fall statistics and dynamical studies, while spectral studies invariably reach opposing conclusions. A variety of solutions to this paradox are discussed by Wetherill and Chapman (1988; also see the chapters by Gaffey et al., Lipschutz et al.); here we assume that *most* S class asteroids are differentiated stony-iron bodies. The reader is warned that the rest of this chapter is critically dependent on the accuracy of this assumption and that our model will collapse utterly if S asteroids *in general* turn out to be undifferentiated objects.

Table I also illustrates how Tholen's classes have been grouped into three larger associations called superclasses (Bell 1986). This system divides as-

TABLE I
Assumed Compositional Interpretations of Asteroid Taxonomic Types

Bell Superclass	Tholen Class	Inferred Minerals	Analogous Meteorites
Primitive	D	organics + ? (ice??)	(none)
	P	organics + ? (ice??)	(none)
	C	clays, C, organics	CI, CM chondrites
	K	ol, pyx, carbon	CV, CO chondrites
	Q	pyx, ol, gray NiFe	H, L, LL chondrites ?
	?	Fe-free pyx, gray NiFe	EH, EL chondrites
Metamorphic	T	?	highly altered C Cs ??
	B + G + F	clays, opaques	highly altered C Cs ?
Igneous	V	plag, pyx, ol	basaltic achondrites
	R	ol, pyx	ol-rich achondrites?
	S	pyx, ol, red NiFe	pallasites, lodranites, irons ?
	A	ol	brachinites
	M	NiFe	irons
	E	Fe-free pyx	aubrites
	(Mars)		(SNC meteorites)
	(Moon)		(lunar meteorites)

teroids according to the degree of metamorphic heating they have undergone, rather than composition. The three superclasses are:

1. The primitive objects that have undergone little or no heating;
2. The metamorphosed objects that have been heated sufficiently to exhibit spectral changes;
3. The igneous objects whose current surface mineralogy was formed from a melt.

Note that the superclasses do not in any way represent a higher level of taxonomy in the traditional system, but are a result of *classifying the meteoritic interpretations* of the Tholen classes. For example, V class and E class asteroids have very different spectra and albedos; they are put into the same superclass because basaltic and enstatite achondrites have similar histories of crystallization from a melt.

The Stratigraphy of the Asteroid Belt

In recent years, it has progressively been realized that asteroids of different mineralogical compositions occur at different characteristic distances from the Sun, and that this property severely restricts possible models of asteroid evolution (Zellner 1979; Gradie and Tedesco 1982; Bell 1986; Chapman 1987; chapter by Gradie et al.). In Fig. 1a we have plotted the abundance of the Tholen taxonomic types against average distance from the Sun. This plot is based on the raw numbers from Table X of Tholen (1984) and therefore exag-
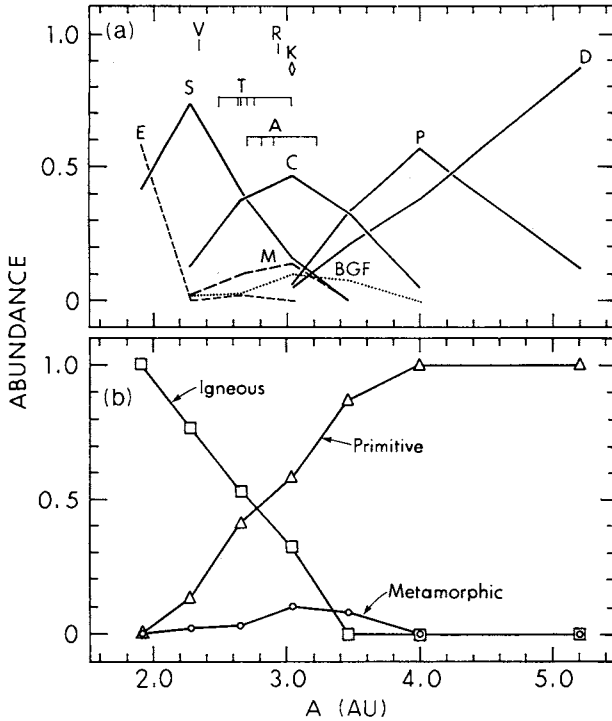
Fig. 1. (a) Distribution in the asteroid belt of the taxonomic types of Tholen (1984), plus K class of Bell (1988). (b) Distribution in the asteroid belt of the asteroid superclasses of Bell (1986).

gerates the abundance of S types and E types because there is no correction for albedo bias. The strong stratification of the asteroid belt is clearly apparent, with each abundant taxonomic class occupying a roughly Gaussian distribution with a FWHM of about 1 AU. Table I and Fig. 1a combined, form a mineralogical map of the asteroid belt which will be our principal tool in reconstructing its history in Sec. IV below.

A plot of the distribution of the superclasses (Fig. 1b) is equally revealing. It shows that the igneous types dominate the belt sunward of 2.7 AU, the metamorphosed types lie in a zone around 3.0 AU, and the primitive types are dominant outside 3.4 AU (Bell 1986; Gaffey 1988). From this, it appears that the heating mechanism which metamorphosed the chondrites and melted the achondrites was one which rapidly declined in efficiency with solar distance. There are only two mechanisms that are capable of melting such small objects in the very earliest days of the solar system: decay of a short-lived radionuclide (probably [26]Al), or magnetic induction heating during the Sun's T Tauri phase when the solar magnetic field was much more intense than today. [26]Al decay can explain the observed pattern only if planetesimal formation

began close to the Sun, and slowly spread outward to reach the region of Jupiter over many half-lives of ^{26}Al. Most models of planetesimal formation do in fact predict such a pattern, but the time required seems excessive. Alternatively, magnetic induction heating would produce the pattern seen (see the chapter by Scott et al.). Whatever the cause, it is clear that the asteroid belt preserves a transition between unaltered chondritic matter and highly evolved igneous materials, and this pattern was overlaid upon any compositional gradient in the original nebular condensate.

The Compositional Meaning of Tholen-Space

A persistent theme in asteroid remote sensing is a tendency to parameterize complex high-resolution spectra and plot the parameters in order to compress vast amounts of data into easily understandable 2-D graphs. In Fig. 2, we show the latest attempt at this (Tholen 1984, his Fig. 8; see also the chapter by Tholen and Barucci). Since the two parameters were determined by means of a mathematical analysis without any reference to particular compositional interpretations, the results provide an independent test of the interpretive scheme in Table I. If the positions of the various classes and superclasses in this parameter space ("Tholen-space") are consistent with the mineralogical and thermal histories implied by Table I, we would have increased confidence in our interpretations.

In Fig. 2a, we show only members of the primitive and metamorphic superclasses. The primitive asteroids (classes D, P and C) lie on a line which may be interpreted as a portion of the original condensation sequence in the solar nebula. The position of asteroids along this line is well correlated with solar distance. In fact, it appears that the C-P-D sequence is actually a continuous trend. The C/P distinction is purely arbitrary (Tholen 1984, p. 67) since the precise location of the boundary in Tholen-space is defined in terms of the unrelated E and M asteroids for historical reasons. Some more recent taxonomic systems deal very differently with this problem (Barucci et al. 1988; Tedesco et al. 1989). The P/D boundary is defined by a real density gap in Tholen-space, but this corresponds to the gap in asteroid density between the outer main belt and the Trojan clouds. There were probably many primordial planetesimals with compositions intermediate to P's and D's. The cause of progressive reddening of the primitive asteroids with increasing solar distance may be an increasing abundance of organic polymers which replace the elemental carbon common in known carbonaceous chondrites (Gradie and Veverka 1980). This trend may continue into the outer solar system, as suggested by the D-like spectrum of the dark hemisphere of the Saturn satellite Iapetus (Bell et al. 1985).

Classes K (CO/CV chondrites) and Q (ordinary chondrites) are not part of this simple trend, because they are higher-albedo objects in which carbon and carbon compounds do not control the spectrum. Since only a few objects
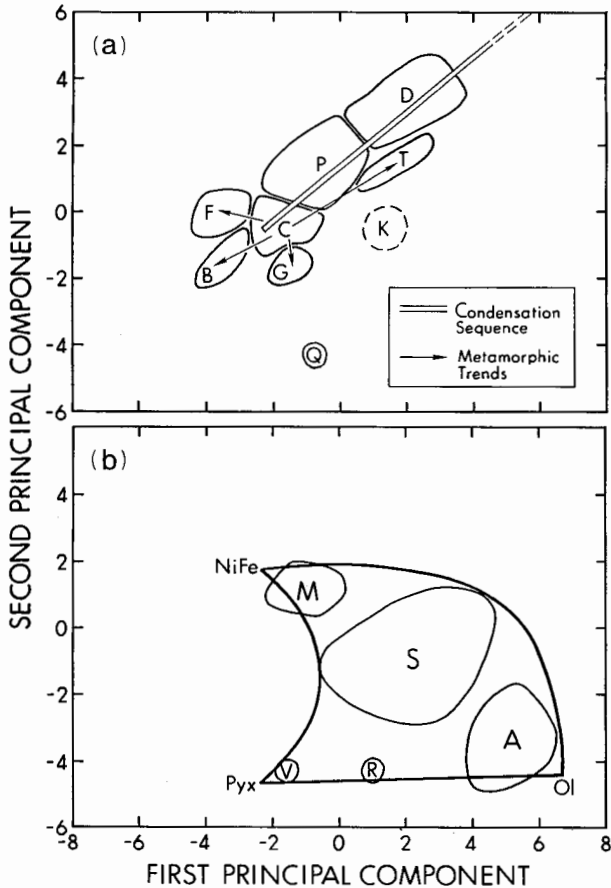
Fig. 2. (a) Distribution of primitive and metamorphic asteroid classes in spectral parameter space (after Fig. 8 of Tholen [1984]), with possible trends due to condensation temperature variations and metamorphism superimposed. (b) Distribution of igneous asteroid classes in spectral parameter space (after Fig. 8 of Tholen [1984]), with olivine/pyroxene/NiFe metal compositional triangle (see Fig. 3 of Chapman [1979]) superimposed.

of either class are currently known, future discoveries may fill in gaps in this graph.

The classes F, B, G and T are all low-albedo classes introduced by Tholen to describe variations within the formerly somewhat ill-defined C class which are generally interpreted as due to post-accretionary alteration. Fig. 1a supports this interpretation: all members of this clan occur in the same zone of the belt as C class objects. Apparently many primordial C class asteroids at the inner edge of the nonmelted region were strongly heated and meta-morphosed, while more organic-rich objects farther out escaped this process.

Additional evidence supporting this genetic relationship is the Themis asteroid family, which contains asteroids with spectra ranging from B to C to F, with many intermediate types (Tholen 1984, his Table XIV; Bell 1989). The thin arrows in Fig. 2a suggest hypothetical metamorphic trends that may link the metamorphic classes F, B, G and T to their parental C class material. Some of these trends could represent hydrous alteration as seen in the petrologic grade 1 and 2 carbonaceous chondrites, while others may indicate high-temperature anhydrous metamorphism as seen in such meteorites as Coolidge and Karoonda. (Unfortunately, the carbonaceous chondrite suite does not exhibit the full range of spectral curves seen in the F-B-C-G-T clan, suggesting that these asteroids, in general, have been exposed to a wider variety of alteration environments than seen in the meteorite samples currently being delivered to the surface of the Earth.)

In Fig. 2b are shown the igneous asteroid classes. The well-characterized mono-mineralic asteroids of the V, A and M classes surround the highly varied S types. This seems to be an expression of the olivine / pyroxene / NiFe metal triangle shown in Chapman (1979, his Fig. 3). In our figure we have superimposed this compositional triangle. Note that plagioclase does not show up in this plot because the ECAS spectra used by Tholen to define the parameters do not detect the feldspar absorption band at 1.2 μm. Also note that Q class would plot on the 0% metal axis of the triangle (between V and R), despite our interpretation of Q types as metal-bearing ordinary chondrites. This is consistent with the spectral difference discovered by Gaffey (1984) between red differentiated NiFe and gray chondritic NiFe.

In summary, Tholen's principal-components analysis seems to provide completely independent support for the interpretive framework in Table I, as well as new information on the genetic interrelationship of many asteroid classes.

Collisional and Dynamical History

Sizes, shapes and spins of main-belt asteroids which we observe today, ranging from km-sized bodies up to nearly 1000-km diameter Ceres, are the product of collisional modification of a primordial population. In the zone between Mars and Jupiter, the accretion process was interrupted by an unknown mechanism (but one likely driven by massive and nearby Jupiter) which pumped up orbital eccentricities and inclinations of the planetesimals in this zone. These orbits produce high-speed collisions, hence collisional grinding has been going on in the asteroid belt since that time.

Another characteristic of the asteroid zone is the low-mass density relative to the rest of the solar system. If all the mass of asteroids were incorporated into a single body it would be only 1400 km in diameter, less than half the size of the Earth's Moon. The mass density must have been higher in the earliest stage of planet formation; otherwise the time to accrete a Ceres-sized body would exceed the age of the solar system (Davis et al. 1979). Assuming

there was an Earth-mass or so initially in the asteroid zone, the question then becomes, what happened to it? Two possibilities are most likely: (1) the same process that stirred up orbits, also removed most of the mass in this zone; or (2) orbits were stirred up sufficiently for subsequent collisional grinding to transform the large bodies into dust which was removed by nongravitational forces, e.g., gas drag, radiation pressure, T-Tauri wind, etc.

Collisional evolution studies by Davis et al. (1985) indicate that the latter scenario is unlikely provided that Vesta is the eucrite parent body and that it formed near its present location. Given this constraint, then the "initial" asteroid population at the time orbits were pumped up enough to give a mean impact speed of 5 km s^{-1} was only several times more massive than the current belt—far short of an Earth mass of material. Furthermore, the removal mechanism in a collisional grinding scenario usually involves gas drag or radiation forces acting on small particles. Gas drag or Poynting-Robertson drag will cause the mass to spiral inward where much of it could be accreted by Mars. But Mars is already an undersized planet, so it is hard to imagine that significant mass could have been removed from the asteroid zone and deposited onto Mars. On the other hand, radiation pressure or the Yarkovsky-Peterson effect can cause very small particles in a selected size range and rotation state to spiral outward from the asteroid zone where they would be incorporated into Jupiter. While such a mechanism operates in principle, it seems unlikely that it would be sufficiently effective to remove nearly an Earth mass of matter from the asteroid zone.

With the hypothesis that the time of mass depletion and the period of orbital stirring were coeval early in solar system history, we may ask which characteristics of the asteroid population are "original" and which are the results of over 4 Gyr of collisional bashing. The asteroid size distribution has larger numbers of bodies at decreasing size, but cannot be represented by a simple power-law size distribution with a single exponent. Furthermore, the size distribution of different asteroid spectral classes, e.g., C and S appears to be quite different (see the chapter by Gradie et al). If we can strip away collisional modifications to the asteroid population, we can learn about the size distribution of accreting planetsimals and help understand how planets grew.

Some features of the present asteroid belt are not primordial. For example, the existence of M class asteroids, widely regarded as the exposed cores of differentiated parent bodies, demand some mechanism by which the overlying mantles are shattered and stripped away. Collisions are the only viable mechanism for accomplishing this. Dynamical families did not exist in the primordial population. These clusterings are the result of large, disruptive impacts during asteroid evolution.

Collisional modeling is a field fraught with uncertainties and unknowns. We have never seen, nor will we likely see, a major collision between two large asteroids; they are extremely rare events. Hence modeling of asteroid

collisional outcomes, the essential step in constructing an asteroid collisional history, involves extrapolating laboratory experiments (involving more or less homogenous, usually spherical, targets of basalt, granite or concrete) over 6 to 8 orders of magnitudes in size to apply to calculate the outcomes of possibly very inhomogeneous, and frequently nonspherical target bodies. This scaling problem is a formidable one and currently presents a major obstacle to further advances in collisional studies (see the chapter by Fujiwara et al.).

Shapes

A paradigm of asteroid research has been that asteroids in general have undergone a long collision history, and that many elongated shapes are associated with fragmentation events that created splinter-like pieces. However, the traditional idea that the original accretionary planetesimals were roughly spherical, and that odd shapes are produced only by fragmentation has recently been challenged on several fronts: (1) Theoretical work on collisions and rotations increases the chance that some highly elongated objects are spinning rubble piles with elongated equilibrium shapes (see the chapter by Weidenschilling et al.). (2) Trojan and possibly Hilda asteroids apparently have more elongated shapes than belt asteroids of the same sizes (Hartmann et al. 1988; French 1987; see also the chapter by French et al.). Comet nuclei also apparently have more elongated shapes than belt asteroids of the same sizes (Jewitt and Meech 1988).

Quantitative observations summarized in Table II expand upon these

TABLE II
Observed and Theoretical Lightcurve Amplitudes
for Different Populations of Bodies[a]

	Seen in Equatorial Plane[b] (aspect = 90)	Seen at Random Orientation[b] (aspect = 60)
Samples of main-belt asteroids:		
<32 km diam.	0.40	0.2 ±0.2
32–64 km diam.	0.66	0.33 ±0.17
50–100 km diam.	0.42	0.21 ±0.02
100–200 km diam.	0.36	0.18 ±0.01
25 C types; 42–188 km diam.	0.32	0.16 ±0.08
19 Trojans; 42–188 km diam.	0.68	0.34 ±0.13
12 Apollo-Amors; 1–16 km diam.	0.94	0.47 ±0.50
Av. of 6 reported comet nuclei	1.14	0.57 ±0.17[c]
Impact-generated rock fragments	0.41 ±0.05	0.21

[a]Using original data and values adapted from Hartmann et al. (1988); Binzel and Mulholland (1983); Jewitt and Meech (1988).
[b]Values with error bars are original observed data. Values without errors are calculated from the former values.
[c]P/Halley represented by 0.32 mag. at random epoch.

points. The shapes may give us important clues about the evolution history of different populations of asteroids. We see, for example, that the mean amplitudes among mid-sized belt asteroids are consistent with amplitudes observed among rock fragments observed at random orientations, in support of the idea that many irregular belt asteroids may be such fragments. Interestingly, nearly identical rock-fragmentation results have been reported by three independent teams (Fujiwara et al. 1977; Hartmann and Cruikshank 1978; Capaccioni et al. 1984). That the larger asteroids above 100 km diameter begin to have smaller amplitudes than the rock fragments may denote a tendency toward hydrostatic equilibrium, especially if some of them have weak, rubble-pile structures. Gravitational stresses exceed typical crushing strengths of chondrites at diameters exceeding about 150 km for weak chondrite materials and as much as 1000 km for strong chondrites (Hartmann 1983, pp. 201ff.). Empirically, strongly irregular shapes occur only among solar system bodies smaller than about 500 km diameter.

That the Trojan asteroids and comet nuclei have higher mean lightcurve amplitudes than expected for collisional fragments suggests a different origin for these extreme shapes. It is as yet unclear whether the whole distribution is shifted to higher amplitudes in these populations, or whether a subset of highly elongate objects is grafted onto distributions like those in the belt.

Body shape for collisionally derived fragments may also reflect differences in compositionally controlled strength within differentiated planetesimals. For completely differentiated bodies (core-mantle-crust) or for those which underwent melting and differentiation of a surficial layer (a silicate surface atop of a metal layer overlying an undifferentiated core), erosion or disruption should be halted or impeded at the metal-silicate boundary. Spherically symmetric differentiated parent bodies may produce asteroidal fragments with a size- and composition-dependent shape distribution.

Recent discussions of irregular shapes (Weidenschilling 1980; French 1987; Hartmann et al. 1988; Jewitt and Meech 1988; the chapter by Binzel et al.) have produced a number of suggestions about causes of various shapes. These can be grouped and summarized as follows:

SPHERICAL SHAPES

(A) Spherical shapes of large, slowly rotating objects, due to hydrostatic equilibrium.

(B) Spherical shapes of small, weak objects due to "sandblasting" by small impactors (French 1987).

ELONGATED SHAPES

(A) Splinter-shaped fragments. Capaccioni et al. (1984) find evidence from impact fragments that many belt asteroids are to be so explained.

(B) Elongated shapes associated with rapid rotation and low strength or rubble-pile structure (Weidenschilling 1980).

(C) Asymmetric sublimation of initially spherical bodies (Jewitt and Meech 1988).

(D) Exaggeration of local topography during sublimation (Colwell and Jakosky 1987).

(E) Exaggeration of axis ratio during sublimation on bodies of initially non-spherical shape (Hartmann, in preparation).

(F) Preservation of primordial irregular shapes produced by low-velocity collisions among similar-sized objects, producing "compound" planetesimals (Hartmann and Cruikshank 1978; French 1987; Hartmann et al. 1988).

In summary, the unexamined paradigm that the original asteroid parent bodies were spherical, and that irregular shapes always indicate collisional fragmentation, seems less convincing upon examination. Current thinking in this area does not provide any generally accepted model for using shape data to constrain the history of the asteroid belt. This is particularly unfortunate since a large fraction of the available observational data on asteroids consists of lightcurves.

III. SOME BAFFLING PARADOXES

Previous attempts to make sense out of the great mass of asteroid data have exposed at least two severe contradictions or paradoxes between different lines of research which many workers in the field regard as severe problems. We prefer to think of them as touchstones for the validity of possible paradigms for asteroid evolution. Only those models which explain the following problems in a straightforward way are worthy of consideration.

The Ordinary-Chondrite Mystery

For many years, the principal problem in asteroid spectroscopy has been the location of the ordinary chondrite parent bodies. In Table I we have followed the current understanding (McFadden et al. 1984,1985; Bell and Keil 1988) and associated them with Tholen's Q class, of which 1862 Apollo is the only well-observed example. Several Earth-crossing asteroids also appear to be of this class. However, no examples are found among the over 500 main-belt objects observed. Instead, the only main-belt class which could remotely be ordinary chondrite (OC) parents, the S class, fails every test so far applied: their metal component has a red spectrum unlike the flat spectrum of OC metal; many of them have no 2-μm pyroxene band (i.e., grossly nonchondritic pure-olivine silicate component); and even 8 Flora which has about the right olivine/pyroxene ratio has surface variations difficult to reconcile with well-known chondritic trends (Gaffey 1984). In addition, systematic trends in spectral properties with solar distance exist within the S zone of the asteroid belt which are in the opposite sense to those expected from chondritic trends. All this observational evidence seemingly conflicts with a variety of cosmo-

chemical evidence that OCs formed in a region of the solar nebula intermediate between the enstatite chondrites/achondrites and the carbonaceous chondrites (which is exactly where many S types, but no Q types, are found in the asteroid belt).

The Great Dunite Shortage

Chapman (1986) has pointed out a second paradox in our current understanding of the inner belt, which he refers to as the olivine problem. Olivine is by far the most common mineral in most chondritic meteorites. Complete differentiation of an ordinary chondrite or carbonaceous chondrite parent body would result in a body with a NiFe metal core, a thick olivine-dominated mantle, and a thin plagioclase/pyroxene crust. Vesta appears to be a rare surviving example of this classic differentiated parent body. Spectral observations have revealed a window in the plagioclase/pyroxene crust which reveals the olivine mantle (Gaffey 1983). (This is probably a deep impact crater; several lunar craters similarly excavate olivine.) A few other objects could represent mantles completely stripped of their crusts. 349 Dembowska has a predominantly olivine composition, and the A class asteroids are apparently pure olivine. But a very much larger number of inner-belt asteroids appear to represent very deep metal-rich assemblages (class M and class S). Similarly, there are a variety of classes of iron and stony-iron meteorites but only one non-Martian olivine meteorite, Brachina. Both asteroid and meteorite studies agree (for once) that mantle material is very rare in the main asteroid belt.

Actually the shortage is not of olivine *per se,* but of olivine-dominated metal-free silicate rocks (i.e., dunites). Many S-type asteroids are rich in olivine (indeed, as first shown by Feierberg et al. [1982], it is one of the reasons they cannot as a class be ordinary chondrites); however, it is mixed with considerable amounts of metal and thus cannot represent a classic planetary mantle. It appears that collisional evolution in the inner main belt has been very severe, and only a few lucky asteroids have managed to retain their pure-silicate upper layers.

This conclusion raises two questions which have no obvious answer: (1) Where did all those bright green olivine rocks go after they were knocked off the asteroids? Dunite has one of the most distinctive visual spectra of any rock, but only a few A class asteroids with this spectrum turned up in the ECAS. (2) If olivine was too fragile to survive to the present, why has a large population of C class asteroids composed of carbonaceous chondrite material survived right next door in the middle belt?

IV. THE MODEL

In this section, we present a tentative model for the thermal and mineralogical evolution of the asteroid belt which attempts to integrate all the reliable data on asteroids and meteorites into a coherent scenario. This model has

been developed by the principal author over the past 4 yr with input from many other scientists whose comments have guided it towards its present form. The intent is not to provide a rigid framework to be memorized by all graduate students, but to provoke asteroid observers, dynamicists, collision modelers and meteorite geochemists to lift their eyes occasionally from the technical details of their daily work and think about the "Big Picture." We hope that it will serve this purpose even if (as we confidently expect) many of its details are proven wrong as a result. The means of presentation will be a series of cross-sections of the asteroid belt at various stages of its development in which the horizontal axis is semimajor axis *a* and the vertical axis is the radius of the parent body or asteroid under consideration.

Condensation Locations

In Fig. 3a is depicted the original sequence of chondritic material in the asteroid belt. The sunward portion of this distribution follows traditional meteoritical precepts with the important exception that the chondrite classes are compressed into a much smaller region than usual. The traditional means of locating chondrites in the solar nebula is to compare their FeO fraction (oxidation state) with those inferred for the terrestrial planets. This has led to the belief that E's come from somewhere near Mercury, H/L/LL's from around Earth and Mars, and only carbonaceous chondrites are native to the asteroid belt. The only way this could be reconciled with the current derivation of all chondrites from the belt was to postulate that the belt was a dumping ground for all the solar system's rejected planetesimals, and contains a variety of materials from widely different condensation locations in the original solar nebula. The systematic mineralogical stratification of the belt shown in Fig. 1a leads us to reject this concept. Readers who feel uncomfortable with this are invited to regard the horizontal scales in Figs. 3 and 4 as flexible.

Along the top of Fig. 3a are portrayed several parameters of chondrites which indicate variations in the characteristics of the solar nebula. Oxidation state and condensation temperature follow traditional patterns, but both trends are much steeper than usually allowed.

The right half of Fig. 3a contains two hypothetical classes of chondrites which are postulated to explain the class P and D asteroids. VCC stands for Very Carbonaceous Chondrites and UCC for Ultra-Carbonaceous Chondrites. This material is ultra-carbonaceous in the sense that it probably contains a spectrally dominant reddish organic phase. Either declining temperatures or longer times below some key temperature (possibly that at which Fischer-Tropsch reactions could occur) produce the increasing abundance of this phase with distance from the Sun.

A major uncertainty in this portion of the diagram is the role of water. Many asteroids in the middle belt show the 3-μm absorption band due to bound water in hydrated silicates (Lebofsky 1980). From fragmentary data available, it seems that this band disappears in the P and D zones (Feierberg et
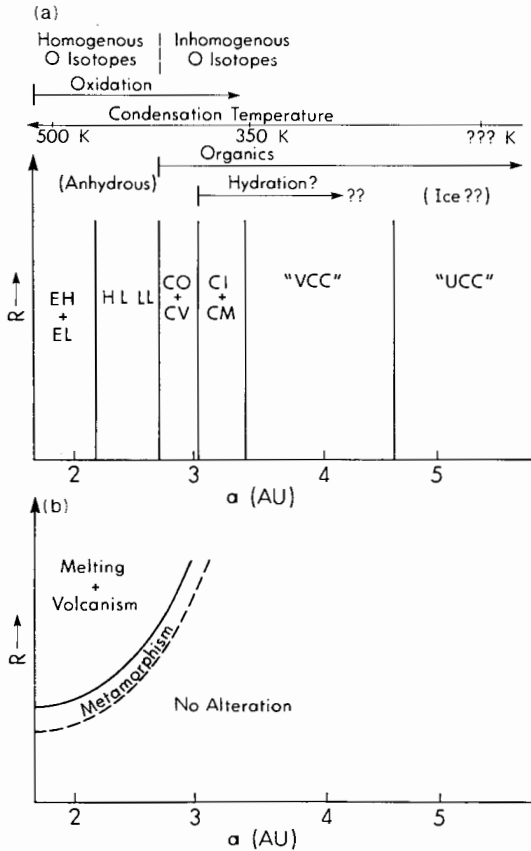
Fig. 3. (a) Cross section of the asteroid belt at the end of condensation and planetesimal accretion, with position of parent bodies of various known and unknown chondrite types. (b) Pattern of metamorphic heating in the early asteroid belt.

al. 1985; Jones et al. 1987). It is currently believed that the hydration of the silicates in meteorites did not occur in the nebula, but in the asteroid parent bodies after a minor ice component melted. Since the post-accretionary heating event declined rapidly with increasing solar distance, the apparent lack of hydrated silicates in the P and D asteroids may represent the absence of sufficient heating to melt and mobilize the original ice. It therefore appears possible that the P and D asteroids still retain ice in their interiors, despite the absence of ice absorptions in their spectra.

The Heating Episode

In Sec. II, we showed that the spatial distribution of the three asteroid superclasses requires an asteroidal heating mechanism which declined rapidly

with solar distance. Since the surface area of a body increases as the square of the diameter while the volume increases as the cube, small asteroids lose heat much more readily than large ones. The degree of metamorphic heating in asteroid parent bodies must have also declined with decreasing parent-body size. (In addition to these major trends, there may be others characteristic of particular heating mechanisms. For instance, electromagnetic heating could actually decline in efficiency for the largest asteroids, as well as showing wide variations in a particular body. Since our current picture of the pre-collisional asteroid belt is too dim to resolve such second-order effects, we will not include them in this graph.) Therefore, we can say that the distribution of melted asteroid parent bodies was something like that shown in Fig. 3b. The upper left region of the diagram contains objects which were at least mostly molten and in which significant segregation of metal and silicates took place. In some unknown fraction of these objects, considerable petrologic evolution of the silicate component and basaltic volcanism also occurred. Surrounding this region of the diagram is a boundary region in which various degrees of metamorphic alteration occurred. The boundary in Fig. 3b is intended to indicate the limit of metamorphism resulting in detectable spectral variations; the region of metamorphism recognized by meteoriticists would be much larger. At large solar distances or for very small parent-body sizes, there were no perceptible thermal effects.

To see what mineralogies would be produced in this heating episode, we overlay Figs. 3a and 3b, with the result shown in Fig. 4a. Enstatite chondrites have brought forth enstatite achondrites (aubrites). The petrologically more complex ordinary chondrites can produce a variety of achondritic mineralogies depending on the degree of segregation of olivine, pyroxene, plagioclase and metal which takes place during a particular asteroid's igneous evolution. A small region of the diagram is reserved for the ureilites and Eagle Station pallasites, which are the only achondrites that seem to have carbonaceous chondrites as parent material (i.e., outer-solar-system oxygen isotopes). Beyond the middle asteroid belt all parent bodies are unaltered. In the inner belt, only small parent bodies for the enstatite and ordinary chondrites can survive, and most of them are significantly metamorphosed (as we see in the meteorites today).

For the benefit of those confused by meteoritical terminology, we present Fig. 4b which is simply Fig. 4a relabeled with the asteroid taxonomic types according to the scheme in Table I. A comparison with Fig. 1a shows that in at least the upper part of the diagram, there is now a close correspondence with the currently observed spatial distribution of asteroid taxonomic types.

Collisional Evolution

There are two features of the modern asteroid belt which cannot be accounted for by the two processes considered above. First, many of the asteroid classes in the upper left region of Fig. 4b occur only in the deep interior
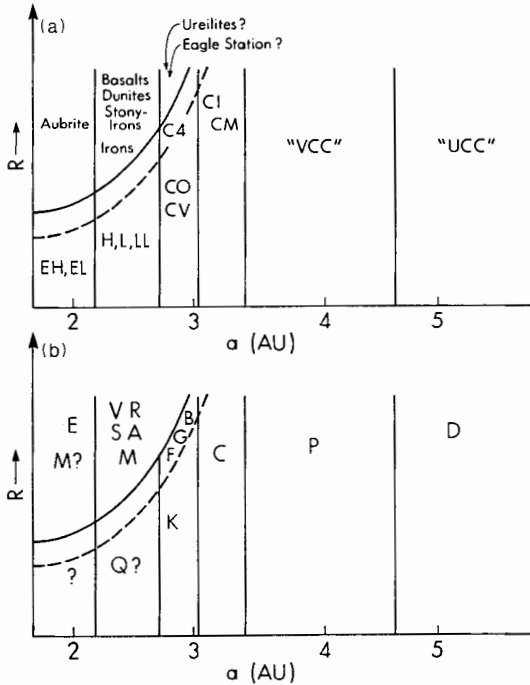
Fig. 4. (a) Combination of Figs. 3a and b illustrating distribution of meteorite mineralogies in the asteroid belt after the heating episode. (b) Same as Fig. 4a with meteorite terminology converted to asteroid taxonomic types using the scheme of Table I.

of the parent bodies and must be liberated by collisional erosion or disruption. This proves that at least the inner belt has undergone massive collisional events. Secondly, the great dunite shortage implies that once disrupted, the metal-rich core regions of the parent bodies survive while the silicate mantles are very efficiently destroyed. Only some process such as this can explain the rarity of metal-free achondritic rocky asteroids (classes V, R, A, E) relative to metal-rich objects (classes S and M) in the inner belt.

Can current mainstream collisional models produce the kind of asteroid belt we see today, starting from the stage portrayed in Fig. 4b? The first-order requirement is a collision scenario which preserves Vesta's basaltic crust while also stripping away the crust and mantle of other differentiated bodies in order to expose their cores as M- and S-type asteroids.

We first consider the minimum mass collisional scenario favored by Davis et al. (1985). This model has a 15% chance of preserving Vesta's crust by starting with an initial belt that is only ~3 times as massive as the present one. The initial size distribution is one characteristic of a runaway planetesimal growth case—there is one large planetesimal (Ceres) which is beginning

to run away from the remaining bodies (Ceres mass is about five times that of the second largest asteroid, 2 Pallas). However, the bulk of the mass in the initial population is in small bodies, ≤ 85 km diameter. While this case does not match exactly the observed asteroid size distribution, it does evolve to one reasonably close (see the chapter by Davis et al.).

Other essential features of this collisional scenario are:

1. A significant fraction (50%) of large asteroids (at ~100 km diameter) are shattered survivors from the primordial population;
2. Only Ceres and Vesta are unshattered surviving planetesimals;
3. The primordial rotation rates of asteroids > 100 km diameter have been little altered by mutual collisions over asteroid history;
4. Asteroid shapes for many 100 to 250 km sized bodies have likely been substantially altered due to formation of gravitationally bound rubble piles;
5. It predicts collisional destruction of 9 bodies > 200-km diameter which is in good agreement with the 8 observed families thought to be formed by disruption of parent bodies larger than this size.

Formation of S and M Asteroids.   The size distribution of large S- and M- type asteroids are given in Table III; these bodies are presumably exposed cores. The largest asteroids that are collisionally exposed cores in this scenario are 15 Eunomia (S) and 16 Psyche (M), both having diameters around 270 km. Smaller asteroids of these classes could be either cores themselves or fragments of disrupted cores. Assuming that these large cores contain ~30% of the parent-body mass, one finds that at least 37 bodies > 150 km diameter must have had their crust and mantles stripped away to produce the observed large S and M type asteroids.

Collisional evolution models (see the chapter by Davis et al.) show that at least this many and likely an even larger number of original bodies in these size ranges have been eroded or disrupted such that they lost >50% of their

TABLE III
Number of Large S- and M-Type Asteroids

| | | Size Range (km) | | |
	Type	>200	150–200	100–150
Observed population	S	5	6	20
	M	1	1	4
	Total	6	7	24
Estimated parent body size		300–400	225–300	150–225
Number of bodies disrupted in collisional models[a]		approx 6	approx 21	approx 100

[a]Data on disrupted bodies are from the RG3B initial population, $S_0 = 3 \times 10^7$ erg cm^{-3}, no strain-rate scaling case of the Davis et al. chapter.

original mass. While there are as yet considerable uncertainties in the collisional studies, even a minimal initial mass belt produces adequate collisional disruption to produce the observed large S and M asteroids (Table III).

The number of shattered parent asteroids substantially exceeds the observed number of S and M cores, as it should. First, not all of the asteroids in these size ranges differentiated (outer belt bodies were never heated sufficiently to cause melting). Second, some of the cores that were formed must have been subsequently shattered in order to form the observed small diameter population of these bodies. While the collisional models do not keep track of the subsequent evolution of exposed cores, it seems likely that some of them have been collisionally shattered.

The Great Dunite Shortage. If so many differentiated parent bodies were shattered, where are all the dunite fragments from their mantles? The collision models do not give a straightforward answer but neither do they indicate a major problem in accounting for this material. First, the largest body that is a fragment from disruption of a larger parent body is 100 km in diameter—but models predict only about one at this size. Even at 50 km, there are only ~10 direct fragments surviving in the population today (see the chapter by Davis et al. for additional discussion of the collision history of asteroids as a function of size). Some of these should be mantle fragments and indeed this is just the size range in which we first observe A class asteroids (246 Asporina: D ~64 km; 446 Aeternitas and 289 Nenetta: both ~43 km in diameter) which are thought to be fragments of disrupted mantle material. Most of the fragments from disruption and large erosive cratering collisions are of even smaller sizes (25 km or less). But at $D = 25$ km, only about 15% of the current population are direct fragments, according to this collisional scenario. However, this number is a lower bound to the actual number of fragments at any size due to the inability of the computer simulation to track multigeneration evolution of fragments. For example, disruption of a 300 km parent body could produce a 35-km fragment which in turn could be whittled down to 25 km diameter by cratering erosion. Such a body would be recorded as an eroded body rather than a fragment and would not be distinguished from a primordial 35-km body which was eroded to 25 km. Additional modeling is needed to provide this more refined resolution.

The Ordinary Chondrite Mystery. Collisional disruption and erosion can potentially explain the lack of observable ordinary chondrite parent bodies in the belt. As shown in Fig. 4b, the OC parent bodies started out even smaller than any differentiated objects, and therefore were even more vulnerable to complete collisional disruption. In terms of our collisional scenario, we ask what is the largest size bin for which the primordial population is essentially all collisionally ground down to below the size limit of the "deepest" comprehensive spectral survey (currently the ECAS)? This size then fixes the

boundary separating the Q-asteroid regime from that of the igneous types in Fig. 4b. With present modeling capabilities, we can only place some constraints on this limiting size; additional capability to follow the multigenerational evolution of fragments is needed to address this question. However, the existing models do show that survivors from the primordial population begin to appear in the final population at around diameters of 50 km or so. Hence the upper limit to the radius of unmelted bodies could not have been larger than this size. Subsequent collisional evolution could have reduced this population to below the ECAS detection limit (about 20 km at the relevant distances and albedos). Traditionally, the OC parent bodies have been thought to be somewhat larger (around 200 to 300 km) on the basis of metallographic cooling rates. But these results could be made consistent with ~50 km parent bodies by assuming a modest insulating regolith. Thus, it is not unreasonable that Q class asteroids have, to date, been found only among the Earth-approaching population, the only place where objects a few kilometers across can be observed with current equipment.

Some Possible Wild Cards.   There are at least two aspects of collisional evolution that are not well treated in current models, and would probably tend to skew them in the direction of producing the odd distribution of types we see in the inner belt. One is the role of strength differences in preserving metal-dominated asteroids. The meteorites associated with the S class are composed of discrete regions of silicates in a continuous metal matrix and are much stronger mechanically than stony meteorites. This suggests that a differentiated or semi-differentiated asteroid parent body will be rapidly stripped of its weak outer silicate layers by collisions with other asteroids; once a metal-dominated layer is reached, fragmentation will proceed more slowly. While there is not a large body of experimental data on collisional shattering of metal, a few experiments have been carried out (Mizutani, personal communication) which show that metal has impact strengths 1 to 2 orders of magnitude larger than stony silicates. Metal targets require projectiles 4 to 5 times larger than silicate ones to produce the same degree of shattering. Thus, it takes longer to shatter strong targets because there are fewer large projectiles in the asteroid population.

Two features of the current asteroid/meteorite population strongly support the idea that mechanical strength (i.e., metal/silicate ratio) is a major controlling factor in asteroid fragmentation:

1. There is a very large difference in cosmic-ray exposure ages between stone meteorites (~10 Myr) and iron meteorites (~500 Myr). The traditional explanation for this difference has been that iron meteorites are much more resistant to collisional destruction than stones. There seems no reason why this should not apply to asteroid-size objects as well as meter-sized ones.
2. The S-type asteroid population shows a significantly different size distribu-

tion than the C-type population, and both types vary somewhat with position in the belt (see the chapter by Gradie et al.). The S population shows a nearly power-law-like distribution while that of the C asteroids contains a distinctive hump. Numerical studies by Davis et al. (1985) clearly showed that a hump will form in a collisionally evolving population at sizes where the gravitational binding energy starts to exceed the material strength of a body. Hence, the size distribution of C asteroids could be a collisional product. On the other hand, the purely power-law size distribution of the S asteroids is typical of collisional shattering in a purely strength-controlled regime. This speculative interpretation implies that the impact strength of S asteroids is significantly higher than that of C asteroids which is consistent with our interpretation of S types as the cores of differentiated parent bodies. We must await results of further models to quantify these strength parameters and test this suggestion.

Another possible "wild card" is an initial asteroid size distribution very different from those we are familiar with in the modern solar system. Quoting Chapman (1986, p. 109), "A projectile population not accompanied by a steep fragmental size distribution of smaller projectiles is just what is required to smash up most bodies, while leaving (by chance) a small number of bodies (e.g., Vesta and Dembowska) relatively undisturbed." A fragmentation-controlled distribution of projectile sizes could not have existed until after many collisions had already occurred; the early populations of both targets and projectiles consisted of original accretionary planetesimals whose size spectrum was probably much narrower than the current one.

In summary, collisional models using homogeneous targets having the impact strength of laboratory basalt predict that the largest fragments from shattered mantles have sizes similar to the observed largest A asteroids. The bulk of the mantle mass, though, is at smaller sizes, ~25 km. The large strength difference between metal and silicates probably biases the collisional evolution of the actual asteroid belt even more toward the survival of metal-rich cores and the rapid destruction of mantle, crust and chondrite material. More refined modeling is needed to calculate how much silicate-rich material may be hidden among asteroids <25 km diameter which we have not yet observed spectroscopically and how much has been ground down to dust and removed from the belt.

Delivery of Asteroids to the Earth

The last stage in the life of an asteroid which we need to explain is their delivery to the Earth. If one compares the distribution of meteorite types in the *observed* asteroid belt (i.e., the larger bodies which have survived the long epoch of mutual collisions) with the statistics of observed meteorite falls, it appears that there is a massive bias in the sampling of meteorite parent bodies. There seems to be a large excess of metal-rich source bodies in the >20-km-

size range relative to the proportion of stony-iron and iron meteorites reaching the Earth. There are many possible biases which may affect the flux of meteorites to the Earth's surface. Are any of them large enough to reconcile the observed meteorite and asteroid type distributions? We suggest (following Fig. 5 of Greenberg and Chapman [1983]; see also the chapter by Greenberg and Nolan) that the strength effects discussed above are largely responsible. Stony and chondritic material is broken down by collisional evolution much more rapidly than stony-iron or iron material. This effect may skew the size distribution of the two classes of material so that the meter-size population (meteorites) is dominated by fragile material, the 100-km-size population (observed belt asteroids) is dominated by strong material, and the 1- to 10-km-size population (observed Earth-crossing asteroids) has some of both. Ordinary chondrites are so common because their parent bodies have been more completely dispersed into many small fragments than any other inner-belt type, and their dominance of the current flux at the Earth is the logical consequence of the absence of a source asteroid in our current highly size-biased sample of the asteroid population, rather than a puzzle.

V. PREDICTIONS AND GUIDELINES FOR THE FUTURE

Predictions of the Model

The model outlined above seems to reconcile most of the current hard data available on asteroids in a superficially appealing way. However, many equally appealing scenarios in other fields have later turned out to be nonsense. The true test of any descriptive model is whether it makes specific predictions about observable parameters which have not as yet been observed. With considerable trepidation, the principal author has compiled the following list of predictions which fall out of the model, and whose confirmation would increase our confidence that it approximates the truth:

1. New classes of chondritic material rich in organic compounds (corresponding to P-type and D-type asteroids) will be found in meteoritic breccias or cosmic dust collection experiments.
2. Parent bodies for the CO and CV chondrites will be found near the transition zone between C types and S types in the asteroid belt.
3. The composition of inner-belt asteroids will be found to vary with asteroid size, in the sense that classes V, R and A will be more common at smaller sizes.
4. Small (<10 km) ordinary-chondrite source bodies (= Q-class asteroids?) will be found in the inner main belt.
5. A few very small objects at the inner edge of the main belt will be found to be source bodies of the enstatite chondrites, and perhaps also enstatite stony-irons such as Mount Egerton.

6. The Earth-crossing asteroid population will be found to resemble closely the inner belt in composition when equal-size distributions are compared.
7. In contrast to the inner belt, the outer belt and Trojan asteroid population will be found to have uniform composition as a function of asteroid size.
8. Body shape for metallic objects should correlate with degree of differentiation; that is, strongest heating (as indicated by degree of silicate re-equilibration) will produce most nearly spherically symmetric metal distributions.

In fact, the first two of these predictions have at least partially come true since this table was first compiled for a presentation in November 1985. Both the Brownlee particles and the dust of Comet Halley appear to exhibit ultracarbonaceous composition predicted for D class asteroids. The CV/CO analogs (i.e., new K class asteroids) have appeared at 3.1 AU exactly where Fig. 4 predicts them, although the 1986 version of this figure erroneously showed them as falling into the old C class even though it had been shown years before that such asteroids would fall into the old S class (Gaffey 1976).

Implications for Future Asteroid Research

The predictions above obviously have implications for the kinds of research that will produce the greatest dividends in terms of real understanding of the complicated story the asteroids are telling us. The following are a few promising areas of inquiry which we commend to both scientists and their funding agencies:

1. Larger telescopes and more sensitive instruments should be used to obtain a spectroscopic sample of smaller main-belt asteroids.
2. A systematic program of observing Earth-crossers should be reinstituted.
3. Asteroid scientists need to become more familiar with recent meteorite research, and use meteoritical terminology correctly. Much of the apparent confusion in asteroid science is really due to lack of mutual understanding between the various communities of scientists who study these objects.
4. Realistic information about asteroid collisions needs to be collected by means of impact experiments using real meteoritic minerals, especially NiFe alloys. There has been little research on metal-metal or rock-metal collisions, much less on collisions between objects with complex internal structures.
5. The asteroid family problem needs to be completely re-examined. There is a persistent schism between dynamical analysts and asteroid spectroscopists as to the significance of many asteroid families.
6. Modelers of the solar nebula need to think about models which can explain the very steep local gradient in composition of the original chondrite material implied by the asteroid observations.

Acknowledgments. Discussions with many asteriod and meteorite researchers over the past four years contributed to the thoughts embodied in this chapter. Extensive reviews by C. Chapman, J. Lewis and K. Keil significantly improved the original manuscript.

REFERENCES

Barucci, M. A., Capria, M. T., Coradini, A., and Fulchignoni, M. 1988. Classification of asteroids using G-mode analysis. *Icarus* 72:304–324.

Bell, J. F. 1986. Mineralogical evolution of meteorite parent bodies. *Lunar and Planet. Sci.* XVII:985–986 (abstract).

Bell, J. F. 1988. A probable asteroidal parent body for the CV or CO chondrites. *Meteoritics* 23:256–257 (abstract).

Bell, J. F. 1989. Mineralogical clues to the origin of asteroid families. *Icarus,* submitted.

Bell, J. F., and Keil, K. 1988. Spectral alteration effects in chondritic gas-rich breccias; Implications for S-class and Q-class asteroids. *Proc. Lunar Planet. Sci. Conf.* 18:573–580.

Bell, J. F., Cruikshank, D. P., and Gaffey, M. J. 1985. The composition and origin of the Iapetus dark material. *Icarus* 61:192–207.

Binzel, R., and Mulholland, J. D. 1983. A photoelectric lightcurve survey of small main-belt asteroids. *Icarus* 56:519–541.

Capaccioni, F., Cerroni, P., Coradini, M., Farinella, P., Flamini, E., Martelli, G., Paolicchi, P., Smith, P., and Zappalà, V. 1984. Shapes of asteroids compared with fragments from hypervelocity impact experiments. *Nature* 308:832–834.

Chapman, C. R. 1979. The asteroids: Nature, interrelations, origin, and evolution. In *Asteroids,* ed. T. Gehrels (Tucson: Univ. of Arizona Press), pp. 25–60.

Chapman, C. R. 1986. Implications of the inferred compositions of the asteroids for their collisional evolution. *Mem. Soc. Astron. Italiana* 57:103–114.

Chapman, C. R. 1987. Distributions of asteroid compositional types with solar distance, body diameter, and solar distance. *Meteoritics* 22:353–354 (abstract).

Colwell, J. E., and Jakosky, B. M. 1987. The evolution of topography on a comet. *Icarus* 72:128–134.

Davis, D. R., Chapman, C. R., Greenberg, R., Weidenschilling, S. J., and Harris, A. W. 1979. Collisional evolution of asteroids: Populations, rotations, and velocities. In *Asteroids,* ed. T. Gehrels (Tucson: Univ. of Arizona Press), pp. 528–557.

Davis, D. R., Chapman, C. R., Weidenschilling, S. J., and Greenberg, R. 1985. Collisional history of asteroids: Evidence from Vesta and the Hirayama families. *Icarus* 63:30–53.

Feierberg, M. A., Larson, H. P., and Chapman, C. R. 1982. Spectroscopic evidence for undifferentiated S-type asteroids. *Astrophys. J.* 257:361–372.

Feierberg, M. A., Lebofsky, L. A., and Tholen, D. J. 1985. The nature of C-class asteroids from 3-micron spectrophotometry. *Icarus* 63:183–191.

French, L. M. 1987. Rotation properties of four L5 Trojan asteroids from CCD photometry. *Icarus* 72:325–341.

Fujiwara, A., Kaminoto, G., and Tsukamoto, A. 1977. Destruction of basaltic bodies by highvelocity impact. *Icarus* 31:277–288.

Gaffey, M. J. 1976. Spectral reflectance of the meteorite classes. *J. Geophys. Res.* 81:905–920.

Gaffey, M. J. 1983. The asteroid (4) Vesta: Rotational spectral variations, surface material heterogeneity, and implications for the origin of the basaltic achondrites. *Lunar Planet. Sci.* XIV:231–232 (abstract).

Gaffey, M. J. 1984. Rotational spectral variations of asteroid (8) Flora: Implications for the nature of the S-type asteroids and for the parent bodies of the ordinary chondrites. *Icarus* 60:83–114.

Gaffey, M. J. 1988. Thermal history of the asteroid belt: Implications for accretion of the terrestrial planets. *Lunar Planet. Sci.* XIX:369–370 (abstract).

Gradie, J. C., and Tedesco, E. F. 1982. Compositional structure of the asteroid belt. *Science* 216:1405–1407.

Gradie, J. C., and Tedesco, E. F. 1989. Asteroid diameters and albedos from IRTF 10 and 20-μm radiometry). *Astron. J.,* in preparation.

Gradie, J. C., and Veverka, J. 1980. The composition of the Trojan asteroids. *Nature* 283:840–842.

Greenberg, R., and Chapman, C. R. 1983. Asteroids and meteorites: Parent bodies and delivered samples. *Icarus* 55:455–481.

Hartmann, W. K. 1983. *Moons and Planets: An Introduction to Planetary Science* (Belmont, CA: Wadsworth Publishing).

Hartmann, W. K., and Cruikshank, D. P. 1978. The nature of Trojan asteroid 624 Hektor. *Icarus* 36:353–366.

Hartmann, W. K., Tholen, D., Goguen, J., Binzel, R., and Cruikshank, D. P. 1988. Trojan and Hilda asteroid lightcurves. 1. Anomalously elongated shapes among Trojans (and Hildas?). *Icarus* 73:487–498.

Jewitt, D., and Meech, K. 1988. Optical properties of cometary nuclei and a preliminary comparison with asteroids. *Astrophys. J.* 328:974–986.

Jones, T. D., Lebofsky, L. A., and Lewis, J. A. 1987. Mid-IR reflectance spectra of C-class asteroids. *Bull. Amer. Astron. Soc.* 19:841 (abstract).

Kerridge, J. F., and Matthews, M. S., eds. 1988. *Meteorites and the Early Solar System* (Tucson: Univ. of Arizona Press).

Lebofsky, L. A. 1980. Infrared reflection spectra of asteroids: A search for water of hydration. *Astron. J.* 85:573–585.

McFadden, L. A., Gaffey, M. J., and McCord, T. B. 1984. Mineralogical-petrological characterization of near-Earth asteroids. *Icarus* 59:25–40.

McFadden, L. A., Gaffey, M. J., and McCord, T. B. 1985. Near-Earth asteroids: Possible sources from reflectance spectroscopy. *Science* 229:160–163.

Ostro, S. J., Campbell, D. B., and Shapiro, I. I. 1985. Mainbelt asteroids: Dual-polarization radar observations. *Science* 229:442–446.

Tedesco, E. F., Williams, J. G., Matson, D. L., Veeder, G. J., Gradie, J. C., and Lebofsky, L. A. 1989. A three-parameter asteroid taxonomy. *Astron. J.*, 97:580–606.

Tholen, D. J. 1984. Asteroid Taxonomy from Cluster Analysis of Photometry. Ph.D. Thesis, Univ. of Arizona.

Weidenschilling, S. J. 1980. Hektor: Nature and origin of a binary asteroid. *Icarus* 44:807–809.

Wetherill, G. W., and Chapman, C. R. 1988. Asteroids and meteorites. In *Meteorites and the Early Solar System*, eds. J. F. Kerridge and M. S. Matthews (Tucson: Univ. of Arizona Press), pp. 35–67.

Zellner, B. 1979. Asteroid taxonomy and the distribution of the compositional types. In *Asteroids*, ed. T. Gehrels (Tucson: Univ. of Arizona Press), pp. 783–806.

Zellner, B., Tholen, D. J., and Tedesco, E. F. 1985. The eight-color asteroid survey: Results for 589 minor planets. *Icarus* 61:355–416.

PART V
Space Studies

ASTEROID OBSERVATIONS WITH THE HUBBLE SPACE TELESCOPE AND THE SPACE INFRARED TELESCOPE FACILITY

B. ZELLNER, EDDIE N. WELLS
Computer Sciences Corporation

CLARK R. CHAPMAN
Planetary Science Institute

and

D. P. CRUIKSHANK
NASA Ames Research Center

The Hubble Space Telescope will provide asteroid observers with exceptional opportunities to make observations not possible from the ground. It will provide expanded wavelength coverage in the ultraviolet, plus high spatial resolution permitting observations of body shape, configuration and compositional variations at geophysically and cosmochemically relevant scales for the nearest and largest objects. There are also opportunities for making important observations of asteroids fainter than can be practically observed from the ground. Other second-generation Earth-orbiting observatories are planned for later years. One of these, the Space Infrared Telescope Facility, has particular potential for asteroids.

I. INTRODUCTION

The asteroids, to date, have been studied only by groundbased and Earth-orbital telescopes. We are entering an era of spacecraft exploration of asteroids, which will permit close-up observations and *in situ* studies. However, such missions will never explore more than a handful of asteroids, whereas an

[949]

essential element of asteroid exploration is study of the great diversity within the asteroid population—diversity in mineralogy, size, spin and shape, Hirayama family membership, and location in the solar system. The Hubble Space Telescope (HST), currently scheduled for launch in early 1990, provides the only capability extant or planned to study asteroids at geophysically relevant spatial scales for a number of bodies sufficient to sample the known range of diversity that is of fundamental interest in solar system science. Likewise, the Space Infrared Telescope Facility (SIRTF), planned for launch in the late 1990s, will provide a capability for infrared observations, some of them quite revolutionary, for large numbers of asteroids and related objects.

In this chapter we consider all small solar system bodies that have observable solid surfaces. Thus, we include bodies of an essentially cometary nature but which do not exhibit active cometary phenomena, either because they are too far from the Sun for their constituent ices to volatilize or because they have already devolatilized, and are "dead." We also treat small planetary satellites as "asteroids." Actually, some may be captured asteroids, as suspected in the case of the outer Jovian satellites (see, e.g., Tholen and Zellner 1984). Only the HST can observe both satellites of Mars and main-belt asteroids by the same techniques, with the same high precision and freedom from systematic error. Such satellites are likely to be primitive bodies in the same sense that asteroids are, and they are likely to provide similar kinds of clues about primordial conditions in the solar system.

II. ASTEROID SCIENCE WITH THE HUBBLE SPACE TELESCOPE

The HST is a 94-inch telescope, in low Earth orbit, with spectral throughput running from Lyman-α into the near infrared. It uses five science instruments: the Wide Field Planetary Camera (WFPC); the Faint Object Camera (FOC); the High Speed Photometer (HSP); the Faint Object Spectrograph (FOS); and the High Resolution Spectrograph (HRS). Instrument handbooks are available which describe the science instruments and their capabilities in detail (see Ebbets [1985]; Ford [1985]; Griffiths [1985]; Paresce [1985]; White [1985]). The science justification for HST observations of asteroids has been examined in detail by Chapman et al. (1985), and much of the discussion in this section is based upon that report.

Spectrophotometry

Groundbased spectral-reflectance observations of asteroids taken from the near-ultraviolet through the visible into the mid-infrared reveal broad absorption features characteristic of electronic transitions in solid materials. Most observations have been made in the wavelength range 0.3 to 1.1 μm. This spectral region, most of which is accessible to science instruments aboard HST, is partially diagnostic for several mafic minerals common in meteorites, including various pyroxenes and olivines. The spectral slope in

the visible is due to the long-wavelength wing of deep charge-transfer absorptions which should be centered at wavelengths in the near-ultraviolet accessible to the HST. Laboratory results for a suite of astronomically significant minerals and frosts in the deeper ultraviolet have been reported, for example, by Hapke et al. (1981) and by Wagner et al. (1987).

Spectral reflectance characteristics of asteroids are quite subtle and depend on photometric precision of 2% or better. Some ultraviolet spectrometry of asteroids was obtained with the International Ultraviolet Explorer (IUE) (Butterworth et al. 1985). Because of the limited dynamic range of the IUE together with the extreme steepness and grassiness of the solar spectrum in this wavelength range, that work was of limited use. The HST carries a much more powerful suite of instruments; below we describe some possibilities for high-precision measurements of spectral reflectance.

Spatial Resolution of Surfaces

While we must wait for close-up spacecraft imagery to study detailed geologic structure, the HST can provide our first resolved images of asteroid compositional heterogeneity. From the ground, all but the very largest asteroids are below the resolution limits allowed by atmospheric seeing. Even the largest ones can barely be resolved by speckle interferometry.

For the HST the Rayleigh diffraction limit of resolution is about 0.04 arcsec in blue light. Tracking is by interferometric lock-up on a pair of guide stars, and tracking jitter is not expected to exceed 0.007 arcsec. According to Macchetto et al. (1982), the Faint Object Camera (FOC) onboard the HST should be able to map Ceres (the largest asteroid with a diameter of 950 km) to a resolution of at least 30 km. If pictures are taken several times during Ceres' 9 hr spin period, a global map of several thousand resolution elements could be produced. There are about three dozen asteroids with diameters $\geq$ 200 km which can be mapped globally in 100 pixels or more.

Asteroid Shapes, Spins and Configurations

Most asteroids are nonspherical bodies, with shapes and spins influenced by collisions. The determination of body shapes and spin-axis directions by inversion of telescopic lightcurves is problematical, and it is difficult to evaluate the reliability of the results without some ground-truth of the sort that can be provided by the HST.

Of particular interest for HST observations are the large asteroids ($D >$ 100 km) with spin periods in the range of 4 to 6 hr which have large-amplitude lightcurve amplitudes. Shapes of asteroids believed to be composed of nickel-iron alloy may be different from those made of ordinary hard rock or of the weaker carbonaceous material so prevalent in the asteroid belt. HST observations of asteroids should be carried out in coordination with groundbased lightcurve observing programs, which can define the epochs and precise times when critical profiles will be presented for imagery. In many cases, several

images during each of two adjacent HST orbits can define the profile at one epoch, and such observations at several different epochs over an asteroid's 4 yr orbital period (during which different aspects are presented) can define the shape and spin-axis orientation of an asteroid to high precision. For asteroids with known surface scattering properties (see the subsection below), photoclinometry may be applied to infer the orientation of surface elements in each pixel to provide shape information in addition to the directly observable profile.

Several dozen asteroids are sufficiently large and/or approach the Earth closely enough to be mapped by the Planetary Camera or Faint Object Camera, through spectral filters in the visible, near-ultraviolet and near-infrared, with 20 or more pixels on each diameter. The potential value of such compositional maps is great. There is already evidence of mineralogical variations on 4 Vesta; with the HST, Vesta's basaltic lava flows could be mapped on a geologically relevant scale. By analogy with the distribution of flow units on the Moon, the HST resolution is sufficient to produce a map adequate to demonstrate the morphological style of volcanism on a small body, or the degree to which volcanic units have been blurred by regolith processes. A great mystery about Vesta is how it has been able to preserve its basaltic crust through aeons of bombardment. High-resolution spectral maps can reveal the degree to which impacts have punctured through the crust to the olivine mantle below; this would constrain the cumulative bombardment rate in the asteroid belt and set limits on the original mass distribution of asteroids at the epoch when Vesta's surface solidified.

All spectral work so far, of course, has been restricted to unresolved asteroids. High-precision studies of spectral and polarimetric variations with rotation for about a dozen asteroids indicate minor heterogeneities on a hemispheric scale of resolution. A detailed study of Vesta has yielded a very coarse map of compositional units on that object, but it is evident that resolution much better than hemispheric scale cannot be achieved from disk-averaged data. Apparently most asteroids are rather homogeneous in surface composition. However, differences in at least one case (8 Flora; see, e.g., Gaffey 1984) are said to be incompatible with undifferentiated mineralogical assemblages and, instead, imply a high degree of geochemical processing. Observations of such heterogeneity would provide a fundamental test of competing models for S-type asteroids, as either homogeneous ordinary chondrites, or alternatively, as stony-iron cores of differentiated bodies that have been collisionally stripped of their crusts and mantles.

Some C-type asteroids are thought to contain a high proportion of organics and volatiles, including water. A map showing bright polar units on Ceres, for example, would be very suggestive of frost.

Detection of Asteroid Satellites

The presence of satellites about asteroids has been a controversial topic, supported by data of generally questionable validity. Nevertheless, some as-

teroids have been discovered that have extremely slow spins. Some of them may have tidally interacted with small satellites and spun down, the same way the Earth's spin is slowing due to lunar tides (chapter by Weidenshilling et al.). Some asteroids, such as those with eclipsing-binary-like lightcurves, may be contact binaries.

Many of the candidates are reasonably large bodies. For example, radar data for 216 Kleopatra seem to indicate a bifurcated shape, suggesting that it may be a contact binary. Typical separations on the sky would range from several hundredths of an arcsec to a couple of arcsec; the HST is ideally suited for searching at such distances. A search would require several exposures over a time baseline during a single HST orbit, in order to permit a potential satellite to be distinguished from the background star-field, and to permit approximate characterization of the orbit.

The FOC has a special capability to optimize searches for faint, nearby asteroid satellites, namely a Lyot-type coronagraph. Operating at f/288, a coronographic finger 0''.4 in radius can be used to occult the central asteroid and the apodizing mask can be employed to reduce the diffracted light dramatically, permitting a search for satellites of about 1 km in size at a distance of several hundred km from large main-belt asteroids. It is also plausible that recent large cratering events might have ejected clouds or rings of debris into orbit around some asteroids. Long exposures in the coronographic mode could sensitively reveal such debris clouds, providing important constraints on asteroidal cratering processes as well as providing practical information about potential hazards of flying spacecraft close to asteroids during the next two decades.

Normal Reflectance and Limb Darkening

Near opposition, a complete description of the photometric function of a particulate surface, such as an asteroid regolith, requires only two parameters: the normal reflectance and the limb darkening. Groundbased observations provide the geometric albedo plus a quantity that is a simple combination of the normal reflectance and limb darkening. Although such data have been obtained for a number of asteroids, it is not possible to determine either the normal reflectance or the limb darkening unambiguously because we cannot resolve their disks. Voyager images of outer-planet satellites have been used to characterize the photometric functions of these icy bodies, but a quantitative comparison with asteroid-scattering properties requires the resolution of asteroid disks afforded by the HST. The photometric function of a surface depends on its composition, particle size and porosity, only the first of which is sensed by colorimetry. These important physical characteristics of the regolith may vary with mineralogy (rock vs metal) and with diameter of the asteroid (since gravity dominates regolith processes). A useful estimate of both geometric albedo and limb darkening may be possible from a single disk-resolved image.

Small and Distant Objects

Since asteroids move rapidly across a background of faint stars, it is extremely difficult to do good spectrophotometry from the ground for asteroids fainter than about 17th magnitude. The perfect seeing available to the HST, in combination with excellent instrumentation, opens up the possibility for measuring reflectance spectra for a representative sample of faint main-belt asteroids only a few km in diameter. Such data would permit us to assess the spectral types of bodies with masses 1000 times smaller than have been sampled so far, including the smallest members of important Hirayama families.

The first essential task for the study of small faint asteroids is to discover them. A coordinated groundbased program would have to be arranged in order to provide precise ephemerides for the HST. The required ephemeris accuracy is a few arcsec.

The Earth-approaching asteroids are a sample of faint asteroids that may be important targets for the HST. These bodies, that range down to just 300 m diameter, are usually very faint, and can be studied from the ground only during very rare, short-duration close approaches to the Earth (which often occur with a viewing geometry that is awkward for observations). Some Earth approachers are being considered as prime targets for the first asteroid rendezvous and sample-return missions but several top prospects have not yet been observed at all for physical properties and will not return for a favorable apparition until it is too late for the proposed missions. The HST, with its much fainter limiting magnitude, can provide diagnostic information during most apparitions, enabling intelligent choices to be made for these spacecraft missions.

Concerning work on very faint objects, a note of caution may be in order. In some respects, the HST is *only* a 94-inch telescope. With a conventional fixed-aperture photometer at a groundbased observatory, we dare not use focal-plane diaphragms smaller than about 10 arcsec because of atmospheric seeing and dispersion. Thus, the effective sky brightness under the best conditions is about magnitude 16. By contrast, the HST can use much smaller apertures, and the sky limit will be at least 5 magnitudes fainter. However, the Poisson noise in the signal itself is no different from that using an equivalent groundbased telescope. With one-arcsec seeing, a groundbased telescope using area-resolving detectors such as CCDs may do as well as the HST down to magnitude 20 or 21. Proposals to use the HST for visible-light spectrophotometry will require careful justification.

Also, we do not think that polarimetry of asteroids and faint comets will be prime work for the HST. In visible light, at groundbased telescopes in the 2-meter class, polarimetry can be done to about magnitude 15 (see the chapter by Dollfus et al.). For fainter objects, adequate precision would generally require exposure times that are too long to be considered practical for the

HST. Disk-resolved polarimetry of the largest asteroids might be of interest, but polarimetry with the WFPC will be difficult to calibrate because of its 45-degree pickoff mirror, and as noted below the FOC is not primarily a photometric instrument.

III. THE HST AND ITS GROUND SYSTEM

With some simplification, the elements of the HST ground system that will be of interest to asteroid observers are as follows:

1. The Proposal Entry Processor (PEP): accepts proposals and translates them into data-base records for further processing.
2. The Science Planning and Scheduling System (SPSS): schedules approved observations. A schedule of observations is turned into actual spacecraft commands by the Science Commanding System (SCS) and other Project elements.
3. The Moving Object Support System (MOSS): accepts proposal input from PEP for moving targets and generates ephemerides and target-local visibility windows for input to SPSS.
4. The Observation Support System (OSS): monitors science and engineering data from HST in near-real-time, and makes real-time target acquisitions.
5. The Post-Observation Data Processing System (PODPS): generates output products in the form of calibrated science data.

It may be important to realize some limitations of the ground system. Generally, the HST works on a stored command load, which has been generated up to several weeks before the observations, based on proposals that were entered into PEP up to 18 months before the observation. Aside from target acquisition in the OSS, there will be essentially no real-time commanding based on considerations of science data quality or utility. One cannot, for example, expect to change a filter in real time.

Some observational requests that make good sense scientifically (like "Give me observations of any five Trojan asteroids, I don't care which.") are simply not within the capabilities of the system. Observations will be easiest to schedule which can be carried out on a single pair of guide stars and which can be completed within a single HST orbit. For objects near the ecliptic, the useful part of a spacecraft orbit will range up to 50 min of time, but guide-star acquisition and target acquisition may leave only 20 to 30 min per orbit for the actual taking of science data. Manpower will not generally be available for optimizing the schedule provided by SPSS, and human intervention in that process is not likely to be encouraged. In the OSS, by contrast, the observer will be welcomed to watch his data come down.

MOSS uses "JPL's best" numerically-integrated ephemerides for the major planets and satellites, and a data base of orbital elements for comets and asteroids also provided by the Jet Propulsion Laboratory. It can also accept

user-supplied heliocentric ephemerides in a variety of formats. MOSS provides ephemerides to SPSS as heliocentric state vectors, which can in principle describe any motion of whatever complexity; the HST can track the body center of an object, or a specified point on its surface, with equal ease.

MOSS is a powerful system not only for generating ephemerides but also for testing the feasibility of a moving-target program. Its windowing functions will allow the identification of all time intervals when a particular target bears a specified geometric relationship to the Sun, the Earth, or another body. It can display the apparent motion of any solar-system target and the HST focal plane against the guide-star field at any time, with correct rendition of occultations and eclipses. Can MOSS be used to *pre-craft* a proposal which can be assured of astronomical feasibility and will have a high probability of successfully being scheduled by SPSS? In principle, yes, and we expect that such work would be encouraged whenever possible, but there is no guarantee that the necessary manpower and computer resources will be available.

Planetary Campaigns

Planetary Campaigns, in which the HST may spend up to several days executing various projects on a *single solar-system target,* have been endorsed in principle by the HST project, and may provide a profitable mechanism for enhancing both the observational data return rate of the HST and the scientific value of observations obtained. It is expected that the Space Telescope Science Institute will announce the opportunity for a campaign along with the regular call for proposals. Proposals for work to be carried out during a campaign will be submitted via the usual channels, and will be judged individually by the Telescope Allocation Committee, which will have the power to accept or reject any or all proposals, or the entire campaign. Individual proposals should carefully state the *enhanced scientific merit* that will accrue from participation in the campaign; enhancement of observational efficiency will not be a consideration at this point. Personnel at the Science Institute will attempt to combine all approved proposals into a coordinated campaign for maximum data and scientific return. Some questions, such as the matter of exclusive data rights for individual investigators within the campaign, remain to be explored.

Target Acquisition and Tracking with the HST

Over 3 arcmin of motion, tracking of moving targets is expected to be accurate at the level of 0.02 arcsec *rms,* for objects moving at rates up to 0.02 arcsec/sec, and at the level of 0.03 arcsec for rates up to 0.21 arcsec/sec. (The latter limit was picked to represent P/Halley at its closest approach to the Earth during the recent apparition.) Much faster motions are possible, but the tracking precision would be expected to degrade substantially.

The positions of the guide stars are expected to be precise to within 0.3 arcsec *rms* in a relative sense, from one guide star to the next, but there may

remain systematic errors of up to 3 arcsec between the tabulated coordinates of the stars and their true directions in inertial space. Several of the science instruments on board the HST, by contrast, use apertures of size one arcsec or smaller. Thus, some form of target acquisition will generally be needed for observations other than simple wide-field imaging.

Mode I target acquisition is done on the ground. An image is produced with the WFPC or FOC, or possibly with some other science instrument in one of several "pseudo-imaging" modes. The image is then downlinked to the ground, and the object of interest is located on the image by personnel in the Observation Support System, with the assistance of the General Observer, if available. The necessary correction in the telescope pointing is computed and uplinked to the spacecraft. The science observation will proceed at the observation time specified in the stored command load.

The distinction between real-time target *acquisition* and real-time target *selection* is a vital one. Provision is being made for real-time target selection only in the case of planetary surface features. It will be possible to select a feature from a target-acquisition image, and to track it according to a precomputed rigid-body rotation law. However, it will not be possible to *discover* a faint satellite, for example, and then track its motion in real time.

A Mode I acquisition is expected to be slow, requiring 15 to 25 min of interaction with the ground system, and the necessary data links are expected to be available only about 20% of the time. For observations requiring the precise location of surface features on extended objects such as major planets, no alternative is available. For small objects such as asteroids, however, many observations should be possible with Mode II acquisitions, in which the target will be located autonomously onboard the spacecraft, either by the science instrument which will make the science observation, or possibly by another instrument. It appears that both the FOS and the HSP can autonomously locate and "peak up" on targets that are not larger than about 1 arcsec in diameter and within their search areas of about 5 arcsec square for the FOS and 10 arcsec square for the HSP.

The tracking of moving targets by HST has additional limitations. Guide stars will be lost after 3 to 10 arcmin of motion. It is not expected that a capability to make handoffs to a second pair of guide stars will be implemented in the flight software at launch; the first pair of guide stars must be dropped, and a second pair acquired, without preserving positional information from any previous Mode I or Mode II acquisition. Alternative methods are under consideration but are expected to provide only a limited degree of improvement.

IV. SPECTROPHOTOMETRY WITH THE HST

For obtaining the spectral reflectance of a solar system body, we may use either filter photometry or dispersive techniques. Onboard the HST, the for-

mer is provided by the High-Speed Photometer, the latter by the Faint-Object Spectrograph and, perhaps for special purposes, by the High-Resolution Spectrograph.

Figure 1 illustrates the steepness of the solar spectrum in the near ultraviolet. The precipitous drop at wavelengths near 2100 Å provides the effective limit for reflected-light spectrophotometry with the HST. We expect that the solar spectrum can be quantified, to adequate precision in terms of the throughput of any filter or dispersive element and detector onboard HST, only by observations of solar-type stars with the same instruments. Such considerations clearly make it desirable to settle on a single observational strategy for carrying out most HST observations of the reflectance spectrum of atmosphereless solar-system bodies. While we are not prepared to recommend a single strategy at this time, we describe below some of the better possibilities. Also, asteroids show rotational lightcurve variations, and it is highly desirable to make multi-wavelength observations within a short time span and in a symmetrical fashion over time. That will generally be difficult with HST instruments, especially for combining ultraviolet with visible passbands. We should perhaps assume that groundbased lightcurve data will provide the necessary corrections for all spectrophotometric work on asteroids with the HST.

The High-Speed Photometer

The High-Speed Photometer is the prime photometric instrument aboard the HST. It uses fixed-aperture filter plates, and the choice of aperture and filter is made by moving the telescope. There are five detectors: two "solar-
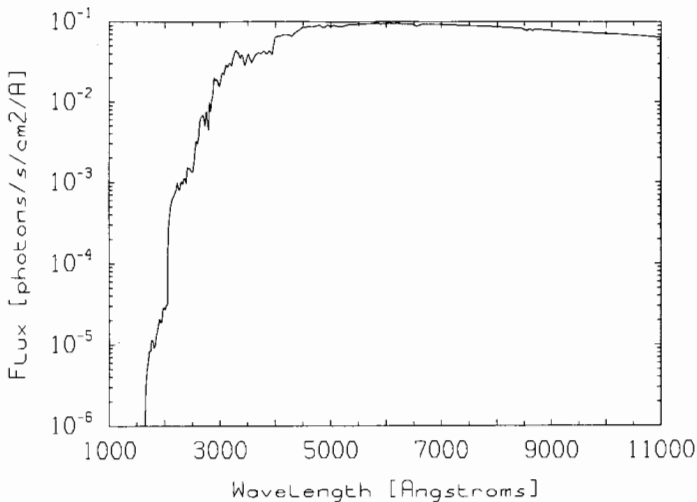
Fig. 1. The spectrum of the Sun. The abscissa gives the flux for a solar-type star of visual magnitude 10.0.

blind" ultraviolet Image Dissector Tubes (IDTs) labelled UV1 and UV2; two IDTs with bialkalai cathodes for sensitivity in visible light; plus one GaAs photomultiplier. The aperture plate for each IDT has a ten-arcsec aperture for target acquisition, a set of one-arcsec apertures for ordinary photometry, and other apertures for special purposes.

The ultraviolet IDTs have useful sensitivity down to Lyman-α, but many of the filter passbands are unsuitable for photometry of objects that are seen by reflected sunlight; the extreme steepness of the solar spectrum plus the red leak of the filters yield profiles that are too ragged and ill defined for useful spectrophotometry. In fact, no filter centered shortward of 2200 Å gives a well-behaved profile; asteroid science with the HSP starts at about 2200 Å. There are four ultraviolet filters which we think could be useful. Table I lists their approximate effective wavelengths for sunlight, their locations on the HSP detectors, and the approximate integration time for 1% counting statistics on an object of visual magnitude 10.0. For work in visible light, the filters F355M, F419N, F450W, F551W and F620W on the visual IDT should be suitable for asteroid work.

The Faint Object Spectrograph

The FOS works in the visible and ultraviolet and is designed to observe faint astronomical objects with a broad spectral coverage, a moderate spectral resolution, a linear photometric response over a large dynamic range, and low background noise. It uses a "red" Digicon detector that is sensitive to light from 1800 Å to 8500 Å and a "blue" Digicon detector sensitive between 1100 Å and 5500 Å. A low-resolution mode with its dispersions ranging from 6.5 to 25 Å per diode makes the FOS a good choice for spectral measurements of asteroids and other atmosphereless bodies. The maximum counting rate of 100,000 counts per s per diode means that only the few brightest asteroids at their most favorable oppositions will be too bright.

Estimates of exposure times for asteroids in the visible and near ultraviolet indicate that the FOS can be used to obtain reflectance spectra over the

TABLE I
Filters for Ultraviolet Spectrophotometry with the High-Speed Photometer

Filter	Effective[a] Wavelength (A°)	FWHM[a]	IDT	Integration Time[b] (S)
F218M	2200A	150	Both	82
F220W	2250	300	UV1	41
F248M	2600	300	Both	19
F284M	2850	300	UV2	11

[a]Numbers are approximate.
[b]For 10,000 counts on an object of visual magnitude 10.0 and a solar spectrum. Exposure times were computed by using the HSP simulator developed at the Space Telescope Science Institute.

wavelength range of 2500 Å to 8000 Å with signal to noise ratios (SNR) of 10 and a resolution of better than 100 Å for asteroids of visual magnitude 14 to 15 with total exposures of < 15 min. That would require at least two exposures for each object: one with the red Digicon and the G650L grating, and one with either the red or blue Digicon and a prism. The observations could be completed within one spacecraft orbit. Measurements could be extended down to 2000 Å for 10th magnitude asteroids with exposure times of about 25 min.

For work in visible light only, the FOS with red detector and grating should provide a well-exposed spectrum in the 4000 Å to 6000 Å range, with an exposure of a few 100 s, for an object at magnitude 20. With the red prism instead of the grating, it should be possible to reach magnitude 20 in the 4000 Å to 7000 Å spectral range in about 15 min. Similar conclusions will apply to filter photometry with the HSP over the UBVR wavelength range at magnitude 20.

The High Resolution Spectrograph

The HRS is an ultraviolet astronomical spectrometer designed to give higher spectral and spatial resolutions than achievable from the ground. The high resolution and consequent low spectral coverage make the HRS difficult to use for our purposes. Coverage of the wavelength range 2200 to 3200 Å would require 22 exposures with a total exposure time of about 15 min for a solar system object of visual magnitude 5. Thus, we do not see effective ways to employ the HRS for spectral reflectance measurements of surfaces of asteroids or other small solar system bodies.

V. IMAGING WITH THE HST

With any imaging device, the maximum exposure time available without sacrificing the highest resolution is limited by rotation of the object. Of course, it is possible to track on a surface point instead of the body-center, at the expense of rotation blur at the limb, or to ignore the rotation blur if one is only interested in a measurement of average diameter or limb darkening. In Table II, we have listed some numbers for the largest main-belt asteroids near mean opposition. The table gives the maximum exposure without rotation blurring for the FOC. For the Planetary Camera of the WFPC, pixel sizes are about twice that of the FOC at f/96, and, correspondingly, the maximum exposures are about twice as long. Other columns in the table are explained below.

The Faint Object Camera

The FOC was designed to utilize fully the spatial resolution of the HST, and to detect the faintest possible objects. It contains two complete cameras, with focal ratios of f/48 and f/96. The f/96 camera also has a high-resolution

TABLE II
Asteroid Images with the FOC

Object	Visual Mag per arcsec²	Period hr	f/96			f/288		
			Pixel Size km	Maximum Exposure min	Max SNR	Pixel Size km	Maximum Exposure min	Max SNR
Ceres	5.2	9.1	28.3	5.2	41	9.0	1.6	11
Pallas	4.6	7.9	28.3	7.9	50	9.0	2.5	14
Juno	4.6	7.2	26.7	14.8	69	8.5	4.7	19
Vesta	3.3	10.6	21.8	7.9	50	6.9	2.5	14
Hygeia	6.3	18.0	34.2	26.5	92	10.9	8.4	26
Interamnia	6.4	8.7	32.9	16.2	72	10.5	5.2	20
Eunomia	4.4	6.1	26.2	11.7	61	8.3	3.7	17
Davida	6.6	5.2	34.9	10.3	57	11.1	3.3	16
Bamberga	6.0	8.0	27.0	16.1	72	8.6	5.1	20
Psyche	5.5	4.3	30.7	10.2	57	9.8	3.2	16

apodizer that can be inserted into the beam to provide imaging with a focal ratio of f/288. On a 512 × 512 image, the f/48 camera provides a field of view of 22.5 arcsec square with pixel size 0.044 arcsec; the resolution is essentially identical to that of the Planetary Camera. The f/96 camera has a field of view of 11.2 arcsec square and pixel size 0.022 arcsec. The f/288 mode covers a field only 3.8 arcsec square, and heavily oversamples the resolution of the HST with a pixel size of 0.007 arcsec. A wide variety of filters are available and can be used in any combination to give the desired bandpass and attenuation. The f/96 camera has five neutral-density filters, with attenuations of 1, 2, 4, 6 and 8 magnitudes.

The high sensitivity of the FOC is provided by an imaging detector working in a photon-counting mode. A single photon event produces a burst of visible light that is detected on a TV tube; only one photon event can be counted at a particular location for each complete scan of the TV tube. The maximum counting rate is 5.3 counts per pixel per s for the f/96 mode covering a 128 × 128 image, and only 1.3 counts per s for the f/288 mode.

Thus the FOC, being optimized for detection of very faint objects, is not a prime instrument for photometric observations. One might think of doing spectrophotometry with the FOC by taking a series of exposures in various filters, perhaps even without Mode I or Mode II target acquisition, but that is impractical because of the slow instrumental counting rates and implied low signal-to-noise ratio.

For images of asteroids with the FOC, three factors must be considered: excessive brightness, body rotation and red leak. At all visible wavelengths and even into the near ultraviolet, the surface brightnesses of main-belt asteroids together with the slow counting rates imply that neutral-density filters must be used. Since surface brightness is the limiting factor, similar conclu-

sions will apply for any solid body in the inner solar system large enough to make imaging an attractive possibility, independently of the integrated magnitude of the object. The f/48 camera has no ND filters, and will have little or no applicability for asteroids.

The solar-like flux distributions of asteroids create problems with red leaks in the ultraviolet and near-ultraviolet filters. We have used a FOC Simulator developed at the Space Telescope Science Institute (STScI) by S. Ewald and F. Paresce to calculate the flux distribution of detected light and the amount of red leak in all the FOC filters with wavelength maxima below 3000 Å. No filters or combinations of filters were found to be useable below an effective wavelength of about 2200 Å. The shortest usable combination was a 2200 Å-wide filter plus a 2310 Å-medium-bandwidth filter. With those filters, an image could be made of an asteroid with surface brightness of 6.6 visual magnitudes per arcsec^2 with SNR = 25 in ~ 20 min. Two additional filter combinations were found that would appear to be useful below 3000 Å.

In Table II, the surface brightnesses range from 3.3 (for Vesta) to 6.6 (for Davida). A dark-surfaced Trojan asteroid would have a surface brightness about one magnitude below that of a C-type asteroid in the outer main belt. For the maximum counting rate supported by the FOC, the signal-to-noise ratio for the longest unblurred exposure would range from about 50 to about 90 in each pixel. We must emphasize that these numbers were computed assuming that filters, attenuators, etc. could be chosen to get *exactly* the maximum counting rate. Further, concerning the f/288 mode, we should re-emphasize that the resolution of the HST is *not* 0.007 arcsec. Nevertheless, the results are gratifying: with exposures that are adequate for imaging purposes (though generally not for high-precision photometry), one can expect to get at least one, and perhaps many, unblurred visible-light exposures of a large main-belt asteroid per HST orbit. Rotation blurring will become important only for the shortest useable ultraviolet filters.

The Wide Field and Planetary Camera

The WFPC was designed to provide photometrically and geometrically accurate images over a relatively wide field-of-view with high angular resolution and a wide spectral range. The Wide Field Camera (WFC) covers 2.6 × 2.6 arcmin, and the Planetary Camera (PC) 66 × 66 arcsec. The detectors consist of mosaics of four CCD arrays of 800 × 800 pixels each. The resulting pixel sizes correspond to 0.1 arcsec for the WFC and 0.043 arcsec for the PC. The CCDs have a range of useful sensitivity from 1150 Å to 11,000 Å, giving the only near-infrared sensitivity on the HST.

The bright end of the dynamic range is determined by the minimum exposure time of 0.11 s combined with the maximum allowed count of 30,000 electrons per pixel, which was selected to prevent blooming of the CCD images. With the WFC, most asteroids will be too bright. With the PC, Vesta at mean opposition will be too bright for the widest visible filters, but all of the

narrow- or medium-width filters will give counts below the limit for short exposures.

The ultraviolet filters of the WFPC have red leaks which, combined with the high-visible and near-infrared sensitivity of the CCDs, make many of them unuseable for objects with solar-like flux distributions. All of the filters with mean wavelength below 2000 Å have excessive red leaks. The shortest useable filter has a mean wavelength of 2300 Å and a red leak of $< 10\%$.

Except for Vesta, as described above, all asteroids should have surface brightnesses in the range observable by the Planetary Camera for all the filters not excluded by red leaks. Through the 2300 Å filter, for example, a dark object like 511 Davida in the outer part of the main belt will give a counting rate of 6 electrons per pixel per s, and hence SNR = 30 per pixel in < 3 min. Thus rotation blurring of asteroid imaging will not be a concern with the Planetary Camera.

If it can be photometrically calibrated to the required precision ($< 2\%$), the red-infrared grating on the PC is potentially very valuable for studying the highly diagnostic variations in absorption bands of olivines and pyroxenes in the 0.9 to 1.1 μm region. We have not considered that in detail, nor have we considered the possibility of doing filter spectrophotometry with the WFPC. While both options could be very attractive, much will depend on the degree to which the flat-field spectral response of the CCDs can be calibrated and controlled over a time period long enough to include observations both of asteroids and of solar-type comparison stars. Table III summarizes some of our conclusions for images of asteroids with the HST.

VI. TARGETS OF OPPORTUNITY AND SERENDIPITY

The HST will be capable of observing very small solar system objects and objects at great distances from the Sun. This presents the possibility that interesting new objects, or even new types of objects, may be discovered. The WFPC and FOC will take several thousand images per year, most of them for purposes of stellar and galactic astronomy. Many of the images will inevitably include trails produced by asteroids and comets. The necessary minimum exposure to produce a visible trail ranges from about 2 min with the FOC at f/96 to about 12 min with the WFC.

There should be a subset of objects detected that will be interesting for subsequent analysis and follow-up. The follow-up should mostly be groundbased, but in exceptional cases by the HST itself. Within 15° of the anti-solar point, "interesting" objects would include those which move slower than 4 or 5 arcmin per day, or about 10 arcsec per hour (C. Kowal, personal communication). The slowest objects we might expect to see will move perhaps 0.5 arcmin per day. The recognition of interesting objects at other solar elongations may be much more difficult, though probably any slow-moving object at high ecliptic latitude would be of interest.

TABLE III
Asteroid Imaging with HST

	WFPC	FOC
Wavelength range	2300 Å–10,800 Å	2300 Å–6400 Å
Pixel size	WF: 0.10 arcsec; many asteroids too bright	F/48: 0.44 arcsec; all asteroids too bright
		f/96: 0.022 arcsec
	PC: 0.043 arcsec	f/288: 0.007 arcsec
Dynamic range	all, except very brightest asteroids in visual filter; exposures short	all asteroids require ND filters; slow counting implies long exposures

Limiting magnitudes will range from about magnitude 22, for a motion of 5 arcmin per day, to magnitude 25 for the slowest-moving objects. The numbers imply diameters ranging from 4 to 15 km for an object of albedo 0.05 at distance 10 AU. For comparison, the limiting magnitude for the 48-inch Schmidt is about 20 to 21. Observationally, there could be whole populations of objects that are beyond the magnitude limits of groundbased surveys but within the limits of deep WF/PC and FOC images made with the HST.

It is expected that within a few minutes after each downlink, practically every WFPC and FOC image taken by the HST will be given a quick examination for science utility by personnel on duty in the Observation Support System. The evaluation will include a quick look for asteroid trails. Possible actions following the discovery of an exceptional trail might cover a wide range. If an object is felt to be of such significance that its mere existence represents a major addition to our inventory of the solar system, and if effective groundbased follow-up appears unlikely, a request that the HST schedule be broken for follow-up images and physical studies would be appropriate. Such drastic action would require the previous approval of a Target of Opportunity Proposal, with stringent criteria in place to prevent false alarms, and would be considered only under compelling circumstances.

VII. THE SPACE INFRARED TELESCOPE FACILITY AND THE ASTEROIDS

The SIRTF is currently projected for launch in late 1997 or early 1998. It will consist of an earth-orbiting 85-cm cryogenic telescope that will be outfitted with three imaging and spectroscopic instruments to permit background-limited measurements at thermal wavelengths of faint sources in the solar system and beyond.

The SIRTF Observatory

The baseline capabilities of the SIRTF telescope facility are as follows:

Orbit altitude: 900 km;
Orbital inclination: 28°5;
Facility lifetime: 5 yr with 10 yr goal;
Spectral range: 1.8 to 700 μm;
Aperture: 85 cm;
Field of view: 7 arcmin;
Sensitivity: Natural background limited, 2 to 200 μm;
Image quality: Diffraction limited over the full infrared field of view at >5 μm and over a reduced field of view at 2.5 to 5 μm;
Pointing accuracy/stability: 0.15 arcsec/0.15 arcsec (1 sigma);
Tracking nonsidereal targets: Up to 0.21 arcsec/sec without degradation of performance;
Viewing constraints: Telescope cannot point to closer than 59° from the Sun or Earth limb.

Those parameters of the telescope and facility having a direct bearing upon observations of solar system bodies are the orbital inclination, the viewing-angle constraints, and the tracking of nonsidereal targets. The nominal orbital inclination of 28°5 permits the observation of solar system objects at and near opposition. The viewing-angle constrains observations to solar elongations of 59°, and thereby eliminates Mercury, Venus, and comets and asteroids in certain parts of their orbits. The nonsidereal tracking parameter is more than adequate for comets at large distances from the Earth and for all main-belt asteroids. Rarely, some comets and Earth-crossing asteroids will have motions exceeding the SIRTF tracking rate for a few days. The field of view of the telescope is 7 arcmin, fully adequate for asteroid observations even in cases where the ephemeris is imperfect, as for newly discovered objects. Image quality and pointing accuracy are adequate for photometric and spectroscopic studies of asteroids.

Instrumentation

Three instruments selected for the SIRTF are as follows:

Infrared Array Camera (IRAC): G. Fazio, SAO, Principal Investigator.
Multiband Imaging Photometer for SIRTF (MIPS): G. Rieke, Univ. of Arizona, Principal Investigator.
Infrared Spectrograph (IRS): J. Houck, Cornell University, Principal Investigator.

Considered together, these instruments provide the following range of photometric, imaging and spectroscopic capability:

1. Photometry with diffraction-limited beams, 2 to 700 μm, using broadband and selectable narrowband filters. Diffraction-limited beam size (FWHM) = 3 arcsec (wavelength = 10 μm).
2. Low-resolution dispersive spectroscopy (resolving power about 100), 4 to

120 μm, using diffraction-limited apertures and detector arrays sampling as much as one octave of the spectrum simultaneously. The option of extending the short-wavelength limit of this instrument to 2.5 μm is discussed further below. ·

3. Moderate-resolution dispersive spectroscopy (resolving power up to 2000), 4 to 120 μm, using diffraction-limited apertures and detector arrays sampling 50 or more spectral resolution elements. The 120 to 200 μm spectral region will be covered by one spectrograph with a resolving power of 500 to 1000.

4. Wide-field and diffraction-limited imaging, mapping and surveying at 2.5 to 200 μm, using arrays with as many as 128 × 128 pixels. A variety of modes will be available which will permit diffraction-limited imaging over most or all of the 7-arcmin field of view at wavelengths between 10 and 120 μm, and over a smaller portion of the field at shorter and longer wavelengths.

5. Polarimetric capability for use in conjunction with both the imaging and photometric instrumentation.

SIRTF Capabilities for Solar System Science

Sensitivity. As an illustration of the sensitivity of SIRTF at spectral resolution 1000 (IRS), 50 and 2 (MIPS), the thermal and reflected solar fluxes from various small bodies in the outer solar system are plotted for wavelengths 2 to 500 μm in Fig. 2. This shows the thermal and reflected sunlight components of the radiation from asteroids, Pluto and Triton, and the nucleus of Comet Halley at 5 AU. There are approximately 25 Trojan asteroids with diamaters > 100 km, and in the main belt there are approximately 1000 bodies of diameter ≥ 40 km. Not all of these asteroids are of special interest, but representatives of all the major and several minor taxonomic types, and some identified with specific meteorite types, are within range of SIRTF at spectral resolutions suitable for diagnostic compositional studies. Spectral observations with SIRTF will extend the compositional studies into wavelength regions that cannot be studied from groundbased observatories because of atmospheric absorptions. With this high sensitivity of SIRTF and the requirements of the science, we anticipate that much of SIRTF's work on solar system objects will be done at spectroscopic resolution ($R > 50$). SIRTF can achieve spectral resolution better than 1000 throughout the thermal wavelength region for large Trojans and main-belt asteroids. We give spectroscopic capabilities particular emphasis in the discussion that follows.

Spectroscopy in the Region 4 to 25 μm. The baseline spectral region for the spectrometer on SIRTF has its short-wavelength limit at 4 μm. Spectroscopy in this region at resolutions afforded by the IRS are expected to be useful in further analysis of mineral and volatile surfaces on small bodies of the solar system, as well as in defining their thermal properties related to
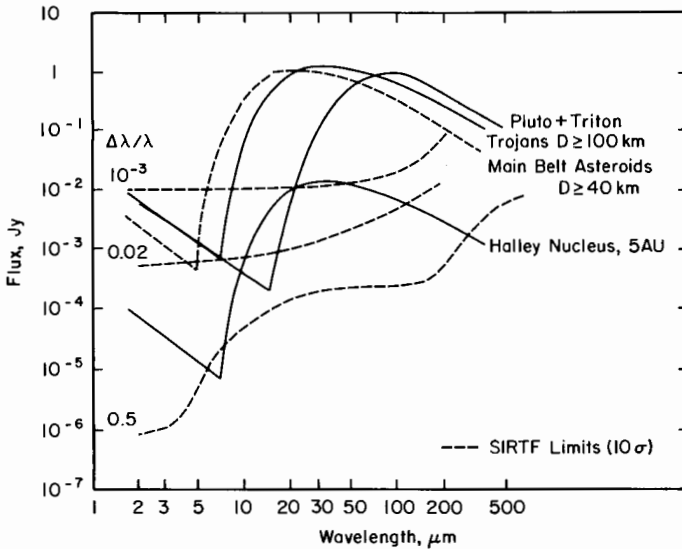
Fig. 2. The predicted brightness of various solar system objects in comparison with the SIRTF 10-sigma measurement limits for 900 s of integration. The curve for resolution 0.02 (50) is based on the original Infrared Spectrometer proposal; reduced read noise will improve performance at wavelengths $\lesssim 5$ μm.

regolith development and rotation. The silicate band near 11 μm is a diagnostic feature in some solar system bodies, particularly comets. In the laboratory, this spectral region has not been thoroughly studied for solid materials such as minerals and ices, but it is of growing interest in the context of organic components of the interstellar medium and related implications for asteroids and comets. Organics with structures representative of low-formation temperatures show extensive spectral features in this region.

Spectroscopy in the Region 2.5 to 5 μm. The SIRTF project and the IRS team are considering extending the wavelength range of the Infrared Spectrometer (IRS) shortward to 2.5 μm rather than the baseline cutoff at 4 μm. The spectral region beginning at about 2.5 μm contains diagnostic absorption bands in reflectance spectra of minerals and ices of cosmochemical relevance in planetary studies. Most of the work on the mineralogy of asteroid and planetary satellites and the study of ices on these bodies (also Mars) has been accomplished in the 0.3 to 2.5 μm region because of accessibility to groundbased telescopes (see the chapter by Gaffey et al.), but preliminary studies of OH and CH spectral features in asteroids beyond 2.5 μm are now being reported (see, e.g., Cruikshank and Brown 1987; Piscitelli et al. 1988).

Laboratory work in the region longward of 2.5 μm on minerals and ices of cosmochemical interest is in its infancy, but is being propelled forward by

the near prospect of spacecraft remote-sensing reflectance data out to 5.2 μm (Galileo, Mars Observer, CRAF and Cassini). The goal of the laboratory programs in progress is not only to extend the wavelength beyond the earlier work, but to increase the resolution to between 1000 and 2000.

Of central importance is the occurrence and distribution of those spectral features related to organic activity on solid surfaces and in the atmospheres of planets and planetary satellites. In particular, the C-H band complex at 3.4 μm in comets, on asteroids and on planetary satellites is of considerable importance to issues of the origin of the dark material that is distributed throughout the solar system. The CN band at 4.5 to 4.6 μm is similarly of great importance, as the combination of the C-H and the CN bands bear directly on questions of the origin and distribution of life in the solar system and elsewhere. A C-H/CN survey of the small bodies of the solar system can only be accomplished with SIRTF because of the difficulties in groundbased measurements of these two band complexes.

SIRTF instrumentation is optimized for spectral regions where the extremely low background radiation from a cryogenic telescope offers the maximum advantage over telescopes at ambient temperature. At wavelengths $\lesssim 3$ μm for SOFIA and 3.5 μm for the Keck Telescope, these larger instruments are superior to SIRTF. However, the residual telluric spectrum from Mauna Kea and SOFIA altitudes is sufficiently complex to disturb measurements in some wavelength bands. In addition, the broader wavelength coverage that would be available by an extension of the IRS spectral range to 2.5 μm would be of great value in numerous observations, and would provide a good wavelength overlap with groundbased data sets.

REFERENCES

Butterworth, P. S., and Meadows, A. J. 1985. Ultraviolet reflectance properties of asteroids. *Icarus* 62:305–318.

Chapman, C. R., Goguen, J., Gradie, J., Lebofsky, L., Tholen, D. J., Veeder, G., and Vilas, F. 1985. Observations of asteroids, small planetary satellites, and inactive comet nuclei. In *Report of the Space Telescope Scientific Working Group for Solar System Science Regarding Key Projects and Planetary Campaigns* (Baltimore: Space Telescope Science Inst.), Appendix.

Cruikshank, D. P., and Brown, R. H. 1987. Organic matter on Asteroid 130 Elektra. *Science* 238:183–184.

Ebbets, D. 1985. *High Resolution Spectrograph Instrument Handbook* (Baltimore: Space Telescope Science Inst.).

Ford, H. C. 1985. *Faint Object Spectrograph Instrument Handbook* (Baltimore: Space Telescope Science Inst.).

Gaffey, M. J. 1984. Rotational spectral variations of asteroid (8) Flora: Implications for the nature of the S-type asteroids and for the parent bodies of the ordinary chondrites. *Icarus* 60:83–114.

Griffiths, R. 1985. *Instrument Handbook for the Wide Field and Planetary Camera* (Baltimore: Space Telescope Science Inst.).

Hapke, B., Wells, E., Wagner, J., and Partlow, W. 1981. Far-UV, visible, and near-IR reflectance spectra of frosts of H_2O, CO_2, NH_3, and SO_2. *Icarus* 47:361–367.

Macchetto, F. 1982. The faint object camera. In *The Space Telescope Observatory*, ed. D. N. B. Hall, NASA CP-2244, pp. 40–54.

Paresce, F. 1985. *Faint Object Camera Instrument Handbook* (Baltimore: Space Telescope Science Inst.).

Piscitelli, J. R., Cruikshank, D. P., Brown, R. H., Tokunaga, A., and Bell, J. F. 1988. The search for macromolecular carbon on asteroids. *Bull. Amer. Astron. Soc.* 20:864 (abstract).

Tholen, D. J., and Zellner, B. 1984. Multicolor photometry of outer Jovian satellites. *Icarus* 58:246–253.

Wagner, J. K., Hapke, B. W., and Wells, E. N. 1987. Atlas of reflectance spectra of terrestrial, lunar, and meteoritic powders and frosts from 92 to 1800 nm. *Icarus* 69:14–28.

White, R. L. 1985. *High Speed Photometer Instrument Handbook* (Baltimore: Space Telescope Science Inst.).

SPACECRAFT EXPLORATION OF ASTEROIDS: THE 1988 PERSPECTIVE

J. VEVERKA
Cornell University

Y. LANGEVIN
Laboratoire Réné Bernais

R. FARQUHAR
NASA Headquarters

and

M. FULCHIGNONI
Istituto di Astrofisica Spaziale

After two decades of spacecraft exploration, we still await the first direct inves-
tigation of an asteroid. Fortunately, a growing international interest in the solar
system's more primitive bodies should remedy this deficiency soon. Plans are
under way in Europe for a dedicated asteroid mission (Vesta—a joint So-
viet/French/ESA venture) which will include multiple flybys with in situ penetra-
tor studies. Possible targets include 4 Vesta, 8 Flora and 46 Hestia; launch is
scheduled for 1994 or 1996. In the United States, NASA plans include flybys of
asteroids en route to outer solar system targets. Indeed, before its most recent
postponement, Galileo was scheduled to have flown by 29 Amphitrite in Decem-
ber 1986. As now rescheduled, Galileo will be launched in the Fall of 1989, and
on its way to Jupiter will encounter asteroids 951 Gaspra (d = 16 km; S type) in
October 1991 and 243 Ida (d = 32 km; S type) in August 1993. The first Mar-
iner Mark II mission, CRAF, includes an asteroid flyby as a major mission ob-
jective, as do plans for the subsequent Cassini mission to the Saturn system. In
Japan, there is interest in multiple-flyby missions to asteroid/cometary targets.

[970]

*In addition, a very strong case can be made for a near-term rendezvous mission
to a near-Earth asteroid. Such a mission could be carried out within the modest
cost and complexity envelope of the "Observer Class" of NASA missions, and
would provide much-needed fundamental data.*

In 1989, the visit of Voyager 2 to Neptune will complete the first survey
of the major planets and satellites of our solar system, with the exception of
distant Pluto-Charon. On the other hand, up to now, only two small bodies
have been investigated: comet Giacobini-Zinner, with the retargeted ISEE
3/ICE spacecraft, and Comet Halley, with the five flybys performed by
Giotto, VEGA 1 and 2, Suisei and Sakigake. The first flyby of an asteroid (by
NASA's Galileo), scheduled for December 1986, has been postponed by at
least five years. The exploration of small bodies therefore constitutes one of
the scientific priorities of the next twenty years, a fact demonstrated by the
prominence given to missions such as CRAF (Comet Rendezvous Asteroid
Flyby) within NASA, or CNSR (Comet Nucleus Sample Return)/Rosetta
within ESA.

I. LOOKING BACK: PROSPECTS FOR THE 1980s

The prospects for asteroid studies from space in the 1980s were aptly
summarized in a chapter by Morrison and Niehoff in the *Asteroids* book
(Gehrels 1979). That review presents succinct summaries of several topics
which remain pertinent today. The interested reader will find there discussions
of such topics as why are spacecraft missions to asteroids necessary to com-
plement data obtainable from the ground and from Earth orbit; what are the
principal science objectives for missions to asteroids; what would be a typical
science payload on such a mission, etc. Above all, the article contains a clear
description of several mission options (flyby, orbiter, lander, and sample re-
turn) and their relative characteristics and merits. Since today we are in much
the same position as Morrison and Niehoff were a decade ago—still awaiting
the first mission to an asteroid—their discussion of these topics remains valid
and will not be duplicated here.

Ten years ago Morrison and Niehoff summarized the prospects for as-
teroid research in the 1980s. How these prospects have squared with reality is
the subject of Table I. First, in the area of groundbased observations their
predictions have been fulfilled: indeed there has been a continuous and spec-
tacular increase in our knowledge of asteroids from groundbased data. As an
illustration, we note that while in 1979 only a handful of asteroids had been
studied by radar, by 1988 almost 50 have been studied in considerable detail,
and some spectacular discoveries have been made (e.g., that 1986 DA is a
metallic body). (See the chapter by Ostro.)

In the area of Earth-orbit observations Morrison and Niehoff focused on
a triad of missions (IRAS, HST, SIRTF) that would provide the bulk of funda-

TABLE I
Prospects for 1980s vs Reality

Prospects for 1980s[a]	1989 Reality
Groundbased Remote Sensing	
Continued Vigorous Growth	Yes
Observations from Earth Orbit	
IRAS	Yes
HST	Delayed: late 1989?
SIRTF	Mid-1990s?
Space Missions (U.S.)	
Multiple Asteroid Rendez-	Vanished from
vous Mission	NASA's capability
Rendezvous with Near-Earth	Vanished from
Asteroid	NASA's planning
	horizon

[a]Morrison and Niehoff 1979

mental new data. Indeed, the Infrared Astronomy Satellite (IRAS) was a huge success and has made lasting contributions to asteroid and related science. The Hubble Space Telescope (HST), which will provide imaging able to resolve some of the larger asteroids, and possibly provide further constraints on the existence of putative satellites of asteroids, still awaits launch. HST is now scheduled to be launched in December 1989; one would expect that routine operations would not begin until well into 1990. The Space Infrared Telescope Facility (SIRTF), which would provide infrared data supplementary to IRAS, is still awaiting a new start decision and is unlikely to materialize before the mid-1990s. Asteroid studies with HST and SIRTF are discussed in detail in the chapter by Zellner et al.

In the area of space missions to asteroids, no progress has been made. Focusing on the NASA program, Morrison and Niehoff looked forward to two important asteroid-dedicated ventures. The first, a Multiple Asteroid Rendezvous mission, would have studied several main-belt objects in detail, but was predicated on the availability of an ion-drive propulsion system. In spite of the optimism expressed by Morrison and Niehoff: "Ion-drive propulsion systems now under development will provide the capability to carry out a variety of exciting multi-target rendezvous missions during the 1980s," NASA has failed to develop such a capability, making multiple rendezvous missions practically impossible. In an attempt to preserve some aspects of the Multiple Asteroid Rendezvous mission, the Solar System Exploration Committee (SSEC) recommended in 1983 a modification that would combine a rendezvous with one main-belt asteroid with flybys of several others (SSEC 1983). Even so, such a "Mainbelt Asteroid Orbiter/Flyby Mission" called for the use of a Shuttle/Centaur launch combination. With the cancellation of the
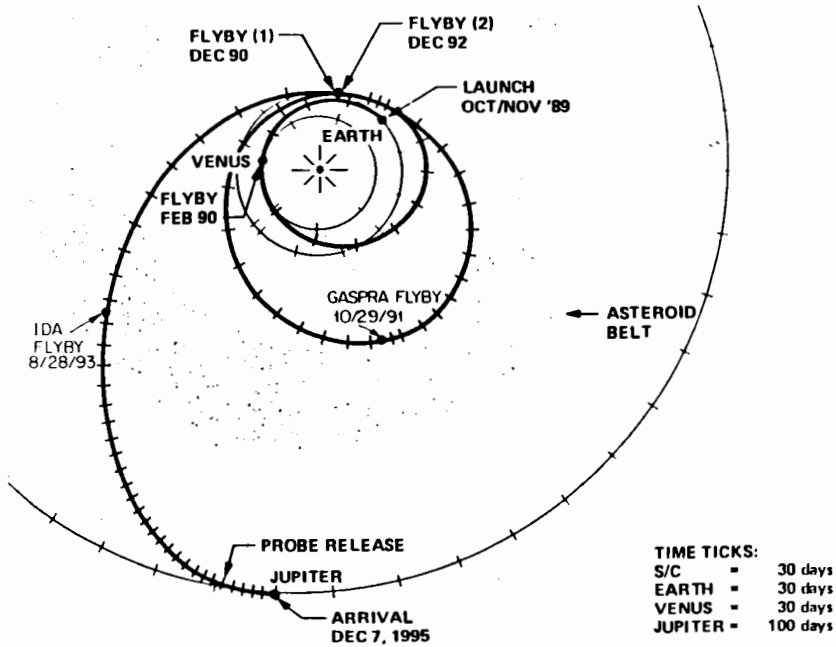
Fig. 1. Planned Galileo trajectory that will take the spacecraft past two S asteroids: 951 Gaspra and 243 Ida.

Shuttle-compatible Centaur upper stage program in 1986, NASA's ability to deliver significant payloads to deep space suffered another dramatic erosion. Currently, only single rendezvous missions are possible, and even then complex trajectories involving planetary swingbys (à la Galileo; see Fig. 1) are necessary. Such trajectories add demonstrably to mission complexity, duration and cost; in less quantifiable, but nonetheless real ways, they also add to mission risk.

To complement the investigation of main-belt asteroids to be accomplished by the Multiple Asteroid Rendezvous Mission, Morrison and Niehoff discussed a rendezvous, including possible sample return, with a near-Earth asteroid. While such a mission remains of high interest, recent emphasis has been on simpler scenarios which include a rendezvous, but do not involve a sample return; these more modest efforts could be carried out within the envelope of NASA's Observer Class of missions.

Not all developments during the past decade have been bleak. In part due to the success of efforts to investigate Comet Halley on its return in 1986, a strong international interest in exploring comets and asteroids has arisen. There is evidence that Japan, possibly in conjunction with the United States, is interested in follow-on missions to comets, and perhaps asteroids. The

Soviets, in conjunction with ESA (European Space Agency) and CNES (Centre National d'Etudes Spatiales), are planning an elaborate effort (Vesta) to study main-belt asteroids.

The Phobos missions launched to Mars in July 1988 offered great potential not only to increase substantially our knowlege of Phobos an Deimos, but also to affect our concepts of what asteroids are like (Zakharov 1988). Their unfortunate loss before completing their mission objectives still leaves many questions unanswered about the surfaces of small bodies.

In the United States, the major positive development was the announcement in 1984 of a NASA policy whereby all future spacecraft flying through the asteroid belt will involve flybys of at least one asteroid en route. The implementation of this policy would have begun with the flyby of the large S asteroid 29 Amphitrite in December 1986, had Galileo been launched as scheduled in the spring of 1986.

II. THE SOLAR SYSTEM EXPLORATION COMMITTEE PROGRAM

The current NASA plans for exploring the solar system are still based officially on a strategy developed in the early 1980s by the Solar System Exploration Committee (SSEC) and published in two reports: *Planetary Exploration Through Year 2000, Core Program;* and *Planetary Exploration Through Year 2000, Augmented Program.* It is difficult to judge the extent to which NASA as an agency takes the program outlined by the SSEC seriously, since it has yet to implement the key enabling step on which the program is based, namely the initiation of the Mariner Mark II spacecraft series of missions. Nevertheless, the SSEC core program involves two asteroid-dedicated missions in addition to missions such as CRAF which include flyby asteroid studies as a major objective. In fact, the SSEC Core Report underscores that the first characterization of main-belt asteroids is to be achieved by flybys during missions destined to other targets (CRAF and Cassini, and of course, Galileo). These are referred to as "initial core missions." Two "subsequent core missions" dedicated to asteroids are recommended. The first, the Multiple Mainbelt Asteroid Rendezvous/Flyby is described in the following terms: "In order to obtain a detailed characterization of at least one such body while at the same time sampling the diversity of chemical and physical types, the recommended mission includes multiple asteroid encounters, some orbiters, some flybys." This type of mission is discussed in Sec. III below. The second asteroid-dedicated mission (see Sec. V) advocated by the SSEC for its core program is a rendezvous with an Earth-approaching asteroid in order to "characterize one chosen member of this set of bodies."

The SSEC augmented program (SSEC 1986), designed to complement the more modest missions within the "core," recommends that sample return

missions to Mars and to a comet receive primary attention. The return of samples from an asteroid is mentioned only in passing.

III. THE MULTIPLE MAINBELT ASTEROID ORBITER/FLYBY: THE ASTEROID GEM OF THE SSEC PROGRAM

Without doubt the key of the SSEC program in terms of asteroid exploration was to have been the Mainbelt Asteroid Multiple Orbiter/Flyby mission. The hope expressed in the report that such a mission would be undertaken in the early 1990's will not be realized. Mission scenarios depended on the use of a Shuttle-compatible Centaur upper stage, the development of which was abandoned by NASA in 1986. With the loss of adequate propulsion systems, demanding missions of this sort cannot be carried out in their original form. Compromises must be made and even then one must accept the higher risks and longer flight times that are involved in the various clever ways of traveling to the asteroid belt and beyond that have now become necessary (Sec. IV).

The specific objectives stated by the SSEC for a multiple asteroid mission are summarized in Table II, as is the core payload of instruments. As envisaged by the SSEC, such a mission would have involved a Shuttle-Centaur launch and a flight time of some four years to the first asteroid target, making use of a planetary gravity assist (Mars or Jupiter) on the way. A propulsive maneuver would match spacecraft and asteroid velocities and result in orbital capture. After about two months of observations, the spacecraft would

TABLE II
Mainbelt Asteroid Multiple Orbiter/Flyby[a]
Science Objectives/Instruments

Science Objectives:
1. Characterize asteroids of various types, including determinations of size, shape, rotation, albedo, mass, density, surface morphology, surface composition, magnetic field and solar wind interaction
2. Provide a more detailed study of one or two selected main-belt asteroids, emphasizing elemental and mineralogical composition and detailed morphology

Instruments and Expected Results:

Imaging:	Size, shape, rotation, surface morphology
X-ray and gamma-ray spectrometers:	Elemental composition (rendezvous)
IR reflectance spectral mapper:	Mineralogical composition
Magnetometer:	Intrinsic magnetic field, nature of solar wind interaction
Radio Science:	Mass determination

[a]From SSEC Report (1983).

be placed in a new trajectory that would take it past several asteroids on its way, and perhaps to a final rendezvous. Examples of similar missions involving the use of an ion-drive upper stage are discussed by Morrison and Niehoff (1979). Unfortunately, lacking as we do adequate upper-stage capabilities, multiple asteroid rendezvous missions of the sort envisaged by the SSEC become very unlikely in the time frame of the next decade. In fact, right now any Mariner Mark II mission of this sort would have to come after Cassini, now optimistically scheduled for launch in 1996. However, to some extent the Vesta mission discussion in Sec. VI is similar in concept.

IV. FLYBYS OF MAIN-BELT ASTEROIDS

As soon as it was generally appreciated that flybys of main-belt asteroids as part of missions to the outer solar system were possible at a very modest cost of resources, NASA established a policy that such flybys would be a part of all future missions. A key to this appreciation was the development at Jet Propulsion Laboratory of efficient computer routines that could find asteroid flyby opportunities on trajectories to outer solar system targets. The increased interest in such flyby opportunities stems from several factors. First, it has always been clear that given the great diversity of asteroids, dedicated missions to all interesting types were unlikely. Second, interest has been piqued by the realization that we are unlikely to see any NASA asteroid-dedicated missions in the coming decade. Finally, such encounters provide interim data returns during the extremely long cruise times that have become necessary to reach the outer solar system.

The asteroid flyby policy is an integral part of CRAF and Cassini and was applied retroactively to Galileo. In fact, on its 1986 launch schedule, Galileo would have made the first asteroid encounter. Even with the current 3-yr delay, if Galileo is launched as now scheduled in the fall of 1989, it will still be the first spacecraft to encounter an asteroid: 951 Gaspra in late 1991. The current Galileo trajectory will include a second asteroid encounter (243 Ida) in 1993 (Fig. 1). The characteristics of the target asteroids are summarized in Table III.

TABLE III
Characteristics of Galileo Target Asteroids

	951 Gaspra	243 Ida[b]
Diameter (km)	16	32
Type	S[a]	S
Flyby Speed (km s^{-1})	8	12.5
Approach phase angle (deg)	32	19

[a]Gaspra is an "unusual" S type (Chapman, personal communication).
[b]Spin period of Ida = 4^{h}6; Δm > 0.4 (Binzel, personal communication).

TABLE IV
Galileo Type Flyby

ASTEROID SCIENCE OBJECTIVES:

Characterization of Global Properties
Accurate size/shape
Mass estimate
Rotation period
Pole orientation (precession?)
Cratering statistics and "age" of surface
Search for close satellites

Characterization of Compositional Properties
Mass—volume—density estimates
Surface composition (minerals, metals, etc.)
    Global properties
    Heterogeneities
    Stratigraphy in craters

Characterization of Surface Morphology
Morphology of craters as function of diameter
Evidence of past internal activity (volcanism, tectonism, etc.)
Search for spallation features
Ejecta patterns

Characterization of Regolith Properties
Stratigraphy
Ejecta dispersal
Photometric properties
Polarimetric properties
Radiometric/thermophysical properties

SCIENCE DATA:

Radio Science (CRMS)

Imaging (SSI)

Mapping Spectrometer (NIMS)

Photopolarimeter/Radiometer (PPR)
Ultraviolet Spectrometer
Magnetometer, etc.
Dust experiment

Mass determination
Bulk properties (e.g., volume)
Surface detail (resolution better than 100 m/lp)
Global map (204 channels: 0.7–5.0 μm)
From 800 km ca at Gaspra get about 10 nimsels/diameter
Thermal properties of regolith
Colors, albedos and phase curves
Interaction with solar wind. Intrinsic field (?)
Circum-asteroid dust (?)

Major science objectives and the instrument complement relevant to the asteroid encounter are summarized in Table IV. The data in these tables can be considered representative of asteroid encounters on upcoming NASA missions (CRAF and Cassini).

The miss distance of the Galileo asteroid encounters remains to be decided, but will be in the range of 500 to 2000 km. Two major factors, spacecraft safety and expected science return, need to be considered to determine the optimum distance for an asteroid flyby. After much effort by several study groups, the Galileo and CRAF/Cassini projects have adopted the position that no "circum-asteroid" dust hazard will be encountered beyond 100 radii of the target. This position may have to be relaxed because there are scientific reasons for wanting to get much closer, especially in the case of small asteroids. For an asteroid as small as 951 Gaspra ($d = 16$ km) the Radio Science Experiment requires a flyby distance of 200 km to achieve a mass determination within about $\pm$ 10%; for a 500-km flyby the accuracy of the mass determination falls to $\pm$ 50%. Scan platform instruments, especially NIMS (Near Infrared Mapping Spectrometer) and Imaging, prefer larger flyby distances (800 to 2000 km), in order to maximize the tradeoff between highest resolution achieved and maximum areal coverage of the asteroid's surface. Since the typical flyby geometries involve approaches at low phase angle, optimum for NIMS but not for imaging, the imaging experiment attaches great significance to targeting frames successfully near the time of closest approach, at which lower Sun (larger phase angle) illuminations are available. Given the possibility of significant downtrack errors in the position of the asteroid, the imaging
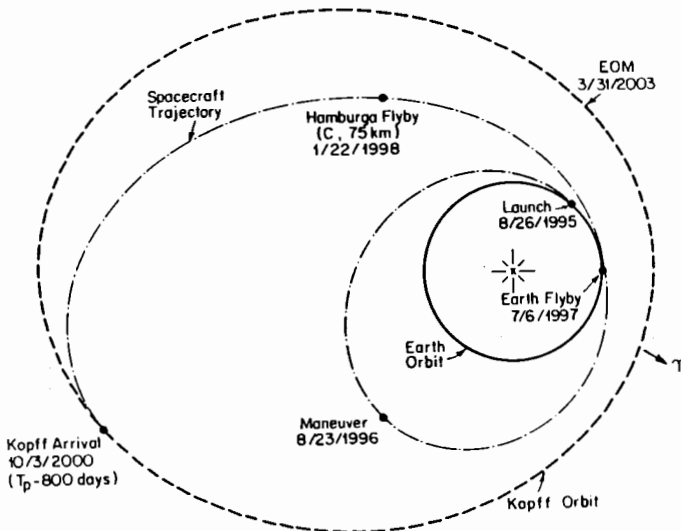
Fig. 2. Possible CRAF trajectory to P/Kopff, involving the close flyby of at least one asteroid.
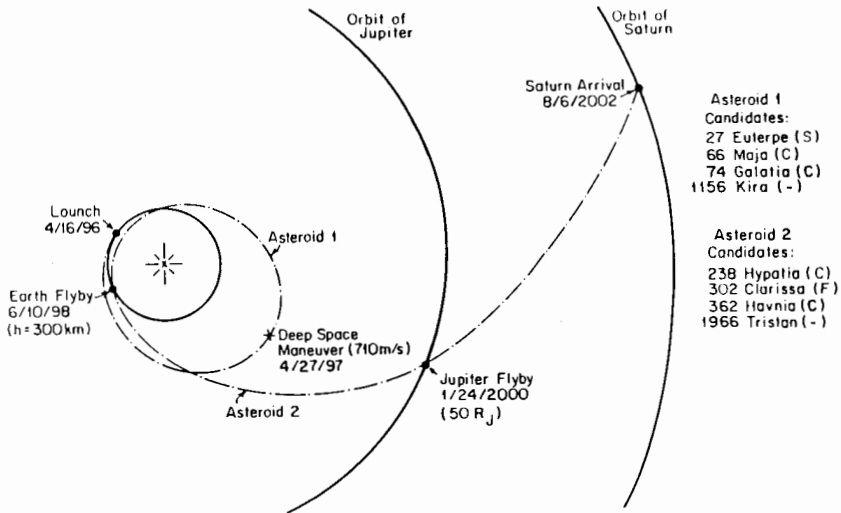
Fig. 3. Baseline trajectory for 1996 launch of Cassini. A number of possible asteroid flyby candidates are indicated.

targeting strategy is actually optimized by flying by at a somewhat greater distance than is desired by NIMS (e.g., 2000 km vs 800 km in the case of 951 Gaspra).

Plans for CRAF and Cassini remain indefinite. For example, if CRAF is launched to P/Kopff in 1995, it could encounter the C asteroid 449 Hamburga ($d = 75$ km) in 1998; the trajectory is summarized in Fig. 2. The payload and objectives for asteroid science on CRAF will be similar to those of Galileo outlined above. The baseline trajectory for a 1996 launch of Cassini to Saturn is shown in Fig. 3. Encounters with two asteroids are possible, but the baseline mission contains a single flyby (e.g., of asteroid 66 Maja in 1997). In all of the above scenarios, long cruise times and gravity assists from the inner planets are involved. In all cases, there is some choice in the type of asteroid that is encountered, but generally it is difficult to arrange to fly by a large asteroid ($d > 100$ km) without paying a penalty in overall mission performance. Critical to the science return on such flybys is the flyby speed, which is often near 15 km s^{-1}. Missions that involve flybys of asteroids, but fall outside the Mariner Mark II category of NASA spacecraft, are discussed in Secs. VI and VII below.

V. MISSIONS TO NEAR-EARTH ASTEROIDS

Earth-approaching asteroids have long been considered attractive targets for space missions. A fundamental reason is that energetically the near-Earth asteroids, or NEAs, are relatively easy targets; some, in fact, are easier to

reach than the Moon. As more remote-sensing data become available, it is clear that this population spans a great diversity of fascinating bodies ranging widely in mineralogy and therefore likely origin (McFadden et al. 1984,1985 and their chapter in this book), as well as in the surface characteristics. A related interest in the NEAs involves the likely link between some of them and some of our meteorite samples (see, e.g., Levin et al. 1976). Another traditional interest has focused on the exploitation of NEAs as potential resources. The recent discovery that at least one of these objects (1986 DA) is a km-sized chunk of metal will certainly sharpen this interest. Since the NEAs have been viewed as easy targets, there have been many past proposals involving them, including manned missions (Alfvén and Arrhenius 1970), as well as full-scale retrieval, ranging from the fancifully plausible (O'Leary 1977) to the downright bizarre (Herrick 1979).

The exploitation of NEAs for space resources, especially those of carbonaceous (source of volatiles) and metallic composition, is discussed in the SSEC's (1986) Augmented Program Report. The report stresses that, "We know much less about the asteroids than we do about the Moon; and it is therefore harder to plan for eventual use of asteroids as resources . . . there is much to be done to find out exactly what materials are out there before we can plan the details of how to use them." While some of this information can be obtained remotely, the type of data needed to land and operate on an asteroid's surface can only come from a precursor spacecraft mission. Such studies could be part of the SSEC's recommended rendezvous with an Earth-approaching asteroid "to characterize one chosen member of this set of bodies" (SSEC 1983). Morrison and Niehoff (1979) describe one scenario for a mission to a NEA which involves the return of a sample to Earth. With the decline of launch capability within NASA, recent discussions in the United States have focused on more modest goals.

As part of the "Planetary Observer" sequence envisaged by the SSEC, consideration has been given to a rendezvous-type mission (without sample return). The results of one study are summarized in the Near-Earth Asteroid Rendezvous (NEAR) Science Working Group Report (Veverka et al. 1986).

Constraints on the launch energy, solar power, and spacecraft life make it impossible to consider all NEAs as potential targets. Specifically, objects that have either very inclined or very eccentric orbits are inaccessible. This consideration excludes bodies, such as 2201 Oljato or 3200 Phaethon, which are suspected of being "dead comets." (See the chapter by Weissman et al.)

Suitable targets are available every year (and with the current rate of discovery of NEAs, even more opportunities can be expected in the future) and include asteroids ranging in average diameter from 21 km (433 Eros) to 500 meters (1982 DB). The best opportunity identified involves a 1994 launch to asteroid 3361 1982 HR, an object about 1 km in diameter. The trajectory to 1982 HR for a 1994 launch shown in Fig. 4 is an exceptional opportunity for several reasons: it is energetically very favorable with a large mass margin
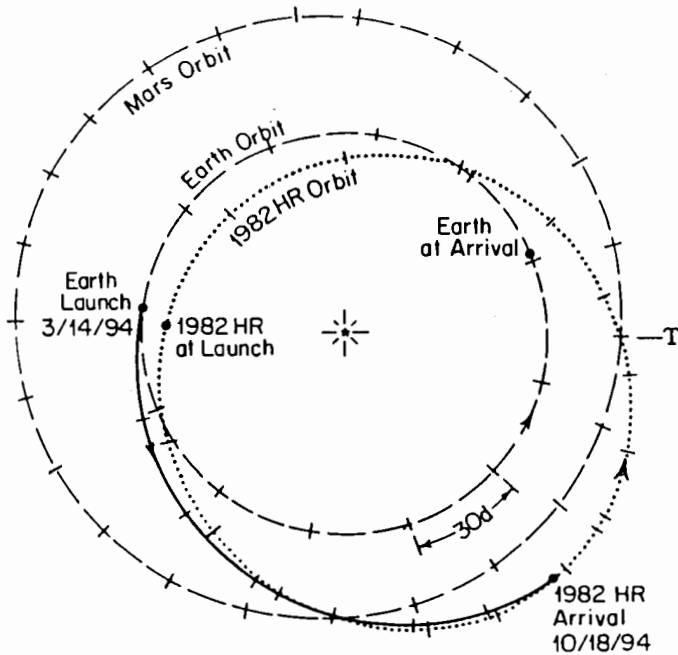
Fig. 4. NEAR trajectory to asteroid 1982 HR for a launch in 1994. Note the short flight time and the low range to Earth throughout the proposed 1-yr rendezvous phase of the mission.

(>100 kg); it involves an extremely short interplanetary flight time (218 days); and it has nearly optimum solar and Earth range distances, allowing good power and telecommunications performance. Furthermore, 1982 HR has been recovered, so the ability to locate the asteroid precisely at any time in the future is assured. In view of the extensive adaptability of a rendezvous mission, the Working Group concluded that from mission operations considerations almost any dynamically accessible NEA is a suitable target. Given our rudimentary state of knowledge, almost any NEA target would provide the opportunity to answer many fundamental questions, and a relatively more accessible target might permit a more comprehensive payload and a more elaborate observational strategy.

The suggested payload for NEAR is based on the assessment that in order to address fundamental questions concerning near-Earth asteroids and their relationship to other bodies of the solar system, the NEAR spacecraft must be equipped to measure the characteristics of the target asteroid summarized in Table V. Determinations of the bulk and surface properties were deemed to be equal first-order objectives—a particularly important goal being the determination of the asteroid's mean density. The NEAR report demonstrates that some of the objectives outlined in Table V are difficult or impossi-

TABLE V
NEAR Science Objectives and Proposed Payload[a]

MAJOR SCIENCE OBJECTIVES

Bulk properties	Size, shape, volume, mass, gravity field and spin state
Surface properties	Elemental and mineral composition, geology, morphology and texture
Internal properties	Mass distribution; possible magnetic field
Environment	Possible near-asteroid gas and dust; solar wind interaction

POSSIBLE PAYLOAD

Essential instruments	Imager (CCD)
	Spectral mapper
	Gamma-ray spectrometer
	X-ray spectrometer
	Radio science package[b]
Highly desirable, but not essential	IR radiometer[c]
	Altimeter[d]
	Magnetometer
Other useful instruments	Penetrator
	Dust collector/analyzer
	Dust counter
	Mass spectrometer

[a]From NEAR Report (Veverka et al. 1986).
[b]Part of telecommunication system. Weight and power negligibly different from minimum required for communication.
[c]Could be part of spectral mapper.
[d]Either radar or laser.

ble to achieve during flybys; consequently a NEA-dedicated rendezvous is essential.

The rendezvous propulsion maneuver needed can be accomplished without prior on-board detection of the target asteroid. Following the initial orbit-matching maneuver, the asteroid would be located using the imager, and a slow approach trajectory established, during which crucial physical parameters such as mass, gravity field, and shape would be measured. With these parameters determined approximately, the spacecraft would be placed into a polar orbit at a distance of about 30 radii to accomplish the major goals of imaging and spectral mapping. Even from 100 km, spectral maps having a resolution of 10 m and images at resolutions better than 1 m can be achieved. Later in the mission the orbit size would be reduced to three or four radii to gather the crucial gamma-ray and X-ray data, and to refine the determination of the gravity field. Assuming an orbit of 1 to 2 km and an integration time of 500 hr or more, the X-ray/gamma-ray combination spectrograph would be able to

distinguish among all major meteorite types. The post-rendezvous mission should last approximately 1 yr. The NEAR Science Working Group recommended that the mission end with a trial descent to the asteroid surface, as a precursor to future sample return and eventual resource utilization missions. The spacecraft would not be required to survive the experimental descent.

A major advantage of studying a very small object such as 1982 HR is that in terms of surface properties and processes a 1-km asteroid is further removed from the types of small bodies that will be studied by flybys (Galileo and CRAF) or that have been studied on previous missions (Viking and Phobos studies of the satellites of Mars, for instance). Note that searches were made for energetically modest mission opportunities that involve flybys of other NEAs on the way to the rendezvous target, but none were identified.

While a NEAR mission fits well into the Observer Class in terms of spacecraft capability, it does involve significant differences from the other Observer-type missions proposed for Mars and the Moon. NEAR will not be mapping a large spherical object that had been investigated previously. The NEAR undertaking will involve both first-order exploration as well as systematic data acquisition. Accordingly, sufficient flexibility in Mission Operations and Data Acquisition must exist to take advantage of unanticipated results. Furthermore, since typical NEAs are small, irregularly-shaped bodies, presumably with similarly irregular gravity fields, navigation and operations in the near-asteroid environment will be substantially more complex than would be the case for Mars or the Moon. While the imager and the near-infrared spectrometer could obtain important data from relatively large stand-off distances, the gamma-ray and X-ray spectrometers must operate within a few body radii for extended periods. Preliminary studies (see, e.g., Friedlander et al. 1979) have shown that operations are possible, down to the distance of the highest point on the surface from the center of gravity, even for very irregular bodies. However, the task will be a demanding one, and work must continue to assess optimum methods for navigating and operating in the proximity of small, irregular objects. In this context, the Soviet Phobos mission should provide much useful experience.

The recognition that in terms of mission operations and spacecraft design a NEAR mission differs from one involving the routine, systematic orbital mapping of a large spherical body such as Mars or the Moon, coupled with the fact that the NEAR spacecraft would involve some asteroid-specific instrumentation, has led to considered neglect of a NEAR-type mission in current NASA planning. Rather, the next Observer Class mission being discussed is a Lunar Orbiter. That mission, both in terms of spacecraft and payload design, as well as in terms of mission operations, would be similar to a Mars Observer. Fortunately, in Europe interest remains in an Observer-class mission to a near-Earth asteroid. The concept being studied in Italy under the name of Piazzi bears some similarity to NEAR, except that it involves a very slow flyby rather than a rendezvous (see Sec. VII below).

VI. EXPLORATION OF SMALL BODIES; THE EUROPEAN PERSPECTIVE

A stated goal of the Soviet space program is the systematic investigation of the solar system's small bodies. This aspect of the Soviet space program got off to a start with the VEGA missions to Halley and continued with the Phobos missions to Mars and its satellites. An essential element of the program involves flybys of small bodies en route to other targets.

A similar emphasis on small bodies is emerging within ESA, building on the success of Giotto. Not surprisingly, a cooperative effort among the USSR, ESA and CNES is emerging as the next major step in exploration of small bodies in the solar system.

A first exploratory mission to asteroids must take into account the extreme diversity of these objects in terms of size and spectral/compositional types. As none of these objects can be resolved spatially from the ground, spacecraft missions are essential to discern any geological/geochemical heterogeneities on their surfaces, which may preserve clues to important internal and external processes. The European scientific community has consistently favored a survey of as many asteroids as possible, with a broad range in size and type. This strategy resulted in the proposal of Asterex (a multiple flyby mission) and Agora (a multiple rendezvous mission) to the European Space Agency in 1980 and 1984. The Vesta project, a multiple flyby mission with *in situ* studies, is based on the same scientific strategy. Initially proposed as a bilateral collaboration between Interkosmos and CNES, it is now developing into a possible collaboration between Interkosmos, CNES and ESA.

The Vesta project takes advantage of specific aspects of the vigorous Soviet planetary program. First each mission is performed by two identical spacecraft, making it feasible to visit 7 to 10 small bodies. Second, landers and penetrators developed for the Phobos mission could be used on Vesta to perform *in situ* investigations on two large asteroids (one for each spacecraft). In order to keep the mass budget and technical complexity of such a module to an acceptable level, the relative spacecraft-asteroid velocity must be less than 4 km s^{-1}. This requirement has led to mission scenarios involving one or two swingbys of Mars. By raising the perihelion of the spacecraft trajectory, such maneuvers greatly reduce the spacecraft-asteroid approach velocity. However, the strategy restricts launch dates to Mars launch windows; the target launch date for Vesta is either Fall 1994 or, more likely, 1996.

In the proposed collaboration, Interkosmos would provide the two launches and the asteroid penetrators, while CNES and ESA would have the responsibility of the small-body spacecraft and operations. The scientific instruments are to be selected jointly.

The results of the Halley flybys led to a re-assessment of the possible connections between asteroids and short-period comets: the distinctions between the nuclei of short-period comets and the darker asteroids may not

TABLE VI
Vesta Major Science Objectives

1. *In situ* chemical and physical characterization of 2 large asteroids with the penetrators

2. Characterization of 6 or 7 asteroids and 1 or 2 comet nuclei by remote sensing

3. Studies of the dust, gas and plasma environment of short-period comets and asteroids

TABLE VII
Vesta Proposed Payload

REMOTE SENSING	RESOLUTION/ACCURACY (Flyby Distance = 500 km)
Imaging system	
high resolution camera	8 m
wide angle camera	120 m
Infrared imaging spectrometer	200 m
(0.5 to 5.5 μm)	
Radar altimeter/radiometer	100 m vertical
(4 frequencies, dual polarization)	5 km footprint
Mass determination	5% accuracy for asteroids larger than 50 km

ENVIRONMENT

Dust counter	Plasma wave system
Dust mass spectrometer	Electron analyzer
Magnetometer	Energetic ion telescope

ASTEROID PENETRATOR (8 kg)
Chemical analysis package (gamma-ray, X-ray, α-backscattering)
Accelerometer—uniaxial seismometer
Electro-conductivity probe
Temperature probe
Magnetometer
Small camera (if data link adequate)

POSSIBLE ADDITIONAL INSTRUMENTS

Photopolarimeter	Gamma-ray burst monitor
UV spectrometer	Stellar oscillation detector
X-ray spectrometer	Cosmic-ray detector

always be as sharp as previously believed. Such considerations have led to the broadening of the scope of the Vesta mission to include 1 or 2 short-period comets among the 7 to 9 small bodies to be visited. The major scientific objectives of Vesta, divided in three categories, are summarized in Table VI.

Given that the two Vesta spacecraft will spend 5 yr between 1 and 3 AU from the Sun, with a relative spacing of up to 3 AU, the configuration provides an ideal basis for studying the interplanetary medium in correlation with scientific observations in the vicinity of the Earth (Soho, Wind) and possibly out of the ecliptic (Ulysses, depending on its launch date and lifetime). The long baseline between the two spacecraft and the long cruise phases between asteroids (typically $1/2$ to 1 yr) are well suited for astrophysical experiments such as gamma-ray burst monitoring or the study of stellar oscillations.

The Vega (small-body) spacecraft is to be three-axis stabilized, with a dry mass of 800 kg, with a minimum of 130 kg for the core science payload. The nominal lifetime is to be 5.5 yr. The minimum telemetry rate expected is 2 kbits s^{-1} at 3.5 AU with a 35-m antenna. A scan platform with 2 deg of freedom will accommodate the remote sensing instruments, and is expected to have a pointing accuracy of $0°1$. A possible payload is summarized in Table VII.

The Soviet penetrator module has a wet mass (propellant included) of 500 kg. After release from the main spacecraft, a braking module reduces the velocity of 100 m s^{-1} at 20 km from the surface. Two penetrators, each carrying 4 kg of scientific payload, are released and reach the surface within a few km of each other. A data link of 60 bits s^{-1} is expected during at least 1 hr.

The double Mars swingby strategy gives great flexibility to the trajectories at minimal Δv cost. An Apollo-Amor asteroid, a Mars-grazing asteroid or a short-period comet can be visited between the two Mars swingbys, at a heliocentric distance of 1.4 to 1.7 AU. After the second Mars swingby, the spacecraft crosses the main belt on a low-eccentricity orbit with a semimajor axis of 1.8 to 2.1 AU, which provides low encounter velocities with main-belt asteroids. These encounters at 2 to 7 km s^{-1} provide 10 to 30 times more observing time than did the Halley flybys.

Baseline trajectories for Vega were selected on the basis of their technical characteristics (total Δv, total duration, phase angle range, communication link), and of their scientific interest. Two scientific selection criteria were used:

1. Diversity in types and sizes of asteroids visited, with at least one "primitive" asteroid (C and related class) and one "evolved" asteroid (S,M,V and related class), larger than 100 km in diameter. Preference was given to missions for which *in situ* penetrator studies of these two major classes were possible.
2. At least one comet on one of the two trajectories. The orbit of this comet must be reliable (good recovery rate).

TABLE VIII
Vesta Trajectory Options

BASELINE MISSIONS FOR 1994

Trajectory 1
  Penetrator on 4 Vesta (type V; 576 km) at 3.35 km s^{-1}; flybys of 2335 James (Mars grazer; ~8 km) at 15 km s^{-1}; 109 Felicitas (C; 76 km) at 6.3 km s^{-1}; 739 Mandeville (C; 70 km) at 7 km s^{-1}. Duration 4.62 yr; total $\Delta v = 450$ m s^{-1}.

Trajectory 2
  Penetrator on 46 Hestia (F; 165 km) at 3.6 km s^{-1}; flybys of 1204 Renzia (Mars grazer; 13 km) at 4.3 km s^{-1}; 435 Ella (U; 32 km) at 3.5 km s^{-1}; P/Tempel 1 at 7.1 km s^{-1}. Duration 5.2 yr; total $\Delta v = 720$ m s^{-1}.

BASELINE MISSIONS FOR 1996

Trajectory 1
  Penetrator on 46 Hestia (F; 165 km) at 3.5 km s^{-1}; flybys of 2285 Ron Helin (Apollo-Amor; 6 km) at 5.6 km s^{-1}; P/Bus at 6.3 km s^{-1}; 317 Roxane (M; 38 km) at 5.2 km s^{-1}; 2335 James (X; 8 km) at 13.7 km s^{-1}. Duration 6 yr; total $\Delta v = 750$ m s^{-1}.

Trajectory 2
  Penetrator on 7 Iris (S; 210 km) at 2.8 km s^{-1}; flybys of 2435 Horemheb (4 km) at 5.9 km s^{-1}; 1879 Broederstroom (12 km) at 3.4 km s^{-1}; P/Dutoit-Neujmin-Delporte at 14 km s^{-1}. Duration 5.5 yr; total $\Delta v = 780$ m s^{-1}.

All comet encounters occur within 40° of perihelion, with relative speeds ranging from 6 to 13 km s^{-1}, 5 to 10 times slower than in the case of Halley. Being short-period comets, the target comets are a factor of 5 to 20 less active than Halley. Thus, a minimum approach distance of 500 km appears compatible with spacecraft safety, in particular in those mission scenarios in which the comet is the last body to be visited.

The characteristics of the baseline missions for 1994 and 1996 are summarized in Table VIII. The two trajectories for the 1994 baseline mission allow one flyby of a comet and seven flybys of asteroids (types C, S, V and U) with diameters ranging from 8 to 576 km. Two are Mars grazers and five are main-belt objects; penetrators would be deployed on 4 Vesta (evolved) and on 46 Hestia (primitive).

The trajectories for the 1996 baseline mission permit flybys of two comets: P/Bus at 6 km s^{-1}, and P/Dutoit-Neujmin-Delporte at 14 km s^{-1}. Both comets have perihelia near 2 AU, significantly more distant than Halley (0.6 AU). *In situ* studies can be performed on two large asteroids: 46 Hestia ($d = 165$ km; F type) and 7 Iris ($d = 210$ km; S type). The trajectories also include visits to the M type asteroid 317 Roxane and four smaller bodies. The latter include both an Amor (2355 James) and inner main-belt objects. By providing a comprehensive survey of a broad spectrum of small solar system ob-
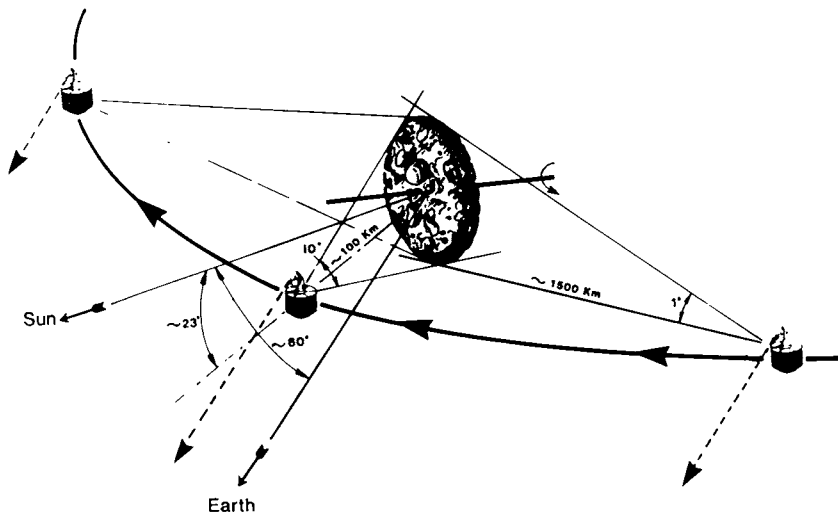
Fig. 5. Schematic of the Piazzi encounter phase. This mission would carry out a slow flyby (~ 100 m s^{-1}) of an Amor-Apollo-Aten asteroid such as 433 Eros.

jects, both the 1994 and 1996 missions fully meet the objectives of the Vesta program.

VII. PIAZZI: AN ITALIAN ASTEROID MISSION

The Italian asteroid community has proposed a dedicated small-body mission called Piazzi that would involve a slow flyby of an Apollo-Amor-Aten asteroid using a Giotto-derived spacecraft. A typical mission scenario might involve a flyby of asteroid 433 Eros at a speed of only 100 m s^{-1} (Fig. 5). Piazzi, a partial acronym, stands for "Probe for Inner Asteroid Zone," and also honors Giuseppe Piazzi, the discoverer of the first asteroid. Piazzi is an important complement to other planned flybys (e.g., Galileo and CRAF) which will not only involve main-belt asteroid targets but significantly higher flyby speeds.

Piazzi is envisaged as a one-axis, spin-stabilized spacecraft that would accommodate a payload of 50 kg. The science package would include a complement of instruments very similar to those proposed for NEAR: an imaging camera, a reflectance spectrometer, a thermal radiometer, a radar altimeter, as well as possibly an X-ray spectrometer. In addition, there would be three instruments optimized for cruise science: a plasma analyzer, a magnetometer and a dust detector. Due to the low velocity of the encounter, an accurate mass determination of the target asteroid is possible, which when combined with a volume estimate would yield an accurate mean density. One idea is to measure

the deflection of a test mass, deployed from the main spacecraft during the slow flyby of the asteroid.

Piazzi represents an intermediate step between very rapid flybys (e.g., Giotto), and more elaborate rendezvous missions such as NEAR. It has the advantage that the mission is modest enough that it could be carried out within the national budget base of Italy; clearly, substantial enhancements would occur if it were implemented as an international effort.

VIII. MULTIPLE FLYBY MISSIONS: POSSIBLE JAPANESE INTEREST

It has long been recognized that a multiple flyby mission provides a rapid means of obtaining some much-needed data on the diversity of asteroids (Morrison and Niehoff 1979). Indeed, the Asterex mission discussed in Europe during the past decade was of this type. In the United States, such missions have received less consideration for at least two reasons. First, was the conviction among most scientists that certain fundamental objectives (e.g., the thorough elemental characterization of surface materials) cannot be achieved at the high flyby speeds associated with multi-asteroid trajectories. Second, was the belief that the more scientifically rewarding concept of a multiple-rendezvous asteroid mission was within our grasp (see Sec. III). Even with the realization that NASA currently lacks the capability to launch multiple-rendezvous missions, interest in multiple flybys has not increased significantly, almost certainly because of the promise of achieving such flybys as parts of other missions such as Galileo, CRAF and Cassini.

However, the interest has increased elsewhere, especially in Europe in conjunction with the proposed "Comet Coma Sample Return" mission, and in Japan (ISAS). The success of the Halley flybys has prompted the question of whether opportunities exist to visit several small bodies (comets and asteroids) on a single mission trajectory, and perhaps even to return the spacecraft to the vicinity of Earth.

Considerable work on such concepts has been done by the group at Goddard which was responsible for finding the opportunity that led to the retargetting of the ISEE-3 spacecraft to a flythrough of the tail of P/Giacobini-Zinner in 1985; the interested reader is referred to a recent paper by Farquhar et al. (1987). Part of the motivation involves the eventual return of a coma sample to Earth from one, or perhaps even two, comets. However, another aspect involves trajectories which include flybys of three comets and two asteroids. An Observer-class spacecraft is involved, and use is made of successive Earth swingbys as well as of propulsive maneuvers. A sample 12-yr mission which would visit three comets (Tempel 1, Tempel 2, Encke) and two asteroids (46 Hestia and 433 Eros) is outlined in Table IX. Note that at least in the case of the two asteroids, the flyby speeds are relatively low. In principle, the spacecraft could be three-axis stabilized (unlike ISEE-3) and carry a payload of 100 kg.

TABLE IX
TABLE IX
Multi-Comet/Asteroid Tour 1994–2005[a]
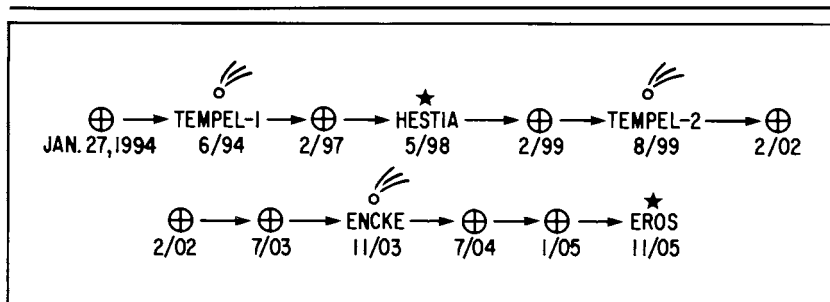
EARTH-SWINGBY MANEUVERS

Swingby Date	Perigee (Earth Radii)	Bend Angle (Deg)	Heliocentric Inclination After Swingby (Deg)
Feb. 13, 1997	2.48	58.4	2.0
Feb. 8, 1999	4.19	41.6	5.6
Feb. 8, 2002	2.42	53.5	0.0
July 29, 2003	1.36	71.1	10.9
July 29, 2004	8.84	19.3	11.6
Jan. 26, 2005	3.18	40.4	8.5

PROPULSIVE MANEUVERS

Maneuver Date	ΔV (m s^{-1})	
July 4, 1994	350	
Aug. 18, 1996	79	Launch C_3: 15.2 km^2 s^{-2}
Aug. 11, 2000	472	Total ΔV: 1063 m s^{-1}
July 29, 2003	152	

SMALL-BODY ENCOUNTERS

Encounter Date	Sun Distance (AU)	Earth Distance (AU)	Phase Angle (Deg)	Flyby Speed (km s^{-1})
Tempel-1: 6-24-94	1.50	0.81	53.6	11.2
Hestia: 5-10-96	2.10	2.68	115.9	6.5
Tempel-2: 8-27-99	1.49	0.77	63.6	12.5
Encke: 11-13-03	1.06	0.26	13.1	28.0
Eros: 11-3-05	1.78	2.23	89.7	1.2

[a]Table from Farquhar et al. 1987
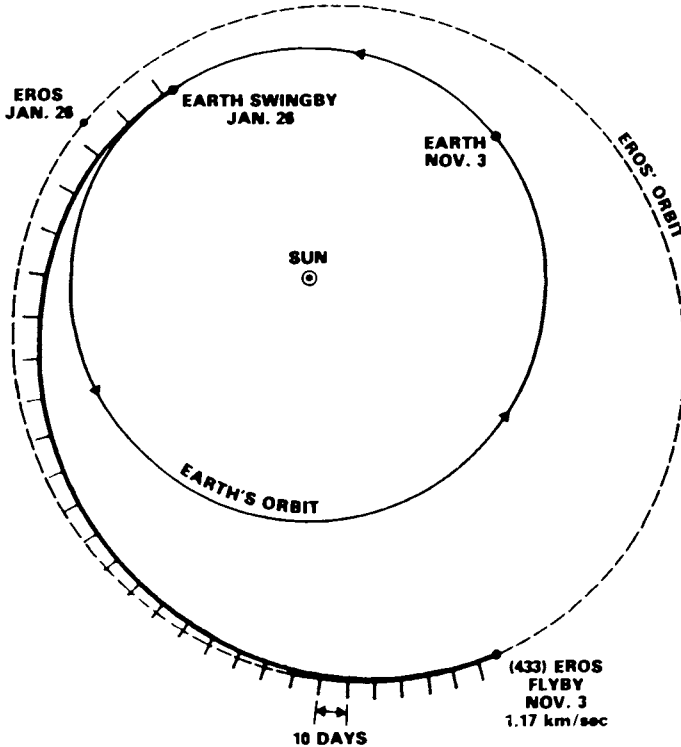
Fig. 6. Ecliptic plane view of the main spacecraft trajectory Earth to Eros (2005) part of the Encke/Eros mission under joint study by ISAS (Japan) and NASA.

Currently a ISAS/NASA study team is considering possible cooperative missions to comets and asteroids. One proposal involves a cometary flyby and a coma sample return mission. ISAS would supply the launch vehicle as well as the spacecraft, but NASA support would be required for the retrieval of the spacecraft in the year 2000. NASA participation would also include responsibility for the gas and dust collectors, DSN tracking support and possibly some spacecraft hardware such as the far-encounter nucleus-sensor and the deployable aerobrake.

A second mission concept calls for an Encke flyby followed by a rendezvous with the well-observed asteroid Eros. This plan was derived from the multibody tour described above (Table IX). The launch would occur in July 2003 with a fast flyby of Encke in November 2005 (Fig. 6). Two Earth-swingby maneuvers would then be used to position the spacecraft for a rendezvous with Eros in 2005 (final $\Delta v \sim 1.2$ km s^{-1}). NASA would furnish a launch vehicle and the main spacecraft bus. ISAS would provide a coma probe that would be deployed during the Encke flyby, and two or three pen-

etrators that would be targeted for Eros after the rendezvous has been achieved.

IX. CONCLUSION

In spite of considerable planning, the direct exploration of asteroids has made no progress during the past decade. This unfortunate situation is in sharp contrast with the remarkable success in gathering new data on the part of the groundbased observers and on the part of Earth-orbital missions such as IRAS. The situation is a dangerous one: no matter how clever one is in obtaining and interpreting spatially unresolved data, one cannot deduce the complexity, for example, of a Miranda, or fully understand the environment of a place like Io. Some asteroids, in their own way, may be just as complex. Nor can one discard fashionable but untenable ideas without the brutal arbitration of observational fact. One suspects that even some cherished ideas of current asteroid discussions, such as Macclaurin ellipsoid-shaped objects and binary asteroids (see the chapter by Weidenschilling et al.), will end up in the dust bin of irrelevancy once facts are available. Theoreticians never tire of proposing quaint ideas, and observations are needed constantly to sort out the few correct ideas from the deluge of strange ones. The long-awaited first spacecraft encounter with an asteroid will be a major event in the history of our science. However, that event (the scheduled December 1991 encounter of Galileo with Gaspra) is still three years off.

REFERENCES

Alfvén, H., and Arrhenius, G. 1970. Mission to an asteroid. *Science* 167:139–141.

Farquhar, R. W., Dunham, D. W., and Hsu, S. C. 1987. A Voyager-style tour of comets and asteroids 1994–2005. *J. Astron. Sci.* 35, in press.

Friedlander, A. L., Wells, W. C., Davies, D. R., Housen, K., and Wilkening, L. L. 1979. *Asteroid Mission Study.* Science Applications, Inc. Report No. 1-120-839-M11.

Gehrels, T., ed. 1979. *Asteroids* (Tucson: Univ. of Arizona Press).

Herrick, S. 1979. Exploration and 1994 exploitation of Geographos. In *Asteroids,* ed. T. Gehrels (Tucson: Univ. of Arizona Press), pp. 222–226.

Levin, B. J., Simonenko, A. N., and Anders, E. 1976. Farmington meteorite: A fragment of an Apollo asteroid? *Icarus* 28:307–324.

McFadden, L. A., Gaffey, M. J., and McCord, T. B. 1984. Mineralogical-petrological characterization of near-earth asteroids. *Icarus* 59:25–40.

McFadden, L. A., Gaffey, M. J., and McCord, T. B. 1985. Near-earth asteroids: Possible sources from reflectance spectroscopy. *Science* 229:160–163.

Morrison, D., and Niehoff, J. 1979. Future exploration of the asteroids. In *Asteroids,* ed. T. Gehrels (Tucson: Univ. of Arizona Press), pp. 227–250.

O'Leary, B. T. 1977. Moving the Apollo and Amor asteroids. *Science* 197:363–366.

Piazzi: A Space Mission to the Apollo-Amor Asteroids. 1988. Aeritalia (Società aerospaziale italiana) Report.

Solar System Exploration Committee. 1983. *Planetary Exploration through the Year 2000: A Core Program* (Washington, DC: U.S. Government Printing Office).

Solar System Exploration Committee. 1986. *Planetary Exploration through the Year 2000: An Augmented Program* (Washington, DC: U.S. Government Printing Office).

Veverka, J., Harris, A. L., and Randolph, J., eds. 1986. *Near-Earth Asteroid Rendezvous (NEAR) Science Working Group Report.* JPL Document 86-7.

Zakharov, A. 1988. Close encounters with Phobos. *Sky and Telescope* 76:17–21.

PART VI

Tabulation

INTRODUCTION TO THE *ASTEROIDS II* DATA BASE

EDWARD F. TEDESCO

Jet Propulsion Laboratory

The Asteroids II *data base presented herein is a compilation of asteroid data published, or in press, as of March 1988 with some updates in early 1989. It is by no means all-inclusive. Excluded are data sets which have remained essentially unchanged since their publication in* Asteroids *(Gehrels 1979). These include the spectral reflectance and spectral parameter data sets (Chapman and Gaffey 1979), and the polarimetric and groundbased radiometric data sets (Morrison and Zellner 1979). Included in this book are asteroid names and discovery circumstances, proper elements and family identifications, asteroid lightcurve parameters, asteroid pole determinations, taxonomic classes, absolute magnitudes and slope parameters,* UBV *color indices, and albedos and diameters from the* IRAS Asteroid and Comet Survey.

The rationale for this data base arose early in 1987 when it was decided to hold an asteroid conference in Tucson, Arizona in March 1988 and to publish a comprehensive book on Asteroids to update the one published nearly ten years earlier (Gehrels 1979). In order to provide participants at the conference, and authors of chapters in the book, with an up-to-date and convenient set of asteroid data, it was agreed to compile a machine-readable version of these data. Consequently, eight people were requested to provide files of data on what was felt to be a core data set. These machine-readable files were made available to the community in December 1987 and an updated version (March 1988) was distributed following the asteroid conference. The purpose of this introduction is to describe the machine-readable version of the data base and list the data sets presented in Part VI of this book.

The floppy-disk version of the machine-readable data set was assembled by the author in March 1988 from files provided by the contributors noted

below. These files constitute the machine-readable version of a preliminary version of the table presented in the tabulation section (Part VI) of this book. Each tabulation contribution contains a brief introduction followed by the tabular material. In some cases, the published tabulation sections are a subset of the machine-readable form of the data set. Readers should note that descriptions of the differences (such as updates or corrections), if any, between the machine-readable and printed versions are presented by the authors of the tabulations.

Because the data from a machine-readable data set may differ from that contained in the printed version, references to data obtained from these electronic files should be made explicitly and the source and version used should be noted. For example a reference to the machine-readable lightcurve data base should read "Lagerkvist et al. 1987" in the text and (for the floppy disk version) "Lagerkvist, C.-I., Harris, A. W., and Zappalà, V. 1987. Asteroids II machine-readable data base: March 1988 floppy disk version." in the references section.

Both the December 1987 and March 1988 versions of the floppy disk data sets have been deposited with the National Space Science Data Center (NSSDC), Code 633.4, Goddard Space Flight Center, Greenbelt MD 20771 under the data set name: "Asteroids II machine-readable data base: December 1987 (or March 1988) version." This data set will be available from NSSDC only on 9-track magnetic tape. If the NSSDC version of this data set is used, then the full reference should read, for example, "Lagerkvist, C.-I., Harris, A. W., and Zappalà, V. 1987. Asteroids II machine-readable data base: March 1988 version, National Space Science Data Center, Greenbelt MD." Naturally, a datum on an individual asteroid, at least one that is being discussed in detail, should reference the original source.

The Asteroids II machine-readable data base: March 1988 version consists of the following files.

Data Set(s)	Provider(s)
Asteroid Names and Discovery Circumstances	F. Pilcher
Proper Elements and Family Identifications	J.G. Williams
Asteroid Lightcurve Parameters	C.-I. Lagerkvist, A.W. Harris and V. Zappalà
Asteroid Pole Determinations	P. Magnusson
Asteroid Taxonomic Classifications	D.J. Tholen
Asteroid Magnitudes, UBV colors, Albedos, and Diameters.	E.F. Tedesco

The machine-readable data sets are provided as the following files:

General Documentation

File		Size (in bytes)	Date	Time	Description
-INTRO	DOC	5130	1-07-88	10:10a	A file similar to the text in this chapter.

Asteroid Names and Discovery Circumstances

File		Size (in bytes)	Date	Time	Description
DISCOVER	DAT	329780	3-20-88	4:46p	Data for asteroids 1–3774
DISCOVER	DOC	4224	11-30-87	9:10a	Discovery documentation file
DISCOVER	NOT	16110	3-20-88	4:54p	Notes

Proper Elements and Family Identifications

File		Size (in bytes)	Date	Time	Description
FAMILY	DAT	17961	12-02-87	12:48p	Williams' family identifications
FAMILY	DOC	2048	12-04-87	10:41a	Documentation file for FAMILY.DAT
PROPER	DAT	129313	3-30-88	5:20p	Williams' proper orbital elements
PROPER	DOC	5376	12-04-87	10:42a	Documentation file for PROPER.DAT

Asteroid Lightcurve Parameters

File		Size (in bytes)	Date	Time	Description
LIGHTCRV	DAT	30208	12-07-87	4:24p	Lightcurve data file
LIGHTCRV	DOC	3712	3-29-88	12:21p	Lightcurve documentation file
LIGHTCRV	REF	26240	12-07-87	2:38p	Lightcurve references file

Asteroid Pole Determinations

File		Size (in bytes)	Date	Time	Description
POLE	DAT	26054	3-29-88	1:03p	Pole orientation data file
POLE	DOC	4422	3-29-88	12:37p	Pole orientation documentation file
POLE	REF	8749	3-29-88	1:06p	Pole orientation references file

Asteroid Taxonomic Classifications

TAXONOMY	DAT	34432	3-29-88	12:28p	Taxonomic classification data file
TAXONOMY	DOC	3456	3-29-88	12:33p	Taxonomic class documentation file
TAXONOMY	NOT	1664	3-29-88	12:34p	Notes to taxonomic class data file

Asteroid Magnitudes, UBV colors, Albedos, and Diameters

MAG-ETAL	DAT	264448	11-30-87	6:17p	Mag, color, albedo, diam data file
MAG-ETAL	DOC	3413	11-30-87	7:07p	Documentation file for MAG-ETAL.DAT

Questions regarding any of the above files should be directed to the provider(s).

Note that additional groundbased asteroid data files, not included in or superseded by the Asteroids II data base, are contained in IRAS Asteroid and Comet Final Data Product 13 (Tedesco 1986), also available from the NSSDC. These include: 24-color reflectances for 284 asteroids from Chapman and Gaffey (1979) and McFadden et al. (1984), eight-color survey color indices for 589 asteroids from Zellner et al. (1985), and polarimetric parameters for 111 asteroids from Ben Zellner's 1979 "TRIAD" file in a slightly modified format (cf. Morrison and Zellner 1979).

REFERENCES

Chapman, C. R., and Gaffey, M. J. 1979. Spectral reflectances of the asteroids. In *Asteroids,* ed. T. Gehrels (Tucson: Univ. of Arizona Press), pp. 1064–1089.

Gehrels, T., ed. 1979. *Asteroids* (Tucson: Univ. of Arizona Press).

Infrared Astronomical Satellite Asteroid and Comet Survey: Preprint Version No. 1. 1986. ed. D. L. Matson, JPL Document No. 3698.

McFadden, L. A., Gaffey, M. J., and McCord, T. B. 1984. Mineralogical-petrological characterization of near-Earth asteroids. *Icarus* 59:25–40.

Morrison, D., and Zellner, B. 1979. Polarimetry and radiometry of the asteroids. In *Asteroids,* ed. T. Gehrels (Tucson: Univ. of Arizona Press), pp. 1090–1097.

Tedesco, E. F. 1986. Ground-based data for asteroids. In *Infrared Astronomical Satellite Asteroid and Comet Survey: Preprint Version No. 1*. 1986, ed. D. L. Matson, JPL Document No. 3698.

Zellner, B., Tholen, D. J., and Tedesco, E. F. 1985. The eight-color asteroid survey: Results for 589 minor planets. *Icarus* 61:355–416.

Editor's note added in proof: Two additional data sets have become available just as this book goes to press. These sets are new proper elements computed by Kneževič and Milani and a new taxonomic classification by Tedesco et al. 1989 (*Astron. J.* 97:580). Both new tables have been added to the tabulation section in this book. (See their descriptions for information on obtaining machine-readable versions.) Readers should note that because of their recent availability, these data sets are not fully referred to within the body of this book.

THE CIRCUMSTANCES OF MINOR PLANET DISCOVERY

FREDERICK PILCHER
Illinois College

This tabulation of minor planet discovery data has also been prepared in machine-readable form for NSSDC. The machine-readable list contains complete data for all numbered minor planets. The table published here contains complete data only for planets 2125 and forward, and notes pertaining to these planets. Those for the preceding planets were published by the writer in *Asteroids*, (1979), ed. T. Gehrels (Tucson: University of Arizona Press), pp. 1130–1154. A few mistakes in the table in the first book have since been found and corrected in the machine readable version, and the reader will note small changes in the numbering of some of the Notes. Diacritical marks for the names of planets, increasingly omitted from machine-readable lists, have been retained in this printed version.

The first column contains the permanent number; the second, the official name; the third, for planets 330 and forward, the provisional designation attached to the discovery apparition; the fourth, the year, month and day of discovery according to criteria explained below; the fifth, the name of the discoverer, discoverers or institution of discovery; the sixth, the discovery place. The seventh column is used when needed for notes referencing two or more discoverers with names of combined length too great to fit in the discoverer column, to give a more complete description of programs involving several persons, and to reference cases in which two numbered planets were subsequently discovered to be identical and the number and name of one of these was re-assigned to a newly discovered planet. Notes in the last column (see end of table) have also been used to reference conflicting discovery

claims and list important independent discoveries which are no longer regarded as official.

The discovery date is in local mean time prior to 1 January 1925, and in UT thereafter, and refers to the time of mid-exposure for planets discovered by photographic means. In many cases, the permanent number was assigned only when several unnumbered planets observed in different years were found to be identical, often many years after the discovery photographs were made. In these cases, the discovery date is the first of that series of photographic observations from which the preliminary orbit was computed, and the provisional designation is that associated with this particular set of observations. Often earlier observations exist, but they are considered prediscoveries. In some cases the discovery and subsequent observations permitted images to be found on photographs obtained at the same observatory earlier in the discovery apparition; these earlier observations are considered prediscoveries.

The following literature has been examined comprehensively to determine the discovery data:

STRACKE, G., *Identifizierungsnachweis der Kleinen Planeten* (Berlin, 1938);
HERGET, P., *Names of Minor Planets* (University of Cincinnati Observatory, 1957, 1967);
Astronomische Nachrichten;
Astronomische Nachrichten Indices;
Monthly Notices of the Royal Astronomical Society;
Rechen-Institut Circulars;
Beobachtungs Zircular;
Minor Planet Circulars;
Lick Research Surveys on Minor Planets;
Turku Informo.

No.	Name*	No.	Name	No.	Name	No.	Name
1	Ceres	2	Pallas	3	Juno	4	Vesta
5	Astraea	6	Hebe	7	Iris	8	Flora
9	Metis	10	Hygiea	11	Parthenope	12	Victoria
13	Egeria	14	Irene	15	Eunomia	16	Psyche
17	Thetis	18	Melpomene	19	Fortuna	20	Massalia
21	Lutetia	22	Kalliope	23	Thalia	24	Themis
25	Phocaea	26	Proserpina	27	Euterpe	28	Bellona
29	Amphitrite	30	Urania	31	Euphrosyne	32	Pomona
33	Polyhymnia	34	Circe	35	Leukothea	36	Atalante
37	Fides	38	Leda	39	Laetitia	40	Harmonia
41	Daphne	42	Isis	43	Ariadnë	44	Nysa
45	Eugenia	46	Hestia	47	Aglaja	48	Doris
49	Pales	50	Virginia	51	Nemausa	52	Europa
53	Kalypso	54	Alexandra	55	Pandora	56	Melete
57	Mnemosyne	58	Concordia	59	Elpis	60	Echo
61	Danaë	62	Erato	63	Ausonia	64	Angelina
65	Cybele	66	Maja	67	Asia	68	Leto
69	Hesperia	70	Panopaea	71	Niobe	72	Feronia
73	Klytia	74	Galatea	75	Eurydike	76	Freia
77	Frigga	78	Diana	79	Eurynome	80	Sappho
81	Terpsichore	82	Alkmene	83	Beatrix	84	Klio
85	Io	86	Semele	87	Sylvia	88	Thisbe
89	Julia	90	Antiope	91	Aegina	92	Undina
93	Minerva	94	Aurora	95	Arethusa	96	Aegle
97	Klotho	98	Ianthe	99	Dike	100	Hekate
101	Helena	102	Miriam	103	Hera	104	Klymene
105	Artemis	106	Dione	107	Camilla	108	Hecuba
109	Felicitas	110	Lydia	111	Ate	112	Iphigenia
113	Amalthea	114	Kassandra	115	Thyra	116	Sirona
117	Lomia	118	Peitho	119	Althaea	120	Lachesis
121	Hermione	122	Gerda	123	Brunhild	124	Alkeste
125	Liberatrix	126	Velleda	127	Johanna	128	Nemesis
129	Antigone	130	Elektra	131	Vala	132	Aethra
133	Cyrene	134	Sophrosyne	135	Hertha	136	Austria
137	Meliboea	138	Tolosa	139	Juewa	140	Siwa
141	Lumen	142	Polana	143	Adria	144	Vibilia
145	Adeona	146	Lucina	147	Protogeneia	148	Gallia
149	Medusa	150	Nuwa	151	Abundantia	152	Atala
153	Hilda	154	Bertha	155	Scylla	156	Xanthippe
157	Dejanira	158	Koronis	159	Aemilia	160	Una
161	Athor	162	Laurentia	163	Erigone	164	Eva
165	Loreley	166	Rhodope	167	Urda	168	Sibylla
169	Zelia	170	Maria	171	Ophelia	172	Baucis
173	Ino	174	Phaedra	175	Andromache	176	Iduna
177	Irma	178	Belisana	179	Klytaemnestra	180	Garumna
181	Eucharis	182	Elsa	183	Istria	184	Dejopeja
185	Eunike	186	Celuta	187	Lamberta	188	Menippe
189	Phthia	190	Ismene	191	Kolga	192	Nausikaa
193	Ambrosia	194	Prokne	195	Eurykleia	196	Philomela
197	Arete	198	Ampella	199	Byblis	200	Dynamene
201	Penelope	202	Chryseïs	203	Pompeja	204	Kallisto
205	Martha	206	Hersilia	207	Hedda	208	Lacrimosa
209	Dido	210	Isabella	211	Isolda	212	Medea
213	Lilaea	214	Aschera	215	Oenone	216	Kleopatra
217	Eudora	218	Bianca	219	Thusnelda	220	Stephania
221	Eos	222	Lucia	223	Rosa	224	Oceana
225	Henrietta	226	Weringia	227	Philosophia	228	Agathe
229	Adelinda	230	Athamantis	231	Vindobona	232	Russia
233	Asterope	234	Barbara	235	Carolina	236	Honoria
237	Coelestina	238	Hypatia	239	Adrastea	240	Vanadis
241	Germania	242	Kriemhild	243	Ida	244	Sita
245	Vera	246	Asporina	247	Eukrate	248	Lameia
249	Ilse	250	Bettina	251	Sophia	252	Clementina
253	Mathilde	254	Augusta	255	Oppavia	256	Walpurga
257	Silesia	258	Tyche	259	Aletheia	260	Huberta
261	Prymno	262	Valda	263	Dresda	264	Libussa
265	Anna	266	Aline	267	Tirza	268	Adorea
269	Justitia	270	Anahita	271	Penthesilea	272	Antonia
273	Atropos	274	Philagoria	275	Sapientia	276	Adelheid
277	Elvira	278	Paulina	279	Thule	280	Philia
281	Lucretia	282	Clorinde	283	Emma	284	Amalia
285	Regina	286	Iclea	287	Nephthys	288	Glauke
289	Nenetta	290	Bruna	291	Alice	292	Ludovica
293	Brasilia	294	Felicia	295	Theresia	296	Phaëtusa
297	Caecilia	298	Baptistina	299	Thora	300	Geraldina
301	Bavaria	302	Clarissa	303	Josephina	304	Olga
305	Gordonia	306	Unitas	307	Nike	308	Polyxo
309	Fraternitas	310	Margarita	311	Claudia	312	Pierretta
313	Chaldaea	314	Rosalia	315	Constantia	316	Goberta
317	Roxane	318	Magdalena	319	Leona	320	Katharina

*Complete discovery circumstances for these objects have been previously published by Pilcher in *Asteroids* (1979), ed. T. Gehrels (Tucson: University of Arizona Press), pp. 1130–1154.

No.	Name*	No.	Name	No.	Name	No.	Name
321	Florentina	322	Phaeo	323	Brucia	324	Bamberga
325	Heidelberga	326	Tamara	327	Columbia	328	Gudrun
329	Svea	330	Adalberta	331	Etheridgea	332	Siri
333	Badenia	334	Chicago	335	Roberta	336	Lacadiera
337	Devosa	338	Budrosa	339	Dorothea	340	Eduarda
341	California	342	Endymion	343	Ostara	344	Desiderata
345	Tercidina	346	Hermentaria	347	Pariana	348	May
349	Dembowska	350	Ornamenta	351	Yrsa	352	Gisela
353	Ruperto-Carola	354	Eleonora	355	Gabriella	356	Liguria
357	Ninina	358	Apollonia	359	Georgia	360	Carlova
361	Bononia	362	Havnia	363	Padua	364	Isara
365	Corduba	366	Vincentina	367	Amicitia	368	Haidea
369	Aëria	370	Modestia	371	Bohemia	372	Palma
373	Melusina	374	Burgundia	375	Ursula	376	Geometria
377	Campania	378	Holmia	379	Huenna	380	Fiducia
381	Myrrha	382	Dodona	383	Janina	384	Burdigala
385	Ilmatar	386	Siegena	387	Aquitania	388	Charybdis
389	Industria	390	Alma	391	Ingeborg	392	Wilhelmina
393	Lampetia	394	Arduina	395	Delia	396	Aeolia
397	Vienna	398	Admete	399	Persephone	400	Ducrosa
401	Ottilia	402	Chloë	403	Cyane	404	Arsinoë
405	Thia	406	Erna	407	Arachne	408	Fama
409	Aspasia	410	Chloris	411	Xanthe	412	Elisabetha
413	Edburga	414	Liriope	415	Palatia	416	Vaticana
417	Suevia	418	Alemannia	419	Aurelia	420	Bertholda
421	Zähringia	422	Berolina	423	Diotima	424	Gratia
425	Cornelia	426	Hippo	427	Galene	428	Monachia
429	Lotis	430	Hybris	431	Nephele	432	Pythia
433	Eros	434	Hungaria	435	Ella	436	Patricia
437	Rhodia	438	Zeuxo	439	Ohio	440	Theodora
441	Bathilde	442	Eichsfeldia	443	Photographica	444	Gyptis
445	Edna	446	Aeternitas	447	Valentine	448	Natalie
449	Hamburga	450	Brigitta	451	Patientia	452	Hamiltonia
453	Tea	454	Mathesis	455	Bruchsalia	456	Abnoba
457	Alleghenia	458	Hercynia	459	Signe	460	Scania
461	Saskia	462	Eriphyla	463	Lola	464	Megaira
465	Alekto	466	Tisiphone	467	Laura	468	Lina
469	Argentina	470	Kilia	471	Papagena	472	Roma
473	Nolli	474	Prudentia	475	Ocllo	476	Hedwig
477	Italia	478	Tergeste	479	Caprera	480	Hansa
481	Emita	482	Petrina	483	Seppina	484	Pittsburghia
485	Genua	486	Cremona	487	Venetia	488	Kreusa
489	Comacina	490	Veritas	491	Carina	492	Gismonda
493	Griseldis	494	Virtus	495	Eulalia	496	Gryphia
497	Iva	498	Tokio	499	Venusia	500	Selinur
501	Urhixidur	502	Sigune	503	Evelyn	504	Cora
505	Cava	506	Marion	507	Laodica	508	Princetonia
509	Iolanda	510	Mabella	511	Davida	512	Taurinensis
513	Centesima	514	Armida	515	Athalia	516	Amherstia
517	Edith	518	Halawe	519	Sylvania	520	Franziska
521	Brixia	522	Helga	523	Ada	524	Fidelio
525	Adelaide	526	Jena	527	Euryanthe	528	Rezia
529	Preziosa	530	Turandot	531	Zerlina	532	Herculina
533	Sara	534	Nassovia	535	Montague	536	Merapi
537	Pauly	538	Friederike	539	Pamina	540	Rosamunde
541	Deborah	542	Susanna	543	Charlotte	544	Jetta
545	Messalina	546	Herodias	547	Praxedis	548	Kressida
549	Jessonda	550	Senta	551	Ortrud	552	Sigelinde
553	Kundry	554	Peraga	555	Norma	556	Phyllis
557	Violetta	558	Carmen	559	Nanon	560	Delila
561	Ingwelde	562	Salome	563	Suleika	564	Dudu
565	Marbachia	566	Stereoskopia	567	Eleutheria	568	Cheruskia
569	Misa	570	Kythera	571	Dulcinea	572	Rebekka
573	Recha	574	Reginhild	575	Renate	576	Emanuela
577	Rhea	578	Happelia	579	Sidonia	580	Selene
581	Tauntonia	582	Olympia	583	Klotilde	584	Semiramis
585	Bilkis	586	Thekla	587	Hypsipyle	588	Achilles
589	Croatia	590	Tomyris	591	Irmgard	592	Bathseba
593	Titania	594	Mireille	595	Polyxena	596	Scheila
597	Bandusia	598	Octavia	599	Luisa	600	Musa
601	Nerthus	602	Marianna	603	Timandra	604	Tekmessa
605	Juvisia	606	Brangäne	607	Jenny	608	Adolfine
609	Fulvia	610	Valeska	611	Valeria	612	Veronika
613	Ginevra	614	Pia	615	Roswitha	616	Elly
617	Patroclus	618	Elfriede	619	Triberga	620	Drakonia
621	Werdandi	622	Esther	623	Chimaera	624	Hektor
625	Xenia	626	Notburga	627	Charis	628	Christine
629	Bernardina	630	Euphemia	631	Philippina	632	Pyrrha
633	Zelima	634	Ute	635	Vundtia	636	Erika
637	Chrysothemis	638	Moira	639	Latona	640	Brambilla
641	Agnes	642	Clara	643	Scheherezade	644	Cosima
645	Agrippina	646	Kastalia	647	Adelgunde	648	Pippa
649	Josefa	650	Amalasuntha	651	Antikleia	652	Jubilatrix

*Complete discovery circumstances for these objects have been previously published by Pilcher in *Asteroids* (1979), ed. T. Gehrels (Tucson: University of Arizona Press), pp. 1130–1154.

No.	Name*	No.	Name	No.	Name	No.	Name
653	Berenike	654	Zelinda	655	Briseis	656	Beagle
657	Gunlöd	658	Asteria	659	Nestor	660	Crescentia
661	Cloelia	662	Newtonia	663	Gerlinde	664	Judith
665	Sabine	666	Desdemona	667	Denise	668	Dora
669	Kypria	670	Ottegebe	671	Carnegia	672	Astarte
673	Edda	674	Rachele	675	Ludmilla	676	Melitta
677	Aaltje	678	Fredegundis	679	Pax	680	Genoveva
681	Gorgo	682	Hagar	683	Lanzia	684	Hildburg
685	Hermia	686	Gersuind	687	Tinette	688	Melanie
689	Zita	690	Wratislavia	691	Lehigh	692	Hippodamia
693	Zerbinetta	694	Ekard	695	Bella	696	Leonora
697	Galilea	698	Ernestina	699	Hela	700	Auravictrix
701	Oriola	702	Alauda	703	Noëmi	704	Interamnia
705	Erminia	706	Hirundo	707	Steina	708	Raphaela
709	Fringilla	710	Gertrud	711	Marmulla	712	Boliviana
713	Luscinia	714	Ululu	715	Transvaalia	716	Berkeley
717	Wisibada	718	Erida	719	Albert	720	Bohlinia
721	Tabora	722	Frieda	723	Hammonia	724	Hapag
725	Amanda	726	Joëlla	727	Nipponia	728	Leonisis
729	Watsonia	730	Athanasia	731	Sorga	732	Tjilaki
733	Mocia	734	Benda	735	Marghanna	736	Harvard
737	Arequipa	738	Alagasta	739	Mandeville	740	Cantabia
741	Botolphia	742	Edisona	743	Eugenisis	744	Aguntina
745	Mauritia	746	Marlu	747	Winchester	748	Simeisa
749	Malzovia	750	Oskar	751	Faïna	752	Sulamitis
753	Tiflis	754	Malabar	755	Quintilla	756	Lilliana
757	Portlandia	758	Mancunia	759	Vinifera	760	Massinga
761	Brendelia	762	Pulcova	763	Cupido	764	Gedania
765	Mattiaca	766	Moguntia	767	Bondia	768	Struveana
769	Tatjana	770	Bali	771	Libera	772	Tanete
773	Irmintraud	774	Armor	775	Lumière	776	Berbericia
777	Gutemberga	778	Theobalda	779	Nina	780	Armenia
781	Kartvelia	782	Montefiore	783	Nora	784	Pickeringia
785	Zwetana	786	Bredichina	787	Moskva	788	Hohensteina
789	Lena	790	Pretoria	791	Ani	792	Metcalfia
793	Arizona	794	Irenaea	795	Fini	796	Sarita
797	Montana	798	Ruth	799	Gudula	800	Kressmannia
801	Helwerthia	802	Epyaxa	803	Picka	804	Hispania
805	Hormuthia	806	Gyldenia	807	Ceraskia	808	Merxia
809	Lundia	810	Atossa	811	Nauheima	812	Adele
813	Baumeia	814	Tauris	815	Coppelia	816	Juliana
817	Annika	818	Kapteynia	819	Barnardiana	820	Adriana
821	Fanny	822	Lalage	823	Sisigambis	824	Anastasia
825	Tanina	826	Henrika	827	Wolfiana	828	Lindemannia
829	Academia	830	Petropolitana	831	Stateira	832	Karin
833	Monica	834	Burnhamia	835	Olivia	836	Jole
837	Schwarzschilda	838	Seraphina	839	Valborg	840	Zenobia
841	Arabella	842	Kerstin	843	Nicolaia	844	Leontina
845	Naëma	846	Lipperta	847	Agnia	848	Inna
849	Ara	850	Altona	851	Zeissia	852	Wladilena
853	Nansenia	854	Frostia	855	Newcombia	856	Backlunda
857	Glasenappia	858	El Djezaïr	859	Bouzaréah	860	Ursina
861	Aïda	862	Franzia	863	Benkoela	864	Aase
865	Zubaida	866	Fatme	867	Kovacia	868	Lova
869	Mellena	870	Manto	871	Amneris	872	Holda
873	Mechthild	874	Rotraut	875	Nymphe	876	Scott
877	Walküre	878	Mildred	879	Ricarda	880	Herba
881	Athene	882	Swetlana	883	Matterania	884	Priamus
885	Ulrike	886	Washingtonia	887	Alinda	888	Parysatis
889	Erynia	890	Waltraut	891	Gunhild	892	Seeligeria
893	Leopoldina	894	Erda	895	Helio	896	Sphinx
897	Lysistrata	898	Hildegard	899	Jokaste	900	Rosalinde
901	Brunsia	902	Probitas	903	Nealley	904	Rockefellia
905	Universitas	906	Repsolda	907	Rhoda	908	Buda
909	Ulla	910	Anneliese	911	Agamemnon	912	Maritima
913	Otila	914	Palisana	915	Cosette	916	America
917	Lyka	918	Itha	919	Ilsebill	920	Rogeria
921	Jovita	922	Schlutia	923	Herluga	924	Toni
925	Alphonsina	926	Imhilde	927	Ratisbona	928	Hildrun
929	Algunde	930	Westphalia	931	Whittemora	932	Hooveria
933	Susi	934	Thüringia	935	Clivia	936	Kunigunde
937	Bethgea	938	Chlosinde	939	Isberga	940	Kordula
941	Murray	942	Romilda	943	Begonia	944	Hidalgo
945	Barcelona	946	Poësia	947	Monterosa	948	Jucunda
949	Hel	950	Ahrensa	951	Gaspra	952	Caia
953	Painleva	954	Li	955	Alstede	956	Elisa
957	Camelia	958	Asplinda	959	Arne	960	Birgit
961	Gunnie	962	Aslög	963	Iduberga	964	Subamara
965	Angelica	966	Muschi	967	Helionape	968	Petunia
969	Leocadia	970	Primula	971	Alsatia	972	Cohnia
973	Aralia	974	Lioba	975	Perseverantia	976	Benjamina
977	Philippa	978	Aidamina	979	Ilsewa	980	Anacostia

*Complete discovery circumstances for these objects have been previously published by Pilcher in *Asteroids* (1979), ed. T. Gehrels (Tucson: University of Arizona Press), pp. 1130–1154.

No.	Name*	No.	Name	No.	Name	No.	Name
981	Martina	982	Franklina	983	Gunila	984	Gretia
985	Rosina	986	Amelia	987	Wallia	988	Appella
989	Schwassmannia	990	Yerkes	991	McDonalda	992	Swasey
993	Moultona	994	Otthild	995	Sternberga	996	Hilaritas
997	Priska	998	Bodea	999	Zachia	1000	Piazzia
1001	Gaussia	1002	Olbersia	1003	Lilofee	1004	Belopolskya
1005	Arago	1006	Lagrangea	1007	Pawlowia	1008	La Paz
1009	Sirene	1010	Marlene	1011	Laodamia	1012	Sarema
1013	Tombecka	1014	Semphyra	1015	Christa	1016	Anitra
1017	Jacqueline	1018	Arnolda	1019	Strackea	1020	Arcadia
1021	Flammario	1022	Olympiada	1023	Thomana	1024	Hale
1025	Riema	1026	Ingrid	1027	Aesculapia	1028	Lydina
1029	La Plata	1030	Vitja	1031	Arctica	1032	Pafuri
1033	Simona	1034	Mozartia	1035	Amata	1036	Ganymed
1037	Davidweilla	1038	Tuckia	1039	Sonneberga	1040	Klumpkea
1041	Asta	1042	Amazone	1043	Beate	1044	Teutonia
1045	Michela	1046	Edwin	1047	Geisha	1048	Feodosia
1049	Gotho	1050	Meta	1051	Merope	1052	Belgica
1053	Vigdis	1054	Forsytia	1055	Tynka	1056	Azalea
1057	Wanda	1058	Grubba	1059	Mussorgskia	1060	Magnolia
1061	Paeonia	1062	Ljuba	1063	Aquilegia	1064	Aethusa
1065	Amundsenia	1066	Lobelia	1067	Lunaria	1068	Nofretete
1069	Planckia	1070	Tunica	1071	Brita	1072	Malva
1073	Gellivara	1074	Beljawskya	1075	Helina	1076	Viola
1077	Campanula	1078	Mentha	1079	Mimosa	1080	Orchis
1081	Reseda	1082	Pirola	1083	Salvia	1084	Tamariwa
1085	Amaryllis	1086	Nata	1087	Arabis	1088	Mitaka
1089	Tama	1090	Sumida	1091	Spiraea	1092	Lilium
1093	Freda	1094	Siberia	1095	Tulipa	1096	Reunerta
1097	Vicia	1098	Hakone	1099	Figneria	1100	Arnica
1101	Clematis	1102	Pepita	1103	Sequoia	1104	Syringa
1105	Fragaria	1106	Cydonia	1107	Lictoria	1108	Demeter
1109	Tata	1110	Jaroslawa	1111	Reinmuthia	1112	Polonia
1113	Katja	1114	Lorraine	1115	Sabauda	1116	Catriona
1117	Reginita	1118	Hanskya	1119	Euboea	1120	Cannonia
1121	Natascha	1122	Neith	1123	Shapleya	1124	Stroobantia
1125	China	1126	Otero	1127	Mimi	1128	Astrid
1129	Neujmina	1130	Skuld	1131	Porzia	1132	Hollandia
1133	Lugduna	1134	Kepler	1135	Colchis	1136	Mercedes
1137	Raissa	1138	Attica	1139	Atami	1140	Crimea
1141	Bohmia	1142	Aetolia	1143	Odysseus	1144	Oda
1145	Robelmonte	1146	Biarmia	1147	Stavropolis	1148	Rarahu
1149	Volga	1150	Achaia	1151	Ithaka	1152	Pawona
1153	Wallenbergia	1154	Astronomia	1155	Aënna	1156	Kira
1157	Arabia	1158	Luda	1159	Granada	1160	Illyria
1161	Thessalia	1162	Larissa	1163	Saga	1164	Kobolda
1165	Imprinetta	1166	Sakuntala	1167	Dubiago	1168	Brandia
1169	Alwine	1170	Siva	1171	Rusthawelia	1172	Aneas
1173	Anchises	1174	Marmara	1175	Margo	1176	Lucidor
1177	Gonnessia	1178	Irmela	1179	Mally	1180	Rita
1181	Lilith	1182	Ilona	1183	Jutta	1184	Gaea
1185	Nikko	1186	Turnera	1187	Afra	1188	Gothlandia
1189	Terentia	1190	Pelagia	1191	Alfaterna	1192	Prisma
1193	Africa	1194	Aletta	1195	Orangia	1196	Sheba
1197	Rhodesia	1198	Atlantis	1199	Geldonia	1200	Imperatrix
1201	Strenua	1202	Marina	1203	Nanna	1204	Renzia
1205	Ebella	1206	Numerowia	1207	Ostenia	1208	Troilus
1209	Pumma	1210	Morosovia	1211	Bressole	1212	Francette
1213	Algeria	1214	Richilde	1215	Boyer	1216	Askania
1217	Maximiliana	1218	Aster	1219	Britta	1220	Crocus
1221	Amor	1222	Tina	1223	Neckar	1224	Fantasia
1225	Ariane	1226	Golia	1227	Geranium	1228	Scabiosa
1229	Tilia	1230	Riceia	1231	Auricula	1232	Cortusa
1233	Kobresia	1234	Elyna	1235	Schorria	1236	Thais
1237	Geneviève	1238	Predappia	1239	Queteleta	1240	Centenaria
1241	Dysona	1242	Zambesia	1243	Pamela	1244	Deira
1245	Calvinia	1246	Chaka	1247	Memoria	1248	Jugurtha
1249	Rutherfordia	1250	Galanthus	1251	Hedera	1252	Celestia
1253	Frisia	1254	Erfordia	1255	Schilowa	1256	Normannia
1257	Móra	1258	Sicilia	1259	Ögyalla	1260	Walhalla
1261	Legia	1262	Sniadeckia	1263	Varsavia	1264	Letaba
1265	Schweikarda	1266	Tone	1267	Geertruida	1268	Libya
1269	Rollandia	1270	Datura	1271	Isergina	1272	Gefion
1273	Helma	1274	Delportia	1275	Cimbria	1276	Ucclia
1277	Dolores	1278	Kenya	1279	Uganda	1280	Baillauda
1281	Jeanne	1282	Utopia	1283	Komsomolia	1284	Latvia
1285	Julietta	1286	Banachiewicza	1287	Lorcia	1288	Santa
1289	Kutaissi	1290	Albertine	1291	Phryne	1292	Luce
1293	Sonja	1294	Antwerpia	1295	Deflotte	1296	Andrée
1297	Quadea	1298	Nocturna	1299	Mertona	1300	Marcelle
1301	Yvonne	1302	Werra	1303	Luthera	1304	Arosa
1305	Pongola	1306	Scythia	1307	Cimmeria	1308	Halleria
1309	Hyperborea	1310	Villigera	1311	Knopfia	1312	Vassar

*Complete discovery circumstances for these objects have been previously published by Pilcher in *Asteroids* (1979), ed. T. Gehrels (Tucson: University of Arizona Press), pp. 1130–1154.

No.	Name*	No.	Name	No.	Name	No.	Name
1313	Berna	1314	Paula	1315	Bronislawa	1316	Kasan
1317	Silvretta	1318	Nerina	1319	Disa	1320	Impala
1321	Majuba	1322	Copernicus	1323	Tugela	1324	Knysna
1325	Inanda	1326	Losaka	1327	Namaqua	1328	Devota
1329	Eliane	1330	Spiridonia	1331	Solvejg	1332	Marconia
1333	Cevenola	1334	Lundmarka	1335	Demoulina	1336	Zeelandia
1337	Gerarda	1338	Duponta	1339	Désagneauxa	1340	Yvette
1341	Edmée	1342	Brabantia	1343	Nicole	1344	Caubeta
1345	Potomac	1346	Gotha	1347	Patria	1348	Michel
1349	Bechuana	1350	Rosselia	1351	Uzbekistania	1352	Wawel
1353	Maartje	1354	Botha	1355	Magoeba	1356	Nyanza
1357	Khama	1358	Gaika	1359	Prieska	1360	Tarka
1361	Leuschneria	1362	Griqua	1363	Herberta	1364	Safara
1365	Henyey	1366	Piccolo	1367	Nongoma	1368	Numidia
1369	Ostanina	1370	Hella	1371	Resi	1372	Haremari
1373	Cincinnati	1374	Isora	1375	Alfreda	1376	Michelle
1377	Roberbauxa	1378	Leonce	1379	Lomonosowa	1380	Volodia
1381	Danubia	1382	Gerti	1383	Limburgia	1384	Kniertje
1385	Gelria	1386	Storeria	1387	Kama	1388	Aphrodite
1389	Onnie	1390	Abastumani	1391	Carelia	1392	Pierre
1393	Sofala	1394	Algoa	1395	Aribeda	1396	Outeniqua
1397	Umtata	1398	Donnera	1399	Teneriffa	1400	Tirela
1401	Lavonne	1402	Eri	1403	Idelsonia	1404	Ajax
1405	Sibelius	1406	Komppa	1407	Lindelöf	1408	Trusanda
1409	Isko	1410	Margret	1411	Brauna	1412	Lagrula
1413	Roucarie	1414	Jérôme	1415	Malautra	1416	Renauxa
1417	Walinskia	1418	Fayeta	1419	Danzig	1420	Radcliffe
1421	Esperanto	1422	Strömgrenia	1423	Jose	1424	Sundmania
1425	Tuorla	1426	Riviera	1427	Ruvuma	1428	Mombasa
1429	Pemba	1430	Somalia	1431	Luanda	1432	Ethiopia
1433	Geramtina	1434	Margot	1435	Garlena	1436	Salonta
1437	Diomedes	1438	Wendeline	1439	Vogtia	1440	Rostia
1441	Bolyai	1442	Corvina	1443	Ruppina	1444	Pannonia
1445	Konkolya	1446	Sillanpää	1447	Utra	1448	Lindbladia
1449	Virtanen	1450	Raimonda	1451	Granö	1452	Hunnia
1453	Fennia	1454	Kalevala	1455	Mitchella	1456	Saldanha
1457	Ankara	1458	Mineura	1459	Magnya	1460	Haltia
1461	Jean-Jacques	1462	Zamenhof	1463	Nordenmarkia	1464	Armisticia
1465	Autonoma	1466	Mündleria	1467	Mashona	1468	Zomba
1469	Linzia	1470	Carla	1471	Tornio	1472	Muonio
1473	Ounas	1474	Beira	1475	Yalta	1476	Cox
1477	Bonsdorffia	1478	Vihuri	1479	Inkeri	1480	Aunus
1481	Tübingia	1482	Sebastiana	1483	Hakoila	1484	Postrema
1485	Isa	1486	Marilyn	1487	Boda	1488	Aura
1489	Attila	1490	Limpopo	1491	Balduinus	1492	Oppolzer
1493	Sigrid	1494	Savo	1495	Helsinki	1496	Turku
1497	Tampere	1498	Lahti	1499	Pori	1500	Jyväskylä
1501	Baade	1502	Arenda	1503	Kuopio	1504	Lappeenranta
1505	Koranna	1506	Xosa	1507	Vaasa	1508	Kemi
1509	Esclangona	1510	Charlois	1511	Daléra	1512	Oulu
1513	Mátra	1514	Ricouxa	1515	Perrotin	1516	Henry
1517	Beograd	1518	Rovaniemi	1519	Kajaani	1520	Imatra
1521	Seinäjoki	1522	Kokkola	1523	Pieksämäki	1524	Joensuu
1525	Savonlinna	1526	Mikkeli	1527	Malmquista	1528	Conrada
1529	Oterma	1530	Rantaseppä	1531	Hartmut	1532	Inari
1533	Saimaa	1534	Näsi	1535	Päijänne	1536	Pielinen
1537	Transylvania	1538	Detre	1539	Borrelly	1540	Kevola
1541	Estonia	1542	Schalén	1543	Bourgeois	1544	Vinterhansenia
1545	Thernöe	1546	Izsák	1547	Nele	1548	Palomaa
1549	Mikko	1550	Tito	1551	Argelander	1552	Bessel
1553	Bauersfelda	1554	Yugoslavia	1555	Dejan	1556	Wingolfia
1557	Roehla	1558	Järnefelt	1559	Kustaanheimo	1560	Strattonia
1561	Fricke	1562	Gondolatsch	1563	Noël	1564	Srbija
1565	Lemaître	1566	Icarus	1567	Alikoski	1568	Aisleen
1569	Evita	1570	Brunonia	1571	Cesco	1572	Posnania
1573	Väisälä	1574	Meyer	1575	Winifred	1576	Fabiola
1577	Reiss	1578	Kirkwood	1579	Herrick	1580	Betulia
1581	Abanderada	1582	Martir	1583	Antilochus	1584	Fuji
1585	Union	1586	Thiele	1587	Kahrstedt	1588	Descamisada
1589	Fanatica	1590	Tsiolkovskaja	1591	Baize	1592	Mathieu
1593	Fagnes	1594	Danjon	1595	Tanga	1596	Itzigsohn
1597	Laugier	1598	Paloque	1599	Giomus	1600	Vyssotsky
1601	Patry	1602	Indiana	1603	Neva	1604	Tombaugh
1605	Milankovitch	1606	Jekhovsky	1607	Mavis	1608	Muñoz
1609	Brenda	1610	Mirnaya	1611	Beyer	1612	Hirose
1613	Smiley	1614	Goldschmidt	1615	Bardwell	1616	Filipoff
1617	Alschmitt	1618	Dawn	1619	Ueta	1620	Geographos
1621	Druzhba	1622	Chacornac	1623	Vivian	1624	Rabe
1625	The NORC	1626	Sadeya	1627	Ivar	1628	Strobel
1629	Pecker	1630	Milet	1631	Kopff	1632	Sieböhme
1633	Chimay	1634	Ndola	1635	Bohrmann	1636	Porter
1637	Swings	1638	Ruanda	1639	Bower	1640	Nemo

*Complete discovery circumstances for these objects have been previously published by Pilcher in *Asteroids* (1979), ed. T. Gehrels (Tucson: University of Arizona Press), pp. 1130–1154.

No.	Name*	No.	Name	No.	Name	No.	Name
1641	Tana	1642	Hill	1643	Brown	1644	Rafita
1645	Waterfield	1646	Rosseland	1647	Menelaus	1648	Shajna
1649	Fabre	1650	Heckmann	1651	Behrens	1652	Hergé
1653	Yakhontovia	1654	Bojeva	1655	Comas Solá	1656	Suomi
1657	Roemera	1658	Innes	1659	Punkaharju	1660	Wood
1661	Granule	1662	Hoffmann	1663	van den Bos	1664	Felix
1665	Gaby	1666	van Gent	1667	Pels	1668	Hanna
1669	Dagmar	1670	Minnaert	1671	Chaika	1672	Gezelle
1673	van Houten	1674	Groeneveld	1675	Simonida	1676	Kariba
1677	Tycho Brahe	1678	Hveen	1679	Nevanlinna	1680	Per Brahe
1681	Steinmetz	1682	Karel	1683	Castafiore	1684	Iguassú
1685	Toro	1686	De Sitter	1687	Glarona	1688	Wilkens
1689	Floris-Jan	1690	Mayrhofer	1691	Oort	1692	Subbotina
1693	Hertzsprung	1694	Kaiser	1695	Walbeck	1696	Nurmela
1697	Koskenniemi	1698	Christophe	1699	Honkasalo	1700	Zvezdara
1701	Okavango	1702	Kalahari	1703	Barry	1704	Wachmann
1705	Tapio	1706	Dieckvoss	1707	Chantal	1708	Pólit
1709	Ukraina	1710	Gothard	1711	Sandrine	1712	Angola
1713	Bancilhon	1714	Sy	1715	Salli	1716	Peter
1717	Arlon	1718	Namibia	1719	Jens	1720	Niels
1721	Wells	1722	Goffin	1723	Klemola	1724	Vladimir
1725	CrAO	1726	Hoffmeister	1727	Mette	1728	Goethe Link
1729	Beryl	1730	Marceline	1731	Smuts	1732	Heike
1733	Silke	1734	Zhongolovich	1735	ITA	1736	Floirac
1737	Severny	1738	Oosterhoff	1739	Meyermann	1740	Paavo Nurmi
1741	Giclas	1742	Schaifers	1743	Schmidt	1744	Harriet
1745	Ferguson	1746	Brouwer	1747	Wright	1748	Mauderli
1749	Telamon	1750	Eckert	1751	Herget	1752	van Herk
1753	Mieke	1754	Cunningham	1755	Lorbach	1756	Giacobini
1757	Porvoo	1758	Naantali	1759	Kienle	1760	Sandra
1761	Edmondson	1762	Russell	1763	Williams	1764	Cogshall
1765	Wrubel	1766	Slipher	1767	Lampland	1768	Appenzella
1769	Carlostorres	1770	Schlesinger	1771	Makover	1772	Gagarin
1773	Rumpelstilz	1774	Kulikov	1775	Zimmerwald	1776	Kuiper
1777	Gehrels	1778	Alfvén	1779	Paraná	1780	Kippes
1781	Van Biesbroeck	1782	Schneller	1783	Albitskij	1784	Benguella
1785	Wurm	1786	Raahe	1787	Chiny	1788	Kiess
1789	Dobrovolsky	1790	Volkov	1791	Patsayev	1792	Reni
1793	Zoya	1794	Finsen	1795	Woltjer	1796	Riga
1797	Schaumasse	1798	Watts	1799	Koussevitzky	1800	Aguilar
1801	Titicaca	1802	Zhang Heng	1803	Zwicky	1804	Chebotarev
1805	Dirikis	1806	Derice	1807	Slovakia	1808	Bellerophon
1809	Prometheus	1810	Epimetheus	1811	Bruwer	1812	Gilgamesh
1813	Imhotep	1814	Bach	1815	Beethoven	1816	Liberia
1817	Katanga	1818	Brahms	1819	Laputa	1820	Lohmann
1821	Aconcagua	1822	Waterman	1823	Gliese	1824	Haworth
1825	Klare	1826	Miller	1827	Atkinson	1828	Kashirina
1829	Dawson	1830	Pogson	1831	Nicholson	1832	Mrkos
1833	Shmakova	1834	1969 QP	1835	Gajdariya	1836	Komarov
1837	Osita	1838	Ursa	1839	Ragazza	1840	Hus
1841	Masaryk	1842	Hynek	1843	Jarmila	1844	Susilva
1845	Helewalda	1846	Bengt	1847	Stobbe	1848	Delvaux
1849	Kresák	1850	Kohoutek	1851	Lacroute	1852	Carpenter
1853	McElroy	1854	Skvortsov	1855	Korolev	1856	Ruzena
1857	Parchomenko	1858	Lobachevskij	1859	Kovalevskaya	1860	Barbarossa
1861	Komenský	1862	Apollo	1863	Antinous	1864	Daedalus
1865	Cerberus	1866	Sisyphus	1867	Deiphobus	1868	Thersites
1869	Philoctetes	1870	Glaukos	1871	Astyanax	1872	Helenos
1873	Agenor	1874	Kacivelia	1875	1969 QQ	1876	Napolitania
1877	Marsden	1878	Hughes	1879	Broederstroom	1880	McCrosky
1881	Shao	1882	Rauma	1883	Rimito	1884	Skip
1885	Herero	1886	Lowell	1887	Virton	1888	Zu Chong-Zhi
1889	Pakhmutova	1890	Konoshenkova	1891	Gondola	1892	Lucienne
1893	Jakoba	1894	Haffner	1895	Larink	1896	Beer
1897	Hind	1898	Cowell	1899	Crommelin	1900	Katyusha
1901	Moravia	1902	Shaposhnikov	1903	Adzhimushkaj	1904	Massevitch
1905	Ambartsumian	1906	Naef	1907	Rudneva	1908	Pobeda
1909	Alekhin	1910	Mikhailov	1911	Schubart	1912	Anubis
1913	Sekanina	1914	Hartbeespoortdam	1915	Quetzálcoatl	1916	Boreas
1917	Cuyo	1918	Aiguillon	1919	Clemence	1920	Sarmiento
1921	Pala	1922	Zulu	1923	Osiris	1924	Horus
1925	Franklin-Adams	1926	Demiddelaer	1927	Suvanto	1928	Summa
1929	Kollaa	1930	Lucifer	1931	1969 QB	1932	Jansky
1933	Tinchen	1934	Jeffers	1935	Lucerna	1936	Lugano
1937	Locarno	1938	Lausanna	1939	Loretta	1940	Whipple
1941	Wild	1942	Jablunka	1943	Anteros	1944	Gunter
1945	Wesselink	1946	Walraven	1947	Iso-Heikkilä	1948	Kampala
1949	Messina	1950	Wempe	1951	Lick	1952	Hesburgh
1953	Rupertwildt	1954	Kukarkin	1955	McMath	1956	Artek
1957	Angara	1958	Chandra	1959	Karbyshev	1960	Guisan
1961	Dufour	1962	Dunant	1963	Bezovec	1964	Luyten
1965	van de Kamp	1966	Tristan	1967	Menzel	1968	Mehltretter
1969	Alain	1970	1954 ER	1971	Hagihara	1972	Yi Xing

*Complete discovery circumstances for these objects have been previously published by Pilcher in *Asteroids* (1979), ed. T. Gehrels (Tucson: University of Arizona Press), pp. 1130–1154.

No.	Name*	No.	Name	No.	Name	No.	Name
1973	Colocolo	1974	Caupolican	1975	Pikelner	1976	Kaverin
1977	Shura	1978	Patrice	1979	Sakharov	1980	Tezcatlipoca
1981	Midas	1982	Cline	1983	Bok	1984	Fedynskij
1985	Hopmann	1986	1935 SV1	1987	Kaplan	1988	Delores
1989	Tatry	1990	Pilcher	1991	Darwin	1992	Galvarino
1993	Guacolda	1994	Shane	1995	Hajek	1996	Adams
1997	Leverrier	1998	Titius	1999	Hirayama	2000	Herschel
2001	Einstein	2002	Euler	2003	Harding	2004	Lexell
2005	Hencke	2006	Polonskaya	2007	McCuskey	2008	Konstitutsiya
2009	Voloshina	2010	Chebyshev	2011	Veteraniya	2012	Guo Shou-Jing
2013	Tucapel	2014	Vasilevskis	2015	Kachuevskaya	2016	Heinemann
2017	Wesson	2018	Schuster	2019	1935 SX1	2020	Ukko
2021	Poincaré	2022	West	2023	Asaph	2024	McLaughlin
2025	1953 LG	2026	Cottrell	2027	Shen Guo	2028	Janequeo
2029	Binomi	2030	Belyaev	2031	BAM	2032	Ethel
2033	Basilea	2034	Bernoulli	2035	Stearns	2036	Sheragul
2037	Tripaxeptalis	2038	Bistro	2039	Payne-Gaposchkin	2040	Chalonge
2041	Lancelot	2042	Sitarski	2043	Ortutay	2044	Wirt
2045	Peking	2046	Leningrad	2047	Smetana	2048	Dwornik
2049	Grietje	2050	Francis	2051	Chang	2052	Tamriko
2053	Nuki	2054	Gawain	2055	Dvořák	2056	Nancy
2057	Rosemary	2058	Róka	2059	Baboquivari	2060	Chiron
2061	Anza	2062	Aten	2063	Bacchus	2064	Thomsen
2065	Spicer	2066	Palala	2067	Aksnes	2068	Dangreen
2069	Hubble	2070	Humason	2071	Nadezhda	2072	Kosmodemyanskaya
2073	Janáček	2074	Shoemaker	2075	Martinez	2076	Levin
2077	Kiangsu	2078	Nanking	2079	Jacchia	2080	Jihlava
2081	Sázava	2082	Galahad	2083	Smither	2084	Okayama
2085	Henan	2086	Newell	2087	Kochera	2088	Sahlia
2089	Cetacea	2090	Mizuho	2091	Sampo	2092	Sumiana
2093	Genichesk	2094	Magnitka	2095	Parsifal	2096	Väinö
2097	1953 PV	2098	Zyskin	2099	Öpik	2100	Ra-Shalom
2101	Adonis	2102	Tantalus	2103	1960 FL	2104	Toronto
2105	Gudy	2106	Hugo	2107	Ilmari	2108	Otto Schmidt
2109	Dhotel	2110	Moore-Sitterly	2111	Tselina	2112	Ulyanov
2113	Ehrdni	2114	Wallenquist	2115	Irakli	2116	Mtskheta
2117	Danmark	2118	Flagstaff	2119	Schwall	2120	Tyumenia
2121	Sevastopol	2122	Pyatiletka	2123	Vltava	2124	Nissen

*Complete discovery circumstances for these objects have been previously published by Pilcher in *Asteroids* (1979), ed. T. Gehrels (Tucson: University of Arizona Press), pp. 1130–1154.

No.	Name	pd	dd	d	dp	
2125	Karl-Ontjes	2005 P-L	1960 Sep 24	PLS	Palomar	107
2126	Gerasimovich	1970 QZ	1970 Aug 30	T. Smirnova	Nauchnyj	
2127	Tanya	1971 KB1	1971 May 29	L. Chernykh	Nauchnyj	
2128	Wetherill	1973 SB	1973 Sep 26	E. F. Helin	Palomar	
2129	Cosicosi	1973 SJ	1973 Sep 27	P. Wild	Zimmerwald	
2130	Evdokiya	1974 QH1	1974 Aug 22	L. Zhuravleva	Nauchnyj	
2131	Mayall	1975 RA	1975 Sep 3	A. R. Klemola	Mount Hamilton	
2132	Zhukov	1975 TW3	1975 Oct 3	L. Chernykh	Nauchnyj	
2133	Franceswright	1976 WB	1976 Nov 20	Harvard College	Agassiz Station	
2134	Dennispalm	1976 YB	1976 Dec 24	C. Kowal	Palomar	
2135	Aristaeus	1977 HA	1977 Apr 17	E. F. Helin and S. J. Bus	Palomar	
2136	Jugta	1933 OC	1933 Jul 24	K. Reinmuth	Heidelberg	
2137	Priscilla	1936 QZ	1936 Aug 24	K. Reinmuth	Heidelberg	
2138	Swissair	1968 HB	1968 Apr 17	P. Wild	Zimmerwald	
2139	Makharadze	1970 MC	1970 Jun 30	T. Smirnova	Nauchnyj	
2140	Kemerovo	1970 PE	1970 Aug 3	L. Chernykh	Nauchnyj	
2141	Simferopol	1970 QC1	1970 Aug 30	T. Smirnova	Nauchnyj	
2142	Landau	1972 GA	1972 Apr 3	L. Chernykh	Nauchnyj	
2143	Jimarnold	1973 SA	1973 Sep 26	E. F. Helin	Palomar	
2144	Marietta	1975 BC1	1975 Jan 18	L. Chernykh	Nauchnyj	
2145	Blaauw	1976 UF	1976 Oct 24	R. M. West	La Silla	
2146	Stentor	1976 UQ	1976 Oct 24	R. M. West	La Silla	
2147	Kharadze	1976 US	1976 Oct 25	R. M. West	La Silla	122
2148	Epeios	1976 UW	1976 Oct 24	R. M. West	La Silla	
2149	Schwambraniya	1977 FX	1977 Mar 22	N. Chernykh	Nauchnyj	
2150		1977 TA	1977 Oct 13	W. Sebok	Palomar	
2151	Hadwiger	1977 VX	1977 Nov 3	P. Wild	Zimmerwald	
2152	Hannibal	1978 WK	1978 Nov 19	P. Wild	Zimmerwald	
2153	Akiyama	1978 XD	1978 Dec 1	Harvard College	Agassiz Station	113
2154	Underhill	2015 P-L	1960 Sep 24	PLS	Palomar	107
2155	Wodan	6542 P-L	1960 Sep 24	PLS	Palomar	107

No.	Name	pd	dd	d	dp	
2156	Kate	A917 SH	1917 Sep 23	S. Belyavskij	Simeis	
2157	Ashbrook	A924 EF	1924 Mar 7	K. Reinmuth	Heidelberg	
2158		1933 OS	1933 Jul 24	K. Reinmuth	Heidelberg	
2159	Kukkamäki	1941 UX	1941 Oct 16	L. Oterma	Turku	
2160	Spitzer	1956 RL	1956 Sep 7	Goethe Link Observatory	Brooklyn	103
2161	Grissom	1963 UD	1963 Oct 17	Goethe Link Observatory	Brooklyn	103
2162	Anhui	1966 BE	1966 Jan 30	Purple Mountain Observatory	Nanking	
2163	Korczak	1971 SP1	1971 Sep 16	Crimean Astrophysical Obs.	Nauchnyj	
2164	Lyalya	1972 RM2	1972 Sep 11	N. Chernykh	Nauchnyj	
2165	Young	1956 RJ	1956 Sep 7	Goethe Link Observatory	Brooklyn	103
2166	Handahl	1936 QB	1936 Aug 13	G Neujmin	Simeis	
2167	Erin	1971 LA	1971 Jun 1	Perth Observatory	Perth	
2168	Swope	1955 RF1	1955 Sep 14	Goethe Link Observatory	Brooklyn	103
2169	Taiwan	1964 VP1	1964 Nov 9	Purple Mountain Observatory	Nanking	
2170	Byelorussia	1971 SZ	1971 Sep 16	Crimean Astrophysical Obs.	Nauchnyj	
2171	Kiev	1973 QD1	1973 Aug 28	T. Smirnova	Nauchnyj	
2172	Plavsk	1973 QA2	1973 Aug 31	T. Smirnova	Nauchnyj	
2173	Maresjev	1974 QG1	1974 Aug 22	L. Zhuravleva	Nauchnyj	
2174	Asmodeus	1975 TA	1975 Oct 8	S. J. Bus and J. Huchra	Palomar	
2175	Andrea Doria	1977 TY	1977 Oct 12	P. Wild	Zimmerwald	
2176	Donar	2529 P-L	1960 Sep 24	PLS	Palomar	107
2177	Oliver	6551 P-L	1960 Sep 24	PLS	Palomar	107
2178	Kazakhstania	1972 RA2	1972 Sep 11	N. Chernykh	Nauchnyj	
2179	Platzeck	1965 MA	1965 Jun 28	A. R. Klemola	El Leoncito	
2180	Marjaleena	1940 RJ	1940 Sep 8	H. Alikoski	Turku	
2181	Fogelin	1942 YA	1942 Dec 28	K. Reinmuth	Heidelberg	
2182	Semirot	1953 FH1	1953 Mar 21	Goethe Link Observatory	Brooklyn	103
2183		1959 OB	1959 Jul 26	C. Hoffmeister	Bloemfontein	
2184	Fujian	1964 TV2	1964 Oct 9	Purple Mountain Observatory	Nanking	
2185	Guangdong	1965 WO	1965 Nov 20	Purple Mountain Observatory	Nanking	
2186	Keldysh	1973 SQ4	1973 Sep 27	L. Chernykh	Nauchnyj	
2187	La Silla	1976 UH	1976 Oct 24	R. M. West	La Silla	
2188	Orlenok	1976 UL4	1976 Oct 28	L. Zhuravleva	Nauchnyj	
2189	Zaragoza	1975 QK	1975 Aug 30	Felix Aguilar Observatory	El Leoncito	
2190	Coubertin	1976 GV3	1976 Apr 2	N. Chernykh	Nauchnyj	
2191	Uppsala	1977 PA1	1977 Aug 6	C.-I. Lagerkvist	Mount Stromlo	
2192	Pyatigoriya	1972 HP	1972 Apr 18	T. Smirnova	Nauchnyj	
2193	Jackson	1926 KB	1926 May 18	H. E. Wood	Johannesburg (UO)	
2194	Arpola	1940 GE	1940 Apr 3	Y. Vaisala	Turku	
2195	Tengström	1941 SP1	1941 Sep 27	L. Oterma	Turku	
2196	Ellicott	1965 BC	1965 Jan 29	Goethe Link Observatory	Brooklyn	103
2197	Shanghai	1965 YN	1965 Dec 30	Purple Mountain Observatory	Nanking	
2198	Ceplecha	1975 VF	1975 Nov 7	Harvard College	Agassiz Station	113
2199	Klet	1978 LA	1978 Jun 6	A. Mrkos	Klet	
2200	Pasadena	6090 P-L	1960 Sep 24	PLS	Palomar	107
2201	Oljato	1947 XC	1947 Dec 12	H. L. Giclas	Flagstaff (LO)	
2202	Pele	1972 RA	1972 Sep 7	A. R. Klemola	Mount Hamilton	
2203		1935 SQ1	1935 Sep 28	H. Van Gent	Johannesburg (LS)	
2204	Lyyli	1943 EQ	1943 Mar 3	Y. Vaisala	Turku	
2205	Glinka	1973 SU4	1973 Sep 27	L. Chernykh	Nauchnyj	
2206	Gabrova	1976 GR3	1976 Apr 1	N. Chernykh	Nauchnyj	
2207	Antenor	1977 QH1	1977 Aug 19	N. Chernykh	Nauchnyj	
2208	Pushkin	1977 QL3	1977 Aug 22	N. Chernykh	Nauchnyj	
2209	Tianjin	1978 US1	1978 Oct 28	Purple Mountain Observatory	Nanking	
2210	Lois	9597 P-L	1960 Sep 24	PLS	Palomar	107
2211		1951 WO2	1951 Nov 26	L. E. Cunningham	Mount Wilson	
2212	Hephaistos	1978 SB	1978 Sep 27	L. Chernykh	Nauchnyj	
2213	Meeus	1935 SO1	1935 Sep 24	E. Delporte	Uccle	
2214	Carol	1953 GF	1953 Apr 7	K. Reinmuth	Heidelberg	
2215	Sichuan	1964 VX2	1964 Nov 12	Purple Mountain Observatory	Nanking	
2216	Kerch	1971 LF	1971 Jun 12	T. Smirnova	Nauchnyj	
2217	Eltigen	1971 SK2	1971 Sep 26	T. Smirnova	Nauchnyj	
2218	Wotho	1975 AK	1975 Jan 10	P. Wild	Zimmerwald	
2219	Mannucci	1975 LU	1975 Jun 13	Felix Aguilar Observatory	El Leoncito	
2220	Hicks	1975 VB	1975 Nov 4	E. F. Helin	Palomar	
2221	Chilton	1976 QC	1976 Aug 25	Harvard College	Agassiz Station	113
2222	Lermontov	1977 ST1	1977 Sep 19	N. Chernykh	Nauchnyj	
2223	Sarpedon	1977 TL3	1977 Oct 4	Purple Mountain Observatory	Nanking	
2224	Tucson	2528 P-L	1960 Sep 24	PLS	Palomar	107
2225	Serkowski	6546 P-L	1960 Sep 24	PLS	Palomar	107
2226	Cunitza	1936 QC1	1936 Aug 26	A. Bohrmann	Heidelberg	
2227	Otto Struve	1955 RX	1955 Sep 13	Goethe Link Observatory	Brooklyn	103
2228	Soyuz-Apollo	1977 OH	1977 Jul 19	N. Chernykh	Nauchnyj	
2229	Mezzarco	1977 RO	1977 Sep 7	P. Wild	Zimmerwald	
2230	Yunnan	1978 UT1	1978 Oct 29	Purple Mountain Observatory	Nanking	
2231	Durrell	1941 SG	1941 Sep 21	S. Arend	Uccle	
2232	Altaj	1969 RD2	1969 Sep 15	B. Burnasheva	Nauchnyj	
2233	Kuznetsov	1972 XE1	1972 Dec 3	L. Zhuravleva	Nauchnyj	
2234	Schmadel	1977 HD	1977 Apr 27	H.-E. Schuster	La Silla	
2235	Vittore	A924 GA	1924 Apr 5	K. Reinmuth	Heidelberg	
2236	Austrasia	1933 FX	1933 Mar 23	K. Reinmuth	Heidelberg	
2237	Melnikov	1938 TB	1938 Oct 2	G. Neujmin	Simeis	
2238	Steshenko	1972 RQ1	1972 Sep 11	N. Chernykh	Nauchnyj	

No.	Name	pd	dd	d	dp	
2239	Paracelsus	1978 RC	1978 Sep 13	P. Wild	Zimmerwald	
2240	Tsai	1978 YA	1978 Dec 30	Harvard College	Agassiz Station	113
2241		1979 WM	1979 Nov 22	C. Kowal	Palomar	
2242		1936 TG	1936 Oct 13	G. Kulin	Budapest	
2243	Lönnrot	1941 SA1	1941 Sep 25	Y. Vaisala	Turku	
2244	Tesla	1952 UW1	1952 Oct 22	M. B. Protitch	Belgrade	
2245	Hekatostos	1968 BC	1968 Jan 24	L. Chernykh	Nauchnyj	
2246	Bowell	1979 XH	1979 Dec 14	E. Bowell	Flagstaff (AM)	119
2247	Hiroshima	6512 P-L	1960 Sep 24	PLS	Palomar	107
2248	Kanda	1933 DE	1933 Feb 27	K. Reinmuth	Heidelberg	
2249	Yamamoto	1942 GA	1942 Apr 6	K. Reinmuth	Heidelberg	
2250	Stalingrad	1972 HN	1972 Apr 18	T. Smirnova	Nauchnyj	
2251	Tikhov	1977 SU1	1977 Sep 19	N. Chernykh	Nauchnyj	
2252	CERGA	1978 VT	1978 Nov 1	K. Tomita	Caussols	
2253	Espinette	1932 PB	1932 Jul 30	G. Van Biesbroeck	Williams Bay	
2254	Requiem	1977 QJ1	1977 Aug 19	N. Chernykh	Nauchnyj	
2255	Qinghai	1977 VK1	1977 Nov 3	Purple Mountain Observatory	Nanking	
2256		4519 P-L	1960 Sep 24	PLS	Palomar	107
2257	Kaarina	1939 QB	1939 Aug 18	H. Alikoski	Turku	
2258	Viipuri	1939 TA	1939 Oct 7	Y. Vaisala	Turku	
2259	Sofievka	1971 OG	1971 Jul 19	B. Burnasheva	Nauchnyj	
2260	Neoptolemus	1975 WM1	1975 Nov 26	Purple Mountain Observatory	Nanking	
2261	Keeler	1977 HC	1977 Apr 20	A. R. Klemola	Mount Hamilton	
2262	Mitidika	1978 RB	1978 Sep 10	P. Wild	Zimmerwald	
2263	Shaanxi	1978 UW1	1978 Oct 30	Purple Mountain Observatory	Nanking	
2264	Sabrina	1979 YK	1979 Dec 16	E. Bowell	Flagstaff (AM)	119
2265	Verbaandert	1950 DB	1950 Feb 17	S. Arend	Uccle	
2266	Tchaikovsky	1974 VK	1974 Nov 12	L. Chernykh	Nauchnyj	
2267	Agassiz	1977 RF	1977 Sep 9	Harvard College	Agassiz Station	113
2268	Szmytowna	1942 VW	1942 Nov 6	L. Oterma	Turku	
2269	Efremiana	1976 JA2	1976 May 2	N. Chernykh	Nauchnyj	
2270	Yazhi	1980 ED	1980 Mar 14	E. Bowell	Flagstaff (AM)	119
2271	Kiso	1976 UV5	1976 Oct 22	H. Kosai and K. Hurukawa	Kiso Station	
2272		1972 FA	1972 Mar 16	T. Gehrels	Palomar	
2273	Yarilo	1975 EV1	1975 Mar 6	L. Chernykh	Nauchnyj	
2274	Ehrsson	1976 EA	1976 Mar 2	C.-I. Lagerkvist	Kvistaberg	
2275		1979 MH	1979 Jun 16	H.-E. Schuster	La Silla	
2276	Warck	1933 QA	1933 Aug 18	E. Delporte	Uccle	
2277	Moreau	1950 DS	1950 Feb 18	S. Arend	Uccle	
2278		1953 GE	1953 Apr 7	K. Reinmuth	Heidelberg	
2279	Barto	1968 DL	1968 Feb 25	L. Chernykh	Nauchnyj	
2280	Kunikov	1971 SL2	1971 Sep 26	T. Smirnova	Nauchnyj	
2281		1971 UQ1	1971 Oct 26	L. Kohoutek	Bergedorf	
2282	Andrés Bello	1974 FE	1974 Mar 22	C. Torres	Cerro El Roble	
2283	Bunke	1974 SV4	1974 Sep 26	L. Zhuravleva	Nauchnyj	
2284	San Juan	1974 TG1	1974 Oct 10	Felix Aguilar Observatory	El Leoncito	
2285	Ron Helin	1976 QB	1976 Aug 27	S. J. Bus	Palomar	
2286	Fesenkov	1977 NH	1977 Jul 14	N. Chernykh	Nauchnyj	
2287	Kalmykia	1977 QK3	1977 Aug 22	N. Chernykh	Nauchnyj	
2288	Karolinum	1979 UZ	1979 Oct 19	L. Brozek	Klet	
2289		6567 P-L	1960 Sep 24	PLS	Palomar	107
2290		1932 CD1	1932 Feb 14	K. Reinmuth	Heidelberg	
2291	Kevo	1941 FS	1941 Mar 19	L. Oterma	Turku	
2292	Seili	1942 RM	1942 Sep 7	Y. Vaisala	Turku	
2293	Guernica	1977 EH1	1977 Mar 13	N. Chernykh	Nauchnyj	
2294		1977 PL1	1977 Aug 14	N. Chernykh	Nauchnyj	
2295		1977 QD1	1977 Aug 19	N. Chernykh	Nauchnyj	
2296		1975 BA1	1975 Jan 18	L. Chernykh	Nauchnyj	
2297	Daghestan	1978 RE	1978 Sep 1	N. Chernykh	Nauchnyj	
2298	Cindijon	A915 TA	1915 Oct 2	M. Wolf	Heidelberg	
2299	Hanko	1941 SZ	1941 Sep 25	Y. Vaisala	Turku	
2300	Stebbins	1953 TG2	1953 Oct 10	Goethe Link Observatory	Brooklyn	103
2301	Whitford	1965 WJ	1965 Nov 20	Goethe Link Observatory	Brooklyn	103
2302	Florya	1972 TL2	1972 Oct 2	N. E. Kurochkin	Nauchnyj	
2303	Retsina	1979 FK	1979 Mar 24	P. Wild	Zimmerwald	
2304	Slavia	1979 KB	1979 May 18	A. Mrkos	Klet	
2305	King	1980 RJ1	1980 Sep 12	Harvard College	Agassiz Station	113
2306		1939 PM	1939 Aug 15	K. Reinmuth	Heidelberg	
2307		1957 HJ	1957 Apr 18	- - -	La Plata	
2308	Schilt	1967 JM	1967 May 6	C. U. Cesco and A. R. Klemola	El Leoncito	
2309	Mr. Spock	1971 QX1	1971 Aug 16	J. Gibson	El Leoncito	
2310	Olshaniya	1974 SU4	1974 Sep 26	L. Zhuravleva	Nauchnyj	
2311	El Leoncito	1974 TA1	1974 Oct 10	Felix Aguilar Observatory	El Leoncito	
2312	Duboshin	1976 GU2	1976 Apr 1	N. Chernykh	Nauchnyj	
2313		1976 TA	1976 Oct 15	H. L. Giclas	Flagstaff (AM)	119
2314	Field	1977 VD	1977 Nov 12	Harvard College	Agassiz Station	113
2315	Czechoslovakia	1980 DZ	1980 Feb 19	Z. Vavrova	Klet	
2316	Jo-Ann	1980 RH	1980 Sep 2	E. Bowell	Flagstaff (AM)	119
2317	Galya	2524 P-L	1960 Sep 24	PLS	Palomar	107
2318	Lubarsky	6521 P-L	1960 Sep 24	PLS	Palomar	107
2319		7631 P-L	1960 Oct 17	PLS	Palomar	107
2320		1979 QJ	1979 Aug 29	P. Wild	Zimmerwald	

No.	Name	pd	dd	d	dp	
2321	Luznice	1980 DB1	1980 Feb 19	Z. Vavrova	Klet	
2322	Kitt Peak	1954 UQ2	1954 Oct 28	Goethe Link Observatory	Brooklyn	103
2323	Zverev	1976 SF2	1976 Sep 24	N. Chernykh	Nauchnyj	
2324	Janice	1978 VS4	1978 Nov 7	E. F. Helin and S. J. Bus	Palomar	
2325	Chernykh	1979 SP	1979 Sep 25	A. Mrkos	Klet	
2326	Tololo	1965 QC	1965 Aug 29	Goethe Link Observatory	Brooklyn	103
2327	Gershberg	1969 TQ4	1969 Oct 13	B. Burnasheva	Nauchnyj	
2328	Robeson	1972 HW	1972 Apr 19	T. Smirnova	Nauchnyj	
2329	Orthos	1976 WA	1976 Nov 19	H.-E. Schuster	La Silla	
2330	Ontake	1977 DS3	1977 Feb 18	H. Kosai and K. Hurukawa	Kiso Station	
2331	Parvulesco	1936 EA	1936 Mar 12	E. Delporte	Uccle	
2332	Kalm	1940 GH	1940 Apr 4	L. Oterma	Turku	
2333	Porthan	1943 EP	1943 Mar 3	Y. Vaisala	Turku	
2334	Cuffey	1962 HD	1962 Apr 27	Goethe Link Observatory	Brooklyn	103
2335	James	1974 UB	1974 Oct 17	E. F. Helin	Palomar	
2336	Xinjiang	1975 WL1	1975 Nov 26	Purple Mountain Observatory	Nanking	
2337		1976 UH1	1976 Oct 22	P. Wild	Zimmerwald	
2338	Bokhan	1977 QA3	1977 Aug 22	N. Chernykh	Nauchnyj	
2339		2509 P-L	1960 Sep 24	PLS	Palomar	107
2340	Hathor	1976 UA	1976 Oct 22	C. Kowal	Palomar	
2341	Aoluta	1976 YU1	1976 Dec 16	L. Chernykh	Nauchnyj	
2342	Lebedev	1968 UQ	1968 Oct 22	T. Smirnova	Nauchnyj	
2343	Siding Spring	1979 MD4	1979 Jun 25	E. F. Helin and S. J. Bus	Siding Spring	
2344	Xizang	1979 SC1	1979 Sep 27	Purple Mountain Observatory	Nanking	
2345	Fučik	1974 OS	1974 Jul 25	T. Smirnova	Nauchnyj	
2346	Lilio	1934 CB	1934 Feb 5	K. Reinmuth	Heidelberg	
2347		1936 TK	1936 Oct 7	H. L. Giclas	Flagstaff (LO)	
2348	Michkovitch	1939 AA	1939 Jan 10	M. B. Protitch	Belgrade	
2349	Kurchenko	1970 OG	1970 Jul 30	T. Smirnova	Nauchnyj	
2350	von Lude	1938 CG	1938 Feb 6	A. Bohrmann	Heidelberg	
2351	O'Higgins	1964 VD	1964 Nov 3	Goethe Link Observatory	Brooklyn	103
2352	Kurchatov	1969 RY	1969 Sep 10	L. Chernykh	Nauchnyj	
2353		1975 UD	1975 Oct 27	P. Wild	Zimmerwald	
2354	Lavrov	1978 PZ3	1978 Aug 9	L. Chernykh and N. Chernykh	Nauchnyj	
2355	Nei Monggol	1978 UV1	1978 Oct 30	Purple Mountain Observatory	Nanking	
2356	Hirons	1979 UJ	1979 Oct 17	E. Bowell	Flagstaff (AM)	119
2357	Phereclos	1981 AC	1981 Jan 1	E. Bowell	Flagstaff (AM)	119
2358	Bahner	1929 RE	1929 Sep 2	K. Reinmuth	Heidelberg	
2359	Debehogne	1931 TV	1931 Oct 5	K. Reinmuth	Heidelberg	
2360	Volgo-Don	1975 VD3	1975 Nov 2	T. Smirnova	Nauchnyj	
2361	Gogol	1976 GQ1	1976 Apr 1	N. Chernykh	Nauchnyj	
2362	Mark Twain	1976 SH2	1976 Sep 24	N. Chernykh	Nauchnyj	
2363	Cebriones	1977 TJ3	1977 Oct 4	Purple Mountain Observatory	Nanking	
2364	Seillier	1978 GD	1978 Apr 14	H. Debehogne	La Silla	
2365	Interkosmos	1980 YQ	1980 Dec 30	Z. Vavrova	Klet	
2366	Aaryn	1981 AC1	1981 Jan 10	N. G. Thomas	Flagstaff (AM)	119
2367	Praha	1981 AK1	1981 Jan 8	A. Mrkos	Klet	
2368	Beltrovata	1977 RA	1977 Sep 4	P. Wild	Zimmerwald	
2369	Chekhov	1976 GC8	1976 Apr 4	N. Chernykh	Nauchnyj	
2370	van Altena	1965 LA	1965 Jun 10	A. R. Klemola	El Leoncito	
2371	Dimitrov	1975 VR3	1975 Nov 2	T. Smirnova	Nauchnyj	
2372	Proskurin	1977 RA8	1977 Sep 13	N. Chernykh	Nauchnyj	
2373		1929 PC	1929 Aug 4	M. Wolf	Heidelberg	
2374	Vladvysotskij	1974 QE1	1974 Aug 22	L. Zhuravleva	Nauchnyj	
2375		1975 AA	1975 Jan 8	L. Kohoutek	Bergedorf	
2376	Martynov	1977 QG3	1977 Aug 22	N. Chernykh	Nauchnyj	
2377	Shcheglov	1978 QT1	1978 Aug 31	N. Chernykh	Nauchnyj	
2378		1935 CY	1935 Feb 13	H. Van Gent	Johannesburg (LS)	
2379	Heiskanen	1941 ST	1941 Sep 21	Y. Vaisala	Turku	
2380	Heilongjiang	1965 SN	1965 Sep 18	Purple Mountain Observatory	Nanking	
2381	Landi	1976 AF	1976 Jan 3	Felix Aguilar Observatory	El Leoncito	
2382	Nonie	1977 GA	1977 Apr 13	Perth Observatory	Perth	
2383	Bradley	1981 GN	1981 Apr 5	E. Bowell	Flagstaff (AM)	119
2384	Schulhof	1943 EC1	1943 Mar 2	M. Laugier	Nice	
2385	Mustel	1969 VW	1969 Nov 11	L. Chernykh	Nauchnyj	
2386	Nikonov	1974 SN1	1974 Sep 19	L. Chernykh	Nauchnyj	
2387		1975 FX	1975 Mar 17	Purple Mountain Observatory	Nanking	
2388	Gase	1977 EA2	1977 Mar 13	N. Chernykh	Nauchnyj	
2389	Dibaj	1977 QC1	1977 Aug 19	N. Chernykh	Nauchnyj	
2390	Nežárka	1980 PA1	1980 Aug 14	Z. Vavrova	Klet	
2391	Tomita	1957 AA	1957 Jan 9	K. Reinmuth	Heidelberg	
2392	Jonathan Murray	1979 MN1	1979 Jun 25	E. F. Helin and S. J. Bus	Siding Spring	
2393	Suzuki	1955 WB	1955 Nov 17	M. Laugier	Nice	
2394	Nadeev	1973 SZ2	1973 Sep 22	N. Chernykh	Nauchnyj	
2395	Aho	1977 FA	1977 Mar 17	Harvard College	Agassiz Station	113
2396	Kochi	1981 CB	1981 Feb 9	T. Seki	Geisei	
2397	Lappajarvi	1938 DV	1938 Feb 22	Y. Vaisala	Turku	
2398	Jilin	1965 UD2	1965 Oct 24	Purple Mountain Observatory	Nanking	
2399	Terradas	1971 MA	1971 Jun 17	C. U. Cesco	El Leoncito	
2400	Derevskaya	1972 KJ	1972 May 17	T. Smirnova	Nauchnyj	
2401	Aehlita	1975 VM2	1975 Nov 2	T. Smirnova	Nauchnyj	
2402	Satpaev	1979 OR13	1979 Jul 31	N. Chernykh	Nauchnyj	
2403	Šumava	1979 SQ	1979 Sep 25	A. Mrkos	Klet	

No.	Name	pd	dd	d	dp	
2404	Antarctica	1980 TE	1980 Oct 1	A. Mrkos	Klet	
2405	Welch	1963 UF	1963 Oct 18	Goethe Link Observatory	Brooklyn	103
2406	Orelskaya	1966 QG	1966 Aug 20	Crimean Astrophysical Obs.	Nauchnyj	
2407		1973 DH	1973 Feb 27	L. Kohoutek	Bergedorf	
2408	Astapovich	1978 QK1	1978 Aug 31	N. Chernykh	Nauchnyj	
2409	Chapman	1979 UG	1979 Oct 17	E. Bowell	Flagstaff (AM)	119
2410	Morrison	1981 AF	1981 Jan 3	E. Bowell	Flagstaff (AM)	119
2411	Zellner	1981 JK	1981 May 3	E. Bowell	Flagstaff (AM)	119
2412	Wil	3537 P-L	1960 Oct 17	PLS	Palomar	107
2413	van de Hulst	6816 P-L	1960 Sep 24	PLS	Palomar	107
2414	Vibeke	1931 UG	1931 Oct 18	K. Reinmuth	Heidelberg	
2415		1978 UJ	1978 Oct 28	H. L. Giclas	Flagstaff (AM)	119
2416	Sharonov	1979 OF13	1979 Jul 31	N. Chernykh	Nauchnyj	
2417	McVittie	1964 CD	1964 Feb 15	Goethe Link Observatory	Brooklyn	103
2418		1971 UV	1971 Oct 26	L. Kohoutek	Bergedorf	
2419	Moldavia	1974 SJ	1974 Sep 19	L. Chernykh	Nauchnyj	
2420	Čiurlionis	1975 TN	1975 Oct 3	N. Chernykh	Nauchnyj	
2421	Nininger	1979 UD	1979 Oct 17	E. Bowell	Flagstaff (AM)	119
2422	Perovskaya	1968 HK1	1968 Apr 28	T. Smirnova	Nauchnyj	
2423	Ibarruri	1972 NC	1972 Jul 14	L. Zhuravleva	Nauchnyj	
2424	Tautenburg	1973 UT5	1973 Oct 27	F. Borngen and K. Kirsch	Tautenburg	
2425		1975 FW	1975 Mar 17	Purple Mountain Observatory	Nanking	
2426	Simonov	1976 KV	1976 May 26	N. Chernykh	Nauchnyj	
2427	Kobzar	1976 YQ7	1976 Dec 20	N. Chernykh	Nauchnyj	
2428	Kamenyar	1977 RZ6	1977 Sep 11	N. Chernykh	Nauchnyj	
2429		1977 TZ	1977 Oct 12	P. Wild	Zimmerwald	
2430	Bruce Helin	1977 VC	1977 Nov 8	E. F. Helin and E. Shoemaker	Palomar	
2431	Skovoroda	1978 PF3	1978 Aug 8	N. Chernykh	Nauchnyj	
2432	Soomana	1981 FA	1981 Mar 30	E. Bowell	Flagstaff (AM)	119
2433	Sootiyo	1981 GJ	1981 Apr 5	E. Bowell	Flagstaff (AM)	119
2434	Bateson	1981 KA	1981 May 27	A. Gilmore and P. Kilmartin	Mount John	
2435	Horemheb	4578 P-L	1960 Sep 24	PLS	Palomar	107
2436	Hatshepsut	6066 P-L	1960 Sep 24	PLS	Palomar	107
2437	Amnestia	1942 RZ	1942 Sep 14	M. Vaisala	Turku	
2438	Oleshko	1975 VO2	1975 Nov 2	T. Smirnova	Nauchnyj	
2439	Ulugbek	1977 QX2	1977 Aug 21	N. Chernykh	Nauchnyj	
2440	Educatio	1978 VQ4	1978 Nov 7	E. F. Helin and S. J. Bus	Palomar	
2441	Hibbs	1979 MN2	1979 Jun 25	E. F. Helin and S. J. Bus	Siding Spring	
2442	Corbett	1980 TO	1980 Oct 3	Z. Vavrova	Klet	
2443	Tomeileen	A906 BJ	1906 Jan 24	M. Wolf	Heidelberg	
2444	Lederle	1934 CD	1934 Feb 5	K. Reinmuth	Heidelberg	
2445	Blazhko	1935 TC	1935 Oct 3	P. Shajn	Simeis	
2446	Lunacharsky	1971 TS2	1971 Oct 14	L. Chernykh	Nauchnyj	
2447	Kronstadt	1973 QY1	1973 Aug 31	T. Smirnova	Nauchnyj	
2448	Sholokhov	1975 BU	1975 Jan 18	L. Chernykh	Nauchnyj	
2449		1978 GC	1978 Apr 8	W. Liller	Cerro Tololo	
2450	Ioannisiani	1978 RP	1978 Sep 1	N. Chernykh	Nauchnyj	
2451	Dollfus	1980 RQ	1980 Sep 2	E. Bowell	Flagstaff (AM)	119
2452	Lyot	1981 FE	1981 Mar 30	E. Bowell	Flagstaff (AM)	119
2453		A921 SA	1921 Sep 30	K. Reinmuth	Heidelberg	
2454	Olaus Magnus	1941 SS	1941 Sep 21	Y. Vaisala	Turku	
2455	Somville	1950 TO4	1950 Oct 5	S. Arend	Uccle	
2456	Palamedes	1966 BA1	1966 Jan 30	Purple Mountain Observatory	Nanking	
2457	Rublyov	1975 TU2	1975 Oct 3	L. Chernykh	Nauchnyj	
2458		1977 RC7	1977 Sep 11	N. Chernykh	Nauchnyj	
2459	Spellmann	1980 LB1	1980 Jun 11	C. Shoemaker	Palomar	123
2460	Mitlincoln	1980 TX4	1980 Oct 1	L. G. Taff and D. Beatty	Socorro	
2461		1981 EC1	1981 Mar 5	H. Debehogne	La Silla	124
2462	Nehalennia	6578 P-L	1960 Sep 24	PLS	Palomar	107
2463		1934 FF	1934 Mar 10	G. Van Biesbroeck	Williams Bay	
2464	Nordenskiöld	1939 BF	1939 Jan 19	Y. Vaisala	Turku	
2465		1949 PK	1949 Aug 2	K. Reinmuth	Heidelberg	
2466	Golson	1959 RJ	1959 Sep 7	Goethe Link Observatory	Brooklyn	103
2467	Kollontai	1966 PJ	1966 Aug 14	L. Chernykh	Nauchnyj	
2468	Repin	1969 TO1	1969 Oct 8	L. Chernykh	Nauchnyj	
2469	Tadjikistan	1970 HA	1970 Apr 27	T. Smirnova	Nauchnyj	
2470	Agematsu	1976 UW15	1976 Oct 22	H. Kosai and K. Hurukawa	Kiso Station	
2471	Ultrajectum	6545 P-L	1960 Sep 24	PLS	Palomar	107
2472		1973 DG	1973 Feb 27	L. Kohoutek	Bergedorf	
2473	Heyerdahl	1977 RX7	1977 Sep 12	N. Chernykh	Nauchnyj	
2474	Ruby	1979 PB	1979 Aug 14	Z. Vavrova	Klet	
2475	Semenov	1972 TF2	1972 Oct 8	L. Zhuravleva	Nauchnyj	
2476	Andersen	1976 JF2	1976 May 2	N. Chernykh	Nauchnyj	
2477	Biryukov	1977 PY1	1977 Aug 14	N. Chernykh	Nauchnyj	
2478	Tokai	1981 JC	1981 May 4	T. Furuta	Tokai	
2479	Sodankyla	1942 CB	1942 Feb 6	Y. Vaisala	Turku	
2480	Papanov	1976 YS1	1976 Dec 16	L. Chernykh	Nauchnyj	
2481		1977 UQ	1977 Oct 18	P. Wild	Zimmerwald	
2482	Perkin	1980 CO	1980 Feb 13	Harvard College	Agassiz Station	113
2483	Guinevere	1928 QB	1928 Aug 17	M. Wolf	Heidelberg	
2484	Parenago	1928 TK	1928 Oct 7	G. Neujmin	Simeis	
2485		1932 BH	1932 Jan 29	K. Reinmuth	Heidelberg	

No.	Name	pd	dd	d	dp	
2486	Metsahovi	1939 FY	1939 Mar 22	Y. Vaisala	Turku	
2487	Juhani	1940 RL	1940 Sep 8	H. Alikoski	Turku	
2488	Bryan	1952 UT	1952 Oct 23	Goethe Link Observatory	Brooklyn	103
2489	Suvorov	1975 NY	1975 Jul 11	L. Chernykh	Nauchnyj	
2490	Bussolini	1976 AG	1976 Jan 3	Felix Aguilar Observatory	El Leoncito	
2491		1977 CB	1977 Feb 15	W. Sebok	Palomar	
2492	Kutuzov	1977 NT	1977 Jul 14	N. Chernykh	Nauchnyj	
2493	Elmer	1978 XC	1978 Dec 1	Harvard College	Agassiz Station	113
2494	Inge	1981 LF	1981 Jun 4	E. Bowell	Flagstaff (AM)	119
2495	Noviomagum	7071 P-L	1960 Oct 17	PLS	Palomar	107
2496	Fernandus	1953 TC1	1953 Oct 8	Goethe Link Observatory	Brooklyn	103
2497	Kulikovskij	1977 PZ1	1977 Aug 14	N. Chernykh	Nauchnyj	
2498	Tsesevich	1977 QM3	1977 Aug 23	N. Chernykh	Nauchnyj	
2499	Brunk	1978 VJ7	1978 Nov 7	E. F. Helin and S. J. Bus	Palomar	
2500		1926 GC	1926 Apr 2	K. Reinmuth	Heidelberg	
2501	Lohja	1942 GD	1942 Apr 14	L. Oterma	Turku	
2502	Nummela	1943 EO	1943 Mar 3	Y. Vaisala	Turku	
2503	Liaoning	1965 UB1	1965 Oct 16	Purple Mountain Observatory	Nanking	
2504	Gaviola	1967 JC	1967 May 6	C. U. Cesco and A. R. Klemola	El Leoncito	
2505	Hebei	1975 UJ	1975 Oct 31	Purple Mountain Observatory	Nanking	
2506	Pirogov	1976 QG1	1976 Aug 26	N. Chernykh	Nauchnyj	
2507	Bobone	1976 WB1	1976 Nov 18	Felix Aguilar Observatory	El Leoncito	
2508	Alupka	1977 ET1	1977 Mar 13	N. Chernykh	Nauchnyj	
2509	Chukotka	1977 NG	1977 Jul 14	N. Chernykh	Nauchnyj	
2510	Shandong	1979 TH	1979 Oct 10	Purple Mountain Observatory	Nanking	
2511	Patterson	1980 LM	1980 Jun 11	C. Shoemaker	Palomar	123
2512	Tavastia	1940 GG	1940 Apr 3	Y. Vaisala	Turku	
2513	Baetsle	1950 SH	1950 Sep 19	S. Arend	Uccle	
2514	Taiyuan	1964 TA1	1964 Oct 8	Purple Mountain Observatory	Nanking	
2515	Gansu	1964 TX1	1964 Oct 9	Purple Mountain Observatory	Nanking	
2516	Roman	1964 VY	1964 Nov 6	Goethe Link Observatory	Brooklyn	103
2517		1968 SB	1968 Sep 28	P. Wild	Zimmerwald	
2518	Rutllant	1974 FG	1974 Mar 22	C. Torres	Cerro El Roble	
2519	Annagerman	1975 VD2	1975 Nov 2	T. Smirnova	Nauchnyj	
2520	Novorossijsk	1976 QF1	1976 Aug 26	N. Chernykh	Nauchnyj	
2521		1979 DK	1979 Feb 28	P. Wild	Zimmerwald	
2522		1980 PP	1980 Aug 6	Z. Vavrova	Klet	
2523		1980 PV	1980 Aug 6	Z. Vavrova	Klet	
2524	Budovicium	1981 QB1	1981 Aug 28	Z. Vavrova	Klet	
2525	O'Steen	1981 VG	1981 Nov 2	B. A. Skiff	Flagstaff (AM)	119
2526	Alisary	1979 KX	1979 May 19	R. M. West	La Silla	
2527	Gregory	1981 RE	1981 Sep 3	N. G. Thomas	Flagstaff (AM)	119
2528	Mohler	1953 TF1	1953 Oct 8	Goethe Link Observatory	Brooklyn	103
2529	Rockwell Kent	1977 QL2	1977 Aug 21	N. Chernykh	Nauchnyj	
2530	Shipka	1978 NC3	1978 Jul 9	L. Chernykh	Nauchnyj	
2531	Cambridge	1980 LD	1980 Jun 11	E. Bowell	Flagstaff (AM)	119
2532	Sutton	1980 TU5	1980 Oct 9	C. Shoemaker	Palomar	123
2533		A905 VA	1905 Nov 3	M. Wolf	Heidelberg	
2534	Houzeau	1931 VD	1931 Nov 2	E. Delporte	Uccle	
2535	Hameenlinna	1939 DH	1939 Feb 17	Y. Vaisala	Turku	
2536	Kozyrev	1939 PJ	1939 Aug 15	G. Neujmin	Simeis	
2537	Gilmore	1951 RL	1951 Sep 4	K. Reinmuth	Heidelberg	
2538	Vanderlinden	1954 UD	1954 Oct 30	S. Arend	Uccle	
2539	Ningxia	1964 TS2	1964 Oct 8	Purple Mountain Observatory	Nanking	
2540	Blok	1971 TH2	1971 Oct 13	L. Chernykh	Nauchnyj	
2541		1973 DE	1973 Feb 27	L. Kohoutek	Bergedorf	
2542	Calpurnia	1980 CF	1980 Feb 11	E. Bowell	Flagstaff (AM)	119
2543	Machado	1980 LJ	1980 Jun 1	H. Debehogne	La Silla	
2544	Gubarev	1980 PS	1980 Aug 6	Z. Vavrova	Klet	
2545	Verbiest	1933 BB	1933 Jan 26	E. Delporte	Uccle	
2546		1950 FC	1950 Mar 23	E. L. Johnson	Johannesburg (UO)	
2547	Hubei	1964 TC2	1964 Oct 9	Purple Mountain Observatory	Nanking	
2548	Leloir	1975 DA	1975 Feb 16	Felix Aguilar Observatory	El Leoncito	
2549	Baker	1976 UB	1976 Oct 23	Harvard College	Agassiz Station	113
2550	Houssay	1976 UP20	1976 Oct 21	Felix Aguilar Observatory	El Leoncito	
2551	Decabrina	1976 YX1	1976 Dec 16	L. Chernykh	Nauchnyj	
2552	Remek	1978 SP	1978 Sep 24	A. Mrkos	Klet	
2553	Viljev	1979 FS2	1979 Mar 29	N. Chernykh	Nauchnyj	
2554	Skiff	1980 OB	1980 Jul 17	E. Bowell	Flagstaff (AM)	119
2555	Thomas	1980 OC	1980 Jul 17	E. Bowell	Flagstaff (AM)	119
2556	Louise	1981 CS	1981 Feb 8	N. G. Thomas	Flagstaff (AM)	119
2557	Putnam	1981 SL1	1981 Sep 26	B. A. Skiff and N. G. Thomas	Flagstaff (AM)	119
2558	Viv	1981 SP1	1981 Sep 26	N. G. Thomas	Flagstaff (AM)	119
2559		1981 UH	1981 Oct 23	A. Mrkos	Klet	
2560		1932 CW	1932 Feb 14	K. Reinmuth	Heidelberg	
2561	Margolin	1969 TK2	1969 Oct 8	L. Chernykh	Nauchnyj	
2562		1973 FF1	1973 Mar 27	L. Zhuravleva	Nauchnyj	
2563	Boyarchuk	1977 FZ	1977 Mar 22	N. Chernykh	Nauchnyj	
2564	Kayala	1977 QX	1977 Aug 19	N. Chernykh	Nauchnyj	
2565		1977 TB1	1977 Oct 12	P. Wild	Zimmerwald	
2566	Kirghizia	1979 FR2	1979 Mar 29	N. Chernykh	Nauchnyj	
2567	Elba	1979 KA	1979 May 19	O. Pizarro and G. Pizarro	La Silla	

No.	Name	pd	dd	d	dp	
2568	Maksutov	1980 GH	1980 Apr 13	Z. Vavrova	Klet	
2569	Madeline	1980 MA	1980 Jun 18	E. Bowell	Flagstaff (AM)	119
2570	Porphyro	1980 PG	1980 Aug 6	E. Bowell	Flagstaff (AM)	119
2571	Geisei	1981 UC	1981 Oct 23	T. Seki	Geisei	
2572		1950 DL	1950 Feb 17	K. Reinmuth	Heidelberg	
2573	Hannu Olavi	1953 EN	1953 Mar 10	H. Alikoski	Turku	
2574	Ladoga	1968 UP	1968 Oct 22	T. Smirnova	Nauchnyj	
2575	Bulgaria	1970 PL	1970 Aug 4	T. Smirnova	Nauchnyj	
2576	Yesenin	1974 QL	1974 Aug 17	L. Zhuravleva	Nauchnyj	
2577	Litva	1975 EE3	1975 Mar 12	N. Chernykh	Nauchnyj	
2578	Saint-Exupéry	1975 VW3	1975 Nov 2	T. Smirnova	Nauchnyj	
2579	Spartacus	1977 PA2	1977 Aug 14	N. Chernykh	Nauchnyj	
2580	Smilevskia	1977 QP4	1977 Aug 18	N. Chernykh	Nauchnyj	
2581		1980 VX	1980 Nov 11	Z. Vavrova	Klet	
2582	Harimaya-Bashi	1981 SA	1981 Sep 26	T. Seki	Geisei	
2583	Fatyanov	1975 XA3	1975 Dec 3	T. Smirnova	Nauchnyj	
2584	Turkmenia	1979 FG2	1979 Mar 23	N. Chernykh	Nauchnyj	
2585	Irpedina	1979 OJ15	1979 Jul 21	N. Chernykh	Nauchnyj	
2586	Matson	1980 LO	1980 Jun 17	C. Shoemaker	Palomar	123
2587	Gardner	1980 OH	1980 Jul 17	E. Bowell	Flagstaff (AM)	119
2588	Flavia	1981 VQ	1981 Nov 2	B. A. Skiff	Flagstaff (AM)	119
2589	Daniel	1979 QU2	1979 Aug 22	C.-I. Lagerkvist	La Silla	
2590	Mourão	1980 KJ	1980 May 22	H. Debehogne	La Silla	
2591		1949 PS	1949 Aug 2	K. Reinmuth	Heidelberg	
2592	Hunan	1966 BW	1966 Jan 30	Purple Mountain Observatory	Nanking	
2593	Buryatia	1976 GB8	1976 Apr 2	N. Chernykh	Nauchnyj	
2594		1978 TB	1978 Oct 4	C. Kowal	Palomar	
2595	Gudiachvili	1979 KL	1979 May 19	R. M. West	La Silla	
2596	Vainu Bappu	1979 KN	1979 May 19	R. M. West	La Silla	
2597	Arthur	1980 PN	1980 Aug 8	E. Bowell	Flagstaff (AM)	119
2598	Merlin	1980 RY	1980 Sep 7	E. Bowell	Flagstaff (AM)	119
2599	Veselí	1980 SO	1980 Sep 29	Z. Vavrova	Klet	
2600	Lumme	1980 VP	1980 Nov 9	E. Bowell	Flagstaff (AM)	119
2601	Bologna	1980 XA	1980 Dec 8	Osservatorio San Vittore	Bologna	
2602	Moore	1982 BR	1982 Jan 24	E. Bowell	Flagstaff (AM)	119
2603	Taylor	1982 BW1	1982 Jan 30	E. Bowell	Flagstaff (AM)	119
2604	Marshak	1972 LD1	1972 Jun 13	T. Smirnova	Nauchnyj	
2605	Sahade	1974 QA	1974 Aug 16	Felix Aguilar Observatory	El Leoncito	
2606	Odessa	1976 GX2	1976 Apr 1	N Chernykh	Nauchnyj	
2607	Yakutia	1977 NR	1977 Jul 14	N. Chernykh	Nauchnyj	
2608	Seneca	1978 DA	1978 Feb 17	H.-E. Schuster	La Silla	
2609	Kiril-Metodi	1978 FB4	1978 Aug 9	L. Chernykh and N. Chernykh	Nauchnyj	
2610	Tuva	1978 RO1	1978 Sep 5	N. Chernykh	Nauchnyj	
2611	Boyce	1978 VQ5	1978 Nov 7	E. F. Helin and S. J. Bus	Palomar	
2612	Kathryn	1979 DE	1979 Feb 28	N. G. Thomas	Flagstaff (AM)	119
2613	Plzeň	1979 QE	1979 Aug 30	L. Brozek	Klet	
2614	Torrence	1980 LP	1980 Jun 11	C. Shoemaker	Palomar	123
2615	Saito	1951 RJ	1951 Sep 4	K. Reinmuth	Heidelberg	
2616	Lesya	1970 QV	1970 Aug 28	T. Smirnova	Nauchnyj	
2617	Jiangxi	1975 WO1	1975 Nov 26	Purple Mountain Observatory	Nanking	
2618	Coonabarabran	1979 MX2	1979 Jun 25	E. F. Helin and S. J. Bus	Siding Spring	
2619	Skalnaté Pleso	1979 MZ3	1979 Jun 25	E. F. Helin and S. J. Bus	Siding Spring	
2620		1980 TN	1980 Oct 3	Z. Vavrova	Klet	
2621	Goto	1981 CA	1981 Feb 9	T. Seki	Geisei	
2622	Bolzano	1981 CM	1981 Feb 9	L. Brozek	Klet	
2623		A919 SA	1919 Sep 22	K. Reinmuth	Heidelberg	
2624	Samitchell	1962 RE	1962 Sep 7	Goethe Link Observatory	Brooklyn	103
2625	Jack London	1976 JQ2	1976 May 2	N. Chernykh	Nauchnyj	
2626	Belnika	1978 PP2	1978 Aug 8	N. Chernykh	Nauchnyj	
2627	Churyumov	1978 PP3	1978 Aug 8	N. Chernykh	Nauchnyj	
2628	Kopal	1979 MS8	1979 Jun 25	E. F. Helin and S. J. Bus	Siding Spring	
2629		1980 RB1	1980 Sep 13	C. Kowal	Palomar	
2630		1980 TF3	1980 Oct 14	- - -	Haute Provence	
2631	Zhejiang	1980 TY5	1980 Oct 7	Purple Mountain Observatory	Nanking	
2632	Guizhou	1980 VJ1	1980 Nov 6	Purple Mountain Observatory	Nanking	
2633	Bishop	1981 WR1	1981 Nov 24	E. Bowell	Flagstaff (AM)	119
2634	James Bradley	1982 DL	1982 Feb 21	E. Bowell	Flagstaff (AM)	119
2635	Huggins	1982 DS	1982 Feb 21	E. Bowell	Flagstaff (AM)	119
2636	Lassell	1982 DZ	1982 Feb 20	E. Bowell	Flagstaff (AM)	119
2637	Bobrovnikoff	A919 SB	1919 Sep 22	K. Reinmuth	Heidelberg	
2638	Gidolin	1939 SG	1939 Sep 19	Y. Vaisala	Turku	
2639	Planman	1940 GN	1940 Apr 9	Y. Vaisala	Turku	
2640	Hallstrom	1941 FN	1941 Mar 18	L. Oterma	Turku	
2641	Lipschutz	1949 GJ	1949 Apr 4	Goethe Link Observatory	Brooklyn	103
2642	Vésale	1961 RA	1961 Sep 14	S Arend	Uccle	
2643		1973 SD	1973 Sep 19	T. Gehrels	Palomar	
2644	Victor Jara	1973 SO2	1973 Sep 22	N. Chernykh	Nauchnyj	
2645	Daphne Plane	1976 QD	1976 Aug 30	E. F. Helin	Palomar	
2646	Abetti	1977 EC1	1977 Mar 13	N. Chernykh	Nauchnyj	
2647		1980 SP	1980 Sep 29	Z. Vavrova	Klet	
2648	Owa	1980 VJ	1980 Nov 8	E. Bowell	Flagstaff (AM)	119
2649	Oongaq	1980 WA	1980 Nov 29	E. Bowell	Flagstaff (AM)	119
2650		1931 EG	1931 Mar 14	M. Wolf	Heidelberg	

No.	Name	pd	dd	d	dp	
2651	Karen	1949 QD	1949 Aug 28	E. L. Johnson	Johannesburg (UO)	
2652	Yabuuti	1953 GM	1953 Apr 7	K. Reinmuth	Heidelberg	
2653	Principia	1964 VP	1964 Nov 4	Goethe Link Observatory	Brooklyn	103
2654	Ristenpart	1968 OG	1968 Jul 18	C. Torres	Cerro El Roble	
2655	Guangxi	1974 XX	1974 Dec 14	Purple Mountain Observatory	Nanking	
2656	Evenkia	1979 HD5	1979 Apr 25	N. Chernykh	Nauchnyj	
2657	Bashkiria	1979 SB7	1979 Sep 23	N. Chernykh	Nauchnyj	
2658	Gingerich	1980 CK	1980 Feb 13	Harvard College	Agassiz Station	113
2659	Millis	1981 JX	1981 May 5	E. Bowell	Flagstaff (AM)	125
2660	Wasserman	1982 FG	1982 Mar 21	E. Bowell	Flagstaff (AM)	125
2661		1982 FC1	1982 Mar 23	Z. Vavrova	Klet	
2662	Kandinsky	4021 P-L	1960 Sep 24	PLS	Palomar	107
2663		6561 P-L	1960 Sep 24	PLS	Palomar	107
2664	Everhart	1934 RR	1934 Sep 8	K. Reinmuth	Heidelberg	
2665		1938 DW1	1938 Feb 24	A. Bohrmann	Heidelberg	
2666	Gramme	1951 TA	1951 Oct 8	S Arend	Uccle	
2667		1967 UO	1967 Oct 30	L. Kohoutek	Bergedorf	
2668	Tataria	1976 QV	1976 Aug 26	N. Chernykh	Nauchnyj	
2669	Shostakovich	1976 YQ2	1976 Dec 16	L. Chernykh	Nauchnyj	
2670	Chuvashia	1977 PW1	1977 Aug 14	N. Chernykh	Nauchnyj	
2671	Abkhazia	1977 QR2	1977 Aug 21	N. Chernykh	Nauchnyj	
2672	Pisek	1979 KC	1979 May 31	J. Kveton	Klet	
2673		1980 KN	1980 May 22	H. Debehogne	La Silla	
2674	Pandarus	1982 BC3	1982 Jan 27	Oak Ridge Observatory	Oak Ridge	113
2675	Tolkien	1982 GB	1982 Apr 14	M. Watt	Flagstaff (AM)	119
2676	Aarhus	1933 QV	1933 Aug 25	K Reinmuth	Heidelberg	
2677		1935 FF	1935 Mar 25	M. Laugier	Nice	
2678	Aavasaksa	1938 DF1	1938 Feb 24	Y. Vaisala	Turku	
2679	Kittisvaara	1939 TG	1939 Oct 7	Y Vaisala	Turku	
2680	Mateo	1975 NF	1975 Jul 1	Felix Aguilar Observatory	El Leoncito	
2681	Ostrovskij	1975 VF2	1975 Nov 2	T. Smirnova	Nauchnyj	
2682	Soromundi	1979 MF4	1979 Jun 25	E. F Helin and S. J. Bus	Siding Spring	
2683	Brian	1981 AD1	1981 Jan 10	N. G Thomas	Flagstaff (AM)	119
2684	Douglas	1981 AH1	1981 Jan 3	N. G. Thomas	Flagstaff (AM)	119
2685	Masursky	1981 JN	1981 May 3	E. Bowell	Flagstaff (AM)	119
2686	Linda Susan	1981 JW1	1981 May 5	C Shoemaker	Palomar	123
2687		1982 HG	1982 Apr 18	M. Watt	Flagstaff (AM)	119
2688	Halley	1982 HG1	1982 Apr 25	E Bowell	Flagstaff (AM)	119
2689	Bruxelles	1935 CF	1935 Feb 3	S. Arend	Uccle	
2690	Ristiina	1938 DG1	1938 Feb 24	Y. Vaisala	Turku	
2691	Sersic	1974 KB	1974 May 18	Felix Aguilar Observatory	El Leoncito	
2692	Chkalov	1976 YT3	1976 Dec 16	L Chernykh	Nauchnyj	
2693	Yan'an	1977 VM1	1977 Nov 3	Purple Mountain Observatory	Nanking	
2694	Pino Torinese	1979 QL1	1979 Aug 22	C.-I. Lagerkvist	La Silla	
2695	Christabel	1979 UE	1979 Oct 17	E. Bowell	Flagstaff (AM)	119
2696	Magion	1980 HB	1980 Apr 16	L. Brozek	Klet	
2697	Albina	1969 TC3	1969 Oct 9	B. Burnasheva	Nauchnyj	
2698	Azerbajdzhan	1971 TZ	1971 Oct 11	Crimean Astrophysical Obs	Nauchnyj	
2699	Kalinin	1976 YX	1976 Dec 16	L. Chernykh	Nauchnyj	
2700	Baikonur	1976 YP7	1976 Dec 20	N. Chernykh	Nauchnyj	
2701	Cherson	1978 RT	1978 Sep 1	N. Chernykh	Nauchnyj	
2702		1978 SZ2	1978 Sep 26	L. Zhuravleva	Nauchnyj	
2703	Rodari	1979 FT2	1979 Mar 29	N. Chernykh	Nauchnyj	
2704	Julian Loewe	1979 MR4	1979 Jun 25	E. F. Helin and S. J. Bus	Siding Spring	
2705	Wu	1980 TD4	1980 Oct 9	C. Shoemaker	Palomar	
2706		1980 VW	1980 Nov 11	Z. Vavrova	Klet	
2707	Ueferji	1981 QS3	1981 Aug 28	H. Debehogne	La Silla	
2708	Burns	1981 WT	1981 Nov 24	E Bowell	Flagstaff (AM)	119
2709	Sagan	1982 FH	1982 Mar 21	E. Bowell	Flagstaff (AM)	119
2710	Veverka	1982 FQ	1982 Mar 23	E. Bowell	Flagstaff (AM)	119
2711	Aleksandrov	1978 QB2	1978 Aug 31	N. Chernykh	Nauchnyj	
2712		1937 YD	1937 Dec 29	G. Kulin	Budapest	
2713	Luxembourg	1938 EA	1938 Feb 19	E. Delporte	Uccle	
2714	Matti	1938 GC	1938 Apr 5	H. Alikoski	Turku	
2715	Mielikki	1938 US	1938 Oct 22	Y. Vaisala	Turku	
2716	Tuulikki	1939 TM	1939 Oct 7	Y. Vaisala	Turku	
2717	Tellervo	1940 WJ	1940 Nov 29	L. Oterma	Turku	
2718		1951 OM	1951 Jul 30	E. L. Johnson	Johannesburg (UO)	
2719		1965 SU	1965 Sep 22	Purple Mountain Observatory	Nanking	
2720	Pyotr Pervyj	1972 RV3	1972 Sep 6	L. Zhuravleva	Nauchnyj	
2721	Vsekhsvyatskij	1973 SP2	1973 Sep 22	N. Chernykh	Nauchnyj	
2722	Abalakin	1976 GM2	1976 Apr 1	N. Chernykh	Nauchnyj	
2723	Gorshkov	1978 QL2	1978 Aug 31	N. Chernykh	Nauchnyj	
2724	Orlov	1978 RZ5	1978 Sep 13	N. Chernykh	Nauchnyj	
2725	David Bender	1978 VG3	1978 Nov 7	E. F. Helin and S. J. Bus	Palomar	
2726	Kotelnikov	1979 SE9	1979 Sep 22	N. Chernykh	Nauchnyj	
2727	Paton	1979 SO9	1979 Sep 22	N. Chernykh	Nauchnyj	
2728	Yatskiv	1979 ST9	1979 Sep 22	N. Chernykh	Nauchnyj	
2729		1979 UA2	1979 Oct 18	Purple Mountain Observatory	Nanking	
2730	Barks	1981 QH	1981 Aug 30	E. Bowell	Flagstaff (AM)	119
2731	Cucula	1982 KJ	1982 May 21	P. Wild	Zimmerwald	
2732	Witt	1926 FG	1926 Mar 19	M Wolf	Heidelberg	
2733	Hamina	1938 DQ	1938 Feb 22	Y Vaisala	Turku	

No.	Name	pd	dd	d	dp	
2734	Hašek	1976 GJ3	1976 Apr 1	N. Chernykh	Nauchnyj	
2735	Ellen	1977 RB	1977 Sep 13	S. J. Bus and T. Lauer	Palomar	
2736	Ops	1979 OC	1979 Jul 23	E. Bowell	Flagstaff (AM)	119
2737	Kotka	1938 DU	1938 Feb 22	Y. Vaisala	Turku	
2738		1940 EC	1940 Mar 12	G. Kulin	Budapest	
2739		1952 UZ1	1952 Oct 17	J. L. Brady	Mount Wilson	
2740		1974 SY4	1974 Sep 26	L. Zhuravleva	Nauchnyj	
2741	Valdivia	1975 XG	1975 Dec 1	C. Torres	Cerro El Roble	
2742	Gibson	1981 JG3	1981 May 6	C. Shoemaker	Palomar	123
2743		1965 WR	1965 Nov 21	Purple Mountain Observatory	Nanking	
2744	Birgitta	1975 RB	1975 Sep 4	C.-I. Lagerkvist	Kvistaberg	
2745		1976 SR10	1976 Sep 25	Felix Aguilar Observatory	El Leoncito	
2746	Hissao	1979 SJ9	1979 Sep 22	N. Chernykh	Nauchnyj	
2747		1980 DW	1980 Feb 19	A. Mrkos	Klet	
2748	Patrick Gene	1981 JF2	1981 May 5	C. Shoemaker	Palomar	123
2749		1937 TD	1937 Oct 11	K. Reinmuth	Heidelberg	
2750	Loviisa	1940 YK	1940 Dec 30	Y. Vaisala	Turku	
2751	Campbell	1962 RP	1962 Sep 7	Goethe Link Observatory	Brooklyn	103
2752		1965 SP	1965 Sep 20	Purple Mountain Observatory	Nanking	
2753	Duncan	1966 DH	1966 Feb 18	Goethe Link Observatory	Brooklyn	103
2754	Efimov	1966 PD	1966 Aug 13	T. Smirnova	Nauchnyj	
2755	Avicenna	1973 SJ4	1973 Sep 26	L. Chernykh	Nauchnyj	
2756	Dzhangar	1974 SG1	1974 Sep 19	L. Chernykh	Nauchnyj	
2757	Crisser	1977 VN	1977 Nov 11	S. Barros	Cerro El Roble	
2758	Cordelia	1978 RF	1978 Sep 1	N. Chernykh	Nauchnyj	
2759	Idomeneus	1980 GC	1980 Apr 14	E. Bowell	Flagstaff (AM)	119
2760	Kacha	1980 TU6	1980 Oct 8	L. Zhuravleva	Nauchnyj	
2761	Eddington	1981 AE	1981 Jan 1	E. Bowell	Flagstaff (AM)	119
2762	Fowler	1981 AT	1981 Jan 14	E Bowell	Flagstaff (AM)	119
2763	Jeans	1982 OG	1982 Jul 24	E. Bowell	Flagstaff (AM)	119
2764	Moeller	1981 CN	1981 Feb 8	N. G. Thomas	Flagstaff (AM)	119
2765		1981 EY	1981 Mar 4	H. Debehogne	La Silla	124
2766		1982 FE1	1982 Mar 23	Z. Vavrova	Klet	
2767		1967 UM	1967 Oct 30	L. Kohoutek	Bergedorf	
2768	Gorky	1972 RX3	1972 Sep 6	L. Zhuravleva	Nauchnyj	
2769	Mendeleev	1976 GZ2	1976 Apr 1	N. Chernykh	Nauchnyj	
2770	Tsvet	1977 SM1	1977 Sep 19	N Chernykh	Nauchnyj	
2771	Polzunov	1978 SP7	1978 Sep 26	L. Zhuravleva	Nauchnyj	
2772	Dugan	1979 XE	1979 Dec 14	E. Bowell	Flagstaff (AM)	119
2773		1981 JZ2	1981 May 6	C. Shoemaker	Palomar	123
2774	Tenojoki	1942 TJ	1942 Oct 3	L. Oterma	Turku	
2775	Odishaw	1953 TX2	1953 Oct 14	Goethe Link Observatory	Brooklyn	103
2776	Baikal	1976 SZ7	1976 Sep 25	N. Chernykh	Nauchnyj	
2777	Shukshin	1979 SY11	1979 Sep 24	N. Chernykh	Nauchnyj	
2778		1979 XP	1979 Dec 14	Purple Mountain Observatory	Nanking	
2779	Mary	1981 CX	1981 Feb 6	N. G. Thomas	Flagstaff (AM)	119
2780	Monnig	1981 DO2	1981 Feb 28	S. J. Bus	Siding Spring	
2781		1982 QH	1982 Aug 19	Z. Vavrova	Klet	
2782		2605 P-L	1960 Sep 24	PLS	Palomar	107
2783	Chernyshevskij	1974 RA2	1974 Sep 14	N. Chernykh	Nauchnyj	
2784	Domeyko	1975 GA	1975 Apr 15	C. Torres	Cerro El Roble	
2785	Sedov	1978 QN2	1978 Aug 31	N. Chernykh	Nauchnyj	
2786	Grinevia	1978 RR5	1978 Sep 6	N. Chernykh	Nauchnyj	
2787	Tovarishch	1978 RC6	1978 Sep 13	N Chernykh	Nauchnyj	
2788		1981 EL	1981 Mar 1	H. Debehogne	La Silla	124
2789		1956 XA	1956 Dec 6	Purple Mountain Observatory	Nanking	
2790		1965 UU1	1965 Oct 19	Purple Mountain Observatory	Nanking	
2791	Paradise	1977 CA	1977 Feb 13	S. J. Bus	Palomar	
2792	Ponomarev	1977 EY1	1977 Mar 13	N Chernykh	Nauchnyj	
2793	Valdaj	1977 QV	1977 Aug 19	N. Chernykh	Nauchnyj	
2794	Kulik	1978 PS3	1978 Aug 8	N. Chernykh	Nauchnyj	
2795	Lepage	1979 YM	1979 Dec 16	H. Debehogne	La Silla	126
2796	Kron	1980 EC	1980 Mar 13	E. Bowell	Flagstaff (AM)	119
2797	Teucer	1981 LK	1981 Jun 4	E. Bowell	Flagstaff (AM)	119
2798		2009 P-L	1960 Sep 24	PLS	Palomar	107
2799	Justus	3071 P-L	1960 Sep 25	PLS	Palomar	107
2800		4585 P-L	1960 Sep 24	PLS	Palomar	107
2801		1935 SU1	1935 Sep 28	H. Van Gent	Johannesburg (LS)	
2802	Weisell	1939 BU	1939 Jan 19	Y. Vaisala	Turku	
2803	Vilho	1940 WG	1940 Nov 29	L. Oterma	Turku	
2804	Yrjo	1941 HF	1941 Apr 19	L. Oterma	Turku	
2805	Kalle	1941 UM	1941 Oct 15	L. Oterma	Turku	
2806		1953 GG	1953 Apr 7	K. Reinmuth	Heidelberg	
2807	Karl Marx	1969 TH6	1969 Oct 15	L. Chernykh	Nauchnyj	
2808		1976 HS	1976 Apr 23	Felix Aguilar Observatory	El Leoncito	
2809	Vernadskij	1978 QW2	1978 Aug 31	N. Chernykh	Nauchnyj	
2810	Lev Tolstoj	1978 RU5	1978 Sep 13	N. Chernykh	Nauchnyj	
2811		1980 JA	1980 May 10	A. Mrkos	Klet	
2812	Scaltriti	1981 FN	1981 Mar 30	E. Bowell	Flagstaff (AM)	119
2813	Zappalà	1981 WZ	1981 Nov 24	E. Bowell	Flagstaff (AM)	119
2814	Vieira	1982 FA3	1982 Mar 18	H. Debehogne	La Silla	124
2815	Soma	1982 RL	1982 Sep 15	E. Bowell	Flagstaff (AM)	119

No.	Name	pd	dd	d	dp	
2816	Pien	1982 SO	1982 Sep 22	E. Bowell	Flagstaff (AM)	119
2817	Perec	1982 UJ	1982 Oct 17	E. Bowell	Flagstaff (AM)	119
2818		2580 P-L	1960 Sep 24	PLS	Palomar	107
2819	Ensor	1933 UR	1933 Oct 20	E. Delporte	Uccle	
2820	Iisalmi	1942 RU	1942 Sep 8	Y. Vaisala	Turku	
2821		1978 SQ	1978 Sep 24	Z. Vavrova	Klet	
2822	Sacajawea	1980 EG	1980 Mar 14	E. Bowell	Flagstaff (AM)	119
2823	van der Laan	2010 P-L	1960 Sep 24	PLS	Palomar	107
2824	Franke	1934 CZ	1934 Feb 4	K. Reinmuth	Heidelberg	
2825		1938 SD1	1938 Sep 19	C. Jackson	Johannesburg (UO)	
2826	Ahti	1939 UJ	1939 Oct 18	Y. Vaisala	Turku	
2827	Vellamo	1942 CC	1942 Feb 11	L. Oterma	Turku	
2828	Iku-Turso	1942 DL	1942 Feb 18	L. Oterma	Turku	
2829		1948 PK	1948 Aug 9	E. L. Johnson	Johannesburg (UO)	
2830	Greenwich	1980 GA	1980 Apr 14	E. Bowell	Flagstaff (AM)	119
2831		1930 SZ	1930 Sep 17	H. Van Gent	Johannesburg (LS)	
2832	Lada	1975 EC1	1975 Mar 6	N. Chernykh	Nauchnyj	
2833	Radishchev	1978 PC4	1978 Aug 9	L. Chernykh and N. Chernykh	Nauchnyj	
2834	Christy Carol	1980 TB4	1980 Oct 9	C. Shoemaker and S. J. Bus	Palomar	
2835	Ryoma	1982 WF	1982 Nov 20	T. Seki	Geisei	
2836	Sobolev	1978 YQ	1978 Dec 22	N. Chernykh	Nauchnyj	
2837	Griboedov	1971 TJ2	1971 Oct 13	L. Chernykh	Nauchnyj	
2838		1971 UM1	1971 Oct 26	L. Kohoutek	Bergedorf	
2839	Annette	1929 TP	1929 Oct 5	C W. Tombaugh	Flagstaff (LO)	
2840	Kallavesi	1941 UP	1941 Oct 15	L. Oterma	Turku	
2841	Puijo	1943 DM	1943 Feb 26	L Oterma	Turku	
2842	Unsöld	1950 OD	1950 Jul 25	Goethe Link Observatory	Brooklyn	103
2843		1975 XQ	1975 Dec 7	P. Wild	Zimmerwald	
2844	Hess	1981 JP	1981 May 3	E. Bowell	Flagstaff (AM)	119
2845	Franklinken	1981 OF	1981 Jul 26	E. Bowell	Flagstaff (AM)	119
2846	Ylppo	1942 CJ	1942 Feb 12	L Oterma	Turku	
2847		1959 CC1	1959 Feb 1	Lowell Observatory	Flagstaff (LO)	
2848	ASP	1959 VF	1959 Nov 8	Goethe Link Observatory	Brooklyn	103
2849	Shklovskij	1976 GN3	1976 Apr 1	N. Chernykh	Nauchnyj	
2850		1978 TM7	1978 Oct 2	L. Zhuravleva	Nauchnyj	
2851		1978 UQ2	1978 Oct 30	Purple Mountain Observatory	Nanking	
2852		1981 QU2	1981 Aug 23	H. Debehogne	La Silla	
2853	Harvill	1963 RG	1963 Sep 14	Goethe Link Observatory	Brooklyn	103
2854		1964 JE	1964 May 6	D. McLeish	Cordoba	
2855		1931 TB2	1931 Oct 10	K. Reinmuth	Heidelberg	
2856		1933 GB	1933 Apr 14	K. Reinmuth	Heidelberg	
2857		1942 DA	1942 Feb 17	L. Oterma	Turku	
2858	Carlosporter	1975 XB	1975 Dec 1	H. Wroblewski	Cerro El Roble	
2859	Paganini	1978 RW1	1978 Sep 5	N. Chernykh	Nauchnyj	
2860	Pasacentennium	1978 TA	1978 Oct 8	E. F. Helin	Palomar	
2861	Lambrecht	1981 VL2	1981 Nov 3	F. Borngen and K. Kirsch	Tautenburg	
2862	Vavilov	1977 JP	1977 May 15	N. Chernykh	Nauchnyj	
2863	Ben Mayer	1981 QG2	1981 Aug 30	E. Bowell	Flagstaff (AM)	119
2864	Soderblom	1983 AZ	1983 Jan 12	B. A. Skiff	Flagstaff (AM)	119
2865		1935 OK	1935 Jul 31	C. Jackson	Johannesburg (UO)	
2866		1961 TA	1961 Oct 7	S. Arend	Uccle	
2867	Steins	1969 VC	1969 Nov 4	N. Chernykh	Nauchnyj	
2868		1972 UA	1972 Oct 30	P. Wild	Zimmerwald	
2869	Nepryadva	1980 RM2	1980 Sep 7	N. Chernykh	Nauchnyj	
2870	Haupt	1981 LD	1981 Jun 4	E. Bowell	Flagstaff (AM)	119
2871	Schober	1981 QC2	1981 Aug 30	E. Bowell	Flagstaff (AM)	119
2872	Gentelec	1981 RU	1981 Sep 5	Oak Ridge Observatory	Oak Ridge	113
2873	Binzel	1982 FR	1982 Mar 28	E. Bowell	Flagstaff (AM)	119
2874	Jim Young	1982 TH	1982 Oct 13	E. Bowell	Flagstaff (AM)	119
2875	Lagerkvist	1983 CL	1983 Feb 11	E. Bowell	Flagstaff (AM)	119
2876	Aeschylus	6558 P-L	1960 Sep 24	PLS	Palomar	107
2877	Likhachev	1969 TR2	1969 Oct 8	L. Chernykh	Nauchnyj	
2878	Panacea	1980 RX	1980 Sep 7	E. Bowell	Flagstaff (AM)	119
2879	Shimizu	1932 CB1	1932 Feb 14	K. Reinmuth	Heidelberg	
2880	Nihondaira	1983 CA	1983 Feb 8	T. Seki	Geisei	
2881		1983 AA1	1983 Jan 12	B. A. Skiff	Flagstaff (AM)	119
2882	Tedesco	1981 OG	1981 Jul 26	E. Bowell	Flagstaff (AM)	119
2883	Barabashov	1978 RG6	1978 Sep 13	N Chernykh	Nauchnyj	
2884	Reddish	1981 ES22	1981 Mar 2	S. J. Bus	Siding Spring	
2885		1939 TC	1939 Oct 7	Y. Vaisala	Turku	
2886		1965 YG	1965 Dec 20	Purple Mountain Observatory	Nanking	
2887	Krinov	1977 QD5	1977 Aug 22	N. Chernykh	Nauchnyj	
2888	Hodgson	1982 TO	1982 Oct 13	E Bowell	Flagstaff (AM)	119
2889		1981 WT1	1981 Nov 17	A. Mrkos	Klet	
2890	Vilyujsk	1978 SY7	1978 Sep 26	L. Zhuravleva	Nauchnyj	
2891	McGetchin	1980 MD	1980 Jun 18	C. Shoemaker	Palomar	123
2892	Filipenko	1983 AX2	1983 Jan 13	L. G. Karachkina	Nauchnyj	
2893	Peiroos	1975 QD	1975 Aug 30	Felix Aguilar Observatory	El Leoncito	
2894	Kakhovka	1978 SH5	1978 Sep 27	L. Chernykh	Nauchnyj	
2895	Memnon	1981 AE1	1981 Jan 10	N. G. Thomas	Flagstaff (AM)	119
2896		1931 RN	1931 Sep 15	K. Reinmuth	Heidelberg	
2897	Ole Rømer	1932 CK	1932 Feb 5	K. Reinmuth	Heidelberg	
2898		1938 DN	1938 Feb 20	Y. Vaisala	Turku	
2899		1964 TR2	1964 Oct 8	Purple Mountain Observatory	Nanking	
2900	Luboš Perek	1972 AR	1972 Jan 14	L. Kohoutek	Bergedorf	

No.	Name	pd	dd	d	dp	
2901		1973 DP	1973 Feb 27	L. Kohoutek	Bergedorf	
2902	Westerlund	1980 FN3	1980 Mar 16	C.-I. Lagerkvist	La Silla	
2903		1981 UV9	1981 Oct 23	Purple Mountain Observatory	Nanking	
2904	Millman	1981 YB	1981 Dec 20	E. Bowell	Flagstaff (AM)	119
2905	Plaskett	1982 BZ2	1982 Jan 24	E. Bowell	Flagstaff (AM)	119
2906	Caltech	1983 AE2	1983 Jan 13	C. Shoemaker	Palomar	
2907	Nekrasov	1975 TT2	1975 Oct 3	L. Chernykh	Nauchnyj	
2908	Shimoyama	1981 WA	1981 Nov 18	T. Furuta	Tokai	
2909	Hoshi-No-Ie	1983 JA	1983 May 9	S. Sei	Chirorin	
2910	Yoshkar-Ola	1980 TK13	1980 Oct 11	N. Chernykh	Nauchnyj	
2911		1938 GJ	1938 Apr 8	H. Alikoski	Turku	
2912		1942 DM	1942 Feb 18	L. Oterma	Turku	
2913	Horta	1931 TK	1931 Oct 12	E. Delporte	Uccle	
2914		1965 SB	1965 Sep 19	P. Wild	Zimmerwald	
2915	Moskvina	1977 QY2	1977 Aug 22	N. Chernykh	Nauchnyj	
2916	Voronveliya	1978 PW2	1978 Aug 8	N. Chernykh	Nauchnyj	
2917	Sawyer Hogg	1980 RR	1980 Sep 2	E. Bowell	Flagstaff (AM)	119
2918	Salazar	1980 TU4	1980 Oct 9	C. Shoemaker	Palomar	
2919	Dali	1981 EX18	1981 Mar 2	S. J. Bus	Siding Spring	
2920	Automedon	1981 JR	1981 May 3	E. Bowell	Flagstaff (AM)	119
2921	Sophocles	6525 P-L	1960 Sep 24	PLS	Palomar	107
2922	Dikan'ka	1976 GY1	1976 Apr 1	N. Chernykh	Nauchnyj	
2923	Schuyler	1977 DA	1977 Feb 22	Harvard College	Agassiz Station	113
2924	Mitake-mura	1977 DJ2	1977 Feb 18	H. Kosai and K. Hurukawa	Kiso Station	
2925	Beatty	1978 VC5	1978 Nov 7	E. F. Helin and S. J. Bus	Palomar	
2926	Caldeira	1980 KG	1980 May 22	H. Debehogne	La Silla	
2927	Alamosa	1981 TM	1981 Oct 5	N. G. Thomas	Flagstaff (AM)	119
2928	Epstein	1976 GN8	1976 Apr 5	Felix Aguilar Observatory	El Leoncito	
2929	Harris	1982 BK1	1982 Jan 24	E Bowell	Flagstaff (AM)	119
2930	Euripides	6554 P-L	1960 Sep 24	PLS	Palomar	107
2931	Mayakovsky	1969 UC	1969 Oct 16	L. Chernykh	Nauchnyj	
2932	Kempchinsky	1980 TK4	1980 Oct 9	C. Shoemaker	Palomar	
2933	Amber	1983 HN	1983 Apr 18	N. G. Thomas	Flagstaff (AM)	119
2934	Aristophanes	4006 P-L	1960 Sep 25	PLS	Palomar	107
2935	Naerum	1976 UU	1976 Oct 24	R. M. West	La Silla	
2936		1979 SF	1979 Sep 17	A. Mrkos	Klet	
2937	Gibbs	1980 LA	1980 Jun 14	E. Bowell	Flagstaff (AM)	119
2938	Hopi	1980 LB	1980 Jun 14	E. Bowell	Flagstaff (AM)	119
2939	Coconino	1982 DP	1982 Feb 21	E. Bowell	Flagstaff (AM)	119
2940	Bacon	3042 P-L	1960 Sep 24	PLS	Palomar	107
2941	Alden	1930 YV	1930 Dec 24	C. W. Tombaugh	Flagstaff (LO)	
2942		1932 BG	1932 Jan 29	K. Reinmuth	Heidelberg	
2943		1933 QU	1933 Aug 25	K. Reinmuth	Heidelberg	
2944		1935 QF	1935 Aug 31	K. Reinmuth	Heidelberg	
2945		1935 ST1	1935 Sep 28	H. Van Gent	Johannesburg (LS)	
2946		1941 UV	1941 Oct 15	L. Oterma	Turku	
2947		1955 QP1	1955 Aug 22	I. Groeneveld	Heidelberg	
2948	Amosov	1969 TD2	1969 Oct 8	L. Chernykh	Nauchnyj	
2949	Kaverznev	1970 PR	1970 Aug 9	Crimean Astrophysical Obs.	Nauchnyj	
2950		1974 VQ2	1974 Nov 9	P. Wild	Zimmerwald	
2951		1977 RB8	1977 Sep 13	N. Chernykh	Nauchnyj	
2952	Lilliputia	1979 SF2	1979 Sep 22	N. Chernykh	Nauchnyj	
2953	Vysheslavia	1979 SV11	1979 Sep 24	N. Chernykh	Nauchnyj	
2954	Delsemme	1982 BT1	1982 Jan 30	E. Bowell	Flagstaff (AM)	119
2955	Newburn	1982 BX1	1982 Jan 30	E. Bowell	Flagstaff (AM)	119
2956	Yeomans	1982 HN1	1982 Apr 28	E. Bowell	Flagstaff (AM)	119
2957		1934 CB1	1934 Feb 5	K. Reinmuth	Heidelberg	
2958		1981 DG	1981 Feb 28	H. Debehogne	La Silla	124
2959	Scholl	1983 RE2	1983 Sep 4	E. Bowell	Flagstaff (AM)	119
2960	Ohtaki	1977 DK3	1977 Feb 18	H. Kosai and K. Hurukawa	Kiso Station	
2961	Katsurahama	1982 XA	1982 Dec 7	T. Seki	Geisei	
2962		1940 YF	1940 Dec 28	Y. Vaisala	Turku	
2963		1964 VM1	1964 Nov 9	Purple Mountain Observatory	Nanking	
2964		1974 OA1	1974 Jul 16	Felix Aguilar Observatory	El Leoncito	
2965	Surikov	1975 BX	1975 Jan 18	L. Chernykh	Nauchnyj	
2966	Korsunia	1977 EB2	1977 Mar 13	N. Chernykh	Nauchnyj	
2967	Vladisvyat	1977 SS1	1977 Sep 19	N. Chernykh	Nauchnyj	
2968	Iliya	1978 QJ	1978 Aug 31	N. Chernykh	Nauchnyj	
2969	Mikula	1978 RU1	1978 Sep 5	N. Chernykh	Nauchnyj	
2970		1978 UC	1978 Oct 27	P. Wild	Zimmerwald	
2971		1980 YL	1980 Dec 30	A. Mrkos	Klet	
2972		1939 TB	1939 Oct 7	Y. Vaisala	Turku	
2973	Paola	1951 AJ	1951 Jan 10	S. Arend	Uccle	
2974		1955 QK	1955 Aug 23	Goethe Link Observatory	Brooklyn	103
2975		1970 AF1	1970 Jan 8	H. Potter and A. Lokalov	Cerro El Roble	
2976	Lautaro	1974 HR	1974 Apr 22	C. Torres	Cerro El Roble	
2977	Chivilikhin	1974 SP	1974 Sep 19	L. Chernykh	Nauchnyj	
2978		1978 SR	1978 Sep 26	Harvard College	Agassiz Station	113
2979	Murmansk	1978 TB7	1978 Oct 2	L Zhuravleva	Nauchnyj	
2980		1981 EU17	1981 Mar 2	S. J. Bus	Siding Spring	
2981	Chagall	1981 EE20	1981 Mar 2	S. J. Bus	Siding Spring	
2982	Muriel	1981 JA3	1981 May 6	C. Shoemaker	Palomar	
2983	Poltava	1981 RW2	1981 Sep 2	N. Chernykh	Nauchnyj	
2984	Chaucer	1981 YD	1981 Dec 30	E. Bowell	Flagstaff (AM)	119
2985	Shakespeare	1983 TV1	1983 Oct 12	E. Bowell	Flagstaff (AM)	119

No.	Name	pd	dd	d	dp	
2986	Mrinalini	2525 P-L	1960 Sep 24	PLS	Palomar	107
2987	Sarabhai	4583 P-L	1960 Sep 24	PLS	Palomar	107
2988		1943 EM	1943 Mar 1	L. Oterma	Turku	
2989		1976 UF1	1976 Oct 22	P. Wild	Zimmerwald	
2990	Trimberger	1981 EN27	1981 Mar 2	S. J. Bus	Siding Spring	
2991		1982 HV	1982 Apr 21	M. Watt	Flagstaff (AM)	119
2992	Vondel	2540 P-L	1960 Sep 24	PLS	Palomar	107
2993		1970 PA	1970 Aug 4	- - -	Perth	
2994		1975 PA	1975 Aug 14	- - -	Perth	
2995	Taratuta	1978 QK	1978 Aug 31	N. Chernykh	Nauchnyj	
2996	Bowman	1954 RJ	1954 Sep 5	Goethe Link Observatory	Brooklyn	103
2997		1974 MJ	1974 Jun 17	Felix Aguilar Observatory	El Leoncito	
2998	Berendeya	1975 TR3	1975 Oct 3	L. Chernykh	Nauchnyj	
2999	Dante	1981 CY	1981 Feb 6	N. G. Thomas	Flagstaff (AM)	119
3000	Leonardo	1981 EG19	1981 Mar 2	S J. Bus	Siding Spring	
3001	Michelangelo	1982 BC1	1982 Jan 24	E. Bowell	Flagstaff (AM)	119
3002		1982 FB3	1982 Mar 20	H. Debehogne	La Silla	
3003		1983 YH	1983 Dec 28	A. Mrkos	Klet	
3004		1976 DD	1976 Feb 27	R. M. West	La Silla	
3005	Pervictoralex	1979 QK2	1979 Aug 22	C.-I. Lagerkvist	La Silla	
3006	Livadia	1979 SF11	1979 Sep 24	N. Chernykh	Nauchnyj	
3007	Reaves	1979 UC	1979 Oct 17	E. Bowell	Flagstaff (AM)	119
3008	Nojiri	1938 WA	1938 Nov 17	K. Reinmuth	Heidelberg	
3009	Coventry	1973 SM2	1973 Sep 22	N. Chernykh	Nauchnyj	
3010	Ushakov	1978 SB5	1978 Sep 27	L. Chernykh	Nauchnyj	
3011		1978 WM14	1978 Nov 26	Purple Mountain Observatory	Nanking	
3012	Minsk	1979 QU9	1979 Aug 27	N. Chernykh	Nauchnyj	
3013	Dobrovoleva	1979 SD7	1979 Sep 23	N. Chernykh	Nauchnyj	
3014		1979 TM	1979 Oct 11	Purple Mountain Observatory	Nanking	
3015	Candy	1980 VN	1980 Nov 9	E. Bowell	Flagstaff (AM)	119
3016		1981 EK	1981 Mar 1	H. Debehogne	La Silla	124
3017		1981 UL	1981 Oct 25	A. Mrkos	Klet	
3018	Godiva	1982 KM	1982 May 21	E. Bowell	Flagstaff (AM)	119
3019		1940 AC	1940 Jan 7	G. Kulin	Budapest	
3020		1949 PR	1949 Aug 2	K. Reinmuth	Heidelberg	
3021		1967 CB	1967 Feb 6	P. Wild	Zimmerwald	
3022		1980 SH	1980 Sep 16	Z. Vavrova	Klet	
3023	Heard	1981 JS	1981 May 5	E. Bowell	Flagstaff (AM)	119
3024		1981 UW9	1981 Oct 23	Purple Mountain Observatory	Nanking	
3025	Higson	1982 QR	1982 Aug 20	C. Shoemaker and E. Shoemaker	Palomar	
3026		1977 TA1	1977 Oct 12	P. Wild	Zimmerwald	
3027	Shavarsh	1978 PQ2	1978 Aug 8	N. Chernykh	Nauchnyj	
3028		1978 TA2	1978 Oct 9	Purple Mountain Observatory	Nanking	
3029	Sanders	1981 EA8	1981 Mar 1	S. J. Bus	Siding Spring	
3030	Vehrenberg	1981 EH16	1981 Mar 1	S. J. Bus	Siding Spring	
3031	Houston	1984 CX	1984 Feb 8	E. Bowell	Flagstaff (AM)	119
3032	Evans	1984 CA1	1984 Feb 8	E. Bowell	Flagstaff (AM)	119
3033	Holbaek	1984 EJ	1984 Mar 5	K. Augustesen	Brorfelde	127
3034	Climenhaga	A917 SE	1917 Sep 24	M. Wolf	Heidelberg	
3035		A924 EJ	1924 Mar 7	K. Reinmuth	Heidelberg	
3036	Krat	1937 TO	1937 Oct 11	G Neujmin	Simeis	
3037		1944 BA	1944 Jan 17	Y. Vaisala	Turku	
3038	Bernes	1978 QB3	1978 Aug 31	N. Chernykh	Nauchnyj	
3039	Yangel	1978 SP2	1978 Sep 26	L. Zhuravleva	Nauchnyj	
3040	Kozai	1979 BA	1979 Jan 23	W. Liller	Cerro Tololo	
3041	Webb	1980 GD	1980 Apr 15	E Bowell	Flagstaff (AM)	119
3042	Zelinsky	1981 EF10	1981 Mar 1	S J. Bus	Siding Spring	
3043	San Diego	1982 SA	1982 Sep 20	E. F. Helin	Palomar	
3044		1983 RE3	1983 Sep 2	N. V. Metlova	Crimea	128
3045	Alois	1984 AW	1984 Jan 8	J. Wagner	Flagstaff (AM)	119
3046	Molière	4120 P-L	1960 Sep 24	PLS	Palomar	107
3047	Goethe	6091 P-L	1960 Sep 24	PLS	Palomar	107
3048		1964 TH1	1964 Oct 8	Purple Mountain Observatory	Nanking	
3049	Kuzbass	1968 FH	1968 Mar 28	T Smirnova	Nauchnyj	
3050	Carrera	1972 NW	1972 Jul 13	C. Torres	Cerro El Roble	
3051		1974 YP	1974 Dec 19	Purple Mountain Observatory	Nanking	
3052	Herzen	1976 YJ3	1976 Dec 16	L. Chernykh	Nauchnyj	
3053	Dresden	1977 QS	1977 Aug 18	N. Chernykh	Nauchnyj	
3054	Strugatskia	1977 RE7	1977 Sep 11	N Chernykh	Nauchnyj	
3055	Annapavlova	1978 TR3	1978 Oct 4	T. Smirnova	Nauchnyj	
3056	INAG	1978 VD1	1978 Nov 1	K Tomita	Caussols	
3057	Malaren	1981 EG	1981 Mar 9	E. Bowell	Flagstaff (AM)	119
3058	Delmary	1981 EO17	1981 Mar 1	S. J. Bus	Siding Spring	
3059	Pryor	1981 EF23	1981 Mar 3	S. J Bus	Siding Spring	
3060		1982 RD1	1982 Sep 12	P. Wild	Zimmerwald	
3061	Cook	1982 UB1	1982 Oct 21	E Bowell	Flagstaff (AM)	119
3062	Wren	1982 XC	1982 Dec 14	E Bowell	Flagstaff (AM)	119
3063	Makhaon	1983 PV	1983 Aug 4	L. G. Karachkina	Nauchnyj	
3064	Zimmer	1984 BB1	1984 Jan 28	E. Bowell	Flagstaff (AM)	119
3065	Sarahill	1984 CV	1984 Feb 8	E. Bowell	Flagstaff (AM)	119
3066	McFadden	1984 EO	1984 Mar 1	E Bowell	Flagstaff (AM)	119
3067	Akhmatova	1982 TE2	1982 Oct 14	L. G. Karachkina	Nauchnyj	129
3068	Khanina	1982 YJ1	1982 Dec 23	L. G Karachkina	Nauchnyj	

No.	Name	pd	dd	d	dp	
3069		1982 UG2	1982 Oct 16	Z. Vavrova	Klet	
3070		1949 GK	1949 Apr 4	Goethe Link Observatory	Brooklyn	103
3071	Nesterov	1973 FT1	1973 Mar 28	T. Smirnova	Nauchnyj	
3072	Vilnius	1978 RS1	1978 Sep 5	N. Chernykh	Nauchnyj	
3073	Kursk	1979 SW11	1979 Sep 24	N. Chernykh	Nauchnyj	
3074	Popov	1979 YE9	1979 Dec 24	L. Zhuravleva	Nauchnyj	
3075	Bornmann	1981 EY15	1981 Mar 1	S. J. Bus	Siding Spring	
3076		1982 RB1	1982 Sep 13	Oak Ridge Observatory	Oak Ridge	113
3077	Henderson	1982 SK	1982 Sep 22	E. Bowell	Flagstaff (AM)	119
3078	Horrocks	1984 FG	1984 Mar 31	E. Bowell	Flagstaff (AM)	119
3079	Schiller	2578 P-L	1960 Sep 24	PLS	Palomar	107
3080	Moisseiev	1935 TE	1935 Oct 3	P. Shajn	Simeis	
3081		1971 UP	1971 Oct 26	L. Kohoutek	Bergedorf	
3082	Dzhalil	1972 KE	1972 May 17	T. Smirnova	Nauchnyj	
3083		1974 MH	1974 Jun 17	Felix Aguilar Observatory	El Leoncito	
3084	Kondratyuk	1977 QB1	1977 Aug 19	N. Chernykh	Nauchnyj	
3085		1980 DA	1980 Feb 18	Harvard College	Agassiz Station	113
3086	Kalbaugh	1980 XE	1980 Dec 4	E. Bowell	Flagstaff (AM)	119
3087	Beatrice Tinsley	1981 QJ1	1981 Aug 30	A. Gilmore and P. Kilmartin	Mount John	
3088		1981 UX9	1981 Oct 24	Purple Mountain Observatory	Nanking	
3089		1981 XK2	1981 Dec 3	Purple Mountain Observatory	Nanking	
3090	Tjossem	1982 AN	1982 Jan 4	J. Gibson	Palomar	
3091	van den Heuvel	6081 P-L	1960 Sep 24	PLS	Palomar	107
3092	Herodotus	6550 P-L	1960 Sep 24	PLS	Palomar	107
3093	Bergholz	1971 MG	1971 Jun 28	T Smirnova	Nauchnyj	
3094	Chukokkala	1979 FE2	1979 Mar 23	N Chernykh	Nauchnyj	
3095	Omarkhayyam	1980 RT2	1980 Sep 8	L. Zhuravleva	Nauchnyj	
3096		1981 QC1	1981 Aug 28	Z. Vavrova	Klet	
3097	Tacitus	2011 P-L	1960 Sep 24	PLS	Palomar	107
3098	van Sprang	4579 P-L	1960 Sep 24	PLS	Palomar	107
3099		1940 GF	1940 Apr 3	Y. Vaisala	Turku	
3100	Zimmerman	1977 EQ1	1977 Mar 13	N. Chernykh	Nauchnyj	
3101	Goldberger	1978 GB	1978 Apr 11	E. F. Helin and G. Grueff	Palomar	130
3102		1981 QA	1981 Aug 21	L. Brozek	Klet	
3103		1982 BB	1982 Jan 20	M. Lovas	Piszkesteto	
3104	Dürer	1982 BB1	1982 Jan 24	E. Bowell	Flagstaff (AM)	119
3105		A907 FB	1907 Aug 8	A. Kopff	Heidelberg	
3106	Morabito	1981 EE	1981 Mar 9	E. Bowell	Flagstaff (AM)	119
3107	Weaver	1981 JG2	1981 May 5	C. Shoemaker	Palomar	
3108	Lyubov	1972 QM	1972 Aug 18	L. Zhuravleva	Nauchnyj	
3109		1974 DC	1974 Feb 19	L. Kohoutek	Bergedorf	
3110		1975 SC	1975 Sep 28	H. L. Giclas	Flagstaff (AM)	119
3111	Misuzu	1977 DX8	1977 Feb 19	H. Kosai and K. Hurukawa	Kiso Station	
3112	Velimir	1977 QC5	1977 Aug 22	N. Chernykh	Nauchnyj	
3113	Chizhevskij	1978 RO	1978 Sep 1	N. Chernykh	Nauchnyj	
3114	Ercilla	1980 FB12	1980 Mar 19	C. Torres	Cerro El Roble	
3115	Baily	1981 PL	1981 Aug 3	E. Bowell	Flagstaff (AM)	119
3116	Goodricke	1983 CF	1983 Feb 11	E. Bowell	Flagstaff (AM)	119
3117	Niepce	1983 CM1	1983 Feb 11	N. G. Thomas	Flagstaff (AM)	119
3118		1974 OD	1974 Jul 19	Felix Aguilar Observatory	El Leoncito	
3119	Dobronravin	1972 YX	1972 Dec 30	T. Smirnova	Nauchnyj	
3120	Dangrania	1979 RZ	1979 Sep 14	N. Chernykh	Nauchnyj	
3121		1981 EV	1981 Mar 2	H. Debehogne	La Silla	124
3122		1981 ET3	1981 Mar 2	S. J. Bus	Siding Spring	
3123	Dunham	1981 QF2	1981 Aug 30	E. Bowell	Flagstaff (AM)	119
3124	Kansas	1981 VB	1981 Nov 3	D. J. Tholen	Kitt Peak	131
3125	Hay	1982 BJ1	1982 Jan 24	E. Bowell	Flagstaff (AM)	119
3126	Davydov	1969 TP1	1969 Oct 8	L. Chernykh	Nauchnyj	
3127	Bagration	1973 ST4	1973 Sep 27	L. Chernykh	Nauchnyj	
3128	Obruchev	1979 FJ2	1979 Mar 23	N. Chernykh	Nauchnyj	
3129	Bonestell	1979 MK2	1979 Jun 25	E. F. Helin and S. J. Bus	Siding Spring	
3130		1981 YO	1981 Dec 20	A. Mrkos	Klet	
3131	Mason-Dixon	1982 BM1	1982 Jan 24	E. Bowell	Flagstaff (AM)	119
3132	Landgraf	1940 WL	1940 Nov 29	L. Oterma	Turku	
3133	Sendai	A907 TC	1907 Oct 4	A. Kopff	Heidelberg	
3134	Kostinsky	A921 VA	1921 Nov 5	S. Belyavskij	Simeis	
3135	Lauer	1981 EC9	1981 Mar 1	S. J. Bus	Siding Spring	
3136		1981 WD4	1981 Nov 18	Purple Mountain Observatory	Nanking	
3137		1982 SM1	1982 Sep 16	A. Mrkos	Klet	
3138		1980 KL	1980 May 22	H. Debehogne	La Silla	
3139		1980 VL1	1980 Nov 11	Purple Mountain Observatory	Nanking	
3140	Stellafane	1983 AO	1983 Jan 9	B. A. Skiff	Flagstaff (AM)	119
3141		1984 RH	1984 Sep 2	A. Mrkos	Klet	
3142	Kilopi	1937 AC	1937 Jan 9	A. Patry	Nice	
3143		1980 UA	1980 Oct 31	Harvard College	Agassiz Station	
3144		1931 TY1	1931 Oct 10	K. Reinmuth	Heidelberg	
3145		1955 RY	1955 Sep 14	Goethe Link Observatory	Brooklyn	103
3146	Dato	1972 KG	1972 May 17	T. Smirnova	Nauchnyj	
3147	Samantha	1976 YU3	1976 Dec 16	L. Chernykh	Nauchnyj	
3148	Grechko	1979 SA12	1979 Sep 24	N. Chernykh	Nauchnyj	
3149	Okudzhava	1981 SH	1981 Sep 22	Z. Vavrova	Klet	
3150	Tosa	1983 CB	1983 Feb 11	T Seki	Geisei	

No.	Name	pd	dd	d	dp	
3151	Talbot	1983 HF	1983 Apr 18	N G. Thomas	Flagstaff (AM)	119
3152	Jones	1983 LF	1983 Jun 7	A. Gilmore and P. Kilmartin	Mount John	
3153		1984 SH3	1984 Sep 28	B. A. Skiff	Flagstaff (AM)	119
3154		1984 SO3	1984 Sep 28	B. A. Skiff	Flagstaff (AM)	119
3155		1984 SP3	1984 Sep 28	B. A. Skiff	Flagstaff (AM)	119
3156		1953 EE	1953 Mar 15	A. Schmitt	Uccle	
3157	Novikov	1973 SX3	1973 Sep 25	L. Zhuravleva	Nauchnyj	
3158	Anga	1976 SU2	1976 Sep 24	N. Chernykh	Nauchnyj	
3159	Prokof'ev	1976 US2	1976 Oct 26	T. Smirnova	Nauchnyj	
3160	Angerhofer	1980 LE	1980 Jun 14	E. Bowell	Flagstaff (AM)	119
3161	Beadell	1980 TB5	1980 Oct 9	C. Shoemaker	Palomar	
3162	Nostalgia	1990 YH	1980 Dec 16	E. Bowell	Flagstaff (AM)	119
3163		1981 QM	1981 Aug 28	C. Kowal	Palomar	
3164	Prast	6562 P-L	1960 Sep 24	PLS	Palomar	107
3165	Mikawa	1984 QE	1984 Aug 31	K. Suzuki and T. Urata	JCPM Oi Station	
3166		1940 FG	1940 Mar 30	Y. Vaisala	Turku	
3167		1955 RS	1955 Sep 13	Goethe Link Observatory	Brooklyn	103
3168		1980 XM	1980 Dec 1	A. Mrkos	Klet	
3169	Ostro	1981 LA	1981 Jun 4	E. Bowell	Flagstaff (AM)	119
3170	Dzhanibekov	1979 SS11	1979 Sep 24	N. Chernykh	Nauchnyj	
3171		1979 WO	1979 Nov 19	Purple Mountain Observatory	Nanking	
3172	Hirst	1981 WW	1981 Nov 24	E. Bowell	Flagstaff (AM)	119
3173	McNaught	1981 WY	1981 Nov 24	E. Bowell	Flagstaff (AM)	119
3174	Alcock	1984 UV	1984 Oct 26	E. Bowell	Flagstaff (AM)	119
3175	Netto	1979 YP	1979 Dec 16	H. Debehogne	La Silla	126
3176	Paolicchi	1980 VR1	1980 Nov 13	Z. Knezevic	Piszkesteto	
3177		1934 AK	1934 Jan 8	H. L Giclas	Flagstaff (LO)	
3178		1984 WA	1984 Nov 21	K. Suzuki and T. Urata	Toyota	
3179		1962 FA	1962 Mar 31	- - -	La Plata	
3180		1962 RO	1962 Sep 7	Goethe Link Observatory	Brooklyn	103
3181	Ahnert	1964 EC	1964 Mar 8	F. Borngen	Tautenburg	
3182	Shimanto	1984 WC	1984 Nov 27	T. Seki	Geisei	
3183		1949 PP	1949 Aug 2	K. Reinmuth	Heidelberg	
3184		1949 QC	1949 Aug 22	E. L Johnson	Johannesburg (UO)	
3185		1953 VY1	1953 Nov 11	Goethe Link Observatory	Brooklyn	103
3186	Manuilova	1973 SD3	1973 Sep 22	N. Chernykh	Nauchnyj	
3187		1977 TO3	1977 Oct 10	Purple Mountain Observatory	Nanking	
3188		1978 OM	1978 Jul 28	Perth Observatory	Perth	
3189	Penza	1978 RF'6	1978 Sep 13	N. Chernykh	Nauchnyj	
3190	Aposhanskij	1978 SR6	1978 Sep 26	L. Zhuravleva	Nauchnyj	
3191	Svanetia	1979 SX9	1979 Sep 22	N. Chernykh	Nauchnyj	
3192	A'Hearn	1982 BY1	1982 Jan 30	E. Bowell	Flagstaff (AM)	119
3193	Elliot	1982 DJ	1982 Feb 20	E. Bowell	Flagstaff (AM)	119
3194	Dorsey	1982 KD1	1982 May 27	C. Shoemaker and E. Shoemaker	Palomar	
3195	Fedchenko	1978 PT2	1978 Aug 8	N. Chernykh	Nauchnyj	
3196	Maklaj	1978 RY	1978 Sep 1	N. Chernykh	Nauchnyj	
3197	Weissman	1981 AD	1981 Jan 1	E. Bowell	Flagstaff (AM)	119
3198	Wallonia	1981 YH1	1981 Dec 30	F. Dossin	Haute Provence	
3199	Nefertiti	1982 RA	1982 Sep 13	C. Shoemaker and E. Shoemaker	Palomar	
3200	Phaethon	1983 TB	1983 Oct 11	IRAS		
3201	Sijthoff	6560 P-L	1960 Sep 24	PLS	Palomar	107
3202		A908 AA	1908 Jan 3	M Wolf	Heidelberg	
3203		1938 SL	1938 Sep 18	C Hoffmeister	Sonneberg	
3204	Lindgren	1978 RH	1978 Sep 1	N. Chernykh	Nauchnyj	
3205	Boksenberg	1979 MO6	1979 Jun 25	E. F. Helin and S. J. Bus	Siding Spring	
3206		1980 VN1	1980 Nov 13	Purple Mountain Observatory	Nanking	
3207		1981 EY25	1981 Mar 2	S J. Bus	Siding Spring	
3208	Lunn	1981 JM	1981 May 3	E. Bowell	Flagstaff (AM)	119
3209	Buchwald	1982 BL1	1982 Jan 24	E. Bowell	Flagstaff (AM)	119
3210	Lupishko	1983 WH1	1983 Nov 29	E. Bowell	Flagstaff (AM)	119
3211		1931 CE	1931 Feb 10	G. Van Biesbroeck	Williams Bay	
3212		1938 DH2	1938 Feb 19	Y. Vaisala	Turku	
3213	Smolensk	1977 NQ	1977 Jul 14	N. Chernykh	Nauchnyj	
3214	Makarenko	1978 TZ6	1978 Oct 2	L. Zhuravleva	Nauchnyj	
3215	Lapko	1980 BQ	1980 Jan 23	L. G. Karachkina	Nauchnyj	
3216	Harrington	1980 RB	1980 Sep 4	E. Bowell	Flagstaff (AM)	119
3217	Seidelmann	1980 RK	1980 Sep 2	E. Bowell	Flagstaff (AM)	119
3218	Delphine	6611 P-L	1960 Sep 24	PLS	Palomar	107
3219	Komaki	1934 CX	1934 Feb 4	K. Reinmuth	Heidelberg	
3220	Murayama	1951 WF2	1951 Nov 22	M. Laugier	Nice	
3221		1981 XF2	1981 Dec 2	Purple Mountain Observatory	Nanking	
3222	Liller	1983 NJ	1983 Jul 10	E. Bowell	Flagstaff (AM)	119
3223		1942 RN	1942 Sep 7	Y. Vaisala	Turku	
3224	Irkutsk	1977 RL6	1977 Sep 11	N. Chernykh	Nauchnyj	
3225	Hoag	1982 QQ	1982 Aug 20	C. Shoemaker and E. Shoemaker	Palomar	
3226		6565 P-L	1960 Sep 24	PLS	Palomar	107
3227	Hasegawa	1928 DF	1928 Feb 24	K. Reinmuth	Heidelberg	
3228	Pire	1935 CL	1935 Feb 8	S Arend	Uccle	
3229		A916 PC	1916 Aug 9	H. Thiele	Bergedorf	
3230	Vampilov	1972 LE	1972 Jun 8	N. Chernykh	Nauchnyj	
3231	Mila	1972 RU2	1972 Sep 4	L. Zhuravleva	Nauchnyj	
3232	Brest	1974 SL	1974 Sep 19	L. Chernykh	Nauchnyj	
3233	Krišbarons	1977 RA6	1977 Sep 9	N. Chernykh	Nauchnyj	

No.	Name	pd	dd	d	dp	
3234	Hergiani	1978 QO2	1978 Aug 31	N. Chernykh	Nauchnyj	
3235		1981 EL1	1981 Mar 6	H. Debehogne	La Silla	124
3236	Strand	1982 BH1	1982 Jan 24	E. Bowell	Flagstaff (AM)	119
3237	Victorplatt	1984 SA5	1984 Sep 25	J. Platt	Palomar	
3238	Timresovia	1975 VB9	1975 Nov 8	N. Chernykh	Nauchnyj	
3239		1978 UJ2	1978 Oct 29	Purple Mountain Observatory	Nanking	
3240	Laocoon	1978 VG6	1978 Nov 7	S. J. Bus	Palomar	132
3241		1978 WH14	1978 Nov 28	Purple Mountain Observatory	Nanking	
3242	Bakhchisaraj	1979 SG9	1979 Sep 22	N. Chernykh	Nauchnyj	
3243		1980 DC	1980 Feb 19	Harvard College	Agassiz Station	113
3244		4008 P-L	1960 Sep 24	PLS	Palomar	107
3245	Jensch	1973 UL5	1973 Oct 27	F. Borngen and K. Kirsch	Tautenburg	
3246		1976 GQ3	1976 Apr 1	N. Chernykh	Nauchnyj	
3247	Di Martino	1981 YE	1981 Dec 30	E. Bowell	Flagstaff (AM)	119
3248	Farinella	1982 FK	1982 Mar 21	E. Bowell	Flagstaff (AM)	119
3249	Musashino	1977 DT4	1977 Feb 18	H. Kosai and K. Hurukawa	Kiso Station	
3250	Martebo	1979 EB	1979 Mar 6	C.-I. Lagerkvist	Mount Stromlo (US)	
3251		6536 P-L	1960 Sep 24	PLS	Palomar	107
3252		1981 EM4	1981 Mar 2	S. J. Bus	Siding Spring	
3253	Gradie	1982 HQ1	1982 Apr 28	E. Bowell	Flagstaff (AM)	119
3254	Bus	1982 UM	1982 Oct 17	E. Bowell	Flagstaff (AM)	119
3255	Tholen	1980 RA	1980 Sep 2	E. Bowell	Flagstaff (AM)	119
3256	Daguerre	1981 SJ1	1980 Sep 26	B. A. Skiff and N. G. Thomas	Flagstaff (AM)	119
3257		1982 GG	1982 Apr 15	A. Mrkos	Klet	
3258		1983 RJ	1983 Sep 8	P. Wild	Zimmerwald	
3259		1984 SZ4	1984 Sep 25	J. Platt	Palomar	
3260	Vizbor	1974 SO2	1974 Sep 20	L. Zhuravleva	Nauchnyj	
3261	Tvardovskij	1979 SF9	1979 Sep 22	N. Chernykh	Nauchnyj	
3262	Miune	1983 WB	1983 Nov 28	T. Seki	Geisei	
3263		1932 CN	1932 Feb 5	K. Reinmuth	Heidelberg	
3264		1934 AF	1934 Jan 7	K. Reinmuth	Heidelberg	
3265		1953 VN2	1953 Nov 9	K. Reinmuth	Heidelberg	
3266		1978 PA	1978 Aug 11	H.-E. Schuster	La Silla	
3267	Glo	1981 AA	1981 Jan 3	E. Bowell	Flagstaff (AM)	119
3268	De Sanctis	1981 DD	1981 Feb 26	H. Debehogne	La Silla	124
3269	Vibert-Douglas	1981 EX16	1981 Mar 6	S. J. Bus	Siding Spring	
3270	Dudley	1982 DA	1982 Feb 18	C. Shoemaker and S. J. Bus	Palomar	
3271		1982 RB	1982 Sep 14	H.-E. Schuster	La Silla	
3272		1938 DB1	1938 Feb 24	Y. Vaisala	Turku	
3273	Drukar	1975 TS2	1975 Oct 3	L. Chernykh	Nauchnyj	
3274		1981 QO2	1981 Aug 23	H. Debehogne	La Silla	
3275	Oberndorfer	1982 HE1	1982 Apr 25	E. Bowell	Flagstaff (AM)	119
3276		1982 RZ1	1982 Sep 15	A. Mrkos	Klet	
3277	Aaronson	1984 AF1	1984 Jan 8	E. Bowell	Flagstaff (AM)	119
3278		1984 BT	1984 Jan 27	A. Mrkos	Klet	
3279		9103 P-L	1960 Oct 17	PLS	Palomar	107
3280	Grétry	1933 SJ	1933 Sep 17	F. Rigaux	Uccle	
3281		1938 DZ	1938 Feb 24	Y Vaisala	Turku	
3282		1949 DA	1949 Feb 19	Goethe Link Observatory	Brooklyn	103
3283		1979 QA10	1979 Aug 27	N. Chernykh	Nauchnyj	
3284		1953 NB	1953 Jul 13	J. A. Bruwer	Johannesburg (UO)	
3285	Ruth Wolfe	1983 VW1	1983 Nov 5	C. Shoemaker and E. Shoemaker	Palomar	
3286	Anatoliya	1980 BV	1980 Jan 23	L. G. Karachkina	Nauchnyj	
3287		1981 DK1	1981 Feb 28	S. J. Bus	Siding Spring	
3288	Seleucus	1982 DV	1982 Feb 28	H.-E. Schuster	La Silla	
3289		1934 RP	1934 Sep 7	K. Reinmuth	Heidelberg	
3290	Azabu	1973 SZ1	1973 Sep 19	C. J. van Houten	Palomar	133
3291	Dunlap	1982 VX3	1982 Nov 14	H. Kosai and K. Hurukawa	Kiso Station	
3292	Sather	2631 P-L	1960 Sep 24	PLS	Palomar	107
3293	Rontaylor	4650 P-L	1960 Sep 24	PLS	Palomar	107
3294	Carlvesely	6563 P-L	1960 Sep 24	PLS	Palomar	107
3295	Murakami	1950 DH	1950 Feb 17	K. Reinmuth	Heidelberg	
3296		1975 SF	1975 Sep 30	Felix Aguilar Observatory	El Leoncito	
3297		1978 WN14	1978 Nov 26	Purple Mountain Observatory	Nanking	
3298		1979 OB15	1979 Jul 21	N. Chernykh	Nauchnyj	
3299	Hall	1980 TX5	1980 Oct 10	C. Shoemaker	Palomar	
3300		1928 NA	1928 Jul 10	H. E. Wood	Johannesburg (UO)	
3301		1978 CT	1978 Feb 6	Perth Observatory	Perth	
3302		1977 RS6	1977 Sep 11	N Chernykh	Nauchnyj	
3303		1967 UN	1967 Oct 30	L Kohoutek	Bergedorf	
3304	Pearce	1981 EQ21	1981 Mar 2	S. J. Bus	Siding Spring	
3305		1985 KB	1985 May 21	A. Gilmore and P. Kilmartin	Mount John	
3306	Byron	1979 SM11	1979 Sep 24	N. Chernykh	Nauchnyj	
3307		1981 DE1	1981 Feb 28	S. J. Bus	Siding Spring	
3308	Ferreri	1981 EP	1981 Mar 1	H. Debehogne	La Silla	124
3309	Brorfelde	1982 BH	1982 Jan 28	K. Jensen and K. Augustesen	Brorfelde	
3310	Patsy	1931 TS2	1931 Oct 9	C. W. Tombaugh	Flagstaff (LO)	
3311		1976 QM1	1976 Aug 26	N. Chernykh	Nauchnyj	
3312	Pedersen	1984 SN	1984 Sep 24	K. Augustesen	Brorfelde	127
3313		1980 DG	1980 Feb 19	A. Mrkos	Klet	
3314	Beals	1981 FH	1981 Mar 30	E. Bowell	Flagstaff (AM)	119
3315	Chant	1984 CZ	1984 Feb 8	E. Bowell	Flagstaff (AM)	119

No.	Name	pd	dd	d	dp	
3316	Herzberg	1984 CN1	1984 Feb 6	E. Bowell	Flagstaff (AM)	119
3317	Paris	1984 KF	1984 May 26	C Shoemaker and E. Shoemaker	Palomar	
3318	Blixen	1985 HB	1985 Apr 23	P. Jensen	Brorfelde	
3319	Kibi	1977 EJ5	1977 Mar 12	H. Kosai and K. Hurukawa	Kiso Station	
3320	Namba	1982 VZ4	1982 Nov 14	H. Kosai and K. Hurukawa	Kiso Station	
3321	Dasha	1975 TZ2	1975 Oct 3	L. Chernykh	Nauchnyj	
3322		1975 XY1	1975 Dec 1	T. Smirnova	Nauchnyj	
3323		1979 SY9	1979 Sep 22	N. Chernykh	Nauchnyj	
3324		1983 CW1	1983 Feb 4	A. Mrkos	Klet	
3325		1984 JZ	1984 May 3	B. A. Skiff	Flagstaff (AM)	119
3326		1985 FL	1985 Mar 20	A. Mrkos	Klet	
3327	Campins	1985 PW	1985 Aug 14	E. Bowell	Flagstaff (AM)	119
3328		1985 QD1	1985 Aug 21	T. Schildknecht	Zimmerwald	
3329		1985 RT1	1985 Sep 12	P. Wild	Zimmerwald	
3330		1985 RU1	1985 Sep 12	T. Schildknecht	Zimmerwald	
3331	Kvistaberg	1979 QS	1979 Aug 22	C.-I. Lagerkvist	La Silla	
3332	Raksha	1978 NT1	1978 Jul 4	L. Chernykh	Nauchnyj	
3333	Schaber	1980 TG5	1980 Oct 9	C. Shoemaker	Palomar	
3334		1981 YR	1981 Dec 20	A. Mrkos	Klet	
3335		1966 AA	1966 Jan 1	Purple Mountain Observatory	Nanking	
3336		1971 UX	1971 Oct 26	L. Kohoutek	Bergedorf	
3337		1971 UG1	1971 Oct 26	L. Kohoutek	Bergedorf	
3338	Richter	1973 UX5	1973 Oct 28	F. Borngen and K Kirsch	Tautenburg	
3339		1978 LB	1978 Jun 6	A. Mrkos	Klet	
3340		1979 TK	1979 Oct 12	Purple Mountain Observatory	Nanking	
3341	Hartmann	1980 OD	1980 Jul 17	E. Bowell	Flagstaff (AM)	119
3342		1982 BD3	1982 Jan 27	Oak Ridge Observatory	Oak Ridge	113
3343	Nedzel	1982 HS	1982 Apr 28	L. G. Taff	Socorro	
3344	Modena	1982 JA	1982 May 15	Osservatorio San Vittore	Bologna	
3345	Tarkovskij	1982 YC1	1982 Dec 23	L. G. Karachkina	Nauchnyj	
3346		1951 SD	1952 Sep 27	S. Arend	Uccle	
3347		1975 VN1	1975 Nov 2	T. Smirnova	Nauchnyj	
3348	Pokryshkin	1978 EA3	1978 Mar 6	N. Chernykh	Nauchnyj	
3349		1979 FH2	1979 Mar 23	N. Chernykh	Nauchnyj	
3350	Scobee	1980 PJ	1980 Aug 8	E Bowell	Flagstaff (AM)	119
3351	Smith	1980 RN1	1980 Sep 7	E. Bowell	Flagstaff (AM)	119
3352	McAuliffe	1981 CW	1981 Feb 6	N. G. Thomas	Flagstaff (AM)	119
3353	Jarvis	1981 YC	1981 Dec 20	E. Bowell	Flagstaff (AM)	119
3354	McNair	1984 CW	1984 Feb 8	E. Bowell	Flagstaff (AM)	119
3355	Onizuka	1984 CC1	1984 Feb 8	E. Bowell	Flagstaff (AM)	119
3356	Resnik	1984 EU	1984 Mar 6	E. Bowell	Flagstaff (AM)	119
3357		1984 FT	1984 Mar 21	A. Mrkos	Klet	
3358		1978 RX	1978 Sep 1	N Chernykh	Nauchnyj	
3359		1978 RA6	1978 Sep 13	N. Chernykh	Nauchnyj	
3360		1981 VA	1981 Nov 4	E. F. Helin and R. S. Dunbar	Palomar	
3361	Orpheus	1982 HR	1982 Apr 24	C. Torres	Cerro El Roble	
3362	Khufu	1984 QA	1984 Aug 30	R. S Dunbar and M. Barucci	Palomar	
3363		1960 EE	1960 Mar 6	Goethe Link Observatory	Brooklyn	103
3364		1984 GF	1984 Apr 5	A Mrkos	Klet	
3365		1985 CG2	1985 Feb 13	H. Debehogne	La Silla	
3366		1985 SD1	1985 Sep 22	T Schildknecht	Zimmerwald	
3367	Alex	1983 CA3	1983 Feb 15	N. G. Thomas	Flagstaff (AM)	119
3368	Duncombe	1985 QT	1985 Aug 22	E. Bowell	Flagstaff (AM)	119
3369	Freuchen	1985 UZ	1985 Oct 18	P. Jensen and K. Augustesen	Brorfelde	
3370	Kohsai	1934 CU	1934 Feb 4	K. Reinmuth	Heidelberg	
3371		1955 RZ	1955 Sep 14	Goethe Link Observatory	Brooklyn	103
3372		1976 SP4	1976 Sep 24	N. Chernykh	Nauchnyj	
3373		1978 QQ2	1978 Aug 31	N Chernykh	Nauchnyj	
3374		1980 KO	1980 May 22	H. Debehogne	La Silla	
3375	Amy	1981 JY1	1981 May 5	C. Shoemaker	Palomar	
3376	Armandhammer	1982 UJ8	1982 Oct 21	L. Zhuravleva	Nauchnyj	
3377		4122 P-L	1960 Sep 24	PLS	Palomar	107
3378		A922 WB	1922 Nov 25	G. Van Biesbroeck	Williams Bay	
3379	Oishi	1931 TJ1	1931 Oct 6	K. Reinmuth	Heidelberg	
3380		1940 EF	1940 Mar 15	G. Kulin	Budapest	
3381		1941 UG	1941 Oct 15	L. Oterma	Turku	
3382		1948 RD	1948 Sep 7	H. L. Giclas	Flagstaff (LO)	
3383	Koyama	1951 AB	1951 Jan 9	K. Reinmuth	Heidelberg	
3384	Daliya	1974 SB1	1974 Sep 19	L. Chernykh	Nauchnyj	
3385		1979 SK11	1979 Sep 24	N. Chernykh	Nauchnyj	
3386		1980 FA	1980 Mar 16	L. Brozek	Klet	
3387	Greenberg	1981 WE	1981 Nov 20	E. Bowell	Flagstaff (AM)	119
3388		1981 YR1	1981 Dec 21	Purple Mountain Observatory	Nanking	
3389		1984 DU	1984 Feb 25	H. Debehogne	La Silla	
3390		1984 ES1	1984 Mar 2	H. Debehogne	La Silla	
3391	Sinon	1977 DD3	1977 Feb 18	H. Kosai and K. Hurukawa	Kiso Station	
3392	Setouchi	1979 YB	1979 Dec 17	H. Kosai and G. Sasaki	Kiso Station	
3393	Štúr	1984 WY1	1984 Nov 28	M. Antal	Piszkesteto	
3394		1986 DB	1986 Feb 16	S. Inoda and T. Urata	Karasuyama	
3395		1985 UN	1985 Oct 20	A. Mrkos	Klet	
3396	Muazzez	A915 TE	1915 Oct 15	M. Wolf	Heidelberg	
3397		1964 XA	1964 Dec 8	R. Burnham and N. G. Thomas	Flagstaff (LO)	
3398		1978 PC	1978 Aug 10	H.-E. Schuster	LaSilla	

No.	Name	pd	dd	d	dp	
3399		1979 SZ9	1979 Sep 22	N. Chernykh	Nauchnyj	
3400		1981 GX	1981 Apr 2	A. Gilmore and P. Kilmartin	Mount John	
3401		1981 PA	1981 Aug 1	Harvard College	Agassiz Station	113
3402	Wisdom	1981 PB	1981 Aug 5	E. Bowell	Flagstaff (AM)	119
3403	Tammy	1981 SW	1981 Sep 25	L. G. Taff	Socorro	
3404		1934 CY	1934 Feb 4	K. Reinmuth	Heidelberg	
3405		1964 UQ	1964 Oct 30	Purple Mountain Observatory	Nanking	
3406		1969 DA	1969 Feb 21	B. Burnasheva	Nauchnyj	
3407		1973 DT	1973 Feb 28	L. Kohoutek	Bergedorf	
3408		1977 QG4	1977 Aug 18	N. Chernykh	Nauchnyj	
3409		1977 RE6	1977 Sep 9	N. Chernykh	Nauchnyj	
3410		1978 SZ7	1978 Sep 26	L. Zhuravleva	Nauchnyj	
3411		1980 LK	1980 Jun 2	H. Debehogne	La Silla	
3412	Kafka	1983 AU2	1983 Jan 10	R. Kirk and D. Rudy	Palomar	
3413	Andriana	1983 CB3	1983 Feb 15	N. G. Thomas	Flagstaff (AM)	119
3414	Champollion	1983 DJ	1983 Feb 19	E. Bowell	Flagstaff (AM)	119
3415	Danby	1928 SL	1928 Sep 22	K. Reinmuth	Heidelberg	
3416	Dorrit	1931 VP	1931 Nov 8	K. Reinmuth	Heidelberg	
3417	Tamblyn	1937 GG	1937 Apr 1	K. Reinmuth	Heidelberg	
3418		1973 QZ1	1973 Aug 31	T. Smirnova	Nauchnyj	
3419		1981 JZ	1981 May 8	L. Brozek	Klet	
3420	Standish	1984 EB	1984 Mar 1	E. Bowell	Flagstaff (AM)	119
3486	Fulchignoni	1984 CR	1984 Feb 5	E. Bowell	Flagstaff (AM)	119
3487		1978 UF	1978 Oct 28	H. L. Giclas	Flagstaff (AM)	119
3488	Brahic	1980 PM	1980 Aug 8	E. Bowell	Flagstaff (AM)	119
3489	Lottie	1983 AT2	1983 Jan 10	K. Herkenhoff	Palomar	135
3490		1984 SV	1984 Sep 20	A. Mrkos	Klet	
3491		1984 SM4	1984 Sep 30	P. Wild	Zimmerwald	
3492		1985 DQ	1985 Feb 16	M. Mahrova	Klet	
3493		1976 GR6	1976 Apr 3	N. Chernykh	Nauchnyj	
3494		1980 XW	1980 Dec 7	Purple Mountain Observatory	Nanking	
3495	Colchagua	1981 NU	1981 Jul 2	L. E. Gonzalez	Cerro El Roble	
3496	Arieso	1977 RC	1977 Sep 5	H.-E. Schuster	La Silla	
3497		1941 HJ	1941 Apr 19	L. Oterma	Turku	
3498		1981 EG14	1981 Mar 1	S. J. Bus	Siding Spring	
3499	Hoppe	1981 VW1	1981 Nov 3	F. Borngen and K. Kirsch	Tautenburg	
3500	Kobayashi	A919 SD	1919 Sep 18	K. Reinmuth	Heidelberg	
3501		1971 QU	1971 Aug 18	T. Smirnova	Nauchnyj	
3502		1964 TR1	1964 Oct 9	Purple Mountain Observatory	Nanking	
3503		1981 EF17	1981 Mar 1	S. J. Bus	Siding Spring	
3504		1981 RV3	1981 Sep 3	N. Chernykh	Nauchnyj	
3505		1983 AM	1983 Jan 9	B. A. Skiff	Flagstaff (AM)	119
3506	French	1984 CO1	1984 Feb 6	E. Bowell	Flagstaff (AM)	119
3507	Vilas	1982 UX	1982 Oct 21	E. Bowell	Flagstaff (AM)	119
3508	Pasternak	1980 DO5	1980 Feb 21	L. G. Karachkina	Nauchnyj	
3509		1978 UH2	1978 Oct 28	Purple Mountain Observatory	Nanking	
3510	Veeder	1982 TP	1982 Oct 13	E. Bowell	Flagstaff (AM)	119
3511	Tsvetaeva	1982 TC2	1982 Oct 14	L. G. Karachkina	Nauchnyj	129
3512		1984 AC1	1984 Jan 8	J. Wagner	Flagstaff (AM)	119
3513		1965 UZ	1965 Oct 16	Purple Mountain Observatory	Nanking	
3514		1971 UJ	1971 Oct 26	L. Kohoutek	Bergedorf	
3515		1982 UH2	1982 Oct 16	Z. Vavrova	Klet	
3516	Rusheva	1982 UH7	1982 Oct 21	L. G. Karachkina	Nauchnyj	
3517		1976 SE1	1976 Sep 24	N. Chernykh	Nauchnyj	
3518		1977 QC4	1977 Aug 18	N. Chernykh	Nauchnyj	
3519		1984 DO	1984 Feb 23	H. Debehogne	La Silla	
3520		1952 SG	1952 Sep 16	Goethe Link Observatory	Brooklyn	103
3521		1982 MH	1982 Jun 26	A. Gilmore and P. Kilmartin	Mount John	
3522		1941 SW	1941 Sep 21	Y. Vaisala	Turku	
3523	Arina	1975 TV2	1975 Oct 3	L. Chernykh	Nauchnyj	
3524		1981 EE27	1981 Mar 2	S. J. Bus	Siding Spring	
3525	Paul	1983 CX2	1983 Feb 15	N. G. Thomas	Flagstaff (AM)	119
3526	Jeffbell	1984 CN	1984 Feb 5	E. Bowell	Flagstaff (AM)	119
3527	McCord	1985 GE1	1985 Apr 15	E. Bowell	Flagstaff (AM)	119
3528		1981 EW3	1981 Mar 2	S. J. Bus	Siding Spring	
3529		1981 EQ19	1981 Mar 2	S. J. Bus	Siding Spring	
3530		1981 EC20	1981 Mar 2	S. J. Bus	Siding Spring	
3531	Cruikshank	1981 FB	1981 Mar 30	E. Bowell	Flagstaff (AM)	119
3532	Tracie	1983 AS2	1983 Jan 10	K. Herkenhoff	Palomar	135
3533	Toyota	1986 UE	1986 Oct 30	K. Suzuki and T. Urata	Toyota	
3534	Sax	1936 XA	1936 Dec 15	E. Delporte	Uccle	
3535		1979 SN11	1979 Sep 24	N. Chernykh	Nauchnyj	
3536		1981 EV20	1981 Mar 2	S. J. Bus	Siding Spring	
3537	Jürgen	1982 VT	1982 Nov 15	E. Bowell	Flagstaff (AM)	119
3538		6548 P-L	1960 Sep 24	PLS	Palomar	107
3539	Weimar	1967 GF1	1967 Apr 11	F. Borngen	Tautenburg	
3540	Protesilaos	1973 UF5	1973 Oct 27	F. Borngen	Tautenburg	
3541		1984 ML	1984 Jun 18	Perth Observatory	Perth	
3542		1964 TN2	1964 Oct 9	Purple Mountain Observatory	Nanking	
3543		1964 VA3	1964 Nov 11	Purple Mountain Observatory	Nanking	
3544		1977 RD4	1977 Sep 7	N. Chernykh	Nauchnyj	
3545	Gaffey	1981 WK2	1981 Nov 20	E. Bowell	Flagstaff (AM)	119

No.	Name	pd	dd	d	dp	
3546	Atanasoff	1983 SC	1983 Sep 28	E. F. Helin and V. Shkodrav	Rozhen	136
3547		1978 TM6	1978 Oct 2	L. Zhuravleva	Nauchnyj	
3548		1973 SO	1973 Sep 19	C. J. van Houten	Palomar	133
3549	Hapke	1981 YH	1981 Dec 30	E. Bowell	Flagstaff (AM)	119
3550		1981 YS	1981 Dec 20	A. Mrkos	Klet	
3551		1983 RD	1983 Sep 12	R. S. Dunbar	Palomar	
3552		1983 SA	1983 Sep 26	P Wild	Zimmerwald	
3553	Mera	1985 JA	1985 May 14	C. Shoemaker	Palomar	
3554	Amun	1986 EB	1986 Mar 4	C. Shoemaker and E. Shoemaker	Palomar	
3555		1931 TC1	1931 Oct 6	K. Reinmuth	Heidelberg	
3556		1964 UO	1964 Oct 30	Purple Mountain Observatory	Nanking	
3557		1977 QE1	1977 Aug 19	N. Chernykh	Nauchnyj	
3558		1978 SQ2	1978 Sep 26	L. Zhuravleva	Nauchnyj	
3559	Violaumayer	1980 PH	1980 Aug 8	E. Bowell	Flagstaff (AM)	119
3560		1980 RZ2	1980 Sep 3	Purple Mountain Observatory	Nanking	
3561	Devine	1983 HO	1983 Apr 18	N. G. Thomas	Flagstaff (AM)	119
3562		1984 AZ	1984 Jan 8	J. Wagner	Flagstaff (AM)	119
3563		1985 FE	1985 Mar 23	A. Gilmore and P. Kilmartin	Mount John	
3564	Talthybius	1985 TC1	1985 Oct 15	E. Bowell	Flagstaff (AM)	119
3565	Ojima	1986 YD	1986 Dec 22	T. Niijima and T. Urata	Ojima	
3566		1979 YA9	1979 Dec 24	L. Zhuravleva	Nauchnyj	
3567		1930 VD	1930 Nov 15	E. Delporte	Uccle	
3568	ASCII	1936 UB	1936 Oct 17	M. Laugier	Nice	
3569	Kumon	1938 DN1	1938 Feb 20	K. Reinmuth	Heidelberg	
3570		1979 XO	1979 Dec 14	Purple Mountain Observatory	Nanking	
3571		1982 EJ	1982 Mar 15	A. Mrkos	Klet	
3572		1954 UJ2	1954 Oct 28	Goethe Link Observatory	Brooklyn	103
3573	Holmberg	1982 QO1	1982 Aug 16	C.-I. Lagerkvist	La Silla	
3574	Rudaux	1982 TQ	1982 Oct 13	E. Bowell	Flagstaff (AM)	119
3575		1984 DU2	1984 Feb 26	N. Chernykh	Nauchnyj	
3576		1984 DB3	1984 Feb 26	N. Chernykh	Nauchnyj	
3577		1969 TK	1969 Oct 7	L. Chernykh	Nauchnyj	
3578		1977 CC	1977 Feb 11	Felix Aguilar Observatory	El Leoncito	
3579		1977 YA	1977 Dec 18	M. Lovas	Piszkesteto	
3580		1983 CS2	1983 Feb 15	N. G. Thomas	Flagstaff (AM)	119
3581	Alvarez	1985 HC	1985 Apr 23	C. Shoemaker and E. Shoemaker	Palomar	
3582		1986 TT5	1986 Oct 2	P. Wild	Zimmerwald	
3583	Burdett	1929 TQ	1929 Oct 5	C. W. Tombaugh	Flagstaff (LO)	
3584		1981 TW	1981 Oct 5	N. G. Thomas	Flagstaff (AM)	119
3585		1987 BE	1987 Jan 28	T. Niijima and T. Urata	Ojima	
3586		1978 SW6	1978 Sep 26	L. Zhuravleva	Nauchnyj	
3587		1981 RK5	1981 Sep 8	L. Zhuravleva	Nauchnyj	
3588	Kirik	1981 TH4	1981 Oct 8	L. Chernykh	Nauchnyj	
3589		1984 AB1	1984 Jan 8	J. Wagner	Flagstaff (AM)	119
3590	Holst	1984 CQ	1984 Feb 5	E. Bowell	Flagstaff (AM)	119
3591		1978 QJ2	1978 Aug 31	N. Chernykh	Nauchnyj	
3592		1980 CT	1980 Feb 15	Z. Vavrova	Klet	
3593		1981 EB20	1981 Mar 2	S. J. Bus	Siding Spring	
3594	Scotti	1983 CN	1983 Feb 11	E. Bowell	Flagstaff (AM)	119
3595	Gallagher	1985 TF1	1985 Oct 15	E. Bowell	Flagstaff (AM)	119
3596	Meriones	1985 VO	1985 Nov 14	P. Jensen and K. Augustesen	Brorfelde	
3597		1941 UL	1941 Oct 15	L. Oterma	Turku	
3598	Saucier	1977 KK1	1977 May 18	E. S. Bus	Palomar	
3599		1978 PB3	1978 Aug 8	N. Chernykh	Nauchnyj	
3600		1978 SL7	1978 Sep 26	L. Zhuravleva	Nauchnyj	
3601		1979 SP9	1979 Sep 22	N. Chernykh	Nauchnyj	
3602		1981 DQ2	1981 Feb 28	S. J. Bus	Siding Spring	
3603		1981 RM	1981 Sep 5	L. Brozek	Klet	
3604		5550 P-L	1960 Oct 17	FLS	Palomar	107
3605	Davy	1932 WB	1932 Nov 28	E. Delporte	Uccle	
3606		1939 SF	1939 Sep 19	Y. Vaisala	Turku	
3607	Naniwa	1977 DO4	1977 Feb 18	H Kosai and K. Hurukawa	Kiso Station	
3608	Kataev	1978 SD1	1978 Sep 27	L. Chernykh	Nauchnyj	
3609		1980 VM1	1980 Nov 13	Purple Mountain Observatory	Nanking	
3610		1981 EA1	1981 Mar 5	H. Debehogne	La Silla	124
3611		1981 YY1	1981 Dec 20	Purple Mountain Observatory	Nanking	
3612	Peale	1982 TW	1982 Oct 13	E. Bowell	Flagstaff (AM)	119
3613		1982 VJ11	1982 Nov 10	Purple Mountain Observatory	Nanking	
3614		1983 AE1	1983 Jan 12	N. G. Thomas	Flagstaff (AM)	119
3615	Safronov	1983 WZ	1983 Nov 29	E. Bowell	Flagstaff (AM)	119
3616		1984 JJ2	1984 May 3	L Zhuravleva	Nauchnyj	
3617		1984 LJ	1984 Jun 2	B. A. Skiff	Flagstaff (AM)	119
3618		1979 QP8	1979 Aug 20	N. Chernykh	Nauchnyj	
3619		1981 EU35	1981 Mar 2	S. J. Bus	Siding Spring	
3620	Platonov	1981 RU2	1981 Sep 7	L. G. Karachkina	Nauchnyj	
3621		1981 SQ1	1981 Sep 26	N. G. Thomas	Flagstaff (AM)	119
3622	Ilinsky	1981 SX7	1981 Sep 29	L. Zhuravleva	Nauchnyj	
3623	Chaplin	1981 TG2	1981 Oct 4	L. G. Karachkina	Nauchnyj	
3624	Mironov	1982 TH2	1982 Oct 14	L. Zhuravleva	Nauchnyj	137
3625	Fracastoro	1984 HZ1	1984 Apr 27	W. Ferreri	La Silla	
3626	Ohsaki	1929 PA	1929 Aug 4	M. Wolf	Heidelberg	
3627		1973 DS	1973 Feb 28	L. Kohoutek	Bergedorf	
3628		1979 WD	1979 Nov 25	Z. Vavrova	Klet	

No.	Name	pd	dd	d	dp	
3629		1982 WK	1982 Nov 21	A. Mrkos	Klet	
3630		1984 QN	1984 Aug 28	A. Mrkos	Klet	
3631	Sigyn	1987 BV1	1987 Jan 25	E. W. Elst	La Silla	
3632		1976 SJ4	1976 Sep 24	N. Chernykh	Nauchnyj	
3633		1980 EE2	1980 Mar 13	Felix Aguilar Observatory	El Leoncito	
3634		1980 FV	1980 Mar 16	C.-I. Lagerkvist	La Silla	
3635		1981 WO1	1981 Nov 21	L. Kohoutek	Calar Alto	
3636		1982 UJ2	1982 Oct 17	A. Mrkos	Klet	
3637		1984 UQ	1984 Oct 23	B. A. Skiff	Flagstaff (AM)	119
3638	Davis	1984 WX	1984 Nov 20	E. Bowell	Flagstaff (AM)	119
3639	Weidenschilling	1985 TX	1985 Oct 15	E. Bowell	Flagstaff (AM)	119
3640	Gostin	1985 TR3	1985 Oct 11	C. Shoemaker and E. Shoemaker	Palomar	
3641		A922 WC	1922 Nov 24	G. Van Biesbroeck	Williams Bay	
3642	Frieden	1953 XL1	1953 Dec 4	H. Gessner	Sonneberg	
3643		1978 UN2	1978 Oct 29	Purple Mountain Observatory	Nanking	
3644		1931 TW	1931 Oct 5	K. Reinmuth	Heidelberg	
3645		1981 QZ	1981 Aug 28	A. Mrkos	Klet	
3646		1985 RK4	1985 Sep 11	H. Debehogne	La Silla	
3647	Dermott	1986 AD1	1986 Jan 11	E. Bowell	Flagstaff (AM)	119
3648		1957 HK	1957 Apr 24	- - -	La Plata	
3649		1976 HQ	1976 Apr 26	Felix Aguilar Observatory	El Leoncito	
3650		1978 UO2	1978 Oct 30	Purple Mountain Observatory	Nanking	
3651	Friedman	1978 VB5	1978 Nov 7	E. F Helin and S. J. Bus	Palomar	
3652		1981 TC3	1981 Oct 6	T. Smirnova	Nauchnyj	
3653		1979 HF5	1979 Apr 25	N. Chernykh	Nauchnyj	
3654		1949 QH1	1949 Aug 21	Goethe Link Observatory	Brooklyn	103
3655	Eupraksia	1978 SA3	1978 Sep 26	L. Zhuravleva	Nauchnyj	
3656		1978 QX	1978 Aug 31	N. Chernykh	Nauchnyj	
3657		1978 ST6	1978 Sep 26	L. Zhuravleva	Nauchnyj	
3658	Feldman	1982 TR	1982 Oct 13	E. Bowell	Flagstaff (AM)	119
3659	Bellingshausen	1969 TE2	1969 Oct 8	L. Chernykh	Nauchnyj	
3660	Lazarev	1978 QX2	1978 Aug 31	N. Chernykh	Nauchnyj	
3661		1979 UY3	1979 Oct 16	N. Chernykh	Nauchnyj	
3662		1980 RU2	1980 Sep 8	L. Zhuravleva	Nauchnyj	
3663	Tisserand	1985 GK1	1985 Apr 15	E. Bowell	Flagstaff (AM)	119
3664		4260 P-L	1960 Sep 24	PLS	Palomar	107
3665		1979 FE	1979 Mar 19	A. Mrkos	Klet	
3666		1979 HP	1979 Apr 19	J. C. Muzzio	Cerro Tololo	
3667	Anne-Marie	1981 EF	1981 Mar 9	E. Bowell	Flagstaff (AM)	119
3668	Ilfpetrov	1982 UM7	1982 Oct 21	L. G. Karachkina	Nauchnyj	
3669		1982 UO7	1982 Oct 21	L. G. Karachkina	Nauchnyj	
3670	Northcott	1983 BN	1983 Jan 22	E. Bowell	Flagstaff (AM)	119
3671	Dionysius	1984 KD	1984 May 27	C. Shoemaker and E. Shoemaker	Palomar	
3672	Stevedberg	1985 QQ	1985 Aug 22	E. Bowell	Flagstaff (AM)	119
3673	Levy	1985 QS	1985 Aug 22	E. Bowell	Flagstaff (AM)	119
3674	Erbisbuhl	1963 RH	1963 Sep 13	C. Hoffmeister	Sonneberg	
3675	Kemstach	1982 YP1	1982 Dec 23	L. G. Karachkina	Nauchnyj	
3676	Hahn	1984 GA	1984 Apr 3	E. Bowell	Flagstaff (AM)	119
3677	Magnusson	1984 QJ1	1984 Aug 31	E. Bowell	Flagstaff (AM)	119
3678		1966 BO	1966 Jan 20	Purple Mountain Observatory	Nanking	
3679		1984 DT	1984 Feb 24	H. Debehogne	La Silla	
3680	Sasha	1987 MY	1987 Jun 28	E. F. Helin	Palomar	
3681		1974 QO2	1974 Aug 27	L. Chernykh	Nauchnyj	
3682		A923 NB	1923 Jul 12	K. Reinmuth	Heidelberg	
3683	Baumann	1987 MA	1987 Jun 23	W. Landgraf	La Silla	
3684		1983 AK	1983 Jan 9	B. A. Skiff	Flagstaff (AM)	119
3685		1981 EH14	1981 Mar 1	S. J. Bus	Siding Spring	
3686		1987 EB	1987 Mar 3	T. Niijima and T. Urata	Ojima	
3687	Dzus	A908 TC	1908 Oct 7	A. Kopff	Heidelberg	
3688	Navajo	1981 FD	1981 Mar 30	E. Bowell	Flagstaff (AM)	119
3689	Yeates	1981 JJ2	1981 May 5	C. Shoemaker	Palomar	
3690	Larson	1981 PM	1981 Aug 3	E. Bowell	Flagstaff (AM)	119
3691		1982 FT	1982 Mar 29	L. E. Gonzalez	Cerro El Roble	
3692	Rickman	1982 HF1	1982 Apr 25	E. Bowell	Flagstaff (AM)	119
3693	Barringer	1982 RU	1982 Sep 15	E. Bowell	Flagstaff (AM)	119
3694		1984 SH5	1984 Sep 27	A. Grossman	Palomar	
3695		1973 UU4	1973 Oct 21	H. L. Giclas	Flagstaff (AM)	119
3696	Herald	1980 OF	1980 Jul 17	E. Bowell	Flagstaff (AM)	119
3697	Guyhurst	1984 EV	1984 Mar 6	E. Bowell	Flagstaff (AM)	119
3698	Manning	1984 UA2	1984 Oct 29	E. Bowell	Flagstaff (AM)	119
3699	Milbourn	1984 UC2	1984 Oct 29	E. Bowell	Flagstaff (AM)	119
3700	Geowilliams	1984 UL2	1984 Oct 23	C. Shoemaker and E. Shoemaker	Palomar	
3701		1985 DW	1985 Feb 20	A. Mrkos	Klet	
3702	Trubetskaya	1970 NB	1970 Jul 3	L. Chernykh	Nauchnyj	
3703	Volkonskaya	1978 PU3	1978 Aug 9	L. Chernykh	Nauchnyj	
3704		1981 YX1	1981 Dec 20	Purple Mountain Observatory	Nanking	
3705		1984 ET1	1981 Mar 4	H. Debehogne	La Silla	
3706		1984 SE3	1984 Sep 28	B. A. Skiff	Flagstaff (AM)	119
3707		1934 CC	1934 Feb 5	K. Reinmuth	Heidelberg	
3708		1974 FV1	1974 Mar 21	- - -	Cerro El Roble	
3709	Polypoites	1985 TL3	1985 Oct 14	C. Shoemaker and E. Shoemaker	Palomar	
3710		1978 RD6	1978 Sep 13	N. Chernykh	Nauchnyj	

No.	Name	pd	dd	d	dp	
3711		1983 QD	1983 Aug 31	J. Gibson	Palomar	
3712		1984 YC	1984 Dec 22	A. R. Klemola	Lick Observatory	
3713	Pieters	1985 FA2	1985 Mar 22	E. Bowell	Flagstaff (AM)	119
3714	Kenrussell	1983 TT1	1983 Oct 12	E. Bowell	Flagstaff (AM)	119
3715		1980 DS	1980 Feb 19	A. Mrkos	Klet	
3716		1980 TG	1980 Oct 2	A. Mrkos	Klet	
3717		1964 CG	1964 Feb 15	Goethe Link Observatory	Brooklyn	103
3718	Dunbar	1978 VS10	1978 Nov 7	E. F. Helin and S. J. Bus	Palomar	
3719	Karamzin	1976 YO1	1976 Dec 16	L. Chernykh	Nauchnyj	
3720	Hokkaido	1987 UR1	1987 Oct 28	S. Ueda and H. Kaneda	Kushiro	
3721	Widorn	1982 TU	1982 Oct 13	E. Bowell	Flagstaff (AM)	119
3722		1927 UE	1927 Oct 29	K. Reinmuth	Heidelberg	
3723		1976 GK2	1976 Apr 1	N. Chernykh	Nauchnyj	
3724		1979 YN8	1979 Dec 23	L. Zhuravleva	Nauchnyj	
3725		1981 EA11	1981 Mar 1	S. J. Bus	Siding Spring	
3726	Johnadams	1981 LJ	1981 Jun 4	E. Bowell	Flagstaff (AM)	119
3727		1981 PQ	1981 Aug 7	A. Mrkos	Klet	
3728		1983 QF	1983 Aug 23	IRAS		
3729		1983 VP7	1983 Nov 1	Purple Mountain Observatory	Nanking	
3730	Hurban	1983 XM1	1983 Dec 4	M. Antal	Piszkesteto	
3731		1984 DH1	1984 Feb 20	- - -	Perth	
3732		1984 SR1	1984 Sep 27	Z. Vavrova	Klet	
3733		1985 AF	1985 Jan 15	K. Suzuki and T. Urata	Toyota	
3734		9527 P-L	1960 Oct 17	PLS	Palomar	
3735		1983 XS	1983 Dec 4	Z. Vavrova	Klet	
3736	Rokoske	1987 SY3	1987 Sep 26	E. Bowell	Flagstaff (AM)	119
3737		1983 PA	1983 Aug 8	E. F. Helin	Palomar	
3738		1977 QA1	1977 Aug 19	N. Chernykh	Nauchnyj	
3739		1977 RE2	1977 Sep 8	N. Chernykh	Nauchnyj	
3740		1981 EM	1981 Mar 1	H. Debehogne	La Silla	124
3741		1981 EL19	1981 Mar 2	S. J. Bus	Siding Spring	
3742		1981 EQ27	1981 Mar 2	S. J. Bus	Siding Spring	
3743		1983 EW	1983 Mar 10	E. Barr	Flagstaff (AM)	119
3744	Horn-d'Arturo	1983 VE	1983 Nov 5	Osservatorio San Vittore	Bologna	
3745		1949 SF	1949 Sep 23	K. Reinmuth	Heidelberg	
3746		1964 TC1	1964 Oct 8	Purple Mountain Observatory	Nanking	
3747	Belinskij	1975 VY5	1975 Nov 5	L. Chernykh	Nauchnyj	
3748	Tatum	1981 JQ	1981 May 3	E. Bowell	Flagstaff (AM)	119
3749	Balam	1982 BG1	1982 Jan 24	E. Bowell	Flagstaff (AM)	119
3750		1982 TD1	1982 Oct 14	L. G Karachkina	Nauchnyj	
3751	Kiang	1983 NK	1983 Jul 10	E. Bowell	Flagstaff (AM)	119
3752		1985 PA	1985 Aug 15	E. F. Helin and M. Barucci	Caussols	138
3753		1986 TO	1986 Oct 10	D. Waldron	Siding Spring	
3754		1931 FM	1931 Mar 16	C. W. Tombaugh	Flagstaff (LO)	
3755		1950 SJ	1950 Sep 19	S. Arend	Uccle	
3756		1979 MV6	1979 Jun 25	E. F. Helin and S. J. Bus	Siding Spring	
3757		1982 XB	1982 Dec 14	E. F. Helin	Palomar	
3758	Karttunen	1983 WP	1983 Nov 28	E. Bowell	Flagstaff (AM)	119
3759	Piironen	1984 AF	1984 Jan 8	E Bowell	Flagstaff (AM)	119
3760	Poutanen	1984 AQ	1984 Jan 8	E Bowell	Flagstaff (AM)	119
3761		1936 OH	1936 Jul 25	G Neujmin	Simeis	
3762		1976 QN1	1976 Aug 26	N. Chernykh	Nauchnyj	
3763		1980 TA6	1980 Oct 14	Purple Mountain Observatory	Nanking	
3764		1980 TL15	1980 Oct 10	- - -	Perth	
3765		1982 SU1	1982 Sep 16	K Tomita	Caussols	
3766	Junepatterson	1983 BF	1983 Jan 16	E Bowell	Flagstaff (AM)	119
3767		1986 LC	1986 Jun 3	E. F. Helin	Palomar	
3768		1937 RB	1937 Sep 5	C. Jackson	Johannesburg (UO)	
3769		1967 UV	1967 Oct 30	L. Kohoutek and A. Kriete	Bergedorf	
3770		1974 QT1	1974 Aug 24	L. Chernykh	Nauchnyj	
3771		1974 SB3	1974 Sep 20	L. Zhuravleva	Nauchnyj	
3772		1982 UR7	1982 Oct 21	L. G. Karachkina	Nauchnyj	
3773		1984 YY	1984 Dec 23	Oak Ridge Observatory	Oak Ridge	
3774	Megumi	1987 YC	1987 Dec 20	T. Kojima	Chiyoda	
3775		1931 TC4	1931 Oct 6	C. W. Tombaugh	Flagstaff (LO)	
3776		1938 GG	1938 Apr 5	H. Alikoski	Turku	
3777	McCauley	1981 JD2	1981 May 5	C. Shoemaker	Palomar	
3778	Regge	1984 HK1	1984 Apr 26	W. Ferreri	La Silla	
3779	Kieffer	1985 JV1	1985 May 13	C. Shoemaker and E. Shoemaker	Palomar	
3780	Maury	1985 RL	1985 Sep 14	E. Bowell	Flagstaff (AM)	119
3781		1986 RG1	1986 Sep 2	A. Mrkos	Klet	
3782		1986 TE	1986 Oct 3	P. Jensen	Brorfelde	
3783	Morris	1986 TW1	1986 Oct 7	E. Bowell	Flagstaff (AM)	119
3784	Chopin	1986 UL1	1986 Oct 31	E. W. Elst	Haute Provence	
3785	Kitami	1986 WM	1986 Nov 30	T. Seki	Geisei	
3786		1988 AE	1988 Jan 10	T. Kojima	Chiyoda	
3787		1977 RG7	1977 Sep 11	N. Chernkyh	Nauchnyj	
3788		1986 QM3	1986 Aug 29	H. Debehogne	La Silla	
3789	Zhongguo	1928 UF	1928 Oct 25	Y. C. Chang	Williams Bay	65
3790		1937 UE	1937 Oct 26	K. Reinmuth	Heidelberg	
3791		1981 WV1	1981 Nov 17	A. Mrkos	Klet	
3792	Preston	1985 FA	1985 Mar 22	C. Shoemaker and E Shoemaker	Palomar	
3793	Leonteus	1985 TE3	1985 Oct 11	C. Shoemaker and E. Shoemaker	Palomar	

No.	Name	pd	dd	d	dp	
3794	Sthenelos	1985 TF3	1985 Oct 12	C. Shoemaker and E. Shoemaker	Palomar	
3795		1986 GV1	1986 Apr 8	E. F. Helin	Palomar	
3796		1986 XJ	1986 Dec 6	P. Jensen	Brorfelde	
3797		1987 YL	1987 Dec 22	Oak Ridge Observatory	Oak Ridge	
3798		2402 T-3	1977 Oct 16	I. van Houten-Groeneveld	Palomar	139
3799		1979 SL9	1979 Sep 22	N. Chernkyh	Nauchnyj	
3800		1984 AB	1984 Jan 4	E. F. Helin	Palomar	
3801	Thrasymedes	1985 VS	1985 Nov 6	SPACEWATCH	Kitt Peak	
3802	Dornburg	1986 PJ4	1986 Aug 7	F. Borngen	Tautenburg	
3803		1981 TP1	1981 Oct 2	L. Zhuravleva	Nauchnyj	
3804		1969 TB2	1969 Oct 8	L Chernykh	Nauchnyj	
3805		1981 DK3	1981 Feb 28	S. J. Bus	Siding Spring	
3806		1981 EW32	1981 Mar 1	S. J. Bus	Siding Spring	
3807		1981 SE1	1981 Sep 26	B. A. Skiff and N. G. Thomas	Flagstaff (AM)	119
3808	Tempel	1982 FQ2	1982 Mar 24	F. Borngen	Tautenburg	
3809	Amici	1984 FA	1984 Mar 26	Osservatorio San Vittore	Bologna	
3810		1985 DX	1985 Feb 20	A. Gilmore and P. Kilmartin	Mount John	
3811		1953 TH	1953 Oct 13	L. Oterma	Turku	
3812		1965 AK1	1965 Jan 11	Purple Mountain Observatory	Nanking	
3813		1970 QA1	1970 Aug 30	T. Smirnova	Nauchnyj	
3814		1981 JA	1981 May 4	T. Furuta	Tokai	
3815	König	1959 GG	1959 Apr 15	A König and G. Jakisch	Heidelberg	140
3816		1975 VG9	1975 Nov 8	N. Chernykh	Nauchnyj	
3817	Lencarter	1979 MK1	1979 Jun 25	E. F. Helin and S. J. Bus	Siding Spring	
3818		1979 QL8	1979 Aug 20	N. Chernykh	Nauchnyj	
3819		1983 AR	1983 Jan 12	B. A. Skiff	Flagstaff (AM)	119
3820		1984 DV	1984 Feb 25	H. Debehogne	La Silla	
3821		1985 RC3	1985 Sep 6	H. Debehogne	La Silla	
3822		1988 DP1	1988 Feb 21	T. Seki	Geisei	
3823	Yorii	1988 EC1	1988 Mar 10	M. Arai and H Mori	Yorii	
3824		1929 TK	1929 Oct 5	C. W. Tombaugh	Flagstaff (LO)	
3825		1967 UR	1967 Oct 30	L. Kohoutek	Bergedorf	
3826	Handel	1973 UV5	1973 Oct 27	F. Borngen	Tautenburg	
3827		1986 VU	1986 Nov 3	A. Mrkos	Klet	
3828		1986 WC	1986 Nov 22	K. Suzuki and T. Urata	Toyota	
3829		1988 EM	1988 Mar 10	T. Kojima	Chiyoda	
3830		1986 RL	1986 Sep 11	P. Jensen	Brorfelde	
3831	Pettengill	1986 TP2	1986 Oct 7	E. Bowell	Flagstaff (AM)	119
3832	Shapiro	1981 QJ	1981 Aug 30	E. Bowell	Flagstaff (AM)	119
3833		1971 SC	1971 Sep 27	J. Gibson and C. U. Cesco	El Leoncito	
3834		1980 JE	1980 May 11	L. Brozek	Klet	
3835		1977 SD3	1977 Sep 23	N. Chernykh	Nauchnyj	
3836		1979 SR9	1979 Sep 22	N. Chernykh	Nauchnyj	
3837	Carr	1981 JU2	1981 May 6	C. Shoemaker	Palomar	
3838		1986 WA	1986 Nov 27	A. Maury	Palomar	
3839		1971 OU	1971 Jul 26	N. Chernykh	Nauchnyj	
3840		1980 TN4	1980 Oct 9	C. Shoemaker	Palomar	
3841		1983 VG7	1983 Nov 4	B. A. Skiff	Flagstaff (AM)	119
3842	Harlansmith	1985 FC1	1985 Mar 21	E. Bowell	Flagstaff (AM)	119
3843	OISCA	1987 DM	1987 Feb 28	Y. Oshima	Gekko	
3844		1966 BZ	1966 Jan 30	Purple Mountain Observatory	Nanking	
3845		1979 SA10	1979 Sep 22	N. Chernykh	Nauchnyj	
3846		1980 TK5	1980 Oct 9	C. Shoemaker	Palomar	
3847		1982 DY1	1982 Feb 16	A. Mrkos	Klet	
3848		1982 FH3	1982 Mar 21	H. Debehogne	La Silla	
3849	Incidentia	1984 FC	1984 Mar 31	E. Bowell	Flagstaff (AM)	119
3850		1986 TK2	1986 Oct 7	E. Bowell	Flagstaff (AM)	119
3851		1986 UZ	1986 Oct 30	T. Seki	Geisei	
3852		1987 DR6	1987 Feb 24	H. Debehogne	La Silla	
3853		1981 WG1	1981 Nov 24	E. Bowell	Flagstaff (AM)	119
3854		1983 EA	1983 Mar 13	C. Shoemaker	Palomar	
3855	Pasasymphonia	1986 NF1	1986 Jul 4	E. F. Helin	Palomar	
3856		1976 QX	1976 Aug 26	N. Chernykh	Nauchnyj	
3857	Cellino	1984 CD1	1984 Feb 8	E. Bowell	Flagstaff (AM)	119
3858		1986 TG	1986 Oct 3	P. Jensen	Brorfelde	
3859	Börngen	1987 EW	1987 Mar 4	E. Bowell	Flagstaff (AM)	119
3860	Plovdiv	1986 PM4	1986 Aug 8	E. W. Elst and V. Ivanova	Rozhev	
3861		A910 FA	1910 Mar 30	J. Helffrich	Heidelberg	
3862		1972 KM	1972 May 18	T. Smirnova	Nauchnyj	
3863		1978 SJ3	1978 Sep 26	L. Zhuravleva	Nauchnyj	
3864		1986 XF	1986 Dec 6	P. Jensen	Brorfelde	
3865		1988 AY4	1988 Jan 13	H. Debehogne	La Silla	
3866		1988 BH4	1988 Jan 20	H Debehogne	La Silla	
3867	Shiretoko	1988 HG	1988 Apr 16	M. Yanai and K. Watanabe	Kitami	
3868		4575 P-L	1960 Sep 24	PLS	Palomar	107
3869		1981 JE	1981 May 3	E. Bowell	Flagstaff (AM)	119
3870	Mayre	1988 CG3	1988 Feb 13	E. W. Elst	La Silla	
3871		1982 DR2	1982 Feb 18	R. M. West	La Silla	
3872		1983 AV	1983 Jan 12	B. A. Skiff	Flagstaff (AM)	119
3873		1984 WB	1984 Nov 21	C. Shoemaker	Palomar	
3874	Stuart	1986 TJ1	1986 Oct 4	E. Bowell	Flagstaff (AM)	119
3875		1988 KE	1988 May 17	E. F. Helin	Palomar	

No.	Name	pd	dd	d	dp	
3876		1988 KJ	1988 May 19	E. F. Helin	Palomar	
3877		3108 P-L	1960 Sep 24	PLS	Palomar	107
3878		1982 VR4	1982 Nov 14	H. Kosai and K. Hurukawa	Kiso Station	
3879		1983 QA	1983 Aug 16	Z. Vavrova	Klet	
3880		1984 WK	1984 Nov 21	C. Shoemaker and E. Shoemaker	Palomar	
3881		1925 VF	1925 Nov 15	B. Jekhowsky	Algiers	
3882		1962 RN	1962 Sep 7	Goethe Link Observatory	Brooklyn	103
3883		1972 RQ	1972 Sep 7	N. Chernykh	Nauchnyj	
3884		1977 EM1	1977 Mar 13	N. Chernykh	Nauchnyj	
3885		1979 HG5	1979 Apr 25	N. Chernykh	Nauchnyj	
3886		1981 RU3	1981 Sep 3	N. Chernykh	Nauchnyj	
3887		1985 QX	1985 Aug 22	A. Mrkos	Klet	
3888		1984 FO	1984 Mar 28	C. Shoemaker	Palomar	
3889		1972 RT3	1972 Sep 6	L. Zhuravleva	Nauchnyj	
3890		1976 YU5	1976 Dec 18	L. Chernykh	Nauchnyj	
3891		1981 EY31	1981 Mar 3	S. J. Bus	Siding Spring	
3892		1941 HD	1941 Apr 19	L. Oterma	Turku	
3893		1980 FG12	1980 Mar 20	Perth Observatory	Perth	
3894		1980 PQ2	1980 Aug 14	Perth Observatory	Perth	
3095		1987 DE	1987 Feb 23	C. Shoemaker	Palomar	
3896	Pordenone	1987 WB	1987 Nov 18	J. M. Baur	Chions	
3897		1942 RT	1942 Sep 8	Y Vaisala	Turku	
3898		1981 SF9	1981 Sep 26	Perth Observatory	Perth	
3899		1982 SN1	1982 Sep 17	M. Mahrova	Klet	
3900	Kneževic	1985 RK	1985 Sep 14	E Bowell	Flagstaff (AM)	119
3901		1958 GH	1958 Apr 7	Purple Mountain Observatory	Nanking	
3902		1986 AL	1986 Jan 14	S. Inoda and T. Urata	Karasuyama	
3903	Kliment Ohridski	1987 SV2	1987 Sep 20	E. W. Elst	Rozhen	
3904		1988 DQ	1988 Feb 22	R. H. McNaught	Siding Spring	
3905		1984 QO	1984 Aug 28	A. Mrkos	Klet	
3906		1987 KE1	1987 May 31	C. Shoemaker	Palomar	
3907		A904 PC	1904 Aug 14	M. Wolf	Heidelberg	
3908		1980 PA	1980 Aug 6	H.-E Schuster	La Silla	
3909		1988 JD1	1988 May 15	K. W. Zeigler	Flagstaff (AM)	119
3910		1988 SF	1988 Sep 16	E. W. Elst	Haute Provence	
3911		1940 QB	1940 Aug 31	K. Reinmuth	Heidelberg	
3912	Troja	1988 SG	1988 Sep 16	E W. Elst	Haute Provence	
3913		1986 XO2	1986 Dec 2	- - -	Caussols	
3914		1987 SE	1987 Sep 16	T. Seki	Geisei	
3915	Fukushima	1988 PA1	1988 Aug 15	M. Yanai and K. Watanabe	Kitami	
3916		1981 QA3	1981 Aug 24	H. Debehogne	La Silla	
3917	Franz Schubert	1961 CX	1961 Feb 15	F. Borngen	Tautenburg	
3918	Brel	1988 PE1	1988 Aug 13	E. W. Elst and G. Sause	Haute Provence	
3919		1984 DS	1984 Feb 23	H. Debehogne	La Silla	
3920		1948 WF	1948 Nov 28	S. Arend	Uccle	
3921		1971 OH	1971 Jul 19	B. Burnasheva	Nauchnyj	
3922		1971 SP3	1971 Sep 26	C. Torres	Cerro El Roble	
3923		1976 SN3	1976 Sep 24	N. Chernykh	Nauchnyj	
3924	Birch	1977 CU	1977 Feb 11	E. Bowell	Palomar	141
3925		1977 SS2	1977 Sep 19	L. Zhuravleva	Nauchnyj	
3926		1978 VQ3	1978 Nov 7	E. F. Helin and S. J. Bus	Palomar	
3927		1981 JA2	1981 May 5	C. Shoemaker	Palomar	
3928		1981 FG	1981 Aug 4	P. Wild	Zimmerwald	
3929		1981 WG9	1981 Nov 16	- - -	Perth	
3930		1982 UV10	1982 Oct 25	L. Zhuravleva	Nauchnyj	
3931	Batten	1984 EN	1984 Mar 1	E. Bowell	Flagstaff (AM)	119
3932		1984 SC5	1984 Sep 27	M. Nolan	Palomar	
3933		1986 EN4	1986 Mar 12	R. M. West	La Silla	
3934		1987 DF1	1987 Feb 23	P. Jensen	Brorfelde	
3935		1987 PB	1987 Aug 14	T. Seki	Geisei	
3936		2321 T-3	1977 Oct 16	C. J. van Houten	Palomar	139
3937		1932 EO	1932 Mar 14	K. Reinmuth	Heidelberg	
3938		1949 PL	1949 Aug 2	K. Reinmuth	Heidelberg	
3939		1953 GO	1953 Apr 7	K. Reinmuth	Heidelberg	
3940		1973 FE1	1973 Mar 27	L. Zhuravleva	Nauchnyj	
3941	Haydn	1973 UU5	1973 Oct 27	F. Borngen	Tautenburg	
3942		1977 RH7	1977 Sep 11	N. Chernykh	Nauchnyj	
3943	Silbermann	1981 RG1	1981 Sep 3	F. Borngen	Tautenburg	
3944		1981 WP1	1981 Nov 24	E Bowell	Flagstaff (AM)	119
3945		1982 PL	1982 Aug 14	N Chernykh	Nauchnyj	
3946		1983 EL2	1983 Mar 5	L. G. Karachkina	Nauchnyj	
3947		1983 XD	1983 Dec 1	E. Bowell	Flagstaff (AM)	119
3948		1985 RF	1985 Sep 15	P. Jensen	Brorfelde	
3949		1985 UL	1985 Oct 20	A. Mrkos	Klet	
3950		1986 CH	1986 Feb 8	S Inoda and T. Urata	Karasuyama	
3951		1986 CK1	1986 Feb 13	Osservatorio San Vittore	Bologna.	
3952		1986 EM2	1986 Mar 14	Bulgarian National Obs.	Rozhev	
3953		1986 VB6	1986 Nov 6	E. Bowell	Flagstaff (AM)	119
3954	Mendelssohn	1987 HU	1987 Apr 24	F. Borngen	Tautenburg	
3955	Bruckner	1988 RF3	1988 Sep 9	F. Borngen	Tautenburg	
3956		1988 VL1	1988 Nov 3	P. Jensen	Brorfelde	
3957		1933 OD	1933 Jul 24	K Reinmuth	Heidelberg	
3958		1953 TC	1953 Oct 10	P F. Schajn	Simeis	

No.	Name	pd	dd	d	dp	
3959		1954 UN2	1954 Oct 28	Goethe Link Observatory	Brooklyn	
3960		1955 BG	1955 Jan 20	Purple Mountain Observatory	Nanking	
3961		1962 OB	1962 Jul 31	Goethe Link Observatory	Brooklyn	
3962		1967 CC	1967 Feb 8	T Smirnova	Nauchnyj	
3963		1969 TP2	1969 Oct 8	L Chernykh	Nauchnyj	
3964		1974 RG1	1974 Sep 12	L. Zhuravleva	Nauchnyj	
3965		1975 VA9	1975 Nov 8	N Chernykh	Nauchnyj	
3966		1976 SD3	1976 Sep 24	N. Chernykh	Nauchnyj	
3967		1976 YW2	1976 Dec 16	L. Chernykh	Nauchnyj	
3968		1978 TU5	1978 Oct 8	L. Chernykh	Nauchnyj	
3696		1978 TQ8	1978 Oct 9	L. Zhuravleva	Nauchnyj	
3970		1979 ME9	1979 Jun 28	C. Torres	Cerro El Roble	
3971		1979 YM8	1979 Dec 23	L. Zhuravleva	Nauchnyj	
3972		1981 JD3	1981 May 6	C. Shoemaker	Palomar	
3973		1981 UC1	1981 Oct 30	L. G. Taff	Socorro	
3974		1982 FS	1982 Mar 28	E. Bowell	Flagstaff (AM)	119
3975		1982 UR3	1982 Oct 19	F. Borngen	Tautenburg	
3976		1983 JM	1983 May 6	N. G. Thomas	Flagstaff (AM)	119
3977		1983 LM	1983 Jun 14	C. Shoemaker	Palomar	
3978		1983 VP1	1983 Nov 7	Z. Vavrova	Klet	
3979		1983 VV1	1983 Nov 8	A. Mrkos	Klet	
3980		1983 XU	1983 Dec 4	A. Mrkos	Klet	
3981		1984 BL	1984 Jan 26	A. Mrkos	Klet	
3982		1984 JP1	1984 May 2	L. G. Karachkina	Nauchnyj	
3983		1984 SX	1984 Sep 20	A. Mrkos	Klet	
3984		1984 SB6	1984 Sep 21	H. Debehogne	La Silla	
3985		1985 CX	1985 Feb 12	C. Shoemaker	Palomar	
3986		1985 SF2	1985 Sep 19	N. Chernykh	Nauchnyj	
3987		1986 EL1	1986 Mar 5	E. Bowell	Flagstaff (AM)	119
3988		1986 LA	1986 Jun 4	E. F. Helin	Palomar	
3989		1986 RM	1986 Sep 8	P. Jensen	Brorfelde	
3990		1987 SO3	1987 Sep 25	P. Jensen	Brorfelde	
3991		1987 SW3	1987 Sep 26	E. Bowell	Flagstaff (AM)	119
3992		1987 SA7	1987 Sep 29	F. Borngen	Tautenburg	
3993		1988 VV5	1988 Nov 4	A. Mrkos	Klet	
3994		1988 XF	1988 Dec 2	M. Koishikawa	Sendai	
3995		1988 XM	1988 Dec 5	T. Kojima	Chiyoda	
3996		1988 XG1	1988 Dec 5	M. Arai and H. Mori	Yorii	
3997		1988 XP1	1988 Dec 6	J. Sugie	Taga-Cho	
3998		1989 AB	1989 Jan 1	T. Kojima	Chiyoda	
3999		1989 AL	1989 Jan 5	T. Kojima	Chiyoda	
4000		1989 AV	1989 Jan 4	S. Ueda and H. Kaneda	Kushiro	
4001		1949 PV	1949 Aug 2	K. Reinmuth	Heidelberg	
4002		1950 JB	1950 May 14	K. Reinmuth	Heidelberg	
4003		1964 ED	1964 Mar 8	F. Borngen	Tautenburg	
4004		1971 SN1	1971 Sep 16	Crimean Astrophysical Obs.	Nauchnyj	
4005		1972 TC2	1972 Oct 8	L. Zhuravleva	Nauchnyj	
4006		1972 YR	1972 Dec 29	T. Smirnova	Nauchnyj	
4007		1973 SR	1973 Sep 19	C. J. van Houten	Palomar	133
4008		1977 BY	1977 Jan 22	Felix Aguilar Observatory	El Leoncito	
4009		1977 EN1	1977 Mar 13	N. Chernykh	Nauchnyj	
4010		1977 QJ2	1977 Aug 21	N. Chernykh	Nauchnyj	
4011		1978 SC6	1978 Sep 28	N. Chernykh	Nauchnyj	
4012		1978 VK9	1978 Nov 7	E. F. Helin and S. J. Bus	Palomar	
4013		1979 OM15	1979 Jul 21	N. Chernykh	Nauchnyj	
4014		1979 SG10	1979 Sep 28	N. Chernykh	Nauchnyj	
4015		1979 VA	1979 Nov 15	E. F. Helin	Palomar	
4016		1979 XK	1979 Dec 15	H. Debehogne	La Silla	126
4017		1980 DL5	1980 Feb 21	L. G. Karachkina	Nauchnyj	
4018		1980 YM	1980 Dec 30	A. Mrkos	Klet	
4019		1981 EK14	1981 Mar 1	S. J. Bus	Siding Spring	
4020		1981 ET38	1981 Mar 1	S. J. Bus	Siding Spring	
4021		1981 QD2	1981 Aug 30	E. Bowell	Flagstaff (AM)	119
4022		1981 TL4	1981 Oct 8	L. Chernykh	Nauchnyj	
4023		1981 UN	1981 Oct 25	L. Brozek	Klet	
4024		1981 WQ	1981 Nov 24	E. Bowell	Flagstaff (AM)	119
4025		1981 WU	1981 Nov 24	E. Bowell	Flagstaff (AM)	119
4026		1982 BU1	1982 Jan 30	E. Bowell	Flagstaff (AM)	119
4027		1982 DN	1982 Feb 21	E. Bowell	Flagstaff (AM)	119
4028		1982 DV2	1982 Feb 18	L. G. Taff	Socorro	
4029		1982 KC1	1982 May 24	C. Shoemaker	Palomar	
4030		1984 EO1	1984 Mar 2	H. Debehogne	La Silla	
4031		1985 CL	1985 Feb 12	C. Shoemaker	Palomar	
4032		1985 UT4	1985 Oct 22	L. Zhuravleva	Nauchnyj	
4033		1986 FA	1986 Mar 16	M. Inoue and O. Muramatsu	Kobuchizawa	
4034		1986 PA	1986 Aug 2	E. F. Helin	Palomar	
4035		1986 WD	1986 Nov 22	K. Suzuki and T. Urata	Toyota	
4036		1987 DW5	1987 Feb 21	H. Debehogne	La Silla	
4037		1987 EC	1987 Mar 2	K. Suzuki and T. Urata	Toyota	
4038		1987 QH2	1987 Aug 21	E. W. Elst	La Silla	
4039		1987 SH	1987 Sep 17	T. Seki	Geisei	
4040		1987 SN1	1987 Sep 21	E. Bowell	Flagstaff (AM)	119

No.	Name	pd	dd	d	dp	
4041		1988 DN1	1988 Feb 19	T. Kojima	Chiyoda	
4042		1989 AT1	1989 Jan 15	K. Endate and K. Watanabe	Kitami	
4043		1175 T-3	1977 Oct 17	C. J. van Houten	Palomar	139
4044		5142 T-3	1977 Oct 16	C. J. van Houten	Palomar	139

NOTES

65. Planets 1125 and 3789. The original planet 1125 China was discovered 1928 Oct. 25 as 1928 UF by Y. C. Chang at Williams Bay and not observed again for many years. It was believed to have been recovered as 1957 UN1 on 1957 Oct. 30 by Chang at Nanking, but this identification was found to be incorrect. In agreement with the discoverer, the designation 1125 China was assigned to planet 1957 UN1. In 1986 C. M. Bardwell and S. Nakano independently identified planet 1986 QK1 with 1928 UF, and subsequently the permanent number 3789 was assigned to 1928 UF = 1986 QK1.

103. Planets discovered by the Indiana Asteroid Program, Goethe Link Observatory, University of Indiana. This program was conceived and directed by F. K. Edmondson; the plates were blinked and measured astrometrically by B. Potter and, following her retirement, by D. Owings; and the photometry was performed under the direction of T. Gehrels. During the years 1947–1967, in which the plates were exposed, a large number of people participated in various aspects of the program.

107. These planets have all been discovered as a result of the Palomar survey of faint minor planets and subsequently identified with planets observed at other oppositions. In Sept. and Oct. 1960, T. Gehrels exposed 130 plates with the 122 cm Schmidt camera at Palomar. In the following years C. J. van Houten and I. van Houten-Groeneveld measured these plates astrometrically and photometrically at Leiden. P. Herget, Cincinnati, computed the orbits of the planets found on the NORC computer, Dahlgren, Virginia, USA.

113. Planets discovered at Oak Ridge Observatory (until 1981 Harvard College's Agassiz Station). The principal observers are R. E. McCrosky, C.-Y. Shao, G. Schwartz, and J. H. Bulger, with some assistance from others.

119. Planets discovered at the Anderson Mesa station, which is operated by the Lowell Observatory.

122. Planet 2147. Oct. 24 observations should be considered a prediscovery.

123. on plates by E. F. Helin and S. J. Bus.

124. and G. de Sanctis.

125. on plates taken by B. A. Skiff at the Anderson Mesa station of the Lowell Observatory.

126. and E. Rangel Netto.

127. and P. Jensen and H. J. Fogh Olsen.

128. Planet 3044. and N. E. Kurochkin at the Sternberg Crimean Station.

129. Planets 3067 and 3511. and L. Zhuravleva.

130. Planet 3101. and J. Wall.

131. Planet 3124. at Steward Observatory's Kitt Peak Station.

132. Planet 3240. on Palomar Schmidt plates taken by E. F. Helin and E. Shoemaker.

133. Planets 3290, 3548, 4007. and I. van Houten-Groeneveld on Palomar Schmidt plates taken by T. Gehrels.

134. Planet 3432. and T. Urata at Yatsugatake-Kobuchizawa.

135. Planets 3489 and 3532. and G. Ojakangas.

136. Planet 3546. and V. Ivanova and A. Georgieva.

137. Planet 3624. and L. G. Karachkina.

138. Planet 3752. and J.-L. Heudier.

139. Planets discovered in the course of the Third Trojan Survey by C. J. van Houten and I. van Houten-Groeneveld on Palomar Schmidt Plates taken by T. Gehrels.

140. Planet 3815. and W. Wenzel.

141. Planet 3924. on plates taken by C. Kowal.

ASTEROID FAMILY IDENTIFICATIONS AND PROPER ELEMENTS

J. G. WILLIAMS
Jet Propulsion Laboratory

Asteroid families and proper elements are discussed in general in the chapters by Chapman et al. and Valsecchi et al. The table given here is a listing of proper elements and family memberships for the first 2065 numbered asteroids plus 20 higher numbered objects (most are planet crossers). The proper elements and family assignments for the first 1796 numbered objects are mostly identical to those given in Williams (1979). However, proper elements were recalculated for 68 objects in the earlier list and entries were made for asteroids omitted from that list (mostly Hilda and Trojan asteroids). All proper elements were calculated using the theory of Williams (1969). Family identifications have changed for several objects as a result of the improvement of the osculating elements, and a recalculation of the proper elements, of asteroids which formerly had poor orbits: 561, 637, 1037, 1265, 1381 and 1686. Asteroid numbers 330 and 864 have had peculiar histories and were not included in the earlier list; the asteroid now assigned to 864 is a member of a family while the one assigned to 330 is not. Thirteen new families have been added as a result of examining the additional and revised material. The former family 174 was split into two families: 174 and 196.

The tabulation for each asteroid contains thirteen columns. The first and last columns contain the asteroid number. The proper semimajor axis (AU) has several major short-period terms removed from it. The proper eccentricity and proper sine of inclination are defined at the zero proper argument of perihelion phase of the free oscillations; the former is a minimum and the latter is a maximum of the free oscillations. Different definitions are common so that proper e and sin i values from different sources should not be expected to

match. The proper longitude of perihelion and node (degrees) are measured from the equinox of B1950.0 and, after the computation at the above phase of the free oscillations, were referenced to the epoch of B1950.0 as though they were linear functions of time. These angles should match those from other sources. The average rates of the proper longitude of perihelion and node are in $''\text{yr}^{-1}$. The resonance column notes secular resonances, commensurabilities or other special characteristics. A number from 1 to 10 indicates a secular resonance arising from one of the ten frequencies governing the secular perturbations of the eccentricities and longitudes of perihelia of the major planets (Brouwer and van Woerkom 1950) while numbers 11–14 and 16–18 refer to the frequencies involved in the secular perturbations of the inclinations and nodes of the major planets. A secular resonance note can mean either that libration about the resonance is taking place or that the proper element calculation failed to converge satisfactorily due to the proximity of the resonance. The strong resonances are 5, 6 and 16 and the line of proper elements is blanked out for asteroids with this notation; the nonresonant rate, usually the node rate, is normally left but is untrustworthy. For the weaker resonances, the proper elements should be treated as noisy. For the frequent tenth resonance, which is known to be enough in error in Brouwer and van Woerkom's calculations to cause trouble, the noise in the proper eccentricity is of the order of 0.01. Minor planet 1866 is in the unusual secular resonance where twice the argument of perihelion rate plus the longitude of perihelion rate equals the sixth rate. Commensurabilities with Jupiter are indicated as 1 : 1 (Trojans), 3 : 2 (Hildas), ... Thus, 153 is a Hilda, 588 is a Trojan, 677 is in the 7 : 3 Kirkwood gap and 887 is in the 3 : 1 gap. A "W L" note in the resonance column indicates argument of perihelion libration, "JXR" means Jupiter crosser, and "SXR" means Saturn crosser. Minor planet 944 is both a Jupiter crosser and is temporarily in the 6 : 7 commensurability while 2335 is both an argument of perihelion librator and is in a secular resonance. The closest distances of approach to Mars and Jupiter are calculated along the straight Sun-Mars-asteroid and Sun-asteroid-Jupiter lines. These minima include the effects of secular perturbations on both the asteroid and planet. A negative value means that the orbits can intersect at some time and impact is possible. Blank distance values mean that a secular resonance caused the distance calculation to fail. The family column indicates the identity of any family to which the asteroid is known to belong.

Each family is designated by a number. Family numbers less than 100 correspond to families previously found by other researchers, but often altered here. Families 1–4 were found by Hirayama (1918a,b,1919,1923,1928, 1933), 21 and 24 are due to Brouwer (1951), families 36, 37, 38, 40 and 43 were found by Lindblad and Southworth (1971), and 67 and 75 are due to Arnold (1969). Family 1, Themis, has a core which is designated 1A here. Family numbers 101–191 are from Williams (1979). Families 192–204 are new here and in Williams and Hierath (1987). Virtually all of the families are

statistically significant, but the reliability and uniqueness of families varies considerably from family to family depending on the number of members and the crowding of families in the proper element space.

Generally the proper elements are more accurate in the inner belt than in the outer belt, but there are several causes for loss of accuracy and some of these influence only restricted regions of the proper element space or minor numbers of asteroids. Accuracy is degraded for minor planets near secular resonances or commensurabilities. Commensurabilities are abundant in the outermost part of the belt and cause a degradation there. Beyond the 2:1 Kirkwood gap there are relatively few asteroids and no recognized families. For planet crossers the proper elements are not constant; they change at times of close approach. For Mars crossers it is possible to get meaningful proper elements, but they are noisier than noncrossers. For deep Earth crossers it is necessary to disregard the perturbations from the Earth and the calculations are quite coarse. Contributions to the secular perturbations can come from second-order influences of short-period terms, but the theory employed does not allow for these. This is the cause of the degradation of accuracy near commensurabilities and in the outer belt. The most widespread effect is to change the rate of precession of the longitude of perihelion and virtually all asteroids beyond about 3 AU have perihelion rates significantly larger than given in the table. Consequently, the locations of the secular resonances will also shift and none of the outer belt asteroids marked as being resonant is trustworthy as demonstrated by the integrations of Froeschlé and Scholl (1987). Major influences on the other elements are more localized and, though the proper elements must be degraded, Themis family members are recognizable less than 0.02 AU from the edge of the 2:1 Kirkwood gap. Proper elements for Hildas and Trojans are not given here, but see Schubart (1982) and Bien and Schubart (1987).

Among the files of the Asteroids II machine-readable data base, a table of family identifications (up to number 1796 and up to family 191) is given as file FAMILY.DAT and the proper elements are in PROPER.DAT. The documentation files are FAMILY.DOC and PROPER.DOC, respectively. A tabulation of proper elements and family identifications for Palomar-Leiden survey (PLS) minor planets is given by Williams and Hierath (1987).

REFERENCES

Arnold, J. R. 1969. Asteroid families and jet streams. *Astron. J.* 74:1235–1242.
Bien, R., and Schubart, J. 1987. Three characteristic orbital parameters for the Trojan group of asteroids. *Astron. Astrophys.* 175:292–298.

Brouwer, D. 1951. Secular variations of the orbital elements of minor planets. *Astron. J.* 56:9–32.

Brouwer, D., and van Woerkom, A. J. J. 1950. The secular variations of the orbital elements of the principal planets. *Astron. Papers Amer. Ephemeris* 13, part 2:85–107.

Froeschlé, C., and Scholl, H. 1987. Orbital evolution of asteroids near the secular resonance ν_6. *Astron. Astrophys.* 179:294–303.

Hirayama, K. 1918a. Groups of asteroids probably of common origin. *Proc. Phys.-Math. Soc. Japan II* 9:354–361.

Hirayama, K. 1918b. Groups of asteroids probably of common origin. *Astron. J.* 31:185–188.

Hirayama, K. 1919. Further notes on the families of asteroids. *Proc. Phys.-Math. Soc. Japan III* 1:52–59.

Hirayama, K. 1923. Families of asteroids. *Japan J. Astron. Geophys.* 1:55–93.

Hirayama, K. 1928. Families of asteroids. Second paper. *Japan J. Astron. Geophys.* 5:137–162.

Hirayama, K. 1933. Present state of the families of asteroids. *Proc. Imp. Acad. Japan* 9:482–485.

Lindblad, B. A., and Southworth, R. B. 1971. A study of asteroid families and streams by computer techniques. In *Physical Studies of Minor Planets,* ed. T. Gehrels, NASA SP-267, pp. 337–352.

Schubart, J. 1982. Three characteristics parameters of orbits of Hilda-type asteroids. *Astron. Astrophys.* 114:200–204.

Williams J. G. 1969. Secular Perturbations in the Solar System. Ph.D. Thesis, Univ. of California at Los Angeles.

Williams, J. G. 1979. Proper elements and family memberships of the asteroids. In *Asteroids,* ed. T. Gehrels (Tucson: Univ. of Arizona Press), pp. 1040–1063.

Williams J. G., and Hierath, J. 1987. Palomar-Leiden minor planets: Proper elements, frequency distributions, belt boundaries, and family memberships. *Icarus* 72:276–303.

numb	a	e	sin i	wbar	node	wbar rate	node rate	res	Mars	Jup	fam	numb
1	2.767	.097	.169	147.8	78.7	50.6	−58.3		.611	1.918	67	1
2	2.771	.180	.584	156.1	184.3	1.5	−50.1		.013	1.773	129	2
3	2.670	.218	.245	63.6	172.6	40.5	−60.5		.234	1.770		3
4	2.362	.097	.112	228.0	107.1	36.8	−39.5		.308	2.422	169	4
5	2.578	.215	.083	143.5	152.7	47.3	−58.5		.197	1.868		5
6	2.425	.146	.258	39.0	140.2	30.9	−41.2		.141	2.157		6
7	2.386	.210	.115	54.2	264.3	37.8	−46.2		.055	2.127		7
8	2.201	.141	.097	60.0	116.9	31.8	−35.0		.024	2.457	189	8
9	2.386	.125	.083	91.6	65.5	38.6	−41.8		.273	2.321	170	9
10	3.144	.136	.092	224.5	285.1	85.7	−99.5		.865	1.465	110	10
11	2.452	.072	.068	302.6	133.7	41.5	−43.0		.463	2.374		11
12	2.334	.172	.167	293.4	236.8	33.9	−40.6		.081	2.266	171	12
13	2.576	.121	.281	135.1	41.0	32.6	−45.6		.370	2.094		13
14	2.588	.191	.153	181.1	86.0	44.3	−55.2		.259	1.924	150	14
15	2.644	.143	.231	41.2	292.6	39.7	−52.0		.428	1.994	140	15
16	2.922	.100	.045	20.2	171.4	69.1	−73.4		.802	1.810		16
17	2.469	.141	.088	247.3	133.1	41.8	−46.3		.304	2.186		17
18	2.296	.174	.179	29.7	153.2	32.1	−39.0		.023	2.285		18
19	2.442	.131	.039	43.6	233.6	41.7	−44.8		.312	2.243	158	19
20	2.408	.162	.026	114.4	242.5	40.5	−44.9		.210	2.206	162	20
21	2.435	.127	.038	322.4	76.7	41.5	−44.3		.315	2.261	158	21
22	2.910	.109	.222	71.7	63.9	50.7	−65.6		.679	1.718		22
23	2.626	.249	.180	130.9	61.1	44.8	−63.7		.126	1.732		23
24	3.133	.159	.020	155.3	315.1	90.6	−105.5		.794	1.409	1A	24
25	2.400	.183	.417	295.4	214.6	17.0	−38.4		.192	2.071		25
26	2.656	.134	.052	222.1	28.4	51.9	−56.7		.425	1.940		26
27	2.347	.187	.012	102.2	104.6	38.2	−43.6		.094	2.226		27
28	2.776	.176	.153	138.5	151.9	53.4	−66.6		.432	1.735		28
29	2.554	.066	.110	87.8	347.2	44.5	−47.0		.568	2.278		29
30	2.366	.103	.050	49.6	295.9	38.4	−40.4		.309	2.398		30
31	3.156	.099	.469	84.1	23.9	.9	−60.4		.925	1.509		31
32	2.588	.114	.109	189.9	228.9	46.2	−50.5		.468	2.121		32
33	2.865	.300	.039	341.6	334.0	68.9	−104.1		.166	1.308		33
34	2.687	.153	.100	167.7	197.4	51.9	−59.5		.383	1.852		34
35	2.997	.254	.158	200.5	341.2	68.9	−105.0		.366	1.278		35
36	2.747					27.8	−45.2	6				36
37	2.642	.165	.061	80.4	350.4	51.3	−62.3	10			142	37
38	2.740	.163	.141	120.5	293.8	52.4	−63.1		.424	1.795		38
39	2.769	.088	.172	10.3	162.7	50.2	−57.7		.661	1.963	67	39
40	2.267	.019	.064	82.2	99.3	34.6	−34.9		.399	2.702		40
41	2.765	.279	.291	211.9	176.0	40.5	−75.3		.111	1.493		41
42	2.441	.186	.137	314.1	81.4	39.0	−47.0		.155	2.120	157	42
43	2.203	.140	.071	260.7	261.0	32.4	−35.2		.046	2.473	185	43
44	2.422	.177	.054	124.2	145.5	40.7	−46.4		.178	2.158	24	44
45	2.721	.115	.107	217.5	155.8	53.1	−58.6		.563	1.961	133	45
46	2.525	.134	.044	355.8	206.0	45.4	−49.2		.372	2.139		46
47	2.881	.111	.092	302.1	351.5	63.6	−69.9		.729	1.819		47
48	3.112	.064	.116	113.4	194.7	78.1	−84.9		1.067	1.722		48
49	3.090	.193	.085	40.7	287.9	83.1	−105.8		.643	1.352		49
50	2.650	.236	.048	12.7	198.0	52.4	−66.6		.167	1.704		50
51	2.366	.111	.177	170.4	180.6	34.1	−39.0		.259	2.383		51
52	3.097	.119	.113	124.9	135.6	78.4	−90.0		.879	1.569		52
53	2.618	.215	.083	104.0	157.7	49.4	−61.2		.213	1.810		53
54	2.710	.179	.221	289.9	311.7	43.8	−59.6		.383	1.813	138	54
55	2.760	.102	.124	15.4	1.8	53.9	−59.6		.633	1.962		55
56	2.598	.208	.160	287.9	201.1	44.4	−57.4		.219	1.870		56
57	3.153	.095	.271	61.4	202.7	50.1	−77.8		.944	1.547	108	57
58	2.700	.088	.083	189.7	173.5	53.0	−56.1		.623	2.053	132	58
59	2.713	.094	.147	27.9	177.1	49.7	−55.6		.615	2.015		59
60	2.393	.201	.076	111.7	206.3	39.2	−46.3		.092	2.136		60

numb	a	e	sin i	wbar	node	wbar rate	node rate	res	Mars	Jup	fam	numb
61	2.984	.122	.319	341.4	330.6	36.4	−65.0		.730	1.686		61
62	3.122	.146	.023	47.6	151.2	88.8	−101.0		.825	1.462	1A	62
63	2.395	.119	.110	254.1	330.5	38.1	−41.7		.289	2.327	165	63
64	2.682	.151	.041	141.3	293.1	53.7	−59.9		.443	1.912		64
65	3.429	.129	.056	244.9	175.6	126.6	−146.6		1.122	1.189		65
66	2.646	.171	.059	41.4	326.1	51.3	−58.8	10	.330	1.869	142	66
67	2.421	.152	.119	298.7	211.0	38.8	−44.1		.226	2.223		67
68	2.782	.144	.132	343.8	39.0	55.0	−64.4		.536	1.827	126	68
69	2.979	.174	.160	124.7	195.4	64.8	−84.0		.607	1.526		69
70	2.616	.146	.198	289.7	43.0	41.8	−51.9		.396	2.017	138	70
71	2.755	.117	.434	222.7	314.3	13.6	−46.0		.642	1.859		71
72	2.266	.077	.105	292.1	212.4	33.7	−35.4		.255	2.564	174	72
73	2.665	.038	.044	136.9	342.8	52.2	−52.8		.709	2.206		73
74	2.780	.199	.077	10.7	214.5	58.9	−72.2		.393	1.683		74
75	2.671	.267	.091	331.3	348.5	52.6	−72.3		.092	1.607		75
76	3.390	.186	.053	105.8	232.3	125.9	−164.2		.890	1.043		76
77	2.668	.109	.048	80.8	338.0	52.5	−55.7		.530	2.025	141	77
78	2.620	.232	.166	132.2	330.3	45.3	−61.5		.169	1.780		78
79	2.444	.175	.090	57.0	216.4	40.8	−47.1		.196	2.134	75	79
80	2.296	.147	.162	7.2	223.4	32.7	−38.0		.095	2.353		80
81	2.854	.179	.149	57.8	351.9	58.2	−73.5		.496	1.649		81
82	2.765	.246	.051	142.1	5.9	59.6	−78.8		.251	1.576		82
83	2.431	.120	.081	187.7	18.2	40.4	−43.5		.324	2.281		83
84	2.362	.190	.169	340.9	321.9	34.8	−43.0		.068	2.204	171	84
85	2.654	.143	.225	320.5	209.2	40.6	−52.7		.440	1.980	140	85
86	3.108	.176	.067	35.7	85.9	85.8	−105.1		.711	1.385		86
87	3.486	.051	.171	320.0	71.3	98.7	−121.6		1.440	1.390		87
88	2.768	.143	.111	297.5	275.5	55.7	−63.9		.532	1.846		88
89	2.552	.089	.296	37.9	308.4	29.9	−42.2		.289	2.068		89
90	3.148	.150	.024	295.7	43.3	91.7	−105.5		.832	1.419	1A	90
91	2.590	.113	.039	100.1	343.3	48.6	−51.5		.474	2.114		91
92	3.193	.061	.152	311.3	102.4	78.8	−90.0		1.152	1.644	106	92
93	2.755	.138	.158	41.4	135.6	51.3	−61.0	10	.313	1.661	127	93
94	3.158	.068	.145	77.5	355.4	77.1	−87.5		1.100	1.658	106	94
95	3.068	.112	.241	46.7	247.4	54.3	−76.3		.858	1.605	116	95
96	3.051	.164	.298	162.2	317.2	43.9	−77.7		.676	1.469		96
97	2.668	.228	.222	75.6	164.9	42.9	−62.7		.212	1.736		97
98	2.687	.225	.280	156.1	352.6	37.6	−61.2		.217	1.733		98
99	2.664	.215	.231	225.9	36.1	41.6	−60.3		.244	1.779		99
100	3.096	.145	.094	296.0	135.0	81.1	−95.1		.799	1.488	114	100
101	2.584	.104	.182	322.9	338.8	41.5	−48.0		.485	2.159	144	101
102	2.661	.234	.105	1.2	225.4	51.3	−66.5	10	.138	1.663		102
103	2.702	.058	.081	293.2	145.5	53.1	−55.1		.707	2.132	134	103
104	3.149	.141	.044	80.5	16.0	90.6	−103.2		.861	1.447		104
105	2.374	.168	.387	234.7	187.0	19.1	−37.1		.217	2.131		105
106	3.172	.136	.064	39.8	52.3	91.2	−104.3		.890	1.440		106
107	3.488	.084	.171	139.4	182.8	100.2	−128.0		1.318	1.273		107
108	3.218	.123	.086	177.2	337.4	93.6	−107.0		.970	1.427	101	108
109	2.696	.277	.167	64.1	351.9	49.6	−74.4		.076	1.553		109
110	2.733	.047	.090	315.0	49.9	54.3	−56.3		.776	2.139	130	110
111	2.593	.124	.102	126.1	300.4	46.8	−51.6		.446	2.087		111
112	2.434	.090	.056	335.4	309.5	41.1	−42.9		.403	2.350	161	112
113	2.376	.123	.077	190.0	130.1	38.4	−41.3		.268	2.342	170	113
114	2.676	.181	.083	165.4	178.6	52.2	−61.4		.325	1.816		114
115	2.380	.171	.223	66.3	307.7	32.2	−41.5		.083	2.184	163	115
116	2.768	.176	.050	162.0	51.9	58.9	−68.6		.454	1.761		116
117	2.991	.028	.264	135.6	345.4	45.3	−62.8		1.056	1.952		117
118	2.439	.164	.128	92.2	40.8	39.2	−45.6		.210	2.174		118
119	2.581	.049	.108	26.8	212.7	45.7	−47.8		.634	2.294		119
120	3.118	.088	.135	204.6	332.9	76.1	−86.6		.992	1.643		120

numb	a	e	sin i	wbar	node	wbar rate	node rate	res	Mars	Jup	fam	numb
121	3.451	.089	.116	1.5	71.3	114.6	−132.3		1.268	1.297		121
122	3.222	.071	.033	183.6	220.0	97.5	−101.3		1.152	1.590		122
123	2.696	.125	.130	84.6	304.7	50.3	−57.0		.490	1.937		123
124	2.630	.080	.056	229.3	207.2	50.2	−52.2		.572	2.127	141	124
125	2.743	.086	.079	250.1	183.0	55.7	−58.9		.678	2.026	132	125
126	2.439	.069	.046	349.2	5.2	41.4	−42.5		.460	2.396		126
127	2.756	.092	.139	152.6	24.8	52.4	−58.4		.636	1.974		127
128	2.750	.088	.091	24.0	73.2	55.5	−59.1		.677	2.015	132	128
129	2.872	.228	.226	41.4	310.0	51.3	−79.0	10	.112	1.258		129
130	3.119					27.8	−76.7	6				130
131	2.431	.098	.073	205.0	60.9	40.6	−42.8		.380	2.339	161	131
132	2.611	.212	.533	143.0	253.6	8.1	−47.2		.089	1.701		132
133	3.065	.148	.150	237.6	315.3	71.4	−88.8		.760	1.510		133
134	2.565	.105	.211	91.6	342.1	38.5	−46.4		.459	2.183		134
135	2.427	.174	.048	315.8	323.6	41.1	−46.5		.191	2.158	160	135
136	2.287	.023	.173	286.2	189.5	31.7	−34.4		.364	2.632		136
137	3.119	.159	.264	296.9	208.2	53.1	−86.2		.719	1.399	113	137
138	2.447	.138	.044	304.4	42.1	41.9	−45.5		.298	2.220	158	138
139	2.785	.200	.195	166.9	357.1	50.2	−68.6		.344	1.642	198	139
140	2.732	.201	.036	291.7	112.9	57.3	−69.0		.357	1.732		140
141	2.666	.162	.233	18.7	313.8	40.8	−54.9		.390	1.917	140	141
142	2.419	.159	.058	210.9	286.1	40.5	−45.1		.223	2.201	24	142
143	2.761	.094	.212	205.0	328.5	45.8	−56.0		.671	1.984		143
144	2.655	.196	.072	10.5	70.0	51.3	−56.9	10			136	144
145	2.673	.160	.208	128.6	74.2	43.4	−56.1		.410	1.905	138	145
146	2.719	.086	.211	212.0	84.0	43.9	−53.1		.658	2.056		146
147	3.137	.011	.053	195.1	260.5	86.6	−87.6		1.265	1.865		147
148	2.771	.098	.433	22.3	145.0	12.5	−45.0		.711	1.902		148
149	2.175	.079	.025	96.8	183.2	32.0	−32.8		.159	2.635		149
150	2.982	.090	.050	354.1	231.1	73.5	−77.6		.883	1.777		150
151	2.592	.069	.103	171.6	31.3	46.6	−49.1		.592	2.230		151
152	3.140	.074	.204	117.8	35.7	64.5	−81.4		1.053	1.662		152
153	3.969							3:2				153
154	3.184					27.8		6				154
155	2.759	.262	.212	91.1	31.7	48.5	−75.7		.164	1.528		155
156	2.729	.246	.196	214.6	249.5	48.2	−70.7		.198	1.609		156
157	2.579	.209	.210	114.5	56.9	40.0	−54.6		.196	1.900		157
158	2.869	.045	.038	103.7	277.8	65.1	−66.1		.917	2.020	3	158
159	3.106	.117	.091	126.8	143.8	81.6	−91.5		.893	1.565	112	159
160	2.728	.052	.069	95.0	352.7	55.1	−56.6		.760	2.134	134	160
161	2.379	.095	.155	300.3	13.9	35.6	−39.4		.319	2.414		161
162	3.022	.206	.105	154.6	29.9	75.4	−98.7		.546	1.389		162
163	2.368	.208	.082	107.5	174.0	38.1	−45.6		.053	2.149	166	163
164	2.633	.213	.463	1.8	79.9	15.2	−49.7		.241	1.726		164
165	3.130	.075	.215	264.5	301.5	61.7	−79.6		1.049	1.660		165
166	2.686	.167	.208	39.5	132.3	43.7	−57.3		.393	1.885	138	166
167	2.854	.043	.037	236.7	197.2	64.0	−64.9		.909	2.042	3	167
168	3.379	.025	.089	54.5	221.3	109.4	−114.9		1.439	1.585		168
169	2.358	.093	.096	321.4	346.3	37.2	−39.3		.320	2.434	197	169
170	2.554	.099	.266	121.2	299.6	33.1	−43.8		.425	2.188	4	170
171	3.134	.161	.024	160.0	101.8	90.6	−106.1		.787	1.401	1A	171
172	2.380	.070	.178	324.7	327.8	34.5	−38.3		.378	2.469		172
173	2.743	.160	.243	16.3	150.2	42.4	−58.9		.455	1.835		173
174	2.861	.133	.235	244.4	324.9	47.3	−63.9		.633	1.769		174
175	3.212	.176	.057	330.8	2.5	98.5	−121.0		.794	1.268		175
176	3.178	.153	.393	16.3	203.6	23.7	−76.4		.768	1.211		176
177	2.770	.198	.040	28.1	314.7	59.6	−71.7		.393	1.700		177
178	2.460	.059	.022	224.4	24.8	42.6	−43.3		.507	2.395		178
179	2.972	.070	.157	350.3	255.8	62.9	−71.1		.926	1.840	121	179
180	2.722	.190	.034	136.4	290.5	56.6	−66.9		.378	1.772		180

numb	a	e	sin i	wbar	node	wbar rate	node rate	res	Mars	Jup	fam	numb
181	3.132	.195	.325	114.4	151.8	42.0	−88.7		.613	1.293		181
182	2.416	.175	.019	67.9	123.9	40.9	−46.1		.183	2.164	162	182
183	2.795	.183	.503	40.2	141.1	8.8	−52.8		.366	1.585		183
184	3.183	.113	.038	187.4	304.0	93.8	−102.2		.979	1.499	103	184
185	2.739	.099	.389	356.3	154.7	20.0	−46.0		.681	1.900		185
186	2.362	.075	.222	334.3	12.3	31.3	−36.8		.282	2.409		186
187	2.732	.256	.183	210.0	12.8	49.9	−73.5		.155	1.561		187
188	2.762	.141	.227	295.6	242.6	44.6	−58.8		.533	1.860		188
189	2.450	.011	.098	89.8	211.9	40.5	−41.6		.611	2.526		189
190	3.969							3:2				190
191	2.896	.047	.192	38.0	164.9	53.5	−62.4		.909	1.976		191
192	2.403	.207	.130	16.6	333.5	37.9	−46.5		.072	2.114		192
193	2.600	.265	.252	80.0	345.7	38.2	−61.5		.043	1.741		193
194	2.616	.166	.306	322.2	164.1	31.5	−49.6		.241	1.902		194
195	2.879	.068	.123	154.5	358.5	60.7	−65.6		.848	1.943		195
196	3.114	.039	.108	216.7	68.5	79.1	−83.9		1.151	1.798		196
197	2.739	.130	.137	309.3	78.7	52.2	−60.0		.511	1.881	133	197
198	2.458	.175	.193	.0	268.4	36.6	−46.0		.189	2.131		198
199	3.167	.189	.249	252.6	90.9	60.5	−100.3		.686	1.268		199
200	2.737	.084	.136	70.7	318.8	51.8	−56.9		.608	1.975		200
201	2.678	.140	.094	315.3	168.2	51.6	−57.9		.372	1.856		201
202	3.072	.127	.139	146.0	143.1	72.9	−86.8		.827	1.572		202
203	2.737	.039	.064	84.2	331.5	55.8	−56.9		.809	2.162		203
204	2.671	.177	.156	247.7	210.0	47.9	−59.3		.359	1.858		204
205	2.777	.019	.195	94.9	217.1	47.8	−54.8		.891	2.176		205
206	2.740	.050	.056	135.2	161.2	56.1	−57.4		.777	2.130		206
207	2.284	.064	.058	183.8	20.5	35.3	−36.1		.317	2.586		207
208	2.893	.045	.037	170.8	332.1	66.8	−67.8		.938	1.997	3	208
209	3.148	.076	.132	227.1	351.5	79.1	−88.5		1.059	1.648		209
210	2.722	.095	.085	60.2	20.8	54.1	−57.7		.632	2.019	132	210
211	3.044	.149	.088	90.4	268.2	77.3	−90.3		.745	1.533		211
212	3.113	.090	.094	74.2	307.7	81.4	−88.8		.989	1.642		212
213	2.754	.143	.103	267.8	128.7	55.4	−63.1		.521	1.861		213
214	2.611	.057	.069	143.7	328.0	48.8	−50.2		.639	2.234	143	214
215	2.767	.015	.029	252.3	346.9	58.5	−58.7		.905	2.203		215
216	2.795	.224	.235	40.1	220.8	46.6	−71.0		.310	1.590		216
217	2.869	.276	.188	312.1	175.0	57.5	−91.8		.208	1.363		217
218	2.667	.130	.264	208.6	173.0	36.8	−50.9		.459	2.013	137	218
219	2.354	.164	.198	346.8	206.7	32.9	−40.5		.101	2.251		219
220	2.349	.203	.159	334.0	258.2	34.9	−43.5		.029	2.191	171	220
221	3.012	.071	.174	318.9	147.0	62.8	−73.2		.957	1.796	2	221
222	3.135	.157	.019	247.0	57.7	90.7	−105.3		.801	1.412	1A	222
223	3.089	.136	.027	124.4	10.8	85.0	−95.1		.831	1.525	1	223
224	2.645	.048	.107	233.9	343.5	48.9	−51.1		.690	2.219		224
225	3.382	.150	.421	300.7	203.1	15.0	−88.8		1.004	1.048		225
226	2.712	.172	.268	279.9	140.2	38.5	−56.8		.384	1.855		226
227	3.145	.214	.201	221.9	321.1	70.7	−109.9		.591	1.226		227
228	2.201	.183	.053	330.7	299.5	32.6	−37.0		−.049	2.382		228
229	3.411	.120	.036	319.3	356.5	125.4	−141.2		1.139	1.236		229
230	2.382	.038	.177	65.5	241.5	34.5	−37.8		.456	2.542		230
231	2.919	.166	.105	244.3	339.6	66.3	−79.4		.593	1.620		231
232	2.553	.205	.100	194.2	159.7	45.5	−55.4		.205	1.927	152	232
233	2.660	.064	.147	343.2	228.0	47.3	−51.4		.664	2.168		233
234	2.386	.162	.251	340.0	147.3	30.5	−40.6		.050	2.143		234
235	2.882	.073	.141	242.5	62.1	59.1	−65.3		.840	1.921		235
236	2.800	.149	.134	358.4	195.9	55.9	−66.0		.539	1.796	126	236
237	2.763	.092	.152	247.6	83.1	51.9	−58.4		.622	1.939		237
238	2.907	.103	.218	41.4	185.0	51.3	−65.3	10	.666	1.712		238
239	2.970	.196	.107	32.0	191.0	70.4	−89.4		.536	1.481		239
240	2.664	.180	.020	64.6	136.5	53.3	−61.6		.348	1.853		240

numb	a	e	sin i	wbar	node	wbar rate	node rate	res	Mars	Jup	fam	numb
241	3.050	.065	.118	333.6	272.4	72.9	−79.2		1.009	1.782		241
242	2.864	.127	.214	131.7	213.3	50.0	−64.7		.635	1.755		242
243	2.862	.045	.036	122.6	300.6	64.6	−65.6		.909	2.026	3	243
244	2.174	.103	.060	39.8	212.5	31.6	−33.2		.096	2.574	193	244
245	3.091	.168	.074	33.5	53.5	83.1	−99.7		.729	1.424		245
246	2.695	.100	.269	230.2	165.8	36.7	−50.1		.566	2.064		246
247	2.742	.151	.446	42.9	353.7	13.9	−48.3		.519	1.776		247
248	2.472	.075	.086	225.8	251.2	41.9	−43.7		.475	2.344	156	248
249	2.378	.173	.181	23.5	328.2	34.6	−42.4		.120	2.225		249
250	3.148	.114	.229	112.3	19.9	60.5	−84.6		.930	1.519		250
251	3.094	.095	.176	108.5	163.2	67.8	−81.8		.953	1.641	115	251
252	3.157	.037	.181	359.7	209.0	70.1	−82.5		1.198	1.759		252
253	2.647	.230	.120	334.5	192.9	49.4	−64.4		.184	1.737		253
254	2.195	.116	.070	231.1	22.9	32.1	−34.1		.088	2.531	188	254
255	2.746	.107	.164	167.2	7.9	50.0	−57.6		.593	1.943		255
256	3.001	.100	.233	211.2	187.4	52.7	−70.5		.826	1.696	120	256
257	3.114	.102	.057	79.2	15.5	84.9	−91.3		.954	1.606		257
258	2.616	.159	.255	8.7	213.3	36.7	−50.9		.342	1.995	21	258
259	3.139	.140	.170	237.8	88.1	73.3	−93.9		.840	1.455	109	259
260	3.445	.084	.105	323.4	178.9	116.4	−131.4		1.285	1.322		260
261	2.331	.132	.050	162.3	99.9	37.2	−40.0		.212	2.370	172	261
262	2.555	.197	.130	70.4	29.2	44.2	−54.2		.220	1.950	43	262
263	2.887	.042	.037	23.3	245.1	66.3	−67.3		.943	2.010	3	263
264	2.798	.090	.167	37.3	45.6	52.2	−59.8		.674	1.923	67	264
265	2.419	.175	.485	218.6	329.8	10.1	−37.1		.177	2.077		265
266	2.804	.125	.247	37.9	240.4	43.3	−59.0		.607	1.862		266
267	2.774	.113	.087	247.9	69.0	57.2	−62.3		.631	1.925		267
268	3.097	.170	.025	185.6	139.2	86.7	−102.4		.732	1.413	1	268
269	2.616	.204	.096	265.6	169.4	48.7	−59.6		.244	1.848		269
270	2.198	.092	.053	334.8	250.6	32.5	−33.7		.151	2.585	193	270
271	3.006	.067	.076	42.9	322.4	73.6	−77.3		.972	1.816		271
272	2.778	.050	.069	151.1	24.1	58.0	−59.6		.815	2.095	38	272
273	2.395	.149	.364	279.8	162.9	21.1	−37.3		.275	2.141		273
274	3.044	.158	.046	205.6	92.8	80.3	−93.2		.725	1.512		274
275	2.771	.201	.071	173.4	142.7	58.7	−71.8		.383	1.688		275
276	3.115	.042	.380	170.1	214.4	19.1	−59.3		1.165	1.687		276
277	2.886	.051	.037	3.7	254.0	66.3	−67.6		.915	1.984	3	277
278	2.755	.172	.125	197.3	58.9	54.3	−65.6		.430	1.779	131	278
279	4.294							4:3				279
280	2.943	.112	.133	116.3	2.6	64.4	−73.6		.771	1.751		280
281	2.188	.134	.084	75.2	26.6	31.6	−34.3		.026	2.484	189	281
282	2.339	.099	.153	108.3	150.4	34.4	−38.0		.270	2.438		282
283	3.046	.105	.162	352.7	300.6	67.3	−79.7		.880	1.661	118	283
284	2.358	.189	.159	277.8	235.0	34.9	−42.8		.063	2.207	171	284
285	3.089	.169	.316	316.4	308.5	41.3	−80.0		.672	1.424		285
286	3.194	.021	.297	140.5	152.7	42.4	−72.0		1.255	1.780		286
287	2.353	.047	.170	183.9	146.2	34.0	−37.0		.404	2.547		287
288	2.760	.242	.066	199.8	126.8	58.8	−77.5		.254	1.590		288
289	2.874	.166	.115	11.2	193.0	62.2	−74.7		.553	1.670		289
290	2.337	.188	.406	127.8	12.0	17.5	−36.7		.145	2.128		290
291	2.222	.141	.036	140.7	183.9	33.5	−36.1		.078	2.467	187	291
292	2.529	.018	.248	179.2	41.1	33.8	−41.3		.628	2.434		292
293	2.863	.120	.263	154.8	59.6	43.0	−61.1		.664	1.819	125	293
294	3.148	.213	.092	312.1	146.2	89.3	−120.7		.616	1.223		294
295	2.797	.152	.068	75.2	278.6	59.9	−67.9		.543	1.794		295
296	2.229	.123	.026	26.4	143.7	33.8	−35.7		.129	2.505	187	296
297	3.171	.110	.144	314.6	326.3	79.7	−94.2		.970	1.514		297
298	2.264	.145	.107	147.4	2.6	33.6	−37.3		.094	2.412	180	298
299	2.434	.041	.043	66.9	252.4	41.3	−41.7		.524	2.468		299
300	3.208	.011	.018	282.8	316.0	95.8	−96.1		1.332	1.796		300

numb	a	e	sin i	wbar	node	wbar rate	node rate	res	Mars	Jup	fam	numb
301	2.725	.083	.074	236.6	154.1	54.7	−57.5		.672	2.051	132	301
302	2.406	.105	.061	81.5	352.7	39.8	−42.0		.343	2.346	161	302
303	3.122	.045	.130	92.1	336.4	76.6	−83.6		1.136	1.772		303
304	2.403	.118	.263	339.6	162.8	29.7	−38.8		.108	2.168		304
305	3.089	.198	.098	114.7	220.6	82.0	−106.4		.621	1.337		305
306	2.358	.117	.120	296.5	148.4	36.4	−39.8		.254	2.383	165	306
307	2.908	.125	.087	78.1	103.7	66.1	−73.6		.711	1.751		307
308	2.750	.045	.078	238.1	196.3	55.9	−57.5		.800	2.133	130	308
309	2.665	.116	.073	271.5	342.0	51.7	−55.7		.437	1.941	139	309
310	2.762	.153	.073	190.4	243.5	57.5	−65.3		.511	1.828		310
311	2.898	.041	.037	180.2	73.1	67.1	−68.0		.954	2.005	3	311
312	2.782	.173	.169	249.8	358.6	52.1	−66.1		.409	1.707		312
313	2.376	.226	.214	139.0	184.9	33.0	−45.2		−.039	2.078		313
314	3.151	.144	.210	358.7	175.8	65.5	−91.7		.839	1.420	202	314
315	2.242	.120	.044	331.4	178.4	34.0	−36.1		.149	2.501	186	315
316	3.175	.134	.024	96.4	149.1	94.2	−105.6		.906	1.442	1	316
317	2.287	.042	.031	331.8	174.8	35.7	−36.0		.375	2.631		317
318	3.199	.075	.178	126.7	168.8	74.0	−89.6		1.107	1.597		318
319	3.392	.184	.198	49.0	192.1	89.0	−141.0		.874	1.036		319
320	3.013	.074	.175	10.9	226.6	62.7	−73.3		.949	1.787	2	320
321	2.886	.046	.038	120.5	14.3	66.2	−67.3		.930	2.000	3	321
322	2.783	.180	.172	4.6	257.4	52.0	−66.9		.388	1.685		322
323	2.383	.195	.438	32.5	101.5	15.3	−38.1		.137	2.068	168	323
324	2.683	.285	.230	10.9	318.3	43.8	−72.1		.061	1.566		324
325	3.206	.128	.168	67.6	337.9	78.3	−99.4		.936	1.421		325
326	2.318	.165	.412	256.5	28.0	16.2	−34.4		.177	2.211		326
327	2.776	.056	.130	262.5	346.7	54.1	−58.2		.782	2.073		327
328	3.106	.105	.291	120.1	350.6	44.3	−73.4		.915	1.592		328
329	2.476	.113	.284	154.7	182.0	29.8	−40.8		.168	2.090		329
330	2.468	.220	.116	42.7	142.9	41.2	−51.5		.096	1.999		330
331	3.025	.063	.102	349.6	11.5	72.8	−77.6		.999	1.811		331
332	2.773	.064	.045	306.2	8.9	58.6	−60.2		.773	2.061		332
333	3.124	.130	.075	13.7	336.8	85.3	−96.8		.872	1.505	112	333
334	3.891	.049	.064	233.0	142.4	228.8	−246.3		1.802	1.009		334
335	2.472	.166	.084	276.1	160.3	42.1	−48.0		.245	2.120	154	335
336	2.252	.091	.110	232.3	235.9	33.0	−35.1		.206	2.540	174	336
337	2.383	.153	.143	109.2	350.1	36.5	−42.2		.185	2.270		337
338	2.913	.025	.125	155.6	286.2	62.4	−66.3		1.010	2.036	124	338
339	3.012	.067	.170	318.6	181.3	63.3	−73.1		.970	1.808	2	339
340	2.748	.102	.079	87.1	13.3	56.0	−59.9		.639	1.979	132	340
341	2.199	.129	.092	318.2	25.5	31.9	−34.5		.053	2.489	189	341
342	2.567	.142	.146	109.6	236.5	43.5	−50.5		.374	2.076	149	342
343	2.412	.211	.049	55.6	20.5	40.5	−48.3		.089	2.087		343
344	2.595	.224	.320	265.5	41.1	30.7	−53.6		.015	1.734		344
345	2.325	.092	.181	114.9	215.3	32.6	−36.8		.253	2.449		345
346	2.796	.062	.134	32.8	92.1	55.0	−59.5		.787	2.039		346
347	2.612	.191	.198	170.7	85.1	42.1	−55.5		.269	1.905		347
348	2.970	.079	.151	124.3	89.2	63.7	−72.0		.898	1.814	121	348
349	2.925	.052	.136	24.9	25.3	62.2	−67.6		.937	1.944	124	349
350	3.116	.119	.400	76.6	91.6	19.2	−65.9		.912	1.442		350
351	2.765	.178	.145	138.9	98.0	53.5	−66.5		.417	1.741	128	351
352	2.194	.130	.070	54.4	247.6	32.1	−34.5		.054	2.499	188	352
353	2.736	.307	.084	68.8	111.1	57.4	−86.5		.055	1.443		353
354	2.796	.159	.309	148.2	142.6	35.1	−58.4		.459	1.775		354
355	2.540	.112	.082	114.6	340.7	45.1	−48.4		.439	2.176		355
356	2.757	.173	.163	41.4	303.5	51.3	−64.1	10	.278	1.629		356
357	3.148	.035	.247	47.3	141.5	54.6	−75.1		1.177	1.764		357
358	2.877	.134	.062	76.9	190.9	65.5	−72.7		.664	1.760		358
359	2.729	.117	.119	333.4	357.6	52.8	−59.0		.555	1.941	133	359
360	3.002	.147	.197	73.9	138.1	60.0	−79.1		.703	1.584		360

numb	a	e	sin i	wbar	node	wbar rate	node rate	res	Mars	Jup	fam	numb
361	3.969							3:2				361
362	2.579	.042	.134	104.4	20.7	44.3	−47.1		.654	2.316		362
363	2.748	.032	.088	349.6	58.9	55.2	−56.9		.832	2.171	130	363
364	2.221	.154	.096	79.0	111.5	32.5	−36.2		.028	2.426	180	364
365	2.802	.127	.226	46.6	189.5	45.9	−60.0		.607	1.851		365
366	3.142	.047	.193	276.3	341.7	66.7	−80.6		1.147	1.743		366
367	2.219	.147	.040	144.0	86.0	33.3	−36.2		.061	2.456	187	367
368	3.070	.170	.163	308.0	233.2	70.5	−92.6		.690	1.438		368
369	2.649	.055	.204	10.2	94.6	41.9	−48.7		.675	2.220		369
370	2.324	.046	.148	20.0	287.9	34.1	−36.4		.382	2.576		370
371	2.727	.062	.148	240.7	282.8	50.1	−54.8		.710	2.081		371
372	3.146	.156	.453	99.4	332.9	11.7	−70.0		.789	1.287		372
373	3.116	.129	.268	.6	.9	51.3	−79.8	10	.743	1.424		373
374	2.780	.105	.169	41.4	39.8	51.3	−59.6	10	.397	1.694	67	374
375	3.127	.073	.284	309.3	334.1	45.5	−72.3		1.039	1.667	111	375
376	2.289	.168	.111	241.7	298.6	34.4	−39.3		.066	2.337	175	376
377	2.691	.068	.126	66.3	217.8	50.0	−53.8		.657	2.106		377
378	2.777	.091	.136	38.7	239.2	53.8	−59.7		.679	1.974		378
379	3.137	.148	.032	348.1	216.8	90.1	−103.2		.832	1.440	1	379
380	2.678	.087	.089	292.9	94.4	51.6	−54.7		.512	1.990		380
381	3.212	.111	.205	253.3	129.6	69.7	−92.9		.991	1.473		381
382	3.121	.192	.165	216.2	310.6	74.8	−103.7		.655	1.317		382
383	3.135	.148	.025	61.7	90.8	90.2	−103.3		.828	1.439	1A	383
384	2.651	.159	.088	89.0	37.1	50.5	−57.7		.360	1.883		384
385	2.847	.162	.246	171.6	340.2	45.8	−65.7		.532	1.709		385
386	2.896					27.8	−51.7	6				386
387	2.742	.200	.303	278.7	133.4	35.9	−60.3		.306	1.733		387
388	3.006	.042	.119	286.7	345.5	69.4	−74.1		1.044	1.894		388
389	2.608	.098	.162	180.7	281.3	44.0	−49.7		.527	2.141	144	389
390	2.653	.155	.230	140.5	302.1	40.3	−53.5		.402	1.948	140	390
391	2.320	.255	.420	3.3	220.0	17.9	−40.9		−.039	1.984		391
392	2.885	.109	.254	31.5	214.5	44.9	−62.2		.721	1.821	125	392
393	2.775	.241	.318	293.7	215.5	36.1	−67.8		.197	1.577		393
394	2.762	.189	.100	329.7	62.1	56.5	−68.6		.399	1.730		394
395	2.786	.095	.078	247.5	264.2	58.2	−62.1		.695	1.959		395
396	2.742	.167	.063	255.6	258.0	56.7	−65.5		.453	1.814		396
397	2.636	.197	.243	12.9	234.8	39.1	−56.1		.266	1.866		397
398	2.739	.224	.187	87.6	282.3	49.2	−68.7		.265	1.648		398
399	3.053	.112	.236	176.4	341.8	54.7	−75.4		.849	1.623	116	399
400	3.129	.137	.206	194.3	322.1	65.1	−88.7		.834	1.479	202	400
401	3.342	.045	.095	233.3	25.9	104.1	−110.7		1.335	1.555		401
402	2.556	.152	.195	149.2	132.1	39.8	−49.3		.334	2.069	148	402
403	2.812	.088	.181	41.4	145.2	51.3	−59.8	10	.540	1.772	67	403
404	2.593	.211	.246	204.8	95.1	37.6	−54.7		.188	1.888		404
405	2.584	.258	.252	198.4	261.7	37.5	−59.3		.049	1.781		405
406	2.916	.142	.092	347.4	306.5	66.6	−76.3		.664	1.691		406
407	2.625	.036	.148	34.7	292.2	45.3	−48.8		.712	2.281		407
408	3.164	.106	.183	52.1	297.6	71.6	−89.9		.971	1.534	204	408
409	2.576	.093	.213	214.7	244.9	38.7	−46.3		.502	2.202		409
410	2.727	.232	.170	262.3	98.8	50.1	−69.4		.219	1.623		410
411	2.935	.104	.245	272.7	109.0	48.2	−65.6		.773	1.771		411
412	2.763	.071	.222	184.8	107.8	44.3	−54.3		.737	2.051		412
413	2.583					27.8	−67.1	6				413
414	3.503	.070	.145	102.9	114.9	110.9	−132.2		1.385	1.310		414
415	2.788	.277	.144	70.5	136.7	56.7	−84.8		.152	1.460		415
416	2.787	.227	.210	245.8	52.8	49.1	−72.1		.293	1.576		416
417	2.799	.174	.124	184.8	211.0	56.9	−69.0		.469	1.729		417
418	2.593	.084	.137	23.6	252.6	44.8	−48.9		.551	2.197		418
419	2.596	.247	.086	263.1	235.7	48.4	−63.4		.118	1.763	146	419
420	3.418	.044	.135	143.6	250.0	103.5	−116.9		1.402	1.482		420

numb	a	e	sin i	wbar	node	wbar rate	node rate	res	Mars	Jup	fam	numb
421	2.538	.258	.141	41.8	193.3	43.3	−59.5		.041	1.820		421
422	2.228	.161	.082	346.4	1.6	33.0	−36.8		.027	2.406	184	422
423	3.068	.052	.178	229.3	66.9	65.3	−76.0		1.069	1.801	200	423
424	2.774	.099	.124	91.9	101.0	54.7	−60.4		.660	1.958		424
425	2.886	.097	.057	184.4	49.7	65.9	−69.8		.781	1.854		425
426	2.889					27.8	−55.0	6				426
427	2.974	.103	.108	288.9	294.1	68.8	−76.0		.827	1.748		427
428	2.308	.153	.104	44.7	9.3	35.2	−39.5		.126	2.357	175	428
429	2.607	.096	.176	39.9	225.3	42.9	−49.2		.530	2.151	144	429
430	2.841	.252	.272	75.2	252.4	44.4	−78.2		.241	1.472		430
431	3.129	.151	.013	321.5	148.3	90.0	−103.3		.815	1.437	1	431
432	2.370	.139	.198	242.5	89.3	33.3	−39.9		.181	2.299		432
433	1.458	.219	.187	126.2	314.5	15.5	−18.7	13	−.439	3.095		433
434	1.944	.067	.358	285.7	183.1	15.0	−22.6		.094	2.833	190	434
435	2.449	.119	.029	355.3	351.9	42.2	−44.7		.347	2.262	158	435
436	3.197	.038	.326	84.8	347.9	34.4	−69.5		1.125	1.682		436
437	2.386	.198	.155	318.8	262.1	36.2	−44.7		.073	2.163		437
438	2.554	.080	.117	227.7	43.1	44.2	−47.2		.531	2.245		438
439	3.132	.081	.339	116.2	205.1	32.0	−67.7		.885	1.582		439
440	2.210	.151	.039	124.3	278.9	33.1	−36.0		.039	2.451	187	440
441	2.807	.086	.161	121.7	256.2	53.1	−60.3		.716	1.946	67	441
442	2.345	.101	.099	198.1	141.2	36.6	−39.1		.286	2.431	197	442
443	2.215	.095	.080	157.6	183.1	32.6	−34.2		.162	2.565	195	443
444	2.771	.140	.184	351.7	203.5	49.6	−61.2		.525	1.836		444
445	3.194	.104	.404	353.1	290.5	16.0	−67.8		1.036	1.425		445
446	2.788	.093	.178	322.4	37.4	50.6	−58.9		.641	1.907	67	446
447	2.986	.015	.066	91.4	64.9	72.5	−73.8		1.110	1.994		447
448	3.144	.130	.223	323.0	35.0	62.2	−87.4		.878	1.473		448
449	2.555	.194	.037	139.6	78.9	47.2	−55.2		.242	1.950	151	449
450	3.015	.065	.174	13.1	8.4	62.8	−73.0		.979	1.811	2	450
451	3.063	.059	.243	104.5	89.2	52.5	−70.7		.998	1.751		451
452	2.865	.063	.036	168.3	90.0	64.9	−66.5		.862	1.973	3	452
453	2.183	.136	.091	199.8	5.0	31.4	−34.2		.010	2.477	189	453
454	2.628	.139	.103	200.4	22.8	48.6	−54.6		.430	2.003		454
455	2.657	.233	.216	347.9	74.8	42.8	−62.4		.195	1.734		455
456	2.784	.203	.265	224.7	232.7	42.0	−65.6		.353	1.676		456
457	3.090	.125	.248	26.9	254.4	54.3	−79.4		.831	1.542	116	457
458	2.994	.188	.227	56.9	139.6	55.8	−83.0		.566	1.463		458
459	2.621	.185	.175	54.9	22.3	44.2	−56.2		.300	1.904		459
460	2.718	.064	.089	5.4	217.4	53.6	−56.0		.710	2.105	134	460
461	3.112	.159	.025	114.3	209.4	88.1	−102.7		.774	1.431	1A	461
462	2.874	.050	.036	345.2	110.5	65.5	−66.6		.908	2.001	3	462
463	2.398	.172	.223	16.4	35.5	32.8	−42.4		.108	2.173	163	463
464	2.802	.152	.166	356.1	102.7	53.2	−65.3		.518	1.769		464
465	3.092	.233	.119	217.2	300.1	81.3	−115.8		.501	1.228		465
466	3.358					27.8	−85.4	6				466
467	2.944	.086	.130	73.6	316.9	64.4	−71.3		.854	1.827		467
468	3.140	.153	.022	348.3	298.9	91.1	−105.1		.819	1.420	1A	468
469	3.166	.200	.226	178.5	326.3	65.7	−105.5		.660	1.235		469
470	2.405	.123	.127	203.2	179.4	37.8	−42.0		.285	2.311		470
471	2.888	.197	.248	47.8	87.2	48.2	−73.8		.451	1.555		471
472	2.542	.103	.264	98.0	130.7	33.0	−43.6		.405	2.190	4	472
473	2.983	.121	.503	10.7	324.6	1.1	−53.8		.626	1.651		473
474	2.454	.173	.151	312.5	169.9	38.8	−46.5		.196	2.138		474
475	2.596	.251	.334	350.9	38.4	30.1	−56.5		−.102	1.630		475
476	2.650	.065	.207	257.3	285.5	41.7	−49.0		.648	2.193		476
477	2.416	.150	.091	328.4	1.6	39.5	−44.2		.237	2.226	75	477
478	3.017	.093	.248	120.6	237.0	50.3	−69.7		.842	1.683	120	478
479	2.721	.214	.153	49.3	140.9	51.3	−67.2	10	.225	1.632	135	479
480	2.644	.012	.376	130.2	238.3	19.8	−39.8		.845	2.237		480

numb	a	e	sin i	wbar	node	wbar rate	node rate	res	Mars	Jup	fam	numb
481	2.741	.174	.156	41.4	38.6	51.3	−63.9	10	.340	1.718		481
482	3.000	.087	.253	242.2	183.7	48.6	−67.6		.877	1.753	120	482
483	3.426	.015	.317	203.0	178.5	36.9	−85.2		1.418	1.558		483
484	2.668	.033	.202	277.4	130.4	42.6	−49.1		.751	2.260		484
485	2.750	.183	.264	115.7	198.6	40.5	−60.5		.384	1.774		485
486	2.352	.184	.187	203.8	96.7	33.5	−41.9		.060	2.215		486
487	2.670	.062	.162	56.6	117.7	46.5	−51.4		.679	2.168		487
488	3.155	.188	.198	159.2	82.0	70.8	−103.9		.687	1.294		488
489	3.152	.079	.220	173.9	172.8	61.7	−81.2		1.054	1.624		489
490	3.175	.052	.159	20.5	186.3	76.1	−86.9		1.164	1.693	106	490
491	3.196	.055	.322	95.0	178.9	35.7	−70.9		1.089	1.646		491
492	3.112	.147	.023	329.2	.7	87.7	−100.0		.813	1.469	1A	492
493	3.120	.128	.278	46.7	352.5	48.4	−78.9		.831	1.509		493
494	2.986	.084	.115	226.3	29.4	68.8	−75.3		.896	1.789		494
495	2.488	.106	.045	44.0	209.3	43.6	−45.9		.414	2.247		495
496	2.199	.128	.077	124.4	212.8	32.1	−34.6		.064	2.499	189	496
497	2.850	.262	.088	8.7	350.6	64.5	−90.7		.259	1.432		497
498	2.650	.183	.156	332.7	95.9	46.8	−58.6		.327	1.866		498
499	3.969							3:2				499
500	2.613	.098	.192	7.5	288.2	41.7	−49.0		.527	2.145	144	500
501	3.155					27.8	−68.1	.6				501
502	2.384	.173	.420	151.2	132.5	16.4	−37.1		.206	2.116		502
503	2.723	.187	.076	120.5	60.0	55.3	−66.1		.379	1.774		503
504	2.721	.165	.216	348.6	104.3	44.4	−58.9		.434	1.836	138	504
505	2.685	.239	.153	73.9	93.5	49.6	−67.9		.182	1.664		505
506	3.041	.156	.313	115.3	313.4	40.3	−74.1		.684	1.520		506
507	3.153	.058	.187	41.5	293.1	68.9	−82.9		1.122	1.696		507
508	3.161	.047	.220	210.5	40.7	61.3	−79.3		1.167	1.716		508
509	3.065	.057	.276	25.5	222.1	45.3	−67.6		1.024	1.795		509
510	2.611	.163	.183	280.0	208.1	42.9	−53.4		.349	1.975	148	510
511	3.178	.171	.253	96.5	111.9	58.9	−96.3		.751	1.312		511
512	2.190	.174	.152	13.8	108.7	30.0	−35.3		−.145	2.320		512
513	3.014	.056	.171	68.0	191.7	63.2	−72.5		1.008	1.841	2	513
514	3.047	.011	.088	81.7	271.2	75.6	−78.0		1.180	1.947		514
515	3.120	.154	.019	66.3	151.1	89.0	−102.6		.800	1.440	1A	515
516	2.680	.261	.277	215.9	323.2	38.5	−65.8		.101	1.656		516
517	3.146	.166	.079	62.6	278.8	88.2	−106.7		.773	1.369		517
518	2.537	.186	.135	314.5	212.3	43.0	−52.2		.234	2.001	150	518
519	2.790	.154	.186	352.6	42.3	50.6	−63.9		.454	1.730		519
520	3.006	.082	.184	70.0	28.7	61.1	−72.9		.915	1.770	2	520
521	2.741	.287	.179	41.4	86.4	51.3	−80.2	10	.003	1.399		521
522	3.629	.039	.057	347.1	126.2	158.6	−164.8		1.613	1.298		522
523	2.966	.178	.097	99.2	264.8	70.8	−86.7		.593	1.533		523
524	2.635	.102	.160	60.6	321.6	45.2	−51.4		.540	2.099		524
525	2.245	.143	.117	122.3	208.6	32.7	−36.5		.074	2.426	183	525
526	3.121	.162	.026	147.9	173.0	89.2	−104.6		.772	1.412	1A	526
527	2.726	.125	.151	317.9	123.5	50.2	−58.3		.523	1.906		527
528	3.397	.033	.206	174.5	47.1	78.7	−102.7		1.422	1.543		528
529	3.017	.065	.174	55.9	62.5	63.0	−73.1		.980	1.809	2	529
530	3.210	.174	.128	318.1	133.5	88.4	−114.9		.780	1.278		530
531	2.784	.154	.584	222.0	188.7	−1.3	−47.8		.115	1.848	129	531
532	2.772	.184	.286	176.7	107.1	38.4	−61.2		.399	1.745		532
533	2.981	.077	.114	199.5	191.0	68.4	−74.4		.914	1.816		533
534	2.884	.053	.037	107.4	93.3	66.2	−67.5		.910	1.982	3	534
535	2.569	.059	.101	164.4	83.9	45.5	−47.6		.601	2.277		535
536	3.500	.038	.316	28.0	58.4	37.1	−92.5		1.409	1.409		536
537	3.063	.222	.152	294.8	124.9	73.5	−105.3		.519	1.291		537
538	3.165	.124	.101	.5	149.8	86.2	−99.3		.921	1.481	104	538
539	2.739	.145	.146	41.4	302.4	51.3	−60.8	10	.433	1.803		539
540	2.219	.145	.109	168.2	207.9	32.1	−35.6		.038	2.441	183	540

numb	a	e	sin i	wbar	node	wbar rate	node rate	res	Mars	Jup	fam	numb
541	2.815	.068	.124	231.5	269.7	56.9	−61.3		.791	2.004		541
542	2.906	.096	.199	4.3	157.6	53.5	−65.7		.767	1.823		542
543	3.062	.115	.172	56.7	294.9	66.9	−81.9		.859	1.613	118	543
544	2.593	.143	.163	267.0	296.7	43.5	−51.5		.392	2.044	149	544
545	3.189	.163	.214	291.2	332.4	68.2	−99.9		.805	1.320	102	545
546	2.597	.145	.261	142.9	19.7	35.3	−48.6		.355	2.043		546
547	2.773	.203	.293	31.5	196.0	38.0	−63.3		.339	1.696		547
548	2.282	.188	.055	81.9	117.3	35.3	−40.5		.027	2.306		548
549	2.682	.256	.089	97.8	291.3	53.1	−71.6		.138	1.630		549
550	2.589	.186	.198	305.6	268.9	41.1	−53.4		.264	1.948		550
551	2.966	.114	.022	91.7	297.6	73.4	−78.8		.798	1.724		551
552	3.154	.101	.157	232.6	270.5	75.6	−90.4		.984	1.558		552
553	2.231	.123	.083	91.1	72.9	33.1	−35.6		.116	2.490	182	553
554	2.375	.148	.066	77.0	290.4	38.6	−42.4		.208	2.284		554
555	3.169	.189	.031	134.9	156.3	95.6	−119.3		.724	1.277	107	555
556	2.467	.117	.108	118.1	283.1	41.0	−44.8		.360	2.250	155	556
557	2.442	.133	.060	140.0	285.7	41.4	−44.8		.303	2.239	159	557
558	2.908	.058	.133	138.4	150.8	61.4	−66.7		.905	1.946	124	558
559	2.712	.077	.145	219.7	115.0	49.7	−54.8		.659	2.061		559
560	2.751	.174	.129	121.2	106.6	53.7	−65.4		.415	1.774	131	560
561	3.167	.143	.026	124.4	211.1	93.4	−106.4		.871	1.420	1	561
562	3.019	.066	.177	310.8	68.1	62.6	−73.1		.980	1.805	2	562
563	2.713	.231	.160	67.9	87.1	50.2	−68.7		.208	1.635		563
564	2.748	.246	.299	272.1	64.5	37.9	−67.7		.186	1.609		564
565	2.442	.169	.213	156.8	230.1	34.8	−44.4		.176	2.159	163	565
566	3.387	.065	.066	27.4	75.7	115.4	−122.1		1.308	1.445		566
567	3.138	.123	.148	194.4	55.3	76.3	−92.5		.900	1.508		567
568	2.883	.171	.337	78.3	252.3	33.2	−63.5		.441	1.610		568
569	2.657	.173	.041	98.2	291.6	52.4	−59.8		.348	1.862	142	569
570	3.429	.068	.047	21.5	248.8	124.4	−130.8		1.335	1.394		570
571	2.410	.212	.097	35.5	350.0	39.3	−47.8		.077	2.088	166	571
572	2.400	.127	.189	38.6	198.7	34.6	−40.9		.252	2.309		572
573	3.014	.073	.180	13.0	337.2	61.9	−73.0		.951	1.789	2	573
574	2.252	.229	.115	66.1	328.9	33.1	−41.2		−.118	2.226		574
575	2.555	.077	.262	320.0	346.5	33.4	−43.1		.489	2.248	4	575
576	2.987	.165	.197	315.4	296.2	59.5	−80.6		.635	1.549		576
577	3.117	.139	.110	281.4	322.2	81.0	−95.6		.829	1.488		577
578	2.750	.185	.109	277.1	19.0	55.1	−66.8		.394	1.752		578
579	3.013	.062	.171	282.2	81.1	63.1	−72.8		.986	1.821	2	579
580	3.220	.089	.042	82.7	100.8	97.0	−102.9		1.090	1.536		580
581	3.214					27.8	−87.6	6				581
582	2.611					4.3	−41.2	5				582
583	3.180	.170	.179	156.4	259.5	75.8	−104.8		.770	1.319		583
584	2.374	.170	.216	17.4	281.1	32.5	−41.3		.090	2.203	163	584
585	2.431	.165	.137	153.2	189.2	38.5	−45.1		.199	2.183		585
586	3.041	.086	.046	140.4	249.7	78.6	−82.8		.946	1.730	119	586
587	2.335	.174	.427	154.3	322.0	15.3	−35.3		.162	2.173		587
588	5.201							1:1				588
589	3.133	.023	.185	94.8	184.6	67.5	−79.4		1.219	1.827		589
590	3.001	.078	.174	111.2	107.8	62.2	−72.8		.925	1.788	2	590
591	2.678	.235	.241	184.9	326.4	41.6	−63.6		.192	1.711		591
592	3.023	.106	.177	77.6	174.7	63.5	−77.1		.854	1.681		592
593	2.700	.223	.289	109.4	71.3	36.9	−61.3		.224	1.728		593
594	2.627	.107	.617	216.6	145.3	−6.3	−38.5		.124	2.077		594
595	3.202	.051	.303	246.2	21.1	41.3	−73.4		1.160	1.683		595
596	2.932	.212	.243	41.4	234.9	51.3	−80.5	10	.176	1.214		596
597	2.672	.099	.216	342.6	33.4	41.8	−51.0		.579	2.075		597
598	2.762	.203	.208	28.7	94.1	47.6	−66.5		.342	1.692	198	598
599	2.772	.209	.305	340.0	45.3	36.7	−63.5		.307	1.678		599
600	2.660	.067	.167	219.7	144.2	45.6	−50.8		.658	2.164		600

numb	a	e	sin i	wbar	node	wbar rate	node rate	res	Mars	Jup	fam	numb
601	3.130	.073	.273	318.6	174.9	48.1	−73.5		1.026	1.671	111	601
602	3.087	.187	.292	11.6	324.8	47.5	−86.2		.623	1.355		602
603	2.552	.199	.151	146.3	338.0	42.9	−53.8		.210	1.953	150	603
604	3.151	.162	.082	48.2	354.5	88.2	−106.2		.790	1.377		604
605	3.000					27.8	−60.0	6				605
606	2.587	.176	.174	19.3	312.5	42.8	−53.5		.297	1.969		606
607	2.852	.060	.197	190.9	284.9	50.9	−60.1		.720	1.872		607
608	3.024	.075	.186	1.8	292.2	61.7	−73.5		.955	1.775	2	608
609	3.088	.050	.068	231.0	182.6	81.1	−83.9		1.097	1.790		609
610	3.085	.222	.215	20.7	15.0	64.3	−102.4		.529	1.256		610
611	2.979	.114	.243	93.6	194.8	50.3	−69.4		.748	1.663	120	611
612	3.132	.194	.412	324.2	212.8	23.5	−79.9		.591	1.144		612
613	2.920	.047	.139	100.7	347.2	61.4	−66.9		.949	1.966	124	613
614	2.695	.107	.135	79.5	223.7	49.9	−55.6		.554	2.003		614
615	2.631	.104	.049	246.1	352.1	50.5	−53.4		.493	2.048	141	615
616	2.553	.096	.264	134.1	353.6	33.3	−43.7		.436	2.201	4	616
617	5.201							1:1				617
618	3.188	.035	.274	333.8	112.3	48.6	−74.7		1.197	1.730		618
619	2.520	.037	.241	30.4	191.0	34.2	−41.4		.579	2.402		619
620	2.435	.095	.134	330.3	353.6	38.6	−42.1		.379	2.346		620
621	3.118	.154	.026	113.7	39.4	88.5	−102.2		.796	1.442	1A	621
622	2.414	.212	.152	46.4	147.3	37.5	−47.4		.066	2.091		622
623	2.459	.146	.263	103.0	308.0	31.3	−42.4		.185	2.135		623
624	5.201							1:1				624
625	2.647	.191	.194	320.6	129.9	44.0	−58.0		.300	1.861		625
626	2.574	.182	.448	10.2	335.0	15.0	−44.2		.303	1.879		626
627	2.900	.045	.100	280.0	151.4	63.9	−66.9		.940	1.990		627
628	2.582	.023	.184	253.2	114.2	40.9	−45.6		.699	2.371		628
629	3.130	.177	.148	127.9	83.5	77.9	−102.7		.714	1.348		629
630	2.624	.141	.228	146.7	105.2	39.4	−50.9		.416	2.022	140	630
631	2.791					27.8		6				631
632	2.662	.221	.052	236.0	332.4	52.8	−65.6		.221	1.742		632
633	3.017	.059	.177	316.9	152.9	62.5	−72.6		.999	1.827	2	633
634	3.047	.141	.199	347.3	135.9	61.7	−82.0		.756	1.555		634
635	3.140	.055	.193	66.0	189.8	66.8	−80.9		1.117	1.720		635
636	2.910	.138	.135	324.0	28.5	62.2	−73.4		.664	1.714		636
637	3.165	.170	.025	172.4	289.6	94.3	−112.3		.783	1.338	1	637
638	2.735	.189	.122	221.9	107.1	53.7	−66.3		.364	1.751	131	638
639	3.016	.068	.171	333.9	279.9	63.4	−73.4		.971	1.801	2	639
640	3.163	.088	.247	237.6	238.5	56.3	−80.4		1.021	1.585		640
641	2.220	.131	.021	80.5	22.9	33.5	−35.7		.099	2.492	187	641
642	3.183	.150	.149	132.7	1.7	81.0	−103.1		.844	1.375		642
643	3.352	.080	.261	128.3	255.3	58.6	−94.4		1.201	1.425		643
644	2.599	.128	.005	23.6	196.0	49.5	−53.1		.436	2.054		644
645	3.200	.147	.137	102.1	352.7	84.7	−105.9		.861	1.373		645
646	2.325	.163	.135	338.7	297.3	34.8	−40.3		.108	2.310		646
647	2.444	.191	.144	81.3	257.4	38.8	−47.4		.142	2.105	157	647
648	3.184	.223	.196	112.7	292.2	75.2	−120.1		.586	1.151		648
649	2.551	.233	.218	346.1	353.8	38.7	−55.4		.109	1.875		649
650	2.458	.161	.056	41.9	231.4	42.2	−47.2		.249	2.152	24	650
651	3.024	.065	.177	41.9	33.1	63.0	−73.5		.986	1.801	2	651
652	2.555	.072	.258	22.9	86.1	33.7	−43.1		.510	2.267	4	652
653	3.014	.079	.182	183.2	136.9	61.7	−73.3		.933	1.772	2	653
654	2.297	.192	.332	133.0	275.0	22.9	−37.1		.077	2.134		654
655	2.989	.064	.098	73.1	137.4	70.6	−74.9		.963	1.844		655
656	3.160	.158	.025	161.5	257.0	93.3	−108.8		.820	1.382	1A	656
657	2.611	.142	.202	175.8	294.6	41.2	−51.2		.403	2.036	138	657
658	2.854	.045	.037	85.6	320.1	64.1	−65.1		.902	2.034	3	658
659	5.201							1:1				659
660	2.535	.088	.262	224.4	160.1	32.9	−42.7		.436	2.234	4	660

numb	a	e	sin i	wbar	node	wbar rate	node rate	res	Mars	Jup	fam	numb
661	3.016	.071	.173	166.6	330.6	63.1	−73.5		.960	1.792	2	661
662	2.554	.197	.061	291.6	148.6	46.7	−55.3		.229	1.944	151	662
663	3.062	.162	.342	184.3	239.7	34.7	−74.1		.614	1.449		663
664	3.175	.234	.171	255.9	182.2	80.6	−126.1		.549	1.124		664
665	3.148	.152	.286	249.6	301.2	48.6	−84.8		.787	1.385		665
666	2.594	.209	.142	33.2	223.5	45.4	−57.7		.216	1.869		666
667	3.198	.120	.432	121.4	160.0	11.1	−68.4		.969	1.367		667
668	2.797	.192	.145	319.2	223.9	55.3	−70.7		.411	1.676	128	668
669	3.012	.074	.185	257.6	177.4	61.0	−72.5		.946	1.790	2	669
670	2.803	.154	.127	8.6	183.6	56.7	−67.1		.528	1.778	126	670
671	3.097	.076	.144	132.9	353.8	72.6	−82.4		1.020	1.692		671
672	2.555	.112	.204	278.8	340.1	38.9	−46.6		.434	2.174		672
673	2.815	.041	.065	169.9	240.7	60.5	−61.9		.878	2.083		673
674	2.924	.158	.230	41.4	349.8	51.3	−71.9	10	.473	1.507		674
675	2.770	.190	.191	64.0	267.3	49.7	−66.2		.375	1.698	198	675
676	3.059	.099	.210	321.8	155.5	59.8	−76.8		.910	1.656	117	676
677	2.956	.079	.170	186.3	273.9	60.0	−69.5	7:3	.883	1.828	199	677
678	2.573	.191	.132	50.2	283.0	44.8	−54.7		.251	1.942	43	678
679	2.586	.186	.449	12.1	111.7	15.1	−45.1		.300	1.856		679
680	3.147	.221	.337	267.2	30.7	41.2	−95.6		.515	1.202		680
681	3.110	.082	.219	270.0	184.5	60.2	−78.4		1.007	1.659		681
682	2.632	.132	.213	269.4	196.8	40.8	−51.2		.454	2.030		682
683	3.116	.095	.343	150.5	260.6	31.4	−67.8		.794	1.534		683
684	2.432	.047	.103	216.3	328.1	39.7	−41.2		.502	2.459		684
685	2.236	.146	.079	306.9	238.1	33.3	−36.6		.071	2.435	184	685
686	2.589	.130	.306	337.8	244.8	30.2	−45.6		.243	1.958		686
687	2.723	.207	.293	29.1	327.8	36.7	−60.5		.284	1.745		687
688	2.698	.110	.178	298.1	177.8	46.6	−54.7		.567	2.010		688
689	2.316	.187	.098	358.4	177.5	35.7	−41.6		.055	2.266		689
690	3.148	.121	.225	12.0	257.5	61.6	−86.1		.911	1.498		690
691	3.012	.082	.207	43.9	88.6	57.3	−71.6		.913	1.767		691
692	3.369	.092	.447	106.6	58.0	−.8	−72.8		1.113	1.318		692
693	2.944	.035	.251	211.8	347.8	46.4	−61.4		.997	1.970		693
694	2.670	.210	.321	346.9	236.0	32.0	−56.2		.157	1.730		694
695	2.538	.088	.263	5.0	275.1	32.9	−42.8		.438	2.231	4	695
696	3.182	.171	.272	54.1	300.5	54.0	−94.3		.730	1.303		696
697	2.881	.116	.258	349.8	12.7	44.3	−62.3		.695	1.807	125	697
698	2.869	.132	.196	154.0	37.5	52.8	−66.6		.621	1.752		698
699	2.616	.235	.337	339.3	245.3	29.8	−55.6		−.072	1.623		699
700	2.229	.148	.111	181.2	99.6	32.4	−36.2		.043	2.426	183	700
701	3.013	.070	.143	195.0	249.4	67.0	−74.9		.967	1.798		701
702	3.194	.041	.371	274.6	289.7	20.6	−64.1		1.212	1.597		702
703	2.175	.117	.053	54.0	217.7	31.7	−33.6		.067	2.544	186	703
704	3.062	.081	.324	40.0	281.2	34.7	−64.7		.881	1.693		704
705	2.923	.045	.425	161.0	1.3	9.6	−47.5		.968	1.925		705
706	2.729	.146	.264	352.2	321.0	39.1	−55.5		.475	1.902		706
707	2.180	.075	.081	50.8	276.1	31.4	−32.6		.146	2.615		707
708	2.671	.136	.068	192.0	337.9	52.2	−57.5		.443	1.938		708
709	2.914	.075	.291	332.9	321.7	38.7	−58.7		.835	1.902		709
710	3.135	.154	.021	227.7	183.5	90.6	−104.7		.810	1.421	1A	710
711	2.237	.152	.109	283.7	351.1	32.7	−36.6		.047	2.415	183	711
712	2.576	.173	.235	62.4	234.7	37.6	−50.7		.277	2.006		712
713	3.399	.108	.196	345.4	227.3	85.2	−116.3		1.154	1.285		713
714	2.535	.091	.264	124.8	235.6	32.8	−42.8		.426	2.225	4	714
715	2.768	.042	.228	341.8	43.1	43.6	−53.2		.822	2.127		715
716	2.811	.125	.139	192.7	152.0	56.0	−64.5		.617	1.849	126	716
717	3.146	.216	.047	2.6	315.0	93.4	−123.9		.614	1.219		717
718	3.056	.236	.114	207.7	29.6	78.7	−111.8		.468	1.261		718
719	2.583	.483	.228	338.3	205.5	43.7	−107.9		−.561	1.208		719
720	2.887	.051	.036	172.9	6.8	66.4	−67.7		.917	1.983	3	720

numb	a	e	sin i	wbar	node	wbar rate	node rate	res	Mars	Jup	fam	numb
721	3.551	.083	.135	41.1	32.4	121.4	−145.8		1.373	1.213		721
722	2.172	.085	.088	281.1	46.2	31.1	−32.5		.113	2.597		722
723	2.994	.038	.082	88.8	177.3	72.0	−74.5		1.049	1.916		723
724	2.451	.234	.217	56.5	206.8	35.4	−49.7		.018	1.993		724
725	2.573	.195	.050	36.6	61.1	47.9	−56.3		.248	1.922	151	725
726	2.566	.186	.301	9.3	246.9	31.2	−49.0		.125	1.884		726
727	2.568	.087	.250	76.3	136.2	34.9	−44.4		.494	2.227		727
728	2.254	.133	.063	143.8	83.4	34.2	−36.8		.128	2.456	181	728
729	2.760	.113	.303	186.3	125.7	34.0	−52.5		.560	1.937		729
730	2.243	.206	.064	203.2	99.5	33.9	−39.7		−.053	2.297		730
731	2.988	.100	.180	320.6	42.2	60.9	−73.4		.844	1.736		731
732	2.457	.068	.192	195.4	177.4	36.1	−41.0		.457	2.397		732
733	3.398	.061	.359	184.4	339.1	22.9	−80.0		1.251	1.284		733
734	3.151	.076	.107	87.4	352.8	82.9	−90.4		1.066	1.646		734
735	2.730	.252	.301	357.1	46.0	37.3	−67.1		.160	1.616		735
736	2.202	.106	.073	337.6	144.2	32.3	−34.1		.118	2.546	188	736
737	2.590	.195	.229	314.4	192.3	38.7	−53.5		.239	1.924		737
738	3.035	.096	.046	179.6	147.3	78.2	−83.3		.910	1.706	119	738
739	2.738					27.8		6				739
740	3.050	.141	.175	167.7	117.3	66.2	−84.4		.764	1.547		740
741	2.720	.127	.130	181.0	101.3	51.7	−58.8		.444	1.850	133	741
742	3.013	.072	.181	340.9	61.5	61.7	−72.8		.953	1.793	2	742
743	2.793	.043	.099	91.9	237.6	57.3	−59.7		.847	2.097		743
744	3.173	.153	.122	176.5	148.3	84.7	−104.8		.823	1.385		744
745	3.238	.099	.219	147.3	129.1	66.6	−92.2		1.059	1.471		745
746	3.109	.166	.324	309.2	2.8	39.8	−80.6		.680	1.420		746
747	2.998	.245	.363	56.8	135.1	34.5	−84.2		.276	1.275		747
748	3.969							3:2				748
749	2.243	.186	.087	221.0	115.9	33.4	−38.5		−.014	2.337		749
750	2.442	.168	.056	147.3	62.5	41.6	−46.8		.219	2.155	24	750
751	2.552	.114	.256	39.1	79.4	34.2	−44.8		.402	2.171		751
752	2.463	.095	.088	129.4	83.7	41.5	−44.0		.417	2.306	156	752
753	2.330	.211	.161	249.4	56.5	34.1	−42.7		−.015	2.182		753
754	2.988	.053	.416	168.1	183.3	11.4	−51.1		1.020	1.827		754
755	3.175	.178	.057	214.3	197.9	94.1	−116.2		.758	1.304	105	755
756	3.200	.172	.363	199.3	211.7	32.6	−85.3		.626	1.230		756
757	2.373	.109	.139	88.2	16.3	36.1	−39.9		.285	2.389		757
758	3.202	.115	.078	74.6	110.1	92.5	−103.6		.985	1.471	101	758
759	2.618					27.8	−52.6	6				759
760	3.158	.255	.243	166.7	325.5	65.0	−121.5		.459	1.070		760
761	2.863	.047	.037	285.0	353.4	64.7	−65.8		.907	2.021	3	761
762	3.157	.124	.248	139.4	303.8	57.1	−85.1		.895	1.479		762
763	2.241	.130	.084	33.2	284.9	33.4	−36.1		.112	2.467	182	763
764	3.187	.086	.195	79.1	262.0	69.6	−88.0		1.056	1.577		764
765	2.546	.248	.126	43.7	317.6	44.3	−59.1		.077	1.832		765
766	3.021	.081	.180	101.3	1.9	62.6	−74.3		.933	1.757	2	766
767	3.117	.150	.025	336.7	63.2	88.3	−101.3		.808	1.454	1A	767
768	3.142	.135	.271	62.0	35.4	51.3	−83.0	10	.687	1.335		768
769	3.181	.162	.130	271.1	29.7	84.6	−107.6		.798	1.348		769
770	2.221	.157	.067	81.5	38.0	33.0	−36.5		.031	2.425	184	770
771	2.652	.232	.292	90.2	217.7	35.4	−59.1		.157	1.753		771
772	3.001	.090	.467	312.0	153.0	2.7	−52.1	7	.922	1.646		772
773	2.858	.047	.301	260.0	320.4	35.3	−53.6		.848	2.030		773
774	3.050	.170	.117	264.4	254.5	75.3	−93.5		.675	1.466		774
775	3.012	.086	.182	129.6	296.0	61.8	−73.8		.909	1.753	2	775
776	2.933	.119	.299	42.5	81.0	39.0	−63.0		.713	1.753		776
777	3.210	.136	.262	171.5	284.4	56.2	−90.5		.890	1.388		777
778	3.177	.243	.270	103.8	328.4	59.3	−115.8		.501	1.087		778
779	2.667	.158	.278	324.7	281.2	35.5	−52.6		.364	1.925	137	779
780	3.116	.041	.315	.4	147.9	36.7	−66.0		1.092	1.789		780

numb	a	e	sin i	wbar	node	wbar rate	node rate	res	Mars	Jup	fam	numb
781	3.223	.067	.319	253.8	142.8	37.6	−74.3		1.091	1.595		781
782	2.180	.104	.083	152.4	83.8	31.4	−33.2		.089	2.558		782
783	2.343	.190	.158	286.1	149.0	34.4	−42.2		.044	2.218	171	783
784	3.107	.228	.239	240.1	5.8	61.7	−105.0		.516	1.216		784
785	2.575	.225	.219	198.8	74.0	39.4	−56.1		.149	1.864		785
786	3.177	.173	.247	221.1	92.6	60.5	−97.3		.748	1.308		786
787	2.540	.063	.264	288.6	187.9	32.7	−42.0		.502	2.289	153	787
788	3.129	.154	.251	207.4	181.2	56.2	−87.5		.769	1.416	113	788
789	2.686	.141	.203	257.1	235.0	44.0	−55.2		.468	1.951	138	789
790	3.406	.169	.391	275.0	249.2	25.0	−100.4		.815	.869		790
791	3.124	.159	.261	320.4	131.3	54.0	−87.0		.733	1.401	113	791
792	2.623	.153	.175	137.9	264.9	44.0	−53.6		.388	1.984		792
793	2.796	.074	.265	346.6	33.4	39.8	−53.9		.739	2.027		793
794	3.139	.277	.106	279.5	181.0	90.8	−145.1		.395	1.043		794
795	2.750	.154	.332	183.0	14.1	30.7	−54.1		.327	1.747		795
796	2.636	.264	.319	11.0	35.6	32.9	−61.2		.019	1.661		796
797	2.537	.078	.094	208.4	244.4	44.5	−46.8		.524	2.266		797
798	3.015	.060	.171	223.7	220.8	63.2	−72.8		.996	1.828	2	798
799	2.542	.024	.089	129.7	175.5	44.8	−45.9		.669	2.397		799
800	2.193	.144	.076	303.7	316.6	32.0	−34.9		.018	2.466	189	800
801	2.605	.118	.250	165.2	190.9	36.4	−47.6		.447	2.116		801
802	2.196	.138	.087	135.0	2.2	31.9	−34.8		.030	2.472	189	802
803	3.204	.041	.169	258.6	254.9	75.9	−88.1		1.225	1.698		803
804	2.839	.101	.269	325.1	344.7	40.8	−57.5		.695	1.906	125	804
805	3.207	.103	.275	221.4	105.5	51.3	−82.8	10	.781	1.296		805
806	3.203	.111	.243	166.2	43.0	59.8	−87.7		.982	1.473		806
807	3.019	.081	.180	136.4	136.6	62.3	−73.9		.932	1.762	2	807
808	2.745	.131	.087	111.1	195.2	55.7	−61.8		.553	1.904	40	808
809	2.283	.143	.121	353.6	160.7	33.8	−37.9		.113	2.396		809
810	2.179	.124	.047	355.3	166.0	31.9	−33.9		.061	2.530	186	810
811	2.897	.062	.040	277.8	148.3	67.1	−68.8		.892	1.946	3	811
812	2.659	.131	.228	359.1	3.3	40.3	−52.1		.474	2.005	140	812
813	2.223	.038	.099	129.8	51.9	32.4	−33.4		.292	2.680		813
814	3.157	.192	.407	22.2	94.1	24.3	−81.9		.590	1.099		814
815	2.659	.093	.230	131.3	54.3	39.9	−49.7		.575	2.111		815
816	3.002	.139	.235	155.5	129.6	53.3	−75.0		.714	1.588	120	816
817	2.590	.154	.190	62.6	129.9	41.4	−51.3		.355	2.027	148	817
818	3.172	.037	.254	11.5	69.4	53.6	−76.0		1.182	1.732		818
819	2.197	.112	.087	252.8	326.3	31.9	−34.0		.092	2.530		819
820	3.128	.052	.085	267.8	124.2	83.2	−87.2		1.125	1.742		820
821	2.778	.231	.105	232.1	218.7	57.8	−76.2		.292	1.599		821
822	2.256	.181	.025	109.2	237.2	34.7	−39.0		.026	2.350	178	822
823	2.221	.136	.078	127.3	253.4	32.9	−35.7		.077	2.469	185	823
824	2.795	.132	.132	263.8	149.7	55.6	−64.2		.583	1.847	126	824
825	2.226	.111	.051	189.0	109.2	33.4	−35.2		.146	2.528	186	825
826	2.713	.213	.141	41.4	21.2	51.3	−66.8	10	.104	1.538	135	826
827	2.275	.117	.063	17.6	184.6	34.9	−37.0		.184	2.477	179	827
828	3.189	.039	.031	248.1	319.1	93.4	−94.7		1.224	1.725		828
829	2.580	.071	.150	50.7	345.5	43.5	−47.5		.575	2.243		829
830	3.205	.062	.079	85.5	328.5	91.4	−96.5		1.161	1.634		830
831	2.212	.136	.091	65.4	184.4	32.3	−35.2		.056	2.468	182	831
832	2.864	.044	.037	18.7	266.7	64.8	−65.8		.916	2.027	3	832
833	3.010	.083	.179	36.9	346.8	62.1	−73.6		.917	1.763	2	833
834	3.174	.217	.078	262.0	198.4	94.3	−127.9		.627	1.184		834
835	3.210	.068	.084	18.2	302.8	91.4	−97.4		1.146	1.610		835
836	2.191	.142	.093	39.2	205.2	31.6	−34.7		.008	2.461	189	836
837	2.298	.027	.126	100.6	204.2	34.1	−35.5		.405	2.650		837
838	2.898	.078	.201	350.3	244.3	52.6	−63.7		.800	1.870		838
839	2.615	.119	.226	308.7	335.0	39.0	−49.1		.468	2.090		839
840	3.134	.099	.195	255.6	274.6	66.8	−84.6		.969	1.590	204	840

numb	a	e	sin i	wbar	node	wbar rate	node rate	res	Mars	Jup	fam	numb
841	2.255	.109	.065	131.7	344.5	34.2	−36.1		.184	2.510	179	841
842	3.233	.077	.253	6.1	1.8	57.3	−84.4		1.115	1.549		842
843	2.279	.155	.138	315.7	359.8	33.1	−38.0		.071	2.363		843
844	3.196	.053	.162	319.3	342.7	76.9	−88.8		1.180	1.668	106	844
845	2.939	.034	.208	294.6	39.4	53.4	−64.0		.983	1.968	122	845
846	3.129	.144	.027	36.8	278.4	89.4	−101.6		.836	1.459	1A	846
847	2.783	.066	.063	57.7	273.7	58.6	−60.6		.775	2.046	37	847
848	3.106	.138	.034	322.5	247.3	86.4	−97.1		.835	1.504	1	848
849	3.151	.124	.351	258.9	229.0	31.4	−73.3		.699	1.396		849
850	2.998	.121	.259	242.3	125.2	48.4	−70.5		.767	1.655	120	850
851	2.228	.140	.040	150.7	158.9	33.6	−36.3		.086	2.463	187	851
852	2.363	.196	.427	307.9	27.5	16.2	−37.7		.127	2.087	168	852
853	2.312	.121	.166	213.8	186.1	33.1	−37.6		.178	2.403		853
854	2.369	.162	.116	258.0	197.7	37.0	−42.4		.156	2.262		854
855	2.362	.177	.190	231.3	10.3	33.7	−41.8		.086	2.221		855
856	2.437	.151	.244	178.7	126.3	32.4	−42.3		.188	2.179		856
857	2.190	.027	.086	300.4	88.0	31.7	−32.3		.271	2.722		857
858	2.808	.132	.139	228.3	63.8	55.8	−64.8		.595	1.834	126	858
859	3.212	.095	.229	57.2	32.0	63.0	−87.5		1.047	1.512		859
860	2.796	.076	.245	315.9	307.0	42.6	−55.1		.746	2.010		860
861	3.144	.082	.120	284.9	118.6	80.6	−89.5		1.037	1.635		861
862	2.803	.075	.259	91.0	299.2	41.0	−54.7		.749	2.012		862
863	3.200	.060	.419	229.3	119.0	6.9	−61.0		1.038	1.662		863
864	2.208	.137	.096	6.7	170.1	32.1	−35.1		.046	2.465	189	864
865	2.416	.235	.249	127.8	185.1	32.2	−47.2		−.050	1.992		865
866	3.123	.024	.129	332.9	90.7	76.6	−82.8		1.208	1.838		866
867	3.065	.143	.098	131.9	37.6	78.0	−91.2		.778	1.528		867
868	2.704	.112	.087	52.9	121.4	53.2	−57.8		.559	1.986	132	868
869	2.693	.204	.143	251.8	163.7	50.1	−64.1		.276	1.735	135	869
870	2.322	.226	.094	311.2	125.3	36.1	−44.4		−.032	2.170		870
871	2.222	.147	.076	202.3	166.4	32.9	−36.1		.053	2.444	184	871
872	2.731	.135	.135	205.0	203.2	52.0	−59.9		.473	1.860	133	872
873	2.627	.150	.087	246.1	161.5	49.3	−55.7		.397	1.966		873
874	3.156	.110	.197	191.5	198.0	68.2	−88.1		.950	1.533	204	874
875	2.555	.083	.263	302.2	199.8	33.3	−43.3		.470	2.230	4	875
876	3.011	.073	.185	353.5	156.3	61.0	−72.4		.947	1.793	2	876
877	2.486	.132	.061	42.2	123.7	43.3	−47.0		.347	2.189		877
878	2.363	.191	.037	2.8	200.6	38.6	−44.5		.097	2.196	164	878
879	2.530	.093	.260	24.5	270.4	33.1	−42.8		.422	2.230	4	879
880	3.002	.217	.331	6.8	267.0	38.9	−81.1		.443	1.382		880
881	2.612	.157	.266	306.8	275.1	35.5	−50.2		.334	1.994	21	881
882	3.132	.216	.140	22.5	266.3	81.1	−115.1		.587	1.228		882
883	2.238	.144	.095	323.3	280.3	33.1	−36.4		.072	2.433	180	883
884	5.201							1:1				884
885	3.097	.146	.046	347.8	170.3	85.2	−97.4		.804	1.486		885
886	3.169	.198	.302	3.2	62.4	47.9	−95.7		.645	1.220		886
887	2.500							3:1				887
888	2.709	.170	.233	74.9	129.0	42.3	−58.1		.404	1.843	140	888
889	2.445	.185	.137	60.7	138.5	39.2	−47.2		.160	2.115	157	889
890	3.023	.077	.183	218.9	166.6	62.1	−73.8		.947	1.768	2	890
891	2.861	.024	.216	114.5	107.3	48.5	−58.4		.957	2.072		891
892	3.229	.022	.365	93.5	179.1	21.6	−65.8		1.279	1.613		892
893	3.052	.100	.283	4.3	147.3	44.8	−70.1		.885	1.665		893
894	3.114	.089	.229	284.5	197.0	58.5	−78.6		.983	1.632		894
895	3.219	.130	.456	83.9	265.5	6.9	−69.7		.870	1.246		895
896	2.286	.160	.157	234.6	254.6	32.6	−38.3		.053	2.332		896
897	2.544	.075	.261	245.4	258.2	33.1	−42.6		.482	2.263	4	897
898	2.728	.343	.219	282.4	237.5	48.4	−89.5		−.090	1.350		898
899	2.908	.155	.243	27.4	257.5	48.5	−69.4		.591	1.651		899
900	2.473	.117	.209	288.0	188.0	35.7	−42.9		.342	2.258		900

numb	a	e	sin i	wbar	node	wbar rate	node rate	res	Mars	Jup	fam	numb
901	2.224	.164	.077	331.5	262.7	33.0	−36.9		.017	2.403	184	901
902	2.447	.145	.116	26.2	343.6	39.9	−45.1		.267	2.207		902
903	3.239	.021	.193	273.3	165.4	72.7	−88.1		1.324	1.733		903
904	2.993	.083	.272	114.2	202.5	44.4	−65.3		.883	1.792		904
905	2.216	.122	.082	38.6	34.0	32.6	−35.0		.101	2.503	182	905
906	2.894	.048	.196	302.3	36.2	53.0	−62.2		.895	1.967		906
907	2.801	.206	.358	135.1	41.8	30.0	−62.1		.134	1.493		907
908	2.474	.171	.220	119.2	83.4	35.3	−45.9		.198	2.120		908
909	3.540	.038	.312	40.9	149.9	38.4	−96.7		1.455	1.378		909
910	2.926	.170	.149	241.6	42.8	62.4	−78.5		.582	1.595		910
911	5.201							1:1				911
912	3.124	.166	.339	132.8	32.5	36.1	−80.0		.648	1.374		912
913	2.197	.135	.091	262.3	98.4	31.8	−34.7		.037	2.477	189	913
914	2.454	.181	.456	284.6	251.2	13.4	−39.3		.214	2.019		914
915	2.228	.134	.094	70.9	1.5	32.7	−35.7		.083	2.464	182	915
916	2.365	.181	.210	19.6	323.8	32.6	−41.7		.059	2.190	163	916
917	2.381	.161	.094	340.3	333.7	38.2	−43.2		.177	2.244	75	917
918	2.865	.158	.221	341.6	325.9	49.8	−67.8		.545	1.670		918
919	2.772	.017	.155	32.5	235.1	51.7	−56.2		.800	2.095		919
920	2.622	.116	.210	119.4	198.1	40.8	−49.9		.480	2.092		920
921	3.173	.152	.303	250.0	207.4	45.4	−85.3		.801	1.377		921
922	2.690	.159	.141	328.3	214.7	49.6	−59.2		.411	1.868		922
923	2.615	.168	.258	46.0	200.6	36.5	−51.6		.314	1.970	21	923
924	2.938	.117	.147	7.9	156.4	62.3	−72.9		.756	1.737		924
925	2.700	.063	.375	152.9	298.1	21.0	−43.2		.745	2.031		925
926	2.983	.205	.272	215.1	47.4	48.1	−81.6		.480	1.428		926
927	3.213	.142	.256	168.9	5.7	58.1	−92.8		.875	1.365		927
928	3.136	.171	.292	151.6	129.9	48.2	−87.1		.709	1.342		928
929	2.239	.118	.080	227.3	233.5	33.4	−35.7		.139	2.497	182	929
930	2.430	.019	.267	256.3	338.2	29.5	−37.1		.335	2.345		930
931	3.168	.205	.188	72.0	119.7	74.9	−112.4		.640	1.223		931
932	2.420	.087	.139	89.2	8.7	37.8	−41.0		.387	2.380		932
933	2.370	.204	.088	155.2	149.9	38.0	−45.3		.064	2.158	166	933
934	2.748	.156	.275	36.6	321.3	38.2	−57.1		.449	1.854		934
935	2.219	.136	.072	65.8	335.9	32.9	−35.6		.076	2.473	185	935
936	3.136	.151	.029	302.5	35.9	90.2	−104.0		.819	1.429	1	936
937	2.231	.166	.082	307.9	245.0	33.1	−37.2		.020	2.394	184	937
938	3.161	.149	.027	334.6	134.2	93.0	−107.0		.847	1.407	1A	938
939	2.247	.129	.050	329.8	312.5	34.1	−36.6		.132	2.473	186	939
940	3.379	.116	.097	331.6	63.8	111.1	−129.1		1.117	1.281		940
941	2.784	.160	.102	31.1	46.1	57.4	−67.0		.502	1.783		941
942	3.160	.133	.167	40.4	70.2	75.1	−95.2		.883	1.454	109	942
943	3.126	.221	.192	122.6	116.1	71.5	−110.8		.554	1.223		943
944	5.764							JXR				944
945	2.636					4.3	−49.7	5				945
946	3.122	.149	.013	119.9	13.0	89.1	−101.8		.817	1.453	1	946
947	2.752	.212	.104	29.1	42.2	56.0	−70.9		.325	1.679		947
948	3.036	.194	.158	164.5	351.5	69.6	−94.1		.588	1.406		948
949	2.998	.212	.226	203.0	315.5	57.1	−88.6		.496	1.388		949
950	2.371	.172	.404	178.1	184.5	17.6	−36.8		.212	2.128		950
951	2.210	.143	.084	40.4	254.0	32.4	−35.4		.042	2.458	189	951
952	2.987	.211	.168	12.9	12.2	65.3	−91.5		.497	1.413		952
953	2.790	.168	.152	282.0	29.1	54.1	−66.8		.470	1.744		953
954	3.139	.147	.024	297.5	224.7	90.6	−103.6		.836	1.439	1A	954
955	2.594	.259	.224	264.5	348.4	40.2	−61.1		.070	1.754		955
956	2.298	.157	.115	310.6	201.0	34.5	−39.2		.100	2.353	175	956
957	2.919	.087	.275	113.1	235.4	41.9	−60.9		.805	1.863		957
958	3.969							3:2				958
959	3.185	.179	.063	28.0	49.6	94.8	−117.5		.763	1.292	105	959
960	2.248	.115	.068	335.3	249.7	33.9	−36.0		.162	2.501	179	960

numb	a	e	sin i	wbar	node	wbar rate	node rate	res	Mars	Jup	fam	numb
961	2.693	.065	.186	289.5	21.8	45.3	−51.9		.690	2.141		961
962	2.906	.062	.035	9.9	171.5	67.9	−69.6		.900	1.935	3	962
963	2.248	.152	.128	87.8	60.7	32.4	−36.8		.049	2.398	183	963
964	3.053	.085	.151	50.2	23.8	69.1	−79.2		.952	1.712		964
965	3.159					27.8	−78.6	6				965
966	2.720	.141	.233	237.1	71.3	42.2	−56.0		.497	1.910	140	966
967	2.226	.118	.083	303.2	83.7	32.9	−35.2		.121	2.505	182	967
968	2.868	.148	.219	150.0	216.2	50.0	−67.0		.572	1.689		968
969	2.463	.171	.061	21.7	284.1	42.4	−48.1		.226	2.120	24	969
970	2.562	.239	.117	52.0	307.1	45.4	−59.3		.116	1.834		970
971	2.641	.169	.223	99.6	82.3	40.8	−54.2		.357	1.925	138	971
972	3.062	.175	.186	14.7	282.3	66.3	−91.0		.662	1.434		972
973	3.227	.066	.283	94.5	344.8	47.8	−78.7		1.142	1.583		973
974	2.534	.085	.078	41.8	85.3	44.9	−47.1		.505	2.254		974
975	2.834	.049	.038	141.4	13.1	62.7	−63.7		.874	2.045	3	975
976	3.186	.148	.159	192.4	252.5	79.5	−102.4		.851	1.377		976
977	3.118	.056	.245	180.6	74.9	54.2	−74.2		1.080	1.728		977
978	3.221	.146	.403	354.0	224.0	20.5	−77.1		.887	1.234		978
979	3.153	.095	.197	332.8	236.8	67.3	−85.4		.998	1.584	204	979
980	2.741	.117	.306	360.0	284.5	33.3	−51.6		.522	1.937		980
981	3.100	.165	.029	337.0	12.5	86.7	−101.6		.750	1.426	1	981
982	3.072	.221	.258	280.3	300.2	55.5	−96.3		.499	1.276		982
983	3.162	.100	.276	230.1	253.9	49.2	−78.5		.949	1.542	108	983
984	2.803	.125	.178	359.5	309.8	51.7	−62.4		.518	1.770		984
985	2.300	.227	.095	349.7	284.2	35.3	−43.4		−.058	2.197		985
986	3.142	.129	.251	352.1	93.0	55.8	−84.1		.863	1.479		986
987	3.150	.195	.170	327.0	317.5	76.3	−108.5		.664	1.274		987
988	3.153	.188	.024	15.2	352.3	93.9	−116.4		.714	1.298	107	988
989	2.660	.234	.270	57.9	248.3	38.0	−60.7		.168	1.752		989
990	2.669	.180	.157	2.1	346.6	47.6	−59.0		.347	1.854		990
991	3.145	.137	.024	298.4	31.4	91.0	−102.2		.874	1.465	1	991
992	3.024	.128	.201	194.8	219.5	60.2	−78.2		.781	1.616		992
993	2.861	.046	.036	117.8	218.2	64.6	−65.6		.906	2.023	3	993
994	2.530	.061	.261	351.2	359.6	32.7	−41.7		.498	2.304	153	994
995	2.615	.111	.243	344.4	226.1	37.3	−48.1		.480	2.118		995
996	3.093	.161	.028	143.0	301.4	86.0	−100.2		.756	1.444	1	996
997	2.670	.156	.203	283.8	248.0	43.5	−55.6		.412	1.931	138	997
998	3.122	.129	.306	12.1	299.3	42.2	−76.5		.838	1.513		998
999	2.612	.169	.189	341.0	222.3	42.5	−53.8		.334	1.960	148	999
1000	3.181	.157	.421	246.0	325.7	18.0	−75.0	4	.837	1.247		1000
1001	3.200	.107	.183	58.4	263.4	73.8	−93.3		.997	1.496		1001
1002	2.788	.120	.193	334.6	339.2	49.3	−60.3		.598	1.875		1002
1003	3.150	.151	.022	108.0	183.7	92.0	−106.0		.833	1.414	1A	1003
1004	3.397	.060	.043	14.7	179.3	119.6	−124.2		1.338	1.453		1004
1005	3.164	.089	.343	90.7	346.9	31.5	−70.1		.856	1.504		1005
1006	3.151	.263	.272	19.2	295.7	58.9	−119.5		.408	1.057		1006
1007	2.708	.072	.063	31.9	297.9	54.2	−56.2		.685	2.098	36	1007
1008	3.093	.047	.153	59.5	13.4	70.7	−79.5		1.111	1.789		1008
1009	2.629	.434	.284	58.2	232.6	40.6	−97.1		−.418	1.269		1009
1010	2.931	.067	.048	19.8	100.1	69.4	−71.7		.908	1.895	123	1010
1011	2.394	.383	.084	129.5	146.0	39.8	−67.1		−.356	1.709		1011
1012	2.483	.139	.055	112.0	66.5	43.3	−47.3		.325	2.174		1012
1013	2.684	.217	.220	133.7	25.0	43.5	−62.3		.257	1.746		1013
1014	2.807	.216	.064	131.4	258.1	61.7	−77.6		.367	1.607		1014
1015	3.203	.061	.147	52.1	125.1	80.5	−91.4		1.160	1.634	106	1015
1016	2.219	.137	.103	85.9	2.2	32.2	−35.4		.061	2.462		1016
1017	2.606	.111	.124	181.1	122.4	46.3	−51.1		.490	2.110		1017
1018	2.537	.215	.135	339.0	353.1	43.2	−54.8		.155	1.928		1018
1019	1.912	.065	.422	259.3	147.2	10.6	−20.8		.059	2.879	191	1019
1020	2.787	.045	.076	193.8	195.4	58.2	−59.9		.838	2.096	38	1020

numb	a	e	sin i	wbar	node	wbar rate	node rate	res	Mars	Jup	fam	numb
1021	2.738	.227	.286	51.5	120.4	38.5	-64.5		.248	1.665		1021
1022	2.805					27.8	-76.4	6				1022
1023	3.168	.069	.178	42.8	201.3	71.8	-85.8		1.102	1.647		1023
1024	2.866	.170	.271	13.9	59.5	42.9	-66.3		.512	1.678		1024
1025	1.979	.055	.419	171.6	168.2	11.2	-22.0		.141	2.828		1025
1026	2.250	.134	.082	308.7	108.1	33.7	-36.6		.116	2.452	182	1026
1027	3.161	.159	.025	169.0	334.3	93.4	-109.1		.816	1.378	1A	1027
1028	3.402	.101	.150	94.8	59.5	98.9	-122.3		1.190	1.302		1028
1029	2.890	.063	.039	178.6	2.1	66.6	-68.4		.882	1.948	3	1029
1030	3.123	.159	.260	189.8	193.7	54.2	-86.8		.737	1.405	113	1030
1031	3.046	.092	.321	169.8	223.5	35.6	-65.2		.848	1.689		1031
1032	3.131	.150	.146	249.5	73.8	77.2	-96.9		.806	1.431		1032
1033	3.003	.086	.188	57.0	195.3	60.2	-72.7		.898	1.762	2	1033
1034	2.292	.220	.082	317.8	295.6	35.3	-42.6		-.044	2.223		1034
1035	3.140	.146	.319	327.6	1.1	40.5	-79.7		.777	1.447		1035
1036	2.662	.382	.577	355.0	235.6	14.0	-73.0		-.445	1.210		1036
1037	2.255	.151	.110	20.2	207.2	33.2	-37.2		.071	2.404	180	1037
1038	3.969					27.8		3:2				1038
1039	2.680	.132	.094	194.9	232.9	51.6	-57.4		.394	1.874		1039
1040	3.118	.185	.307	91.6	282.7	44.8	-86.8		.656	1.329		1040
1041	3.072	.109	.224	52.8	58.3	57.6	-77.7		.886	1.615	116	1041
1042	3.225					27.8	-70.2	6				1042
1043	3.093	.028	.147	262.3	167.1	71.4	-79.1		1.170	1.845		1043
1044	2.578	.130	.060	273.0	49.3	47.6	-51.8		.423	2.084	145	1044
1045	2.359	.161	.021	87.9	267.9	38.6	-42.6		.167	2.271	162	1045
1046	2.984	.049	.139	98.4	2.5	65.5	-71.7		.998	1.895		1046
1047	2.241	.157	.087	30.5	79.9	33.3	-37.1		.051	2.406	184	1047
1048	2.731	.202	.261	225.3	49.9	40.7	-62.0		.320	1.743		1048
1049	3.095	.088	.274	23.3	338.9	47.4	-72.4		.949	1.662		1049
1050	2.625	.142	.235	60.1	337.4	38.7	-50.8		.410	2.020	140	1050
1051	3.213	.080	.401	324.8	186.0	14.3	-65.9		1.131	1.493		1051
1052	2.236	.125	.072	57.0	105.4	33.4	-35.9		.122	2.485	188	1052
1053	2.615	.086	.143	78.8	10.5	45.5	-50.0		.570	2.162		1053
1054	2.921	.095	.172	26.6	85.9	58.2	-68.3		.803	1.818		1054
1055	2.198	.145	.089	319.6	154.9	31.9	-35.1		.018	2.455	189	1055
1056	2.230	.128	.084	307.4	108.1	33.0	-35.7		.105	2.481	182	1056
1057	2.893	.205	.091	11.2	265.9	66.1	-83.6		.457	1.541		1057
1058	2.197	.127	.078	307.2	224.9	32.0	-34.5		.060	2.501	189	1058
1059	2.644	.159	.193	273.7	205.2	43.5	-54.6		.387	1.948		1059
1060	2.237	.149	.120	293.4	224.3	32.4	-36.4		.047	2.415	183	1060
1061	3.121	.182	.024	36.9	88.1	89.9	-108.9		.709	1.354	107	1061
1062	3.007	.065	.109	111.0	332.9	70.8	-76.0		.973	1.822		1062
1063	2.314	.078	.092	180.2	98.1	35.6	-37.3		.314	2.518		1063
1064	2.547	.149	.180	288.3	279.0	40.5	-49.0		.337	2.082	148	1064
1065	2.361	.252	.152	319.1	325.3	35.6	-47.7		-.085	2.061		1065
1066	2.403	.171	.090	3.4	333.6	39.1	-44.7		.174	2.193	75	1066
1067	2.871	.155	.211	41.4	278.6	51.3	-68.3	10	.572	1.688		1067
1068	2.908	.125	.116	211.4	312.3	63.8	-72.6		.701	1.751		1068
1069	3.132	.135	.225	172.4	145.7	61.2	-86.7		.851	1.473		1069
1070	3.219	.067	.286	348.1	169.7	46.8	-77.9		1.133	1.593		1070
1071	2.801	.104	.082	98.4	42.2	58.9	-63.7		.682	1.920		1071
1072	3.173	.209	.140	69.6	25.1	84.1	-119.3		.630	1.213		1072
1073	3.178	.164	.026	320.7	354.2	95.8	-113.6		.810	1.343	1	1073
1074	3.155	.151	.020	65.3	321.8	92.6	-106.6		.837	1.409	1A	1074
1075	3.014	.069	.182	342.3	101.3	61.6	-72.6		.965	1.803	2	1075
1076	2.477	.147	.051	99.9	161.7	43.1	-47.4		.302	2.163	24	1076
1077	2.393	.158	.099	1.4	336.1	38.4	-43.5		.193	2.237	75	1077
1078	2.270	.187	.118	141.1	93.3	33.6	-39.5		-.004	2.307	177	1078
1079	2.874	.047	.036	119.4	304.0	65.5	-66.5		.917	2.009	3	1079
1080	2.421	.239	.092	66.7	347.8	40.0	-50.7		.014	2.012		1080

numb	a	e	sin i	wbar	node	wbar rate	node rate	res	Mars	Jup	fam	numb
1081	3.091	.122	.069	43.7	13.8	82.6	−91.9		.872	1.567		1081
1082	3.128	.144	.025	323.7	192.8	89.3	−101.5		.837	1.461	1A	1082
1083	2.329	.212	.076	121.0	77.1	36.7	−43.9		.014	2.193		1083
1084	2.689	.124	.074	274.8	202.7	53.0	−57.8		.515	1.969		1084
1085	3.183	.066	.102	238.4	148.6	86.4	−93.2		1.125	1.645		1085
1086	3.164	.069	.164	145.5	309.4	74.3	−86.7		1.101	1.649	106	1086
1087	3.015	.071	.170	78.2	24.2	63.6	−73.6		.963	1.795	2	1087
1088	2.202	.154	.122	32.2	55.2	31.2	−35.3		−.024	2.414		1088
1089	2.214	.139	.053	87.4	72.0	33.0	−35.6		.069	2.474	186	1089
1090	2.360	.196	.360	135.1	152.3	22.1	−39.2		.118	2.061		1090
1091	3.420	.071	.007	129.2	349.1	125.9	−131.1		1.319	1.392		1091
1092	2.901	.096	.114	239.2	303.5	63.1	−69.6		.783	1.840		1092
1093	3.134	.142	.462	293.8	48.8	8.6	−66.3		.816	1.347		1093
1094	2.548	.148	.238	115.1	154.8	36.1	−47.3		.315	2.096		1094
1095	3.025	.059	.173	180.8	185.9	63.5	−73.4		1.007	1.820	2	1095
1096	2.601	.155	.153	320.8	78.7	44.7	−53.1		.369	2.000	149	1096
1097	2.641	.275	.019	300.3	188.4	52.7	−71.9		.064	1.622		1097
1098	2.689	.090	.247	72.6	326.0	38.9	−50.3		.601	2.094		1098
1099	3.167	.245	.200	5.4	20.9	74.6	−124.1		.502	1.103		1099
1100	2.898	.047	.037	292.6	290.0	67.2	−68.3		.938	1.987	3	1100
1101	3.243	.050	.371	251.4	204.4	20.4	−67.5		1.228	1.523		1101
1102	3.066	.062	.288	325.7	220.9	42.9	−67.0		1.019	1.775		1102
1103	1.934	.073	.360	323.4	271.4	14.8	−22.5		.071	2.832	190	1103
1104	2.630	.319	.119	49.5	136.8	49.7	−77.1		−.077	1.524		1104
1105	3.013	.069	.171	323.8	119.4	63.2	−73.2		.965	1.802	2	1105
1106	2.597	.154	.245	185.7	323.1	37.1	−49.9		.348	2.031	147	1106
1107	3.191	.125	.103	120.8	113.8	88.5	−102.4		.936	1.452	104	1107
1108	2.428	.163	.468	297.0	231.3	11.3	−36.8		.235	2.096		1108
1109	3.210	.134	.095	251.0	272.4	91.9	−107.5		.925	1.402		1109
1110	2.218	.173	.122	314.9	242.6	31.8	−36.7		−.038	2.368		1110
1111	2.994	.062	.052	2.9	145.9	74.1	−76.5		.979	1.848		1111
1112	3.021	.065	.177	39.0	300.8	62.6	−73.1		.985	1.807	2	1112
1113	3.113	.128	.249	106.6	324.0	55.1	−81.6		.840	1.511	116	1113
1114	3.092	.049	.190	61.0	202.2	64.5	−76.9		1.097	1.785		1114
1115	3.101	.164	.269	131.3	68.8	51.3	−85.0	10	.701	1.414	113	1115
1116	2.925	.184	.321	92.4	354.1	37.2	−69.5		.482	1.567		1116
1117	2.248	.161	.074	285.5	158.8	33.8	−37.6		.054	2.395	184	1117
1118	3.210	.037	.257	253.3	316.6	54.2	−78.7		1.220	1.697		1118
1119	2.612	.142	.125	272.3	51.0	46.7	−53.4		.408	2.020		1119
1120	2.216	.121	.073	35.1	167.4	32.8	−35.0		.106	2.507	188	1120
1121	2.546	.139	.114	58.3	348.0	44.2	−49.8		.367	2.103		1121
1122	2.605	.236	.068	36.2	57.2	49.4	−63.0		.148	1.773		1122
1123	2.225	.140	.101	57.3	82.7	32.5	−35.8		.063	2.453		1123
1124	2.927	.044	.132	228.9	14.1	62.7	−67.6		.966	1.967	124	1124
1125	3.136	.220	.032	116.7	94.3	93.3	−124.0		.597	1.218		1125
1126	2.272	.195	.116	141.7	355.4	33.7	−40.1		−.020	2.286	177	1126
1127	2.594	.223	.265	62.0	133.4	36.0	−55.4		.141	1.848		1127
1128	2.789	.047	.012	243.9	338.9	60.2	−60.9		.837	2.090		1128
1129	3.022	.059	.170	68.9	271.4	63.8	−73.4		1.005	1.822	2	1129
1130	2.229	.146	.050	326.0	226.3	33.5	−36.5		.071	2.448	186	1130
1131	2.229	.234	.045	350.0	104.5	33.7	−40.9		−.126	2.253		1131
1132	2.686	.242	.140	294.4	22.0	50.3	−68.7		.148	1.638		1132
1133	2.186	.138	.083	20.2	59.1	31.6	−34.4		.016	2.478	189	1133
1134	2.684	.411	.279	337.6	12.5	42.8	−98.9		−.323	1.245		1134
1135	2.666	.108	.086	5.1	338.7	51.3	−55.0	10	.463	1.959	139	1135
1136	2.565	.214	.169	357.7	218.9	42.5	−55.7		.179	1.899		1136
1137	2.424	.058	.060	357.2	76.4	40.5	−41.5		.471	2.441		1137
1138	3.146	.063	.264	51.2	284.2	50.8	−74.9		.989	1.599	111	1138
1139	1.947	.220	.245	55.3	202.3	20.9	−28.2		−.221	2.502		1139
1140	2.772	.078	.228	36.8	71.3	44.1	−54.9		.723	2.022		1140

numb	a	e	sin i	wbar	node	wbar rate	node rate	res	Mars	Jup	fam	numb
1141	2.271	.132	.065	33.8	111.4	34.7	−37.4		.144	2.445	181	1141
1142	3.179	.120	.026	223.8	172.8	94.1	−103.1		.954	1.482	103	1142
1143	5.201							1:1				1143
1144	3.755	.047	.159	12.2	165.7	134.6	−172.0		1.688	1.141		1144
1145	2.424	.124	.116	233.5	338.9	39.0	−42.9		.300	2.286		1145
1146	3.047	.207	.327	258.0	212.7	39.8	−83.0		.495	1.367		1146
1147	2.271	.208	.082	267.7	264.1	34.5	−41.1		−.040	2.262		1147
1148	3.016	.089	.175	304.8	151.4	63.0	−74.7		.905	1.740	2	1148
1149	2.898	.063	.224	29.6	263.5	49.4	−61.6		.864	1.915		1149
1150	2.191	.147	.052	350.3	216.6	32.3	−35.1		.020	2.470	186	1150
1151	2.406	.228	.139	347.7	233.9	37.8	−48.3		.022	2.062		1151
1152	2.427	.079	.097	180.2	323.0	39.7	−41.8		.420	2.388	156	1152
1153	2.196	.109	.066	295.6	273.1	32.2	−34.0		.108	2.549	188	1153
1154	3.399	.067	.059	239.9	78.8	118.4	−124.8		1.313	1.426		1154
1155	2.462	.188	.107	219.5	29.6	41.1	−48.7		.176	2.082		1155
1156	2.237	.076	.015	121.5	111.4	34.1	−34.8		.245	2.603		1156
1157	3.195	.118	.184	269.2	333.6	73.7	−94.5		.956	1.466		1157
1158	2.564	.087	.266	72.2	340.7	33.3	−43.7		.467	2.209	4	1158
1159	2.380	.031	.226	201.5	344.4	31.4	−36.6		.410	2.501		1159
1160	2.560	.078	.256	20.7	.1	34.0	−43.5		.503	2.250	4	1160
1161	3.164	.059	.146	22.6	70.0	77.3	−87.3		1.134	1.678	106	1161
1162	3.969							3:2				1162
1163	3.215	.022	.138	301.8	132.6	82.8	−91.0		1.299	1.757		1163
1164	2.306	.192	.426	148.4	160.4	15.6	−35.5		.095	2.163		1164
1165	3.130	.162	.251	285.7	209.4	56.7	−89.2		.746	1.392	113	1165
1166	2.542					27.8	−75.2	6				1166
1167	3.413	.073	.114	248.1	234.3	109.5	−122.9		1.294	1.387		1167
1168	2.551	.161	.242	342.9	223.7	35.9	−48.2		.293	2.062		1168
1169	2.318	.160	.086	86.8	256.9	36.0	−40.4		.123	2.327		1169
1170	2.326	.212	.409	53.9	354.8	17.8	−38.0		.071	2.087		1170
1171	3.167	.176	.039	56.2	138.3	94.1	−113.7		.765	1.318		1171
1172	5.201							1:1				1172
1173	5.201							1:1				1173
1174	3.022	.079	.178	346.7	355.1	62.8	−74.2		.940	1.763	2	1174
1175	3.215	.025	.297	269.2	240.1	42.6	−73.6		1.263	1.747		1175
1176	2.692	.142	.136	79.0	274.1	49.9	−58.0		.452	1.910		1176
1177	3.350	.037	.278	146.5	255.4	50.5	−86.1		1.271	1.518		1177
1178	2.680	.203	.119	160.6	180.1	50.8	−62.6		.207	1.703		1178
1179	2.617	.188	.160	228.7	357.7	45.1	−56.6		.290	1.899		1179
1180	3.969							3:2				1180
1181	2.664	.187	.117	64.2	265.2	49.9	−60.3		.305	1.824		1181
1182	2.259	.110	.166	73.1	332.0	31.5	−35.3		.131	2.454		1182
1183	2.383	.158	.048	207.8	354.1	39.3	−43.5		.194	2.247	167	1183
1184	2.668	.049	.200	275.4	350.8	42.8	−49.5		.707	2.217		1184
1185	2.237	.124	.088	97.3	71.9	33.2	−35.8		.120	2.482	182	1185
1186	3.021	.071	.179	326.3	38.6	62.5	−73.5		.963	1.787	2	1186
1187	2.640	.177	.217	49.4	322.9	41.3	−55.3		.335	1.903	138	1187
1188	2.191	.140	.079	28.8	358.1	31.8	−34.7		.022	2.474	189	1188
1189	2.931	.065	.194	14.1	276.0	55.3	−65.7		.893	1.892		1189
1190	2.432	.127	.051	83.4	8.8	41.1	−44.1		.311	2.266	159	1190
1191	2.893	.085	.306	168.8	136.3	35.8	−57.1		.761	1.884		1191
1192	2.365	.224	.422	146.4	5.0	17.5	−40.1		.064	2.011		1192
1193	2.646	.144	.233	220.2	46.5	39.6	−52.1		.426	1.989	140	1193
1194	2.914	.127	.216	180.1	289.3	52.1	−68.2		.652	1.689		1194
1195	2.258	.197	.146	231.7	281.3	32.3	−39.0		−.057	2.275		1195
1196	2.653	.103	.297	20.2	101.4	32.2	−47.1		.474	2.053		1196
1197	2.883	.230	.280	172.0	259.0	44.4	−76.9		.354	1.468		1197
1198	2.249	.281	.074	343.7	261.8	34.0	−45.2		−.222	2.123		1198
1199	3.019	.063	.170	174.3	241.3	63.7	−73.4		.989	1.814	2	1199
1200	3.059	.133	.090	236.1	217.8	78.0	−89.1		.808	1.567		1200

numb	a	e	sin i	wbar	node	wbar rate	node rate	res	Mars	Jup	fam	numb
1201	2.699	.021	.130	48.3	211.3	50.1	−52.9		.793	2.223		1201
1202	3.969							3:2				1202
1203	2.884	.223	.117	44.1	235.4	64.0	−85.3		.390	1.500		1203
1204	2.263	.248	.034	315.9	341.6	35.0	−43.5		−.127	2.190		1204
1205	2.532	.244	.148	12.8	17.2	42.5	−57.2		.072	1.865		1205
1206	2.865	.066	.241	212.2	321.3	45.5	−58.7		.837	1.960		1206
1207	3.021	.070	.179	85.9	14.1	62.5	−73.4		.969	1.792	2	1207
1208	5.201							1:1				1208
1209	3.175	.132	.100	251.9	89.1	87.6	−102.1		.899	1.445	104	1209
1210	3.011	.069	.177	240.2	108.9	62.3	−72.8		.962	1.804	2	1210
1211	2.930	.120	.204	329.5	132.4	54.6	−69.4		.719	1.733		1211
1212	3.969							3:2				1212
1213	3.132	.077	.252	28.1	273.4	53.6	−76.4		1.013	1.643	111	1213
1214	2.711	.091	.189	303.4	284.6	46.0	−53.9		.631	2.050		1214
1215	2.579	.094	.265	54.3	125.9	33.8	−44.6		.470	2.183	4	1215
1216	2.232	.160	.128	245.4	127.3	32.0	−36.6		.007	2.386	183	1216
1217	2.353	.169	.087	225.0	157.3	37.3	−42.4		.133	2.260		1217
1218	2.263	.153	.043	140.1	58.1	34.8	−38.1		.090	2.404		1218
1219	2.213	.138	.068	88.7	36.7	32.8	−35.5		.066	2.474	185	1219
1220	3.005	.072	.178	112.9	116.1	61.7	−72.4		.945	1.800	2	1220
1221	1.921	.448	.223	199.3	168.5	21.7	−42.1		−.697	2.095		1221
1222	2.792					27.8	−22.0	6				1222
1223	2.869	.043	.037	90.2	14.7	65.1	−66.1		.923	2.025	3	1223
1224	2.304	.168	.155	41.6	260.7	33.4	−39.4		.062	2.306		1224
1225	2.233	.116	.049	129.9	.9	33.7	−35.6		.147	2.515	186	1225
1226	2.584	.140	.170	160.4	13.0	42.6	−50.6		.391	2.063	149	1226
1227	3.201	.150	.307	294.7	1.5	44.9	−86.9		.825	1.355		1227
1228	2.769	.076	.075	168.8	300.1	57.3	−60.0		.734	2.030	37	1228
1229	3.215	.135	.032	346.4	246.6	98.6	−111.4		.936	1.396	1	1229
1230	2.572	.151	.188	32.5	206.2	40.9	−50.2		.353	2.049	148	1230
1231	2.669	.104	.211	208.3	337.0	42.2	−51.3		.564	2.063		1231
1232	3.181	.159	.207	225.8	267.1	68.7	−98.9		.801	1.356	102	1232
1233	2.555	.068	.115	230.8	288.8	44.3	−47.0		.562	2.272		1233
1234	3.013	.055	.168	50.7	302.1	63.5	−72.5		1.010	1.844	2	1234
1235	1.910	.075	.435	49.6	6.8	9.8	−20.7		.037	2.861	191	1235
1236	2.430	.183	.223	1.7	48.2	33.8	−44.5		.116	2.124	163	1236
1237	2.612	.041	.155	12.5	54.6	44.4	−48.2		.686	2.283		1237
1238	2.667	.159	.210	150.2	49.1	42.7	−55.5		.397	1.927	138	1238
1239	2.664	.241	.014	117.1	34.7	53.8	−68.9		.184	1.697		1239
1240	2.868	.133	.190	337.8	318.8	53.7	−67.1		.627	1.756		1240
1241	3.185	.082	.420	286.6	322.6	9.4	−62.7		1.070	1.538		1241
1242	2.736	.157	.193	49.5	343.0	47.4	−60.0		.464	1.842		1242
1243	3.099	.048	.248	240.4	248.6	52.8	−72.2		1.073	1.756		1243
1244	2.344	.138	.171	169.3	275.6	33.8	−39.3		.171	2.340		1244
1245	2.893	.043	.042	349.7	175.3	66.6	−67.7		.943	2.003	3	1245
1246	2.620	.193	.318	346.1	286.8	30.8	−51.9		.134	1.797		1246
1247	3.138	.160	.031	283.2	205.8	90.7	−106.1		.795	1.402	1	1247
1248	2.722	.028	.141	127.7	77.8	50.2	−53.9		.797	2.175		1248
1249	2.224	.128	.099	134.0	256.9	32.5	−35.3		.088	2.476	182	1249
1250	2.551	.308	.312	146.6	283.9	32.4	−62.0		−.166	1.647		1250
1251	2.717	.116	.093	352.0	148.7	53.6	−58.7		.564	1.966	132	1251
1252	2.696	.095	.579	178.3	131.4	−6.6	−39.5		.363	2.012		1252
1253	3.169	.169	.024	40.3	341.9	94.8	−112.8		.789	1.335	1	1253
1254	3.134	.070	.145	182.9	286.9	75.5	−85.5		1.070	1.675		1254
1255	3.153	.121	.169	10.3	245.0	73.8	−92.1		.915	1.499	109	1255
1256	3.904	.024	.090	307.7	249.9	213.1	−234.0		1.909	1.094		1256
1257	2.488	.108	.080	210.2	224.6	42.8	−45.6		.406	2.246		1257
1258	3.185	.009	.154	316.6	297.7	77.3	−86.4		1.316	1.818		1258
1259	3.100	.166	.024	216.0	55.2	87.1	−102.7		.745	1.425	1	1259
1260	2.614	.017	.155	254.5	301.4	44.5	−47.9		.752	2.344		1260

numb	a	e	sin i	wbar	node	wbar rate	node rate	res	Mars	Jup	fam	numb
1261	3.145	.212	.029	170.5	48.0	94.0	−122.6		.631	1.234		1261
1262	3.002	.033	.211	192.5	127.4	55.6	−67.8		1.065	1.911		1262
1263	2.665	.085	.508	102.1	163.4	−.3	−37.8		.640	2.020		1263
1264	2.862	.162	.443	249.4	234.1	15.1	−55.3		.574	1.604		1264
1265	3.025	.064	.182	100.1	311.6	62.1	−73.1		.991	1.806	2	1265
1266	3.363	.038	.313	199.4	319.3	39.3	−82.5		1.323	1.559		1266
1267	2.465	.170	.082	279.0	12.8	41.9	−47.9		.230	2.120	154	1267
1268	3.969							3:2				1268
1269	3.969							3:2				1269
1270	2.235	.155	.097	3.2	100.3	32.9	−36.7		.041	2.410	180	1270
1271	3.135	.096	.104	44.4	132.5	82.3	−91.2		.987	1.600	203	1271
1272	2.783	.126	.160	308.3	316.5	52.4	−61.8		.565	1.850	127	1272
1273	2.394	.120	.110	341.9	291.5	38.1	−41.6		.284	2.327	165	1273
1274	2.229	.148	.084	192.5	317.3	33.0	−36.4		.056	2.434	184	1274
1275	2.680	.136	.225	30.2	192.9	41.7	−53.8		.478	1.967	140	1275
1276	3.172	.071	.378	105.8	116.7	20.6	−64.8		1.104	1.526		1276
1277	2.699	.215	.145	286.8	248.3	50.4	−65.9		.238	1.687	135	1277
1278	2.405	.211	.181	323.3	87.9	35.6	−46.0		.054	2.109		1278
1279	2.370	.197	.115	260.0	329.3	37.2	−44.5		.072	2.179		1279
1280	3.413	.018	.134	34.3	292.6	103.0	−114.4		1.493	1.577		1280
1281	2.560	.187	.147	271.2	215.1	43.4	−53.4		.249	1.971	150	1281
1282	3.118	.080	.330	80.9	322.8	34.0	−67.6		.943	1.649		1282
1283	3.202	.164	.150	31.3	162.9	83.0	−108.9		.811	1.309		1283
1284	2.646	.150	.211	71.4	302.4	41.7	−53.3		.416	1.965	138	1284
1285	2.993	.021	.115	74.1	312.0	68.8	−72.6		1.098	1.970		1285
1286	3.023	.074	.178	278.2	207.7	62.8	−73.9		.956	1.777	2	1286
1287	3.012	.075	.180	140.4	209.9	61.9	−73.0		.943	1.785	2	1287
1288	2.885	.028	.150	330.6	296.6	58.1	−63.4		.977	2.048		1288
1289	2.860	.052	.037	270.3	226.8	64.5	−65.7		.890	2.010	3	1289
1290	2.366	.120	.113	38.0	301.9	36.9	−40.4		.256	2.362	165	1290
1291	3.012	.061	.171	309.5	222.3	63.1	−72.7		.990	1.827	2	1291
1292	2.543	.089	.057	156.8	271.6	45.9	−47.9		.503	2.231		1292
1293	2.227	.206	.118	334.6	239.9	32.2	−38.7		−.097	2.293		1293
1294	2.687	.215	.138	39.9	82.7	50.2	−65.1		.232	1.714	135	1294
1295	3.388	.132	.056	122.4	210.1	120.3	−139.5		1.076	1.221		1295
1296	2.418	.159	.088	113.8	233.8	39.7	−44.8		.216	2.201	75	1296
1297	3.021	.058	.176	94.4	294.9	62.8	−72.9		1.005	1.826	2	1297
1298	3.128	.105	.118	355.2	295.9	79.9	−90.7		.946	1.580		1298
1299	2.803	.164	.139	75.8	173.7	55.7	−67.6		.499	1.746	126	1299
1300	2.782	.038	.148	182.2	81.7	52.8	−57.4		.830	2.101		1300
1301	2.767	.163	.579	136.7	174.4	.0	−48.1		.095	1.837	129	1301
1302	3.122	.162	.024	94.7	83.0	89.3	−104.6		.775	1.413	1A	1302
1303	3.230	.109	.332	180.9	72.2	36.7	−79.1		.940	1.443		1303
1304	3.196	.125	.315	219.7	89.9	41.3	−80.9		.896	1.451		1304
1305	3.014	.107	.026	203.0	37.3	77.4	−82.9		.859	1.690		1305
1306	3.140	.089	.280	76.1	276.1	47.1	−75.1		.980	1.618	108	1306
1307	2.251	.118	.082	103.7	236.0	33.7	−36.1		.154	2.490	182	1307
1308	2.909	.049	.104	180.8	343.7	64.2	−67.6		.937	1.969		1308
1309	3.220	.121	.194	104.5	211.1	73.4	−96.9		.966	1.432		1309
1310	2.393	.236	.424	318.2	225.2	18.0	−42.2	4	.023	1.939		1310
1311	2.426	.078	.065	146.4	250.5	40.5	−42.0		.425	2.391		1311
1312	3.093					27.8	−68.4	6				1312
1313	2.657	.161	.248	49.1	298.0	38.7	−53.5		.379	1.937		1313
1314	2.295	.163	.107	63.4	266.1	34.7	−39.4		.087	2.345	175	1314
1315	3.212	.082	.140	237.6	242.3	82.6	−94.9		1.099	1.558		1315
1316	2.411	.264	.435	31.3	245.5	18.3	−45.4		−.036	1.858		1316
1317	3.192					27.8	−114.5	6				1317
1318	2.308	.217	.422	190.8	354.4	16.7	−37.5		.033	2.101		1318
1319	2.987	.242	.076	207.0	268.7	76.0	−104.5		.419	1.325		1319
1320	2.986	.221	.325	263.6	67.4	39.9	−81.0		.428	1.385		1320

numb	a	e	sin i	wbar	node	wbar rate	node rate	res	Mars	Jup	fam	numb
1321	2.941	.153	.183	290.5	315.3	58.9	−75.6		.639	1.629		1321
1322	2.422	.238	.423	270.7	249.6	18.4	−43.5		.057	1.910		1322
1323	3.204	.176	.330	185.7	47.8	40.8	−90.6		.734	1.265		1323
1324	2.185	.136	.086	249.3	298.2	31.5	−34.3		.017	2.481	189	1324
1325	2.538	.224	.127	349.7	7.9	43.7	−55.9		.136	1.905		1325
1326	2.666	.160	.275	32.2	103.5	35.8	−52.9		.361	1.922	137	1326
1327	2.781	.131	.091	315.0	50.0	57.5	−64.2		.584	1.866	40	1327
1328	3.496	.109	.113	40.9	235.0	122.9	−146.9		1.230	1.182		1328
1329	2.617	.140	.241	284.3	136.0	37.9	−50.0		.406	2.040	140	1329
1330	3.176	.111	.269	172.6	162.9	51.3	−81.7	10	.905	1.471	108	1330
1331	3.104	.171	.036	291.1	137.2	87.3	−104.4		.729	1.403	201	1331
1332	3.063	.094	.046	354.4	347.1	80.8	−85.8		.940	1.681	119	1332
1333	2.633	.146	.238	105.7	118.0	38.8	−51.4		.406	2.002	140	1333
1334	2.914	.101	.187	241.7	137.8	55.8	−67.4		.770	1.806		1334
1335	2.241	.116	.049	23.1	186.6	33.9	−35.9		.155	2.509	186	1335
1336	2.851	.047	.036	278.0	98.4	63.9	−64.9		.893	2.031	3	1336
1337	2.911	.057	.301	4.2	163.8	36.6	−56.8		.873	1.956		1337
1338	2.264	.126	.091	97.7	318.8	34.0	−36.7		.143	2.460	182	1338
1339	3.021	.063	.171	126.3	289.9	63.5	−73.4		.991	1.812	2	1339
1340	3.183	.167	.028	206.8	295.1	96.4	−114.9		.805	1.330	1	1340
1341	2.742	.089	.211	228.9	109.7	45.2	−54.8		.667	2.018		1341
1342	2.289	.179	.382	180.5	308.3	18.8	−35.0		.128	2.202		1342
1343	2.568	.113	.097	256.7	32.3	45.8	−49.8		.459	2.142		1343
1344	2.248	.163	.089	181.3	58.3	33.5	−37.6		.043	2.385	184	1344
1345	3.969							3:2				1345
1346	2.627	.148	.247	67.2	169.6	37.7	−50.9		.391	2.010		1346
1347	2.572	.070	.221	98.8	231.9	37.7	−45.0		.556	2.271		1347
1348	2.791	.148	.096	118.1	85.3	58.0	−66.5		.543	1.807		1348
1349	3.013	.159	.205	241.2	306.8	59.5	−81.3		.673	1.538		1349
1350	2.858	.051	.039	23.9	160.4	64.3	−65.5		.889	2.013	3	1350
1351	3.192	.057	.171	92.1	3.7	74.8	−87.9		1.160	1.660	106	1351
1352	2.778	.039	.068	68.7	203.0	58.0	−59.3		.846	2.125	38	1352
1353	3.012	.073	.172	280.9	218.3	63.1	−73.4		.952	1.792	2	1353
1354	3.134	.207	.112	266.2	16.6	85.1	−115.0		.617	1.259		1354
1355	1.853	.070	.403	213.8	230.5	11.5	−20.2		−.003	2.930	191	1355
1356	3.083	.012	.120	349.6	65.8	74.9	−79.7		1.210	1.911		1356
1357	3.190	.094	.229	11.5	83.2	62.1	−85.6		1.033	1.538		1357
1358	2.475	.148	.037	298.1	355.2	43.2	−47.4		.299	2.162		1358
1359	3.120	.041	.175	66.9	61.3	68.8	−79.8		1.148	1.782		1359
1360	2.633	.160	.429	263.5	332.3	16.4	−45.1		.425	1.869		1360
1361	3.084					27.8	−67.1	6				1361
1362	3.276							2:1				1362
1363	2.903	.047	.034	291.5	247.0	67.7	−68.7		.943	1.982	3	1363
1364	3.012	.073	.183	253.3	60.8	61.4	−72.7		.949	1.790	2	1364
1365	2.249	.141	.104	213.6	258.9	33.1	−36.6		.090	2.434	180	1365
1366	2.875	.116	.167	290.9	18.2	56.5	−67.0		.699	1.806		1366
1367	2.344	.152	.396	258.2	271.2	17.6	−34.9		.241	2.203		1367
1368	2.523	.056	.253	222.5	14.9	33.3	−41.5		.517	2.337	153	1368
1369	3.109	.162	.269	305.1	187.9	51.3	−85.1	10	.668	1.378	113	1369
1370	2.251	.128	.091	297.9	299.3	33.6	−36.4		.127	2.462	182	1370
1371	3.203	.085	.292	248.8	190.0	45.8	−78.2		1.056	1.555		1371
1372	2.767	.119	.304	80.6	325.9	34.2	−53.3		.549	1.913		1372
1373	3.409							W L				1373
1374	2.251	.224	.115	9.0	295.6	33.1	−40.8		−.108	2.239		1374
1375	2.448	.079	.090	111.0	46.4	40.8	−42.8		.443	2.363	156	1375
1376	2.228	.165	.063	313.2	177.2	33.4	−37.1		.025	2.403	184	1376
1377	2.260	.125	.118	197.0	226.3	33.1	−36.2		.129	2.455		1377
1378	2.375	.162	.053	230.4	29.5	38.9	−43.3		.175	2.248	167	1378
1379	2.528	.129	.270	180.2	172.1	32.4	−44.1		.309	2.128		1379
1380	3.148	.125	.193	223.8	352.8	69.0	−90.0		.894	1.494	202	1380

numb	a	e	sin i	wbar	node	wbar rate	node rate	res	Mars	Jup	fam	numb
1381	2.488	.148	.088	26.9	339.2	42.6	−47.7		.304	2.145		1381
1382	2.220	.147	.029	218.2	325.9	33.4	−36.2		..063	2.456	187	1382
1383	3.083	.148	.023	355.1	276.8	84.8	−96.4		.790	1.496	1	1383
1384	2.677	.160	.209	80.9	158.7	43.2	−56.2		.404	1.913	138	1384
1385	2.741	.064	.104	17.1	119.0	54.0	−57.1		.728	2.085	134	1385
1386	2.364	.228	.205	309.6	169.1	33.1	−45.0		−.051	2.089		1386
1387	2.258	.155	.109	325.1	210.3	33.3	−37.5		.067	2.394	180	1387
1388	3.019	.071	.182	284.6	50.1	61.9	−73.1		.961	1.790	2	1388
1389	2.866	.043	.037	167.3	206.8	64.9	−65.8		.919	2.027	3	1389
1390	3.435					27.8	−85.8	6				1390
1391	2.549	.194	.123	181.6	105.0	44.3	−53.8		.225	1.963	43	1391
1392	2.608	.167	.225	49.2	351.6	39.5	−52.3		.334	1.972	147	1392
1393	2.435	.130	.090	217.4	51.6	40.3	−44.0		.300	2.253		1393
1394	2.439	.064	.050	263.2	197.6	41.4	−42.4		.474	2.408		1394
1395	3.201	.028	.169	296.9	249.8	75.5	−87.1		1.267	1.744		1395
1396	2.248	.153	.081	246.9	349.4	33.7	−37.3		.070	2.411	184	1396
1397	2.685	.249	.044	272.6	64.5	54.7	−71.6		.182	1.657		1397
1398	3.159	.056	.227	12.9	295.7	59.9	−79.1		1.135	1.690		1398
1399	2.216	.136	.118	45.6	166.5	31.7	−35.1		.046	2.455	183	1399
1400	3.114	.160	.308	315.9	216.1	43.2	−81.3		.726	1.421		1400
1401	2.227	.110	.142	359.8	274.5	31.3	−34.4		.099	2.483		1401
1402	2.684	.145	.264	261.6	267.3	37.6	−53.0		.435	1.958	137	1402
1403	2.718	.271	.167	350.5	163.0	50.7	−75.5		.052	1.485		1403
1404	5.201							1:1				1404
1405	2.252	.139	.133	70.8	308.2	32.4	−36.4		.082	2.422	183	1405
1406	2.696	.081	.228	84.1	329.8	41.4	−51.1		.646	2.101		1406
1407	2.763	.233	.138	20.1	273.3	54.6	−74.2		.258	1.606		1407
1408	3.110	.056	.151	33.6	210.1	72.7	−81.8		1.095	1.745		1408
1409	2.676	.037	.116	50.1	186.9	49.8	−52.3		.735	2.208		1409
1410	3.020	.073	.177	54.1	177.4	62.7	−73.6		.958	1.784	2	1410
1411	3.003	.017	.161	29.0	284.3	63.7	−70.9		1.119	1.966		1411
1412	2.215	.138	.071	101.4	64.8	32.8	−35.5		.066	2.470	185	1412
1413	3.022	.079	.178	143.1	186.6	62.9	−74.2		.939	1.762	2	1413
1414	2.785	.193	.143	151.5	150.4	54.8	−69.8		.398	1.687	128	1414
1415	2.224	.125	.064	188.5	317.4	33.2	−35.5		.110	2.496	188	1415
1416	3.018	.079	.184	75.3	346.8	61.5	−73.4		.936	1.768	2	1416
1417	2.973	.093	.125	236.4	97.1	66.8	−74.5		.856	1.778		1417
1418	2.242	.147	.124	313.7	350.3	32.4	−36.4		.054	2.414	183	1418
1419	2.293	.165	.114	100.5	218.1	34.4	−39.3		.076	2.340	175	1419
1420	2.749	.048	.080	305.8	264.4	55.8	−57.5		.789	2.125	130	1420
1421	3.093	.113	.161	198.3	38.2	70.7	−85.5		.895	1.586		1421
1422	2.247	.130	.055	23.2	213.0	34.1	−36.5		.130	2.471	186	1422
1423	2.860	.044	.037	25.9	39.7	64.5	−65.5		.910	2.030	3	1423
1424	3.187	.025	.149	336.5	37.1	78.4	−87.4		1.268	1.766		1424
1425	2.612	.138	.229	168.1	191.6	38.8	−50.1		.412	2.044	140	1425
1426	2.581	.162	.178	235.2	330.0	42.1	−51.8		.328	2.014	148	1426
1427	2.750	.180	.152	304.2	74.4	52.1	−64.9		.366	1.724		1427
1428	2.810	.079	.287	15.3	116.9	36.9	−53.6		.727	2.002		1428
1429	2.550	.295	.139	342.9	46.2	44.3	−65.3		−.050	1.712		1429
1430	2.559	.175	.069	309.7	315.1	46.6	−53.6		.290	1.995		1430
1431	2.620	.138	.229	334.7	118.5	39.1	−50.5		.421	2.035	140	1431
1432	2.381	.181	.132	338.6	125.7	36.9	−43.9		.115	2.204		1432
1433	2.786	.132	.164	71.6	318.0	52.3	−62.3		.546	1.827	127	1433
1434	3.018	.059	.179	259.9	158.9	62.2	−72.5		.999	1.827	2	1434
1435	2.648	.267	.088	41.4	139.5	51.3	−70.3	10	.045	1.598		1435
1436	3.146	.076	.259	254.6	262.1	52.2	−76.5		.997	1.608	111	1436
1437	5.201							1:1				1437
1438	3.177	.180	.058	4.0	257.1	94.1	−116.1		.750	1.297	105	1438
1439	3.969							3:2				1439
1440	3.153	.159	.032	44.1	12.7	92.3	−108.0		.810	1.386	1	1440

numb	a	e	sin i	wbar	node	wbar rate	node rate	res	Mars	Jup	fam	numb
1441	2.632	.171	.273	19.8	258.1	35.4	−52.0		.306	1.931	21	1441
1442	2.875	.045	.038	330.7	248.1	65.5	−66.5		.923	2.014	3	1442
1443	2.938	.036	.036	300.2	209.9	70.2	−71.0		1.006	1.977		1443
1444	3.158	.100	.335	235.5	304.5	34.2	−72.0		.902	1.541		1444
1445	3.114	.149	.021	356.0	79.7	88.1	−100.7		.808	1.461	1A	1445
1446	2.246	.136	.086	193.7	9.5	33.5	−36.5		.105	2.450	182	1446
1447	2.536	.057	.076	135.4	25.0	45.0	−46.4		.577	2.321		1447
1448	2.372	.214	.099	126.5	37.1	37.8	−45.9		.039	2.134	166	1448
1449	2.223	.151	.110	218.7	116.0	32.2	−36.0		.029	2.424	183	1449
1450	2.611	.179	.069	97.7	67.9	49.3	−57.3		.308	1.913		1450
1451	2.203	.146	.095	200.6	180.8	31.9	−35.2		.019	2.448	189	1451
1452	3.117	.179	.268	130.9	20.2	53.0	−89.9		.646	1.339		1452
1453	1.897	.041	.416	229.5	1.4	10.8	−20.4		.095	2.942	191	1453
1454	2.365	.177	.094	135.4	344.1	37.6	−43.3		.123	2.228		1454
1455	2.247	.147	.132	204.5	132.6	32.3	−36.5		.056	2.406	183	1455
1456	3.190	.179	.220	331.9	282.0	68.0	−103.6		.748	1.268		1456
1457	2.695	.159	.133	222.1	294.8	50.4	−59.7		.389	1.844		1457
1458	2.627	.152	.230	266.3	186.5	39.4	−51.8		.389	1.991	140	1458
1459	3.148	.144	.278	9.7	40.1	51.3	−84.2	10	.659	1.303		1459
1460	2.541	.189	.100	80.2	70.7	44.8	−53.3		.238	1.983		1460
1461	3.127	.045	.245	119.0	106.2	54.4	−74.2		1.125	1.753		1461
1462	3.152	.138	.025	203.8	323.0	91.7	−103.5		.874	1.452	1	1462
1463	3.147	.159	.153	51.6	324.5	77.5	−99.9		.788	1.386		1463
1464	3.002	.075	.183	160.4	85.9	60.8	−72.1		.934	1.795	2	1464
1465	3.024	.202	.175	207.6	170.9	66.5	−93.5		.551	1.395		1465
1466	2.377	.171	.230	203.7	156.5	31.6	−41.2		.066	2.172	163	1466
1467	3.386	.129	.392	309.6	327.7	19.7	−87.3		1.081	1.115		1467
1468	2.195	.133	.176	345.3	305.0	29.2	−33.7		−.151	2.301		1468
1469	3.124	.032	.234	74.5	194.1	56.6	−74.5		1.173	1.798		1469
1470	3.160	.042	.063	295.2	340.4	88.3	−90.9		1.187	1.743		1470
1471	2.716	.096	.253	79.5	319.7	39.2	−51.7		.609	2.050		1471
1472	2.234	.155	.069	11.9	40.9	33.5	−36.9		.054	2.421	184	1472
1473	2.574	.176	.257	348.8	222.5	35.4	−50.0		.263	1.995		1473
1474	2.735	.154	.601	47.5	320.7	−1.9	−45.9		.039	1.902		1474
1475	2.349	.148	.087	53.3	209.0	37.1	−41.1		.180	2.314		1475
1476	2.281	.144	.113	313.7	324.2	34.0	−37.9		.114	2.400	180	1476
1477	3.187	.212	.332	75.9	322.4	42.9	−98.2		.596	1.164		1477
1478	2.464	.126	.150	132.9	314.2	39.1	−44.4		.325	2.238		1478
1479	2.676	.199	.135	105.0	9.8	49.6	−62.3		.282	1.784	135	1479
1480	2.202	.165	.075	135.8	61.1	32.3	−36.1		−.015	2.415	194	1480
1481	3.017	.040	.071	255.5	337.5	74.6	−76.8		1.066	1.887		1481
1482	2.872	.049	.035	236.4	57.1	65.4	−66.5		.909	2.005	3	1482
1483	2.717	.215	.066	163.6	65.1	55.7	−69.2		.300	1.711		1483
1484	2.737	.213	.306	196.2	75.7	35.7	−61.6		.265	1.702		1484
1485	3.026	.080	.175	326.6	295.3	63.5	−74.8		.942	1.756	2	1485
1486	2.198	.072	.010	313.0	239.7	32.8	−33.4		.204	2.637		1486
1487	3.143	.154	.023	195.2	97.8	91.3	−105.6		.817	1.414	1A	1487
1488	3.038	.128	.193	126.3	350.5	61.9	−79.6		.793	1.603		1488
1489	3.189	.191	.036	172.5	188.5	97.9	−123.1		.728	1.249	107	1489
1490	2.353	.091	.192	350.0	254.6	32.9	−37.6		.278	2.425		1490
1491	3.216	.174	.085	122.1	307.8	95.5	−119.1		.798	1.266		1491
1492	2.173	.156	.106	188.7	142.5	30.8	−34.4		−.063	2.422		1492
1493	2.430	.165	.055	327.2	314.6	41.0	−46.1		.213	2.175	24	1493
1494	2.190	.100	.052	43.5	202.1	32.2	−33.6		.122	2.574	193	1494
1495	2.640	.127	.228	264.5	8.4	39.7	−50.8		.470	2.040	140	1495
1496	2.206	.125	.051	277.3	283.7	32.8	−34.8		.090	2.512	186	1496
1497	2.895	.057	.038	301.4	288.3	67.0	−68.5		.906	1.962	3	1497
1498	3.100	.153	.264	359.3	267.7	52.4	−83.1		.709	1.421	113	1498
1499	2.671	.140	.236	301.0	241.3	40.3	−53.1		.456	1.973	140	1499
1500	2.243	.170	.125	52.6	13.4	32.4	−37.4		.000	2.360		1500

numb	a	e	sin i	wbar	node	wbar rate	node rate	res	Mars	Jup	fam	numb
1501	2.547	.205	.126	34.1	6.6	44.0	−54.6		.193	1.938	43	1501
1502	2.732	.106	.083	136.4	218.2	54.8	−59.2		.613	1.982	132	1502
1503	2.627	.135	.230	141.0	313.7	39.2	−50.6		.433	2.034	140	1503
1504	2.399	.196	.184	147.1	93.2	35.3	−44.7		.083	2.148		1504
1505	2.659	.149	.272	218.6	251.5	36.1	−51.7		.395	1.965	137	1505
1506	2.566	.244	.241	266.5	233.6	37.6	−57.0		.079	1.835		1506
1507	2.331	.183	.182	342.3	288.7	33.0	−40.9		.045	2.238		1507
1508	2.768	.154	.587	122.2	19.0	−1.3	−47.3		.096	1.863	129	1508
1509	1.866	.042	.417	208.7	284.1	10.5	−19.8		.062	2.970	191	1509
1510	2.670	.182	.219	142.8	328.3	42.4	−57.1		.345	1.858	138	1510
1511	2.358	.148	.057	174.1	80.7	38.1	−41.7		.193	2.304	167	1511
1512	3.969							3:2				1512
1513	2.193	.159	.067	157.5	145.1	32.1	−35.5		−.013	2.435	194	1513
1514	2.241	.152	.075	321.0	155.9	33.6	−37.0		.065	2.421	184	1514
1515	2.566	.212	.171	46.5	45.7	42.4	−55.5		.184	1.902		1515
1516	2.620	.206	.149	211.5	130.1	46.1	−59.0		.243	1.843		1516
1517	2.717	.050	.076	243.6	56.8	54.1	−55.8		.752	2.145	134	1517
1518	2.226	.154	.112	85.6	21.7	32.2	−36.2		.024	2.414	183	1518
1519	3.134	.195	.215	352.7	13.8	66.1	−101.5		.654	1.283		1519
1520	3.108	.057	.283	28.0	255.9	45.0	−69.7		1.078	1.739		1520
1521	2.850	.112	.265	74.3	7.7	42.0	−59.4		.676	1.859	125	1521
1522	2.368	.090	.080	115.7	55.9	38.0	−39.8		.341	2.425	197	1522
1523	2.242	.147	.096	153.9	319.5	33.2	−36.7		.071	2.425	180	1523
1524	3.107	.090	.226	346.5	343.9	58.9	−78.4		.974	1.636		1524
1525	2.696	.227	.132	41.4	339.2	51.3	−67.3	10	.177	1.653		1525
1526	2.315	.172	.120	63.1	329.4	35.0	−40.5		.081	2.304		1526
1527	2.227	.144	.087	314.3	9.9	32.9	−36.1		.063	2.445	184	1527
1528	2.415	.177	.143	188.3	142.9	37.7	−44.9		.156	2.173		1528
1529	3.969							3:2				1529
1530	2.249	.155	.094	20.4	281.8	33.4	−37.2		.060	2.401	180	1530
1531	2.628	.143	.234	77.8	280.4	38.9	−51.1		.411	2.014	140	1531
1532	3.005	.063	.166	131.4	325.9	63.4	−72.6		.977	1.827	2	1532
1533	3.013	.074	.177	170.5	162.9	62.3	−73.1		.949	1.789	2	1533
1534	2.730	.253	.171	110.1	46.5	51.3	−91.2	10				1534
1535	3.148	.191	.129	286.7	265.5	83.2	−110.8		.677	1.295		1535
1536	2.204	.151	.035	16.0	213.0	32.9	−35.8		.034	2.457	187	1536
1537	3.050	.259	.091	19.1	248.5	81.6	−119.8		.401	1.203		1537
1538	2.361	.173	.168	358.2	337.2	34.7	−41.9		.110	2.247	171	1538
1539	3.147	.151	.021	33.3	188.6	91.8	−105.6		.831	1.417	1A	1539
1540	2.850	.131	.200	41.4	280.7	51.3	−64.9	10	.376	1.550		1540
1541	2.769	.106	.089	188.7	348.7	56.7	−61.4		.645	1.947		1541
1542	3.095	.074	.060	11.7	232.1	82.6	−86.6		1.029	1.708		1542
1543	2.628	.296	.215	305.3	282.9	42.9	−69.5		−.002	1.610		1543
1544	2.373	.096	.045	77.3	51.3	38.8	−40.5		.334	2.404		1544
1545	2.771	.267	.046	146.1	34.4	60.6	−83.4		.198	1.513		1545
1546	3.172	.113	.293	123.7	197.0	45.9	−79.3		.942	1.497		1546
1547	2.645	.256	.226	94.3	294.0	42.0	−64.6		.115	1.693		1547
1548	2.788	.101	.273	187.4	118.3	38.9	−54.8		.647	1.964		1548
1549	2.231	.118	.086	114.2	87.4	33.0	−35.3		.128	2.502	182	1549
1550	2.548	.265	.148	19.3	65.6	43.4	−60.8		.028	1.791		1550
1551	2.395	.029	.052	326.1	113.8	39.5	−39.9		.517	2.540		1551
1552	3.010	.070	.173	62.6	3.5	62.7	−72.9		.958	1.801	2	1552
1553	2.907	.125	.037	146.1	118.3	68.5	−74.6		.715	1.754		1553
1554	2.620	.150	.228	349.7	223.0	39.3	−51.4		.389	2.004	140	1554
1555	2.690	.252	.131	41.4	344.8	51.3	−70.5	10	.103	1.594		1555
1556	3.420	.058	.257	349.0	92.6	61.9	−98.9		1.346	1.424		1556
1557	3.010	.070	.183	349.3	349.7	61.2	−72.3		.959	1.804	2	1557
1558	3.217	.039	.163	106.6	113.5	78.0	−89.8		1.244	1.691		1558
1559	2.390	.173	.069	178.6	313.8	39.2	−44.5		.162	2.206		1559
1560	2.684	.184	.136	28.2	287.9	49.9	−61.1		.328	1.811		1560

numb	a	e	sin i	wbar	node	wbar rate	node rate	res	Mars	Jup	fam	numb
1561	3.191	.147	.093	254.5	240.8	90.7	−108.1		.865	1.381	104	1561
1562	2.226	.116	.082	187.8	136.3	32.9	−35.2		.126	2.509	182	1562
1563	2.191	.148	.096	160.2	53.1	31.6	−34.9		−.002	2.453	189	1563
1564	3.161	.166	.200	49.9	182.6	69.9	−98.9		.764	1.352		1564
1565	2.393	.242	.435	18.6	267.0	17.2	−42.5		.013	1.933		1565
1566	1.078					4.3	−21.9	5				1566
1567	3.219	.084	.288	173.4	49.4	47.0	−79.6		1.073	1.536		1567
1568	2.352	.197	.430	.6	143.1	15.8	−37.4		.114	2.098	168	1568
1569	3.152	.080	.195	336.7	100.1	67.4	−83.9		1.047	1.631		1569
1570	2.844	.043	.036	94.9	223.7	63.4	−64.3		.898	2.050	3	1570
1571	3.141	.112	.274	87.4	293.5	49.8	−78.9		.887	1.516	108	1571
1572	3.111	.168	.229	359.2	1.9	61.1	−90.9		.723	1.393		1572
1573	2.370	.212	.422	14.7	204.9	17.2	−39.3		.085	2.032		1573
1574	3.537	.059	.272	169.8	249.7	58.3	−108.0		1.434	1.306		1574
1575	2.375	.196	.430	201.1	209.9	16.0	−38.1		.135	2.074	168	1575
1576	3.135	.152	.022	58.7	234.4	90.4	−104.1		.817	1.429	1A	1576
1577	2.230	.141	.071	46.1	131.6	33.3	−36.2		.080	2.455	185	1577
1578	3.969							3:2				1578
1579	3.424	.132	.163	117.7	196.3	99.7	−132.9		1.089	1.175		1579
1580	2.196					4.3		5				1580
1581	3.164	.153	.025	188.9	111.9	93.6	−108.3		.837	1.392	1A	1581
1582	3.162	.141	.189	215.3	96.7	71.3	−94.9		.854	1.429	202	1582
1583	5.201							1:1				1583
1584	2.376	.195	.458	133.8	302.8	13.5	−37.5		.118	2.079		1584
1585	2.932	.156	.487	47.3	149.8	7.9	−56.4		.569	1.501		1585
1586	2.429	.144	.059	157.9	135.0	40.9	−44.7		.265	2.229	159	1586
1587	2.547	.156	.146	108.9	351.8	42.7	−50.3		.319	2.064	149	1587
1588	3.030	.049	.175	289.1	99.2	63.4	−73.1		1.045	1.847	200	1588
1589	2.417	.062	.077	35.9	91.4	39.9	−41.2		.457	2.436		1589
1590	2.230	.134	.088	258.0	228.7	32.9	−35.8		.089	2.465	182	1590
1591	2.393	.186	.413	335.5	173.0	17.3	−38.4	3	.215	2.062		1591
1592	2.768	.289	.212	276.7	109.2	49.6	−81.9		.080	1.431		1592
1593	2.225	.208	.157	296.8	122.9	30.9	−38.2		−.151	2.245		1593
1594	2.269	.155	.143	275.1	67.0	32.6	−37.5		.055	2.366		1594
1595	2.642	.083	.055	296.0	118.6	50.9	−52.9		.513	2.045	141	1595
1596	2.891	.112	.247	64.0	252.3	46.2	−62.9		.715	1.805	125	1596
1597	2.845	.095	.198	190.6	163.3	50.7	−61.6		.655	1.824		1597
1598	2.332	.097	.145	210.2	294.9	34.5	−37.8		.269	2.452		1598
1599	3.135	.105	.095	48.4	33.7	83.5	−92.9		.958	1.573	203	1599
1600	1.849	.027	.339	151.2	54.6	14.9	−20.7		.086	3.008		1600
1601	2.234	.118	.074	246.3	75.2	33.3	−35.6		.136	2.503	188	1601
1602	2.245	.154	.061	150.3	74.0	33.9	−37.2		.071	2.418		1602
1603	2.755	.048	.134	38.8	135.2	52.5	−56.4		.766	2.099		1603
1604	3.024	.066	.180	328.2	305.9	62.4	−73.3		.982	1.799	2	1604
1605	3.014	.077	.182	120.5	181.3	61.7	−73.1		.939	1.779	2	1605
1606	2.690	.283	.151	333.2	205.1	51.3	−75.6	10	.028	1.514		1606
1607	2.546	.265	.146	356.0	122.9	43.4	−60.7		.028	1.794		1607
1608	2.214	.119	.066	302.6	348.0	32.8	−34.9		.109	2.515	188	1608
1609	2.585					27.8	−43.9	6				1609
1610	2.202	.160	.038	26.2	339.3	32.8	−36.1		.010	2.438	187	1610
1611	3.187	.128	.095	291.9	246.0	89.3	−103.0		.925	1.447	104	1611
1612	3.102	.104	.313	186.6	316.3	39.1	−70.7		.893	1.622		1612
1613	2.736	.249	.164	41.4	266.4	51.3	−72.8	10	.143	1.539		1613
1614	2.996	.121	.240	169.9	167.8	51.7	−71.9		.685	1.576	120	1614
1615	3.113	.158	.025	49.7	197.8	88.1	−102.5		.779	1.434	1A	1615
1616	2.911	.033	.135	158.4	42.5	61.2	−65.9		.981	2.014	124	1616
1617	3.204	.156	.223	179.7	157.8	66.6	−99.0		.837	1.325	102	1617
1618	2.869	.046	.036	223.9	107.0	65.1	−66.1		.915	2.018	3	1618
1619	2.241	.151	.095	45.3	61.0	33.1	−36.8		.061	2.417	180	1619
1620	1.244	.323	.282	252.6	336.3	9.6	−15.3		−.309	3.243		1620

numb	a	e	sin i	wbar	node	wbar rate	node rate	res	Mars	Jup	fam	numb
1621	2.230	.123	.062	83.1	192.1	33.4	−35.7		.122	2.496	188	1621
1622	2.234	.153	.113	238.6	357.1	32.5	−36.5		.038	2.411	183	1622
1623	3.133	.155	.025	86.3	133.5	90.2	−104.5		.806	1.422	1A	1623
1624	3.180	.143	.021	159.2	170.8	95.2	−108.6		.879	1.407	1	1624
1625	3.183	.184	.327	236.4	322.2	41.6	−90.7		.698	1.260		1625
1626	2.364	.233	.446	77.9	283.7	15.7	−40.4		.016	1.998		1626
1627	1.864	.424	.149	297.3	141.4	22.4	−38.9		−.674	2.213		1627
1628	3.014	.103	.339	140.1	186.5	32.0	−63.1		.722	1.638		1628
1629	2.238	.162	.169	208.6	136.3	30.8	−36.4		−.039	2.328		1629
1630	3.030	.197	.073	155.3	44.5	78.3	−99.1		.588	1.406		1630
1631	2.235	.152	.125	331.1	13.2	32.2	−36.4		.033	2.406	183	1631
1632	2.656	.106	.109	319.0	210.5	49.5	−54.1		.533	2.048		1632
1633	3.169	.185	.029	178.2	124.9	95.5	−118.3		.734	1.288	107	1633
1634	2.246	.136	.120	261.7	92.3	32.6	−36.2		.089	2.440	183	1634
1635	2.855	.045	.037	277.8	217.8	64.1	−65.1		.903	2.033	3	1635
1636	2.235	.120	.082	70.5	176.5	33.2	−35.6		.129	2.495	182	1636
1637	3.070	.075	.241	219.3	16.8	53.5	−72.5		.974	1.712		1637
1638	2.749	.186	.022	273.2	261.5	58.4	−68.2		.410	1.756		1638
1639	2.574	.137	.163	84.4	320.8	42.5	−50.0		.397	2.077	149	1639
1640	2.289	.291	.123	350.8	347.7	34.3	−47.7		−.234	2.048		1640
1641	3.019	.073	.174	315.6	326.7	63.1	−73.8		.959	1.785	2	1641
1642	2.751	.095	.198	143.3	335.0	46.6	−56.0		.651	1.999		1642
1643	2.490	.163	.084	20.2	285.3	42.9	−48.7		.268	2.106	154	1643
1644	2.546	.178	.144	118.8	270.3	42.9	−51.9		.261	2.011	150	1644
1645	3.059	.077	.039	8.4	273.4	80.5	−83.8		.991	1.738	119	1645
1646	2.361	.099	.137	60.9	124.2	35.8	−39.1		.296	2.427	169	1646
1647	5.201							1:1				1647
1648	2.236	.194	.076	248.8	140.9	33.4	−38.7		−.036	2.328		1648
1649	3.021	.081	.176	168.3	150.8	63.1	−74.5		.933	1.757	2	1649
1650	2.437	.168	.057	241.6	215.1	41.3	−46.6		.213	2.161	24	1650
1651	2.180	.135	.098	156.1	193.5	31.1	−34.0		.008	2.478	189	1651
1652	2.251	.144	.069	244.5	252.1	34.0	−37.1		.098	2.432	185	1652
1653	2.610	.292	.108	36.3	299.9	48.7	−70.6		−.002	1.631		1653
1654	3.017	.052	.176	354.6	19.8	62.5	−72.2		1.023	1.851	2	1654
1655	2.783	.218	.151	83.7	117.3	54.5	−73.0		.322	1.619		1655
1656	1.878	.087	.410	123.5	181.1	11.4	−20.8		−.015	2.871	191	1656
1657	2.349	.189	.413	155.9	102.4	17.1	−37.0		.138	2.114		1657
1658	2.560	.173	.139	273.2	95.5	43.8	−52.4		.286	2.004	150	1658
1659	2.783	.200	.306	12.8	331.9	36.6	−62.9		.342	1.691		1659
1660	2.395	.212	.411	135.1	216.7	18.3	−40.5		.116	2.004		1660
1661	2.184	.120	.064	197.4	258.1	31.9	−33.9		.065	2.529	188	1661
1662	2.743	.135	.091	39.4	320.0	55.3	−61.8		.538	1.895	40	1662
1663	2.240	.131	.084	5.8	84.9	33.3	−36.1		.109	2.466	182	1663
1664	2.339	.263	.106	152.7	39.3	36.5	−48.0		−.110	2.062		1664
1665	2.414	.226	.174	105.8	90.9	36.4	−48.0		.027	2.059		1665
1666	2.185	.122	.059	352.9	258.5	32.0	−34.0		.063	2.524	188	1666
1667	2.190	.130	.070	252.7	80.3	32.0	−34.4		.049	2.502	188	1667
1668	2.806	.180	.076	345.4	175.5	60.4	−72.0		.468	1.706		1668
1669	3.140	.150	.026	194.6	319.3	90.8	−104.3		.828	1.429	1A	1669
1670	2.902	.095	.169	97.2	54.9	57.4	−67.0		.786	1.840		1670
1671	2.588	.249	.075	73.4	191.1	48.5	−63.2		.110	1.768	146	1671
1672	3.178	.257	.028	75.6	235.7	101.3	−149.2		.505	1.060		1672
1673	3.101	.157	.073	61.9	224.3	84.2	−99.3		.770	1.449		1673
1674	3.187	.139	.025	106.3	93.9	95.7	−108.5		.898	1.412	1	1674
1675	2.233	.149	.113	100.6	24.6	32.4	−36.3		.045	2.421	183	1675
1676	2.236	.181	.094	241.2	49.4	33.0	−37.9		−.014	2.355		1676
1677	2.532	.063	.263	259.6	335.6	32.6	−41.7		.493	2.296	153	1677
1678	3.165	.113	.186	133.6	347.8	71.3	−90.7		.951	1.513	204	1678
1679	3.125	.111	.319	240.6	180.6	38.5	−72.8		.882	1.573		1679
1680	2.724	.209	.056	230.2	81.0	56.3	−69.2		.323	1.718		1680

numb	a	e	sin i	wbar	node	wbar rate	node rate	res	Mars	Jup	fam	numb
1681	2.698	.204	.107	106.9	94.3	52.6	−65.4		.284	1.741		1681
1682	2.239	.140	.075	333.7	315.8	33.5	−36.5		.091	2.449	185	1682
1683	2.735	.151	.228	305.1	324.0	43.4	−57.9		.482	1.863	140	1683
1684	3.092	.149	.044	240.0	112.0	84.9	−97.4		.790	1.482		1684
1685	1.368	.397	.244	237.2	185.5		−18.7	13				1685
1686	3.163	.148	.025	287.7	306.2	93.3	−107.0		.854	1.410	1A	1686
1687	3.158	.151	.025	60.9	91.6	92.8	−106.9		.839	1.406	1A	1687
1688	2.618	.220	.226	274.5	244.9	40.4	−58.0		.197	1.822		1688
1689	2.449	.176	.102	34.1	128.5	40.7	−47.3		.195	2.126		1689
1690	3.041	.050	.239	40.3	234.5	52.5	−69.0		1.009	1.801		1690
1691	3.165	.142	.025	48.7	233.4	93.3	−106.0		.874	1.426	1	1691
1692	2.788	.117	.052	294.3	222.2	59.6	−64.3		.636	1.900		1692
1693	2.804	.226	.207	299.2	63.6	50.4	−73.7		.265	1.534		1693
1694	2.396	.217	.186	13.5	8.8	35.1	−46.1		.026	2.103		1694
1695	2.784	.222	.312	4.2	227.1	36.5	−65.8		.269	1.625		1695
1696	2.262	.145	.100	175.6	15.2	33.7	−37.3		.094	2.416	180	1696
1697	2.374	.112	.108	83.4	324.7	37.4	−40.5		.284	2.370	165	1697
1698	3.155	.150	.029	158.9	341.9	92.3	−106.3		.839	1.412	1A	1698
1699	2.211	.112	.046	319.0	266.0	33.0	−34.7		.127	2.535	186	1699
1700	2.361	.188	.082	15.9	343.6	37.8	−43.9		.096	2.206		1700
1701	3.170	.124	.282	307.1	59.1	49.1	−82.2		.898	1.446		1701
1702	2.858	.102	.157	334.5	104.6	56.4	−65.0		.727	1.863		1702
1703	2.215	.117	.071	319.7	118.6	32.8	−34.8		.114	2.518	188	1703
1704	2.223	.136	.031	170.7	256.5	33.5	−35.9		.091	2.479	187	1704
1705	2.299	.193	.139	346.4	197.0	33.9	−40.8		.005	2.259	177	1705
1706	2.125	.110	.038	213.3	264.3	30.4	−31.8		−.008	2.564		1706
1707	2.219	.163	.070	66.6	354.2	32.9	−36.7		.016	2.413	184	1707
1708	2.916	.287	.131	85.4	200.2	67.0	−104.8		.212	1.280		1708
1709	2.379	.165	.149	339.9	295.2	36.1	−42.5		.148	2.251		1709
1710	2.322	.217	.147	330.5	352.4	34.5	−43.2		−.032	2.183		1710
1711	3.015	.069	.180	32.3	139.2	62.0	−72.8		.965	1.801	2	1711
1712	3.176	.151	.348	233.8	240.1	34.2	−80.4		.738	1.360		1712
1713	2.228	.136	.055	309.2	57.8	33.5	−36.1		.092	2.469	186	1713
1714	2.565	.160	.160	248.0	299.5	42.5	−51.1		.328	2.029	149	1714
1715	2.399	.245	.193	234.5	31.2	35.1	−48.4		−.045	2.029		1715
1716	2.733	.133	.120	196.1	250.3	53.1	−60.4		.519	1.897	133	1716
1717	2.195	.180	.113	113.7	335.7	31.3	−36.2		−.084	2.366		1717
1718	2.366	.224	.151	335.0	212.2	35.8	−45.7		−.010	2.125		1718
1719	2.657	.159	.276	27.6	318.9	35.7	−52.2		.362	1.937	137	1719
1720	2.188	.130	.015	101.3	180.2	32.5	−34.5		.062	2.516		1720
1721	3.148	.060	.294	123.4	315.9	43.1	−71.6		1.093	1.695		1721
1722	2.514	.065	.094	129.4	178.9	43.4	−45.3		.536	2.324		1722
1723	3.013	.077	.179	168.4	155.4	62.1	−73.3		.939	1.778	2	1723
1724	2.711	.074	.208	129.3	169.5	44.0	−52.3		.677	2.102		1724
1725	2.903	.057	.037	334.2	131.4	67.6	−69.1		.913	1.953	3	1725
1726	2.787	.046	.076	246.8	241.5	58.2	−60.0		.837	2.094	38	1726
1727	1.854	.079	.349	101.0	135.5	14.5	−21.2		−.010	2.905		1727
1728	2.562	.071	.141	279.6	244.0	43.3	−46.9		.561	2.262		1728
1729	2.230	.092	.038	240.6	353.5	33.7	−34.9		.197	2.570		1729
1730	2.784	.178	.167	40.2	176.6	52.6	−66.9		.417	1.710		1730
1731	3.174	.081	.092	342.1	164.0	87.3	−94.5		1.070	1.607		1731
1732	3.012	.076	.177	.7	161.5	62.3	−73.3		.943	1.784	2	1732
1733	2.193	.136	.081	124.4	168.7	31.9	−34.6		.034	2.482	189	1733
1734	2.777	.191	.144	6.9	190.6	54.3	−69.0		.395	1.697	128	1734
1735	3.145	.086	.278	263.3	6.1	47.6	−75.4		.992	1.617	108	1735
1736	2.229	.161	.082	66.3	168.6	33.0	−36.9		.027	2.406	184	1736
1737	3.013	.081	.179	186.0	322.4	62.2	−73.6		.928	1.768	2	1737
1738	2.183	.135	.077	326.8	41.9	31.6	−34.3		.022	2.488	189	1738
1739	2.261	.102	.069	261.4	211.0	34.3	−36.1		.201	2.518	179	1739
1740	2.467	.151	.054	19.0	287.9	42.7	−47.1		.282	2.164	24	1740

numb	a	e	sin i	wbar	node	wbar rate	node rate	res	Mars	Jup	fam	numb
1741	2.885	.039	.038	59.0	35.4	66.2	−67.1		.949	2.020	3	1741
1742	2.889	.059	.036	.8	180.2	66.6	−68.1		.897	1.960	3	1742
1743	2.470	.180	.117	182.9	199.2	41.0	−48.4		.199	2.094		1743
1744	2.229	.170	.070	173.7	19.6	33.3	−37.4		.012	2.389	184	1744
1745	2.846	.042	.038	96.5	70.1	63.5	−64.3		.903	2.051	3	1745
1746	3.969							3:2				1746
1747	1.709	.121	.420	249.3	270.0	9.9	−18.3		−.222	2.988		1747
1748	3.969							3:2				1748
1749	5.201							1:1				1749
1750	1.926	.116	.394	23.3	278.0	13.2	−22.7		−.033	2.756		1750
1751	2.790	.123	.161	11.0	246.0	52.6	−62.0		.584	1.856	127	1751
1752	2.238	.146	.077	334.0	240.4	33.4	−36.6		.075	2.435	184	1752
1753	3.015	.079	.183	259.4	54.3	61.6	−73.3		.934	1.772	2	1753
1754	3.969							3:2				1754
1755	3.093	.068	.177	153.1	163.8	67.2	−79.2		1.038	1.724	115	1755
1756	2.548	.197	.116	38.2	289.6	44.5	−54.2		.216	1.955	43	1756
1757	2.351	.166	.061	182.4	29.1	37.8	−42.3		.143	2.272		1757
1758	3.007	.063	.170	206.5	116.3	62.9	−72.4		.977	1.826	2	1758
1759	2.648	.253	.071	358.5	171.3	51.7	−68.7		.069	1.617		1759
1760	3.157	.149	.167	200.8	241.5	75.5	−98.1		.825	1.405	109	1760
1761	3.168	.258	.029	135.2	54.2	100.1	−147.5		.495	1.067		1761
1762	2.876	.046	.036	54.5	191.4	65.6	−66.7		.922	2.010	3	1762
1763	2.189	.138	.080	333.1	296.3	31.8	−34.6		.022	2.478	189	1763
1764	3.089	.155	.032	221.6	184.6	85.2	−98.3		.772	1.468	1	1764
1765	3.169	.068	.337	334.7	69.3	32.0	−68.9		.959	1.583		1765
1766	2.749	.047	.094	352.4	200.8	55.0	−57.2		.789	2.125	130	1766
1767	3.020	.066	.176	309.8	199.8	62.8	−73.2		.980	1.804	2	1767
1768	2.450	.154	.057	39.0	353.9	41.9	−46.4		.260	2.179	24	1768
1769	2.179	.084	.030	349.9	297.6	32.1	−33.0		.151	2.620		1769
1770	2.457	.058	.088	98.9	12.0	41.2	−42.7		.503	2.401		1770
1771	3.125	.140	.177	54.9	87.7	71.0	−91.7		.827	1.471	109	1771
1772	2.530	.133	.087	176.5	88.1	44.5	−48.9		.377	2.136		1772
1773	2.435	.148	.079	226.9	72.1	40.7	−45.1		.258	2.215		1773
1774	2.877	.058	.035	98.7	210.4	65.8	−67.3		.886	1.972	3	1774
1775	2.603	.156	.234	263.2	199.4	38.4	−50.8		.354	2.010	147	1775
1776	3.104	.044	.162	162.5	184.7	70.2	−79.7		1.127	1.789		1776
1777	2.626	.042	.066	144.1	320.7	49.7	−50.7		.684	2.247	143	1777
1778	3.146	.158	.023	224.1	116.9	91.8	−107.0		.807	1.397	1A	1778
1779	2.176	.147	.027	242.6	248.9	32.0	−34.6		.010	2.484		1779
1780	3.016	.067	.178	235.3	290.6	62.3	−72.9		.972	1.805	2	1780
1781	2.395	.081	.110	43.7	39.8	38.1	−40.3		.383	2.419		1781
1782	3.118	.164	.025	248.9	205.7	88.9	−104.5		.766	1.411	1A	1782
1783	2.662	.160	.209	151.9	197.2	42.5	−55.3		.390	1.931	138	1783
1784	2.405	.125	.010	262.6	108.7	40.4	−43.1		.297	2.297		1784
1785	2.236	.118	.078	162.7	277.7	33.3	−35.6		.137	2.500	182	1785
1786	3.021	.070	.178	2.0	10.7	62.6	−73.5		.967	1.790	2	1786
1787	3.002	.080	.176	203.3	304.2	62.0	−72.9		.920	1.781	2	1787
1788	3.111	.147	.020	289.6	244.3	87.8	−100.0		.813	1.469	1A	1788
1789	2.213	.140	.025	308.3	116.9	33.3	−35.7		.072	2.478	187	1789
1790	2.238	.154	.088	150.8	354.3	33.2	−36.9		.052	2.414	184	1790
1791	2.746	.150	.103	254.7	208.9	55.0	−63.2		.494	1.850		1791
1792	2.777	.243	.141	41.2	74.0	55.5	−77.0		.248	1.558		1792
1793	2.224	.144	.039	176.9	235.8	33.5	−36.2		.073	2.459	187	1793
1794	3.124	.198	.275	200.2	229.0	52.6	−93.8		.575	1.267		1794
1795	2.784	.195	.146	256.0	199.2	54.6	−70.0		.389	1.681	128	1795
1796	3.359	.071	.387	195.0	190.8	14.3	−74.7		1.280	1.378		1796
1797	2.237	.037	.046	128.1	22.6	33.8	−34.2		.330	2.689		1797
1798	2.199	.126	.099	77.0	42.0	31.7	−34.4		.055	2.492	189	1798
1799	3.025	.088	.188	340.1	162.5	61.5	−74.5		.913	1.733	2	1799
1800	2.357	.094	.090	333.7	130.0	37.3	−39.4		.317	2.429	197	1800

numb	a	e	sin i	wbar	node	wbar rate	node rate	res	Mars	Jup	fam	numb
1801	3.018	.074	.173	113.5	75.7	63.3	−73.8		.953	1.782	2	1801
1802	2.843	.044	.036	134.7	166.8	63.3	−64.2		.895	2.049	3	1802
1803	2.349	.199	.411	226.1	332.7	17.5	−37.8		.122	2.088		1803
1804	2.410	.040	.072	198.9	315.2	39.8	−40.6		.505	2.497		1804
1805	3.133	.157	.026	171.1	63.5	90.2	−104.8		.800	1.416	1A	1805
1806	2.237	.145	.081	119.6	267.6	33.3	−36.5		.075	2.438	184	1806
1807	2.226	.142	.073	30.0	240.5	33.1	−36.1		.071	2.454	185	1807
1808	2.748	.160	.041	70.5	342.1	57.7	−65.4		.482	1.827		1808
1809	2.927	.074	.036	311.9	100.7	69.5	−71.9		.885	1.879	123	1809
1810	2.224	.131	.084	117.0	252.6	32.8	−35.5		.090	2.478	182	1810
1811	3.141	.090	.145	279.2	177.3	76.4	−88.2		1.011	1.605		1811
1812	3.008	.073	.179	108.3	185.8	61.8	−72.6		.948	1.797	2	1812
1813	2.684	.108	.133	192.8	28.8	49.4	−55.1		.548	2.018		1813
1814	2.226	.157	.072	103.5	10.9	33.1	−36.7		.037	2.421	184	1814
1815	3.159	.195	.027	113.6	123.5	94.8	−119.4		.696	1.271	107	1815
1816	2.340	.210	.437	144.2	157.5	15.4	−37.8		.065	2.083		1816
1817	2.372	.183	.436	238.4	93.1	15.1	−37.0		.162	2.108	168	1817
1818	2.164	.109	.064	319.7	245.3	31.3	−33.0		.061	2.560	193	1818
1819	3.140					27.8	−79.8	6				1819
1820	2.199	.150	.085	306.3	153.9	32.0	−35.3		.008	2.445	189	1820
1821	2.377	.187	.052	274.9	289.1	39.0	−44.8		.117	2.187	164	1821
1822	2.170	.154	.028	227.1	229.7	31.8	−34.6		−.014	2.471		1822
1823	2.226	.144	.061	224.1	300.4	33.3	−36.2		.071	2.453		1823
1824	2.885	.048	.037	130.4	342.8	66.2	−67.4		.923	1.994	3	1824
1825	2.677	.082	.089	119.6	286.8	51.5	−54.5		.483	1.964		1825
1826	2.997	.078	.181	102.6	275.3	60.9	−72.1		.921	1.793	2	1826
1827	2.709	.183	.098	112.3	229.2	53.5	−64.0		.366	1.796		1827
1828	3.060	.078	.250	41.4	173.8	51.3	−71.4	10	.938	1.703		1828
1829	2.251	.141	.122	97.0	290.5	32.7	−36.6		.082	2.423	183	1829
1830	2.188	.115	.071	136.8	156.8	31.9	−33.8		.079	2.535	188	1830
1831	2.239	.130	.086	231.4	72.6	33.3	−36.0		.111	2.470	182	1831
1832	3.216	.053	.280	63.3	293.5	47.9	−77.2		1.178	1.634		1832
1833	2.634	.088	.168	296.3	164.5	44.5	−50.3		.579	2.140		1833
1834	3.024	.088	.185	240.1	270.3	61.9	−74.5		.914	1.736	2	1834
1835	2.833	.052	.037	20.3	286.1	62.6	−63.8		.862	2.035	3	1835
1836	2.783	.192	.142	270.8	273.0	54.8	−69.6		.400	1.690	128	1836
1837	2.206	.108	.077	202.7	276.0	32.4	−34.2		.118	2.540	188	1837
1838	3.210	.042	.367	225.4	42.5	22.0	−65.6		1.203	1.565		1838
1839	2.800	.134	.162	48.7	46.8	53.1	−63.5		.570	1.824	127	1839
1840	2.918	.031	.035	158.9	12.5	68.6	−69.3		1.002	2.013		1840
1841	3.425	.135	.038	174.3	19.4	128.6	−149.2		1.101	1.173		1841
1842	2.266	.160	.095	262.1	162.9	34.0	−38.2		.068	2.381		1842
1843	2.653	.152	.165	285.3	266.7	45.9	−55.5		.416	1.946		1843
1844	3.017	.078	.187	176.4	100.1	61.0	−73.1		.938	1.773	2	1844
1845	2.971	.070	.173	138.1	148.2	60.4	−70.0		.922	1.843	199	1845
1846	2.338	.159	.054	107.8	3.1	37.4	−41.4		.151	2.297	167	1846
1847	2.611	.044	.177	193.5	108.7	42.7	−47.5		.675	2.284		1847
1848	2.871	.053	.041	239.7	308.3	65.2	−66.6		.895	1.993	3	1848
1849	3.053	.050	.174	186.1	46.4	64.9	−75.0		1.061	1.821	200	1849
1850	2.251	.126	.058	236.6	67.5	34.1	−36.5		.142	2.476	186	1850
1851	3.108	.148	.031	6.2	342.8	87.1	−99.6		.806	1.470	1	1851
1852	3.014	.067	.175	114.5	95.8	62.7	−73.0		.971	1.805	2	1852
1853	3.064	.031	.290	90.6	298.0	41.8	−65.1		1.113	1.875		1853
1854	2.540	.147	.094	116.1	201.2	44.8	−50.3		.346	2.088		1854
1855	2.247	.131	.062	171.4	202.6	34.0	−36.5		.126	2.467	181	1855
1856	2.237	.099	.089	208.0	191.8	33.1	−35.0		.178	2.540		1856
1857	2.243	.130	.089	71.1	238.6	33.3	−36.2		.115	2.465	182	1857
1858	2.699	.082	.048	257.3	273.4	54.2	−56.3		.651	2.082	36	1858
1859	3.221	.104	.151	219.8	335.3	82.1	−98.7		1.030	1.478		1859
1860	2.564	.188	.161	285.8	138.8	42.7	−53.3		.252	1.957		1860

numb	a	e	sin i	wbar	node	wbar rate	node rate	res	Mars	Jup	fam	numb
1861	3.019	.065	.179	250.9	17.6	62.4	−73.0		.982	1.807	2	1861
1862	1.470	.549	.155	319.3	28.8	14.4	−37.0		−.946	2.607		1862
1863	2.261	.475	.544	253.1	343.6	15.3	−60.1		−.744	1.569		1863
1864	1.461					12.1	−25.7	16				1864
1865	1.080	.473	.338	182.5	230.0	6.3	−12.8		−.271	3.320		1865
1866	1.893					−4.6	−20.8	6				1866
1867	5.201							1:1				1867
1868	5.201							1:1				1868
1869	5.201							1:1				1869
1870	5.201							1:1				1870
1871	5.201							1:1				1871
1872	5.201							1:1				1872
1873	5.201							1:1				1873
1874	3.143	.254	.075	349.7	175.2	93.2	−137.4		.482	1.108		1874
1875	3.130	.123	.243	328.3	200.7	57.0	−83.0		.878	1.510		1875
1876	1.964	.051	.439	192.2	303.1	9.6	−21.3		.134	2.852		1876
1877	3.969							3:2				1877
1878	2.846	.042	.037	169.0	220.8	63.5	−64.4		.903	2.051	3	1878
1879	2.246	.152	.044	81.4	252.2	34.2	−37.4		.079	2.423	187	1879
1880	2.675	.075	.068	263.9	123.5	52.1	−54.3		.612	2.093	36	1880
1881	3.168	.096	.186	260.8	223.5	70.8	−88.0		1.009	1.562	204	1881
1882	3.006	.065	.173	306.9	208.8	62.5	−72.3		.972	1.822	2	1882
1883	2.414	.219	.421	51.6	78.3	17.9	−41.6		.111	1.963		1883
1884	2.424	.188	.403	116.1	355.3	18.6	−40.0		.205	2.029		1884
1885	2.250	.196	.104	329.4	318.5	33.2	−39.1		−.037	2.307		1885
1886	2.627	.132	.240	281.8	80.4	38.2	−50.0		.438	2.049	140	1886
1887	3.006	.074	.175	20.9	342.5	62.2	−72.8		.942	1.795	2	1887
1888	2.549	.182	.125	126.4	247.3	44.1	−52.8		.256	1.993	43	1888
1889	3.090	.121	.224	148.0	52.7	58.7	−80.8		.861	1.558	116	1889
1890	3.235	.100	.155	103.3	66.5	81.9	−98.2		1.057	1.478		1890
1891	2.706	.040	.211	310.8	318.4	43.1	−50.8		.774	2.195		1891
1892	2.461	.095	.255	92.4	314.0	31.7	−40.3		.328	2.268		1892
1893	2.708	.039	.159	266.3	61.3	48.3	−52.9		.775	2.183		1893
1894	2.887	.036	.036	21.3	268.8	66.4	−67.1		.959	2.026	3	1894
1895	3.184	.162	.027	116.4	5.0	96.3	−113.8		.823	1.345	1	1895
1896	2.368	.181	.043	4.1	206.6	38.7	−44.1		.124	2.212	164	1896
1897	2.283	.097	.059	326.9	60.4	35.2	−36.8		.240	2.514	179	1897
1898	3.120	.134	.021	44.0	229.6	88.2	−98.3		.862	1.502	1	1898
1899	2.265	.154	.118	172.0	50.4	33.3	−37.6		.068	2.386		1899
1900	2.209	.158	.126	89.4	280.3	31.3	−35.6		−.023	2.401		1900
1901	3.232	.093	.395	238.7	97.8	16.8	−69.3		1.089	1.423		1901
1902	3.969							3:2				1902
1903	3.002	.075	.176	149.0	139.9	61.9	−72.5		.935	1.796	2	1903
1904	2.744	.036	.205	21.1	107.5	45.1	−52.7		.813	2.174		1904
1905	2.223	.156	.055	242.3	210.9	33.3	−36.6		.042	2.429		1905
1906	2.373	.098	.114	17.2	346.9	37.2	−39.9		.319	2.407	169	1906
1907	2.545	.076	.050	196.3	170.0	46.1	−47.6		.539	2.260		1907
1908	2.891	.068	.083	207.8	.6	64.7	−67.9		.866	1.931		1908
1909	2.424	.247	.047	222.2	245.8	41.1	−51.9		.006	1.990		1909
1910	3.047	.082	.187	176.0	208.4	62.7	−75.9		.948	1.730		1910
1911	3.969							3:2				1911
1912	2.903	.064	.037	47.8	65.8	67.6	−69.5		.893	1.934	3	1912
1913	2.880	.047	.036	54.0	325.5	65.9	−66.9		.923	2.004	3	1913
1914	2.406	.139	.088	264.3	127.5	39.2	−43.2		.256	2.265		1914
1915	2.500							3:1				1915
1916	2.274	.345	.223	314.7	341.7	30.2	−50.3		−.501	1.830		1916
1917	2.149	.477	.408	17.2	183.6	20.0	−55.0		−.697	1.726		1917
1918	3.189	.112	.171	85.2	203.1	75.7	−94.1		.973	1.490		1918
1919	1.936	.068	.365	116.3	349.6	14.6	−22.4		.082	2.839	190	1919
1920	1.930	.077	.358	20.3	56.9	14.9	−22.5		.060	2.828	190	1920

numb	a	e	sin i	wbar	node	wbar rate	node rate	res	Mars	Jup	fam	numb
1921	3.276							2:1				1921
1922	3.276							2:1				1922
1923	2.435	.086	.090	124.2	343.2	40.3	−42.4		.412	2.361	156	1923
1924	2.339	.172	.053	146.9	333.0	37.4	−42.1		.123	2.268	167	1924
1925	2.552	.139	.121	354.3	115.9	44.1	−50.0		.371	2.097		1925
1926	2.656	.131	.228	179.4	93.9	40.3	−51.9		.471	2.008	140	1926
1927	2.651	.161	.237	133.6	24.2	39.7	−53.6		.381	1.939	140	1927
1928	2.478	.162	.082	333.0	195.0	42.4	−48.0		.262	2.123	154	1928
1929	2.363	.112	.124	145.9	63.4	36.4	−39.7		.270	2.388	165	1929
1930	2.896	.122	.258	288.4	317.0	44.7	−63.6		.686	1.776	125	1930
1931	2.542	.229	.145	343.2	193.1	43.0	−56.3		.121	1.890		1931
1932	2.372	.192	.042	138.2	215.8	38.9	−45.0		.101	2.182	164	1932
1933	2.353	.090	.120	33.1	171.5	36.2	−38.8		.314	2.452	196	1933
1934	2.390	.206	.417	24.4	90.6	17.6	−39.7		.132	2.025		1934
1935	2.627	.200	.172	43.6	205.3	44.8	−58.2		.262	1.856		1935
1936	2.676	.159	.209	159.9	265.7	43.1	−56.0		.406	1.917	138	1936
1937	2.378	.110	.202	288.2	77.8	33.2	−39.0		.258	2.356		1937
1938	2.236	.176	.062	218.2	183.1	33.7	−37.9		.010	2.373		1938
1939	3.129	.152	.020	220.9	324.4	89.8	−103.3		.813	1.436	1A	1939
1940	3.060	.071	.135	116.6	266.5	71.4	−79.5		.999	1.756		1940
1941	3.969							3:2				1941
1942	2.318	.172	.410	348.6	343.8	16.6	−34.9		.160	2.193		1942
1943	1.431	.265	.168	226.1	259.8	16.2	−23.5		−.470	3.036		1943
1944	2.240	.178	.110	337.2	219.5	32.7	−37.8		−.011	2.352		1944
1945	2.555	.145	.063	332.7	155.7	46.5	−51.4		.366	2.074		1945
1946	2.294	.187	.135	1.6	12.8	33.8	−40.3		.014	2.279	177	1946
1947	3.152	.071	.188	206.4	91.6	68.8	−83.7		1.078	1.658		1947
1948	2.530	.207	.099	199.2	11.9	44.5	−54.4		.180	1.950		1948
1949	2.384	.187	.103	326.3	264.4	38.1	−44.7		.114	2.181		1949
1950	2.178	.143	.064	133.2	70.3	31.7	−34.4		.010	2.480		1950
1951	1.390	.049	.606	294.4	133.3	−3.5	−11.6		−.150	3.414		1951
1952	3.107	.123	.227	66.6	78.3	59.4	−82.3		.868	1.536	116	1952
1953	3.115	.144	.025	46.8	55.7	87.9	−99.8		.825	1.475	1A	1953
1954	2.937	.215	.318	342.4	275.3	39.4	−75.9		.403	1.474		1954
1955	2.855	.046	.037	88.1	268.4	64.2	−65.2		.900	2.029	3	1955
1956	3.201	.135	.023	139.3	210.2	97.3	−109.6		.925	1.411	1	1956
1957	3.009	.075	.182	232.4	46.3	61.4	−72.7		.940	1.788	2	1957
1958	3.108	.138	.198	293.0	342.0	65.4	−87.4		.817	1.499	202	1958
1959	2.316	.093	.120	303.9	281.6	34.9	−37.4		.271	2.485	196	1959
1960	2.525	.115	.144	265.5	16.0	41.6	−46.6		.409	2.197		1960
1961	3.198	.105	.113	97.9	19.4	87.1	−98.9		1.005	1.508		1961
1962	3.184	.194	.036	20.7	333.4	97.5	−123.3		.714	1.245	107	1962
1963	2.424	.192	.407	107.0	108.0	18.3	−40.2		.195	2.020		1963
1964	2.467	.169	.057	49.5	250.1	42.6	−48.2		.236	2.120	24	1964
1965	2.569	.104	.021	86.6	84.1	47.8	−50.0		.487	2.158		1965
1966	2.447	.129	.032	178.0	143.3	42.1	−45.1		.321	2.241	158	1966
1967	2.233	.129	.056	65.4	55.2	33.6	−36.0		.115	2.483	186	1967
1968	2.740	.139	.063	221.5	65.1	56.4	−62.5		.531	1.887		1968
1969	3.091	.191	.072	192.3	230.0	84.1	−106.0		.653	1.356		1969
1970	2.779	.191	.144	150.9	306.4	54.4	−69.1		.398	1.697	128	1970
1971	2.994	.065	.170	87.4	298.6	62.2	−71.6		.961	1.834	2	1971
1972	2.418	.172	.064	91.0	33.9	40.4	−45.8		.190	2.172	24	1972
1973	3.180	.048	.183	341.1	190.5	71.0	−84.7		1.180	1.704		1973
1974	3.169	.099	.176	238.3	174.9	72.9	−89.3		1.003	1.551		1974
1975	2.802	.080	.106	349.1	181.1	57.5	−61.6		.748	1.985		1975
1976	2.381	.107	.026	195.0	94.0	39.4	−41.2		.319	2.370		1976
1977	2.781	.081	.148	248.9	326.7	53.0	−59.0		.707	1.985		1977
1978	2.194	.153	.067	318.4	51.2	32.2	−35.4		.004	2.449	194	1978
1979	2.374	.098	.115	85.8	208.9	37.1	−39.9		.317	2.404	169	1979
1980	1.709	.231	.526	7.6	254.7	6.4	−20.9		−.477	2.785		1980

numb	a	e	sin i	wbar	node	wbar rate	node rate	res	Mars	Jup	fam	numb
1981	1.776							W L				1981
1982	2.309	.202	.117	316.5	37.1	35.0	−41.9		.006	2.240		1982
1983	2.622	.066	.157	15.9	18.0	44.7	−49.2		.628	2.209		1983
1984	3.013	.070	.087	287.9	200.6	73.3	−77.6		.970	1.803		1984
1985	3.122	.164	.334	164.1	300.8	37.4	−80.0		.674	1.396		1985
1986	3.097	.160	.029	15.2	179.9	86.2	−100.2		.763	1.445	1	1986
1987	2.382	.194	.418	337.4	308.7	17.1	−38.5		.149	2.064		1987
1988	2.154	.035	.075	15.5	114.6	30.8	−31.3		.195	2.713		1988
1989	2.351	.109	.130	130.9	20.2	35.7	−39.2		.263	2.413		1989
1990	2.174	.103	.065	173.5	198.8	31.6	−33.1		.093	2.572	193	1990
1991	2.249	.160	.107	305.9	322.1	33.1	−37.4		.044	2.389		1991
1992	2.994	.055	.184	232.8	189.1	60.0	−70.1		.988	1.863		1992
1993	3.059	.050	.191	272.2	164.3	62.3	−74.2		1.063	1.816		1993
1994	2.679	.155	.208	326.9	247.8	43.3	−55.8		.421	1.924	138	1994
1995	2.528	.094	.177	174.7	44.1	39.8	−45.3		.466	2.243		1995
1996	2.558	.094	.258	1.0	357.7	34.0	−44.0		.458	2.210	4	1996
1997	2.209	.152	.102	1.1	346.7	32.0	−35.6		.012	2.433		1997
1998	2.418	.086	.136	209.7	344.9	37.9	−41.0		.388	2.383		1998
1999	3.115	.145	.206	150.5	154.0	64.3	−88.6		.795	1.470	202	1999
2000	2.381	.226	.424	71.5	296.9	17.6	−40.8		.068	1.988		2000
2001	1.933	.106	.419	205.3	349.4	11.4	−22.1		−.006	2.772		2001
2002	2.417	.095	.151	205.4	184.1	37.2	−40.9		.361	2.368		2002
2003	3.064	.147	.020	143.2	28.4	83.0	−94.1		.776	1.520		2003
2004	2.172	.102	.038	99.0	352.9	31.8	−33.1		.102	2.583	192	2004
2005	2.621	.134	.235	57.8	291.4	38.5	−50.1		.429	2.047	140	2005
2006	2.325	.162	.088	34.1	349.4	36.2	−40.7		.125	2.314		2006
2007	2.384	.151	.051	193.0	358.5	39.2	−43.1		.212	2.264	167	2007
2008	3.229					27.8	−71.5	6				2008
2009	3.118	.156	.029	128.1	114.1	88.4	−102.5		.791	1.437	1	2009
2010	3.094	.153	.050	45.4	341.4	84.8	−98.0		.781	1.470		2010
2011	2.387	.108	.112	339.0	330.9	37.7	−40.8		.307	2.364	165	2011
2012	2.328	.145	.066	303.4	273.0	36.8	−40.3		.175	2.345		2012
2013	2.290	.173	.121	331.3	96.6	34.1	−39.5		.051	2.323		2013
2014	2.401	.218	.420	276.6	203.2	17.8	−41.1		.104	1.982		2014
2015	2.336	.095	.211	214.7	340.5	31.4	−36.7		.217	2.393		2015
2016	3.139	.143	.025	352.2	317.4	90.4	−102.7		.848	1.451	1A	2016
2017	2.252	.142	.090	296.4	181.1	33.6	−36.9		.097	2.431	184	2017
2018	2.183	.133	.052	348.5	197.1	32.0	−34.3		.040	2.505	186	2018
2019	2.241	.146	.083	257.9	251.6	33.4	−36.7		.077	2.431	184	2019
2020	3.023	.088	.182	143.0	155.1	62.3	−74.7		.913	1.736	2	2020
2021	2.309	.180	.092	312.6	165.5	35.6	−40.9		.068	2.291		2021
2022	2.706	.077	.103	53.9	351.6	52.3	−55.6		.641	2.063	134	2022
2023	2.881					27.8	−68.4	6				2023
2024	2.325	.096	.115	8.8	68.3	35.4	−37.9		.277	2.468	196	2024
2025	3.163	.116	.142	252.9	325.1	78.9	−94.5		.943	1.502		2025
2026	2.445	.157	.059	162.6	298.9	41.6	−46.3		.246	2.176	24	2026
2027	3.021	.073	.177	67.8	51.4	62.9	−73.8		.959	1.782	2	2027
2028	2.297	.102	.151	240.7	243.3	33.1	−36.5		.211	2.463		2028
2029	2.350	.082	.113	344.0	275.6	36.3	−38.6		.332	2.471	196	2029
2030	2.247	.117	.049	207.2	183.5	34.2	−36.2		.160	2.500	186	2030
2031	2.234	.141	.086	37.4	177.1	33.1	−36.2		.078	2.446	184	2031
2032	3.067	.106	.027	311.4	345.3	82.1	−87.9		.907	1.642		2032
2033	2.225	.173	.157	116.2	319.0	30.8	−36.5		−.070	2.323		2033
2034	2.246	.208	.155	98.9	13.1	31.6	−39.1		−.109	2.245		2034
2035	1.884	.142	.432	264.8	71.3	10.7	−22.0		−.113	2.754		2035
2036	2.245	.152	.073	278.0	336.4	33.7	−37.1		.070	2.417	184	2036
2037	2.301	.090	.070	.8	359.4	35.7	−37.3		.276	2.508		2037
2038	2.436	.092	.243	219.0	73.1	32.0	−39.6		.329	2.317		2038
2039	3.178	.161	.023	150.9	91.3	95.8	−112.9		.820	1.352	1	2039
2040	3.115	.181	.269	139.9	36.8	52.8	−89.0		.637	1.334		2040

numb	a	e	sin i	wbar	node	wbar rate	node rate	res	Mars	Jup	fam	numb
2041	3.161	.165	.040	57.0	153.8	93.0	−110.2		.795	1.359		2041
2042	2.753	.137	.095	86.0	4.8	55.7	−62.7		.539	1.878	40	2042
2043	3.107	.072	.071	19.5	310.3	82.9	−87.4		1.044	1.700		2043
2044	2.379	.256	.439	335.5	282.6	17.3	−43.3	3	−.033	1.905		2044
2045	2.380	.089	.117	189.4	3.8	37.2	−39.9		.345	2.418	196	2045
2046	3.150	.148	.031	348.1	58.9	91.6	−105.2		.840	1.423	1	2046
2047	1.872	.022	.421	219.8	31.5	10.2	−19.7		.108	3.005		2047
2048	1.954	.049	.364	249.2	163.0	14.7	−22.5		.137	2.859	190	2048
2049	1.949	.056	.413	332.4	206.6	11.4	−21.5		.113	2.858		2049
2050	2.326	.255	.441	244.0	74.2	16.4	−40.7		−.061	1.993		2050
2051	2.841	.044	.038	46.1	243.5	63.1	−64.1		.892	2.049	3	2051
2052	3.008	.063	.176	83.0	220.1	62.1	−72.1		.980	1.826	2	2052
2053	2.802	.121	.157	84.8	200.1	53.6	−62.8		.614	1.859	127	2053
2054	2.964	.119	.087	134.2	289.6	70.2	−77.8		.775	1.709		2054
2055	2.311	.250	.427	219.3	333.1	17.2	−40.0		−.051	2.016		2055
2056	2.218	.100	.079	29.8	228.5	32.7	−34.4		.153	2.552	195	2056
2057	3.079	.198	.035	37.5	330.1	85.7	−107.3		.626	1.352		2057
2058	3.119	.159	.023	260.8	93.1	88.9	−103.6		.780	1.424	1A	2058
2059	2.646	.503	.197	33.9	204.9	49.9	−130.1		−.615	1.031		2059
2060	13.650							SXR				2060
2061	2.264	.483	.088	5.7	234.8	34.4	−69.8		−.698	1.648		2061
2062	.966	.200	.330	254.6	110.0	6.3	−12.0		.162	3.732		2062
2063	1.077	.319	.189	84.5	19.6	10.6	−17.6	14				2063
2064	2.178	.262	.107	297.0	296.1	31.1	−40.3		−.288	2.197		2064
2065	2.699	.233	.140	38.5	319.6	51.3	−68.5	10	.131	1.584		2065
2074	1.800					4.3	−17.8	5				2074
2077	2.326	.267	.456	57.7	72.0	15.7	−41.6		−.105	1.965		2077
2099	2.304	.325	.482	22.4	223.6	15.5	−45.8		−.291	1.838		2099
2100	.832					4.3	−9.7	5				2100
2101	1.870	.724	.078	30.8	309.0	18.1	−63.4		−1.230	1.695		2101
2102	1.290							W L				2102
2128	2.731	.330	.304	330.0	2.3	39.5	−82.0		−.070	1.400		2128
2131	1.887	.080	.588	317.6	303.1	−2.7	−19.0		−.090	2.850		2131
2135	1.600	.386	.494	127.5	207.0	8.8	−23.6		−.820	2.657		2135
2202	2.293	.467	.170	31.6	168.1	33.5	−68.7		−.680	1.629		2202
2212	2.164	.847	.518	234.9	345.1	17.2	−139.0		−1.548	.944		2212
2329	2.406	.569	.557	317.0	194.5	18.9	−89.6		−.936	1.139		2329
2335	2.123					−25.7	−25.7	16				2335
2340	.844	.424	.119	241.6	220.2	5.5	−8.3	1	.047	3.647		2340
2368	2.106	.229	.111	341.2	280.3	28.8	−35.4		−.510	2.112		2368
2423	2.188	.213	.093	348.8	263.8	31.5	−37.5		−.156	2.309		2423
2608	2.500							3:1				2608
2744	2.299	.274	.145	1.2	306.5	33.9	−46.4		−.195	2.070		2744
2938	3.143							W L				2938
3040	1.843							W L				3040

ASTEROID PROPER ELEMENTS FROM AN ANALYTICAL SECOND ORDER THEORY

Z. KNEŽEVIĆ

Astronomska Opservatorija Beograd

and

A. MILANI

Università di Pisa

We have computed by a fully analytical method a new set of proper elements for 3322 numbered main-belt asteroids. They are presented in the following format: asteroid number, proper semimajor axis (AU), proper eccentricity, sine of proper inclination and quality code (see below).

This new set is significantly more accurate than all the previous ones at low to moderate eccentricities and inclinations, and especially near the main mean-motion resonances (e.g., in the Themis region). This is because the short periodic perturbations are rigorously removed, and the main effects of the second-order (containing the square of the ratio [the mass of Jupiter/ mass of the Sun]) are accounted for. Effects arising from the terms in the Hamiltonian of degree up to four in the eccentricity and inclination of both the asteroid and Jupiter are taken into account, and the fundamental frequencies g (for the perihelion) and s (for the node) of the asteroid are computed with a new iterative algorithm consistent with the basic results of modern dynamics (e.g., Kolmogorov-Arnold-Moser theory). The theory has been further improved by reducing the elements to the invariable plane, and by using a seminumerical secular perturbation theory derived from the LONGSTOP computations of the orbits of the outer planets.

This set of proper elements is also much larger than previous ones; it has been computed starting from a set of osculating orbital elements for the first 3495 numbered asteroids, as listed in the 1987 edition of the *Leningrad Ephemerides of the Minor Planets*. After discarding 218 Hildas, Trojans and Earth-approachers ($q < 1.1$ AU), our algorithm, which is implemented in a totally automated computer program (written in standard Fortran), was able to compute proper elements for all but 55 asteroids.

Since the algorithm we used involves an iterative procedure, a quality code QC was formed as follows. A QC in the range 1 to 20 indicates the number of iterations needed to achieve a satisfactory convergence, which was defined by requiring a change from the previous iteration by less than 0.01 arcsec yr^{-1} in both the fundamental frequencies g and s. Within this range, although a higher number could indicate that the computation of the proper elements was more difficult and the iterative procedure more beneficial, it does not necessarily imply a lower accuracy for the final result. On the contrary, a quality code in the range from 51 to 99 indicates nonconvergence of the algorithm within 20 iterations. In this case the quality code is defined by computing the distance in the frequency space between the last two iterations: $d = \sqrt{(g_{20} - g_{19})^2 + (s_{20} - s_{19})^2}$, then by encoding d in a logarithmic scale:

$$QC = 50 - 10 \log_{10} d. \tag{1}$$

Thus, a QC between 51 and about 70, i.e., an oscillation in the frequencies below about 1 arcsec yr^{-1}, indicates problems in the computation (e.g., the effect of a nearby secular resonance of higher order), but the proper elements are still of acceptable quality, since our convergence criterion was very strict. A quality code above about 70, on the contrary, indicates low accuracy and reliability proper elements, and these should probably be excluded (or at least given reduced weight) in family identification algorithms. This occurs for 33 asteroids, all but 7 with inclination above 20°. For the 55 asteroids for which the algorithm is strongly divergent (to the point that the proper elements are not defined at all), we give a separate list containing the mean elements; the latter can be used to identify the regions of the phase space where our algorithm fails, but cannot be used to identify asteroid families. Most of the rejected cases had large inclinations (all but 3 had inclinations above 20°). For high inclinations and eccentricities (e.g., above the ν_6 secular resonance), the proper elements of Williams are more accurate and reliable. However, this occurs in a sparsely populated region of the asteroid belt.

A full description of the algorithm is contained in the following references. For the elimination of the short periodic perturbations see Knežević (1988); for an assessment of the accuracy in the removal of the short periodic terms, see Knežević et al (1988). For the second-order terms, see Knežević (1989). For the effects of degree 4, see Knežević, in preparation. For a full discussion of the iterative algorithm and for internal and external tests of the

accuracy of the proper elements (e.g., by comparison with numerical integrations), see Milani and Knežević, in preparation. For a discussion of the relationship between proper elements, divergence of the perturbative series and KAM theory, see Milani (1988,1989). For a discussion of proper elements, see the chapter by Valsecchi et al.; however, the proper elements presented here are a later and significantly improved version with respect to the one discussed in Sec. III. C of that chapter.

These proper elements can also be obtained from the authors in computer readable form by sending an electronic mail message to TWIN2@ICN-UCEVM.BITNET. It is also possible to obtain supplementary information (e.g., proper longitudes of perihelia and nodes, fundamental frequencies, mean elements). In the same way it will be possible later to obtain larger proper element sets, since we plan to update regularly the list by adding recently discovered and/or numbered asteroids, and to improve the proper elements especially for asteroids whose orbital parameters are improved by later observations.

REFERENCES

Knežević, Z. 1988. Asteroid mean-orbital elements. *Bull. Obs. Astron. Belgrade* 139:1–6.

Knežević, Z. 1989. Asteroid long-periodic perturbations: The second order Hamiltonian. *Celest. Mech.* in press.

Knežević, Z., Carpino, M., Farinella, P., Froeschlé, C., Froeschlé, C., Gonczi, R., Jovanovic, B., Paolicchi, P., and Zappalà, V. 1988. *Astron. Astrophys.* 192:360–369.

Milani, A. 1988. Secular perturbations of planetary orbits and their representation as series. In *Long-Term Dynamical Behaviour of Natural and Artificial N-Body Systems*, ed. A. E. Roy (Dordrecht: Kluwer), pp. 73–108.

Milani, A. 1989. Planetary orbits: Emerging stability and chaos. *Nature* 338:207–208.

no;	a (AU);	ecc ;	sinI;	QC
1	2.76709	.1053	.1673	3
3	2.66941	.2259	.2288	4
4	2.36151	.1025	.1058	2
5	2.57627	.2172	.0769	3
6	2.42528	.1714	.2449	3
7	2.38611	.2095	.1123	3
8	2.20140	.1326	.0869	2
9	2.38643	.1173	.0807	2
10	3.14224	.1335	.0876	3
11	2.45224	.0835	.0639	2
12	2.33426	.2012	.1629	3
13	2.57632	.1019	.2773	3
14	2.58758	.1978	.1444	3
15	2.64367	.1469	.2278	4
16	2.92216	.1030	.0431	2
17	2.47102	.1386	.0818	2
18	2.29563	.1886	.1649	3
19	2.44199	.1345	.0383	2
20	2.40861	.1517	.0254	2
21	2.43523	.1391	.0366	2
22	2.90984	.0928	.2176	4
23	2.62785	.2482	.1678	3
24	3.13429	.1520	.0189	3
25	2.40036	.2081	.4029	10
26	2.65567	.1131	.0531	3
27	2.34702	.1743	.0089	2
28	2.77736	.1752	.1457	3
29	2.55434	.0595	.1123	2
30	2.36562	.1027	.0540	2
32	2.58702	.1183	.1068	3
33	2.86738	.3022	.0357	3
34	2.68681	.1382	.0954	3
35	2.99617	.2581	.1457	3
36	2.74777	.2580	.3299	6
37	2.64214	.1627	.0595	3
38	2.74078	.1659	.1362	3
39	2.76876	.0815	.1684	3
40	2.26728	.0166	.0566	2
41	2.76454	.3052	.2637	5
42	2.44124	.2024	.1319	3
43	2.20326	.1658	.0760	2
44	2.42277	.1635	.0490	2
45	2.72073	.1077	.1036	3
46	2.52581	.1283	.0420	2
47	2.88012	.1140	.0913	3
48	3.11262	.0640	.1133	3
49	3.08872	.2011	.0779	4
50	2.65015	.2510	.0478	60
51	2.36571	.0988	.1693	3
52	3.09699	.1189	.1099	3
53	2.61903	.2071	.0776	2
54	2.71068	.1954	.2121	4
55	2.75974	.1112	.1239	3
56	2.59797	.2188	.1509	3
57	3.15394	.0977	.2628	5
58	2.69994	.0799	.0811	55
59	2.71334	.0868	.1434	3
60	2.39320	.1903	.0687	3
61	2.98462	.1661	.3061	7
62	3.12170	.1521	.0222	3
63	2.39530	.1281	.1125	2
64	2.68181	.1477	.0406	3
65	3.42802	.1291	.0524	5
66	2.64599	.1495	.0585	3
67	2.42100	.1679	.1143	2
68	2.78211	.1528	.1286	3
69	2.97964	.1763	.1521	4
70	2.61477	.1619	.1947	4
72	2.26621	.1025	.1033	2
73	2.66472	.0367	.0467	2
74	2.77952	.2031	.0729	3
75	2.67209	.2756	.0861	4
76	3.40339	.1769	.0466	4
77	2.66871	.1162	.0498	3
78	2.62123	.2314	.1572	68
79	2.44425	.1748	.0856	3
80	2.29586	.1688	.1608	3
81	2.85413	.1830	.1445	3
82	2.76211	.2469	.0475	3
83	2.43150	.1120	.0817	2
84	2.36212	.2123	.1674	3
85	2.65369	.1596	.2171	3
86	3.10769	.1847	.0633	3
87	3.48591	.0516	.1661	7
88	2.76810	.1471	.1092	3

no;	a (AU);	ecc ;	sinI;	QC
89	2.55163	.1428	.2905	4
90	3.14607	.1540	.0241	2
91	2.58999	.1056	.0431	3
92	3.19573	.0700	.1512	3
93	2.75470	.1396	.1556	3
94	3.15843	.0745	.1434	3
95	3.06882	.1334	.2332	5
96	3.05226	.1760	.2824	6
97	2.66889	.2319	.2072	3
98	2.68722	.2381	.2605	5
99	2.66357	.2317	.2202	4
100	3.09449	.1496	.0907	3
101	2.58328	.1168	.1820	3
102	2.66143	.2171	.0988	3
103	2.70209	.0597	.0792	2
104	3.14791	.1468	.0428	3
105	2.37318	.1893	.3578	19
106	3.17084	.1475	.0634	3
107	3.48652	.0945	.1614	7
108	3.21076	.1159	.0847	3
109	2.69626	.2718	.1506	4
110	2.73287	.0507	.0909	2
111	2.59416	.1187	.1020	3
112	2.43397	.1027	.0596	2
113	2.37601	.1154	.0722	2
114	2.67657	.1703	.0779	2
115	2.37988	.1651	.2226	3
116	2.76839	.1716	.0485	2
117	2.99128	.0204	.2643	3
118	2.43794	.1583	.1242	3
119	2.58137	.0468	.1063	3
120	3.11733	.0841	.1325	3
121	3.45104	.0930	.1113	5
122	3.22211	.0542	.0313	3
123	2.69505	.1123	.1288	3
124	2.62989	.0948	.0480	62
125	2.74323	.0661	.0553	70
126	2.43886	.0793	.0491	2
127	2.75594	.0863	.1380	3
128	2.75007	.0926	.0906	3
129	2.86970	.2215	.2070	4
130	3.11749	.1941	.3690	13
131	2.43159	.0919	.0711	2
132	3.06288	.1518	.1452	4
133	3.06288	.1518	.1452	4
134	2.56406	.1012	.1213	3
135	2.42845	.1846	.0493	2
136	2.28678	.0635	.1675	2
137	3.11835	.1861	.2492	4
138	2.44812	.1469	.0453	2
139	2.78310	.2161	.1845	4
140	2.73240	.2026	.0341	3
141	2.66594	.1712	.2251	7
142	2.41867	.1579	.0589	2
143	2.76156	.0969	.2123	3
144	2.65503	.1982	.0673	3
145	2.67270	.1614	.2028	3
146	2.71880	.0937	.2076	3
147	3.13710	.0056	.0520	3
148	2.17469	.0520	.0178	2
149	2.98220	.0936	.0479	3
151	2.59175	.0699	.1035	3
152	3.13982	.0768	.2017	4
154	3.18268	.1349	.3406	5
155	2.75841	.2649	.1958	4
156	2.72985	.2611	.1793	4
157	2.57983	.2062	.1996	4
158	2.86881	.0447	.0375	2
159	3.10475	.1167	.0884	3
160	2.72772	.0532	.0702	2
161	2.37936	.1178	.1565	2
162	3.01980	.2078	.0997	3
163	2.36716	.1963	.0787	3
164	2.63292	.2560	.5575	82
165	3.12925	.0814	.2109	3
166	2.68589	.1728	.1991	3
167	2.85357	.0414	.0355	2
168	3.38052	.0269	.0870	5
169	2.35817	.1079	.1004	2
170	2.55371	.0839	.2635	4
171	3.13644	.1513	.0240	3
172	2.37985	.0937	.1827	3
173	2.74324	.1719	.2318	4
174	2.85985	.1491	.2287	4
175	3.20390	.1982	.0543	3
176	3.17715	.2127	.3587	11

no;	a (AU);	ecc ;	sinI;	QC
177	2.76997	.2021	.0387	2
178	2.46017	.0546	.0246	2
179	2.97236	.0762	.1547	4
180	2.72196	.1882	.0331	3
181	3.12702	.2272	.2932	7
182	2.41621	.1711	.0164	2
184	3.18253	.1023	.0369	3
185	2.73860	.1106	.3787	79
186	2.36183	.1254	.2255	3
187	2.73153	.2753	.1725	3
188	2.76190	.1603	.2254	66
189	2.45035	.0120	.0966	2
191	2.89558	.0577	.1897	3
192	2.40287	.2169	.1266	3
193	2.60157	.2677	.2335	4
194	2.61644	.2261	.2922	5
195	2.87802	.0668	.1237	3
196	3.11447	.0325	.1083	3
197	2.73985	.1345	.1361	3
198	2.45905	.1950	.1881	3
199	3.16934	.1996	.2348	5
200	2.73752	.1087	.1367	3
201	2.67823	.1518	.0884	3
202	3.07240	.1252	.1347	3
203	2.73717	.0399	.0656	2
204	2.67112	.1871	.1499	3
205	2.77733	.0128	.1933	3
206	2.74072	.0474	.0537	2
207	2.28399	.0555	.0618	2
208	2.89290	.0423	.0382	2
209	3.14779	.0718	.1304	3
210	2.72209	.0992	.0851	3
211	3.04440	.1511	.0844	3
212	3.11321	.0932	.0923	3
213	2.75293	.1455	.0988	3
214	2.61140	.0542	.0709	2
215	2.76667	.0140	.0309	2
216	2.79467	.2335	.2187	4
217	2.87027	.2870	.1685	4
218	2.66723	.1384	.2573	7
219	2.35403	.1936	.1923	3
220	2.34860	.2243	.1566	4
221	3.01240	.0792	.1716	3
222	3.13477	.1535	.0192	2
223	3.08994	.1349	.0273	3
224	2.64525	.0541	.1082	7
225	3.37705	.1945	.3882	20
226	2.71251	.2029	.2533	4
227	3.14384	.2195	.1846	4
228	2.20145	.2146	.0582	3
229	3.41422	.1181	.0351	3
230	2.38233	.0361	.1784	3
231	2.92038	.1683	.1012	3
232	2.55311	.2108	.0950	3
233	2.66011	.0673	.1455	3
234	2.38577	.2291	.2378	4
235	2.88203	.0727	.1403	3
236	2.79980	.1567	.1291	3
237	2.76258	.0780	.1495	3
238	2.90704	.0632	.2119	4
239	2.97020	.2011	.1013	3
240	2.66459	.1857	.0187	2
241	3.04981	.0701	.1164	3
242	2.86291	.1336	.2066	4
243	2.86163	.0443	.0369	2
244	2.17449	.1086	.0583	2
245	3.09237	.1730	.0724	3
246	2.69468	.1101	.2652	4
247	2.74125	.3146	.2742	86
248	2.47089	.0753	.0865	2
249	2.37755	.1865	.1787	3
250	3.14630	.1249	.2222	5
251	3.09504	.0975	.1721	4
252	3.15786	.0513	.1782	3
253	2.64737	.2348	.1141	4
254	2.19482	.1290	.0747	2
255	2.74579	.1157	.1628	3
256	3.00016	.0950	.2270	4
257	3.11545	.1046	.0585	3
258	2.61548	.1743	.2442	62
259	3.13841	.1429	.1639	4
260	3.44693	.0836	.1000	5
261	2.33156	.1187	.0455	2
262	2.55364	.1940	.1246	3
263	2.88657	.0442	.0364	2

no	a (AU)	ecc	sinI	QC
264	2.79817	.1098	.1656	3
266	2.80444	.1353	.2405	5
267	2.77414	.1110	.0863	2
268	3.09600	.1660	.0242	3
269	2.61538	.2158	.0897	3
270	2.19833	.1230	.0588	2
271	3.00626	.0700	.0756	3
272	2.77784	.0475	.0706	2
273	2.39510	.1279	.3458	5
274	3.04330	.1538	.0442	3
275	2.77128	.1986	.0664	3
276	3.11631	.0430	.3731	12
277	2.88563	.0553	.0368	2
278	2.75474	.1694	.1201	3
280	2.94315	.1124	.1323	3
281	2.18776	.1146	.0857	2
282	2.33927	.0811	.1458	3
283	3.04617	.1145	.1584	3
284	2.35843	.2132	.1545	3
285	3.08786	.2139	.2954	7
286	3.19635	.0066	.2940	5
287	2.35299	.0394	.1622	2
288	2.75850	.2423	.0602	3
289	2.87393	.1717	.1100	3
290	2.33738	.2547	.3643	80
291	2.22205	.1156	.0298	2
292	2.52987	.0230	.2472	3
293	2.86182	.1221	.2584	4
294	3.14280	.2254	.0876	4
295	2.79670	.1537	.0657	3
296	2.22886	.1307	.0161	2
297	3.17062	.1197	.1415	4
298	2.26389	.1223	.1100	2
299	2.43419	.0403	.0444	2
300	3.21025	.0121	.0175	2
301	2.72532	.0793	.0728	3
302	2.40563	.0995	.0631	2
303	3.12231	.0471	.1300	3
304	2.40364	.2072	.2519	4
305	3.09303	.1985	.0891	4
306	2.35802	.1353	.1123	3
307	2.90858	.1269	.0851	3
308	2.74956	.0428	.0759	2
309	2.66468	.1020	.0721	3
310	2.76179	.1502	.0698	3
311	2.89766	.0372	.0378	2
312	2.78218	.1636	.1645	3
313	2.37577	.2033	.1986	3
314	3.15126	.1616	.2022	5
315	2.24140	.1413	.0380	2
316	3.17197	.1375	.0230	3
317	2.28656	.0590	.0250	2
318	3.20326	.0708	.1744	3
319	3.40029	.1900	.1804	7
320	3.01332	.0820	.1716	3
321	2.88563	.0447	.0393	2
322	2.78253	.2054	.1639	3
323	2.38208	.2456	.4160	9
324	2.68364	.2963	.2103	4
325	3.20251	.1500	.1611	4
326	2.31766	.2042	.4008	12
327	2.77601	.0564	.1312	3
328	3.10668	.1143	.2836	5
329	2.47561	.0344	.2724	4
330	2.46994	.2263	.1084	3
331	3.02524	.0673	.1021	3
332	2.77304	.0662	.0461	2
333	3.12402	.1382	.0739	3
335	2.47476	.1695	.0785	3
336	2.25179	.1030	.1113	2
337	2.38308	.1408	.1436	3
338	2.91266	.0217	.1248	3
339	3.01191	.0751	.1664	3
340	2.74641	.1042	.0784	3
341	2.19942	.1693	.0947	2
342	2.56797	.1364	.1417	3
343	2.41161	.2103	.0496	3
344	2.59455	.2932	.3110	6
345	2.32534	.0637	.1779	2
346	2.79621	.0681	.1330	3
347	2.61302	.1925	.1908	3
348	2.96959	.0799	.1486	3
349	2.92490	.0578	.1360	3
350	3.11441	.2151	.3612	19
351	2.76600	.1770	.1394	3
352	2.19409	.1250	.0746	2
353	2.73482	.3099	.0763	4
354	2.79807	.1621	.2920	5
355	2.53868	.1121	.0830	2
356	2.75696	.2216	.1583	4
357	3.14864	.0545	.2446	4
358	2.87783	.1349	.0596	2
359	2.72908	.1261	.1180	3
360	3.00159	.1569	.1894	4
362	2.57881	.0373	.1357	3
363	2.74746	.0376	.0883	2
364	2.22064	.1361	.0870	2
365	2.80268	.1323	.2178	4
366	3.14264	.0533	.1916	3
367	2.21942	.1203	.0348	2
368	3.06792	.1801	.1549	4
369	2.64893	.0592	.2024	3
370	2.32443	.0599	.1547	2
371	2.72688	.0771	.1476	3
372	3.15310	.2734	.3893	56
373	3.11685	.1351	.2586	5
374	2.77963	.1058	.1649	3
375	3.12876	.1004	.2794	5
376	2.28864	.1807	.1118	2
377	2.69045	.0566	.1240	3
378	2.77671	.1004	.1343	3
379	3.13587	.1573	.0294	2
380	2.67841	.0854	.0873	3
381	3.20957	.1190	.1994	3
382	3.12213	.1923	.1535	4
383	3.13422	.1542	.0252	3
384	2.65208	.1429	.0743	3
385	2.84644	.1722	.2369	5
386	2.89636	.1533	.3305	6
387	2.73883	.2434	.2822	4
388	3.00566	.0441	.1190	3
389	2.60850	.0981	.1618	3
390	2.65189	.1638	.2233	4
392	2.88454	.1217	.2466	5
393	2.77528	.2857	.2933	6
394	2.76270	.1951	.0963	3
395	2.78524	.0950	.0763	3
396	2.74193	.1668	.0607	2
397	2.63547	.2108	.2321	4
398	2.73845	.2240	.1759	3
399	3.05274	.1112	.2318	5
400	3.13200	.1321	.1992	5
401	3.34635	.0286	.0957	3
402	2.55763	.1494	.1868	3
403	2.80968	.1204	.1763	3
404	2.59227	.2290	.2309	3
405	2.58279	.2781	.2303	4
406	2.91600	.1469	.0902	3
407	2.62473	.0354	.1499	3
408	3.16472	.1224	.1782	4
409	2.57623	.1010	.2090	3
410	2.72683	.2515	.1604	3
411	2.93494	.1213	.2387	11
412	2.76294	.0714	.2200	3
413	2.58335	.2700	.3259	6
414	3.50450	.0727	.1381	7
415	2.79028	.2826	.1296	4
416	2.78806	.2448	.1985	4
417	2.79767	.1753	.1179	3
418	2.59296	.0840	.1362	3
419	2.59420	.2581	.0758	65
420	3.41927	.0426	.1305	5
421	2.53926	.2554	.1299	4
422	2.22836	.1856	.0853	3
423	3.06852	.0501	.1770	3
424	2.77394	.1017	.1216	3
425	2.88664	.0944	.0562	3
426	2.88854	.1434	.3433	7
427	2.97339	.1050	.1066	3
428	2.30791	.1541	.1046	3
429	2.60732	.0959	.1733	3
430	2.84451	.2610	.2471	5
431	3.12984	.1569	.0129	2
432	2.36928	.1576	.1878	3
434	1.94426	.0910	.3855	4
435	2.44946	.1286	.0320	2
436	3.19935	.0599	.3222	5
437	2.38560	.2225	.1491	3
438	2.55408	.0860	.1162	3
439	3.13127	.0574	.3310	6
440	2.21034	.1221	.0445	2
441	2.80669	.0870	.1586	3
442	2.34532	.0961	.0924	2
443	2.21549	.0700	.0725	2
444	2.77071	.1442	.1782	3
445	3.18967	.1469	.3964	6
446	2.78776	.0991	.1770	3
447	2.98634	.0163	.0663	3
448	3.14218	.1530	.2154	4
449	2.55355	.1945	.0360	2
450	3.01574	.0728	.1735	3
451	3.06240	.0721	.2401	4
452	2.84697	.0462	.0364	2
453	2.18324	.1296	.0970	3
454	2.62718	.1466	.1023	3
455	2.65684	.2464	.2046	4
456	2.78623	.2231	.2481	5
457	3.09061	.1508	.2392	5
458	2.99308	.2065	.2137	4
459	2.62060	.1876	.1691	3
460	2.71765	.0701	.0869	3
461	3.11405	.1564	.0225	3
462	2.87375	.0524	.0357	2
463	2.39833	.1976	.2192	3
464	2.80299	.1635	.1617	3
465	3.09395	.2324	.1861	4
466	3.36690	.0736	.3445	7
467	2.94411	.0894	.1289	3
468	3.14107	.1602	.0209	2
469	3.16100	.2029	.2119	5
470	2.40471	.1199	.1219	2
471	2.88837	.2078	.2338	5
472	2.54308	.0842	.2575	4
474	2.45390	.1917	.1428	3
475	2.59325	.3243	.3252	5
476	2.64978	.0785	.2069	3
477	2.41546	.1643	.0918	2
478	3.01644	.0914	.2432	5
479	2.72093	.1884	.1411	3
480	2.64405	.0883	.3765	15
481	2.74059	.1412	.1506	3
482	2.99884	.0992	.2495	5
483	3.42782	.0351	.3072	8
484	2.66776	.0442	.1990	3
485	2.74988	.1866	.2517	4
486	2.35197	.1863	.1765	3
487	2.67006	.0591	.1599	3
488	3.15348	.1885	.1872	5
489	3.15377	.0711	.2150	4
490	3.17521	.0648	.1561	3
491	3.19392	.0600	.3188	5
492	3.11193	.1521	.0229	2
493	3.12087	.1425	.2676	6
494	2.98668	.0820	.1147	3
495	2.48667	.1267	.0428	3
496	2.19890	.0922	.0747	2
497	2.85118	.2654	.0825	4
498	2.65070	.1900	.1484	3
500	2.61293	.1053	.1911	3
501	3.15442	.1806	.3382	10
502	2.38306	.1980	.3947	56
503	2.72424	.1861	.0725	3
504	2.72146	.1657	.2005	70
505	2.68539	.2341	.1431	3
506	3.04340	.1750	.2934	6
507	3.15439	.0722	.1851	4
508	3.16213	.0367	.2190	3
509	3.06471	.0766	.2705	5
510	2.60931	.1786	.1768	3
511	3.17414	.1887	.2416	5
512	2.18950	.2192	.1387	3
513	3.01454	.0905	.1673	3
514	3.04676	.0126	.0873	3
515	3.12112	.1571	.0178	3
516	2.67925	.2837	.2585	5
517	3.14477	.1729	.0748	3
518	2.53494	.1952	.1282	3
519	2.79013	.1504	.1814	3
520	3.00660	.0878	.1812	4
521	2.74169	.2551	.1605	4
522	3.63044	.0377	.0532	7
523	2.96765	.1775	.0912	3
524	2.63547	.1010	.1586	3
525	2.24521	.1142	.1120	2
526	3.12283	.1552	.0239	3

```
no; a (AU); ecc ; sinI; QC        no; a (AU); ecc ; sinI; QC        no; a (AU); ecc ; sinI; QC
----------------------------      ----------------------------      ----------------------------
527 2.72533 .1306 .1463   3       616 2.55257 .0798 .2632   3       704 3.06094 .1037 .3230   4
528 3.39778 .0350 .2036   5       618 3.18963 .0588 .2724   4       705 2.92286 .5383 .5808  98
529 3.01768 .0713 .1730   3       619 2.52022 .0342 .2364   3       706 2.72833 .1677 .2565   4
530 3.20041 .1929 .1259   3       620 2.43543 .1123 .1364   2       707 2.18036 .0785 .0922   2
532 2.77164 .1955 .2732   5       621 3.11898 .1512 .0265   3       708 2.67053 .1204 .0684   2
533 2.98055 .0749 .1116   3       622 2.41460 .2161 .1424   3       709 2.91439 .1020 .2874   4
534 2.88424 .0523 .0370   2       623 2.46034 .1128 .2590   4       710 3.13302 .1511 .0195   2
535 2.56923 .0586 .0995   3       625 2.64643 .2053 .1832   3       711 2.23723 .1822 .1121   3
536 3.49956 .0845 .2989  18       626 2.57364 .2728 .4202  75       712 2.57520 .1758 .2247   4
537 3.06580 .2271 .1428   4       627 2.89998 .0465 .0984   3       713 3.40353 .1203 .1853   5
538 3.16477 .1352 .0975   3       628 2.58178 .0332 .1809   3       714 2.53522 .0700 .2610   3
539 2.73892 .1724 .1435   3       629 3.12725 .1782 .1418   3       715 2.76779 .0511 .2281   3
540 2.21892 .1207 .1029   2       630 2.62348 .1418 .2208   3       716 2.81069 .1234 .1344   3
541 2.81422 .0691 .1231   3       631 2.79261 .0969 .3379   5       717 3.14474 .2273 .0434   3
542 2.90603 .1102 .1950   3       632 2.66243 .2107 .0500   2       718 3.05853 .2333 .1064   3
543 3.06192 .1238 .1678   4       633 3.01731 .0659 .1742   3       719 2.57918 .5036 .1847   6
544 2.59173 .1565 .1605   3       634 3.04732 .1538 .1930   4       720 2.88734 .0482 .0372   2
545 3.18326 .1837 .2031   5       635 3.13955 .0647 .1888   4       721 3.55297 .0814 .1275   8
546 2.59789 .1378 .2551   5       636 2.91021 .1438 .1321   3       722 2.17188 .1291 .0897   2
547 2.77329 .2238 .2730   5       637 3.16265 .1638 .0231   3       723 2.99323 .0397 .0796   3
548 2.28211 .1755 .0493   2       638 2.73446 .1867 .1157   3       724 2.45130 .2413 .2008   4
549 2.68358 .2588 .0838   3       639 3.01672 .0742 .1694   3       725 2.57276 .1883 .0485   3
550 2.59024 .1994 .1923   4       640 3.16375 .0858 .2422   3       726 2.56672 .2230 .2945   5
551 2.96678 .1140 .0219   2       641 2.21992 .1156 .0247   2       727 2.56738 .0782 .2463   3
552 3.15465 .0997 .1319   3       642 3.18078 .1506 .1434   3       728 2.25375 .1119 .0576   2
553 2.23084 .1025 .0774   2       643 3.35593 .0775 .2532   6       729 2.75994 .1119 .2974   4
554 2.37470 .1410 .0691   2       644 2.59934 .1209 .0046   2       730 2.24365 .2029 .0563   2
555 3.16909 .1838 .0288   3       645 3.19678 .1567 .1294   4       731 2.98806 .1096 .1769   3
556 2.46545 .1099 .1088   2       646 2.32483 .1851 .1359   3       732 2.45664 .0594 .1870   2
557 2.44136 .1199 .0615   2       647 2.44272 .1878 .1395   3       733 3.39407 .1248 .3373   8
558 2.90787 .0549 .1311   3       648 3.18107 .2287 .1821   5       734 3.15161 .0792 .1062   3
559 2.71165 .0888 .1432   3       649 2.54892 .2497 .2090   4       735 2.72878 .2817 .2796   5
560 2.75139 .1740 .1238   3       650 2.45821 .1638 .0546   2       736 2.20198 .1380 .0622   2
561 3.16753 .1382 .0241   3       651 3.02452 .0725 .1758   3       737 2.59182 .2127 .2153   5
562 3.01909 .0721 .1768   3       652 2.55528 .0806 .2561   4       738 3.03492 .0930 .0451   3
563 2.71305 .2217 .1503   3       653 3.01408 .0761 .1790   3       739 2.73748 .1844 .3336   7
564 2.74882 .2799 .2779   5       654 2.29696 .2701 .3231   5       740 3.05138 .1408 .1698   4
565 2.44321 .1513 .2056   3       655 2.98910 .0665 .0963   3       741 2.71999 .1002 .1277   3
566 3.38890 .0687 .0651   5       656 3.15598 .1531 .0222   3       742 3.01286 .0755 .1774  68
567 3.13504 .1210 .1451   3       657 2.61070 .1418 .1988   3       743 2.79320 .0438 .0975   3
568 2.88351 .1866 .3113   7       658 2.85429 .0454 .0380   2       744 3.17604 .1401 .1179   3
569 2.65767 .1774 .0405   3       660 2.53458 .1097 .2564   4       745 3.21860 .1117 .2304   4
570 3.43024 .0692 .0447   5       661 3.01567 .0697 .1718   3       746 3.11207 .2170 .3052   7
571 2.41010 .2157 .0947   3       662 2.55380 .2043 .0554   3       747 2.99625 .2752 .3276   9
572 2.40064 .1359 .1820   3       663 3.06294 .1844 .3150   7       749 2.24346 .1916 .0773   2
573 3.01382 .0812 .1795   4       664 3.17651 .2412 .1527   4       750 2.44340 .1536 .0541   2
574 2.25256 .2193 .1149   2       665 3.14931 .1791 .2710   5       751 2.55127 .1165 .2516   4
575 2.55477 .1069 .2621   3       666 2.59317 .2098 .1346   3       752 2.46319 .0822 .0855   2
576 2.98587 .1769 .1896   7       667 3.19374 .2105 .3962   9       753 2.32937 .2297 .1556   3
577 3.11779 .1416 .1052   3       668 2.79668 .2017 .1355   3       755 3.17335 .1715 .0538   3
578 2.75011 .1859 .1064   3       669 3.01152 .1006 .1928  72       756 3.20358 .1833 .3371   5
579 3.01284 .0656 .1714   3       670 2.80322 .1616 .1225   3       757 2.37315 .0986 .1392   2
580 3.21865 .1011 .0428   3       671 3.09482 .0672 .1442   3       758 3.20123 .1245 .0759   3
581 3.21590 .0278 .3530   4       672 2.55522 .1275 .2021   3       759 2.61767 .2129 .3313   5
583 3.18234 .1663 .1668   4       673 2.81492 .0388 .0639   2       760 3.14740 .2670 .2209   5
584 2.37365 .1935 .2133   4       674 2.92408 .1921 .2223   4       761 2.86324 .0455 .0383   2
585 2.42987 .1568 .1294   3       675 2.76966 .1892 .1835  10       762 3.15649 .1263 .2387   5
586 3.04114 .0825 .0441   3       676 3.05938 .1102 .2047   5       763 2.24074 .1361 .0906   2
587 2.33510 .2144 .4114  10       677 2.95581 .0792 .1675   3       764 3.18719 .0966 .1901   5
589 3.13374 .0255 .1832   4       678 2.57332 .1885 .1272   3       765 2.54686 .2456 .1182   4
590 3.00071 .0796 .1715   4       679 2.58648 .2017 .4279  19       766 3.02151 .0842 .1786   4
591 2.67939 .2441 .2275   4       680 3.14230 .2661 .3106   8       767 3.11826 .1559 .0247   3
592 3.02267 .1132 .1727   4       681 3.11025 .0860 .2156   4       768 3.13984 .2034 .2587   6
593 2.69881 .2291 .2697   4       682 2.65241 .1565 .2067   4       769 3.18038 .1706 .1234   3
595 3.20450 .0602 .3028   5       683 3.11678 .0549 .3350   6       770 2.22099 .1395 .0666   2
596 2.93019 .1953 .2253   5       684 2.43199 .0467 .1072   2       771 2.65235 .2380 .2704   4
597 2.67201 .1110 .2136   3       685 2.23594 .1748 .0797   2       773 2.85772 .0795 .2985   4
598 2.76174 .2090 .1985   4       686 2.58935 .2070 .3030   5       774 3.04839 .1726 .1112   3
599 2.77266 .2411 .2904   5       687 2.72259 .2258 .2763   5       775 3.01194 .0851 .1771  65
600 2.65991 .0729 .1635   3       688 2.69855 .1199 .1731   3       776 2.93258 .1398 .2913   6
601 3.13112 .1019 .2670   5       689 2.31584 .2001 .0911   3       777 3.20156 .1444 .2487   5
602 3.08849 .2089 .2745   6       690 3.14907 .1463 .2155   5       778 3.17015 .2715 .2400   5
603 2.54235 .2031 .1440   3       691 3.01188 .0935 .2050   4       779 2.66551 .1945 .2687   5
604 3.15110 .1706 .0800   3       692 3.37809 .0761 .5285  93       780 3.11719 .0834 .3082   6
605 3.00024 .1464 .3281   8       693 2.94405 .0381 .2519   4       781 3.22798 .1060 .3110   5
606 2.58739 .1790 .1691   3       694 2.67097 .2581 .3079   6       782 2.17983 .0684 .0757   2
607 2.85211 .1041 .1966   3       695 2.53913 .1081 .2425   3       783 2.34258 .2186 .1468   3
608 3.02452 .0833 .1835   4       696 3.18255 .2138 .2508   5       784 3.10162 .2440 .2211   5
609 3.08764 .0470 .0666   3       697 2.88132 .1352 .2526   5       785 2.57264 .2425 .2051   3
610 3.08359 .2397 .2005   5       698 2.86848 .1312 .1932   3       786 3.17365 .1852 .2302   5
611 2.97897 .1090 .2363   4       699 2.61278 .3333 .3192   7       787 2.53963 .1013 .2577   4
612 3.14239 .2309 .3701  13       700 2.22951 .1326 .1019   2       788 3.12794 .1569 .2407   5
613 2.92035 .0463 .1404   2       701 3.01429 .0678 .1404   3       789 2.68595 .1542 .1981   3
614 2.69406 .0983 .1315   2       702 3.19530 .0257 .3661   5       790 3.40077 .1860 .3418  10
615 2.63134 .1251 .0519   2       703 2.17489 .1125 .0527   2       791 3.12181 .1879 .2511   5
```

no	a (AU)	ecc	sinI	QC	no	a (AU)	ecc	sinI	QC	no	a (AU)	ecc	sinI	QC
792	2.62201	.1546	.1698	3	878	2.36307	.2001	.0345	2	969	2.46273	.1797	.0615	2
793	2.79603	.0916	.2631	5	879	2.53063	.1013	.2595	4	970	2.56133	.2385	.1109	3
794	3.14122	.2822	.0904	4	880	3.00268	.2500	.3079	7	971	2.64035	.1709	.2139	4
795	2.75011	.1550	.3148	5	881	2.61195	.1888	.2587	4	972	3.06238	.1899	.1740	4
796	2.63495	.2989	.2962	5	882	3.13280	.2292	.1272	4	973	3.22488	.0818	.2793	5
797	2.53629	.0880	.0936	2	883	2.23820	.1736	.0995	3	974	2.53403	.0773	.0765	2
798	3.01460	.0596	.1685	3	885	3.09771	.1518	.0446	3	975	2.83417	.0459	.0392	2
799	2.54163	.0221	.0857	2	886	3.16226	.2450	.2785	6	976	3.18903	.1414	.1498	3
800	2.19266	.1831	.0843	3	887	2.48388	.5755	.1152	6	977	3.11814	.0438	.2438	4
801	2.60539	.1155	.2414	4	888	2.70926	.1734	.2239	4	978	3.20627	.2256	.3681	8
802	2.19614	.0997	.0917	3	889	2.44609	.1852	.1294	3	979	3.15218	.1167	.1909	4
803	3.20538	.0349	.1674	3	890	3.02341	.0751	.1799	3	980	2.74102	.1492	.3002	5
804	2.83923	.1267	.2651	5	891	2.86047	.0215	.2145	3	981	3.10103	.1688	.0287	3
805	3.20646	.1666	.2637	5	892	3.23234	.0860	.3592	6	982	3.07285	.2424	.2365	6
806	3.20227	.1099	.2339	5	893	3.05228	.1202	.2751	5	983	3.16145	.1194	.2670	3
807	3.01855	.0813	.1772	3	894	3.11477	.1000	.2235	4	984	2.80397	.1580	.1774	3
808	2.74514	.1316	.0830	2	895	3.21190	.1982	.4262	11	985	2.29982	.2443	.0924	3
809	2.28311	.1638	.1119	3	896	2.28521	.1779	.1548	2	986	3.14124	.1549	.2441	5
810	2.17878	.1505	.0378	2	897	2.54319	.1020	.2607	4	987	3.14541	.2120	.1622	4
811	2.89696	.0617	.0385	2	898	2.72963	.3621	.1903	5	988	3.15193	.1988	.0240	3
812	2.65938	.1415	.2239	4	899	2.90798	.1647	.2336	4	989	2.65946	.2447	.2509	4
813	2.22320	.0060	.0980	2	900	2.47204	.1490	.2032	3	990	2.66914	.1845	.1525	3
814	3.16271	.2739	.3539	10	901	2.22422	.1299	.0797	3	991	3.14367	.1398	.0241	2
815	2.65883	.0883	.2276	3	902	2.44664	.1537	.1166	3	992	3.02495	.1289	.1931	3
816	3.00381	.1397	.2260	5	903	3.24592	.0131	.1931	4	993	2.86128	.0447	.0350	2
817	2.58965	.1527	.1837	3	904	2.99312	.0806	.2665	5	994	2.53028	.0833	.2640	3
818	3.17355	.0644	.2520	4	905	2.21595	.1259	.0834	2	995	2.61560	.1282	.2393	4
819	2.19763	.1393	.0966	3	906	2.89467	.0550	.1956	3	996	3.09412	.1561	.0268	3
820	3.12830	.0512	.0837	3	907	2.80050	.1582	.3366	5	997	2.66985	.1718	.1977	4
821	2.77560	.2329	.0980	3	908	2.47528	.1530	.2112	4	998	3.12390	.1587	.2964	6
822	2.25563	.1614	.0254	2	909	3.54216	.0573	.2935	56	999	2.61252	.1798	.1819	3
823	2.22134	.1062	.0801	2	910	2.92484	.1733	.1454	3	1000	3.18935	.1970	.3885	11
824	2.79379	.1355	.1273	3	912	3.12465	.1676	.3187	7	1001	3.19778	.1264	.1785	5
825	2.22595	.1017	.0421	2	913	2.19754	.1664	.0810	2	1002	2.78791	.1296	.1903	3
826	2.71400	.2158	.1342	4	914	2.45562	.2438	.4159	65	1003	3.14843	.1524	.0206	3
827	2.27452	.1269	.0568	2	915	2.22772	.1211	.0978	2	1004	3.39834	.0606	.0413	3
828	3.19087	.0333	.0306	3	916	2.36470	.2049	.2045	3	1005	3.16442	.0953	.3345	5
829	2.57996	.0687	.1507	3	917	2.38135	.1742	.0954	3	1006	3.14241	.3081	.2339	5
830	3.20684	.0681	.0783	3	918	2.86589	.1654	.2137	4	1007	2.70774	.0777	.0629	2
831	2.21226	.1258	.0832	2	919	2.77226	.0558	.1542	3	1008	3.09302	.0526	.1522	3
832	2.86442	.0463	.0367	2	920	2.62227	.1099	.2054	3	1009	2.62467	.4473	.2439	5
833	3.01012	.0904	.1756	68	921	3.17527	.1712	.2909	15	1010	2.93106	.0697	.0482	2
834	3.16684	.2195	.0719	3	922	2.68954	.1618	.1364	2	1011	2.39434	.3696	.0730	4
835	3.21054	.0861	.0829	3	923	2.61491	.1774	.2448	5	1012	2.47910	.1414	.0532	3
836	2.19005	.1490	.0881	3	924	2.93755	.1231	.1423	3	1013	2.68288	.2246	.2088	4
837	2.29824	.0140	.1224	2	925	2.70036	.1480	.3658	10	1014	2.80256	.2204	.0589	3
838	2.89825	.0965	.1978	3	926	2.98329	.2306	.2526	5	1015	3.20225	.0774	.1447	3
839	2.61465	.1371	.2233	3	927	3.19793	.1488	.2488	5	1016	2.21938	.1157	.1068	2
840	3.13372	.1060	.1893	4	928	3.13870	.1772	.2763	6	1017	2.60609	.1109	.1210	2
841	2.25513	.0869	.0717	2	929	2.23870	.1262	.0806	2	1018	2.53908	.2158	.1304	3
842	3.22882	.1175	.2504	5	930	2.43103	.1329	.2675	66	1019	1.91158	.0792	.4554	7
843	2.27914	.1868	.1401	3	931	3.16644	.2233	.1737	5	1020	2.79023	.0741	.0701	2
844	3.19680	.0682	.1608	3	932	2.41990	.0803	.1407	2	1021	2.73794	.2417	.2681	4
845	2.93957	.0386	.2085	3	933	2.36866	.1938	.0815	3	1022	2.80785	.1728	.3468	5
846	3.12750	.1528	.0254	2	934	2.74833	.1714	.2658	4	1023	3.16797	.0825	.1745	4
847	2.78275	.0684	.0629	2	935	2.21882	.1256	.0790	2	1024	2.86675	.1905	.2608	4
848	3.10670	.1425	.0321	3	936	3.13823	.1532	.0292	3	1025	1.97911	.0589	.4520	64
849	3.15474	.1809	.3453	7	937	2.23157	.1957	.0818	3	1026	2.25038	.1594	.0747	3
850	2.99858	.1401	.2505	5	938	3.16085	.1594	.0270	2	1027	3.15903	.1504	.0244	3
851	2.22831	.1173	.0315	2	939	2.24693	.1508	.0571	2	1028	3.40528	.1046	.1445	5
852	2.36270	.2181	.4143	9	940	3.38455	.1200	.0922	5	1029	2.89035	.0599	.0403	2
853	2.31236	.1231	.1599	2	941	2.78460	.1642	.0993	3	1030	3.12339	.1606	.2452	6
854	2.36821	.1745	.1107	2	942	3.16069	.1477	.1617	4	1031	3.04692	.0895	.3100	5
855	2.36146	.1897	.1893	3	943	3.12191	.2280	.1786	4	1032	3.13402	.1495	.1419	4
856	2.43618	.1367	.2352	4	946	3.12353	.1445	.0133	3	1033	3.00298	.0922	.1839	4
857	2.19036	.0668	.0758	2	947	2.75227	.2178	.0995	3	1034	2.29259	.2402	.0828	3
858	2.80953	.1295	.1362	3	948	3.03534	.1967	.1496	4	1035	3.14172	.2001	.3012	7
859	3.21150	.1172	.2259	5	949	2.99741	.2201	.2120	5	1036	2.65947	.4710	.4843	75
860	2.79648	.0903	.2431	4	951	2.20974	.1455	.0887	3	1037	2.25489	.1622	.1058	3
861	3.14441	.0845	.1186	3	952	2.98745	.2196	.1607	4	1039	2.68003	.0954	.0909	3
862	2.80316	.0728	.2571	4	953	2.78892	.1736	.1483	3	1040	3.11702	.2107	.2837	7
863	3.19866	.0387	.4160	10	954	3.13684	.1510	.0217	2	1041	3.07196	.1321	.2180	5
864	2.20835	.1606	.0867	3	955	2.59325	.2824	.2077	4	1042	3.22374	.0934	.3417	4
865	2.41663	.2079	.2307	4	956	2.29810	.1811	.1097	2	1043	3.09320	.0287	.1451	3
866	3.12373	.0301	.1301	3	957	2.91938	.0864	.2686	4	1044	2.57678	.1384	.0610	2
867	3.06609	.1421	.0956	3	959	3.18094	.1933	.0617	3	1045	2.35875	.1522	.0227	2
868	2.70738	.1212	.0839	3	960	2.24836	.1372	.0706	2	1046	2.98413	.0500	.1390	5
869	2.69204	.2248	.1333	2	961	2.69298	.0738	.1870	3	1047	2.24100	.1632	.0823	3
870	2.32161	.2446	.0857	3	962	2.90569	.0650	.0339	2	1048	2.73204	.2212	.0780	3
871	2.22209	.1435	.0675	2	963	2.24767	.1307	.1229	2	1049	3.09551	.1072	.2677	5
872	2.73146	.1136	.1299	3	964	3.05243	.0913	.1495	3	1050	2.62514	.1441	.2311	4
873	2.62751	.1609	.0863	3	965	3.15565	.2404	.3642	14	1051	3.21067	.1208	.3893	6
874	3.15798	.1018	.1907	3	966	2.71922	.1561	.2253	4	1052	2.23611	.1204	.0644	2
875	2.55389	.1184	.2584	4	967	2.22550	.1484	.0775	2	1053	2.61486	.0797	.1437	3
877	2.48713	.1498	.0581	3	968	2.86766	.1606	.2108	4	1054	2.92119	.1027	.1699	3

no	a (AU)	ecc	sinI	QC
1055	2.19848	.1842	.0792	3
1056	2.23001	.1572	.0755	3
1057	2.89260	.2104	.0842	4
1058	2.19633	.1656	.0780	2
1059	2.64271	.1749	.1857	4
1060	2.23777	.1834	.1173	2
1061	3.12193	.1899	.0230	3
1062	3.00670	.0659	.1087	3
1063	2.31413	.0683	.0864	2
1064	2.54542	.1653	.1784	3
1065	2.36011	.2783	.1462	3
1066	2.40271	.1790	.0911	3
1067	2.87102	.1635	.2059	6
1068	2.90837	.1230	.1141	3
1069	3.13238	.1330	.2167	5
1070	3.21852	.0923	.2834	5
1071	2.80096	.1058	.0815	3
1072	3.17471	.2182	.1312	3
1073	3.17614	.1756	.0252	2
1074	3.15627	.1563	.0195	3
1075	3.01369	.0775	.1812	3
1076	2.47527	.1438	.0467	2
1077	2.39236	.1689	.1001	3
1078	2.26970	.1618	.1110	3
1079	2.87390	.0460	.0369	2
1080	2.42017	.2393	.0894	3
1081	3.09170	.1267	.0683	3
1082	3.12921	.1487	.0232	2
1083	2.32904	.1956	.0720	3
1084	2.68875	.1231	.0708	3
1085	3.18291	.0615	.1006	3
1086	3.16588	.0608	.1612	3
1087	3.01505	.0745	.1685	4
1088	2.20157	.1670	.1188	3
1089	2.21393	.1185	.0490	3
1090	2.35916	.2822	.3334	7
1091	3.42094	.0710	.0074	2
1092	2.90126	.0974	.1132	9
1094	2.54658	.1425	.2298	4
1095	3.02525	.0552	.1699	3
1096	2.60198	.1611	.1493	3
1097	2.64113	.2757	.0151	3
1098	2.68881	.0893	.2467	4
1099	3.16679	.2674	.1859	4
1100	2.89851	.0481	.C372	2
1101	3.24699	.0547	.4345	87
1102	3.06704	.0850	.2832	4
1103	1.93364	.0581	.3168	7
1104	2.62916	.3142	.1039	3
1105	3.01234	.0756	.1699	3
1106	2.59767	.1567	.2406	4
1107	3.19016	.1227	.1005	3
1109	3.20842	.1308	.0915	3
1110	2.21829	.2155	.1213	3
1111	2.99391	.0651	.0514	3
1112	3.02053	.0714	.1760	3
1113	3.11177	.1413	.2415	73
1114	3.09246	.0560	.1875	4
1115	3.10134	.1727	.2532	6
1116	2.92453	.1924	.3069	6
1117	2.24779	.1852	.0654	3
1118	3.21054	.0471	.2558	3
1119	2.61239	.1494	.1235	3
1120	2.21628	.1271	.0635	2
1121	2.54677	.1324	.1133	3
1122	2.60613	.2263	.0644	3
1123	2.22512	.1342	.0942	2
1124	2.92707	.0411	.1327	3
1125	3.13711	.2175	.0311	3
1126	2.27211	.1722	.1153	3
1127	2.59492	.2258	.2507	4
1128	2.78755	.0469	.0133	2
1129	3.02242	.0635	.1680	3
1130	2.22876	.1711	.0508	2
1131	2.22848	.2544	.0390	3
1132	2.68571	.2587	.1298	4
1133	2.18604	.1566	.0802	3
1134	2.68505	.4356	.2407	5
1135	2.66595	.0825	.0868	3
1136	2.56551	.2193	.1609	3
1137	2.42378	.0683	.0584	2
1138	3.14726	.0465	.2605	4
1139	1.94746	.2562	.2277	4
1140	2.77233	.0825	.2261	4
1141	2.27058	.1365	.0576	2
1142	3.18017	.1098	.0242	2
1145	2.42433	.1272	.1186	2
1146	3.04809	.2408	.3059	8
1147	2.27105	.2295	.0818	3
1148	3.01574	.1141	.1814	72
1149	2.89845	.0615	.2224	3
1150	2.19094	.1740	.0517	2
1151	2.40626	.2432	.1328	4
1152	2.42684	.0701	.1006	2
1153	2.19589	.1433	.0746	2
1154	3.39730	.0673	.0581	3
1155	2.46153	.1869	.1046	3
1156	2.23700	.0532	.0072	2
1157	3.19536	.1282	.1777	3
1158	2.56389	.0798	.2656	3
1159	2.37962	.0472	.2321	3
1160	2.56044	.0898	.2560	3
1161	3.16589	.0727	.1445	3
1163	3.21774	.0342	.1379	3
1164	2.30617	.2117	.3964	51
1165	3.13274	.1817	.2381	4
1166	2.53892	.2118	.2893	5
1167	3.41494	.0728	.1101	5
1168	2.55188	.1768	.2348	4
1169	2.31841	.1484	.0859	2
1171	3.16306	.1857	.0357	3
1174	3.02202	.0877	.1761	3
1175	3.22089	.0354	.2935	5
1176	2.69205	.1332	.1326	3
1177	3.35390	.0254	.2739	5
1178	2.67858	.2219	.1110	3
1179	2.61599	.1963	.1566	3
1181	2.66414	.1771	.1128	3
1182	2.25958	.0935	.1738	2
1183	2.38356	.1549	.0505	2
1184	2.66809	.0594	.2015	3
1185	2.23751	.1019	.0830	2
1186	3.02046	.0761	.1770	3
1187	2.64031	.1842	.2076	4
1188	2.19051	.1513	.0842	2
1189	2.93170	.0757	.1925	3
1190	2.43133	.1219	.0533	2
1191	2.89223	.0779	.3012	5
1192	2.36584	.4347	.3867	85
1193	2.64701	.1565	.2268	4
1194	2.91354	.1197	.2104	4
1195	2.25764	.2147	.1419	3
1196	2.65277	.1265	.2925	4
1197	2.88154	.2506	.2612	5
1198	2.25083	.3024	.0713	3
1199	3.01860	.0607	.1674	3
1200	3.05990	.1299	.0865	3
1201	2.69852	.0020	.1275	4
1203	2.88502	.2230	.1095	4
1204	2.26331	.2696	.0360	3
1205	2.53454	.2406	.1407	3
1206	2.86583	.0703	.2406	4
1207	3.02076	.0741	.1779	4
1208	3.17444	.1312	.0982	3
1209	3.01120	.0713	.1745	3
1210	2.92982	.1338	.1992	3
1211	3.13222	.1048	.2471	4
1215	2.71085	.1012	.1879	3
1216	2.57884	.0926	.2608	3
1217	2.23238	.1838	.1160	3
1218	2.35290	.1718	.0809	2
1219	2.26302	.1315	.0419	2
1220	2.21307	.1157	.0679	2
1221	3.00490	.0740	.1756	3
1222	2.79222	.2228	.3476	9
1223	2.86953	.0437	.0384	2
1224	2.30419	.1711	.1551	3
1225	2.23323	.0907	.0547	2
1226	2.58302	.1474	.1677	3
1227	3.19689	.1989	.2907	5
1228	2.76900	.0721	.0757	2
1229	3.20279	.1646	.0290	3
1230	2.57250	.1518	.1809	3
1231	2.66895	.1100	.2101	3
1232	3.17738	.1637	.1943	5
1233	2.55518	.0738	.1160	2
1234	3.01288	.0605	.1671	3
1235	1.91027	.1470	.4090	4
1236	2.43019	.2120	.2176	4
1237	2.61234	.0421	.1548	3
1238	2.66651	.1634	.2032	3
1239	2.66209	.2419	.0159	3
1240	2.86800	.1458	.1863	3
1241	3.18997	.1462	.3957	11
1242	2.73584	.1584	.1876	3
1243	3.09890	.0421	.2444	3
1244	2.34332	.1247	.1716	2
1245	2.89319	.0463	.0406	2
1246	2.62153	.2597	.2994	5
1247	3.13862	.1599	.0283	2
1248	2.72179	.0294	.1409	3
1249	2.22433	.0961	.1018	2
1250	2.55113	.3076	.2798	4
1251	2.71757	.1227	.0899	3
1253	3.16670	.1829	.0231	3
1254	3.13513	.0600	.1433	3
1255	3.15250	.1368	.1631	3
1257	2.48432	.1003	.0765	4
1258	3.18614	.0182	.1529	3
1259	3.10217	.1580	.0240	2
1260	2.61395	.0257	.1566	3
1261	3.14670	.2002	.0276	3
1262	3.00257	.0300	.2090	3
1263	2.66611	.1716	.5548	86
1264	2.86465	.2293	.4006	80
1265	3.02545	.0656	.1814	3
1266	3.36471	.0359	.3082	5
1267	2.46666	.1756	.0833	2
1270	2.23469	.1757	.0885	3
1271	3.13538	.1030	.0990	3
1272	2.78384	.1327	.1575	3
1273	2.39368	.1337	.1123	3
1274	2.22922	.1395	.0904	2
1275	2.68022	.1440	.2165	3
1276	3.16891	.1478	.3591	8
1277	2.69818	.2318	.1361	3
1278	2.40517	.2330	.1733	4
1279	2.37015	.2102	.1139	3
1280	3.41492	.0189	.1300	5
1281	2.55862	.2018	.1404	3
1282	3.11998	.0831	.3274	6
1283	3.19968	.1844	.1447	3
1284	2.64511	.1507	.2081	4
1285	2.99305	.0226	.1156	3
1286	3.02241	.0785	.1750	3
1287	3.01162	.0747	.1763	3
1288	2.88521	.0299	.1500	4
1289	2.86059	.0513	.0354	3
1290	2.36639	.1249	.1159	2
1291	3.01308	.0666	.1684	3
1292	2.54272	.0897	.0572	2
1293	2.22765	.2426	.1145	3
1294	2.68710	.2038	.1316	3
1295	3.38873	.1311	.0521	5
1296	2.41811	.1496	.0853	2
1297	3.02087	.0612	.1747	3
1298	3.12825	.1158	.1162	3
1299	2.80334	.1676	.1342	3
1300	2.78187	.0314	.1472	3
1302	3.12029	.1631	.0244	3
1303	2.31631	.1246	.3204	5
1304	3.19404	.1445	.3022	5
1305	3.01366	.1054	.0270	2
1306	3.14121	.0985	.2724	5
1307	2.25049	.0970	.0823	2
1308	2.90927	.0451	.1042	3
1309	3.21660	.1333	.1864	5
1310	2.39220	.2521	.3972	74
1311	2.42663	.0651	.0659	2
1313	2.65669	.1688	.2435	4
1314	2.29543	.1563	.1080	3
1315	3.21339	.0726	.1370	3
1316	2.41162	.2436	.4776	83
1317	3.18220	.2397	.3417	9
1318	2.30787	.2501	.4008	55
1319	2.98712	.2391	.0692	4
1320	2.98534	.2617	.2978	7
1321	2.94224	.1610	.1756	4
1323	3.19941	.2032	.3047	5
1324	2.18494	.1642	.0936	2
1325	2.53975	.2231	.1222	3
1326	2.66672	.1753	.2666	4
1327	2.78083	.1351	.0896	3
1328	3.49735	.1096	.1054	5
1329	2.61714	.1691	.2279	4

```
no; a (AU); ecc ; sinI; QC       no; a (AU); ecc ; sinI; QC       no; a (AU); ecc ; sinI; QC
------------------------------   ------------------------------   ------------------------------
1330 3.17570 .0940 .2607  5      1420 2.74872 .0512 .0797  3      1509 1.86625 .0447 .3833  4
1331 3.10600 .1719 .0340  2      1421 3.09229 .1132 .1579  3      1510 2.67113 .1838 .2093 66
1332 3.06307 .0981 .0457  3      1422 2.24735 .1379 .0535  2      1511 2.35788 .1383 .0542  2
1333 2.63355 .1449 .2294  4      1423 2.86016 .0471 .0380  2      1512 3.19268 .1285 .0567  2
1334 2.91508 .1029 .1831  3      1424 3.18830 .0406 .1493  3      1513 2.24043 .1758 .0665  3
1335 2.24047 .1245 .0429  2      1425 2.61218 .1405 .2208  3      1514 2.57104 .2119 .1643  3
1336 2.85081 .0488 .0356  2      1426 2.57962 .1759 .1746  2      1515 2.62116 .2144 .1402  3
1337 2.91050 .0840 .2943  4      1427 2.75080 .1848 .1470  3      1516 2.71692 .0466 .0768  2
1338 2.26392 .1088 .0968  2      1428 2.80991 .0958 .2831  4      1517 2.22551 .1326 .1121  3
1339 3.02124 .0635 .1694  3      1429 2.55300 .2978 .1282  4      1518 3.13398 .2170 .2038  6
1340 3.18114 .1584 .0256  3      1430 2.56017 .1766 .0695  3      1519 3.10740 .0758 .2797  4
1341 2.74243 .0969 .2074  3      1431 2.61933 .1529 .2216  3      1520 2.85020 .1156 .2612  4
1343 2.56920 .1182 .0972  3      1432 2.38175 .1986 .1244  3      1521 2.36814 .0774 .0795  2
1344 2.24785 .1506 .0848  3      1433 2.79702 .1455 .1623  3      1522 2.24206 .1226 .1010  2
1346 2.62807 .1487 .2379  3      1434 3.01778 .0621 .1761  3      1523 3.11356 .0978 .2229  5
1347 2.57138 .0633 .2177  3      1435 2.64606 .2512 .0783  3      1524 2.69613 .2286 .1271  4
1348 2.79251 .1466 .0942  3      1436 3.14603 .0719 .2553  4      1525 2.31495 .1663 .1219  2
1349 3.01513 .1678 .1952  4      1438 3.17358 .1982 .0538  3      1526 2.27741 .1749 .0896  2
1350 2.85810 .0540 .0377  2      1440 3.15219 .1693 .0318  3      1527 2.41501 .1705 .1357  2
1351 3.19369 .0639 .1696  4      1441 2.63172 .1908 .2648  4      1528 2.24861 .1668 .0979  3
1352 2.77813 .0404 .0668  2      1442 2.87491 .0473 .0366  2      1530 2.62718 .1447 .2296  4
1353 3.01200 .0770 .1692  3      1443 2.93823 .0372 .0342  2      1531 3.00466 .0638 .1652  3
1354 3.13386 .2098 .1044  4      1444 3.15832 .1431 .3194  7      1532 3.01195 .0714 .1740  3
1355 1.85350 .0613 .3963 68      1445 3.11419 .1533 .0205  3      1533 2.72954 .2566 .1594  4
1356 3.08322 .0177 .1210  3      1446 2.24573 .1285 .0896  2      1534 3.15069 .1951 .1234  3
1357 3.19101 .1227 .2240  4      1447 2.53519 .0578 .0772  2      1535 2.20415 .1646 .0344  2
1358 2.47719 .1556 .0394  2      1448 2.37271 .2002 .0948  2      1536 3.05083 .2650 .0807  4
1359 3.11990 .0486 .1750  3      1449 2.22246 .1581 .0991  2      1537 2.35240 .1917 .1665  3
1360 2.63370 .1925 .4126 11      1450 2.61234 .1698 .0665  3      1538 3.14743 .1597 .0197  3
1361 3.08402 .1545 .3388 11      1451 2.20327 .1405 .0869  2      1539 2.84894 .1152 .1959  3
1362 3.23317 .3136 .4143  6      1452 3.11788 .1943 .2507  6      1540 2.76857 .1038 .0898  3
1363 2.90286 .0480 .0331  2      1453 1.89701 .0427 .3958  5      1541 3.09539 .0810 .0581  3
1364 3.01229 .0749 .1822  4      1454 2.36452 .1641 .0944  2      1542 2.62992 .3107 .1968  4
1365 2.24872 .1431 .1048  2      1455 2.24672 .1453 .1221  2      1543 2.37339 .0903 .0446  2
1366 2.87446 .1217 .1639  3      1456 3.18738 .2043 .2077  4      1544 2.76973 .2662 .0426  3
1368 2.52372 .0693 .2554  3      1457 2.69573 .1810 .1282  3      1545 3.17252 .1204 .2811  5
1369 3.10999 .1960 .2514  5      1458 2.62589 .1706 .2226  4      1546 2.64454 .2617 .2094  4
1370 2.25042 .1544 .0973  3      1459 3.14915 .2223 .2645  6      1547 2.78789 .1025 .2701  4
1371 3.20670 .1014 .2844  5      1460 2.54240 .1796 .0965  3      1548 2.23084 .0903 .0793  2
1372 2.76719 .1151 .3016  4      1461 3.12710 .0463 .2424  4      1549 2.54625 .2693 .1365 64
1374 2.25068 .2437 .1139  3      1462 3.15365 .1277 .0237  2      1550 2.39464 .0407 .0474  2
1375 2.44777 .0704 .0896  2      1463 3.14543 .1729 .1458  4      1551 3.00966 .0763 .1724  3
1376 2.22800 .1925 .0570  2      1464 3.00359 .0717 .1807 17      1552 2.90681 .1229 .0358  3
1377 2.26022 .1193 .1153  2      1465 3.03101 .2063 .1653 56      1553 2.61938 .1641 .2216  3
1378 2.37484 .1656 .0539  2      1466 2.37719 .1723 .2223  3      1554 2.68965 .2388 .1245  3
1379 2.52644 .1346 .2602  4      1467 3.38574 .1812 .3547 15      1555 3.42182 .0708 .2496  7
1380 3.14631 .1236 .1883  4      1468 2.19580 .2468 .1799  3      1556 3.01026 .0785 .1821 17
1381 2.48873 .1754 .0892  3      1469 3.12451 .0433 .2305  5      1557 3.22149 .0371 .1620  3
1382 2.21986 .1496 .0369  2      1470 3.16045 .0453 .0632  3      1558 2.39010 .1651 .0700  2
1383 3.08240 .1535 .0213  2      1471 2.71643 .0946 .2520  4      1559 2.68460 .1765 .1337  3
1384 2.67712 .1622 .2001  3      1472 2.23409 .1682 .0685  2      1560 3.18092 .1531 .0888  3
1385 2.74097 .0689 .1004 57      1473 2.57479 .1933 .2463 62      1561 2.22636 .1049 .0715  2
1386 2.36510 .2657 .1925  4      1475 2.34920 .1469 .0825  3      1562 2.19151 .1159 .0926  2
1387 2.25839 .1813 .1053  2      1476 2.28111 .1696 .1181  3      1563 3.15712 .1856 .1883  5
1388 3.01905 .0752 .1816  3      1477 3.17911 .2609 .2958  6      1564 2.39253 .2887 .4122 18
1389 2.86607 .0410 .0358  2      1478 2.46515 .1092 .1498  3      1565 3.22101 .0823 .2831  5
1390 3.43572 .0375 .3246 10      1479 2.67489 .1954 .1309  3      1567 2.35196 .2471 .4272 74
1391 2.54852 .2004 .1166  3      1480 2.20233 .1302 .0716  2      1568 3.15420 .0954 .1932  4
1392 2.60776 .1715 .2183  3      1481 3.01723 .0390 .0698  3      1569 2.84377 .0435 .0350  2
1393 2.43443 .1262 .0875  2      1482 2.87234 .0473 .0356  2      1570 3.14030 .1203 .2643  5
1394 2.43899 .0718 .0474  2      1483 2.71715 .2113 .0639  3      1571 3.11000 .1886 .2184  5
1395 3.20296 .0388 .1669  3      1484 2.73787 .2371 .2835  5      1572 3.53770 .0674 .2556  9
1396 2.24797 .1688 .0853  3      1485 3.02595 .0868 .1733  3      1574 2.37458 .2389 .3966 11
1397 2.68398 .2499 .0435  3      1486 2.19841 .1018 .0183  2      1575 3.13619 .1562 .0198  3
1398 3.15886 .0743 .2251  4      1487 3.13942 .1492 .0227  2      1576 2.23035 .1401 .0616  2
1399 2.21609 .1393 .1063  3      1488 3.03853 .1314 .1887  4      1577 3.42931 .1390 .1503  7
1400 3.11590 .1986 .2918  6      1489 3.17639 .1906 .0334  3      1579 3.16434 .1428 .0240  3
1401 2.22672 .1467 .1471  3      1490 2.35267 .1203 .1941  3      1581 3.16060 .1433 .1812  3
1402 2.68499 .1692 .2555  4      1491 3.21058 .1673 .0810  3      1582 2.37574 .2574 .4260 10
1403 2.71860 .2635 .1531  4      1492 2.17310 .1407 .0944  2      1584 2.43012 .1306 .0543  2
1405 2.25172 .1257 .1391  2      1493 2.42965 .1782 .0569  2      1586 2.54499 .1556 .1440  3
1406 2.69618 .0774 .2284  3      1494 2.19017 .1035 .0483  2      1587 3.03001 .0518 .1744  3
1407 2.76357 .2435 .1278  4      1495 2.63921 .1436 .2257  4      1588 2.41723 .0657 .0734  2
1408 3.11060 .0644 .1481  3      1496 2.20575 .1522 .0594  2      1589 2.23019 .1557 .0877  2
1409 2.67638 .0256 .1137  3      1497 2.89528 .0583 .0378  2      1590 2.39167 .3141 .3048 82
1410 3.01968 .0793 .1737  4      1498 3.09859 .1919 .2519  4      1591 2.76672 .3126 .1950  4
1411 3.00357 .0229 .1596  3      1499 2.67063 .1577 .2312  4      1592 2.22485 .2675 .1464  4
1412 2.21470 .1116 .0673  2      1500 2.24249 .1674 .1244  3      1593 2.26908 .1861 .1391  3
1413 3.02204 .0790 .1740  3      1501 2.54617 .2050 .1218  3      1594 2.64507 .1000 .0513  3
1414 2.78658 .1909 .1350  3      1502 2.73214 .1051 .0793  3      1595 2.89079 .1172 .2397  6
1415 2.22376 .1139 .0725  2      1503 2.62631 .1361 .2255  3      1596 2.84643 .1204 .1950  4
1416 3.01797 .1021 .1914 72      1504 2.39950 .1801 .1754  3      1597 2.33197 .0989 .1489  2
1417 2.97362 .0928 .1227  3      1505 2.65994 .1683 .2602  4      1598 3.13510 .1125 .0946  3
1418 2.24165 .1820 .1280  3      1506 2.57003 .2652 .2265  4      1599 1.84891 .0119 .3530  5
1419 2.29274 .1474 .1094  3      1507 2.33141 .2135 .1795  3      1600 2.23397 .1332 .0691  2
                                                                 1601 2.23397 .1332 .0691  2
```

no;	a (AU);	ecc ;	sinI;	QC
1602	2.24463	.1310	.0572	2
1603	2.75521	.0616	.1327	3
1604	3.02378	.0734	.1794	3
1605	3.01345	.0769	.1787	4
1606	2.69065	.2839	.1375	4
1607	2.54876	.2676	.1379	59
1608	2.21395	.1505	.0732	2
1609	2.58355	.2141	.2981	5
1610	2.20252	.1690	.0441	2
1611	3.18719	.1343	.0911	3
1612	3.10238	.0986	.3070	6
1613	2.73560	.2593	.1529	4
1614	2.99598	.1087	.2307	4
1615	3.11380	.1626	.0227	3
1616	2.91061	.0291	.1361	3
1617	3.20072	.1535	.2138	5
1618	2.86881	.0439	.0361	2
1619	2.24110	.1508	.0923	3
1621	2.23008	.1073	.0568	2
1622	2.23444	.1686	.1179	3
1623	3.13438	.1552	.0237	3
1624	3.18052	.1322	.0200	3
1625	3.17771	.2257	.3008	6
1626	2.36350	.2951	.4087	58
1627	1.86307	.3692	.1244	4
1628	3.01331	.0769	.3279	6
1629	2.23824	.1687	.1582	2
1630	3.03146	.1947	.0682	3
1631	2.23530	.1866	.1275	3
1632	2.65591	.1098	.1060	2
1633	3.17295	.1725	.0272	3
1634	2.24578	.1604	.1118	2
1635	2.85339	.0452	.0358	2
1636	2.23466	.1093	.0739	2
1637	3.06943	.0690	.2395	4
1638	2.74848	.1869	.0209	2
1639	2.57338	.1365	.1621	3
1640	2.28916	.3132	.1176	4
1641	3.01902	.0802	.1725	3
1642	2.75148	.0942	.1965	3
1643	2.48870	.2051	.0827	3
1644	2.54752	.1716	.1386	3
1645	3.05897	.0814	.0382	3
1646	2.36034	.0961	.1303	2
1648	2.23559	.2117	.0661	3
1649	3.02055	.0807	.1726	3
1650	2.43635	.1719	.0539	2
1651	2.17968	.0966	.0904	2
1652	2.25142	.1565	.0708	2
1653	2.60988	.2891	.0979	4
1654	3.01634	.0603	.1754	3
1655	2.78258	.2245	.1424	3
1656	1.87763	.1055	.4301	5
1657	2.34839	.1828	.3881	53
1658	2.56017	.1835	.1339	3
1659	2.78358	.2270	.2871	5
1661	2.18369	.1125	.0697	2
1662	2.74296	.1403	.0899	3
1663	2.23968	.1483	.0776	2
1664	2.33853	.2519	.0995	3
1665	2.41500	.2150	.1626	3
1666	2.18546	.1519	.0658	3
1667	2.19001	.1552	.0626	2
1668	2.80610	.1836	.0714	3
1669	3.14082	.1405	.0249	2
1670	2.90147	.0978	.1668	3
1671	2.58827	.2410	.0694	3
1672	3.17721	.2626	.0244	4
1673	3.10162	.1600	.0690	3
1674	3.18409	.1422	.0256	3
1675	2.23327	.1226	.1134	2
1676	2.23566	.1963	.0929	3
1677	2.53232	.0969	.2650	3
1678	3.16482	.1135	.1820	4
1679	3.12238	.1253	.3132	6
1680	2.72469	.2057	.0537	3
1681	2.69690	.2102	.1017	3
1682	2.23876	.1650	.0810	3
1683	2.73524	.1684	.2217	4
1684	3.09071	.1482	.0429	3
1686	3.16569	.1490	.0235	2
1687	3.15796	.1568	.0249	3
1688	2.61965	.2375	.2144	4
1689	2.44960	.1809	.0967	2
1690	3.04021	.0743	.2352	4
1691	3.16562	.1499	.0228	3
1692	2.78801	.1190	.0505	2
1693	2.80250	.2476	.1940	4
1694	2.39572	.2342	.1798	3
1695	2.78293	.2555	.2905	5
1696	2.26175	.1301	.1013	2
1697	2.37412	.1054	.1115	2
1698	3.15763	.1404	.0280	3
1699	2.21134	.1417	.0522	2
1700	2.36106	.1951	.0826	3
1701	3.17249	.1530	.2730	5
1702	2.85787	.1086	.1540	3
1703	2.21477	.1474	.0608	3
1704	2.22283	.1176	.0345	2
1705	2.29918	.2163	.1328	3
1706	2.12551	.1234	.0492	2
1707	2.21911	.1517	.0736	2
1708	2.91602	.2929	.1150	4
1709	2.37823	.1856	.1484	3
1710	2.32177	.2438	.1449	3
1711	3.01489	.0768	.1770	4
1712	3.16922	.1932	.3259	6
1713	2.22827	.1626	.0532	2
1714	2.56596	.1697	.1565	3
1715	2.39963	.2564	.1849	3
1716	2.73369	.1254	.1167	3
1717	2.19569	.1368	.1166	3
1718	2.36553	.2458	.1430	4
1719	2.65706	.1769	.2667	4
1720	2.18842	.1018	.0094	2
1721	3.14773	.0605	.2898	4
1722	2.51265	.0720	.0910	2
1723	3.01363	.0742	.1757	3
1724	2.71142	.0704	.2042	3
1725	2.90329	.0594	.0366	2
1726	2.78740	.0450	.0751	2
1727	1.85414	.0765	.3907	6
1728	2.56288	.0783	.1409	3
1729	2.22960	.1045	.0461	2
1730	2.78448	.1942	.1593	3
1731	3.17510	.0915	.0903	3
1732	3.01176	.0843	.1741	4
1733	2.19290	.0970	.0715	2
1734	2.77779	.1998	.1361	3
1735	3.14502	.1066	.2748	5
1736	2.22870	.1505	.0737	2
1737	3.01246	.0794	.1772	4
1738	2.18348	.1761	.0771	2
1739	2.26116	.1197	.0671	2
1740	2.46709	.1634	.0556	2
1741	2.88500	.0406	.0387	2
1742	2.88922	.0610	.0344	2
1743	2.47020	.1667	.1107	3
1744	2.22954	.1523	.0716	2
1745	2.84592	.0421	.0387	2
1750	1.92644	.1897	.3434	72
1751	2.78991	.1384	.1574	3
1752	2.23812	.1719	.0783	3
1753	3.01552	.0795	.1820	5
1755	3.09252	.0663	.1737	3
1756	2.54839	.1952	.1123	3
1757	2.35175	.1565	.0608	2
1758	3.00652	.0610	.1685	3
1759	2.64838	.2793	.0657	4
1760	3.15374	.1497	.1584	4
1761	3.17188	.2498	.0270	3
1762	2.87613	.0476	.0343	2
1763	2.18868	.1771	.0885	3
1764	3.09196	.1495	.0305	2
1765	3.16519	.1413	.3371	6
1766	2.74938	.0530	.0921	3
1767	3.02006	.0739	.1724	3
1768	2.45012	.1572	.0588	2
1769	2.17861	.1130	.0420	2
1770	2.45767	.0510	.0901	2
1771	3.12524	.1535	.1711	4
1772	2.53005	.1370	.0823	3
1773	2.43593	.1458	.0760	2
1774	2.87700	.0586	.0332	2
1775	2.60304	.1754	.2272	4
1776	3.10391	.0386	.1601	3
1777	2.62619	.0431	.0680	2
1778	3.14421	.1527	.0227	2
1779	2.17553	.1660	.0319	2
1780	3.01606	.0689	.1753	3
1781	2.39489	.0831	.1097	2
1782	3.12075	.1598	.0232	2
1783	2.66192	.1630	.1996	3
1784	2.40511	.1315	.0069	2
1785	2.23608	.0982	.0838	2
1786	3.02091	.0798	.1772	3
1787	3.00256	.0785	.1741	4
1788	3.11136	.1501	.0182	2
1789	2.21353	.1669	.0164	2
1790	2.23812	.1290	.0914	2
1791	2.74673	.1488	.0994	3
1792	2.77731	.2508	.1330	4
1793	2.22391	.1277	.0402	2
1794	3.12053	.2043	.2511	5
1795	2.78520	.1953	.1371	3
1796	3.35738	.0946	.3720	7
1797	2.23660	.0127	.0504	2
1798	2.19906	.1055	.0970	2
1799	3.02503	.0981	.1848	4
1800	2.35728	.1089	.0837	2
1801	3.01841	.0760	.1709	4
1802	2.84318	.0420	.0347	2
1803	2.34881	.2221	.4001	15
1804	2.41046	.0361	.0772	2
1805	3.13316	.1498	.0263	3
1806	2.23671	.1185	.0839	2
1807	2.22623	.1489	.0756	3
1808	2.74805	.1603	.0410	3
1809	2.92739	.0752	.0365	2
1810	2.22400	.1014	.0864	2
1811	3.14132	.0919	.1418	3
1812	3.00761	.0738	.1756	4
1813	2.68338	.1165	.1323	3
1814	2.22597	.1314	.0747	2
1815	3.15547	.1955	.0261	3
1816	2.33894	.2480	.4019	18
1817	2.37150	.2593	.3972	71
1818	2.16407	.1535	.0691	2
1819	3.14223	.2665	.3514	11
1820	2.19828	.1899	.0745	3
1821	2.37820	.1969	.0530	3
1822	2.17025	.1651	.0296	2
1823	2.22590	.1498	.0670	2
1824	2.88464	.0468	.0378	2
1825	2.67712	.1068	.0888	3
1826	2.99723	.0796	.1775	4
1827	2.70888	.1846	.0918	3
1828	3.06001	.0898	.2440	5
1829	2.25112	.1182	.1262	2
1830	2.18835	.0775	.0599	2
1831	2.23921	.1396	.0810	2
1832	3.21568	.0778	.2762	5
1833	2.63460	.0967	.1637	3
1834	3.02306	.0936	.1825	61
1835	2.83308	.0553	.0370	2
1836	2.78337	.1953	.1362	3
1837	2.20570	.1057	.0846	2
1838	3.21219	.0199	.3641	4
1839	2.80007	.1450	.1590	3
1840	2.91753	.0294	.0364	2
1841	3.42559	.1323	.0368	3
1842	2.26645	.1776	.0862	3
1843	2.65236	.1633	.1619	3
1844	3.01646	.0754	.1846	5
1845	2.97024	.0713	.1707	3
1846	2.33854	.1462	.0560	2
1847	2.61058	.0466	.1747	3
1848	2.87126	.0525	.0408	2
1849	3.05348	.0454	.1740	3
1850	2.25096	.1352	.0548	2
1851	3.10929	.1547	.0307	2
1852	3.01459	.0681	.1726	3
1853	3.06406	.0288	.2891	3
1854	2.53840	.1484	.0903	4
1855	2.24752	.1146	.0575	2
1856	2.23688	.0981	.0840	2
1857	2.24362	.1183	.0896	2
1858	2.69859	.0787	.0482	2
1859	3.21594	.1055	.1458	3
1860	2.56544	.1973	.1525	3
1861	3.01896	.0658	.1786	3
1874	3.13975	.2677	.0697	4
1875	3.13106	.1492	.2320	5
1876	1.96427	.0507	.3985	3
1878	2.84569	.0399	.0362	2

no	a (AU)	ecc	sinI	QC	no	a (AU)	ecc	sinI	QC	no	a (AU)	ecc	sinI	QC
1879	2.24571	.1380	.0460	2	1972	2.41905	.1631	.0627	2	2064	2.17821	.3140	.1067	3
1880	2.67469	.0671	.0658	2	1973	3.18051	.0659	.1807	3	2065	2.69904	.1994	.1316	3
1881	3.16949	.0984	.1817	4	1974	3.16893	.0972	.1721	4	2066	2.39427	.1501	.0489	2
1882	3.00657	.0710	.1701	3	1975	2.80225	.0845	.1033	3	2068	2.77197	.0859	.2022	3
1884	2.42460	.1964	.3818	66	1976	2.38092	.1025	.0232	2	2069	3.15601	.1912	.1534	5
1885	2.24979	.2228	.1062	4	1977	2.78084	.0773	.1483	3	2070	2.24992	.1253	.0519	2
1886	2.62637	.1514	.2351	4	1978	2.19422	.1891	.0659	2	2071	2.25198	.1441	.0782	2
1887	3.00588	.0816	.1746	4	1979	2.37400	.0900	.1113	2	2072	2.45012	.1528	.0800	2
1888	2.54754	.1835	.1196	3	1982	2.31010	.2237	.1147	3	2073	2.71654	.1105	.0328	2
1889	3.08861	.1257	.2181	8	1983	2.62161	.0666	.1580	3	2074	1.79976	.0931	.4948	70
1890	3.22662	.1183	.1532	3	1984	3.01242	.0710	.0845	3	2075	2.40338	.2778	.3969	61
1891	2.70618	.0490	.2126	3	1985	3.12451	.1606	.3144	8	2076	2.27347	.1302	.1008	2
1892	2.46173	.0748	.2579	4	1986	3.09730	.1657	.0272	3	2077	2.32686	.3269	.4096	59
1893	2.70804	.0466	.1587	3	1987	2.38215	.2568	.4072	75	2078	2.36915	.2917	.4064	13
1894	2.88675	.0389	.0353	2	1988	2.15379	.0739	.0575	2	2079	2.59854	.1143	.2335	3
1895	3.18102	.1623	.0268	3	1989	2.35129	.0912	.1315	2	2080	2.17674	.0610	.0639	2
1896	2.36796	.1908	.0404	2	1990	2.17405	.0797	.0592	2	2081	2.45016	.1589	.0535	2
1897	2.28314	.1160	.0573	2	1991	2.24878	.1891	.1113	3	2082	2.92208	.1903	.0330	2
1898	3.11997	.1397	.0194	3	1992	2.99376	.0544	.1819	3	2083	1.87203	.8253	.8901	93
1899	2.26495	.1373	.1148	3	1993	3.05959	.0548	.1881	3	2084	2.39545	.0799	.0744	2
1900	2.20944	.1266	.1302	2	1994	2.67794	.1692	.2010	3	2085	2.69912	.0659	.0485	2
1901	3.23360	.1041	.3913	7	1995	2.52963	.0935	.1756	3	2086	2.40136	.1045	.0993	2
1903	3.00145	.0741	.1727	3	1996	2.55871	.1122	.2573	3	2087	2.20592	.0479	.0146	2
1904	2.74394	.0371	.2035	3	1997	2.20942	.1773	.1073	3	2088	2.20708	.0853	.1002	2
1905	2.22347	.1696	.0525	2	1998	2.41878	.0831	.1397	2	2089	2.53434	.1163	.2498	4
1906	2.37359	.1063	.1168	2	1999	3.11608	.1447	.1971	5	2090	3.06945	.1283	.2105	5
1907	2.54529	.0814	.0472	2	2000	2.38048	.2586	.4044	72	2091	3.01433	.0600	.1765	3
1908	2.89128	.0658	.0841	3	2001	1.93342	.1201	.3827	5	2092	2.84821	.0448	.0371	2
1909	2.42340	.2461	.0435	3	2002	2.41713	.0914	.1459	2	2093	2.26918	.1687	.0996	3
1910	3.04636	.0817	.1831	3	2003	3.06285	.1450	.0204	3	2094	2.23227	.1261	.1064	2
1912	2.90304	.0655	.0373	2	2004	2.17215	.0711	.0471	2	2095	2.64140	.0259	.0759	2
1913	2.87960	.0482	.0372	2	2005	2.62157	.1360	.2326	4	2096	2.44500	.2050	.0361	2
1914	2.40553	.1479	.0811	2	2006	2.32459	.1654	.0891	2	2097	3.13112	.2277	.0919	4
1916	2.27298	.4282	.2127	4	2007	2.38372	.1452	.0532	2	2098	2.42391	.1057	.1219	2
1918	3.18854	.1238	.1639	4	2008	3.22254	.1073	.3464	5	2099	2.30349	.3867	.4189	67
1920	1.92998	.0912	.3796	5	2009	3.11915	.1504	.0286	3	2103	3.15127	.2081	.1593	4
1921	3.25509	.3921	.3286	5	2010	3.09345	.1582	.0484	3	2104	3.19336	.1133	.3341	7
1922	3.01229	.5926	.5744	91	2011	2.38697	.1234	.1156	2	2106	2.70344	.0700	.1294	3
1923	2.43521	.0732	.0932	2	2012	2.32869	.1603	.0683	2	2107	2.62690	.0551	.1634	3
1924	2.33947	.1573	.0551	2	2013	2.29000	.1967	.1137	3	2108	2.43625	.0223	.1993	3
1925	2.55168	.1398	.1168	3	2014	2.40235	.2531	.4012	19	2109	2.69157	.2297	.1220	70
1926	2.65646	.1354	.2224	3	2015	2.33543	.1076	.2164	3	2110	2.19802	.1507	.0143	2
1927	2.65054	.1625	.2315	3	2016	3.13810	.1536	.0246	2	2111	3.01870	.0638	.1747	4
1928	2.47596	.1838	.0807	4	2017	2.25206	.1680	.0827	3	2112	2.25376	.1160	.0738	2
1929	2.36265	.0977	.1213	2	2018	2.18328	.1625	.0481	2	2113	2.47378	.0778	.1083	2
1930	2.89652	.1452	.2516	5	2019	2.24113	.1659	.0851	2	2114	3.20045	.1634	.0251	3
1931	2.54268	.2335	.1362	3	2020	3.02317	.0868	.1781	3	2115	3.01047	.0875	.1713	3
1932	2.37181	.1798	.0392	2	2021	2.30949	.1978	.0851	3	2116	2.58872	.0277	.1524	3
1933	2.35296	.0959	.1131	2	2022	2.70634	.0903	.1030	3	2117	2.87027	.0505	.0384	2
1934	2.39010	.2493	.4004	19	2023	2.87848	.2915	.3357	8	2118	2.54590	.2072	.1265	3
1935	2.62654	.2037	.1631	3	2024	2.32540	.1071	.1124	2	2119	2.25128	.1512	.0829	2
1936	2.67520	.1637	.2018	4	2025	3.16486	.1155	.1371	3	2120	3.06240	.1034	.3146	6
1937	2.37755	.1422	.1979	3	2026	2.44573	.1446	.0599	2	2121	2.18357	.1620	.0655	3
1938	2.23629	.1793	.0558	2	2027	3.02167	.0791	.1753	4	2122	2.40176	.0103	.1192	2
1939	3.12640	.1465	.0195	2	2028	2.29659	.1190	.1516	2	2123	2.86023	.0423	.0363	2
1940	3.06013	.0697	.1325	3	2029	2.35006	.0985	.1165	2	2124	3.02345	.0817	.1757	3
1942	2.31839	.2478	.3713	78	2030	2.24733	.1152	.0430	2	2125	2.78669	.0809	.0465	2
1944	2.24000	.2060	.1079	3	2031	2.23420	.1456	.0779	3	2126	2.39003	.0953	.1614	2
1945	2.55449	.1489	.0589	3	2032	3.06664	.1090	.0272	2	2127	3.20961	.0427	.2060	3
1946	2.29360	.2073	.1341	3	2033	3.22537	.1210	.1589	3	2128	2.73400	.3602	.2727	6
1947	3.15250	.0646	.1858	3	2034	2.24615	.1760	.1500	3	2129	2.18094	.1448	.0819	3
1948	2.53090	.2147	.0966	2	2035	1.88407	.1797	.4453	66	2130	2.25286	.1682	.1027	3
1949	2.38340	.2030	.1019	3	2036	2.24454	.1760	.0779	3	2131	1.88723	.2197	.5323	66
1950	2.17851	.1043	.0591	2	2037	2.30133	.1025	.0745	2	2132	2.78098	.0675	.0829	3
1951	1.39052	.1431	.5881	16	2038	2.43523	.1062	.2363	3	2133	2.41050	.1534	.1050	2
1952	3.10780	.1377	.2198	5	2039	3.17465	.1566	.0237	3	2136	3.02074	.0761	.1709	3
1953	3.11592	.1497	.0252	3	2040	3.11108	.1924	.2550	6	2137	3.18256	.0719	.2162	5
1954	2.93564	.2511	.2954	6	2041	3.16223	.1716	.0372	3	2138	2.68618	.0770	.0840	3
1955	2.85507	.0470	.0367	2	2042	2.75310	.1389	.0943	3	2139	2.46043	.1709	.0568	2
1956	3.19814	.1294	.0210	3	2043	3.10712	.0790	.0709	3	2140	2.98827	.0286	.1411	2
1957	3.00841	.0746	.1801	5	2044	2.38070	.2606	.3998	70	2141	2.80390	.1048	.1235	3
1958	3.10769	.1533	.1905	4	2045	2.37991	.0839	.1203	2	2142	3.17371	.1339	.0169	3
1959	2.31606	.1148	.1246	3	2046	3.15051	.1574	.0311	3	2143	2.28081	.2072	.1367	3
1960	2.52512	.1215	.1462	3	2047	1.87194	.0120	.4190	5	2144	2.87554	.0458	.0357	2
1961	3.19979	.1079	.1116	3	2048	1.95362	.0542	.4036	5	2145	3.21770	.1050	.2803	5
1962	3.17527	.2147	.0338	3	2049	1.94909	.0936	.4157	6	2147	3.17139	.0642	.1594	3
1963	2.42338	.7351	.5025	89	2051	2.84121	.0469	.0366	2	2149	2.54964	.1019	.1190	3
1964	2.46642	.1763	.0564	2	2052	3.00857	.0666	.1726	3	2150	1.91315	.0481	.4343	7
1965	2.56866	.0973	.0199	2	2053	2.80219	.1288	.1516	3	2151	2.56198	.0738	.2623	3
1966	2.44753	.1187	.0278	2	2054	2.96429	.1180	.0849	3	2152	3.13485	.1984	.2485	5
1967	2.23318	.1197	.0544	2	2055	2.31040	.2939	.4045	61	2153	3.11695	.1541	.0190	3
1968	2.73952	.1377	.0625	2	2056	2.21782	.1094	.0809	2	2154	2.63548	.1447	.1390	3
1969	3.09253	.1877	.0660	3	2057	3.07897	.2034	.0327	3	2155	2.85630	.0460	.0388	2
1970	2.77966	.1911	.1376	3	2058	3.11910	.1580	.0230	2	2156	2.24239	.1740	.0892	3
1971	2.99392	.0687	.1694	3	2059	2.64715	.4977	.1644	6	2157	2.78351	.1246	.1608	3

no;	a (AU);	ecc ;	sinI;	QC		no;	a (AU);	ecc ;	sinI;	QC		no;	a (AU);	ecc ;	sinI;	QC
2158	3.07291	.1743	.0339	2		2250	3.17553	.1752	.0232	2		2342	3.20333	.1402	.0217	3
2159	2.48266	.0432	.0647	2		2251	2.71072	.1168	.1290	3		2343	2.33442	.2246	.0438	2
2160	2.89852	.0687	.0346	2		2252	2.61639	.0404	.0796	2		2344	2.75410	.1573	.0484	2
2161	2.74821	.1257	.1111	3		2253	2.28400	.2548	.0537	3		2345	3.01715	.0768	.1757	3
2162	2.22729	.1086	.0398	2		2254	2.34225	.1196	.0974	2		2346	2.37122	.1247	.1212	3
2163	3.14913	.1534	.0244	2		2255	3.10011	.1340	.2240	69		2347	3.09381	.1747	.2508	5
2164	3.17594	.1334	.0257	2		2256	3.09725	.1544	.0128	2		2348	2.39762	.1864	.0850	2
2165	3.13369	.1440	.0252	3		2257	2.48530	.2343	.1048	4		2349	2.76963	.0926	.2813	4
2166	2.34653	.2038	.0851	3		2258	2.69388	.1015	.0483	63		2350	2.24208	.1187	.0777	2
2167	2.54234	.2197	.1279	3		2259	2.29382	.1788	.0969	3		2351	2.52992	.1515	.0804	2
2168	2.45199	.1371	.0969	2		2262	2.58678	.2564	.2177	4		2352	3.10621	.0858	.2700	2
2169	2.78860	.0464	.0132	2		2263	3.01597	.0729	.1784	69		2353	2.80465	.0900	.0806	3
2170	2.40451	.1519	.0555	2		2264	3.13068	.1545	.0226	2		2354	2.73069	.0705	.0549	2
2171	2.25563	.1643	.1100	3		2265	2.61659	.2550	.3041	5		2355	3.02085	.0859	.1621	3
2172	2.89626	.1205	.0383	2		2266	3.38402	.1836	.2330	7		2356	3.24164	.0173	.2680	5
2173	3.13363	.1108	.2396	5		2267	2.21747	.1427	.0475	2		2358	3.02331	.0680	.1783	3
2174	2.53728	.2346	.1367	3		2268	2.94075	.0927	.0374	2		2359	2.42528	.1138	.0836	2
2175	2.21572	.1757	.0767	3		2269	3.12884	.0837	.2488	5		2360	2.67249	.1670	.0516	3
2176	2.93139	.0671	.0332	2		2270	3.15143	.1499	.0200	2		2361	3.14344	.1531	.0244	3
2177	3.18659	.0956	.0205	2		2271	2.75940	.0474	.0446	2		2362	2.19541	.1629	.0682	2
2178	2.20765	.1247	.0539	2		2272	1.86675	.0689	.4195	5		2364	3.18355	.1588	.1704	4
2179	3.01147	.0841	.1822	70		2273	2.45170	.1725	.0135	2		2365	2.54311	.1453	.1114	3
2180	3.01144	.0622	.1751	3		2274	2.40924	.2614	.0497	3		2366	2.24070	.1144	.0353	2
2181	2.59054	.1468	.2242	3		2275	2.29621	.1401	.1148	2		2367	2.20656	.1208	.0388	2
2182	3.13009	.1511	.0308	2		2276	2.37480	.1744	.0533	2		2368	2.10539	.3808	.1094	4
2183	2.99910	.3211	.3073	8		2277	2.60127	.1549	.1847	2		2369	2.78290	.0507	.0372	2
2184	3.17621	.0765	.1093	3		2278	2.45166	.1606	.0612	2		2370	2.71394	.1591	.1438	2
2185	2.70894	.1340	.1554	3		2279	2.45981	.1811	.0395	2		2371	2.44086	.0401	.0465	2
2186	2.68090	.0855	.0609	2		2280	2.17885	.1112	.0457	2		2372	3.11099	.1606	.0266	3
2187	2.53591	.0833	.2137	3		2281	2.18826	.1243	.0365	2		2373	2.79523	.1402	.1592	3
2188	2.90241	.0613	.0332	2		2282	2.20317	.0833	.0949	2		2374	3.08764	.1972	.2532	6
2189	2.40326	.2010	.2207	4		2283	2.24888	.1186	.1207	3		2375	3.18133	.2178	.2518	5
2190	2.47189	.1057	.0335	2		2284	2.32556	.0774	.0813	2		2376	3.20285	.0948	.0526	3
2191	3.01820	.0778	.1719	3		2285	2.22026	.1791	.0827	3		2377	2.87914	.0471	.0371	2
2192	3.13665	.0610	.1737	3		2286	2.19265	.0665	.0140	2		2378	2.88937	.1293	.2496	4
2193	3.10809	.0836	.1932	3		2287	2.24014	.1535	.0733	2		2379	3.18308	.2452	.0175	3
2194	2.32780	.0687	.1378	2		2288	2.90949	.1817	.2416	4		2380	2.19194	.0590	.0465	2
2195	2.22180	.0831	.0625	2		2289	2.63539	.1706	.0413	2		2381	2.61077	.1472	.2295	3
2196	3.43457	.0993	.1818	7		2290	2.59113	.2118	.1996	3		2383	2.21788	.1347	.0620	2
2197	3.15166	.1418	.0328	3		2292	2.61912	.2144	.2516	3		2384	2.61012	.1603	.2324	4
2198	2.59291	.1715	.0733	3		2293	3.13744	.1545	.0209	3		2385	2.24254	.1323	.0616	2
2199	2.24135	.1918	.1319	3		2294	2.58117	.0908	.1286	3		2386	2.81368	.1397	.1601	3
2200	2.40521	.1771	.0893	2		2295	2.90317	.0606	.0619	3		2387	3.02283	.0767	.1774	4
2202	2.29107	.4792	.1399	5		2296	3.19398	.1741	.0203	3		2388	2.45126	.2017	.0564	2
2203	3.10990	.1512	.0218	2		2297	3.16393	.1547	.0177	2		2389	2.44353	.2188	.1412	4
2204	2.59203	.3678	.3813	12		2298	2.40624	.1437	.0950	2		2390	2.61960	.1288	.1885	3
2205	3.00540	.0894	.1968	3		2299	2.58557	.2632	.0835	65		2391	2.44016	.1349	.0483	2
2206	3.01547	.0792	.1726	3		2300	2.83849	.0478	.0379	2		2392	2.34454	.1518	.0476	2
2208	3.49868	.0397	.0724	5		2301	3.15794	.2280	.1760	5		2393	3.19881	.1934	.1938	4
2209	2.84648	.0488	.0363	2		2302	2.64559	.1499	.2321	4		2394	3.18201	.1928	.0137	3
2210	2.40354	.2007	.0335	2		2303	2.99631	.1670	.3146	5		2395	3.08098	.0677	.0152	2
2211	3.17682	.0861	.2806	5		2304	2.61271	.1483	.2380	4		2396	2.79436	.1051	.2079	4
2213	2.19820	.1962	.0765	3		2305	2.78614	.0095	.1259	3		2397	3.08908	.1672	.1657	4
2214	3.15887	.2445	.2473	5		2306	2.73207	.0349	.0892	3		2398	2.39172	.2428	.0450	3
2215	2.79193	.2417	.1598	4		2307	3.04591	.0862	.1512	3		2399	2.23970	.1534	.0780	3
2216	3.01914	.0758	.1681	3		2308	2.54754	.1798	.2392	4		2400	3.00165	.0836	.1753	68
2217	3.15809	.1565	.0223	2		2309	3.01248	.0757	.1808	4		2401	2.77038	.0645	.0645	2
2218	3.04280	.1575	.2306	5		2310	3.15016	.1538	.0278	3		2402	2.22210	.1091	.1007	2
2219	3.15435	.0858	.1141	3		2311	3.63575	.0227	.0966	9		2403	2.54708	.1018	.0758	2
2220	3.14977	.1375	.0250	2		2313	2.45815	.1638	.0483	2		2404	3.12710	.1459	.0267	2
2221	2.59093	.1025	.2575	4		2314	2.26092	.0530	.0930	2		2405	3.19559	.1580	.0220	3
2222	3.11584	.1619	.0236	3		2315	3.00982	.0892	.1793	66		2406	2.19257	.1331	.0412	2
2224	2.88102	.0472	.0367	2		2316	2.45157	.1565	.0247	2		2407	2.92320	.1857	.0543	3
2225	2.85247	.0470	.0375	2		2317	2.52399	.1295	.0729	2		2408	2.63715	.2176	.3150	5
2226	2.86898	.0473	.0373	2		2318	2.25229	.1082	.0550	2		2409	2.26608	.1612	.0482	2
2227	2.23603	.1672	.0871	3		2319	2.90591	.0585	.0325	2		2410	2.21556	.0930	.0281	2
2228	3.14327	.1629	.0232	3		2320	3.16290	.1057	.1821	4		2411	2.22545	.0965	.0168	2
2229	2.69400	.2571	.2278	4		2321	3.00536	.0460	.1245	3		2412	2.67969	.1485	.1394	3
2230	2.85827	.0433	.0365	2		2322	2.29238	.0194	.0478	2		2413	3.01688	.0885	.1806	73
2231	2.72867	.2167	.1498	4		2323	3.13117	.1653	.0858	3		2414	3.20984	.0956	.2921	5
2232	2.66734	.1259	.0770	2		2324	3.09049	.1879	.0264	2		2415	2.65947	.0416	.0223	2
2233	2.77827	.0645	.0753	2		2325	3.14315	.1488	.0217	3		2416	3.01330	.0649	.1700	3
2235	3.21361	.1880	.3374	6		2326	2.86111	.1245	.2567	4		2417	3.19397	.2161	.0343	3
2236	2.34485	.1976	.1796	3		2327	2.36836	.1033	.0678	2		2418	3.11723	.1523	.0257	3
2237	3.15427	.1796	.0234	3		2328	2.34167	.1781	.1699	3		2419	2.29603	.0846	.1076	2
2238	3.06509	.1504	.0235	2		2330	3.18273	.0344	.1350	3		2420	2.56078	.1141	.2537	3
2239	3.19378	.0890	.1847	3		2331	2.42486	.2378	.0834	3		2421	3.23064	.0482	.1577	3
2240	3.15337	.1471	.0134	3		2332	3.07241	.0595	.2358	4		2422	2.32885	.2262	.1037	3
2242	2.20815	.1162	.0536	2		2333	2.64608	.1582	.2016	3		2423	2.18846	.2499	.0938	3
2243	2.24825	.1709	.1164	2		2334	2.26856	.0961	.0558	2		2424	2.34968	.1507	.1515	3
2244	2.81139	.1529	.1177	3		2336	3.18799	.1713	.0292	3		2425	3.00128	.0873	.1764	4
2245	2.63688	.1101	.1855	3		2337	2.59421	.1564	.2370	4		2426	2.91031	.1447	.1588	3
2247	2.44919	.0886	.1056	2		2338	2.83322	.0488	.0365	2		2427	2.74061	.1377	.0840	2
2248	3.09964	.1499	.0274	3		2339	2.52646	.1610	.0832	3		2428	3.17073	.0623	.1622	3
2249	3.18624	.1017	.0598	3		2341	2.21191	.1344	.0563	2		2429	2.57194	.0805	.2559	3

no	a (AU)	ecc	sinI	QC
2430	2.36272	.2313	.3940	69
2431	2.64621	.2639	.0626	3
2432	2.35146	.1139	.1205	2
2433	2.60750	.2287	.1854	4
2434	3.08543	.1351	.2710	5
2435	2.20329	.1753	.0620	2
2436	3.16917	.1382	.0878	3
2437	2.18874	.1183	.0626	2
2438	2.24393	.1333	.0730	2
2439	3.13051	.1595	.0154	3
2440	2.21565	.1468	.0852	2
2441	2.40917	.1633	.0513	2
2442	2.38767	.1088	.0925	2
2443	3.00658	.0865	.1806	4
2444	2.72827	.1337	.2741	4
2445	2.26904	.1386	.0866	2
2446	2.35478	.1626	.0581	2
2447	2.53924	.2242	.1340	3
2448	2.79145	.1358	.2926	4
2449	1.90887	.1309	.4369	65
2450	3.11529	.1427	.0252	2
2451	2.72473	.1440	.1605	3
2452	3.15740	.1533	.2032	5
2453	3.01949	.0842	.1768	3
2454	2.25182	.1773	.1009	3
2455	2.72787	.0705	.1494	3
2457	2.64002	.0965	.0957	3
2458	3.13426	.1221	.0200	2
2459	3.02089	.0628	.1772	4
2460	2.25728	.1275	.0649	2
2461	3.17730	.1469	.0241	2
2462	2.40903	.1674	.0336	2
2463	2.60033	.1431	.2344	3
2464	3.16757	.2085	.0257	3
2465	2.75300	.0699	.0857	3
2466	2.63751	.1315	.0786	2
2467	2.21339	.1371	.1141	2
2468	2.32667	.1352	.1118	2
2469	3.11255	.1280	.1565	3
2470	2.88790	.0440	.0361	2
2471	2.99817	.0799	.1796	3
2472	2.26506	.1212	.0963	2
2473	2.24180	.1211	.0918	2
2474	2.68588	.2397	.1380	3
2475	3.03841	.0800	.1628	3
2476	3.02383	.0824	.1706	3
2477	2.55709	.1438	.1157	3
2478	2.22555	.0801	.0851	2
2479	2.38905	.2092	.0647	2
2480	2.22571	.1025	.0449	2
2481	2.57002	.2323	.0406	2
2482	2.92855	.0754	.0341	2
2484	2.34281	.2234	.0334	2
2485	3.19914	.2237	.0266	3
2486	2.26838	.0905	.1497	3
2487	2.39697	.1562	.0592	2
2488	2.26377	.1926	.1064	3
2489	3.11016	.1479	.0226	2
2490	2.60973	.1203	.2301	3
2491	1.87769	.0435	.3874	5
2492	3.17543	.1575	.0232	2
2493	2.78892	.1380	.1567	3
2494	3.16096	.0381	.2189	4
2495	1.91766	.1258	.3662	6
2496	2.17039	.0475	.0184	2
2497	2.53927	.2261	.1144	3
2498	2.91767	.0589	.0373	2
2499	3.10077	.1485	.0240	2
2500	2.24038	.1283	.1099	3
2501	2.42069	.2152	.0623	3
2502	2.93743	.2635	.2946	5
2503	2.19242	.1876	.1205	3
2504	2.76181	.1216	.0730	2
2505	3.15115	.1746	.0255	2
2506	2.89971	.0399	.0342	2
2507	2.78004	.1079	.1641	3
2508	2.36815	.1094	.1099	2
2509	2.45543	.1711	.0584	2
2510	2.25306	.1776	.0721	3
2511	2.29853	.1073	.1212	2
2512	2.24393	.1220	.0951	2
2513	2.28643	.1492	.0745	3
2514	2.65085	.0659	.0484	2
2515	3.17559	.1818	.0560	3
2516	2.27971	.1598	.0085	2
2517	3.17069	.1601	.0292	3
2518	2.30888	.1900	.1080	3
2519	3.14731	.1522	.0236	2
2520	3.10805	.0726	.1112	3
2521	2.79388	.1209	.1562	3
2522	3.01853	.0804	.1729	4
2523	3.01701	.0681	.1750	3
2524	3.12039	.1454	.0250	2
2525	3.14045	.1581	.0290	3
2526	3.13691	.1713	.0606	3
2527	2.46581	.1585	.0476	2
2528	3.14641	.1464	.0187	2
2529	2.53538	.0714	.0855	2
2530	3.01876	.0971	.1773	14
2531	3.00964	.0784	.1711	4
2532	2.37259	.1425	.0829	2
2533	3.09711	.1529	.0360	3
2534	3.14367	.1447	.0199	2
2535	2.23972	.0994	.0584	2
2536	2.30609	.1940	.1077	3
2537	2.65680	.1449	.2286	3
2538	2.23926	.1275	.0721	2
2539	2.26225	.1505	.0724	3
2540	2.19650	.0575	.0275	2
2541	2.93588	.0570	.0378	2
2542	3.12635	.1135	.0672	3
2543	3.08986	.2436	.2689	5
2544	2.37371	.1885	.4185	10
2545	2.22926	.1178	.1175	2
2546	2.60227	.2207	.1997	4
2547	2.38548	.1000	.1141	2
2548	2.63316	.1091	.3320	5
2549	3.19819	.1505	.0208	3
2550	3.19713	.1436	.1721	4
2551	3.14374	.1578	.0242	3
2552	2.14679	.1629	.0269	2
2553	3.08674	.0202	.0722	3
2554	2.26374	.1489	.1008	2
2555	2.86974	.0488	.0359	2
2556	2.16271	.0564	.0354	2
2557	2.35001	.1283	.1051	3
2558	2.21594	.1300	.0808	2
2559	2.78798	.1430	.1655	3
2560	2.74996	.0378	.0914	3
2561	2.43253	.1338	.0408	2
2562	3.00876	.0747	.1891	3
2563	3.20433	.1511	.0158	3
2564	2.23722	.1125	.0291	2
2565	2.35686	.2047	.0479	2
2566	2.45002	.0953	.0776	2
2567	2.73742	.1152	.1379	3
2568	2.20505	.1855	.1188	3
2569	2.62629	.1330	.1802	3
2570	2.76646	.0874	.2947	4
2571	2.22819	.1637	.0360	2
2572	2.39139	.1600	.0945	2
2573	3.01656	.1424	.2073	3
2574	2.85075	.0482	.0380	2
2575	2.24019	.1358	.0964	2
2576	3.08684	.1285	.2214	5
2577	1.90438	.1072	.3954	6
2578	3.00310	.0687	.1678	2
2579	2.21037	.0874	.1176	2
2580	2.18257	.1662	.0133	2
2581	2.23610	.1047	.0602	2
2582	3.20738	.0460	.2967	4
2583	2.25216	.1788	.1084	3
2584	2.22789	.0631	.0184	2
2585	2.42599	.2064	.0919	3
2586	2.38695	.0698	.0714	2
2587	3.17545	.1517	.0255	2
2588	2.45758	.1847	.0583	2
2589	2.87983	.0493	.0354	2
2590	2.34249	.0938	.1172	3
2591	2.93936	.0557	.0376	2
2592	3.12269	.1496	.0340	2
2593	2.16977	.1044	.0142	2
2594	2.78578	.1272	.1617	3
2595	3.03235	.0376	.1623	3
2596	3.00570	.1231	.0066	2
2597	2.78178	.1962	.1368	3
2598	2.53504	.1399	.2628	4
2599	3.01353	.0829	.1816	60
2600	3.13050	.0737	.1851	4
2601	2.38460	.1304	.0890	2
2603	2.78047	.0333	.0474	2
2604	2.38791	.2358	.2427	4
2605	3.09258	.0540	.1566	3
26C6	2.76120	.3128	.2020	4
2607	2.37649	.2009	.0417	2
2609	2.22139	.1170	.1164	2
2610	2.15927	.1145	.0235	2
2611	3.04159	.0857	.0410	3
2612	2.89582	.2191	.3080	7
2613	3.04014	.0636	.2431	5
2614	2.33830	.1416	.1019	3
2615	3.17408	.1470	.0883	3
2616	2.16236	.0471	.0197	2
2617	3.15089	.2337	.1914	5
2618	3.02453	.0779	.1813	4
2619	3.00873	.0593	.0312	2
2620	2.85864	.0423	.0370	2
2621	3.08617	.1321	.2117	64
2622	3.00378	.0705	.1734	4
2623	2.25487	.2042	.0776	2
2625	2.19590	.1290	.0628	2
2626	2.85029	.0488	.0365	2
2627	3.11314	.1542	.0230	3
2628	2.90807	.1167	.0351	2
2629	1.74029	.2065	.4096	6
2630	3.07545	.0917	.0417	3
2631	2.79766	.1366	.1602	3
2632	3.03920	.0838	.1794	3
2633	2.22485	.1137	.0416	2
2634	3.45480	.0755	.0911	5
2635	2.23167	.1078	.0911	2
2636	3.00516	.0965	.1607	3
2637	2.25492	.2076	.0873	3
2638	2.55514	.0748	.2608	4
2639	2.44621	.2000	.1322	69
2640	2.39781	.1184	.1177	2
2641	2.37817	.1664	.1486	3
2642	2.42604	.1682	.2469	3
2643	2.37784	.2186	.4016	13
2644	2.17037	.1533	.0548	2
2645	2.39139	.0944	.2466	3
2646	3.01373	.0652	.1749	3
2647	2.24393	.1212	.0861	2
2648	2.25029	.1570	.1014	2
2649	2.62670	.1320	.2217	3
2650	2.63553	.1726	.2455	4
2651	2.98283	.2636	.3160	7
2652	2.63606	.0501	.1071	3
2653	2.44353	.1059	.0868	2
2654	3.04631	.1225	.1346	3
2655	3.19303	.1679	.2644	5
2656	2.25557	.1102	.0383	2
2657	3.17474	.1402	.0308	3
2658	3.05804	.3317	.1723	5
2659	3.12320	.1305	.0209	3
2660	2.61836	.1552	.2248	4
2661	3.02633	.0893	.1865	65
2662	2.43903	.1549	.0631	2
2663	2.23373	.1515	.1050	2
2664	2.38050	.1535	.0518	2
2665	2.24754	.1122	.1001	2
2666	3.17228	.2141	.2281	5
2667	3.19566	.1906	.0264	3
2668	2.31686	.0480	.0723	2
2669	2.77961	.1814	.1610	4
2670	3.17365	.0730	.1887	5
2671	2.60874	.0871	.0404	2
2672	2.61228	.1523	.2256	4
2673	3.18957	.1812	.0237	3
2674	2.21287	.0721	.0508	2
2675	2.40339	.1016	.0975	2
2676	2.99288	.0836	.1758	3
2677	2.25979	.0958	.0488	2
2678	2.62094	.1223	.1844	3
2679	2.40309	.1876	.0463	2
2680	2.74662	.2121	.0564	3
2681	2.27033	.1530	.0785	3
2682	2.91564	.0263	.0396	2
2683	3.04964	.0610	.1605	3
2684	2.56802	.1382	.2214	3
2685	3.00405	.0797	.1749	3
2686	2.51998	.1055	.1641	3
2687	3.15677	.1596	.0387	2
2688	2.23242	.1480	.0972	2
2690	3.03479	.0847	.1839	4

no; a (AU); ecc ; sinI; QC

no	a (AU)	ecc	sinI	QC
2691	2.24442	.1315	.0779	2
2692	2.58120	.2171	.1806	3
2693	2.23935	.1629	.1102	3
2694	2.30812	.1260	.0445	2
2695	2.70949	.0413	.2423	3
2696	2.45109	.1381	.4346	71
2697	3.55861	.0543	.0787	7
2698	2.66234	.0588	.1271	3
2699	2.63882	.1267	.2654	4
2700	2.90707	.0498	.0401	2
2701	3.16942	.1362	.1115	3
2702	3.43028	.1173	.0458	5
2703	2.19350	.0830	.0939	2
2704	2.38488	.1044	.0873	2
2705	2.19003	.1314	.0786	2
2706	3.01873	.0689	.1759	3
2707	3.18588	.1188	.0279	3
2708	3.08533	.1669	.0276	3
2709	2.19546	.0992	.0628	2
2710	2.42431	.1610	.0426	2
2711	3.00681	.0674	.1663	3
2712	2.16202	.0637	.0190	2
2713	2.85459	.0427	.0380	2
2714	2.24386	.2030	.0924	3
2715	2.73543	.1200	.1225	3
2716	2.36919	.0804	.1133	2
2717	2.21475	.1919	.0527	2
2718	3.11276	.1497	.0228	2
2719	2.18803	.1255	.0095	2
2720	2.33041	.1737	.0396	2
2721	3.21307	.1749	.0199	3
2722	3.20223	.1622	.0163	3
2723	3.12507	.1622	.0275	3
2724	2.92382	.1166	.0601	3
2725	3.03341	.1514	.2496	5
2726	2.85934	.0495	.0378	2
2727	2.61016	.1211	.0691	2
2728	2.45812	.1543	.0538	2
2729	2.88809	.0474	.0409	2
2730	2.72007	.1332	.1179	2
2731	3.16951	.2024	.2215	5
2732	2.76003	.0298	.1000	3
2733	2.34709	.1551	.1609	3
2734	3.16298	.0427	.2747	4
2735	1.85699	.0391	.3854	4
2736	2.29062	.0646	.1465	2
2737	2.74692	.1886	.1674	3
2738	2.72002	.1480	.0401	2
2739	2.45742	.1174	.0386	2
2740	3.00231	.0648	.1669	3
2741	2.60730	.2005	.1734	3
2742	2.91019	.0452	.0372	2
2743	2.65407	.1469	.2274	4
2744	2.30218	.2975	.1351	4
2745	2.28856	.2366	.3618	54
2746	2.24808	.1092	.0687	2
2747	3.10339	.1214	.1125	3
2748	2.80612	.1071	.0813	2
2749	3.18510	.1528	.0225	3
2750	2.21245	.0965	.0808	2
2751	2.40725	.1725	.0421	2
2752	3.02439	.0810	.1724	3
2753	2.78984	.0577	.1287	3
2754	2.22797	.1981	.1226	3
2755	2.84896	.2218	.0932	3
2756	2.55156	.0773	.1069	2
2757	3.17351	.1786	.0244	3
2758	2.55115	.2444	.0662	3
2761	3.07974	.2041	.0522	3
2762	2.33084	.1742	.0970	3
2763	2.40356	.1894	.0781	3
2764	2.24670	.1134	.0529	2
2765	3.14950	.0695	.2477	4
2766	2.54727	.2008	.1237	3
2767	3.02175	.0651	.1730	3
2768	2.23421	.1460	.0950	3
2769	3.14316	.1503	.0234	3
2770	2.17016	.0942	.0430	2
2771	2.67751	.1872	.2565	4
2772	2.31443	.2022	.1551	3
2773	2.32797	.1191	.0459	2
2774	3.19058	.1129	.1678	4
2775	2.42165	.1662	.0462	2
2776	2.36791	.2004	.0857	2
2777	2.37056	.1117	.0789	2

no	a (AU)	ecc	sinI	QC
2778	2.28127	.0927	.0629	2
2779	2.21200	.0915	.0515	2
2780	2.19401	.1378	.1132	2
2781	3.15304	.1575	.0299	3
2782	2.68083	.1973	.0676	3
2783	2.56045	.1275	.0235	3
2784	2.24156	.1677	.0963	3
2785	2.87338	.0402	.0403	2
2786	2.60644	.1488	.2249	3
2787	3.01995	.0632	.1738	3
2788	2.55970	.1330	.0472	3
2789	2.22755	.1365	.0819	3
2790	2.65270	.1699	.2321	4
2791	2.27683	.1283	.1631	3
2792	3.16415	.0625	.3750	9
2794	2.44474	.1934	.1491	2
2795	2.29574	.0543	.1143	2
2796	2.64305	.1440	.2330	4
2798	2.41778	.0381	.1033	2
2799	2.38829	.1162	.1092	2
2800	3.14655	.1509	.0320	2
2801	2.80081	.1410	.1575	3
2802	3.11706	.1457	.1508	4
2803	3.14807	.1551	.0291	3
2804	3.01443	.0833	.1732	3
2805	2.69397	.1110	.1079	3
2806	2.37873	.0442	.0241	2
2807	2.79537	.1954	.1369	3
2808	3.00666	.0747	.1720	3
2809	2.42819	.1523	.0491	2
2810	2.60663	.1474	.2274	3
2811	2.86517	.0438	.0343	2
2812	2.22444	.1212	.1046	3
2813	3.13844	.1423	.2735	6
2814	2.86839	.0489	.0348	2
2815	2.23303	.1379	.0835	2
2816	2.72693	.1510	.1179	3
2817	2.35777	.1486	.0588	2
2818	2.37618	.1798	.0389	2
2819	2.75842	.1686	.0427	2
2820	2.22935	.1330	.0618	2
2821	2.43874	.1799	.0999	3
2822	2.58154	.1464	.2331	3
2823	2.41058	.0632	.0835	2
2824	2.32583	.1775	.0774	2
2825	2.24588	.1554	.0755	2
2826	3.22769	.0472	.2583	4
2827	2.30905	.0612	.1572	2
2828	2.24183	.0990	.0419	2
2829	3.08908	.1920	.2496	6
2831	2.22545	.1664	.0577	2
2832	2.47732	.0988	.0659	2
2833	2.87583	.0495	.0380	2
2834	2.54099	.1806	.1232	3
2835	2.74568	.0476	.0316	2
2836	3.00100	.0835	.1765	11
2837	2.90346	.0485	.0367	2
2838	2.34114	.1718	.0196	2
2839	2.21656	.1334	.0732	2
2840	2.39845	.0715	.1351	2
2841	2.25250	.1147	.0687	2
2842	2.61779	.1340	.2178	3
2843	2.29850	.1550	.1144	2
2844	2.22113	.1689	.0372	2
2845	2.26098	.1599	.0943	3
2846	3.23430	.0630	.1833	3
2847	2.16911	.1251	.0577	2
2848	3.20793	.1671	.0329	3
2849	2.56616	.0260	.1085	2
2850	2.44925	.0564	.1181	2
2851	2.47823	.1192	.1345	3
2852	2.78527	.0511	.0106	2
2853	2.34470	.1256	.0784	2
2854	2 20513	.1467	.1195	2
2855	2.45412	.1625	.1543	3
2856	3.02789	.0353	.1703	3
2857	2.40034	.1130	.0891	2
2858	2.26675	.1774	.0982	3
2859	2.23865	.1449	.0575	2
2860	2.33234	.1700	.3969	13
2861	2.47159	.0625	.0728	2
2862	2.20103	.1403	.0743	2
2863	3.17388	.1613	.0158	2
2864	2.74764	.1772	.0388	3
2865	2.56056	.0848	.2615	3

no	a (AU)	ecc	sinI	QC
2866	2.91093	.1751	.1550	3
2867	2.36354	.1283	.1618	3
2868	2.81487	.1454	.1191	3
2869	2.63591	.1576	.2314	3
2870	2.39200	.1802	.0556	2
2871	2.25819	.1098	.0940	2
2872	2.74098	.1374	.0673	3
2873	2.25111	.1627	.0832	2
2874	2.24473	.1133	.0679	2
2875	2.79771	.1346	.1646	3
2876	2.60208	.1224	.2621	4
2877	3.11204	.1749	.0231	2
2878	3.04518	.0651	.1918	3
2879	2.76782	.1821	.1700	3
2880	2.20333	.1604	.0936	3
2881	2.24776	.1794	.0779	2
2882	3.16576	.1653	.0246	2
2883	2.24564	.1114	.0184	2
2884	3.11537	.1508	.0300	3
2885	2.23757	.1688	.0594	2
2886	2.36634	.1514	.0054	3
2887	2.25906	.1544	.0597	2
2888	2.25755	.1226	.1404	3
2889	3.02190	.0854	.1764	3
2890	2.26010	.1402	.1212	3
2891	3.36891	.0831	.1404	5
2892	3.16122	.1806	.3159	6
2894	3.11440	.1553	.0259	3
2896	2.22019	.1757	.1036	3
2897	2.24741	.1274	.0918	2
2898	2.55613	.0241	.2291	3
2899	2.26218	.1327	.0550	2
2900	3.02395	.0878	.1762	4
2901	2.86429	.0416	.0395	2
2902	2.20320	.1703	.0752	2
2903	2.56195	.0741	.2621	3
2904	2.60299	.1283	.2431	4
2905	2.80378	.1243	.1562	3
2907	3.01700	.0627	.1699	3
2908	2.97889	.1341	.2382	56
2909	3.02078	.0804	.1803	3
2910	2.20241	.1263	.0419	2
2911	2.79416	.1256	.1559	3
2912	2.28926	.1004	.1100	2
2913	2.70497	.1844	.2633	4
2914	2.26148	.1040	.0481	2
2915	2.56306	.1587	.2249	4
2916	2.23492	.1276	.0789	2
2917	2.79536	.0801	.2287	4
2918	3.17642	.1397	.0227	2
2919	3.13342	.1528	.0235	2
2921	3.20707	.1768	.0194	3
2922	2.37163	.1751	.0548	2
2923	2.45328	.1608	.0580	2
2924	2.88771	.0442	.0350	2
2925	2.38635	.2126	.0528	2
2926	2.27454	.1307	.0713	2
2927	2.53352	.1431	.2714	4
2928	3.00746	.0824	.1822	66
2929	3.12329	.0936	.2400	5
2930	2.78022	.0427	.0770	3
2931	2.87506	.0476	.0387	2
2932	3.62476	.0678	.0339	7
2933	2.60890	.0217	.1080	2
2934	3.16736	.0582	.1581	3
2935	2.59889	.1293	.2115	3
2936	2.67878	.0703	.1591	3
2937	2.32039	.2794	.4047	12
2939	2.43975	.1854	.0795	2
2940	2.78448	.1987	.1350	4
2941	2.15157	.0874	.0577	2
2942	2.23861	.1565	.1011	3
2943	2.44826	.1298	.2385	3
2944	2.64954	.1344	.1852	3
2945	2.66920	.1086	.0254	3
2946	2.45492	.1619	.0275	2
2947	2.30796	.1282	.0717	2
2948	2.86338	.1040	.2226	4
2949	2.19469	.1296	.0803	2
2950	2.75675	.2312	.1520	4
2951	3.12682	.1470	.2487	5
2952	2.31349	.1479	.0737	2
2953	2.82802	.0496	.0375	2
2954	2.28716	.2224	.0625	3
2955	2.18025	.1208	.0579	2

no;	a (AU);	ecc ;	sinI;	QC
2956	2.76503	.1171	.0310	2
2957	3.02209	.0764	.1682	3
2958	2.87354	.0433	.0376	2
2960	2.22087	.1249	.0645	2
2961	2.26812	.1246	.0892	2
2962	2.56789	.0750	.2577	3
2963	2.87079	.0478	.0383	2
2964	2.59354	.1572	.2517	4
2965	2.39150	.1845	.4113	7
2966	2.44917	.1526	.0360	2
2967	3.20951	.1170	.2961	5
2968	2.36703	.2946	.1706	4
2969	2.84529	.0437	.0357	2
2970	2.63869	.1273	.2232	4
2971	2.24632	.1111	.1042	2
2972	2.15111	.1399	.0304	2
2973	2.46872	.1450	.0412	2
2974	2.31229	.1106	.1221	2
2975	2.24831	.1243	.1343	3
2976	3.36254	.0940	.1703	5
2977	2.78470	.1410	.1558	3
2978	3.09982	.1518	.0347	2
2979	3.12607	.1328	.1789	4
2980	2.56862	.1626	.1254	3
2981	3.14561	.1767	.0242	2
2982	2.99939	.0607	.1679	3
2983	2.84710	.0344	.0919	3
2984	2.47221	.1443	.0359	2
2985	2.84791	.0396	.0424	2
2986	3.17601	.1294	.0342	3
2987	2.88682	.0933	.0212	2
2988	2.60762	.1485	.2361	3
2989	2.23830	.1501	.0478	2
2990	2.43885	.1427	.0473	2
2991	2.33768	.2108	.0684	3
2992	2.74623	.1866	.1269	3
2993	2.58666	.1514	.2354	4
2994	2.41799	.2084	.0488	2
2995	2.61509	.1714	.2449	15
2996	2.78231	.0455	.0773	3
2997	2.55502	.1679	.1265	3
2998	2.42258	.1666	.0451	2
2999	2.27081	.1207	.1019	2
3000	2.35121	.1518	.0543	2
3001	2.35651	.0902	.3283	5
3002	2.23973	.1448	.0908	2
3003	3.02360	.0862	.1823	3
3005	2.36832	.1969	.0418	2
3006	2.43303	.1600	.0556	2
3007	2.36838	.1100	.1307	2
3008	3.17078	.1447	.0203	3
3009	2.19659	.1804	.0798	2
3010	3.20886	.1784	.0190	3
3011	3.21388	.1757	.1128	3
3012	3.22119	.0683	.3172	5
3013	2.35867	.1484	.0675	2
3014	2.36408	.2052	.0137	2
3015	3.39094	.1475	.2843	7
3016	2.83455	.0501	.0340	2
3017	2.60748	.1450	.2222	3
3018	2.36834	.1732	.0969	2
3019	2.86365	.0446	.0360	2
3020	2.76156	.0359	.0951	3
3021	3.17897	.2353	.3022	7
3022	1.93109	.0788	.4023	6
3023	2.21598	.1115	.0824	2
3024	3.42365	.0971	.2386	7
3025	3.20658	.0740	.3706	5
3026	3.03036	.0198	.1764	3
3027	2.67313	.1852	.0418	2
3028	3.01934	.0623	.1650	2
3029	2.23974	.1352	.0761	2
3030	2.26963	.2216	.0814	3
3031	2.23605	.1253	.0909	2
3032	2.89361	.0476	.0369	2
3033	2.23562	.1158	.0784	2
3034	2.32412	.1870	.0861	3
3035	2.63445	.1647	.0450	2
3036	3.20895	.1062	.3807	6
3037	2.67451	.2035	.2935	5
3038	2.43886	.1764	.0873	3
3039	2.55895	.1489	.2670	4
3041	2.58570	.1491	.2286	3
3042	2.27739	.1979	.1010	2
3043	1.92653	.1347	.3609	8
3044	2.85215	.1334	.2520	4
3045	3.13401	.0786	.0520	3
3046	3.13394	.1242	.3224	7
3047	2.64281	.0191	.0451	2
3048	2.39857	.1623	.0462	2
3049	3.12201	.1445	.0225	2
3050	2.22487	.1644	.0395	2
3051	2.59374	.2021	.2641	4
3052	2.37454	.2096	.0868	2
3053	2.37951	.1836	.0819	3
3054	3.10043	.1791	.0254	3
3055	2.56122	.0906	.2631	3
3056	2.41958	.0884	.0977	2
3057	2.26042	.1036	.1109	3
3058	2.24907	.1436	.0693	2
3059	2.26823	.1181	.0433	2
3060	2.27779	.1539	.1349	3
3061	3.09247	.1624	.0369	3
3062	3.01857	.0784	.1782	3
3064	2.45532	.1443	.0437	2
3065	2.71836	.0954	.0933	3
3066	2.52645	.0995	.2584	3
3067	2.24554	.1384	.0865	2
3068	2.22973	.1315	.1086	2
3069	2.35207	.2124	.0440	2
3070	2.30602	.2222	.0383	2
3071	3.19358	.1266	.0237	3
3072	2.23870	.1697	.0900	3
3073	2.24262	.1326	.0948	2
3074	2.33883	.1359	.0506	2
3075	2.27359	.1058	.1803	3
3076	2.23790	.1603	.1348	3
3077	2.24073	.0451	.0425	2
3078	3.15073	.1289	.1156	3
3079	2.68504	.2356	.0709	3
3080	2.61008	.1581	.2281	4
3081	2.41044	.1600	.0847	2
3082	2.57702	.0427	.1614	3
3083	2.28445	.1627	.1238	3
3084	2.43691	.2019	.0747	2
3085	2.38807	.0945	.0844	2
3087	3.07626	.0776	.3537	8
3088	3.01939	.0750	.1709	3
3089	2.93163	.2088	.2527	5
3090	3.16972	.0619	.1590	3
3091	2.34962	.1858	.0481	2
3092	3.54166	.0777	.1792	12
3093	2.67676	.1682	.2434	4
3094	2.64818	.1036	.2460	4
3095	3.49718	.0490	.0699	5
3096	2.66779	.1705	.1979	4
3097	2.93041	.0882	.1338	68
3098	2.30229	.1925	.0086	2
3099	2.88155	.2506	.2487	5
3100	2.25906	.1063	.0463	2
3101	1.97887	.0805	.4749	8
3102	2.15165	.4170	.1392	5
3104	2.96364	.1561	.3899	82
3105	2.26198	.1664	.0972	3
3106	3.14999	.2057	.2430	5
3107	2.20212	.1842	.0458	2
3108	2.22912	.1419	.0518	2
3109	2.45157	.0863	.1229	2
3110	2.56159	.1084	.0507	2
3111	2.22375	.1344	.0173	2
3112	2.37830	.1768	.0548	2
3113	2.42729	.0503	.0874	2
3114	2.41930	.1950	.0407	2
3115	2.57924	.1340	.1901	3
3116	2.22806	.1685	.0803	3
3117	2.84667	.0447	.0365	2
3118	3.03571	.0807	.2488	5
3119	3.06034	.1939	.0606	3
3120	3.02758	.0673	.2334	4
3121	2.22783	.1116	.0967	2
3123	2.46166	.1099	.0188	2
3124	2.74562	.0546	.0947	3
3125	2.60218	.2325	.1956	3
3126	3.00535	.0749	.1726	3
3127	2.59751	.1767	.1012	3
3128	3.11578	.1534	.0295	2
3129	2.69753	.2492	.1079	3
3130	2.46604	.1721	.0554	2
3131	2.92409	.0757	.0347	2
3132	3.14784	.0952	.0582	3
3133	2.18083	.1383	.1041	3
3135	2.41997	.1286	.1216	2
3136	3.15735	.1492	.0605	3
3137	2.40098	.1773	.0615	2
3138	2.22562	.1047	.0925	3
3139	3.19366	.0242	.3646	6
3140	3.01571	.0725	.1767	3
3141	3.41143	.0802	.1992	7
3142	2.55363	.1307	.2559	4
3143	2.84652	.0608	.0356	2
3144	2.22512	.1772	.1160	3
3145	2.19227	.2106	.1047	3
3146	2.43336	.2008	.1497	3
3147	2.62275	.1986	.0738	3
3148	3.10810	.1604	.0270	3
3149	2.24777	.1465	.1266	3
3150	3.20647	.0850	.3851	6
3151	2.76417	.1751	.3209	8
3152	2.62634	.1106	.2161	3
3153	2.42289	.1064	.1233	2
3154	3.10298	.1440	.0223	3
3155	2.34262	.0871	.1199	2
3156	2.85472	.2212	.2736	5
3157	3.14917	.1201	.1209	3
3158	2.54927	.0819	.2526	3
3159	2.56975	.1113	.2625	4
3160	2.37710	.1543	.1034	2
3161	2.57060	.1780	.2708	5
3162	3.16143	.1552	.2821	6
3163	2.39498	.3107	.0643	2
3164	3.15036	.1786	.0280	3
3165	2.24450	.1536	.0511	2
3166	2.23778	.1474	.0761	3
3167	2.54207	.1030	.2688	4
3168	2.99379	.0807	.1812	3
3169	1.89185	.0748	.4146	60
3170	2.92917	.0976	.0935	2
3171	3.18205	.1287	.1895	5
3172	2.42661	.1923	.0471	2
3173	2.20384	.1973	.1177	3
3174	3.15455	.1565	.0251	3
3175	2.36391	.1885	.0247	2
3176	2.87598	.0334	.2977	4
3177	2.63357	.1402	.2689	64
3178	2.71170	.3952	.1490	5
3179	3.09179	.1597	.0340	3
3180	2.23037	.1248	.0978	2
3181	2.22911	.0944	.0806	2
3182	2.61398	.1306	.2285	3
3183	3.17952	.1210	.0215	2
3184	2.66573	.2318	.1261	3
3185	2.36571	.1633	.0540	2
3186	3.10991	.1420	.0202	2
3187	2.28352	.0485	.0634	2
3188	2.28943	.1039	.0916	2
3189	3.10293	.1639	.1332	4
3190	2.99749	.0865	.1751	3
3191	2.87448	.0429	.0378	2
3192	2.37705	.1954	.0390	2
3193	2.29581	.1075	.1010	2
3194	3.01194	.0769	.1754	3
3195	2.91136	.0404	.0352	2
3196	3.02864	.0146	.1558	3
3197	2.66554	.1730	.2604	4
3198	2.18054	.2653	.2929	4
3201	2.25799	.1171	.0351	2
3203	2.32286	.2310	.1053	3
3204	3.17305	.2472	.0158	3
3205	2.68240	.1656	.2009	3
3206	2.55473	.2195	.1271	3
3207	2.90825	.0461	.0361	2
3208	3.11616	.1439	.0262	3
3209	2.19247	.0824	.0772	2
3210	3.11217	.0806	.2162	5
3211	2.73528	.2202	.2053	4
3212	2.25634	.1787	.1180	3
3213	3.19327	.1415	.0209	3
3214	3.01354	.0764	.1785	3
3215	3.12661	.1114	.1098	3
3216	2.39570	.2770	.0658	3
3217	2.38709	.2360	.1096	3
3218	2.52384	.1906	.0468	3
3219	3.03776	.1548	.1415	4
3220	2.22554	.1572	.1098	3
3221	2.20409	.1349	.0475	2

no;	a (AU);	ecc ;	sinI;	QC
3222	3.08860	.0634	.2636	5
3223	2.60729	.1489	.1706	3
3224	2.78516	.1926	.0859	3
3225	1.87979	.0546	.4299	6
3226	2.87375	.0502	.0332	2
3227	2.44605	.1543	.0593	2
3228	2.46290	.1469	.0515	2
3229	2.31403	.1330	.1766	3
3230	3.13285	.2920	.2639	6
3231	2.44613	.1003	.1256	2
3232	3.02300	.0653	.1735	3
3233	2.22655	.0882	.0709	2
3234	3.10610	.1557	.0089	3
3235	2.68701	.2912	.2237	4
3236	2.20180	.1384	.0316	2
3237	3.01528	.0818	.1774	3
3238	2.66584	.1603	.2056	3
3239	2.18446	.1936	.0352	2
3241	3.04559	.1514	.0139	3
3242	2.67993	.1452	.2192	3
3243	3.03787	.1031	.1723	4
3244	2.24379	.1377	.0770	2
3245	3.13010	.1436	.0230	3
3246	3.19677	.0430	.3700	5
3247	2.37750	.1586	.0583	2
3248	3.18832	.1549	.1885	4
3249	2.34659	.2183	.0411	2
3250	3.01604	.0770	.1690	3
3251	3.11524	.1256	.0138	2
3252	2.66384	.1439	.2289	4
3253	2.24807	.1860	.1168	3
3255	2.37256	.2732	.4086	12
3256	2.77825	.0934	.1334	3
3257	2.25060	.1527	.0934	2
3258	2.20606	.1655	.1226	3
3259	3.16466	.1524	.2793	5
3260	2.23451	.1186	.1080	2
3261	2.90433	.0558	.0356	2
3262	3.00972	.0839	.1474	3
3263	2.41433	.0728	.1172	2
3264	3.15146	.1653	.0133	3
3265	2.41077	.1127	.1046	2
3266	1.90830	.0875	.4432	6
3267	2.32966	.2486	.3994	65
3268	2.34677	.1165	.1226	2
3269	2.78511	.1283	.3008	4
3270	2.14892	.3442	.4171	12
3271	2.10165	.4932	.3985	73
3272	2.24397	.1049	.0506	2
3273	3.40470	.0534	.2272	5
3274	3.14853	.1299	.0258	2
3275	2.33269	.2027	.1350	3
3276	3.12167	.1483	.0296	3
3277	3.14929	.2351	.1317	4
3278	3.21296	.0507	.1493	3
3279	2.20268	.1433	.0590	2
3280	2.58191	.1550	.0541	2
3281	2.34973	.1198	.1129	2
3282	2.18953	.0727	.0508	2
3283	2.39663	.0739	.1237	2
3284	2.76910	.3482	.1108	4
3285	2.52639	.2301	.3423	6
3286	2.63649	.1326	.2166	3
3287	2.36626	.2648	.2344	4
3288	2.03489	.4891	.1050	4
3289	2.32694	.1838	.0239	2
3291	3.15281	.0798	.0269	2
3292	3.16809	.1497	.0268	3
3293	2.39848	.1651	.0421	2
3294	2.69777	.1044	.1229	3
3295	2.69572	.2213	.1420	4
3296	2.65472	.1517	.2294	4
3297	3.14323	.1404	.0217	3
3298	2.35352	.1652	.0638	2
3299	2.28032	.1006	.1123	2
3300	3.16580	.1609	.3329	6
3301	2.23360	.1629	.0767	2
3302	2.45307	.0789	.0507	2
3303	2.89705	.0480	.0379	2
3304	3.05317	.2434	.0593	4
3305	2.60332	.1534	.2281	4
3306	2.24749	.1441	.0883	2
3307	2.25923	.0807	.1276	2
3309	1.81755	.0888	.3512	5
3310	3.01001	.0811	.1722	3
3311	2.78928	.0729	.0177	2
3312	3.00467	.0886	.1773	3
3313	2.65459	.1511	.2125	3
3314	2.21820	.0320	.1319	2
3315	2.64063	.1193	.1622	3
3316	3.11433	.1338	.1474	3
3318	3.00999	.0735	.1807	4
3319	3.16137	.1335	.0872	3
3320	2.45936	.0699	.0816	2
3321	2.54580	.1651	.1164	3
3322	2.39199	.2078	.4027	7
3323	2.56259	.1571	.0214	2
3324	2.69922	.0563	.2018	3
3325	3.18350	.0140	.3669	7
3326	2.36818	.1683	.0646	2
3327	3.17482	.0826	.0145	2
3328	3.01748	.0788	.1860	4
3329	2.99701	.0789	.1821	4
3330	3.14406	.1933	.1812	4
3331	2.41956	.1023	.0588	2
3332	2.54415	.0673	.2443	3
3333	3.13128	.2073	.2261	5
3334	2.84962	.0426	.0375	2
3335	2.61038	.1448	.2433	4
3336	2.32438	.1560	.0329	2
3337	2.84320	.0521	.0362	2
3338	2.14648	.1542	.0090	2
3339	3.18591	.1496	.2810	5
3340	2.23354	.1710	.0925	2
3341	3.02428	.1991	.1697	60
3342	3.13757	.0801	.0932	3
3343	2.34903	.3463	.4141	67
3344	2.41637	.1171	.1451	2
3345	2.47347	.2198	.2776	5
3346	3.18137	.0700	.3644	7
3347	3.12505	.0850	.0858	3
3348	3.18178	.1655	.1806	4
3349	2.73889	.0658	.0602	2
3350	2.31069	.1814	.0644	2
3351	3.04204	.2482	.2076	5
3352	1.87890	.3992	.0635	4
3353	1.86294	.1186	.3790	5
3354	2.32464	.0927	.1250	2
3355	2.18634	.0688	.0603	2
3356	2.19285	.1195	.0541	2
3357	3.02147	.0866	.1816	5
3358	3.19430	.1787	.0270	3
3359	2.25655	.1132	.0965	2
3363	2.77727	.1246	.0594	2
3364	2.19885	.1152	.0873	2
3365	2.71116	.1620	.1410	3
3366	3.00530	.0620	.1700	3
3367	2.78527	.0916	.1117	3
3368	3.38149	.1031	.3172	8
3369	3.04477	.1159	.1556	3
3370	2.21564	.1114	.1136	3
3371	2.73844	.0343	.1867	3
3372	2.69428	.1128	.0571	3
3373	2.24569	.1223	.0561	2
3374	2.94814	.0489	.0354	2
3375	2.17191	.0552	.0215	2
3376	2.34881	.0924	.1267	2
3377	2.91385	.0467	.0361	2
3378	2.31614	.0839	.1513	3
3379	2.35471	.1337	.0405	2
3380	2.84270	.0477	.0366	2
3381	2.45388	.1825	.0917	2
3382	2.24215	.1557	.1057	3
3383	2.56545	.0525	.2388	3
3384	2.38477	.1874	.0367	2
3385	2.22078	.0526	.1231	2
3386	2.83795	.0549	.0352	2
3387	2.60040	.1491	.2372	4
3388	2.36329	.1710	.3897	68
3389	2.77243	.1188	.1132	3
3390	2.25270	.1321	.0697	2
3392	2.13965	.2327	.4697	52
3393	2.58552	.0794	.1589	3
3394	2.31758	.2292	.1240	3
3395	2.79226	.0723	.0748	2
3396	3.38905	.1528	.1328	5
3398	2.28730	.1762	.3721	73
3399	3.09686	.1482	.0217	2
3400	1.93500	.0569	.3548	8
3401	2.36792	.2910	.4060	14
3402	2.13183	.2621	.0903	3
3403	2.41193	.1820	.0895	2
3404	2.66813	.1575	.1897	3
3405	2.60995	.1007	.2435	4
3406	2.79445	.1633	.1662	3
3407	2.68680	.1638	.2010	3
3408	2.37164	.2007	.0343	2
3409	2.85576	.0488	.0366	2
3410	2.26006	.1217	.0911	2
3411	2.24295	.1349	.0794	2
3412	2.22471	.0952	.0674	2
3413	2.25177	.1461	.1188	2
3414	2.19019	.1032	.0888	2
3416	1.91771	.1989	.3845	7
3417	2.42288	.2546	.1241	3
3418	3.15231	.1615	.0145	2
3419	3.20325	.0867	.2853	5
3420	3.10670	.1084	.2297	5
3421	2.23361	.0968	.0583	2
3422	2.69128	.1408	.2162	3
3423	3.05097	.1366	.0256	3
3424	2.54766	.0430	.1070	2
3425	3.00028	.0802	.1784	68
3426	2.61915	.1004	.2315	4
3427	2.28074	.1076	.0621	2
3428	2.66459	.1963	.1705	3
3429	2.33871	.1611	.0284	2
3430	2.75907	.0767	.0688	2
3431	3.09535	.0197	.2283	3
3432	3.16917	.2559	.2434	5
3433	2.39369	.1672	.0928	2
3434	2.63906	.1956	.0425	2
3435	2.32383	.0616	.1305	2
3436	2.86353	.0395	.0359	2
3437	2.27146	.0912	.0627	2
3438	3.05076	.1884	.2505	6
3439	2.74352	.1313	.0872	3
3440	2.90348	.0417	.1253	65
3441	3.10173	.1556	.0290	2
3442	3.15501	.1082	.1910	4
3443	2.39188	.2798	.2360	4
3444	2.55734	.2417	.1300	3
3445	2.68828	.1643	.2048	3
3446	2.37665	.1766	.1293	3
3447	1.99080	.1086	.3574	68
3448	2.19206	.0952	.0492	2
3449	3.07981	.1376	.0172	3
3450	2.74506	.0455	.0953	3
3452	2.26923	.0515	.0285	2
3453	2.38708	.0964	.0960	2
3454	2.26776	.1532	.0982	3
3455	2.24326	.0947	.0588	2
3456	2.16408	.0391	.0158	2
3457	2.85423	.0457	.0364	2
3458	2.45071	.1719	.0314	2
3459	2.24530	.1576	.0714	2
3460	3.16990	.2025	.0223	3
3461	2.37804	.1140	.0433	2
3462	2.45363	.1839	.0846	2
3463	2.44742	.1385	.0432	2
3464	2.23986	.0699	.1305	2
3465	2.31432	.0682	.0887	2
3466	2.33802	.1804	.0124	2
3467	2.41011	.1522	.0519	2
3468	3.01992	.0548	.1713	3
3469	3.01998	.0830	.1706	3
3470	2.34626	.1747	.0609	2
3471	3.19462	.0697	.2732	5
3472	2.72532	.1433	.0945	3
3473	2.36302	.1878	.0097	2
3474	2.55828	.2051	.1033	3
3475	3.18030	.1166	.2756	6
3476	3.16909	.1958	.3413	11
3477	2.34554	.1088	.1192	2
3478	2.23625	.1391	.0530	2
3479	3.04705	.0953	.2216	4
3480	3.03549	.3232	.0619	4
3481	2.24055	.1352	.0980	3
3482	2.78154	.1361	.0657	2
3483	1.93284	.0963	.3966	5
3484	2.59083	.1855	.2367	4
3485	2.44022	.1563	.0469	2
3486	2.43116	.1699	.0466	2
3487	2.60736	.1457	.2230	4
3488	2.60671	.1445	.2339	3

```
DISCARDED ASTEROIDS
no;   a (AU); mean e; mean I(deg)
------------------------------------
   2   2.77064 0.23306   34.216
  31   3.15420 0.22083   26.019
  71   2.75503 0.17544   24.661
 132   2.61113 0.38632   26.436
 148   2.77139 0.18612   24.072
 183   2.79194 0.35039   25.131
 265   2.42113 0.26531   26.743
 391   2.32026 0.30660   23.622
 433   1.45824 0.22287   12.351
 473   2.97977 0.25629   28.825
 531   2.78513 0.19595   34.074
 582   2.61097 0.22404   28.939
 594   2.62771 0.35250   31.567
 754   2.98739 0.05114   24.110
 772   3.00050 0.09493   27.687
 876   3.01051 0.11130   10.264
 945   2.63762 0.16218   34.203
 950   2.37141 0.15960   23.099
1093   3.13838 0.26448   24.287
1108   2.42697 0.25785   25.895
1170   2.32564 0.30014   22.708
1252   2.69507 0.20458   32.584
1301   2.76534 0.27200   33.105
1312   3.09383 0.21553   20.465
1322   2.42394 0.23239   24.659
1342   2.28898 0.20252   22.375
1367   2.34412 0.13083   23.990
1373   3.41155 0.32149   40.439
1474   2.73437 0.48995   27.968
1508   2.76915 0.41841   28.836
1573   2.37042 0.23195   24.739
1580   2.19658 0.48953   50.942
1585   2.93117 0.30595   25.086
1660   2.39419 0.30260   21.041
1747   1.70911 0.11044   22.912
1883   2.41451 0.26205   24.137
1919   1.93600 0.09501   19.943
2050   2.32513 0.23808   25.305
2105   2.38915 0.15047   30.852
2134   2.63842 0.25575   31.492
2234   2.69976 0.20047   25.583
2261   2.37758 0.23800   21.150
2291   3.04518 0.06122   23.765
2335   2.12326 0.36019   36.283
2382   2.76190 0.32920   32.187
2791   2.39693 0.17188   32.122
2830   2.37761 0.20743   24.548
2906   3.16017 0.11244   29.305
2938   3.13920 0.33693   39.916
3004   2.59070 0.26414   31.508
3040   1.84072 0.20084   45.366
3086   1.93577 0.02668   20.546
3199   1.57469 0.28371   33.961
3308   3.14945 0.18152   22.976
3397   2.34948 0.29833   21.809
```

ASTEROID MAGNITUDES, UBV COLORS, AND IRAS ALBEDOS AND DIAMETERS

EDWARD F. TEDESCO
Jet Propulsion Laboratory

Absolute magnitudes and slope parameters on the system adopted by the International Astronomical Union (IAU) in November 1985 (see the Appendix to the chapter by Bowell et al.) are presented for known asteroids numbered through 3318. The values presented here are those used in reducing asteroid infrared flux data obtained with the International Astronomical Satellite (IRAS). U-B colors are given for 938 asteroids and B-V colors for 945. IRAS albedos and diameters are tabulated for 1790 asteroids.

The set of asteroid orbital elements used as input to the IRAS Asteroid Data Analysis System included asteroids numbered through 3318. An additional 135 orbits of, at that time unnumbered asteroids, were included as well and 21 of these were observed by IRAS. These results do not appear here.

This contribution was assembled primarily from IRAS Asteroid and Comet Survey final data product Nos. 2, 4, 6 and 13 (IRAS Asteroid and Comet Survey 1986). Its contents are described below.

The absolute magnitudes were computed by the author using as input data an augmented version of the B magnitude data set used by Gehrels and Tedesco (1979) and which the author assembled in 1985. This augmented data set contained over 10,000 observations 9195 of which were used in computing the absolute magnitudes given herein.

The deadline for completing the groundbased IRAS input data file was October 1985. Because of the decision, made in real time at the November 1985 IAU meeting, to use V, rather than B, as the band for absolute magnitudes the H and G values used in reducing the IRAS asteroid data are, strictly speaking, not on the IAU system. The reason for this is that the H and G

values were computed using B, rather than V, magnitudes. The difference in the value of G caused by this discrepancy is small, and in reality only affects the 317 asteroids for which values of G were explicitly computed. Furthermore, in many cases the H and G values given here differ from those published in the 1988 Russian *Ephemerides of Minor Planets* due to the incorporation of additional data and recomputation of H and G, and/or changes in the adopted values of G, made by B. Marsden in September 1986.

An additional, and more significant, difference between the IRAS magnitude set and that appearing in the 1988 Russian *Ephemerides of Minor Planets* was caused by the decision, reached at the final IRAS Asteroid Workshop in June 1986, to use adopted values for G when the computed value fell outside the range 0 to 0.5. This affected 79 of the 317 asteroids for which G had been explicitly computed.

As is evident from the above discussion, a "final" set of asteroid absolute magnitudes and slope parameters (G) does not yet exist. An internally consistent set, using the additional photographic magnitudes provided by Marsden in 1986, additional photoelectric and photographic data published since mid-1985, and the V band will be generated following publication of the paper describing the magnitude system. In the mean time, the set presented here serves the purpose of documenting the magnitude data set used in producing the IRAS albedos and diameters which appear in this same table.

The quality codes for the UBV colors have the following meanings:

Quality Code	For Uncertainty
0	> 0.05 magnitude
1	≤ 0.05 but > 0.03 magnitude
2	≤ 0.03 but > 0.02 magnitude
3	≤ 0.02 magnitude
4	≤ 0.02 magnitude and good agreement between results from references 1 and 2.

The UBV references have the following meanings:

Code	Reference
1	Bowell et al. (1979). ["TRIAD"]
2	Computed from u-v and b-v colors given in Zellner et al. (1985). ["ECAS"]
3	Weighted mean of values from references 1 and 2.

Remarks

The H magnitudes given here are equal to the blue absolute magnitudes (H_B) given in final data product No. 4 minus the B-V color. The values for G are identical to those given in final data product No. 4.

Column	FDP No.	Description
M.P.		Asteroid number.
H	2	The visual absolute magnitude.
G	2	The slope parameter.
No. Obs.*	2	The number of magnitude observations upon which the absolute magnitude and slope parameter are based.
Min Phase*		The minimum phase angle of the magnitude observations used in determining the H and G.
Max Phase*		The maximum phase angle of the magnitude observations used in determining the H and G.
U-B	13	The U-B color index.
UQ	13	The quality code for the U-B color index. [See below.]
B-V	4	The B-V color index.
BQ	4	The quality code for the B-V color index. [See below.]
UBV Ref	4	The reference for the UBV color(s). [See below.]
Albedo	4	Visual geometric albedo.
Albedo Unc.	4	One sigma formal uncertainty in the visual geometric albedo.
D	4	Diameter (in km).
D Unc	4	One sigma formal uncertainty in the diameter.
No. Obs Pre*	6	Number of times the satellite was predicted to observe the given asteroid.
No. Obs Acc	4	Number of "accepted" IRAS observations, i.e., the number of observations actually used in computing the average albedo and diameter.

*Not in the machine-readable version.

For additional details refer to the appropriate chapters in the IRAS Asteroid and Comet Survey (1986).

REFERENCES

Bowell, E., Gehrels, T., and Zellner, B. 1979. Magnitudes, colors, types, and adopted diameters of the asteroids. In *Asteroids,* ed. T. Gehrels (Tucson: Univ. of Arizona Press), pp. 1108–1129.

Gehrels, T., and Tedesco, E. 1979. Minor planets and related objects. XXVIII. Asteroid magnitudes and phase relations. *Astron. J.* 84:1079–1087.

Infrared Astronomical Satellite Asteroid and Comet Survey: Preprint Version No. 1. 1986. Ed. D. L. Matson, JPL Internal Document No. D-3698.

Zellner, B., Tholen, D. J., and Tedesco, E. F. 1985. The eight-color asteroid survey: Results for 589 minor planets. *Icarus* 61:355–416.

Magnitudes, UBV Colors, IRAS Albedos and Diameters

M P	H	G	No Obs.	Min Phase	Max Phase	U-B	UQ	B-V	BQ	UBV Ref	Albedo	Albedo Unc	D	D Unc	No. Obs Pre	No. Obs Acc
1	3.32	0.111	35	1.7	22 6	0 43	4	0.72	4	3	0.10	0.01	913	43	6	4
2	4 13	0 148	56	0 2	25.7	0 29	4	0 66	4	3	0 14	0 01	523	20	11	8
3	5 31	0 300	18	7 7	25 8	0.41	4	0.81	4	3	0.22	0 02	244	12	9	8
4	3.16	0 338	28	1 7	24.7	0 50	4	0 80	4	3	0.38	0 03	501	24	2	1
5	7.24	0.672	8	10.7	24 1	0 41	4	0.83	4	3	0.14	0.01	125	7	3	3
6	5 70	0 240	27	1 3	28.9	0.38	4	0 83	4	3	0.25	0 01	192	4	9	7
7	5.76	0.509	9	4.2	32 3	0.48	4	0.85	4	3	0.21	0.01	203	5	7	3
8	6 48	0.327	16	7 5	26 0	0 48	4	0 89	4	3	0.22	0 01	141	3	7	6
9	6.32	0 293	24	2.4	26 9	0 51	4	0.86	4	3						
10	5.27	- 039	9	4.8	18.3	0.35	4	0.69	4	3	0 075	0.003	429	8	9	8
11	6 62	0.272	9	6.6	25.6	0 42	4	0.85	4	3	0 15	0.01	162	3	4	4
12	7 23	0.240	18	2 2	22 4	0 51	4	0.88	4	3	0 16	0 01	117	4	2	2
13	6 47	-.020	7	9.6	24.7	0 46	4	0.75	4	3	0 099	0 006	215	7	3	1
14	6.27	0.092	22	1 1	23.0	0 39	4	0.84	4	3						
15	5.22	0.199	20	4 8	25.9	0 46	4	0.84	4	3	0.19	0 01	272	6	7	6
16	5.99	0 217	85	1.0	21.4	0 25	4	0.70	4	3	0.10	0.01	264	4	10	10
17	7 77	0.134	24	0 6	23.9	0.42	4	0.83	4	3	0.15	0 01	93.2	2.5	4	3
18	6 41	0 175	7	3 4	27.8	0.39	4	0.85	4	3	0.22	0 01	148	3	4	3
19	7.09	0 104	29	1.1	22.7	0.39	3	0.75	3	3						
20	6 52	0.263	43	0.6	28 1	0.42	4	0 81	4	3	0 19	0.02	151	11	3	3
21	7 34	0 163	21	2 8	24.9	0.20	4	0 70	4	3	0.20	0.02	99.5	5.5	5	5
22	6.50	0 215	32	0.4	18 8	0.25	4	0.69	4	3	0 12	0 01	187	4	8	3
23	7 07	0.370	12	1 6	28.8	0.43	4	0.85	4	3	0 21	0.01	111	3	6	6
24	7 07	0 098	11	0 2	18.4	0.35	4	0 68	4	3						
25	7 78	0 095	6	10 0	25 4	0 51	4	0.94	4	3	0 22	0.01	78 2	2.0	8	6
26	7 61	0.40	6	1.5	21.5	0.51	3	0 88	4	3	0.16	0.01	98.7	2.2	7	4
27	6 78	- 016	6	5 9	26 2	0.49	4	0.87	4	3						
28	7.17	0.221	10	1.7	22.7	0.46	4	0 85	4	3	0.15	0.01	126	2	8	7
29	5.84	0.208	53	0.5	23 9	0.42	4	0 83	4	3	0.16	0.01	219	5	5	5
30	7.74	0.413	6	1.7	24 9	0.47	2	0.87	2	3	0 13	0.01	104	2	7	5
31	6.53	0.15	4	1 6	7.4	0.32	1	0 67	1	1	0.070	0.031	248	54	8	8
32	7.50	0.110	10	3 5	24.0	0.43	4	0 86	4	3	0.25	0.01	82.6	2.0	12	9
33	8.43	0.239	14	1 4	15.7	0.47	2	0.86	3	3						
34	8.37	0.035	7	2.4	21 3	0.37	3	0.70	3	3	0.057	0.003	118	3	7	7
35	8 54	0.15	3	0 3	3.8	0.33	1	0 70	2	3	0 058	0.004	108	3	2	2
36	8 23	-.054	5	7.4	19.6	0.35	2	0.73	2	1	0 076	0.008	109	6	3	2
37	7.28	0 251	15	2.4	22 9	0.42	4	0.84	4	3	0 17	0.01	112	2	8	8
38	8.31	0.054	7	4.4	18.3	0.41	3	0 72	3	3	0.058	0.002	120	2	9	9
39	5 94	- 029	17	6.1	21.8	0.50	4	0 89	4	3	0 29	0.02	159	5	3	2
40	7.14	0 307	7	3.7	19.0	0.43	4	0.85	4	3	0 20	0.02	111	7	6	6
41	7.16	-.057	13	7 3	18.4	0.37	4	0 73	4	3	0.073	0.014	182	18	3	2
42	7.75	0 587	11	5 9	23.1	0.46	4	0 88	4	3	0.12	0.01	107	3	3	3
43	7.89	-.048	12	2.5	19.0	0.49	4	0 87	4	3	0.28	0.02	65.3	3.0	2	2
44	7.05	0.440	26	2 0	23.4	0.24	4	0.70	4	3	0.49	0.05	73.3	3.7	6	6
45	7.27	0.15	9	2.9	20.2	0.27	4	0 66	4	3	0.048	0 004	214	8	7	1
46	8 38	0.106	13	4.9	19.0	0.22	4	0.70	4	3	0.046	0.005	131	7	3	3
47	7 86	0.125	9	2.0	18.6	0.31	3	0 66	3	3	0.072	0.009	133	8	8	7
48	6.83	-.047	12	3.8	17.9	0.43	4	0.72	4	3	0.064	0.006	225	11	6	4
49	7 91	0.389	5	2.5	19.6	0.39	2	0.75	2	3	0.051	0.003	154	5	2	1
50	9 20	0.15	4	2.2	23 7	0 35	2	0.71	2	3					2	
51	7 36	0 061	10	1.8	22.2	0.47	4	0.77	4	3	0 086	0.004	153	3	6	6
52	6 25	- 004	9	1.6	16.8	0.33	4	0.66	4	3	0.057	0.002	312	7	7	7
53	8 61	- 101	10	3.3	26.6	0 32	3	0.71	2	1	0 045	0.002	119	3	5	4
54	7 70	0.149	9	4.8	25.5	0.36	4	0.70	4	3	0.050	0.002	101	3	7	6
55	7 68	0.347	6	3.0	15.1	0.25	2	0.69	3	3	0 32	0.03	67.5	3.6	2	1
56	8 30	0.15	7	2.8	28.0	0.32	4	0.69	4	3	0.062	0.002	117	2	8	8
57	6.95	0.071	5	2.7	18.5	0.44	4	0.83	4	3	0 21	0.01	116	3	2	1
58	8.79	0.15	7	1.1	13.3	0.37	3	0 69	2	3	0.056	0.004	97.7	3.0	3	3
59	7 72	0.014	5	1.0	21.5	0 29	4	0.67	4	3	0.048	0.005	173	8	4	4
60	8.68	0.332	8	1.5	12.4	0.44	4	0.85	4	3	0 15	0 01	61.6	1.8	3	2
61	7.66	0.076	7	2.9	15.7	0.40	4	0.85	4	3	0.21	0 01	83.6	3.5	16	8
62	8.24	0.25	4	1 0	17.9	0 36	4	0 71	4	3	0 090	0 004	99.3	2.1	5	5
63	7.35	-.018	21	1.4	21 0	0 48	3	0.90	3	3	0.17	0 01	108	3	4	3
64	7.65	0.369	7	4 8	16 4	0 26	4	0 75	4	3						
65	6 79	0 15	10	1 8	11.0	0 27	4	0 67	4	3	0.057	0.003	245	6	7	7
66	9.39	0 15	9	2 6	9.9	0.36	3	0.71	3	3	0 050	0.009	78.3	6.6	8	7
67	8.36	0.247	5	7.1	20.8	0.43	4	0.86	4	3	0 21	0 01	60.3	1.5	3	3
68	6 84	0 110	9	2.7	17.6	0.48	4	0 84	3	3	0.20	0 01	127	4	8	6
69	7.10	0 153	10	1.3	16.0	0.23	2	0.70	3	3	0 12	0.01	143	4	2	1
70	7.99	0 15	6	4 3	21.6	0 38	3	0.74	4	3	0.070	0.004	127	4	4	2
71	7.26	0 370	6	1 3	13.8	0 43	3	0 82	4	3	0 28	0 01	87.3	1.7	5	5
72	9.00	0.232	5	2.3	15 3	0 38	2	0 78	3	1	0 056	0.004	89 3	2.8	8	8
73	9 00	0 25	1		4.8	0.43	1	0 82	1	1	0.21	0.02	45.5	2.0	9	6

Magnitudes, UBV Colors, IRAS Albedos and Diameters

M.P.	H	G	No. Obs.	Min Phase	Max Phase	U-B	UQ	B-V	BQ	UBV Ref	Albedo	Albedo Unc.	D	D Unc	No. Obs Pre	No Obs Acc
74	8.84	0.15	5	2 0	6.9	0.32	1	0 69	2	1	0 034	0.002	123	3	3	3
75	9.02	0.25	5	2.7	14.7	0.26	4	0.71	3	3	0.12	0.02	58 3	4.5	7	7
76	8.08	0.438	7	0.6	20 2	0.29	4	0.70	4	3	0.029	0.001	190	4	5	4
77	8.57	0 259	5	6.7	23.3	0 24	4	0.75	4	3	0 13	0.01	71.0	2.0	6	3
78	8.11	0 079	6	1.9	27.8	0 36	4	0.71	4	3	0.064	0.003	125	3	9	9
79	7.83	0.178	12	4.5	23 9	0.43	4	0.88	4	3	0 27	0.01	68.8	1.8	4	4
80	8.10	0.300	6	7.6	27.6	0.50	4	0.90	4	3	0.15	0.01	81.7	1.2	11	11
81	8.49	0.15	5	2.1	12.2	0.35	3	0.71	3	3	0.046	0.002	124	2	12	11
82	8.51	0.336	16	2.3	27 2	0.38	3	0 81	4	3	0.17	0.01	63.6	1.7	5	5
83	8.89	0.301	5	2 5	21.3	0 26	3	0.70	3	3	0 069	0.003	84.2	1.8	7	7
84	8.91	-.224	5	1.8	26.1	0.44	1	0.73	3	1	0 070	0.004	83.0	2.0	4	3
85	7 56	0.053	13	6.3	20.7	0.28	4	0 66	4	3	0.068	0.004	157	5	2	2
86	8 51	0.115	8	3 9	17.2	0.33	4	0.71	4	3	0 043	0.002	127	3	4	4
87	6 95	0.275	10	5.1	15.6	0 25	4	0 70	4	3	0.040	0 004	271	12	9	7
88	7.05	0.169	7	2 9	19.7	0.29	4	0.66	4	3					2	
89	6.57	0.144	17	3.8	25.5	0.48	4	0.88	4	3	0.16	0.01	159	3	5	4
90	8.37	0.260	7	0.4	16.3	0.32	4	0.69	4	3	0.051	0.003	125	4	1	1
91	8.79	0.15	4	2.3	21.2	0.32	3	0.73	3	1	0.042	0.002	114	3	2	2
92	6.75	0.326	5	2.8	19.3	0.26	4	0.73	4	3	0.20	0 01	132	4	2	2
93	7.47	-.113	13	2.0	23.1	0 25	3	0 73	2	3	0.085	0.006	146	5	2	2
94	7.55	0.085	5	2.4	17 1	0.30	4	0 66	4	3	0.038	0.001	212	4	6	6
95	7 84	0.078	9	4.6	20 5	0 37	4	0.71	4	3	0.062	0.010	145	11	7	4
96	7 97	0.15	5	0.3	13.6	0 34	2	0.77	2	1	0.038	0.002	174	4	7	7
97	7 70	0.255	7	3 3	23.8	0 22	4	0.70	4	3	0.19	0.03	87.1	7.6	8	8
98	8.92	0.15	3	8 3	21.2	0.38	1	0 75	1	3	0.041	0.002	109	2	9	8
99	9.42	0.15	3	3.8	15.2	0.33	4	0.70	4	3					2	
100	7 79	0.25	6	2.9	11 6	0 34	1	0 83	2	1	0.16	0.01	92.0	2.0	8	8
101	8.45	0.497	6	2.6	24.7	0.43	3	0 87	4	3	0.15	0.01	68.3	1.5	5	5
102	9 23	0.15	6	2.8	27.1	0.37	1	0.72	3	3	0.049	0.002	86.0	2.0	5	5
103	7.59	0 107	10	3 7	22.6	0.44	4	0.86	4	3	0.17	0.01	95.2	5.0	9	9
104	8.31	0.196	7	1 4	11.5	0.34	4	0.68	4	3	0.052	0.004	127	5	6	6
105	8 89	0.292	11	11.1	27.0	0.31	2	0.70	3	3	0.032	0.002	123	3	3	3
106	7.42	0.168	6	4.3	20.2	0.47	4	0 74	4	3	0.083	0.004	152	3	6	6
107	6.80	-.173	5	4.2	17.9	0.30	4	0.70	4	3	0.060	0.007	237	14	10	8
108	8.27	0.25	5	1 7	10 7	0.48	2	0 86	2	3	0.19	0.03	67.2	6 0	5	4
109	8.87	0.110	5	8 5	26.2	0 39	4	0 73	4	3	0.060	0.003	91.6	2.3	9	6
110	7.79	0.184	25	0.6	19.7	0.27	4	0.71	4	3	0.17	0.01	89.1	2.3	5	5
111	7.39	0.043	7	9.7	24 9	0.39	4	0.70	4	3	0.064	0 006	139	6	1	1
112	9.80	0.15	4	3.5	18.8	0.29	2	0.70	2	1	0.037	0.004	75.5	4.1	13	13
113	8.63	0.263	17	4.2	25.5	0.52	4	0.94	4	3	0.27	0.03	47.6	2 7	3	3
114	8.24	0.098	5	1.4	22.6	0.35	4	0.76	4	3	0.084	0 003	103	2	7	7
115	7.51	0.144	12	9.8	30.1	0 43	3	0.86	3	3	0.25	0.01	83.5	2.5	7	7
116	7.86	0.25	4	2.5	18.3	0.41	1	0.87	1	3	0.22	0.04	75.5	6.8	2	2
117	8.18	0.484	8	6.2	17.5	0 30	4	0.68	4	3	0.040	0.005	154	9	4	4
118	9 01	0 25	4	3.4	13.7	0.43	1	0.86	2	3	0.20	0.01	45 7	1.2	13	10
119	8 61	0.574	5	5.0	23.8	0.47	3	0.89	2	3	0 17	0.01	60.7	1.1	8	6
120	7.73	0.172	8	0 8	16.3	0.38	4	0.70	4	3	0.045	0 002	178	3	9	8
121	7.39	0.150	6	3.2	18.9	0.39	3	0.72	4	3	0.042	0 002	217	4	6	6
122	7.68	0.25	4	1.1	15.9	0.41	1	0 78		3	0.20	0.01	86.5	2.0	3	3
123	8.93	0.25	6	3.0	20.3	0.39	2	0.85	2	1	0.19	0.02	49.8	3.2	5	5
124	8.13	0.311	13	0.7	13.2	0.42	4	0 85	4	3	0.15	0.01	79.5	1.8	4	4
125	9.06	0.357	9	2 1	19.2	0.24	2	0.68	3	3	0.18	0.01	47.5	1.5	5	5
126	9.31	0.25	6	2.9	17.5	0 49	2	0.87	3	1	0.15	0.01	46.5	1.3	2	2
127	8.48	0.15	4	4 3	8.4	0.35	2	0.70	2	1						
128	7.55	0.15	4	5.7	19.0	0.36	3	0.68	3	3	0.045	0.002	194	4	4	3
129	7.05	0.366	17	5.3	18.7	0 25	3	0.72	3	1	0.17	0.01	125	4	2	2
130	6.86	-.036	9	8.3	22.1	0 47	4	0.75	4	3	0.089	0.013	189	13	7	7
131	9.99	0.25	3	3.6	12.8	0 39	2	0.77	2	3	0.095	0.011	43.3	2.5	5	2
132	9.35	0.117	5	7.5	26.9	0.19	3	0.68	3	2	0.14	0.01	47.0	1.8	7	2
133	8.05	0.242	14	0.6	13.2	0.53	2	0.92	2	1	0.21	0.02	70.1	4.0	5	3
134	8.67	0.064	5	8.3	25.7	0.34	4	0.68	4	3	0.041	0.014	122	21	8	7
135	8.21	0.194	10	1.2	30 3	0.27	3	0.70	4	3	0.13	0.01	82.0	2.5	5	5
136	9 71	0.25	3	4.5	10 0	0.23	1	0 74	1	1	0.13	0.01	41.7	1.0	3	3
137	8.04	0.098	8	7 2	17.7	0.33	4	0.70	4	3	0.048	0.002	150	4	4	4
138	9.04	0.25	4	4 0	9.5	0.49	2	0 88	2	1	0.18	0.02	47.5	3.1	2	2
139	7.79	0.15	6	4.9	10 9	0.29	1	.0.70	1	1	0 051	0.002	162	3	8	7
140	8.20	0.15	4	4.4	13.7	0.30	2	0.72	2	1	0.071	0.004	114	3	2	2
141	8.56	0.15	1		2.2	0.29	1	0.66	2	1	0.036	0 002	135	3	3	3
142	10.26	0.145	7	1.3	25.9	0.23	4	0.62	4	3	0.042	0.003	57.1	1.6	2	2
143	9.24	0 15	5	1.3	16.0	0.34	2	0.74	2	1	0.041	0.002	92.8	2 3	8	4
144	7 87	0 081	9	1.9	27.8	0.39	4	0 72	4	3	0.059	0.003	146	4	7	6
145	8 05	0 013	6	6.9	24 1	0.36	3	0.69	3	3	0.044	0.002	155	4	4	3
146	8 15	0 135	12	4.9	21.9	0.40	4	0 68	4	3	0.052	0.002	137	3	9	5

Magnitudes, UBV Colors, IRAS Albedos and Diameters

M.P.	H	G	No. Obs.	Min Phase	Max Phase	U-B	UQ	B-V	BQ	UBV Ref	Albedo	Albedo Unc.	D	D Unc	No. Obs Pre	No. Obs Acc
147	8 76	0 15	6	1 0	3 4	0.28 2		0.69 2		3	0 029	0.002	137	5	4	4
148	7.60	0.130	11	9.4	22 0	0.41 4		0.86 3		3	0 14	0 01	104	2	4	4
149	10.90	0.25	3	1.4	3 7	0.50 2		0 80 2		1	0 15	0.03	22.0	2.0	9	6
150	8 32	0 15	4	0 9	9.5	0 27 2		0 71 2		1	0.034	0.001	157	3	6	6
151	9.34	0.25	7	3.2	16.3	0 50 2		0.87 3		1	0.14	0.01	46.7	1.0	7	7
152	8 58	0.25	6	3.5	17.5	0 37 3		0 68 3		1						
153	7 46	0.031	7	2 3	12.6	0.25 4		0 67 4		3	0.060	0.003	175	4	7	6
154	7.09	0.15	1		2 5						0.070	0.003	192	4	6	5
155	11 34	0.15	2	8 2	16.9	0.23 1		0 68 2		1	0.021	0.002	49.5	2.7	9	3
156	8.61	0 15	12	3.1	12 8	0 32 4		0 70 4		3	0.040	0.002	126	3	7	4
157	11.2	0.15	1								0.15	0.04	19.1	2.7	3	2
158	9.49	0.25	11	0.6	20 8	0.41 3		0.80 3		3	0.17	0.02	39.8	2.3	5	3
159	8.07	0.15	4	2.1	9.8	0.38 4		0.69 4		3	0.061	0.003	131	3	7	6
160	9.04	0.15	5	2.7	6.9	0.36 1		0.72 2		1	0.059	0.004	85.0	2.5	2	2
161	9.55	0.731	10	5.2	22.5	0.23 3		0.72 3		3	0.12	0.02	45.7	4.5	11	9
162	8 84	0.25	8	3.3	10.9	0.39 2		0.76 2		1	0.047	0 003	105	3	4	3
163	9.51	0.15	5	1.1	18 3	0.33 2		0.70 2		1	0.047	0.006	76.5	4.7	6	5
164	8 60	0.011	5	5.9	26.6	0.32 3		0.68 3		1	0.053	0 003	110	3	8	4
165	7.49	0.15	5	0.9	18 2	0 31 1		0.74 2		1	0.069	0.005	160	6	2	2
166	9.85	0.15	3	5.8	11.9	0.42 1		0.72 1		1						
167	9.16	0.25	4	1.2	18 1	0.40 2		0.86 3		3	0.21	0.02	42.2	2.1	2	2
168	7 93	0.155	6	1.4	17.7	0.38 4		0.75 4		3	0.050	0.003	154	4	2	2
169	9.60	0.25	3	0.9	1.8	0.46 3		0 85 3		2	0.19	0.03	36.5	2.8	5	4
170	9.42	0.25	1		5 9	0.45 2		0 89 3		2	0 14	0.01	46.2	1.0	4	3
171	8.39	0.244	6	2.1	13.3	0.33 4		0.69 4		3	0.053	0.008	121	9	4	4
172	8 80	0.25	7	3.7	25.1	0.49 2		0.90 3		1	0.12	0.01	64.5	1.3	7	7
173	7.79	0 121	6	7.3	20.3	0.32 4		0 70 4		3	0 053	0.003	159	4	5	5
174	8 40	0.25	7	4.1	17 7	0.48 2		0 86 2		1	0 14	0.01	71.7	4.2	8	8
175	8.43	0 15	4	1 3	6.2	0.33 2		0 70 2		1	0.065	0.004	107	3	6	6
176	8 3	0 15	1								0 053	0 002	125	2	11	11
177	9.54	0 15	3	6.2	6.4	0.35 1		0 73 1		1	0.048	0.003	75.3	2.2	5	2
178	9.41	0.25	6	2.4	20.5	0.49 2		0.90 3		1	0 21	0.01	37.8	0.7	6	6
179	8.20	0.25	6	3.5	6.2	0.41 4		0.83 4		3	0.14	0.01	81.0	1.5	16	11
180	10.39	0.25	4	2.7	9.4	0.45 2		0.83 2		1	0.11	0.01	32.7	1.8	6	1
181	7.77	0.053	6	4.7	23.7	0.37 3		0.80 4		3	0.12	0.02	107	12	7	6
182	9 30	0.296	5	1.7	27.2	0.43 2		0 89 2		1	0.16	0.03	45.3	4.5	5	5
183	9.78	0.25	4	3 2	8.9	0.36 2		0.84 2		1	0.16	0.04	36.0	4.2	9	3
184	8.29	-.060	8	0 2	14 0	0.24 3		0.71 4		3	0.18	0.01	68.2	2.2	4	3
185	7.73	0.273	5	7.5	23.8	0 33 4		0.68 4		3	0.053	0.002	165	3	11	10
186	9.08	0.287	7	11.2	22 9	0.36 4		0.84 4		3	0.15	0.01	52.3	2.0	3	3
187	8.16	0 128	6	4.9	19 8	0.34 4		0.71 '4		3	0.053	0.002	135	3	5	4
188	9 31	0.25	3	4.6	15.0	0.39 1		0.89 1		2	0.19	0.01	41.3	1.0	7	7
189	9.51	0.25	4	1.8	17.5	0.48 4		0 90 4		3	0.18	0.03	38.5	3.3	6	4
190	7.56	-.018	5	0.9	15.8	0.28 3		0.68 3		2						
191	8.98	0.15	3	6.2	9.8	0.26		0.68 1		1	0.041	0.003	105	4	2	2
192	7 13	0.029	12	10.7	24.2	0.48 4		0.94 4		3	0.21	0.01	107	2	6	6
193	9 80	0.15	4	4.2	4.9											
194	7.66	0 15	4	5.3	25 1	0.35 4		0.73 4		3	0.050	0.003	174	5	3	2
195	9 05	0 15	7	2.3	8.6	0 39 4		0.69 4		3	0 053	0 002	89.7	1.7	10	9
196	6 64	0.475	9	2.0	18 2	0.46 4		0.86 4		3	0.18	0 01	146	4	7	7
197	9.44	0.25	3	4.5	4 9	0 47 1		0.89 1		1	0.27	0 03	32.6	1.7	10	7
198	8.55	0.373	5	7.3	26.9	0 41 3		0.88 4		3	0 19	0.02	58.7	3 1	11	6
199	8 80	0.15	2	5 1	6 0						0 13	0 01	63.0	4.1	2	1
200	8 20	0.059	5	2.1	17 0	0 37 4		0 71 4		3	0 053	0 002	132	3	9	9
201	8.48	0 139	14	3.6	20.2	0 25 3		0 71 3		3	0 14	0.01	70.5	2.1	5	5
202	7.83	0 25	7	4.8	12 1	0 46 2		0.86 2		1	0.17	0.02	85.5	5.3	2	2
203	9.08	0.15	6	1 3	8 4	0.29 2		0.70 1		1	0.029	0 001	120	3	5	5
204	9 00	0.25	4	4.1	14 7	0.41 2		0.82 3		1	0.17	0.01	50.8	1.0	11	9
205	9.04	0.15	3	3 3	9 9	0.32 1		0 69 1		1	0.061	0.002	83.5	1.5	7	7
206	8.65	0.103	6	2.2	15.0	0 36 4		0.70 4		3						
207	9.96	0.15	4	5 0	11 2	0.36 2		0.73 2		1	0.050	0.002	60.7	1.3	3	3
208	9.05	0.25	6	0 8	15.9	0.40 3		0.80 4		3	0 21	0.01	44 3	1.3	2	2
209	8 15	-.086	5	3 0	12.3	0.29 4		0.69 4		3	0.044	0.036	149	62	8	6
210	9.32	0.15	4	1.6	21.5	0.26 4		0.67 4		3	0.041	0.003	90.0	2.7	2	1
211	7.84	0.032	7	1 6	20.8	0.36 4		0 72 4		3	0 059	0.003	148	4	21	20
212	8.22	0.15	6	1 7	7.3	0.29 1		0 70 1		1	0 046	0.002	140	3	5	5
213	8.83	0.15	5	4.0	13.6	0 21 4		0.64 4		3	0.072	0 005	84.6	2.7	2	2
214	9.45	0.480	10	1.5	13.5	0.23 3		0.70 4		3	0.40	0.03	26.8	1.2	6	5
215	9.62	0.25	5	4.4	10.5	0.45 2		0.84 2		1	0.18	0.01	37.3	1.1	6	6
216	7.53	0.247	6	6.5	25 1	0.24 4		0.70 4		3	0.088	0 006	140	5	7	2
217	9.87	0.15	2	1.4	5.3										2	
218	8.68	0.25	4	3.9	12.0	0 42 1		0.86 1		1	0.15	0.01	62 0	1.2	4	4
219	9.43	0 25	3	3.3	10.0	0.49 1		0.87 2		3	0 15	0.01	43.6	2.0	8	7

Magnitudes, UBV Colors, IRAS Albedos and Diameters

M.P.	H	G	No. Obs.	Min Phase	Max Phase	U-B	UQ	B-V	BQ	UBV Ref	Albedo	Albedo Unc.	D	D Unc	No. Obs Pre	No. Obs Acc
220	11.14	0.25	2	3.8	9.8						0.066	0.015	30.6	3.5	3	3
221	7.69	0.157	7	2.0	13.8	0.40	4	0.79	4	3	0.12	0.01	110	2	8	6
222	9 52	0.651	5	1.1	12 3	0.39	3	0.66	4	3	0.082	0.013	58.0	4.5	14	11
223	9.95	0.15	4	0.8	9.9	0.29	2	0.71	3	2	0.022	0.002	90.7	4.0	7	6
224	8.71	0.25	7	2.9	11 8	0 20	3	0.75	3	1					2	
225	8 62	0.15	4	4.4	24.0	0.27	3	0.66	2	3	0.041	0.002	124	3	7	6
226	9.84	0.15	1		2.5						0.13	0.01	39.2	1.3	5	3
227	8.97	0.15	5	3.4	5 4						0.056	0.005	90.1	3.7	6	4
228	12.67	0.25	4	2.0	23.2	0.60	1	0.92	3	2	0.12	0.01	10.7	0.5	10	1
229	9.29	0.25	2	1.9	10.2	0.25	2	0.71	2	2	0.037	0.006	96.0	7.8	1	1
230	7.47	0.354	7	6.8	26.1	0.44	3	0.85	4	3	0.14	0.01	113	2	6	6
231	9.40	0.15	1		3.5						0.042	0.002	85.1	2.2	3	3
232	10.27	0.15	5	3.6	7.7	0.35	4	0.70	4	3	0.045	0.002	55.2	1.0	8	8
233	8.30	0.168	8	2.6	20.1	0.33	3	0.78	3	3	0.073	0.011	108	8	14	14
234	8.97	0.043	8	0.8	16.0	0.49	4	0.87	4	3	0.22	0.01	44.6	1.5	4	4
235	8.76	0.25	4	0.7	8.3	0.54	2	0.90	2	1	0 15	0.01	60.2	2.5	4	3
236	8.29	0.192	8	3.0	20.2	0.44	4	0.85	4	3	0 10	0.01	90.5	2.0	7	7
237	9.43	0.25	2	2.3	2.9	0.41		0.79	1	1	0.15	0.01	44.0	1.2	4	3
238	8.38	0.507	8	3.0	18.2	0.38	4	0.73	4	3	0.032	0.001	156	3	8	7
239	10.62	0.15	2	3.0	3.4						0.054	0.006	43.0	2.5	4	4
240	8.99	0.134	7	0.7	25.2	0.34	3	0.70	2	3	0.039	0.002	108	3	3	3
241	7.50	0.043	6	3.0	18.3	0.29	3	0.69	4	3	0.062	0.004	169	5	6	1
242	9.61	0.15	3	5.7	6.8						0.14	0.03	41.5	5.3	2	2
243	10.02	0.203	9	0.9	14.6	0.44	3	0.81	4	3	0.16	0.03	32.5	3.8	7	5
244	12.35	0.25	1		3.0						0.10	0.01	13.8	0.5	10	2
245	7.92	0.393	5	5.5	16.5	0.47	4	0.84	4	3	0.16	0.01	84.8	2.3	4	3
246	8.74	0.400	5	5.1	16.6	0.59	3	0.99	3	3	0.13	0.01	63.8	4.1	7	7
247	8.00	0.073	8	5.5	18.9	0.26	2	0.69	3	1	0.059	0.003	137	3	6	4
248	10.14	0.15	4	2.8	14.1						0.057	0.005	52.0	2.3	4	4
249	11.22	0.25	3	6.1	17.8						0.041	0.002	37.2	1.0	5	5
250	7.80	0.705	8	2.2	19.1	0.26	4	0.72	4	3	0.18	0.03	85.5	9.1	5	5
251	10 06	0.15	2	3.0	6.9						0 17	0.03	31.1	3.0	6	1
252	9.53	0.15	1		3.6						0 052	0.008	72.1	5.6	4	4
253	10 30	0.15	2	3.6	5.3						0.036	0.002	61.0	2.0	7	7
254	12.08	0.25	4	1.5	9.9	0.50	1	0.85	2	1	0 13	0.01	14.1	0.8	6	1
255	10.35	0.15	5	1.5	3.0	0.25	2	0.68	1	1	0.038	0.004	58.3	3.2	4	2
256	9.90	0 15	4	2.6	5.9						0.044	0.003	66.1	1.8	3	3
257	9.18	0.25	3	1.1	7.7	0.38	1	0 76	1	1	0.070	0.005	73.5	2.6	2	2
258	8.47	0.461	6	7.4	25.7	0.45	4	0 86	4	3	0.15	0.01	67.7	1.5	8	4
259	7.86	0.15	4	2.0	12.4	0 28	1	0.67	1	1	0.037	0.003	185	7	2	2
260	9.26	0.15	5	0.2	7.6	0 31	1	0 71	1	1	0.034	0.005	101	2	2	2
261	9.50	0.25	7	2.5	15.7	0.31	3	0.69	4	3	0 10	0.01	52.6	1.5	3	3
262	11.72	0.25	1		6.7	0.53	1	0.84	1	1					5	
263	10.52	0.25	3	1.9	15.0						0.14	0.03	28.0	3.2	6	3
264	8.40	0.25	5	4.6	12.8	0.42	4	0.84	4	3	0.27	0.06	53 5	6.0	11	3
265	11.36	0.25	1		5.2						0.054	0.005	30.5	1.3	3	2
266	8.52	0.15	3	5.1	8.5	0.34	2	0.71	2	2	0 054	0.003	113	3	3	2
267	10.63	0.25	1		7 8			0.80	1	1	0.034	0.005	53.6	4 2	5	5
268	8.40	0.15	7	1.0	16 9	0.26	4	0.64	4	3	0.038	0.003	142	5	2	2
269	9.84	0.15	2		3.7						0.068	0.003	54.7	1.2	4	4
270	8.79	0.25	4	2.3	12.5	0.53	3	0.87	3	1	0 19	0.02	52.2	3.2	6	6
271	9.77	0.15	6	1.3	10.9	0.33	2	0.71	1	1	0.058	0.008	61.2	4.0	7	7
272	10.79	0.15	1		2.6						0.10	0.02	29.0	3.3	4	4
273	10.35	0.15	4	3 4	10.0	0.38	2	0.76	2	1	0.12	0 01	32.1	1.0	3	3
274	10.12	0.25	2	5 8	6.4						0.17	0.03	30.3	3.0	5	5
275	8.82	0 15	7	2.2	15.8	0.33	4	0.72	4	3	0.036	0.002	121	4	2	2
276	8.57	0.154	8	1.2	17.4	0.27	4	0.71	4	3	0.041	0.006	127	9	8	8
277	9.96	0.25	7	2.8	9.4	0.42	2	0 83	3	3	0.21	0.01	29.5	0.8	6	5
278	9.38	0.15	2	0.2	3.5						0.21	0.02	38.0	2.2	5	4
279	8 77	0.520	10	0.4	13.2	0.21	2	0.75	4	3	0.030	0.004	135	9	7	3
280	10 87	0.15	3	2.0	2.4						0.033	0.007	48.6	4.7	6	4
281	12 08	0.399	7	3.6	21.7	0.49	2	0.95	2	1	0.14	0.02	13.1	1.1	9	3
282	10.98	0.25	4	5.0	23.1	0.27	1	0.63	1	3	0.043	0.002	40.5	1.0	10	7
283	8.73	0.15	5	3.7	18.0	0.30	1	0.71	1	1	0.025	0.002	150	5	2	2
284	10.06	0.15	5	5.3	21.4	0.38	2	0.70	3	1	0.055	0 002	55.1	1.1	9	8
285	10.78	0 15	1		1.9						0.037	0 005	48.3	3.0	3	3
286	9.10	0.15	3	7.3	8.7	0.30	1	0.67	1	1	0 043	0.003	96.5	2.8	5	5
287	8.32	0.295	5	4.4	21.1	0.47	3	0.87	3	3	0.16	0.01	70 1	1.5	4	4
288	10.08	0.438	6	1.4	17.3	0 41	3	0 85	3	3	0.11	0.01	37.5	2.0	2	1
289	9.60	0.40	3	1.5	20.1	0 65	3	1.05	3	2	0.14	0.01	41.5	2.0	5	3
290	12.0	0.25	1												6	
291	11.48	0.25	2		12.7						0.14	0.01	17.5	1.0	14	2

Magnitudes, UBV Colors, IRAS Albedos and Diameters

M.P.	H	G	No. Obs.	Min Phase	Max Phase	U-B	UQ	B-V	BQ	UBV Ref	Albedo	Albedo Unc.	D	D Unc	No. Obs Pre	No Obs Acc
292	10.28	0.15	1		1.1						0.11	0.01	35.0	1.0	10	5
293	9.95	0.15	4	4.7	10 8	0.35	2	0.72	3	1	0.055	0.009	58.0	4 8	11	7
294	10.11	0 15	1		3.3						0.045	0 003	59.6	1.7	5	4
295	10.23	0 25	3	1.4	2 4	0.50	2	0.85	2	1	0 15	0 02	30.6	2.1	10	3
296	12 63	0.25	4	2.3	10 0	0.46	3	0.88	3	2					6	
297	9.43	0.15	3	3.1	3 5						0.14	0.01	45 8	1.8	5	3
298	11.24	0.25	3	5.3	5.6											
299	11.72	0.25	2	1.0	11.1						0 081	0 008	21.1	1.0	8	3
300	9.83	0 15	2		1.5						0.033	0 005	79 1	5.3	2	2
301	10.03	0.15	1		3.0						0.056	0.003	55.5	1.5	11	3
302	10.94	0.15	4	2.0	24.7	0.28	3	0.65	3	3	0.045	0.006	40.5	2.5	7	4
303	8.88	0.15	2	3.8	5.1						0.047	0.002	103	2	5	5
304	9.76	0.089	15	1.8	22.1	0.26	4	0.71	3	3	0.047	0.004	68.5	3.0	3	1
305	9.02	0.25	4	1.1	14 6	0.49	2	0.89	2	1	0.16	0.01	50.7	1.5	8	8
306	9.05	0.509	6	1.7	22.6	0.46	4	0.86	4	3	0.17	0.01	49.2	2.0	11	11
307	10.00	0.15	3	3.3	9.1	0.30	1	0.67	1	1	0.053	0.009	58.0	4.8	6	6
308	8.18	0.283	13	1.4	19.3	0.37	4	0.79	4	3	0.043	0.002	148	4	6	4
309	10.49	0.15	3	4.6	7.5						0.037	0.010	54.7	7.2	7	5
310	10.47	0.15	2		2.2						0.087	0.010	36.3	2.0	11	1
311	10.09	0.25	5	2.5	17.8	0.43	1	0.83	1	1	0.20	0.02	27.8	1.5	2	2
312	8.93	0.25	4	6.2	9.8	0.41	2	0.84	1	1	0.18	0.02	51.0	3.2	11	4
313	8.86	0.045	11	3.4	30.7	0.33	3	0.71	3	3	0.050	0.002	101	2	6	6
314	9.77	0.15	1		4.0						0.057	0.004	61.6	2.1	3	2
315	13.43	0.25	2	2.2	9.6										6	
316	11.52	0.15	1		1.0						0.018	0.002	49.3	2.0	2	2
317	10.18	0.40	4	0.2	27.3	0.23	1	0.67	1	3	0.29	0.03	22.6	1.2	6	1
318	9.27	0.15	5	3 8	6.8	0.29	1	0.68	1	1						
319	10.1	0.15	1								0.028	0.005	73.3	6.8	9	5
320	10.63	0.25	3	0.4	4 9										4	
321	10.20	0.25	8	1.0	10.6	0.41	2	0.79	2	1	0.15	0.03	31.2	3.2	10	4
322	9.02	0.15	5	5.3	25.7	0.23	2	0.72	3	2	0.080	0.004	73.8	1.6	12	10
323	9.67	0.25	4	11.4	33.2	0 48	2	0.90	3	3	0 16	0.01	37.7	1.2	2	1
324	6.82	0.104	16	10.4	29.5	0.30	3	0.70	3	1	0.057	0.003	242	7	2	2
325	9.00	0.25	3	3.9	9.0	0 24	1	0.70	1	1	0.073	0 004	78.0	2.0	6	6
326	9.13	-.109	5	8.7	22.9	0.32	4	0.71	4	3	0.039	0.005	100	7	4	2
327	10.23	0.15	4	1.7	8.9						0.11	0.02	35.5	4.5	3	2
328	9.11	0.25	1		2.6	0.42	1	0.89	1	1	0.028	0.003	120	7	3	1
329	9.66	0.15	2	9.7	10.8	0.31	3	0.69	3	3	0.037	0.002	80.5	1.8	5	3
330	12.7	0.25	1													
331	9 63	0.15	3	3.3	5 4	0.30	2	0.70	2	1	0.040	0.004	78.5	3.3	4	4
332	9.24	0.15	3	3.1	6.3						0.17	0 02	45.0	2.6	2	2
333	9.51	0.15	2	2.2	7.1	0.37	1	0 75	1	1	0.042	0.002	81.5	2.0	4	4
334	7.46	-.057	7	1.8	14.2	0.36	4	0.72	3	3	0.064	0 012	170	16	7	3
335	8.95	0.140	6	1.4	21.2	0.23	4	0 62	4	3	0 053	0 003	93 6	2.5	6	6
336	9.78	0.173	6	7.2	20.3	0.27	2	0 73	2	3	0.042	0 004	72.0	3.1	9	8
337	8.76	0.25	4	4.4	23.9	0.31	2	0 69	2	3	0 13	0.01	63.2	2.8	8	2
338	8.54	0.25	3	1.3	13.7	0.24	3	0.70	3	3	0 17	0.07	62.1	13.6	6	5
339	9.34	0.249	8	3.4	19.6	0.41	4	0 77	4	3	0 16	0.01	43.7	2.5	6	2
340	10.38	0.25	1		3.2						0 11	0.01	32.5	1.2	3	3
341	10.96	0.25	3	3.7	22.1			0.92	1	1	0.26	0.01	16.6	0.5	16	6
342	10.15	0.15	4	4.0	8.7	0.36	2	0.71	2	1	0.036	0.005	65.0	4.1	2	2
343	11.55	0.15	3	6.7	9.5	0.46	1	0.77	2	1	0 099	0.015	20.6	1.5	2	1
344	8.11	0.172	9	3.9	23.9	0.38	2	0.71	3	3	0.053	0.002	138	3	10	9
345	8.75	0.15	11	3.8	10.9	0.41	4	0 72	4	3	0 056	0.007	100	6	9	5
346	7.59	0.570	6	3.4	19.8	0.49	3	0.85	3	3	0.13	0 01	110	2	5	5
347	9.03	0.25	2	4.7	10.2	0.26	3	0.68	3	2	0.14	0.02	54.1	4.0	10	10
348	9.50	0.15	2	3.4	3.5						0.036	0.002	88 3	3.0	7	3
349	5.98	0.325	10	2.3	18 1	0.54	4	0.93	4	3	0 34	0.01	143	3	6	6
350	8.48	0.15	4	4.3	8.2	0.37	4	0.69	4	3	0.047	0.002	123	3	13	11
351	9.12	0.25	3	4.9	17.2	0.40	2	0 84	2	1	0.20	0.05	44.3	5.5	4	4
352	10.11	0.25	4	2.8	25.9	0.52	4	0.90	4	3	0.31	0.08	22.5	2.8	2	2
353	11.22	0.15	3	2.3	4.0											
354	6.32	0.321	41	1.5	20.8	0.54	4	0.95	4	3	0.19	0.02	162	10	15	14
355	10.49	0.15	2		2.3						0 16	0.02	25.7	1.6	15	5
356	7.99	-.081	8	4.6	19 1	0.35	3	0.73	3	1	0.062	0.003	135	4	7	7
357	8.71	0.15	4	4.6	9.5	0.35	2	0 72	3	1	0 048	0.002	110	3	4	4
358	9.06	0.15	2	3.8	5 3						0.050	0 003	91.8	2.2	6	6
359	9.29	0.25	4	3.5	17.2	0.30	2	0.70	2	3	0.15	0.03	47.5	5.1	4	4
360	8.41	0.15	5	4.6	14.0	0.28	2	0 68	3	3	0.052	0.010	121	12	7	6
361	8.27	0.15	4	1.2	8.6	0.19	4	0.75	4	3	0.039	0.002	149	4	8	5
362	8.95	0.098	5	4.5	18.5	0.35	2	0 71	2	1						
363	8.97	0.15	6	1.7	10.2	0 37	2	0.75	3	1						
364	9.85	0.25	5	3.6	26.5	0.52	3	0.89	3	3	0.20	0.01	31.0	0.8	11	7

E.F. TEDESCO

Magnitudes, UBV Colors, IRAS Albedos and Diameters

M.P.	H	G	No. Obs.	Min Phase	Max Phase	U-B	UQ	B-V	BQ	UBV Ref	Albedo	Albedo Unc.	D	D Unc	No. Obs Pre	No. Obs Acc
365	9.27	0.299	6	6.3	19.6	0.32	4	0.72	4	3	0.029	0.001	110	2	12	12
366	8.46	0.15	1		6.0						0.076	0.004	98.1	2.6	13	9
367	10.95	0.25	2	3.1	3.3						0.14	0.01	22.3	1.0	2	1
368	9.99	0.15	6	3.0	4.3	0.29	3	0.73	3	2	0.032	0.002	74.5	2.0	4	3
369	8.55	0.219	7	6.0	17.4	0.26	4	0.71	4	3	0.17	0.01	62.2	1.5	9	9
370	10.69	0.25	6	3.2	9.8	0.29	1	0.71	1	1						
371	8.79	0.25	3	5.0	10.5	0.51	1	0.82	1	1	0.16	0.01	56.7	1.2	7	7
372	7.3	0.25	1								0.054	0.002	195	4	6	6
373	9.17	0.15	4	3.6	21.5	0.36	2	0.67	2	3	0.038	0.003	99.6	4.2	7	7
374	8.95	0.25	7	4.3	19.7	0 44	3	0 85	3	3	0 19	0.01	48.2	1.5	4	3
375	7.43	0.233	8	8.1	17.3	0.34	2	0.68	2	1					2	
376	9 41	0.25	5	4.9	16.9	0.47	2	0.88	3	3	0.22	0.01	37.0	1.1	5	2
377	8.98	0.305	5	4.6	14.4	0.28	2	0.75	2	1	0.051	0.003	94.5	2.5	4	3
378	9.99	0 25	3	2.8	3.8	0.39	1	0.84	1	1	0.17	0.04	31.6	4.0	4	3
379	9.08	0.25	3	1.1	19.8	0.29	1	0.67	1	1	0.045	0.002	96.1	2.0	6	6
380	9.43	0.15	5	0.9	15.9	0.37	3	0.71	3	3	0.051	0.002	76.3	1.5	11	11
381	8.50	0.15	7	1.3	13.7	0.32	3	0.67	3	3	0.045	0.003	124	4	8	8
382	8.86	0.25	3	8.0	12.8	0.25	2	0.69	2	3	0.13	0.01	60.6	1.6	6	6
383	9.98	0.244	5	0.8	18.2	0.35	2	0.67	2	3	0.072	0.005	49.7	1.6	5	4
384	9.68	0.25	4	0.8	16.7	0.41	2	0.85	2	1	0.16	0.02	38.5	2.5	6	6
385	7.46	0.184	6	5.6	23.0	0.44	1	0 90	2	1	0.20	0.01	94.1	1.8	9	8
386	7.42	0.228	18	3.2	20.6	0.40	4	0.74	4	3	0.063	0 002	173	3	8	8
387	7.48	0.237	7	5.1	23.3	0 46	4	0.88	4	3	0.16	0.01	106	5	2	1
388	8.41	0.15	5	2.2	7.3	0.29	4	0.72	3	3	0.053	0.008	120	9	4	4
389	7.77	-.062	5	1.8	20.6	0.41	4	0.86	4	3	0.20	0.01	81.6	1.7	9	9
390	10.25	0.15	3	3.7	5.7	0.29	1	0.79	1	1	0.19	0.04	26.8	2.6	8	7
391	11.1	0.25	1												3	
392	9.79	0.15	1		1.7						0 051	0.003	64.6	1.6	3	3
393	8.40	0 15	4	4.6	22.4	0.32	2	0.74	3	1	0 069	0.065	106	50	3	3
394	9.75	0.278	5	3.4	18.4	0 40	3	0.83	3	2	0.16	0.01	36.2	1.5	5	3
395	10.42	0.259	5	1.7	11.1	0.38	2	0.73	3	1	0.041	0.004	54.2	2.3	1	1
396	9 77	0.15	1		1.4						0.17	0.04	34.8	4.0	8	3
397	9.36	0.220	5	5.4	21.2	0.37	2	0 81	3	1	0.15	0.02	46 0	3.5	11	9
398	10.46	0.15	1		19.7						0.045	0.007	50 5	3.8	6	2
399	9.14	0.15	2	5.0	5 4						0.14	0.02	52.8	5.2	5	5
400	10.00	0.25	1		7.0						0.14	0.04	34.3	5.1	7	3
401	9.35	0.15	3	3.3	4.7						0.030	0.001	103	2	4	4
402	9.06	0.163	6	0.9	21.2	0.40	3	0.80	3	3	0 12	0.01	57.6	1.8	8	8
403	9.34	0 25	2	5.1	5.3			0.90	1	1	0 12	0.01	51.3	1.0	9	9
404	9.05	0.189	5	3.6	20.0	0.33	3	0.66	3	3	0.041	0.002	101	2	9	9
405	8.43	0.121	7	2.4	27.2	0.37	4	0.69	4	3	0.045	0.002	129	3	5	5
406	10.38	0.15	5	3.3	9.5	0.28	3	0.73	3	2	0.043	0 003	53.8	1.5	4	4
407	8.92	0.15	6	3.9	17.9	0.38	2	0.70	2	3	0.050	0.006	97.6	6.1	11	11
408	9.61	0.15	1		6 4						0.12	0.01	45.5	1.5	13	6
409	7.60	0.284	9	3.2	19.4	0.34	2	0.72	3	1	0 057	0.005	168	8	5	3
410	8.26	0.083	6	7.2	15.6	0.40	2	0.75	2	3	0.054	0.002	128	2	21	21
411	9.06	0.15	2	4.4	5.5						0.066	0.003	79.6	2.0	7	7
412	9.19	0.15	2	5.0	10.6						0.043	0 003	93.3	2.7	5	5
413	10.24	0.25	1		11.3	0.22	1	0.68	1	1	0.12	0.02	34.3	3.5	4	4
414	9.55	0.15	2	0.9	11.5	0.38	2	0.75	3	2	0.047	0.008	75 2	6.6	6	6
415	9.38	0.315	5	3.0	17.6	0.23	2	0.71	3	1	0.049	0.006	80.1	5.0	11	11
416	7.87	0 257	6	5.1	15.2	0.46	3	0.88	4	3	0.15	0.01	89.5	2.0	7	5
417	9.31	0.25	2	2.5	7.7	0.36	1	0.76	2	2	0.17	0.01	43.3	2.0	2	2
418	9.84	0.25	4	2.7	21.8	0.25	3	0.69	3	3	0.13	0.03	38.5	4.7	11	5
419	8.39	0.145	9	3.5	18.2	0.24	3	0.64	3	3	0.044	0.002	133	2	12	11
420	8.35	0.042	5	1.1	16.9	0.23	3	0.69	3	3	0.038	0.005	146	9	10	10
421	11.87	0.25	1		19.6	0 45	1	0.85	1	2					4	
422	10.89	0.40	10	2.2	4.8	0.28	2	0.70	2	1					3	
423	7.48	0.681	5	2.6	19.1	0 30	4	0.67	4	3	0.038	0.002	217	6	3	3
424	9 63	0.15	1		4.8						0.030	0.001	90.5	1.8	6	5
425	9.83	0.15	2	1.1	1.8						0.046	0.002	66.8	1.7	5	5
426	8.56	0.15	2	4.8	10.5	0.34	1	0.71	1	1	0.037	0.002	134	6	5	5
427	9.41	0.15	2	3.1	5.7						0.26	0.03	33.8	2.0	9	4
428	11.93	0.25	2		2.9						0 067	0.007	21.0	1.0	4	3
429	9.77	0.15	2	5.4	6.3	0.35	3	0.74	2	2	0 044	0.012	70.3	9.6	7	7
430	10.40	0.15	1		3.3						0.10	0.01	34.6	1.0	5	5
431	8.97	0.25	3	1.5	5.4	0.33	3	0.64	3	2	0.048	0.002	97.7	2.1	8	7
432	9.09	0.25	3	8.6	15.3	0.45	2	0 87	2	1	0.17	0 01	48.6	1.0	9	9
433	11.24	0.625	46	8.7	44.3	0.52	4	0.90	4	3						
434	11.47	0.376	7	8.9	29.1	0.25	4	0.71	4	3						
435	10.23	0.15	5	1.5	8.6	0.29	3	0.70	3	1	0.077	0 005	43.0	1.5	2	2
436	9.91	0.15	3	5.1	6.7						0.048	0.007	63.0	4.7	9	9
437	10.44	0.25	4	3.7	7.4						0.56	0.03	14.3	0.5	5	3

Magnitudes, UBV Colors, IRAS Albedos and Diameters

M.P.	H	G	No. Obs.	Min Phase	Max Phase	U-B	UQ	B-V	BQ	UBV Ref	Albedo	Albedo Unc.	D	D Unc	No. Obs Pre	No. Obs Acc
438	9.97	0.15	3	1 1	12.6	0.20	1	0.61	1	1	0 045	0.005	63.6	3.7	9	9
439	9.72	0.15	2	1.1	5.9	0.24	1	0 72	1	1	0 036	0.002	79.3	2.2	2	2
440	11.82	0.25	3	13.0	14.2										7	
441	8 40	0 25	9	1.0	3.1	0 27	2	0.69	3	1	0.14	0.01	73.2	2 5	2	1
442	9.87	-.015	5	3.9	17.8	0.33	3	0.69	3	2	0.044	0.004	67.5	3.1	8	8
443	10 23	0.25	6	4.6	9 7	0.48	3	0.90	3	2	0.17	0 01	28 3	0.7	8	8
444	7.85	0.226	11	1.3	14.5	0.30	4	0.68	4	3	0.044	0.005	170	10	6	4
445	9 25	0.15	4	2.4	19 4	0.37	2	0.68	2	1	0.044	0 003	89.8	3.0	9	2
446	8.57	-.374	5	3.6	14.5	0.62	2	1.03	2	3	0.35	0 08	43 0	5.0	6	3
447	9.25	0.15	4	0.5	15.6	0.36	1	0.78	1	1	0.052	0.007	82 0	5.2	15	13
448	10 39	0.243	5	4.7	16 5	0.30	3	0.66	3	1	0.050	0.003	49.7	1.6	2	2
449	9.66	0.15	3	4.0	22.7	0.38	3	0.70	2	3	0.031	0.001	88.6	1.6	7	7
450	10.37	0.25	4	4.1	9 9	0.48	1	0.78	1	1	0 099	0.005	35.6	1.0	6	4
451	6 65	0.204	14	1.7	19.0	0.33	4	0.65	4	3	0.073	0.013	230	20	8	7
452	12.2	0.25	1												6	
453	10.81	0.25	3	2.5	7.0						0.14	0.01	24.2	0.8	3	3
454	9.06	0.15	4	4.2	13.2	0.35	2	0.66	2	1	0 059	0 004	84.5	3.1	2	1
455	8.96	0.15	4	2.4	7.7	0.31	2	0.70	2	1	0 060	0.009	87.5	6.6	6	6
456	9.90	0.15	2	4.7	5.6						0.10	0.01	43.1	1.5	7	2
457	11.19	0.15	1		16.8										4	
458	9.51	0.25	3	3 9	19.2	0 47	1	0.88	1	1	0.17	0.01	40.0	1.0	3	3
459	10.46	0.25	2	5.3	10.2	0.45	1	0.87	2	2	0.15	0.02	27.5	1.7	5	1
460	10.76	0.15	3	2.5	5.1						0.037	0.002	76.6	1.6	2	
461	10.54	0 15	8	0.3	3.9	0 31	2	0.61	2	1	0.051	0.011	45.7	4.7	2	2
462	9.01	-.080	5	1.9	15.7	0 42	4	0.84	4	3	0.30	0.02	38.0	1.2	7	3
463	11.73	0.25	3	1.1	10 0	0 29	1	0.71	1	1	0.077	0.006	21.5	0.8	10	3
464	9.55	0.15	6	4.1	8 3			0.64	1	1	0.046	0.009	76.5	7.5	6	6
465	9.77	0.15	2	2.2	2.3						0.037	0.002	76.6	1.6	6	6
466	8.34	0.15	3	6.0	16.7	0.34	2	0.66	2	3	0.056	0.003	121	3	12	11
467	10.86	0.15	4	3.9	6.3						0.036	0.007	47.5	4.5	9	6
468	9.60	0.15	9	0.2	11.5	0.31	2	0.67	3	1	0.050	0.004	71.7	2.8	2	2
469	8.89	0.15	4	1.1	8.6	0.27	3	0.65	3	2	0 030	0.001	129	3	7	7
470	10.10	0.25	4	4.9	11.2	0.47	3	0.89	3	2	0.19	0.01	28.5	0.5	11	8
471	6.61	0.285	9	6.1	25.4	0.49	4	0.83	4	3	0 20	0.01	139	3	4	4
472	8.76	- 007	5	9.4	17.0	0.46	3	0.88	4	3	0.24	0.03	47.6	3.6	7	5
473	10.0	0 25	1													
474	10.52	0.25	1		3 7						0 077	0.017	37.5	4.2	7	5
475	11.86	0.15	2	20.9	21.4	0.30	1	0.70	1	2	0.033	0.005	31.0	2.0	6	1
476	8 71	0.15	6	3 6	14.4	0.37	2	0.71	2	3	0.039	0.002	121	3	4	4
477	10.25	0.25	5	3.8	23.3	0.47	2	0 89	3	3	0.21	0.03	25.2	2.0	7	6
478	7.99	0.139	6	2.7	18.4	0.44	3	0.86	3	3	0.16	0.01	82.0	1.8	9	7
479	9 63	0.15	3	3.1	5.0						0 041	0.002	77.5	1.7	6	4
480	8.71	0.471	5	5.5	22.4	0.43	4	0.87	4	3	0.17	0.02	58.0	3.5	6	4
481	8.75	0.15	2	6.9	9.2	0.32	1	0.70	1	1	0 041	0.003	116	4	1	1
482	9.09	0.25	2	5.0	14.1	0.46	1	0.87	1	1	0 15	0.03	51.6	5.6	2	2
483	8.45	0.25	2	3.2	8.6	0.41	3	0.86	3	2	0.13	0.01	73.5	1.8	10	10
484	10.09	0.15	2	2.0	4.9										2	
485	8.69	0.15	2	2.7	3.2						0.12	0.01	68.2	3 1	7	4
486	11.03	0.25	3	6.5	8.9						0.11	0.01	24.5	2.0	2	2
487	8.21	0.078	6	3.6	14.3	0 43	2	0.85	2	1	0.22	0.01	64.2	1.6	8	8
488	7.83	0.15	5	5.2	17.3	0.36	3	0 70	3	3	0.052	0.003	158	4	8	8
489	8.36	0.15	3	6.5	8.3	0 36	1	0.69	2	1	0.038	0.002	144	3	4	4
490	8.32	0.15	4	2.0	12.7	0 37	1	0.75	2	1	0.057	0.005	121	5	5	5
491	8 81	0.15	1		3 5						0.052	0.004	101	4	2	1
492	10 26	0.25	2	4.4	6.2						0.047	0 003	54.5	1.5	8	4
493	10 6	0.15	1								0.036	0 002	52 0	1.5	10	4
494	8.94	0.094	7	1.6	14 7	0.37	2	0.73	3	1	0.059	0 003	89.1	2.0	7	6
495	10 97	0.25	4	0.5	16.0						0 041	0 004	41.7	1.7	8	7
496	11.89	0.25	3	3.0	12.1	0.51	3	0.86	3	2	0 10	0.01	17.5	1.0	6	2
497	10.01	0 107	7	1.1	18.3	0.25	1	0.70	1	3	0 085	0.010	45.3	2.5	7	1
498	8.82	-.049	5	0.7	22.0	0.38	4	0.75	4	3	0.073	0.005	84 8	2.8	7	6
499	9.64	0.420	8	1.4	16 6	0 29	3	0.67	3	2	0.033	0.002	86.0	2.5	4	3
500	9.37	0.15	2		5 9						0 15	0.01	45.1	1 0	9	8
501	9.02	0.15	1		4.0						0.068	0.004	80.1	2.5	4	3
502	10.76	0.25	4	9.0	20.4	0 48	2	0.87	2	1	0.20	0.01	20.7	1.0	4	1
503	8.98	0.15	4	2.7	17.8	0.32	1	0.72	1	1	0.071	0.005	79.5	2.6	2	1
504	10 08	0.15	1		4.6						0.16	0.02	31.2	2.6	14	12
505	8.80	0.15	2		24.7	0 23	1	0.66	1	3						
506	8.82	0.107	7	6.4	19.2	0 33	3	0.71	4	3	0.044	0.002	109	2	6	5
507	9.48	0.15	2	5 6	8.5						0.12	0.03	48.5	6.5	14	9
508	8.30	0.15	6	1.1	7.9	0 33	4	0.73	4	3	0.039	0.001	147	2	10	9
509	8.51	0.25	7	2.6	12.1	0.42	4	0.82	4	3	0.20	0.01	59.0	2.1	4	2
510	9.71	0.15	8	4.1	11.1	0.25	2	0.73	2	1	0.065	0.008	59.3	3.5	8	8

Magnitudes, UBV Colors, IRAS Albedos and Diameters

M.P.	H	G	No. Obs.	Min Phase	Max Phase	U-B	UQ	B-V	BQ	UBV Ref	Albedo	Albedo Unc.	D	D Unc	No. Obs Pre	No. Obs Acc
511	6.17	0.020	13	1.6	17.1	0.36	4	0.72	4	3	0.053	0.002	337	5	9	8
512	10.79	0.25	4	5.4	29.6	0.54	3	0.94	3	3	0.15	0.01	23.3	1.3	4	1
513	9.72	0.25	5	4.5	8.2	0.44	1	0 81	1	1	0.083	0 006	52.5	1.7	2	2
514	9.25	0.15	3	2.3	7.8	0.26	3	0 65	3	3	0.029	0.003	110	5	5	5
515	11.23	0.15	1		9.5	0.41	1	0.88	2	2	0.031	0.002	43.0	1.5	4	4
516	8.25	0.25	4	3.9	27.1	0.27	3	0 74	3	1	0.15	0.01	75.7	2.1	2	2
517	9.38	0.221	5	2.3	13.5	0.29	2	0.71	3	1	0.034	0.002	95.5	2.2	6	5
518	11.44	0.15	2		9.5						0.15	0.04	17.6	2.3	6	3
519	9.24	0.25	3	1.1	5.3	0.36	3	0.83	3	2	0.12	0.02	53.1	4.5	2	2
520	10.93	0.25	5	3.5	5.6	0.57	1	0.74	1	1	0.081	0.022	30.3	4.0	4	2
521	8.81	0.536	14	3.1	25.0	0.35	3	0.71	4	3	0.036	0.002	121	3	15	7
522	9.28	0.364	5	2 6	13.8	0.24	3	0.67	3	3	0.027	0 009	113	19	7	5
523	9.62	0.15	2		1.2						0.18	0.01	36.7	1.3	7	3
524	9.81	0.15	8	2.5	13 3	0.32	2	0 72	2	1	0.038	0 004	74.1	3.5	1	1
525	12.55	0.25	3	3 2	14.8	0.56	1	0 95	1	1						
526	10.36	0.25	3	0.8	19 1	0.37	3	0.64	3	2	0.058	0.010	46.7	3.8	7	6
527	10.31	0.15	4	2.1	9.7						0.043	0.003	55.2	1.7	2	2
528	9.10	0.15	1		1.1						0.054	0.004	86.2	3.5	3	2
529	10.15	0.25	6	0 7	15.5	0.45	3	0.79	3	2	0.10	0.01	38.2	3.3	9	4
530	9.27	0.15	4	3.9	15.5	0.30	3	0.65	3	3	0.043	0.003	89 3	3.3	4	2
531	11.1	0.25	1								0.19	0.08	17.8	3.7	7	2
532	5.78	0.247	14	4.0	22.8	0.41	4	0 85	4	3	0.16	0.01	231	4	12	10
533	9.71	0.25	4	3.4	14.5	0.42	1	0.87	2	1	0.19	0.04	34.8	4.5	5	5
534	9.81	0.25	10	0.3	12.9	0.39	2	0 83	2	1	0.14	0.02	37.5	3.2	7	6
535	9.50	0.15	3	0.5	4.4	0 39	1	0.74	2	1	0.047	0.007	77.0	5.5	8	8
536	8.08	0.15	2	7.2	9.1	0.28	3	0.69	3	3	0.042	0.005	158	10	11	4
537	8.79	0.15	2	3.8	5.2			0.82		1	0.23	0 05	47.5	5.0	5	4
538	9.39	0.15	3	0.7	3.0						0.051	0 007	77.8	5.2	2	2
539	9.85	0.15	2	2.1	4.9						0.066	0.010	55.3	4.1	6	5
540	10.75	0.25	3	3.8	6.4	0 49	1	0.91	2	3	0.19	0.04	21.0	2.5	14	6
541	10.22	0.15	2	3.2	3.5						0 041	0.002	59.1	1.6	4	4
542	9.22	0.25	4	1.3	13.1	0 38	1	0.80	1	1	0.19	0.01	43.5	1.0	7	5
543	9.57	0.15	2	3.4	3.6						0.13	0 01	44.2	2.0	6	3
544	10.18	0.15	2	4.3	7.0						0.22	0.06	26.0	3.8	3	3
545	8.56	-.095	6	1.8	14.2	0.30	1	0.69	2	1	0.050	0 003	115	3	4	4
546	9.68	0.15	4	3.3	17.6	0.38	2	0 77	3	1	0.049	0 002	69.7	1.5	11	7
547	9.73	0.15	3	6.2	20.8	0.25	1	0.76	1	1	0.042	0.004	73.0	3.1	2	1
548	11.43	0.25	3	3.7	19.4	0.49	3	0.88	3	2					2	
549	11.04	0.25	1		5.2	0.36	3	0.83	3	2	0.16	0.03	20.5	2.1	8	4
550	9.21	0.25	5	3.1	5.6	0.39	1	0.85	1	1	0.22	0.04	39.8	3.6	4	3
551	9.54	0.15	5	1.3	9.6	0.30	3	0.67	3	3	0.041	0.006	81.2	5.7	4	4
552	9.76	0.15	2		3.6						0.034	0.003	81.0	3.0	2	1
553	12.41	0.25	1		4.9										7	
554	8.89	0.15	5	3.3	23.7	0.34	4	0.66	4	3	0.051	0.002	98.5	1.8	17	14
555	10.53	0.15	1		1.9						0.060	0.004	42.5	1 2	2	2
556	9.32	0.25	3	3.5	25.7	0.41	3	0.83	2	3	0.21	0.01	39.5	1.0	5	5
557	12.21	0.25	1		2.2											
558	9.07	0.25	5	3.7	10.1	0.28	3	0.73	3	2	0.10	0.01	61.6	1.8	2	2
559	9.44	0.15	4	4.5	14.1	0.37	4	0.74	4	3	0.046	0.003	80.0	2.5	4	1
560	10.60	0.15	1		5.4						0.060	0.004	41.0	1.2	9	8
561	11.49	0.25	3	7.1	12.1			0.75	1	1	0.067	0.006	25.7	1.1	5	3
562	10.02	0.360	6	2.4	13.6	0.41	4	0.80	3	3	0.13	0.02	35.8	3.6	8	4
563	8.61	0.25	7	3.8	17.3	0.45	4	0.87	4	3	0.21	0.01	54.8	1.3	9	9
564	10.42	0.15	1		8.4	0.31	1	0.73	1	1	0.047	0.012	50.7	6.5	9	9
565	11.05	0.25	5	5.8	15.6	0.42	2	0.81	3	1	0.076	0.005	29.6	0.8	6	5
566	8.15	0.431	11	2.2	17.8	0.30	4	0.70	4	3	0.032	0.003	175	8	2	1
567	9.33	0.15	4	3.0	5.0	0.31	1	0.65	1	1	0.035	0.002	97.0	2.3	9	5
568	9.40	0.15	3	7.1	7.5						0.038	0.002	89.7	2.0	6	6
569	10.10	0.088	6	1.4	18.2	0.38	2	0.74	2	1	0.028	0.001	75.6	1.6	4	4
570	8.70	-.044	5	0.2	15.8	0.37	3	0.78	4	3	0.052	0.003	106	3	2	2
571	11.69	0.25	3	1.2	6.8	0.44	2	0.87	3	2	0.019	0.002	44.5	2.6	9	1
572	10.91	0.25	5	6.5	12.2	0.29	2	0.69	2	1	0.080	0.005	30.8	1.0	2	2
573	9.42	0.25	1		4.5						0.11	0.02	50.5	4.5	6	5
574	12.6	0.25	1								0.19	0.05	8.81	1.29	6	2
575	11.22	0.25	2	4.8	5.9						0.10	0.03	23.1	4.0	4	2
576	9.93	0.15	2		2.5						0.025	0.003	86.8	4.7	8	6
577	9.84	0.15	2	1.8	2.4						0.10	0.01	44.2	3.2	2	1
578	9.51	0.15	3	3.3	4.2						0.054	0 003	71.6	2.0	2	2
579	7.78	0.051	9	4.8	16.1	0.42	4	0.82	4	3	0.17	0.01	89.6	1.8	7	7
580	9.83	0.15	2	2.6	4.4						0.069	0.004	54.7	1.6	7	3
581	9.57	0.15	3	4.4	4.7						0.058	0.006	67.1	3.1	9	7
582	9.03	0.25	3	5.7	26.6	0.56	1	0.89	1	3	0.19	0.03	47.0	4.0	10	10
583	9.16	0.15	4	0.4	6.4	0.31	2	0.66	2	2	0.052	0 006	86.0	5.0	8	7
584	8.74	0.339	6	8.2	29.9	0.51	3	0.89	4	3	0.17	0.01	56.2	1.7	4	4

Magnitudes, UBV Colors, IRAS Albedos and Diameters

M.P.	H	G	No. Obs.	Min Phase	Max Phase	U-B	UQ	B-V	BQ	UBV Ref	Albedo	Albedo Unc.	D	D Unc	No. Obs Pre	No. Obs Acc
585	10.34	0.15	4	4.8	19.3	0 32	1	0 70	1	1	0.035	0 001	60.3	1.2	7	7
586	9.24	0.15	3	3.4	4.7	0.37	1	0.66	1	1	0.049	0 002	85.0	2.0	4	4
587	12.3	0.25	1												7	
588	8.59	0.15	6	2.7	3.6	0.23	3	0.77	2	3	0.030	0.004	147	9	7	5
589	9.06	0.15	3	3.6	5.5	0.36	2	0 72	2	1	0.049	0 003	92.5	2.5	4	4
590	10.14	0.435	5	7 0	17 7						0.095	0.008	40.5	1.5	4	2
591	10.74	0.15	3	3.7	4.4	0.20	2	0.69	2	1	0 030	0.002	54.7	1.3	8	8
592	9.63	0 15	1		1.8										3	
593	9.33	0.067	5	3.2	14.8	0.32	4	0.65	3	3	0.053	0.005	78 2	3.2	5	5
594	12 6	0 15	1								0.15	0.04	10.0	1.2	20	14
595	8.09	0.15	1		4.6						0.080	0 003	114	2	7	4
596	8.89	0.15	2	6.0	7 9	0.18	2	0 72	2	1	0 036	0 002	117	3	7	5
597	9 33	0.15	1		0.3						0.22	0.01	37.7	1 5	5	4
598	9 65	0.15	3	5.6	20.8	0.38	1	0.74	1	1	0.044	0.005	74.7	4.5	2	2
599	8.48	0 25	2	3.0	21 2	0 45	2	0.88	3	2	0 14	0.01	69.6	1.7	5	5
600	10.24	0.15	4	5.3	7.5						0.17	0.01	28.3	1.0	7	6
601	9.66	0.15	2	1.7	3.9	0.24	1	0.66	1	1	0.042	0.002	76.0	1.7	9	9
602	8.41	0 308	8	2.8	19.2	0.34	4	0.70	4	3	0 045	0.003	130	4	6	2
603	12.96	0.15	1		0.8						0.049	0.005	15.2	0.7	7	1
604	9.36	0.15	3	0.6	3.3						0.075	0.017	65.3	7.3	4	4
605	9.4	0.15	1								0.058	0.003	72.0	1.5	7	4
606	10.40	0.15	2	4.5	11.2	0.39	1	0.77	1	2	0.076	0.008	40.0	2.1	4	3
607	9.79	0.15	3	3.9	5.2						0.050	0.005	65.5	3.2	4	3
608	10.69	0.25	2	3.3	3.6										5	
609	10.04	0.15	4	1.4	7.7						0.054	0.006	56.3	3.1	2	1
610	12.1	0.15	1												2	
611	9.36	0.25	3	0.6	4.0	0.41	1	0.82	2	1	0.091	0.005	59.0	1.6	6	4
612	11.1	0.15	1								0.036	0.004	40.5	2.5	8	6
613	9.83	0.15	5	3 1	15.3	0.29	2	0 64	3	3	0.031	0.002	82.0	2.0	4	4
614	10.93	0.15	3	5.4	5.7						0 089	0.018	29.0	3.0	6	4
615	10.37	0.15	4	2.5	8.1	0 31	3	0.71	2	1	0.051	0.003	49.5	1.2	6	3
616	10.75	0.25	4	9.5	14.4	0.44	3	0.88	4	3	0.15	0.03	23 5	2.5	7	3
617	8.17	0 15	6	2.5	8 7	0 21	3	0.70	4	3	0.043	0.003	149	5	4	4
618	8.24	0 15	5	4.5	11.4	0.32	4	0.70	4	3	0.058	0.007	124	8	1	1
619	10.20	0.461	5	5.2	17.6	0.46	1	0.86	1	1					1	
620	11.37	0.40	2	1.5	8.0	0.24	1	0.68	1	1					1	
621	10.60	0.15	5	1.9	13 6	0.28	1	0.65	1	1	0 10	0.02	31.2	4.2	5	3
622	10.30	0 25	2	10.2	24.5	0.44	2	0.81	2	2					4	
623	10.87	0.25	3	2.2	10 7	0.33	2	0.71	1	1	0.037	0.002	46.0	1.5	3	2
624	7.47	0.15	11	3 6	7.8	0.24	3	0.79	4	3						
625	10.40	0.15	2	7.1	7 2						0.12	0.01	31.3	1.2	2	1
626	8 99	0.15	2	15.9	19.0	0.31	3	0.70	3	3	0.041	0.002	104	2	8	8
627	10.10	0.15	4	1.9	3.1	0.26	1	0.68	1	1	0.062	0.003	51.0	1.2	11	9
628	9.18	0.25	4	2.9	9.1	0.30	1	0.82	1	1	0.14	0.01	51.2	1.3	10	5
629	9.67	0.15	3	3.8	4.7										2	
630	11.2	0.15	1								0.13	0.01	20.3	0.7	5	3
631	8.96	0.586	6	2.2	15.3	0.44	4	0.87	4	3	0.12	0.01	60.5	1.2	4	4
632	11.74	0.15	4	1.5	11.8										2	
633	9.94	0.25	5	2.2	9.9	0.42	1	0.79	1	1	0.12	0.01	38.8	1.0	3	3
634	9 9	0.15	1								0.040	0.002	69.1	1.8	7	6
635	9.06	0.15	4	2.9	17.2	0.32	3	0 68	3	3	0 042	0.003	100	3	5	5
636	9.66	0.15	2	3.5	4 2						0 039	0.008	78.3	8.0	9	8
637	11.00	0 15	1		0 5						0.037	0.009	43.5	5.2	4	2
638	9 75	0.15	3	3.3	9.4						0.048	0.002	68.0	1.5	9	5
639	8 35	0.431	8	1.2	16.9	0.47	4	0 84	4	3	0 14	0.01	74.5	2.0	5	5
640	8.97	0.15	2	2.2	15.2	0.47	3	0.75	3	2	0.063	0.003	84.8	2.3	4	4
641	12.4	0.25	1												2	
642	10.06	0.25	2	4 4	4.5	0 40	2	0.88	1	1	0.10	0.01	40.0	1.6	4	2
643	9.83	0.314	5	3.7	15.3	0 33	1	0.71	3	3	0.036	0 002	76.1	2.0	8	5
644	10.91	0.25	7	1.7	12.1	0.41	2	0.81	2	1	0.14	0.02	23.2	1.7	2	1
645	10.00	0 25	5	2.6	14.6	0.41	1	0 86	2	1	0 17	0.02	32.0	1.8	6	4
646	13.1	0.25	1												4	
647	11.49	0.25	3	4.1	6.0	0.27	2	0.73	2	1					8	
648	9 72	0.15	5	3.1	16 5	0.28	1	0 68	1	3	0 046	0.003	70.5	1.8	4	4
649	12.30	0.15	1		6.2										4	
650	13.03	0.15	3	2.4	15 4	0 27		0 53		2					2	
651	10.02	0.035	6	2.6	19.7	0.49	2	0.85	2	3	0.12	0 01	36.8	1.5	4	3
652	11.47	0.25	1		2.3						0.092	0.012	22.1	1.5	6	1
653	9.31	0.25	4	1.3	17.3	0.44	3	0.84	3	3	0.17	0.01	43.3	1.2	8	8
654	8.43	0.054	6	4.6	22.3	0.33	3	0.68	4	3	0.043	0.002	132	3	5	5
655	10.16	0.15	2	3.0	3.1						0.11	0.02	37.2	4.3	10	4
656	9.64	0.25	2	2.8	4.0						0.075	0 016	57.5	6.2	8	5
657	10.92	0.15	4	7.5	12.0						0.040	0.003	43.6	1.5	3	3

Magnitudes, UBV Colors, IRAS Albedos and Diameters

M.P.	H	G	No. Obs	Min Phase	Max Phase	U-B	UQ	B-V	BQ	UBV Ref	Albedo	Albedo Unc.	D	D Unc	No. Obs Pre	No. Obs Acc
658	10.56	0.25	4	2.8	8.5	0.36	1	0.87	1	1	0.15	0.01	26.0	1 3	5	2
659	8.80	0.15	6	0.7	8.0	0.25	1	0.72	1	2	0.040	0.006	115	8	6	6
660	9.45	0.25	5	4.8	19.7	0.47	4	0.85	4	3	0.15	0.01	44.2	1.6	4	1
661	9.64	0.25	6	4.2	11.7	0 40	3	0.81	4	3	0.091	0.009	52.0	2.6	7	7
662	10.46	0.15	4	3.1	8.9						0.15	0.01	27.2	1.1	2	1
663	9.23	0.15	3	5.4	13.2	0.31	2	0 68	2	3	0.033	0.002	104	3	8	3
664	9.99	0.15	6	3.8	10.4	0.26	3	0.71	3	3					2	
665	8.52	0.15	2		2.6						0.21	0.01	56.1	2.1	5	3
666	10.80	0.15	2	3.2	5.7						0.095	0.005	29.7	0.7	9	5
667	9.12	0.15	2		8.0						0.057	0.003	83.5	2.0	6	5
668	12.13	0.15	1		4.9						0.032	0.002	28.0	0.7	3	2
669	10.24	0.25	4	1.2	9.6	0.47	1	0 82	1	1	0.10	0.01	36.5	1.5	4	2
670	9.33	0.15	1		4.9						0.24	0.01	36.5	0.8	8	6
671	10 35	0.15	2	3.2	3.5						0.031	0.007	63.7	6.8	7	6
672	11.41	0.15	3		5.8						0.040	0.010	34.8	4 3	2	2
673	10.27	0.25	4	2.1	3.8	0.43	1	0.78	1	1	0.089	0.009	39.3	2.0	8	5
674	7.43	0.25	4	0.9	9.3	0.43	2	0.88	1	1	0.18	0.01	101	4	9	9
675	8.05	0.15	3	1.8	9.0	0.44	1	0.85	1	2					9	
676	9.46	0.15	3	3.8	4.8						0.042	0.002	82.6	1.7	8	8
677	9.74	0.15	1		1.8						0.25	0.03	29 3	1.7	3	1
678	8.69	0.15	2	2.9	3.0						0.30	0.03	44.0	2.5	5	3
679	9.01	0.15	2	13.2	16.1	0.43	1	0.86	1	1					2	
680	9.41	0.15	4	1.7	7.6	0.27	2	0.69	2	1	0.040	0.002	86.7	1.7	10	9
681	10.73	0.25	1		4.1										4	
682	12.3	0.15	1								0.082	0.010	15.5	0.8	4	1
683	8.55	0.15	3	6.4	8.9						0.050	0.003	116	3	3	1
684	10.92	0.25	2	6.0	13.2										4	
685	11.78	0.25	1		1.7						0.20	0.02	13.0	0.6	2	2
686	9.75	0.25	4	5.6	20.4	0.42	3	0.84	3	3	0.11	0 02	44.1	4.5	6	6
687	11.72	0.15	4	8.3	20.0	0.25	2	0.68	3	2					5	
688	10.51	0.15	3	1.6	18.5						0 057	0.008	44.0	3.1	5	5
689	12.19	0.15	2	6.0	15.0	0 31	1	0.71	1	1	0.10	0.03	15.0	2.6	4	2
690	7.66	0.15	6	4.2	22.2	0.28	2	0.66	2	1	0.078	0.005	140	4	2	2
691	9.35	0.15	3	5.9	17.7	0.31	1	0.74	1	1	0 037	0.002	92.6	2.0	6	6
692	9 08	0.25	4	10.1	14.2	0 43	3	0.86	4	3	0.18	0.02	47.7	3.0	6	2
693	9.21	0.25	3	3.2	11.2	0.41	1	0.78	1	1	0.076	0.004	69.1	1.5	8	5
694	9 01	0.15	3	5.4	9.1	0.35	1	0.72	1	1	0.051	0.006	92.7	5.1	9	6
695	9.03	0.25	2	7.7	10.6	0.41	2	0.87	2	2	0.16	0 01	51.2	1.7	4	3
696	9.32	0.15	3	4.4	6.0						0.052	0.003	79.3	2.1	3	3
697	9.61	0.15	2	11 5	14 8	0.39	1	0 73	1	1	0.037	0.002	82.5	1.7	4	4
698	10.7	0 15	1												4	
699	11.99	0 40	4	22.8	28.0	0.38	3	0.86	3	2					2	
700	11.43	0.25	2	3.8	14.1						0.16	0.04	17.1	2.2	12	7
701	9.33	0.15	4	2 2	8.4	0.30	1	0.66	2	1	0 15	0.04	46.0	6.0	7	7
702	7.23	0.130	6	3 4	14.8	0.32	4	0.66	4	3	0 056	0.003	202	5	9	4
703	12.4	0.25	1												14	
704	6 00	0.019	22	9 2	22.6	0.26	4	0 64	4	3	0 064	0.002	333	6	10	8
705	8.46	0.15	5	6 1	8.0	0.29	2	0.70	2	3	0.038	0.002	139	3	8	5
706	10.9	0.15	1								0.075	0.009	32.0	1.8	3	2
707	12.90	0.15	1		0.5										7	
708	10.65	0.25	3	2 2	9.5	0.38	2	0.88	2	1	0.15	0.01	25.0	1.5	4	1
709	9.00	0.15	4	1.7	16.6	0 33	3	0.72	3	1	0.045	0.003	99.6	3.0	4	4
710	11 14	0.15	2	4.1	5.1						0.065	0.014	30.8	3.2	7	4
711	12.10	0.25	2	5 9	13.9										4	
712	8.35	0.064	5	5 6	19.5	0 36	4	0 73	4	3	0 046	0.002	132	2	17	15
713	8 90	0.15	3	3 3	5.1	0.28	3	0.66	3	2	0.041	0.003	109	4	2	2
714	9.09	0 25	5	4 5	13.2	0 45	3	0.88	3	3	0.24	0.03	41.0	2.5	5	4
715	9.97	0.15	3	4.9	6.8						0.18	0.02	31.5	2.5	9	5
716	10.81	0 25	5	4.7	6.2	0 33	2	0.86	1	1	0.12	0.01	25 5	1.6	2	1
717	11.04	0 15	5	1.5	9.1	0.24	2	0 70	1	1	0 051	0.014	36 5	5.1	10	8
718	9.76	0.15	2	3.7	3 9						0.038	0.005	76.5	4.7	7	7
719	15.6	0 25	1													
720	9.53	-.225	5	2.6	13.6	0.44	1	0 81	3	1	0.18	0.01	37.8	1.1	8	6
721	9.28	0.15	4	2.6	14 6	0.24	3	0.78	3	3	0 050	0.010	82.6	8.3	7	1
722	12.17	0 25	3	3.4	5.2										6	
723	9.99	0.15	1		2 8						0.12	0 01	38.3	2 5	4	3
724	13.6	0 25	1												6	
725	11.69	0 15	2	3 8	20.4	0.42	1	0.74	1	2	0.037	0 004	31.8	2.0	4	1
726	10 78	0.15	2	3.1	9.7						0.038	0.002	47.2	1.5	4	4
727	9 87	0.15	4	4.0	14.4	0.30	1	0.78	1	1	0.14	0.01	37.5	2.3	9	5
728	12.6	0.25	1												6	
729	9 36	0.25	2		11.1	0.38	1	0.78	1	1	0.11	0.01	53.3	2.7	6	1
730	13 5	0.25	1												6	

Magnitudes, UBV Colors, IRAS Albedos and Diameters

M.P.	H	G	No. Obs.	Min Phase	Max Phase	U-B	UQ	B-V	BQ	UBV Ref	Albedo	Albedo Unc.	D	D Unc	No. Obs Pre	No Obs Acc
731	9 50	0.15	7	2.0	11.6	0 30	2	0 69	2	1	0.12	0.01	46.6	1.5	5	4
732	10.76	0 25	2		7.7						0.058	0 004	39.0	1 1	2	1
733	9.07	0 15	3	4.3	15.6	0.29	3	0 68	3	3	0.049	0.009	92 0	8.3	5	5
734	10.03	0.15	3	2.5	6.7						0.028	0.004	78.6	5.2	11	5
735	9.57	0.15	4	2.1	15.3	0.32	2	0.70	2	1	0 044	0 002	77.0	1.5	8	7
736	11.55	0.25	2	4.6	4 7	0.51	1	0 90	1	1	0 11	0.02	19.0	1 7	14	11
737	8.84	0 25	3	6.2	29.9	0.39		0.83	1	1	0.23	0 01	46 3	1.5	2	2
738	9.96	0.15	3	1.6	2.1	0 50	1	0.76	1	1	0 044	0 002	64.8	1 1	10	8
739	9 20	0.935	9	4.6	18.6	0.32	4	0.71	4	3	0 030	0.002	110	3	5	4
740	9.02	0.15	5	4.5	14.1	0.31	3	0.72	3	3	0.049	0 002	94.5	1.7	9	9
741	10.39	0 15	1		4.3						0 11	0.01	32.5	1.2	3	2
742	9.59	0.25	5	3 3	5.5	0.45	1	0 84	3	1	0.11	0 03	46 7	5.8	9	9
743	10.22	0.15	2	1.5	5 8						0 046	0 002	55.7	1 1	6	6
744	10.19	0 15	2	4 3	5.1	0.16	1	0 66	1	1	0.039	0.010	62.0	7.6	10	9
745	10.38	0.15	2	1.7	2 4										4	
746	9.77	0 15	4	3 4	12.9	0.28	1	0 73	2	2	0.038	0 002	75.5	1.8	6	5
747	7.68	0.15	2	9 4	9.8	0.32	2	0.71	2	1	0.047	0 002	178	4	10	9
748	8.99	0 15	5	2.0	4 5	0 21	3	0 69	3	2	0.039	0 002	107	2	4	4
749	11 85	0 25	1		5 5	0 50	1	0 86	1	1					7	
750	12 13	0.15	4	3.2	13.9	0 21	3	0.60	3	3	0 043	0 004	24 0	1.1	4	2
751	8.64	0.15	4	2.7	21.6	0.36	4	0.68	4	3	0.047	0.002	115	2	7	6
752	10.22	0.25	1		7.0						0.033	0.001	65.7	1.5	8	5
753	10.34	0.25	4	2.5	13.4	0.49	1	0.94	1	1					4	
754	9.18	0.15	2		12.6	0.34	1	0.70	2	1	0.047	0.007	89.1	6.6	11	7
755	9.93	0.523	5	1 7	16.5	0.22	3	0.70	4	3	0.11	0.01	41.0	1.7	4	3
756	10.0	0.15	1								0.031	0.001	73.8	1.5	5	5
757	10.36	0.25	4	5.1	27.0	0.23	2	0 70	2	3	0.11	0.01	34.0	2.1	3	3
758	8.39	0.15	4	2.4	8.2	0.42	1	0.74	1	1	0.10	0.02	86.5	10.1	7	5
759	10.55	0.15	1		6.1						0.038	0.003	52.7	1.8	5	4
760	8.23	0.25	6	4.6	9.0	0.52	2	0 95	1	1	0.16	0.01	74.8	2.0	4	3
761	10.91	0.25	3	1.3	1.9	0.41	2	0.76	2	2					6	
762	8 58	0.496	6	2.6	19.6	0.31	1	0.65	2	3	0.032	0.002	142	4	5	4
763	12.39	0.25	1		6.9						0.064	0.006	17.3	0.7	8	1
764	9.49	0.15	3	1.5	2.0	0.40	2	0.72	2	1	0.077	0.004	60.5	1.5	5	4
765	12.29	0.15	2	1.1	10.9										5	
766	9.99	0.25	7	3.3	8.3			0 81	1	1	0.12	0.01	37.1	1.3	6	3
767	10.41	0.15	1		1.2						0.073	0.009	40.6	2.5	5	1
768	10.19	0.15	1		15.5	0.24	1	0.72	1	2					8	
769	8.84	0.15	1		1.3						0.049	0.016	102	17	4	4
770	10.93	0.25	4	4.0	11.2	0.55	2	0.88	2	1	0.22	0.01	18.5	0.5	3	3
771	10.33	0.25	3	5.4	17.0	0.25	1	0 66	1	2	0.14	0.01	30.5	1.2	2	2
772	8.32	0.15	3	15.6	16.3	0.36	2	0 67	2	3	0.055	0.003	123	3	10	8
773	9.34	0.15	4	7.3	11.9	0.29	3	0 70	3	2	0.033	0.001	99.1	1.8	6	6
774	8 86	0.15	2	0.9	5.5						0.15	0.01	57.0	2.0	2	1
775	10 44	0.25	6	0 7	8.3	0 43	3	0.81	2	3	0.096	0.009	35.0	1.6	6	2
776	7.68	0.341	9	1 5	12.3	0.39	4	0.70	4	3					2	
777	10.02	0.15	1		4.0						0.037	0.003	68.7	3.0	5	5
778	9.58	0.008	7	2.7	21.1	0.26	4	0.62	4	3	0.057	0.003	67.3	2.0	7	3
779	8.5	0.15	1								0.12	0.07	72.7	21.7	7	4
780	8.99	0.15	2	8.8	11.1						0.047	0.002	97.1	2.3	6	3
781	9.44	0.15	1		6.3						0.082	0.017	60.0	6.0	6	2
782	11.53	0.25	2		6.8						0.23	0.02	13.5	0.5	6	2
783	10.98	0.25	2	7.1	7.2						0.042	0.002	41.3	0.7	5	5
784	9.13	0.15	4	4.1	5.8						0.049	0.004	90.0	3.8	2	1
785	9.24	-.003	5	13.9	29.5	0.18	4	0.64	4	3	0.13	0.01	52.1	1.7	2	2
786	8.71	0.15	5	2.3	12.2	0.25	3	0.69	3	2	0.067	0.012	93.2	8.2	7	6
787	10.2	0.25	1								0.15	0.03	30.3	3.0	6	5
788	8.23	0.15	2	3.9	5.7						0.076	0.005	109	4	2	2
789	11.09	0.15	3	3.8	9.6										4	
790	8.05	0.15	5	5.3	11.3	0.30	3	0.70	3	3	0.034	0.001	176	3	10	8
791	9.33	0.15	3	4.5	8.3	0.28	3	0.71	3	2	0.029	0.001	107	2	7	6
792	10.13	0.15	2	4.2	12.9						0.039	0.002	63.5	1.3	5	5
793	10.17	0.15	2	4.8	5.2			0.82	1	1	0.15	0.01	30.8	0.8	3	3
794	11.20	0.15	3		5 9						0.035	0.004	41.0	2.5	7	1
795	9.81	0.15	3		3.3						0.034	0.003	78.7	3.6	6	2
796	9.11	0.15	5	2.4	27.9	0.27	1	0.70	2	1	0.18	0.01	46.7	1.5	2	2
797	10.45	0.25	5	2.8	9.7	0.51	2	0.89	2	1					2	
798	9.64	0.237	5	6 0	15.5	0.39		0.69		2	0.11	0.01	46.2	2.5	15	11
799	10.35	0.15	3	2.9	6.0						0.059	0.003	46.5	1.1	8	7
800	11.60	0.25	2	3.6	5.9	0.52	1	0 92	1	1					6	
801	11.39	0.15	3	2.6	6.0	0 27	1	0.73	1	2	0.039	0.006	35.3	2.7	12	9
8Q2	12.4	0.25	1												9	
803	9.69	0.15	2		1 6						0.087	0.007	51.8	2.0	5	3

Magnitudes, UBV Colors, IRAS Albedos and Diameters

M.P.	H	G	No. Obs.	Min Phase	Max Phase	U-B	UQ	B-V	BQ	UBV Ref	Albedo	Albedo Unc.	D	D Unc	No. Obs Pre	No. Obs Acc
804	7 87	0.221	7	0.9	12.5	0.38	4	0.71	4	3	0.049	0.003	161	5	10	9
805	9.72	0.15	2	6.0	13.1	0.28	2	0.70	3	2	0.043	0.003	73.0	2.7	4	3
806	10.81	0.15	1		13.3						0.020	0.001	65.2	1.5	5	5
807	10.62	0.298	8	3.6	15.1	0.46	2	0.85	2	1	0.10	0.01	31.3	2.5	6	5
808	9.62	0.15	1		1.5						0.21	0.02	34.3	1.8	4	2
809	12.08	0.25	2	2.4	5.6										7	
810	13.0	0.25	2												2	
811	10.82	0.25	4	3.8	9.3	0.42	2	0.86	2	3	0.14	0.01	23.6	1.3	6	1
812	11.3	0.15	1												7	
813	12.27	0.25	2		6.3						0.084	0.010	16.1	1.0	7	2
814	9.08	0.524	10	5.4	16.0	0 34	3	0.68	3	1	0.031	0.002	116	3	2	2
815	10.82	0.15	2	12.0	12.1						0.13	0.01	24.5	1.5	5	1
816	10.25	0.15	3	4.2	10.3						0.036	0.002	62.5	1.3	8	6
817	10.80	0.15	1		4.8						0.13	0.02	25.0	2.2	6	2
818	9.35	0.15	1		5.2						0.11	0.02	53.0	4.6	2	2
819	12.09	0.25	3	4.0	8.6										3	
820	10.38	0.15	1		3.1						0.033	0.003	61.1	2.8	10	9
821	11.84	0.15	1		1.5	0.32	3	0.71	3	2					2	
822	12.18	0.15	1		6.1			0.77	1	1						
823	11.46	0 25	2	3.8	8.5						0.11	0.01	20.2	1.2	11	1
824	10.46	0.25	4	2.8	6.9	0.41	1	0.85	1	1	0.089	0.028	36.0	5.6	5	2
825	11.79	0.25	6	3.7	10.4	0.54	2	0 91	3	1	0.21	0.01	12.5	0.5	9	1
826	11.63	0.15	1		4 9						0.085	0.027	21.5	3.3	7	6
827	12.98	0.25	2	2.1	3.7										4	
828	10.26	0.15	3	1.1	5.3			0.67	1	1	0.044	0.005	55.8	3.0	12	7
829	11.07	0.15	3	4.9	6.6						0.034	0.002	44.0	1.5	2	2
830	9.36	0.25	5	1.6	9.6	0.50	1	0.90	2	1	0.14	0.01	47.1	1.5	9	6
831	12.3	0.25	1													
832	11.20	0.25	5	2.8	9.1										7	
833	11.1	0.25	1												8	
834	9.33	0.15	4	1.5	6.3	0.47	1	0.75	2	1	0.068	0.004	69.2	1.7	11	11
835	11.12	0.15	1		2.3						0.037	0.009	41.3	5.2	6	2
836	13.1	0.25	1												6	
837	11.8	0.25	1												3	
838	10.13	0.15	4	1.1	8.7	0.31	2	0.71	3	2	0.039	0.002	63.1	2.0	4	3
839	10.77	0.25	1		7.2						0.17	0.01	22.3	0.6	12	7
840	9.4	0.15	1								0.34	0.07	30.0	3.0	7	2
841	13.02	0.25	3	4.5	21.2										8	
842	10.6	0.15	1								0.054	0.008	43.2	3 3	9	3
843	13.1	0.25	1												5	
844	9.67	0.15	3	2.0	8.9						0.055	0.056	66.1	33.6	8	2
845	10.46	0.15	1		3.8						0.035	0.005	57.5	3.7	6	5
846	10.47	0.15	5	2.4	5.3	0.39	1	0.61	1	1	0.039	0.002	54.2	1.3	3	3
847	10.27	0.25	2	2.3	3.6	0.46	1	0 90	1	1	0.13	0.02	32.1	2.5	5	3
848	11.09	0.15	2	0.1	2.9										2	
849	8.19	0.25	4	14.8	21.8	0.25	4	0.70	4	3					2	
850	9.53	0.15	3	3.4	4.4						0.038	0.002	84.5	2.0	4	3
851	11.75	0 25	4	3.0	5.5	0.48	1	0.86	2	2	0.17	0.01	14.2	0.6	13	1
852	10.16	0.25	2	8.1	10.2						0.25	0.03	24.6	1.5	3	3
853	11.68	0.25	8	2.2	16 6	0.29	1	0 73	2	1	0.048	0.002	28.0	0.6	6	5
854	12.41	0.25	3	4.8	6.1										2	
855	12.05	0.25	1		5.7										3	
856	10.62	0.25	2	1.2	8.7						0.037	0 004	52.0	2.8	2	1
857	11.38	0.25	1		11.5	0.14	1	0.63	1	1	0.17	0.01	16.5	0.7	13	5
858	10.17	0 25	1		4.5						0 28	0.03	23.1	1.2	7	2
859	9.91	0.15	3	5.6	10.7						0.032	0.002	77.5	2.0	6	6
860	10.36	0.25	1		20.2	0.21	1	0.66	1	2	0.11	0.02	32.8	3.0	4	1
861	9.91	0.15	4	3.1	3.7						0.039	0.002	70.1	1.7	17	14
862	10.1	0 15	1								0 18	0.01	29.2	1 0	5	4
863	9.13	0.40	5	5.9	15.7	0.61	3	1.08	4	3	0.39	0.03	31.5	1.3	4	2
864	12.98	0.25	2	17.8	28.8	0.55	2	0 91	2	2					11	
865	12.10	0.25	2	7.0	7.9						0.059	0.005	20.7	0.8	4	3
866	9.42	0 15	2		3 6						0.036	0.002	91.7	2.0	4	4
867	10.9	0.15	1								0.087	0.013	28.5	2.0	6	2
868	10.17	0 15	5	1.9	8.5	0 36	1	0.71	1	1	0.050	0 003	54.7	1.7	4	3
869	12.1	0.15	1								0.057	0 012	21.0	2.1	5	4
870	11.8	0.25	1												4	
871	12.5	0 25	1								0 10	0.01	12.2	0.6	4	1
872	9.95	0.25	5	0 2	9.3	0.28	1	0.73	1	1	0 16	0 03	33.5	4.0	3	3
873	11 39	0 15	3	3.9	11.8	0.32	2	0.68	2	2	0 044	0.004	33.5	1.5	2	2
874	9 77	0.15	1		5.5						0 064	0.010	58 3	4.5	5	5
875	11 75	0 25	2	7 0	10 2						0.15	0.01	14.8	0.5	2	2
876	10.95	0.25	5	1.8	15.0	0 43	1	0.81	2	1	0.11	0.01	25.8	1.5	6	1

Magnitudes, UBV Colors, IRAS Albedos and Diameters

M.P	H	G	No. Obs.	Min Phase	Max Phase	U-B	UQ	B-V	BQ	UBV Ref	Albedo	Albedo Unc.	D	D Unc	No. Obs Pre	No. Obs Acc
877	10.94	0 398	6	5.2	22.2	0.24	3	0.64	3	3	0.047	0.004	39.6	1.6	2	2
878	15.4	0.25	1													
879	11.5	0.25	1													
880	11.45	0.15	1		15.0	0 30	2	0.63	2	2	0.036	0.005	36.0	2.5	4	1
881	12.4	0.15	1												3	
882	10.61	0.15	2	2.1	2.6						0.042	0.003	48.8	1.8	6	1
883	12.86	0.25	2	0.9	13.9	0.48	1	0.86	1	1					5	
884	8.89	0.15	10	1.0	6.1	0 20	2	0 71	2	3						
885	10 83	0.15	2	3.4	4.7						0.060	0 018	37.0	5 5	2	2
886	8 52	0.15	2		4.5						0.079	0 028	93.3	16 7	14	12
887	13.83	-.084	7	5.8	27.8	0.43	1	0.84	2	3					6	
888	9.52	0.25	4	4.8	17 3	0.50	3	0.88	3	1	0 13	0 04	44.8	6.6	10	7
889	11.58	0.25	1		7.7						0 080	0.011	22 6	1 5	7	1
890	10.79	0.25	3	6.7	7.0	0.33	2	0.77	1	1	0 095	0.010	30.0	1.5	2	2
891	10.23	0.15	4	5.0	7 0						0.050	0.013	53.6	7.0	3	3
892	9.45	0 15	1		5 9						0.048	0.002	78.5	1.7	6	6
893	9 75	0 15	4	4.0	7.4	0.23	1	0 67	1	1	0.036	0.002	78.2	2.0	7	6
894	9.80	0.15	1		5 7						0.12	0.01	40.8	1.6	4	2
895	8 6	0.15	1								0 029	0 002	147	4	2	2
896	11 79	0 25	1		7.0						0 16	0 02	14 5	1.2	6	5
897	10 40	0.25	2	4.6	5.9	0 39	3	0 83	3	2	0 21	0.02	24 0	1 3	5	5
898	12.2	0.15	1												16	
899	10 17	0.15	5	3 2	12.7	0 26	2	0.68	3	1	0 16	0.02	30 0	2.3	9	7
900	11 94	0.25	2	6 6	16.1						0 057	0 015	22 7	2.8	4	2
901	11.79	0.25	3	4.3	22.5	0.55	3	0.90	2	2					6	
902	12.4	0.25	1												5	
903	9.6	0.15	1								0.056	0.004	65.7	2.5	6	5
904	10.2	0 15	1								0.036	0.002	62.5	1.8	6	3
905	11.80	0.25	2	1.4	8.5						0.076	0.007	21.0	1.0	8	1
906	9.98	0.15	5	2.9	5.8										2	
907	9.64	0.15	4	8.0	9.8	0.27	3	0.71	3	2	0.057	0.003	65.8	1.7	4	4
908	10.89	0.25	3	7.5	8.7						0.099	0.013	28.0	1.8	7	3
909	8.81	0.15	2	3.8	8.3	0.28	2	0.69	2	2	0.037	0.002	120	3	4	3
910	10.17	0.15	2		5.7						0.054	0.009	53.0	4.2	4	4
911	7.88	0.15	2	2.0	8.4	0.22	2	0.77	3	1	0.041	0.002	175	4	7	6
912	9.12	0.15	3	5.8	7.6						0 053	0.003	86.6	2.3	4	3
913	12.5	0.25	1												4	
914	8.82	0.15	4	9.9	25.8	0.35	3	0.74	3	3	0.084	0.004	79.0	2.0	6	3
915	11.97	0.25	1		4.0										10	
916	11.55	0.25	1		7 8						0.032	0.005	36.5	2.5	7	4
917	11.51	0.25	2	3.6	8.0						0.047	0.013	30.5	4.3	7	4
918	10.84	0.15	2	1.5	7 1						0.13	0 02	24.5	2.3	2	1
919	11.33	0.15	3	5.1	5.7						0.055	0.004	30.5	1.0	2	1
920	11.19	0.15	1		6.8	0.30	1	0.80	1	1	0.082	0.009	26.7	1.3	7	7
921	10.03	0.15	1		5.2						0.047	0.004	60.5	2.5	2	2
922	11.94	0.15	2	1.1	1.5										5	
923	11.5	0.15	1								0.037	0.002	33.6	0.8	5	5
924	9.39	0.15	4	3.4	6.7	0.34	1	0.72	2	1	0.040	0.002	87.6	2.0	9	7
925	8.41	0.25	4	2.3	19.8	0 42	2	0.84	4	3	0.23	0.03	57.0	4.0	13	12
926	10.5	0.15	1								0.043	0.003	50.5	1.5	9	5
927	9.31	0.15	2	5.8	6.5	0.34	1	0.67	1	1	0.068	0.003	70.0	1.7	6	5
928	10.10	0.15	2		1.6						0.033	0.002	69.7	1.7	7	5
929	12.42	0.25	1		6.3										5	
930	11.3	0.25	1								0.032	0.002	39.1	1.2	3	2
931	9.26	0.25	3	4.7	22.6	0.22	3	0.68	3	2	0.12	0.03	52.6	7.0	12	7
932	10.05	0.15	4	5.2	14.4	0.33	2	0.67	2	1						
933	12.60	0.25	2	4.8	7.0						0.024	0.004	26.0	2.1	6	1
934	10.3	0.15	1								0.040	0.008	57.1	5.7	14	10
935	13.27	0.25	1		3.8						0.11	0.01	8.69	0.51	8	2
936	10.08	0.25	3	0.7	4 8						0.084	0.004	44.1	1.0	13	6
937	11 70	0.25	4	2.0	12.2	0.53	2	0.94	2	2	0.049	0.005	27.5	1.2	8	1
938	11.2	0.15	3								0.072	0.012	28.0	2.2	3	2
939	12.06	0.25	2	3.8	7.7	0.54	1	0.93	1	1	0.083	0.010	17.8	1.0	5	1
940	9.33	0.15	2	2.8	4.8	0.36	1	0.58	1	1					2	
941	11.55	0.15	1		6.1	0.31	1	0.70	1	1					5	
942	10.3	0.15	1								0.11	0.01	32.7	1.3	2	1
943	9.73	0.25	4	2.7	7.5	0.39	1	0.78	1	1	0.044	0 003	72.0	2.5	4	4
944	10.54	-.084	7	4.4	26 9	0.22	2	0.75	2	1					12	
945	10.09	0.25	3	1.3	1.9	0.39	2	0.81	2	2	0.18	0.02	29.5	1.5	2	1
946	10.51	0.15	5	0.8	20.4	0.34	4	0.66	4	3	0.044	0.013	50.0	7.0	16	6
947	10 17	0.15	1		4.9						0.19	0.03	27.7	2.2	8	7
948	11.42	0.15	3	4.9	6.8										2	
949	9.59	0.15	2	1.5	4.5						0.051	0 003	71.0	1.8	6	6

Magnitudes, UBV Colors, IRAS Albedos and Diameters

M.P.	H	G	No. Obs.	Min Phase	Max Phase	U-B	UQ	B-V	BQ	UBV Ref	Albedo	Albedo Unc.	D	D Unc	No. Obs Pre	No. Obs Acc
950	11.3	0.25	1								0 17	0.04	17.5	2.2	7	7
951	11.67	0.25	2	5.4	19.5	0.55	1	0.87	1	2	0.15	0.02	15.5	1.0	3	1
952	9.12	0.15	1		3.4						0.055	0.007	84.5	5.0	4	4
953	10.40	0.15	3	1.8	8.7						0.12	0.01	31.5	1.0	4	4
954	9.94	0.15	2	2.1	8.4	0.31	2	0.62	2	1	0.052	0.002	59.7	1.1	6	6
955	11.5	0.15	1								0.12	0.01	18.7	0.5	7	5
956	12.61	0.25	2	3.8	4.6										8	
957	9.85	0.15	1		6.8						0.034	0.002	76.6	2.1	4	1
958	10.73	0.15	2	4.8	6.9	0.19		0.83		2	0.031	0.009	53.7	7.5	4	3
959	10.7	0.15	1								0.026	0.001	59.1	1.2	8	7
960	13.12	0.25	2	6.5	8.8										5	
961	11.39	0.15	1		6.9						0.032	0.002	39.3	1.0	7	4
962	11.61	0.25	4	1.5	9.6	0.41	2	0.82	3	2	0.026	0.010	39.5	7.5	5	2
963	12.55	0.25	2	10.2	10.8	0.53	1	0.90	2	1	0.12	0.01	11.5	0.6	11	1
964	10.94	0.15	3	1.0	1.3										11	
965	10.23	0.15	1		1.3						0.048	0.003	54.5	1.6	4	4
966	10.02	0.25	5	8.8	16.0	0.45	2	0.87	3	1	0.23	0.02	27.3	1.5	4	3
967	12.56	0.25	2		4.8						0.076	0.008	14.7	0.7	7	2
968	10.05	0.25	1		5.7	0.37	1	0.87	1	1	0.17	0.05	31.0	4.7	9	2
969	12.59	0.15	3	5.8	6.5	0.23	2	0.62	2	3	0.038	0.002	20.5	0.6	2	2
970	12.3	0.15	1												3	
971	9.91	0.15	2	4.0	7.0						0.043	0.003	66.7	2.0	5	4
972	9.50	0.15	2	3.3	3.5						0.045	0.002	79.0	2.0	6	5
973	9.86	0.15	2	4.4	5.5						0.067	0.004	54.7	1.5	5	5
974	10.40	0.25	4	1.9	20.7	0.48	3	0.90	2	2	0.19	0.05	24.8	3.0	5	3
975	10.38	0.25	3	0.7	8.0	0.39	1	0.85	1	1					4	
976	9.35	0.15	2	2.1	7.6	0.25	1	0.74	1	1	0.043	0.004	86.6	4.0	2	1
977	9.74	0.15	3	5.7	8.8	0.39	2	0.71	2	1	0.050	0.008	67.0	5.5	8	5
978	9.72	0.15	2	0.9	1.1	0.24	1	0.67	2	1	0.034	0.002	82.5	2.0	6	6
979	10.03	0.15	1		2.7						0.10	0.01	40.6	2.3	12	6
980	7.76	0.058	5	7.4	25.4	0.54	4	0.91	4	3	0.17	0.01	89.0	1.6	7	6
981	10.84	0.15	2	1.4	13.8	0.33	1	0.62	1	1	0.083	0.011	31.2	2.0	2	2
982	10.27	0.15	2	4.5	6.9										2	
983	9.58	0.15	2	8.8	9.0	0.28	2	0.74	1	1	0.043	0.002	77.3	1.6	9	5
984	9.23	0.15	6	1.2	8.0						0.31	0.06	33.6	3.3	5	5
985	13.08	0.25	2		5.2										4	
986	9.43	0.15	4	3.7	8.0						0.10	0.01	53.0	2.0	7	4
987	9.46	0.15	4	1.1	6.8						0.14	0.01	44.6	1.1	5	5
988	11.2	0.15	1								0.064	0.017	29.0	3.8	9	7
989	12.2	0.15	1								0.11	0.01	14.3	0.6	2	1
990	11.61	0.15	1		3.4						0.097	0.014	20.3	1.5	4	2
991	11.35	0.15	3	0.6	11.3	0.37	1	0.66	1	1	0.043	0.009	34.5	3.5	6	5
992	10.88	0.15	1		3.9						0.082	0.008	30.8	1.5	8	4
993	12.02	0.25	1		9.4										8	
994	10.28	0.15	3	3.2	6.7						0.18	0.03	27.2	2.7	4	3
995	10.37	0.15	2	3.8	7.6						0.11	0.01	32.6	0.5	9	7
996	11.00	0.25	2	4.3	6.3	0.39	3	0.69	3	3	0.060	0.007	34.1	2.0	11	6
997	11.8	0.15	1								0.056	0.007	23.5	1.5	4	1
998	11.0	0.15	1								0.057	0.016	35.0	5.0	9	1
999	10.79	0.15	1		3.1						0.18	0.02	21.2	1.2	2	1
1000	10.1	0.15	1								0.051	0.010	54.0	5.0	10	7
1001	9.55	-.060	7	3.6	19.9	0.26	4	0.70	4	3	0.044	0.005	78.3	4.6	4	1
1002	10.9	0.15	1								0.023	0.002	57.1	2.5	12	1
1003	10.57	0.15	1		1.6										9	
1004	9 82	0 15	5	1.0	5.0	0.12	1	0.72	1	1	0.035	0.003	76.6	3.0	4	2
1005	9.73	0.15	1		4.5						0.057	0.008	62.7	4.3	10	6
1006	11.64	0.15	2	6.3	10.3						0.030	0.004	35.7	2.1	10	1
1007	11.52	0.15	1		4.9						0.071	0 017	24.6	3.0	7	1
1008	10.56	0.15	2	2.7	6.1						0 063	0.007	41.0	2.3	4	3
1009	14.1	0.15	1													
1010	10.76	0.15	2	1.8	2.0						0.043	0.002	45.2	1.1	5	5
1011	12.85	0.25	2	22.6	32.8	0.52	2	0.90	2	1						
1012	12.33	0.15	6	4.2	26.0	0.22	2	0.66	3	3	0.039	0.010	23.0	3.0	5	3
1013	9.83	0 15	3	4.6	25.3	0.36	2	0.74	1	1	0.16	0.03	35.6	3.7	10	3
1014	11.92	0.15	1		2.4										8	
1015	9.10	0.15	5	3.7	8.4	0.32	2	0.69	3	1	0.039	0.002	101	3	9	9
1016	12.22	0.25	1		2.2											
1017	11.0	0.15	1								0.043	0.009	39.0	4.1	4	4
1018	11.01	0.15	3	1.0	10 7						0.24	0.02	16.7	0.8	3	2
1019	12.73	0 244	5	9.3	24.7	0.50	4	0.94	4	3	0.15	0.01	9.55	0.57	7	2
1020	12.06	0.15	2	1.3	11.9										2	
1021	8.89	0.039	5	5.9	28.5	0.23	3	0.66	3	3	0.046	0.003	103	3	4	4
1022	10.1	0.15	1								0.16	0.01	31.1	1.3	2	1

Magnitudes, UBV Colors, IRAS Albedos and Diameters

M.P.	H	G	No. Obs.	Min Phase	Max Phase	U-B	UQ	B-V	BQ	UBV Ref	Albedo	Albedo Unc.	D	D Unc	No. Obs Pre	No. Obs Acc
1023	9 73	0.15	4	2.6	7.6	0 49	2	0 74	2	1	0.062	0 005	60.2	2.5	4	4
1024	10.58	0.15	1		2.2						0.055	0.004	43.2	1.7	6	2
1025	12.87	0 40	1		29.0	0.29	2	0.71	2	2					6	
1026	13.4	0.25	1													
1027	10.7	0.15	4								0.068	0.004	36.1	1 0	9	3
1028	9.41	0.15	4	2.5	19.3	0.28	1	0.68	1	2	0.052	0.002	76.3	1.6	10	10
1029	10.95	0.342	5	2.8	12.6	0.40	2	0.79	3	1	0.12	0.01	24.5	1.3	6	1
1030	10.42	0.15	2		1 4						0.028	0.003	65.5	3.3	4	4
1031	9.56	0.15	2		7.9	0.32	1	0.68	1	1	0.043	0.002	78.0	1.7	7	7
1032	9.90	0 15	1		5.5						0.055	0.006	59.1	3.2	6	4
1033	11.12	0.25	2	3.3	7.3						0.096	0.034	25.5	4.5	4	2
1034	12.5	0.25	1								0 21	0.02	8 85		7	2
1035	10 5	0 15	1								0.032	0 003	56.8	2 5	2	2
1036	9.42	0.307	5	10.0	24 4	0.42	3	0 84	3	3	0.17	0 02	41.0	2.3	4	1
1037	13.24	0.25	1		4.3										4	
1038	10.82	0.15	1		5.8	0.23		0 77		2					4	
1039	11.22	0.15	2	1.9	4.4										5	
1040	10 01	0 15	1		4.7						0 097	0.013	42.5	2.7	6	1
1041	10.01	0 15	1		4 9						0 048	0 003	60.6	1.5	6	5
1042	10.21	0.15	3	6.0	9.4						0.025	0.001	76.7	1 8	7	6
1043	9 84	0.25	4	4.8	6.1	0 45	1	0 90	1	1	0.14	0 02	37.3	3.2	8	6
1044	10.87	0.15	3	2 9	4.3						0.19	0 03	20.0	2.0	4	2
1045	13 09	0 25	1		0 2										13	
1046	10.41	0.15	4	3.0	5.4										6	
1047	12.00	0.25	2	5.8	14 9	0.54	3	0 91	2	2					6	
1048	9.68	0.15	5	1.7	21 1	0.32	3	0.71	3	1	0 045	0 003	72 5	2 1	3	3
1049	10.6	0.15	1								0 029	0 007	58.2	6 6	7	7
1050	12 7	0 15	1												8	
1051	9.87	0.15	1		6.1						0.042	0.002	68.6	1.7	4	4
1052	12.02	0.25	1		8.2	0.54	1	0.90	1	1					3	
1053	12.56	0.15	2	7 2	7.4										14	
1054	10.49	0.15	3	4 5	8.1						0.045	0.009	49.6	5.0	7	7
1055	12.10	0.25	2	5.3	6.2										5	
1056	11.62	0 25	1		5.7										2	
1057	11.06	0.15	3	2.2	6 7						0.027	0.003	49.1	2.5	9	2
1058	11.99	0.25	5	4.5	20.6						0.13	0.02	14.6	1.5	5	2
1059	10.56	0.15	1		5.9										7	
1060	13.1	0.25	1												3	
1061	12 07	0.15	1		18.4	0.34	1	0.68	3	2					4	
1062	10.10	0.15	3	3 4	12.2										2	
1063	11.41	0.25	2	3.7	23.4						0 14	0.02	18.0	1.2	7	3
1064	11 1	0.15	1								0.15	0 02	19.8	1.3	3	3
1065	12.6	0.25	1												4	
1066	12.34	0.25	1		2 6											
1067	10.83	0.15	5	4.1	7 0										12	
1068	10.58	0.15	1		14.9						0.14	0.01	26.8	1.6	4	1
1069	9.6	0.15	1								0.13	0.01	43.2	1.6	2	2
1070	10.91	0.15	1		2.5						0.048	0.007	40.0	2.7	7	6
1071	10.10	0.15	3	2 4	4 2						0.058	0.003	52.7	1.5	2	2
1072	10.87	0.15	1		0.5						0 037	0 002	46.5	1.1	10	10
1073	11.46	0 15	1		1.1										2	
1074	10.16	0 15	1		2.8						0 052	0.003	53.8	1.7	11	5
1075	10.21	0.25	4	2.5	8.3	0.37	2	0.76	2	1	0.089	0.021	40.5	4.7	6	2
1076	12.51	0.495	7	1.1	22.4	0.24	4	0.63	4	3	0.029	0 003	24.5	1.0	9	1
1077	12.8	0.25	2												5	
1078	11.61	0 25	5	1.5	9.0	0.49	3	0.89	2	2					7	
1079	11 25	0.25	4	2.3	12.1	0.40	2	0.80	1	1	0.099	0 010	23.7	1.1	9	4
1080	12 32	0.15	3	6.4	11.4	0.21	2	0.62	2	2	0 027	0.007	27.8	3.3	8	6
1081	11.65	0.15	1		3.7						0.024	0 001	40.3	1.2	8	8
1082	10.41	0.15	2	5.3	11.4	0.32	2	0.70	2	1	0.055	0.005	47.0	2.0	2	2
1083	12.8	0.25	1												4	
1084	10 69	0.15	3	2.9	9 7						0.091	0.026	32.0	4.5	4	3
1085	9 72	0.15	3	2.1	8.2						0 044	0.002	72 3	1.5	8	7
1086	9 55	0.15	2	4.7	6.4						0 054	0.006	70.5	4 1	6	5
1087	9.80	0.25	6	2.3	7.0	0.37	2	0.80	1	3	0 12	0 01	40.8	2.3	6	1
1088	11.45	0.25	5	3.5	10.1	0.48	2	0.93	4	3					8	
1089	11 78	0.25	3	1 9	4.6						0.17	0.02	14.1	0.8	7	4
1090	12.8	0.25	1												10	
1091	10.7	0.15	1								0.067	0.004	36.3	1.1	2	1
1092	10.61	0.15	2	3.6	5.2						0 044	0.004	47.6	2 0	4	2
1093	8 82	0.15	4	7.6	10.8	0.36	2	0 68	2	1	0 036	0.002	120	3	3	3
1094	12 02	0.15	3	8 4	24.2						0 083	0 010	18.1	1 0	6	2
1095	10.59	0.25	2	3.6	9.9						0.11	0 04	29.5	6.1	6	3

Magnitudes, UBV Colors, IRAS Albedos and Diameters

M.P.	H	G	No. Obs	Min Phase	Max Phase	U-B	UQ	B-V	BQ	UBV Ref	Albedo	Albedo Unc.	D	D Unc	No. Obs Pre	No. Obs Acc
1096	10.20	0.15	2	4.6	7.0						0.069	0.007	46.2	2.3	6	3
1097	11.71	0.15	1		2.0						0.057	0.005	25.3	1.0	6	2
1098	10.60	0.15	1		3.5						0.12	0 01	28.5	1.2	7	2
1099	10.04	0.15	2	5.7	11.9						0.13	0.07	35.8	9.5	11	2
1100	11.25	0.25	5	1.0	7.8										2	
1101	10.8	0.15	1								0.047	0.003	41.0	1.3	9	5
1102	9.69	0.15	4	0.8	8.0	0.39	1	0.72	1	1	0.12	0.03	43.5	5.5	5	4
1103	12.49	0.40	2	18.5	19 1	0.24	3	0.73	3	2					3	
1104	12.4	0.15	1								0.033	0.002	24.2	0.6	8	5
1105	10.20	0.25	4	4.7	6.6	0.42	2	0.77	2	2	0.081	0.018	42.5	4.7	7	7
1106	11.7	0.15	1												4	
1107	8.96	0.15	2	3.8	7.1						0.070	0.008	81.0	4.7	4	1
1108	11.88	0.15	1		17.5	0.31	1	0.68	2	2					2	
1109	10.04	0.15	6	0.6	8.3	0.29		0.60	2	1	0.035	0.001	69.5	1.3	6	6
1110	12.16	0.25	1		5.8										6	
1111	10.74	0.15	4	3.1	6.5			0.63	1	1					5	
1112	10.15	0.25	5	1.6	9.3	0.44	1	0.78	2	1	0.095	0.006	40.3	1.2	5	5
1113	9.52	0.15	3	3.6	7.5						0.13	0.01	44.7	2.8	2	1
1114	9.72	0.15	2	5.8	6.8						0.057	0.004	63.0	2.3	3	2
1115	9.31	0.15	3	4.3	6.0						0.066	0.004	71.1	2.0	3	3
1116	9.65	0.15	1		5.1						0.14	0.01	40.7	0.8	8	6
1117	12.13	0.25	2	5.4	9.0										4	
1118	9.79	0.15	2	4.9	5.5						0.033	0.001	80.7	1.5	11	9
1119	11.51	0.15	1		3.4						0.022	0.003	44.8	3.3	3	1
1120	12.2	0.25	1												4	
1121	11.4	0 15	1												5	
1122	11.6	0.15	1								0.20	0.02	13.8	1.0	2	1
1123	11.62	0.25	2	9.3	9.4										6	
1124	10.79	0.15	2	6.3	7.7	0.22	3	0.70	3	2	0 10	0.01	28.6	2.1	4	1
1125	12.01	0.15	3	0.4	5.1										6	
1126	12.6	0.25	1								0.085	0.007	13.7	0.5	3	1
1127	10.92	0.15	2		11.1	0.30	2	0.70	2	1	0.030	0.007	50.3	6.0	9	8
1128	10.79	0.15	5	0.6	4.0						0.052	0.004	40 2	1.5	2	1
1129	10.04	0.25	5	4.1	7.4	0.41	1	0.78	1	1	0.11	0.01	38.3	1.1	2	2
1130	12.0	0.25	2												1	
1131	14.2	0.25	1												2	
1132	11.07	0.15	1		5.5						0.056	0.009	34.2	2.5	3	1
1133	12.30	0.25	4	1.1	17.4	0.51	1	0.88	2	2					4	
1134	13.66	0.15	1		5.2										7	
1135	10.37	0.15	2		5.5						0.047	0 006	51.5	3.5	5	4
1136	11.00	0.15	4	2.2	8.5						0.094	0.009	27.2	1.2	2	1
1137	11.16	0.25	4	3.3	4 8						0.089	0.007	26.1	1.0	3	2
1138	11.1	0.15	1												11	
1139	12.55	0.25	1		7.9	0.50	3	0 92	3	2					7	
1140	10.33	0.25	2	6.2	6.7	0.48	2	0.91	2	1	0 13	0.01	31.5	1.1	8	5
1141	13.4	0.25	1								0.056	0.007	11.6	0.7	11	1
1142	10.48	0.15	4	2 0	7.2										10	
1143	8.43	0.15	6	1.0	4.9	0.24	2	0.80	2	3	0.041	0.003	135	5	6	3
1144	10.12	0 15	4	1.9	10.0	0.24	3	0.71	3	2					10	
1145	11.10	0.25	3	3.8	5.5						0.098	0.006	25.5	0.7	6	4
1146	9.80	0.15	2	9.7	14.3	0.23	3	0 68	3	3	0.17	0.01	34.5	1.2	4	3
1147	12.04	0.25	1		4.5										7	
1148	10.10	0.25	4	2.7	18.7	0.44	3	0.86	3	3	0.16	0.01	31.7	1.8	3	1
1149	10.29	0.15	6	2 6	10.8						0.041	0.002	57.3	1.0	9	8
1150	13.3	0.25	2													
1151	13 7	0.25	1								0.012	0.002	22.0	1.5	4	1
1152	11.1	0.25	1								0.18	0.01	18.2	0.6	5	3
1153	12.26	0.25	2	1.3	3.7										2	
1154	10.50	0.15	2	2.2	15.9	0.23	1	0.66	1	2	0.027	0.002	64.3	2.7	9	7
1155	11.81	0.25	2	7.1	7.2						0.14	0.05	15.2	2.6	9	3
1156	12.7	0.25	1												4	
1157	10.09	0.15	3	5.2	6.8										8	
1158	11.03	0.25	1		7.3						0.14	0.02	21.7	1.5	3	2
1159	11.54	0.25	2	6.4	8.1						0.044	0.002	31.0	0.7	6	6
1160	11.14	0.25	1		0.8										2	
1161	11.14	0.15	1		3.8						0.040	0.004	39.0	2.0	5	1
1162	9.58	0.25	4	0.6	9.2	0.26	3	0 77	3	3	0.080	0.012	56.8	4.1	2	2
1163	10.62	0.15	4	2.7	6.3						0.082	0.022	34.8	4.5	7	3
1164	13.16	0.25	1		15 2										10	
1165	10.65	0.15	1		1.7						0.032	0.008	54.6	6.6	10	5
1166	11.4	0.15	1								0 078	0.008	24.0	1 1	3	1
1167	9.94	0.15	5	1.7	11.5	0.20	2	0.74	2	2	0.039	0.006	69.0	5.2	6	3
1168	12.41	0.15	2	3.9	18.6						0 12	0.01	12.5	0.6	7	2

Magnitudes, UBV Colors, IRAS Albedos and Diameters

M.P.	H	G	No. Obs.	Min Phase	Max Phase	U-B	UQ	B-V	BQ	UBV Ref	Albedo	Albedo Unc.	D	D Unc	No. Obs Pre	No. Obs Acc
1169	13.1	0.25	1												5	
1170	12.52	0.25	1		19.2	0.45	2	0.86	2	2	0.11	0.01	12.3	0.6	5	1
1171	9.84	0.15	5	0.7	8.9	0.25	4	0.69	4	3	0 038	0.002	73.6	2.2	4	4
1172	8.26	0.15	7	2.9	10 0	0.26	4	0.73	4	3	0.038	0.002	151	5	4	3
1173	8.91	0.15	7	1.1	8.1	0.26	3	0.71	2	3	0 026	0.006	135	16	5	4
1174	11.7	0.25	1												2	
1175	10.41	0.15	2	2.1	2.5										2	
1176	11.0	0.15	1								0 064	0.003	32.0	0.7	8	8
1177	9.25	0.15	3	2.4	11.7	0.24	2	0 67	2	2	0 039	0.002	95.5	2.6	6	4
1178	11.82	0.15	1		4.5						0 070	0.015	21.6	2.3	12	8
1179	13.9	0.25	1													
1180	9.15	0.15	5		16.2	0.22	3	0 70	3	2					2	
1181	11.5	0.15	1													
1182	11.44	0.25	1		1.8						0.14	0.03	18.0	2.0	8	3
1183	11.96	0.25	3	0.9	4.8						0.068	0.010	20.6	1.5	6	3
1184	11.39	0.15	4	4.9	9.0										10	
1185	12.11	0.25	4	5.7	9.0	0 51	3	0.92	2	2					9	
1186	9.52	0.25	3	2.7	11.1	0.43	1	0 79	1	1	0 18	0.02	39.0	2.5	2	2
1187	11 35	0 15	2	0 4	3.2						0.037	0.004	37.0	2 0	7	4
1188	12.11	0 25	4	2.8	4.7						0.13	0.01	13.8	0.5	9	6
1189	9.98	0.15	3	0.5	9.1						0 053	0.003	58.3	1.7	2	2
1190	12.0	0.25	1								0.065	0.006	20.1	0.8	4	2
1191	10.5	0.15	1								0.052	0.003	45.6	1.0	6	4
1192	12 93	0.25	1		3.5										8	
1193	12.1	0.15	1												9	
1194	10.62	0.15	2		4.4						0 031	0.002	56.8	1.3	3	3
1195	13.4	0.25	1												2	
1196	10.36	0.15	3	2.4	13 0						0.11	0.01	33.8	2 5	18	7
1197	10.15	0.15	2	5.8	8.4						0.064	0.011	49.0	4 1	6	6
1198	15.5	0.25	1												6	
1199	10.49	0.25	3	2.8	5.1	0 33	1	0.76	1	1	0.089	0 011	35.5	2.1	6	4
1200	10.68	0.15	2	1.2	2 6						0 054	0 008	42.0	3.2	11	10
1201	11 50	0.15	2	2.9	3.7						0 030	0.006	38.3	3.8	12	11
1202	10.2	0.15	1								0.033	0.003	66.3	2.7	9	2
1203	11.76	0.15	4	2.7	12.5						0.017	0.005	44.7	6.6	7	2
1204	12.27	0.25	1		1.5										2	
1205	14.0	0.15	1												6	
1206	9.48	0.15	1		2.8										6	
1207	11.22	0.25	1		10.6						0.074	0.007	27.7	1.3	4	2
1208	9.00	0.15	3	3.3	9.4	0.32	1	0.69	1	3	0.036	0.002	111	4	4	3
1209	10.3	0.15	1												5	
1210	10.08	0.25	3	8.2	14.7			0.83	1	1	0.13	0.01	34.5	2.2	7	2
1211	10.94	0.15	2	6 1	10.2						0.043	0 005	41.6	2.5	3	2
1212	9.38	0.15	5	2.2	12 5	0 22	4	0.70	4	3	0.038	0.005	90 7	5.5	5	5
1213	11.0	0.15	1								0.036	0.010	43.2	5.8	5	1
1214	11 01	0.15	2	5.5	6.6						0.051	0.009	37.0	3.3	12	9
1215	11 39	0.40	2	11.3	24.8	0.46	2	0 88	2	3					6	
1216	12 73	0.25	2	2 8	7.6	0.53		0 90	1	1					6	
1217	13 3	0.25	1												15	
1218	13.08	0.25	2		1.6										9	
1219	12.11	0.25	2	4.9	7.3						0 14	0.02	13.1	1.0	4	1
1220	11.1	0.25	1												2	
1221	17.9	0.25	1												5	
1222	12.0	0.15	1								0.055	0.012	22.0	2.5	8	5
1223	10.66	0.25	4	1.5	16.4	0.40	1	0.84	2	1					7	
1224	11.47	0.25	1		17.1	0.41	1	0.90	1	1	0.19	0.01	15.5	0.3	6	6
1225	12.5	0.25	2												5	
1226	12.1	0.15	1								0.074	0.018	18.5	2.2	9	3
1227	10.28	0.15	2	2.8	6.4						0.058	0.008	48.2	3.1	6	2
1228	11.6	0.15	1												3	
1229	11.04	0.15	1		10.0						0.070	0.005	31.0	1.0	4	3
1230	13.5	0.15	1												6	
1231	11 5	0.15	1								0.084	0.036	22.0	4.6	5	3
1232	10.21	0.15	4	2.8	4 5						0.093	0.020	39.6	4.2	2	1
1233	11.2	0.15	1								0.048	0.003	34.5	0.8	13	7
1234	10.77	0.25	1		8.8						0.10	0.02	28.3	3.0	9	2
1235	12.96	0.15	2	30.1	31.8	0.33	1	0.75	1	1					12	
1236	11.92	0 25	5	4.2	19.4	0.38	2	0.76	2	2	0.043	0.004	26.3	1.1	7	2
1237	10.85	0.15	3	4.3	8.0						0.046	0.002	42.0	1.0	7	7
1238	11.9	0.15	1								0.059	0.005	22.5	0.8	3	2
1239	12.5	0.15	3								0.056	0.010	17.1	1.5	3	2
1240	9.80	0.15	2	3.0	6.3						0.058	0.004	60.5	2.0	5	4
1241	9.45	0.15	1		2.1	0.29	1	0.75	1	1	0.039	0.005	86.2	5.3	6	6

Magnitudes, UBV Colors, IRAS Albedos and Diameters

M.P.	H	G	No. Obs.	Min Phase	Max Phase	U-B	UQ	B-V	BQ	UBV Ref	Albedo	Albedo Unc.	D	D Unc	No. Obs Pre	No Obs Acc
1242	10.31	0.15	1		5.2						0.055	0.005	49.2	2.3	2	2
1243	9.80	0.15	5	2.8	13.3						0.037	0.006	75.5	6.5	8	8
1244	11.41	0.25	1		7.2						0.049	0.013	31.2	4.1	5	5
1245	10.05	0.488	5	1.2	13.3	0.44	3	0.83	4	3	0.20	0.02	28.3	1.6	2	1
1246	10.77	0.15	2	11.0	15.4						0.22	0.03	19.8	1.5	6	5
1247	10.64	0.15	3	0.9	5.6	0.29	1	0.68	2	1	0.059	0.005	40.6	1.5	2	2
1248	9.84	0.15	3	8.5	8.8											
1249	11.77	0.25	4	4.9	6.0	0.48	2	0.88	3	2	0.15	0.03	14.6	1.5	7	5
1250	12.26	0.15	1		4.4						0 046	0.006	21.7	1.2	6	1
1251	10.71	0.40	4	4.0	24.2	0.26	2	0 71	3	3						
1252	10.97	0.25	2		14.0	0.42	1	0.89	1	1					4	
1253	12.1	0.15	1								0.027	0.003	30.1	1.7	2	1
1254	10.92	0.15	2	1 8	5.2						0.031	0 007	49.2	5.1	7	7
1255	10.41	0.15	2	1.7	5.7						0.10	0.01	34.6	2.5	5	4
1256	9.69	0.15	5	4.9	10.2	0.24	3	0.73	3	2	0.039	0.003	78.0	2.5	6	3
1257	11.90	0.25	2	2.1	2.2											
1258	10.53	0.15	3	2.4	4.5						0.048	0.006	47.5	3.0	7	6
1259	10.83	0.25	1		3.9						0.063	0.012	36.2	3.5	8	6
1260	11.7	0.15	1													
1261	10.7	0.15	1								0.077	0.008	34.2	1.8	4	4
1262	10.18	0.15	1		16.1						0.043	0.005	58.7	3.6	3	2
1263	10.48	0.15	2	18.2	21.8	0.29	1	0.73	1	1	0.044	0.002	50.7	1.2	4	4
1264	9.7	0.15	1								0.037	0.002	77.5	1.5	7	6
1265	10.80	0.25	1		13.2										10	
1266	9.27	-.079	5	2.0	12.6	0.34	2	0.73	3	3	0.060	0.009	76.0	5.7	6	6
1267	12.27	0.25	2	4.4	7.7						0.030	0.003	26.8	1.3	6	2
1268	9.17	0.15	5	0.8	3.9	0.24	3	0.66	3	3	0.040	0.002	97.5	2.6	4	4
1269	8.73	0.15	2	2.3	15.2	0.27	2	0.77	3	2	0.047	0.002	109	2	6	6
1270	12.73	0.25	2	3.1	3.6						0.15	0.01	9.58	0.57	7	2
1271	10.52	0.15	1		3.7						0.045	0.008	49.5	4.5	5	5
1272	12.4	0.15	1												2	
1273	13.05	0.25	2	2.8	9.5						0.011	0.001	30.5	1.6	7	1
1274	11.89	0.25	3	1 0	4.8	0.53	1	0 90	2	1					11	
1275	10.72	0.15	5	4.2	8.8	0.29	3	0.70	3	3	0.084	0.029	33.0	5.6	9	3
1276	10.7	0.15	1								0.068	0.009	36.2	2.5	3	2
1277	11.12	0.15	2	1 4	11.4	0.38	3	0.73	3	2	0.070	0.013	30.0	2.7	8	7
1278	11.05	0.25	1		7.0										2	
1279	12.57	0.25	2	6.2	8.7										6	
1280	10.30	0.15	3	2.9	10.7	0.36	1	0.67	1	2	0.044	0.006	55.3	3.8	6	6
1281	11.51	0.15	2		4.7										2	
1282	10.07	0.15	4	6.4	6.6						0.053	0.007	55.7	3.6	6	6
1283	10.8	0.15	1								0.093	0.006	29.8	1.0	7	4
1284	10.23	0.15	3	3.7	19.8	0.35	2	0.77	2	2	0.088	0.005	40.2	1.0	6	6
1285	10.2	0.15	1								0 068	0.004	45.5	1.3	7	6
1286	10.67	0.25	4	4.3	13.4	0.43	1	0.85	1	1	0 083	0.023	33.8	4.6	5	2
1287	11.06	0.25	3	2.6	7.2						0.090	0.011	27.0	1.5	4	1
1288	11.33	0.15	1		3.3						0.034	0.009	39.2	5.5	2	1
1289	10.64	0.25	4	0.1	16.4	0.38	1	0.78	1	1					2	
1290	12.5	0.25	1												9	
1291	10.36	0.25	7	2.6	7.3										4	
1292	11.41	0.15	1		5.4											
1293	14.0	0.25	1								0.059	0.019	8.52	1.36	7	1
1294	10.51	0.15	2		7.5						0.074	0.011	38.5	2.8	5	5
1295	10.5	0.15	1								0.040	0.003	52.0	1.6	2	2
1296	11.5	0.25	1								0.061	0.010	26.5	2.2	8	7
1297	11.2	0.25	1								0.012	0.001	66.0	3.7	11	1
1298	10.90	0.15	1		2.4						0.034	0.002	47.3	1.3	3	3
1299	11.91	0.15	1		3.6										6	
1300	11.11	0.15	2	4.5	5 8						0.061	0.010	32.1	2.6	8	3
1301	10.6	0.15	1								0.15	0.01	24.7	1.1	11	6
1302	10.7	0.15	1												6	
1303	9.3	0.15	1								0 041	0.002	88.8	2 3	4	3
1304	9 19	0.15	2		3.4						0.16	0.01	47.8	1.7	3	2
1305	10.49	0.15	4	0 9	2.5						0.13	0.01	29.5	2.0	6	2
1306	9 62	0.25	5	1.6	4.8	0.40	1	0.85	1	1	0.052	0.007	69.5	4.7	6	6
1307	12.33	0.25	2	5.7	17.7	0 55	2	0.88	2	2					7	
1308	10.76	0.15	2	0.9	1.3						0.043	0.003	45.0	1.3	5	5
1309	10.24	0.15	2	1.2	1.6						0 039	0.005	59 8	3.7	6	6
1310	11 55	0.25	1		25.0	0.44	3	0.91	3	2						
1311	12.6	0.25	1												12	
1312	11.02	0.15	1		3.3						0.047	0.003	38.3	1.2	2	2
1313	11.8	0.15	1												4	
1314	12.73	0.25	1		8.8	0.46	1	0 87	1	1	0.071	0.015	14.1	1.5	10	1

Magnitudes, UBV Colors, IRAS Albedos and Diameters

M.P.	H	G	No. Obs.	Min Phase	Max Phase	U-B	UQ	B-V	BQ	UBV Ref	Albedo	Albedo Unc.	D	D Unc	No. Obs Pre	No. Obs Acc
1315	9.95	0.15	1		4.5						0.043	0.002	65.5	1.6	5	5
1316	13.6	0 25	1												7	
1317	9.93	0.15	3	5 1	8.0	0.34	1	0.72	1	1					4	
1318	12.0	0.25	1								0.12	0 03	14.5	1.7	10	8
1319	10.6	0 15	1												6	
1320	10.7	0.15	1								0.041	0.004	45.6	2.2	3	2
1321	10.29	0.15	3	3.1	9 7						0 10	0.01	36.3	2.1	4	1
1322	12.9	0.25	1												10	
1323	10.26	0.15	3	3.3	6.5						0 038	0.007	60.1	5.6	2	2
1324	12.4	0.25	1												7	
1325	12.1	0 15	1								0.16	0.01	12.5	0.5	6	1
1326	10.96	0.25	2		5 7	0.48	1	0 78	1	1					2	
1327	12 17	0.15	1		2.4						0.021	0.003	33.5	2.0	4	1
1328	10.35	0.15	2		8 1	0.16	1	0.70	1	1	0.036	0.007	59.6	5.5	7	7
1329	10.80	0.25	3	6.0	11.0	0.53	1	0.87	2	1	0 11	0.02	27.5	3.0	4	1
1330	10 18	0.15	2	14.5	14 8	0.17	1	0.67	1	1	0 044	0.008	58.0	5.3	12	11
1331	10 35	0.25	2	2.1	11.6	0.35	1	0.64	1	1	0 094	0.019	37.0	3.7	6	6
1332	10.2	0 15	2								0.059	0.013	49.5	5.3	5	5
1333	11.71	0 15	3	5.5	8.5										4	
1334	10 01	0.15	2	3.8	5.8						0 21	0.09	28 3	6.0	8	2
1335	13.7	0.25	1												5	
1336	10.93	0.25	3	1 8	3.2	0.37	2	0.81	2	2	0.11	0.02	25.1	2.7	2	1
1337	11 00	0.15	2	5.9	11.2						0.042	0.008	41.0	4 1	12	8
1338	12.91	0.25	1		4 7										7	
1339	10 84	0 25	2	4.3	13 0	0.43	2	0 79	2	1	0.10	0.01	27.6	1 5	7	2
1340	11.32	0.15	4	0.1	8.3						0.060	0.016	29.5	4.0	4	1
1341	10 59	0.15	5	7.6	15 7	0 26	2	0.68	2	1	0.10	0.02	30.7	3.0	7	6
1342	11.45	0.25	1		20.4	0.30	3	0 71	3	2	0.11	0.03	20.1	2.6	11	7
1343	11.42	0 15	2	3.9	4 1						0.059	0.006	28 3	1.3	3	2
1344	13.00	0.25	1		1 9										4	
1345	9.74	0.15	3	4.4	10.8	0.30	2	0.71	2	3	0.036	0.003	79.3	3.1	6	4
1346	11.29	0.15	1		8.5						0.23	0.02	15.1	0.7	2	2
1347	11.73	0.15	1		10.6						0.028	0.002	36.0	1.0	9	6
1348	11.20	0 15	3	2 1	4.6										2	
1349	10 66	0 15	2		4 3										2	
1350	10 62	0.25	2	1 1	5 9	0 37	1	0.85	3	2	0.14	0.01	26 1	1.3	2	1
1351	10 05	0.15	1		0.8						0.037	0.005	67.1	4.5	4	4
1352	11.25	0.15	1		2.6						0.097	0.013	24.0	1.5	7	1
1353	10 00	0.25	1		4.3						0.12	0.03	37.5	4.5	7	6
1354	10.32	0 15	1		8.1						0.048	0.012	52.5	6.8	7	5
1355	13.18	0.25	2	14.6	19.7	0.26	1	0.71	1	2					8	
1356	10.26	0.15	1		1.8						0 031	0 005	67.2	5.8	4	4
1357	11.03	0.15	1		6.3			0.73	1	1	0 033	0.003	45.1	2.0	6	1
1358	12 52	0.25	3	3.4	22.0						0.030	0.004	24.0	1.5	2	2
1359	10.53	0.15	2		13.5	0.36	1	0.72	1	1	0 035	0.002	55.5	1.3	7	7
1360	11.3	0.15	1		10.9						0.054	0.015	31.0	4.2	7	4
1361	11.40	0.15	1		10.9						0.040	0.010	34.7	4.5	9	6
1362	11.10	0.15	2	5.4	15.9	0.36	2	0.72	2	1	0.066	0.008	31.1	2.0	2	2
1363	11.60	0.25	1		2 3										8	
1364	10.97	0.25	1		4.4						0.084	0.011	29.3	1.8	6	1
1365	12.23	0.25	2	4.5	7.5										3	
1366	10.39	0.15	2	5.2	7.8						0.12	0.01	31.7	1.5	7	2
1367	13 1	0.25	1												4	
1368	10 96	0.15	3	5.0	7.9						0 14	0.01	22.3	0.8	8	4
1369	10.69	0.15	1		9.0						0.045	0.009	45.5	4.7	5	3
1370	13 7	0.25	1												2	
1371	11.1	0 15	1								0.049	0.012	35.2	4.2	1	1
1372	11.6	0.15	1												3	
1373	13.1	0.15	1												13	
1374	13.6	0.25	1												2	
1375	11 88	0.25	2	4 1	5.5						0 055	0.008	23.7	1.5	6	1
1376	12 48	0.25	1		6.6										4	
1377	13 0	0.25	1												11	
1378	12 25	0.25	1		1.4										2	
1379	10.96	0.15	5	3.4	10.3						0.16	0.01	21.0	1.0	3	1
1380	11.9	0.15	1												7	
1381	11 96	0.25	5	2.7	13.5						0.050	0.006	24.0	1.5	5	1
1382	12.26	0.25	2		4.5										2	
1383	11.77	0.15	1		3 0						0.059	0.012	24.2	2.5	10	7
1384	11.6	0.15	4								0 045	0.007	29 0	2.2	3	3
1385	10.92	0 15	2	2 2	4.8						0 12	0.01	25.0	1.3	4	2
1386	13 5	0.25	1												3	
1387	13.2	0.25	1												3	
1388	11.10	0 25	1		23.2						0 074	0.018	29.3	3.5	2	1

Magnitudes, UBV Colors, IRAS Albedos and Diameters

M.P.	H	G	No. Obs	Min Phase	Max Phase	U-B	UQ	B-V	BQ	UBV Ref	Albedo	Albedo Unc.	D	D Unc	No. Obs Pre	No. Obs Acc
1389	11.64	0.25	3	2.1	4.4						0.049	0.007	28.1	2.0	7	1
1390	9.24	-.221	7	1.1	15.4	0.21	2	0 71	3	3	0.033	0.002	104	3	4	3
1391	12.08	0.25	5	6.9	18.4	0 46	3	0.87	4	3					7	
1392	11.72	0 15	1		6.2	0.23	1	0.76	1	1	0.040	0.003	30.0	1.1	8	3
1393	12.28	0.25	2	3.5	7.3										2	
1394	11.89	0.25	1		4.8										3	
1395	11.5	0.15	1								0.095	0.012	20.8	1.2	6	1
1396	11.87	0.25	2	4 3	5.0						0 16	0.06	14.0	2.5	15	2
1397	11.49	0.15	4	1.5	13.8										4	
1398	10.31	0.25	2		5.6						0.11	0 01	34.5	2.1	6	1
1399	14 0	0.25	1												3	
1400	11 7	0.15	1												1	
1401	12.29	0.25	2	6.0	6.4	0.48	2	0.88	2	1					4	
1402	12.94	0.15	1		12.6										4	
1403	11.29	0.15	1		4.6										4	
1404	9.0	0.15	1								0.049	0.005	92.0	4.8	6	6
1405	12.52	0.25	1		22 6										9	
1406	11.3	0.15	2								0.054	0.018	31.0	5.0	9	4
1407	11.22	0.15	1		4.2						0.10	0.02	23.1	2.5	9	6
1408	10.9	0.15	1								0.046	0.011	41.0	4.8	8	1
1409	10.57	0.15	1		2.8						0.077	0.013	36.8	3.0	6	6
1410	11.32	0.25	3	2.8	10.1						0.10	0.01	22.6	1.3	2	1
1411	10.88	0.15	2	2.7	4.2						0.066	0.008	34.3	2.0	14	8
1412	12.4	0.25	1												4	
1413	11.41	0.25	2	5.4	10.1						0.077	0.021	25.0	3.5	2	2
1414	12.6	0 15	1								0.039	0.012	20.0	3.0	5	3
1415	12.43	0.25	3	6.3	9.2	0.48	1	0.86	2	1	0.064	0.009	17.0	1 0	7	1
1416	10.47	0.25	2	3.1	5.6	0.41	1	0.79	1	1					3	
1417	11.19	0.15	2		4.3										5	
1418	12.01	0.25	5	3.8	29.2	0.48	1	0.92	1	2	0.22	0 02	11.0	0.5	12	1
1419	11.47	0.25	3	0.1	5.1						0.14	0.01	17.5	1.0	5	1
1420	11.7	0.15	1								0 064	0.007	23.8	1.2	6	3
1421	10.36	0.15	2		4.8										2	
1422	13.43	0.25	1		0.7	0.52	1	0.87	1	2					10	
1423	11.23	0.25	2	1.0	3.6						0.056	0.006	31.8	1.7	8	1
1424	9 48	0 15	1		4.9						0.052	0.003	74.0	2.0	4	3
1425	11.6	0.15	1												7	
1426	10.9	0.15	1								0.21	0.03	18.5	1.3	10	5
1427	10.72	0.15	1		6.8						0.059	0.002	39.2	0.6	11	10
1428	10.36	0.15	1		3.3						0.035	0.007	60.0	5.6	4	3
1429	12.0	0.15	2												2	
1430	12.0	0.15	1												2	
1431	11.4	0.15	1												8	
1432	12.26	0.25	1		7.2										4	
1433	11.6	0.15	1												8	
1434	10.42	0.25	7	2.7	10.8	0.40	2	0.81	2	3	0.12	0.04	31.0	5.0	6	2
1435	12.76	0.15	1		2.3						0 035	0.006	20.0	1.6	8	2
1436	10.70	0.15	1		5.5						0.023	0.001	63.6	1.6	4	4
1437	8 30	0.15	2	3.5	5 8	0 24	2	0.70	2	1	0.029	0.001	171	4	8	6
1438	11.22	0.15	1		7.9						0.033	0.002	41.7	1.0	3	3
1439	10.65	0 15	3	9 7	10.6	0.32	1	0.75	1	1	0.027	0.003	60.1	2.8	6	4
1440	11.7	0.15	1												2	
1441	13.0	0.15	1								0.035	0.004	17.6	1.0	8	1
1442	11.62	0.25	1		7.9	0 44	1	0 87	1	2					4	
1443	11 2	0.15	1												4	
1444	11 0	0 15	1								0.069	0.008	31.2	1.8	4	1
1445	11.85	0.15	2	3 8	19.0	0.33	2	0.66	2	2					6	
1446	13.18	0.25	1		2.2										5	
1447	11.12	0.15	1		5.6										7	
1448	13.1	0.25	1								0.017	0.002	23.0	1.3	7	2
1449	12 6	0 25	1												2	
1450	11.79	0.15	3	2.6	10.1						0.11	0 02	17.2	2.0	3	2
1451	12.6	0.25	1													
1452	11.9	0.15	1												8	
1453	12.58	0.25	4	12.0	23.5	0.53	2	0.94	2	3					6	
1454	13 1	0.25	1												5	
1455	13.3	0.25	1												11	
1456	10.92	0.15	1		15.4	0.34	1	0 69	1	1	0 036	0.001	45.5	0.8	8	8
1457	11.2	0.15	1												2	
1458	11.64	0.15	2	3.0	6.1						0.11	0.02	18.7	2.1	9	6
1459	10.7	0.15	1								0.079	0.021	33.2	4.2	7	2
1460	12.6	0.15	1												5	
1461	10.07	0.25	3	5.1	19.1	0.20	2	0.71	2	3	0.11	0.01	38.2	1.5	4	3

Magnitudes, UBV Colors, IRAS Albedos and Diameters

M.P.	H	G	No. Obs.	Min Phase	Max Phase	U-B	UQ	B-V	BQ	UBV Ref	Albedo	Albedo Unc.	D	D Unc	No. Obs Pre	No. Obs Acc
1462	10.9	0.25	1								0.072	0.015	31.5	3.1	7	3
1463	10.9	0.15	1								0.028	0.002	51.7	2.0	4	3
1464	11.14	0.25	4	2.6	7.5						0.082	0.011	27.5	1.8	6	1
1465	11 0	0.15	1												2	
1466	12.9	0.25	1								0.022	0.001	23.5	0.7	9	4
1467	8.55	0.15	4	5.8	11.5	0.38	2	0.72	2	3	0.054	0.006	112	6	2	1
1468	13.49	0.25	3	7.2	10.8						0.022	0.003	17.7	1.1	4	1
1469	9.77	0.15	4	4.8	9.6						0.060	0.009	60.2	4.3	9	5
1470	11.0	0.15	1								0.039	0.002	40.5	1.0	8	6
1471	11.2	0.15	4								0.050	0.008	33.1	2.7	8	6
1472	12.63	0.25	1		5.2										5	
1473	12.4	0.15	1								0.052	0.008	19.0	1.5	11	5
1474	12.61	0.15	3	16.9	17.2	0.20	1	0	63	3	1				6	
1475	12.9	0.25	1												6	
1476	13.6	0.25	1												4	
1477	11.59	0.15	2	12.2	13.6			0.72	1	1	0.042	0.003	31.0	1.0	4	3
1478	12.75	0.25	1		13.6										2	
1479	11.71	0.15	5	3.8	13.9			0.69	2	1					13	
1480	13.38	0.25	1		5.1											
1481	10.47	0.15	2	2.9	8.3						0.085	0.006	36.6	1.2	2	2
1482	10.97	0.25	5	3.1	7.0										8	
1483	11.70	0.15	3	2.2	5.7										7	
1484	11.1	0.15	1								0.029	0.004	46.3	3.2	4	4
1485	11.3	0.25	1								0.072	0.009	26.3	1.6	7	1
1486	13.47	0.25	1		5.2										10	
1487	10.53	0.15	3	2.4	5.2						0 085	0.019	35.6	4.0	2	1
1488	10.8	0.15	1												9	
1489	11.47	0.15	1		11.8						0.046	0.015	31.5	5.0	8	3
1490	12.15	0.25	1		11.4						0.058	0.014	20.5	2.5	8	2
1491	11.4	0.25	1								0.061	0.009	27.3	2.0	5	2
1492	12.98	0.25	3	9.0	15.0						0.051	0.016	15.0	2.2	7	1
1493	11.43	-.203	5	7.9	25.9	0.23	3	0.64	3	3	0.069	0.014	26.1	2.6	8	3
1494	13.16	0.25	1		2.6										10	
1495	11.72	0.15	4	6.0	13.8										4	
1496	12.46	0.25	2		6.6										6	
1497	11 8	0.25	2												2	
1498	11.9	0.15	1												2	
1499	11.44	0.15	1		8.6						0.036	0.004	36.2	2.0	13	1
1500	13.12	0.25	1		11.7	0.52	1	0.92	1	1					6	
1501	12.43	0.15	2	5.7	6.2						0.12	0 01	12.2	0.5	2	1
1502	11.6	0.15	1								0.033	0.002	34.8	1.0	6	4
1503	10.64	0.15	2	2 0	6.5						0 18	0.02	23.0	1.7	7	3
1504	11.89	0.25	2	3.8	13.5	0.42	1	0.88	1	1	0.11	0.01	16.5	1.0	5	1
1505	11.39	0.15	1		6 4						0 086	0.014	23.8	1.8	14	9
1506	12 04	0.15	1		8.0										4	
1507	·13 4	0 25	1												5	
1508	11.90	0.25	2	4.3	13.7	0.25	3	0.64	3	2					7	
1509	12.74	0.25	2	19.8	19.9	0.47	2	0.89	2	2	0.095	0.028	12.1	1.7	15	3
1510	11.40	0.15	3	2.1	5.1						0.067	0.017	27.0	3.3	9	6
1511	12.9	0.25	1								0.020	0.003	23.8	1.5	12	1
1512	9.59	0.15	4	1.6	3.7	0 20	2	0.72	3	3	0 032	0 001	90.0	2.0	17	16
1513	13.40	0.25	1		11.8										6	
1514	12.4	0 25	1												8	
1515	12.7	0.15	1												4	
1516	12 04	0.15	3	7.1	8.2						0.046	0.011	24.2	2.8	2	2
1517	11.0	0.15	1								0.046	0.005	38.7	2.0	7	7
1518	12.42	0.25	1		4.5										7	
1519	11.2	0.15	1								0.065	0.009	29.6	2.1	2	1
1520	10.37	0.15	2		4 4						0.039	0 002	56.5	1.2	8	6
1521	12.0	0.15	1												4	
1522	12.54	0.25	1		2.3										5	
1523	12.54	0.25	2	4.5	9.2										10	
1524	10.74	0.15	3	5.4	6 3						0.043	0.003	45.8	1.6	5	2
1525	12.4	0.15	1								0.096	0.023	13.6	1.6	7	2
1526	13.6	0.25	1												2	
1527	12.07	0.25	1		10.9										2	
1528	12.4	0.25	1												6	
1529	10.04	0.15	3	8.3	10.2	0.32	1	0.76	2	3						
1530	13.3	0.25	1													
1531	11.9	0.25	1												4	
1532	11.01	0.25	5	0.7	9.3	0.36	1	0.84	1	1	0.085	0.011	28.5	1.8	7	1
1533	10.92	0.25	3	3.4	5.4	0.48	1	0 80	1	1	0.072	0.008	32.3	1.7	5	2
1534	11.88	0.15	3		2.9						0.053	0.004	24.3	0.7	3	2

Magnitudes, UBV Colors, IRAS Albedos and Diameters

M.P.	H	G	No. Obs.	Min Phase	Max Phase	U-B	UQ	B-V	BQ	UBV Ref	Albedo	Albedo Unc.	D	D Unc	No. Obs Pre	No. Obs Acc
1535	11.7	0.15	1								0.044	0.005	29.0	1.6	7	5
1536	13.07	0.25	1		3.7										4	
1537	11.9	0.15	1								0.12	0.03	15.0	2.0	7	3
1538	14.3	0.25	1												12	
1539	11.12	0.15	2	3.2	7.2										6	
1540	10.6	0.15	3								0.042	0.002	47.5	1.1	6	6
1541	11.30	0.15	3	0.5	6.2						0.10	0.01	22.2	1.2	6	1
1542	10.40	0.15	3	2.5	4.3						0.049	0.003	50.1	1.2	8	8
1543	12.4	0.15	1												6	
1544	11.89	0.25	4	2.5	3.7						0.052	0.004	24.2	1.0	1	1
1545	11.60	0.15	2		3.1						0.085	0.008	21.7	1.0	2	2
1546	10.5	0.15	1												4	
1547	10.75	0.15	4	7.1	15.0	0.34	2	0.78	2	1					2	
1548	11.6	0.15	5								0.043	0.009	29.5	3.0	4	2
1549	12.5	0.25	1								0.13	0.02	11.3	0.8	7	1
1550	11.80	0.15	1		10.9										8	
1551	12.54	0.25	2	1.8	10.7						0.031	0.006	23.3	2.1	13	1
1552	11.5	0.25	1								0 093	0.010	21.5	1.1	2	1
1553	11.6	0.15	4												2	
1554	11 57	0.15	1		3.3										2	
1555	11.55	0.15	2	6.2	6.5										4	
1556	10.57	0.15	4	3.3	3.4	0.20	3	0.71	3	2	0.10	0 03	30.8	5.5	6	4
1557	11.25	0 25	2	0.7	5.2										4	
1558	10.29	0.15	3	5.4	6.4						0.029	0.007	68.1	7.6	2	2
1559	11.9	0.25	1												7	
1560	11.82	0.15	3	0.7	11.4						0.075	0.009	21.0	1.2	8	1
1561	10.8	0.15	1								0.071	0.015	33.1	3.5	4	1
1562	11.80	0.25	1		3 2						0.20	0.02	12.8	0.6	7	2
1563	12.6	0.25	1												6	
1564	10.87	0.15	1		13.7	0.33	2	0 70	1	2						
1565	12.5	0.25	1												3	
1566	15 95	-.041	12	38.6	103	0.54	1	0.80	1	1					6	
1567	9.57	0.15	4	1.8	8.7			0 72	2	1	0.052	0.003	71.0	2.1	4	4
1568	12.0	0.25	1												1	
1569	12.09	0.15	1		9.5						0.019	0.003	36.5	2.5	2	1
1570	12.07	0.25	4	0.3	7.1						0.099	0.012	16.2	1.0	8	1
1571	12.0	0.15	1								0.023	0.003	34.5	2.2	5	1
1572	10.05	0.15	1		3.6										2	
1573	12.6	0.25	1								0.11	0.01	12.0	0.6	7	1
1574	10.4	0.15	1								0.030	0.002	64.2	1.6	10	6
1575	12.6	0.25	1												10	
1576	11.07	0.25	2	0.9	6.7	0 32	1	0.63	1	3	0.065	0.007	31.7	1.7	4	1
1577	14.1	0.25	1												5	
1578	10.33	0.15	4	0.8	5.2	0.30	2	0.79	3	2	0.040	0.002	57.0	1.6	6	6
1579	10.69	0.15	1		2.7	0.29	2	0.64	3	2	0.040	0.007	48.5	4.2	7	4
1580	14.55	0.017	47	8.4	39.7	0.27	2	0.66	2	1					14	
1581	10.88	0.25	1		3.6	0.35	1	0.66	1	2	0.049	0.004	40.0	1.6	4	3
1582	10.93	0.15	4	3.3	9.0						0.048	0.007	39.6	2.6	6	5
1583	8.66	0.15	6	2.0	7.9	0.24	2	0.75	4	3	0.051	0.003	109	3	11	10
1584	10.81	0.25	2	17.7	24.7	0.44	3	0.89	3	3	0.13	0.02	24.7	2.0	6	3
1585	10.46	0.15	1		8.6						0.042	0.003	52.1	1.7	2	2
1586	12.4	0.25	2								0.074	0.009	16.0	1.0	2	1
1587	11.7	0.15	1												6	
1588	10.9	0.15	2												7	
1589	12.13	0.25	4	4.1	5.7										8	
1590	11.87	0.25	2	4.1	5.5						0.14	0.01	14.8	0.5	12	6
1591	11.91	0.25	1		9.5						0.065	0.008	21.5	1.2	4	1
1592	11.62	0.15	1		8.0						0.16	0.02	15.5	1.1	12	4
1593	13.50	0.25	1		10.1										5	
1594	12.2	0.25	1								0.12	0.01	13.1	0.8	8	4
1595	11.94	0.15	2	12.6	12.7	0.48	1	0.66	1	1	0.037	0.003	28.0	1.0	3	3
1596	10.6	0.15	1								0.037	0.002	51.1	1.2	9	8
1597	12.1	0.15	1												13	
1598	13.2	0.25	1								0.043	0.005	14.5	0.7	9	1
1599	11.01	0.15	2	2.9	3.1						0.036	0.008	44.0	4.6	5	3
1600	13.0	0.25	1													
1601	12.50	0.25	3	5.2	12.3	0.49	1	0.95	1	2					7	
1602	12.56	0.25	1		10.7	0.55	1	0.93	1	1	0.11	0.01	12.2	0.5	9	2
1603	10.94	0.15	3	2.3	4.0						0.048	0.010	39.3	4.1	6	5
1604	10.58	0.245	6	1.6	16.0	0.37	3	0.75	3	3	0.090	0.011	33.8	2.0	5	3
1605	10.21	0.25	3	3.6	5.2						0.098	0.016	38.5	3.0	4	2
1606	11 99	0.15	5	7.6	23 0	0.39	2	0.73	3	2	0.041	0.005	26.1	1.5	4	1
1607	11.76	0.15	5	3.2	12.3						0.15	0.01	14.8	0.8	2	1

Magnitudes, UBV Colors, IRAS Albedos and Diameters

M.P.	H	G	No Obs.	Min Phase	Max Phase	U-B	UQ	B-V	BQ	UBV Ref	Albedo	Albedo Unc.	D	D Unc	No. Obs Pre	No. Obs Acc
1608	12.62	0.25	1		2.4											
1609	10.72	0.15	3	6.0	8.7						0.087	0.016	32.2	2.8	6	2
1610	13.5	0.25	4												7	
1611	10 7	0.15	4												6	
1612	11.0	0.15	1													
1613	11.75	0.15	2	4.9	6.3						0.072	0.005	22.0	0.6	3	2
1614	10.45	0.15	2	6.6	7.3						0.048	0.003	49.5	1.3	4	3
1615	11.36	0.25	5	1 2	10.1	0 32	2	0 69	3	3	0 048	0 006	32.3	2.0	7	2
1616	11.1	0.25	4								0.079	0 008	28.0	1.3	2	2
1617	10.9	0.15	1												5	
1618	11.6	0.25	4												6	
1619	12.21	0.25	3	4.2	18.3	0.55	1	0.90	1	2					4	
1620	14.97	-.129	5	17.3	53.2	0.50	2	0.89	2	3					8	
1621	11.64	0.25	1		2.3	0.47	1	0.90	1	1	0.32	0.03	11.0	0.5	2	1
1622	12.3	0.25	4												6	
1623	10.6	0.25	1								0.081	0.009	34.1	1.8	2	2
1624	11.24	0.15	1		0.5						0.072	0.009	28.0	1.6	3	1
1625	10.32	0.15	2	5.1	5.2	0.33	3	0.75	3	3					2	
1626	11.40	0.25	1		3.2										6	
1627	12.88	0.25	5	9.7	19.1	0.47	4	0 87	3	3					2	
1628	10.06	0.15	1		6 4						0.048	0.005	59.1	3.1	4	4
1629	12.9	0.25	1								0.10	0.01	11.0	0.5	7	1
1630	11.4	0.15	1								0.083	0.008	23.8	1.0	11	2
1631	12.4	0.25	1								0.13	0.05	11.5	2.1	2	2
1632	11.5	0.15	1								0.046	0.004	30.7	1.3	2	1
1633	10.4	0.15	1								0.072	0.014	40.3	3.7	2	1
1634	12.94	0 25	1		8.8										3	
1635	11.6	0.25	1								0.078	0.010	22.5	1.3	7	1
1636	12.2	0.25	1								0.14	0.01	12.1	0.6	9	1
1637	10.1	0.15	1								0.062	0.004	49.7	1.5	9	3
1638	11.6	0.15	1												5	
1639	10.97	0.15	2	6.9	7.2	0.37	2	0.68	2	1	0.043	0.015	41.0	7.0	8	2
1640	13.5	0.25	1												2	
1641	10.68	0.25	1		18.6						0.11	0.02	29.0	3.3	7	6
1642	11.2	0.15	1								0.085	0.010	26.1	1.5	6	1
1643	12.5	0.25	1												3	
1644	12.01	0.25	2	5.4	14.5	0.40	1	0.87	2	2					2	
1645	11.4	0.15	1												3	
1646	12.05	0.25	2	9 5	10.7										4	
1647	10.2	0.15	1								0.028	0.004	72.0	5.0	4	1
1648	12.63	0.25	1		15.9	0.50		0.79	1	1					3	
1649	11.6	0.25	1								0.049	0.007	28.7	2.0	6	1
1650	11.56	0.15	4	7.5	12.8	0.21	3	0.63	4	3	0.042	0.007	31.6	2.6	2	2
1651	12.2	0.25	1													
1652	12.6	0.25	1												2	
1653	11.5	0.15	1												10	
1654	10.9	0.15	1								0.078	0.008	30.8	1.5	2	1
1655	11.03	0.15	1		12.2	0.26	2	0.64	3	2					7	
1656	13 1	0.25	1								0.11	0.03	9.31	1.32	8	2
1657	12.79	0.25	2	20.2	20.4			0.86	1	3	0.14	0.01	9.61	0.56	14	1
1658	11.41	0.25	3	7.6	15.9	0.61	1	0.96	2	1					2	
1659	10.0	0.15	1								0 16	0.01	31.6	1.8	4	1
1660	13.0	0.25	1								0.033	0.004	18.1	1.0	18	1
1661	12.9	0.25	1								0.058	0.007	14.5	0.8	10	1
1662	11.8	0.15	1												2	
1663	13.6	0.25	1								0.034	0.005	13.2	0.8	9	2
1664	12.6	0.25	1								0.018	0.002	29.7	1.6	6	1
1665	11 88	0.25	2		19.2	0.48	2	0.85	2	2					7	
1666	12.91	0.25	1		7.1											
1667	11.95	0.25	1		2.5										2	
1668	12.3	0.15	1												2	
1669	10.75	0.15	2	10.1	11.7	0.46	1	0.73	1	1	0.051	0.009	41.5	3.7	7	4
1670	11.22	0.15	1		1.8						0.072	0.029	28.1	5.5	8	2
1671	12.40	0.15	3	1.1	10.5										5	
1672	11.9	0.15	1												7	
1673	11.0	0.15	1												7	
1674	11 05	0.15	1		2.1						0.076	0.008	29.6	1.5	5	3
1675	11.9	0.25	1								0.15	0.01	13.5	0.6	6	2
1676	13 0	0.25	1								0.070	0.010	12.3	0.8	6	1
1677	12 2	0.25	1													
1678	10.8	0.15	1								0.038	0.004	45.2	2.3	6	4
1679	10.4	0.15	1												2	
1680	11.3	0.15	1								0.19	0.01	16.3	0.5	7	2

Magnitudes, UBV Colors, IRAS Albedos and Diameters

M.P.	H	G	No. Obs.	Min Phase	Max Phase	U-B	UQ	B-V	BQ	UBV Ref	Albedo	Albedo Unc.	D	D Unc	No Obs Pre	No Obs Acc
1681	11.60	0.25	2	6.7	7.9	0.45	2	0.88	1	1	0.083	0.013	22.0	1.6	5	1
1682	12.89	0.25	1		7.6										2	
1683	11.7	0.15	1												2	
1684	10.85	0.15	2	7.7	9.4						0.093	0.009	29.5	1.3	9	1
1685	13.96	0.034	5	39.2	98.6	0.47	2	0.88	2	1	0.030	0.007	12.2	1.3	12	2
1686	10.8	0.25	1								0.063	0.008	36.3	2.2	5	1
1687	10.15	0.25	1		5.2						0.084	0.018	42.6	4.6	3	1
1688	12.2	0.15	1												2	
1689	11.73	0.25	1		7.0										17	
1690	10.7	0.15	1								0.071	0.008	36.1	2.0	10	2
1691	10.95	0.15	1		0.8	0.32	1	0.68	2	2	0.044	0.006	40.6	2.8	6	1
1692	11.2	0.15	1								0.037	0.003	38.5	1.3	4	4
1693	11.03	0.15	4	6.4	12.2	0.33	2	0.74	2	3	0.044	0.006	39.5	2.6	2	1
1694	12.13	0.15	2	13.5	13.9	0.42	2	0.74	2	1					2	
1695	11.9	0.15	1								0.069	0.005	21.0	0.7	2	1
1696	13.2	0.25	1												5	
1697	12.1	0.25	1												11	
1698	11.1	0.15	1												2	
1699	13.2	0.25	1												7	
1700	12.49	0.25	2	1.1	1.3	0.32	3	0.72	3	2	0.032	0.008	23.5	2.8	8	5
1701	10.4	0.15	1								0.13	0.01	29.7	1.7	2	1
1702	11.03	0.15	2	12.0	12.1	0.20	1	0.74	1	1	0.050	0.005	36.8	1.8	2	1
1703	13.1	0.25	1								0.086	0.007	10.8	0.3	8	3
1704	12.7	0.25	1												3	
1705	13.1	0.25	1								0.071	0.016	12.0	1.3	6	2
1706	12.7	0.25	1												7	
1707	12.61	0.25	1		14.0	0.53	1	0.87	1	1					9	
1708	11.6	0.15	1								0.036	0.009	33.5	4.1	8	4
1709	12.98	0.25	1		7.3										9	
1710	13.4	0.25	1												14	
1711	11.04	0.25	2	14.1	14.7	0.43	1	0.85	2	2					4	
1712	9.9	0.15	1								0.044	0.011	66.2	8.0	2	2
1713	13.1	0.25	1												5	
1714	11.6	0.15	1								0.10	0.01	19.2	1.2	6	1
1715	12.1	0.25	1								0.042	0.002	24.5	0.5	10	8
1716	11.9	0.15	1								0.035	0.008	29.3	3.3	8	5
1717	12.44	0.25	2	2.7	4.8										6	
1718	13.6	0.25	1												2	
1719	11.4	0.15	1								0.10	0.01	21.0	1.0	2	1
1720	13.1	0.25	1													
1721	10.6	0.15	1								0.052	0.004	44.3	1.5	4	3
1722	12 53	0.15	2	3.3	5.1						0.025	0.004	26.2	1.8	8	2
1723	10.10	0.25	2	7.0	7.5	0.44	1	0.76	1	1	0.13	0.03	35.0	4.5	5	3
1724	11.29	0 15	2		20.7	0.26		0.69	1	2	0.037	0.002	38.2	1.2	6	2
1725	11.0	0.25	1												8	
1726	11.9	0.15	1								0.034	0.003	30.0	1.2	7	2
1727	13.1	0.40	1												9	
1728	11.6	0.15	1												5	
1729	12.3	0.25	1												3	
1730	11.5	0.15	1												2	
1731	9.9	0.15	1								0.061	0.003	56.2	1.1	6	5
1732	10.7	0.25	1								0.14	0.01	24.2	1.5	3	1
1733	13.0	0.25	1													
1734	11.4	0.15	1								0.048	0.003	31.0	1.0	7	3
1735	9.6	0.15	1								0.058	0.008	66.0	4.5	3	3
1736	12.2	0.25	1								0.026	0.003	30.1	2.0	9	1
1737	11.0	0.25	1								0.10	0.01	26.5	1.5	4	1
1738	12.6	0.25	1												4	
1739	13.53	0.25	1		12.3						0.090	0.014	8.71	0.65	9	1
1740	13.25	0.15	2		7.1	0.19	3	0.61	3	2					4	
1741	11.5	0.25	1								0.064	0.007	26.2	1.5	4	1
1742	11.88	0.25	1		9.6										6	
1743	12.31	0.25	1		1.9						0.050	0.018	20.5	3.5	4	2
1744	13.7	0.25	1								0.027	0.004	14.1	0.8	11	1
1745	12.0	0.25	1												8	
1746	9.91	0.15	2	11.9	13.0	0.23	3	0.72	3	2					3	
1747	13.38	0.25	1		6.0	0.48		1.28		1	0.11	0.03	8.11	1.04	8	3
1748	10.52	0.15	3	2.0	19.1	0.26	1	0.73	1	2					2	
1749	10.1	0.15	1								0.012	0.001	115	5	8	1
1750	13.52	0.25	2	12.7	13.1	0.50	2	0.88	2	1						
1751	12.2	0.15	1								0.11	0.01	14.3	0.8	6	1
1752	13.5	0.25	1												7	
1753	11.1	0.25	1												2	

Magnitudes, UBV Colors, IRAS Albedos and Diameters

M.P	H	G	No. Obs.	Min Phase	Max Phase	U-B	UQ	B-V	BQ	UBV Ref	Albedo	Albedo Unc.	D	D Unc	No. Obs Pre	No Obs Acc
1754	9.74	0 15	3	6.0	6.3	0.25	2	0.67	2	3	0.033	0.002	82.6	2.7	7	6
1755	10.81	0.25	2	4.9	9.9	0.36	1	0.92	2	1	0.10	0.03	29.0	4.3	14	3
1756	12.8	0.15	1												4	
1757	13 45	0.25	1		17.8										6	
1758	10.7	0.25	1								0.11	0.01	29.0	1.6	4	1
1759	13.15	0.15	1		13.4										6	
1760	11.5	0.15	1								0.028	0.005	40.1	3.7	5	4
1761	11.5	0.15	1												4	
1762	11.7	0.25	1												3	
1763	13.1	0.25	1												3	
1764	11.2	0.25	1								0.064	0.013	30.1	3.0	5	3
1765	9 92	0.15	2	7 0	7.2	0.27	2	0.75	2	1	0 090	0.008	45.8	2.0	8	6
1766	11.97	0.15	1		11.7						0.048	0.004	24.5	1.0	6	1
1767	12.26	0.25	1		10.9	0.34	1	0.75	1	1					3	
1768	12.45	0.15	3	2.5	5.7	0.23	1	0.61	1	2					7	
1769	12.7	0.25	1												2	
1770	12.39	0.25	1		3.4										8	
1771	10.1	0.15	1								0.047	0.002	58.7	1.1	6	5
1772	12.93	0.15	1		3.9										2	
1773	11.42	0.25	1		19.3										3	
1774	12.2	0.25	1												2	
1775	12.2	0.15	1												2	
1776	11.0	0.15	1								0.044	0.003	39.7	1.5	4	3
1777	11.8	0.15	1												6	
1778	11.8	0.15	1												6	
1779	14.3	0.25	1												2	
1780	10.69	0.25	1		2.2						0.093	0.020	31.7	3.5	10	9
1781	12.7	0.25	1												7	
1782	10.85	0.15	1		9.7						0.073	0.009	33.1	2.0	7	1
1783	11.94	0.15	1		3.9						0.043	0.004	26.3	1.2	10	2
1784	11.81	0.25	1		3.1						0.13	0.04	15.5	2.7	9	3
1785	12.8	0.25	1												2	
1786	11.0	0.25	1								0.12	0.01	23.5	1.3	8	1
1787	11.3	0.25	1								0.060	0.007	29.8	1.8	6	1
1788	11.7	0.15	1												5	
1789	12.54	0.25	2	6.6	8.6										2	
1790	12.61	0.25	1		9.9										6	
1791	12.0	0.15	1								0.032	0.003	29.3	1.5	6	3
1792	12.05	0.15	1		2.3	0.34	1	0.74	1	1					4	
1793	12.6	0.25	1								0.046	0.006	18.6	1.2	2	1
1794	11.08	0.15	1		6.0	0.31	2	0.70	2	2	0.035	0.004	43.1	2.3	5	4
1795	11.9	0.15	1								0.036	0.002	28.7	0.8	3	3
1796	9.66	0.15	1		21.3	0.29	2	0.68	2	2	0.041	0.003	76.5	2.5	4	2
1797	12.8	0.25	1												2	
1798	12.6	0.25	1												6	
1799	11.3	0.25	1								0 067	0.013	28.2	2.6	2	1
1800	12.7	0.25	1												2	
1801	11.2	0.25	1												6	
1802	11 7	0.25	1												5	
1803	12.2	0.25	1												8	
1804	12.3	0.25	1												1	
1805	11 2	0.15	1								0.051	0.020	33.7	6.5	5	2
1806	12.7	0.25	1												4	
1807	12.7	0.25	1												4	
1808	12.2	0.15	1								0.078	0.011	17.0	1.1	10	5
1809	11.7	0.15	1												6	
1810	12.7	0.25	1												3	
1811	11.1	0.15	1												6	
1812	11.6	0.25	1								0.056	0.008	26.6	1.7	8	1
1813	12.5	0.15	1								0.022	0.003	27.8	2.0	2	1
1814	13.1	0.25	1												8	
1815	11.36	0.15	1		0.9	0.33	2	0.62	1	2	0.044	0.008	34.0	3.0	7	2
1816	13.6	0.25	1												10	
1817	12.2	0.25	1								0.081	0.027	17.0	2.8	9	6
1818	14.1	0.25	1												12	
1819	10.7	0.15	1								0.046	0.006	44.6	2.6	2	1
1820	13.5	0.25	1												3	
1821	13.7	0.25	1												7	
1822	13.04	0.25	1		4.3										3	
1823	13.0	0.25	1												7	
1824	11.7	0.25	1								0.072	0.010	22.6	1.5	5	1
1825	11.8	0.15	1												6	
1826	11.84	0.15	1		3.8						0.042	0.009	27.6	2.8	4	2

Magnitudes, UBV Colors, IRAS Albedos and Diameters

M.P.	H	G	No. Obs.	Min Phase	Max Phase	U-B	UQ	B-V	BQ	UBV Ref	Albedo	Albedo Unc.	D	D Unc	No. Obs Pre	No. Obs Acc
1827	12.41	0.15	2	5.6	6.1			0.81	1	1					6	
1828	11.1	0.15	1								0.069	0.007	30.5	1.3	2	1
1829	12.6	0.25	1												7	
1830	12.53	0.25	1		14.9	0.50	1	0.91	1	1					3	
1831	12.84	0.25	1		6.2						0.040	0.006	17.8	1.1	2	1
1832	11.28	0.15	1		3.2						0.041	0.010	36.3	4.3	4	2
1833	11.97	0.15	1		8.9										3	
1834	11.6	0.25	1												4	
1835	11.6	0.25	1												6	
1836	11.5	0.15	1												6	
1837	13.47	0.25	1		3.7										5	
1838	10.8	0.15	1								0.054	0.008	39.5	3.0	2	2
1839	11.6	0.15	1												4	
1840	11.7	0.15	1												7	
1841	11.37	0.15	2		1.5						0.018	0.001	53.3	2.0	4	3
1842	12.75	0.25	2	4.8	6.7	0.52	2	0.87	3	2					8	
1843	11.5	0.15	1								0.056	0.003	28.0	0.6	9	8
1844	11.2	0.25	1												2	
1845	11.8	0.15	1												2	
1846	13.5	0.25	1								0.041	0.005	12.7	0.7	5	1
1847	10.7	0.15	1								0.13	0.01	26.5	1.0	5	2
1848	11.41	0.25	1		4.7										1	
1849	11.1	0.15	1												1	
1850	13.1	0.25	1												9	
1851	12.0	0.15	1								0.065	0.031	20.7	5.0	6	5
1852	10.7	0.25	1												5	
1853	10.5	0.15	1								0.17	0.01	25.3	1.0	5	4
1854	12.89	0.15	1		4.6										10	
1855	12.7	0.25	1												2	
1856	12.3	0 25	1												2	
1857	12.6	0.25	1												7	
1858	11.7	0.15	1												7	
1859	10.84	0.15	2	4.4	14.5						0.034	0.002	48.6	1.3	7	7
1860	11.5	0.15	1												4	
1861	11.8	0.25	1												4	
1862	16.23	0.122	10	5.6	59.8	0.50	3	0.82	3	2					6	
1863	15.81	0.40	3	21.7	25.0	0.37	3	0.77	3	2					3	
1864	15.02	0.25	1		30.0	0.50	2	0.83	2	1					4	
1865	16.91	0.25	5	8.3	11.5	0.40	2	0.79	3	2					4	
1866	13.2	0.25	1													
1867	8.60	0.15	6	0.5	9.6	0.24	4	0.72	4	3	0.037	0.002	131	3	5	4
1868	9.6	0.15	1													
1869	11.2	0.15	1												6	
1870	10.8	0.15	1												4	
1871	11.2	0.15	1												4	
1872	10.2	0.15	1												4	
1873	10.6	0.15	1								0.024	0.002	64.8	3.2	5	1
1874	11.0	0.15	1												4	
1875	12.2	0.15	1												4	
1876	14.7	0.25	1													
1877	11.3	0.15	1								0.021	0.003	50.3	3.3	2	1
1878	11.88	0.25	2	2.0	10.7						0.070	0.009	21.0	1.3	10	1
1879	13.0	0.25	1													
1880	12.13	0.15	1		2.6						0.036	0.005	26.2	1.7	13	2
1881	11.0	0.15	1								0.072	0.011	31.2	2.3	5	1
1882	11.0	0.25	1								0.12	0.02	23.8	1.8	2	1
1883	13.2	0.25	1												4	
1884	13.2	0.25	1								0.059	0.006	12.5	0.6	7	2
1885	13.6	0.25	1													
1886	11.6	0.15	1								0.094	0.017	20.7	1.7	15	2
1887	11.53	0.25	1		15.5										4	
1888	12.0	0.15	1												10	
1889	10.7	0.15	1								0.068	0.005	36.8	1.3	2	1
1890	11.2	0.15	1								0.060	0.004	31.1	1.0	6	3
1891	11.7	0.15	1								0.10	0.01	18.8	1.0	3	2
1892	12.28	0.25	1		18.0										3	
1893	11.3	0.15	1								0.11	0.01	21.2	1.2	10	1
1894	12.3	0.25	1												4	
1895	12.34	0.15	1		3.9						0.048	0.007	20.6	1.3	3	1
1896	13.7	0.25	1												2	
1897	13.79	0.25	1		7.6										6	
1898	12.2	0.15	1												2	
1899	12.7	0.25	1												7	

Magnitudes, UBV Colors, IRAS Albedos and Diameters

M.P.	H	G	No. Obs.	Min Phase	Max Phase	U-B	UQ	B-V	BQ	UBV Ref	Albedo	Albedo Unc.	D	D Unc	No. Obs Pre	No. Obs Acc
1900	12.2	0.25	1												7	
1901	11.2	0 15	1												6	
1902	9 49	0.15	2	5.0	8.0	0.19	2	0.70	2	2	0.028	0.002	101	3	2	2
1903	10.7	0.25	1								0.10	0.02	29.7	3.5	9	2
1904	11.7	0.15	1								0.085	0.019	20.7	2.3	3	1
1905	13.54	0.25	1	1.5											2	
1906	12.7	0.25	1												6	
1907	12.1	0.15	1												6	
1908	11.2	0.15	1								0.085	0.010	26.1	1.5	2	2
1909	12.3	0.25	1								0.056	0.003	19.5	0.5	9	4
1910	10.6	0.15	1								0 078	0.006	36.0	1.3	2	2
1911	10.11	0.15	1	0.5		0.22	2	0.70	2	2	0.023	0.001	83.0	2.0	4	4
1912	12.0	0.25	1												5	
1913	11.2	0.25	1												2	
1914	12.5	0.25	1												2	
1915	19.05	0.157	5	9.2	42.2	0.41		0.74		2					4	
1916	15.03	0.25	4	12.7	27.7	0.41	1	0.85	2	1					6	
1917	15.2	0.25	1													
1918	11.2	0.15	1												7	
1919	13.77	0.40	1		32.6	0.25	2	0.75	3	2						
1920	14.34	0.40	1		11.7	0.26	2	0 72	3	2					7	
1921	14.5	0.15	1												4	
1922	11.8	0.15	1												5	
1923	13.5	0.25	1								0.026	0.003	16.2	0.7	6	2
1924	13.2	0.25	1								0.046	0.004	14.0	0.5	5	3
1925	12.2	0.15	1												7	
1926	12.1	0.15	1												10	
1927	11.8	0.15	1												4	
1928	12.95	0.25	1	11.9											4	
1929	12.2	0.25	1												8	
1930	11.2	0.15	1								0.071	0.017	28.6	3.5	6	4
1931	13.4	0.15	1			0.32	1	0.69	1	1					3	
1932	13.5	0.25	1													
1933	13.3	0.25	1												4	
1934	12.7	0.25	1								0.27	0.01	7.25	0.22	15	6
1935	13.3	0.15	1												7	
1936	11.2	0.15	1								0.085	0.012	26.2	1.7	5	5
1937	12.2	0.25	1								0.095	0.026	15.5	2.0	14	3
1938	12.7	0.25	1													
1939	10.7	0.25	1								0.074	0.010	35.3	2.2	7	4
1940	11.2	0.15	1								0.039	0.006	38.6	3.0	10	6
1941	11.2	0.25	1												5	
1942	13.1	0.25	1								0.046	0.003	14.8	0.5	2	1
1943	15.83	0.25	2	15.9	17.1	0.45	2	0.84	2	2					2	
1944	13.7	0.25	1												2	
1945	12.2	0.15	1												10	
1946	12.7	0.25	1												7	
1947	10.2	0.15	1								0.12	0.01	35.0	1.7	2	1
1948	12.2	0.15	1												6	
1949	13.5	0.25	1												5	
1950	13.84	0.25	1	0.5												
1951	16.1	0.25	1								0.026	0.009	4.98	0.88	10	3
1952	10.59	0.15	4	2.3	9.7	0.31	1	0.74	1	1	0.062	0 009	40.5	2.8	7	3
1953	11.8	0.15	1												7	
1954	12.1	0.15	1												2	
1955	12.08	0 25	3	2.2	8.1										2	
1956	11.7	0.15	1													
1957	11.53	0 25	4	2.7	7.9										2	
1958	11.0	0.15	1								0.039	0.004	42.6	2.0	6	1
1959	12.7	0.25	1												8	
1960	11 85	0.15	1	5.3							0.038	0.005	28.8	1.8	4	3
1961	11.2	0.15	1								0.019	0.002	55.5	2.2	9	3
1962	12.2	0.15	1												B	
1963	10.89	0.15	1		20.4	0.33	2	0.74	2	2	0.036	0.002	46.5	1.0	10	7
1964	13.3	0.15	1												6	
1965	12.3	0.15	1												5	
1966	14.0	0.25	1												7	
1967	12.15	0.25	1	8.5											7	
1968	11.7	0.15	1												7	
1969	11.5	0.15	1								0.066	0.008	25.8	1.5	7	1
1970	12.20	0.15	3	14.8	17.5						0.029	0.005	28.5	2.3	8	3
1971	12.3	0.25	1												4	
1972	13.2	0.25	1												2	

Magnitudes, UBV Colors, IRAS Albedos and Diameters

M.P.	H	G	No Obs.	Min Phase	Max Phase	U-B	UQ	B-V	BQ	UBV Ref	Albedo	Albedo Unc.	D	D Unc	No. Obs Pre	No. Obs Acc
1973	11.7	0.15	1													
1974	12.0	0.15	1								0.039	0.005	26.6	1.6	5	1
1975	12.1	0.15	1												9	
1976	13.49	0.25	4	1.3	10.2										3	
1977	11.3	0.15	1								0.014	0.002	60.8	4.2	8	1
1978	13.1	0.25	1												4	
1979	13.5	0.25	1													
1980	14.07	0.25	1		53.3	0.46	1	0.96	1	1	0.024	0.003	13.0	0.8	8	1
1981	16.9	0.25	1												2	
1982	12.90	0.25	2	4.0	6.3										2	
1983	12.7	0.15	1												7	
1984	11.2	0.15	1								0.038	0.007	39.3	3.7	5	5
1985	11.2	0.15	1								0.038	0.010	39.3	5.3	2	2
1986	12.0	0.15	1								0.011	0.001	49.5	2.7	7	2
1987	11.8	0.25	1								0.11	0.01	16.8	1.0	4	1
1988	13.6	0.25	1								0.011	0.002	23.6	1.5	10	1
1989	12.2	0.25	1													
1990	13.15	0.25	3	2.1	3.6	0.50	1	0.86	2	2					4	
1991	13.5	0.25	1												6	
1992	12.1	0.15	1												16	
1993	12.2	0.15	1												9	
1994	12.2	0.15	1								0.035	0.004	26.0	1.5	7	4
1995	12.6	0.15	1												6	
1996	12.1	0.25	1												3	
1997	13.3	0.25	1								0.11	0.01	8.53	0.46	2	1
1998	12.50	0.25	4	3.4	13.8										4	
1999	10.7	0.15	1								0.065	0.007	37.6	2.1	2	1
2000	11.36	0.25	4	21.6	26.8	0.49	2	0.89	2	1						
2001	12.96	0.25	2	24.4	28.5	0	27	3	0.71	3	2					
2002	12.2	0.25	1								0.068	0.012	18.5	1.5	2	1
2003	11.8	0.15	1												3	
2004	12.8	0.25	1												2	
2005	12.2	0.15	1												4	
2006	13.0	0.25	1												7	
2007	11.7	0.25	1								0.057	0.005	25.3	1.0	4	1
2008	10.1	0.15	1								0.058	0.003	52.5	1.3	7	5
2009	11.0	0.25	1								0.043	0.004	40.5	1.8	7	2
2010	11.54	0.25	2	1.7	15.3	0.34	1	0.70	1	2					4	
2011	12.7	0.25	1												6	
2012	13.2	0.25	1													
2013	12.1	0.25	1												6	
2014	12.54	0.25	1		16.6										5	
2015	12.3	0.25	1												4	
2016	11.2	0.15	1								0.094	0.006	25.0	0.7	7	4
2017	12.71	0.25	1		19.4										4	
2018	14.5	0.25	1												3	
2019	12.2	0.25	1								0.077	0.010	17.3	1.0	2	1
2020	11.49	0.25	5	2.4	13.1						0.068	0.008	25.6	1.5	5	1
2021	13.6	0.25	1												2	
2022	12.14	0.15	1		3.9						0.035	0.004	26.5	1.3	4	1
2023	11.6	0.15	1												5	
2024	13.3	0.25	1												6	
2025	10.7	0.15	1								0.046	0.003	45.0	1.6	2	2
2026	13.2	0.15	1												3	
2027	11.7	0.25	1												5	
2028	14.1	0.25	1												2	
2029	13.2	0.25	1												9	
2030	13.6	0.25	1												3	
2031	13.3	0.25	1												2	
2032	11.6	0.15	1								0.023	0.002	42.0	1.5	6	4
2033	13.7	0.25	1												4	
2034	12.7	0.25	1												2	
2035	12.78	0.40	3	7.9	14.6	0.28	1	0.81	1	3					9	
2036	12.7	0.25	1												6	
2037	13.7	0.25	1												13	
2038	12.2	0.25	1												17	
2039	12.7	0.15	1								0.019	0.002	27.5	1.6	4	1
2040	11.7	0.15	1								0.031	0.008	34.3	4.5	2	2
2041	12.5	0.15	1												3	
2042	12.9	0.15	1												4	
2043	11.0	0.15	1								0.029	0.004	49.6	3.2	6	6
2044	13.2	0.25	1								0.14	0.01	7.87	0.35	3	1
2045	12.3	0.25	1												2	

Magnitudes, UBV Colors, IRAS Albedos and Diameters

M P	H	G	No. Obs.	Min Phase	Max Phase	U-B	UQ	B-V	BQ	UBV Ref	Albedo	Albedo Unc.	D	D Unc	No. Obs Pre	No. Obs Acc
2046	11.0	0.15	1								0.094	0.012	27.3	1.6	8	1
2047	13.7	0.25	1												12	
2048	13.79	0.40	3	21.4	25.3	0.24	3	0.71	3	2					4	
2049	15.1	0.25	1												7	
2050	12.79	0.25	1		22.5	0.42	2	0.87	3	2					2	
2051	11.7	0.25	1								0.057	0.008	25.2	1.6	4	1
2052	10.53	0.25	1		8.8	0.43	2	0.83	2	2	0.087	0.010	35.1	1.8	4	2
2053	12.14	0.15	1		7.7										11	
2054	12.5	0.15	1								0.029	0.004	24.5	1.5	5	2
2055	13.5	0.25	1												3	
2056	12 2	0.25	1												7	
2057	14.7	0.15	1												7	
2058	10 7	0.15	1								0.092	0.012	31.7	2.0	6	1
2059	14.7	0 15	1												3	
2060	6 62	0.25	11	0.4	2.9	0 28	2	0.70	2	2					2	
2061	16.7	0.15	1			0.35	1	0 76	1	1					4	
2062	16.96	0.25	1		59.7	0.46	1	0.93	1	1						
2063	17.6	0.25	1													
2064	13.7	0.25	1												6	
2065	12.2	0.15	1								0.048	0.006	22.0	1.3	6	1
2066	13.0	0.25	1								0.024	0.003	21.6	1.2	4	1
2067	10.49	0.15	2	8.9	9.1	0 24	2	0.66	2	2	0.044	0.004	50.3	2.0	4	2
2068	11.7	0.15	1								0.029	0.001	35.7	0.7	6	5
2069	11.2	0.15	1								0.037	0.008	40 0	4.1	6	3
2070	13.6	0.25	1												3	
2071	13.2	0.25	1												5	
2072	12.64	0.25	1		3.5										4	
2073	12.7	0.15	1													
2074	13.8	0.40	1												11	
2075	13.7	0.25	1												8	
2076	14 2	0.25	1												7	
2077	13.2	0.25	1												4	
2078	12.7	0.25	1												4	
2079	12.2	0.15	1												3	
2080	13.6	0.25	1												5	
2081	12.13	0.15	1		7.3	0.22	2	0.60	3	2	0.036	0.003	26.1	1.0	6	3
2082	12.6	0.15	1												4	
2083	13.33	0.25	3	8.3	21.3	0.22	3	0.70	3	3					5	
2084	12.5	0.25	1								0.037	0.009	22.0	2.5	8	7
2085	11.85	0.15	1		1.3										2	
2086	11.9	0.25	1												7	
2087	13.2	0.25	1													
2088	12.48	0.25	1		8.8										8	
2089	11.25	0.25	2	22.0	22.2	0.40	1	0.82	2	1					5	
2090	11.02	0.25	4	1.4	2.3	0.50	2	0.87	3	2	0.041	0.005	41.2	2.2	4	1
2091	10.7	0.25	1								0.077	0.010	34.7	2.2	10	4
2092	11.6	0.25	1												5	
2093	13.2	0.25	1												2	
2094	12.79	0.25	1		13.5										7	
2095	12.8	0.15	1												2	
2096	13.2	0.25	1												5	
2097	11.7	0.15	1												4	
2098	12.1	0.25	1								0.080	0.011	17.8	1.2	8	1
2099	15.44	0.25	2		16.4	0.35	1	0.83	1	1					6	
2100	16.12	0.168	8	3.2	30.9	0.31	2	0.72	4	3						
2101	18.2	0.25	1												5	
2102	16.2	0.25	1													
2103	10 63	0.15	2	12.6	12.8						0.17	0.01	24.0	1.2	7	2
2104	9.9	0 15	1													
2105	12.4	0.25	1								0 034	0.002	24.0	0.7	8	7
2106	11.7	0.15	1												5	
2107	11 7	0.15	1								0 11	0.02	17.8	1.5	8	1
2108	11.5	0.25	1								0.080	0.016	23.5	2.3	3	1
2109	11.91	0.15	1		11.2										4	
2110	13.6	0.25	1												7	
2111	10.53	0.25	1		18.1	0.46	1	0.80	2	2	0.11	0.01	30.1	1.5	4	2
2112	12.6	0.25	1												2	
2113	13.23	0.25	1		3.3										7	
2114	11.2	0.15	1								0.055	0.005	32.6	1.5	4	1
2115	11.2	0.25	1								0.095	0.013	24.8	1.6	6	1
2116	12.2	0.15	1								0 045	0.009	22.8	2.2	6	5
2117	11.7	0.25	1												8	
2118	11.87	0.15	1		4.9										2	

Magnitudes, UBV Colors, IRAS Albedos and Diameters

M.P.	H	G	No. Obs	Min Phase	Max Phase	U-B	UQ	B-V	BQ	UBV Ref	Albedo	Albedo Unc.	D	D Unc	No. Obs Pre	No. Obs Acc
2119	13.7	0.25	1												7	
2120	10.6	0.15	1								0.055	0.007	43.0	2.7	4	4
2121	12.5	0.25	1												6	
2122	12.1	0.25	1												2	
2123	11.05	0.25	1		18 1										4	
2124	12.05	0.25	1		6.1										4	
2125	12.71	0.15	3	2.4	7.8						0.058	0.006	15.8	0.7	5	1
2126	12.4	0.25	1												6	
2127	11.56	0.15	1		5.1						0.023	0.001	42.5	1.2	6	6
2128	14.0	0.15	1												3	
2129	14.0	0.25	1												2	
2130	13.7	0.25	1								0.018	0.002	18.0	1.0	7	2
2131	12.97	0.40	2	11.1	32.5	0.44	3	0.87	3	2	0.14	0.01	9.01	0.53	4	1
2132	11.2	0.15	1								0.051	0.010	34.0	3.3	8	3
2133	13.2	0.25	1												9	
2134	12.9	0.15	1					0.94	1	1					8	
2135	18.0	0.25	1												23	
2136	11.6	0.25	1												4	
2137	11.2	0.15	1								0.029	0.004	44.5	2.7	2	2
2138	11.6	0.15	1								0.16	0.02	15.5	1.0	6	1
2139	12.81	0.15	2	4.5	5.1	0.23	1	0.64	1	2					2	
2140	11.0	0.15	1								0.054	0.008	36.0	2.5	4	3
2141	11.2	0.15	1								0.081	0.041	26.7	6.7	9	2
2142	11.7	0.15	1								0.077	0.009	21.8	1.2	5	1
2143	14.1	0.25	1												8	
2144	11.54	0.25	2	6.2	6.3						0.13	0.01	18.0	1.1	3	1
2145	10.5	0.15	1								0.081	0.005	37.0	1.1	4	3
2146	10.2	0.15	1												7	
2147	11.7	0.15	1								0.032	0.006	33.7	3.0	6	1
2148	10.7	0.15	1												6	
2149	12.2	0.15	1												2	
2150	13.7	0.25	1													
2151	10.7	0.25	1			0.50	1	0.77	1	1	0.22	0.02	20.2	1.2	4	1
2152	11.2	0.15	1								0.024	0.001	49.0	1.0	10	10
2153	11.7	0.15	1								0.090	0.011	20.2	1.1	2	1
2154	12.6	0.15	1								0.035	0.005	21.5	1.5	6	1
2155	12.4	0.25	1								0.022	0.006	29.5	4.2	5	2
2156	12.67	0 25	2	5.7	16.9	0.53	1	0.92	1	2	0.029	0.007	22.7	2.6	7	1
2157	11.5	0.15	1												2	
2158	11.4	0.15	1												2	
2159	12.16	0.25	1		4.2										8	
2160	11.96	0.25	1		2.5										4	
2161	12.2	0.15	1												4	
2162	12.7	0.25	1												8	
2163	11.6	0.15	1												2	
2164	11.9	0.15	1												5	
2165	10.7	0.15	1												7	
2166	13 2	0.25	1												10	
2167	11.7	0.15	1												10	
2168	13.2	0.15	1												2	
2169	12.1	0.15	1								0.064	0.008	20.0	1.2	2	2
2170	13.5	0.25	1												2	
2171	13.7	0.25	1												10	
2172	11.5	0.15	1												4	
2173	11.4	0.15	1												4	
2174	13.2	0.15	1												10	
2175	13.7	0.25	1												6	
2176	12.2	0.15	1												3	
2177	11.7	0.15	1												4	
2178	13.7	0.25	1												2	
2179	11.7	0.25	1								0.069	0.006	23.1	1.0	2	1
2180	10.7	0.25	1												2	
2181	12.2	0.15	1												4	
2182	11.2	0.15	1								0.060	0.010	31.2	2.5	6	1
2183	11.4	0.15	1								0.035	0.004	37.5	2.2	5	1
2184	10.7	0.15	1								0.10	0.02	29.7	3.5	7	4
2185	11.34	0.15	1		7 6						0.12	0.01	20.2	1.5	3	1
2186	12.2	0.15	1												6	
2187	13.48	0.15	1		8.9										4	
2188	11.7	0.25	1												4	
2189	12.7	0.25	1												3	
2190	13.58	0.25	1		0.1						0.020	0.002	18.0	0.8	5	1
2191	11.2	0.25	1								0.12	0.01	21.2	1.3	7	3

Magnitudes, UBV Colors, IRAS Albedos and Diameters

M.P.	H	G	No. Obs.	Min Phase	Max Phase	U-B	UQ	B-V	BQ	UBV Ref	Albedo	Albedo Unc.	D	D Unc	No. Obs Pre	No. Obs Acc
2192	11.2	0.15	1								0.062	0.016	30.6	4.0	7	2
2193	10.96	0.15	1		3.5						0.027	0.002	51.5	1.8	2	2
2194	12.2	0.25	1												9	
2195	12.2	0.25	1												9	
2196	10.24	0.15	1		14.3	0.25	1	0.67	1	2	0.036	0.002	62.2	1.8	2	2
2197	11.28	0.15	5	2.0	11.6						0.076	0.009	26.6	1.5	4	2
2198	14.5	0.15	1												7	
2199	13.2	0.25	1												2	
2200	12.7	0.25	1												4	
2201	15.41,	0.25	1		33.4						0.33	0.07	1.90	0.19	8	4
2202	17.2	0.25	1													
2203	12.01	0.15	1		1.7										4	
2204	12.80	0.15	1		3.0						0.018	0.005	27.5	3.5	5	2
2205	11 7	0.15	1												4	
2206	11.6	0.25	1												5	
2207	8.87	0.15	3	1.4	4.6	0.24	3	0.73	3	2	0.058	0.004	92.6	3.3	6	4
2208	10 96	0.15	3	2.1	2.2	0.24	2	0.75	2	2	0.036	0.003	45.2	1.6	6	3
2209	11.2	0.25	1								0.15	0.04	19.2	2.5	4	2
2210	14.4	0.25	1												3	
2211	12.7	0.15	1												8	
2212	14.0	0.25	1			0.41	2	0.77	2	1					2	
2213	13.2	0.25	1												7	
2214	11.7	0.15	1								0.045	0.003	28.5	0.8	8	8
2215	11.6	0.15	1								0.13	0.01	17.2	1.0	2	1
2216	11.2	0.25	1								0.12	0.01	21.8	1.2	6	2
2217	11.20	0.15	3	5.3	14.1						0.066	0.011	29.8	2.5	2	1
2218	11.7	0.15	1								0.037	0.003	31.5	1.5	11	3
2219	10.7	0.15	1								0.046	0.004	45.0	2.0	2	2
2220	12.0	0.15	1												4	
2221	13.1	0.15	1												8	
2222	11.2	0.15	1								0.073	0.019	28.2	3.6	2	2
2223	9.41	0.15	3	5.3	7.8	0 22	2	0.79	3	2	0.027	0.004	105	8	4	3
2224	11.9	0.25	1												8	
2225	12.0	0.25	1												7	
2226	11.75	0.25	2	8.7	14.7										5	
2227	13.7	0.25	1												5	
2228	11.85	0.15	2		5.4						0.036	0.005	29.7	1.7	5	2
2229	12.7	0.15	1												4	
2230	12.0	0.25	1												2	
2231	12.2	0.15	1												7	
2232	12.2	0.15	1												2	
2233	12.69	0.25	4	2.5	19.9											
2234	12.2	0.15	1												2	
2235	11.26	0.15	1		5.1						0.019	0.003	54.6	3.7	7	2
2236	12.2	0.25	1												6	
2237	11.2	0.15	1								0.10	0.02	23.6	2.3	6	5
2238	11.7	0.15	1								0.078	0.018	21.6	2.3	6	3
2239	11.46	0.15	1		1.2						0.025	0.002	43.1	1.5	9	5
2240	11.7	0.15	1								0.048	0.013	27.6	3.7	7	2
2241	8.66	0.15	3	0.9	9.8	0.21	3	0.74	3	2	0.040	0.003	123	5	4	1
2242	13.2	0.25	1												7	
2243	12.7	0.25	1												7	
2244	12.2	0.15	1								0.026	0.003	29.6	1.8	4	1
2245	11.2	0.15	1								0.052	0.011	33.6	3.6	7	2
2246	10.71	0.15	5	1.4	11.2	0.24	3	0.74	3	2	0.034	0.008	52.1	6.0	8	3
2247	13.6	0.25	1												6	
2248	11.06	0.15	2	1.0	9.6						0.074	0.016	30.0	3.3	10	1
2249	11.40	0.15	1		1.8						0.023	0.004	46.0	4.1	8	7
2250	11.2	0.15	1												4	
2251	11.6	0.15	1								0.047	0.004	29.5	1.1	4	3
2252	12.85	0.15	1		1.3										2	
2253	13.2	0.25	1												4	
2254	12.7	0.25	1												5	
2255	11.2	0.15	1								0.071	0 006	28.5	1.1	2	1
2256	11.9	0.15	1												2	
2257	13.1	0.25	1												3	
2258	11.7	0.15	1								0 048	0.004	27.6	1.1	3	3
2259	12.7	0.25	1								0.024	0.003	25.0	1.7	3	1
2260	8.95	0.15	5	3.4	9.5	0.34		0.79		2	0.064	0.004	85.0	2.8	7	5
2261	13.43	0.25	1		6.6										3	
2262	12 2	0.15	1												2	
2263	11.2	0.25	1								0.10	0.03	23.5	3 2	7	5
2264	10.59	0 15	3	1.4	11.6						0.10	0.01	30.8	1.0	5	5

Magnitudes, UBV Colors, IRAS Albedos and Diameters

M.P.	H	G	No. Obs.	Min Phase	Max Phase	U-B	UQ	B-V	BQ	UBV Ref	Albedo	Albedo Unc.	D	D Unc	No. Obs Pre	No. Obs Acc
2265	12.7	0.15	1													
2266	10.81	0.15	2	3.4	4.6	0.26	3	0.75	3	2	0.029	0.008	53.6	7.7	4	2
2267	13.2	0.25	1								0.036	0.005	16.0	1.0	10	1
2268	11.7	0.15	1												2	
2269	10.7	0.15	1								0.10	0.03	30.2	4.5	8	5
2270	10.81	0.15	6	3.7	15.8										4	
2271	10.7	0.15	1								0.079	0.006	34.1	1.2	5	3
2272	14.04	0.25	1		22.6	0.49	2	0 88	2	2					3	
2273	13.34	0.25	1		9.0										10	
2274	12 70	0.25	1		8.0	0.41	1	0.77	1	1					6	
2275	13.60	0.25	3	5.0	9.3										6	
2276	12.7	0.25	1												6	
2277	12.11	0.15	1		10.6										6	
2278	14.27	0.15	2	4.7	5.1	0.23	1	0.64	2	2					6	
2279	12.97	0.15	1		1.1	0.22	3	0.62	3	2	0.040	0.008	17.0	1.6	6	3
2280	14.14	0.25	1		4.3										7	
2281	13.5	0.25	1												7	
2282	13.7	0.25	1													
2283	12.70	0.25	7	6.9	19.5										5	
2284	12.7	0.25	1												5	
2285	13.7	0.25	1												2	
2286	13.2	0 25	1												11	
2287	13.2	0.25	1												6	
2288	10.7	0.15	1												5	
2289	13.4	0.15	1												2	
2290	11.98	-.086	5	3.6	16.8										9	
2291	10.61	0.25	3	3.4	9.4						0.068	0.005	38.5	1.2	4	4
2292	11.7	0.15	1												5	
2293	10.7	0.15	1												7	
2294	11.4	0.15	1												5	
2295	11.7	0.15	1												2	
2296	11.2	0.15	1												11	
2297	11.2	0.15	1								0.069	0.019	29.1	4.0	9	6
2298	14.7	0.25	1												2	
2299	13.2	0.15	1												2	
2300	11 76	0.25	8	3.2	14.8										2	
2301	11.2	0.15	1												5	
2302	12.20	0.408	6	2.6	18.6										5	
2303	12.2	0.15	1												2	
2304	12.22	0.15	1		8.0										11	
2305	11.2	0.15	1												5	
2306	12.42	0.15	1		8.1						0.035	0.006	23.3	1.8	7	2
2307	11.19	0.15	1		8.7						0.029	0.002	45.1	1.1	5	4
2308	11.87	0.15	2	11.2	12.2						0.081	0.015	19.6	1.8	10	8
2309	11.2	0.25	1												2	
2310	11.2	0.15	1												11	
2311	10.55	0.15	5	2.6	11.2	0.21	1	0.75	1	2	0.029	0.005	61.0	5.3	5	3
2312	10.24	0.15	6	2.2	13.0	0.25	3	0.73	3	2	0.039	0.010	60.0	7.6	4	4
2313	13.12	0.15	5	6.2	17.4						0.032	0.003	17.6	0.8	5	2
2314	12.7	0.25	1												6	
2315	10.7	0.25	1								0.13	0.01	26.0	1.2	2	2
2316	12.39	-.104	6	3.9	19.3										5	
2317	13.46	0.15	1		4.6										13	
2318	13.85	0.25	1		6.0										19	
2319	12.15	0.25	1		8.7										4	
2320	10.7	0.15	1								0.056	0.014	40.5	5.0	12	7
2321	11.7	0.15	1								0.075	0.009	22.0	1.2	3	1
2322	12.7	0.25	1								0.042	0.004	18.7	0.8	6	2
2323	10.7	0.15	1													
2324	11.64	0.15	1		7.6										5	
2325	12 05	0.15	3	1.9	6.6										9	
2326	10.61	0.15	3	4.8	10.9						0.048	0.006	45.6	2.7	15	11
2327	13.76	0.25	2	3.0	13.1										7	
2328	12.7	0.25	1								0.073	0.009	14.1	0.8	9	1
2329	15.1	0.25	1												4	
2330	10.7	0.15	1								0.061	0.012	39.0	3.6	5	2
2331	12.37	0.25	3	2.4	15.2						0.046	0.006	20.7	1.3	8	1
2332	10.64	0.15	5	2.1	9.9						0.083	0.023	34.2	4.7	5	4
2333	11.88	0.15	2	15.7	18.5						0.055	0.005	23.8	1.0	6	1
2334	13.2	0.25	1												9	
2335	13.1	0.25	1												5	
2336	11.44	0.15	1		10.0										4	
2337	12.05	0.15	1		12.2						0.042	0.006	25.2	1.7	11	1

Magnitudes, UBV Colors, IRAS Albedos and Diameters

M.P.	H	G	No. Obs	Min Phase	Max Phase	U-B	UQ	B-V	BQ	UBV Ref	Albedo	Albedo Unc.	D	D Unc	No. Obs Pre	No. Obs Acc
2338	11.7	0.25	1												3	
2339	13.55	0.15	1		10.9										7	
2340	20.2	0.15	1			0.50	1	0.77	1	1					1	
2341	12.7	0.25	1													
2342	11.97	0.15	2	0.5	4.5										9	
2343	13.7	0.25	1												8	
2344	11.7	0.15	1												9	
2345	10.80	0.25	3	1.5	16.7	0 43	3	0 81	2	2	0.067	0.020	35.5	5.3	6	2
2346	12.2	0.25	1												12	
2347	11.42	0 15	1		2.7										11	
2348	12.2	0.25	1													
2349	11.58	0.15	2	11.4	11.5						0.089	0.011	21.5	1.2	8	1
2350	13.2	0.25	1								0 043	0.006	14.7	1.0	5	1
2351	13.2	0.15	1												11	
2352	10 79	0.15	1		6.6											
2353	11.7	0.15	1												7	
2354	11.7	0.15	1												6	
2355	11.2	0.15	1								0.11	0.02	22.5	2.3	8	2
2356	10.67	0.15	6	7.6	16.5						0.039	0.005	49.2	3.2	7	5
2357	8.99	0.15	5	1.3	10.7	0.23	2	0.72	2	2	0.042	0.004	103	4	4	2
2358	10.7	0.25	1												2	
2359	12.93	0.25	3	4.6	11.7										12	
2360	12.43	0.15	3	10.3	14.7										9	
2361	11.91	0.15	3	10.7	13 7										6	
2362	13.7	0.25	1												3	
2363	8.7	0.15	1			0 25	2	0.75	2	2	0.066	0.023	91.7	15.8	4	3
2364	10.77	0.15	2	8.9	9.6						0.17	0.02	22.3	1.2	6	1
2365	11.96	0.15	2	5.4	9.3										4	
2366	13.95	0.25	4	2.5	16.8										6	
2367	13.75	0.25	1		11.6										6	
2368	15.5	0.25	1			0.52	1	0.83	3	1					7	
2369	12.00	0 15	2	4.6	8.3										2	
2370	10.2	0.15	1								0.44	0.06	18.0	1.1	7	3
2371	12.72	0.25	3	3 5	14.6										2	
2372	11.7	0.15	1								0 061	0.007	24.6	1.3	3	1
2373	13.2	0.15	1												6	
2374	11.21	0.15	1		13.3										4	
2375	10.51	-.046	7	6.9	20.4	0.23	3	0 73	3	2						
2376	10.78	0.15	4	2.4	13.3						0.052	0.003	40.6	1.1	6	5
2377	12 44	0.25	4	0.9	4.7										4	
2378	10.59	0.15	1		13.8						0.072	0.010	37.7	2.5	3	3
2379	10.93	0.15	2	6.6	9.7	0.34	3	0.65	3	2	0.071	0.013	32.5	3.0	11	2
2380	12.7	0.25	1												3	
2381	11.2	0.15	1								0.30	0.03	13.8	0.8	7	2
2382	10.7	0.15	1												2	
2383	13.47	0.25	4	3.0	17.9										2	
2384	12.40	0.301	6	1.6	25.1										6	
2385	13.2	0.25	1												2	
2386	11.7	0.25	1								0.15	0.01	15.5	0.8	7	1
2387	11.58	0.25	3	1.0	10.5										5	
2388	12.97	0.25	3	4.7	16.2										2	
2389	13.2	0.25	1												4	
2390	12.33	0.15	1		15.4										5	
2391	12.2	0.25	1													
2392	13.39	0.25	1		0.9										4	
2393	10.6	0.15	1								0.039	0.006	50.8	3.8	7	7
2394	11.49	0.15	1		16.6						0.014	0.002	56.0	3.8	7	2
2395	12.4	0.15	1												6	
2396	11.36	0.15	1		20.6										6	
2397	11.25	0.15	2	4.2	11.2										6	
2398	13.58	0.25	1		13 8											
2399	13.27	0.25	2	16.7	17 9										4	
2400	12.43	0.25	1		4.4										9	
2401	12.2	0.15	1												5	
2402	13.30	0.25	2	2.5	6.2										4	
2403	12.2	0.15	1												2	
2404	11.14	0 15	2	4.0	9.8										7	
2405	12.09	0.25	1		1.1	0 31	1	0.70	1	2	0.030	0.003	29.3	1.3	4	1
2406	13.7	0.25	1												2	
2407	10.77	0.15	1		6.0	0.25	1	0 70	2	2					4	
2408	12.7	0.15	1								0.023	0.003	25.3	1.6	4	3
2409	13.04	0.25	2	4.7	11.1										2	
2410	12.99	0.25	1		23.9										2	

Magnitudes, UBV Colors, IRAS Albedos and Diameters

M.P.	H	G	No. Obs.	Min Phase	Max Phase	U-B	UQ	B-V	BQ	UBV Ref	Albedo	Albedo Unc.	D	D Unc	No. Obs Pre	No Obs Acc
2411	12.98	0.25	5	1.8	24.9	0.55	1	0.93	1	2						
2412	11.7	0.15	1												2	
2413	10.63	0.25	1		9.3						0.13	0.03	26.6	3.0	5	3
2414	10.9	0.15	1								0.068	0.006	33.5	1.3	9	7
2415	12.13	0.15	1		5.7										2	
2416	11.0	0.25	1								0.090	0.012	27.8	1.8	8	1
2417	12.25	0.15	2	5.9	6.6										6	
2418	12.2	0.15	1												2	
2419	13.45	0.25	1		6.0										5	
2420	12.7	0.25	1													
2421	10.82	0.15	7	4.7	16.1						0.044	0.010	43.3	4.7	9	5
2422	13.7	0.25	1			0.50	1	0.85	1	1					6	
2423	13.7	0.15	1												6	
2424	12.7	0.25	1												8	
2425	11.72	0.25	3	1.3	11.3										2	
2426	11.55	0.15	3	6.4	14.5						0.053	0.006	28.2	1.5	2	2
2427	12.7	0.15	1												9	
2428	11.2	0.15	1								0.061	0.004	31.0	0.8	7	4
2429	12.33	0.25	1		12.1										4	
2430	12.1	0.25	1			0.42	2	0.82	2	1					6	
2431	12.2	0.15	1												2	
2432	13.08	0.25	4	3.3	8.3						0.10	0.01	10.0	0.5	2	1
2433	11.88	0.330	6	3.5	29.5										2	
2434	11.61	0.15	1		10.7										2	
2435	14.7	0.25	1												7	
2436	12.2	0.15	1												6	
2437	13.5	0.25	1												6	
2438	13.69	0.25	1		3.5											
2439	11.2	0.15	1								0.10	0.02	23.8	2.2	7	5
2440	13.7	0.25	1												6	
2441	13.2	0.25	1								0.065	0.007	11.8	0.5	4	2
2442	12.73	0.25	1		9.1										13	
2443	10.47	0.25	3	4.2	14.0						0.092	0.007	35.1	1.3	3	2
2444	11.86	0.15	3	3.5	12.7										10	
2445	12.94	0.25	1		4.2											
2446	12.99	0.25	2	0.6	4.2										2	
2447	13.05	0.15	3	4.6	13.5										4	
2448	10.85	0.15	2	1.7	8.7						0.073	0.016	33.2	3.5	5	5
2449	14.47	0.40	4	18.8	32.2	0.34	2	0.70	3	2					4	
2450	11.55	0.15	4	1.7	12.2						0.035	0.005	35.0	2.2	7	1
2451	12.02	0.15	6	1.9	18.8										7	
2452	12.02	0.15	6	2.0	20.9										7	
2453	11.09	0.25	1		16.7						0.031	0.023	45.7	16.7	10	2
2454	13.68	0.25	2	3.4	14.4										4	
2455	11.78	0.15	3	2.9	14.0										4	
2456	9.2	0.15	1								0.035	0.002	103	3	7	5
2457	12.7	0.15	1												6	
2458	11.59	0.15	2	1.8	17.0						0.052	0.008	28.0	2.0	8	3
2459	11.7	0.25	1								0.062	0.008	24.3	1.5	11	1
2460	11.96	0.25	1		14.3										7	
2461	11.2	0.15	1								0.072	0.014	28.5	2.6	4	3
2462	13.98	0.25	2	2.6	4.6										2	
2463	12.2	0.15	1								0.14	0.01	12.6	0.5	3	2
2464	11.92	0.15	1		4.1						0.075	0.009	20.0	1.1	2	1
2465	12.2	0.15	1								0.047	0.006	22.2	1.3	6	1
2466	12.2	0.15	1								0.038	0.005	24.6	1.5	4	1
2467	12.65	0.25	1		8.5										2	
2468	12.7	0.25	1								0.16	0.02	9.53	0.62	4	1
2469	11.7	0.15	1												2	
2470	11.2	0.25	1												4	
2471	11.66	0.15	2	2.8	6.0										4	
2472	13.7	0.25	1												4	
2473	13.51	0.25	3	5 5	8.6										8	
2474	11.7	0.15	1								0.082	0.031	21.1	4.0	8	4
2475	11.1	0.25	1												2	
2476	10.99	0.25	2	7.2	17.3						0.11	0.02	24.8	2.3	7	4
2477	12.01	0.15	1		8.4										4	
2478	12.54	0.25	3	6.0	11.8											
2479	12.7	0.25	1								0.037	0.005	20.0	1.2	10	1
2480	13.49	0.25	3	2.5	4.5										2	
2481	13.93	0.15	4	3.7	12.0										4	
2482	11.2	0.15	1												4	
2483	11.18	0.15	3	4.7	4.8						0.021	0.002	53.3	2.5	7	1

Magnitudes, UBV Colors, IRAS Albedos and Diameters

M.P.	H	G	No. Obs.	Min Phase	Max Phase	U-B	UQ	B-V	BQ	UBV Ref	Albedo	Albedo Unc.	D	D Unc	No. Obs Pre	No Obs Acc
2484	13.2	0.25	1								0.060	0.006	12.3	0.5	7	1
2485	12.54	0.15	2	2.4	4.1										4	
2486	12.98	0.25	1		7.9										7	
2487	12.7	0.25	1												4	
2488	13.7	0.25	1												3	
2489	12.00	0.15	4	2.5	8.2										7	
2490	12.19	0.15	1		3.1						0.12	0.01	13.6	0.7	3	1
2491	13.74	0.25	2	13.5	28.6	0.26	2	0	76	2	2				9	
2492	11.16	0.15	1		5.1						0.086	0.024	26.5	3.6	4	2
2493	12.7	0.15	1												1	
2494	10.70	0.15	6	3.2	14.0						0.028	0.002	57.7	2.0	2	2
2495	15.2	0.40	1												2	
2496	13.2	0.25	1													
2497	13.28	0.15	1		14.2										4	
2498	12.03	0.15	2	4.8	6.8										2	
2499	12.25	0.15	2	4.9	7.8										6	
2500	12.84	0.25	4	1.4	14.8										11	
2501	12.15	0 25	1		11.9	0.58	1	1.06	2	2					6	
2502	11.56	0.15	2	1.0	3.9						0.11	0.03	18.8	2.7	7	5
2503	14 2	0 25	1												5	
2504	11.93	0.15	4	6.2	19.4										2	
2505	11.31	0.15	5	0 4	6.5										4	
2506	11.86	0.25	5	1.3	9.0										5	
2507	11.63	0.15	6	5.3	13.2										7	
2508	13.7	0 25	1													
2509	13.15	0.15	2	10.3	14.3										7	
2510	12.28	0.25	2	6.1	12.9	0.47	2	0.89	2	2					2	
2511	12.82	0.25	1		4.6						0.041	0.006	18.0	1.1	6	1
2512	12.7	0.25	1												8	
2513	12.7	0.25	1												4	
2514	12.95	0.15	3	1.8	14.1						0.019	0.003	24.5	1.6	5	1
2515	12.34	0.15	2	2 4	2.5										4	
2516	13.76	0.25	5	3.2	21.9										7	
2517	11.75	0.15	2	2.6	14.2						0.016	0.002	47.5	3.1	4	1
2518	13.69	0.25	2	3.9	9 5										2	
2519	11.40	0.15	4	2.3	11.6										5	
2520	11.73	0.15	1		7.9										2	
2521	11.7	0.15	1												10	
2522	11.7	0.25	1												8	
2523	11.58	0.25	1		10.6						0.073	0.009	23.6	1.5	4	1
2524	11.08	0.15	3	1.0	10.4						0.048	0.006	36.7	2.2	12	4
2525	10.76	0.15	4	1.4	13.0										5	
2526	12.2	0.15	1												3	
2527	13.04	0.15	4	3.2	11.8										4	
2528	11.6	0.15	1												4	
2529	13 1	0.15	1												7	
2530	11.7	0.25	1												13	
2531	11.01	0.25	10	1.7	13.8						0.10	0.01	25.6	1.0	4	1
2532	12.7	0.25	1												7	
2533	11.76	0.15	4	2.7	15.9										6	
2534	10.67	0.15	4	5.1	10.7						0.081	0.025	34.2	5.2	5	2
2535	12.65	0.329	5	5.3	25.6										7	
2536	13 11	0.25	2	14.8	24 5										4	
2537	12.2	0.15	1												7	
2538	13.76	0.338	5	3.2	17 2										9	
2539	14.39	0.25	4	2.3	15.3										6	
2540	13.2	0.25	1												7	
2541	12.2	0.15	1												4	
2542	11.48	0.137	5	6.8	19.9						0.040	0.008	33.6	3.3	5	2
2543	11.2	0.15	1												3	
2544	12.7	0.25	1								0.14	0.01	10.1	0.3	11	3
2545	13.21	0.25	1		3.2										6	
2546	12.2	0.15	1								0.070	0.009	18.2	1.1	4	1
2547	13.2	0.25	1												2	
2548	12.2	0.15	1												4	
2549	12.7	0.15	1												7	
2550	11.34	0.15	1		2.5										2	
2551	12.40	0.427	5	2.1	16.7										4	
2552	14.98	0.25	1		10.6										6	
2553	11 2	0.15	1												4	
2554	12.91	0.127	6	3.8	20.3										2	
2555	12.03	0.314	11	1.2	15.4										6	
2556	13.70	0.25	4	1.4	17.7										2	

Magnitudes, UBV Colors, IRAS Albedos and Diameters

M.P.	H	G	No. Obs.	Min Phase	Max Phase	U-B	UQ	B-V	BQ	UBV Ref	Albedo	Albedo Unc.	D	D Unc	No. Obs Pre	No. Obs Acc
2557	12.49	0.25	4	3.8	21.1										2	
2558	13.87	0.25	3	9.0	13.8										7	
2559	12.2	0.15	1								0.025	0.004	30.5	2.5	2	1
2560	11.81	0.15	4	4.1	8.2										10	
2561	13.12	0.25	5	2.5	9.8										15	
2562	10.56	0.25	1		1.3						0.17	0.02	24.5	1.3	4	1
2563	11.42	0.15	4	5.4	8.8						0.041	0.004	34.0	1.5	7	3
2564	13.53	0.25	1		2.8										9	
2565	14.7	0.25	1												4	
2566	12.71	0.25	3	6.7	15.9										7	
2567	11.75	0.15	7	2.3	11.7						0.058	0.021	24.5	4.5	10	2
2568	13.7	0.25	1												5	
2569	11.34	0.15	5	6.3	16.1						0.047	0.007	33.0	2.5	5	4
2570	12.21	0.15	6	7.8	16.5						0.026	0.006	30.0	3.2	5	3
2571	13.21	0.25	4	5.7	22.0										4	
2572	12.7	0.25	1												4	
2573	11.2	0.15	1												2	
2574	12.56	0.25	1		1.3										2	
2575	13.2	0.25	1								0.026	0.003	18.8	1.1	6	1
2576	11.22	0.15	2	4.0	8.4										5	
2577	12.7	0.40	1			0.34	3	0.79	3	2					12	
2578	11.70	0.25	3	4.6	13.2										4	
2579	13.2	0.25	1												9	
2580	13.49	0.25	1		0.9										9	
2581	13.7	0.25	1												7	
2582	10.7	0.15	1								0.064	0.016	37.8	4.6	7	4
2583	13.12	0.25	1		12.4						0.028	0.006	18.8	2.0	6	1
2584	13.65	0.25	1		8.6						0.043	0.006	11.8	0.7	10	1
2585	12.6	0.25	1												7	
2586	13.10	0.25	3	4.9	18.5										3	
2587	11.19	0.15	6	2.9	15.7										6	
2588	13.43	0.15	4	0.8	14.1										6	
2589	12.05	0.25	1		6.0										10	
2590	12.84	0.25	1		18.6										4	
2591	11.58	0.15	4	1.0	11.3										7	
2592	10.7	0.15	1												4	
2593	14.01	0.25	3	6.8	10.4										6	
2594	11.2	0.15	1												4	
2595	12.37	0.15	5	2.7	7.9						0.014	0.002	38.2	2.2	7	1
2596	12.2	0.15	1												4	
2597	11.74	0.15	4	2.6	16.6										5	
2598	12.59	0.15	4	3.9	12.3										6	
2599	12.27	0.15	1		4.9										7	
2600	11.29	0.25	4	1.9	16.1										4	
2601	11.30	0.15	2	12.5	14.7						0.10	0.01	22.7	1.3	8	1
2602	13.08	0.25	5	2.5	9.2										10	
2603	11.98	0.15	3	2.6	6.7										13	
2604	12.7	0.25	1								0.045	0.006	18.0	1.0	10	1
2605	12.7	0.15	1												4	
2606	11.42	0.15	1		16.0										6	
2607	13.47	0.25	2	10.6	14.3										4	
2608	17.57	0.25	1		22.2	0.41	1	0.80	2	1					5	
2609	13.27	0.25	2	5.0	18.4										2	
2610	13.7	0.25	1												4	
2611	11.96	0.15	1		9.3										6	
2612	11.20	0.15	1		3.0											
2613	11.38	0.15	2	5.0	16.5										6	
2614	13.2	0.25	1												8	
2615	12.2	0.15	1												4	
2616	12.4	0.25	1								0.23	0.02	9.01	0.52	8	1
2617	10.66	0.15	2	0.5	6.8						0.027	0.005	59.2	5.8	4	3
2618	12.2	0.25	1								0.022	0.007	32.6	5.1	6	1
2619	12.6	0.15	1												4	
2620	12.61	0.25	1		4.8										8	
2621	10.75	0.15	2	5.4	14.6						0.035	0.002	50.1	1.0	9	8
2622	11.6	0.25	1												8	
2623	13.2	0.25	1												6	
2624	10.7	0.15	1												4	
2625	12.7	0.25	1												5	
2626	11.7	0.25	1												7	
2627	11.93	0.15	1		4.0										6	
2628	12.7	0.15	1												9	
2629	14.76	0.25	1		17.9										2	

Magnitudes, UBV Colors, IRAS Albedos and Diameters

M P.	H	G	No. Obs.	Min Phase	Max Phase	U-B	UQ	B-V	BQ	UBV Ref	Albedo	Albedo Unc.	D	D Unc	No. Obs Pre	No. Obs Acc
2630	11.68	0.15	2	0.9	5.1										4	
2631	11.79	0.15	1		8.6						0.029	0.004	34.0	2.0	6	1
2632	11.2	0.25	1								0.054	0.007	32.7	2.0	5	2
2633	13.42	1.184	5	1.7	14.3										7	
2634	10.36	0.15	3	4.9	14.5						0.058	0.005	46.5	2.0	5	2
2635	13.25	0.25	3	4.5	15.4										2	
2636	11.46	0.15	3	6.4	14.7										6	
2637	13.2	0.25	1								0.024	0.003	19.6	1.2	15	1
2638	12.2	0.15	1												9	
2639	13.34	0.25	1		11.9										4	
2640	13.31	0.25	4	2.0	8.7										4	
2641	13.16	0.25	3	3.9	11.2										4	
2642	12.7	0.25	1												11	
2643	15.2	0.25	1												14	
2644	13.86	0.25	2	4.0	8.0										2	
2645	12.2	0.25	1								0.075	0.009	17.5	1.0	8	1
2646	11.2	0.25	1								0.073	0.010	28.2	1.8	11	1
2647	12.80	0.25	1		13.1										7	
2648	13.02	0.25	4	4.4	25.2										8	
2649	11.79	0.15	5	15.2	23.7						0.031	0.003	33.1	1.5	13	1
2650	11.2	0.15	1												6	
2651	12.2	0.15	1												4	
2652	11 7	0.15	1												4	
·2653	12.2	0.25	1								0.055	0.008	20.5	1.3	6	1
2654	12.2	0.15	1								0.043	0.009	23.1	2.5	8	2
2655	11.30	0.15	3	6 4	14.9						0.032	0 009	40.7	5.5	6	1
2656	13.84	0.25	2	2.5	6.4										6	
2657	11.93	0.15	1		5 8										7	
2658	11.7	0.15	1												4	
2659	11.15	0.15	4	5.4	11.7						0.063	0.008	31.0	1.8	6	2
2660	12.09	0.15	1		3.1						0.14	0.02	13.3	1.1	9	1
2661	11.7	0.25	1												17	
2662	13.7	0.15	1								0.052	0.006	10.5	0.6	9	1
2663	13.86	0.25	1		5.8										8	
2664	13.7	0.25	1								0.034	0.004	13.1	0.7	5	1
2665	13.34	0.25	3	5.6	20.0										4	
2666	11.7	0.15	1								0.024	0.005	39.3	4.2	12	2
2667	12.2	0.15	1								0.029	0.006	28.5	3.0	7	3
2668	13.52	0.25	1		6.8										5	
2669	12.77	0.15	3	6.0	11.9										5	
2670	10.70	0.15	1		6.2										4	
2671	13.7	0.15	1												6	
2672	12.34	0.15	1		10.0						0.044	0.007	21.5	1.6	6	3
2673	12.2	0.15	1												2	
2674	9.05	0.15	2		10.9	0.25	2	0.76	2	2	0.041	0.003	102	4	6	3
2675	12.45	0.25	2	7.6	12 6										2	
2676	12.7	0.25	1												2	
2677	11.87	0.15	3	1.7	13.3						0.062	0.008	22.5	1.3	6	1
2678	12.2	0.25	1												9	
2679	11.7	0.15	1												5	
2680	13.2	0.25	1												10	
2681	12.58	0.15	2	2.0	3.4										7	
2682	13.76	0.25	2	4.5	5.3										4	
2683	11.97	0.15	6	1.4	11.5										6	
2684	11.92	0.626	5	2.3	14.7										8	
2685	12.36	0.15	3	1.9	13.0										2	
2686	11.7	0.25	1												4	
2687	12.07	0.15	4	2.9	15.3										8	
2688	11.84	0.15	4	5.8	14.1						0.069	0.008	21.5	1.2	4	1
2689	13.87	0.25	3	1.8	18.4										4	
2690	10.7	0.25	1								0.20	0.02	21.2	1.0	6	3
2691	13.61	0.25	4	5.4	18.9										4	
2692	12.33	0.15	4	0.8	14.0										4	
2693	13.22	0.25	1		6.8										7	
2694	13.94	0.25	2	0.4	4.4										6	
2695	12.10	0.15	4	5.6	13.5										4	
2696	11.7	0.25	1												2	
2697	10.62	0.15	2	9.5	11.2						0.034	0.003	54.0	2.0	6	5
2698	12.15	0.15	1		3.7										7	
2699	12.0	0.15	1												9	
2700	12.31	0.25	1		4.8										5	
2701	12.2	0.15	1												7	
2702	11.5	0.15	1												9	

Magnitudes, UBV Colors, IRAS Albedos and Diameters

M.P.	H	G	No. Obs.	Min Phase	Max Phase	U-B	UQ	B-V	BQ	UBV Ref	Albedo	Albedo Unc.	D	D Unc	No. Obs Pre	No. Obs Acc
2703	13.46	0.25	1		8.2										2	
2704	12.93	0.25	2	5.9	7.2										2	
2705	13.7	0.25	1								0.062	0.006	9.71	0.44	11	1
2706	11.9	0.25	1												6	
2707	11.6	0.15	1								0.046	0.012	29.7	4.0	6	4
2708	11.98	0.316	5	4.1	20.9										4	
2709	13.44	0.25	3	4.4	16.1						0.018	0.003	20.2	1.3	4	1
2710	13.43	0.15	4	2.7	17.1											
2711	11.88	0.25	1		7.7										7	
2712	13.7	0.25	1												7	
2713	11.68	0.25	1		7.7										7	
2714	12.86	0.25	1		5.8										2	
2715	12.24	0.15	1		2.4						0.098	0.009	15.0	0.6	6	2
2716	13.2	0.25	1												2	
2717	12.76	0.25	3	2.7	13.5										3	
2718	11.7	0.15	1								0.043	0.005	29.2	1.6	8	2
2719	13.2	0.25	1												8	
2720	14.2	0.25	1								0.042	0.005	9.39	0.55	2	1
2721	11.7	0.15	1												8	
2722	12.27	0.15	4	5.1	13.6										6	
2723	12.93	0.15	1		4.0										6	
2724	12.32	0.15	1		2.7						0.022	0.003	30.7	2.0	4	1
2725	10.69	0.15	1		8.6						0.053	0.003	42.0	1.1	12	11
2726	12.2	0.25	1								0.020	0.003	34.0	2.3	7	1
2727	12 2	0.15	1												5	
2728	12.59	0.15	2	4.3	4.9						0.048	0.011	18.5	2.1	11	2
2729	11.62	0.25	1		6.9						0.083	0.011	21.8	1.3	9	2
2730	11.71	0.15	5	2.0	9.8										4	
2731	10.90	0.15	4	2.0	9.7						0.029	0.002	51.1	1.3	4	3
2732	12.27	0.15	1		6.9										4	
2733	13.39	0.328	5	3.3	17.8										7	
2734	11.2	0.15	1								0.081	0.010	26.8	1.5	6	1
2735	14.41	0.25	3	21.8	24.0	0.41		0.83		2						
2736	12.98	0.25	5	3.8	14.0										6	
2737	11.2	0.15	1												6	
2738	12.0	0.15	1												2	
2739	12.55	0.25	1		14.8						0.090	0.012	13.6	0.8	2	1
2740	11.2	0.25	1								0.087	0.011	26.0	1.5	9	1
2741	11.6	0.15	1												3	
2742	12.0	0.25	1								0.062	0.035	21.1	5.8	7	2
2743	12.35	0.15	1		0.4										2	
2744	15.09	0.25	2	11.9	13.1	0.47	1	0.86	1	3						
2745	13.37	0.25	3	15.3	27.4										6	
2746	13.68	0.25	3	2.6	4.8										3	
2747	11.2	0.15	1												2	
2748	12.7	0.15	1												2	
2749	12.26	0.15	1		5.2										3	
2750	12.85	0.25	1		18.0										2	
2751	12.7	0.25	1								0.037	0.005	20.0	1.1	10	1
2752	10.7	0.25	1												3	
2753	11.81	0.15	1		6.1						0.079	0.008	20.5	1.0	2	2
2754	12.7	0.25	1												2	
2755	12.2	0.15	1												2	
2756	13 19	0.15	1		8.7										2	
2757	11.56	0.15	2	7.9	8.5										2	
2758	13.85	0.15	1		9.6											
2759	9.77	0.15	8	4.3	9.4						0.041	0.004	73.3	3.5	6	1
2760	10.04	0.15	4	4.4	11.3	0.26	3	0.72	3	2	0.043	0.003	62.6	2.1	5	4
2761	12.08	0.15	4	3.0	14.6						0.025	0 003	32.3	2.0	7	1
2762	13.69	0.25	2	1.0	10.2										6	
2763	12.43	0.25	3	3.4	16.1										2	
2764	13.48	0.25	4	3.6	15.8										2	
2765	11.7	0.15	1								0.017	0.002	46.6	3.0	6	1
2766	12.2	0.15	1												6	
2767	11.60	0.25	3	4.2	11.7										2	
2768	12.79	0.25	3	5.8	16.3											
2769	12.12	0.15	3	1.4	12.5										6	
2770	13.2	0.25	1												6	
2771	13.03	0.15	1		12.8										3	
2772	13.09	-.122	5	3.2	24.2											
2773	13.24	0.25	4	2.3	16.1											
2774	11.08	0.15	6	3.5	11.9						0.043	0.006	39.0	2.6	4	4
2775	13.7	0.15	1												3	

Magnitudes, UBV Colors, IRAS Albedos and Diameters

M.P.	H	G	No. Obs.	Min Phase	Max Phase	U-B	UQ	B-V	BQ	UBV Ref	Albedo	Albedo Unc.	D	D Unc	No. Obs Pre	No. Obs Acc
2776	12.62	0.25	1		9.6											
2777	13.40	0.25	3	1.8	3.9										2	
2778	13.06	0.25	6	4.3	17.5											
2779	13.53	0.25	4	8.7	19.8										2	
2780	12.7	0.25	1												2	
2781	12.03	0.15	2	4.6	7.0										2	
2782	13.2	0.15	1								0.013	0.002	26.8	1.7	2	1
2783	13.2	0.15	1												3	
2784	13.1	0.25	1												3	
2785	11.7	0.25	1												5	
2786	12.1	0.15	1												2	
2787	11.4	0.25	1												5	
2788	13.0	0.15	1												6	
2789	13.7	0.25	1												2	
2790	12.85	0.15	2	12.1	15.4										2	
2791	11.4	0.25	1					1.02	1	1					8	
2792	13 00	0.25	3	1.0	16.3											
2793	10.7	0.15	1								0 087	0 027	32.5	5.0	5	2
2794	12 7	0.25	1													
2795	13.19	0.25	3	1.5	15.1										1	
2796	12.51	0.498	7	5.9	19.5										3	
2797	8.51	0.15	4	3.0	9.8						0.046	0.003	123	4	7	4
2798	12.7	0.25	1												2	
2799	14.2	0.25	1								0.011	0.001	18.1	1.1	2	1
2800	12.2	0.15	1												6	
2801	12.31	0.15	2	5.2	7.1										2	
2802	10.7	0.15	1												4	
2803	11.7	0.15	1												9	
2804	11.2	0.25	1								0.086	0.019	26.0	3.0	8	1
2805	12.2	0.15	1												4	
2806	12.2	0.25	1								0.057	0.005	20.1	0.8	8	1
2807	12.2	0.15	1												6	
2808	11.44	0.25	1		2.6										9	
2809	13.69	0.25	2	9.5	24.8	0.24	1	0.65	1	2					3	
2810	12.7	0.15	1												2	
2811	12.11	0.25	3	0 6	11.2										2	
2812	14.14	1.529	5	5.3	23.0										2	
2813	11.41	0.645	5	2.5	18.8						0.036	0 007	36.7	3.3	3	3
2814	12.44	0.25	1		2.7										7	
2815	12.80	-.201	5	4.8	19.7											
2816	11.87	0.15	3	6 3	15.5						0.046	0.006	26.1	1.7	2	1
2817	13.91	0.25	3	2.2	16.8										1	
2818	13.89	0.25	2	13.4	17.1										2	
2819	12.2	0.15	1								0.12	0.01	13.3	0.7	9	1
2820	12.7	0.25	1													
2821	13.7	0.25	1													
2822	12.53	0 15	9	8.3	17.9											
2823	13.2	0.25	1												2	
2824	13.58	0.25	2	7 5	11.0											
2825	12.7	0.25	1								0 046	0.006	17.7	1.0	6	1
2826	11.60	0.15	2	1 1	5.7						0 023	0.004	42.0	3.5	10	7
2827	12 2	0.25	1												3	
2828	12.7	0.25	1												9	
2829	11.08	0.15	1		4.8						0.029	0.007	47.3	5.5	7	2
2830	12.55	0.25	6	8.3	25.0	0.44	3	0.87	3	2					4	
2831	12.15	0.25	1		11.6										6	
2832	12.5	0.25	1												8	
2833	12.15	0.25	2	0.8	3.3										4	
2834	12.0	0.15	1												8	
2835	11 9	0.15	1								0.033	0.007	30.6	3.2	3	1
2836	11.1	0.25	1												2	
2837	11.94	0.25	2	6.4	8.5										4	
2838	14.27	0.25	1		10.9										7	
2839	12.2	0.25	1												11	
2840	12.96	0.25	1		11.3											
2841	12.7	0.25	1												3	
2842	11.7	0.15	1												14	
2843	12.94	0.25	1		18.6										8	
2844	13.61	0.25	3	3.5	17.5										3	
2845	13.51	0.25	3	17.3	20.2										4	
2846	10.6	0.15	1								0.10	0 02	31.6	3.2	8	6
2847	12.6	0.25	1												2	
2848	11 50	0.15	2	6.7	10.5						0.070	0.008	25.2	1.5	5	1

Magnitudes, UBV Colors, IRAS Albedos and Diameters

M.P.	H	G	No. Obs	Min Phase	Max Phase	U-B	UQ	B-V	BQ	UBV Ref	Albedo	Albedo Unc.	D	D Unc	No. Obs Pre	No. Obs Acc
2849	12.5	0.15	1							0 056	0.007		17.7	1.0	8	2
2850	12.0	0.25	1												2	
2851	12.36	0.25	1		8.4										4	
2852	12.2	0.15	1												5	
2853	13.61	0.25	1		9.6										8	
2854	13.0	0.25	1												7	
2855	12.7	0.25	1												4	
2856	11.2	0.15	1								0.078	0.005	27.2	0.8	9	5
2857	12 7	0.25	1												4	
2858	14.2	0.25	1												6	
2859	12.7	0.25	1												6	
2860	13.02	0.25	1		15.9										6	
2861	12 73	0.25	2	1.3	9.9										4	
2862	13.57	0.25	2	5.8	17.3										7	
2863	12.31	0.15	3	4.9	10.6										6	
2864	12.68	0.15	4	1.3	13.0						0.042	0.004	18.8	0.7	8	5
2865	11.50	0.25	1		10.0						0.14	0.02	17.5	1.5	2	2
2866	11.79	0.15	3	1.5	2.7										4	
2867	12.81	0.25	2	12.0	14.0										7	
2868	13.22	0.15	1		2.7						0.014	0.002	25.3	1.5	6	1
2869	12.37	0.15	2	2.8	10.5										4	
2870	13.48	1.146	6	4.9	24.3										4	
2871	12.75	0.25	5	3.2	27.2						0.036	0.005	19.6	1.1	6	1
2872	12.62	0.15	2	6.4	12.1						0.056	0.005	16.7	0.7	6	1
2873	13.13	0.394	5	5.1	26.5										6	
2874	13.58	0.25	4	4.4	18.3											
2875	12.39	0.15	5	2.1	12.5										6	
2876	12.68	0.15	2	1.7	12.2										4	
2877	12.2	0.15	1								0.017	0.004	37.0	4.0	4	2
2878	11.57	0.15	5	3.4	16.4										5	
2879	11.2	0.15	1								0.057	0.011	32.0	3.0	7	3
2880	12.7	0.25	1								0.043	0.005	18.5	1.0	6	1
2881	13.64	0.25	4	3.8	14.9										4	
2882	12.03	0.222	5	0.1	15.3										1	
2883	13.19	0.25	1		2.0										5	
2884	11.7	0.15	1												8	
2885	13.7	0.25	1												3	
2886	13.2	0.25	1												6	
2887	13.07	0.25	4	3.4	7.1										2	
2888	13.2	0.25	1													
2889	11.50	0.25	2	4.1	6.0										6	
2890	12.96	0.25	3	3.4	13.2										6	
2891	11.11	0.15	1		8.2										2	
2892	10.2	0.15	1								0.043	0.003	58.5	1.8	4	3
2893	8.92	0.15	1		1.6	0.24	2	0.73	3	2	0.055	0.016	92.8	13.5	4	3
2894	12.2	0.15	1												4	
2895	9.23	0.15	2	5.1	6.4										5	
2896	12.85	0.25	2	1.9	5.1										2	
2897	13.79	0.25	1		3.4										7	
2898	11.7	0.15	1												5	
2899	13.57	0.25	5	2.2	21.1										6	
2900	11.7	0.25	1												4	
2901	12.28	0.25	2	5.1	8.2										4	
2902	14.43	0.25	5	1.9	8.5										5	
2903	11.7	0.25	1													
2904	11.70	0.15	4	9.9	23.2										7	
2905	11.99	0.15	5	3.1	8.4										6	
2906	9 7	0.15	1								0.060	0.010	62.0	5.2	5	2
2907	11.2	0.25	1												4	
2908	11.65	0.15	4	9.0	19.8						0.034	0.002	33.7	1.0	7	4
2909	11.49	0.25	1		13.5						0.066	0.008	26.0	1.5	8	1
2910	13.91	0.25	1		4.8										11	
2911	11.7	0.15	1												2	
2912	12.2	0.25	1												2	
2913	12.7	0 15	1												14	
2914	13.95	0.25	2	1.5	5.7										1	
2915	13.39	0.15	3	3.5	16.6										6	
2916	13.2	0.25	1													
2917	12.12	0.554	5	3.2	16.1										4	
2918	12.2	0.15	1												4	
2919	12.09	0.15	1		1.9										4	
2920	8.83	0.15	7	1.5	7.9						0.034	0.007	123	13	7	4
2921	13.2	0.15	1												7	

Magnitudes, UBV Colors, IRAS Albedos and Diameters

M.P.	H	G	No. Obs	Min Phase	Max Phase	U-B	UQ	B-V	BQ	UBV Ref	Albedo	Albedo Unc.	D	D Unc	No. Obs Pre	No Obs Acc
2922	13.2	0.25	1								0.065	0.009	12.0	0.7	4	1
2923	12.7	0.15	1												7	
2924	11 7	0.25	1												9	
2925	13.7	0.25	1												7	
2926	13.2	0.25	1												5	
2927	12 23	0.15	4	2.8	21.0										6	
2928	11.67	0.25	1		2.3						0.035	0.005	33.0	2.2	4	1
2929	11.70	0.427	6	1.3	11.9										13	
2930	12.52	0.15	2	1.1	8.9										4	
2931	11.82	0.25	4	0.9	11.4										4	
2932	11.7	0.15	1								0.015	0.002	48.7	3.0	5	1
2933	11.64	0.15	3	4.5	10.8						0.068	0.011	24.0	1.8	10	5
2934	11.2	0.15	1								0.058	0.011	31.7	3.0	9	5
2935	13.03	0.15	3	7.3	9.3										4	
2936	12.43	0.15	2	4.7	4.9										9	
2937	13 09	0 25	8	16.5	22.8										6	
2938	11.44	0.15	9	3.3	15.0										7	
2939	12.69	0.25	6	1.7	21.2										7	
2940	13.7	0.15	1												5	
2941	13.54	0.25	2	2.5	15.4										8	
2942	13.49	0.25	1		3.4										10	
2943	12.74	0.25	1		15.1										8	
2944	12.7	0.15	1												2	
2945	11.7	0.15	1												5	
2946	13.24	0.25	4	0.8	13.4										4	
2947	13.2	0.25	1												5	
2948	12.2	0.15	1												2	
2949	13.69	0.25	4	3.1	7.9										9	
2950	12.08	0.15	3	9.6	11.7						0.081	0.011	17.8	1.1	7	1
2951	10 2	0.15	1								0.054	0.012	52.1	5.5	6	6
2952	14.2	0.25	1												2	
2953	11.68	0 15	2	12.5	13.1										10	
2954	13.83	0.25	4	6.5	23.7										5	
2955	13 19	0 25	4	3.9	17.4										5	
2956	12.40	0.15	7	2.2	11.2										4	
2957	10.2	0.25	1								0.17	0.03	29.0	3.0	8	2
2958	11.7	0.25	1												4	
2959	11.09	0.15	5	2.4	5.6						0.036	0.009	42.1	5.0	4	3
2960	13.9	0.25	1													
2961	13.0	0.25	1												2	
2962	11.39	0.15	4	4.8	17.8										6	
2963	12.50	0.25	1		1.9										8	
2964	12.2	0 15	1												7	
2965	13.2	0.25	1												12	
2966	13.58	0.25	2	0.4	16.0										3	
2967	11.18	0.15	2	5.2	8.4						0.047	0.010	35.5	3.8	6	5
2968	14.2	0.25	1												2	
2969	12.63	0.25	3	2.1	7.4										4	
2970	12.76	0.15	3	4.3	9.0										3	
2971	13.2	0.25	1												4	
2972	14.13	0.25	1		25.8										9	
2973	12 53	0.25	2	1.4	4.7										8	
2974	13.7	0.25	1												6	
2975	12.2	0.25	1													
2976	10 88	0.15	2	1.4	7.7						0.044	0.006	42.1	2.8	4	2
2977	12.73	0.15	2	6.1	12.0										8	
2978	11.7	0.15	1												6	
2979	11.75	0.15	2	14.2	15.8						0.039	0.005	30.0	2.0	7	1
2980	12.7	0.15	1												4	
2981	11.83	0.15	3	1.3	12.1										4	
2982	12.00	0.25	3	3.4	6.7										6	
2983	11.12	0.15	2	2.6	10.9						0.055	0.010	33.7	3.0	8	5
2984	13.16	0.178	5	2.4	16.0						0.013	0.002	27.2	1.6	12	1
2985	12.29	0.25	3	3.9	5.7										9	
2986	12.04	0.15	3	4.6	5.1						0.051	0.009	23.0	2.0	9	4
2987	11.83	0.15	1		5.8										9	
2988	11.7	0.15	1												6	
2989	13.05	0.25	6	1.9	14.7						0.050	0.007	14.5	1.0	2	1
2990	13.2	0.25	1												6	
2991	13.77	0.25	3	4.4	14.4										2	
2992	13.2	0.15	1												12	
2993	12.67	0.15	1		11.7						0.099	0.008	12.2	0.5	8	1
2994	14.2	0.25	1												3	

Magnitudes, UBV Colors, IRAS Albedos and Diameters

M.P.	H	G	No. Obs.	Min Phase	Max Phase	U-B	UQ B-V	BQ	UBV Ref	Albedo	Albedo Unc.	D	D Unc	No. Obs Pre	No. Obs Acc
2995	12.7	0.15	1							0.062	0.011	15.3	1.3	3	2
2996	11.87	0.15	3	1.8	6.4									2	
2997	13.16	0.15	1		5.1									2	
2998	13.7	0.25	1											3	
2999	13.36	0.181	8	0.9	20.2									2	
3000	12.7	0.25	1											2	
3001	12.40	0.25	3	6.4	9.2									9	
3002	12.7	0.25	1											1	
3003	11.38	0.15	4	1.1	12.3					0.061	0.008	28.3	1.7	2	1
3004	14.7	0.15	1											2	
3005	13.88	0.25	2	4.1	9.6									4	
3006	13.61	0.25	3	2.7	16.1					0.051	0.006	11.1	0.6	2	1
3007	12.76	0.25	5	6.6	12.0									2	
3008	12.11	0 678	7	0.5	13.9									2	
3009	13.82	0.25	1		12.5					0.10	0.01	7.10	0.44	10	1
3010	12.43	0.15	1		5.7									8	
3011	11.7	0.15	1											6	
3012	10.7	0.15	1							0.022	0.007	64.1	10.5	9	1
3013	13.54	0.25	4	1.5	7.5					0.044	0.004	12.3	0.5	3	1
3014	13.18	0.25	4	1.4	14.1									2	
3015	11.15	0.15	7	4.9	14.3									4	
3016	12.22	0.15	3	2.4	4.8										
3017	11.99	0.15	1		8.7									5	
3018	12.92	0.25	10	1.0	14.4									2	
3019	11.95	0.15	4	1.5	12.1										
3020	12.17	0.15	4	1.3	12.2									11	
3021	12.15	0.716	7	2.3	12.4										
3022	13.7	0.25	1											2	
3023	13.75	0.431	7	5.1	14 3										
3024	10.74	0.15	2	3.6	6.0					0.053	0.010	41.1	3.8	4	3
3025	11.7	0.15	1							0.014	0.001	52.1	1.8	2	1
3026	11.99	0.15	1		4.7					0.062	0.008	21.3	1.2	2	1
3027	13.2	0.15	1											2	
3028	10.7	0.15	1							0.11	0.01	28.5	1.1	6	4
3029	13.2	0.25	1											3	
3030	14.2	0.25	1											3	
3031	13.14	0.25	4	2.2	15.5									1	
3032	11.38	0.15	4	1.6	10.2					0.065	0.014	27.5	3.0	6	2
3033	12.51	0.25	3	0.8	14.6									5	
3034	12.28	0.25	3	13.4	22.0									4	
3035	12.62	0.15	3	0.6	14.5										
3036	9.7	0.15	1							0.11	0.01	44.8	2.0	4	2
3037	11.33	0.15	1		10.1					0.11	0.01	21.2	0.8	4	3
3038	13.45	0.25	1		11.5									1	
3039	12.2	0.15	1											2	
3040	15.7	0.25	1												
3041	12.53	0.117	7	6.3	21.0									2	
3042	13 2	0.25	1											2	
3043	13.75	0.25	1		6.0										
3044	11.7	0.15	1							0.063	0.014	24.2	2.7	3	3
3045	11.45	0.15	3	2.8	4.6									2	
3046	12.2	0.15	1							0.056	0.008	20.2	1.5	2	1
3047	12.91	0.15	1		1.7									2	
3048	13.75	0.25	1		8.6									2	
3049	11.48	0.15	5	1.9	12.7									6	
3050	14.65	0.25	1		4.1									2	
3051	12.7	0.15	1							0.055	0.007	16.2	1.0	4	1
3052	13.2	0.25	1							0.050	0.006	13.6	0.8	7	2
3053	12.53	0.25	3	13.2	21.5									6	
3054	11.46	0.637	8	1.0	12.0					0.059	0.006	28.0	1.3	2	2
3055	12.2	0.15	1											3	
3056	12.69	0.25	2	0 3	1.7									10	
3057	13.84	0.781	5	8.0	20.2									2	
3058	14.2	0.25	1											3	
3059	13.63	0.25	3	2.1	17.2									3	
3060	13.2	0.25	1											2	
3061	11.92	0.15	1		5.8					0.042	0.005	26.5	1.6	2	1
3062	10.96	0.15	5	3.2	16.8					0.094	0.024	27.7	3.5	5	4
3063	8.7	0.15	1							0.037	0.002	125	4	6	4
3064	13.36	0.516	5	3.4	19.4									2	
3065	12.09	0.15	4	2.0	12.5										
3066	11.39	0.15	3	1.6	10.5										
3067	13.2	0 25	1												

Magnitudes, UBV Colors, IRAS Albedos and Diameters

M.P.	H	G	No. Obs	Min Phase	Max Phase	U-B	UQ	B-V	BQ	UBV Ref	Albedo	Albedo Unc.	D	D Unc	No. Obs Pre	No Obs Acc
3068	13.2	0.25	1												6	
3069	13.2	0.25	1													
3070	14.11	0.25	3	2.1	17.0											
3071	11.2	0.15	1												2	
3072	13.57	0.25	2	4 6	15.5										4	
3073	13.57	0.25	3	2.6	13 0											
3074	13.60	0.25	1		7.2											
3075	13.7	0.25	1												3	
3076	13.84	0.25	4	3.7	27.8											
3077	12.96	0.398	7	1.0	24.0											
3078	11.47	0.15	3	1.3	11.1						0.045	0.014	31.6	5.0	5	4
3079	13.22	0.15	4	2.9	17.1											
3080	11.67	0.15	4	6.8	15.2										4	
3081	14.07	0.25	2	4.2	5.2										2	
3082	12.38	0.15	3	0.4	12.3										4	
3083	13.95	0.25	1		8.6										4	
3084	13.54	0.25	4	2.0	15.3										4	
3085	13.39	0.25	1		10.4											
3086	13.60	0.25	8	6.8	25.0											
3087	12.7	0.15	1												2	
3088	11.63	0.15	2	5.2	8.5										5	
3089	10.7	0.15	1								0.058	0.015	39.8	5.0	4	2
3090	12.2	0.15	1												4	
3091	13.7	0.25	1												2	
3092	10.68	0.15	2	3.0	3.5						0.065	0.008	38.0	2.3	4	1
3093	11 2	0.15	1												5	
3094	11.7	0.15	1								0.061	0.008	24.5	1.5	4	2
3095	11.2	0.15	1												6	
3096	12.49	0.15	2	9.3	13.2										4	
3097	12.31	0.15	2	4.2	4.4						0.034	0.006	25.0	2.3	4	1
3098	14.7	0.25	1												4	
3099	11.16	0.15	1		14.8										2	
3100	14.2	0.25	1													
3101	13 7	0.25	1												5	
3102	16.04	0.25	7	24.3	26 5	0.52	2	0.84	3	2					6	
3103	14.7	0.25	1													
3104	11.17	0.15	3	6.2	8.3						0.12	0 01	22.3	1.2	9	1
3105	13.0	0.25	1												2	
3106	10 81	0.15	5	5 2	13.5										6	
3107	13.2	0 25	1												5	
3108	13.7	0.25	1													
3109	11.2	0.25	1								0 099	0.011	24.2	1.2	4	1
3110	12.96	0.15	3	2.5	5.4										2	
3111	13.7	0.25	1													
3112	13.55	0.25	1		2.5										6	
3113	13.17	0.25	2	5.2	8.8											
3114	14 13	0.25	1		4.4										4	
3115	11 18	-.049	6	7.0	17.3						0.14	0.01	20.5	1.0	6	3
3116	12.34	0.25	4	3.5	6.7										7	
3117	12.31	0.15	5	1.5	6.8										4	
3118	11.03	0.15	2	9.8	16.0						0.048	0.008	37.5	3.0	5	4
3119	12.24	0.15	3	2.0	10.5										1	
3120	11 86	0.15	1		1.2										9	
3121	13 62	0.25	2	2.0	14.7										2	
3122	14 2	0.25	1												5	
3123	13.36	0.15	10	3.0	13.7	0.28	2	0.60	3	2					4	
3124	13.24	0.15	3		21.3	0.38	1	0.75	1	2					4	
3125	12.11	0.008	5	3.7	24.0										7	
3126	12.30	0 15	1		8.5										6	
3127	12 16	0.15	3	3.0	8.9						0.025	0.004	31.0	2.2	5	1
3128	11.34	0.15	5	2.3	7.4										9	
3129	12.51	0.15	1		13.3										8	
3130	12.7	0.25	1												7	
3131	12.03	0.15	5	1.1	10.3										7	
3132	11.72	0.15	4	1.1	14.7						0.024	0.008	39.0	6.5	8	2
3133	13.53	0.25	1		6.6										5	
3134	10.34	0.15	1		9.8						0.041	0.004	55.8	2.6	4	1
3135	13.7	0 25	1												6	
3136	11.7	0.15	1												5	
3137	13.4	0.25	1													
3138	13.07	0.25	1		10.9										6	
3139	10.7	0.15	1								0.044	0.003	45.6	1.5	6	3
3140	10.96	0.346	6	2.1	15.6						0.082	0.008	29.7	1.5	4	4

Magnitudes, UBV Colors, IRAS Albedos and Diameters

M.P.	H	G	No. Obs.	Min Phase	Max Phase	U-B	UQ	B-V	BQ	UBV Ref	Albedo	Albedo Unc.	D	D Unc	No. Obs Pre	No Obs Acc
3141	10.2	0.15	1								0.078	0.018	43.5	5.0	9	6
3142	12.43	0.15	4	4.7	9.8										10	
3143	12.7	0.15	1												8	
3144	13.2	0 25	1								0.012	0.001	28.2	1.6	6	1
3145	14.2	0.25	1												6	
3146	13.06	0.25	1		11.3										7	
3147	13.2	0.15	1								0.011	0.001	29.0	2.0	7	1
3148	11.7	0.15	1								0.014	0.002	51.5	3.0	6	1
3149	13.75	0.25	1		8.6										5	
3150	10.97	0.15	4	2.3	17.2						0.065	0.019	33.5	4.7	4	3
3151	11.99	0.15	3	1.2	12.7										7	
3152	11.2	0.15	1								0.047	0.002	35.1	0.6	9	8
3153	13.11	0 25	3	4.4											10	
3154	12.62	0.15	3	5.0	7.7										8	
3155	11.7	0.25	1												6	
3156	11.56	0.15	4	4.0	20.0						0.040	0.003	32.5	1.2	8	3
3157	11.67	0.15	3	3.0	13.1						0.032	0.005	34.2	2.5	10	2
3158	12.54	0.15	2	8.0	9.3										12	
3159	12.53	0.15	2	3.1	7.0										10	
3160	13.72	0.401	11	2.3	19.1										6	
3161	12.29	0.15	3	1.6	13.1						0.087	0.018	15.6	1.5	11	5
3162	11.46	0.382	7	3.4	16.5										7	
3163	13.7	0.25	1												4	
3164	11.74	0.15	1		3.8						0.090	0.011	19.8	1.1	5	1
3165	12 7	0.25	1												5	
3166	12.7	0.25	1								0.10	0.01	12.0	0.5	7	1
3167	11.2	0.15	1												8	
3168	11.88	0.15	3	1.0	9.5						0.034	0.024	30.3	10.5	8	2
3169	12.32	0.15	5	7.5	24.7	0.30	3	0.77	3	2					5	
3170	11.7	0.15	1												4	
3171	10.7	0.15	1								0.041	0.004	47.3	2.0	7	1
3172	13.61	0.698	5	0 6	20 0										2	
3173	12 7	0.25	1												7	
3174	11.7	0.15	1												6	
3175	13.2	0.25	1								0.030	0.003	17.6	1.0	3	1
3176	10.7	0.15	1								0.066	0.014	37.3	3.8	9	3
3177	12.12	0.15	3	3.5	7.1										8	
3178	12.2	0.15	1												9	
3179	12.2	0.15	1												4	
3180	14.2	0.25	1													
3181	12.7	0.25	1												2	
3182	12.2	0.15	1								0.031	0.005	27.5	2.3	7	1
3183	11.7	0.15	1												6	
3184	12.90	0.15	1		13.7										8	
3185	13.7	0.25	1													
3186	12.52	0.15	2	5.7	8.2										7	
3187	12.7	0.25	1								0.050	0.006	17.0	1.0	10	1
3188	13.2	0.25	1												2	
3189	12.7	0.15	1												7	
3190	13.01	0.15	1		4.3										4	
3191	12.39	0.15	4	0.9	4.4										7	
3192	13.2	0.25	1												7	
3193	13.26	0.147	5	3.6	16.3						0.014	0.002	25.2	1.5	9	1
3194	11.7	0.15	1								0.10	0.01	18.8	1.0	4	1
3195	12.61	0.15	3	0.7	11.7										3	
3196	12.7	0.15	1												2	
3197	11.88	0.332	6	0.5	19.5						0.050	0.009	25.0	2.1	8	1
3198	13.53	0.25	2	24.3	31.6										8	
3199	15.03	0.25	5	45.7	57.0	0.38	2	0.94	2	2					9	
3200	14.65	0.25	1		47.7						0.089	0.025	5.23	0.72	7	6
3201	13.7	0.25	1								0.011	0.001	22.7	1.5	13	1
3202	10.2	0.15	1												8	
3203	14.17	0.25	2	14.2	17.1										4	
3204	12.29	0.15	2	2.7	3.5										6	
3205	13 22	0.15	1		10.4										9	
3206	13.7	0.15	1												7	
3207	12.64	0.15	1		2.4						0.040	0.005	19.6	1.1	5	1
3208	12.17	0.15	3	1.4	11.4										5	
3209	13.91	0.961	5	2.1	17.0										8	
3210	11.28	0.15	3	5.2	9.1										4	
3211	12.7	0.15	1								0.014	0.002	32.5	2.1	7	1
3212	13.89	0.25	3	5.7	14.7										8	
3213	12.28	0.15	3	0.8	8.7											

Magnitudes, UBV Colors, IRAS Albedos and Diameters

M.P.	H	G	No. Obs.	Min Phase	Max Phase	U-B	UQ	B-V	BQ	UBV Ref	Albedo	Albedo Unc.	D	D Unc	No. Obs Pre	No. Obs Acc
3214	10.7	0.15	1							0.10	0.01	29.5	1.7	6	1
3215	11.7	0 15	1											6	
3216	13.87	0.019	5	10.5	24.3									5	
3217	14.2	0.25	1											8	
3218	13.7	0.15	1											9	
3219	11.2	0.15	1											10	
3220	13.2	0.25	1											11	
3221	13.28	0.25	3	3.9	5.6									4	
3222	11.42	0.15	6	5.5	9.3					0.042	0.003	33.5	1.0	9	3
3223	11.37	0.15	2	6.2	7.5					0.083	0.011	24.5	1.5	9	1
3224	11.35	0.15	1		7.3					0.042	0.004	34.8	1.7	3	1
3225	13.40	0.25	1		3.2										
3226	13 2	0.15	1											10	
3227	12.2	0.25	1											11	
3228	12.7	0.25	1											2	
3229	12.2	0.25	1											9	
3230	11.7	0.15	1							0.051	0.005	26.8	1.3	12	3
3231	12.7	0.25	1											9	
3232	11.82	0.15	1		1.5									9	
3233	12.7	0.25	1											6	
3234	12.2	0.15	1							0.026	0.003	30.0	1.8	7	1
3235	13.2	0.15	1											4	
3236	13.81	0.25	4	5.2	11.6									9	
3237	11.2	0.15	1							0.061	0.005	31.0	1.2	8	3
3238	13.2	0.15	1							0.037	0.005	15.6	1.0	9	1
3239	14.66	0.25	3	5.2	19.0									5	
3240	10.2	0.15	1											5	
3241	12.09	0.15	3	2.4	14.1					0.060	0.008	20.6	1.2	6	1
3242	12.7	0.15	1											5	
3243	11.2	0.15	1											2	
3244	14.2	0.25	1											7	
3245	12.7	0.15	1											7	
3246	11.47	0.15	2	4.2	5.9									7	
3247	13.01	0.25	3	1.9	14.0					0.035	0.004	17.7	1.0	9	1
3248	10.97	0.15	4	2.4	8.9					0.029	0.006	50.1	5.0	9	1
3249	13.56	0.25	2	2.5	3.8									2	
3250	11.1	0.15	1											4	
3251	12.2	0.15	1											5	
3252	12.14	0 15	2	6 9	10.5									5	
3253	13 37	-.093	7	0.6	13.8									2	
3254	10.99	0.15	4	1.4	10.3									2	
3255	13.72	0.298	6	2.0	21.9									7	
3256	12.38	0.15	4	2.4	11.9					0.023	0.002	29.0	1.5	4	1
3257	13.50	0 25	1		10.1									6	
3258	13.36	0.25	4	9.4	17.6									6	
3259	10.2	0.15	1							0.10	0.01	37.5	2.5	7	1
3260	12.79	0.25	2		17.5					0.041	0.013	18.1	2.7	12	2
3261	11.77	0.15	3	4.8	7.3									6	
3262	11.02	0.635	8	0.7	13.4									3	
3263	13.36	0.782	8	1.4	17.5									2	
3264	12 32	0.15	6	0.3	12.2					0.036	0.003	24.1	1.0	2	1
3265	13 25	0.494	6	0.8	16.9									2	
3266	13.50	0.25	2	10.5	15.6									8	
3267	12.90	0.25	4	9.3	26.0									11	
3268	13.2	0.25	1											2	
3269	12.74	0.15	1		5.5									5	
3270	14.7	0.25	1											8	
3271	16.7	0.25	1											3	
3272	12.7	0.25	1												
3273	11 2	0.15	1							0.045	0.010	35.8	4.0	9	2
3274	11.7	0.15	1											2	
3275	13.59	0.25	3	6.9	22.0					0.025	0.003	16.0	1.0	7	1
3276	12.01	0.15	3	1.4	8.2									2	
3277	11.27	0.15	4	3.0	8.4									2	
3278	11.2	0.15	1							0.046	0.004	35.6	1.5	2	1
3279	13.78	0.25	3	7.2	7.9									7	
3280	12.2	0.15	1											5	
3281	12.2	0.25	1											4	
3282	12.7	0.25	1											9	
3283	12.7	0.25	1							0.061	0.021	15.5	2.5	7	3
3284	12.84	0.15	4	3.2	17.6									4	
3285	12.39	0.15	1		11.1					0.19	0.02	10.0	0.5	8	5
3286	13.06	0.15	4	0.6	1.8									2	

Magnitudes, UBV Colors, IRAS Albedos and Diameters

M.P.	H	G	No. Obs	Min Phase	Max Phase	U-B	UQ	B-V	BQ	UBV Ref	Albedo	Albedo Unc.	D	D Unc	No. Obs Pre	No Obs Acc
3287	13.7	0.25	1												2	
3288	15.34	0.25	5	29.9	34.7	0.50	3	0.92	3	2					6	
3289	14.2	0.25	1												12	
3290	11.5	0.15	1												3	
3291	12.2	0.15	1												2	
3292	12.2	0.15	1												2	
3293	13.7	0.25	1												2	
3294	12.6	0.15	1												3	
3295	12.7	0.15	1												9	
3296	13.04	0.15	2	0.8	2.0										7	
3297	12.52	0.15	1		4.1										4	
3298	13.2	0.25	1								0.032	0.004	16.8	1.0	10	1
3299	13.2	0.25	1												8	
3300	10.2	0.15	1												4	
3301	13.2	0.25	1												2	
3302	12.9	0.25	1												5	
3303	11.2	0.15	1												4	
3304	12.7	0.15	1												10	
3305	12.2	0.15	1												2	
3306	12.6	0.25	1												2	
3307	13.5	0.25	1								0.038	0.005	13.5	0.7	3	1
3308	11.72	0.15	2	2.6	10.9										8	
3309	13.9	0.25	1												6	
3310	10.7	0.15	1								0.12	0.01	27.1	1.6	5	1
3311	12.2	0.15	1								0.047	0.006	22.3	1.3	4	1
3312	11.7	0.15	1								0.034	0.018	32.7	8.5	12	2
3313	12.2	0.15	1												2	
3314	14.02	0.25	4	1.6	7.4										2	
3315	12.50	0.15	4	2.1	13.2											
3316	11.57	0.15	4	3.9	13.6						0.075	0.009	23.5	1.5	4	1
3317	8.35	0.15	2	1.7	3.1						0.050	0.006	127	8	4	3
3318	11.2	0.15	1												2	

ASTEROID TAXONOMIC CLASSIFICATIONS

D. J. THOLEN

University of Hawaii

Since *Asteroids* was published (Gehrels 1979), there have been three taxonomic classification schemes developed and applied to the body of available color and albedo data (Tholen 1984; Barucci et al. 1987; Tedesco et al. 1989). Asteroid taxonomic classifications according to the first two of these schemes are reproduced in this table. The Tedesco et al. classifications were unavailable at the time this table was prepared; they are described in the chapter by Tedesco et al. The Barucci et al. classifications have been copied directly from the paper they published in *Icarus*. Their classifications are based on a combination of eight-color photometry and IRAS albedos. The Tholen classifications are essentially the same as those supplied to the IRAS Asteroid Advisory Group in November 1983 and, as such, are not based on the IRAS albedos. This list consists of the classifications tabulated in Tholen (1984) but extended by a rigorous application of the classification scheme to those objects with *UBV* colors (Bowell et al. 1979), and a nonrigorous application to those objects with 24-color spectra (Chapman and Gaffey 1979). A few of the classifications given here differ from the ones given by Tholen (1984). These discrepancies are explained in the footnotes to the table. In some cases, the classifications of objects in the X and C spectral classes are based on unpublished albedos provided by Tedesco and Gradie. Although IRAS albedos that would permit the elimination of some classification ambiguities are available, caution is advised when applying IRAS albedos, because in many cases the IRAS fluxes have been overestimated, resulting in underestimated albedos.

Two differences between Tholen's 1984 list and this list are apparent. The letter X has been used to stand for E or M or P. Tholen (1984) used EMP,

which could be misinterpreted as meaning E is most likely, M is next most likely, and P is least likely. Note that the E, M, and P classes are spectrally degenerate, so in the absence of albedo information, their similar spectra can be represented by a single letter. Also, the letter I has been introduced to stand for inconsistent data. In Tholen (1984), 515 Athalia was given a stand-alone U classification, due to its S-type spectrum but uniquely low albedo. However, because of the desire to use U as only a suffix, the letter I was introduced. The following notation appears in the classifications:

U Suffix indicating an unusual spectrum; falls far from cluster center;
: Suffix indicating noisy data;
:: Suffix indicating very noisy data;
--- Indicates data that are too noisy to permit classification (essentially all types would be allowed).

Due to popular demand, orbital group designations have been included in this table. The two- or three-letter abbreviations stand for the following groups:

ATE	Aten	PHO	Phocaea
APO	Apollo	GRI	Griqua
AMO	Amor	CYB	Cybele
MC	Mars crosser	HIL	Hilda
HUN	Hungaria	TRO	Trojan

Explanatory footnotes and references follow the table. This list was revised as of March 20, 1988 and therefore supercedes earlier tabulations.

Editors' note added in proof: The Tedesco et al. 1989 tabulation has become available as this book goes to press and is included in a separate following table.

REFERENCES

Barucci, M. A., Capria, M. T., Coradini, A., and Fulchignoni, M. 1987. Classification of asteroids using G-mode analysis. *Icarus* 72:304–324.

Bowell, E., Gehrels, T., and Zellner, B. 1979. Magnitudes, colors, types, and adopted diameters of the asteroids. In *Asteroids,* ed. T. Gehrels (Tucson: Univ. of Arizona Press), pp. 1108–1129.

Chapman, C. R., and Gaffey, M. J. 1979. Reflectance spectra for 277 asteroids. In *Asteroids,* ed. T. Gehrels (Tucson: Univ. of Arizona Press), pp. 655–687.

Gehrels, T., ed. 1979. *Asteroids* (Tucson: Univ. of Arizona Press).

Hartmann, W. K., Tholen, D. J., and Cruikshank, D. P. 1987. The relationship of active comets, "extinct" comets, and dark asteroids. *Icarus* 69:33–50.

Tedesco, E. F., Williams, J. G., Matson, D. L., Veeder, G. J., Gradie, J. C., and Lebofsky, L. A. 1989. A three-parameter asteroid taxonomy. *Astron. J.* 97:580–606.

Tholen, D. J. 1984. Asteroid Taxonomy from Cluster Analysis of Photometry. Ph.D. Thesis, Univ. of Arizona.

Tholen, D. J. 1985. (3200) 1983 T 13. *IAU Circular* No. 4034.

Tholen, D. J., Hartmann, W. K., and Cruikshank, D. P. 1988. 1980 PA and 1985 DO2. *IAU Circ.* No. 4655.

Minor Planet	Tholen Class	Barucci Class	Group	Minor Planet	Tholen Class	Barucci Class	Group
1 Ceres	G	G0		58 Concordia	C	C0	
2 Pallas	B	B3		59 Elpis	CP	C0	
3 Juno	S	S0		60 Echo	S	S0	
4 Vesta	V	V0		61 Danae	S	S0	
5 Astraea	S	S0		62 Erato	BU	B3	
6 Hebe	S	S0		63 Ausonia	S	S0	
7 Iris	S	S0		64 Angelina·	E		
8 Flora	S	S0		65 Cybele	P	C0	CYB
9 Metis	S			66 Maja	C	C0	
10 Hygiea	C	C0		67 Asia	S	S0	
11 Parthenope	S	S0		68 Leto	S	S0	
12 Victoria	S	S0		69 Hesperia	M	M0	
13 Egeria[1]	G			70 Panopaea	C	C0	
14 Irene	S			71 Niobe	S	S0	
15 Eunomia	S	S0		72 Feronia	TDG		
16 Psyche	M	M0		73 Klytia	S		
17 Thetis	S	S0		74 Galatea	C		
18 Melpomene	S	S0		75 Eurydike	M	M0	
19 Fortuna	G			76 Freia	P	C0	CYB
20 Massalia	S	S0		77 Frigga	MU	D2	
21 Lutetia	M	M0		78 Diana	C	C0	
22 Kalliope	M	M0		79 Eurynome	S	S0	
23 Thalia	S	S0		80 Sappho	S	S0	
24 Themis	C			81 Terpsichore	C	C0	
25 Phocaea	S	S2	PHO	82 Alkmene	S	S0	
26 Proserpina	S	S0		83 Beatrix	X	M0	
27 Euterpe	S			84 Klio	G		
28 Bellona	S	S0		85 Io	FC	C0	
29 Amphitrite	S	S0		86 Semele	C	C0	
30 Urania	S	S0		87 Sylvia	P	C0	CYB
31 Euphrosyne	C			88 Thisbe	CF		
32 Pomona	S	S0		89 Julia	S	S0	
33 Polyhymnia	S			90 Antiope	C	C0	
34 Circe	C	C0		91 Aegina	CP		
35 Leukothea	C	C0		92 Undina	X	M0	
36 Atalante	C			93 Minerva	CU	B3	
37 Fides	S	S0		94 Aurora	CP	C0	
38 Leda	C	C0		95 Arethusa	C	C0	
39 Laetitia	S	S0		96 Aegle	T		
40 Harmonia	S	S0		97 Klotho	M	M0	
41 Daphne	C	C0		98 Ianthe	CG	C0	
42 Isis	S	S0		99 Dike	C		
43 Ariadne	S	S0		100 Hekate	S		
44 Nysa	E	E0		101 Helena	S	S0	
45 Eugenia	FC	C0		102 Miriam	P	D2	
46 Hestia	P	C0		103 Hera	S	S0	
47 Aglaja	C	C0		104 Klymene	C	C0	
48 Doris	CG			105 Artemis	C	C0	PHO
49 Pales	CG	C0		106 Dione	G	G0	
50 Virginia	X			107 Camilla	C	C0	CYB
51 Nemausa	CU	S1		108 Hecuba	S	S0	
52 Europa	CF	C0		109 Felicitas	GC	C0	
53 Kalypso	XC			110 Lydia	M	M0	
54 Alexandra	C	C0		111 Ate	C	C0	
55 Pandora	M	E0		112 Iphigenia	DCX		
56 Melete	P	C0		113 Amalthea	S	S2	
57 Mnemosyne	S	S0		114 Kassandra	T	D3	

Minor Planet	Tholen Class	Barucci Class	Group	Minor Planet	Tholen Class	Barucci Class	Group
115 Thyra	S	S1		174 Phaedra	S		
116 Sirona	S	S0		175 Andromache	C		
117 Lomia	XC	C0		176 Iduna	G		
118 Peitho	S	S0		177 Irma	C:		
119 Althaea	S	S2		178 Belisana	S		
120 Lachesis	C	C0		179 Klytaemnestra	S	S0	
121 Hermione	C	C0	CYB	180 Garumna	S		
122 Gerda	ST			181 Eucharis	S		
123 Brunhild	S			182 Elsa	S		
124 Alkeste	S	S0		183 Istria	S		
125 Liberatrix	M	M0		184 Dejopeja	X		
126 Velleda	S			185 Eunike	C	C0	
127 Johanna	CX			186 Celuta	S	S0	
128 Nemesis	C	C0		187 Lamberta	C	C0	
129 Antigone	M			188 Menippe	S	S0	
130 Elektra	G	G0		189 Phthia	S		
131 Vala	SU	S1		190 Ismene	P		HIL
132 Aethra	M	M0	MC	191 Kolga	XC:		
133 Cyrene	SR			192 Nausikaa[2]	S	V0	
134 Sophrosyne	C	C0		194 Prokne	C	C0	
135 Hertha	M	M0		195 Eurykleia	C	C0	
136 Austria	M			196 Philomela	S	S0	
137 Meliboea	C	C0		197 Arete	S		
138 Tolosa	S			198 Ampella	S	S0	
139 Juewa	CP			200 Dynamene	C	C0	
140 Siwa	P			201 Penelope	M	M0	
141 Lumen	CPF			202 Chryseis	S		
142 Polana	F	B1		203 Pompeja	DCX:		
143 Adria	C			204 Kallisto	S	S0	
144 Vibilia	C	C0		205 Martha	C		
145 Adeona	C	C0		206 Hersilia	C		
146 Lucina	C	C0		207 Hedda	C		
147 Protogeneia	C	C0		208 Lacrimosa	S		
148 Gallia	GU	S1		209 Dido	C	C0	
149 Medusa	S			210 Isabella	CF		
150 Nuwa	CX			211 Isolda	C	C0	
151 Abundantia	S			212 Medea	DCX:		
152 Atala	D			213 Lilaea	F	B1	
153 Hilda	P	C0	HIL	214 Aschera	E	E0	
155 Scylla	XFC			215 Oenone	S		
156 Xanthippe	C	C0		216 Kleopatra	M	M0	
158 Koronis	S	S0		217 Eudora	X		
159 Aemilia	C	C0		218 Bianca	S		
160 Una	CX			219 Thusnelda	S	S0	
161 Athor	M	M0		220 Stephania	XC		
162 Laurentia	STU			221 Eos	S	S0	
163 Erigone	C			222 Lucia	BU	B0	
164 Eva	CX			223 Rosa	X		
165 Loreley	CD			224 Oceana	M		
166 Rhodope	GC:			225 Henrietta	F	C0	CYB
167 Urda	S			228 Agathe	S	S2	
168 Sibylla	C	C0	CYB	229 Adelinda	BCU	C0	CYB
169 Zelia	S	S0		230 Athamantis	S	S0	
170 Maria	S	S0		232 Russia	C	C0	
171 Ophelia	C	C0		233 Asterope	T	D3	
172 Baucis	S			234 Barbara	S	S0	
173 Ino	C	C0		235 Carolina	S		

Minor Planet	Tholen Class	Barucci Class	Group	Minor Planet	Tholen Class	Barucci Class	Group
236 Honoria	S	S0		328 Gudrun	S		
237 Coelestina	S			329 Svea	C	C0	
238 Hypatia	C	C0		331 Etheridgea	CX		
240 Vanadis	C	C0		333 Badenia	C:		
241 Germania	CP	C0		334 Chicago	C	C0	HIL
243 Ida	S	S0		335 Roberta	FP	C0	
245 Vera	S	S0		336 Lacadiera	D	D0	
246 Asporina	A	A0		337 Devosa	X	M0	
247 Eukrate	CP			338 Budrosa	M	M0	
250 Bettina	M	M0		339 Dorothea	S	S1	
254 Augusta	S •			340 Eduarda	S		
255 Oppavia	X			341 California	S		
257 Silesia	SCTU			342 Endymion	C		
258 Tyche	S	S0		343 Ostara	CSGU		
259 Aletheia	CP			344 Desiderata[3]	C	C0	
260 Huberta	CX:		CYB	345 Tercidina	C	C0	
261 Prymno	B	B3		346 Hermentaria	S	S0	
262 Valda	S			347 Pariana	M	M0	
264 Libussa	S	S0		349 Dembowska	R	V0	
266 Aline	C	C0		350 Ornamenta	C	C0	
267 Tirza	DU			351 Yrsa	S		
268 Adorea	FC	C0		352 Gisela	S	S0	
270 Anahita	S			354 Eleonora	S	S2	
271 Penthesilea	PC			356 Liguria	C		
273 Atropos	SCTU		PHO	357 Ninina	CX		
275 Sapientia	X			359 Georgia	CX	M0	
276 Adelheid	X	C0		360 Carlova	C	C0	
277 Elvira	S	S0		361 Bononia	DP		HIL
279 Thule	D	D0		362 Havnia	XC		
281 Lucretia	SU			363 Padua	XC		
282 Clorinde	BFU::	B0		364 Isara	S	S0	
283 Emma	X			365 Corduba	X	C0	
284 Amalia	CX			368 Haidea	D	D2	
286 Iclea	CX			369 Aeria	M	M0	
287 Nephthys	S	S0		370 Modestia	X		
288 Glauke	S	S0		371 Bohemia	QSV		
289 Nenetta	A	A0		372 Palma	BFC		
293 Brasilia	CX			373 Melusina	C	C0	
295 Theresia	S			374 Burgundia	S	S0	
296 Phaetusa	S			375 Ursula	C		
302 Clarissa	F	C0		376 Geometria	S	S0	
304 Olga	C	C0		377 Campania	PD		
305 Gordonia	S			378 Holmia	S		
306 Unitas	S	S0		379 Huenna	B	C0	
307 Nike	CX			380 Fiducia	C	C0	
308 Polyxo	T	D3		381 Myrrha	C	C0	
311 Claudia	S			382 Dodona	M	M0	
312 Pierretta	S			383 Janina	B	B3	
313 Chaldaea	C	C0		384 Burdigala	S		
317 Roxane	E	E0		385 Ilmatar	S		
318 Magdalena	CXF			386 Siegena	C	C0	
321 Florentina	S			387 Aquitania	S	S0	
322 Phaeo	X	M0		388 Charybdis	C	C0	
323 Brucia	S	S0		389 Industria	S	S0	
324 Bamberga	CP			390 Alma	DT		
325 Heidelberga	M			391 Ingeborg	S		PHO
326 Tamara	C	C0	PHO	393 Lampetia	C		

Minor Planet	Tholen Class	Barucci Class	Group	Minor Planet	Tholen Class	Barucci Class	Group
394 Arduina	S	S0		475 Ocllo	X	M0	MC
395 Delia	C			476 Hedwig	P	C0	
397 Vienna	S			477 Italia	S	S0	
402 Chloe	S	S0		478 Tergeste	S	S0	
403 Cyane	S			480 Hansa	S	S0	
404 Arsinoe	C	C0		481 Emita	C		
405 Thia	C	C0		482 Petrina	S		
406 Erna	P	M0		483 Seppina	S	S0	CYB
407 Arachne	C	C0		487 Venetia	S		
409 Aspasia	CX			488 Kreusa	C		
410 Chloris	C	C0		489 Comacina	C		
413 Edburga	M			490 Veritas	C		
414 Liriope	C	C0	CYB	494 Virtus	C		
415 Palatia	DP			496 Gryphia	S	S0	
416 Vaticana	S	S0		497 Iva	M		
417 Suevia	X			498 Tokio	M	D3	
418 Alemannia	M	M0		499 Venusia	P	C0	HIL
419 Aurelia	F	C0		502 Sigune	S		PHO
420 Bertholda	P	M0	CYB	503 Evelyn	XC		
421 Zahringia	S			505 Cava	FC		
422 Berolina	DX			506 Marion	XC	C0	
423 Diotima	C	C0		508 Princetonia	C	C0	
426 Hippo	F			509 Iolanda	S	S0	
429 Lotis	C	C0		510 Mabella	PD		
431 Nephele	B	C0		511 Davida	C	C0	
432 Pythia	S			512 Taurinensis	S	S2	MC
433 Eros	S		AMO	513 Centesima	S		
434 Hungaria	E		HUN	514 Armida	XC	C0	
435 Ella	DCX			515 Athalia[4]	I	S0	
438 Zeuxo	F:			516 Amherstia	M		
439 Ohio	X:			517 Edith	X		
441 Bathilde	M			519 Sylvania	S	S0	
442 Eichsfeldia	C	C0		520 Franziska	CGU		
443 Photographica	S	S3		521 Brixia	C	C0	
444 Gyptis	C	C0		522 Helga	X	C0	CYB
445 Edna	C			524 Fidelio	XC		
446 Aeternitas	A	A0		525 Adelaide	SU		
447 Valentine	TD			526 Jena	B	C0	
448 Natalie	C			529 Preziosa	S	S0	
449 Hamburga	C	C0		530 Turandot	F	C0	
450 Brigitta	CSU			532 Herculina	S	S0	
451 Patientia	CU	B3		533 Sara	S		
453 Tea	S			534 Nassovia	S		
454 Mathesis	CB			535 Montague	C		
455 Bruchsalia	CP			536 Merapi	X	C0	CYB
458 Hercynia	S			537 Pauly	DU:		
459 Signe	S	S0		540 Rosamunde	S	S0	
461 Saskia	FCX			542 Susanna	S		
462 Eriphyla	S			545 Messalina	CD		
463 Lola	X			546 Herodias	TDG		
464 Megaira	FXU:			547 Praxedis	XD:		
466 Tisiphone	C	C0	CYB	548 Kressida	S		
468 Lina	CPF			549 Jessonda	S	S0	
469 Argentina	X			550 Senta	S		
470 Kilia	S	S0		551 Ortrud	XC	C0	
471 Papagena	S	S0		554 Peraga	FC	C0	
472 Roma	S	S0		556 Phyllis	S	S0	

Minor Planet	Tholen Class	Barucci Class	Group	Minor Planet	Tholen Class	Barucci Class	Group
558 Carmen	M	M0		650 Amalasuntha	---		
559 Nanon	C	C0		651 Anukleia	S	S3	
560 Delila	---			653 Berenike	S	S0	
561 Ingwelde	XCU			654 Zelinda	C	C0	PHO
562 Salome	S	S0		658 Asteria	S		
563 Suleika	S	S0		659 Nestor	XC	C0	TRO
564 Dudu	CDX:			660 Crescentia	S	S0	
565 Marbachia	S			661 Cloelia	S	S0	
566 Stereoskopia	C	C0	CYB	663 Gerlinde	X	C0	
567 Eleutheria	CFB			664 Judith	XC		
569 Misa	C			669 Kypria	S		
570 Kythera	ST	S0	CYB	673 Edda	S		
571 Dulcinea	S	S0		674 Rachele	S		
572 Rebekka	XDC			675 Ludmilla	S		
574 Reginhild	S			676 Melitta	XC		
579 Sidonia	S	S0		679 Pax	I		
582 Olympia	S	S0		680 Genoveva	XC		
583 Klotilde	C	C0		686 Gersuind	S	S0	
584 Semiramis	S	S0		687 Tinette	X		
585 Bilkis	C			689 Zita	CX:		
586 Thekla	C:			690 Wratislavia	CPF		
588 Achilles	DU	D1	TRO	691 Lehigh	CD:		
589 Croatia	CX			692 Hippodamia	S	S0	CYB
591 Irmgard	X			693 Zerbinetta	ST		
593 Titania	C	C0		694 Ekard	CP:		
596 Scheila	PCD			695 Bella	S		
598 Octavia	C:			696 Leonora	XC		
599 Luisa	S	S0		697 Galilea	C:		
601 Nerthus	X			699 Hela	S		MC
602 Marianna	C	C0		701 Oriola	C		
606 Brangane	TSD	D3		702 Alauda	C	C0	
611 Valeria	S			704 Interamnia	F	C0	
613 Ginevra	P	C0		705 Erminia	X	C0	
615 Roswitha	CX			708 Raphaela	S		
616 Elly	S	S0		709 Fringilla	X		
617 Patroclus	P	C0	TRO	712 Boliviana	C	C0	
618 Elfriede	C	C0		713 Luscinia	C	C0	CYB
619 Triberga	S			714 Ulula	S	S0	
620 Drakonia	E			716 Berkeley	S		
621 Werdandi	FCX:			717 Wisibada	DX:		
622 Esther	S			720 Bohlinia	S		
623 Chimaera	XC			721 Tabora	D	D0	CYB
624 Hektor	D		TRO	725 Amanda	CSU	C0	
626 Notburga	CX	C0		727 Nipponia	DT		
627 Charis	XB:			729 Watsonia	STGD		
628 Christine	SD			731 Sorga	CD		
631 Philippina	S	S0		733 Mocia	CF	C0	CYB
633 Zelima	S			735 Marghanna	C		
635 Vundtia	C	C0		736 Harvard	S		
639 Latona	S	S0		737 Arequipa	S		
640 Brambilla	G	G0		738 Alagasta	CGSU		
642 Clara	S			739 Mandeville	X	C0	
643 Scheherezade	P	C0	CYB	740 Cantabia	CX	C0	
644 Cosima	S			741 Botolphia	X		
645 Agrippina	S			742 Edisona	S		
647 Adelgunde	X			744 Aguntina	FX:		
648 Pippa	XC	C0		746 Marlu	P	C0	

Minor Planet	Tholen Class	Barucci Class	Group	Minor Planet	Tholen Class	Barucci Class	Group
747 Winchester	PC			860 Ursina	M	M0	
748 Simeisa	P	C0	HIL	863 Benkoela	A	A0	
749 Malzovia	S			864 Aase	S		
750 Oskar	F	B1		868 Lova	C:		
751 Faina	C	C0		872 Holda	M		
753 Tiflis	S			873 Mechthild .	PC	C0	
754 Malabar	XC			876 Scott	S		
755 Quintilla	M	M0		877 Walkure	F	C0	
757 Portlandia	XF	M0		880 Herba	F	C0	
758 Mancunia	X			883 Matterania	S		
760 Massinga	SU			884 Priamus	D		TRO
761 Brendelia	SC			887 Alinda	S		AMO
762 Pulcova	F	C0		888 Parysatis	S		
764 Gedania	C			890 Waltraut	CTGU:		
766 Moguntia	MU			893 Leopoldina	XF		
768 Struveana	X			895 Helio	FCB		
770 Bali	S			897 Lysistrata	S	S0	
771 Libera	X	M0		899 Jokaste	XB		
772 Tanete	C	C0		901 Brunsia	S		
773 Irmintraud	D	D0		907 Rhoda	C	C0	
775 Lumiere	S	S0		909 Ulla	X	C0	CYB
776 Berberica	C			911 Agamemnon	D		TRO
778 Theobalda	F	C0		914 Palisana	CU	D3	PHO
781 Kartvelia	CPU:			920 Rogeria	DTU		
782 Montefiore	S			924 Toni	CX		
783 Nora	---			925 Alphonsina	S	S0	
785 Zwetana	M	B2		927 Ratisbona	CB:		
786 Bredichina	C	C0		931 Whittemora	M	M0	
790 Pretoria	P	C0	CYB	932 Hooveria	CB		
791 Ani	C	C0		937 Bethgea	S	S2	
793 Arizona	DU:			939 Isberga	S		
796 Sarita	XD			940 Kordula	FC:		CYB
797 Montana	S			941 Murray	CX		
798 Ruth	M			943 Begonia	ST		
800 Kressmannia	S			944 Hidalgo	D		
801 Helwerthia	XC	C0		945 Barcelona	S	S0	
804 Hispania	PC	C0		946 Poesia	FU	C0	
805 Hormuthia	CX	C0		951 Gaspra	S	S0	
807 Ceraskia	S			954 Li	FCX		
811 Nauheima	S	S0		958 Asplinda	---		HIL
814 Tauris	C			962 Aslog	S	S0	
821 Fanny	C			963 Iduberga	S		
822 Lalage	DXCU			966 Muschi	S		
824 Anastasia	S			968 Petunia	S		
825 Tanina	SR			969 Leocadia	FXU:	B2	
828 Lindemannia	XFU			974 Lioba	S	S0	
830 Petropolitana	S			975 Perseverantia	S		
834 Burnhamia	GS:			976 Benjamina	XD:		
838 Seraphina	P	C0		977 Philippa	C		
839 Valborg	S			978 Aidamina	PF		
846 Lipperta	CBU:			980 Anacostia	SU	S3	
847 Agnia	S			981 Martina	CFU:		
849 Ara	M			983 Gunila	XD		
851 Zeissia	S	S0		991 McDonalda	C:		
853 Nansenia	XD			996 Hilaritas	B	C0	
857 Glasenappia	MU			1001 Gaussia	PC	C0	
858 El Djezair	S			1004 Belopolskya	PC		CYB

Minor Planet	Tholen Class	Barucci Class	Group	Minor Planet	Tholen Class	Barucci Class	Group
747 Winchester	PC			860 Ursina	M	M0	
748 Simeisa	P	C0	HIL	863 Benkoela	A	A0	
749 Malzovia	S			864 Aase	S		
750 Oskar	F	B1		868 Lova	C:		
751 Faina	C	C0		872 Holda	M		
753 Tiflis	S			873 Mechthild	PC	C0	
754 Malabar	XC			876 Scott	S		
755 Quintilla	M	M0		877 Walkure	F	C0	
757 Portlandia	XF	M0		880 Herba	F	C0	
758 Mancunia	X			883 Matterania	S		
760 Massinga	SU			884 Priamus	D		TRO
761 Brendelia	SC			887 Alinda	S		AMO
762 Puleova	F	C0		888 Parysatis	S		
764 Gedania	C			890 Waltraut	CTGU		
766 Moguntia	MU			893 Leopoldina	XF		
768 Struveana	X			895 Helio	FCB		
770 Bali	S			897 Lysistrata	S	S0	
771 Libera	X	M0		899 Jokaste	XB		
772 Tanete	C	C0		901 Brunsia	S		
773 Irmintraud	D	D0		907 Rhoda	C	C0	
775 Lumiere	S	S0		909 Ulla	X	C0	CYB
776 Berbericia	C			911 Agamemnon	D		TRO
778 Theobalda	F	C0		914 Palisana	CU	D3	PHO
781 Kartvelia	CPU·			920 Rogeria	DTU		
782 Montefiore	S			924 Toni	CX		
783 Nora	---			925 Alphonsina	S	S0	
785 Zwetana	M	B2		927 Ratisbona	CB:		
786 Bredichina	C	C0		931 Whittemora	M	M0	
790 Pretoria	P	C0	CYB	932 Hooveria	CB		
791 Ani	C	C0		937 Bethgea	S	S2	
793 Arizona	DU:			939 Isberga	S		
796 Sarita	XD			940 Kordula	FC:		CYB
797 Montana	S			941 Murray	CX		
798 Ruth	M			943 Begonia	ST		
800 Kressmannia	S			944 Hidalgo	D		
801 Helwerthia	XC	C0		945 Barcelona	S	S0	
804 Hispania	PC	C0		946 Poesia	FU	C0	
805 Hormuthia	CX	C0		951 Gaspra	S	S0	
807 Ceraskia	S			954 Li	FCX		
811 Nauheima	S	S0		958 Asplinda	---		HIL
814 Tauris	C			962 Aslog	S	S0	
821 Fanny	C			963 Iduberga	S		
822 Lalage	DXCU			966 Muschi	S		
824 Anastasia	S			968 Petunia	S		
825 Tanina	SR			969 Leocadia	FXU:	B2	
828 Lindemannia	XFU			974 Lioba	S	S0	
830 Petropolitana	S			975 Perseverantia	S		
834 Burnhamia	GS:			976 Benjamina	XD:		
838 Seraphina	P	C0		977 Philippa	C		
839 Valborg	S			978 Aidamina	PF		
846 Lipperta	CBU:			980 Anacostia	SU	S3	
847 Agnia	S			981 Martina	CFU:		
849 Ara	M			983 Gunila	XD		
851 Zeissia	S	S0		991 McDonalda	C:		
853 Nansenia	XD			996 Hilaritas	B	C0	
857 Glasenappia	MU			1001 Gaussia	PC	C0	
858 El Djezair	S			1004 Belopolskya	PC		CYB

Minor Planet	Tholen Class	Barucci Class	Group	Minor Planet	Tholen Class	Barucci Class	Group
1011 Laodamia	S		MC	1199 Geldonia	CGTP:		
1012 Sarema	F			1208 Troilus	FCU	C0	TRO
1013 Tombecka	XSC			1210 Morosovia	MU:		
1015 Christa	C			1212 Francette	P	M0	HIL
1019 Strackea	S	S2	HUN	1215 Boyer	S		
1021 Flammario	F	C0		1216 Askania	S		
1023 Thomana	G			1223 Neckar	S		
1025 Riema	E		HUN	1224 Fantasia	S		
1028 Lydina	C	C0	CYB	1235 Schorria	CX:		HUN
1029 La Plata	S			1236 Thais	T	D3	
1031 Arctica	CX:			1241 Dysona	PDC		
1036 Ganymed	S	S0	AMO	1245 Calvinia	S	S0	
1038 Tuckia	DTU:		HIL	1247 Memoria	CXF		
1043 Beate	S			1249 Rutherfordia	S		
1047 Geisha	S			1251 Hedera	E		
1048 Feodosia	XC			1252 Celestia	S		
1052 Belgica	S			1256 Normannia	D	D0	HIL
1055 Tynka	S			1263 Varsavia	X		
1058 Grubba	S			1266 Tone	P	C0	CYB
1061 Paeonia	C			1268 Libya	P	C0	HIL
1075 Helina	SU			1269 Rollandia	D	D0	HIL
1076 Viola	F	B1		1274 Delportia	S		
1078 Mentha	S			1275 Cimbria	X	M0	
1079 Mimosa	S			1277 Dolores	C	C0	
1080 Orchis	F	B1		1280 Baillauda	X		CYB
1082 Pirola	C			1284 Latvia	T	D3	
1087 Arabis	S	S0		1286 Banachiewicza	S		
1088 Mitaka	S			1289 Kutaissi	S		
1093 Freda	C			1306 Scythia	S		
1102 Pepita	C			1307 Cimmeria	S		
1103 Sequoia	E		HUN	1310 Villigera	S		PHO
1105 Fragaria	ST	S0		1314 Paula	S		
1108 Demeter	CX		PHO	1317 Silvretta	CX:		
1109 Tata	FC			1326 Losaka	CSU		
1111 Reinmuthia	FXU:			1328 Devota	X		CYB
1112 Polonia	S			1329 Eliane	S		
1124 Stroobantia	X	M0		1330 Spiridonia	P		
1127 Mimi	CX			1331 Solvejg	BC:		
1129 Neujmina	S			1336 Zeelandia	S	S0	
1133 Lugduna	S			1339 Desagneauxa	S		
1139 Atami	S		MC	1341 Edmee	XB		
1140 Crimea	S			1342 Brabantia	X		PHO
1143 Odysseus	D		TRO	1345 Potomac	X		HIL
1144 Oda	D		HIL	1350 Rosselia	S		
1146 Biarmia	X	M0		1355 Magoeba	X		HUN
1148 Rarahu	S			1357 Khama	XCU		
1154 Astronomia	FXU:	C0	CYB	1359 Prieska	CX:		
1162 Larissa	P	M0	HIL	1362 Griqua	CP		GRI
1167 Dubiago	D	D0	CYB	1364 Safara	---		
1170 Siva	S	S0	PHO	1390 Abastumani	P	C0	CYB
1171 Rusthawelia	P	C0		1391 Carelia	S		
1172 Aneas	D	D0	TRO	1392 Pierre	DX		
1173 Anchises	P	C0	TRO	1401 Lavonne	S		
1177 Gonnessia	XFU	C0	CYB	1415 Malautra	S		
1180 Rita	P		HIL	1416 Renauxa	S		
1185 Nikko	S			1418 Fayeta	S	S0	
1186 Turnera	S			1422 Stromgrenia	S		

Minor Planet	Tholen Class	Barucci Class	Group	Minor Planet	Tholen Class	Barucci Class	Group
1434 Margot	S			1681 Steinmetz	S		
1437 Diomedes	DP		TRO	1685 Toro	S		APO
1439 Vogtia	XFU	B2	HIL	1691 Oort	CU	C0	
1442 Corvina	S			1693 Hertzsprung	CBU	C0	
1445 Konkolya	C			1694 Kaiser	GC		
1449 Virtanen	S			1700 Zvezdara	X	C0	
1453 Fennia	S		HUN	1702 Kalahari	D		
1456 Saldanha	C:			1707 Chantal	S		
1461 Jean-Jacques	M	M0		1711 Sandrine	S		
1467 Mashona	GC	C0	CYB	1717 Arlon	S		
1474 Beira	FX		MC	1723 Klemola	S		
1477 Bonsdorffia	XU			1724 Vladimir	FBCU :	B0	
1479 Inkeri	XFU			1727 Mette	S		HUN
1493 Sigrid	F	C0		1740 Paavo Nurmi	F		
1500 Jyvaskyla	S			1746 Brouwer	D		HIL
1504 Lappeenranta	S			1747 Wright	AU:		MC
1508 Kemi	BCF			1748 Mauderli	D		HIL
1509 Esclangona	S	S0	HUN	1750 Eckert	S		HUN
1512 Oulu	P	M0	HIL	1754 Cunningham	P	C0	HIL
1529 Oterma	P:		HIL	1755 Lorbach	S		
1532 Inari	S			1765 Wrubel	DX		
1533 Saimaa	S			1767 Lampland	XC		
1547 Nele	TD			1768 Appenzella	F		
1556 Wingolfia	XC	M0	CYB	1792 Reni	C:		
1564 Srbija	X			1794 Finsen	C	C0	
1566 Icarus	---		APO	1796 Riga	XFCU	C0	CYB
1567 Alikoski	PU			1815 Beethoven	F	C0	
1576 Fabiola	BU	B0		1827 Atkinson	DU		
1578 Kirkwood	D	D1	HIL	1830 Pogson	S		
1579 Herrick	F	C0	CYB	1842 Hynek	S		
1580 Betulia	C		AMO	1862 Apollo	Q		APO
1581 Abanderada	BCU	B0		1863 Antinous	SU		APO
1583 Antilochus	D	D0	TRO	1864 Daedalus	SQ		APO
1584 Fuji	S	S0	PHO	1865 Cerberus	S		APO
1595 Tanga	C:			1867 Deiphobus	D	D0	TRO
1601 Patry	S			1902 Shaposhnikov	X		HIL
1602 Indiana	S			1911 Schubart	P	C0	HIL
1604 Tombaugh	XSCU	D3		1915 Quetzalcoatl	SMU		AMO
1606 Jekhovsky	C	C0		1916 Boreas	S		AMO
1615 Bardwell	B	C0		1919 Clemence	X		HUN
1619 Ueta	S			1920 Sarmiento	X		HUN
1620 Geographos	S		APO	1931 1969 QB	C		
1621 Druzhba	S			1943 Anteros	S		AMO
1625 The NORC	C			1952 Hesburgh	CD:		
1627 Ivar	S		AMO	1963 Bezovec	C	C0	PHO
1636 Porter	S			1980 Tezcatlipoca	SU		AMO
1639 Bower	C			1990 Pilcher	S		
1644 Rafita	S			2000 Herschel	S		PHO
1645 Waterfield	XDC			2001 Einstein	X		HUN
1648 Shajna	S			2010 Chebyshev	BU:		
1650 Heckmann	F	B1		2035 Stearns	E		MC
1655 Comas Sola	XFU			2048 Dwornik	E		HUN
1656 Suomi	S		HUN	2050 Francis	S		PHO
1657 Roemera	S		PHO	2052 Tamriko	S	S0	
1658 Innes	AS			2060 Chiron	B		
1665 Gaby	S			2061 Anza	TCG:		AMO
1669 Dagmar	G:			2062 Aten	S		ATE

Minor Planet	Tholen Class	Barucci Class	Group	Minor Planet	Tholen Class	Barucci Class	Group
2067 Aksnes	P	M0	HIL	2411 Zellner	S		
2081 Sazava	F	B1		2430 Bruce Helin	S		PHO
2083 Smither	X		HUN	2449 1978 GC	E		HUN
2089 Cetacea	S			2491 1977 CB	X		HUN
2090 Mizuho	S	S0		2501 Lohja	A		
2099 Opik	S		MC	2510 Shandong	S		
2100 Ra-Shalom	C		ATE	2577 Litva	EU		HUN
2111 Tselina	S	S0		2608 Seneca	S		AMO
2131 Mayall	S	S0	MC	2674 Pandarus	D		TRO
2134 Dennispalm	DSU:			2735 Ellen	SDU::		HUN
2139 Makharadze	F			2744 Birgitta	S		MC
2156 Kate	S	S2		2760 Kacha	X		HIL
2196 Ellicott	CFXU	C0	CYB	2791 Paradise	SU		PHO
2207 Antenor	D	D0	TRO	2809 Vernadskij	BFX		
2208 Pushkin	D	D0	CYB	2830 Greenwich	S		PHO
2212 Hephaistos	SG		APO	2893 Peiroos	D		TRO
2223 Sarpedon	DU		TRO	3102 1981 QA	QRS		AMO
2241 1979 WM	D	D0	TRO	3123 Dunham	F		
2246 Bowell	D	D0	HIL	3124 Kansas	CG		
2260 Neoptolemus	DTU·	D1	TRO	3169 Ostro	TS		HUN
2266 Tchaikovsky	D	D0	CYB	3199 Nefertiti	S		AMO
2272 1972 FA	S		HUN	3200 Phaethon[5]	F		APO
2274 Ehrsson	SG			3288 Seleucus	S		AMO
2278 1953 GE	FC			3551 1983 RD[6]	V		AMO
2279 Barto	F			3552 1983 SA[6]	D		AMO
2311 El Leoncito	D	D0	CYB	3757 1982 XB	S		AMO
2312 Duboshin	D	D0	HIL	3908 1980 PA[7]	V		AMO
2340 Hathor	CSU		ATE	4015 1979 VA	CF		APO
2345 Fucik	S	S0		4055 1985 DO2[7]	V		AMO
2357 Phereclos	D	D0	TRO	1975 EA	CSU		
2363 Cebriones	D		TRO	1975 GB	S		
2368 Beltrovata	SQ		AMO	1975 U2[8]	S		
2375 1975 AA	D			1977 VA	XC		
2379 Heiskanen	C	C0		1978 CA	S		AMO
2405 Welch	BCU:	B3		1980 WF	QU		AMO
2407 1973 DH	C			1984 BC[6]	D		MC

[1]13 Egeria. Tholen (1984) listed classification as CG. C eliminated on the basis of 24-color data.

[2]192 Nausikaa. Tholen (1984) listed classification as RS. R eliminated on the basis of 24-color data.

[3]344 Desiderata. Tholen (1984) listed classification as CSU. SU eliminated on the basis of 24-color data.

[4]515 Athalia. Tholen (1984) listed classification as U. Changed to I as explained in the introduction.

[5]3200 Phaethon. From Tholen (1985).

[6]3551 1983 RD, 3552 1983 SA, and 1984 BC. Unpublished data of Tholen cited in Hartmann et al. (1987).

[7]3908 1980 PA and 4055 1985 DO2. From Tholen et al. (1988).

[8]1975 U2. Not a proper provisional designation. Data taken from TRIAD *UBV* table as published by Bowell et al. (1979). In turn, they took the data from unpublished observations by Tedesco. It is not known what this object really is.

THREE-PARAMETER ASTEROID TAXONOMY CLASSIFICATIONS

EDWARD F. TEDESCO, JAMES G. WILLIAMS, DENNIS L. MATSON,
GLENN J. VEEDER
Jet Propulsion Laboratory

JONATHAN C. GRADIE
University of Hawaii

and

LARRY A. LEBOFSKY
University of Arizona

This contribution contains a listing of the classifications for the 357 asteroids with both high-quality visual (U, V, x) photometry and high-quality IRAS albedos used by Tedesco et al. (1989) to define the three-parameter taxonomic system. See the chapter by Tedesco, Matson and Veeder for a summary of this method and Tedesco et al. (1989) for complete details.

All but one of the three-parameter classes are similar to those previously recognized using other classification schemes. Eleven classes are found: the C, S, M and E classes have been known for a long time, the A, F, P, D, T and G classes have been generally accepted in recent years, and the K class is new. The P class is contiguous with the C's, but is distinguishable from a change in morphology of the distribution of the three parameters. The distribution of P's may be bimodal in U-V. The D's are slightly separated from the P's. The G's are slightly separated from the C's; they are not end members of the C distribution. The F's are adjacent to the C's, but seem distinct. The K's lie at the low-color, low-albedo side of the S distribution. The small number of K's

makes it unclear whether the K's are end members of the S's or are slightly separated.

Of the 14 asteroids in the defining sample which are not associated with a class, indicated in the table by one of the lower-case letters "l", "m" or "r" (see below), three (2 Pallas, 4 Vesta and 349 Dembowska) have long been known to have unique surface compositions. Another three which are not associated with a class (308 Polyxo, 570 Kythera and 785 Zwetana) also probably have unique surface mineralogies. Some of the remaining eight may fail to classify due to erroneous or spurious data, in spite of small formal observational uncertainties, while others may represent new taxons. The classification algorithm explicitly accounts for the observational uncertainties in each of the classification parameters, thus the derived classification depends upon both the parameter values and their uncertainties.

The results are summarized in the following table. In this table we give, respectively, asteroid number and name, IRAS diameter (in km), IRAS visual geometric albedo, the U-V and v-x color indices, the 1 σ uncertainties in IRAS albedo, the U-V and v-x colors, and the three-parameter classification. Certain matches, i.e., for cases in which the error box of the observation falls entirely within a class volume, are indicted with a single letter. Possible matches have either a multiple-letter designation or a single letter followed by a question mark. The symbols "l" (low albedo, i.e., ≤ 0.10), "r" (red, i.e., U-$V \geq 1.25$), or "m" (moderate to high albedo, i.e., > 0.10 and U-$V < 1.25$) are used when no match is found, i.e., when the error box of the observation falls entirely outside of all defined class volumes.

Most of the uncertain matches are either near the edge of their class distributions, have relatively large errors, or both. In most of these cases, the single letter, or the first of two letters, is the most probable class. The many objects classified PC or CP are the result of the defined contiguous nature of these two groups. Most of the other double possibilities result from the relatively narrow separation between the paired classes involved. It appears that many of the uncertain classes could be resolved given measurements with improved accuracies. (The reader is cautioned to be wary of combining classifications derived from different methods.)

The classification scheme is automated and accommodates data with a variety of observational accuracies. Readers wishing to obtain a copy of the three-parameter classification program for use on IBM PC compatible microcomputers can do so by sending a blank, formatted 3.5-inch or 5.25-inch floppy disk and return address label to E. Tedesco.

REFERENCES

Gradie, J. C and Tedesco, E. F. 1989. Radiometric albedos and diameters for 350 asteroids. *Astron. J.* (to be submitted).

IRAS Asteroid and Comet Survey: Preprint Version No. 1. 1986. Ed. D. L. Matson, JPL Internal Document No. D-3698.

Tedesco, E. F., Williams, J. G., Matson, D. L., Veeder, G. J., Gradie, J. C., and Lebofsky, L. A. 1989. A three-parameter asteroid taxonomy. *Astron. J.* 97:580–606

Zellner, B., Tholen, D. J., and Tedesco, E. F. 1985. The eight-color asteroid survey: Results for 589 minor planets. *Icarus* 61:355–416.

Asteroid	IRAS Diam.	IRAS p_V	U-V	v-x	σ_{p_V}	σ_{U-V}	σ_{v-x}	CLASS	Notes
1 Ceres	913	0.10	1.15	-0.005	0.01	0.02	0.006	G?	
2 Pallas	523	0.14	0.95	-0.023	0.01	0.02	0.006	m	
3 Juno	244	0.22	1.22	0.079	0.02	0.02	0.010	S	
4 Vesta	501	0.38	1.30	-0.168	0.03	0.02	0.009	r	6
5 Astraea	125	0.14	1.24	0.083	0.01	0.02	0.014	S	5
6 Hebe	192	0.25	1.21	0.084	0.01	0.02	0.008	S	
7 Iris	203	0.21	1.33	0.135	0.01	0.02	0.008	S	
8 Flora	141	0.22	1.37	0.181	0.01	0.02	0.009	S	
10 Hygiea	429	0.075	1.04	-0.024	0.003	0.02	0.009	C	
11 Parthenope	162	0.15	1.27	0.126	0.01	0.02	0.033	S	5
12 Victoria	117	0.16	1.39	0.254	0.01	0.02	0.016	S	
13 Egeria	215	0.099	1.21	0.037	0.006	0.02	0.009	G	5 6
15 Eunomia	272	0.19	1.30	0.184	0.01	0.02	0.022	S	5
16 Psyche	264	0.10	0.95	0.128	0.01	0.02	0.012	M	
17 Thetis	93.2	0.15	1.25	0.142	0.01	0.02	0.035	S	5
18 Melpomene	148	0.22	1.24	0.171	0.01	0.02	0.028	S	
20 Massalia	151	0.19	1.23	0.104	0.02	0.02	0.015	S	5
21 Lutetia	99.5	0.20	0.90	0.073	0.02	0.02	0.009	M	
22 Kalliope	187	0.12	0.94	0.080	0.01	0.02	0.009	M	5
23 Thalia	111	0.21	1.28	0.121	0.01	0.02	0.012	S	
25 Phocaea	78.2	0.22	1.45	0.189	0.01	0.02	0.017	S	5
26 Proserpina	98.7	0.16	1.39	0.196	0.01	0.02	0.028	S	5
28 Bellona	126	0.15	1.31	0.149	0.01	0.02	0.009	S	5
29 Amphitrite	219	0.16	1.25	0.185	0.01	0.02	0.007	S	
30 Urania	104	0.13	1.34	0.240	0.01	0.03	0.041	S	2 5
32 Pomona	82.6	0.25	1.29	0.131	0.01	0.02	0.020	S	5
34 Circe	118	0.057	1.07	0.000	0.003	0.02	0.024	C	5
35 Leukothea	108	0.058	1.03	0.016	0.004	0.05	0.045	C	1 2 5
37 Fides	112	0.17	1.26	0.123	0.01	0.02	0.015	S	
38 Leda	120	0.058	1.13	0.021	0.002	0.02	0.023	C	
39 Laetitia	159	0.29	1.39	0.173	0.02	0.02	0.016	S	5
40 Harmonia	111	0.20	1.28	0.170	0.02	0.02	0.009	S	5
41 Daphne	182	0.073	1.10	0.040	0.014	0.02	0.034	C	5
42 Isis	107	0.12	1.34	0.178	0.01	0.02	0.014	S	
43 Ariadne	65.3	0.28	1.36	0.085	0.02	0.02	0.021	S	5
44 Nysa	73.3	0.49	0.94	0.041	0.05	0.02	0.010	E	
45 Eugenia	214	0.048	0.93	0.018	0.004	0.02	0.013	C	6
46 Hestia	131	0.046	0.92	0.091	0.005	0.02	0.014	C	
47 Aglaja	133	0.072	0.97	-0.018	0.009	0.02	0.015	C	
48 Doris	225	0.064	1.15	-0.015	0.006	0.02	0.023	C	5
49 Pales	154	0.051	1.14	0.041	0.003	0.03	0.045	C	2 5 6
51 Nemausa	153	0.086	1.24	0.071	0.004	0.02	0.011	G	
52 Europa	312	0.057	0.99	-0.032	0.002	0.02	0.010	C	5
54 Alexandra	171	0.050	1.06	0.019	0.002	0.02	0.020	C	5
55 Pandora	67.5	0.32	0.94	0.073	0.03	0.03	0.032	E?	5 6
56 Melete	117	0.062	1.01	0.134	0.002	0.02	0.014	1	5
57 Mnemosyne	116	0.21	1.27	0.167	0.01	0.02	0.024	S	5 6
58 Concordia	97.7	0.056	1.06	0.007	0.004	0.03	0.038	C	5
59 Elpis	173	0.048	0.96	0.043	0.005	0.02	0.018	C	5
60 Echo	61.6	0.15	1.29	0.114	0.01	0.02	0.026	S	5

Asteroid	IRAS Diam.	IRAS p_V	U-V	v-x	σ_{p_V}	σ_{U-V}	σ_{v-x}	CLASS	Notes
61 Danae	83.6	0.21	1.25	0.130	0.01	0.02	0.018	S	5
62 Erato	99.3	0.090	1.07	-0.074	0.004	0.02	0.039	C?	5
63 Ausonia	108	0.17	1.38	0.216	0.01	0.02	0.022	S	5
64 Angelina	59.8	0.430	1.01	0.143	0.030	0.02	0.008	E	4
65 Cybele	245	0.057	0.94	0.041	0.003	0.02	0.007	C	
66 Maja	78.3	0.050	1.07	-0.018	0.009	0.02	0.015	C	5
67 Asia	60.3	0.21	1.29	0.135	0.01	0.02	0.024	S	5
68 Leto	127	0.20	1.32	0.121	0.01	0.02	0.022	S	5
69 Hesperia	143	0.12	0.93	0.142	0.01	0.03	0.038	M	5 6
70 Panopaea	127	0.070	1.12	0.044	0.004	0.02	0.028	C	5
71 Niobe	87.3	0.28	1.25	0.195	0.01	0.02	0.012	S	
75 Eurydike	58.3	0.12	0.97	0.100	0.02	0.02	0.018	M	5
76 Freia	190	0.029	0.99	0.108	0.001	0.02	0.033	CP	5
77 Frigga	71.0	0.13	0.99	0.175	0.01	0.02	0.016	M?	5
78 Diana	125	0.064	1.07	-0.008	0.003	0.02	0.023	C	5
79 Eurynome	68.8	0.27	1.31	0.145	0.01	0.02	0.034	S	5
80 Sappho	81.7	0.15	1.40	0.198	0.01	0.02	0.016	S	
81 Terpsichore	124	0.046	1.06	0.007	0.002	0.02	0.023	C	5
82 Alkmene	63.6	0.17	1.19	0.116	0.01	0.02	0.027	S	5
83 Beatrix	84.2	0.069	0.96	0.154	0.003	0.02	0.019	I	
85 Io	157	0.068	0.94	-0.011	0.004	0.02	0.013	C	
86 Semele	127	0.043	1.04	0.022	0.002	0.02	0.018	C	
87 Sylvia	271	0.040	0.95	0.119	0.004	0.02	0.012	PC	
89 Julia	159	0.16	1.36	0.225	0.01	0.02	0.033	S	5
90 Antiope	125	0.051	1.01	0.007	0.003	0.02	0.021	C	6
92 Undina	132	0.20	0.99	0.103	0.01	0.02	0.035	M	5
93 Minerva	146	0.085	0.98	0.004	0.006	0.03	0.025	C?	
94 Aurora	212	0.038	0.96	0.054	0.001	0.02	0.013	C	
95 Arethusa	145	0.062	1.08	0.015	0.010	0.02	0.015	C	
97 Klotho	87.1	0.19	0.92	0.109	0.03	0.02	0.015	M	
98 Ianthe	109	0.041	1.13	0.012	0.002	0.05	0.029	C	1 5
101 Helena	68.3	0.15	1.32	0.172	0.01	0.02	0.018	S	
102 Miriam	86.0	0.049	1.09	0.200	0.002	0.03	0.033	I	5
103 Hera	95.2	0.17	1.30	0.140	0.01	0.02	0.009	S	
104 Klymene	127	0.052	1.02	0.000	0.004	0.02	0.019	C	5
105 Artemis	123	0.032	1.01	0.015	0.002	0.03	0.023	C	
106 Dione	152	0.083	1.21	-0.004	0.004	0.02	0.025	G	
107 Camilla	237	0.060	1.00	0.056	0.007	0.02	0.014	C	
108 Hecuba	67.2	0.19	1.34	0.185	0.03	0.03	0.028	S	5
109 Felicitas	91.6	0.060	1.12	0.003	0.003	0.02	0.014	C	
110 Lydia	89.1	0.17	0.98	0.126	0.01	0.02	0.025	M	5
111 Ate	139	0.064	1.09	0.024	0.006	0.02	0.012	C	6
113 Amalthea	47.6	0.27	1.46	0.178	0.03	0.02	0.011	S	5
114 Kassandra	103	0.084	1.11	0.187	0.003	0.02	0.030	T	
116 Sirona	75.5	0.22	1.28	0.113	0.04	0.05	0.026	S	1 5
117 Lomia	154	0.040	0.98	0.026	0.005	0.02	0.017	C	
118 Peitho	45.7	0.20	1.29	0.208	0.01	0.05	0.021	S	1 5
119 Althaea	60.7	0.17	1.36	0.190	0.01	0.03	0.032	S	5
120 Lachesis	178	0.045	1.08	0.037	0.002	0.02	0.019	C	5
121 Hermione	217	0.042	1.11	-0.005	0.002	0.02	0.024	C	5

Asteroid	IRAS Diam.	IRAS p_V	U-V	v-x	σ_{p_V}	σ_{U-V}	σ_{v-x}	CLASS	Notes
124 Alkeste	79.5	0.15	1.27	0.158	0.01	0.02	0.012	S	
125 Liberatrix	47.5	0.18	0.92	0.068	0.01	0.03	0.034	M	5
128 Nemesis	194	0.045	1.04	0.071	0.002	0.02	0.016	C	5
130 Elektra	189	0.089	1.22	-0.001	0.013	0.02	0.014	G	5
131 Vala	43.3	0.095	1.16	0.066	0.011	0.03	0.032	KCT	5
132 Aethra	47.0	0.14	0.87	0.087	0.01	0.02	0.011	M?	
134 Sophrosyne	122	0.041	1.02	0.017	0.014	0.02	0.015	C	3
135 Hertha	82.0	0.13	0.97	0.100	0.01	0.02	0.009	M	
137 Meliboea	150	0.048	1.03	0.057	0.002	0.02	0.030	C	
142 Polana	57.1	0.042	0.85	-0.044	0.003	0.02	0.018	F	
144 Vibilia	146	0.059	1.11	0.008	0.003	0.02	0.014	C	5
145 Adeona	155	0.044	1.05	0.068	0.002	0.02	0.016	C	5
146 Lucina	137	0.052	1.08	-0.008	0.002	0.02	0.019	C	5
147 Protogeneia	137	0.029	0.97	0.043	0.002	0.03	0.044	C	2 5
148 Gallia	104	0.14	1.27	-0.029	0.01	0.02	0.047	r	2 5
153 Hilda	175	0.060	0.92	0.101	0.003	0.02	0.008	C	
156 Xanthippe	126	0.040	1.02	0.053	0.002	0.02	0.011	C	5
158 Koronis	39.8	0.17	1.21	0.110	0.02	0.02	0.017	S	
159 Aemilia	131	0.061	1.07	-0.008	0.003	0.02	0.016	C	5
161 Athor	45.7	0.12	0.95	0.101	0.02	0.02	0.023	M	5
167 Urda	42.2	0.21	1.26	0.135	0.02	0.03	0.014	S	5
168 Sibylla	154	0.050	1.13	0.048	0.003	0.02	0.013	C	
170 Maria	46.2	0.14	1.34	0.165	0.01	0.03	0.043	S	2 5
171 Ophelia	121	0.053	1.02	-0.014	0.008	0.02	0.024	C	
173 Ino	159	0.053	1.02	0.044	0.003	0.02	0.026	C	5
179 Klytaemnestra	81.0	0.14	1.24	0.139	0.01	0.02	0.021	S	5
181 Eucharis	107	0.12	1.17	0.176	0.02	0.02	0.021	K	5
184 Dejopeja	68.2	0.18	0.95	0.107	0.01	0.02	0.017	M	5
185 Eunike	165	0.053	1.01	0.004	0.002	0.02	0.013	C	5
186 Celuta	52.3	0.15	1.20	0.147	0.01	0.02	0.034	SK	5
187 Lamberta	135	0.053	1.05	0.045	0.002	0.02	0.014	C	
188 Menippe	41.3	0.19	1.28	0.193	0.01	0.05	0.050	S	1 2 5
189 Phthia	38.5	0.18	1.38	0.274	0.03	0.02	0.010	S	5
194 Prokne	174	0.050	1.08	-0.002	0.003	0.02	0.021	C	5
195 Eurykleia	89.7	0.053	1.08	0.002	0.002	0.02	0.011	C	5
196 Philomela	146	0.18	1.32	0.199	0.01	0.02	0.016	S	5
198 Ampella	58.7	0.19	1.29	0.183	0.02	0.02	0.019	S	
200 Dynamene	132	0.053	1.08	0.015	0.002	0.02	0.012	C	5
201 Penelope	70.5	0.14	0.96	0.100	0.01	0.02	0.012	M	5
204 Kallisto	50.8	0.17	1.23	0.174	0.01	0.03	0.020	S	5
208 Lacrimosa	44.3	0.21	1.20	0.145	0.01	0.02	0.011	S	5
209 Dido	149	0.044	0.98	0.012	0.036	0.02	0.040	C?	3 5
210 Isabella	90.0	0.041	0.93	-0.004	0.003	0.02	0.011	CF	5 6
211 Isolda	148	0.059	1.08	0.001	0.003	0.02	0.010	C	
213 Lilaea	84.6	0.072	0.85	-0.018	0.005	0.02	0.023	F	5
214 Aschera	23.7	0.52	0.93	0.013	0.03	0.02	0.011	E	4
216 Kleopatra	140	0.088	0.94	0.125	0.006	0.02	0.004	M	
219 Thusnelda	43.6	0.15	1.36	0.203	0.01	0.05	0.039	S	1 5
221 Eos	110	0.12	1.19	0.113	0.01	0.02	0.018	K	
222 Lucia	58.0	0.082	1.05	-0.079	0.013	0.02	0.037	C?	5

Asteroid	IRAS Diam.	IRAS p_V	U-V	v-x	σ_{p_V}	σ_{U-V}	σ_{v-x}	CLASS	Notes
223 Rosa	90.7	0.022	1.00	0.114	0.002	0.03	0.012	CP	5
225 Henrietta	124	0.041	0.93	0.031	0.002	0.03	0.034	C	5
229 Adelinda	96.0	0.037	0.96	0.005	0.006	0.03	0.039	C	5
230 Athamantis	113	0.14	1.29	0.148	0.01	0.02	0.051	S	2 5
232 Russia	55.2	0.045	1.05	0.041	0.002	0.02	0.014	C	5
233 Asterope	108	0.073	1.11	0.203	0.011	0.02	0.013	T	
234 Barbara	44.6	0.22	1.36	0.254	0.01	0.02	0.015	S	5
236 Honoria	90.5	0.10	1.29	0.252	0.01	0.02	0.012	S	
238 Hypatia	156	0.032	1.11	0.047	0.001	0.02	0.029	C	5
240 Vanadis	108	0.039	1.04	0.017	0.002	0.03	0.025	C	5
241 Germania	169	0.062	0.98	0.003	0.004	0.02	0.041	C	2 5 6
245 Vera	84.8	0.16	1.31	0.134	0.01	0.02	0.034	S	5
246 Asporina	63.8	0.13	1.58	0.276	0.01	0.02	0.024	r	5
250 Bettina	85.5	0.18	0.98	0.124	0.03	0.02	0.031	M	5
258 Tyche	67.7	0.15	1.31	0.136	0.01	0.02	0.033	S	5
261 Prymno	52.6	0.10	1.00	-0.036	0.01	0.02	0.025	1	5
264 Libussa	53.5	0.27	1.26	0.111	0.06	0.02	0.017	S	3 5
266 Aline	113	0.054	1.05	-0.025	0.003	0.03	0.036	C	5
268 Adorea	142	0.038	0.90	-0.025	0.003	0.02	0.022	FC	5
275 Sapientia	121	0.036	1.05	0.107	0.002	0.02	0.006	C	
276 Adelheid	127	0.041	0.98	0.123	0.006	0.02	0.015	PC	5
279 Thule	135	0.030	0.96	0.257	0.004	0.02	0.029	D	
287 Nephthys	70.1	0.16	1.34	0.142	0.01	0.02	0.009	S	
288 Glauke	37.5	0.11	1.26	0.155	0.01	0.02	0.011	SK	6
302 Clarissa	40.5	0.045	0.93	0.025	0.006	0.02	0.043	C	2 5
304 Olga	68.5	0.047	0.97	0.012	0.004	0.02	0.025	C	5 6
306 Unitas	49.2	0.17	1.32	0.141	0.01	0.02	0.017	S	
308 Polyxo	148	0.043	1.16	0.254	0.002	0.02	0.018	1	
313 Chaldaea	101	0.050	1.04	0.046	0.002	0.02	0.024	C	5
322 Phaeo	73.8	0.080	0.95	0.150	0.004	0.03	0.019	M	
323 Brucia	37.7	0.16	1.38	0.182	0.01	0.03	0.022	S	6
326 Tamara	100	0.039	1.03	0.034	0.005	0.02	0.007	C	
329 Svea	80.5	0.037	1.00	0.025	0.002	0.02	0.020	C	5
334 Chicago	170	0.064	1.08	0.055	0.012	0.02	0.009	C	
335 Roberta	93.6	0.053	0.85	0.030	0.003	0.02	0.026	F	5
336 Lacadiera	72.0	0.042	1.00	0.241	0.004	0.03	0.022	D	5
337 Devosa	63.2	0.13	1.00	0.125	0.01	0.03	0.029	M	5
338 Budrosa	62.1	0.17	0.94	0.103	0.07	0.02	0.038	M	3 5
339 Dorothea	43.7	0.16	1.18	0.123	0.01	0.02	0.025	SK	
344 Desiderata	138	0.053	1.09	0.081	0.002	0.03	0.037	C?	5
345 Tercidina	100	0.056	1.13	-0.011	0.007	0.02	0.019	C	5
346 Hermentaria	110	0.13	1.34	0.116	0.01	0.02	0.030	S	5
347 Pariana	54.1	0.14	0.94	0.089	0.02	0.02	0.031	M	5
349 Dembowska	143	0.34	1.47	-0.042	0.01	0.02	0.011	r	
350 Ornamenta	123	0.047	1.06	-0.011	0.002	0.02	0.019	C	5
354 Eleonora	162	0.19	1.49	0.237	0.02	0.02	0.018	S	5
359 Georgia	47.5	0.15	1.02	0.110	0.03	0.02	0.016	M	5
360 Carlova	121	0.052	0.96	0.026	0.010	0.03	0.019	C	5
361 Bononia	149	0.039	0.94	0.232	0.002	0.02	0.010	D	
365 Corduba	110	0.029	1.04	0.097	0.001	0.02	0.017	C	5

Asteroid	IRAS Diam.	IRAS P_V	U-V	v-x	σ_{P_V}	σ_{U-V}	σ_{v-x}	CLASS	Notes
368 Haidea	74.5	0.032	1.02	0.183	0.002	0.02	0.032	PD	
369 Aeria	62.2	0.17	0.97	0.123	0.01	0.02	0.028	M	
373 Melusina	99.6	0.038	1.03	0.028	0.003	0.03	0.039	C	5
374 Burgundia	48.2	0.19	1.29	0.156	0.01	0.02	0.025	S	
376 Geometria	37.0	0.22	1.35	0.187	0.01	0.03	0.019	S	5
379 Huenna	96.1	0.045	0.96	0.022	0.002	0.05	0.040	C	1 5
380 Fiducia	76.3	0.051	1.08	0.000	0.002	0.02	0.032	C	
381 Myrrha	124	0.045	0.99	-0.004	0.003	0.02	0.023	C	5
382 Dodona	60.6	0.13	0.94	0.130	0.01	0.03	0.032	M	5
383 Janina	49.7	0.072	1.02	-0.088	0.005	0.03	0.028	C?	
386 Siegena	173	0.063	1.14	0.044	0.002	0.02	0.016	C	5
387 Aquitania	106	0.16	1.34	0.249	0.01	0.02	0.023	S	5 6
388 Charybdis	120	0.053	1.01	0.000	0.008	0.02	0.031	C	5
389 Industria	81.6	0.20	1.27	0.166	0.01	0.02	0.018	S	
402 Chloe	57.6	0.12	1.20	0.178	0.01	0.02	0.018	K	5
404 Arsinoe	101	0.041	0.99	0.004	0.002	0.02	0.033	C	5
405 Thia	129	0.045	1.06	-0.024	0.002	0.02	0.018	C	5
406 Erna	53.8	0.043	1.01	0.164	0.003	0.02	0.020	P	
407 Arachne	97.6	0.050	1.08	-0.012	0.006	0.03	0.017	C	
410 Chloris	128	0.054	1.15	-0.028	0.002	0.03	0.032	C	5
414 Liriope	75.2	0.047	1.13	0.040	0.008	0.03	0.032	C	5
417 Suevia	43.3	0.17	1.12	0.123	0.01	0.05	0.013	KS	1 5
419 Aurelia	133	0.044	0.88	0.004	0.002	0.02	0.013	F	
420 Bertholda	146	0.038	0.92	0.165	0.005	0.02	0.014	P	
423 Diotima	217	0.038	0.97	0.026	0.002	0.02	0.019	C	5
429 Lotis	70.3	0.044	1.09	0.071	0.012	0.03	0.053	C?	2 3 5
431 Nephele	97.7	0.048	0.97	-0.012	0.002	0.02	0.028	C	5
434 Hungaria	10.0	0.46	0.96	0.113	0.04	0.02	0.012	E	4
442 Eichsfeldia	67.5	0.044	1.02	0.030	0.004	0.02	0.018	C	
443 Photographica	28.3	0.17	1.38	0.290	0.01	0.02	0.016	S	
444 Gyptis	170	0.044	0.98	-0.008	0.005	0.02	0.022	C	5
446 Aeternitas	43.0	0.35	1.65	0.248	0.08	0.03	0.025	A	3 5
449 Hamburga	88.6	0.031	1.08	0.061	0.001	0.03	0.019	C	5
451 Patientia	230	0.073	0.98	-0.060	0.013	0.02	0.019	C	5
462 Eriphyla	38.0	0.30	1.26	0.140	0.02	0.02	0.011	S	5
466 Tisiphone	121	0.056	1.00	-0.012	0.003	0.03	0.038	C	5
469 Argentina	129	0.030	0.92	0.059	0.001	0.02	0.007	C	5
470 Kilia	28.5	0.19	1.36	0.196	0.01	0.02	0.022	S	5
471 Papagena	139	0.20	1.32	0.087	0.01	0.02	0.017	S	
472 Roma	47.6	0.24	1.34	0.137	0.03	0.02	0.023	S	5
476 Hedwig	121	0.039	1.08	0.096	0.002	0.03	0.010	C	5
478 Tergeste	82.0	0.16	1.30	0.248	0.01	0.02	0.021	S	5
480 Hansa	58.0	0.17	1.30	0.094	0.02	0.02	0.011	S	
483 Seppina	73.5	0.13	1.27	0.248	0.01	0.02	0.015	S	
488 Kreusa	158	0.052	1.06	0.019	0.003	0.02	0.009	C	5
497 Iva	45.3	0.085	0.95	0.122	0.010	0.05	0.049	M	1 2 5
498 Tokio	84.8	0.073	1.13	0.128	0.005	0.02	0.018	T	5
499 Venusia	86.0	0.033	0.96	0.080	0.002	0.02	0.016	C	
506 Marion	109	0.044	1.04	0.062	0.002	0.02	0.034	C	5
508 Princetonia	147	0.039	1.06	-0.014	0.001	0.02	0.020	C	5

Asteroid	IRAS Diam.	IRAS p_V	U-V	v-x	σ_{p_V}	σ_{U-V}	σ_{v-x}	CLASS	Notes
509 Iolanda	59.0	0.20	1.24	0.099	0.01	0.02	0.026	S	
511 Davida	337	0.053	1.08	0.045	0.002	0.02	0.016	C	5
514 Armida	110	0.029	0.91	0.062	0.003	0.02	0.029	C	5
519 Sylvania	53.1	0.12	1.19	0.078	0.02	0.02	0.024	K	5
521 Brixia	121	0.036	1.06	0.049	0.002	0.02	0.016	C	5
522 Helga	113	0.027	0.91	0.028	0.009	0.02	0.034	CF	3
530 Turandot	89.3	0.043	0.95	-0.022	0.003	0.02	0.034	C	5
532 Herculina	231	0.16	1.26	0.120	0.01	0.02	0.023	S	
536 Merapi	158	0.042	0.97	0.070	0.005	0.02	0.028	C	5
551 Ortrud	81.2	0.041	0.97	0.012	0.006	0.02	0.031	C	5
554 Peraga	98.5	0.051	1.00	-0.005	0.002	0.02	0.022	C	5
556 Phyllis	39.5	0.21	1.24	0.165	0.01	0.03	0.021	S	5
558 Carmen	61.6	0.10	1.01	0.103	0.01	0.02	0.009	M	
559 Nanon	80.0	0.046	1.11	0.058	0.003	0.02	0.022	C	5
563 Suleika	54.8	0.21	1.32	0.160	0.01	0.02	0.028	S	5
566 Stereoskopia	175	0.032	1.00	0.041	0.003	0.02	0.020	C	
570 Kythera	106	0.052	1.15	0.209	0.003	0.02	0.025	I	
571 Dulcinea	44.5	0.019	1.31	0.110	0.002	0.03	0.029	r	5 6
579 Sidonia	89.6	0.17	1.24	0.191	0.01	0.02	0.008	S	
582 Olympia	47.0	0.19	1.45	0.243	0.03	0.05	0.025	S	1 5
583 Klotilde	86.0	0.052	0.97	0.013	0.006	0.03	0.013	C	5
584 Semiramis	56.2	0.17	1.40	0.113	0.01	0.02	0.044	S	2 5
593 Titania	78.2	0.053	0.97	0.041	0.005	0.02	0.018	C	5
599 Luisa	69.6	0.14	1.33	0.272	0.01	0.03	0.032	S	5
602 Marianna	130	0.045	1.04	0.018	0.003	0.02	0.011	C	
606 Brangane	40.0	0.076	1.16	0.222	0.008	0.05	0.023	TK	1 5
613 Ginevra	82.0	0.031	0.93	0.065	0.002	0.03	0.027	C	5
617 Patroclus	149	0.043	0.91	0.158	0.003	0.02	0.030	P	
618 Elfriede	124	0.058	1.02	0.066	0.007	0.02	0.025	C	5
626 Notburga	104	0.041	1.01	0.049	0.002	0.02	0.017	C	5
631 Philippina	60.5	0.12	1.31	0.159	0.01	0.02	0.017	S	5
635 Vundtia	100	0.042	1.00	0.043	0.003	0.02	0.027	C	
639 Latona	74.5	0.14	1.31	0.238	0.01	0.02	0.027	S	
640 Brambilla	84.8	0.063	1.22	-0.014	0.003	0.02	0.027	G?	5
648 Pippa	70.5	0.046	0.96	0.069	0.003	0.05	0.046	C	1 2 5
654 Zelinda	132	0.043	1.01	0.023	0.002	0.02	0.013	C	
660 Crescentia	44.2	0.15	1.32	0.204	0.01	0.02	0.021	S	5
661 Cloelia	52.0	0.091	1.21	0.151	0.009	0.02	0.009	K	5
663 Gerlinde	104	0.033	0.99	0.082	0.002	0.03	0.021	C	5
692 Hippodamia	47.7	0.18	1.29	0.121	0.02	0.02	0.045	S	2 5
695 Bella	51.2	0.16	1.28	0.120	0.01	0.03	0.017	S	5
702 Alauda	202	0.056	0.98	0.004	0.003	0.02	0.015	C	
704 Interamnia	333	0.064	0.90	-0.034	0.002	0.02	0.010	F	
705 Erminia	139	0.038	0.99	0.057	0.002	0.03	0.026	C	5
712 Boliviana	132	0.046	1.09	0.069	0.002	0.02	0.016	C	
713 Luscinia	109	0.041	0.94	0.002	0.003	0.02	0.036	C	5
714 Ulula	41.0	0.24	1.33	0.197	0.03	0.02	0.010	S	5
721 Tabora	82.6	0.050	1.02	0.252	0.010	0.02	0.031	D	
733 Mocia	92.0	0.049	0.97	0.023	0.009	0.02	0.021	C	
739 Mandeville	110	0.030	1.03	0.114	0.002	0.02	0.009	CP	

Asteroid	IRAS Diam.	IRAS p_V	U-V	v-x	σ_{p_V}	σ_{U-V}	σ_{v-x}	CLASS	Notes
740 Cantabia	94.5	0.049	1.03	0.076	0.002	0.02	0.026	C	5
746 Marlu	75.5	0.038	1.01	0.123	0.002	0.05	0.048	PC	1 2 5
748 Simeisa	107	0.039	0.90	0.148	0.002	0.02	0.023	P	
751 Faina	115	0.047	1.04	-0.032	0.002	0.02	0.019	C	5
757 Portlandia	34.0	0.11	0.93	0.093	0.01	0.03	0.025	M	5
762 Pulcova	142	0.032	0.96	-0.019	0.002	0.05	0.041	CF	1 2 5
771 Libera	30.5	0.14	0.91	0.111	0.01	0.05	0.036	M	1 5
772 Tanete	123	0.055	1.03	-0.003	0.003	0.03	0.032	C	5
773 Irmintraud	99.1	0.033	0.99	0.222	0.001	0.02	0.016	D	
778 Theobalda	67.3	0.057	0.88	-0.046	0.003	0.02	0.020	F	
785 Zwetana	52.1	0.13	0.82	0.068	0.01	0.02	0.007	m	
786 Bredichina	93.2	0.067	0.94	-0.006	0.012	0.02	0.014	C	
790 Pretoria	176	0.034	1.00	0.134	0.001	0.02	0.026	PC	5
791 Ani	107	0.029	0.99	0.022	0.001	0.02	0.044	C	2 5
804 Hispania	161	0.049	1.09	0.057	0.003	0.02	0.021	C	5
805 Hormuthia	73.0	0.043	0.98	0.002	0.003	0.03	0.037	C	5
838 Seraphina	63.1	0.039	1.02	0.145	0.002	0.03	0.036	PC	5
863 Benkoela	28.3	0.49	1.69	0.269	0.03	0.02	0.018	A	4
877 Walkure	39.6	0.047	0.88	-0.002	0.004	0.02	0.011	F	
907 Rhoda	65.8	0.057	0.98	0.009	0.003	0.02	0.028	C	5
909 Ulla	120	0.037	0.97	0.015	0.002	0.03	0.039	C	5
914 Palisana	79.0	0.084	1.09	0.099	0.004	0.02	0.018	T	
925 Alphonsina	57.0	0.23	1.26	0.147	0.03	0.02	0.017	S	5
937 Bethgea	27.5	0.049	1.47	0.241	0.005	0.03	0.028	r	5 6
980 Anacostia	89.0	0.17	1.45	0.329	0.01	0.02	0.021	S	
1001 Gaussia	78.3	0.044	0.96	0.073	0.005	0.02	0.019	C	
1021 Flammario	103	0.046	0.89	0.025	0.003	0.02	0.028	FC	
1028 Lydina	76.3	0.052	0.96	0.040	0.002	0.05	0.043	C	1 2 5
1103 Sequoia	6.1	0.48	0.97	0.075	0.040	0.02	0.021	E	4
1143 Odysseus	135	0.041	1.04	0.274	0.003	0.03	0.020	D	5
1146 Biarmia	34.5	0.17	0.91	0.099	0.01	0.02	0.025	M	5
1167 Dubiago	69.0	0.039	0.94	0.253	0.006	0.03	0.026	D	
1171 Rusthawelia	73.6	0.038	0.94	0.086	0.002	0.02	0.029	C	5
1172 Aneas	151	0.038	0.99	0.235	0.002	0.02	0.037	DP	
1177 Gonnessia	95.5	0.039	0.91	0.122	0.002	0.03	0.038	PC	5
1212 Francette	90.7	0.038	0.92	0.190	0.005	0.02	0.015	P	
1245 Calvinia	28.3	0.20	1.27	0.088	0.02	0.02	0.025	S	5
1251 Hedera	15.0	0.41	0.97	0.091	0.03	0.03	0.035	E	4
1256 Normannia	78.0	0.039	0.97	0.260	0.003	0.02	0.018	D	
1266 Tone	76.0	0.060	1.07	0.083	0.009	0.03	0.037	C?	
1268 Libya	97.5	0.040	0.90	0.061	0.002	0.02	0.033	CF	
1269 Rollandia	109	0.047	1.04	0.264	0.002	0.03	0.026	D	5
1390 Abastumani	104	0.033	0.92	0.079	0.002	0.03	0.037	C	5
1467 Mashona	112	0.054	1.10	0.028	0.006	0.03	0.038	C	5
1512 Oulu	90.0	0.032	0.92	0.173	0.001	0.03	0.037	PD	5
1583 Antilochus	109	0.051	0.99	0.279	0.003	0.02	0.032	D	5
1693 Hertzsprung	39.5	0.044	1.07	-0.002	0.006	0.03	0.040	C	5
1796 Riga	76.5	0.041	0.97	0.095	0.003	0.03	0.045	CP	2 5
1867 Deiphobus	131	0.037	0.96	0.290	0.002	0.02	0.023	D	
1902 Shaposhnikov	101	0.028	0.89	0.127	0.002	0.03	0.020	PC	

Asteroid	IRAS Diam.	IRAS p_V	U-V	v-x	σ_{p_V}	σ_{U-V}	σ_{v-x}	CLASS	Notes
1911 Schubart	83.0	0.023	0.92	0.106	0.001	0.03	0.053	CP	2 5
1963 Bezovec	46.5	0.036	1.07	0.018	0.002	0.03	0.030	C	5
2241 1979 WM	123	0.040	0.95	0.300	0.003	0.02	0.023	D	
2311 El Leoncito	61.0	0.029	0.96	0.285	0.005	0.05	0.034	D	1 5
2357 Phereclos	103	0.042	0.95	0.321	0.004	0.03	0.035	D	
2674 Pandarus	102	0.041	1.01	0.306	0.003	0.03	0.025	D	
2760 Kacha	62.6	0.043	0.98	0.163	0.003	0.02	0.010	P	

Notes: 1. σU-$V > 0.03$ mag.
2. σv-$x > 0.04$ mag.
3. $\sigma pv > 20\%$
4. pv and Diam. from Gradie and Tedesco (1989).
5. Single eight-color observation (cf., Zellner et al. 1985).
6. Single IRAS observation (cf., *IRAS Asteroid and Comet Survey,* 1986 or the tabulation contribution containing magnitudes, *UBV* colors, and IRAS albedos and diameters).

ASTEROID LIGHTCURVE PARAMETERS

C.-I. LAGERKVIST
Astronomiska Observatoriet

A. W. HARRIS
Jet Propulsion Laboratory

and

V. ZAPPALÀ
Osservatorio Astronomico di Torino

The lightcurve data file consists of three parts: this explanatory introduction, the asteroid list with footnotes at the end, and the reference list. The reference list is numbered and sorted by first author plus date. Each citation includes the year, all authors, journal or book name, volume and first and last page numbers. The asteroid list is ordered by asteroid number, followed by the asteroid name, the period in hours, amplitude of variation or range of amplitude observed, and a reliability code as follows:

1. Very tentative result, may be completely wrong.
2. Reasonably secure result, based on over half coverage of the lightcurve.
3. Secure result, full lightcurve coverage, no ambiguity of period.
4. Multiple apparition coverage, pole position reported.

Following the reliability code is a space for remarks, with the following meanings:

3 Number of extrema per rotation cycle (e.g., 1, 3). Unless otherwise noted, two per cycle is assumed.

A Ambiguous period. The "most likely" period is listed, with other possibilities listed in a footnote ordered by asteroid number, below.

D Rotation period "determined" from published data, but not given by author(s) of original data.

F Footnote, below, ordered by asteroid number, containing additional information.

N No lightcurve published.

P Photographic photometry.

V Visual photometry.

Following the remarks columns, all references to the asteroid are cited, by number from the reference list, in chronological order. That is, the last few citations are the most recent, and should therefore be the most useful for evaluating the current state of knowledge of a given asteroid.

Asteroid Lightcurve List Updated 1 December, 1987.

	Period	Amplitude	Q	Notes	References						
1 Ceres	9.075	0.04	3		12	1	75	194	237	34	24
2 Pallas	7.811	0.03-0.16	4		83	33	270	23	101	141	22
					34	25	30	16	282	26	26
					144	127					
3 Juno	7.210	0.14-0.22	4		83	32	75	221	282	144	6
4 Vesta	5.342	0.12	4	F	227	40	82	100	31	32	7
					236	237	53	55	21	73	14
					146	144	127	151			
5 Astraea	16.812	0.10-0.30	4		161	32	75	239	162	285	15
6 Hebe	7.274	0.05-0.20	4		12	1	271	265	79	292	5
					144						
7 Iris	7.139	0.04-0.29	4		82	258	75	33	238	292	12
					285	127					
8 Flora	12.790	0.02-0.10	2		161	173	1	258	264	280	29
					261	106					
9 Metis	5.078	0.04-0.36	4	F	82	83	32	75	257	271	20
					287	57	282	61	267	151	
10 Hygiea	18.4	0.09-0.18	2		83	261	128				
11 Parthenope	7.83	0.07-0.12	2		12	258	270	280	7		
12 Victoria	8.654	0.08-0.33	3		252	26	261				
13 Egeria	7.045	0.12	3		33						
14 Irene	9.35	0.04-0.1	2		12	173	83	265	188	34	
15 Eunomia	6.083	0.4 -0.56	4		82	258	31	257	176	34	16
					126	144	149	127	267		
16 Psyche	4.196	0.03-0.42	4		12	258	237	130	34	133	29
					250	282	292	251	293	126	14
					127	267					
17 Thetis	12.275	0.13-0.36	4		82	258	129	285			
18 Melpomene	11.572	0.22-0.35	3		75	13	34	261	287	126	12
19 Fortuna	7.445	0.22-0.35	3		271	259	131	128	267		
20 Massalia	8.098	0.17-0.27	4		12	74	32	75	134	292	
					146	144					
21 Lutetia	8.167	0.15-0.25	3		33	136	281	138			
22 Kalliope	4.147	0.04-0.30	4		1	75	182	273	133	4	29
					282	144	233	152	267		
23 Thalia	12.308	0.10-0.18	2		271	259	93	288	261		
24 Themis	8.38	0.10-0.14	3		55	247	259	93			
25 Phocaea	9.945	0.18	3		12	82	258				
26 Proserpina	10.60	0.15	2	A	185	34					
27 Euterpe	8.500	0.15	3		32						
28 Bellona	15.695	0.03-0.28	4		259	93	282				
29 Amphitrite	5.390	0.01-0.15	4		33	44	259	248	131	145	28
					144	150	267				
30 Urania	13.686	0.14-0.45	3		3	12	173	75	91		
31 Euphrosyne	5.531	0.09-0.13	4		203	7	146				
32 Pomona	9.443	0.13-0.30	4		193	34	285	61			
33 Polyhymnia	18.601	0.14	3		276						
34 Circe	>12.	>0.25	2		261	128					
35 Leukothea					128						
36 Atalante	9.93	0.15-0.17	3		91	209	61				
37 Fides	7.332	0.10-0.25	4		183	208	277	288	144		
38 Leda		>0.08		N	93						
39 Laetitia	5.138	0.08-0.53	4		12	82	83	258	75	271	26
					34	145	282	146	261	144	26
40 Harmonia	9.136	0.22	3		75	111	146				
41 Daphne	5.988	0.16-0.38	4		180	5	7	144	285	267	
42 Isis	13.59	0.29-0.32	3		89	51	261				
43 Ariadne	5.751	0.13-0.66	4		24	140	259	145	57	8	6
44 Nysa	6.422	0.22-0.55	4		10	11	161	173	83	224	3
					271	273	20	164	93	143	24
					144	61	127				
45 Eugenia	5.699	0.08-0.41	3		89	48	52	267			
46 Hestia	21.04	0.11	3		187						
47 Aglaja	13.	<0.05-0.20	1		46	93	29				
48 Doris	11.89	0.35	3		91	209	51				
49 Pales	10.42	0.15-0.20	3		247	199					
50 Virginia	>24.	>0.15	1		91						
51 Nemausa	7.785	0.14-0.25	3	3	33	265	71	72	61		

		Period	Amplitude	Q	Notes	References					
52	Europa	5.631	0.09-0.10	4		179	279	8			
53	Kalypso	26.56	>0.1	2		93	50	231			
54	Alexandra	7.04	0.12	2		259	104	61			
55	Pandora	4.804	0.07-0.33	4		197	7	57	285	61	267
56	Melete	13.7	0.06	2	A	89					
59	Elpis	13.69	0.1	3		45					
60	Echo	25.208	0.22	3		75	93	280	68	261	287
61	Danae	11.45	0.30	3		270					
63	Ausonia	9.298	0.15-0.95	4		173	181	117	280	57	282 14
						138					
64	Angelina	8.752	0.05-0.44	3		116	170				
65	Cybele	6.07	0.04-0.12	3		203	267				
67	Asia	15.89	0.23	3		91					
68	Leto	14.848	0.15-0.19	3	3	91	230				
69	Hesperia	5.655	0.20	3		171	61				
70	Panopaea	15.87	0.12	2		222					
71	Niobe	11.21	0.12	1		140	7				
74	Galatea	9.0	0.14	2		91					
75	Eurydike	8.92	0.12	2	3	114	280				
76	Freia	9.98	0.15-0.2	3		125	128				
77	Frigga	9.012	0.07-0.19	3		122	280				
78	Diana	8.	0.14	2		237	280				
79	Eurynome	5.979	0.05-0.24	3		177	192	7	57		
80	Sappho	14.05	0.07-0.37	3		183	93	26			
82	Alkmene	12.999	0.40-0.54	3		95					
83	Beatrix	10.16	0.18-0.27	3		280	102				
85	Io	6.875	0.15	3		271	118				
86	Semele	16.634	0.18	3		231					
87	Sylvia	5.183	0.30-0.62	3		202	91	267			
88	Thisbe	6.042	0.08-0.21	4		199	37	57	285	267	61 15
89	Julia	11.387	0.10-0.25	3		263	189	261			
91	Aegina	6.025	0.15	3		91					
92	Undina	15.94	0.17	3		199					
93	Minerva	5.97	0.10	2		51	156				
94	Aurora	7.22	0.12	3		93	60				
95	Arethusa	8.688	0.24	3		93	29				
97	Klotho	35.	0.07-0.25	3		12	82	183	93		
99	Dike	>24.	>0.25	1		103					
100	Hekate	>10.	>0.05	1	D	247					
101	Helena	23.16	0.13	2		119					
103	Hera	23.74	0.42	2		89	93				
104	Klymene	9.	>0.2	2		247					
105	Artemis	>24.	>0.1	1		247	51	218			
107	Camilla	4.840	0.32-0.52	3		60	267				
108	Hecuba		0.2	1	V	3					
109	Felicitas	26.3	>0.06	1		280					
110	Lydia	10.927	0.10-0.20	3		235	134				
111	Ate	22.2	0.1	2		93					
113	Amalthea	9.935	0.19-0.26	3		93	231	261			
114	Kassandra	20.	>0.17	1	N	93					
115	Thyra	7.241	0.14-0.20	3		187	34	88	146		
116	Sirona	12.028	0.42	3		3	91	287			
118	Peitho	7.78	0.33	3		226					
120	Lachesis	>20.	>0.1	1		52					
121	Hermione	6.1	0.03	1		44	61				
123	Brunhild	10.04	0.16	3		7					
124	Alkeste	9.921	0.15	3		93					
125	Liberatrix	3.969	0.29-0.71	3		247	275	123	125	267	
128	Nemesis	39.	0.10	3		43	184				
129	Antigone	4.957	0.21-0.49	4		180	57	7	261	144	61 26
130	Elektra	5.225	0.19-0.58	3		267					
133	Cyrene	12.708	0.26	3		96	116				
135	Hertha	8.40	0.15-0.30	3		91	117	93	125		
136	Austria	11.5	>0.40	3		211					
137	Meliboea	>20.	>0.15	1		93	280				
138	Tolosa		>0.28			261					
139	Juewa	41.8	0.18	2	A	81	49	102			
140	Siwa	>22.	>0.05	1		201	91				
144	Vibilia	13.810	0.13	3		280					
145	Adeona	8.1	0.08	2		93	51	26			
146	Lucina	18.54	0.08	3		93	213				

	Period	Amplitude	Q	Notes	References						
147 Protogeneia					128						
148 Gallia	20.664	0.32	3		229						
150 Nuwa	8.14	0.09	2		58						
152 Atala	5.282	0.50	3		209						
156 Xanthippe	22.5	0.12	3		50						
158 Koronis	14.18	0.32	3		19						
161 Athor	7.288	0.1 -0.27	3		49	30					
162 Laurentia	12.98	0.29	3		234	261					
164 Eva	13.66	0.07-0.36	3		195	207					
165 Loreley	7.6	0.12	2	N	215						
167 Urda	16.	0.24	2		247						
171 Ophelia	13.4	0.16	2		247						
173 Ino	5.93	0.04-0.11	3		197	57					
179 Klytaemnestra	11.173	0.35	3		93						
181 Eucharis	>7.	>0.08	1		57						
182 Elsa	80.	0.7	2		90						
183 Istria	11.77	0.31	3		93						
184 Dejopeja	6.7	0.25	2		247						
185 Eunike	10.83	>0.12	3		44						
186 Celuta	19.6	0.4	2		3	111	112				
192 Nausikaa	13.622	0.20-0.40	4		271	177					
194 Prokne	15.67	0.27	2		185						
196 Philomela	8.333	0.07-0.33	3		271	280					
197 Arete	6.54	0.10	3		60						
200 Dynamene	19.	0.10	2		196						
201 Penelope	3.747	0.15-0.73	3		120	121	232	60 163 267			
203 Pompeja	46.6	>0.10	2		58						
208 Lacrimosa	13.5	0.15	2		19						
209 Dido	8.	0.20	2		247						
211 Isolda		>0.07			280						
213 Lilaea	7.85	0.07	2		290						
214 Aschera	6.835	0.22	3		93						
216 Kleopatra	5.385	0.13-1.18	4		183	254	84 107 167 278	3			
					144	138	267				
218 Bianca	6.43	0.22	2		28						
219 Thusnelda	29.76	0.20	3		124						
221 Eos	10.436	0.04-0.11	4		91	93					
222 Lucia	7.	0.33	2		247						
224 Oceana	18.933	0.10	2		91	93					
230 Athamantis	23.99	0.2	2		271	287					
233 Asterope	19.70	0.35	3		93						
234 Barbara	26.5	>0.24	2		204	93					
235 Carolina	17.56	>0.25	2		222						
236 Honoria	12.34	0.08-0.15	2		93	128					
238 Hypatia	8.9	0.12	3		211						
243 Ida	4.65	0.45	3		19						
245 Vera	14.38	0.26	3		51						
246 Asporina	16.222	0.40	3		93						
247 Eukrate	12.10	0.10	2		202	91					
248 Lameia	12.00	0.10	2		19						
249 Ilsie	85.24	0.33	1	A	15	19					
250 Bettina	5.105	0.33-0.60	3		121	57 125					
254 Augusta	6.0	0.56	2	P	111						
255 Oppavia					128						
261 Prymno	8.00	0.20	3	N	93						
263 Dresda	14.32	0.32	2		19						
267 Tirza	5.9	0.4	2	P	111						
268 Adorea	6.1	0.15	1		247	28					
270 Anahita	15.06	0.32	3		183	91					
273 Atropos	20.	0.65	2		247						
276 Adelheid		>0.6?	1	N	30						
277 Elvira	30.	0.45	2		19						
280 Philia	64.	0.19	1		19						
281 Lucretia	4.348	0.38	4		237						
282 Clorinde	6.42	0.09	3		15						
283 Emma	6.888	0.31	3		225						
287 Nephthys	7.603	0.20	2		185	93					
288 Glauke	1150.	>0.6	2	F	94	19					
291 Alice	4.32	0.15-0.25	3		108	15					
292 Ludovica	8.93	0.45	3		19						
302 Clarissa	>10.	>0.3	1	P	111						

		Period	Amplitude	Q Notes		References						
304	Olga	18.36	0.20	3		92						
306	Unitas	8.75	0.26	3		93						
308	Polyxo	12.032	0.20	3		47	93					
311	Claudia	11.48	0.32	2		19						
313	Chaldaea	10.08	0.17-0.23	2		183	50					
317	Roxane	8.16	0.67	3		123						
321	Florentina	2.870	0.36-0.40	3		258						
322	Phaeo		>0.07	N		93						
323	Brucia	10.	0.36	2		247						
324	Bamberga	29.43	0.07	3		75	186					
328	Gudrun	>12.	0.15	1 PN		111						
332	Siri	7.0	0.32	2 P		111						
335	Roberta	8.03	0.05	2		19						
336	Lacaderia	13.70	0.34	3		58						
337	Devosa	4.610	0.08-0.75	3 3		198	19	128	267			
338	Budrosa		>0.05			128						
340	Eduarda	7.7	0.17	2 P		111						
343	Ostara	6.42	0.23	1		19						
344	Desiderata	10.53	0.17	3		93	7	42				
345	Tercidina	12.371	0.15	3		3	93					
349	Dembowska	4.701	0.08-0.47	4		33	55	247	274	102	146	14
						61	138	267				
352	Gisela	6.7	0.25	2 P		111						
354	Eleonora	4.277	0.12-0.30	4		173	83	33	274	132	282	2
356	Liguria	31.82	0.22	3		91						
357	Ninina	>20.	0.08	1		247						
359	Georgia	7.3	0.3	2 P		111						
360	Carlova	6.183	0.30-0.37	3		93	60					
362	Havnia	18.	0.1	2		91						
363	Padua	>10.	>0.3	2 P		111						
364	Isara	9.155	0.40	3		271						
369	Aeria	14.	0.02	1 N		119	125	217				
372	Palma	6.58	0.12	2 1A		280	104					
375	Ursula	16.83	0.05-0.17	2		215	155	219				
376	Geometria	7.74	0.16-0.18	3		7	290					
377	Campania	15.	0.16	2		247	128					
379	Huenna	6.6	0.06	1		247						
382	Dodona	4.116	0.39-0.42	3		59	125					
383	Janina	6.4	0.17	3		247						
385	Ilmatar	62.35	0.50	3		289						
386	Siegena	9.763	0.11	3		276	93					
387	Aquitania	24.0	>0.09	2 A		200	7					
389	Industria	11.	0.15	1		102						
393	Lampetia	38.7	0.14	2 A		184						
396	Aeolia	>12.	>0.3	1 P		111						
397	Vienna	15.48	0.20	3		93						
404	Arsinoe	8.93	0.36	3		206	261					
405	Thia	10.08	0.15	3		91						
409	Aspasia	9.03	0.10-0.14	3		117	87	56	283			
410	Chloris	32.50	0.28	3		93	213					
416	Vaticana		>0.19			128						
418	Alemannia	5.82	0.14	1		128						
419	Aurelia		>0.1			93	128					
422	Berolina	>15.0	0.15	1 N		214	56	283	285			
423	Diotima	4.622	0.06-0.18	4		214	56	283	285			
431	Nephele		<0.02			29						
432	Pythia	8.287	0.15	3		119						
433	Eros	5.270	0.05-1.5	4		3	27	174	9	35	36	3
						153	159	169	178	244	241	
434	Hungaria	26.51	0.70	3		93						
437	Rhodia	56.	0.38	1		7	19					
439	Ohio	19.2	0.24	2 1A		128						
441	Bathilda	10.35	0.13	2		91						
444	Gyptis	6.214	0.15	3		95						
451	Patientia	9.727	0.05-0.10	4		237	93	60	285			
454	Mathesis	7.7	0.37	2 P		111						
458	Hercynia	22.3	0.33	2		19						
459	Signe	6.38	0.25	2 P		111						
462	Eriphyla	8.6	0.23	2		19						
464	Megaira		>0.06	N		93						
468	Lina	8.3	0.10	1		247						

	Period	Amplitude	Q	Notes	References
470 Kilia		<0.2	1	P	256
471 Papagena	7.113	0.11-0.13	3		142 183 228 57
476 Hedwig	27.33	0.13	3		216
484 Pittsburghia	10.63	0.33	3		19
485 Genua	17.59	0.12	3		28
495 Eulalia	29.2	0.30	4		19
497 Iva	4.620	0.38-0.50	3		93
502 Sigune	10.5	0.35	2		247
505 Cava	8.180	0.23	3		111 91 272
510 Mabella	19.5	0.3	1	N	93
511 Davida	5.130	0.06-0.25	4		82 75 33 257 261 60 28
512 Taurinensis	5.582	0.21	3		124
513 Centesima	5.23	0.45	3		247
514 Armida	>20.	>0.3	1	P	111
516 Amherstia	7.49	0.15-0.48	3		91 128
520 Franziska	14.0	0.51	2		19
521 Brixia	>24.	>0.09	1		231
529 Preziosa	27.	0.56	2		19
532 Herculina	9.405	0.08-0.18	4		173 83 33 89 41 62 24
534 Nassovia	9.39	0.35-0.37	3		247 19
545 Messalina	7.2	0.22	3		58
554 Peraga	13.63	0.22	3		185
556 Phyllis	4.28	0.24	3		280
558 Carmen	10.	0.25	2		89
562 Salome	10.4	0.14	1		19
563 Suleika	5.69	0.13-0.21	3		230 61
579 Sidonia	16.50	0.02-0.28	4		247 19
584 Semiramis	5.068	0.18-0.44	3		267
588 Achilles					115
590 Tomyris	5.562	0.21	3		19
591 Irmgard	7.35	0.26	3		128
593 Titania	9.89	0.24	3		280
599 Luisa	9.566	0.18	3		43
600 Musa	5.92	0.28	3		19
619 Triberga	13.95	0.30	2		19
621 Werdandi	>10.	>0.4	1	P	111
622 Esther	47.5	>0.6	2		280
624 Hektor	6.921	0.1 -1.1	4		63 99 143 282 144
628 Christine	>14.	>0.4	1		206
631 Philippina	5.92	0.20	3		213
632 Pyrrha	4.6	0.4	1	PD	111
633 Zelima	10.	>0.26	1	PN	111
639 Latona	6.22	0.35	2		19
641 Agnes	8.9	0.18	1	P	111
644 Cosima	15.13	0.16	1		19
645 Agrippina	32.6	0.18	2		19
653 Berenike	14.14	0.08	2		19
654 Zelinda	31.9	0.3	2		191
657 Gunlod	15.7	0.20	2		166 19
658 Asteria	28.	0.32	1		19
660 Crescentia	7.92	0.33	3		91
674 Rachele	16.66	0.15	1		91 280 289
675 Ludmilla	7.717	0.28-0.38	3		190 34
677 Aaltje	>10.	<0.1		P	111
679 Pax	7.625	0.07	3		205
683 Lanzia	4.322	0.12	2	A	28
684 Hildburg	11.92	0.23	2		19
688 Melanie		<0.05			19
694 Ekard	5.925	0.50	3		286 287 267
699 Hela	3.656	0.60	3		168 19
700 Auravictrix	6.0	0.4	2	P	114
702 Alauda	8.36	0.07-0.10	2		93 60 163
704 Interamnia	8.727	0.03-0.11	4	F	271 253 141
709 Fringilla	52.4	0.18	3		91
712 Boliviana	11.87	0.11	2		280
716 Berkeley	>17.	>0.2	1	P	113
720 Bohlinia	14.49	0.16	2		19
726 Joella	13.04	0.12	3		15
736 Harvard	6.7	0.32	3		247 55
737 Arequipa	14.13	0.15	3		91
739 Mandeville	15.9	0.15	2		280

	Period	Amplitude	Q	Notes	References
747 Winchester	9.40	0.13	3		91 280 261
753 Tiflis	9.85	0.35-0.8	3		256 19
766 Moguntia	3.446	0.23	3		19
771 Libera	5.92	0.53	3		19
775 Lumiere	6.96	0.25	3		19
776 Berbericia	7.672	0.13-0.23	2		200 52 61
778 Theobalda	11.659	0.18	3		15
790 Pretoria	10.37	0.16	3		201
792 Metcalfia	9.17	0.62	3		28
796 Sarita	7.75	0.29	3		205
800 Kressmannia	4.464	0.20	3		59
804 Hispania	7.42	0.19	2	A	93 52
807 Ceraskia	7.4	0.25	2		19
811 Nauheima	5.58	0.20	3		19
814 Tauris	35.8	0.20	2		52
832 Karin	18.82	0.32	3		19
838 Seraphina	16.2	0.30	2		19
841 Arabella	3.39	0.26	3		15
846 Lipperta	>24.	>0.02			247
852 Wladilena	4.56	0.31	3		247 57
853 Nansenia	9.31	0.13	2		19
856 Backlunda	12.08	0.29	2		19
873 Mechthild	10.6	0.33	2	P	111
876 Scott	>14.	>0.3		P	115
877 Walkure	17.49	0.40	2		19
887 Alinda	73.97	0.35	2		67
900 Rosalinde	16.5	0.52	2		19
905 Universitas	10.	0.22	2		247
908 Buda	18.20	0.09	2		19
911 Agamemnon	7.	0.2 -0.4	1	N	63 234
914 Palisana	>14.	<0.02	1		247
916 America	38.	0.28	1		59
925 Alphonsina	7.92	0.18	2		86
939 Isberga	>20.	>0.2	1		247
944 Hidalgo	10.064	0.35-0.60	3	F	245 55
952 Caia	7.51	0.13	2		226 91
974 Lioba	38.7	0.37	3		19
980 Anacostia	21.	0.1	2		147
984 Gretia	5.781	0.4 -0.63	3		256 58
987 Wallia	10.	>0.3	1	P	114
994 Otthild	5.95	0.13	2		19
1012 Sarema	10.32	0.81	3		19
1018 Arnolda	11.97	0.42	1		19
1029 La Plata	15.37	0.44-0.53	2		111 19
1036 Ganymed	10.308	0.45	3		97 105 139
1057 Wanda	28.8	0.41	2		19
1058 Grubba	>18.	>0.10			261
1062 Ljuba	36.	0.20	1		19
1063 Aquilegia	5.79	0.93	2		19
1067 Lunaria	7.74	0.13	2		19
1068 Nofretete	6.15	0.04	2		19
1076 Viola	7.336	0.12	3		15
1078 Mentha				N	15
1079 Mimosa	7.3	0.10	1		19
1084 Tamariwa	7.08	0.27	2		19
1092 Lilium	17.63	0.16	1		19
1095 Tulipa	2.77	0.21	3		19
1111 Reinmuthia	4.02	0.61	3		19
1129 Neujmina	7.61	0.06	2		19
1137 Raissa	37.	0.34	1		19
1149 Volga	27.5	0.26	2		19
1159 Granada	31.	0.28	2		19
1168 Brandia	11.444	0.62	3		19
1173 Anchises	11.60	0.57	3		69
1178 Irmela	19.17	0.34	2		19
1192 Prisma	6.558	0.85	3		15
1196 Sheba	7.08	0.21	2		19
1197 Rhodesia	15.89	0.22	2		19
1207 Ostenia	8.4	0.5 -0.7	2	P	111 114
1208 Troilus	>24.	>0.2			69
1210 Morosovia	15.3	0.53	3		59
1212 Francette	>16.	>0.03	1		237
1219 Britta	5.575	0.60-0.70	3		18

	Period	Amplitude	Q	Notes	References
1220 Crocus	737.	0.87	2	F	17 19
1223 Neckar	8.78	0.20-0.45	3		247 19
1224 Fantasia	>12.	0.06	1		7
1234 Elyna	17.6	0.16	1		19
1236 Thais	>72.	>0.08			212
1237 Genevieve	16.37	0.23	3		19
1240 Centenaria	14.	0.08	1		58
1245 Calvinia	4.855	0.63	3		111 113 247 55
1250 Galanthus	3.92	0.28	3		15
1257 Mora	5.28	0.43	3		19
1259 Ogyalla	12.	>0.3	1	PD	111
1262 Sniadeckia	17.57	0.16	3		19
1267 Geertruida	5.50	0.5	2	P	114
1279 Uganda	23.2	0.16	1		19
1284 Latvia	>18.	>0.1	1		15
1288 Santa	8.28	0.46	2		19
1289 Kutaissi	3.60	0.40	3		19
1291 Phryne	5.55	0.86	3		19
1305 Pongola	8.03	0.18	2		19
1317 Silvretta	7.048	0.30	3		212
1321 Majuba	6.78	>0.43	2		19
1331 Solvejg	>10.	>0.3	1	P	111
1337 Gerarda	12.52	0.23	2		19
1346 Gotha	11.19	0.12	2		19
1350 Rosselia	6.0	0.3	2	P	111
1362 Griqua	7.	0.20	1	D	237
1366 Piccolo	16.57	0.33	2		19
1368 Numidia	3.64	0.35	3		19
1379 Lomonsowa	24.71	>0.51	2		19
1389 Onnie	22.5	0.34	2		19
1397 Umtata	30.	0.13	1		19
1416 Renauxa	4.3	0.4	2	PD	111
1434 Margot	8.17	0.52	3		19
1437 Diomedes	18.	0.35-0.42	1	N	63 234
1468 Zomba	2.77	0.3	2		268
1478 Vihuri	19.5	0.23	1		19
1481 Tubingia	160.	0.55	1		19
1482 Sebastiana	10.45	0.70	3		19
1504 Lappeenranta	10.44	0.29	2		19
1513 Matra	>24.	>0.1	1		15
1522 Kokkola	5.83	0.29	3		19
1523 Pieksamaki	5.33	0.5	2	P	114
1533 Saimaa	7.08	0.18	3		19
1562 Gondolatsch	8.2	0.4	2	P	114
1566 Icarus	2.273	0.05-0.22	4		158 77 262
1576 Fabiola	6.7	0.2	2	P	111
1580 Betulia	6.130	0.21-0.50	4 3		2 110 246
1584 Fuji	10.	0.30	1		247
1585 Union	9.38	0.22	2		19
1590 Tsiolkovskaja	6.7	0.4	2	P	111
1604 Tombaugh	7.04	0.20	2		111 19
1609 Brenda	19.46	0.16	2		19
1615 Bardwell	>18.	>0.2	1	D	247
1620 Geographos	5.223	1.10-2.03	4		65
1627 Ivar	4.798	0.35	3		97 137
1628 Strobel	11.80	0.22	2		19
1641 Tana	6.01	0.33	2		19
1646 Rosseland	69.2	0.13	2		15
1670 Minnaert	3.79	0.25	2		19
1672 Gezelle		>0.2			111
1674 Groeneveld	8.1	0.19	2		247
1685 Toro	10.196	0.6 -0.8	4		64
1687 Glarona	6.3	0.75	3		247
1689 Floris-Jan	145.	0.4	3		210
1707 Chantal	>10.	>0.2		PN	111
1709 Ukraina	7.28	0.62	3		19
1715 Salli	>11.	>0.5	1	P	111
1722 Goffin	31.	0.63	3		19
1723 Klemola	5.57	0.22	3		19
1727 Mette	2.63	0.3	2		268
1742 Schaifers	8.56	1.46	3		19
1743 Schmidt	17.45	0.36	3		19

	Period	Amplitude	Q	Notes		References	
1753 Mieke	8.8	0.2	2	P	111		
1757 Porvoo	4.89	0.30	3		15		
1759 Kienle	29.25	0.30	2		15		
1772 Gagarin	10.96	0.24	2		19		
1780 Kippes	18.0	0.23	2		19		
1789 Dobrovolsky	5.8	0.7	2	P	111		
1793 Zoya	7.0	0.4	2	P	111		
1862 Apollo	3.065	0.15-0.60	4		85	98	
1863 Antinous	4.02	0.12	1		19		
1864 Daedalus	8.57	0.85	3		78		
1867 Deiphobus	>24.	>0.1			69		
1892 Lucienne	9.31	0.42	2		19		
1915 Quetzalcoatl	4.9	0.26	2		14		
1928 Summa	9.66	>0.14	1		19		
1946 1931 PH	10.223	0.6	2	P	255		
1957 Angara	3.67	0.52	3		19		
1960 Guisan	8.46	0.52	3		19		
1972 Yi Zing	14.183	0.18	2		18		
2061 Anza	11.50	0.3	2		172		
2072 Kosmodemyanska	4.4	0.09	2		15		
2088 Sahlia	10.37	0.12	2		15		
2100 Ra-shalom	19.79	0.3	3		160		
2109 Dhotel	32.	0.3	1		15		
2113 Ehrdni	13.2	0.22	1		19		
2156 Kate	5.62	0.60	3		15		
2159 Kukkamaki	4.06	0.32	3		115	19	
2167 Erin	7.0	0.3	2	P	111		
2201 Oljato	24.	>0.1	1		93		
2317 Galya	2.60	0.24	2		19		
2339 2509 P-L	>24.	>0.05	1		19		
2368 Beltrovata	5.9	0.84	2	N	22		
2608 Seneca	8.	0.5	2		54	223	
2674 Pandarus	8.480	0.58	3		69		
2687 1982 HG	21.75	0.19	2		19		
2744 Birgitta	9.02	0.4	2	P	109		
3103 1982 BB	5.71	0.9	3		269		
3199 Nefertiti	2.82	0.12	2		97	269	
3288 Seleucus	>16.	>0.4	1		52		
3551 1983 RD	4.930	0.11-0.15	2		97	19 269	
3552 1983 SA	3.	>0.41	1	A	19		
76EB 1976 EB	7.7	0.31	2	P	111		
78CA 1978 CA	3.756	0.8	3		54	223	
78EC 1978 EC		<0.2		P	115		
78ED 1978 ED	>12.	>0.3	1	P	115		
78EE 1978 EE				P	115		
78EF 1978 EF	6.2	0.2	1	P	115		
79VA 1979 VA	3.556	0.06	1		93		
82XB 1982 XB	9.012	0.20	3		97	19	
84KD 1984 KD	2.4	0.26	2		287	97	
86DA 1986 DA	3.58	0.32	3		269		
86JK 1986 JK		0.05			269		
86RA 1986 RA		0.02			269		

FOOTNOTES AND ALTERNATE VALUES FOR AMBIGUOUS PERIODS

4 Degewij and Zellner (1978) and Degewij et al. (1979) show that varia-
tion is primarily due to albedo and not due to shape. Taylor (1985)
found no asymmetry in the 10-hr lightcurve as claimed by Taylor (1973)
when he reobserved at similar aspect. Magnusson (1986) obtains a bet-
ter solution for the pole position of Vesta with a 5-hr period than with a
10-hr period.

9 Correct period is 5.079 hr. Other values resulted from cycle errors in compositing lightcurves.

26 $P = 10.60$ or 13.13 hr.

56 $P = 13.7$ or 19.0 hr.

139 $P = 20.9$ or 41.8 hr.

249 $P = 42.62$ or 85.24 hr.

288 Period may be a precession period (see 1220 footnote).

372 $P = 6.58, 8.67$ or 12.83 hr.

387 $P = 16.0, 24.0$ or 48.0 hr.

393 $P = 19.35$ or 38.7 hr.

439 $P = 19.2$ or 38.4 hr.

683 $P = 4.3, 5.3$ or 8.6 hr.

704 Pole position inferred from YANG 65 observation.

804 $P = 7.42$ or 14.851 hr.

944 Accurate period quoted by Tedesco (in *Asteroids,* ed. T. Gehrels, Tucson: Univ. Ariz. Press, pp 1098–1107).

1220 A modulation of $P = 7.90$ hr, Ampl $= 0.15$ mag was observed near minimum light of the longer-period variation. Binzel (1984) interprets this as the real rotation period, with the long period being a precession period caused by an unseen satellite. 288 Glauke may be another case of the same phenomenon.

3552 $P = 3$ or 7 hr.

Lightcurve Reference List, Updated 1 December, 1987.

1   Ahmad, I.I.: 1954, Astrophys. J. 120, 551–560.
2   Austin, R.D.: 1976, Southern Stars 26, 228–230.
3   Bailey, S.J.: 1913, Ann Harvard Coll. Obs. 72, 165–189.
4   Barucci, M.A., Dipaoloantonio, A.: 1983, Astron. Astrophys. 117, 1–2.
5   Barucci, M.A.: 1983, Astron. Astrophys. Suppl. Ser. 54, 471–473.
6   Barucci, M.A., Di Martino, M.: 1984, Astron. Astrophys. Suppl. Ser. 57, 103–106.
7   Barucci, M.A., Fulchignoni, M., Burchi, R., D'Ambrosio, V.: 1985, Icarus 61, 152–162.
8   Barucci, M.A., Bockelee-Morvan, D., Brahic, A., Clairemidi, S., Lecacheux, J., Roques, F.: 1986, Astron. Astrophys. 163, 261–268.
9   Beyer, M.: 1953, Astron. Nachr. 281, 121–130.
10 Bianchi, E.: 1920, Mem. Soc. Astron. Ital. 1, 39–55.
11 Bianchi, E., Padova, E.: 1920, Mem. Soc. Astron. Ital. 1, 56–65.
12 Bianchi, E., Padova, E.: 1921, Mem. Soc. Astron. Ital. 2, 45–54.
13 Binzel, R.P., Harris, A.W.: 1980, Icarus 42, 43–45.
14 Binzel, R.P., Tholen, D.J.: 1983, Icarus 55, 495–497.
15 Binzel, R.P., Mulholland J.D.: 1983, Icarus 56, 519–533.
16 Binzel, R.P.: 1984, Icarus 59, 456–461.
17 Binzel, R.P.: 1985, Icarus 63, 1, 99–108.
18 Binzel, R.P., Cochran, A.L., Barker, E.S., Tholen, D.J., Barucci, A., DiMartino, M., Greenberg, R., Weidenschilling, S.J., Chapman, C.R., Davis, D.R.: 1987, Icarus 71, 148–158.
19 Binzel, R.P.: 1987, Icarus 72, 135–208.
20 Birch, P.V., Tedesco, E.F., Taylor, R.C., Binzel, R.P., Blanco,

C., Catalano, S., Hartigan, P., Scaltriti, F., Tholen, D.J., Zappala, V.: 1983, Icarus 54, 1-12.

21 Blanco, C., Catalano, S.: 1979, Icarus 40, 359-363.

22 Bowell, E.: 1977, IAUC 3111.

23 Burchi, R.: 1972, Mem. Soc. Astron. Ital., Nuova Ser. 43, 27-32.

24 Burchi, R., Milano, I.: 1974, Astron. Astrophys. Suppl. Ser. 15, 173-180.

25 Burchi, R., Milano, L.: 1983, Moon Planets 28, 17-21.

26 Burchi, R., D'Ambrosio, V., Tempesti, P., Lanciano, N.: 1985, Astron. Astrophys. Suppl. Ser. 60, 1, 9-15.

27 Campa, M.: 1938, Mem. Soc. Astron. Ital. 11, 285-301.

28 Carlsson, M., Lagerkvist, C.-I.: 1981, Astron. Astrophys. Suppl. Ser. 44, 15-22.

29 Carlsson, M., Lagerkvist, C.-I.: 1981, Astron. Astrophys. Suppl. Ser. 45, 1-4.

30 Carlsson, M, Lagerkvist, C.-I.: 1983, Astron. Astrophys. Suppl. Ser. 53, 157-159.

31 Chang, Y.C., Hsu W.-t., Ku F.-y.: 1959, Acta Astron. Sin. 7, 204-207.

32 Chang, Y.C., Chang, C.-s.: 1962, Acta Astron. Sin. 10, 101-111.

33 Chang, Y.C., Chang, C.-s.: 1963, Acta Astron. Sin. 11, 139-149.

34 Chang, Y.C., Zhou, X.-h., Yang, X.-y., Zhang, Y.-y., Li X.-q., Wu, Z.-x.: 1981, Acta Astron. Sin. 22, 169-173 (Chin. Astron. Astrophys. 5, 434-437).

35 Chen, D.-h., Yang, X.-y., Wu, Z.-x.: 1975, Acta Astron. Sin. 16, 131-137.

36 Chen, D-h., Wu, Z-x, Yang, X-y: 1976, Acta Astron. Sin. 17, 176-184.

37 Choloniewski, J.: 1979, Acta Astron. 29, 105-107.

38 Cristescu, C.: 1972, Stud. Cerc. Astron. 17, 177-181.

39 Cristescu, C.: 1976, Icarus 28, 39-42.

40 Cuffey, J.: 1953, Astron. J. 58, 212.

41 Cunningham, C.: 1983, Minor Planet Bull. 10,1, 3-5.

42 Cunningham, C.J.: 1986, in Asteroids, Comets, Meteors II. Eds. C.-I. Lagerkvist, B.A. Lindblad, M. Lundstedt and H. Rickman, Uppsala, pp. 85-87.

43 Debehogne, H., Surdej, A., Surdej, J.: 1977, Astron. Astrophys. Suppl. Ser. 30, 375-379.

44 Debehogne, H., Surdej, A., Surdej, J.: 1978, Astron. Astrophys. Suppl. Ser. 32, 127-133.

45 Debehogne, H., Surdej, A., Surdej, J.: 1978, Astron. Astrophys. Suppl. Ser. 33, 1-5.

46 Debehogne, H.: 1979, Messenger 18, 27-28.

47 Debehogne, H., Zappala, V.: 1980, Astron. Astrophys. Suppl. Ser. 39, 163-165.

48 Debehogne, H., Zappala, V.: 1980, Astron. Astrophys. Suppl. Ser. 40, 257-258.

49 Debehogne, H., Zappala, V.: 1980, Astron. Astrophys. Suppl. Ser. 42, 85-89.

50 Debehogne, H., De Sanctis, G., Zappala, V.: 1982, Astron. Astrophys. 108, 197-200.

51 Debehogne, H., Lagerkvist, C.-I., Zappala, V.: 1982, Astron. Astrophys. Suppl. Ser. 50, 277-281.

52 Debehogne, H., De Sanctis, G., Zappala, V.: 1983, Icarus 55, 236-244.

53 Degewij, J., Zellner, B.: 1978, Lunar Science IX, 235-237.

54 Degewij, J.: 1978, Messenger 13, 5.

55 Degewij, J., Tedesco, E.F., Zellner, B.: 1979, Icarus 40, 364-374.

56 Di Martino, M., Cacciatori, S.: 1984, Astron. Astrophys. 130, 206-207.

57 Di Martino, M., Cacciatori, S.: 1984, Icarus 60, 75-82.

58 Di Martino, M.: 1984, Icarus 60, 541-546.

59 Di Martino, M.: 1986, in Asteroids, Comets, Meteors II. Eds. C.-I. Lagerkvist, B.A. Lindblad, M. Lundstedt and H. Rickman, Uppsala, pp. 81-84.

60 Di Martino, M., Zappala, V., De Campos, J.A., Debehogne, H., Lagerkvist, C.-I.: 1987, Astron. Astrophys. Suppl. Ser. 67, 95-101.

61 Di Martino, M., Zappala, V., De Sanctis, G., Cacciatori, S.:
    1987, Icarus 69, 338-353.
62 Drummond, J.D., Cocke, W.J., Hege, E.K., Strittmatter, P.A.,
    Lambert, J.V.: 1985, Icarus 61, 132-151.
63 Dunlap, J.L., Gehrels, T.: 1969, Astron. J. 74, 796-803.
64 Dunlap, J.L., Gehrels, T., Howes, M.L.: 1973, Astron. J. 78,
    491-501.
65 Dunlap, J.L.: 1974, Astron. J. 79, 324-332.
66 Dunlap, J.L.: 1976, Icarus 28, 69-78.
67 Dunlap, J.L., Taylor, R.C.: 1979, Astron. J. 84, 269-273.
68 Florence W.B., Zeigler, K.W.: 1984, Minor Planet Bull. 11,
    33-34.
69 French, L.M.: 1987, Icarus 72, 325-341.
70 Gaffey, M.J.: 1984, Icarus 60, 83-114.
71 Gammelgaard, P., Kristensen, L.K.: 1983, Messenger, 32, 29-30.
72 Gammelgaard, P., Kristensen, L.K.: 1986, in Asteroids, Comets,
    Meteors II. Eds. C.-I. Lagerkvist, B.A. Lindblad, M.
    Lundstedt and H. Rickman, Uppsala, pp. 77-80.
73 Geffert, M., Hoffmann, M.: 1981, Minor Planet Bull. 8, 17-19.
74 Gehrels, T.: 1956, Astrophys. J. 123, 331-338.
75 Gehrels, T., Owings D.: 1962, Astrophys. J. 135, 906-924.
76 Gehrels, T.: 1967, Astron. J. 72, 929-938.
77 Gehrels, T., Roemer, E., Taylor, R.C., Zellner, B.H.: 1970,
    Astron. J. 75, 186-195.
78 Gehrels, T., Roemer, E. and Marsden, B.G.: 1971, Astron. J. 76,
    607-608.
79 Gehrels, T., Taylor, R.C.: 1977, Astron. J. 82, 229-237.
80 Giclas, H..L.: 1951, Lowell Obs. Rep. N. 9, 33-71.
81 Goguen, J., Veverka, J., Elliot, J.L., Church, C.: 1976, Icarus
    29, 137-142.
82 Groeneveld, I., Kuiper, G.P.: 1954, Astrophys. J. 120, 200-220.
83 Groeneveld, I., Kuiper, G.P.: 1954, Astrophys. J. 120, 529-546.
84 Grossmann, M., Hoffmann, M., Duerbeck, H.W.: 1981, Minor Planet
    Bull. 8, 14-15.
85 Hahn, G.: 1983, in Asteroids, Comets, Meteors. Eds. C.-I.
    Lagerkvist and H. Rickman, Uppsala, pp.35-44.
86 Hanslmeier, A.: 1980, Mitt. Univ. Graz No. 70.
87 Hanslmeier, A.: 1982, Anz. Osterr. Akad. Wiss.
    Math.-Naturwiss. Kl. 119, 5-8.
88 Hanslmeier, A., Denzel, R.: 1985, Anz. Osterr. Akad. Wiss.
    Math.-Naturwiss. Kl., 122, 151-154.
89 Harris, A.W., Young, J.: 1979, Icarus 38, 100-105.
90 Harris, A.W., Young, J.W., Scaltriti, F., Zappala, V.: 1980,
    Icarus 41, 316-317.
91 Harris, A.W., Young, J.W.: 1980, Icarus 43, 20-32.
92 Harris, A.W., Young, J.W., Bowell, E.: 1980, Icarus 43,
    181-183.
93 Harris, A.W., Young, J.W.: 1983, Icarus 54, 59-109.
94 Harris, A.W.: 1983, Sky Telescope 65, 504.
95 Harris, A.W., Young, J., Scaltriti, F., Zappala, V.: 1984,
    Icarus 57, 251-258.
96 Harris, A.W., Carlsson, M., Young, J., Lagerkvist, C.-I.: 1984,
    Icarus 58, 377-382.
97 Harris, A.W.: 1985, Bull. Amer. Astron. Soc. 17, 726.
98 Harris, A.W., Young, J.W., Goguen, J., Hammel, H.B., Hahn, G.:
    1987, Icarus 70, 246-256.
99 Hartmann, W.K., Cruikshank, D.P.: 1978, Icarus 36, 353-366.
100 Haupt, H.: 1958, Sitzber. Osterr. Akad. Wiss. Math.-Naturwiss.
    Kl. Abteilung II 167, 303-341.
101 Haupt, H., Schroll, A.: 1974, Mitt. Univ.-Sternw. Graz 16,
    1-10.
102 Haupt, H.: 1980, Mitt. Univ. Graz No. 69.
103 Haupt, H.: 1982, Anz. Osterr. Akad. Wiss. Math.-Naturwiss. Kl.
    119, 47-49.
104 Haupt, H., Hanslmeier, A.: 1984, Anz. Osterr. Akad. Wiss.
    Math.-Naturwiss. Kl. 121, 69-74.
105 Hoffmann, M.: 1986, Minor Planet Bull. 13, 27.
106 Hollis, A.J., Bembrick, C.S., Dumont, M., Miles, R.: 1987, J.
    Brit. Astron. Assoc. 97, 220-223.

107 Kennedy, H.D., Tholen, D.J.: 1982, Proc. Astron. Soc. Aust. 4, 414-417.
108 Lagerkvist, C.-I.: 1976, Icarus 27, 157-160.
109 Lagerkvist, C.-I.: 1976, Icarus 29, 143-145.
110 Lagerkvist, C.-I.: 1977, Icarus 32, 233-234.
111 Lagerkvist, C.-I.: 1978, Astron. Astrophys. Suppl. Ser. 31, 361-381.
112 Lagerkvist, C.-I., Pettersson, B.: 1978, Astron. Astrophys. Suppl. Ser. 32, 339-342.
113 Lagerkvist, C.-I.: 1978, Astron. Astrophys. Suppl. Ser. 34, 203-205.
114 Lagerkvist, C.-I.: 1979, Icarus 38, 106-114.
115 Lagerkvist, C.-I., Sjolander, N.-G.: 1979, Acta Astron. 29, 455-461.
116 Lagerkvist, C.-I.: 1980, Messenger 22, 5-7.
117 Lagerkvist, C.-I.: 1981, Astron. Astrophys. Suppl. Ser. 44, 345-347.
118 Lagerkvist, C.-I., Schober, H.J.: 1981, Astron. Astrophys. Suppl. Ser. 44, 401-404.
119 Lagerkvist, C.-I., Rickman, H.: 1981, Astron. Astrophys. Suppl. Ser. 45, 177-179.
120 Lagerkvist, C.-I., Rickman, H., Scaltriti, F., Zappala, V.: 1981, Astron. Astrophys. 104, 148-149.
121 Lagerkvist, C.-I., Rickman, H.: 1981, Moon Planets 24, 437-440.
122 Lagerkvist, C.-I., Rickman, H.: 1982, Moon Planets 27, 107-110.
123 Lagerkvist, C.-I., Rickman, H.: 1982, in Sun and Planetary System, Eds. W. Fricke and G. Teleki, pp. 289-290.
124 Lagerkvist, C.-I., Kamel, L.: 1982, Moon Planets 27, 463-466.
125 Lagerkvist, C.-I., Hahn, G., Magnusson, P., Rickman, H., Hammarback, G.: 1986, in Asteroids, Comets, Meteors II. Eds. C.-I. Lagerkvist, B.A. Lindblad, M. Lundstedt and H. Rickman, Uppsala, pp. 67-72.
126 Lagerkvist, C.-I., Williams I.P.: 1986, Upps. Astron. Obs. Rep. 40, 13pp.
127 Lagerkist, C.-I., Williams, I.P.: 1987, Astron. Astrophys. Suppl. Ser. 68, 295-315.
128 Lagerkvist, C.-I., Hahn, G., Magnusson, P., Rickman, H.: 1987, Astron. Astrophys. Suppl. Ser. 70, 21-32.
129 Lupishko, D.F., Kiselev N.N., Chernova G.N.: 1979, Pis'ma Astron. Zh. 5, 201-205 (Sov. Astron. Lett. 5, 108-110).
130 Lupishko, D.F., Kiselev, N.N., Chernova, G.P., Bel'skaya, I.N.: 1980, Pis'ma Astron. Zh. 6, 184-188 (Sov. Astron. Lett. 6, 102-104).
131 Lupishko, D.F., Tupieva, F.A., Velichko, F.P., Kiselev N.N., Chernova G.P.: 1981, Astron. Vestn. 15, 25-31 (Solar System Res. 15, 19-24.
132 Lupishko, D.F., Velichko, F.P., Tupieva, F.A., Chernova, G.P.: 1981, Pis'ma Astron. Zh. 7, 437-442 (Sov. Astron. Lett. 7, 241-244).
133 Lupishko, D.F., Bel'skaya, I.N., Tupieva, F.A., Chernova, G.P.: 1982, Astron. Vestn. 16, 101-108 (Solar System Res. 16, 75-80).
134 Lupishko, D.F., Bel'skaya, I.N., Tupieva, F.A., Chernova, G.P.: 1982, Vestn. Khar'kov Univ. 232, 54-58.
135 Lupishko, D.F., Belskaya, I.N.: 1983, in Asteroids, Comets, Meteors. Eds. C.-I. Lagerkvist and H. Rickman, Uppsala, pp. 55-61.
136 Lupishko, D.F., Bel'skaya, I.N., Tupieva, F.A.: 1983, Pis'ma Astron. Zh. 9, 691-694 (Sov. Astron. Lett. 9, 358-360).
137 Lupishko, D.F., Velichko, F.P., Shevchenko, V.G.: 1986, Kinematika Fiz. Nebesn. Tel 2, 39-43 (Kin. Phys. Celest. Bodies 2, 47-51).
138 Lupishko, D.F., Velichko, F.P.: 1987, Kinematika Fiz. Nebesn. Tel 3, 57-65 (Kin. Phys. Celest. Bodies 3, -).
139 Lupishko, D.F., Velichko, F.P., Kazakov, V.V., Shevchenko, V.G.: 1987, Kinematika Fiz. Nebesn. Tel 3, 92-93 (Kin. Phys. Celest. Bodies 3, -).
140 Lustig, G., Dvorak, R.: 1975, Acta Phys. Austriaca 43, 89-97.
141 Lustig, G., Hahn, G.: 1976, Acta Physica Austriaca 44, 199-205.

142 Lustig, G.: 1977, Astron. Astrophys. Suppl. Ser. 30, 117-119.
143 Magnusson, P.: 1983, in Asteroids, Comets, Meteors. Eds. C.-I.
     Lagerkvist and H. Rickman, Uppsala, pp. 77-85.
144 Magnusson, P.: 1986, Icarus 68, 1-39.
145 McCheyne, R.S., Eaton, N., Green, S.F., Meadows, A.J.: 1984,
     Icarus 59, 286-295.
146 McCheyne, R.S., Eaton, N., Meadows, A.J.: 1985, Icarus 61,
     443-460.
147 McFaul T.G.: 1981, Minor Planet Bull. 8, 19-21.
148 Melillo, F.J.: 1985, Minor Planet Bull. 12, 38.
149 Melillo, F.J.: 1986, Minor Planet Bull. 13, 21-22.
150 Melillo, F.J.: 1987, Minor Planet Bull. 14, 13-14.
151 Melillo, F.J.: 1987, Minor Planet Bull. 14, 21-22.
152 Melillo, F.J.: 1987, Minor Planet Bull. 14, 42-43.
153 Millis, R.L., Bowell, E., Thompson, D.T.: 1976, Icarus 28,
     53-67.
154 Millis, R.L., Wasserman, L.H., Bowell, E., Franz, O.G., White,
     N.M., Lockwood, G.W., Nye, R., Bertram, R., Klemola, A.,
     Dunham, E., Baron, R.L., Elliot, J.L., Harris, A., Young,
     J.W., Faulkner, J., Stanton, R., Reitsema, H.J., Hubbard,
     W.B., Zellner, B., Lebofsky, L., Cruikshank, D.P., Macknick,
     L.S., Becklin, E.E., Morrison, D., Lonsdale, C.J., Kunkle,
     T.D., Lee, T., Gatley, I., A'Hearn, M.F., DuPuy, D.L.,
     Nolthenius, R., Ford, H., McKenna, D., Placova, Z., Horne,
     K., Sandmann, W.H., Taylor, G.E., Tucker, R.: 1981, Astron.
     J. 86, 306-313.
155 Millis, R.L., Wasserman, L.H., Bowell, E., Franz, O.G.,
     Klemola A., Dunham, D.W.: 1984, Astron. J. 89, 592-596.
156 Millis, R.L., Wasserman, L.H., Bowell, E., Franz, O.G., Nye,
     R., Osborn, W., Klemola, A.: 1985, Icarus 61, 124-131.
157 Millis, R.L., Wasserman, L.H., Franz, O.G., Nye, R.A., Oliver,
     R.C., Kreidl, T.J., Jones, S.E., Hubbard, W., Lebofsky, L.,
     Goff, R., Marcialis, R., Sykes, M., Frecker, J., Hunten, D.,
     Zellner, B., Reitsema, H., Schneider, G., Dunham, E.,
     Klavetter, J., Meech, K., Oswalt, T., Rafert, J., Strother,
     E., Smith, J., Povenmire, H., Jones, B., Kornbluh, D., Reed,
     L., Izor, K., A'Hearn, M.F., Schnurr, R., Osborn, W.,
     Parker, D., Douglas, W.T., Beish, J.D., Klemola, A.R., Rios,
     M.: 1987, Icarus 72, in press.
158 Miner, E., Young, J.: 1969, Icarus 10, 436-440.
159 Miner, E., Young, J.: 1976, Icarus 28, 43-51.
160 Ostro, S.J., Harris, A.W., Campbell, D.B., Shapiro, I.I.,
     Young, J.: 1984, Icarus 60, 391-403.
161 Padova, E.: 1921, Mem. Soc. Astron. Ital. 2, 82.
162 Pavlovski, K., Knezevic, Z., Muminovic, M.: 1981, Publ.
     Astron. Obs. Sarajevo 1, 225-230.
163 Pfleiderer, J., Pfleiderer, M., Hanslmeier, A.: 1987, Astron.
     Astrophys. Suppl. Ser. 69, 117-122.
164 Piironen, J.O.: 1982, Astron. Astrophys. 112, 172-173.
165 Piironen, J.O., Poutanen, M., Di Martino, M., Zappala, V.:
     1985, Astron. Astrophys. Suppl. Ser. 61, 299-302.
166 Pilcher, F.: 1980, Minor Planet Bull. 7, 26-27.
167 Pilcher, F., Tholen, D.J.: 1982, Minor Planet Bull. 9, 13-14.
168 Pilcher, F.: 1983, Minor Planet Bull. 10, 18-20.
169 Pop, V., Chis, D.: 1976, Icarus 28, 37-38.
170 Poutanen, M.: 1983, in Asteroids, Comets, Meteors. Eds. C.-I.
     Lagerkvist and H. Rickman, Uppsala, pp. 45-48.
171 Poutanen, M., Bowell, E., Martin, L.J., Thompson, D.T.: 1985,
     Astron. Astrophys. Suppl. Ser. 61, 291-297.
172 Rakos, K.D.: 1960, Lowell Obs. Bull. 5, No. 109, 28-29.
173 Rigollet, R.: 1950, C. R. 230, 2077-2078.
174 Roach, F.E., Stoddard, L.G.: 1938, Astrophys. J. 88, 305-312.
175 Sather, R.E.: 1976, Astron. J. 81, 67-73.
176 Scaltriti, F., Zappala, V.: 1975, Astron. Astrophys. Suppl.
     Ser. 19, 249-255.
177 Scaltriti, F., Zappala, V.: 1976, Astron. Astrophys. Suppl.
     Ser. 23, 167-179.
178 Scaltriti, F., Zappala, V.: 1976, Icarus 28, 29-35.

179 Scaltriti, F., Zappala, V.: 1977, Astron. Astrophys. Suppl.
     Ser. 30, 169-174.
180 Scaltriti, F., Zappala, V.: 1977, Astron. Astrophys. 56, 7-11.
181 Scaltriti, F., Zappala, V.: 1977, Icarus 31, 498-502.
182 Scaltriti, F., Zappala, V., Stanzel, R.: 1978, Icarus 34,
     93-98.
183 Scaltriti, F., Zappala, V.: 1978, Icarus 34, 428-435.
184 Scaltriti, F., Zappala, V., Schober, H.J.: 1979, Icarus 37,
     133-141.
185 Scaltriti, F., Zappala, V.: 1979, Icarus 39, 124-130.
186 Scaltriti, F., Zappala, V., Stanzel, R., Blanco, C., Catalano,
     S., Young, J.W.: 1980, Icarus 43, 391-398.
187 Scaltriti, F., Zappala, V., Harris, A.W.: 1981, Icarus 46,
     275-280.
188 Scaltriti, F., Zappala, V., Schober, H.J., Hanslmeier, A.,
     Sudy, A., Piironen, J., Blanco, C., Catalano, S.: 1981,
     Astron. Astrophys. 100, 326-329.
189 Schober, H.J., Lustig, G.: 1975, Icarus 25, 339-343.
190 Schober, H.J., Dvorak, R.: 1975, Astron. Astrophys. 44, 81-84.
191 Schober, H.J.: 1975, Astron. Astrophys. 44, 85-89.
192 Schober, H.J.: 1976, Icarus 28, 415-420.
193 Schober, H.J.: 1976, Astron. Astrophys. 53, 115-119.
194 Schober, H.J.: 1976, Mitt. Astr. Gesellschaft 40, 207-210.
195 Schober, H.J., Scaltriti, F., Zappala, V.: 1977, Icarus 31,
     175-179.
196 Schober, H.J.: 1978, Astron. Astrophys. Suppl. Ser. 31,
     175-178.
197 Schober, H.J.: 1978, Astron. Astrophys. Suppl. Ser. 34,
     377-381.
198 Schober, H.J.: 1979, Astron. Astrophys. Suppl. Ser. 35,
     337-343.
199 Schober, H.J., Scaltriti, F., Zappala, V.: 1979, Astron.
     Astrophys. Suppl. Ser. 36, 1-8.
200 Schober, H.J.: 1979, Astron. Astrophys. Suppl. Ser. 38, 91-99.
201 Schober, H.J., Stanzel, R.: 1979, Astron. Astrophys. Suppl.
     Ser. 38, 265-268.
202 Schober, H.J., Surdej, J.: 1979, Astron. Astrophys. Suppl. Ser.
     38, 269-274.
203 Schober, H.J., Scaltriti, F., Zappala, V., Harris, A.W.: 1980,
     Astron. Astrophys. 91, 1-6.
204 Schober, H.J.: 1981, Astron. Astrophys. 96, 302-305.
205 Schober, H.J.: 1981, Astron. Astrophys. 99, 199-201.
206 Schober, H.J.: 1981, Astron. Astrophys. 100, 311-313.
207 Schober, H.J.: 1982, Astron. Astrophys. Suppl. Ser. 48, 57-62.
208 Schober, H.J.: 1982, Astron. Astrophys. 105, 419-421.
209 Schober, H.J., Schroll, A.: 1982, Astron. Astrophys. 107,
     402-405.
210 Schober, H.J., Surdej, J, Harris, A.W., Young, J.W.: 1982,
     Astron. Astrophys. 115, 257-262.
211 Schober, H.J.: 1983, Astron. Astrophys. 117, 362-364.
212 Schober, H.J., Schroll, A.: 1983, Astron. Astrophys. 120,
     106-108.
213 Schober, H.J.: 1983, Astron. Astrophys. Suppl. Ser. 53, 71.
214 Schober, H.J.: 1983, Astron. Astrophys. 127, 301-303.
215 Schober, H.J.: 1983, in Asteroids, Comets, Meteors. Eds. C.-I.
     Lagerkvist and H. Rickman, Uppsala, p.21-26.
216 Schober, H.J., Schroll, A.: 1985, Astron. Astrophys. Suppl.
     Ser. 62, 2, 187-189.
217 Schober, H.J.: 1986, in Asteroids, Comets, Meteors II. Eds.
     C.-I. Lagerkvist, B.A. Lindblad, M. Lundstedt and H. Rickman,
     Uppsala, p. 73.
218 Schober, H.J., Schroll, A.: 1986, in Asteroids, Comets, Meteors
     II. Eds. C.-I. Lagerkvist, B.A. Lindblad, M. Lundstedt and
     H. Rickman, Uppsala, pp. 75-76.
219 Schober, H.J.: 1987, Astron. Astrophys. 183, 151-155.
220 Schroll, A., Haupt, H.F., Maitzen, H.M.: 1976, Icarus 27,
     147-156.
221 Schroll, A., Schober, H.J., Lagerkvist, C.-I.: 1981, Astron.
     Astrophys. 104, 296-299.

222 Schroll, A., Schober, H.J.: 1983, Astron. Astrophys. Suppl.
     Ser. 53, 77-79.
223 Schuster, H.E., Surdej, A., Surdej, J.: 1979, Astron.
     Astrophys. Suppl. Ser. 37, 483-486.
224 Shatzel, A.V.: 1954, Astrophys. J. 120, 547-550.
225 Stanzel, R.: 1978, Astron. Astrophys., Suppl. Ser. 34, 373-376.
226 Stanzel, R., Schober, H.J.: 1980, Astron. Astrophys. Suppl.
     Ser. 39, 3-5.
227 Stephenson, C.B.: 1951, Astrophys. J. 114, 500-504.
228 Surdej, A., Surdej, J.: 1977, Astron. Astrophys. Suppl. Ser.
     30, 121-124.
229 Surdej, A., Surdej, J.: 1979, Astron. Astrophys. Suppl. Ser.
     37, 471-474.
230 Surdej, J., Schober, H.J.: 1980, Astron. Astrophys. Suppl.
     Ser. 41, 335-338.
231 Surdej, J., Surdej, A., Louis, B.: 1983, Astron. Astrophys.
     Suppl. Ser. 52, 203-211.
232 Surdej, J., Louis, R., Cramer, N., Rufener, F., Waelkens C.,
     Barbier, R., Birch, P.V.: 1983, Astron. Astrophys. Suppl.
     Ser. 54, 371-378.
233 Surdej, J., Pospieszalska-Surdej, A., Michalowski, T., Schober,
     H.J.: 1986, Astron. Astrophys. 170, 167-173.
234 Taylor, R.C.: 1971, in Physical Studies of Minor Planets, Ed.
     T. Gehrels, NASA SP-267, Washington, D.C., 117-131.
235 Taylor, R.C., Gehrels, T., Silvester, A.B.: 1971, Astron. J.
     76, 141-146.
236 Taylor, R.C.: 1973, Astron. J. 78, 1131-1139.
237 Taylor, R.C., Gehrels, T., Capen, R.C.: 1976, Astron. J. 81,
     778-786.
238 Taylor, R.C.: 1977, Astron. J. 82, 441-444.
239 Taylor, R.C.: 1978, Astron. J. 83, 201-204.
240 Taylor, R.C., Tedesco, E.F.: 1983, Icarus 54, 13-22.
241 Taylor, R.C.: 1985, Icarus 61, 3, 490-496.
242 Taylor, R.C., Tapia S., Tedesco, E.F.: 1985, Icarus 62,
     298-304.
243 Taylor, R.C., Birch, P.V., Drummond, J., Pospieszalska-Surdej,
     A., Surdej, J.: 1987, Icarus 69, 354-369.
244 Tedesco, E.F.: 1976, Icarus 28, 21-28.
245 Tedesco, E.F., Drummond, J.D.: 1976, IAUC 3007.
246 Tedesco, E.F., Drummond, J., Candy, M., Birch, P., Nikoloff,
     I., Zellner, B.: 1978, Icarus 35, 344-359.
247 Tedesco, E.F.: 1979, PhD Dissertation, New. Mex. State Univ.
     280pp.
248 Tedesco, E.F., Sather, R.E.: 1981, Astron. J. 86, 1553-1558.
249 Tedesco, E.F., Taylor, R.C., Drummond, J., Harwood, D.,
     Nickoloff, I., Scaltriti, F., Schober, H.J., Zappala, V.:
     1983, Icarus 54, 23-29.
250 Tedesco, E.F., Taylor, R.C., Drummond, J., Harwood, D.,
     Nickoloff, I., Scaltriti, F., Zappala, V.: 1983, Icarus 54,
     30-37.
251 Tedesco, E.F., Taylor, R.C.: 1985, Icarus 61, 2, 241-251.
252 Tempesti, P., Burchi, R.: 1969, Mem. Soc. Astron. Ital. N. S.
     40, 415-432.
253 Tempesti, P.: 1975, Mem. Soc. Astron. Ital. N. S. 46, 397-405.
254 Tholen, D.J.: 1980, Sky Telescope 60, 203.
255 Van Gent, H.: 1933, Bull. Astron. Inst. Netherlands 7, 65-66.
256 Van Houten, C.J.: 1962, Bull. Astron. Inst. Netherlands 16,
     160-162.
257 Van Houten, C.J.: 1963, Stern und Weltraum 2, 228-230.
258 Van Houten-Groeneveld, I., van Houten, C.J.: 1958, Astrophys.
     J. 127, 253-273.
259 Van Houten-Groeneveld, I., van Houten, C.J., Zappala, V.: 1979,
     Astron. Astrophys. Suppl. Ser. 35, 223-232.
260 Van Houten-Groeneveld, I.: 1981, Astron. Astrophys. 98,
     203-204.
261 Vesely, C.D., Taylor, R.C.: 1985, Icarus 64, 37-52.
262 Veverka, J., Liller, W.: 1969, Icarus 10, 441-444.
263 Veverka, J.: 1970, PhD Dissertation, Harvard.
264 Veverka, J.: 1971, Icarus 15, 454-458.

265 Wamsteker, W., Sather, R.E.: 1974, Astron. J. 79, 1465-1470.
266 Wasserman, L.H., Millis, R.L., Franz, O.G., Bowell, E., White,
     N.M., Giclas, H.L., Martin, L.J., Elliot, J.L., Dunham, E.,
     Mink, D., Baron, R., Honeycutt, R.H., Henden, A.A., Kephart,
     J.E., A'Hearn, M.F., Reitsema, H.J., Radick, R., Taylor,
     G.E.: 1979, Astron. J. 84, 259-268.
267 Weidenschilling, S.J., Chapman, C.R., Davis, D.R., Greenberg,
     R., Levy, D.H., Vail, S.: 1987, Icarus 70, 191-245.
268 Wisniewski, W.Z.,McMillan, R.S.: 1987, Astron. J. 93, 5,
     1264-1267.
269 Wisniewski, W.Z.: 1987, Icarus 70, 566-572.
270 Wood, H.J., Kuiper, G.P.: 1963, Astrophys. Journ. 137,
     1279-1285.
271 Yang, X.-y., Zhang, Y.-y., Li X.-q.: 1965, Acta Astron. Sin.
     13, 66-74.
272 Young, J., Harris, A.W.: 1985, Icarus 64, 528-530.
273 Zappala, V., van Houten-Groeneveld, I.: 1979, Icarus 40,
     289-296.
274 Zappala, V., van Houten-Groeneveld, I., van Houten, C.J.: 1979,
     Astron. Astrophys. Suppl. Ser. 35, 213-221.
275 Zappala, V., Debehogne, H., Lagerkvist, C.-I., Rickman, H.:
     1982, Astron. Astrophys. Suppl. Ser. 50, 23-26.
276 Zappala, V., Scaltriti, F., Lagerkvist, C.-I., Rickman, H.,
     Harris, A.W.: 1982, Icarus 52, 196-201.
277 Zappala, V., Di Martino, M., Scaltriti, F., Burchi, R., Milano,
     L., Young, J., Wahlgren, G., Pavlovski, K.: 1983, Astron.
     Astrophys. 123, 326-330.
278 Zappala, V., Di Martino, M., Scaltriti, F., Djurasevic, G.,
     Knezevic, Z.: 1983, Icarus 53, 458-464.
279 Zappala, V., Di Martino, M., Cacciatori, S.: 1983, Icarus 56,
     319-324.
280 Zappala, V., Scaltriti, F., Di Martino, M.: 1983, Icarus 56,
     325-344.
281 Zappala, V., Di Martino, M., Knezevic, Z., Djurasevic, G.:
     1984, Astron. Astrophys. 130, 208-210.
282 Zappala, V., Knezevic, Z.: 1984, Icarus 59, 436-455.
283 Zappala, V., Di Martino, M., Hanslmeier, A., Schober, H.J.:
     1985, Astron. Astrophys. 147, 1, 35-38.
284 Zappala, V., Knezevic, Z.: 1986, Icarus 65, 122-128.
285 Zappala, V., Di Martino, M.: 1986, Icarus 68, 40-54.
286 Zeigler, K.W., Tomlinson, D.: 1984, Minor Planet Bull. 11,
     21-22.
287 Zeigler, K.W., Florence W.B.: 1985, Icarus 62, 512-517.
288 Zeigler, K.W., Florence W.B.: 1985, Minor Planet Bull. 12,
     21-23.
289 Zeigler, K.W., Florence, W.B., Blanco, E.J., McGaughey, J.:
     1986, Minor Planet Bull. 13, 25-26.
290 Zeigler, K.W.: 1987, Minor Planet Bull. 14, 11-12.
291 Zhou, X.-h., Yang, X.-y.: 1981, Acta Astron. Sin. 22, 378-382
     (Chin. Astron. Astrophys. 6, 57-59, 1982).
292 Zhou, X.-z., Yang, X.-y., Wu, Z.-x.: 1982, Acta Astron. Sin.
     23, 349-352 (Chin. Astron. Astrophys. 7, 129-131, 1983).
293 Zhou, X.-h.: 1985, Publ. Purple Mt. Obs. 4, 46-51.

POLE DETERMINATIONS OF ASTEROIDS

PER MAGNUSSON
Uppsala Universitet

This is a comprehensive tabulation of asteroid pole orientations and the sense of rotation. No weeding out of vague or uncertain results has been done. An indication of the reliability (or lack thereof) of the solutions may be obtained by comparing results derived from different sources of data (see column 2). Discussions of the methods of individual pole determination including weaknesses and error sources are given in the chapter by Magnusson et al.

EXPLANATION OF TABLE COLUMNS

No. Asteroid Number.

Basic Data from which pole coordinates, senses of rotation and rejection of spurious solutions are based are designated by the letters:

A = Amplitudes of lightcurves;
D = Individual data-points of photometric lightcurves;
E = Epochs (e.g., times of lightcurve extrema);
F = Fourier coefficients of photometric lightcurves;
I = Infrared pre- and post-opposition differences;
M = Magnitudes (usually at maximum light);
O = Occultation observations;
P = Infrared polarimetry;
R = Radar observations;
S = Speckle interferometry;
V = Visual position angles;
Z = Zero and nonzero amplitude apparitions implying pole-on view in former case.

Pole Coordinates are given in the ecliptical reference frame of equinox 1950. For symmetry reasons, two pole solution often result for main-belt asteroids, thus two sub-columns are tabulated. Simple comparison is achieved by tabulating coordinates referring to the pole which is above the orbital plane and occasionally giving the longitude outside the range 0–360 deg. The spin direction is indicated by preceding the coordinates with the letter "N" if they refer to the north pole (direction of spin-vector) and the letter "S" if the coordinates refer to the south pole (anti-direction of spin-vector). The word "rejected" indicates a pole solution shown to be inconsistent with observations. A pole solution within parenthesis is significantly less likely than the other solution.

Sense of Rotation:

– Sense of rotation not determined;
P Prograde rotation;
R Retrograde rotation;
I Indeterminate case.

The sense of rotation is termed indeterminate (I) when the spin direction is known, but the accuracy of the pole coordinates is insufficient to give an unambigous sense of rotation, or the pole is so close to the ecliptic and/or orbital plane that forced precession will cause the sense of rotation to alternate with time.

Sidereal Period in days. Due to the usually nonuniform time distribution of the observations, sidereal periods tend to be either very accurate or, when the number of rotation cycles is incorrectly determined, erroneous by hundreds of times the expected uncertainty.

Model.   Many pole determination methods are based on a tri-axial ellipsoid model with semi-axes $a \geqslant b \geqslant c$ which rotates about the c axis. Correction for nongeometric scattering and albedo variegation has often not been made. A warning must therefore be made against direct identification of the model axis-ratios with the asteroid shape. Values within parenthesis are assumed and not determined. The table is not a comprehensive list of asteroid shapes and albedo models, but includes models obtained as by-products of pole determinations.

Reference Code refers to the reference list.

No.	Basic data	Pole coordinates						Sense of rotation	period (days)	Model Shape		Albedo varieg.	Reference code
		λ_0	β_0	P	λ_0	β_0	P			a/b	b/c		
1	I							P	- - - - -				Mor77
	I							P	- - - - -				Han77
	P				270°	+36°	N	P	- - - - -				Joh+83
	R	concentric ring region						−	- - - - -				Ost87
2	EZ				228°	+43°	N	P	0 325440				Sch+76
	I							P	- - - - -				Han77
	Z				211°	+38°	−	−	- - - - -				Bur+83
	AM	44°	+4°	−	(148°	+55°	−)	−	- - - - -	1 14	(1 0)		Zap+84
	A				200°	+40°	−	−	- - - - -				Bin84
	A				220°	+15°	−	−	- - - - -				Bin84
	A	49°	+6°	−	(157°	+53°	−)	−	- - - - -	1 14	(1 0)		Bur+85
	R	aspect circle						−	- - - - -				Ost85
	R	concentric ring region						−	- - - - -				Ost87
	OEAI	rejected			227°	+20°	N	I	0 325995	1 11	1.03		Lam85
	OEA	54°	−6°	N	rejected			I	0.32555136	1 06	1 05		Mag86
	S	100°	−22°	N	295°	+16°	N	I	- - - - -	1 10	1 01		Dr+89a*
	O	71°	−19°	−	251°	+19°	−	−	- - - - -	1 11	1 29		Dr+89b*
	SOEA	74°	−17°	−				I	- - - - -	1 09	1 09		Dr+89b*
3	EA	71°	+49°	N				P	0 3004950				Cha+62
	AM	101°	+29°	−	(321°	+57°	−)		- - - - -	1.23	(1 0)		Zap+84
	OEA	110°	+40°	N	rejected			P	0 30040	1 20	1 02		Mag86
4	EA	14°	+80°	N				P	0 2227006				Cai56
	EA		+90°	S		+90°	S	R	0 4453666	1.14	(1 0)		Hau58
	EA	57°	+74°	N				P	0 2225884				Cha+62
	E	126°	+65°	N	rejected			P	0.22258871				Geh67
	E	139°	+47°	N	333°	+39°	N	P	0.4451021	1 15	1	flat region	Tay73
	I							P	- - - - -				Han77
	E	103°	+43°	N	301°	+33°	N	P	0 2225889				Tay+85
	E	120°	+65°	N	325°	+55°	N	P	0 22258849	1.01	1 4[1]		Mag86
	AM	85°	+58°	−	310°	+60°	−	−	- - - - -	(1.0)	1 27	see ref.	Cel+87
	S				336°	+55°	N	P	0.2225887	1 10	1 14	see ref.	Dr+88a
	S				311°	+67°	N	P	- - - - -	1 07	1 14		Dr+89a*
5	E	148°	+9°	N	rejected			I	0 7005047				Tay78
	AM	131°	+49°	−	328°	+46°	−	−	- - - - -	1 29	(1 0)		Za+86b
	R	concentric ring region						−	- - - - -				Ost87
6	A	145°	+15°	−				−	- - - - -				Geh+62
	E	rejected			365°	+50°	N	P	0 3031020	1 15	(1)		Geh+77
	AM	130°	+33°	−	344°	+30°	−	−	- - - - -	1 24	(1.0)		Zap+84
	OEA	rejected			355°	+50°	N	P	0 3031025	1 14	1 2		Mag86
	R	concentric ring region						−	- - - - -				Ost87
	E				363°	+60°	N	P	0.3031024				Mic88*
7	EA				184°	+55°	N	P	0 2967853	"kettle"			Cai56
	AM				193°	+15°	−	−	- - - - -				Geh+62
	AM	11°	+41°	−	rejected			−	- - - - -	1.31	1 35		Tay77
	EA	15°	+25°	N	195°	+15°	N	P	0 29745197	1 18	1 40		Mag86
	AM	18°	+33°	−	193°	+16°	−	−	- - - - -	1 19	1.21		Za+86b
	R	concentric ring region						−	- - - - -				Ost87
8	A	157°	+10°	−				−	- - - - -				Geh+62
	A	140°			320°			−	- - - - -				Zap+83
	A	148°			328°			−	- - - - -				Hol+87
9	AM				156°	+15°	−	−	- - - - -				Geh+62
	A	−12°	+76°	−				−	- - - - -				Cha+62
	I							I	- - - - -				Mor77
	AM				191°	+56°	−	−	- - - - -	1.30	1.70		Zap+79
	AM	2°	+26°	−	186°	+43°	−	−	- - - - -	1.32	1.34		Zap+84
	R	concentric ring region						−	- - - - -				Ost87
	EAM	1°	+9°	N	183°	+25°	N	P	0 2116324	1.27	1.26		Dr+88b
	EAM	0°	+20°	N	180°	+30°	N	P	0 2116322	1.27	1.26		Mag89

No.	Basic data	Pole coordinates						Sense of rotation	Sidereal period (days)	Model Shape a/b	b/c	Albedo varieg.	Reference code
		λ_0	β_0	P	λ_0	β_0	P						
10	I							R	- - - - -				Mor77
12	A				242°	+17°	–	--	0 36060				Tem+69
	R		concentric ring region					–	- - - - -				Ost87
15	EA		+90°	S		+90°	S	R	0 253448				Gro+54
	EA	157°	+82°	S				R	0 25344810	1 51	?		Cai56
	EA		+90°	S		+90°	S	R	0 253448				HG+58
	EA				250°	+74°	S	R	0 25344810				Cai60
	EA		+90°	S		+90°	S	R	0 25336				Sca+75
	A	164°	+52°	–		rejected		–	- - - - -	1 6	(1 0)		Pu+85
	A	170°	+57°	–		rejected		--	- - - - -	1 6	(1 4)		Pu+85
	E							P	0 25336				Lup+85
	EA	171°	+61°	S	286°	+73°	S	R	0 25344806	1 50	1 0		Mag86
	E	180°	+50°	S	311°	+71°	S	R	0 25344810	1 40	1 06		Mic88*
	EAM	172°	+61°	S	262°	+78°	S	R	0 25344805	1 44	1 0		Dr+88b
	EA	170°	+59°	S	288°	+74°	S	R	0 25344808				Mag89
16	Z				222°	+4°	–	–	0 174831	1 3	1 3		Lup+83
	EZ		rejected		225°	+5°	N	I	0 17483120				Zho+82
	AM	40°	+23°	–	217°	+31°	–	–	- - - - -	1 32	1 26		Zap+84
	R		concentric ring region					–	- - - - -				Ost87
	E	41°	+33°	N	223°	+37°	N	P	0 1748143				Ted+85
	AM	39°	+35°	–	220°	+40°	–	–	- - - - -	1 33	1 33		Ted+85
	EA	37°	+14°	S	216°	+21°	S	R	0 17483113	1 19	1 16		Mag86
	EAM	35°	+17°	S		rejected		R	0 17483117	1.27	1 35		Dr+88b
	EAM	36°	+12°	S	215°	+19°	S	R	0 17483106	1 16	1 34		Mag89
17	AM	69°	+43°	–	268°	+55°	–	–	- - - - -	1 25	(1 35)		Za+86b
19	I							P	- - - - -				Han77
	R		concentric ring region					–	- - - - -				Ost87
	E							P	0 310125				Lup+85
	EAM	65°	+48°	N		rejected		P	0 3101343	1 24	0 94		Dr+88b
	E	70°	+50°	N	250°	+50°	N	P	0 3101342	1 21	1 1		Mag89
20	A	10°	+78°	–				--	- - - - -				Cha+62
	AM	(30°	+49°	–)	207°	+51°	–	–	- - - - -	1 27	(1 0)		Bar+85
	A	30°	+54°	–	205°	+79°	–	–	- - - - -	1 25	?		McC'+85
	E							R	0 337419				Lup+85
	EA	20°	+80°	N	200°	+80°	N	P	0 3373993	1 16			Mag86
21	E							P	0 340277				Lu+87a
	AM	42°	+40°	–	223°	+48°	–	–	- - - - -	1 25	1 09		Lu+87c
22	AM				215°	+45°	–	–	- - - - -	1 34	1 23		Sca+78
	AM	13°	+17°	–	214°	+42°	–	–	- - - - -	1 34	1 18		Zap+84
	EAM	19°	−11°	N	199°	+14°	N	I	0 1728092	1 4	1 18		Mag86
	A				203°	+29°	–	–	- - - - -	1 33	1 24		Sur+86
	M				201°	+22°	–	–	- - - - -	1 32	1 13		Sur+86
	EAM	14°	+8°	S		rejected		I	0 17284164	1 32	1 27		Dr+88b
	EAM	15°	−2°	S	(200°	+23°	S)	I	0.1728416	1 6	1.2		Mag89
28	AM	93°	+18°	–	285°	+37°	–	–	- - - - -	1 31	1 18		Zap+84
20	A	165°	+45°	–	345°	+45°	–	–	- - - - -	1 14	(1 0)		Ted+81
	A	160°	+53°	–	320°	+45°	–	–	- - - - -	1 13	1 00		McC'84
	AM	142°	+50°	–	308°	+40°	–	–	- - - - -	1 13	(1 0)		Zap+84
	EAM	140°	+25°	S	315°	+15°	S	R	0 22458835	1.06	1 06		Mag86
	EAM		rejected		316°	+33°	S	R	0 2245882	1 13	1 14		Dr+88b
	EAM	138°	+25°	S	313°	+17°	S	R	0 22458829	1 05	1 16		Mag89
	S		rejected		314°	+36°	S	R	- - - - -	1 22	1 06		Dr+89a*
31	AM	(186°	+67°	–)	317°	+4°	–	–	- - - - -	1 12	(1 0)		Bar+85
	A	178°	+72°	–	315°	+5°	–	–	- - - - -	1 12	1 00		McC'+85
32	AM	91°	+34°	–	263°	+46°	–	–	- - - - -	1 34	(1 0)		Za+86b
37	EA	100°	+5°	N	280°	−5°	N	I	0 305573	1 2			Mag86

No.	Basic data	Pole coordinates						Sense of rotation	Sidereal period (days)	Model		Albedo varieg.	Refer- ence code
		λ_0	β_0	P	λ_0	β_0	P			Shape a/b	b/c		
39	EA	100°	+66°	S				R	0 2144712	"kettle"			Cai56
	A	114°	+28°	–				–	- - - - -				HG+58
	EA	103°	+61°	S				R	0 2144712	1 7	3 3		Cai60
	AM	130°	+10°	–				–	- - - - -				Geh+62
	M	121°	+37°	–				–	- - - - -	1 64	1 80		Sat76
	A	128°	+38°	–	339°	+48°	-	–	- - - - -	1 53	1 31[1]		McC+84
	AM	116°	+49°	–	338°	+57°	–	–	- - - - -	1 58	2 08		Zap+84
	A	111°	+56°	–	365°	+70°	–	–	- - - - -	1 53	3 1[1]		McC+85
	E							P	0 21409				Lup+85
	EAM	(129°	+30°	N)	324°	+35°	N	P	0 21409332	1 49	1 49		Mag86
	EAM	rejected			318°	+26°	N	P	0 21409327	1 45	1 48		Dr+88b
	EAM	130°	+29°	N	325°	+37°	N	P	0 21409333	1 50	1 50		Mag89
41	AM	15°	+36°	–	157°	+28°	–	–	- - - - -	1 51	1 00		Bar83
	AM	19°	+35°	–	159°	+32°	–	–	- - - - -	1 44	(1 0)		Bar+85
	R	concentric ring region						–	- - - - -				Ost87
	EA	6°	+40°	S	(155°	+33°	S)	R	0 2495001	1 30	1 0		Mag86
	AM	(18°	+48°	–)	135°	+43°	–	–	- - - - -	1 31	1 16		Za+86b
	EAM	rejected			154°	+32°	S	R	0 2494996	1 28	1 23		Dr+88b
	EA	17°	+36°	S	(164°	+38°	S)	R	0 2494994	1 28	1 00		Mag89
43	A	73°	+40°	–	249°	+43°	–	–	- - - - -	1 69	1 8[1]		McC+84
	AM	73°	+25°	–	248°	+20°	–	–	- - - - -	1 79	1 10		Bar+84
	E	61°	+21°	S	235°	+16°	S	R	0 2400784				Mic88*
	EAM	78°	+13°	N	256°	+13°	N	P	0 2400924	1 40	1 10		Dr+88b
	EA	71°	+16°	S	248°	+14°	S	R	0 2400828	1 76	1 01		Mag89
44	EA				358°	+84°	S	R	0 26737846	1 47	"kettle"		Cai56
	AM	105°	+30°					–	- - - - -				Geh+62
	EA				358°	+84°	N	P	0 26730938				Cha+62
	AM	100°	+50°	–				–	- - - - -	1 58	1 30		Zap+79
	E	100°	+60°	N	265°	+55°	N	P	0 26755902				Tay+83
	EA	94°	+59°	N	288°	+63°	N	P	0.26755895				Mag83
	AM	99°	+49°	–	295°	+54°	–	–	- - - - -	1 51	1 18		Zap+84
	EAM	(105°	+57°	N)	300°	+61°	N	P	0 26755902	1 37	1 4		Mag86
45	E	106°	+26°	S	295°	+34°	S	R	0 2374645				Tay+88
	EAM	rejected			307°	+44°	S	R	0 2374646	1 33	1 65		Dr+88b
	EAM	116°	+26°	S	305°	+35°	S	R	0 2374646	1 36	1 48		Mag89
52	A	0°	+37°	–	(203°	+38°	–)	–	- - - - -	1 12	(1 0)		Bar+86
55	AM	36°	+32°	–	226°	+19°	–	–	- - - - -	1 27	1 10		Za+86b
	EAM	22°	+26°	S	rejected			R	0 2001593	1 76	1 52		Dr+88b
63	AM	130°			310°			–	- - - - -	2.4	1 0		Zap+83
	AM	127°	+38°	–	298°	+28°	-	–	- - - - -	2 25	(1 0)		Zap+84
	EAM	125°	+30°	S	300°	+30°	S	R	0 3873987	2.06	1.04		Mag86
	E							R	0 387230				Lu+87a
65	EAM	rejected			206°	+52°	S	R	0 1661266	1 08	1 74		Dr+88b
80	R	concentric ring region						–	- - - - -				Ost87
87	EAM	89°	+52°	N	288°	+40°	N	P	0 2159852	1 41	1 17		Dr+88b
	EAM	66°	+67°	N	296°	+59°	N	P	0.2159851	1 44	1 5		Mag89
88	AM	32°	+69°	–	205°	+54°	–	–	- - - - -	1.13	(1 0)		Za+86b
	EAM	rejected			129°	+78°	N	P	0 2517222	1 12	1 30		Dr+88b
	EA	40°	+70°	N	200°	+70°	N	P	0 2517223	1 13			Mag89
107	EAM	71°	+61°	N	233°	+74°	N	P	0 2018306	1 45	1 72		Dr+88b
	EAM	74°	+55°	N	239°	+76°	N	P	0 2018305	1 46	1 6		Mag89
125	EAM	80°	+74°	N	rejected			P	0.1653422	1 28	2 68		Dr+88b
	E		+70°	N		+70°	N	P	0 1653425				Mag89

No.	Basic data	Pole coordinates						Sense of rotation	Sidereal period (days)	Model			Reference code
		λ_0	β_0	P	λ_0	β_0	P			Shape a/b	b/c	Albedo varieg.	
129	AM	(133°	+48°	−)	331°	+30°	−	−	- - - - -	1 37	(1 0)		Bar+85
	EA	(20°	+50°	N)	180°	+72°	N	P	0 2065566	1 27	1 0		Mag86
	EAM	rejected			196°	+64°	N	P	0 2065486	1 27	1 05		Dr+88b
	EA	38°	+27°	N	202°	+53°	N	P	0 2065485	1 32	1 02		Mag89
130	EAM	10°	+81°	S	rejected			R	0 2176951	1 29	1 63		Dr+88b
	EAM	(60°	+40°	S)	360°	+85°	S	R	0 2176942	1 41	1 2		Mag89
133	E							P	0 5295				Har+84
144	R	concentric ring region						−	- - - - -				Ost87
192	A	130°	+40°	−				−	- - - - -				Sc+76a
201	EAM	78°	−4°	S	258°	+3°	S	I	0 1561283[1]	1 47	1 22		Dr+88b
	EAM	80°	+25°	S	260°	+35°	S	R	0 1561443	1 50	1 23		Mag89
210	EA	71°	+21°	N	(234°	+38°	N)	P	0 2243864				Mag83
	A	67°	+15°	−	231°	+31°	−	−	- - - - -	2 83			Zap+84
	E	71°	+21°	N	234°	+38°	N	P	?				Kos86
	EA	72°	+20°	N	(235°	+34°	N)	P	0 2243865	2 78	1 5[1]		Mag86
	E							P	0 22438596				Lu+87a
	EAM	69°	+10°	N	rejected			P	0 2243870	2 54	1.32		Dr+88b
	EAM	71°	+19°	N	(236°	+34°	N)	P	0 2243868	2 71	1 30		Mag89
281	A		+90°	−		+90°	−	−	- - - - -				Tay+76
349	E	150°	+25°	N	330°	+5°	N	P	0 1958834	<1 3			Mag86
	AM	163°	+49°	−	330°	+29°	−	−	- - - - -	1 28	1 15		Za+86b
	E							P	0 195895				Lu+87a
	EAM	153°	+35°	N	rejected			P	0 19588337	1 30	1 12		Dr+88b
	EAM	157°	+30°	N	331°	+15°	N	P	0 1958835	1.29	1 11		Mag89
354	EA				360°	+35°	N	P	- - - - -				Lup+81
	A	132°	+45°	−	357°	+38°	−	−	- - - - -	1 36	(1 0)		Zap+84
	A	(137°	+44°	−)	363°	+28°	−	−	- - - - -	1 35	(1 0)		Bur+85
	A		355°	+36°			−	−	- - - - -				Pii+85
	EA	159°	+22°	N	339°	+2°	N	P	0 1782160	1 23	1 0		Mag86
	EAM	170°	+39°	N	366°	+2°	N	P	0 17821593	1 17	1 24		Dr+88b
	EAM	148°	+35°	N	350°	+21°	N	P	0 1782161	1 21	1 11		Mag89
356	R	concentric ring region						−	- - - - -				Ost87
423	AM	170°	+63°	−	345°	+31°	−	−	- - - - -	1 14	1 50		Za+86b
433	V	29°	+22°	N				P	- - - - -				Zes32
	A	4°	+45°	−				−	- - - - -				Ros32
	AM	2°	+53°	−				−	- - - - -	1 79	1 18		Kru+36
	V A	−11°	+62°	S				R	- - - - -				Wat37
	VEA	moving						P	0 2195937				Sto40
	EA	−7°	+13°	N				I	0.21959390				Bey53
	EA	10°	+46°	N				P	0 21959386	4 0	(1 0)		Cai56
	E	13°	+28°	N				P	- - - - -				Ves71
	A	17°	+10°	−				−	0 21959				Sc+76b
	A	15°	+9°	−				−	- - - - -	2 3			Mil+76
	E	16°	+12°	N				I	0 219599	2 6	rnd cyl		Dun76
	A	moving						−	- - - - -	4 0	1 25		Che+77
	AM	15°	+20°	−				−	- - - - -	2 33	1.00		Lum+81
	S	23°	+37°	N				P	- - - - -	2 79	1 03		Dr+85a
	E	22°	+9°	N				I	0 219588				Tay85
	E	16°	+6°	N				I	- - - - -				Kos86
451	AM	153°	+67°	−	345°	+25°	−	−	- - - - -	1 07	1 0		Za+86b
495	Z				224°	+2°	−	−	- - - - -				Bin87
505	Z	113°	+4°	−				−	- - - - -				You+85

No	Basic data	Pole coordinates						Sense of rotation	Sidereal period (days)	Model Shape		Albedo varieg.	Reference code
		λ_0	β_0	P	λ_0	β_0	P			a/b	b/c		
511	AM	122°	+10°	–				–	- - - - -				Geh+62
	A	rejected			306°	+34°	–	–	- - - - -				Cha+63
	E				285°	+45°	?	?	- - - - -				Ves+85
	AM	92°	+33°	–	303°	+34°	–	–	- - - - -	1 19	1 13		Za+86a
	S	rejected			291°	+37°	N	P	- - - - -	1 30	1 4		Dru+86
	AM				307°	+32°	–	–	- - - - -	1 25	1 14		Dru+86
	EAM	rejected			300°	+32°	N	P	0 21372345	1 25	1 16		Dr+88b
	EAM	(99°	+26°	N)	299°	+26°	N	P	0 21372348	1 22	1 13		Mag89
532	S				312°	+59°	S	R	- - - - -	1 21	1 01	see ref	Dr+85b
	E				276°	+1°	S	I	0 3918711	(1 0)	(1 0)	see ref	Tay+87
554	R	concentric ring region						–	- - - - -				Ost87
579	Z	96°	+7°	–				–	- - - - -				Bin87
584	EAM	147°	+55°	S	rejected			R	0 2112053	1 19	1 28		Dr+88b
	EAM	140°	+30°	S	290°	+40°	S	R	0 211206	1 17	1 1		Mag89
624	E	rejected			324°	+10°	N	P	0 28843884	2 7	rnd cyl		Dun+69
	A				314°	+10°	–	–	- - - - -	2 01	?		Pou81
	EA	144°	+10°	N	322°	–4°	N	I	0 2884382				Mag83
	AM	152°	+29°	–	314°	+15°	–	–	- - - - -	2 66	1 13		Zap+84
	A	152°	+27°	–	315°	+16°	–	–	- - - - -	2 26	1 35[1]		Pos+85
	EA	150°	+30°	S	(314°	+15°	S)	R	0 2883544	2 70	1 43		Mag86
	EAMD				314°	+17°	N	P	0 288335	2 22	1 19		Uch+87
	E	156°	+32°	S	314°	+17°	S	R	0 2883546				Mic88*
694	R	concentric ring region						–	- - - - -				Ost87
	EAM	96°	+32°	N	rejected			P	0 246744	1 42	1 38		Dr+88b
704	Z	70°	+10°	–				–	- - - - -				Har+79
1036	E							P	0 42951				Lu+87b
1219	E							R	0 232290				Bin+87
1566	E	49°	0°	N	229°	0°	N	I	0 09471				Geh+70
1580	A	140°	+20°	–				–	- - - - -	1 21	complex		Ted+78
1620	E				200°	+60°	S	R	0 2176378	2 7	rnd cyl		Dun74
1627	E							P	0 19991				Lup+86
1685	EA				200°	+55°	N	P	0 42481	3 2			Dun+73
1862	EA				236°	+26°	S	R	0 1277265				Har+87

Footnotes: * New or altered material not present in the digital version
          [1] Mean value of two significantly different solutions

REFERENCES

Bar83   Barucci, M. A. 1983. Estimate of the shape and pole coordinates for the asteroid 41 Daphne. *Astron. Astrophys. Suppl.* 54:471–473.

Bar+85   Barucci, M. A., Fulchignoni, M., Burchi, R., and D'Ambrosio, V. 1985. Rotational properties of ten main belt asteroids: Analysis of the results obtained by photoelectric photometry. *Icarus* 61:152–162.

Bar+86   Barucci, M. A., Bockelee-Morvan, D., Brahic, A., Clairemidi, S., Lecacheux, J., and Roques, F. 1986. Asteroid spin axes: Two additional pole determinations and theoretical implications. *Astron. Astrophys.* 163:261–268.

Bey53   Beyer, M. 1953. Der Lichtwechsel und die Lage der Rotationachse des Planeten 433 Eros während der Opposition 1951–52. *Astron. Nachr.* 281:121–130.

Bin84   Binzel, R. P. 1984. 2 Pallas: 1982 and 1983 lightcurves and a new pole solution. *Icarus* 59:456–461.

Bin87   Binzel, R. P. 1987. A photometric survey of 130 asteroids. *Icarus* 72:135–208.

Bin+87   Binzel, R. P., Cochran, A. L., Barker, E. S., Tholen, D. J., Barucci, A., Di Martino, M., Greenberg, R., Weidenschilling, S. J., Chapman, C. R., and Davis, D. R. 1987. Coordinated observations of asteroids 1219 Britta and 1972 Yi Xing. *Icarus* 71:148–158.

Bur+83   Burchi, R., and Milano, L. 1983. 2 Pallas pole revisited. *Moon and Planets* 28:17–21.

Bur+85   Burchi, R., D'Ambrosio, V., Tempesti, P., and Lanciano, N. 1985. Rotational properties of asteroids 2, 12, 80, 145 and 354 obtained by photoelectric photometry. *Astron. Astrophys. Suppl.* 60:9–15.

Cai56   Cailliate, C. 1956. Contribution à l'étude des astéroïdes variables. *Publ. Obs. Lyon* 3, fasc. 28.

Cai60   Cailliate, C. 1960. Contribution; à l'étude des astéroïdes variables. *Bull. Astron.* 23, fasc. 3.

Cel+87   Cellino, A., Zappalà, P., Di Martino, M., Farinella P., and Paolicchi, P. 1987. Flattening, pole and albedo features of 4 Vesta from photometric data. *Icarus* 70:546–565.

Cha+62   Chang, Y. C., and Chang, C.-S. 1962. Photometric investigations of seven variable asteroids. *Acta Astron. Sin.* 10:101–111. In Chinese.

Cha+63   Chang, Y. C., and Chang, C.-S. 1963. Photometric observations of variable asteroids, II. *Acta Astron. Sin.* 11:139–149. In Chinese.

Che+77   Chen, D.-H., Wu, Z.-X., and Yang, X-Y. 1977. Motion in space of the rotation axis of asteroid Eros (433). *Chinese Astron.* 1:321–329.

Dru+86   Drummond, J. D., and Hege, E. K. 1986. Speckle interferometry of asteroids. III. 511 Davida. *Icarus* 67:251–263.

Dr+85a   Drummond, J. D., Cocke, W. J., Hege, E. K., and Strittmatter, P. A. 1985a. Speckle interferometry of asteroids. I. 433 Eros. *Icarus* 61:132–151.

Dr+85b   Drummond, J. D., Hege, E. K., Cocke, W. J., Freeman, J. D., and Christou, J. C. 1985b. Speckle interferometry of asteroids. II. 532 Herculina. *Icarus* 61:232–240.

Dr+88a   Drummond, J. D., Eckart, A., and Hege, E. K. 1988a. Speckle interferometry of asteroids. IV. Reconstructed images of 4 Vesta. *Icarus* 73:1–14.

Dr+88b   Drummond, J. D., Weidenschilling, S. J., Chapman, C. R., and Davis, D. R. 1988b. Photometric geodesy of main-belt asteroids. II. Analysis of lightcurves for poles and shapes. *Icarus* 76:19–77.

Dr+89a*   Drummond, J. D., and Hege, E. K. 1989. Speckle interferometry of asteroids. See their chapter.

Dr+89b*   Drummond, J. D., and Cocke, W. J. 1989. Triaxial ellipsoid dimensions and rotational pole of 2 Pallas from two stellar occultations. *Icarus*, in press.

Dun74   Dunlap, J. L. 1974. Minor planets and related objects. XV. Asteroid (1620) Geographos. *Astron. J.* 79:324–332.

Dun76   Dunlap, J. L. 1976. Lightcurves and the axis of rotation of 433 Eros. *Icarus* 28:69–78.

Dun+69   Dunlap, J. L., and Gehrels, T. 1969. Minor planets. III. Lightcurves of a Trojan asteroid. *Astron J.* 74:796–804.

Dun+73   Dunlap, J. L., Gehrels, T., and Howes, M. L. 1973. Minor planets and related objects. IX. Photometry and polarimetry of (1685) Toro. *Astron. J.* 78:491–501.

Geh67   Gehrels, T. 1967. Minor planets. I. The rotation of Vesta. *Astron. J.* 72:929–938.

Geh+62   Gehrels, T., and Owings, D. 1962. Photometric studies of asteroids. IX. Additional light-curves. *Astrophys. J.* 135:906–924.

Geh+77   Gehrels, T., and Taylor, R. C. 1977. Minor planets and related objects. XXII. Phase functions for (6) Hebe. *Astron. J.* 82:229–237.

Geh+70   Gehrels, T., Roemer, E., Taylor, R. C., and Zellner, B. H. 1970. Minor planets and related objects. IV. Asteroid (1566) Icarus. *Astron. J.* 75:186–195.

Gro+54   Groeneveld, I., and Kuiper, G. P. 1954. Photometric studies of asteroids. I. *Astrophys. J.* 120:200–220.

Han77   Hansen, O. 1977. On the prograde rotation of asteroids. *Icarus* 32:458–460.

Har+79   Harris, A. W., and Burns, J. A. 1979. Asteroid rotation. I. Tabulation and analysis of rates, pole positions and shapes. *Icarus* 40:115–144.

Har+84   Harris, A. W., Carlsson, M., Young, J. W., and Lagerkvist, C. I. 1984. The lightcurve and phase relation of the asteroid 133 Cyrene. *Icarus* 58:377–382.

Har+87   Harris, A. W., Young, J. W., Goguen, J., Hammel, H., Hahn, G., Tedesco, E. F., and Tholen, D. 1987. Photoelectric lightcurves of the asteroid 1862 Apollo. *Icarus* 70:246–256.

Hau58   Haupt, H. 1958. Photoelektrisch-photometrische Studie an Vesta. *Mitt. Sonnenobs. Kanzelhohe* 14:303.

Hol+87   Hollis, A. J., Bembrick, C. S., Dumont, M., and Miles, R. 1987. Photometric properties of the minor planets: Observations of (8) Flora in 1984. *J. British Astron. Assoc.* 97:220–223.

HG+58   van Houten-Groeneveld, I., and van Houten, C. J. 1958. Photometric studies of asteroids. VII. *Astrophys. J.* 127:253–272.

Joh+83   Johnson, P. E., Kemp, J. C., Lebofsky, M. J., and Rieke, G. H. 1983. 10 μm polarimetry of Ceres. *Icarus* 56:381–392.

Kos86   Koshkin, N. I. 1986. The determination of parameters of asteroids with large amplitudes of variation. *Kinem. Phys. Celest. Bodies* 2:44–50.

Kru+36   Krug, W., and Schrutka-Rechtenstamm, G. 1936. Untersuchung über Gestalt und Grösse des Planetoiden Eros. *Z. Astrophys.* 13:1–12.

Lam85   Lambert, J. V. 1985. Occultation and Lightcurve Analysis: The Figure of 2 Pallas. Ph.D. Thesis, New Mexico State Univ.

Lum+81   Lumme, K., Poutanen, M., and Bowell, E. 1981. Photometric determination of asteroid shapes and spin axial directions. *Bull. Amer. Astron. Soc.* 13:719 (abstract).

Lup+83   Lupishko, D. F., and Belskaja, I. N. 1983. Surface, shape and rotation of the M-type asteroid 16 Psyche from UBV photometry in 1978 and 1979. In *Asteroids, Comets, Meteors,* eds. C.-I. Lagerkvist and H. Rickman (Uppsala: Uppsala University), pp. 55–61.

Lu+87a   Lupishko, D. F., and Velichko, F. P. 1987a. Sense of rotation of asteroids 21, 63, 216 and 349. *Kinem. Phys. Celest. Bodies* 3:57–65.

Lup+81   Lupishko, D. F., Velichko, F. P., Tupieva, F. A., and Chernova, G. P. 1981. Asteroid 354 Eleonora: Orientation of rotation axis and U, B, V, photometry. *Soviet Astron. Lett.* 7:241–243.

Lup+85   Lupishko, D. F., Belskaja, I. N., and Velichko, F. P. 1985. *Vestn. Kharkov Univ.* 278:51–56.

Lup+86   Lupishko, D. F., Velichko, F. P., and Shevchenko, V. G. 1986. Asteroid 1627 Ivar. UBV photometry, period and sense of rotation. *Kinem. Phys. Celest. Bodies* 2:39–43.

Lu+87b   Lupishko, D. F., Velichko, F. P., Kazakov, V. V., and Shevchenko, V. G. 1987b. Asteroid 1036 Ganymede, lightcurves, period and sense of rotation. *Kinem. Phys. Celest. Bodies* 3:92–93.

Lu+87c   Lupishko, D. F., Velichko, F. P., Belskaja, I. N., and Shevchenko, V. G. 1987c. Pole coordinates and phase dependence of brightness of the asteroid 21 Lutetia. *Kinem. Phys. Celest. Bodies* 3:36–38.

Mag83   Magnusson, P. 1983. Determination of spin axis orientation for asteroids 44 Nysa, 216 Kleopatra and 624 Hektor. In *Asteroids, Comets, Meteors,* eds. C.-I. Lagerkvist and H. Rickman (Uppsala: Uppsala University), pp. 77–85.

Mag86   Magnusson, P. 1986. Distribution of spin axes and senses of rotation for 20 large asteroids. *Icarus* 68:1–39.

Mag89   Magnusson, P. 1989. Spin vectors of 22 large asteroids. *Icarus*, submitted.

McC+84   McCheyne, R. S., Eaton, N., Green, S. F., and Meadows, A. J. 1984. B and V lightcurves and pole positions of three S-class asteroids. *Icarus* 59:286–295.

McC+85   McCheyne, R. S., Eaton, N., and Meadows, A. J. 1985. Visible and near-infrared lightcurves of eight asteroids. *Icarus* 61:443–460.

Mic88*   Michalowski, T. 1988. Photometric astrometry applied to asteroids: 6, 15, 43, and 624. *Acta Astron.* 38:455–468.

Mil+76 Millis, R. L., Bowell, E., and Thompson, D. T. 1976. UBV photometry of asteroid 433 Eros. *Icarus* 28:53–67.

Mor77 Morrison, D. 1977. Asteroid sizes and albedos. *Icarus* 31:185–220.

Ost85 Ostro, S. J. 1985. Radar observations of asteroids and comets. *Publ. Astron. Soc. Pacific* 97:877–884.

Ost87 Ostro, S. J. 1987. Physical properties of asteroids from radar observations. In *The Evolution of the Small Bodies of the Solar System*, XCVIII Corso (Bologna: Soc. Italiana di Fisica), pp. 131–146.

Pii+85 Piironen, J. O., Poutanen, P., Di Martino, M., and Zappalà, V. 1985. UBV observations and pole determinations of asteroids 15 Eunomia and 354 Eleonora. *Astron. Astrophys. Suppl.* 61:299–302.

Pos+85 Pospieszalska-Surdej, A., and Surdej, J. 1985. Determination of the pole orientation of an asteroid. The amplitude-aspect relation revisited. *Astron. Astrophys.* 149:186–194.

Pou+81 Poutanen, M., Bowell, E., and Lumme, K. 1981. A physically plausible ellipsoidal model of Hektor? *Bull. Amer. Astron. Soc.* 13:725 (abstract).

Ros32 Rosenhagen, J. 1932. Einige Bemerkungen zur Helligkeit und zum Lichtwechsel des Planeten Eros. *Mitt. Wien. Sternw.* 1(2):45–52.

Sat76 Sather, R. E. 1976. Minor planets and related objects. XIX. Shape and pole orientation of (39) Laetitia. *Astron. J.* 81:67–73.

Sca+75 Scaltriti, F., and Zappalà, V. 1975. A photoelectric study of the minor planet 15 Eunomia. *Astron. Astrophys. Suppl.* 19:249–255.

Sc+76a Scaltriti, F., and Zappalà, V. 1976a. A photometric study of the minor planets 192 Nausikaa and 79 Eurynome. *Astron. Astrophys. Suppl.* 23:167–179.

Sc+76b Scaltriti, F., and Zappalà, V. 1976b. Photometric lightcurves and pole determination of 433 Eros. *Icarus* 28:29–35.

Sca+78 Scaltriti, F., Zappalà, V., and Stanzel, R. 1978. Lightcurves, phase function and pole of the asteroid 22 Kalliope. *Icarus* 34:93–98.

Sch+76 Schroll, A., Haupt, H. F., and Maitzen, H. M. 1976. Rotation and photometric characteristics of Pallas. *Icarus* 27:147–156.

Sto40 Stobbe, J. 1940. Die Lichtwechsel des Eros. Teil II: Die Rotation des Eros und ihr Einfluss auf den Lichtwechsel. *Astron. Nachr.* 270:1–24.

Sur+86 Surdej, J., Pospieszalska-Surdej, A., Michalowski, T., and Schober, H. J. 1986. Photoelectric photometry of 22 Kalliope during the 1985 opposition and determination of its pole orientation: The "magnitude-aspect" relations revisited. *Astron. Astrophys.* 170:167–173.

Tay73 Taylor, R. C. 1973. Minor planets and related objects. XIV. Asteroid (4) Vesta. *Astron. J.* 78:1131–1139.

Tay77 Taylor, R. C. 1977. Minor planets and related objects. XXIII. Photometry of asteroid (7) Iris. *Astron. J.* 82:441–444.

Tay78 Taylor, R. C. 1978. Minor planets and related objects. XXIV. Photometric observations for (5) Astraea. *Astron. J.* 83:201–204.

Tay79 Taylor, R. C. 1979. Pole orientations of asteroids. In *Asteroids,* ed. T. Gehrels (Tucson: Univ. of Arizona Press), pp. 480—493.

Tay85 Taylor, R. C. 1985. The pole orientation of asteroid 433 Eros determined by photometric astrometry. *Icarus* 61:490—496.

Tay+83 Taylor, R. C., and Tedesco, E. F. 1983. Pole orientation of asteroid 44 Nysa via photometric astrometry, including a discussion of the method's application and its limitations. *Icarus* 54:13–22.

Tay+76 Taylor, R. C., Gehrels, T., and Capen, R. C. 1976. Minor planets and related objects. XXI. Photometry of eight asteroids. *Astron. J.* 81:778–786.

Tay+85 Taylor, R. C., Tapia, S., and Tedesco, E. F. 1985. The rotation period and pole orientation of asteroid 4 Vesta. *Icarus* 62:298–304.

Tay+87 Taylor, R. C., Birch, P. V., Drummond, J., Pospieszalska-Surdej, A., and Surdej, J. 1987. Asteroid 532 Herculina: Lightcurves, pole orientation and a model. *Icarus* 69:354–369.

Tay+88 Taylor, R. C., Birch, P. V., Pospieszalska-Surdej, A., and Surdej, J. 1988. Asteroid 45 Eugenia. Lightcurves, and the pole orientation. *Icarus* 73:314–323.

Ted+81 Tedesco, E. F., and Sather, R. E. 1981. Minor planets and related objects. XXIX. Asteroid 29 Amphitrite. *Astron. J.* 86:1553–1558.

Ted+85 Tedesco, E. F., and Taylor, R. C. 1985. Pole orientation of 16 Psyche by two independent methods. *Icarus* 61:241–251.

Ted+78   Tedesco, E. F., Drummond, J., Candy, M., Birch, P., Nikoloff, I., and Zellner, B. H. 1978. 1580 Betulia: An unusual asteroid with an extraordinary lightcurve. *Icarus* 35:344–359.

Tem+69   Tempesti, P., and Burchi, R. 1969. A photometric research on the minor planet 12 Victoria. *Mem. Soc. Astron. Italiana* 40:415.

Uch+87   Uchida, K., and Goguen, J. D. 1987. A new method for determining asteroid shapes and rotation poles from lightcurves and its application to 624 Hektor. *Bull. Amer. Astron. Soc.* 19:842 (abstract).

Ves71   Vesely, C. D. 1971. Summary on orientations of rotation axes. In *Physical Studies of Minor Planets*, ed. T. Gehrels, NASA SP-267, pp. 133–140.

Ves+85   Vesely, C. D., and Taylor, R. C. 1985. Photometric lightcurves of 21 asteroids. *Icarus* 64:37–52.

Wat37   Watson, F. 1937. The physical nature of Eros. *Harvard Coll. Obs. Circ.* 419:1–14.

You+85   Young, J. W., and Harris, A. W. 1985. Photoelectric lightcurves and phase relation of the asteroid 505 Cava. *Icarus* 64:528–530.

Zap+84   Zappalà, V., and Knežević, Z. 1984. Rotation axes of asteroids: Results for 14 objects. *Icarus* 59:436–455.

Za+86a   Zappalà, V., and Knežević, Z. 1986a. Pole coordinates of the asteroid 511 Davida as determined via the amplitude-magnitude method. *Icarus* 65:122–128.

Za+86b   Zappalà, V., and Di Martino, M. 1986b. Rotation axes of asteroids via the amplitude-magnitude method: Results for 10 objects. *Icarus* 68:40–54.

Zap+79   Zappalà, V., and van Houten-Groeneveld, I. 1979. Pole coordinates of the asteroids 9 Metis, 22 Kalliope, and 44 Nysa. *Icarus* 40:289–296.

Zap+83   Zappalà, V., Scaltriti, F., and Di Martino, M. 1983. Photoelectric photometry of 21 asteroids. *Icarus* 56:325—344.

Zes32   Zessewitsch, W. 1932. Die Bestimmung der Winkelelemente der Inneren Bewegung von Eros. *Astron. Nachr.* 246:441–450.

Zho+82   Zhou X.-H., and Yang, X.-Y. 1982. The rotation of asteroid (16) Psyche. *Chinese Astron. Astrophys.* 6:57–59.

Glossary

GLOSSARY*

Compiled by Melanie Magisos

a	semimajor axis of an orbit.
A	bolometric Bond or spherical albedo. $A = pq$, where p is the bolometric geometric albedo and q the phase integral.
Å	Ångstrom = 10^{-8} cm.
AAAO	Apollo, Amor, Aten objects. Also called NEA, AAA, Earth-approaching, or planet-crossing asteroids.
ablation	removal of material by attrition, e.g., by passage through the atmosphere.
absolute magnitude	the magnitude of an asteroid at zero phase angle and at unit heliocentric and geocentric distances.
accretion	the process by which matter assembles to form larger bodies such as stars, planets and satellites.
accumulation	*see* accretion.
achondrite	meteorite of nonsolar composition, also known as differentiated stony meteorite.
A class	a rare asteroid taxonomic classification denoted by moderately high albedos and extremely reddish spectra short-

[1193]

	ward of 0.7 μm. A very strong near-infrared absorption feature centered around 1.05 μm is interpreted as being due to olivine.
aeon (AE)	10^9 yr; *see* Gyr.
agglutinate	small objects consisting of glass and fragments of minerals or rocks, all welded together into an aggregate; they are produced by micrometeorite impact into fine-grained unconsolidated regolith.
albedo, Bond	fraction of the total incident light reflected by a spherical body. Bolometric Bond albedo refers to reflectivity over all wavelengths.
albedo, geometric	ratio of planet brightness at zero phase angle to the brightness of a perfectly diffusing disk with the same position and apparent size as the planet. Bolometric geometric albedo refers to reflectivity over all wavelengths.
albedo, hemispherical	fraction of incident light scattered by a surface as a function of angle of incidence.
albedo, normal	the brightness of a surface at zero phase angle relative to a perpendicularly illuminated, perfectly diffusing (Lambert) surface at the same distance as the surface.
albedo, physical	*see* albedo, geometric.
albedo, single-particle scattering	the fraction of incident light scattered by a particle.
albedo, spherical	*see* albedo, Bond.
α	*see* phase angle.
Amor asteroids	asteroids having perihelion distance 1.017 AU $< q \leq 1.3$ AU.
angular momentum	the angular momentum of a system about a specified origin is the sum over all the particles in the system (or an integral over the different elements of the system if it is

continuous) of the vector products of the radius vector joining each particle to the origin and the momentum of each particle. For a closed system it is conserved by virtue of the isotropy of space.

anorthosite — an igneous rock made up almost entirely of plagioclase feldspar.

aphelion — Q, distance of greatest heliocentric separation for a body in an eccentric orbit.

Apollo asteroids — asteroids having semimajor axis $a \geq 1.0$ AU, and perihelion distance $q \leq 1.017$ AU.

arcsec — second of arc, equal to $1/3600$ degree.

aspect — angle between the rotation axis of the body and the radius vector to the Earth.

asteroid — one of a number of objects ranging in size from sub-km to about 1000 km, most of which lie between the orbits of Mars and Jupiter.

asteroid belt — a region of space lying between Mars and Jupiter, where the great majority of the asteroids are found.

asthenosphere — a weak spherical shell located below the lithosphere, in which isostatic adjustments take place, magmas may be generated, and seismic waves are strongly attenuated.

Aten asteroids — asteroids having semimajor axis $a < 1.0$ AU, and aphelion distance $Q > 0.983$ AU.

AU — astronomical unit. The mean distance of the Earth from the Sun, equal to 1.496×10^{13} cm.

aubrite — alternate name for enstatite achondrite. A differentiated stony meteorite consisting predominantly of enstatite with very low Fe content, highly reduced, possibly related to enstatite chondrites.

$B(a,0)$ — mean opposition magnitude in the B band, defined by $B(a,0) = B(1,0) + 5\log a(a - 1)$, where $B(1,0)$ is the

old-style absolute magnitude and a is the semimajor axis in AU.

B(1,0)   old-style B-band absolute magnitude, now superseded by H. $H \approx B(1,0) - 1.0$ mag.

backscatter   scattering of radiation (or particles) through angles greater than 90° with respect to the original direction of motion.

barycenter   the center of mass of a system.

basalt   a dark, fine-grained, mafic igneous rock composed primarily of plagioclase and pyroxene.

basaltic achondrite   collective name for eucrites and howardites which superficially resemble terrestrial basalts or their fragmentation products.

B class   a subclass of the C asteroids, distinguished by higher albedos than the average C type.

blackbody   an idealized body that absorbs all radiation of all wavelengths incident on it. The radiation emitted by a blackbody is a function of temperature only. Because it is a perfect absorber, it is also a perfect emitter.

bolometric   including radiation over all wavelengths.

breccia   a clastic rock composed of angular, broken rock fragments that are embedded into a finer-grained matrix. *See also* genomict, monomict and polymict.

brecciation   breakage of a rock into smaller fragments.

brightness temperature   the temperature that a blackbody would have to have in order to emit radiation of the observed intensity at a given wavelength. This quantity is particularly useful when the Rayleigh-Jeans approximation is valid (as it often is in radio astronomy) because in this approximation it is directly proportional to the specific intensity. It is useful whenever there is reason to believe that it corresponds to a physical temperature; in other cases it merely indicates the radiation's intensity at a given wavelength.

Brownlee particles	*see* IDP.
c	speed of light in a vacuum = 2.998 $\times$ 10^{10} cm s^{-1}.
CAI	calcium, aluminum-rich inclusions. Inclusions rich in these elements are abundant in CV and, to a lesser degree, CM chondrites.
carbonaceous chondrite	a chondritic meteorite, generally containing more than about 0.2 wt% C. Most such chondrites are highly oxidized and have nearly solar composition for all but the most volatile elements. It is the most primitive (least processed) type of meteorite.
cataclastic	a type of structure produced in a rock by severe deformation resulting in fracturing and rotation of mineral grains.
catastrophic disruption	term applied to collisional breakup when the mass of the largest post-impact fragment is $\leq$ 50% of the original target mass.
CCD	charge-coupled device. A solid state detector used for low-light level imaging.
C class	a very common asteroid type in the outer part of the main belt; they typically have flat spectra longward of 0.4 μm and are presumably similar in surface composition to some carbonaceous chondrites. The relative strength of a UV absorption feature may be correlated with the presence of water of hydration. B, F and G are subclasses of the C class.
celestial equator	the projection of the Earth's equator onto the celestial sphere.
chaotic orbit	unpredictable orbit characterized by at least one Lyapunov characteristic exponent strictly positive.
chassignite	a very rare type of achondrite (one known, Chassigny) consisting of olivine with minor amounts of pyroxene, plagioclase, chromite and sulfide.
chondrite	originally defined as a meteorite that contained chond-

	rules; now also implies a chemical composition similar to that of the Sun, for all but the most volatile elements.
chondrite, equilibrated	chondrite that has closely approached or reached internal equilibrium, presumably as a result of thermal metamorphism, so that individual grains of the same mineral have similar compositions.
chondrules	approximately spherical assemblages, characteristic of most chondrites, that existed independently prior to incorporation in the meteorite and that also show evidence for partial or complete melting.
CHON particles	light-element particles rich in carbon, hydrogen, oxygen and nitrogen that are thought to exist in comets.
clast	a rock fragment produced by mechanical weathering of a larger rock and included in another rock.
clathrate	a structure formed by the systematic inclusion of certain molecules in cavities within a crystal lattice.
clinopyroxene	a mineral of the pyroxene group that crystallizes in the monoclinic system.
cm	centimeter.
color index	the difference in magnitudes between any two spectral regions. Color index is always defined as the short-wavelength magnitude minus the long-wavelength magnitude. In the UBV system, the color index for an A0 star is defined as $B-V = U-B = 0$; it is negative for hotter stars and positive for cooler ones.
column density	number of atoms or molecules per cm^2 in the line of sight.
coma	the usually spherical region of diffuse gas, typically 150,000 km in diameter, which surrounds the nucleus of a comet. Together, the coma and the nucleus form the comet's head.
comet	a diffuse body of gas and solid particles (such as CN, C_2, NH_3 and OH), which orbits the Sun. The orbit is usually

highly elliptical or even parabolic (average perihelion distance less than 1 AU; average aphelion distance, roughly 10^4 AU). Comets are unstable bodies with masses on the order of 10^{18} g whose average lifetime is about 100 perihelion passages. Periodic comets comprise only ~4% of all known comets.

comet nucleus — the solid part of a comet, typically a few kilometers (up to tens of kilometers) in diameter, consisting of a mixture of ices and solid silicate and carbonaceous grains.

commensurate orbits — a term applied to two bodies orbiting around a common barycenter when the period of one is an integral multiple of that of the other.

comminution — the reduction of a rock to progressively smaller particles by weathering, impacts, erosion, etc.

condensation — transformation from the gaseous to a solid or liquid phase. In the context of this book, it is generally taken to refer to the formation of solid grains from nebular gas.

conjunction — *see* elongation.

cosmic-ray exposure age — the period of time during which a meteorite was exposed to cosmic radiation, commonly the time between its final reduction in size by impact and its arrival on Earth. More generally, it is the time spent within a few m of the space environment. Nuclear reactions between the radiation and nuclides in the meteorite produce new nuclides, or associated phenomena such as tracks, whose abundances can be used to estimate the exposure age.

cosmic rays — atomic nuclei (mostly protons) that are observed to strike the Earth's atmosphere with exceedingly high energies.

CRAF mission — Comet Rendezvous Asteroid Flyby. A proposed NASA mission to orbit a comet nucleus with at least one asteroid flyby en route. See the chapter by Veverka et al.

crust — the outermost, highly differentiated, solid layer of a planet or satellite, mostly consisting of crystalline rock or ice.

D class	an asteroid type that is rare in the main belt, but becomes increasingly dominant beyond the 2 : 1 Jovian resonance. Their spectra are neutral to slightly reddish shortward of 0.5μm, very red longward of 0.55μm, and for some objects the spectrum tends to flatten longward of 0.95μm. Coloring may be due to kerogen-like materials.
depolarization	randomization of polarization by multiple scattering or single scattering off wavelength-scale structure.
differentiation (in a planet)	a process whereby the primordial substances are separated. Generally metal sinks to the center to form a core, displacing the lighter silicates which form the crust plus mantle.
Doppler spectrum	spectrum of radar echo Doppler shifts due primarily to planet rotation.
dunite	an ultramafic rock composed of at least 90% olivine.
dynamical family	a statistically significant cluster of asteroids in proper element space.
e	eccentricity of an elliptical orbit. The amount by which the orbit deviates from circularity: $e = c/a$, where c is the distance from the center to a focus and a is the semimajor axis.
ECAS	Eight-Color Asteroid Survey (see the chapter by Tholen and Barucci).
E class	a rare asteroid type with featureless 0.3 to 1.1μm spectra (identical to M and P classes) but distinguished by high albedos. Surface composition may be similar to enstatite achondrites.
ecliptic	plane of the Earth's orbit.
ejecta	materials ejected from a crater either by the action of volcanism or a meteoroid impact.
ejecta blanket	the deposit surrounding an impact crater composed of material ejected from the crater during its formation.

elongation	the angle planet-Earth-Sun. Eastern elongations appear east of the Sun in the evening; western elongations, west of the Sun in the morning. An elongation of 0° is called conjunction; one of 180° is called opposition; and one of 90° is called quadrature.
emissivity	ratio of the radiation emitted by a body to that emitted by a blackbody at the same temperature.
EMP	*Ephemerides of Minor Planets,* published yearly by the Russian Academy of Sciences, Institute of Theoretical Astronomy, Leningrad, U.S.S.R.
endogenic	originating within a planetary or planetesimal object.
enstatite chondrite	collective name for the EH and EL classes of chondritic meteorite, highly reduced chondrites with Mg/Si around 0.83.
ephemeris	(pl., ephemerides) a list of computed positions occupied by a celestial body over successive intervals of time.
equilibrium condensation model	a model for the chemical composition of the planets in which solids are hypothesized to have condensed from an initially hot nebula of solar composition, which cools slowly enough so that chemical equilibrium is maintained, and in which accretion takes place rapidly enough so that the solids may be characterized as being due to condensates at a particular temperature, which decreases with increasing distance of the planet from the Sun.
escape velocity	the velocity required to escape entirely from the gravitational field of an object; also the minimum impact velocity for any body arriving from a very great distance.
eucrite	class of achondritic meteorite consisting of Ca-pyroxene and plagioclase.
eV	electron volt $= 1.602 \times 10^{-12}$ ergs.
exogenic	originating externally to a planetary or planetesimal object.

exposure age   *see* cosmic-ray exposure age.

fall   a meteorite that was seen to fall. Such meteorites are usually recovered soon after the fall and are relatively free of terrestrial contamination and weathering effects.

family   a statistically significant cluster of asteroids in proper element space which may share a common origin, perhaps by the collisional disruption of a larger parent body. Members of a "real" family in this sense should have compositions consistent with this interpretation. *See also* Hirayama family.

F class   a subclass of the C asteroids, distinguished by a weak to nonexistent UV absorption feature.

feldspars   common aluminous silicate minerals in meteorites and other rocks. Plagioclase feldspars are members of a solid solution series which varies continuously from sodium-rich to calcium-rich compositions.

find   a meteorite that was not seen to fall but was found and recognized subsequently.

fireball   *see* meteor.

Fourier analysis   the analysis of a periodic function into its simple harmonic components.

g   gram.

g   local gravitational acceleration.

G V-band slope parameter in the H,G magnitude system. $G \approx 0$ pertains to steep phase curves, such as those of low-albedo asteroids; $G \approx 1$ to shallow phase curves, such as those of icy satellites.

gardening   reworking and overturning of a regolith, principally by micrometeoroid bombardment.

gas-retention   the age of a meteorite as calculated from the abundance
  ages   of gaseous daughter products.

G class	a subclass of the C asteroids, distinguished by a strong UV absorption feature.
genomict	a breccia in which the components originated in distinct but genetically closely related rocks.
geocentric	Earth-centered.
granite	an igneous rock associated primarily with the Earth's continental crust, composed chiefly of quartz and alkali feldspar.
gravitational constant, G	the constant of proportionality in the attraction between two unit masses a unit distance apart. $G = 6.668 \times 10^{-8}$ dyn cm^2 g^{-2}.
gravitationally bound rubble pile	an asteroid that has experienced an impact with enough energy to shatter it, but not enough to disperse the fragments, which remain held together by their own gravity.
Gyr	gigayear $= 10^9$ yr.
H	absolute magnitude in the H,G magnitude system. H pertains to the V band unless subscripted otherwise (e.g., H_B). It is the time-averaged magnitude of an asteroid, calculated at zero phase angle and unit heliocentric and geocentric distances. (see the Appendix to the chapter on photometric models by Bowell et al.).
half-life	the time required for half of the radioactive atoms in a sample to disintegrate.
$H(\alpha)$	reduced V-band magnitude of an asteroid at phase angle α as calculated using the H,G magnitude system: $$H(\alpha) = H - 2.5\log[(1 - G)\Phi_1(\alpha) + G\Phi_2(\alpha)],$$ where H is the absolute magnitude, G is the slope parameter and Φ_1 and Φ_2 are specified phase functions (see the Appendix to the chapter on photometric models by Bowell et al.).
heavy bombardment	the period of time, beginning during planetary formation and apparently lasting until about 3.8 billion years ago,

when the cratering rate was high throughout at least the inner solar system.

heliocentric — Sun-centered.

H-function — (the Chandrasekhar H-function) the solution to an integral equation that appears in radiative transfer problems. The H-function describes the results of multiple-scattering in an atmosphere or surface, and depends on the angle of incident or emitted radiation, and on the single-scattering albedo.

H,G magnitude system — a means of calculating the magnitudes of asteroids adopted by the IAU in 1985 (described in the Appendix to the chapter on photometric models by Bowell et al.).

Hill sphere — the approximately spherical region within which a planet, rather than the Sun, dominates the motion of particles.

Hirayama family — same as "family" although it may refer specifically to one of the clusters first noted by K. Hirayama in the early twentieth century.

horseshoe orbit — the motion of an orbiting particle that alternately nearly overtakes another body and then slows down so as to be nearly overtaken by the other body. In a reference frame rotating with the orbit of the other body's orbital motion, the particle follows a horseshoe-shaped path.

howardite — polymict brecciated achondrite consisting predominantly of lithic units similar to eucrites and diogenites, though more extreme compositions are also found.

HST — Hubble Space Telescope (see the chapter by Zellner et al.).

i — inclination of an orbit. The angle between an asteroid's orbit and the plane of the ecliptic (or between a satellite's orbit and the planet's equatorial plane).

IAU — International Astronomical Union.

IAUC — *International Astronomical Union Circulars.*

IDP   interplanetary dust particle, also known as a microme-
                        teoroid or, after entry into the Earth's atmosphere, a mi-
                        crometeorite. Sometimes called Brownlee particle.

igneous   a term used to describe the melting and subsequent solid-
                        ification of a rock.

impact melt   target material that was melted by the heat generated by
                        an impact.

impact strength   energy density (specific energy times target density ρ)
    (S_0)   required to produce a barely catastrophic outcome.

inclusions   aggregates of mineral grains that existed independently
                        prior to incorporation in the meteorite. *See* CAI.

infrared (IR)   that part of the electromagnetic spectrum that lies beyond
                        the red, having wavelengths from about 7500 Å to a few
                        millimeters (about $10^{11} - 10^{14}$ Hz). Infrared radiation
                        can be produced by atomic transitions, or by vibrational
                        (near-IR) and rotational (far-IR) transitions in molecules.
                        Planetary thermal emissions peak in the infrared.

interstellar grains   small solid particles (including silicates) that exist in in-
                        terstellar space; some may have become incorporated
                        into comets and meteorite parent bodies and preserved
                        (i.e., not melted or vaporized through the formative and
                        later periods of solar system history).

IRAS   Infrared Astronomical Satellite (see the chapter by Mat-
                        son et al.).

iron meteorite   a meteorite composed primarily of metallic iron and
                        nickel and thought to represent material from the core of
                        a differentiated parent body.

isochemical   without change in bulk chemical composition.

isomer   one of a number of molecules that all have the same ele-
                        mental composition but which differ from each other in
                        structure.

isothermal   a simplistic thermal model for asteroids and other airless
  latitude model   bodies that assumes the ideal situation of a rapidly rotat-

ing and/or rocky spherical body with the Sun and Earth in the equatorial plane. Thus, the body has a temperature distribution that is isothermal in longitude, i.e., the thermal flux is a function only of equatorial distance (latitude).

isotope | any of two or more forms of the same elements, whose atoms all have the same number of protons but different numbers of neutrons.

IUE | International Ultraviolet Explorer, an Earth-orbiting observatory.

Jacobi ellipsoid | a triaxial figure assumed by a rapidly rotating body of low strength if its specific angular momentum exceeds a critical value. Its shape is determined by self-gravity and centrifugal force, and depends only on the body's density and rotation rate.

Jy | Jansky; $1\ Jy = 10^{-26}\ W\ m^{-2}\ Hz^{-1}$.

k | Boltzmann constant $= 1.38 \times 10^{-16}\ erg\ deg^{-1}$; alternately, $= 8.62 \times 10^{-5}\ eV\ deg^{-1}$.

K | degrees Kelvin, $0\ K = -273C$.

kamacite | Fe,Ni alloy of 7 wt% Ni or less with the body-centered-cubic structure. It occurs as large plates or single crystals in iron meteorites, abundant grains in chondrites and rare grains in most achondrites.

Kepler's laws | 1. Each planetary orbit is an ellipse with the Sun at one focus. 2. (law of areas) Equal areas are swept out in equal times. 3. (harmonic law) The square of the period is proportional to the cube of the distance. Newton's generalized formula for the third law is $P^2 = 4\pi^2 a^3/[G(m_1 + m_2)]$.

Kepler velocity | the orbital velocity of a gravitationally bound object around the central object, i.e., the velocity that leads to a centrifugal force exactly balancing the gravitational attraction between the two objects.

kerogen | insoluble macromolecular organic matter, operationally

defined as the organic residue left after acid demineralization of a rock.

Kirkwood gaps

regions in the asteroid zone which have been swept clear of asteroids by the perturbing effects of Jupiter. They were named for the American astronomer Daniel Kirkwood, who first noted them in 1866.

km

kilometer $= 10^5$ cm.

KREEP

lunar basaltic material rich in radioactive elements (K for potassium, REE for rare earth elements, P for phosphorus).

K/T event

the major break in the history of life on Earth (a mass extinction) that occurred 65 million years ago, between the Cretaceous and Tertiary periods, apparently due to the impact of an asteroidal object.

$L4$

one of the five Lagrangian points.

$L_\odot$

solar luminosity $= 3.826 \times 10^{33}$ erg s^{-1}.

Lagrangian orbit

an orbit in which a particle oscillating about one of the stable Lagrangian equilibrium points defined by the restricted three-body problem moves.

Lagrangian points

the five equilibrium points in the restricted three-body problem. Two of the Lagrange points ($L4$ and $L5$) are located at the vertices of equilateral triangles formed by the two primaries (e.g., Sun and Jupiter) and are stable; the other three are unstable and lie on the line connecting the two primaries. *See* Trojans.

Lambert's law

a simple scattering law according to which the intensity of scattered light is independent of the emission angle. An ideal Lambert surface scatters light uniformly in all directions (i.e., a diffuse scatterer).

late-heavy bombardment

a period of time from about 4.2 to 3.8 Gyr ago when most of the basins and other craters were formed on the Moon and terrestrial planets.

lava

molten rock erupted onto the surface of a planet.

libration   a small oscillation around an equilibrium configuration,
                     such as the angular change in the face that a syn-
                     chronously rotating satellite presents towards the focus
                     of its orbit.

lightcurve   brightness values plotted as a function of time. Note that
                     this plot does not necessarily have to show variability.
                     Lightcurve amplitude: peak-to-peak value in magnitudes
                     of a lightcurve showing variability.

limb   the edge of the apparent disk of a celestial body, as of the
                     Sun, the Moon, a planet or a satellite.

lithology   the physical character of a rock.

lithophile   one of the geochemical classes of elements. Lithophile
                     elements are those which tend to concentrate in the sili-
                     cate phase; e.g., Si, Mg, Ca, Al, Na, K and rare-earth
                     elements.

lithosphere   the stiff upper layer of a planetary body, including the
                     crust and part of the upper mantle, lying above the
                     weaker asthenosphere.

lithostatic   pressure due to the weight of overlying rock.
  pressure

Lommel-Seeliger   a surface with large-scale roughness where shadowing
  surface   effects are important.

Lyapunov   numbers which indicate how fast nearby orbits diverge
  characteristic   and thus the degree of unpredictability of such orbits.
  exponents
  (LCE)

$M_\odot$ mass of Sun $= 1.989 \times 10^{33}$ g.

$M_\oplus$ mass of Earth $= 5.976 \times 10^{27}$ g.

mafic   term used to describe a silicate mineral whose cations are
                     predominantly Mg and/or Fe. It is also used for rocks
                     made up principally of such minerals.

magma   mobile or fluid rock material, lava, generalized to refer

to any material that behaves like silicate magma in the Earth.

magnitude

an arbitrary number, measured on a logarithmic scale, used to indicate the brightness of an object. If l_i is the brightness of star i, and m_i its magnitude, then $m_1 - m_2 = 2.5 \log (l_2/l_1)$. Two stars differing by 5 magnitudes differ in luminosity by a factor of 100. One magnitude difference is the fifth root of 100, or a factor of about 2.512. The brighter the star, the lower the numerical value of the magnitude and very bright objects have negative magnitudes. The star Vega (α Lyrae) is defined to be magnitude zero in the *UBV* system.

main-belt asteroids

asteroids that occupy the main asteroid belt between Mars and Jupiter, sometimes limited specifically to the most populous parts of the belt, from 2.2 to 3.3 AU from the Sun.

mantle

the interior zone of a planet or satellite below the crust and above the core, which is divided into the upper mantle and the lower mantle with a transition zone in between.

mare

(pl., maria) an area on the Moon or Mars that appears darker and smoother than its surroundings. Lunar maria are scattered basaltic flows.

matrix

the fine-grained material that occupies the space in a rock, such as a meteorite, between the larger, well-characterized components such as chondrules, inclusions, etc.

M class

a fairly common asteroid type in the main belt with featureless 0.3 to 1.1 μm spectra (identical to E and P classes) but distinguished by moderate albedos. Presumed to have metallic (Ni-Fe) compositions, but with varying metal contents.

mean motion

usually denoted by μ or n. Average daily motion for an orbiting body $= 2\pi/P$ radians day^{-1} or $360/P$ deg day^{-1}, where P is the orbital period. P may be derived from the semimajor axis using Kepler's third law.

mean motion resonance	a situation in which the ratio of the mean motions of two bodies (or the reciprocals of the revolution periods) is a simple fraction. For example, an asteroid with a semimajor axis of 2.5 AU has an orbital period which is $1/3$ that of Jupiter and is said to be in a $3:1$ resonance. The gravitational influence for the resulting repeated alignments tends to be large and such resonances with Jupiter tend to result in depletions or concentrations of asteroids (see the chapter by Froeschlé and Greenberg).
megaregolith	regolith structure throughout the asteroid.
mesosiderite	class of stony-iron meteorite consisting of subequal proportions of silicate material (related to eucrites and diogenites) and Fe-Ni metal.
metamorphic rock	any rock produced by the physical and chemical alteration (without melting) of another rock that has been subjected to high temperature and pressure.
metamorphism	solid-state modification of a rock, e.g., recrystallization, caused by elevated temperature (and possibly pressure).
meteor	the light phenomenon produced by a meteoroid experiencing frictional heating when entering a planetary atmosphere; also used for the glowing meteoroid itself. If particularly large, it is described as a fireball.
meteorite	a natural object of extraterrestrial origin that survives passage through the atmosphere.
meteoroid	a natural small (sub-km) object in an independent orbit in the solar system.
meteor shower	many meteors appearing to radiate from a common point in the sky caused by the collision of the Earth with a swarm of meteoritic particles.
micrometeorite	a small extraterrestrial particle that has survived entry into the Earth's atmosphere. The actual size is not rigorously constrained but is operationally defined by the collection procedure because small particles are more abundant than large ones. In practice, the microme-

teorites being studied in the laboratory after collection in the stratosphere are rarely as large as 50 μm.

microwave — an electromagnetic wave (in the radio region just beyond the infrared) with a wavelength of from about 1 mm to 30 cm (about 10^9-10^{11} Hz).

Mie theory — a theory of light scattering by small spherical particles.

minor satellite — a satellite of an asteroid.

moment of inertia — the product of the mass of a body and the square of its radius of gyration.

monoclinic — a crystal system characterized by either a single twofold symmetry axis, a single symmetry plane or a combination of the two.

monomict — a breccia in which all components originated in the same type of rock.

Monte Carlo technique — a computational procedure in which random numbers are used to approximate the solution to otherwise intractable mathematical or physical problems.

MPC — *Minor Planet Circulars* (see chapter by Bowell, Chernykh and Marsden).

msec — millisecond = 10^{-3} s.

μm — 1μm = 1 micrometer = 1 micron = 10^{-4} cm.

Myr — 10^6 yr.

nakhlite — a rare type of achondritic meteorite consisting of calcic pyroxene (augite) and olivine.

NEAs — near-Earth asteroids. Specifically Apollo, Amor and Aten asteroids.

nm — nanometer = 10^{-7} cm.

noble gases — the gases He, Ar, Kr, Ne, Xe, Rn which rarely undergo

chemical reactions, also known as inert gases and rare gases.

nodes

the points at which a planet's orbit crosses the plane of the ecliptic. The longitude of the ascending node is one of the six orbital elements and measures the angle between the ascending node and vernal equinox, measured in the plane of the ecliptic.

ν_5

the secular resonance at which the apsidal motion of an asteroid is equal to the fifth secular apsidal frequency. Across the asteroid belt this resonance occurs at a proper inclination near 30° and tends to limit the asteroidal proper inclinations to smaller values.

ν_6

the secular resonance at which the apsidal motion of an asteroid is equal to the sixth secular apsidal frequency. This resonance occurs at a proper inclination that rapidly increases from near 0° just inside the inner edge of the main asteroid belt to a broad maximum around 20° and therefore separates the main belt from the Hungaria and Phocaea regions.

ν_{16}

the secular resonance at which the nodal motion of an asteroid is equal to the sixth secular nodal frequency. This resonance remains near heliocentric distance 2.0 AU even for high proper inclination and divides the Hungaria and Phocaea regions.

obliquity

the angle between a planet's axis of rotation and the pole of its orbit.

occultation

the cutoff of light or radiation from a celestial body (or spacecraft) due to its passage behind another body.

Ockham's razor

Entia non sunt multiplicanda praeter necessitatem ("Things should not be multiplied beyond necessity."). A doctrine formulated by William of Ockham in the fourteenth century. Any hypothesis should be shorn of all unnecessary assumptions; if two hypotheses fit equally well, the one that makes the fewest assumptions should be chosen.

olivine

the most abundant mineral in chondritic meteorites, $(Mg,Fe)_2SiO_4$.

ω	argument of perihelion or periapse for a planet or satellite. Angular distance (measured in the plane of a body's orbit) in the direction of motion from the ascending node to the perihelion point.
ῶ	longitude of perihelion or periapse for a planet or satellite = Ω + ω.
Ω	longitude of ascending node. The angle between some line in the reference plane (usually the direction to the vernal equinox) and the point where the body crosses the reference plane moving south to north.
onion-shell	a hypothetical chondrite parent body in which petrographic types are arranged concentrically.
Oort cloud	a spherical cloud of comets having semimajor axes ≳ 20,000 AU found by J. H. Oort in his empirical study of the orbits of long-period comets. Comets in this shell can be sufficiently perturbed by passing stars or giant molecular clouds so that a fraction of them acquire orbits that take them within the orbits of Jupiter and Saturn.
opacity	a loosely defined term referring to the ability of a medium to extinguish radiation of any given wavelength. In various applications, opacity has been used to mean: (a) optical thickness divided by physical thickness; (b) optical or radio thickness; or (c) mass extinction coefficient.
opposition	*see* elongation.
opposition effect	an enhancement in the brightness of an object when observed at phase angles ≤7°, in excess of that predicted by a linear extrapolation of the brightness vs phase relation from larger phase angles (see the chapter on photometric models by Bowell et al.).
orbital elements	six quantities that fully describe an orbit; along with time, they specify the position of an orbiting body along its path. A typical set of orbital elements are: (1) semimajor axis a; (2) eccentricity e; (3) inclination i; (4) longitude of the ascending node Ω; (5) argument of periapse ω; and (6) the time of passage through periapse, T. An alternative set, as in the *Ephemerides of Minor Planets*

gives the mean anomaly M at an epoch t. These are related by $M = \mu(t - T)$ where μ is the mean motion.

ordinary
chondrite
collective name for the most common variety of chondritic meteorite, subdivided into H, L and LL groups on the basis of Fe content and distribution.

orthopyroxene
a mineral of the pyroxene group that crystallizes in the orthorhombic form.

orthorhombic
a crystal system characterized by three mutually perpendicular two-fold symmetry axes.

osculating orbit
the path that an asteroid would follow if it were subject only to the inverse-square attraction of the Sun or other central body. In practice, secondary bodies such as Jupiter produce perturbations. Thus osculating orbital elements are subject to variations over time.

oxidation
the process of adding O to, or removing H from, an element (or of increasing the element's valence, i.e., oxidation state).

p
geometric albedo. The ratio of the brightness of an asteroid to that of a perfectly scattering screen of the same cross-sectional area and in the same place, both being illuminated and viewed normally.

p_H
V-band geometric albedo calculated using the H,G magnitude system.

p_V
geometric albedo; p_V, the geometric albedo with the V filter of the UBV system.

paired falls
meteorite specimens originally recovered some distance apart and hence given separate names, but later recognized as fragments of a single parent mass, on the basis of classification, cosmic-ray or gas-retention age, texture, or other diagnostic features.

pallasite
class of stony-iron meteorites in which the Fe-Ni metal forms a continuous framework enclosing nodules of the silicate olivine.

parent body   the object on or in which a given meteorite or class of meteorites was located prior to ejection as ~meter-sized objects. Also used to refer to the precursor body of an asteroid family.

P class   a fairly common asteroid type in the outer main belt with a heliocentric distribution that peaks near the 3 : 2 Jovian resonance. Their spectra are featureless from 0.3 to 1.1μm (identical to E and M classes) but the class is distinguishable by low albedos.

perihelion q, distance of least heliocentric separation for a body in an eccentric orbit.

permanent designation   the numbers and names, beginning with 1 Ceres, given to asteroids for which orbits are accurately determined. Asteroid 4000 was numbered in February 1989. The numbers are supplied by the Minor Planet Center after orbits have been fitted to observations at several different oppositions. Names are proposed by discoverers to the Minor Planet Names committee of IAU Commission 20 and cannot be adopted until at least two months after an asteroid is numbered. If the discoverer is deceased there is a waiting period of six months, and names are usually proposed by the orbit identifier or by the discoverer's former colleagues.

perturbation   the gravitational effect of one object on the orbit of another, if this effect is very small.

phase angle α, the solar phase angle: the angle subtended at the center of the planet by the vectors direction to the Sun and observer.

phase angle bisector   the direction, or position in the sky, which is the mean between the geocentric position and the heliocentric position of the asteroid. If one were to bisect the angle formed by the lines to the Sun and the Earth, from the asteroid, the resultant line would be in the direction of the phase angle bisector.

phase curve   a plot showing the brightness (reduced to common heliocentric and observer distances) of a planet, satellite, or asteroid vs phase angle.

phase integral   the relationship between the geometric and Bond albedos
                     of a body: $A = pq$, where A is the bolometric Bond al-
                     bedo, p is the bolometric geometric albedo and q is the
                     phase integral.

photometry   the measurement of light intensities.

phyllosilicate   one of a family of silicate minerals characterized by a
                     structure that consists of sheets or layers, invariably
                     hydrated.

pixel   picture element. Electronic images are composed of
                     pixels arranged in rows and columns.

plagioclase   a mineral group, formula $(Na,Ca)Al(Si,Al)Si_2O_8$; a solid
                     solution series from $NaAlSi_3O_8$ (albite) to $CaAl_2Si_2O_8$
                     (anorthite), triclinic. It is one of the most common rock-
                     forming minerals.

planetesimal   small rocky or icy body formed from the primordial solar
                     nebula, perhaps having sizes ranging up to 10 km, out of
                     which all larger solar system members are presumed to
                     have accumulated.

planetocentric   centered on a planet. A satellite is in a planetocentric (as
                     opposed to heliocentric) orbit. A planetocentric coordi-
                     nate system is subtended at the planet's center.

plasma   the completely ionized gas, the so-called fourth state of
                     matter in which the temperature is too high for atoms, as
                     such, to exist and which consists of free electrons and
                     free atomic nuclei.

PLS   Palomar-Leiden Survey of Faint Asteroids (see chapter
                     by Bowell, Chernykh and Marsden).

polarization   the action or process of affecting radiation, especially
                     light, such that the vibrations assume some definite
                     form. Light which has encountered an index of refraction
                     boundary will have different reflection coefficients de-
                     pending on the orientation of the electric vector. Polariz-
                     ation is defined as negative if the light reflected from a
                     boundary is greater in the plane given by the scattering
                     plane (source-boundary-observer) than in the perpen-

dicular plane. If the light intensity is the same in both perpendicular and parallel directions, the light is unpolarized, and if it is greater in the perpendicular direction, the polarization is called positive (see the chapter by Dollfus et al.).

polymict	a breccia in which the components originated in two or more rocks of differing compositions.
Poynting-Robertson effect	an effect of radiation on a small particle orbiting the Sun that causes it to spiral slowly toward the Sun. It occurs because the orbiting particle absorbs energy and momentum streaming radially outward from the Sun, but reradiates this energy isotropically in its own frame of reference.
ppm	parts per million, generally by weight. This type of measurement is also often given by the term $\mu g/g$.
precession	a slow, periodic conical motion of the rotation axis of a spinning body.
preliminary designation	the system for designating asteroids upon discovery and before their orbits are well-enough determined that they can be given a permanent number and name. The designations are supplied by the Minor Planet Center and consist of the year of discovery, an upper case letter to indicate the halfmonth in that year (A = Jan. 1–15, B = Jan. 16–31, . . ., Y = Dec. 16–31, I being omitted), a second upper case letter in sequence, and when this sequence of 25 (I again being omitted) has been completed it is repeated and followed by a sequential number (written as a subscript, if possible). Before 1925 the system consisted simply of a sequential pair of letters (and initially only a single letter), and the subsequent interpolation of additional objects was troublesome. The modern system is therefore now also used for unnumbered pre-1925 objects, except that the initial 1 in the year is replaced by A.
primitive	in planetary science and meteoritics, a type of object or rock that is little changed chemically since its formation, hence representative of the conditions in the solar nebula at the time of formation of the solar system.

prograde motion

motion in the same direction as the prevailing direction of motion. As viewed from the north, prograde motion is counter-clockwise, or west to east.

proper elements

orbital elements from which the effects of planetary perturbations have been removed.

protoplanet

a precursor body from which a planet develops.

pyroxenes

a group of common rock-forming silicates which have ratios of metal oxides (MgO, FeO or CaO) to SiO_2 of $1:1$. These are called metasilicates. Pure members of this group are $MgSiO_3$ (enstatite), $FeSiO_3$ (ferrosilite). Pure $CaSiO_3$ does not crystallize with the pyroxene structure. Ca does substitute for up to 50% of the Mg and Fe in the pyroxene structure.

q

perihelion distance, $q = a(1 - e)$.

q

phase integral. The brightness of an asteroid summed over all phase angles.

Q

aphelion distance, $Q = a(1 + e)$.

Q class

a rare asteroid classification denoted by moderate albedos and spectra with a strong absorption feature shortward of 0.7 μm and a modest absorption feature centered near 1 μm. The spectra are interpreted as being similar to ordinary chondrites. At present this asteroid type has only been identified for 1862 Apollo and a few other near-Earth asteroids.

quadrature

see elongation.

$R_\odot$

solar radius $= 6.96 \times 10^{10}$ cm.

radar cross section

effective projected area of a radar target calculated on the assumption of a perfect, isotropic reflector. It is often expressed as a dimensionless quantity normalized by the true projected area of the target (planet or asteroid).

radioactive age dating

the technique of determining the ages of rocks, meteorites, or other specimens by the amount of decay of certain radioactive elements contained therein.

rare-earth element (REE)	one of the elements with atomic numbers from 57 to 71, inclusive, in the lanthanide series of the periodic table.
Rayleigh-Jeans law	an approximation of Planck's blackbody formula valid at long wavelengths ($h\nu \ll kT$): $B_\nu(T) \approx 2kT\nu^2/c^2$. It is often used in radio astronomy; the brightness temperature of a source observed with a radio telescope is the temperature required to fit the observed specific intensity with the Rayleigh-Jeans formula.
R class	a rare asteroid classification exemplified by 349 Dembowska and denoted by moderately high albedos and spectra with a strong absorption feature shortward of 0.7 μm and a fairly strong absorption feature centered near 1 μm.
RD objects	an old term used to describe asteroids with very low albedos and reddish spectra; now called D asteroids.
refractory	term describing the high-temperature stability of an element or phase. The opposite of volatile.
regolith	the layer of fragmental incoherent rocky debris that nearly everywhere forms the surface terrain; it is produced by meteoritic impact on the surfaces of the planets, satellites or asteroids.
regolith breccia	fragmental breccias containing some identifiable regolith component such as solar-wind gas.
resonance	the enhanced response of any oscillating system to an external stimulus that has the same driving frequency as the natural frequency of the system; higher-order resonances occur when these frequencies are commensurable.
restricted three-body problem	two bodies assumed to be point masses and called primaries revolve around their center of mass under the influence of their mutual attraction. The problem is to determine the motion of a third body attracted by the previous two but not influencing their motion.
retrograde motion	the opposite of prograde motion.
rms	root mean square. The square root of the mean square value of a set of numbers.

Roche limit — the minimum distance at which a fluid satellite influenced by its own gravitation and that of a central mass can be in mechanical equilibrium. For a satellite of zero tensile strength, and the same mean density as its primary, in a circular orbit around its primary, this critical distance is 2.44 times the radius of the primary.

saturation equilibrium — the case where a surface has accumulated so many craters (of a particular size) that subsequent craters tend to destroy (by overlapping and other processes) roughly equal numbers of pre-existing craters.

Schmidt telescope — a type of reflecting telescope (more accurately, a large camera) in which the coma produced by a spherical concave mirror is compensated for by a thin correcting lens placed at the opening of the telescope tube. The Palomar 122-cm Schmidt has a usable field of 6°.

S class — a very common asteroid class in the inner main belt with moderate albedos and reddish spectra shortward of 0.7 μm and moderate to nonexistent absorption features in the near-infrared. May be similar to stony-iron meteorites, but their meteoritical interpretation is uncertain.

secular perturbations — averaged perturbations experienced by planets and asteroids when the effects that depend upon the actual positions of the objects in their orbits are eliminated. The classical procedure, due originally to Lagrange, expresses the long-term variations of the eccentricities and perihelion longitudes in terms of constant "proper" eccentricities, one corresponding to each object, and "proper" perihelion longitudes that are linear functions of the time. An analogous process gives the long-term variations of the inclinations and nodal longitudes in terms of constant "proper" inclinations and "proper" nodal longitudes that are linear functions of the time. In this scheme there are, by definition, no secular changes in the semimajor axis.

secular resonance — a situation in which the rate of the precession of the proper longitudes of the nodes or perihelion of an asteroid's orbit (called nodal and apsidal frequencies) is equal to one of the nodal or apsidal frequencies associated with the mutual secular perturbations of the major planets. Over a long period of time an asteroid near a

secular resonance can experience large perturbations. For orbits of low (proper) eccentricity and inclination, the principal secular resonances, largely arising from the mutual perturbations of Jupiter and Saturn, occur at a heliocentric distance of about 2.0 AU (see the chapter by Scholl et al.).

shergottite — a rare type of meteorite, consisting of pyroxene (pigeonite) and maskelynite.

shock wave (or shock front) — discontinuity in temperature and pressure propagating in a solid, liquid or gas with supersonic velocity, caused by impact or explosion.

sidereal period — the time it takes for a planet or satellite to make one complete rotation or revolution relative to the stars.

siderophile — one of the geochemical classes of elements. Siderophile elements are those which tend to go into the metal phase, e.g., Ni, Co, Au, As, Ge, Ga, Ir, Os, Re.

silicate — any of a wide range of rocks and minerals composed in part of silica (silicon and oxygen).

SIRTF — Space Infrared Telescope Facility (see the chapter by Zellner et al.).

SNC meteorites — a group of uncommon, but apparently genetically related meteorite types which are highly differentiated (the shergottites, nahklites, and Chassigny). They may originate from Mars.

solar nebula — the gas-dust disk that surrounded the protosun. Mass of the solar nebula is usually assumed to be in the range from 0.02 to 0.05 $M_\odot$ The term protoplanetary cloud is also sometimes used as a synonym for the solar nebula.

solar wind — the energetic charged particles that flow radially outward from the solar corona, carrying mass and angular momentum away from the Sun.

solidification age — the most common age determined by radioactive dating techniques—the time since the rock or mineral grain being tested solidified from the molten state, thus isolating itself from further chemical changes.

specific energy   kinetic energy per unit mass.

standard thermal   a simplistic thermal model for asteroids and other airless
   model   bodies that assumes the ideal situation of a nonrotating
                         spherical body in instantaneous equilibrium with insola-
                         tion. It also assumes that the sub-solar and sub-Earth
                         points on the body coincide. The thermal emission is a
                         function only of sub-solar distance

steradian   the solid angle which, having its vertex in the center of a
                         sphere, cuts out an area of the surface of the sphere equal
                         to that of a square with sides of length equal to the radius
                         of the sphere. A complete sphere contains 4π steradians.

Stokes   four parameters to describe fully a beam of polarized
   parameters   light. They involve the maximum and minimum inten-
                         sity, the ellipticity, and the direction of polarization.

stony-iron   a fairly rare kind of differentiated meteorite, composed
   meteorite   of a mixture of silicates with metallic iron-nickel, thought
                         to have originated near the core-mantle boundary of a
                         differentiated parent body.

sub-Earth point   point on the surface of a body from which the Earth is
                         seen at the zenith.

sub-solar point   point on the surface of a body from which the Sun is seen
                         at the zenith.

superclasses   groupings of asteroid taxonomic classes into large cate-
                         gories such as primitive, igneous and metamorphic (see
                         the chapter by Bell et al.).

surface of section   sub-space of the phase space of a dynamical system or
                         more generally the set of the successive in intersections
                         of a trajectory with this subspace.

synchronous   rotation of a body so that it always keeps the same face
   rotation   toward another object; the situation where the periods of
                         rotation and revolution of an orbiting body are equal.

synodic period   the period of revolution of one body about another with
                         respect to the Earth (synodic period)$^{-1}$ $= \pm$ (sidereal
                         period)$^{-1}$ $\mp$ (Earth's period)$^{-1}$.

taxonomic
classifications

a system for categorizing similar observed properties of asteroids, such as color or spectral properties and albedo. Letters such as A, B, C, D, E, F, G, M, P, Q, S, T, V are used to denote currently recognized distinct classes (see the chapter by Tholen and Barruci).

T class

a class of low albedo asteroids having spectra with a moderate absorption feature shortward of 0.85μm and generally flat in the near-infrared.

terrestrial age

the period of time since the fall of a meteorite.

thermal
conductivity

the proportionality constant that gives the amount of heat conducted through a unit cross section in unit time under the influence of unit heat gradient. cal cm^{-2} s^{-1} k^{-1}.

thermal emission

the emission of electromagnetic radiation from a body due to its temperature and emissivity.

thermal emission
spectrum

the thermal emission from a body measured as a function of wavelength.

thermal inertia

a material parameter which indicates the rate at which a body's temperature responds to changing heat input. It is proportional to the square root of the product of thermal conductivity and volume heat capacity.

thermophysical
model

a thermal model for asteroids and other airless bodies that lies between the standard thermal and isothermal latitude models. It takes into account the thermophysical properties of the body and may also include spin axis and direction as well as shape.

tisserand
invariant

a pseudo-constant of the motion in the restricted three-body problem based on the Jacobi integral, used to identify returning short-period comets, even though their orbits may have been perturbed by a close Jupiter encounter:

$$T = a_J/a + 2\sqrt{(a/a_J)\,(1 - e^2)}\,\cos i$$

where a, e, and i are the semimajor axis, eccentricity, and inclination (to the plane of Jupiter's orbit), respec-

tively, of the comet's orbit, and a_J is Jupiter's semimajor axis.

Titius-Bode law   a mnemonic device discovered by Titius in 1776 and advanced by Bode in 1772, used for remembering the distances of the planets from the Sun. Take the series 0, 3, 6, 12, . . . ; add 4 to each member of the series, and divide by 10. The resulting sequence 0.4, 0.7, 1.0, 1.6, . . . gives the approximate distance from the Sun (in AU) of Mercury, Venus, Earth, Mars, . . . , out to Uranus. The law fails for Neptune and beyond. Its value at 2.8 spurred a search for a "missing" planet between Mars and Jupiter.

TRIAD   Tucson Revised Index of Asteroid Data, published in the book *Asteroids,* ed. T. Gehrels (Tucson: Univ. of Arizona Press, 1979), pp. 1011–1154.

Trojans   Trojan asteroids occur in orbits librating around two of the Lagrangian points, namely the ones preceding and following Jupiter in its orbit, equidistant from the Sun and Jupiter.

T Tauri stars   young, late-type stars that are precursors to solar-mass stars characterized by emission line spectra, infrared excesses, and irregular variability. The prototype for this class of stars is T Tauri.

T Tauri wind   outflow from a T Tauri star.

UBV system   a system of stellar magnitudes devised by Johnson and Morgan at the Yerkes Observatory which consists of measuring an object's apparent magnitude through three color filters: the ultraviolet (U) at 3600 Å; the blue (B) at 4200 Å; and the "visual" (V) in the green-yellow spectral region at 5400 Å. It is defined so that, for A0 stars, $B - V = U - B = 0$; it is negative for hotter stars and positive for cooler stars. Filters at other wavelengths are also used and indicated with letters R, I, H, J, K, L, M, etc.

UCAS   United Kingdom Schmidt-California Institute of Technology Asteroid Survey (see chapter by Bowell, Chernykh and Marsden).

ultramafic   an igneous rock consisting predominantly of mafic sili-
                  cate minerals.

ultraviolet (UV) that part of the electromagnetic spectrum that lies at
                  wavelengths shortward of about 3500Å. UV absorption
                  features in asteroid spectra result from charge transfer
                  mechanisms. X rays and gamma rays occur at wave-
                  lengths shortward of 300Å.

Universal Time   the local mean time of the prime meridian. It is the same
  (UT)   as Greenwich mean time, counted from 0 hr beginning at
                  Greenwich mean midnight.

ureilite   class of carbon-rich achondritic meteorite in which the
                  silicates consist of olivine and pigeonite.

$V(\alpha)$ reduced magnitude. The observed magnitude of an as-
                  teroid at phase angle α converted to unit heliocentric and
                  geocentric distances. In the V band $V(\alpha) = V_{obs}(\alpha) -$
                  $5\log r\Delta$, when r and Δ are, respectively, the heliocentric
                  and geocentric distances in AU.

Väisälä orbits   orbits computed on the assumption that the heliocentric
                  radial velocity is zero, i.e., the object is taken to be at peri-
                  helion or aphelion (or in a circular orbit as a special case).
                  Series of Väisälä orbits with different eccentricities can be
                  derived very simply from only two observations, and they
                  are often useful in identifying further observations.

V class   a rare asteroid classification exemplified by 4 Vesta.
                  Spectra are very red shortward of 0.5 μm, moderately
                  red from 0.5 to 0.7 μm, and show a strong near-infrared
                  absorption feature centered around 0.95 μm. Surface
                  composition may be similar to basaltic achondrites.

vernal equinox   the intersection of ecliptic and celestial equator where
                  the Sun is moving from south to north.

volatile   an element that condenses from a gas or evaporates from
                  a solid at a relatively low temperature.

xenolith   fragment in a rock or meteorite foreign to its host.

Yarkovsky effect the effect of rotation on the trajectory of a small particle

orbiting the Sun (compare Poynting-Robertson effect). If the orbiting body is rotating, there is a temperature variation over its surface, and it will reradiate the incident radiation anisotropically.

zodiac

a belt around the sky that is 18° wide and centered on the ecliptic, within which are found the Moon and planets.

zodiacal light

a faint glow that extends away from the Sun in the ecliptic plane of the sky, visible to the naked eye in the western sky shortly after sunset or in the eastern sky shortly before sunrise. Its spectrum indicates it to be sunlight scattered by interplanetary dust. The zodiacal light contributes about a third of the total light in the sky on a moonless night.

Acknowledgments and List of Contributors

ACKNOWLEDGMENTS AND
LIST OF CONTRIBUTORS

Many people contributed to the production of this book, as members of the organizing committee, authors, referees, conference participants, or otherwise. Their names and addresses follow.

J. Abraham, *Saturday Evening Post,* 8111 W. 8th St., Zionsville, IN 46077

M. F. A'Hearn, Astronomy Program, University of Maryland, College Park, MD 20742

M. A. Allen, MS 183-601, Jet Propulsion Laboratory, 4800 Oak Grove Dr., Pasadena, CA 91109

E. Anders, Enrico Fermi Institute, 5630 S. Ellis Ave, University of Chicago, Chicago, IL 60637

L. Anselmo, CNRCE/CNR, via S. Maria 36, I-56100, Pisa, Italy

S. K. Atreya, Space Research Bldg., University of Michigan, Ann Arbor, MI 48109

M. A. Barucci, Observatoire de Paris, DAEC, 5, Place J. Janssen, 92195 Meudon Principal, France

A. T. Basilevsky, V. I. Vernadsky Institute of Geochemistry, Kosygin St. 19, 117975, GSP-1, V-334 Moscow, USSR

J. F. Bell, Planetary Geosciences Division, Hawaii Institute of Geophysics, 2525 Correa Rd., Honolulu, HI 96822

M. J. S. Belton, Kitt Peak National Observatory, P.O. Box 26732, Tucson, AZ 85726

R. P. Binzel, Mail Code 54-418, Massachusetts Institute of Technology, Cambridge, MA 02139

M. Blaine, The Composing Room of Michigan Inc., Box 2048, Grand Rapids, MI 49501

D. D. Bogard, NASA Johnson Space Flight Center, Code SN4, Houston, TX 77058

E. L. G. Bowell, Lowell Observatory, P.O. Box 1269, Flagstaff, AZ 86002

W. V. Boynton, Lunar and Planetary Laboratory, University of Arizona, Tucson, AZ 85721

A. Brahic, Observatoire de Paris, 92190 Meudon, France

D. Britt, Dept. of Geological Science, Box 1846, Brown University, Providence, RI 02912

R. H. Brown, MS 183-501, Jet Propulsion Laboratory, 4800 Oak Grove Dr., Pasadena, CA 91109

R. Burchi, Osservatorio Collurania, 63100 Teramo, Italy

J. A. Burns, Space Science Bldg., Cornell University, Ithaca, NY 14853

E. Bus, Lunar and Planetary Laboratory, University of Arizona, Tucson, AZ 85721

S. J. Bus, Lowell Observatory, 1400 W. Mars Hill Rd., Flagstaff, AZ 86001

H. Campins, Planetary Science Institute, 2030 E. Speedway Blvd., Suite 201, Tucson, AZ 85719

F. Capaccioni, Reparto di Planetolgia, viale dell' Università n. 11, 00185 Rome, Italy

M. T. Capria, CNR-IAS, CP 67, 00022 Frascati, Italy

M. Carpino, Osservatorio Astronomico di Brera, via Brera 28, I-20121 Milano, Italy

A. Carusi, Istituto di Astrofisica Spaziale, Reparto di Planetologia, viale dell' Università 11, 00185 Rome, Italy

C. Casacci, Aeritalia Space Systems Group, Corso Marche 41, Torino, Italy

P. Cassen, MS 245-3, NASA Ames Research Center, Moffett Field, CA 94035

V. Castellani, Osservatorio Teramo, Teramo, Italy

A. Cellino, Osservatorio Astronomico di Torino, Strada Osservatorio 20, 10025 Pino Torinese, Italy

P. Cerroni, Istituto di Astrofisica Spaziale, Reparto di Planetologia, viale dell' Università 11, 00185 Rome, Italy

C. R. Chapman, Planetary Science Institute, 2030 E. Speedway Blvd., Suite 201, Tucson, AZ 85719

N. S. Chernykh, Crimean Astrophysical Observatory, Nauchnyj, 334413 Crimea, USSR

J. M. Cline, 4277 Chula Bend, Flintridge, CA 91011

A. L. Cochran, Dept. of Astronomy, University of Texas, Austin, TX 78712

W. D. Cochran, Dept. of Astronomy, University of Texas, Austin, TX 78712

K. Cole, Science Applications International Corp., 1701 E. Woodfield Rd., Suite 819, Schaumburg, IL 60173

C. Cook, University of Arizona Press, 1230 N. Park, Suite 102, Tucson, AZ 85719

S. F. Cox, University of Arizona Press, 1230 N. Park, Suite 102, Tucson, AZ 85719

D. P. Cruikshank, MS 245-6, NASA Ames Research Center, Moffett Field, CA 94035

C. J. Cunningham, 250 Frederick St., Apt. 101, Kitchener, Ontario N2H 2NI, Canada

J. K. Davies, Royal Observatory, Blackford Hill, Edinburgh EH 17 8BP, Scotland

D. R. Davis, Planetary Science Institute, 2030 E. Speedway Blvd., Suite 201, Tucson, AZ 85719

K. Denomy, Lunar and Planetary Laboratory, University of Arizona, Tucson, AZ 85721

I. DePater, Astronomy Dept., Campbell Hall, University of California, Berkeley, CA 94720

F. Marzari, Dipartimento di Fisica "G. Galilei," via F. Marzolo, 8, I-35131 Padova, Italy

D. L. Matson, MS 183-501, Jet Propulsion Laboratory, 4800 Oak Grove Dr., Pasadena, CA 91109

M. S. Matthews, Lunar and Planetary Laboratory, University of Arizona, Tucson, AZ 85721

A. Maury, Palomar Observatory, 105-24, California Institute of Technology, Pasadena, CA 91125

L. A. McFadden, California Space Institute, A016, University of California at San Diego, La Jolla, CA 92093

E. McFarlane, Lunar and Planetary Laboratory, University of Arizona, Tucson, AZ 85721

D. W. McGarvie, Dept. of Earth Sciences, The Open University, Walton Hall, Milton Keynes, MK7 6AA, England

D. S. McKay, Code SN4, NASA Johnson Space Center, Houston, TX 77058

W. B. McKinnon, Dept. of Earth and Planetary Science, Washington University, St. Louis, MO 63130

R. S. McMillan, Lunar and Planetary Laboratory, University of Arizona, Tucson, AZ 85721

H. J. Melosh, Lunar and Planetary Laboratory, University of Arizona, Tucson, AZ 85721

J. Miller, Lunar and Planetary Laboratory, University of Arizona, Tucson, AZ 85721

R. L. Millis, Lowell Observatory, P.O. Box 1269, Flagstaff, AZ 86001

H. Mizutani, Institute of Space and Astronautical Science, Tokyo, Japan

D. Möhlmann, Institut für Kosmosforschung, Rudower Chassee 5, DDR-1199 Berlin-Adlershof, East Germany

D. Morrison, Institute for Astronomy, 2680 Woodlawn Dr., Honolulu, HI 96822

C. Murray, Dept. of Physics, Mile End Road, Queen Mary College, London E1 4NS, England

M. Nelson, Planetary Geosciences Div., Hawaii Institute of Geophysics, 2525 Correa Rd., Honolulu, HI 96822

H. E. Newsom, Institute of Meteoritics, University of New Mexico, Albuquerque, NM 87131

P. D. Nicholson, Astronomy Dept., Space Science Bldg., Cornell University, Ithaca, NY 14853

A. M. Nobili, Gruppo di Meccanica Spaziale, Dipartimento di Matematica, Università di Pisa, via Buonarroti 2, I-56100 Pisa, Italy

M. C. Nolan, Lunar and Planetary Laboratory, University of Arizona, Tucson, AZ 85721

J. Oberst, Institute for Geophysics, University of Texas, Austin, TX 78751

G. Ojakangas, Lunar and Planetary Laboratory, University of Arizona, Tucson, AZ 85721

D. Olsson-Steel, Institute for Astronomy, Lunds Universitet, Lund Observatory, Sweden

S. J. Ostro, MS 300-233, Jet Propulsion Laboratory, 4800 Oak Grove Dr., Pasadena, CA 91130

P. D. Owensby, Hawaii Institute of Geophysics, 2525 Correa Rd., Honolulu, HI 96822

P. Paolicchi, Istituto di Astronomia, Piazza Torricelli 2, I-56100 Pisa, Italy

C. Patterson, MS J569, Los Alamos National Laboratory, P.O. Box 1663, Los Alamos, NM 87545

P. Pellas, Laboratoire de Minéralogie du Museum, 61 Rue Buffon, F-75005 Paris, France

J. Peltoniemi, Observatory and Astrophysical Laboratory, University of Helsinki, Tähtitornin-mäki, 00130 Helsinki, Finland

E. Perozzi, Osservatorio Astronomico Collurania, I-64100, Teramo, Italy

A. Perret, CNES, 18 ave. Ed. Belin, 31055 Toulouse, France

C. Pieters, Geology Dept., Brown University, Providence, RI 02912

F. Pilcher, Illinois College, Jacksonville, IL 62650

J. R. Piscitelli, Institute of Astronomy, University of Hawaii, Honolulu, HI 96822

C. Porco, Lunar and Planetary Laboratory, University of Arizona, Tucson, AZ 85721

A. Porter, National Optical Astronomy Observatories, 950 N. Cherry, Tucson, AZ 85719

S. D. Price, OPI/Stop 30, Air Force Geophysics Lab, Hanscom Air Force Base, MA 011731

M. Prinz, Dept. of Mineralogy, American Museum of Natural History, Central Park West at 79th St., New York, NY 10024

J. Rahe, Code EL, NASA Headquarters, Washington, DC 20546

J. Raitala, Dept. of Astronomy, University of Oulu, 90570 Oulu, Finland

J. J. Rawal, Nehru Planetarium, Nehru Centre, Dr. Annie Besant Road, Worli, Bombay 400018, India

R. O. Redman, Radio Astronomy Section, Herzberg Institute of Astrophysics, NRC of Canada, 1200 Sussex Dr., Ottawa, K1A, OR6, Canada

H. Reitsema, Ball Aerospace Systems Group, P.O. Box 1062, Boulder, CO 80306

H. Rickman, Astronomiska Observatoriet, Box 515, S-75120 Uppsala, Sweden

E. Roemer, Lunar and Planetary Laboratory, University of Arizona, Tucson, AZ 85721

D. J. Rudy, Dept. of Earth and Space Sciences, University of California, Los Angeles, CA 90024

K. Russell, U.K. Schmidt Telescope, Private Bag, Coonabarabran NSW 2357, Australia

A. Ruzicka, Lunar and Planetary Laboratory, University of Arizona, Tucson, AZ 85721

T. V. Ruzmaikina, Institute of Physics of the Earth, B Gruzushaya 10, Moscow 123242, USSR

E. Ryan, Planetary Science Institute, 2030 Speedway Blvd., Suite 201, Tucson, AZ 85719

V. S. Safronov, Institute of Physics of the Earth, B Gruzushaya 10, Moscow 123242, USSR

S. Sawyer, Astronomy Dept., University of Texas, Austin, TX 78712

T. Schemenauer, Lunar and Planetary Laboratory, University of Arizona, Tucson, AZ 85721

H. Scholl, Observatoire de Nice, BP 139, 06003 Nice-Cedex, France

J. Schubart, Astronomisches Rechen-Institut, Monchhofstrasse 12–14, D-6900 Heidelberg, West Germany

L. Schultz, Max-Planck-Institut für Chemie, Saarstrasse 23, D-6500 Mainz, West Germany

E. R. D. Scott, Dept. of Geology, University of New Mexico, Albuquerque, NM 87131

J. V. Scotti, Lunar and Planetary Laboratory, University of Arizona, Tucson, AZ 85721

C. S. Shoemaker, U.S. Geological Survey, 2255 N. Gemini Dr., Flagstaff, AZ 86001

E. M. Shoemaker, U.S. Geological Survey, 2255 N. Gemini Dr., Flagstaff, AZ 86001

R. B. Singer, Lunar and Planetary Laboratory, University of Arizona, Tucson, AZ 85721

C. P. Sonett, Lunar and Planetary Laboratory, University of Arizona, Tucson, AZ 85721

D. Spaute, Planetary Science Institute, 2030 E. Speedway Blvd., Suite 201, Tucson, AZ 85719

J. R. Spencer, Institute for Astronomy, University of Hawaii, 2680 Woodlawn Dr., Honolulu, HI 96822

N. Sperling, 5248 Lawton Ave., Oakland, CA 94618

J. Stam, 534 Lake Rd., London, KY 40741

E. M. Standish, MS 301-150, Jet Propulsion Laboratory, 4800 Oak Grove Dr., Pasadena, CA 91109

J. Stansbury, Lunar and Planetary Laboratory, University of Arizona, Tucson, AZ 85721

A. Stern, LASP/Campus Box 392, University of Colorado, Boulder, CO 80309

R. Strom, Lunar and Planetary Laboratory, University of Arizona, Tucson, AZ 85721

J. Surdej, Institut d'Astrophysique, Université de Liège, 5, ave. de Cointe, B-4200 Cointe-Ougrée, Belgium

T. D. Swindle, Lunar and Planetary Laboratory, University of Arizona, Tucson, AZ 85721

M. V. Sykes, Steward Observatory, University of Arizona, Tucson, AZ 85721

Y. Takagi, Nagoya University, Chikusa, Nagoya, Japan

H. Takeda, Mineralogical Institute, Faculty of Science, University of Tokyo, Hongo, Tokyo 113, Japan

G. J. Taylor, Dept. of Geology, Institute of Meteoritics, University of New Mexico, Albuquerque, NM 87131

R. C. Taylor, Lunar and Planetary Laboratory, University of Arizona, Tucson, AZ 85721

S. R. Taylor, Research School of Earth Science, Australian National University, Canberra Act, Australia 2601

E. F. Tedesco, Earth and Planetary Science, MS 100-22, Jet Propulsion Laboratory, 4800 Oak Grove Dr., Pasadena, CA 91109

D. J. Tholen, Institute for Astronomy, 2680 Woodlawn Drive, Honolulu, HI 96822

S. Uras, GNA-CNR, Stazione Astronomica, via Ospedale 72, 09100 Cagliari, Italy

R. Vaidyanath, Lunar and Planetary Laboratory, University of Arizona, Tucson, AZ 85721

G. B. Valsecchi, Istituto di Astrofisica Spaziale, Reparto di Planetolgia, viale dell' Università 11, 00185 Rome, Italy

C. J. van Houten, Sterrewacht, Leiden, The Netherlands

V. Vanzani, Dipartimento di Fisica, Università di Padova, via Marzolo, 8, 35131 Padova, Italy

G. J. Veeder, Jr., Earth and Planetary Science, MS 183-501, Jet Propulsion Laboratory, 4800 Oak Grove Dr., Pasadena, CA 91109

J. Veverka, Space Science Bldg., Cornell University, Ithaca, NY 14853

F. Vilas, SN3, NASA Johnson Space Center, Houston, TX 77058

S. C. Wang, Institute of Geophysics and Planetary Physics, University of California at Los Angeles, Los Angeles, CA 90024

L. Wasserman, Lowell Observatory, 1400 W. Mars Hill Rd., Flagstaff, AZ 86001

J. T. Wasson, Institute of Geophysics and Planetary Physics, University of California, Los Angeles, CA 90024

W. J. Webster, Jr., Goddard Space Flight Center, Code 622, Greenbelt, MD 20771

S. J. Weidenschilling, Planetary Science Institute, 2030 E. Speedway Blvd., Suite 201, Tucson, AZ 85719

P. R. Weissman, MS 183-301, Jet Propulsion Laboratory, 4800 Oak Grove Dr., Pasadena, CA 91109

W. Welker, Rt. 1, Box 237A, Solon, IA 52333

E. N. Wells, Computer Sciences Corp., Space Telescope Science Institute, 3700 San Martin Dr., Homewood Campus, Baltimore, MD 21218

R. Werner, Rt. 1, Box 237A, Solon, IA 52333

G. W. Wetherill, Dept. of Terrestrial Magnetism, Carnegie Institute of Washington, 5241 Broad Branch Rd. NW, Washington, DC 20015

A. Whipple, Nautical Almanac Office, U.S. Naval Observatory, Washington, DC 20392

L. L. Wilkening, 301 Administration Bldg., AH-20, University of Washington, Seattle, WA 98195

A. Williams, Dept. of Geology and Planetary Science, University of Pittsburgh, Pittsburgh, PA 15260

J. G. Williams, MS 238-332, Jet Propulsion Laboratory, 4800 Oak Grove Dr., Pasadena, CA 91109

J. Wisdom, Dept. of Planetary Science, Massachusetts Institute of Technology, Mail Code 54-414, Cambridge, MA 02178

W. Wisniewski, Lunar and Planetary Laboratory, University of Arizona, Tucson, AZ 85721

R. F. Wolfe, U.S. Geological Survey, 2255 N. Gemini Dr., Flagstaff, AZ 86001

M. Wolff, 1600 Nelson, Manhattan Beach, CA 90266

J. A. Wood, Center for Astrophysics, 60 Garden St., Cambridge, MA 02138

D. K. Yeomans, MS 301-150 G, Jet Propulsion Laboratory, 4800 Oak Grove Dr., Pasadena, CA 91109

M. Yoshikawa, MS 238-332, Jet Propulsion Laboratory, California Institute of Technology, Pasadena, CA 91109

V. Zappalà, Osservatorio Astronomico di Torino, I-10025 Pino Torinese, Italy

K. W. Zeigler, Gila Astronomical Research Institute, P.O. Box 362, Claypool, AZ 85532

B. Zellner, Computer Sciences Corp., Space Telescope Science Institute, 3700 San Martin Dr., Homewood Campus, Baltimore, MD 21218

M. Zolensky, NASA Johnson Space Center, Code SN2, Houston, TX 77058

Index

INDEX